Mathematical Problems in Engineering

Robust Control with Engineering Applications

Guest Editors: Tao Li, Baoyong Zhang, Zhiguang Feng, and Bochao Zheng

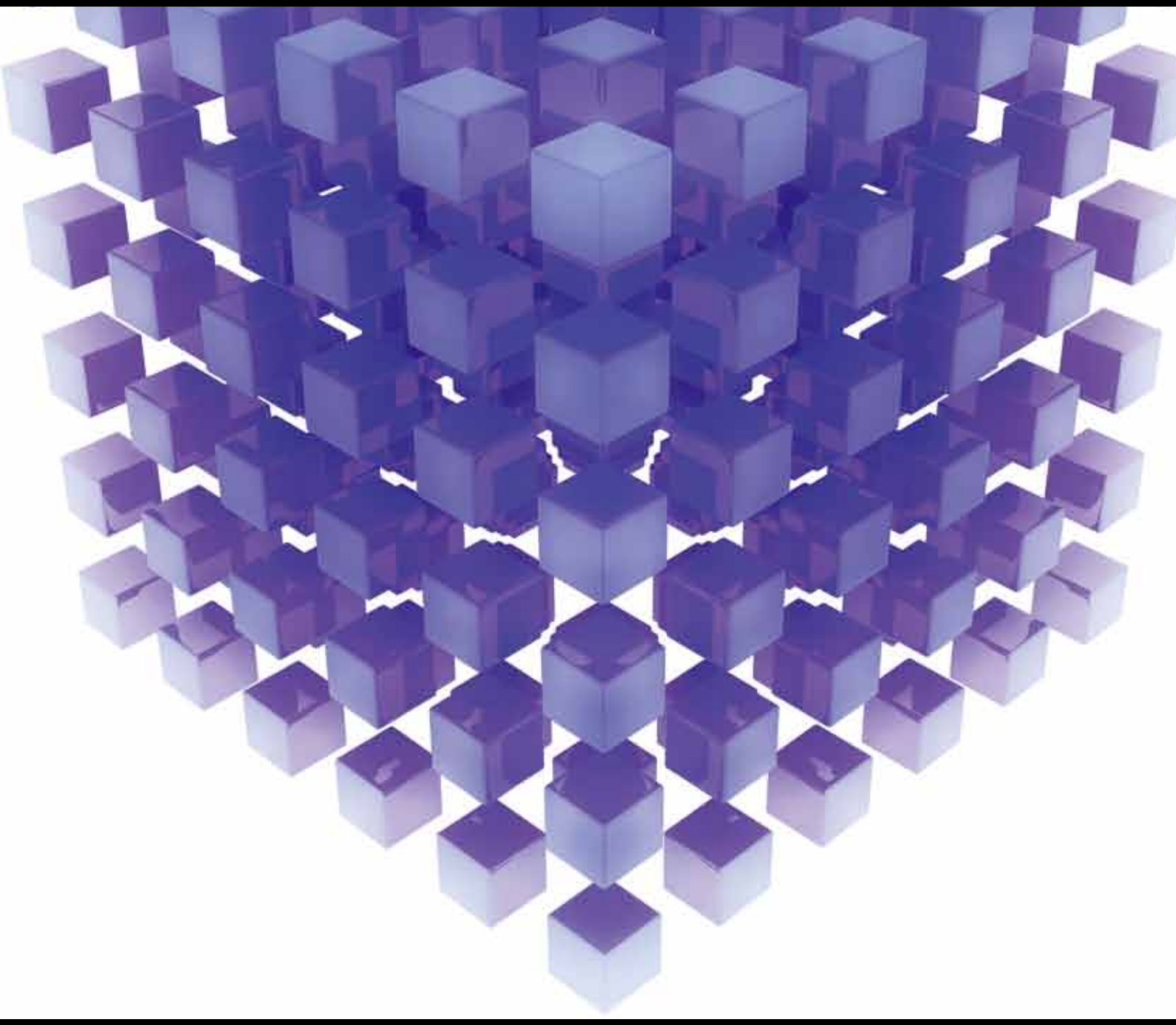

Robust Control with Engineering Applications

Mathematical Problems in Engineering

Robust Control with Engineering Applications

Guest Editors: Tao Li, Baoyong Zhang, Zhiguang Feng, and Bochao Zheng

Editorial Board

Contents

Hindawi Publishing Corporation
Mathematical Problems in Engineering
Volume 2014, Article ID 567672, 2 pages
http://dx.doi.org/10.1155/2014/567672

Editorial
Robust Control with Engineering Applications

Tao Li,[1] Baoyong Zhang,[2] Zhiguang Feng,[3] and Bochao Zheng[1]

[1] *School of Information and Control, Nanjing University of Information Science & Technology, Nanjing 210044, China*
[2] *School of Automation, Nanjing University of Science and Technology, Nanjing 210094, China*
[3] *Department of Mechanical Engineering, The University of Hong Kong, Hong Kong*

Correspondence should be addressed to Tao Li; litaojia@nuist.edu.cn

Received 12 January 2014; Accepted 12 January 2014; Published 14 April 2014

Robust control is an important branch of control theory that explicitly deals with uncertainty in its approach to controller design. Over the past several decades, there has been an increasing interest in robust control. On one hand, uncertain parameters or disturbances exist inherently in the aeronautics and astronautics, advanced manufacturing, and other complex engineering systems. On the other hand, uncertain parameters or disturbances seriously affect the stability, accuracy, and reliability of underlying control systems. Therefore, robust control has become a challenging problem in international control filed, for example, H_∞ control, H_2 control, guaranteed cost control (GCC), adaptive control (AC), variable structure control (VSC), antidisturbance control (ADC), fault-tolerant control (FTC), and so forth.

This special issue contain sixty-seven papers, which covers currently hot topics on robust control from theoretical methods to practical applications. Figure 1 shows their distribution about the topics. Moreover, we will summarize the typical papers about every topic.

H_∞ Control. "*H_∞ control theory using in the air pollution control systems*" by T. Yang et al. shows H_∞ control theory for the air pollution control systems. "*H_∞ filter design for large-scale systems with missing measurements*" by Y. Zhou et al. deals with the H_∞ filter design problem for large-scale systems with missing measurements, where the occurrence of missing measurements is assumed to be a Bernoulli distributed sequence with known probability. "*Delay-probability-distribution-dependent H_∞ FIR filtering design with envelope constraints*" by C. Peng et al. employs the information of the delay size and delay probability distribution and gives a novel delay-probability-distribution-dependent filter design method.

H_2 Control. "*H_2 control for continuous-time Markovian jump linear uncertain systems with partly known transition rates and quantization*" by X.-G. Zhao et al. proposes sufficient conditions in terms of linear matrix inequalities for H_2 control of Markov jump linear uncertain systems. "*A novel approach to l_2-l_∞ filtering design for T-S fuzzy systems with multiple time-varying delays*" by X. Zhang et al. proposes the full-order and reduced-order filter design schemes for T-S fuzzy systems with multiple time-varying delays by using the free-weighting matrices method.

Guaranteed Cost Control. "*Switching fuzzy guaranteed cost control for nonlinear networked control systems*" by L. Cai et al. introduces a switching mechanism to handle the uncertainties of networked control systems and presents guaranteed cost controller design method. "*Convergence guaranteed nonlinear constraint model predictive control via I/O linearization*" by X. Kong et al. presents iterative quadratic program routine on the continuous-time system to guarantee its convergence.

Adaptive Control. "*Characteristic modeling and control of servo systems with backlash and friction*" by Y. Wu et al. investigates an approach for modeling and adaptive control of servo systems with backlash and friction based on the characteristic model. "*Robust adaptive PID control of robot manipulator with bounded disturbances*" by J. Xu and L. Qiao gives two novel robust adaptive PID control schemes for

robot manipulator with bounded disturbances and larger external disturbances can be tolerated by comparing with the existing adaptive PD control. "*Global harmonic current rejection of nonlinear backstepping control with multivariable adaptive internal model principle for grid-connected inverter under distorted grid voltage*" by Y. Yu et al. investigates the global harmonic current rejection problem of grid-connected inverter under distorted grid voltage and a multivariable adaptive state feedback control method is designed to guarantee the global stability of the closed-loop system.

Variable Structure Control. "*Sliding sector-based variable structure control of continuous-time Markov jump linear systems subject to unknown transition rates*" by Y.-M. Xue et al. presents a sufficient condition for variable structure control design based on sliding sector technique for a class of Markov jump systems with unknown transition rates.

Anti-Disturbance Control. "*Active disturbance rejection with sliding mode control based course and path following for underactuated ships*" by R. Li at el. investigates the path following problem of underactuated surface ship with uncertainties and external disturbances and active-disturbance-rejection control with sliding mode is provided to improve the performance of the closed-loop system. "*Robust coordinated control algorithm for multiple marine vessels with external disturbances*" by W. X. Liu et al. considers the coordinated control problem for multiple marine vessels with external disturbances and a robust coordinated control algorithm is given based on dynamic surface control method.

Fault-Tolerant Control. "*Fault-tolerant control for civil structures based on LMI approach*" by C. Qu et al. designs a filter to perform the fault detection and isolation and then forms a control strategy to achieve the fault-tolerant control. "*Robust adaptive switching fault-tolerant control of a class of uncertain systems against actuator faults*" by X.-Z. Jin deals with the fault-tolerant control problem for a class of linear time-invariant systems with time-varying actuator faults and uncertainties. "*Fault-tolerant control in redundant inertial navigation system*" by X. Dai studies the robust fault-tolerant control problem for the redundant inertial navigation system and an improved control algorithm which considers the unknown noise characteristics, model inaccuracies, and the drift factor to improve the control performance.

This special issue also includes riches of collections of engineering applications related to robust control theory, such as spacecraft and flight control, robots, power systems, networked systems, servo systems, autonomous underwater vehicles, and energy systems.

Of course, the selected topics and papers are not a comprehensive representation of the area of this special issue. Nonetheless, they represent the rich and much faceted knowledge that we have the pleasure of sharing with the readers.

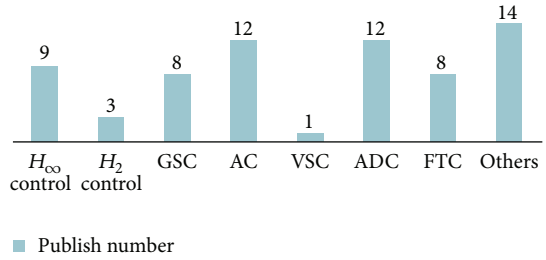

Figure 1

Acknowledgments

We would like to express appreciation to the authors for their excellent contributions and patience in assisting us. Finally, the fundamental work of all reviewers on these papers is also very greatly acknowledged.

Tao Li
Baoyong Zhang
Zhiguang Feng
Bochao Zheng

Hindawi Publishing Corporation
Mathematical Problems in Engineering
Volume 2014, Article ID 589381, 16 pages
http://dx.doi.org/10.1155/2014/589381

Research Article

Robust Control for Autonomous Spacecraft Evacuation with Model Uncertainty and Upper Bound of Performance with Constraints

Dian Sheng,[1] Xuebo Yang,[2] and Hamid Reza Karimi[3]

[1] *Space Control and Inertial Technology Research Center, Harbin Institute of Technology, Harbin 150001, China*
[2] *Bohai University, Jinzhou 121013, China*
[3] *Department of Engineering, Faculty of Engineering and Science, University of Agder, 4898 Grimstad, Norway*

Correspondence should be addressed to Xuebo Yang; yangxuebo@gmail.com

Received 4 September 2013; Accepted 30 October 2013; Published 8 April 2014

Academic Editor: Zhiguang Feng

This paper studies the problem of guaranteed cost control for spacecraft evacuation. The relative dynamic model is established based on Clohessy-Wiltshire (C-W) equations. The paper has taken parameter uncertainty, output tracking, disturbance attenuation, and fuel cost into consideration. The paper introduces a new Lyapunov approach, so the controller design problem can be transferred into a convex optimization problem subject to linear matrix inequality (LMI) constraints. By using the controller, the spacecraft evacuation can be completed in a safe extent. Meanwhile, the fuel cost also has an upper bound. Then the paper analyzes the approach of evacuation and discusses possible initial states of the spacecraft for the controller design. An illustrative example is applied to show the effectiveness of the proposed control design method, and different performances caused by different initial states of spacecraft (-V-bar, -R-bar, and +H-bar) are simulated.

1. Introduction

With the development of aerospace science, the research of space exploration is deepening gradually. Among them, manned space technology has been in the limelight of the aerospace around the world. In addition, most tracking spacecrafts need to be evacuated safely after completing autonomous spacecrafts rendezvouz. Furthermore, evacuation segment can be divided into three stages: unlocking, separation, and orbital transformation. In the study of evacuation, Fehse has introduced the process and the bounds of the evacuation [1]. Besides, he has also compared the evacuation from V-bar and R-bar and has discussed the security of the two means. Yin et al. also review most popular data-driven PM-FD methods with recent developments [2, 3]. Hablani et al. has studied the target spacecraft by using a kind of multiplepulse linear guidance control method applicable to arbitrary direction approach and evacuation [4]. Bergez et al. has reached the conclusion which is based on an assumption, where the safe evacuation theory is happening in the failure of capture lock while the ATV is docking with the Russian Mir space station [5]. However, some correlative issues have not yet been fully explained because of their complexity and uncertainty, and many existing studies have left considerable room for improvement. This leads us to look for a new method to control the evacuation phase of spacecraft.

Moreover, spacecraft relative motion problems are often took over based on Clohssey and Wiltshire (C-W) equations in 1960 [6, 7]. Generally speaking, the equations are transformed into a state function based on $\dot{\mathbf{x}}(t) = A\mathbf{x}(t) + B\mathbf{u}(t)$, where $\mathbf{x}(t)$ is the relative position and velocity states vector and $\mathbf{u}(t)$ is the control input vector. This description has been used widely to study the spacecraft rendezvous problems [8–11]. But due to many uncertain factors, the state matrix A and the control input matrix B are not easy to be determined accurately. Besides, the elements of matrix A are related to the angle velocity of the target spacecraft which is susceptible to many inevitable factors such as errors of detection. Besides, the conceivable mass variation of fuel causes the input of thrusters inaccuracy, which can be

regarded as the uncertainty of the input matrix B [12]. These uncertainties may lessen stability of spacecraft evacuation phase. In the past decades, many researches about uncertain system papers [13–18]. Petersen presents an algorithm for the stabilization of a class of uncertain linear systems. The uncertain systems under consideration are described by state equations which depend on time-varying unknown-but-bounded uncertain parameters [19]. Singla et al. has developed an output feedback structured model reference adaptive control law for spacecraft rendezvous and docking problems [20]. However, the parameter uncertainties have not attracted enough attention to the research of spacecraft evacuation phase control problems. This leads to our desire to think over uncertainties and find a proper method to handle them.

The evacuation phase and short-range phase all belong to the relative navigation phase, both of them based on the relative phase. Evacuation phase is an opposite movement process to short-range phase with the final approach phase. Spacecraft rendezvous and docking are unusual complex fields of aerospace work, which must be measured accurately to the relative position and relative attitude of the two spacecrafts. Rendezvous and docking phases ask for a very high requirement of accuracy, reliability, and control system robustness of the independent measurement system. The slightest mistake could result in docking failure. However, the researches of the spacecraft evacuation seem too few compared with the researches of spacecraft rendezvous and docking. That is because spacecraft evacuation needs less automaticity than rendezvous, which is primarily based on orbit control to ensure the security of the process. In that case, the chaser will not collide with the target spacecraft even when the thrust equipment is out of control. So the study of spacecraft rendezvous and docking has a significant reference for the control of evacuation phase.

Besides, rendezvous and docking not only need the orbital maneuvering control, but also are based on the advanced attitude control. Nevertheless, the evacuation phase is mainly based on the orbital maneuvering control. To sum up, research of orbital maneuvering control for the rendezvous has a very important significance of the evacuation phase. In recent 50 years, related researchers have done in-depth research for spacecraft rendezvous and docking and made a lot of research achievements in the orbital maneuvering control problem. In addition, spacecraft autonomous rendezvous (RVD) has been recognized as a crucial issue for many progressive astronautic missions. Besides, spacecraft autonomous rendezvous is also very important in the field of the manned space flight project. Manned space flight project generally requires the technique of spacecraft autonomous rendezvous, such as the spacecraft orbit service, space rescue, repair, and the space station supplies. Nowadays, United States, Russia, Europe, Japan, and other countries are involving to the area of spacecraft autonomous rendezvous and have experiment successfully for hundreds of times. As manned space technology develops, the theory of spacecraft autonomous rendezvous will be more mature than the past [8–11, 20, 21].

The paper provides a systematic research of the control problem aiming at the orbit of the spacecraft autonomous evacuation and gives a new method to control the evacuation phase of spacecraft. Based on the two-body problem, the paper has constructed the relative motion equation for the process of evacuation, which is the C-W equation, and makes a brief introduction about the bound that the spacecraft has to comply with. Then it gives the new controller calculated by the bound of guaranteed cost output [22–27]. Firstly, the paper analyzes the characteristic of the holding point. Then it uses the state error variables to replace the state vector. Transform the tracking problem of constant reference signal into the problem of asymptotically stability under the feedback control [28]. However, the spacecraft has to receive many disturbances during the flight, such as solar radiation pressure perturbation and electromagnetic radiation. Thus the paper takes the uncertainty into consideration when it designs the controller. Besides, the paper considers the limited constraint condition and the quadratic performance index, transforms the problem into convex optimization of the LMI by the method of Lyapunov, and then receives the guaranteed cost output with the minimal upper bound. Verify the solution by simulation with MATLAB. In the end of the paper, we compare the fuel consumers under the different levels of the disturbance and simulate the output tracking of the chaser spacecraft by three cases (-V-bar, -R-bar, and +H-bar). The result proves that the model has good dynamic response, reliability, and self-adaptability. Therefore, the model can be applied to control system of spacecraft.

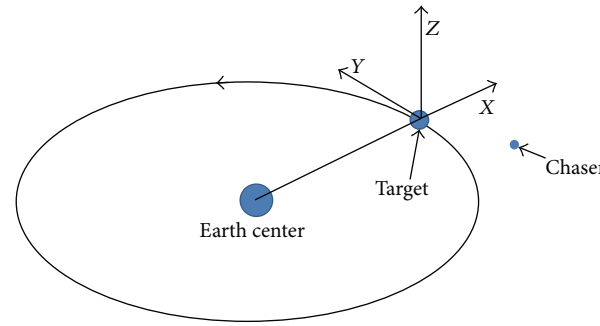

Figure 1: Spacecraft rendezvous and the utilized coordinate.

2. Problem Formulation

A right-handed Cartesian coordinate can be established based on the structure of the target. As shown in Figure 1, the origin attaches to the mass center of the target, the x-axis is along the vector from earth center to the origin, the y-axis is along the target orbit circumference, and the z-axis sets up the right-handed frame [29].

In this coordinate system, the evacuation phase described in this paper can be depicted in Figure 2.

Define R_0 as the radius of the target circular orbit and n as the angular velocity of the target equals $(\mu_e/R_0^3)^{1/2}$, where μ_e is the gravitational parameter of the earth. Considering the C-W equations and proposing the mathematical description

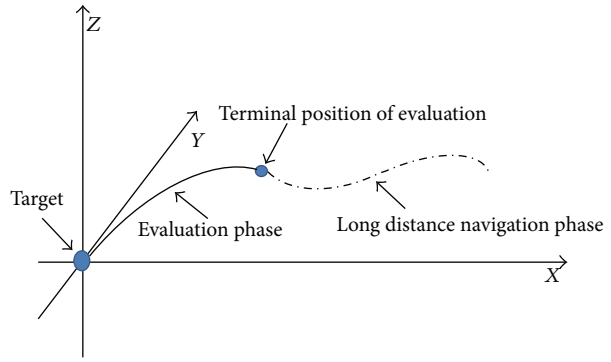

Figure 2: Evacuation phases of rendezvous in the target frame coordinate.

of the relative motion for two adjacent spacecrafts, the relative dynamic model can be described by C-W's equations as

$$\begin{aligned} \ddot{x} - 2n\dot{y} - 3n^2 x &= \frac{1}{m}T_x, \\ \ddot{y} + 2n\dot{x} &= \frac{1}{m}T_y, \\ \ddot{z} + n^2 z &= \frac{1}{m}T_z, \end{aligned} \tag{1}$$

where x, y, and z are the components of the relative position in corresponding axes, m is the mass of the chaser, and T_i ($i = x, y, z$) is the ith component of the control thrust applied on the spacecraft [30].

2.1. Transfer of Evacuation Phase. By defining the state vector $x(t) = [x, y, z, \dot{x}, \dot{y}, \dot{z}]^T$, control input vector $u(t) = [T_x, T_y, T_z]^T$, and output vector $y(t) = [x, y, z]^T$, we have

$$\begin{aligned} \dot{x}(t) &= Ax(t) + Bu(t), \\ y(t) &= Cx(t), \end{aligned} \tag{2}$$

where

$$A = \begin{bmatrix} 0 & 0 & 0 & 1 & 0 & 0 \\ 0 & 0 & 0 & 0 & 1 & 0 \\ 0 & 0 & 0 & 0 & 0 & 1 \\ 3n^2 & 0 & 0 & 0 & 2n & 0 \\ 0 & 0 & 0 & -2n & 0 & 0 \\ 0 & 0 & -n^2 & 0 & 0 & 0 \end{bmatrix},$$

$$B = \begin{bmatrix} 0 & 0 & 0 \\ 0 & 0 & 0 \\ 0 & 0 & 0 \\ \frac{1}{m} & 0 & 0 \\ 0 & \frac{1}{m} & 0 \\ 0 & 0 & \frac{1}{m} \end{bmatrix}, \tag{3}$$

$$C = \begin{bmatrix} 1 & 0 & 0 \\ 0 & 1 & 0 \\ 0 & 0 & 1 \\ 0 & 0 & 0 \\ 0 & 0 & 0 \\ 0 & 0 & 0 \end{bmatrix}^T.$$

Thus, the specific relative motion of chaser and target can be realized by designing proper control input thrust $u(t)$.

2.2. Uncertainty. Due to the measure the complex external perturbations among the objects in space, the target angle velocity n can be described accurately. Besides, inevitable input uncertainties still exist because of the error of the thrust and fuel. Having taken these modeling uncertainties into consideration, the system functions can be expressed as follows:

$$\begin{aligned} \dot{x}(t) &= (A + \Delta A)x(t) + (B + \Delta B)u(t), \\ y(t) &= Cx(t). \end{aligned} \tag{4}$$

The two norm-bounded uncertain matrices ΔA and ΔB have proper dimensions and are in the form of $[\Delta A \ \ \Delta B] = \lambda\varphi(t)[\sigma_1 \ \ \sigma_2]$, where λ, σ_1, and σ_2 are the constant matrices with proper dimensions, which can reflect the uncertainty structure; $\varphi(t)$ is an unknown real-time varying matrix with Lebesgue measurable elements bounded by $\varphi^T(t)\varphi(t) \le I$. The introduced matrices can be regarded as the following patterns because of the structures of A and B:

$$\begin{aligned} \lambda &= \Upsilon \times \begin{bmatrix} 0 & 0 & 0 & 1 & 0 & 0 \\ 0 & 0 & 0 & 0 & 1 & 0 \\ 0 & 0 & 0 & 0 & 0 & 1 \end{bmatrix}, \\ \sigma_1 &= \Xi \times \begin{bmatrix} 0 & 0 & 0 & 1 & 1 & 0 \\ 1 & 0 & 0 & 1 & 0 & 0 \\ 0 & 0 & 0 & 0 & 0 & 0 \end{bmatrix}, \\ \sigma_2 &= \Omega \times \begin{bmatrix} 0 & 0 & 0 \\ 0 & 0 & 0 \\ 1 & 1 & 1 \end{bmatrix}. \end{aligned} \tag{5}$$

Define $\varphi(t) = \mathrm{diag}[\varphi_1(t), \varphi_2(t), \varphi_3(t)]$, where $\varphi_1(t)$, $\varphi_2(t)$, and $\varphi_3(t)$ are three varying scalars within the boundary of $[0, 1]$. And Υ, Ξ, and Ω signify magnitudes of the uncertainties.

Then, the system state functions with modeling uncertainty can be rewritten as

$$\begin{aligned} \dot{x}(t) &= \widetilde{A}x(t) + \widetilde{B}u(t), \\ y(t) &= Cx(t), \end{aligned} \tag{6}$$

where $\widetilde{A} = A + \lambda\varphi(t)\sigma_1$ and $\widetilde{B} = B + \lambda\varphi(t)\sigma_2$. It can be seen that matrices λ, σ_1, and σ_2 reflect the structural information of uncertainties.

2.3. Output Tracking. Considering the evacuation phase of spacecraft rendezvous, the terminal position of the chaser is a certain point that can be defined as a fixed reference output signal $x_r = (x_r, y_r, z_r, 0, 0, 0)^T$. Therefore, the evacuation phase orbital control problem can be solved by designing an output tracking controller. The output $x(t)$ of the closed-loop system tracks the reference signal x_r, which means that

$$\lim_{t \to \infty} [x(t) - x_r] = 0. \tag{7}$$

We introduce the error integral action in the controller for eliminating the steady-state tracking error. Then we define

$$e(t) = \int_0^t \left[x(\tau) - x_r\right] d\tau \tag{8}$$

and then we have $\dot{e}(t) = x(t) - x_r$.

Therefore, we obtain the augmented system

$$\begin{aligned} \dot{\xi}(t) &= \widetilde{\Lambda}\xi(t) + \widetilde{\Gamma}u(t) + \widetilde{\Psi}\xi_r, \\ f(t) &= \widetilde{\Phi}\xi(t) + \widetilde{\Phi}\xi_r, \end{aligned} \tag{9}$$

where

$$\begin{aligned} \widetilde{\Lambda} &= \begin{bmatrix} \widetilde{A} & 0 \\ C & 0 \end{bmatrix}, \qquad \widetilde{\Gamma} = \begin{bmatrix} \widetilde{B} \\ 0 \end{bmatrix}, \qquad \widetilde{\Psi} = \begin{bmatrix} 0 \\ -I \end{bmatrix}, \\ \widetilde{\Phi} &= \begin{bmatrix} C & 0 \end{bmatrix}, \qquad \xi(t) = \begin{bmatrix} q(t) \\ e(t) \end{bmatrix}. \end{aligned} \tag{10}$$

Considering the uncertainties described in (4), the augmented matrices $\widetilde{\Lambda}$ and $\widetilde{\Gamma}$ can be further transformed into $\widetilde{\Lambda} = \Lambda + \Delta\Lambda$, $\widetilde{\Gamma} = \Gamma + \Delta\Gamma$, where

$$\begin{aligned} \Lambda &= \begin{bmatrix} A & 0 \\ C & 0 \end{bmatrix}, \qquad \Gamma = \begin{bmatrix} B \\ 0 \end{bmatrix}, \qquad \Delta\Lambda = \Pi\varphi(t)\sigma_{1A}, \\ \Delta\Gamma &= \Pi\varphi(t)\sigma_2, \quad \Pi = \begin{bmatrix} D \\ 0 \end{bmatrix}, \quad \sigma_{1A} = \begin{bmatrix} E_1 & 0 \end{bmatrix}. \end{aligned} \tag{11}$$

Use the state feedback control law, and define $K = [K_q \ K_d]$, then we obtain $u(t) = K\xi(t) = K_q q(t) + K_d d(t)$.

Then the augmented closed-loop system can be described as

$$\dot{\xi}(t) = \left[\widetilde{\Lambda} + \widetilde{\Gamma}K\right]\xi(t) + \widetilde{\Psi}f_r. \tag{12}$$

The output tracking requirement in (7) can be satisfied if the closed-loop system in (12) is stable. Thus, the output tracking control problem studied in this paper can be transformed into the stabilization problem of the system in (9). If there has a controller K guarantee the system stable in (9), then the output $\varphi(t)$ of (6) can track the reference signal f_r.

2.4. Control Performance. Primarily, we take the rendezvous control performances into consideration. Because of the weight boundary of spacecraft, the minimal fuel cost has to be chosen as one control performance index for evacuation. Then, by defining a control weighting matrix $R_{3\times3}$, the fuel cost performance index can be expressed as $J_1 = \int_0^\infty u^T(t)Ru(t)dt$.

Secondly, there should not be violent shake during the orbital transfer for the security. Define a control weighting matrix Q, and then the smooth transfer trajectory control performance index can be written as $J_2 = \int_0^\infty \xi^T(t)Q\xi(t)dt$.

Then, consider the two performance indexes together. The comprehensive control performance cost can be described as

$$J = J_1 + J_2 = \int_0^\infty \left[u^T(t)Ru(t) + \xi^T(t)Q\xi(t)\right] dt. \tag{13}$$

For $u(t) = K\zeta(t)$, the equality (13) can be redescribed as

$$J = \int_0^\infty \left[\zeta^T(t)K^TRK\zeta(t) + \zeta^T(t)Q\zeta(t)\right] dt. \tag{14}$$

Then, the guaranteed cost control design problem can be depicted as follows: to find an admissible controller K, which makes the system performance cost J meets a minimal upper bound μ.

Besides, the dynamic performance of a system is correlated to the location of its poles, and the satisfactory transient responses can be ensured by constraining the poles to position in a prescribed region. In this paper, we consider the disk regional poles constraint, which has been proved efficient in both theory and practice. Consider the uncertain rendezvous dynamic model (9); design a guaranteed cost output tracking controller K, such that the closed-loop system in (12) is asymptotically stable (meaning that the output tracking requirement in (7) is satisfied); meanwhile, the performance cost in (14) is below a prescribed upper bound for all admissible uncertainties.

2.5. Description of the Control Law

Lemma 1. *To the given symmetric matrix* $A = \left[\begin{smallmatrix} A_{11} & A_{12} \\ A_{21} & A_{22} \end{smallmatrix}\right]$, *the following conditions are equivalent:*

(i) $A < 0$;

(ii) $A_{11} < 0$, $A_{22} - A_{12}^T A_{11}^{-1} A_{12} < 0$;

(iii) $A_{22} < 0$, $A_{11} - A_{12}A_{11}^{-1}A_{12}^T < 0$.

Lemma 2. *$u(t) = Kx(t)$ is a guaranteed cost controller if there exist symmetric positive-definite matrices P, $S \in R^{3\times3}$ such that for all uncertain matrices φ satisfying $\varphi^T(t)\varphi(t) \leqslant I$,*

$$\begin{bmatrix} \Sigma & P\left[\widetilde{A} + \lambda\varphi\left(\sigma_1 + \sigma_2\right)\right] \\ \left[\widetilde{A} + \lambda\varphi\left(\sigma_1 + \sigma_2\right)\right]^T P & -S \end{bmatrix} < 0, \tag{15}$$

where $\Sigma = Q + K^TRK + S + \mathrm{sym}\{\mathrm{P}[\mathbf{A} + \mathbf{B}\mathrm{K} + \lambda\varphi(\sigma_1 + \sigma_2)]\}$ [31].

Based on Lyapunov stable theory, the controller design requirements such as input constraint and the guaranteed cost are formulated as some LMI conditions, and the controller design problem is cast into a convex optimization problem subject to the LMI constraints.

Presume $x_r = 0$. Define the Lyapunov function $V(\xi(t)) = \xi(t)^T P\xi(t)$, where P is a positive symmetry matrix. Then,

$$\dot{V}(\xi(t)) = \xi(t)^T \mathrm{sym}\left\{P\left(\widetilde{\Lambda} + \widetilde{\Gamma}K\right)\right\}\xi(t). \tag{16}$$

If a controller K can satisfy the following equation,

$$\mathrm{sym}\left\{P\left(\widetilde{\Lambda} + \widetilde{\Gamma}K\right)\right\} < 0, \tag{17}$$

then the system begins to stabilize.

Besides, the target function should satisfy some constraints like Lemma 2 as follows:

$$\dot{V}(\xi(t)) < -\xi^T(t)\left(Q + K^TRK\right)\xi(t) < 0. \tag{18}$$

Then the system not only begins to stabilize, but also has a certain upper constraint.

Consider the following:

$$J = \int_0^\infty \left[\xi^T(t) Q\xi(t) + u^T(t) Ru(t)\right] dt < v(\xi(0)) = \xi^T(0) P\xi(0), \tag{19}$$

where $\xi(0)$ means the error in the system.

The quadratic performance index is restrained by $V(\xi(e)) = \xi(t)^T P\xi(t)$. This upper bound form of the performance index can qualitatively describe the consumption of fuel and concussion of trace.

The function can be transferred as based on Lemma 2.

Consider the following:

$$\text{sym}\left\{P\left(\widetilde{\Lambda} + \widetilde{\Gamma}K\right)\right\} + Q + K^T RK < 0. \tag{20}$$

However P and K are not independent. Therefore the function above is not a LMI. But based on Lemma 1 and define $\chi = \text{sym}\{P(\widetilde{\Lambda} + \widetilde{\Gamma}K)\}$, $\varrho = \text{diag}(R^{-1}, Q^{-1})$, and $\varpi = [K^T, I]$, it equals

$$\begin{bmatrix} \chi & \varpi \\ * & \varrho \end{bmatrix} < 0. \tag{21}$$

Define $X = P^{-1}$, $Y = KP^{-1}$, $\eth = \text{sym}\{\widetilde{\Lambda}X + \widetilde{\Gamma}Y\}$, and $\widehat{H} = [Y^T, I]$. We obtain the function

$$\begin{bmatrix} \eth & \widehat{H} \\ * & \varrho \end{bmatrix} < 0. \tag{22}$$

The function is a LMI about X and Y to the certain system matrix $\widetilde{\Lambda}$ and the input matrix $\widetilde{\Gamma}$. Using the LMI box in the Matlab can readily solve the function.

First, introduce the matrix $U_x = [1,0,0]^T[1,0,0]$; $U_y = [0,1,0]^T[0,1,0]$; $U_z = [0,0,1]^T[0,0,1]$.

Then, we obtain

$$\begin{aligned} u_x^2(t) &= \left[U_x u(t)\right]^T \left[U_x u(t)\right] \leqslant u_{x,\max}^2, \\ u_y^2(t) &= \left[U_y u(t)\right]^T \left[U_y u(t)\right] \leqslant u_{y,\max}^2, \\ u_z^2(t) &= \left[U_z u(t)\right]^T \left[U_z u(t)\right] \leqslant u_{z,\max}^2, \end{aligned} \tag{23}$$

where $u_{x,\max}$, $u_{y,\max}$, and $u_{z,\max}$ are the maximum inputs of the system.

According to $u(t) = K\xi(t)$, we have the constraint of the system

$$\begin{aligned} u_i^2(t) &= \left[U_i K\xi(t)\right]^T \left[U_i K\xi(t)\right] \\ &= \xi^T(t) K^T U_i^T U_i K\xi(t) \leqslant u_{i,\max}^2, \end{aligned} \tag{24}$$

where $i = x, y, z$.

Because the LMI has already guaranteed that the closed system has the upper bound, then

$$V(\xi(t)) = \xi(t)^T P\xi(t) < V(\xi(0)). \tag{25}$$

Thus, when the x_r has been given, the function $V(\xi(0)) = \xi(0)^T P\xi(0)$ has the constraint $V(\xi(0)) < \mu$.

Then, we have

$$u_{i,\max}^{-2} \xi^T(t) K^T U_i^T U_i K\xi(t) < \mu^{-1} \xi^T(t) P\xi(t). \tag{26}$$

Because we know if the target constraint is less than the Lyapunov function, the controller can satisfy the requirement. Then, we obtain

$$u_{i,\max}^{-2} K^T U_i^T U_i K < \mu^{-1} P. \tag{27}$$

However, the function above is not the LMI. According to Lemma 1, we have

$$\begin{bmatrix} -\mu^{-1}P & (U_i K)^T \\ * & -u_{i,\max}^2 \end{bmatrix} < 0. \tag{28}$$

Take the left and right by matrix $\text{diag}\{P^{-1}, I\}$, then the LMI can be described as follows:

$$\begin{bmatrix} -\mu^{-1}X & (U_i Y)^T \\ * & -u_{i,\max}^2 \end{bmatrix} < 0. \tag{29}$$

Besides, we can alter the function above:

$$\begin{bmatrix} -\mu & \xi(0)^T \\ * & -X \end{bmatrix} < 0. \tag{30}$$

By solving the LMI above and using the (X, Y), we can obtain the matrix K, then we can design the controller $u(t)$, in which $K = YX^{-1}$.

Meanwhile, we can also obtain the upper bound of the system

$$J_{\max} = \xi(0) X^{-1} \xi(0). \tag{31}$$

Next, we consider the obtained performance cost upper bound. Apart from the obtainable upper bounds of the performance consumers, it is also hopeful to make the bounds as low as possible to the practical engineering. We introduce another matrix Θ satisfying

$$\begin{bmatrix} -\Theta & I \\ * & -X \end{bmatrix} < 0 \tag{32}$$

which means $\Theta > X^{-1} > 0$. Then, the lower performance cost bound can be obtained by solving the following optimization problem:

$$\begin{aligned} &\min \quad \xi(0)^T \Theta \xi(0) \\ &\text{s.t.} \quad \text{LMIs } (22), (29), (30) \text{ and } (32). \end{aligned} \tag{33}$$

According to the results shown above, we can find that the solution of the optimization problem does not totally depend on the exact value of the uncertain matrix $\varphi(t)$, and the magnitudes of the uncertainties can be adjusted by changing the values of Υ, Ξ, and Ω. Thus, the effects of the parameter errors can be analyzed according to these three parameters. Particularly, when we assume $\Upsilon = \Xi = \Omega = 0$, which means that there is no parameter error in the model, the uncertain matrices λ, σ_1, and σ_2 will be transformed into zero matrices. At the same time, the system takes exactly the form of the nominal system of no uncertainty. Correspondingly, the LMI constraints will alter, and the relative optimization problem can also be solved readily. The conditions are all formulated in the form of linear matrix inequalities, and the controller design is transformed into a convex optimization problem subject to LMI constraints that can be solved by Matlab. However, the conditions we obtained here are sufficient conditions for the existence of a proper controller. Thus, even if there is no parameter error, the result is not the unique solution of the controller design problem. This is because the guaranteed cost and the poles constraint of the closed-loop system are considered simultaneously. It is still hard to solve this kind of multiobjective optimization problem, and finding a necessary and sufficient condition for the existence of the proper controller is difficult. However, the correlative problems are significant and worth investigating in our further studies. For the orbital control system, there are many other performances that can be adopted for the controller design. The orbital controller design problems with these kinds of performance measures for spacecraft rendezvous are worth studying in the future.

3. Illustrative Example

Because the target spacecraft has 3 methods to evacuation (-V-bar, -R-bar, and +H-bar), this chapter discussed and simulated the guaranteed cost control low based on these methods separately. In this section, we provide an example to illustrate the usefulness and advantage of the controller design method proposed in the above sections. We consider a couple of adjacent spacecrafts, where the chaser is being transferred towards the target along the homing phase orbit. Assume the mass of the chaser is 600 kg, and the target is moving in a geosynchronous orbit of radius $r = 42241$ km with an orbital period of 24 hours. Thus, we have the angle velocity $n = 1.117 \times 10^{-3}$ rad/s. Assume that the maximum input control force is 130 N.

3.1. -V-bar. According to the coordinate based on target frame, we presume that the chaser transfers to position $(135, 0, 0)$. Therefore, the initial error state can be expressed as $(-135, 0, 0, 0, 0, 0, 0, 0, 0)^T$.

For simplicity, we presume the thrust can vary continuously. First, we analyze the situation with $\Upsilon = \Xi = \Omega = 0.03$. In the coordinate based on target frame, assume the initial state of homing phase is $[0, 0, 0, 0, 0, 0, 0, 0, 0]$. And by considering the construction of uncertainties in the form of (9), we make the following assumptions:

$$X = \begin{bmatrix} 0.0001 & 0.0000 & 0.0000 & -0.0000 & -0.0000 & -0.0000 & -0.0020 & -0.0001 & -0.0001 \\ 0.0000 & 0.0001 & 0.0000 & -0.0000 & -0.0000 & -0.0000 & -0.0003 & -0.0020 & -0.0005 \\ 0.0000 & 0.0000 & 0.0001 & -0.0000 & -0.0000 & -0.0000 & -0.0002 & -0.0005 & -0.0021 \\ -0.0000 & -0.0000 & -0.0000 & 0.0000 & 0.0000 & 0.0000 & 0.0000 & 0.0000 & 0.0000 \\ -0.0000 & -0.0000 & -0.0000 & 0.0000 & 0.0000 & 0.0000 & 0.0000 & 0.0000 & 0.0000 \\ -0.0000 & -0.0000 & -0.0000 & 0.0000 & 0.0000 & 0.0000 & 0.0000 & 0.0000 & 0.0000 \\ -0.0020 & -0.0003 & -0.0002 & 0.0000 & 0.0000 & 0.0000 & 0.0626 & 0.0029 & 0.0015 \\ -0.0001 & -0.0020 & -0.0005 & 0.0000 & 0.0000 & 0.0000 & 0.0029 & 0.0604 & 0.0076 \\ -0.0001 & -0.0005 & -0.0021 & 0.0000 & 0.0000 & 0.0000 & 0.0015 & 0.0076 & 0.0621 \end{bmatrix}, \tag{34}$$

$$Y = 10^{-3} \times \begin{bmatrix} -0.0198 & -0.0002 & -0.0001 & -0.0002 & 0.0000 & 0.0000 & 0.3065 & -0.0200 & -0.0097 \\ 0.0053 & -0.0063 & -0.0058 & -0.0002 & -0.0005 & -0.0003 & -0.1446 & 0.0986 & 0.0035 \\ 0.0075 & -0.0050 & -0.0061 & -0.0002 & -0.0003 & -0.0006 & -0.1492 & -0.0014 & 0.0904 \end{bmatrix}.$$

Therefore, the gain matrix for the augmented feedback controller is given by

$$K = Y \times X^{-1} = \begin{bmatrix} -0.8725 & 0.0156 & -0.0023 & -19.6879 & -0.0475 & -0.0355 & -0.0156 & -0.0000 & -0.0002 \\ -0.1172 & -0.7895 & -0.2242 & -1.8656 & -21.4237 & -1.1423 & -0.0032 & -0.0140 & -0.0073 \\ 0.0174 & -0.1945 & -0.7776 & -0.5884 & -0.2998 & -20.7360 & -0.0010 & -0.0066 & -0.0142 \end{bmatrix}. \tag{35}$$

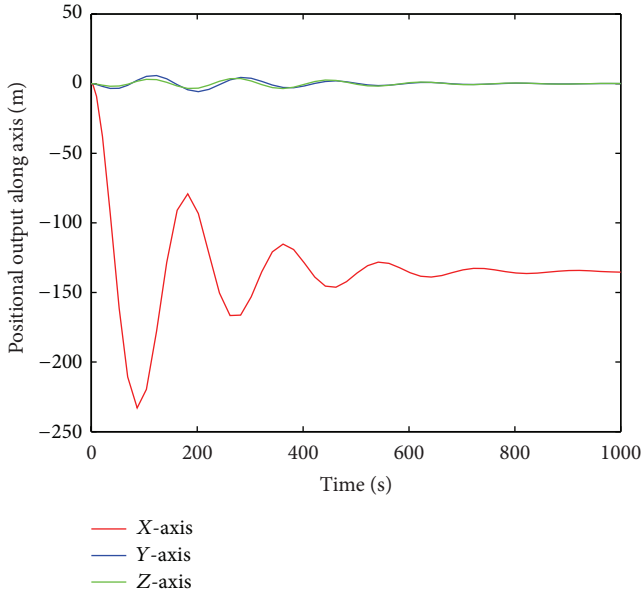

Figure 3: Chaser's positional output of closed-loop control.

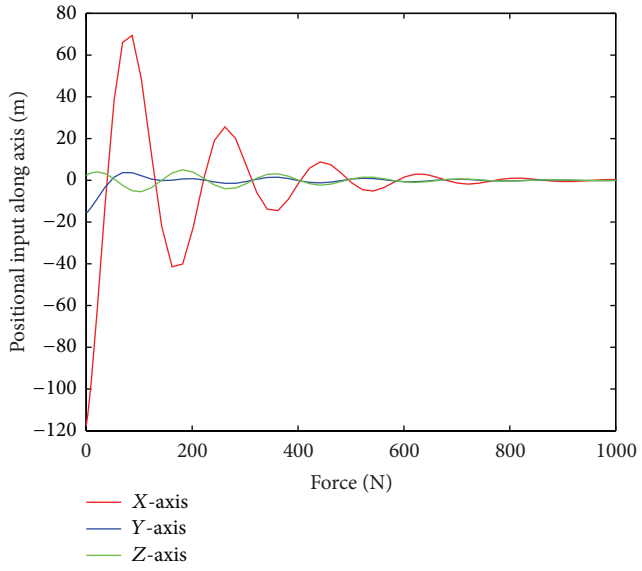

Figure 4: Chaser's input thrust of closed-loop control.

The output of the system which means the relative position of the two spacecrafts is depicted in Figure 3.

It can be seen that the output of the system is asymptotically convergent to the reference signal, which means that the chaser keeps at the terminal point. We can also obtain the relevant control thrusts needed for these methods in Figure 4.

Besides the nonzero initial velocity, the coupling action brought by parameter uncertainties is another source for the fluctuation in z-axis. It can be seen that the fluctuation finally restrained and the positional output in z-axis asymptotically converged to the reference signal. We can see that the controller can effectively stabilize the system in spite of the existence of parameter uncertainties.

Next, we change the magnitudes of uncertainties by considering the following four conditions:

$$\begin{aligned} &\text{Case A: } \Upsilon = \Xi = \Omega = 0; \\ &\text{Case B: } \Upsilon = 0.03, \quad \Xi = \Omega = 0.015; \\ &\text{Case C: } \Upsilon = 0.06, \quad \Xi = \Omega = 0.03; \\ &\text{Case D: } \Upsilon = \Xi = \Omega = 0.0652. \end{aligned} \tag{36}$$

The proper controllers for these conditions can be obtained by solving the convex optimization problems as follows:

$$\begin{aligned} K_{\text{Case A}} &= \begin{bmatrix} -0.8726 & 0.0168 & -0.0012 & -19.6631 & -0.0165 & -0.0238 & -0.0156 & 0.0001 & -0.0001 \\ -0.0510 & -0.8183 & -0.1570 & -0.7472 & -22.4896 & -0.5307 & -0.0021 & -0.0140 & -0.0052 \\ -0.0232 & -0.1522 & -0.8247 & -1.0570 & -0.5274 & -22.3842 & -0.0012 & -0.0052 & -0.0144 \end{bmatrix}, \\ K_{\text{Case B}} &= \begin{bmatrix} -0.8728 & 0.0137 & -0.0035 & -19.6836 & -0.0418 & -0.0430 & -0.0157 & -0.0001 & -0.0003 \\ -0.0886 & -0.7852 & -0.2359 & -1.5512 & -21.3489 & -1.2784 & -0.0029 & -0.0140 & -0.0074 \\ -0.0103 & -0.2165 & -0.7832 & -1.1239 & -0.8532 & -20.8999 & -0.0015 & -0.0071 & -0.0143 \end{bmatrix}, \\ K_{\text{Case C}} &= \begin{bmatrix} -0.8723 & 0.0153 & -0.0014 & -19.7047 & -0.0793 & -0.0305 & -0.0156 & -0.0001 & -0.0002 \\ -0.1809 & -0.7652 & -0.2506 & -2.9144 & -20.5827 & -1.3472 & -0.0042 & -0.0138 & -0.0083 \\ 0.0635 & -0.2401 & -0.7132 & -0.0714 & -0.5607 & -19.1985 & -0.0007 & -0.0075 & -0.0132 \end{bmatrix}, \\ K_{\text{Case D}} &= \begin{bmatrix} -0.8702 & 0.0296 & 0.0013 & -19.6788 & -0.0089 & 0.0016 & -0.0154 & 0.0004 & 0.0000 \\ -0.3263 & -0.7475 & -0.1084 & -2.9313 & -22.6185 & -0.2819 & -0.0036 & -0.0106 & -0.0041 \\ 0.2335 & 0.0512 & -0.7417 & 3.9454 & 4.0154 & -19.6471 & 0.0032 & -0.0009 & -0.0129 \end{bmatrix}, \end{aligned} \tag{37}$$

and the positional outputs of the closed-loop systems with these controllers in three axes are depicted in Figures 5, 7, and 9 separately. We can also obtain the four relevant control thrusts needed for these two methods in

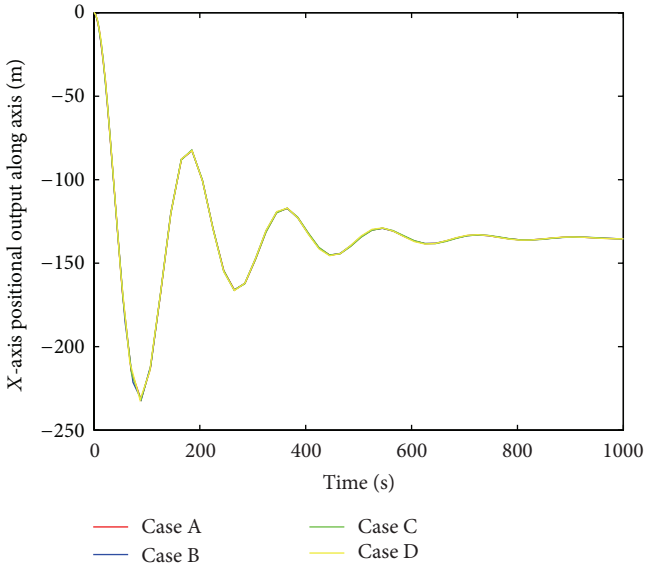

Figure 5: X-axis positional output of closed-loop system for the four different uncertainty cases.

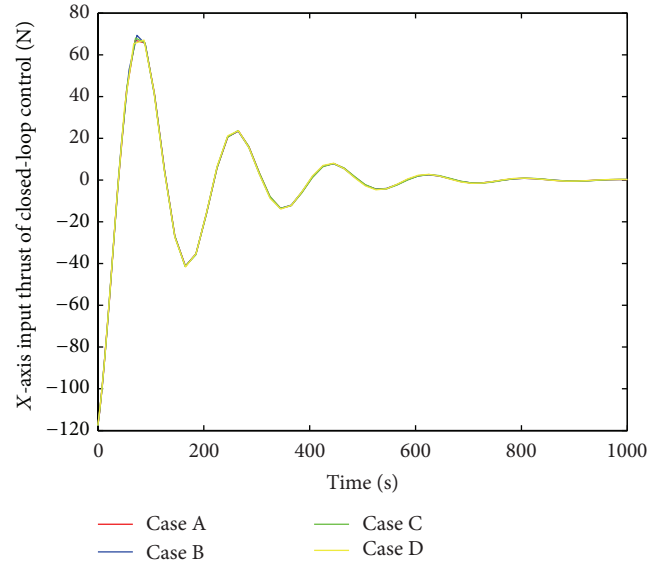

Figure 6: X-axis input of closed-loop system for the four different uncertainty cases.

Figures 6, 8, and 10 separately. We can see that the closed-loop systems with the controllers K are all stable and the output tracking requirement can be guaranteed. From these figures and the data, we can also find that the larger uncertainties will extend the stabilizing time and bring larger fluctuations in z-axis input thrust, and the performance cost bound will also be elevated by larger uncertainties.

Finally, the terminal segment close to the target is depicted clearly in Figure 11. It can be seen that the chaser will asymptotically move to the evacuation point eventually, which means that the output tracking requirements can be satisfied by the designed controller K.

3.2. -R-bar. According to the coordinate based on target frame, we presume that the chaser transfers to position $(0, -135, 0)$. Therefore, the initial error state can be expressed as $(0, 135, 0, 0, 0, 0, 0, 0, 0)^T$.

For simplicity, we presume the thrust can vary continuously. First, we analyze the situation with $\Upsilon = \Xi = \Omega = 0.03$. In the coordinate based on target frame, assume the initial state of homing phase is $[0, 0, 0, 0, 0, 0, 0, 0, 0]$. And by considering the construction of uncertainties in the form of (9), we make the following assumptions:

$$X = \begin{bmatrix} 0.0001 & 0.0000 & 0.0000 & -0.0000 & -0.0000 & -0.0000 & -0.0019 & -0.0002 & -0.0005 \\ 0.0000 & 0.0001 & 0.0000 & -0.0000 & -0.0000 & -0.0000 & -0.0003 & -0.0020 & -0.0002 \\ 0.0000 & 0.0000 & 0.0001 & -0.0000 & -0.0000 & -0.0000 & -0.0005 & -0.0002 & -0.0021 \\ -0.0000 & -0.0000 & -0.0000 & 0.0000 & 0.0000 & 0.0000 & 0.0000 & 0.0000 & 0.0000 \\ -0.0000 & -0.0000 & -0.0000 & 0.0000 & 0.0000 & 0.0000 & 0.0000 & 0.0000 & 0.0000 \\ -0.0000 & -0.0000 & -0.0000 & 0.0000 & 0.0000 & 0.0000 & 0.0000 & 0.0000 & 0.0000 \\ -0.0019 & -0.0003 & -0.0005 & 0.0000 & 0.0000 & 0.0000 & 0.0590 & 0.0035 & 0.0086 \\ -0.0002 & -0.0020 & -0.0002 & 0.0000 & 0.0000 & 0.0000 & 0.0035 & 0.0630 & 0.0028 \\ -0.0005 & -0.0002 & -0.0021 & 0.0000 & 0.0000 & 0.0000 & 0.0086 & 0.0028 & 0.0618 \end{bmatrix}, \quad (38)$$

$$Y = 10^{-3} \times \begin{bmatrix} -0.0068 & 0.0065 & -0.0062 & -0.0005 & -0.0002 & -0.0003 & 0.0595 & -0.1188 & -0.0113 \\ -0.0004 & -0.0194 & -0.0005 & -0.0000 & -0.0002 & -0.0000 & -0.0014 & 0.2965 & -0.0121 \\ -0.0051 & 0.0077 & -0.0059 & -0.0003 & -0.0002 & -0.0006 & 0.0089 & -0.1633 & 0.1018 \end{bmatrix}.$$

Therefore, the gain matrix for the augmented feedback controller is given by

$$K = Y \times X^{-1} = \begin{bmatrix} -0.8013 & -0.0073 & -0.2275 & -20.7499 & -2.1876 & -1.2217 & -0.0148 & -0.0009 & -0.0077 \\ -0.0521 & -0.8723 & -0.0134 & -0.1245 & -19.6957 & -0.0528 & -0.0009 & -0.0157 & -0.0007 \\ -0.2448 & 0.0160 & -0.7531 & -0.8687 & -0.3932 & -20.6737 & -0.0075 & -0.0008 & -0.0134 \end{bmatrix}. \quad (39)$$

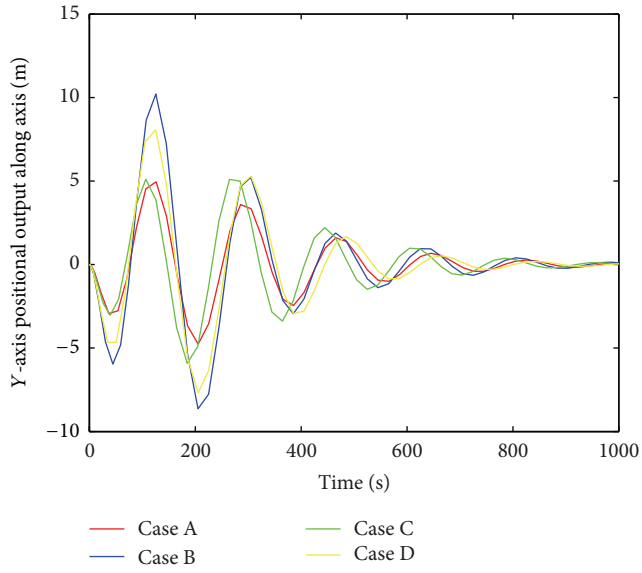

Figure 7: Y-axis positional output of closed-loop system for the four different uncertainty cases.

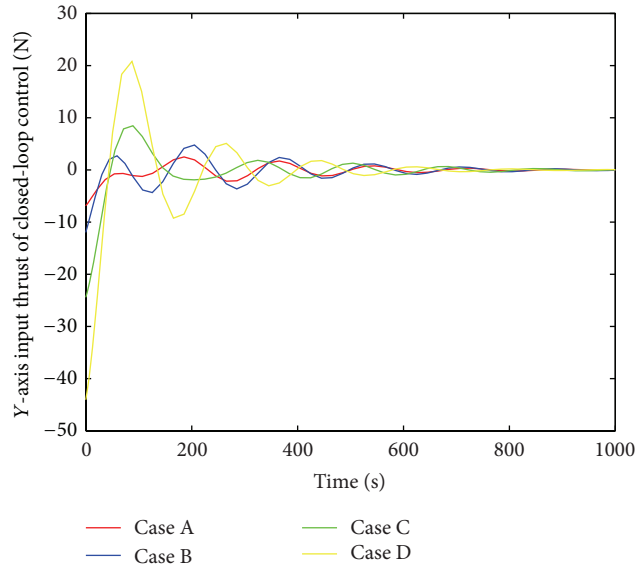

Figure 8: Y-axis input of closed-loop system for the four different uncertainty cases.

The output of the system which means the relative position of the two spacecraft is depicted in Figure 12.

It can be seen that the output of the system is asymptotically convergent to the reference signal, which means that the chaser keeps at the terminal point. We can also obtain the relevant control thrusts needed for these methods in Figure 13.

Besides the nonzero initial velocity, the coupling action brought by parameter uncertainties is another source for the fluctuation in z-axis. It can be seen that the fluctuation is finally restrained and the positional output in z-axis asymptotically converged to the reference signal. We can see that the controller can effectively stabilize the system in spite of the existence of parameter uncertainties.

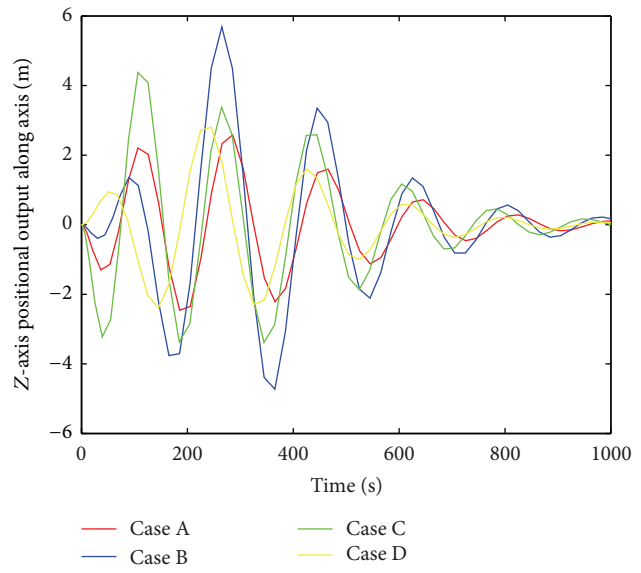

Figure 9: Z-axis positional output of closed-loop system for the four different uncertainty cases.

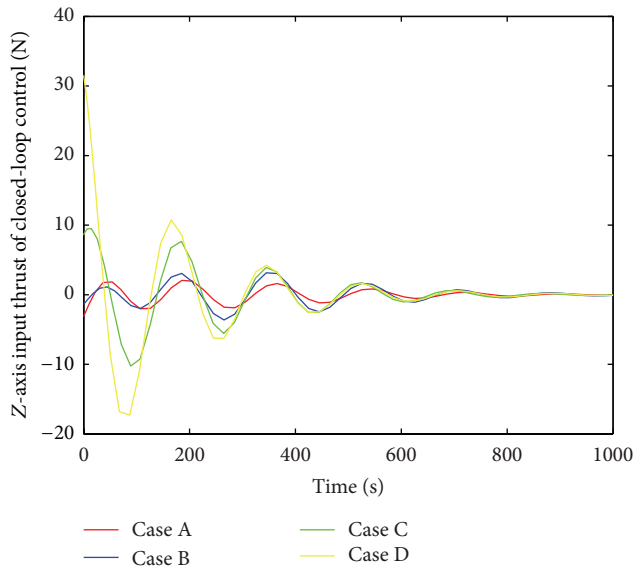

Figure 10: Z-axis input of closed-loop system for the four different uncertainty cases.

Next, we change the magnitudes of uncertainties by considering the following four conditions:

$$\begin{aligned} &\text{Case A: } \Upsilon = \Xi = \Omega = 0; \\ &\text{Case B: } \Upsilon = 0.03, \quad \Xi = \Omega = 0.015; \\ &\text{Case C: } \Upsilon = 0.06, \quad \Xi = \Omega = 0.03; \\ &\text{Case D: } \Upsilon = \Xi = \Omega = 0.0652. \end{aligned} \tag{40}$$

The proper controllers for these conditions can be obtained by solving the convex optimization problems as follows:

$$K_{\text{Case A}} = \begin{bmatrix} -0.8255 & 0.0128 & -0.1707 & -22.1674 & -1.1565 & -0.6244 & -0.0146 & -0.0002 & -0.0058 \\ -0.0275 & -0.8714 & -0.0092 & -0.0469 & -19.6785 & -0.0279 & -0.0007 & -0.0156 & -0.0005 \\ -0.1763 & -0.0132 & -0.8192 & -0.6430 & -0.7610 & -22.3625 & -0.0058 & -0.0010 & -0.0143 \end{bmatrix},$$

$$K_{\text{Case B}} = \begin{bmatrix} -0.7953 & -0.0035 & -0.2394 & -20.8135 & -1.9250 & -1.3488 & -0.0147 & -0.0009 & -0.0078 \\ -0.0425 & -0.8720 & -0.0144 & -0.1018 & -19.6821 & -0.0528 & -0.0010 & -0.0157 & -0.0007 \\ -0.2562 & -0.0016 & -0.7652 & -1.2303 & -0.7713 & -20.9066 & -0.0078 & -0.0011 & -0.0137 \end{bmatrix},$$

$$K_{\text{Case C}} = \begin{bmatrix} -0.8103 & -0.0211 & -0.2089 & -20.2798 & -2.8811 & -1.0569 & -0.0151 & -0.0013 & -0.0076 \\ -0.0766 & -0.8730 & -0.0122 & -0.2170 & -19.7221 & -0.0484 & -0.0011 & -0.0158 & -0.0007 \\ -0.2670 & 0.0462 & -0.6986 & -1.1317 & 0.1392 & -19.6532 & -0.0075 & -0.0003 & -0.0122 \end{bmatrix},$$

$$K_{\text{Case D}} = \begin{bmatrix} -0.8509 & -0.0492 & -0.1465 & -20.3975 & -4.1579 & -0.5316 & -0.0154 & -0.0016 & -0.0062 \\ -0.1433 & -0.8744 & -0.0109 & -0.5140 & -19.7942 & -0.0420 & -0.0014 & -0.0159 & -0.0007 \\ -0.1512 & 0.1218 & -0.6620 & 0.6308 & 2.0097 & -18.6886 & -0.0048 & -0.0013 & -0.0108 \end{bmatrix}, \quad (41)$$

and the positional outputs of the closed-loop systems with these controllers in three axes are depicted in Figures 14, 16, and 18 separately. We can also obtain the four relevant control thrusts needed for these two methods in Figures 15, 17, and 19 separately. We can see that the closed-loop systems with the controllers K are all stable and the output tracking requirement can be guaranteed. From these figures and the table, we can also find that larger uncertainties will extend the stabilizing time and bring larger fluctuations in z-axis input thrust, and the performance cost bound will also be elevated by larger uncertainties.

Finally, the terminal segment close to the target is depicted clearly in Figure 20. It can be seen that the chaser will asymptotically move to the evacuation point eventually, which means that the output tracking requirements can be satisfied by the designed controller K.

3.3. +H-bar. Due to the poor security and the accident of collision, the application of the H-bar is less than those of the methods discussed above. However, H-bar evacuation is easy to accomplish because the z-axis is uncorrelated with x-axis and y-axis. Besides, H-bar evacuation consumers less fuel and can move along the H-bar automatically. So, we consider H-bar evacuation as a kind of illustrative example.

According to the coordinate based on target frame, we presume that the chaser transfers to position $(0, 0, 135)$. Therefore, the initial error state can be expressed as $(0, 0, -135, 0, 0, 0, 0, 0, 0)^T$.

For simplicity, we presume the thrust can vary continuously. First, we analyze the situation with $\Upsilon = \Xi = \Omega = 0.03$. In the coordinate based on target frame, assume the initial state of homing phase is $[0, 0, 0, 0, 0, 0, 0, 0, 0]$. And by considering the construction of uncertainties in the form of (9), we make the following assumptions:

$$X = \begin{bmatrix} 0.0001 & 0.0001 & 0.0000 & -0.0000 & -0.0000 & -0.0000 & -0.0017 & -0.0008 & -0.0004 \\ 0.0001 & 0.0001 & 0.0000 & -0.0000 & -0.0000 & -0.0000 & -0.0010 & -0.0018 & -0.0004 \\ 0.0000 & 0.0000 & 0.0001 & -0.0000 & -0.0000 & -0.0000 & -0.0003 & -0.0003 & -0.0021 \\ -0.0000 & -0.0000 & -0.0000 & 0.0000 & 0.0000 & 0.0000 & 0.0000 & 0.0000 & 0.0000 \\ -0.0000 & -0.0000 & -0.0000 & 0.0000 & 0.0000 & 0.0000 & 0.0000 & 0.0000 & 0.0000 \\ -0.0000 & -0.0000 & -0.0000 & 0.0000 & 0.0000 & 0.0000 & 0.0000 & 0.0000 & 0.0000 \\ -0.0017 & -0.0010 & -0.0003 & 0.0000 & 0.0000 & 0.0000 & 0.0541 & 0.0169 & 0.0056 \\ -0.0008 & -0.0018 & -0.0003 & 0.0000 & 0.0000 & 0.0000 & 0.0169 & 0.0559 & 0.0057 \\ -0.0004 & -0.0004 & -0.0021 & 0.0000 & 0.0000 & 0.0000 & 0.0056 & 0.0057 & 0.0638 \end{bmatrix}, \quad (42)$$

$$Y = 10^{-3} \times \begin{bmatrix} -0.0070 & -0.0068 & 0.0019 & -0.0005 & -0.0004 & -0.0004 & 0.0599 & 0.0242 & -0.0729 \\ -0.0070 & -0.0070 & 0.0017 & -0.0004 & -0.0004 & -0.0004 & 0.0306 & 0.0444 & -0.0716 \\ -0.0024 & -0.0023 & -0.0180 & -0.0001 & -0.0001 & -0.0003 & -0.0459 & -0.0436 & 0.2483 \end{bmatrix}.$$

Therefore, the gain matrix for the augmented feedback controller is given by

$$K = Y \times X^{-1} = \begin{bmatrix} -0.6798 & -0.3389 & -0.1329 & -18.4530 & -3.9755 & -2.1891 & -0.0130 & -0.0093 & -0.0044 \\ -0.4350 & -0.6511 & -0.1324 & -4.1696 & -18.1157 & -2.1782 & -0.0106 & -0.0123 & -0.0044 \\ -0.0448 & -0.0400 & -0.8411 & 0.3381 & 0.3693 & -18.7812 & -0.0029 & -0.0026 & -0.0158 \end{bmatrix}. \quad (43)$$

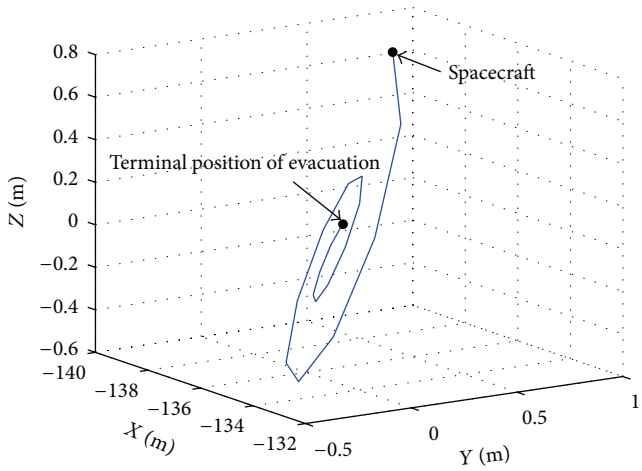

Figure 11: Terminal segment of the transfer orbit in rendezvous homing phase.

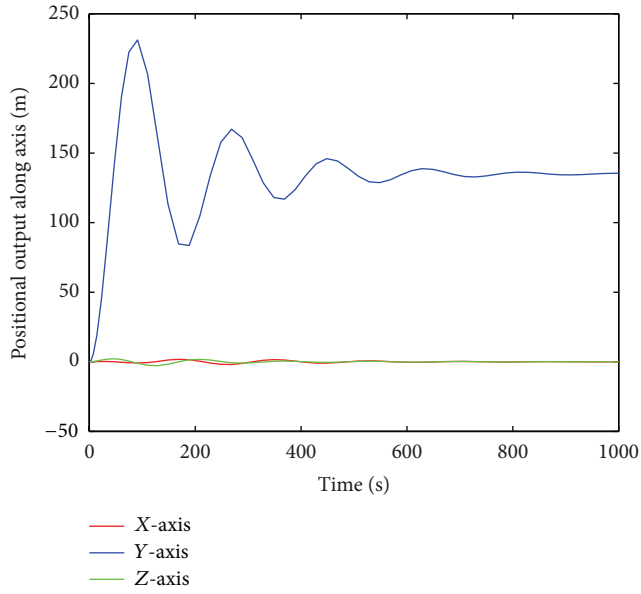

Figure 12: Chaser's positional output of closed-loop control.

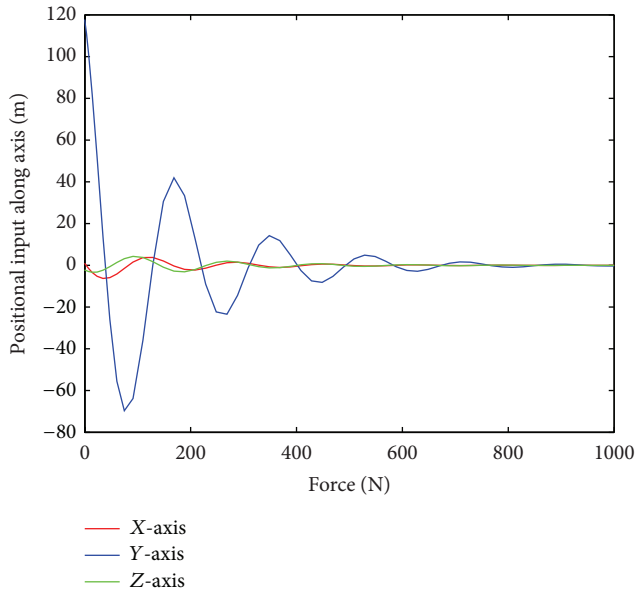

Figure 13: Chaser's input thrust of closed-loop control.

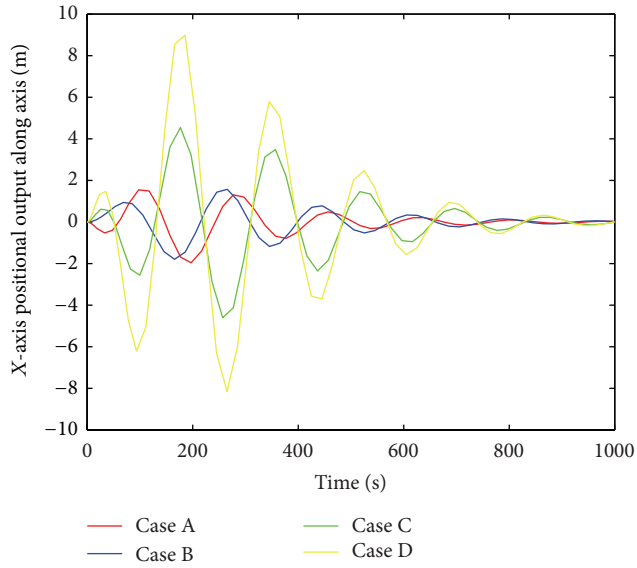

Figure 14: X-axis positional output of closed-loop system for the four different uncertainty cases.

The output of the system which means the relative position of the two spacecrafts is depicted in Figure 21.

It can be seen that the output of the system is asymptotically convergent to the reference signal, which means that the chaser keeps at the terminal point. We can also obtain the relevant control thrusts needed for these methods in Figure 22.

Besides the nonzero initial velocity, the coupling action brought by parameter uncertainties is another source for the fluctuation in z-axis. It can be seen that the fluctuation finally restrained and the positional output in z-axis asymptotically converged to the reference signal. We can see that the controller can effectively stabilize the system in spite of the existence of parameter uncertainties.

Next, we change the magnitudes of uncertainties by considering the following four conditions:

$$\begin{aligned} &\text{Case A: } \Upsilon = \Xi = \Omega = 0; \\ &\text{Case B: } \Upsilon = 0.03, \quad \Xi = \Omega = 0.015; \\ &\text{Case C: } \Upsilon = 0.06, \quad \Xi = \Omega = 0.03; \\ &\text{Case D: } \Upsilon = \Xi = \Omega = 0.0652. \end{aligned} \tag{44}$$

The proper controllers for these conditions can be obtained by solving the convex optimization problems as follows:

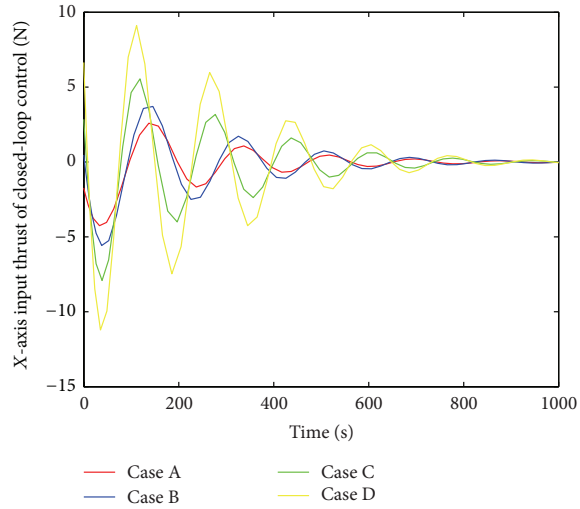

FIGURE 15: X-axis input of closed-loop system for the four different uncertainty cases.

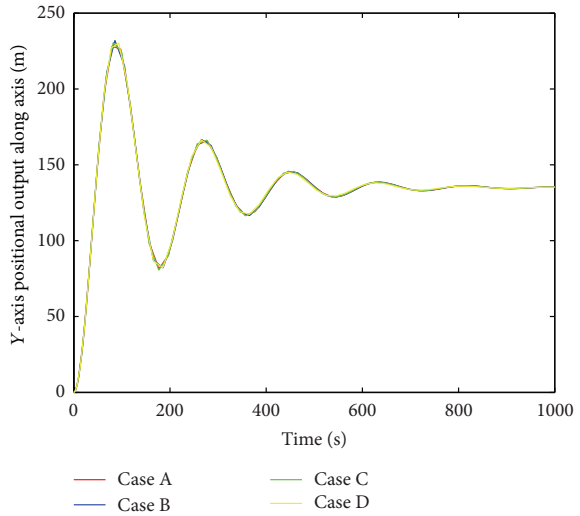

FIGURE 16: Y-axis positional output of closed-loop system for the four different uncertainty cases.

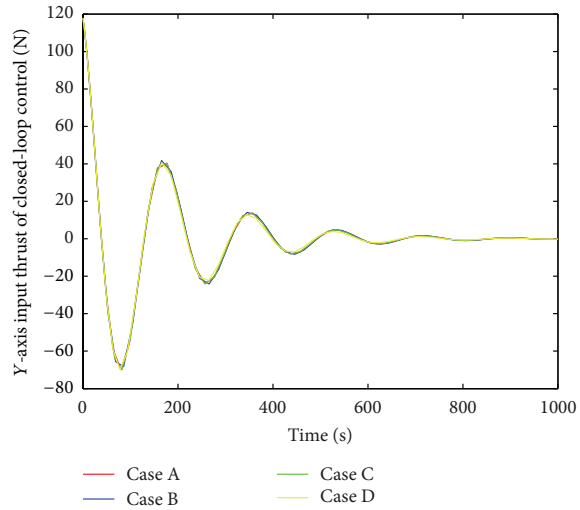

FIGURE 17: Y-axis input of closed-loop system for the four different uncertainty cases.

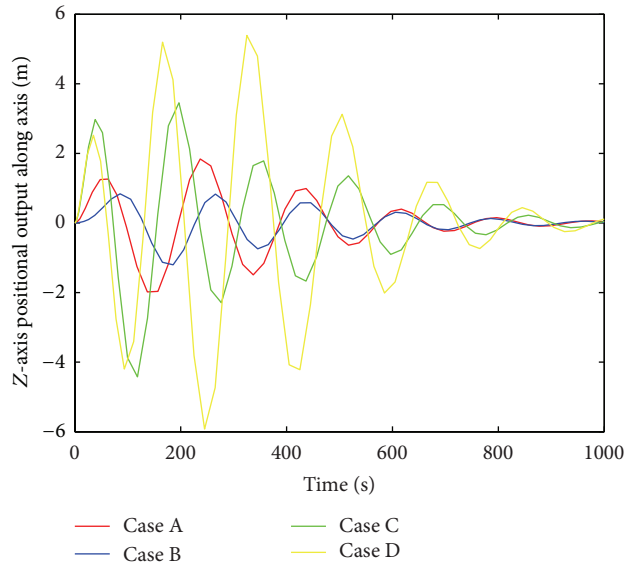

FIGURE 18: Z-axis positional output of closed-loop system for the four different uncertainty cases.

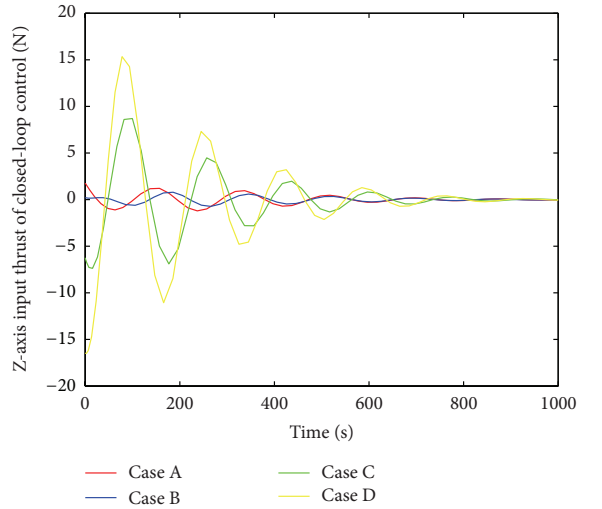

FIGURE 19: Z-axis input of closed-loop system for the four different uncertainty cases.

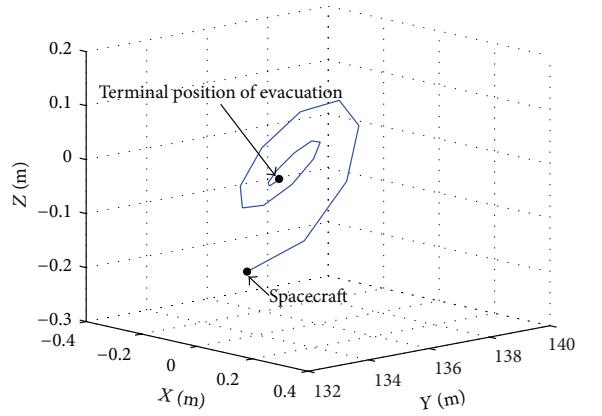

FIGURE 20: Terminal segment of the transfer orbit in rendezvous homing phase.

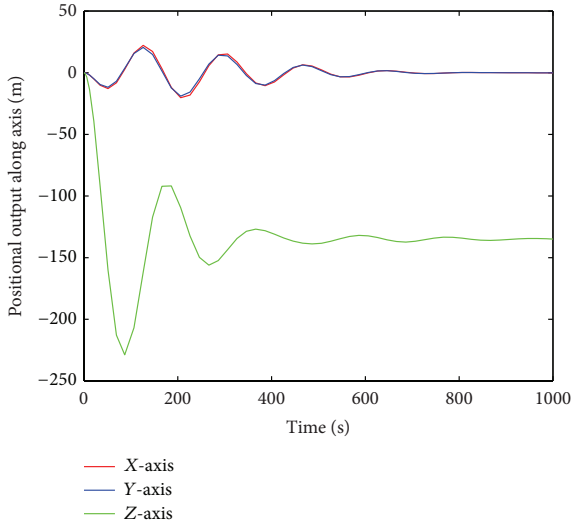

Figure 21: Chaser's positional output of closed-loop control.

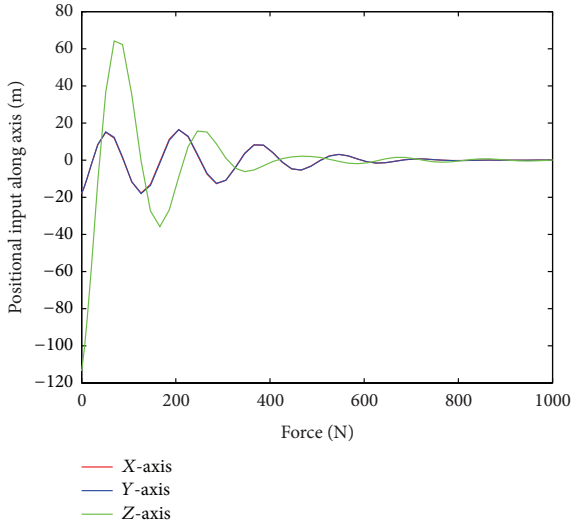

Figure 22: Chaser's input thrust of closed-loop control.

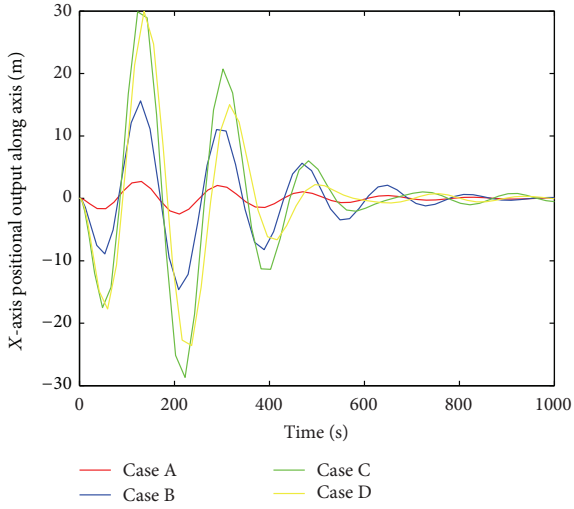

Figure 23: X-axis positional output of closed-loop system for the four different uncertainty cases.

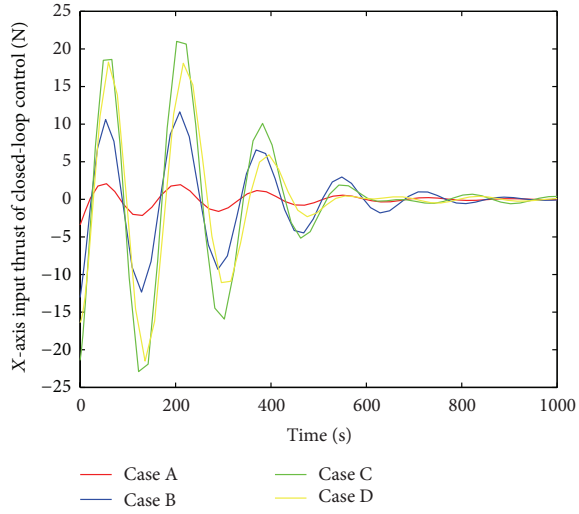

Figure 24: X-axis input of closed-loop system for the four different uncertainty cases.

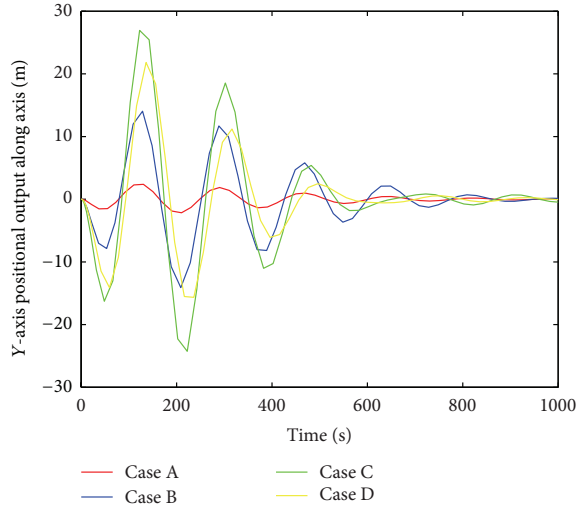

Figure 25: Y-axis positional output of closed-loop system for the four different uncertainty cases.

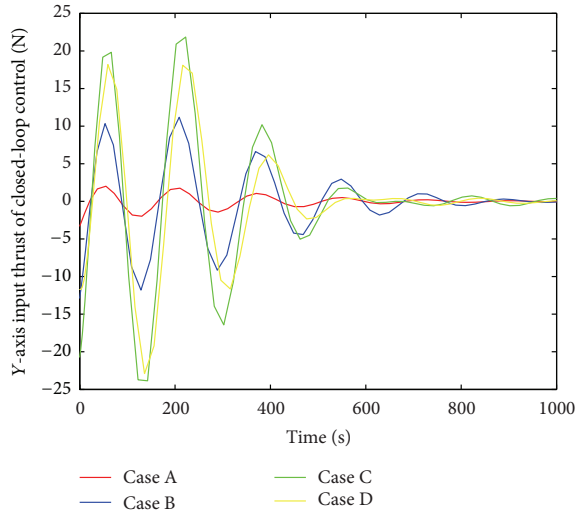

Figure 26: Y-axis input of closed-loop system for the four different uncertainty cases.

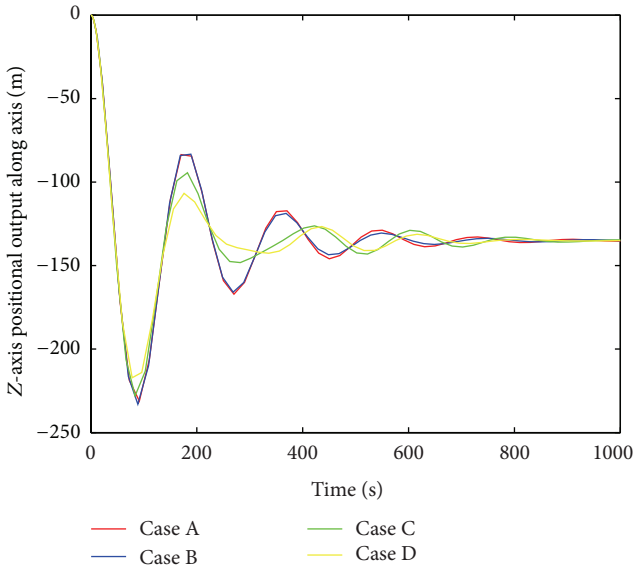

FIGURE 27: Z-axis positional output of closed-loop system for the four different uncertainty cases.

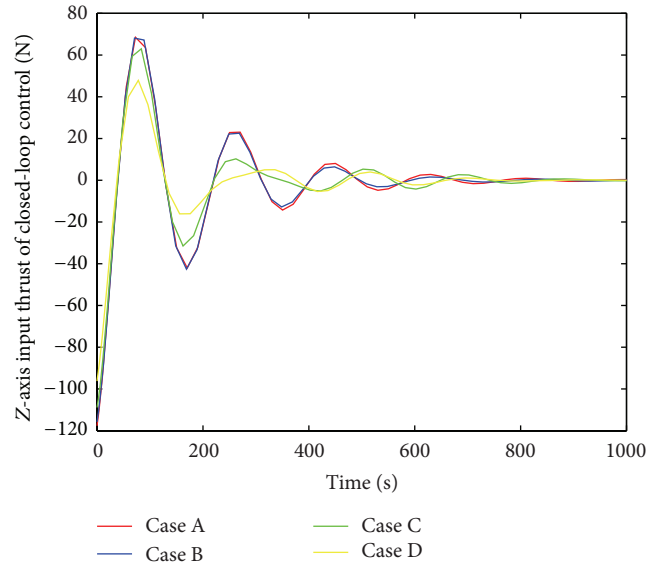

FIGURE 28: Z-axis input of closed-loop system for the four different uncertainty cases.

$$
\begin{aligned}
K_{\text{Case A}} &= \begin{bmatrix} -0.8726 & 0.0168 & -0.0012 & -19.6631 & -0.0165 & -0.0238 & -0.0156 & 0.0001 & -0.0001 \\ -0.0510 & -0.8183 & -0.1570 & -0.7472 & -22.4896 & -0.5307 & -0.0021 & -0.0140 & -0.0052 \\ -0.0232 & -0.1522 & -0.8247 & -1.0570 & -0.5274 & -22.3842 & -0.0012 & -0.0052 & -0.0144 \end{bmatrix}, \\
K_{\text{Case B}} &= \begin{bmatrix} -0.8728 & 0.0137 & -0.0035 & -19.6836 & -0.0418 & -0.0430 & -0.0157 & -0.0001 & -0.0003 \\ -0.0886 & -0.7852 & -0.2359 & -1.5512 & -21.3489 & -1.2784 & -0.0029 & -0.0140 & -0.0074 \\ -0.0103 & -0.2165 & -0.7832 & -1.1239 & -0.8532 & -20.8999 & -0.0015 & -0.0071 & -0.0143 \end{bmatrix}, \\
K_{\text{Case C}} &= \begin{bmatrix} -0.8723 & 0.0153 & -0.0014 & -19.7047 & -0.0793 & -0.0305 & -0.0156 & -0.0001 & -0.0002 \\ -0.1809 & -0.7652 & -0.2506 & -2.9144 & -20.5827 & -1.3472 & -0.0042 & -0.0138 & -0.0083 \\ 0.0635 & -0.2401 & -0.7132 & -0.0714 & -0.5607 & -19.1985 & -0.0007 & -0.0075 & -0.0132 \end{bmatrix}, \\
K_{\text{Case D}} &= \begin{bmatrix} -0.8702 & 0.0296 & 0.0013 & -19.6788 & -0.0089 & 0.0016 & -0.0154 & 0.0004 & 0.0000 \\ -0.3263 & -0.7475 & -0.1084 & -2.9313 & -22.6185 & -0.2819 & -0.0036 & -0.0106 & -0.0041 \\ 0.2335 & 0.0512 & -0.7417 & 3.9454 & 4.0154 & -19.6471 & 0.0032 & -0.0009 & -0.0129 \end{bmatrix},
\end{aligned} \tag{45}
$$

and the positional outputs of the closed-loop systems with these controllers in three axes are depicted in Figures 23, 25, and 27 separately. We can also obtain the four relevant control thrusts needed for these two methods in Figures 24, 26, and 28 separately. We can see that the closed-loop systems with the controllers K are all stable and the output tracking requirement can be guaranteed. From these figures and the table, we can also find that larger uncertainties will extend the stabilizing time and bring smaller fluctuations in z-axis input thrust, and the performance cost bound will also be diminished by larger uncertainties.

Finally, the terminal segment close to the target is depicted clearly in Figure 20. It can be seen that the chaser will asymptotically move to the evacuation point eventually, which means that the output tracking requirements can be satisfied by the designed controller K (Figure 29).

4. Conclusions

The paper has demonstrated a robust guaranteed cost output tracking control design method for the evacuation phase of spacecraft rendezvous with parameter uncertainties. Tracking control problem has been altered into a stabilization problem of an augmented system by taking the reference signal of the output into consideration. By using Lyapunov method, the controller K design problem has progressively been transformed into a convex optimization problem with linear matrix inequality constraints. The output tracking requirement can be satisfied with performance cost upper bound, and the poles of the augmented closed-loop system lie in the desired region. An illustrative example has shown the effectiveness of the proposed controller design method.

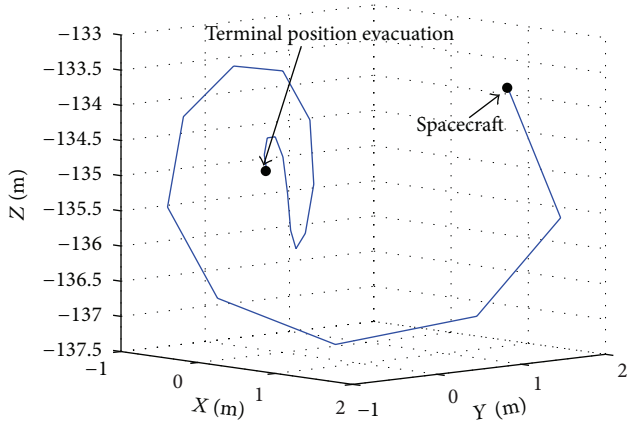

Figure 29: Terminal segment of the transfer orbit in rendezvous homing phase.

Conflict of Interests

The authors declare that there is no conflict of interests regarding the publication of this paper.

Acknowledgment

This work was partially supported by the National Natural Science Foundation of China (61203122), the China Postdoctoral Science Foundation (2012M510961), the Doctoral Fund of Ministry of Education of China (20122302120028), the Natural Science Foundation of Liaoning Province of China (2013020023) and the Key Laboratory Open Foundation of HIT (HIT.KLOF.2012.080).

References

[1] W. Fehse, *Automated Rendezvous and Docking of Spacecraft*, Cambridge University Press, Cambridge, UK, 2003.

[2] S. Yin, S. Ding, and H. Luo, "Real-time implementation of fault tolerant control system with performance optimization," *IEEE Transactions on Industrial Electronics*, vol. 61, no. 5, pp. 2402–2411, 2013.

[3] S. Yin, S. Ding, A. Haghani, H. Hao, and P. Zhang, "A comparison study of basic data-driven fault diagnosis and process monitoring methods on the benchmark Tennessee Eastman process," *Journal of Process Control*, vol. 22, no. 9, pp. 1567–1581, 2012.

[4] H. B. Hablani, M. L. Tapper, and D. J. Dana-Bashian, "Guidance algorithms for autonomous rendezvous of spacecraft with a target vehicle in circular orbit," *Journal of Guidance, Control, and Dynamics*, vol. 25, no. 3, pp. 553–562, 2002.

[5] G. Bergez, O. Mongrard, C. Santini, and R. Lainé, "ATV separation and departure strategy from uncontrolled international space station," in *Proceedings of the 18th International Symposium on Space Flight Dynamics (ESA SP-548)*, pp. 85–90, Munich, Germany, October 2004.

[6] W. H. Clohessy and R. S. Wiltshire, "Terminal guidance system for satellite rendezvous," *Journal of Aerospace Science*, vol. 27, no. 9, pp. 653–658, 1960.

[7] W. H. Clohessy and R. S. Wiltshire, "Terminal guidance system for satellite rendezvous," in *Proceedings of the American Institute of the Aerospace Sciences Summer Meeting*, pp. 59–93, Los-Angeles, Calif, USA, 1959.

[8] Y. Z. Luo and G. J. Tang, "Spacecraft optimal rendezvous controller design using simulated annealing," *Aerospace Science and Technology*, vol. 9, no. 8, pp. 732–737, 2005.

[9] D. J. Jezewski and J. D. Donaldson, "An analytical approach to optimal rendezvous using Clohessy–Wiltshire equations," *Journal of the Astronautical Sciences*, vol. 27, no. 3, pp. 293–310, 1979.

[10] Y. Z. Luo, G. J. Tang, and Y. J. Lei, "Optimal multi-objective linearized impulsive rendezvous," *Journal of Guidance, Control, and Dynamics*, vol. 30, no. 2, pp. 383–389, 2007.

[11] G. L. Tang, Y. Z. Luo, and H. Y. Li, "Optimal robust linearized impulsive rendezvous," *Aerospace Science and Technology*, vol. 11, no. 7-8, pp. 563–569, 2007.

[12] S. Yin, S. Ding, A. Haghani, and H. Hao, "Data-driven monitoring for stochastic systems and its application on batch process," *International Journal of Systems Science*, vol. 44, no. 7, pp. 1366–1376, 2013.

[13] M. Basin and D. Calderon-Alvarez, "Optimal LQG controller for linear stochastic systems with unknown parameters," *Journal of the Franklin Institute*, vol. 345, no. 3, pp. 293–302, 2008.

[14] M. Basin and D. Calderon-Alvarez, "Optimal filtering over linear observations with unknown parameters," *Journal of the Franklin Institute*, vol. 347, no. 6, pp. 988–1000, 2010.

[15] H. Gao and C. Wang, "A delay-dependent approach to robust H_∞ filtering for uncertain discrete-time state-delayed systems," *IEEE Transactions on Signal Processing*, vol. 52, no. 6, pp. 1631–1640, 2004.

[16] P. Shi, E. Boukas, and R. K. Agarwal, "Control of Markovian jump discrete-time systems with norm bounded uncertainty and unknown delay," *IEEE Transactions on Automatic Control*, vol. 44, no. 11, pp. 2139–2144, 1999.

[17] J. Wang, P. Shi, H. Gao, and J. Wang, "Gain-scheduled stabilisation of linear parameter-varying systems with time-varying input delay," *IET Control Theory and Applications*, vol. 1, no. 5, pp. 1276–1285, 2007.

[18] J. Zhang, P. Shi, and J. Qiu, "Non-fragile guaranteed cost control for uncertain stochastic nonlinear time-delay systems," *Journal of the Franklin Institute*, vol. 346, no. 7, pp. 676–690, 2009.

[19] I. R. Petersen, "A stabilization algorithm for a class of uncertain linear systems," *Systems and Control Letters*, vol. 8, no. 4, pp. 351–357, 1987.

[20] P. Singla, K. Subbarao, and J. L. Junkins, "Adaptive output feedback control for spacecraft rendezvous and docking under measurement uncertainty," *Journal of Guidance, Control, and Dynamics*, vol. 29, no. 4, pp. 892–902, 2006.

[21] B. Ebrahimi, M. Bahrami, and J. Roshanian, "Optimal sliding-mode guidance with terminal velocity constraint for fixed-interval propulsive maneuvers," *Acta Astronautica*, vol. 62, no. 10-11, pp. 556–562, 2008.

[22] G. W. Hughes and C. R. McInnes, "Solar sail hybrid trajectory optimization for non-Keplerian orbit transfers," *Journal of Guidance, Control, and Dynamics*, vol. 25, no. 3, pp. 602–604, 2002.

[23] C. A. Kluever, "Optimal low-thrust interplanetary trajectories by direct method techniques," *Journal of the Astronautical Sciences*, vol. 45, no. 3, pp. 247–262, 1997.

[24] C. A. Kluever, "Comet rendezvous mission design using solar electric propulsion spacecraft," *Journal of Spacecraft and Rockets*, vol. 37, no. 5, pp. 698–700, 2000.

[25] G. Mengali and A. A. Quarta, "Fuel-optimal, power-limited rendezvous with variable thruster efficiency," *Journal of Guidance, Control, and Dynamics*, vol. 28, no. 6, pp. 1194–1199, 2005.

[26] D. S. Naidu, "Fuel-optimal trajectories of aeroassisted orbital transfer with plane change," *IEEE Transactions on Aerospace and Electronic Systems*, vol. 27, no. 2, pp. 361–369, 1991.

[27] W. A. Scheel and B. A. Conway, "Optimization of very-low-thrust, many-revolution spacecraft trajectories," *Journal of Guidance, Control, and Dynamics*, vol. 17, no. 6, pp. 1185–1192, 1994.

[28] X. Yang, H. Gao, and P. Shi, "Robust orbital transfer for low earth orbit spacecraft with small-thrust," *Journal of the Franklin Institute*, vol. 347, no. 10, pp. 1863–1887, 2010.

[29] X. Yang, X. Cao, and H. Gao, "Sampled-data control for relative position holding of spacecraft rendezvous with thrust nonlinearity," *IEEE Transactions on Industrial Electronics*, vol. 59, no. 2, pp. 1146–1153, 2012.

[30] X. Yang and H. Gao, "Guaranteed cost output tracking control for autonomous homing phase of spacecraft rendezvous," *Journal of Aerospace Engineering*, vol. 24, no. 4, pp. 478–487, 2011.

[31] L. Yu and J. Chu, "LMI approach to guaranteed cost control of linear uncertain time-delay systems," *Automatica*, vol. 35, no. 6, pp. 1155–1159, 1999.

Hindawi Publishing Corporation
Mathematical Problems in Engineering
Volume 2014, Article ID 136497, 17 pages
http://dx.doi.org/10.1155/2014/136497

Research Article

Quantitative Feedback Control of Multiple Input Single Output Systems

Javier Rico-Azagra,[1] Montserrat Gil-Martínez,[1] and Jorge Elso[2]

[1] *Electrical Engineering Department, University of La Rioja, 26004 Logroño, Spain*
[2] *Automatic Control and Computer Science Department, Public University of Navarra, 31006 Pamplona, Spain*

Correspondence should be addressed to Javier Rico-Azagra; javier.rico@unirioja.es

Received 24 September 2013; Revised 9 December 2013; Accepted 13 December 2013; Published 7April 2014

Academic Editor: Baoyong Zhang

This paper presents a robust feedback control solution for systems with multiple manipulated inputs and a single measurable output. A structure of parallel controllers achieves robust stability and robust disturbance rejection. Each controller uses the least possible amount of feedback at each frequency. The controller design is carried out in the Quantitative Feedback Theory framework. The method pursues a smart load sharing along the frequency spectrum, where each branch must either collaborate in the control task or be inhibited at each frequency. This reduces useless fatigue and saturation risk of actuators. Different examples illustrate the ability to deal with complex control problems that current MISO methodologies cannot solve. Main control challenges arise due to the uncertainty of plant and disturbance models and when a fast-slow hierarchy of plants cannot be uniquely established.

1. Introduction

This paper deals with systems where multiple inputs are used to govern a single output. Although scientific literature refers to them with diverse names, here they will simply be called MISO systems. In some cases, each individual output is accessible, as in distributed energy generation systems [1], decentralised production systems [2], or unmanned fleets [3]. Usually, this leads to complex multiloop control structures [4]. However, a lot of engineering MISO systems lack physical individual outputs or sensors to measure them. Such systems are common in process industry [5], where the MISO control sometimes pursues the management of the global production system [6], whereas other times it governs low-level process variables (typical examples are two pumps or a pump and a valve, used as actuators in pressure or flow control [7–9]). In other cases the MISO control attends certain subsystems in a process, such as chemical reactors [10–12] or biological reactors [13–15]. More specific usages can be found in drying sections of paper machines [7, 16] or in aerobic digesters of waste water treatment plants [17]. Heat exchangers [18–20], chemical reactors in polymerization processes [9, 18], or distillation columns [9, 20–23] are repeated references in the scientific literature as MISO control applications. The automotive industry has also adopted these principles, firstly for the government of internal combustion engines [24–27] and recently for HCCI (Homogeneous Charge Compression Ignition) engines [28–30]. Another area devoted to MISO control is the consumer electronics, and particularly the massive data storage devices [31–33]. And finally, biological engineering applications can be found in [18, 34].

Within those MISO systems with nonindividual measurable outputs, the control strategies can be divided into noncollaborative and collaborative ones. Noncollaborative control selects a plant inside a battery of them, which covers a wide range of operating points for the output. The selection criterion is based on the stationary capacity of each plant. Thus, the control law is designed for an equivalent SISO system. A selector splits online the control action to the plant or plants with capacity to regulate the output in the actual operating point. The *split-range control* [35, 36] is the most representative of this methodology. A simpler method reduces to a pure SISO control system, which closes a single feedback loop around a plant. The inputs to the other plants are manipulated manually or are left constant [37].

On the other hand, collaborative strategies benefit from the dynamic strengths of each plant to improve the controlled output performance considering the restrictions of manipulated variables and individual outputs. In the scientific literature collaborative MISO systems appear under diverse designations: VPC (*Valve Position Control*) [8, 9, 21–23], *habituating control* [10–12, 17, 18, 34, 38], *main-vernier control* [39–42], *cooperative-feedback control* [20, 43, 44], *load sharing control* [2, 45–47], or *PQ design method* [27, 48, 49]. *Midranging control* [7, 13, 15, 16, 35, 50–54] is frequently found in process control literature.

The controlled collaboration of parallel plants can be performed by serial (Figure 1(a)) or parallel (Figure 1(b)) structures of controllers. Serial collaboration is based on a qualitative organization of plants: the *main* loop $c_n p_n$ corresponds to the fastest plant p_n, the first one to react to output deviations. The *vernier* loops are arranged to produce a chained intervention of gradually slower plants. The last loop, which incorporates the slowest plant, is in charge of the steady state. In this way, each system collaborates to the extent it provides benefits, avoiding useless actuator fatigue and risk of saturation. This is also the goal of parallel structures. However, the involvement of each plant is determined by its preceding controller, instead of by its position in the overall scheme. Thus, the design of each open-loop transfer function $c_m c_i p_i$ becomes more complex, since it has to define both the actuation domain and the action itself. However, unlike serial structures, parallel designs can cope with systems where the fast-slow hierarchy cannot be uniquely established.

In addition to all this, a proper design must pay some attention to the pervasive presence of uncertainty. In this sense, some solutions for the MISO control problem come from the Quantitative Feedback Theory (QFT). Horowitz [4, 55] did not pay much attention to the MISO problem with no individual measurable outputs. His work suggests the reduction of the MISO system to a SISO equivalent by plant summation. Then, a master controller (c_m in Figure 1(b)) is designed for the equivalent plant, and no individual controller is used ($c_i = 1, i = 1, \ldots, n$). The master control strategy can extract the maximum dynamic potential of each plant under certain restrictions for their phases. Nevertheless, its main drawback is that the same control action reaches all plant actuators. This entails using more feedback than necessary at certain frequencies on each branch, which leads to different negative effects in real-life actuators. In particular, an excess of noise amplification arises in the control actions to the slowest plants and steady-state offsets reduce the available actuation range for the fastest ones. Another drawback of plant summation strategy is that feedback is allocated by the plant instead of by the designer, losing some flexibility. This might have some importance in certain systems [7] whose high operation expenses suggest to arrange plant interventions according to monetary criteria rather than dynamic ones. Further QFT developments include the approaches in [25, 56], which detail a collaborative control of parallel plants with uncertainties and restrictions for particular applications, and the approach in [3], which adds feedback loops of actuations inside a parallel structure as described in [57].

However, a general robust methodology to deal with MISO collaborative systems through QFT tools has not been presented yet. Such is the goal of this paper. In particular, it focuses on the disturbance rejection or regulation problem. The new technique is fitted to the parallel structure. This is the most versatile one since other arrangements can always be transformed into it while the inverse transformation is not always feasible. Besides, some examples will show that main-vernier design philosophy cannot cope with certain types of MISO plants. The new methodology seeks a quantitative division of feedback amongst parallel loops in the frequency domain. In absence of restrictions, this distribution leads to the accomplishment of the specifications with minimum use of feedback, that is, each loop only contributes at those frequencies where its plant favours the output performance.

2. MISO QFT Design Methodology

2.1. Robust MISO Regulation Problem. Consider Figure 1(b) with $c_m = 1$. Each parallel plant p_i, $i = 1, \ldots, n$, defines the effect of each manipulated variable u_i over the single measurable output y. The plant p_d defines the way in which the nonmeasurable disturbance d deviates the single output y from its desired constant set-point r. A set of parallel controllers c_i, $i = 1, \ldots, n$ are designed to minimize such deviation. Each c_i fixes its corresponding u_i based on a common output measurement y, which is corrupted by the noise signal n. For this regulation problem, the closed loop functions are

$$\begin{aligned} y &= \frac{p_d}{1 + l_t} d - \frac{l_t}{1 + l_t} n, \\ y_i &= -\frac{l_i p_d}{1 + l_t} d - \frac{l_i}{1 + l_t} n, \\ u_i &= -\frac{c_i p_d}{1 + l_t} d - \frac{c_i}{1 + l_t} n, \end{aligned} \tag{1}$$

where $l_i = p_i c_i$ are the individual open-loop transfer functions and

$$l_t = \sum_{i=1}^{n} l_i \tag{2}$$

is the global open-loop transfer function.

All plants are assumed to present parametric uncertainty. Let us define $\mathbf{q} = [q_1, q_2, \ldots, q_m]$ as the vector of all parameters appearing in the transfer functions $p_1, p_2, \ldots, p_n, p_d$. Each q_i varies within certain lower and upper limits. Therefore, the uncertainty vector $\mathbf{q}$ belongs to a hyperrectangle in $\mathbb{R}^m$ called the uncertainty space $\mathcal{Q}$; that is,

$$\mathbf{q} \in \mathcal{Q} \triangleq \left\{ \mathbf{q} \in \mathbb{R}^m \mid q_i^- \le q_i \le q_i^+, i = 1, \ldots, m \right\}. \tag{3}$$

The purpose of QFT control is to enforce the specifications for all elements in the uncertainty space. In this case, the specifications include robust stability,

$$\left| \frac{l_t}{1 + l_t} \right| \le W_s \quad \forall \mathbf{q} \in \mathcal{Q}, \tag{4}$$

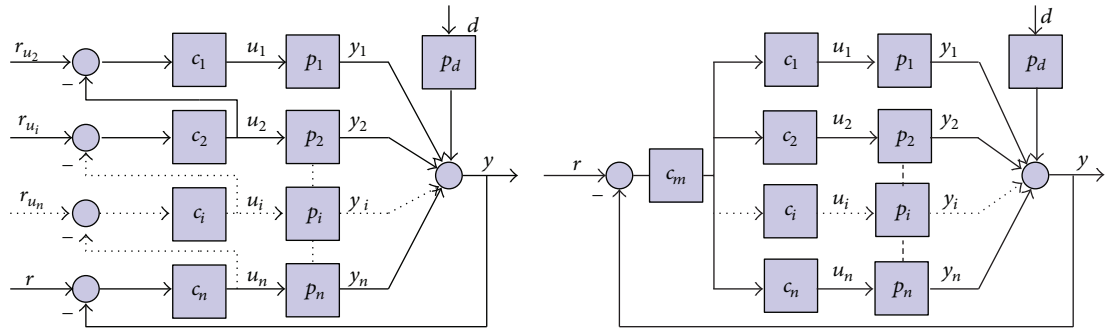

(a) Serial structure or *main-vernier*

(b) Parallel structure

Figure 1: Control structures for MISO plant.

and robust disturbance rejection,

$$\left|\frac{p_d}{1+l_t}\right| \leq W_d \qquad \forall \mathbf{q} \in \mathcal{Q}, \tag{5}$$

where W_s and W_d are upper tolerances for each closed-loop frequency response.

As long as feedback control guarantees expected specifications at a certain price, QFT advocates for that control solution with the minimum amount of feedback, which will be denoted as the QFT optimum. In SISO control, the bounds express the minimal gain requirements on the nominal open-loop transfer function for the accomplishment of the specifications. Consequently, an QFT optimal loop-shaping tries first a narrow fulfilment of the bounds, and then an abrupt roll-off to minimize the presence of noise in the control signals [58].

In the MISO case, the search for the QFT optimum is not so obvious. There is a minimal gain of the nominal open-loop global function l_{t_o} that meets (4) and (5). However, it can be achieved by several combinations of l_{i_o} in (2). That combination of minimum gains of each c_i at each frequency is the solution that demands the minimum amount of feedback. Then, one option is splitting the global problem in several designs l_{i_o} in such a way that each bound arrangement shows the minimum amount of feedback solution. If so, each loop-shaping reduces to a narrow fulfilment of the bounds and a maximal reduction of gain in the frequencies where no restrictions are imposed.

In practice, the new methodology looks for a wise distribution of feedback, which exploits the power of each plant frequency response to achieve controllers of minimum gain. This minimizes the presence of noise in the control signals to the slowest plants, which usually exhibit the most powerful actuators and provide the bias action. In this way, faster plant actuators preserve their full range of operation for output regulation in response to disturbances.

2.2. Parallel Plants and the Amount of Feedback. The core of the method is to quantify the amount of feedback, which is evaluated with the controller gain. For a better understanding, let us take a single frequency, exclude the uncertainty, and consider solely the specification of robust disturbance rejection. Then, certain l_t will be a solution to (5). Two parallel structures from Figure 1(b) will be studied: a master control, which sintonizes c_m , and does each $c_i = 1$, and a strictly parallel control, which sintonizes each c_i and does $c_m = 1$.

To achieve l_t, we are firstly comparing the controller gain necessities for plants of similar characteristics. For simplification purposes, let us take two plants p. As expected, if the system power to regulate the output was increased from p to $2p$, feedback necessities would reduce in the same proportion from $|l_t/p|$ to $|l_t/2p|$, independently if a master controller or two parallel controllers were used.

Secondly, control necessities to achieve l_t are being evaluated for plants with very different gains at the same phase. Let us take two plants as $|p_1| \gg |p_2|$. Note that, if p_1 plant worked alone, the feedback demand would be considerably inferior to the case of p_2 working alone: $|l_t/p_1| \ll |l_t/p_2|$. Therefore, there is no sense in using the p_2 actuation unless you consider other criteria different from meeting the performance with the minimum feedback. In the case of a master controller, its control demand is $|l_t/(p_1 + p_2)|$, which approaches to $|l_t/p_1|$. Thus, p_1 is the only plant contributing to the performance and p_2 actuator is being excited unnecessarily. A parallel controller structure can overcome this drawback as follows. Basing on the formulation, $l_t = c_1p_1 + c_2p_2$ can be achieved by different combinations of c_1, c_2. However, as long as p_2 powerfulness is negligible, any attempt of collaboration with p_1 to the performance will require a huge control demand in the second branch. Then, the best option is to achieve the performance with the p_1-branch, whose control demand will be $|l_t/p_1|$. Simultaneously, tuning $c_2 \approx 0$ avoids that useless signals reach the p_2 actuators.

One of the above two situations (plants that should collaborate or not) arises in the loop-shaping of controllers at each frequency. In a first stage of the proposed methodology, special QFT bounds guide the designer to define when several plants are similar enough to collaborate at certain frequency or when they are different enough such that some must take the whole responsibility and others must be inhibited. Model uncertainty and the whole set of specifications are included in the method. In a second stage, the feedback is

shared accordingly through the sequential loop-shaping of controllers in the parallel structure.

2.3. First Stage: Load Sharing Planning at Each Frequency of Design. The proposed method firstly evaluates the amount of controller gain $|c_i|$ that each plant p_i would demand to fulfil the specifications (4), and (5) by itself, that is, assuming $c_{j\neq i} = 0$. The required gain is expressed graphically by a QFT bound at each frequency ω, denoted by $\beta_{c_i}(\omega)$. Note that, unlike common QFT bounds, these are bounds on the controller gain, not on the nominal open-loop gain $|l_{i_o}|$, in the vertical axis. This is so, because their purpose is not to serve as design guidelines, but to allow a graphical comparison among the controller gains that are being demanded at subsequent design phase $\angle l_{i_o}$ by each plant. Once all the bounds for a single frequency ω are computed and a design phase Θ_d is selected for comparisons, a conclusion is reached according to the following criteria.

(a) If one of the bounds, say $\beta_{c_k}(\omega)$, is *sensibly* lower than the others at Θ_d, then regulation at that frequency must be accomplished through the open-loop function l_k, and the other branches must be inhibited by decreasing the gain of $c_{i\neq k}(j\omega)$ as much as possible. The quantity of 20 log n dB is a practical guideline to establish the bound height difference. It is funded on the ideal collaboration of n equal plants, which would reduce n times the amount of feedback, as Section 2.2 details. Figure 2 shows the analysis for a 2-branch structure, which suggests that the controller c_2 should carry the burden of control at ω_1 whatever the chosen Θ_d is.

(b) If several bounds are located at the bottom and their heights do not differ too much from each other at Θ_d, then their associated controllers must share the regulating task. The branches whose bounds locate above this bound group must be inhibited. In this case, the practical rule of thumb is that any set of m bounds within a range of ±20 log m dB are suitable for cooperation. According to this, Figure 2 suggests that controllers c_1 and c_2 should collaborate at ω_2 whatever the chosen Θ_d is to fulfil the specification.

Remark 1. The first stage of the new methodology arranges the best load sharing amongst parallel plants at each frequency for minimum amount of feedback in each branch to meet the control specifications. This approach is completely new inside the MISO control literature.

2.4. Second Stage: Feedback Sharing in Parallel Structure of Controllers. Once it is decided which plants or plants must deal with the specifications at each frequency, the n parallel controllers are designed sequentially. The procedure presented here aims to minimize the number of iterations required to reach a feasible solution. At each step, one of the controllers is tuned by QFT loop-shaping, while the remaining ones are considered constant components of the overall uncertain system. This rotating nature of the tunable controller is enabled by the *genbnds* command of the Terasoft QFT Toolbox [59], which admits general specifications in the form

$$\left|\frac{A+BG}{C+DG}\right| \leq W. \tag{6}$$

Thus, if at some point the controller c_k is to be adjusted, the robust stability (4) bounds can be computed by choosing $A = \sum_{i\neq k} l_i, B = p_k, C = 1+\sum_{i\neq k} l_i, D = p_k, G = c_k$, and $W = W_s$, while the robust disturbance rejection (5) bounds require the choice $A = p_d, B = 0, C = 1 + \sum_{i\neq k} l_i$, $D = p_k, G = c_k$, and $W = W_d$. Note that these are common QFT bounds, since they are imposed on the open-loop transfer function l_{k_o}, and consequently denoted $\beta_{l_k}(\omega)$, which represent all the specifications to meet at ω.

The design procedure begins with all controllers set to zero. Subsequently, in the first step of design, the loop-shaping of the branch/branches that should work at the lowest frequency is performed fully. In an increasing order of frequencies, the last step corresponds with the design of branch/branches working at the highest frequency. During any loop-shaping design, the course of action at certain frequency depends on the result of the load sharing planning stage. As common in QFT for each loop-shaping, the design begins satisfying the bounds in an increasing order of frequencies, and finally, a fast roll-off of the open-loop gain is shaped in the high frequency range. A novelty of MISO control is that the open-loop gain must also be cut or reduced in the frequencies where the branch should be noncollaborating. Following, there are some hints of guide for both goals of design: when the branch must achieve the performance at ω and when the branch must be inhibited at ω because other branches do the work or because ω is the roll-off frequency for the branch.

At the frequencies where the branch/branches must perform the regulation task, two different cases are detailed next. Figures 3 and 4 show examples of both cases. Superscripts in bound designation indicate the step in the sequential design.

(a) A single plant p_k will be responsible for the regulating task at ω (see the two-branch example in Figure 3). Thus, l_{k_o} is placed above the bound $\beta_{l_k}(\omega)$ (see l_{1_o} and $\beta^0_{l_1}$). After this, the k bound arrangement does not change (see $\beta^{\mathrm{I}}_{l_1}$). However, since the accomplishment of the specifications has just been secured by c_k, the bounds $\beta_{l_{i\neq k}}(\omega)$ delimit now closed forbidden regions, which will allow a reduction of the $l_{i_o\neq k_o}$ gains for feedback saving at ω when these designs are faced (compare $\beta^{\mathrm{I}}_{l_2}$ with $\beta^0_{l_2}$). Note also that, an excess of l_{k_o} gain to meet β_{l_k} would imply a major contraction of $\beta_{l_{i\neq k}}$ if this was necessary in the design of the other loops.

(b) A group of m plants will share the control task at ω (see the four-branch example in Figure 4, where $m = 3$). Their loop shaping is carried out jointly as follows. For convenience, let us denote the group $p_{k_1}, p_{k_2}, \ldots, p_{k_m}$. Let us assume as well that c_{k_1} is tuned first. The purpose of the designer is to place

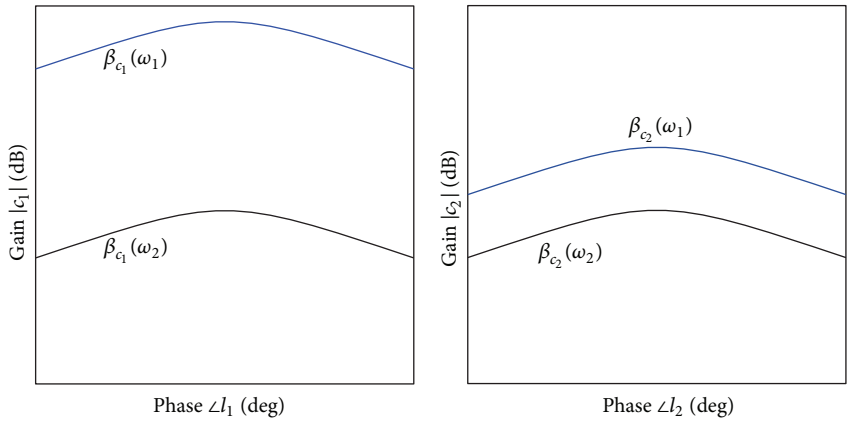

FIGURE 2: Feedback demand comparisons in a 2 × 1 system.

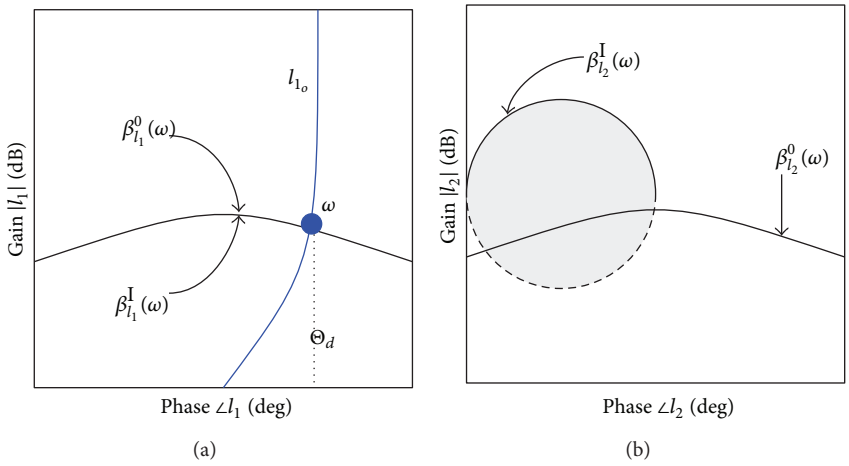

FIGURE 3: Single brach achieves the specifications at ω in a 2 × 1 system.

$l_{k_{1_o}}$ around 20 log m decibels below the bound $\beta_{l_{k_1}}(\omega)$ at the design phase of interest Θ_d (see l_{1_o} and $\beta^0_{l_1}$). The consequences are that $\beta_{l_{k_1}}(\omega)$ bound does not change (see $\beta^{\mathrm{I}}_{l_1}$) and that a dip appears at Θ_d in bounds $\beta_{l_{k_j}}(\omega)$, $j = 2, \ldots, m$ (see $\beta^{\mathrm{I}}_{l_2}$ and $\beta^{\mathrm{I}}_{l_3}$). Then, tuning of $l_{k_{2_o}}$ takes place, and the goal is to place $l_{k_{2_o}}$ around 20 log$(m - j + 1)$, $j = 2$, decibels below the bound $\beta_{l_{k_2}}(\omega)$; (see l_{2_o} and $\beta^{\mathrm{I}}_{l_2}$). Once achieved, the $\beta_{l_{k_2}}(\omega)$ bound does not change (see $\beta^{\mathrm{II}}_{l_2}$), but it extends the depth of the dip in $\beta_{l_{k_j}}(\omega)$, $j \neq 2$ (see $\beta^{\mathrm{II}}_{l_1}$ and $\beta^{\mathrm{II}}_{l_3}$). The process goes on in this manner, temporarily violating their bo-unds, until the tuning of $l_{k_{m_o}}$ is reached. In this case, the purpose is simply to meet the bound $\beta_{l_{k_m}}(\omega)$, whose dip has been repeatedly enlarged by each one of the controllers c_j, $j = 1, \ldots, m - 1$ (see l_{3_o} and $\beta^{\mathrm{II}}_{l_3}$). Once this step is completed, all previously violated bounds are now met (see $\beta^{\mathrm{III}}_{l_1}$, $\beta^{\mathrm{III}}_{l_2}$, and $\beta^{\mathrm{III}}_{l_3}$).

If the m plants were identical at ω and Θ_d, the gain of each controller $c_{k_{1,\ldots,m}}$ would be 20 log m dB lower. Nevertheless, differences between plant gains up to ±20 log m dB are acceptable for successful cooperation and controller gain reduction, as Section 2.3(b) reports. In consequence, some extra adjustments are usually necessary to meet each $\beta_{l_{k_j}}$. After the design of the m controllers with control responsibilities at ω, the bounds of the remaining loops will delimit closed forbidden regions (see $\beta^{\mathrm{III}}_{l_4}$).

At the frequencies where the branch/branches has/have no regulation responsibilities, a great deal of different situations may arise, specially when there are more than two inputs in the MISO system. Some of the most frequent ones are being described. In any case, the bound recalculation after any design step contributes to value the tradeoffs, which are inherent to any design with multiple degrees of freedom.

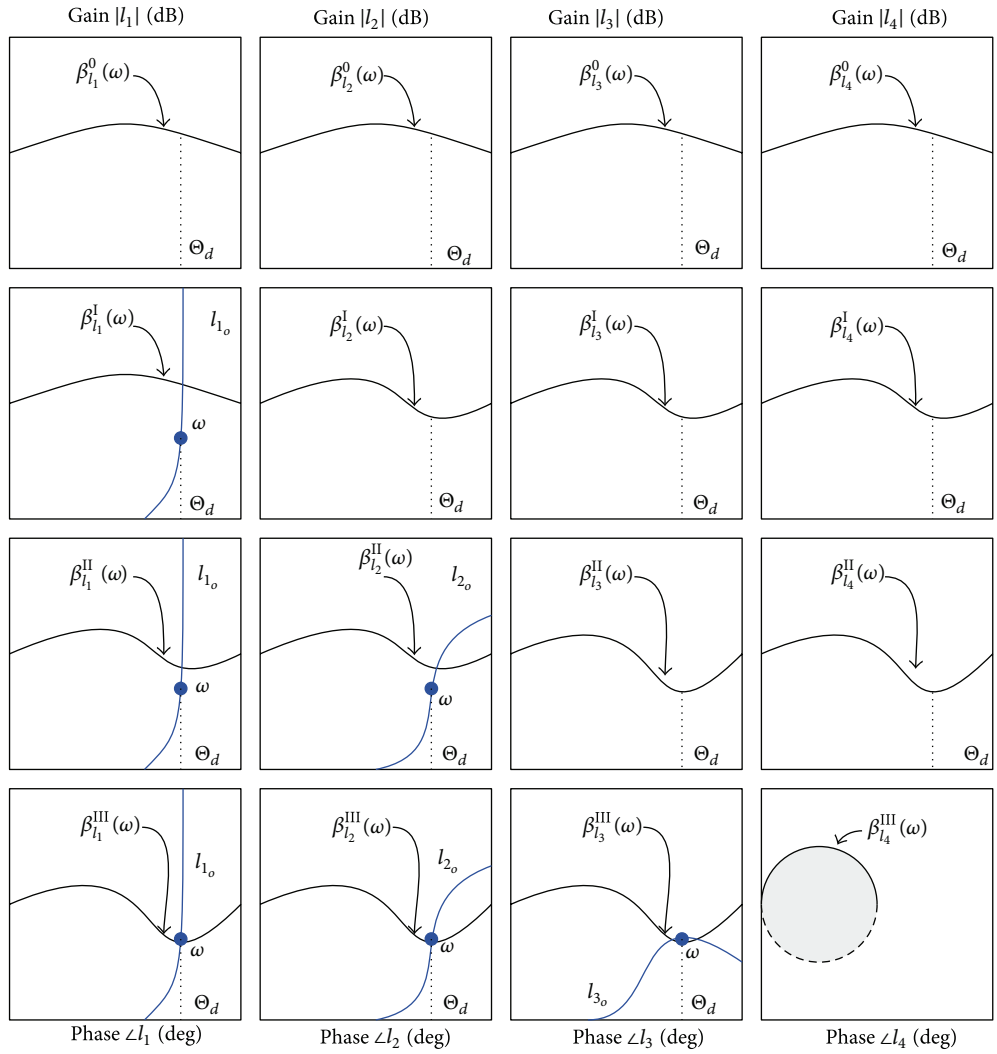

Figure 4: Three plants collaborate to achieve the specifications at ω in a 4×1 system.

(i) Design hints for the roll-off frequencies ω of the k loop. The l_{k_o} gain reduction is usually a tradeoff between a maximum noise amplification and a minimum controller order. One case is that the bounds β_{l_k} demand certain feedback at ω. This happens if there are other loops with control responsibilities at ω that have not been designed yet. In this circumstance, the l_{k_o} design is performed temporarily violating its bounds at the roll-off frequencies ω. After the design of the loops with control responsibilities at ω, the bounds β_{l_k} are automatically reshaped and now demarcate forbidden closed regions. In the new picture, l_{k_o} will usually meet its bounds. Nevertheless, further iterations may be required to optimize the gain reduction at these roll-off frequencies. Other case is if the k loop is the last one to be designed. In this circumstance, β_{l_k} bounds, which already delimit forbidden closed regions, are the definitive restrictions to be met in the l_{k_o} gain reduction at its roll-off frequencies.

(ii) Design hints for the frequencies ω where the k plant participation must be inhibited. The bounds β_{l_k} currently demarcate fobidden closed regions at ω, since other loops have already achieved the prescribed specifications. The restrictions for the l_{k_o} gain reduction at frequencies ω are the bounds β_{l_k} at frequencies higher than ω, where the k plant will have to achieve or collaborate in the regulation task. The controller complexity is another reason to take into account in the gain saving procedure.

Remark 2. The second stage of quantitative MISO control details the QFT framework and procedure for the sequential loopshaping of parallel controllers in order to meet the predefined load-sharing arrangement. A set of branches collaborate in the control tasks or are inhibited for feedback saving. A standard method is given to deal with n-input single-output systems from a quantitative feedback control point of view, which remained unsolved till now.

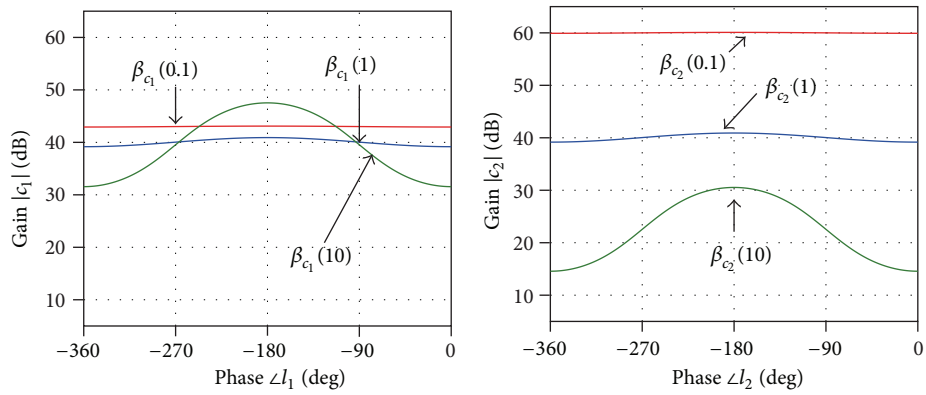

Figure 5: Feedback demands for single plant intervention.

3. Design Examples

3.1. Example 1. A simple MISO system illustrates the new methodology and its potential benefits. The uncertainty-free plant models are

$$p_1 = \frac{1}{10s+1}, \qquad p_2 = \frac{0.1}{0.1s+1}, \qquad p_d = 1. \tag{7}$$

Inside a parallel disposition (Figure 1(b) with $c_m = 1$), the regulatory problem aims to design $c_{i=1,2}$ to meet certain stability (4) and performance (5) specifications with minimum controller gains at each frequency. For a minimum stability phase margin of 45°, the tolerance choice is

$$W_s = \left| \frac{0.5}{\cos\left(\pi\left(180 - PM\right)/360\right)} \right|, \qquad PM = 45. \tag{8}$$

And for disturbance rejection, the performance upper model is

$$W_d = \left| \frac{1.4167s\left(s+30\right)}{\left(s+10\right)\left(s+42.5\right)} \right|. \tag{9}$$

For bound computation and loop-shaping guide, a suitable vector of discrete frequencies is chosen:

$$\Omega = \{0.1, 0.5, 1, 5, 10, 100\} \left[\frac{\text{rad}}{\text{s}}\right]. \tag{10}$$

3.1.1. First Stage: Load Sharing Planning at Each Frequency. According to explanations in Section 2.3, the required amount of feedback at Ω is computed in case that a single system regulated the output: p_1 or p_2, in Figure 5(a) and Figure 5(b), respectively (only three frequencies in Ω are drawn to illustrate the three potential outcomes). Compare controller bounds of both systems as follow.

(i) At low frequencies ($\omega < 0.5$), the bounds β_{c_1} are over 20 log 2 dB lower than the bounds β_{c_2}; see $\omega = 0.1$. Thus, p_1 branch should assume y regulation and p_2 branch should be switched off. Subsequent loop-shaping goals are $l_t \approx l_1$, $l_2 \approx 0$ at $\omega < 0.5$.

Table 1: Load-sharing planning for minimum amount of feedback.

ω	0.1	0.5	1	5	10	100
p_1	×	×	×			
p_2		×	×	×	×	×

(ii) At medium frequencies ($0.5 \le \omega < 2$), the bound heights differ less than 20 log 2; see $\omega = 1$. Thus, the collaboration of both plants is suggested. Subsequent loop-shaping goals are $l_1 \approx l_2$ at $0.5 \le \omega < 2$.

(iii) At high frequencies ($\omega \ge 2$), the bounds β_{c_2} are over 20 log 2 dB lower than the bounds β_{c_1}; see $\omega = 10$. Subsequent loop-shaping goals are $l_t \approx l_2$, $l_1 \approx 0$ at $\omega \ge 2$.

Accordingly, Table 1 summarises the load sharing planning at design frequencies Ω.

3.1.2. Second Stage: Design of Parallel Controllers. Sequential loop-shaping of c_1 and c_2 is performed with Table 1 aims. Figure 6 illustrates the procedure in detailed steps. Steps 0, I, and II belong to the same first iteration, which explains the design of c_1 and c_2 (marked with superscripts). Further iterations (step III) are required to optimize both designs looking for the strictly minimum amount of feedback at each frequency, which usually trades off with a reasonable order of the controllers. General guidelines were described in Section 2.4.

(0) Initial bound computation is drawn with $c_2^0 = 0$ for the loop 1 (Figure 6(a)) and with $c_1^0 = 0$ for the loop 2 (Figure 6(b)).

(I) Loop-shaping of l_1 (see Figure 6(c)). To achieve $l_t \approx l_1$ at $\omega < 0.5$, l_1 is located onto bound $\beta_{l_1}(0.1)$. For plant collaboration at $0.5 \le \omega < 2$, l_1 is shaped 20 log 2 dB below $\beta_{l_1}(0.5)$ and $\beta_{l_1}(1)$. At $\omega \ge 2$, the goal becomes $l_t \approx l_2$. Then, $\omega \ge 2$ are the roll-off frequencies for l_1. Its gain is reduced as much as possible, even momentary violating bounds $\beta_{l_1}(5)$, $\beta_{l_1}(10)$, and $\beta_{l_1}(100)$,

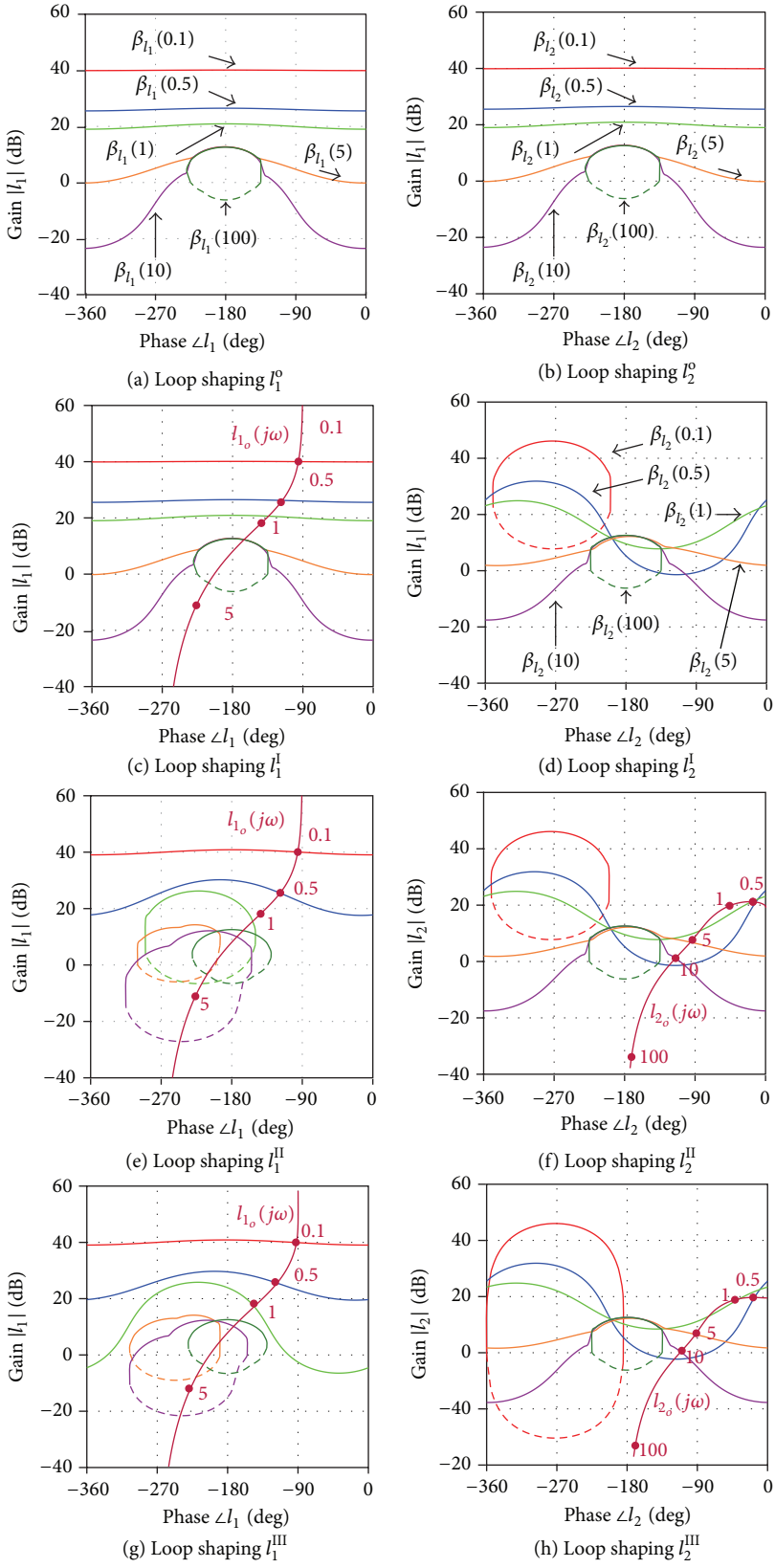

Figure 6: Sequential loop-shaping.

since control requirements will be achieved by l_2. As this reduction is not bound guided, it could require later a l_1 reshaping at these high frequencies. After step I, the controllers are

$$c_1^{\mathrm{I}} = \frac{417\,(s+0.1)}{s(s+2)^2}, \qquad c_2^{\mathrm{I}} = c_2^0 = 0. \tag{11}$$

As a consequence, suitable bounds β_{l_2} arise for the subsequent loop-shaping of l_2. Let us compare new bounds in Figure 6(d) with initial bounds in Figure 6(b): closed exclusion regions appear in $\beta_{l_2}(0.1)$ for l_2 feedback saving at $\omega < 0.5$, since l_1 has already achieved the feedback requirements; dips arise in $\beta_{l_2}(0.5)$ and $\beta_{l_2}(1)$, where l_2 has to collaborate with previous l_1 contribution; the bounds at $\omega = \{5, 10, 100\}$ are not modified since l_2 must assume the whole control tasks.

(II) Loop-shaping of l_2 (see Figure 6(f)). Firstly, reduce l_2 gain at $\omega < 0.5$ to meet $|l_2| \ll |l_m|$, since $l_t \approx l_1$ was achieved. This example does not need adding a lag network, which favours a lower order of controller c_2. Secondly, locate l_2 onto its bounds β_{l_2} at $\omega = \{0.5, 1, 5, 10\}$; note that the purpose of an excess of feedback at $\omega = 1$ is the illustration of subsequent optimization iterations. Finally, reduce the high frequency gain of l_2 at $\omega \geq 100$ (roll-off frequencies) as much as possible as in any *classical* QFT design. After step II, the controllers are

$$c_2^{\mathrm{II}} = \frac{193.2\,(s+0.4)\,(s+6.3)}{(s+11)\left(s^2+1.2s+0.51\right)}, \qquad c_1^{\mathrm{II}} = c_1^{\mathrm{I}}. \tag{12}$$

As a consequence, let us compare new bounds β_{l_1} in Figure 6(e) with bounds of the previous step in Figure 6(c). Note that l_1 now meets all its bounds. Pay special attention to collaboration frequencies in Figures 6(e) and 6(f): the feedback sharing is close to the optimum at $\omega = 0.5$ (l_1 and l_2 lie on their respective bounds), but it is not the case at $\omega = 1$. Thus, small adjustments are required to economize feedback.

(III) Both loops are iteratively redesigned in Figures 6(g) and 6(h). Thanks to the help of software tools, this is usually a simple procedure. The final controllers are

$$c_1 = c_1^{\mathrm{III}} = \frac{329.7\,(s+0.088)}{s\,(s+1.5)\,(s+2)}, \tag{13}$$

$$c_2 = c_2^{\mathrm{III}} = \frac{225.13\,(s+1.1)\,(s+6.95)}{(s+14.81)\left(s^2+1.77s+1.22\right)}. \tag{14}$$

Note that l_1 achieves by itself the control requirements at $\omega = 0.1$ and shares this task with l_2 at $\omega = \{0.5, 1\}$. Thus, l_1 lies on β_{l_1} at $\omega = \{0.1, 0.5, 1\}$. Alongside, l_2 achieves by itself the performance load at $\omega = \{5, 10\}$. Thus, l_2 lies on β_{l_2} at $\omega = \{0.5, 1, 5, 10\}$. It's also necessary to remark how the bound disposition eases the reduction of the open-loop gains, in particular at $\omega > 1$ for l_1 and at $\omega < 0.5$, $\omega > 10$ for l_2. Nevertheless, the feedback saving at these frequencies trades off with a minimum order of controllers.

3.1.3. Analysis and Comparisons. Parallel control, $c_{i=1,2}$ (13) and (14), is being compared with master control, c_m, which is designed for the equivalent plant $p_e = p_1 + p_2$ in order to satisfy the same performance and stability specifications. QFT design yields the single controller

$$c_m = \frac{192.6\,(s+0.1)\,(s+4.4)}{s\,(s+1)\,(s+8.9)}. \tag{15}$$

For a fairer comparison, $l_m = c_m p_e$ lies exactly on its bounds and reduces its high frequency gain as much as possible. Thus, it is the solution of minimum amount of feedback at each frequency if the system was single input; Figure 7(a) depicts the minimum $|c_m|$. This QFT optimal loop-shaping is easily achievable as there is no uncertainty and there is a single controller. For the MISO solution, the exact meeting of bounds with controllers (13) and (14) required a second iteration to reshape the former controllers (11) and (12). Nevertheless, the main feedback saving is not so much to lie exactly on the bounds but to share conveniently the feedback between branches. Note that $|c_2| \ll |c_m|$ at low frequencies, where p_1 regulates the output, and $|c_1| \ll |c_m|$ at high frequencies, where p_2 works. In this way, c_2 filters low frequencies, which avoids unnecessary offsets of p_2 actuation. And c_1 filters high frequencies, which reduces the amplification of high frequency signals (sensor noise) in p_1 actuator (usually labelled as cost of feedback in SISO QFT [58]).

Figure 8 clearly demonstrates these benefits in the time domain. External inputs are a unity step disturbance $d(t)$ at $t = 0.5$ s and the sensor noise $n(t)$ built with a white-noise source (noise power = 0.001, sample time = 0.01). All response signals are depicted with and without noise intervention in blue and green lines, respectively. As long as $l_1 + l_2 \approx l_m$ (a better agreement could be achieved with higher order of controllers), the closed-loop transfer functions y/n and y/d are similar for both control strategies. Accordingly, the $y(t)$ performance coincides for master and parallel control (only one is depicted in Figure 8), in presence (blue line) or absence (green line) of noise. However, the control effort strikes the differences as setting forward by closed-loop frequency responses in Figure 7(b). Let us compare the pair $u_1(t)$-$u_2(t)$ with the signal $u_m(t)$ in Figure 8. Actuation $u_1(t)$ is hardly affected by sensor noise amplifications, which avoids unnecessary fatigue of p_1 actuator; the exact quantification of this benefit is on the distance

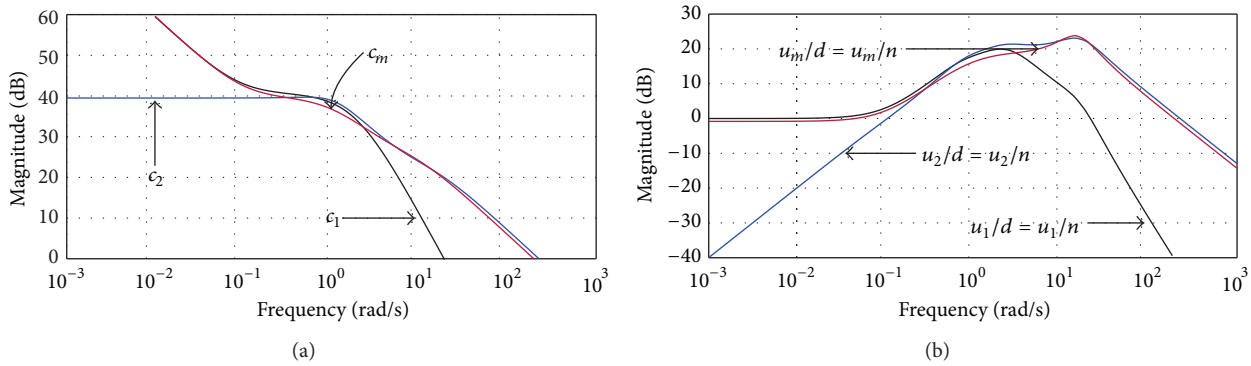

Figure 7: (a) Amount of feedback. (b) Closed-loop feedback cost.

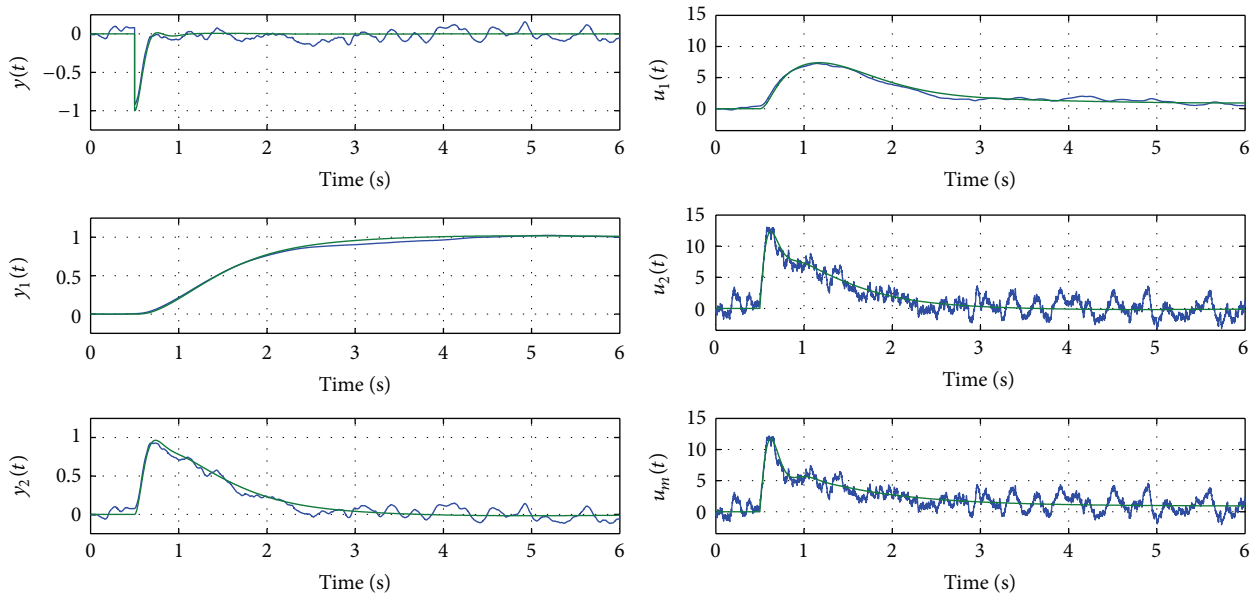

Figure 8: Time domain behaviour.

between $|u_1/n|$ and $|u_m/n|$, which mainly depends on the affordable bandwidth saving during the l_1 shaping. On the other hand, the noise $n(t)$ affects similarly to both $u_2(t)$ and $u_m(t)$. However, $u_2(t)$ recovers the initial stationary state and $u_m(t)$ does not: see $u_2(t = \infty) \approx 0$, $u_m(t = \infty) = u_1(t = \infty)$ in time-domain, and $|u_2/d|_{\omega=0} \approx -\infty$, $|u_m/d|_{\omega=0} \approx |u_1/d|_{\omega=0}$ in the frequency domain. Thus, for accumulative disturbances, the fast time actuation of $u_2(t)$ starts out always from zero, and consequently, the full range of u_2 signal is available to speed up the transient response with a less saturation risk. Both improvements (the noise release of $u_1(t)$ and the zero steady state of $u_2(t)$) are more valuable in practice, where real-life plants, actuators, and sensors have physical limitations.

As some final comparisons, once c_1 and c_2 are achieved, there are equivalences in other MISO control topologies (Eitelberg's master-slaves [46] and Lurie's serial structure [39]) for this particular example. Designs according to those other structures and methodologies can always be transformed into the strictly parallel structure, while the inverse transformation is not always feasible. In any case, the same QFT optimal solutions (13) and (14) would not probably be attainable since those other design methodologies do not quantify neither the amount of feedback nor the collaboration degree. Besides, some MISO plants or design-condition arrangements are only affordable with the new parallel design methodology; as following examples are discussing.

Remark 3. Firstly, this example details the two stages of the proposed MISO control methodology. Then analysis and comparisons show the expected benefits of a parallel structure of controllers in comparison with a single master controller: the reduction of useless fatigue and saturation risk of actuators. In comparison with other MISO control strategies (master-slaves or serial structures), the new one offers the minimum amount of feedback to govern each plant for prescribed specifications.

3.2. Example 2. Heat exchangers are common engineering applications of MISO control [18–20]. Figure 9 outlines

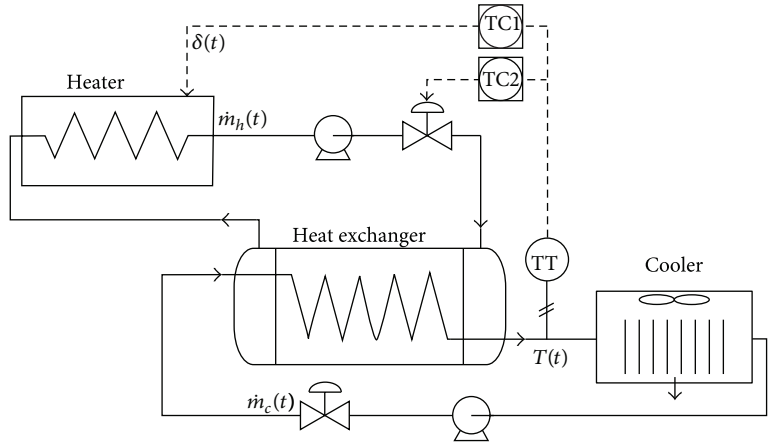

Figure 9: Thermal process control.

a heat-exchanger where the output temperature $T(t)$, can be regulated through two manipulated variables: the hot flow $\dot{m}_h(t)$ and the heating power control $\delta(t)$ (which conditions the input temperature of the hot flow). The cold flow $\dot{m}_c(t)$ acts as a disturbance since the production rate changes on demand. A laboratory-scale plant commercialised by Feedback Systems Inc. agrees with this arrangement [60].

Around certain operating conditions, linear plant models of the form

$$p(s) = \frac{b_3 s^3 + b_2 s^2 + b_1 s + b_0}{s^4 + a_3 s^3 + a_2 s^2 + a_1 s + a_0} \tag{16}$$

are identified [61]. They express the relationships from the two manipulated variables to the output ($p_1 = T/\delta$ and $p_2 = T/\dot{m}_h$) and from the disturbance to the output ($p_d = T/\dot{m}_c$). A total amount of 112 cases are defined for each output/input relation, which generate the uncertainty of numerator and denominator coefficients in (16). Figure 10 depicts the envelopes of the plant frequency responses. As long as all the p-models are minimum phase, only magnitude Bode diagrams are included.

The robust stability control specification is (4) with tolerance (8) for a minimum phase margin of 45°. The specification for robust disturbance rejection is (5) with upper tolerance model

$$W_d = \left| \frac{1.2s\,(s+1.6)\,(s+5)}{(s+6)\,(s^2+1.6s+1.778)} \right|. \tag{17}$$

After computing the demand of feedback if p_1 or p_2 worked alone, Table 2 resumes the load-sharing planning at discrete frequencies to meet the robust control specifications with the minimum amount of feedback.

Consequently, the loop-shaping of l_{1_o} and l_{2_o} are performed (see Figure 11) and yield

$$c_1 = \frac{69.5\,(s+0.0044)\,(s+0.058)}{s\,(s+0.018)\,(s+0.49)\,(s+2.94)}, \tag{18}$$

$$c_2 = \frac{278.2\,(s+0.003)\,(s+0.052)\,(s+0.54)}{(s+0.0027)\,(s+0.016)\,(s+4)\,(s+20)}. \tag{19}$$

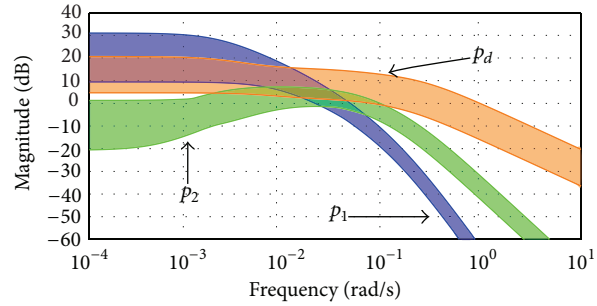

Figure 10: Frequency response magnitude plots of plants.

Table 2: Load-sharing planning along the frequency band.

Ω	0.005	0.02	0.05	0.2	0.5	1	10
p_1	×	×					
p_2		×	×	×	×	×	×

In Figure 12, closed-loop frequency responses illustrate the achievement of control specifications and the control effort that is used for it. Only the envelopes of a set of 112 frequency responses are depicted for each plant. In summary, the originality of this example relapses in the engineering character of the MISO plant, the robustness of the new methodology (model uncertainty consideration), and the challenge of disturbance incorporation through a dynamical model with uncertainty.

For comparison purposes, a master controller is firstly designed for the summation of plants $p_e = p_1 + p_2$ in order to meet the same robust control specifications

$$c_m = \frac{280\,(s+0.0044)\,(s+0.058)\,(s+0.38)\,(s+0.58)}{s\,(s+0.018)\,(s+0.49)\,(s+4)\,(s+20)}. \tag{20}$$

The parallel arrangement and the master controller behave equally attending to the prescribed stability and performance. However, the parallel one is superior in terms

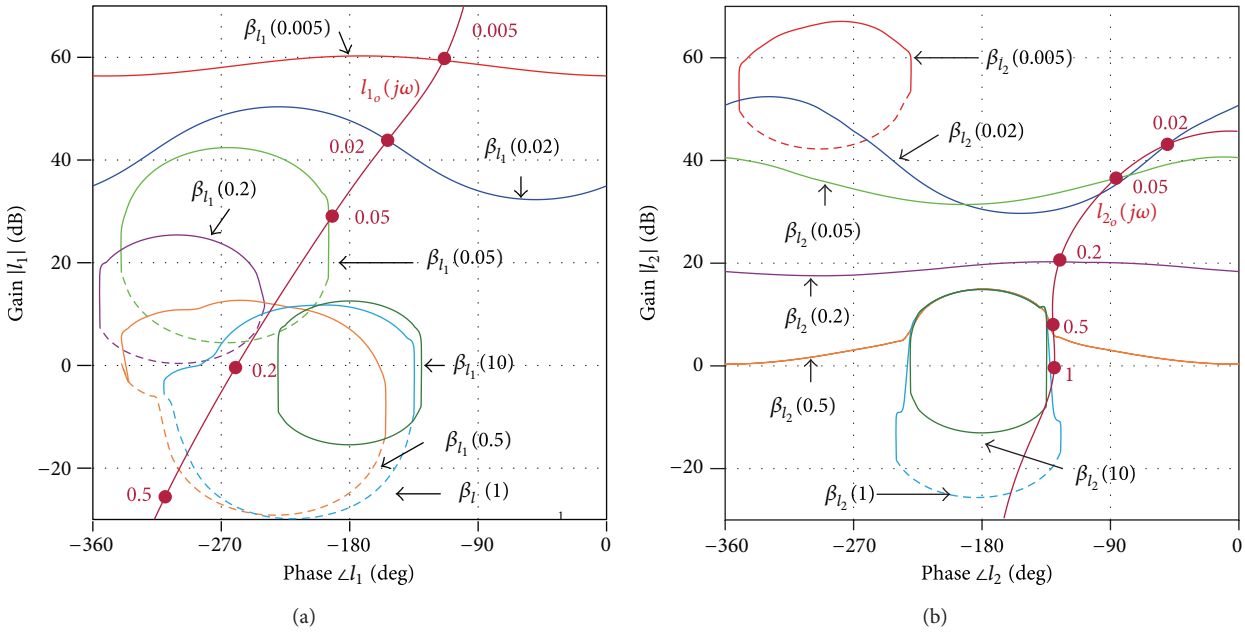

Figure 11: Loop-shaping of controllers.

of the actuation signals. The same reasoning and benefits of example 1 can be extended to this example.

Secondly, comparisons of the parallel arrangement and the master-slaves structures are shown. The master-slaves structure (Figure 1(b) with $c_m \neq 1$, $c_1 \neq 1$, and $c_2 \neq 1$) can be considered a particular case of the parallel structure ($c_m = 1$), since this last one will be demonstrated more versatile. Attending their functionality as filters, let us rename slave c_1 as filter f_1 and slave c_2 as filter f_2. Let us suppose that c_1 (18) and c_2 (19) have already been designed for a parallel control structure. Then, there would not be a single equivalence for them in the master-slaves structure. Equivalents should meet: $c_m f_1 = c_1$ and $c_m f_2 = c_2$. A practical solution would be firstly to assume the master c_m of (20), as long as its output performance matches that of the set c_1 (18) and c_2 (19). And secondly, to overcome the drawbacks of master control for parallel plants, filters are computed as $f_1 = c_1/c_m$ and $f_1 = c_1/c_m$ with c_1 (18) and c_2 (19). This equivalence procedure is also reliable in example 1. The inverse procedure, that is, the direct design of f_1, f_2, and c_m can be successfully done in example 1; however, it would become extremely difficult in example 2 for the following reasons. The master-slaves method firstly addresses the design of the filters and then the master. As a first difficulty, the filters have to perform the load sharing in frequency terms, but their manual open-loop design would not meet quantitative closed-loop criteria. Besides, the uncertainty in parallel plant models (p_1, p_2) hinders the choice of the cut-off frequency and the roll-off of the filters. Another difficulty is that the disturbance participation through dynamical models (p_d) makes impossible to guess the best load sharing along the frequencies between the parallel plants (p_1, p_2), and then it hinders a suitable parametrization of filters. At a second step of the master-slave method of design, the master would be designed, taking into account the initial MISO plant and the branch filters. In this stage, filter roll-offs may add serious problems: a high roll-off improves the filtering power but the branch phase deviates far from the original plant phase. Thus, branches can reach counter-phase conditions at certain frequencies. In such a case, a master controller spoils plant collaborations, since the vectorial sum $l_t = l_1 + l_2$ yields a smaller modulus than l_1 and l_2.

Remark 4. A common engineering problem is solved: the robust regulation of output-flow temperature in a heat exchanger manipulating the input-flow heating power and the input heating flow itself, for different production rates (output-flows). Model uncertainty is fully considered to obtain the minimum amount of feedback controllers, whose benefits are detailed in previous examples. Additionally, the difficulties exhibited by the master-slaves strategy are overcome. The challenge is due to plant uncertainty and to the dynamical incorporation of disturbances.

3.3. Example 3. Despite the large number of engineering systems that have more than two manipulated inputs and single regulated output, few applications of this kind have been solved [40] so far. In fact, only a few scientific works incorporate a control theory for n inputs [25, 26, 45, 48, 56] because of its complexity. In this sense, the following example tries to demonstrate the potential of the new methodology. Consider a system with three manipulated inputs and a single regulated output, whose transfer function models are

$$p_i = \frac{k_i (a_i s + 1)}{(b_i s + 1)(c_i s + 1)}, \quad i = 1, 2, 3, \tag{21}$$

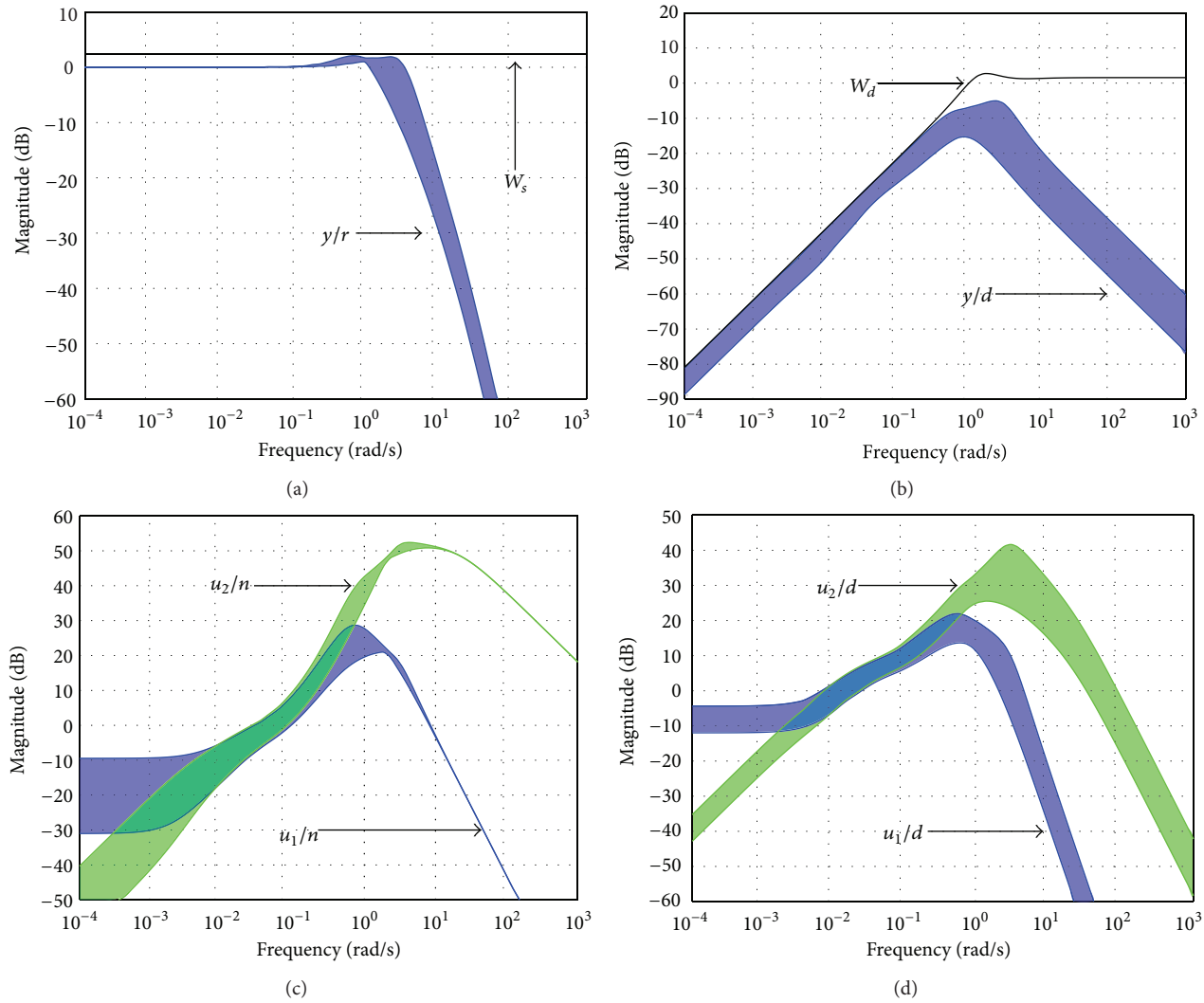

Figure 12: Closed-loop frequency response magnitude plots.

which are particularised for each i input by $k_1 = 100$, $k_2 = 10$, $k_3 = 1$, $a_1 = 10$, $a_2 = a_3 = 0$, $b_1 = 1000$, $b_2 = b_3 = 0.01$, and $c_1 = 0.1$, $c_2 = c_3 = 0$. Disturbances come into the single output straightforward, $p_d = 1$. As the difficulty of this example relapses on dealing with three actuators, parameter uncertainty has been intentionally omitted in the p_i plant models. Stability and disturbance rejection have to be attended meeting (4), (8) and (5), (9), respectively.

Upper section of Table 3 shows the amount of feedback $|c_i|$ that a single branch $c_i p_i$ would demand at the design phase $\Theta_d \approx -90^\circ$ to meet the specifications by itself. Note that the selection of design phase is part of the designer tasks. Previous examples depicted control necessities on the Nichols chart, that is, for all possible design phases $[-360^\circ, 0^\circ]$. Consequently with the upper part, the bottom of Table 3 shows the planning on load sharing along the frequencies; revise the criteria in Section 2.3 to decide plant collaborations or not as a function of feedback demand $|c_i|$.

Accordingly to results and choices on Table 3, the loop-shaping of each l_i, $i = 1, 2, 3$ is sequentially performed

Table 3: (Up) Feedback demand; (down) load-sharing planning.

Ω	0.001	0.01	0.05	0.1	0.5	1	5	10	100
$\lvert c_1 \rvert$	43	40	39	37	26	20	6	−3	20
$\lvert c_2 \rvert$	60	40	27	23	20	20	19	13	40
$\lvert c_3 \rvert$	80	60	46	40	26	20	5	−6	3
Ω	0.001	0.01	0.05	0.1	0.5	1	5	10	100
p_1	×	×			×	×	×	×	
p_2		×	×	×	×	×			
p_3					×	×	×	×	×

(see the final arrangements in Figure 13). The achieved controllers are

$$c_1 = \frac{584.7(s + 0.0007)(s + 0.39)(s + 7.68)\left(s^2 + 0.132s + 0.009\right)}{s(s + 0.0068)(s + 0.08)(s + 9)(s + 86)\left(s^2 + 0.98s + 0.33\right)}, \quad (22)$$

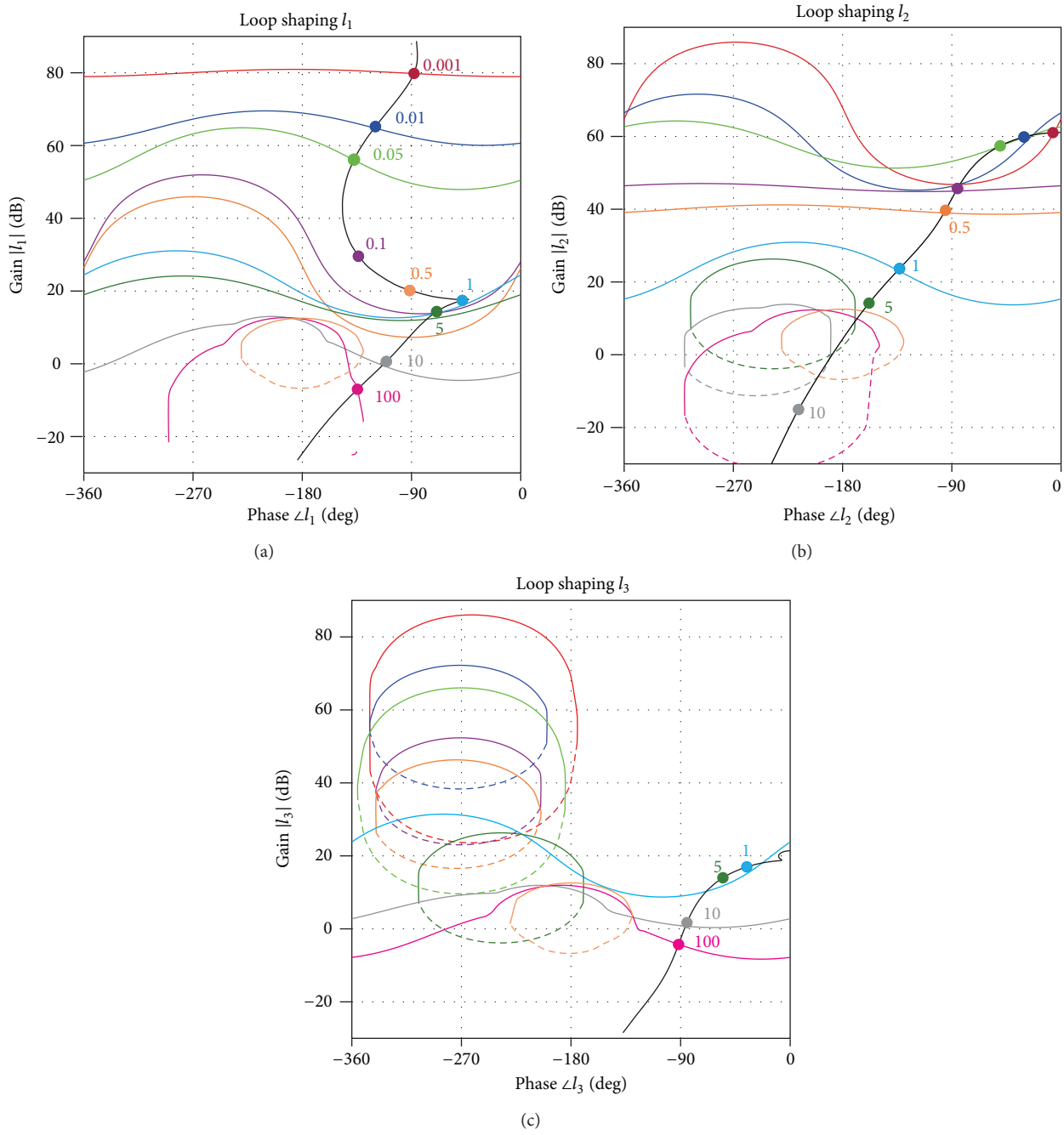

Figure 13: Loop-shaping of three parallel controllers.

$$c_2 = \frac{32.4\,(s+0.1)}{(s+0.0087)\,(s+0.63)\,(s+5.27)}, \tag{23}$$

$$c_3 = \frac{6.155\,(s+0.01)}{(s+0.007355)\,(s+0.7128)}. \tag{24}$$

Figure 14 depicts the expected feedback sharing along the frequency band (Table 3) in terms of branch open-loop functions $|l_i|$ and their contribution to the global open-loop function $|l_t| = |l_1 + l_2 + l_3|$ in dB units.

The originality of this theoretical example relapses mainly in two challenges: facing regulatory problems with more than two manipulated inputs and dealing with parallel plants when some of them must work in disjoint bands of frequencies. Note that p_1 joins first at $\omega \in [0.001, 0.01]$ and later on at $\omega \in [0.5, 10]$. This causes that there is not an equivalent for c_1 (22), c_2 (23), and c_3 (24) in a serial structure (Figure 1(a)). Let us rename serial controllers as c_1^s, c_2^s, and c_3^s. The equivalents can be computed as $c_1^s = c_1$, and $c_2^s = -c_2/c_1$, $c_3^s = -c_3/c_2$, which would yield a nonproper controller c_3^s. On the other hand, it is not feasible either a straight away design of the serial controllers c_i^s using a main-vernier strategy, since the load sharing planning (Table 3) does not allow sorting the

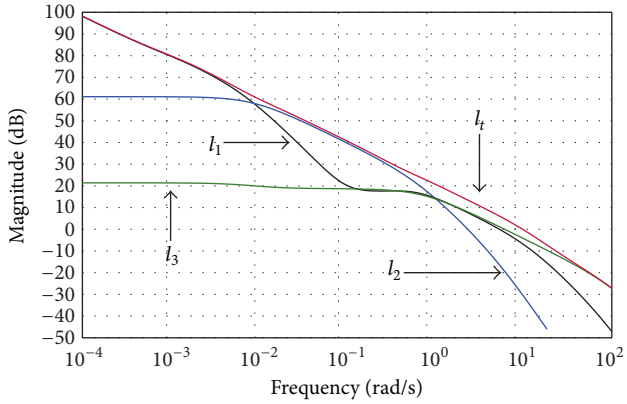

Figure 14: Open-loop responses on magnitude Bode diagram.

plants from faster to slower (p_1 joins at discontinuous intervals of frequencies). That is, the serial strategy is conceived for that each plant works in one and only one frequency interval.

Remark 5. This example tries to illustrate the new methodology ability (i) to solve regulatory problems of more than two manipulated inputs, which are frequent in engineering applications but are not so common in the scientific literature and (ii) to deal with parallel plants when some of them must work in disjoint bands of frequencies. For this last case, a serial structure of controllers (main-vernier) fails.

4. Conclusions

In attention to engineering application demands, a parallel structure of controllers has been proposed to solve MISO regulatory problems, which concern robust stability and robust disturbance rejection. MISO plant models included parametric uncertainty. Inside a QFT framework, a new methodology of design was proposed with the aim of tuning a set of controllers that met the robust specifications, and simultaneously, each controller used the least possible gain at each frequency. The keypoint was to quantify the feedback demanded by each plant at each frequency to meet the specifications by itself. This allowed a planning of the best load sharing along the frequency band. At each frequency, either one or several plants in collaboration must assume feedback responsibilities to meet the specifications or the plant/s participation must be inhibited for feedback saving. To accomplish it, a sequential design of the parallel controllers was fully detailed, using current QFT software tools for bound computations and for loop-shapings.

The abilities and engineering interest of the new methodology were demonstrated through several examples. The first one illustrated the methodology and detailed the benefits of a parallel structure of robust controllers in comparison with a single robust master controller. The main advantages are (i) to reduce the sensor noise amplification in the actuators of the slowest plants, which are conceived to work in the band of lower frequencies and provide the stationary and (ii) to avoid unnecessary offsets in the actuators of the faster plants, and consequently, that their full range of actuation is available to speed up the response with less risk of saturation. Nevertheless, these are also the aims of current MISO methodologies, whose weak points have been also overcome by the new technique. In particular, a second engineering example exhibited the difficulties of tuning a parallel control using the master-slave philosophy. The challenge is mainly the filter (slaves) design due to plant uncertainties and the dynamic incorporation of disturbances, which are common in real-life plants. A third example illustrated the weak points of a chained serial structure of controllers (main-vernier), which fails when plants must work in disjoint bands of frequencies. In any case, the proposed parallel structure can always be converted to both master-slaves or main-vernier structures. The inverse procedure was demonstrated as not always being possible. In addition, the third example showed the difficulty of facing a MISO problem with three manipulabled variables, which are not common in the scientific literature but are frequent in engineering applications.

Conflict of Interests

The authors declare that there is no conflict of interests regarding the publication of this paper.

Acknowledgment

The authors are grateful for the assistance provided by La Rioja Government through Project IMPULSA 2010/01 and through ADER Grant 2012-I-IDD-00093.

References

[1] M. N. Marwali, J.-W. Jung, and A. Keyhani, "Control of distributed generation systems—part II: load sharing control," *IEEE Transactions on Power Electronics*, vol. 19, no. 6, pp. 1551–1561, 2004.

[2] E. Eitelberg, "Macrodynamic feedback interaction between trade and production," *International Journal of Robust and Nonlinear Control*, vol. 17, no. 2-3, pp. 203–224, 2007.

[3] M. Garcia-Sanz and F. Y. Hadaegh, "Load-sharing robust control of spacecraft formations: deep space and low Earth elliptic orbits," *IET Control Theory and Applications*, vol. 1, no. 2, pp. 475–484, 2007.

[4] I. Horowitz, *Synthesis of Feedback Systems*, 1963.

[5] M. Kano and M. Ogawa, "The state of the art in chemical process control in Japan: good practice and questionnaire survey," *Journal of Process Control*, vol. 20, no. 9, pp. 969–982, 2010.

[6] S. K. Jha and N. Kaistha, "Valve positioning control for process through-put maximization," *Chemical Engineering Research and Design*, vol. 85, no. 11, pp. 1465–1475, 2007.

[7] B. J. Allison and A. J. Isaksson, "Design and performance of mid-ranging controllers," *Journal of Process Control*, vol. 8, no. 5-6, pp. 469–474, 1998.

[8] B. J. Allison and S. Ogawa, "Design and tuning of valve position controllers with industrial applications," *Transactions of the Institute of Measurement and Control*, vol. 25, no. 1, pp. 3–16, 2003.

[9] C.-C. Yu and W. L. Luyben, "Analysis of valve-position control for dual-input processes," *Industrial and Engineering Chemistry Fundamentals*, vol. 25, no. 3, pp. 344–350, 1986.

[10] R. B. McLain, M. J. Kurtz, M. A. Henson, and F. J. Doyle III, "Habituating control for nonsquare nonlinear processes," *Industrial and Engineering Chemistry Research*, vol. 35, no. 11, pp. 4067–4077, 1996.

[11] R. Monroy-Loperena, R. Solar, and J. Alvarez-Ramirez, "Balanced control scheme for reactor/separator processes with material recycle," *Industrial and Engineering Chemistry Research*, vol. 43, no. 8, pp. 1853–1862, 2004.

[12] A. Velasco-Perez, J. Alvarez-Ramirez, A. Velasco, and R. Solar-Gonzalez, "Control múltiple entrada una salida (miso) de un cstr," *Revista Mexicana De Ingeniería Química*, vol. 10, no. 2, pp. 321–331, 2011.

[13] O. A. Prado-Rubio, S. B. Jorgensen, and G. Jonsson, "Ph control structure design for a periodically operated membrane separation process," *Computers and Chemical Engineering*, vol. 43, pp. 120–129, 2012.

[14] S. Haugwitz, P. Hagander, and T. Norén, "Modeling and control of a novel heat exchange reactor, the open plate reactor," *Control Engineering Practice*, vol. 15, no. 7, pp. 779–792, 2007.

[15] S. Velut, L. de Maré, and P. Hagander, "Bioreactor control using a probing feeding strategy and mid-ranging control," *Control Engineering Practice*, vol. 15, no. 2, pp. 135–147, 2007.

[16] M. Karlsson, O. Slätteke, B. Wittenmark, and S. Stenström, "Reducing moisture transients in the paper-machine drying section with the mid-ranging control technique," *Nordic Pulp and Paper Research Journal*, vol. 20, no. 2, pp. 150–155, 2005.

[17] A. Velasco-Pérez and J. Alvarez-Ramírez, "Algorithm for parallel control for an aerobic reactor with a recirculation current," *Revista Mexicana De Ingeniería Química*, vol. 6, no. 2, pp. 229–236, 2007.

[18] M. A. Henson, B. A. Ogunnaike, and J. S. Schwaber, "Habituating control strategies for process control," *AIChE Journal*, vol. 41, no. 3, pp. 604–618, 1995.

[19] D. F. Marselle, M. Morari, and D. F. Rudd, "Design of resilient processing plants-II design and control of energy management systems," *Chemical Engineering Science*, vol. 37, no. 2, pp. 259–270, 1982.

[20] L. Giovanini, "Cooperative-feedback control," *ISA Transactions*, vol. 46, no. 3, pp. 289–302, 2007.

[21] G. F. Fauth and F. G. Shinskey, "Advanced control of distillation columns," *Chemical Engineering Progress*, vol. 71, no. 6, pp. 49–54, 1975.

[22] F. G. Shinskey, "Energy-conserving control systems for distillation units," *Chemical Engineering Progress*, vol. 72, no. 5, pp. 73–78, 1976.

[23] F. G. Shinskey, "Control systems can save energy," *Chemical Engineering Progress*, vol. 74, no. 5, pp. 43–46, 1978.

[24] S. J. Williams, D. Hrovat, C. Davey, D. Maclay, J. W. V. Crevel, and L. F. Chen, "Idle speed control design using an H-infinity approach," in *Proceedings of the American Control Conference*, pp. 1950–1956, June 1989.

[25] S. Jayasuriya and M. A. Franchek, "A qft-type design methodology for a parallel plant structure and its application in idle speed control," *International Journal of Control*, vol. 60, no. 5, pp. 653–670, 1994.

[26] V. Besson and A. T. Shenton, "Interactive parameter space design for robust performance of MISO control systems," *IEEE Transactions on Automatic Control*, vol. 45, no. 10, pp. 1917–1924, 2000.

[27] P. Gorzelic, E. Hellstrom, A. Stefanopoulou, L. Jiang, and S. Gopinath, "A coordinated approach for throttle and wastegate control in turbocharged spark ignition engines," in *Proceedings of the 24th Control and Decision Conference (CCDC '12)*, pp. 1524–1529, 2012.

[28] N. Ravi, H.-H. Liao, A. F. Jungkunz, and J. C. Gerdes, "Mid-ranging control of a multi-cylinder HCCI engine using split fuel injection and valve timings," in *Proceedings of the 6th IFAC Symposium Advances in Automotive Control (AAC '10)*, pp. 797–802, July 2010.

[29] S. Jade, E. Hellstrom, L. Jiang, and A. G. Stefanopoulou, "Fuel governor augmented control of recompression hcci combustion during large load transients," in *Proceedings of the American Control Conference*, pp. 2084–2089, 2012.

[30] S. Jade, J. Larimore, E. Hellstrom, L. Jiang, and A. G. Stefanopoulou, "Enabling large load transitions on multicylinder recompression hcci engines using fuel governors," in *Proceedings of the American Control Conference*, pp. 4423–4428, 2013.

[31] J. Zhai, Y. Huang, S. Schroeck, W. Messner, D. D. Stancil, and T. E. Schlesinger, "High bandwidth electro-optic scanner for optical data storage," *Japanese Journal of Applied Physics*, vol. 39, no. 2, pp. 883–887, 2000.

[32] A. Al Mamun, I. Mareels, T. H. Lee, and A. Tay, "Dual stage actuator control in hard disk drive—a review," in *Proceedings of the 29th Annual Conference of the IEEE Industrial Electronics Society*, pp. 2132–2137, November 2003.

[33] T. Gao, C. Du, C. P. Tan, Z. He, J. Yang, and L. Xie, "High bandwidth control design and implementation for a dual-stage actuation system with a microthermal actuator," *IEEE Transactions on Magnetics*, vol. 49, no. 3, pp. 1082–1087, 2013.

[34] J. Sun, F. Cameron, and B. W. Bequette, "A habituating blood glucose control strategy for the critically ill," *Journal of Process Control*, vol. 22, no. 8, pp. 1411–1421.

[35] K. Aström and T. Hägglund, *Control Pid Avanzado*, Pearson Prentice Hall, 2009.

[36] V. Lersbamrungsuk, T. Srinophakun, S. Narasimhan, and S. Skogestad, "Control structure design for optimal operation of heat exchanger networks," *AIChE Journal*, vol. 54, no. 1, pp. 150–162, 2008.

[37] J. Alvarez-Ramirez and H. Puebla, "On classical PI control of chemical reactors," *Chemical Engineering Science*, vol. 56, no. 6, pp. 2111–2121, 2001.

[38] J. Alvarez-Ramirez, A. Velasco, and G. Fernandez-Anaya, "A note on the stability of habituating process control," *Journal of Process Control*, vol. 14, no. 8, pp. 939–945, 2004.

[39] B. J. Lurie and P. Enright, *Classical Feedback Control: With MATLAB*, Control Engineering, Taylor & Francis, 2000.

[40] R. L. Grogan, G. H. Blackwood, and R. J. Calvet, "Optical delay line nanometer level pathlength control law design for space-based interferometry," in *Proceedings of the International Society for Optical Engineering (SPIE '98)*, pp. 14–25, March 1998.

[41] G. W. Neat and A. Abramovici, "Control technology lessons learned: case study using the micro-precision interferometer testbed," in *Proceedings of the American Control Conference*, vol. 2, 1998.

[42] J. Daeges, B. Lurie, and A. Bhanji, "An improved high-voltage dc regulator for a radar and communication transmitter," in *Proceedings of the 18th IEEE Conference Record of the Power Modulator Symposium*, pp. 106–108, 1988.

[43] Q.-G. Wang, Y. Zhang, W.-J. Cai, Q. Bi, and C.-C. Hang, "Cooperative control of multi-input single-output processes: on-line strategy for releasing input saturation," *Control Engineering Practice*, vol. 9, no. 5, pp. 491–500, 2001.

[44] L. L. Giovanini, "Flexible-structure control: a strategy for releasing input constraints," *ISA Transactions*, vol. 43, no. 3, pp. 361–376, 2004.

[45] E. Eitelberg, *Load Sharing Control*, NOYB Press, 1999.

[46] E. Eitelberg, "Load sharing in a multivariable temperature control system," *Control Engineering Practice*, vol. 7, no. 11, pp. 1369–1377, 1999.

[47] E. Eitelberg, "Some peculiarities of load sharing control," *International Journal of Robust and Nonlinear Control*, vol. 13, no. 7, pp. 607–618, 2003.

[48] S. J. Schroeck, W. C. Messner, and R. J. McNab, "On compensator design for linear time-invariant dual-input single-output systems," *IEEE/ASME Transactions on Mechatronics*, vol. 6, no. 1, pp. 50–57, 2001.

[49] S. Brennan and A. Alleyne, "Integrated vehicle control via coordinated steering and wheel torque inputs," in *Proceedings of the American Control Conference*, pp. 7–12, June 2001.

[50] B. J. Allison and J. B. Ball, "Constrained model predictive control of blow tank consistency," *Control Engineering Practice*, vol. 12, no. 7, pp. 837–845, 2004.

[51] S. Haugwitz, M. Karlsson, S. Velut, and P. Hagander, "Anti-windup in mid-ranging control," in *Proceedings of the 44th IEEE Conference on Decision and Control, and the European Control Conference (CDC-ECC '05)*, pp. 7570–7575, December 2005.

[52] M. Karlsson, O. Slatteke, T. Hagglund, and S. Stenstrom, "Feedforward control in the paper machine drying section," in *Proceedings of the American Control Conference*, 2006.

[53] S. Gayadeen and W. Heath, "An internal model control approach to mid-ranging control," in *Proceedings of the 7th IFAC International Symposium on Advanced Control of Chemical Processes (ADCHEM '09)*, pp. 542–547, July 2009.

[54] W. P. Heath and S. Gayadeen, "Simple robustness measures for control of miso and simo plants," in *IFAC Proceedings*, vol. 18, pp. 11356–11361, 2011.

[55] I. Horowitz, *Quantitative Feedback Design Theory (QFT)*, QFT Publications, Boulder, Colorado, USA, 1993.

[56] P.-O. Gutman, E. Horesh, R. Guetta, and M. Borshchevsky, "Control of the aero-electric power station—an exciting qft application for the 21st century," *International Journal of Robust and Nonlinear Control*, vol. 13, no. 7, pp. 619–636, 2003.

[57] F. G. Shinskey and J. H. P. Castellanos, "Sistemas de control de procesos: aplicación, diseño y sintonización," in *Sistemas De Control De Procesos: Aplicación, Diseño Y Sintonización*, McGraw-Hill, 1996.

[58] A. Gera and I. Horowitz, "Optimization of the loop transfer function," *International Journal of Control*, vol. 31, no. 2, pp. 389–398, 1980.

[59] C. Borghesani, Y. Chait, and O. Yaniv, *Quantitative Feedback Theory Toolbox. For Use With Matlab*, Terasoft, 2nd edition, 2002.

[60] F. Instruments, Limited Proces control, http://www.fbk.com.

[61] J. Rico and M. Gil-Martinez, "Multivariable QFT robust control of a heat exchanger," in *Proceedings of the 19th Mediterranean Conference on Control and Automation (MED '11)*, pp. 588–593, June 2011.

Research Article

An Improved Phase Disposition SPWM Strategy for Cascaded Multilevel Inverter

Jinbang Xu,[1] Zhizhuo Wu,[1] Xiao Wu,[2] Fang Wu,[1] and Anwen Shen[1]

[1] *Huazhong University of Science and Technology, Wuhan, Hubei 430074, China*
[2] *Guangdong University of Technology, Guangzhou, Guangdong 510006, China*

Correspondence should be addressed to Anwen Shen; sawyi@mail.hust.edu.cn

Received 21 August 2013; Revised 2 December 2013; Accepted 4 December 2013; Published 19 March 2014

Academic Editor: Tao Li

The Carrier Phase Shifted (CPS) strategy is conventional for cascaded multilevel inverter, because it can naturally ensure all cascaded cells to output balanced power. However, in point of spectra of the output line voltage, CPS is suboptimal to Phase Disposition (PD) strategy, because the latter can not naturally ensure power balance. This paper presents an improved PD strategy, inspiration from the disposition of CPS strategy triangle carriers. Just reconstructing the triangle carriers of PD strategy, it can not only reserve the waveform quality of the line voltage to be optimal, but also naturally ensure the output power of each cascaded cells to be balanced.

1. Introductions

The cascaded multilevel inverters are widely implemented in the high power AC drivers and power management systems with a medium or high voltage level [1–5]. The structure of the cascaded multilevel inverters is shown in Figure 1. It is constructed with several full bridge inverters with the same topology. The advantages of the cascaded multilevel inverters include being simple to control, being easy in output voltage level extension, modular design and implementation, and the fault tolerance control realization [6–10].

The Carriers Phase Shift (CPS) control is one of the conventional control schemes employed in the cascaded multilevel inverters. The control signals for each cascaded unit are generated by comparison between N (N is the number of cascaded units) triangle carrier and the modulated signal. The carrier waveform is chosen with a phase shift of $360/N$ degree. The fundamental component amplitude of each unit driving signal is the same. So the output power of each unit is balanced [11–14].

Except for the CPS control method, Phase Disposition (PD), Phase Opposite Disposition (POD), and Alternative Phase Opposite Disposition (APOD) are three other carry deposition control strategies used in multilevel inverters [15]. In [10], under the condition of same switching frequency, the output line voltage waveforms with both the CPS and PD control methods are compared. It is indicated that the experiment result with the PD control method is better than that with the CPS control.However, PD cannot achieve power balance spontaneously. According to [16], each cascaded unit outputs the PWM under the previous setting cycle and the output power will be balanced after $N/2$ output periods. This balance strategy is easy, but the power balance time increases with the cascade units increasing.

To shorten the time of power balance, this paper proposes an improved PD control strategy. By improving the carrier wave for modulation, the output power of each cascaded unit can be balanced in an output cycle, and the switching frequency of each switch tube is equal to each other at the same time. The output line voltage waveform quality is maintained to be optimized as that of the PD control. An experimental prototype of a 5 kW three-phase cascaded multilevel inverter is designed to verify the validity of this improved PD control.

2. CPS and PD Control Strategy

2.1. Principle. The principle of the CPS control strategy based on a two-unit cascaded multilevel inverter is shown in Figure 2(a). The triangular carrier of tri.1~tri.4 and the reference signal v_{ref} are combined to generate the control

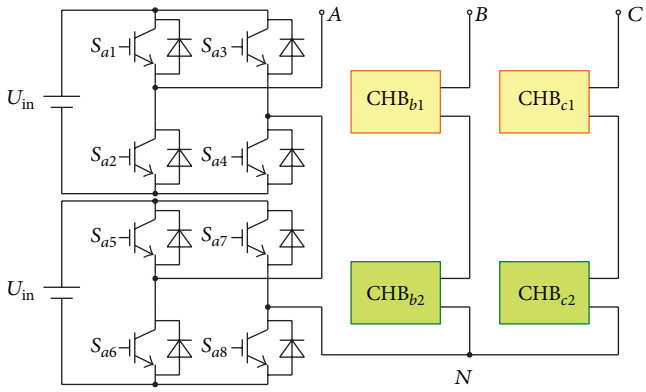

FIGURE 1: Cascaded five-level inverter.

signal for the bridges. The triangular carrier signal is arranged with 90 degree phase shift between the adjacent ones. The control signal modulation is performed with the following principle.

The drive signal for H_{a1} is generated by comparing v_{ref} with tri.1 and tri.3. And the drive signal for H_{a2} is generated by comparing v_{ref} with tri.2 and tri.4. As is shown in Figure 2(a), the u_{Ha1} and u_{Ha2} are the output voltage of the full bridges, respectively. And the u_{AN} is the output voltage of phase A.

In Figure 2(b), the modulation principle of the PD control strategy is illustrated. Like that of CPS, a combination of four triangular carrier signals is implemented with the same phase but different amplitude range. The amplitude of the carrier is distributed evenly in the whole carrier amplitude. The modulation of PD strategy is comparing the v_{ref} with tri.1 and tri.4 to obtain the drive signal of H_{a1} and with tri.2 and tri.3 to obtain the drive signal of H_{a2}. In Figure 2(b), the full bridge output voltage of each inverter unit is shown as u_{Ha1} and u_{Ha2}. And the output voltage of phase A is shown as u_{AN}.

It is obvious that the switching frequencies of the two units are identical in the CPS strategy. But with the PD strategy, the drive signal shows much difference between the two units. The switching frequencies of the two bridges are different. And at the same time, when the PD strategy is employed, the amplitudes of fundamental component in the output voltage of the two units are different. This means that the output power of the two units is not balanced. So when the PD strategy is directly implemented in the cascaded multilevel inverter, the output power and the switching frequency of the cascaded units are not the sameThis brings a lot of practical design problems. The rated power and the cooling design of the power units is hard to determine.

2.2. Voltage Harmonics Comparison. With the different triangular carrier waveform used in the two modulation strategies of PD and CPS, the output voltage of phase A, u_{AN} produced is different. The voltage harmonic is analyzed to reveal the difference and the Flourier transformation is implemented to illustrate the spectral characteristics of the two voltage waveforms.

The modulation of the SPWM control is performed by comparison between the reference signal and the triangular carrier. The Flourier expression of the phase voltage can be divided into three parts: The first part is the integer order harmonics of the reference signal; the second part is the integer order harmonics of the triangular carrier signal; the third part is the sideband harmonics which are centralized to integer order harmonics of the carrier signal.

The extended Flourier expression of the voltage waveform is shown in

$$\begin{aligned} u_{AN}(t) = {} & \frac{A_{00}}{2} \\ & + \sum_{n=1}^{\infty} \left[A_{0n} \cos\left(n\omega_o t\right) + B_{0n} \sin\left(n\omega_o t\right)\right] \\ & + \sum_{m=1}^{\infty} \sum_{n=-\infty}^{\infty} \left[A_{mn} \cos\left(n\omega_o t + m\omega_c t\right)\right. \\ & \left. + B_{mn} \sin\left(n\omega_o t + m\omega_c t\right)\right], \end{aligned} \tag{1}$$

in which ω_o and ω_c are the frequency of the sinusoidal reference signal and the triangular carrier, m and n are integer, and A_{00} is the dc component, while A_{mn} and B_{mn} are the harmonic coefficient of the integer order harmonics and the sideband harmonics.

Then the output voltage of PD modulation is analyzed with Double Fourier series expansion as follows:

$$\begin{aligned} u_{\text{PD\_}AN}(t) = {} & NM_r U_{\text{in}} \sin\left(\omega_o t\right) \\ & + \sum_{m=1}^{\infty} \sum_{n=-\infty}^{+\infty} \left\{B_{p1}(m,n)\right. \\ & \left. \times \sin\left[\left(2m-1\right)\omega_c t + 2n\omega_o t\right]\right\} \\ & + \sum_{m=1}^{\infty} \sum_{n=-\infty}^{\infty} \left\{C_{p1}(m,n)\right. \\ & \left. \times \sin\left[2m\omega_c t + \left(2n-1\right)\omega_o t\right]\right\}, \end{aligned} \tag{2}$$

in which N is the cascaded unit number and U_{in} is the input voltage. Assuming that U_{om} is the amplitude of the fundamental component in the output voltage of each unit, the voltage transfer ratio of each unit M_r can be calculated as

$$M_r = \frac{U_{om}}{U_{\text{in}}}. \tag{3}$$

The $B_{p1}(m, n)$ and $C_{p1}(m, n)$ in (2) are the amplitude of the odd harmonics and the even harmonics

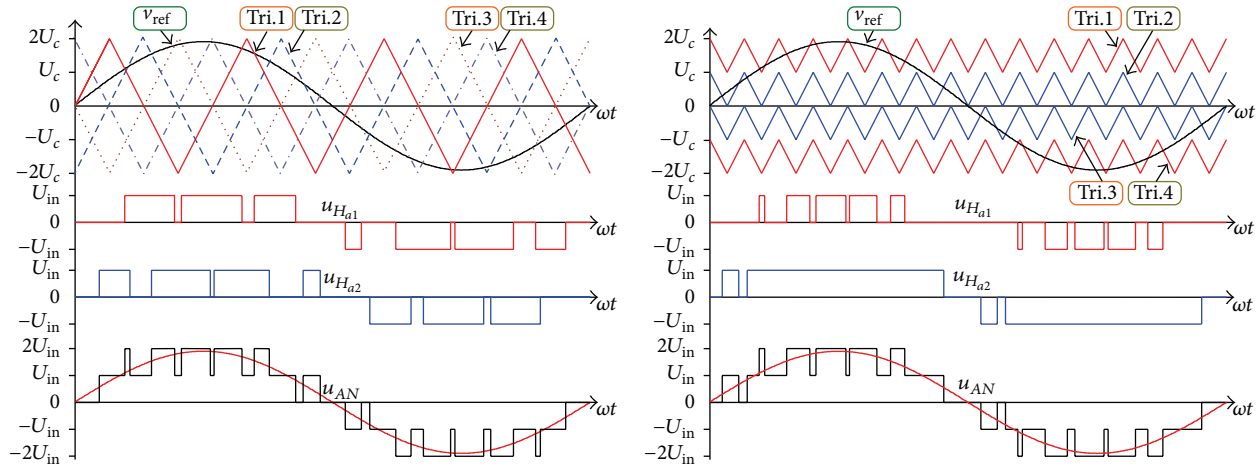

(a) CPS strategy (b) PD strategy

Figure 2: Modulation of CPS and PD control strategy.

of the reference signal. The value can be expressed as follows:

$$
\begin{aligned}
&B_{p1}(m,n)\\
&=\sum_{k=0}^{\infty}\left\{\frac{4U_{\text{in}}(-1)^k J_{(2k+1)}\left[(2m-1)\pi NM_r\right]}{\pi^2(2m-1)}\right.\\
&\quad\cdot\left[\frac{1}{2n-2k-1}\right.\\
&\qquad\times\left(-\sin\left[(2n-2k-1)\frac{\pi}{2}\right]\right.\\
&\qquad\quad+2\sum_{h=0}^{N-1}\left\{\cos(h\pi)\right.\\
&\qquad\qquad\cdot\sin\left[(2n-2k\ -1)\right.\\
&\qquad\qquad\quad\left.\left.\left.\left.\times\ \arccos\left(\frac{h}{NM_r}\right)\right]\right\}\right)\\
&\qquad+\frac{1}{2n+2k+1}\\
&\qquad\times\left(-\sin\left[(2n+2k+1)\frac{\pi}{2}\right]\right.\\
&\qquad\quad+2\sum_{h=0}^{N-1}\left\{\cos(h\pi)\right.\\
&\qquad\qquad\cdot\sin\left[(2n+2k+1)\right.\\
&\qquad\qquad\quad\left.\left.\left.\left.\left.\times\arccos\left(\frac{h}{NM_r}\right)\right]\right\}\right)\right]\Bigg\},\\
&C_{p1}(m,n)=\frac{U_{\text{in}}}{\pi m}J_{(2n-1)}(2m\pi NM_r).
\end{aligned}
\tag{4}
$$

In accordance with the phase voltage, the line voltage $u_{\text{PD\_}AB}$ can be expressed as follows:

$$
\begin{aligned}
u_{\text{PD\_}AB}(t)&=\sqrt{3}NM_rU_{\text{in}}\sin\left(\omega_o t+\frac{\pi}{6}\right)\\
&\quad+\sum_{m=1}^{\infty}\sum_{n=-\infty}^{+\infty}\left\{B_{l1}(m,n)\right.\\
&\qquad\times\sin\left[(2m-1)\omega_c t\right.\\
&\qquad\quad\left.\left.+2n\omega_o t-\frac{2n\pi}{3}\right]\right\}\\
&\quad+\sum_{m=1}^{\infty}\sum_{n=-\infty}^{\infty}\left\{C_{l1}(m,n)\right.\\
&\qquad\times\sin\left[2m\omega_c t+(2n-1)\omega_o t\right.\\
&\qquad\quad\left.\left.-\frac{(2n-1)\pi}{3}\right]\right\}.
\end{aligned}
\tag{5}
$$

In which, $B_{l1}(m,n)$ and $C_{l1}(m,n)$ are the amplitude of the line voltage harmonics. The value can be express in (6) and (7)

$$
B_{l1}(m,n)=2\sin\left(\frac{2n\pi}{3}\right)\cdot B_{p1}(m,n),
\tag{6}
$$

$$
C_{l1}(m,n)=2\sin\left[\frac{(2n-1)\pi}{3}\right]\cdot C_{p1}(m,n).
\tag{7}
$$

With the same principle, the phase voltage of CPS control strategy $u_{\mathrm{CPS\_}AN}$ can be expanded as follows:

$$u_{\mathrm{CPS\_}AN}(t) = NM_r U_{\mathrm{in}} \sin(\omega_o t) + \sum_{m=1}^{\infty}\sum_{n=-\infty}^{\infty}\left\{B_{p2}(m,n)\sin\left[2mN\omega_c' t + (2n-1)\omega_o t\right]\right\}, \tag{8}$$

in which, $B_{p2}(m,n)$ is the amplitude of the integer multiple harmonics with carrier frequency. The value can be expressed:

$$B_{p2}(m,n) = \frac{2U_{\mathrm{in}}}{\pi m} J_{(2n-1)}(m\pi NM_r). \tag{9}$$

And the output line voltage $u_{\mathrm{CPS\_}AB}$ can be expressed as follows:

$$u_{\mathrm{CPS\_}AB}(t) = NM_r U_{\mathrm{in}} \sin(\omega_o t) + \sum_{m=1}^{\infty}\sum_{n=-\infty}^{\infty}\left\{B_{l2}(m,n) \times \sin\left[2mN\omega_c' t + (2n-1)\left(\omega_o t - \frac{\pi}{3}\right)\right]\right\}, \tag{10}$$

in which

$$B_{l2}(m,n) = 2\sin\left[\frac{(2n-1)\pi}{3}\right]\cdot B_{p2}(m,n). \tag{11}$$

It is shown, through the comparison of (5) and (8), that when the following situation is satisfied, the major harmonics of the two control methods will appear with the same frequency

$$\omega_c = 2N\omega_c'. \tag{12}$$

When m is 1, the harmonics of PD and CPS control with the highest amplitude are around the carrier frequency ω_c. The high frequency filter design can be directly determined by the amplitude of the harmonic at this frequency. So the carrier frequency harmonics are compared. And for convenience, the amplitude with the carrier frequency of both two control strategies is defined as follows:

$$\begin{aligned} H_{\mathrm{PD\_}AN} &= \frac{\sqrt{\sum_{n=1}^{10} B_{p1}^2(1,n)}}{NM_r U_{\mathrm{in}}}, \\ H_{\mathrm{PD\_}AB} &= \frac{\sqrt{\sum_{n=1}^{10} B_{l1}^2(1,n)}}{\sqrt{3}NM_r U_{\mathrm{in}}}, \\ H_{\mathrm{CPS\_}AN} &= \frac{\sqrt{\sum_{n=1}^{10} B_{p2}^2(1,n)}}{NM_r U_{\mathrm{in}}}, \\ H_{\mathrm{CPS\_}AB} &= \frac{\sqrt{\sum_{n=1}^{10} B_{l2}^2(1,n)}}{\sqrt{3}NM_r U_{\mathrm{in}}}. \end{aligned} \tag{13}$$

Taking two unit cascaded inverters as an example ($N = 2$), (13) is calculated to obtain the relationship between the amplitude of the carrier harmonic and the voltage transfer ratio M_r in the range of $[0, 1]$. The result is shown in Figure 3.

Figure 3(a) shows that the phase voltage harmonics produced by the two control strategies are with the same amplitude. And in Figure 3(b), it is indicated that with both the two control schemes, the line voltage of is better than the phase voltage. This can be verified by (6) and (11). For that when n is an integral multiple of 3 in (6), the harmonic amplitude is 0, the harmonics with these frequencies are naturally eliminated in the line voltage. The same situation can be observed in (11), assuming that $(2n-1)$ is an integral multiple of 3.

And in Figure 3(b), the line voltage of the PD control method contains fewer harmonic than that of the CPS control. For a multilevel cascaded inverter implementation in the three-phase-three-wire system, the quality of the line voltage is an important performance requirement. And PD control method shows obvious advantages with this consideration.

3. Improved PD Control

As is analyzed above, although the line voltage quality of PD control is better than that of a CPS control, the PD control cannot be directly implemented. Because the disadvantages of the PD control method are unbalanced output power and different switching frequencies of the cascaded units. The PD control method has to be improved to be implemented in the multi-level cascaded inverter.

The improvement of the PD control can be done by changing the carrier signal waveform with observation of the difference between the PD and CPS modulation. The carrier signal of the CPS control in a carrier period is shown in Figure 4 for comparison.

As is shown in Figures 4(a) and 4(b), the waveform of the carrier signals in both CPS and PD control is equally divided into 8 parts, which is shown in dash grid in Figures 4(a) and 4(b). Through comparison of the carrier signal in the corresponding parts of the period, the following pattern can be discovered.

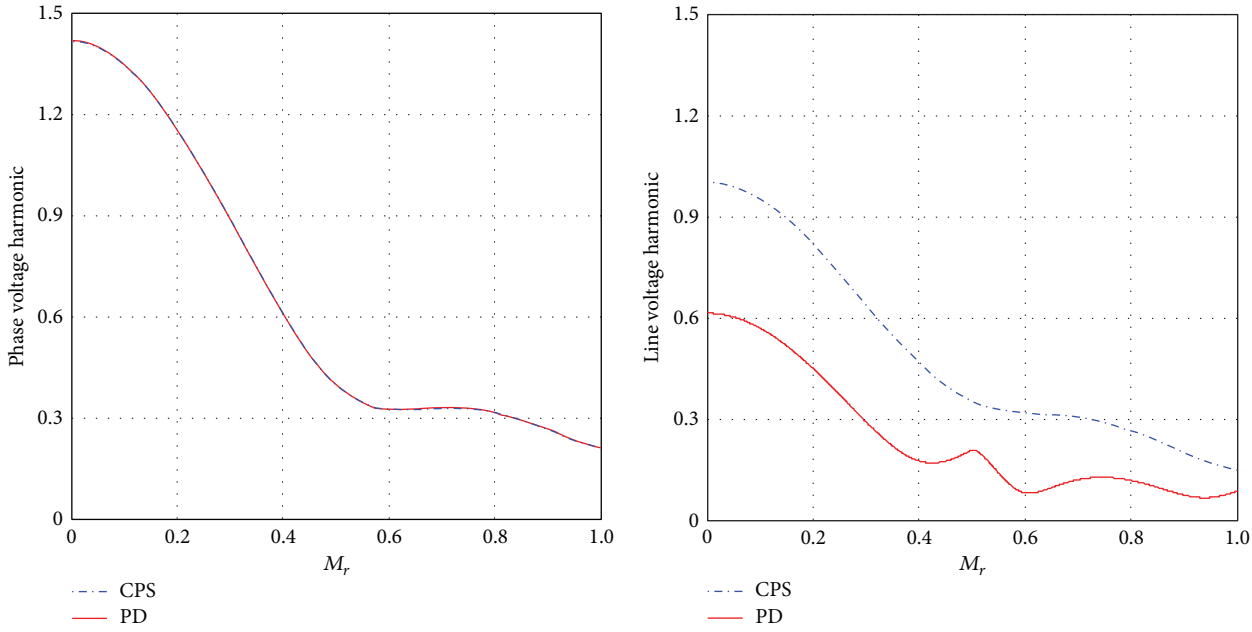

(a) Amplitude of ω_c voltage harmonic in phase voltage

(b) Amplitude of ω_c voltage harmonic in line voltage

FIGURE 3: Amplitude of ω_c voltage harmonic comparison of PD and CPS control.

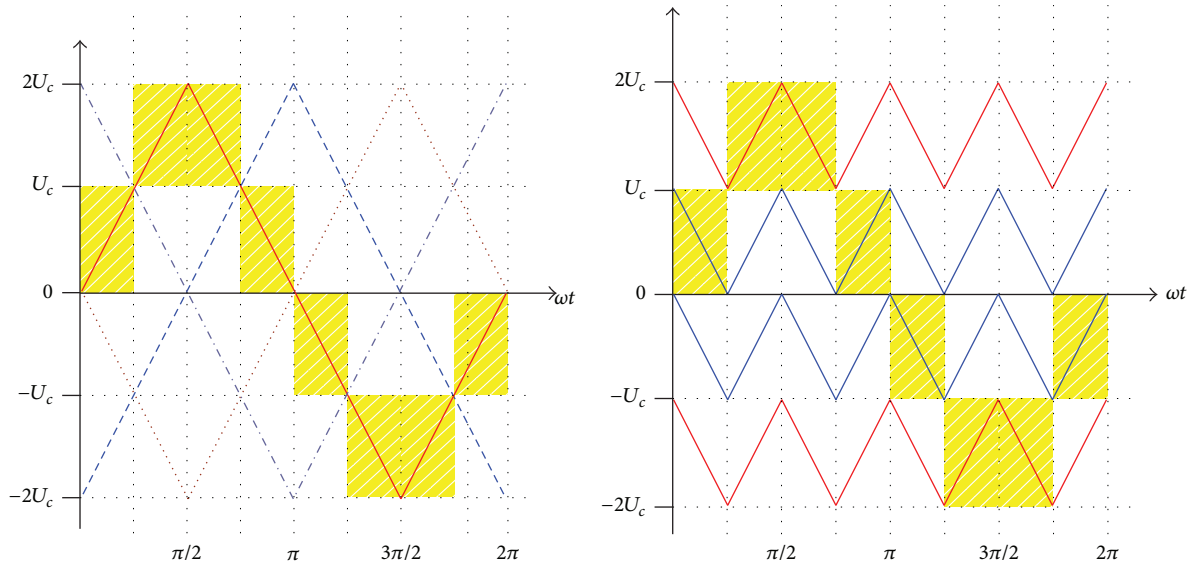

(a) CPS carrier signal

(b) PD carrier signal

FIGURE 4: Carrier signal comparison of CPS and PD control.

(1) In the parts of $\omega t \in [0, \pi/4] \cup [3\pi/4, \pi] \cup [5\pi/4, 7\pi/4]$, the slope of the CPS and PD carrier signal is the same.

(2) In the part of $\omega t \in [\pi/4, 3\pi/4] \cup [\pi, 5\pi/4] \cup [7\pi/4, 2\pi]$, the slope of the CPS and PD carrier signal is the opposite.

The shadow part of Figure 4(b) carrier waveform is separately arranged as a set of carriers, which is shown in Figure 5(a). Defined as Ca.1, compared with tri.1 in CPS control, the carrier signal set is no longer a triangular carrier. And the frequency of this carrier signal is the same as that of the CPS triangular carrier. The same separation can be done in the other parts of the PD carrier signal with the same

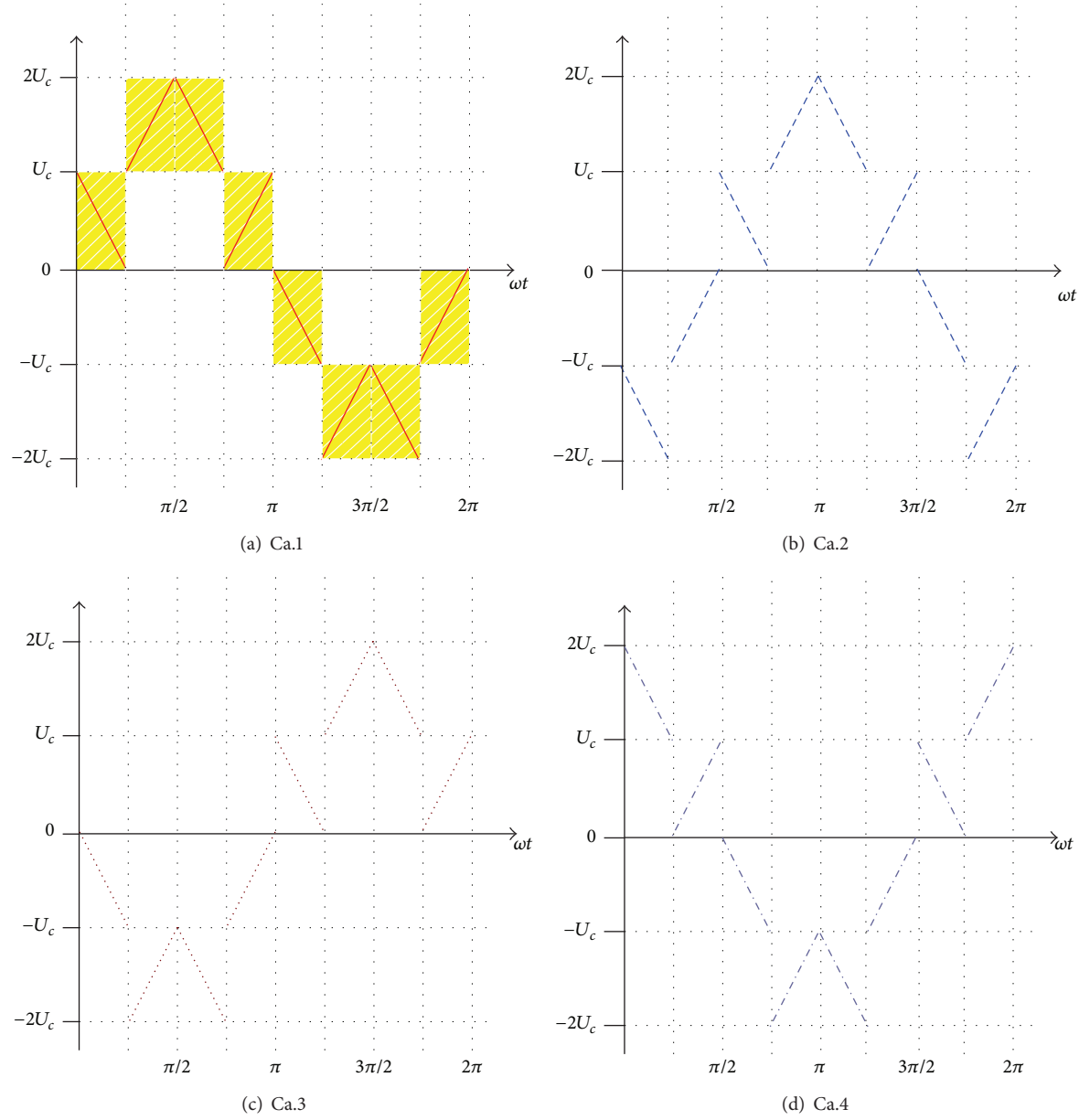

Figure 5: Carrier signal sets of the improved PD control method.

principle. The results are shown in Figures 5(b), 5(c), and 5(d), which are defined as Ca.2, Ca.3, and Ca.4. It is obvious that the phase shift of 90 degrees is the same pattern of that in the CPS control.

Then, the modulation of the improved PD control is designed to be similar to that of CPD control. The reference signal v_{ref} is compared with Ca.1 and Ca.3 to generate the drive signal for full bridge unit H_{a1}. The reference signal v_{ref} is compared with Ca.2 and Ca.4 to generate the drive signal for full bridge unit H_{a2}. The u_{Ha1} and u_{Ha2} are the output voltage of the full bridge unit, and u_{AN} is the output phase voltage of the cascaded inverter, which has been shown in Figure 6.

It can be observed in Figure 6 that the switching frequencies of the two bridge units are the same. This is important for heat dissipation design of the power unit. At the same time, the fundamental component of the output voltage for each unit can be measured to be the same. The reason is that the four sets of carrier signals are developed from CPS control, only with different sequence. It means that the output power of each unit is balanced. These two factors are essential for practical implementation of this modulation method. Because only with the balanced output power and equal switching frequency, the practical consideration of rated power and heat cooling design of the power unit can be determined. So this improved PD control method can be used in cascaded multilevel inverter. In the following section, the experimental prototype and measured results will verify the theory.

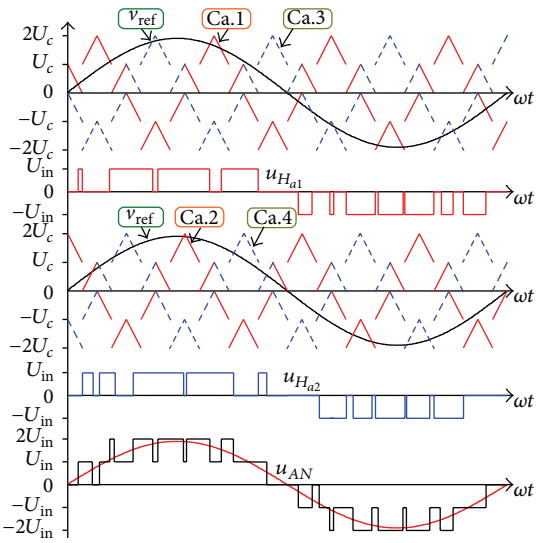

Figure 6: Modulation of improved PD control.

Figure 7: Three phase cascaded multilevel inverter experimental prototype.

Table 1: Output power measure in different situations.

Output power	Output power of unit 1	Output power of unit 2
1.5 kW	750 w	751 w
2 kW	999 w	1001 w

4. Experiment Results and Analysis

To verify the conclusion above, a five-level three phase cascaded inverter is built with two cascaded units, which is shown in Figure 7. The microcontroller is the TMS320LF2812 from Taxes Instruments. The rated power is 5 kW and the switching frequency is 5 kHz. The input dc voltage for each bridge unit is 180 V. The rated output phase voltage is 220 V, with the frequency of 50 Hz. The output filter inductor is 400 μH, and the output filter capacitor is 15 μF.

The experiment result is shown is Figure 8 with measured output voltage, output current, and the instantaneous power waveform. In Figure 8(a), the u_{AN} represents the phase voltage in the inverter side, while the filtered output line voltage is defined as u_o. The load current i_o is shown in the brown color. The inverter output line voltage u_{AB} is also shown in Figure 8(a). The spectrum analysis of the phase voltage shows that the highest amplitude of phase voltage harmonic is at the switching frequency. But in the line voltage, this harmonic is naturally eliminated. It means that the improved PD control method remains the advantage of PD control. The harmonic of output line voltage is optimized. In Figure 8(b), the output instantaneous power waveform under rated power condition is measured and shown. The driving signals of both units are shown in Figure 8(b). The output inductor current is also shown in Figure 8(b). The average output power of bridge units is measured using a power analyzer and shown in Table 1. It is clear that the improved PD control method can balance the output power of each unit.

Figure 9 shows the spectrum analysis results of the phase voltage and line voltage with the improved PD method. In Figure 9(a), major harmonics below 50 kHz are shown for the phase voltage and line voltage separately. The highest amplitude harmonics around the 4 times of the switching frequency (20 kHz) are magnified in Figure 9(b) for a clearer view. The analysis result for phase voltage is shown in the up side and line voltage in the low side. It can be observed that, in the situation of phase voltage, the highest amplitude voltage harmonic appears with the frequency of 20 kHz, while in the situation of line voltage, the voltage harmonic at 20 kHz is naturally eliminated with inconsiderable amplitude. The analysis result shows clearly that the improved PD control method retains the PD control's advantage of optimized line voltage harmonic.

5. Conclusions

In this paper, a Fourier series expansion method is used to analyze the output phase voltage and line voltage of the PD and CPS control. The spectrum character of the two control methods is analyzed to come to the conclusion that in the range of the whole modulation ratio, the line voltage quality of PD control is better than that of CPS control. The carrier signals of CPS and PD control are compared and an improved PD control method is discussed in this paper. The new method can be practically implemented in the cascaded multilevel invert. With the improved PD control method, the output power of each full bridge unit is balanced and the switching frequencies of the units are kept the same. At the same time, the improved PD method retains the advantage of PD control, the optimized line voltage harmonic. To verify the theory, a 5 kW three phase cascaded multilevel inverter prototype is built in the laboratory. The experiment results show the feasibility of the improved PD control method and the advantages of this novel control method.

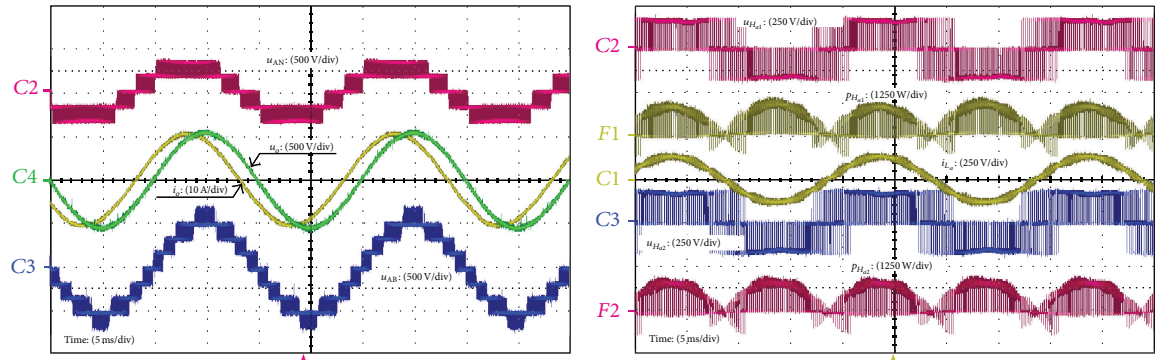

(a) Output voltage and current waveform

(b) Phase *A* output voltage and instantaneous output power of each unit

Figure 8: Experiment waveform for improved PD control method.

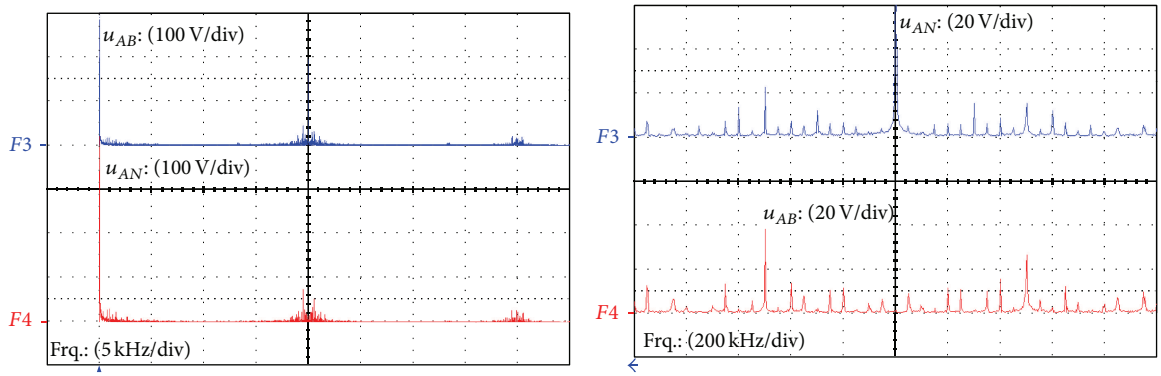

(a) Major harmonic spectrum

(b) Harmonic spectrum around 4 times of the switching frequency

Figure 9: Spectrum analysis result of output phase voltage and line voltage.

Conflict of Interests

The authors declare that there is no conflict of interests regarding the publication of this paper.

References

[1] M. Malinowski, K. Gopakumar, J. Rodriguez, and M. A. Perez, "A survey on cascaded multilevel inverters," *IEEE Transactions on Industrial Electronics*, vol. 57, no. 7, pp. 2197–2206, 2010.

[2] J. Ebrahimi, E. Babaei, and G. B. Gharehpetian, "A new multilevel converter topology with reduced number of power electronic components," *IEEE Transactions on Industrial Electronics*, vol. 59, no. 2, pp. 655–667, 2012.

[3] Z. Du, B. Ozpineci, and L. M. Tolbert, "Modulation extension control of hybrid cascaded H-bridge multilevel converters with 7-level fundamental frequency switching scheme," in *Proceedings of the 38th IEEE Annual Power Electronics Specialists Conference (PESC '07)*, pp. 2361–2366, June 2007.

[4] C. Buccella, C. Cecati, and H. Latafat, "Digital control of power converters—a survey," *IEEE Transactions on Industrial Informatics*, vol. 3, no. 8, pp. 437–4447, 2012.

[5] R. Rathore, H. Holtz, and T. Boller, "Generalized optimal pulsewidth modulation of multilevel inverters for low switching frequency control of medium voltage high power industrial ac drives," *IEEE Transactions on Industrial Electronics*, vol. 10, no. 60, pp. 4215–4224, 2013.

[6] L. M. Tolbert, F. Z. Peng, and T. G. Habetier, "A multilevel converter-based universal power conditioner," *IEEE Transactions on Industry Applications*, vol. 36, no. 2, pp. 596–603, 2000.

[7] Z. Wu, Y. Zou, and K. Ding, "Analysis of output voltage spectra in a hybrid diode-clamp cascade 13-level inverter," in *Proceedings of the 36th IEEE Power Electronics Specialists Conference (PESC '05)*, pp. 873–8879, 2005.

[8] J. Wang and F. Z. Peng, "Unified power flow controller using the cascade multilevel inverter," *IEEE Transactions on Power Electronics*, vol. 19, no. 4, pp. 1077–1084, 2004.

[9] H. Akagi, S. Inoue, and T. Yoshii, "Control and performance of a transformerless cascade PWM STATCOM with star configuration," *IEEE Transactions on Industry Applications*, vol. 43, no. 4, pp. 1041–1049, 2007.

[10] S. Yin, H. Luo, and S. X. Ding, "Real-time implementation of fault-tolerant control systems with performance optimization," *IEEE Transactions on Industrial Electronics*, vol. 61, no. 5, pp. 2402–2411, 2014.

[11] X. Wang, Y. Zang, B. Xu, and J.-Q. Lin, "Research on switch-based control method for cascaded H-bridge inverter failures," *Proceeding of the CSEE*, vol. 27, no. 7, pp. 76–81, 2007.

[12] P. W. Hammond, "Enhancing the reliability of modular medium-voltage drives," *IEEE Transactions on Industrial Electronics*, vol. 49, no. 5, pp. 948–954, 2002.

[13] Y.-F. Sun and X.-B. Ruan, "Power balance control schemes for cascaded multilevel inverters," *Proceeding of the CSEE*, vol. 26, no. 4, pp. 126–133, 2006.

[14] Y.-F. Sun and X.-B. Ruan, "Power balance control schemes for cascaded multilevel inverters," *Proceeding of the CSEE*, vol. 26, no. 4, pp. 126–133, 2006.

[15] Z.-Y. Yang, J.-F. Zhao, X.-J. Ni, J.-M. Lu, and B. Chen, "Eliminating common-mode voltage of cascaded medium-voltage variable frequency driver with phase-difference STS-SVM," *Proceeding of the CSEE*, vol. 28, no. 15, pp. 32–38, 2008.

[16] P. Lezana and G. Ortiz, "Extended operation of cascade multicell converters under fault condition," *IEEE Transactions on Industrial Electronics*, vol. 56, no. 7, pp. 2697–2703, 2009.

Hindawi Publishing Corporation
Mathematical Problems in Engineering
Volume 2014, Article ID 328450, 21 pages
http://dx.doi.org/10.1155/2014/328450

Research Article

Characteristic Modeling and Control of Servo Systems with Backlash and Friction

Yifei Wu, Zhihong Wang, Yuanyuan Li, Wei Chen, Renhui Du, and Qingwei Chen

School of Automation, Nanjing University of Science and Technology, Nanjing 210094, China

Correspondence should be addressed to Yifei Wu; wuyifei0911@163.com

Received 23 August 2013; Revised 4 December 2013; Accepted 8 December 2013; Published 19 February 2014

Academic Editor: Bo-Chao Zheng

A novel approach for modeling and control of servo systems with backlash and friction is proposed based on the characteristic model. Firstly, to deal with friction-induced nonlinearities, a smooth Stribeck friction model is introduced. The backlash is modeled by a continuous and derivable mathematical function. Secondly, a characteristic model in the form of a second-order slowly time-varying difference equation is established and verified by simulations. Thirdly, a composite controller including the golden-section adaptive control law and the integral control law is designed and the stability of the closed-loop system is analyzed. The simulation and experimental results show that the proposed control scheme is effective and can improve the steady-state precision and the dynamic performance of the servo system with backlash and friction.

1. Introduction

Servo systems have been widely used in various applications, such as machine tools, robots, semiconductor manufacturing manipulators, radars, and satellite antennas. With the development of technology, there is an increasing demand for high precision position controllers, which should have fast tracking behavior, disturbance rejection ability, and robustness to uncertainties. However, the nonsmooth nonlinearities including backlash and friction are often present in servo systems, which can lead to steady-state tracking errors, undesired stick-slip motion, and limit cycles [1, 2]. Although some control approaches [1, 2], such as PD control, fuzzy control, adaptive control, robust adaptive control, neural networks control, and sliding mode control, have been given to reduce the backlash and friction effect, it is still a challenging problem because of the nondifferentiable nature of the backlash and friction. In addition, backlash and friction have previously been studied separately [1, 2], more rarely together. In many servo systems, a controller designed to compensate only for friction may perform poor performance in the presence of backlash, and vice versa, because they coexist in these systems. Thus, both of them should be taken into consideration in the controller design.

Backlash is present in servo systems with gear transmissions, where the motor temporarily loses direct contact with the load when the backlash gap opens. It may often cause delays, oscillations, and steady-state errors. Since backlash is characterized by nondifferentiable nonlinearity, which is poorly known, the control system with unknown backlash is a difficult problem. Therefore, a number of different approaches to model and compensate for backlash have been investigated for several decades. A recent survey paper [2] summarizes the backlash models and the compensation methods. Different mathematical models have been developed to describe the backlash phenomenon, such as dead-zone model and hysteresis model [2]. The dead-zone model is a static, scalar nonlinear function, which means that it is relatively easy to be analyzed. In this paper, we will adopt it as the backlash model. Many papers deal with the compensation for the backlash. An adaptive control scheme developed by Tao and Kokotović for the systems with unknown backlash is given in [3]. The scheme of Selmic and Lewis [4] implements a dynamic inversion compensation for backlash using the backstepping technique with neural networks. In [5], an optimal control scheme is employed for backlash compensation and a feedback linearization is designed to decouple the multivariable nonlinear dynamics

so that backlash compensation and tracking control can be both achieved. In [6], a novel adaptive control design is achieved by introducing a smooth inverse function of the dead zone and using it in the controller design with the backstepping technique. A hybrid model based on model predictive control (MPC) scheme for backlash compensation is introduced in [7]. A second-order sliding mode observer ensuring the finite time convergence of estimated state values towards real state values in a nonlinear mechanical system with backlash is given in [8]. A linear estimator for the fast and accurate estimation of the position and velocity in the presence of backlash in automotive power trains is described in [9]. In [10], an adaptive dynamic surface control scheme combined with sliding mode control to compensate for backlash nonlinearities in a linear stage motion system is present. In [11], an extended state observer (ESO) combined with the adaptive sliding mode control theory is proposed to deal with a nonlinear pneumatic servo system characterized with input backlash.

Friction is one of the most important limitations in high precision position systems. It can cause tracking errors, self-excited vibration, and limit cycles [1]. Friction modeling and compensation have been studied extensively in the past few decades but is still full of interesting problems due to their practical significance and the complex behavior of friction. Satisfactory friction compensation can be obtained if a good friction model is available. However, friction is a highly nonlinear phenomenon, which is difficult to be described by a simple model [1]. Some models, which include both static and dynamic, have been proposed by researchers. A classical static friction model contains the property such as Coulomb friction, stiction, Stribeck effect, and viscous friction [1]. Dynamic friction models, mainly including the Dahl model [12] and the LuGre model [13], have been proposed and shown to be more beneficial. However, experimental measurements have proved that a good static friction model can approximate the real friction force with a degree of 90% fidelity [14]. The dynamic friction behaviour can be introduced in the static model as a bounded additive model uncertainty [1]. Therefore, the static friction model with Stribeck effect has a great significance for practical applications. The control methods for friction compensation are divided into three categories [1, 15]: the model-oriented friction compensation scheme, the adaptive compensation scheme, and the soft computing approach. In [16], a nonlinear proportional-integral-derivative (NPID) control has been designed to improve compensation for friction by applying a state feedback NPID control law with time-varying state feedback gains. In [17–19], a fuzzy system is utilized to adaptively learn unknown friction behavior and compensate for it. In [20], an adaptive friction compensator structure is proposed in which the Stribeck friction term is approximated by RBF-type neural network. To handle model uncertainties, robust adaptive control techniques [21, 22] are also very popular for friction compensation.

From the preceding discussion, it can be found that the majority of previous studies have addressed either the friction compensation problem or the backlash compensation problem. Very few papers deal with the control of systems in the presence of backlash and friction [23, 24]. This motivates us to carry out present work. In this paper, we adopt a new adaptive control method based on a characteristic model to handle both friction and backlash. The characteristic modeling theory and methods, proposed by Wu in the 1990s, are an integrated and practical modeling and control theory based on the control-oriented design thought, and improved gradually in the recent 20 years, which has already been applied successfully in more than 400 systems belonging to nine kinds of engineering plants in the field of astronautics and industry [25–27]. The characteristic modeling is based on the dynamics characteristics and control performance requirements of the plants, rather than being only based on accurate plant dynamics analysis. This method provides a feasible low-order intelligent controller design method for various complicated plants with nonlinearities and uncertainties, and whose output variables cannot be measured online continuously. Currently, it has not been applied in servo systems with backlash and friction. Therefore, we will attempt to use a characteristic model to describe the servo system with backlash and friction and design the controller.

The remainder of this paper is organized as follows. In Section 2, we describe the original dynamic model and the characteristic model of the servo system with backlash and friction. In Section 3, the composite controller including the golden-section adaptive control law and the integral control law is designed, and the stability of the closed-loop system is analyzed. Sections 4 and 5 present consecutively the simulation and experimental results. Finally, the conclusion is given in Section 6.

2. Characteristic Modeling

The characteristic modeling is based on the dynamics characteristics and control performance requirements of the plants, rather than being only based on accurate plant dynamics analysis. This method provides a feasible low-order intelligent controller design method for various complicated plants with nonlinearities and uncertainties.

A characteristic model has the following features [25].

(1) For the same input, a plant characteristic model is equivalent to its practical plant in output. In a dynamic process, the output error can be maintained within a permitted range. In the steady state, their outputs are equal.

(2) Besides plant characteristics, the form and order of a characteristic model mainly rely on control performance requirements.

(3) The structure of a characteristic model should be simpler, than an original dynamic equation, easier, and more convenient to be realized in engineering.

(4) A characteristic model is different from the reduced-order model of a high-order system. It compresses all the information of the high-order model into several characteristic parameters. In the bandwidth of the control system, no information is lost. In general,

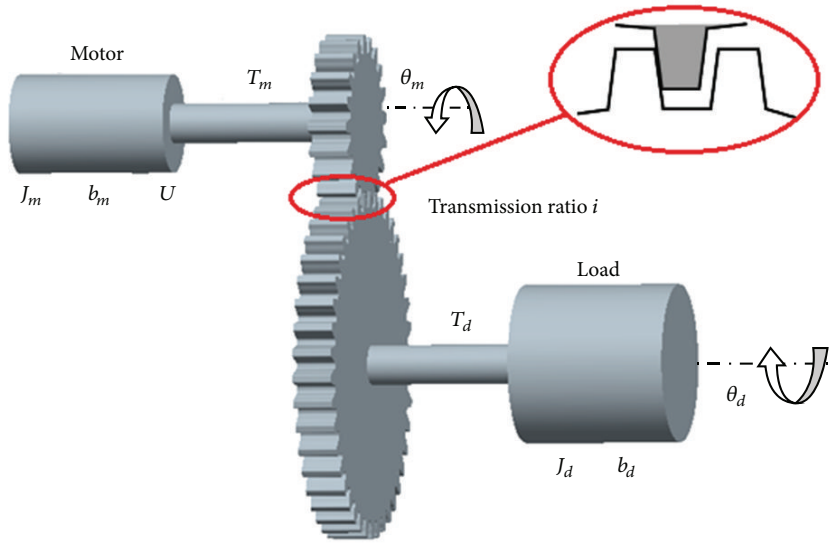

Figure 1: Structure of a typical electromechanical system driven by gears.

a characteristic model is represented by a slowly time-varying difference equation.

Characteristic modeling mainly considers the characteristic relation between control input and output. There are two approaches to establish characteristic model. One is to establish the characteristic model directly according to the dynamic features of the practical plant and the control performance requirements. And the other is to establish the characteristic model based on the original dynamic model. The latter one is applied in this paper; that is, the original dynamic model containing backlash and friction seems as the standard plant model of the system. Then the characteristic model is established based on it.

2.1. Dynamic Model. The structure of a typical electromechanical system driven by gears is shown in Figure 1. θ_m and $\dot{\theta}_m$ denote the angular displacement and the angular velocity of the motor, respectively. θ_d and $\dot{\theta}_d$ denote the angular displacement and the angular velocity of the load, respectively, J_m and J_d denote the rotational inertia of the motor and the load, respectively, T_m and T_d denote the torque of the motor and the load, respectively, b_m and b_d denote the viscous friction coefficient of the motor and the load, respectively, and i denotes the gear ratio.

The dead-zone model is used to model the backlash in Figure 1, and τ_1 can be expressed as

$$\tau_1 = k_b f(z) \tag{1}$$

$$f(z) = \begin{cases} z + \alpha & z < \alpha \\ 0 & |z| \le \alpha \\ z - \alpha & z > \alpha, \end{cases} \tag{2}$$

where τ_1 denotes the elastic torque between the motor and the load, k_b denotes the stiffness, $f(z)$ denotes the dead-zone function, z ($z = \theta_m - i\theta_d$) denotes the relative angular displacement between the motor and the load, and α denotes half of the backlash width.

Besides the backlash nonlinearity, the friction nonlinearity should be also considered in the system. The Stribeck model is used to describe the friction in this paper. So the friction torque τ_2 can be expressed as

$$\tau_2 = \left[F_c + (F_s - F_c) e^{-(\dot{\theta}_m/\dot{\theta}_s)^{\delta}} \right] \operatorname{sgn}(\dot{\theta}_m) + B\dot{\theta}_m, \tag{3}$$

where F_c, F_s, B, $\dot{\theta}_m$, and $\dot{\theta}_s$ represent the Coulomb friction, the maximum static friction, the viscous damping coefficient, the angular velocity of the motor, and the Stribeck speed, respectively, and sgn(·) represents the sign function. $\dot{\theta}_s$ and δ are empirical constants, which are usually assumed to be 0.05 and 2, respectively.

The dynamic equations of a typical electromechanical system driven by gears can be expressed as

$$U(t) = k_e \dot{\theta}_m(t) + RI(t) + L\frac{dI(t)}{dt}$$

$$J_m \ddot{\theta}_m(t) + b_m \dot{\theta}_m(t) = T_m - \tau_1 - \tau_2$$

$$J_d \ddot{\theta}_d(t) + b_d \dot{\theta}_d(t) = i\tau_1$$

$$T_m = k_d I(t)$$

$$\tau_1 = k_b f(z)$$

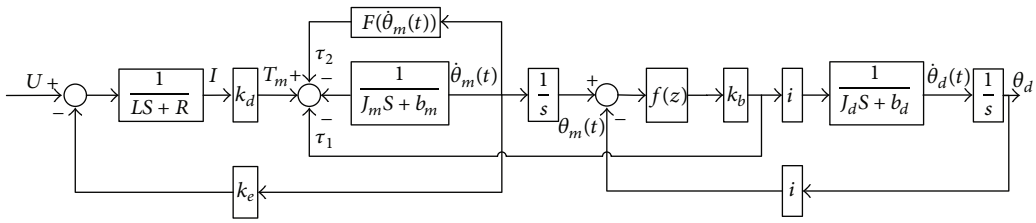

Figure 2: Structure diagram of the electromechanical system.

$$f(z) = \begin{cases} z+\alpha & z < -\alpha \\ 0 & |z| \le \alpha \\ z-\alpha & z > \alpha \end{cases}$$

$$\tau_2 = \left[F_c + (F_s - F_c)\, e^{-(\dot{\theta}_m/\dot{\theta}_s)^{\delta}}\right] \operatorname{sgn}\left(\dot{\theta}_m\right) + B\dot{\theta}_m, \tag{4}$$

where $U(t)$ denotes the armature voltage, $I(t)$ denotes the armature current, R and L denote the resistance and the inductance, respectively, k_e denotes the back electromotive force coefficient of the motor, and k_d denotes the torque coefficient of the motor.

The system (2.1) can also be represented by the structure diagram as shown in Figure 2.

2.2. Characteristic Model. The nonlinear system is expressed as

$$\dot{x}(t) = f\left(x, \dot{x}, \ldots, x^{(n)}, u, \dot{u}, \ldots, u^{(m)}\right). \tag{5}$$

Let $x = x_1, \dot{x} = x_2, \ldots, x^{(n)} = x_{n+1}$ and $u = u_1, \dot{u} = u_2, \ldots, u^{(m)} = u_{m+1}$; then (5) can be rewritten as

$$\dot{x}(t) = f\left(x_1, \ldots, x_{n+1}, u_1, \ldots, u_{m+1}\right). \tag{6}$$

This nonlinear system (6) is assumed as follows (see [28]).

Assumption 1. The system is a SISO system.

Assumption 2. The order of control input u is 1.

Assumption 3. If all the variables x_i and u_i in $f(\cdot)$ are zero, $f(\cdot) = 0$.

Assumption 4. $f(\cdot)$ is continuous differentiable to all the variables, and all partial derivatives are bounded.

Assumption 5. $|f(x(t+\Delta t), u(t+\Delta t))| - |f(x(t), u(t))| < M\Delta t$, where M is positive constant and Δt is sample period.

Assumption 6. All the variables x_i and u_i are bounded. This assumption can be satisfied easily in practical engineering.

Lemma 7 (see [28]). *If the system* (5) *satisfies the above Assumptions 1–4 and sample time Δt satisfies some certain conditions, the characteristic model of the system can be established in the form of a second-order time-varying difference equation as*

$$\begin{aligned} x(k+1) = {} & \alpha_1(k)\, x(k) + \alpha_2(k)\, x(k-1) \\ & + \beta_0(k)\, u(k) + \beta_1(k)\, u(k-1), \end{aligned} \tag{7}$$

where $\alpha_1(k)$, $\alpha_2(k)$, $\beta_0(k)$, and $\beta_1(k)$ are coefficients.

When the controlled system is stable and satisfies Assumptions 5 and 6, the following conclusions can be drawn.

(1) In a dynamic process, under the same input, the output of the characteristic model is equal to that of the practical plant (suitably selected sampling period Δt can make sure that the output error is kept within a permitted range). In the steady state, both outputs are equal.

(2) The coefficients $\alpha_1(k)$, $\alpha_2(k)$, $\beta_0(k)$, and $\beta_1(k)$ are slowly time-varying.

(3) The range of these coefficients can be determined beforehand.

If the system is a minimum phase system, $\beta_1(k)u(k-1)$ in (7) *can be left out.*

According to Lemma 7, the characteristic model only can be applied to the system which is continuous differentiable to all the variables and where all partial derivatives are bounded. But in the system dynamic equations (2.1), the dead-zone function of the backlash model and the sign function sgn(·) in the friction model are both indifferentiable. Thus, to establish the characteristic model of the system, the backlash model and the friction model should be smoothed.

According to the modeling method of backlash (see [29]), a continuous approximate dead-zone function is introduced as

$$f^*(z) = z - a\alpha\left(\frac{2}{1+e^{-rz}} - 1\right), \tag{8}$$

where $a > 0$ and $r > 0$ are undetermined parameters in the backlash model. For analysing the degree of the approximation of the function (8) to (2), $\Delta f(z)$ is defined to be the difference between the two functions:

$$\Delta f(z) = \begin{cases} -a\alpha\left(\dfrac{2}{1+e^{-rz}} - 1\right) - \alpha, & z < -\alpha, \\ z - a\alpha\left(\dfrac{2}{1+e^{-rz}} - 1\right), & |z| \le \alpha, \\ -a\alpha\left(\dfrac{2}{1+e^{-rz}} - 1\right) + \alpha, & z > \alpha. \end{cases} \tag{9}$$

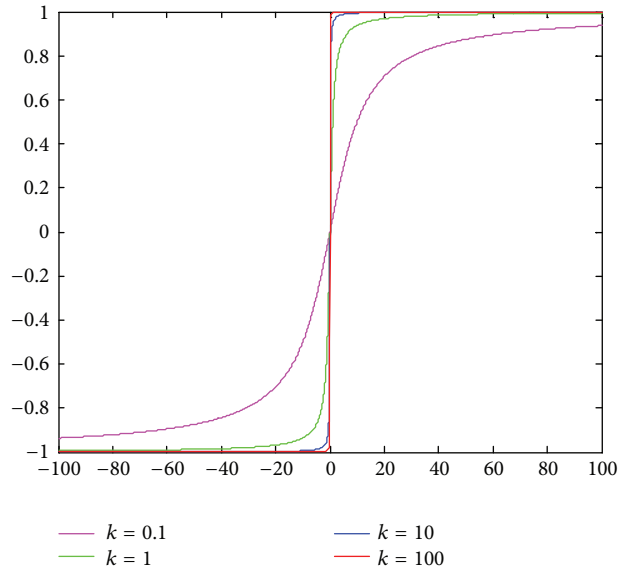

FIGURE 3: $(2/\pi)\arctan(kv)$.

Lemma 8 (see [29]). *When $a = 1$ and $r = 2/\alpha$, the following conclusions can be obtained:*

(1) $\lim_{z\to\infty}\Delta f(z) = 0$;

(2) $f^*(z)$ *is a monotonous increasing function;*

(3) the area enclosed by $f^*(z)$ *and* $f(z)$ *is the minimum;*

(4) $|\Delta f(z)| \le 2\alpha e^{-r\alpha}/(1+e^{-r\alpha})$.

Thus, the approximate dead-zone function $f^*(z)$ can be used to replace the dead-zone function in the system dynamic equations (2.1)*, and τ_1 can be rewritten as*

$$\tau_1 = k_b\left[z - \alpha\left(\frac{2}{1+e^{-rz}} - 1\right)\right]. \tag{10}$$

To make the friction model smooth, the function $(2/\pi)\arctan(kv)$ is used to replace the sign function $\mathrm{sgn}(\cdot)$ in the friction model. $\Delta g2(k, \dot\theta_m)$ is defined as

$$\Delta g\left(k, \dot\theta_m\right) = \mathrm{sgn}\left(\dot\theta_m\right) - \frac{2}{\pi}\arctan\left(k\dot\theta_m\right). \tag{11}$$

As shown in Figure 3, the function $\Delta\mathbf{g}(k, \dot\theta_m)$ is smaller and smaller with k increasing.

Thus, the friction torque τ_2 can be rewritten as

$$\tau_2 = \left[F_c + \left(F_s - F_c\right)e^{-\left(\dot\theta_m/\dot\theta_s\right)^\delta}\right]\frac{2}{\pi}\arctan\left(k\theta_m\right) + B\dot\theta_m. \tag{12}$$

Define $x_1 = \theta_m(t)$, $x_2 = \dot\theta_m(t)$, $x_3 = \theta_d(t)$, $x_4 = \dot\theta_d(t)$, and $x_5 = I(t)$; then

$$\begin{aligned}\tau_1 &= k_b\left[\left(x_1 - ix_3\right) - \alpha\left(\frac{2}{1+e^{-r(x_1-ix_3)}} - 1\right)\right]\\ \tau_2 &= \left[F_c + \left(F_s - F_c\right)e^{-\left(x_2/\dot\theta_s\right)^\delta}\right]\frac{2}{\pi}\arctan\left(kx_2\right) + Bx_2.\end{aligned} \tag{13}$$

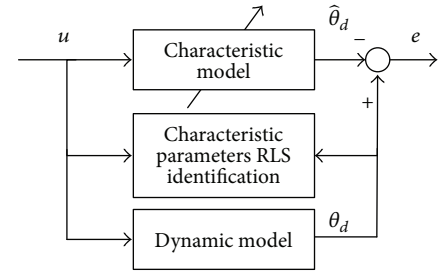

FIGURE 4: Scheme of verifying the characteristic model.

The system (2.1) can be expressed by state

$$\begin{aligned}\dot x_1 &= x_2\\ \dot x_2 &= \frac{1}{J_m}\left(k_d x_5 - \tau_1 - \tau_2 - b_m x_2\right)\\ \dot x_3 &= x_4\\ \dot x_4 &= \frac{1}{J_d}\left(i\tau_1 - b_d x_4\right)\\ \dot x_5 &= \frac{1}{L}\left(U - k_e x_2 - Rx_5\right)\\ y &= x_3.\end{aligned} \tag{14}$$

The characteristic model of the system can be obtained based on Lemma 7 as

$$\begin{aligned}y(k) &= \alpha_1(k)\,y(k-1) + \alpha_2(k)\,y(k-2)\\ &\quad + \beta_0(k)\,u(k-1) = \phi^T(k-1)\,\theta(k),\end{aligned} \tag{15}$$

where

$$\begin{aligned}\phi^T(k-1) &= \left[y(k-1)\quad y(k-2)\quad u(k-1)\right]\\ \theta^T(k) &= \left[\alpha_1(k)\quad \alpha_2(k)\quad \beta_0(k)\right],\end{aligned} \tag{16}$$

where the parameters $\alpha_1(k)$, $\alpha_2(k)$, and $\beta_0(k)$ are all bounded and the bound can be determined beforehand according to Lemma 7. These coefficients are time-varying and need to be estimated online, so the recursive least squares (RLS) method with forgetting factor f is applied. The recursive formula is shown as

$$\begin{aligned}K(k) &= \frac{P(k-1)\,\phi(k-1)}{f + \phi^T(k-1)\,P(k-1)\,\phi(k-1)}\\ \hat\theta(k) &= \hat\theta(k-1) + K(k)\left[y(k) - \phi^T(k-1)\,\hat\theta(k-1)\right]\\ P(k) &= \frac{1}{f}\left[I - K(k)\,\phi^T(k)\right]P(k-1).\end{aligned} \tag{17}$$

To verify the effectiveness of the proposed characteristic model, the simulations of verifying the characteristic model are performed based on MATLAB. The output of the dynamic model is as the standard output. The scheme of verifying the characteristic model is shown in Figure 4.

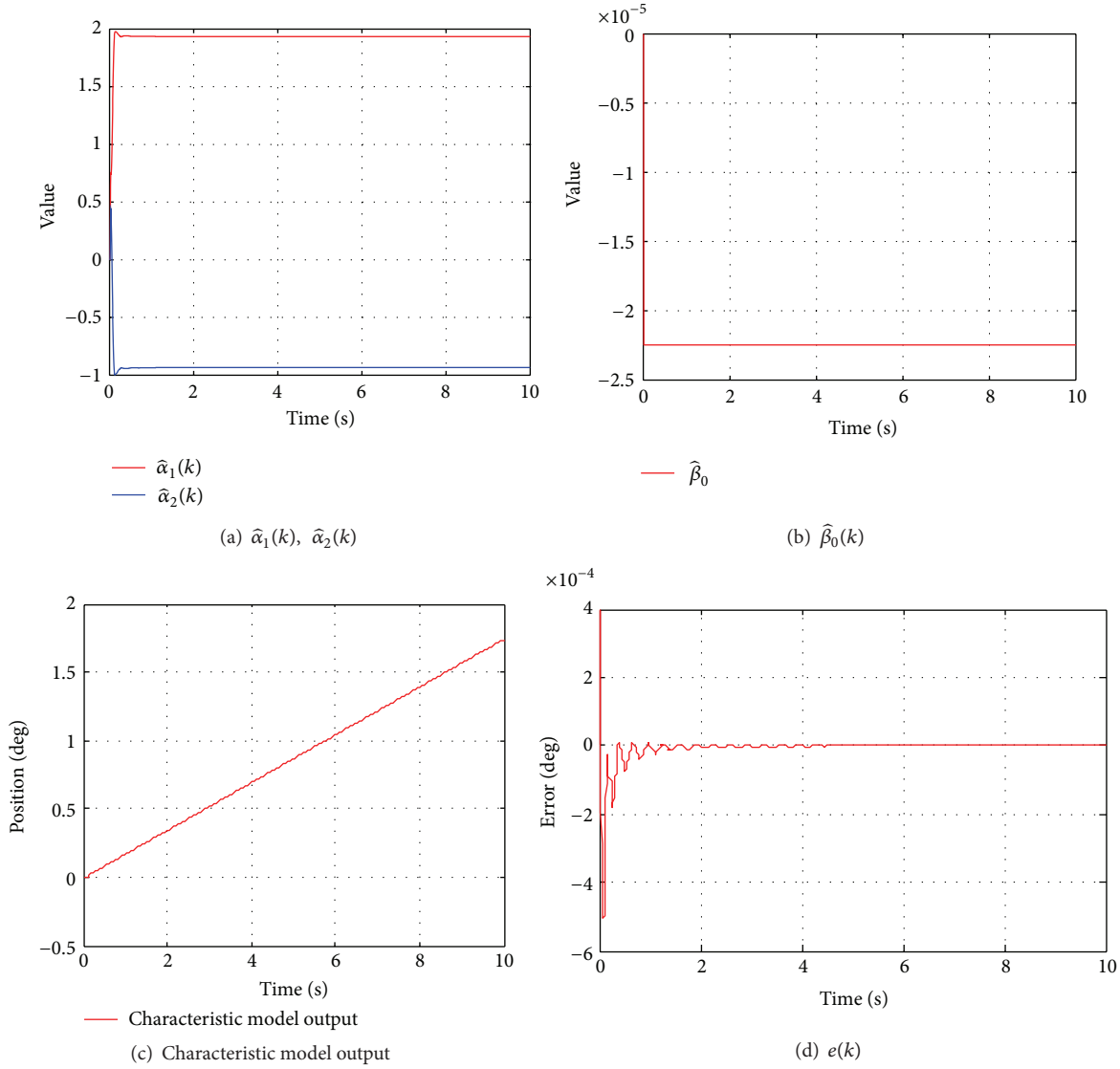

FIGURE 5: Verification results when $u(t) = 10$ V.

The system parameters are as $L = 0.0375$ H, $R = 1.3\,\Omega$, $k_e = 67.2$ V/krpm, $k_d = 1.11$ N·m/A, $k_b = 7 \times 10^4$ N·m/rad, $J_m = 0.00259$ kg·m^2, $J_d = 23.12$ kg·m^2, $b_m = 0.015$ N·m/krpm, $b_d = 0.024$ N·m/krpm, $i = 238$, $\alpha = 0.18^\circ$, and $r = 1.7/\alpha$, $k = 10$.

The sampling period Δt is 5 ms. Define the error $e(k)$ between the output of the characteristic model θ_d and the standard output $\widehat{\theta}_d$ as

$$e(k) = \theta_d(k) - \widehat{\theta}_d(k) = \theta_d(k) - \phi^T(k-1)\,\widehat{\theta}(k). \quad (18)$$

The RLS method expressed in (17) is used to estimate the characteristic parameters; the initial values are selected as $\widehat{\boldsymbol{\theta}}(0) = 10^{-3} \times [1 \;\; 1 \;\; 1]^T$, $\mathbf{P}(0) = 10^6 \times \mathbf{I}_{3\times 3}$, and the forgetting factor f is 0.99.

The results of verifying the characteristic model are shown in Figures 5–7.

(1) When $u(t) = 10$ V, the results are shown in Figure 5.

(2) When $u(t) = 10t$ V, the results are shown in Figure 6.

(3) When $u(t) = 30\sin(t)$ V, the results are shown in Figure 7.

According to Figures 5–7, the error between the characteristic model and the dynamic model is very small. The results indicate that the characteristic model can well describe the electromechanical system.

3. Controller Design and Stability Analysis

According to [25], the system error characteristic equation can be expressed as a second-order slowly time-varying difference equation:

$$y_e(k+1) = \alpha_1(k)\,y_e(k) + \alpha_2(k)\,y_e(k-1) + \beta_0(k)\,u(k), \quad (19)$$

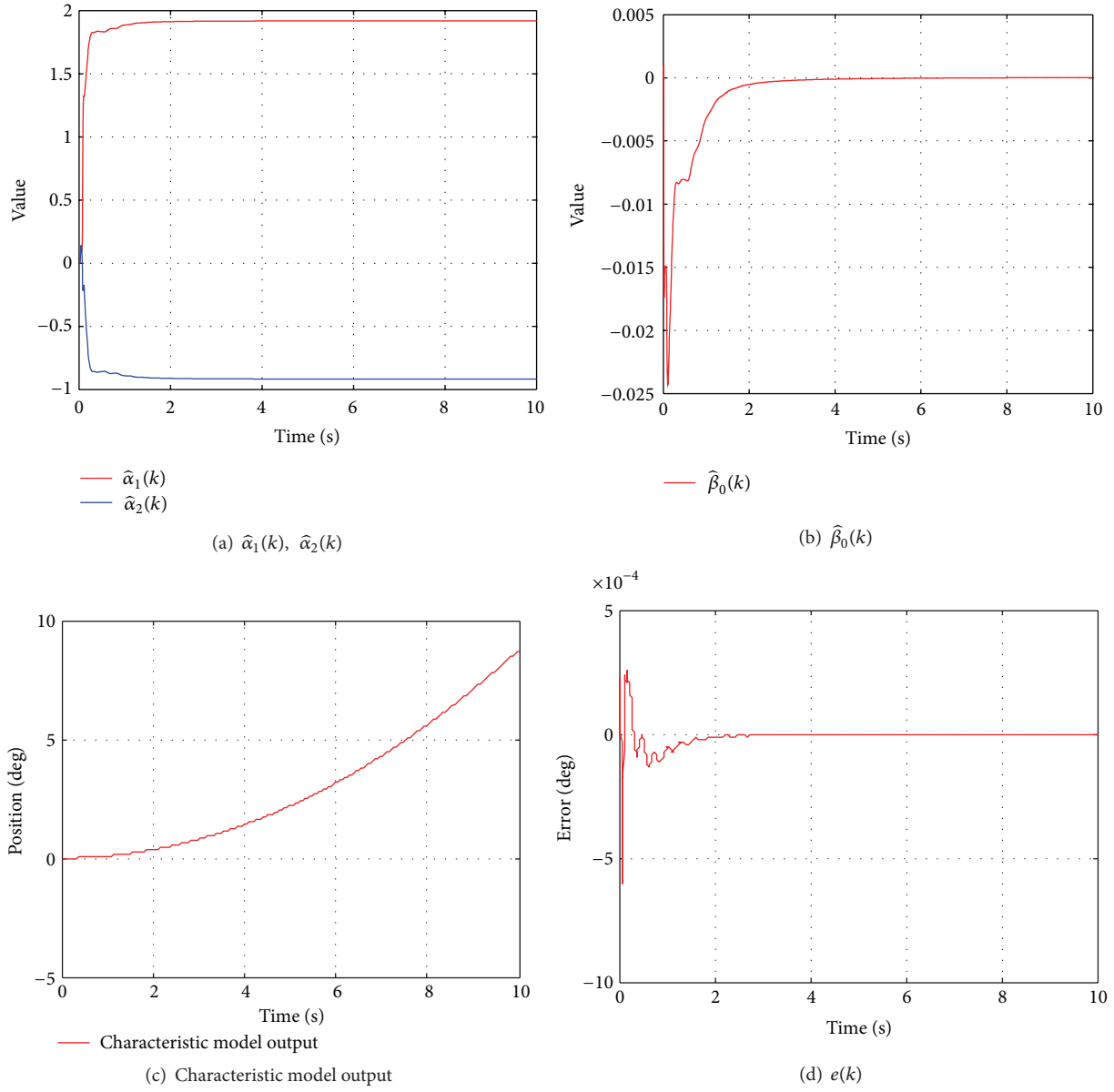

FIGURE 6: Verification results when $u(t) = 10t$ V.

where $y_e(k)$ ($y_e(k) = y(k) - y_r(k)$) is the error output, $y(k)$ is the system input, and $u(k)$ is the controller input which is designed as

$$u(k) = u_1(k) + u_2(k), \tag{20}$$

where $u_1(k)$ and $u_2(k)$ are the golden-section adaptive control law, and the integral control law, respectively, which satisfy

$$u_1(k) = -\frac{[l_1\widehat{\alpha}_1(k)\, y_e(k) + l_2\widehat{\alpha}_2(k)\, y_e(k-1)]}{\widehat{\beta}_0(k)},$$

$$\begin{aligned} u_2(k) &= u_2(k-1) + \alpha_0(k)\, y_e(k) \\ &= u_2(k-2) + \alpha_0(k-1)\, y_e(k-1) + \alpha_0(k)\, y_e(k), \end{aligned} \tag{21}$$

where $l_1 = 0.382$ and $l_2 = 0.618$ are the golden-section feedback coefficients, $\widehat{\alpha}_1(k)$, $\widehat{\alpha}_2(k)$, and $\widehat{\beta}_0(k)$ are the estimates of $\alpha_1(k)$, $\alpha_2(k)$, and $\beta_0(k)$, and $-1 < \alpha_0(k) < 0$ is a variable integral coefficient. Take (20) and (21) into (19) to obtain

$$\begin{aligned} y_e(k+1) = &-f_1(k)\, y_e(k) - f_2(k)\, y_e(k-1) \\ &- f_3(k)\, u_2(k-2), \end{aligned} \tag{22}$$

where

$$f_1(k) = l_1\frac{\beta_0(k)\,\widehat{\alpha}_1(k)}{\widehat{\beta}_0(k)} - \alpha_1(k) - \alpha_0(k)\,\beta_0(k),$$

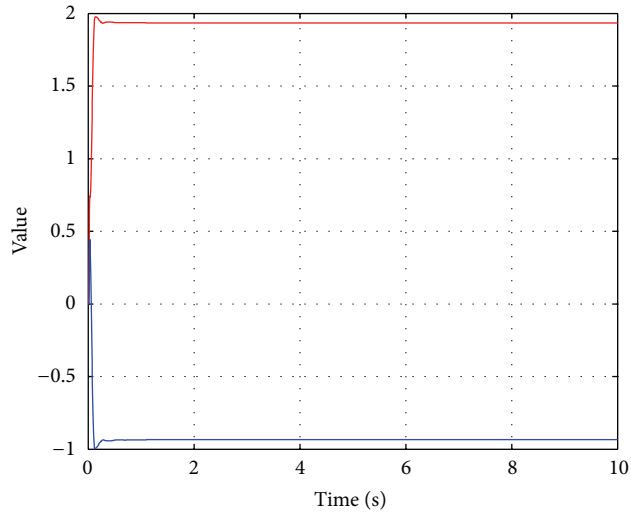

(a) $\widehat{\alpha}_1(k)$, $\widehat{\alpha}_2(k)$

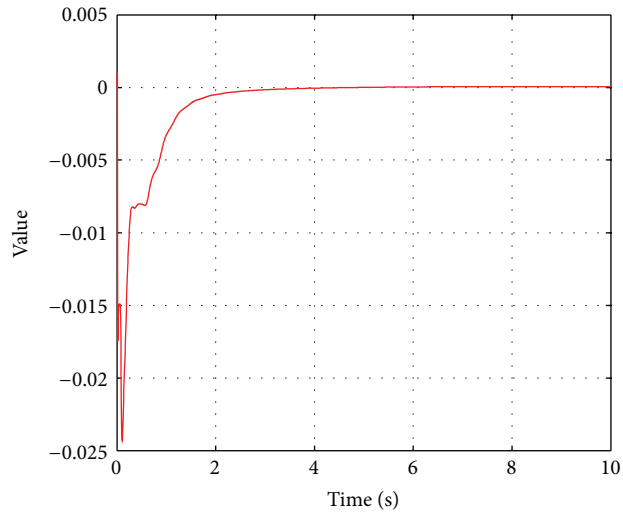

(b) $\widehat{\beta}_0(k)$

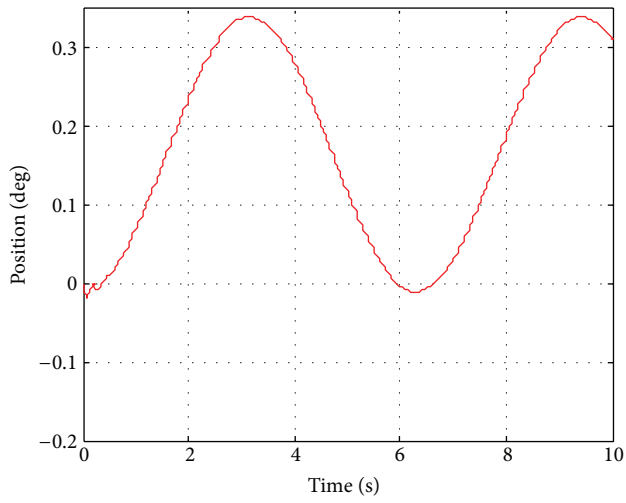

(c) Characteristic model output

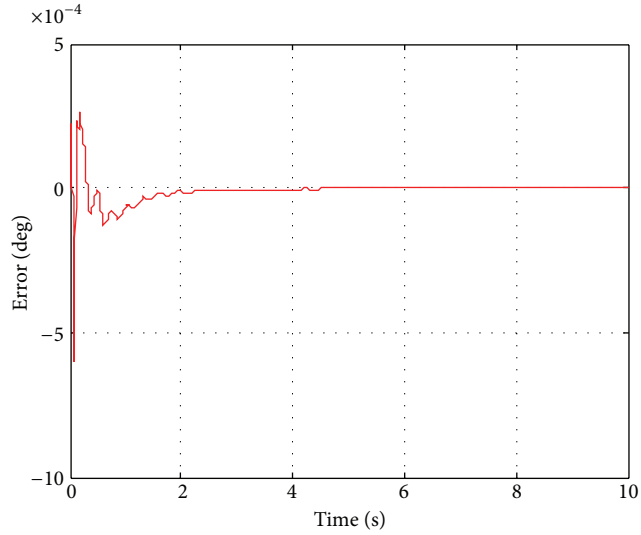

(d) $e(k)$

Figure 7: Verification results when $u(t) = 30\sin(t)$ V.

$$f_2(k) = l_2 \frac{\beta_0(k)\,\widehat{\alpha}_2(k)}{\widehat{\beta}_0(k)} - \alpha_2(k) - \alpha_0(k-1)\,\beta_0(k),$$
$$f_3(k) = -\beta_0(k). \tag{23}$$

Define $Y(k) = [y_0(k-1) \;\; y_e(k) \;\; y_e(k+1)]^T$, where $y_0(k-1) = u_2(k-1)$ so that the system (22) can be expressed as

$$Y(k+1) = A(k+1)\,Y(k), \tag{24}$$

where

$$A(k+1) = \begin{bmatrix} 1 & \alpha_0 & 0 \\ 0 & 0 & 1 \\ -f_3(k+1) & -f_2(k+1) & -f_1(k+1) \end{bmatrix}. \tag{25}$$

In order to analyze the uniform asymptotic stability of system (22), the following three lemmas are introduced.

Lemma 9 (see [30]). *Assume that a linear time-varying discrete system can be written as*

$$Y(k+1) = A(k+1)\,Y(k), \tag{26}$$

where $A(k+1) \in R^{n\times n}$, $Y(k) \in R^{n\times 1}$, and the origin is the equilibrium state of the system. For a given uniformly bounded, positive definite symmetric matrix $P(k)$, if $Q(k)$ which can be obtained by

$$A^T(k+1)P(k+1)A(k+1) - P(k) = -Q(k) \tag{27}$$

is a uniformly bounded, positive definite symmetric matrix, then the equilibrium state of the system (26) *is uniformly asymptotically stable according to Lyapunov theory.*

Lemma 10 (see [30]). *Assume that $B(k) = (b_{ij}(k))$ is a symmetric matrix which satisfies*

(1) every element and principal minor of $B(k)$ can be expressed as a continuous function about $f_i(k)$ or a constant;

(2) $f_i(k)$ $(i = 1, 2, \ldots, N)$ belongs to a finite closed interval, where N is a finite positive integer;

(3) all principal minors of $B(k)$ are greater than zero.

Then $B(k)$ is a uniformly bounded, positive definite symmetric matrix.

Lemma 11 (see [30]). *Assume that $M(k) \in R$ and $0 < M(k) < M$, where M is a positive constant. Assume that $B(k+1)$, $C(k+1)$, $D(k)$, $E_0(k)$, $E_1(k)$, and $F(k)$ satisfy*

$$E_0(k) = M(k)B^2(k+1) + E_1(k)B(k+1) - M(k)C^2(k+1) + F(k)C(k+1) + D(k), \tag{28}$$

$$E_1(k) = -2M(k)B(k+1) - 2M(k)C(k+1) + F(k). \tag{29}$$

The quadratic trinomial about $Z(k)$ is

$$-M(k)Z^2(k) + E_1(k)Z(k) + E_0(k) \tag{30}$$

whose discriminant root is $\Delta(k) = E_1^2(k) + 4M(k)E_0(k) = F^2(k) + 4M(k)D(k)$. When

$$\Delta(k) > 0$$
$$\frac{E_1(k) - \sqrt{\Delta(k)}}{2M(k)} < Z(k) < \frac{E_1(k) + \sqrt{\Delta(k)}}{2M(k)}, \tag{31}$$

the quadratic trinomial (30) *is greater than zero.*

Design the symmetric matrix $P(k)$ as

$$p_{ii}(k) = p_{ii} \quad (i = 1, 2, 3), \tag{32}$$

where p_{11}, p_{22}, and p_{33} are all positive constants and $0 < p_{11} < p_{22} < p_{33}$:

$$p_{12}(k) = p_{21}(k) = \varepsilon_3 f_3(k),$$
$$p_{13}(k) = p_{31}(k) = \varepsilon_2 f_2(k), \tag{33}$$
$$p_{23}(k) = p_{32}(k) = \varepsilon_1 f_1(k),$$

where $\varepsilon_1, \varepsilon_2$, and ε_3 are positive constants and $0 < \varepsilon_i \le (p_{11}/M_i\sqrt{5})$ $(i = 1, 2, 3)$, where M_i is the bound of $f_i(k)$; that is, $|f_i(k)| < M_i$.

Then the $Q(k)$ can be calculated as

$$\left(Q_{ij}(k)\right)_{3\times 3} \triangleq Q(k) = -A^T(k+1)P(k+1)A(k+1) + P(k), \tag{34}$$

where

$$\begin{aligned}
Q_{11}(k) &= 2p_{13}(k+1)f_3(k+1) - p_{33}f_3^2(k+1),\\
Q_{12}(k) &= Q_{21}(k)\\
&= p_{12}(k) - \alpha_0 p_{11} + \alpha_0 p_{13}(k+1)f_3(k+1)\\
&\quad + p_{13}(k+1)f_2(k+1) - p_{33}f_2(k+1)f_3(k+1),\\
Q_{13}(k) &= Q_{31}(k)\\
&= p_{13}(k) - p_{12}(k+1) + p_{23}(k+1)f_3(k+1)\\
&\quad + p_{13}(k+1)f_1(k+1) - p_{33}f_1(k+1)f_3(k+1),\\
Q_{22}(k) &= p_{22} - \alpha_0^2 p_{11} + 2\alpha_0^2 p_{13}(k+1)f_2(k+1)\\
&\quad - p_{33}f_2^2(k+1),\\
Q_{23}(k) &= Q_{32}(k)\\
&= p_{23}(k) - \alpha_0 p_{12}(k+1) + \alpha_0 p_{13}(k+1)f_1(k+1)\\
&\quad + p_{23}(k+1)f_2(k+1) - p_{33}f_1(k+1)f_2(k+1),\\
Q_{33}(k) &= p_{33} - p_{22} + 2p_{23}(k+1)f_1(k+1)\\
&\quad - p_{33}f_1^2(k+1).
\end{aligned} \tag{35}$$

Theorem 12. *The sufficient conditions which guarantee the uniform asymptotic stability of the time-varying discrete system* (15) *are*

(1) $f_1(k)$, $f_2(k)$, and $f_3(k)$ satisfy

$$|f_1(k)| < \sqrt{\frac{p_{33} - p_{22}}{p_{33}}} = M_1 \tag{36}$$

$$|f_2(k)| < \sqrt{\frac{p_{22} - \alpha_0^2 p_{11}}{p_{33}}}, \quad f_2(k) \neq 0 \tag{37}$$

$$\frac{\varepsilon_2}{p_{33}}\left(f_2(k+1) - |f_2(k+1)|\right) < f_3(k) < \frac{\varepsilon_2}{p_{33}}\left(f_2(k+1) + |f_2(k+1)|\right). \tag{38}$$

(2) The change rate of $f_1(k)$, $f_2(k)$, and $f_3(k)$ satisfy

$$\frac{(S_{23}/2) - \sqrt{M_{Q2}(k)\left(Q_{11}(k)Q_{33}(k) - Q_{13}^2(k)\right)}}{Q_{11}(k)} < -\varepsilon_1 \Delta f_1(k) < \frac{(S_{23}/2) + \sqrt{M_{Q2}(k)\left(Q_{11}(k)Q_{33}(k) - Q_{13}^2(k)\right)}}{Q_{11}(k)} \tag{39}$$

$$\frac{S_{13}}{2} - \sqrt{Q_{11}(k)Q_{33}(k)} < -\varepsilon_2 \Delta f_2(k) < \frac{S_{13}}{2} + \sqrt{Q_{11}(k)Q_{33}(k)} \tag{40}$$

$$\frac{S_{12}}{2} - \sqrt{Q_{11}(k)Q_{22}(k)} < -\varepsilon_3 \Delta f_3(k) < \frac{S_{12}}{2} + \sqrt{Q_{11}(k)Q_{22}(k)}, \tag{41}$$

where

$$\begin{aligned} S_{23} = &-2Q_{11}(k)p_{23}(k+1) - 2Q_{11}(k) \\ &\times \left(-\alpha_0 p_{12}(k+1) + \alpha_0 p_{13}(k+1) f_1(k+1) \right. \\ &+ p_{23}(k+1) f_2(k+1) \\ &\left. - p_{33} f_1(k+1) f_2(k+1)\right) + 2Q_{12}(k)Q_{13}(k), \\ S_{13} = &-2p_{13}(k+1) \\ &-2\left(-p_{12}(k+1) + p_{23}(k+1) f_3(k+1)\right. \\ &+ p_{13}(k+1) f_1(k+1) \\ &\left. - p_{33} f_1(k+1) f_3(k+1)\right), \\ S_{12} = &-2p_{12}(k+1) \\ &-2\left(-\alpha_0 p_{11} + \alpha_0 p_{13}(k+1) f_3(k+1)\right. \\ &+ p_{13}(k+1) f_2(k+1) \\ &\left. - p_{33} f_2(k+1) f_3(k+1)\right) \end{aligned} \tag{42}$$

$$M_{Q2}(k) = Q_{11}(k)Q_{22}(k) - Q_{12}^2(k) \tag{43}$$

$$\Delta f_i(k) = f_i(k+1) - f_i(k) \quad (i = 1, 2, 3). \tag{44}$$

Remark 13. Due to $-1 < \alpha_0(k) < 0$, we obtain $|f_2(k)| < \sqrt{(p_{22} - \alpha_0^2\ p_{11})/p_{33}} < \sqrt{p_{22}/p_{33}} = M_2$ by (37). According to (38), we get

$$\begin{aligned} &0 < f_3(k) < \frac{2\varepsilon_2}{p_{33}} f_2(k+1) \quad f_2(k+1) > 0 \\ &\frac{2\varepsilon_2}{p_{33}} f_2(k+1) < f_3(k) < 0 \quad f_2(k+1) < 0. \end{aligned} \tag{45}$$

So $|f_3(k)| < (2\varepsilon_2/p_{33})|f_2(k+1)| < (2/p_{33})(p_{11}/M_2\sqrt{5})M_2 = 2\sqrt{5}p_{11}/5p_{33} = M_3$.

Remark 14. The bound of $f_2(k)$ and $f_3(k)$ is related to $\alpha_0(k)$ and $f_2(k+1)$, respectively, in (37) and (38). In order to make the conditions (37) and (38) possible to be satisfied in the operation of the system, we reduce the range for

$$\begin{aligned} &\delta < |f_2(k)| < \sqrt{\frac{p_{22} - p_{11}}{p_{33}}} \\ &0 < f_3(k) < \frac{2\varepsilon_2}{p_{33}}\delta \quad f_2(k+1) > 0 \\ &-\frac{2\varepsilon_2}{p_{33}}\delta < f_3(k) < 0 \quad f_2(k+1) < 0, \end{aligned} \tag{46}$$

where δ is a positive constant. In this way, the upper bound and lower bound of $f_2(k)$ and $f_3(k)$ are constant and they are possible to implement in real system.

Proof of Theorem 12. The first-order principal minor of $P(k)$ satisfies

$$M_{p1}(k) = p_{11}, \quad p_{11} > 0. \tag{47}$$

The second-order principal minor of $P(k)$ satisfies

$$\begin{aligned} M_{p2}(k) &= p_{11}p_{22} - p_{12}^2(k) = p_{11}p_{22} - \varepsilon_3^2 f_3^2(k) \\ &> p_{11}p_{22} - \frac{p_{11}^2}{5M_3^2}M_3^2 > p_{11}^2 - \frac{p_{11}^2}{5} > 0. \end{aligned} \tag{48}$$

The third-order principal minor of $P(k)$ satisfies

$$\begin{aligned} M_{p3}(k) &= p_{11}p_{22}p_{33} + 2\varepsilon_1\varepsilon_2\varepsilon_3 f_1(k) f_2(k) f_3(k) \\ &\quad - p_{11}\varepsilon_1^2 f_1^2(k) - p_{22}\varepsilon_2^2 f_2^2(k) - p_{33}\varepsilon_3^2 f_3^2(k) \\ &> p_{11}p_{22}p_{33} - 2\frac{p_{11}}{M_1\sqrt{5}}\frac{p_{11}}{M_2\sqrt{5}}\frac{p_{11}}{M_3\sqrt{5}}M_1M_2M_3 \\ &\quad - p_{11}\frac{p_{11}^2}{5M_1^2}M_1^2 - p_{22}\frac{p_{11}^2}{5M_2^2}M_2^2 - p_{33}\frac{p_{11}^2}{5M_3^2}M_3^2 \\ &> \frac{2}{5}p_{11}^3 + \frac{1}{5}p_{11}^3 + \frac{1}{5}p_{22}p_{11}^2 + \frac{1}{5}p_{33}p_{11}^2 - \frac{2}{5\sqrt{5}}p_{11}^3 \\ &\quad - \frac{1}{5}p_{11}^3 - \frac{1}{5}p_{22}p_{11}^2 - \frac{1}{5}p_{33}p_{11}^2 > 0. \end{aligned} \tag{49}$$

As a result, $P(k)$ is a uniformly bounded, positive definite symmetric matrix by Lemma 10.

The first-order principal minor of $Q(k)$ is

$$\begin{aligned} M_{Q1}(k) = Q_{11}(k) &= 2\varepsilon_2 f_2(k+1) f_3(k+1) - p_{33} f_3^2(k+1) \\ &= -p_{33}\left[f_3(k+1) - \frac{\varepsilon_2 f_2(k+1) + \varepsilon_2 |f_2(k+1)|}{p_{33}}\right] \\ &\quad \times \left[f_3(k+1) - \frac{\varepsilon_2 f_2(k+1) - \varepsilon_2 |f_2(k+1)|}{p_{33}}\right]. \end{aligned} \tag{50}$$

According to (38) and $f_2(k) \neq 0$ in (37), we can obtain $M_{Q1}(k) = Q_{11}(k) > 0$.

Define

$$\begin{aligned} a_{12}(k+1) &= Q_{12}(k) - p_{12}(k) \\ &= -\alpha_0 p_{11} + \alpha_0 p_{13}(k+1) f_3(k+1) \\ &\quad + p_{13}(k+1) f_2(k+1) \\ &\quad - p_{33} f_2(k+1) f_3(k+1). \end{aligned} \tag{51}$$

According to (43), the second-order principal minor of $Q(k)$ is

$$\begin{aligned} M_{Q2}(k) &= -\left[p_{12}(k) + a_{12}(k+1)\right]^2 + Q_{11}(k) Q_{22}(k) \\ &= -\left[p_{12}(k) - p_{12}(k+1)\right]^2 \\ &\quad + S_{12}\left[p_{12}(k) - p_{12}(k+1)\right] + T_{12}, \end{aligned} \tag{52}$$

where

$$\begin{aligned} S_{12} &= -2p_{12}(k+1) - 2a_{12}(k+1), \\ T_{12} &= p_{12}^2(k+1) + S_{12} p_{12}(k+1) \\ &\quad - a_{12}^2(k+1) + Q_{11}(k) Q_{22}(k). \end{aligned} \tag{53}$$

S_{12} and T_{12} can be expressed in the form of (29) and (28):

$$\begin{aligned} &B(k+1) = p_{12}(k+1), \qquad C(k+1) = a_{12}(k+1), \\ &D(k) = Q_{11}(k) Q_{22}(k), \qquad F(k) = 0, \qquad M(k) = 1. \end{aligned} \tag{54}$$

Then the discriminant root of the quadratic trinomial (52) about $[p_{12}(k) - p_{12}(k+1)]$ is

$$\begin{aligned} \Delta_{12}(k) &= F^2(k) + 4M(k) D(k) = 4Q_{11}(k) Q_{22}(k) \\ &= 4M_{Q1}(k) Q_{22}(k), \end{aligned} \tag{55}$$

where

$$Q_{22}(k) = p_{22} - \alpha_0^2 p_{11} + 2\alpha_0^2 \varepsilon_2 f_2^2(k+1) - p_{33} f_2^2(k+1). \tag{56}$$

We can get $Q_{22}(k) > 0$ by (37), so $\Delta_{12}(k) > 0$. Then we have $M_{Q2}(k) > 0$ according to (41) and Lemma 11.

The third-order principal minor of $P(k)$ is

$$\begin{aligned} M_{Q3}(k) &= -Q_{11}(k) Q_{23}^2(k) + 2Q_{12}(k) Q_{13}(k) Q_{23}(k) \\ &\quad - Q_{22}(k) Q_{13}^2(k) + Q_{33}(k) M_{Q2}(k). \end{aligned} \tag{57}$$

Define

$$\begin{aligned} a_{23}(k+1) &= Q_{23}(k) - p_{23}(k) \\ &= -\alpha_0 p_{12}(k+1) + \alpha_0 p_{13}(k+1) f_1(k+1) \\ &\quad + p_{23}(k+1) f_2(k+1) \\ &\quad - p_{33} f_1(k+1) f_2(k+1). \end{aligned} \tag{58}$$

We get

$$\begin{aligned} M_{Q3}(k) &= -Q_{11}(k)\left[p_{23}(k) + a_{23}(k+1)\right]^2 \\ &\quad + 2Q_{12}(k) Q_{13}(k) a_{23}(k+1) - Q_{22}(k) Q_{13}^2(k) \\ &\quad + Q_{33}(k) M_{Q2}(k) \\ &= -Q_{11}(k)\left[p_{23}(k) - p_{23}(k+1)\right]^2 \\ &\quad + S_{23}\left[p_{23}(k) - p_{23}(k+1)\right] + T_{23}, \end{aligned} \tag{59}$$

where

$$\begin{aligned} S_{23} &= -2Q_{11}(k) p_{23}(k+1) - 2Q_{11}(k) a_{23}(k+1) \\ &\quad + 2Q_{12}(k) Q_{13}(k), \\ T_{23} &= Q_{11}(k) p_{23}^2(k+1) + S_{23} p_{23}(k+1) \\ &\quad - Q_{11}(k) a_{23}^2(k+1) + 2Q_{12}(k) Q_{13}(k) a_{23}(k+1) \\ &\quad - Q_{22}(k) Q_{13}^2(k) + Q_{33}(k) M_{Q2}(k). \end{aligned} \tag{60}$$

S_{23} and T_{23} can be expressed in the form of (29) and (28):

$$\begin{aligned} &M(k) = Q_{11}(k), \qquad B(k+1) = p_{23}(k+1), \\ &C(k+1) = a_{23}(k+1), \\ &D(k) = -Q_{22}(k) Q_{13}^2(k) + Q_{33}(k) M_{Q2}(k), \\ &F(k) = 2Q_{12}(k) Q_{13}(k). \end{aligned} \tag{61}$$

Then the discriminant root of the quadratic trinomial (59) about $[p_{23}(k) - p_{23}(k+1)]$ is

$$\begin{aligned} \Delta_{23}(k) &= F^2(k) + 4M(k) D(k) = 4Q_{12}^2(k) Q_{13}^2(k) \\ &\quad + 4Q_{11}(k)\left[-Q_{22}(k) Q_{13}^2(k) + Q_{33}(k) M_{Q2}(k)\right] \\ &= 4Q_{13}^2(k)\left[Q_{12}^2(k) - Q_{11}(k) Q_{22}(k)\right] \\ &\quad + 4Q_{11}(k) Q_{33}(k) M_{Q2}(k) \\ &= 4M_{Q2}(k)\left[Q_{11}(k) Q_{33}(k) - Q_{13}^2(k)\right]. \end{aligned} \tag{62}$$

Define

$$\begin{aligned} a_{13}(k+1) &= Q_{13}(k) - p_{13}(k) \\ &= -p_{12}(k+1) + p_{23}(k+1) f_3(k+1) \\ &\quad + p_{13}(k+1) f_1(k+1) \\ &\quad - p_{33} f_1(k+1) f_3(k+1). \end{aligned} \tag{63}$$

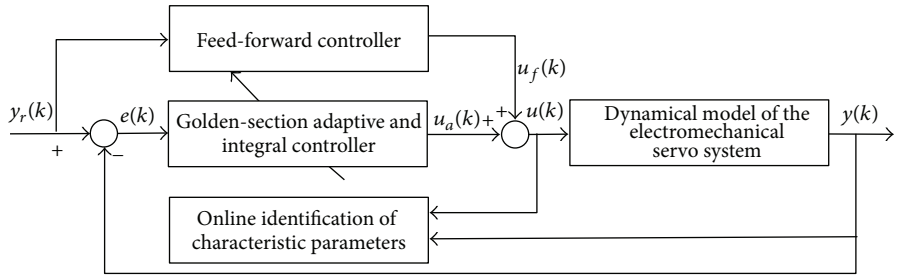

Figure 8: Structure of the closed-loop system.

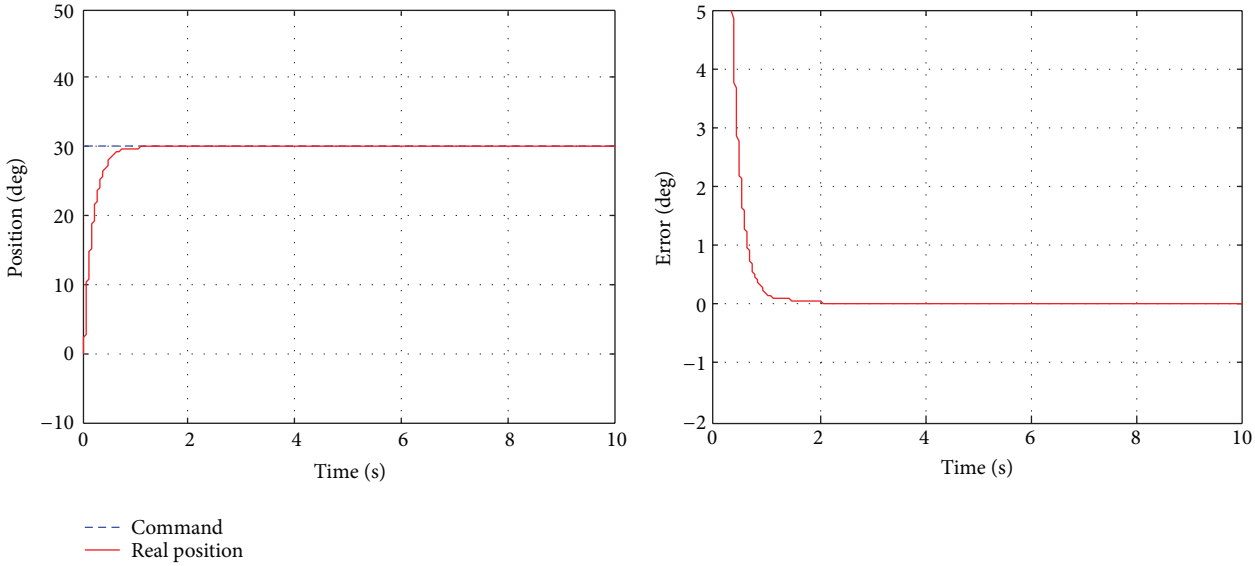

(a) Position tracking response

(b) Tracking error

Figure 9: Simulation results for the step signal input.

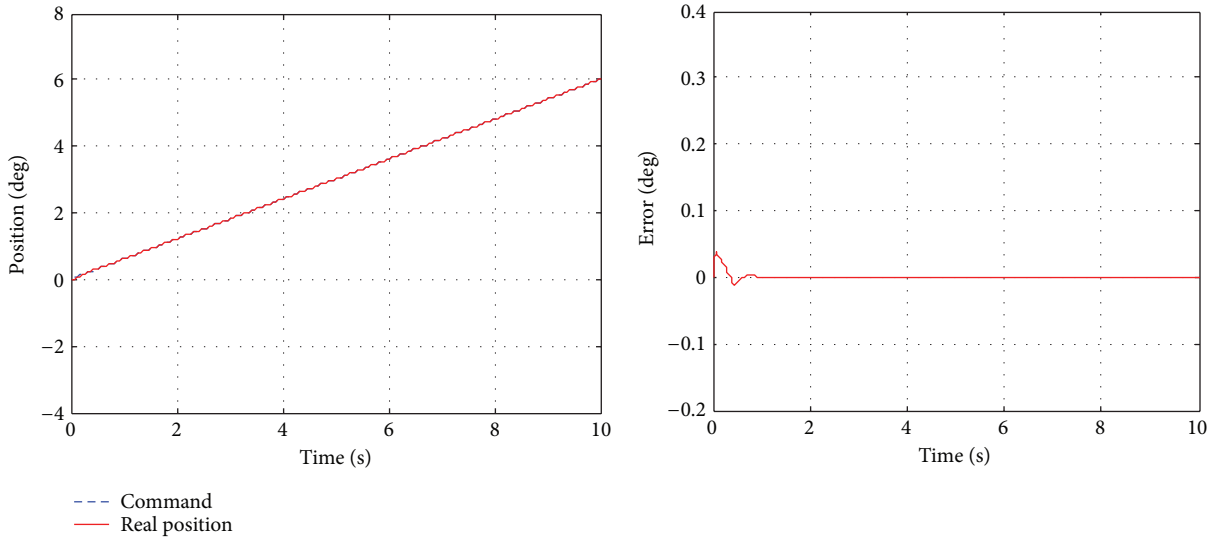

(a) Position tracking response

(b) Tracking error

Figure 10: Simulation results for the 0.6°/s slope signal input.

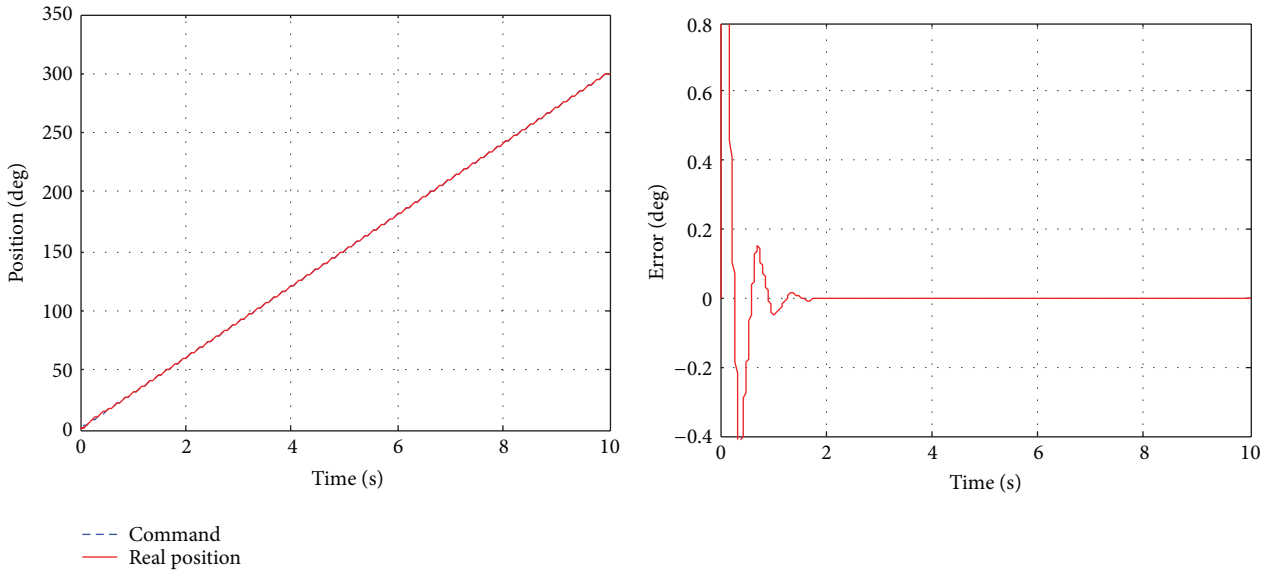

(a) Position tracking response (b) Tracking error

FIGURE 11: Simulation results for the 30°/s slope signal input.

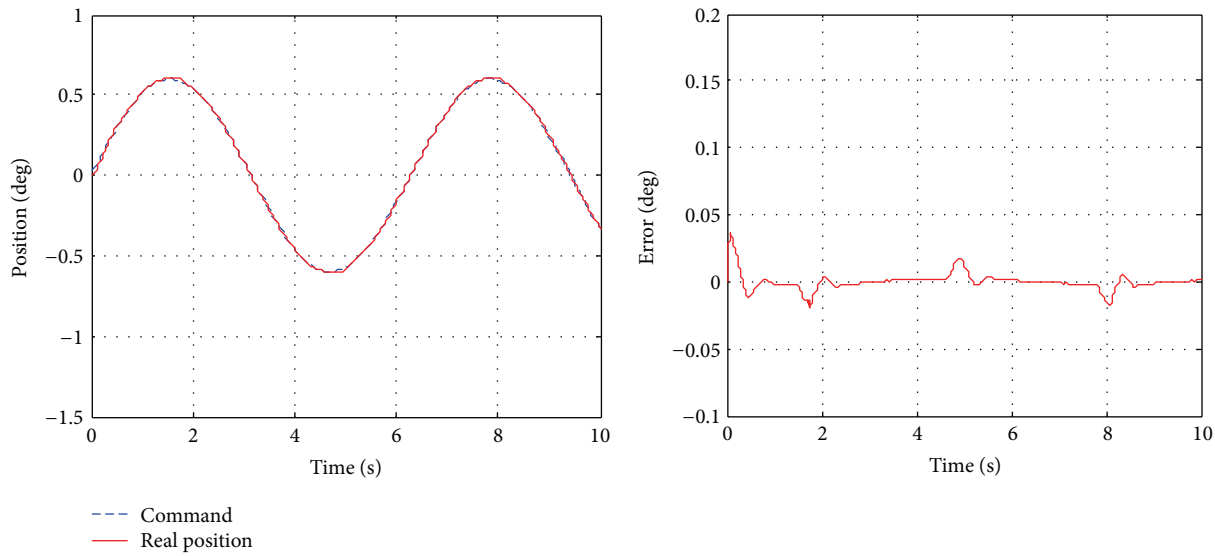

(a) Position tracking response (b) Tracking error

FIGURE 12: Simulation results for the 0.6°/s and 0.6°/s^2 sine signal input.

We get

$$\begin{aligned} &Q_{11}(k)\,Q_{33}(k) - Q_{13}^2(k) \\ &\quad = -\left[p_{13}(k) + a_{13}(k+1)\right]^2 + Q_{11}(k)\,Q_{33}(k) \\ &\quad = -\left[p_{13}(k) - p_{13}(k+1)\right]^2 \\ &\qquad + S_{13}\left[p_{13}(k) - p_{13}(k+1)\right] + T_{13}, \end{aligned} \tag{64}$$

where

$$\begin{aligned} S_{13} &= -2p_{13}(k+1) - 2a_{13}(k+1), \\ T_{13} &= p_{13}^2(k+1) + S_{13}p_{13}(k+1) \\ &\quad - a_{13}^2(k+1) + Q_{11}(k)\,Q_{33}(k). \end{aligned} \tag{65}$$

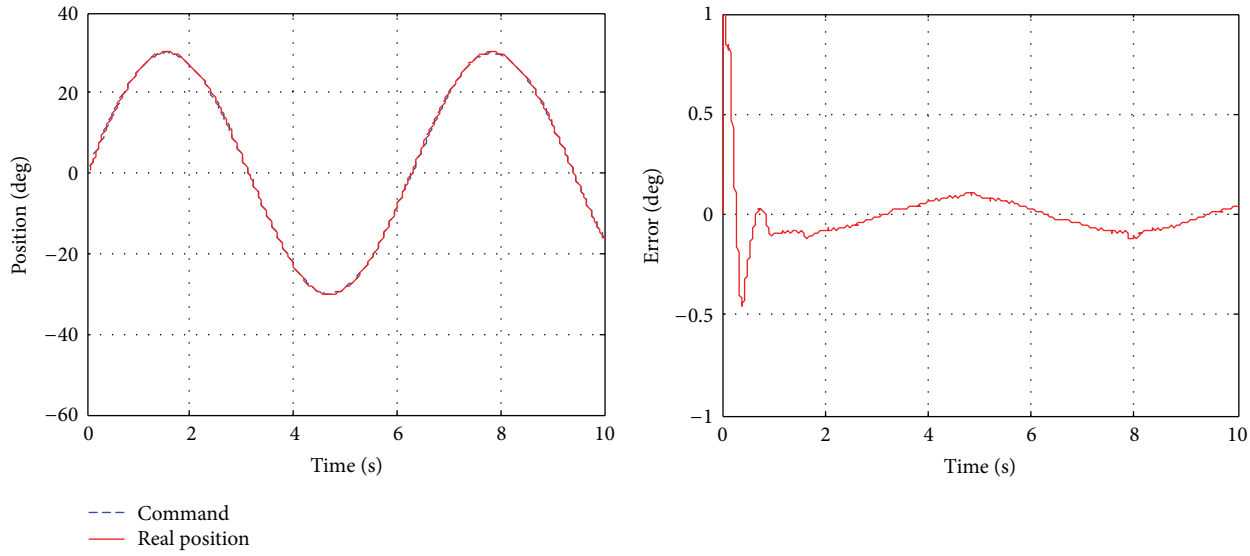

(a) Position tracking response (b) Tracking error

FIGURE 13: Simulation results for the 30°/s and 30°/s^2 sine signal input.

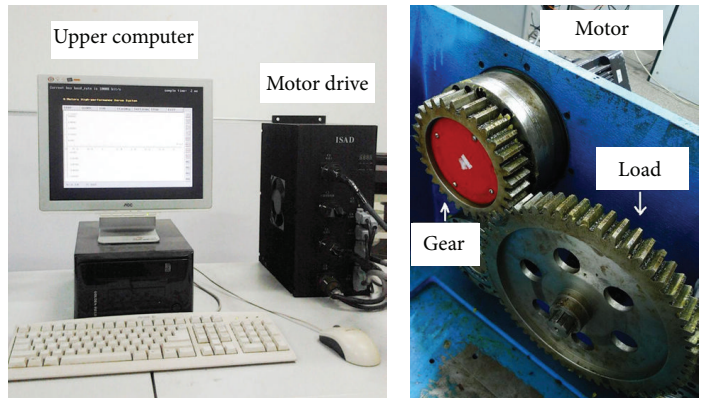

(a) Upper computer and servo drive (b) Motor and load

FIGURE 14: Experimental system.

S_{13} and T_{13} can be expressed in the form of (29) and (28):

$$B(k+1) = p_{13}(k+1), \quad C(k+1) = a_{13}(k+1),$$
$$D(k) = Q_{11}(k) Q_{33}(k), \quad F(k) = 0, \quad M(k) = 1. \tag{66}$$

Then the discriminant root of the quadratic trinomial (64) about $[p_{13}(k) - p_{13}(k+1)]$ is

$$\begin{aligned} \Delta_{13}(k) &= F^2(k) + 4M(k) D(k) \\ &= 4Q_{11}(k) Q_{33}(k) = 4M_{Q1}(k) Q_{33}(k), \end{aligned} \tag{67}$$

where

$$Q_{33}(k) = p_{33} - p_{22} + 2\varepsilon_1 f_1^2(k+1) - p_{33} f_1^2(k+1). \tag{68}$$

We can get $Q_{33}(k) > 0$ by (44), so $\Delta_{13}(k) > 0$. According to (40) and Lemma 11, we obtain

$$Q_{11}(k) Q_{33}(k) - Q_{13}^2(k) > 0. \tag{69}$$

So we get $\Delta_{23}(k) > 0$ by (62). Then we have $M_{Q3}(k) > 0$, according to (39) and Lemma 11.

Thus, $Q(k)$ is a uniformly bounded, positive definite symmetric matrix by Lemma 10. Furthermore, the time-varying discrete system (22) is uniformly asymptotically stable by Lemma 9. The proof is completed. □

4. Simulation Results

Considering the characters of the servo system, a composite controller which is composed of golden-section adaptive control law, integral control law, and feed-forward control

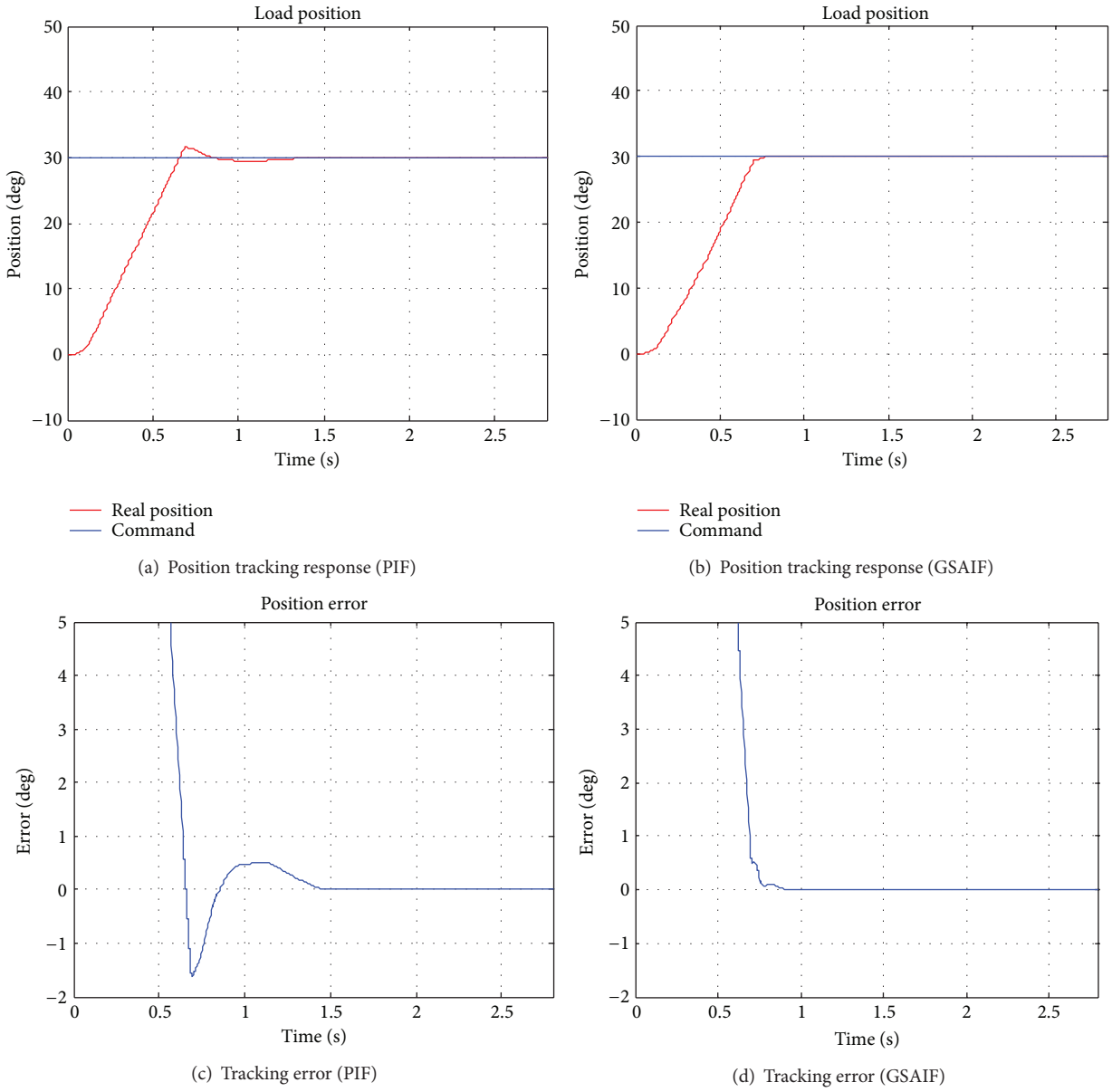

(a) Position tracking response (PIF)

(b) Position tracking response (GSAIF)

(c) Tracking error (PIF)

(d) Tracking error (GSAIF)

FIGURE 15: 30° step response.

law is applied in the system simulation. The structure of the closed-loop system is shown in Figure 8.

The golden-section adaptive control law $u_l(k)$ is given as

$$u_l(k) = \frac{1}{\widehat{\beta}_0(k) + \lambda}\left[l_1\widehat{\alpha}_1(k)\, e(k) + l_2\widehat{\alpha}_2(k)\, e(k-1)\right], \quad (70)$$

where $e(k) = y_r(k) - y(k)$, $l_1 = 0.382$, $l_2 = 0.618$, and λ is a small positive constant which ensures that the golden-section adaptive control law is bounded when $\beta_0(k) = 0$.

The integral control law is given as

$$u_i(k) = u_i(k-1) + k_i e(k). \quad (71)$$

The feed-forward control law is given as

$$u_f(k) = k_f\left(y_r(k) - y_r(k-1)\right), \quad (72)$$

where k_f is the feed-forward coefficient.

In summary, the composite controller is

$$u(k) = u_a(k) + u_f(k) = u_l(k) + u_i(k) + u_f(k). \quad (73)$$

The values of the controller parameters are $\lambda = 2 \times 10^{-3}$, $k_i = 0.6$, and $k_f = 50$.

In order to verify the effectiveness of the servo system, step signal, slope signal, and sine signal, which are often used in the performance test of servo systems, are used as input signals in this paper. In the simulations, the system responses under 30° step signal input, 0.6°/s slope signal input, 30°/s slope signal input, 0.6°/s, 0.6°/s^2 sine signal input, and 30°/s, 30°/s^2 sine signal input are tested, respectively.

(1) When the input signal is $y_r(t) = 30°$, the results are shown in Figure 9.

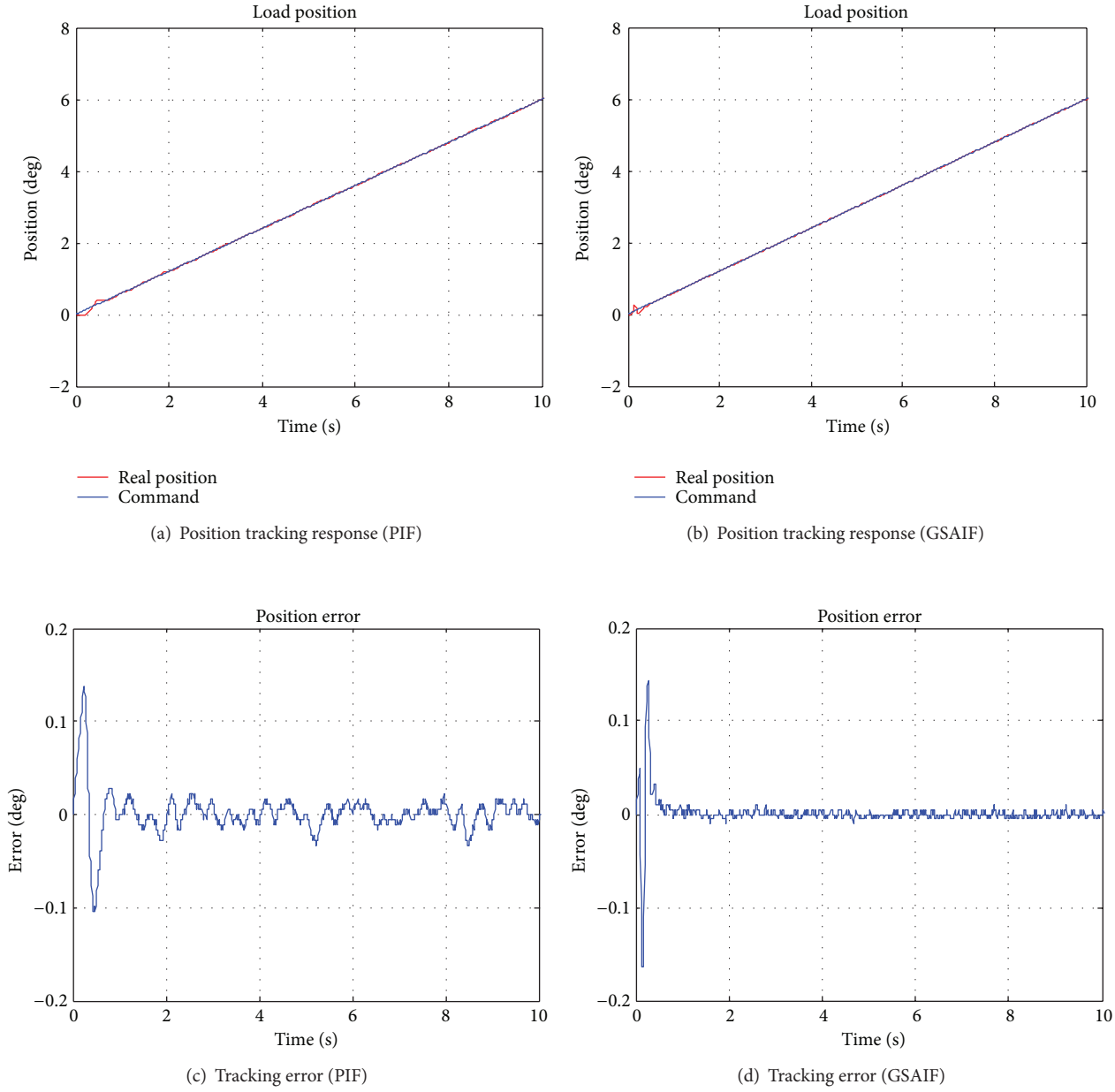

(a) Position tracking response (PIF)

(b) Position tracking response (GSAIF)

(c) Tracking error (PIF)

(d) Tracking error (GSAIF)

Figure 16: 0.6°/s slope response.

(2) When the input signal is $y_r(t) = 0.6^\circ/\text{s}$, the results are shown in Figure 10.

(3) When the input signal is $y_r(t) = 30^\circ/\text{s}$, the results are shown in Figure 11.

(4) When the input signal is $y_r(t) = 0.6^\circ \sin(t)$, the results are shown in Figure 12.

(5) When the input signal is $y_r(t) = 30^\circ \sin(t)$, the results are shown in Figure 13.

5. Experimental Results

To verify the effectiveness of the proposed control scheme, the experiments are conducted on the experimental system as shown in Figure 14. The experimental system consisted of an upper computer, a servo drive, a servo motor, a reducer, and a load. The PC104 (SCM/SPT4) module is used as the upper computer, and it is mainly used for sending instructions and monitoring the status of the system. The servo drive is designed by us based on the DSP TMS320F28335, which has a CAN communication interface and can receive the position instruction from the upper computer in real time. In the running process, the drive implements the control of current,

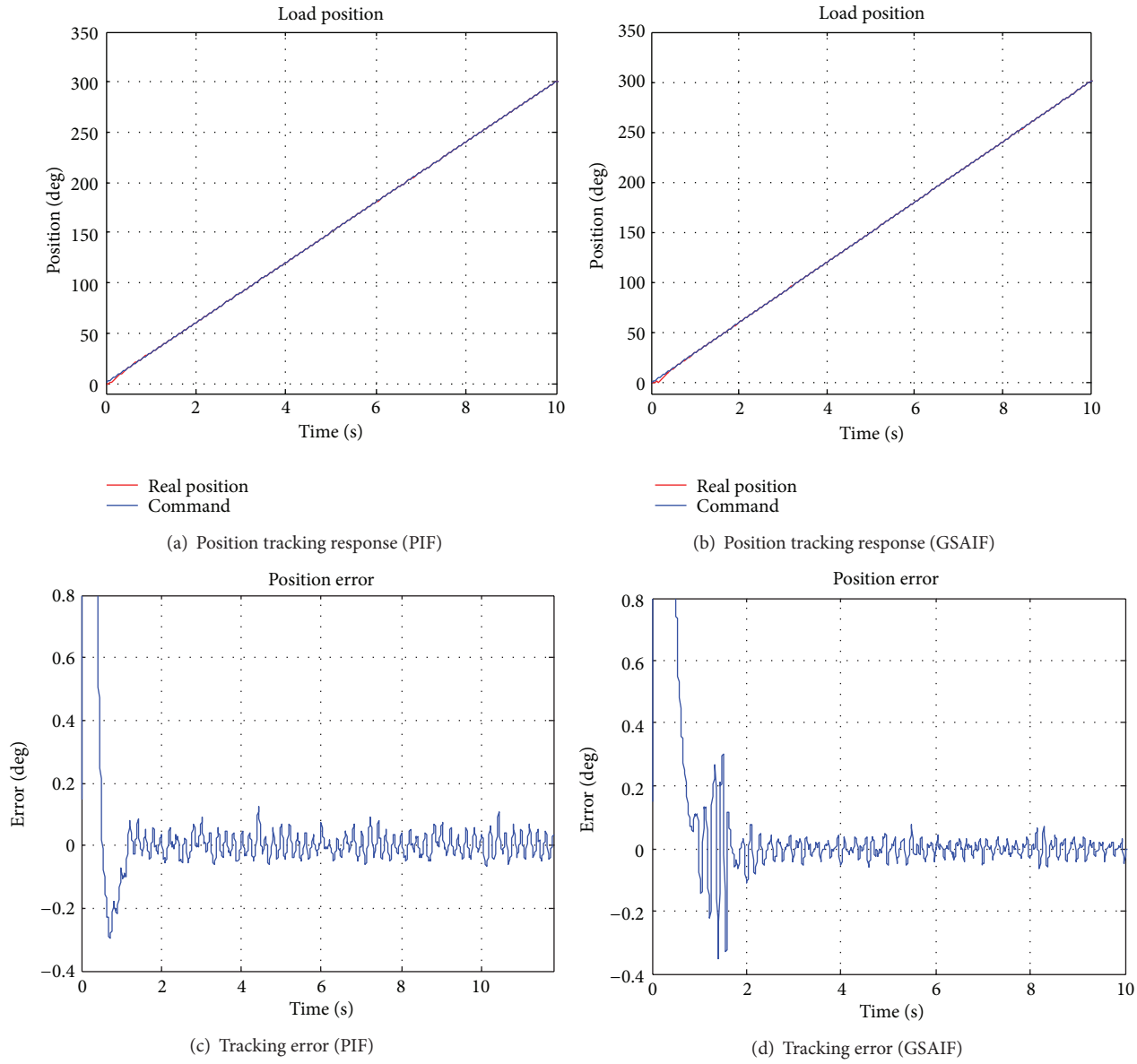

(a) Position tracking response (PIF)

(b) Position tracking response (GSAIF)

(c) Tracking error (PIF)

(d) Tracking error (GSAIF)

FIGURE 17: 30°/s slope response.

speed, and position of the motor. The PMSM (M-403-B) produced by Kollmorgen Company is selected as the servo motor in the experiment. The parameters of the motor are listed in Table 1. The high speed and high rigidity planetary gear reducer (FIC-A35-119) produced by Sumitomo Heavy Machinery Company is utilized in the experiment, whose reduction ratio is 1 : 119, and the reduction ratio of the final gears is 1 : 2.

The backlash between the motor and the load is 0.36°. PI control scheme is used in the speed controller and current controller of the motor drive; the proportion and integral gains of the speed controller and current controller are 1.2, 0.02, 1.5, and 0.02, respectively, after adjustment. For the sake of comparison, the position controller based on PI control scheme with feed-forward compensation (PIF) and the composite position controller including the golden-section adaptive control law, the integral control law, and feed forward compensation (GSAIF) are tested, respectively, in the

TABLE 1: Parameters of the servo motor (M-403-B).

Name	Units	Value
Rated power	kW	2.5
Rated speed	rpm	3000
Torque coefficient	N·m/A	1.11
EMF	V/krpm	67.2
Line resistance	ohms	2.6
Line induction	mH	50
Inertia	Kg·m^2	0.00259
Static friction	N·m	0.24
Viscous friction	N·m/krpm	0.015

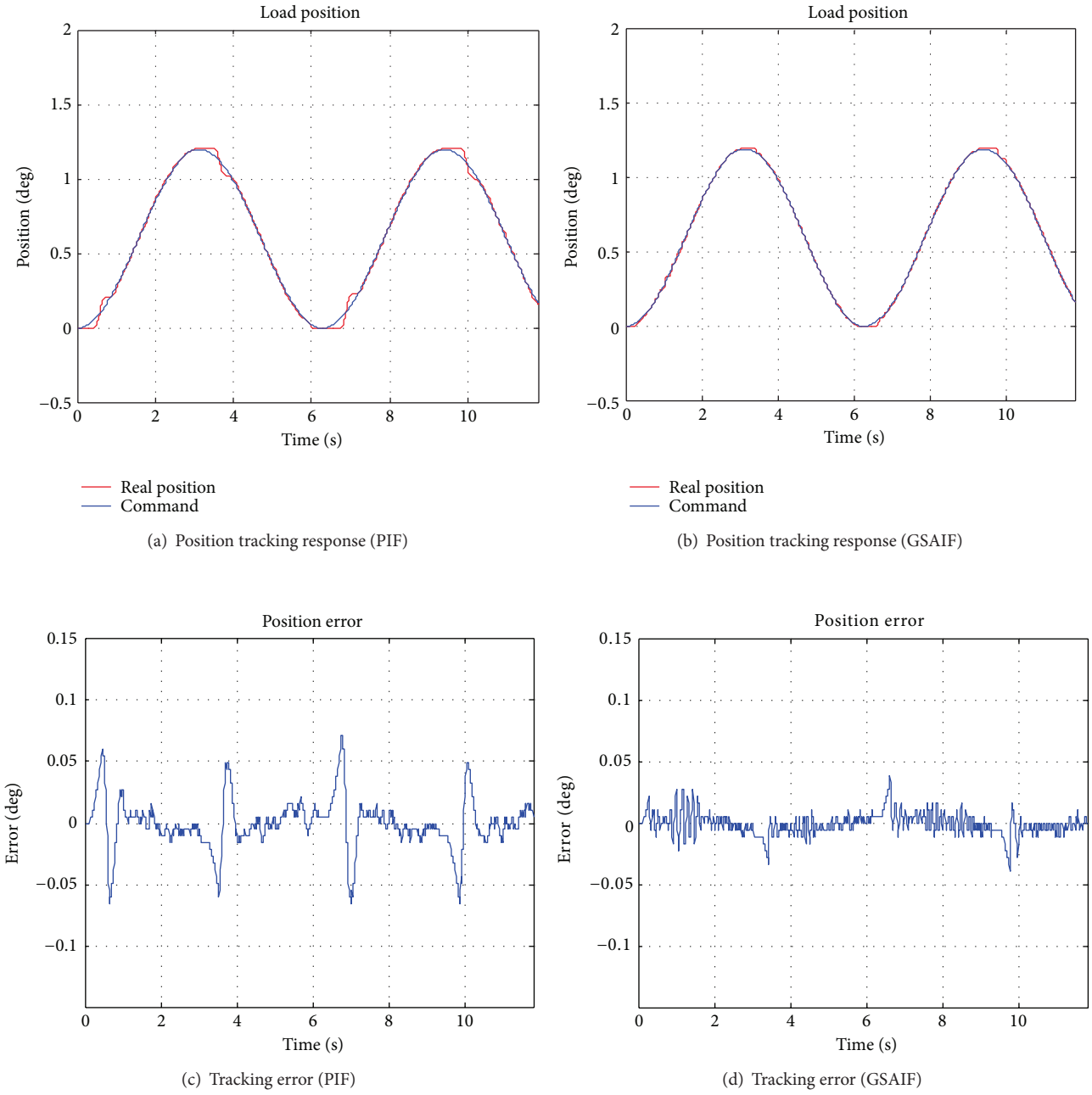

(a) Position tracking response (PIF)

(b) Position tracking response (GSAIF)

(c) Tracking error (PIF)

(d) Tracking error (GSAIF)

Figure 18: 0.6°/s and 0.6°/s^2 sine response.

experiment. In the PIF scheme, the proportion and integral gains are 4.2 and 0.23, respectively, and the feed-forward gain is 0.25. In the GSAIF scheme, $f = 0.995$, and $\lambda = 0.01$, the coefficients of integral gain and feed forward gain are 0.29 and 0.25. Position step, slope, and sine signals are used in the experiments to test the system performance. The experimental results are shown in Figures 15–19.

(1) Tracking the 30° Step Signal. From Figure 15 it can be obtained that the system overshoot is 1.8° using PIF control scheme; after 1.5 s the system is in a stable state and the tracking error is zero. When using GSAIF control scheme, the overshoot does not appear, and after 0.8 s the system is in a stable state and the stable tracking error is zero too. The comparison results show that the GSAIF scheme has a better dynamic performance and the response speed is much better than the PIF scheme.

(2) Tracking the 0.6°/s and the 30°/s Slope Signal. As shown in Figures 16 and 17, the system is tested for tracking 0.6°/s and 30°/s position slope signal. In the 0.6°/s tracking experiment, the maximum stable error is 0.023° using PIF scheme. When the system tracks the command signal using GSAIF, the maximum tracking error is only 0.01°. In the 30°/s tracking test, the stable error increases using both of the control schemes. The maximum stable tracking error

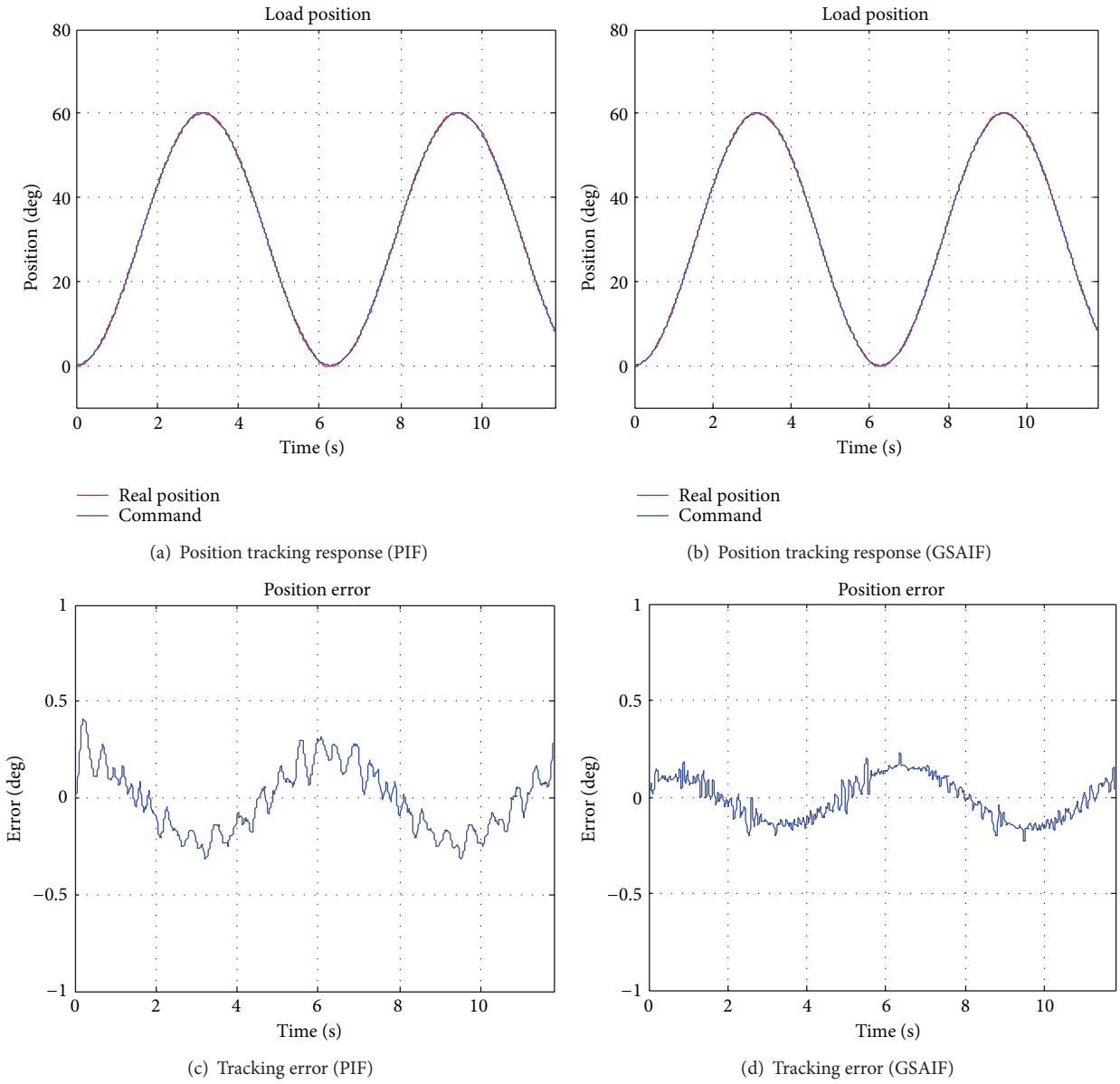

(a) Position tracking response (PIF)

(b) Position tracking response (GSAIF)

(c) Tracking error (PIF)

(d) Tracking error (GSAIF)

FIGURE 19: 30°/s and 30°/s^2 sine response.

using PIF scheme is 0.12°. When using GSAIF scheme, the maximum tracking error is 0.08°. The comparison results show that the GSAIF scheme has better smoothness and higher precision tracking performance compared with PIF scheme when tracking the position slope signals.

(3) Tracking the 0.6°/*s,* 0.6°/s^2 *and* 30°/*s,* 30°/s^2 *Sine Signal.* As shown in Figures 18 and 19, the system is tested for tracking position sine signal; the maximum speed and acceleration of the command signals are 0.6°/s, 0.6°/s^2 and 30°/s, 30°/s^2, respectively. In the 0.6°/s, 0.6°/s^2 sine signal tracking test, the maximum tracking error is 0.06° when using PIF scheme. However, using GSAIF scheme, the maximum tracking error is 0.04°. In the 30°/s, 30°/s^2 sine signal tracking test, the tracking error vibrates severely using the PIF scheme and the maximum tracking error reaches 0.42°. Using GSAIF scheme, there is no obvious vibrations and the maximum tracking error is only 0.26°. The comparison results show that the GSAIF scheme possesses a better suppression ability of nonlinear uncertainties such as backlash and friction when tracking sine signals, and it improves the system tracking precision.

6. Conclusions

In this paper, the characteristic modeling technique is applied for modeling and control of the servo system with backlash and friction. To meet the demands of characteristic modeling,

a continuous approximation of dead-zone function is introduced to describe the backlash model, and the sgn(·) function is replaced by $(2/\pi)\arctan(kv)$ to make the Stribeck friction model smooth. The characteristic model of the system is established based on a second-order slowly time-varying difference equation and verified by simulations. The composite controller based on golden-section adaptive law, feedforward compensation, and integral law is proposed, and the stability of the closed-loop system is analyzed by Lyapunov theory. It is shown by both simulation and experimental results that it is feasible to establish the characteristic model of the servo system with backlash and friction. The GSAIF controller is also effective, and it can reduce the effect of backlash and friction and improve the steady-state precision and the dynamic performance of the servo system.

Conflict of Interests

The authors declare that there is no conflict of interests regarding the publication of this paper.

Acknowledgment

This work was supported by the National Natural Science Foundation of China under Grant nos. 61074023 and 60974027.

References

[1] B. Armstrong-Hélouvry, P. Dupont, and C. C. de Wit, "A survey of models, analysis tools and compensation methods for the control of machines with friction," *Automatica*, vol. 30, no. 7, pp. 1083–1138, 1994.

[2] M. Nordin and P.-O. Gutman, "Controlling mechanical systems with backlash—a survey," *Automatica*, vol. 38, no. 10, pp. 1633–1649, 2002.

[3] G. Tao and P. V. Kokotović, "Continuous-time adaptive control of systems with unknown backlash," *IEEE Transactions on Automatic Control*, vol. 40, no. 6, pp. 1083–1087, 1995.

[4] R. R. Selmic and F. L. Lewis, "Neural net backlash compensation with Hebbian tuning using dynamic inversion," *Automatica*, vol. 37, no. 8, pp. 1269–1277, 2001.

[5] G. Tao, X. Ma, and Y. Ling, "Optimal and nonlinear decoupling control of systems with sandwiched backlash," *Automatica*, vol. 37, no. 2, pp. 165–176, 2001.

[6] J. Zhou, C. Wen, and Y. Zhang, "Adaptive output control of nonlinear systems with uncertain dead-zone nonlinearity," *IEEE Transactions on Automatic Control*, vol. 51, no. 3, pp. 504–511, 2006.

[7] P. Rostalski, T. Besselmann, M. Barić, F. van Belzen, and M. Morari, "A hybrid approach to modelling, control and state estimation of mechanical systems with backlash," *International Journal of Control*, vol. 80, no. 11, pp. 1729–1740, 2007.

[8] R. Merzouki, J. A. Davila, L. Fridman, and J. C. Cadiou, "Backlash phenomenon observation and identification in electromechanical system," *Control Engineering Practice*, vol. 15, no. 4, pp. 447–457, 2007.

[9] A. Lagerberg and B. Egardt, "Backlash estimation with application to automotive powertrains," *IEEE Transactions on Control Systems Technology*, vol. 15, no. 3, pp. 483–493, 2007.

[10] S. I. Han and J. M. Lee, "Adaptive dynamic surface control with sliding mode control and RWNN for robust positioning of a linear motion stage," *Mechatronics*, vol. 22, no. 2, pp. 222–238, 2012.

[11] Y.-T. Liu, T.-T. Kung, K.-M. Chang, and S.-Y. Chen, "Observer-based adaptive sliding mode control for pneumatic servo system," *Precision Engineering*, vol. 37, no. 3, pp. 522–530.

[12] B. A. Bucci, J. S. Vipperman, D. G. Cole, and S. J. Ludwick, "Evaluation of a servo settling algorithm," *Precision Engineering*, vol. 37, no. 1, pp. 10–22, 2013.

[13] C. Canudas de Wit, H. Olsson, K. J. Åström, and P. Lischinsky, "A new model for control of systems with friction," *IEEE Transactions on Automatic Control*, vol. 40, no. 3, pp. 419–425, 1995.

[14] L. Márton and B. Lantos, "Control of mechanical systems with Stribeck friction and backlash," *Systems & Control Letters*, vol. 58, no. 2, pp. 141–147, 2009.

[15] B. Bona and M. Indri, "Friction compensation in robotics: an overview," in *Proceedings of the 44th IEEE Conference on Decision and Control, and the European Control Conference (CDC-ECC '05)*, pp. 4360–4367, Seville, Spain, December 2005.

[16] B. Armstrong, D. Neevel, and T. Kusik, "New results in NPID control: tracking, integral control, friction compensation and experimental results," *IEEE Transactions on Control Systems Technology*, vol. 9, no. 2, pp. 399–406, 2001.

[17] D. Garagić and K. Srinivasan, "Adaptive friction compensation for precision machine tool drive," *Control Engineering Practice*, vol. 12, no. 11, pp. 1451–1464, 2004.

[18] H. Chaoui and P. Sicard, "Adaptive fuzzy logic control of permanent magnet synchronous machines with nonlinear friction," *IEEE Transactions on Industrial Electronics*, vol. 59, no. 2, pp. 1123–1133, 2012.

[19] Y. Wang, D. Wang, and T. Chai, "Extraction and adaptation of fuzzy rules for friction modeling and control compensation," *IEEE Transactions on Fuzzy Systems*, vol. 19, no. 4, pp. 682–693, 2011.

[20] S. N. Huang, K. K. Tan, and T. H. Lee, "Adaptive motion control using neural network approximations," *Automatica*, vol. 38, no. 2, pp. 227–233, 2002.

[21] S.-W. Lee, "Robust adaptive stick slip compensation," *Industrial Electronics*, vol. 22, no. 5, pp. 747–779, 1995.

[22] H. Xu and P. A. Ioannou, "Robust adaptive control of linearizable nonlinear single input systems with guaranteed error bounds," *Automatica*, vol. 40, no. 11, pp. 1905–1911, 2004.

[23] K. Menon and K. Krishnamurthy, "Control of low velocity friction and gear backlash in a machine tool feed drive system," *Mechatronics*, vol. 9, no. 1, pp. 33–52, 1999.

[24] S. Suraneni, I. N. Kar, O. V. R. Murthy, and R. K. P. Bhatt, "Adaptive stick-slip friction and backlash compensation using dynamic fuzzy logic system," *Applied Soft Computing Journal*, vol. 6, no. 1, pp. 26–37, 2005.

[25] H. Wu, J. Hu, and Y. Xie, "Characteristic model-based all-coefficient adaptive control method and its applications," *IEEE Transactions on Systems, Man and Cybernetics C*, vol. 37, no. 2, pp. 213–221, 2007.

[26] B. Meng and H.-X. Wu, "A unified proof of the characteristic model of linear time-invariant systems," in *Proceedings of the American Control Conference (ACC '07)*, pp. 935–940, New York, NY, USA, July 2007.

[27] Y. Wang, "Stability analysis of characteristic model based all-coefficient adaptive control for a class of minimum-phase linear system," *Procedia Engineering*, vol. 29, pp. 2410–2420, 2012.

[28] H. Wu, J. Hu, and Y. Xie, *Characteristic Model-Based Intelligent Adaptive Control*, Chinese Science and Technology Press, Beijing, China, 2008.

[29] R.-H. Du, Y.-F. Wu, W. Chen, and Q.-W. Chen, "Adaptive backstepping fuzzy control for servo systems with backlash," *Control Theory and Applications*, vol. 30, no. 2, pp. 254–260, 2013.

[30] D.-Q. Sun and H.-X. Wu, "Uniform asymptotic stability of 3rd-order time-variant discrete systems," *Journal of Astronautics*, vol. 25, no. 5, pp. 502–506, 2004.

Hindawi Publishing Corporation
Mathematical Problems in Engineering
Volume 2014, Article ID 539617, 12 pages
http://dx.doi.org/10.1155/2014/539617

Research Article

Switching Fuzzy Guaranteed Cost Control for Nonlinear Networked Control Systems

Linqin Cai,[1,2] Zhuo Yang,[2] Jimin Yu,[2] and Zhenhua Zhang[2]

[1] *Key Laboratory of Industrial Internet of Things & Networked Control, Ministry of Education, Chongqing University of Posts and Telecommunications, Chongqing 400065, China*
[2] *Research Center on Complex System Analysis and Control, Chongqing University of Posts and Telecommunications, Chongqing 400065, China*

Correspondence should be addressed to Linqin Cai; cailq@cqupt.edu.cn

Received 17 August 2013; Accepted 21 November 2013; Published 9 February 2014

Academic Editor: Bo-Chao Zheng

This paper deals with the problem of guaranteed cost control for a class of nonlinear networked control systems (NCSs) with time-varying delay. A guaranteed cost controller design method is proposed to achieve the desired control performance based on the switched T-S fuzzy model. The switching mechanism is introduced to handle the uncertainties of NCSs. Based on Lyapunov functional approach, some sufficient conditions for the existence of state feedback robust guaranteed cost controller are presented. Simulation results show that the proposed method is effective to guarantee system's global asymptotic stability and quality of service (QoS).

1. Introduction

As network technology advanced in the last decade, networked control system (NCS) has increasingly become a research focus. Considerable attention on the modeling and controller design of NCSs has been paid in [1–5]. There are many advantages to NCSs, such as reduced system wiring, facilitated system maintenance, and increased systems flexibility.

However, due to the insertion of communication channels, this brings many challenging problems such as network-induced delay and data packet dropout. Regardless of the type of network used, these special issues degrade the system dynamic performance and are a source of potential instability. There are a number of design methods that have been proposed to deal with these problems. One of the most general methods is to model the NCS as a system with time-varying delays. So the stability of an NCS is equivalent to the stability of a system with time-varying delays [2]. Moreover, the sampling behavior has also an important impact on the design of the NCS controller because the states of the feedback controller are not continuous as a result of the existence of zeroth-order hold (ZOH). In [1], a model of NCS was provided considering network-induced delay and packet dropout in the transmission. In [3], an observer-based stabilizing controller was designed for the NCSs involving both random measurement and actuation delays. Robust controllers for uncertain NCSs were also obtained in [4, 5]. However, how to analyze the stability of nonlinear NCSs has increasingly become a challenging topic. Some results about the stability of nonlinear NCSs were obtained in [6, 7]. In [8], a stochastic optimal controller design for nonlinear NCSs with uncertain dynamics via neurodynamic programming was proposed. The closed-loop stability of the nonlinear NCSs was demonstrated by selecting neural network (NN) update laws. However, these methods often require some strict assumptions for a system model, so it is difficult for practical applications.

In the last few years, the fuzzy control is a useful approach to solve the control problems of nonlinear systems. The Takagi-Sugeno (T-S) fuzzy system proposed in [9] is widely applied to industrial control fields because of its simple structure with local dynamics. In the T-S fuzzy model, local dynamics in different state-space regions are represented by many linear models so that linear system theory can conveniently be employed to analyze the stability of overall closed-loop system and to design the feedback controller. The typical design approaches are carried out based on fuzzy model

via the so-called parallel distributed compensation (PDC) method [10]. Considering the time-delay characteristic of nonlinear systems, many results about the T-S fuzzy model with a time-delay term are obtained to deal with stability and stabilization problems of nonlinear systems with time delays [2, 11–13]. The guaranteed cost control for a T-S fuzzy system with time delays was presented in [2, 11, 12]. In [13], robust control problem was studied for a class of large-scale NCSs, and the decentralized design was presented using T-S fuzzy approach.

Nevertheless, an inherent drawback remains since the number of fuzzy rules of a T-S model increases exponentially with the number of nonlinearities constituting the matched nonlinear system [14]. This makes fuzzy controller design and implementation difficult as the complexity of the nonlinear system to be controlled increases [15]. To outline the problem of rules explosion in fuzzy T-S modeling, some authors have proposed to combine the merit of switched systems with T-S ones to deal with nonlinear control problems [16–18]. To do so, partitioning the state space of a nonlinear system allows defining a switched nonlinear system. Then, inside each partition, a T-S model can be obtained. As stated in [18], the resulting switched T-S system inherits some essential features of hybrid systems and maintains all the information and knowledge representation capacity of fuzzy systems. However, few papers have studied stabilization issues of switched fuzzy systems based on switching Lyapunov functions [16] or quadratic approaches [17]. In [19], based on barrier Lyapunov functions (BLFs), a new control design for constrained nonlinear switched systems was investigated to achieve output tracking. By ensuring the boundedness of the BLFs in the closed loop, the proposed approaches can guarantee that all states in the switched systems do not violate the desired constraints and that all closed-loop signals are bounded. For many nonlinear systems, some of the premise variables of the corresponding T-S fuzzy models are measurable when they are modeled as T-S fuzzy models, while the parts with unmeasurable premise variables can be modeled as uncertainties. Thus, the overall systems can be described by T-S fuzzy parts with measurable premise variables and uncertainty parts. In [20], a switching stabilizing controller is designed for a nonlinear system with unknown parameters or unmeasurable premise variables. However, the uncertainties cannot be well handled. In [21], a switching fuzzy dynamic output feedback control scheme is proposed, where the switching mechanism is introduced to handle the unknown parameters.

In designing a controller for a real plant, it is invariably necessary to design a control system which not only is stable but also possesses a strong robust performance. One way to deal with this is the so-called guaranteed cost control approach [2]. This addresses the robust performance problem and has the advantage of providing an upper bound on a given performance index guaranteeing that system performance degradation incurred by uncertainty is less than this bound. For the NCSs, the quality of service (QoS) is one of the most important performance indexes. Therefore, it is vital to design a guaranteed cost controller such that the NCSs are stable as well as satisfactory with the required QoS.

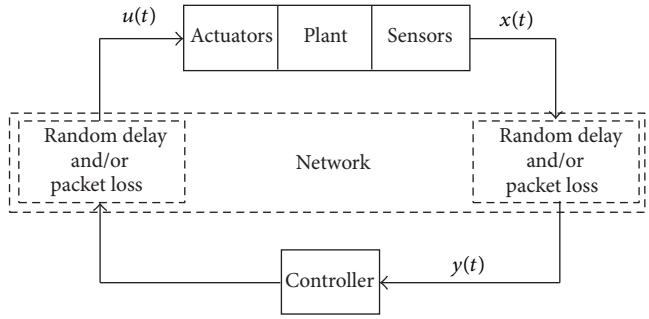

Figure 1: A general NCS.

In this paper, we aim at the problem of guaranteed cost control for a class of uncertain nonlinear NCSs with time delays. Considering the QoS of NCSs, we propose a guaranteed cost control scheme to achieve the desired control performance based on switched T-S fuzzy control method, where the switching mechanism is introduced to handle the uncertainties. Moreover, the sufficient condition for the existence of the robust guaranteed cost controller and the design method of the corresponding switching control law are obtained via Lyapunov functions. Comparing with [2, 11, 12], the proposed switching fuzzy approach inherits some essential features of hybrid systems to deal with the uncertain nonlinear NCSs and avoids the inherent drawback of rules explosion in modeling a fuzzy T-S model. In addition, we consider the stabilization problem of the switched fuzzy T-S system with time delays in NCSs.

The innovations of this paper are as follows: (1) the guaranteed cost controller is proposed for nonlinear NCSs with time-varying delay to achieve the desired control performance based on the switched T-S fuzzy model with uncertain parameters, and (2) the sufficient condition for the robust guaranteed cost control law is presented to uncertain nonlinear NCSs.

The paper is organized as follows. The basic problem formulation of the nonlinear networked control system is given in Section 2. The switching fuzzy controller via state feedback is analyzed in Section 3. In Section 4, the sufficient stability conditions and guaranteed cost control law are discussed by Lyapunov functions. Section 5 provides simulation results to demonstrate the effectiveness of the proposed method. Finally, concluding remarks are given in Section 6.

2. Problem Formulation

A general NCS configuration is illustrated in Figure 1, which is composed of a controller and a remote system containing a physical plant, sensors, and actuators. The controller and the plant are physically located at different locations and are directly linked by a data network in order to perform remote closed-loop control.

In Figure 1, the nonlinear networked control system can be described as follows:

$$\begin{aligned} \dot{x}(t) &= f(x(t), u(t)), \\ y(t) &= g(x(t), u(t)), \end{aligned} \tag{1}$$

where $x(t) \in R^n$ is the state variation, $u(t) \in R^m$ is the control input, $y(t) \in R^s$ is the regulated output, $f(x,u)$ and $g(x,u)$ are the nonlinear functions. Currently, it has been proved that the T-S fuzzy models are universal approximations of many nonlinear dynamic systems. So we introduce a T-S fuzzy system to model a class of nonlinear NCSs. Without considering the disturbance input, we use the following T-S fuzzy model to approximate $f(x(t),u(t))$ and $g(x(t),u(t))$:

$$R_i\text{: IF } \theta_1(t) \text{ is } N_{i1},\ldots,\text{and } \theta_g(t) \text{ is } N_{ig},$$
$$\text{THEN } \begin{cases} \dot{x}(t) = A_i x(t) + B_i u(t), \\ y(t) = C_i x(t), \end{cases} \tag{2}$$

where $i = 1,2,\ldots,r$ is the index number of fuzzy rules, $\theta_1(t),\theta_2(t),\ldots,\theta_g(t)$ are the known premise variables, N_{ik} is the fuzzy sets ($k = 1,2,\ldots,g$), $x(t) \in R^n$ is the state vector, $y(t) \in R^s$ is the output vector, $u(t) \in R^m$ is the control input, $A_i \in R^{n\times n}$ is known system matrices, $B_i \in R^{n\times m}$ is the input matrix, and $C_i \in R^{n\times s}$ is the output matrix.

Before designing the controller, we make the following reasonable assumptions.

Assumption 1. The sensor is clock-driven. The controller and actuator are event-driven. The clocks among them are synchronized.

Assumption 2. Time-varying network-induced delay is less than one sampling period.

Assumption 3. The computational delay is negligible.

Assumption 4. The signal is single-packet transmission without packet drop.

Assuming the node sampling period is T, so we can obtain the discrete T-S fuzzy model of nonlinear networked control systems with time-varying delay:

$$R_i\text{: IF } \theta_1(k) \text{ is } N_{i1},\ldots,\text{and } \theta_g(k) \text{ is } N_{ig},$$
$$\text{THEN } \begin{cases} x(k+1) \\ \quad = \Phi_i x(k) + \Gamma_{i0}(\tau_k) u(k) \\ \quad\quad + \Gamma_{i1}(\tau_k) u(k-1), \\ y(k) = C_i x(k), \end{cases} \tag{3}$$

where $\Phi_i = e^{A_i T}$, $\Gamma_{i0}(\tau_k) = \int_0^{T-\tau_k} e^{A_i T} dt \cdot B_i$, $\Gamma_{i1}(\tau_k) = \int_{T-\tau_k}^{T} e^{A_i T} dt \cdot B_i$, and τ_k is the network-induced delay, $i = 0,1,2,\ldots,r$.

Furthermore, (3) can be transformed into the following form with uncertain parameters:

$$\begin{aligned} x(k+1) &= \Phi_i x(k) + \left(\Gamma_{i0} + D_i F_i(\tau_k) E_i\right) u(k) \\ &\quad + \left(\Gamma_{i1} - D_i F_i(\tau_k) E_i\right) u(k-1), \\ y(k) &= C_i x(k), \end{aligned} \tag{4}$$

where D_i, E_i are known constant matrices of appropriate dimensions and F_i is an unknown matrix function satisfying

$$\begin{aligned} F^T F &\le I, \\ \Gamma_{i0}(\tau_k) &= \Gamma_{i0} + D_i F_i(\tau_k) E_i, \\ \Gamma_{i1}(\tau_k) &= \Gamma_{i1} - D_i F_i(\tau_k) E_i. \end{aligned} \tag{5}$$

For any given $x(k)$ and $u(k)$, by using a weighted-average defuzzifier, product inference, and singleton fuzzifier, the local models can be integrated into a global nonlinear model:

$$\begin{aligned} x(k+1) &= \sum_{i=1}^{r} \mu_i(\theta(k)) \left[\Phi_i x(k) + \Gamma_{i0}(\tau_k) u(k) \right. \\ &\quad \left. + \Gamma_{i1}(\tau_k) u(k-1)\right], \\ y(k) &= C_i x(k), \end{aligned} \tag{6}$$

where

$$\begin{aligned} \theta(k) &= \left[\theta_1^T(k), \theta_2^T(k), \ldots, \theta_g^T(k)\right]^T, \\ \mu_i(\theta(k)) &= \frac{\prod_{l=1}^{g} N_{il}(q_l(k))}{\sum_{i=1}^{r} \prod_{l=1}^{g} N_{il}(\theta_l(k))}. \end{aligned} \tag{7}$$

$N_{il}(\theta_l(k))$ is the grade of membership of $\theta_l(k)$ in the fuzzy set N_{il}. Notice the following facts:

$$\mu_i(\theta(k)) \ge 0, \qquad \sum_{i=1}^{r} \mu_i(\theta(k)) = 1. \tag{8}$$

The guaranteed cost function associated with system (3) is given by

$$J = \sum_{k=0}^{\infty} \left[x^T(k) Q x(k) + u_\sigma^T(k) R u_\sigma(k)\right]. \tag{9}$$

Definition 5. Consider the uncertain system (3) and cost function (9). If there exists a control law $u_\sigma^*(k)$ and a positive scalar J^* such that for all admissible uncertainties, the closed-loop system is asymptotically stable and the value of the cost function (9) satisfies $J \le J^*$, then J^* is said to be a guaranteed cost and $u_\sigma^*(k)$ is said to be a guaranteed cost control law.

3. Controller Design

We assume that switched fuzzy controller is constituted with N switching rules. The σth subfuzzy controller is

$$R^\sigma{}_i\text{: IF } \theta_1(t) \text{ is } N_{i1},\ldots,\text{and } \theta_g(t) \text{ is } N_{ig},$$
$$\text{THEN } u_\sigma(k) = K_{\sigma i} x(k), \tag{10}$$

where $\sigma = 1,2,\ldots,N$ is a piecewise constant function representing the switching signal and R_i^σ represents ith fuzzy

rule of the σth subfuzzy controller. The switching control law is constituted by the following fuzzy controller:

$$\begin{aligned} u_1(k) &= \sum_{i=1}^{r} \mu_i(\theta(k)) K_{1i} x(k), \\ u_2(k) &= \sum_{i=1}^{r} \mu_i(\theta(k)) K_{2i} x(k), \\ &\vdots \\ u_N(k) &= \sum_{i=1}^{r} \mu_i(\theta(k)) K_{Ni} x(k). \end{aligned} \tag{11}$$

When the controlled system is in σth switching subsystem, the global fuzzy equation is as follows

$$\begin{aligned} & x(k+1) \\ &= \sum_{i=1}^{r} \mu_i \left[\Phi_i x(k) + \Gamma_{i0}(\tau_k) u(k) + \Gamma_{i1}(\tau_k) u(k-1)\right] \\ &= \sum_{i=1}^{r} \mu_i \Phi_i x(k) \\ &\quad + \sum_{i=1}^{r}\sum_{j=1}^{r} \mu_i \mu_j \left[\Gamma_{i0}(\tau_k) K_{\sigma j} x(k) + \Gamma_{i1}(\tau_k) K_{\sigma j} x(k-1)\right] \\ &= \sum_{i=1}^{r}\sum_{j=1}^{r} \mu_i \mu_j \\ &\qquad \times \left[\Phi_i x(k) + \Gamma_{i0}(\tau_k) K_{\sigma j} x(k) \right. \\ &\qquad\quad \left. + \Gamma_{i1}(\tau_k) K_{\sigma j} x(k-1)\right] \\ &= \sum_{i=1}^{r}\sum_{j=1}^{r} \mu_i \mu_j \\ &\qquad \times \left\{\left[\Phi_i + \Gamma_{i0}(\tau_k) K_{\sigma j}\right] x(k) \right. \\ &\qquad\quad \left. + \Gamma_{i1}(\tau_k) K_{\sigma j} x(k-1)\right\} \\ &= \sum_{i=1}^{r}\sum_{j=1}^{r} \mu_i \mu_j \left\{\left[\Phi_i + \left(\Gamma_{i1} - D_i F_i(\tau_k) E_i\right) K_{\sigma j}\right] x(k) \right. \\ &\qquad\quad \left. + \left(\Gamma_{i1} - D_i F_i(\tau_k) E_i\right) K_{\sigma j} x(k-1)\right\}. \end{aligned} \tag{12}$$

Let $\Omega_1, \Omega_2, \ldots, \Omega_N$ be a partition of the set R^n; then $\bigcup_{i=1}^{N} \Omega_i = R^n \setminus \{0\}$, $\Omega_i \bigcap \Omega_j = \Phi$, $i = j$. The switching law that is determined by $\Omega_1, \Omega_2, \ldots$, and Ω_N is $\sigma = \sigma(x(t)) = i$, when $x(t) \in \Omega_i$. This switching law can be completely described by the following function:

$$v_\sigma(x(t)) = \begin{cases} 1, & x(t) \in \Omega_\sigma, \\ 0, & x(t) \notin \Omega_\sigma, \end{cases} \quad \sigma = 1, 2, \ldots, N. \tag{13}$$

Thus, we have

$$\begin{aligned} x(k+1) = \sum_{\sigma=1}^{N}\sum_{i=1}^{r}\sum_{j=1}^{r} & v_\sigma \mu_i \mu_j \\ & \times \left\{\left[\Phi_i + \left(\Gamma_{i1} - D_i F_i(\tau_k) E_i\right) K_{\sigma j}\right] x(k) \right. \\ & \left. + \left(\Gamma_{i1} - D_i F_i(\tau_k) E_i\right) K_{\sigma j} x(k-1)\right\}, \end{aligned} \tag{14}$$

where τ_k is the network-induced delay.

4. Sufficient Condition for Guaranteed Cost Control

Lemma 6 (see [22] (Schur complement)). *For a given symmetric matrix,*

$$S = \begin{bmatrix} S_{11} & S_{12} \\ S_{21} & S_{22} \end{bmatrix}. \tag{15}$$

Then, the following three conditions are mutually equivalent:

(1) $S < 0$,

(2) $S_{11} < 0$, $S_{22} - S_{12}^T S_{11}^{-1} S_{12} < 0$,

(3) $S_{22} < 0$, $S_{11} - S_{12} S_{22}^{-1} S_{12}^T < 0$.

Lemma 7 (see [23]). *Given matrices Y, D, E, and I of appropriate dimensions and with Y and I symmetrical and $I > 0$, then*

$$Y + DFE + E^T F^T D^T < 0 \tag{16}$$

for all F satisfying $F^T F \le I$, if and only if there exists some $\varepsilon > 0$ such that

$$Y + \varepsilon^2 DD^T + \varepsilon^{-2} E^T E < 0. \tag{17}$$

Theorem 8. *Consider the uncertain nonlinear networked control systems* (3) *and the cost function* (9). *If there exist some constants $\lambda_\sigma \in [0,1]$, $\sum_{\sigma=1}^{l} \lambda_\sigma = 1$, a group of positive constants $\varepsilon_\sigma > 0$, and positive definite matrices X, Z, $Y_{\sigma i}$, $\sigma = 1, \ldots, l$, $i = 1, \ldots, r$, such that the following matrix inequalities* (18) *hold:*

$$\sum_{\sigma=1}^{l} \lambda_\sigma \begin{bmatrix} L & U & V & 0 & 0 & 0 & 0 \\ * & -2X + 2Z & 0 & 2X & \left(Y_{\sigma i} + Y_{\sigma j}\right)^T & \left(E_i Y_{\sigma j}\right)^T & \left(E_j Y_{\sigma i}\right)^T \\ * & * & -2Z & 0 & 0 & -\left(E_i Y_{\sigma j}\right)^T & -\left(E_j Y_{\sigma i}\right)^T \\ * & * & * & -2Q^{-1} & 0 & 0 & 0 \\ * & * & * & * & -2R^{-1} & 0 & 0 \\ * & * & * & * & * & -\varepsilon_\sigma I & 0 \\ * & * & * & * & * & * & -\varepsilon_\sigma I \end{bmatrix} < 0, \quad 1 \le i \le j \le r, \tag{18}$$

where

$$X = P^{-1}, \qquad Y_{\sigma i} = k_{\sigma i} X,$$
$$Z = XSX,$$
$$L = -2X + \varepsilon_\sigma \left(D_i D_i^T + D_j D_j^T \right), \tag{19}$$
$$U = \Phi_i + \Phi_j + \Gamma_{i0} Y_{\sigma j} + \Gamma_{j0} Y_{\sigma i},$$
$$V = \Gamma_{i1} Y_{\sigma j} + \Gamma_{j1} Y_{\sigma i},$$

then close-loop system (14) *with the guaranteed cost controller* (11) *and the switching law* $\sigma = \sigma(x(k))$ *is globally asymptotically stable. The guaranteed cost function* (9) *satisfies the following bound:*

$$J \le x^T(0) P x(0) + x^T(-1) S x(-1). \tag{20}$$

Proof. For the networked control system (3), we lead the performance index as follows:

$$\begin{aligned} J &= \sum_{k=0}^{\infty} \left[x^T(k) Q x(k) + u_\sigma^T(k) R u_\sigma(k) \right] \\ &= \sum_{k=0}^{\infty} \left[\sum_{i=1}^{r} \sum_{j=1}^{r} \mu_i \mu_j x^T(k) \left(Q + K_{\sigma i}^T R K_{\sigma j} \right) x(k) \right] \\ &= \sum_{k=0}^{\infty} \left[\sum_{i=1}^{r} \mu_i^2 x^T(k) \left(Q + K_{\sigma i}^T R K_{\sigma i} \right) x(k) \right. \\ &\qquad \left. + 2 \sum_{i=1}^{r} \sum_{j>i}^{r} \mu_i \mu_j x^T(k) \left(Q + K_{\sigma i}^T R K_{\sigma j} \right) x(k) \right] \\ &= \sum_{k=0}^{\infty} \left[\sum_{i=1}^{r} \mu_i^2 x^T(k) \left(Q + K_{\sigma i}^T R K_{\sigma i} \right) x(k) \right. \\ &\qquad + 2 \sum_{i=1}^{r} \sum_{j>i}^{r} \mu_i \mu_j x^T(k) \\ &\qquad \left. \times \left(Q + \frac{\left(K_{\sigma i} + K_{\sigma j} \right)^T}{2} R \frac{\left(K_{\sigma i} + K_{\sigma j} \right)}{2} \right) x(k) \right]. \end{aligned} \tag{21}$$

Consider the Lyapunov function as

$$\begin{aligned} V(x(k)) &= x^T(k) P x(k) \\ &\quad + x^T(k-1) S x(k-1). \end{aligned} \tag{22}$$

Let

$$\begin{aligned} \Theta &= \begin{bmatrix} G_{\sigma ij}^T P G_{\sigma nm} - P + S & G_{\sigma ij}^T P H_{\sigma nm} \\ H_{\sigma ij}^T P G_{\sigma nm} & H_{\sigma ij}^T P H_{\sigma nm} - S \end{bmatrix}, \\ G_{\sigma ij} &= \Phi_i + \Gamma_{i0} K_{\sigma j} + D_i F_i(\tau_k) E_i K_{\sigma j}, \\ \alpha_{\sigma ij} &= G_{\sigma ij} + G_{\sigma ji}, \\ H_{\sigma ij} &= \Gamma_{i1} K_{\sigma j} - D_i F_i(\tau_k) E_i K_{\sigma j}, \\ \beta_{\sigma ij} &= H_{\sigma ij} + H_{\sigma ji}. \end{aligned} \tag{23}$$

Along any trajectory of the closed-loop system (14), the forward difference of $V(k)$ is

$$\begin{aligned} \Delta V(x(k)) &= V(x(k+1)) - V(x(k)) \\ &= x^T(k+1) P x(k+1) + x^T(k) S x(k) - x^T(k) P x(k) - x^T(k-1) S x(k-1) \\ &= \sum_{\sigma=1}^{N} \sum_{i=1}^{r} \sum_{j=1}^{r} \sum_{n=1}^{r} \sum_{m=1}^{r} \nu_\sigma \mu_i \mu_j \mu_n \mu_m \begin{bmatrix} x(k) \\ x(k-1) \end{bmatrix}^T \Theta \begin{bmatrix} x(k) \\ x(k-1) \end{bmatrix} \\ &\le \sum_{\sigma=1}^{N} \nu_\sigma \left\{ \frac{1}{4} \sum_{i=1}^{r} \sum_{j=1}^{r} \mu_i \mu_j \begin{bmatrix} x(k) \\ x(k-1) \end{bmatrix}^T \begin{bmatrix} \alpha_{\sigma ij}^T P \alpha_{\sigma ij} - 4P + 4S & \alpha_{\sigma ij}^T P \beta_{\sigma ij} \\ \beta_{\sigma ij}^T P \alpha_{\sigma ij} & \beta_{\sigma ij}^T P \beta_{\sigma ij} - 4S \end{bmatrix} \begin{bmatrix} x(k) \\ x(k-1) \end{bmatrix} \right\} \\ &= \sum_{\sigma=1}^{N} \nu_\sigma \left\{ \sum_{i=1}^{r} \mu_i^2 \begin{bmatrix} x(k) \\ x(k-1) \end{bmatrix}^T \begin{bmatrix} G_{\sigma ii}^T P G_{\sigma ii} - P + S & G_{\sigma ii}^T P H_{\sigma ii} \\ H_{\sigma ii}^T P G_{\sigma ii} & H_{\sigma ii}^T P H_{\sigma ii} - S \end{bmatrix} \begin{bmatrix} x(k) \\ x(k-1) \end{bmatrix} \right. \\ &\qquad \left. + 2 \sum_{i=1}^{r} \sum_{j>i}^{r} \mu_i \mu_j \begin{bmatrix} x(k) \\ x(k-1) \end{bmatrix}^T \begin{bmatrix} \left[\frac{\alpha_{\sigma ij}}{2} \right]^T P \frac{\alpha_{\sigma ij}}{2} - P + S & \left[\frac{\alpha_{\sigma ij}}{2} \right]^T P \frac{\beta_{\sigma ij}}{2} \\ \left[\frac{\beta_{\sigma ij}}{2} \right]^T P \frac{\alpha_{\sigma ij}}{2} & \left[\frac{\beta_{\sigma ij}}{2} \right]^T P \frac{\beta_{\sigma ij}}{2} - S \end{bmatrix} \begin{bmatrix} x(k) \\ x(k-1) \end{bmatrix} \right\}. \end{aligned} \tag{24}$$

Thus

$$
\begin{aligned}
&\Delta V(x(k)) + x^T(k) Q x(k) + u_\sigma^T(k) R u_\sigma(k) \\
&\quad \le \sum_{\sigma=1}^{N} \nu_\sigma \left\{ \sum_{i=1}^{r} \mu_i^2 \begin{bmatrix} x(k) \\ x(k-1) \end{bmatrix}^T \right. \\
&\qquad \times \begin{bmatrix} G_{\sigma ii}^T P G_{\sigma ii} - P + S & G_{\sigma ii}^T P H_{\sigma ii} \\ H_{\sigma ii}^T P G_{\sigma ii} & H_{\sigma ii}^T P H_{\sigma ii} - S \end{bmatrix} \begin{bmatrix} x(k) \\ x(k-1) \end{bmatrix} \\
&\qquad + 2 \sum_{i=1}^{r} \sum_{j>i}^{r} \mu_i \mu_j \begin{bmatrix} x(k) \\ x(k-1) \end{bmatrix}^T \begin{bmatrix} \left[\frac{\alpha_{\sigma ij}}{2}\right]^T P \frac{\alpha_{\sigma ij}}{2} - P + S & \left[\frac{\alpha_{\sigma ij}}{2}\right]^T P \frac{\beta_{\sigma ij}}{2} \\ \left[\frac{\beta_{\sigma ij}}{2}\right]^T P \frac{\alpha_{\sigma ij}}{2} & \left[\frac{\beta_{\sigma ij}}{2}\right]^T P \frac{\beta_{\sigma ij}}{2} - S \end{bmatrix} \begin{bmatrix} x(k) \\ x(k-1) \end{bmatrix} \\
&\qquad + \sum_{i=1}^{r} \mu_i^2 x^T(k) \left(Q + K_{\sigma i}^T R K_{\sigma i}\right) x(k) \\
&\qquad \left. + 2 \sum_{i=1}^{r} \sum_{j>i}^{r} \mu_i \mu_j x^T(k) \left(Q + \frac{(K_{\sigma i} + K_{\sigma j})^T}{2} R \frac{\left(K_{\sigma i} + K_{\sigma j}\right)}{2} \right) x(k) \right\} \qquad (25) \\
&\quad = \sum_{\sigma=1}^{N} \nu_\sigma \left\{ \sum_{i=1}^{r} \mu_i^2 \begin{bmatrix} x(k) \\ x(k-1) \end{bmatrix}^T \right. \\
&\qquad \times \begin{bmatrix} G_{\sigma ii}^T P G_{\sigma ii} - P + S + Q + K_{\sigma i}^T R K_{\sigma i} & G_{\sigma ii}^T P H_{\sigma ii} \\ H_{\sigma ii}^T P G_{\sigma ii} & H_{\sigma ii}^T P H_{\sigma ii} - S \end{bmatrix} \begin{bmatrix} x(k) \\ x(k-1) \end{bmatrix} \\
&\qquad + 2 \sum_{i=1}^{r} \sum_{j>i}^{r} \mu_i \mu_j \begin{bmatrix} x(k) \\ x(k-1) \end{bmatrix}^T \\
&\qquad \times \begin{bmatrix} \left[\frac{\alpha_{\sigma ij}}{2}\right]^T P \frac{\alpha_{\sigma ij}}{2} - P + S + Q + \frac{(K_{\sigma i} + K_{\sigma j})^T}{2} R \frac{\left(K_{\sigma i} + K_{\sigma j}\right)}{2} & \left[\frac{\alpha_{\sigma ij}}{2}\right]^T P \frac{\beta_{\sigma ij}}{2} \\ \left[\frac{\beta_{\sigma ij}}{2}\right]^T P \frac{\alpha_{\sigma ij}}{2} & \left[\frac{\beta_{\sigma ij}}{2}\right]^T P \frac{\beta_{\sigma ij}}{2} - S \end{bmatrix} \\
&\qquad \left. \times \begin{bmatrix} x(k) \\ x(k-1) \end{bmatrix} \right\}.
\end{aligned}
$$

Thus, if the matrix inequalities (26) and (27) hold

$$
\begin{bmatrix} G_{\sigma ii}^T P G_{\sigma ii} - P + S + Q + K_{\sigma i}^T R K_{\sigma i} & G_{\sigma ii}^T P H_{\sigma ii} \\ H_{\sigma ii}^T P G_{\sigma ii} & H_{\sigma ii}^T P H_{\sigma ii} - S \end{bmatrix} < 0, \quad 1 \le i \le r, \qquad (26)
$$

$$
\begin{bmatrix} \left[\frac{\alpha_{\sigma ij}}{2}\right]^T P \frac{\alpha_{\sigma ij}}{2} - P + S + Q + \frac{(K_{\sigma i} + K_{\sigma j})^T}{2} R \frac{\left(K_{\sigma i} + K_{\sigma j}\right)}{2} & \left[\frac{\alpha_{\sigma ij}}{2}\right]^T P \frac{\beta_{\sigma ij}}{2} \\ \left[\frac{\beta_{\sigma ij}}{2}\right]^T P \frac{\alpha_{\sigma ij}}{2} & \left[\frac{\beta_{\sigma ij}}{2}\right]^T P \frac{\beta_{\sigma ij}}{2} - S \end{bmatrix} < 0, \quad 1 \le i < j \le r, \qquad (27)
$$

then, the following inequality can hold:

$$\Delta V(x(k)) + x^T(k) Q x(k) + u_\sigma^T(k) R u_\sigma(k) < 0, \tag{28}$$

and (26) is the special case of (27) when $i = j$. Thus, when (27) holds, the inequality (28) can hold. Consider

$$\theta_{\sigma ij} = \begin{bmatrix} \left[\frac{\alpha_{\sigma ij}}{2}\right]^T P \frac{\alpha_{\sigma ij}}{2} - P + S + Q + \frac{\left(K_{\sigma i} + K_{\sigma j}\right)^T}{2} R \frac{\left(K_{\sigma i} + K_{\sigma j}\right)}{2} & \left[\frac{\alpha_{\sigma ij}}{2}\right]^T P \frac{\beta_{\sigma ij}}{2} \\ \left[\frac{\beta_{\sigma ij}}{2}\right]^T P \frac{\alpha_{\sigma ij}}{2} & \left[\frac{\beta_{\sigma ij}}{2}\right]^T P \frac{\beta_{\sigma ij}}{2} - S \end{bmatrix} < 0, \quad 1 \le i \le j \le r. \tag{29}$$

Let

$$\Omega_{\sigma ij} = -4P + 4S + 4Q + \left(K_{\sigma i} + K_{\sigma j}\right)^T R \left(K_{\sigma i} + K_{\sigma j}\right),$$

$$\theta_{\sigma ij} = \begin{bmatrix} \Omega_{\sigma ij} + \alpha_{\sigma ii}^T P \alpha_{\sigma ij} & \alpha_{\sigma ii}^T P \beta_{\sigma ij} \\ \beta_{\sigma ii}^T P \alpha_{\sigma ij} & \beta_{\sigma ii}^T P \beta_{\sigma ij} - 4S \end{bmatrix} < 0, \quad 1 \le i \le j \le r. \tag{30}$$

Therefore, according to the fact of $\mu_i(\theta(k)) \ge 0$ in (8), the inequality (30) and the equality (24), we can obtain $\Delta V < 0$.

Define sets $\Omega_\sigma = \{y \in R^{2n} : y^T \theta_{\sigma ij} y < 0\}$; thus $\cup \Omega_i = R^{2n} \setminus \{0\}$. Construct the sets $\widetilde{\Omega}_1 = \Omega_1, \ldots, \widetilde{\Omega}_\sigma = \Omega_\sigma - \bigcup_{i=1}^{\sigma-1} \widetilde{\Omega}_i, \ldots$.

Obviously, we have $\bigcup_{i=1}^{l} \widetilde{\Omega}_i = R^{2n} \setminus \{0\}$, $\widetilde{\Omega}_i \cap \widetilde{\Omega}_j = \Phi$, $i \ne j$.

Construct a switching law as follows:

$$\sigma(x(k)) = i, \quad \text{when } x(k) \in \widetilde{\Omega}_i,\ \sigma \in M. \tag{31}$$

Thus, $\Delta V(x(k)) + x^T(k) Q x(k) + u_\sigma^T(k) R u_\sigma(k) \le \xi^T(k) \theta_{\sigma ij} \xi(k) < 0$, $\forall \xi(k) \ne 0$, where $\xi(k) = [x^T(k) \;\; x^T(k-1)]^T$.

Notice that $F^T F \le I$. Applying Lemmas 6 and 7 to the inequality (29), we have

$$\begin{bmatrix} \Psi & \Lambda & \Pi & 0 & 0 & 0 & 0 \\ * & -2P + 2S & 0 & 2I & (k_{\sigma i} + k_{\sigma j})^T & (E_i k_{\sigma j})^T & (E_j k_{\sigma i})^T \\ * & * & -2S & 0 & 0 & -(E_i k_{\sigma j})^T & (E_j k_{\sigma i})^T \\ * & * & * & -2Q^{-1} & 0 & 0 & 0 \\ * & * & * & * & -2R^{-1} & 0 & 0 \\ * & * & * & * & * & -\varepsilon_\sigma I & 0 \\ * & * & * & * & * & * & -\varepsilon_\sigma I \end{bmatrix} < 0, \tag{32}$$

where

$$\Psi = -2P^{-1} + \varepsilon_\sigma \left(D_i D_i^T + D_j D_j^T\right),$$
$$\Lambda = \Phi_i + \Phi_j + \Gamma_{i0} k_{\sigma j} + \Gamma_{j0} k_{\sigma i}, \tag{33}$$
$$\Pi = \Gamma_{i1} k_{\sigma j} + \Gamma_{j1} k_{\sigma i}.$$

By inequality (32) left-multiplied and right-multiplied by diag($I \;\; P^{-1} \;\; P^{-1} \;\; I \;\; I \;\; I \;\; I$) and defining new variables $X = P^{-1}$, $Y_{\sigma i} = k_{\sigma i} X$, and $Z = XSX$, we have

$$\begin{bmatrix} L & U & V & 0 & 0 & 0 & 0 \\ * & -2X + 2Z & 0 & 2X & \left(Y_{\sigma i} + Y_{\sigma j}\right)^T & \left(E_i Y_{\sigma j}\right)^T & \left(E_j Y_{\sigma i}\right)^T \\ * & * & -2Z & 0 & 0 & -\left(E_i Y_{\sigma j}\right)^T & \left(E_j Y_{\sigma i}\right)^T \\ * & * & * & -2Q^{-1} & 0 & 0 & 0 \\ * & * & * & * & -2R^{-1} & 0 & 0 \\ * & * & * & * & * & -\varepsilon_\sigma I & 0 \\ * & * & * & * & * & * & -\varepsilon_\sigma I \end{bmatrix} < 0, \tag{34}$$

where

$$\begin{aligned} L &= -2X + \varepsilon_\sigma \left(D_i D_i^T + D_j D_j^T\right), \\ U &= \Phi_i + \Phi_j + \Gamma_{i0} Y_{\sigma j} + \Gamma_{j0} Y_{\sigma i}, \\ V &= \Gamma_{i1} Y_{\sigma j} + \Gamma_{j1} Y_{\sigma i}. \end{aligned} \tag{35}$$

Taking (28) into account, for all admissible uncertainties, we can infer that as follows:

$$\Delta V\left(x\left(k\right)\right) \le -x^T\left(k\right) Q x\left(k\right) - u_\sigma^T\left(k\right) R u_\sigma\left(k\right). \tag{36}$$

According to (18), we can infer that there exists at least one σ such that (29) is established. Therefore, the closed-loop system (14) is asymptotically stable under the controller (11) and the switching law (31). Moreover, we have

$$\begin{aligned} \Delta V < & \sum_{i=1}^{r} \mu_i^2 x^T\left(k\right)\left(Q + K_{\sigma i}^T R K_{\sigma i}\right) x\left(k\right) \\ & + 2\sum_{i=1}^{r}\sum_{j>i}^{r} \mu_i \mu_j x^T\left(k\right) \\ & \times \left(Q + \frac{\left(K_{\sigma i} + K_{\sigma j}\right)^T}{2} R \frac{\left(K_{\sigma i} + K_{\sigma j}\right)}{2}\right) x\left(k\right), \end{aligned} \tag{37}$$

thus

$$\begin{aligned} & \sum_{i=1}^{r} \mu_i^2 x^T\left(k\right)\left(Q + K_{\sigma i}^T R K_{\sigma i}\right) x\left(k\right) \\ & + 2\sum_{i=1}^{r}\sum_{j>i}^{r} \mu_i \mu_j x^T\left(k\right) \\ & \times \left(Q + \frac{\left(K_{\sigma i} + K_{\sigma j}\right)^T}{2} R \frac{\left(K_{\sigma i} + K_{\sigma j}\right)}{2}\right) x\left(k\right) < -\Delta V. \end{aligned} \tag{38}$$

The inequalities (38) are added up together in the case that k is $0, 1, 2, \ldots, \infty$; we have

$$\begin{aligned} J = & \sum_{k=0}^{\infty} \left[\sum_{i=1}^{r} \mu_i^2 x^T\left(k\right)\left(Q + K_{\sigma i}^T R K_{\sigma i}\right) x\left(k\right) \right. \\ & + 2\sum_{i=1}^{r}\sum_{j>i}^{r} \mu_i \mu_j x^T\left(k\right) \\ & \left. \times \left(Q + \frac{\left(K_{\sigma i} + K_{\sigma j}\right)^T}{2} R \frac{\left(K_{\sigma i} + K_{\sigma j}\right)}{2}\right) x\left(k\right) \right] \\ & \le x^T\left(0\right) P x\left(0\right) + x^T\left(-1\right) S x\left(-1\right). \end{aligned} \tag{39}$$

Therefore, Theorem 8 is proved. □

Theorem 9. *Consider the uncertain nonlinear networked control systems* (3) *and the cost function* (9)*. If there exist some nonpositive or nonnegative constants $\delta_{\sigma\lambda}$ $(\sigma, \lambda = 1, 2, \ldots, l)$, a group of positive constants $\varepsilon_\sigma > 0$, and positive-definite matrices X_σ, Z_σ, matrix $Y_{\sigma i}$, $\sigma = 1, \ldots, l$, $i = 1, \ldots, r$, such that the following matrix inequalities:*

$$\begin{bmatrix} L & U & V & 0 & 0 & 0 & 0 \\ * & \Xi + \sum_{\lambda=1, \lambda\neq\sigma}^{l} \delta_{\sigma\lambda}\left(X_\lambda - X_\sigma\right) & 0 & 2X & \left(Y_{\sigma i} + Y_{\sigma j}\right)^T & \left(E_i Y_{\sigma j}\right)^T & \left(E_j Y_{\sigma i}\right)^T \\ * & * & -2Z & 0 & 0 & -\left(E_i Y_{\sigma j}\right)^T & -\left(E_j Y_{\sigma i}\right)^T \\ * & * & * & -2Q^{-1} & 0 & 0 & 0 \\ * & * & * & * & -2R^{-1} & 0 & 0 \\ * & * & * & * & * & -\varepsilon_\sigma I & 0 \\ * & * & * & * & * & * & -\varepsilon_\sigma I \end{bmatrix} < 0, \quad 1 \le i \le j \le r, \tag{40}$$

hold, where

$$\begin{aligned} \Xi &= -2X_\sigma + 2Z_\sigma, \qquad X_\sigma = P_\sigma^{-1}, \\ Y_{\sigma i} &= k_{\sigma i} X_\sigma, \qquad Z_\sigma = X_\sigma S_\sigma X_\sigma, \\ L &= -2X_\sigma + \varepsilon_\sigma \left(D_i D_i^T + D_j D_j^T\right), \\ U &= \Phi_i + \Phi_j + \Gamma_{i0} Y_{\sigma j} + \Gamma_{j0} Y_{\sigma i}, \\ V &= \Gamma_{i1} Y_{\sigma j} + \Gamma_{j1} Y_{\sigma i}, \end{aligned} \tag{41}$$

then system (14) *with the guaranteed cost controller* (11) *and the switching law $\sigma = \sigma(x(k))$ is globally asymptotically stable. The guaranteed cost function* (9) *satisfies the following bound:*

$$J \le x^T\left(0\right) P_\sigma x\left(0\right) + x^T\left(-1\right) S_\sigma x\left(-1\right). \tag{42}$$

Proof. By the Lemmas 6 and 7, and $X_\sigma = {P_\sigma}^{-1}$, $Y_{\sigma i} = k_{\sigma i} X_\sigma$, $Z_\sigma = X_\sigma S_\sigma X_\sigma$, from (40), we have

$$\begin{bmatrix} \left[\frac{\alpha_{\sigma ij}}{2}\right]^T P_\sigma \frac{\alpha_{\sigma ij}}{2} - P_\sigma + S_\sigma + Q + \frac{(K_{\sigma i}+K_{\sigma j})^T}{2} R \frac{\left(K_{\sigma i}+K_{\sigma j}\right)}{2} + \sum_{\lambda=1,\lambda\neq\sigma}^{l} \delta_{\sigma\lambda}\left(P_\lambda - P_\sigma\right) & \left[\frac{\alpha_{\sigma ij}}{2}\right]^T P_\sigma \frac{\beta_{\sigma ij}}{2} \\ \left[\frac{\beta_{\sigma ij}}{2}\right]^T P_\sigma \frac{\alpha_{\sigma ij}}{2} & \left[\frac{\beta_{\sigma ij}}{2}\right]^T P_\sigma \frac{\beta_{\sigma ij}}{2} - S_\sigma \end{bmatrix} < 0. \tag{43}$$

Without loss of generality, we assume that $\delta_{\sigma\lambda} \geq 0$.

Obviously, there exists at least one $\sigma \in M$ when $x(k) \in R^n \setminus \{0\}$, such that $x^T(k)(P_\lambda - P_\sigma)x(k) \geq 0, \forall \lambda \in M$.

Let $\Omega_\sigma = \{x(k) \in R^n \mid x^T(k)(P_\lambda - P_\sigma)x(k) \geq 0, \forall \lambda \in M, \lambda \neq \sigma, x(k) \neq 0\}$; thus $\cup\Omega_i = R^n \setminus \{0\}$.

Construct the sets $\widetilde{\Omega}_1 = \Omega_1, \ldots, \widetilde{\Omega}_\sigma = \Omega_\sigma - \bigcup_{i=1}^{\sigma-1} \widetilde{\Omega}_i, \ldots$.

Obviously, we have $\bigcup_{i=1}^{l} \widetilde{\Omega}_i = R^n \setminus \{0\}$, $\widetilde{\Omega}_i \cap \widetilde{\Omega}_j = \Phi, i \neq j$. Construct a switched law by

$$\sigma(x(k)) = i, \quad \text{when } x(k) \in \widetilde{\Omega}_i,\ \sigma \in M. \tag{44}$$

Thus, from (43), we have

$$\begin{bmatrix} x(k) \\ x(k-1) \end{bmatrix}^T \begin{bmatrix} \left[\frac{\alpha_{\sigma ij}}{2}\right]^T P_\sigma \frac{\alpha_{\sigma ij}}{2} - P_\sigma + S_\sigma + Q + \frac{\left(K_{\sigma i}+K_{\sigma j}\right)^T}{2} R \frac{\left(K_{\sigma i}+K_{\sigma j}\right)}{2} & \left[\frac{\alpha_{\sigma ij}}{2}\right]^T P_\sigma \frac{\beta_{\sigma ij}}{2} \\ \left[\frac{\beta_{\sigma ij}}{2}\right]^T P_\sigma \frac{\alpha_{\sigma ij}}{2} & \left[\frac{\beta_{\sigma ij}}{2}\right]^T P_\sigma \frac{\beta_{\sigma ij}}{2} - S \end{bmatrix} \begin{bmatrix} x(k) \\ x(k-1) \end{bmatrix} < 0, \quad 1 \leq i \leq j \leq r. \tag{45}$$

Following the similar lines as in the proof of Theorem 8, we have

$$\theta_{\sigma ij} = \begin{bmatrix} \left[\frac{\alpha_{\sigma ij}}{2}\right]^T P_\sigma \frac{\alpha_{\sigma ij}}{2} - P_\sigma + S_\sigma + Q + \frac{\left(K_{\sigma i}+K_{\sigma j}\right)^T}{2} R \frac{\left(K_{\sigma i}+K_{\sigma j}\right)}{2} & \left[\frac{\alpha_{\sigma ij}}{2}\right]^T P_\sigma \frac{\beta_{\sigma ij}}{2} \\ \left[\frac{\beta_{\sigma ij}}{2}\right]^T P_\sigma \frac{\alpha_{\sigma ij}}{2} & \left[\frac{\beta_{\sigma ij}}{2}\right]^T P_\sigma \frac{\beta_{\sigma ij}}{2} - S \end{bmatrix} < 0, \quad 1 \leq i \leq j \leq r, \tag{46}$$

then, $\Delta V_\sigma(x(k)) + x^T(k)Qx(k) + u_\sigma^T(k)Ru_\sigma(k) < 0$. Thus,

$$\begin{aligned} &\sum_{i=1}^{r} \mu_i^2 x^T(k)\left(Q + K_{\sigma i}^T R K_{\sigma i}\right) x(k) \\ &+ 2\sum_{i=1}^{r}\sum_{j>i}^{r} \mu_i\mu_j x^T(k)\left(Q + \frac{\left(K_{\sigma i}+K_{\sigma j}\right)^T}{2} R \frac{\left(K_{\sigma i}+K_{\sigma j}\right)}{2}\right) x(k) \\ &< -\Delta V_\sigma. \end{aligned} \tag{47}$$

The above inequality (47) is added up together in the case that k is $0, 1, 2, \ldots, \infty$, according to the stability of the system, then

$$J \leq x^T(0) P_\sigma x(0) + x^T(-1) S_\sigma x(-1). \tag{48}$$

Theorem 9 is proved. □

5. Simulation Example

Consider the nonlinear system with the following differential equation [24]:

$$\ddot{s}(t) + f(s(t), \dot{s}(t)) - 0.1s(t) = F(t), \tag{49}$$

where $f(s(t), \dot{s}(t)) = 0.5s(t) + 0.75\sin(\dot{s}(t)/0.5)$.

Choose the state variable and the input variable as $x(t) = [s(t), \dot{s}(t)]^T$, $u(t) = F(t)$, respectively. It can be represented by the following fuzzy model consisting of two rules:

$$\begin{aligned} R^1&: \text{ IF } x_2(t) \text{ is } M_1, \\ &\text{THEN } \dot{x}(t) = A_1 x(t) + B_1 u(t), \\ R^2&: \text{ IF } x_2(t) \text{ is } M_2, \\ &\text{THEN } \dot{x}(t) = A_2 x(t) + B_2 u(t), \end{aligned} \tag{50}$$

where $x(t) = [x_1(t), x_2(t)]^T$

$$\begin{aligned} A_1 &= \begin{bmatrix} 0 & 1 \\ 0.1 & -2 \end{bmatrix}, \qquad A_2 = \begin{bmatrix} 0 & 1 \\ 0.1 & -0.5 - 1.5\beta \end{bmatrix}, \\ B_1 &= B_2 = [-0.1 \ \ -0.2]^T, \qquad \beta = \frac{0.01}{\pi}, \end{aligned} \tag{51}$$

and β is used to avoid system matrices being singular.

The sampling period $T = 0.3$ s, then the discrete model of the system is as follows:

$$\begin{aligned} R^1&: \text{ IF } \frac{x_2(t)}{0.5} \text{ is about } 0, \\ &\text{THEN } x(k+1) = \Phi_1 x(k) + \left(\Gamma_{10} + D_1 F_1(\tau_k) E_1\right) u(k) \\ &\qquad + \left(\Gamma_{11} - D_1 F_1(\tau_k) E_1\right) u(k-1), \\ R^2&: \text{ IF } \frac{x_2(t)}{0.5} \text{ is about } \pi \text{ or } -\pi, \\ &\text{THEN } x(k+1) = \Phi_2 x(k) + \left(\Gamma_{20} + D_2 F_2(\tau_k) E_2\right) u(k) \\ &\qquad + \left(\Gamma_{21} - D_2 F_2(\tau_k) E_2\right) u(k-1), \end{aligned} \tag{52}$$

where

$$\begin{aligned} \Phi_1 &= \begin{bmatrix} 1.0037 & 0.2259 \\ 0.0226 & 0.5519 \end{bmatrix}, \qquad \Phi_2 = \begin{bmatrix} 1.0043 & 0.2788 \\ 0.0279 & 0.8635 \end{bmatrix}, \\ \Gamma_{10} &= \begin{bmatrix} -10.0018 \\ -0.0001 \end{bmatrix}, \qquad \Gamma_{11} = \begin{bmatrix} -10.0390 \\ -0.2260 \end{bmatrix}, \\ \Gamma_{20} &= \begin{bmatrix} -10 \\ 0 \end{bmatrix}, \qquad \Gamma_{21} = \begin{bmatrix} -10.0432 \\ -0.2788 \end{bmatrix}, \\ D_1 &= \begin{bmatrix} 20.7693 & 0.2141 \\ 1.0137 & -0.4386 \end{bmatrix}, \\ D_2 &= \begin{bmatrix} 6.8691 & 0.6676 \\ 0.3353 & -1.3678 \end{bmatrix}, \\ E_1 &= \begin{bmatrix} 0.4773 \\ 1.0869 \end{bmatrix}, \qquad E_2 = \begin{bmatrix} 1.2500 \\ 1.4786 \end{bmatrix}, \\ F_1(\tau_k) &= \begin{bmatrix} e^{-0.0488\tau_k} & 0 \\ 0 & e^{-2.0488(0.3-\tau_k)} \end{bmatrix}, \\ F_2(\tau_k) &= \begin{bmatrix} e^{-0.1522\tau_k} & 0 \\ 0 & e^{-0.6570(0.3-\tau_k)} \end{bmatrix}. \end{aligned} \tag{53}$$

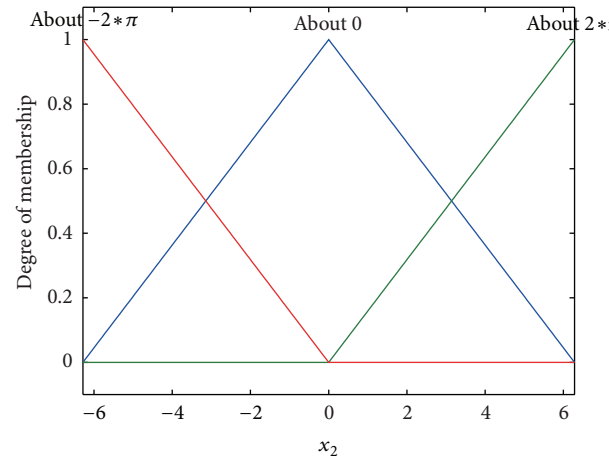

FIGURE 2: The membership function of input x_2.

Obviously, $F_1(\tau_k)$ and $F_2(\tau_k)$ satisfy the uncertain matching conditions:

$$F_1^T(\tau_k) F_1(\tau_k) \le I, \qquad F_2^T(\tau_k) F_2(\tau_k) \le I. \tag{54}$$

The membership functions of "about 0" and "about π or $-\pi$" are selected as in Figure 2.

Suppose the switched fuzzy feed-back controllers are the following fuzzy controllers:

$$\begin{aligned} u_1(k) &= \sum_{i=1}^{2} \mu_i(x_2(k)) k_{1i} x_i(k), \\ u_2(k) &= \sum_{i=1}^{2} \mu_i(x_2(k)) k_{2i} x_i(k). \end{aligned} \tag{55}$$

Choose $Q = 0.1 I_{2\times 2}$, $R = 1$. Carrying out computations for matrices inequality (40), we obtain

$$\begin{aligned} P_1 &= \begin{bmatrix} 8.0177 & 5.2362 \\ 5.2362 & 8.5369 \end{bmatrix}, \\ P_2 &= \begin{bmatrix} 7.8926 & 5.4026 \\ 5.4026 & 9.1487 \end{bmatrix}. \end{aligned} \tag{56}$$

The controller gain:

$$\begin{aligned} k_{11} &= [-0.6138 \ \ -0.4204], \\ k_{12} &= [-0.2936, \ \ -0.3036], \\ k_{21} &= [-0.4156 \ \ -0.3852], \\ k_{22} &= [-0.0893, \ \ -0.1025]. \end{aligned} \tag{57}$$

Let

$$\begin{aligned} \Omega_1 &= \left\{x(k) \in R^2 \mid x^T(k)(P_2 - P_1) x(k) \ge 0, x(k) \ne 0\right\}, \\ \Omega_2 &= \left\{x(k) \in R^2 \mid x^T(k)(P_1 - P_2) x(k) \ge 0, x(k) \ne 0\right\}. \end{aligned} \tag{58}$$

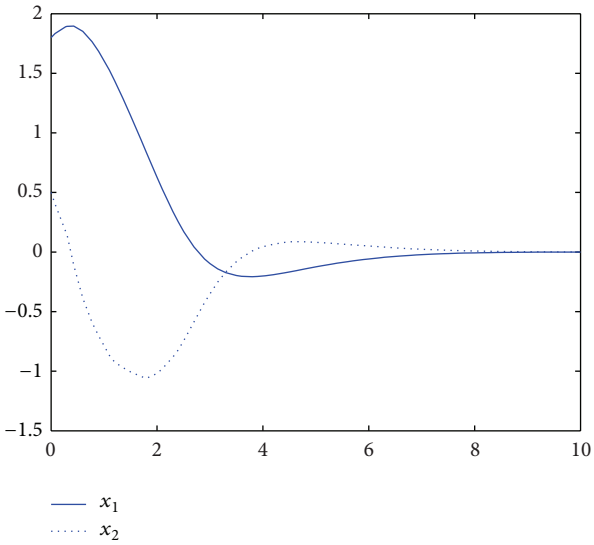

Figure 3: The state trajectory using fuzzy controller 1.

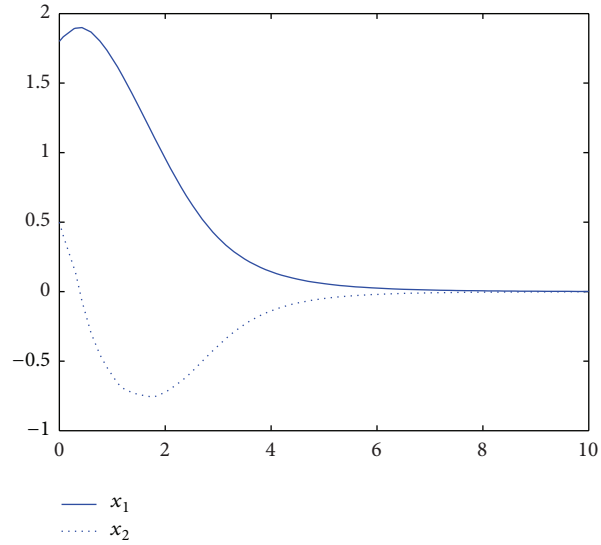

Figure 4: The state trajectory using fuzzy controller 2.

Then $\Omega_1 \cup \Omega_2 = R^2 \setminus \{0\}$. We design a switched law as follows:

$$\sigma(x(k)) = \begin{cases} 1, & x(k) \in \Omega_1, \\ 2, & x(k) \in \Omega_2 \setminus \Omega_1. \end{cases} \tag{59}$$

The initial condition is $[1.8 \quad 0.5]^T$, guaranteed cost bound $J^* = 36.53$.

Figures 3 and 4 show the system state trajectories that use fuzzy controller 1 and fuzzy controller 2, respectively. Figure 5 shows the simulating results for the proposed switched fuzzy controller method. In Figure 5, the system state trajectories indicate that nonlinear networked control system is asymptotically stable and satisfies the performance index via the designed guaranteed cost controller and the switching law. From the simulating results, we can confirm that the guaranteed cost controller in the switched fuzzy model is able to stabilize the nonlinear delay system via switching T-S fuzzy method. In addition, the performance of switching fuzzy controller is better than that of the fuzzy controllers.

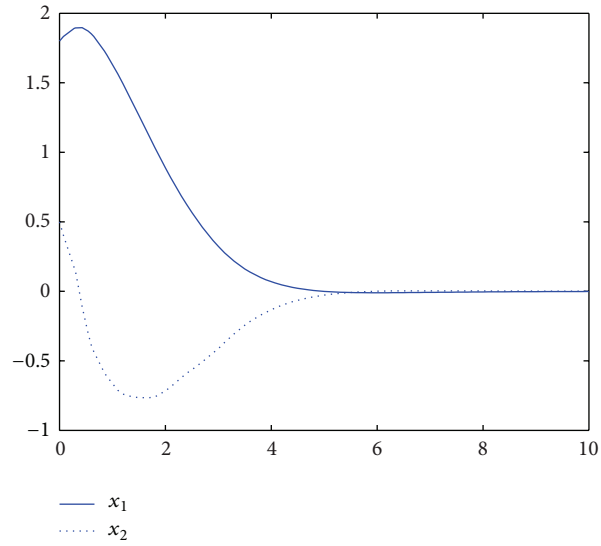

Figure 5: The state trajectory using switched fuzzy controller.

6. Conclusions

In this paper, we have presented a novel controller design methodology for a class of nonlinear NCSs based on switched T-S fuzzy model. By introducing the switching mechanism into the fuzzy T-S systems, the proposed methods can deal with the uncertainties of nonlinear NCSs with time delays and furthermore avoid the inherent drawback of a fuzzy T-S model in controller design and implementation of nonlinear systems. In addition, considering QoS of nonlinear NCSs, some sufficient conditions for the existence of the robust guaranteed cost control law have been built via Lyapunov functional approach. Simulation results have verified and confirmed the effectiveness of the guaranteed cost controller based on the switched T-S fuzzy model for nonlinear NCSs.

At present, this paper only presents a numerical example to show the validity of our control scheme on the nonlinear NCS with time delays. In next step, we plan to further verify this control scheme via practical NCSs and investigate the stability analysis and controller design with multiple-packet transmission in nonlinear NCSs. Moreover, the boundedness of the parameter constraints for NCSs will be studied. The switched dynamics of nonlinear NCSs will also be considered in future investigation.

Conflict of Interests

The authors declare that there is no conflict of interests regarding the publication of this paper.

Acknowledgments

This work is supported by National Natural Science Foundation of China (Grant no. 50804061) and Scientific and Technological Research Program of Chongqing Municipal Education Commission (Grant no. KJ130522).

References

[1] D. Yue, Q.-L. Han, and C. Peng, "State feedback controller design of networked control systems," *IEEE Transactions on Circuits and Systems II*, vol. 51, no. 11, pp. 640–644, 2004.

[2] H. Zhang, D. Yang, and T. Chai, "Guaranteed cost networked control for T-S fuzzy systems with time delays," *IEEE Systems, Man, and Cybernetics Society*, vol. 37, no. 2, pp. 160–172, 2007.

[3] X. Luan, P. Shi, and F. Liu, "Stabilization of networked control systems with random delays," *IEEE Transactions on Industrial Electronics*, vol. 58, no. 9, pp. 4323–4330, 2011.

[4] B. Rahmani and A. H. D. Markazi, "Variable selective control method for networked control systems," *IEEE Transactions on Control Systems Technology*, vol. 21, no. 3, pp. 975–982, 2012.

[5] D. Nešić and A. R. Teel, "Input-to-state stability of networked control systems," *Automatica*, vol. 40, no. 12, pp. 2121–2128, 2004.

[6] H. Chu, S. Fei, D. Yue, C. Peng, and J. Sun, "H_∞ quantized control for nonlinear networked control systems," *Fuzzy Sets and Systems*, vol. 174, pp. 99–113, 2011.

[7] J. Gao, H. Su, X. Ji, and J. Chu, "Robust stabilization for a class of nonlinear networked control systems," *Journal of Control Theory and Applications*, vol. 6, no. 3, pp. 300–304, 2008.

[8] H. Xu and S. Jagannathan, "Stochastic optimal controller design for uncertain nonlinear networked control system neuro dynamic programming," *IEEE Transactions On Neural Networks And Learning Systems*, vol. 24, no. 3, pp. 471–484, 2013.

[9] T. Takagi and M. Sugeno, "Fuzzy identification of systems and its applications to modeling and control," *IEEE Transactions on Systems, Man and Cybernetics*, vol. 15, no. 1, pp. 116–132, 1985.

[10] R.-J. Wang, W.-W. Lin, and W.-J. Wang, "Stabilizability of linear quadratic state feedback for uncertain fuzzy time-delay systems," *IEEE Transactions on Systems, Man, and Cybernetics B*, vol. 34, no. 2, pp. 1288–1292, 2004.

[11] B. Chen and X. Liu, "Fuzzy guaranteed cost control for nonlinear systems with time-varying delay," *IEEE Transactions on Fuzzy Systems*, vol. 13, no. 2, pp. 238–249, 2005.

[12] X.-P. Guan and C.-L. Chen, "Delay-dependent guaranteed cost control for T-S fuzzy systems with time delays," *IEEE Transactions on Fuzzy Systems*, vol. 12, no. 2, pp. 236–249, 2004.

[13] C. Hua and S. X. Ding, "Decentralized networked control system design using T-S fuzzy approach," *IEEE Transactions on Fuzzy Systems*, vol. 20, no. 1, pp. 9–21, 2012.

[14] F. Delmotte, T. M. Guerra, and M. Ksantini, "Continuous Takagi-Sugeno's models: reduction of the number of LMI conditions in various fuzzy control design technics," *IEEE Transactions on Fuzzy Systems*, vol. 15, no. 3, pp. 426–438, 2007.

[15] D. Jabri, K. Guelton, N. Manamanni et al., "Robust stabilization of nonlinear systems based on a switched fuzzy control law," *Control Engineering And Applied Informatics*, vol. 14, no. 2, pp. 40–49, 2012.

[16] H. Ohtake, K. Tanaka, and H. O. Wang, "Switching fuzzy controller design based on switching lyapunov function for a class of nonlinear systems," *IEEE Transactions on Systems, Man, and Cybernetics B*, vol. 36, no. 1, pp. 13–23, 2006.

[17] H. K. Lam, "Stability analysis of sampled-data fuzzy controller for nonlinear systems based on switching T-S fuzzy model," *Nonlinear Analysis*, vol. 3, no. 4, pp. 418–432, 2009.

[18] H. Yang and J. Zhao, "Robust control for a class of uncertain switched fuzzy systems," *Journal of Control Theory and Applications*, vol. 5, no. 2, pp. 184–188, 2007.

[19] B. Niu and J. Zhao, "Barrier Lyapunov functions for the output tracking control of constrained nonlinear switched systems," *Systems & Control Letters*, vol. 62, no. 10, pp. 963–971, 2013.

[20] H. K. Lam, F. H. F. Leung, and Y. S. Lee, "Design of a Switching Controller for Nonlinear Systems With Unknown Parameters Based on a Fuzzy Logic Approach," *IEEE Transactions on Systems, Man, and Cybernetics B*, vol. 34, no. 2, pp. 1068–1074, 2004.

[21] G.-H. Yang and J. Dong, "Switching fuzzy dynamic output feedback H∞ control for nonlinear systems," *IEEE Transactions on Systems, Man, and Cybernetics B*, vol. 40, no. 2, pp. 505–516, 2010.

[22] Y. Sun and J. Xu, "Stability analysis and controller design for networked control systems with random time delay," in *Proceedings of the 9th International Conference on Electronic Measurement and Instruments (ICEMI '09)*, pp. 136–141, August 2009.

[23] L. Xie, "Output feedback H_∞ control of systems with parameter uncertainty," *International Journal of Control*, vol. 63, no. 4, pp. 741–750, 1996.

[24] X.-P. Guan and C.-L. Chen, "Delay-dependent guaranteed cost control for T-S fuzzy systems with time delays," *IEEE Transactions on Fuzzy Systems*, vol. 12, no. 2, pp. 236–249, 2004.

Research Article

Fusion Control of Flexible Logic Control and Neural Network

Lihua Fu and Dan Wang

College of Computer Science, Beijing University of Technology, Beijing 100124, China

Correspondence should be addressed to Lihua Fu; fulihuapaper@sohu.com

Received 26 August 2013; Revised 12 November 2013; Accepted 15 November 2013; Published 20 January 2014

Academic Editor: Bo-Chao Zheng

Based on the basic physical meaning of error E and error variety EC, this paper analyzes the logical relationship between them and uses *Universal Combinatorial Operation Model* in *Universal Logic* to describe it. Accordingly, a flexible logic control method is put forward to realize effective control on multivariable nonlinear system. In order to implement fusion control with artificial neural network, this paper proposes a new neuron model of *Zero-level Universal Combinatorial Operation* in *Universal Logic*. And the artificial neural network of flexible logic control model is implemented based on the proposed neuron model. Finally, stability control, anti-interference control of double inverted-pendulum system, and free walking of cart pendulum system on a level track are realized, showing experimentally the feasibility and validity of this method.

1. Introduction

In recent years, fuzzy control has made a rapid development, and it has found a considerable number of successful industrial applications [1–3]. But fuzzy control has two shortcomings in the process of controlling some practical complex systems. One is that the number of control rules increases exponentially with the increase of the number of inputs, and the other one is that the precision of control system is low [4].

To reduce the dimension of control model, hierarchical fuzzy logic control divides the collection of control rules into several collections based on different functions [5, 6]. Compound control combines fuzzy control and other relatively mature control methods to realize the effective control [7], such as Fuzzy-PID Compound Control [8], fuzzy predication control [9], adaptive fuzzy H_∞ control [10], and so forth. The basic idea of adaptive fuzzy control based on variable universe [11, 12] is to keep the form of rules and varies universe of discourse according to the control error. Though a great deal of research has been done to improve the performance of fuzzy control, most of these methods are based on the basic idea that fuzzy controller is a piecewise approximator. However, to date, there has been relatively little research conducted on the internal relations among input variables of fuzzy controllers.

Based on analysis of the logical relationship between the system's error E and error variety EC, this paper indicates that the relationship is just universal combinatorial relation in *Universal Logic* [13], and the simple *Universal Combinatorial Operation* can be used instead of complex fuzzy rule-based reasoning process. As a result, a flexible logic control method is proposed to realize effective control on multivariable nonlinear system.

Artificial neural network is widely used in modelling and controlling thanks to its properties of self-learning, self-organizing, and self-adapting [14]. In order to realize fusion control with artificial neural network, this paper attempts to study the neuron model of *Zero-level Universal Combinatorial Operation* in *Universal Logic* and propose a new neural model. Based on this neuron model, the artificial neural network of flexible logic control model is implemented. Finally, stability control, anti-interference control of double inverted-pendulum system, and free walking of cart pendulum system on a level track are realized to prove the feasibility and validity of this method.

The rest of the paper is organized as follows. Section 2 introduces necessary background on *Universal Combinatorial Operation Model* and flexible logic control method and gives and proves some important theorems of *Universal Combinatorial Operation Model* in the interval $[a, b]$. Section 3 puts forward a new neuron model of *Zero-level Universal*

Combinatorial Operation. Based on this neuron model, the artificial neural network of flexible logic control model is implemented in Section 4. The designed flexible logic control model is applied to treat the double inverted-pendulum system in Section 5. Finally, concluding remarks are given in Section 6.

2. Universal Combinatorial Operation Model

2.1. Universal Combinatorial Operation Model. In order to deal reasonably with the complex relation between factors in complex system, T-norm, S-norm or *Mean* operators are taken as Aggregation Operators.

However, T-norm result is not bigger than the minimum value, and S-norm result is not less than the maximum value. As a result, T-norm, or S-norm can only handle mutually conflictive relation. In contrast, *Mean* operators can vary only between the minimum and maximum values based on its "tradeoff" concept, so it can only handle mutually consistent relation [13].

Universal Logic [13], proposed by Professor He et al., is a kind of flexible logic. It considers the continuous change of not only the truth value of propositions, which is called truth value flexibility, but also the relation between propositions, which is called relation flexibility. Based on fuzzy logic, it puts forward two important coefficients: *generalized correlation coefficient* "h" and *generalized self-correlation coefficient* "k". The flexible change of universal logic operations is based on "h" and "k". So *Universal Logic* provides a new theoretical foundation to realize more effective control for complex systems.

Universal Combinatorial Operation Model is the combinatorial connective of *Universal Logic*. In this paper, we will only consider *generalized correlation coefficient h*. So *Zero-level Universal Combinatorial Operation Model* is defined as follows.

Definition 1 (see [13]). Set mapping $C^e : [0,1] \times [0,1] \to [0,1]$ and

$$\begin{aligned} &C^e(x,y,h) \\ &= \text{ite}\left\{ \Gamma^e\left[\left(x^m + y^m - e^m\right)^{1/m}\right] \mid x + y < 2e; \right. \\ &\qquad 1 - \left(\Gamma^{1-e}\left[(1-x)^m + (1-y)^m - (1-e)^m\right]\right)^{1/m} \mid x \\ &\qquad \left. + y > 2e; e \right\}. \end{aligned} \tag{1}$$

So C^e is *Zero-level Universal Combinatorial Operation Model*, denoted by C_h^e, where $m = (3-4h)/(4h(1-h))$, $h \in [0,1]$, $m \in R$, $e \in [0,1]$.

Note 1. Conditional expression $\text{ite}\{\beta \mid \alpha; \gamma\}$ means if α is true, then β; otherwise γ. $\text{ite}\{\beta_1 \mid \alpha_1; \beta_2 \mid \alpha_2; \gamma\} = \text{ite}\{\beta_1 \mid \alpha_1; \text{ite}\{\beta_2 \mid \alpha_2; \gamma\}\}$. Amplitude limiting function $\Gamma^1[x] = \text{ite}\{1 \mid x > 1; 0 \mid x < 0 \text{ or imaginary number}; x\}$.

Universal Combinatorial Operation Model is a cluster of combinatorial operators, which is determined by *general correlation coefficient h* between propositions. In practical application, according to general correlation between propositions, we can take the corresponding one from the cluster. As *generalized correlation coefficient h* is equal to some special values, the corresponding combinatorial operators are given as follows.

(1) When $h = 1$, it means two propositions attract each other to the maximum extent. And $C^e(x,y,1) = \text{ite}\{\min(x,y) \mid x + y < 2e; \max(x,y) \mid x + y > 2e; e\}$ is *Zadeh* combination $\mathbf{C}_3^e$.

(2) When $h = 0.75$, it means two propositions are independently correlated. And $C^e(x,y,0.75) = \text{ite}\{xy/e \mid x + y < 2e; (x + y - xy - e)/(1-e) \mid x + y > 2e; e\}$ is probability combination $\mathbf{C}_2^e$.

(3) When $h = 0.5$, it means two propositions reject each other to the maximum extent or restrain each other to the minimum extent. And $C^e(x,y,0.5) = \Gamma^1[x+y-e]$ is bounded combination $\mathbf{C}_1^e$.

(4) When $h = 0$, it means two propositions restrain each other to the maximum extent. And $C^e(x,y,0) = \text{ite}\{0 \mid x, y < e; 1 \mid x, y > e; e\}$ is drastic combination $\mathbf{C}_0^e$.

2.2. Universal Combinatorial Operation Model in Any Interval $[a,b]$. In practical control application, fuzzy domain of fuzzy variables, E and EC, is mostly symmetrical, such as $[-6,6]$. However, the conventional *Universal Combinatorial Operation Model* has been limited in the interval $[0,1]$. To this end, Chen, based on the basic idea of *Universal Logic*, sets up *Fractal Logic* in his doctoral dissertation [15], which can make inference in any interval $[a,b]$.

The combinatorial operation model in *Fractal Logic* is described below.

Definition 2 (see [15]). Set mapping $GN : [a,b] \to [a,b]$ and

$$GN(x) = b + a - x. \tag{2}$$

Then GN is normal universal *Not* operation model in any interval $[a,b]$, denoted by GN.

For the above definition, normal universal *Not* operation model has the following characters.

(1) *Closure:*

$$GN(x) \in [a,b]. \tag{3}$$

(2) *Two polar law:*

$$GN(a) = b, \qquad GN(b) = a. \tag{4}$$

(3) *Symmetric involution:*

$$GN(GN(x)) = x. \tag{5}$$

Definition 3 (see [15]). Set mapping $GC^e : [a,b] \times [a,b] \to [a,b]$ and

$$\begin{aligned} &GC^e(x,y,h) \\ &= \text{ite}\Big\{ \min\Big(e, (b-a) \\ &\quad \times \Big[\max\Big(0, \big((x-a)^m + (y-a)^m \\ &\qquad - (e-a)^m\big) \\ &\qquad \times \big((b-a)^m\big)^{-1}\big)\Big]^{1/m} + a\Big) \mid \\ &\quad x+y < 2e; b+a \\ &\quad - \min\Big(e', (b-a) \\ &\quad \times \Big[\max\Big(0, \big((b-x)^m + (b-y)^m \\ &\qquad - (b-e)^m\big) \\ &\qquad \times \big((b-a)^m\big)^{-1}\big)\Big]^{1/m} + a\Big) \mid \\ &\quad x+y > 2e; e\Big\}. \end{aligned} \tag{6}$$

Then GC^e is *Zero-level Universal Combinatorial Operation Model* in any interval $[a,b]$, denoted by GC_h^e, where $m = (3-4h)/(4h(1-h))$, $h \in [0,1]$, $m \in R$, $e, e' \in [a,b]$, and $e' = GN(e)$.

2.3. Demonstration of Attributes of Universal Combinatorial Operation Model in Any Interval. According to the definition of *Universal Combinatorial Operation Model* in any interval, the following characters [15] are attained.

(1) $GC^e(x,y,h)$ conforms to the combination axiom:

(i) *Boundary condition GC*1:
If $x, y < e$, then $GC^e(x,y,h) \le \min(x,y)$.
If $x, y > e$, then $GC^e(x,y,h) \ge \max(x,y)$.
If $x + y = 2e$, then $GC^e(x,y,h) = e$.
Otherwise, $\min(x,y) \le GC^e(x,y,h) \le \max(x,y)$.

(ii) *Monotonicity GC*2:
$GC^e(x,y,h)$ increases monotonously along with x and y.

(iii) *Continuity GC*3:
When $h \in (0,1)$, $GC^e(x,y,h)$ is continuous for all x and y.

(iv) *Commutative law GC*4:

$$GC^e(x,y,h) = GC^e(y,x,h). \tag{7}$$

(v) *Law of identical element GC*5:

$$GC^e(x,e,h) = x. \tag{8}$$

(2) *Closure*:

$$GC^e(x,y,h) \in [a,b]. \tag{9}$$

(3) *Inverse law*:

$$GC^e(x, 2e-x, h) = e. \tag{10}$$

(4) *Renunciation law*

$$GC^e(e,e,h) = e. \tag{11}$$

Theorem 4. $GN(GC^{GN(e)}(GN(x), GN(y), h)) = GC^e(x,y,h)$, $x, y \in [a,b], e \in [a,b]$.

Proof. $x, y \in [a,b], e \in [a,b]$, according to the closure of normal universal *Not* operation and universal combinatorial operation: $GN(x), GN(y) \in [a,b], GN(e) \in [a,b]$ and $GC^{GN(e)}(GN(x), GN(y), h) \in [a,b]$ and according to the definition of universal combinatorial operation:

(1) when $x + y < 2e$

$$\begin{aligned} GN(x) + GN(y) &= (b+a-x) + (b+a-y) \\ &= 2(b+a) - (x+y) \\ &> 2(b+a-e) = 2GN(e). \end{aligned} \tag{12}$$

Then, according to the definition of $GC^e(x,y,h)$:

$$\begin{aligned} &GC^{GN(e)}(GN(x), GN(y), h) \\ &= b + a \\ &\quad - \min\Bigg(ab + a - GN(e), (b-a) \\ &\qquad \times \Big[\max\Big(0, \big((b-GN(x))^m \\ &\qquad + (b-GN(y))^m - (b-GN(e))^m\big) \\ &\qquad \times \big((b-a)^m\big)^{-1}\big)\Big]^{1/m} + a\Bigg). \end{aligned} \tag{13}$$

According to the definition of central generalized negation operation:

$$GN(x) = b + a - x, \tag{14}$$

$$GN(y) = b + a - y, \tag{15}$$

$$GN(e) = b + a - e. \tag{16}$$

Substituting (14), (15), and (16) separately into (13):

$$\begin{aligned} &GC^{GN(e)}\left(GN\left(x\right),GN\left(y\right),h\right)\\ &=b+a\\ &\quad-\min\Big(e,(b-a)\\ &\qquad\times\Big[\max\Big(0,\big((x-a)^m+(y-a)^m\\ &\qquad\qquad-(e-a)^m\big)\\ &\qquad\qquad\times\big((b-a)^m\big)^{-1}\big)\Big]^{1/m}+a\Big). \end{aligned} \tag{17}$$

And then

$$\begin{aligned} &GN\left(GC^{GN(e)}\left(GN\left(x\right),GN\left(y\right),h\right)\right)\\ &=b+a-\Big(b+a\\ &\qquad-\min\Big(e,(b-a)\\ &\qquad\qquad\times\Big[\max\Big(0,\big((x-a)^m+(y-a)^m\\ &\qquad\qquad\qquad-(e-a)^m\big)\\ &\qquad\qquad\qquad\times\ \big((b-a)^m\big)^{-1}\big)\Big]^{1/m}+a\Big)\Big)\\ &=\min\Big(e,(b-a)\\ &\qquad\times\Big[\max\Big(0,\big((x-a)^m+(y-a)^m\\ &\qquad\qquad-(e-a)^m\big)\times\big((b-a)^m\big)^{-1}\big)\Big]^{1/m}+a\Big)\\ &=GC^e\left(x,y,h\right) \end{aligned} \tag{18}$$

(2) when $x+y>2e$

$$\begin{aligned} &GN\left(x\right)+GN\left(y\right)\\ &\quad=(b+a-x)+\left(b+a-y\right)\\ &\quad=2\left(b+a\right)-\left(x+y\right)\\ &\quad<2\left(b+a-e\right)=2GN\left(e\right). \end{aligned} \tag{19}$$

So, according to the definition of $GC^e(x,y,h)$:

$$\begin{aligned} &GC^{GN(e)}\left(GN\left(x\right),GN\left(y\right),h\right)\\ &=\min\Big(GN\left(e\right),(b-a)\\ &\qquad\times\Big[\max\Big(0,\big((GN\left(x\right)-a)^m+\left(GN\left(y\right)-a\right)^m\\ &\qquad\qquad-(GN\left(e\right)-a)^m\big)\\ &\qquad\qquad\times\big((b-a)^m\big)^{-1}\big)\Big]^{1/m}+a\Big). \end{aligned} \tag{20}$$

Substituting (14), (15), and (16) separately into (20):

$$\begin{aligned} &GC^{GN(e)}\left(GN\left(x\right),GN\left(y\right),h\right)\\ &=\min\Big(b+a-e,(b-a)\\ &\qquad\times\Big[\max\Big(0,\big((b-x)^m+(b-y)^m\\ &\qquad\qquad-(b-e)^m\big)\times\big((b-a)^m\big)^{-1}\big)\Big]^{1/m}+a\Big). \end{aligned} \tag{21}$$

And then

$$\begin{aligned} &GN\left(GC^{GN(e)}\left(GN\left(x\right),GN\left(y\right),h\right)\right)\\ &=b+a\\ &\quad-\min\Big(b+a-e,(b-a)\\ &\qquad\times\Big[\max\Big(0,\big((b-x)^m+(b-y)^m\\ &\qquad\qquad-(b-e)^m\big)\times\big((b-a)^m\big)^{-1}\big)\Big]^{1/m}+a\Big)\\ &=GC^e\left(x,y,h\right) \end{aligned} \tag{22}$$

(3) when $x+y=2e$

$$\begin{aligned} &GN\left(x\right)+GN\left(y\right)\\ &\quad=(b+a-x)+\left(b+a-y\right)\\ &\quad=2\left(b+a\right)-\left(x+y\right)\\ &\quad=2\left(b+a-e\right)\\ &\quad=2GN\left(e\right). \end{aligned} \tag{23}$$

According to the definition of $GC^e(x,y,h)$:

$$GC^{GN(e)}\left(GN\left(x\right),GN\left(y\right),h\right)=GN\left(e\right). \tag{24}$$

Then:

$$GN\left(GC^{GN(e)}\left(GN\left(x\right),GN\left(y\right),h\right)\right)=GN\left(GN\left(e\right)\right)=e. \tag{25}$$

From the above, the theorem is true. □

Lemma 5. $GC^{GN(e)}(GN(x),GN(y),h)=GN(GC^e(x,y,h))$.

Table 1: Fuzzy rules defining the fuzzy composed variable GE_θ.

Error of pendulum rod	Angle speed of pendulum rod						
	NB	NM	NS	ZE	PS	PM	PB
Angle of pendulum rod							
NB	**NB**	**NB**	**NB**	NM	**NM**	**NS**	**ZE**
NM	**NB**	**NB**	**NM**	NM	**NS**	**ZE**	**PS**
NS	**NB**	**NM**	**NM**	NS	**ZE**	**PS**	**PM**
ZE	NM	NM	NS	ZE	PS	PM	PM
PS	**NM**	**NS**	**ZE**	PS	**PM**	**PM**	**PB**
PM	**NS**	**ZE**	**PS**	PM	**PM**	**PB**	**PB**
PB	**ZE**	**PS**	**PM**	PM	**PB**	**PB**	**PB**

Proof. According to Theorem 4 and involution law of normal universal *Not* operation in any interval $[a, b]$, the theorem can be proved simply. □

Lemma 6. $C^e(x, y, h) = 1 - C^{1-e}(1 - x, 1 - y, h)$.

Proof. Setting the interval $[a, b]$ of x, y as $[0, 1]$, the lemma can be proved simply. □

Lemma 7. *If the interval $[a, b]$ is symmetrical about e, then $GC^e(x^*, y^*, h) = (GC^e(x, y, h))^*$, where x^* and x are symmetrical about e, namely, $x^* = 2e - x$, y^*, e^*, and $(GC^e(x, y, h))^*$ are similar, $e \in [a, b]$, $h \in [0, 1]$.*

Proof. Since the interval $[a, b]$ is symmetrical about e, then $a + b = 2e$ and $GN(x) = a + b - x = 2e - x$; thus

$$GN(x) = x^*. \tag{26}$$

Similarly

$$\begin{aligned} GN(y) &= y^*, \\ GN(e) &= a + b - e = 2e - e = e. \end{aligned} \tag{27}$$

From (26) and (27) the following could be obtained:

$$\begin{aligned} GC^{GN(e)}(GN(x), GN(y), h) &= GC^e(x^*, y^*, h), \\ GN(GC^e(x, y, h)) &= (GC^e(x, y, h))^*. \end{aligned} \tag{28}$$

And then from Lemma 5

$$GC^e(x^*, y^*, h) = (GC^e(x, y, h))^*. \tag{29}$$

So the theorem is true. □

Lemma 8. $C^{0.5}(1 - x, 1 - y, h) = 1 - C^{0.5}(x, y, h)$, *where* $h \in [0, 1]$.

Lemma 9. *If the interval $[a, b]$ is symmetrical about the original point, then $GC^0(-x, -y, h) = -GC^0(x, y, h)$, $h \in [0, 1]$.*

This lemma indicates that, when the interval $[a, b]$ is symmetrical about the origin and identity element e is 0, *Universal Combinatorial Operation* $GC^e(x, y, h)$ is also symmetrical about the origin.

As pointed out in the literature [4], the logical relationship between input variables, error E and error variety EC of normal two-dimensional fuzzy controller, is universal combinatorial relation in *Universal Logic*. Consequently, the complex reasoning process based on fuzzy rule can be replaced by the simple universal combinatorial operation, and a flexible logic control model is presented accordingly. In fuzzy control, the domains of input variables and output variable are generally symmetric to the origin, such as $[-5, 5]$. Obviously, it is the prerequisite of control model that the operation model be symmetric to the origin. Therefore, Lemma 9 provides a basis for the *Universal Combinatorial Operation*'s application in control.

2.4. Flexible Logic Control Method. Xiao et al. have put forward a concept of fuzzy composed variable to reduce effectively fuzzy control rules in multivariable nonlinear system [16]. According to the characteristics of controlled system and the internal relationship between input variables, the core is to construct a fuzzy composed variable by the fuzzy logic system to synthetically reflect the deviation between reference and the process output.

Four output variables in single inverted pendulum are considered, which are the displacement and speed of cart, x and x', and the angle and angle speed between pendulum bar and vertical line, θ and θ'. Four input variables are involved for the fuzzy controller. In the input variables of control system, the angle and angle speed, θ and θ', directly reflected the motion of pendulum. Therefore, according to the angle and angle speed of pendulum and the language rules shown in Table 1, a fuzzy composed variable, the error GE_θ of pendulum, can be defined to synthetically describe the motion of pendulum with the fuzzy logic system. Similarly, a fuzzy composed variable, the error GE_x of cart, can be defined according to the displacement and speed of cart, x and x', so as to synthetically describe the motion of cart. For multivariable system, it need not define, respectively, fuzzy logic system for every fuzzy composed variable. We can use a uniform fuzzy rule table, such as Table 1, and just select different quantization factors to obtain different fuzzy composed variables.

Note 2. In the paper, the fuzzy controller discussed has inputs, such as error e and error variety ec, and output variable u is the control signal. The variables, e,ec, and u, are crisp values from the practical process. The fuzzy language variables, E, EC, and U, are the corresponding fuzzy ones, and the fuzzy domains are unified as $[-1, 1]$ with fuzzy subsets, such as negative big (NB), negative middle (NM), negative small (NS), zero (ZE), positive small (PS), positive middle (PM), and positive big (PB).

Obviously, the language rules shown in Table 1 actually reflect the essential relationship between error E and error variety EC. The contents in Table 1 can be approximately divided into four parts, which separately give the language rules used to define composed variables under four conditions, such as error E and error variety EC are both negative, error E is negative but error variety EC is positive, error E is positive but error variety EC is negative, and error E and error variety EC are both positive.

Both error E and error variety EC reflect the deviation between the reference and the output; and then a composed variable E' can be defined to synthetically describe the control deviation of system, based on the essential relationship between them.

According to the physical meanings of error E and error variety EC, we can get the following conclusions.

(1) When error E and error variety EC are both positive, the control deviation of system is positive and tends to further increase positively. So the value of composed variable E' should not be smaller than their maximum value and the direction is positive. The combination rules are shown by the lower right bold corner of Table 1.

(2) When error E is positive but error variety EC is negative, the control deviation of system is positive but tends to decrease. So the value of composed variable E' should be between E and EC in this case. The combination rules are shown by the lower left bold corner of Table 1.

(3) Similarly, the value of composed variable E' under two other conditions can also be obtained.

Through above analysis, it is easy to know that the essential relationship among error E, error variety EC and the composed variable E' is just a kind of universal combinatorial one in *Universal Logic*. As a result, we have

$$E' = GC^e(E, EC, h). \tag{30}$$

Obviously, now the identity element e is zero.

Moreover, according to the concept of negative feedback control, there is only a difference of a single sign between composed variable E' describing control deviation and the output variable U of controller, namely;

$$U = -E'. \tag{31}$$

Therefore, the relationship among error E, error variety EC, and the output variable U is

$$U = -GC^e(E, EC, h), \tag{32}$$

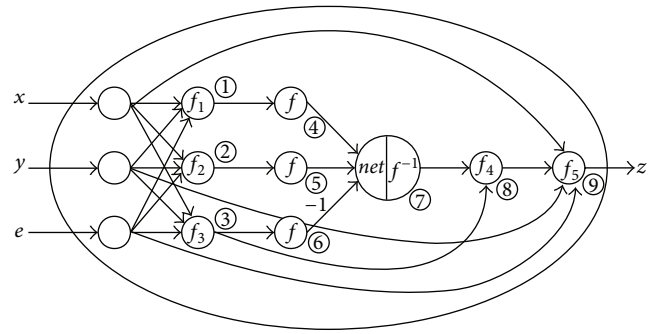

Figure 1: The neuron model of zero-level universal combinatorial operation.

where $E, EC, U \in [-1, 1]$, $e = 0$, and $h \in [0, 1]$. The control method is called *Flexible Logic Control Method* [4].

At the same time, a weighted factor $\alpha, \alpha \in [0, 1]$ is introduced to meet the requirements of different controlled objects. By adjusting the value of α, it is possible to change the weighting degrees for error E and error variety EC. When the *general correlation coefficient* h is 0.5, there is

$$\begin{aligned} U &= -GC^e(\alpha E, (1-\alpha)EC, 0.5) \\ &= \Gamma_{-1}^1[\alpha E + (1-\alpha)EC - e] \\ &= \alpha E + (1-\alpha)EC. \end{aligned} \tag{33}$$

And the formula (33) is just the fuzzy control method proposed by Long and Wang [17]. He used a linear equation, such as (33), to describe fuzzy control rules. But the relationship among E, EC, and U is not only linear. So (32) is a cluster of operators determined by *general correlation coefficient* h, and (33) is only a special operator in the cluster as h is equal to 0.5. As a result, flexible logic control method can realize the effective control for complex system.

3. Neuron Model of Zero-Level Universal Combinatorial Operation

The uniform neuron model of generalized logic operators in any intervals $[a, b]$ is established in the literature [18]. Seven neuron models of logic operation are given separately, such as *Not*, *And*, *Or*, *Implication*, *Equation*, *Average*, and *Combination*.

But the neuron model of combination logic operation is too complicated for practical applications.

In this section, a new neuron model of zero-level universal combinatorial operation is constructed based on Lemma 6 in Section 2.3.

It is learnt from Lemma 6 in Section 2.3 that

$$C^e(x, y, h) = 1 - C^{1-e}(1-x, 1-y, h). \tag{34}$$

Therefore, the model of zero-level universal combinatorial operation can be represented by the neuron shown in Figure 1.

The neuron model is composed of several subneurons which are interconnected. In the model, there are three input

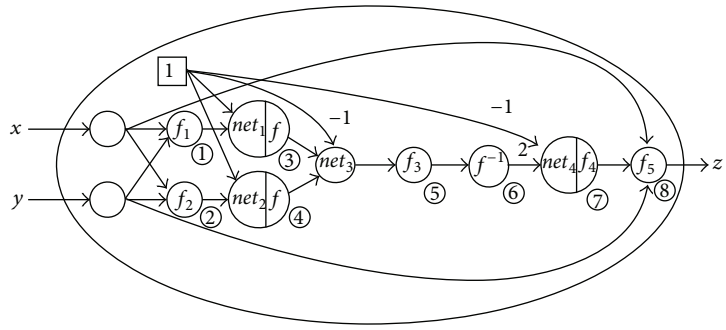

Figure 2: The neuron model of zero-level universal combinatorial operation in the interval $[-1, 1]$.

parameters: x, y, and e. And the output z, *net* denotes the weighted sum of all inputs, and all unmarked weights are 1. The transfer functions of the subneurons marked ④, ⑤, ⑥ are $f(x) = x^m$ with the parameter m and $m = (3-4h)/(4h(1-h))$. And the transfer function of the sub-neuron marked ⑦ is $f^{-1}(x)$. The sub-neurons marked ①, ②, ③, ⑧, and ⑨ have the following transfer functions, respectively:

$$f_1(u, v, e) = \begin{cases} u & u + v < 2e \\ 1 - u & u + v > 2e \\ e & \text{otherwise,} \end{cases}$$

$$f_2(u, v, e) = \begin{cases} v & u + v < 2e \\ 1 - v & u + v > 2e \\ e & \text{otherwise,} \end{cases}$$

$$f_3(u, v, e) = \begin{cases} e & u + v < 2e \\ 1 - e & u + v > 2e \\ e & \text{otherwise,} \end{cases} \tag{35}$$

$$f_4(u, v) = \Gamma^v[u],$$

$$f_5(u, v, w, e) = \begin{cases} w & u + v < 2e \\ 1 - w & u + v > 2e \\ w & \text{otherwise.} \end{cases}$$

We will discuss if the neuron model shown in Figure 1 has realized zero-level universal combinatorial operation.

(1) $x + y < 2e$. According to the definition of transfer functions f_1, f_2, and f_3, it is easy to find that the outputs of the sub-neurons marked ①, ②, ③ separately are x, y, and e. According to the definition of transfer function f, it is found that the outputs of the sub-neuron marked ④, ⑤, ⑥ separately are x^m, y^m, and e^m. Therefore, the output of the sub-neuron marked ⑦ is $(x^m + y^m - e^m)^{1/m}$. According to the definition of transfer function f_4, the output of the sub-neuron marked ⑧ is $\Gamma^e[(x^m + y^m - e^m)^{1/m}]$. According to the definition of transfer function f_5, the output of the sub-neuron marked ⑨ is $\Gamma^e[(x^m + y^m - e^m)^{1/m}]$. When $x + y < 2e$, the output of the neuron is

$$\Gamma^e\left[\left(x^m + y^m - e^m\right)^{1/m}\right] \tag{36}$$

(2) $x + y > 2e$. It is similarly learnt that the output of the sub-neuron marked ⑦ is $((1-x)^m + (1-y)^m - (1-e)^m)^{1/m}$, the output of the sub-neuron marked ⑧ is $\Gamma^{1-e}[((1-x)^m + (1-y)^m - (1-e)^m)^{1/m}]$, and the output of the sub-neuron marked ⑨ is $1 - \Gamma^{1-e}[((1-x)^m + (1-y)^m - (1-e)^m)^{1/m}]$. When $x + y > 2e$, the output of the neuron is

$$1 - \Gamma^{1-e}\left[\left((1-x)^m + (1-y)^m - (1-e)^m\right)^{1/m}\right]. \tag{37}$$

(3) $x + y = 2e$. It is similarly learnt that the output of the sub-neuron marked ⑦ is e, the output of the sub-neuron marked ⑧ is e, and the output of the sub-neuron marked ⑨ is e. When $x + y = 2e$, the output of neuron is e.

In summary, the neuron model shown in Figure 1 has fully realized the model of zero-level universal combinatorial operation.

In practical control application, the fuzzy domains of system variables are generally expressed as $[-n, n]$, for example, $[-6, 6]$. To simplify the neuron model, we can unify the fuzzy domains of system variables as $[-1, 1]$. Obviously, the identity element e is 0. Therefore, the model of zero-level universal combinatorial operation in the interval $[-1, 1]$ can be obtained by the definition of universal combinatorial operation model in any intervals $[a, b]$ in Section 2.2,

$$\begin{aligned} &GC^0(x, y, h) \\ &= \text{ite}\left\{\min\left(0, 2\left[\max\left(0, \frac{(x+1)^m + (y+1)^m - 1}{2^m}\right)\right]^{1/m} - 1\right) \mid x + y < 0; \right. \\ &\quad \left. -\min\left(0, 2\left[\max\left(0, \frac{(1-x)^m + (1-y)^m - 1}{2^m}\right)\right]^{1/m} - 1\right) \mid x + y > 0; 0\right\}. \end{aligned} \tag{38}$$

Therefore, it is easy to obtain the neuron model of zero-level universal combinatorial operation in the interval $[-1, 1]$

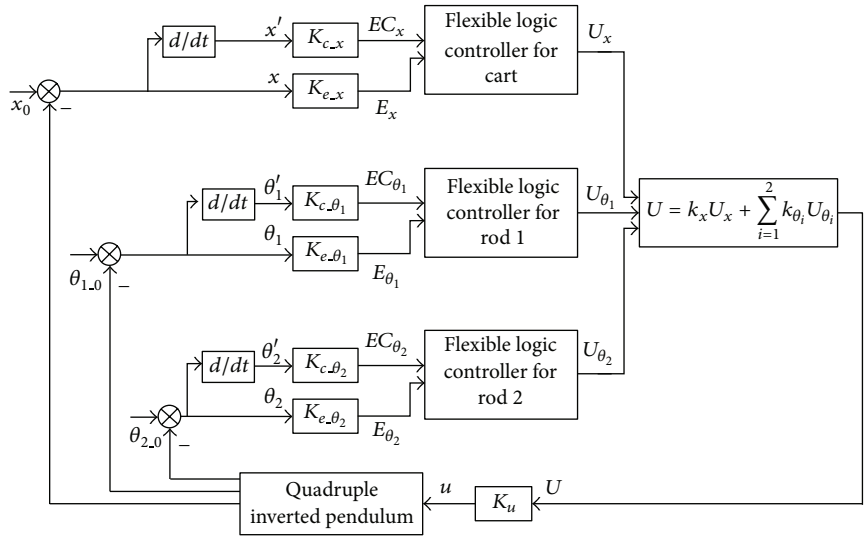

Figure 3: The flexible logic control model of double inverted-pendulum.

according to the neuron model given in Figure 1, as shown in Figure 2.

The neuron model is composed of interconnected multiple sub-neurons, and its internal structure is a small artificial neural network. In the model, x and y are the inputs, z is the output, net_1, net_2, net_3, and net_4 are the weighted sum of all inputs, the values of connecting weights without specific marking are 1, and ①, ②,..., ⑧ are marks of some sub-neurons for convenient discussion. The sub-neurons marked ③ and ④ have the transfer function $f(x) = x^m$ with the parameter m. And the sub-neuron marked ⑤ also has the transfer function $f_3(x) = \max(0, x/(2^m))$ with the parameter m, where $m = (3 - 4h)/(4h(1 - h))$. The sub-neuron marked ⑥ also has the transfer function $f^{-1}(x)$ with the parameter m, and the sub-neurons marked ①, ②, ⑦, and ⑧ have the following transfer functions, respectively:

$$f_1(u, v) = \begin{cases} u & u + v < 0 \\ -u & u + v > 0 \\ 0 & \text{otherwise,} \end{cases}$$

$$f_2(u, v) = \begin{cases} v & u + v < 0 \\ -v & u + v > 0 \\ 0 & \text{otherwise,} \end{cases} \tag{39}$$

$$f_4(u) = \min(0, u),$$

$$f_5(u, v, w) = \begin{cases} w & u + v < 0 \\ -w & u + v > 0 \\ w & \text{otherwise.} \end{cases}$$

4. Realization of Artificial Neural Network of Flexible Logic Control Model

In the practical complex system, the control objects are always not less than one, so multiple system variables are selected for feedback control. The basic idea of flexible logic control model presented in Section 2.4 is to design sub-goal controller based on the control object, and each subgoal controller is designed with the flexible logic control method. Then the output variable of control system is the weighted sum of the outputs of these sub-goal controllers.

Obviously, most of the operators involved in this model are universal combinatorial operation. Therefore, it is easy to implement the artificial neural network of the flexible logic control model by using the neuron model of zero-level universal combinatorial operation in Section 3. In this section, the artificial neural network structure of flexible logic control model is presented using the double inverted-pendulum system as the control object.

The objective is to maintain the rods in an upright position and the cart in an appointed position in the rail. There are six output variables and one input variable in double inverted-pendulum, which are x, x', θ_1, $\theta_1{}'$, θ_2, $\theta_2{}'$, and u. The variables, E_x, EC_x, E_{θ_1}, EC_{θ_1}, E_{θ_2}, EC_{θ_2}, and U, are the corresponding fuzzy ones, and the fuzzy domains are unified as $[-1, 1]$.

We can design three subcontrollers with the flexible logic control method. One is to maintain the cart in an appointed position with two input variables, E_x and EC_x. The other ones are to maintain, respectively, the rods in an upright position with two input variables E_{θ_i} and EC_{θ_i} $(i = 1, 2)$. And we lead into weighted factors, such as α_x, α_{θ_1}, and α_{θ_2}. The three sub-controllers are designed as follows:

$$U_x = -GC^0(\alpha_x E_x, (1 - \alpha_x) EC_x, h_x), \tag{40}$$

$$\alpha_x = (\alpha_{s\_x} - \alpha_{0\_x}) |E_x| + \alpha_{0\_x}, \tag{41}$$

$$U_{\theta_i} = -GC^0(\alpha_{\theta_i} E_{\theta_i}, (1 - \alpha_{\theta_i}) EC_{\theta_i}, h_{\theta_i}), \tag{42}$$

$$\alpha_{\theta_i} = (\alpha_{s\_\theta_i} - \alpha_{0\_\theta_i}) |E_{\theta_i}| + \alpha_{0\_\theta_i}. \tag{43}$$

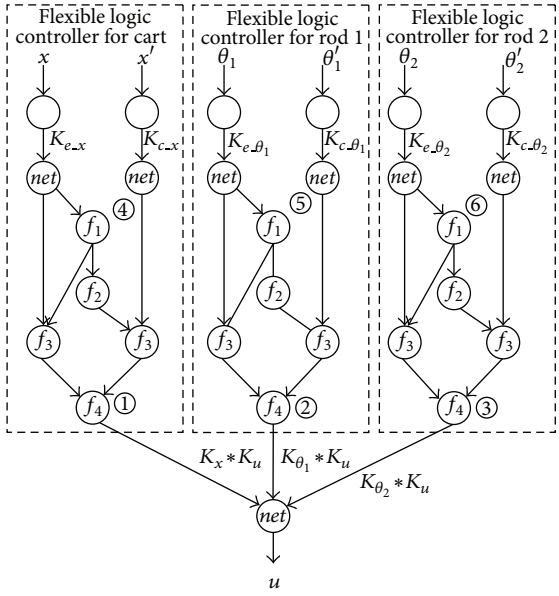

Figure 4: The neural network structure of flexible logic control model.

When the control signal U is combined, we lead into three weighted factors, such as k_x, k_{θ_1}, and k_{θ_2}, for the three sub-controllers. According to (40) and (42), we can get the output of the controller as follows:

$$\begin{aligned} U &= k_x U_x + k_{\theta_1} U_{\theta_1} + k_{\theta_2} U_{\theta_2} \\ &= k_x \left(-GC^0 \left(\alpha_x E_x, \left(1-\alpha_x\right) EC_x, h_x\right)\right) \\ &\quad + \sum_{i=1}^{2} k_{\theta_i} \left(-GC^0 \left(\alpha_{\theta_i} E_{\theta_i}, \left(1-\alpha_{\theta_i}\right) EC_{\theta_i}, h_{\theta_i}\right)\right), \end{aligned} \tag{44}$$

where E_x, EC_x, E_{θ_i}, EC_{θ_i}, and $U \in [-1, 1]$, $GC^0(x, y, h)$ is (38), h_x, h_{θ_1}, and h_{θ_2} are general correlation coefficients, h_x, h_{θ_1}, and $h_{\theta_2} \in [0, 1]$, α_x, α_{θ_1}, and $\alpha_{\theta_2} \in [0, 1]$, k_x, k_{θ_1}, and $k_{\theta_2} \in [-1, 1]$, $0 \le \alpha_{0\_x} \le \alpha_{s\_x} \le 1$, $0 \le \alpha_{0\_\theta_1} \le \alpha_{s\_\theta_1} \le 1$, and $0 \le \alpha_{0\_\theta_2} \le \alpha_{s\_\theta_2} \le 1$.

By the above analysis, we can obtain the control model of double inverted-pendulum, as shown in Figure 3. Based on the neuron model of zero-level universal combinatorial operation, the artificial neural network structure of the control model could be obtained, as shown in Figure 4.

The displacement and speed of cart, x and x', the angle and angle speed between the lower pendulum bar and vertical line, θ_1 and $\theta_1{}'$, and the angle and angle speed between the upper pendulum bar and vertical line, θ_2 and $\theta_2{}'$, are the input variables of the artificial neural network. The output variable is the control signal. ①, ②,. . ., ⑥ are marks of some sub-neurons for convenient discussion. *Net* is the weighted sum of these inputs of the corresponding sub-neurons. The connection weight values of the unmarked sub-neurons are 1. The sub-neurons marked ①, ②, and ③ are the neuron model of zero-level universal combinatorial operation in the interval $[-1, 1]$, as given in Section 3. The other sub-neurons have the following transfer functions, respectively:

$$\begin{aligned} f_1(u) &= \left(\alpha_s - \alpha_0\right)|u| + \alpha_0, \\ f_2(u) &= 1 - u, \qquad f_3(u, v) = uv, \end{aligned} \tag{45}$$

where the transfer function f_1 has the parameters such as α_0 and α_s, and the transfer functions of the sub-neurons marked ④, ⑤, and ⑥ separately have the parameters α_{0_x}, α_{s_x}, $\alpha_{0\_\theta_1}$, $\alpha_{s\_\theta_1}$, $\alpha_{0\_\theta_2}$, and $\alpha_{s\_\theta_2}$.

From the Figure 4, we can see that the artificial neural network structure of the control model is a feed forward neural network. *Genetic algorithms* (*GAs*) are a robust and efficient optimization technique based on the mechanism of natural selection and natural genetics [19]. One of the important features of *GAs* is that they are a population-based search technique. Instead of moving from one single point to another like traditional mathematical programming techniques, *GAs* always maintain and manipulate a solution set. Therefore, *GAs* are used to train the artificial neural network.

Table 2: The physical parameters of the double inverted-pendulum.

Symbol	Value
m_0	0.924 kg
m_1	0.185 kg
m_2	0.2 kg
l_1	0.283 m
l_2	0.245 m
L_1	0.483 m
f_0	0.1 N·s/m
J_1	0.00547 kg·m^2
J_2	0.00549 kg·m^2

5. Results of Experiments

This section takes a double inverted-pendulum physical system, for example, to show the feasibility and validity of the flexible logic control method based on artificial neural network.

Owing to the rapidity and the absolute instability of the inverted-pendulum system, it requires a high real-time processing frequency. Therefore, the sampling interval of this system is set as 5 ms. When the system is running for 20 s, the control effect comparison could be conducted. The physical parameters of the system are given in Table 2.

The flexible logic control method based on artificial neural network is applied into the above double inverted-pendulum physical system. The network parameters are optimized by genetic algorithms. The definition of the fitness

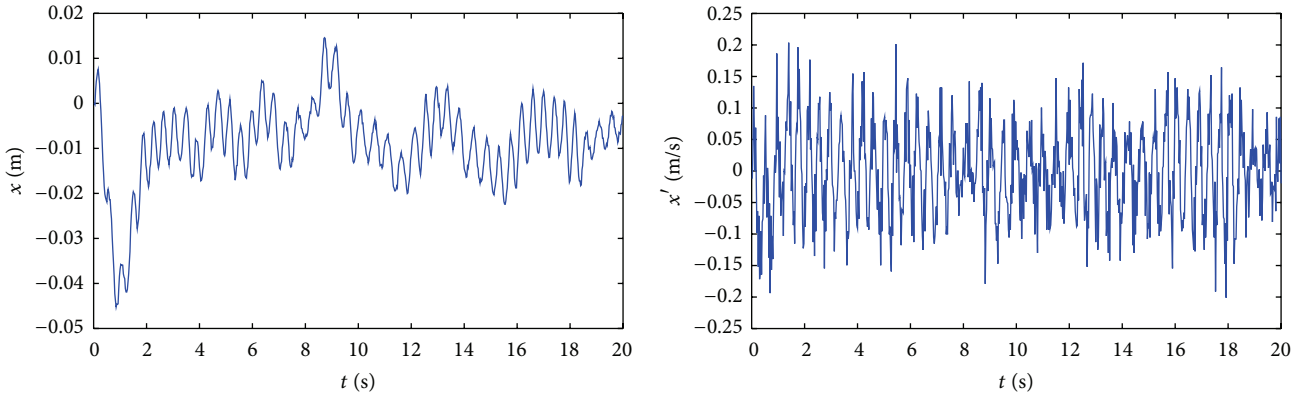

(a) The cart displacement curve

(b) The cart speed curve

Figure 5: The car displacement and speed curve when the system is steady.

Table 3: The control parameters of the control model.

Symbol	Value	Description
K_{e_x}	29.4118	Quantification factor for E_x
K_{c_x}	16.3529	Quantification factor for EC_x
h_x	0.2902	General correlation coefficient between E_x and EC_x
a_{0_x}	0.2157	Minimum value of a_x
a_{s_x}	0.5258	Maximum value of a_x
$K_{e\_\theta 1}$	73.3333	Quantification factor for $E_{\theta 1}$
$K_{c\_\theta 1}$	8.0000	Quantification factor for $EC_{\theta 1}$
$h_{\theta 1}$	0.8275	General correlation coefficient between $E_{\theta 1}$ and $EC_{\theta 1}$
$a_{0\_\theta 1}$	0.7569	Minimum value of $a_{\theta 1}$
$a_{s\_\theta 1}$	0.7701	Maximum value of $a_{\theta 1}$
$K_{e\_\theta 2}$	47.4510	Quantification factor for $E_{\theta 1}$
$K_{c\_\theta 2}$	14.9412	Quantification factor for $EC_{\theta 1}$
$h_{\theta 2}$	0.5674	General correlation coefficient between $E_{\theta 2}$ and $EC_{\theta 2}$
$a_{0\_\theta 2}$	0.6745	Minimum value of $a_{\theta 2}$
$a_{s\_\theta 2}$	0.7530	Maximum value of $a_{\theta 2}$
K_x	0.4902	Weighted factor of the subcontroller for cart
$K_{\theta 1}$	−0.3645	Weighted factor of the subcontroller for rod1
$K_{\theta 2}$	0.9686	Weighted factor of the subcontroller for rod2
K_u	8.7843	Proportion factor for U

function is shown as (46) and the control parameters of the system are shown in Table 3. Consider

$$\text{Dis} = \sum_{i=0}^{N} \left(\left(\left(\frac{x^2(i)}{25} \right) + \left(\frac{x'^2(i)}{50} \right) + \left(\frac{\theta_1^2(i)}{5} \right) + \left(\frac{\theta_1'^2(i)}{10} \right) + \theta_2^2(i) + \theta_2'^2(i) \right) \times (N)^{-1} \right),$$
$$\text{fitness} = \frac{1}{(\text{Dis}/10)}. \tag{46}$$

Three experiments as the stability control, anti-interference control, and the free movement in a level track of cart pendulum system for the above double inverted-pendulum physical system are carried out by using the controller made of these control parameters.

5.1. Stability Control Experiment. Under the same initial state such as $x(0) = 0$ m, $\theta_1(0) = 0.05$ rad and $\theta_2(0) = 0.05$ rad, the stability control of the double inverted-pendulum physical system has been realized. The experimental results are shown in Figures 5, 6, 7, and 8 (running time: 20 s).

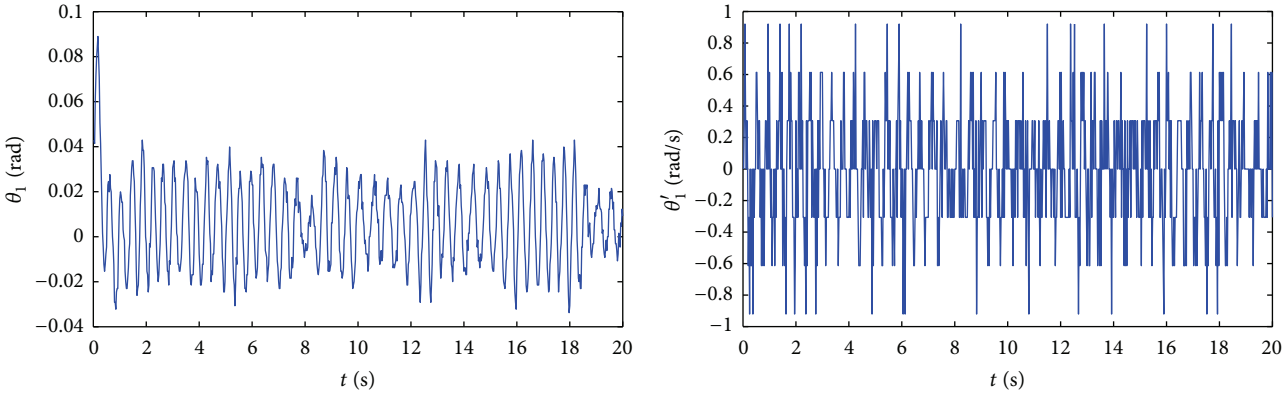

(a) The lower rod angle curve

(b) The lower rod angular velocity curve

Figure 6: The lower rod angle curve and angular velocity curve when the system is steady.

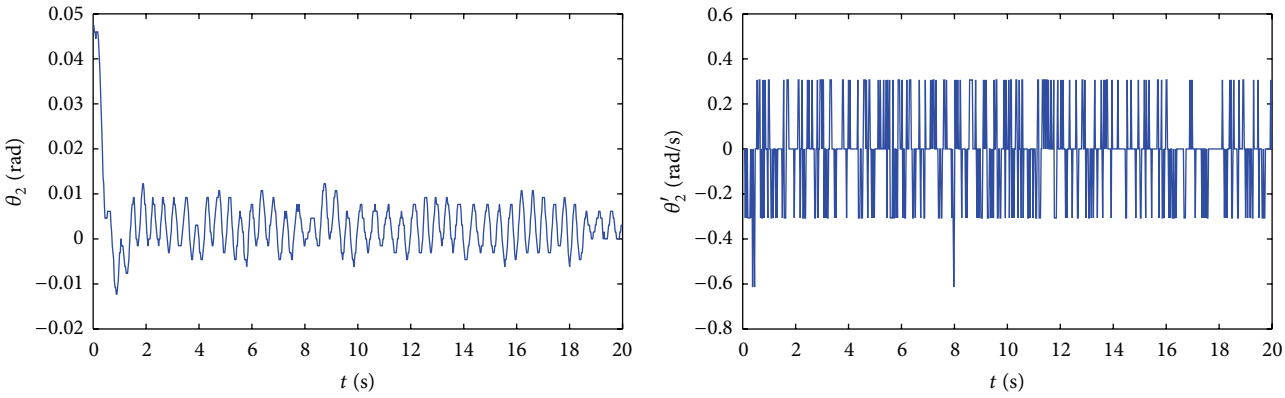

(a) The upper rod angle curve

(b) The upper rod angular velocity curve

Figure 7: The upper rod angle curve and angular velocity curve when the system is steady.

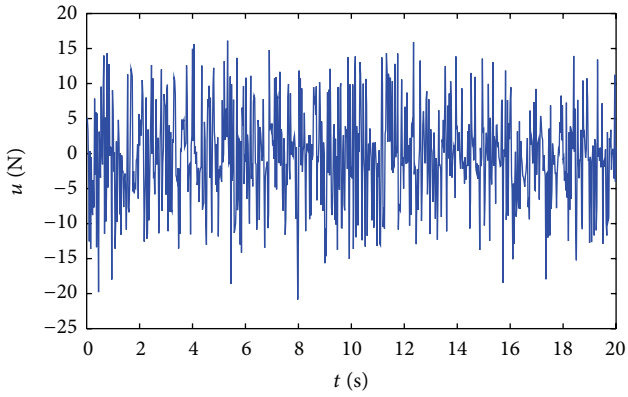

Figure 8: The controlled quantity curve when the system is steady.

From the experimental results, we can find when the system is in a stable state, the deviation of the cart displacement could be about 0.01 m with a good stability control effect.

5.2. Anti-Interference Control Experiment. After knocking the upper pendulum twice when the system reaches a steady state, it shows strong anti-interference ability. The experimental results are shown in Figures 9, 10, 11, and 12.

From the experimental results, we can find the system becomes stable again after 1.9 s.

5.3. Free Movement Control Experiment of Cart Pendulum System. When the system reaches a steady state, the target position x_d is changed on-line, such as from 0 m to −0.2 m. So the free movement control of cart pendulum on a level track could be realized. The experimental results are shown in Figures 13, 14, 15, and 16.

From the experimental results, we can see the cart moves to the new target location after 2.7 s and the system remains stable.

5.4. Self-Adaptive Experiment of Control Model. Some physical parameters have been changed in another double inverted-pendulum physical system. The physical parameters of the system are shown in Table 4. The control model

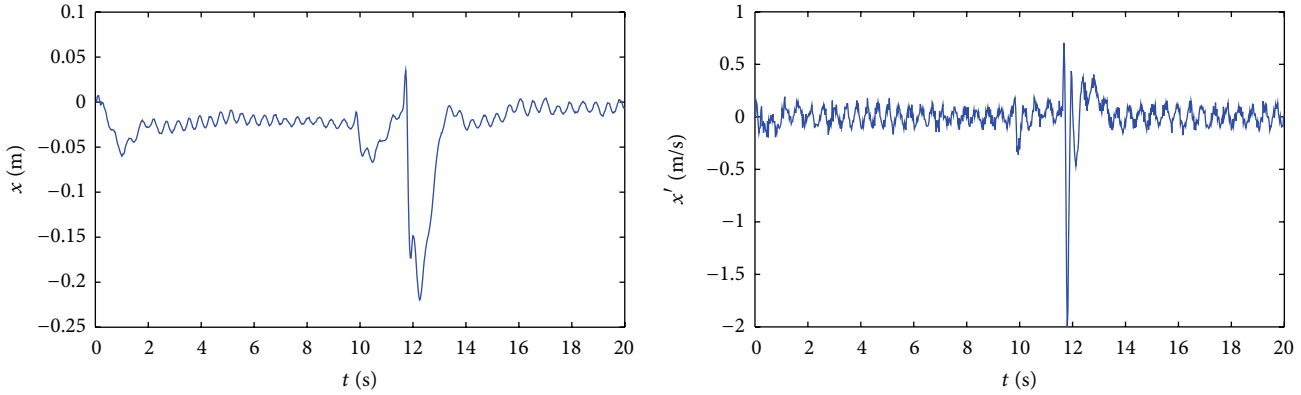

(a) The cart displacement curve (b) The cart speed curve

Figure 9: The car displacement and speed curve when the system is interfered.

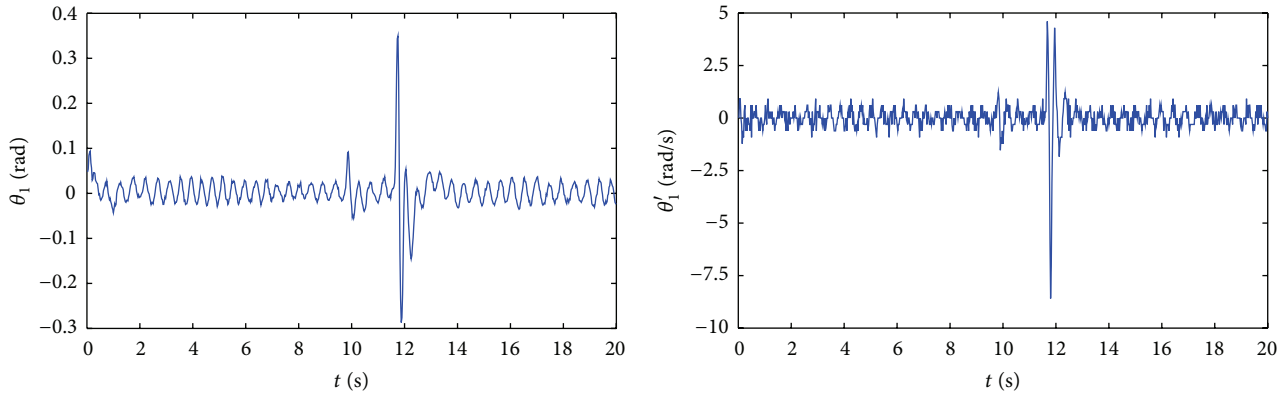

(a) The lower rod angle curve (b) The lower rod angular velocity curve

Figure 10: The lower rod angle curve and angular velocity curve when the system is interfered.

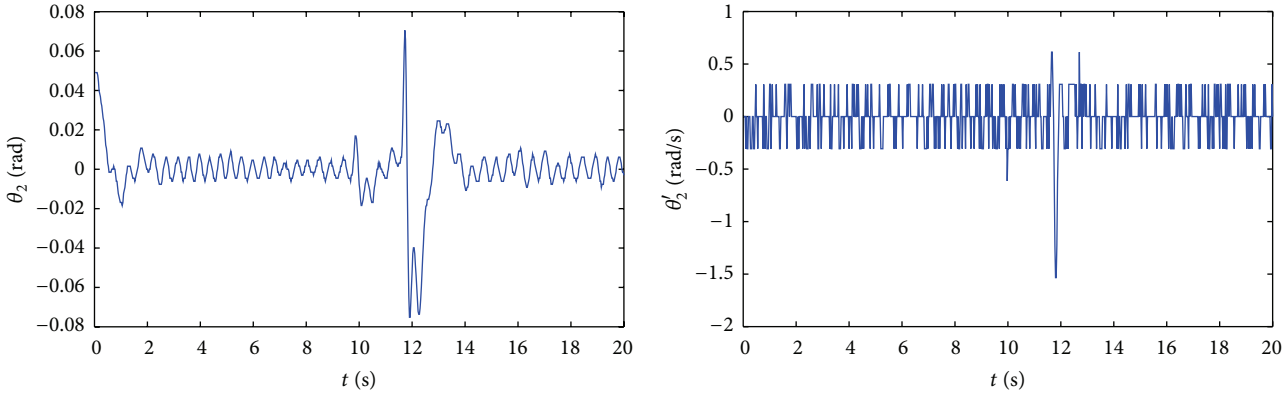

(a) The upper rod angle curve (b) The upper rod angular velocity curve

Figure 11: The upper rod angle curve and angular velocity curve when the system is interfered.

also can realize the stability control of the new double inverted-pendulum after changing some parameters. The experimental results are shown in Figures 17, 18, 19, and 20. The experimental results show that the control model based on artificial neural network has excellent self-adaptability and portability.

5.5. Comparison of the Experimental Results. Cheng et al. [20] put forward a parameter fuzzy control method in 1996. The core idea of this method is to find the synthetical relationship among state variables by using modern control theory and form composed error and composed variety of error so as to construct a fuzzy controller.

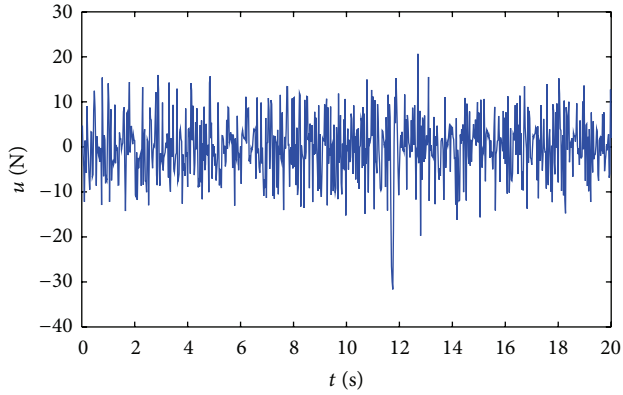

Figure 12: The controlled quantity curve when the system is interfered.

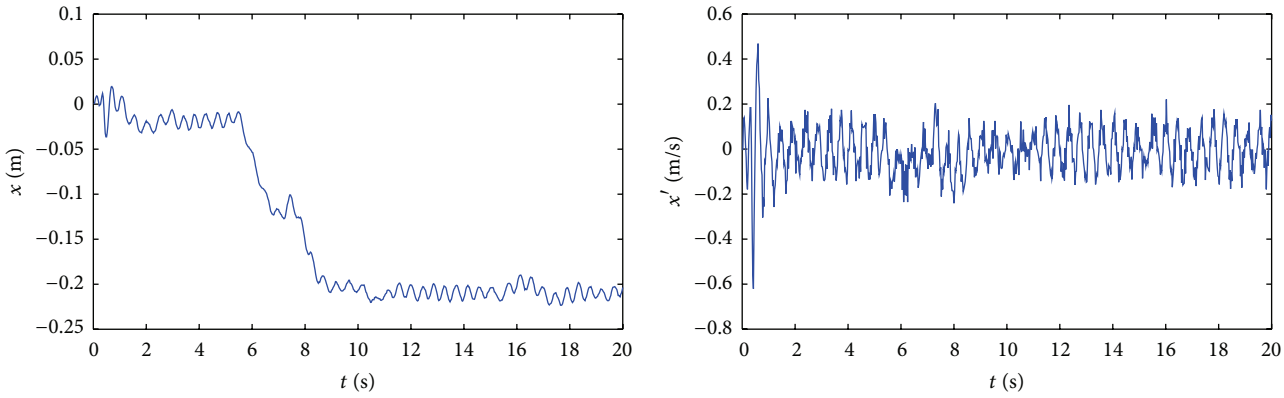

(a) The cart displacement curve

(b) The cart speed curve

Figure 13: The car displacement and speed curve when the cart is moving in a level track.

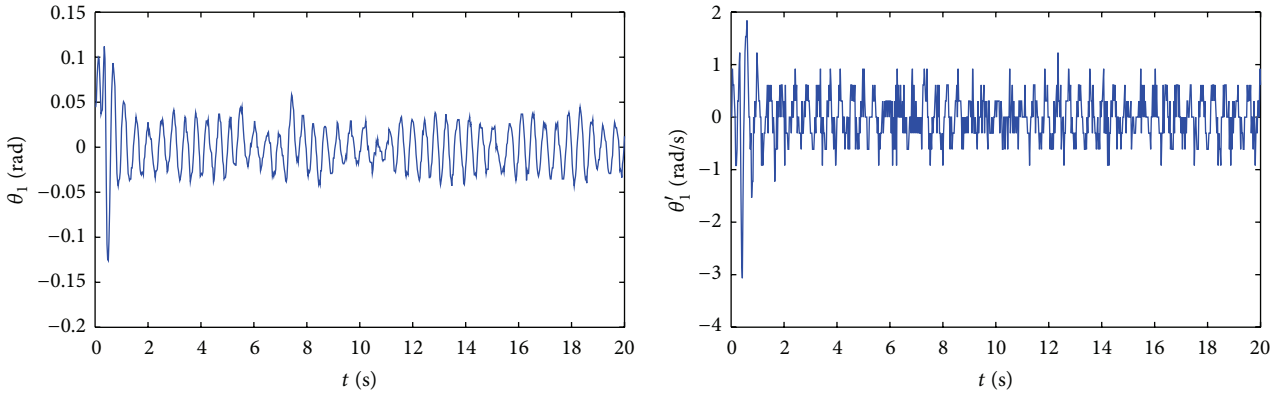

(a) The lower rod angle curve

(b) The lower rod angular velocity curve

Figure 14: The lower rod angle curve and angular velocity curve when the cart is moving in a level track.

The parameter fuzzy control method is used to stabilize the above double inverted-pendulum physical system. The control parameters of this system are shown in Table 5.

Real-time control is carried out in the above double inverted-pendulum physical system. When the initial state of the system is $x(0) = 0$ m, $\theta_1(0) = 0.05$ rad, and $\theta_2(0) = 0.05$ rad, the running time is 20 s. The comparison of the experimental results for two control methods is shown in Table 6.

From Table 6, the adjusting time and the steady-state errors of the displacement and the angle are compared with

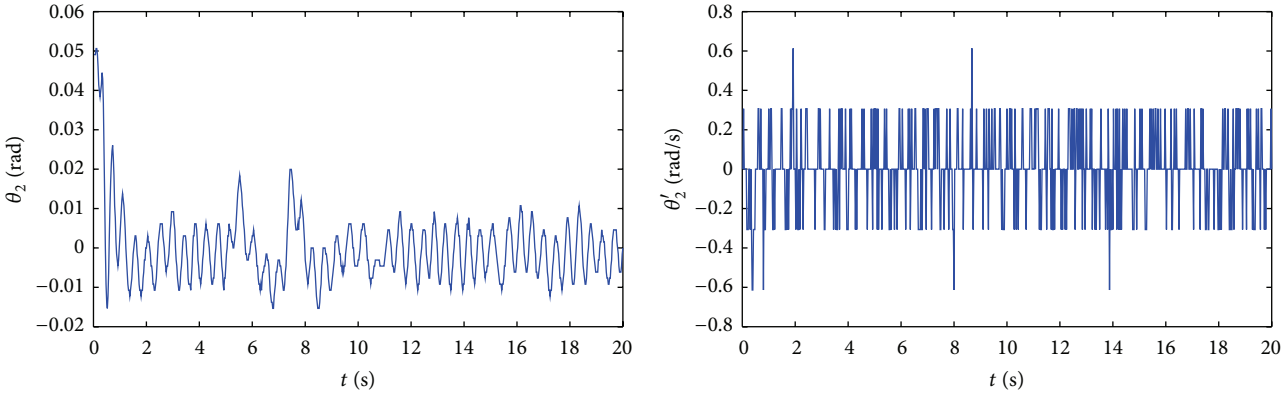

(a) The upper rod angle curve

(b) The upper rod angular velocity curve

Figure 15: The upper rod angle curve and angular velocity curve when the cart is moving in a level track.

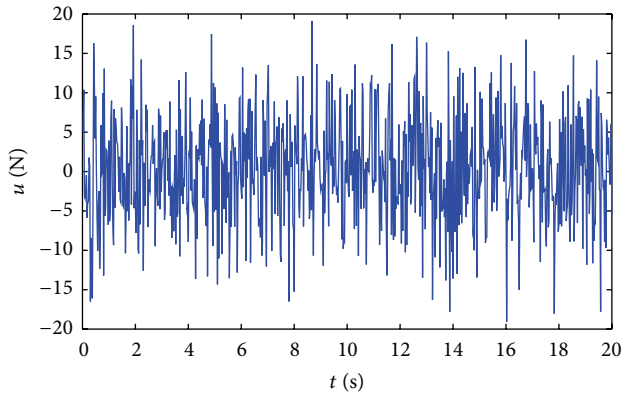

Figure 16: The controlled quantity curve when the cart is moving in a level track.

Table 4: The physical parameters of another double inverted-pendulum.

Symbol	Value
m_0	0.595 kg
m_1	0.158 kg
m_2	0.142 kg
l_1	0.1237 m
l_2	0.2265 m
L_1	0.151 m
f_0	0.1 N·s/m
J_1	0.0028394 kg·m^2
J_2	0.0024329 kg·m^2

Table 5: The control parameters of the parameter fuzzy controller.

Symbol	Value
k_1	8.3089
k_2	33.4311
k_3	−114.1740
k_4	0.0978
k_5	26.8817
k_6	−22.1896
a_0	0.3333
a_s	0.7518

parameter fuzzy control method about the stability control in double inverted-pendulum physical system.

In summary, the flexible logic control model based on artificial neural networks has good control effects. And the controlling system has good stability and anti-interference ability.

6. Conclusion

Based on the basic physical meaning of error E and error variety EC, this paper analyzes the logical relationship between them and uses universal combinational operation model to describe it. And a flexible logic control method is put forward to realize effective control on multivariable nonlinear system.

In order to implement the fusion control of *Universal Logic* and artificial neural networks, this paper puts forward a new neuron model of zero-level universal combinational

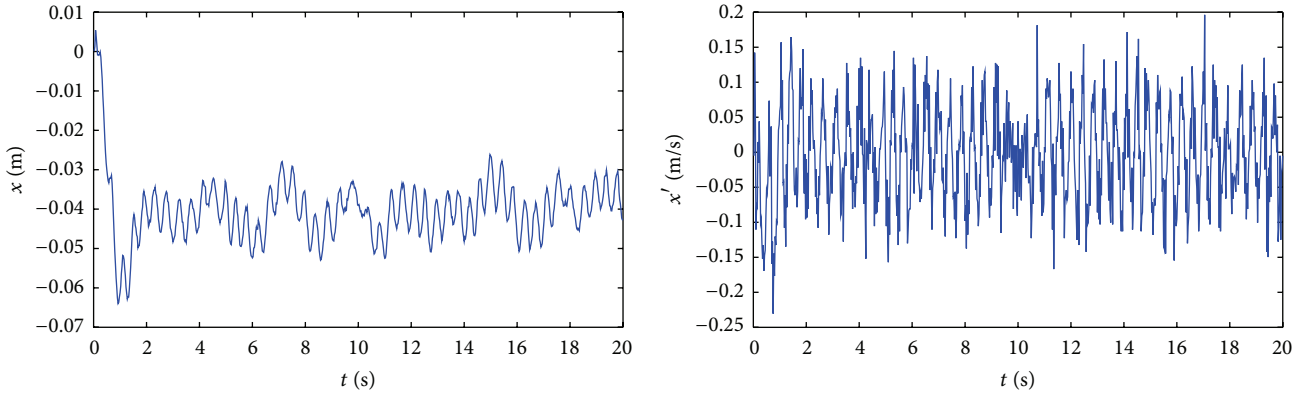

(a) The cart displacement curve (b) The cart speed curve

Figure 17: The car displacement and speed curve when the system is steady.

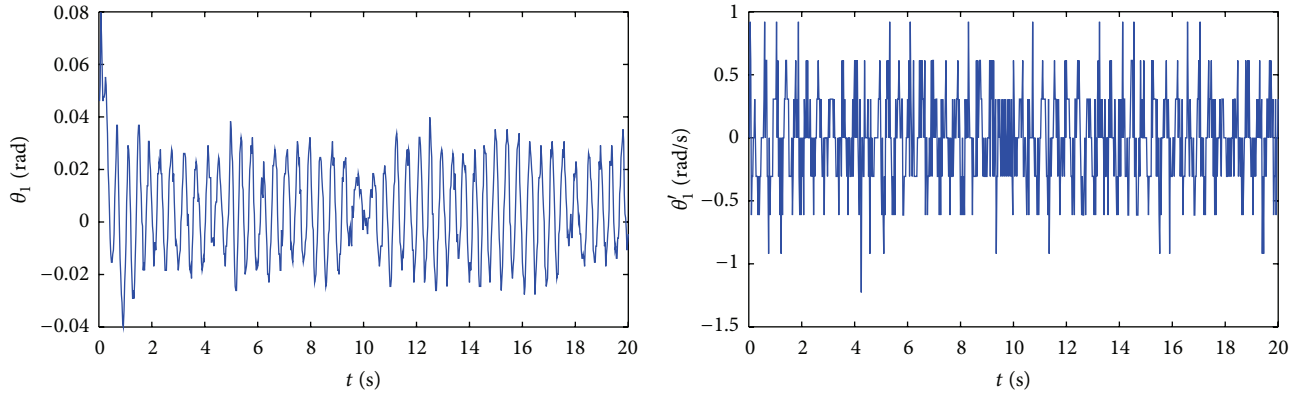

(a) The lower rod angle curve (b) The lower rod angular velocity curve

Figure 18: The lower rod angle curve and angular velocity curve when the system is steady.

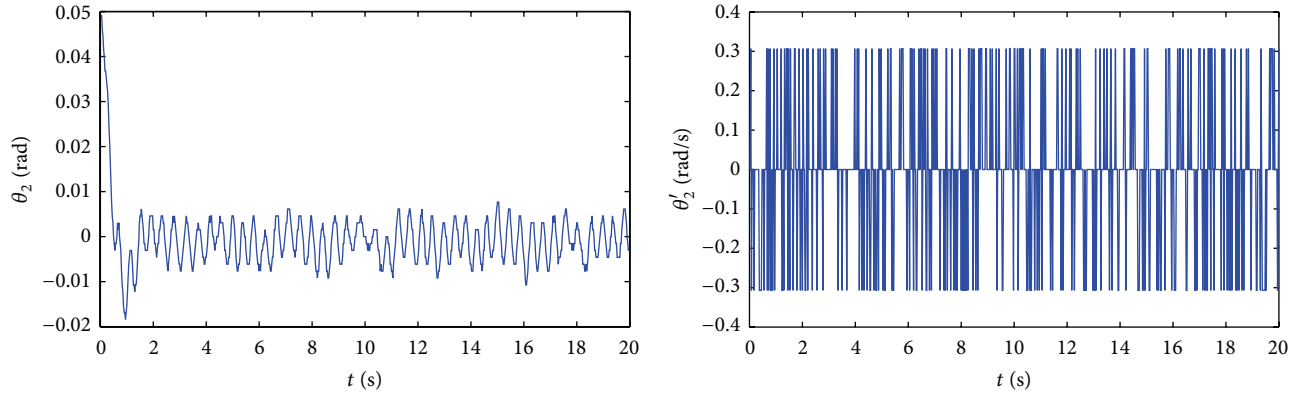

(a) The upper rod angle curve (b) The upper rod angular velocity Curve

Figure 19: The upper rod angle curve and angular velocity curve when the system is steady.

Table 6: The comparison of the control effects for two control methods.

Control method	Control effects Evaluation indexes Steady state deviation			Adjusting time (s)
	The cart displacement (m)	The angle of the lower rod (rod)	The angle of the upper rod (rod)	
Fuzzy control parameter method	0.125	0.01	0.004	2.37
Flexible logic control method	0.01	0.004	0.002	1.7

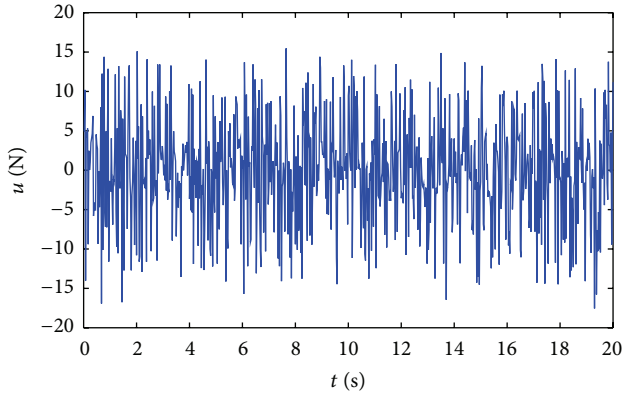

Figure 20: The controlled quantity curve when the system is steady.

operation. Based on this neuron model, artificial neural network is designed for flexible logic control model. Meanwhile, the stability control of the double inverted-pendulum physical system, anti-interference control, and free movement of the cart pendulum have been realized in a level track by using the proposed control model.

Conflict of Interests

The authors declare that there is no conflict of interests regarding the publication of this paper.

Acknowledgments

This work is supported by the Beijing Municipal Natural Science Foundation of China (nos. 4113069 and 4122007) and the Beijing Municipal Education Commission Foundation (no. 007000546311501).

References

[1] L. Hou, H. Zhang, X. Liu, E. Chu, and Q. Wang, "The PMSM passive control of the speed sensor with self-adaptive soft switching fuzzy sliding mode," *Domination and Decision*, vol. 25, pp. 686–690, 2010.

[2] H.-L. Hung and J.-H. Wen, "Reduce-complexity fuzzy-inference-based iterative multiuser detection for wireless communication systems," *International Journal of Communication Systems*, vol. 25, no. 4, pp. 478–490, 2012.

[3] D.-Q. Zhou, Y.-S. Huang, K.-J. Long, and Q.-X. Zhu, "Decentralised direct adaptive output feedback fuzzy controller for a class of large-scale nonaffine nonlinear systems and its applications," *International Journal of Systems Science*, vol. 43, no. 5, pp. 939–951, 2012.

[4] L. Fu and H. He, "A study of control methods based on flexible logic," *Computer Science*, vol. 36, pp. 158–161, 2009.

[5] I.-H. Li and L.-W. Lee, "A hierarchical structure of observer-based adaptive fuzzy-neural controller for MIMO systems," *Fuzzy Sets and Systems*, vol. 185, pp. 52–82, 2011.

[6] W.-Y. Wang, M.-C. Chen, and S.-F. Su, "Hierarchical *T*-*S* fuzzy-neural control of anti-lock braking system and active suspension in a vehicle," *Automatica*, vol. 48, no. 8, pp. 1698–1706, 2012.

[7] J. Wen and F. Liu, "Aggregation-based fuzzy dual-mode control for nonlinear systems with mixed constraints," *International Journal of Systems Science*, vol. 43, no. 5, pp. 834–844, 2012.

[8] O. Karasakal, M. Guzelkaya, L. Eksin, E. Yesil, and T. Kumbasar, "Online tuning of fuzzy PID controllers via rule weighing based on normalized acceleration," *Engineering Applications of Artificial Intelligence*, vol. 26, pp. 184–197, 2013.

[9] Y. Li, J. Shen, K. Lee, and X. Liu, "Offset-free fuzzy model predictive control of a boiler-turbine system based on genetic algorithm," *Simulation Modelling Practice and Theory*, vol. 26, pp. 77–95, 2012.

[10] J.-W. Wang, H.-N. Wu, L. Guo, and Y.-S. Luo, "Robust H_{∞} fuzzy control for uncertain nonlinear Markovian jump systems with time-varying delay," *Fuzzy Sets and Systems*, vol. 212, pp. 41–61, 2013.

[11] Y. Zhang, J. Wang, and H. Li, "Stabilization of the quadruple inverted pendulum by variable universe adaptive fuzzy controller based on variable gain H_{∞} regulator," *Journal of Systems Science & Complexity*, vol. 25, no. 5, pp. 856–872, 2012.

[12] H. Guo, H. Li, W. Zhao, and Z. Song, "Direct adaptive fuzzy sliding mode control with variable universe fuzzy switching term for a class of MIMO nonlinear systems," *Mathematical Problems in Engineering*, vol. 2012, Article ID 543039, 21 pages, 2012.

[13] H. He, H. Wang, Y. Liu, Y. Wang, and Y. Du, *The Principle of the Universal Logic*, Science Press, Beijing, China, 2001.

[14] M. Borenovic, A. Neskovic, and D. Budimir, "Multi-system-multi-operator localization in PLMN using neural networks," *International Journal of Communication Systems*, vol. 25, no. 2, pp. 67–83, 2012.

[15] Z. Chen, *Related Reasoning Study about the Fractal Chaos and Logic in Complex System*, Northwestern Polytechnical University, Shaanxi, China, 2004.

[16] J. Xiao, S. Zhang, and X. Xu, "The adaptive weighting control based on fuzzy combination of variable," *Control and Decision*, vol. 16, pp. 191–194, 2001.

[17] S. Long and P. Wang, "The self-adjustment of fuzzy control rules," *Fuzzy Mathematics*, vol. 3, pp. 105–112, 1982.

[18] M.-Y. Mao, Z.-C. Chen, and H.-C. He, "A new uniform neuron model of generalized logic operators based on [*a, b*]," *International Journal of Pattern Recognition and Artificial Intelligence*, vol. 20, no. 2, pp. 159–171, 2006.

[19] D. Gözüpek and F. Alagöz, "Genetic algorithm-based scheduling in cognitive radio networks under interference temperature constraints," *International Journal of Communication Systems*, vol. 24, no. 2, pp. 239–257, 2011.

[20] F. Cheng, G. Zhong, Y. Li, and Z. Xu, "Fuzzy control of a double-inverted pendulum," *Fuzzy Sets and Systems*, vol. 79, no. 3, pp. 315–321, 1996.

Hindawi Publishing Corporation
Mathematical Problems in Engineering
Volume 2014, Article ID 101473, 15 pages
http://dx.doi.org/10.1155/2014/101473

Research Article

Stability Analysis and H_∞ Model Reduction for Switched Discrete-Time Time-Delay Systems

Zheng-Fan Liu, Chen-Xiao Cai, and Wen-Yong Duan

School of Automation, Nanjing University of Science and Technology, Nanjing 210094, China

Correspondence should be addressed to Zheng-Fan Liu; senseblaze900@163.com

Received 2 September 2013; Accepted 21 November 2013; Published 2 January 2014

Academic Editor: Bo-Chao Zheng

This paper is concerned with the problem of exponential stability and H_∞ model reduction of a class of switched discrete-time systems with state time-varying delay. Some subsystems can be unstable. Based on the average dwell time technique and Lyapunov-Krasovskii functional (LKF) approach, sufficient conditions for exponential stability with H_∞ performance of such systems are derived in terms of linear matrix inequalities (LMIs). For the high-order systems, sufficient conditions for the existence of reduced-order model are derived in terms of LMIs. Moreover, the error system is guaranteed to be exponentially stable and an H_∞ error performance is guaranteed. Numerical examples are also given to demonstrate the effectiveness and reduced conservatism of the obtained results.

1. Introduction

Switched systems belong to a special class of hybrid control systems, which comprises a collection of subsystems described by dynamics differential or difference equations, together with a switching law that specifies the switching rule among the subsystems. Due to the theoretical development as well as practical applications, analysis and synthesis of switched systems have recently gained considerable attention [1–4].

Furthermore, the time-delay phenomenon is frequently encountered in a variety of industrial and engineering systems [5–7], for instance, chemical process, long distance transmission line, communication networks, and so forth. Moreover, time-delay is a predominant source of the poor performance and instability. In the last two decades, there has been increasing interest in the stability analysis for the systems; see, for example, [8, 9] and the references cited there in. For switched delay systems, due to the impact of time-delays, the behavior of switched delay systems is usually much more complicated than that of switched systems or delay systems [10, 11].

The average dwell time (ADT) technique [12] and multiple Lyapunov function approach [13] are two powerful and effective tools for studying the problems of stability for switched systems under controlled switching. By applying ADT scheme, the disturbance attenuation properties of time-controlled switched systems are investigated in [14]. In [15], the exponential stability and L_2-gain of switched delay systems are studied by using ADT approach. Furthermore, based on ADT method, in [16–18] the stability of switched systems with stable and unstable subsystems co existing was considered. Using the ADT scheme, switching design for exponential stability was proposed in [19] for a class of switched discrete-time constant time-delay systems. By using the multiple Lyapunov function approach and ADT technique, the literature [20] studied the problem of state feedback stabilization of a class of discrete-time switched singular systems with time-varying state delay under asynchronous switching. However, many free weighing matrices were introduced, which made the stability result complicated. In [11], the problem of stabilization and robust H_∞ control via ADT method switching for discrete switched system with time-delay was considered. However, the procedures given in [11] could not be applied to the case of asynchronous switching or the case of switching delay systems with stable and unstable subsystems co existing. This motivates the present study.

On another research front line, it is well known that mathematical modeling of physical systems often results in complex high-order models. However, this causes the great difficulties in analysis and synthesis of the systems. Therefore, in practical applications it is desirable to replace high-order models with reduced-order ones for reducing the computational complexities in some given criteria without incurring much loss of performance or information. The purpose of model reduction is to obtain a lower-order system which approximates a high-order system according to certain criterion. Recently, much attention has been focused on the model reduction problem [21–25]. Many important results have been reported, which involve various efficient approaches, such as the balanced truncation method [24], the optimal Hanker norm reduction method [25], the cone complementarily linearization method [26], and sequential linear programming matrix method [27]. In terms of LMIs with inverse constraints or other non convex conditions, the model reduction of the discrete-time context has been investigated in [28, 29]. However, it is difficult to obtain the numerical solutions. In [30], the existence conditions for H_∞ model reduction for discrete-time uncertain switched systems are derived in terms of strict LMIs by using switched Lyapunov function method. However, time delays are not taken into account. In the literature [31], a novel idea to approximate the original time-delay system by a reduced time-delay model has been proposed recently. However, the unstable subsystems are not taken into account.

Motivated by the preceding discussion, the main contributions of this paper are highlighted as follows. The problem of exponential stability and H_∞ model reduction for a class of switched linear discrete-time systems with time-varying delay have been investigated. To lessen the computation complexity and to reduce the conservatism, new discrete LKF are constructed and the delay interval is divided into two unequal subintervals by the delay decomposition method. The switching law is given by ADT scheme, such that even if one or more subsystem is unstable the overall switched system still can be stable. For the high-order systems, sufficient conditions for the existence of the desired reduced-order model are derived in terms of strict LMIs, which can be easily solved by using MATLAB LMI control toolbox. Finally, numerical examples are given to show the effectiveness of the proposed methods.

The remainder of this paper is structured as follows. In Section 2, the problem formulation and some preliminaries are introduced. In Section 3, the main results are presented on the exponential stability of switched discrete-time systems with time-varying delay. In Section 4, the main results on the H_∞ model reduction for the high-order systems are presented. Numerical examples are given in Section 5. The last section concludes the work.

Notations. We use standard notations throughout the paper. $\lambda_{\min}(M)$ ($\lambda_{\max}(M)$) stands for the minimal (maximum) eigenvalue of M. M^T is the transpose of the matrix M. The relation $M > N$ ($M < N$) means that the matrix $M - N$ is positive (negative) definite. $\|x\|$ denotes the Euclidian-norm of the vector $x \in R^n$. R^n represents the n-dimensional real Euclidean space. $R^{n\times m}$ is the set of all real $n \times m$ matrices. diag$\{\cdots\}$ stands for a block-diagonal matrix. In symmetric block matrices or long matrix expressions, we use an asterisk "$*$" to represent a term that is induced by symmetry. I denotes the identity matrix.

2. Problem Description and Preliminaries

Consider a class of switched linear discrete-time systems with time-varying state delay of the form

$$\begin{aligned} x(k+1) &= A_i x(k) + A_{di} x(k - d(k)) + B_i u(k), \\ y(k) &= C_i x(k) + C_{di} x(k - d(k)) + D_i u(k), \\ x(\theta) &= \phi(\theta), \quad \theta = -h, -h+1, \ldots, 1, \end{aligned} \tag{1}$$

where $x(k) \in R^n$ denotes the system state, $y(k) \in R^m$ is the measured output, $u(k) \in R^p$ is the disturbance input vector which belongs to $l_2[0, \infty)$. $\phi(\theta) \in R^n$ is a vector-valued initial function. The switching signal σ (denoting $\sigma(k)$ for simplicity) : $[0, \infty) \to \overline{N} = \{1, 2, \ldots, T\}$ is a piecewise constant function and depends on time. $\sigma = i$ means that the ith subsystem is activated. T is the number of subsystems. The system matrices $A_i, A_{di}, B_i, C_i, C_{di}$, and D_i are a set of known real matrices with appropriate dimensions.

For a given finite positive integer $h > 0$, $d(k)$ is time-varying delay and satisfies the following condition

$$0 \le d(k) \le h, \quad \forall k \in N^+. \tag{2}$$

To facilitate theoretical development, we introduce the following definitions and lemmas.

Definition 1 (see [19]). The system (1) with disturbance input $u(k) = 0$ is said to be exponentially stable if there exist a switching function $\sigma(\cdot)$ and positive number c such that every solution $x(k, \phi)$ of the system satisfies

$$\|x(k)\| \le c\lambda^{k-k_0} \|\phi\|_s, \quad \forall k \ge k_0, \tag{3}$$

for any initial conditions $(k_0, \phi) \in R^+ \times C^n$. $c > 0$ is the decay coefficient, $0 < \lambda \le 1$ is the decay rate, and $\|\phi\|_s = \sup\{\|\phi(l)\|, l = k_0 - h, k_0 - h + 1, \ldots, k_0\}$.

Definition 2 (see [11]). Consider the system (1) with the following conditions.

(1) With $u(k) = 0$, the system (1) is exponentially stable with convergence rate $\lambda > 0$.

(2) The H_∞ performance $\|y(k)\|_2 < \gamma \|u(k)\|_2$ is guaranteed for all nonzero $u(k) \in L_2[0, \infty)$ and a prescribed $\kappa > 0$ under the zero condition.

In the above conditions, the system (1) is exponentially stabilizable with H_∞ performance γ and convergence rate λ.

Here γ characterizes the disturbance attenuation performance. The smaller the γ is, the better the performance is.

Definition 3 (see [12]). For a switching signal $\sigma(k)$ and any $T_2 > k > T_1 \ge 0$, let $N_\sigma(T_1, T_2)$ denote the number of

switching of $\sigma(k)$ over (T_1, T_2). If for any given $N_0 \geq 1$ and $T_a > 0$, we have $N_\sigma(T_1, T_2) \leq N_0 + (T_2 - T_1)/T_a$, then T_a and N_0 are called the ADT and the chatter bound, respectively.

Lemma 4 (see [9]). *For any matrix $R = R^T > 0$, integers $a \leq b$, vector function $\xi(k) : \{-b, -b+1, \ldots, -a\} \to R^n$, then*

$$(a-b)\sum_{s=k-b}^{k-a-1} z^T(s) R z(s) \leq \xi^T(k) \begin{bmatrix} -R & R \\ & -R \end{bmatrix} \xi(k). \quad (4)$$

Here

$$z(k) = x(k+1) - x(k),$$
$$\xi^T(k) = \begin{bmatrix} x^T(k-a) & x^T(k-b) \end{bmatrix}. \quad (5)$$

Lemma 5 (Schur complement [32]). *Let M, P, Q be given matrices such that $Q > 0$. Then*

$$\begin{bmatrix} P & M \\ * & -Q \end{bmatrix} < 0 \Longleftrightarrow P + MQ^{-1}M^T < 0. \quad (6)$$

The aim of this paper is to find a class of time-based switching signals for the discrete-time switched time-delay systems (1), whose subsystem is not necessarily stable, to guarantee the system to be exponentially stable. For a high-order system, we are interested in constructing a reduced-order switched system to approximate the system.

3. Stability Analysis

With the preliminaries given in the previous section we are ready to state the exponential stability and H_∞ performance of switched systems (1). To obtain the exponential stability of switched systems (1), we construct following discrete LKF:

$$V_i(k) = V_{i1}(k) + V_{i2}(k) + V_{i3}(k), \quad \forall i \in \overline{N}. \quad (7)$$

Here

$$\begin{aligned} V_{i1}(k) &= x^T(k) P_i x(k), \\ V_{i2}(k) &= \sum_{s=k-\vartheta}^{k-1} (1+\alpha_i)^{k-1-s} x^T(s) Q_{i1} x(s) \\ &\quad + \sum_{s=k-h}^{k-\vartheta-1} (1+\alpha_i)^{k-1-s} x^T(s) Q_{i2} x(s) \\ &\quad + \sum_{s=k-d(k)}^{k-1} (1+\alpha_i)^{k-1-s} x^T(s) Q_{i3} x(s), \\ V_{i3}(k) &= \sum_{\theta=-\vartheta}^{-1} \sum_{s=k+\theta}^{k-1} (1+\alpha_i)^{k-1-s} z^T(s) R_{i1} z(s) \\ &\quad + \sum_{\theta=-h}^{-\vartheta-1} \sum_{s=k+\theta}^{k-1} (1+\alpha_i)^{k-1-s} z^T(s) R_{i2} z(s) \\ &\quad + \sum_{\theta=-d(k)}^{-1} \sum_{s=k+\theta}^{k-1} (1+\alpha_i)^{k-1-s} z^T(s) R_{i3} z(s), \end{aligned} \quad (8)$$

where P_i, Q_{im}, R_{im} $(i \in \overline{N},\ m = 1,2,3)$ are symmetric positive definite matrices with appropriate dimensions, $z(k) = x(k+1) - x(k)$, and integer $\vartheta \in (0, h)$ and α_i are given constants.

Remark 6. In order to derive less conservative criteria than the existing ones, the delay interval $[0, h]$ is divided into two unequal subintervals: $[0, \vartheta]$ and $[\vartheta, h]$, where $\vartheta \in (0, h)$ is a tuning parameter. The information about $x(t-\vartheta)$ can be taken into account. This plays a vital role in deriving less conservative results. Thus, for any $k \in Z^+$, we have $d(k) \in [0, \vartheta]$ or $d(k) \in [\vartheta, h]$.

Firstly, we will provide a decay estimation of the system LKF in (7) along the state trajectory of switched system (1) without disturbance input (i.e., $u(k) = 0$).

Lemma 7. *Given constants $-1 < \alpha_i \leq 0$, $h > 0$ and $\vartheta \in (0, h)$, if there exist some symmetric positive definite matrices P_i, Q_{im}, R_{im} $(i \in \overline{N},\ m = 1,2,3)$ such that the following LMIs hold:*

$$\begin{bmatrix} \Psi_{i11} & \Psi_{i12} \\ & \Psi_{i22} \end{bmatrix} < 0, \quad (9)$$

$$\begin{bmatrix} \Phi_{i11} & \Phi_{i12} \\ & \Phi_{i22} \end{bmatrix} < 0, \quad (10)$$

where

$$\Psi_{i11} = \begin{bmatrix} \psi_{11}^i & \psi_{12}^i & 0 & 0 \\ & \psi_{22}^i & \psi_{23}^i & 0 \\ & * & \psi_{33}^i & \psi_{34}^i \\ & * & * & \psi_{44}^i \end{bmatrix},$$

$$\Phi_{i11} = \begin{bmatrix} \psi_{11}^i & 0 & \phi_{13}^i & 0 \\ & \phi_{22}^i & \phi_{23}^i & \phi_{24}^i \\ & * & \phi_{33}^i & 0 \\ & * & * & \psi_{44}^i \end{bmatrix},$$

$$\Psi_{i12} = \begin{bmatrix} A_i^T P_i & (A_i - I)^T W_{1i}^T \\ A_{di}^T P_i & A_{di}^T W_{1i}^T \\ 0 & 0 \\ 0 & 0 \end{bmatrix},$$

$$\Phi_{i12} = \begin{bmatrix} A_i^T P_i & (A_i - I)^T W_{2i}^T \\ A_{di}^T P_i & A_{di}^T W_{2i}^T \\ 0 & 0 \\ 0 & 0 \end{bmatrix},$$

$$\Psi_{i22} = \operatorname{diag}\{-P_i \ \ -W_{1i}\}, \qquad \Phi_{i22} = \operatorname{diag}\{-P_i \ \ -W_{2i}\},$$

$$\psi_{11}^i = -(1+\alpha_i) P_i - \frac{(1+\alpha_i)^\vartheta}{\vartheta}(R_{i1} + R_{i3}) + Q_{i1} + Q_{i3},$$

$$\psi_{12}^i = \frac{(1+\alpha_i)^\vartheta}{\vartheta}(R_{i1} + R_{i3}),$$

$$\psi_{22}^i = -(1+\alpha_i)^\vartheta Q_{i3} - \frac{(1+\alpha_i)^\vartheta}{\vartheta}(2R_{i1} + R_{i3}),$$

$$\psi_{23}^{i} = \frac{(1+\alpha_i)^{\vartheta}}{\vartheta} R_{i1},$$

$$\psi_{33}^{i} = (1+\alpha_i)^{\vartheta}(Q_{i2} - Q_{i1}) - \frac{(1+\alpha_i)^{h}}{h-\vartheta} R_{i2} - \frac{(1+\alpha_i)^{\vartheta}}{\vartheta} R_{i1},$$

$$\psi_{34}^{i} = \frac{(1+\alpha_i)^{h}}{h-\vartheta} R_{i2},$$

$$\psi_{44}^{i} = -(1+\alpha_i)^{h} Q_{i2} - \frac{(1+\alpha_i)^{h}}{h-\vartheta} R_{i2},$$

$$\phi_{13}^{i} = \frac{(1+\alpha_i)^{\vartheta}}{\vartheta}(R_{i1} + R_{i3}),$$

$$\phi_{22}^{i} = -(1+\alpha_i)^{h} Q_{i3} - \frac{(1+\alpha_i)^{h}}{h-\vartheta}(2R_{i2} + R_{i3}),$$

$$\phi_{23}^{i} = \frac{(1+\alpha_i)^{h}}{h-\vartheta}(R_{i2} + R_{i3}),$$

$$\phi_{24}^{i} = \frac{(1+\alpha_i)^{h}}{h-\vartheta} R_{i2},$$

$$\phi_{33} = -\frac{(1+\alpha_i)^{h}}{h-\vartheta}(R_{i2} + R_{i3}) - \frac{(1+\alpha_i)^{\vartheta}}{\vartheta}(R_{i1} + R_{i3}) - (1+\alpha_i)^{\vartheta}(Q_{i1} - Q_{i2}),$$

$$W_{1i} = (h-\vartheta) R_{i2} + \vartheta R_{i1} + \vartheta R_{i3},$$

$$W_{2i} = (h-\vartheta) R_{i2} + \vartheta R_{i1} + h R_{i3}. \tag{11}$$

Then, by means of LKF (7)*, along the trajectory of the systems* (1) *without disturbance input, one has*

$$\Delta V_i(k) = V_i(k+1) - V_i(k) \le \alpha_i V_i(k). \tag{12}$$

Proof. Let us choose the system LKF (7). Define

$$V_i(k+1) - (1+\alpha_i) V_i(k) = \sum_{m=1}^{3} \widetilde{\Delta} V_{im}(k), \tag{13}$$

where

$$\widetilde{\Delta} V_{im}(k) = V_{im}(k+1) - (1+\alpha_i) V_{im}(k). \tag{14}$$

Therefore, the following equality holds along the solution of (1):

$$\widetilde{\Delta} V_{i1}(k) = x^T(k+1) P_i x(k+1) - (1+\alpha_i) x^T(k) P_i x(k), \tag{15}$$

$$\widetilde{\Delta} V_{i2}(k) = x^T(k)(Q_{i1} + Q_{i3}) x(k) - (1+\alpha_i)^{h} x^T(k-h) Q_{i2} x(k-h) - (1+\alpha_i)^{d(k)} x^T(k-d(k)) Q_{i3} x(k-d(k)) - (1+\alpha_i)^{\vartheta} x^T(k-\vartheta)(Q_{i1} - Q_{i2}) x(k-\vartheta), \tag{16}$$

$$\widetilde{\Delta} V_{i3}(k) = z^T(k)((h-\vartheta) R_{i2} + \vartheta R_{i1} + d(k) R_{i3}) z(k) - \sum_{s=k-\vartheta}^{k-1} (1+\alpha_i)^{k-s} z^T(s) R_{i1} z(s) - \sum_{s=k-h}^{k-\vartheta-1} (1+\alpha_i)^{k-s} z^T(s) R_{i2} z(s) - \sum_{s=k-d(k)}^{k-1} (1+\alpha_i)^{k-s} z^T(s) R_{i3} z(s). \tag{17}$$

For any $k \in Z^+$, we have $d(k) \in [0, \vartheta]$ or $d(k) \in [\vartheta, h]$.

(1) If $d(k) \in [0, \vartheta]$, it gets

$$-\sum_{s=k-\vartheta}^{k-1} (1+\alpha_i)^{k-s} z^T(s) R_{i1} z(s) = -\sum_{s=k-\vartheta}^{k-1-d(k)} (1+\alpha_i)^{k-s} z^T(s) R_{i1} z(s) - \sum_{s=k-d(k)}^{k-1} (1+\alpha_i)^{k-s} z^T(s) R_{i1} z(s). \tag{18}$$

So (17) could be

$$\widetilde{\Delta} V_{i3}(k) \le z^T(k)((h-\vartheta) R_{i2} + \vartheta R_{i1} + \vartheta R_{i3}) z(k) - \sum_{s=k-h}^{k-\vartheta-1} (1+\alpha_i)^{k-s} z^T(s) R_{i2} z(s) - \sum_{s=k-\tau(k)}^{k-1} (1+\alpha_i)^{k-s} z^T(s)(R_{i1} + R_{i3}) z(s) - \sum_{s=k-\vartheta}^{k-1-\tau(k)} (1+\alpha_i)^{k-s} z^T(s) R_{i1} z(s). \tag{19}$$

From Lemma 4, we have

$$
\begin{aligned}
&-\sum_{s=k-h}^{k-\vartheta-1}(1+\alpha_i)^{k-s}z^T(s)R_{i2}z(s)\\
&\le\frac{(1+\alpha_i)^h}{h-\vartheta}\xi_1^T(t)\begin{bmatrix}-R_{i2} & R_{i2}\\ & -R_{i2}\end{bmatrix}\xi_1(t),
\end{aligned}
\tag{20}
$$

$$
\begin{aligned}
&-\sum_{s=k-d(k)}^{k-1}(1+\alpha_i)^{k-s}z^T(s)(R_{i1}+R_{i3})z(s)\\
&\le\frac{(1+\alpha_i)^{\tau(k)}}{\tau(k)}\xi_2^T(k)\begin{bmatrix}-R_{i1}-R_{i3} & R_{i1}+R_{i3}\\ & -R_{i1}-R_{i3}\end{bmatrix}\xi_2(k)\\
&\le\frac{(1+\alpha_i)^{\vartheta}}{\vartheta}\xi_2^T(k)\begin{bmatrix}-R_{i1}-R_{i3} & R_{i1}+R_{i3}\\ & -R_{i1}-R_{i3}\end{bmatrix}\xi_2(k),
\end{aligned}
\tag{21}
$$

$$
\begin{aligned}
&-\sum_{s=k-\vartheta}^{k-1-d(k)}(1+\alpha_i)^{k-s}z^T(s)R_{i1}z(s)\\
&\le\frac{(1+\alpha_i)^{\vartheta}}{\vartheta-\tau(k)}\xi_3^T(k)\begin{bmatrix}-R_{i1} & R_{i1}\\ & -R_{i1}\end{bmatrix}\xi_3(k)\\
&\le\frac{(1+\alpha_i)^{\vartheta}}{\vartheta}\xi_3^T(k)\begin{bmatrix}-R_{i1} & R_{i1}\\ & -R_{i1}\end{bmatrix}\xi_3(k),
\end{aligned}
\tag{22}
$$

where

$$
\begin{aligned}
\xi_1^T(k)&=\left[x^T(k-\vartheta)\quad x^T(k-h)\right],\\
\xi_2^T(k)&=\left[x^T(k)\quad x^T(k-d(k))\right],\\
\xi_3^T(k)&=\left[x^T(k-d(k))\quad x^T(k-\vartheta)\right].
\end{aligned}
\tag{23}
$$

Combining (13)–(22), it yields

$$
\begin{aligned}
&V_i(k+1)-(1+\alpha_i)V_i(k)\\
&\le\xi^T(k)\Psi_{i11}\xi(k)\\
&\quad+x^T(k+1)P_ix(k+1)+z^T(k)W_{1i}z(k),
\end{aligned}
\tag{24}
$$

where

$$
\xi^T(k)=\left[x^T(k)\quad x^T(k-d(k))\quad x^T(k-\vartheta)\quad x^T(k-h)\right].
\tag{25}
$$

Multiplying (9) both from left and right by diag $\left\{0\ \ 0\ \ 0\ \ 0\ \ P_i^{-1}\ \ W_i^{-T}\right\}$, by *Schur Complement*, further, considering (24), one can infer that (12) holds.

(2) If $d(k)\in[\vartheta,h]$, it gets

$$
\begin{aligned}
&-\sum_{s=k-d(k)}^{k-1}(1+\alpha_i)^{k-s}z^T(s)R_{i3}z(s)\\
&=-\sum_{s=k-\vartheta}^{k-1}(1+\alpha_i)^{k-s}z^T(s)R_{i3}z(s)\\
&\quad-\sum_{s=k-d(k)}^{k-\vartheta-1}(1+\alpha_i)^{k-s}z^T(s)R_{i3}z(s).
\end{aligned}
\tag{26}
$$

One obtains

$$
\begin{aligned}
\widetilde{\Delta}V_{i3}(k)&\le z^T(k)\left((h-\vartheta)R_{i2}+\vartheta R_{i1}+hR_{i3}\right)z(k)\\
&\quad-\sum_{s=k-\vartheta}^{k-1}(1+\alpha_i)^{k-s}z^T(s)(R_{i1}+R_{i3})z(s)\\
&\quad-\sum_{s=k-d(k)}^{k-\vartheta-1}(1+\alpha_i)^{k-s}z^T(s)(R_{i2}+R_{i3})z(s)\\
&\quad-\sum_{s=k-h}^{k-d(k)-1}(1+\alpha_i)^{k-s}z^T(s)R_{i2}z(s).
\end{aligned}
\tag{27}
$$

Similarly, it is easy to get that

$$
\begin{aligned}
&V_i(k+1)-(1+\alpha_i)V_i(k)\\
&\le\xi^T(k)\Phi_{i11}\xi(k)\\
&\quad+x^T(k+1)P_ix(k+1)+z^T(k)W_{2i}z(k).
\end{aligned}
\tag{28}
$$

If (10) holds, by *Schur Complement*, then we have (12). This completes the proof. □

Remark 8. Our LKF does not include free-weighing matrices as in previous investigations, and this may lead to reduce the computational complexity and get less conservation results.

Remark 9. In order to get less conservative results, the delay interval $[0,h]$ can be divided into much more subintervals. However, when the number of dipartite numbers increases, the matrix formulation becomes more complex and the time-consuming grows bigger.

Now we have the following theorem.

Theorem 10. *If there exist some constants* $-1<\alpha_i<0$ *and positive definite symmetric matrices* P_i,Q_{im},R_{im} $(i\in\overline{N},m=1,2,3)$ *and* $\mu\ge1$ *such that* (9), (10), *and the following inequalities hold:*

$$
\begin{aligned}
&P_i\le\mu P_j,\quad Q_{im}\le\mu Q_{jm},\quad R_{im}\le\mu R_{jm},\\
&\forall i,j\in\overline{N}.
\end{aligned}
\tag{29}
$$

Then, the switched system (1) *with* $u(k)=0$ *and ADT satisfies* $\tau_a>-\ln\mu/\ln\alpha$ *which is exponentially stable.*

Proof. By Lemma 7, we have

$$
\Delta V_i(k)=V_i(k+1)-V_i(k)\le\alpha_iV_i(k),\quad\forall i\in\overline{N}.
\tag{30}
$$

Therefore,

$$V_i(k_0+n) \le (\alpha_i+1)^n V_i(k_0). \tag{31}$$

There exists $\mu_i \ge 1$ $(i \in \overline{N})$, such that

$$V_i(k) \le \mu_i V_j(k), \quad \forall i, j \in \overline{N}. \tag{32}$$

We let $\tau_1, \ldots, \tau_{N_{\sigma(k_0,k_0+k)}}$ denote the switching times of σ in (k_0, k_0+k), and let $N_{\sigma(k_0,k+k_0)}$ be the switching number of σ in $(k_0, k+k_0)$, by (31) and (32), one obtains

$$\begin{aligned} V_{\sigma(k+k_0)}(k+k_0) &\le \mu_{\sigma(\tau_1)} \cdots \mu_{\sigma(\tau_{N_{\sigma(k_0,k_0+k)}})} \left(\alpha_{\sigma(k+k_0)}+1\right)^{m_1} \cdots \\ &\left(\alpha_{\sigma(k_0)}+1\right)^{m_{N_{\sigma(k_0,k+k_0)}}} V_{\sigma(k_0)}(k_0), \end{aligned} \tag{33}$$

where $m_1 + \cdots + m_{N_{\sigma(k_0,k+k_0)}} = k$.

By $-1 < \alpha_i < 0$, for all $i \in \overline{N}$, we know that there exists $\alpha \triangleq \max_{i\in\overline{N}}\{\alpha_i+1\} \in (0,1)$. Let $\mu = \max_{i\in\overline{N}}\{\mu_i\}$; from (33), one obtains

$$V_i(k+k_0) \le \alpha^k \mu^{N_\sigma} V_j(k_0) = \alpha^{k+N_\sigma(\ln\mu/\ln\alpha)} V_j(k_0). \tag{34}$$

By Definition 2, for any $k_0 < k$, it follows that

$$V_i(k) \le \alpha^{k+N_\sigma(\ln\mu/\ln\alpha)} V_j(k_0) \le \alpha^{k(1+(\ln\mu/T_a\ln\alpha))} V_j(k_0). \tag{35}$$

By the system LKF (7), there always exist two positive constants c_1, c_2 such that

$$c_1\|x(k)\|^2 \le V_i(k), \qquad V_i(k_0) \le c_2\|x(k_0)\|_s^2, \tag{36}$$

where

$$\begin{aligned} c_1 &= \min_{i\in\overline{N}} \{\lambda_{\min}(P_i)\}, \\ c_2 &= \max_{i\in\overline{N}} \left\{\lambda_{\max}(P_i) + \sum_{m=1}^{3} \left(\lambda_{\max}(Q_{im}) + \lambda_{\max}(R_{im})\right)\right\}. \end{aligned} \tag{37}$$

Therefore,

$$\|x(k)\|^2 \le \frac{c_2}{c_1}\alpha^{k(1+(\ln\mu/T_a\ln\alpha))}\|x(k_0)\|_s^2. \tag{38}$$

If the average dwell time τ_a satisfies $\tau_a > -\ln\mu/\ln\alpha$ for $\mu \ge 1$, then the switched system (1) with $u(k) = 0$ is exponentially stable with $\lambda = \alpha^{1/2} = \max_{i\in\overline{N}}\{(\alpha_i+1)^{1/2}\} \in (0,1)$ stability degree. □

Remark 11. The case $\alpha = 0$ implies the asymptotic stability.

The following theorem provides exponential stability analysis with H_∞ performance of the system (1).

Theorem 12. *For given constants $\gamma > 0$, $\lambda > 0$ and $-1 < \alpha_i < 0$, if there exist positive definite symmetric matrices P_i, Q_{im}, R_{im} $(i \in \overline{N}, m = 1,2,3)$ and $\mu \ge 1$ such that* (29) *and the following LMIs hold:*

$$\begin{bmatrix} \Psi_{i11} & 0 & \Psi_{i13} \\ & -\gamma^2 I & \Psi_{i23} \\ & * & \Psi_{i33} \end{bmatrix} < 0, \tag{39}$$

$$\begin{bmatrix} \Phi_{i11} & 0 & \Phi_{i13} \\ & -\gamma^2 I & \Phi_{i23} \\ & * & \Phi_{i33} \end{bmatrix} < 0, \tag{40}$$

where

$$\Psi_{i13} = \begin{bmatrix} A_i^T P_i & (A_i - I)^T W_{1i}^T & C_i^T \\ A_{di}^T P_i & A_{di}^T W_{1i}^T & C_{di}^T \\ 0 & 0 & 0 \\ 0 & 0 & 0 \end{bmatrix},$$

$$\Phi_{i13} = \begin{bmatrix} A_i^T P_i & (A_i - I)^T W_{2i}^T & C_i^T \\ A_{di}^T P_i & A_{di}^T W_{2i}^T & C_{di}^T \\ 0 & 0 & 0 \\ 0 & 0 & 0 \end{bmatrix},$$

$$\Psi_{i33} = \operatorname{diag}\{-P_i \ \ -W_{1i} \ \ -I\},$$

$$\Phi_{i33} = \operatorname{diag}\{-P_i \ \ -W_{2i} \ \ -I\},$$

$$\Psi_{i23} = \begin{bmatrix} B_i^T P_i & B_i^T W_{1i}^T & D_i^T \end{bmatrix}, \qquad \Phi_{i23} = \begin{bmatrix} B_i^T P_i & B_i^T W_{2i}^T & D_i^T \end{bmatrix}. \tag{41}$$

Then, the system (1) *with average dwell time satisfies $\tau_a > -\ln\mu/\ln\alpha$ which is globally exponentially stable with convergence rate λ and H_∞ performance γ.*

Proof. Choose the LKF (7); the result is carried out by using the techniques employed for proving Lemma 7 and Theorem 10. If $d(k) \in [0, \vartheta]$, by (24), we have

$$\begin{aligned} &V_i(k+1) - \alpha V_i(k) + y^T(k)\,y(k) - \gamma^2 u^T(k)\,u(k) \\ &\quad \le x^T(k+1)\,P_i\,x(k+1) \\ &\qquad + z^T(k)\,W_i\,z(k) + y^T(k)\,y(k) \\ &\qquad + \zeta_1^T(k) \begin{bmatrix} \Psi_{i11} & 0 \\ 0 & -\gamma^2 \end{bmatrix} \zeta_1(k), \end{aligned} \tag{42}$$

where

$$\zeta_1^T(k) = \begin{bmatrix} \xi^T(k) & u^T(k) \end{bmatrix}. \tag{43}$$

If $d(k) \in [\vartheta, h]$, by (28), we have

$$\begin{aligned} &V_i(k+1) - \alpha V_i(k) + y^T(k)\,y(k) - \gamma^2 u^T(k)\,u(k) \\ &\quad \le x^T(k+1)\,P_i\,x(k+1) + z^T(k)\,W_i\,z(k) + y^T(k)\,y(k) \\ &\qquad + \zeta_1^T(k) \begin{bmatrix} \Phi_{i11} & 0 \\ 0 & -\gamma^2 \end{bmatrix} \zeta_1(k). \end{aligned} \tag{44}$$

Combining (39) and (40), by *Schur Complement*, one can obtain

$$V_i(k+1) - \alpha V_i(k) + y^T(k)\,y(k) - \gamma^2 u^T(k)\,u(k) \le 0. \tag{45}$$

Let

$$J(k) = y^T(k)\,y(k) - \gamma^2 u^T(k)\,u(k); \tag{46}$$

we have

$$V_i(k+1) \le \alpha V_i(k) - J(k). \tag{47}$$

By Definition 2 and Theorem 10, it is sufficient to show that $\sum_{k=0}^{\infty} J(k) < 0$ for any nonzero $u(k)$. Combining (35) and (47), it can be shown that

$$V_\sigma(k) \le \alpha^k \mu^{N_{\sigma(0,k)}} V_\sigma(0) - \sum_{s=0}^{k-1} \alpha^{k-s-1} \mu^{N_{\sigma(s,k)}} J(s). \tag{48}$$

Under the zero initial condition, we have

$$V(0) = 0, \quad V(\infty) \ge 0. \tag{49}$$

Combining (48), we have

$$\sum_{s=0}^{k-1} \alpha^{k-s-1} \mu^{N_{\sigma(s,k)}} J(s) = \sum_{s=0}^{k-1} \alpha^{-1} e^{\ln\alpha + \ln\mu/\tau_a} J(s) \le 0. \tag{50}$$

Now, we consider

$$\sum_{k=1}^{\infty}\sum_{s=0}^{k-1} \alpha^{-1} e^{\ln\alpha + \ln\mu/\tau_a} J(s). \tag{51}$$

Exchanging the double-sum region, by $\tau_a > -\ln\mu/\ln\alpha$ and $\alpha \in (0,1)$, one can easily get

$$\begin{aligned}
&\sum_{k=1}^{\infty}\sum_{s=0}^{k-1} \alpha^{-1} e^{\ln\alpha + \ln\mu/\tau_a} J(s) \\
&\quad = \sum_{s=0}^{\infty} J(s) \sum_{k=s+1}^{\infty} \alpha^{-1} e^{\ln\alpha + \ln\mu/\tau_a} \\
&\quad = \frac{e^{\ln\alpha + \ln\mu/\tau_a}\alpha^{-1}}{1 - e^{\ln\alpha + \ln\mu/\tau_a}} \sum_{s=1}^{\infty} J(s) \le 0,
\end{aligned} \tag{52}$$

which means that $\sum_{s=1}^{\infty} J(s) \le 0$. Then, by Definition 2, the system (1) with average dwell time satisfies $\tau_a > -\ln\mu/\ln\alpha$ which is globally exponentially stable with convergence rate λ and H_∞ performance γ. This completes the proof. □

If there exist some unstable subsystems in the switched system (1) with $u(k) = 0$, in this case, we need to estimate the growth rate of the system LKF in (7) along the state trajectory of switched system (1). And the corresponding $\alpha_j > 0$ ($j \in \overline{N}$). By using the techniques employed for proving Lemma 7, one can easily obtain the following Lemma.

Lemma 13. *Given constants $\alpha_j > 0$, $h > 0$ and $\vartheta \in (0,h)$, if there exist some symmetric positive definite matrices P_j, Q_{jm}, R_{jm} ($j \in \overline{N}$, $m = 1,2,3$) such that the following LMIs hold:*

$$\begin{bmatrix} \overline{\Psi}_{j11} & \Psi_{j12} \\ & \Psi_{j22} \end{bmatrix} < 0, \qquad \begin{bmatrix} \overline{\Phi}_{j11} & \Phi_{j12} \\ & \Phi_{j22} \end{bmatrix} < 0, \tag{53}$$

where

$$\overline{\Psi}_{j11} = \begin{bmatrix} \overline{\psi}_{11}^j & \overline{\psi}_{12}^j & 0 & 0 \\ & \overline{\psi}_{22}^j & \overline{\psi}_{23}^j & 0 \\ & * & \overline{\psi}_{33}^j & \overline{\psi}_{34}^j \\ & * & * & \overline{\psi}_{44}^j \end{bmatrix},$$

$$\overline{\Phi}_{j11} = \begin{bmatrix} \overline{\psi}_{11}^j & 0 & \overline{\phi}_{13}^j & 0 \\ & \overline{\phi}_{22}^j & \overline{\phi}_{23}^j & \overline{\phi}_{24}^j \\ & * & \overline{\phi}_{33}^j & 0 \\ & * & * & \overline{\psi}_{44}^j \end{bmatrix},$$

$$\overline{\psi}_{11}^j = -\left(1+\alpha_j\right)P_j + Q_{j1} + Q_{j3} - \frac{1}{\vartheta}\left(R_{j1} + R_{j3}\right),$$

$$\overline{\psi}_{12}^j = \frac{1}{\vartheta}\left(R_{j1} + R_{j3}\right), \qquad \overline{\psi}_{22}^j = -Q_{j3} - \frac{1}{\vartheta}\left(2R_{j1} + R_{j3}\right),$$

$$\overline{\psi}_{23}^j = \frac{1}{\vartheta}R_{j1}, \qquad \overline{\psi}_{34}^j = \frac{\left(1+\alpha_j\right)^{\vartheta}}{h-\vartheta}R_{j2},$$

$$\overline{\psi}_{33}^j = \left(1+\alpha_j\right)^{\vartheta}\left(Q_{j2} - Q_{j1}\right) - \frac{\left(1+\alpha_j\right)^{\vartheta}}{h-\vartheta}R_{j2} - \frac{1}{\vartheta}R_{j1},$$

$$\overline{\psi}_{44}^j = -\left(1+\alpha_j\right)^{h}Q_{j2} - \frac{\left(1+\alpha_j\right)^{\vartheta}}{h-\vartheta}R_{i2}, \qquad \overline{\phi}_{11}^j = \overline{\psi}_{11}^j,$$

$$\overline{\phi}_{13}^j = \frac{\left(1+\alpha_j\right)}{\vartheta}\left(R_{j1} + R_{j3}\right),$$

$$\overline{\phi}_{22}^j = -\left(1+\alpha_j\right)^{\vartheta}Q_{j3} - \frac{\left(1+\alpha_j\right)^{\vartheta}}{h-\vartheta}\left(2R_{j2} + R_{j3}\right),$$

$$\overline{\phi}_{23}^j = \frac{\left(1+\alpha_j\right)^{\vartheta}}{h-\vartheta}\left(R_{j2} + R_{j3}\right), \qquad \overline{\phi}_{24}^j = \frac{\left(1+\alpha_j\right)^{\vartheta}}{h-\vartheta}R_{j2},$$

$$\begin{aligned}
\overline{\phi}_{33}^j = &-\frac{\left(1+\alpha_j\right)^{\vartheta}}{h-\vartheta}\left(R_{j2} + R_{j3}\right) \\
&- \frac{\left(1+\alpha_j\right)}{\vartheta}\left(R_{j1} + R_{j3}\right) - \left(1+\alpha_j\right)^{\vartheta}\left(Q_{j1} - Q_{j2}\right).
\end{aligned} \tag{54}$$

Then, by means of LKF (7)*, along the trajectory of the systems* (1) *without disturbance input, one has*

$$\Delta V_j(k) = V_j(k+1) - V_j(k) \le \alpha_j V_j(k). \tag{55}$$

Remark 14. The proof of Lemma 13 is similar to that of Lemma 7 and is thus omitted here. Based on Lemmas 7 and 13, one can easily design the stabilizing switching law to guarantee the system (1) with $u(k) = 0$ to be exponentially stable, although some subsystems are unstable.

Without loss of generality, we can assume that $\overline{N}_u = \{j_1, j_2, \ldots, j_s\}$ is the set of all unstable subsystems and $\overline{N}_s = \{i_{s+1}, i_{s+2}, \ldots, i_p\}$ is the set of all stable subsystems. For simplicity, the LKF (7) is defined as $V_i(\alpha_i, k) \triangleq V_i(k)$. Choose the LKF $V_i(\alpha_i, k)$ $(-1 < \alpha_i < 0, i \in \overline{N}_s)$ for the stable subsystem and choose the LKF $V_j(\alpha_j, k)$ $(\alpha_j > 0, j \in \overline{N}_u)$ for the unstable subsystem. Then, we have the following conclusion.

Theorem 15. *If there exist some constants $-1 < \alpha_i < 0$, $\alpha_j > 0$ $(j \neq i, i \in \overline{N}_s,\ j \in \overline{N}_u)$ and positive definite symmetric matrices P_i, $Q_{im}, R_{im}, P_j, Q_{jm}, R_{jm}$ $(m = 1, 2, 3)$ and $\mu \geq 1$ such that Lemmas 7 and 13 and the following LMIs hold:*

$$P_l \leq \mu P_s, \quad Q_{lm} \leq \mu Q_{sm}, \quad R_{lm} \leq \mu R_{sm}, \quad \forall l, s \in \overline{N}. \tag{56}$$

Then, the switched system (1) *with $u(k) = 0$ and the average dwell time satisfies $\tau_a > \ln\mu/-\kappa$, $T^{\alpha}_{k_0,n+k_0}/T^{\beta}_{k_0,n+k_0} \geq (\ln\beta - \kappa)/(-\ln\alpha + \kappa)$, $\kappa \in (\ln\alpha, 0)$ which is exponentially stable.*

Proof. Consider the following LKF candidate:

$$V_{\sigma(k)}(k) = \begin{cases} V_i(\alpha_i, k), & \sigma(k) = i \in \overline{N}_s, \\ V_j(\alpha_j, k), & \sigma(k) = j \in \overline{N}_u. \end{cases} \tag{57}$$

By Lemmas 7 and 13, we have

$$V_{\sigma(k+1)}(k+1) \leq (\alpha_{\sigma(k+1)} + 1) V_{\sigma(k+1)}(k). \tag{58}$$

Let $T^{\alpha}_{k_0,n+k_0}$ be the total activity time in which all subsystems satisfied $0 > \alpha_i > -1$ on the interval $(k_0, n + k_0)$ and $T^{\beta}_{k_0,n+k_0} \triangleq n - T^{\alpha}_{k_0,n+k_0}$ the total activity time in which all subsystems satisfied $\alpha_j > 0$ on the interval $(k_0, n + k_0)$. By using the techniques employed for proving Theorem 10, combining (56) and (58), we derive that

$$\begin{aligned} &V_{\sigma(n+k_0)}(n + k_0) \\ &\leq \mu^{N_{\sigma(n+k_0)}} \alpha^{T^{\alpha}_{k_0,n+k_0}} \beta^{T^{\beta}_{k_0,n+k_0}} V_{\sigma(k_0)}(k_0) \\ &= e^{T^{\alpha}_{k_0,n+k_0} \ln\alpha + T^{\beta}_{k_0,n+k_0} \ln\beta + N_{\sigma(k_0,n+k_0)} \ln\mu} V_{\sigma(k_0)}(k_0), \end{aligned} \tag{59}$$

where

$$\alpha \triangleq \max_{i \in \overline{N}_s} \{\alpha_i + 1\} \in (0, 1), \qquad \beta \triangleq \max_{j \in \overline{N}_u} \{\alpha_j + 1\} > 1. \tag{60}$$

By $T^{\alpha}_{k_0,n+k_0}/T^{\beta}_{k_0,n+k_0} \geq (\ln\beta - \kappa)/(-\ln\alpha + \kappa)$, $\kappa \in (\ln\alpha, 0)$, one obtains

$$T^{\alpha}_{k_0,n+k_0} \ln\alpha + T^{\beta}_{k_0,n+k_0} \ln\beta \leq \kappa n. \tag{61}$$

So we have

$$V_{\sigma(n+k_0)}(n + k_0) \leq e^{\kappa n + N_{\sigma(k_0,n+k_0)} \ln\mu} V_{\sigma(k_0)}(k_0). \tag{62}$$

By Definition 2, for any $n + k_0 > k_0$, it follows that

$$\begin{aligned} V_{\sigma(n+k_0)}(n + k_0) &\leq e^{\kappa n + N_{\sigma(k_0,n+k_0)} \ln\mu} V_{\sigma(k_0)}(k_0) \\ &\leq e^{n(\kappa + (\ln\mu/\tau_a))} V_{\sigma(k_0)}(k_0). \end{aligned} \tag{63}$$

By $\tau_a > \ln\mu/-\kappa$, we have $\lim_{k\to\infty} V_{\sigma}(k) = 0$. Moreover, the overall system is exponentially stable. This completes the proof. □

Remark 16. From the proof of Theorem 15, one can see that the obtained exponential stability for the switched system (1) with $u(k) = 0$ is exponential stable with $e^{-1/2}$ stability degree. In order to get a free decay rate, we can replace the condition $\tau_a > \ln\mu/-\kappa$, $T^{\alpha}_{k_0,n+k_0}/T^{\beta}_{k_0,n+k_0} \geq (\ln\beta - \kappa)/(-\ln\alpha + \kappa)$, $\kappa \in (\ln\alpha, 0)$ by $\tau_a > \log^{\mu}_{\epsilon}/-\kappa$, $T^{\alpha}_{k_0,n+k_0}/T^{\beta}_{k_0,n+k_0} \geq (\log^{\beta}_{\epsilon} - \kappa)/(-\log^{\alpha}_{\epsilon} + \kappa)$, $\kappa \in (\log^{\alpha}_{\epsilon}, 0)$, $\epsilon > 1$; then the switched system (1) with $u(k) = 0$ is exponentially stable with $\epsilon^{-1/2}$ stability degree.

Theorem 17. *For given constants $\gamma > 0$, $-1 < \alpha_i < 0$, $\alpha_j > 0$ $(j \neq i,\ i \in \overline{N}_s,\ j \in \overline{N}_u)$, if there exist positive definite symmetric matrices P_i, $Q_{im}, R_{im}, P_j, Q_{jm}, R_{jm}$ $(m = 1, 2, 3)$ and $\mu \geq 1$ such that* (56), (39), (40)*, and the following LMIs hold:*

$$\begin{bmatrix} \overline{\Psi}_{j11} & 0 & \Psi_{j13} \\ & -\gamma^2 I & \Psi_{j23} \\ & * & \Psi_{j33} \end{bmatrix} 0, \qquad \begin{bmatrix} \overline{\Phi}_{j11} & 0 & \Phi_{j13} \\ & -\gamma^2 I & \Phi_{j23} \\ & * & \Phi_{j33} \end{bmatrix} < 0, \tag{64}$$

and $T^{\alpha}_{k_0,n+k_0}/T^{\beta}_{k_0,n+k_0} \geq (\ln\beta - \kappa)/(-\ln\alpha + \kappa)$, $\kappa \in (\ln\alpha, 0)$, and the average dwell time satisfies $\tau_a > \ln\mu/-\kappa$; then the switched system (1) *is exponentially stable and with H_∞ performance γ.*

Remark 18. The proof of Theorem 17 is similar to that of Theorems 12 and 15 and is thus omitted here.

4. H_∞ Model Reduction

In this section, we will approximate system (1) by a reduced-order switched system described by

$$\begin{aligned} \widehat{x}(k+1) &= A_{ri}\widehat{x}(k) + A_{rdi}\widehat{x}(k - d(k)) + B_{ri}u(k), \\ \widehat{y}(k) &= C_{ri}\widehat{x}(k) + C_{rdi}\widehat{x}(k - d(k)) + D_{ri}u(k), \end{aligned} \tag{65}$$

where $\widehat{x}(k) \in R^q$ is the state vector of the reduced-order system with $q < n$ and $\widehat{y}(k) \in R^m$ is the output of reduced-order system. $A_{ri}, A_{rdi}, C_{ri}, C_{rdi}, B_{ri}$, and D_{ri} are the matrices with compatible dimensions to be determined. The system (65) is assumed to be switched synchronously by switching signal $\sigma(k)$ in system (1).

Augmenting the model of system (1) to include the states of (65), we can obtain the error system as follows:

$$\begin{aligned}\widetilde{x}(k+1) &= \widetilde{A}_i\widetilde{x}(k) + \widetilde{A}_{di}\widetilde{x}(k-d(k)) + \widetilde{B}_i u(k),\\ \widetilde{e}(k) &= \widetilde{C}_i\widetilde{x}(k) + \widetilde{C}_{di}\widetilde{x}(k-d(k)) + \widetilde{D}_i u(k).\end{aligned} \tag{66}$$

Here

$$\begin{aligned}\widetilde{A}_i &= \begin{bmatrix} A_i & 0 \\ 0 & A_{ri}\end{bmatrix}, \qquad \widetilde{A}_{di} = \begin{bmatrix} A_{di} & 0 \\ 0 & A_{rdi}\end{bmatrix},\\ \widetilde{B}_i &= \begin{bmatrix} B_i \\ B_{ri}\end{bmatrix}, \qquad \widetilde{x}(k) = \begin{bmatrix} x(k) \\ \widehat{x}(k)\end{bmatrix},\\ \widetilde{C}_i &= \begin{bmatrix} C_i & -C_{ri}\end{bmatrix}, \qquad \widetilde{C}_{di} = \begin{bmatrix} C_{di} & -C_{rdi}\end{bmatrix},\\ \widetilde{D}_i &= D_i - D_{rdi}, \qquad \widetilde{e}(k) = y(k) - \widehat{y}(k).\end{aligned} \tag{67}$$

The following theorem gives a sufficient condition for the existence of an admissible H_∞ reduced-order model (65) for system (1).

Theorem 19. *Given constants $0 < \alpha < 1$, $\gamma > 0$, $\mu \geq 1$, $h > 0$, and ϑ $(0 < \vartheta < h)$, if there exist some symmetric positive definite matrices $\widetilde{P}_i, \widetilde{Q}_{im}, \widetilde{R}_{im}$ $(m = 1, 2, 3)$ and matrices X_i, Y_i, L_i, H_i, F_i $(i \in \overline{N})$ such that the following LMIs hold*

$$\begin{bmatrix} \Pi_{i1} & \Pi_{i2} \\ * & \Pi_{i3}\end{bmatrix} < 0, \tag{68}$$

$$\begin{bmatrix} \overline{\Pi}_{i1} & \Pi_{i2} \\ * & \overline{\Pi}_{i3}\end{bmatrix} < 0, \tag{69}$$

$$\widetilde{P}_i \leq \mu\widetilde{P}_j, \quad \widetilde{Q}_{im} \leq \mu\widetilde{Q}_{jm}, \quad \widetilde{R}_{im} \leq \mu\widetilde{R}_{jm}, \quad \forall i, j \in \overline{N}. \tag{70}$$

Then system (66) *with the average dwell time τ_a satisfies $\tau_a > -\ln\mu/\ln\alpha$ which is exponentially stable with an H_∞ norm bound γ.*

Here

$$\Pi_{i1} = \begin{bmatrix} \varphi_{11}^i & \varphi_{12}^i & 0 & 0 & 0 \\ & \varphi_{22}^i & \varphi_{23}^i & 0 & 0 \\ & * & \varphi_{33}^i & \varphi_{34}^i & 0 \\ & * & * & \varphi_{44}^i & 0 \\ & * & * & * & \varphi_{55}^i \end{bmatrix},$$

$$\overline{\Pi}_{i1} = \begin{bmatrix} \varphi_{11}^i & 0 & \overline{\varphi}_{13}^i & 0 & 0 \\ & \overline{\varphi}_{22}^i & \overline{\varphi}_{23}^i & \overline{\varphi}_{24}^i & 0 \\ & * & \overline{\varphi}_{33}^i & 0 & 0 \\ & * & * & \varphi_{44}^i & 0 \\ & * & * & * & \varphi_{55}^i \end{bmatrix},$$

$$\Pi_{i2} = \begin{bmatrix} \varphi_{i16}^T & \varphi_{i17}^T & \varphi_{i18}^T \\ \varphi_{i26}^T & \varphi_{i27}^T & \varphi_{i28}^T \\ 0 & 0 & 0 \\ 0 & 0 & 0 \\ \varphi_{i56}^T & \varphi_{i57}^T & \varphi_{i58}^T \end{bmatrix},$$

$$\Pi_{i3} = \operatorname{diag}\left\{\widetilde{P}_i - 2\widetilde{U}_i \;\; \widetilde{W}_i - 2\widetilde{U}_i \;\; -I\right\},$$

$$\overline{\Pi}_{i3} = \operatorname{diag}\left\{\widetilde{P}_i - 2\widetilde{U}_i \;\; \widehat{W} - 2\widetilde{U}_i \;\; -I\right\},$$

$$\varphi_{11}^i = \widetilde{Q}_{i1} + \widetilde{Q}_{i3} - \alpha\widetilde{P} - \frac{\alpha^\vartheta}{\vartheta}\left(\widetilde{R}_{i1} + \widetilde{R}_{i3}\right),$$

$$\varphi_{12}^i = \frac{\alpha^\vartheta}{\vartheta}\left(\widetilde{R}_{i1} + \widetilde{R}_{i3}\right), \qquad \varphi_{22}^i = -\alpha^\vartheta\widetilde{Q}_{i3} - \frac{\alpha^\vartheta}{\vartheta}\left(2\widetilde{R}_{i1} + \widetilde{R}_{i3}\right),$$

$$\varphi_{23}^i = \frac{\alpha^\vartheta}{\vartheta}\widetilde{R}_{i1}, \qquad \varphi_{34}^i = \frac{\alpha^h}{h-\vartheta}\widetilde{R}_{i2},$$

$$\varphi_{33}^i = \alpha^\vartheta\left(\widetilde{Q}_{i2} - \widetilde{Q}_{i1}\right) - \frac{\alpha^h}{h-\vartheta}\widetilde{R}_{i2} - \frac{\alpha^\vartheta}{\vartheta}\widetilde{R}_{i1},$$

$$\varphi_{44}^i = -\alpha^h\widetilde{Q}_{i2} - \frac{\alpha^h}{h-\vartheta}\widetilde{R}_{i2},$$

$$\varphi_{55}^i = -\gamma^2 I, \qquad \overline{\varphi}_{13}^i = \varphi_{12}^i,$$

$$\overline{\varphi}_{22}^i = -\alpha^h\widetilde{Q}_{i3} - \frac{\alpha^h}{h-\vartheta}\left(2\widetilde{R}_{i2} + \widetilde{R}_{i3}\right),$$

$$\overline{\varphi}_{23}^i = \frac{\alpha^h}{h-\vartheta}\left(\widetilde{R}_{i2} + \widetilde{R}_{i3}\right), \qquad \overline{\varphi}_{24}^i = \varphi_{34}^i,$$

$$\overline{\varphi}_{33} = \alpha^\vartheta\left(\widetilde{Q}_{i2} - \widetilde{Q}_{i1}\right) - \frac{\alpha^\vartheta}{\vartheta}\left(\widetilde{R}_{i1} + \widetilde{R}_{i3}\right) - \frac{\alpha^h}{h-\vartheta}\left(\widetilde{R}_{i2} + \widetilde{R}_{i3}\right),$$

$$\widetilde{W}_i = (h-\vartheta)\widetilde{R}_{i2} + \vartheta\widetilde{R}_{i1} + \vartheta\widetilde{R}_{i3},$$

$$\widehat{W}_i = (h-\vartheta)\widetilde{R}_{i2} + \vartheta\widetilde{R}_{i1} + h\widetilde{R}_{i3},$$

$$\varphi_{i16}^T = \begin{bmatrix} A_i^T X_i^T & A_i^T E^T Y_i \\ 0 & L_i^T \end{bmatrix},$$

$$\varphi_{i17}^T = \begin{bmatrix} A_i^T X_i^T - X_i^T & A_i^T E^T Y_i - E^T Y \\ 0 & L_i^T - Y_i^T \end{bmatrix},$$

$$\varphi_{i18}^T = \begin{bmatrix} C_i^T \\ -C_{ri}^T \end{bmatrix},$$

$$\varphi_{i26}^T = \varphi_{i27}^T = \begin{bmatrix} A_{id}^T X_i^T & A_{id}^T E^T Y_i \\ 0 & H_i^T \end{bmatrix},$$

$$\varphi_{i28}^T = \begin{bmatrix} C_{di}^T \\ -C_{rdi}^T \end{bmatrix},$$

$$\varphi_{i56} = \varphi_{i57} = \begin{bmatrix} X_i B_i \\ F_i + Y_i^T E B_i \end{bmatrix},$$

$$\varphi_{i58} = D_i - D_{rdi}. \tag{71}$$

Furthermore, if a feasible solution to the above LMIs (68), (69), *and* (70) *exists, then the system matrices of an admissible H_∞ reduced-order model in the form of* (65) *are given by*

$$A_{ri} = Y_i^{-1}L_i, \qquad A_{rdi} = Y_i^{-1}H_i, \qquad B_{ri} = Y_i^{-1}F_i. \tag{72}$$

Proof. Consider the following LKF for the switched system (66):

$$V_i(k) = V_{i1}(k) + V_{i2}(k) + V_{i3}(k). \tag{73}$$

Here

$$\begin{aligned}
V_{i1}(k) &= \tilde{x}^T(k)\,\widetilde{P}_i\tilde{x}(k),\\
V_{i2}(k) &= \sum_{s=k-\vartheta}^{k-1}\alpha^{k-1-s}\tilde{x}^T(s)\,\widetilde{Q}_{i1}\tilde{x}(s)\\
&\quad+\sum_{s=k-h}^{k-\vartheta-1}\alpha^{k-1-s}\tilde{x}^T(s)\,\widetilde{Q}_{i2}\tilde{x}(s)\\
&\quad+\sum_{s=k-d(k)}^{k-1}\alpha^{k-1-s}\tilde{x}^T(s)\,\widetilde{Q}_{i3}\tilde{x}(s),\\
V_{i3}(k) &= \sum_{\theta=-\vartheta}^{-1}\sum_{s=k+\theta}^{k-1}\alpha^{k-1-s}\tilde{z}^T(s)\,\widetilde{R}_{i1}\tilde{z}(s)\\
&\quad+\sum_{\theta=-h}^{-\vartheta-1}\sum_{s=k+\theta}^{k-1}\alpha^{k-1-s}\tilde{z}^T(s)\,\widetilde{R}_{i2}\tilde{z}(s)\\
&\quad+\sum_{\theta=-d(k)}^{-1}\sum_{s=k+\theta}^{k-1}\alpha^{k-1-s}\tilde{z}^T(s)\,\widetilde{R}_{i3}\tilde{z}(s),
\end{aligned} \tag{74}$$

where $\tilde{z}(k) = \tilde{x}(k+1) - \tilde{x}(k)$ and $\widetilde{P}_i, \widetilde{Q}_{im}, \widetilde{R}_{im}$ ($i \in \overline{N}$, $m = 1,2,3$) are symmetric positive definite matrices with appropriate dimensions; integer ϑ and α are given constants.

By using the techniques employed for proving Lemma 7, one can easily obtain the result. Calculate the difference of $V_i(k)$ in (73) along the state trajectory of system (66).

(1) If $d(k) \in [0, \vartheta]$, it gets

$$\begin{aligned}
&V_i(k+1) - \alpha V_i(k) + \tilde{e}^T(k)\,\tilde{e}(k) - \gamma^2 u^T(k)\,u(k)\\
&\quad\le \tilde{\xi}^T(k)\,\Pi_{i1}\tilde{\xi}(k)\\
&\qquad+\tilde{x}^T(k+1)\,\widetilde{P}_i\tilde{x}(k+1)\\
&\qquad+z^T(k)\,\widetilde{W}_i z(k) + \tilde{e}^T(k)\,\tilde{e}(k),
\end{aligned} \tag{75}$$

where

$$\begin{aligned}
&\tilde{\xi}^T(k)\\
&= \left[\tilde{x}^T(k)\ \ \tilde{x}^T(k-d(k))\ \ \tilde{x}^T(k-\vartheta)\ \ \tilde{x}^T(k-h)\ \ u^T(k)\right].
\end{aligned} \tag{76}$$

For any appropriately dimensioned matrices $\widetilde{P}_i > 0$ and nonsingular matrices $\widetilde{U}_i$, we have

$$\left(\widetilde{P}_i - \widetilde{U}_i\right)^T\widetilde{P}_i^{-1}\left(\widetilde{P}_i - \widetilde{U}_i\right) \ge 0. \tag{77}$$

Thus

$$-\widetilde{U}_i^T\widetilde{P}_i^{-1}\widetilde{U}_i \le \widetilde{P}_i - 2\widetilde{U}_i. \tag{78}$$

If (68) holds, we have

$$\begin{bmatrix}\Pi_{i1} & \Pi_{i2}\\ & \Theta_{i3}\end{bmatrix} < 0, \tag{79}$$

where

$$\Theta_{i3} = \operatorname{diag}\left\{-\widetilde{U}_i^T\widetilde{P}_i^{-1}\widetilde{U}_i\ \ \widetilde{U}_i^T\widetilde{W}_i^{-1}\widetilde{U}_i\ \ -I\right\}. \tag{80}$$

Let

$$\begin{aligned}
&\widetilde{U}_i = \begin{bmatrix}X_i & 0\\ Y_i^T E & Y_i\end{bmatrix}, \qquad E = \begin{bmatrix}I & 0\end{bmatrix},\\
&Y_i A_{ri} = L_i, \qquad Y_i A_{rdi} = H_i, \qquad Y_i B_{ri} = F_i.
\end{aligned} \tag{81}$$

Multiplying (79) both from left and right by $\operatorname{diag}\left\{0\ 0\ 0\ 0\ 0\ \widetilde{U}_i^{-T}\ \widetilde{U}_i^{-T}\ -I\right\}$, by Schur Complement, further, considering (75), one can infer

$$V_i(k+1) - \alpha V_i(k) + \tilde{e}^T(k)\,\tilde{e}(k) - \gamma^2 u^T(k)\,u(k) \le 0. \tag{82}$$

Similarly, for the case of $d(k) \in [\vartheta, h]$, the fact that (69) holds means that (82) is true. Set

$$\Gamma(k) = \tilde{e}^T(k)\,\tilde{e}(k) - \gamma^2 u^T(k)\,u(k), \tag{83}$$

we have

$$V_i(k+1) \le \alpha V_i(k) - \Gamma(k). \tag{84}$$

Let $N_{\sigma(k_0,k)}$ be the number of switching times in (k_0, k). From (84) and (70), we can obtain

$$\begin{aligned}
V_i(k+k_0) &\le \alpha^k\mu^{N_{\sigma(k_0,k)}}V_i(k_0)\\
&\quad-\sum_{s=k_0}^{k-1}\alpha^{k-s-1}\mu^{N_{\sigma(s,k)}}\Gamma(s)\\
&\le \alpha^{k+N_{\sigma(k_0,k)}(\ln\mu/\ln\alpha)}V_j(k_0)\\
&\quad-\sum_{s=k_0}^{k-1}\alpha^{k-s-1+N_{\sigma(s,k)}(\ln\mu/\ln\alpha)}\mu^{N_{\sigma(s,k)}}\Gamma(s).
\end{aligned} \tag{85}$$

Assume the zero disturbances input $u(k) = 0$ to the state equation of system (66). By Definition 2, for any $k_0 < k$, it follows that

$$V_i(k) \le \alpha^{k+N_\sigma(\ln\mu/\ln\alpha)}V_j(k_0) \le \alpha^{k(1+(\ln\mu/\tau_a\ln\alpha))}V_j(k_0). \tag{86}$$

From $\tau_a > -\ln\mu/\ln\alpha$, one obtains $\lim_{k\to\infty}V_i(k) = 0$. There exist $c_n > 0$, $n = 1,2$, such that

$$c_1\|\tilde{x}(k)\|^2 \le V_i(k), \qquad V_i(k_0) \le c_2\|\tilde{x}(k_0)\|_s^2. \tag{87}$$

Here

$$\begin{aligned}
&\|\tilde{x}(k)\|_s = \max_{\theta=-h,\dots,0}\|\tilde{x}(k+\theta)\|, \qquad c_1 = \lambda_{\min}(P_i),\\
&c_2 = \lambda_{\max}(P_i) + \sum_{k=1}^{3}\left(\lambda_{\max}(Q_{ik}) + \lambda_{\max}(R_{ik})\right).
\end{aligned} \tag{88}$$

Therefore

$$\|\tilde{x}(k)\|^2 \le \frac{c_2}{c_1}\alpha^{k(1+(\ln\mu/\tau_a\ln\alpha))}\|\tilde{x}(k_0)\|_s^2. \tag{89}$$

If the average dwell time τ_a satisfies $\tau_a > -\ln\mu/\ln\alpha$, then the switched system (66) is exponentially stable with $\lambda = \alpha^{1/2}$ stability degree. For any nonzero $u(k) \in l_2[0,\infty)$, under zero initial condition, combining (68), (69), (70), (85), and (89), one can easily obtain

$$J = \sum_{k=0}^{\infty} \left[\widetilde{e}^T(k)\,\widetilde{e}(k) - \gamma^2 u^T(k)\,u(k)\right] \le 0. \tag{90}$$

Therefore $\|\widetilde{e}(k)\|_2 \le \gamma\|u(k)\|_2$. This completes the proof. □

Remark 20. Recently, authors in [30, 31] have studied the problem of model reduction for discrete-time switched systems. In those papers, time delays are not taken into account. However, in most of the cases in engineering problems, there always exist unknown time-varying delays; moreover, the case of stable and unstable subsystems co exists. Motivated by this, in this paper, we discussed the problem of H_∞ model reduction for switched linear discrete-time systems with time-varying delays via delay decomposition approach [10–12]. Accordingly, numerical results are given for time-varying delay cases.

If there exist some unstable subsystems in the switched system (1), we have the following conclusion.

Theorem 21. *Given constants $0 < \alpha < 1$, $\beta > 1$, $\gamma > 0$, $\mu \ge 1$, $h > 0$, and ϑ $(0 < \vartheta < h)$, if there exist some symmetric positive definite matrices $\widetilde{P}_i, \widetilde{Q}_{im}, \widetilde{R}_{im}$ $(m = 1,2,3)$ and matrices X_i, Y_i, L_i, H_i, F_i $(i \in \overline{N})$ such that* (68), (69), (70), *and the following LMIs hold:*

$$\begin{bmatrix} \widetilde{\Pi}_{i1} & \Pi_{i2} \\ * & \Pi_{i3} \end{bmatrix} < 0,$$
$$\begin{bmatrix} \widehat{\Pi}_{i1} & \Pi_{i2} \\ * & \overline{\Pi}_{i3} \end{bmatrix} < 0. \tag{91}$$

And $T^{\alpha}_{k_0,n+k_0}/T^{\beta}_{k_0,n+k_0} \ge (\ln\beta - \kappa)/(-\ln\alpha + \kappa)$, $\kappa \in (\ln\alpha, 0)$; then system (66) *with the average dwell time τ_a satisfies $\tau_a > -\ln\mu/\ln\alpha$ which is exponentially stable with an H_∞ norm bound γ. Furthermore, if a feasible solution to the above LMIs* (68), (69), (70), *and* (91) *exists, then the system matrices of an admissible H_∞ reduced-order model in the form of* (65) *are given by* (72).

Here,

$$\widetilde{\Pi}_{i1} = \begin{bmatrix} \widetilde{\varphi}^i_{11} & \widetilde{\varphi}^i_{12} & 0 & 0 & 0 \\ & \widetilde{\varphi}^i_{22} & \widetilde{\varphi}^i_{23} & 0 & 0 \\ & * & \widetilde{\varphi}^i_{33} & \widetilde{\varphi}^i_{34} & 0 \\ & * & * & \widetilde{\varphi}^i_{44} & 0 \\ & * & * & * & \widetilde{\varphi}^i_{55} \end{bmatrix},$$

$$\widehat{\Pi}_{i1} = \begin{bmatrix} \widetilde{\varphi}^i_{11} & 0 & \widetilde{\varphi}^i_{13} & 0 & 0 \\ & \widetilde{\varphi}^i_{22} & \widetilde{\varphi}^i_{23} & \widetilde{\varphi}^i_{24} & 0 \\ & * & \widehat{\varphi}^i_{33} & 0 & 0 \\ & * & * & \widetilde{\varphi}^i_{44} & 0 \\ & * & * & * & \widetilde{\varphi}^i_{55} \end{bmatrix},$$

$$\widetilde{\varphi}^i_{11} = \widetilde{Q}_{i1} + \widetilde{Q}_{i3} - \beta\widetilde{P} - \frac{1}{\vartheta}\left(\widetilde{R}_{i1} + \widetilde{R}_{i3}\right),$$

$$\widetilde{\varphi}^i_{12} = \frac{1}{\vartheta}\left(\widetilde{R}_{i1} + \widetilde{R}_{i3}\right), \qquad \widetilde{\varphi}^i_{22} = -\widetilde{Q}_{i3} - \frac{1}{\vartheta}\left(2\widetilde{R}_{i1} + \widetilde{R}_{i3}\right),$$

$$\widetilde{\varphi}^i_{23} = \frac{1}{\vartheta}\widetilde{R}_{i1}, \qquad \widetilde{\varphi}^i_{33} = \beta^{\vartheta}\left(\widetilde{Q}_{i2} - \widetilde{Q}_{i1}\right) - \frac{\beta^{\vartheta}}{h-\vartheta}\widetilde{R}_{i2} - \frac{1}{\vartheta}\widetilde{R}_{i1},$$

$$\widetilde{\varphi}^i_{34} = \frac{\beta^{\vartheta}}{h-\vartheta}\widetilde{R}_{i2}, \qquad \widetilde{\varphi}^i_{44} = -\beta^h\widetilde{Q}_{i2} - \frac{\beta^{\vartheta}}{h-\vartheta}\widetilde{R}_{i2},$$

$$\widetilde{\varphi}^i_{55} = -\gamma^2 I, \qquad \widetilde{\varphi}^i_{13} = \frac{\beta}{\vartheta}\left(\widetilde{R}_{i1} + \widetilde{R}_{i3}\right),$$

$$\widetilde{\varphi}^i_{22} = -\beta^{\vartheta}\widetilde{Q}_{i3} - \frac{\beta^{\vartheta}}{h-\vartheta}\left(2\widetilde{R}_{i2} + \widetilde{R}_{i3}\right),$$

$$\widetilde{\varphi}^i_{23} = \frac{\beta^{\vartheta}}{h-\vartheta}\left(\widetilde{R}_{i2} + \widetilde{R}_{i3}\right), \qquad \widehat{\varphi}^i_{24} = \frac{\beta^{\vartheta}}{h-\vartheta}\left(\widetilde{R}_{i2}\right),$$

$$\widehat{\varphi}^i_{33} = \beta^{\vartheta}\left(\widetilde{Q}_{i2} - \widetilde{Q}_{i1}\right) - \frac{\beta}{\vartheta}\left(\widetilde{R}_{i1} + \widetilde{R}_{i3}\right) - \frac{\beta^{\vartheta}}{h-\vartheta}\left(\widetilde{R}_{i2} + \widetilde{R}_{i3}\right). \tag{92}$$

Remark 22. The proof of Theorem 21 is carried out by using the techniques employed in the previous section and is thus omitted here.

5. Examples

In this section, we consider some numerical examples to illustrate the benefits of our results.

Example 1 (see [20]). Consider the discrete-time switched system (1) with $u(k) = 0$ and the following parameters:

$$A_1 = \begin{bmatrix} 0 & 0.3 \\ -0.2 & 0.1 \end{bmatrix}, \qquad A_{d1} = \begin{bmatrix} 0 & 0.1 \\ 0 & 0.2 \end{bmatrix},$$
$$A_2 = \begin{bmatrix} 0 & 0.3 \\ -0.2 & -0.1 \end{bmatrix}, \qquad A_{d2} = \begin{bmatrix} 0 & 0.1 \\ 0 & 0 \end{bmatrix}. \tag{93}$$

For this system, we choose $\mu = 1.1$ and $\lambda = 0.931$. Applying Theorem 10, by solving the LMIs (9) and (10) and (29), we can obtain the allowable delay upper bound $h = 20$. It is reported, with decay rate $\lambda = 0.931$, that the upper bound h can be obtained as 14 in [19] and 16 in [20]. Therefore, the result in this brief can indeed provide larger delay bounds than the results in [19, 20]. This supports the effectiveness of the proposed idea in Theorem 10 in reducing the conservatism of stability criteria.

Example 2. Consider the discrete-time switched system (1) with $u(k) = 0$ and parameters as follows:

$$A_1 = \begin{bmatrix} 0 & 0.3 \\ -0.2 & 0.1 \end{bmatrix}, \qquad A_{d1} = \begin{bmatrix} 0 & 0.1 \\ 0 & 0.2 \end{bmatrix},$$
$$A_2 = \begin{bmatrix} 0 & 0.3 \\ -0.2 & -0.1 \end{bmatrix}, \qquad A_{d2} = \begin{bmatrix} 1.3 & 0.1 \\ 0 & 0.9 \end{bmatrix}. \tag{94}$$

It is easy to check that the $A_2 + A_{d2}$ is unstable. In this case, we need to find a class of switching signals to guarantee

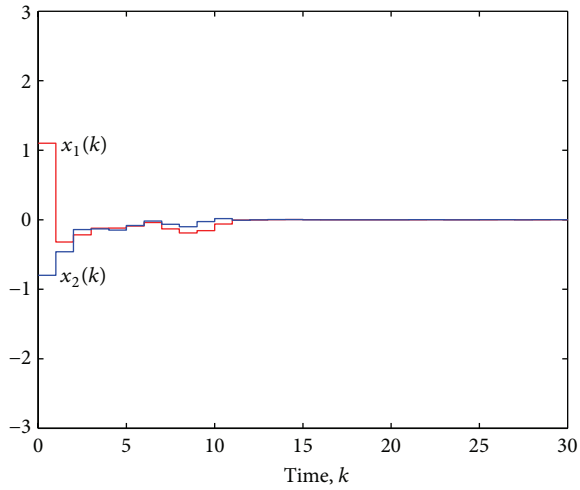

FIGURE 1: The state response.

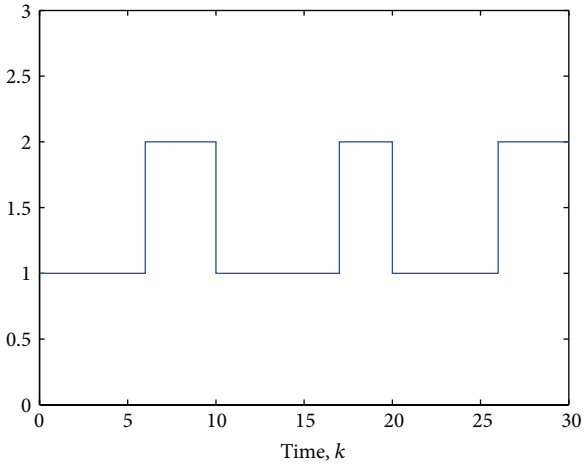

FIGURE 2: Switching law.

the overall switched system to be exponentially stable. Set $d(k) = [|3\sin(k\pi/6)|]$ and $\alpha = 0.5329$, according to Theorem 15 and by solving the LMIs (9), (10), (53), and (29), set $\vartheta = 1$; we have $\mu = 2.4$ and $\beta = 2.01$. Choosing $\gamma' = -0.18$, we have $T^{\alpha}_{k_0,n+k_0}/T^{\beta}_{k_0,n+k_0} \geq (\ln\beta - \gamma')/(-\ln\alpha + \gamma') = 1.953$ and $\tau_a > \ln\mu/-\gamma' = 4.9$. The simulation result of the switched system is shown in Figure 1, where the initial condition $\phi(\theta) = [1.1 \quad -0.8]^T$ and the switching law is shown in Figure 2. It can be seen from Figure 1 that the designed switching signals are effective although one subsystem is unstable. However, the results in [20] cannot find any feasible solution to guarantee the exponential stability of system (1).

Example 3 (see [31]). Consider the system (1) with parameters as follows:

$$A_1 = \begin{bmatrix} 0.13 & 0.22 & -0.13 & 0.08 \\ 0.05 & -0.03 & 0.19 & 0.06 \\ -0.07 & -0.05 & -0.04 & -0.12 \\ -0.17 & 0.21 & 0.03 & 0.28 \end{bmatrix},$$

$$A_2 = \begin{bmatrix} 0.11 & 0.22 & -0.13 & 0.08 \\ 0.05 & -0.03 & 0.15 & 0.06 \\ -0.07 & -0.03 & -0.04 & -0.12 \\ -0.17 & 0.21 & 0.03 & 0.2 \end{bmatrix},$$

$$A_{d1} = A_{d2} = \begin{bmatrix} 0.02 & 0.01 & 0 & 0 \\ 0 & 0.02 & 0 & 0 \\ 0 & 0 & 0.02 & 0.01 \\ 0 & 0 & 0 & 0.02 \end{bmatrix},$$

$$B_1 = [0.19 \quad -0.18 \quad 0.16 \quad -0.08]^T,$$

$$B_2 = [0.23 \quad -0.13 \quad 0.16 \quad -0.04]^T,$$

$$C_1 = C_2 = [1.2 \quad 0.5 \quad 0.03 \quad 0.28],$$

$$C_{d1} = C_{d2} = [0.02 \quad 0.05 \quad 0.01 \quad 0.09],$$

$$D_1 = D_2 = 0.1. \tag{95}$$

When the decay rate α is fixed, the maximum value of the time-delay h and the minimum value of the performance index γ can computed by solving the LMIs (68)–(70) procedure in Theorem 19, which is listed in Table 1 via different methods. Here, we choose $\mu = 1.001$. Assume that decay rate $\alpha = 0.9$; we can compute the maximum value of allowed delay $h = 42$ and the minimum value of the performance index $\gamma = 1.67$. From ADT $\tau_a > -\ln\mu/\ln\alpha$, we have $\tau_a > 0.0095$. When $h = 2$ and $\alpha = 0.9$, we can compute the minimum value of performance index $\gamma = 0.53$. On the other hand, assume that maximum allowed delay $h = 2$ and performance index $\gamma = 2$; we can compute the minimum value of the decay rate $\alpha = 0.59$ and $\tau_a > 0.0019$.

Let $\alpha = 0.9$; here, we are interested in designing a q-order ($q < 4$) system (65) and choose the ADT $\tau_a = 2$ switching signals such that the model error system (66) is exponentially stable with H_∞ norm bound $\gamma = 2$. By solving the corresponding LMIs (68)–(70) procedure in Theorem 19. For comparison with [31], we set the delay $d(k) = 2$, and the following reduced-order models can be given.

Third Order Model

$$A_{r1} = \begin{bmatrix} 0.2753 & 0.0282 & -0.0033 \\ 0.0097 & 0.2507 & -0.0033 \\ -0.0045 & -0.0124 & 0.2569 \end{bmatrix},$$

$$A_{r2} = \begin{bmatrix} 0.2799 & 0.0259 & -0.0058 \\ 0.0074 & 0.2581 & -0.0025 \\ -0.0051 & -0.01 & 0.2611 \end{bmatrix},$$

$$A_{rd1} = \begin{bmatrix} -0.005 & 0.0069 & -0.0023 \\ 0.0037 & -0.0046 & 0.003 \\ -0.0011 & 0.0002 & -0.0006 \end{bmatrix},$$

$$A_{rd2} = \begin{bmatrix} -0.001 & 0.0066 & -0.0025 \\ 0.0039 & -0.0044 & 0.0033 \\ -0.0018 & 0.001 & -0.0024 \end{bmatrix},$$

Table 1: Comparison of parameters via different methods.

	α	γ	h	τ_a
[31]	0.9	2	2	>1.7305
Theorem 19	0.9	1.67	42	>0.0095
Theorem 19	0.9	0.53	2	>0.0095
Theorem 19	0.59	2	2	>0.0019
Theorem 19	0.6	1.8	2	>0.002

$$
\begin{aligned}
B_{r1} &= \left[-0.171 \quad 0.1795 \quad -0.111\right]^T,\\
B_{r2} &= \left[-0.191 \quad 0.148 \quad -0.1285\right]^T,\\
C_{r1} &= \left[-0.3016 \quad -0.1328 \quad -0.0149\right],\\
C_{r2} &= \left[-0.2987 \quad -0.1265 \quad -0.0173\right],\\
D_{r1} &= -0.1754,\\
C_{rd1} &= \left[-0.0314 \quad -0.0047 \quad -0.0182\right],\\
C_{rd2} &= \left[-0.0361 \quad -0.0011 \quad -0.0199\right],\\
D_{r2} &= -0.2396.
\end{aligned}
\tag{96}
$$

Second Order Model

$$
\begin{aligned}
A_{r1} &= \begin{bmatrix} 0.2419 & 0.0355 \\ 0.015 & 0.2141 \end{bmatrix}, \quad A_{rd1} = \begin{bmatrix} -0.0028 & 0.0088 \\ 0.0052 & -0.007 \end{bmatrix},\\
B_{r1} &= \begin{bmatrix} -0.1528 \\ 0.1617 \end{bmatrix}, \quad C_{r1} = \begin{bmatrix} -0.3109 \\ -0.1453 \end{bmatrix}^T,\\
A_{r2} &= \begin{bmatrix} 0.2382 & 0.0324 \\ 0.0147 & 0.2183 \end{bmatrix}, \quad A_{rd2} = \begin{bmatrix} -0.0023 & 0.0076 \\ 0.0046 & -0.006 \end{bmatrix},\\
B_{r2} &= \begin{bmatrix} -0.1667 \\ 0.1203 \end{bmatrix}, \quad C_{r2} = \begin{bmatrix} -0.3076 \\ -0.1362 \end{bmatrix}^T,\\
C_{rd1} &= \left[-0.0488 \quad 0.0034\right], \quad D_{r1} = -0.2422,\\
C_{rd2} &= \left[-0.05 \quad 0.0057\right], \quad D_{r2} = -0.3605.
\end{aligned}
\tag{97}
$$

First Order Model

$$
\begin{aligned}
&A_{r1} = 0.2528, \quad A_{rd1} = -0.0057, \quad B_{r1} = -0.1498,\\
&C_{r1} = -0.2769, \quad C_{rd1} = 0.0301, \quad D_{r1} = -0.1792,\\
&A_{r2} = 0.2606, \quad A_{rd2} = -0.005, \quad B_{r2} = -0.1787,\\
&C_{r2} = -0.2851, \quad C_{rd2} = -0.04, \quad D_{r2} = -0.2624.
\end{aligned}
\tag{98}
$$

To illustrate the model reduction performances of the obtained reduced-order models, let the initial condition be zero; the exogenous input is given as $u(k) = 1.8\exp(-0.4k)$. The output errors between the original system and the corresponding three reduced models obtained in this paper (shown by the blue line) and the literature [31] (shown by the red line) are displayed in Figures 3, 4, and 5. The switching signal is shown in Figure 6. The simulation result of the switched system is shown in Figures 3–5. It can be seen from Figures 3–5 that the output errors between the original system and the reduced-order models obtained in this paper are smaller than that in [31].

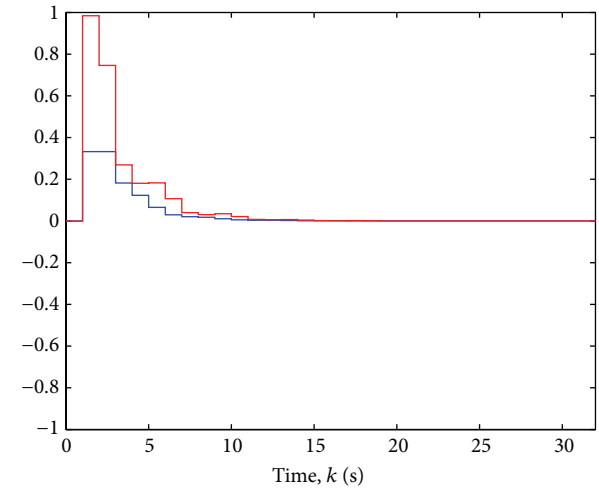

Figure 3: Output errors between the original system and the 3rd model.

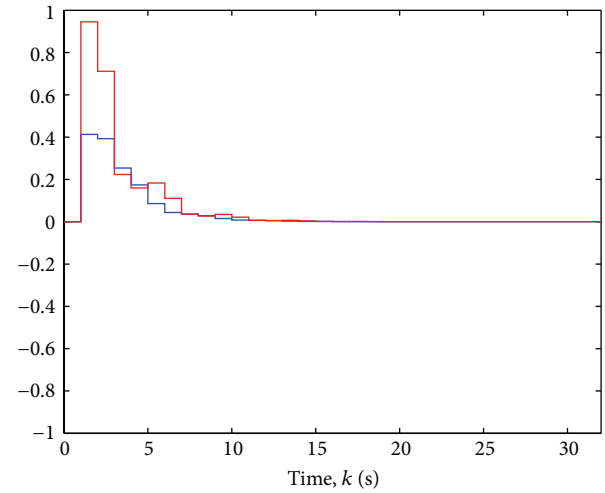

Figure 4: Output errors between the original system and the 2nd model.

6. Conclusions

The problem of exponential stability with H_∞ performance and H_∞ model reduction for a class of switched linear discrete-time systems with time-varying delay have been investigated in this paper. The switching law is given by ADT technique, such that even if one or more subsystem is unstable the overall switched system can still be exponentially stable. Sufficient conditions for the existence of the desired

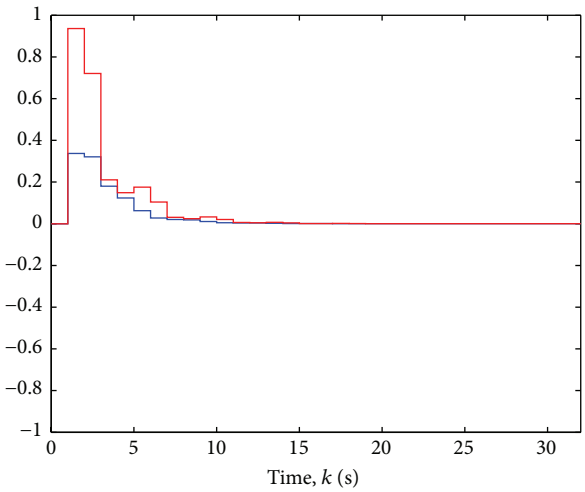

Figure 5: Output errors between the original system and the 1st model.

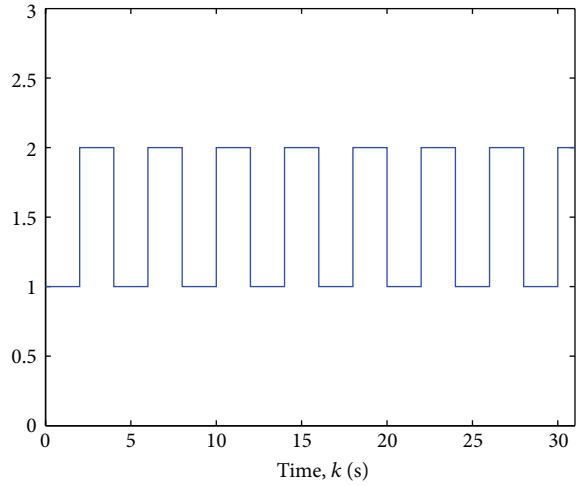

Figure 6: Switching law.

reduced-order model are derived and formulated in terms of strict LMIs. By solving the LMIs, the system of reduced-order model can be obtained, which also provides an H_∞ gain for the error system between the original system and the reduced-order model. Finally, numerical examples are provided to illustrate the effectiveness and less conservativeness of the proposed method. A potential extension of this method to nonlinear case deserves further research.

Conflict of Interests

The authors declare that there is no conflict of interests regarding the publication of this paper.

Acknowledgment

This work was supported by the National Natural Science Foundation of China under Grant no. 61104064 and no. 61174038.

References

[1] Z. Sun, *Stability Theory of Switched Dynamical Systems*, Springer, New York, NY, USA, 2011.

[2] D. Liberzon and A. S. Morse, "Basic problems in stability and design of switched systems," *IEEE Control Systems Magazine*, vol. 19, no. 5, pp. 59–70, 1999.

[3] H. Lin and P. J. Antsaklis, "Stability and stabilizability of switched linear systems: a survey of recent results," *IEEE Transactions on Automatic Control*, vol. 54, no. 2, pp. 308–322, 2009.

[4] A.-G. Wu, G. Feng, G.-R. Duan, and H. Gao, "Stabilising slow-switching laws for switched discrete-time linear systems," *IET Control Theory & Applications*, vol. 5, no. 16, pp. 1843–1858, 2011.

[5] J. K. Hale and S. M. Verduyn Lunel, *Introduction to Functional-Differential Equations*, vol. 99, Springer, New York, NY, USA, 1993.

[6] O. Arino, M. Lhassan Hbid, and E. Ait Dads, *Delay Differential Equations and Applications*, vol. 205, Springer, New York, NY, USA, 2006.

[7] V. L. Kharitonov, "Robust stability analysis of time delay systems: a survey," *Annual Reviews in Control*, vol. 23, pp. 185–196, 1999.

[8] X.-M. Zhang and Q.-L. Han, "A delay decomposition approach to delay-dependent stability for linear systems with time-varying delays," *International Journal of Robust and Nonlinear Control*, vol. 19, no. 17, pp. 1922–1930, 2009.

[9] S. B. Stojanovic et al., "Delay-dependent stability of discrete-time systems with time-varying delay: delay decomposition approach," With Emphasis on the Integration of Three Technologies, 214, 2012.

[10] P. Yan and H. Özbay, "Stability analysis of switched time delay systems," *SIAM Journal on Control and Optimization*, vol. 47, no. 2, pp. 936–949, 2008.

[11] Y. Song, J. Fan, M. Fei, and T. Yang, "Robust H_∞ control of discrete switched system with time delay," *Applied Mathematics and Computation*, vol. 205, no. 1, pp. 159–169, 2008.

[12] D.-W. Ding and G.-H. Yang, "H_∞ static output feedback control for discrete-time switched linear systems with average dwell time," *IET Control Theory & Applications*, vol. 4, no. 3, pp. 381–390, 2010.

[13] M. S. Branicky, "Multiple Lyapunov functions and other analysis tools for switched and hybrid systems," *IEEE Transactions on Automatic Control*, vol. 43, no. 4, pp. 475–482, 1998.

[14] G. Zhai, B. Hu, K. Yasuda, and A. N. Michel, "Disturbance attenuation properties of time-controlled switched systems," *Journal of the Franklin Institute*, vol. 338, no. 7, pp. 765–779, 2001.

[15] X.-M. Sun, J. Zhao, and D. J. Hill, "Stability and L_2-gain analysis for switched delay systems: a delay-dependent method," *Automatica*, vol. 42, no. 10, pp. 1769–1774, 2006.

[16] G. Zhai, B. Hu, K. Yasuda, and A. N. Michel, "Stability analysis of switched systems with stable and unstable subsystems: an average dwell time approach," *International Journal of Systems Science*, vol. 32, no. 8, pp. 1055–1061, 2001.

[17] X.-M. Sun, D. Wang, W. Wang, and G.-H. Yang, "Stability analysis and L_2-gain of switched delay systems with stable and unstable subsystems," in *Proceedings of the IEEE 22nd International Symposium on Intelligent Control (ISIC '07)*, pp. 208–213, October 2007.

[18] R. Chen and K. Khorasani, "Stability analysis of a class of switched time-delay systems with unstable subsystems," in *Proceedings of the IEEE International Conference on Control and Automation (ICCA '07)*, pp. 265–270, June 2007.

[19] W.-A. Zhang and L. Yu, "Stability analysis for discrete-time switched time-delay systems," *Automatica*, vol. 45, no. 10, pp. 2265–2271, 2009.

[20] J. Lin, S. Fei, and Z. Gao, "Stabilization of discrete-time switched singular time-delay systems under asynchronous switching," *Journal of the Franklin Institute*, vol. 349, no. 5, pp. 1808–1827, 2012.

[21] H. Gao, J. Lam, and C. Wang, "Model simplification for switched hybrid systems," *Systems & Control Letters*, vol. 55, no. 12, pp. 1015–1021, 2006.

[22] X. Shi, D.-W. Ding, X. Li, and Z. Shi, "Model reduction of discrete-time switched linear systems over finite-frequency ranges," *Nonlinear Dynamics*, vol. 71, no. 1-2, pp. 361–370, 2013.

[23] A. Birouche, B. Mourllion, and M. Basset, "Model order-reduction for discrete-time switched linear systems," *International Journal of Systems Science*, vol. 43, no. 9, pp. 1753–1763, 2012.

[24] B. C. Moore, "Principal component analysis in linear systems: controllability, observability, and model reduction," *IEEE Transactions on Automatic Control*, vol. 26, no. 1, pp. 17–32, 1981.

[25] K. Glover, "All optimal Hankel-norm approximations of linear multivariable systems and their L^{∞}-error bounds," *International Journal of Control*, vol. 39, no. 6, pp. 1115–1193, 1984.

[26] L. El Ghaoui, F. Oustry, and M. AitRami, "A cone complementarity linearization algorithm for static output-feedback and related problems," *IEEE Transactions on Automatic Control*, vol. 42, no. 8, pp. 1171–1176, 1997.

[27] F. Leibfritz, "A LMI-based algorithm for designing suboptimal static H_2/H_{∞} output feedback controllers," *SIAM Journal on Control and Optimization*, vol. 39, no. 6, pp. 1711–1735, 2001.

[28] S. Xu and J. Lam, "H_{∞} model reduction for discrete-time singular systems," *Systems & Control Letters*, vol. 48, no. 2, pp. 121–133, 2003.

[29] H. Gao, J. Lam, C. Wang, and S. Xu, "H_{∞} model reduction for discrete time-delay systems: delay-independent and dependent approaches," *International Journal of Control*, vol. 77, no. 4, pp. 321–335, 2004.

[30] L. Zhang, P. Shi, E.-K. Boukas, and C. Wang, "H_{∞} model reduction for uncertain switched linear discrete-time systems," *Automatica*, vol. 44, no. 11, pp. 2944–2949, 2008.

[31] Q. Liu, W. Wang, and D. Wang, "New results on model reduction for discrete-time switched systems with time delay," *International Journal of Innovative Computing, Information and Control*, vol. 8, no. 5, pp. 3431–3440, 2012.

[32] S. Boyd, L. El Ghaoui, E. Feron, and V. Balakrishnan, *Linear Matrix Inequalities in System and Control Theory*, vol. 15 of *Society for Industrial and Applied Mathematics*, 1987.

Hindawi Publishing Corporation
Mathematical Problems in Engineering
Volume 2013, Article ID 468168, 10 pages
http://dx.doi.org/10.1155/2013/468168

Research Article

Robust Distributed Model Predictive Load Frequency Control of Interconnected Power System

Xiangjie Liu,[1] Huiyun Nong,[1] Ke Xi,[1] and Xiuming Yao[2]

[1] *State Key Laboratory of Alternate Electrical Power System with Renewable Energy Sources, North China Electric Power University, Beijing 102206, China*
[2] *Department of Automation, North China Electric Power University, Baoding 071003, China*

Correspondence should be addressed to Xiangjie Liu; liuxj@ncepu.edu.cn

Received 10 August 2013; Accepted 20 September 2013

Academic Editor: Zhiguang Feng

Considering the load frequency control (LFC) of large-scale power system, a robust distributed model predictive control (RDMPC) is presented. The system uncertainty according to power system parameter variation alone with the generation rate constraints (GRC) is included in the synthesis procedure. The entire power system is composed of several control areas, and the problem is formulated as convex optimization problem with linear matrix inequalities (LMI) that can be solved efficiently. It minimizes an upper bound on a robust performance objective for each subsystem. Simulation results show good dynamic response and robustness in the presence of power system dynamic uncertainties.

1. Introduction

The load frequency control (LFC) has long been a much concerned research interest for power system engineers over the past forty years [1]. In modern power system, undesirable frequency and scheduled tie-line power changes in multiarea power system are a direct result of the imbalance between generated power and system demand plus associated system losses. The main objectives of the LFC are to keep the system frequency at the scheduled value and regulate the generator units to make the area control error tend to zero under the continuous adjustment of active power, so that the generation of the entire system and the load power well match.

In a practical power system, there exist different kinds of uncertainties, such as changes in parameter. And each control area contains various disturbances due to increased complexity, system modeling errors, and changing power system structure. Thus the robustness must be taken into theoretical consideration in the LFC design procedure to promise high power quality. A fixed controller based on classical theory is not very suitable for the LFC problem. It is necessary that a flexible controller should be developed [2–4]. Robust LFC was early designed based on the Riccati equation approach [5], which is simple and effective and can ensure the overall system to be asymptotically stable for all admissible uncertainties. Motivated by the large uncertainty in dynamic models of power system components and their interconnections, paper [6] proposes a physically motivated passivity objective as a means to achieve effective closed-loop control. Recently, robust LFC can be realized using linear matrix inequalities [7], fuzzy logic [8], neural networks [9], and genetic algorithms [10].

Model predictive control (MPC) has been an attracting method for power system LFC, which can perform an optimization procedure to calculate optimal control actions within the realistic power system constrains. In LFC research, there is the practical limit on the rate of change in the generating power, called the generation rate constraints (GRC), which can result in the LFC to be a constraint optimal problem. Traditional MPC is unable to explicitly incorporate plant uncertainty. Thus, robust MPC has been well developed recently [11, 12].

Most existing MPCs assume that all subsystems are identical, which is not the case of actual power systems. Subsequently, a number of decentralized/distributed load frequency controllers were developed to eliminate the above

drawback. In [13], the distributed model predictive control (DMPC) is used in LFC, which offers an effective means of achieving the desired controller coordination and performance improvements. A decentralized MPC framework for multiarea power system has been presented in [14]. Accordingly, the robustness of DMPC strategies to model errors has been identified as a key factor for the successful application of DMPC [15].

In this paper, a robust distributed MPC (RDMPC) strategy for load frequency control in interconnected power system is presented. The entire power system is composed of several subareas and the problem is formulated as convex optimization problem with linear matrix inequalities (LMI) that can be solved efficiently using the algorithm. The method shows good dynamic response and robustness in the presence of power system model dynamic uncertainties.

2. Mathematical Model of Power System

The interconnected power system consists of at least two control areas connected by tie lines. Usually the subsystem contains thermal power system, hydro power system, nuclear power system, and renewable power system, in which thermal power system and hydro power system generally participate in load frequency control. Figures 1 and 2 show, respectively, the structures of thermal power plant and hydro power plant in power system LFC. The original model has been given in [16]. Comparing to [16], the model in this article contains the reheater part, which is quite common in modern thermal power plant. Each control area has its own controller. The variables and parameters are given in Table 1.

When load change happens in one area, all the interconnected areas will be affected, and the controllers act to adjust the frequency deviation and tie-line active power to return to steady state. The LFC using RDMPC will be applied to the whole control areas.

The time-varying linearized mathematical model of thermal and hydro plant used in interconnected power system can be described as

$$\dot{\mathbf{x}}_i(t) = \mathbf{A}_{ii}(t)\,\mathbf{x}_i(t) + \sum_j \mathbf{A}_{ij}(t)\,\mathbf{x}_j(t) + \mathbf{B}_{ii}(t)\,\mathbf{u}_i(t) + \mathbf{F}_{ii}(t)\,\mathbf{d}_i(t), \tag{1}$$

where i represents the control area; $\mathbf{x}_i \in \mathbb{R}^{n_i}$, $\mathbf{u}_i \in \mathbb{R}^{m_i}$, and $\mathbf{d}_i \in \mathbb{R}^{z_i}$ represent the state, input, and disturbance vector in the i's subsystem, respectively. $\mathbf{x}_j \in \mathbb{R}^{n_j}$ is a state vector of the neighbor system.

Define the area control error (ACE) to be

$$\mathrm{ACE}_i = \mathbf{y}_i(t) = \mathbf{C}_{ii}\mathbf{x}_i(t) = B_i\Delta f_i(t) + \Delta P_{\mathrm{tie}i}(t), \tag{2}$$

where $\mathbf{y}_i \in \mathbb{R}^{v_i}$ represents system output signal. Matrices in (1) and (2) have dimensions

$$\mathbf{A}_{ii} \in \mathbb{R}^{n_i\times n_i}, \quad \mathbf{A}_{ij} \in \mathbb{R}^{n_i\times n_j}, \quad \mathbf{B}_{ii} \in \mathbb{R}^{n_i\times m_i}, \quad \mathbf{F}_{ii} \in \mathbb{R}^{n_i\times z_i}, \quad \mathbf{C}_{ii} \in \mathbb{R}^{v_i\times n_i}. \tag{3}$$

In Figure 1, the state variable in the thermal power system is

$$\mathbf{x}_i(t) = \left[\Delta f_i(t)\ \ \Delta P_{\mathrm{tie}i}(t)\ \ \Delta P_{gi}(t)\ \ \Delta X_{gi}(t)\ \ \Delta P_{ri}(t)\right]^T; \tag{4}$$

while the state variable in the hydro power system is

$$\mathbf{x}_i(t) = \left[\Delta f_i(t)\ \ \Delta P_{\mathrm{tie}i}(t)\ \ \Delta P_{gi}(t)\ \ \Delta X_{gi}(t)\ \ \Delta X_{ghi}(t)\right]^T. \tag{5}$$

The control signal and disturbance in both the thermal power system and the hydro power system are as follows:

$$\mathbf{u}_i(t) = \Delta P_{ci}(t), \qquad \mathbf{d}_i(t) = \Delta P_{di}(t). \tag{6}$$

The state, control, and disturbance matrix in thermal power system are

$$\mathbf{A}_{ii} = \begin{bmatrix} -\frac{1}{T_{pi}} & -\frac{K_{pi}}{T_{pi}} & \frac{K_{pi}}{T_{pi}} & 0 & 0 \\ \sum_{j\neq i} T_{sij} & 0 & 0 & 0 & 0 \\ 0 & 0 & -\frac{1}{T_{Ti}} & 0 & \frac{1}{T_{Ti}} \\ -\frac{1}{T_{Gi}R_i} & 0 & 0 & -\frac{1}{T_{Gi}} & 0 \\ -\frac{K_{ri}}{R_iT_{Gi}} & 0 & 0 & \frac{1}{T_{ri}} - \frac{K_{ri}}{T_{Gi}} & -\frac{1}{T_{ri}} \end{bmatrix}, \quad \mathbf{B}_{ii} = \begin{bmatrix} 0 \\ 0 \\ 0 \\ \frac{1}{T_{Gi}} \\ 0 \end{bmatrix}, \quad \mathbf{F}_{ii} = \begin{bmatrix} -\frac{K_{pi}}{T_{pi}} \\ 0 \\ 0 \\ 0 \\ 0 \end{bmatrix}, \tag{7}$$

while the state, control, and disturbance matrix in hydro power system are

$$\mathbf{A}_{ii} = \begin{bmatrix} -\frac{1}{T_{Pi}} & -\frac{K_{Pi}}{T_{Pi}} & \frac{K_{Pi}}{T_{Pi}} & 0 & 0 \\ \sum_{j\neq i} T_{sij} & 0 & 0 & 0 & 0 \\ 2\alpha & 0 & -\frac{2}{T_{Wi}} & 2\kappa & 2\beta \\ -\alpha & 0 & 0 & -\frac{1}{T_{2i}} & -\beta \\ -\frac{1}{T_{1i}R_i} & 0 & 0 & 0 & -\frac{1}{T_{1i}} \end{bmatrix}, \quad \mathbf{B}_{ii} = \begin{bmatrix} 0 \\ 0 \\ -2R_i\beta \\ R_i\beta \\ \frac{1}{T_{1i}} \end{bmatrix}, \quad \mathbf{F}_{ii} = \begin{bmatrix} -\frac{K_{Pi}}{T_{Pi}} \\ 0 \\ 0 \\ 0 \\ 0 \end{bmatrix}, \tag{8}$$

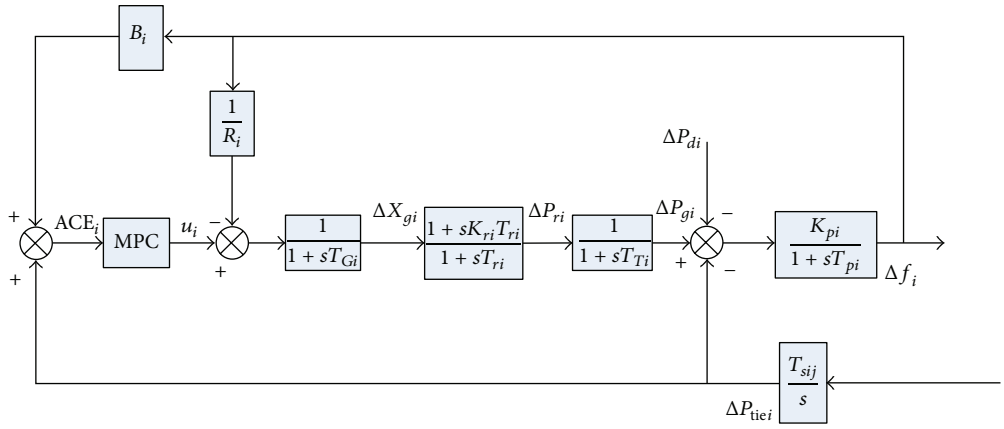

Figure 1: The block diagram of thermal power plant in area i.

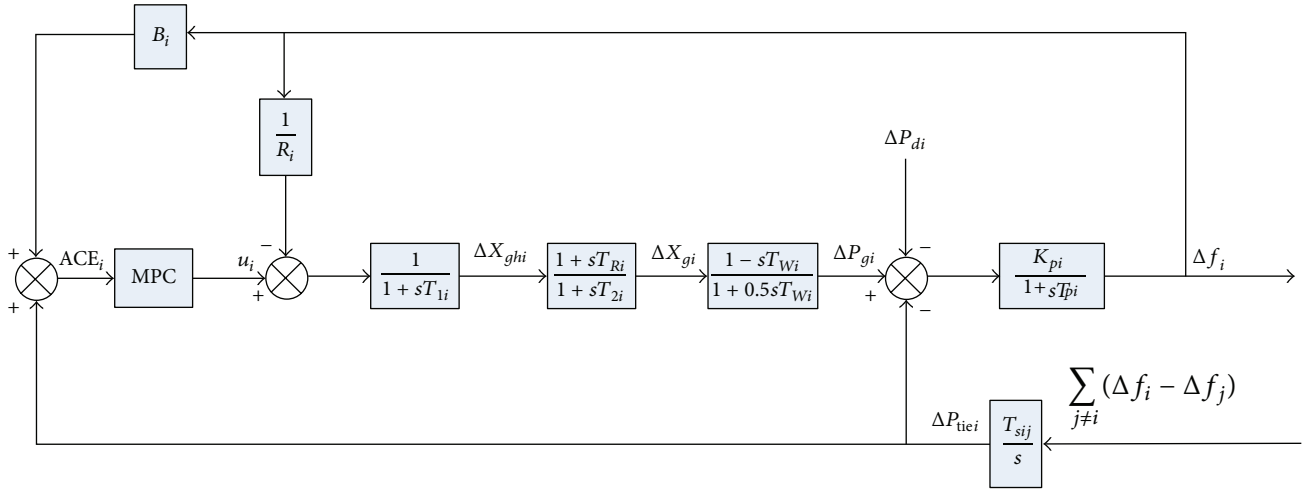

Figure 2: The block diagram of hydro power plant in area i.

where $\alpha = T_{Ri}/T_{1i}T_{2i}R_i$, $\beta = (T_{Ri} - T_{1i})/T_{1i}T_{2i}$, $\kappa = (T_{2i} + T_{Wi})/T_{2i}T_{Wi}$.

Here A_{ij} have 5×5 dimensions. All their elements are equal to zero, except for the element at position $(1, 2)$, which is equal to $-T_{sij}$.

For the whole power system, the state-space equation is as follows:

$$\begin{aligned} \dot{\mathbf{x}}(t) &= \mathbf{A}(t)\,x(t) + \mathbf{B}(t)\,u(t) + \mathbf{F}(t)\,d(t), \\ \mathbf{y}(t) &= \mathbf{C}(t)\,x(t), \end{aligned} \tag{9}$$

where

$$\begin{aligned} \mathbf{x}(t) &= \begin{bmatrix} \mathbf{x}_1(t) \\ \mathbf{x}_2(t) \\ \vdots \\ \mathbf{x}_M(t) \end{bmatrix} \qquad \mathbf{u}(t) = \begin{bmatrix} \mathbf{u}_1(t) \\ \mathbf{u}_2(t) \\ \vdots \\ \mathbf{u}_M(t) \end{bmatrix}, \\ \mathbf{d}(t) &= \begin{bmatrix} \mathbf{d}_1(t) \\ \mathbf{d}_2(t) \\ \vdots \\ \mathbf{d}_M(t) \end{bmatrix} \qquad \mathbf{y}(t) = \begin{bmatrix} \mathbf{y}_1(t) \\ \mathbf{y}_2(t) \\ \vdots \\ \mathbf{y}_M(t) \end{bmatrix}. \end{aligned} \tag{10}$$

This is a general continuous-time linear system with added disturbance. M is the number of control areas of the interconnected power system. After using the zero-order hold (ZOH) discretization method, each control area's distributed discrete-time linear model is expressed as follows:

$$\begin{aligned} x_i(k+1) &= \widetilde{A}_{ii}(k)\,x_i(k) + \widetilde{B}_{ii}(k)\,u_i(k) \\ &\quad + \sum_{j\neq i}^{M} \left(\widetilde{A}_{ij}(k)\,x_j(k) + \widetilde{B}_{ij}(k)\,u_j(k)\right), \\ y_i(k) &= \widetilde{C}_{ii}x_i(k). \end{aligned} \tag{11}$$

From (11), the polytopic model of each control area is

$$\begin{aligned} &\left[\widetilde{A}_{ii}(k)\,\widetilde{B}_{ii}(k)\cdots\widetilde{A}_{ij}(k)\,\widetilde{B}_{ij}(k)\cdots\right] \\ &\quad = \sum_{\ell=1}^{L}\beta_\ell\left[\widetilde{A}_{ii}^{(\ell)}\widetilde{B}_{ii}^{(\ell)}\cdots\widetilde{A}_{ij}^{(\ell)}\widetilde{B}_{ij}^{(\ell)}\cdots\right] \in \Omega \\ &\qquad \forall j \in \{1,\ldots,M\}, \quad j \neq i. \end{aligned} \tag{12}$$

Table 1: Variables and parameters used in thermal and hydro power plant.

Parameter/variable	Description	Unit
$\Delta f\,(t)$	Frequency deviation	Hz
$\Delta P_g\,(t)$	Generator output power deviation	p.u.MW
$\Delta X_g\,(t)$	Governor valve position deviation	p.u.
$\Delta P_r(t)$	Reheater output deviation	p.u.
$\Delta X_{gh}\,(t)$	Governor valve servomotor position deviation	p.u.
$\Delta P_{\text{tie}}\,(t)$	Tie-line active power deviation	p.u.MW
$\Delta P_d\,(t)$	Load disturbance	p.u.MW
$\Delta\delta\,(t)$	Rotor angle deviation	rad
K_P	Power system gain	Hz/p.u.MW
K_r	Reheater gain	p.u.
T_P	Power system time constant	s
T_W	Water starting time	s
T_1, T_2, T_R	Hydrogovernor time constants	s
T_G	Thermal governor time constant	s
T_T	Turbine time constant	s
T_r	Reheater time constant	s
T_s	Interconnection gain between CAs	p.u.MW
B	Frequency bias factor	p.u.MW/Hz
R	Speed droop due to governor action	Hz/p.u.MW
ACE	Area control error	p.u.MW

$\widetilde{A}_{ii}(k)$, $\widetilde{B}_{ii}(k)$, $\widetilde{A}_{ij}(k)$, $\widetilde{B}_{ij}(k)$, and $\widetilde{C}_{ii}$ are the relative matrices in the discrete-time model (11). Ω is the model parameter uncertainty set. β_ℓ's are used to represent a convex combination of the model vertices since the convex hull (the polytope) is the extreme model vertices. Each vertex ℓ corresponds to a linear model. The states are assumed to be available.

3. Robust Distributed Model Predictive Control Algorithm

Considering the distributed discrete-time power system model (11), the min-max problem to be solved for each subsystem is expressed as

$$\min_{u_i(k+l|k)} \max_{\left[\widetilde{A}_{ii}(k+l)\widetilde{B}_{ii}(k+l)\cdots\widetilde{A}_{ij}(k+l)\widetilde{B}_{ij}(k+l)\cdots\right],\, l\geq 0} J_i\,(k) \tag{13}$$

$$\text{s.t.}\ \left|u_i\,(k+l\mid k)\right| \leq u_i^{\max}, \quad l\geq 0, \tag{14}$$

where $J_i(k)$ is an object function for subsystem i to guarantee the cooperation of subsystem controllers, defined as

$$\begin{aligned} J_i\,(k) = \sum_{l=0}^{\infty} \Big[& x_i'\,(k+l\mid k)\,S_i x_i\,(k+l\mid k) \\ & + u_i'\,(k+l\mid k)\,R_i u_i\,(k+l\mid k)\Big] \\ + \sum_{j\neq i}^{M}\sum_{l=0}^{\infty} \Big[& x_j'\,(k+l\mid k)\,S_j x_j\,(k+l\mid k) \\ & + u_j'\,(k+l\mid k)\,R_j u_j\,(k+l\mid k)\Big], \end{aligned} \tag{15}$$

where $x_i(k+l\mid k)$ and $u_i(k+l\mid k)$ are the predicted state and input variables for the ith subsystem at time instant $k+l, l\geq 0$, based on data at time k. S_i, R_i, S_j, and R_j are the weighting matrices.

The maximization is to choose time-varying model $[\widetilde{A}_{ii}(k+l)\widetilde{B}_{ii}(k+l)\cdots\widetilde{A}_{ij}(k+l)\widetilde{B}_{ij}(k+l)\cdots]$ in the uncertainty set Ω to get the worst situation of $J_i(k)$, and this worst situation will be minimized on the current and the future horizons.

To solve the optimal problem (13), it is necessary to find an upper bound of the object function (15). Considering the quadratic function

$$V_i\,(\overline{x}) = \overline{x}^T P_i \overline{x}, \quad P_i > 0, \tag{16}$$

where $\overline{x} = [x_1'\ \ x_2'\ \ \cdots\ \ x_M']'$. For all the subsystem i, $V_i(\overline{x})$ should satisfy the following stability constraint:

$$\begin{aligned} & V_i\,(\overline{x}\,(k+l+1\mid k)) - V_i\,(\overline{x}\,(k+l\mid k)) \\ & \leq -\Big[x_i'\,(k+l\mid k)\,S_i x_i\,(k+l\mid k) \\ & \quad + u_i'\,(k+l\mid k)\,R_i u_i\,(k+l\mid k) \\ & \quad + \sum_{j\neq i}^{M}\Big(x_j'\,(k+l\mid k)\,S_j x_j\,(k+l\mid k) \\ & \quad + u_j'\,(k+l\mid k)\,R_j u_j\,(k+l\mid k)\Big)\Big]. \end{aligned} \tag{17}$$

For $l = 0, 1, \ldots, \infty$, the accumulation of (17) is

$$V_i\,(\overline{x}\,(k\mid k)) \geq J_i\,(k). \tag{18}$$

So the upper bound of object function can be proved to be

$$\max_{[\widetilde{A}_{ii}(k+l)\widetilde{B}_{ii}(k+l)\cdots\widetilde{A}_{ij}(k+l)\widetilde{B}_{ij}(k+l)\cdots],l\geq 0} J_i(k) \leq V_i(\overline{x}(k\mid k)). \quad (19)$$

A state-feedback law is sought for each subsystem i as follows:

$$\begin{aligned} u_i(k+l\mid k) &= f_{ii}x_i(k+l\mid k) + \sum_{j\neq i}^{M} f_{ij}x_j(k+l\mid k) \\ &= f_i\overline{x}(k+l\mid k), \end{aligned} \quad (20)$$

where $f_i = [f_{i1} \;\; f_{i2} \;\; \cdots \;\; f_{iM}]$.

When solving optimization problem of the subsystem i, the state-feedback law of the neighboring subsystem j $(j\neq i)$ is expressed as

$$\begin{aligned} u_j(k+l\mid k) &= f_{jj}^{*}x_j(k+l\mid k) + \sum_{j\neq s}^{M} f_{js}^{*}x_s(k+l\mid k) \\ &= f_j^{*}\overline{x}(k+l\mid k), \end{aligned} \quad (21)$$

where $f_j^{*} = [f_{j1}^{*} \;\; f_{j2}^{*} \;\; \cdots \;\; f_{jM}^{*}]$.

The RDMPC algorithm will be redefined using state-feedback law (20) to minimize the upper bound

$$\min_{u_i(k+l|k)} V_i(\overline{x}(k\mid k)) = \min_{f_i} \overline{x}'(k\mid k)P_i\overline{x}(k\mid k), \quad P_i > 0. \quad (22)$$

For the whole power system, the expression of $\overline{x}$ is

$$\begin{aligned} \overline{x}(k+1) &= \begin{bmatrix} x_1(k+1) \\ x_2(k+1) \\ \vdots \\ x_M(k+1) \end{bmatrix} \\ &= \begin{bmatrix} \widetilde{A}_{11}(k) & \widetilde{A}_{12}(k) & \cdots & \widetilde{A}_{1M}(k) \\ \widetilde{A}_{21}(k) & \widetilde{A}_{22}(k) & \cdots & \widetilde{A}_{2M}(k) \\ \vdots & \vdots & & \vdots \\ \widetilde{A}_{M1}(k) & \widetilde{A}_{M2}(k) & \cdots & \widetilde{A}_{MM}(k) \end{bmatrix} \begin{bmatrix} x_1(k) \\ x_2(k) \\ \vdots \\ x_M(k) \end{bmatrix} \\ &\quad + \begin{bmatrix} \widetilde{B}_{11}(k) \\ \widetilde{B}_{21}(k) \\ \vdots \\ \widetilde{B}_{M1}(k) \end{bmatrix} u_1(k) + \begin{bmatrix} \widetilde{B}_{12}(k) \\ \widetilde{B}_{22}(k) \\ \vdots \\ \widetilde{B}_{M2}(k) \end{bmatrix} u_2(k) \\ &\quad + \cdots + \begin{bmatrix} \widetilde{B}_{1M}(k) \\ \widetilde{B}_{2M}(k) \\ \vdots \\ \widetilde{B}_{MM}(k) \end{bmatrix} u_M(k). \end{aligned} \quad (23)$$

Define

$$A(k) = \begin{bmatrix} \widetilde{A}_{11}(k) & \widetilde{A}_{12}(k) & \cdots & \widetilde{A}_{1M}(k) \\ \widetilde{A}_{21}(k) & \widetilde{A}_{22}(k) & \cdots & \widetilde{A}_{2M}(k) \\ \vdots & \vdots & & \vdots \\ \widetilde{A}_{M1}(k) & \widetilde{A}_{M2}(k) & \cdots & \widetilde{A}_{MM}(k) \end{bmatrix}, \quad (24)$$

$$B_i(k) = \begin{bmatrix} \widetilde{B}_{1i}(k) \\ \widetilde{B}_{2i}(k) \\ \vdots \\ \widetilde{B}_{Mi}(k) \end{bmatrix}. \quad (25)$$

Using (20) and (21), the state (23) can be simplified as

$$\overline{x}(k+1) = \left[\overline{A}(k) + B_i(k)f_i\right]\overline{x}(k) \quad (26)$$

in which $\overline{A}(k) = A(k) + \sum_{j\neq i}^{M} B_j(k)f_j^{*}$.

The robust stability constraint in (17) becomes

$$\begin{aligned} &\left[\overline{A}^{(\ell)}(k+l) + B_i^{(\ell)}(k+l)f_i\right]' \\ &\quad \times P_i\left[\overline{A}^{(\ell)}(k+l) + B_i^{(\ell)}(k+l)f_i\right] - P_i \\ &\leq -\left(\overline{S}_i + \sum_{j\neq i}^{M} f_j^{*\prime}R_jf_j^{*} + f_i'R_if_i\right), \end{aligned} \quad (27)$$

where

$$\overline{S}_i = \begin{bmatrix} S_1 & & & \\ & S_2 & & \\ & & \ddots & \\ & & & S_M \end{bmatrix}. \quad (28)$$

By defining an upper bound,

$$J_i(k) \leq V_i(\overline{x}(k\mid k)) \leq \gamma_i. \quad (29)$$

The optimal problem (22) is equivalent to

$$\begin{aligned} \min_{\gamma_i,P_i} \quad & \gamma_i \\ \text{s.t.} \quad & \overline{x}'(k\mid k)P_i\overline{x}(k\mid k) \leq \gamma_i. \end{aligned} \quad (30)$$

Substituting $P_i = \gamma_iQ_i^{-1} > 0$, $Y_i = f_iQ_i$, with the input constraints given in (13) and the stability constraint (27), followed by a Schur complement decomposition, the minimization of $J_i(k)$ can be replaced by the minimization

problem (30) as in the following linear minimization problem with LMI constraints:

$$\begin{aligned}
&\min_{\gamma_i, P_i, Q_i} \quad \gamma_i \\
&\text{s.t.} \quad \begin{bmatrix} 1 & \overline{x}'(k \mid k) \\ \overline{x}(k \mid k) & Q_i \end{bmatrix} \geq 0, \\
&\begin{bmatrix} Q_i & Q_i \overline{A}^{\prime(\ell)} + Y_i' B_i^{\prime(\ell)} & Q_i \overline{S}_i^{1/2} & Y_i R_i^{1/2} \\ \overline{A}^{(\ell)} Q_i + B_i^{(\ell)} Y_i & Q_i & 0 & 0 \\ \overline{S}_i^{1/2} Q_i & 0 & \gamma_i I & 0 \\ R_i^{1/2} Y_i & 0 & 0 & \gamma_i I \end{bmatrix} \geq 0 \\
&\qquad\qquad \ell = 1, 2, \ldots, L, \\
&\begin{bmatrix} (u_i^{\max})^2 I & Y_i \\ Y_i' & Q_i \end{bmatrix} \geq 0.
\end{aligned} \tag{31}$$

For the constraints on power system state

$$\max_{[\widetilde{A}_{ii}(k+l)\widetilde{B}_{ii}(k+l)\cdots\widetilde{A}_{ij}(k+l)\widetilde{B}_{ij}(k+l)\cdots]\in\Omega,\, l\geq 0} \left\| y_i(k+l \mid k) \right\|_2 \leq y_{i,\max}. \tag{32}$$

Transform it to LMI form as

$$\begin{aligned}
&\begin{bmatrix} Q_i & \left(\overline{A}^{(\ell)} Q_i + B_i^{(\ell)} Y_i\right)' \widetilde{C}_{ii}' \\ \widetilde{C}_{ii}\left(\overline{A}^{(\ell)} Q_i + B_i^{(\ell)} Y_i\right) & y_{i,\max}^2 I \end{bmatrix} \geq 0 \\
&\qquad\qquad \ell = 1, 2, \ldots, L.
\end{aligned} \tag{33}$$

4. The Simulation

Two examples are considered to demonstrate the effectiveness of the proposed RDMPC. In the first one, the RDMPC is utilized in a two-control area thermal power system, while in the second one, a three-area thermal-hydro power system is considered.

Case 1 (a two-control area thermal power system). A two-control area thermal power system is shown in Figure 3. The parameters used in the simulation is as follows:

$$\begin{aligned}
&K_{P1} = 120\ \text{Hz/p.u.MW}; \quad K_{P2} = 75\ \text{Hz/p.u.MW}; \\
&T_{P1} = 20\ \text{s}; \quad T_{P2} = 15\ \text{s}; \quad K_{r1} = K_{r2} = 0.5\ \text{Hz/p.u.MW}; \\
&R_1 = 2.4\ \text{Hz/p.u.MW}; \quad R_2 = 3\ \text{Hz/p.u.MW}; \\
&B_1 = 0.425\ \text{p.u.MW/Hz}; \quad B_2 = 0.347\ \text{p.u.MW/Hz}; \\
&T_{G1} = 0.08\ \text{s}; \quad T_{G2} = 0.2\ \text{s}; \quad T_{T1} = T_{T2} = 0.3\ \text{s}; \\
&T_{s12} = 0.545\ \text{p.u.MW}; \quad T_{r1} = T_{r2} = 10\ \text{s}.
\end{aligned} \tag{34}$$

The power system model in Figure 1 with included GRC is shown in Figure 4. In simulations, GRC was set to $|\Delta \dot{P}_{gi}| \leq r = 0.0017$ p.u.MW/s.

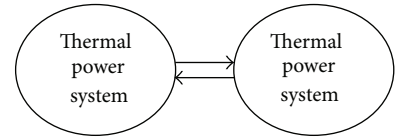

Figure 3: The two-control area interconnected thermal power system.

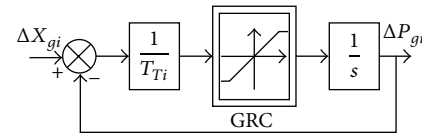

Figure 4: GRC in power system LFC.

In real time power system LFC, the power system time constant T_P and turbine time constant T_T can change frequently. Thus the robustness study is performed by applying intentional changes in these two parameters. The maximum range of parameter variation is chosen to be 40%. The polytopic of uncertain LFC system has four vertices, which are

$$\begin{aligned}
&A_i^{(1)}\left(0.6T_{Pi}, 0.6T_{Ti}\right); \quad A_i^{(2)}\left(1.4T_{Pi}, 1.4T_{Ti}\right); \\
&A_i^{(3)}\left(0.6T_{Pi}, 1.4T_{Ti}\right); \quad A_i^{(4)}\left(1.4T_{Pi}, 0.6T_{Ti}\right).
\end{aligned} \tag{35}$$

Under the parameter changes, the performance of the RDMPC is assessed by applying load disturbance. At $t = 2$ s, a step load disturbance on control area is added to be $\Delta P_{d1} = 0.01$ p.u. Choose the sample time to be $T_s = 0.1$ s, $S_i = 1$, and $R_i = 0.05$.

The proposed RDMPC is compared with two other schemes, for example, the conventional robust centralized MPC, which solves the min-max optimization problem using the centralized model by the formulation of a linear matrix inequality and also with the communicated-based MPC, which utilizes the objective function for local subsystem only. Figures 5, 6, and 7 show the comparison results of the ACE signals, the frequency deviations, and the tie-line power flow, respectively. It is clear that the proposed RDMPC has the best performance, since the MPC controllers cooperate with each other in achieving system-wide objectives. The performance of the robust centralized MPC is quite close to that of the RDMPC, since it is also robust to parameter changes. The only shortcoming of the centralized MPC is its high computation burden. The performance of the communicated-based MPC is the worst, since it can neither realize the cooperation of the subsystems nor adapt to parameter changes.

Case 2 (a three-area thermal-hydro power system). The three-control area interconnected power system containing thermal and hydro power plant is showed in Figure 8.

The power system model in Figures 1 and 2 with included GRC in hydro power plant is shown in Figure 9, where $|\Delta \dot{P}_{gi}| \leq r = 0.045$ p.u.MW/s.

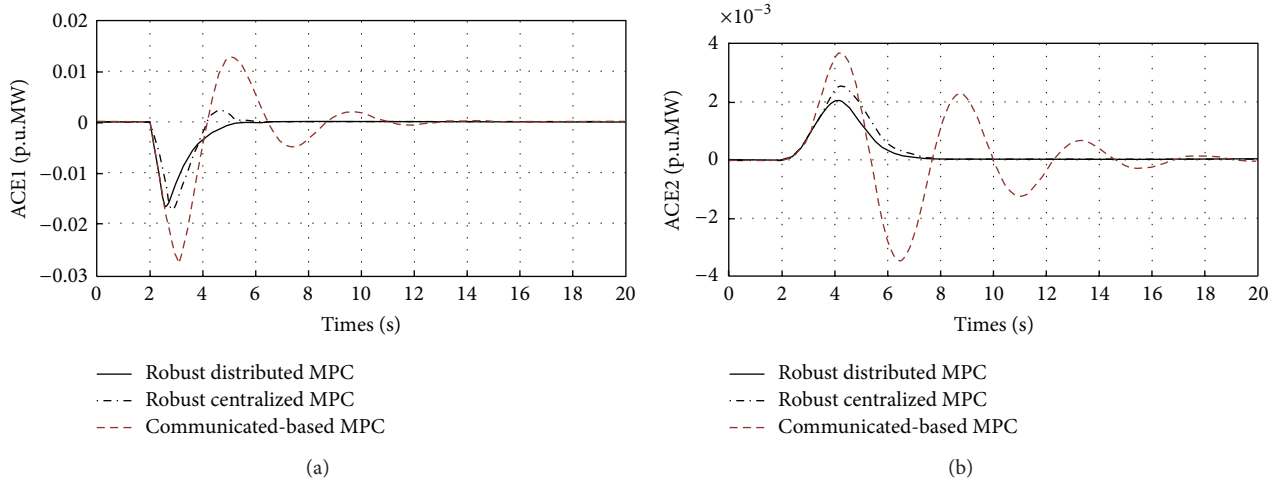

Figure 5: ACE signals in the two subsystems.

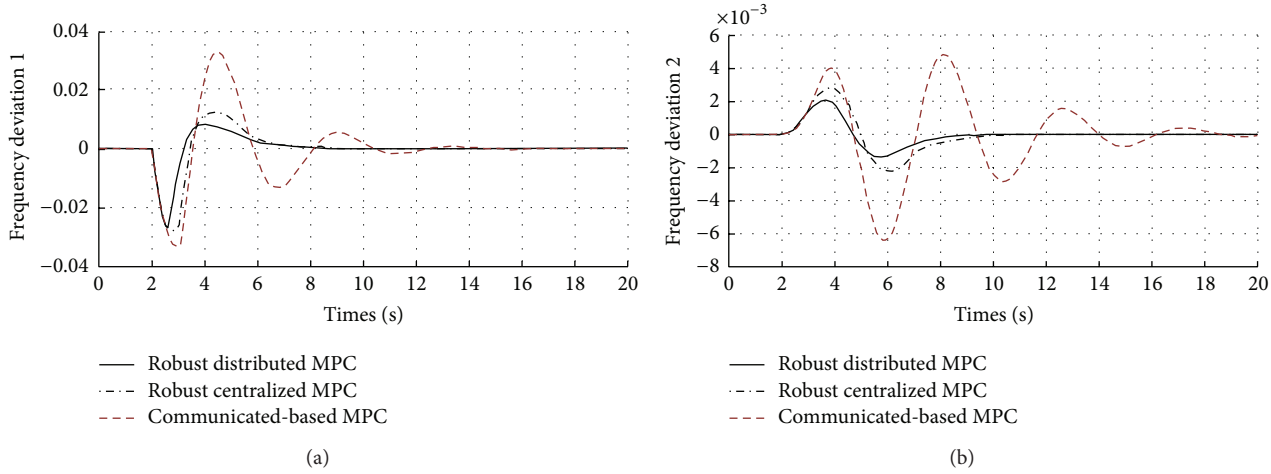

Figure 6: The frequency deviations.

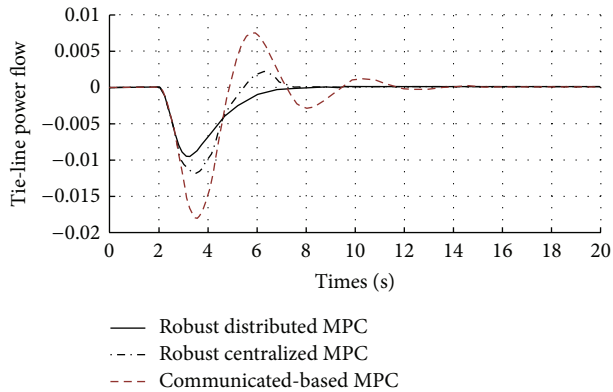

Figure 7: The tie-line power flow between two control areas.

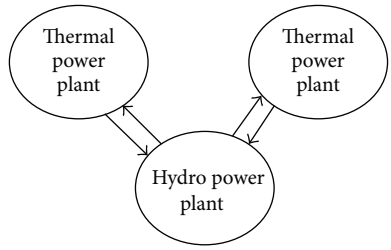

Figure 8: The three-control area interconnected thermal-hydro power system.

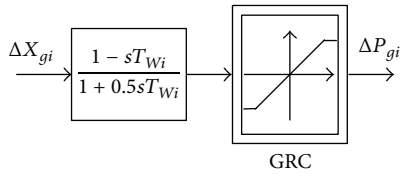

Figure 9: GRC in hydro power system.

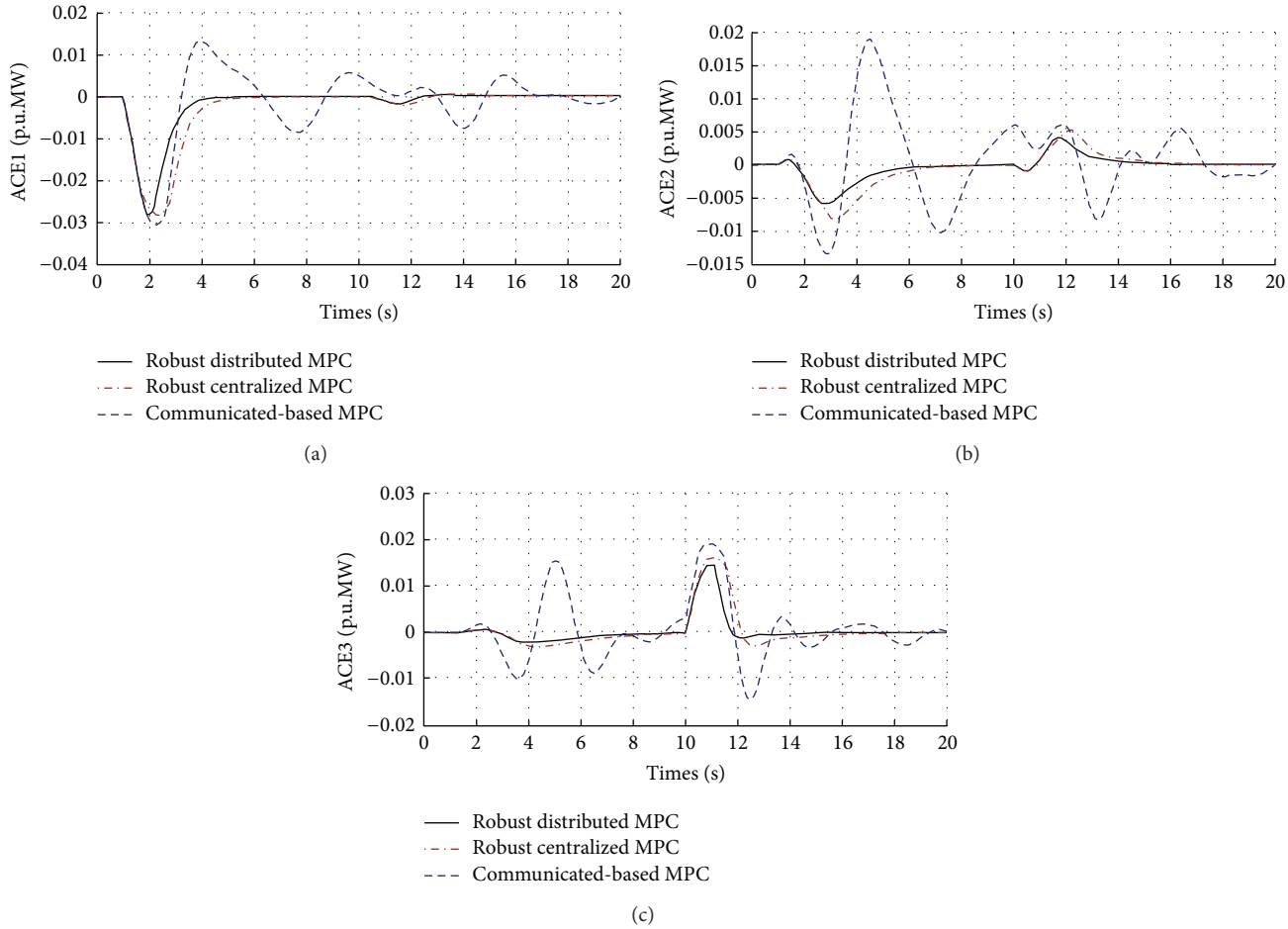

Figure 10: ACE signals in three-area thermal-hydro power system.

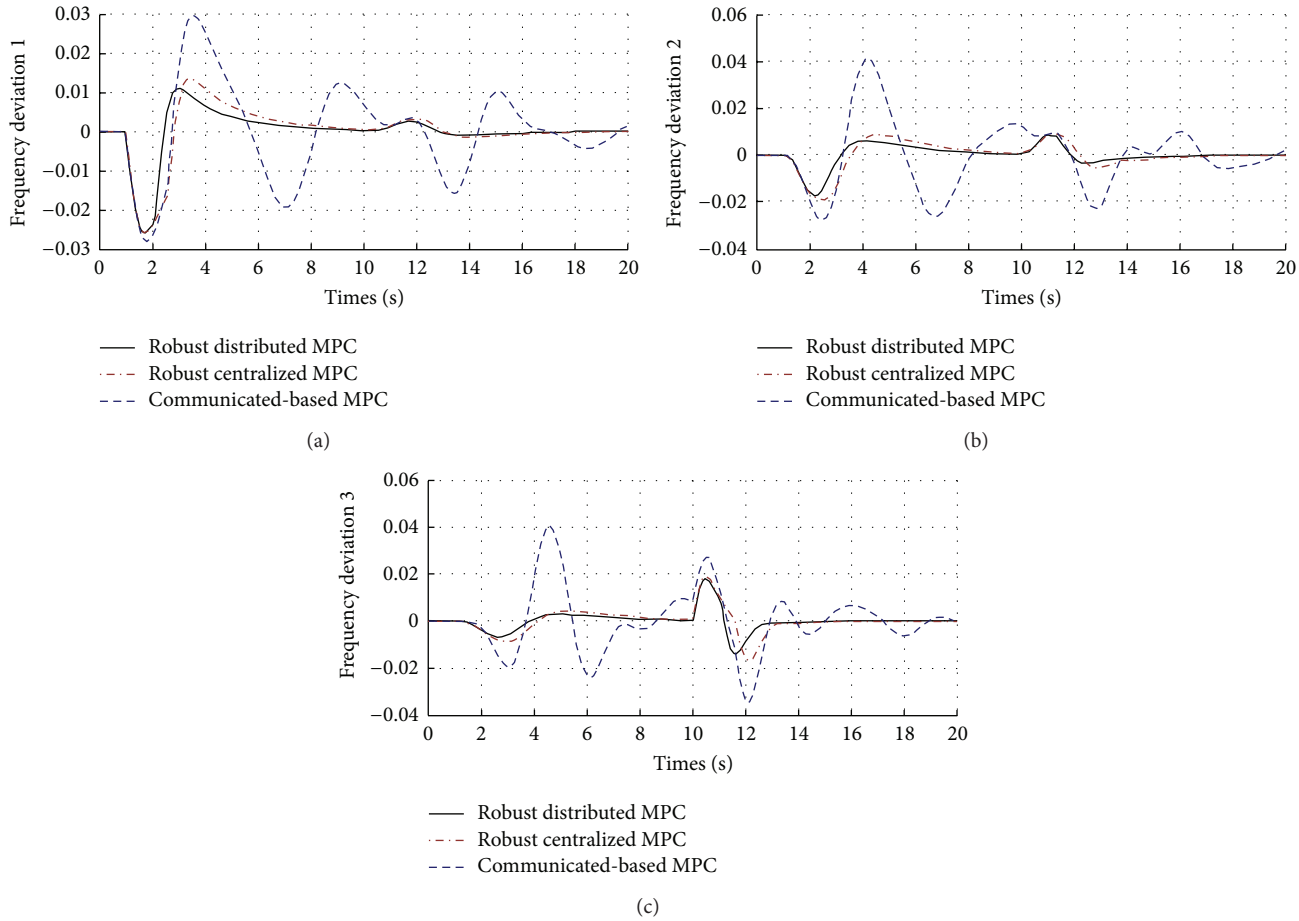

FIGURE 11: The frequency deviation in the three-area thermal-hydro power system.

The parameters used in the simulation are as follows:

$$K_{P1} = 120\,\text{Hz/p.u.MW}; \quad K_{P3} = 115\,\text{Hz/p.u.MW};$$
$$K_{P3} = 75\,\text{Hz/p.u.MW}; \quad T_{P1} = 20\,\text{s}; \quad T_{P2} = 20\,\text{s};$$
$$T_{P3} = 15\,\text{s}; \quad K_{r1} = K_{r3} = 0.5\,\text{Hz/p.u.MW};$$
$$R_1 = 2.4\,\text{Hz/p.u.MW}; \quad R_2 = 2.5\,\text{Hz/p.u.MW};$$
$$R_3 = 3\,\text{Hz/p.u.MW}; \quad B_1 = 0.425\,\text{p.u.MW/Hz};$$
$$B_2 = 0.494\,\text{p.u.MW/Hz}; \quad B_3 = 0.347\,\text{p.u.MW/Hz};$$
$$T_{R2} = 0.6\,\text{s}; \quad T_{1(2)} = 48.7\,\text{s}; \quad T_{2(2)} = 5\,\text{s};$$
$$T_{W2} = 1\,\text{s}; \quad T_{G1} = 0.08\,\text{s}; \quad T_{G3} = 0.2\,\text{s};$$
$$T_{T1} = T_{T3} = 0.3\,\text{s}; \quad T_{r1} = T_{r3} = 10\,\text{s};$$
$$T_{s12} = 0.545\,\text{p.u.MW}; \quad T_{s23} = 0.545\,\text{p.u.MW}. \tag{36}$$

Since the maximum range of parameter variation is also chosen to be 40% for hydro power system, the polytope is

$$A_2^{(1)}\left(0.6T_{P2}\right); \quad A_2^{(2)}\left(1.4T_{P2}\right). \tag{37}$$

At $t = 1\,\text{s}$, a step load disturbance on control area 1 is added as $\Delta P_{d1} = 0.01\,\text{p.u.}$, and at $t = 10\,\text{s}$, a step load disturbance on control area 3 is added as $\Delta P_{d3} = -0.01\,\text{p.u.}$ Figures 10 and 11 show the comparison results of the ACE signals and the frequency deviations, demonstrating clearly the advantage of the proposed RDMPC.

5. Conclusion

In this paper, a robust distributed MPC scheme for load frequency control of interconnected power system is presented. The overall system consisted of at least two control areas, which either can be thermal-thermal power system or thermal-hydro power system. Each control area has its own polytopic distributed model in order to consider the uncertainty because of parameter variation. A min-max cost function is used for the optimization problem, and the LMI method is involved to solve this problem. The simulation results illustrate the advantage of the proposed RDMPC, due to its cooperative function. Thus it is suitable for LFC of power system, which is large-scale complex system and subject to parameter uncertainty.

Conflict of Interests

The authors declare that there is no conflict of interests regarding the publication of this paper.

Acknowledgments

This work was supported by National Natural Science Foundation of China under Grants 60974051, 61273144, and 61203041, Natural Science Foundation of Beijing under Grant 4122071, Chinese National Postdoctoral Science Foundation under Grants 2011M500217 and 2012T50036, and the Doctoral Fund of Ministry of Education of China under Grant 20120036120013.

References

[1] R. K. Cavin, M. C. Budge, and P. Rasmussen, "An optimal linear system approach to load-frequency control," *IEEE Transactions on Power Apparatus and Systems*, vol. 90, no. 6, pp. 2472–2482, 1971.

[2] S. Yin, H. Luo, and S. Ding, "Real-time implementation of fault tolerant control system with performance optimization," *IEEE Transactions on Industrial Electronics*, vol. 61, no. 5, pp. 2402–2411, 2013.

[3] S. Ding, S. Yin, K. Peng, H. Hao, and B. Shen, "A novel scheme for key performance indicator prediction and diagnosis with application to an industrial hot strip mill," *IEEE Transactions on Industrial Informatics*, vol. 9, no. 4, pp. 2239–2247, 2012.

[4] T. Li, W. X. Zheng, and C. Lin, "Delay-slope-dependent stability results of recurrent neural networks," *IEEE Transactions on Neural Networks*, vol. 22, no. 12, pp. 2138–2143, 2011.

[5] Y. Wang, R. Zhou, and C. Wen, "Robust load-frequency controller design for power systems," *IEE Proceedings C*, vol. 140, no. 1, pp. 11–16, 1993.

[6] A. M. Stanković, G. Tadmor, and T. A. Sakharuk, "On robust control analysis and design for load frequency regulation," *IEEE Transactions on Power Systems*, vol. 13, no. 2, pp. 449–455, 1998.

[7] X. Yu and K. Tomsovic, "Application of linear matrix inequalities for load frequency control with communication delays," *IEEE Transactions on Power Systems*, vol. 19, no. 3, pp. 1508–1515, 2004.

[8] H. J. Lee, J. B. Park, and Y. H. Joo, "Robust load-frequency control for uncertain nonlinear power systems: a fuzzy logic approach," *Information Sciences*, vol. 176, no. 23, pp. 3520–3537, 2006.

[9] H. Shayeghi, H. A. Shayanfar, and O. P. Malik, "Robust decentralized neural networks based LFC in a deregulated power system," *Electric Power Systems Research*, vol. 77, no. 3-4, pp. 241–251, 2007.

[10] D. Rerkpreedapong, A. Hasanović, and A. Feliachi, "Robust load frequency control using genetic algorithms and linear matrix inequalities," *IEEE Transactions on Power Systems*, vol. 18, no. 2, pp. 855–861, 2003.

[11] M. V. Kothare, V. Balakrishnan, and M. Morari, "Robust constrained model predictive control using linear matrix inequalities," *Automatica*, vol. 32, no. 10, pp. 1361–1379, 1996.

[12] X. Liu, S. Feng, and M. Ma, "Robust MPC for the constrained system with polytopic uncertainty," *International Journal of Systems Science*, vol. 43, no. 2, pp. 248–258, 2012.

[13] A. N. Venkat, I. A. Hiskens, J. B. Rawlings, and S. J. Wright, "Distributed MPC strategies with application to power system automatic generation control," *IEEE Transactions on Control Systems Technology*, vol. 16, no. 6, pp. 1192–1206, 2008.

[14] T. H. Mohamed, H. Bevrani, A. A. Hassan, and T. Hiyama, "Decentralized model predictive based load frequency control in an interconnected power system," *Energy Conversion and Management*, vol. 52, no. 2, pp. 1208–1214, 2011.

[15] W. Al-Gherwi, H. Budman, and A. Elkamel, "A robust distributed model predictive control algorithm," *Journal of Process Control*, vol. 21, no. 8, pp. 1127–1137, 2011.

[16] K. Vrdoljak, N. Perić, and I. Petrović, "Sliding mode based load-frequency control in power systems," *Electric Power Systems Research*, vol. 80, no. 5, pp. 514–527, 2010.

Hindawi Publishing Corporation
Mathematical Problems in Engineering
Volume 2013, Article ID 265895, 9 pages
http://dx.doi.org/10.1155/2013/265895

Research Article

Analysis and Optimization of Dynamic Measurement Precision of Fiber Optic Gyroscope

Hui Li, Liyang Cui, Zhili Lin, and Chunxi Zhang

School of Instrument Science and Optoelectronics Engineering, Beihang University, Beijing 100191, China

Correspondence should be addressed to Hui Li; lihui@buaa.edu.cn

Received 26 August 2013; Accepted 16 November 2013

Academic Editor: Bo-Chao Zheng

In order to improve the dynamic performance of high precision interferometer fiber optic gyroscope (IFOG), the influencing factors of the fast response characteristics are analyzed based on a proposed assistant design setup, and a high dynamic detection method is proposed to suppress the adverse effects of the key influencing factors. The assistant design platform is built by using the virtual instrument technology for IFOG, which can monitor the closed-loop state variables in real time for analyzing the influence of both the optical components and detection circuit on the dynamic performance of IFOG. The analysis results indicate that nonlinearity of optical Sagnac effect, optical parameter uncertainty, dynamic characteristics of internal modules and time delay of signal detection circuit are the major causes of dynamic performance deterioration, which can induce potential system instability in practical control systems. By taking all these factors into consideration, we design a robust control algorithm to realize the high dynamic closed-loop detection of IFOG. Finally, experiments show that the improved 0.01 deg/h high precision IFOG with the proposed control algorithm can achieve fast tracking and good dynamic measurement precision.

1. Introduction

Interferometer fiber optic gyroscope (IFOG) has become a new and highly stable angular velocity sensor with the development of optical fiber sensing technology [1, 2]. IFOG is very competitive in the field of inertial device, owing to its advantages over traditional inertial devices, such as no moving parts, simpler structure, higher detection accuracy, and better reliability [3, 4].

As digital closed-loop detection scheme becomes the mainstream of current high precision IFOG scheme, optimization of closed-loop control algorithm is of great significance for improving performance in temperature and vibration environment [5, 6]. In [7], Spammer and Swart analyzed the influence of loop gain on the dynamic characteristic of system and investigated a control algorithm to eliminate steady-state error. Japan Aviation Electronics Industry Limited (JEA) corporation from Japan focused on the winding method of optical fiber coil and closed-loop control technology to improve the temperature and vibration characteristics [8]. An implemented signal processing scheme was proposed to promote the reduction of the source intensity noise around the proper frequency of birefringent IFOG for a better signal-to-noise ratio [9]. Thus, the importance of optimization of closed-loop control algorithm is apparent in order to further enhance the system performance.

However, the closed-loop control period of IFOG is in a time scale of several microseconds, while the refresh time of the system output is in a time scale of milliseconds [10, 11]. Hence, it is difficult to analyze the working process of IFOG only by the test data of IFOG, especially in the environment of high frequency vibration and shock. By taking the environmental factors into consideration, Litef GmbH established a simulation system for IFOG and optimized the optical components and design of closed-loop control [11, 12]. To realize the environmentally insensitive IFOG, Honeywell International proposed a compensating error component by testing the frequency responses of optical path and closed-loop circuit [13]. However, if the inner state variables of closed-loop detection system cannot be monitored in real time, the influence of optical parameters

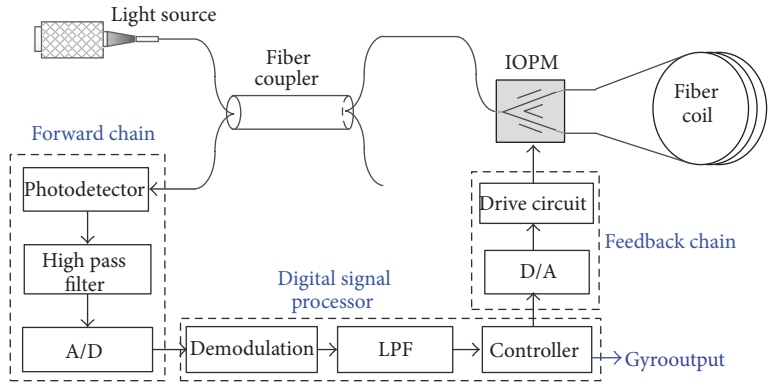

Figure 1: The signal detection flowchart of the designed high precision IFOG, which includes a high pass filter to eliminate the DC component in the interference intensity, demodulation, and a low-pass filter (LPF) to extract the modulated nonlinear closed-loop error precisely; a closed-loop controller is needed to obtain the feedback of IFOG and to generate digital phase ramp.

and circuit parameters on the performance of high precision IFOG cannot be analyzed accurately.

In addition, the optical parameters and circuit parameters varying with time and environment can also cause the deterioration of dynamic performance of high precision IFOG. For improving the performance of IFOG, Honeywell International proposed an apparatus for eliminating or reducing vibration-induced errors by applying a variable weighting function at the demodulator or analog-to-digital converter to change the size of the demodulator reference signal or the converter gain, respectively [14]. In respect of the temperature dependency, a precision calibration procedure was described for reducing the resulting errors [15]. In [16], a method based on a radial basis function (RBF) neural network was presented for dynamic angular velocity modeling and error compensation. However, most of the above methods adopted are to compensate error of IFOG according to the built model based on closed-loop output of IFOG. And few works have considered the optical parameters and circuit parameters uncertainty in the dynamic model of the closed-loop system, so that performance of IFOG may not be able to be controlled precisely due to parameter variance with time and environment in engineering practice. With this background, we study the high dynamic model of IFOG with parameters uncertainty and design robust control algorithm to suppress the influence of parameters uncertainty for improving the dynamic characteristics of high precision IFOG.

In this paper, we establish an assistant design platform for high precision IFOG by using the virtual instrument technology, which can monitor the real-time closed-loop state variables and test the dynamic performance of closed-loop system. With the assistant design platform, we analyze the influence of optical sensing and detection circuit on the dynamic performance of high precision IFOG. Furthermore, with the consideration of these factors, the high dynamic mathematic model of IFOG with parameters uncertainty is derived and a robust controller is designed to enhance the dynamic measurement performance of high precision IFOG for applications in navigation and aerospace fields.

2. Analysis Setup of Dynamic Performance of IFOG

The optical path scheme for high precision IFOG is illustrated in Figure 1. The light from the light source is split by the coupler into two beams, one of which is propagating into integrated optical modulator (IOPM). The light polarized by the IOPM is divided into two light beams that pass through the fiber coil clockwise and anticlockwise, respectively. With the induced Sagnac phase $\Delta\varphi_s$, the two beams of light interfere coherently at the IOPM. The time of the light propagating through the fiber coil is τ, which restricts the minimum closed-loop period.

To achieve higher accuracy in angular velocity measurement, we design a signal detection scheme, and the working diagram of the closed-loop detection for IFOG is shown in Figure 1. With the square wave modulation and the phase ramp feedback, the interference intensity can be given by

$$I = \alpha I_0 \left\{1 + f_b(t) \cdot \sin\left[\Delta\varphi_s(t) - \Delta\varphi_f(t)\right]\right\}, \quad (1)$$

where α is the total loss of the full optical path, I_0 is the output power of the light source, $\Delta\varphi_f(t)$ is the feedback phase stair of the digital phase ramp used to counteract $\Delta\varphi_s(t)$, $\Delta\varphi_s(t)$ is the Sagnac phase, and $f_b(t)$ is the modulating square wave with amplitude ± 1 and period 2τ. We here introduce a quantity $\Delta\varphi$ that represents the closed-loop error of the IFOG, which is defined by $\Delta\varphi(t) = \Delta\varphi_s(t) - \Delta\varphi_f(t)$.

To further improve the dynamic measurement precision of IFOG, the influence of optical parameters and signal detection circuits on dynamic performance should be analyzed. However, by the traditional analysis that is only based on the output data of IFOG, the complex closed-loop process of IFOG cannot be manifested. And it is also difficult to assess and verify the influence of inner elements' parameters of closed-loop system on the performance of IFOG. In fact, it is difficult to experimentally analyze the dynamic variation of error signal between input and output signals, especially when the system is in high frequency vibration and shock environment. In order to assess the main factors that influence the dynamic characteristics and

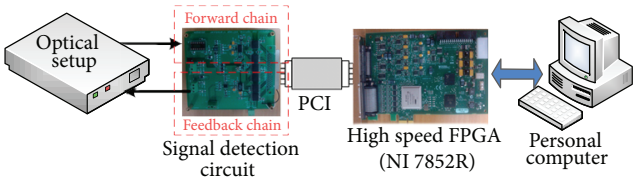

Figure 2: The constituent components of the proposed assistant design setup of IFOG, which is composed of four parts: optical setup, signal detection circuit, computer, and NI7852R with an embedded high-speed FPGA.

to optimize the dynamic measurement performance of high precision IFOG, we develop an assistant design setup based on virtual instrument technology as illustrated in Figure 2. The assistant design setup can achieve the high-speed closed-loop control with microsecond closed-loop period to detect interference intensity signal and exert the modulating square wave and feedback phase ramp on IOPM. Besides, the proposed detection setup can monitor the output signal of detector and the closed-loop state variables in real time through the digital communication between the embedded high-speed field programmable gate array (FPGA) and the personal computer.

The dynamic performance tests also can be conducted based on this platform. The embedded high-speed FPGA of national instruments (NI) 7852R is utilized to generate a frequency adjustable and phase steerable excitation signal, which is added to the stair ramp to substitute input angular speed in considering the fact that stair ramp imposed on IOPM can introduce phase shift with the same effect as Sagnac phase. We can evaluate the dynamic characteristics by comparing the excitation and output signals since the signal processing unit can generate the excitation signal and process the output data of IFOG simultaneously.

3. Analysis of Influencing Factors on Dynamic Performance

3.1. Influence of Optical Characteristics on the Dynamic Performance of High Precision IFOG. The output of photoelectric detector, also served as the input of signal detection unit, is of great importance to the stability and dynamic performance of IFOG. From (1), it is noted that the optical characteristics contain the interference intensity and the physical intrinsic nonlinearity of interference link.

Due to the varying external environment factors, the changing optical parameters result in the fluctuation of interference intensity, such as the unavoidable light power drift with temperature and the attenuation of light power after long-term working. We analyze the relationship between the power variation of light source and the environmental temperature, and the obtained experiment results are shown in Figure 3. Together with the loss of light power in other optical devices, the range of light power variation can reach ±10% under the condition of temperature varying from −45°C to +70°C. As verified by the conducted experiments

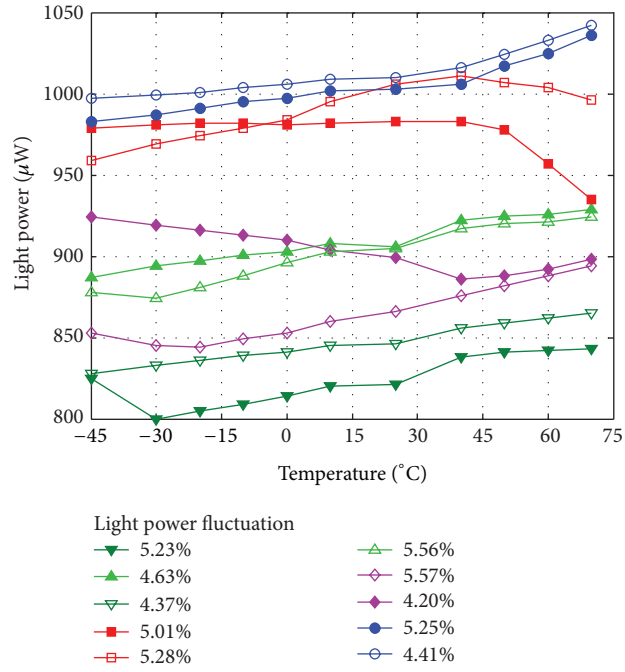

Figure 3: The results of experiment tests on the relationship between the light power variation and temperature.

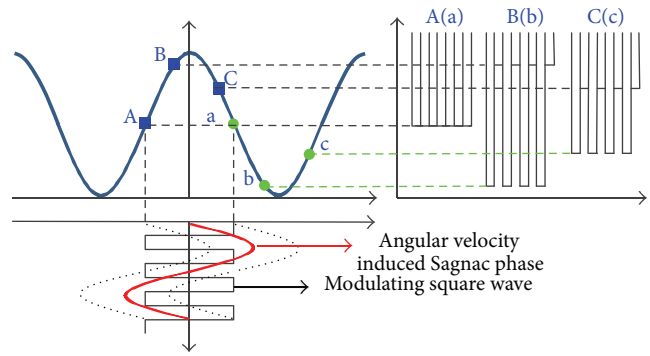

Figure 4: The principle of nonlinearity that influences the dynamic performance of the IFOG that adopts the closed-loop scheme of square wave modulation and feedback phase ramp.

based on the assistant design setup, we know that the detection sensitivity of IFOG is not determined by the light power, because the light power is translated into one factor of the gain of forward chain, while the dynamic performance of high precision IFOG is apparently different from the gain variation of forward chain.

The interference link generates a nonlinear sine function, which confines the IFOG's dynamic measurement range. Although the closed-loop scheme of square wave modulation and feedback phase ramp is adopted to suppress the closed-loop error near the zero point and to improve the linear characteristic, the IFOG system is a nonlinear system as determined by (1). According to the working principle of our scheme, the linear model used to approximate the nonlinear

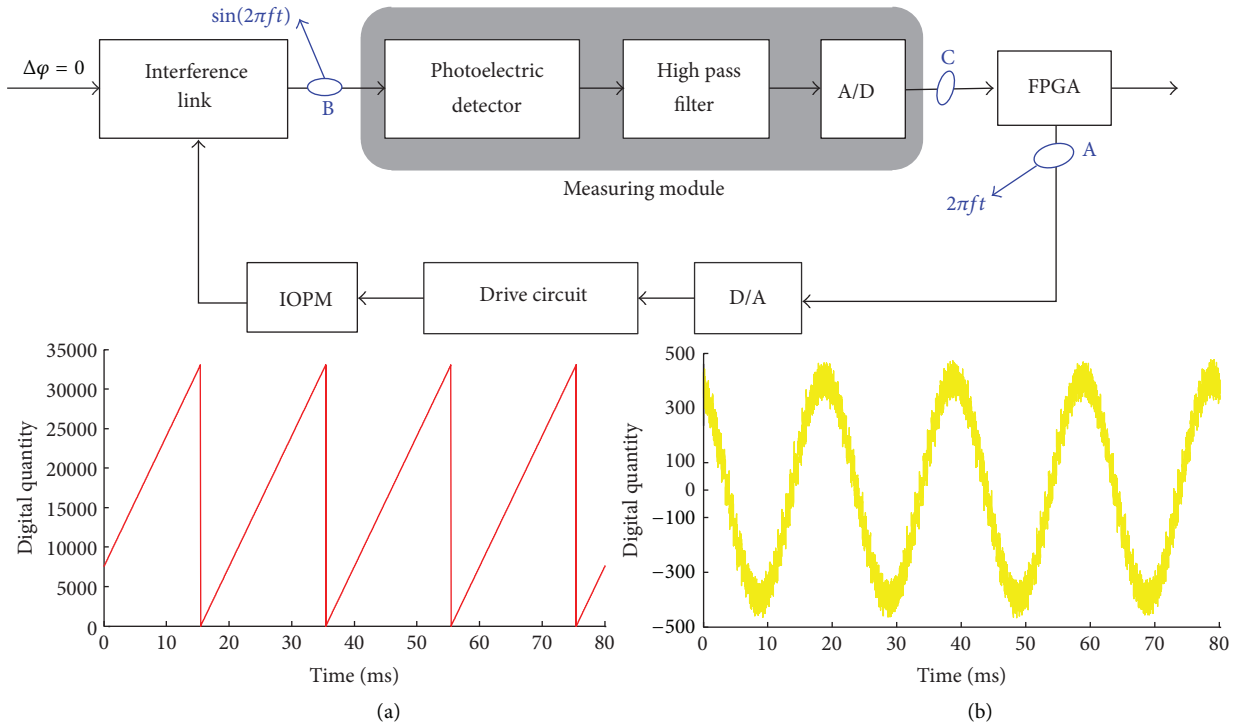

FIGURE 5: The testing principle of the frequency characteristic of the whole forward chain; (a) the signal observed at A point; (b) the signal observed at C point.

system is effective only when the IFOG works near a balance point, such as point A, as denoted in Figure 4. However, when it works at the state of point B or point C due to high frequency or high impulse angular velocity input, the nonlinear characteristic of optical interference link can cause the deterioration of dynamic performance and the potential system instability. In engineering practice, IFOG is not able to precisely measure the high frequency or high impulse angular velocity signal due to the nonlinearity, which might also cause system instability.

3.2. Influence of the Hardware Detection on the Dynamic Performance of the High Precision IFOG. The proposed detection equipment for signal processing can be divided into three parts: the forward chain, the feedback chain, and modulation-demodulation component. To improve the bandwidth of the forward chain and eliminate the DC component of the interference intensity signal, we design a high pass filter in the forward chain. The dynamic characteristics and bandwidth of the forward chain can significantly affect the dynamic performance of the high precision IFOG. However, besides the high pass filter and an A/D converter, the forward chain also includes an optical device—photoelectric detector. It is difficult to analyze the dynamic characteristics of forward chain by using frequency characteristic analyzer.

To solve this problem, we use the assistant design setup to measure the model of the whole forward chain. As illustrated in Figure 5, the assistant design setup is utilized to generate ramp signals at point A. The ramp signal is $u(t) = 2\pi ft$, where f is the frequency of target excitation signal. Then, we make the ingenious application of the nonlinear characteristic of interference link in translating the ramp signal into a sinusoidal signal $\sin(2\pi ft)$ at point B. The ramp signal has to be reset periodically at the level of 2π when it reaches the full scale of DA converter, and the digital signal processor receives the interference signal synchronously at point C. Moreover, the frequency of the sinusoidal signal is controlled by the commercial software Laboratory Virtual Instrument Engineering Workbench (LabVIEW) installed in the computer. Thus the frequency characteristics of the whole forward chain can be calculated based on the assistant design setup. The obtained results demonstrate that the bandwidth of forward chain can reach 10 MHz and satisfy the requirement for high-frequency angular velocity measurement.

To accurately extract the closed-loop error, the output of A/D converter is demodulated by multiplying a digital square wave that has the same frequency and phase as that of $f_b(t)$, and it also needs a low-pass filter to remove the high frequency components and noise. The response function of the designed low-pass filter is $H(z) = 1 + \beta_1 z^{-1} + \beta_2 z^{-2} + \cdots + \beta_d z^{-d}$, where z^{-1} represents the time of one closed-loop period and $\beta_1, \ldots, \beta_d$ are the coefficients of filter. The higher order of filter can arouse better signal to noise ratio. However, the higher-order items of filter introduce larger time-delay at the same time. The time-delay can intrinsically influence the dynamic performance of the closed-loop system. The feedback chain contains a D/A converter, a D/A drive circuit,

and the previously mentioned IOPM. A 16 bit D/A converter is adopted and its theoretical bandwidth is up to 50 MHz. The D/A drive circuit is essentially a translation circuit with bandwidth designed as wide as possible and its practically measured bandwidth is up to 4.547 MHz. The IOPM is a conversion circuit that can convert modulation voltage into modulation phase shift and its modulation bandwidth can reach as high as 1 GHz. So the feedback chain can be considered as a linear module.

4. Mathematic Model Establishment and Robust Control Algorithm Design

The analysis results about the dynamic performance of the optical components and signal detection circuits of high precision IFOG are important for guiding the design of closed-loop control algorithm. Prior to the question on how to design an optimized control algorithm, we need to establish the mathematic model of the dynamic performance of closed-loop system by taking the influencing factors into consideration, which are obtained from the results of dynamic performance analysis based on the assistant design setup.

Firstly, we analyze the forward chain where the influence of optical parameter uncertainty works. Its bandwidth is much larger than the required bandwidth of high precision IFOG. Therefore the forward chain can be considered as a proportional component with uncertain parameters. The proportional factor of the forward chain, denoted as k_1, is determined not only by the parameters of detection circuit but also by the interference intensity. We define the variation of proportional factor k_1 as Δk_1, which reflects the effect of temperature drift on the forward channel. Because the variation range of the gain of the forward channel is bounded, we can denote $\Delta k = HFE$, where H and E are constant matrices with appropriate dimensions describing the parameters' variation of the optical path and detection circuit caused by temperature drift in the forward channel, respectively, and F is an uncertain matrix with appropriate dimension that satisfies $F^T F \le I$. As for the interference intensity I_0, the gain of high pass filter k_H, and the gain of A/D converter k_{AD}, respectively, we can derive $k_1 = I_0 \cdot k_H \cdot k_{\mathrm{AD}}$. In the feedback chain, due to the limited range of D/A converter, the digital phase is reset periodically at the digital level of $2^{n_{\mathrm{DA}}}$ corresponding to 2π, where n_{DA} is the conversion bit of the D/A converter. The proportional factor of the feedback chain k_m is a constant value satisfying $k_m = 2\pi/2^{n_{\mathrm{DA}}} = K_{\mathrm{D/A}} \cdot K_{\mathrm{dri}} \cdot K_{\mathrm{IOPM}}$, where $K_{\mathrm{D/A}}$, K_{dri}, and K_{IOPM} are the proportional factors of D/A converter, D/A drive circuit, and IOPM, respectively. Then, the feedback phase can be described as $\Delta\varphi_f(k) = k_m u(k)$, where $u(k)$ is the linear controller described by $u(k) = -k_m K_c x(k)$. $K_c \in R^{1\times n}$ is the feedback-gain matrix. The time-delay of the low-pass filter is confined by the closed-loop period, and the nonlinear characteristic of optical interference link deteriorates the high precision IFOG's dynamic performance.

Based on the proposed detection equipment, in consideration of the influence of optical nonlinearity, optical parameter uncertainty, and time-delay of low-pass filter, the mathematic model of high precision IFOG can be described by

$$\begin{aligned} x(k+1) = {} & Ax(k) + B(k_1 + \Delta k_1)\sin\left(-k_m K_c x(k)\right) \\ & + B(k_1 + \Delta k_1)\sum_{i=1}^{d}\beta_i \sin\left(-k_m K_c x(k-i)\right), \end{aligned} \tag{2}$$

where $x \in R^n$ is the state vector with the initial condition $x(k_0)$ for the zero sampling time,

$$A = \begin{bmatrix} 1 & 1 & 0 & \cdots \\ 0 & 1 & 1 & \cdots \\ \cdots & \cdots & \cdots & \cdots \\ 0 & \cdots & 0 & 1 \end{bmatrix}, \qquad B = \begin{bmatrix} 0 \\ 0 \\ \cdots \\ 1 \end{bmatrix}. \tag{3}$$

To extract the closed-loop error quickly and optimize the dynamic response characteristic, we assume that the order of low-pass filter is $d = 1$.

Now, we investigate the method of designing feedback-gain matrix K_c for improving the dynamic performance of system (2) with the initial condition $x(k_0)$. Before the discussion of the main theorem for the design of feedback-gain matrix, some useful definition and lemmas are first elucidated.

Definition 1 (see [17]). System (2) is said to be exponentially stable, if there exist some scalars $\kappa \ge 0$ and $0 < \alpha < 1$, such that the solution $x(k)$ of system (2) satisfies $\|x(k)\|^2 < \kappa(1-\alpha)^{k-k_0}\|x(k_0)\|^2$, for all $k \ge k_0$.

Lemma 2 (see [18] (the Schur complement)). *For a given symmetric matrix S with the form $S = [S_{ij}]$, $S_{11} \in R^{r\times r}$, $S_{12} \in R^{r\times(n-r)}$, and $S_{22} \in R^{(n-r)\times(n-r)}$, $S < 0$ if and only if $S_{11} < 0$, $S_{22} - S_{21}S_{11}^{-1}S_{12} < 0$ or $S_{22} < 0$, $S_{11} - S_{12}S_{22}^{-1}S_{21} < 0$.*

Lemma 3 (see [18]). *Suppose that $x \in R^p$, $y \in R^q$, and H and E are constant matrices with appropriate dimensions. For any appropriate dimension matrix F satisfying $F^T F \le I$, one has that $2x^T DFEy \le \varepsilon x^T DD^T x + (1/\varepsilon)y^T E^T Ey$ for any $\varepsilon > 0$.*

In the following discussions, we are interested in analyzing the stability of the IFOG and finding the design rules of the feedback-gain matrix K_c to guarantee that the high precision IFOG achieves exponentially dynamic response characteristic.

Theorem 4. *System* (2) *locally solves the exponential stability problem, if there exist positive definite matrices $P, Q, R \in R^{n\times n}$, the feedback-gain matrix $K_c \in R^{1\times n}$, and positive scalars α, ε_1, ε_2 such that*

$$\psi = \begin{bmatrix} \varphi & \varsigma_1^T R & \varsigma_2^T R & 0 \\ * & -P & 0 & PH \\ * & * & -R & RH \\ * & * & * & -\varepsilon_3 I \end{bmatrix} < 0, \tag{4}$$

where

$$\varsigma_1 = \begin{bmatrix} A & 0 & Bk_1 & Bk_1 \end{bmatrix},$$

$$\varsigma_2 = \begin{bmatrix} A - I & 0 & Bk_1 & Bk_1 \end{bmatrix},$$

$$\varphi = \begin{bmatrix} -(1-\alpha)P + Q - (1-\alpha)R & (1-\alpha)R & \frac{1}{2}\varepsilon_1 k_m K_c^T & 0 \\ * & -(1-\alpha)(Q+R) & 0 & \frac{1}{2}\varepsilon_2 k_m K_c^T \\ * & * & -\varepsilon_1 I + \varepsilon_3 E^T E & \varepsilon_3 E^T E \\ * & * & * & -\varepsilon_2 I \end{bmatrix}. \tag{5}$$

Proof. See the Appendix. □

We use a Lyapunov-based approach to analyze the convergence and the dynamic performance analysis of the high precision IFOG. Theorem 4 provides a sufficient condition to design the control matrix K_c for the high precision IFOG with time-delay, nonlinearity, and uncertainty, which guarantees that the system can achieve exponential stabilization. It also should be pointed out that, as deduced from the theoretical analysis on the stability of IFOG, the designed controller can make the dynamic errors of nonlinear IFOG within $(-\pi, \pi)$ exponentially converge to zeros, which are only dependent on the uncertain intensity of light power and the range of time-delay of the low-pass filter. At the same time, the results reveal that the proposed controller has strong robustness, so that the interference intensity is tolerant of temperature shift in a certain range. The theoretical result is of significant importance to the design of good dynamic detection method for the high precision IFOG under complex conditions of engineering application.

5. Experiment Results

Experiments are conducted to demonstrate the effectiveness of the previously obtained theoretical results and the dynamic measurement precision of the 0.01 deg/h IFOG using the optimized control algorithm. In the experiments, the light power is placed in a temperature control chamber where the temperature varies 5°C per minute to force the light power changeable in a certain range. We monitor the closed-loop state variables in real time to verify the ability of the designed high precision IFOG in suppressing the influence of parameter uncertainty, nonlinearity and time-delay on dynamic performance.

To validate the dynamic response characteristics of IFOG, the experiments are conducted to test the 50 Hz and 2 kHz frequency response, respectively. The excitation signal is generated by adding digital sinusoidal signal to the feedback phase ramp. We can control the applying time of excitation signal through the detection equipment. The digital signal processor synchronously receives the excitation signal and the output of IFOG so that the precise amplitude attenuation and phase delay can be measured. For the result of 50 Hz frequency response tests, the deterioration of amplitude is 0.3% and the phase delay is 0.4° as shown in Figure 6. In the 2 kHz frequency response tests with the results shown in Figure 7, the relative measurement error is 0.77% in amplitude and 3° in phase.

Then, to further validate the dynamic performance of IFOG with the proposed controller, the ramp response of the new high precision IFOG is compared with that of the previous high precision IFOG based on the assistant design setup. The results shown in Figure 8 demonstrate that there exists a dynamic tracking error in the previous high precision IFOG, which explains that the previous scheme of high precision detection reduces the dynamic performance of optical sensing. In contrast, the optimized detection scheme of the high precision IFOG can track the ramp signal rapidly without dynamic tracking error and better tracking performance is achieved as shown in Figure 9.

Furthermore, we conduct the experiments of tracking angular acceleration with 0.01 deg/h high precision IFOG utilizing the angular rotating platform. Angular rotating platform oscillates at frequency of 28 Hz so that the output of IFOG forms a sinusoidal trace at various oscillating points. The sinusoidal curve near the zero point can approximate to ramp response, and amplitude of angular acceleration can be controlled by the oscillating amplitude of angular rotating platform. On adopting previous control algorithm and our optimized control algorithm, the results are shown in Figures 10 and 11, respectively. We can see that the experiment results based on the angular rotating platform agree well with the results utilizing the assistant design setup, both of which verify that the optimized robust control algorithm can track the angular acceleration better than the previous control algorithm. All the above experiments demonstrate that the high precision IFOG system with our optimized control algorithm can effectively suppress the influence of parameter uncertainty, nonlinearity, and time-delay, so that a

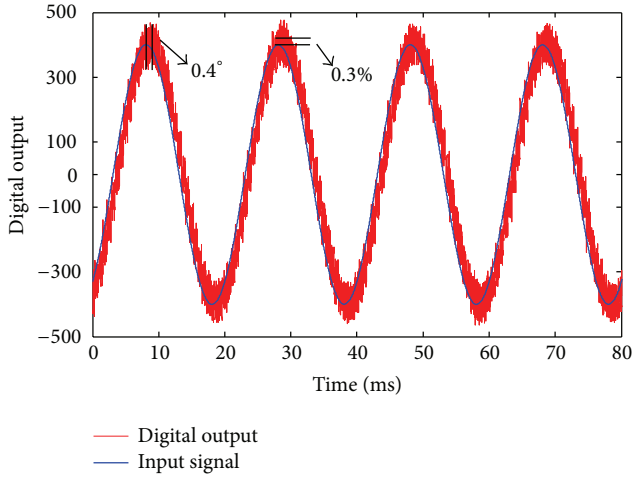

Figure 6: The result of the 50 Hz frequency response test of the optimized IFOG.

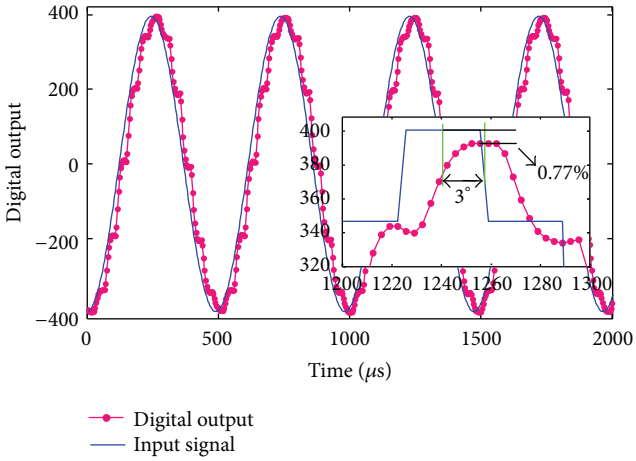

Figure 7: The result of the 2 kHz frequency response test of the optimized IFOG.

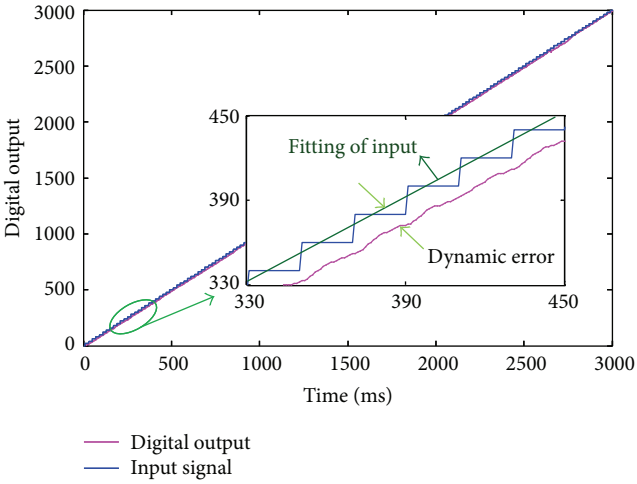

Figure 8: The result of the ramp response test of the previous 0.01 deg/h IFOG.

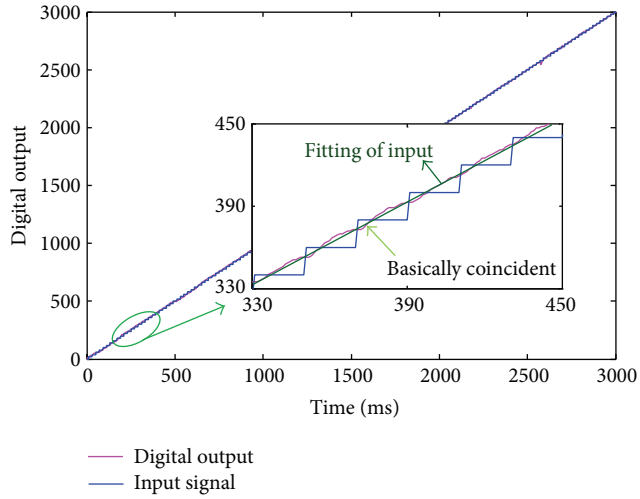

Figure 9: The result of the ramp response test of the optimized 0.01 deg/h IFOG.

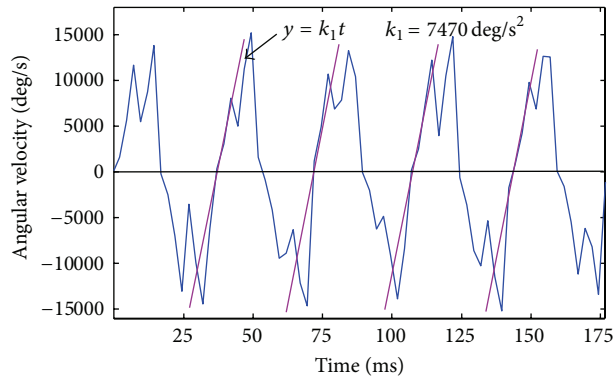

Figure 10: The output of 0.01 deg/h IFOG adopting previous control algorithm when the angular acceleration is 7470 deg/s^2.

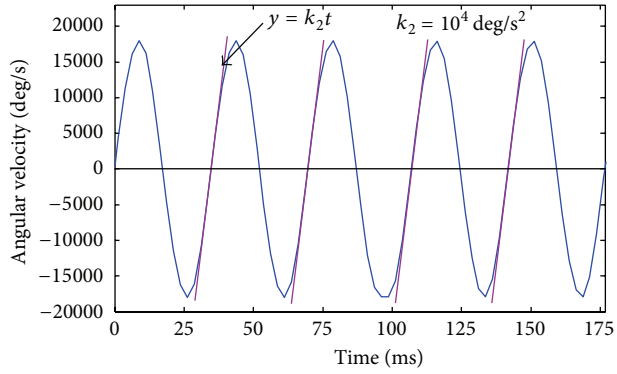

Figure 11: The output of 0.01 deg/h IFOG adopting our optimized control algorithm, when the angular acceleration is 10000 deg/s^2.

better dynamic measurement performance is achieved. These strategies could be applied in the engineering systems of high precision IFOGs to improve their dynamic measurement precision meeting the demand of inertial navigation systems.

6. Conclusion

In engineering practice, the closed-loop detection scheme can improve the measurement precision of IFOG. In this work, the influence of optical sensing and closed-loop signal detection on the dynamic performance of high precision IFOG is analyzed based on the established assistant design platform. We find that the several important facts that restrict the high dynamic property of IFOG include that (1) the interference link introduces the nonlinearity, (2) the optical parameter variation causes the light power fluctuation, and (3) the time of the light propagating through the fiber coil limits the closed-loop period and the time-delay of the low-pass filter. By taking these influencing factors into consideration, we propose a robust control algorithm to improve the dynamic characteristics of high precision IFOG. The obtained experiment results demonstrate the effectiveness of the proposed closed-loop design method. The improved dynamic measurement precision is of great significance in expanding the scope of application of IFOG.

Appendix

Proof of Theorem 4. We consider the main influencing factors to obtain the exponential stability condition of the high precision IFOG system. The following Lyapunov function is chosen for system (2):

$$V(k) = x^T(k) Px(k) + \sum_{s=k-d}^{k-1} x^T(s) (1-\alpha)^{k-s-1} Qx(s) + d \sum_{s=-d}^{-1} \sum_{m=k+s}^{b-1} \eta^T(k) (1-\alpha)^{k-m-1} R\eta(k), \tag{A.1}$$

where $\eta(k) = x(k+1) - x(k)$ and P, Q, and R are defined as those in Theorem 4.

Calculating $\Delta V(k) = V(k+1) - V(k)$ along the solution of system (2), we have that

$$\begin{aligned} &\Delta V(k) + \alpha \Delta V(k) \\ &\quad = x^T(k+1) Px(k+1) - (1-\alpha) x^T(k) Px(k) \\ &\qquad + x^T(k) Qx(k) - (1-\alpha)^d x^T(k-d) Qx(k-d) \\ &\qquad + d^2 \eta^T(k) R\eta(k) - d(1-\alpha)^d \sum_{m=k-d}^{k-1} \eta^T(m) R\eta(m). \end{aligned} \tag{A.2}$$

As $d = 1$ in the digital filter of the high precision IFOG, we have

$$\begin{aligned} &-d \sum_{m=k-d}^{k-1} \eta^T(m) R\eta(m) \\ &\quad = -(x(k) - x(k-1))^T R(x(k) - x(k-1)). \end{aligned} \tag{A.3}$$

We find that $\sin(x)$ satisfies the Lipschitz condition and is a monotonically ascending function for $x \in (-\pi, \pi)$. That is, there exists a function $M(k)$, such that $\sin(\Delta\varphi_f(k)) = M(k)\Delta\varphi_f(k)$ for $\Delta\varphi_f(k) \in (-\pi, \pi)$, where $\|M(k)\| \le l_f$ with $l_f = 1$. Then, the following inequality holds:

$$\sin\left(\Delta\varphi_f(k)\right)^T \left(\sin\left(\Delta\varphi_f(k)\right) - l_f \Delta\varphi_f(k)\right) \le 0, \tag{A.4}$$

where $\Delta\varphi_f(k) \in (-\pi, \pi)$.

For any two scalars $\varepsilon_1 > 0$ and $\varepsilon_2 > 0$, we have that

$$\begin{aligned} &\Delta V(k) + \alpha \Delta V(k) \\ &\quad \le \Delta V(k) + \alpha \Delta V(k) \\ &\qquad - \varepsilon_1 \sin\left(\Delta\varphi_f(k)\right)^T \left(\sin\left(\Delta\varphi_f(k)\right) - l_f \Delta\varphi_f(k)\right) \\ &\qquad - \varepsilon_2 \sin\left(\Delta\varphi_f(k-1)\right)^T \left(\sin\left(\Delta\varphi_f(k-1)\right) - l_f \Delta\varphi_f(k-1)\right) \\ &\quad \le \xi^T(k) \left(\widetilde{\varphi} + \widetilde{\varsigma}_1^T P \widetilde{\varsigma}_1 + \widetilde{\varsigma}_2^T P \widetilde{\varsigma}_2\right) \xi(k), \end{aligned} \tag{A.5}$$

where

$$\begin{aligned} \widetilde{\varsigma}_1 &= \left[A \;\; 0 \;\; B\left(k + \Delta k_1\right) \;\; B\left(k + \Delta k_1\right)\right], \\ \widetilde{\varsigma}_2 &= \left[A - I \;\; 0 \;\; B\left(k + \Delta k_1\right) \;\; B\left(k + \Delta k_1\right)\right], \\ \xi(k) &= \left[x^T(k) \;\; x^T(k-1) \;\; \sin^T\left(\Delta\varphi_f(k)\right) \;\; \sin^T\left(\Delta\varphi_f(k-1)\right)\right]^T, \\ \widetilde{\varphi} &= \begin{bmatrix} -(1-\alpha)P + Q - (1-\alpha)R & (1-\alpha)R & \frac{1}{2}\varepsilon_1 k_m K_c^T & 0 \\ * & -(1-\alpha)(Q+R) & 0 & \frac{1}{2}\varepsilon_2 k_m K_c^T \\ * & * & -\varepsilon_1 I & 0 \\ * & * & * & -\varepsilon_2 I \end{bmatrix}. \end{aligned} \tag{A.6}$$

By Lemma 2, we can see that $\widetilde{\varphi}+\widetilde{\varsigma}_1^T P\widetilde{\varsigma}_1+\widetilde{\varsigma}_2^T P\widetilde{\varsigma}_2 < 0$, if and only if

$$\begin{bmatrix} \widetilde{\varphi} & \widetilde{\varsigma}_1^T P & \widetilde{\varsigma}_2^T R \\ * & -P & 0 \\ * & * & -R \end{bmatrix} < 0. \tag{A.7}$$

Because $\Delta k = HFE$, (A.7) can be rewritten as

$$\begin{bmatrix} \widetilde{\varphi} & \varsigma_1^T P & \varsigma_2^T R \\ * & -P & 0 \\ * & * & -R \end{bmatrix} + M^T F(k) N + N^T F^T(k) M < 0, \tag{A.8}$$

where ς_1 and ς_2 are defined as that in Theorem 4, $N = [0\ \ 0\ \ E\ \ E\ \ 0\ \ 0]$, and $M = [0\ \ 0\ \ 0\ \ 0\ \ H^T P\ \ H^T R]$.

By Lemma 3, (A.8) holds if and only if there exists a positive constant ε_3 such that

$$\begin{bmatrix} \widetilde{\varphi} & \varsigma_1^T P & \varsigma_2^T R \\ * & -P & 0 \\ * & * & -Q \end{bmatrix} + \varepsilon_3^{-1} M^T M + \varepsilon_3 N^T N < 0. \tag{A.9}$$

Thus a sufficient condition for $\Delta V(k) + \alpha V(k) < 0$ is equivalent to $\psi < 0$ by the Schur complement lemma. If $\Delta V(k) + \alpha V(k) < 0$, we have that $V(k) \le (1-\alpha)^{k-k_0} V(k_0)$ along any trajectory of system (2). Then, IFOG can obtain the exponential stability.

Furthermore, we have that

$$\begin{aligned} \lambda_1 x^T(k)\, x(k) &\le V(k) \\ &\le (1-\alpha)^{k-k_0} V(k) \\ &\le \lambda_2 (1-\alpha)^{k-k_0} x^T(k_0)\, x(k_0), \end{aligned} \tag{A.10}$$

where $\lambda_1 = \min \lambda(P)$ is the minimum eigenvalue of P, $\lambda_2 = \max \lambda(P) + d \max \lambda(Q) + 2d^2(d+1) \max \lambda(R)$, and $\max \lambda(\cdot)$ is the maximum eigenvalue of the matrix.

That means that $\|x(k)\| \le \sqrt{\lambda_1/\lambda_2}(1-\alpha)^{k-k_0}\|x(k_0)\|$ by (A.10) and we can conclude that system (2) is locally and exponentially stable. This completes the proof. □

Acknowledgments

This work was supported by the National Aeronautics Foundation of China (no. 20100851016) and the National Natural Science Foundation of China (no. 61101007).

References

[1] G. M. Williams and E. J. Friebele, "Space radiation effects on erbium-doped fiber devices: sources, amplifiers, and passive measurements," *IEEE Transactions on Nuclear Science*, vol. 45, no. 3, pp. 1531–1536, 1998.

[2] J. Jin, H. Tian, N. Song, and C. Zhang, "Stellar sensor assistant fiber optic gyroscope drift extraction," *Transactions of the Japan Society for Aeronautical and Space Sciences*, vol. 53, no. 179, pp. 40–46, 2010.

[3] H. C. Lefevre, *The Fiber-Optic Gyroscope*, Artech House, London, UK, 1993.

[4] N. Barbour and G. Schmidt, "Inertial sensor technology trends," *IEEE Sensors Journal*, vol. 1, no. 4, pp. 332–339, 2001.

[5] R. Zhu, Y. Zhang, and Q. Bao, "A novel intelligent strategy for improving measurement precision of FOG," *IEEE Transactions on Instrumentation and Measurement*, vol. 49, no. 6, pp. 1183–1188, 2000.

[6] R. Azor, I. Y. Bar-Itzhack, J. K. Deutschmann, and R. R. Harman, "Angular-rate estimation using delayed quaternion measurements," *Journal of Guidance, Control, and Dynamics*, vol. 24, no. 3, pp. 436–443, 2001.

[7] S. J. Spammer and P. L. Swart, "Open-loop fibre optic gyroscope with wide dynamic range and source variation insensitivity," in *Proceedings of the 15th Anniversary Conference on SPIE Fiber Optic Gyros*, vol. 1585, pp. 215–225, 1992.

[8] A. Ohno, S. Motohara, S. Usul et al., "Development of fiber-optic-gyroscope with environmental ruggedness," in *Proceedings of the 15th Anniversary Conference on SPIE Fiber Optic Gyros*, pp. 82–88, 1992.

[9] R. C. Rabelo, R. T. de Carvalho, and J. Blake, "SNR enhancement of intensity noise-limited FOGs," *Journal of Lightwave Technology*, vol. 18, no. 12, pp. 2146–2150, 2000.

[10] J. Jin and S. Lin, "Parameters optimization of interferometric fiber optic gyroscope for improvement of random walk coefficient degradation in space radiation environment," *Optics and Lasers in Engineering*, vol. 50, pp. 1106–1112, 2013.

[11] J. Kunz, M. W. Kemmier, G. Spahlinger et al., "Design of an ASIC for a commercial small volume fiber optic gyro," in *Proceedings of the 20th Anniversary Conference on SPIE Fiber Optic Gyros*, vol. 2837, pp. 98–105, 1996.

[12] G. Spahlinger, M. Kemniler, M. Ruf et al., "Error compensation via signal correlation in high precision closed-loop fiber optic gyros," in *Proceedings of the 20th Anniversary Conference on SPIE Fiber Optic Gyros*, vol. 2837, pp. 218–227, 1996.

[13] S. J. Sanders, J. E. Lewis, S. Mosor et al., "Systems and methods for environmentally insensitive high-performance fiber-optic gyroscopes," US 2013/0044328 A1.

[14] G. A. Sanders, R. C. Dankwort, and R. A. Bergh, "Vibration rectification error reducer for fiber optic gyroscope," US 5,946,097.

[15] H. Chung, L. Ojeda, and J. Borenstein, "Sensor fusion for mobile robot dead-reckoning with a precision-calibrated fiber optic gyroscope," in *Proceedings of the IEEE International Conference on Robotics and Automation (ICRA '01)*, pp. 3588–3593, May 2001.

[16] Y.-S. Zhang, Y. Wang, T. Yang, R. Yin, and J. Fang, "Dynamic angular velocity modeling and error compensation of one-fiber fiber optic gyroscope (OFFOG) in the whole temperature range," *Measurement Science and Technology*, vol. 23, no. 2, Article ID 025101, 2012.

[17] D. Zhang, L. Yu, and W. A. Zhang, "Exponential H_∞ filtering for a class of switched stochastic hybrid systems with mixed time delays and random missing measurements," *Asian Journal of Control*, vol. 14, no. 3, pp. 807–816, 2013.

[18] S. Boyd, L. El Ghaoui, E. Feron, and V. Balakrishnan, *Linear Matrix Inequalities in System and Control Theory*, vol. 15, Society for Industrial and Applied Mathematics (SIAM), Philadelphia, Pa, USA, 1994.

Hindawi Publishing Corporation
Mathematical Problems in Engineering
Volume 2013, Article ID 967574, 13 pages
http://dx.doi.org/10.1155/2013/967574

Research Article

Finite-Time Anti-Disturbance Inverse Optimal Attitude Tracking Control of Flexible Spacecraft

Chutiphon Pukdeboon and Anuchit Jitpattanakul

Department of Mathematics, Faculty of Applied Science, King Mongkut's University of Technology North Bangkok, Bangkok 10800, Thailand

Correspondence should be addressed to Chutiphon Pukdeboon; cpd@kmutnb.ac.th

Received 4 September 2013; Accepted 25 November 2013

Academic Editor: Baoyong Zhang

We propose a new robust optimal control strategy for flexible spacecraft attitude tracking maneuvers in the presence of external disturbances. An inverse optimal control law is designed based on a Sontag-type formula and a control Lyapunov function. An adapted extended state observer is used to compensate for the total disturbances. The proposed controller can be expressed as the sum of an inverse optimal control and an adapted extended state observer. It is shown that the developed controller can minimize a cost functional and ensure the finite-time stability of a closed-loop system without solving the associated Hamilton-Jacobi-Bellman equation directly. For an adapted extended state observer, the finite-time convergence of estimation error dynamics is proven using a strict Lyapunov function. An example of multiaxial attitude tracking maneuvers is presented and simulation results are included to show the performance of the developed controller.

1. Introduction

Optimal control for spacecraft rotational problems has attracted a great deal of interest. The problem of optimal attitude control has been studied by many researchers (see, e.g., [1–4]). The main objective of optimal attitude control is to design a controller that stabilizes the attitude of a spacecraft system to an equilibrium state and minimizes some performance criterion for the stabilization process. Generally for linear systems, the linear quadratic regulator (LQR) is able to ensure an optimal and asymptotically stable solution. In [5] the LQR method was extended to a nonlinear control problem but more constraints were required to meet the optimality and stability conditions. Various nonlinear optimal control methods have been proposed for solving the attitude control problem. Sharma and Tewari [6] devised a Hamilton-Jacobi formulation for tracking attitude maneuvers of spacecraft to derive a nonlinear optimal control law. In [7] optimal controllers for a programmed motion of a rigid spacecraft were designed using the optimal Lyapunov approach. In [8, 9] state-dependent Riccati equation (SDRE) techniques were successfully applied to spacecraft attitude control. In [10] a class of globally asymptotically stabilizing controllers was developed for the complete attitude motion of a nonsymmetric rigid body. An inverse optimal control approach was presented in [11] to construct the optimal controller for regulation of the rigid body. Recently, attitude controller designs for rigid spacecraft using inverse optimal control schemes have been developed [12]. The inverse optimal control method incorporates the task of solving a Hamilton-Jacobi-Bellman equation and offers a globally asymptotically stabilizing control law which is optimal with respect to a performance index. Sontag's formula [13] uses the directional information supplied by a control Lyapunov function (CLF). Freeman and Kokotovic [14] have shown that every CLF solves the Hamilton-Jacobi-Bellman (HJB) equation associated with a meaningful cost. In other words, if we have a CLF for a nonlinear system, we can compute the resulting optimal control law without solving the HJB equation.

As extensions of the above studies, optimal control and robust control have been merged to obtain robust optimal control laws. Various methods for developing robust optimal controllers for the attitude control of a rigid spacecraft have

been proposed in the literature. Kang [15] used nonlinear H_∞ control to design a stabilizing feedback control for the spacecraft tracking problem. Luo et al. [16] developed an H_∞ inverse optimal adaptive controller for attitude tracking of spacecraft. Adaptive control and nonlinear H_∞ control have also been merged to design robust optimal controllers. Park [17] proposed a robust optimal control scheme for attitude stabilization and used a minimax approach and inverse optimal approach to examine the optimality property of this control law. Due to its lower dependence on model information and its strong capability for estimating disturbance and simple structure, an extended state observer (ESO) [18] has been widely used to deal with various kinds of engineering control problems such as flight control and chemical process control. In [19] the ESO based disturbance rejection control approach has been addressed for attitude tracking of a rigid spacecraft. The vibration effect of flexible appendages was not considered in the attitude control design. An alternative way to design a robust optimal controller is to use an optimal sliding mode controller design scheme. Sliding mode control (SMC) is a very effective approach when applied to a system with disturbances which satisfy the matched uncertainty condition [20]. Pukdeboon and Zinober [21, 22] have developed robust optimal control laws based on the optimal sliding mode control technique for attitude tracking of spacecraft. However, since the attitude control system of flexible spacecraft is quite complicated, optimal sliding mode control has rarely been studied for attitude control design. SDRE-based optimal sliding mode (SM) control and optimal Lyapunov-based SM control approaches have been used in [23] to design optimal controllers for attitude stabilization of flexible spacecraft. However, the optimal controllers developed in that paper contain some drawbacks. The SDRE approach usually provides only local asymptotic stability while for the optimal Lyapunov approach it is a formidable task to choose a Lyapunov function to satisfy the partial differential equation derived from the Krasovskii theorem [24].

In this paper, a novel control methodology for flexible spacecraft attitude maneuvers is proposed in the presence of external disturbances. First, an inverse optimal controller for stabilizing systems is designed based on a Sontag-type formula [25, 26] and a finite-time control Lyapunov function (FTCLF) [27, 28]. Then, the total disturbance is estimated by an adapted ESO which is a modified version of the traditional ESO in [18, 29]. The stability of the traditional ESO [18] has been proved using the self-stable region (SSR) approach [30], but this approach takes many steps and is rather complicated. In this paper the finite-time convergence of an adapted ESO is proved by using a strict Lyapunov function. The proposed new attitude controller for flexible spacecraft enforces tracking motion, robustness, and optimality with respect to a family of cost functionals and achieves disturbance rejection.

The main contributions of this paper are as follows.

(i) An inverse optimal control method for flexible spacecraft attitude tracking maneuvers is proposed for the first time in this paper.

(ii) A second-order sliding mode based disturbance compensator is developed and combined with the proposed attitude controller. The necessity of a compensator is also discussed.

(iii) The hybrid control method is used to develop a controller with complete robustness under the system uncertainty and external disturbances.

This paper is organized as follows. Section 2 introduces some preliminary results which are required for the following discussion. In Section 3 the dynamic equations of a flexible spacecraft and the attitude kinematics [31, 32] are described. Section 4 provides the problem statement and control objective. Section 5 proposes a finite-time inverse optimal control design with the FTCLF concepts. We design an inverse optimal controller that provides the convergence of system states to the desired attitude motion. In Section 6, an adapted ESO method is used to develop an anti-disturbance feedback controller. The finite-time convergence of estimation error dynamics is proved using a strict Lyapunov function. In Section 7, an example of spacecraft attitude maneuvers is presented to illustrate the performance of the developed control law. In Section 8, we present conclusions.

2. Mathematical Preliminaries

2.1. Finite-Time Stability. We now restate the concepts related to finite-time stability [33, 34].

Definition 1 (see [33]). Consider a time invariant system in the form of

$$\dot{x} = f(x), \quad f(0) = 0 \quad x \in \mathscr{R}^n, \tag{1}$$

where $f : \widehat{U}_0 \to \mathscr{R}^n$ is continuous on an open neighborhood $\widehat{U}_0$ of the origin. The equilibrium $x = 0$ of the system is (locally) finite-time stable if (i) it is asymptotically stable, in $\widehat{U}$, an open neighborhood of the origin, with $\widehat{U} \subset \widehat{U}_0$ and (ii) it is finite-time convergent in $\widehat{U}$; that is, for any initial condition $x_0 \in \widehat{U} \setminus \{0\}$, there is a settling time $T > 0$ such that every solution $x(t, x_0)$ of system (1) is defined with $x(t, x_0) \in \widehat{U} \setminus \{0\}$ for $t \in [0, T]$ and satisfies

$$\lim_{t \to T(x_0)} x(t, x_0) = 0 \tag{2}$$

and $x(t, x_0) = 0$, if $t \geq T$. Moreover, if $\widehat{U} = \mathscr{R}^n$, the origin is globally finite-time stable.

Definition 2. Consider a controlled system

$$\dot{x} = f(x) + b(x)u, \quad x \in \mathscr{R}^n, \ u \in \mathscr{R}^m, \tag{3}$$

with $b(x) \neq 0$. It is finite-time stabilizable if there is a feedback law $u(x)$ such that $x = 0$ is a (locally) finite-time stable equilibrium of the closed-loop system.

Lemma 3 (see [34]). *Consider the nonlinear system described in* (1). *Suppose there is a* C^1 *function* $V(x)$ *defined on a neighborhood* $\widehat{U} \subset U_0 \subset \mathscr{R}^n$ *of the origin such that the*

following conditions hold: (i)$V(x)$ *is positive definite on* $\widehat{U}$ *and* (ii) *there are real numbers* $\varrho > 0$ *and* $0 < \iota < 1$, *such that*

$$\dot{V}(x) + \varrho(V(x))^{\iota} \leq 0, \quad x \in \widehat{U} \setminus \{0\}. \tag{4}$$

Then, the origin of system (1) *is locally finite-time stable, with its settling time*

$$T \leq \frac{V(x_0)^{1-\iota}}{\varrho(1-\iota)}. \tag{5}$$

If $\widehat{U} = \mathcal{R}^n$ *and* $V(x)$ *is radially unbounded, then the origin of system* (1) *is globally finite-time stable.*

2.2. Finite-Time Control Lyapunov Function. Based on the definition of a finite-time control Lyapunov function (FTCLF) in [27, 28], we provide the following definitions.

Definition 4 (see [27, 28]). Let U_0 be a neighborhood of the origin. A positive-definite and C^1 function $V : U_0 \to R^+$ is called a finite-time control Lyapunov function (FTCLF) of system (3) if there exist real numbers $c_1 > 0$ and $\alpha \in (0, 1)$ such that for all $x \in U_0 \setminus \{0\}$,

$$\inf_u \left\{ L_f V(x) + L_b V(x) u \right\} \leq -c_1 (V(x))^{\alpha}, \tag{6}$$

where $L_f V(x)$ and $L_b V(x)$ are the Lie derivatives of V along the solution of system (3).

Note that the Lie derivative of V with respect to $h : R^n \to R^n$ is defined as the inner product of h and the gradient of V; that is, $L_h V(x) = (\partial V/\partial x)h$.

Obviously, if (6) holds, then for all $\in U_0 \setminus \{0\}$, the condition that $V(x)$ is a FTCLF of (3) is precisely the statement

$$L_b V = 0 \Longrightarrow L_f V < -c_1 (V(x))^{\alpha}. \tag{7}$$

In fact, if there exists a positive-definite and C^1 function $V : U_0 \to R^+$ such that (7) holds, then V is a FTCLF of system (3). Note that if $V(x)$ is a continuous positive-definite function, then $L_f V(x)$ and $L_b V(x)$ can be seen as Dini derivatives.

Definition 5 (see [27]). $V(x)$ is said to satisfy the extended small control property with respect to system (3) if, for all $\epsilon > 0$, there exists $\varepsilon > 0$ such that if $x \neq 0$ and $\|x\| < \varepsilon$, then there exists a certain u with $\|u\| < \epsilon$, such that $L_f V(x) + L_b V(x) u \leq -c_1 (V(x))^{\alpha}$, where $c_1 > 0$ and $\alpha \in (0, 1)$.

2.3. The Inverse Optimal Control Problem. This subsection considers the design of finite-time inverse optimal control. A feedback control law $u(x)$ for the system (3) will be designed such that the closed-loop system is finite-time stable at the equilibrium $x = 0$ and minimizes the cost functional

$$I(u, x, x_0) = \int_0^{T(x)} \left(l(x) + u^T R u \right) dt, \tag{8}$$

where $l(x) \geq 0$ and $R(x) > 0$ for all x and $T(x)$ is the settling time function.

According to the theorem in [11, 27], if $V(x)$ is a FTCLF for the system (3), then a stabilizing control law

$$u(x) = \alpha^*(x) = -\frac{1}{2} R^{-1}(x) \left(L_b V(x) \right)^T \tag{9}$$

solves an inverse optimal control problem for the system (3) with respect to the cost functional (8).

Moreover, if we choose

$$l(x) = -L_f V(x) - \frac{1}{2} L_b V(x) \alpha^*(x), \tag{10}$$

then $l(x) \geq 0$ is achieved with the control law $u = (1/2)\alpha^*$. Next, substituting $u = (1/2)\alpha^*$ into (10), we obtain the HJB equation

$$l(x) = -L_f V(x) + \frac{1}{4} L_b V(x) R^{-1}(x) \left(L_b V(x) \right)^T \geq 0. \tag{11}$$

Then, using the concept in [27], we have that $V(x)$ is the solution of the HJB equation (11).

Remark 6. In the inverse optimal approach, a finite-time stabilizing feedback control law $u(x)$ is designed first and then it is shown that the feedback law is to find $l(x) \geq 0$ and $R(x) > 0$ such that u optimizes (8). The problem is inverse because the functions $l(x)$ and $R(x)$ are a posteriori found by the stabilizing feedback law, rather than a priori selected by the designer.

3. Mathematical Model of Flexible Spacecraft

We now briefly explain the use of quaternions for description of the attitude error. We define the quaternion $Q = [q^T \ \ q_4]^T \in \mathcal{R}^3 \times \mathcal{R}$ with $q = [q_1 \ \ q_2 \ \ q_3]^T \in \mathcal{R}^3$ and

$$Q_d = \left[q_d^T \ \ q_{4d} \right]^T, \tag{12}$$

where $q_d = [q_{1d} \ \ q_{2d} \ \ q_{3d}]^T \in \mathcal{R}^3$ is the desired reference attitude. The quaternion for the attitude error is $Q_e = [q_e^T \ \ q_{4e}]^T \in \mathcal{R}^3 \times \mathcal{R}$ with $q_e = [q_{1e} \ \ q_{2e} \ \ q_{3e}]^T \in \mathcal{R}^3$. Using the multiplication law for quaternions, we then obtain

$$Q_e = \begin{bmatrix} q_{4d} q - q_4 q_d - q_d^{\times} q \\ q_4 q_{4d} + q^T q_d \end{bmatrix} \tag{13}$$

subject to the constraint

$$Q_e^T Q_e = \left(q^T q + q_4^2 \right) \left(q_d^T q_d + q_{4d}^2 \right) = 1. \tag{14}$$

In (13) $q_d^{\times}$ is given by

$$q_d^{\times} = \begin{bmatrix} 0 & -q_{3d} & q_{2d} \\ q_{3d} & 0 & -q_{1d} \\ -q_{2d} & q_{1d} & 0 \end{bmatrix}. \tag{15}$$

Remark 7. A quaternion consists of the scalar q_4 and the three-dimensional vector q, so it has four components. The scalar term is used for avoidance of singular points in the attitude representation [35]. The quaternion kinematics equation is required to be solved for all four components. However, to indicate the maneuver of the spacecraft, it is sufficient to use only the vector q because this vector properly represents both Euler axis and Euler angle. Furthermore, the scalar q_4 can be calculated easily using the vector q and the condition $\|Q\| = 1$. For more details of quaternion and other attitude representation see [31, 35].

The kinematic equation for the attitude error can then be expressed as (see, [31, 36])

$$\dot{Q}_e = \frac{1}{2}\begin{bmatrix} T(Q_e) \\ -q_e^T \end{bmatrix}\omega_e, \tag{16}$$

where $T(Q_e) = q_e^{\times} + q_{4e}I_3$ with I_3being the 3×3 identity matrix.

The equation governing a flexible spacecraft is expressed as [32]

$$J\dot{\omega} + \delta^T\ddot{\eta} = -\omega^{\times}\left(J\omega + \delta^T\dot{\eta}\right) + u + d, \tag{17a}$$

$$\ddot{\eta} + C\dot{\eta} + K\eta = -\delta\dot{\omega}, \tag{17b}$$

where $J = J^T$ is the total inertia matrix of the spacecraft, η is the modal displacement, and δ is the coupling matrix between the central rigid body and the flexible attachments. $u \in \mathcal{R}^3$ denotes the control input, $d \in \mathcal{R}^3$ represents the external disturbances, and K and C denote the stiffness and damping matrices, respectively, which are defined as

$$K = \operatorname{diag}\left(\omega_{ni}^2, i = 1, 2, \ldots, N\right), \tag{18}$$

$$C = \operatorname{diag}\left(2\zeta_i\omega_{ni}, i = 1, 2, \ldots, N\right) \tag{19}$$

with damping ζ_i and natural frequency ω_{ni}.

We denote by $\omega_d = [\omega_{1d} \;\; \omega_{2d} \;\; \omega_{3d}]^T$ the desired angular velocity and by $\omega_e = \omega - \omega_d$ as the angular velocity error. Let

$$\vartheta = \begin{bmatrix} \eta \\ \psi \end{bmatrix}, \tag{20}$$

where $\psi = \dot{\eta} + \delta\omega_e$. The relative dynamic equation can be written as [36]

$$\begin{aligned}\dot{\omega}_e = J_{mb}^{-1}\Big[&-\left(\omega_e^{\times} + \omega_d^{\times}\right)\left(J_{mb}\omega_e + \delta^T\psi + J\omega_d\right) \\ &+\delta^T\left(C\psi + K\eta - C\delta\omega_e\right) + u + d\Big] - \dot{\omega}_d,\end{aligned} \tag{21}$$

$$\dot{\vartheta} = A\vartheta + B\omega_e + D\dot{\omega}_d,$$

where $\dot{\omega}_d$ is the first time derivative of ω_d. The matrices J_{mb}, AB, and D are given as

$$\begin{aligned} J_{mb} &= J - \delta^T\delta, \\ A &= \begin{bmatrix} 0_{4\times4} & I_4 \\ -K & -C \end{bmatrix}, \qquad B = \begin{bmatrix} -\delta \\ C\delta \end{bmatrix}, \qquad D = \begin{bmatrix} 0_{4\times3} \\ -\delta \end{bmatrix}. \end{aligned} \tag{22}$$

Clearly, A is a Hurwitz matrix.

If we let

$$x(t) = \left[\omega_e^T \;\; q_{4e} \;\; q_e^T \;\; \vartheta^T\right]^T, \tag{23}$$

then the spacecraft systems (16), (17a), and (17b) can be expressed in the state space form as

$$\dot{x} = f(x) + b(x)u + b(x)d, \qquad x(0) = x_0, \tag{24}$$

$$f(x) = \begin{bmatrix} J_{mb}^{-1}\Xi\left(\omega_e, \omega_d, \dot{\omega}_d\right) \\ -0.5q_e^T\omega_e \\ 0.5\left(q_e^{\times} + q_{4e}I_3\right)\omega_e \\ A\vartheta + B\omega_e + D\dot{\omega}_d \end{bmatrix}, \qquad b(x) = \begin{bmatrix} J_{mb}^{-1} \\ 0_{1\times3} \\ 0_{3\times3} \\ 0_{8\times3} \end{bmatrix}, \tag{25}$$

where

$$\begin{aligned}\Xi\left(\omega_e, \omega_d, \dot{\omega}_d\right) = &-\omega_e^{\times}J_{mb}\omega_e - \omega_e^{\times}\delta^T\psi - \omega_e^{\times}J\omega_d - \omega_d^{\times}J_{mb}\omega_e \\ &- \omega_d^{\times}\delta^T\psi - \omega_d^{\times}J\omega_d + \delta^T\left(C\psi + K\eta - C\delta\omega_e\right) \\ &- J_{mb}\dot{\omega}_d.\end{aligned} \tag{26}$$

4. Problem Statement

In this work we consider tracking maneuvers. The control objective is to realize desired rotations of flexible spacecraft in the presence of external disturbances and minimize a cost functional. In other words, we shall find a controller u subject to (24) such that for all initial conditions the desired rotations are achieved

$$\lim_{t\to T} q_e = 0, \quad \lim_{t\to T} q_{4e} = 1, \quad \lim_{t\to T} \omega_e = 0 \tag{27}$$

and the cost functional (8) is minimized. Note that, when $q_e \to 0$, we have $q_{4e} \to 1$, due to the constraint relation $q_e^T q_e + q_{4e}^2 = 1$.

5. Inverse Optimal Controller Design for Flexible Spacecraft

In this section, we first propose a finite-time inverse optimal controller for stabilizing the complete attitude motion of flexible spacecraft in the presence of external disturbances.

In order to design this controller for solving the finite-time inverse optimal problem we first choose a FTCLF for the system (24) as the following candidate positive-definite function:

$$\begin{aligned}V(x) = &\frac{1}{2}\omega_e^T J_{mb}\omega_e + \beta\left(q_{4e} - 1\right)^2 + \beta q_e^T q_e \\ &+ \frac{1}{2}\vartheta^T P\vartheta + \gamma q_e^T J_{mb}\omega_e,\end{aligned} \tag{28}$$

where β and γ are nonnegative constants and P is a positive-definite matrix that is a solution of the Lyapunov equation $A^T P + PA = -Q_A$ with a positive-definite matrix Q_A.

Assumption 8. The desired angular velocity vector and its first time derivative are bounded and satisfy the following conditions:

$$\|\omega_d\| \le W_1, \qquad \|\dot{\omega}_d\| \le W_2, \tag{29}$$

where W_1 and W_2 are positive constants.

We next show that the function $V(x)$ defined in (28) is a FTCLF for the system (24) by using the following lemma.

Lemma 9. *In the absence of disturbance vector, under Assumption 8, the positive definite V defined in* (28) *is a FTCLF for the spacecraft tracking system* (24).

Proof. Since J_{mb} is symmetric positive definite, we can write $V(x)$ as

$$V = \overline{x}^T \Omega \overline{x} + \beta(q_{4e} - 1)^2, \tag{30}$$

where $\overline{x}(t) = \begin{bmatrix} \omega_e^T & q_e^T & \vartheta^T \end{bmatrix}^T$, and

$$\Omega = \frac{1}{2}\begin{bmatrix} J_{mb} & \gamma J_{mb} & 0_{3\times 8} \\ \gamma J_{mb} & 2\beta I_3 & 0_{3\times 8} \\ 0_{8\times 3} & 0_{8\times 3} & P \end{bmatrix}. \tag{31}$$

The conditions for $V(x)$ to be positive definite are

$$\beta > 0, \quad 2\beta J_{mb} > \gamma^2 J_{mb}^2. \tag{32}$$

Also, using (28) we can obtain the following inequalities:

$$\begin{aligned} &\sigma_{\min}(\Omega)\|\overline{x}\|^2 + \beta(q_{4e} - 1)^2 \\ &\le V \le \sigma_{\max}(\Omega)\|\overline{x}\|^2 + \beta(q_{4e} - 1)^2, \end{aligned} \tag{33}$$

where $\|\overline{x}\|$ denotes the Euclidean norm of $\overline{x}$ and $\sigma_{\min}(\Omega)$ and $\sigma_{\max}(\Omega)$ denote the minimum and maximum singular values of the matrix Ω.

The first time derivative of V can be obtained as

$$\frac{\partial V(x)}{\partial x} = \begin{bmatrix} J_{mb}\omega_e + \gamma J_{mb} q_e \\ 2\beta(q_{4e} - 1) \\ 2\beta J_{mb}\omega_e + \gamma q_e \\ \vartheta^T P \end{bmatrix}, \tag{34}$$

$$\begin{aligned} &\left[\frac{\partial V(x)}{\partial x}\right]^T \\ &= \begin{bmatrix} \omega_e^T J_{mb} + \gamma q_e^T J_{mb} & 2\beta(q_{4e} - 1) & \omega_e^T J_{mb}\beta + q_e^T\gamma & \vartheta^T P \end{bmatrix}. \end{aligned} \tag{35}$$

Thus, we have

$$\begin{aligned} &L_b V \\ &= \begin{bmatrix} \omega_e^T J_{mb} + \gamma q_e^T J_{mb} & 2\beta(q_{4e} - 1) & \omega_e^T \beta J_{mb} + q_e^T\gamma & \vartheta^T P \end{bmatrix} \\ &\quad \times \begin{bmatrix} J_{mb}^{-1} \\ 0_{1\times 3} \\ 0_{3\times 3} \\ 0_{8\times 3} \end{bmatrix} \\ &= \omega_e^T + q_e^T\gamma. \end{aligned} \tag{36}$$

Therefore, if $L_b V = 0$, we have

$$\omega_e^T = -\gamma q_e^T. \tag{37}$$

Next, we show that for all $x \neq 0$, if $L_b V = 0$, then $L_f V < -c_2 V^{1/2}$ with $c_2$being a positive constant. Here, $L_f V$ can be expressed as

$$\begin{aligned} L_f V &= \left(\omega_e^T J_{mb} + \gamma q_e^T J_{mb}\right)\left(J_{mb}^{-1}\Xi(\omega_e, \omega_d, \dot{\omega}_d)\right) \\ &\quad + 2\beta(q_{4e} - 1)\left(-\frac{1}{2}q_e^T\omega_e\right) + \beta q_e\left(q_e^{\times} + q_{4e}I_3\right)\omega_e \\ &\quad + \vartheta^T P\left(A\vartheta + B\omega_e + D\dot{\omega}_d\right). \end{aligned} \tag{38}$$

Substituting (37) in (38), we obtain

$$\begin{aligned} L_f V &= \beta(q_{4e} - 1)\gamma q_e^T q_e + \beta q_e\left(q_e^{\times} + q_{4e}I_3\right)(-\gamma q_e) \\ &\quad + \vartheta^T PA\vartheta + \vartheta^T PB(-\gamma q) + \vartheta^T PD\dot{\omega}_d. \end{aligned} \tag{39}$$

Since $q_e^{\times} q_e = 0$, (39) becomes

$$\begin{aligned} L_f V &\le -\beta\gamma q_e^T q_e - \frac{1}{2}\vartheta^T Q_A\vartheta - \gamma\vartheta^T PBq_e + \|\vartheta\|\,\|PD\|\,W_2 \\ &\le -\varpi^T\Pi_1\varpi + \|\vartheta\|\,\|PD\|\,W_2, \end{aligned} \tag{40}$$

where

$$\varpi = \begin{bmatrix} q_e \\ \vartheta \end{bmatrix}, \qquad \Pi_1 = \begin{bmatrix} \beta\gamma & \frac{\gamma}{2}PB \\ \frac{\gamma}{2}PB & \frac{1}{2}Q_A \end{bmatrix}. \tag{41}$$

With proper parameters β and γ, one can obtain that Π_1 is positive definite

$$\begin{aligned} L_f V &\le -\sigma_{\min}(\Pi_1)\|\varpi\|^2 + \|\varpi\|\,\|PD\|\,W_2 \\ &\le -\left(\sigma_{\min}(\Pi_1)\|\varpi\| - \|PD\|\,W_2\right)\|\varpi\|. \end{aligned} \tag{42}$$

From (33) we have $\sigma_{\min}(\Omega)\|\overline{x}\|^2 \le V$. Using $\|\varpi\| \le \|\overline{x}\|$, one has $\sigma_{\min}(\Omega)\|\varpi\|^2 \le V$ and it follows that $\|\varpi\| \le V^{1/2}/\sqrt{\sigma_{\min}(\Omega)}$. Thus, (42) becomes

$$L_f V \le -\left(\sigma_{\min}(\Pi_1)\|\varpi\| - \|PD\|\,W_2\right)\frac{V^{1/2}}{\sqrt{\sigma_{\min}(\Omega)}} \le -c_2 V^{1/2}, \tag{43}$$

where $c_2 = (\sigma_{\min}(\Pi_1)\|\varpi\| - \|PD\|W_2)/\sqrt{\sigma_{\min}(\Omega)}$.

We know that there exist proper parameters β and γ such that Π_1 is positive definite and $\|\varpi\| > \|PD\|W_2/\sigma_{\min}(\Pi_1)$ can be achieved with these parameters. So, if $L_b V = 0$, then for all $x \neq 0$ we can obtain $L_f V \le -c_2 V^{1/2}$. This guarantees that the candidate $V(x)$ is a FTCLF for system (24). □

Next, the main results of our proposed anti-disturbance inverse optimal control for the spacecraft model are presented.

Theorem 10. *Let Assumption 8 hold. The following dynamic feedback control law*

$$u = u^* - \widehat{d} \tag{44}$$

with

$$u^* = \begin{cases} -\varphi^T(x)\dfrac{\psi(x)+c_3(V(x))^{1/2}+\sqrt{\left(\psi(x)+c_3(V(x))^{1/2}\right)^2+\|\varphi(x)\|^4}}{\|\varphi(x)\|^2}, & if\ \|\varphi(x)\|\neq 0 \\ 0, & if\ \|\varphi(x)\|=0, \end{cases} \tag{45}$$

where c_3 is a positive constant, $\hat{d}$ is an estimated value of d which will be defined later, $\psi(x) = L_f V$, and $\varphi(x) = L_b V$, finite-time stabilizes the spacecraft system (24).

Proof. We show that the control law u in (44) is a stabilizing controller for attitude control system in (24). Consider the smooth positive-definite radially unbounded function $V(x)$ in (28) as the Lyapunov function. The time derivative of the $V(x)$ is

$$\begin{aligned} \dot{V} &= \frac{\partial V}{\partial x}\left(f(x)+b(x)u+b(x)d\right) \\ &= L_f V + L_b V\left(u^*-\hat{d}\right)+\varphi(x)d \\ &= \psi(x)-\varphi^T(x)\varphi(x) \\ &\quad \times \frac{\psi(x)+c_3(V(x))^{1/2}+\sqrt{\left(\psi(x)+c_3(V(x))^{1/2}\right)^2+\|\varphi(x)\|^4}}{\|\varphi(x)\|^2} \\ &= -\sqrt{\left(\psi(x)-c_3(V(x))^{1/2}\right)^2+\|\varphi(x)\|^4} \\ &\quad -c_3(V(x))^{1/2}-\varphi^T(x)\left(\hat{d}-d\right) \\ &\le -c_3(V(x))^{1/2}-\varphi^T(x)\left(\hat{d}-d\right). \end{aligned} \tag{46}$$

It has been shown that if $\hat{d}$ converges to d, then $e_2 = \hat{d} - d$ converges to zero in finite time. This means that an appropriate c_3 can be selected such that $\dot{V} \le -c_3(V(x))^{1/2}$is achieved. By Lemma 3, the finite-time stability of closed-loop system is ensured. This completes the proof. □

Next, we show that if the disturbance estimate $\hat{d}$ in (44) and disturbance term d in (24) are ignored, then the feedback stabilizing controller u in (44) solves the inverse optimal control problem.

Theorem 11. *Consider the system* (24) *for which Assumption 8 holds. Then the following dynamic feedback control law*

$$\begin{aligned} u^* &= -R(e,e_0,\omega_e)^{-1}\varphi(x) \\ &= \begin{cases} -\varphi^T(x)\dfrac{\psi(x)+c_3(V(x))^{1/2}+\sqrt{\left(\psi(x)+c_3(V(x))^{1/2}\right)^2+\|\varphi(x)\|^4}}{\|\varphi(x)\|^2}, & if\ \|\varphi(x)\|\neq 0 \\ 0, & if\ \|\varphi(x)\|=0 \end{cases} \end{aligned} \tag{47}$$

solves the inverse optimal assignment problem for the attitude tracking system (24) *by minimizing the cost functional* (8).

Proof. With $\tilde{d} = 0$, using the control law u one obtains $\dot{V} \le -c_3(V(x))^{1/2}$. Letting $u_1 = (1/2)u^*$ we also obtain $\dot{V} \le -c_3(V(x))^{1/2} \le 0$. Next, choosing

$$l(x) = -\psi(x) - \varphi(x)u_1, \tag{48}$$

it can be ensured that $l(x) \ge 0$. This shows that $l(x)$ is positive semidefinite in q_e, q_{4e}, and ω_e. Therefore this $l(x)$ is a meaningful cost function for the attitude control problem, penalizing on q_e, q_{4e}, and ω_e, as well as the control effort u. Substituting $l(x)$ into the cost functional (8), we obtain the optimal cost

$$I(u^*, x, x_0) = V(x_0) \tag{49}$$

for every $x_0 \in D$. □

Remark 12. It should be noted that most existing inverse optimal attitude control approaches have been developed for attitude motions of a rigid spacecraft [16, 17]. For a flexible spacecraft the vibration of flexible appendages induced by an orbiting attitude slewing operation may degrade the attitude pointing accuracy. In this paper, we develop an inverse optimal attitude maneuver controller for a flexible spacecraft system which is significantly different from the controllers in [16, 17], where the effects of vibration of flexible appendages were not considered.

6. Anti-Disturbance Inverse Optimal Control with Extended State Observer

Due to the great advances in nonlinear control theory, the observer-based controller is now one of the most common schemes in industrial applications. The extended state observer (ESO) mentioned in [18, 28] has high efficiency

in accomplishing nonlinear dynamic estimation. We know that use of the ESO dynamics of the observer error gives convergence into a residual set of zero. The convergence proof has been shown using the SSR approach [30]. However, this method takes many steps and is quite complicated. In this paper an adapted ESO which is a modified version of the traditional ESO is presented and the finite-time stability of the adapted ESO system is investigated using the strict Lyapunov function.

We now consider the coordinate transformation of the spacecraft model into the following form:

$$z = \omega_e + \lambda q_e, \tag{50}$$

where λ is a positive constant. The time derivative of z is

$$\dot{z} = \dot{\omega}_e + \lambda \dot{q}_e. \tag{51}$$

Substituting (14) and (17a) into (51), we obtain the auxiliary dynamics

$$\dot{z} = J_{mb}^{-1}\Xi\left(\omega_e, \omega_e, \dot{\omega}_d\right) + J_{mb}^{-1}u + J_{mb}^{-1}d + \frac{\lambda}{2}\left(q_e^{\times} + q_{4e}I_3\right)\omega_e, \tag{52}$$

which can be rewritten as

$$\dot{z} = F + \overline{B}u + \overline{d}, \tag{53}$$

where

$$F = J_{mb}^{-1}\Xi\left(\omega_e, \omega_d, \dot{\omega}_d\right) + \frac{\lambda}{2}\left(q_e^{\times} + q_{4e}I_3\right)\omega_e,$$
$$\overline{B} = J_{mb}^{-1}, \qquad \overline{d} = J_{mb}^{-1}d. \tag{54}$$

Here, the new disturbance variable $\overline{d}$ is introduced. Although we need to estimate d in (24), it is simpler to first estimate $\overline{d}$ and then use the results to estimate d. Thus, we now consider the estimate for $\overline{d}$ in the ESO design.

We next consider the auxiliary system (53) with the adapted ESO technique. The ESO views the system model uncertainties and external disturbances as an added state to be estimated. Using this idea, a nonlinear ESO can be designed for estimating the disturbances $\overline{d}(t)$. We add an extended state χ to the state equations to represent the total disturbances $\overline{d}$. The system (53) then becomes

$$\dot{z} = F + \overline{B}u + \chi,$$
$$\dot{\chi} = g\left(t\right), \tag{55}$$

where the function $g(t)$ is the estimated derivative of the disturbances $\overline{d}(t)$.

Assumption 13. The ith component of $g(t)$ is bounded; that is, $g_i(t) \le \overline{g}_1$, $i = 1, 2, 3$.

Then the adapted ESO for the system (53) is proposed to be as follows:

$$E_1 = Z_1 - \eta,$$
$$\dot{Z}_1 = Z_2 + F + \overline{B}u - \lambda_2 E_1, \tag{56}$$
$$\dot{Z}_2 = -\lambda_1 E_1 - \mu\,\mathrm{sign}^r\left(E_1\right),$$

where E_1 is the estimation error of the ESO, Z_1 and Z_2 are the observer output, $\lambda_1 = \mathrm{diag}(\lambda_{11}, \lambda_{12}, \lambda_{13})$, and $\lambda_2 = \mathrm{diag}(\lambda_{21}, \lambda_{22}, \lambda_{23})$ with $\lambda_{1i} > 0$ and $\lambda_{2i} > 0$ being the observer gains. Here, the function $\mathrm{sign}^r(E_1)$ is defined as

$$\mathrm{sign}^r\left(E_1\right) = \left[\left|E_{11}\right|^r\ \mathrm{sign}\left(E_{11}\right)\ \left|E_{12}\right|^r\ \mathrm{sign}\left(E_{12}\right)\ \left|E_{13}\right|^r\ sign\left(E_{13}\right)\right]^T \tag{57}$$

with $r \in (0, 1)$.

Theorem 14. *Let Assumption 13 hold. Consider the system* (55) *with the adaptive ESO* (56)*. Then there exist positive observer gains λ_{1i}, λ_{2i}, and $\mu_i (i = 1, 2, 3)$ and $r \in (0, 1)$ such that the estimated states Z_1 and Z_2 finite-time converge into a residual set of actual states z and $\overline{d}$, respectively.*

Proof. To investigate the stability of the ESO system, one must consider an expression for the observer dynamics. We first define the observer errors $E_1 = Z_1 - \eta$ and $E_2 = Z_2 - x_2 = Z_2 - \overline{d}$. The observer error dynamics are also expressed as

$$\dot{E}_1 = E_2 - \lambda_2 E_1,$$
$$\dot{E}_2 = -g\left(t\right) - \lambda_1 E_1 - \mu\,\mathrm{sign}^r\left(E_1\right). \tag{58}$$

Letting $E_1 = e_1$ and $E_2 = e_2 + \lambda_2 e_1$ the observer error dynamics (58) can be transformed to the scalar form ($i = 1, 2, 3$) as

$$\dot{e}_{1i} = e_{2i},$$
$$\dot{e}_{2i} = -g_i\left(t\right) - \lambda_{1i}e_{1i} - \lambda_{2i}e_{2i} - \mu_i\left|e_{1i}\right|^r\ \mathrm{sign}\left(e_{1i}\right). \tag{59}$$

We define $\nu = \left[\left|e_{1i}\right|^{(r+1)/2}\ \mathrm{sign}(e_{1i})\ \ e_{1i}\ \ e_{2i}\right]^T$. To prove the stability, we select the Lyapunov function

$$\overline{V} = \frac{1}{2}\nu^T\Lambda\nu, \tag{60}$$

where

$$\Lambda = \begin{bmatrix} \dfrac{\mu_i}{r+1} & 0 & 0 \\ 0 & \lambda_{1i} & \dfrac{\lambda_{2i}}{2} \\ 0 & \dfrac{\lambda_{2i}}{2} & 1 \end{bmatrix}. \tag{61}$$

The matrix Λ is positive definite if λ_{2i} and λ_{1i} are chosen to satisfy the condition

$$\lambda_{1i} > \frac{1}{4}\lambda_{2i}^2. \tag{62}$$

Taking the time derivative of $\overline{V}$ and using (60), we obtain

$$\dot{\overline{V}} = \begin{bmatrix} e_{1i} & e_{2i} \end{bmatrix}\begin{bmatrix} \lambda_{1i} & \dfrac{\lambda_{2i}}{2} \\ \dfrac{\lambda_{2i}}{2} & 1 \end{bmatrix}\begin{bmatrix} \dot{e}_{1i} \\ \dot{e}_{2i} \end{bmatrix} + \mu_i\left|e_{1i}\right|^r\ \mathrm{sign}\left(e_1\right)\dot{e}_{1i}, \tag{63}$$

which can be further written as

$$\begin{aligned}\dot{\overline{V}} = &\begin{bmatrix} e_{1i} & e_{2i} \end{bmatrix} \begin{bmatrix} \lambda_{1i} & 0.5\lambda_{2i} \\ 0.5\lambda_{2i} & 1 \end{bmatrix} \\ &\times \begin{bmatrix} e_{2i} \\ -g_i(t) - \lambda_{1i}e_{1i} - \lambda_{2i}e_{2i} - \mu_i |e_{1i}|^r \ \operatorname{sign}(e_1) \end{bmatrix} \\ &+ \mu_i |e_{1i}|^r \ \operatorname{sign}(e_1)\, \dot{e}_{1i}. \end{aligned} \tag{64}$$

After some manipulation, the derivative of V can be written as follows:

$$\dot{\overline{V}} = -\frac{\lambda_{2i}}{2} \nu^T \Pi_2 \nu + \varrho \nu, \tag{65}$$

where

$$\Pi_2 = \begin{bmatrix} \mu_i & 0 & 0 \\ 0 & \lambda_{1i} & \dfrac{\lambda_{2i}}{2} \\ 0 & \dfrac{\lambda_{2i}}{2} & 1 \end{bmatrix}, \qquad \varrho = \begin{bmatrix} 0 & -\dfrac{\lambda_{2i}}{2} g_i(t) & -g_i(t) \end{bmatrix}. \tag{66}$$

Letting $L = \begin{bmatrix} 0 & (\lambda_{2i}/2)\overline{g}_1 & \overline{g}_1 \end{bmatrix}$, one obtains

$$\begin{aligned} \dot{\overline{V}} &\le -\frac{\lambda_{2i}}{2} \sigma_{\min}(\Pi_2) \|\nu\|^2 + \|L\| \|\vartheta\| \\ &= -\left(0.5\lambda_{2i}\sigma_{\min}(\Pi_2) \|\nu\| - \|L\|\right) \|\nu\|. \end{aligned} \tag{67}$$

Using (60) we know that $\overline{V}/\sigma_{\max}(\Lambda) \le \|\nu\|^2 \le \overline{V}/\sigma_{\min}(\Lambda)$. We obtain

$$\dot{\overline{V}} \le -\left(\sigma_{\min}(\Pi_2) \|\nu\| - \|L\|\right) \frac{\overline{V}^{1/2}}{\sqrt{\sigma_{\max}(\Lambda)}}. \tag{68}$$

If $\sigma_{\min}(\Pi_2)\|\nu\| > \|L\|$, the error system (59) will finite-time converge to the region

$$\|\nu\| \le \left(\frac{\|L\|}{\sigma_{\min}(\Lambda)}\right). \tag{69}$$

It is obvious that the estimation errors are determined by the parameters λ_{2i}, λ_{1i}, and μ_i. Basically, these parameters can be chosen such that (62) is satisfied. This makes the error states converge to region (69) in finite time. □

Remark 15. It should be noticed that conditions for the stability of the adapted ESO (56) have been obtained in terms of positive gains λ_{2i},λ_{1i}, and μ_i and $r \in (0, 1)$ in (59) for the estimation errors. When suitable gains are chosen, Z_2 will be a precise estimate of $\overline{d}$ and the estimation error E_2 will converge to region (69) in finite time.

Using the results from the ESO system, the estimated disturbance $\hat{d}$ is determined by $\hat{d} = \overline{B}^{-1} Z_2$. Thus, the proposed anti-disturbance inverse optimal control can be obtained as

$$u = u^* - \overline{B}^{-1} Z_2. \tag{70}$$

With suitable control gains defined by the inverse optimal control approach based on FTCLF concept, the optimal feedback controller (70) contains both optimality and robustness performance to attenuate external disturbances.

7. Simulation Results

An example of attitude control of flexible spacecraft is presented with numerical simulations. The performance of our proposed controller (70) is compared with the performances of the optimal Lyapunov sliding mode (SM) controller (4.3) in [23] and robust finite-time controller (23) in [37]. The spacecraft is assumed to have the nominal inertia matrix [38]

$$J = \begin{bmatrix} 350 & 3 & 4 \\ 3 & 270 & 10 \\ 4 & 10 & 190 \end{bmatrix} \text{kg} \cdot \text{m}^2 \tag{71}$$

and coupling matrices

$$\delta = \begin{bmatrix} 6.45637 & 1.27814 & 2.15629 \\ -1.25619 & 0.91756 & -1.67264 \\ 1.11678 & 2.48901 & -0.83674 \\ 1.23637 & -2.6581 & -1.12503 \end{bmatrix} \text{kg}^{1/2} \cdot \text{m/s}^2, \tag{72}$$

respectively. The first four elastic modes that have been considered in the model used for simulating a spacecraft are $\omega_{n1} = 0.7681$, $\omega_{n2} = 1.1038$, $\omega_{n3} = 1.8733$, and $\omega_{n4} = 2.5496$ rad/sec with damping $\xi_1 = 0.0056$, $\xi_2 = 0.0086$, $\xi_3 = 0.013$, and $\xi_1 = 0.025$. The initial states of the rotation motion are given by $Q(0) = [0.3 \ \ -0.1 \ \ 0.2 \ \ 0.9274]^T$, $\omega(0) = [0 \ \ 0 \ \ 0]^T$ rad/sec, and $\vartheta(0) = [0 \ \ 0 \ \ 0 \ \ 0 \ \ 0 \ \ 0 \ \ 0]^T$. For the FTCLF (29), the parameters β and γ are set as $\beta = 10$ and $\gamma = 2.5$. The adapted ESO parameters are selected as $\lambda = 0.5$, $\lambda_{1i} = 2.0$, $\lambda_{2i} = 1.5$, and $\mu_i = 5.0 (i = 1, 2, 3)$. The attitude control problem is considered in the presence of external disturbance $d(t)$. The external disturbances are described as

$$d(t) = \begin{bmatrix} 0.3\cos(0.1t) + 0.1 \\ 0.15\sin(0.1t) + 0.3\cos(0.1t) \\ 0.3\sin(0.1t) + 0.1 \end{bmatrix} \text{Nm} \tag{73}$$

and the desired angular velocity tracking is given by

$$\omega_d(t) = \begin{bmatrix} -0.04\cos(0.2t) \\ -0.04\sin(0.2t) \\ 0.05\sin(0.2t) + \cos(0.2t) \end{bmatrix} \text{rad/sec} \tag{74}$$

together with

$$q_d(0) = \begin{bmatrix} 0 & 0 & 0 \end{bmatrix}^T. \tag{75}$$

Note that the optimal Lyapunov SM controller (4.3) in [23] was designed for optimal attitude stabilization. To apply this controller to the tracking problem, we define the total disturbance as

$$\begin{aligned} \tau_d(t) = &-\omega_e^{\times} J \omega_d - \omega_d^{\times} J_{mb} \omega_e - \omega_d^{\times} J \omega_d - \omega_d^{\times} \delta^T \psi \\ &- J_{mb} \dot{\omega}_d + d(t) \end{aligned} \tag{76}$$

and use it as the disturbance in the spacecraft model (24). Also, the corresponding parameters in the optimal Lyapunov SM controller (4.3) in [23] are selected. In this paper, to apply controller (23) in [37] to the attitude control problem we use quaternions instead of Euler angles to describe the attitude of

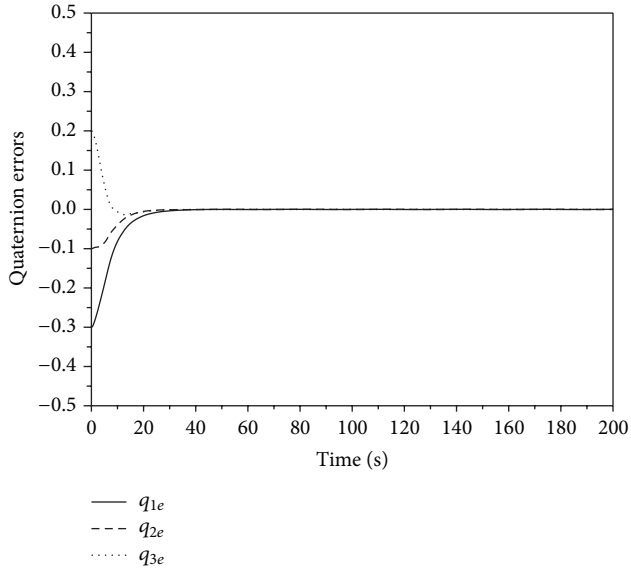

Figure 1: Quaternion tracking errors—controller (4.3) in [23].

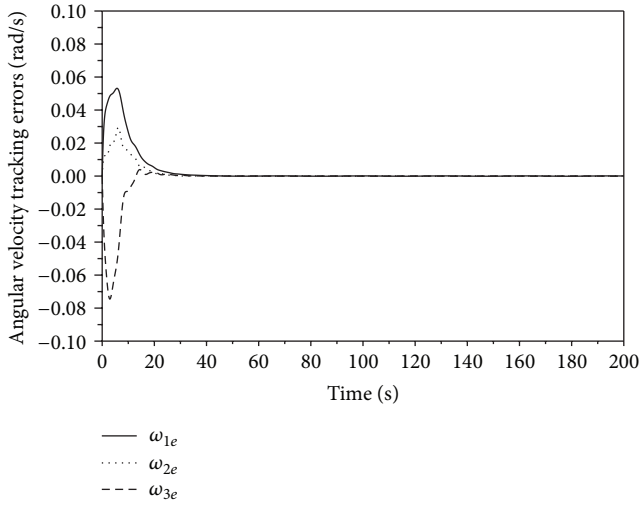

Figure 2: Angular velocity tracking errors—controller (4.3) in [23].

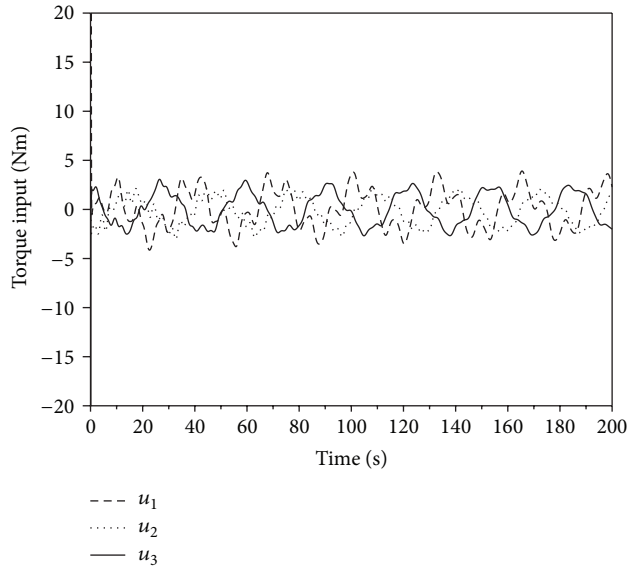

Figure 3: Control torques—controller (4.3) in [23].

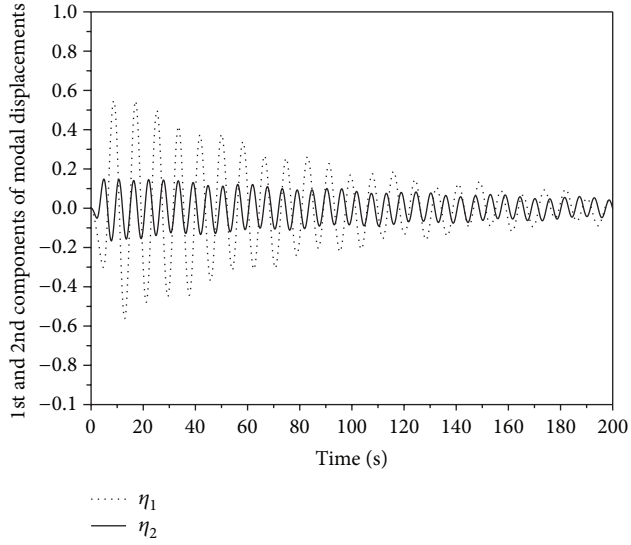

Figure 4: Modal displacements—controller (4.3) in [23].

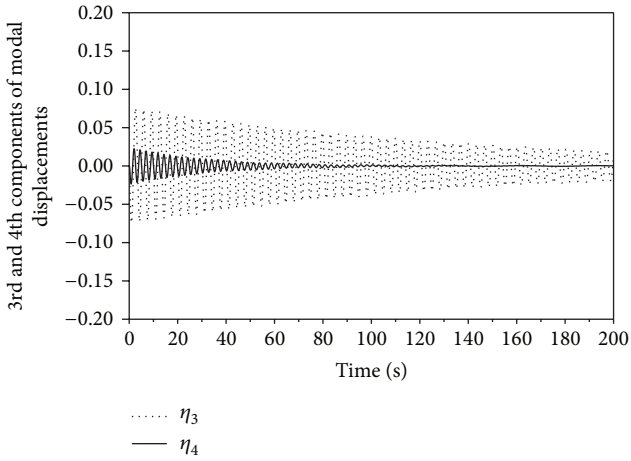

Figure 5: Modal displacements—controller (4.3) in [23].

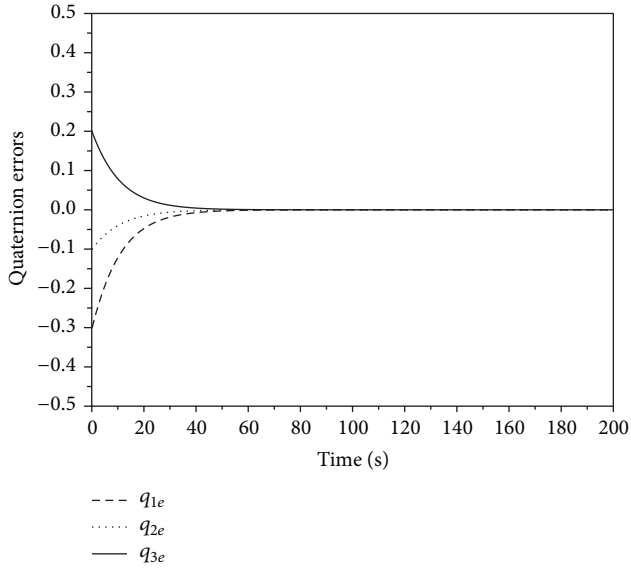

Figure 6: Quaternion tracking errors—controller (70).

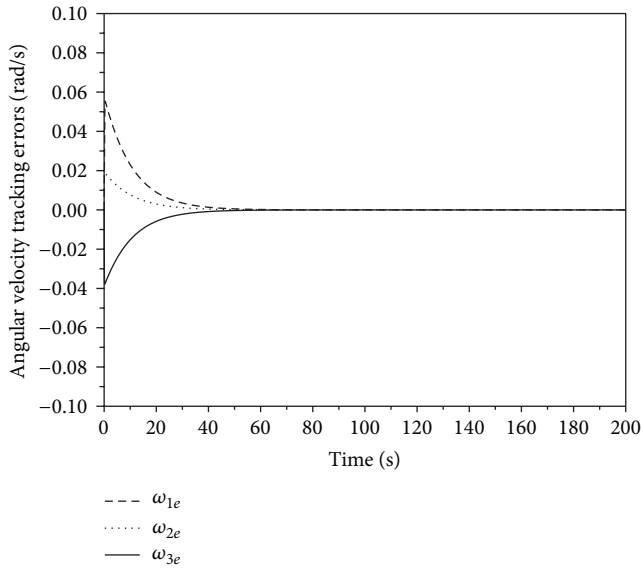

Figure 7: Angular velocity tracking errors—controller (70).

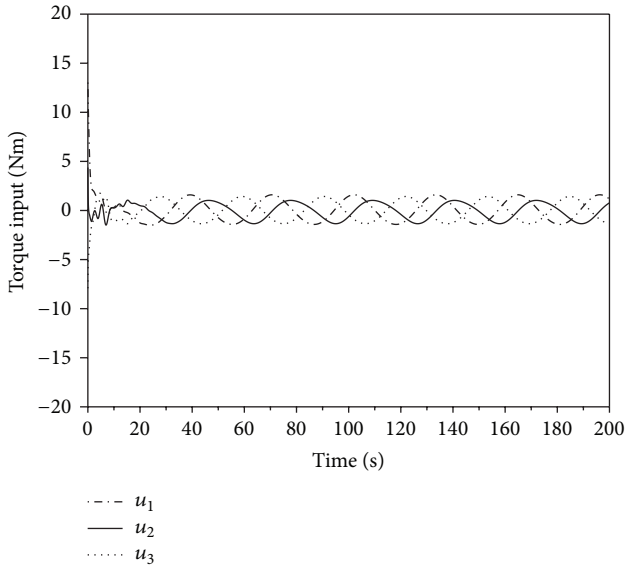

Figure 8: Control torques—controller (70).

the flexible spacecraft. For controller (23) in [37], the control parameters were selected as $\lambda = 0.5$, $\beta = 1$, $a = 5$, $b = 7$, and $k^* = 10I_3$.

Simulation studies have been performed to test all controllers. Figures 1 and 2 show the performance of controller (4.3) in [23]. The responses of quaternion and angular velocity tracking errors reach zero after 40 seconds. The components of angular velocity tracking error vector are smooth. From Figure 3 it can be seen that the optimal Lyapunov SM controller (4.3) in [23] stabilizes the closed-loop system of flexible spacecraft. As shown in Figures 4 and 5 the modal displacements ($\eta_1 - \eta_4$) converge to the neighborhood of zero.

On the other hand Figure 6 shows that controller (70) provides good trajectories of the quaternion error and they

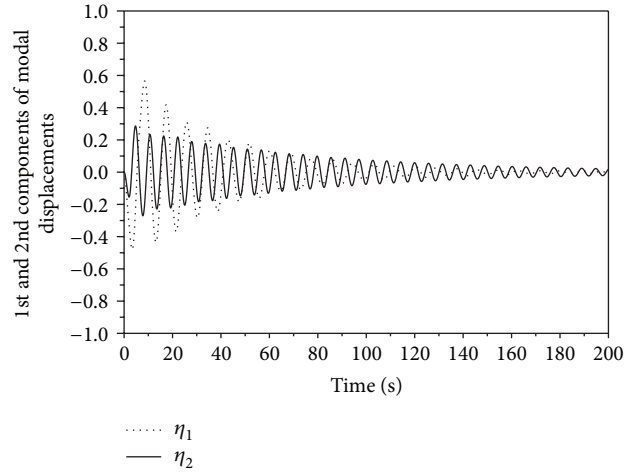

Figure 9: Modal displacements—controller (70).

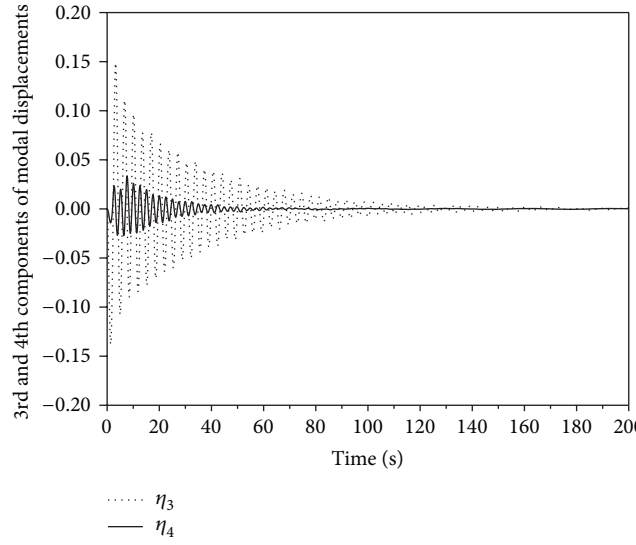

Figure 10: Modal displacements—controller (70).

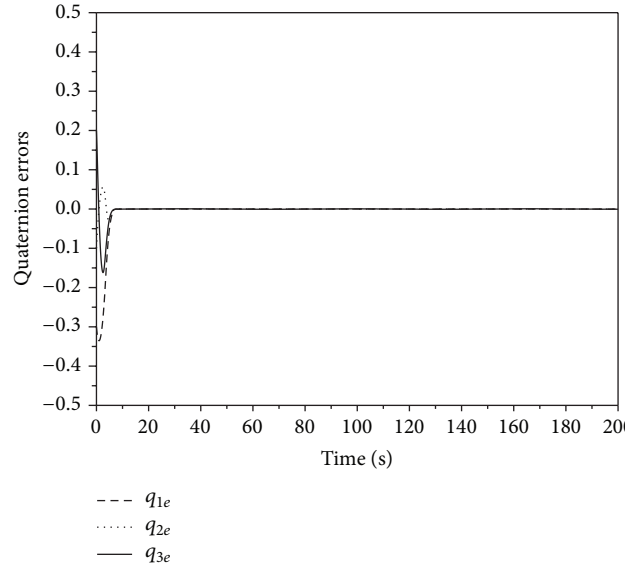

Figure 11: Quaternion tracking errors—controller (23) in [37].

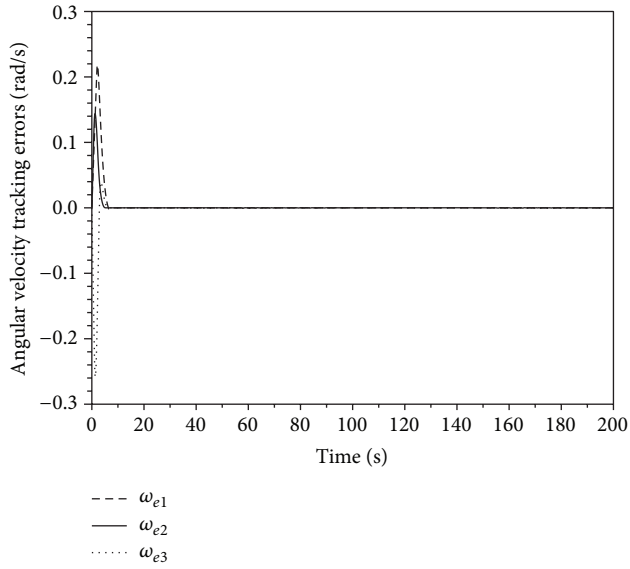

Figure 12: Angular velocity tracking errors—controller (23) in [37].

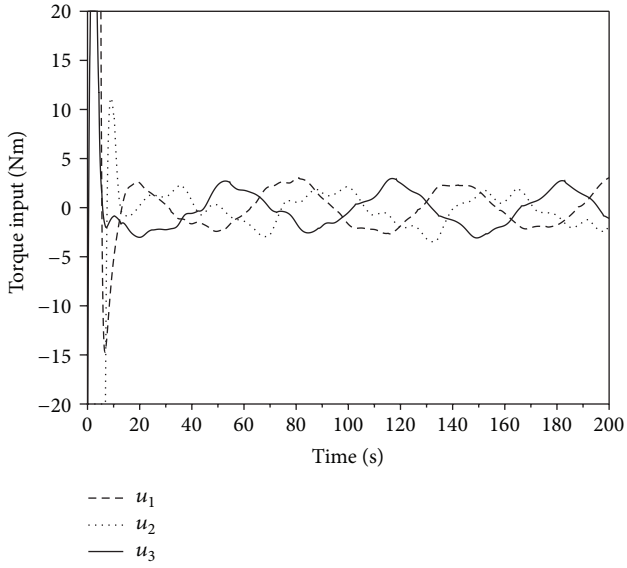

Figure 13: Control torques—controller (23) in [37].

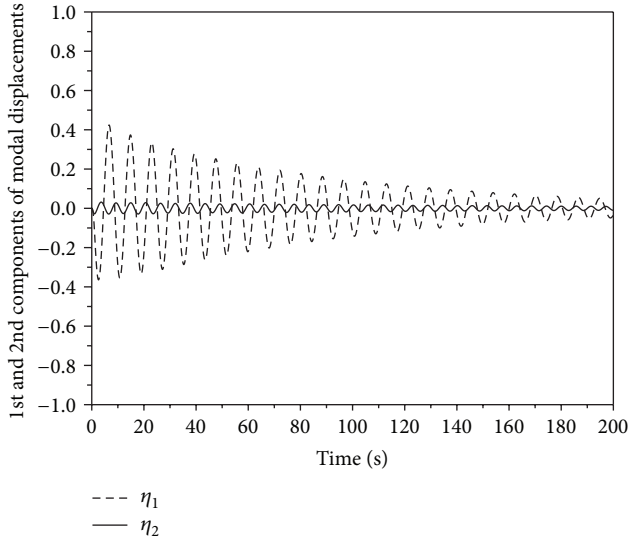

Figure 14: Modal displacements—controller (23) in [37].

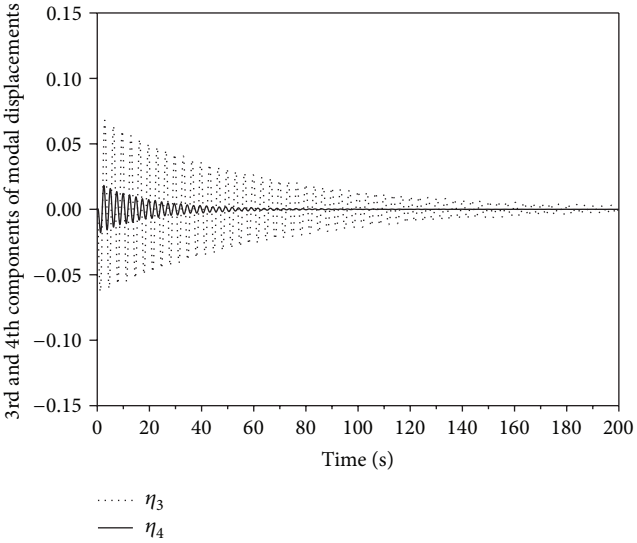

Figure 15: Modal displacements—controller (23) in [37].

reach zero in about 50 seconds. Similarly, from Figure 7 it can be seen that the angular velocity tracking errors reach zero after 80 seconds. The responses of angular velocity tracking errors at the first 20 seconds are smoother when compared with those obtained from controller (4.3) in [23]. As shown in Figure 8 the control torques obtained by controller (70) are quite smooth even though the external disturbances are taken into account. The responses of modal displacements shown in Figures 9 and 10 converge to a smaller region around the zero when compared to controller (4.3) in [23]. Figures 11–15 show the simulation results of controller (23) in [37]. As shown in Figures 11 and 12 quaternion and angular velocity tracking errors converge to zero in about 10 seconds. Figure 13 depicts the control torques which approximate the harmonic curves. The responses of modal displacements for controller (23) in [37] are shown in Figures 14 and 15.

A comparison of the simulation results obtained by control law (4.3) in [23], our proposed controller (70), and controller (23) in [37] shows the following. It can be seen that our proposed control law (70) provides smoother attitude velocity tracking error responses and control input responses than those of controller (4.3) in [23]. It can be seen that the vibration of flexible appendages of the spacecraft is obviously reduced by applying the proposed controller (70) rather than through the use of (4.3) in [23]. Next, we compare the performance of (70) and controller (23) in [37]. Although tracking responses obtained by our proposed control law (70) converge more slowly to zero than (23) in [37], smaller values of control torques are required in (70) than in (29). Our proposed control law is based on the inverse optimal control concept that minimizes the performance index, so

it usually requires smaller values of control torques. In addition, the proposed controller gives smoother control torque signals. This shows that our controller (70) achieves better disturbance rejection performance than (23) in [37]. In view of these simulation results, controller (70) seems to give the best overall control for practical inverse optimal attitude tracking control of a flexible spacecraft.

8. Conclusion

We have studied a finite-time anti-disturbance inverse optimal controller design of attitude tracking of a flexible spacecraft in the presence of external disturbances. The concepts of inverse optimal control and the FTCLF have been employed to develop a novel finite-time inverse optimal attitude tracking control law. An adapted ESO has been designed by modifying the structure of the traditional ESO. The finite-time convergence of an adapted ESO has been proven using the strict Lyapunov function. A finite-time anti-disturbance inverse optimal controller can be expressed as the sum of a finite-time inverse optimal control and adapted ESO. It has been shown that the developed controller solves the inverse optimal control problem and converges to the reference attitude states in finite time. An example of multiaxial attitude maneuver is presented and simulation results are given and compared with the results from controller (4.3) in [23] and controller (23) in [37] to verify the usefulness of the developed controller.

References

[1] S. R. Vadali, L. G. Kraige, and J. L. Junkins, "New results on the optimal spacecraft attitude maneuver problem," *Journal of Guidance, Control, and Dynamics*, vol. 7, no. 3, pp. 378–380, 1984.

[2] S. Bharadwaj, M. Osipchuk, K. D. Mease, and F. C. Park, "Geometry and inverse optimality in global attitude stabilization," *Journal of Guidance, Control, and Dynamics*, vol. 21, no. 6, pp. 930–939, 1998.

[3] C. K. Carrington and J. L. Junkins, "Optimal nonlinear feedack control for spacecraft attitude maneuvers," *Journal of Guidance, Control, and Dynamics*, vol. 9, no. 1, pp. 99–107, 1986.

[4] C.-C. Yang and C.-J. Wu, "Optimal large-angle attitude control of rigid spacecraft by momentum transfer," *IET Control Theory and Applications*, vol. 1, no. 3, pp. 657–664, 2007.

[5] S.-P. Shue, M. E. Sawan, and K. Rokhsaz, "Optimal feedback control of a nonlinear system: wing rock example," *Journal of Guidance, Control, and Dynamics*, vol. 19, no. 1, pp. 166–171, 1996.

[6] R. Sharma and A. Tewari, "Optimal nonlinear tracking of spacecraft attitude maneuvers," *IEEE Transactions on Control Systems Technology*, vol. 12, no. 5, pp. 677–682, 2004.

[7] A. El-Gohary, "Optimal control of a programmed motion of a rigid spacecraft using redundant kinematics parameterizations," *Chaos, Solitons and Fractals*, vol. 26, no. 4, pp. 1053–1063, 2005.

[8] D. K. Parrish and D. B. Ridgely, "Attitude control of a satellite using the SDRE method," in *Proceedings of the American Control Conference*, pp. 942–946, Albuquerque, NM, USA, June 1997.

[9] D. T. Stansbery and J. R. Cloutier, "Position and attitude control of a spacecraft using the state-dependent Riccati equation technique," in *Proceedings of the American Control Conference*, pp. 1867–1871, Chicago, Ill, USA, June 2000.

[10] P. Tsiotras, "Stabilization and optimality results for the attitude control problem," *Journal of Guidance, Control, and Dynamics*, vol. 19, no. 4, pp. 772–779, 1996.

[11] M. Krstić and P. Tsiotras, "Inverse optimal stabilization of a rigid spacecraft," *IEEE Transactions on Automatic Control*, vol. 44, no. 5, pp. 1042–1049, 1999.

[12] Y. Park, "Inverse optimal and robust nonlinear attitude control of rigid spacecraft," *Aerospace Science and Technology*, vol. 28, no. 1, pp. 257–265, 2013.

[13] E. D. Sontag, "A "universal" construction of Artstein's theorem on nonlinear stabilization," *Systems and Control Letters*, vol. 13, no. 2, pp. 117–123, 1989.

[14] R. A. Freeman and P. V. Kokotovic, "Inverse optimality in robust stabilization," *SIAM Journal on Control and Optimization*, vol. 34, no. 4, pp. 1365–1391, 1996.

[15] W. Kang, "Nonlinear H_{∞} control and its application to rigid spacecraft," *IEEE Transactions on Automatic Control*, vol. 40, no. 7, pp. 1281–1285, 1995.

[16] W. Luo, Y.-C. Chu, and K.-V. Ling, "Inverse optimal adaptive control for attitude tracking of spacecraft," *IEEE Transactions on Automatic Control*, vol. 50, no. 11, pp. 1639–1654, 2005.

[17] Y. Park, "Robust and optimal attitude stabilization of spacecraft with external disturbances," *Aerospace Science and Technology*, vol. 9, no. 3, pp. 253–259, 2005.

[18] J. Han, "From PID to active disturbance rejection control," *IEEE Transactions on Industrial Electronics*, vol. 56, no. 3, pp. 900–906, 2009.

[19] Y. Xia, Z. Zhu, M. Fu, and S. Wang, "Attitude tracking of rigid spacecraft with bounded disturbances," *IEEE Transactions on Industrial Electronics*, vol. 58, no. 2, pp. 647–659, 2011.

[20] V. I. Utkin, *Sliding Modes in Control and Optimization*, Springer, Berlin, Germany, 1992.

[21] C. Pukdeboon and A. S. I. Zinober, "Optimal sliding mode controllers for attitude tracking of spacecraft," in *Proceedings of the IEEE International Conference on Control Applications*, pp. 1708–1713, Saint Petersburg, Russia, July 2009.

[22] C. Pukdeboon and A. S. I. Zinober, "Control Lyapunov function optimal sliding mode controllers for attitude tracking of spacecraft," *Journal of the Franklin Institute*, vol. 349, no. 2, pp. 456–475, 2012.

[23] C. Pukdeboon, "Optimal sliding mode controllers for attitude stabilization of flexible spacecraft," *Mathematical Problems in Engineering*, vol. 2011, Article ID 863092, 20 pages, 2011.

[24] N. N. Krasovskii, "On the stabilization of unstable motions by additional forces when the feedback loop is incomplete," *Journal of Applied Mathematics and Mechanics*, vol. 27, no. 4, pp. 971–1004, 1963.

[25] E. D. Sontag, "Mathematical control theory," in *Deterministic Finite Dimensional Systems*, vol. 6 of *Texts in Applied Mathematics*, Springer, New York, NY, USA, 2nd edition, 1998.

[26] J. A. Primbs, V. Nevistić, and J. C. Doyle, "Nonlinear optimal control : a control Lyapunov function and receding horizon perspective," *Asian Journal of Control*, vol. 1, no. 1, pp. 14–24, 1999.

[27] X. Cai, "Finite time inverse optimal control of affine nonlinear systems," in *Proceedings of the 24th Chinese Control and Decision Conference*, Taiyuan, China, May 2012.

[28] L. Mo, "Finite-time H_∞ inverse optimal control of affine nonlinear systems," *Circuits, Systems, and Signal Processing*, vol. 32, no. 1, pp. 47–60, 2013.

[29] S. Li, X. Yang, and D. Yang, "Active disturbance rejection control for high pointing accuracy and rotation speed," *Automatica*, vol. 45, no. 8, pp. 1854–1860, 2009.

[30] Y. Huang and J. Han, "Analysis and design for the second order nonlinear continuous extended states observer," *Chinese Science Bulletin*, vol. 45, no. 21, pp. 1938–1944, 2000.

[31] J. R. Wertz, *Spacecraft Attitude Determination and Control*, Kluwer Academic, Dordrecht, The Netherlands, 1978.

[32] S. Di Gennaro, "Passive attitude control of flexible spacecraft from quaternion measurements," *Journal of Optimization Theory and Applications*, vol. 116, no. 1, pp. 41–60, 2003.

[33] V. T. Haimo, "Finite time controllers," *SIAM Journal on Control and Optimization*, vol. 24, no. 4, pp. 760–770, 1986.

[34] S. P. Bhat and D. S. Bernstein, "Finite-time stability of continuous autonomous systems," *SIAM Journal on Control and Optimization*, vol. 38, no. 3, pp. 751–766, 2000.

[35] M. D. Shuster, "Survey of attitude representations," *Journal of the Astronautical Sciences*, vol. 41, no. 4, pp. 439–517, 1993.

[36] S. Di Gennaro, "Output attitude tracking for flexible spacecraft," *Automatica*, vol. 38, no. 10, pp. 1719–1726, 2002.

[37] S. Wu, G. Radice, and Z. Sun, "Robust finite-time control for flexible spacecraft attitude maneuver," *Journal of Aerospace Engineering*, 2012.

[38] Q. Hu, "Sliding mode attitude control with L2-gain performance and vibration reduction of flexible spacecraft with actuator dynamics," *Acta Astronautica*, vol. 67, no. 5-6, pp. 572–583, 2010.

Hindawi Publishing Corporation
Mathematical Problems in Engineering
Volume 2013, Article ID 840648, 9 pages
http://dx.doi.org/10.1155/2013/840648

Research Article

Power-Split Hybrid Electric Vehicle Energy Management Based on Improved Logic Threshold Approach

Zhumu Fu,[1,2] Bin Wang,[1] Xiaona Song,[1] Leipo Liu,[1] and Xiaohong Wang[1]

[1] *Information Engineering College, Henan University of Science and Technology, Luoyang 471023, China*
[2] *School of Control Science and Engineering, Shandong University, Jinan 250061, China*

Correspondence should be addressed to Zhumu Fu; fzm1974@163.com

Received 22 July 2013; Revised 3 November 2013; Accepted 6 November 2013

Academic Editor: Baoyong Zhang

We design an improved logic threshold approach of energy management for a power-split HEV assisted by an integrated starter generator (ISG). By combining the efficiency map and the optimum torque curve of internal combustion engine (ICE) with the state of charge (SOC) of batteries, the improved logic threshold controller manages the ICE within its peak efficiency region at first. Then the electrical power demand is established based on the ICE energy output. On that premise, a variable logic threshold value K is defined to achieve the power distribution between the ISG and the electric motor/generator (EMG). Finally, simulation models for the power-split HEV with improved logic threshold controller are established in ADVISOR. Compared to the equally power-split HEV with the logic threshold controller, when using the improved logic threshold controller, the battery power consumption, the ICE efficiency, the fuel consumption, and the motor driving system efficiency are improved.

1. Introduction

To improve the efficiency and fuel economy of hybrid electric vehicle (HEV), many researchers focus on power-split HEVs [1–5] as they can achieve a potential of higher fuel economy and reduce the electrical system loss. The power-split hybrid system, which usually uses an ICE with integrated starter generator (ISG) [6, 7] and an electric motor/generator (EMG), combines the benefits of both the parallel- and series-type hybrid systems without the cost effectiveness of this hybrid system.

Since the structure of power-split HEV is more complicated [5, 8], traditional control methods (such as optimal control [9] and robust control [10]) cannot deal with this kind of system efficiently. So it needs a sophisticated control system to manage the power-split HEV power trains. Such control system requires a reasonable control strategy at first to improve the fuel-saving capability of the ICE, (see [11, 12]). To solve this problem, studies such as logic threshold approach applied to the design of the control strategy for HEV have been used to achieve the power or torque distribution [2, 13]. However, due to the individual characters of the power-split HEVs [5] and even different driving performance under different driving cycles to the same power-split HEV [14, 15], it is necessary to consider the individual ICE, structure, and other driving conditions like SOC and vehicles' speed of the HEV when designing the control strategy [16].

In this case, by analyzing the structure of a power-split HEV and its operation, we have designed an improved logic threshold controller to achieve the power distribution in the ICE and electrical system. Furthermore, to obtain the actual torque distributed in electrical system, a variable logic threshold value K is defined to achieve the power distribution between the ISG and the EMG. The improved logic threshold controller behaviors in simulation under different driving conditions are compared with the performances of logic threshold controller system. Results clearly demonstrate that the improved logic threshold approach can significantly improve the efficiency of the ICE and electrical system behavior.

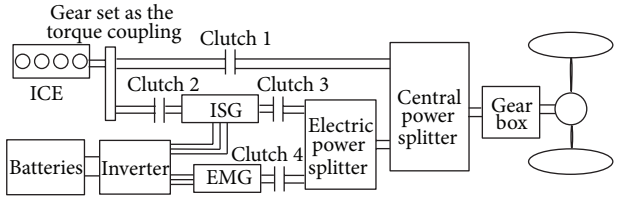

Figure 1: Structure of power-split HEV.

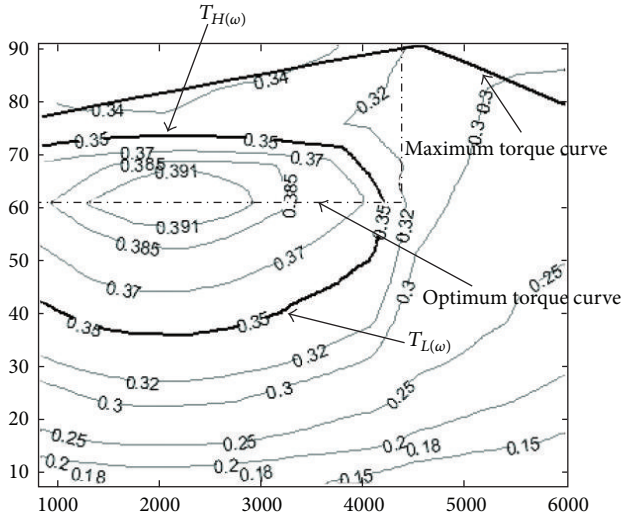

Figure 2: Efficiency map of an operating ICE.

2. Power-Split HEV Structure and Its Operation with Logic Threshold Approach

The structure of power-split HEV studied [5] is shown in Figure 1. To reduce inefficiencies of a single motor driving system, the power-split HEV adopts two motors in its electrical system, and that is, the ISG and the EMG. The former is integrated with the ICE by a gear set and the latter is downsized and integrated with the ISG and the ICE. Both of them can work as driving motor and generator. Since this structure increases the complexity of the electrical system, an electric power splitter and a central power splitter are used in it. To insure the independences of the ICE, the ISG, and the EMG, it adds the clutches 1–4.

To meet the power demand, the central power splitter distributes the power between the ICE and the electrical system and the electrical power splitter distributes the power between the ISG and the EMG. How to distribute the power among the ICE, the ISG, and the EMG is very important, so the main objective is to obtain the highest efficiency of the ICE. Figure 2 shows the efficiency map of an ICE, of which the maximum torque curve represents the highest ICE torque achievable for any speed. The contours show constant efficiencies, whose value will increase toward inner contours, so the points in dashed line are the highest efficiency operating points of the ICE at any corresponding speed. The dashed line can be called the ICE optimum torque curve. Notice that the ICE optimum torque curve must be limited within its peak efficiency region ($\eta_{\mathrm{ICE}} \geq 0.35$), or else the optimal ICE output torque will change suddenly.

When driving the power-split HEV, ICE optimum torque curve can be used as a logic threshold value and ICE is operating at the optimum torque curve. By neglecting energy losses, the relationship among the ICE, the ISG, and the EMG can be expressed as

$$\begin{aligned} k_1 T_{\mathrm{isg}} &= T_{\mathrm{ele}} = T_{\mathrm{ice}}^{\mathrm{req}} - T_{\mathrm{ice}}^{\mathrm{opt}}, \quad T_{\mathrm{ice}}^{\mathrm{opt}} > T_{\mathrm{ice}}^{\mathrm{req}} > 0, \\ k_1 T_{\mathrm{isg}} + k_2 T_{\mathrm{emg}} &= T_{\mathrm{ele}} = T_{\mathrm{ice}}^{\mathrm{req}} - T_{\mathrm{ice}}^{\mathrm{opt}}, \quad \text{else}, \end{aligned} \tag{1}$$

$$\begin{aligned} \omega_{\mathrm{isg}} &= k_1 \omega_{\mathrm{ice}}, \qquad \omega_{\mathrm{emg}} = k_2 \omega_{\mathrm{ice}}, \qquad T_{\mathrm{ice}}^{\mathrm{opt}} \neq 0, \\ k_2 \omega_{\mathrm{isg}} &= k_1 \omega_{\mathrm{emg}}, \qquad T_{\mathrm{ice}}^{\mathrm{opt}} = 0, \end{aligned} \tag{2}$$

where T_{isg} is the output torque from the ISG; T_{ele} is the output torque of the electrical system; $T_{\mathrm{ice}}^{\mathrm{req}}$ is the torque demand on the ICE; $T_{\mathrm{ice}}^{\mathrm{opt}}$ is the optimum output torque of the ICE, when the ICE is stopped; $T_{\mathrm{ice}}^{\mathrm{opt}} = 0$; T_{emg} is the output torque from the EMG; k_1 and k_2 are the gear ratios; ω_{isg} is the speed demand on the ISG; ω_{ice} is the actual speed of the ICE, which depends on the power-split HEV speed and the gear ratios; ω_{emg} is the speed demand on the EMG.

Equations (1) and (2) reflect the relationship between the ICE, the ISG, and the EMG when driving the power-split HEV. It is easy to calculate the power distribution of every component on the basis of obtaining the torque and speed. For instance, the optimum output power $P_{\mathrm{ice}}^{\mathrm{opt}}$ from the ICE can be calculated by using $T_{\mathrm{ice}}^{\mathrm{opt}}$ and optimum output speed $\omega_{\mathrm{ice}}^{\mathrm{opt}}$ of the ICE as follows:

$$T_{\mathrm{ice}}^{\mathrm{opt}} \omega_{\mathrm{ice}}^{\mathrm{opt}} = P_{\mathrm{ice}}^{\mathrm{opt}}. \tag{3}$$

By combining (1) and (3), the output power of the ICE can be controlled at the highest efficiency by changing the output torque of the ISG or the EMG. Since $P_{\mathrm{ice}}^{\mathrm{opt}}$ is known, the power demand on electrical system can be obtained by

$$\begin{aligned} P_{\mathrm{ele}} &= P_{\mathrm{ice}}^{\mathrm{req}} - P_{\mathrm{ice}}^{\mathrm{opt}}, \\ P_{\mathrm{ice}}^{\mathrm{req}} &= T_{\mathrm{ice}}^{\mathrm{req}} \omega_{\mathrm{ice}}, \end{aligned} \tag{4}$$

where P_{ele} denotes the power demand on electrical system and $P_{\mathrm{ice}}^{\mathrm{req}}$ is the power demand to the ICE.

It can distribute the power between the ISG and the EMG in the electrical system by the known parameter P_{ele}. At a certain speed, when P_{ele} is less than the peak power of the ISG, the electrical power is supplied by the ISG. While P_{ele} is up to the peak power of the ISG and less than the peak power of the EMG, the electrical power is supplied by the EMG. While P_{ele} is up to the peak power of the EMG, the electrical power is supplied by the ISG and the EMG.

It can be seen that the power distribution among the ICE, the ISG, and the EMG is very easy when using simple logic threshold approach. However, the ICE may fail to achieve the best efficiency on account of the complex nature of power-split HEV. For example, the inertial additional torque of the running/stopping of the ICE, the SOC of batteries, and

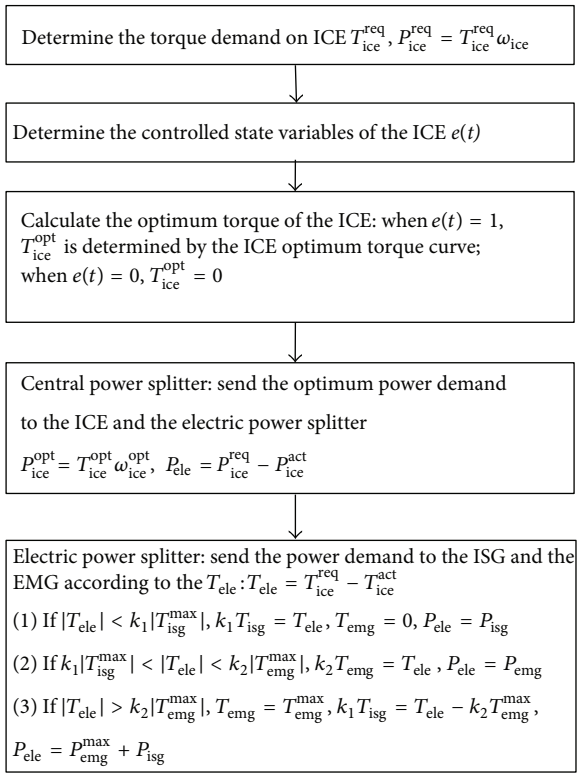

Figure 3: The control flow chart of the logic threshold approach.

the driving cycles are usually important factors affecting the ICE output. In this condition, the ICE is operating at region near the optimum torque curve. The relationship among the ICE, the ISG, and the EMG can be described as

$$\begin{aligned} k_1T_{isg} = T_{ele} = T_{ice}^{req} - T_{ice}^{act}, \quad T_{ice}^{opt} > T_{ice}^{req} > 0, \\ k_1T_{isg} + k_2T_{emg} = T_{ele} = T_{ice}^{req} - T_{ice}^{act}, \quad \text{else}, \end{aligned} \tag{5}$$

where T_{ice}^{act} is the actual output torque of the ICE and $T_{ice}^{act} \geq 0$. The power demand on electrical system P_{ele} in (4) should be changed into $P_{ele} = P_{ice}^{req} - P_{ice}^{act}$, $P_{ice}^{act} = T_{ice}^{act}\omega_{ice}$.

In order to give a detailed introduction of the logic threshold approach, the control flow chart is shown in Figure 3. We can see that the power distribution between the ISG and the EMG is also determined by some logic control conditions.

Equation (5) and Figure 3 reflect the actual torque distribution among the ICE, the ISG, and the EMG. One can see the logic threshold value T_{ice}^{opt} is very important to design the highest efficiency of the ICE. Because the threshold value T_{ice}^{opt} is changed into the actual output torque T_{ice}^{act}, the control strategy fails to achieve the best efficiency of the ICE. On the other hand, the electric power splitter distributes the power on the basis of the output torque of the electrical system T_{ele}, but it does not consider the efficiency of the overall electrical system. In this way, the control strategy fails to achieve the best efficiency of the system. Since simple logic threshold approach is not available to achieve the best efficiency of the system, we propose an improved logic threshold approach of energy management by taking into account the factors such as the character of ICE, the SOC, and the speed of the power-split HEV.

3. Design of the Improved Logic Threshold Approach

The control system uses an ICE logic threshold controller with three inputs and one output, where the first input is the torque demand on the ICE, the second input is the SOC, and the third input is the current ICE speed. The schematic of control system is shown in Figure 4. To design the improved logic threshold approach, we analyze the main effects of the traditional logic threshold approach. Combined with Figure 3, the main controlling parameters are the state variables of the ICE $e(t)$, the actual output torque and the power of the ICE T_{ice}^{act} and P_{ice}^{act}, and the electrical power distribution P_{ele} between the ISG and EMG. To sum up, the basic idea of the improved logic threshold approach should consider the influenced factors about the main effects and then correct the main controlling parameters to improve the efficiency of the components.

The ICE logic threshold controller calculates the torque distribution to the ICE and the first objective is the prejudgment for running/stopping of the ICE. The state running/stopping of the ICE is determined by three logic threshold values: the minimum speed demand on the ICE, the minimum torque demand on the ICE, and the current SOC, respectively. When the ICE is operating, the output speed and torque must be controlled in the peak efficiency region ($\eta_{ICE} \geq 0.35$). To ensure the efficiency, the minimum speed demand on the ICE is designed as 800 rpm and the maximum speed to the ICE is designed as 4100 rpm. On the other hand, the lowest and highest output torque of the ICE are designed as $T_{L(\omega)}$ and $T_{H(\omega)}$, respectively, as shown in Figure 2.

Next, the second objective is the calculation of T_{ice}^{act}. To calculate T_{ice}^{act}, it is very important to consider SOC of batteries firstly because SOC is related to the ICE output torque. The resistance curves and the voltage curve corresponding to SOC of the single NI-MH battery used in this study are shown in Figure 5. To ensure the batteries charging/discharging efficiency, we define that, when SOC is over 0.8, the ICE must be stopped to avoid the overcharging the batteries. When SOC is lower than 0.2, the ICE must be started to avoid the over discharge of batteries.

When SOC is in the region $[0.2, 0.8]$, the running/stopping of the ICE is determined by a binary variable, which is expressed as follows:

$$\begin{aligned} e(t-1) = 0, \quad e(t) = \begin{cases} 1, & 0.2 \leq \text{SOC} \leq 0.5 \\ 0, & \text{else}, \end{cases} \\ e(t-1) = 1, \quad e(t) = \begin{cases} 0, & 0.5 \leq \text{SOC} \leq 0.8 \\ 1, & \text{else}, \end{cases} \end{aligned} \tag{6}$$

where $e(t)$ is the binary variable, $e(t) = 0$ indicates that the ICE stops, the actual output torque is 0, and $e(t) = 1$ indicates that the ICE runs.

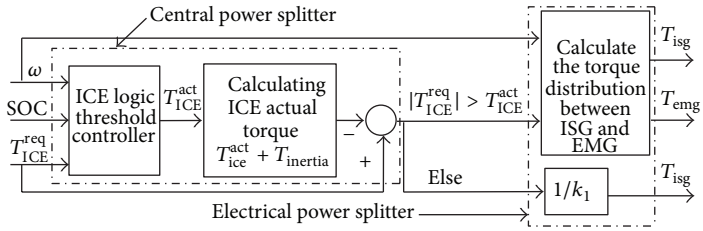

Figure 4: Schematic of control system with logic threshold controller.

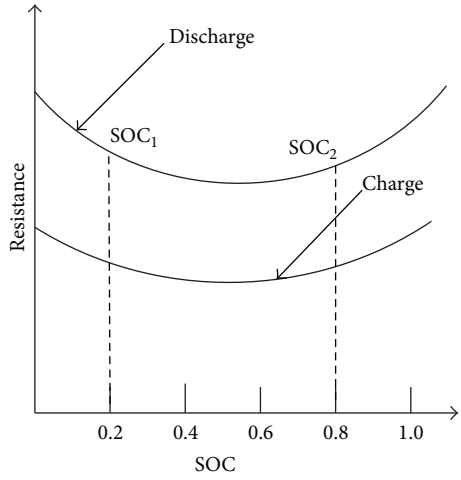

Figure 5: The resistance curves corresponding to SOC.

We can see that 0.5 can be used as a logic threshold value of SOC to change the state of ICE. However, the state of ICE may be changed quite frequently when SOC is changed in regions around SOC = 0.5. So the single logic threshold value of SOC is improved and the single value SOC = 0.5 is changed to the region [0.45, 0.55]. In this region, the state of the ICE is maintained, and the binary variable $e(t)$ is expressed as follows:

$$e(t-1) = 0, \qquad e(t) = \begin{cases} 1, & 0.2 \le \text{SOC} \le 0.45 \\ 0, & \text{else}, \end{cases}$$
$$e(t-1) = 1, \qquad e(t) = \begin{cases} 0, & 0.55 \le \text{SOC} \le 0.8 \\ 1, & \text{else}. \end{cases} \tag{7}$$

From (7), we can see that the batteries should be charged when SOC is lower than 0.45 and be discharged when SOC is more than 0.55. The ICE provides the charge or discharge power, so the actual output torque of the ICE T_{ice}^{act} must be related to the value of SOC and the modes of the vehicle.

When $e(t) = 0$, it can be known that $T_{ice}^{act} = 0$ because the ICE is turned off. When $e(t) = 1$, $T_{ice}^{act} > 0$, the calculation of T_{ice}^{act} should be determined by the modes of the vehicle. The modes of the vehicle are determined by ΔT as follows:

$$\Delta T = T_{ice}^{act} - T_{ice}^{req}. \tag{8}$$

(a) When $\Delta T > 0$ and $T_{ice}^{req} < T_{L(\omega)}$, operating the ICE within the low torque region is uneconomical. It is avoidable by activating the recharging mode so that the ICE can operate in its peak efficiency, T_{ice}^{act} can be calculated as

$$T_{ice}^{act} = T_{L(\omega)} + \frac{0.45 - \text{SOC}}{0.45 - 0.2}\left(T_{ice}^{opt} - T_{L(\omega)}\right), \quad \text{SOC} \le 0.45,$$
$$T_{ice}^{act} = T_{L(\omega)}, \quad 0.45 < \text{SOC} < 0.55. \tag{9}$$

(b) When $\Delta T < 0$ and $T_{ice}^{req} > T_{H(\omega)}$, the ICE is operated at the highest output torque by activating the hybrid mode. T_{ice}^{act} is limited as

$$T_{ice}^{act} = T_{H(\omega)}. \tag{10}$$

(c) When $\Delta T = 0$ and $T_{L(\omega)} < T_{ice}^{req} < T_{H(\omega)}$, since operating the ICE alone within the peak efficiency region is economical, the pure ICE mode is activated. T_{ice}^{act} can be calculated as

$$T_{ice}^{act} = T_{ice}^{opt}, \quad 0.45 < \text{SOC} < 0.5,$$
$$T_{ice}^{act} = T_{ice}^{req} + \frac{0.45 - \text{SOC}}{0.45 - 0.2}\left(T_{H(\omega)} - T_{ice}^{req}\right), \quad \text{SOC} \le 0.45. \tag{11}$$

When we get T_{ice}^{act}, we should consider the inertia torque of ICE to calculate the electrical system power demand P_{ele}. The relation of the power between the ICE and the electrical system can be expressed by rewriting (4) as follows:

$$P_{ele} = P_{ice}^{req} - P_{ice}^{act},$$
$$P_{ice}^{act} = \left(T_{ice}^{act} + T_{inertia}\right)\omega_{ice}, \tag{12}$$

where $T_{inertia}$ is the inertia torque of ICE, $T_{inertia} = mr^2(d\omega)/(dt)$, m is the mass of ICE flywheel, r is the radius of ICE flywheel, and ω is the angular speed of ICE flywheel.

To distribute the torque or power between the ISG and the EMG, we define a variable logic threshold value K to achieve the distribution; it is shown as follows:

$$K = \frac{P_{isg}}{P_{ele}}, \tag{13}$$

where $K = \{0, 0.1, 0.2, 0.3, 0.4, 0.5, 0.6, 0.7, 0.8, 0.9, 1\}$ and P_{isg} is the power contribution of the ISG to the electrical power demand P_{ele}. The power contribution of the EMG can be calculated as

$$P_{\text{emg}} = (1 - K) P_{\text{ele}}, \tag{14}$$

where P_{emg} is the power contribution of the EMG.

The efficiency of electrical system can be calculated as

$$\begin{aligned} \eta_{\text{ele}} &= \left\{ \frac{T_{\text{isg}} \omega_{\text{isg}} \eta_{\text{isg}}^{i} + T_{\text{emg}} \omega_{\text{emg}} \eta_{\text{emg}}^{i}}{P_{\text{isg}} + P_{\text{emg}}} \right\}^{i} \\ &= \left\{ \frac{P_{\text{isg}} \eta_{\text{isg}}^{i} + P_{\text{emg}} \eta_{\text{emg}}^{i}}{P_{\text{ele}}} \right\}^{i}, \end{aligned} \tag{15}$$

where η_{isg}^{i} is the efficiency of the ISG; η_{emg}^{i} is the efficiency of the EMG; $i = 1$ when the ISG and the EMG work in recharge state; and $i = -1$ when they work in discharge state.

By combining (13)–(15), the best efficiency $\eta_{\text{ele max}}$ of electrical system can be calculated as

$$\begin{aligned} \eta_{\text{ele}} &= \left\{ K \eta_{\text{isg}}^{i} + (1 - K) \eta_{\text{emg}}^{i} \right\}^{i}, \\ \eta_{\text{ele max}} &= \arg\max_{K \in (K_{\min}, K_{\max})} \left\{ K \eta_{\text{isg}}^{i} + (1 - K) \eta_{\text{emg}}^{i} \right\}^{i}. \end{aligned} \tag{16}$$

For a particular K, P_{isg} and P_{emg} can be calculated by (13) and (14). On the other hand, ω_{isg} and ω_{emg} can be obtained by knowing the wheel speed corresponding to driving cycles, η_{isg}^{i} and η_{emg}^{i}, by the calculation

$$\begin{aligned} \eta_{\text{isg}}^{i} &= f\left(T_{\text{isg}}, \omega_{\text{isg}}\right), \qquad T_{\text{isg}} = \frac{P_{\text{isg}}}{\omega_{\text{isg}}}, \\ \eta_{\text{emg}}^{i} &= f\left(T_{\text{emg}}, \omega_{\text{emg}}\right), \qquad T_{\text{emg}} = \frac{P_{\text{emg}}}{\omega_{\text{emg}}}. \end{aligned} \tag{17}$$

From (16) and (17), we can get the efficiency of electrical system to any specific K. At the same time, we can get the maximum efficiency $\eta_{\text{ele max}}$ by searching the maximum value of η_{ele}, then the value K corresponding to $\eta_{\text{ele max}}$ is used to calculate P_{isg} and P_{emg}.

From (6)~(17), the underlying reasons of the improvements can be summarized as follows: (1) the corrected $e(t)$ can reduce the running/stopping times and improve the output stability of the ICE; (2) the designed $T_{\text{ice}}^{\text{act}}$ combined the peak region of the ICE, the modes of the vehicle, and the SOC of the batteries; it can improve the efficiency of overall vehicle control and energy management system in any modes; (3) the variable logic threshold value K can achieve the best efficiency of the electrical system.

4. Simulation and Comparative Analysis

The Urban Dynamometer Driving Schedule (UDDS) and the New European Driving Cycle (NEDC) are chosen to demonstrate the improved logic threshold approach. The important parameters of power-split HEV are listed in Table 1. The selected driving cycles are shown in Figure 6.

Table 1: Parameters of vehicles.

Component	Parameter	Power-split HEV value
ICE (Honda-Insight)	Peak power	50 kw
	Optimum torque	60 Nm
	Peak efficiency	0.4
EMG (Insight)	Peak power	30 kw
	Peak torque	±220 Nm
ISG (Insight)	Peak power	10 kw
	Peak torque	±100 Nm
NIHM battery	Voltage	288 V
	Capacity	6.5 Ah
Power-split HEV data	Radius of wheel	0.275 m
	Frontal area	1.92 m^2
	Total mass	1350 Kg

The ICE performance of the power-split HEV is shown in Figure 7. We can see that the ICE can operate in its peak efficiency region and near its optimum curve with both the logic threshold controller and the improved logic threshold controller. From Figure 7(b), the operating points of them not only behave in peak efficiency region, but also behave closer to the ICE optimum torque curve than to the ICE operating points with logic threshold controller. When the ICE is starting or running in the low speed area, some output torque points of the ICE with logic threshold controller are higher than those expected, some points even present beyond the peak efficiency region. So the operating points of the ICE with logic threshold are of less efficiency than the operating points of the ICE with improved logic threshold control.

The performances of the EMG are shown in Figures 8(a) and 8(b). It is apparent that the ICE is less efficient in two regions: (1) higher output torque in low speed and (2) lower braking torque in low speed. From Figure 8, the EMG with improved logic threshold controller behaves with higher efficiency than the ICE with logic threshold controller because it avoids the higher output torque and lower braking torque in low speed. On the other hand, the operating points of the EMG are closer to the red curve which presents the highest efficiency. So the improved logic threshold controller can improve the efficiency of the EMG. The performance of the ISG is shown in Figures 8(c) and 8(d). It should be noticed that the ISG efficiency is different from the EMG in different speed. The efficiency is higher when the ISG is operating in low output torque and low braking torque. However, the ISG is of low efficiency in high output or braking torque when it is operating at about 500 rpm. We can see that the ISG with improved logic threshold controller is operating in low output torque or braking torque region when the speed of the ISG is operating at about 500 rpm. So it avoids low efficiency in operating and higher efficiency than the ISG with logic threshold controller.

Table 2: Comparison of simulation results.

Driving cycle	ICE efficiency		The variation of the SOC (initial SOC~final SOC)		Motor driving system efficiency		Fuel consumption	
	Logic threshold	Improved logic threshold	Logic threshold	Improved logic threshold	Logic threshold	Improved logic threshold	Logic threshold	Improved logic threshold
NEDC	35.8%	37.6%	0.70~0.51	0.70~0.59	81.0%	87.1%	3.41 L	3.36 L
UDDS	34.7%	36.4%	0.70~0.47	0.70~0.56	79.5%	85.7%	3.73 L	3.64 L

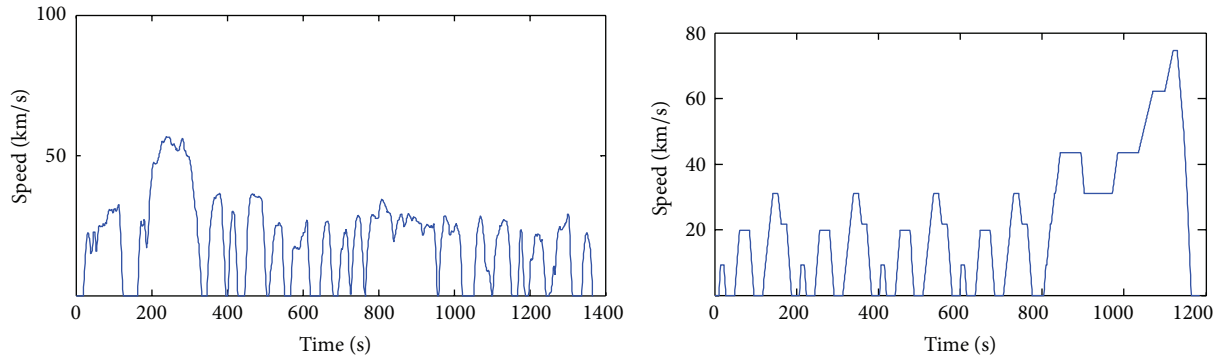

(a) UDDS (b) NEDC

Figure 6: Driving cycles.

Figure 9 shows the comprehensive results of the power-split HEV in NEDC. The torque outputs of the ICE, the ISG, and the EMG reflect that the ICE controlled by both logic threshold controller and improved logic threshold controller can work in the peak efficiency region. When the electrical system responds to high regenerative braking torque, the ISG and the EMG controlled by improved logic threshold controller can work more harmonically than logic threshold controller since the logic threshold variable K is used to achieve the torque distribution between the ISG and the EMG. In other words, it reflects the change of SOC; the initial value of SOC is set to 0.7. The final value is 0.51 when the logic threshold controller is used, but the final value is up to 0.59 when the improved logic threshold controller is used. So the improved logic threshold controller reduces the energy consumption of batteries up to 8%.

To have more specific comparative analysis, we list the ICE efficiency, the variation of SOC, and the motor driving system efficiency calculated from ADVISOR in the two driving cycles. They are shown in Table 2. We can see that the improved logic threshold controller improves the ICE efficiency and reduces the variation of SOC. The motor driving system efficiency is improved apparently. The ICE efficiency is increased by 1.7%, the fuel consumption is reduced down to 1.4%, and the motor driving system efficiency is increased by 6.1% when using the improved logic threshold controller when compared to the power-split HEV with the logic threshold controller.

5. Conclusions

This paper designs an improved logic threshold approach of energy management for a power-split HEV assisted by an ISG. By analyzing the power-split HEV structure and its operation with logic threshold approach, combining the ICE characters and the demand torque with the value of SOC to manage the ICE within its peak efficiency region, the logic threshold controller is improved. Furthermore, a variable logic threshold value K is defined to achieve the best efficiency of electrical system and achieve the power distribution between the ISG and the EMG.

Results have shown that the ICE efficiency and the efficiency of battery charging and discharging with improved logic threshold controller are improved when compared to the equally power-split HEV with the logic threshold controller. The comprehensive results show that battery power consumption reduces down to 8%, the ICE efficiency improves up to 1.7%, the fuel consumption is reduced down to 1.4%, and the motor driving system efficiency improves up to 6.1% of a power-split HEV with the improved logic threshold approach when compared with one with the logic threshold approach. The comprehensive results show the effectiveness and the validity of the improved logic threshold approach.

Acknowledgments

The authors would like to thank the anonymous reviewers for their constructive and insightful comments for further

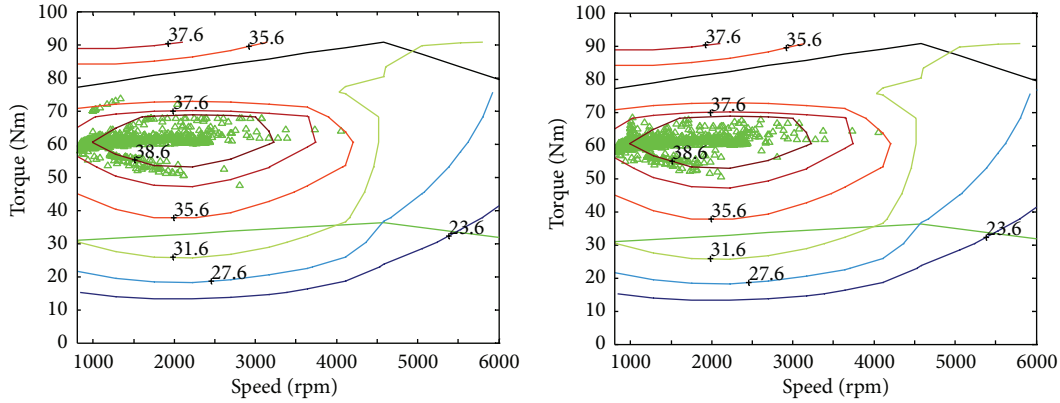

(a) Operating points of the ICE with logic threshold

(b) Operating points of the ICE with improved logic threshold

Figure 7: ICE performances in UDDS.

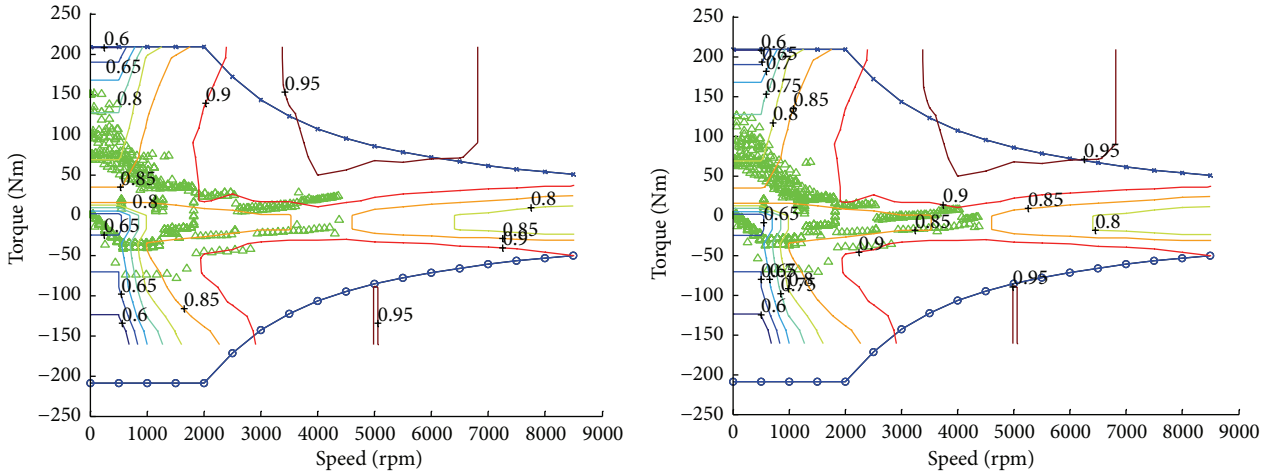

(a) Operating points of the EMG with logic threshold

(b) Operating points of the EMG with improved logic threshold

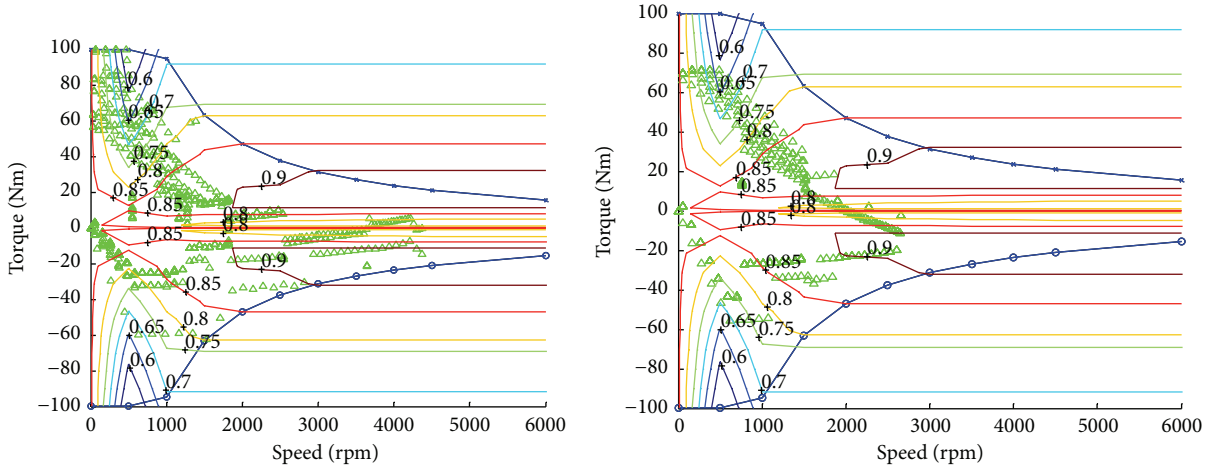

(c) Operating points of the ISG with logic threshold

(d) Operating points of the ISG with improved logic threshold

Figure 8: EMG and ISG performances in UDDS.

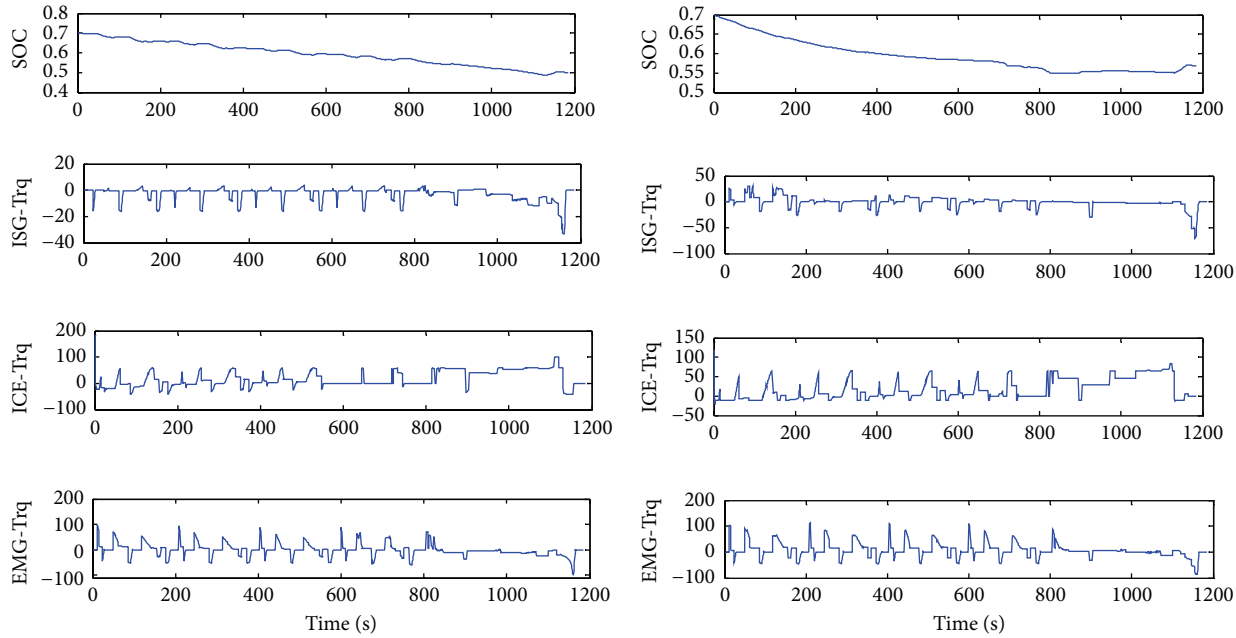

(a) Comprehensive results with logic threshold

(b) Comprehensive results with improved logic threshold

Figure 9: Comprehensive results in NEDC.

improving the quality of this paper. This work was partially supported by National Natural Science Foundation of China under Grant nos. 60904023, 51277116, and 61203047, China Postdoctoral Science Foundation under Grant no. 2013T60670, the Science and Technology Programme Foundation for the Innovative Talents of Henan Province University under Grant no. 13HASTIT038 and the Key Scientific and Technological Project of Henan Province under Grant no. 132102210247.

References

[1] H. Borhan, A. Vahidi, A. M. Phillips, M. L. Kuang, I. V. Kolmanovsky, and S. Di Cairano, "MPC-based energy management of a power-split hybrid electric vehicle," *IEEE Transactions on Control Systems Technology*, vol. 20, no. 3, pp. 593–603, 2012.

[2] L. Chen, F. Zhu, M. Zhang, Y. Huo, C. Yin, and H. Peng, "Design and analysis of an electrical variable transmission for a series-parallel hybrid electric vehicle," *IEEE Transactions on Vehicular Technology*, vol. 60, no. 5, pp. 2354–2363, 2011.

[3] F. U. Syed, M. L. Kuang, M. Smith, S. Okubo, and H. Ying, "Fuzzy gain-scheduling proportional-integral control for improving engine power and speed behavior in a hybrid electric vehicle," *IEEE Transactions on Vehicular Technology*, vol. 58, no. 1, pp. 69–84, 2009.

[4] F. U. Syed, M. L. Kuang, J. Czubay, and H. Ying, "Derivation and experimental validation of a power-split hybrid electric vehicle model," *IEEE Transactions on Vehicular Technology*, vol. 55, no. 6, pp. 1731–1747, 2006.

[5] S. Adhikari, S. K. Halgamuge, and H. C. Watson, "An online power-balancing strategy for a parallel hybrid electric vehicle assisted by an integrated starter generator," *IEEE Transactions on Vehicular Technology*, vol. 59, no. 6, pp. 2689–2699, 2010.

[6] H.-U. Rehman, "An integrated starter-alternator and low-cost high-performance drive for vehicular applications," *IEEE Transactions on Vehicular Technology*, vol. 57, no. 3, pp. 1454–1465, 2008.

[7] J. T. B. A. Kessels, M. W. T. Koot, P. P. J. van den Bosch, and D. B. Kok, "Online energy management for hybrid electric vehicles," *IEEE Transactions on Vehicular Technology*, vol. 57, no. 6, pp. 3428–3440, 2008.

[8] O. Reyss, G. Duc, P. Pognant-Gros, and G. Sandou, "Multivariable torque tracking control for E-IVT hybrid powertrain," *International Journal of Systems Science*, vol. 40, no. 11, pp. 1181–1195, 2009.

[9] A. Sciarretta, M. Back, and L. Guzzella, "Optimal control of parallel hybrid electric vehicles," *IEEE Transactions on Control Systems Technology*, vol. 12, no. 3, pp. 352–363, 2004.

[10] B. Zhang and S. Xu, "Delay-dependent Robust H∞ control for uncertain discrete-time fuzzy systems with time-varying delays," *IEEE Transactions on Fuzzy Systems*, vol. 17, no. 4, pp. 809–823, 2009.

[11] M. Montazeri-Gh and M. Asadi, "Intelligent approach for parallel HEV control strategy based on driving cycles," *International Journal of Systems Science*, vol. 42, no. 2, pp. 287–302, 2011.

[12] L. Wu, Y. Wang, X. Yuan, and Z. Chen, "Multiobjective optimization of HEV fuel economy and emissions using the self-adaptive differential evolution algorithm," *IEEE Transactions on Vehicular Technology*, vol. 60, no. 6, pp. 2458–2470, 2011.

[13] A. L. Shen, W. H. Yuan, Q. S. Zuo et al., "Intelligent optimization for logic threshold control parameter on parallel hybrid electric vehicle," *Zhongnan Daxue Xuebao*, vol. 43, no. 11, pp. 4306–4312, 2012.

[14] B. Mashadi and S. A. M. Emadi, "Dual-mode power-split transmission for hybrid electric vehicles," *IEEE Transactions on Vehicular Technology*, vol. 59, no. 7, pp. 3223–3232, 2010.

[15] J. Kim, T. Kim, B. Min, S. Hwang, and H. Kim, "Mode control strategy for a two-mode hybrid electric vehicle using electrically variable transmission (EVT) and fixed-gear mode," *IEEE Transactions on Vehicular Technology*, vol. 60, no. 3, pp. 793–803, 2011.

[16] F. Yan, J. Wang, and K. Huang, "Hybrid electric vehicle model predictive control torque-split strategy incorporating engine transient characteristics," *IEEE Transactions on Vehicular Technology*, vol. 61, no. 6, pp. 2458–2467, 2012.

Hindawi Publishing Corporation
Mathematical Problems in Engineering
Volume 2013, Article ID 609523, 12 pages
http://dx.doi.org/10.1155/2013/609523

Research Article

Active Disturbance Rejection Approach for Robust Fault-Tolerant Control via Observer Assisted Sliding Mode Control

John Cortés-Romero,[1] Harvey Rojas-Cubides,[1] Horacio Coral-Enriquez,[1] Hebertt Sira-Ramírez,[2] and Alberto Luviano-Juárez[3]

[1] *Departamento de Ingeniería Eléctrica y Electrónica, Universidad Nacional de Colombia, Carrera 45 No. 26-85, Bogotá, Colombia*
[2] *Centro de Investigación y de Estudios Avanzados del Instituto Politécnico Nacional (CINVESTAV-IPN), Avenida Instituto Politécnico Nacional, No. 2508, Departamento de Ingeniería Eléctrica, Sección de Mecatrónica, Colonia San Pedro Zacatenco A.P. 14740, 07300 México, DF, Mexico*
[3] *Unidad Profesional Interdisciplinaria en Ingeniería y Tecnologías Avanzadas (UPIITA), Instituto Politécnico Nacional, Avenida Instituto Politécnico Nacional 2580, Barrio La Laguna Ticomán, Gustavo A. Madero 07340, México, DF, Mexico*

Correspondence should be addressed to John Cortés-Romero; jacortesr@unal.edu.co

Received 23 August 2013; Revised 4 November 2013; Accepted 6 November 2013

Academic Editor: Baoyong Zhang

This work proposes an active disturbance rejection approach for the establishment of a sliding mode control strategy in fault-tolerant operations. The core of the proposed active disturbance rejection assistance is a Generalized Proportional Integral (GPI) observer which is in charge of the active estimation of lumped nonlinear endogenous and exogenous disturbance inputs related to the creation of local sliding regimes with limited control authority. Possibilities are explored for the GPI observer assisted sliding mode control in fault-tolerant schemes. Convincing improvements are presented with respect to classical sliding mode control strategies. As a collateral advantage, the observer-based control architecture offers the possibility of chattering reduction given that a significant part of the control signal is of the continuous type. The case study considers a classical DC motor control affected by actuator faults, parametric failures, and perturbations. Experimental results and comparisons with other established sliding mode controller design methodologies, which validate the proposed approach, are provided.

1. Introduction

The main challenge of the Fault-Tolerant Control is to guarantee high performance and reliability in the most adverse operations such as the presence of perturbations, disturbances, dynamic miss-modeling, and actuator faults among others. In general, the techniques employed on the Fault-tolerant Control (FTC) can be classified into active and passive. Active FTC is characterized by the controller reconfiguration assisted by fault detection and isolation (FDI) schemes [1]. On the other hand, passive techniques exploit the robustness of some types of controllers without requiring changes in their structure and can operate satisfactorily without information about system failures. These techniques are usually simple in implementation but are not usually suitable for severe cases of failures [1].

The robust characteristics of the sliding mode technique provide a natural environment for the use of such techniques on passive FTC schemes. This technique has been properly used in different control schemes and assisted by other effective control strategies which have shown proper performance under fault-tolerant operations (see [1–4] as representative examples). Over the past years, considerable attention has been paid to the design of linear/nonlinear disturbance observers for sliding mode controller assistance in order to overcome several issues like chattering [5–8], disturbances and system uncertainties [8–10], coupling of MIMO systems [11], or uncertainties, disturbances, and actuator faults [12].

Even though the performance of the aforementioned control proposals is accurate, there are still complexities in the design that are a consequence of dealing with the system faults and disturbances separately, on the one hand, and, on the other hand, the need for precise knowledge of the system model.

In the active disturbance rejection control (ADRC) philosophy, system fault and disturbances can be dealt with unitedly rendering a simplified linear control structure based on a simplified model like the classical passive fault-tolerant scheme. From the ADRC point of view, the disturbances must be rejected in an active manner, so the control system actively produces accurate estimates and reduces the causes of the output errors. ADRC as a potential solution has been explored in several domains of control engineering (see [13–15]). In accordance with this field, Generalized Proportional Integral (GPI) observers were introduced in [16]. Despite of grand ADRC applications reported in the literature, the potential of this technique for fault-tolerant performance has been scarcely considered. Under the ADRC setup, a GPI disturbance observer assisted sliding mode control approach can be used to deal with fault-tolerant operation. In this paper, the linear GPI observers are used as a part of an active disturbance rejection scheme for the sliding mode creation problem on nonlinear systems with low switching authority.

We are interested in a proper local sliding mode creation with the aid of a GPI disturbance observer. In the establishment of the slide surface, unknown inputs (state dependent or external) impact the correct evolution of the sliding regime demanding greater bound of the control input; when the sliding surface dynamics include an active disturbance cancellation of the influence of that kind of unknown inputs, the required switching input amplitude can be decreased. Furthermore, risk for deviations from the sliding surface, due to unexpected control input saturations, is practically avoided. The proposed GPI observer can be related to either the system dynamics or sliding surface dynamics disturbance inputs; in both cases, it is possible to correctly design a suitable assisted sliding mode control law with fault-tolerant capabilities.

It is assumed that the effect of additive state-dependent and exogenous nonlinearities, that affect the sliding mode regime, may be approximately but accurately canceled from the nonlinear system behavior via the injection of a precise and exogenously generated time-varying signal.

In this work we propose an approach of passive fault-tolerant control based on a classic sliding mode controller assisted by a GPI observer under the context of the active disturbance rejection. This scheme has been validated with the control of a DC motor subject to perturbations in the load torque, actuator faults, and parametric failures.

This paper is organized as follows. Section 2 explores the possibilities of the ADRC in GPI based observer sliding mode control for fault-tolerant operation and two related useful cases are presented. Section 3 describes the study case, states the formulation of the problem, and presents its corresponding proposed design. Section 4 is devoted to the presentation of the experimental results describing experimental platform and the experiments that were carried out to enhance the advantages of using the linear estimation of the disturbance functions during the sliding mode creation problem. Finally, Section 5 contains the conclusions.

2. Possibilities of ADRC for Sliding Mode Control Assistance

It is possible to assist the creation of a sliding mode regime for a wide variety of sliding mode control strategies. The idea is to inject a continuous term via a suitably defined observer, in an active fashion, at the controller stage to ensure the correct establishment or continuation of the sliding mode regime.

The objective of the proposed fault-tolerant control design is to accurately track a desired reference trajectory, even in the presence of the unknown disturbances caused by actuator faults, parameter uncertainty, the presence of unmodeled state-dependent nonlinearities, or the combination of these previous cases with the presence of uncertain exogenous time-varying signals.

This is explained in this section by using a GPI observer-based sliding mode controller. From this point of view, all those terms are considered as a single, lumped, unstructured, time-varying disturbance term. In the establishment of the sliding mode control law, it is necessary to have an estimation of the related disturbance term. Two main benefits of using this strategy can be highlighted: (1) GPI observers allow the estimation of the state of the system, the related disturbance function, and a certain number of its time derivatives; (2) the control law is composed of a discontinuous term plus a continuous injection provided by the GPI observer. The amplitude of the switching part (W) acts as a weighting factor allowing the chattering reduction.

In the following section, two approaches for the creation of the sliding mode regimes assisted by GPI observers, suitable for fault-tolerant operation, are explained.

It should be noted that our approach is not the only possibility; it is merely a preferred approach with ease of analysis, (e.g., it is possible to propose a GPI observer assisted strategy of high-order sliding mode).

2.1. On Observer Assisted First Order Sliding Mode Creation. In this subsection a conventional first order sliding mode control is appropriately adapted by a GPI observer. Consider the following n-dimensional, nonlinear, single-input single-output system:

$$\dot{x} = f(x) + g(x)u, \qquad \sigma = h(x), \tag{1}$$

where the drift vector field $f(x)$ is a smooth but uncertain vector field on $T\mathbb{R}^n$, $g(x)$ is known and a smooth vector field on $T\mathbb{R}^n$, and u is the control input taking values on the closed interval $[-U, U], U > 0$. The function $h(x)$ is a smooth function $h : \mathbb{R}^n \to \mathbb{R}$. The zero level set for the scalar output σ,

$$S = \{x \in \mathbb{R}^n \mid \sigma = h(x) = 0\}, \tag{2}$$

represents a smooth, $n - 1$ dimensional manifold acting as a sliding surface, where σ is the sliding surface coordinate function.

The state-dependent unperturbed sliding surface dynamics are characterized by

$$\dot{\sigma} = L_f h(x) + L_g h(x) u, \tag{3}$$

where L_f and L_g are the Lie derivatives or the directional derivatives of h, along the directions of the vectors f and g, respectively.

Actuator faults, exogenous disturbances, modeled and non modeled internal dynamics, and possible parameter variation can be treated as an equivalent additive lumped disturbance function, ξ_σ, affecting the sliding surface dynamic σ:

$$\dot{\sigma} = \xi_\sigma + L_g h(x) u. \tag{4}$$

2.1.1. Assumptions

Assumption 1. The amplitude, W, of the switching part of the control input u satisfies $W < U$.

Assumption 2. The disturbance function, ξ_σ, and a finite number of its time derivatives, $\xi_\sigma^{(k)}$, $k = 0, 1, 2, \ldots, m$, for a sufficiently large m, are assumed to be uniformly and absolutely bounded; that is, $0 \le |\xi_\sigma^{(k)}| \le \delta_k < \infty$ for any feedback control input stabilizing the sliding surface coordinate dynamics.

Assumption 3. We assume that $L_g h(x) > 0$ is perfectly known and locally strictly positive.

The key observation for the robust operation of the proposed sliding regimes is based on the accurate, yet approximate, on-line estimation of the scalar uncertain disturbance function ξ_σ in the form $\widehat{\xi}_\sigma$. The incorporation of that estimation in the sliding mode control law may result in a substantially enhanced possibility for the creation of a sliding motion via the active disturbance cancelation strategy:

$$u = \frac{1}{L_g h(x)} \left[-\widehat{\xi}_\sigma - W \operatorname{sign}(\sigma) \right]. \tag{5}$$

An extended state representation can be proposed to cope with the disturbance function estimation $\widehat{\xi}_\sigma$. The augmented representation is based on the internal model of the disturbance function ξ_σ. When there is no previous knowledge about the disturbance term ξ_σ, a general signal oriented approach can be quite effective for on-line estimation purposes. Associated with ADRC and specialized by GPI approaches, unknown input signals can be approximated by $d^m \xi_\sigma / dt^m \approx 0$. For that realization, the extended state vector $x_\sigma = [\sigma \ \xi_\sigma \ \xi_\sigma^{(1)} \ \cdots \ \xi_\sigma^{(m-1)}]^T$ is considered. Therefore, the extended state space representation is given by

$$\dot{x}_\sigma = A_1 x_\sigma + B_\sigma L_g h(x) u + E_\sigma \xi^{(m)}, \tag{6}$$

where

$$A_1 = \begin{bmatrix} 0 & 1 & 0 & \cdots & 0 \\ 0 & 0 & 1 & & 0 \\ \vdots & & & \ddots & \vdots \\ 0 & 0 & 0 & \cdots & 1 \\ 0 & 0 & 0 & \cdots & 0 \end{bmatrix}, \quad B_\sigma = \begin{bmatrix} 1 \\ 0 \\ \vdots \\ 0 \\ 0 \end{bmatrix}, \quad E_\sigma = \begin{bmatrix} 0 \\ 0 \\ \vdots \\ 0 \\ 1 \end{bmatrix}. \tag{7}$$

The disturbance function estimation is given by the following GPI observer.

Theorem 1. *Letting* $z = [z_1 \ z_2 \ \cdots \ z_{m+1}]^T$ *and* $\Gamma = [\gamma_m \ \gamma_{m-1} \ \cdots \ \gamma_0]^T$, *with Assumptions 1–3, the following observer for system* (4)*:*

$$\dot{z} = A_1 z + B_\sigma L_g h(x) u + \Gamma e_\sigma \tag{8}$$

with m being a sufficiently large integer, produces exponentially asymptotic estimation of $\sigma, \xi_\sigma, \ldots, \xi_\sigma^{(m-1)}$ *given by the observer variables* $z_1, z_2, \ldots, z_m$, *respectively. The estimation errors* $(\sigma - z_1), (\xi_\sigma - z_2), \ldots, (\xi_\sigma^{(m-1)} - z_{m+1})$ *are ultimately uniformly bounded given the design parameters* $\gamma_0, \ldots, \gamma_m$ *that are chosen so that the following characteristic polynomial is Hurwitz:*

$$p_{e_\sigma}(s) = s^{m+1} + \gamma_m s^m + \cdots + \gamma_1 s + \gamma_0. \tag{9}$$

Proof. The corresponding estimation error vector is defined as $\widetilde{e}_\sigma = x_\sigma - z$ and satisfies

$$\dot{\widetilde{e}}_\sigma = (A_1 - LC)\widetilde{e}_\sigma + E_\sigma \xi^{(m)} = A_\sigma \widetilde{e}_\sigma + E_\sigma \xi^{(m)}, \tag{10}$$

with

$$A_\sigma = \begin{bmatrix} -\gamma_m & 1 & 0 & \cdots & 0 \\ -\gamma_{m-1} & 0 & 1 & & 0 \\ \vdots & & & \ddots & \\ -\gamma_1 & 0 & 0 & \cdots & 1 \\ -\gamma_0 & 0 & 0 & \cdots & 0 \end{bmatrix} \in \mathbb{R}^{(1+m)\times(1+m)}, \tag{11}$$

and its characteristic polynomial in the complex variable s is given by

$$p_{e_\sigma}(s) = \det(sI - A_\sigma) = s^{m+1} + \gamma_m s^m + \cdots + \gamma_1 s + \gamma_0, \tag{12}$$

where the eigenvalues of A_σ can be placed as desired by selecting the gain vector Γ. The Hurwitzian character of A_σ implies that, for every constant, $(1+m)\times(n+m)$, symmetric, positive definite matrix $Q = Q^T > 0$, there exists a symmetric, positive definite $(1+m)\times(1+m)$ matrix $P = P^T > 0$, so that $A_\sigma^T P + P A_\sigma = -Q$. The Lyapunov function candidate $V(x) = (1/2) e_\sigma^T P e_\sigma$ exhibits a time derivative, along with the solutions of the closed loop system given by

$$\dot{V}(\widetilde{e}_\sigma, t) = \frac{1}{2}\widetilde{e}_\sigma^T \left(A_\sigma^T P + P A_\sigma \right) \widetilde{e}_\sigma + \widetilde{e}_\sigma^T P E_\sigma \xi_\sigma^{(m)}(t). \tag{13}$$

For $Q = I$, that is, an $(1+m)\times(1+m)$ identity matrix, this function satisfies

$$\begin{aligned} \dot{V}(x_\sigma, t) &= \frac{1}{2}\widetilde{e}_\sigma^T (-Q)\widetilde{e}_\sigma + \widetilde{e}_\sigma^T P E_\sigma \xi_\sigma^{(m)}(t) \\ &\le \frac{1}{2}\|\widetilde{e}_\sigma\|_2^2 + \|\widetilde{e}_\sigma\|_2 \|P\|_2 \|E\|_2 \delta_m. \end{aligned} \tag{14}$$

Given that $\|E\|_2 = 1$ and according to Assumption 2, this function is strictly negative everywhere outside the sphere S_σ, given by

$$S_\sigma = \left\{ \widetilde{e}_\sigma \in R^{1+m} \mid \left\| \widetilde{e}_\sigma \right\|_2 \leq 2\delta_m \|P\|_2 \right\}. \tag{15}$$

Hence, all trajectories $\widetilde{e}_\sigma(t)$ starting outside this sphere converge towards its interior, and all those trajectories starting inside S_σ will never abandon it. □

Corollary 2. *Under all the previous assumptions, the discontinuous active disturbance rejection feedback controller*

$$u = \frac{1}{L_g h(x)} \left[-z_1 - W \operatorname{sign}(\sigma) \right] \tag{16}$$

locally creates a sliding regime for any amplitude, W, satisfying: $W > \delta_0$, with δ_0 as the ultimate bound for the disturbance estimation error e_σ.

Proof. The observer-based control law renders the following closed loop sliding surface dynamics:

$$\dot{\sigma} = \left(\xi_\sigma - \widehat{\xi}_\sigma \right) - W \operatorname{sign}(\sigma) \tag{17}$$

with $\widehat{\xi}_\sigma = z_1$, which would require a smaller control input switching amplitude W than in the case where the observer is not used. According to Theorem 1, the disturbance estimation error, e_σ, is bounded by δ_1, and the local existence of a sliding regime $\sigma = 0$ is guaranteed even if W is rather small.

Consider the following Lyapunov function candidate:

$$V = \frac{1}{2}\sigma^2. \tag{18}$$

Differentiating the Lyapunov function (18) with respect to time and using (17) yield

$$\begin{aligned} \dot{V} &= \sigma\dot{\sigma}, \\ \dot{V} &= \sigma \left(\xi_\sigma - \widehat{\xi}_\sigma - W \operatorname{sign}(\sigma) \right), \\ \dot{V} &= \sigma \left(\xi_\sigma - \widehat{\xi}_\sigma \right) - W|\sigma|, \\ \dot{V} &\leq |\sigma| \delta_0 - W|\sigma|. \end{aligned} \tag{19}$$

$\dot{V}$ is strictly negative if $W > \delta_0$. Therefore, if $W > \delta_0$, locally it creates a sliding regime (see [17]). □

2.2. Observer Assisted Nonlinear Controlled Systems in Input-Output Representation. In the previous subsection, the power of the GPI observer injections for a proper establishment and development of a first order sliding mode regimen was demonstrated. In this subsection, the GPI observer is used in a wider perspective allowing both sliding surface coordinate function (σ) and disturbance function (ξ_σ) constructions. These constructions are conducted by means of the system state estimation and disturbance function estimation related to system dynamics; all are supplied by the GPI observer.

Consider the nonlinear, scalar, differentially flat system

$$y^{(n)} = \psi(t, y)\, u + \phi\left(t, y, \dot{y}, \ldots, y^{(n-1)}\right) \tag{20}$$

with the following set of initial conditions: $Y_0 = \{y(t_0), \dot{y}(t_0), \ldots, y^{(n-1)}(t_0)\}$. We refer to the function $\psi(t, y)$ as the control input gain of the system. The term $\phi(t, y, \dot{y}, \ldots, y^{(n-1)})$ will be addressed as the drift function.

For a given smooth control input function, $u(t)$, let $y(t) = \Theta(t, t_0, Y_0, u(t))$ denote the solution trajectory of system (20) from the set of initial conditions, Y_0. We denote by the time function $\xi(t)$ the additive disturbance function, regardless of any particular internal structure.

It is desired to drive the flat output y of the system

$$y^{(n)} = \psi(t, y)\, u + \xi(t) \tag{21}$$

to track a given smooth reference trajectory $y^*(t)$, regardless of the unknown but uniformly bounded nature of the disturbance function $\xi(t)$. As in the previous case, ξ takes into account, in a lumped way, faults and exogenous and endogenous disturbances affecting the system dynamics. It is important to note that the disturbance functions ξ and ξ_σ are defined in different dynamics but catch the same essential disturbance behavior. Indeed, it will be showed that it is possible to form an estimate of ξ_σ from an estimate of ξ and some others estimates provided by the GPI observer.

Regarding controlled system (21), we make the following assumptions.

Assumption 4. The disturbance function $\xi(t)$ is completely unknown, while the control input gain $\psi(t, y)$ is perfectly known. Let ϵ be a strictly positive real number. The control input gain $\psi(t, y)$ is assumed to be uniformly bounded away from zero; that is, $\inf_t |\psi(t, y)| \geq \epsilon > 0$ for any solution $y(t)$ of the controlled system. In particular, it is bounded away from zero for the given output reference trajectory $y^*(t)$.

Assumption 5. It is assumed that a solution $y(t)$ exists, uniformly in t for every given set of initial conditions Y_0, specified at time $t = t_0$ and for a given, sufficiently smooth control input function $u(t)$. Given a desired flat output reference trajectory $y^*(t)$, the flatness of the system, and the previous assumption, a straightforward calculation of the corresponding (unique) open loop control input $u^*(t)$ is possible (see [18]).

Assumption 6. Let m be a given integer. As a time function, the mth, time derivative of $\xi(t)$, is uniformly absolutely bounded. In other words, there exists a constant K_m so that

$$\sup_t \left| \xi^{(m)}(t) \right| \leq K_m. \tag{22}$$

Remark 3. Assumption 6 cannot be verified a priori when $\xi(t)$ is completely unknown. However, in cases where the nonlinearity is known except for some of its parameters, its validity can be assessed with some work. Also, if $\xi^{(m)}(t)$ is not uniformly absolutely bounded almost everywhere, then solutions $y(t)$ for (21) do not exist for any finite $u(t)$ (see [19]).

2.2.1. Observer-Based Approach. With reference to simplified system (21), in order to propose a GPI observer for a related state and disturbance function estimation, it is considered that the internal model of the disturbance function, ξ, is approximated by $d^m\xi(t)/dt^m \approx 0$ at the observer stage. This model is embedded into the augmented model which is characterized by an extended state composed of the phase variables $x_1, x_2, \ldots, x_n$, associated with the flat output $x_1 = y$, and augmented by the m output estimation error iterated integral injections $x_{n+1}, \ldots, x_{n+m}$. As a result, setting the state vector $x = [x_1 \;\; x_2 \;\; \cdots \;\; x_{n+m}]$ with $x_1 = y$, $x_2 = \dot{y}, \ldots, x_n = y^{(n-1)}$, $x_{n+1} = \xi, \ldots, x_{n+m} = \xi^{(m-1)}$, the augmented state space model is given by

$$\begin{aligned} \dot{x} &= Ax + B\psi(t, y)\, u + E\xi^{(m)}, \\ y &= Cx \end{aligned} \tag{23}$$

with

$$A = \begin{bmatrix} 0 & 1 & 0 & \cdots & 0 \\ 0 & 0 & 1 & & 0 \\ \vdots & & & \ddots & \\ 0 & 0 & 0 & \cdots & 1 \\ 0 & 0 & 0 & \cdots & 0 \end{bmatrix} \in \mathbb{R}^{(n+m)\times(n+m)},$$

$$B = \begin{bmatrix} 0 \\ \vdots \\ 1_{(n\text{th position})} \\ \vdots \\ 0 \end{bmatrix} \in \mathbb{R}^{(n+m)\times 1},$$

$$C = \begin{bmatrix} 1 & 0 & \cdots & 0 \end{bmatrix} \in \mathbb{R}^{1\times(n+m)}, \qquad E = \begin{bmatrix} 0 \\ 0 \\ \vdots \\ 0 \\ 1 \end{bmatrix} \in \mathbb{R}^{(n+m)\times 1}. \tag{24}$$

Now, the GPI observer for the state, x, is proposed:

$$\begin{aligned} \dot{\hat{x}} &= A\hat{x} + B\psi(t, y)\, u + L(y - \hat{y}), \\ \hat{y} &= C\hat{x}, \end{aligned} \tag{25}$$

where $\hat{x} = [\hat{x}_1 \;\; \hat{x}_2 \;\; \cdots \;\; \hat{x}_{n+m}]^T$ is the estimation state vector and the observer gain vector is $L = [l_{n+m-1} \;\; \cdots \;\; l_1 \;\; l_0]^T$.

The estimation error vector, $\tilde{e}_x = [\tilde{e}_{x1} \;\; \tilde{e}_{x2} \;\; \cdots \;\; \tilde{e}_{x(n+m)}]^T$, defined as $\tilde{e}_x = x - \hat{x}$, satisfies

$$\begin{aligned} \dot{\tilde{e}}_x &= (A - LC)\,\tilde{e}_x + E\xi^{(m)}, \\ \dot{\tilde{e}}_x &= A_e\tilde{e}_x + E\xi^{(m)}, \end{aligned} \tag{26}$$

where

$$A_e = \begin{bmatrix} -l_{n+m-1} & 1 & 0 & \cdots & 0 \\ -l_{n+m-2} & 0 & 1 & & 0 \\ \vdots & & & \ddots & \\ -l_1 & 0 & 0 & \cdots & 1 \\ -l_0 & 0 & 0 & \cdots & 0 \end{bmatrix}, \tag{27}$$

with $A_e \in \mathbb{R}^{(n+m)\times(n+m)}$, and its characteristic polynomial in the complex variable s is given by

$$\begin{aligned} p_{e_x}(s) &= \det(sI - A_e) \\ &= s^{n+m} + l_{n+m-1}s^{n+m-1} + \cdots + l_1 s + l_0. \end{aligned} \tag{28}$$

Theorem 4. *Suppose that all previous assumptions are valid. Let the coefficients, l_j, with $j = 0, 1, \ldots, n+m-1$, of the polynomial $p_{e_x}(s)$ be chosen so that all their roots are exhibited to the left of the complex plane $\mathbb{C}$. Then, the trajectories of the estimation error vector $\tilde{e}_x(t)$ globally converge towards a small as-desired sphere of radius ρ, denoted by $S(0, \rho)$, centered at the origin of the estimation error phase space $\{\tilde{e}_{x1}, \tilde{e}_{x2}, \ldots, \tilde{e}_{x(n+m)}\}$, where they remain ultimately bounded.*

Proof. This problem has already been proposed with slightly different notation in [20]. In a recent work [21], it is shown that the estimation error vector is uniformly ultimately bounded. □

Remark 5. Consequently with Theorem 4, the variables $\hat{x}_{n+1}, \hat{x}_{n+2}, \ldots, \hat{x}_{n+m}$ track arbitrarily and closely the unknown time functions $\xi(t)$ and their time derivatives $\xi^{(j)}(t)$, $j = 1, \ldots, m-1$.

2.2.2. Sliding Surface Design. Regarding controlled systems (21), a conventional sliding surface can be chosen as (in order to decrease the stable error, an integral term of the tracking error e_y can be introduced (see [12]), but it is preferred to maintain a conventional surface to enhance the GPI observer capabilities)

$$\sigma = e_y^{(n-1)} + \lambda_{n-2}e_y^{(n-2)} + \cdots + \lambda_0 e_y \tag{29}$$

with $e_y = y - y^*$ being flat output tracking error. The design parameters $\lambda_0, \ldots, \lambda_{n-2}$ are chosen so that the characteristic polynomial $p_\sigma(s) = s^{(n-1)} + \lambda_{n-2}s^{(n-2)} + \cdots + \lambda_0$ is Hurwitz.

An estimated version of the previous surface can be given by

$$\begin{aligned} \hat{\sigma} = \hat{x}_n - [y^*]^{(n-1)} + \lambda_{n-2}\left(\hat{x}_{n-1} - [y^*]^{(n-2)}\right) \\ + \cdots + \lambda_0(\hat{x}_1 - y^*), \end{aligned} \tag{30}$$

where $\hat{y} = \hat{x}_1, \ldots, \widehat{y^{(n-1)}} = \hat{x}_n$ are estimates provided by GPI observer (8). The use of $\hat{x}_1$ instead of x_1 is preferred for chattering reduction purposes (see [17]).

The sliding surface dynamics of $\hat{\sigma}$ is given by

$$\begin{aligned} \dot{\hat{\sigma}} = \dot{\hat{x}}_n - [y^*]^{(n)} + \lambda_{n-2}\left(\dot{\hat{x}}_{n-1} - [y^*]^{(n-1)}\right) \\ + \cdots + \lambda_0\left(\dot{\hat{x}}_1 - \dot{y}^*\right). \end{aligned} \tag{31}$$

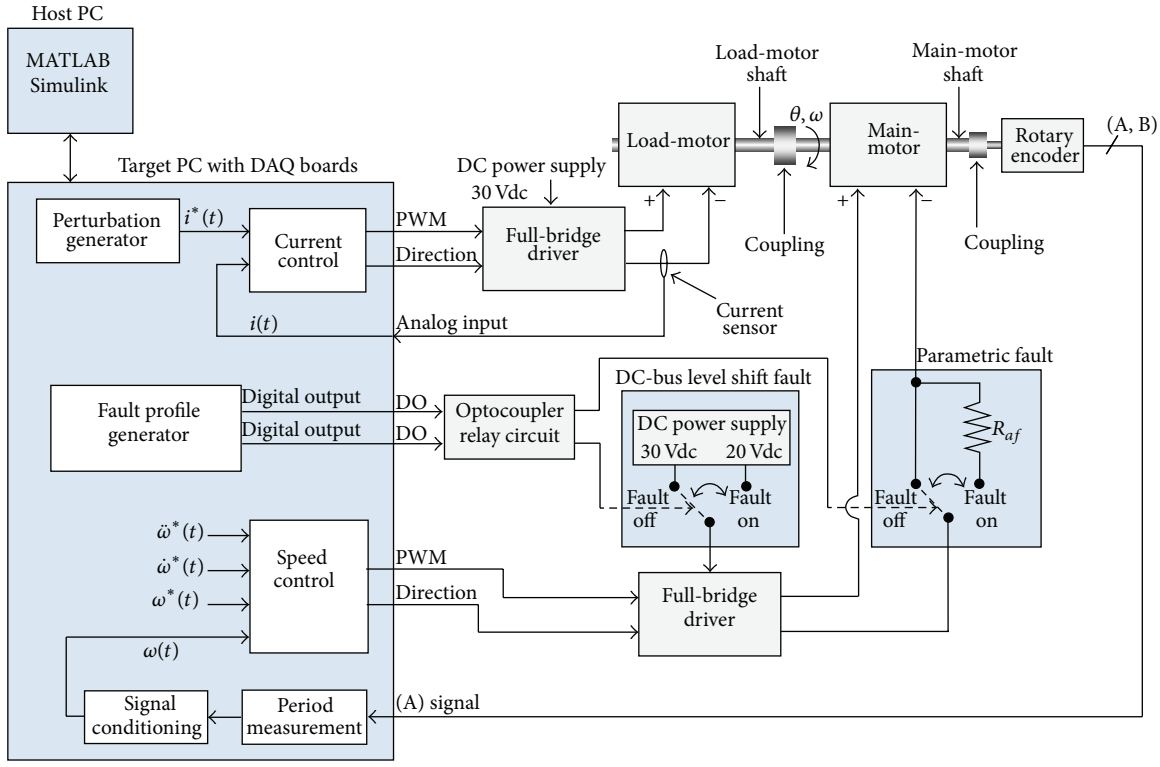

Figure 1: General scheme of the experimental setup.

On the other hand from the GPI Observer we have

$$\dot{\hat{x}}_n = \psi(t, y)\, u + \hat{x}_{n+1} + l_m (x_1 - \hat{x}_1), \tag{32}$$

therefore,

$$\dot{\hat{\sigma}} = \psi(t, y)\, u + \hat{\xi}_\sigma \tag{33}$$

with

$$\hat{\xi}_\sigma = \hat{x}_{n+1} + l_m (x_1 - \hat{x}_1) - [y^*]^{(n)} + \lambda_{n-2} \left(\dot{\hat{x}}_{n-1} - [y^*]^{(n-1)} \right) + \cdots + \lambda_0 \left(\dot{\hat{x}}_1 - [y^*]^{(1)} \right), \tag{34}$$

where the estimates $\dot{\hat{x}}_{n-1}, \ldots, \dot{\hat{x}}_1$ are also provided by the GPI observer. Remember that as stated by the GPI observer state notation $\hat{x}_{n+1} = \hat{\xi}$ as announced at the beginning of this subsection, the disturbance function estimation related to sliding regime (33) $\hat{\xi}_\sigma$ is given in terms of $\hat{\xi}$, which is related to system dynamics (21).

According to (5) the control law is

$$u = \frac{1}{\psi(t, y)} \left[-\hat{\xi}_\sigma - W \operatorname{sign}(\hat{\sigma}) \right]. \tag{35}$$

Now, consider the following Lyapunov function candidate:

$$V_1 = \frac{1}{2} \hat{\sigma}^2. \tag{36}$$

Differentiating the Lyapunov function (36) with respect to time and using (33) and (35), we obtained

$$\dot{V}_1 = \hat{\sigma} \dot{\hat{\sigma}} = \hat{\sigma} \left(\psi(t, y)\, u + \hat{\xi}_\sigma \right) = -W |\hat{\sigma}| \tag{37}$$

which assures the sliding mode regime provided that $W > 0$.

3. Case Study

The system used for the experimental comparison of the proposed control strategies is a mechatronic system composed of two directly coupled DC motors. The first motor (also called the main-motor) acts as the system to be controlled. The second motor (also called the load-motor) generates perturbation loads to the main-motor. Hence, the proposed control strategies are applied to control the angular speed of the main-motor, while the load-motor acts as the load-torque perturbation generator by means of a current control loop. Figure 1 shows a detailed scheme of the mechatronic system, control loops, and the experimental setup. This figure also shows the implementation scheme of two faults: armature resistance fault (fault 1) and DC-bus level shift fault (fault 2). These faults are typical in systems as the one under study (as it will be explained later), and all controllers will be assessed under these faults.

3.1. Fault-Tolerant Control for DC Motors. The most common faults in DC-motor drives can be classified as actuator, parametric, and sensor faults [22]. The actuator faults are mainly due to the reduction in the performance of amplifiers,

malfunction of power semiconductors and failures in regulatory stages in the power supply [23, 24]. Parametric faults are caused by degradation of brushes, inertia and friction changes, and variations in resistance or inductance of the armature [22]. This paper will consider two faults in the mechatronic system:

(1) parametric fault due to a change in the resistance of DC-motor armature and

(2) actuator fault due to level shift of the DC-bus voltage that feeds the full-bridge drive of the main-motor.

3.2. Problem Formulation. Consider the following dynamic model describing a DC-motor controlled by armature voltage $u(t)$, with state variables given by $\omega(t)$ describing the rotor angular speed and $i(t)$ representing the armature current:

$$\begin{aligned} L_a \frac{di(t)}{dt} &= k_{\text{pwm}} u(t) - R_a i(t) - K_b \omega(t), \\ J_m \frac{d\omega(t)}{dt} &= K_T i(t) - \tau_L(t) - B\omega(t) - \delta(\omega(t)). \end{aligned} \tag{38}$$

The parameters L_a and R_a represent the armature inductance and armature resistance, J_m is the moment of inertia, K_b is the back-emf constant, K_T is the torque constant, B is the viscous friction coefficient, k_{pwm} is the conversion gain of PWM, τ_L represents the unknown load-torque perturbation input, $u(t)$ is the control signal, and $\delta(\omega(t))$ represents a nonlinear model of dry friction, where T_c, T_s, and α are terms associated with coulomb friction (see [25]). Consider

$$\delta(\omega) = \omega\left[> T_c \left\{\text{sign}(\omega) + \left(T_s - T_c\right) e^{-\alpha|\omega|} \text{sign}(\omega)\right\}\right]. \tag{39}$$

By rewriting and lumping together some terms of (38), the following representation of the system (typical of the ADRC paradigm) is obtained:

$$\ddot{\omega}(t) = \kappa u(t) + \xi(t), \tag{40}$$

where

$$\begin{aligned} \kappa &= \frac{K_T k_{\text{pwm}}}{J_m L_a}, \\ \xi(t) &= \frac{K_T}{J_m L_a}\left[-R_a i(t) - K_b \omega(t)\right] \\ &\quad - \frac{1}{J_m}\frac{d\tau_L}{dt} - \frac{B}{J_m}\frac{d\omega(t)}{dt} - \frac{1}{J_m}\frac{d\delta(\omega(t))}{dt}. \end{aligned} \tag{41}$$

The problem is as follows. Consider a DC-motor described by the dynamics presented in (40), where the rotor angular speed $\omega(t)$ is available for measurement. Given a smooth reference trajectory, $\omega^*(t)$, for the angular velocity of the motor shaft, find a control law $u(t)$ such that $\omega(t)$ is forced to track the given reference trajectory $\omega^*(t)$. This objective must be achieved even in the presence of unknown disturbances represented by the load input torque τ_L, and the effect of parametric and actuator faults.

3.3. Disturbance GPI Observer Design. The following approximation concerning the internal model of the disturbance function $d^2\xi(t)/dt^2 \approx 0$ is considered. According to this approximation, the extended state vector is given by $[\omega\ \dot{\omega}\ \xi\ \dot{\xi}]^T$ thus we obtain the following augmented plant model:

$$\begin{bmatrix} \dot{\omega} \\ \ddot{\omega} \\ \dot{\xi} \\ \ddot{\xi} \end{bmatrix} = \begin{bmatrix} 0 & 1 & 0 & 0 \\ 0 & 0 & 1 & 0 \\ 0 & 0 & 0 & 1 \\ 0 & 0 & 0 & 0 \end{bmatrix} \begin{bmatrix} \omega \\ \dot{\omega} \\ \xi \\ \dot{\xi} \end{bmatrix} + \kappa \begin{bmatrix} 0 \\ 1 \\ 0 \\ 0 \end{bmatrix} u + \begin{bmatrix} 0 \\ 0 \\ 0 \\ 1 \end{bmatrix} \xi^{(2)}. \tag{42}$$

It is defined as an estimation error: $\widetilde{e}_\omega = \omega - \widehat{\omega}$. In order to observe the augmented state, a GPI observer is proposed:

$$\begin{bmatrix} \dfrac{d\widehat{\omega}}{dt} \\ \dfrac{d\widehat{\dot{\omega}}}{dt} \\ \dfrac{d\widehat{\xi}}{dt} \\ \dfrac{d\widehat{\dot{\xi}}}{dt} \end{bmatrix} = \begin{bmatrix} 0 & 1 & 0 & 0 \\ 0 & 0 & 1 & 0 \\ 0 & 0 & 0 & 1 \\ 0 & 0 & 0 & 0 \end{bmatrix} \begin{bmatrix} \widehat{\omega} \\ \widehat{\dot{\omega}} \\ \widehat{\xi} \\ \widehat{\dot{\xi}} \end{bmatrix} + \kappa \begin{bmatrix} 0 \\ 1 \\ 0 \\ 0 \end{bmatrix} u + \begin{bmatrix} l_3 \\ l_2 \\ l_1 \\ l_0 \end{bmatrix} \widetilde{e}_\omega, \tag{43}$$

where $[l_3\ l_2\ l_1\ l_0]^T$ is the observer gains vector. The characteristic polynomial which describes the estimation error dynamics is defined as

$$p_{\widetilde{e}_x}(s) = s^4 + l_3 s^3 + l_2 s^2 + l_1 s + l_0. \tag{44}$$

Given the previously described uncertain model (42), linear GPI observer (43) estimates the augmented state: $[\omega\ \dot{\omega}\ \xi\ \dot{\xi}]^T$ with an arbitrary small phase space estimation error, provided that the set of observer design coefficients $\{l_3, l_2, l_1, l_0\}$ is chosen in such a manner that the roots of the characteristic polynomial $p_{\widetilde{e}_\omega}(s)$, on the complex variable s, are located sufficiently far from the imaginary axis, in the left half side of the complex plane.

3.4. Sliding Control Law Design. By defining the tracking error as $e_\omega(t) = \omega(t) - \omega^*(t)$, the following sliding surface in terms of the tracking error e_ω are proposed:

$$\sigma = \dot{e}_\omega + \lambda e_\omega. \tag{45}$$

A modified version of the sliding surface that uses estimates of ω and $\dot{\omega}$ is proposed:

$$\widehat{\sigma} = \widehat{\dot{\omega}} - \left[\omega^*\right]^{(1)} + \lambda_0\left(\widehat{\omega} - \omega^*\right), \tag{46}$$

where $\widehat{\dot{\omega}}(t)$ and $\widehat{\omega}(t)$ are estimations provided by a GPI observer (43).

Applying time derivative to (46), the following dynamics is obtained:

$$\dot{\widehat{\sigma}} = \kappa u + \widehat{\xi}_\sigma \tag{47}$$

with

$$\widehat{\xi}_\sigma = \widehat{\xi} + l_2\left(\omega - \widehat{\omega}\right) - \left[\omega^*\right]^{(2)} + \lambda_0\left(\frac{d\widehat{\omega}}{dt} - \left[\omega^*\right]^{(1)}\right), \tag{48}$$

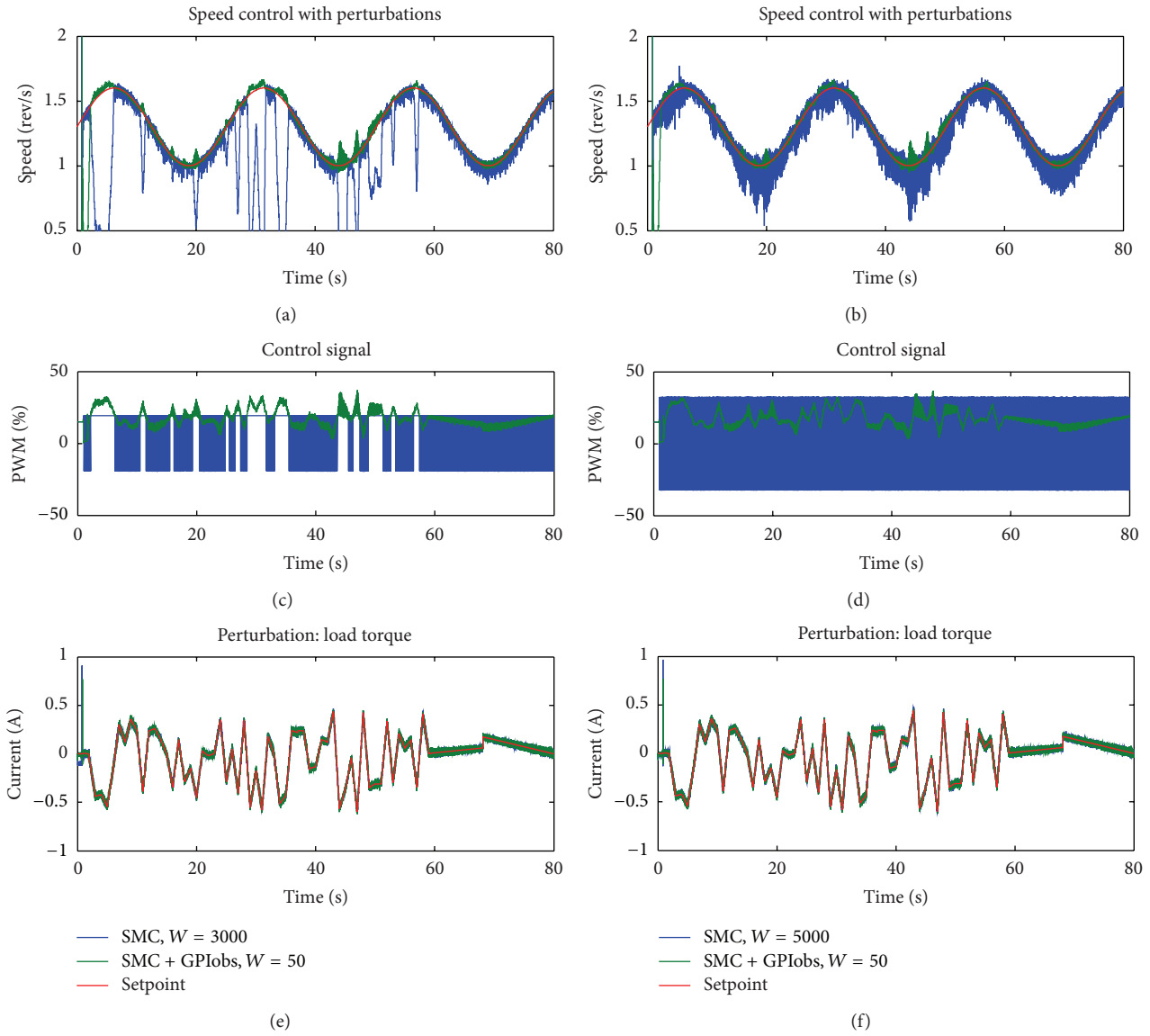

FIGURE 2: Time response of the control systems under the load-torque perturbations. From top to bottom: speed control response, control signal, and load-torque perturbation.

where the estimates $\widehat{\omega}$, $\widehat{\xi}$, and $d\widehat{\omega}/dt$ are also provided by GPI observer (43).

Finally, the following discontinuous feedback control law is considered:

$$u = \frac{1}{\kappa}\left[-\widehat{\xi}_{\sigma} - W\,\mathrm{sign}\,(\sigma)\right]. \tag{49}$$

4. Experimental Results

In this section, we describe the experiments that were carried out to assess the performance of the proposed GPI observer assisted sliding mode control (SMC+GPIobs) against the classic sliding mode control (SMC) applied to a mechatronic system affected by perturbations and faults. First, the experimental setup is described; then two different operation cases are exposed and analyzed under a tracking problem: system with perturbations and system with faults.

4.1. Experimental Setup. The designed controllers were implemented in a MATLAB xPC Target environment using a sampling period of 0.1 ms on a computer equipped with a Pentium D processor. The connection between the mechatronic system and each controller was performed by two National Instruments PCI-6024E data acquisition cards. A PWM output at 8000 Hz and a digital output were both used to command each DC-motor full-bridge driver, one PWM input was used to read the main-motor encoder frequency, two digital outputs were used for enabling/disabling the faults, and an analog input was used to read the load-motor current sensor output.

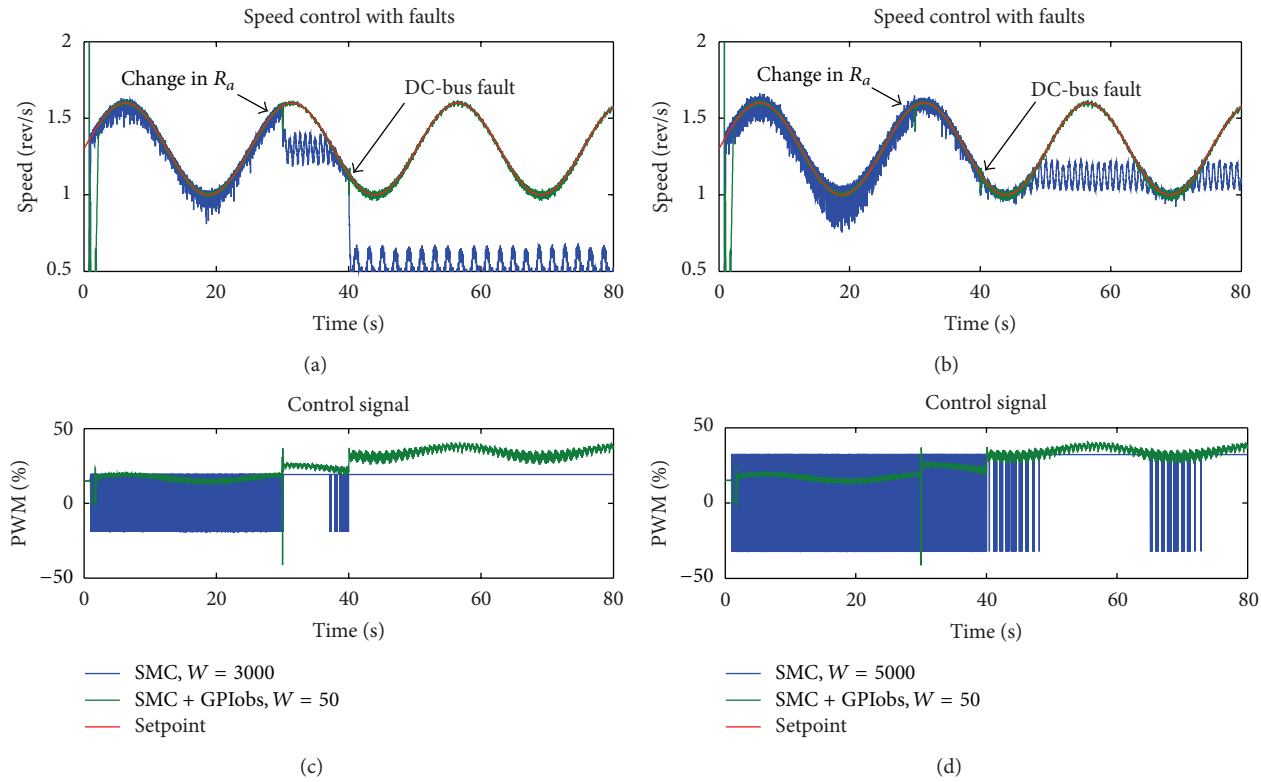

FIGURE 3: Time response of the control systems under faults 1 and 2. Fault 1 is applied at $t = 30$ and fault 2 is applied at $t = 40$.

Fault 1 consists of increasing the armature resistance of the main-motor; when this fault is enabled, the armature resistance of the motor is increased by 80% ($R_{af} = 4.7$ ohms). This fault is enabled (when applicable) at $t = 30$ sec. Fault 2 consists of changing the DC-level of the main-motor full-bridge driver power supply. When this fault goes from disabled to enabled, the DC-level of the power supply changes from 30 Vdc to 20 Vdc. This fault is enabled (when applicable) at $t = 40$ sec.

The parameters of the controller are defined as follows: $\kappa = 155.6$, $\lambda_0 = 100$, $W = 50$, $l_3 = 320$, $l_2 = 26400$, $l_1 = 128000$, and $l_0 = 160000$.

4.2. Experimental Results under Perturbations. Figure 2 shows the experimental results of the control systems under evaluation using a setpoint defined as $\omega_r^*(t) = 0.3\sin(0.25\pi t) + 1.3$. In this case, the control systems are affected by load torque disturbances. The perturbations applied to the main-motor are showed in Figures 2(e) and 2(f). Notice that the same perturbation profile is applied to all control schemes in evaluation.

The plots of (a), (c), and (e) in the first column of Figure 2 depict the experiments of the control systems using $W = 3000$ for SMC and $W = 50$ for SMC+GPIobs. The plots (b), (d), and (f) of Figure 2 in the last column depict the experiments using $W = 5000$ for SMC and $W = 50$ for SMC+GPIobs. Figure 2(a) shows that the classic SMC (in blue) is highly affected by the perturbations. Although the switching gain was fixed in $W = 3000$, the control system gets out of the sliding mode many times and the tracking performance is reduced. Notice that the tracking performance and disturbance rejection may be improved by increasing the switching gain W; however, under this condition the chattering phenomenon will be more problematic (see Figure 2(b)).

On the other hand, the proposed GPI observer assisted SMC was capable of rejecting the perturbations and the tracking performance was maintained. In this case, the switching gain W was reduced to $W = 50$, which was allowed by the use of the GPI observer that assists the sliding mode controller. Figures 2(c) and 2(d) show that the control signal for SMC+GPIobs (in green) has less control effort than the classic SMC scheme. The chattering in the controlled speed was attenuated even in the presence of unknown perturbations as seen in Figures 2(a) and 2(b) (in green).

4.3. Experimental Results under Faults. Figure 3(a) shows that in presence of fault 1 at $t = 30$, the tracking performance of the classic SMC (in blue) is degraded. The selection of $W = 3000$ in the classic SMC allows setpoint tracking with no faults; however, it is not possible to maintain the sliding mode for the tracking trajectory when the fault is enabled. Meanwhile, the GPI observer assisted SMC (in green) is capable of tolerating the first fault and even of keeping the tracking performance almost with no change. Note that the switching gain of the proposed strategy is very low ($W = 50$), which is beneficial for chattering reduction. It is important to observe that, at

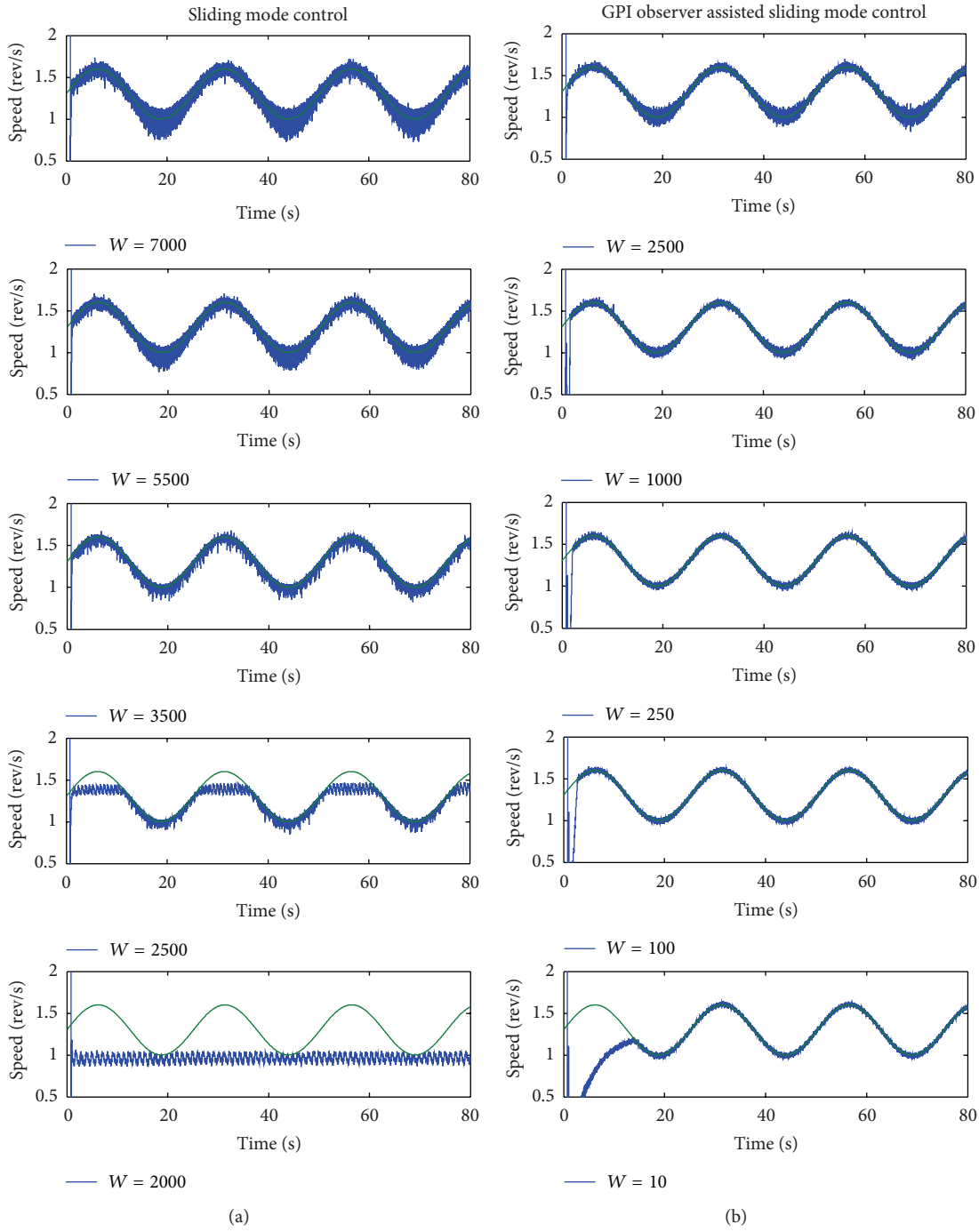

FIGURE 4: Time response of the control systems (no faults and no perturbations) under variations in the switching gain W. In the first column: sliding mode control; in the second column: GPI observer assisted sliding mode control.

the time of the fault ($t = 30$), there is a tiny transient response in the controlled speed to recover the sliding regime again.

Figure 3(a) also shows the effect of fault 2 in the controlled speed at $t = 40$. At this point, it is noticed that after the fault is applied, the classic SMC (in blue) is not capable of maintaining the sliding regime and its tracking performance is highly degraded. Moreover, the GPI observer assisted SMC (in green) tolerates the fault and quickly restores its tracking performance without increasing the chattering.

Figures 3(b) and 3(d) show the experimental results using $W = 5000$ for the classic SMC compared to the proposed GPI observer assisted SMC. In this case, the classic SMC can tolerate fault 1 at $t = 30$; however, a notable increasing in the chattering is observed. On the other hand, when fault 2 is applied at $t = 40$, the classic SMC cannot tolerate it.

4.4. Chattering Reduction. Figure 4 shows that both control systems in evaluation track the setpoint when no faults and no perturbations are applied. However, the classic SMC requires larger switching gains to track the given setpoint. This issue notably increases the chattering phenomenon in the main-motor controlled speed compared to the proposed GPI observer assisted SMC. In the proposed assisted SMC scheme, the chattering is alleviated by reducing the switching gain down to $W = 10$ without loss of the sliding mode. Figure 4 shows that the use of the GPI observer to assist the SMC allows reducing the switching gain W; thus the chattering problem is alleviated.

5. Conclusions

In this paper, an extension of Generalized Proportional Integral observer-based control has been proposed to the problem of robust creation of sliding regimes for nonlinear single-input single-output systems, with limited switching control input authority for fault-tolerant operation. The approach considers the use of a GPI observer for the accurate (linear) estimation of nonlinear endogenous, as well as exogenous, disturbance inputs affecting the existence of local sliding regimes on a given smooth sliding manifold. Active, on-line disturbance estimation and subsequent cancellation of state-dependent and time-dependent disturbances, significantly contribute to reducing the required switching control amplitude needed to sustain a sliding regime. As an additional bonus it experimented a chattering reduction.

It was shown through the experimental tests that the proposed GPI observer assisted sliding mode control strategy is capable of maintaining the sliding regime even under hard operating conditions such as system uncertainties, perturbations, actuator faults, parametric failures, and small switching control input authority. This demonstrates the robustness of the proposed strategy accomplished by a simple linear GPI observer-based control working on an ADRC paradigm.

It was experimentally probed that (a) the proposed GPI observer-based SMC strategy allows reducing the chattering in the controlled variable (limited by the lumped perturbation estimation error) and (b) the proposed strategy forces the system to approximately keep its nominal performance in the presence of perturbations, faults, and uncertainties.

Acknowledgments

The authors gratefully acknowledge the support for the realization of this work from the following institutions: Universidad Nacional de Colombia, Cinvestav-IPN, and UPIITA-IPN.

References

[1] C. Edwards, H. Alwi, and C. P. Tan, "Sliding mode methods for fault detection and fault tolerant control," in *Proceedings of the 1st Conference on Control and Fault-Tolerant Systems (SysTol '10)*, pp. 106–117, Nice, France, October 2010.

[2] H. Alwi and C. Edwards, "Fault detection and fault-tolerant control of a civil aircraft using a sliding-mode-based scheme," *IEEE Transactions on Control Systems Technology*, vol. 16, no. 3, pp. 499–510, 2008.

[3] B. Xiao, Q. Hu, and Y. Zhang, "Adaptive sliding mode fault tolerant attitude tracking control for flexible spacecraft under actuator saturation," *IEEE Transactions on Control Systems Technology*, vol. 20, no. 6, pp. 1605–1612, 2012.

[4] M. T. Hamayun, C. Edwards, and H. Alwi, "Integral sliding mode fault tolerant control incorporating on-line control allocation," in *Proceedings of the 11th International Workshop on Variable Structure Systems (VSS '10)*, pp. 100–105, Mexico City, Mexico, June 2010.

[5] M. Chen and W.-H. Chen, "Sliding mode control for a class of uncertain nonlinear system based on disturbance observer," *International Journal of Adaptive Control and Signal Processing*, vol. 24, no. 1, pp. 51–64, 2010.

[6] W. Wang and Z.-M. Bai, "Sliding mode control based on disturbance observer for servo system," in *Proceedings of the 2nd International Conference on Computer and Automation Engineering (ICCAE '10)*, vol. 2, pp. 26–29, Singapore, February 2010.

[7] D. Tian, D. Yashiro, and K. Ohnishi, "Improving transparency of bilateral control system by sliding mode assist disturbance observer," *IEEJ Transactions on Electrical and Electronic Engineering*, vol. 8, no. 3, pp. 277–283, 2013.

[8] J. Yang, S. Li, and X. Yu, "Sliding-mode control for systems with mismatched uncertainties via a disturbance observer," *IEEE Transactions on Industrial Electronics*, vol. 60, no. 1, pp. 160–169, 2013.

[9] M. Shi, X. Liu, Y. Shi, W. Chen, and Q. Zhao, "Research on the sliding mode based ADRC for hydraulic active suspension of a six-wheel off-road vehicle," in *Proceedings of the International Conference on Electronic and Mechanical Engineering and Information Technology (EMEIT '11)*, vol. 2, pp. 1066–1069, Heilongjiang, China, August 2011.

[10] V. S. Deshpande, M. Bhaskara, and S. B. Phadke, "Sliding mode control of active suspension systems using a disturbance observer," in *Proceedings of the 12th International Workshop on Variable Structure Systems (VSS '12)*, pp. 70–75, 2012.

[11] Y. Cao and X. B. Chen, "Disturbance-observer-based sliding-mode control for a 3-dof nanopositioning stage," in *Proceedings of the IEEE/ASME Transactions on Mechatronics*, vol. PP, no. 99, pp. 1–8, Mumbai, India, 2013.

[12] D.-J. Zhao, Y.-J. Wang, L. Liu, and Z.-S. Wang, "Robust fault-tolerant control of launch vehicle via GPI observer and integral sliding mode control," *Asian Journal of Control*, vol. 15, no. 2, pp. 614–623, 2013.

[13] Z. Gao, Y. Huang, and J. Han, "An alternative paradigm for control system design," in *Proceedings of the 40th IEEE Conference on Decision and Control (CDC '01)*, vol. 5, pp. 4578–4585, December 2001.

[14] G. Tian and Z. Gao, "From poncelet's invariance principle to active disturbance rejection," in *Proceedings of the American Control Conference (ACC '09)*, pp. 2451–2457, June 2009.

[15] J. Han, "From PID to active disturbance rejection control," *IEEE Transactions on Industrial Electronics*, vol. 56, no. 3, pp. 900–906, 2009.

[16] H. Sira-Ramírez and V. F. Batlle, "Robust $\Sigma - \Delta$ modulation-based sliding mode observers for linear systems subject to time polynomial inputs," *International Journal of Systems Science*, vol. 42, no. 4, pp. 621–631, 2011.

[17] V. Utkin, J. Guldner, and J. Shi, *Sliding Mode Control in Electro-Mechanical Systems*, CRC Press, Boca Raton, Fla, USA, 2nd edition, 2009.

[18] H. Sira-Ramírez and S. K. Agrawal, *Differentially Flat Systems*, Marcel Dekker, 2004.

[19] Y. Gliklikh, "Necessary and suffcient conditions for global-in-time existence of solutions of ordinary, stochastic, and parabolic differential equations," *Abstract and Applied Analysis*, vol. 2006, Article ID 39786, 17 pages, 2006.

[20] H. Sira-Ramírez, A. Luviano-Juárez, and J. Cortés-Romero, "Control lineal robusto de sistemas no lineales diferencialmente planos," *RIAI: Revista Iberoamericana de Automàtica e Informàtica Industrial*, vol. 8, no. 1, pp. 14–28, 2011.

[21] H. Coral-Enriquez, J. Cortés-Romero, and A. G. Ramos, "Robust active disturbance rejection control approach to maximize energy capture in variable-speed wind turbines," *Mathematical Problems in Engineering*, vol. 2013, Article ID 396740, 12 pages, 2013.

[22] R. Isermann, *Fault-Diagnosis Applications*, Springer, Berlin, Germany, 2011.

[23] J. H. Lee and J. Lyou, "Fault diagnosis and fault tolerant control of dc motor driving system," in *Proceedings of the IEEE International Symposium on Industrial Electronics (ISIE '01)*, vol. 3, pp. 1719–1723, 2001.

[24] G. Grandi, P. Sanjeevikumar, Y. Gritli, and F. Filippetti, "Fault-tolerant control strategies for quad inverter induction motor drives with one failed inverter," in *Proceedings of the 20th International Conference on Electrical Machines (ICEM '12)*, pp. 959–966, 2012.

[25] C. C. de Wit, H. Olsson, K. J. Åström, and P. Lischinsky, "A new model for control of systems with friction," *IEEE Transactions on Automatic Control*, vol. 40, no. 3, pp. 419–425, 1995.

Hindawi Publishing Corporation
Mathematical Problems in Engineering
Volume 2013, Article ID 913458, 14 pages
http://dx.doi.org/10.1155/2013/913458

Research Article

Effective and Robust Generalized Predictive Speed Control of Induction Motor

Patxi Alkorta,[1] Oscar Barambones,[2] Asier Zubizarreta,[3] and José Antonio Cortajarena[1,4]

[1] *Department of Automatic Control and Systems Engineering, EUITI de Eibar, University of the Basque Country (UPV/EHU), Otaola Hiribidea 29, 20600 Eibar, Spain*
[2] *Department of Automatic Control and Systems Engineering, EUI de Vitoria-Gasteiz, University of the Basque Country (UPV/EHU), Nieves Cano 12, 01006 Vitoria-Gasteiz, Spain*
[3] *Department of Automatic Control and Systems Engineering, ETSI de Bilbao, University of the Basque Country (UPV/EHU), Alameda Urquijo s/n, 48013 Bilbao, Spain*
[4] *Department of Electronics Technology, EUITI de Eibar, University of The Basque Country (UPV/EHU), Otaola Hiribidea 29, 20600 Eibar, Spain*

Correspondence should be addressed to José Antonio Cortajarena; josean.cortajarena@ehu.es

Received 20 June 2013; Revised 30 September 2013; Accepted 16 October 2013

Academic Editor: Bo-Chao Zheng

This paper presents and validates a new proposal for effective speed vector control of induction motors based on linear Generalized Predictive Control (GPC) law. The presented GPC-PI cascade configuration simplifies the design with regard to GPC-GPC cascade configuration, maintaining the advantages of the predictive control algorithm. The robust stability of the closed loop system is demonstrated by the poles placement method for several typical cases of uncertainties in induction motors. The controller has been tested using several simulations and experiments and has been compared with Proportional Integral Derivative (PID) and Sliding Mode (SM) control schemes, obtaining outstanding results in speed tracking even in the presence of parameter uncertainties, unknown load disturbance, and measurement noise in the loop signals, suggesting its use in industrial applications.

1. Introduction

The Model Predictive Control (MPC) groups a set of controllers which are based on the model of the system and the known future reference for optimal control signal calculation. The operational principle of predictive control is to calculate in advance the control signal required by the system, when the future input reference that will be applied is known beforehand [1]. In this sense, the system is able to react to the input reference, anticipating its changes and avoiding the effects of delay in system response [2]. There are countless applications in industry where the input reference is known beforehand, such as robotic systems, and machine tools. Therefore, in all these systems predictive control algorithms can be implemented. Since Clarke et al. proposed the design principles of Generalized Predictive Control [3, 4], many authors have used this advanced technique for induction motor control in the last two decades. There is extensive research related to the application of predictive controllers in electric drives, and, for this reason, predictive algorithms compete with other advanced control techniques such as fuzzy control [5], sliding mode control [6, 7], and nonlinear $H^{\inf}$ control [8].

Predictive algorithms are often implemented using two or more GPC blocks to control several loops of the electrical machine, and usually they are connected in cascade form [9–11]. Frequently, only one predictive regulator for the control of the main variable of the machine is implemented, such as speed [12–15] or position [16], while the rest of the variables are controlled with classical algorithms, usually PI/PID and hysteresis comparators. Some authors use more complex formulations in order to control several variables of

the engine, such as the multivariable GPC [17], and others implement a predictive algorithm in the current loops [18, 19], using the classic PI regulators for the main variables such as speed and rotor flux.

All predictive control schemes are based on the minimization of a cost function. In the GPC this implies solving a quadratic programming problem in the case where physical constraints are introduced in the optimization. If no constraints are considered, an analytical solution can be obtained. In this sense, it is known that all real systems have constraints, such as saturation values, frequencies, and time limits of the actuators [13, 16, 20]. Hence, a numerical method is required to solve the quadratic programming problem, which implies a high computation cost for the processor where the controller is implemented. For this reason, the sample period of a predictive controller is usually greater than other types of controllers [9], which limit its applicability to quick response systems. Due to this issue, some works do not consider constraints, implementing the analytical solution with acceptable results [15, 17]. Moreover, constraints can be considered after the predictive control law is obtained [15].

In addition, even if the delay time of the electric motor systems is usually small, sometimes it can be long enough so that its compensation improves significantly the system behaviour [21], and in this way it can be used in precision applications. In this sense, the predictive algorithms allow to compensate easily the delay time of the controlled system, because this aspect is included in the implementation of these algorithms.

Finally, the robustness of the GPC regulator is another aspect included by some authors in the controller design [16, 20], obtaining relevant results, but with an arduous controller design process. In this sense, it is known that all closed loop controlled systems have inherent robustness [22] that in the presented GPC speed controller is enough to overcome the typical uncertainty cases of induction motor, without having to design an explicit robust controller nor to include any method for the adaptive identification of the motor parameters.

After all these considerations and taking into account the complexity in the design of predictive controllers and their important computational costs, this paper presents an induction motor speed indirect vector control that combines the GPC algorithm with PI regulators, proposing a simple, robust, and effective design which provides better dynamical behaviour than other speed regulators such as other GPC, PID, and Sliding Mode (SM). The rest of the paper is organized as follows. In Section 2 the design of the proposed GPC speed regulator is presented, detailing the objectives, the dynamics of the induction motor, the design of the controller and its tuning, and finally its robust stability. Section 3 contains a brief description of the used experimental platform and the simulation and experimental tests carried out by implementing the proposed regulator. Comparative results are given of the presented speed GPC regulator with other GPC, PI/PID, and SM speed controllers. Finally, Section 4 summarizes the most important ideas.

2. Linear GPC Speed Controller for Induction Motor

2.1. Objective and Description. The objective of this paper is to demonstrate experimentally that the GPC algorithm can be used in speed regulation of induction motors in an effective way with a simple, robust, and stable design, offering faster speed tracking than other algorithms such as PID or SM, allowing being implemented in industrial applications.

The proposed speed regulator combines a GPC scheme with two PI current regulators. The dynamics of the induction motor is regulated using a distributed control in cascade form: the stator, (1), (2), is regulated with the PI current regulators and the rotor, (4), (5), with a GPC speed controller. The PI current regulators are very effective, simple, and provide fast response, offering similar results to the ones obtained by implementing a GPC-based current regulator. These are combined with a Space Vector Pulse Width Modulation (SVPWM), which is a standard modulator that is implemented in many commercial Digital Signal Process (DSP) processors, even in many low-cost processors. The proposed GPC controller is designed taking into account the first order transfer function (mechanical equation, (4), (5)) of the induction motor, considering the delay time, but without considering the constraints. Therefore, it is a simpler approach to GPC-based controllers than previous works.

2.2. Induction Motor Dynamics. The dynamics of the motor can be described by the stator voltage equations and the rotor flux equation, expressed all in the d-q synchronous rotating reference frame [23], assuming that the quadrature component of rotor flux is null, $\psi_{rq} \approx 0$, and consequently the rotor flux is formed only by its direct component, $\psi_r \approx \psi_{rd}$:

$$v_{sd} = R_s i_{sd} + \sigma L_s \frac{di_{sd}}{dt} + \frac{L_m}{L_r}\frac{d\psi_{rd}}{dt} - \omega_e \sigma L_s i_{sq}, \quad (1)$$

$$v_{sq} = R_s i_{sq} + \sigma L_s \frac{di_{sq}}{dt} + \omega_e \frac{L_m}{L_r}\psi_{rd} + \omega_e \sigma L_s i_{sd}, \quad (2)$$

$$\frac{d\psi_{rd}}{dt} = \frac{R_r}{L_r} L_m i_{sd} - \frac{R_r}{L_r}\psi_{rd}, \quad (3)$$

$$T_e - T_L = J\frac{d\omega_m}{dt} + B_v \omega_m, \quad (4)$$

$$T_e = \frac{3}{4} p \frac{L_m}{L_r}\psi_{rd} i_{sq}. \quad (5)$$

The employed symbols are described as follows:

B_v: viscous friction coefficient,

J: moment of inertia,

L_m: magnetizing inductance,

L_s: stator inductance,

L_r: rotor inductance,

R_r: rotor resistance,

R_s: stator resistance,

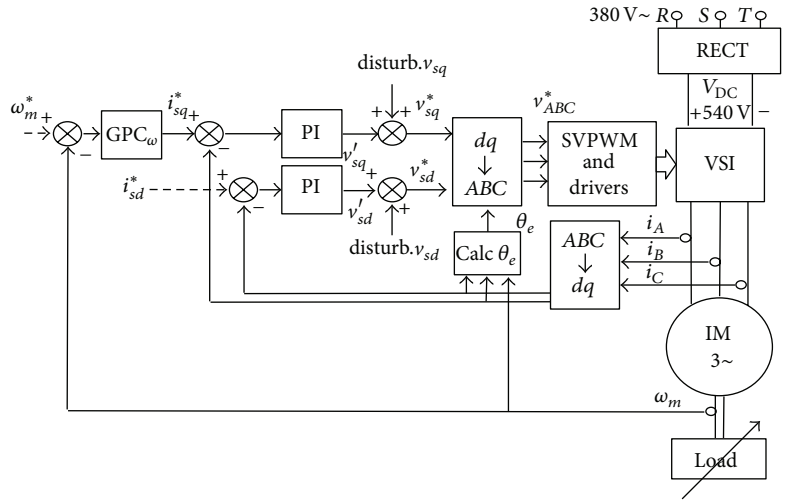

Figure 1: Diagram of GPC speed control of induction motor with the PI current control and SVPWM.

p: number of poles,

σ: leakage factor,

T_e: electromagnetic torque,

T_L: load or disturbance torque,

ω_e: synchronous rotating speed,

ω_m: mechanical rotor speed,

ω_r: electrical rotor speed,

ψ_r: rotor flux vector,

ψ_{rd}, ψ_{rq}: direct and quadrature components of the rotor flux vector,

i_s: stator current vector,

i_{sd}, i_{sq}: direct and quadrature components of the stator current vector,

v_s: stator voltage vector,

v_{sd}, v_{sq}: direct and quadrature components of the stator voltage vector.

2.3. GPC Speed Controller Design. Figure 1 shows the speed vector control diagram of an induction motor, where the GPC$_\omega$ block is the proposed GPC controller for the speed loop whose algorithm will be detailed later. The two PI blocks are a pair of PI controllers for the two current loops. Their function is to convert the i_{sd} and i_{sq} current commands in their respective v_{sd} and v_{sq} voltage commands. This conversion is necessary because the inverter needs voltage commands, instead of current commands. The VSI block is the three-phase Voltage Sourced Inverter, $ABC \rightarrow dq$ block gets the i_s space vector in the d-q synchronous rotating reference frame from the i_A, i_B, and i_C motor stator three-phase currents measured with Hall effect sensors, using Park's transformation [23, 24], while the $dq \rightarrow ABC$ block makes the reverse Park's transformation. It should be noted that this transformation uses the rotor flux angular position, θ_e, and therefore this angle is calculated using the indirect method, obtained by integrating the ω_e synchronous speed.

Next, the dynamics of the induction motor system will be calculated in order to design the GPC.

As it is known that the synchronous speed can be expressed as follows:

$$\omega_e = \omega_s + \omega_r, \tag{6}$$

where ω_s is the slip speed, and ω_r is the rotor speed. As it is assumed that the d direct and q quadrature components of the rotor flux are decoupled, then $\psi_{rq} \approx 0$, and $d\psi_{rq}/dt \approx 0$, and consequently the rotor flux is formed only by the direct component [23, 24]. In this context, the slip speed is obtained from the following:

$$\omega_s = \frac{L_m}{\psi_r}\frac{R_r}{L_r} i_{sq}, \tag{7}$$

where the rotor flux is calculated by (3),

$$\frac{R_r}{L_r}\frac{d\psi_r}{dt} + \psi_r = L_m i_{sd}, \tag{8}$$

while the rotor speed is proportional to the ω_m mechanical rotor speed, which is measured using a incremental encoder:

$$\omega_r = \omega_m \frac{p}{2}. \tag{9}$$

From diagram of Figure 1 it is possible to obtain the external representation of the induction motor (Figure 2).

Usually the rotor flux is held constant, fixing the rotor flux current command (i_{sq}^*) to a constant value, that is, I_{sd}; see Figures 1 and 2. Then the pole associated to the electrical time constant can be neglected and consequently (3) in a steady state takes the following expression:

$$\psi_r = L_m I_{sd}. \tag{10}$$

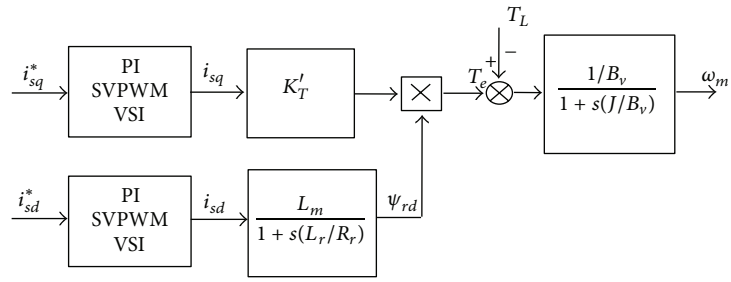

Figure 2: External representation of the induction motor with the PI current control and SVPWM.

The electromagnetic torque of the induction motor in steady state, taking into account that torque and rotor flux current components are decoupled in the *d-q* rotating reference frame, (5), also can be expressed as follows [24]:

$$T_e = \frac{3p}{4}\frac{L_m}{L_r}\psi_{rd} i_{sq} = K_T i_{sq}, \tag{11}$$

where K_T is the torque constant (12) and ψ_{rd} is the rotor flux:

$$K_T = \frac{3p}{4}\frac{L_m}{L_r}\psi_{rd} = K_T' \psi_{rd} = K_T' L_m I_{sd}. \tag{12}$$

Considering that the SVPWM and the VSI modules have neither dynamics nor gain in diagram of Figure 1, it is possible to obtain the following transfer function:

$$\frac{\omega_m(s)}{I_{sq}^*(s)} = \frac{K_T'\psi_{rd}/B_v}{(1+s\tau_r)(1+s\tau_m)} \times \left(\frac{Kp_i s + Ki_i}{\sigma L_s s^2 + (R_s + Kp_i)s + Ki_i}\right)^2, \tag{13}$$

where the mechanical time constant and the rotor electrical time constant are, respectively,

$$\tau_m = \frac{J}{B_v}, \qquad \tau_r = \frac{L_r}{R_r}. \tag{14}$$

Now, if the dynamics associated to the two current loops are neglected, because they are much faster than the rest, the following second order transfer function of the induction motor is obtained as follows:

$$\frac{\omega_m(s)}{I_{sq}^*(s)} = \frac{K_T/B_v}{(1+s\tau_m)(1+s\tau_r)} e^{-\tau_d s}, \tag{15}$$

where τ_d is the delay time of the induction motor.

Taking into account the consideration to obtain (10) from (3), Figure 2, and also considering that the dynamics associated to the rotor electrical time constant is much faster than the mechanical time constant, then the electrical pole is neglected. Thus, the following first order transfer function of the induction motor is obtained

$$\frac{\omega_m(s)}{I_{sq}^*(s)} = \frac{K_T/B_v}{(1+s\tau_m)} e^{-\tau_d s}. \tag{16}$$

The design of the GPC controller is carried out using the first order transfer function of the motor. As the GPC controller is defined in discrete time, the transfer function must be transformed into a discrete time transfer function. Then, using the ZOH (Zero-Order Hold) discretization method, it is obtained that

$$\frac{\omega_m(z^{-1})}{I_{sq}^*(z^{-1})} = \frac{B(z^{-1})}{A(z^{-1})} z^{-d} = \frac{b_0}{(1-az^{-1})} z^{-d}. \tag{17}$$

Taking into account GPC theory and employing the CARIMA model [1], it is possible to obtain the following equation of the system, in which the output ω_m is replaced by y, the input i_{sq}^* is replaced by u, and white noise is included in the previous transfer function (17):

$$A(z^{-1})\, y(t) = B(z^{-1}) z^{-d} u(t-1) + C(z^{-1}) \frac{\varepsilon(t)}{\Delta}, \tag{18}$$

where d is the delay time of the system and it is multiple of the sample time chosen, ε is the white noise with null average, $\Delta = 1 - z^{-1}$, and the $C(z^{-1})$ is the noise polynomial that is chosen to be 1 for simplicity in this design [1].

The GPC algorithm involves applying a control sequence that minimizes a multistage cost function of the form:

$$J_c = \sum_{j=N_1}^{N_2} \delta(j)\left[\hat{y}(t+j \mid t) - w(t+j)\right]^2 + \sum_{j=1}^{N_u} \lambda(j)\left[\Delta u(t+j-1)\right]^2, \tag{19}$$

where $\hat{y}(t+j \mid t)$ is the predicted output j step ahead of actual time t, N_1 is the minimum cost horizon, N_2 is the maximum cost horizon, N_u is the control horizon, $\delta(t)$ and $\lambda(t)$ are the weighting sequences, and $w(t+j)$ is the future reference trajectory. The GPC regulator design requires tuning the prediction horizons and the two weighting factors. If one takes into account the possibility that the plant has a delay time, then the minimum and maximum horizons are, respectively, $N_1 = 1 + d$ and $N_2 = N + d$ [1], where N is the prediction horizon. Since a high value for the control horizon produces an undesirable oscillation in the control signal [3, 4], which could cause the chattering phenomenon in the induction motor, then it is assumed that $N_u = 1$.

The prediction of the future output is as follows:

$$\hat{y}(t+j+d \mid t) = F_{j+d}\left(z^{-1}\right) y(t) + E_{j+d}\left(z^{-1}\right) B\left(z^{-1}\right) \Delta u(t+j-1), \tag{20}$$

where $F(z^{-1})$ and $E(z^{-1})$ polynomials are calculated by operating $1/\widetilde{A}(z^{-1})N_2$ times, where $\widetilde{A}(z^{-1}) = A(z^{-1})\Delta$, according to the following Diophantine identity:

$$1 = E_j\left(z^{-1}\right)\widetilde{A}\left(z^{-1}\right) + z^{-j}F_j\left(z^{-1}\right). \tag{21}$$

Taking into account that

$$G_j\left(z^{-1}\right) = E_j\left(z^{-1}\right) B\left(z^{-1}\right) \tag{22}$$

the following set of j ahead optimal predictions for the system expressed in matrix form (23) can be obtained:

$$y = G\mathbf{u} + F\left(z^{-1}\right) y(t) + G'\left(z^{-1}\right) \Delta u(t+j-1) = G\mathbf{u} + \mathbf{f}, \tag{23}$$

where, for an N prediction horizon, one obtains the G matrix, which contains values of the step sequence of the plant (induction motor), with $N \times N$ dimension:

$$G = \begin{bmatrix} g_{N_1} & 0 & \cdots & 0 \\ g_{N_1+1} & g_{N_1} & \ddots & \vdots \\ \vdots & g_{N_1+1} & \ddots & 0 \\ g_{N_2} & \cdots & \cdots & g_{N_1} \end{bmatrix} = \begin{bmatrix} G_{N_1}\left(z^{-1}\right) \\ \vdots \\ \vdots \\ G_{N_2}\left(z^{-1}\right) \end{bmatrix}. \tag{24}$$

Thus, from (22) and (24) we can see that the G matrix depends only on the process parameters, while the $\mathbf{f}$ term is the free response of the system, and it is easy to deduce that it is a vector of N elements:

$$\mathbf{f} = \begin{bmatrix} F_{N_1,0} + F_{N_1,1}z^{-1} \\ \vdots \\ F_{N_2,0} + F_{N_2,1}z^{-1} \end{bmatrix} y(t) + \begin{bmatrix} g_{N_1+1} + g_{N_1+2}z^{-1} + \cdots + g_{N_1+d}z^{-(d-1)} \\ \vdots \\ g_{N_2+1} + g_{N_2+2}z^{-1} + \cdots + g_{N_2+d}z^{-(d-1)} \end{bmatrix} \Delta u(t-1),$$

$$\mathbf{f} = \begin{bmatrix} F_{N_1}\left(z^{-1}\right) \\ \vdots \\ F_{N_2}\left(z^{-1}\right) \end{bmatrix} y(t) + \begin{bmatrix} G'_{N_1}\left(z^{-1}\right) \\ \vdots \\ G'_{N_1}\left(z^{-1}\right) \end{bmatrix} \Delta u(t-1). \tag{25}$$

Assuming that the $\delta(t)$ control weighting sequence is constant and equal to 1, then the cost function (19) can be written in the following form:

$$J_c = (G\mathbf{u} + \mathbf{f} - \mathbf{w})^T (G\mathbf{u} + \mathbf{f} - \mathbf{w}) + \lambda \mathbf{u}^T \mathbf{u}. \tag{26}$$

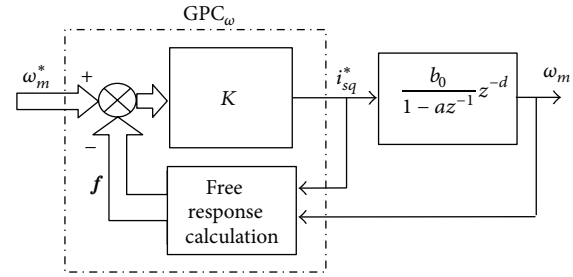

Figure 3: Diagram of the induction motor speed control scheme using GPC linear regulator.

The minimum of the cost function (26) when no constraints are considered can be calculated by equalling 0 the gradient of J_c, obtaining the following analytical expression:

$$\mathbf{u} = \left(G^T G + \lambda I\right)^{-1} G^T (\mathbf{w} - \mathbf{f}), \tag{27}$$

where $\mathbf{u}$ and $\mathbf{w}$ are two vectors of N elements:

$$\mathbf{u} = \begin{bmatrix} \Delta u(t) \\ \vdots \\ \Delta u(t+N-1) \end{bmatrix}, \qquad \mathbf{w} = \begin{bmatrix} w(t+N_1) \\ \vdots \\ w(t+N_2) \end{bmatrix}. \tag{28}$$

As the receding horizon strategy is used, the control signal applied to the process is obtained from the first element of $\mathbf{u}$, where the following expression must be employed:

$$\Delta u(t) = K(\mathbf{w} - \mathbf{f}), \tag{29}$$

where $K = [K_1 K_2 \cdots K_N]$, that is, the first row of the $(G^T G + \lambda I)^{-1} G^T$ matrix in (27).

Now replacing the variables $y(t)$ and $u(t)$, by ω_m^* and i_{sq}^*, respectively, it is obtained that

$$\Delta i_{sq}^*(t) = K\left(\omega_m^* - \mathbf{f}\right), \tag{30}$$

where finally the control law for the induction motor GPC speed regulation (31) is obtained, Figure 3 as follows:

$$i_{sq}^*(t) = K\left(\omega_m^* - \mathbf{f}\right) + i_{sq}^*(t-1). \tag{31}$$

The analytical solution of the cost function minimization is possible only if the control signal (31) is not restricted or limited [1]. As induction motors can support stator overcurrents up to 2.5 times the rated value in short periods, this GPC design does not need to limit the stator currents. That is, the i_{sq}^* control signal is not limited, allowing the implementation of the more simple, low computational cost analytical solution. With regard to the i_{sd}^* current, it is fixed to a value to produce the nominal rotor flux, I_{sd}. Finally, the calculation of the K, G, F, and G' parameters is carried out off-line, without using any identification algorithm, because the usual variation of the main parameters of the motor should be overcome in an effective form by the inherent robustness of any closed loop controller [22].

Table 1: Induction motor parameters (manufacturer).

Parameter	Symbol	Value
Stator resistance	R_s	0.81 Ω
Rotor resistance	R_r	0.57 Ω
Magnetizing inductance	L_m	0.117774 H
Stator inductance	L_s	0.120416 H
Rotor inductance	L_r	0.121498 H
Nominal rotor flux	ψ_r	1.01 Wb
Number of poles	p	4
Nominal torque	T_N	49.3 N m
Moment of inertia	J	0.057 kg m^2
Viscous friction coefficient	B_v	0.015 N m/(rad/s)
Temperature coeff. Al/Cu	α	0.0039 K^{-1}

Table 2: Several stable cases of GPC speed regulator designs.

GPC speed regulator design	
D1 (efficient 1)	D2 (efficient 2)
Nominal mech. parameters	Nominal mech. parameters
$\tau_m = 3.8$ s	$\tau_m = 1.9$ s ($J = 0.0285$ kgm^2)
$T_s = 100$ μs, $N = 5$, $d = 7$,	$T_s = 700$ μs, $N = 5$, $d = 1$,
$N_1 = 8$, $N_2 = 12$, $N_u = 1$,	$N_1 = 2$, $N_2 = 6$, $N_u = 1$, $\lambda = 1$
$\lambda = 0.17$	$GM_\omega = 12$ dB, $PM_\omega = 35^\circ$
$GM_\omega = 15$ dB, $PM_\omega = 8^\circ$	
U1	U1
IM: τ_m higher	IM: τ_m higher
$\tau_m = 7.6$ s ($J = 0.114$ kgm^2)	$\tau_m = 3.8$ s ($J = 0.057$ kgm^2)
$GM_\omega = 25$ dB, $PM_\omega = 5^\circ$	$GM_\omega = 25$ dB, $PM_\omega = 25^\circ$
U2	U2
IM: τ_m smaller	IM: τ_m smaller
$\tau_m = 0.38$ s ($B_v = 0.15$ Nms)	$\tau_m = 0.19$ s ($B_v = 0.15$ Nms)
$GM_\omega = 15$ dB, $PM_\omega = 9^\circ$	$GM_\omega = 12$ dB, $PM_\omega = 35^\circ$
PI currents regulators design	
Stator nominal electr. parameters $\tau_s = 0.1487$ s ($T = 20^\circ$C)	
$T_s = 100$ μs, $\omega_{ci} = 3000$ rad/s $PM_i = 1.5707$ (90°)	
Us1: τ_s higher $\tau_s = 0.1612$ s ($T = 0^\circ$C)	
$PM_i = 90^\circ$	
Us2: τ_s smaller $\tau_s = 0.1040$ s ($T = 130^\circ$C)	
$PM_i = 90^\circ$	

2.4. Regulator Tuning

2.4.1. PID and PI Controllers. The two current PI regulators use the same tuning values. The higher the bandwidth chosen for these controllers, the faster the current loops dynamics are. However, in practice, any real system's bandwidth is limited physically. In the employed experimental platform (Section 3.1), which uses the induction motor described in Table 1, this limit is located at 4000 rad/s; up to this value, the platform produces the undesirable chattering phenomenon and dangerous mechanical vibrations that can damage the machine.

As to the speed regulation, in the first case, a PID speed controller has been used to measure the delay time of the system. This PID speed regulator has also been designed in the frequency domain, using a bandwidth which is 10 times smaller than the PI current loop regulators [24]. Then, the optimal tuning of the PID speed regulator has been obtained taking into account this ratio of bandwidths and the physical limit of the experiment platform. Thus, the most efficient PID-PI (speed currents) controller system has been designed with the following parameter values: $\omega_{c\omega} = 300$ rad/s with a margin phase of $PM_\omega = 1.4311$ rad (82°) and $\omega_{ci} = 3000$ rad/s with a margin phase of $PM_i = 1.5707$ rad (90°). The D action of the speed loop is added after PI is tuned, and a small value is enough to do faster the response but without any overshot, where $K_d = 0.02$ and the PID-PI controller is obtained. The delay time measured in the experiment platform using this PID-PI speed regulator tuning is 700 μs, using the sample time of 100 μs, (Section 3.2).

2.4.2. SM Controller. A sliding-mode speed regulator for induction motor is also implemented in order to be compared with the proposed GPC regulator. This advanced speed regulator was presented by the authors in [7], where the parameters used in its design for the induction motor (Table 1) are obtained considering an uncertainty around 50% in the system parameters: $a = 0.3947$, $b = 77.601$, $f = 17.544 * T_L$, $k = 400$, $\gamma = 1.3$, and $\zeta = 2.5$. This speed scheme uses the same two current PI regulators employed in GPC and PI speed schemes and detailed in the previous subsection.

2.4.3. GPC Controller. The tuning of the GPC regulator requires choosing the values of two horizons and two weighting factors. The control horizon, N_u, and the output error weighting factor, δ, both have been fixed to 1 (Section 2.1). The prediction horizon, N, determines the size of the G matrix and the $\mathbf{f}$ vector, and, as a consequence, the number of the GPC controller's coefficients. A larger value for N increases the anticipative effect, involving a better control and performance of the system. However, this increases the number of the coefficients and the computational cost of the control law, which requires increasing the sample time. So N should be selected to ensure proper dynamic behaviour and low computational cost. In this design it has been set to 5. From Section 2.1, it is known that the minimum and maximum horizons take into account the delay time of the system, $N_1 = 1 + d$ and $N_2 = N + d$. Considering two GPC speed regulator designs, D1 and D2, using sample times of 100 μs and 700 μs, respectively, and taking into account that the measured experimental delay time is 700 μs (Section 3.2), then the delay values are $d = 7$ for D1 and $d = 1$ for D2 (Table 2).

The control weighting factor, λ, has a direct impact on the response of the controlled system. Hence, the higher its value, the slower the resulting controlled system. On the other hand, if its value is too small, it can produce the chattering phenomenon that can damage the motor in a real case. Then, it is desirable to find a value for λ to provide

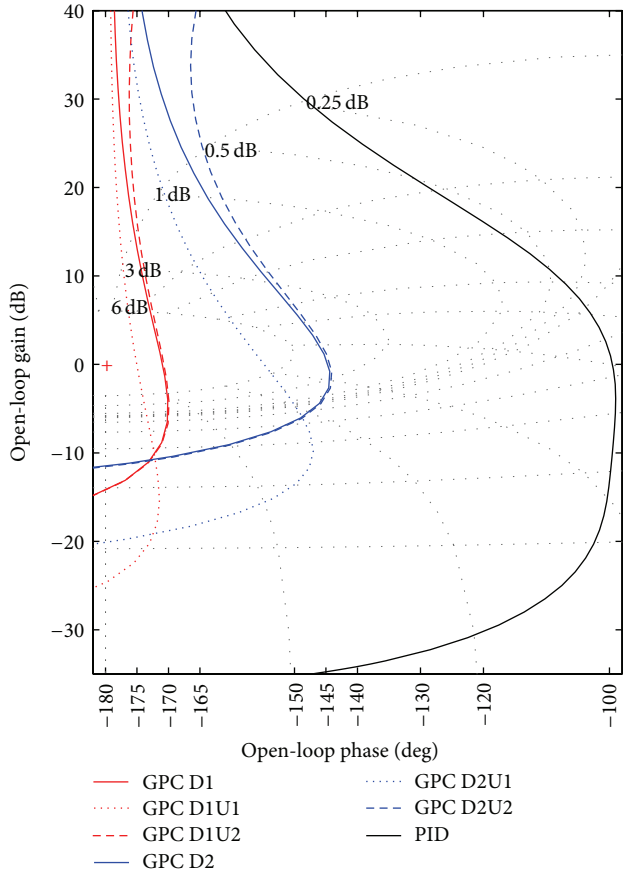

Figure 4: Nichols diagram of the GPC and PID speed loops.

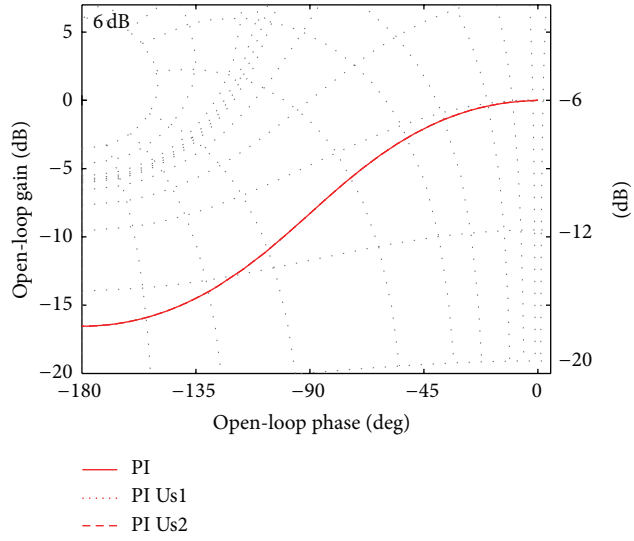

Figure 5: Nichols diagram of the PI current loops.

an effective response of the controlled system. Taking into account the recommendation in [15], an easy way to obtain an effective and stable value for λ factor is applying the following empirical expression:

$$\lambda_{\text{opt}} = m \,\text{trace}\left(G^T G\right), \tag{32}$$

where m takes a value inversely proportional to the sample time. For D1 design the m parameter results in a value of 60, and for D2, m equals 2 (tens for 100 μs, units for 700 μs).

2.5. Robust Stability Analysis. The closed loop stability of the motor d-q currents with the PI controllers is guaranteed if the PM_i phase margins are positive and sufficiently high. As to the speed loop, the stability of the controlled system is analysed using the classic RST poles placement scheme [25], where the control law is obtained as

$$i_{sq}^*(t) = \frac{1}{r_0}\left[T\left(z^{-1}\right)\omega_m^*(t)\,T - S\left(z^{-1}\right)\omega_m(t) - i_{sq}^*(t-1)\,R'\left(z^{-1}\right)\right]. \tag{33}$$

In this sense, it is necessary to translate the GPC controlled system parameters to its equivalent RST controlled system parameters [1], to check the stability of the system. Identifying the terms between (31) and (33), we can obtain the general expression of equivalence in both RST and GPC algorithms for any first order plant with delay time:

$$\begin{aligned}
R\left(z^{-1}\right) &= r_0 + r_1 z^{-1} + \cdots + r_{d+1} z^{-(d+1)} = r_0 + z^{-1} R'\left(z^{-1}\right),\\
S\left(z^{-1}\right) &= s_0 + s_1 z^{-1},\\
T\left(z^{-1}\right) &= t_0 z^{-N_1} + t_1 z^{-(N_1+1)} + \cdots + t_{N-1} z^{-N_2},
\end{aligned} \tag{34}$$

$$\begin{aligned}
r_0 &= 1,\\
r_1 &= K\left[g_{N_1+1} \;\cdots\; g_{N_2+1}\right]^T - 1,\\
r_2 &= K\left(\left[g_{N_1+2} \;\cdots\; g_{N_2+2}\right]^T - \left[g_{N_1+1} \;\cdots\; g_{N_2+1}\right]^T\right),\\
r_d &= K\left(\left[g_{N_1+d} \;\cdots\; g_{N_2+d}\right]^T - \left[g_{N_1+d-1} \;\cdots\; g_{N_2+d-1}\right]^T\right),\\
r_{d+1} &= -K\left[g_{N_1+d} \;\cdots\; g_{N_2+d}\right]^T,\\
s_0 &= K\left[F_{N_1,0} \;\cdots\; F_{N_2,0}\right]^T,\\
s_1 &= K\left[F_{N_1,1} \;\cdots\; F_{N_2,1}\right]^T,
\end{aligned}$$

$$t_0 = K_1,$$
$$t_1 = K_2,$$
$$\vdots$$
$$t_{N-1} = K_N, \tag{35}$$

where it should be noted that the polynomial T multiplies the future references vector (33). Thus, the controller should be designed so that the controlled system presents all the poles inside the unit circle. In order to achieve this a graphical representation (Nichols chart) of the open loop system is more appropriate as GM_ω gain margin and PM_ω phase margin can be observed.

The robust stability is analysed taking into account the parametric uncertainties of the induction motor in two limit real cases of each control loop detailed in Table 2. These limits are used to determine the robustness of the speed and current regulators, as these limits are both critical in real cases. Hence, as the controller is lineal, any uncertainty case located into the defined limits has the stability guaranteed.

First, the following two uncertainty cases for the limits of robustness, related with the mechanical parameters of the induction motor, are considered in the proposed GPC. The U1 takes J a 100% higher, and the U2 that considers B_v 10 times higher, increasing 2 times and reducing 10 times, respectively, the τ_m mechanical time constant of the machine. The D1 and D2 designs are presented for the speed GPC regulator. The D1 uses a sample time of 100 μs and nominal J of 0.057 kg m^2, and D2, a sample time of 700 μs and a nominal J of 0.0285 kg m^2. On the other hand, another two limit cases are considered for the PI current controllers, which are related with the stator windings resistances (R_s) modified by their temperature. Us1 determines the uncertainty when the temperature of the windings is 0°C (before starting in a cold place), and Us2 considers the heating case of the stator windings when the induction motor is working at rating power for half an hour or more, where the stator windings are around 130°C. As it is known, the temperature variation produces the proportional increase of the stator windings resistance:

$$R_f = R_0\left(1 + \alpha\left(T_f - T_0\right)\right) \tag{36}$$

and the proportional decrease of the τ_s stator electrical time constant:

$$\tau_s = \frac{L_s}{R_s}. \tag{37}$$

Table 2 shows the two efficient designs for the GPC speed regulator, D1 and D2, taking into account different nominal moments of inertia of the induction motor and sample times in each case. The two uncertainties cases, U1 and U2, have been based in the D1 and D2 designs, but even so, the stability of the controlled system is guaranteed observing the gain and phase margins obtained from Figure 4. In Table 2, the efficient design for the two PI current controllers is detailed, with Us1 and Us2 uncertainties cases. Figure 5 shows that the temperature variations in the stator windings practically have not any effect.

3. Simulation and Experimental Results

3.1. Experiment Platform. The employed platform is composed by a PC with *MatLab7/Simulink R2007a*, *dsControl 3.2.1,* and the *DS1103 Controller Board* real time interface of *dSpace*, with a floating point *PowerPC* processor to 1 GHz; and a set of electric machines that includes a *M2AA 132M4ABB* commercial induction motor of 7.5 kW of die-cast aluminium squirrel-cage type (1445 rpm), Table 1, connected to a DC bus of 540 V by VSI inverter, and a *190U2 Unimotor* synchronous AC servo in motor of 10.6 kW to generate the load torque (controlled in torque), presented in [15]. An incremental encoder of 4096 pulses is employed to measure the mechanical speed of the induction motor. The rotor flux of the induction motor has been set to its nominal value of 1.01 Wb, keeping the flux current command i_{sq}^*, that is, I_{sd}, to a constant value of 8.61 A. Finally, as the SVPWM modulator frequency is fixed at 10 kHz, then the sample time employed for the PI current controllers is 100 μs.

3.2. Speed Tracking. Using D1 design for the GPC controller, simulation and experimental tests are carried out with a trapezoidal speed reference of 1445 rpm and 0.33 Hz, adding an square form load torque of 30 Nm (starting from the second period of the speed reference).

Results are shown in Figure 6, where very satisfactory speed tracking can be observed, obtaining a stationary speed error of about 2 rpm (0.138%) in the experimental case, both without and with load torque. In addition, the electromagnetic torque does not present any aggressiveness, and consequently it will not generate the undesirable chattering phenomenon, as seen in the third graph. Moreover, around $t = 4$ s and $t = 5.5$ s, the motor is working at nominal speed and torque (Table 2), obtaining an excellent speed tracking. Considering the electromagnetic torque reference current, i_{sq}^*, it should be noted that it is not limited, which justifies the employed analytical. Moreover, it can be seen that the rotor flux current, i_{sd}, takes the value imposed by its reference in accordance with the previous assumption of the theoretical section (see Section 2.3), and consequently that the rotor flux remains constant at its nominal value for a short time after it is requested, verifying the decoupling of its components. The great similarity between the simulation and the experimental tests validates the presented GPC speed regulator, and they show that the choice of the first order model for the induction motor is correct.

Figure 7 shows the speed response and the electromagnetic torque reference current for D1 of GPC speed controller and PID speed regulator cases. It can be observed that the PI regulator has a delay of 700 μs ($d = 7$) and that the GPC controller generates the control signal 12 sample times (N_2) before the speed reference, compensating for the delay time of the system and anticipating 5 steps (N) the reaction of the speed response.

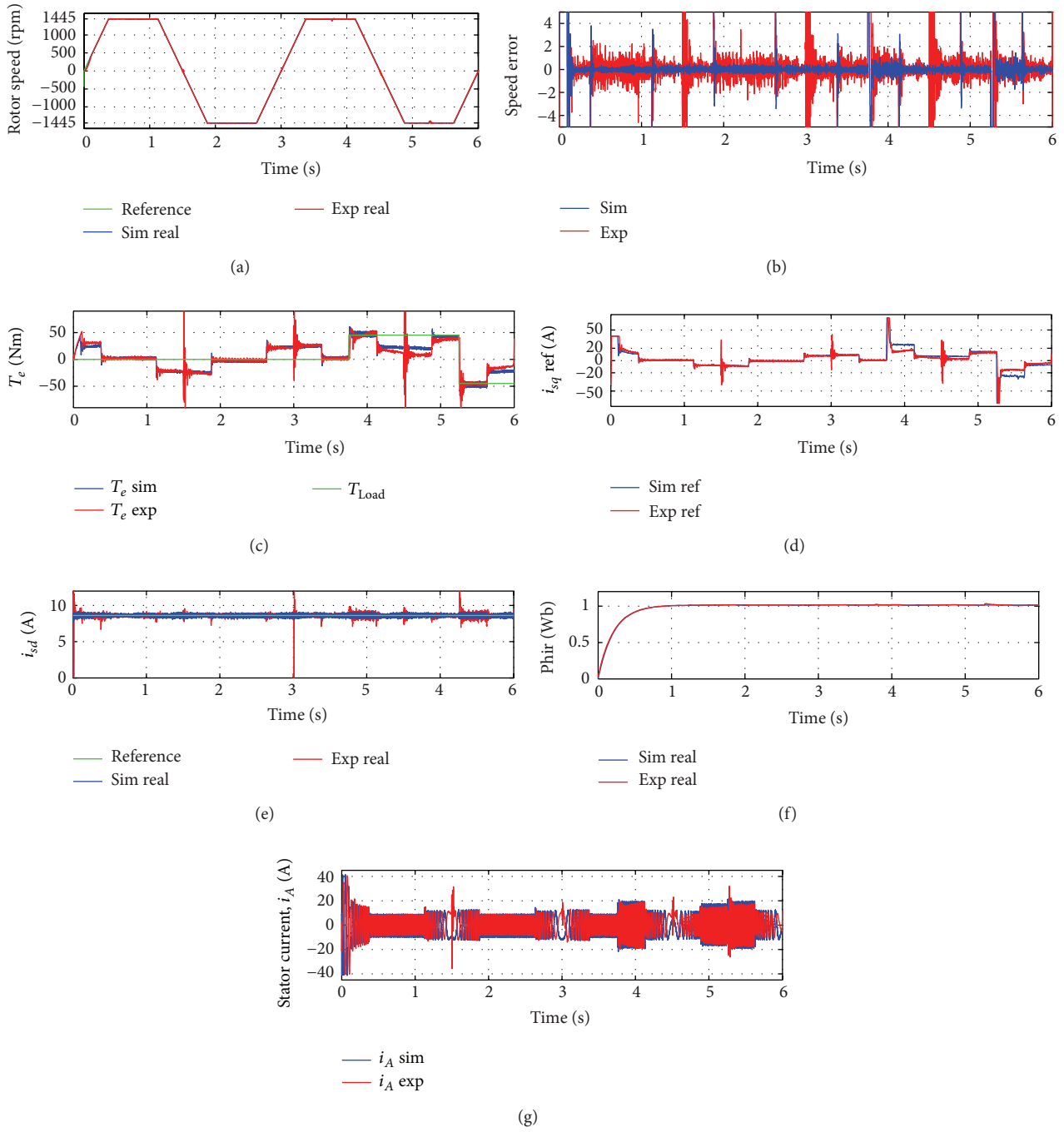

FIGURE 6: Simulation and real tests of the GPC-PI model with D1 design with unknown load torque.

In Figure 8 the performance comparison between the regulator proposed in this paper, GPC1, and a previously proposed GPC one [15] based on a second order transfer function (15), GPC2, can be observed. The tests are based on a 1200 rpm and 0.75 Hz a saw-toothed speed reference and an unknown load torque of 25 Nm starting from 1.65 s. Comparing the two speed responses, it is possible to appreciate that the proposed GPC speed regulator (GPC1) is better than the previous version (GPC2), because the speed response is similar but is less oscillatory.

Figure 9 compares the GPC1, SM, PI, and PID speed regulators, in the same test conditions as in the previous case. Comparing the responses of the GPC1 and SM regulators, it can be observed that the predictive response is a little faster than sliding modes' response. Moreover, the effect of the load torque in the GPC1 case is minor than the SM case, which

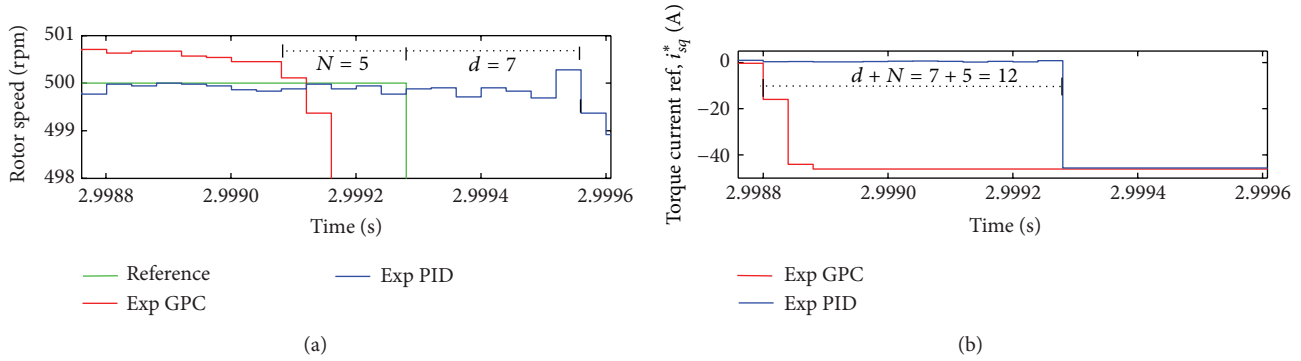

FIGURE 7: Comparative experimental tests: speed responses (a) and torque reference currents (b) of GPC D1 controller versus PI regulator.

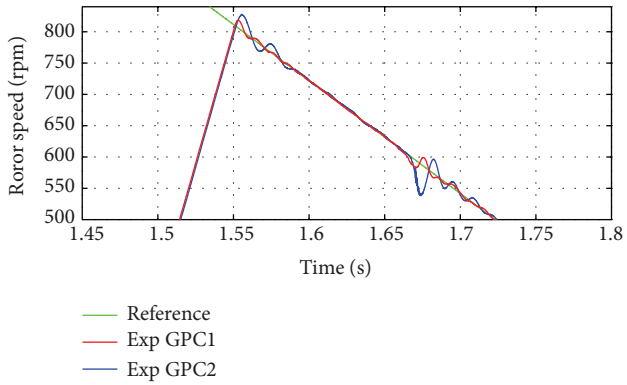

FIGURE 8: Comparative experimental tests: speed responses of GPC1 D1 controller versus GPC2 D1 regulator.

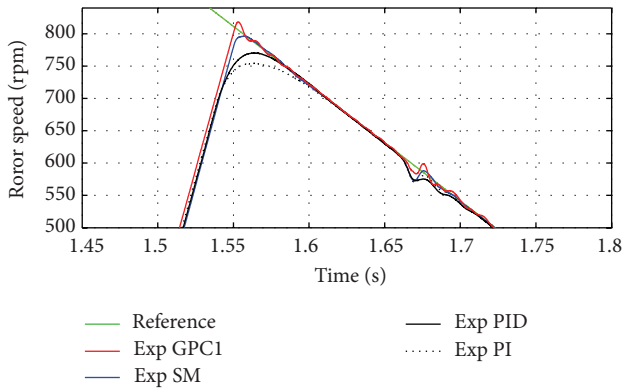

FIGURE 9: Comparative experimental tests: speed responses of GPC1 D1, SM, PI, and PID speed regulators.

demonstrates the robustness of the approach when varying load torques are applied. In addition, it can be seen that the PID is faster than PI due to derivative effect. Also, it can be observed that the GPC1 regulator's response is considerably faster than PID's response.

Figures 10 and 11 show the comparative experimental tests of the GPC1, SM, and PID speed regulators using constant acceleration and variable acceleration cases, respectively. Figure 10 shows that the speed tracking without any load torque (between 0 and 2.25 s) is very similar for the three regulators though it can be observed that the speed error is about 2 rpm for GPC while its magnitude is increased to 4 and 5 rpm in the SM and PID cases. When the load torque is considered, the speed tracking is considerably worse for SM and PID cases, while the GPC maintains a good speed tracking (fourth graph (a)). Moreover, GPC regulator supports better than the SM and PID controllers the load torque changes (fourth graph on the right (b)). Figure 11 shows that the speed tracking without any load torque (between 0 and 2.25 s) is similar for the three regulators although the speed error is 2 rpm for GPC while it increases to 4 an 5 rpm in the SM cases, and about 8 rpm in the PID case. Moreover, the GPC regulator provides a faster response in the initial half period (fourth graph on the left (a)). When the load torque appears, the speed tracking is considerably worse for PID case, while the GPC and SM maintain a good speed tracking (fourth graph on the right (b)), though the GPC response is a little faster than sliding mode's response.

Therefore, the use of the first order transfer function model is justified because the first order model simplifies the computational cost and the controlled performance contains less oscillations than the second order case.

3.3. Load Disturbance, Uncertainties, and Measurement Noise Rejection. One of the issues that usually exists in real applications is load disturbance, and, in the previous tests, the proposed GPC speed controller has demonstrated its performance even in presence of this effect. Moreover, parametric uncertainties that is, the change of values in the induction motor parameters can arise. These have been considered as U1 and U2 in Table 2. Finally, the measurement noise in the two loop signals, in the rotor speed, and in the stator current has a negative impact on the controllers.

In this sense, the graphs of Figure 12 show the simulation and real tests, using a 1200 rpm and 0.33 Hz trapezoidal speed reference and an unknown square form load disturbance

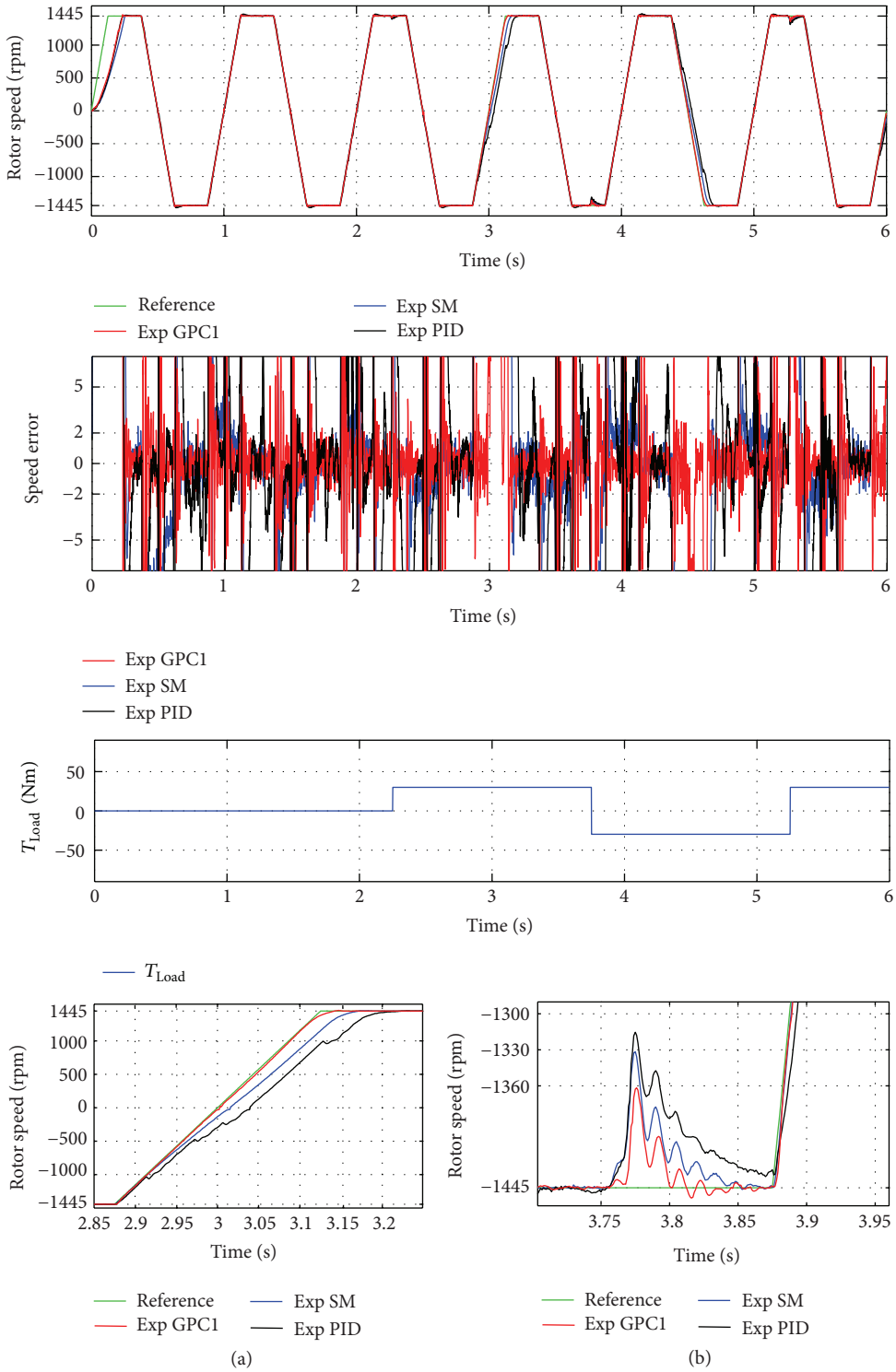

FIGURE 10: Comparative experimental tests: speed responses of GPC1 D1, SM, PI, and PID speed regulators for constant acceleration case.

of 30 Nm. The GPC speed regulator is designed taking into account the nominal parameters of the motor, D2 design (Table 2). In the simulation case the induction motor has the nominal values in its parameters, and the unknown load disturbance in its shaft only is considered. In the experimental case, an additional, software based, measurement white noise is induced in the two feedback signals, ω_m and i_A (using MatLab/dSControl). In this way, robustness against measurement noises is demonstrated. Additionally, in this case parameter uncertainties and load disturbances are introduced, this is, a greater stator (Cu) resistance, at 130°C and a 100% greater moment of inertia, Us2 and U2 cases for D2 design in Table 2.

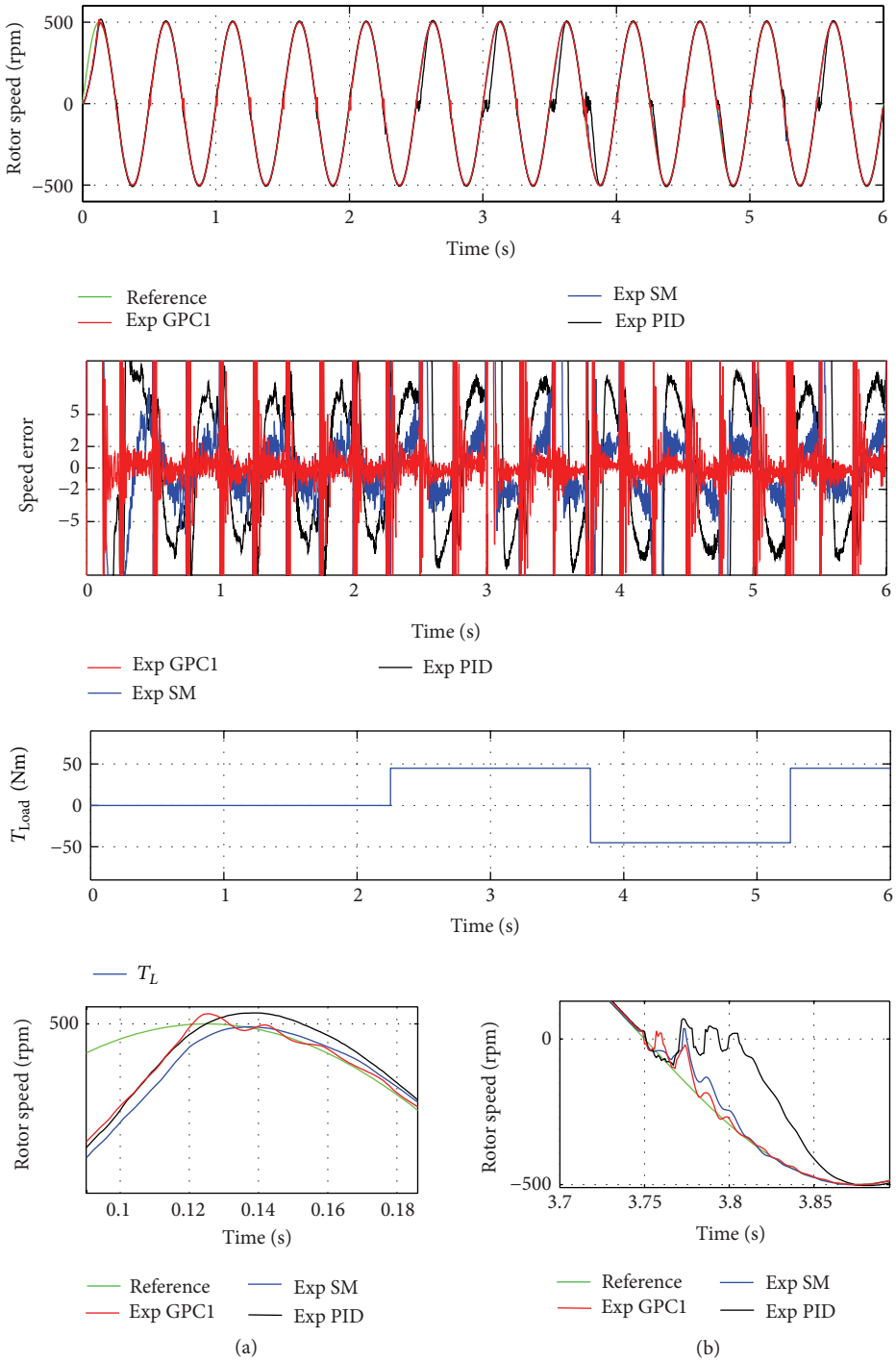

Figure 11: Comparative experimental tests: speed responses of GPC1 D1, SM, PI, and PID speed regulators for variable acceleration case.

Observing the graphs of Figure 10, it can be seen that the motor response is very good in spite of all the adversities, and a satisfactory speed tracking is achieved. The electromagnetic torque manifests some activity due to the sensor noises, but not due to the controller action, as observed in the simulation test in the second graph. As to real computational cost of the GPC-PI controller, as the calculation of the parameters K, G, F, and G' is realized offline, its value is the same as the PI-PI controller: 10 μs employing a *PowerPC* processor at 1 GHz.

4. Conclusions

The contribution of this work consists of the combination of the GPC algorithm in the speed loop with a PI based control

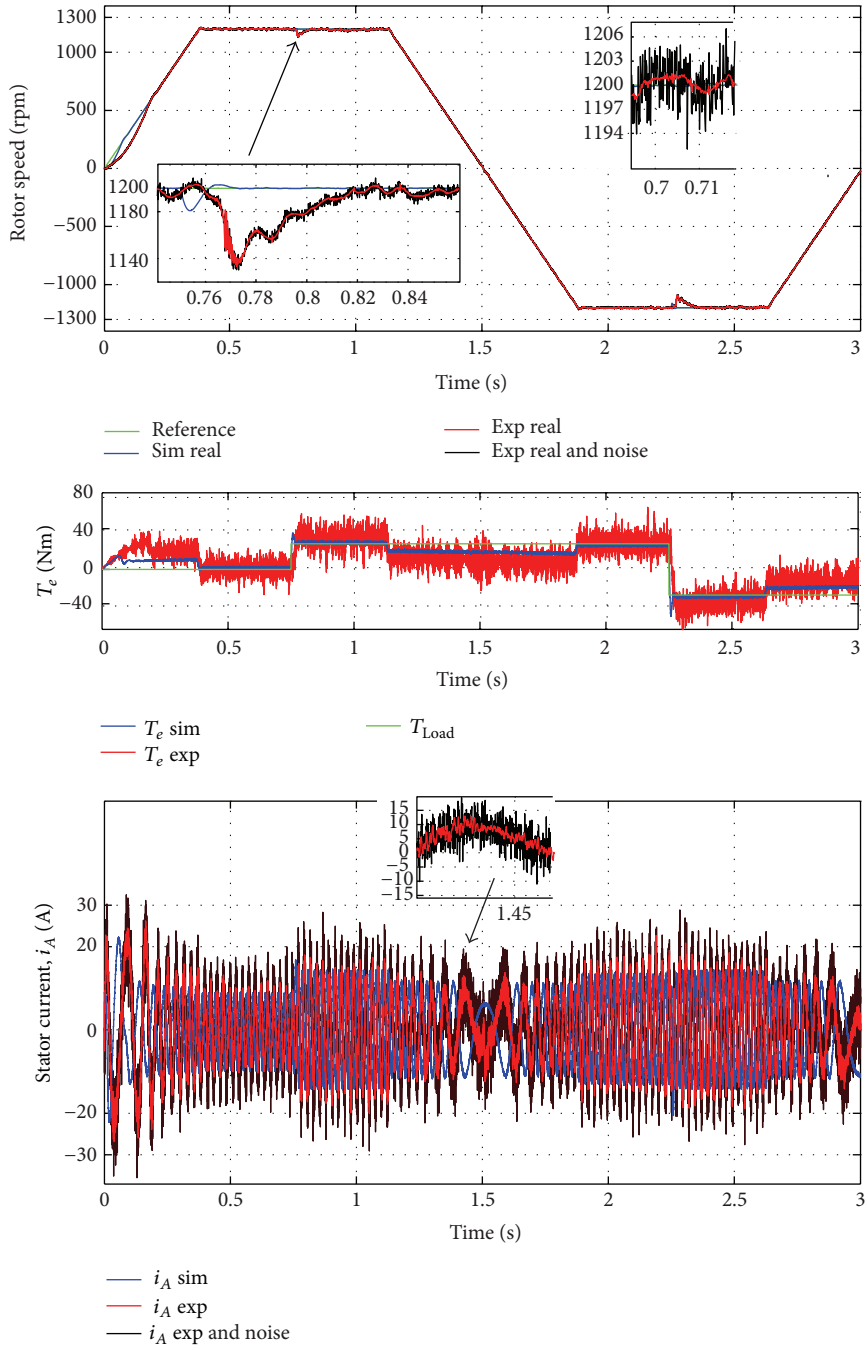

FIGURE 12: Simulation and real tests of the proposed GPC (D2 design) speed regulator with high-level noise in the two feedback loops and unknown load torque.

in the current loops, using an easy and effective design, where the robust stability is demonstrated for typical induction motors' parametric uncertainties. The GPC speed controller design is based on the first order model of the induction motor with a delay time, which is compensated. This regulator design is simpler to implement than other predictive proposed schemes, as neither constraints nor robustness terms have been taken into account.

The proposed controller has been tested using various simulation and experimental tests in the presence of the parametric uncertainties, unknown load disturbance, and measurement noise in the loop signals: the rotor speed and the stator current. The experiment demonstrates the effectiveness of the approach. Moreover, the presented results also show that the GPC speed regulator is considerably faster than the classic PID and slightly faster than the advanced

SM speed controller, using the same computational cost. This work demonstrates that the GPC-PI controller is an effective speed control algorithm, in both adverse and acceptable conditions, its robustness is clearly shown, the proposed control scheme is also easy to tune and to implement in a real system, and therefore it can be used in industrial applications.

Acknowledgments

The authors are very grateful to the UPV/EHU for its support throughout the project GUI07/08 and the Basque Government for the support to this work throughout the project S-PE09UN12.

References

[1] E. F. Camacho and C. Bordons, *Model Predictive Control*, Springer, London, UK, 2nd edition, 2007.

[2] Y. Xia, G.-P. Liu, M. Fu, and D. Rees, "Predictive control of networked systems with random delay and data dropout," *Control Theory and Applications*, vol. 3, no. 11, pp. 1476–1486, 2009.

[3] D. W. Clarke, C. Mohtadi, and P. S. Tuffs, "Generalized predictive control—part I. The basic algorithm," *Automatica*, vol. 23, no. 2, pp. 137–148, 1987.

[4] D. W. Clarke, C. Mohtadi, and P. S. Tuffs, "Generalized predictive control—part II. Extensions and interpretations," *Automatica*, vol. 23, no. 2, pp. 149–160, 1987.

[5] J. Yu, J. Gao, Y. Ma, and H. Yu, "Adaptive fuzzy tracking control for a permanent magnet synchronous motor via backstepping approach," *Mathematical Problems in Engineering*, vol. 2010, Article ID 391846, 13 pages, 2010.

[6] C.-F. Huang, J.-S. Lin, T.-L. Liao, C.-Y. Chen, and J.-J. Yan, "Quasi-sliding mode control of chaos in permanent magnet synchronous motor," *Mathematical Problems in Engineering*, vol. 2011, Article ID 964240, 10 pages, 2011.

[7] O. Barambones and P. Alkorta, "A robust vector control for induction motor drives with an adaptive sliding-mode control law," *Journal of the Franklin Institute*, vol. 348, no. 2, pp. 300–314, 2011.

[8] S. Zeng, "Adaptive speed control design for brushed permanent magnet DC motor based on worst-case analysis approach," *Mathematical Problems in Engineering*, vol. 2013, Article ID 698050, 15 pages, 2013.

[9] R. Kennel, A. Linder, and M. Linke, "Generalized Predictive Control (GPC)-ready for use in drive applications?" in *Proceedings of the IEEE 32nd Annual Power Electronics Specialists Conference*, pp. 1839–1844, Vancouver, Canada, June 2001.

[10] R. Hedjar, R. Toumi, P. Boucher, and D. Dumur, "Cascaded nonlinear predictive control of induction motor," *European Journal of Control*, vol. 10, no. 1, pp. 65–80, 2004.

[11] K. Barra and K. Benmahammed, "New extended cascaded predictive control with multiple reference models ECGPC/MRM of an induction motor drive with efficiency optimization," *Journal of Electrical Engineering*, vol. 58, no. 2, pp. 71–78, 2007.

[12] M. Tonnes and H. Rasmussen, "Robust self-tuning control of AC-servo drive," in *Proceedings of the European Conference on Power Electronics and Application*, pp. 3049–3053, November 1991.

[13] P. Boucher, D. Dumur, and A. Ehrlinger, "Unified approach of equality and inequality constraints in G.P.C," in *Proceedings of the IEEE International Conference on Control Applications*, pp. 894–899, Dearborn, Mich, USA, September 1996.

[14] M. A. Gama and M. Mahfouf, "Speed control of an experimental hot-rolling mill using generalized predictive control," in *Proceedings of the International Control Conference (CCA '06)*, pp. 1–6, September 2006.

[15] P. Alkorta, O. Barambones, A. J. Garrido, and I. Garrido, "SVPWM linear Generalized Predictive Control of induction motor drives," in *Proceedings of the IEEE International Symposium on Industrial Electronics (ISIE '08)*, pp. 588–593, Cambridge, UK, July 2008.

[16] P. Rodríguez and D. Dumur, "Generalized predictive control robustification under frequency and time-domain constraints," *IEEE Transactions on Control Systems Technology*, vol. 13, no. 4, pp. 577–587, 2005.

[17] E. S. de Santana, E. Bim, and W. C. do Amaral, "A predictive algorithm for controlling speed and rotor flux of induction motor," *IEEE Transactions on Industrial Electronics*, vol. 55, no. 12, pp. 4398–4407, 2008.

[18] P. Cortés, L. Vattuone, and J. Rodríguez, "Predictive current control with reduction of switching frequency for three phase voltage source inverters," in *Proceedings of the IEEE International Symposium on Industrial Electronics (ISIE '11)*, pp. 1817–1822, Gdansk, Poland, June 2011.

[19] J. Guzinski and H. Abu-Rub, "Speed sensorless induction motor drive with predictive current controller," *IEEE Transactions on Industrial Electronics*, vol. 60, no. 2, pp. 699–709, 2013.

[20] E. F. Camacho, "Constrained generalized predictive control," *IEEE Transactions on Automatic Control*, vol. 38, no. 2, pp. 327–332, 1993.

[21] C.-W. Park and W.-H. Kwon, "Time-delay compensation for induction motor vector control system," *Electric Power Systems Research*, vol. 68, no. 3, pp. 238–247, 2004.

[22] K. Ogata, *Modern Control Engineering*, Prentice Hall, Upper Saddle River, NJ, USA, 3rd edition, 1997.

[23] N. Mohan, *Advanced Electric Drives*, University of Minnesota, Mineapolis, Minn, USA, 1st edition, 2001.

[24] B. K. Bose, *Modern Power Electronics and AC Drives*, Prentice Hall, Upper Saddle River, NJ, USA, 2002.

[25] K. J. Åström and B. Wittenmark, *Computer Controller Systems: Theory and Designs*, Prentice Hall, Upper Saddle River, NJ, USA, 3rd edition, 1997.

Hindawi Publishing Corporation
Mathematical Problems in Engineering
Volume 2013, Article ID 617054, 9 pages
http://dx.doi.org/10.1155/2013/617054

Research Article

Angle Displacement Robust Controller for the Port Plate of the Hydraulic Transformer

Wei Shen,[1] Jihai Jiang,[1] Xiaoyu Su,[2] and Hamid Reza Karimi[3]

[1] *School of Mechatronics Engineering, Harbin Institute of Technology, Harbin 150080, China*
[2] *College of Automation, Harbin Engineering University, Harbin 150001, China*
[3] *Department of Engineering, Faculty of Technology and Science, University of Agder, 4898 Grimstad, Norway*

Correspondence should be addressed to Wei Shen; shenw@hit.edu.cn

Received 21 August 2013; Accepted 15 October 2013

Academic Editor: Tao Li

The hydraulic transformer is used in the hydraulic system to enhance the efficiency. However, how to control the angle displacement of the port plate is becoming a critical issue because of the new structure of the hydraulic transformer. This paper presents a new method for the angle displacement control system. Firstly, the basic principle of the system is presented. Then, the disturbance which is mainly the friction torque between the port plate and the cylinder block is calculated to estimate the range. Furthermore, the guaranteed cost control (GCC) is analyzed and combined with the disturbance and the characteristics of parameter uncertainties. Finally, the proposed control method is compared with the traditional PI control and the simulation result shows the effectiveness of the proposed design method.

1. Introduction

Energy saving research in the field of hydraulic system is becoming a hot point [1–6]. Common pressure rail (CPR) is one promising hydraulic architecture because of its many advantages, for instance, not only that it eliminates the throttling loss in the theoretical aspect, but also has the module characteristic [7, 8]. In CPR, the constant pressure variable pump and hydraulic accumulator constitute the high pressure oil sources, and multiple different loads connect in parallel between the high pressure and the low pressure oil pipe [9–12]. Basically, there are two kinds of actuators in CPR. They are hydraulic variable displacement motors and cylinders. For the rotating load, the control target such as position, velocity, or power can be reached by regulating the displacement of hydraulic pump/motor. However, because it is hard to change the displacement of the hydraulic cylinder, hydraulic transformer (HT) is introduced to control the hydraulic cylinder for adapting to load change without throttling loss from the theoretical aspect. The detailed information about HT can be found in [13]. Hence, HT is used to control the hydraulic cylinder by regulating the angle of the port plate. However, because the structure of the port plate is different from the traditional axial piston type component, how to control the angle of port plate is a new challenge. For the traditional axial piston pump, the port plate is fixed with the case and it cannot be moved. Hence, the force applied on the swash plate from the cylinder block and some other components of the pump is balanced by the case. However, the torque applied on the port plate of HT should be considered because of the rotation motion during controlling its angle. Figure 1 shows the structure of the HT [14]. The external load torque, which is mainly the friction torque between the cylinder block and the port plate, is also changing during the regulating process. This can be explained by introducing the working principle of HT.

Figure 1(b) shows the structure of the port plate which has three ports [13]. They are connected with the high pressure pipe of CPR, the load, and the low pressure pipe of CPR, respectively. The cylinder block of the HT is driven by the sum of torque generated by the three ports of the SHT. The sum of torque among three ports is

$$\Delta T = J_{\mathrm{HT}}\dot{\omega}_{\mathrm{HT}} = T_A + T_B + T_T, \tag{1}$$

where J_{HT} is the moment of inertia of HT and ω_{HT} is the angular speed of the cylinder block of HT.

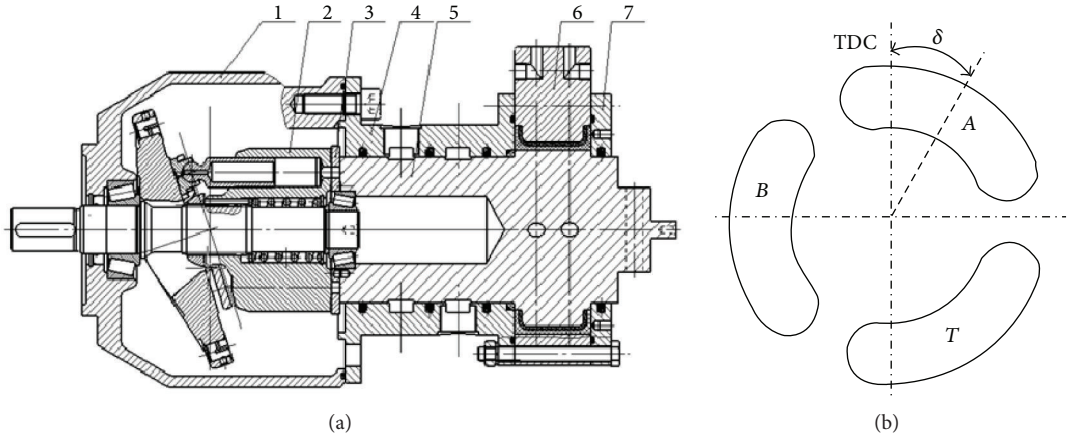

Figure 1: Structure of HT. (1) Case of original pump. (2) Cylinder block. (3) New port plate. (4) Case of swing motor. (5) Rotor of swing motor. (6) Stator of swing motor. (7) Rear cover of swing motor.

The torque applied on the port plate should be changing because of the changing load and then the difficulty for a good control performance is increased. Until now, there are already many papers which are focusing on the robust control [15–21]; for instance, in [22], the authors deal with the robust control problem with parametric uncertainties for delayed singular systems. In [23], the paper describes robust force sensorless control system in motion control. In addition, the robust control theory is applied on diesel engine selective catalytic reduction (SCR) systems to enhance the performance [24]. Because the guaranteed cost control (GCC) not only stabilizes the uncertain system robustly but also ensures an adequate level of performance, in which an upper bound on the closed-loop value of a quadratic cost function can be guaranteed by using a fixed Lyapunov function [25], the GCC becomes an effective method for enhancing the system performance [26–30]. However, there is no method that focuses on the angle displacement control of the port plate. In general, the critical problems can be described by how to resist the interference which was applied on the port plate and eliminated the influence of the uncertain model. In this paper, the GCC is introduced to the field of the angle displacement control for the port plate. Firstly, the mathematical model of the angle displacement system is constructed. Secondly, the range of the disturbance and the uncertain parameter must be estimated in order to apply the GCC theory. Moreover, the simulation about the GCC control and the PI control is conducted by using Matlab. Finally, the simulation result is explained.

2. Modeling

The basic schematic is shown in Figure 2. The main components of the system are (1) pump and (2) servovalve, and both (3-1) swing motor and (3-2) HT main part are one piece in practical applications. However, this paper is focused on the valve controlling the motor, and the information about other parts can be found in [31].

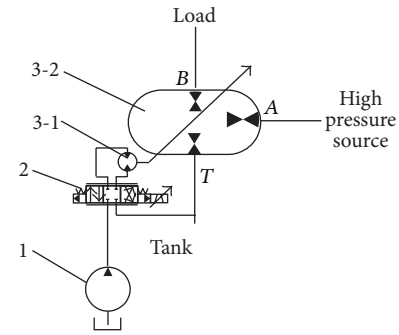

Figure 2: Hydraulic schematic of the system.

2.1. Servovalve Flow Rate Equation. The linearized servovalve flow equation is

$$Q_L = K_q K_i K_s u_i - K_c p, \tag{2}$$

where Q_L and u_i are, respectively, cylinder flow and input control voltage, K_i, K_s, K_q, and K_c are different kinds of gain listed as gain of the amplifier, servovalve coefficient, servovalve flow gain, and servovalve flow-pressure coefficient, respectively, and p represents cylinder pressure difference.

2.2. Continuity Equation in the Motor. Applying the continuity equation to each chamber of motor,

$$\begin{aligned} \dot{p}_1 &= \frac{\beta_e}{V_0}\left(Q_1 - D_m\dot{\theta} - C_{\text{ic}}\left(p_1 - p_2\right) - C_{\text{ec}}p_1\right), \\ \dot{p}_2 &= \frac{\beta_e}{V_0}\left(-Q_2 + D_m\dot{\theta} + C_{\text{ic}}\left(p_1 - p_2\right) - C_{\text{ec}}p_2\right), \end{aligned} \tag{3}$$

where D_m represents the displacement volume of motor, θ is the angle displacement of the valve plate, and β_e, C_{ic}, C_{ec}, and V_0 are coefficients defined as effective bulk modulus of system, internal or cross-port leakage coefficient of motor, external leakage coefficient of motor, and total volume of fluid

under compression in both chambers, respectively. We define that $p_L = p_1 - p_2$ and $Q_L = Q_1 = Q_2$; thus,

$$\dot{p}_L = Q_L - D_m\omega - Q_l\left(p_1, p_2, \omega\right), \tag{4}$$

where C_{tc} means total leakage coefficient of variables in cylinder:

$$Q_L = C_d l_v \sqrt{\frac{1}{2}\left(p_s - p_L\right)}, \tag{5}$$

where C_d is the flow coefficient and l_v represents the displacement of the valve.

2.3. Torque Motion Equation at the Load. The torque balance equation for the valve plate is expressed as

$$J_{vp}\frac{d^2\theta}{dt^2} = D_m p_L - d_r \cdot \frac{d\theta}{dt} - T_f - T_e, \tag{6}$$

where θ denotes angular position of the secondary component, J_{vp} represents equivalent moment of inertia of the port plate, besides, T_f is the total friction torque, T_e is the disturbance torque, and d_r is the kinematic coefficient of viscosity.

2.4. System State-Space Model. State variables are selected as $X = [x_1 \;\; x_2 \;\; x_3]^T = [\theta \;\; \dot{\theta} \;\; p_L]^T$, where x_1 is the angular displacement of valve plate, x_2 is the rotating velocity of valve plate, and x_3 is the differential pressure of the two chambers. Thus, a state-space equation of the system under consideration can be given by

$$\dot{x} = \begin{pmatrix} x_2 \\ \dfrac{D_m}{J_{vp}}x_3 \\ -\dfrac{D_m\beta_e}{V_0}x_2 - \dfrac{\beta_e C_{ei}}{V_0}x_3 \end{pmatrix} + \begin{bmatrix} 0 \\ 0 \\ \dfrac{\beta_e}{V_0} \end{bmatrix} u + \begin{bmatrix} 0 \\ -T_e - T_f \\ 0 \end{bmatrix},$$
$$y = \begin{bmatrix} 1 & 0 & 0 \end{bmatrix}^T x. \tag{7}$$

About the equation, there exist parameter uncertainty and external disturbance in the system. In detail, β_e can change from $0.8\beta_e$ to $1.2\beta_e$, and C_{ei} can also change from $0.5C_{ei}$ to $2C_{ei}$. For the disturbance T_f and T_e, it is noted that T_f is the friction torque between the cylinder block and the port plate which should be calculated in the following section to estimate the range; then, T_e is the small disturbance caused by other factors. The main external disturbance torque is the friction torque, and the following part will focus on calculating the range of the disturbance torque.

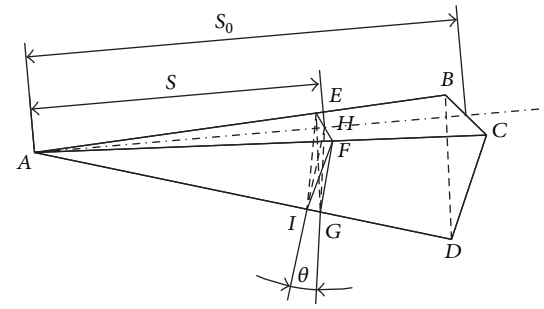

Figure 3: Structure of the triangular groove.

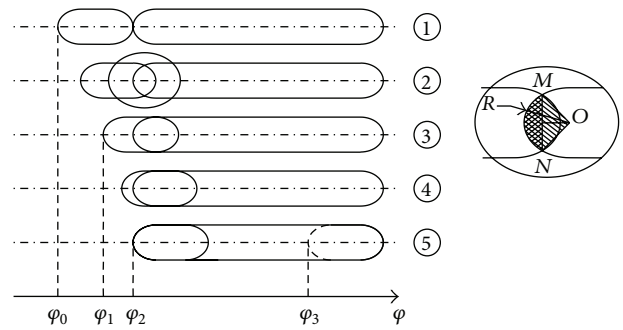

Figure 4: The position relationship between the plunger hole and the kidney slot.

2.5. Range Estimation of the Disturbance Torque

2.5.1. Calculation of Triangular Groove. The triangular groove is one common kind of dampening groove in practical engineering, which is depicted in Figure 3. It can be found that the flow area is changing with the relative location.

The flow area can be defined as the minimum area which is vertical with the flow direction; hence the flow area A_3 should be the area of ΔEFI through the geometric calculation:

$$A_3 = S_{\Delta EFI} = S_{\Delta EFG}\cos\theta = \frac{s}{s_0}\frac{\sqrt{3}}{4}a^2\cos\theta, \tag{8}$$

where ΔBCD is the equilateral triangle and the side length is a, ΔABC is the isosceles triangle, and in addition, the plane ABC is vertical with the plane BCD. s_0 is the total length of the triangular groove and s is the effective length. ΔEFG is through the H point and parallel ΔBCD.

2.5.2. Flow Area Calculation of the Waist Type Groove. The profile and dimensions of the three waist type grooves are all the same except for the different location. Defining the radius of the distribution circle of the waist type groove and the plunger hole is r. All of the three flow area calculation methods are similar. The position relationship between the hole of the plunger hole and the waist type groove during the piston is rotating as shown in Figure 4. ①, ③, and ⑤ are the critical positions in Figure 4 and the corresponding angles are φ_0, φ_1, and φ_2, respectively.

(a) When $\varphi_0 < \varphi < \varphi_1$, the flow area is overlying through two arches. And the area of the single arch can be obtained by subtracting the area of ΔOMN from the area of OMN.

The flow area can be obtained from

$$A = 2\left(A' - A''\right) = R^2 \arccos\left(\frac{(\varphi - \varphi_0) r}{2R}\right) - (\varphi - \varphi_0) r \sqrt{R^2 - \left(\frac{(\varphi - \varphi_0) r}{2}\right)^2}, \tag{9}$$

where the central angle is

$$\angle MON = 2\arccos\left(\frac{(\varphi - \varphi_0) r}{2R}\right). \tag{10}$$

And the sector can be calculated as

$$A' = \frac{R^2}{2} \arccos\left(\frac{(\varphi - \varphi_0) r}{2R}\right). \tag{11}$$

The area of the triangle is

$$A'' = \frac{(\varphi - \varphi_0) r}{2} \sqrt{R^2 - \left(\frac{(\varphi - \varphi_0) r}{2}\right)^2}. \tag{12}$$

(b) When $\varphi_1 < \varphi < \varphi_2$, the flow area is equal to the difference of the entire circle area and the two sector areas; hence the flow area is

$$A = \pi R^2 + \frac{\varphi - \varphi_1}{2}\left(\left(r + \frac{R}{2}\right)^2 - \left(r - \frac{R}{2}\right)^2\right). \tag{13}$$

(c) When $\varphi_2 < \varphi < \varphi_3$, the entire plunger hole is contained in the waist type groove; hence the flow area is the area of the plunger hole:

$$A = \pi R^2 + \frac{\varphi_{\text{con}}}{2}\left(\left(r + \frac{R}{2}\right)^2 - \left(r - \frac{R}{2}\right)^2\right), \tag{14}$$

where φ_{con} is the central angle of the sector of the plunger hole.

(d) When $\varphi > \varphi_3$ the method is the same as above; hence the period is omitted.

2.5.3. Flow Continuity Equation. Figure 5 shows the motion analysis of the axial piston pump which has piston shoes.

There are nine plungers which are doing the alternative liner motion. The radius of the distribution circle is r, and the plane Oxy is vertical with the axis of the cylinder. The plane $O'x'y'$ is the same plane with the swash plate and the angle between the two planes is φ, which is the tilt angle of the swash plate. During the working period, the plungers not only rotate around the z-axis, but also do the liner alternating motion with the z-axis. Points A and B are the top and bottom dead points, respectively, during the plungers moving, and point C is the position while the plungers at the t time. Hence, the position of the plunger is

$$x = r \sin\alpha, \qquad y = r \cos\alpha, \qquad z = -r \tan\varphi \cos\alpha. \tag{15}$$

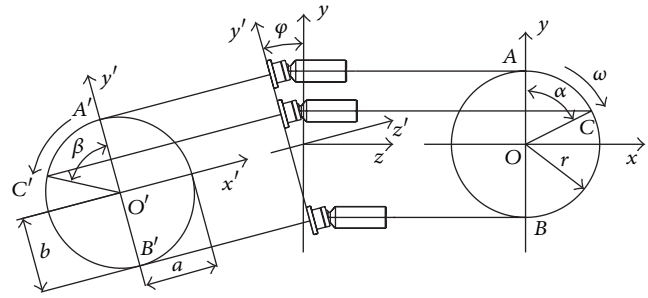

Figure 5: The motion analysis of the plunger.

We can also get the velocity of the plunger relative to the cylinder as follows:

$$v = \frac{dz}{dt} = \frac{d\left(-r \tan\varphi \cos\alpha\right)}{dt} = \omega r \tan\varphi \sin\alpha, \tag{16}$$

where ω is the angular velocity of the cylinder (rad/s).

Then, the flow rate of the plunger hole caused by the motion of the plunger is calculated by

$$Q_v = v A_z = \frac{\omega \pi r d^2}{4} \tan\varphi \sin\alpha, \tag{17}$$

where A_z is the area of the plunger (m^2) and d is the diameter of the plunger (m).

The compression flow rate inside the plunger hole can be obtained by

$$Q_E = \frac{d\Delta V}{dt} = \frac{V_0}{E}\frac{dP}{dt}, \tag{18}$$

where V_0 is the oil volume corresponding to the time of t (m^3) and E is the volumetric modulus of elasticity (MPa).

The equation for calculating the flow rate through the throttle valve is below:

$$Q_T = C_d A \sqrt{\frac{2\Delta P}{\rho}}, \tag{19}$$

where A is the flow area and ρ is the density of the oil and then ΔP is the pressure difference.

Then, the flow continuity equations are

$$Q_v = Q_E + Q_T,$$

$$\frac{\omega \pi r d^2}{4} \tan\varphi \sin\alpha = \frac{V_0}{E}\frac{dP}{dt} + C_d A \sqrt{\frac{2\left(p - p_A\right)}{\rho}},$$

$$\frac{\omega \pi r d^2}{4} \tan\varphi \sin\alpha = \frac{V_0}{E}\frac{dP}{dt} + C_d A \sqrt{\frac{2\left(p - p_B\right)}{\rho}}, \tag{20}$$

$$\frac{\omega \pi r d^2}{4} \tan\varphi \sin\alpha = \frac{V_0}{E}\frac{dP}{dt} + C_d A \sqrt{\frac{2\left(p - p_T\right)}{\rho}}.$$

The pressure inside the plunger can be got by solving the equations above. Then, the friction torque can be obtained

by introducing the friction coefficient between the two kinds of materials. It should be noticed that the value of the friction torque maybe less than the value above because the oil film could be generated. However, it is reasonable to use this big value to design the robust controller because on one side the exact value with the influence of the oil film is difficult to calculate and the other side is that if the controller can be adaptive to the worst working condition, the controller should also work for other situations.

3. The Main Results

Consider the state-space model of the system with parameter uncertainties as follows:

$$\begin{aligned}\dot{\mathbf{x}}(t) &= (\mathbf{A}+\Delta\mathbf{A})\,\mathbf{x}(t)+(\mathbf{B}+\Delta\mathbf{B})\,\mathbf{u}(t)+\mathbf{w}(t),\\ \mathbf{z}_0(t) &= \mathbf{C}_0\mathbf{x}(t)+\mathbf{D}_0\mathbf{u}(t),\\ \mathbf{z}_1(t) &= \mathbf{C}_1\mathbf{x}(t)+\mathbf{D}_1\mathbf{u}(t),\end{aligned} \tag{21}$$

where $\mathbf{x}(t)$ is the state vector, $\mathbf{u}(t)$ is the control input, $\mathbf{w}(t)$ is the disturbance input, $\mathbf{z}_0(t)$, $\mathbf{z}_1(t)$ are the controlled outputs, $\mathbf{A}$, $\mathbf{B}$, $\mathbf{C}_0$, $\mathbf{D}_0$, $\mathbf{C}_1$, $\mathbf{D}_1$ are known constant matrices of appropriate dimensions, and $\Delta\mathbf{A}$, $\Delta\mathbf{B}$ are matrices of appropriate dimensions representing parameter uncertainties, which are supposed to be in the following form:

$$\begin{bmatrix}\Delta\mathbf{A} & \Delta\mathbf{B}\end{bmatrix} = \mathbf{D}\mathbf{F}(t)\begin{bmatrix}\mathbf{E}_1 & \mathbf{E}_2\end{bmatrix}, \tag{22}$$

where $\mathbf{D}$, $\mathbf{E}_1$, $\mathbf{E}_2$ are known real constant matrices and $\mathbf{F}(t)$ is an unknown real time-varying matrix with Lebesgue measurable elements satisfying

$$\mathbf{F}(t) \in \Omega_F := \{\mathbf{F}(t) : \|\mathbf{F}(t)\| \le \mathbf{I}\}. \tag{23}$$

Assume that the desired trajectory is $\mathbf{y}_d(t)$ and the error vector is defined as

$$\mathbf{e}(t) = \mathbf{y}(t) - \mathbf{y}_d(t) = \mathbf{x}(t) - \mathbf{y}_d(t), \tag{24}$$

and we can obtain $\mathbf{x}(t) = \mathbf{e}(t) + \mathbf{y}_d(t)$. Generalized error feedback control is used to be a control input:

$$\mathbf{u}(t) = \mathbf{K}\mathbf{e}(t) + \upsilon(t), \tag{25}$$

where $\upsilon(t) = \mathbf{B}^{+}(-\mathbf{A}\mathbf{y}_d(t)+\dot{\mathbf{y}}_d(t))$ and $\mathbf{B}^{+}$ is the pseudoinverse of matrix $\mathbf{B}$. According to above equations, the following equation can be obtained:

$$\dot{\mathbf{e}}(t) = \left(\overline{\mathbf{A}}+\overline{\mathbf{B}}\mathbf{K}\right)\mathbf{e}(t)+\mathbf{w}(t). \tag{26}$$

Define $\mathbf{u}_e = \mathbf{u}(t) - \upsilon(t)$; the cost function associated with the system (21) is

$$\mathbf{J}_e = \int_0^{\infty} \mathbf{e}^T(t)\,\mathbf{Q}\mathbf{e}(t) + \mathbf{u}_e^T(t)\,\mathbf{R}\mathbf{u}_e(t)\,dt, \tag{27}$$

where $\mathbf{Q}$ and $\mathbf{R}$ are the weighing positive matrices.

The purpose of this paper is to study an $\mathbf{H}_2/\mathbf{H}_\infty$ guaranteed cost control for all admissible uncertainties such that

(1) the closed-loop system is asymptotically stable;

(2) under zero initial condition, the closed-loop system guarantees that $\|\mathbf{z}\|_2 < \gamma\|\mathbf{w}\|_2$ for all nonzero $\mathbf{w} \in \mathbf{L}_2[0,\infty)$ and a prescribed scalar $\gamma > 0$;

(3) the input constraint (7) is satisfied.

For obtaining the main conclusions of this paper, the following lemma will be adopted to handle the parameter uncertainties in the system.

Lemma 1. *Given matrices with appropriate dimensions* $\mathbf{Y}$, $\mathbf{C}$, *and* $\mathbf{D}$ *and that* $\mathbf{Y}$ *is the symmetric matrix, then*

$$\mathbf{Y} + \mathbf{C}\mathbf{F}\mathbf{D} + \mathbf{D}^T\mathbf{F}^T\mathbf{C}^T < 0. \tag{28}$$

For all $\mathbf{F}$ satisfying $\mathbf{F}^T\mathbf{F} \le \mathbf{I}$, if and only if there exists a scalar $\varepsilon > 0$ such that

$$\mathbf{Y} + \varepsilon\mathbf{C}\mathbf{C}^T + \varepsilon^{-1}\mathbf{D}^T\mathbf{D} < 0. \tag{29}$$

Theorem 2. *Given constant* $\gamma > 0$, *if there exist scalars* $\alpha > 0$, $\beta > 0$, $\mathbf{P} = \mathbf{P}^T > 0$ *satisfying the following inequality:*

$$\begin{aligned}&(\mathbf{A}+\mathbf{B}\mathbf{K})^T\mathbf{P} + \mathbf{P}(\mathbf{A}+\mathbf{B}\mathbf{K}) + \mathbf{P}\left(\boldsymbol{\alpha}\mathbf{D}\mathbf{D}^T + \boldsymbol{\beta}\boldsymbol{\gamma}^{-2}\mathbf{B}_{\mathbf{w}}\mathbf{B}_{\mathbf{w}}^T\right)\mathbf{P}\\ &\quad + \boldsymbol{\alpha}^{-1}(\mathbf{E}_1+\mathbf{E}_2\mathbf{K})^T(\mathbf{E}_1+\mathbf{E}_2\mathbf{K})\\ &\quad + \boldsymbol{\beta}^{-1}(\mathbf{C}_1+\mathbf{D}_1\mathbf{K})^T(\mathbf{C}_1+\mathbf{D}_1\mathbf{K})\\ &\quad + (\mathbf{C}_0+\mathbf{D}_0\mathbf{K})^T(\mathbf{C}_0+\mathbf{D}_0\mathbf{K}) < 0,\end{aligned} \tag{30}$$

then the controller in the form of (25) *exists, such that*

(1) *the closed-loop system* (21) *with* $\mathbf{w}(t) = 0$ *is asymptotically stable;*

(2) *under zero initial condition, the closed-loop system guarantees that* $\|\mathbf{z}\|_2 < \gamma\|\mathbf{w}\|_2$ *for all nonzero* $\mathbf{w} \in \mathbf{L}_2[0,\infty)$ *and a prescribed scalar* $\gamma > 0$;

(3) *if* (30) *has a symmetric positive definite solution* $\mathbf{P}$, *then for all admissible parameter uncertainties,* $0 \le \overline{\mathbf{P}} \le \mathbf{P}$, *where* $\overline{\mathbf{P}} = \overline{\mathbf{P}}^T \ge 0$ *is a solution to Lyapunov equation:*

$$\begin{aligned}&\mathbf{P}\left(\mathbf{A}+\mathbf{D}\mathbf{F}(t)\left(\mathbf{E}_1+\mathbf{E}_2\mathbf{K}\right)\right)+\left(\mathbf{A}+\mathbf{D}\mathbf{F}(t)\left(\mathbf{E}_1+\mathbf{E}_2\mathbf{K}\right)\right)^T\\ &\quad + (\mathbf{C}_0+\mathbf{D}_0\mathbf{K})^T(\mathbf{C}_0+\mathbf{D}_0\mathbf{K}) = 0.\end{aligned} \tag{31}$$

Proof. From [23], it follows that system (21) with $\mathbf{w}(t) = 0$ is asymptotically stable and $\|\mathbf{z}\|_2 < \gamma\|\mathbf{w}\|_2$ if there exists a symmetric positive definite matrix $\overline{\mathbf{P}}$ such that

$$\begin{aligned}&\left(\mathbf{A}+\mathbf{B}\mathbf{K}+\mathbf{D}\mathbf{F}(t)\left(\mathbf{E}_1+\mathbf{E}_2\mathbf{K}\right)\right)^T\overline{\mathbf{P}}\\ &\quad + \overline{\mathbf{P}}\left(\mathbf{A}+\mathbf{B}\mathbf{K}+\mathbf{D}\mathbf{F}(t)\left(\mathbf{E}_1+\mathbf{E}_2\mathbf{K}\right)\right) + \boldsymbol{\gamma}^{-2}\overline{\mathbf{P}}\mathbf{B}_{\mathbf{w}}\mathbf{B}_{\mathbf{w}}^T\overline{\mathbf{P}}\\ &\quad + (\mathbf{C}_1+\mathbf{D}_1\mathbf{K})^T(\mathbf{C}_1+\mathbf{D}_1\mathbf{K}) < 0.\end{aligned} \tag{32}$$

The above inequality is equivalent to the fact that there exists a scalar $\beta > 0$ such that

$$\begin{aligned}&(\mathbf{A}+\mathbf{BK}+\mathbf{DF}(t)(\mathbf{E}_1+\mathbf{E}_2\mathbf{K}))^T\overline{\mathbf{P}}\\&\quad+\overline{\mathbf{P}}(\mathbf{A}+\mathbf{BK}+\mathbf{DF}(t)(\mathbf{E}_1+\mathbf{E}_2\mathbf{K}))\\&\quad+\boldsymbol{\gamma}^{-2}\overline{\mathbf{P}}\mathbf{B}_\mathbf{w}\mathbf{B}_\mathbf{w}^T\overline{\mathbf{P}}+(\mathbf{C}_1+\mathbf{D}_1\mathbf{K})^T(\mathbf{C}_1+\mathbf{D}_1\mathbf{K})\\&\quad+\boldsymbol{\beta}(\mathbf{C}_0+\mathbf{D}_0\mathbf{K})^T(\mathbf{C}_0+\mathbf{D}_0\mathbf{K})<0.\end{aligned}\tag{33}$$

Define $\mathbf{P}=\beta^{-1}\overline{\mathbf{P}}$; the above inequality can be described as

$$\begin{aligned}&(\mathbf{A}+\mathbf{BK})^T\mathbf{P}+\mathbf{P}(\mathbf{A}+\mathbf{BK})\\&\quad+\boldsymbol{\beta}\boldsymbol{\gamma}^{-2}\mathbf{P}\mathbf{B}_\mathbf{w}\mathbf{B}_\mathbf{w}^T\mathbf{P}+\boldsymbol{\beta}^{-1}(\mathbf{C}_1+\mathbf{D}_1\mathbf{K})^T(\mathbf{C}_1+\mathbf{D}_1\mathbf{K})\\&\quad+(\mathbf{C}_0+\mathbf{D}_0\mathbf{K})^T(\mathbf{C}_0+\mathbf{D}_0\mathbf{K})+\mathbf{PDF}(\mathbf{E}_1+\mathbf{E}_2\mathbf{K})\\&\quad+(\mathbf{E}_1+\mathbf{E}_2\mathbf{K})^T\mathbf{F}^T\mathbf{D}^T\mathbf{P}<0.\end{aligned}\tag{34}$$

According to Lemma 1, the above inequality holds for all $\mathbf{F}$ satisfying $\mathbf{F}^T\mathbf{F}\le\mathbf{I}$ if and only if there exists $\alpha>0$ such that

$$\begin{aligned}&(\mathbf{A}+\mathbf{BK})^T\mathbf{P}+\mathbf{P}(\mathbf{A}+\mathbf{BK})+\boldsymbol{\beta}\boldsymbol{\gamma}^{-2}\mathbf{P}\mathbf{B}_\mathbf{w}\mathbf{B}_\mathbf{w}^T\mathbf{P}\\&\quad+\boldsymbol{\beta}^{-1}(\mathbf{C}_1+\mathbf{D}_1\mathbf{K})^T(\mathbf{C}_1+\mathbf{D}_1\mathbf{K})\\&\quad+(\mathbf{C}_0+\mathbf{D}_0\mathbf{K})^T(\mathbf{C}_0+\mathbf{D}_0\mathbf{K})\\&\quad+\boldsymbol{\alpha}\mathbf{P}\mathbf{D}\mathbf{D}^T\mathbf{P}+\boldsymbol{\alpha}^{-1}(\mathbf{E}_1+\mathbf{E}_2\mathbf{K})^T(\mathbf{E}_1+\mathbf{E}_2\mathbf{K})<0.\end{aligned}\tag{35}$$

So, we obtain (30). Suppose that (30) has a symmetric positive definite solution $\mathbf{P}$, define

$$\begin{aligned}\boldsymbol{\Delta}=&\boldsymbol{\alpha}\mathbf{P}\mathbf{D}\mathbf{D}^T\mathbf{P}+\boldsymbol{\alpha}^{-1}(\mathbf{E}_1+\mathbf{E}_2\mathbf{K})^T(\mathbf{E}_1+\mathbf{E}_2\mathbf{K})\\&-\mathbf{PDF}(\mathbf{E}_1+\mathbf{E}_2\mathbf{K})-(\mathbf{E}_1+\mathbf{E}_2\mathbf{K})^T\mathbf{F}^T\mathbf{D}^T\mathbf{P}.\end{aligned}\tag{36}$$

According to [24] and considering $\|\mathbf{F}(t)\|\le\mathbf{I}$, it follows that $\boldsymbol{\Delta}\ge 0$; then subtracting

$$\begin{aligned}&\mathbf{P}(\mathbf{A}+\mathbf{DF}(t)(\mathbf{E}_1+\mathbf{E}_2\mathbf{K}))+(\mathbf{A}+\mathbf{DF}(t)(\mathbf{E}_1+\mathbf{E}_2\mathbf{K}))^T\\&\quad+(\mathbf{C}_0+\mathbf{D}_0\mathbf{K})^T(\mathbf{C}_0+\mathbf{D}_0\mathbf{K})=0\end{aligned}\tag{37}$$

from (30), we can get

$$\begin{aligned}&(\mathbf{A}+\mathbf{BK}+\mathbf{DF}(t)(\mathbf{E}_1+\mathbf{E}_2\mathbf{K}))^T(\mathbf{P}-\overline{\mathbf{P}})\\&\quad+(\mathbf{P}-\overline{\mathbf{P}})(\mathbf{A}+\mathbf{BK}+\mathbf{DF}(t)(\mathbf{E}_1+\mathbf{E}_2\mathbf{K}))\\&\quad+\boldsymbol{\beta}\boldsymbol{\gamma}^{-2}\mathbf{P}\mathbf{B}_\mathbf{w}\mathbf{B}_\mathbf{w}^T\mathbf{P}+\boldsymbol{\beta}^{-1}(\mathbf{C}_1+\mathbf{D}_1\mathbf{K})^T(\mathbf{C}_1+\mathbf{D}_1\mathbf{K})\\&\quad+\boldsymbol{\Delta}<0.\end{aligned}\tag{38}$$

Since $\boldsymbol{\beta}\boldsymbol{\gamma}^{-2}\mathbf{P}\mathbf{B}_\mathbf{w}\mathbf{B}_\mathbf{w}^T\mathbf{P}+\boldsymbol{\beta}^{-1}(\mathbf{C}_1+\mathbf{D}_1\mathbf{K})^T(\mathbf{C}_1+\mathbf{D}_1\mathbf{K})+\boldsymbol{\Delta}\ge 0$ and system (21) with $\mathbf{w}(t)=0$ is asymptotically stable according to the Lyapunov stability theory, we can get $\mathbf{P}-\overline{\mathbf{P}}\ge 0$ or $\overline{\mathbf{P}}\le\mathbf{P}$; then the proof is completed. □

If there exist two scalars $\alpha>0$, $\beta>0$ such that the matrix inequality (30) has a symmetric positive definite solution $\mathbf{P}$, then the closed-loop system is asymptotically stable for all admissible parameter uncertainties and satisfies an $\mathbf{H}_\infty$ disturbance attenuation constraint. In addition, this solution $\mathbf{P}$ will guarantee the worst $\mathbf{H}_2$ performance index that satisfies $\mathbf{J}_0(\mathbf{K})\le\mathbf{J}(\mathbf{K},\mathbf{P})=\mathrm{tr}(\mathbf{B}_\mathbf{w}^T\mathbf{P}\mathbf{B}_\mathbf{w})$. $\mathbf{J}(\mathbf{K},\mathbf{P})$ is considered as an $\mathbf{H}_2/\mathbf{H}_\infty$ guaranteed cost bound of the closed-loop system.

Theorem 3. *Given a constant $\gamma>0$, the system (21) is asymptotically stable and satisfies $\|\mathbf{z}\|_2<\gamma\|\mathbf{w}\|_2$ for any nonzero $\mathbf{w}\in\mathbf{L}_2[0,\infty)$, and the input constraint is guaranteed if there exist scalars $\alpha>0$, $\beta>0$, a symmetric positive definite matrix $\mathbf{X}$, and a matrix $\mathbf{W}$ satisfying*

$$\begin{bmatrix}\mathbf{V}&(\mathbf{E}_1\mathbf{X}+\mathbf{E}_2\mathbf{W})^T&(\mathbf{C}_1\mathbf{X}+\mathbf{D}_1\mathbf{W})^T&(\mathbf{C}_0\mathbf{X}+\mathbf{D}_0\mathbf{W})^T\\\mathbf{E}_1\mathbf{X}+\mathbf{E}_2\mathbf{W}&-\boldsymbol{\alpha}\mathbf{I}&0&0\\\mathbf{C}_1\mathbf{X}+\mathbf{D}_1\mathbf{W}&0&-\boldsymbol{\beta}\mathbf{I}&0\\\mathbf{C}_0\mathbf{X}+\mathbf{D}_0\mathbf{W}&0&0&-\mathbf{I}\end{bmatrix}<0,\tag{39}$$

$$\mathbf{e}_0^T\mathbf{P}\mathbf{e}_0\le\boldsymbol{\rho},\tag{40}$$

$$\begin{bmatrix}-\mathbf{I}&\sqrt{\rho}\mathbf{W}\\*&-\mathbf{u}_{\max}^2\mathbf{X}\end{bmatrix}<0,\tag{41}$$

where $\mathbf{V}=(\mathbf{A}\mathbf{X}+\mathbf{B}\mathbf{W})^T+\mathbf{A}\mathbf{X}+\mathbf{B}\mathbf{W}+\boldsymbol{\alpha}\mathbf{D}\mathbf{D}^T+\boldsymbol{\beta}\boldsymbol{\gamma}^{-2}\mathbf{B}_\mathbf{w}\mathbf{B}_\mathbf{w}^T$. In addition, if the above inequalities have a feasible solution $(\boldsymbol{\alpha},\boldsymbol{\beta},\mathbf{X},\mathbf{W})$, the state feedback controller can be given by $\mathbf{u}(t)=\mathbf{W}\mathbf{X}^{-1}\mathbf{e}(t)+\upsilon(t)$, and the $\mathbf{H}_2/\mathbf{H}_\infty$ guaranteed cost bound of the closed-loop system is described by $\mathbf{J}(\mathbf{K},\mathbf{X}^{-1})=\mathrm{tr}(\mathbf{B}_\mathbf{w}^T\mathbf{X}^{-1}\mathbf{B}_\mathbf{w})$.

Proof. It follows from Theorem 2 that there exists a controller $\mathbf{u}(t)=\mathbf{K}\mathbf{e}(t)+\upsilon(t)$ such that the design criteria (1) and (2) are satisfied if and only if there exist two scalars $\alpha>0$, $\beta>0$ and a symmetric positive definite matrix $\mathbf{P}$ which guarantees that the matrix inequality (30) holds. Pre- and postmultiplying

both sides of (30) by $\mathbf{P}^{-1}$ and using Schur's complement yield that (30) is equivalent to

$$\begin{bmatrix} \overline{\mathbf{V}} & \mathbf{P}^{-1}(\mathbf{E}_1\mathbf{X}+\mathbf{E}_2\mathbf{W})^T & \mathbf{P}^{-1}(\mathbf{C}_1\mathbf{X}+\mathbf{D}_1\mathbf{W})^T & \mathbf{P}^{-1}(\mathbf{C}_0\mathbf{X}+\mathbf{D}_0\mathbf{W})^T \\ (\mathbf{E}_1\mathbf{X}+\mathbf{E}_2\mathbf{W})\mathbf{P}^{-1} & -\boldsymbol{\alpha}\mathbf{I} & 0 & 0 \\ (\mathbf{C}_1\mathbf{X}+\mathbf{D}_1\mathbf{W})\mathbf{P}^{-1} & 0 & -\boldsymbol{\beta}\mathbf{I} & 0 \\ (\mathbf{C}_0\mathbf{X}+\mathbf{D}_0\mathbf{W})\mathbf{P}^{-1} & 0 & 0 & -\mathbf{I} \end{bmatrix} < 0, \tag{42}$$

where $\overline{\mathbf{V}} = \mathbf{P}^{-1}(\mathbf{A}+\mathbf{BK})^T + (\mathbf{A}+\mathbf{BK})\mathbf{P}^{-1} + \boldsymbol{\alpha}\mathbf{D}\mathbf{D}^T + \boldsymbol{\beta}\boldsymbol{\gamma}^{-2}\mathbf{B}_\mathbf{w}\mathbf{B}_\mathbf{w}^T$. Defining $\mathbf{X} = \mathbf{P}^{-1}$, $\mathbf{W} = \mathbf{K}\mathbf{P}^{-1}$, the matrix inequality (39) can be easily obtained from (42).

In addition, we will show that the input constraint is satisfied. Define $\mathbf{V} = \mathbf{e}^T\mathbf{P}\mathbf{e}$; we can easily know $\dot{\mathbf{V}} < 0$ and thus $\mathbf{e}^T\mathbf{P}\mathbf{e} \le \mathbf{e}_0^T\mathbf{P}\mathbf{e}_0$; we can also obtain

$$\begin{aligned} \max_{t>0}|\mathbf{u}(t)|^2 &< \max_{t>d(t)}\left\|\mathbf{e}^T(t)\mathbf{K}^T\mathbf{K}\mathbf{e}(t)\right\|_2 \\ &= \max_{t>d(t)}\left\|\mathbf{e}^T(t)\mathbf{P}^{1/2}\mathbf{P}^{-1/2}\mathbf{K}^T\mathbf{K}\mathbf{P}^{-1/2}\mathbf{P}^{1/2}\mathbf{e}(t)\right\|_2 \\ &< \rho\cdot\theta_{\max}\left(\mathbf{P}^{-1/2}\mathbf{K}^T\mathbf{K}\mathbf{P}^{-1/2}\right), \end{aligned} \tag{43}$$

where $\theta_{\max}(\cdot)$ shows the maximal eigenvalue. From the above inequality, the input constraint is established if $\boldsymbol{\rho}\mathbf{P}^{-1/2}\mathbf{K}^T\mathbf{K}\mathbf{P}^{-1/2} < \mathbf{u}_{\max}^2\mathbf{I}$. By Schur complements, the above inequality is equivalent to (41). This completes the proof. □

Theorem 3 provides a characterization of all controllers that guarantee the design criteria (1) and (2) to be achieved, and the controller $\mathbf{u}(t) = \mathbf{W}\mathbf{X}^{-1}\mathbf{e}(t) + \upsilon(t)$ provides a $\mathbf{H}_2/\mathbf{H}_\infty$ guaranteed cost bound $\mathrm{tr}(\mathbf{B}_\mathbf{w}^T\mathbf{X}^{-1}\mathbf{B}_\mathbf{w})$.

4. Simulation Results

According to (7) combined with the uncertain parameter, consider the system with the following state-space matrices:

$$\begin{aligned} \dot{x}(t) &= \begin{pmatrix} 0 & 1 & 0 \\ 0 & 0 & 0.0085 \\ 0 & -1.68e8 & -1.7 \end{pmatrix} x(t) \\ &+ \begin{pmatrix} 0 & 0 & 0 \\ 0 & 0 & 0 \\ 0 & -0.85e8 & -0.856 \end{pmatrix} x(t) \\ &+ \begin{bmatrix} 0 \\ 0 \\ 3.41e12 \end{bmatrix} u(t) + \begin{bmatrix} 0 \\ 0 \\ 1.71e12 \end{bmatrix} u(t) + \begin{bmatrix} 0 \\ -T_e - T_f \\ 0 \end{bmatrix} \\ z_0(t) &= \begin{bmatrix} 1 & 1 & 1 \end{bmatrix} x(t) + u(t) \\ z_1(t) &= \begin{bmatrix} 1 & 0 & 0 \end{bmatrix} x(t), \end{aligned} \tag{44}$$

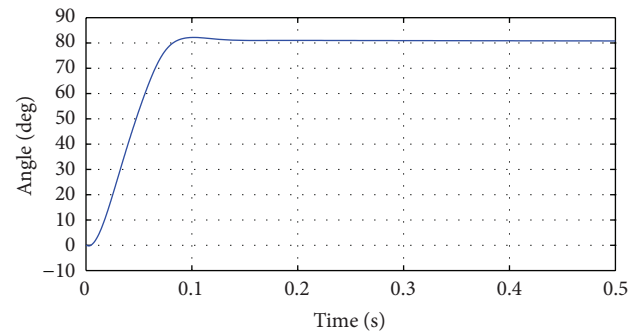

Figure 6: Step response of the PI control.

with

$$\mathbf{D} = \begin{bmatrix} 0 & 0 & 0 \\ 0 & 0 & 0 \\ 1 & 1 & 1 \end{bmatrix}, \quad \mathbf{E}_1 = \begin{bmatrix} 0 & 0 & 0 \\ 0 & 0 & 0 \\ 0 & -0.85e8 & -0.856 \end{bmatrix},$$

$$\mathbf{E}_2 = \begin{bmatrix} 0 \\ 0 \\ 1.71e12 \end{bmatrix}, \tag{45}$$

$$\mathbf{F} = \begin{bmatrix} r_1 & & \\ & r_2 & \\ & & s_1 \end{bmatrix}, \quad -1 \le r_1, r_2, s_1 \le 1.$$

The angle displacement control system of the port plate is simulated according to the result above and the comparison with the traditional PI control is conducted. During the working condition of HT, the port plate angle should change to meet the requirement of the servosystem. Hence, the extreme working condition is the period that the port plate angle is varying because the disturbance, which is the friction torque mainly, is varying greatly. The other working conditions are chosen as the step response to reveal the dynamic response. The model is constructed in Simulink and Figures 6–9 show the simulation result.

According to Figures 6 and 7, it can be found that the step responses of both the two control methods are fast to meet the practical requirement. PI control can get a faster response; however, the overshot is larger. The GCC does not show the obvious advantage to the PI control. This is because the friction torque disturbance acts the least influence compared with the changing working condition. Hence, the good performance can be got by adjusting PI coefficients. However, the coefficients should be changed corresponding to different

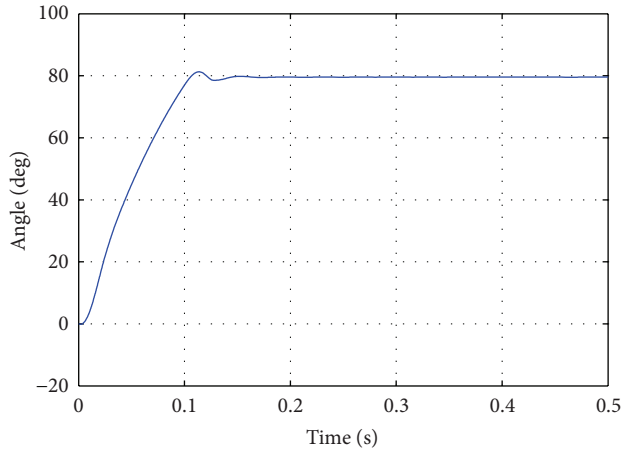

Figure 7: Step response of the GCC.

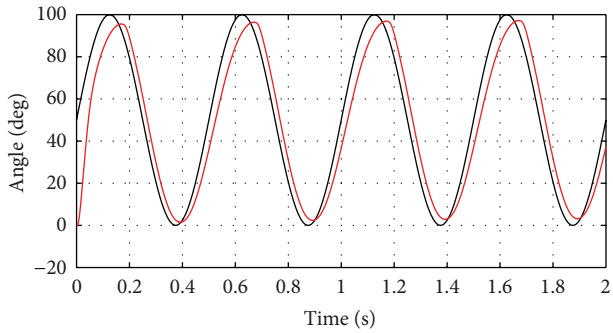

Figure 8: Sinusoidal signal response of the PI control.

loads, which is difficult in practice. This phenomenon can be explained by using sinusoidal response simulation. The sinusoidal signal responses are depicted by Figures 8 and 9. The black curve is the command signal and the red curve is the response. The GCC follows the command much better than the traditional PI control. The results can be shown clearly through Figures 10 and 11 which show the tracking error of the two control methods. The reason is mainly about the better robustness of the GCC. The improvement over the traditional PI control is dramatic.

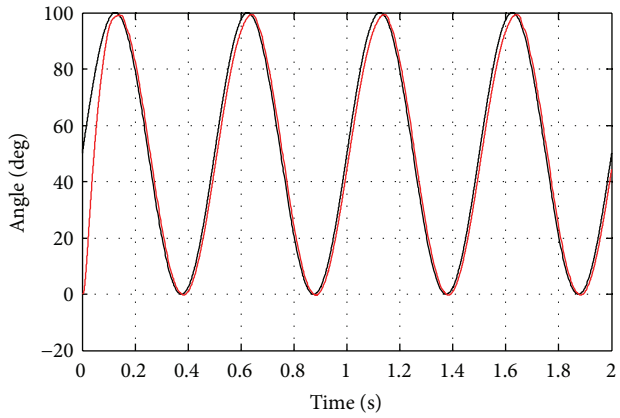

Figure 9: Sinusoidal signal response of the GCC.

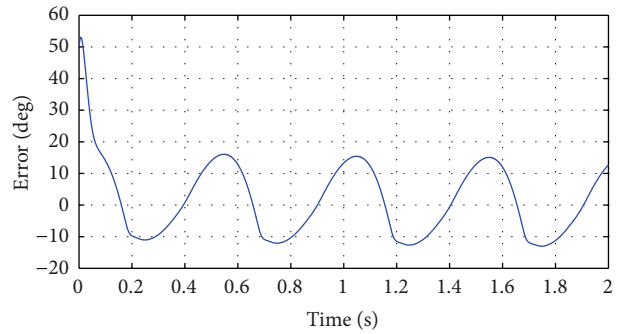

Figure 10: Tracking error of the PI control.

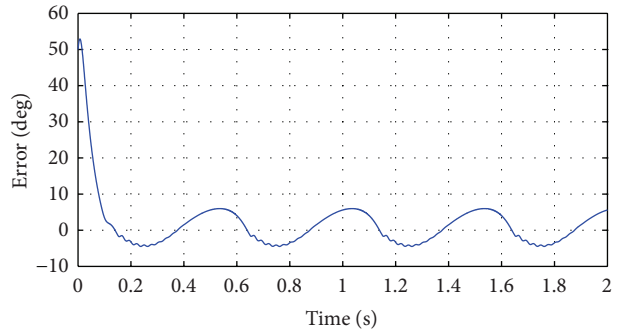

Figure 11: Tracking error of the GCC.

5. Conclusion

This paper is focused on the robust control for the port plate angle displacement control system with parameter uncertainties and load disturbance. The critical problem about the angle displacement control is analyzed and the main disturbance range is calculated by studying the stress relationship between the port plate and the cylinder. The analysis result shows that the friction torque is changing with different port plate angles, differential pressures, and the rotating speed. Furthermore, the guaranteed cost control for the system is designed. Simulation results show that both the GCC and PI control can get a good response under running the step response simulation. Especially, the GCC achieves much better robustness than PI control during the sinusoidal signal response simulation which is because the disturbance changes greatly is while the port plate is moving all the time. In order to prove the effectiveness of the proposed control method, the next step for this project is to construct the test rig.

Conflict of Interests

The authors declare that there is no conflict of interests regarding the publication of this paper.

Acknowledgments

The authors acknowledge the contribution of the National Natural Science Foundation of China (50875054, 51275123)

and open fund of State Key Laboratory of Fluid Power Transmission and Control, Zhejiang University (GZKF-2008003).

References

[1] I. Y. Jong, K. K. Ahn, and Q. T. Dinh, "A study on an energy saving electro-hydraulic excavator," in *Proceedings of the ICROS-SICE International Joint Conference (ICCAS-SICE '09)*, pp. 3825–3830, August 2009.

[2] J. Yang, L. Quan, and Y. Yang, "Excavator energy-saving efficiency based on diesel engine cylinder deactivation technology," *Chinese Journal of Mechanical Engineering*, vol. 25, no. 5, pp. 897–904, 2012.

[3] T. Lin, Q. Wang, B. Hu, and W. Gong, "Development of hybrid powered hydraulic construction machinery," *Automation in Construction*, vol. 19, no. 1, pp. 11–19, 2010.

[4] H. Kim, J. Choi, and K. Yi, "Development of supervisory control strategy for optimized fuel consumption of the compound hybrid excavator," *Journal of Automobile Engineering*, vol. 226, no. 12, pp. 1652–1666, 2012.

[5] K. K. Ahn, H. O. TH, and Q. T. Dinh, "A study on energy saving potential of hydraulic on energy saving potential of hydraulic control system using switching type closed loop constant pressure system," in *Proceedings of the 7th JFPS International Symposium on Fluid Power*, pp. 317–322, 2008.

[6] Q. Xiao, Q. Wang, and Y. Zhang, "Control strategies of power system in hybrid hydraulic excavator," *Automation in Construction*, vol. 17, no. 4, pp. 361–367, 2008.

[7] S. Sgro, M. Inderelst, and H. Murrenhoff, "Energy efficiency of mobile working machines," in *Proceedings of the 7th International Fluid Power Conference*, 2010.

[8] J. Jiang, A. Yu, and W. Shen, "The review of full hydraulic hybrid excavator based on common pressure rail network," *Chinese Hydraulics and Pneumatics*, vol. 9, pp. 44–49, 2010.

[9] P. Achten, G. Vael, H. Murrenhoff, T. Kohmäscher, and M. Inderelst, "Low-emission hydraulic hybrid for passenger cars," *Automobiltechnische Zeitschrift*, vol. 111, pp. 378–384, 2009.

[10] W. Shen and J. Jiang, "Analysis and development of the hydraulic secondary regulation system based on the CPR," in *Proceedings of the International Conference on Fluid Power and Mechatronics (FPM '11)*, pp. 117–122, August 2011.

[11] P. A. J. Achten, G. E. M. Vael, and F. Zhao, "The Innas hydraulic transformer—the key to the hydrostatic common pressure rail," SAE paper 2000-01-2561.

[12] W. Shen and J.-H. Jiang, "Analysis of energy recovery efficiency of hydraulic hybrid excavator," *Journal of South China University of Technology*, vol. 40, no. 1, pp. 82–87, 2012.

[13] P. A. J. Achten, F. Zhao, and G. E. M. Vael, "Transforming future hydraulics: a new design of a hydraulic transformer," in *Proceedings of the The 5th Scandinavian International Conference on Fluid Power*, 1997.

[14] W. Shen, J. Jiang, X. Su, and H. R. Karimi, "Energy-saving analysis of hydraulic hybrid excavator based on common pressure rail," *The Scientific World Journal*, vol. 2013, Article ID 560694, 12 pages, 2013.

[15] H. Zhang, Y. Shi, and A. Saadat Mehr, "Robust static output feedback control and remote PID design for networked motor systems," *IEEE Transactions on Industrial Electronics*, vol. 58, no. 12, pp. 5396–5405, 2011.

[16] H. Li, H. Liu, H. Gao, and P. Shi, "Reliable fuzzy control for active suspension systems with actuator delay and fault," *IEEE Transactions on Fuzzy Systems*, vol. 20, no. 2, pp. 342–357, 2012.

[17] Z. Wang, D. W. C. Ho, Y. Liu, and X. Liu, "Robust H_∞ control for a class of nonlinear discrete time-delay stochastic systems with missing measurements," *Automatica*, vol. 45, no. 3, pp. 684–691, 2009.

[18] J. Jiang, Y. Han, and D. Wang, "The intelligent PID control in Hydrostatic drive system with secondary regulation," *Journal of Harbin Institute of Technology*, vol. 30, pp. 36–38, 1998.

[19] H. Li, J. Yu, C. Hilton, and H. Liu, "Adaptive sliding mode control for nonlinear active suspension vehicle systems using T-S fuzzy approach," *IEEE Transactions on Industrial Electronics*, vol. 60, no. 8, pp. 3328–3338, 2013.

[20] C. S. Kim and C. O. Lee, "Robust speed control of a variable-displacement hydraulic motor considering saturation nonlinearity," *Journal of Dynamic Systems, Measurement and Control, Transactions of the ASME*, vol. 122, no. 1, pp. 196–201, 2000.

[21] W. Shen, J. Jiang, and H. R. Karimi, "Observer-based robust control for hydraulic velocity control system," *Mathematical Problems in Engineering*, vol. 2013, Article ID 689132, 9 pages, 2013.

[22] S. Zhou and W. X. Zheng, "Robust H_∞ control of delayed singular systems with linear fractional parametric uncertainties," *Journal of the Franklin Institute*, vol. 346, no. 2, pp. 147–158, 2009.

[23] A. Kato and K. Ohnishi, "Robust force sensorless control in motion control system," in *Proceedings of the 9th IEEE International Workshop on Advanced Motion Control*, pp. 165–170, March 2006.

[24] H. Zhang, J. Wang, and Y. Wang, "Robust filtering for ammonia coverage estimation in Diesel engine selective catalytic reduction (SCR) Systems," *ASME Transactions, Journal of Dynamic Systems, Measurement, and Control*, vol. 135, no. 6, Article ID 064504, 7 pages, 2013.

[25] S. Xu and J. Lam, "Guaranteed cost control," *Lecture Notes in Control and Information Science*, vol. 332, pp. 107–118, 2006.

[26] S. O. R. Moheimani and I. R. Petersen, "Optimal guaranteed cost control of uncertain systems via static and dynamic output feedback," *Automatica*, vol. 32, no. 4, pp. 575–579, 1996.

[27] J. Doyle, K. Zhou, K. Glover, and B. Bodenheimer, "Mixed H_2 and H_∞ performance objectives II: optimal control," *IEEE Transactions on Automatic Control*, vol. 39, no. 8, pp. 1575–1587, 1994.

[28] J. Abedor, K. Nagpal, P. P. Khargonekar, and K. Poolla, "Robust regulation in the presence of norm-bounded uncertainty," *IEEE Transactions on Automatic Control*, vol. 40, no. 1, pp. 147–153, 1995.

[29] J. Ren and Q. Zhang, "Robust normalization and guaranteed cost control for a class of uncertain descriptor systems," *Automatica*, vol. 48, pp. 1693–1697, 2012.

[30] H. Mukaidani, "An LMI approach to guaranteed cost control for uncertain delay systems," *IEEE Transactions on Circuits and Systems I*, vol. 50, no. 6, pp. 795–800, 2003.

[31] P. A. J. Achten and J. O. Palmberg, "What a difference a hole makes: the commercial value of the innas hydraulic transformer," in *Proceedings of the 6th Scandinavian International Conference on Fluid Power*, pp. 873–886, 1999.

Hindawi Publishing Corporation
Mathematical Problems in Engineering
Volume 2013, Article ID 159279, 12 pages
http://dx.doi.org/10.1155/2013/159279

Research Article

Robust and Passive Constrained Fuzzy Control for Discrete Fuzzy Systems with Multiplicative Noises and Interval Time Delay

Wen-Jer Chang,[1] Cheung-Chieh Ku,[1] and Zong-Guo Fu[2]

[1] *Department of Marine Engineering, National Taiwan Ocean University, Keelung 202, Taiwan*
[2] *School of Naval Architecture and Marine Engineering, Zhejiang Ocean University, Zhoushan, Zhejiang 316022, China*

Correspondence should be addressed to Wen-Jer Chang; wjchang@mail.ntou.edu.tw

Received 18 August 2013; Accepted 1 November 2013

Academic Editor: Baoyong Zhang

The passive fuzzy control for discrete-time uncertain Takagi-Sugeno (T-S) fuzzy models with multiplicative noises and time delay is investigated subject to robust asymptotical stability. Applying Jensen's inequality and free-weighting matrix technique, less conservative sufficient conditions are derived via choosing Lyapunov function to analyze and synthesize the robust asymptotical stability and passivity of closed-loop system. The derived conditions are not strictly linear matrix inequality (LMI) problems, thus the cone complementarity technique is employed to propose a suboptimal technique to solve the proposed nonstrictly LMI problems. An algorithm is developed in this paper to design the fuzzy controller which can be accomplished by state-feedback scheme or output-feedback scheme. Finally, numerical examples are provided to demonstrate the feasibility and applicability of the proposed fuzzy controller design technique.

1. Introduction

The delay-dependent stability analysis and synthesis of T-S fuzzy model with time delay has been extensively discussed in [1–4]. The time delay is an inherent and unavoidable effect on many practical dynamic nonlinear systems. In literature, the stability conditions of T-S fuzzy model with time delay were derived in terms of LMI problem [5] that can be solved by convex optimization technique. Furthermore, many relaxed techniques have been proposed to extend the maximum allowable delay range. For example, the piecewise Lyapunov function technique, fuzzy Lyapunov function approach, and free-weighting matrix approach have been used in [6–10] to reduce the conservatism of stability and stabilization problems for T-S fuzzy model with time delay. Although the conservatism of concerned problems can be decreased by such approaches, too many variables are needed to be found for satisfying their stability conditions. It is known that the complications of control synthesis and computational demands are increasing when the number of free variables is increased. Hence, the less conservative stability criteria with few free variables for dealing with T-S fuzzy model with time delay are worth to be discussed and investigated.

As well known, the performance requirement is the most important issue in the stability analysis and synthesis of control systems. For attenuating the effect of the external disturbance on systems, many efforts [11–17] proposed useful techniques such that the attenuation performance of system can be achieved. From [17], it can be found that the dissipativity and its particular case of passivity can be defined as H_∞ performance constraint, positive real performance constraint, strictly input passive performance constraint, strictly output passive performance constraint, and strictly vary passive performance constraint by setting different power supply function [18]. Based on the power supply function, the passivity theory proposes a general and elastic tool for dealing with the effect of disturbance on the systems. On the other hand, uncertainty is often an existing phenomenon which is caused by modeling errors and internal perturbations. Generally, the parameter uncertainties of system are considered as norm-bounded time-varying function [1, 2, 12]. Considering

external disturbances and uncertainties, the robust stability and passivity become important performances of control systems.

Recently, the stochastic systems have received much attention based on the stochastic modeling approach [19]. Therefore, many efforts have been devoted to expand the stability criteria [20, 21] from deterministic systems to stochastic ones. Applying the fuzzy modeling approach, the nonlinear stochastic systems can be approximated by blending linear stochastic subsystems with corresponding membership functions. In literature [22–27], the nonlinear stochastic systems were represented by T-S fuzzy models in which the consequent part is structured by Itô stochastic differential equations. Since the consequent part of stochastic fuzzy mode belongs to linear stochastic systems, the Itô formula can also be employed to analyze the stability of stochastic T-S fuzzy systems. And then, the parallel distributed compensation (PDC) technique [17] was employed to design the fuzzy controller such that stability of nonlinear stochastic system is achieved. In case of continuous-time T-S fuzzy model, the delay-dependent stability and stabilization problems were studied in [23], robust fuzzy controller problems were discussed in [24–26], and robust fuzzy filtering design problem was addressed in [27, 28]. However, only few efforts [29–32] have been proposed for solving the stability and stabilization problems of discrete-time stochastic nonlinear systems.

From the above motivations, the fuzzy controller design of discrete uncertain T-S fuzzy model with multiplicative noise and time delay is investigated in this paper subject to passivity and robust asymptotical stability. The time delay effect is concerned as an interval time-varying delay [9] in this paper. Based on the discrete type Jensen inequality [33] and free-weighting matrix technique, the less conservative sufficient conditions are derived via Lyapunov function to achieve the robust asymptotical stability. In addition, the passivity theory is applied to discuss the external disturbance effect on the system. While deriving the conditions, none of the model transportation is used to avoid the potential conservatism of stability criteria in time delay systems. Since the proposed sufficient conditions belong to nonstrictly LMI problems, an algorithm based on cone complementarity technique [34] is developed in this paper. With the proposed algorithm, the feasible solutions of the conditions and allowable maximum upper bound of interval time-varying delay can be found by LMI technique. The main contributions of this paper can be summarized as follows. (1) Achieving passivity performance constraint, a robust fuzzy controller is developed in this paper for discrete uncertain T-S fuzzy model with multiplicative noise and time delay. (2) Comparing previous researches, the proposed fuzzy control method provides less conservatism because it can find bigger allowable maximum upper bound of time delay and its less desired unknown variables reduce the mathematical complexity. At last, two numerical examples are employed to demonstrate the effectiveness and application of the proposed design method.

Notation. The following notations are applied throughout this paper. The $\mathrm{tr}(\mathbf{A})$ denotes the trace of matrix $\mathbf{A}$. The $\mathbf{I}$ is identity matrix with appropriate dimension. The $\mathrm{diag}\{\cdots\}$ means block-diagonal matrix. The * denotes the transposed elements of matrices for symmetric position. The $E\{Q(\cdot)\}$ denotes the expected value of function $Q(\cdot)$. Moreover, let $(\Omega, \mathscr{F}, \{\mathscr{F}_t\}_{t\geq 0}, \mathscr{P})$ be a complete probability space with filtration $\{\mathscr{F}_t\}_{t\geq 0}$ satisfying the usual conditions (i.e., the filtration contains all $\mathscr{P}$-null sets and is right continuous).

2. System Description and Problem Statement

Applying the fuzzy modeling approach, the nonlinear stochastic systems can be represented by the T-S fuzzy model with multiplicative noise. Hence, the uncertain T-S fuzzy model with interval time-varying delay and multiplicative noise can be structured as follows:

$$x(k+1) = \sum_{i=1}^{r} h_i(\theta(k)) \left\{ f_i(k) + \overline{f}_i(k)\beta(k) \right\}, \tag{1a}$$

$$z(k) = \sum_{i=1}^{r} h_i(\theta(k)) \left\{ \mathbf{C}_{1i}x(k) + \mathbf{C}_{di}x(k-\tau(k)) + \mathbf{D}_i v(k) \right\}, \quad i = 1, 2, \ldots, r, \tag{1b}$$

$$y(k) = \sum_{i=1}^{r} h_i(\theta(k)) \left\{ \mathbf{C}_{2i}x(k) \right\}, \tag{1c}$$

$$x(k) = \varphi(k), \quad k = 0, -1, \ldots, -\tau(k), \tag{1d}$$

where

$$\begin{aligned} f_i(k) = {} & \left(\mathbf{A}_i + \Delta\mathbf{A}_i\right) x(k) + \left(\mathbf{A}_{di} + \Delta\mathbf{A}_{di}\right) x(k-\tau(k)) \\ & + \left(\mathbf{B}_i + \Delta\mathbf{B}_i\right) u(k) + \left(\mathbf{E}_i + \Delta\mathbf{E}_i\right) v(k), \end{aligned} \tag{2a}$$

$$\begin{aligned} \overline{f}_i(k) = {} & \left(\overline{\mathbf{A}}_i + \overline{\Delta}\,\overline{\mathbf{A}}_i\right) x(k) + \left(\overline{\mathbf{A}}_{di} + \overline{\Delta}\,\overline{\mathbf{A}}_{di}\right) x(k-\tau(k)) \\ & + \left(\overline{\mathbf{B}}_i + \overline{\Delta}\,\overline{\mathbf{B}}_i\right) u(k) + \left(\overline{\mathbf{E}}_i + \overline{\Delta}\,\overline{\mathbf{E}}_i\right) v(k). \end{aligned} \tag{2b}$$

Besides, $\sum_{i=1}^{r} h_i(\theta(k)) = 1$, $h_i(\theta(k)) \geq 0$ is the grade of membership function, $\theta(k)$ is the set of premise variables, r is the number of fuzzy rules, and $\mathbf{A}_i$, $\mathbf{A}_{di}$, $\mathbf{B}_i$, $\mathbf{E}_i$, $\overline{\mathbf{A}}_i$, $\overline{\mathbf{A}}_{di}$, $\overline{\mathbf{B}}_i$, $\overline{\mathbf{E}}_i$, $\mathbf{C}_{1i}$, $\mathbf{C}_{2i}$, $\mathbf{C}_{di}$ and $\mathbf{D}_i$ are known constant matrices with appropriate dimensions. $x(k) \in \mathfrak{R}^{n_x}$, $x(k-\tau(k)) \in \mathfrak{R}^{n_x}$, $u(k) \in \mathfrak{R}^{n_u}$, $z(k) \in \mathfrak{R}^{n_z}$, $y(k) \in \mathfrak{R}^{n_z}$, $v(k) \in \mathfrak{R}^{n_z}$, and $\varphi(k)$ are state vector, state delay vector, controller input vector, controlled output vector, measurable output vector, external disturbance input vector, and initial condition, respectively. In addition, the $\beta(k)$ denotes standard scalar discrete Wiener process (Brownian motion) [19] on $(\Omega, \mathscr{F}, \mathscr{P})$ with $E\{\beta(k)\} = 0$ and $E\{\beta^2(k)\} = 1$. The time-varying delay $\tau(k)$ is a positive integer and satisfies $\tau_{\min} \leq \tau(k) \leq \tau_{\max}$. Here, $\tau_{\min}$ and $\tau_{\max}$ are known lower and upper bounds of delay,

respectively. Moreover, $\Delta\mathbf{A}_i$, $\Delta\mathbf{A}_{di}$, $\Delta\mathbf{B}_i$, $\Delta\mathbf{E}_i$, $\overline{\Delta}\,\overline{\mathbf{A}}_i$, $\overline{\Delta}\,\overline{\mathbf{A}}_{di}$, $\overline{\Delta}\,\overline{\mathbf{B}}_i$, and $\overline{\Delta}\,\overline{\mathbf{E}}_i$ are defined as follows:

$$\begin{bmatrix} \Delta\mathbf{A}_i & \Delta\mathbf{A}_{di} & \Delta\mathbf{B}_i & \Delta\mathbf{E}_i \\ \overline{\Delta}\,\overline{\mathbf{A}}_i & \overline{\Delta}\,\overline{\mathbf{A}}_{di} & \overline{\Delta}\,\overline{\mathbf{B}}_i & \overline{\Delta}\,\overline{\mathbf{E}}_i \end{bmatrix} = \begin{bmatrix} \mathbf{H}_i & 0 \\ 0 & \overline{\mathbf{H}}_i \end{bmatrix} \begin{bmatrix} \Delta(k) & 0 \\ 0 & \overline{\Delta}(k) \end{bmatrix} \begin{bmatrix} \mathbf{R}_i & \mathbf{R}_{di} & \mathbf{R}_{Bi} & \mathbf{R}_{Ei} \\ \overline{\mathbf{R}}_i & \overline{\mathbf{R}}_{di} & \overline{\mathbf{R}}_{Bi} & \overline{\mathbf{R}}_{Ei} \end{bmatrix}, \tag{3}$$

where $\mathbf{H}_i$, $\overline{\mathbf{H}}_i$, $\mathbf{R}_i$, $\mathbf{R}_{di}$, $\mathbf{R}_{Bi}$, $\mathbf{R}_{Ei}$, $\overline{\mathbf{R}}_i$, $\overline{\mathbf{R}}_{di}$, $\overline{\mathbf{R}}_{Bi}$, and $\overline{\mathbf{R}}_{Ei}$ are known constant matrices and $\Delta(k)$ and $\overline{\Delta}(k)$ are unknown time-varying function with $\Delta(k)\Delta(k) \le \mathbf{I}$ and $\overline{\Delta}(k)\overline{\Delta}(k) \le \mathbf{I}$. In the following statements, the $h_i(\theta(k))$, $\Delta(k)$, and $\overline{\Delta}(k)$ are denoted as $\widehat{h}_i$, Δ, and $\overline{\Delta}$, respectively, for simplifying the context of this paper.

With state-feedback control scheme, the PDC-based fuzzy controller can be designed as follows:

$$u(k) = \sum_{i=1}^{r} \widehat{h}_i \left(\mathbf{F}_i x(k)\right). \tag{4}$$

Substituting (4) into (1a), the closed-loop uncertain T-S fuzzy model with interval time-varying delay and multiplicative noise can be inferred as follows:

$$\begin{aligned} & x(k+1) \\ &= \sum_{i=1,j=1}^{r} \widehat{h}_i\widehat{h}_j \left\{\left(\mathbf{f}_{ij} + \mathbf{H}_i\Delta\mathbf{f}_{Rij} + \left(\overline{\mathbf{f}}_{ij} + \overline{\mathbf{H}}_i\overline{\Delta}\,\overline{\mathbf{f}}_{Rij}\right)\beta(k)\right)\xi(k)\right\} \\ &= \sum_{i=1}^{r}\sum_{j=1}^{r} \widehat{h}_i\widehat{h}_j \left\{\frac{1}{2}\left(\mathbf{f}_{ij} + \mathbf{H}_i\Delta\mathbf{f}_{Rij} + \mathbf{f}_{ji} + \mathbf{H}_j\Delta\mathbf{f}_{Rji}\right.\right. \\ &\qquad \left.\left. + \left(\overline{\mathbf{f}}_{ij} + \overline{\mathbf{H}}_i\overline{\Delta}\,\overline{\mathbf{f}}_{Rij} + \overline{\mathbf{f}}_{ji} + \overline{\mathbf{H}}_j\overline{\Delta}\,\overline{\mathbf{f}}_{Rji}\right)\beta(k)\right)\xi(k)\right\}, \end{aligned} \tag{5}$$

where

$$\begin{aligned} \xi(k) &= \left[x^T(k) \;\; x^T(k-\tau(k)) \;\; v^T(k) \;\; x^T(k-\tau_{\max}) \;\; x^T(k-\tau_{\min}) \;\; \eta(k)\right], \\ \mathbf{f}_{ij} &= \left[\mathbf{G}_{ij} \;\; \mathbf{A}_{di} \;\; \mathbf{E}_i \;\; 0_{1\times 3}\right], \\ \overline{\mathbf{f}}_{ij} &= \left[\overline{\mathbf{G}}_{ij} \;\; \overline{\mathbf{A}}_{di} \;\; \overline{\mathbf{E}}_i \;\; 0_{1\times 3}\right], \\ \mathbf{f}_{Rij} &= \left[\mathbf{R}_{ij} \;\; \mathbf{R}_{di} \;\; \mathbf{R}_{Ei} \;\; 0_{1\times 3}\right], \\ \overline{\mathbf{f}}_{Rij} &= \left[\overline{\mathbf{R}}_{ij} \;\; \overline{\mathbf{R}}_{di} \;\; \overline{\mathbf{R}}_{Ei} \;\; 0_{1\times 3}\right], \\ \mathbf{G}_{ij} &= \mathbf{A}_i + \mathbf{B}_i\mathbf{F}_j, \qquad \overline{\mathbf{G}}_{ij} = \overline{\mathbf{A}}_i + \overline{\mathbf{B}}_i\mathbf{F}_j, \\ \mathbf{R}_{ij} &= \mathbf{R}_i + \mathbf{R}_{Bi}\mathbf{F}_j, \qquad \overline{\mathbf{R}}_{ij} = \overline{\mathbf{R}}_i + \overline{\mathbf{R}}_{Bi}\mathbf{F}_j, \\ \eta(k) &= x(k) - x(k-\tau(k)). \end{aligned} \tag{6}$$

For deriving the stability criteria of this paper, the following definitions and lemmas are necessary to be introduced. Based on the energy concept, the passivity theory provides a useful tool to discuss the effect of external disturbance for achieving attenuation performance. Here, the passivity property is introduced in the following definition.

Definition 1 (see [18]). If there exist constant matrices $\mathbf{S}_1$, $\mathbf{S}_2$, and $\mathbf{S}_3$ for satisfying the following inequality, then the closed-loop system (5) is called passive with the disturbance $v(k)$ and controlled output $z(k)$ for all terminal time $k_q > 0$:

$$\begin{aligned} & E\left\{2\sum_{k=0}^{k_q} z^T(k)\,\mathbf{S}_1 v(k)\right\} \\ &\qquad > E\left\{\sum_{k=0}^{k_q} z^T(k)\,\mathbf{S}_2 z(k) + \sum_{k=0}^{k_q} v^T(k)\,\mathbf{S}_3 v(k)\right\}. \end{aligned} \tag{7}$$

Via the well-known mathematical definition of power supply function [18], the passivity theory includes several performance constraints with setting matrices $\mathbf{S}_1$, $\mathbf{S}_2$, and $\mathbf{S}_3$. In this paper, the generalized power supply function (7) is proposed to be the constraint index. Besides, for illustrating the concerned stability concept clearly, the following definition is introduced.

Definition 2 (see [19]). For the closed-loop system (5) without external disturbance input, that is, $v(k) = 0$, the solution with admissible uncertainties is robustly asymptotically stable in the mean square if $E\{x(k)\}$ and state correlation matrix $E\{x^T(k)x(k)\}$ converge to zero as $t \to \infty$.

For analyzing the uncertainties of systems, the following lemma is proposed to convert the uncertain matrices into deterministic matrices.

Lemma 3 (see [26]). *Given real compatible dimension matrices* $\mathbf{A}$, $\mathbf{H}$, *and* $\mathbf{R}$ *for any matrix* $\mathbf{X} > 0$, $\varepsilon > 0$, Δ *with* $\Delta^T\Delta \le \mathbf{I}$, *one can find the following results:*

$$\begin{aligned} & (\mathbf{A} + \mathbf{H}\Delta\mathbf{R})^T\mathbf{X}(\mathbf{A} + \mathbf{H}\Delta\mathbf{R}) \\ &\qquad \le \mathbf{A}^T\left(\mathbf{X}^{-1} - \varepsilon\mathbf{H}\mathbf{H}^T\right)^{-1}\mathbf{A} + \varepsilon^{-1}\mathbf{R}^T\mathbf{R}, \end{aligned} \tag{8}$$

where $\mathbf{X}^{-1} - \varepsilon\mathbf{H}\mathbf{H}^T > 0$.

In this paper, the following discrete type Jensen inequality is employed to derive the less conservative sufficient conditions.

Lemma 4 (see [33]). *For any compatible constant matrices* $\mathbf{Q} = \mathbf{Q}^T > 0$, *scalars* $\tau_{\min} > 0$ *and* $\tau_{\max} > 0$ *satisfying* $\tau_{\min} < \tau_{\max}$ *and vector function* $\varpi : [\tau_{\min}, \tau_{\min}+1, \ldots, \tau_{\max}] \to \Re^{n_x}$ *such that the following sums are well defined, it holds that*

$$\begin{aligned} & -(\tau_{\max} - \tau_{\min} + 1)\sum_{k=\tau_{\min}}^{\tau_{\max}} \varpi^T(k)\,\mathbf{Q}\,\varpi(k) \\ &\qquad \le -\left(\sum_{k=\tau_{\min}}^{\tau_{\max}} \varpi(k)\right)^T \mathbf{Q} \sum_{k=\tau_{\min}}^{\tau_{\max}} \varpi(k). \end{aligned} \tag{9}$$

From the above definitions and lemmas, the sufficient conditions are derived in the following section for guaranteeing the robust asymptotical stability and passivity of closed-loop system (5).

3. Stabilization Criteria and Robust Fuzzy Controller Design

In this section, the stability criteria for closed-loop system (5) are derived with both of state-feedback control scheme and output-feedback control scheme. The sufficient conditions derived in this paper are nonstrictly LMI problems. In order to solve the proposed nonstrictly LMI problems, an algorithm is also developed in this section.

Theorem 5. *Given performance parameters* $\mathbf{S}_1$, $\mathbf{S}_2 \geq 0$, *and* $\mathbf{S}_3$; *positive scalars* $\tau_{\min} > 0$ *and* $\tau_{\max} > 0$, *if there exist positive definite matrices* $\mathbf{P}_1 > 0$, $\mathbf{P}_2 > 0$, $\mathbf{P}_3 > 0$, $\mathbf{P}_4 > 0$, *and* $\mathbf{P}_5 > 0$, *any matrices* $\mathbf{N}_1$, $\mathbf{N}_2$, *and* $\mathbf{N}_3$, *scalars* $\varepsilon_{ij} > 0$ *and* $\bar{\varepsilon}_{ij} > 0$, *and state-feedback gains* $\mathbf{F}_i$ *for satisfying the following conditions, then the closed-loop system* (5) *is passive and robustly asymptotically stable in the mean square:*

$$\mathbf{\Phi} < 0 \quad \text{for } i, j \leq r, \tag{10}$$

where

$$\mathbf{\Phi} = \begin{bmatrix} \mathbf{\Phi}_{11ij} & \mathbf{\Phi}_{12} & \mathbf{\Phi}_{13} & \mathbf{\Phi}_{14} & \mathbf{\Phi}_{15} \\ * & \mathbf{\Phi}_{22} & 0 & 0 & 0 \\ * & * & \mathbf{\Phi}_{33} & 0 & 0 \\ * & * & * & \mathbf{\Phi}_{44} & 0 \\ * & * & * & * & \mathbf{\Phi}_{55} \end{bmatrix}, \tag{11}$$

$$\begin{aligned}
\mathbf{\Phi}_{11ij} &= \overline{\mathbf{\Phi}} + \frac{1}{2}\left(\mathbf{W}_{ij} + \mathbf{W}_{ji}\right), \\
\mathbf{\Phi}_{12} &= \frac{1}{2}\left[\mathbf{\Phi}_{12ij} \quad \mathbf{\Phi}_{12ji}\right], \qquad \mathbf{\Phi}_{13} = \sqrt{\tau_{\max}}\mathbf{\Phi}_{12}, \\
\mathbf{\Phi}_{14} &= \frac{1}{2}\left[\mathbf{\Phi}_{14ij} \quad \mathbf{\Phi}_{14ji}\right], \qquad \mathbf{\Phi}_{15} = \sqrt{\tau_{\max}}\mathbf{\Phi}_{14}, \\
\mathbf{\Phi}_{22} &= \operatorname{diag}\left\{\mathbf{\Phi}_{22ij}, \mathbf{\Phi}_{22ji}\right\}, \qquad \mathbf{\Phi}_{33} = \operatorname{diag}\left\{\mathbf{\Phi}_{33ij}, \mathbf{\Phi}_{33ji}\right\}, \\
\mathbf{\Phi}_{44} &= \operatorname{diag}\left\{\mathbf{\Phi}_{44ij}, \mathbf{\Phi}_{44ji}\right\}, \qquad \mathbf{\Phi}_{55} = \operatorname{diag}\left\{\mathbf{\Phi}_{55ij}, \mathbf{\Phi}_{55ji}\right\},
\end{aligned} \tag{12a}$$

$$\begin{aligned}
&\overline{\mathbf{\Phi}} \\
&= \begin{bmatrix} \overline{\mathbf{\Phi}}_{11} & \tau_{\max}^{-1}\mathbf{P}_5 - \mathbf{N}_1 + \mathbf{N}_2^T & 0 & 0 & 0 & -\mathbf{N}_1 + \mathbf{N}_3^T \\ * & -\tau_{\max}^{-1}\mathbf{P}_5 - \mathbf{P}_4 - \mathbf{N}_2^T - \mathbf{N}_2 & 0 & 0 & 0 & -\mathbf{N}_2 - \mathbf{N}_3^T \\ * & * & 0 & 0 & 0 & 0 \\ * & * & * & -\mathbf{P}_2 & 0 & 0 \\ * & * & * & * & -\mathbf{P}_3 & 0 \\ * & * & * & * & * & -\mathbf{N}_3^T - \mathbf{N}_3 \end{bmatrix}, \\
&\mathbf{W}_{ij} \\
&= \begin{bmatrix} \mathbf{C}_{1i}^T\mathbf{S}_2\mathbf{C}_{1j} & \mathbf{C}_{1i}^T\mathbf{S}_2\mathbf{C}_{dj} & \mathbf{C}_{1i}^T\mathbf{S}_2\mathbf{D}_j - \mathbf{C}_{1i}^T\mathbf{S}_1 & 0 & 0 & 0 \\ * & \mathbf{C}_{di}^T\mathbf{S}_2\mathbf{C}_{dj} & \mathbf{C}_{di}^T\mathbf{S}_2\mathbf{D}_j - \mathbf{C}_{di}^T\mathbf{S}_1 & 0 & 0 & 0 \\ * & * & \mathbf{S}_3 - \mathbf{D}_i^T\mathbf{S}_1 - \mathbf{S}_1^T\mathbf{D}_i + \mathbf{D}_i^T\mathbf{S}_2\mathbf{D}_j & 0 & 0 & 0 \\ * & * & * & 0 & 0 & 0 \\ * & * & * & * & 0 & 0 \\ * & * & * & * & * & 0 \end{bmatrix},
\end{aligned}$$

$$\begin{aligned}
\overline{\mathbf{\Phi}}_{11} &= \mathbf{P}_2 + \mathbf{P}_3 + \left(\tau_{\max} - \tau_{\min} + 1\right)\mathbf{P}_4 - \mathbf{P}_1 - \tau_{\max}^{-1}\mathbf{P}_5 \\
&\quad + \mathbf{N}_1^T + \mathbf{N}_1, \\
\mathbf{\Phi}_{12ij} &= \left[\mathbf{f}_{ij}^T \quad \mathbf{f}_{Rij}^T\right], \qquad \mathbf{\Phi}_{14ij} = \left[\bar{\mathbf{f}}_{ij}^T \quad \bar{\mathbf{f}}_{Rij}^T\right], \\
\mathbf{\Phi}_{22ij} &= \operatorname{diag}\left\{\varepsilon_{ij}\mathbf{H}_i\mathbf{H}_i^T - \mathbf{P}_1^{-1}, -\varepsilon_{ij}\mathbf{I}\right\}, \\
\mathbf{\Phi}_{33ij} &= \operatorname{diag}\left\{\varepsilon_{ij}\mathbf{H}_i\mathbf{H}_i^T - \mathbf{P}_5^{-1}, -\varepsilon_{ij}\mathbf{I}\right\}, \\
\mathbf{\Phi}_{44ij} &= \operatorname{diag}\left\{\bar{\varepsilon}_{ij}\overline{\mathbf{H}}_i\overline{\mathbf{H}}_i^T - \mathbf{P}_1^{-1}, -\bar{\varepsilon}_{ij}\mathbf{I}\right\}, \\
\mathbf{\Phi}_{55ij} &= \operatorname{diag}\left\{\bar{\varepsilon}_{ij}\overline{\mathbf{H}}_i\overline{\mathbf{H}}_i^T - \mathbf{P}_5^{-1}, -\bar{\varepsilon}_{ij}\mathbf{I}\right\}.
\end{aligned} \tag{12b}$$

Proof. Choose the following Lyapunov function:

$$V(x(k)) = V_1(x(k)) + V_2(x(k)) + V_3(x(k)) + V_4(x(k)), \tag{13}$$

where

$$V_1(x(k)) = x^T(k)\mathbf{P}_1x(k), \tag{14a}$$

$$\begin{aligned}
V_2(x(k)) &= \sum_{\ell=k-\tau_{\max}}^{k-1} x^T(\ell)\mathbf{P}_2x(\ell) + \sum_{\ell=k-\tau_{\min}}^{k-1} x^T(\ell)\mathbf{P}_3x(\ell) \\
&\quad + \sum_{\ell=k-\tau(k)}^{k-1} x^T(\ell)\mathbf{P}_4x(\ell),
\end{aligned} \tag{14b}$$

$$V_3(x(k)) = \sum_{s=-\tau_{\max}+1}^{-\tau_{\min}} \sum_{\ell=k+s}^{k-1} x^T(\ell)\mathbf{P}_4x(\ell), \tag{14c}$$

$$V_4(x(k)) = \sum_{s=-\tau_{\max}+1}^{-1} \sum_{\ell=k+s}^{k-1} \Delta x^T(\ell)\mathbf{P}_5\Delta x(\ell), \tag{14d}$$

where $\Delta x(k) = x(k+1) - x(k)$. Firstly, calculating the difference of $V_1(x(k))$ in (14a) along the trajectory of closed-loop system (5) and taking the mathematical expectation, the following inequality can be obtained with relations $\widehat{h}_i\widehat{h}_j\widehat{h}_m\widehat{h}_n \leq \widehat{h}_i\widehat{h}_j$ and $0 \leq \widehat{h}_i \leq 1$:

$$\begin{aligned}
&E\{\Delta V_1(x(k))\} \\
&\leq E\left\{\sum_{i=1}^{r}\sum_{j=1}^{r}\widehat{h}_i\widehat{h}_j\right. \\
&\qquad \times \left\{\xi^T(k)\left(\left(\mathbf{f} + \mathbf{H}\widetilde{\Delta}\mathbf{f}_R\right)^T\widetilde{\mathbf{P}}_1\left(\mathbf{f} + \mathbf{H}\widetilde{\Delta}\mathbf{f}_R\right)\right.\right. \\
&\qquad\qquad \left.\left. + \left(\bar{\mathbf{f}} + \overline{\mathbf{H}}\,\widetilde{\bar{\Delta}}\,\bar{\mathbf{f}}_R\right)^T \times \widetilde{\mathbf{P}}_1\left(\bar{\mathbf{f}} + \overline{\mathbf{H}}\,\widetilde{\bar{\Delta}}\bar{\mathbf{f}}_R\right)\right) \\
&\qquad\qquad \left.\left. \times \xi(k) - x^T(k)\mathbf{P}_1x(k)\right\}\right\},
\end{aligned} \tag{15}$$

where $\mathbf{f} = (1/2)\left[\mathbf{f}_{ij}^T \ \mathbf{f}_{ji}^T\right]^T$, $\mathbf{f}_R = (1/2)\left[\mathbf{f}_{Rij}^T \ \mathbf{f}_{Rji}^T\right]^T$, $\bar{\mathbf{f}} = (1/2)\left[\bar{\mathbf{f}}_{ij}^T \ \bar{\mathbf{f}}_{ji}^T\right]^T$, $\bar{\mathbf{f}}_R = (1/2)\left[\bar{\mathbf{f}}_{Rij}^T \ \bar{\mathbf{f}}_{Rji}^T\right]^T$, $\mathbf{H} = \mathrm{diag}\{\mathbf{H}_i, \mathbf{H}_j\}$, $\overline{\mathbf{H}} = \mathrm{diag}\{\overline{\mathbf{H}}_i, \overline{\mathbf{H}}_j\}$, $\widetilde{\Delta} = \mathrm{diag}\{\Delta, \Delta\}$, $\widetilde{\overline{\Delta}} = \mathrm{diag}\{\overline{\Delta}, \overline{\Delta}\}$, and $\widetilde{\mathbf{P}}_1 = \mathrm{diag}\{\mathbf{P}_1, \mathbf{P}_1\}$. According to Lemma 3, the following inequalities always hold:

$$\begin{aligned}&\left(\mathbf{f} + \mathbf{H}\widetilde{\Delta}\mathbf{f}_R\right)^T \widetilde{\mathbf{P}}_1 \left(\mathbf{f} + \mathbf{H}\widetilde{\Delta}\mathbf{f}_R\right) \\ &\quad \le \mathbf{f}^T\left(\widetilde{\mathbf{P}}_1^{-1} - \widetilde{\varepsilon}\mathbf{H}\mathbf{H}\right)^{-1}\mathbf{f} + \widetilde{\varepsilon}^{-1}\mathbf{f}_R^T\mathbf{f}_R,\end{aligned} \tag{16a}$$

$$\begin{aligned}&\left(\bar{\mathbf{f}} + \overline{\mathbf{H}}\widetilde{\overline{\Delta}}\bar{\mathbf{f}}_R\right)^T \widetilde{\mathbf{P}}_1 \left(\bar{\mathbf{f}} + \overline{\mathbf{H}}\widetilde{\overline{\Delta}}\bar{\mathbf{f}}_R\right) \\ &\quad \le \bar{\mathbf{f}}^T\left(\widetilde{\mathbf{P}}_1^{-1} - \widetilde{\overline{\varepsilon}}\,\overline{\mathbf{H}}\,\overline{\mathbf{H}}\right)^{-1}\bar{\mathbf{f}} + \widetilde{\overline{\varepsilon}}^{-1}\bar{\mathbf{f}}_R^T\bar{\mathbf{f}}_R,\end{aligned} \tag{16b}$$

where $\widetilde{\varepsilon} = \mathrm{diag}\{\varepsilon_{ij}, \varepsilon_{ji}\}$ and $\widetilde{\overline{\varepsilon}} = \mathrm{diag}\{\overline{\varepsilon}_{ij}, \overline{\varepsilon}_{ji}\}$. According to (16a) and (16b), one can obtain the following inequality from (15):

$$\begin{aligned}&E\{\Delta V_1(x(k))\} \\ &\le E\left\{\sum_{i=1}^{r}\sum_{j=1}^{r}\widehat{h}_i\widehat{h}_j \right. \\ &\qquad \times\left\{\xi^T(k)\left(\mathbf{f}^T\left(\widetilde{\mathbf{P}}_1^{-1} - \widetilde{\varepsilon}\mathbf{H}\mathbf{H}\right)^{-1}\mathbf{f}\right.\right. \\ &\qquad\qquad + \widetilde{\varepsilon}^{-1}\mathbf{f}_R^T\mathbf{f}_R + \bar{\mathbf{f}}^T\left(\widetilde{\mathbf{P}}_1^{-1} - \widetilde{\overline{\varepsilon}}\,\overline{\mathbf{H}}\,\overline{\mathbf{H}}\right)^{-1}\bar{\mathbf{f}} \\ &\qquad\qquad \left.\left. + \widetilde{\overline{\varepsilon}}^{-1}\bar{\mathbf{f}}_R^T\bar{\mathbf{f}}_R\right)\xi(k) - x^T(k)\,\mathbf{P}_1 x(k)\right\}\Bigg\}.\end{aligned} \tag{17}$$

Furthermore, the difference of other Lyapunov functions, that is, $V_2(x(k))$, $V_3(x(k))$, and $V_4(x(k))$, can be obtained as follows:

$$\begin{aligned}&E\{\Delta V_2(x(k))\} \\ &\le E\left\{x^T(k)\left(\mathbf{P}_2 + \mathbf{P}_3 + \mathbf{P}_4\right)x(k)\right. \\ &\qquad - x^T\left(k - \tau_{\max}\right)\mathbf{P}_2 x\left(k - \tau_{\max}\right) - x^T\left(k - \tau_{\min}\right) \\ &\qquad \times \mathbf{P}_3 x\left(k - \tau_{\min}\right) - x^T\left(k - \tau(k)\right)\mathbf{P}_4 x\left(k - \tau(k)\right) \\ &\qquad \left. + \sum_{s=k-\tau_{\max}+1}^{k-\tau_{\min}} x^T(s)\,\mathbf{P}_4 x(s)\right\},\end{aligned} \tag{18}$$

$$\begin{aligned}&E\{\Delta V_3(x(k))\} \\ &= E\left\{\left(\tau_{\max} - \tau_{\min}\right)x^T(k)\,\mathbf{P}_4 x(k) - \sum_{s=k-\tau_{\max}+1}^{k-\tau_{\min}} x^T(s)\,\mathbf{P}_4 x(s)\right\},\end{aligned} \tag{19}$$

$$\begin{aligned}&E\{\Delta V_4(x(k))\} \\ &= E\left\{\tau_{\max}(x(k+1) - x(k))^T\mathbf{P}_5\left(x(k+1) - x(k)\right)\right. \\ &\qquad \left. - \sum_{s=-\tau_{\max}+1}^{-1}\Delta x^T(s)\,\mathbf{P}_5\Delta x(s)\right\}.\end{aligned} \tag{20}$$

Substituting (5) into the first term of the right-hand side of (20) and using the relation $h_i h_j h_m h_n \le h_i h_j$, one has

$$\begin{aligned}&E\left\{\tau_{\max}(x(k+1) - x(k))^T\mathbf{P}_5\left(x(k+1) - x(k)\right)\right\} \\ &\le E\left\{\sum_{i=1}^{r}\sum_{j=1}^{r}\widehat{h}_i\widehat{h}_j\tau_{\max}\right. \\ &\qquad \times\left\{\xi^T(k)\left(\left(\left(\mathbf{f} - \mathbf{I}_2\right) + \mathbf{H}\widetilde{\Delta}\mathbf{f}_R\right)^T\widetilde{\mathbf{P}}_5\right.\right. \\ &\qquad\qquad \times\left(\left(\mathbf{f} - \mathbf{I}_2\right) + \mathbf{H}\widetilde{\Delta}\mathbf{f}_R\right) + \left(\bar{\mathbf{f}} + \overline{\mathbf{H}}\widetilde{\overline{\Delta}}\bar{\mathbf{f}}_R\right)^T \\ &\qquad\qquad \left.\left.\left.\times\widetilde{\mathbf{P}}_5\left(\bar{\mathbf{f}} + \overline{\mathbf{H}}\widetilde{\overline{\Delta}}\bar{\mathbf{f}}_R\right)\right)\xi(k)\right\}\Bigg\},\end{aligned} \tag{21}$$

where $\widetilde{\mathbf{P}}_5 = \mathrm{diag}\{\mathbf{P}_5, \mathbf{P}_5\}$, $\mathbf{I}_2 = \left[\begin{smallmatrix}\mathbf{I}_1 \\ \mathbf{I}_1\end{smallmatrix}\right]$, and $\mathbf{I}_1 = \left[\mathbf{I} \ \ 0 \ \ 0 \ \ 0 \ \ 0 \ \ 0\right]$. With the similar relations from (15) to (17), one can also obtain the following inequality:

$$\begin{aligned}&E\left\{\tau_{\max}(x(k+1) - x(k))^T\mathbf{P}_5\left(x(k+1) - x(k)\right)\right\} \\ &\le E\left\{\sum_{i=1}^{r}\sum_{j=1}^{r}\widehat{h}_i\widehat{h}_j\tau_{\max}\right. \\ &\qquad \times\left\{\xi^T(k)\left(\left(\mathbf{f} - \mathbf{I}_2\right)^T\right.\right. \\ &\qquad\qquad \times\left(\widetilde{\mathbf{P}}_5^{-1} - \widetilde{\varepsilon}\mathbf{H}\mathbf{H}\right)^{-1}\left(\mathbf{f} - \mathbf{I}_2\right) + \widetilde{\varepsilon}^{-1}\mathbf{f}_R^T\mathbf{f}_R \\ &\qquad\qquad + \bar{\mathbf{f}}^T\left(\widetilde{\mathbf{P}}_5^{-1} - \widetilde{\overline{\varepsilon}}\,\overline{\mathbf{H}}\,\overline{\mathbf{H}}\right)^{-1}\bar{\mathbf{f}} \\ &\qquad\qquad \left.\left. + \widetilde{\overline{\varepsilon}}^{-1}\bar{\mathbf{f}}_R^T\bar{\mathbf{f}}_R\right)\xi(k)\right\}\Bigg\}.\end{aligned} \tag{22}$$

On the other hand, using Lemma 4, one has the following relation from the second term of the right-hand side of (20):

$$\begin{aligned}&-\sum_{s=-\tau_{\max}+1}^{-1}\Delta x^T(s)\,\mathbf{P}_5\Delta x(s) \\ &\le -\tau_{\max}^{-1}\left(\sum_{s=-\tau(k)+1}^{-1}\Delta x(s)\right)^T\mathbf{P}_5\left(\sum_{s=-\tau(k)+1}^{-1}\Delta x(s)\right) \\ &= -\tau_{\max}^{-1}(x(k) - x(k - \tau(k)))^T\mathbf{P}_5\left(x(k) - x(k - \tau(k))\right).\end{aligned} \tag{23}$$

Thus, the following inequality can be obtained due to (22) and (23):

$$\begin{aligned} &E\{\Delta V_4(x(k))\} \\ &\le E\left\{\sum_{i=1}^{r}\sum_{j=1}^{r}\widehat{h}_i\widehat{h}_j\tau_{\max}\right. \\ &\qquad\times\left\{\xi^T(k)\left((\mathbf{f}-\mathbf{I}_2)^T\left(\widetilde{\mathbf{P}}_5^{-1}-\widetilde{\varepsilon}\mathbf{H}\mathbf{H}\right)^{-1}(\mathbf{f}-\mathbf{I}_2)\right.\right. \\ &\qquad\qquad+\widetilde{\varepsilon}^{-1}\mathbf{f}_R^T\mathbf{f}_R+\overline{\mathbf{f}}^T\left(\widetilde{\mathbf{P}}_5^{-1}-\widetilde{\overline{\varepsilon}}\overline{\mathbf{H}}\,\overline{\mathbf{H}}\right)^{-1}\overline{\mathbf{f}} \\ &\qquad\qquad\left.\left.+\widetilde{\overline{\varepsilon}}^{-1}\overline{\mathbf{f}}_R^T\overline{\mathbf{f}}_R\right)\xi(k)\right\}\Bigg\} \\ &\quad-\tau_{\max}^{-1}(x(k)-x(k-\tau(k)))^T\times\mathbf{P}_5(x(k)-x(k-\tau(k))). \end{aligned} \tag{24}$$

For reducing the conservatism, the following equation is introduced with the concept of free-weighting matrices technique [10]. For any matrices with approximate dimensions, the following equation always holds:

$$\begin{aligned} &2\left(x^T(k)\mathbf{N}_1+x^T(k-\tau(k))\mathbf{N}_2+\eta^T(k)\mathbf{N}_3\right) \\ &\quad\times\left(x(k)-x(k-\tau(k))-\eta(k)\right)=0. \end{aligned} \tag{25}$$

From (17), (18), (19), (24), and (25), one has

$$\begin{aligned} &E\{\Delta V(x(k))\} \\ &=E\{\Delta V_1(x(k))+\Delta V_2(x(k))+\Delta V_3(x(k))+\Delta V_4(x(k))\} \\ &\le E\left\{\sum_{i=1}^{r}\sum_{j=1}^{r}\widehat{h}_i\widehat{h}_j\left\{\xi^T(k)\mathbf{\Pi}_{ij}\xi(k)\right\}\right\}, \end{aligned} \tag{26}$$

where

$$\begin{aligned} \mathbf{\Pi}_{ij}=\overline{\mathbf{\Phi}}-\left(\mathbf{\Phi}_{12}\mathbf{\Phi}_{22}^{-1}\mathbf{\Phi}_{12}^T+\mathbf{\Phi}_{13}\mathbf{\Phi}_{33}^{-1}\mathbf{\Phi}_{13}^T+\mathbf{\Phi}_{14}\mathbf{\Phi}_{44}^{-1}\mathbf{\Phi}_{14}^T\right. \\ \left.+\mathbf{\Phi}_{15}\mathbf{\Phi}_{55}^{-1}\mathbf{\Phi}_{15}^T\right). \end{aligned} \tag{27}$$

Let us consider the following performance function to achieve the attenuation performance of system for all $w(k)\neq 0$ with zero initial condition:

$$\begin{aligned} &J(x(k)) \\ &=E\left\{\sum_{k=0}^{k_q}\left(z^T(k)\mathbf{S}_2z(k)+v^T(k)\mathbf{S}_3v(k)-2z^T(k)\mathbf{S}_1v(k)\right)\right\} \\ &\le E\left\{\sum_{k=0}^{k_q}\left(z^T(k)\mathbf{S}_2z(k)+v^T(k)\mathbf{S}_3v(k)\right.\right. \\ &\qquad\left.\left.-2z^T(k)\mathbf{S}_1v(k)+\Delta V(x(k))\right)\right\}. \end{aligned} \tag{28}$$

According to (26), the following inequality can be obtained via (28):

$$\begin{aligned} &J(x(k)) \\ &<E\sum_{k=0}^{k_q}\left\{\sum_{i=1}^{r}\sum_{j=1}^{r}\widehat{h}_i\widehat{h}_j\left\{\xi^T(k)\left(\mathbf{\Pi}_{ij}+\frac{1}{2}\left(\mathbf{W}_{ij}+\mathbf{W}_{ji}\right)\right)\xi(k)\right\}\right\}. \end{aligned} \tag{29}$$

Using the Schur complement, one can find the following inequality from (10):

$$\mathbf{\Pi}_{ij}+\frac{1}{2}\left(\mathbf{W}_{ij}+\mathbf{W}_{ji}\right)<0. \tag{30}$$

Obviously, if condition (10) is held then (29) is strictly negative that is, $J(x(k))<0$, due to (30). And the following relation can be obtained from (28) according to $J(x(k))<0$:

$$\begin{aligned} &E\left\{\sum_{k=0}^{k_q}\left(z^T(k)\mathbf{S}_2z(k)+v^T(k)\mathbf{S}_3v(k)-2z^T(k)\mathbf{S}_1v(k)\right)\right\} \\ &\quad<0 \end{aligned} \tag{31}$$

or

$$\begin{aligned} &E\left\{2\sum_{k=0}^{k_q}\left(z^T(k)\mathbf{S}_1v(k)\right)\right\} \\ &\qquad>E\left\{\sum_{k=0}^{k_q}\left(z^T(k)\mathbf{S}_2z(k)+v^T(k)\mathbf{S}_3v(k)\right)\right\}. \end{aligned} \tag{32}$$

Since (32) is equivalent to (7) defined in Definition 1, the closed-loop system is passive for all nonzero external disturbance; that is, $v(t)\neq 0$.

Next, we will show that the closed-loop system (5) with all admissible uncertainties is robustly asymptotically stable in the mean square. By assuming $v(t)=0$, the following inequality can be obtained from (30):

$$\begin{aligned} \mathbf{\Pi}_{ij}<\frac{-1}{2}\left\{\left(\mathbf{C}_{1i}x(k)+\mathbf{C}_{di}x(k-\tau(k))\right)^T\right. \\ \times\mathbf{S}_2\left(\mathbf{C}_{1j}x(k)+\mathbf{C}_{dj}x(k-\tau(k))\right) \\ +\left(\mathbf{C}_{1j}x(k)+\mathbf{C}_{dj}x(k-\tau(k))\right)^T \\ \left.\times\mathbf{S}_2\left(\mathbf{C}_{1i}x(k)+\mathbf{C}_{di}x(k-\tau(k))\right)\right\}. \end{aligned} \tag{33}$$

Obviously, if $\mathbf{S}_2\ge 0$ is held, then $\mathbf{\Pi}_{ij}<0$. Hence, from (26), the $E\{\Delta V(x(k))\}<0$ can be obtained due to $\mathbf{\Pi}_{ij}<0$. In this case, the closed-loop system is robustly asymptotically stable in the mean square from Definition 2. The proof of this theorem is completed. □

In Theorem 5, condition (10) simultaneously includes variables $\mathbf{P}_1$, $\mathbf{P}_1^{-1}$, $\mathbf{P}_5$, and $\mathbf{P}_5^{-1}$ such that (10) is not a strictly

LMI problem. For applying the LMI technique, let us introduce two new variables, that is, $\mathbf{X}_1$ and $\mathbf{X}_5$, such that

$$\mathbf{P}_1\mathbf{X}_1 = \mathbf{I}, \qquad \mathbf{P}_5\mathbf{X}_5 = \mathbf{I}, \tag{34}$$

and use $\mathbf{X}_1$ and $\mathbf{X}_5$ to substitute $\mathbf{P}_1^{-1}$ and $\mathbf{P}_5^{-1}$ in condition (10), respectively. Based on the cone complementarity technique [34], the following nonlinear minimization problem is proposed instead of the original nonconvex condition (10):

$$\begin{aligned} &\text{Minimize} \quad \operatorname{tr}\left(\mathbf{P}_1\mathbf{X}_1 + \mathbf{P}_5\mathbf{X}_5\right) \\ &\text{Subject to} \quad (10)\left(\mathbf{P}_1^{-1} \text{ and } \mathbf{P}_5^{-1} \text{ are replaced}\right. \\ &\qquad\qquad \left.\text{by } \mathbf{X}_1 \text{ and } \mathbf{X}_5, \text{resp.}\right), \\ &\qquad \begin{bmatrix} \mathbf{P}_1 & \mathbf{I} \\ \mathbf{I} & \mathbf{X}_1 \end{bmatrix} \geq 0, \qquad \begin{bmatrix} \mathbf{P}_5 & \mathbf{I} \\ \mathbf{I} & \mathbf{X}_5 \end{bmatrix} \geq 0. \end{aligned} \tag{35}$$

Although the above minimization problem gives suboptimal solutions for original problem (10), it is much easier to solve (35) than the original nonconvex problem. In order to find the feasible solutions of (35), the following algorithm is proposed.

Algorithm 6.

Step 1. Choose the time delay values $\tau_{\min}$, $\tau_{\max}$ and performance matrices $\mathbf{S}_1$, $\mathbf{S}_2 \geq 0$, and $\mathbf{S}_3$. Set $t = 0$, and find the initial feasible solution set $\{\mathbf{P}_1, \mathbf{P}_5, \mathbf{X}_1, \mathbf{X}_5\}^t$ to satisfy condition (10) with $\mathbf{P}_1^{-1} \triangleq \mathbf{X}_1$ and $\mathbf{P}_5^{-1} \triangleq \mathbf{X}_5$.

Step 2. Solve the following LMI problem:

$$\begin{aligned} &\text{Minimize} \quad \operatorname{tr}\left(\mathbf{P}_1\mathbf{X}_1^t + \mathbf{X}_1\mathbf{P}_1^t + \mathbf{P}_5\mathbf{X}_5^t + \mathbf{X}_5\mathbf{P}_5^t\right) \\ &\text{Subject to} \quad (10)\left(\mathbf{P}_1^{-1} \text{ and } \mathbf{P}_5^{-1} \text{ are replaced}\right. \\ &\qquad\qquad \left.\text{by } \mathbf{X}_1 \text{ and } \mathbf{X}_5, \text{resp.}\right), \\ &\qquad \begin{bmatrix} \mathbf{P}_1 & \mathbf{I} \\ \mathbf{I} & \mathbf{X}_1 \end{bmatrix} \geq 0, \qquad \begin{bmatrix} \mathbf{P}_5 & \mathbf{I} \\ \mathbf{I} & \mathbf{X}_5 \end{bmatrix} \geq 0. \end{aligned} \tag{36}$$

Step 3. Substitute the feasible solutions obtained from Step 2 into (10). If condition (10) is satisfied, then go back to Step 2 after increasing the $\tau_{\max}$ until (10) is not satisfied with specified $\tau_{\max}$. In this case, the feasible solutions are obtained and the algorithm can be stopped. Otherwise, go to the next step.

Step 4. Set $t = t + 1$ and $\{\mathbf{P}_1, \mathbf{P}_5, \mathbf{X}_1, \mathbf{X}_5\}^t = \{\mathbf{P}_1, \mathbf{P}_5, \mathbf{X}_1, \mathbf{X}_5\}$; then go to Step 2.

Remark 7. In order to apply the LMI technique, Algorithm 6 is a useful tool to find the feasible solutions of conditions of Theorem 5. In Algorithm 6, the number of desired unknown variables in fuzzy controller design process is $2r^2 + r + 8$. From Theorem 3 of [9], one can find that the number of desired unknown variables is $72r^3 + 7r^2 + 11r + 6$. Obviously, the number of desired unknown variables of the proposed method is less than that developed in [9].

Remark 8. In [9], the quadratic transformation inequality "$\mathbf{W} + \mathbf{W} + \mathbf{P} \geq \mathbf{W}\mathbf{P}^{-1}\mathbf{W}$" is often applied for converting the bilinear matrix inequalities into linear matrix inequalities. During the transformation process, the conservatisms arise to find the solutions of sufficient conditions of Theorems 2 and 3 in [9]. Oppositely, the similar bilinear matrix inequalities are solved via the cone complement technique in this paper. Applying the cone complement technique, the bilinear matrix inequalities are converted into nonstrictly linear matrix inequalities that can be solved by a suboptimal algorithm, that is, Algorithm 6.

Remark 9. In Theorem 5, the free-weighting matrix technique is applied to reduce the conservatism of considered fuzzy controller design problems. By applying the free-weighting matrix technique, more free matrices are added to reduce the conservatism of derived sufficient conditions. However, adding free matrices also increases the computational complexity. In order to balance the incompatible case, it is recommended to use the free-weighting matrix technique as less as possible.

Theorem 5 provides the sufficient conditions (10) to design state-feedback fuzzy controller for guaranteeing robust asymptotical stability and passivity of closed-loop system (5) in mean square. In the following, with the few modifications, Theorem 5 can also be applied to find the output-feedback gains for structuring the fuzzy controller. Based on (1c), the output-feedback fuzzy controller can also be structured via PDC technique such as

$$u(k) = \sum_{i=1}^{r} \widehat{h}_i\left(\mathbf{K}_i y(k)\right). \tag{37}$$

Introducing (37) into (1a), the closed-loop system can be obtained as follows:

$$\begin{aligned} &x(k+1) \\ &= \sum_{i=1,j=1,p=1}^{r} \widehat{h}_i\widehat{h}_j\widehat{h}_p \\ &\qquad \times \left\{\left(\mathbf{g}_{ijp} + \mathbf{H}_i\Delta\mathbf{g}_{Rijp} + \left(\overline{\mathbf{g}}_{ijp} + \overline{\mathbf{H}}_i\overline{\Delta}\overline{\mathbf{g}}_{Rijp}\right)\beta(k)\right)\xi(k)\right\} \\ &= \sum_{i=1}^{r}\sum_{j=1}^{r}\sum_{p=1}^{r} \widehat{h}_i\widehat{h}_j\widehat{h}_p \\ &\qquad \times \left\{\frac{1}{3}\left(\mathbf{g}_{ijp} + \mathbf{H}_i\Delta\mathbf{g}_{Rijp} + \mathbf{g}_{jpi}\right.\right. \\ &\qquad\quad + \mathbf{H}_j\Delta\mathbf{g}_{Rjpi} + \mathbf{g}_{pij} + \mathbf{H}_p\Delta\mathbf{g}_{Rpij} \\ &\qquad\quad + \left(\overline{\mathbf{g}}_{ijp} + \overline{\mathbf{H}}_i\overline{\Delta}\overline{\mathbf{g}}_{Rijp} + \overline{\mathbf{g}}_{jpi} + \overline{\mathbf{H}}_j\overline{\Delta}\overline{\mathbf{g}}_{Rjpi}\right. \\ &\qquad\quad \left.\left.\left.+\overline{\mathbf{g}}_{pij} + \overline{\mathbf{H}}_p\overline{\Delta}\overline{\mathbf{g}}_{Rpij}\right)\beta(k)\right)\xi(k)\right\}, \end{aligned} \tag{38}$$

where $\mathbf{g}_{ijp} = \left[\mathbf{G}_{ijp}\ \mathbf{A}_{di}\ \mathbf{E}_i\ 0_{1\times 3}\right]$, $\overline{\mathbf{g}}_{ijp} = \left[\overline{\mathbf{G}}_{ijp}\ \overline{\mathbf{A}}_{di}\ \overline{\mathbf{E}}_i\ 0_{1\times 3}\right]$, $\mathbf{g}_{Rijp} = \left[\mathbf{R}_{ijp}\ \mathbf{R}_{di}\ \mathbf{R}_{Ei}\ 0_{1\times 3}\right]$, $\overline{\mathbf{g}}_{Rijp} = \left[\overline{\mathbf{R}}_{ijp}\ \overline{\mathbf{R}}_{di}\ \overline{\mathbf{R}}_{Ei}\ 0_{1\times 3}\right]$, $\mathbf{G}_{ijp} = \mathbf{A}_i + \mathbf{B}_i\mathbf{K}_j\mathbf{C}_{2p}$, $\overline{\mathbf{G}}_{ijp} = \overline{\mathbf{A}}_i + \overline{\mathbf{B}}_i\mathbf{K}_j\mathbf{C}_{2p}$, $\mathbf{R}_{ijp} = \mathbf{R}_i + \mathbf{R}_{Bi}\mathbf{K}_j\mathbf{C}_{2p}$, and $\overline{\mathbf{R}}_{ijp} = \overline{\mathbf{R}}_i + \overline{\mathbf{R}}_{Bi}\mathbf{K}_j\mathbf{C}_{2p}$.

Theorem 10. *Given performance parameters* $\mathbf{S}_1$, $\mathbf{S}_2 \geq 0$, *and* $\mathbf{S}_3$ *and values* $\tau_{\min} > 0$ *and* $\tau_{\max} > 0$, *the closed-loop system* (38) *is robustly asymptotically stable and passive in the sense of mean square, if there exist positive definite matrices* $\mathbf{P}_1 > 0$, $\mathbf{P}_2 > 0$, $\mathbf{P}_3 > 0$, $\mathbf{P}_4 > 0$ *and* $\mathbf{P}_5 > 0$, *any matrices* $\mathbf{N}_1$, $\mathbf{N}_2$ *and* $\mathbf{N}_3$, *scalars* $\varepsilon_{ijp} > 0$ *and* $\overline{\varepsilon}_{ijp} > 0$, *and output-feedback gains* $\mathbf{K}_i$ *such that*

$$\mathbf{\Omega} < 0 \quad \text{for } i, j, p \leq r, \tag{39}$$

where

$$\mathbf{\Omega} = \begin{bmatrix} \mathbf{\Omega}_{11} & \mathbf{\Omega}_{12} & \mathbf{\Omega}_{13} & \mathbf{\Omega}_{14} & \mathbf{\Omega}_{15} \\ * & \mathbf{\Omega}_{22} & 0 & 0 & 0 \\ * & * & \mathbf{\Omega}_{33} & 0 & 0 \\ * & * & * & \mathbf{\Omega}_{44} & 0 \\ * & * & * & * & \mathbf{\Omega}_{55} \end{bmatrix}, \tag{40}$$

$$\begin{aligned} \mathbf{\Omega}_{11} &= \overline{\mathbf{\Phi}} + \frac{1}{3}\left(\mathbf{W}_{ii} + \mathbf{W}_{jj} + \mathbf{W}_{ij}\right), \\ \mathbf{\Omega}_{12} &= \frac{1}{3}\left[\mathbf{\Omega}_{12ijp} \;\; \mathbf{\Omega}_{12jpi} \;\; \mathbf{\Omega}_{12pij}\right], \\ \mathbf{\Omega}_{13} &= \sqrt{\tau_{\max}}\mathbf{\Omega}_{12}, \\ \mathbf{\Omega}_{14} &= \frac{1}{3}\left[\mathbf{\Omega}_{14ijp} \;\; \mathbf{\Omega}_{14jpi} \;\; \mathbf{\Omega}_{14pij}\right], \qquad \mathbf{\Omega}_{15} = \sqrt{\tau_{\max}}\mathbf{\Omega}_{14}, \\ \mathbf{\Omega}_{22} &= \operatorname{diag}\left\{\mathbf{\Omega}_{22ijp}, \mathbf{\Omega}_{22jpi}, \mathbf{\Omega}_{22pij}\right\}, \\ \mathbf{\Omega}_{33} &= \operatorname{diag}\left\{\mathbf{\Omega}_{33ijp}, \mathbf{\Omega}_{33jpi}, \mathbf{\Omega}_{33pij}\right\}, \\ \mathbf{\Omega}_{44} &= \operatorname{diag}\left\{\mathbf{\Omega}_{44ijp}, \mathbf{\Omega}_{44jpi}, \mathbf{\Omega}_{44pij}\right\}, \\ \mathbf{\Omega}_{55} &= \operatorname{diag}\left\{\mathbf{\Omega}_{55ijp}, \mathbf{\Omega}_{55jpi}, \mathbf{\Omega}_{55pij}\right\}, \end{aligned} \tag{41}$$

$$\begin{aligned} \mathbf{\Omega}_{12ijp} &= \left[\mathbf{f}_{ijp}^T \;\; \mathbf{f}_{Rijp}^T\right], \qquad \mathbf{\Omega}_{14ijp} = \left[\overline{\mathbf{f}}_{ijp}^T \;\; \overline{\mathbf{f}}_{Rijp}^T\right], \\ \mathbf{\Omega}_{33ijp} &= \operatorname{diag}\left\{\varepsilon_{ijp}\mathbf{H}_i\mathbf{H}_i^T - \mathbf{P}_5^{-1}, -\varepsilon_{ijp}\mathbf{I}\right\}, \\ \mathbf{\Omega}_{22ijp} &= \operatorname{diag}\left\{\varepsilon_{ijp}\mathbf{H}_i\mathbf{H}_i^T - \mathbf{P}_1^{-1}, -\varepsilon_{ijp}\mathbf{I}\right\}, \\ \mathbf{\Omega}_{44ijp} &= \operatorname{diag}\left\{\overline{\varepsilon}_{ijp}\overline{\mathbf{H}}_i\overline{\mathbf{H}}_i^T - \mathbf{P}_1^{-1}, -\overline{\varepsilon}_{ijp}\mathbf{I}\right\}, \\ \mathbf{\Omega}_{55ijp} &= \operatorname{diag}\left\{\overline{\varepsilon}_{ijp}\overline{\mathbf{H}}_i\overline{\mathbf{H}}_i^T - \mathbf{P}_5^{-1}, -\overline{\varepsilon}_{ijp}\mathbf{I}\right\}. \end{aligned} \tag{42}$$

With the same Lyapunov function (13), the proof of Theorem 10 can be obtained with similar procedure of proof of Theorem 5. Hence, the proof of Theorem 10 is omitted here. Although the feasible solutions condition (39) of Theorem 10 cannot be directly obtained by using LMI technique, one can also apply Algorithm 6 by substituting sufficient condition (39) for (10). And then, the feasible solutions can be obtained for satisfying condition (39) and hence the modified algorithm is omitted here.

In the following section, the two numerical examples are provided to apply the proposed fuzzy controller design technique in this paper.

4. Numerical Examples

In this section, two numerical examples apply the proposed fuzzy controller design method in this paper. In the first example, the less conservatism of stability criteria in this paper can be shown and demonstrated. On the other hand, in Example 2, both of Theorems 5 and 10 are applied to design the state-feedback fuzzy controller and output-feedback fuzzy controller, respectively.

Example 1. Referring to [9], the following T-S fuzzy model without multiplicative noise term is proposed to apply the proposed design technique in Theorem 5:

$$\begin{aligned} x(k+1) = \sum_{i=1}^{2} \widehat{h}_i \{ &\left(\mathbf{A}_i + \Delta\mathbf{A}_i\right) x(k) \\ &+ \left(\mathbf{A}_{di} + \Delta\mathbf{A}_{di}\right) x(k - \tau(k)) \\ &+ \left(\mathbf{B}_i + \Delta\mathbf{B}_i\right) u(k) + \left(\mathbf{E}_i + \Delta\mathbf{E}_i\right) v(k) \}, \end{aligned} \tag{43a}$$

$$z(k) = \sum_{i=1}^{2} \widehat{h}_i \left\{\mathbf{C}_{1i} x(k) + \mathbf{C}_{di} x(k - \tau(k)) + \mathbf{D}_i v(k)\right\}, \tag{43b}$$

$$x(k) = \varphi(k), \quad k = 0, -1, \ldots, -\tau(k), \tag{43c}$$

where $\mathbf{A}_1 = \left[\begin{smallmatrix} 0.5 & 0.3 \\ 0.1 & 1 \end{smallmatrix}\right]$, $\mathbf{A}_2 = \left[\begin{smallmatrix} -0.5 & 0.3 \\ 0.1 & 1 \end{smallmatrix}\right]$, $\mathbf{A}_{d1} = \left[\begin{smallmatrix} -0.05 & 0.1 \\ 0 & 0.05 \end{smallmatrix}\right]$, $\mathbf{B}_1 = \left[\begin{smallmatrix} 1 & 0 \\ 0 & 0.5 \end{smallmatrix}\right]$, $\mathbf{E}_1 = \left[\begin{smallmatrix} -0.5 \\ 0 \end{smallmatrix}\right]$, $\mathbf{A}_{d2} = -\mathbf{A}_{d1}$, $\mathbf{B}_2 = \mathbf{B}_1$, $\mathbf{E}_2 = -\mathbf{E}_1$, $\mathbf{C}_{11} = \left[-0.05 \;\; 0\right]$, $\mathbf{C}_{12} = -\mathbf{C}_{11}$, $\mathbf{H}_i = \left[\begin{smallmatrix} -0.05 & 0.1 \\ 0.1 & 0 \end{smallmatrix}\right]$, $\mathbf{R}_i = \left[\begin{smallmatrix} 0 & 0.2 \\ 0 & 0 \end{smallmatrix}\right]$, $\mathbf{R}_{di} = \left[\begin{smallmatrix} 0 & 0 \\ 0 & 0.1 \end{smallmatrix}\right]$, $\mathbf{R}_{Bi} = \mathbf{R}_{Ei} = 0$, $\mathbf{C}_{di} = \left[0 \;\; 0.2\right]$, and $\mathbf{D}_i = 0.1$ for $i = 1, 2$.

And the membership function of (43a), (43b), and (43c) is chosen as $\widehat{h}_1 = (1 - 2x_1(k))/2$ and $\widehat{h}_2 = 1 - \widehat{h}_1$. For comparing the proposed method with that developed in [9], the passivity performance is chosen as H_∞ performance constraint by setting $\mathbf{S}_1 \triangleq 0$, $\mathbf{S}_2 \triangleq \mathbf{I}$, and $\mathbf{S}_3 \triangleq -\gamma^2\mathbf{I}$. For finding maximum allowable $\tau_{\max}$, let us study different cases with $\tau_{\min} = 2$, $\tau_{\min} = 5$, and $\tau_{\min} = 10$. From Table 1, one can find that the allowed upper bound of delay $\tau_{\max}$ controlled by the proposed design method is bigger than that of [9]. It means that the proposed design method can provide bigger maximum delay bound than the approach developed in [9]. Besides, the smaller H_∞ performance level γ can be found by using the proposed design method. It should be noted that the stability criterion of this paper possesses less conservatism than that proposed in [9].

Next, we apply the proposed design techniques to find both of state-feedback fuzzy controller and output-feedback fuzzy controller for nonlinear delay Hénon system.

Example 2. In this example, the nonlinear delay Hénon system is proposed to apply the proposed fuzzy controller design techniques. Referring to [10], the nonlinear delay Hénon system with external disturbance can be proposed as follows:

$$\begin{aligned} x_1(k+1) = &\left(0.8x_1(k) + 0.2x_1(k - \tau(k))\right)^2 \\ &+ 0.3x_2(k) + 1.4 + \widetilde{u}(k), \end{aligned} \tag{44a}$$

Table 1: Comparisons between proposed method and [9].

$\tau_{\min}$	Design method	$\tau_{\max} = 12$	$\tau_{\max} = 13$	$\tau_{\max} = 14$	$\tau_{\max} = 15$	$\tau_{\max} = 16$
10	γ in [9]	0.3408	0.4085	0.4897	0.5909	Infeasible
	γ in Theorem 5	0.3351	0.338	0.3481	0.3515	0.3595
5	γ in [9]	0.4882	0.806	0.6963	0.8468	Infeasible
	γ in Theorem 5	0.3691	0.3712	0.383	0.394	0.4012
2	γ in [9]	0.5818	0.6932	0.8369	Infeasible	Infeasible
	γ in Theorem 5	0.4124	0.4087	0.5124	0.598	0.612

$$x_2(k+1) = 0.8x_1(k) + 0.2x_1(k-\tau(k)) + 0.1v(k), \tag{44b}$$

$$z(k) = 0.8x_1(k) + 0.2x_1(k-\tau(k)) + v, \tag{44c}$$

$$y(k) = x_1, \tag{44d}$$

$$x(k) = \varphi(k), \quad k = 0, -1, \ldots, -\tau(k), \tag{44e}$$

where $v(k)$ is chosen as a zero-mean white noise with variance 0.5. Based on the fuzzy modeling in [10], the considered discrete uncertain stochastic T-S fuzzy model of (44a), (44b), (44c), (44d), and (44e) can be obtained by adding the uncertainties and stochastic behaviors

$$\begin{aligned} & x(k+1) \\ &= \sum_{i=1}^{2} \widehat{h}_i \Big\{ \left(\mathbf{A}_i + \Delta\mathbf{A}_i\right) x(k) \\ &\qquad + \left(\mathbf{A}_{di} + \Delta\mathbf{A}_{di}\right) x(k-\tau(k)) \\ &\qquad + \left(\mathbf{B}_i + \Delta\mathbf{B}_i\right) u(k) + \mathbf{E}_i v(k) \\ &\qquad + \left(\overline{\mathbf{A}}_i x(k) + \overline{\mathbf{A}}_{di} x(k-\tau(k)) + \overline{\mathbf{B}}_i u(k)\right) \beta(k) \Big\}, \end{aligned} \tag{45a}$$

$$z(k) = \sum_{i=1}^{2} \widehat{h}_i \left\{ \mathbf{C}_{1i} x(k) + \mathbf{D}_i v(k) \right\}, \tag{45b}$$

$$y(k) = \sum_{i=1}^{2} \widehat{h}_i \left\{ \mathbf{C}_{2i} x(k) \right\}, \tag{45c}$$

where $u(k) = 1.4 + \widetilde{u}(k)$, premise variable $\theta(k) = 0.8x_1(k) + 0.2x_1(k-\tau(k))$, membership function $\widehat{h}_1 = (1/2)(1 - (\theta(k)/2))$ and $\widehat{h}_2 = 1 - \widehat{h}_1$, $\mathbf{A}_1 = \left[\begin{smallmatrix} 1.6 & 0.3 \\ 0.8 & 0 \end{smallmatrix}\right]$, $\mathbf{A}_2 = \left[\begin{smallmatrix} -1.8 & 0.3 \\ 0.8 & 0 \end{smallmatrix}\right]$, $\mathbf{A}_{d1} = \left[\begin{smallmatrix} 0.4 & 0 \\ 0.2 & 0 \end{smallmatrix}\right]$, $\mathbf{A}_{d1} = \left[\begin{smallmatrix} -0.4 & 0 \\ 0.2 & 0 \end{smallmatrix}\right]$, $\mathbf{B}_i = \left[\begin{smallmatrix} 1 \\ 0 \end{smallmatrix}\right]$, $\mathbf{E}_i = \left[\begin{smallmatrix} 0 \\ 0.1 \end{smallmatrix}\right]$, $\mathbf{C}_{1i} = \begin{bmatrix} 0.8 & 0 \end{bmatrix}$, $\mathbf{C}_{di} = \begin{bmatrix} 0.2 & 0 \end{bmatrix}$, $\mathbf{C}_{2i} = \begin{bmatrix} 1 & 0 \end{bmatrix}$, $\mathbf{D}_i = 1$, $\overline{\mathbf{A}}_i = 0.1\mathbf{A}_i$, $\overline{\mathbf{A}}_{di} = 0.1\mathbf{A}_{di}$, $\overline{\mathbf{B}}_i = 0.1\mathbf{B}_i$, $\overline{\mathbf{E}}_i = 0$ and $\left[\begin{smallmatrix} \Delta\mathbf{A}_i & \Delta\mathbf{A}_{di} & \Delta\mathbf{B}_i & \Delta\mathbf{E}_i \\ \Delta\overline{\mathbf{A}}_i & \Delta\overline{\mathbf{A}}_{di} & \Delta\overline{\mathbf{B}}_i & \Delta\overline{\mathbf{E}}_i \end{smallmatrix}\right] = \left[\begin{smallmatrix} \mathbf{H}_i & 0 \\ 0 & 0 \end{smallmatrix}\right] \left[\begin{smallmatrix} \sin(k) & 0 \\ 0 & 0 \end{smallmatrix}\right] \left[\begin{smallmatrix} \mathbf{R}_i & \mathbf{R}_{di} & \mathbf{R}_{Bi} & 0 \\ 0 & 0 & 0 & 0 \end{smallmatrix}\right]$ with $\mathbf{H}_i = 0.1 \times \mathbf{I}$, $\mathbf{R}_i = 0.01\mathbf{A}_i$, and $\mathbf{R}_{di} = 0.01\mathbf{A}_{di}$ and $\mathbf{R}_{Bi} = 0.01\mathbf{B}_i$, for $i = 1, 2$.

In the following, both design methods in Theorems 5 and 10 will be applied to design the PDC-based fuzzy controller in the terms of (4) and (37), respectively, such that closed-loop system is robustly asymptotically stable and passive in mean square.

Case A: State-Feedback. Through Theorem 5 and Algorithm 6 of this paper, the following feasible solutions can be found with the range of time-varying delay between $\tau_{\max} = 5$ and $\tau_{\min} = 1$ and chosen passivity (7) with $\mathbf{S}_1 \triangleq \mathbf{I}$, $\mathbf{S}_2 \triangleq 0.8$, and $\mathbf{S}_3 \triangleq 0.8$:

$$\mathbf{P}_1 = \begin{bmatrix} 30.3351 & -0.3962 \\ -0.3962 & 0.9253 \end{bmatrix}, \quad \mathbf{P}_2 = \begin{bmatrix} 0.008 & 0.0001 \\ 0.0001 & 0.0029 \end{bmatrix},$$

$$\mathbf{P}_3 = \begin{bmatrix} 0.008 & 0.0001 \\ 0.0001 & 0.0029 \end{bmatrix}, \quad \mathbf{P}_4 = \begin{bmatrix} 5.6071 & -0.0167 \\ -0.0167 & 0.0003 \end{bmatrix},$$

$$\mathbf{P}_5 = \begin{bmatrix} 0.2488 & 0.0858 \\ 0.0858 & 0.1773 \end{bmatrix},$$

$$\mathbf{N}_1 = \begin{bmatrix} -3.2735 & -0.011 \\ -0.0111 & -3.3647 \end{bmatrix} \times 10^3,$$

$$\mathbf{N}_2 = \begin{bmatrix} 3.2735 & 0.0111 \\ 0.0111 & 3.3647 \end{bmatrix} \times 10^3,$$

$$\mathbf{N}_3 = \begin{bmatrix} 3.2735 & 0.0111 \\ 0.0111 & 3.3647 \end{bmatrix} \times 10^3,$$

$$\varepsilon_{11} = 0.0127, \quad \varepsilon_{22} = 0.0246,$$

$$\mathbf{F}_1 = \begin{bmatrix} -1.5878 & -0.2669 \end{bmatrix}, \quad \mathbf{F}_2 = \begin{bmatrix} 1.6623 & -0.306 \end{bmatrix}. \tag{46}$$

From PDC concept, the fuzzy controller can be established with sublinear state-feedback gains in (46) and the membership function, such as

$$u(k) = \sum_{i=1}^{3} \widehat{h}_i \left(\mathbf{F}_i x(k)\right). \tag{47}$$

With (47), the responses of system (44a), (44b), (44c), (44d), and (44e) by adding the uncertainties and stochastic behaviors are stated in Figure 1 with initial condition $x(0) = \begin{bmatrix} 1 & 0 \end{bmatrix}^T$. And the time delay effect is chosen by random block in Simulink of MATLAB and bounded as $1 \le \tau(k) \le 5$ in this case. Based on the simulation results in this case, the attenuation performance can be checked by the following equation:

$$\frac{0.8E\left\{\sum_{k=0}^{k_q} z^T(k) z(k) + \sum_{k=0}^{k_q} v^T(k) v(k)\right\}}{E\left\{2\sum_{k=0}^{k_q} z^T(k) v(k)\right\}} = 0.8637. \tag{48}$$

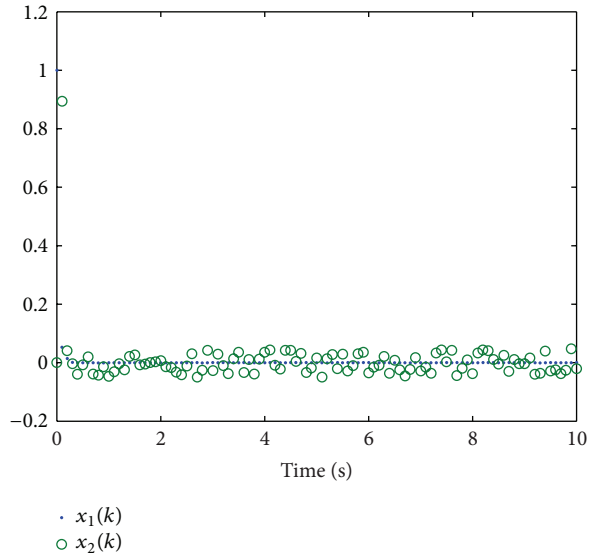

Figure 1: State responses driven by fuzzy controller (47): Case A of Example 2.

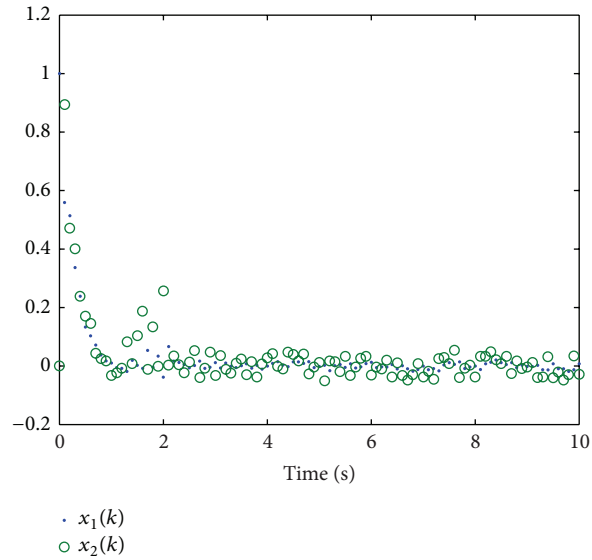

Figure 2: State responses driven by fuzzy controller (50): Case B of Example 2.

Obviously, because the radio value of (48) is smaller than one, the chosen passivity inequality can be satisfied with the simulation results of this case. Hence, from (48) and Figure 1, the robust asymptotical stability and passivity of system (45a), (45b), and (45c) by adding the uncertainties and stochastic behaviors can be achieved by design fuzzy controller (47). Next, the case of output-feedback controller design for the same considered system will be shown.

Case B: Output-Feedback. Considering the system (45a), (45b), and (45c) with $\tau_{\max} = 2$ and $\tau_{\min} = 1$, the following feasible solutions are found to satisfying the Theorem 10 by using modified Algorithm 6:

$$\mathbf{P}_1 = \begin{bmatrix} 6.8827 & -1.2065 \\ -1.2065 & 2.0775 \end{bmatrix},$$

$$\mathbf{P}_2 = \begin{bmatrix} 0.2406 & -0.0869 \\ -0.0869 & 0.1647 \end{bmatrix} \times 10^{-3},$$

$$\mathbf{P}_3 = \begin{bmatrix} 0.2406 & -0.0869 \\ -0.0869 & 0.1647 \end{bmatrix} \times 10^{-3},$$

$$\mathbf{P}_4 = \begin{bmatrix} 1.9831 & -0.3483 \\ -0.3483 & 0.0614 \end{bmatrix}, \qquad \mathbf{P}_5 = \begin{bmatrix} 1.4313 & 0.7436 \\ 0.7436 & 0.6632 \end{bmatrix},$$

$$\mathbf{N}_1 = \begin{bmatrix} -3.2772 & 1.1479 \\ 1.016 & -4.2002 \end{bmatrix} \times 10^{3},$$

$$\mathbf{N}_2 = \begin{bmatrix} 3.2776 & -1.1483 \\ -1.0161 & 4.2003 \end{bmatrix} \times 10^{3},$$

$$\mathbf{N}_3 = \begin{bmatrix} 3.2777 & -1.1483 \\ -1.0156 & 4.1998 \end{bmatrix} \times 10^{3},$$

$$\begin{aligned} \varepsilon_{11} &= 0.0302, \qquad \varepsilon_{22} = 0.0573, \\ \mathbf{K}_1 &= -2.0142, \qquad \mathbf{K}_2 = 2.4929. \end{aligned} \tag{49}$$

With the sublinear output-feedback gains, the PDC-based fuzzy controller can be obtained as follows:

$$u(k) = \sum_{i=1}^{r} \widehat{h}_i \left(\mathbf{K}_i y(k) \right). \tag{50}$$

In Figure 2, the responses of considered system with fuzzy controller (50) are shown with initial condition $x(0) = \begin{bmatrix} 1 & 0 \end{bmatrix}^T$ and random time-varying delay which bounded as $1 \le \tau(k) \le 2$. And the attenuation performance of the system can be checked by the following equation:

$$\frac{0.8E\left\{\sum_{k=0}^{k_q} z^T(k) z(k) + \sum_{k=0}^{k_q} v^T(k) v(k)\right\}}{E\left\{2\sum_{k=0}^{k_q} z^T(k) v(k)\right\}} = 0.9383. \tag{51}$$

Since the value of (51) is smaller than one, the passivity of system can be achieved by the fuzzy controller (50). From (51) and Figure 2, (45a), (45b), and (45c) with design fuzzy controller are robustly asymptotically stable and passive in the mean square.

5. Conclusion

The fuzzy controller design problems of discrete uncertain T-S fuzzy systems with interval time-varying delay and multiplicative noise were discussed and investigated in this paper. With the free-weighting matrices technique and discrete type Jensen inequality, the less conservative stability criterion was derived by applying Lyapunov function. Although the

derived conditions were not strictly convex problems, the cone complementarity method provided a suboptimal technique to solve it with the LMI technique. Through the proposed design method, the PDC-based fuzzy controller can be established by both of state-feedback and output-feedback schemes for guaranteeing the robust asymptotical stability and passivity constraints. Finally, two numerical examples have been provided to demonstrate the effectiveness and usefulness of the proposed design methods.

Acknowledgments

The authors would like to express their sincere gratitude to the anonymous reviewers who gave them some constructive comments, criticisms, and suggestions. This work was supported by the National Science Council of the Republic of China under Contract NSC102-2221-E-019-051.

References

[1] C. Peng and M.-R. Fei, "An improved result on the stability of uncertain T-S fuzzy systems with interval time-varying delay," *Fuzzy Sets and Systems*, vol. 212, no. 2, pp. 97–109, 2013.

[2] G. Wei, G. Feng, and Z. Wang, "Robust H_∞ control for discrete-time fuzzy systems with infinite-distributed delays," *IEEE Transactions on Fuzzy Systems*, vol. 17, no. 1, pp. 224–232, 2009.

[3] Z.-G. Wu, P. Shi, H. Su, and J. Chu, "Reliable H_∞ control for discrete-time fuzzy systems with infinite-distributed delay," *IEEE Transactions on Fuzzy Systems*, vol. 20, no. 1, pp. 22–31, 2012.

[4] P. L. Liu, "New results on stability analysis for time-varying delay systems with non-linear perturbations," *ISA Transactions*, vol. 52, no. 2, pp. 215–222, 2013.

[5] S. Boyd, L. El Ghaoui, E. Feron, and V. Balakrishnan, *Linear Matrix Inequalities in System and Control Theory*, vol. 15 of *SIAM Studies in Applied Mathematics*, SIAM, Philadelphia, Pa, USA, 1994.

[6] M. Chen, G. Feng, H. Ma, and G. Chen, "Delay-dependent H_∞ filter design for discrete-time fuzzy systems with time-varying delays," *IEEE Transactions on Fuzzy Systems*, vol. 17, no. 3, pp. 604–616, 2009.

[7] H. Zhang and C. Dang, "Piecewise H_∞ controller design of uncertain discrete-time fuzzy systems with time delays," *IEEE Transactions on Fuzzy Systems*, vol. 16, no. 6, pp. 1649–1655, 2008.

[8] L. Wu, X. Su, P. Shi, and J. Qiu, "A new approach to stability analysis and stabilization of discrete-time T-S fuzzy time-varying delay systems," *IEEE Transactions on Systems, Man, and Cybernetics, Part B*, vol. 41, no. 1, pp. 273–286, 2011.

[9] B. Zhang and S. Xu, "Delay-Dependent Robust H_∞ control for uncertain discrete-time fuzzy systems with time-varying delays," *IEEE Transactions on Fuzzy Systems*, vol. 17, no. 4, pp. 809–823, 2009.

[10] H. Gao, X. Liu, and J. Lam, "Stability analysis and stabilization for discrete-time fuzzy systems with time-varying delay," *IEEE Transactions on Systems, Man, and Cybernetics, Part B*, vol. 39, no. 2, pp. 306–317, 2009.

[11] S.-M. Wu, C.-C. Sun, H.-Y. Chung, and W.-J. Chang, "Discrete H_2/H_∞ nonlinear controller design based on fuzzy region concept and Takagi-Sugeno fuzzy framework," *IEEE Transactions on Circuits and Systems. I. Regular Papers*, vol. 53, no. 12, pp. 2838–2848, 2006.

[12] P. Vadivel, R. Sakthivel, K. Mathiyalagan, and P. Thangaraj, "Robust stabilisation of non-linear uncertain Takagi-Sugeno fuzzy systems by H_∞ control," *IET Control Theory & Applications*, vol. 6, no. 16, pp. 2556–2566, 2012.

[13] A. H. Besheer, H. M. Emara, and M. M. Abdel Aziz, "Fuzzy-based output-feedback H_∞ control for uncertain nonlinear systems: an LMI approach," *IET Control Theory & Applications*, vol. 1, no. 4, pp. 1176–1185, 2007.

[14] J. Dong and G.-H. Yang, "H_∞ control for fast sampling discrete-time singularly perturbed systems," *Automatica*, vol. 44, no. 5, pp. 1385–1393, 2008.

[15] B. Zhang, W. X. Zheng, and S. Xu, "Passivity analysis and passive control of fuzzy systems with time-varying delays," *Fuzzy Sets and Systems*, vol. 174, no. 1, pp. 83–98, 2011.

[16] A. Bemporad, G. Bianchini, and F. Brogi, "Passivity analysis and passification of discrete-time hybrid systems," *IEEE Transactions on Automatic Control*, vol. 53, no. 4, pp. 1004–1009, 2008.

[17] W.-J. Chang, C.-C. Ku, and P.-H. Huang, "Robust fuzzy control for uncertain stochastic time-delay Takagi-Sugeno fuzzy models for achieving passivity," *Fuzzy Sets and Systems*, vol. 161, no. 15, pp. 2012–2032, 2010.

[18] R. Lozano, B. Brogliato, O. Egeland, and B. Maschke, *Dissipative Systems Analysis and Control Theory and Applications*, Communications and Control Engineering Series, Springer, London, UK, 2000.

[19] G. Eli, S. Uri, and Y. Isaac, H_∞ *Control and Estimation of State-Multiplicative Linear Systems*, vol. 318 of *Lecture Notes in Control and Information Sciences*, Springer, London, UK, 2005.

[20] H. Gao, J. Lam, and Z. Wang, "Discrete bilinear stochastic systems with time-varying delay: stability analysis and control synthesis," *Chaos, Solitons & Fractals*, vol. 34, no. 2, pp. 394–404, 2007.

[21] S. Xu, J. Lam, and T. Chen, "Robust H_∞ control for uncertain discrete stochastic time-delay systems," *Systems & Control Letters*, vol. 51, no. 3-4, pp. 203–215, 2004.

[22] Q. Gao, G. Feng, Y. Wang, and J. Qiu, "Universal fuzzy models and universal fuzzy controllers for stochastic nonaffine nonlinear systems," *IEEE Transactions on Fuzzy Systems*, vol. 21, no. 2, pp. 328–341, 2013.

[23] B. Zhang, S. Xu, G. Zong, and Y. Zou, "Delay-dependent stabilization for stochastic fuzzy systems with time delays," *Fuzzy Sets and Systems*, vol. 158, no. 20, pp. 2238–2250, 2007.

[24] H. Huang and D. W. C. Ho, "Delay-dependent robust control of uncertain stochastic fuzzy systems with time-varying delay," *IET Control Theory & Applications*, vol. 1, no. 4, pp. 1075–1085, 2007.

[25] X. Liu and H. Zhang, "Delay-dependent robust stability of uncertain fuzzy large-scale systems with time-varying delays," *Automatica*, vol. 44, no. 1, pp. 193–198, 2008.

[26] C.-C. Ku, P.-H. Huang, and W.-J. Chang, "Observer-based robust fuzzy controller design for uncertain stochastic T-S fuzzy model with passivity performance," in *Proceedings of the 48th IEEE Conference on Decision and Control Held Jointly with the 28th Chinese Control Conference (CDC/CCC '09)*, pp. 7783–7788, Shanghai, China, December 2009.

[27] C.-S. Tseng, "Robust fuzzy filter design for a class of nonlinear stochastic systems," *IEEE Transactions on Fuzzy Systems*, vol. 15, no. 2, pp. 261–274, 2007.

[28] X. Su, P. Shi, L. Wu, and S. K. Nguang, "Induced l_2 filtering of fuzzy stochastic systems with time-varying delays," *IEEE Transactions on Cybernetics*, vol. 43, no. 4, pp. 1251–1264, 2013.

[29] Y. Tang, J.-A. Fang, M. Xia, and X. Gu, "Synchronization of Takagi-Sugeno fuzzy stochastic discrete-time complex networks with mixed time-varying delays," *Applied Mathematical Modelling. Simulation and Computation for Engineering and Environmental Systems*, vol. 34, no. 4, pp. 843–855, 2010.

[30] W.-J. Chang, S.-S. Jheng, and C.-C. Ku, "Fuzzy control with robust and passive properties for discrete-time Takagi-Sugeno fuzzy systems with multiplicative noises," *Proceedings of the Institution of Mechanical Engineers. Part I: Journal of Systems and Control Engineering*, vol. 226, no. 4, pp. 476–485, 2012.

[31] W. J. Chang, M. W. Chen, and C. C. Ku, "Passive fuzzy controller design for discrete ship steering systems via Takagi-Sugeno fuzzy model with multiplicative noises," *Journal of Marine Science and Technology*, vol. 21, no. 2, pp. 159–165, 2013.

[32] Y. Niu and D. W. C. Ho, "Stabilization of discrete-time stochastic systems via sliding mode technique," *Journal of the Franklin Institute*, vol. 349, no. 4, pp. 1497–1508, 2012.

[33] X.-L. Zhu and G.-H. Yang, "Jensen inequality approach to stability analysis of discrete-time systems with time-varying delay," in *Proceedings of the American Control Conference (ACC '08)*, pp. 1644–1649, June 2008.

[34] L. El Ghaoui, F. Oustry, and M. AitRami, "A cone complementarity linearization algorithm for static output-feedback and related problems," *IEEE Transactions on Automatic Control*, vol. 42, no. 8, pp. 1171–1176, 1997.

Hindawi Publishing Corporation
Mathematical Problems in Engineering
Volume 2013, Article ID 408941, 10 pages
http://dx.doi.org/10.1155/2013/408941

Research Article

Robust l_2-l_∞ Filtering for Discrete-Time Delay Systems

Chengming Yang,[1] Zhandong Yu,[1] Pinchao Wang,[2] Zhen Yu,[1] Hamid Reza Karimi,[3] and Zhiguang Feng[4]

[1] *College of Engineering, Bohai University, Jinzhou, Liaoning 121013, China*
[2] *School of Astronautics, Harbin Institute of Technology, Harbin, Heilongjiang 150001, China*
[3] *Department of Engineering, Faculty of Engineering and Science, University of Agder, 4898 Grimstad, Norway*
[4] *College of Information Science and Technology, Bohai University, Jinzhou, Liaoning 121013, China*

Correspondence should be addressed to Zhiguang Feng; oncharge@hku.hk

Received 11 September 2013; Accepted 8 October 2013

Academic Editor: Baoyong Zhang

The problem of robust l_2-l_∞ filtering for discrete-time system with interval time-varying delay and uncertainty is investigated, where the time delay and uncertainty considered are varying in a given interval and norm-bounded, respectively. The filtering problem based on the l_2-l_∞ performance is to design a filter such that the filtering error system is asymptotically stable with minimizing the peak value of the estimation error for all possible bounded energy disturbances. Firstly, sufficient l_2-l_∞ performance analysis condition is established in terms of linear matrix inequalities (LMIs) for discrete-time delay systems by utilizing reciprocally convex approach. Then a less conservative result is obtained by introducing some variables to decouple the Lyapunov matrices and the filtering error system matrices. Moreover, the robust l_2-l_∞ filter is designed for systems with time-varying delay and uncertainty. Finally, a numerical example is given to demonstrate the effectiveness of the filter design method.

1. Introduction

The uncertainty is unavoidable in practical engineering due to the parameter drafting, modeling error, and component aging. The controllers or filtering obtained based on nominal systems cannot be employed to get the desired performance. Therefore, more and more researchers are devoted to robust control or robust filtering problems; see, for instance, [1–4]. On the other hand, time-delay often exists in the practical engineering systems and is the main reason of the instability and poor performance of the systems. Time-delay systems have been widely studied during the past two decades [5–7]. In order to get less conservative results, more and more approaches have been proposed to develop delay-dependent conditions for discrete-time system with time-varying delay. For examples, Jensen's inequality is proposed in [8]; delay-partitioning method is utilized in [9]; improved results are obtained by using convex combination approach in [10].

In some practical applications, the peak value of the estimation error is required to be within a certain range and the aim of the l_2-l_∞ (energy-to-peak) filtering is to minimize the peak values of the filtering error for any bounded energy disturbance, which has received many attention. By using a parameter-dependent approach, the robust energy-to-peak filtering problem is considered in [11]. An improved robust energy-to-peak filtering condition is proposed by increasing the flexible dimensions in the solution space in [12]. The robust L_2-L_∞ filtering for stochastic systems and the exponential L_2-L_∞ filtering for Markovian jump systems are investigated in [13, 14], respectively. Compared with the corresponding continuous-time systems, discrete-time systems with time-varying delay have more stronger application background [15]. For discrete-time Markovian jumping systems, the reduced-order filter is designed in [16] such that the filtering error system satisfies an energy-to-peak performance. When time-delay appears, the robust energy-to-peak filtering problem for networked systems is tackled in [17]. For discrete-time switched systems with time-varying delay, an improved robust energy-to-peak filtering design method is proposed in [18].

In this paper we consider the problem of robust l_2-l_∞ filtering for uncertain discrete-time systems with time-varying delay. The filter is designed by employing the reciprocally convex approach proposed in [19] such that the filtering error system is asymptotically stable with an l_2-l_∞ performance. Firstly, a sufficient condition of the l_2-l_∞ performance analysis for nominal systems is obtained in terms of LMIs for systems with time-varying delay and uncertainty. Based on this criterion, by introducing some slack matrices, a less conservative result is obtained. Moreover, the desired filter for nominal systems with time-varying delay is obtained by solving a set of LMIs. Then the result is extended to the uncertain systems. A numerical example is given to illustrate the effectiveness of the presented results.

Notation. The notation used throughout the paper is given as follows. $\mathbb{R}^n$ is the n-dimensional Euclidean space and $P > 0$ (≥ 0) denotes that matrix P is real symmetric and positive definite (semidefinite); I and 0 present the identity matrix and zero matrix with compatible dimensions, respectively; $\star$ means the symmetric terms in a symmetric matrix and $\mathrm{sym}(A)$ stands for $A + A^T$; l_2 means the space of square summable infinite vector sequences; for any real function $x \in l_2$, we define $\|x\|_\infty = \sup_k \sqrt{x^T(k)x(k)}$ and $\|x\|_2 = \sqrt{\sum_{k=0}^{\infty} x^T(k)x(k)}$; $\|\cdot\|$ refer to the Euclidean vector norm. Matrices are assumed to be compatible for algebraic operations if their dimensions are not explicitly stated.

2. Problem Statement

Consider a class of uncertain discrete-time systems with time-varying delay described by

$$\begin{aligned} x(k+1) &= A(\sigma)x(k) + A_d(\sigma)x(k-d(k)) + B(\sigma)w(k), \\ y(k) &= C(\sigma)x(k) + C_d(\sigma)x(k-d(k)) + D(\sigma)w(k), \\ z(k) &= L(\sigma)x(k) + L_d(\sigma)x(k-d(k)) + G(\sigma)w(k), \\ x(k) &= \phi(k), \quad k = -d_2, -d_2+1, \ldots, 0, \end{aligned} \tag{1}$$

where $x(k) \in \mathbb{R}^n$ is the state vector; $y(k) \in \mathbb{R}^m$ is the measured output; $z(k) \in \mathbb{R}^p$ represents the signal to be estimated; $w(k) \in \mathbb{R}^l$ is assumed to be an arbitrary noise belonging to l_2 and $\phi(k)$ is a given initial condition sequence; $d(k)$ is a time-varying delay satisfying

$$1 \leq d_1 \leq d(k) \leq d_2 < \infty, \quad k = 1, 2, \ldots \tag{2}$$

$A(\sigma)$, $A_d(\sigma)$, $B(\sigma)$, $C(\sigma)$, $C_d(\sigma)$, $D(\sigma)$, $L(\sigma)$, $L_d(\sigma)$, and $G(\sigma)$ are system matrices and satisfy

$$\begin{aligned} A(\sigma) &= A + \Delta A(\sigma), \qquad A_d(\sigma) = A_d + \Delta A_d(\sigma), \\ B(\sigma) &= B + \Delta B(\sigma), \\ C(\sigma) &= C + \Delta C(\sigma), \qquad C_d(\sigma) = C_d + \Delta C_d(\sigma), \\ D(\sigma) &= D + \Delta D(\sigma), \\ L(\sigma) &= L + \Delta L(\sigma), \qquad L_d(\sigma) = L_d + \Delta L_d(\sigma), \\ G(\sigma) &= G + \Delta G(\sigma). \end{aligned} \tag{3}$$

Matrices $\Delta A(\sigma)$, $\Delta A_d(\sigma)$, $\Delta B(\sigma)$, $\Delta C(\sigma)$, $\Delta C_d(\sigma)$, $\Delta D(\sigma)$, $\Delta L(\sigma)$, $\Delta L_d(\sigma)$, and $\Delta G(\sigma)$ are unknown time-invariant matrix representing the uncertainty of the system satisfying the following conditions:

$$\begin{aligned} &\left[\Delta A(\sigma) \;\; \Delta A_d(\sigma) \;\; \Delta B(\sigma)\right] = M_1 \Delta_1(\sigma) \left[N_A \;\; N_{Ad} \;\; N_B\right], \\ &\qquad \Delta_1^T(\sigma)\Delta_1(\sigma) \leq I, \\ &\left[\Delta C(\sigma) \;\; \Delta C_d(\sigma) \;\; \Delta D(\sigma)\right] = M_2 \Delta_2(\sigma) \left[N_C \;\; N_{Cd} \;\; N_D\right], \\ &\qquad \Delta_2^T(\sigma)\Delta_2(\sigma) \leq I, \\ &\left[\Delta L(\sigma) \;\; \Delta L_d(\sigma) \;\; \Delta G(\sigma)\right] = M_3 \Delta_3(\sigma) \left[N_L \;\; N_{Ld} \;\; N_G\right], \\ &\qquad \Delta_3^T(\sigma)\Delta_3(\sigma) \leq I, \end{aligned} \tag{4}$$

where $\sigma \in \Theta$ and Θ is a compact set in $\mathbb{R}$. The system in (1) is assumed to be asymptotically stable. Our purpose is to design a full order linear filter for the estimate of $z(k)$:

$$\begin{aligned} \hat{x}(k+1) &= A_f \hat{x}(k) + B_f y(k), \quad \hat{x}(0) = 0, \\ \hat{z}(k) &= C_f \hat{x}(k) + D_f y(k), \end{aligned} \tag{5}$$

where A_f, B_f, C_f, and D_f are filter gains to be determined.

Let the augmented state vector $\tilde{x}(k) = \left[x^T(k) \;\; \hat{x}^T(k)\right]^T$ and $\tilde{z}(k) = z(k) - \hat{z}(k)$. Then the filtering error system is described as

$$\begin{aligned} \tilde{x}(k+1) &= \widetilde{A}(\sigma)\tilde{x}(k) + \widetilde{A}_d(\sigma)\Phi\tilde{x}(k-d(k)) + \widetilde{B}(\sigma)w(k) \\ \tilde{z}(k) &= \widetilde{L}(\sigma)\tilde{x}(k) + \widetilde{L}_d(\sigma)\Phi\tilde{x}(k-d(k)) + \widetilde{G}(\sigma)w(k) \\ \tilde{x}(k) &= \left[\phi^T(k) \;\; 0\right]^T, \quad k = -d_2, -d_2+1, \ldots, 0, \end{aligned} \tag{6}$$

where $\Phi = \left[I \;\; 0\right]$ and

$$\begin{aligned} \widetilde{A}(\sigma) &= \begin{bmatrix} A(\sigma) & 0 \\ B_f C(\sigma) & A_f \end{bmatrix}, \qquad \widetilde{A}_d(\sigma) = \begin{bmatrix} A_d(\sigma) \\ B_f C_d(\sigma) \end{bmatrix}, \\ \widetilde{B} &= \begin{bmatrix} B(\sigma) \\ B_f D(\sigma) \end{bmatrix}, \\ \widetilde{L}(k) &= \left[L(\sigma) - D_f C(\sigma) \;\; -C_f\right], \\ \widetilde{L}_d(\sigma) &= L_d(\sigma) - D_f C_d(\sigma), \qquad \widetilde{G}(\sigma) = G(\sigma) - D_f D(\sigma). \end{aligned} \tag{7}$$

The nominal system of (6) is system (6) without uncertainty; that is, $\Delta A(\sigma) = 0$, $\Delta A_d(\sigma) = 0$, $\Delta B(\sigma) = 0$, $\Delta C(\sigma) = 0$, $\Delta C_d(\sigma) = 0$, $\Delta D(\sigma) = 0$, $\Delta L(\sigma) = 0$, $\Delta L_d(\sigma) = 0$, and $\Delta G(\sigma) = 0$.

The following lemmas and definition will be utilized in the derivation of the main results.

Lemma 1 (see [20]). *For any matrices U and $V > 0$, the following inequality holds:*

$$UV^{-1}U^T \geq U + U^T - V. \tag{8}$$

Lemma 2 (see [19]). *Let $f_1, f_2, \ldots, f_N : \mathbb{R}^m \to \mathbb{R}$ have positive values in a subset D of $\mathbb{R}^m$. Then, the reciprocally convex combination of f_i over D satisfies*

$$\min_{\{\alpha_i | \alpha_i > 0, \sum_i \alpha_i = 1\}} \sum_i \frac{1}{\alpha_i} f_i(k) = \sum_i f_i(k) + \max_{g_{i,j}(k)} \sum_{i \neq j} g_{i,j}(k) \tag{9}$$

subject to

$$\left\{ g_{i,j} : \mathbb{R}^m \longrightarrow \mathbb{R}, g_{j,i}(k) = g_{i,j}(k), \begin{bmatrix} f_i(k) & g_{i,j}(k) \\ g_{j,i}(k) & f_j(k) \end{bmatrix} \geq 0 \right\}. \tag{10}$$

Lemma 3. *For any constant matrix $M > 0$, integers $a \leq b$, vector function w: $\{a, a+1, \ldots, b\} \to \mathbb{R}^n$, then*

$$-(b-a+1) \sum_{i=a}^{b} w^T(i) M w(i) \leq -\left(\sum_{i=a}^{b} w(i) \right)^T M \left(\sum_{i=a}^{b} w(i) \right). \tag{11}$$

Lemma 4. *Given a symmetric matrix Q and matrices H, E with appropriate dimensions, then*

$$Q + \operatorname{sym}(HFE) < 0, \tag{12}$$

for all $F^T F \leq I$, if and only if there exists a scalar $\varepsilon > 0$ such that

$$Q + \varepsilon E^T E + \varepsilon^{-1} H H^T < 0. \tag{13}$$

Definition 5. Given a scalar $\gamma > 0$, the filtering error $\tilde{z}(k)$ in (6) is said to satisfy the l_2-l_∞ disturbance attenuation level γ under zero initial state, and the following condition is satisfied:

$$\|\tilde{z}\|_\infty < \gamma \|w\|_2. \tag{14}$$

Our aim is to design a filter in the form of (5) such that the filtering error system in (6) is asymptotically stable and satisfies the l_2-l_∞ performance defined in Definition 5.

3. Main Results

In this section, the sufficient l_2-l_∞ performance analysis condition is first derived for nominal filtering error system of (6). Then an equivalent result is obtained by introducing three slack matrices. Based on these results, a desired filter is designed to render the nominal system of (6) asymptotically stable with an l_2-l_∞ performance. Then the result is extended to the uncertain system in (6).

3.1. l_2-l_∞ Performance Analysis. In this subsection, we first give the result of l_2-l_∞ performance analysis for nominal system of (6).

Theorem 6. *Given a scalar $\gamma > 0$, the nominal system of (6) is asymptotically stable with an l_2-l_∞ performance if there exist matrices $P > 0$, $Q_3 > 0$, $\overline{Q}_i > 0$, $i = 1, 2$, $S_j > 0$, $j = 1, 2$, and M such that the following LMIs hold:*

$$\begin{bmatrix} S_2 & M \\ \star & S_2 \end{bmatrix} \geq 0, \tag{15}$$

$$\begin{bmatrix} P & 0 & 0 & \widetilde{L}^T \\ \star & Q_3 & 0 & \widetilde{L}_d^T \\ \star & \star & I & \widetilde{G}^T \\ \star & \star & \star & \gamma^2 I \end{bmatrix} > 0, \tag{16}$$

$$\widetilde{\Pi} = \begin{bmatrix} \widetilde{\Pi}_{11} & \Phi^T S_1 & 0 & 0 & 0 & \widetilde{\Pi}_{16} S_1 & \widetilde{\Pi}_{17} S_2 & \widetilde{A}^T P \\ \star & \widetilde{\Pi}_{22} & \widetilde{\Pi}_{23} & M^T & 0 & 0 & 0 & 0 \\ \star & \star & \widetilde{\Pi}_{33} & \widetilde{\Pi}_{34} & 0 & d_1 A_d^T S_1 & \tilde{d} A_d^T S_2 & \widetilde{A}_d^T P \\ \star & \star & \star & \widetilde{\Pi}_{44} & 0 & 0 & 0 & 0 \\ \star & \star & \star & \star & -I & d_1 B^T S_1 & \tilde{d} B^T S_2 & \widetilde{B}^T P \\ \star & \star & \star & \star & \star & -S_1 & 0 & 0 \\ \star & \star & \star & \star & \star & \star & -S_2 & 0 \\ \star & \star & \star & \star & \star & \star & \star & -P \end{bmatrix} < 0, \tag{17}$$

where

$$\begin{aligned} \widetilde{\Pi}_{11} &= -P + Q_1 + Q_2 + \left(\tilde{d} + 1\right) \Phi^T Q_3 \Phi - \Phi^T S_1 \Phi, \\ \widetilde{\Pi}_{22} &= -S_2 - \overline{Q}_1 - S_1, \qquad \widetilde{\Pi}_{23} = S_2 - M^T, \\ \widetilde{\Pi}_{33} &= -Q_3 - 2S_2 + \operatorname{sym}(M), \qquad \widetilde{\Pi}_{34} = S_2 - M^T, \\ \widetilde{\Pi}_{44} &= -\overline{Q}_2 - S_2, \\ \widetilde{\Pi}_{16} &= d_1 \Phi^T (A - I)^T, \qquad \widetilde{\Pi}_{17} = \tilde{d} \Phi^T (A - I)^T, \\ Q_i &= \operatorname{diag}\left\{\overline{Q}_i, \overline{Q}_i\right\}, \quad i = 1, 2, \ \tilde{d} = d_2 - d_1. \end{aligned} \tag{18}$$

Proof. First, the asymptotic stability of the nominal system of (6) is proved. We denote $\tilde{\eta}(k) = \tilde{x}(k+1) - \tilde{x}(k)$ and the following Lyapunov functional is chosen:

$$V(k) = V_1(k) + V_2(k) + V_3(k) + V_4(k) + V_5(k), \tag{19}$$

where

$$V_1(k) = \tilde{x}^T(k) P \tilde{x}(k),$$

$$V_2(k) = \sum_{j=1}^{2} \sum_{i=k-d_j}^{k-1} \tilde{x}^T(i) Q_i \tilde{x}(i),$$

$$V_3(k) = \sum_{i=k-d(k)}^{k-1} \tilde{x}^T(i)\Phi^T Q_3 \Phi \tilde{x}(i) + \sum_{j=-d_2+1}^{-d_1} \sum_{i=k+j}^{k-1} \tilde{x}^T(i)\Phi^T Q_3 \Phi \tilde{x}(i),$$

$$V_4(k) = \sum_{j=-d_1}^{-1} \sum_{i=k+j}^{k-1} d_1 \tilde{\eta}^T(i)\Phi^T S_1 \Phi \tilde{\eta}(i),$$

$$V_5(k) = \sum_{j=-d_2}^{-d_1-1} \sum_{i=k+j}^{k-1} \tilde{d}\tilde{\eta}^T(i)\Phi^T S_2 \Phi \tilde{\eta}(i). \tag{20}$$

Calculating the forward difference of $V(k)$ along the trajectories of filtering error system (6) with $w(k) = 0$ yields

$$\begin{aligned}\Delta V_1(k) &= \tilde{x}^T(k+1)P\tilde{x}(k+1) - \tilde{x}^T(k)P\tilde{x}(k)\\ &= \left(\widetilde{A}\tilde{x}(k) + \widetilde{A}_d\Phi\tilde{x}(k-d(k))\right)^T\\ &\quad \times P\left(\widetilde{A}\tilde{x}(k) + \widetilde{A}_d\Phi\tilde{x}(k-d(k))\right)\\ &\quad - \tilde{x}^T(k)P\tilde{x}(k),\end{aligned} \tag{21}$$

$$\begin{aligned}\Delta V_2(k) &= \sum_{j=1}^{2} \tilde{x}^T(k)Q_j\tilde{x}(k)\\ &\quad - \sum_{j=1}^{2} \tilde{x}\left(k-d_j\right)Q_j\tilde{x}\left(k-d_j\right)\\ &\le \sum_{j=1}^{2} \tilde{x}^T(k)Q_j\tilde{x}(k)\\ &\quad - \sum_{j=1}^{2} \tilde{x}\left(k-d_j\right)\Phi^T\overline{Q}_j\Phi\tilde{x}\left(k-d_j\right),\end{aligned} \tag{22}$$

$$\begin{aligned}\Delta V_3(k) &= \left(\tilde{d}+1\right)\tilde{x}^T(k)\Phi^T Q_3\Phi\tilde{x}(k)\\ &\quad + \sum_{i=k+1-d(k+1)}^{k-1} \tilde{x}^T(i)\Phi^T Q_3\Phi\tilde{x}(i)\\ &\quad - \sum_{i=k+1-d(k)}^{k-1} \tilde{x}^T(i)\Phi^T Q_3\Phi\tilde{x}(i)\\ &\quad - \tilde{x}^T(k-d(k))\Phi^T Q_3\Phi\tilde{x}(k-d(k))\\ &\quad - \sum_{i=k-d_2+1}^{k-d_1} \tilde{x}^T(i)\Phi^T Q_3\Phi\tilde{x}(i)\\ &= \left(\tilde{d}+1\right)\tilde{x}^T(k)\Phi^T Q_3\Phi\tilde{x}(k)\\ &\quad + \sum_{i=k+1-d_1}^{k-1} \tilde{x}^T(i)\Phi^T Q_3\Phi\tilde{x}(i)\\ &\quad + \sum_{i=k+1-d(k+1)}^{k-d_1} \tilde{x}^T(i)\Phi^T Q_3\Phi\tilde{x}(i)\\ &\quad - \tilde{x}^T(k-d(k))\Phi^T Q_3\Phi\tilde{x}(k-d(k))\\ &\quad - \sum_{i=k+1-d(k)}^{k-1} \tilde{x}^T(i)\Phi^T Q_3\Phi\tilde{x}(i)\\ &\quad - \sum_{i=k-d_2+1}^{k-d_1} \tilde{x}^T(i)\Phi^T Q_3\Phi\tilde{x}(i)\\ &\le \left(\tilde{d}+1\right)\tilde{x}^T(k)\Phi^T Q_3\Phi\tilde{x}(k)\\ &\quad - \tilde{x}^T(k-d(k))\Phi^T Q_3\Phi\tilde{x}(k-d(k)).\end{aligned} \tag{23}$$

By using Lemma 3, we have

$$\begin{aligned}\Delta V_4(k) &= d_1^2\tilde{\eta}^T(k)\Phi^T S_1\Phi\tilde{\eta}(k)\\ &\quad - d_1\sum_{i=k-d_1}^{k-1} \tilde{\eta}^T(i)\Phi^T S_1\Phi\tilde{\eta}(i)\\ &\le d_1^2\left((A-I)\Phi\tilde{x}(k) + A_d\Phi\tilde{x}(k-d(k))\right)^T\\ &\quad \times S_1\left((A-I)\Phi\tilde{x}(k) + A_d\Phi\tilde{x}(k-d(k))\right)\\ &\quad - \left(\Phi\tilde{x}(k) - \Phi\tilde{x}\left(k-d_1\right)\right)^T\\ &\quad \times S_1\left(\Phi\tilde{x}(k) - \Phi\tilde{x}\left(k-d_1\right)\right).\end{aligned} \tag{24}$$

Since $\begin{bmatrix} S_2 & M \\ \star & S_2 \end{bmatrix} \ge 0$, the following inequality holds:

$$\begin{aligned}&\begin{bmatrix} \sqrt{\frac{\alpha_1}{\alpha_2}}\left(x(k-d(k)) - x\left(k-d_2\right)\right) \\ -\sqrt{\frac{\alpha_2}{\alpha_1}}\left(x\left(k-d_1\right) - x(k-d(k))\right)\end{bmatrix}^T\\ &\times \begin{bmatrix} S_2 & M \\ \star & S_2 \end{bmatrix}\\ &\times \begin{bmatrix} \sqrt{\frac{\alpha_1}{\alpha_2}}\left(x(k-d(k)) - x\left(k-d_2\right)\right) \\ -\sqrt{\frac{\alpha_2}{\alpha_1}}\left(x\left(k-d_1\right) - x(k-d(k))\right)\end{bmatrix} \ge 0,\end{aligned} \tag{25}$$

where $\alpha_1 = (d_2 - d(k))/\tilde{d}$ and $\alpha_2 = (d(k) - d_1)/\tilde{d}$. Then employing Lemma 2, for $d_1 < d(k) < d_2$, we have

$$\begin{aligned}
\Delta V_5(k) &= \tilde{d}^2 \tilde{\eta}^T(k) \Phi^T S_2 \Phi \tilde{\eta}(k) \\
&\quad - \tilde{d} \sum_{i=k-d_2}^{k-d(k)-1} \tilde{\eta}^T(i) \Phi^T S_2 \Phi \tilde{\eta}(i) \\
&\quad - \tilde{d} \sum_{i=k-d(k)}^{k-d_1-1} \tilde{\eta}^T(i) \Phi^T S_2 \Phi \tilde{\eta}(i) \\
&\le \tilde{d}^2 \tilde{\eta}^T(k) \Phi^T S_2 \Phi \tilde{\eta}(k) \\
&\quad - \frac{\tilde{d}}{d_2 - d(k)} \left(\sum_{i=k-d_2}^{k-d(k)-1} \Phi \tilde{\eta}(i) \right)^T S_2 \left(\sum_{i=k-d_2}^{k-d(k)-1} \Phi \tilde{\eta}(i) \right) \\
&\quad - \frac{\tilde{d}}{d(k) - d_1} \left(\sum_{i=k-d(k)}^{k-d_1-1} \Phi \tilde{\eta}(i) \right)^T S_2 \left(\sum_{i=k-d(k)}^{k-d_1-1} \Phi \tilde{\eta}(i) \right) \\
&\le \tilde{d}^2 \left((A - I) \Phi \tilde{x}(k) + A_d \Phi \tilde{x}(k - d(k)) \right)^T \\
&\quad \times S_2 \left((A - I) \Phi \tilde{x}(k) + A_d \Phi \tilde{x}(k - d(k)) \right) \\
&\quad - \begin{bmatrix} x(k - d(k)) - x(k - d_2) \\ x(k - d_1) - x(k - d(k)) \end{bmatrix}^T \begin{bmatrix} S_2 & M \\ \star & S_2 \end{bmatrix} \\
&\quad \times \begin{bmatrix} x(k - d(k)) - x(k - d_2) \\ x(k - d_1) - x(k - d(k)) \end{bmatrix}.
\end{aligned} \tag{26}$$

Note that when $d(k) = d_1$ or $d(k) = d_2$, it yields $x(k - d_1) - x(k - d(k)) = 0$ or $x(k - d(k)) - x(k - d_2) = 0$. Hence, the inequality in (24) still holds. Combining the conditions from (21) to (24), we have

$$\Delta V(k) = \zeta^T(k) \Pi_s \zeta(k), \tag{27}$$

where

$$\begin{aligned}
&\zeta(k) \\
&= \left[\tilde{x}^T(k) \quad \tilde{x}^T(k - d_1) \Phi^T \quad \tilde{x}^T(k - d(k)) \Phi^T \quad \tilde{x}^T(k - d_2) \Phi^T \right]^T, \\
&\Pi_s = \begin{bmatrix} \widetilde{\Pi}_{11} & \Phi^T S_1 & 0 & 0 \\ \star & \widetilde{\Pi}_{22} & \widetilde{\Pi}_{23} & M^T \\ \star & \star & \widetilde{\Pi}_{33} & \widetilde{\Pi}_{34} \\ \star & \star & \star & \widetilde{\Pi}_{44} \end{bmatrix} + \begin{bmatrix} \widetilde{\Pi}_{16} \\ 0 \\ d_1 A_d^T \\ 0 \end{bmatrix} S_1 \begin{bmatrix} \widetilde{\Pi}_{16} \\ 0 \\ d_1 A_d^T \\ 0 \end{bmatrix}^T \\
&\quad + \begin{bmatrix} \widetilde{\Pi}_{17} \\ 0 \\ \tilde{d} A_d^T \\ 0 \end{bmatrix} S_2 \begin{bmatrix} \widetilde{\Pi}_{17} \\ 0 \\ \tilde{d} A_d^T \\ 0 \end{bmatrix}^T + \begin{bmatrix} \widetilde{A}^T \\ 0 \\ \widetilde{A}_d^T \\ 0 \end{bmatrix} P \begin{bmatrix} \widetilde{A}^T \\ 0 \\ \widetilde{A}_d^T \\ 0 \end{bmatrix}^T.
\end{aligned} \tag{28}$$

On the other hand, the following inequality can be obtained from (17):

$$\begin{aligned}
\Pi_{s1} &= \begin{bmatrix} \widetilde{\Pi}_{11} & \Phi^T S_1 & 0 & 0 & \widetilde{\Pi}_{16} S_1 & \widetilde{\Pi}_{17} S_2 & \widetilde{A}^T P \\ \star & \widetilde{\Pi}_{22} & \widetilde{\Pi}_{23} & M^T & 0 & 0 & 0 \\ \star & \star & \widetilde{\Pi}_{33} & \widetilde{\Pi}_{34} & d_1 A_d^T S_1 & \tilde{d} A_d^T S_2 & \widetilde{A}_d^T P \\ \star & \star & \star & \widetilde{\Pi}_{44} & 0 & 0 & 0 \\ \star & \star & \star & \star & -S_1 & 0 & 0 \\ \star & \star & \star & \star & \star & -S_2 & 0 \\ \star & \star & \star & \star & \star & \star & -P \end{bmatrix} \\
&< 0
\end{aligned} \tag{29}$$

which is equivalent to $\Pi_s < 0$. Hence, $\Delta V(k) < 0$ which implies that the filtering error system in (6) with $w(k) = 0$ is asymptotically stable.

Next, we show the l_2-l_∞ performance of system (6). To this end, we define

$$J(k) = V(k) - \sum_{i=0}^{k-1} w^T(i) w(i). \tag{30}$$

Then under the zero initial condition, that is, $x(k) = 0$, $k = -d_2, -d_2 + 1, \ldots, 0$, it can be shown that for any nonzero $w(k) \in l_2[0, \infty)$

$$\begin{aligned}
J(k) &= \sum_{i=0}^{k-1} \left[\Delta V(i) - w^T(i) w(i) \right] \\
&= \sum_{i=0}^{k-1} \xi^T(i) \Big(\overline{\Pi} + \overline{\Pi}_1^T P \overline{\Pi}_1 + d_1^2 \overline{\Pi}_2^T S_1 \overline{\Pi}_2 \\
&\qquad + d_{12}^2 \overline{\Pi}_2^T S_2 \overline{\Pi}_2 \Big) \xi(i),
\end{aligned} \tag{31}$$

where

$$\begin{aligned}
&\xi(i) \\
&= \left[\tilde{x}^T(i) \quad \tilde{x}^T(i - d_1) \Phi^T \quad \tilde{x}^T(i - d(i)) \Phi^T \quad \tilde{x}^T(i - d_2) \Phi^T \quad w(i) \right]^T, \\
&\overline{\Pi} = \begin{bmatrix} \widetilde{\Pi}_{11} & \Phi^T S_1 & 0 & 0 & \widetilde{\Pi}_{15} \\ \star & \widetilde{\Pi}_{22} & \widetilde{\Pi}_{23} & M^T & 0 \\ \star & \star & \widetilde{\Pi}_{33} & \widetilde{\Pi}_{34} & -\widetilde{L}_d^T S \\ \star & \star & \star & \widetilde{\Pi}_{44} & 0 \\ \star & \star & \star & \star & \widetilde{\Pi}_{55} \end{bmatrix}, \\
&\overline{\Pi}_1 = \begin{bmatrix} \widetilde{A} & 0 & \widetilde{A}_d & 0 & \widetilde{B} \end{bmatrix}, \\
&\overline{\Pi}_2 = \begin{bmatrix} (A - I) \Phi & 0 & A_d & 0 & B \end{bmatrix}, \\
&\overline{\Pi}_3 = \begin{bmatrix} \widetilde{L} & 0 & \widetilde{L}_d & 0 & \widetilde{G} \end{bmatrix}.
\end{aligned} \tag{32}$$

By using Schur complement equivalence, the inequality in (17) is equivalent to $\overline{\Pi} + \overline{\Pi}_1^T P \overline{\Pi}_1 + d_1^2 \overline{\Pi}_2^T S_1 \overline{\Pi}_2 + d_{12}^2 \overline{\Pi}_2^T S_2 \overline{\Pi}_2 < 0$. Then we have $J(k) < 0$; that is,

$$V(k) < \sum_{i=0}^{k-1} w^T(i) w(i). \tag{33}$$

On the other hand, it yields from (16) and (33) that

$$\begin{aligned}\widetilde{z}^T(k)\widetilde{z}(k) &= \eta^T(k)\left[\widetilde{L}\ \ \widetilde{L}_d\ \ \widetilde{G}\right]^T\left[\widetilde{L}\ \ \widetilde{L}_d\ \ \widetilde{G}\right]\eta(k)\\ &\le \gamma^2\eta^T(k)\begin{bmatrix}P & 0 & 0\\ \star & Q_3 & 0\\ \star & \star & I\end{bmatrix}\eta(k)\\ &\le \gamma^2\left(V(k)+w^T(k)w(k)\right)\\ &\le \gamma^2\sum_{i=0}^{k}w^T(i)w(i) \le \gamma^2\sum_{i=0}^{\infty}w^T(i)w(i),\end{aligned} \tag{34}$$

where

$$\eta(k) = \begin{bmatrix}\widetilde{x}(k)\\ \Phi\widetilde{x}(k-d(k))\\ w(k)\end{bmatrix}. \tag{35}$$

Then, we have $\|\widetilde{z}\|_\infty < \gamma\|w\|_2$ by taking the supremum over time $k > 0$. By Definition 5, the filtering error $\widetilde{z}(k)$ satisfies a given l_2-l_∞ disturbance attenuation level. This completes the proof. □

Remark 7. The advantage of the results benefits from utilizing the reciprocally convex combination approach proposed in [19]. For the extensively used Jensen inequality [8], the integral term

$$\begin{aligned}&-\sum_{i=k-d_2}^{k-d_1-1}(d_2-d_1)\eta^T(i)S\eta(i)\\ &= -\sum_{i=k-d_2}^{k-d(k)-1}(d_2-d_1)\eta^T(i)S\eta(i)\\ &\quad -\sum_{i=k-d(k)}^{k-d_1-1}(d_2-d_1)\eta^T(i)S\eta(i)\end{aligned} \tag{36}$$

with $d_1 \le d(k) \le d_2$, $\eta(i) = x(i+1) - x(i)$ by the term

$$\begin{aligned}&-\left[x(k-d_1)-x(k-d(k))\right]^T S\left[x(k-d_1)-x(k-d(k))\right]\\ &-\left[x(k-d(k))-x(k-d_2)\right]^T S\left[x(k-d(k))-x(k-d_2)\right]\end{aligned} \tag{37}$$

which is a special case of the following term with $M = 0$

$$\begin{aligned}&-\begin{bmatrix}x(k-d(k))-x(k-d_1)\\ x(k-d(k))-x(k-d_2)\end{bmatrix}^T\\ &\times\begin{bmatrix}S & M\\ \star & S\end{bmatrix}\begin{bmatrix}x(k-d(k))-x(k-d_1)\\ x(k-d(t))-x(k-d_2)\end{bmatrix}\end{aligned} \tag{38}$$

with $\left[\begin{smallmatrix}S & M\\ \star & S\end{smallmatrix}\right] \ge 0$, which is one of the advantages of reciprocally convex combination approach. On the other hand, the delay partitioning method is widely applied to reduce the conservatism of the results [9, 21, 22]. Also, the method can be extended to the problem considered in this paper. However, it will rise significant computation cost with the partitioning number increasing. Therefore, the reciprocally convex method needs less decision variables and can be seen as a tradeoff between the conservatism and the computation cost.

Then, an equivalent condition of LMI (17) is obtained by introducing three slack matrices H_1, H_2, and T, which is presented in the following theorem.

Theorem 8. *Given a scalar $\gamma > 0$, the nominal system of (6) is asymptotically stable with an l_2-l_∞ performance if there exist matrices $P > 0$, $\overline{Q}_i > 0$, $i = 1, 2, 3$, $S_j > 0$, H_j, $j = 1, 2$, T, and M, such that the following LMIs hold:*

$$\begin{bmatrix}S_2 & M\\ \star & S_2\end{bmatrix} \ge 0, \tag{39}$$

$$\begin{bmatrix}P & 0 & 0 & \widetilde{L}^T\\ \star & Q_3 & 0 & \widetilde{L}_d^T\\ \star & \star & I & \widetilde{G}^T\\ \star & \star & \star & \gamma^2 I\end{bmatrix} > 0, \tag{40}$$

$$\widetilde{\Omega} = \begin{bmatrix}\widetilde{\Pi}_{11} & \Phi^T S_1 & 0 & 0 & 0 & \widetilde{\Pi}_{16}H_1^T & \widetilde{\Pi}_{17}H_2^T & \widetilde{A}^T T^T\\ \star & \widetilde{\Pi}_{22} & \widetilde{\Pi}_{23} & M^T & 0 & 0 & 0 & 0\\ \star & \star & \widetilde{\Pi}_{33} & \widetilde{\Pi}_{34} & 0 & d_1 A_d^T H_1^T & \tilde{d}A_d^T H_2^T & \widetilde{A}_d^T T^T\\ \star & \star & \star & \widetilde{\Pi}_{44} & 0 & 0 & 0 & 0\\ \star & \star & \star & \star & -I & d_1 B^T H_1^T & \tilde{d}B^T H_2^T & \widetilde{B}^T T^T\\ \star & \star & \star & \star & \star & S_1 - H_1^T - H_1 & 0 & 0\\ \star & \star & \star & \star & \star & \star & S_2 - H_2^T - H_2 & 0\\ \star & \star & \star & \star & \star & \star & \star & P - T^T - T\end{bmatrix} < 0, \tag{41}$$

where $\widetilde{\Pi}_{ii}$, $i = 1, \ldots, 4$, $\widetilde{\Pi}_{16}$, $\widetilde{\Pi}_{17}$, $\widetilde{\Pi}_{23}$, *and* $\widetilde{\Pi}_{34}$ *are defined in* (17).

Proof. On one hand, if (17) holds, then there exist $H_j = H_j^T = S_j$, $j = 1, 2$, and $T = T^T = P$ such that (41) holds. On the other hand, if (41) holds, we have the following inequality based on Lemma 1:

$$\begin{bmatrix} \widetilde{\Pi}_{11} & \Phi^T S_1 & 0 & 0 & 0 & \widetilde{\Pi}_{16} H_1^T & \widetilde{\Pi}_{17} H_2^T & \widetilde{A}^T T^T \\ \star & \widetilde{\Pi}_{22} & \widetilde{\Pi}_{23} & M^T & 0 & 0 & 0 & 0 \\ \star & \star & \widetilde{\Pi}_{33} & \widetilde{\Pi}_{34} & 0 & d_1 A_d^T H_1^T & \tilde{d} A_d^T H_2^T & \widetilde{A}_d^T T^T \\ \star & \star & \star & \widetilde{\Pi}_{44} & 0 & 0 & 0 & 0 \\ \star & \star & \star & \star & -I & d_1 B^T H_1^T & \tilde{d} B^T H_2^T & \widetilde{B}^T T^T \\ \star & \star & \star & \star & \star & -H_1 S_1^{-1} H_1^T & 0 & 0 \\ \star & \star & \star & \star & \star & \star & -H_2 S_2^{-1} H_2^T & 0 \\ \star & \star & \star & \star & \star & \star & \star & -TP^{-1}T^T \end{bmatrix} < 0. \tag{42}$$

In addition, matrices H_j, $j = 1, 2$, and T are nonsingular due to $S_j - H_j^T - H_j < 0$, $j = 1, 2$, and $P - T^T - T < 0$. Then, pre- and promultiplying (42) by $\mathrm{diag}\{I, I, I, I, I, S_1 H_1^{-1}, S_2 H_2^{-1}, PT^{-1}\}$ and its transpose yields (17). Therefore, the equivalence between (41) and (17) is proved. □

3.2. Robust Filter Design. In this subsection, the filter in the form of (5) is firstly designed such that the nominal filtering error system of (6) is asymptotically stable with an l_2-l_∞ performance. Then the robust filtering problem is solved. Based on the result of Theorem 8, the filter design method for nominal system of (1) is presented in the following theorem.

Theorem 9. *Given a scalar* $\gamma > 0$, *the nominal system of* (6) *is asymptotically stable with an* l_2-l_∞ *performance if there exist matrices* $\begin{bmatrix} P_1 & P_2 \\ \star & P_3 \end{bmatrix} > 0$, $Q_3 > 0$, $\widetilde{Q}_l > 0$, $\overline{Q}_l > 0$, $l = 1, 2$, $S_j > 0$, H_j, F_j, $j = 1, 2$, *diagonal matrix* $N > 0$, T_1, *and* M *such that the following set of LMIs hold:*

$$\begin{bmatrix} S_2 & M \\ \star & S_2 \end{bmatrix} \geq 0 \tag{43}$$

$$\Omega = \begin{bmatrix} \Xi & \Gamma \\ \star & \Lambda \end{bmatrix} < 0 \tag{44}$$

$$\Upsilon = \begin{bmatrix} P_1 & P_2 & 0 & 0 & \left(L - \overline{D}_f C\right)^T \\ \star & P_3 & 0 & 0 & -\overline{C}_f^T \\ \star & \star & Q_3 & 0 & \left(L_d - \overline{D}_f C_d\right)^T \\ \star & \star & \star & I & \left(G - \overline{D}_f C_d\right)^T \\ \star & \star & \star & \star & \gamma^2 I \end{bmatrix} > 0, \tag{45}$$

where

$$\Xi = \begin{bmatrix} \Xi_{11} & -P_2 & S_1 & C^T N C_d & 0 & 0 \\ \star & \Xi_{22} & 0 & 0 & 0 & 0 \\ \star & \star & \Xi_{33} & S_2 - M^T & M^T & 0 \\ \star & \star & \star & \Xi_{44} & S_2 - M^T & 0 \\ \star & \star & \star & \star & \Xi_{55} & 0 \\ \star & \star & \star & \star & \star & -I \end{bmatrix},$$

$$\Gamma = \begin{bmatrix} \Gamma_{11} & \Gamma_{12} & A^T T_1^T + C^T \mathscr{A}_{s0} \overline{B}_f^T & A^T F_1^T + C^T \mathscr{A}_{s0} \overline{B}_f^T \\ 0 & 0 & \overline{A}_f^T & \overline{A}_f^T \\ 0 & 0 & 0 & 0 \\ d_1 A_d^T H_1^T & \tilde{d} A_d^T H_2^T & A_d^T T_1^T + C_d^T \mathscr{A}_{s0} \overline{B}_f^T & A_d^T F_1^T + C_{di}^T \mathscr{A}_{s0} \overline{B}_f^T \\ 0 & 0 & 0 & 0 \\ d_1 B^T H_1^T & \tilde{d} B^T H_2^T & B^T T_1^T + D^T \mathscr{A}_{s0} \overline{B}_f^T & B^T F_1^T + D^T \mathscr{A}_{s0} \overline{B}_f^T \end{bmatrix},$$

$$\Lambda = \begin{bmatrix} S_1 - H_1 - H_1^T & 0 & 0 & 0 \\ \star & S_2 - H_2 - H_2^T & 0 & 0 \\ \star & \star & P_1 - T_1 - T_1^T & P_2 - F_2 - F_1^T \\ \star & \star & \star & P_3 - F_2 - F_2^T \end{bmatrix},$$

$$\Xi_{11} = -\left(P_1 + S_1\right) + \overline{Q}_1 + \overline{Q}_2 + \left(\tilde{d} + 1\right) Q_3,$$

$$\Xi_{22} = -P_3 + \widetilde{Q}_1 + \widetilde{Q}_2,$$

$$\Xi_{33} = -S_2 - \overline{Q}_1 - S_1,$$

$$\Xi_{44} = -Q_3 + \mathrm{sym}\left(M_i - S_{2i}\right),$$

$$\Xi_{55} = -\overline{Q}_2 - S_2,$$

$$\Gamma_{11} = d_1 (A - I)^T H_1^T, \qquad \Gamma_{12} = \tilde{d} (A - I)^T H_2^T. \tag{46}$$

Moreover, a suitable l_2-l_∞ *filter is given by*

$$A_f = \overline{A}_f F_2^{-1}, \qquad B_f = \overline{B}_f, \qquad C_f = \overline{C}_f F_2^{-1}, \qquad D_f = \overline{D}_f. \tag{47}$$

Proof. Firstly, we introduce four matrices T_1, T_2, T_3, and T_4 with T_4 invertible and define

$$J_1 = \begin{bmatrix} I & 0 \\ 0 & T_2 T_4^{-1} \end{bmatrix}, \qquad F_1 = T_2 T_4^{-1} T_3, \qquad F_2 = T_2 T_4^{-T} T_2^T,$$

$$\widetilde{Q}_l = T_2 T_4^{-1} \overline{Q}_l T_4^{-T} T_2^T, \qquad J = \mathrm{diag}\left\{J_1, I, I, I, I, I, I, I, J_1\right\},$$

$$\begin{bmatrix} P_1 & P_2 \\ \star & P_3 \end{bmatrix} = J_1 P J_1^T, \qquad T = \begin{bmatrix} T_1 & T_2 \\ T_3 & T_4 \end{bmatrix},$$

$$J_2 = \mathrm{diag}\left\{J_1, I, I, I\right\},$$

$$\begin{bmatrix} \overline{A}_f & \overline{B}_f \\ \overline{C}_f & \overline{D}_f \end{bmatrix} = \begin{bmatrix} T_2 & 0 \\ 0 & I \end{bmatrix} \begin{bmatrix} A_f & B_f \\ C_f & D_f \end{bmatrix} \begin{bmatrix} T_4^{-T} T_2^T & 0 \\ 0 & I \end{bmatrix}. \tag{48}$$

From (44), we have $F_2 + F_2^T = T_2 T_4^{-T} T_2^T + T_2 T_4^{-1} T_2^T > 0$ which implies that T_2 is nonsingular. Hence, J and J_2 are

nonsingular. The inequality in (45) can be obtained by pre- an promultiplying (33) with J_2 and J_2^T, respectively. Noting that

$$\overline{\Omega} = J\widetilde{\Omega}J^T \tag{49}$$

we have $\widetilde{\Omega} < 0$. On the other hand, because T_2 and T_4 cannot be obtained from (44), we cannot determine the filters from (48). However, we can construct an equivalent filter transfer function from $y(k)$ to $\widetilde{z}(k)$:

$$\begin{aligned} T_{\widetilde{z}y} &= C_f\left(zI - A_f\right)^{-1}B_f + D_f \\ &= \overline{C}_f T_2^{-T}T_4^T\left(zI - T_2^{-1}\overline{A}_f T_2^{-T}T_4^T\right)^{-1}T_2^{-1}\overline{B}_f + \overline{D}_f \\ &= \overline{C}_f\left(zF_2 - \overline{A}_f\right)^{-1}\overline{B}_f + \overline{D}_f \\ &= \overline{C}_f F_2^{-1}\left(zI - \overline{A}_f F_2^{-1}\right)^{-1}\overline{B}_f + \overline{D}_f. \end{aligned} \tag{50}$$

Therefore, the desired filter can be obtained from (47). This completes the proof. □

Then the filter design result for uncertain system (6) is presented in the following theorem.

Theorem 10. *Given a scalar $\gamma > 0$, the system in* (6) *with uncertainty is asymptotically stable with an l_2-l_∞ performance if there exist matrices $\begin{bmatrix} P_1 & P_2 \\ \star & P_3 \end{bmatrix} > 0$, $Q_3 > 0$, $\overline{Q}_l > 0$, $\overline{Q}_l > 0$, $l = 1, 2$, $S_j > 0$, H_j, F_j, $j = 1, 2$, diagonal matrix $N > 0$, T_1, M, and scalars $\varepsilon_i > 0$, $i = 1, \ldots, 4$ such that the following set of LMIs hold:*

$$\begin{bmatrix} S_2 & M \\ \star & S_2 \end{bmatrix} \geq 0, \tag{51}$$

$$\begin{bmatrix} \Omega + \varepsilon_3\Omega_1^T\Omega_1 + \varepsilon_4\Omega_2^T\Omega_2 & \Omega_3 & \Omega_4 \\ \star & -\varepsilon_3 I & 0 \\ \star & \star & -\varepsilon_4 I \end{bmatrix} < 0, \tag{52}$$

$$\begin{bmatrix} \Upsilon_{11} & P_2 & \Upsilon_{13} & \Upsilon_{14} & \left(L - \overline{D}_f C\right)^T & 0 & 0 \\ \star & P_3 & 0 & 0 & -\overline{C}_f^T & 0 & 0 \\ \star & \star & \Upsilon_{33} & \Upsilon_{34} & \left(L_d - \overline{D}_f C_d\right)^T & 0 & 0 \\ \star & \star & \star & \Upsilon_{44} & \left(G - \overline{D}_f C_d\right)^T & 0 & 0 \\ \star & \star & \star & \star & \gamma^2 I & M_3 & 0 \\ \star & \star & \star & \star & \star & \varepsilon_1 I & \overline{D}_f M_2 \\ \star & \star & \star & \star & \star & \star & \varepsilon_2 I \end{bmatrix} > 0, \tag{53}$$

where Ω is defined in (44) *and*

$$\Omega_1 = \begin{bmatrix} N_A & 0 & 0 & N_{Ad} & 0 & N_B & 0 & 0 & 0 & 0 \end{bmatrix},$$

$$\Omega_2 = \begin{bmatrix} N_C & 0 & 0 & N_{Cd} & 0 & N_D & 0 & 0 & 0 & 0 \end{bmatrix},$$

$$\Omega_3 = \begin{bmatrix} 0 & 0 & 0 & 0 & 0 & 0 & d_1 M_1^T H_1^T & \tilde{d} M_1^T H_2^T & M_1^T T_1^T & M_1^T F_1^T \end{bmatrix}^T,$$

$$\Omega_4 = \begin{bmatrix} 0 & 0 & 0 & 0 & 0 & 0 & 0 & 0 & M_2^T \widetilde{B}_f^T & M_2^T \widetilde{B}_f^T \end{bmatrix}^T,$$

$$\begin{aligned} \Upsilon_{11} &= P_1 - \varepsilon_1 N_L^T N_L - \varepsilon_2 N_C^T N_C, \\ \Upsilon_{13} &= -\varepsilon_1 N_L^T N_{Ld} - \varepsilon_2 N_C^T N_{Cd}, \\ \Upsilon_{14} &= -\varepsilon_1 N_L^T N_G - \varepsilon_2 N_C^T N_D, \\ \Upsilon_{33} &= Q_3 - \varepsilon_1 N_{Ld}^T N_{Ld} - \varepsilon_2 N_{Cd}^T N_{Cd}, \\ \Upsilon_{34} &= -\varepsilon_1 N_{Ld}^T N_G - \varepsilon_2 N_{Cd}^T N_D, \\ \Upsilon_{44} &= I - \varepsilon_1 N_G^T N_G - \varepsilon_2 N_D^T N_D. \end{aligned} \tag{54}$$

Moreover, a suitable l_2-l_∞ filter is given by

$$A_f = \overline{A}_f F_2^{-1}, \qquad B_f = \overline{B}_f, \qquad C_f = \overline{C}_f F_2^{-1}, \qquad D_f = \overline{D}_f. \tag{55}$$

Proof. Firstly, replace matrices A, A_d, B, C, C_d, and D in (44) with $A+\Delta A$, $A_d+\Delta A_d$, $B+\Delta B$, $C+\Delta C$, $C_d+\Delta C_d$, and $D+\Delta D$, respectively, and the following inequality is obtained:

$$\Omega + \mathrm{sym}\left(\Omega_1^T\Delta_1^T\Omega_3^T\right) + \mathrm{sym}\left(\Omega_2^T\Delta_2^T\Omega_4^T\right) < 0, \tag{56}$$

where Ω_i, $i = 1, \ldots, 4$ are defined in (52). Then by using Lemma 4, the above inequality holds if and only if

$$\Omega + \varepsilon_3\Omega_1^T\Omega_1 + \varepsilon_3^{-1}\Omega_3\Omega_3^T + \varepsilon_4\Omega_2^T\Omega_2 + \varepsilon_4^{-1}\Omega_4\Omega_4^T < 0. \tag{57}$$

Then by using Schur complement equivalence, the inequality in (57) is equivalent to (44). Substituting L, L_d, and G in (45) with $L + \Delta L$, $L_d + \Delta L_d$, and $G + \Delta G$, respectively, we can get

$$\Upsilon + \mathrm{sym}\left(\Upsilon_1^T\Delta_3^T\Upsilon_3^T\right) + \mathrm{sym}\left(\Upsilon_2^T\Delta_2^T\Upsilon_4^T\right) > 0, \tag{58}$$

where

$$\Upsilon_1 = \begin{bmatrix} N_L & N_{Ld} & N_G & 0 \end{bmatrix}, \qquad \Upsilon_2 = \begin{bmatrix} N_C & N_{Cd} & N_D & 0 \end{bmatrix}$$

$$\Upsilon_3 = \begin{bmatrix} 0 & 0 & 0 & M_3^T \end{bmatrix}, \qquad \Upsilon_4 = \begin{bmatrix} 0 & 0 & 0 & M_2^T\overline{D}_f^T \end{bmatrix}. \tag{59}$$

By following the similar line, the equivalence between (58) and (53) can be proved. □

4. Illustrative Example

In this section, the following example is given to demonstrate the effectiveness of the proposed approach.

Example 1. Firstly, consider a nominal discrete-time delay system in (1) with the following parameters:

$$A = \begin{bmatrix} 0.1 & -0.5 \\ 0.2 & 0.5 \end{bmatrix}, \quad A_d = \begin{bmatrix} 0.1 & 0 \\ 0 & 0.2 \end{bmatrix},$$
$$B = \begin{bmatrix} -1 \\ 1 \end{bmatrix}, \quad C = \begin{bmatrix} -0.1 & -1 \end{bmatrix}, \quad C_d = \begin{bmatrix} -0.1 & 0.6 \end{bmatrix},$$
$$L = \begin{bmatrix} 1 & 0.2 \end{bmatrix}, \quad L_d = \begin{bmatrix} 0.5 & 0.6 \end{bmatrix}, \quad D = 0.1,$$
$$G = -0.5. \tag{60}$$

For different delay cases, the different minima of γ can be calculated by solving the LMIs in Theorem 9. When the upper bound of the time-varying delay is 5, that is, $d_2 = 5$, the minima of γ for a given d_1 are listed in Table 1.

Moreover, when $d_1 = 2$, $d_2 = 5$, the corresponding l_2-l_∞ filter is given as follows:

$$A_f = \begin{bmatrix} 2.6553 & -1.9535 \\ 2.2783 & -1.5631 \end{bmatrix}, \quad B_f = \begin{bmatrix} -1.5405 \\ -1.9024 \end{bmatrix},$$
$$C_f = \begin{bmatrix} -1.3230 & 1.0479 \end{bmatrix}, \quad D_f = 0.2378. \tag{61}$$

When uncertainty appears in the system, Theorem 10 will be used for the desired filter design. The following uncertainty parameters are considered:

$$M_1 = \begin{bmatrix} 0.35 & 0 \\ -0.2 & 0.1 \end{bmatrix}, \quad N_A = \begin{bmatrix} 0.2 & 0.4 \\ 0 & 0.5 \end{bmatrix},$$
$$N_{Ad} = \begin{bmatrix} 0.1 & 0 \\ 0 & 0.2 \end{bmatrix}, \quad N_B = \begin{bmatrix} 0.3 \\ 0.1 \end{bmatrix},$$
$$M_2 = 0.2, \quad N_C = \begin{bmatrix} 0.15 & -0.22 \end{bmatrix}, \tag{62}$$
$$N_{Cd} = \begin{bmatrix} -0.3 & 0.2 \end{bmatrix}, \quad N_D = -0.5,$$
$$M_3 = -0.4, \quad N_L = \begin{bmatrix} -0.25 & -0.2 \end{bmatrix},$$
$$N_{Ld} = \begin{bmatrix} 0.13 & 0.32 \end{bmatrix}, \quad N_D = 0.2.$$

Similarly, the allowed minimal values of γ can be obtained by solving the LMIs in Theorem 10. For $d_2 = 5$, the different minimum allowed γ are listed in Table 2 for the uncertain system with different d_1.

Moreover, when $d_1 = 2$, $d_2 = 5$, the desired filter is given as follows:

$$A_f = \begin{bmatrix} -0.1261 & 0.2147 \\ -0.3333 & 0.5671 \end{bmatrix}, \quad B_f = \begin{bmatrix} -0.1725 \\ -0.2622 \end{bmatrix},$$
$$C_f = \begin{bmatrix} -0.0076 & 0.0125 \end{bmatrix}, \quad D_f = 0.1106. \tag{63}$$

Table 1: Minimum allowed γ for $d_2 = 5$.

Methods	d_1			
	1	2	3	4
Theorem 9	1.8371	1.5652	1.3585	1.1861

Table 2: Minimum allowed γ for $d_2 = 5$.

Methods	d_1			
	1	2	3	4
Theorem 10	3.4157	2.6514	2.1568	1.8405

5. Conclusions

The robust l_2-l_∞ filtering has been studied for uncertain discrete-time systems with time-varying delay in this paper. Based on reciprocally convex approach, the sufficient l_2-l_∞ performance analysis conditions in terms of LMIs have been proposed to render the filtering error systems asymptotically stable with an l_2-l_∞ performance. Then the desired filter has been designed for the filtering error system with time-varying delay. The results presented in this paper are in terms of strict LMIs which make the conditions more tractable. Finally, a numerical example is given to demonstrate the effectiveness of our methods. For future research topic, the results can be extended to the system with actuator/sensor failures which may lead to unsatisfactory performance and has attracted many researchers' attention such as faulty diagnosis [23, 24] and fault tolerant control [25].

Conflict of Interests

None of the authors of the paper has declared any conflict of interests.

Acknowledgment

This work was partially supported by Liaoning Provincial Natural Science Foundation of China (2013020227).

References

[1] H. Gao and C. Wang, "A delay-dependent approach to robust H_∞ filtering for uncertain discrete-time state-delayed systems," *IEEE Transactions on Signal Processing*, vol. 52, no. 6, pp. 1631–1640, 2004.

[2] J. Lam, Z. Shu, S. Xu, and E. K. Boukas, "Robust H_∞ control of descriptor discrete-time Markovian jump systems," *International Journal of Control*, vol. 80, no. 3, pp. 374–385, 2007.

[3] S. Ma, C. Zhang, and Z. Cheng, "Delay-dependent robust H_∞ control for uncertain discrete-time singular systems with time-delays," *Journal of Computational and Applied Mathematics*, vol. 217, no. 1, pp. 194–211, 2008.

[4] L. Wu, P. Shi, H. Gao, and C. Wang, "A new approach to robust H_∞ filtering for uncertain systems with both discrete and distributed delays," *Circuits, Systems, and Signal Processing*, vol. 26, no. 2, pp. 229–247, 2007.

[5] H. Li, X. Jing, and K. H. R, "Output-feedback-based H_∞ control for vehicle suspension systems with control delay," *IEEE*

Transactions on Industrial Electronics, vol. 61, no. 1, pp. 436–446, 2014.

[6] T. Li, W. X. Zheng, and C. Lin, "Delay-slope-dependent stability results of recurrent neural networks," *IEEE Transactions on Neural Networks*, vol. 22, no. 12, pp. 2138–2143, 2011.

[7] Q. Zhou, P. Shi, S. Xu, and H. Li, "Observer-based adaptive neural network control for nonlinear stochastic systems with time-delay," *IEEE Transactions on Neural Networks and Learning Systems*, vol. 24, no. 1, pp. 71–80, 2013.

[8] X. Zhu and G. Yang, "Jensen inequality approach to stability analysis of discrete-time systems with time-varying delay," in *Proceedings of the American Control Conference (ACC '08)*, pp. 1644–1649, Seattle, Wash, USA, June 2008.

[9] X. Meng, J. Lam, H. Gao, and B. Du, "A delay-partitioning approach to the stability analysis of discrete-time systems," *Automatica*, vol. 46, no. 3, pp. 610–614, 2010.

[10] H. Shao and Q. L. Han, "New stability criteria for linear discrete-time systems with interval-like time-varying delays," *IEEE Transactions on Automatic Control*, vol. 56, no. 3, pp. 619–625, 2011.

[11] X. Meng, H. Gao, and S. Mou, "A new parameter-dependent approach to robust energy-to-peak filter design," *Circuits, Systems, and Signal Processing*, vol. 26, no. 4, pp. 451–471, 2007.

[12] H. Zhang, A. S. Mehr, and Y. Shi, "Improved robust energy-to-peak filtering for uncertain linear systems," *Signal Processing*, vol. 90, no. 9, pp. 2667–2675, 2010.

[13] B. Zhang and S. Xu, "Robust L_2-L_∞ filtering for uncertain nonlinearly parameterized stochastic systems with time-varying delays," *Circuits, Systems, and Signal Processing*, vol. 26, no. 5, pp. 751–772, 2007.

[14] B. Zhang and Y. Li, "Exponential L_2-L_∞ filtering for distributed delay systems with markovian jumping parameters," *Signal Processing*, vol. 93, no. 1, pp. 206–216, 2013.

[15] H. Gao and T. Chen, "New results on stability of discrete-time systems with time-varying state delay," *IEEE Transactions on Automatic Control*, vol. 52, no. 2, pp. 328–334, 2007.

[16] H. Liu, F. Sun, and Z. Sun, "Reduced-order filtering with energy-to-peak performance for discrete-time Markovian jumping systems," *IMA Journal of Mathematical Control and Information*, vol. 21, no. 2, pp. 143–158, 2004.

[17] H. Zhang, Y. Shi, and A. S. Mehr, "Robust energy-to-peak filtering for networked systems with time-varying delays and randomly missing data," *IET Control Theory & Applications*, vol. 4, no. 12, pp. 2921–2936, 2010.

[18] J. Qiu, G. Feng, and J. Yang, "New results on robust energy-to-peak filtering for discrete-time switched polytopic linear systems with time-varying delay," *IET Control Theory & Applications*, vol. 2, no. 9, pp. 795–806, 2008.

[19] P. G. Park, J. W. Ko, and C. Jeong, "Reciprocally convex approach to stability of systems with time-varying delays," *Automatica*, vol. 47, no. 1, pp. 235–238, 2011.

[20] E. K. Boukas, *Control of Singular Systems with Random Abrupt Changes*, Communications and Control Engineering Series, Springer, Berlin, Germany, 2008.

[21] Z. Feng, J. Lam, and H. Gao, "α-dissipativity analysis of singular time-delay systems," *Automatica*, vol. 47, no. 11, pp. 2548–2552, 2011.

[22] S. Mou, H. Gao, and T. Chen, "New delay-range-dependent stability condition for linear system," in *Proceedings of the 7th World Congress on Intelligent Control and Automation (WCICA '08)*, pp. 313–316, Chongqing, China, June 2008.

[23] S. Yin, S. Ding, A. Haghani, H. Hao, and P. Zhang, "A comparison study of basic data-driven fault diagnosis and process monitoring methods on the benchmark Tennessee Eastman process," *Journal of Process Control*, vol. 22, no. 9, pp. 1567–1581, 2012.

[24] S. Yin, X. Yang, and H. R. Karimi, "Data-driven adaptive observer for fault diagnosis," *Mathematical Problems in Engineering*, vol. 2012, Article ID 832836, 21 pages, 2012.

[25] S. Yin, S. Ding, and H. Luo, "Real-time implementation of fault tolerant control system with performance optimization," *IEEE Transactions on Industrial Electronics*, vol. 61, no. 5, pp. 2402–2411, 2013.

Hindawi Publishing Corporation
Mathematical Problems in Engineering
Volume 2013, Article ID 747641, 9 pages
http://dx.doi.org/10.1155/2013/747641

Research Article

Nonlinear Robust Disturbance Attenuation Control Design for Static Var Compensator in Power System

Ting Liu, Nan Jiang, Yuanwei Jing, and Siying Zhang

Faculty of Information Science and Engineering, Northeastern University, Box 135 Shenyang, Liaoning 110819, China

Correspondence should be addressed to Ting Liu; liuting_tinka@sina.cn

Received 23 August 2013; Accepted 28 October 2013

Academic Editor: Baoyong Zhang

The problem of designing an adaptive backstepping controller for nonlinear static var compensator (SVC) system is addressed adopting two perspectives. First, instead of artificially assuming an upper bound or inequality scaling, the minimax theory is used to treat the external unknown disturbances. The system is insensitive to effects of large disturbances due to taking into account the worst case disturbance. Second, a parameter projection mechanism is introduced in adaptive control to force the parameter estimate within a prior specified interval. The proposed controller handles the nonlinear parameterization without compromising control smoothness and at the same time the parameter estimate speed is improved and the robustness of system is strengthened. Considering the short-circuit ground fault and mechanical power perturbation, a simulation study is carried out. The results show the effectiveness of the proposed control method.

1. Introduction

With the expansion of the scale of electric network, static var compensators (SVCs) have been employed in power systems for several years in a cost-effective manner [1]. SVCs play important roles in voltage regulation and stability improvement due to simple structures and reactive power compensation [2]. Numerous control techniques with varying levels of success for SVC have been used to enhance power system stability [3, 4]. The fixed-gain PID controllers are designed for improving the dynamic impact of SVCs based on the linearization model without taking nonlinear characteristic into consideration [5]. The exact feedback linearization design depends on the basis of nonlinear SVC model [6]; however, such a solution requires a completely accurate model, which is rarely satisfying from the practical point of view. The Hamiltonian function method cannot only develop nonlinear control for the SVC, but also solve the problem of L_2 disturbance attenuation [7], whereas it is hard work to express the nonlinear system into a Hamiltonian system. Adaptive backstepping technique has received a considerable attention in recent robust control literatures of power systems [8, 9].

Several papers have studied the adaptive backstepping SVC control strategies and gave insights into the effect of external disturbance. There are many causes of variations in a power system's operating conditions, such as continual changes in power consumption and changes in the generation and transmission device structure. Significant progress has been made in disturbance treatment linking with backstepping method; the H_∞ control problem can be solved by inequality-scaling the item including disturbance in energy function [10, 11], while the scaling way may have brought conservativeness. Although many works successfully deal with the disturbances, the disturbances are always restricted with a certain bound or a certain expression [12–14]. The upper bound is difficult to be selected because of the difficulty of exact measurement in some practical applications [15]. It is the objective of this paper to provide an effective way in unknown disturbance treatment to overcome the above disadvantages. The minimax method is an efficient approach to deal with large disturbance attenuation problem by estimating the degree of damage [16, 17]; an in-depth study on the large disturbance attenuation problems of the nonlinear TCSC and STATCOM is conducted via adaptive backstepping and minimax method [18, 19].

References [18, 19] also play a key role in uncertain parameter estimation. However, conventional adaptive controls always ignore the available prior information of the uncertainties, which may lead to poor and slow convergence, because the parameter search process possibly takes place outside the region of true value. It is often reasonable to obtain the knowledge on bounds of unknown parameter of the SVC model. To absorb the prior information, the projection technique can be adopted [20, 21]. A novel adaptive control solution is provided; this approach enforces prior known upper and lower bounds of the uncertain parameters always on their corresponding estimates, without compromising control smoothness or global stability guarantees for the closed-loop dynamics [22].

This paper addresses the nonlinear robust control problem for the SVC system with unknown external disturbances and parameter uncertainties using modified adaptive backstepping and minimax approach. In order to avoid the conservativeness brought by conventional disturbance treatment, a test function related to the performance index is constructed to maximize the impact of the disturbances, and the feedback control is investigated by taking account of the worst case. Moreover, the class-κ functions are used in the design procedure to keep the balance between transient response and controller gain. For the uncertainties, a projection mechanism is applied depending on the available bounds on the plant parameters, which can promote the efficiency of parameter search process. Compared with traditional adaptive backstepping method, numerical simulations of two kinds of disturbances to the SVC system demonstrate that the proposed control gives superiorities on transient performance.

2. Dynamic Model and Problem Statements

Consider the following dynamic model of single-machine infinite-bus (SMIB) power system with SVC as shown in Figure 1 [11].

The mathematical dynamics of SVC control system can be expressed by the following nonlinear differential equations [11]

$$\begin{aligned}\dot{\delta} &= \omega - \omega_0,\\ \dot{\omega} &= \frac{\omega_0}{H}\left(P_m - E_q' V_s y_{\text{svc}} \sin\delta\right) - \frac{D}{H}\left(\omega - \omega_0\right),\\ \dot{y}_{\text{svc}} &= \frac{1}{T_{\text{svc}}}\left(-y_{\text{svc}} + y_{\text{svc0}} + u\right).\end{aligned} \tag{1}$$

In the above equations, δ is the rotor angle; ω is the angular speed; H and D are the inertia constant and damping coefficient; P_m is the mechanical power; E_q' and V_s are the q axis transient reactance and infinite bus voltage; y_{svc} is the susceptance of the overall system, $y_{\text{svc}} = 1/(X_1 + X_2 + X_1X_2(B_L + B_C))$, $X_1 = X_d' + X_T + X_L$, $X_2 = X_L, X_d', X_T$ and X_L are, respectively, the direct axis transient reactance of the generator, the reactance of the transformer, and the line reactance, and B_L and B_C are the susceptance of the inductor

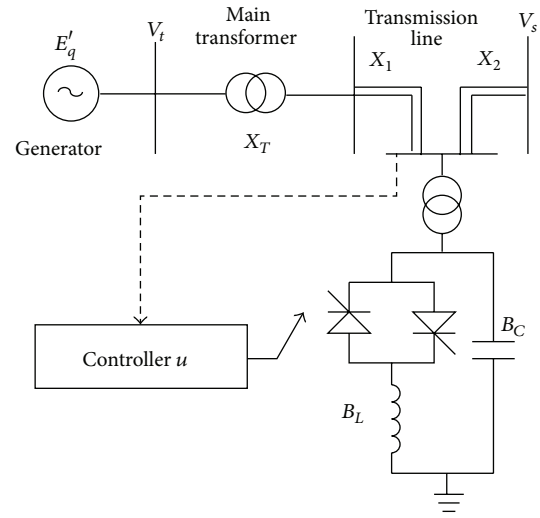

Figure 1: Single machine infinite bus system with SVC.

and the capacitor in SVC; T_{svc} is the time constant of SVC; u is the equivalence input of SVC regulator.

Denote $x_1 = \delta - \delta_0$, $x_2 = \omega - \omega_0$, and $x_3 = y_{\text{svc}} - y_{\text{svc0}}$, where $(\delta_0, \omega_0, y_{\text{svc0}})$ represent an operating point of the power system. Consider the external disturbance vector $\varepsilon = [\varepsilon_1 \quad \varepsilon_2]^T$; ε_1 and ε_2 are unknown functions that belong to L_2 space. Then, system (1) can be transformed into the following form:

$$\dot{x}_1 = x_2, \tag{2a}$$

$$\dot{x}_2 = \theta x_2 + a_0 P_m + b_0\left(x_3 + y_{\text{svc0}}\right)\sin\left(x_1 + \delta_0\right) + \varepsilon_1, \tag{2b}$$

$$\dot{x}_3 = -m_0 x_3 + m_0 u + \varepsilon_2, \tag{2c}$$

where $a_0 = \omega_0/H$, $b_0 = -\omega_0 E_q' V_s/H$, $m_0 = 1/T_{\text{svc}}$. Let $\theta = -D/H$ be an uncertain constant parameter in view of the damping coefficient D that cannot be measured accurately. However, it is reasonable to obtain a prior knowledge on its bound, both from literatures and practice [23–25]. Hence, the upper and lower bounds of θ can also be acquired; we assume $\theta \in (\theta_{\min}, \theta_{\max})$.

3. Adaptive Disturbance Attenuation Design for SVC Control System

In the control of large scale power system, one usually faces limited knowledge on plant parameters and the appearance of sudden large disturbances. A well-designed controller should have the ability to perform its desired function in the presence of changes and uncertainties in the system. The proposed approach is aiming to attenuate the external disturbance and estimate the uncertainty. We adopt the minimax method and parameter projection mechanism based on backstepping technique to deal with the problems.

Step 1. Start with (2a); we define $e_1 = x_1$ and view x_2 as a control variable. Design a virtual control law x_2^* as $x_2^* = -[c_1 + \varphi_1(|e_1|)]e_1$, where $c_1 > 0$, and $\varphi_1(\cdot)$ is a class-κ function; we select $\varphi_1(|e_1|) = k_1 e_1^2$, $k_1 > 0$. Define an error variable $e_2 = x_2 - x_2^*$ representing the difference between the actual and virtual controls. Then, we can derive the dynamics of the new coordinate

$$\dot{e}_1 = -\left[c_1 + \varphi_1\left(|e_1|\right)\right] e_1 + e_2. \tag{3}$$

The objective of this step is to make $e_1 \to 0$, by considering the Lyapunov function as

$$V_1 = \frac{\sigma}{2} e_1^2, \tag{4}$$

where $\sigma > 0$; then the time derivative of V_1 becomes

$$\dot{V}_1 = -\sigma c_1 e_1^2 - \sigma \varphi_1\left(|e_1|\right) e_1^2 + \sigma e_1 e_2. \tag{5}$$

Apparently, if $e_2 = 0$, then $\dot{V}_1 = -\sigma c_1 e_1^2 - \sigma k_1 e_1^4 \le 0$, and e_1 is guaranteed to converge to zero asymptotically. The coupling term $\sigma e_1 e_2$ will be canceled in the next step.

Step 2. Consider (2b) by viewing x_3 as a virtual control variable. Define a virtual control law x_3^* and the error variable $e_3 = x_3 - x_3^*$. Our objective in this step is to make $e_2 \to 0$, and then choose a Lyapunov function by augmenting (4):

$$V_2 = V_1 + \frac{1}{2} e_2^2. \tag{6}$$

Before virtual control law design, we plot out a regulated output $z = [q_1 e_1 \;\; q_2 e_2]^T$ into system (2a), (2b), and (2c), where q_1 and q_2 are nonnegative weighted coefficients representing weighting proportion of e_1 and e_2. Then, construct a performance index based on minimax theory as

$$J_1 = \int_0^\infty \left(\|z\|^2 - \gamma^2 \|\varepsilon_1\|^2\right) dt, \tag{7}$$

where $\gamma > 0$, and γ is disturbance attenuation constant. Further, construct a test function related to the performance index to estimate the worst case disturbance, which means the highest degree of critical disturbance that can be endured by the system:

$$H_1 = \dot{V}_2 + \frac{1}{2}\left(\|z\|^2 - \gamma^2 \|\varepsilon_1\|^2\right). \tag{8}$$

Substituting $\dot{V}_2 = \dot{V}_1 + e_2 \dot{e}_2$ into (8) yields

$$\begin{aligned} H_1 = {} & -\sigma c_1 e_1^2 - \sigma k_1 e_1^4 + \sigma e_1 e_2 \\ & + e_2\left(\theta x_2 + a_0 P_m + b_0\left(x_3 + y_{\text{svc}0}\right)\sin\left(x_1 + \delta_0\right)\right. \\ & \left. + \varepsilon_1 + c_1 x_2 + 3k_1 x_1^2 x_2\right) \\ & + \frac{1}{2} q_1^2 e_1^2 + \frac{1}{2} q_2^2 e_2^2 - \frac{1}{2}\gamma^2 \varepsilon_1^2. \end{aligned} \tag{9}$$

We assume that the upper value of (7) is J_1^*. If a disturbance exists and makes J_1 no larger than J_1^*, then the degree of damage is greatest on the system performance. Thus, our task here is to maximize J_1 by making the first-order derivative of H_1 with respect to ε_1 equal to zero, which is equivalent to $e_2 - \gamma^2 \varepsilon_1 = 0$; then we derive

$$\varepsilon_1^* = \frac{e_2}{\gamma^2}. \tag{10}$$

Furthermore, we compute the second-order derivative; that is, $\partial^2 H_1 / \partial \varepsilon_1^2 = -\gamma^2 < 0$. Therefore, the maximum value of H_1 about ε_1 exists, and

$$\max H_1 = \max\left[\dot{V}_2 + \frac{1}{2}\left(\|z\|^2 - \gamma^2 \|\varepsilon_1\|^2\right)\right]. \tag{11}$$

Integrating both sides of (11) yields

$$\begin{aligned} & \max \int_0^\infty H_1 dt \\ & \quad = \max\left[\int_0^\infty \dot{V}_2 dt + \frac{1}{2}\int_0^\infty \left(\|z\|^2 - \gamma^2 \|\varepsilon_1\|^2\right) dt\right]. \end{aligned} \tag{12}$$

Let $\overline{H}_1 = \int_0^\infty H_1 dt$; then (12) becomes $\max \overline{H}_1 = \max[V_2(\infty) - V_2(0) + (1/2)J_1]$, and then

$$\max\left(\frac{1}{2} J_1\right) = \max\left(\overline{H}_1 - \Delta V_2\right) \le \max\left(\overline{H}_1\right) - \min\left(\Delta V_2\right). \tag{13}$$

When the system suffers sufficiently large disturbances, V_2 will not be reduced, in other words, the disturbance ε_1 is assumed to reduce V_2 to 0; that is, $\min(\Delta V_2) = 0$. Thus, it proves that $\max((1/2)J_1) = \max(\overline{H}_1)$, and ε_1^* is the worst case disturbance for the subsystem.

Remark 1. From the equivalent analysis of $\max(\overline{H}_1)$ and $\max((1/2)J_1)$, it is obvious that if ε_1 allows $\overline{H}_1$ to obtain the maximum value, ε_1 also allows J_1 to obtain the maximum value. That is, system performance damage via ε_1 is the largest.

The stabilizing function x_3^* needs to be designed by undertaking the disturbances with such damage degree into system; our approach is to replace ε_1 in (9) with (10):

$$\begin{aligned} H_1 = {} & -\sigma c_1 e_1^2 - \sigma k_1 e_1^4 + \sigma e_1 e_2 \\ & + e_2\left(\theta x_2 + a_0 P_m + b_0\left(x_3 + y_{\text{svc}0}\right)\sin\left(x_1 + \delta_0\right)\right. \\ & \left. + \frac{e_2}{\gamma^2} + c_1 x_2 + 3k_1 x_1^2 x_2\right) \\ & + \frac{1}{2} q_1^2 e_1^2 + \frac{1}{2} q_2^2 e_2^2 - \frac{1}{2}\gamma^2\left(\frac{e_2}{\gamma^2}\right)^2. \end{aligned} \tag{14}$$

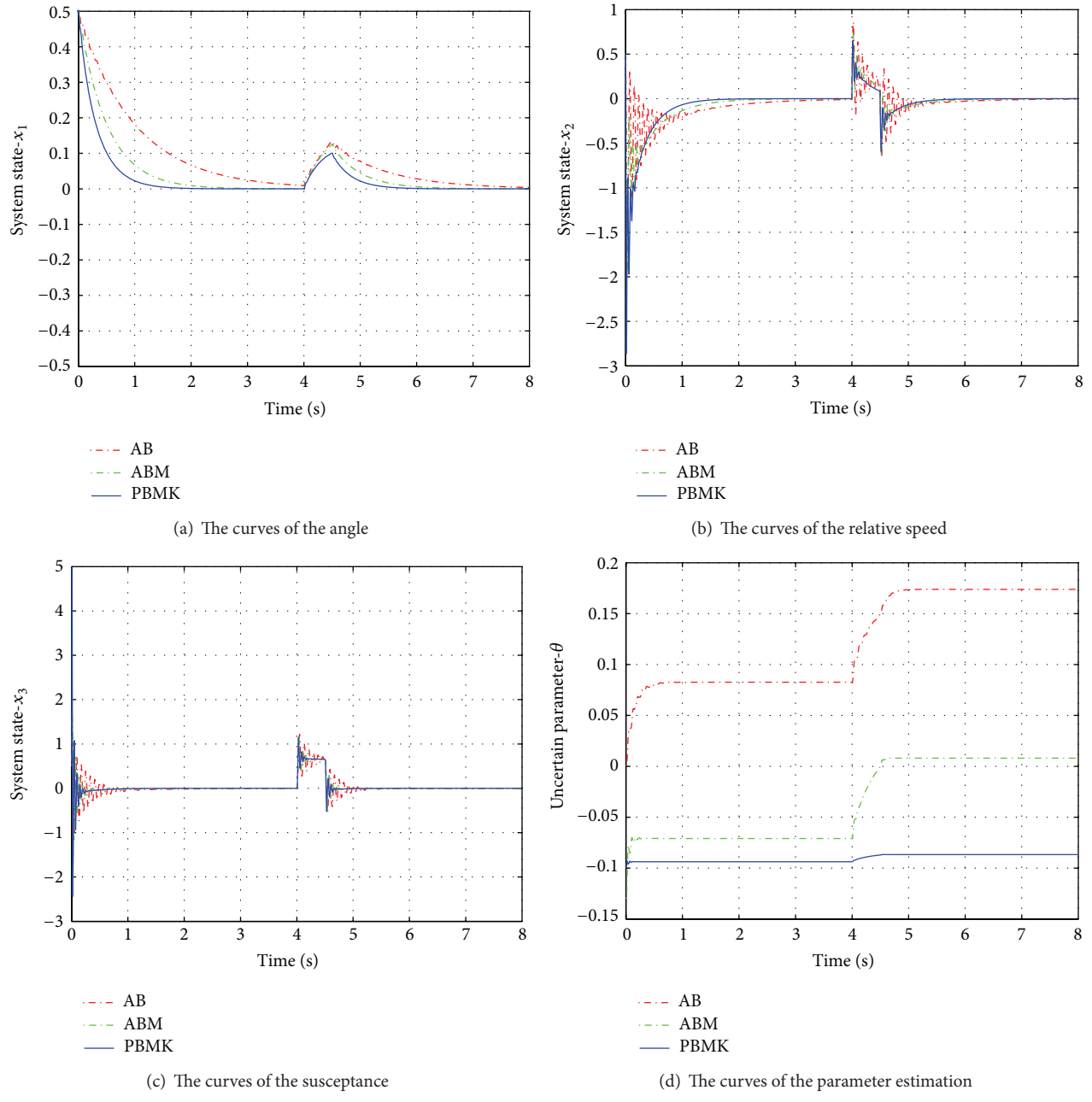

(a) The curves of the angle

(b) The curves of the relative speed

(c) The curves of the susceptance

(d) The curves of the parameter estimation

FIGURE 2: Transient response of closed-loop system under the short circuit ground fault.

Suppose that $h_1 = \sigma c_1 - (1/2)q_1^2$; $h_2 = c_2 + (1/2)q_2^2 + 1/2\gamma^2$, $c_2 > 0$; $f_{\sin} = \sin(x_1 + \delta_0)$. Now we select

$$x_3^* = -\frac{1}{b_0 f_{\sin}}\left[h_2 e_2 + \varphi_2\left(|e_2|\right)e_2 + \sigma e_1 + \widehat{\theta} x_2 + c_1 x_2 + a_0 P_m + 3k_1 x_1^2 x_2\right] - y_{\text{svc}0}, \tag{15}$$

where $\varphi_2(\cdot)$ is a class-κ function; we choose $\varphi_2(|e_2|) = k_2 e_2^2$, $k_2 > 0$; $\widehat{\theta}$ is an estimate of θ, and $\widetilde{\theta} = \theta - \widehat{\theta}$. If the rotor angle $\delta = k\pi$, $k = 0, 1, \ldots$, synchronism of the power system will be lost. Fortunately, under the normal operating conditions in the system $0 < \delta < \pi$ holds, and therefore, the condition $\sin(x_1 + \delta_0) \neq 0$ can be guaranteed.

Then, $H_1 = -h_1 e_1^2 - \sigma k_1 e_1^4 - c_2 e_2^2 - k_2 e_2^4 + e_2\widetilde{\theta} x_2 + b_0 e_2 e_3 f_{\sin}$. In the final step, the coupling term $b_0 e_2 e_3 f_{\sin}$ will be canceled, and the uncertainty item $e_2\widetilde{\theta} x_2$ will be dealt with.

Step 3. For the uncertainty, as mentioned in Section 2, it is reasonable to expect availability of a prior knowledge in terms of lower and upper bounds of θ in (2a), (2b), and (2c). Thereby, we reparameterize the uncertain parameter θ in an associated uncertain variable ϕ as follows [22]:

$$\theta = \frac{1}{2}\left(\theta_{\max} - \theta_{\min}\right)\left(1 - \tanh\phi\right) + \theta_{\min}. \tag{16}$$

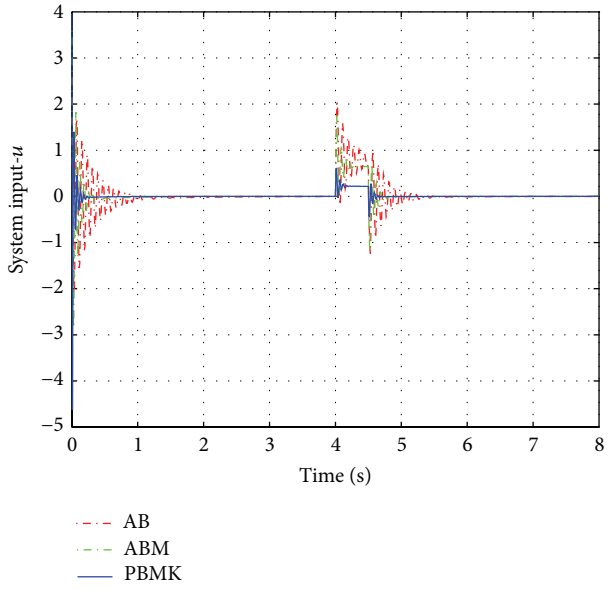

FIGURE 3: Control input curves under the short circuit ground fault.

It is clear that is for all values of $\phi \in R$, $\tanh\phi \in (-1, 1)$, hence, θ is restricted to lie within the region of $(\theta_{\min}, \theta_{\max})$. Consequently, the system governing equation in (2b), which is linear in terms of θ, immediately becomes nonlinear in terms of ϕ. We are in the position to develop a smooth adaptive controller in order to handle the nonlinear parameterization of (16). We define $z = \widehat{\phi} - \phi$, wherein $\widehat{\phi}$ is the estimate of ϕ; then choose the following nonnegative, and therefore, lower-bounded function of z and ϕ as

$$V_z = \frac{1}{2}\left(\theta_{\max} - \theta_{\min}\right)\left[\ln\cosh\left(z + \phi\right) - z\tanh\phi\right]. \quad (17)$$

Consider the candidate Lyapunov function as

$$V_3 = V_2 + \frac{1}{2}e_3^2 + \frac{1}{\rho}V_z. \quad (18)$$

The time derivative of V_3 becomes

$$\dot{V}_3 = \dot{V}_2 + e_3\dot{e}_3 + \frac{1}{2\rho}\left(\theta_{\max} - \theta_{\min}\right)\left[\tanh\left(z + \phi\right) - \tanh\phi\right]\dot{z}. \quad (19)$$

The performance index is expressed as

$$J_2 = \int_0^{\infty}\left(\|z\|^2 - \gamma^2\|\varepsilon\|^2\right)dt. \quad (20)$$

The test function is

$$H_2 = \dot{V}_3 + \frac{1}{2}\left(\|z\|^2 - \gamma^2\|\varepsilon\|^2\right). \quad (21)$$

Substituting (19) into (21) yields

$$\begin{aligned} H_2 = &- h_1e_1^2 - \sigma k_1e_1^4 - c_2e_2^2 - k_2e_2^4 + e_2\widetilde{\theta}x_2 + b_0e_2e_3f_{\sin} \\ &+ e_3\left\{-m_0x_3 + m_0u + \varepsilon_2 + \frac{1}{b_0f_{\sin}}\right. \\ &\times\left[\left(\sigma + \dot{\widehat{\theta}}\right)x_2 + 6k_1x_1x_2^2\right. \\ &+ \left(h_2 + 3k_2e_2^2\right)\left(c_1x_2 + 3k_1e_1^2x_2\right) \\ &+ \left(\widehat{\theta} + c_1 + 3k_1x_1^2 + h_2 + 3k_2e_2^2\right) \\ &\left.\times\left(\theta x_2 + a_0P_m + b_0\left(x_3 + y_{\text{svc0}}\right)f_{\sin} + \frac{e_2}{\gamma^2}\right)\right] \\ &- \frac{f_{\cos}x_2}{b_0f_{\sin}^2}\left(h_2e_2 + k_2e_2^3 + \sigma e_1 + \widehat{\theta}x_2\right. \\ &\left.\left.+ c_1x_2 + a_0P_m + 3k_1x_1^2x_2\right)\right\} \\ &- \frac{1}{2}\gamma^2\varepsilon_2^2 + \frac{1}{2\rho}\left(\theta_{\max} - \theta_{\min}\right) \\ &\times\left[\tanh\left(z + \phi\right) - \tanh\phi\right]\dot{z}, \end{aligned} \quad (22)$$

where $f_{\cos} = \cos(x_1 + \delta_0)$. A similar procedure is employed to make $\partial H_2/\partial\varepsilon_2 = 0$; we can obtain the worst case disturbance $(\partial^2 H_2/\partial\varepsilon_2^2 = -\gamma^2 < 0)$

$$\varepsilon_2^* = \frac{e_3}{\gamma^2}. \quad (23)$$

Taking (23) into account, (22) is rewritten as

$$\begin{aligned} H_2 = &- h_1e_1^2 - \sigma k_1e_1^4 - c_2e_2^2 - k_2e_2^4 \\ &+ e_3\left\{b_0e_2f_{\sin} - m_0x_3 + m_0u + \frac{e_3}{2\gamma^2}\right. \\ &+ \frac{1}{b_0f_{\sin}}\left[\left(\sigma + \dot{\widehat{\theta}}\right)x_2 + 6k_1x_1x_2^2\right. \\ &+ \left(h_2 + 3k_2e_2^2\right)\left(c_1x_2 + 3k_1e_1^2x_2\right) \\ &+ \left(\widehat{\theta} + c_1 + 3k_1x_1^2 + h_2 + 3k_2e_2^2\right) \\ &\left.\times\left(\widehat{\theta}x_2 + a_0P_m + b_0\left(x_3 + y_{\text{svc0}}\right)f_{\sin} + \frac{e_2}{\gamma^2}\right)\right] \\ &- \frac{f_{\cos}x_2}{b_0f_{\sin}^2}\left(h_2e_2 + k_2e_2^3 + \sigma e_1 + \widehat{\theta}x_2\right. \\ &\left.\left.+ c_1x_2 + a_0P_m + 3k_1x_1^2x_2\right)\right\} \end{aligned}$$

$$+\left[e_2x_2+\frac{e_3x_2}{b_0f_{\sin}}\left(\widehat{\theta}+c_1+3k_1x_1^2+h_2+3k_2e_2\right)\right]\widetilde{\theta}$$
$$+\frac{1}{2\rho}\left(\theta_{\max}-\theta_{\min}\right)\left[\tanh\left(z+\phi\right)-\tanh\phi\right]\dot{z}, \tag{24}$$

in which $\widehat{\theta}=(1/2)(\theta_{\max}-\theta_{\min})(1-\tanh\widehat{\phi})+\theta_{\min}$, and then $\widetilde{\theta}=(1/2)(\theta_{\max}-\theta_{\min})(\tanh\widehat{\phi}-\tanh\phi)$.

For the purpose of making $H_2\le 0$, we select an adaptive controller consisting of an actual control input u and a reparameter estimator, which provides the estimate of ϕ:

$$\begin{aligned}u=\ &-\frac{1}{m_0}\\ &\times\left\{\left(c_3+\frac{1}{2\gamma^2}+\varphi_3\left(|e_3|\right)\right)e_3\right.\\ &\quad+\frac{1}{b_0f_{\sin}}\left[\left(\sigma-\frac{1}{2}\left(\theta_{\max}-\theta_{\min}\right)\frac{\dot{\widehat{\phi}}}{\cosh^2\widehat{\phi}}\right)x_2\right.\\ &\qquad+6k_1x_1x_2^2+\left(h_2+3k_2e_2^2\right)\left(c_1x_2+3k_1e_1^2x_2\right)\\ &\qquad+\left(\widehat{\theta}+c_1+3k_1x_1^2+h_2+3k_2e_2^2\right)\\ &\qquad\left.\times\left(\widehat{\theta}x_2+b_0\left(x_3+y_{\text{svc}0}\right)f_{\sin}+a_0P_m+\frac{e_2}{\gamma^2}\right)\right]\\ &\quad-\frac{f_{\cos}x_2}{b_0f_{\sin}^2}\left(h_2e_2+k_2e_2^3+\sigma e_1+\widehat{\theta}x_2\right.\\ &\qquad\left.+c_1x_2+a_0P_m+3k_1x_1^2x_2\right)\\ &\quad\left.+b_0e_2f_{\sin}-m_0x_3\right\},\end{aligned} \tag{25}$$

$$\begin{aligned}\dot{\widehat{\phi}}=-\rho\Bigg[&e_2x_2\\ &+\frac{e_3x_2}{b_0f_{\sin}}\left(\frac{1}{2}\left(\theta_{\max}-\theta_{\min}\right)\left(1-\tanh\widehat{\phi}\right)\right.\\ &\left.+\theta_{\min}+c_1+3k_1x_1^2+h_2+3k_2e_2^2\right)\Bigg],\end{aligned} \tag{26}$$

where $\varphi_3(\cdot)$ is a class-κ function. We choose $\varphi_3(|e_3|)=k_3e_3^2$, $k_3>0$, and then $\widehat{\phi}$ is generated through the solution of the differential equations governed by (26). And $\widehat{\theta}$, the estimate of θ, is indirectly obtained by $\widehat{\phi}$:

$$\widehat{\theta}=\frac{1}{2}\left(\theta_{\max}-\theta_{\min}\right)\left(1-\tanh\widehat{\phi}\right)+\theta_{\min}. \tag{27}$$

Then, we can obtain

$$H_2=-h_1e_1^2-\sigma k_1e_1^4-c_2e_2^2-k_2e_2^4-c_3e_3^2-k_3e_3^4\le 0. \tag{28}$$

If we define $V(x)=2V_3(x)$ as the overall Lyapunov function, then it follows readily that

$$\dot{V}\le\gamma^2\|\varepsilon\|^2-\|z\|^2. \tag{29}$$

Equation (29) indicates that all increased energy of SVC system from $t=0$ to any final time is always smaller than or equal to the ones from outside; that is, the system energy is decreasing.

Theorem 2. *For the given disturbance attenuation constant $\gamma>0$, the L_2 disturbance attenuation problem of system* (1) *can be solved by adaptive controller* (25) *to* (27)*, and a positive storage function $V(x)$ exists such that the dissipation inequality*

$$V\left(x\left(t\right)\right)-V\left(x\left(0\right)\right)\le\int_0^T\left(\gamma^2\|\varepsilon\|^2-\|z\|^2\right)dt \tag{30}$$

holds for any final time T, and the closed-loop system is characteristic with disturbance rejection.

When $\varepsilon_1=0$, $\varepsilon_2=0$, the closed-loop system is asymptotically stable. When $\varepsilon_1\neq 0$, $\varepsilon_2\neq 0$, the L_2 gain from the disturbance to the output of the system is smaller than or equal to γ. According to the definition of virtual control, the x_1, x_2, and x_3 are bounded convergences.

Remark 3. The class-κ function $\varphi_i(\cdot)$ is introduced into the selection of stabilizing function x_i^*, $i=1,2,3$, during the recursive design procedure, in order to keep the balance between transient response and controller gain. This approach promotes convergent speed remarkably without increasing the controller gain.

Remark 4. Exist disturbance treatment usually assumes the plant with bounded disturbance or zooms the items of the energy function about the disturbance, which probably increase the conservativeness. This paper adopts the minimax method to maximize the effects of disturbances. The control law is designed by undertaking the worst case disturbance to ensure the stability of the closed-loop system. Thus, the system is theoretically not sensitive to disturbance effects.

Remark 5. Different from the previous adaptive method in power systems, we fully and properly utilize all the available prior information on the bound of unknown parameter by adopting parameter projection technique. We select a specific uncertain parameter structure to force the parameter estimate to stay within the valid region and generate a smooth adaptive control law. Accordingly, the transient performance is significantly improved.

4. Results and Discussion

We will consider two kinds of disturbances in the digital simulation for the single-machine infinite-bus system with SVC. The physical parameters are selected as follows: $H=5.9$ s, $D=1.0$, $E_q'=1.123$ pu, $V_s=1.0$ pu, $T_{\text{svs}}=0.02$ s, $X_1=0.84$ pu, $X_2=0.52$ pu, and $B_L+B_C=0.3$ pu. The operating point is $\delta_0=0.9$ rad, $\omega_0=314.159$ rad/s, and

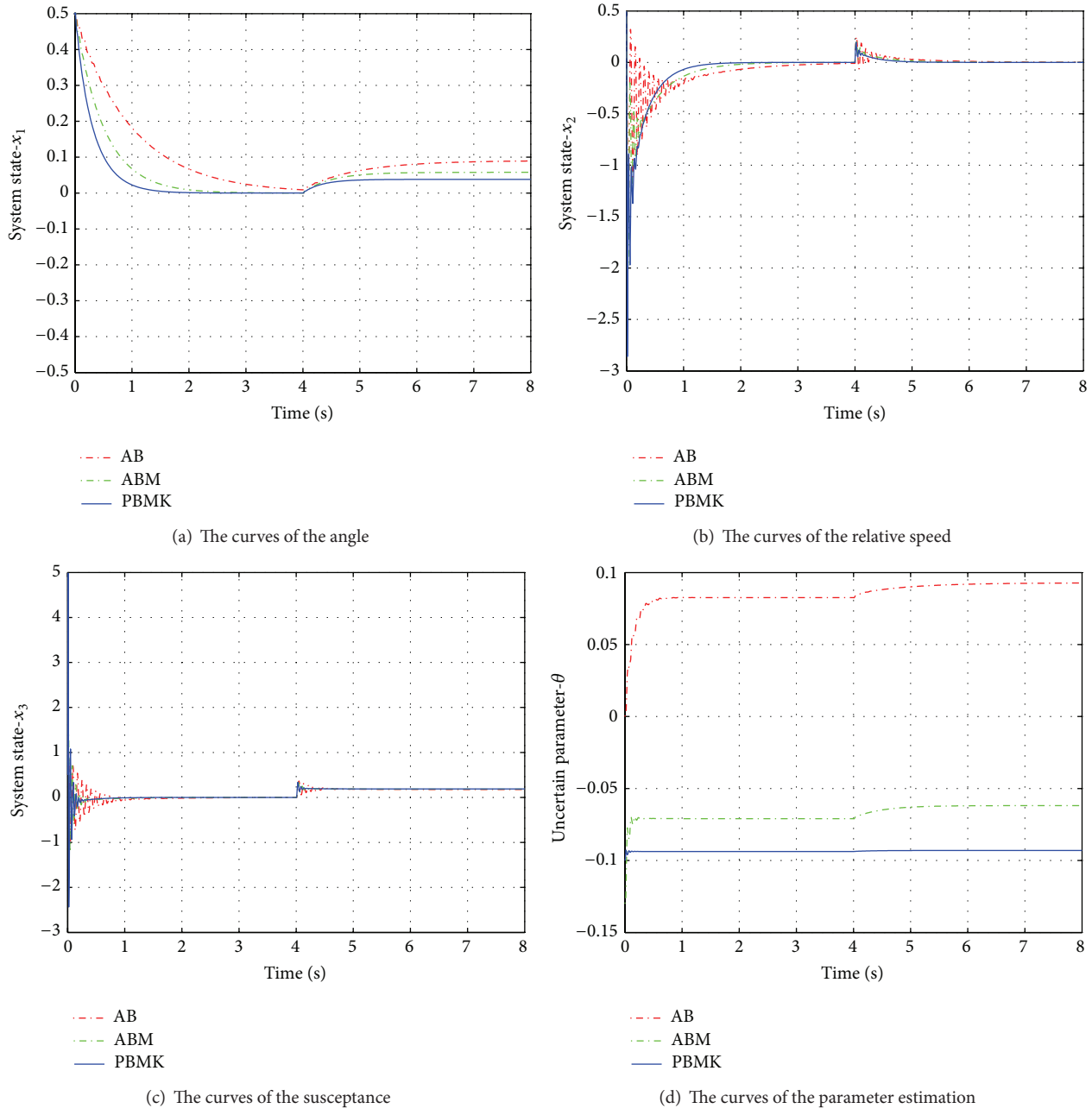

(a) The curves of the angle

(b) The curves of the relative speed

(c) The curves of the susceptance

(d) The curves of the parameter estimation

FIGURE 4: Transient response of closed-loop system under the mechanical power perturbation.

$y_{svc0} = 0.4$ pu. The control parameters are selected as follows: $q_1 = 0.4, q_2 = 0.6, c_1 = 2, c_2 = 2, c_3 = 2, k_1 = 1, k_2 = 1, k_3 = 1, \gamma = 0.2$, and $\rho = 1$. The upper and lower bound of uncertain parameter are $\theta_{max} = 0$ and $\theta_{min} = -0.5$.

In order to show the effectiveness of the proposed modified parameter projection adaptive backstepping minimax (PBMK) controller, we will make comparisons with the adaptive backstepping minimax (ABM) controller [18] and the conventional adaptive backstepping (AB) controller [10] under the same nonzero initial condition. Note that the control parameters for ABM controller and AB controller are selected as $c_1 = 3, c_2 = 3$, and $c_3 = 3$.

4.1. Short Circuit Ground Fault. In 4 s, a transient three-phase short-circuit fault occurred on the transmission line. In 4.5 s, the fault disappears, and the system restores to the normal structure. The reactance of the transformer varies in different stages after a short circuit ground fault as follows:

the period of pre-fault $X_L = 0.52$ pu;

the period of fault procedure $X_L = \infty$;

the period of after-fault $X_L = 0.52$ pu;

the transient response curves of the system are shown in Figures 2 and 3.

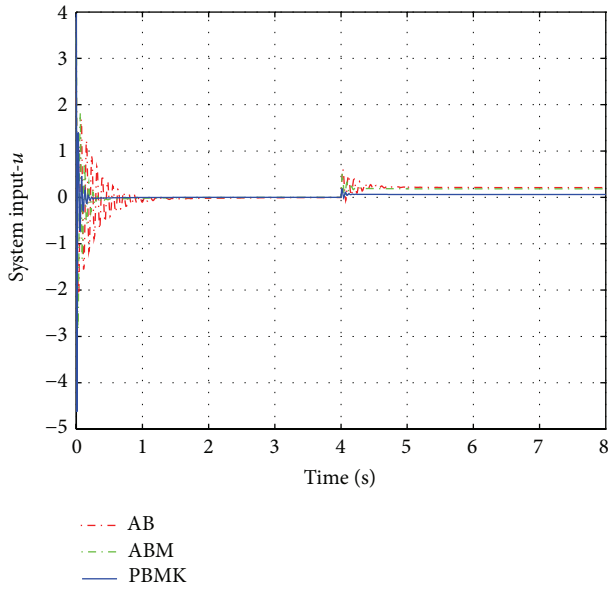

Figure 5: Control input curves under the mechanical power perturbation.

Figures 2(a)–2(c) show that, under the proposed controller PBMK, the response is improved without remarkably increasing the controller gain; the convergent speed is faster; the system reaches the stable state more rapidly than the ones under ABM and AB controller. Moreover, PBMK and ABM controllers, which are both designed by minimax method, have advantages in the ability of disturbance attenuation. Figure 2(d) shows that the proposed adaptive control in this paper ensures that the estimates of the uncertain parameter are always within the prior bounds, while for the ABM and AB controllers, the parameter search process takes place outside the feasible region where the corresponding "true" parameters lie.

Figure 3 shows that, under PBMK controller, the control input requires bigger energy in the initial period, but it reaches the stable state in short time, and the amplitude of oscillation is relatively smaller. The selected class-κ functions converge to zero along with the convergence to zero of the errors. Then the control energy also coincides with that of ABM controller.

4.2. Mechanical Power Perturbation. Unrecoverable mechanical power perturbation occurs at 4 s, and the mechanical power P_m changes to another value; that is,

$$P_m = \begin{cases} 0.9, & 0 \le t < 4.0\,\text{s} \\ 0.9 + \Delta P_m, & 4.0\,\text{s} < t, \end{cases} \qquad \Delta P_m(t) = 30\% P_m. \tag{31}$$

The dynamic responses of closed-loop system are shown in Figures 4 and 5.

Figures 4 and 5 show that, after the presence of mechanical power perturbation, the states are stable in a new equilibrium point. And the proposed PBMK controller on the convergence time and the amplitude of oscillation still has advantages compared with ABM and AB controllers. The dynamic response of the system does not change significantly with the variety of disturbance form. Therefore, the controller is insensitive to the change in disturbance.

5. Conclusions

In this paper, we present an improved robust disturbance attenuation scheme for the nonlinear uncertain SVC system based on improved adaptive backstepping and minimax method. The proposed control strategy gives some advantages, such as the following. (a) The nonlinearities of the SVC system model are completely retained for no linearization process is put on the original system. (b) Our disturbance treatment does not inquire artificially imposing an upper bound on the disturbance or unequally scaling the disturbance items existing in the energy function; then the conservativeness is greatly reduced. (c) The closed-loop system is insensitive to the disturbances because of taking account of the maximum effect of the damage. (d) The class-κ functions introduced into the backstepping procedure are helpful to speed up the response without significantly increasing the control gain. (e) We develop a nonlinear smooth function to map the uncertain parameter θ into ϕ in order to restrict θ to be lying within the prior specified interval, and guarantee that the parameter estimate has a higher convergence rate. Simulation research is under two disturbances that; the results indicate that the proposed control strategy has advantages in terms of the convergence time and oscillation amplitude in comparison with traditional adaptive backstepping approach.

Acknowledgments

This work is supported by the National Natural Science Foundation of China, under Grants 61304021, 61233002, and 61104074, and the Fundamental Research Funds for the Central Universities, under Grants N110404032 and N110417005.

References

[1] P. Pourbeik, A. Boström, and B. Ray, "Modeling and application studies for a modern static VAr system installation," *IEEE Transactions on Power Delivery*, vol. 21, no. 1, pp. 368–377, 2006.

[2] L. Wang and D. N. Truong, "Stability enhancement of a power system with a PMSG-based and a DFIG-based offshore wind farm using a SVC with an adaptive-network-based fuzzy inference system," *IEEE Transactions on Industrial Electronics*, vol. 60, no. 7, pp. 2799–2807, 2013.

[3] S. Robak, "Robust SVC controller design and analysis for uncertain power systems," *Control Engineering Practice*, vol. 17, no. 11, pp. 1280–1290, 2009.

[4] S. Teleke, T. Abdulahovic, T. Thiringer, and J. Svensson, "Dynamic performance comparison of synchronous condenser and SVC," *IEEE Transactions on Power Delivery*, vol. 23, no. 3, pp. 1606–1612, 2008.

[5] J. C. Dermentzoglou and A. D. Karlis, "Development of linear models of static var compensators and design of controllers suitable for enhancing dynamic/transient performance of power systems including wind farms," *Electric Power Systems Research*, vol. 81, no. 4, pp. 922–929, 2011.

[6] Y. Ruan and J. Wang, "The coordinated control of SVC and excitation of generators in power systems with nonlinear loads," *International Journal of Electrical Power and Energy Systems*, vol. 27, no. 8, pp. 550–555, 2005.

[7] Y. Sun, Q. Liu, Y. Song, and T. Shen, "PCH models of facts with adaptive L_2-gain control part one theory," *Automation of Electric Power Systems*, vol. 25, no. 15, pp. 1–6, 2001.

[8] M. Krstic, I. Kanellakopoulos, and P. Kokotovic, *Nonlinear and Adaptive Control Design*, John Wiley & Sons, New York, NY, USA, 1995.

[9] J. Fu, "Extended backstepping approach for a class of non-linear systems in generalised output feedback canonical form," *IET Control Theory and Applications*, vol. 3, no. 8, pp. 1023–1032, 2009.

[10] W. Li, S. Liu, and Y. Jing, "Nonlinear robust control based on adaptive backstepping design for static var compensator," in *Proceedings of the 23th Chinese Control Conference*, pp. 1250–1253, 2004.

[11] L.-Y. Sun, S. Tong, and Y. Liu, "Adaptive backstepping sliding mode Hoo control of static var compensator," *IEEE Transactions on Control Systems Technology*, vol. 19, no. 5, pp. 1178–1185, 2011.

[12] C.-S. Tseng, "Robust fuzzy filter design for nonlinear systems with persistent bounded disturbances," *IEEE Transactions on Systems, Man, and Cybernetics B*, vol. 36, no. 4, pp. 940–945, 2006.

[13] Y. Wang, T. Chai, and Y. Zhang, "State observer-based adaptive fuzzy output-feedback control for a class of uncertain nonlinear systems," *Information Sciences*, vol. 180, no. 24, pp. 5029–5040, 2010.

[14] H. Coral-Enriquez, J. Cortés-Romero, and G. A. Ramos, "Robust active disturbance rejection control approach to maximize energy capture in variable-speed wind turbines," *Mathematical Problems in Engineering*, vol. 2013, Article ID 396740, 12 pages, 2013.

[15] X. Zhang, L. Sun, K. Zhao, and L. Sun, "Nonlinear speed control for PMSM system using sliding-mode control and disturbance compensation techniques," *IEEE Transactions on Power Electronics*, vol. 28, no. 3, pp. 1358–1365, 2013.

[16] I. Petersen, V. Ugrinovskii, and A. Savkin, *Robust Control Design Using H_∞ Methods*, Springer, 2000.

[17] K. Ezal, P. V. Kokotović, A. R. Teel, and T. Başar, "Disturbance attenuating output-feedback control of nonlinear systems with local optimality," *Automatica*, vol. 37, no. 6, pp. 805–817, 2001.

[18] N. Jiang, B. Liu, J. Kang, Y. Jing, and T. Zhang, "The design of nonlinear disturbance attenuation controller for TCSC robust model of power system," *Nonlinear Dynamics*, vol. 67, no. 3, pp. 1863–1870, 2012.

[19] N. Jiang, S. Li, T. Liu, and X. Dong, "Nonlinear large disturbance attenuation controller design for the power systems with STATCOM," *Applied Mathematics and Computation*, vol. 219, pp. 10378–10386, 2013.

[20] K. S. Narendra, "Parameter adaptive control—the end...or the beginning?" in *Proceedings of the 33rd IEEE Conference on Decision and Control*, pp. 2117–2125, 1994.

[21] R. Bakker and A. M. Annaswamy, "Stability and robustness properties of a simple adaptive controller," *IEEE Transactions on Automatic Control*, vol. 41, no. 9, pp. 1352–1358, 1996.

[22] M. R. Akella and K. Subbarao, "A novel parameter projection mechanism for smooth and stable adaptive control," *Systems & Control Letters*, vol. 54, no. 1, pp. 43–51, 2005.

[23] R. T. H. Alden and A. A. Shaltout, "Analysis of damping and synchronizing torques—part 1: a general calculation method," *IEEE Transactions on Power Apparatus and Systems*, vol. 98, no. 5, pp. 1696–1700, 1979.

[24] E. Abu-Al-Feilat, M. Bettayeb, H. Al-Duwaish, M. Abido, and A. Mantawy, "A neural network-based approach for on-line dynamic stability assessment using synchronizing and damping torque coefficients," *Electric Power Systems Research*, vol. 39, no. 2, pp. 103–110, 1996.

[25] M. Ranlöf, J. Bladh, and U. Lundin, "Use of a finite element model for the determination of damping and synchronizing torques of hydroelectric generators," *Electrical Power and Energy Systems*, vol. 44, pp. 844–851, 2013.

Hindawi Publishing Corporation
Mathematical Problems in Engineering
Volume 2013, Article ID 476367, 9 pages
http://dx.doi.org/10.1155/2013/476367

Research Article

Convergence Guaranteed Nonlinear Constraint Model Predictive Control via I/O Linearization

Xiaobing Kong,[1] Xiangjie Liu,[1] and Xiuming Yao[2]

[1] *State Key Laboratory of Alternate Electrical Power System with Renewable Energy Sources, North China Electric Power University, Beijing 102206, China*
[2] *Department of Automation, North China Electric Power University, Baoding 071003, China*

Correspondence should be addressed to Xiangjie Liu; liuxj@ncepu.edu.cn

Received 14 July 2013; Revised 23 October 2013; Accepted 28 October 2013

Academic Editor: Baoyong Zhang

Constituting reliable optimal solution is a key issue for the nonlinear constrained model predictive control. Input-output feedback linearization is a popular method in nonlinear control. By using an input-output feedback linearizing controller, the original linear input constraints will change to nonlinear constraints and sometimes the constraints are state dependent. This paper presents an iterative quadratic program (IQP) routine on the continuous-time system. To guarantee its convergence, another iterative approach is incorporated. The proposed algorithm can reach a feasible solution over the entire prediction horizon. Simulation results on both a numerical example and the continuous stirred tank reactors (CSTR) demonstrate the effectiveness of the proposed method.

1. Introduction

Model predictive control (MPC) is a popular algorithm in process control which online solves an optimization problem at each time step [1]. MPC considers process input, output, and state constraints directly in the control variable calculation. Under the linear model, with a quadratic objective function, MPC utilizes the convex quadratic program (QP), which can easily find the optimal solution [2].

Industrial processes are generally nonlinear, due to the frequent changes of the operating point right across the whole operation range. In general, the nonlinear model predictive control (NMPC) also online solves an optimization problem, by using the sequential quadratic program (SQP). The resulting nonlinear programming problems are usually nonconvex, and the online computational burden is generally large for most complex systems. A general way to solve this nonlinear optimal problem is to use approximate approach. For example, the first control move is calculated exactly, since it is actually implemented. The rest control moves can be approximated, since they are not implemented [3]. Thus the number of decision variables in the online optimization problem is equal to the number of inputs, instead of the number of inputs multiplied by the control horizon for a conventional NMPC algorithm. Paper [4] extended the first prediction of the linear constraints to the whole control horizon. Paper [5] studies the stability and region of attraction properties of a family of nonlinear MPC systems. Paper [6] presents nonlinear multivariable predictive control using neurofuzzy networks.

"Jacobian linearization" and "the input-output feedback linearization (IOFL)" are the two popular approaches in nonlinear control area. While the former can reflect the nonlinear model only at some certain point, the later represents the nonlinear system over a much wider operating range. Thus, IOFL is utilized in this paper for constituting nonlinear MPC, since the IOFL can offer a linear dynamic system so that the total optimal problem can be solved using the QP routine. Nevertheless, this can make the constraints to be nonlinear and state dependent. The approximate method developed in paper [7] can guarantee a feasible solution over the entire prediction horizon. The neural network is utilized to model the nonlinear discrete-time system. Paper [8] also introduces a technique with an affine transformation of the feasible region using feedback linearization scheme for handling input constraints. The neural network is also utilized to model the nonlinear system.

For digital MPC controller design, since the real-time control systems are in discrete-time forms, most NMPC research adopts the discrete-time feedback linearization. It should be noticed that the IOFL in differential geometry has been well developed for continuous-time system. Some famous methods in continuous-time system [9], for example, the extended system method, are not suitable to feedback linearise a general discrete-time system. Direct application of feedback linearization for a general discrete-time system may either be impossible or involve the time-consuming search algorithm. In [10], the authors proposed a linear model predictive control strategy via input/output linearization to the nonlinear process, by using one-step constraint algorithm. This paper aims to make full use of the advantage of continuous-time system IOFL and then try to reach the convergence to a feasible solution over the entire prediction horizon within the available time. Since the input constraints are transferred into nonlinear constraints from initial linear constraints, the convergent algorithm is constituted to guarantee a feasible solution without constraints violation. Simulation results on both a numerical example and the continuous stirred tank reactors (CSTR) demonstrate the effectiveness of the NMPC method.

2. The Linear Control Structure via Input-Output Feedback Linearization

The IOFL is to transform the original nonlinear system into linear input-output relationship, generally by using a static state feedback control law [11]. Consider the SISO affine state-space model as follows:

$$\begin{aligned} \dot{\overline{x}} &= f(\overline{x}) + g(\overline{x})\,u, \\ y &= h(\overline{x}), \end{aligned} \tag{1}$$

where $\overline{x} \in R^n$ is state variables, u is the manipulated input variable, y is the controlled output variable, and f, g, and h are smooth functions in a domain $D \subset R^n$.

Definition 1 (relative degree). The nonlinear system (1) is said to have relative degree γ, $1 \le \gamma \le n$, in a region $D_0 \subset D$ if

$$\begin{aligned} &L_g L_f^i h(\overline{x}) \equiv 0, \quad i = 0, \ldots, \gamma - 2; \\ &L_g L_f^{\gamma-1} h(\overline{x}) \neq 0, \quad \forall \overline{x} \in D_0. \end{aligned} \tag{2}$$

If the relative degree $\gamma = n$, then for every $x_0 \in D$, a neighborhood N of x_0 exists such that the map $\Phi : \overline{x} \to x = [h \quad L_f h \quad \cdots \quad L_f^{n-1} h]^T$ restricted to N is a diffeomorphism on N.

The mapping Φ transfers the system (1) to a new system as follows:

$$\begin{aligned} \dot{x}_1 &= x_2, \\ \dot{x}_2 &= x_3, \\ &\vdots \\ \dot{x}_n &= b(x) + a(x)\,u, \\ y &= x_1, \end{aligned} \tag{3}$$

where $a(\overline{x}) = L_g L_f^{n-1} h(\overline{x})$, $b(\overline{x}) = L_f^n h(\overline{x})$, which can also be expressed as $a(x)$, $b(x)$ in the new coordinates.

The feedback law is

$$u = \frac{1}{a(x)} \left[-b(x) + v \right], \tag{4}$$

where v is the transformed input variable. The new linear system is

$$\begin{aligned} \dot{x} &= Ax + Bv, \\ y &= Cx, \end{aligned} \tag{5}$$

where

$$A = \begin{bmatrix} 0 & 1 & & 0 \\ & \ddots & \ddots & \\ & & \ddots & 1 \\ 0 & & & 0 \end{bmatrix}, \qquad B = \begin{bmatrix} 0 \\ 0 \\ \vdots \\ 1 \end{bmatrix}, \qquad C = \begin{bmatrix} 1 & 0 & \cdots & 0 \end{bmatrix}. \tag{6}$$

The resulting linear state-space system (5) could be used for constituting "standard" linear MPC [1]. Discretization (5) can result in

$$\begin{aligned} x(k+1) &= A_d x(k) + B_d v(k), \\ y(k) &= C_d x(k). \end{aligned} \tag{7}$$

The matrices A_d, B_d, and C_d are expressed as $A_d = e^{AT}$, $B_d = \int_0^T e^{At} dt \cdot B$, $C_d = C$, where T is sampling time.

Define $\Delta x(k+1) = x(k+1) - x(k)$; $\Delta x(k) = x(k) - x(k-1)$; $\Delta v(k) = v(k) - v(k-1)$. Choose a new group of state variables $x_u(k) = [\Delta x(k)^T \quad y(k)]^T$; the augmented system is

$$\begin{aligned} \overbrace{\begin{bmatrix} \Delta x(k+1) \\ y(k+1) \end{bmatrix}}^{x_u(k+1)} &= \overbrace{\begin{bmatrix} A_d & 0_d^T \\ C_d A_d & 1 \end{bmatrix}}^{A_u} \overbrace{\begin{bmatrix} \Delta x(k) \\ y(k) \end{bmatrix}}^{x_u(k)} + \overbrace{\begin{bmatrix} B_d \\ C_d B_d \end{bmatrix}}^{B_u} \Delta v(k), \\ y(k) &= \overbrace{\begin{bmatrix} 0_d & 1 \end{bmatrix}}^{C_u} \begin{bmatrix} \Delta x(k) \\ y(k) \end{bmatrix}, \end{aligned} \tag{8}$$

where $0_d = \overbrace{[0 \quad 0 \quad \cdots \quad 0]}^{n}$. Based on the state-space model (A_u, B_u, C_u), the future outputs along the predictive horizon N_p are calculated sequentially as

$$\begin{aligned} y(k+1 \mid k) &= C_u A_u x_u(k) + C_u B_u \Delta v(k), \\ y(k+2 \mid k) &= C_u A_u^2 x_u(k) + C_u A_u B_u \Delta v(k) \\ &\quad + C_u B_u \Delta v(k+1) \\ &\vdots \\ y\left(k+N_p \mid k\right) &= C_u A_u^{N_p} x_u(k) + C_u A_u^{N_p-1} B_u \Delta v(k) \\ &\quad + C_u A_u^{N_p-2} B_u \Delta v(k+1) + \cdots \\ &\quad + C_u A_u^{N_p-N_c} B_u \Delta v\left(k+N_c-1\right). \end{aligned} \tag{9, 10}$$

Define vectors

$$\begin{aligned} Y &= \left[y(k+1 \mid k) \quad \cdots \quad y\left(k+N_p \mid k\right)\right]^T, \\ \Delta V &= \left[\Delta v(k) \quad \Delta v(k+1 \mid k) \quad \cdots \quad \Delta v\left(k+N_c-1 \mid k\right)\right]^T, \end{aligned} \tag{11}$$

where N_c is the control horizon.

Collect (9) and (10) together in a compact matrix form as

$$Y = F x_u(k) + \Psi \Delta V, \tag{12}$$

where

$$F = \begin{bmatrix} C_u A_u \\ C_u A_u^2 \\ C_u A_u^3 \\ \vdots \\ C_u A_u^{Np} \end{bmatrix}, \qquad \Psi = \begin{bmatrix} C_u B_u & 0 & 0 & \cdots & 0 \\ C_u A_u B_u & C_u B_u & 0 & \cdots & 0 \\ C_u A_u^2 B_u & C_u A_u B_u & C_u B_u & \cdots & 0 \\ \vdots & & & & \\ C_u A_u^{N_p-1} B_u & C_u A_u^{N_p-2} B_u & C_u A_u^{N_p-3} B_u & \cdots & C_u A_u^{N_p-N_c} B_u \end{bmatrix}. \tag{13}$$

Similarly, we can have the future state variables along the predictive horizon N_c based on the model of (A_d, B_d, C_d)

$$X = \widetilde{A} \Delta V + \gamma, \tag{14}$$

where

$$X = \left[x(k) \quad x(k+1 \mid k) \quad \cdots \quad x\left(k+N_c-1 \mid k\right)\right]^T,$$

$$\widetilde{\mathbf{A}} = \begin{bmatrix} 0 & 0 & \cdots & 0 \\ B_d & 0 & \cdots & 0 \\ \left(A_d + I\right) B_d & B_d & \cdots & 0 \\ \vdots & \vdots & \vdots & \vdots \\ \left(\sum_{i=1}^{N_c-1} A_d^{i-1}\right) B_d & \left(\sum_{i=1}^{N_c-2} A_d^{i-1}\right) B_d & \cdots & 0 \end{bmatrix}, \tag{15}$$

$$\gamma = \begin{bmatrix} x(k) \\ x(k) + A_d \Delta x(k) \\ x(k) + \left(\sum_{i=1}^{2} A_d^i\right) \Delta x(k) \\ \vdots \\ x(k) + \left(\sum_{i=1}^{N_c-1} A_d^i\right) \Delta x(k) \end{bmatrix}.$$

The object function to be minimised is a quadratic criterion on ΔV as

$$J = \left(R_s - Y\right)^T \left(R_s - Y\right) + \Delta V^T \overline{R} \Delta V. \tag{16}$$

By using (12), the optimization problem can be attributed to

$$\begin{aligned} J_{\min} &= \min_{\Delta V} \left\{ \frac{1}{2} \Delta V^T H \Delta V + \Gamma^T \Delta V \right\} \\ &\text{subject to} \quad \underline{\Delta V} \le \Delta V \le \overline{\Delta V}, \end{aligned} \tag{17}$$

where $H = \Psi^T \Psi + \overline{R}$, $\Gamma = \Psi^T(-R_s + F x_u(k))$, $\underline{\Delta V}$ and $\overline{\Delta V}$ indicates the minimal and maximum value of ΔV.

3. Convergence Algorithm for Constraint Optimal MPC

3.1. The Nonlinear Constraint Handling. In practice, the process inputs are frequently subjected to the following level inequality constraints:

$$\underline{U} \le U \le \overline{U}, \tag{18}$$

where $U = [u_k \quad \cdots \quad u_{k+N_c-1}]^T$ represents the control inputs, and $\underline{U}$ and $\overline{U}$ indicate the minimal and maximum value of U.

After the realization of the IOFL, the input vector U is transformed into a new one V. With this nonlinear and state dependent input constraint, traditional QP cannot be used to calculate the optimal control sequence. Though the sequential quadratic programming (SQP) technique is generally used on nonlinear constraint MPC, it is often nonconvex and can cause large computation burden. This property will be demonstrated later in the simulation example of CSTR.

In order to solve this nonlinear constraints problem, an iterative QP is first used to try to get the optimal solution. The key issue is to establish the nonlinear relationship between vectors V and U and then get the explicit expression of U from V.

To establish the nonlinear relationship between vectors V and U, expand the feedback law (4) over the control horizon N_c,

$$\begin{aligned} v(k) &= a(x(k))\,u(k) + b(x(k)), \\ v(k+1) &= a(x(k+1))\,u(k+1) + b(x(k+1)), \\ &\vdots \\ v(k+N_c-1) &= a\left(x\left(k+N_c-1\right)\right)u\left(k+N_c-1\right) + b\left(x\left(k+N_c-1\right)\right). \end{aligned} \tag{19}$$

Considering the expression (14), (19) can be rearranged in the matrix form

$$V = G_u\,[U, \Delta V]. \tag{20}$$

The above inequality can be rewritten in the following form:

$$G\,[U, \Delta V] = 0 \tag{21}$$

due to

$$\begin{aligned} V &= \begin{bmatrix} v(k) \\ v(k+1) \\ \vdots \\ v\left(k+N_c-1\right) \end{bmatrix} \\ &= \begin{bmatrix} 1 & & & & 0 \\ 1 & 1 & & & \\ 1 & 1 & 1 & & \\ \vdots & \ddots & \ddots & \ddots & \\ 1 & 1 & \cdots & 1 & 1 \end{bmatrix} \cdot \begin{bmatrix} \Delta v(k) \\ \Delta v(k+1) \\ \vdots \\ \Delta v\left(k+N_c-1\right) \end{bmatrix} + v(k-1). \end{aligned} \tag{22}$$

In general, $v(k+i-1)$ can be rewritten as

$$\begin{aligned} &v(k+i-1) \\ &\quad = v(k-1) + \sum_{j=1}^{i} \Delta v\left(k+j-1\right) \quad \left(i = 1, \ldots, N_c\right), \end{aligned} \tag{23}$$

with the constraints

$$\underline{v} \le v \le \overline{v}, \tag{24}$$

where $\underline{v}$, $\overline{v}$ indicate the minimal and maximum value of v, which are state dependent.

Thus

$$\begin{aligned} &\underline{v}_{k+i-1}\left(x\left(k+i-1\right)\right) - v(k-1) \\ &\quad \le \sum_{j=1}^{i} \Delta v\left(k+j-1\right) \\ &\quad \le \overline{v}_{k+i-1}\left(x\left(k+i-1\right)\right) - v(k-1). \end{aligned} \tag{25}$$

The above inequality can be rewritten over the entire horizon,

$$\Lambda^T \Delta V(k) \le c\left(X\left(\Delta V(k)\right)\right)^T, \tag{26}$$

where

$$\Lambda = \begin{bmatrix} L^T & -L^T \end{bmatrix}, \qquad L = \begin{bmatrix} 1 & & & 0 \\ 1 & 1 & & \\ \vdots & & & \\ 1 & 1 & \cdots & 1 \end{bmatrix}, \tag{27}$$

$$c = \begin{bmatrix} \overline{v}_k - v(k-1) & \cdots & \overline{v}_{k+N_c-1} - v(k-1) & v(k-1) - \underline{v}_k & \cdots & v(k-1) - \underline{v}_{k+N_c-1} \end{bmatrix}.$$

From (26), the above equation can be rewritten as

$$\Lambda^T \Delta V(k) \le c\left(X\left(\Delta V\left(U(k)\right)\right)\right)^T. \tag{28}$$

This iterative QP algorithm is presented below:

Step 1: Initializing $c(X(\Delta V(U^0(k))))$ within the input constraint.

Step 2: Solve QP for $\Delta V^i(k)$ subject to $\Lambda^T \Delta V^i(k) \leq c(X(\Delta V(U^{i-1}(k))))^T$

Step 3: Calculate $c(X(\Delta V(U^i(k))))$

Step 4: Test if $\Lambda^T \Delta V^i(k) \leq c(X(\Delta V(U^i(k))))^T$, end; otherwise, $i = i + 1$, go to Step 2.

The above iterative QP is effective for solving the problem if the initial condition is properly chosen. Nevertheless, it has no guaranteed convergence to a feasible solution. To overcome this problem, another iterative algorithm is needed to guarantee a feasible solution over the entire prediction horizon is incorporated. This idea is previously presented by paper [7] on a input/output model. Extending it to the state-space equation is straightforward.

In order to solve the convergence problem, linear approximation is necessary. Now consider the approximation by linearization through Taylor's expansion about U_0 of the nonlinear constraints (21) as

$$\Delta V = \Delta V_0 + g\left[U_0\right]\left(\widetilde{h}\right) + r\left(\widetilde{h}\right), \tag{29}$$

where U_0 is the chosen initial operating trajectory, ΔV_0 is obtained from (21) when $U = U_0$, the $(N_c \times N_c)$ dimensional matrix $g[U_0]$ represents the Jacobian matrix $\partial \Delta V / \partial U$ in (21) at the operating trajectory, and $r(\widetilde{h})$ corresponds to the higher order terms of the approximation given by

$$r\left(\widetilde{h}\right) = \frac{1}{2}\widetilde{h}^T g\left[U_0 + \theta\widetilde{h}\right]\widetilde{h}, \tag{30}$$

where $\theta \in [0, 1]$, $\widetilde{h} = U - U_0$.

Neglect the higher order terms as

$$\Delta V = \Delta V_0 + g\left[U_0\right]\left(U - U_0\right). \tag{31}$$

Equation (31) can lead to an explicitly linear function relationship between the control sequence U and ΔV:

$$U = g^{-1}\left[U_0\right]\Delta V + U_0 - g^{-1}\left[U_0\right]\Delta V_0. \tag{32}$$

Now the optimization problem is defined as

$$J_{\min} = \min_{\Delta V}\left\{\frac{1}{2}\Delta V^T H \Delta V + \Gamma^T \Delta V\right\}. \tag{33}$$

subject to the convex set of approximate linear constraints

$$\underline{U} \leq M\Delta V + m_0 \leq \overline{U}, \tag{34}$$

with $M = g^{-1}[U_0]$, $m_0 = U_0 - g^{-1}[U_0] \times \Delta V_0$.

In order for the algorithm to reach the convergence to a feasible solution, the optimal problem can be rewritten as

$$\Delta V^* = \arg\min_{\Delta V}\left\{\frac{1}{2}\Delta V^T H \Delta V + \Gamma^T \Delta V\right\} \tag{35}$$

$$\text{subject to} \quad \underline{U} \leq M^\alpha \Delta V + {m_0}^\alpha \leq \overline{U}, \tag{36}$$

where $0 < \alpha < 1$ is decreasing parameter with initial value $\alpha = 1$. Define M^α and m_0^α, respectively, by

$$\begin{aligned} M^\alpha &= \left(g^{-1}\left[U_0\right]\right)^\alpha \left(I - \left(g^{-1}\left[U_0\right]\right)^\alpha\right)^{-1}, \\ m_0^\alpha &= U_0 - \left(g^{-1}\left[U_0\right]\right)^\alpha \left(I - \left(g^{-1}\left[U_0\right]\right)^\alpha\right)^{-1}\Delta V_0. \end{aligned} \tag{37}$$

Define $U_l^* = M^\alpha \Delta V^* + m_0^\alpha$ to be the linear control sequence and U_{nl}^* to be the nonlinear control sequence obtained from $G[U, \Delta V^*] = 0$. Then the major goal is to keep

$$\underline{U} \leq U_{nl}^* \leq \overline{U}. \tag{38}$$

Thus the optimization problem with the approximate constraints ΔV^* is a feasible solution, which can be solved iteratively using QP.

This approximate constraints algorithm is presented follows.

Step 1: assure feasibility of the new operating trajectory: $\underline{U} \leq U_i \leq \overline{U}$. Solve for ΔV_0, M, m_0

Step 2: $\alpha_{i-1} = 1$

Step 3: actualize the squeezing factor α:

$$\alpha = \alpha \times \lambda. \tag{39}$$

Step 4: new linearized constraints at U_0: $\underline{U} \leq M^\alpha \Delta V + m_0^\alpha \leq \overline{U}$.

Step 5: Solve QP for the new linearized constraints:

$$\Delta V_{i+1}^* = \arg\min_{\Delta V} J\left(\Delta V\right). \tag{40}$$

Step 6: test if U_{nl}^* violate the original constraint. If: $\underline{U} \leq U_{nl}^* \leq \overline{U} \Rightarrow End$.

Step 7: let $i = i + 1$, go to 3.

3.2. The Convergence Property. With the object function (35), assume the practical input sequence constraints

$$|U| \leq 1. \tag{41}$$

Assume a given initial vector representing the operating trajectory, U_0, verifying the conditions

$$\left|U_0\right| \leq 1 - \varepsilon_1, \tag{42}$$

where ε_1 is small positive scalar values, $\varepsilon_1 > 0$.

For any given scalar $0 < \alpha < 1$, the solution of the optimization problem (35) is subjected to

$$\left|U_0 + \left(g^{-1}\left[U_0\right]\right)^\alpha \left(I - \left(g^{-1}\left[U_0\right]\right)^\alpha\right)\left(\Delta V^* - \Delta V_0\right)\right| \leq 1. \tag{43}$$

which can be further written as

$$\left|\Delta V^*\right| \leq \left[I - \left(g^{-1}\left[U_0\right]\right)^{-\alpha}\right]\left(g\left[U_0\right]\right)^\alpha \left(1 - U_0\right) + \Delta V_0. \tag{44}$$

In the limit, as $\alpha \to 0$, $(g^{-1}[U_0])^{-\alpha} \to I$, $(g[U_0])^\alpha \to I$, the solution of the optimization problem is given by

$$\lim_{\alpha \to 0}\left|\Delta V^*\right| \leq \Delta V_0. \tag{45}$$

Due to the smooth function $G[U, \Delta V] = 0$ and definition (42), this last result leads to

$$\left|U^*\right| = \left|U_0\right| \leq 1 - \varepsilon_1, \tag{46}$$

signifying that the resulting practical nonlinear control sequence is always within the bounds, and so a feasible solution is always guaranteed.

3.3. The Algorithm for Constraint Optimal MPC. The MPC algorithm, which can guarantee convergence to a feasible solution, has to deal with the constraints as the following steps:

Step 1: $i = 0$.

Step 2: if $(N - i < 0)$, go to 8.

Step 3: assure feasibility of the new operating trajectory: $\underline{U} \le U_i \le \overline{U}$.

Step 4: solve QP at U_i:

$$\Delta V_{i+1}^* = \arg\min_{\Delta V} J(\Delta V) \tag{47}$$

$$\text{subject to } \Lambda^T \Delta V_{i+1}^* \le c\left(X\left(\Delta V\left(U_i\right)\right)\right)^T. \tag{48}$$

Step 5: test if ΔV_{nl}^* violates the constraints: if $\Lambda^T \Delta V \le c(X(\Delta V(U_{i+1})))^T \Rightarrow END$

where $U_{i+1} = U_{nl}^*$ is nonlinear control sequence, obtained from $G[U_{nl}^*, \Delta V_{i+1}^*] = 0$.

Step 6: $i = i + 1$. Go to 2

Step 7: $U_0 = U_i$, $\Delta V_0 = \Delta V_N^*$. Solve for M, m_0.

Step 8: $\alpha = 1$.

Step 9: actualize the squeezing factor α:

$$\alpha = \alpha \times \lambda. \tag{49}$$

Step 10: new linearized constraints at U_0: $\underline{U} \le M^\alpha \Delta V + {m_0}^\alpha \le \overline{U}$

Step 11: Solve QP for the new linearized constraints:

$$\Delta V_{i+1}^* = \arg\min_{\Delta V} J(\Delta V). \tag{50}$$

Step 12: test if U_{nl}^* violate the original constraint. If: $\underline{U} \le U_{nl}^* \le \overline{U} \Rightarrow End$

Step 13: let $i = i + 1$. Go to 9.

The total algorithm performance is quite related to the tuning of two parameters:

N: the number of iterations of the QP algorithm;

λ: the squeezing parameter of the convergence guaranteed algorithm.

The convergence speed of this iterative algorithm can be set using the decreasing rate α, defined here through parameter $0 < \lambda < 1$.

Choosing the initial value U_0 is a key issue in solving the optimal problem, since it is quite related to the resulting computation burden. Suppose that the final input sequence at instant k can be expressed as $U_{nl}^* = [u(0) \ u(1) \ \cdots \ u(N_c - 2)]^T$. Then, the initial value U_0 at instant $k + 1$ should be chosen as $U_0 = [u(1) \ \cdots \ u(N_c - 2) \ 0]^T$; for example, the first $N_c - 1$ factors are taken directly from the prediction of U_{nl}^*.

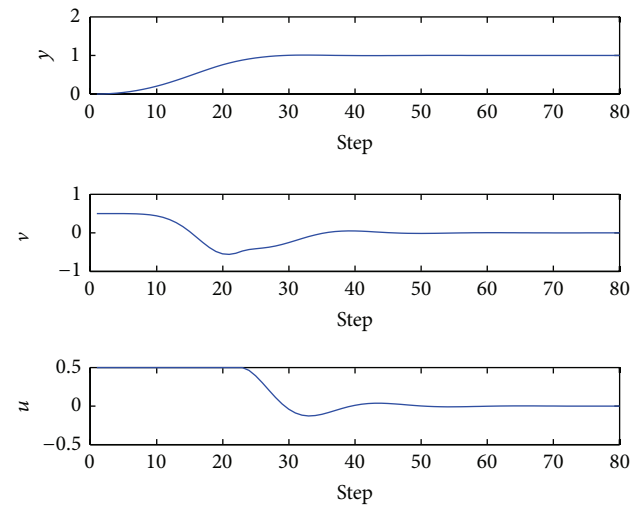

Figure 1: The closed-loop response for a step signal under the proposed IOFL MPC.

4. Case Studies

Two examples are presented to illustrate the implementation and the performance of the proposed nonlinear MPC. In example 1, a numerical state-space equation is used, and in example 2, the control problem of CSTR is considered.

4.1. Numerical Example. Assume the state-space equations to be

$$\begin{aligned} \dot{\overline{x}}_1 &= \overline{x}_2, \\ \dot{\overline{x}}_2 &= -3\overline{x}_1^2 \overline{x}_2 - \overline{x}_1^3 \sin\left(\overline{x}_2\right) + u, \\ y &= \overline{x}_1. \end{aligned} \tag{51}$$

The input constraint is $-0.5 \le u \le 0.5$.

Using (4), the static feedback law: $v = u + (-3x_1^2 x_2 - x_1^3 \sin x_2)$

The resulting feedback linearization linear system is

$$\begin{aligned} \begin{bmatrix} \dot{x}_1 \\ \dot{x}_2 \end{bmatrix} &= \begin{bmatrix} 0 & 1 \\ 0 & 0 \end{bmatrix} \begin{bmatrix} x_1 \\ x_2 \end{bmatrix} + \begin{bmatrix} 0 \\ 1 \end{bmatrix} v, \\ y &= x_1 y = x_1. \end{aligned} \tag{52}$$

Choose the predictive horizon $N_p = 8$, the control horizon $N_c = 5$, and the sampling time $\tau = 1$ s. Figure 1 shows the system response for a step signal using the proposed IOFL MPC method. The algorithm guarantee's that the process input does not violate the constraints. The system reaches stability in 3 seconds without overshoot. Figure 2 shows the number of iterations at each optimization step. From Figure 2, the process needs 65 iterations at the beginning but soon reduces the iteration and finally reaches the convergence using only one iteration.

Simulations were then repeated under different predictive horizons. Table 1 lists the comparison of the control performance. From Table 1, the computing burden increases when

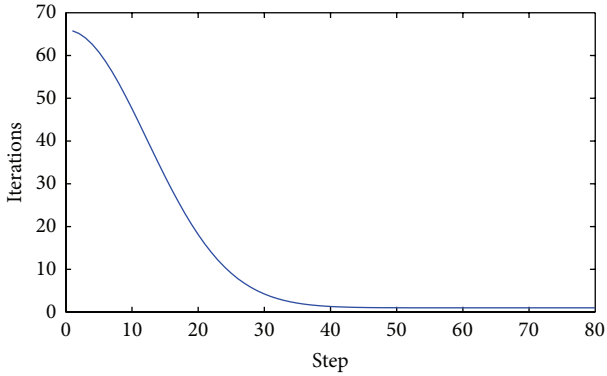

Figure 2: The number of iterations at each optimization step.

Table 1: The comparison of control performance at different prediction horizon.

Prediction horizon	Computing burden (CPU time)	Sum squared error
8	1.0469	11.4042
10	1.1875	11.4036
12	1.2813	11.4032

the prediction horizon increases, meanwhile the tracking property improves with the increment of the prediction horizon.

4.2. The Control of a First-Order CSTR. CSTRs are typical chemical processes representing a variety of complex industry systems. The CSTR problem discussed here represents a first-order, irreversible, exothermic kinetics reaction, which can be described by the following equation [12]:

$$\begin{aligned}\frac{dx_1}{dt} &= -x_1 + D_\alpha \cdot \exp\left(\frac{x_2}{1+x_2/\gamma}\right),\\ \frac{dx_2}{dt} &= -x_2(1+\beta) + H \cdot D_\alpha \cdot (1-x_1) \cdot \exp\left(\frac{x_2}{1+x_2/\gamma}\right)\\ &\quad + \beta u,\\ y &= x_1,\end{aligned} \tag{53}$$

where the two state variables x_1 and x_2 are the reactor temperature and the normalized reactant concentration. The control variable u is the normalized cooling water temperature. D_α, β, and γ are the constants of the system.

The CSTR control objectives contain two aspects: set point tracking and regulation of reactant concentration under the perturbation of feed water temperature.

With the static feedback law,

$$v = au + b, \tag{54}$$

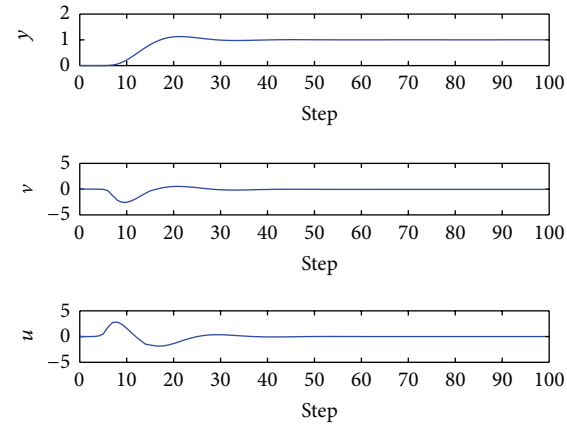

Figure 3: The system output and the control under step changes in the reference signal.

where

$$\begin{aligned}a &= \beta(\xi_1+\xi_2) \cdot \left(1 - \left(\frac{1}{r}\right)\ln\left(\frac{(\xi_1+\xi_2)}{D_\alpha}\right)\right)^2,\\ b &= \xi_1 - (\xi_1+\xi_2) + (\xi_1+\xi_2)\\ &\quad \cdot \left[\frac{\ln((\xi_1+\xi_2)/D_\alpha)}{1-(1/r)\ln((\xi_1+\xi_2)/D_\alpha)}(1+\beta)\right.\\ &\quad \left. + H \cdot (1-\xi_1)(\xi_1+\xi_2)\right].\end{aligned} \tag{55}$$

The resulting feedback linearization linear system is

$$\begin{aligned}\begin{bmatrix}\dot{\xi}_1\\ \dot{\xi}_2\end{bmatrix} &= \begin{bmatrix}0 & 1\\ 0 & 0\end{bmatrix}\begin{bmatrix}\xi_1\\ \xi_2\end{bmatrix} + \begin{bmatrix}0\\ 1\end{bmatrix} v,\\ y &= \begin{bmatrix}1 & 0\end{bmatrix}\begin{bmatrix}\xi_1\\ \xi_2\end{bmatrix}.\end{aligned} \tag{56}$$

Suppose the constraint to be $-3 \le u \le 3$. Let $r, D_\alpha, H = 1$, $\beta = 0.01$, the predictive horizon $N_p = 10$, the control horizon $N_c = 5$, and the sampling time $\tau = 1$ s. Figure 3 shows the system output and the control under step changes in the reference signal.

From the simulation result, the manipulated variable u does not violate the defined constraint. The system reaches stability in 30 steps without obvious overshoot.

As mentioned before, there exist two general approaches for NMPC. One is to use the SQP method. Another is to approximate the first constraints as the constraints over the entire control horizon. The proposed method is then compared with these two methods, considering this CSTR plant. The simulation results using the three predictive control schemes for $N_c = 5$ are given in Figure 4, adopting the best N and λ for each N_p in the proposed IOFL NMPC.

Computation burden is one of the most concerning problems in CSTR real-time control. In using MPC, though choosing larger predictive horizon can improve system performance, it can, meantime, result in the increment of

Table 2: Left: CPU time of the entire simulation. Right: sum squared output error (SSE) in the simulation.

Predictive horizon	CPU time			SSE		
	One-step constraints	IOFL MPC	SQP	One-step constraints	IOFL MPC	SQP
10	0.1563	0.2011	0.3054	11.4181	11.4045	11.4042
12	0.1719	0.2407	0.3602	11.4180	11.4034	11.4031
14	0.2031	0.2795	0.4415	11.4177	11.4026	11.4018
16	0.2614	0.3306	0.5728	11.4130	11.4019	11.4003

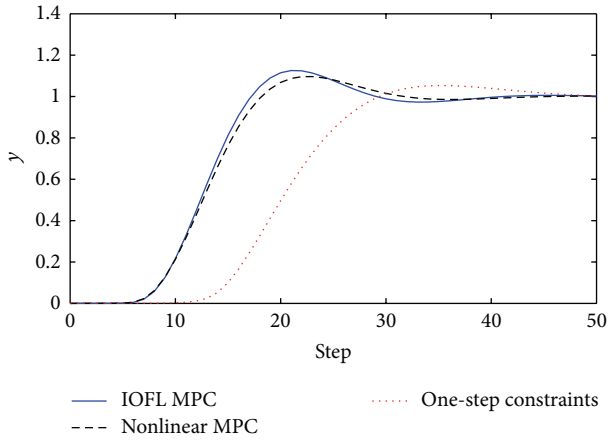

Figure 4: The comparison of the three responses.

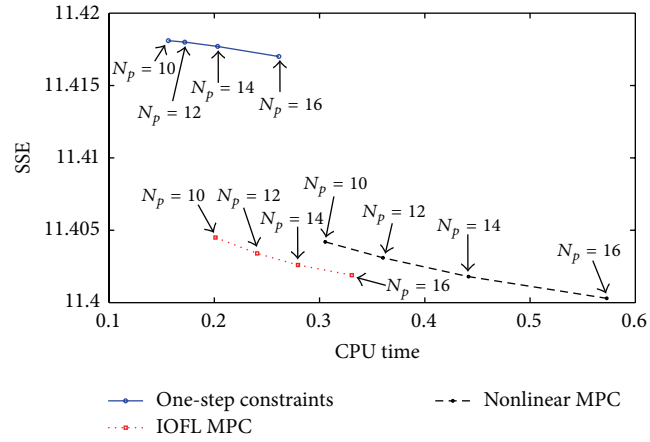

Figure 5: The comparison of control performance.

computation burden, especially in nonlinear system. For further comparison, the controller performance is analysed with respect to two variables, for example, sum squared output error (SSE) and the relative optimization time for the simulation. Table 2 shows the performance of each controller configuration for various prediction horizons. The three methods, namely, the one-step constraints, the MPC with IOFL and the nonlinear MPC, can all guarantee a feasible control solution over the complete prediction horizon. The comparison of the three shows a similar trend performance in terms of the system tracking error, although the one-step constraint is less computational time demanding, as shown in Figure 5. With the increase of the prediction horizon, the time increase in nonlinear MPC is obvious, while the time increase in one-step constraints and MPC with IOFL optimization is quite minor. This is due to the efficient iterative process of the proposed IOFL MPC. The reduced computing burden for the one-step constraints method is obvious, since only the first time-step-ahead inputs are constrained, leaving the other $N_p - 1$ inputs unconstrained. The shortcoming is that the resulting optimum may not be feasible. From Figure 5, the total trade-off between the computational demands and the gain in optimality is obviously favourable to the proposed MPC with IOFL.

5. Conclusions

MPC has been widely used in industrial process. One limitation of MPC is that it is mostly based on a linear model. The performance will deteriorate when the current output is relatively far away from the operating point at which the linear control model was generated, especially in the presence of constrains. The approach presented in this paper aims at combining the nonlinear differential geometry technique with existing MPC technique to avoid nonlinear optimization when using a nonlinear model of the process. Considering the continuous-time system, the detailed routine for reaching a feasible solution through iterative QP optimization is presented in this paper. The initial value is properly chosen to greatly reduce the computation burden. Comparing results on the CSTR considering, both the SSE and the relative optimization time needed for completing the simulation have also been addressed in detail. The advantage is that it avoids a direct nonlinear optimization on a nonlinear model of the process and incorporates the linear optimization technique in the controller design.

Acknowledgments

This work was supported by the National Natural Science Foundation of China under Grants 60974051, 61273144, and 61203041, the Natural Science Foundation of Beijing under Grant 4122071, the Chinese National Postdoctor Science Foundation under Grants 2011M500217 and 2012T50036, the Doctoral Fund of Ministry of Education of China under Grant 20120036120013, and the Fundamental Research Funds for the Central Universities 13XS09.

References

[1] W. Liuping, *Model Predictive Control System Design and Implementation Using MATLAB*, Springer, New York, NY, USA, 2009.

[2] T. Zou, "Offset-free strategy by double-layered linear model predictive control," *Journal of Applied Mathematics*, vol. 2012, Article ID 808327, 14 pages, 2012.

[3] A. Zheng, "A computationally efficient nonlinear MPC algorithm," in *Proceedings of the American Control Conference*, pp. 1623–1627, Albuquerque, NM, USA, June 1997.

[4] M. J. Kurtz, G.-Y. Zhu, and M. A. Henson, "Constrained output feedback control of a multivariable polymerization reactor," *IEEE Transactions on Control Systems Technology*, vol. 8, no. 1, pp. 87–97, 2000.

[5] A. Jadbabaie and J. Hauser, "On the stability of receding horizon control with a general terminal cost," *IEEE Transactions on Automatic Control*, vol. 50, no. 5, pp. 674–678, 2005.

[6] X. J. Liu, P. Guan, and C. W. Chan, "Nonlinear multivariable power plant coordinate control by constrained predictive scheme," *IEEE Transactions on Control Systems Technology*, vol. 18, no. 5, pp. 1116–1125, 2010.

[7] M. A. Botto, T. J. J. Van Den Boom, A. Krijgsman, and J. Sá Da Costa, "Predictive control based on neural network models with I/O feedback linearization," *International Journal of Control*, vol. 72, no. 17, pp. 1538–1554, 1999.

[8] J. Deng, V. Becerra, and R. Stobart, "Input constraints handling in an MPC/feedback linearization scheme," *International Journal of Applied Mathematics and Computer Science*, vol. 19, no. 2, pp. 219–232, 2009.

[9] M. A. Henson and D. E. Seborg, "Input-output linearization of general nonlinear processes," *AIChE Journal*, vol. 36, no. 11, pp. 1753–1757, 1990.

[10] X.-B. Kong, Y.-J. Chen, and X.-J. Liu, "Nonlinear model predictive control with input-output linearization," in *Proceedings of the 24th Chinese Control and Decision Conference (CCDC '12)*, pp. 688–693, Taiyuan, China, May 2012.

[11] H. K. Khalil, *Nonlinear Systems*, Prentice Hall, Upper Saddle River, NJ, USA, 2002.

[12] T. D. Knapp, H. M. Budman, and G. Broderick, "Adaptive control of a CSTR with a neural network model," *Journal of Process Control*, vol. 11, no. 1, pp. 53–68, 2001.

Hindawi Publishing Corporation
Mathematical Problems in Engineering
Volume 2013, Article ID 579137, 9 pages
http://dx.doi.org/10.1155/2013/579137

Research Article

$\mathcal{H}_\infty$ Filter Design with Minimum Entropy for Continuous-Time Linear Systems

Jie Zhang,[1] Hamid Reza Karimi,[2] Zhong Zheng,[3] Ming Lyu,[4] and Yuming Bo[1]

[1] *School of Automation, Nanjing University of Science and Technology, Nanjing 210094, China*
[2] *Department of Engineering, Faculty of Engineering and Science, University of Agder, 4898 Grimstad, Norway*
[3] *Space Control and Inertial Technology Research Center, Harbin Institute of Technology, Harbin, 150001, China*
[4] *Information Overall Department, North Information Control Group Co., Ltd., Nanjing 211153, China*

Correspondence should be addressed to Jie Zhang; zhangjie.njust@gmail.com

Received 1 August 2013; Revised 8 October 2013; Accepted 21 October 2013

Academic Editor: Zhiguang Feng

We deal with the design problem of minimum entropy $\mathcal{H}_\infty$ filter in terms of linear matrix inequality (LMI) approach for linear continuous-time systems with a state-space model subject to parameter uncertainty that belongs to a given convex bounded polyhedral domain. Given a stable uncertain linear system, our attention is focused on the design of full-order and reduced-order robust minimum entropy $\mathcal{H}_\infty$ filters, which guarantee the filtering error system to be asymptotically stable and are required to minimize the filtering error system entropy (at $s_0 = \infty$) and to satisfy a prescribed $\mathcal{H}_\infty$ disturbance attenuation performance. Sufficient conditions for the existence of desired full-order and reduced-order filters are established in terms of LMIs, respectively, and the corresponding filter synthesis is cast into a convex optimization problem which can be efficiently handled by using standard numerical software. Finally, an illustrative example is provided to show the usefulness and effectiveness of the proposed design method.

1. Introduction

Estimation is the process of inferring the value of a quantity of interests from indirect, inaccurate, and uncertain observations [1]. State estimation of dynamic systems with both process and measurement noise inputs is a very important and challenging problem in engineering applications. In the past decades, quite a few attention has been devoted to estimation methods that are based on the minimization of the variance of the estimation error, that is, the well-known Kalman filtering approach [2, 3]. Unfortunately, it is recognized soon that the performance of Kalman filter can deteriorate significantly when the process parameters are subjected to relatively small modeling errors. In order to cope with this problem, over the past few years interest has been devoted to the design of robust estimators. There are essentially two approaches to the robust estimation problem. The first is robust $\mathcal{H}_2$ filtering, which minimizes the upper bound of the estimation error variance for all possible parametric uncertainties under the assumption that the noise processes have known power spectral densities [4, 5]. In many practical situations, however, we may not be able to have exactly known information on the spectral densities of the noise processes. In such cases, an alternative is to reformulate the estimation problem in an $\mathcal{H}_\infty$ filtering framework, which has been well recognized to be most appropriate for systems with noise input whose stochastic information is not precisely known. It minimizes the worst-case energy gain from the noise inputs to the estimation error [6–8]. There are many results reported on the problem of $\mathcal{H}_\infty$ filtering; for example, it has been addressed for linear systems [9], linear systems with uncertain parameters [10, 11], delay systems [6, 12], and stochastic systems [8]. Although the $\mathcal{H}_\infty$ filter is known to be less sensitive to modeling errors than $\mathcal{H}_2$ filter, it is generally so conservative as to lead to a large intolerable estimation error variance when the system is driven by white noise signals.

Similar to $\mathcal{H}_\infty$ control problem, in the $\mathcal{H}_\infty$ filtering problem [13–17], the family of filters that satisfy a filtering error system with an $\mathcal{H}_\infty$-norm bound is characterized by

a linear fractional transformation of a "ball in $\mathscr{H}_\infty$," and then a natural question is which element of this ball to choose. One choice that has been considered in a closely related problem in mathematics is to choose that which minimizes an entropy integral; that is, the filter is well selected such that not only the filtering error system is asymptotically stable and the $\mathscr{H}_\infty$-norm of its transfer function is below a prescribed level, but also the entropy of the filtering error system at infinity is minimized. This kind of optimal filters is referred to as minimum entropy $\mathscr{H}_\infty$ filters in the present paper. In fact, minimum entropy $\mathscr{H}_\infty$ filtering provides a means of trading off some of the features of other filtering problems, namely, $\mathscr{H}_2$ filtering and $\mathscr{H}_\infty$ filtering. As for the minimum entropy $\mathscr{H}_\infty$ control problem, there are many important results that have been reported in the literature; for example, controllers which minimize the entropy of the closed-loop transfer function have been studied extensively for linear time-invariant (LTI) systems, both in the continuous and discrete-time cases [18–20]. Minimum entropy control for time-varying systems has been investigated in [21]. To the best of our knowledge, however, there is not any result reported on minimum entropy $\mathscr{H}_\infty$ filtering problem in the literature; research in this area should be important and challenging; this motivates us to carry out the present study.

In this paper, we make an attempt to investigate the design of minimum entropy $\mathscr{H}_\infty$ filters by using linear matrix inequality (LMI) approach for linear continuous-time systems with a state-space model subject to parameter uncertainty that belongs to a given convex bounded polyhedral domain. Given a stable uncertain linear system, our attention is focused on the design of full-order and reduced-order robust minimum entropy $\mathscr{H}_\infty$ filters, which guarantee the filtering error system to be asymptotically stable and are required to minimize the filtering error system entropy (at $s_0 = \infty$) as well as to satisfy a prescribed $\mathscr{H}_\infty$ disturbance attenuation performance. Sufficient conditions for the existence of desired full-order and reduced-order filters are established in terms of LMIs, respectively, and the corresponding filter synthesis is cast into a convex optimization problem which can be efficiently handled by using the well-known interior-point algorithms [22]. A numerical simulation example is provided to show the usefulness and effectiveness of the proposed design method.

The rest of this paper is organized as follows. In Section 2, the minimum entropy $\mathscr{H}_\infty$ filtering problem is formulated. Section 3 presents our main results of the full-order and reduced-order minimum entropy $\mathscr{H}_\infty$ filters design. Section 4 provides an illustrative example. Finally, conclusions are drawn in Section 5.

Notations. The notation used here is fairly standard except where otherwise stated. A^T represents the transpose of A; $\mathbb{R}^n$ and $\mathbb{R}^{n\times m}$ denote, respectively, the n dimensional Euclidean space and the set of all $n \times m$ real matrices. the notation $P > 0$ means that P is a real symmetric and positive definite matrix; trace(P) represents the trace of P; diag$\{F_1, F_2, \ldots\}$ stands for a block-diagonal matrix whose diagonal blocks are given by $F_1, F_2, \ldots$. I and 0 represent identity matrix and zero matrix; $|\cdot|$ refers to the Euclidean vector norm and $\|\cdot\|_2$ denotes the $\mathscr{L}_2$ norm of a differential signal; The signals that are square integrable over $[0,\infty)$ are denoted by $\mathscr{L}_2[0,\infty)$ with the norm $\|\cdot\|_2$; the symbol $*$ in a matrix means that the corresponding term of the matrix can be obtained by symmetric property.

2. Problem Formulation

Consider the following linear time-invariant (LTI) system (Σ):

$$(\Sigma): \begin{cases} \dot{x}(t) = Ax(t) + B\omega(t), \\ y(t) = Cx(t) + D\omega(t), \\ z(t) = Lx(t), \end{cases} \tag{1}$$

where $x(t) \in \mathbb{R}^n$ is the state vector; $y(t) \in \mathbb{R}^m$ is the measured output; $z(t) \in \mathbb{R}^q$ is a linear combination of the state variables to be estimated; $\omega(t) \in \mathbb{R}^l$ is the disturbance input which belongs to $\mathscr{L}_2[0,\infty)$; A, B, C, D, and L are constant real matrices of appropriate dimensions, where L is a known matrix and A, B, C, D are unknown matrices such that the system matrix

$$\mathscr{G} \triangleq \begin{bmatrix} A & B \\ C & D \end{bmatrix} \tag{2}$$

belongs to a given polytope $\mathscr{D}$ described by

$$\mathscr{D} \triangleq \left\{ \mathscr{G} \mid \mathscr{G} = \sum_{i=1}^{n_s} \lambda_j \mathscr{G}_j; \sum_{i=1}^{n_s} \lambda_j = 1, \lambda_j \geq 0 \right\}; \tag{3}$$

that is, any admissible system matrix $\mathscr{G}$ can be written as an unknown convex combination of n_s vertices $\mathscr{G}_j$, $j = 1, 2, \ldots, n_s$, given by

$$\mathscr{G}_j \triangleq \begin{bmatrix} A_j & B_j \\ C_j & D_j \end{bmatrix}, \tag{4}$$

where A_j, B_j, C_j, and D_j, $j = 1, 2, \ldots, n_s$, are given matrices. Clearly, $n_s = 1$ corresponds to the case where the system (Σ) is perfectly known.

Before formulating the problem of this paper, we first give some definitions and existing results of the minimum entropy problem. Consider the following LTI system (Π):

$$(\Pi): \begin{cases} \dot{x}(t) = Ax(t) + B\omega(t), \\ y(t) = Lx(t), \end{cases} \tag{5}$$

where $y(t)$ is the output; the other notations are defined as in (1), and let $\mathbb{G}$ denote its transfer function.

Definition 1 (entropy at $s_0 \in (0,\infty)$). Let $\mathbb{G} \in \mathscr{RL}_\infty$ and $\gamma > 0$ be a real scalar such that $\|\mathbb{G}\|_\infty < \gamma$. Then the entropy of $\mathbb{G}$ at s_0 is defined by

$$\mathscr{I}(\mathbb{G}; \gamma; s_0) \triangleq -\frac{\gamma^2}{2\pi} \int_{-\infty}^{\infty} \ln \left| \det \left(I - \gamma^{-2} \mathbb{G}^* (j\omega) \mathbb{G} (j\omega) \right) \right| \times \left[\frac{s_0^2}{s_0^2 + \omega^2} \right] d\omega. \tag{6}$$

When $s_0 \to \infty$, we obtain the entropy at infinity of the system, which has the following definition.

Definition 2 (entropy at infinity). Let $\mathbb{G} \in \mathcal{RL}_\infty$ and $\gamma > 0$ be a real scalar such that $\|\mathbb{G}\|_\infty < \gamma$. Then the entropy of $\mathbb{G}$ at infinity is defined by

$$\mathcal{I}(\mathbb{G};\gamma;\infty) \triangleq -\frac{\gamma^2}{2\pi}\int_{-\infty}^{\infty} \ln\left|\det\left(I-\gamma^{-2}\mathbb{G}^*(j\omega)\,\mathbb{G}(j\omega)\right)\right| d\omega. \tag{7}$$

It is well known that for LTI system (Π) in (5), we have the following results for the $\mathcal{H}_2$ optimization problem:

$$\|\mathbb{G}\|_2^2 = \operatorname{trace}\left(B^T Q B\right), \tag{8}$$

where $Q = Q^T \geq 0$ is the solution to the Lyapunov equation

$$A^T Q + QA + L^T L = 0. \tag{9}$$

In fact, Q is just the controllability Gramian.

Now, considering the $\mathcal{H}_\infty$ optimization problem of LTI system, we knew that $\|\mathbb{G}\|_\infty < \gamma$ if there exists a stabilizing solution $P = P^T \geq 0$ to the algebraic Riccati equation

$$A^T P + PA + \gamma^{-2} PBB^T P + L^T L = 0, \tag{10}$$

and it is easy to prove that any P solving (10) overbounds the controllability Gramian Q; that is, $P \geq Q$. To evaluate the entropy cost, we define the following auxiliary cost.

Definition 3 (auxiliary cost). Let $\mathbb{G} \in \mathcal{RL}_\infty$ and $\gamma > 0$ be a real scalar such that $\|\mathbb{G}\|_\infty < \gamma$. Then the auxiliary cost with $\mathbb{G}$ is defined by

$$\mathcal{J}(\mathbb{G};\gamma) \triangleq \operatorname{trace}\left(B^T P B\right), \tag{11}$$

where P is a positive symmetric matrix with the smallest possible maximum singular value among all solutions of the algebraic Riccati equality (10).

The following lemma gives the equivalence between the auxiliary cost and the entropy defined in (7) and (11), respectively, which plays a key role in deriving our main results subsequently.

Lemma 4 (see [20]). *Let $\mathbb{G} \in \mathcal{RL}_\infty$ and $\gamma > 0$ be a real scalar such that $\|\mathbb{G}\|_\infty < \gamma$. Then the entropy equals the auxiliary cost; that is,*

$$\mathcal{I}(\mathbb{G};\gamma;\infty) = \mathcal{J}(\mathbb{G};\gamma). \tag{12}$$

Moreover, according to the result in [22], the minimum entropy $\mathcal{H}_\infty$ optimization problem for the LTI system (Π) can be formulated as follows:

$$\min_{P>0,\,R>0} \operatorname{trace}(R), \tag{13}$$

subject to

$$\begin{bmatrix} A^T P + PA & PB & L^T \\ \star & -\gamma^2 I & 0 \\ \star & \star & -I \end{bmatrix} < 0, \qquad \begin{bmatrix} -R & B^T P \\ \star & -P \end{bmatrix} \leq 0. \tag{14}$$

The objective of this paper is to design a full-order (or reduced-order) minimum entropy $\mathcal{H}_\infty$ filter the system (Σ) in (1) of the following form:

$$\left(\widehat{\Sigma}\right): \begin{cases} \dot{\widehat{x}}(t) = A_f \widehat{x}(t) + B_f y(t), & \widehat{x}(0) = 0, \\ \widehat{z}(t) = L_f \widehat{x}(t), \end{cases} \tag{15}$$

where $\widehat{x}(t) \in \mathbb{R}^k$ is the filter state vector, $A_f \in \mathbb{R}^{k\times k}$, $B_f \in \mathbb{R}^{k\times m}$, and $C_f \in \mathbb{R}^{q\times k}$ are filter parameters to be determined later. In the case where $k = n$, the filter will be referred to as a full-order filter and as a reduced-order filter when $k < n$.

Augmenting the model of (1) to include the state of the filter ($\widehat{\Sigma}$), we obtain the filtering error system as

$$\left(\widetilde{\Sigma}\right): \begin{cases} \dot{\xi}(t) = \widetilde{A}\xi(t) + \widetilde{B}\omega(t), \\ e(t) = \widetilde{L}\xi(t), \end{cases} \tag{16}$$

where $\xi(t) \triangleq [x^T(t)\widehat{x}^T(t)]^T$, $e(t) \triangleq z(t) - \widehat{z}(t)$ and

$$\widetilde{A} \triangleq \begin{bmatrix} A & 0 \\ B_f C & A_f \end{bmatrix}, \qquad \widetilde{B} \triangleq \begin{bmatrix} B \\ B_f D \end{bmatrix}, \qquad \widetilde{L} \triangleq \begin{bmatrix} L & -L_f \end{bmatrix}. \tag{17}$$

Our aim in this paper is to determine the matrices A_f, B_f, and L_f of the full-order (or reduced-order) minimum entropy $\mathcal{H}_\infty$ filter ($\widehat{\Sigma}$) in (15) such that the filtering error system ($\widetilde{\Sigma}$) in (16) is asymptotically stable with a prescribed $\mathcal{H}_\infty$ disturbance attenuation level $\gamma > 0$ and a guaranteed minimum entropy at infinity; that is, $\mathcal{I}(\mathbb{E};\gamma;\infty)$ is minimized for a given scalar $\gamma > 0$ (where $\mathbb{E}$ is defined as the transfer function of the filtering error system ($\widetilde{\Sigma}$) in (16)).

3. Main Results

3.1. Full-Order Robust Filter Design. In this section, we will first study the design of a full-order filter. In order to pave the way for deriving the robust filter, initially we consider the case where the system matrix $\mathcal{G}$ is perfectly known; that is, $n_s = 1$. We first give the following result which will play a key role in deriving our subsequent results. Since the result can be easily obtained according to the analysis in Section 2, we omit the proof.

Theorem 5. *The filtering error system* $(\widetilde{\Sigma})$ *in* (16) *is asymptotically stable with an* $\mathscr{H}_\infty$ *disturbance attenuation level* $\gamma > 0$ *and a guaranteed minimum entropy, if there exist matrices* $P > 0$ *and* $R > 0$ *such that the following optimization problem has feasible solution:*

$$\min_{P>0,\, R>0,\, A_f, B_f, L_f} trace\,(R)\,, \tag{18}$$

subject to

$$\begin{bmatrix} \widetilde{A}^T P + P\widetilde{A} & P\widetilde{B} & \widetilde{L}^T \\ \star & -\gamma^2 I & 0 \\ \star & \star & -I \end{bmatrix} < 0, \tag{19}$$

$$\begin{bmatrix} -R & \widetilde{B}^T P \\ \star & -P \end{bmatrix} \le 0. \tag{20}$$

Notice that the inequalities constraints of (19)-(20) are not convex on the decision variables P, A_f, B_f, and L_f. In what follows, we will present the design method of the minimum entropy $\mathscr{H}_\infty$ filter, and give the following result.

Theorem 6. *Consider the system* (Σ) *with perfectly known system matrix* $\mathscr{G}$. *There exists a full-order minimum entropy* $\mathscr{H}_\infty$ *filter of the form of* (15) *such that the filtering error system* $(\widetilde{\Sigma})$ *in* (16) *is asymptotically stable with an* $\mathscr{H}_\infty$ *disturbance attenuation level* $\gamma > 0$ *and a guaranteed minimum entropy, if there exist matrices* $\mathscr{U} > 0$ *and* $\mathscr{V} > 0$ *and matrices* $\mathscr{A}_f$, $\mathscr{B}_f$, *and* $\mathscr{L}_f$ *such that the following optimization problem has feasible solution:*

$$\min_{\mathscr{U}>0,\, \mathscr{V}>0,\, \mathscr{A}_f, \mathscr{B}_f, \mathscr{L}_f} trace\,(R)\,, \tag{21}$$

subject to

$$\begin{bmatrix} \mathscr{U}A + A^T\mathscr{U} + \mathscr{B}_f C + C^T\mathscr{B}_f^T & \mathscr{A}_f + A^T\mathscr{V} + C^T\mathscr{B}_f^T & \mathscr{U}B + \mathscr{B}_f D & L^T \\ \star & \mathscr{A}_f + \mathscr{A}_f^T & \mathscr{V}B + \mathscr{B}_f D & -\mathscr{L}_f^T \\ \star & \star & -\gamma^2 I & 0 \\ \star & \star & \star & -I \end{bmatrix} < 0, \tag{22}$$

$$\begin{bmatrix} -R & B^T\mathscr{U} + D^T\mathscr{B}_f^T & B^T\mathscr{V} + D^T\mathscr{B}_f^T \\ \star & -\mathscr{U} & -\mathscr{V} \\ \star & \star & -\mathscr{V} \end{bmatrix} \le 0. \tag{23}$$

Moreover, a desired full-order minimum entropy $\mathscr{H}_\infty$ *filter can be computed from*

$$\begin{bmatrix} A_f & B_f \\ L_f & 0 \end{bmatrix} \triangleq \begin{bmatrix} \mathscr{V}^{-1} & 0 \\ 0 & I \end{bmatrix} \begin{bmatrix} \mathscr{A}_f & \mathscr{B}_f \\ \mathscr{L}_f & 0 \end{bmatrix}. \tag{24}$$

Proof. According to Theorem 5, P is nonsingular if the optimization problem of (18)–(20) has feasible solutions since $P > 0$. Now, partition P as

$$P \triangleq \begin{bmatrix} P_1 & P_3 \\ \star & P_2 \end{bmatrix}, \tag{25}$$

where P_1 and P_2 are $n \times n$ symmetric positive definite matrices. Without loss of generality, we assume that P_3 is nonsingular. To see this, let the matrix $Q \triangleq P + \alpha W$, where α is a positive scalar and

$$W \triangleq \begin{bmatrix} 0 & I \\ \star & 0 \end{bmatrix}, \qquad Q \triangleq \begin{bmatrix} Q_1 & Q_3 \\ \star & Q_2 \end{bmatrix}. \tag{26}$$

Observe that, since $P > 0$, we have $Q > 0$ for $\alpha > 0$ in a neighborhood of the origin. Thus, it can be easily verified that there exists an arbitrarily small $\alpha > 0$ such that Q_3 is nonsingular and inequalities (19)-(20) are feasible with P replaced by Q and such that the objective function of (18) will be increased only by an arbitrarily small quantity. Since Q_3 is nonsingular, we thus conclude that there is no loss of generality to assume the matrix P_3 to be nonsingular.

Define the following matrices which are all nonsingular:

$$\Gamma \triangleq \begin{bmatrix} I & 0 \\ 0 & P_2^{-1}P_3^T \end{bmatrix}, \qquad \mathscr{U} \triangleq P_1, \qquad \mathscr{V} \triangleq P_3 P_2^{-1} P_3^T, \tag{27}$$

$$\begin{bmatrix} \mathscr{A}_f & \mathscr{B}_f \\ \mathscr{L}_f & 0 \end{bmatrix} \triangleq \begin{bmatrix} P_3 & 0 \\ 0 & I \end{bmatrix} \begin{bmatrix} A_f & B_f \\ L_f & 0 \end{bmatrix} \begin{bmatrix} P_2^{-1}P_3^T & 0 \\ 0 & I \end{bmatrix}. \tag{28}$$

Performing congruence transformations to (19)-(20) by $\mathrm{diag}(\Gamma, I, I)$ and $\mathrm{diag}(I, \Gamma)$, respectively, we have

$$\begin{bmatrix} \Gamma^T\widetilde{A}^T P\Gamma + \Gamma^T P\widetilde{A}\Gamma & \Gamma^T P\widetilde{B} & \Gamma^T\widetilde{L}^T \\ \star & -\gamma^2 I & 0 \\ \star & \star & -I \end{bmatrix} < 0, \tag{29}$$

$$\begin{bmatrix} -R & \widetilde{B}^T P\Gamma \\ \star & -\Gamma^T P\Gamma \end{bmatrix} \le 0. \tag{30}$$

Considering (17) and (25)–(28), we have

$$\Gamma^T P\widetilde{A}\Gamma \triangleq \begin{bmatrix} \mathscr{U}A + \mathscr{B}_f C & \mathscr{A}_f \\ \mathscr{V}A + \mathscr{B}_f C & \mathscr{A}_f \end{bmatrix}, \qquad \Gamma^T P\widetilde{B} \triangleq \begin{bmatrix} \mathscr{U}B + \mathscr{B}_f D \\ \mathscr{V}B + \mathscr{B}_f D \end{bmatrix},$$

$$\Gamma^T P\Gamma \triangleq \begin{bmatrix} \mathscr{U} & \mathscr{V} \\ \star & \mathscr{V} \end{bmatrix}, \qquad \widetilde{L}\Gamma \triangleq \begin{bmatrix} L & -\mathscr{L}_f \end{bmatrix}. \tag{31}$$

Substituting (31) into (29)-(30) yields (22)-(23), respectively.

On the other hand, (28) is equivalent to

$$\begin{bmatrix} A_f & B_f \\ L_f & 0 \end{bmatrix} = \begin{bmatrix} P_3^{-1} & 0 \\ 0 & I \end{bmatrix} \begin{bmatrix} \mathscr{A}_f & \mathscr{B}_f \\ \mathscr{L}_f & 0 \end{bmatrix} \begin{bmatrix} P_3^{-T}P_2 & 0 \\ 0 & I \end{bmatrix}$$

$$= \begin{bmatrix} \left(P_3^{-T}P_2\right)^{-1}\mathscr{V}^{-1} & 0 \\ 0 & I \end{bmatrix} \begin{bmatrix} \mathscr{A}_f & \mathscr{B}_f \\ \mathscr{L}_f & 0 \end{bmatrix} \begin{bmatrix} P_3^{-T}P_2 & 0 \\ 0 & I \end{bmatrix}. \tag{32}$$

Note that the filter matrices of (15) can be written as (32), which implies that $P_3^{-T}P_2$ can be viewed as a similarity transformation on the state-space realization of the filter and, as such, has no effect on the filter mapping from y to $\widehat{z}$. Without loss of generality, we can set $P_3^{-T}P_2 = I$ and thus obtain (24). This completes the proof. □

Now, we will consider the design of a full-order robust filter. To this end, consider the system (Σ) in (1) and the uncertainty domain $\mathscr{D}$ in (3). According to the previous arguments, we have the following result.

Theorem 7. *Consider the system (Σ) with system matrix $\mathscr{G} \in \mathscr{D}$. There exists a full-order minimum entropy $\mathscr{H}_\infty$ filter of the form of (15) such that the filtering error system $(\widetilde{\Sigma})$ in (16) is asymptotically stable with an $\mathscr{H}_\infty$ disturbance attenuation level $\gamma > 0$ and a guaranteed minimum entropy, if there exist matrices $\mathscr{U} > 0$ and $\mathscr{V} > 0$ and matrices $\mathscr{A}_f$, $\mathscr{B}_f$, and $\mathscr{L}_f$ such that, for $j = 1, 2, \ldots, n_s$, the following optimization problem has a feasible solution:*

$$\min_{\mathscr{U}>0,\mathscr{V}>0,\mathscr{A}_f,\mathscr{B}_f,\mathscr{L}_f} trace\,(R), \tag{33}$$

subject to

$$\begin{bmatrix} \mathscr{U}A_j + A_j^T\mathscr{U} + \mathscr{B}_f C_j + C_j^T\mathscr{B}_f^T & \mathscr{A}_f + A_j^T\mathscr{V} + C_j^T\mathscr{B}_f^T & \mathscr{U}B_j + \mathscr{B}_f D_j & L^T \\ \star & \mathscr{A}_f + \mathscr{A}_f^T & \mathscr{V}B_j + \mathscr{B}_f D_j & -\mathscr{L}_f^T \\ \star & \star & -\gamma^2 I & 0 \\ \star & \star & \star & -I \end{bmatrix} < 0,$$
$$\begin{bmatrix} -R & B_j^T\mathscr{U} + D_j^T\mathscr{B}_f^T & B_j^T\mathscr{V} + D_j^T\mathscr{B}_f^T \\ \star & -\mathscr{U} & -\mathscr{V} \\ \star & \star & -\mathscr{V} \end{bmatrix} \le 0. \tag{34}$$

Moreover, a desired full-order minimum entropy $\mathscr{H}_\infty$ filter can be computed from (24).

Proof. Employing the same arguments as in the proof of Theorem 6, it follows that the optimization problem of (33)-(34) is equivalent to

$$\min_{P>0,\,R>0,\,A_f,\,B_f,\,L_f} \operatorname{trace}(R), \tag{35}$$

subject to $j = 1, 2, \ldots, n_s$,

$$\begin{bmatrix} \widetilde{A}_j^T P + P\widetilde{A}_j & P\widetilde{B}_j & \widetilde{L}^T \\ \star & -\gamma^2 I & 0 \\ \star & \star & -I \end{bmatrix} < 0,$$
$$\begin{bmatrix} -R & \widetilde{B}_j^T P \\ \star & -P \end{bmatrix} \le 0, \tag{36}$$

where $\widetilde{A}_j$ and $\widetilde{B}_j$ are as in (17) with A, B, C, and D replaced by A_j, B_j, C_j, and D_j, respectively.

Now, in view of the convexity of the uncertainty domain and considering that the inequalities (36) are affine in the matrices A_j, B_j, C_j, and D_j, we have the result that the optimization problem of (35)–(36) is equivalent to that of (18)–(20) with system matrix $\mathscr{G} \in \mathscr{D}$. This completes the proof. □

3.2. Reduced-Order Robust Filter Design. In this section, we will consider the design of reduced-order robust filter, that is, the case where the order of the filter k is smaller than the order n of the original system model. As the former, we first consider the case where the system matrix $\mathscr{G}$ is perfectly known, that is, $n_s = 1$, which have the following result.

Theorem 8. *Consider system (Σ) with perfectly known system matrix $\mathscr{G}$. There exists a reduced-order minimum entropy $\mathscr{H}_\infty$ filter of the form of (15) such that the filtering error system $(\widetilde{\Sigma})$ in (16) is asymptotically stable with an $\mathscr{H}_\infty$ disturbance attenuation level $\gamma > 0$ and a guaranteed minimum entropy, if there exist matrices $\mathscr{M} > 0$ and $\mathscr{N} > 0$ and matrices $\mathscr{A}_f$, $\mathscr{B}_f$, and $\mathscr{L}_f$ such that the following optimization problem has feasible solution:*

$$\min_{\mathscr{M}>0,\mathscr{N}>0,\mathscr{A}_f,\mathscr{B}_f,\mathscr{L}_f} trace\,(R), \tag{37}$$

subject to

$$\begin{bmatrix} \Pi_{11} & \mathscr{K}\mathscr{A}_f + A^T\mathscr{K}\mathscr{N} + C^T\mathscr{B}_f^T & \mathscr{M}B + \mathscr{K}\mathscr{B}_f D & L^T \\ \star & \mathscr{A}_f + \mathscr{A}_f^T & \mathscr{N}^T\mathscr{K}^T B + \mathscr{B}_f D & -\mathscr{L}_f^T \\ \star & \star & -\gamma^2 I & 0 \\ \star & \star & \star & -I \end{bmatrix} \tag{38}$$
$$< 0,$$
$$\begin{bmatrix} -R & B^T\mathscr{M} + D^T\mathscr{B}_f^T & B^T\mathscr{K}\mathscr{N} + D^T\mathscr{B}_f^T \\ \star & -\mathscr{M} & -\mathscr{K}\mathscr{N} \\ \star & \star & -\mathscr{N} \end{bmatrix} \le 0, \tag{39}$$

where $\mathscr{K} \triangleq \begin{bmatrix} I_{k\times k} \\ 0_{(n-k)\times k} \end{bmatrix}$ and $\Pi_{11} \triangleq \mathscr{M}A + A^T\mathscr{M} + \mathscr{K}\mathscr{B}_f C + C^T\mathscr{B}_f^T\mathscr{K}^T$. Moreover, a desired reduced-order minimum entropy $\mathscr{H}_\infty$ filter can be computed from

$$\begin{bmatrix} A_f & B_f \\ L_f & 0 \end{bmatrix} \triangleq \begin{bmatrix} \mathscr{N}^{-1} & 0 \\ 0 & I \end{bmatrix} \begin{bmatrix} \mathscr{A}_f & \mathscr{B}_f \\ \mathscr{L}_f & 0 \end{bmatrix}. \tag{40}$$

Proof. The proof is along the same lines as in the proof of Theorem 6. According to Theorem 5, P is nonsingular if the optimization problem of (18)–(20) has feasible solutions since $P > 0$. Now, partition P as

$$P \triangleq \begin{bmatrix} P_1 & P_3 \\ \star & P_2 \end{bmatrix}, \qquad P_3 \triangleq \begin{bmatrix} P_4 \\ 0_{(n-k)\times k} \end{bmatrix}, \tag{41}$$

where $P_1 \in \mathbb{R}^{n\times n}$ and $P_2 \in \mathbb{R}^{k\times k}$ are symmetric positive definite matrices and $P_4 \in \mathbb{R}^{k\times k}$. Without loss of generality,

we assume that P_4 is nonsingular; to see this, let the matrix $\mathcal{Q} \triangleq P + \alpha\mathcal{W}$, where α is a positive scalar and

$$\mathcal{W} \triangleq \left[\begin{array}{c|c} 0_{n\times n} & \mathcal{K} \\ \hline \star & 0_{k\times k} \end{array}\right], \qquad \mathcal{Q} \triangleq \begin{bmatrix} \mathcal{Q}_1 & \mathcal{Q}_3 \\ \star & \mathcal{Q}_2 \end{bmatrix}, \qquad \mathcal{Q}_3 \triangleq \begin{bmatrix} \mathcal{Q}_4 \\ 0_{(n-k)\times k} \end{bmatrix}. \tag{42}$$

With the same principle as in the proof of Theorem 6, it can be seen that there exists an arbitrarily small $\alpha > 0$ such that $\mathcal{Q}_4$ is nonsingular and (18)–(20) have feasible solutions with P replaced by $\mathcal{Q}$; thus, we can conclude that there is no loss of generality to assume the matrix P_4 to be nonsingular.

Define the following matrices:

$$\widetilde{\Gamma} \triangleq \begin{bmatrix} I & 0 \\ 0 & P_2^{-1}P_4^T \end{bmatrix}, \qquad \mathcal{M} \triangleq P_1, \qquad \mathcal{N} \triangleq P_4P_2^{-1}P_4^T, \tag{43}$$

$$\begin{bmatrix} \mathcal{A}_f & \mathcal{B}_f \\ \mathcal{L}_f & 0 \end{bmatrix} \triangleq \begin{bmatrix} P_4 & 0 \\ 0 & I \end{bmatrix} \begin{bmatrix} A_f & B_f \\ L_f & 0 \end{bmatrix} \begin{bmatrix} P_2^{-1}P_4^T & 0 \\ 0 & I \end{bmatrix}. \tag{44}$$

Performing congruence transformations to (19) and (20) by $\mathrm{diag}(\widetilde{\Gamma}, I, I)$ and $\mathrm{diag}(I, \widetilde{\Gamma})$, respectively, we have

$$\begin{bmatrix} \widetilde{\Gamma}^T\widetilde{A}^TP\widetilde{\Gamma} + \widetilde{\Gamma}^TP\widetilde{A}\widetilde{\Gamma} & \widetilde{\Gamma}^TP\widetilde{B} & \widetilde{\Gamma}^T\widetilde{L}^T \\ \star & -\gamma^2 I & 0 \\ \star & \star & -I \end{bmatrix} < 0, \tag{45}$$

$$\begin{bmatrix} -R & \widetilde{B}^TP\widetilde{\Gamma} \\ \star & -\widetilde{\Gamma}^TP\widetilde{\Gamma} \end{bmatrix} \le 0. \tag{46}$$

Considering (17) and (41)–(44), we have

$$\widetilde{\Gamma}^TP\widetilde{A}\widetilde{\Gamma} \triangleq \begin{bmatrix} \mathcal{M}A + \mathcal{K}\mathcal{B}_fC & \mathcal{K}\mathcal{A}_f \\ \mathcal{N}^T\mathcal{K}^TA + \mathcal{B}_fC & \mathcal{A}_f \end{bmatrix},$$

$$\widetilde{\Gamma}^TP\widetilde{B} \triangleq \begin{bmatrix} \mathcal{M}B + \mathcal{K}\mathcal{B}_fD \\ \mathcal{N}^T\mathcal{K}^TB + \mathcal{B}_fD \end{bmatrix}, \tag{47}$$

$$\widetilde{\Gamma}^TP\widetilde{\Gamma} \triangleq \begin{bmatrix} \mathcal{M} & \mathcal{K}\mathcal{N} \\ \star & \mathcal{N} \end{bmatrix}, \qquad \widetilde{L}\widetilde{\Gamma} \triangleq \begin{bmatrix} L & -\mathcal{L}_f \end{bmatrix}.$$

Substituting (47) into (45)-(46), we obtain (38)-(39), respectively.

The remainder of the proof follows along the same lines as in the proof of Theorem 6. □

Now, considering the design of reduced-order robust filter, we give the following result without proof, which can be obtained by employing the same techniques used as those in Theorems 7 and 8.

Theorem 9. *Consider the system (Σ) with system matrix $\mathcal{G} \in \mathcal{D}$. There exists a reduced-order minimum entropy $\mathcal{H}_\infty$ filter of the form of* (15) *such that the filtering error system ($\widetilde{\Sigma}$) in* (16) *is asymptotically stable with an $\mathcal{H}_\infty$ disturbance attenuation level $\gamma > 0$ and a guaranteed minimum entropy, if there exist matrices $\mathcal{M} > 0$ and $\mathcal{N} > 0$ and matrices $\mathcal{A}_f$, $\mathcal{B}_f$, and $\mathcal{L}_f$ such that, for $j = 1, 2, \ldots, n_s$, the following optimization problem has feasible solution:*

$$\min_{\mathcal{M}>0,\, \mathcal{N}>0,\, \mathcal{A}_f, \mathcal{B}_f, \mathcal{L}_f} trace\,(R), \tag{48}$$

subject to

$$\begin{bmatrix} \Pi_{11j} & \mathcal{K}\mathcal{A}_f + A_j^T\mathcal{K}\mathcal{N} + C_j^T\mathcal{B}_f^T & \mathcal{M}B_j + \mathcal{K}\mathcal{B}_fD_j & L^T \\ \star & \mathcal{A}_f + \mathcal{A}_f^T & \mathcal{N}^T\mathcal{K}^TB_j + \mathcal{B}_fD_j & -\mathcal{L}_f^T \\ \star & \star & -\gamma^2 I & 0 \\ \star & \star & \star & -I \end{bmatrix} \le 0,$$

$$\begin{bmatrix} -R & B_j^T\mathcal{M} + D_j^T\mathcal{B}_f^T\mathcal{K}^T & B_j^T\mathcal{K}\mathcal{N} + D_j^T\mathcal{B}_f^T \\ \star & -\mathcal{M} & -\mathcal{K}\mathcal{N} \\ \star & \star & -\mathcal{N} \end{bmatrix} < 0, \tag{49}$$

where $\Pi_{11j} \triangleq \mathcal{M}A_j + A_j^T\mathcal{M} + \mathcal{K}\mathcal{B}_fC_j + C_j^T\mathcal{B}_f^T\mathcal{K}^T$ and $\mathcal{K}$ is defined in (38). *Moreover, a desired reduced-order minimum entropy $\mathcal{H}_\infty$ filter can be computed from* (40).

4. Numerical Example

In this section, we present an illustrative example to demonstrate the effectiveness of the proposed algorithm. Consider the linear continuous-time system (Σ) in (1) with parameter matrix $\mathcal{G}$ belonging to polyhedral domain $\mathcal{D}$, and assume $n_s = 3$, then the system data $\mathcal{G}_j$, $(j = 1, 2, 3)$ are given as follows:

$$A_1 = \begin{bmatrix} -2.3 & 0.2 & -0.3 \\ -0.4 & -0.6 & 0.0 \\ 0.0 & 0.5 & -1.3 \end{bmatrix}, \quad B_1 = \begin{bmatrix} 0.6 \\ 0.3 \\ -0.9 \end{bmatrix}, \quad C_1 = \begin{bmatrix} 1.0 & 0.3 & 1.0 \end{bmatrix}, \quad D_1 = 0.2,$$

$$A_2 = \begin{bmatrix} -2.5 & 0.0 & 0.6 \\ 0.0 & -1.3 & -0.2 \\ -0.2 & 0.5 & -1.6 \end{bmatrix}, \quad B_2 = \begin{bmatrix} -0.4 \\ 0.6 \\ -0.3 \end{bmatrix}, \quad C_2 = \begin{bmatrix} 0.4 & 1.2 & -0.7 \end{bmatrix}, \quad D_2 = 0.8,$$

$$A_3 = \begin{bmatrix} -1.6 & 0.5 & -0.2 \\ 0.3 & -1.6 & 0.2 \\ 0.2 & 0.0 & -0.6 \end{bmatrix}, \quad B_3 = \begin{bmatrix} -0.1 \\ -0.3 \\ 0.6 \end{bmatrix}, \quad C_3 = \begin{bmatrix} 0.3 & -1.5 & 0.8 \end{bmatrix}, \quad D_3 = -0.5,$$

$$L = \begin{bmatrix} 0.3 & 0.5 & 0.8 \end{bmatrix}. \tag{50}$$

First, we consider the full-order filter design; solving the LMIs condition in Theorem 7 by applying the well-developed LMI Toolbox in the MATLAB environment directly, we obtain that the minimum γ is $\gamma^* = 0.4666$, the minimum entropy of

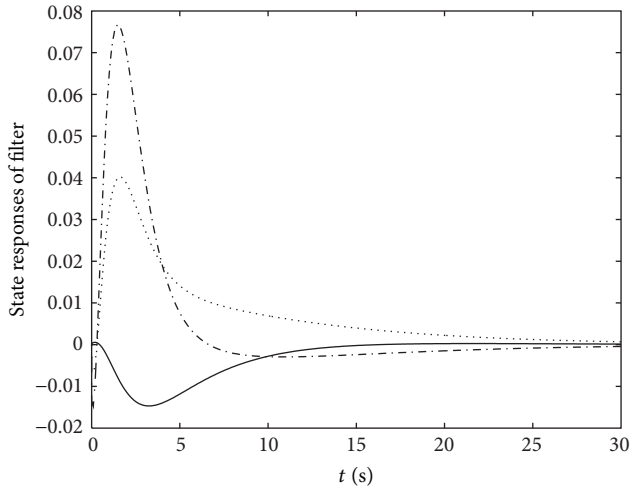

Figure 1: States of the designed full-order filter.

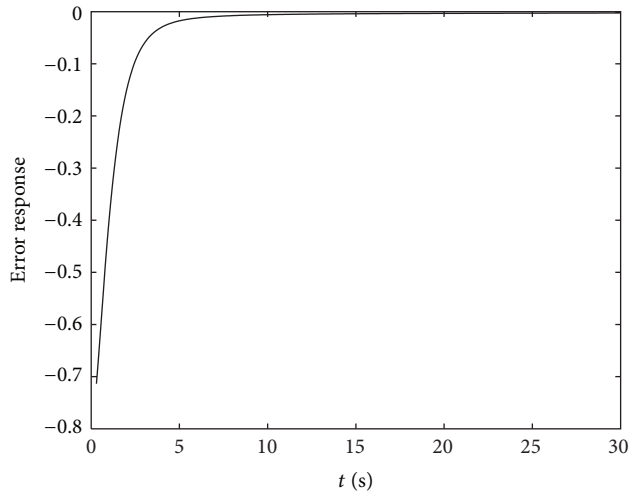

Figure 2: Filtering error of the full-order filtering.

the filtering error system is $\mathcal{I}(\mathbb{E}; \gamma^*; \infty) = 0.3618$ (where $\mathbb{E}$ denotes the transfer function of filtering error system), and

$$A_f = \begin{bmatrix} -0.3015 & -0.0948 & -0.0196 \\ -0.3450 & -1.0629 & -0.6874 \\ -0.2279 & -0.4217 & -0.4166 \end{bmatrix},$$
$$B_f = \begin{bmatrix} 0.0125 \\ -0.5696 \\ -0.2754 \end{bmatrix}, \quad (51)$$
$$L_f = \begin{bmatrix} -0.3007 & -0.5002 & -0.8002 \end{bmatrix}.$$

With $\lambda_1 = 0.7$, $\lambda_2 = 0.1$, and $\lambda_3 = 0.2$ in (3), the states of the full-order designed filter are given in Figure 1, where the initial condition is $\begin{bmatrix} 1.0 & -0.5 & -1.0 \end{bmatrix}^T$, and the exogenous disturbance input $\omega(t)$ is given as $\omega(t) = 1/(0.5 + 1.8t)$, $t \geq 0$. Figure 2 shows the error response of $e(t)$.

Now, we consider the reduced-order filter design, and two cases of such filters are considered.

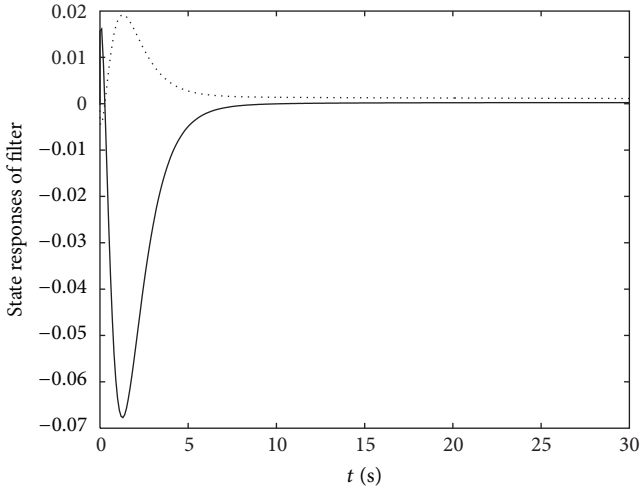

Figure 3: States of the designed reduced-order filter (with the order of $k = 2$).

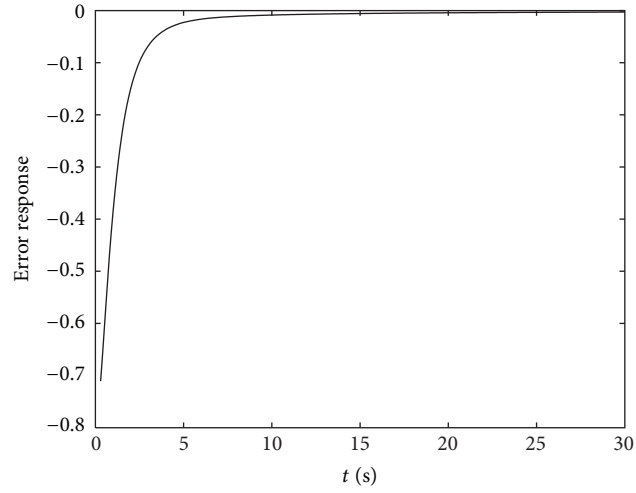

Figure 4: Filtering error of the reduced-order filtering (with the order of $k = 2$).

Case 1. Set $k = 2$; that is, the order of the reduced filter is $k = 2$; solving the LMIs condition in Theorem 9, we obtain that the minimum γ is $\gamma^* = 0.5069$, the minimum entropy of the filtering error system is $\mathcal{I}(\mathbb{E}; \gamma^*; \infty) = 0.9401$, and

$$A_f = \begin{bmatrix} -1.9483 & 0.5354 \\ 0.5302 & -0.1546 \end{bmatrix}, \quad B_f = \begin{bmatrix} 0.6662 \\ -0.1850 \end{bmatrix}, \quad (52)$$
$$L_f = \begin{bmatrix} 1.1058 & -0.3003 \end{bmatrix}.$$

Under the same conditions as in the full-order filter design, the states of the designed reduced-order filter are given in Figure 3. Figure 4 shows the error response of $e(t)$.

Case 2. Set $k = 1$; that is, the order of the reduced filter is $k = 1$; by solving the LMIs condition in Theorem 9, we obtain

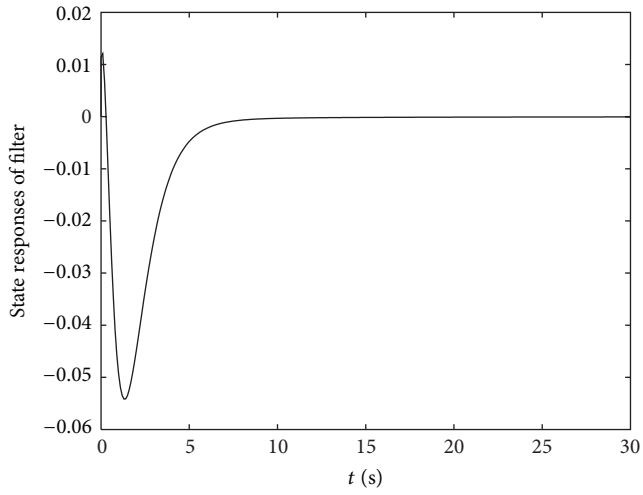

Figure 5: States of the designed reduced-order filter (with the order of $k = 1$).

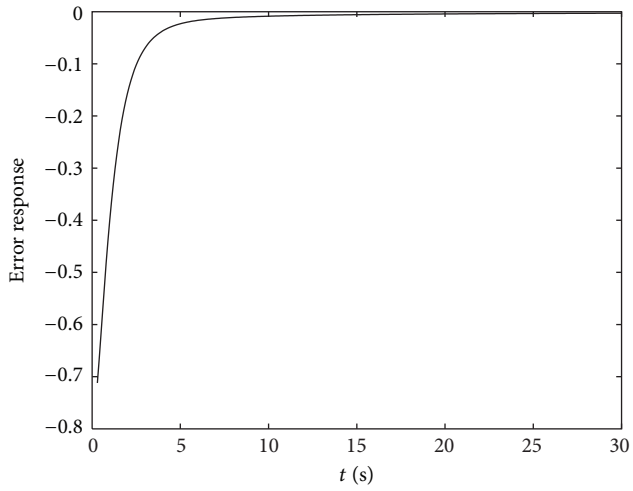

Figure 6: Filtering error of the reduced-order filtering (with the order of $k = 1$).

that the minimum γ is $\gamma^* = 0.5148$, the minimum entropy of the filtering error system is $\mathcal{I}(\mathbb{E}; \gamma^*; \infty) = 0.8677$, and

$$A_f = -1.8368, \qquad B_f = 0.4853, \qquad L_f = 1.2617. \quad (53)$$

The states and the filtering error of the designed reduced-order filter are given in Figures 5 and 6, respectively.

5. Conclusion

In this paper, the robust minimum entropy $\mathscr{H}_\infty$ filter has been designed for linear continuous-time systems with polytopic parameter uncertainty. Sufficient conditions have been established for the existence of general full- and reduced-order minimum entropy $\mathscr{H}_\infty$ filters in terms of LMIs, which guarantee the filtering error system to be robustly asymptotically stable and to have a prescribed $\mathscr{H}_\infty$ performance as well as a guaranteed minimum entropy. The filler design could be cast into a convex optimization problem and a numerical example has been provided to demonstrate the effectiveness of the proposed design method.

Conflict of Interests

The authors declare that there is no conflict of interests regarding the publication of this paper.

Acknowledgments

This work has been supported by the National Natural Science Foundation of China (Grant no. 61104109), the Natural Science Foundation of Jiangsu Province of China (Grant no. BK2011703), the Support of Science and Technology and Independent Innovation Foundation of Jiangsu Province of China (Grant no. BE2012178), and the Doctoral Fund of Ministry of Education of China (Grant no. 20113219110027).

References

[1] L. Wu, P. Shi, and H. Gao, "State estimation and sliding-mode control of Markovian jump singular systems," *IEEE Transactions on Automatic Control*, vol. 55, no. 5, pp. 1213–1219, 2010.

[2] I. R. Petersen and A. V. Savkin, *Robust Kalman Filtering for Signals and Systems with Large Uncertainties*, Control Engineering, Birkhäuser, Boston, Mass, USA, 1999.

[3] P. Shi, "Robust Kalman filtering for continuous-time systems with discrete-time measurements," *IMA Journal of Mathematical Control and Information*, vol. 16, no. 3, pp. 221–232, 1999.

[4] C. E. de Souza and A. Trofino, *An LMI Approach to the Design of Robust $\mathscr{H}_2$ fiLters*, SIAM, Philadelphia, Pa, USA, 1999.

[5] J. C. Geromel and M. C. de Oliveira, "$\mathscr{H}_2$ and $\mathscr{H}_\infty$ robust filtering for convex bounded uncertain systems," *IEEE Transactions on Automatic Control*, vol. 46, no. 1, pp. 100–107, 2001.

[6] H. Gao and C. Wang, "Delay-dependent robust $\mathscr{H}_\infty$ and $\mathscr{L}_2$-$\mathscr{L}_\infty$ filtering for a class of uncertain nonlinear time-delay systems," *IEEE Transactions on Automatic Control*, vol. 48, no. 9, pp. 1661–1666, 2003.

[7] S. Xu, "Robust $\mathscr{H}_\infty$ filtering for a class of discrete-time uncertain nonlinear systems with state delay," *IEEE Transactions on Circuits and Systems I*, vol. 49, no. 12, pp. 1853–1859, 2002.

[8] S. Xu and T. Chen, "Reduced-order $\mathscr{H}_\infty$ filtering for stochastic systems," *IEEE Transactions on Signal Processing*, vol. 50, no. 12, pp. 2998–3007, 2002.

[9] A. Elsayed and M. J. Grimble, "A new approach to the $\mathscr{H}_\infty$ design of optimal digital linear filters," *IMA Journal of Mathematical Control and Information*, vol. 6, no. 2, pp. 233–251, 1989.

[10] S. H. Jin and J. B. Park, "Robust $\mathscr{H}_\infty$ filtering for polytopic uncertain systems via convex optimisation," *IEE Proceedings*, vol. 148, no. 1, pp. 55–59, 2001.

[11] H. Li and M. Fu, "Linear matrix inequality approach to robust $\mathscr{H}_\infty$ filtering," *IEEE Transactions on Signal Processing*, vol. 45, no. 9, pp. 2338–2350, 1997.

[12] H. Gao and C. Wang, "Robust $\mathscr{L}_2$-$\mathscr{L}_\infty$ filtering for uncertain systems with multiple time-varying state delays," *IEEE Transactions on Circuits and Systems. I*, vol. 50, no. 4, pp. 594–599, 2003.

[13] L. Wu, P. Shi, H. Gao, and C. Wang, "$\mathscr{H}_\infty$ filtering for 2D Markovian jump systems," *Automatica*, vol. 44, no. 7, pp. 1849–1858, 2008.

[14] L. Wu, J. Lam, W. Paszke, K. Galkowski, and E. Rogers, "Robust $\mathscr{H}_\infty$ filtering for uncertain differential linear repetitive processes," *International Journal of Adaptive Control and Signal Processing*, vol. 22, no. 3, pp. 243–265, 2008.

[15] L. Wu and J. Lam, "Weighted $\mathscr{H}_\infty$ filtering of switched systems with time-varying delay: average dwell time approach," *Circuits, Systems, and Signal Processing*, vol. 28, no. 6, pp. 1017–1036, 2009.

[16] L. Wu, P. Shi, H. Gao, and C. Wang, "A new approach to robust $\mathscr{H}_\infty$ filtering for uncertain systems with both discrete and distributed delays," *Circuits, Systems, and Signal Processing*, vol. 26, no. 2, pp. 229–248, 2007.

[17] L. Wu, P. Shi, C. Wang, and H. Gao, "Delay-dependent robust $\mathscr{H}_\infty$ and $\mathscr{L}_2$-$\mathscr{L}_\infty$ filtering for LPV systems with both discrete and distributed delays," *IEE Proceedings*, vol. 153, no. 4, pp. 483–492, 2006.

[18] P. A. Iglesias and D. Mustafa, "State-space solution of the discrete-time minimum entropy control problem via separation," *IEEE Transactions on Automatic Control*, vol. 38, no. 10, pp. 1525–1530, 1993.

[19] P. A. Iglesias, D. Mustafa, and K. Glover, "Discrete time $\mathscr{H}_\infty$ controllers satisfying a minimum entropy criterion," *Systems & Control Letters*, vol. 14, no. 4, pp. 275–286, 1990.

[20] D. Mustafa and K. Glover, *Minimum Entropy $\mathscr{H}_\infty$ Control*, vol. 146 of *Lecture Notes in Control and Information Sciences*, Springer, Berlin, Germany, 1990.

[21] M. A. Peters and P. A. Iglesias, *Minimum Entropy Control for Time-Varying Systems*, Systems & Control: Foundations & Applications, Birkhäuser, Boston, Mass, USA, 1997.

[22] S. Boyd, L. El Ghaoui, E. Feron, and V. Balakrishnan, *Linear Matrix Inequalities in System and Control Theory*, vol. 15 of *SIAM Studies in Applied Mathematics*, Society for Industrial and Applied Mathematics (SIAM), Philadelphia, Pa, USA, 1994.

Hindawi Publishing Corporation
Mathematical Problems in Engineering
Volume 2013, Article ID 546520, 4 pages
http://dx.doi.org/10.1155/2013/546520

Research Article

Stability Analysis of Bipedal Robots Using the Concept of Lyapunov Exponents

Liu Yunping,[1] Wang Lipeng,[2] Mei Ping,[1] and Hu Kai[1]

[1] *College of Information and Control, Nanjing University of Information Science & Technology, Nanjing 210044, China*
[2] *Wind Power Business Unit, CSR Zhuzhou Electric Locomotive Research Institute Co., Ltd., Zhuzhou 412001, China*

Correspondence should be addressed to Liu Yunping; liuyunping@nuist.edu.cn

Received 3 September 2013; Accepted 26 October 2013

Academic Editor: Bo-Chao Zheng

The dynamics and stability of passive bipedal robot have an important impact on the mass distribution, leg length, and the angle of inclination. Lyapunov's second method is difficult to be used in highly nonlinear multibody systems, due to the lack of constructive methods for deriving Lyapunov fuction. The dynamics equation is established by Kane method, the relationship between the mass, length of leg, angle of inclination, and stability of passive bipedal robot by the largest Lyapunov exponent. And the Lyapunov exponents of continuous dynamical systems are estimated by numerical methods, which are simple and easy to be applied to the system stability simulation analysis, provide the design basis for passive bipedal robot prototype, and improve design efficiency.

1. Introduction

The walking gait of active bipedal robot is achieved by control and drive system tracking the joint angle trajectories. The huge energy constrains the development of bipedal robot [1]. The passive bipedal robot can walk naturally under the drive of gravity without the outside force. It is important to study the bipedal robot walking in low energy from the bionics [2, 3]; some research by the universities of Cornell, Mit, and Delft was published in the Science [4].

However, the stability of the passive bipedal robot has high sensitivity to its structure parameters; any change of structure parameter will lead to its gait characteristics being fluctuated evidently [5]. Therefore, it is very important to optimize the configuration for the stability of the system [6, 7]. The effect of structure parameters to the stable fixed point and speed of periodic motion was analyzed under the given initial conditions in literature [5]. Asymptotical stability of passive bipedal robot in three dimensional space was researched by the method that combined extended virtual constraints and hybrid zero dynamics [8].

The dynamics equation of passive bipedal robot is modeled using the Kane method in this paper, and the method of Lyapunov exponent is applied to analyze the relationship between the stability of the system and mass, length of leg, and slope angle. This method is simple and reliable for the optimization design of passive bipedal robot prototype and is easy to program.

2. Lyapunov Exponents

Consider the two following equations

$$\begin{aligned} x_{n+1} &= f(x_n), \\ y_{n+1} &= f(y_n). \end{aligned} \tag{1}$$

Suppose that the error of initial value is $|x_0 - y_0|$, through the first iteration by

$$\begin{aligned} |x_1 - y_1| &= |f(x_0) - f(y_0)| \\ &= \frac{|f(x_0) - f(y_0)|}{|x_0 - y_0|} |x_0 - y_0| \\ &\approx \left| \left. \frac{df}{dx} \right|_{x_0} \right| |x_0 - y_0|, \end{aligned} \tag{2}$$

where

$$\left|\frac{df}{dx}\Big|_{x_0}\right| = \lim_{x_0 \to y_0} \frac{|f(x_0) - f(y_0)|}{|x_0 - y_0|}. \quad (3)$$

After the second iteration, we have

$$|x_2 - y_2| \approx \left|\frac{df}{dx}\Big|_{x_1}\right| |x_1 - y_1| \approx \left|\frac{df}{dx}\Big|_{x_1} \frac{df}{dx}\Big|_{x_0}\right| |x_0 - y_0|. \quad (4)$$

And through the n time iteration

$$|x_n - y_n| \approx \left|\prod_{n=0}^{n-1} \frac{df(x_n, \mu)}{dx}\Big|_{x_n}\right| |x_0 - y_0|. \quad (5)$$

From the above, the sensitivity of two systems to initial disturbance is effected by the value of derivative $|df/dx|$ at x_0.

The sensitivity of overall system mapping to initial value is achieved depending on the average of all initial conditions that needs the nth time iteration; the value of every deviation is

$$\left(\left|\prod_{n=0}^{n-1} \frac{df}{dx}\Big|_{x_n}\right|\right)^{1/n}. \quad (6)$$

If there are small deviations from the initial value in the two systems, the result will be divergent along with the time (or times of iteration). The deviation is measured by Lyapunov exponent, the logarithmic of geometric average in following form:

$$\lambda = \frac{1}{n} \ln\left(\left|\prod_{n=0}^{n-1} \frac{df(x_n, \mu)}{dx}\Big|_{x_n}\right|\right), \quad (7)$$

where x_n is the value of n times iteration. The computational formula of Lyapunov exponent (8) is received with n tending to infinity

$$\lambda = \lim_{n \to \infty} \frac{1}{n} \sum_{n=0}^{n-1} \ln\left|\frac{df(x_n, \mu)}{dx}\right|. \quad (8)$$

The stability of system state is related to the divergence or convergence of two adjacent trajectories through the time evolution, which can be measured by Lyapunov exponent.

In phase space, the initial conditions of the system are defined as an infinitesimal m dimensional ball. The ball will naturally deform as a super circle ellipsoid due to the dynamics effects. All the main axes of ellipsoid are arranged according to their length, and the Lyapunov exponent λ_i can be achieved by the following form:

$$\lambda_i = \lim_{n \to \infty} \frac{1}{n} \frac{\varepsilon_i(n)}{\varepsilon_0(n)}, \quad (i = 1, 2, \ldots). \quad (9)$$

The Lyapunov exponent is related to the divergence or convergence of system. The trajectory is convergent in the direction of the value of Lyapunov exponent of less than 0, and the system is stable with no sensitivity to the initial conditions [9]. The trajectory is divergent in the direction of the value of positive Lyapunov exponent, and the system is unstable with sensitivity to the initial conditions. Usually, Lyapunov exponent is arranged according to $\lambda_1 \geq \lambda_2 \geq \lambda_3 \geq \cdots \geq \lambda_m$.

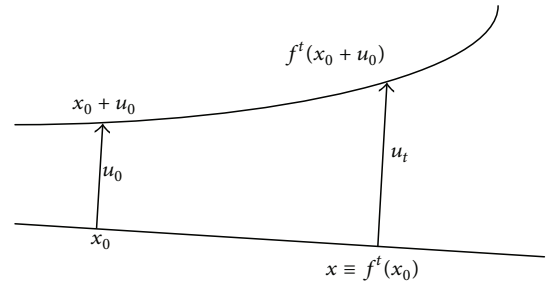

Figure 1: Distance evolution of the adjacent trajectory.

Where the convergence and divergence of two adjacent trajectories in phase space are quantitative description by maximum Lyapunov exponent; the motion is stable when the maximum Lyapunov exponent of system is less than zero.

3. Lyapunov Exponent of Continuous System

An n-dimensional differential equation of continuous smooth dynamics system is defined as the following form:

$$\dot{x} = F(x), \quad (10)$$

where $\dot{x} = dx/dt$, $x(t) \in R^n$ is the state vector. Usually, suppose two close points x_0, $x_0 + u_0$, and the initial point x_0 located in the basin of attraction; u_0 is the disturbance of initial x_0 (Figure 1). After a period of time t, the disturbance u_t is as the following form:

$$u_t \equiv f^t(x_0 + u_0) - f^t(x_0) = D_{x_0} f^t(x_0) \cdot u_0, \quad (11)$$

where u_t is tangent vector in (11), which satisfies vary equation in following form [10]:

$$\dot{\Phi}_t(x_0) = D_x F\left(f^t(x_0)\right) \cdot \Phi_t(x_0), \qquad \Phi_0(x_0) = I, \quad (12)$$

where $\Phi_t(x_0)$ is the derivative at x_0, that is, $\Phi_t(x_0) = D_{x_0} f^t(x_0)$. In order to calculate the trajectory, (13) needs to be integrated. Consider the following:

$$\begin{Bmatrix} \dot{x} \\ \dot{\Phi} \end{Bmatrix} = \begin{Bmatrix} F(x) \\ D_x F(x) \cdot \Phi \end{Bmatrix}, \qquad \begin{Bmatrix} x(t_0) \\ \Phi(t_0) \end{Bmatrix} = \begin{Bmatrix} x_0 \\ I \end{Bmatrix}. \quad (13)$$

Then, the average exponent of two trajectories' divergence or convergence is defined as

$$\lambda(x_0, u_0) = \lim_{t \to \infty} \frac{1}{t} \frac{\|u_t\|}{\|u_0\|} = \lim_{t \to \infty} \frac{1}{t} \ln\left\|D_{x_0} f^t(x_0) \cdot u_0\right\|, \quad (14)$$

where $\|u_t\|$ is the vector of length. If $\lambda > 0$, the exponent will be divergent nearby track. For $x_0 \in M$, (14) can calculate the maximum Lyapunov exponent in a very weak smoothness conditions.

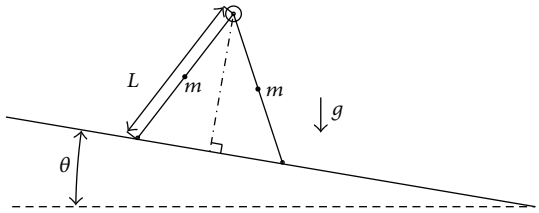

Figure 2: The simplified biped model.

4. Dynamics Model of Passive Bipedal Robot

The simplified biped model is showed in Figure 2. The mass, length, moment of inertia are, respectively, represented with m, L, and I. The two legs are connect with a passive joint. The distance between the center of mass and hip joint is $L_0 = L/2$. The body of leg is rigid. The collision between foot and ground is completely inelastic contact with no friction and slippage. The ground is also rigid. The robot will walk along the slope face automatically under its own gravity and inertia with the leg given an initial speed.

The process of robot's motion is divided into parts. (1) The leg 1 will swing around the hip joint after it left off the ground. The total procedure is only in gravity acting, so the total mechanical energy is conserved. (2) When the swing leg contacts with the ground, it will exchange role with the supporting leg. The collision between the foot and the ground is instantaneous, and there is no sliding during the process of collision. The angular momentum of system is conservation.

The dynamics equations are modeled by Kane method in following form:

$$\begin{bmatrix} M_{11} & M_{12} \\ M_{21} & M_{22} \end{bmatrix} \{\dot{u}\} = f(u),$$

$$\begin{aligned} f(u) = {} & \left[gLm\cos[\theta]\sin[q_1(t)] \right. \\ & + mg(L - L_0)\cos[\theta]\sin[q_1(t)] \\ & + mLL_0\sin[q_1(t) - q_2(t)]u_2^2 \\ & - mgL_0\cos[\theta]\sin[q_2(t)] \\ & \left. + \left(mL_0^2 + mL_0(L_0 - L)\right)\sin[q_1(t) - q_2(t)]u_1^2 \right], \\ M_{11} = {} & -I_0 + mL(L - L_0) - mL_0L + m(L - L_0)^2, \\ M_{12} = {} & mL_0L\cos[q_1(t) - q_2(t)], \\ M_{21} = {} & \left(mL_0(L - L_0) + mL_0^2\right)\cos[q_1(t) - q_2(t)], \\ M_{22} = {} & -I_0 - mL_0^2. \end{aligned} \tag{15}$$

5. Simulation

Supposing $L = 0.62$ m, $\theta = 31^\circ$, and $m = 14$ kg, the Lyapunov exponent spectrum will be received by (14) (showed in Figure 3). The whole calculation is used by software Mathematica. From the Lyapunov exponent spectrum of Figure 3, we can find one of the values of Lyapunov exponent above 0, so the passive biped robot system is unstable. It is greatly important for optimization of the structure parameter and stability of control to analyze the dynamic characteristic of the passive biped robot.

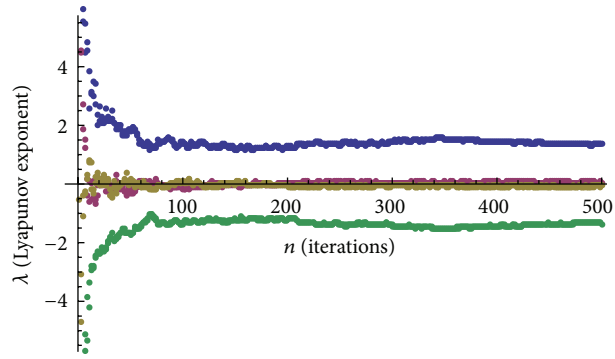

Figure 3: Lyapunov exponent spectrum.

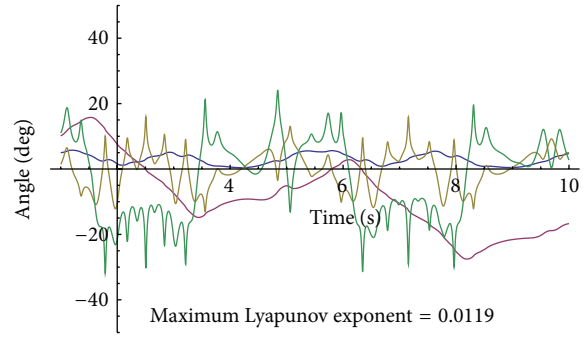

Figure 4: Time series of the variable.

The time series of all variables is showed in Figure 4. The dynamics characteristic of system can be observed by changing one of the structure parameters. From lots of results of simulation, it is concluded that small changes in mass cannot affect the dynamic characteristics of the whole system, but the length of leg and slope angle's effect are obvious.

6. Conclusion

It is significant to optimize t mass distribution, leg length, slope angle, and other parameters of passive bipedal robot for improving the stability of the system. The dynamics equation of passive bipedal robot is modeled by Kane method in this paper, and the method of Lyapunov exponent is applied to analyze the relationship between the stability of the system and mass, length of leg, and slope angle. This method is simple and reliable for the optimization design of passive bipedal robot prototype.

Conflict of Interests

The authors declare that there is no conflict of interests regarding the publication of this paper.

Acknowledgments

This research is supported by the Natural Science Foundation of Jiangsu Province (BK20130999), the Natural Science Foundation of Colleges and Universities in Jiangsu Provincel (13KJB460012), the Postdoctoral Science Foundation of China (230210235), the Open Project (KDX1102) of Jiangsu Key Laboratory of Meteorological Observation and Information Processing, and Nanjing University of Information Science and Technology.

References

[1] Y. Sun and Q. Wu, "Stability analysis via the concept of Lyapunov exponents: a case study in optimal controlled biped standing," *International Journal of Control*, vol. 85, no. 12, pp. 1952–11966, 2012.

[2] B. W. Verdaasdonk, H. F. J. M. Koopman, and F. C. T. Van Der Helm, "Energy efficient walking with central pattern generators: From passive dynamic walking to biologically inspired control," *Biological Cybernetics*, vol. 101, no. 1, pp. 49–61, 2009.

[3] N. Liu, J. Li, and T. Wang, "Passive walker that can walk down steps: simulations and experiments," *Acta Mechanica Sinica*, vol. 24, no. 5, pp. 569–573, 2008.

[4] S. Collins, A. Ruina, R. Tedrake, and M. Wisse, "Efficient bipedal robots based on passive-dynamic walkers," *Science*, vol. 307, no. 5712, pp. 1082–1085, 2005.

[5] Y.-F. Hu, Y.-H. Zhu, X.-G. Wu, and J. Zhao, "Simulation and analysis of simple biped passive dynamic walking model," *Harbin Gongye Daxue Xuebao/Journal of Harbin Institute of Technology*, vol. 42, no. 3, pp. 490–499, 2010.

[6] C. Yang and Q. Wu, "On stabilization of bipedal robots during disturbed standing using the concept of Lyapunov exponents," *Robotica*, vol. 24, no. 5, pp. 621–624, 2006.

[7] S. Aoi and K. Tsuchiya, "Self-stability of a simple walking model driven by a rhythmic signal," *Nonlinear Dynamics*, vol. 48, no. 1-2, pp. 1–16, 2007.

[8] C. Chevallereau, J. W. Grizzle, and C.-L. Shih, "Asymptotically stable walking of a five-link underactuated 3-D bipedal robot," *IEEE Transactions on Robotics*, vol. 25, no. 1, pp. 37–50, 2009.

[9] C. Yang and Q. Wu, "On stability analysis via lyapunov exponents calculated from a time series using nonlinear mapping—a case study," *Nonlinear Dynamics*, vol. 59, no. 1-2, pp. 239–257, 2010.

[10] T. S. Parker and L. O. Chua, *Practical Numerical Algorithms for Chaotic Systems*, Springer, Berlin, Germany, 1989.

Hindawi Publishing Corporation
Mathematical Problems in Engineering
Volume 2013, Article ID 856914, 12 pages
http://dx.doi.org/10.1155/2013/856914

Research Article

Fault Detection for a Class of Uncertain Linear Systems

Qingyu Su and Jian Li

School of Automation Engineering, Northeast Dianli University, Jilin 132012, China

Correspondence should be addressed to Qingyu Su; suqingyuphd@yeah.net

Received 3 July 2013; Accepted 15 August 2013

Academic Editor: Bochao Zheng

Design problem of the fault detection filter for a class of uncertain feedback systems is discussed in this paper. The system under consideration is the model with the nonstandard parameter uncertain regions. The fault detection filter design problem is reduced to an optimized filter design problem, which maximizes the sensitivity of the fault in the fault cases and meets the disturbance attenuation performance in both fault-free cases and fault cases, simultaneously. A numerical example is used to demonstrate the effectiveness of the proposed design method.

1. Introduction

In recent years, fault detection technique is given more and more attentions for the higher demands of safety and reliability of the control systems. A considerable sum of results on fault detection, both in the light of the data-driven and the model-based detection techniques, have been achieved (see [1–3]). Among the model-based techniques, a number of results which depend on the linear matrix inequality (LMI) techniques have appeared to deal with the fault detection problem. References [4–6] investigate the estimation problem of the fault by designing a filter. Recently, a so-called H_∞/H_- design approach for the fault detection problem has received considerable attentions. Further, the fault detection problem associated with some certain H_∞/H_- performance indices is discussed in [7–10]. The fault models considered in the above papers are classical and can describe a large class of the fault types. However, it should be pointed out that the actuator stuck fault also needs to be investigated when the amplitude of the faults are not larger enough to be detected.

At the same time, most of the models are obtained by the identification experiments with some limited input/output data. Identification experiment in the prediction error (PE) framework delivers an uncertain region which contains the true system at some (user-chosen) probability level [11]. The uncertain region can result in an identified parametric ellipsoid set which is regarded as a nonstandard parameter uncertain structure in the related classical papers. The ellipsoidal uncertain structure is studied by some results; see [12–15] which reduce the uncertain region by employing the robust tools. Compared with the stability and the stabilization problems for this particular uncertainty, there are no results that to pay attention to deal with the fault detection problem with the models which have the ellipsoidal uncertainty. Moreover, since the existing approaches about fault detection (FD) are not appropriate for FD problem for this kind of uncertainty, the new FD technique should solve this case.

Motivated by the above reasons, the optimization design problem of the FD filter for uncertain linear feedback system is studied. The design objective is to maximize the sensitivity of the fault in the fault cases, which subjects to the disturbances attenuation performance in both fault-free cases and the fault cases. In practical, the frequency of the disturbance signals and the fault signals are usually in bound. Thus, a notion of the finite-frequency performance indices is introduced to describe the performance indices; LMIs-based sufficient conditions are provided using the finite-frequency approach proposed in [16, 17]. The optimal solution of gain matrices of the FD filter can be obtained.

The main contribution of this paper that the direct design approach of the FD filter proposed to the linear model with elliptical uncertain structure. Unlike other fault detection approaches for the uncertain model, in which the FD filter is achieved not only depending on the known

lower and known upper bounds of the uncertainty but also extracting convex polygons of the uncertain region, a general parametrization for the set of multipliers is introduced to decrease the conservatism. To the best of our knowledge, such a framework for the fault detection with the elliptical parameter uncertainty structure has not been reported in the literature.

The paper is organized as follows. Section 2 introduces the problem under consideration and presents the design objectives. Section 3 illustrates a FD filter design approach in detail. The algorithm is given in Section 4. An illustrative example is given in Section 5 to demonstrate the proposed method. Conclusions to this work are given in the last section.

Notation. For a matrix A, A^T denotes its transpose. For a symmetric matrix, $A > 0$ ($A \geq 0$) and $A < 0$ ($A \leq 0$) denote positive-definiteness (positive semidefinite matrix) and negative-definiteness (negative semi-definite matrix), respectively. The Hermitian part of a square matrix M is denoted by $\mathrm{He}(M) := M + M^T$. The symbol $*$ within a matrix represents the symmetric entries. $\sigma_{\min}(G)$ denotes minimum singular values of the transfer matrix G. The symbol $\otimes$ denotes the Kronecker product, and 0 denotes zero matrix with appropriate dimension. Both I and $\mathcal{I}$ denote identity matrix with appropriate dimension. $\mathcal{I}_0$ and $\mathcal{I}_1$ denote the matrices $[1\ 0; 0\ 0]$ and $[1; 0]$ of appropriate dimensions, respectively.

2. Problem Formulation

2.1. System Model. Consider the following uncertain linear systems:

$$\begin{aligned} \dot{x}(t) &= Ax(t) + B_1 d(t) + B_2 f(t) + L_1 w(t), \\ y(t) &= Cx(t) + D_1 d(t) + D_2 f(t) + L_2 w(t), \\ w(t) &= \Delta z(t), \\ z(t) &= Hx(t) \quad \Delta \in \mathbf{\Delta}, \end{aligned} \tag{1}$$

where $x(t)$ is the state $y(t)$ is the output, $u(t)$ is the input, and $d(t)$ is an energy-bounded disturbance; r_0 is the reference input, $x(t)$ is the state; A, B_1, B_u, C, D, L_1, L_2, and H are known constant matrices of appropriate dimensions. Consider that $\Delta \in \mathbf{\Delta}$, where Δ is defined as

$$\Delta = \mathrm{diag}\left(\underbrace{\theta, \ldots, \theta}_{n_0}\right), \quad \theta = \left[\theta_1^T, \ldots, \theta_{n_\theta}^T\right]^T \in R^{n_\theta}, \tag{2}$$

where n_0 is the number of θ in Δ, then the dimension of the Δ is $n_\theta n_0 \times n_0$, and $\mathbf{\Delta}$ is the parameter set of Δ. The uncertain parameter θ with a certain use-chosen probability ($\mathcal{X}$) is at the uncertain set $\mathcal{U}$. The uncertain set $\mathcal{U}$ is an ellipsoid in the parameter space:

$$\mathcal{U} = \left\{\theta \mid \theta^T \mathcal{R} \theta < \mathcal{X}\right\}, \tag{3}$$

where $\mathcal{R}$ describes the form of the ellipsoid and $\mathcal{X}$ is a constant computed by the desired probability in model identification.

Remark 1. The parameter uncertainty region in (1) is ellipsoidal. This kind of particular uncertainty is derived from classical prediction error identification, and it is a typical parameter uncertainty of the model which is identified. Although the parameter uncertainty can turn into the polytopic uncertainty by extracting convex polygons of the ellipsoidal region, this transformation method enlarges the the uncertain region and increases the conservatism. In this paper, the ellipsoidal uncertainty is disposed directly.

To detect the actuator stuck faults, the FD filter is designed such that the residual $r(t)$ can be obtained as

$$\begin{aligned} \dot{x}_f(t) &= A_f x_f(t) + B_f y(t), \\ r(t) &= C_f x_f(t) + D_f y(t), \end{aligned} \tag{4}$$

where x_f is the state of the FD filter. Consider that $A_f \in R^{n_f \times n_f}$, $B_f \in R^{n_f \times n_m}$, $C_f \in R^{n_f}$, $D_f \in R^m$.

By combining (1) and (4), we have the following augmented systems:

$$\begin{aligned} \xi(t) &= \overline{A}\xi(t) + \overline{B}_d d(t) + \overline{L}_1 w(k) + \overline{B}_f f(t), \\ r(t) &= \overline{C}\xi(t) + \overline{D}_d d(t) + \overline{D}_f f(t) + \overline{L}_2 w(t), \\ w(t) &= \Delta z(t) \\ z(t) &= \overline{H}\xi(t) \qquad \Delta \in \mathbf{\Delta}, \end{aligned} \tag{5}$$

where $\xi(t) = [x(t)^T, x_f(t)^T]^T$,

$$\left[\begin{array}{c|c|c|c} \overline{A} & \overline{B}_d & \overline{B}_f & \overline{L}_1 \\ \hline \overline{C} & \overline{D}_d & \overline{D}_f & \overline{L}_2 \end{array}\right] = \left[\begin{array}{cc|c|c|c} A & 0 & B_1 & B_2 & L_1 \\ B_f C & A_f & B_f D_1 & B_f D_2 & B_f L_2 \\ \hline D_f C & C_f & D_f D_1 & D_f D_2 & D_f L_2 \end{array}\right] \tag{6}$$

$$\overline{H} = [H \ \ 0].$$

2.2. Problem Formulation. The design problem of the FD filter to be addressed in this paper can be expressed as follows.

The design objective: consider a class of uncertain linear systems (1); the FD filter (4) is designed such that the augmented model (5) is stable; the disturbance effects on the residual are minimized in both the fault-free case and the fault cases, while the fault effects on the residual are maximized in the fault cases. To detect actuator faults, our design objective of the FD filter can now be formulated as the following optimization problem:

$$\max \beta \tag{7}$$

$$\text{s.t.} \quad \delta_{\max}\left(G_{rd}(j\omega)\right) < \gamma, \qquad \gamma > 0, \ \forall |\omega| \leq \overline{\omega}_1, \ \Delta \in \mathbf{\Delta} \tag{8}$$

$$\delta_{\min}\left(G_{rf}(j\omega)\right) > \beta \qquad \beta > 0, \ \forall |\omega| \leq \overline{\omega}_2, \ \Delta \in \mathbf{\Delta}, \tag{9}$$

where $\overline{\omega}_1$ is the upper bounds on the frequency for the disturbance and $\overline{\omega}_2$ is the upper bounds on the frequency for the fault. G_{rd} is the transfer function from the disturbance d to the residual signal r with fault-free case and fault cases. G_{rf} is the transfer function from the fault f to the residual signal r with fault cases.

Remark 2. Condition (8) describes the disturbance attenuation condition in both the fault-free case and fault cases. Condition (9) is formulated as the sensitiveness performance in the fault cases.

Before ending this section, the following lemmas and proposition shall be recalled to prove our main results for the FD filter design.

Lemma 3 (see [18]). *Given a symmetric matrix $\Theta \in R^{n\times n}$ and two matrices $\mathscr{M}$ and $\mathscr{H}$ of column dimension n, there exists matrix $\mathscr{F}$ that satisfies $\Theta + \mathscr{M}^T\mathscr{F}\mathscr{H} + \mathscr{H}^T\mathscr{F}^T\mathscr{M} < 0$ if and only if the following two conditions hold:*

$$\mathscr{N}_{\mathscr{M}}^T\Theta\mathscr{N}_{\mathscr{M}} < 0 \qquad \mathscr{N}_{\mathscr{H}}\Theta\mathscr{N}_{\mathscr{H}}^T < 0, \tag{10}$$

where $\mathscr{N}_{\mathscr{M}}$ and $\mathscr{N}_{\mathscr{H}}$ denote arbitrarily bases of null space of $\mathscr{M}$ and $\mathscr{H}$, respectively.

Lemma 4 (see [19]). *Let $\xi \in R^n$, $\mathscr{N} \in R^{n\times n}$, and $\mathscr{M} \in R^{n\times m}$ such that rank $(\mathscr{N}) < n$. The following statements are equivalent:*

(1) $\xi^T\mathscr{M}\xi < 0$, *for* $\forall\ \xi \neq 0$, *subject to* $\mathscr{N}\xi = 0$;

(2) $\mathscr{N}^{\perp T}\mathscr{M}\mathscr{N}^{\perp} < 0$, *where $\mathscr{N}^{\perp}$ is the kernel of $\mathscr{N}$;*

(3) $\mathscr{M} - \varepsilon\mathscr{N}^T\mathscr{N} < 0$, *for some scalar $\varepsilon \in R$;*

(4) $\mathscr{M} + X^T\mathscr{N} + \mathscr{N}^TX < 0$, *for some matrix $X \in R^{n\times m}$.*

Proposition 5 (see [11]). *Consider the uncertainty Δ with $\theta \in \mathscr{U}$ defined in* (3), *$\Gamma \in \mathbf{\Gamma}$ is defined as*

$$\mathbf{\Gamma} := \left\{\Gamma = \begin{bmatrix}\Delta\\ I\end{bmatrix} \mid \Delta \in \mathbf{\Delta}\right\}. \tag{11}$$

Restrict the parametrization of matrices Λ defined as

$$\mathbf{\Lambda} := \left\{\Lambda \mid \Lambda = \begin{bmatrix}\Lambda_{11} & \Lambda_{12}\\ \Lambda_{12}^T & \Lambda_{22}\end{bmatrix}\right\} \tag{12}$$

with Λ_{22} as a positive complex Hermitian matrix of dimension $n \times n$. Consider that $\Lambda_{11} = -(\Lambda_{22} \otimes (R/\mathscr{X}) + \Lambda_1) \in R^{n_\theta n\times n_\theta n}$ and

$$\Lambda_{12} = \begin{pmatrix} 0 & p_{12} & \cdots & p_{1n}\\ -p_{12} & 0 & \cdots & p_{2n}\\ \vdots & \ddots & \ddots & \vdots\\ -p_{1\hat{n}} & \cdots & \cdots & 0\end{pmatrix} \in R^{n_\theta n\times n}, \tag{13}$$

where $\mathscr{R}$ describes the form of the ellipsoid for uncertainty in (3), *and the elements of this parametrization (Λ_a, p_{ij}) can take any values provided. Consider that $\Lambda_a \in R^{n_\theta n\times n_\theta n}$ has the following structure that:*

$$\Lambda_1 \in \mathbf{\Lambda_1} : \left\{ \begin{bmatrix} 0 & k_{12} & \cdots & k_{1n}\\ -k_{12} & 0 & \cdots & \vdots\\ \vdots & \ddots & \ddots & k_{(n-1)n}\\ -k_{1n} & \cdots & -k_{(n-1n)} & 0\end{bmatrix} \mid k_{ij} = -k_{ij}^T \in R^{n_\theta\times n_\theta}\right\} \tag{14}$$

and $p_{ij} \in R^n$, $i = 1,\ldots,n$, $j = 1,\ldots,n$. For $\Lambda \in \mathbf{\Lambda}$, $\Gamma^T\Lambda\Gamma > 0$, $\forall\Gamma \in \mathbf{\Gamma}$.

3. Fault Detection Design

In this section, Lemma 6 and Proposition 7 are first given, and inequality conditions for performance indices (8) and (9) are also given. Based on these conditions, an algorithm based on LMIs is presented.

Lemma 6 (see [16]). *Consider the following uncertain system:*

$$\begin{aligned}\dot{x}(t) &= \left(A + B_1\Delta\left(I - D_{11}\Delta\right)^{-1}C_1\right)x(t) + B_2u(t),\\ y(t) &= \left(C_2 + D_{21}\Delta\left(I - D_{11}\Delta\right)^{-1}C_1\right)x(t) + D_{22}u(t),\end{aligned} \tag{15}$$

with $\Delta \in \mathbf{\Delta}$. Let a real symmetric matrix Π and a positive scalar $\bar{\omega}$ be given. The following robust finite-frequency condition

$$\left[G_1(j\omega)^T \quad I\right]\Pi\left[G_1(j\omega)^T \quad I\right]^T < 0 \quad |\omega| \le \bar{\omega},\ \Delta \in \mathbf{\Delta} \tag{16}$$

holds if there exist real symmetric matrices $\mathscr{P}$, $\mathscr{Q}$, $\Phi \in \mathbf{\Phi}$, and $\Lambda \in \mathbf{\Lambda}$ such that

$$\begin{bmatrix}\mathscr{A} & \mathscr{B}\\ \mathscr{I} & 0\end{bmatrix}^T\begin{bmatrix}-\mathscr{Q} & \mathscr{P}\\ \mathscr{P} & \bar{\omega}^2\mathscr{Q}\end{bmatrix}\begin{bmatrix}\mathscr{A} & \mathscr{B}\\ \mathscr{I} & 0\end{bmatrix} < \begin{bmatrix}\mathscr{C}^T\\ \mathscr{D}^T\end{bmatrix}\Phi\begin{bmatrix}\mathscr{C} & \mathscr{D}\end{bmatrix}, \tag{17}$$

$$\mathscr{Q} \ge \mathscr{C}_1^T\Lambda\mathscr{C}_1, \tag{18}$$

where

$$\mathbf{\Phi} := \left\{\begin{bmatrix}\Psi & 0\\ 0 & \Pi\end{bmatrix} : \begin{bmatrix}\Gamma & 0\\ 0 & \Gamma\end{bmatrix}^T\Psi\begin{bmatrix}\Gamma & 0\\ 0 & \Gamma\end{bmatrix} \le 0,\ \forall\Gamma \in \mathbf{\Gamma}\right\},$$

$$\left[\begin{array}{cc}\mathscr{A} & \mathscr{B}\\ \mathscr{C}_1 & \mathscr{D}_1\\ \mathscr{C}_2 & \mathscr{D}_2\end{array}\right] := \left[\begin{array}{cc|cc} A & B_1 & B_2 & 0\\ 0 & 0 & 0 & I\\ \hline 0 & I & 0 & 0\\ C_1 & D_{11} & 0 & 0\\ \hline C_2 & D_{21} & D_{22} & 0\\ 0 & 0 & I & 0\end{array}\right] \tag{19}$$

$$\left[\mathscr{C} \quad \mathscr{D}\right] := \left[\begin{array}{c|c}\mathscr{C}_{11} & \mathscr{D}_{11}\\ \hline \mathscr{C}_2 & \mathscr{D}_2\end{array}\right] = \left[\begin{array}{c|c}\mathscr{C}_1 & 0\\ \mathscr{C}_1\mathscr{A} & \mathscr{C}_1\mathscr{B}\\ \hline \mathscr{C}_2 & \mathscr{D}_2\end{array}\right].$$

Proposition 7. *Consider the uncertainty Δ with $\theta \in \mathcal{U}$ defined in* (3) *and $\Gamma \in \mathbf{\Gamma}$ defined in* (11). *Restrict the parametrization of matrices Ψ defined as*

$$\Psi = \left[\begin{array}{c|c} \Psi_{11} & \Psi_{12} \\ \hline \Psi_{12}^T & \Psi_{22} \end{array}\right] = \left[\begin{array}{cc|cc} \Psi_{111} & \Psi_{112} & \Psi_{121} & \Psi_{122} \\ \Psi_{112}^T & \Psi_{113} & \Psi_{122}^T & \Psi_{123} \\ \hline \Psi_{121}^T & \Psi_{122} & \Psi_{221} & \Psi_{222} \\ \Psi_{122}^T & \Psi_{123}^T & \Psi_{222}^T & \Psi_{223} \end{array}\right], \quad (20)$$

where $\left[\begin{smallmatrix} \Psi_{113} & \Psi_{123} \\ * & \Psi_{223} \end{smallmatrix}\right]$ are positive complex Hermitian matrices of dimension $2n \times 2n$; Ψ_{111}, Ψ_{121}, and Ψ_{221} of the dimension $n_\theta n \times n_\theta n$ have the structure with $-(\Psi_{113} \otimes (R/\mathcal{X}) + \Psi_1)$, $-(\Psi_{123} \otimes (R/\mathcal{X}) + \Psi_2)$, and $-(\Psi_{223} \otimes (R/\mathcal{X}) + \Psi_3)$, respectively. Moreover

$$\Psi_{p2} = \begin{pmatrix} 0 & p_{p2} & \cdots & p_{pn} \\ -p_{p2} & 0 & \cdots & p_{pn} \\ \vdots & \ddots & \ddots & \vdots \\ -p_{p\hat{n}} & \cdots & \cdots & 0 \end{pmatrix} \in R^{n_\theta n \times n}, \quad p = 11, 12, 22, \quad (21)$$

where $\mathcal{R}$ describes the form of the ellipsoid for uncertainty in (3), *and the elements of this parametrization (Ψ_1, Ψ_2, Ψ_3, p_{1ij}, p_{2ij}, p_{3ij}, $i = 1, \ldots, n$, $j = 1, \ldots, n$) can take any values provided. For $t = 1, 2, 3$, $i = 1, \ldots, n$, and $j = 1, \ldots, n$, $\Psi_t \in R^{n_\theta n \times n_\theta n}$ has the following structure:*

$$\Psi_t \in \mathbf{\Psi_t} : \left\{ \left[\begin{array}{cccc} 0 & k_{t12} & \cdots & k_{t1n} \\ -k_{t12} & 0 & \cdots & \vdots \\ \vdots & \ddots & \ddots & k_{t(n-1)n} \\ -k_{t1n} & \cdots & -k_{t(n-1)n} & 0 \end{array}\right] \Bigg| \; k_{tij} = -k_{tij}^T \in R^{n_\theta \times n_\theta} \right\}, \quad (22)$$

and $p_{tij} \in R^n$. Then, for $\Psi \in \mathbf{\Psi}$, it has

$$\begin{bmatrix} \Gamma & 0 \\ 0 & \Gamma \end{bmatrix}^T \Psi \begin{bmatrix} \Gamma & 0 \\ 0 & \Gamma \end{bmatrix} > 0, \quad \forall \Gamma \in \mathbf{\Gamma}, \quad (23)$$

where Γ is defined in (11).

Proof. Let all Ψ_{p2}, Ψ_t, $p \in \{11, 12, 22\}$, $t \in \{1, 2, 3\}$ have the structure in the statement of the proposition:

$$\Psi_{p2}^T \Delta + \Delta^T \Psi_{p2} = 0, \qquad \Delta^T \Psi_t \Delta = 0. \quad (24)$$

Therefore, for every $\Psi \in \mathbf{\Psi}$, we can have

$$\begin{aligned} \begin{bmatrix} \Gamma & 0 \\ 0 & \Gamma \end{bmatrix}^T \Psi \begin{bmatrix} \Gamma & 0 \\ 0 & \Gamma \end{bmatrix} &= \begin{bmatrix} \Delta & 0 \\ 0 & I \\ \Delta & 0 \\ 0 & I \end{bmatrix}^T \Psi \begin{bmatrix} \Delta & 0 \\ 0 & I \\ \Delta & 0 \\ 0 & I \end{bmatrix} \\ &= \begin{bmatrix} \Delta^T \Psi_{111} \Delta^T + \Psi_{112}^T \Delta + \Delta^T \Psi_{112} + \Psi_{113} & \Delta^T \Psi_{121} \Delta^T + \Psi_{122}^T \Delta + \Delta^T \Psi_{122} + \Psi_{123} \\ * & \Delta^T \Psi_{221} \Delta^T + \Psi_{222}^T \Delta + \Delta^T \Psi_{222} + \Psi_{223} \end{bmatrix} \\ &= \begin{bmatrix} \left(1 - \theta^T \dfrac{R}{\mathcal{X}} \theta\right) \Psi_{111} & \left(1 - \theta^T \dfrac{R}{\mathcal{X}} \theta\right) \Psi_{121} \\ * & \left(1 - \theta^T \dfrac{R}{\mathcal{X}} \theta\right) \Psi_{221} \end{bmatrix}. \end{aligned} \quad (25)$$

When $\theta \in \mathcal{U}$ and $\left[\begin{smallmatrix} \Psi_{113} & \Psi_{123} \\ * & \Psi_{223} \end{smallmatrix}\right] > 0$, we can have

$$\begin{bmatrix} \Gamma & 0 \\ 0 & \Gamma \end{bmatrix}^T \Psi \begin{bmatrix} \Gamma & 0 \\ 0 & \Gamma \end{bmatrix} > 0, \quad \forall \Gamma \in \mathbf{\Gamma}. \quad (26)$$

□

3.1. The Disturbance Attenuation Condition

Theorem 8. *Consider the system in* (5) *with $\Delta \in \mathbf{\Delta}$. A real symmetric matrix $\Pi_a = \left[\begin{smallmatrix} 1 & 0 \\ 0 & -\gamma^2 I \end{smallmatrix}\right]$ is given. Condition*

$$\delta_{\max}(G_{rd}(j\omega)) < \gamma, \quad |\omega| < \overline{\omega}_2, \ \Delta \in \mathbf{\Delta} \quad (27)$$

holds if there exist matrix variables $\widehat{A}$, $\widehat{B}$, $\widehat{C}$, $\widehat{D}$, M, R, Y_a, E_a, L_a, N_a, W_a, S_a,

$$P_a = \begin{bmatrix} P_{a11} & P_{a12} & P_{a13} \\ P_{a21} & P_{a22} & P_{a23} \\ P_{a31} & P_{a32} & P_{a33} \end{bmatrix},$$

$$Q_a = \begin{bmatrix} Q_{a11} & Q_{a12} & Q_{a13} \\ Q_{a21} & Q_{a22} & Q_{a23} \\ Q_{a31} & Q_{a32} & Q_{a33} \end{bmatrix},$$

$$\Psi_a = \begin{bmatrix} \Psi_{a111} & \Psi_{a112} & \Psi_{a121} & \Psi_{a122} \\ \Psi_{a112}^T & \Psi_{a113} & \Psi_{a122^T} & \Psi_{a123} \\ \Psi_{a121}^T & \Psi_{a122} & \Psi_{a221} & \Psi_{a222} \\ \Psi_{a122}^T & \Psi_{a123}^T & \Psi_{a222}^T & \Psi_{a223} \end{bmatrix},$$
$$\Lambda_a = \begin{bmatrix} \Lambda_{a11} & \Lambda_{a12} \\ \Lambda_{a12}^T & \Lambda_{a22} \end{bmatrix} \tag{28}$$

of appropriate dimensions satisfying $Q_a > 0$, $\Psi_a \in \boldsymbol{\Psi}$, *and* $\Lambda_a \in \boldsymbol{\Lambda}$ *such that*

$$\begin{bmatrix} -Q_{a11} & -Q_{a12} & -Q_{a13} & P_{a11} - Y_a^T & P_{a12} + E_a^T & P_{a13} - L_a^T & a_{17} & a_{28} & 0 \\ * & -Q_{a22} & -Q_{a23} & P_{a21} - M^T & P_{a22} - M^T & P_{a23} & a_{27} & a_{28} & 0 \\ * & * & -Q_{a33} & Q_{a31} - W_a^T & P_{a32} - S_a^T & P_{a33} - N_a^T & a_{37} & a_{38} & 0 \\ * & * & * & a_{44} & a_{45} & a_{46} & a_{47} & a_{48} & \left(\widehat{D}C\right)^T \\ * & * & * & * & a_{55} & a_{56} & a_{57} & a_{58} & \widehat{C}^T \\ * & * & * & * & * & a_{66} & a_{67} & a_{68} & \left(\widehat{D}L_2\right)^T \\ * & * & * & * & * & * & a_{77} & a_{78} & \left(\widehat{D}D_1\right)^T \\ * & * & * & * & * & * & * & a_{88} & 0 \\ * & * & * & * & * & * & * & * & I - \mathrm{He}\,(R) \end{bmatrix} < 0 \tag{29}$$

$$\begin{bmatrix} Q_{a11} - H^T \Lambda_{a22} H & Q_{a12} & Q_{a13} - H^T \Lambda_{a12}^T \\ * & Q_{a22} & Q_{a23} \\ * & * & Q_{a33} - \Lambda_{a11} \end{bmatrix} > 0, \tag{30}$$

where

$$\begin{aligned} a_{17} &= -Y_a^T \nu_1, \quad a_{27} = -M^T \nu_1, \quad a_{37} = -W_a^T \nu_1, \\ a_{18} &= -Y_a^T \nu_2, \quad a_{28} = -M^T \nu_2, \quad a_{38} = -W_a^T \nu_2, \\ a_{44} &= \overline{\omega}_1^2 Q_{a11} + H^T \Psi_{a113} H + A^T H^T \Psi_{a223} HA \\ &\quad + \mathrm{He}\left(Y_a A + \widehat{B}C + H^T \Psi_{a123} HA\right), \\ a_{45} &= \overline{\omega}_1^2 Q_{a12} + \widehat{A} - A^T E_a^T + C^T \widehat{B}^T, \\ a_{46} &= \overline{\omega}_1^2 Q_{a13} + H^T \Psi_{a112}^T + A^T H^T \Psi_{a122}^T + H^T \Psi_{a123} HL_1 \\ &\quad + A^T H^T \Psi_{a223} HL_1 + Y_a L_1 + \widehat{B} L_2 + A^T L_a^T, \\ a_{55} &= \overline{\omega}_1^2 Q_{a22} + \mathrm{He}\left(\widehat{A}\right) \quad a_{56} = \overline{\omega}^2{}_1 Q_{a23} - E_a L_1 + \widehat{B} L_2 \\ a_{66} &= \overline{\omega}_1^2 Q_{a33} + \Psi_{a111} + L_1^T H^T \Psi_{a223} HL_1 \\ &\quad + \mathrm{He}\left(\Psi_{a122} HL_1 + L_a L_1\right), \\ a_{47} &= H^T \Psi_{a123} HB_1 + A^T H^T \Psi_{a223} HB_1 + Y_a B_1 \\ &\quad + \widehat{B} D_1 + \left(A^T Y_a^T + C^T \widehat{B}^T\right) \nu_1, \\ a_{48} &= H^T \Psi_{a122}^T + A^T H^T \Psi_{a222}^T + W_a + \left(A^T Y_a^T + C^T \widehat{B}^T\right) \nu_2, \\ a_{57} &= -E_a B_1 + \widehat{B} D_1 + \widehat{A}^T \nu_1, \\ a_{58} &= S_a + \widehat{A}^T \nu_2, \\ a_{67} &= \Psi_{a122} HB_1 + L_1^T H^T \Psi_{a223} HB_1 + L_a B_1 \\ &\quad + \left(L_1^T Y^T + L_2^T \widehat{B}^T\right) \nu_1, \\ a_{68} &= \Psi_{a121} + L_1^T H^T \Psi_{a222}^T + N + \left(L_1^T Y_a^T + L_2^T \widehat{B}^T\right) \nu_2, \\ a_{77} &= -\gamma^2 I + B_1^T H^T \Psi_{a223} HB_1 \\ &\quad + \mathrm{He}\left(\left(B_1^T Y_a^T + D_1^T \widehat{B}^T\right) \nu_1\right), \\ a_{78} &= B_1^T H^T \Psi_{a222}^T + \nu_1^T W_a + \left(B_1^T Y_a^T + D_1^T \widehat{B}^T\right) \nu_2, \\ a_{88} &= \Psi_{a221} + \mathrm{He}\left(\nu_2^T W_a\right), \\ \boldsymbol{\Lambda} &:= \{\Lambda_a : \textit{satisfy (12) in Proposition 5}\}, \\ \boldsymbol{\Psi} &:= \{\Psi_a : \textit{satisfy (20) in Proposition 7}\}, \end{aligned} \tag{31}$$

Proof. Substituting Π_a into (17), $G_{rd}(j\omega)^T G_{rd}(j\omega) < \gamma^2$ which is equivalent to (27). By applying Lemma 6, (27) holds if

$$\begin{bmatrix} \mathscr{A} & \mathscr{B}_a \\ \mathscr{I} & 0 \end{bmatrix}^T \begin{bmatrix} -\mathscr{Q}_a & \mathscr{P}_a \\ \mathscr{P}_a & \overline{\omega}^2 \mathscr{Q}_a \end{bmatrix} \begin{bmatrix} \mathscr{A} & \mathscr{B}_a \\ \mathscr{I} & 0 \end{bmatrix}$$

$$< \begin{bmatrix} \mathscr{C}^T \\ \mathscr{D}^T \end{bmatrix} \begin{bmatrix} \Psi_a & 0 \\ 0 & \Pi_a \end{bmatrix} [\mathscr{C} \quad \mathscr{D}] \tag{32}$$

$$\mathscr{Q}_a > \mathscr{C}_1^T \Lambda_a \mathscr{C}_1, \tag{33}$$

where

$$\begin{bmatrix} \mathscr{A} & \mathscr{B}_a \\ \mathscr{C}_1 & \mathscr{D}_1 \\ \mathscr{C}_2 & \mathscr{D}_2 \end{bmatrix} := \left[\begin{array}{cc|cc} \overline{A} & \overline{L}_1 & \overline{B}_d & 0 \\ 0 & 0 & 0 & I \\ \hline 0 & I & 0 & 0 \\ \overline{H} & 0 & 0 & 0 \\ \hline \overline{C} & \overline{L}_2 & \overline{D}_d & 0 \\ 0 & 0 & I & 0 \end{array}\right], \tag{34}$$

$$[\mathscr{C} \quad \mathscr{D}] := \left[\begin{array}{cc} \mathscr{C}_{11} & \mathscr{D}_{11} \\ \hline \mathscr{C}_2 & \mathscr{D}_2 \end{array}\right] = \left[\begin{array}{cc} \mathscr{C}_1 & 0 \\ \hline \mathscr{C}_1\mathscr{A} & \mathscr{C}_1\mathscr{B}_a \\ \mathscr{C}_2 & \mathscr{D}_2 \end{array}\right].$$

Let

$$\Upsilon_a = \begin{bmatrix} -\mathscr{Q}_a & \mathscr{P}_a & 0 \\ \mathscr{P}_a & \overline{\omega}_2\mathscr{Q}_a + \mathscr{C}_{11}^T\Psi_a\mathscr{C}_{11} + \mathscr{C}_2^T\Pi_a\mathscr{C}_2 & \mathscr{C}_{11}^T\Psi_a\mathscr{D}_{11} + \mathscr{C}_2^T\Pi_a\mathscr{D}_2 \\ 0 & \mathscr{D}_{11}^T\Psi_a\mathscr{C}_{11} + \mathscr{D}_2^T\Pi_a\mathscr{C}_2 & \mathscr{D}_{11}^T\Psi_a\mathscr{D}_{11} + \mathscr{D}_2^T\Pi_a\mathscr{D}_2 \end{bmatrix} \tag{35}$$

(32) is equivalent to

$$\begin{bmatrix} \mathscr{A} & \mathscr{B}_a \\ I & 0 \\ 0 & I \end{bmatrix}^T \Upsilon_a \begin{bmatrix} \mathscr{A} & \mathscr{B}_a \\ I & 0 \\ 0 & I \end{bmatrix} < 0. \tag{36}$$

And on the other hand,

$$[I \quad 0 \quad 0]\,\Upsilon_a [I \quad 0 \quad 0]^T = -\mathscr{Q}_a < 0. \tag{37}$$

By combining (36) with (37), and applying Lemma 3, (32) holds if and only if

$$\Upsilon_a + \begin{bmatrix} -I \\ \mathscr{A}^T \\ \mathscr{B}_a^T \end{bmatrix} \mathscr{X}_a \begin{bmatrix} 0 & I & 0 \\ 0 & 0 & I \end{bmatrix} + \begin{bmatrix} 0 & I & 0 \\ 0 & 0 & I \end{bmatrix}^T \mathscr{X}_a^T \begin{bmatrix} -I \\ \mathscr{A}^T \\ \mathscr{B}_a^T \end{bmatrix}^T < 0, \tag{38}$$

where $\mathscr{X}_a$ introduced by Lemma 3 is the variable matrix of appropriate dimensions. Here, $\mathscr{X}_a$ is defined as $\mathscr{X}_a = [\mathscr{X}_{a1} \quad \mathscr{X}_{a1}V_1]$ and partition $\mathscr{X}_{a1}$ into $\begin{bmatrix} x_{a11} & -x_{a12} & x_{a13} \\ x_{21} & x_{22} & 0 \\ x_{a31} & x_{a32} & x_{a33} \end{bmatrix}$ where x_{21} and x_{22} are nonsingular matrices variable. V_1 is a given matrix, defined as $V_1 = \begin{bmatrix} v_1^T & 0 & 0 \\ v_2^T & 0 & 0 \end{bmatrix}^T$.

Let $J = \operatorname{diag}\{I, x_{22}^{-1}x_{21}, I\}$, and define the linearizing change of the control variables as follows:

$$Q_a = J^T\mathscr{Q}_a J,$$

$$X_{a1} = \begin{bmatrix} Y_a^T & -E_a^T & L_a^T \\ M^T & M^T & 0 \\ W_a^T & S_a^T & N_a^T \end{bmatrix} = \begin{bmatrix} x_{11} & -x_{12}x_{22}^{-1}x_{21} & x_{13} \\ x_{21}^T x_{22}^{-T} x_{21} & x_{21}^T x_{22}^{-T} x_{21} & 0 \\ x_{31} & x_{32}x_{22}^{-1}x_{21} & x_{33} \end{bmatrix}, \tag{39}$$

$$P_a = J^T\mathscr{P}_a J,$$

$$\begin{bmatrix} \widehat{A}_f & \widehat{B}_f \\ \widehat{C}_f & 0 \end{bmatrix} = \begin{bmatrix} x_{21}^T x_{22} & 0 \\ 0 & I \end{bmatrix} \begin{bmatrix} A_f & B_f \\ C_f & 0 \end{bmatrix} \begin{bmatrix} x_{22}^T x_{21} & 0 \\ 0 & I \end{bmatrix}$$

By Pre- and postmultiplying (38) by $\operatorname{diag}\{J^T, J^T, I\}$ and $\operatorname{diag}\{J, J, I\}$ and choos Ψ_a satisfying Proposition 5, (38) is equivalent to □

$$\begin{bmatrix} -Q_a & P_a - X_{a1} & -X_{a1}V_1 \\ * & \overline{\omega}_2 Q_a + \mathscr{C}_{11}^T\Psi_a\mathscr{C}_{11} + \mathscr{C}_2^T\Pi_a\mathscr{C}_2 + \operatorname{He}\left(\mathscr{A}^T X_{a1}\right) & \mathscr{C}_{11}^T\Psi_a\mathscr{D}_{11} + \mathscr{C}_2^T\Pi_a\mathscr{D}_2 + \mathscr{A}^T X_{a1}V_1 + X_{a1}^T\mathscr{B}_a \\ * & * & \mathscr{D}_{11}^T\Psi_a\mathscr{D}_{11} + \mathscr{D}_2^T\Pi_a\mathscr{D}_2 + \operatorname{He}\left(\mathscr{B}_a^T X_{a1}V_1\right) \end{bmatrix} < 0, \tag{40}$$

where $\mathscr{A}$, $\mathscr{B}_a$, $\mathscr{C}_{11}$, $\mathscr{C}_2$ are the matrices which use the new defined variables $\widehat{A}_f, \widehat{B}_f, \widehat{C}_f$ in the matrices $\mathscr{A}, \mathscr{B}_a, \mathscr{C}_{11}, \mathscr{C}_2$.

By simple calculation, we can obtain that

$$\left[\begin{array}{c|c} \mathscr{C}_2^T\Pi_a\mathscr{C}_2 & \mathscr{C}_2^T\Pi_a\mathscr{D}_2 \\ \hline * & \mathscr{D}_2^T\Pi_a\mathscr{D}_2 \end{array}\right] = \left[\begin{array}{cc|cc} 0 & 0 & 0 & 0 \\ 0 & 0 & 0 & 0 \\ \hline 0 & 0 & -\gamma^2 I & 0 \\ 0 & 0 & 0 & 0 \end{array}\right]$$

$$+ \begin{bmatrix} \mathfrak{C}^T \\ \overline{L}_2^T \\ \overline{D}_2^T \\ 0 \end{bmatrix} \left[\begin{array}{c|cc} \mathfrak{C} & \overline{L}_2 & \overline{D}_2 \quad 0 \end{array}\right]$$

$$= \left[\begin{array}{c|c} 0 & 0 \\ \hline 0 & -\gamma^2\mathscr{I}_0 \end{array}\right] + \begin{bmatrix} \mathfrak{C}_1^T \\ \mathfrak{D}_2^T \end{bmatrix} \left[\begin{array}{c|c} \mathfrak{C}_1 & \mathfrak{D}_2 \end{array}\right], \tag{41}$$

where $\mathfrak{C} = \left[D_f C \ \ \widehat{C}_f\right]$, $\mathfrak{C}_1 = \left[\mathfrak{C} \ \ \overline{L}_2\right]$, $\mathfrak{D}_2 = \left[\overline{D}_2 \ \ 0\right]$. By applying the Schur complement formula, the following can be obtained:

$$\begin{bmatrix} -Q_a & P_a - X_{a1} & -X_{a1}V_1 & 0 \\ * & \overline{\omega}_2 Q_a + \mathscr{C}_{11}^T \Psi_a \mathscr{C}_{11} + \mathrm{He}\left(\mathscr{A}^T X_{a1}\right) & \mathscr{C}_{11}^T \Psi_a \mathscr{D}_{11} + \mathscr{A}^T X_{a1} V_1 + X_{a1}^T \mathscr{B}_a & \mathfrak{C}_1^T \\ * & * & \mathscr{D}_{11}^T \Psi_a \mathscr{D}_{11} + \mathrm{He}\left(\mathscr{B}_a^T X_{a1} V_1\right) - \gamma^2 \mathscr{I}_0 & \mathfrak{D}_2^T \\ * & * & * & -I \end{bmatrix} < 0. \tag{42}$$

Then, pre-and postmultiply diag$\{I, I, I, R^T\}$ to (42). Due to $-R^T R \le I - \mathrm{He}(R)$ and defineing $\widehat{A} = M\widehat{A}_f$, $\widehat{B} = M\widehat{B}$, $\widehat{C} = R^T\widehat{C}_f$, $\widehat{D} = R^T D_f$, (29) hold. In addition, and pre- and postmultiplying (33) by J_1^T and J_1, respectively, (33) becomes (30).

Hence, if conditions (29) and (30) holds, the augmented uncertain system (5) is stable and guarantees the H_∞ performance (27), which completes the proof.

3.2. The Fault Sensitiveness Condition for Faulty Case

Theorem 9. *Consider the system in* (5) *with* $\Delta \in \mathbf{\Delta}$. *A real symmetric matrix* $\Pi_b = \left[\begin{smallmatrix} -1 & 0 \\ 0 & \beta^2 I \end{smallmatrix}\right]$. *The following condition*

$$\delta_{\min}\left(G_{rf}\left(j\omega\right)\right) > \beta, \quad |\omega| < \overline{\omega}_2, \ \Delta \in \mathbf{\Delta} \tag{43}$$

holds if there exist matrix variables $\widehat{A}$, $\widehat{B}$, $\widehat{C}$, $\widehat{D}$, M, R, Y_b, E_b, L_b, N_b, W_b, S_b,

$$P_b = \begin{bmatrix} P_{b11} & P_{b12} & P_{b13} \\ P_{b21} & P_{b22} & P_{b23} \\ P_{b31} & P_{b32} & P_{b33} \end{bmatrix},$$

$$Q_b = \begin{bmatrix} Q_{b11} & Q_{b12} & Q_{b13} \\ Q_{b21} & Q_{b22} & Q_{b23} \\ Q_{b31} & Q_{b32} & Q_{b33} \end{bmatrix}$$

$$\Psi_b = \begin{bmatrix} \Psi_{b111} & \Psi_{b112} & \Psi_{b121} & \Psi_{b122} \\ \Psi_{b112}^T & \Psi_{b113} & \Psi_{b122^T} & \Psi_{b123} \\ \Psi_{b121}^T & \Psi_{b122} & \Psi_{b221} & \Psi_{b222} \\ \Psi_{b122}^T & \Psi_{b123}^T & \Psi_{b222}^T & \Psi_{b223} \end{bmatrix}, \tag{44}$$

$$\Lambda_b = \begin{bmatrix} \Lambda_{b11} & \Lambda_{b12} \\ \Lambda_{b12}^T & \Lambda_{b22} \end{bmatrix}$$

of appropriate dimensions satisfying $Q_b > 0$, $\Psi_b \in \mathbf{\Psi}$, *and* $\Lambda_b \in \mathbf{\Lambda}$ *such that*

$$\begin{bmatrix} -Q_{b11} & -Q_{b12} & -Q_{b13} & P_{b11} - Y_b^T & P_{b12} - E_b^T & P_{b13} - L_b^T & -Y_b^T\nu_3 & -Y_b^T\nu_4 & 0 \\ * & -Q_{b22} & -Q_{b23} & P_{b21} - M^T & P_{b22} - M^T & P_{b23} & -M^T\nu_3 & -M^T\nu_4 & 0 \\ * & * & -Q_{b33} & P_{b31} - W_b^T & P_{b32} - S_b^T & P_{b33} - N_b^T & -W_b^T\nu_3 & -W_b^T\nu_4 & 0 \\ * & * & * & c_{44} & b_{45} & b_{46} & b_{47} & b_{48} & -\mathscr{I}_1 R^T \\ * & * & * & * & b_{55} & B_{56} & b_{57} & b_{58} & -\mathscr{I}_1 R^T \\ * & * & * & * & * & b_{66} & b_{67} & b_{69} & -\mathscr{I}_1 R^T \\ * & * & * & * & * & * & b_{77} & b_{78} & 0 \\ * & * & * & * & * & * & * & b_{88} & 0 \\ * & * & * & * & * & * & 0 & 0 & -I \end{bmatrix} < 0, \tag{45}$$

$$\begin{bmatrix} Q_{b11} - H^T\Lambda_{b22}H & Q_{b12} & Q_{b13} - H^T\Lambda_{b12}^T \\ * & Q_{b22} & Q_{b23} \\ * & * & Q_{b33} - \Lambda_{b11} \end{bmatrix} > 0, \tag{46}$$

where

$$b_{44} = \overline{\omega}_2^2 Q_{b11} + H^T\Psi_{113}H + A^T H^T \Psi_{b223} HA + \mathrm{He}\left(Y_b A + \widehat{B}C + \mathscr{I}_1\widehat{D}C + H^T\Psi_{b123}HA\right),$$

$$b_{45} = \overline{\omega}_2^2 Q_{b12} + \widehat{A} + A^T E_b^T + C^T\widehat{B}^T + C^T\widehat{B}^T + \left(\mathscr{I}_1\widehat{D}C\right)^T + \mathscr{I}_1\widehat{C},$$

$$b_{46} = \overline{\omega}_2^2 Q_{b13} + H^T\Psi_{b112}^T + A^T H^T \Psi_{b122}^T$$

$$
\begin{aligned}
&+ H^T\Psi_{b123}HL_1 + A^TH^T\Psi_{b223}HL_1\\
&+ \widehat{B}L_2 + A^TL_b^T + \mathscr{J}_1\widehat{D}L_2 + C^T\widehat{D}^T\mathscr{J}_1^T,\\
b_{55} &= \overline{\omega}_2^2Q_{b22} + \mathrm{He}\left(\widehat{A} + \mathscr{J}_1\widehat{C}\right),\\
b_{56} &= \overline{\omega}_2^2Q_{b23} + EL_1 + \widehat{B}L_2 + \mathscr{J}_1\widehat{D}L_2 + \widehat{C}^T\mathscr{J}_1^T,\\
b_{66} &= \overline{\omega}_2^2Q_{b33} + \Psi_{b111} + L_1^TH^T\Psi_{b223}HL_1\\
&\quad + \mathrm{He}\left(\Psi_{b122}HL_1 + L_bL_1 + \mathscr{J}_1\widehat{D}L_2\right),\\
b_{47} &= H^T\Psi_{b123}HB_2 + A^TH^T\Psi_{b223}HB_2 + Y_bB_2\\
&\quad + \widehat{B}D_2 + \left(Y_bA + \widehat{B}C\right)^T\nu_3 + \mathscr{J}_1\widehat{D}D_2,\\
b_{48} &= H^T\Psi_{b122}^T + A^TH^T\Psi_{b222}^T + W_b + \left(Y_bA + \widehat{B}C\right)^T\nu_4,\\
b_{57} &= E_bB_2 + \widehat{B}D_2 + \widehat{A}^T\nu_3 + \mathscr{J}_1\widehat{D}D_2,\\
b_{58} &= S_b + \widehat{A}^T\nu_4,\\
b_{67} &= \Psi_{b122}HB_2 + L_1^TH^T\Psi_{b223}HB_2 + L_bB_2\\
&\quad + \left(YL_1 + \widehat{B}L_2\right)^T\nu_3 + \mathscr{J}_1\widehat{D}D_2,\\
b_{68} &= \Psi_{b121} + L_1^TH^T\Psi_{b222}^T + N_b + \left(Y_bL_1 + \widehat{B}L_2\right)^T\nu_4,\\
b_{77} &= \beta^2I + B_2^TH^T\Psi_{a223}HB_2 + \mathrm{He}\left(\left(Y_bB_2 + \widehat{B}D_2\right)^T\nu_3\right),\\
b_{78} &= B_2^TH^T\Psi_{b222}^T + \nu_3^TW_b + \left(Y_bB_2 + \widehat{B}D_2\right)^T\nu_4,\\
b_{88} &= \Psi_{b221} + \mathrm{He}\left(\nu_4^TW_b\right),\\
\mathbf{\Lambda} &:= \left\{\Lambda_b : \textit{satisfy (12) in Proposition 5}\right\},\\
\mathbf{\Psi} &:= \left\{\Psi_b : \textit{satisfy (20) in Proposition 7}\right\},
\end{aligned}
\tag{47}
$$

Proof. Substituting Π_b into (17), $G_{rr_{0i}}(j\omega)^TG_{rr_{0i}}(j\omega) < \beta^2I$ which is equivalent to (43). Applying Lemma 6, (43) holds if

$$
\begin{aligned}
&\begin{bmatrix}\mathscr{A} & \mathscr{B}_b\\ \mathscr{I} & 0\end{bmatrix}^T\begin{bmatrix}-\mathscr{Q}_b & \mathscr{P}_b\\ \mathscr{P}_b & \overline{\omega}^2\mathscr{Q}_b\end{bmatrix}\begin{bmatrix}\mathscr{A} & \mathscr{B}_b\\ \mathscr{I} & 0\end{bmatrix}\\
&< \begin{bmatrix}\mathscr{C}^T\\ \mathscr{D}^T\end{bmatrix}\begin{bmatrix}\Psi_b & 0\\ 0 & \Pi_b\end{bmatrix}\begin{bmatrix}\mathscr{C} & \mathscr{D}\end{bmatrix}
\end{aligned}
\tag{48}
$$

$$
\mathscr{Q}_b > \mathscr{C}_1^T\Lambda_b\mathscr{C}_1 \tag{49}
$$

hold.

Where

$$
\begin{bmatrix}\mathscr{A} & \mathscr{B}_b\\ \mathscr{C}_1 & \mathscr{D}_1\\ \mathscr{C}_2 & \mathscr{D}_2\end{bmatrix} := \left[\begin{array}{cc|cc}\overline{A} & \overline{L}_1 & \overline{B}_f & 0\\ 0 & 0 & 0 & I\\ \hline 0 & I & 0 & 0\\ \overline{H} & 0 & 0 & 0\\ \hline \overline{C} & \overline{L}_2 & \overline{D}_f & 0\\ 0 & 0 & I & 0\end{array}\right] \tag{50}
$$

$$
\begin{bmatrix}\mathscr{C} & \mathscr{D}\end{bmatrix} := \left[\begin{array}{c|c}\mathscr{C}_{11} & \mathscr{D}_{11}\\ \hline \mathscr{C}_2 & \mathscr{D}_2\end{array}\right] = \left[\begin{array}{c|c}\mathscr{C}_1 & 0\\ \mathscr{C}_1\mathscr{A} & \mathscr{C}_1\mathscr{B}_b\\ \hline \mathscr{C}_2 & \mathscr{D}_2\end{array}\right].
$$

Let

$$
\Upsilon_b = \begin{bmatrix}-\mathscr{Q}_b & \mathscr{P}_b & 0\\ \mathscr{P}_b & \overline{\omega}_2\mathscr{Q}_b + \mathscr{C}_{11}^T\Psi_b\mathscr{C}_{11} + \mathscr{C}_2^T\Pi_b\mathscr{C}_2 & \mathscr{C}_{11}^T\Psi_b\mathscr{D}_{11} + \mathscr{C}_2^T\Pi_b\mathscr{D}_2\\ 0 & \mathscr{D}_{11}^T\Psi_b\mathscr{C}_{11} + \mathscr{D}_2^T\Pi_b\mathscr{C}_2 & \mathscr{D}_{11}^T\Psi_b\mathscr{D}_{11} + \mathscr{D}_2^T\Pi_b\mathscr{D}_2\end{bmatrix} \tag{51}
$$

(48) is equivalent to

$$
\begin{bmatrix}\mathscr{A} & \mathscr{B}_b\\ I & 0\\ 0 & I\end{bmatrix}^T\Upsilon_b\begin{bmatrix}\mathscr{A} & \mathscr{B}_b\\ I & 0\\ 0 & I\end{bmatrix} < 0, \tag{52}
$$

and on the other hand,

$$
\begin{bmatrix}I & 0 & 0\end{bmatrix}\Upsilon_b\begin{bmatrix}I & 0 & 0\end{bmatrix}^T = -\mathscr{Q}_b < 0. \tag{53}
$$

Combining (52) with (53) and applying Lemma 3, (48) holds if and only if

$$
\Upsilon_b + \begin{bmatrix}-I\\ \mathscr{A}^T\\ \mathscr{B}_b^T\end{bmatrix}\mathscr{X}_b\begin{bmatrix}0 & I & 0\\ 0 & 0 & I\end{bmatrix} + \begin{bmatrix}0 & I & 0\\ 0 & 0 & I\end{bmatrix}^T\mathscr{X}_b^T\begin{bmatrix}-I\\ \mathscr{A}^T\\ \mathscr{B}_b^T\end{bmatrix}^T < 0, \tag{54}
$$

where $\mathscr{X}_b$ introduced by Lemma 3 is the variable matrix of appropriate dimensions. Here, $\mathscr{X}_b$ is defined as $\mathscr{X}_b = [\mathscr{X}_{b1}\ \ \mathscr{X}_{b1}V_2]$, where $\mathscr{X}_{b1} = \begin{bmatrix}x_{b11} & -x_{b12} & x_{b13}\\ x_{21} & x_{22} & 0\\ x_{b31} & x_{b32} & x_{b33}\end{bmatrix}$, where x_{21} and x_{22} are the same as in Theorem 8. V_2 is an given matrix, defined as $V_2 = \begin{bmatrix}\nu_3^T & 0 & 0\\ \nu_4^T & 0 & 0\end{bmatrix}^T$. Pre- and postmultiply (54) by $\mathrm{diag}\{J^T, J^T, I\}$ and $\mathrm{diag}\{J, J, I\}$, where J is defined as Theorem 8 and choose Ψ_b satisfying Proposition 5, (54) is equivalent to

$$
\begin{bmatrix}-Q_b & P_b - X_{b1} & -X_{b1}V_2\\ * & \overline{\omega}_2Q_b - \mathscr{C}_{b2}^T\mathscr{C}_{b2} + \mathscr{C}_{11}^T\Psi_b\mathscr{C}_{11} + \mathrm{He}\left(X_{b1}^T\overline{\mathscr{A}}_b\right) & -\mathscr{C}_{b2}^T\mathscr{D}_{b2} + \mathscr{C}_{11}^T\Psi_b\mathscr{D}_{11} + X_{b1}^T\overline{\mathscr{B}}_b + \overline{\mathscr{A}}_bX_{b1}V_2\\ * & * & -\mathscr{D}_{b2}^T\mathscr{D}_{b2} + \mathscr{D}_{11}^T\Psi_b\mathscr{D}_{11} + \beta^2\mathscr{I}_0 + \mathrm{He}\left(\overline{\mathscr{B}}_b^TX_{b1}V_2\right)\end{bmatrix} < 0, \tag{55}
$$

where

$$\begin{bmatrix} \widehat{A}_f & \widehat{B}_f \\ \widehat{C}_f & 0 \end{bmatrix} = \begin{bmatrix} x_{21}^T x_{22} & 0 \\ 0 & I \end{bmatrix} \begin{bmatrix} A_f & B_f \\ C_f & 0 \end{bmatrix} \begin{bmatrix} x_{22}^T x_{21} & 0 \\ 0 & I \end{bmatrix},$$

$$\mathscr{X}_{b1} = J^T X_1 J = \begin{bmatrix} Y_b^T & E_b^T & L_b^T \\ M^T & M^T & 0 \\ W_b^T & S_b^T & N_b^T \end{bmatrix},$$

$$\overline{\mathscr{A}}_b = J^{-1} \mathscr{A} J = \begin{bmatrix} A & 0 & L_1 \\ \widehat{B}_f C & \widehat{A}_f & \widehat{B}_f L_2 \\ 0 & 0 & 0 \end{bmatrix},$$

$$\overline{\mathscr{B}}_b = J^{-1} \mathscr{B}_b = \begin{bmatrix} B_2 & 0 \\ \widehat{B}_f D_2 & 0 \\ 0 & I \end{bmatrix},$$

$$\mathscr{C}_{b2} = \begin{bmatrix} D_f C & \widehat{C}_f & D_f L_2 \end{bmatrix}, \qquad \mathscr{D}_{b2} = \begin{bmatrix} D_f D_2 & 0 \end{bmatrix}, \tag{56}$$

Condition (55) is nonlinear owing to the product terms $-C_{b2}^T C_{b2}$. To solve this problem, condition (55) is equivalent to

$$\Xi_{b2}^T \Theta \Xi_{b2} < 0, \tag{57}$$

where

$$\Xi_{b2} = \begin{bmatrix} I & 0 & 0 \\ 0 & I & 0 \\ 0 & 0 & I \\ 0 & \mathscr{C}_{b2} & \mathscr{D}_{b2} \end{bmatrix},$$

$$\Theta = \begin{bmatrix} -Q_b & P_b - X_1 & -X_1 V_2 & 0 \\ * & \mathscr{C}_{11}^T \Psi_b \mathscr{C}_{11} + \mathrm{He}\left(X_1^T \overline{\mathscr{A}}_{bi}\right) & X_1^T \overline{\mathscr{B}}_b + \overline{\mathscr{A}}_{bi} X_1 V_2 + \mathscr{C}_{11}^T \Psi_b \mathscr{D}_{11} & 0 \\ * & * & \mathscr{D}_{11}^T \Psi_b \mathscr{D}_{11} + \beta^2 \mathscr{I}_0 + \mathrm{He}\left(\overline{\mathscr{B}}_b^T X_{b1} V_2\right) & 0 \\ 0 & 0 & 0 & -I \end{bmatrix}. \tag{58}$$

Defining $G = \begin{bmatrix} 0 & \mathscr{C}_{b2} & \mathscr{D}_{b2} & -I \end{bmatrix}$ satisfies $G\Xi_{b2} = 0$. Using Lemma 4, and given a matrix T, (57) is equivalent to

$$\Theta + TG + (TG)^T < 0, \tag{59}$$

where one notes T as

$$T = \begin{bmatrix} 0 & \mathscr{R} & 0 & 0 \end{bmatrix}^T, \quad \mathscr{R} = \begin{bmatrix} R\mathscr{I}_1^T & R\mathscr{I}_1^T & R\mathscr{I}_1^T \end{bmatrix}. \tag{60}$$

Defining $\widehat{A} = M\widehat{A}_f$, $\widehat{B} = M\widehat{B}$, $\widehat{C} = R^T\widehat{C}_f$, and $\widehat{D} = R^T D_f$ and after some matrix manipulation, (59) becomes (45). By pre- and postmultiplying (49) by J^T and J, respectively, (49) becomes (46). □

Remark 10. Theorem 8 considers the attenuation performance for the disturbance $d(t)$, and the conservatism comes from the special structure of $\mathscr{X}_{a1}$ and the same one in $\mathscr{X}_a$. Theorem 9 considers the sensitiveness performance for the fault $f(t)$, and the conservatism comes from the special structure of $\mathscr{X}_{b1}$ and the same one in $\mathscr{X}_b$. Then, the conservatism for Theorem 9 comes as the same as Theorem 8. However, in order to obtain the better detection performance, the sensitiveness performance is considered over the conservatism.

3.3. Stability Condition for the Filter. Due to the fault tolerant controller, the closed-loop system is stable both in the fault-free cases and in the fault cases. Then, the condition that the augmented systems (1) is stable can translate into the condition that the FD filter is stable.

Lemma 11 (see [20]). *By considering the FD filter* (4)*, the FD filter is stable, if there exist matrix variables* M*,* $\widehat{A}$ *and* $P_s > 0$ *satisfying*

$$\begin{bmatrix} -\left(M + M^T\right) & \widehat{A} + P_s & M \\ * & -P_s & 0 \\ * & * & -P_s \end{bmatrix} < 0. \tag{61}$$

3.4. Algorithm. In the precious sections, Theorems 8 and 9 and Lemma 11 have formulated the inequality conditions for the performance indexes (8) and (9) and the stable condition, respectively. Summarily, we have the following theorem.

Theorem 12. *By considering the uncertain system model* (1)*, there exists a FD filter* (4) *such that the augmented system model* (5) *is stable and satisfies the performance indices* (8) *and* (9) *if inequality conditions* (29)*,* (30)*,* (45)*,* (46)*, and* (61) *hold.*

Proof. Combining Theorems 8–9 and Lemma 11, it is obviously that the theorem holds. □

Remark 13. In Theorems 8–9, if the matrices v_i, $i \in \{1, \ldots, 4\}$ are given, all conditions (29), (30), (45), and (46) are the LMI conditions. Specially, if the disturbance and the fault are a scalar, respectively, v_i is vector, and it can be easily chosen, which has been further confirmed in the simulink. In addition, Propositions 5 and 7 are used to directly deal with the ellipsoidal uncertainty; the variable structure is complex. However, all the variables in Propositions 5 and 7 is composed of linear matrices, and can be used for LMI conditions.

The gain matrices A_f, B_f, C_f, and D_f defining the FD filter can be derived by the means of a standard procedure. Denote $\widehat{A}$, $\widehat{B}$, $\widehat{C}$, $\widehat{D}$, and M is the optimal solution of (7) with condition (29), (30), (45), (46), and (61):

(1) compute the x_{21}, x_{22} by solving the following factorization problem $M = x_{21}^T x_{22}^{-1} x_{21}$;

(2) compute $\widehat{A}_f$, $\widehat{B}_f$ by $\widehat{A}$, $\widehat{B}$ and M. Compute $\widehat{C}_f$, D_f by $\widehat{C}$, $\widehat{D}$ and R;

(3) finally, obtain the gain matrices of the FD filter

$$\begin{bmatrix} \widehat{A}_f & \widehat{B}_f \\ \widehat{C}_f & 0 \end{bmatrix} = \begin{bmatrix} x_{21}^T x_{22} & 0 \\ 0 & I \end{bmatrix} \begin{bmatrix} A_f & B_f \\ C_f & 0 \end{bmatrix} \begin{bmatrix} x_{22}^T x_{21} & 0 \\ 0 & I \end{bmatrix}. \quad (62)$$

4. Thresholds Computation

After the parameter matrices of the FD filter A_f, B_f, C_f, and D_f are designed, similar to that proposed in [21], the residual evaluation function $J_r(t)$ can be selected as

$$J_r(t) = \sqrt{\frac{1}{t}\int_0^t r^T(\tau)\, r(\tau)\, d\tau}. \quad (63)$$

Under fault-free condition, the residual $r(t)$ becomes

$$r(t) = G_{rd}(j\omega)\, d(t), \quad (64)$$

and namely, the Parseval Theorem (see [22]), one has that

$$J_r(t) \le \left\|G_{rd_0}\right\|_\infty \|d\|_{\text{rms}} \le \left\|G_{rd_0}\right\|_\infty \overline{d}, \quad (65)$$

where $\overline{d}$ is the upper bound on the disturbance. It is assumed that $\overline{d}$ is the known. As a consequence, the following threshold results:

$$J_{\text{th}} = \left\|G_{rd_0}\right\|_\infty \overline{d}. \quad (66)$$

Based on this, the occurrence of faults can be detected by the following logic rule.

$$\begin{aligned} \|J_r\| &\le J_{\text{th}}, \quad \text{no alarm}, \\ \|J_r\| &> J_{\text{th}}, \quad \text{with alarm}. \end{aligned} \quad (67)$$

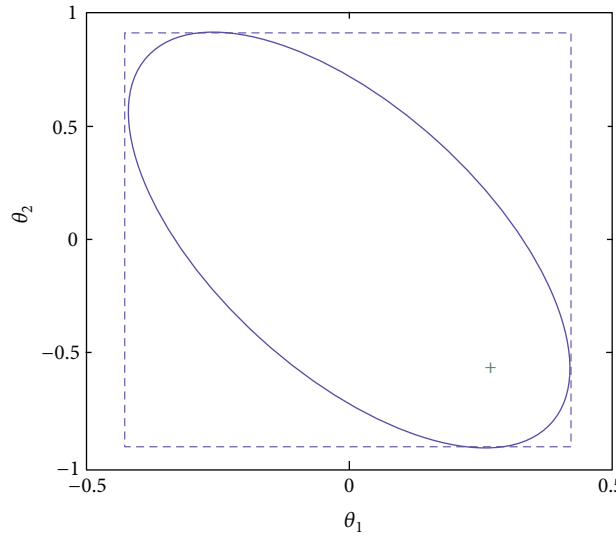

Figure 1: Ellipsoidal uncertainty.

5. Example

In this section, an example is given to illustrate the effectiveness of our design method. Consider the uncertain linear system by

$$\begin{aligned} A &= \begin{bmatrix} 0.5 & 1 \\ -3 & -3 \end{bmatrix}, \quad B_1 = \begin{bmatrix} 0.4 \\ -0.5 \end{bmatrix}, \quad B_2 = \begin{bmatrix} 0.5 \\ -1 \end{bmatrix}, \\ L_1 &= \begin{bmatrix} 0.2 & 0 & 0.1 & 0 \\ 0 & 0 & 0 & 0.2 \end{bmatrix}, \quad C = \begin{bmatrix} 1 & 1 \end{bmatrix}, \\ D_1 &= 0.5, \quad D_2 = 0.5, \\ L_2 &= \begin{bmatrix} 0 & 0 & 0 & 0 \end{bmatrix}, \quad H = \begin{bmatrix} 1 & 0 \\ 0 & 1 \end{bmatrix}, \\ \Delta &= \begin{bmatrix} \theta & 0 \\ 0 & \theta \end{bmatrix}, \quad \theta = \begin{bmatrix} \theta_1 \\ \theta_2 \end{bmatrix}, \end{aligned} \quad (68)$$

and the uncertain parameters $\begin{bmatrix} \theta_1^T \\ \theta_2^T \end{bmatrix} \in \mathcal{U}$ satisfy $\{\theta \mid \theta^T \mathcal{R} \theta < 1\}$, as shown in Figure 1, where $\mathcal{R} = \begin{bmatrix} 1.25 & 0.25 \\ 0.25 & 1.25 \end{bmatrix}$. It is worth pointing out that if the method in this paper is adopted, the uncertain region is only in the ellipsoid (solid lines). Otherwise, the ellipsoid has to translate into the convex bounded polyhedral domain (dashed line) for the existing method to deal with the uncertainty, which enlarges the uncertain region and results in increasing the conservatism.

Given the matrices

$$\begin{aligned} v_1 &= \begin{bmatrix} 0 \\ -0.2 \end{bmatrix}, \quad v_2 = \begin{bmatrix} 0 & 0 & 0 & 0 \\ 0 & 0 & 0 & 0 \end{bmatrix}, \\ v_3 &= \begin{bmatrix} -0.5 \\ -0.5 \end{bmatrix}, \quad v_4 = \begin{bmatrix} 1.5 & 1.5 & 1.5 & -1.5 \\ 1 & 1 & -1 & -1 \end{bmatrix}, \end{aligned} \quad (69)$$

the disturbance is $d(t) = 0.8\sin(0.1t)\exp(-0.05t)$. Then, the upper bounds on the frequency for the disturbance and the reference input can choose $\overline{\omega}_1 = 0.5$ and $\overline{\omega}_2 = 0$, respectively.

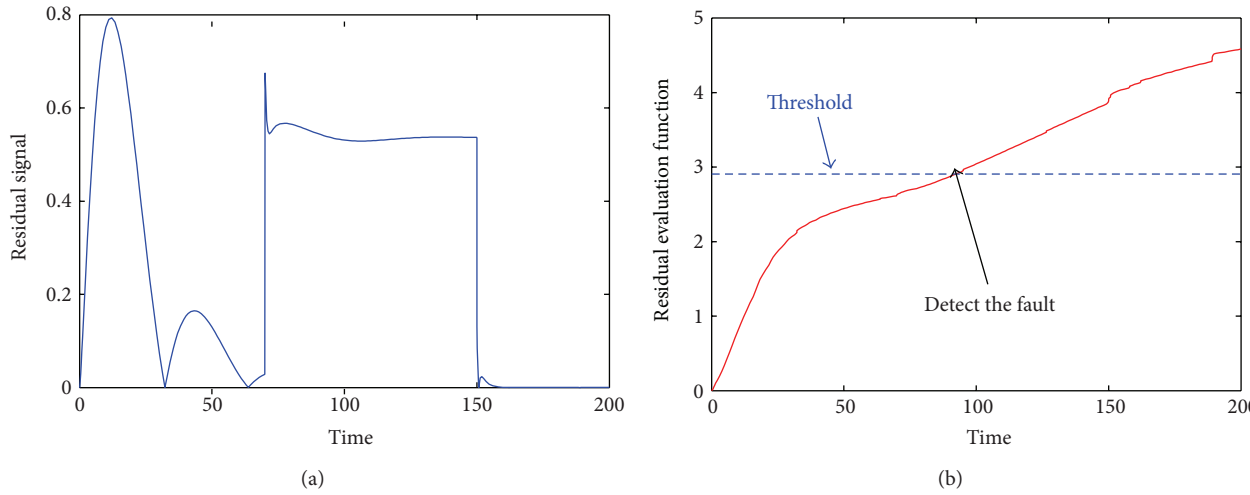

Figure 2: The residual signal and the residual evaluation function J_r.

Given $\gamma = 1$, for the practical needs, we obtain the sensitivity performance $\beta = 0.4234$ by solving the optimization problem (16) with the conditions in Theorem 12 and the FD filter with gain matrices as

$$A_f = \begin{bmatrix} -3.5304 & 0.0850 \\ -6.0843 & -0.2812 \end{bmatrix}, \quad B_f = \begin{bmatrix} 0.0696 \\ 2.5117 \end{bmatrix}, \quad C_f = \begin{bmatrix} -0.0539 & -0.2526 \end{bmatrix}, \quad D_f = -1.3339. \tag{70}$$

Choose $\theta_1 = 0.2$ and $\theta_1 = -0.6$. Considering the case that the fault occurs between 70 sec and 150 sec, the residual signal and the residual evaluation function $J_r(t)$ and the threshold $J_{\text{th}}(t)$ are shown in Figure 2. Consider that $J_r(t) > J_{\text{th}}(t)$ at 92.5 sec, which means that the fault alarms when the outage fault occurs. Hence, the fault can be detected.

6. Conclusions

In this paper, the design problem of the FD filter for uncertain linear systems has been addressed. A method for the design problem is given in terms of the linear matrix inequality (LMI) optimization techniques. The new proposed method has two main advantages. The first one is to resolve the problem of designing FD filters subjected to the model with ellipsoidal parametric uncertainty region, while this problem cannot be directly resolved using the existing method. The second one is that the finite-frequency performances of the fault and the disturbance have been detected.

References

[1] J. Chen and P. R. Patton, *Robust Model-Based Fault Diagnosis For Dynamic Systems*, Kluwer Academic Publishers, Boston, Mass, USA.

[2] T. Li, L. Guo, and L. Y. Wu, "Observer-based optimal fault detection using PDFs for time-delay stochastic systems," *Nonlinear Analysis: Real World Applications*, vol. 9, no. 5, pp. 2337–2349, 2008.

[3] I. Hwang, S. Kim, Y. Kim, and C. E. Seah, "A survey of fault detection, isolation, and reconfiguration methods," *IEEE Transactions on Control Systems Technology*, vol. 18, no. 3, pp. 636–653, 2010.

[4] E. G. Nobrega,, M. O. Abdalla, and K. M. Grigoriadis, "LMI-based filter design for fault detection and isolation," in *Proceedings of the 39th IEEE Confernce on Decision and Control (CDC '00)*, pp. 4329–4334, Sydney, Australia, December 2000.

[5] T. Li and L. Guo, "Optimal fault-detection filtering for non-Gaussian systems via output PDFs," *IEEE Transactions on Systems, Man, and Cybernetics A*, vol. 39, no. 2, pp. 476–481, 2009.

[6] W. Li, F. Jiang, Z. Wang, G. Zhou, and Z. Zhu, "Fault detection of Markov jumping linear systems," *Mathematical Problems in Engineering*, vol. 2012, Article ID 141867, 27 pages, 2012.

[7] M. Hou and R. J. Patton, "A LMI approach to $H_-/H\infty$ fault detection observers," in *Proceedings of the UKACC International Conference on Control*, pp. 305–310, London, UK, September 1996.

[8] I. M. Jaimoukha, Z. Li, and V. Papakos, "A matrix factorization solution to the $H_-/H\infty$ fault detection problem," *Automatica*, vol. 42, no. 11, pp. 1907–1912, 2006.

[9] X. Li and H. H. T. Liu, "Minimum system sensitivity study of linear discrete time systems for fault detection," *Mathematical Problems in Engineering*, vol. 2013, Article ID 276987, 13 pages, 2013.

[10] X. J. Cai and F. Wu, "Robust fault detection and isolation for parameter-dependent LFT systems," *International Journal of Robust and Nonlinear Control*, vol. 20, no. 7, pp. 764–776, 2010.

[11] M. Barenthin, X. Bombois, H. Hjalmarsson, and G. Scorletti, "Identification for control of multivariable systems: controller validation and experiment design via LMIs," *Automatica*, vol. 44, no. 12, pp. 3070–3078, 2008.

[12] R. D. Braatz and O. D. Crisalle, "Robustness analysis for systems with ellipsoidal uncertainty," *International Journal of Robust and Nonlinear Control*, vol. 8, no. 13, pp. 1113–1117, 1998.

[13] X. Bombois, M. Gevers, G. Scorletti, and B. D. O. Anderson, "Robustness analysis tools for an uncertainty set obtained by prediction error identification," *Automatica*, vol. 37, no. 10, pp. 1629–1636, 2001.

[14] X. Bombois, H. Hjalmarsson, and G. Scorletti, "Identification for robust H_2 deconvolution filtering," *Automatica*, vol. 46, no. 3, pp. 577–584, 2010.

[15] A. Sadeghzadeh and H. Momeni, "Fixed-order robust H_∞ control and control-oriented uncertainty set shaping for systems with ellipsoidal parametric uncertainty," *International Journal of Robust and Nonlinear Control*, vol. 21, no. 6, pp. 648–665, 2011.

[16] G.-H. Yang and H. Wang, "Fault detection for a class of uncertain state-feedback control systems," *IEEE Transactions on Control Systems Technology*, vol. 18, no. 1, pp. 201–212, 2010.

[17] T. Iwasaki, S. Hara, and H. Yamauchi, "Dynamical system design from a control perspective: finite frequency positive-realness approach," *IEEE Transactions on Automatic Control*, vol. 48, no. 8, pp. 1337–1354, 2003.

[18] X. J. Li and G. H. Yang, "Fault detection filter design for stochastic time-delay systems with sensor faults," *International Journal of Systems Science*, vol. 43, no. 8, 2012.

[19] K. Hu and J. Yuan, "Improved robust H_∞ filtering for uncertain discrete-time switched systems," *IET Control Theory & Applications*, vol. 3, no. 3, pp. 315–324, 2009.

[20] X. J. Li, *Research on robust adaptive fault detection and isolation approaches [Ph.D. thesis]*, Northeastern University, Liaoning, China.

[21] P. M. Frank and X. Ding, "Frequency domain approach to optimally robust residual generation and evaluation for model-based fault diagnosis," *Automatica*, vol. 30, no. 5, pp. 789–804, 1994.

[22] S. Boyd and C. Barratt, *Linear Controller Design: Limites of Performance*, Prentice Hall, Englewood Cliffs, NJ, USA, 1991.

Hindawi Publishing Corporation
Mathematical Problems in Engineering
Volume 2013, Article ID 696058, 12 pages
http://dx.doi.org/10.1155/2013/696058

Research Article

Delay-Dependent Robust H_∞ Filtering of the Takagi-Sugeno Fuzzy Stochastic Systems

Ze Li[1] and Xin-Hao Yang[2]

[1] *College of Electronic and Information Engineering, Suzhou University of Science and Technology, Suzhou 215009, China*
[2] *School of Mechanical and Electric Engineering, Soochow University, Suzhou 215006, China*

Correspondence should be addressed to Ze Li; lizeing@163.com

Received 1 August 2013; Accepted 22 September 2013

Academic Editor: Baoyong Zhang

This paper is concerned with the problem of the robust H_∞ filtering for the Takagi-Sugeno (T-S) fuzzy stochastic systems with bounded parameter uncertainties. For a given T-S fuzzy stochastic system, this paper focuses on the stochastically mean-square stability of the filtering error system and the H_∞ performance level of the output error and the disturbance input. The design method for delay-dependent filter is developed based on linear matrix inequalities. Finally, the effectiveness of the proposed methods is substantiated with an illustrative example.

1. Introduction

As an efficient technique to linearize the nonlinear differential equations, the T-S fuzzy model [1] has been an active research area over the past three decades. This model is capable of representing linear input-output relations of nonlinear systems by appropriate fuzzy sets, such as the stirred tank reactor system [2] and the truck trailer system [3]. And it has been proved that this model can accurate to a compact set by a family of IF-THEN rules. This way, the stability analysis and synthesis of the nonlinear system turn into the analysis of linear systems, where the linear system theory can be conveniently applied. In recent years, the researches of T-S fuzzy have grown into a great number. To mention a few, the stability and control problem of T-S fuzzy systems have been investigated in [4–14] and the references therein.

Moreover, as a branch of state estimation theory, the filtering problem has become an important research field for many kinds of systems. The H_∞ filtering problems for the T-S fuzzy systems have been addressed in [15–19]; references [20, 21] have considered the $L_2 - L_\infty$ filtering problem for delayed T-S fuzzy systems with different methods.

On the other hand, stochastic system has received considerable attention because uncertain factors are unavoidable in most of the physical systems, for example, signal processing, engineering, finance, economics; biological movement systems, and so forth. Stochastic modeling has become important in many branches of engineering applications [22]. And many results on the study of stochastic systems can be found in the literature. References [23, 24] study the problem of designing delay-dependent controllers and H_∞ output feedback controller for nonlinear stochastic time-delay system with method, respectively. The sliding mode control for the time-delay nonlinear Itô stochastic systems was proposed in [25, 26]. References [26, 27] have investigated the stability of the time-delay stochastic neutral networks. The problem of filtering is considered in [29–31]. Fault detection problem of the stochastic system has been addressed in [32, 33]. And the problem of H_∞ model reduction in stochastic framework is investigated in [34].

Through the above analysis, T-S fuzzy model could be used to represent the nonlinear stochastic system with several subsystems that could easily be analyzed. There have been a few works in this manner; [35] deals with the robust fault detection problem for T-S fuzzy stochastic systems. And [36] considers the stabilization for the stochastic fuzzy systems with delays. However, to the best of the authors knowledge, few results on filtering problem for TCS fuzzy stochastic systems are available which still remains challenging.

Inspired by the above discussions, this paper will focus on the robust fuzzy delay-dependent H_∞ filter design for a T-S fuzzy stochastic system with time-varying delays and

norm-bounded parameter uncertainties. The problem we consider here is to make sure that the fuzzy filters we design could ensure both the robust stochastic mean-square stability and a prescribed H_∞ performance level of the filtering error system. During the proof of the theorems, some useful free-weighting matrices are introduced to reduce the potential conservatism as much as we can. By using the Lyapunov-Krasovskii functional technique, a linear matrix inequality (LMI) approach is proposed to solve the problem.

The remainder of the paper is organized as follows. Section 2 formulates the filter design problem. Section 3 gives the delay-dependent conditions for the stochastic stability problem of the T-S fuzzy stochastic systems. And the solvability of the filtering design problem is obtained in terms of LMIs, which are presented in Section 4. In Section 5, a numerical example is shown to illustrate the effectiveness of the proposed methods. Finally, we conclude the paper in Section 6.

Notation. The notation used in this paper is fairly standard. The superscript "T" stands for matrix transposition. Throughout this paper, for real symmetric matrices X and Y, the notation $X \geq Y$ (resp., $X > Y$) means that the matrix $X - Y$ is positive semidefinite (resp., positive definite). $\mathbf{R}^n$ denotes the n-dimensional Euclidean space, and $\mathbf{R}^{m\times n}$ denotes the set of all $m \times n$ real matrices. I stands for an identity matrix of appropriate dimension, while $I_n \in \mathbf{R}^n$ denotes a vector of ones. The notation $*$ is used as an ellipsis for terms that are induced by symmetry. diag$(\cdots)$ stands for a block-diagonal matrix. $|\cdot|$ denotes the Euclidean norm for vectors, and $\|\cdot\|$ denotes the spectral norm for matrices. $\mathbf{L}_2[0,\infty)$ represents the space of square-integrable vector functions over $[0,\infty)$. $\mathsf{E}(\cdot)$ stands for the mathematical expectation operator. Matrix dimensions, if not explicitly stated, are assumed to be compatible for algebraic operations.

2. Problem Formulation and Preliminaries

Consider a T-S fuzzy stochastic time-delay system with time-varying parameter uncertainties.

Plant rule i: IF $s_1(t)$ is μ_{i1}, and $s_2(t)$ is μ_{i2}, and $\cdots$ and $s_g(t)$ is μ_{ig}, THEN

$$\begin{aligned} dx(t) = {} & \left[\left(A_i + \Delta A_i(t)\right)x(t)\right. \\ & + \left(A_{d1i} + \Delta A_{d1i}(t)\right)x\left(t-\tau_1(t)\right) \\ & \left. + \left(A_{d2i} + \Delta A_{d2i}(t)\right)x\left(t-\tau_2(t)\right) + B_i v(t)\right]dt \\ & + \left[\left(H_i + \Delta H_i(t)\right)x(t)\right. \\ & + \left(H_{d1i} + \Delta H_{d1i}(t)\right)x\left(t-\tau_1(t)\right) \\ & \left. + \left(H_{d2i} + \Delta H_{d2i}(t)\right)x\left(t-\tau_2(t)\right)\right]d\omega(t), \end{aligned} \tag{1}$$

$$\begin{aligned} dy(t) = {} & \left[C_i x(t) + C_{d1i}x\left(t-\tau_1(t)\right)\right. \\ & \left. + C_{d2i}x\left(t-\tau_2(t)\right) + D_i v(t)\right]dt, \end{aligned} \tag{2}$$

$$z(t) = L_i x(t) + L_{d1i}x\left(t-\tau_1(t)\right) + L_{d2i}x\left(t-\tau_2(t)\right), \tag{3}$$

$$x(t) = \varphi(t), \quad t \in \left[-\max\left(h_1,h_2\right),0\right], \ i = 1,2,\ldots,r, \tag{4}$$

where $s(t) = [s_1(t) \ \ s_2(t) \ \cdots \ s_g(t)]$ are the premise variables, μ_{ij} is the fuzzy set, and r is the number of IF-THEN rules; $x(t) \in \mathbf{R}^n$ is the system state; $\varphi(t)$ is a given differential initial function on $[-u_2, 0]$, and $y(t) \in \mathbf{R}^m$ is the measured output; $z(t) \in \mathbf{R}^l$ is a signal to be estimated; $v(t) \in \mathbf{R}^s$ is the noise signal which belongs to $\mathscr{L}_2[0,\infty)$; $\tau_1(t)$ and $\tau_2(t)$ are continuous differentiable functions representing the time-varying delays, which are assumed to satisfy for all $t \geq 0$,

$$0 \leq \tau_1(t) < h_1, \qquad 0 \leq \tau_2(t) < h_2. \tag{5}$$

In the considered system, A_i, A_{d1i}, A_{d2i}, B_i, H_i, H_{d1i}, H_{d2i}, C_i, C_{d1i}, C_{d2i}, D_i, L_i, L_{d1i}, and L_{d2i} are known constant matrices with appropriate dimensions. $\Delta A_i(t)$, $\Delta A_{d1i}(t)$, $\Delta A_{d2i}(t)$, $\Delta H_i(t)$, $\Delta H_{d1i}(t)$, and $\Delta H_{d2i}(t)$ represent the unknown time-varying parameter uncertainties and are assumed to satisfy

$$\begin{aligned} & \begin{bmatrix} \Delta A_i(t) & \Delta A_{d1i}(t) & \Delta A_{d2i}(t) \\ \Delta H_i(t) & \Delta H_{d1i}(t) & \Delta H_{d2i}(t) \end{bmatrix} \\ & = \begin{bmatrix} K_{1i} \\ K_{2i} \end{bmatrix} F_i(t) \begin{bmatrix} T_{1i} & T_{2i} & T_{3i} \end{bmatrix}, \end{aligned} \tag{6}$$

where K_{1i}, K_{2i}, T_{1i}, T_{2i}, and T_{3i} are known real constant matrices and the unknown time-varying matrix function satisfying

$$F_i(t)^T F_i(t) \leq I \quad \forall t. \tag{7}$$

Now, the defuzzied output of the dynamic fuzzy stochastic model in (1)–(4) can be represented as follows:

$$\begin{aligned} (\Sigma):\ dx(t) = {} & \sum_{i=1}^{r} \rho_i(s(t)) \\ & \times \left[\left(A_i + \Delta A_i(t)\right)x(t)\right. \\ & + \left(A_{d1i} + \Delta A_{d1i}(t)\right)x\left(t-\tau_1(t)\right) \\ & + \left(A_{d2i} + \Delta A_{d2i}(t)\right)x\left(t-\tau_2(t)\right) \\ & \left. + B_i v(t)\right]dt \\ & + \left[\left(H_i + \Delta H_i(t)\right)x(t)\right. \\ & + \left(H_{d1i} + \Delta H_{d1i}(t)\right)x\left(t-\tau_1(t)\right) \\ & \left. + \left(H_{d2i} + \Delta H_{d2i}(t)\right)x\left(t-\tau_2(t)\right)\right]d\omega(t), \end{aligned}$$

$$
\begin{aligned}
dy(t) &= \sum_{i=1}^{r} \rho_i(s(t)) \\
&\quad \times \left[C_i x(t) + C_{d1i} x(t-\tau_1(t)) \right. \\
&\quad \left. + C_{d2i} x(t-\tau_2(t)) + D_i v(t)\right] dt, \\
z(t) &= \sum_{i=1}^{r} \rho_i(s(t)) \\
&\quad \times \left[L_i x(t) + L_{d1i} x(t-\tau_1(t)) \right. \\
&\quad \left. + L_{d2i} x(t-\tau_2(t))\right], \\
x(t) &= \varphi(t), \quad t \in [-\max(h_1, h_2), 0],
\end{aligned} \tag{8}
$$

where

$$
\begin{aligned}
\rho_i(s(t)) &= \frac{\overline{\omega}_i(s(t))}{\sum_{j=1}^{r} \overline{\omega}_j(s(t))}, \\
\overline{\omega}_i(s(t)) &= \prod_{j=1}^{g} \mu_{ij}(s_j(t));
\end{aligned} \tag{9}
$$

using the fuzzy theory, it is easy to see that, for all t,

$$
\begin{aligned}
&\rho_i(s(t)) \geq 0, \quad i = 1, 2, \ldots, r, \\
&\sum_{i=1}^{r} h_i(s(t)) = 1.
\end{aligned} \tag{10}
$$

Then, we consider the following fuzzy filters:

$$
\begin{aligned}
d\widehat{x}(t) &= \sum_{i=1}^{r} \rho_i(s(t)) \left[A_{fi} \widehat{x}(t)\, dt + B_{fi} dy(t)\right], \\
\widehat{z}(t) &= \sum_{i=1}^{r} \rho_i(s(t)) \left[L_{fi} \widehat{x}(t)\right],
\end{aligned} \tag{11}
$$

in which, the fuzzy rule has the same representation as in (1)–(4). Now we consider $\widehat{x}(t) \in \mathbf{R}^n$ and $\widehat{z}(t) \in \mathbf{R}^l$. The matrixes A_{fi}, B_{fi}, and L_{fi} are the filters need to be determined.

Let $\xi(t) = [x(t)^T \ \ \widehat{x}(t)^T]^T$, $\widetilde{z}(t) = z(t) - \widehat{z}(t)$.

For convenience, the filtering error dynamic system can be written as

$$
\begin{aligned}
&\left(\widetilde{\Sigma}\right): d\xi(t) \\
&= \left[\left(\widetilde{A} + \Delta\widetilde{A}(t)\right)\xi(t) \right. \\
&\quad + \left(\widetilde{A}_{d1} + \Delta\widetilde{A}_{d1}(t)\right) G\xi(t-\tau_1(t)) \\
&\quad \left. + \left(\widetilde{A}_{d2} + \Delta\widetilde{A}_{d2}(t)\right) G\xi(t-\tau_2(t)) + \widetilde{B} v(t)\right] dt \\
&\quad + \left[\left(\widetilde{H} + \Delta\widetilde{H}(t)\right)\xi(t) + \left(\widetilde{H}_{d1} + \Delta\widetilde{H}_{d1}(t)\right)\right. \\
&\quad \times G\xi(t-\tau_1(t)) \\
&\quad \left. + \left(\widetilde{H}_{d2} + \Delta\widetilde{H}_{d2}(t)\right) G\xi(t-\tau_2(t))\right] d\omega(t), \\
&\widetilde{z}(t) = \widetilde{L}\xi(t) + \overline{L}_{d1} G\xi(t-\tau_1(t)) \\
&\quad + \overline{L}_{d2} G\xi(t-\tau_2(t)),
\end{aligned} \tag{12}
$$

where

$$
\widetilde{A} = \begin{bmatrix} \overline{A} & 0 \\ \overline{B}_f \overline{C} & \overline{A}_f \end{bmatrix}, \qquad \widetilde{A}_{d1} = \begin{bmatrix} \overline{A}_{d1} \\ \overline{B}_f \overline{C}_{d1} \end{bmatrix},
$$

$$
\widetilde{A}_{d2} = \begin{bmatrix} \overline{A}_{d2} \\ \overline{B}_f \overline{C}_{d2} \end{bmatrix}, \qquad \widetilde{H} = \begin{bmatrix} \overline{H} & 0 \\ 0 & 0 \end{bmatrix},
$$

$$
\widetilde{H}_{d1} = \begin{bmatrix} \overline{H}_{d1} \\ 0 \end{bmatrix}, \qquad \widetilde{H}_{d2} = \begin{bmatrix} \overline{H}_{d2} \\ 0 \end{bmatrix},
$$

$$
\widetilde{B} = \begin{bmatrix} \overline{B} \\ \overline{B}_f \overline{D} \end{bmatrix}, \qquad \Delta\widetilde{A}(t) = \begin{bmatrix} \Delta\overline{A}(t) & 0 \\ 0 & 0 \end{bmatrix},
$$

$$
\Delta\widetilde{A}_{d1}(t) = \begin{bmatrix} \Delta\overline{A}_{d1}(t) \\ 0 \end{bmatrix}, \qquad \Delta\widetilde{A}_{d2}(t) = \begin{bmatrix} \Delta\overline{A}_{d2}(t) \\ 0 \end{bmatrix},
$$

$$
\Delta\widetilde{H}(t) = \begin{bmatrix} \Delta\overline{H}(t) & 0 \\ 0 & 0 \end{bmatrix}, \qquad \Delta\widetilde{H}_{d1}(t) = \begin{bmatrix} \Delta\overline{H}_{d1}(t) \\ 0 \end{bmatrix},
$$

$$
\Delta\widetilde{H}_{d2}(t) = \begin{bmatrix} \Delta\overline{H}_{d2}(t) \\ 0 \end{bmatrix}, \qquad \overline{A} = \sum_{i=1}^{r} \rho_i(s(t)) A_i,
$$

$$
\overline{A}_{d1} = \sum_{i=1}^{r} \rho_i(s(t)) A_{d1i}, \qquad \overline{A}_{d2} = \sum_{i=1}^{r} \rho_i(s(t)) A_{d2i},
$$

$$
\overline{H} = \sum_{i=1}^{r} \rho_i(s(t)) H_i, \qquad \overline{H}_{d1} = \sum_{i=1}^{r} \rho_i(s(t)) H_{d1i},
$$

$$
\overline{H}_{d2} = \sum_{i=1}^{r} \rho_i(s(t)) H_{d2i}, \qquad \overline{C} = \sum_{i=1}^{r} \rho_i(s(t)) C_i,
$$

$$
\overline{C}_{d1} = \sum_{i=1}^{r} \rho_i(s(t)) C_{d1i}, \qquad \overline{C}_{d2} = \sum_{i=1}^{r} \rho_i(s(t)) C_{d2i},
$$

$$
\overline{B} = \sum_{i=1}^{r} \rho_i(s(t)) B_i, \qquad \overline{D} = \sum_{i=1}^{r} \rho_i(s(t)) D_i,
$$

$$
\widetilde{L} = \left[\overline{L} \ \ -\overline{L}_f\right], \qquad G = [I \ \ 0],
$$

$$
\overline{A}_f = \sum_{i=1}^{r} \rho_i(s(t)) A_{fi}, \qquad \overline{B}_f = \sum_{i=1}^{r} \rho_i(s(t)) B_{fi},
$$

$$
\overline{L}_f = \sum_{i=1}^{r} \rho_i(s(t)) L_{fi},
$$

$$
\overline{L} = \sum_{i=1}^{r} \rho_i(s(t)) L_i, \qquad \overline{L}_{d1} = \sum_{i=1}^{r} \rho_i(s(t)) L_{d1i},
$$

$$\begin{aligned}
\overline{L}_{d2} &= \sum_{i=1}^{r} \rho_i (s(t)) L_{d2i},\\
\Delta\overline{A}(t) &= \sum_{i=1}^{r} \rho_i (s(t)) \Delta A_i(t),\\
\Delta\overline{A}_{d1}(t) &= \sum_{i=1}^{r} \rho_i (s(t)) \Delta A_{d1i}(t),\\
\Delta\overline{H}(t) &= \sum_{i=1}^{r} \rho_i (s(t)) \Delta H_i(t),\\
\Delta\overline{H}_{d1}(t) &= \sum_{i=1}^{r} \rho_i (s(t)) \Delta H_{d1i}(t),\\
\Delta\overline{A}_{d2}(t) &= \sum_{i=1}^{r} \rho_i (s(t)) \Delta A_{d2i}(t),\\
\Delta\overline{H}_{d2}(t) &= \sum_{i=1}^{r} \rho_i (s(t)) \Delta H_{d2i}(t).
\end{aligned} \tag{13}$$

The purpose of this work is to design a sets of fuzzy filters in the form of (11) such that for any scalar $0 \le h_1$, $0 \le h_2$ and a prescribed level of noise attenuation $\gamma > 0$, the filtering error system $(\widetilde{\Sigma})$ is mean-square stable, and the error system $(\widetilde{\Sigma})$ satisfies H_∞ performance.

Now, we introduce the following definitions and lemmas, which help to complete the proof of the main results.

Definition 1. The system (Σ) is said to be robust stochastic mean-square stable if there exists $\delta(\varepsilon) > 0$ for any $\varepsilon > 0$ such that

$$\mathsf{E}\left(\|x(t)\|^2\right) < \varepsilon, \quad t > 0, \tag{14}$$

when $\sup_{-h\le s\le 0}\mathsf{E}(\|\varphi(s)\|^2) < \delta(\varepsilon)$, for any uncertain variables. In addition,

$$\lim_{t\to\infty} \mathsf{E}\left(\|x(t)\|^2\right) = 0, \tag{15}$$

for any initial conditions.

Definition 2. The robust stochastic mean-square stable system $(\widetilde{\Sigma})$ is said to satisfy the H_∞ performance; for the given scalar $\gamma > 0$ and any nonzero $v(t) \in L_2[0,\infty)$, the system $(\widetilde{\Sigma})$ satisfies

$$\|z(t)\|_{E_2} < \gamma \|v(t)\|_2, \tag{16}$$

for any uncertain variables, where

$$\|z(t)\|_{E_2} = \left(\mathsf{E}\left\{\int_0^\infty |z(t)|^2 dt\right\}\right)^{1/2}. \tag{17}$$

Lemma 3. *For the given matrices D, E, and F with $F^TF \le I$ and positive scalar $\varepsilon > 0$, the following inequality holds:*

$$DFE + (DFE)^T \le \varepsilon DD^T + \varepsilon^{-1}E^TE. \tag{18}$$

3. Robust Stochastic Stabile

First, we derive the robust stochastic mean-square stochastic conditions and the H_∞ conditions for system $(\widetilde{\Sigma})$. Defining the following variables for convenience:

$$\begin{aligned}
\Phi(t) &= \left(\overline{A} + \Delta\overline{A}(t)\right)\xi(t)\\
&\quad + \left(\overline{A}_{d1} + \Delta\overline{A}_{d1}(t)\right)G\xi\left(t-\tau_1(t)\right)\\
&\quad + \left(\overline{A}_{d2} + \Delta\overline{A}_{d2}(t)\right)G\xi\left(t-\tau_2(t)\right) + \overline{B}v(t),\\
g(t) &= \left(\overline{H} + \Delta\overline{H}(t)\right)\xi(t)\\
&\quad + \left(\overline{H}_{d1} + \Delta\overline{H}_{d1}(t)\right)G\xi\left(t-\tau_1(t)\right)\\
&\quad + \left(\overline{H}_{d2} + \Delta\overline{H}_{d2}(t)\right)G\xi\left(t-\tau_2(t)\right).
\end{aligned} \tag{19}$$

Theorem 4. *For given scalars $0 \le h_1$, $0 \le h_2$, the filtering error system $(\widetilde{\Sigma})$ is robust stochastic mean-square stables and* (16) *is satisfied if there exist matrices $P = P^T > 0$, $Q_i = Q_i^T > 0$, $R_i = R_i^T > 0$, N_i, M_i, $i = 1,2$, and $Z_j = Z_j^T > 0$, $j = 1,\ldots,4$, such that the following matrix inequalities hold:*

$$\Psi = \begin{bmatrix} \Omega & \Psi_{12} & \Psi_{13} \\ * & \Psi_{22} & \mathbf{0} \\ * & * & \Psi_{33} \end{bmatrix} < 0, \tag{20}$$

where

$$\Omega = \begin{bmatrix}
\Omega_{11} & 0 & 0 & \Omega_{14} & \Omega_{15} & 0 & 0 & P\widetilde{B} \\
* & \Omega_{22} & 0 & N_2 & M_2 & 0 & 0 & 0 \\
* & * & \Omega_{33} & 0 & 0 & 0 & 0 & 0 \\
* & * & * & \Omega_{44} & 0 & 0 & 0 & 0 \\
* & * & * & * & \Omega_{55} & 0 & 0 & 0 \\
* & * & * & * & * & -\dfrac{R_1}{h_1} & 0 & 0 \\
* & * & * & * & * & * & -\dfrac{R_2}{h_2} & 0 \\
* & * & * & * & * & * & * & -\gamma^2 I
\end{bmatrix},$$

$$\Psi_{12} = \left[\widetilde{N}_1 \;\; \widetilde{N}_2 \;\; h_1\widetilde{N}_1 \;\; h_1\widetilde{N}_2 \;\; \widetilde{M}_1 \;\; \widetilde{M}_2 \;\; h_2\widetilde{M}_1 \;\; h_2\widetilde{M}_2\right],$$

$$\Psi_{22} = \operatorname{diag}\left\{-Z_3, -Z_3, -h_1Z_1, -h_1Z_1, -Z_4, -Z_4, -h_2Z_2, -h_2Z_2\right\},$$

$$\Psi_{13} = \left[\check{A}G^TU_1 \;\; \check{H}G^TU_2 \;\; \check{H}P \;\; \check{L}\right], \qquad \Psi_{33} = \operatorname{diag}\left\{-U_1, -U_2, -P, -I\right\},$$

$$\Omega_{11} = P\left(\widetilde{A} + \Delta\widetilde{A}(t)\right) + \left(\widetilde{A} + \Delta\widetilde{A}(t)\right)^T P + G^T\left(Q_1 + Q_2 + h_1R_1 + h_2R_2\right)G,$$

$$\Omega_{14} = P\left(\widetilde{A}_{d1} + \Delta\widetilde{A}_{d1}(t)\right) + G^TN_1^T, \qquad \Omega_{15} = P\left(\widetilde{A}_{d2} + \Delta\widetilde{A}_{d2}(t)\right) + G^TM_1^T,$$

$$\Omega_{22} = -Q_2 - N_2 - N_2^T, \qquad \Omega_{33} = -Q_2 - M_2 - M_2^T, \qquad \Omega_{44} = -N_1 - N_1^T, \qquad \Omega_{55} = -M_1 - M_1^T,$$

$$\widetilde{N}_1 = \left[0 \;\; 0 \;\; 0 \;\; N_1^T \;\; 0 \;\; 0 \;\; 0 \;\; 0\right]^T, \qquad \widetilde{M}_1 = \left[0 \;\; 0 \;\; 0 \;\; 0 \;\; M_1^T \;\; 0 \;\; 0 \;\; 0\right]^T,$$

$$\widetilde{N}_2 = \left[0 \;\; N_2^T \;\; 0 \;\; 0 \;\; 0 \;\; 0 \;\; 0 \;\; 0\right]^T, \qquad \widetilde{M}_2 = \left[0 \;\; 0 \;\; M_2^T \;\; 0 \;\; 0 \;\; 0 \;\; 0 \;\; 0\right]^T,$$

$$\check{A} = \left[\widetilde{A}^T + \Delta\widetilde{A}^T(t) \;\; 0 \;\; 0 \;\; \widetilde{A}_{d1}^T + \Delta\widetilde{A}_{d1}^T(t) \;\; \widetilde{A}_{d2}^T + \Delta\widetilde{A}_{d2}^T(t) \;\; 0 \;\; 0 \;\; \widetilde{B}^T\right]^T,$$

$$\check{H} = \left[\widetilde{H}^T + \Delta\widetilde{H}^T(t) \;\; 0 \;\; 0 \;\; \widetilde{H}_{d1}^T + \Delta\widetilde{H}_{d1}^T(t) \;\; \widetilde{H}_{d2}^T + \Delta\widetilde{H}_{d2}^T(t) \;\; 0 \;\; 0 \;\; 0\right]^T,$$

$$\check{L} = \left[\widetilde{L}^T \;\; 0 \;\; 0 \;\; \overline{L}_{d1}^T \;\; \overline{L}_{d2}^T \;\; 0 \;\; 0 \;\; 0\right]^T, \qquad U_1 = h_1Z_1 + h_2Z_2, \qquad U_2 = h_1Z_3 + H_2Z_4. \tag{21}$$

Proof. Define the following Lyapunov-Krasovskii candidate for system $(\widetilde{\Sigma})$:

$$\begin{aligned}
&V(\xi(t), t)\\
&= \xi^T(t)P\xi(t) + \int_{t-h_1}^{t}\xi^T(s)G^TQ_1G\xi(s)\,ds\\
&\quad + \int_{t-h_2}^{t}\xi^T(s)G^TQ_2G\xi(s)\,ds\\
&\quad + \int_{-h_1}^{0}\int_{t+\theta}^{t}\xi^T(s)G^TR_1G\xi(s)\,ds\,d\theta\\
&\quad + \int_{-h_2}^{0}\int_{t+\theta}^{t}\xi^T(s)G^TR_2G\xi(s)\,ds\,d\theta\\
&\quad + \int_{-h_1}^{0}\int_{t+\beta}^{t}\Phi^T(s)G^TZ_1G\Phi(s)\,ds\,d\beta\\
&\quad + \int_{-h_2}^{0}\int_{t+\beta}^{t}\Phi^T(s)G^TZ_2G\Phi(s)\,ds\,d\beta\\
&\quad + \int_{-h_1}^{0}\int_{t+\beta}^{t}g^T(s)G^TZ_3Gg(s)\,ds\,d\beta\\
&\quad + \int_{-h_2}^{0}\int_{t+\beta}^{t}g^T(s)G^TZ_4Gg(s)\,ds\,d\beta.
\end{aligned} \tag{22}$$

When $\nu(t) = 0$,

$$dV(\xi(t), t) = \mathbf{L}V(\xi(t), t) + 2\xi^T(t)Pg(t)\,d\omega(t). \tag{23}$$

By the Newton-Leibnitz formula, we can get the following equations for any matrices N_i, M_i, $i = 1, 2$ with any appropriate dimensions:

$$\begin{aligned}
&2\eta^T(t)\overline{N}_1G\left[\xi(t) - \xi\left(t - \tau_1(t)\right) - \int_{t-\tau_1(t)}^{t}\Phi(s)\,ds\right.\\
&\qquad\left. - \int_{t-\tau_1(t)}^{t}g(s)\,d\omega(s)\right] = 0,\\
&2\eta^T(t)\overline{N}_2G\left[\xi\left(t - \tau_1(t)\right) - \xi\left(t - h_1\right)\right.\\
&\qquad\left. - \int_{t-h_1}^{t-\tau_1(t)}\Phi(s)\,ds - \int_{t-h_1}^{t-\tau_1(t)}g(s)\,d\omega(s)\right] = 0,\\
&2\eta^T(t)\overline{M}_1G\left[\xi(t) - \xi\left(t - \tau_2(t)\right) - \int_{t-\tau_2(t)}^{t}\Phi(s)\,ds\right.\\
&\qquad\left. - \int_{t-\tau_2(t)}^{t}g(s)\,d\omega(s)\right] = 0,
\end{aligned}$$

$$
\begin{aligned}
&2\eta^T(t)\overline{M}_2G\Big[\xi(t-\tau_2(t))-\xi(t-h_2)\\
&\qquad-\int_{t-h_2}^{t-\tau_2(t)}\Phi(s)\,ds-\int_{t-h_2}^{t-\tau_2(t)}g(s)\,d\omega(s)\Big]=0,\\
&\tau_1(t)\eta^T(t)\overline{N}_1Z_1^{-1}\overline{N}_1^T\eta(t)\\
&\quad-\int_{t-\tau_1(t)}^{t}\eta^T(t)\overline{N}_1Z_1^{-1}\overline{N}_1^T\eta(t)\,ds=0,\\
&\tau_2(t)\eta^T(t)\overline{M}_1Z_2^{-1}\overline{M}_1^T\eta(t)\\
&\quad-\int_{t-\tau_2(t)}^{t}\eta^T(t)\overline{M}_1Z_2^{-1}\overline{M}_1^T\eta(t)\,ds=0,\\
&(h_1-\tau_1(t))\eta^T(t)\overline{N}_2Z_1^{-1}\overline{N}_1^T\eta(t)\\
&\quad-\int_{t-h_1}^{t-\tau_1(t)}\eta^T(t)\overline{N}_1Z_1^{-1}\overline{N}_1^T\eta(t)\,ds=0,\\
&(h_2-\tau_2(t))\eta^T(t)\overline{M}_2Z_2^{-1}\overline{M}_1^T\eta(t)\\
&\quad-\int_{t-h_2}^{t-\tau_2(t)}\eta^T(t)\overline{M}_2Z_2^{-1}\overline{M}_1^T\eta(t)\,ds=0,
\end{aligned}
\tag{24}
$$

where

$$
\begin{aligned}
\overline{N}_1&=\begin{bmatrix}0&0&0&N_1^T&0&0&0\end{bmatrix}^T,\\
\overline{N}_2&=\begin{bmatrix}0&N_2^T&0&0&0&0&0\end{bmatrix}^T,\\
\overline{M}_1&=\begin{bmatrix}0&0&0&0&M_1^T&0&0\end{bmatrix}^T,\\
\overline{M}_2&=\begin{bmatrix}0&0&M_2^T&0&0&0&0\end{bmatrix}^T,
\end{aligned}
\tag{25}
$$

and $\eta(t)$ is a new vector defined as follows:

$$
\eta^T(t)=\left[\xi^T(t)\ \ \xi^T(t-h_1)G^T\ \ \xi^T(t-h_2)G^T\ \ \xi^T(t-\tau_1(t))G^T\ \xi^T(t-\tau_2(t))G^T\ \ \left(\int_{t-h_1}^{t}\xi(s)\,ds\right)^TG^T\ \ \left(\int_{t-h_2}^{t}\xi(s)\,ds\right)^TG^T\ \right].
\tag{26}
$$

Using the above formulas (24) and Lemma 3, it can be seen that

$$
\begin{aligned}
&\mathbf{L}V(\xi(t),t)\\
&\quad=2\xi^T(t)P\Phi(t)+g^T(t)Pg(t)\\
&\qquad+\xi^T(t)G^TQ_1G\xi(t)+\xi^T(t)G^TQ_2G\xi(t)\\
&\qquad-\xi^T(t-h_1)G^TQ_1G\xi(t-h_1)\\
&\qquad-\xi^T(t-h_2)G^TQ_2G\xi(t-h_2)+h_1\Phi^T(t)G^TZ_1G\Phi(t)\\
&\qquad+h_1\xi^T(t)G^TR_1G\xi(t)+h_2\xi^T(t)G^TR_2G\xi(t)\\
&\qquad+h_2\Phi^T(t)G^TZ_2G\Phi(t)-\int_{t-h_1}^{t}\xi^T(s)G^TR_1G\xi(s)\,ds\\
&\qquad-\int_{t-h_2}^{t}\xi^T(s)G^TR_2G\xi(s)\,ds+h_1g^T(t)G^TZ_3Gg(t)\\
&\qquad-\int_{t-h_1}^{t}\Phi^T(s)G^TZ_1G\Phi(s)\,ds\\
&\qquad-\int_{t-h_2}^{t}\Phi^T(s)G^TZ_2G\Phi(s)\,ds+h_2g^T(t)G^TZ_4Gg(t)\\
&\qquad-\int_{t-h_1}^{t}g^T(s)G^TZ_3Gg(s)\,ds\\
&\qquad-\int_{t-h_2}^{t}g^T(s)G^TZ_4Gg(s)\,ds\\
&\quad\le\eta^T(t)\Big[\overline{\Omega}+\overline{N}_1Z_3^{-1}\overline{N}_1^T\\
&\qquad+\widehat{H}\left(G^Th_1Z_3G+G^Th_2Z_4G+P\right)\widehat{H}\\
&\qquad+\widehat{A}G^T(h_1Z_1+h_2Z_2)G\widehat{A}^T+\overline{N}_2Z_3^{-1}\overline{N}_2^T\\
&\qquad+h_1\overline{N}_1Z_1^{-1}\overline{N}_1^T+h_1\overline{N}_2Z_1^{-1}\overline{N}_2^T+h_2\overline{M}_1Z_2^{-1}\overline{M}_1^T\\
&\qquad+h_2\overline{M}_2Z_2^{-1}\overline{M}_2^T+\overline{M}_1Z_4^{-1}\overline{M}_1^T+\overline{M}_2Z_4^{-1}\overline{M}_2^T\Big]\eta(t)\\
&\qquad-\int_{t-\tau_1(t)}^{t}\left[\eta^T(t)\overline{N}_1+\Phi^T(s)G^TZ_1\right]Z_1^{-1}\\
&\qquad\quad\times\left[Z_1G\Phi(s)+\overline{N}_1^T\eta(t)\right]ds\\
&\qquad-\int_{t-h_1}^{t-\tau_1(t)}\left[\eta^T(t)\overline{N}_2+\Phi^T(s)G^TZ_1\right]Z_1^{-1}\\
&\qquad\quad\times\left[Z_1G\Phi(s)+\overline{N}_2^T\eta(t)\right]ds\\
&\qquad-\int_{t-\tau_2(t)}^{t}\left[\eta^T(t)\overline{M}_1+\Phi^T(s)G^TZ_2\right]Z_2^{-1}\\
&\qquad\quad\times\left[Z_2G\Phi(s)+\overline{M}_1^T\eta(t)\right]ds\\
&\qquad-\int_{t-h_2}^{t-\tau_2(t)}\left[\eta^T(t)\overline{M}_2+\Phi^T(s)G^TZ_2\right]Z_2^{-1}\\
&\qquad\quad\times\left[Z_2G\Phi(s)+\overline{M}_2^T\eta(t)\right]ds
\end{aligned}
$$

$$
\begin{aligned}
&+\left(\int_{t-\tau_1(t)}^{t} g(s)\,d\omega(s)\right)^T G^T Z_3 G\left(\int_{t-\tau_1(t)}^{t} g(s)\,d\omega(s)\right)\\
&-\int_{t-\tau_1(t)}^{t} g^T(s)\,G^T Z_3 G g(s)\,ds\\
&+\left(\int_{t-h_1}^{t-\tau_1(t)} g(s)\,d\omega(s)\right)^T G^T Z_3 G\left(\int_{t-h_1}^{t-\tau_1(t)} g(s)\,d\omega(s)\right)\\
&-\int_{t-h_1}^{t-\tau_1(t)} g^T(s)\,G^T Z_3 G g(s)\,ds\\
&+\left(\int_{t-\tau_2(t)}^{t} g(s)\,d\omega(s)\right)^T G^T Z_4 G\left(\int_{t-\tau_2(t)}^{t} g(s)\,d\omega(s)\right)\\
&-\int_{t-\tau_2(t)}^{t} g^T(s)\,G^T Z_4 G g(s)\,ds\\
&+\left(\int_{t-h_2}^{t-\tau_2(t)} g(s)\,d\omega(s)\right)^T G^T Z_4 G\left(\int_{t-h_2}^{t-\tau_1(t)} g(s)\,d\omega(s)\right)\\
&-\int_{t-h_2}^{t-\tau_1(t)} g^T(s)\,G^T Z_4 G g(s)\,ds,
\end{aligned}
\tag{27}
$$

where

$$
\overline{\Omega}=\begin{bmatrix}
\Omega_{11} & 0 & 0 & \Omega_{14} & \Omega_{15} & 0 & 0\\
* & \Omega_{22} & 0 & 0 & N_2 & M_2 & 0\\
* & * & \Omega_{33} & 0 & 0 & 0 & 0\\
* & * & * & \Omega_{44} & 0 & 0 & 0\\
* & * & * & * & \Omega_{55} & 0 & 0\\
* & * & * & * & * & -\dfrac{R_1}{h_1} & 0\\
* & * & * & * & * & * & -\dfrac{R_2}{h_2}
\end{bmatrix},
\tag{28}
$$

$$
\widehat{A}=\left[\left(\widetilde{A}+\Delta\widetilde{A}(t)\right)^T\ \ 0\ \ 0\ \ \left(\widetilde{A}_{d1}+\Delta\widetilde{A}_{d1}(t)\right)^T\ \ \left(\widetilde{A}_{d2}+\Delta\widetilde{A}_{d2}(t)\right)^T\ \ 0\ \ 0\ \right]^T,
$$

$$
\widehat{H}=\left[\left(\widetilde{H}+\Delta\widetilde{H}(t)\right)^T\ \ 0\ \ 0\ \ \left(\widetilde{H}_{d1}+\Delta\widetilde{H}_{d1}(t)\right)^T\ \ \left(\widetilde{H}_{d2}+\Delta\widetilde{H}_{d2}(t)\right)^T\ \ 0\ \ 0\ \right]^T.
$$

Note that

$$
\begin{aligned}
&\mathsf{E}\left(\int_{t-\tau_1(t)}^{t} g^T(s)\,G^T Z_3 G g(s)\,ds\right)\\
&\quad=\mathsf{E}\left(\left(\int_{t-\tau_1(t)}^{t} g^T(s)\,d\omega(s)\right)^T\right.\\
&\qquad\left.\times G^T Z_3 G\left(\int_{t-\tau_1(t)}^{t} g^T(s)\,d\omega(s)\right)\right),\\
&\mathsf{E}\left(\int_{t-h_1}^{t-\tau_1(t)} g^T(s)\,G^T Z_3 G g(s)\,ds\right)\\
&\quad=\mathsf{E}\left(\left(\int_{t-h_1}^{t-\tau_1(t)} g^T(s)\,d\omega(s)\right)^T\right.\\
&\qquad\left.\times G^T Z_3 G\left(\int_{t-h_1}^{t-\tau_1(t)} g^T(s)\,d\omega(s)\right)\right),\\
&\mathsf{E}\left(\int_{t-\tau_2(t)}^{t} g^T(s)\,G^T Z_4 G g(s)\,ds\right)\\
&\quad=\mathsf{E}\left(\left(\int_{t-\tau_2(t)}^{t} g^T(s)\,d\omega(s)\right)^T\right.\\
&\qquad\left.\times G^T Z_4 G\left(\int_{t-\tau_2(t)}^{t} g^T(s)\,d\omega(s)\right)\right),\\
&\mathsf{E}\left(\int_{t-h_2}^{t-\tau_2(t)} g^T(s)\,G^T Z_4 G g(s)\,ds\right)\\
&\quad=\mathsf{E}\left(\left(\int_{t-h_2}^{t-\tau_2(t)^T} g^T(s)\,d\omega(s)\right)\right.\\
&\qquad\left.\times G^T Z_4 G\left(\int_{t-h_2}^{t-\tau_2(t)} g^T(s)\,d\omega(s)\right)\right).
\end{aligned}
\tag{29}
$$

So, the mathematical expectation of the last eight parts of (27) equals 0. And applying the Schur complement to (3), we can derive the following inequality with $\nu(t)=0$:

$$
\begin{aligned}
&\overline{\Omega}+\overline{N}_1 Z_3^{-1}\overline{N}_1^T+\widehat{H}\left(G^T h_1 Z_3 G+G^T h_2 Z_4 G+P\right)\widehat{H}\\
&+\widehat{A}G^T\left(h_1 Z_1+H_2 Z_2\right)G\widehat{A}^T+\overline{N}_2 Z_3^{-1}\overline{N}_2^T\\
&+h_1\overline{N}_1 Z_1^{-1}\overline{N}_1^T+h_1\overline{N}_2 Z_1^{-1}\overline{N}_2^T+h_2\overline{M}_1 Z_2^{-1}\overline{M}_1^T\\
&+h_2\overline{M}_2 Z_2^{-1}\overline{M}_2^T+\overline{M}_1 Z_4^{-1}\overline{M}_1^T+\overline{M}_2 Z_4^{-1}\overline{M}_2^T<0.
\end{aligned}
\tag{30}
$$

From (27), (29), and (30), we can see that

$$\mathbf{L}V(\xi(t),t) < 0, \tag{31}$$

which, by Definition 2.1 [37, 38], ensures that system $(\widetilde{\Sigma})$ with $v(t) = 0$ is robustly stochastically stable. By Itô's formula, we can derive

$$\mathsf{E}(V(\xi(t),t)) = \mathsf{E}\left(\int_0^t \mathbf{L}V(\xi(s),s)\,ds\right). \tag{32}$$

Now, set a functional J_T as

$$J_T = \mathsf{E}\left(\int_0^T \left[z(t)^T z(t) - \gamma^2 v(t)^T v(t)\right] ds\right), \tag{33}$$

where $t > 0$. From (32) and (33), it is easy to show that

$$\begin{aligned} J_T &= \mathsf{E}\left(\int_0^T \left[z(t)^T z(t) - \gamma^2 v(t)^T v(t) + \mathbf{L}V(\xi(s),s)\right] ds\right) \\ &\quad - \mathsf{E}(V(\xi(t),t)) \\ &\le \mathsf{E}\left(\int_0^T \left[z(t)^T z(t) - \gamma^2 v(t)^T v(t) + \mathbf{L}V(\xi(s),s)\right] ds\right), \end{aligned} \tag{34}$$

for all $t > 0$. By using the Schur complement to (3), there is

$$z(t)^T z(t) - \gamma^2 v(t)^T v(t) + \mathbf{L}V(\xi(s),s) \le \overline{\eta}(t)\,\Psi\overline{\eta}(t) < 0, \tag{35}$$

where

$$\overline{\eta}^T(t) = \left[\xi^T(t)\ \ \xi^T(t-h_1)G^T\ \ \xi^T(t-h_2)G^T\ \ \xi^T(t-\tau_1(t))G^T\ \ \xi^T(t-\tau_2(t))G^T\ \ \left(\int_{t-h_1}^t {}^T\xi(s)\,ds\right)G^T\ \ \left(\int_{t-h_2}^t {}^T\xi(s)\,ds\right)G^T\ \ v(t)\ \right]. \tag{36}$$

It follows from (33) and (34) that

$$J(t) < 0, \tag{37}$$

for all $t > 0$, which implies that (10) is satisfied. This completes the proof. □

Remark 5. The Lyapunov functional (22) contains the information of the uppers bound of the delays; by such a choice, delay-dependent results are obtained.

4. Robust H_∞ Filter Design

In this section, a sufficient condition for the solvability of robust H_∞ filter problem for uncertain T-S fuzzy stochastic time-delay system is investigated. The main result is given in the following theorem by LMI form.

Theorem 6. *Consider the uncertain T-S fuzzy stochastic time-delay system (Σ). The robust H_∞ filtering problem is solvable with disturbance attenuation $\gamma > 0$ if there exist scalars $\varepsilon_i > 0$ and matrices $W > 0$, $X > 0$, $Q_i > 0$, $R_i > 0$, $i = 1, 2$; $Z_j > 0$, $j = 1, 2, 3, 4$; N_{1i}, N_{2i}, M_{1i}, M_{2i}, $i = 1, 2, 3, 4$; $\{\Gamma_i = \Gamma_i^T,\ 1 \le i \le r\}$, $\{\Pi_{ij},\ 1 \le i < j \le r\}$, such that the following LMIs hold:*

$$\begin{bmatrix} \Theta_{ii} - \Gamma_i + \varepsilon_i \Xi_i \Xi_i^T & \varrho_i \\ * & -\varepsilon_i \end{bmatrix} < 0, \quad (1 \le i \le r), \tag{38}$$

$$\begin{bmatrix} \Theta_{ij} + \Theta_{ji} - \Pi_{ij} - \Pi_{ij}^T + \varepsilon_i \Xi_i \Xi_i^T + \varepsilon_j \Xi_j \Xi_j^T & \varrho_i & \varrho_j \\ * & -\varepsilon_i & 0 \\ * & * & -\varepsilon_j \end{bmatrix} < 0, \quad (1 \le i < j \le r), \tag{39}$$

$$\begin{bmatrix} \Gamma_1 & \Pi_{12} & \cdots & \Pi_{1r} \\ * & \Gamma_2 & \cdots & \Pi_{2r} \\ \vdots & \vdots & \ddots & \vdots \\ * & * & \cdots & \Gamma_r \end{bmatrix} < 0, \tag{40}$$

$$X - W > 0, \tag{41}$$

where

$$\varrho_i^T = \left[K_{1i}^T W\ \ K_{1i}^T X\ \ \mathbf{0}_{1*15}\ \ K_{1i}^T U_1\ \ K_{2i}^T U_2\ \ K_{2i}^T X\ \ K_{2i}^T\right],$$

$$\Xi_i^T = \left[T_{1i}^T\ \ T_{1i}^T\ \ 0\ \ 0\ \ T_{2i}^T\ \ T_{3i}^T\ \ \mathbf{0}_{15*1}\right], \qquad \Theta_{ij} = \begin{bmatrix} \Theta_{11} & \Theta_{12} & \Theta_{13} \\ * & \Theta_{22} & \mathbf{0}_{8*8} \\ * & * & \Theta_{33} \end{bmatrix},$$

$$\Theta_{11} = \begin{bmatrix} \Lambda_{11} & \Lambda_{12} & 0 & 0 & \Lambda_{15} & \Lambda_{16} & 0 & 0 & \Lambda_{19} \\ * & \Lambda_{22} & 0 & 0 & \Lambda_{25} & \Lambda_{26} & 0 & 0 & \Lambda_{29} \\ * & * & \Lambda_{33} & 0 & \Lambda_{35} & \Lambda_{36} & 0 & 0 & 0 \\ * & * & * & \Lambda_{44} & 0 & 0 & 0 & 0 & 0 \\ * & * & * & * & -N_1 - N_1^T & 0 & 0 & 0 & 0 \\ * & * & * & * & * & -M_1 - M_1^T & 0 & 0 & 0 \\ * & * & * & * & * & * & -\dfrac{R_1}{h_1} & 0 & 0 \\ * & * & * & * & * & * & * & -\dfrac{R_2}{h_2} & 0 \\ * & * & * & * & * & * & * & * & -\gamma^2 I \end{bmatrix},$$

$$\Lambda_{11} = WA_i + A_i^T W + Q_1 + Q_2 + h_1 R_1 + h_2 R_2,$$

$$\Lambda_{12} = WA_i + A_i^T X + C_j^T \Phi_{1i}^T + \Phi_{2i}^T + Q_1 + Q_2 + h_1 R_1 + h_2 R_2,$$

$$\Lambda_{15} = N_1^T + WA_{d1i}, \quad \Lambda_{16} = M_1^T + WA_{d2i}, \quad \Lambda_{19} = WB_i, \quad \Lambda_{29} = XB_i + \Phi_{1i} D_j,$$

$$\Lambda_{22} = X^T A_i + \Phi_{1i} C_j + C_j^T \Phi_{1i}^T + A_i^T X + Q_1 + Q_2 + h_1 R_1 + h_2 R_2,$$

$$\Lambda_{25} = N_1^T + X^T A_{d1i} + \Phi_{1i} C_{d1j}, \quad \Lambda_{26} = M_1^T + X^T A_{d2i} + \Phi_{1i} C_{d2j},$$

$$\Lambda_{33} = -Q_1 - N_2 - N_2^T, \quad \Lambda_{35} = N_2, \quad \Lambda_{36} = M_2, \quad \Lambda_{44} = -Q_2 - M_2 - M_2^T,$$

$$\Theta_{12} = \begin{bmatrix} 0 & 0 & 0 & 0 & 0 & 0 & 0 & 0 \\ 0 & N_2 & 0 & h_2 N_2 & 0 & 0 & 0 & 0 \\ 0 & 0 & 0 & 0 & 0 & M_2 & 0 & h_2 M_2 \\ N_1 & 0 & h_1 N_1 & 0 & 0 & 0 & 0 & 0 \\ 0 & 0 & 0 & 0 & M_1 & 0 & h_2 M_1 & 0 \\ 0 & 0 & 0 & 0 & 0 & 0 & 0 & 0 \\ 0 & 0 & 0 & 0 & 0 & 0 & 0 & 0 \\ 0 & 0 & 0 & 0 & 0 & 0 & 0 & 0 \\ 0 & 0 & 0 & 0 & 0 & 0 & 0 & 0 \end{bmatrix},$$

$$\Theta_{22} = \operatorname{diag}\{-Z_3, -Z_3, -h_1 Z_1, -h_1 Z_1, -Z_4, -Z_4, -h_2 Z_2, -h_2 Z_2\},$$

$$\Theta_{13} = \begin{bmatrix} h_1 A_i^T Z_1 + H_2 A_i^T Z_2 & h_1 H_i Z_3 + h_2 H_i Z_4 & H_i^T X & H_i^T & L_i^T - \Phi_{3i}^T \\ h_1 A_i^T Z_1 + H_2 A_i^T Z_2 & h_1 H_i Z_3 + h_2 H_i Z_4 & H_i^T X & H_i^T & L_i^T \\ 0 & 0 & 0 & 0 & 0 \\ 0 & 0 & 0 & 0 & 0 \\ h_1 A_{d1i}^T Z_1 + H_2 A_{d1i}^T Z_2 & h_1 H_{d1i} Z_3 + h_2 H_{d1i} Z_4 & H_{d1i}^T X & H_{d1i}^T & 0 \\ h_1 A_{d2i}^T Z_1 + H_2 A_{d2i}^T Z_2 & h_1 H_{d2i} Z_3 + h_2 H_{d2i} Z_4 & H_{d2i}^T X & H_{d2i}^T & 0 \\ 0 & 0 & 0 & 0 & 0 \\ 0 & 0 & 0 & 0 & 0 \\ 0 & 0 & 0 & 0 & 0 \end{bmatrix},$$

$$\Theta_{33} = \operatorname{diag}\left\{-h_1 Z_1 - h_2 Z_2, -h_1 Z_3 - h_2 Z_4, \begin{bmatrix} -X & -I \\ * & -\Phi_4 \end{bmatrix}, -I\right\}. \tag{42}$$

When the LMIs (38)–(41) are feasible, there exist nonsingular matrices σ and β satisfying $\sigma\beta^T = I - XW^{-1}$. Under this condition, a desired time-dependent filter can be chosen as

$$L_{fi} = \Phi_{3i} W^{-1} \beta^{-T}, \quad i = 1, \ldots, r. \tag{43}$$

Proof. From the demonstration in [21], we know that $I - XW^T - 1$ is nonsingular. Therefore, there always exist nonsingular matrices σ and β such that $\sigma\beta^T = I - XW^{-1}$ holds. Then, we define the nonsingular matrices χ_1 and χ_2 as follows:

$$\chi_1 = \begin{bmatrix} W^{-1} & I \\ \beta^T & o \end{bmatrix}; \qquad \chi_2 = \begin{bmatrix} I & X \\ 0 & \sigma^T \end{bmatrix}. \tag{44}$$

Let $P = \chi_2 \chi_1^{-1}$; there is

$$P = \begin{bmatrix} X & \sigma \\ \sigma^T & \beta^{-1} W^{-1} (X_W) W^{-1} \beta^{-T} \end{bmatrix}, \tag{45}$$

which means that $P > 0$.

Now, using Lemma 3 and recalling (40), we can deduce that

$$\begin{aligned}
\kappa &= \sum_{i=1}^{r} \rho_i^2 (s(t)) \left[\Theta_{ii} + \varrho_i F_i(t) \Xi_i^T + \Xi_i F_i(t) \varrho_i^T\right] \\
&\quad + \sum_{i=1}^{r}\sum_{j>i}^{r} \rho_i (s(t)) \rho_j (s(t)) \\
&\qquad \times \left[\Theta_{ij} + \varrho_i F_i(t) \Xi_i^T + \Xi_i F_i(t) \varrho_i^T \right. \\
&\qquad\quad \left. + \Theta_{ji} + \varrho_i F_j(t) \Xi_j^T + \Xi_j F_j(t) \varrho_j^T\right] \\
&< \sum_{i=1}^{r} \rho_i^2 (s(t)) \left[\Theta_{ii} + \varepsilon_i^{-1} \varrho_i \varrho_i^T + \varepsilon_i \Xi_i \Xi_i^T\right] \\
&\quad + \sum_{i=1}^{r}\sum_{j>i}^{r} \rho_i (s(t)) \rho_j (s(t)) \left[\Theta_{ij} + \varepsilon_i^{-1} \varrho_i \varrho_i^T + \varepsilon_i \Xi_i \Xi_i^T \right. \\
&\qquad\quad \left. + \Theta_{ji} + \varepsilon_j^{-1} \varrho_j \varrho_j^T + \varepsilon_j \Xi_j \Xi_j^T\right] \\
&< \sum_{i=1}^{r} \rho_i^2 (s(t)) \Gamma_i + \sum_{i=1}^{r}\sum_{j>i}^{r} \rho_i (s(t)) \rho_j (s(t)) \left[\Pi_{ij} + \Pi_{ji}^T\right] \\
&= \begin{bmatrix} h_1(s(t))I \\ h_2(s(t))I \\ \vdots \\ h_r(s(t))I \end{bmatrix}^T \begin{bmatrix} \Gamma_1 & \Pi_{12} & \cdots & \Pi_{1r} \\ * & \Gamma_2 & \cdots & \Pi_{2r} \\ \vdots & \vdots & \ddots & \vdots \\ * & * & \cdots & \Gamma_r \end{bmatrix} \begin{bmatrix} h_1(s(t))I \\ h_2(s(t))I \\ \vdots \\ h_r(s(t))I \end{bmatrix} < 0.
\end{aligned} \tag{46}$$

Then, it is easy to see that

$$\begin{aligned}
&\left\{\operatorname{diag}\left(\chi_2^{-T}\begin{bmatrix} W^{-1} & 0 \\ 0 & I \end{bmatrix}, I, \ldots, I\right)\right\} \kappa \left\{\operatorname{diag}\left(\chi_2^{-T}\begin{bmatrix} W^{-1} & 0 \\ 0 & I \end{bmatrix}, I, \ldots, I\right)\right\} \\
&= \begin{bmatrix} \Omega & \Psi_{12} & \Psi_{13} \\ * & \Psi_{22} & \mathbf{0} \\ * & * & \Psi_{33} \end{bmatrix} < 0,
\end{aligned} \tag{47}$$

which is equivalent to (3). Therefore, the condition in Theorem 4 is satisfied when the LMIs in (38)–(41) hold. Finally, it can be concluded that the filtering error system $(\widetilde{\Sigma})$ is stochastically stable with H_∞ performance level γ. □

Remark 7. There is more than one time delay appear in the electric system, the network system, and so on. So, it makes sense to investigate the system containing two terms of time delays as shown in this paper. The model we consider here contains two terms of time-varying delay as $\tau_1(t)$ and $\tau_1(t)$ in the state $x(t)$. The method we use can be easily drawn back to the system that has only one time delay. Meanwhile, the result we get can be extended to the system that contains more delays at the same time by developing the Lyapunov function with $h_3, h_4, \ldots$ integral terms in the same way.

5. Numerical Example

In this section, we provide a numerical example to show the effectiveness of the results obtained in the previous section.

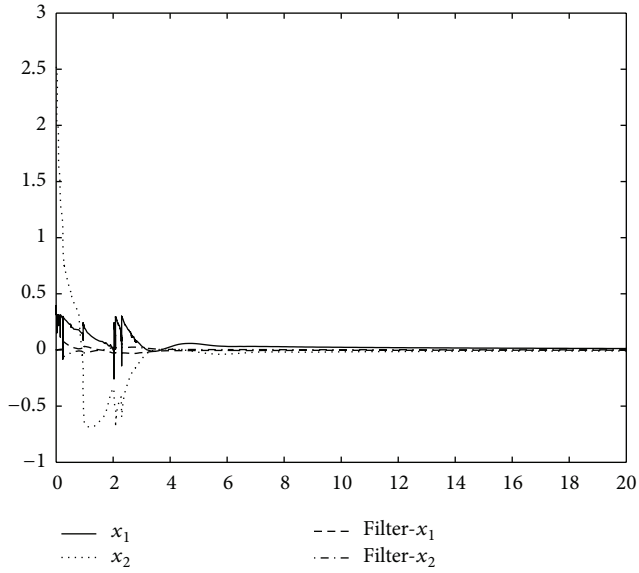

Figure 1: State responses of $x(t)$ and $\widehat{x}(t)$.

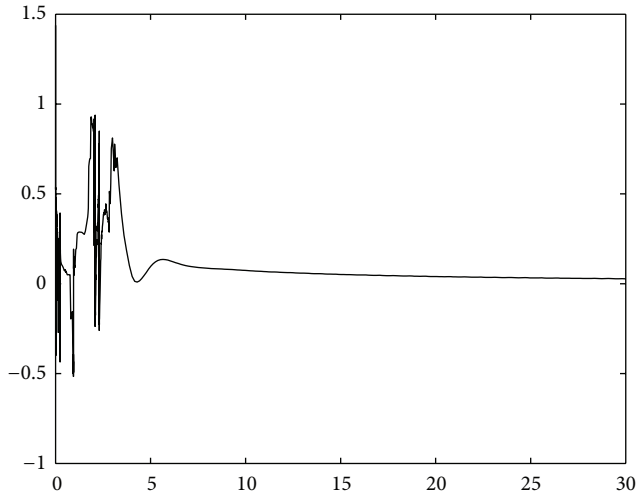

Figure 2: Responses of the signal $\widetilde{z}(t) = z(t) - \widehat{z}(t)$.

Example 1. Consider the T-S fuzzy stochastic system $(\widetilde{\Sigma})$ with model parameters given as follows:

$$A_1 = \begin{bmatrix} -1.9 & 0.4 \\ 0.2 & -1.1 \end{bmatrix}, \quad A_{d11} = \begin{bmatrix} -1.1 & 0.1 \\ -0.8 & -0.9 \end{bmatrix},$$

$$A_{d21} = \begin{bmatrix} -0.02 & 0.01 \\ 0.05 & -0.05 \end{bmatrix}, \quad H_1 = \begin{bmatrix} -0.04 & 0.1 \\ 0.03 & -0.05 \end{bmatrix},$$

$$H_{d11} = \begin{bmatrix} -0.01 & 0.02 \\ 0.01 & -0.05 \end{bmatrix}, \quad H_{d21} = \begin{bmatrix} -0.04 & 0.01 \\ 0.03 & -0.05 \end{bmatrix},$$

$$
\begin{aligned}
C_1 &= \begin{bmatrix}1 & -0.4\end{bmatrix}, \quad C_{d11} = \begin{bmatrix}-0.4 & 0.1\end{bmatrix},\\
C_{d21} &= \begin{bmatrix}-0.1 & -0.4\end{bmatrix}, \quad D_1 = 0.3,\\
L_1 &= \begin{bmatrix}1.0 & -0.5\end{bmatrix}, \quad L_{d11} = \begin{bmatrix}1 & -0.5\end{bmatrix},\\
L_{d21} &= \begin{bmatrix}1 & -0.5\end{bmatrix}, \quad A_2 = \begin{bmatrix}-2.1 & 0.2\\ 0.1 & -1.1\end{bmatrix},\\
A_{d12} &= \begin{bmatrix}-0.9 & 0.1\\ -1.1 & -1.2\end{bmatrix}, \quad A_{d22} = \begin{bmatrix}-0.04 & 0.05\\ 0.02 & -0.04\end{bmatrix},\\
H_2 &= \begin{bmatrix}-0.4 & 0.01\\ 0.03 & -0.05\end{bmatrix}, \quad H_{d12} = \begin{bmatrix}-0.05 & 0.01\\ 0.03 & -0.05\end{bmatrix},\\
H_{d22} &= \begin{bmatrix}-0.06 & 0.02\\ 0.01 & -0.05\end{bmatrix},\\
C_2 &= \begin{bmatrix}0.2 & -0.5\end{bmatrix}, \quad C_{d12} = \begin{bmatrix}-0.4 & 0.5\end{bmatrix},\\
C_{d22} &= \begin{bmatrix}-0.3 & -0.4\end{bmatrix}, \quad L_2 = \begin{bmatrix}-0.2 & 0.3\end{bmatrix},\\
L_{d12} &= \begin{bmatrix}-0.2 & -0.5\end{bmatrix}, \quad L_{d22} = \begin{bmatrix}-0.3 & -0.5\end{bmatrix}\\
B_1 &= \begin{bmatrix}1.0\\ -0.2\end{bmatrix}, \quad B_2 = \begin{bmatrix}0.3\\ 0.1\end{bmatrix}, \quad D_2 = -0.3,
\end{aligned}
\tag{48}
$$

and the parameter uncertainties are shown as

$$
\begin{aligned}
K_{11} &= \begin{bmatrix}1.0\\ -0.5\end{bmatrix}, \quad K_{12} = \begin{bmatrix}-0.2\\ 0.3\end{bmatrix},\\
K_{21} &= \begin{bmatrix}0.8\\ -0.1\end{bmatrix}, \quad K_{22} = \begin{bmatrix}-0.1\\ 0.4\end{bmatrix},\\
T_{11} &= \begin{bmatrix}0 & -0.3\end{bmatrix}, \quad T_{21} = \begin{bmatrix}-0.2 & 0.1\end{bmatrix}\\
T_{31} &= \begin{bmatrix}-0.5 & 0.1\end{bmatrix}, \quad T_{12} = \begin{bmatrix}0 & -0.3\end{bmatrix}\\
T_{22} &= \begin{bmatrix}0 & -0.1\end{bmatrix}, \quad T_{32} = \begin{bmatrix}-0.3 & -0.2\end{bmatrix}.
\end{aligned}
\tag{49}
$$

The two membership functions are, respectively, described as

$$
\begin{aligned}
h_1(x_1(t)) &= \left(1 - \frac{1}{1 + \exp(6x_1(t) + 2)}\right),\\
h_2(x_1(t)) &= 1 - h_1.
\end{aligned}
\tag{50}
$$

In this example, the noise attenuation level γ is set to $\gamma = 0.42$. From Theorem 6, it is to see that the robust H_∞ filtering problem is solvable for any $0 < h_1(t) \le 0.8$, $0 < h_2(t) \le 0.9$. Thus, a desired fuzzy H_∞ filter can be constructed as in the form of (11) with

$$
\left[\begin{array}{c|c|c} A_{f1} & B_{f1} & L_{f1} \\ \hline A_{f2} & B_{f2} & L_{f2} \end{array}\right] = \left[\begin{array}{cc|c|cc} -69.057 & 76.641 & -0.514 & -24.7515 & -26.0768 \\ 48.860 & 53.611 & 0.427 & & \\ \hline 46.823 & 58.857 & -0.083 & -76.7602 & -93.953 \\ -131.781 & -161.087 & 0.116 & & \end{array}\right].
\tag{51}
$$

The simulation results of the state response of the plant and the filter are given in Figure 1, where the initial condition is $x_0(t) = \begin{bmatrix}0.4 & 2.5\end{bmatrix}^T$, $\hat{x}_0(t) = \begin{bmatrix}0 & 0\end{bmatrix}^T$. Figure 2 shows the simulation results of the signal $z(t) - \hat{z}(t)$, and the exogenous disturbance input $v(t)$ is given by $v(t) = 12/(5 + 3.1t)$, $t \ge 0$, which belongs to $\mathscr{L}_2[0, \infty)$.

6. Conclusion

This paper has investigated the filter design problem for the uncertain T-S fuzzy stochastic system with time-varying delays. An LMI approach has been developed to design the fuzzy filter ensuring not only the robust stochastic mean-square stability but also a prescribed H_∞ performance level of the filtering error system for all admissible uncertainties. A numerical example has been provided to show the effectiveness of the proposed filter design methods.

Conflict of Interests

The authors declare that there is no conflict of interests regarding the publication of this paper.

Acknowledgment

This work is supported by the National Natural Science Foundation of China under Grant nos. 61203048 and 61203047.

References

[1] T. Takagi and M. Sugeno, "Fuzzy identification of systems and its applications to modeling and control," *IEEE Transactions on Systems, Man and Cybernetics*, vol. 15, no. 1, pp. 116–132, 1985.

[2] Y.-Y. Cao and P. M. Frank, "Analysis and synthesis of nonlinear time-delay systems via fuzzy control approach," *IEEE Transactions on Fuzzy Systems*, vol. 8, no. 2, pp. 200–211, 2000.

[3] K. Tanaka and M. Sano, "Robust stabilization problem of fuzzy control systems and its application to backing up control of a truck-trailer," *IEEE Transactions on Fuzzy Systems*, vol. 2, no. 2, pp. 119–134, 1994.

[4] W. Assawinchaichote, S. K. Nguang, and P. Shi, "H_∞ output feedback control design for uncertain fuzzy singularly perturbed systems: an LMI approach," *Automatica*, vol. 40, no. 12, pp. 2147–2152, 2004.

[5] C.-W. Chen, K. Yeh, K. R. Liu, and M.-L. Lin, "Applications of fuzzy control to nonlinear time-delay systems using the linear matrix inequality fuzzy Lyapunov method," *Journal of Vibration and Control*, vol. 18, pp. 1561–1574, 2012.

[6] G. Feng, "A survey on analysis and design of model-based fuzzy control systems," *IEEE Transactions on Fuzzy Systems*, vol. 14, no. 5, pp. 676–697, 2006.

[7] S.-W. Kau, H.-J. Lee, C.-M. Yang, C.-H. Lee, L. Hong, and C.-H. Fang, "Robust H_∞ fuzzy static output feedback control of T-S fuzzy systems with parametric uncertainties," *Fuzzy Sets and Systems*, vol. 158, no. 2, pp. 135–146, 2007.

[8] J. Lam and S. Zhou, "Dynamic output feedback H_∞ control of discrete-time fuzzy systems: a fuzzy-basis-dependent Lyapunov

function approach," *International Journal of Systems Science*, vol. 38, no. 1, pp. 25–37, 2007.

[9] C. Lin, Q.-G. Wang, T. H. Lee, and Y. He, "Design of observer-based H_∞ control for fuzzy time-delay systems," *IEEE Transactions on Fuzzy Systems*, vol. 16, no. 2, pp. 534–543, 2008.

[10] S. K. Nguang, P. Shi, and S. Ding, "Fault detection for uncertain fuzzy systems: an LMI approach," *IEEE Transactions on Fuzzy Systems*, vol. 15, no. 6, pp. 1251–1262, 2007.

[11] J. Qiu, G. Feng, and H. Gao, "Fuzzy-model-based piecewise H_∞ static-output-feedback controller design for networked nonlinear systems," *IEEE Transactions on Fuzzy Systems*, vol. 18, no. 5, pp. 919–934, 2010.

[12] B. Zhang, S. Zhou, and T. Li, "A new approach to robust and non-fragile H_∞ control for uncertain fuzzy systems," *Information Sciences*, vol. 177, no. 22, pp. 5118–5133, 2007.

[13] B. Zhang, W. X. Zheng, and S. Xu, "Passivity analysis and passive control of fuzzy systems with time-varying delays," *Fuzzy Sets and Systems*, vol. 174, no. 1, pp. 83–98, 2011.

[14] S. Zhou, T. Li, H. Shao, and W. X. Zheng, "Output feedback H_∞ control for uncertain discrete-time hyperbolic fuzzy systems," *Engineering Applications of Artificial Intelligence*, vol. 19, no. 5, pp. 487–499, 2006.

[15] Z. Li, Y. Chu, and S. Xu, "Delay-dependent nonfragile robust H_∞ filtering of T-S fuzzy time-delay systems," *Circuits, Systems, and Signal Processing*, vol. 29, no. 3, pp. 361–375, 2010.

[16] Z. Li, S. Xu, Y. Zou, and Y. Chu, "Robust H_∞ filter design of uncertain T-S fuzzy neutral systems with time-varying delays," *International Journal of Systems Science*, vol. 42, no. 7, pp. 1231–1238, 2011.

[17] C. Lin, Q.-G. Wang, T. H. Lee, and Y. He, "Fuzzy weighting-dependent approach to H_∞ filter design for time-delay fuzzy systems," *IEEE Transactions on Signal Processing*, vol. 55, no. 6 I, pp. 2746–2751, 2007.

[18] S. Xu, J. Lam, T. Chen, and Y. Zou, "A delay-dependent approach to robust H_∞ filtering for uncertain distributed delay systems," *IEEE Transactions on Signal Processing*, vol. 53, no. 10, pp. 3764–8772, 2005.

[19] S. Zhou, J. Lam, and A. Xue, "H_∞ filtering of discrete-time fuzzy systems via basis-dependent Lyapunov function approach," *Fuzzy Sets and Systems*, vol. 158, no. 2, pp. 180–193, 2007.

[20] Z. Li and S. Xu, "Fuzzy weighting-dependent approach to robust $L_2 - L_\infty$ filter design for delayed fuzzy systems," *Signal Processing*, vol. 89, no. 4, pp. 463–471, 2009.

[21] Z. Li, S. Xu, Y. Zou, and Y. Chu, "Delay-dependent robust $L_2 - L_\infty$ filtering of T-S fuzzy systems with time-varying delays," *International Journal of Adaptive Control and Signal Processing*, vol. 24, no. 7, pp. 529–539, 2010.

[22] D. J. Higham, "An algorithmic introduction to numerical simulation of stochastic differential equations," *SIAM Review*, vol. 43, no. 3, pp. 525–546, 2001.

[23] M. Basin and D. Calderon-Alyarez, "Delay-dependent stability for vector nonlinear stochastic systems with multiple delays," *International Journal of Innovative Computing, Information and Control*, vol. 7, no. 4, pp. 1565–1576, 2011.

[24] W.-B. Wu, P.-C. Chen, M.-H. Hung, K.-Y. Chang, and W.-J. Chang, "LMI robustly decentralized H_∞ output feedback controller design for stochastic large-scale uncertain systems with time-delays," *Journal of Marine Science and Technology*, vol. 17, no. 1, pp. 42–49, 2009.

[25] D. W. C. Ho and Y. Niu, "Robust fuzzy design for nonlinear uncertain stochastic systems via sliding-mode control," *IEEE Transactions on Fuzzy Systems*, vol. 15, no. 3, pp. 350–358, 2007.

[26] Y. Niu, B. Chen, and X. Wang, "Sliding mode control for a class of nonlinear itô stochastic systems with state and input delays," *International Journal of Control, Automation and Systems*, vol. 7, no. 3, pp. 365–370, 2009.

[27] W.-H. Chen and X. Lu, "Mean square exponential stability of uncertain stochastic delayed neural networks," *Physics Letters A*, vol. 372, no. 7, pp. 1061–1069, 2008.

[28] R. Yang, Z. Zhang, and P. Shi, "Exponential stability on stochastic neural networks with discrete interval and distributed delays," *IEEE Transactions on Neural Networks*, vol. 21, no. 1, pp. 169–175, 2010.

[29] B.-S. Chen, W.-H. Chen, and H.-L. Wu, "Robust H_2/H_∞ global linearization filter design for nonlinear stochastic systems," *IEEE Transactions on Circuits and Systems I*, vol. 56, no. 7, pp. 1441–1454, 2009.

[30] H. Gao, J. Lam, and C. Wang, "Robust energy-to-peak filter design for stochastic time-delay systems," *Systems and Control Letters*, vol. 55, no. 2, pp. 101–111, 2006.

[31] M. Liu, D. W. C. Ho, and Y. Niu, "Robust filtering design for stochastic system with mode-dependent output quantization," *IEEE Transactions on Signal Processing*, vol. 58, no. 12, pp. 6410–6416, 2010.

[32] T. Li, L. Guo, and L. Wu, "Observer-based optimal fault detection using PDFs for time-delay stochastic systems," *Nonlinear Analysis: Real World Applications*, vol. 9, no. 5, pp. 2337–2349, 2008.

[33] T. Li and Y. Zhang, "Fault detection and diagnosis for stochastic systems via output PDFs," *Journal of the Franklin Institute*, vol. 348, no. 6, pp. 1140–1152, 2011.

[34] S. Xu and T. Chen, "H_∞ model reduction in the stochastic framework," *SIAM Journal on Control and Optimization*, vol. 42, no. 4, pp. 1293–1309, 2004.

[35] L. Wu and D. W. C. Ho, "Fuzzy filter design for Itô stochastic systems with application to sensor fault detection," *IEEE Transactions on Fuzzy Systems*, vol. 17, no. 1, pp. 233–242, 2009.

[36] J. Yang, S. Zhong, W. Luo, and G. Li, "Delay-dependent stabilization for stochastic delayed fuzzy systems with impulsive effects," *International Journal of Control, Automation and Systems*, vol. 8, no. 1, pp. 127–134, 2010.

[37] S. Xu and T. Chen, "Robust H_∞ control for uncertain stochastic systems with state delay," *IEEE Transactions on Automatic Control*, vol. 47, no. 12, pp. 2089–2094, 2002.

[38] X. Mao, *Stochastic Differential Equations and Their Applications*, Horwood Publishing Limited, Chichester, UK, 1997.

Hindawi Publishing Corporation
Mathematical Problems in Engineering
Volume 2013, Article ID 530198, 12 pages
http://dx.doi.org/10.1155/2013/530198

Research Article

Safety Assessment of High-Risk Operations in Hydroelectric-Project Based on Accidents Analysis, SEM, and ANP

Jian-Lan Zhou,[1] Bai Zhe-Hua,[1] and Zhi-Yu Sun[2]

[1] *Key Laboratory of Ministry of Education for Image Processing and Intelligent Control, Department of Systems Science and Engineering, Huazhong University of Science & Technology, Wuhan, Hubei 430074, China*
[2] *Departments of Science, Technology & Environmental Protection, China Three Gorges Project Corporation, Beijing 100038, China*

Correspondence should be addressed to Jian-Lan Zhou; zhoujl1999@163.com

Received 20 August 2013; Accepted 1 October 2013

Academic Editor: Zhiguang Feng

Safety risk analysis and assessment of high-risk work system in hydroelectric project has an important role in safety management. The interactive relationships between human factors and the importance of factors are analyzed and proposed. We analyze the correlation relationship among the factors by using statistical method, which is more objective than subjective judgment. The HFACS is provided to establish a rational and an applicable index system for investigating human error in accidents; the structural equation modeling (SEM) and accident data are used to construct system model and acquire the path coefficient among the risk factor variables; the ANP model is built to assess the importance of accident factors. 289 pieces of valid questionnaires data are analyzed to obtain the path coefficient between risk factor variables and to build the ANP model's judgment matrix. Finally, the human factors' weights are calculated by ANP model. Combining SEM's results and factor's frequency analysis and building the ANP model, the results show that the four greatest weight values of the factors are, respectively, "personal readiness," "perception and decision errors," "skill-based errors," and "violation operations." The results of ANP model provide a reference for the engineering and construction management.

1. Introductions

Hydroelectric project construction has higher safety risk for the interactive factors like complex geological conditions, small venue, large amount of construction workers, various stages of cross-operation, and frequent aerial work, which is vulnerable to induce safety accidents. In recent years, in order to guarantee the safety of hydroelectric project construction work, a great deal of human, material, and financial resources have been invested, the management and supervision of construction have gradually strengthened, but the overall status remains grim, and the annual total number of hydroelectric project construction accidents and the number of deaths and serious injuries are still high in China. The safety work management is still in a blind state; especially the role of human factors in the accident control still lacks clarity. In order to create a good work environment and improve the safety index of the hydroelectric project construction, we need to find out the safety factors in construction, implement identification of human risk factors, analyze interrelationship between human factors, calculate the weight of every factors, find out the factors need to improve, and minimize or prevent the occurrence of accidents.

In hydroelectric project construction process, a significant proportion of the technical causes of serious accidents are attributed to human factors, to establish a rational and comprehensive safety classification system based on human behavior is important for safety assessment. The classification system is used to provide the types of failure involved in accidents. One of the more widely used approaches is the Human Factors Analysis and Classification System [1] drawn in [2]. HFACS is a commonly utilized tool for investigating human contributions to aviation accidents under a

widespread evaluation scheme. HFACS, and its derivatives, has been adapted, applied, and promoted in several domains (and countries) in addition to commercial and private flying, including mining accident [3, 4], helicopter maintenance [5], maritime accident [6, 7], railroad accident [8], and surgery accident [9]. In [6], the HFACS was extended on an analytical basis in a fuzzy environment to investigate shipping accidents in a consistent manner. A sample of 263 significant mining incidents in Australia across 2007-2008 are analyzed using HFACS and provide a greater understanding of the systemic factors involved in mining accidents [3]. Therefore, we extend the HFACS on an analytical basis in the safety assessment of work system in hydropower project construction to evaluate the faulty behavioral risk value.

In HFACS framework extended for hydroelectric project construction, there are some observed factors and latent factors; some of these are influenced by each other; quantitative analysis on these factors to assess their weight in whole system is needed. Structural equation modeling (SEM) is a modeling technique that can handle a large number of endogenous and exogenous variables, as well as latent (unobserved) variables specified as linear combinations (weighted averages) of the observed variables. Regression, simultaneous equations (with and without error-term correlations), path analysis, and variations of factor analysis and canonical correlation analysis are all special cases of SEM [10]. We can consider the risk as a quantity, which can be measured and expressed by a mathematical relation, under the help of real accidents' data [11–13]. SEM is a relatively new method, and its history can be traced back to the 1970s. Most applications have been in psychology, sociology, the biological sciences, educational research, political science, and market research. Applications in travel behavior research date from 1980. Use of SEM is now rapidly expanding as user-friendly software becomes available, and researchers become comfortable with SEM and regard it as another tool in their arsenal. Chen et al. [14] research the influencing factors of coalmine employees' deliberate violation behaviors in China coalmine fatal accidents.

There are some evaluation methods for hydroelectric project high-risk operations, such as LEC assessment method, Safety Inspection Table, Analytic Hierarchy Process (AHP), Fault Tree Analysis method, Fuzzy Comprehensive Evaluation method, and Neural Network. Many scholars over the world have researched in this area. In [15], the degree of danger was studied when the workers work in potentially dangerous environment, presented the LEC method's formula $D = L*E*C$, where D is the value-at-risk, L is the probability of the accident happening, E is how often exposure to dangerous environment, and C is the possible consequences of the accident. LEC method is greatly dependent on the subjectivity of experts, which is prone to difference in the process of rating value; the results are not very objective. Dongzhi [16] used Accident Tree Analysis, studied risk factors of hydroelectric engineering construction, put forward improvement measures to reduce the incidence of accidents, and improved the safety level of construction. But Accident Tree Analysis method has many calculation steps and is difficult to make quantitatively analysis when the data are less. Dedobbeleer and Béland [17] identified the current safety performance evaluation index of construction work system, understood the practical characteristics of workplace by questionnaire survey, and accordingly analyzed construction of safety environment. In [18, 19], safety warnings were proposed after certain steps, including identification of factors which can influence safety level, assessment of potential changes of those factors, assessment of the impact of those changes and selection of safety-related criteria.

The above studies adopt different evaluation methods to analyze the project safety, but there is no evaluation from a holistic perspective; all the methods have some deficiencies. Application of Analytic Network Process (ANP) in the project construction for safety assessment is a hotspot; this is a method based on Analytic Hierarchical Process (AHP). ANP method considers interrelationship among all factors in the same level and adjacent levels, uses supermatrix to comprehensively analyze the factors affecting each other, and obtains the ultimate hybrid weight. In dealing with complex problems that elements connected with and influenced each other, ANP method is proved to be effective and reasonable by the global studies. In [20], fuzzy ANP method was adopted to evaluate the operation system's risk factors, but the correlations among the factors are simply used by the experts' estimation, which may induce expert's bias. In [21], the "3P + I" model was proposed to evaluate the effectiveness of safety management system, AHP and factor analysis were used to identify the key indicators impacting the construction and eventually the questionnaire and expert scoring method were adopted to determine the weight. In [22] the hydroelectric project risk factors were studied to establish the index system based on the ANP, and five main classes of risk factors were identified: organization and management of risks, technological risks, natural risks, social risk, and economic risk and actually a hydroelectric project was assessed. In contrast with the above studies, there is a little research on hydroelectric project construction, or it only uses a single method to qualitatively analyze correlation coefficient and may cause subjective influence. In [23], it was noted noted that the ANP method has some limitations, cannot exclude the bias of the experts, the model's output depends on the given value of expert and cause inconsistencies in the pairwise comparison process. Therefore, it was mentioned that knowledge should be incorporated. In [24], it was pointed out should make use of statistical methods for the analysis of accident statistics, so as to more accurately determine dependency relationship between elements, which avoid the comparison between factors given by experts with prejudice or inconsistency problem.

Therefore, it is necessary to use ANP method combined with quantitative methods and systematically study the factors from the layers of management to construction workers. Combining ANP and other methods for comprehensive assessment can take advantage of their respective advantages,

develop its advantages, avoid disadvantages, and get better results. In [25], ANP and Bayesian Networks method were used to study the safety classification of nuclear power plants. In [26], the ANP and DEMATEL were combined successfully to solve the evaluation for vehicle fleet maintenance management. In [27], QFD, fuzzy ANP, and fuzzy FMEA (failure modes and effect analysis) were used to identify the important types and causes of hazards in the construction industry, meantime providing risk assessment values of hazard causes and relevant improvement strategies. Above researches combined ANP with other methods, the evaluation process is becoming more refined and more realistic. In this paper, we combined ANP, HFACS, SEM, and synthetic statistical methods to evaluate the high-risk work system in hydroelectric projects.

The rest of this paper is organized as follows. In Section 2, the framework of research methodology is constructed and has been presented in detail. In Section 3, based on the HFACS framework, the questionnaire is designed and SEM is built by AMOS. Section 4 analyzes the correlation factors' interdependence relationships based on accident cases by lambda method and tau-y method. In Section 5, the relative weights of factors are calculated by synthetic matrix in ANP model. Finally, the results were thoroughly analyzed, while in the last section the main conclusions and future research topics were drawn up.

2. Methodology Research

ANP model is based on risk influential factors' classification and layered architecture. This study firstly analyzes the human risk factors; therefore, human factors analysis and classification system framework (HFACS) is used to analyze human factors in construction engineering accidents. The technical thinking of this study is firstly applying HFACS and other standardized documents or results to design questionnaire, which is designed for the Three Gorges project, and Xiluodu project, Xiangjiaba project, and then sends the questionnaire to the management units, design units, construction units, supervision units, and technical and safety management staff. Secondly, we analyze the questionnaire data; SPSS17.0 can analyze reliability and validity of the data and confirm the internal consistency of the data. If the data's reliability is high, use AMOS to establish structural equation modeling (SEM); the path coefficients among the factors can be obtained, thus the relationship can be analyzed among the factors. Thirdly, under the HFACS, structure the previous accident cases of Xiluodu project, Xiangjiaba project, and the Three Gorges project, using statistical methods to analyze human factors of accident, we can get the correlation coefficient between the factors. Finally, based on the preceding analysis, combine judgment matrix achieved by empowerment table with judgment matrix by SEM, use linear weighting method, obtain one synthesized judgment matrix, and then calculate this judgment matrix by Super Decision (SD) tool. Eventually, we obtain the ANP evaluation weight and ranking of various factors. In summary, this study was carried out through interviews, questionnaires, theoretic analysis with modeling and statistic methods, and decision and assessment method. It consists of 3 stages shown in Figure 1.

3. Factors Correlation Analysis Based on Empirical Study

3.1. HFACS Framework. Before designing the questionnaire, firstly make sure of the composition of hydroelectric construction risk factors, determine the classification and hierarchical structure of human factors, and construct hierarchy model of hydroelectric construction risk; then base on the model to implement the study. In this study, the HFACS framework is adopted to analyze the human factors which result in the engineering construction accidents; HFACS considers both unsafe behaviors and potential factors which influence unsafe behaviors, satisfy the characteristics of reliability, diagnostic and comprehensive, in accidents investigation. We revise the standard framework of HFACS to adapt with actual safety management of hydroelectric project construction, technical measurements, personnel quality situation, and so forth; the adjusted risk influential human factor is shown in Figure 2.

3.2. Questionnaire Design. In the HFACS framework shown in Figure 1, there are 4 categories and 17 indicators of human factors in this study. We finally formed a questionnaire with 63 detailed items, which include 9 items about organizational influences, 24 items about safety management, 23 items about site work related factors, and 7 items about construction personal unsafe behaviors. According to the degree of importance, the questionnaire's indicators are in descending order and adopt Likert-3 table scale method to divide indictors into three degrees: "the first class indicator," scheduled for score 3; "the second class indicator," scheduled for score 2 and "the third class indicator," scheduled for score 1. Each item needs to record the corresponding rating value. The questionnaires were issued in 418 pieces; 403 valid pieces were collected. After sorting and filtering data, we finally obtained 289 pieces of valid questionnaires data and based on this to make validity analysis.

3.3. Reliability Analysis and Validity Analysis. SPSS17.0 is used to analyze the reliability and validity of the data. By the SPSS software's "reliability analysis" function, the reliability analysis results of all data can be obtained. α value is closer to 1, the reliability is better. Use SPSS software's "factor analysis" function to precede validity analysis and get validity result of all the data, the reliability and validity of latent variables' analysis results are shown in Table 1, the reliability analysis results are shown in Table 2, and KMO and Bartlett's values are shown in Table 3.

In these tables, Cronbach's alpha coefficient is the internal consistency coefficient, which is one of the most commonly used indicators to test questionnaire's reliability, reflecting the consistency and stability degree of the scale items; Bartlett's test assumes that variable correlation coefficient matrix is the identity matrix; if the original hypothesis denied, it is suitable for factor analysis; KMO is the sampling appropriate

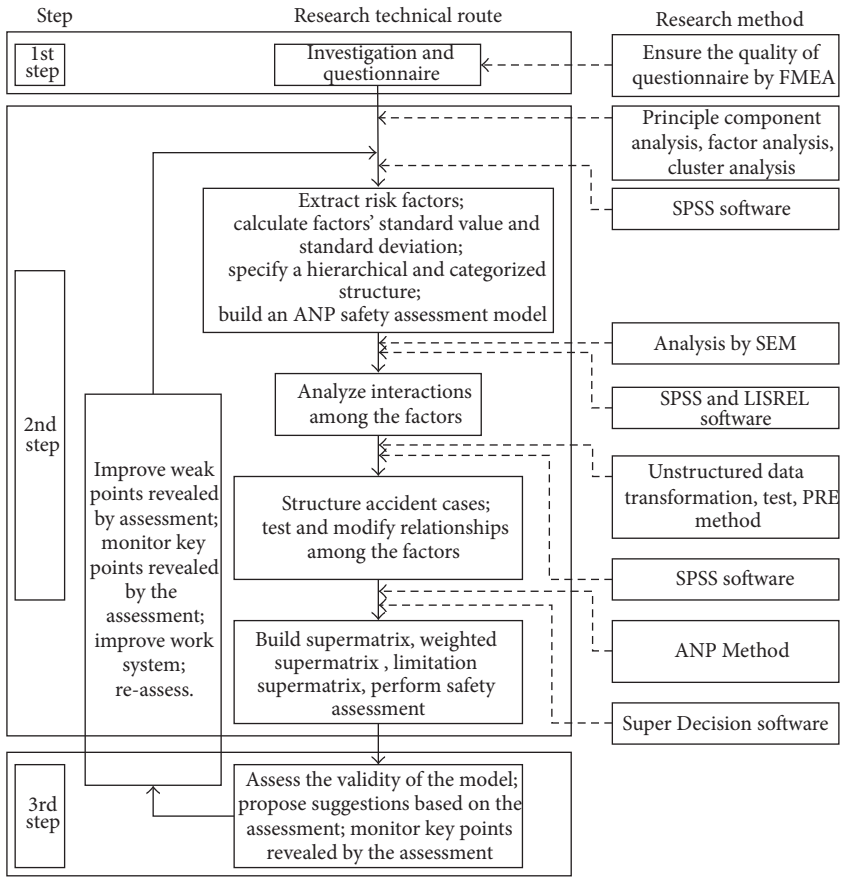

Figure 1: The framework of research methodology.

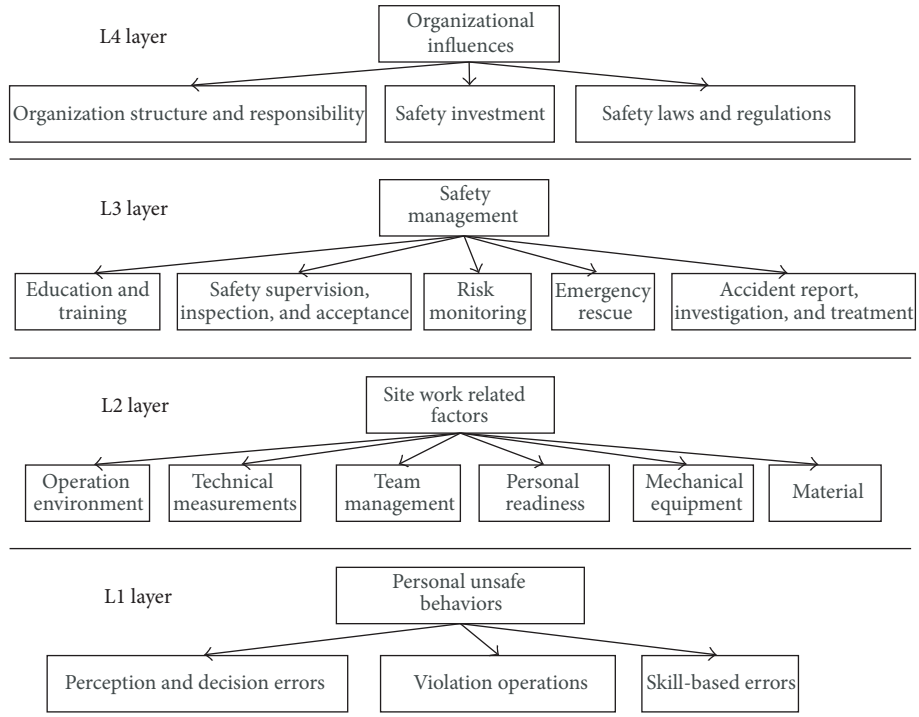

Figure 2: Human factors analysis and classification system framework.

Table 1: The test result of latent variables' reliability and validity.

Latent variable	Measurable variables number	KMO	Bartlett's test			Cronbach's alpha (α value)
			Approx. chi-square	df	Sig.	
Organizational influences	4	0.675	177.907	6	0.000	0.510
Safety management	5	0.854	536.007	10	0.000	0.822
Site work related factors	7	0.918	1074.889	21	0.000	0.883
Workers' unsafe behaviors	3	0.727	342.280	3	0.000	0.816

Table 2: The reliability analysis results of all data.

Cronbach's alpha (α value)	Terms number
0.916	19

Table 3: The KMO and Bartlett's test results of this study.

KMO and Bartlett's test	
Kaiser-Meyer-Olkin measurement of sampling adequacy	0.923
Bartlett's test	
Approx. chi-square	2924.223
df	171
Sig.	0.000

parameter; this when the value is greater than 0.5, means that these variables can make factor analysis; Sig. is significance level and less than 0.05.

We can infer from the parameters in the table data that the value of α for each subscale is good, and the entire questionnaire's Cronbach's alpha coefficient reaches 0.910, close to 1, which indicates the high reliability of the questionnaire data. Each subscale's KMO and Bartlett's test value is good, and the entire questionnaire data's KMO value is 0.928, very close to 1, Sig. <0.05, which shows good questionnaire construction validity. In short, the reliability and validity of the survey data are desirable.

3.4. The Factors Correlation Analysis Based on the SEM Model. Consider organizational influences as SEM model's external latent variable, the corresponding observable variables are exogenous observable variables, safety management, and the site work related factors and construction personal unsafe behaviors are latent variable, and the corresponding observable variables are endogenous observable variable. We try to establish two test models: the first model is the high layer factors which only directly affect their low layers, L4 effects on L3, L3 effects on L2, L2 effect on L1 (more accord with the HFACS theory); the second model is L3 affect L2 and L1, but L2 does not affect L1. By AMOS17.0 software, make comparison of the two models' fit indices; the fitting parameter of the first model is more satisfactory, and the first model is also more in line with the actual significance of this study. Therefore, amend the first model and make the result analysis.

Observe the M.I. value in the AMOS's output. The M.I. value is the revised index, which can discover meaningful information for improving the model's fitting situation; the correction index can predict the reduction of the chi-square value. Before the correction, we must check whether the path is correct in the model and the variable is really relevant; if the regression coefficient is significantly not equal to 0, it represents that the path relationship between the variables is correct. When modifying the model, the higher modification index's value of the path means more conduciveness to improve the model's fitting situation.

After repeatedly estimating the model and constantly checking the output of AMOS software to find out variables with high M.I. value, simultaneously combine with the practical significance of the model to increase the correlation path. Eventually, we get the fixed model as shown in Figure 3, where the path coefficients are marked.

Model-fitted indices after being amended are shown in Table 4. We can see that the correction model's chi-square value is reduced, the path value P is significantly below level 0.01, and all fit indices have been improved greatly, explaining the model's fitting situation that getting better.

The correlation coefficient between the variables is over 0, which means the relationship between each latent variable is positively correlated, indicating that one of the latent variables will have a positive impact on the other latent variable. Similarly, the influence between the latent variable and its corresponding observable variables is positive.

We may acquire analysis result by the AMOS that in the organizational influences layer, the safety laws and regulations' standardization path coefficient is the highest (0.799), which indicates the safety laws and regulations have a very big influence in this level. In safety management layer, emergency rescue's standardization path coefficient is the highest (0.765), followed by risk monitoring (0.755); the next is education and training (0.735). In site work related factors, team management's standardized path coefficient is 0.802, showing the biggest influence in this layer, followed by technical measurements (0.760). In workers' unsafe behaviors layer, perception and decision errors' path coefficient is the highest (0.901); therefore, its influence is the most in this layer, followed by skill-based errors and violation operations. The interrelationship between hidden variables is different: the correlation coefficient between organizational influences and the safety management, the correlation coefficient between safety management and site work related factors, the correlation coefficient between site related factors and construction personal unsafe behaviors are, respectively, 0.872, 0.808, and 0.547; therefore, the organizational influences have the greatest impact on safety management.

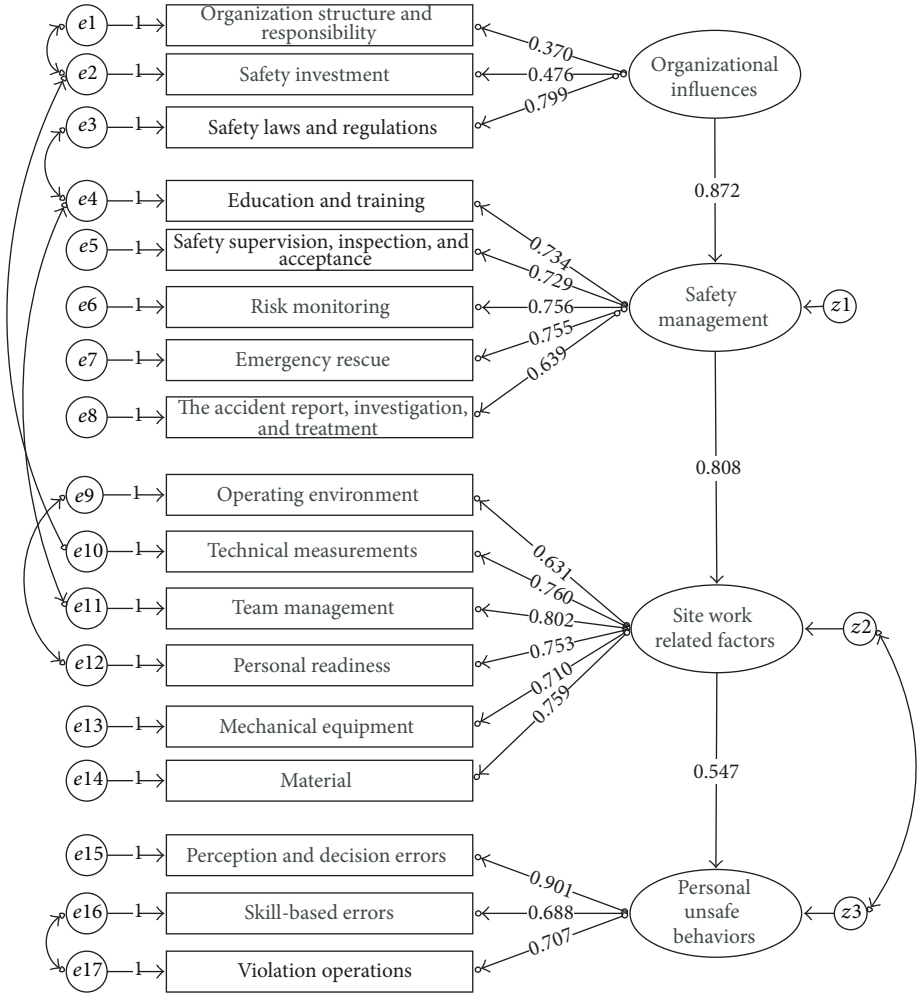

Figure 3: Path analysis graph for SEM revised model.

Table 4: Commonly used fitting index computed result of revised model.

Fit index	Chi-square	FID	CFI	NFI	IFI	RFI	RMSEA	AIC	BCC	GFI	RMR
Result	181.207	108	0.970	0.930	0.970	0.911	0.049	271.207	277.207	0.932	0.124

4. The Correlation Analysis of Factors Based on Accident Cases

Based on the accident data, we count accidents caused by human factors, find out factor categories with big proportion, and analyze their influence on accidents. The data come from "the Xiluodu project accident cases analysis," "the Xiangjiaba project accident cases analysis" and "the Three Gorges project accident cases analysis." Apply Kappa coefficient analysis method to analyze 108 accident cases happened in the above three projects. Determining the human factors' corresponding accident cases and calculating the percentage accounted for the total number of all accidents, this study gets a general understanding of the frequency of occurrence of each factor, as well as the weighting among all the factors. The weights of human factors in Table 5 are calculated on the basis of frequency statistics of all factors resulting in the accident. Empowering values in Table 5 will provide an important reference to build judgment matrix.

Subsequently, statistically analyze the interaction between human factors and use Chi-square test to analyze the correlation and identify the linkages between factors; apply Lambda method and Tau-y method to calculate the proportional reduction in error (PRE), which is correlation analysis. Both Lambda method and Tau-y method are directional statistics, and they can determine the degree of correlation between the human factors. By these methods, we find out how the factors influence each other and how to form a clue between different levels. The more detailed correlation analysis based on accident cases can be referred to in our previous work in the reference. Here, we take an example as follows: the impact of "organization structure and responsibility" on "education and training" is calculated in Table 6. When the Tau-y value exceeds 0.10, the correlation

Table 5: The empowerment for each human factor.

First class index	Weight ai	Second class index	Weight bi	Normalized weight Wi
Organizational influences L4	0.1254	Organization structure and responsibility	0.6019	0.0741
		Safety investment	0.3241	0.0399
		Safety laws and regulations	0.0926	0.0114
Safety management L3	0.3123	Education and training	0.8981	0.1106
		Safety supervision, inspection, and acceptance	0.787	0.0969
		Risk monitoring	0.7222	0.0889
		Emergency rescue	0.0741	0.0091
		Accident report, investigation, and treatment	0.0556	0.0068
Site work related factors L2	0.3945	Operating environment	0.6481	0.0798
		Technical measurements	0.787	0.0969
		Team management	0.6667	0.0821
		Personal readiness	0.9167	0.1129
		Mechanical equipment	0.1296	0.0160
		Material	0.0556	0.0068
Construction personal unsafe behaviors L1	0.1671	Perception and decision errors	0.5278	0.0645
		Skill-based errors	0.3426	0.0422
		Violation operations	0.4907	0.0604

Table 6: The cross table of "organization structure and responsibility" on "education and training."

Count	q1 "organization structure and responsibility"		sum
	Not resulting in accident (0)	Resulting in accident (1)	
A1 "education and training"			
Not resulting in accident (0)	10	1	11
Resulting in accident (1)	33	64	97
Sum	43	65	108

relationship is practical; when it exceeds 0.3, the correlation relationship is strong:

$$\begin{aligned} E1 &= \frac{[(108-97)*97+(108-11)*11]}{108} \\ &= 19.759 \\ E2 &= \frac{[(43-10)*10+(43-33)*33]}{43} \\ &\quad + \frac{[(65-1)*1+(65-64)*64]}{65} = 17.318 \\ \text{Tau-}y = \tau y &= \frac{E1-E2}{E1} = \frac{19.759 - 17.318}{19.759} \\ &= 0.124. \end{aligned} \tag{1}$$

Based on the correlation analysis, we can draw the HFACS framework shown in Figure 4, which reflects the degree of correlation. The thick solid lines indicate strong correlation between the two factors (the Tau-y value exceeds 0.1), and the dashed line indicates the weak correlation between the two factors. In Figure 4, the dashed box means the frequency of the occurring factor in the accident cases is less than 0.1.

In Figure 4, there are some connections between the factors "organization structure and responsibility" in the L4 layer and "education training," "safety supervision, inspection, and acceptance," and "emergency rescue" in the L3 layer; the relationship between "organization structure and responsibility" and "emergency rescue" is weak, which means that safety management facilities, safety management personnel, and safe work responsibility system have limited impact on safety work emergency management and accident rescue but can greatly affect on the staff "education and training" and "safety supervision, inspection, and acceptance," which indicates that safety managers responsibilities' full fulfillments can improve the effect of safety education and training; carefully found hidden danger, strict rectification, and process monitoring can also play an important role in accident prevention.

"Education and training" in L3 layer has relationship with "team management" and "personal readiness" in L2, but the correlation with "team management" is weaker, which indicates that good safety education training of team members has a positive effect on good information communication, team cooperation, and effectiveness of foreknowing dangerous activities. The correlation between "education training" and "personal readiness" is strong, which means that "education training" can greatly improve the "personnel's basic situation"; the workers get enough safety education and skills training, which enhance their safety consciousness; they

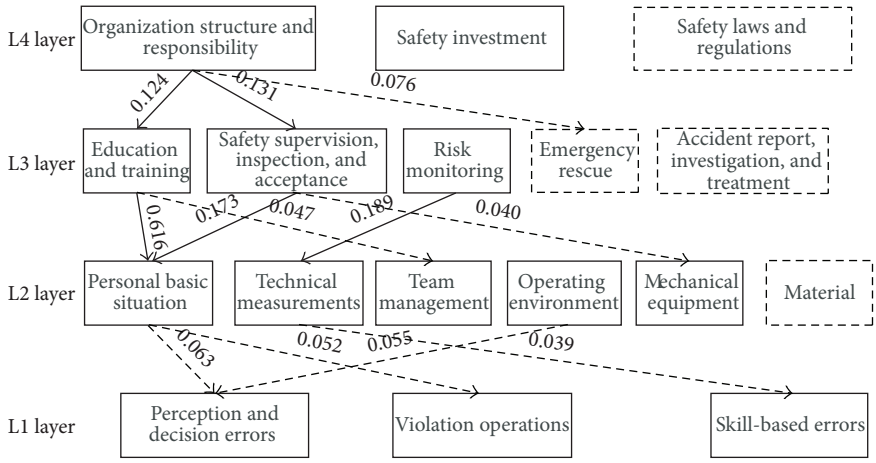

Figure 4: The correlation analysis among the HFACS factors using Tau-y method.

also can understand their objective situation and avoid being involved in the accidents. "Safety supervision, inspection, and acceptance" in L3 layers and "personal readiness" in L2 layer as well as "mechanical equipment" have relationships, which mean "safety supervision, inspection, and acceptance" affects both the workers' situation and the mechanical equipment safety management, but less the latter. "Risk control" in L3 layer and "technical measures" in L2 layers also have relationship, which means that the dangerous places and hazards identification, assessment, and monitoring can lead to more targeted and practical measures. The premise of the safety warning signs set is the hazards identification; the rational allocation of safety measurements and confiding technical intentions are also determined by the hazards identification.

There are relationships between "operation environment" in layer 2 and "perception and decision errors" in layer 1, "technical measures" in layer 2 and "skill-based errors" in layer 1, "Personal readiness" in layer 2 and "perception and decision errors," "violation operation" in layer 1. The dotted lines mean the relationships are weak, indicating that the construction workers' unsafe behavior is little affected by site work related conditions. The capacity of the worker's perception and decision-making, work skills, and operational violations are affected by the individual subjective, individual technical ability, and accidental factors; therefore, there are some relationships between L2 layer factors and L1 layer ones.

5. Safety Assessment Based on the ANP Method

5.1. Molding and Building Judgment Matrix. According to the HFACS framework as well as the mutual correlation among the human factors, build the ANP network hierarchy evaluation model, as shown in Figure 5. The model reflects the relationship between the various factors in the criterion layer.

The core work of the ANP's empowerment and solution is to compute each supermatrix, weighted super matrix, and limitation supermatrix, which is a very complex calculation process. Therefore, we use the Super Decision tool to deal with the calculation.

The judgment matrix constructed in this study is quite different from other studies. The judgment matrix is not from the expert's pairwise comparison but linearly weighs the judgment matrix W' and judgment matrix W''. The next both matrixes are respectively, from the pairwise comparison of empowerment values (see Table 5) and the pairwise comparison of path coefficients of structure equation modeling (see Figure 3). According to the properties of the positive reciprocal matrix, use the following formula to obtain synthetic matrix:

$$W = \alpha W' + (1 - \alpha) W''. \tag{2}$$

In this formula, α is weighted index, $\alpha \in [0, 1]$, $W'$is built by the pairwise comparison of empowerment values in Table 5, W'' is built by the pairwise comparison of path coefficients of structure equation modeling in Figure 3, and W is the final judgment matrix. W',W'', and W are all positive reciprocal matrixes, subjected to $a_{ij} > 0$,$a_{ii} = 1$,$a_{ij} = 1/a_{ji} (i, j = 1, 2, \ldots, n)$. The judgment matrix is from concrete values compared with each other, so the judgment matrix is satisfied with $a_{ij} = a_{ik}/a_{jk}$. Each judgment matrix' consistency ratio CR is equal to zero and is satisfied with full consistency. Using the synthetic matrix, the ANP assessment process is a fully quantitative process.

The value of weighted index α is set to 0.7 on preference. All factors of layers with mutual relationship are carried out pair-wise comparisons. The detailed calculation process is as follows.

Firstly, build the judgment matrixes of "organizational influences," "safety management," "site work related factors" and "personal unsafe behaviors":

$$W_1' = \begin{bmatrix} 1 & 0.40 & 0.32 & 0.75 \\ 2.5 & 1 & 0.79 & 1.86 \\ 3.125 & 1.266 & 1 & 2.35 \\ 1.33 & 0.538 & 0.426 & 1 \end{bmatrix}$$

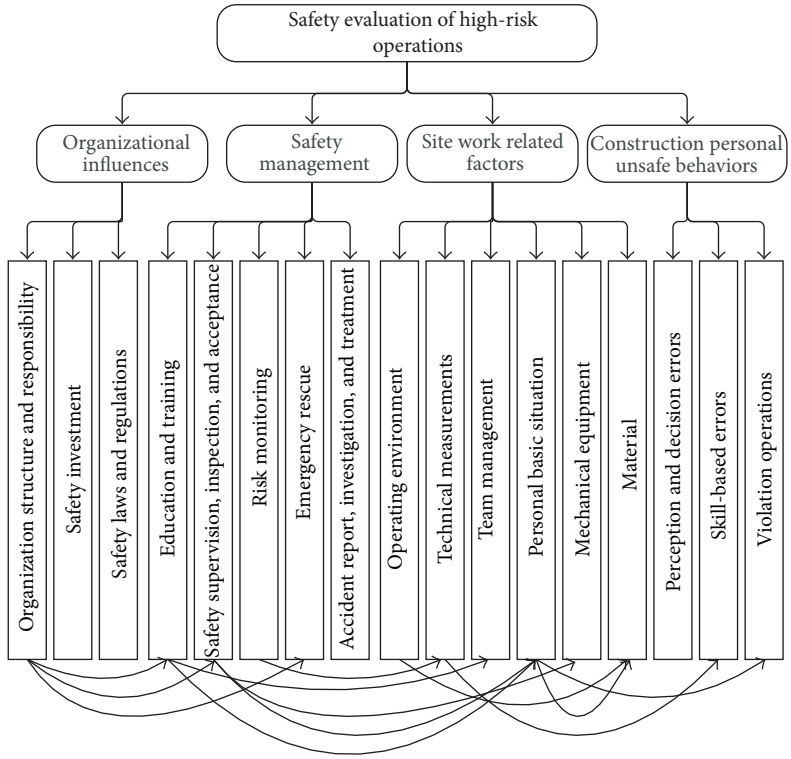

Figure 5: Hierarchical and correlation of the factors in ANP model.

$$W_1'' = \begin{bmatrix} 1 & 1.147 & 1.418 & 2.597 \\ 0.872 & 1 & 1.238 & 2.262 \\ 0.705 & 0.808 & 1 & 1.828 \\ 0.385 & 0.442 & 0.547 & 1 \end{bmatrix}. \tag{3}$$

According to the formula (2), the synthetic matrix is as follows:

$$W_1 = \begin{bmatrix} 1 & 0.62 & 0.65 & 1.30 \\ 1.61 & 1 & 0.92 & 1.98 \\ 1.54 & 1.09 & 1 & 2.19 \\ 0.77 & 0.51 & 0.46 & 1 \end{bmatrix}. \tag{4}$$

The judgment matrix of the elements in "organizational influences" is as follows:

$$W_2 = \begin{bmatrix} 1 & 1.54 & 4.69 \\ 0.65 & 1 & 2.63 \\ 0.21 & 0.38 & 1 \end{bmatrix}. \tag{5}$$

The judgment matrix of the elements in "safety management" is as follows:

$$W_3 = \begin{bmatrix} 1 & 1.10 & 1.16 & 8.80 & 11.73 \\ 0.91 & 1 & 1.05 & 7.75 & 10.32 \\ 0.86 & 0.95 & 1 & 7.14 & 9.50 \\ 0.11 & 0.13 & 0.14 & 1 & 1.29 \\ 0.09 & 0.10 & 0.11 & 0.78 & 1 \end{bmatrix}. \tag{6}$$

The judgment matrix of the elements in "site work related factors" is as follows:

$$W_4 = \begin{bmatrix} 1 & 0.82 & 0.92 & 0.75 & 3.76 & 8.47 \\ 1.22 & 1 & 1.11 & 0.91 & 4.56 & 10.28 \\ 1.09 & 0.90 & 1 & 0.83 & 3.93 & 8.77 \\ 1.33 & 1.10 & 1.20 & 1 & 5.26 & 11.92 \\ 0.27 & 0.22 & 0.25 & 0.19 & 1 & 1.93 \\ 0.12 & 0.10 & 0.11 & 0.08 & 0.52 & 1 \end{bmatrix}. \tag{7}$$

The judgment matrix of the elements in "personal unsafe behaviors" is as follows:

$$W_5 = \begin{bmatrix} 1 & 1.47 & 1.14 \\ 0.68 & 1 & 0.78 \\ 0.88 & 1.28 & 1 \end{bmatrix}. \tag{8}$$

Considering correlation analysis, the judgment matrix of "organizational structure and responsibilities" to its correlation factors is as follows:

$$W_6 = \begin{bmatrix} 1 & 0.947 & 1.632 \\ 1.056 & 1 & 1.724 \\ 0.613 & 0.580 & 1 \end{bmatrix}. \tag{9}$$

Considering correlation analysis, the judgment matrix of "education and training" to its correlation factors is as follows:

$$W_7 = \begin{bmatrix} 1 & 0.076 \\ 13.158 & 1 \end{bmatrix}. \tag{10}$$

Table 7: ANP assessment weights.

First class index	ANP weight	Second class index	ANP weight	ANP rank	Normalized weight Wi	Cases rank
Organizational influences	0.1315	q1 organization structure and responsibility	0.0347	11	0.0741	8
		q2 safety investment	0.0214	13	0.0399	12
		q3 safety laws and regulations	0.0078	15	0.0114	14
Safety Management	0.3474	a1 education and training	0.0693	6	0.1106	2
		a2 safety supervision, inspection, and acceptance	0.0652	7	0.0969	3
		a3 risk monitoring	0.0493	8	0.0889	5
		a4 emergency rescue	0.0146	14	0.0091	15
		a5 accident report, investigation, and treatment	0.0050	16	0.0068	16
Site work related factors	0.3755	x1 operating environment	0.0363	10	0.0798	7
		x2 technical measurements	0.0934	5	0.0969	4
		x3 team management	0.0440	9	0.0821	6
		x4 personal readiness	0.1664	1	0.1129	1
		x5 mechanical equipment	0.0216	12	0.0160	13
		x6 material	0.0044	17	0.0068	17
Construction personal unsafe behaviors	0.1456	d1 perception and decision errors	0.1551	2	0.065	9
		d2 skill-based errors	0.1122	3	0.0422	11
		d3 violation operations	0.0994	4	0.0604	10

Considering correlation analysis, the judgment matrix of "safety supervision, inspection, and acceptance" to its correlation factors is as follows:

$$W_8 = \begin{bmatrix} 1 & 4.325 \\ 0.231 & 1 \end{bmatrix}. \quad (11)$$

Considering correlation analysis, the judgment matrix of "personal basic situation" to its correlation factors is as follows:

$$W_9 = \begin{bmatrix} 1 & 1.212 \\ 0.825 & 1 \end{bmatrix}. \quad (12)$$

According to Figure 5, we use SD tool to build the ANP model. The model reflects the relationship between the variables in the layer factors. At the network layer, we have four categories; each category has several elements (17 evaluation indicators in the sum). Because the factors in the layers are not independent, the circular arrow lines are seen in Figure 5.

5.2. Solutions. Through calculation by the SD software, the weight values of every factor are shown in Table 7.

5.3. Results. In Table 7, the four smallest weight values of the factors are, respectively, "material" (0.0044), "accident report, investigation and treatment" (0.0050), "safety laws and regulations" (0.0078), and "emergency rescue" (0.0146). The normalized weight values based on cases statistics also show that these four factors result in accidents less frequently, which indicate that these four factors less likely to result in accidents in the high-risk construction operations, and the organizations have done well in these four aspects.

The four greatest weight values of the factors are, respectively, "personal readiness" (0.1664), "perception and decision errors" (0.1551), "skill-based errors" (0.1122), and "violation operations" (0.0994). But in of cases statistical analysis, the four greatest weight values are "personal readiness"(0.1129), "education training" (0.1106), "technical measures" (0.0969), and "safety supervision, inspection, and acceptance" (0.0969). Only "personal readiness" is the most greatest in both methods, which shows that in the project construction, when the worker's basic situation greatly influences his safety consciousness, risk awareness, and psychological and physiological conditions. In order to guarantee the safety of construction projects, organizations should strive to improve this factor. The rank of "educating training" drops from the original 2 to 6, indicating that the interaction among the factors will lead to the assessment results change. Because the "education and training" and "personal readiness" have a very strong relationship, the imperfections of the safety education and skills training will lead to personnel's basic situation get worse. In order to avoid the double counting of the associated factors, the assessment weight of "education and training" decreases. The weight of "safety supervision, inspection, and acceptance" drops from the original ranking 3 to 7, which is a result that this factor also directly affects "personal readiness." So with the similar reason, the ANP assessment weight of "safety supervision, inspection, and acceptance" decreases.

After ANP assessment, the weight values of "perception and decision errors," "skill-based errors," and "operation violation" have increased. According to the results of factor analysis, "education training" and "safety supervision, inspection, and acceptance" will influence "personal readiness," "personal readiness" located in L2 layer directly influences "perception and decision-making errors" in L1 layer

and "operation violation," and "risk monitoring" influences "technology measures," "technology measures" in L2 layer influence "skills errors" in L1 layer. It can be seen that construction worker's unsafe behavior is the direct influential factor which may lead to the accident. Three factors in L1 layer "perception and decision-making errors," "skill errors," and "operation irregularities" with higher weight values in ANP assessment, which also indicate the unsafe behavior of construction workers, are the most important factors leading to accidents.

In "organizational influences" layer, the three factors of "organization structure and duties," "safety investments," and "safety laws and regulations," their weight values being relatively smaller, indicate that the organizations have taken complete measurements on these aspects, have invested on safety management institutions, safety management personnel, and have established the safety work responsibility system, series of laws and regulations, and relevant rules and regulations. All the above measures are successful.

In the actual construction project, these 17 assessment factors often influence each other, so the ANP assessment results may be more realistic and can provide a reference for the engineering and construction management. Meanwhile, there are still a lot of factors need to be considered to determine the final management plans and schedules.

6. Conclusions

This study firstly revises the standard HFACS framework to evaluate the risk factors of the high-risk operations in hydroelectric engineering construction, constructs a comprehensive framework system from the organizational layer to personal layer, and is based on the framework to deal with the subsequent research.

Secondly, this study obtains the original data from questionnaire and analyzes the data by the SPSS. The reliability and validity analysis results indicate that the questionnaire data met the realistic requirements. The conceptual model is drawn by AMOS, the raw data is imported from the SPSS to fit, make comparison, revise, and analyze the model. After modeling, analyzing, and revising, we get correlation coefficients between latent variables which may influence hydroelectric construction safety as well as correlation coefficients between latent variables and their corresponding observable variables. The correlation coefficients excess zero, which means the variables have positive relationships; if any variable (factor) is improved, other variables (factors) will also be improved to some degree. The value of correlation coefficient between variables shows the influence on each other. These results give some reference for the organizations to develop management regulations and strategies.

Thirdly, we use the statistical methods such as the PRE method, revise HFACS framework to analyze 108 accident cases, and count the frequency of each risk factor in the accidents. We use the chi-square test to determine correlation between adjacent level factors, in order to determine the concrete association degree between the factors more accurately and calculate the correlation coefficient with the PRE method between the factors. The coefficient values indicate the correlation degree between the two factors.

Finally, we use the ANP method to evaluate the importance of the factors influencing safety work. The traditional safety assessment methods generally use subjective qualitative or semiqualitative principles; not quantitatively assess the safety and risk of construction project. The AHP method cannot consider the interrelationship between the factors they do and is not consistent with the actual situation. However, the ANP method makes up for such deficiency. In this study, the ANP model's judgment matrix is not from the pair-wise comparison method, but from a combination of accident cases analysis results of factor frequency, the correlation coefficient between the factors, and the path coefficient of structural equation modeling. Then, we follow a linear formula to get the final judgment matrix, which can improve the qualitative analysis result relative to the traditional ANP method (the expert rating). Such method makes possible the assessment results more objective and quantitative.

Due to research limitation, there remains a further analysis to satisfy a more realistic factors classification and hierarchical relationships as well as more rational framework. The accident cases data are also limited and cannot cover all characteristics of risk factors. The analysis model is to some extent simple, according to a fixed direction to make factor analysis, and the variables in the analysis process are nominal variables. However, in the actual construction project, the relationships between the factors are complex; there are no such simple relationships in the HFACS model. Therefore, there may some deviations between the analysis results and the realistic situation.

Finally, this study only selects structural equation modeling, accidents statistical analysis, and ANP method to implement the safety assessment research and has not comprehensively compared other more methods, such as Bayesian theory, D-S evidence theory, and neural network. Therefore, the assessment results may not be most accurate and optimal. As a result, we should carry out a variety of assessment methods and select the combination of optimal methods to evaluate in the future.

Conflict of Interests

The authors declare that there is no conflict of interests regarding the publication of this paper.

Acknowledgments

This paper is supported by the National Natural Science Fund Project (50909045, 51079078), and the Fundamental Research Funds for the Central Universities (HUST: 2013QN154).

References

[1] D. A. Wiegmann and S. A. Shappell, "Human error analysis of commercial aviation accidents: application of the human factors

analysis and classification system (HFACS)," *Aviation Space and Environmental Medicine*, vol. 72, no. 11, pp. 1006–1016, 2001.

[2] J. Reason, *Human Error*, Cambridge University Press, New York, NY, USA, 1990.

[3] M. G. Lenné, P. M. Salmon, C. C. Liu, and M. Trotter, "A systems approach to accident causation in mining: an application of the HFACS method," *Accident Analysis and Prevention*, vol. 48, pp. 111–117, 2012.

[4] J. M. Patterson and S. A. Shappell, "Operator error and system deficiencies: analysis of 508 mining incidents and accidents from Queensland, Australia using HFACS," *Accident Analysis and Prevention*, vol. 42, no. 4, pp. 1379–1385, 2010.

[5] H. S. J. Rashid, C. S. Place, and G. R. Braithwaite, "Helicopter maintenance error analysis: beyond the third order of the HFACS-ME," *International Journal of Industrial Ergonomics*, vol. 40, no. 6, pp. 636–647, 2010.

[6] M. Celik and S. Cebi, "Analytical HFACS for investigating human errors in shipping accidents," *Accident Analysis and Prevention*, vol. 41, no. 1, pp. 66–75, 2009.

[7] C. Chauvin, S. Lardjane, G. Morel, and J. P. Clostermann, "Human and organizational factors in maritime accidents: analysis of collisions at sea using the HFACS," *Accident Analysis and Prevention*, vol. 59, pp. 26–37, 2013.

[8] S. Reinach and A. Viale, "Application of a human error framework to conduct train accident/incident investigations," *Accident Analysis and Prevention*, vol. 38, no. 2, pp. 396–406, 2006.

[9] A. W. ElBardissi, D. A. Wiegmann, J. A. Dearani, R. C. Daly, and T. M. Sundt III, "Application of the human factors analysis and classification system methodology to the cardiovascular surgery operating room," *Annals of Thoracic Surgery*, vol. 83, no. 4, pp. 1412–1419, 2007.

[10] T. F. Golob, "Structural equation modeling for travel behavior research," *Transportation Research B*, vol. 37, no. 1, pp. 1–25, 2003.

[11] P. K. Marhavilas and D. Koulouriotis, "Risk Estimation in the Constructions' Worksites by using a Quantitative Assessment Technique and Statistical Information of Accidents," *Scientific Journal of Technical Chamber of Greece*, vol. 1, no. 1-2, pp. 47–60, 2007.

[12] P. K. Marhavilas and D. E. Koulouriotis, "A risk-estimation methodological framework using quantitative assessment techniques and real accidents' data: application in an aluminum extrusion industry," *Journal of Loss Prevention in the Process Industries*, vol. 21, no. 6, pp. 596–603, 2008.

[13] P. K. Marhavilas, D. E. Koulouriotis, and K. Voulgaridou, "Development of a quantitative risk assessment technique and application on an industry's worksite using real accidents' data," *Scientific Journal of Hellenic Association of Mechanical and Electrical Engineers*, vol. 416, pp. 14–20, 2009.

[14] H. Chen, H. Qi, O. Wang, and R.-Y. Long, "The research on the structural equation model of affecting factors of deliberate violation in coalmine fatal accidents in China," *System Engineering Theory and Practice*, vol. 27, no. 8, pp. 127–136, 2007.

[15] K. J. Graham and G. F. Kinney, "Explosive shocks in air," *Journal of the Acoustical Society of America*, vol. 80, no. 2, pp. 708–709, 1986.

[16] Peng Dongzhi, "Four dangers condition identification and control in water and electricity project construction work system," *Construction Technique*, vol. 26, no. 5, pp. 70–72, 2007.

[17] N. Dedobbeleer and F. Béland, "A safety climate measure for construction sites," *Journal of Safety Research*, vol. 22, no. 2, pp. 97–103, 1991.

[18] K. Øien, "Risk indicators as a tool for risk control," *Reliability Engineering and System Safety*, vol. 74, no. 2, pp. 129–145, 2001.

[19] K. Øien, "Risk indicators as a tool for risk control," *Reliability Engineering and System Safety*, vol. 74, no. 2, pp. 147–167, 2001.

[20] M. Dağdeviren, I. Yüksel, and M. Kurt, "A fuzzy analytic network process (ANP) model to identify faulty behavior risk (FBR) in work system," *Safety Science*, vol. 46, no. 5, pp. 771–783, 2008.

[21] E. Ai Lin Teo and F. Yean Yng Ling, "Developing a model to measure the effectiveness of safety management systems of construction sites," *Building and Environment*, vol. 41, no. 11, pp. 1584–1592, 2006.

[22] D. Zhong, S. Cai, and Y. Li, "Risk analysis of hydropower project based on analytic network process and its application," *Journal of Hydroelectric Engineering*, vol. 27, no. 1, pp. 11–17, 2008.

[23] Z. Ayağ and R. G. Özdemir, "A hybrid approach to concept selection through fuzzy analytic network process," *Computers and Industrial Engineering*, vol. 56, no. 1, pp. 368–379, 2009.

[24] K. F. R. Liu and J.-H. Lai, "Decision-support for environmental impact assessment: a hybrid approach using fuzzy logic and fuzzy analytic network process," *Expert Systems with Applications*, vol. 36, no. 3, pp. 5119–5136, 2009.

[25] J. S. Ha and P. H. Seong, "A method for risk-informed safety significance categorization using the analytic hierarchy process and bayesian belief networks," *Reliability Engineering and System Safety*, vol. 83, no. 1, pp. 1–15, 2004.

[26] D. Vujanović, V. Momčilović, N. Bojović, and V. Papić, "Evaluation of vehicle fleet maintenance management indicators by application of DEMATEL and ANP," *Expert Systems with Applications*, vol. 39, no. 12, pp. 10552–10563, 2012.

[27] H.-T. Liu and Y.-L. Tsai, "A fuzzy risk assessment approach for occupational hazards in the construction industry," *Safety Science*, vol. 50, no. 4, pp. 1067–1078, 2012.

Hindawi Publishing Corporation
Mathematical Problems in Engineering
Volume 2013, Article ID 598357, 11 pages
http://dx.doi.org/10.1155/2013/598357

Research Article

Robust Stability and Stabilization for Singular Time-Delay Systems with Linear Fractional Uncertainties: A Strict LMI Approach

Jinxing Lin[1,2] and Lina Rong[1]

[1] *College of Automation, Nanjing University of Posts and Telecommunications, Nanjing 210023, China*
[2] *Key Laboratory of Measurement and Control of Complex Systems of Engineering, Ministry of Education, Southeast University, Nanjing 210096, China*

Correspondence should be addressed to Jinxing Lin; jxlin2004@126.com

Received 21 August 2013; Accepted 24 September 2013

Academic Editor: Tao Li

This paper is concerned with the problems of delay-dependent robust stability and stabilization for a class of continuous singular systems with time-varying delay in range and parametric uncertainties. The parametric uncertainties are assumed to be of a linear fractional form, which includes the norm bounded uncertainty as a special case and can describe a class of rational nonlinearities. In terms of strict linear matrix inequalities (LMIs), delay-range-dependent robust stability criteria for the unforced system are presented. Moreover, a strict LMI design approach is developed such that, when the LMI is feasible, a desired state feedback stabilizing controller can be constructed, which guarantees that, for all admissible uncertainties, the closed-loop dynamics will be regular, impulse free, and robustly asymptotically stable. Numerical examples are provided to demonstrate the effectiveness of the proposed methods.

1. Introduction

Singular time-delay systems, which are known as descriptor time-delay systems, implicit time-delay systems, or generalized differential-difference equations, often appear in various engineering systems, for example, aircraft attitude control, flexible arm control of robots, large-scale electric network control, chemical engineering systems, lossless transmission lines, and so forth [1, 2]. Since singular time-delay systems are matrix delay differential equations coupled with matrix difference equations, the study for such systems is much more complicated than that for standard state-space time-delay systems. Recently, a great deal of attention has been devoted to the study of such more general class of delay systems; see [3–27].

The existing stability criteria for singular time-delay systems can be classified into two types: delay independent [3–5] and delay dependent [6–10]. Generally, delay-dependent conditions are less conservative than the delay-dependent ones, especially when the time delay is small. To obtain delay-dependent conditions, many efforts have been made in the literature, among which the model transformation and bounding technology for cross-terms [8–10] are often used. However, it is known that the bounding technology and the model transformation are the main source of conservation [28]. Recently, some improved stability conditions with less conservatism have been provided by utilizing the free weighting matrix method [11–13], the integral inequality [14], and the delay decomposition approach [15–17], in which neither the bounding technology nor model transformation is involved. However, these conditions in [6–17] were established under the assumption that the delay was time invariant. For the continuous singular systems with time-varying delay, Yue and Han investigated the delay-dependent stability condition by introducing the free weighting matrices [18]. In [19], a delay-dependent stability condition was presented by using the integral inequality method. But the range of the time-varying delay considered in [18, 19] is from 0 to an upper bound. In practice, a time-varying interval delay is often encountered; that is, the range of delay varies in an interval for which the lower bound is not restricted to 0. In this case, the stability criteria in [18, 19] are conservative

because they do not take into account the information of the lower bound of delay. Moreover, when estimating the upper bound of the derivative of Lyapunov functional, some useful terms are ignored in [18, 19]. More recently, continuous singular systems with time-varying delay in a range have been extensively studied; see, for example, [20–27] and references therein.

On the other hand, in recent years, more and more attention has been devoted to derive strict LMI conditions for stability analysis and controller design; see, for example [29, 30] and references therein. The strict LMI conditions, that is, definite LMIs without equality constraints, are highly tractable and reliable when checked by some recently developed algorithms for solving LMIs [31]. However, it should be pointed that the stability conditions derived in [20–27] are formulated in terms of nonstrict LMIs, whose solutions are difficult to calculate since equality constraints are often fragile and usually not met perfectly. Furthermore, up to now, to the best of the authors' knowledge, for a continuous uncertain singular system with a time-varying interval delay, the problems of robust stability, stabilization, and feedback control have not been fully investigated yet [23]. Particularly, strict LMI-based condition has never been reported in the published works.

In this paper, by using a strict LMI approach, we study the robust stability and stabilization problems for a class of singular systems with a time-varying interval delay and uncertainties. Different from the existing results in [13, 19, 21, 23], first, the criteria proposed in our paper do not contain any semidefinite matrix inequality and are expressed as strict LMIs. Second, the new criteria are obtained by only using a well-known integral-inequality and do not employ any free-weighting matrix, which makes our methods more efficient. Third, a new type of uncertainty, namely, linear fractional form, is considered in this paper. Three numerical examples are given to illustrate the effectiveness of the presented method.

Notations. $\mathbf{R}^n$ denotes the n-dimensional Euclidean space, and $\mathbf{R}^{n\times m}$ denotes the sets of all $n\times m$ matrices. I is the identity matrix with appropriate dimensions. For a real symmetric matrix X, X^{T} denotes its transpose, the notation $X \geq 0$ ($X > 0$) means that the matrix X is positive semidefinite (positive-definite), and $\lambda_{\min}(X)$ ($\lambda_{\max}(X)$) denotes the minimum (maximum) eigenvalue of X. $C_{n,\tau} := C([-\tau, 0], R^n)$ denotes the Banach space of continuous vector functions mapping the interval $[-\tau, 0]$ into R^n, $x_t := x(t+\theta)$, $\theta \in [-\tau, 0]$, and $t \geq 0$ denotes the function family defined on $[-\tau, 0]$ which is generated by n-dimensional real vector valued continuous function $x(t)$, $t \in [-\tau, +\infty)$. Obviously, $x_t \in C_{n,\tau}$. $\|\cdot\|$ refers to the Euclidean vector norm or spectral matrix norm, and $\|\varphi\|_c := \sup_{-\tau\leq t\leq 0}\|\varphi(t)\|$ stands for the norm of a function $\varphi \in C_{n,\tau}$. The symmetric terms in a symmetric matrix are denoted by $*$.

2. Problem Formulation and Preliminaries

Consider the following singular time-delay system:

$$\begin{aligned} E\dot{x}(t) = {} & (A + \Delta A)\, x(t) + \left(A_\tau + \Delta A_\tau\right) x(t - \tau(t)) \\ & + (B + \Delta B)\, u(t), \\ x(t) = {} & \phi(t), \quad t \in [-h_2, 0], \end{aligned} \tag{1}$$

where $x(t) \in \mathbf{R}^n$ is the state vector, and $u(t) \in \mathbf{R}^m$ is the control input. E, $A \in \mathbf{R}^{n\times n}$, $A_\tau \in \mathbf{R}^{n\times n}$, and $B \in \mathbf{R}^{n\times m}$ are real constant matrices with appropriate dimensions, and $0 < \operatorname{rank} E = r \leq n$. $\tau(t)$ denotes the time-varying delay which satisfies $h_1 < \tau(t) \leq h_2$, $\dot{\tau}(t) \leq \mu < 1$. Note that h_1 may not be equal to 0. $\phi(t)$ is a compatible continuous vector-valued initial function on $[-h_2, 0]$. ΔA, ΔA_τ and ΔB are matrices with parametric uncertainties satisfying

$$\begin{bmatrix} \Delta A & \Delta A_\tau & \Delta B \end{bmatrix} = D\Delta(t) \begin{bmatrix} E_a & E_\tau & E_b \end{bmatrix}, \tag{2}$$

$$\Delta(t) = F(t)\left(I - JF(t)\right)^{-1}, \tag{3}$$

$$I - J^{\mathrm{T}} J > 0, \tag{4}$$

where D, E_a, E_τ, E_b, and J are known real constant matrices of approximate dimensions and $F(t)$ are unknown time-varying matrix function satisfying

$$F^{\mathrm{T}}(t) F(t) \leq I. \tag{5}$$

The parametric uncertainties ΔA, ΔA_τ, and ΔB satisfying (2)–(5) are said to be admissible.

Remark 1. The above-structured linear fractional form includes the norm-bounded uncertainty as a special case when $J = 0$ [3, 8–11, 13, 19, 23] and can describe a class of rational nonlinearities [32]. Note also that conditions (4) and (5) guarantee that $I - JF(t)$ is invertible.

The nominal unforced system of (2) can be written as

$$\begin{aligned} E\dot{x}(t) &= Ax(t) + A_\tau x(t - \tau(t)), \\ x(t) &= \phi(t), \quad t \in [-h_2, 0]. \end{aligned} \tag{6}$$

The following notations are given.

(i) $S_0 := \{\phi(t) \in C_{n,h_2}, \phi(t)$ is the compatible initial function of system (6)$\}$.

(ii) $S := \{\phi(t) \in C_{n,h_2}$, and there exists a uniquely continuous solution of system (6) on $[0, +\infty)$ for $\phi(t)\}$.

(iii) $B(0, \delta) := \{\phi(t) \mid \phi(t) \in C_{n,h_2}, \|\phi\|_c \leq \delta, \delta > 0\}$.

Definition 2 (see [33]). (1) The pair (E, A) is said to be regular if $\det(sE - A)$ is not identically 0.

(2) The pair (E, A) is said to be impulse-free if $\deg(\det(sE - A)) = \operatorname{rank} E$.

Lemma 3 (see [3]). *If the pair (E, A) is regular and impulse free, then for any compatible initial function $\phi(t) \in C_{n,h_2}$, there exists a uniquely continuous solution of system* (6) *on* $[0, +\infty)$ *for* $\phi(t)$.

Definition 4 (see [3]). The singular system (6) is said to be regular and impulse free, if the pair (E, A) is regular and impulse free.

Definition 5 (see [11]). (1) The system (6) is said to be stable, if for any $\varepsilon > 0$, there exists a scalar $\delta(\varepsilon) > 0$ such that for any compatible initial function $\phi(t) \in B(0,\delta) \cap S$, the solution $x(t)$ of system (6) satisfies $\|x(t)\| \le \varepsilon$, $t > 0$.

(2) The system (6) is said to be asymptotically stable, if its zero solution is stable, and furthermore, there exists a $b_0 > 0$ such that for any compatible initial function $\phi(t) \in B(0,b_0) \cap S$, the solution $x(t) \to 0$ as $t \to \infty$.

The objective of this note is to develop delay-range-dependent robust stability conditions for system (2) with $u(t) = 0$ and to design a state-feedback controller

$$u(t) = Kx(t), \quad K \in \mathbf{R}^{m\times n} \tag{7}$$

so that system (2) is closed-loop *regular*, *impulse-free*, *and* robustly asymptotically stable for admissible linear fractional form uncertainties. To this end, the following lemmas are needed.

Lemma 6 (see [34]). *For any constant matrix $W \in \mathbf{R}^{n\times n}$, $W = W^T > 0$, scalar $0 \le r(t) \le r_M$, and vector function $\dot{x} : [-r_M, 0] \to \mathbf{R}^n$ such that the following integration is well defined, then*

$$\begin{aligned} &-r_M \int_{-r(t)}^{0} \dot{x}^T(t+\xi) W \dot{x}(t+\xi)\, d\xi \\ &\quad \le \begin{pmatrix} x^T(t) & x^T(t-r(t)) \end{pmatrix} \begin{pmatrix} -W & W \\ W & -W \end{pmatrix} \begin{pmatrix} x(t) \\ x(t-r(t)) \end{pmatrix}. \end{aligned} \tag{8}$$

Lemma 7 (see [35]). *Consider the function $\varphi : R^+ \to R$, if $\dot{\varphi}$ is bounded on $[0,\infty)$; that is, there exists a scalar $\alpha > 0$ such that $|\dot{\varphi}(t)| \le \alpha$ for all $t \in [0,\infty)$, and then φ is uniformly continuous on $[0,\infty)$.*

Lemma 8 (see [35]). *Consider the function $\varphi : R^+ \to R$, if $\varphi(t)$ is uniformly continuous and $\int_0^\infty \varphi(s)ds < \infty$, then $\lim_{t\to\infty}\varphi(t) = 0$.*

Lemma 9 (see [32]). *Given matrices $Q = Q^T$, Γ, and Ξ of approximate dimensions, then*

$$Q + \Gamma\Delta(t)\Xi + \Xi^T\Delta^T(t)\Gamma^T < 0, \tag{9}$$

where $\Delta(t)$ is as in (3)*, if and only if there exists scalar $\varepsilon > 0$ such that*

$$Q + \begin{bmatrix} \varepsilon^{-1}\Xi^T & \varepsilon\Gamma \end{bmatrix} \begin{bmatrix} I & -J \\ -J^T & I \end{bmatrix}^{-1} \begin{bmatrix} \varepsilon^{-1}\Xi \\ \varepsilon\Gamma^T \end{bmatrix} < 0. \tag{10}$$

3. Stability Issue

In this section, first of all, we will present new delay-range-dependent stability conditions that guarantee system (6) to be regular, impulse free, and asymptotically stable in terms of LMI, which will play a key role in obtaining the robust stability criterion for the uncertain system (2).

Theorem 10. *Given scalars $0 \le h_1 < h_2$ and μ, the singular system* (6) *is regular, impulse free, and asymptotically stable if there exist positive-definite matrices P, Q_i, $i = 1,2,3$, Z_j, $j = 1,2$ and matrix S with appropriate dimensions such that*

$$\Lambda = \begin{bmatrix} \Lambda_{11} & \Lambda_{12} & 0 & 0 & h_2A^TZ_1 & h_{12}A^TZ_2 \\ * & \Lambda_{22} & \Lambda_{23} & \Lambda_{24} & h_2A_\tau^TZ_1 & h_{12}A_\tau^TZ_2 \\ * & * & \Lambda_{33} & 0 & 0 & 0 \\ * & * & * & \Lambda_{44} & 0 & 0 \\ * & * & * & * & -h_2Z_1 & 0 \\ * & * & * & * & * & -h_{12}Z_2 \end{bmatrix} < 0, \tag{11}$$

where

$$\begin{aligned} \Lambda_{11} &= E^TPA + A^TPE + SR^TA + A^TRS^T \\ &\quad + \sum_{i=1}^{3} Q_i - h_2^{-1}E^TZ_1E, \\ \Lambda_{12} &= E^TPA_\tau + SR^TA_\tau + h_2^{-1}E^TZ_1E, \\ \Lambda_{22} &= -(1-\mu)Q_3 - h_2^{-1}E^TZ_1E \\ &\quad - h_{12}^{-1}E^T(Z_1+Z_2)E - h_{12}^{-1}E^TZ_2E, \\ \Lambda_{23} &= h_{12}^{-1}E^TZ_2E, \\ \Lambda_{24} &= h_{12}^{-1}E^T(Z_1+Z_2)E, \\ \Lambda_{33} &= -Q_1 - h_{12}^{-1}E^TZ_2E, \\ \Lambda_{44} &= -Q_2 - h_{12}^{-1}E^T(Z_1+Z_2)E, \\ h_{12} &= h_2 - h_1, \end{aligned} \tag{12}$$

and $R \in \mathbf{R}^{n\times(n-r)}$ is any matrix with full column rank and satisfies $E^TR = 0$.

Proof. Since $\operatorname{rank} E = r \le n$, there must exist two invertible matrices $\overline{G}$ and $\overline{H}$ such that

$$\overline{E} = \overline{G}E\overline{H} = \begin{bmatrix} I_r & 0 \\ 0 & 0 \end{bmatrix}. \tag{13}$$

Then, R can be parameterized as

$$R = \overline{G}^{\mathrm{T}} \begin{bmatrix} 0 \\ \overline{\Phi} \end{bmatrix}, \tag{14}$$

where $\overline{\Phi} \in \mathbf{R}^{(n-r)\times(n-r)}$ is any nonsingular matrix.

Similar to (13), we define

$$\begin{aligned} \overline{A} &= \overline{G}A\overline{H} = \begin{bmatrix} \overline{A}_{11} & \overline{A}_{12} \\ \overline{A}_{21} & \overline{A}_{22} \end{bmatrix}, \\ \overline{P} &= \overline{G}^{-\mathrm{T}}P\overline{G}^{-1} = \begin{bmatrix} \overline{P}_{11} & \overline{P}_{12} \\ \overline{P}_{21} & \overline{P}_{22} \end{bmatrix}, \\ \overline{S} &= \overline{H}^{\mathrm{T}}S = \begin{bmatrix} \overline{S}_1 \\ \overline{S}_2 \end{bmatrix}, \qquad \overline{R} = \overline{G}^{-\mathrm{T}}R = \begin{bmatrix} 0 \\ \overline{\Phi} \end{bmatrix}, \\ \overline{Z}_1 &= \overline{G}^{-\mathrm{T}}Z_1\overline{G}^{-1} = \begin{bmatrix} \overline{Z}_{1,11} & \overline{Z}_{1,12} \\ \overline{Z}_{1,21} & \overline{Z}_{1,22} \end{bmatrix}. \end{aligned} \tag{15}$$

Since $\Lambda_{11} < 0$ and $Q_i > 0$, $i = 1, 2, 3$, we can formulate the following inequality easily:

$$\Psi = E^{\mathrm{T}}PA + A^{\mathrm{T}}PE + SR^{\mathrm{T}}A + A^{\mathrm{T}}RS^{\mathrm{T}} - h_2^{-1}E^{\mathrm{T}}Z_1E < 0. \tag{16}$$

Pre- and postmultiplying $\Psi < 0$ by $\overline{H}^{\mathrm{T}}$ and $\overline{H}$, respectively, yields

$$\overline{\Psi} = \overline{H}^{\mathrm{T}}\Psi\overline{H} = \begin{bmatrix} \overline{\Psi}_{11} & \overline{\Psi}_{12} \\ * & \overline{A}_{22}^{\mathrm{T}}\overline{\Phi}\,\overline{S}_2^{\mathrm{T}} + \overline{S}_2\overline{\Phi}^{\mathrm{T}}\overline{A}_{22} \end{bmatrix} < 0, \tag{17}$$

where $\overline{\Psi}_{11}$ and $\overline{\Psi}_{12}$ represent the matrices not relevant in the following discussion. From (17), it is easy to see that

$$\overline{A}_{22}^{\mathrm{T}}\overline{\Phi}\,\overline{S}_2^{\mathrm{T}} + \overline{S}_2\overline{\Phi}^{\mathrm{T}}\overline{A}_{22} < 0 \tag{18}$$

which gives that $\overline{A}_{22}$ is nonsingular.

Define

$$\widetilde{G} = \begin{bmatrix} I & -\overline{A}_{12}\overline{A}_{22}^{-1} \\ 0 & I \end{bmatrix}\overline{G}, \qquad \widetilde{H} = \overline{H}\begin{bmatrix} I & 0 \\ -\overline{A}_{22}^{-1}\overline{A}_{21} & \overline{A}_{22}^{-1} \end{bmatrix}. \tag{19}$$

After some algebraic manipulations, we can obtain

$$\widetilde{E} = \widetilde{G}E\widetilde{H} = \begin{bmatrix} I_r & 0 \\ 0 & 0 \end{bmatrix}, \qquad \widetilde{A} = \widetilde{G}A\widetilde{H} = \begin{bmatrix} \widetilde{A}_{11} & 0 \\ 0 & I \end{bmatrix}, \tag{20}$$

where $\widetilde{A}_{11} = \overline{A}_{11} - \overline{A}_{12}\overline{A}_{22}^{-1}\overline{A}_{21}$. Then, it can be shown that

$$\begin{aligned} \det(sE - A) &= \det\left(\widetilde{G}^{-1}\right)\det\left(s\widetilde{E} - \widetilde{A}\right)\det\left(\widetilde{H}^{-1}\right) \\ &= \det\left(\widetilde{G}^{-1}\right)(-1)^{(n-r)}\det\left(sI_r - \widetilde{A}_{11}\right)\det\left(\widetilde{H}^{-1}\right) \end{aligned} \tag{21}$$

which implies that $\det(sE - A)$ is not identically zero and $\deg(\det(sE - A)) = r = \operatorname{rank} E$. Then, the pair of (E, A) is regular and impulse-free, which shows that system (6) is regular and impulse-free. In the following, we will prove that system (6) is also asymptotically stable.

Denote

$$\begin{aligned} \widetilde{A}_\tau &= \widetilde{G}A_\tau\widetilde{H} = \begin{bmatrix} \widetilde{A}_{\tau 11} & \widetilde{A}_{\tau 12} \\ \widetilde{A}_{\tau 21} & \widetilde{A}_{\tau 22} \end{bmatrix}, \\ \widetilde{P} &= \widetilde{G}^{-\mathrm{T}}P\widetilde{G}^{-1} = \begin{bmatrix} \widetilde{P}_{11} & \widetilde{P}_{12} \\ \widetilde{P}_{21} & \widetilde{P}_{22} \end{bmatrix}, \\ \widetilde{R} &= \widetilde{G}^{-\mathrm{T}}R = \begin{bmatrix} 0 \\ \widetilde{\Phi} \end{bmatrix}, \qquad \widetilde{S} = \widetilde{H}^{\mathrm{T}}S = \begin{bmatrix} \widetilde{S}_1 \\ \widetilde{S}_2 \end{bmatrix}, \\ \widetilde{Q}_i &= \widetilde{H}^{\mathrm{T}}Q_i\widetilde{H} = \begin{bmatrix} \widetilde{Q}_{i,11} & \widetilde{Q}_{i,12} \\ \widetilde{Q}_{i,21} & \widetilde{Q}_{i,22} \end{bmatrix}, \quad i = 1, 2, 3, \\ \widetilde{Z}_j &= \widetilde{G}^{-\mathrm{T}}Z_j\widetilde{G}^{-1} = \begin{bmatrix} \widetilde{Z}_{j,11} & \widetilde{Z}_{j,12} \\ \widetilde{Z}_{j,21} & \widetilde{Z}_{j,22} \end{bmatrix}, \quad j = 1, 2. \end{aligned} \tag{22}$$

By using Schur complement and noting that $Q_i > 0$, $i = 1, 2$, $\mu < 1$, it follows from (11) that

$$\begin{bmatrix} \overline{\Lambda}_{11} & \Lambda_{12} \\ * & \overline{\Lambda}_{22} \end{bmatrix} < 0, \tag{23}$$

where

$$\begin{aligned} \overline{\Lambda}_{11} &= E^{\mathrm{T}}PA + A^{\mathrm{T}}PE + SR^{\mathrm{T}}A + A^{\mathrm{T}}RS^{\mathrm{T}} + Q_3 - h_2^{-1}E^{\mathrm{T}}Z_1E, \\ \overline{\Lambda}_{22} &= -Q_3 - h_2^{-1}E^{\mathrm{T}}Z_1E - h_{12}^{-1}E^{\mathrm{T}}\left(Z_1 + Z_2\right)E - h_{12}^{-1}E^{\mathrm{T}}Z_2E. \end{aligned} \tag{24}$$

Pre- and post-multiplying (23) by $\mathrm{diag}\{\widetilde{H}^{\mathrm{T}}, \widetilde{H}^{\mathrm{T}}\}$ and $\mathrm{diag}\{\widetilde{H}, \widetilde{H}\}$, respectively, yields

$$\begin{bmatrix} \widetilde{\overline{\Lambda}}_{11} & \widetilde{\Lambda}_{12} \\ * & \widetilde{\overline{\Lambda}}_{22} \end{bmatrix} < 0, \tag{25}$$

where

$$\begin{aligned} \widetilde{\overline{\Lambda}}_{11} &= \widetilde{E}^{\mathrm{T}}\widetilde{P}\widetilde{A} + \widetilde{A}^{\mathrm{T}}\widetilde{P}\widetilde{E} + \widetilde{S}\widetilde{R}^{\mathrm{T}}\widetilde{A} + \widetilde{A}^{\mathrm{T}}\widetilde{R}\widetilde{S}^{\mathrm{T}} + \widetilde{Q}_3 - h_2^{-1}\widetilde{E}^{\mathrm{T}}\widetilde{Z}\widetilde{E}, \\ \widetilde{\Lambda}_{12} &= \widetilde{E}^{\mathrm{T}}\widetilde{P}\widetilde{A}_\tau + \widetilde{S}\widetilde{R}^{\mathrm{T}}\widetilde{A}_\tau + h_2^{-1}\widetilde{E}^{\mathrm{T}}\widetilde{Z}_1\widetilde{E}, \\ \widetilde{\overline{\Lambda}}_{22} &= -\widetilde{Q}_3 - h_2^{-1}\widetilde{E}^{\mathrm{T}}\widetilde{Z}_1\widetilde{E} - h_{12}^{-1}\widetilde{E}^{\mathrm{T}}\left(\widetilde{Z}_1 + \widetilde{Z}_2\right)\widetilde{E} - h_{12}^{-1}\widetilde{E}^{\mathrm{T}}\widetilde{Z}_2\widetilde{E}. \end{aligned} \tag{26}$$

Substituting (20), (22) into (25), we have

$$\begin{bmatrix} \widetilde{S}_2\widetilde{\Phi}^{\mathrm{T}} + \widetilde{\Phi}\widetilde{S}_2^{\mathrm{T}} + \widetilde{Q}_{3,22} & \widetilde{S}_2\widetilde{\Phi}^{\mathrm{T}}\widetilde{A}_{\tau 22}^{\mathrm{T}} \\ * & -\widetilde{Q}_{3,22} \end{bmatrix} < 0. \tag{27}$$

Pre- and post-multiplying (27) by $\xi = \left[\widetilde{\Phi}^{-\mathrm{T}}\widetilde{S}_2^{-1} \quad -\widetilde{A}_{\tau 22}\widetilde{\Phi}^{-\mathrm{T}}\widetilde{S}_2^{-1}\right]$ and ξ^{T}, respectively, yields

$$\widetilde{A}_{\tau 22}\widetilde{\Theta}\widetilde{A}_{\tau 22}^{\mathrm{T}} - \widetilde{\Theta} < 0, \tag{28}$$

where

$$\widetilde{\Theta} = -\widetilde{\Phi}^{-\mathrm{T}}\widetilde{S}_2^{-1}\left(\widetilde{S}_2\widetilde{\Phi}^{\mathrm{T}} + \widetilde{\Phi}\widetilde{S}_2^{\mathrm{T}} + \widetilde{Q}_{3,22}\right)\widetilde{S}_2^{-\mathrm{T}}\widetilde{\Phi}^{-1} > 0. \tag{29}$$

Therefore,

$$\rho\left(\widetilde{A}_{\tau 22}\right) < 1. \tag{30}$$

Now, let

$$\widetilde{x}(t) = \begin{bmatrix} \widetilde{x}_1(t) \\ \widetilde{x}_2(t) \end{bmatrix} = \overline{H}^{-1}x(t), \tag{31}$$

where $\widetilde{x}_1(t) \in \mathbf{R}^r$ and $\widetilde{x}_2(t) \in \mathbf{R}^{n-r}$. Using the expressions in (20), (22), and (31), system (6) can be decomposed as

$$\dot{\widetilde{x}}_1(t) = \widetilde{A}_{11}\widetilde{x}_1(t) + \widetilde{A}_{\tau 11}\widetilde{x}_1(t - \tau(t)) + \widetilde{A}_{\tau 12}\widetilde{x}_2(t - \tau(t)), \tag{32}$$

$$0 = \widetilde{x}_2(t) + \widetilde{A}_{\tau 21}\widetilde{x}_1(t - \tau(t)) + \widetilde{A}_{\tau 22}\widetilde{x}_2(t - \tau(t)), \tag{33}$$

or equivalently rewritten as

$$\widetilde{E}\dot{\widetilde{x}}(t) = \widetilde{A}\widetilde{x}(t) + \widetilde{A}_\tau \widetilde{x}(t-\tau(t)). \tag{34}$$

It is easy to see that the stability of system (6) is equivalent to that of system (34).

Construct the Lyapunov-Krasovskii functional for system (34) as

$$\begin{aligned}\widetilde{V}(\widetilde{x}_t) = {} & \widetilde{x}^{\mathrm{T}}(t)\widetilde{E}^{\mathrm{T}}\widetilde{P}\widetilde{E}\widetilde{x}(t) \\ & + \sum_{i=1}^{2}\int_{t-h_i}^{t}\widetilde{x}^{\mathrm{T}}(s)\widetilde{Q}_i\widetilde{x}(s)\,ds \\ & + \int_{t-\tau(t)}^{t}\widetilde{x}^{\mathrm{T}}(s)\widetilde{Q}_3\widetilde{x}(s)\,ds \\ & + \int_{-h_2}^{0}\int_{t+\theta}^{t}\dot{\widetilde{x}}^{\mathrm{T}}(s)\widetilde{E}^{\mathrm{T}}\widetilde{Z}_1\widetilde{E}\dot{\widetilde{x}}(s)\,ds\,d\theta \\ & + \int_{-h_2}^{-h_1}\int_{t+\theta}^{t}\dot{\widetilde{x}}^{\mathrm{T}}(s)\widetilde{E}^{\mathrm{T}}\widetilde{Z}_2\widetilde{E}\dot{\widetilde{x}}(s)\,ds\,d\theta.\end{aligned} \tag{35}$$

By Lemma 6, the following inequalities are true

$$\begin{aligned}& -h_2\int_{t-h_2}^{t}\dot{\widetilde{x}}^{\mathrm{T}}(s)\widetilde{E}^{\mathrm{T}}\widetilde{Z}_1\widetilde{E}\dot{\widetilde{x}}(s)\,ds \\ & \quad = -h_2\int_{t-\tau(t)}^{t}\dot{\widetilde{x}}^{\mathrm{T}}(s)\widetilde{E}^{\mathrm{T}}\widetilde{Z}_1\widetilde{E}\dot{\widetilde{x}}(s)\,ds \\ & \qquad - h_2\int_{t-h_2}^{t-\tau(t)}\dot{\widetilde{x}}^{\mathrm{T}}(s)\widetilde{E}^{\mathrm{T}}\widetilde{Z}_1\widetilde{E}\dot{\widetilde{x}}(s)\,ds \\ & \quad \le \begin{pmatrix}\widetilde{x}^{\mathrm{T}}(t) & \widetilde{x}^{\mathrm{T}}(t-\tau(t))\end{pmatrix} \\ & \qquad \times\begin{pmatrix}-\widetilde{E}^{\mathrm{T}}\widetilde{Z}_1\widetilde{E} & \widetilde{E}^{\mathrm{T}}\widetilde{Z}_1\widetilde{E} \\ \widetilde{E}^{\mathrm{T}}\widetilde{Z}_1\widetilde{E} & -\widetilde{E}^{\mathrm{T}}\widetilde{Z}_1\widetilde{E}\end{pmatrix}\begin{pmatrix}\widetilde{x}(t) \\ \widetilde{x}(t-\tau(t))\end{pmatrix} \\ & \qquad + h_{12}^{-1}\begin{pmatrix}\widetilde{x}^{\mathrm{T}}(t-\tau(t)) & \widetilde{x}^{\mathrm{T}}(t-h_2)\end{pmatrix} \\ & \qquad \times\begin{pmatrix}-\widetilde{E}^{\mathrm{T}}\widetilde{Z}_1\widetilde{E} & \widetilde{E}^{\mathrm{T}}\widetilde{Z}_1\widetilde{E} \\ \widetilde{E}^{\mathrm{T}}\widetilde{Z}_1\widetilde{E} & -\widetilde{E}^{\mathrm{T}}\widetilde{Z}_1\widetilde{E}\end{pmatrix}\begin{pmatrix}\widetilde{x}(t-\tau(t)) \\ \widetilde{x}(t-h_2)\end{pmatrix}, \\ & -h_{12}\int_{t-h_2}^{t-h_1}\dot{\widetilde{x}}^{\mathrm{T}}(s)\widetilde{E}^{\mathrm{T}}\widetilde{Z}_2\widetilde{E}\dot{\widetilde{x}}(s)\,ds \\ & \quad = -h_{12}\int_{t-h_2}^{t-\tau(t)}\dot{\widetilde{x}}^{\mathrm{T}}(s)\widetilde{E}^{\mathrm{T}}\widetilde{Z}_2\widetilde{E}\dot{\widetilde{x}}(s)\,ds \\ & \qquad - h_{12}\int_{t-\tau(t)}^{t-h_1}\dot{\widetilde{x}}^{\mathrm{T}}(s)\widetilde{E}^{\mathrm{T}}\widetilde{Z}_2\widetilde{E}\dot{\widetilde{x}}(s)\,ds \\ & \quad \le \begin{pmatrix}\widetilde{x}^{\mathrm{T}}(t-\tau(t)) & \widetilde{x}^{\mathrm{T}}(t-h_2)\end{pmatrix} \\ & \qquad \times\begin{pmatrix}-\widetilde{E}^{\mathrm{T}}\widetilde{Z}_2\widetilde{E} & \widetilde{E}^{\mathrm{T}}\widetilde{Z}_2\widetilde{E} \\ \widetilde{E}^{\mathrm{T}}\widetilde{Z}_2\widetilde{E} & -\widetilde{E}^{\mathrm{T}}\widetilde{Z}_2\widetilde{E}\end{pmatrix}\begin{pmatrix}\widetilde{x}(t-\tau(t)) \\ \widetilde{x}(t-h_2)\end{pmatrix} \\ & \qquad + \begin{pmatrix}\widetilde{x}^{\mathrm{T}}(t-h_1) & \widetilde{x}^{\mathrm{T}}(t-\tau(t))\end{pmatrix} \\ & \qquad \times\begin{pmatrix}-\widetilde{E}^{\mathrm{T}}\widetilde{Z}_2\widetilde{E} & \widetilde{E}^{\mathrm{T}}\widetilde{Z}_2\widetilde{E} \\ \widetilde{E}^{\mathrm{T}}\widetilde{Z}_2\widetilde{E} & -\widetilde{E}^{\mathrm{T}}\widetilde{Z}_2\widetilde{E}\end{pmatrix}\begin{pmatrix}\widetilde{x}(t-h_1) \\ \widetilde{x}(t-\tau(t))\end{pmatrix}.\end{aligned} \tag{36}$$

On the other hand, noticing that $E^{\mathrm{T}}R = 0$, we can deduce that

$$0 = 2\widetilde{x}^{\mathrm{T}}(t)\widetilde{S}\widetilde{R}^{\mathrm{T}}\widetilde{E}\dot{\widetilde{x}}(t), \tag{37}$$

where $\widetilde{S}$ is any matrix with appropriate dimensions.

Taking the derivative of $\widetilde{V}(\widetilde{x}_t)$ with respect to t along the trajectory of system (34) and using (36) and (37), we have

$$\begin{aligned}& \dot{\widetilde{V}}(\widetilde{x}_t) \\ & = \dot{\widetilde{x}}^{\mathrm{T}}(t)\widetilde{E}^{\mathrm{T}}\widetilde{P}\widetilde{E}\widetilde{x}(t) + \widetilde{x}^{\mathrm{T}}(t)\widetilde{E}^{\mathrm{T}}\widetilde{P}\widetilde{E}\dot{\widetilde{x}}(t) \\ & \quad + \sum_{i=1}^{2}\left\{\widetilde{x}^{\mathrm{T}}(t)\widetilde{Q}_i\widetilde{x}(t) - \widetilde{x}^{\mathrm{T}}(t-h_i)\widetilde{Q}_i\widetilde{x}(t-h_i)\right\} \\ & \quad + \widetilde{x}^{\mathrm{T}}(t)\widetilde{Q}_3\widetilde{x}(t) - (1-\dot{\tau}(t))\widetilde{x}^{\mathrm{T}}(t-\tau(t))\widetilde{Q}_3\widetilde{x}(t-\tau(t)) \\ & \quad + h_2\dot{\widetilde{x}}^{\mathrm{T}}(t)\widetilde{E}^{\mathrm{T}}\widetilde{Z}_1\widetilde{E}\dot{\widetilde{x}}(t) - \int_{t-h_2}^{t}\dot{\widetilde{x}}^{\mathrm{T}}(s)\widetilde{E}^{\mathrm{T}}\widetilde{Z}_1\widetilde{E}\dot{\widetilde{x}}(s)\,ds \\ & \quad + (h_2-h_1)\dot{\widetilde{x}}^{\mathrm{T}}(t)\widetilde{E}^{\mathrm{T}}\widetilde{Z}_2\widetilde{E}\dot{\widetilde{x}}(t) - \int_{t-h_2}^{t-h_1}\dot{\widetilde{x}}^{\mathrm{T}}(s)\widetilde{E}^{\mathrm{T}}\widetilde{Z}_2\widetilde{E}\dot{\widetilde{x}}(s)\,ds \\ & \le \widetilde{\psi}^{\mathrm{T}}(t)\widetilde{\Lambda}\widetilde{\psi}(t),\end{aligned} \tag{38}$$

where

$$\begin{aligned}& \widetilde{\psi}(t) = \left[\widetilde{x}^{\mathrm{T}}(t)\ \ \widetilde{x}^{\mathrm{T}}(t-\tau(t))\ \ \widetilde{x}^{\mathrm{T}}(t-h_1)\ \ \widetilde{x}^{\mathrm{T}}(t-h_2)\right]^{\mathrm{T}}, \\ & \widetilde{\Lambda} = \begin{bmatrix}\widetilde{\Lambda}_{11} & \widetilde{\Lambda}_{12} & 0 & 0 \\ * & \widetilde{\Lambda}_{22} & \widetilde{\Lambda}_{23} & \widetilde{\Lambda}_{24} \\ * & * & \widetilde{\Lambda}_{33} & 0 \\ * & * & * & \widetilde{\Lambda}_{44}\end{bmatrix},\end{aligned} \tag{39}$$

with

$$\begin{aligned}\widetilde{\Lambda}_{11} = {} & \widetilde{E}^{\mathrm{T}}\widetilde{P}\widetilde{A} + \widetilde{A}^{\mathrm{T}}\widetilde{P}\widetilde{E} + \widetilde{S}\widetilde{R}^{\mathrm{T}}\widetilde{A} + \widetilde{A}^{\mathrm{T}}\widetilde{R}\widetilde{S}^{\mathrm{T}} \\ & + \sum_{i=1}^{3}\widetilde{Q}_i + h_2\widetilde{A}^{\mathrm{T}}\widetilde{Z}_1\widetilde{A} + h_{12}\widetilde{A}^{\mathrm{T}}\widetilde{Z}_2\widetilde{A} - h_2^{-1}\widetilde{E}^{\mathrm{T}}\widetilde{Z}_1\widetilde{E}, \\ \widetilde{\Lambda}_{12} = {} & \widetilde{E}^{\mathrm{T}}\widetilde{P}\widetilde{A}_\tau + \widetilde{S}\widetilde{R}^{\mathrm{T}}\widetilde{A}_\tau + h_2\widetilde{A}^{\mathrm{T}}\widetilde{Z}_1\widetilde{A}_\tau + h_{12}\widetilde{A}^{\mathrm{T}}\widetilde{Z}_2\widetilde{A}_\tau \\ & + h_2^{-1}\widetilde{E}^{\mathrm{T}}\widetilde{Z}_1\widetilde{E}, \\ \widetilde{\Lambda}_{22} = {} & -(1-\mu)\widetilde{Q}_3 + h_2\widetilde{A}_\tau^{\mathrm{T}}\widetilde{Z}_1\widetilde{A}_\tau + h_{12}\widetilde{A}_\tau^{\mathrm{T}}\widetilde{Z}_2\widetilde{A}_\tau \\ & - h_2^{-1}\widetilde{E}^{\mathrm{T}}\widetilde{Z}_1\widetilde{E} - h_{12}^{-1}\widetilde{E}^{\mathrm{T}}\left(\widetilde{Z}_1+\widetilde{Z}_2\right)\widetilde{E} - h_{12}^{-1}\widetilde{E}^{\mathrm{T}}\widetilde{Z}_2\widetilde{E},\end{aligned}$$

$$\widetilde{\Lambda}_{23} = h_{12}^{-1}\widetilde{E}^{\mathrm{T}}\widetilde{Z}_2\widetilde{E}, \quad \widetilde{\Lambda}_{24} = h_{12}^{-1}\widetilde{E}^{\mathrm{T}}\left(\widetilde{Z}_1 + \widetilde{Z}_2\right)\widetilde{E},$$
$$\widetilde{\Lambda}_{33} = -\widetilde{Q}_1 - h_{12}^{-1}\widetilde{E}^{\mathrm{T}}\widetilde{Z}_2\widetilde{E},$$
$$\widetilde{\Lambda}_{44} = -\widetilde{Q}_2 - h_{12}^{-1}\widetilde{E}^{\mathrm{T}}\left(\widetilde{Z}_1 + \widetilde{Z}_2\right)\widetilde{E}. \tag{40}$$

It is easy to see that (17) guarantees $\dot{\widetilde{V}}(\widetilde{x}_t) < 0$ and

$$\begin{aligned}\lambda_1\left\|\widetilde{x}_1(t)\right\|^2 - \widetilde{V}\left(\widetilde{x}(0)\right) &\le -\widetilde{V}\left(\widetilde{x}(t)\right) - \widetilde{V}\left(\widetilde{x}(0)\right)\\ &= \int_0^t \dot{\widetilde{V}}\left(\widetilde{x}(s)\right)ds \le -\lambda_2\int_0^t \|\widetilde{x}(s)\|^2 ds\\ &\le -\lambda_2\int_0^t \left\|\widetilde{x}_1(s)\right\|^2 ds < 0,\end{aligned} \tag{41}$$

where $\lambda_1 = \lambda_{\min}(\widetilde{P}_{11}) > 0$, $\lambda_1 = -\lambda_{\max}(\widetilde{\Lambda}) > 0$.

Taking into account (41), we can deduce that

$$\lambda_1\left\|\widetilde{x}_1(t)\right\|^2 + \lambda_2\int_0^t \left\|\widetilde{x}_1(s)\right\|^2 ds \le \widetilde{V}\left(\widetilde{x}(0)\right). \tag{42}$$

Therefore,

$$\left\|\widetilde{x}_1(t)\right\|^2 \le m_1, \tag{43}$$

$$\int_0^t \left\|\widetilde{x}_1(s)\right\|^2 ds \le m_2, \tag{44}$$

where $m_1 = (1/\lambda_1)\widetilde{V}(\widetilde{x}(0)) > 0$, $m_2 = (1/\lambda_2)\widetilde{V}(\widetilde{x}(0)) > 0$. Thus, $\|\widetilde{x}_1(t)\|$ is bounded. Considering this and (30), it can be deduced from (33) that $\|\widetilde{x}_2(t)\|$ is bounded;, hence, it follows that from (32) that $\|\dot{\widetilde{x}}_1(t)\|$ is bounded. Therefore, $(d/dt)\|\dot{\widetilde{x}}_1(t)\|^2$ is bounded too. By Lemma 7, we obtain that $\|\dot{\widetilde{x}}_1(t)\|^2$ is uniformly continuous. Therefore, noting (44) and using Lemma 8, we get

$$\lim_{t\to\infty}\left\|\widetilde{x}_1(t)\right\| = 0. \tag{45}$$

This, together with (33), implies that

$$\lim_{t\to\infty}\left\|\widetilde{x}_2(t)\right\| = 0. \tag{46}$$

Thus, according to Definition 5, system (34) is stable. This completes the proof. □

Remark 11. From the proof of Theorem 10, it is clear to see that neither model transformation nor bounding technique for cross-terms is involved. Hence, the conservatism inherited from these ideas will no longer exist in Theorem 10.

Remark 12. Free-weighting matrices in [11–13, 22, 23, 25] plays an important role to reducing the conservatism of delay-dependent stability conditions. However, too many free-weighting matrices will complicate the system analysis and increase the computational demand. It is worth pointing out that no free-weighting matrix is involved in Theorem 10.

Remark 13. Recently, the delay-partitioning or delay-fractioning method [36] was widely used to reduce the conservatism of the delay-dependent results of standard time-delay systems. This method can be extended to study the stability of singular time-delay system (2). Suppose we decompose the delay interval $[h_1, h_2]$ into Nequidistant subintervals. Defining $h^i = h_1 + i(h_2 - h_1)/N$, $i = 1, 2, \ldots, N-1$, and constructing the following Lyapunov-Krasovskii functional:

$$\begin{aligned}\widetilde{V}\left(\widetilde{x}_t\right) = {}& \widetilde{x}^{\mathrm{T}}(t)\widetilde{E}^{\mathrm{T}}\widetilde{P}\widetilde{E}\widetilde{x}(t) + \sum_{i=1}^{2}\int_{t-h_i}^{t}\widetilde{x}^{\mathrm{T}}(s)\widetilde{Q}_i\widetilde{x}(s)\,ds\\ &+ \sum_{j=1}^{N-1}\int_{t-h^j}^{t} x^{\mathrm{T}}(s)\widetilde{Q}_j' x(s)\,ds\\ &+ \int_{-h_2}^{0}\int_{t+\theta}^{t}\dot{\widetilde{x}}^{\mathrm{T}}(s)\widetilde{E}^{\mathrm{T}}\widetilde{Z}_1\widetilde{E}\dot{\widetilde{x}}(s)\,ds\,d\theta\\ &+ \int_{-h^1}^{-h_1}\int_{t+\theta}^{t}\dot{\widetilde{x}}^{\mathrm{T}}(s)\widetilde{E}^{\mathrm{T}}\widetilde{Z}_2\widetilde{E}\dot{\widetilde{x}}(s)\,ds\,d\theta\\ &+ \sum_{l=1}^{N-2}\int_{-h^{l+1}}^{-h^l}\int_{t+\theta}^{t}\dot{\widetilde{x}}^{\mathrm{T}}(s)\widetilde{E}^{\mathrm{T}}\widetilde{Z}_{l+2}\widetilde{E}\dot{\widetilde{x}}(s)\,ds\,d\theta\\ &+ \int_{-h_2}^{-h^{N-1}}\int_{t+\theta}^{t}\dot{\widetilde{x}}^{\mathrm{T}}(s)\widetilde{E}^{\mathrm{T}}\widetilde{Z}_{N+1}\widetilde{E}\dot{\widetilde{x}}(s)\,ds\,d\theta\end{aligned} \tag{47}$$

with $\widetilde{Q}_1 > 0$, $\widetilde{Q}_2 > 0$, $\widetilde{Q}_j' > 0$, $j = 1, 2, \ldots, N-1$, $\widetilde{Z}_1 > 0$, $\widetilde{Z}_2 > 0$ and $\widetilde{Z}_{l+2} > 0$, $l = 1, 2, \ldots, N-2$. Then, by checking the variation of $\dot{\widetilde{V}}(\widetilde{x}_t)$ for the case when $\tau(t) \in [h_1, h^1]$ or $\tau(t) \in [h^j, h^{j+1}]$ $(j = 1, 2, \ldots, N-1)$ or $\tau(t) \in [h^{N-1}, h_2]$, respectively, we can derive the delay-dependent condition, which can guarantee that $\dot{\widetilde{V}}(\widetilde{x}_t) < 0$. Generally, increasing N may result in the reduction of conservatism of the obtained results. However, the corresponding computational complexity will be increased greatly since the dimensions and matrix variables of the involved LMIs will be sharply expanded. For example, in [36], a numerical example has shown that, with N changing from 1 to 3, the allowable upper bounds of h_2 increased 12.9%, but the consumed CPU time increased 9 times.

Theorem 10 presents a delay-range-dependent criterion for system (6) with time-varying delay $\tau(t)$ in a range. If we set $Q_1 = 0$ and $Z_2 = 0$, Theorem 10 yields the following delay-dependent stability criterion.

Corollary 14. *Given scalars $h_2 > 0$, $h_1 = 0$ and μ, system (6) is regular, impulse free, and asymptotically stable if there exist positive-definite matrices P, Q_i, $i = 2, 3$, Z_1, and matrix S with appropriate dimensions such that*

$$\begin{bmatrix} T_{11} & T_{12} & 0 & h_2A^TZ_1 \\ * & T_{22} & h_2^{-1}E^TZ_1E & h_2A_\tau^TZ_1 \\ * & * & T_{33} & 0 \\ * & * & * & -h_2Z_1 \end{bmatrix}, \tag{48}$$

where

$$\begin{aligned}
\mathrm{T}_{11} &= E^T PA + A^T PE + SR^T A + A^T RS^T \\
&\quad + \sum_{i=2}^{3} Q_i - h_2^{-1} E^T Z_1 E, \\
\mathrm{T}_{12} &= E^T PA_\tau + SR^T A_\tau + h_2^{-1} E^T Z_1 E, \\
\mathrm{T}_{22} &= -(1-\mu) Q_3 - 2h_2^{-1} E^T Z_1 E, \\
\mathrm{T}_{33} &= -Q_2 - h_2^{-1} E^T Z_1 E,
\end{aligned} \tag{49}$$

and $R \in \mathbf{R}^{n\times(n-r)}$ *is any matrix with full column rank and satisfies* $E^T R = 0$.

Now, we will present the delay-range-dependent robust stability conditions for the uncertain singular time-delay system (2) with $u(t) = 0$ via Theorem 10.

Theorem 15. *Given scalars* $0 \le h_1 < h_2$ *and* μ, *the uncertain singular time-delay system* (2) *with* $u(t) = 0$ *is regular, impulse free, and robustly asymptotically stable if there exist positive-definite matrices* P, Q_i, $i = 1, 2, 3$, Z_j, $j = 1, 2$, *and matrix* S *with appropriate dimensions and a scalar* $\eta > 0$ *such that the following LMI holds:*

$$\begin{bmatrix}
\Lambda_{11} & \Lambda_{12} & 0 & 0 & h_2 A^T Z_1 & h_{12} A^T Z_2 & \eta E_a^T & \left(E^T P + SR^T\right) D \\
* & \Lambda_{22} & \Lambda_{23} & \Lambda_{24} & h_2 A_\tau^T Z_1 & h_{12} A_\tau^T Z_2 & \eta E_\tau^T & 0 \\
* & * & \Lambda_{33} & 0 & 0 & 0 & 0 & 0 \\
* & * & * & \Lambda_{44} & 0 & 0 & 0 & 0 \\
* & * & * & * & -h_2 Z_1 & 0 & 0 & h_2 Z_1 D \\
* & * & * & * & * & -h_{12} Z_2 & 0 & h_{12} Z_2 D \\
* & * & * & * & * & * & -\eta I & \eta J \\
* & * & * & * & * & * & * & -\eta I
\end{bmatrix} < 0, \tag{50}$$

where Λ_{11}, Λ_{12}, Λ_{22}, Λ_{23}, Λ_{24}, Λ_{33}, Λ_{44}, *and* h_{12} *are defined in* (11).

Proof. Suppose (50) to be true. Let $\varepsilon = 1/\sqrt{\eta}$. Pre- and postmultiplying the left-hand side matrix of (50) by $\mathrm{diag}\{I, I, I, I, I, I, \varepsilon, \varepsilon\}$ and its transpose, respectively, we obtain

$$\Lambda + \begin{bmatrix} \varepsilon^{-1}\Xi^{\mathrm{T}} & \varepsilon\Gamma \end{bmatrix} \begin{bmatrix} I & -J \\ -J^{\mathrm{T}} & I \end{bmatrix}^{-1} \begin{bmatrix} \varepsilon^{-1}\Xi \\ \varepsilon\Gamma^{\mathrm{T}} \end{bmatrix} < 0, \tag{51}$$

where

$$\begin{aligned}
\Gamma &= \begin{bmatrix} D^{\mathrm{T}}(PE + RS^{\mathrm{T}}) & 0 & 0 & 0 & h_2 D^{\mathrm{T}} Z_1 & h_{12} D^{\mathrm{T}} Z_2 \end{bmatrix}^{\mathrm{T}}, \\
\Xi &= \begin{bmatrix} E_a & E_\tau & 0 & 0 & 0 & 0 \end{bmatrix},
\end{aligned} \tag{52}$$

and Λ is defined in (11). Thus, $\Theta = \Lambda + \Gamma\Delta(t)\Xi + \Xi^{\mathrm{T}}\Delta^{\mathrm{T}}(t)\Gamma^{\mathrm{T}} < 0$ holds according to Lemma 9. It can be verified that Θ is exactly the left-hand side of (11) when $A$and A_τ are replaced with $A + D\Delta(t)E_a$and $A_\tau + D\Delta(t)E_\tau$ in (11), respectively. The result then follows from Theorem 10. □

4. Control Design

On the basis of the previous stability conditions, we will present a design method of robustly stabilizing controllers in this section. For simplicity, we first consider system (6).

Theorem 16. *Given scalars* $0 \le h_1 < h_2$ *and* μ, *if there exist scalar* $\alpha > 0$, *positive-definite matrices* P, Q_i, $i = 1, 2, 3$, Z_j, $j = 1, 2$, X, *and matrices* R, S, U *with appropriate dimensions such that*

$$\Psi = \begin{bmatrix}
\Psi_{11} & \Psi_{12} & \Psi_{13} & 0 & 0 & 0 & \Psi_{17} & 0 & \Psi_{19} \\
* & \Psi_{22} & XA_\tau^T & 0 & 0 & h_2 Z_1 & -h_2 X & h_{12} Z_2 & -h_{12} X \\
* & * & \Psi_{33} & \Psi_{34} & \Psi_{35} & 0 & h_2 A_\tau X & 0 & h_{12} A_\tau X \\
* & * & * & \Psi_{44} & 0 & 0 & 0 & 0 & 0 \\
* & * & * & * & \Psi_{55} & 0 & 0 & 0 & 0 \\
* & * & * & * & * & -h_2 Z_1 & 0 & 0 & 0 \\
* & * & * & * & * & * & -h_2 X & 0 & 0 \\
* & * & * & * & * & * & * & -h_{12} Z_2 & 0 \\
* & * & * & * & * & * & * & * & -h_{12} X
\end{bmatrix} < 0, \tag{53}$$

where

$$\begin{aligned}
\Psi_{11} &= AX + XA^T + BU + U^T B^T + \sum_{i=1}^{3} Q_i - h_2^{-1} E Z_1 E^T, \\
\Psi_{12} &= EP + SR^T - X + AX + BU, \\
\Psi_{13} &= XA_\tau^T + h_2^{-1} E Z_1 E^T, \\
\Psi_{17} &= h_2 AX + h_2 BU, \qquad \Psi_{19} = h_{12} AX + h_{12} BU, \\
\Psi_{22} &= -2X + 3aI, \\
\Psi_{33} &= -(1-\mu) Q_3 - h_2^{-1} E Z_1 E^T - h_{12}^{-1} E (Z_1 + Z_2) E^T \\
&\quad - h_{12}^{-1} E Z_2 E^T, \\
\Psi_{34} &= h_{12}^{-1} E Z_2 E^T, \qquad \Psi_{35} = h_{12}^{-1} E (Z_1 + Z_2) E^T, \\
\Psi_{44} &= -Q_1 - h_{12}^{-1} E Z_2 E^T, \\
\Psi_{55} &= -Q_2 - h_{12}^{-1} E (Z_1 + Z_2) E^T
\end{aligned} \tag{54}$$

and $R_1 \in \mathbf{R}^{n\times(n-r)}$ *is any matrix with full column rank and satisfying* $E^T R_1 = 0$, *then there exists a state feedback controller* (7) *such that the resulting closed-loop system of system* (6) *is regular, impulse free, and asymptotically stable. In this case, a suitable controller gain is given by*

$$u(t) = UX^{-1} x(t). \tag{55}$$

Proof. With the control law $u(t) = Kx(t)$, the resultant closed-loop system of system (6) is

$$E\dot{x}(t) = (A + BK) x(t) + A_\tau x(t - \tau(t)). \tag{56}$$

Following the same philosophy as that in [37], we represent system (56) as the following form,

$$\begin{aligned}
&\begin{bmatrix} E & 0 \\ 0 & 0 \end{bmatrix} \begin{bmatrix} \dot{x}(t) \\ \dot{y}(t) \end{bmatrix} \\
&\quad = \begin{bmatrix} 0 & I \\ A + BK & -I \end{bmatrix} \begin{bmatrix} x(t) \\ y(t) \end{bmatrix} + \begin{bmatrix} 0 & 0 \\ A_\tau & 0 \end{bmatrix} \begin{bmatrix} x(t - \tau(t)) \\ y(t - \tau(t)) \end{bmatrix},
\end{aligned} \tag{57}$$

where $y(t) = E\dot{x}(t)$.

For notational convenience, we introduce

$$\overline{E} = \begin{bmatrix} E & 0 \\ 0 & 0 \end{bmatrix}, \qquad \overline{A} = \begin{bmatrix} 0 & I \\ A+BK & -I \end{bmatrix}, \qquad \overline{A}_\tau = \begin{bmatrix} 0 & 0 \\ A_\tau & 0 \end{bmatrix}. \tag{58}$$

Then, by Theorem 10, we can show that system (57) is regular, impulse free, and asymptotically stable if (11) holds, where E, A, A_τ, P, Q_i, and $i = 1, 2, 3$, Z_j, $j = 1, 2$, R, S are replaced by $\overline{E}$, $\overline{A}$, $\overline{A}_\tau$, $\overline{P}$, $\overline{Q}_i$, $i = 1, 2, 3$, $\overline{Z}_j$, and $j = 1, 2$, $\overline{R}$, $\overline{S}$, respectively. For a special issue, we choose $\overline{P}$, $\overline{Q}_i$, $\overline{Z}_j$, $\overline{R}$, and $\overline{S}$ as

$$\begin{aligned} \overline{P} &= \begin{bmatrix} P & 0 \\ 0 & \alpha I \end{bmatrix}, \qquad \overline{Q}_1 = \begin{bmatrix} Q_1 & 0 \\ 0 & \alpha I \end{bmatrix}, \\ \overline{Q}_2 &= \begin{bmatrix} Q_2 & 0 \\ 0 & \alpha I \end{bmatrix}, \qquad \overline{Q}_3 = \begin{bmatrix} Q_3 & 0 \\ 0 & \alpha I \end{bmatrix}, \\ \overline{Z}_1 &= \begin{bmatrix} Z_1 & 0 \\ 0 & X \end{bmatrix}, \qquad \overline{Z}_2 = \begin{bmatrix} Z_2 & 0 \\ 0 & X \end{bmatrix}, \\ \overline{R} &= \begin{bmatrix} R & 0 \\ 0 & X \end{bmatrix}, \qquad \overline{S} = \begin{bmatrix} S & I \\ 0 & I \end{bmatrix}, \end{aligned} \tag{59}$$

where $P \in \mathbf{R}^{n\times n}$, $Q_i \in \mathbf{R}^{n\times n}$, $i = 1, 2, 3$, $Z_j \in \mathbf{R}^{n\times n}$, and $j = 1, 2$, $X \in \mathbf{R}^{n\times n}$ are symmetrical positive-definite matrices, $R \in \mathbf{R}^{n\times(n-r)}$ is with full column rank and satisfies $E^{\mathrm{T}}R = 0$, $S \in \mathbf{R}^{n\times(n-r)}$ is any matrix and $\alpha > 0$ is a scalar. It is easy to verify that $\overline{R}$ is with full column rank and satisfies $\overline{E}^{\mathrm{T}}\overline{R} = 0$. Then, the following LMI can be obtained:

$$\begin{bmatrix} \Phi_{11} & \Phi_{12} & \Phi_{13} & 0 & 0 & 0 & \Phi_{17} & 0 & \Phi_{19} \\ * & \Phi_{22} & XA_\tau & 0 & 0 & h_2Z_1 & -h_2X & h_{12}Z_2 & -h_{12}X \\ * & * & \Phi_{33} & \Phi_{34} & \Phi_{35} & 0 & h_2A_\tau^{\mathrm{T}}X & 0 & h_{12}A_\tau^{\mathrm{T}}X \\ * & * & * & \Phi_{44} & 0 & 0 & 0 & 0 & 0 \\ * & * & * & * & \Phi_{55} & 0 & 0 & 0 & 0 \\ * & * & * & * & * & -h_2Z_1 & 0 & 0 & 0 \\ * & * & * & * & * & * & -h_2X & 0 & 0 \\ * & * & * & * & * & * & * & -h_{12}Z_2 & 0 \\ * & * & * & * & * & * & * & * & -h_{12}X \end{bmatrix} < 0, \tag{60}$$

where

$$\begin{aligned} \Phi_{11} &= X(A+BK) + (A+BK)^{\mathrm{T}}X + \sum_{i=1}^{3} Q_i - h_2^{-1}E^{\mathrm{T}}Z_1E, \\ \Phi_{12} &= E^{\mathrm{T}}P + S_1R_1^{\mathrm{T}} - X + (A+BK)^{\mathrm{T}}\mathrm{X}, \\ \Phi_{13} &= XA_\tau + h_2^{-1}E^{\mathrm{T}}Z_1E, \quad \Phi_{17} = h_2(A+BK)^{\mathrm{T}}X, \\ \Phi_{19} &= h_{12}(A+BK)^{\mathrm{T}}X, \quad \Phi_{22} = -2X + 3aI, \\ \Phi_{33} &= -(1-\mu)Q_3 - h_2^{-1}E^{\mathrm{T}}Z_1E - h_{12}^{-1}E^{\mathrm{T}}(Z_1+Z_2)E \\ &\quad - h_{12}^{-1}E^{\mathrm{T}}Z_2E, \\ \Phi_{34} &= h_{12}^{-1}E^{\mathrm{T}}Z_2E, \quad \Phi_{35} = h_{12}^{-1}E^{\mathrm{T}}(Z_1+Z_2)E, \\ \Phi_{44} &= -Q_1 - h_{12}^{-1}E^{\mathrm{T}}Z_2E, \quad \Phi_{55} = -Q_2 - h_{12}^{-1}E^{\mathrm{T}}(Z_1+Z_2)E. \end{aligned} \tag{61}$$

Note that the pairs $(E, (A+BK))$ and $(E, (A+BK+A_\tau))$ are regular, causal if and only if the pairs $(E^{\mathrm{T}}, (A+BK)^{\mathrm{T}})$ and $(E^{\mathrm{T}}, (A+BK+A_\tau)^{\mathrm{T}})$ are regular, causal. Furthermore, $\det(sE-(A+BK)-e^{-\tau(t)s}A_\tau) = \det(sE^{\mathrm{T}}-(A+BK)^{\mathrm{T}}-e^{-\tau(t)s}A_\tau^{\mathrm{T}})$. Then, as long as the regularity, causality, and stability problems are concerned, we can consider the following system instead of (56):

$$E^{\mathrm{T}}\dot{\zeta}(t) = (A+BK)^{\mathrm{T}}\zeta(t) + A_\tau^{\mathrm{T}}\zeta(t-\tau(t)), \tag{62}$$

where $\zeta(t) \in \mathbf{R}^n$ is the state vector.

In this sense, (53) can be obtained by replacing E, $(A+BK)$, A_τ in (60) by E^{T}, $(A+BK)^{\mathrm{T}}$, A_τ^{T}, respectively, and introducing a matrix $U = KX$. □

The robust stabilizability result for uncertain singular system (2) is presented in the following theorem.

Theorem 17. *Given scalars $0 \le h_1 < h_2$ and μ, if there exist scalar $\alpha > 0$, positive-definite matrices P, Q_i, $i = 1, 2, 3$, Z_j, $j = 1, 2$, X, and matrices R, S, U with appropriate dimensions and scalars $\eta_1 > 0$, $\eta_2 > 0$ such that*

$$\begin{bmatrix} \Psi_{11} & \Psi_{12} & \Psi_{13} & 0 & 0 & 0 & \Psi_{17} & 0 & \Psi_{19} & \Psi_{110} & \eta_1D & \Psi_{112} & 0 \\ * & \Psi_{22} & XA_\tau^T & 0 & 0 & h_2Z_1 & -h_2X & h_{12}Z_2 & \Psi_{29} & \Psi_{210} & 0 & \Psi_{212} & 0 \\ * & * & \Psi_{33} & \Psi_{34} & \Psi_{35} & 0 & h_2A_\tau X & 0 & \Psi_{39} & 0 & 0 & 0 & \eta_2D \\ * & * & * & \Psi_{44} & 0 & 0 & 0 & 0 & 0 & 0 & 0 & 0 & 0 \\ * & * & * & * & \Psi_{55} & 0 & 0 & 0 & 0 & 0 & 0 & 0 & 0 \\ * & * & * & * & * & -h_2Z_1 & 0 & 0 & 0 & 0 & 0 & 0 & 0 \\ * & * & * & * & * & * & -h_2X & 0 & 0 & \Psi_{710} & 0 & \Psi_{712} & 0 \\ * & * & * & * & * & * & * & -h_{12}Z_2 & 0 & 0 & 0 & 0 & 0 \\ * & * & * & * & * & * & * & * & -h_{12}X & \Psi_{910} & 0 & \Psi_{912} & 0 \\ * & * & * & * & * & * & * & * & * & -\eta_1I & \eta_1J & 0 & 0 \\ * & * & * & * & * & * & * & * & * & * & -\eta_1I & 0 & 0 \\ * & * & * & * & * & * & * & * & * & * & * & -\eta_2I & \eta_2J \\ * & * & * & * & * & * & * & * & * & * & * & * & -\eta_2I \end{bmatrix} < 0, \tag{63}$$

where Ψ_{11}, Ψ_{12}, Ψ_{13}, Ψ_{17}, Ψ_{19}, Ψ_{22}, Ψ_{33}, Ψ_{34}, Ψ_{35}, Ψ_{44}, *and* Ψ_{55} *are defined in* (53), $\Psi_{29} = -h_{12}X$, $\Psi_{110} = \Psi_{210} = XE_a^T + U^TE_b^T$, $\Psi_{112} = \Psi_{212} = XE_\tau^T$, $\Psi_{39} = h_{12}A_\tau X$, $\Psi_{710} = h_2(XE_a^T + U^TE_b^T)$, $\Psi_{910} = h_{12}(XE_a^T + U^TE_b^T)$, $\Psi_{712} = h_2XE_\tau^T$, $\Psi_{912} = h_{12}XE_\tau^T$, *and* $R_1 \in \mathbf{R}^{n\times(n-r)}$ *is any matrix with full column rank and satisfying* $E^TR_1 = 0$*; then there exists a state feedback controller* (7) *such that the resulting closed-loop system of system* (2) *is regular, impulse free, and robustly asymptotically stable. In this case, a suitable controller gain is given by*

$$u(t) = UX^{-1}x(t). \tag{64}$$

Proof. Replacing A by $A + D\Delta(t)E_a$, A_τ by $A_\tau + D\Delta(t)E_\tau$ and B by $B + D\Delta(t)E_b$ in (53), respectively, results in the following condition:

$$\Psi + \Gamma_1\Delta(t)\Xi_1 + \Xi_1^{\mathrm{T}}\Delta^{\mathrm{T}}(t)\Gamma_1^{\mathrm{T}} + \Gamma_2\Delta(t)\Xi_2 + \Xi_2^{\mathrm{T}}\Delta^{\mathrm{T}}(t)\Gamma_2^{\mathrm{T}} < 0, \tag{65}$$

where

$$\begin{aligned}
\Gamma_1 &= \left[D^{\mathrm{T}} \;\; 0 \;\; 0 \;\; 0 \;\; 0 \;\; 0 \;\; 0 \;\; 0 \;\; 0\right]^{\mathrm{T}},\\
\Xi_1 &= \left[E_aX + E_bU \;\; E_aX + E_bU \;\; 0 \;\; 0 \;\; 0 \;\; 0 \;\; h_2\left(E_aX + E_bU\right) \;\; 0 \;\; h_{12}\left(E_aX + E_bU\right)\right],\\
\Gamma_2 &= \left[0 \;\; 0 \;\; D^{\mathrm{T}} \;\; 0 \;\; 0 \;\; 0 \;\; 0 \;\; 0 \;\; 0\right]^{\mathrm{T}},\\
\Xi_2 &= \left[E_\tau U \;\; E_\tau U \;\; 0 \;\; 0 \;\; 0 \;\; 0 \;\; h_2E_\tau X \;\; 0 \;\; h_{12}E_\tau X\right],
\end{aligned} \tag{66}$$

and Ψ is defined in (53).

By Lemma 9, (65) holds for $\Delta(t)$ satisfying (3), if there exist scalars $\varepsilon_1 > 0$, $\varepsilon_2 > 0$ such that

$$\begin{aligned}
&\Psi + \left[\varepsilon_1^{-1}\Xi_1^{\mathrm{T}} \;\; \varepsilon_1\Gamma_1\right]\begin{bmatrix} I & -J \\ -J^{\mathrm{T}} & I\end{bmatrix}^{-1}\begin{bmatrix}\varepsilon_1^{-1}\Xi_1 \\ \varepsilon_1\Gamma_1^{\mathrm{T}}\end{bmatrix}\\
&\quad + \left[\varepsilon_2^{-1}\Xi_2^{\mathrm{T}} \;\; \varepsilon_2\Gamma_2\right]\begin{bmatrix} I & -J \\ -J^{\mathrm{T}} & I\end{bmatrix}^{-1}\begin{bmatrix}\varepsilon_2^{-1}\Xi_2 \\ \varepsilon_2\Gamma_2^{\mathrm{T}}\end{bmatrix} < 0.
\end{aligned} \tag{67}$$

Suppose (63) to be true. Let $\varepsilon_i = \sqrt{\eta_i}$, $i = 1, 2$. Pre- and postmultiplying the left-hand side matrix of (63) by $\mathrm{diag}\{I, I, I, I, I, I, \varepsilon_1^{-1}, \varepsilon_1^{-1}, \varepsilon_2^{-1}, \varepsilon_2^{-1}\}$ and its transpose, respectively, and using Schur complement equivalence to (63) yields (67). The result then follows from Theorem 16. □

5. Numerical Examples

In this section, some examples are provided to illustrate the benefits of our results.

Example 1. Consider the nominal unforced part of system (2) with

$$E = \begin{bmatrix}1 & 0\\ 0 & 0\end{bmatrix}, \qquad A = \begin{bmatrix}0.5 & 0\\ 0 & -1\end{bmatrix}, \qquad A_\tau = \begin{bmatrix}-1.1 & 1\\ 0 & 0.5\end{bmatrix}. \tag{68}$$

The case for $h_1 = 0$ and $\mu = 0$ has been studied in [12]. We choose $R = \left[0 \;\; 1\right]^{\mathrm{T}}$. The comparison among Corollary 14 in this note and those in [6–9, 11, 12, 19] is listed in Table 1 for $h_1 = 0$. It should be pointed out that the results of [7] fail to deal with the system because the matrix describing the relationship between the fast and slow variables cannot be chosen beforehand. It can be seen that our method is less conservative than those in [6, 9] and gives the same results as that in [8, 11, 12, 19]. However, when the time delay is a varying delay, our method gives better results than that in [19] for $\mu = 0.3$ and $\mu = 0.75$ since the relationship among h_2, $\tau(t)$, $h_2 - \tau(t)$, and $\tau(t) - h_1$ has been taken into account in Corollary 14. On the other hand, for system with time-varying delay in a range, Table 1 also lists the allowable maximum upper bounds of h_2 for different μ with $h_1 = 0.3$ and $h_1 = 0.6$.

Example 2. Consider the unforced part of uncertain system (2) with

$$\begin{aligned}
E &= \begin{bmatrix}1 & 0\\ 0 & 0\end{bmatrix}, \qquad A = \begin{bmatrix}0.4 & 0.2\\ 0 & -1\end{bmatrix},\\
A_\tau &= \begin{bmatrix}-1 & 1\\ 0 & 0.3\end{bmatrix}, \qquad D = \begin{bmatrix}0.1 & 0\\ 0 & 0.1\end{bmatrix},\\
E_a &= \begin{bmatrix}-0.05 & 0\\ 0 & 0.05\end{bmatrix}, \qquad E_\tau = \begin{bmatrix}0.05 & 0\\ 0 & -0.05\end{bmatrix}.
\end{aligned} \tag{69}$$

We choose $R = \left[0 \;\; 1\right]^{\mathrm{T}}$. For $h_1 = 0$, the comparison among Theorem 15 in this note and that in [19] is listed in Table 2. It is clear that the result in this note is better than that in [19]. The corresponding maximum upper bounds of h_2 for different h_1 and μ derived by Theorem 15 are also listed in Table 2.

Example 3. Consider system (2) with

$$\begin{aligned}
E &= \begin{bmatrix}1 & 1 & 0\\ 1 & -1 & 1\\ 2 & 0 & 1\end{bmatrix}, \qquad A = \begin{bmatrix}1.5 & 0.5 & 1\\ -1 & 0 & 1\\ 0.5 & 0 & 1\end{bmatrix},\\
A_\tau &= \begin{bmatrix}-1 & 0 & 1\\ 1 & -1 & 0.5\\ 0.3 & 0.5 & -1\end{bmatrix}, \qquad B = \begin{bmatrix}1 & 1\\ 1 & 0\\ 0 & 1\end{bmatrix},
\end{aligned}$$

Table 1: Allowable upper bounds of h_2 with given h_1 for different μ.

h_1	Methods	$\mu = 0$	$\mu = 0.3$	$\mu = 0.75$
0	[7]	—	—	—
	[9]	0.5567	—	—
	[6]	0.9680	—	—
	[8, 11, 12]	1.0660	—	—
	[19]	1.0660	1.0130	0.6496
	Corollary 14	1.0660	1.0263	0.7141
0.3	Theorem 10	1.0660	1.0315	0.7376
0.6	Theorem 10	1.0660	1.0421	0.7426

Table 2: Allowable upper bounds of h_2 with given h_1 for different μ.

h_1	Methods	$\mu = 0$	$\mu = 0.3$	$\mu = 0.75$
0	[19]	1.1836	1.1217	1.0307
	Theorem 15 ($J = 0$)	1.1836	1.1348	1.1095
0.3	Theorem 15 ($J = 0$)	1.1836	1.1394	1.1197
	Theorem 15 ($J = 0.1$)	1.1842	1.1400	1.1200
0.6	Theorem 15 ($J = 0$)	1.1836	1.1489	1.1317
	Theorem 15 ($J = 0.1$)	1.1842	1.1494	1.1321

Table 3: Allowable upper bounds of h_2 with given h_1.

h_1	Methods	h_2	K
0	Theorem 17 ($J = -0.1$)	0.9062	$\begin{bmatrix} -0.5515 & -0.1800 & -0.7849 \\ -1.0962 & -0.7997 & -0.2503 \end{bmatrix}$
0.3	Theorem 17 ($J = -0.1$)	1.0482	$\begin{bmatrix} -0.5845 & -0.1547 & -0.8065 \\ -1.1257 & -0.7953 & -0.2363 \end{bmatrix}$
0.6	Theorem 17 ($J = -0.1$)	1.1919	$\begin{bmatrix} -0.6093 & -0.1360 & -0.8218 \\ -1.1582 & -0.7942 & -0.2136 \end{bmatrix}$

$$D = \begin{bmatrix} 0.1 & 0.1 & 0.1 \end{bmatrix}^{\mathrm{T}}, \quad E_a = \begin{bmatrix} 0.2 & 0.1 & 0.3 \end{bmatrix},$$
$$E_\tau = \begin{bmatrix} 0.1 & 0.2 & 0.1 \end{bmatrix}, \quad E_b = \begin{bmatrix} 0.1 & 0.1 \end{bmatrix}, \quad \mu = 0.1. \tag{70}$$

We choose $R = \begin{bmatrix} -1 & 1 & 2 \end{bmatrix}^{\mathrm{T}}$. According to Theorem 17, Table 3 shows the allowed maximum upper bounds of h_2 and the corresponding state feedback gain K for different h_1.

6. Conclusions

In this note, the delay-range-dependent robust stability and stabilization for singular time-delay systems with linear fractional uncertainty and time-varying delay in a range are studied. The results are obtained by using the strict LMI approach and constructing an appropriate Lyapunov-Krasovskii functional. Numerical examples have been given to demonstrate the effectiveness of the presented criteria and their improvement over existing results.

Acknowledgments

This work was supported by the opening Foundation of the Key Laboratory of Measurement and Control of Complex Systems of Engineering, Ministry of Education, Southeast University (MCCSE2012A06), and the Scientific Research Foundation of Nanjing University of Posts and Telecommunications (NY210080).

References

[1] J. K. Hale and S. M. Verduyn Lunel, *Introduction to Functional Differential Equations*, Springer, New York, NY, USA, 1993.

[2] V. B. Kolmanovskii and V. R. Nosov, *Stability of Functional Differential Equations*, Academic, New York, NY, USA, 1986.

[3] S. Y. Xu, P. Van Dooren, R. Ştefan, and J. Lam, "Robust stability and stabilization for singular systems with state delay and parameter uncertainty," *IEEE Transactions on Automatic Control*, vol. 47, no. 7, pp. 1122–1128, 2002.

[4] S. S. Zhou and J. Lam, "Robust stabilization of delayed singular systems with linear fractional parametric uncertainties," *Circuits, Systems, and Signal Processing*, vol. 22, no. 6, pp. 579–588, 2003.

[5] S. Xu, J. Lam, and L. Zhang, "Robust D-stability analysis for uncertain discrete singular systems with state delay," *IEEE Transactions on Circuits and Systems I*, vol. 49, no. 4, pp. 551–555, 2002.

[6] E. Fridman and U. Shaked, "H_∞ control of linear state-delay descriptor systems: an LMI approach," *Linear Algebra and Its Applications*, vol. 351-352, pp. 271–302, 2002.

[7] E. K. Boukas and Z. K. Liu, "Delay-dependent stability analysis of singular linear continuous-time system," *IEE Proceedings*, vol. 150, no. 4, pp. 325–330, 2003.

[8] H. Su, X. Ji, and J. Chu, "Delay-dependent robust control for uncertain singular time-delay systems," *Asian Journal of Control*, vol. 8, no. 2, pp. 180–189, 2006.

[9] R. Zhong and Z. Yang, "Delay-dependent robust control of descriptor systems with time delay," *Asian Journal of Control*, vol. 8, no. 1, pp. 36–44, 2006.

[10] Z. P. Wu and W. Zhou, "Delay-dependent robust H_∞ control for uncertain singular time-delay systems," *IET Control Theory and Applications*, vol. 1, no. 5, pp. 1234–1241, 2007.

[11] S. Zhu, C. Zhang, Z. Cheng, and J. Feng, "Delay-dependent robust stability criteria for two classes of uncertain singular time-delay systems," *IEEE Transactions on Automatic Control*, vol. 52, no. 5, pp. 880–885, 2007.

[12] Z. Wu and W. Zhou, "Delay-dependent robust stabilization for uncertain singular systems with state delay," *Acta Automatica Sinica*, vol. 33, no. 7, pp. 714–718, 2007.

[13] M. Fang, "Delay-dependent robust H_∞ control for uncertain singular systems with state delay," *Acta Automatica Sinica*, vol. 35, no. 1, pp. 65–70, 2009.

[14] Z. Wu, H. Su, and J. Chu, "Improved results on delay-dependent H_∞ control for singular time-delay systems," *Acta Automatica Sinica*, vol. 35, no. 8, pp. 1101–1106, 2009.

[15] Y.-F. Feng, X.-L. Zhu, and Q.-L. Zhang, "Delay-dependent stability criteria for singular time-delay systems," *Acta Automatica Sinica*, vol. 36, no. 3, pp. 433–437, 2010.

[16] S. Zhu, Z. Li, and C. Zhang, "Delay decomposition approach to delay-dependent stability for singular time-delay systems," *IET Control Theory and Applications*, vol. 4, no. 11, pp. 2613–2620, 2010.

[17] Z. Feng, J. Lam, and H. Gao, "α-Dissipativity analysis of singular time-delay systems," *Automatica*, vol. 47, no. 11, pp. 2548–2552, 2011.

[18] D. Yue and Q.-L. Han, "A delay-dependent stability criterion of neutral systems and its application to a partial element equivalent circuit model," *IEEE Transactions on Circuits and Systems II*, vol. 51, no. 12, pp. 685–689, 2004.

[19] H. Wang, A. Xue, R. Lu, and J. Wang, "Delay-dependent robust stability and stabilization for uncertain singular system with time-varying delay," in *Proceedings of the American Control Conference*, pp. 1327–1331, Washington, DC, USA, 2008.

[20] A. Haidar and E. K. Boukas, "Exponential stability of singular systems with multiple time-varying delays," *Automatica*, vol. 45, no. 2, pp. 539–545, 2009.

[21] Z. Wu, H. Su, and J. Chu, "Delay-dependent H_∞ filtering for singular Markovian jump time-delay systems," *Signal Processing*, vol. 90, no. 6, pp. 1815–1824, 2010.

[22] Z. Wu, H. Su, and J. Chu, "H_∞ filtering for singular systems with time-varying delay," *International Journal of Robust and Nonlinear Control*, vol. 20, no. 11, pp. 1269–1284, 2010.

[23] J. Lin and S. Fei, "Reliable control for a class of uncertain singular systems with interval time-varying delay," *Asian Journal of Control*, vol. 13, no. 4, pp. 542–552, 2011.

[24] X. Zhu, Y. Wang, and Y. Gan, "H_∞ filtering for continuous-time singular systems with time-varying delay," *International Journal of Adaptive Control and Signal Processing*, vol. 25, no. 2, pp. 137–154, 2011.

[25] L. Chen, M.-Y. Zhong, and M.-Y. Zhang, "H_∞ fault detection for linear singular systems with time-varying delay," *International Journal of Control, Automation and Systems*, vol. 9, no. 1, pp. 9–14, 2011.

[26] F. Li and X. Zhang, "A delay-dependent bounded real lemma for singular LPV systems with time-variant delay," *International Journal of Robust and Nonlinear Control*, vol. 22, no. 5, pp. 559–574, 2012.

[27] Y. Ding, H. Zhu, S. Zhong, and Y. Zeng, "Exponential mean-square stability of time-delay singular systems with Markovian switching and nonlinear perturbations," *Applied Mathematics and Computation*, vol. 219, no. 4, pp. 2350–2359, 2012.

[28] T. Li, L. Guo, and Y. Zhang, "Delay-range-dependent robust stability and stabilization for uncertain systems with time-varying delay," *International Journal of Robust and Nonlinear Control*, vol. 18, no. 13, pp. 1372–1387, 2008.

[29] Y. Xia, E. Boukas, P. Shi, and J. Zhang, "Stability and stabilization of continuous-time singular hybrid systems," *Automatica*, vol. 45, no. 6, pp. 1504–1509, 2009.

[30] G. I. Bara, "Robust analysis and control of parameter-dependent uncertain descriptor systems," *Systems and Control Letters*, vol. 60, no. 5, pp. 356–364, 2011.

[31] S. Boyd, L. E. Ghaoui, E. Feron, and V. Balakrishnan, *Linear Matrix Inequalities in System and Control Theory*, SIAM, Pennsylvania, Pa, USA, 1994.

[32] L. Xie, "Output feedback H_∞ control of systems with parameter uncertainty," *International Journal of Control*, vol. 63, no. 4, pp. 741–750, 1996.

[33] L. Dai, *Singular Control Systems*, Springer, New York, NY, USA, 1989.

[34] Q.-L. Han and D. Yue, "Absolute stability of Lur'e systems with time-varying delay," *IET Control Theory and Applications*, vol. 1, no. 3, pp. 854–859, 2007.

[35] M. Krstic and H. Deng, *Stabilization of Nonlinear Uncertain Systems*, Springer, London, UK, 1998.

[36] X.-M. Zhang and Q.-L. Han, "A delay decomposition approach to delay-dependent stability for linear systems with time-varying delays," *International Journal of Robust and Nonlinear Control*, vol. 19, no. 17, pp. 1922–1930, 2009.

[37] E. Fridman and U. Shaked, "A descriptor system approach to H_∞ control of linear time-delay systems," *IEEE Transactions on Automatic Control*, vol. 47, no. 2, pp. 253–270, 2002.

Hindawi Publishing Corporation
Mathematical Problems in Engineering
Volume 2013, Article ID 150129, 7 pages
http://dx.doi.org/10.1155/2013/150129

Research Article

Modeling Analysis of DC Magnetic Bias of Iron Core Reactor of APF

Zujun Ding,[1] Lutao Liu,[2] and Baolian Liu[1]

[1] *Department of Electronic and Electrical Engineering, Huaiyin Institute of Technology, Huai'an 223001, China*
[2] *College of Information and Telecommunication, Harbin Engineering University, Harbin 150001, China*

Correspondence should be addressed to Lutao Liu; liulutao@msn.com

Received 13 September 2013; Revised 21 October 2013; Accepted 30 October 2013

Academic Editor: Zhiguang Feng

As one of the main power devices of active power filter (APF), iron core reactor DC magnetic bias would affect the performance of APF. Based on the study of DC magnetic bias mechanism of APF iron core reactor, the data model was established in this paper. The performance of APF device impacted by iron core reactor DC magnetic bias was analysed through the simulation in different DC current conditions, and optimization scheme was proposed to reduce DC magnetic bias to improve working performance of APF. To reduce DC magnetic bias, main circuit parameters and control characteristics were uniform, and reluctance of iron core was increased. Results of the simulations and experiments validated that the improved method could restrain reactor DC magnetic bias to reduce even harmonic current in APF output current, which could greatly optimize APF performance.

1. Introduction

Nowadays, with the increase of power electronic devices application, the voltage and current of electric power system have been distorted and it caused serious pollution problems of power supply quality [1, 2]. Power system harmonics suppression, to improve power quality, has become an urgent problem to be resolved [3, 4]. Active power filter (APF) is a kind of power electronic devices that is currently used to suppress harmonic and compensate reactive power [5, 6]. Figure 1 shows a parallel APF structure diagram. Because of the nonlinear load, load current I_l has harmonic component, with harmonic suppression current I_c of APF. Harmonic component of the system current I_s would be reduced. It is clearly seen that APF consists of two parts, including current detection and control units and four-leg inverter main circuit. Through current detection, APF obtains harmonic and reactive current reference value, and through pulse width modulation (PWM) control and drive circuit, inverter main circuit would generate the compensation current to realize harmonic suppression and reactive power compensation function [7, 8]. As the main power components, the filter reactor L is connected to power system with converter, and working current of APF device is undertaken. Therefore, the reactor feature is very important to decide the performance of APF [9]. APF filter reactance according to the magnetic medium can be divided into two categories [10, 11], which are air core reactor and iron core reactor. Due to the advantages of simple structure and low price, air core reactors were widely applied in the traditional APF, but insulation aging and magnetic leakage problem are the two largest unavoidable defects. So, iron core reactors have got more application in APF instead of air core reactor. DC magnetic bias of converter transformer was researched in documents [12, 13], but the study of iron core reactor DC magnetic bias mechanism in APF as high frequency converter is not sufficient [14]. In the actual application process, magnetic bias DC excitation of iron core can lead working current of APF to have large even harmonic current [15] and cause the core saturation. Thereby, it would increase the loss of reactor and reduce the efficiency of APF, which seriously affected the performance of the APF [16]. In this paper, based on study of DC magnetic bias mechanism of iron core reactor of APF, data model was established. The performance of the APF device impacted by the DC magnetic bias was analysed through simulation, and optimization scheme was proposed. Experimental results showed that the optimization could greatly reduce the DC

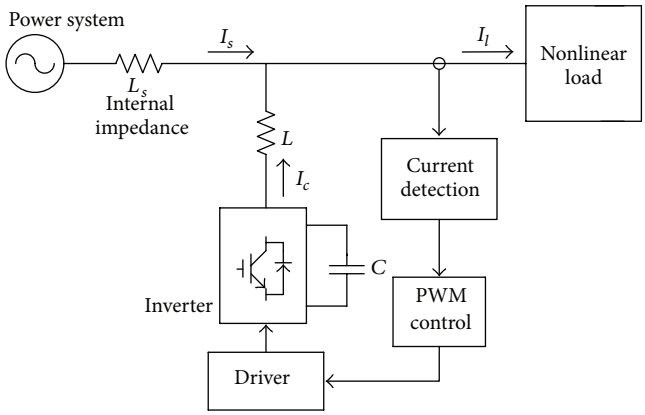

Figure 1: APF structure diagram.

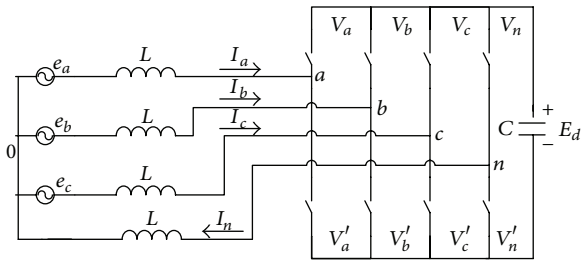

Figure 2: Main circuit configuration diagram of APF.

bias magnetic content of core reactor, even harmonic output was reduced to below 1%, and the performance of APF would be greatly optimized. Data-driven fault diagnosis methods become hot topic in industry sectors. So a combination of the proposed method and data-driven techniques is the future work to realize DC magnetic bias compression for APF operation [17–20].

The paper is organized as follows. In the next section, we introduce DC magnetic bias Mechanism of iron core reactor in APF. DC magnetic bias modeling process is extended in Section 3. In Section 4, we give simulation analysis of APF DC magnetic bias. Improved method and experiment of APF are supplied in Section 5 before summarising in Section 6.

2. Research on DC Magnetic Bias Mechanism of Iron Core Reactor in APF

Because the imbalance of forward and reverse volt second area of the transformer or reactor was inevitable in positive and negative pulse process, work hysteresis loop center of the magnetic core deviated from the coordinate origin, and this asymmetrical magnetic working state caused DC magnetic bias. In ideal conditions magnetization process of APF device iron core reactor should be two-way, excitation current should be pure alternating current (AC), and each cycle of iron core magnetic would reset in each repetition period. But because of the actual operation factors of APF, magnetic bias DC excitation of iron core would have DC component, which lead to DC magnetic bias. Specific factors of generating DC magnetic bias are as follows.

(1) The given reference sine wave and triangular wave signal of control system have DC component.

(2) The power electronics devices (IGBT) characteristics and the driving signal transmission delay are different.

(3) The feedback control systems had zero drift.

(4) The application of amplitude limiting in detection and current protection method would cause the imbalance of excitation current.

(5) The magnetic circuit of iron core reactor of APF was asymmetric.

3. DC Magnetic Bias Modeling of APF

The main circuit configuration diagram of APF was shown in Figure 2. In this figure, three-phase power system could be expressed as e_a, e_b, and e_c and zero line could be expressed as o. The filter reactor L could be expressed as L, and the output currents of APF could be expressed as I_a, I_b, I_c, and I_n. The three-phase four-leg inverter of APF was composed of IGBT devices ($V_a, V_a', \ldots, V_n, V_n'$) and DC capacitor ($C$). DC-bus voltage of capacitor could be expressed as E_d. As research object, DC magnetic bias of three-phase four wire APF was modeled, the mathematical expression was established, and the output performance of the DC bias condition of APF device was analysed as follows. The output voltage of APF converter could be expressed as

$$U_{an} = U_d + mE_d \sin(\omega_0 t + \varphi) + \sum_{n=1}^{\infty} \frac{4}{n\pi} \left\{ \frac{n\pi}{2} \left[m \sin(\omega_0 t + \varphi) - 1 \right] \right\} \cos n\omega_s t, \quad (1)$$

where U_d was DC component of output voltage, m was modulation ration, E_d was DC-bus voltage, ω_0 was fundamental frequency, and ω_s was carrier wave frequency. Assume resistance of core reactor was r; the DC current of reactor coil could be as follows:

$$I_d = \frac{U_d}{r}, \quad (2)$$

DC current would generate DC bias magnetic flux (ψ_d) and magnetic induction (B_d), which could be given as

$$\psi_d = \mu H_d S = \frac{\mu S N_i}{l_i} \cdot I_d, \qquad B_d = \frac{\psi_d}{S}, \quad (3)$$

where N_i and l_i were the number of windings and magnetic path length of the reactor, μ was magnetic permittivity of iron core, and S was cross-sectional areas of iron core. According to (1), the following equation could be obtained:

$$N_1 \frac{d\psi_1}{dt} = mE_d \sin(\omega_0 t + \varphi), \quad (4)$$

where ψ_1 was fundamental magnetic flux. Both sides of (4) were integrated with time t; then

$$\psi_1 = \frac{mE_d}{N_1\omega_0}\sin\left(\omega_0 t + \phi - \frac{\pi}{2}\right). \tag{5}$$

So, variation amplitude of fundamental magnetic flux ($\Delta\psi_1$) and induction (ΔB_1) can be given by

$$\begin{aligned}\Delta\psi_1 &= \frac{mE_d}{N_1\omega_0},\\ \Delta B_1 &= \frac{\Delta\psi_1}{S}.\end{aligned} \tag{6}$$

In order to improve the utilization ratio of iron core, the maximum magnetic induction intensity would be set near the saturated magnetic induction intensity (B_s). Normally, variation range of flux was between $-\Delta\psi_1$ and $+\Delta\psi_1$, and variation range of magnetic induction intensity was between $-\Delta B_1$ and $+\Delta B_1$. Because DC magnetic bias induction intensity existed, magnetic induction intensity ranges between $B_d - \Delta B_1$ and $B_d + \Delta B_1$. It led the core work saturation magnetization area and the current to be distorted, which was shown in Figure 3. In this figure, the dotted line was the ideal magnetic excitation process, in which the magnetic induction intensity was sine wave and it was in linearity area of the magnetization curve. So the output current was sine wave, too. However, existence of the DC magnetic bias induction intensity made the magnetic excitation process move to the saturated range of the magnetization curve. The negative and positive half wave curve of the magnetic induction intensity was asymmetric, which was shown as the solid line in Figure 3. The output current of APF was severely distorted. From Figure 3, it can be clearly seen that, with DC magnetic bias, APF working current had large even harmonic current, and it caused output current of APF half-wave asymmetry, which decayed the APF performance.

4. Simulation Analysis of APF DC Magnetic Bias

In order to analyze APF DC magnetic bias model, the simulation system was established to study the influence of DC magnetic bias. Iron core reactor was selected as APF filter reactor. Silicon steel sheet was usually chosen as iron core material of APF device, and its saturated induction intensity was normally between 1.9 T and 2.0 T. The expression for the $B-H$ function could be fitted according to the magnetization curve. Consider the following:

$$B = \alpha_1 \arctan\frac{H}{K} + \alpha_2 H, \tag{7}$$

where $\alpha_1 = 1.121$ and $\alpha_2 = 5.937 \times 10^{-6}$ were the fitting coefficients. H was magnetic field intensity and K was 204.4. The fitting curve was shown in Figure 4.

According to the definition of magnetic field intensity,

$$H = \frac{N_j}{l_j} i(t), \tag{8}$$

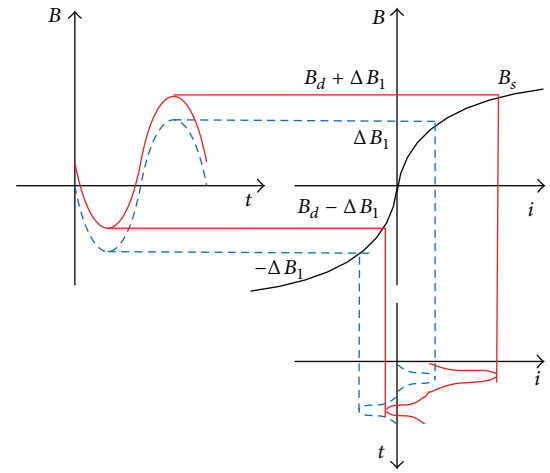

Figure 3: Current and flux based on DC magnetic bias of APF.

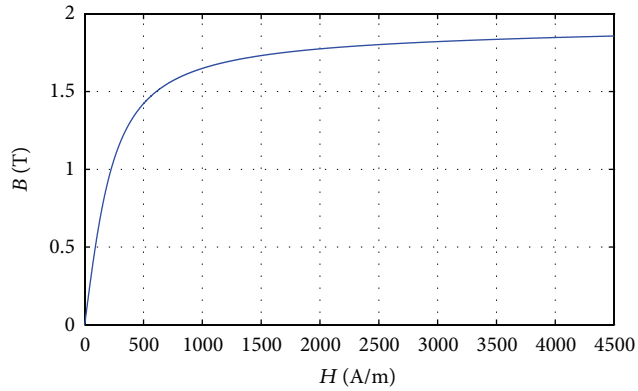

Figure 4: Magnetization curve of silicon steel sheet.

where N_j and l_j were the number of windings and magnetic path length of reactor, and $i(t)$ was output current of APF. Assumed APF mainly suppressed 5th, 7th, and 11th harmonic currents; output current of phase A would be

$$\begin{aligned}i(t) = {} & I_d + \sqrt{2}I_5\sin(5\omega_0 t) + \sqrt{2}I_7\sin(7\omega_0 t)\\ & + \sqrt{2}I_{11}\sin(11\omega_0 t),\end{aligned} \tag{9}$$

where I_d was DC current and $I_n\,(n = 5, 7, 11)$ was each order harmonic current amplitude. According to (7) and (9), magnetic induction intensity could be expressed as

$$B = f(t) = \alpha_1 \arctan\frac{N_i i(t)}{Kl_i} + \alpha_2\frac{N_i}{l_i} i(t). \tag{10}$$

According to the law of electromagnetic induction, magnetic induction intensity in the iron core of APF reactor would induce electromotive voltage and produce induced current $i(t)$, and it could be expressed as

$$i(t) = -\frac{N_i S}{r}\cdot\frac{dB}{dt}. \tag{11}$$

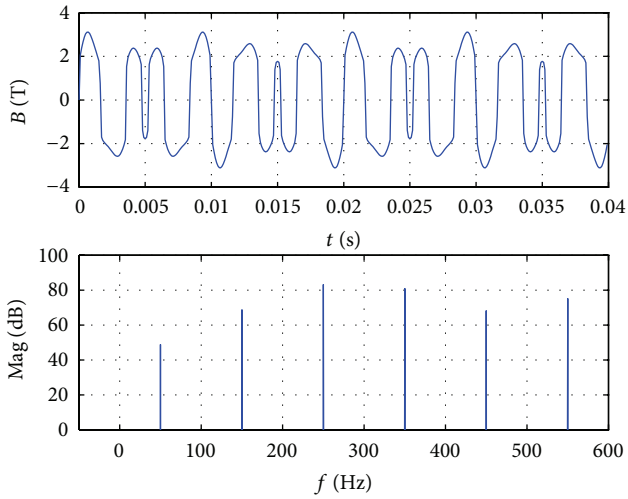

(a) Waveform and frequency spectrum when I_d is zero

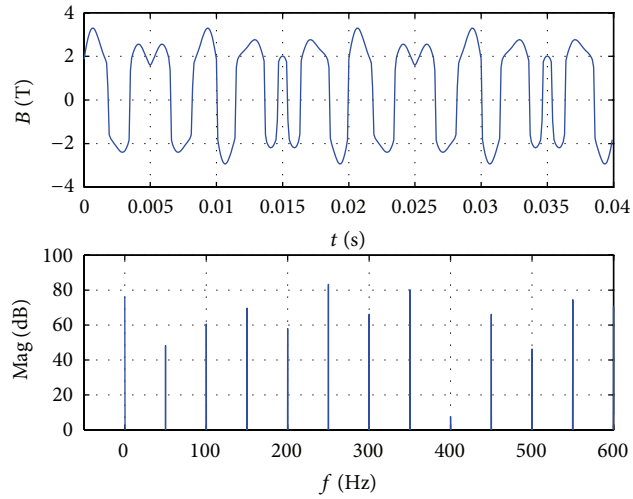

(b) Waveform and frequency spectrum when I_d is 5 A

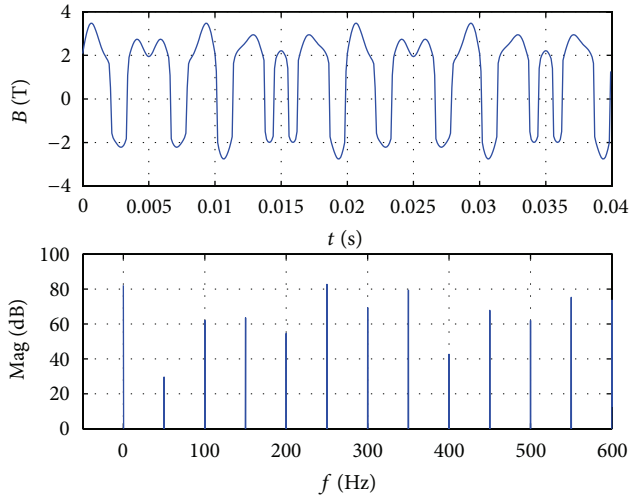

(c) Waveform and frequency spectrum when I_d is 10 A

Figure 5: Magnetic induction intensity via the different DC magnetic bias.

From (11), harmonic components in induction current were equivalent to harmonic components in magnetic induction intensity. According to Fourier decomposition of (10), frequency spectrogram of magnetic induction could be obtained. Therefore, thing $N_i = 300$ turn, $l_i = 0.5$ m, $I_5 = 20$ A, $I_7 = 14.29$ A, and $I_{11} = 9.1$ A, the relation between magnetic induction intensity and DC current (I_d) would be analyzed. And the simulation result with different I_d was shown in Figure 5. When $I_d = 0$, there are only odd harmonics in magnetic induction intensity. If DC current existed, even harmonics in magnetic induction intensity were created. With the DC current increasing, DC magnetic bias became more and more serious and even harmonics of induction intensity increased (second harmonic was the most significant in the even harmonics). And output current of APF was distorted at same time, which worsened the APF performance. So more even harmonics current were injected into the power system and reduced the power quality. From the simulation results with different DC magnetic bias conditions, we could see that the DC magnetic bias would decay the magnetic excitation process, which would reduce the performance of APF.

5. Improved Method and Experiment of APF

Iron core reactor of APF would lead DC magnetic bias while running and it could produce more even harmonics current and reduce the performance of APF. Particular attention should be paid to loss and overheat of the reactor when DC magnetic bias was serious. So, improved methods of DC magnetic bias were proposed and the improved methods were listed as follows.

(1) Main circuit parameters of APF devices and reactor characteristics may be uniform and reluctance of iron core was increased to enhance the ability against DC magnetic bias.

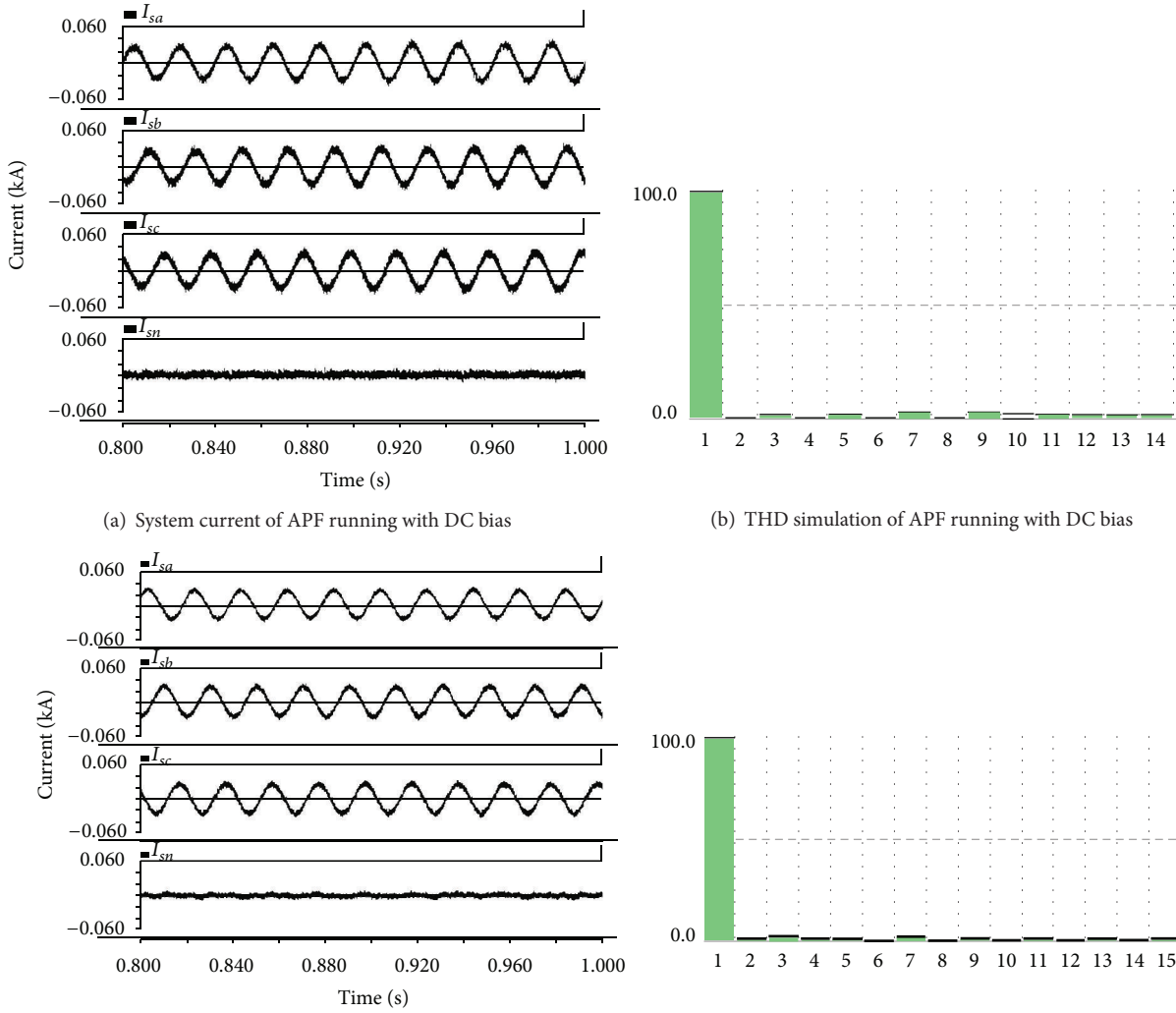

(a) System current of APF running with DC bias

(b) THD simulation of APF running with DC bias

(c) System current of APF running with improved methods

(d) THD simulation of APF running with improved methods

Figure 6: Simulation results of APF performance.

(2) Three-phase control parameters must be uniform and maximum variation rate of reference current in APF should be limited to ensure current symmetry in positive and negative half-wave region.

(3) Soft start technology can be used to prevent starting transient saturation and the minimum duty ratio of driving signal should be limited.

The simulation system of APF with DC magnetics bias influence was established in PSCAD environment, which could verify improved methods. In the simulation, AC power frequency was 50 Hz, phase voltage amplitude was 220 V, and the main circuit topology was three-phase four-leg inverter. The nonlinear load was three-phase rectifier, and the load was 10 Ω resistor series-wound to the 5 mH inductance. The DC current signal would be added to the reference current of APF to simulate DC magnetics bias, and simulation results were shown in Figure 6. System current of APF running with DC bias was shown in Figure 6(a), system current of APF running with improved methods was shown in Figure 6(b), and the system current total harmonic distortion (THD) simulation result of APF by improved methods was given in Figure 6(c). In Figure 6, I_{sa}, I_{sb}, and I_{sc} were system phase current after APF running, and I_{sn} was the zero-line current of system side. From Figure 6, it could be seen that, because of DC magnetic bias of APF, the operation performance was affected, and the system current contained the even harmonic components. The improved method could reduce DC magnetic bias, and even harmonic components of system current were reduced, which improved the APF operation performance. The system current with DC bias deviated from the coordinate origin and was asymmetric, which brought more even harmonic components, see Figures 6(a) and 6(b). However, the system current was symmetrical after processing by the proposed methods, which compressed even harmonic currents, see Figures 6(c) and 6(d). So, the proposed method could restrain DC magnetic bias to improve the APF performance.

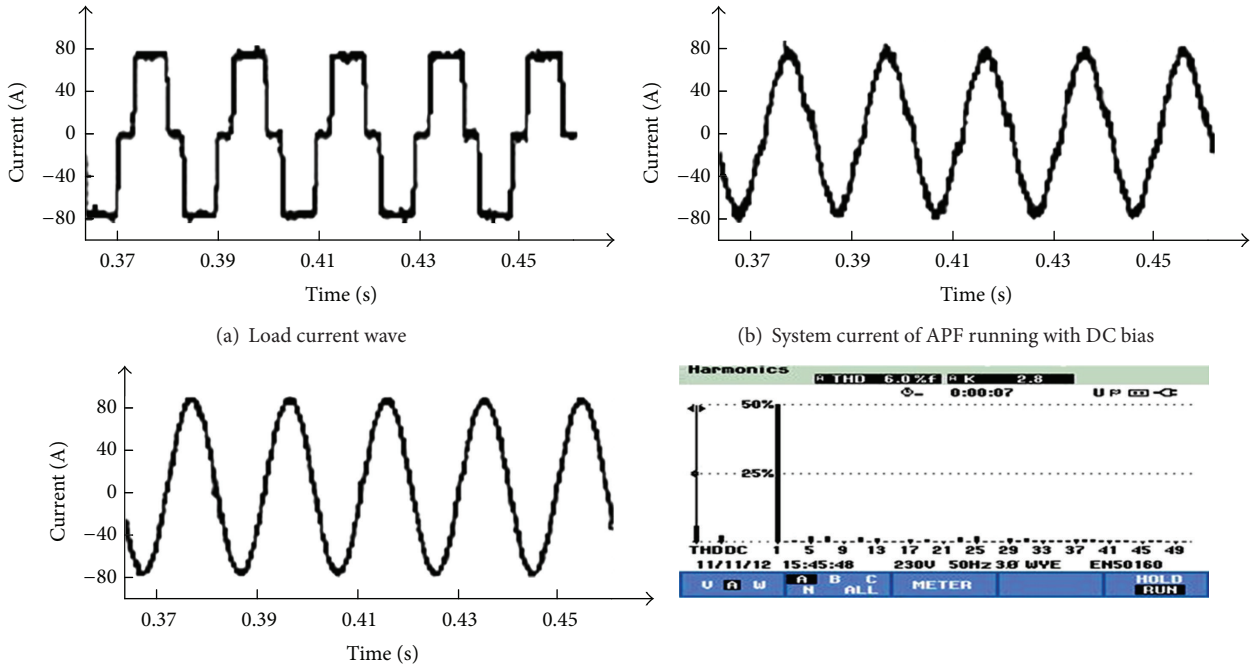

(a) Load current wave

(b) System current of APF running with DC bias

(c) System current of APF running with improved method

(d) THD simulation of APF running with improved method

Figure 7: Simulation result of APF performance.

In order to verify DC magnetics bias influence and improved methods, experiment platform was established. Iron core inductors, intelligent power module (PM75-RSE120), and capacitors are used to design main circuit of the three-phase four-wire APF device. AC power frequency was 50 Hz and voltage amplitude was 220 V. The iron core reactor was selected as the filter reactor of APF and the inductance was 4 mH. To produce harmonic current, the nonlinear load was three-phase rectifier, and the load was 8 Ω resistor series-wound to the 5 mH inductance. When APF was running, the DC current would be added to the reference current of APF to simulate DC magnetics bias of iron reactor. The experimental results were shown in Figure 7. The waveform in Figure 7(a) was the nonlinear load current of the phase A, the waveform in Figure 7(b) was the system current of phase A after compensation of APF with DC magnetic bias, and the waveform in Figure 7(c) was system current of phase A after compensation of APF with DC magnetic bias improved method. In order to validate the performance of the proposed method, total harmonic distortion (THD) analysis was shown in Figure 7(d).

From Figure 7, because of the nonlinear load, the load current was distorted. It contained many harmonic components. With reactor DC magnetic bias of APF, output current contained the even harmonic components, the filtering performance was affected, and distortion rate of power system side current after filtering by APF was 13.54%. With DC magnetic bias optimization method, even harmonic current in APF device output current was reduced. The distortion rate of power system side current after filtering by APF was only 5.4%. So, filtering performance of APF was improved obviously.

Table 1: Harmonic analysis of system side current.

Harmonic order	Nonoptimization	Optimization
2	4.78	0.55
3	1.16	0.36
4	1.57	0.30
5	0.56	0.52
6	1.28	0.22
7	0.08	0.06
8	0.78	0.17
9	1.18	0.09
10	1.37	0.18
11	0.95	0.63
12	1.26	0.04
13	0.27	0.23
THD	13.54%	5.4%

In order to analyse the proposed method of DC magnetic bias of APF, the harmonic analytical data of two operational conditions was shown in Table 1. From Table 1, it can be seen that while APF was working, DC magnetic bias would generate even harmonic current components, such as second and fourth harmonic. The even harmonic current amplitude was large and it would cause power system side current to be distorted, which affected the performance of APF.

Optimization method must be used to suppress the reactor DC bias to improve APF performance.

6. Conclusion

As one of the main power devices of APF, iron core reactor would cause DC magnetic bias at running time, which would cause loss of reactor increasing, output current containing even harmonic currents. APF device performance was decayed. The mechanism of DC bias and mathematical model were analysed in this paper. From the three-phase four-leg APF simulation, it was shown that DC magnetic bias caused by iron core reactor would produce even harmonics injected into the power grid and reduce the performance of APF. The improved method was proposed, and experimental platform was established. Experimental results shown that the improved method can reduce reactor DC magnetic bias and even harmonic current and greatly optimize APF performance. The study of this issue is quite significant for APF application.

Acknowledgments

This research has been supported by the National Natural Science Foundation of China (no. 61201410) and the Natural Science Fund for Colleges and Universities in Jiangsu Province (11KJB470002). The authors are grateful to the reviewers for their valuable comments.

References

[1] Z. Wang, J. Yang, and J. Liu, *Harmonics Suppression and Reactive Power Compensation*, China Machine Press, Beijing, China, 1998.

[2] P. Mattavelli and F. P. Marafao, "Repetitive-based control for selective harmonic compensation in active power filters," *IEEE Transactions on Industrial Electronics*, vol. 51, no. 5, pp. 1018–1024, 2004.

[3] Z. Ding, B. Liu, and Y. Zhang, "Optimal control for DC side voltage of active power filter based on auto-disturbance rejection control," *Power System Technology*, vol. 37, no. 7, pp. 2030–2034, 2013.

[4] J. Le and K. Liu, "Parameters optimization method of three-phase four-wire shunt active power filter based on unified mathematical model," *Transactions of China Electrotechnical Society*, vol. 27, no. 10, pp. 220–227, 2012.

[5] X. Wei, K. Dai, B. Xie, Y. Kang, and H.-L. Peng, "Control scheme for three-phase three-wire shunt active power filter with unbalanced loads," *Proceedings of the Chinese Society of Electrical Engineering*, vol. 28, no. 24, pp. 64–69, 2008.

[6] H. Pan, A. Luo, and C. Tu, "Development of a shunt type of high power quality regulating device," *Power System Technology*, vol. 33, no. 1, pp. 11–16, 2009.

[7] M. Izhar, C. M. Hadzer, M. Syafrudin, S. Taib, and I. Idris, "Performance for passive and active power filter in reducing harmonics in the distribution system," in *Proceedings of the National Power and Energy Conference (PECon '04)*, pp. 104–108, Kuala Lumpur, Malaysia, November 2004.

[8] G. Y. Jeong, T. J. Park, and B. H. Kwon, "Line-voltage-sensorless active power filter for reactive power compensation," *IEE Proceedings of Electric Power Applications*, vol. 147, no. 5, pp. 385–390, 2000.

[9] M. Marius, P. Florin, and S. B. Liliana, "Modeling and simuling power active filter using method of generalized reactive power theory," in *Proceedings of the IEEE International Conference on Computer Science and Automation Engineering (CSAE '11)*, vol. 2, pp. 213–218, Shanghai, China, June 2011.

[10] G. Zhang, C. Zhao, M. Ding, J.-H. Su, and H.-N. Wang, "Simulation analysis of output filter in PAPF system," *Journal of System Simulation*, vol. 21, no. 4, pp. 969–972, 2009.

[11] G. Zhang, G. Qi, J. Su, M. Ding, L. Chen, and X.-A. Zhang, "A new method of output inductance selection in shunt active power filter," *The Chinese Society of Electrical Engineering Proceedings*, vol. 30, no. 6, pp. 22–27, 2010.

[12] A. V. Makarov, O. V. Talamanov, and M. E. Kuznethova, "The mathematical model of flexible transmission systems on the magnetic bias controlled reactors basis," in *Proceedings of the IEEE Russia Power Tech*, St. Petersburg, Russia, June 2005.

[13] R. P. Price, "Geomagnetically induced current effects on transformers," *IEEE Transactions on Power Delivery*, vol. 17, no. 4, pp. 1002–1008, 2002.

[14] K. Dizheng, L. Chengmin, and D. Wan, "Experiment and research of the influence of direct-current magnetic bias on transformer," *Electric Power*, vol. 37, no. 8, pp. 12–13, 2004.

[15] A. Dovzhenko, Y. Yanovskaya, V. Pilinsky, and V. Shvaichenko, "Research of influencing of DC magnetic bias process of core of inductive slements of converters on the radiofrequency interferences of equipments," in *Proceedings of the International Conference on Modern Problems of Radio Engineering and Telecommunications and Computer Science*, vol. 1, p. 231, Lviv-Slavsko, Ukraine, February 2008.

[16] Z. Linsuo, Z. Zhanxin, B. Baodong, and Y. Song, "Research on influence of DC magnetic bias on a converter transformer," in *Proceedings of the International Conference on Electrical Machines and Systems (ICEMS '07)*, vol. 1, pp. 1346–1349, Seoul, Republic of Korea, October 2007.

[17] S. Yin, S. Ding, A. Haghani, H. Hao, and P. A. Zhang, "Comparison study of basic data-driven fault diagnosis and process monitoring methods on the benchmark Tennessee Eastman process," *Journal of Process Control*, vol. 22, no. 9, pp. 1567–1581, 2012.

[18] S. Yin, S. Ding, and H. Luo, "Real-time implementation of fault-tolerant control system with performance optimization," *IEEE Transactions on Industrial Electronics*, vol. 61, no. 5, pp. 2402–2411, 2013.

[19] S. Yin, S. Ding, A. Haghani, and H. Hao, "Data-driven monitoring for stochastic systems and its application on batch process," *International Journal of Systems Science*, vol. 44, no. 7, pp. 1366–1376, 2013.

[20] S. Yin, X. Yang, and H. Karimi, "Data-driven adaptive observer for fault diagnosis," *Mathematical Problems in Engineering*, vol. 2012, Article ID 832836, 21 pages, 2012.

Hindawi Publishing Corporation
Mathematical Problems in Engineering
Volume 2013, Article ID 714320, 8 pages
http://dx.doi.org/10.1155/2013/714320

Research Article

Congestion Control Based on Multiple Model Adaptive Control

Xinhao Yang[1] and Ze Li[2]

[1] *Department of Mechanical and Electric Engineering, Soochow University, Suzhou 215006, China*
[2] *College of Electronic and Information Engineering, Suzhou University of Science and Technology, Suzhou 215009, China*

Correspondence should be addressed to Xinhao Yang; yangxinhao@163.com

Received 13 August 2013; Accepted 11 October 2013

Academic Editor: Baoyong Zhang

The congestion controller based on the multiple model adaptive control is designed for the network congestion in TCP/AQM network. As the conventional congestion control is sensitive to the variable network condition, the adaptive control method is adopted in our congestion control. The multiple model adaptive control is introduced in this paper based on the weight calculation instead of the parameter estimation in past adaptive control. The model set is composed by the dynamic model based on the fluid flow. And three "local" congestion controllers are nonlinear output feedback controller based on variable RTT, H_2 output feedback controller, and proportional-integral controller, respectively. Ns-2 simulation results in section 4 indicate that the proposed algorithm restrains the congestion in variable network condition and maintains a high throughput together with a low packet drop ratio.

1. Introduction

In recent years, with the rapid growth of network size and network applications, congestion control has been exposed as an essential factor in communication network design. Congestion [1] occurs when the aggregate demand for a resource exceeds the available capacity of the resource, which may deteriorate the performance and the reliability of the network. Resulting effects from such congestion include long delays in data delivery, wasted resources due to lost or dropped packets, and even possible congestion collapse [2], in which all communications cease in the entire network.

TCP can only provide best effort service, in which the traffic is processed as quickly as possible, but there is no guarantee as to timeliness or actual delivery [3]. Moreover, it is difficult for the data source to perceive the network condition. When the incoming packet rate is higher than the router's outgoing packet rate, the queue size will increase and eventually give rise to the congestion. The queue management scheme in router will use queue to smooth spike in the incoming packet rates. In the Drop Tail (DT) policy which is the most extensive dropping policy, the packet will be dropped when it arrives and finds the queue full. It has been shown that the DT mechanism interacts badly with TCP's congestion control mechanisms and could lead to a poor performance [3].

In the same time, Active Queue Management (AQM) is the early notification of incipient congestion so that TCP senders can reduce their transmission rate before the queue overflows [4]. Random Early Detection (RED) [5, 6] is an important AQM mechanism, which is recommended by Internet Engineering Task Force (IETF) [7]. The basic idea behind RED queue management is to detect incipient congestion early and convey congestion notification to the end hosts, allowing them to reduce their transmission rates before queues in the network overflow and packets are dropped. To fulfill this aim, RED maintains an exponentially weighted moving average of the queue length which it uses to detect congestion. RED takes an average measure of the queue length and randomly drop packets that are within a threshold between $\min_{th}$ and $\max_{th}$. As a result, RED requires a wide range of parameters to operate correctly under different congestion scenarios. When RED parameters are not correctly defined, RED may perform even worse than the traditional tail drop policy [8, 9].

To solve the problem of the parameter setting in RED, application of the control theory to solve the congestion problem has been considered since late 1990s [10]. In such

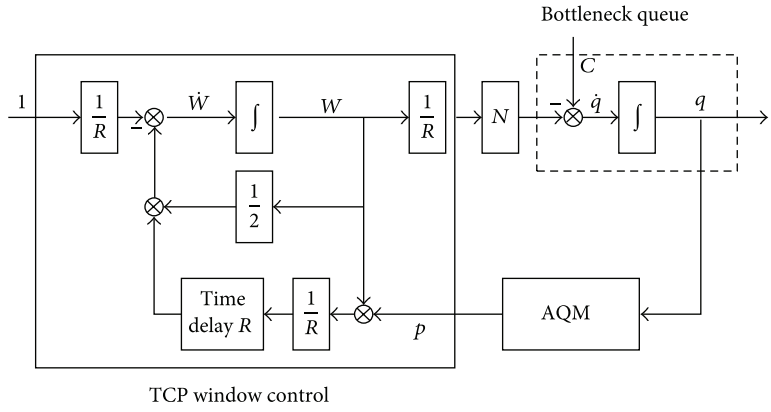

Figure 1: Block diagram of TCP's congestion avoidance flow-control mode.

approach, the main idea is to analyses the dynamic of TCP/AQM networks, build the mathematical models, and use the available tools to design and analyze suitable congestion controllers [11]. Based on the close loop system for the communication networks, several conventional controllers such as P, PI [12], PID [13], Lyapunov Drifts [14], and variable structure control (VSC) [15] have been designed as AQM scheme in TCP/AQM networks.

Due to inevitability of the time-variable parameters in network, some limitations and disadvantages are presented in the controllers mentioned above. For example, PI controllers are very sensitive to system parameter variations, and PID controller would generate a high fluctuation in queue length of router buffers [13]. Consequently, the controller seems necessary, which is of better performance in variable network condition. In [16], a self-regulating AQM controller has been proposed, which has been compared with RED and PI controllers in variable network parameters. However, it is known that self-regulatory control performs weakly in the presence of noise. In order to overcome this, congestion controller based on adaptive controller is presented in [17–23]. The parameters in conventional adaptive controllers would be considered as the infinite model identification [24].

Through the analysis above, the congestion control based on multiple model adaptive control (MMAC) is designed in this paper. Multiple model adaptive control [25–28] is considered as the finite model identification method, which uses the weight calculation rather than the parameters estimation. Simulation results indicate that the proposed multiple model adaptive congestion control (MMACC) is superior from queue length in bottleneck router, throughput for the data source, and drop ratio for the whole communication network of the conventional congestion control.

We believe that three aspects of this paper will make it interesting to general readers. Firstly, the congestion control algorithm based on the adaptive control is proposed in variable network condition. Secondly, the multiple model adaptive control is introduced in this paper based on the weight calculation instead of the parameter estimation in traditional adaptive control. Finally, the model set is introduced in the paper, which is composed by the dynamic model based on the fluid flow. The rest of the paper is structured as follows. The dynamic model of TCP/AQM in congestion control is discussed in Section 2. Section 3 investigates the design of our proposed MMACC for congestion control. Simulation results are presented in Section 4. Finally, Section 5 concludes the paper.

2. A Fluid-Flow Model of TCP Behavior

In this section, we overview the system model [29] for TCP and queue dynamics based on fluid-flow and stochastic differential equation analysis. This model describes a sample path of each long-lived TCP connection with an additive increase and multiplicative decrease (AIMD) strategy and is given by the following coupled, nonlinear differential equations:

$$\dot{W}(t) = \frac{1}{R(t)} - \frac{W(t)}{2}\frac{W(t-R(t))}{R(t-R(t))}p(t-R(t)),$$
$$\dot{q}(t) = -C(t) + \frac{N(t)}{R(t)}W(t), \tag{1}$$

where W is the average congestion window size (packets), q is the average queue length (packets), $R(t) = q(t)/C(t) + T_p$ is the round trip time (secs), and p is the probability of packet mark/drop in AQM, which takes value only in $[0, 1]$. C, T_p and N denote the link capacity (packets/sec), the propagation delay (secs), and the connection number, respectively. $1/R(t)$ indicates the additive increase strategy, and $W(t)/2$ means the multiplicative decrease strategy. Simulation results demonstrated that this model accurately captured the dynamics of TCP. Hollot et al. [30] illustrated these differential equations in the block diagram of Figure 1 which highlights TCP window-control and queue dynamics.

Taking (W, q) as the state variables and p as the reference input, the equilibrium point (W_0, q_0, p_0) is defined by $\dot{W} = 0$ and $\dot{q} = 0$, so that

$$W_0 = \sqrt{\frac{2}{p_0}} = \frac{R_0 C_0}{N_0} = \frac{q_0 + C_0 T_p}{N_0},$$
$$p_0 = \frac{2N_0^2}{(R_0 C_0)^2} = \frac{2N_0^2}{(q_0 + C_0 T_p)^2}, \quad (2)$$
$$R_0 = \frac{q_0}{C_0} + T_p,$$

where the steady sate queue length q_0 is the desired queue length in the buffer and $N(t) \equiv N_0$ and $C(t) \equiv C_0$ are assumed as constants.

Employing small signal linearization, we linearize the model (1) about equilibrium point and ignore the delay term. The simplified dynamics is given as

$$\dot{x}_1(t) = -\frac{N_0}{R_0^2 C_0}(x_1(t) + x_1(t - R_0)) - \frac{R_0 C_0^2}{2N_0^2} u(t - R_0) - \frac{1}{R_0^2 C_0}(x_2(t) - x_2(t - R_0)),$$
$$\dot{x}_2(t) = \frac{N_0}{R_0} x_1(t) - \frac{1}{R_0} x_2(t), \quad (3)$$

where $x_1(t) = \delta W = W(t) - W_0$, $x_2(t) = \delta q = q(t) - q_0$, $u(t) = \delta p = p(t) - p_0$.

Based on (3) and assuming $R_0 \gg N_0/C_0$ (which allows us to ignore the delay), the open loop transfer function of linearized system can be obtained as

$$P(s) = \frac{K}{(T_1 s + 1)(T_2 s + 1)}, \quad (4)$$

where $K = (R_0 C_0)^3 / 4N_0^2$, $T_1 = R_0$, $T_2 = R_0^2 C_0 / 2N_0$.

Remark 1. For typical network condition, $W_0 \gg 1$ is a reasonable assumption. Based on formula (2), we can get $W_0 = R_0 C_0 / N_0$, so $R_0 \gg N_0/C_0$.

Discrediting (4) with sampling period T_s using the bilinear Z-transformation $s = (2/T)((1 - z^{-1})/(1 + z^{-1}))$, the equivalent discrete system model of the linearized TCP/AQM can be written as follows:

$$P(z) = \frac{b_0 + b_1 z^{-1} + b_2 z^{-2}}{1 + a_1 z^{-1} + a_2 z^{-2}}, \quad (5)$$

where

$$a_1 = \frac{2(T_s^2 - 4T_1 T_2)}{(T_s + 2T_1)(T_s + 2T_2)},$$
$$a_2 = \frac{(T_s - 2T_1)(T_s - 2T_2)}{(T_s + 2T_1)(T_s + 2T_2)},$$
$$b_0 = b_2 = \frac{K T_s^2}{(T_s + 2T_1)(T_s + 2T_2)}, \quad (6)$$
$$b_1 = \frac{2K T_s^2}{(T_s + 2T_1)(T_s + 2T_2)}.$$

3. Congestion Control Based on Multiple Model Adaptive Control

In this section, we present the proposed multiple model adaptive congestion controller. First, we describe the multiple model adaptive control taken into consideration. Then, we introduce the "local" congestion controller assigned in MMAC.

3.1. The MMAC Controller. Now, the system equation with input $u(k)$, output $y(k)$, and the system noise $e(k)$ can be written as

$$A(z^{-1}) y(k) = B(z^{-1}) u(k) + e(k), \quad (7)$$

where $A(z^{-1}) = 1 + a_1 z^{-1} + \cdots + a_n z^{-n}$ is a single polynomial of order n with coefficients a_i and $B(z^{-1}) = b_0 + b_1 z^{-1} + \cdots + b_m z^{-m}$ is a general polynomial of order m with coefficients b_i.

Remark 2. According to the statistics of MCI, 95% of bytes and 90% of packets are transported within the TCP scheme [31]. So the non-TCP data traffics, such as UDP, are considered as the noise in congestion control model.

In order to estimate the online parameters, the output $y(k)$ can be rewritten as

$$y(k) = \theta \varphi^T(k), \quad (8)$$

where

$$\theta = [-a_1, \ldots, -a_n, b_0, b_1, \ldots, b_m],$$
$$\varphi(k) = [y(k-1), \ldots, y(k-n), u(k), \ldots, u(k-m)], \quad (9)$$

where $\mathbf{M} = \{M_i, i = 1, 2, \ldots, N\}$ is the model set that may include the true model of the unknown plant $\mathbf{P}$. Further, define y_i as the output of M_i. For each model $M_i \in \mathbf{M}$, its output error is given by

$$e_i = y(k) - y_i(k). \quad (10)$$

A concise block diagram is shown in Figure 2 to represent an MMAC system, where "local" controller C_i is designed

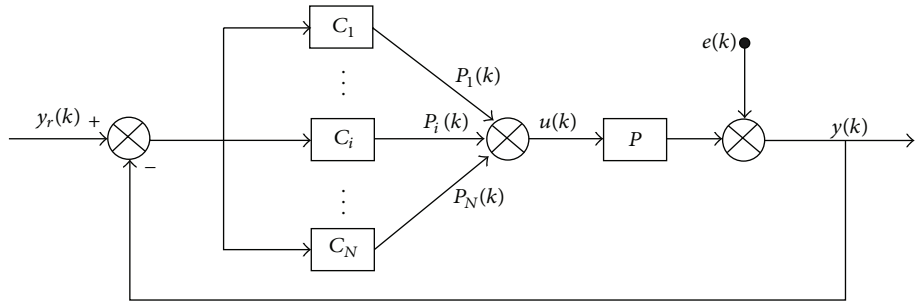

Figure 2: Block diagram of MMAC system.

according to any possible control strategies, if C_i stabilizes model M_i. Then, the global control $u(k)$ is obtained by

$$u(k) = \sum_{i=1}^{N} p_i(k)\, u_i(k), \tag{11}$$

where $u_i(k)$ is the output of the "local" controller C_i.

Typically, controller weights $p_i(k)$ are calculated through a bank of Kalman filters [32]. But in [28], a new algorithm is proposed which is simpler in $p_i(k)$ calculation; that is,

$$\begin{aligned} p_i(0) &= l_i(0) = \frac{1}{N}, \\ l_i'(k) &= 1 + \frac{1}{k}\sum_{r=1}^{k} e_i^2(r), \\ l_{\min}'(k) &= \min_i \left\{ l_i'(k) \right\}, \\ l_i(k) &= \frac{l_{\min}'(k)}{l_i'(k)} l_i(k-1), \\ p_i(k) &= \frac{l_i(k)}{\sum_{r=1}^{N} l_r(k)}. \end{aligned} \tag{12}$$

3.2. "Local" Congestion Controller. The model set $\mathbf{M}$ is composed by three kinds of congestion models including nonlinear model, local linearization model, and the model without time delay. The model set is described as follows:

$$\mathbf{M} = \{ M_i, i = 1, 2, 3 \}. \tag{13}$$

In other words, three "local" congestion controllers (C_1, C_2, and C_3) should be designed to stabilize the submodel M_i, respectively.

Firstly, nonlinear output feedback control based on variable RTT (NOFC-VRTT, C_1) [33] is designed according to nonlinear dynamic model (1); that is,

$$\begin{aligned} p_1(k) = 2 \Big[& N_0 \overline{q}(k) + \left(N_0 \widehat{W}(k)\, \overline{q}(k) - 1 \right) \left(k_1 \overline{q}^* - 1 \right) \\ & + k_2 \overline{q}(k) \left(N_0 \widehat{W}(k)\, \overline{q}(k) - 1 - k_1 \left(\overline{q}(k) - \overline{q}^* \right) \right) \Big] \\ & \times \left(N_0 \widehat{W}^2(k)\, \overline{q}(k) \right)^{-1}. \end{aligned} \tag{14}$$

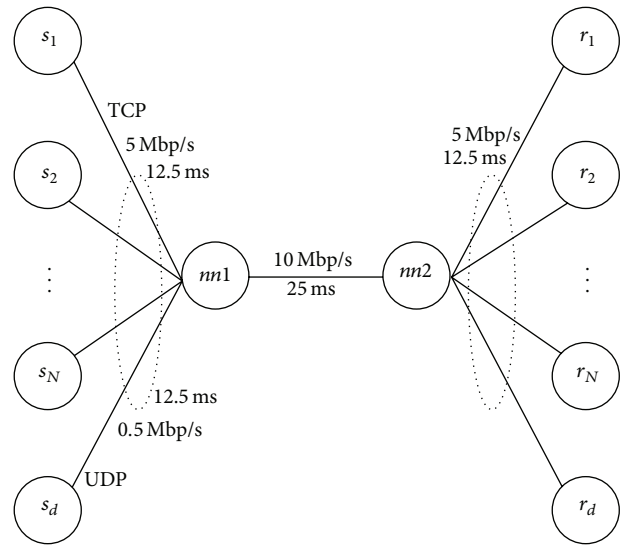

Figure 3: Network topology.

The congestion window observer is chosen as

$$\dot{\widehat{W}}(k) = C_0 \overline{q}(k) - \frac{C_0}{2} \widehat{W}^2(k)\, \overline{q}(k)\, p(k), \tag{15}$$

where

$$\overline{q} = \frac{1}{q + T_p C}, \qquad \overline{q}^* = \frac{1}{q_0 + T_p C_0}. \tag{16}$$

The control parameters k_1 and k_2 should satisfy the following inequalities:

$$\begin{aligned} & 1 \le k_1 \overline{q}^* + k_2 \overline{q} \le 2, \\ & 0 \le N_0 \overline{q} + 1 - k_1 \overline{q}^* - k_2 \overline{q} - k_1 k_2 \overline{q} z_2 \\ & \quad \le 2 N_0 \overline{q} \left(2 - k_1 \overline{q}^* - k_2 \overline{q} \right). \end{aligned} \tag{17}$$

Secondly, based on the linear state space model (3), the H_2 output feedback controller (H_2OFC, C_2) could be presented as

$$\begin{aligned} \dot{\widehat{x}}(t) &= \widehat{A}_0 \widehat{x}(t) + \widehat{A}_1 \widehat{x}(t - R_0) + \widehat{B} y(t), \\ u(t) &= \widehat{C}_0 \widehat{x}(t) + \widehat{C}_1 \widehat{x}(t - R_0) + \widehat{D} y(t). \end{aligned} \tag{18}$$

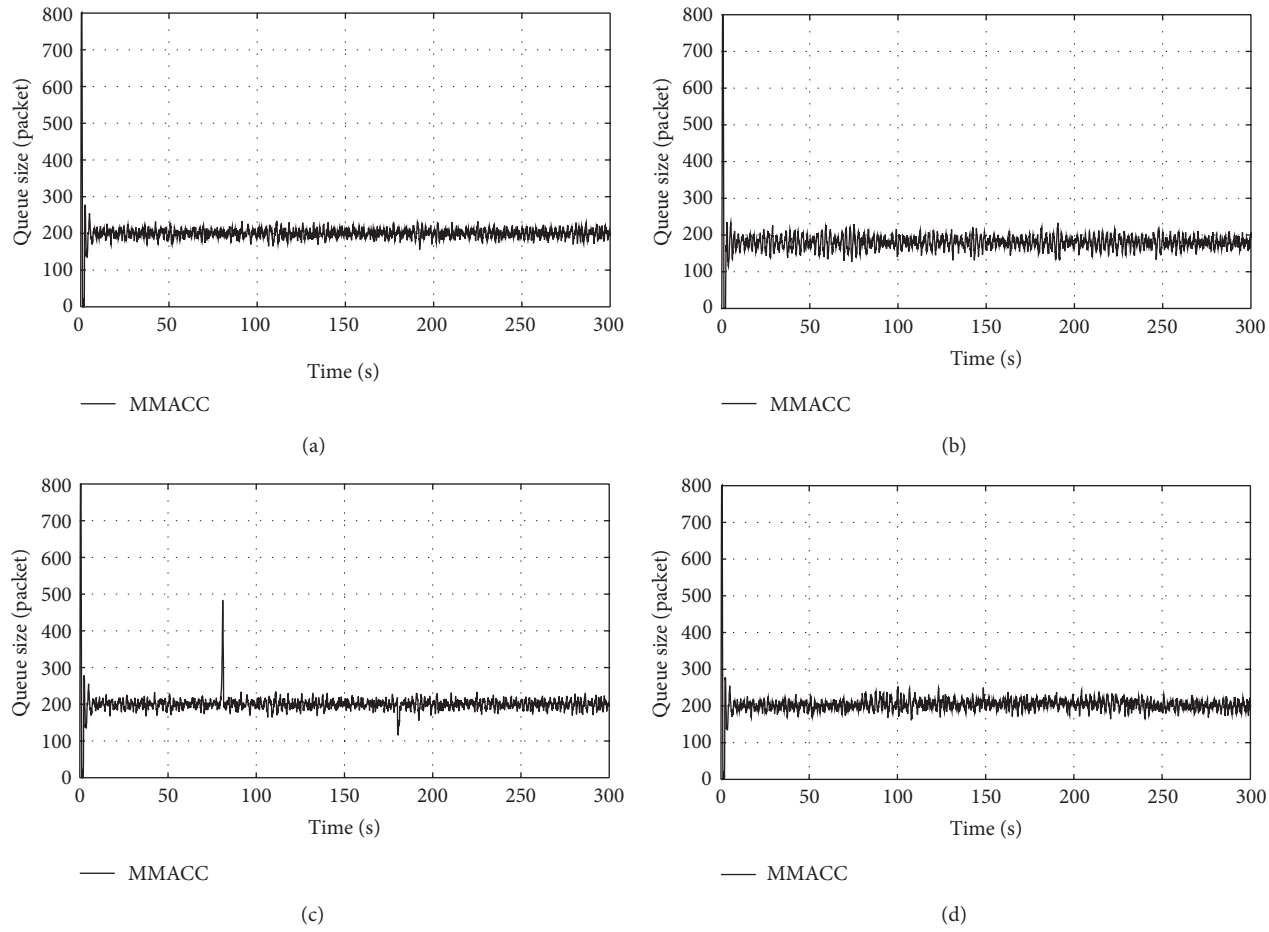

Figure 4: Robustness of MMACC.

This controller could also be described in the frequency domain by the nonrational transfer function

$$C_2(s) = \left(\widehat{C}_0 + \widehat{C}_1 e^{-sR_0}\right)\left(sI - \widehat{A}_0 - \widehat{A}_1 e^{-sR_0}\right)^{-1}\widehat{B} + \widehat{D}, \quad (19)$$

where the parameter matrices $\widehat{A}_0$, $\widehat{A}_1$, $\widehat{B}$, $\widehat{C}_0$, $\widehat{C}_1$, and $\widehat{D}$ are regulated by the linear matrix inequalities. A detailed description of the regulation could be seen in Section 3 of [34]. In the same time, the transfer function in the z-domain is obtained by the bilinear Z-transformation.

Lastly, the classical proportional integral control (PI, C_3) is adopted in the transfer function model (4), and the parameter tuning is discussed in paper [35]:

$$C_3(s) = K_p + \frac{K_i}{s} = K_{PI}\frac{(s/z+1)}{s}. \quad (20)$$

4. Simulation

In this section, we verify the proposed MMACC via simulation using the Ns-2 simulator. The benchmark network topology is addressed as shown in Figure 3. The following numerical values are considered as the system parameters: $N = 30$ TCP sessions, $T_p = 0.1$ s, $q_0 = 200$ packets, and buffer size is 800 packets. Also, the bottleneck link bandwidth is 10 Mb/s with an average packet size of 500 byte which results in $C = 2500$ packets/s. Using these parameters, we can calculate other parameters such as R_0, W_0, and p_0 according to formula (2). Node S_d is set up as the UDP sender with a 0.5 Mb/s bandwidth as discussed in Section 3.1. The sample frequency is 160 Hz, and the simulation period equals to 300 s. The parameters of the three "local" controllers are designed by the network simulation condition above.

In detail, the parameters of C_1 are as follows:

$$k_1 = 224, \qquad k_2 = \frac{11}{3}. \quad (21)$$

The parameters of C_2 are calculated as

$$a = 1.547e-9, \qquad b = 0.3607. \quad (22)$$

And the parameters of C_3 are

$$K_p = 1.822e-5, \qquad K_i = 1.816e-5. \quad (23)$$

Experiment 3. Now we look at the bottleneck router *nn*1 running MMACC and router *nn*2 running drop tail algorithm. In order to verify the robustness of the proposed MMACC, the network condition is changed as follows: (a) initial condition; (b) propagation delay T_p is converted from 0.1 s to 0.15 s;

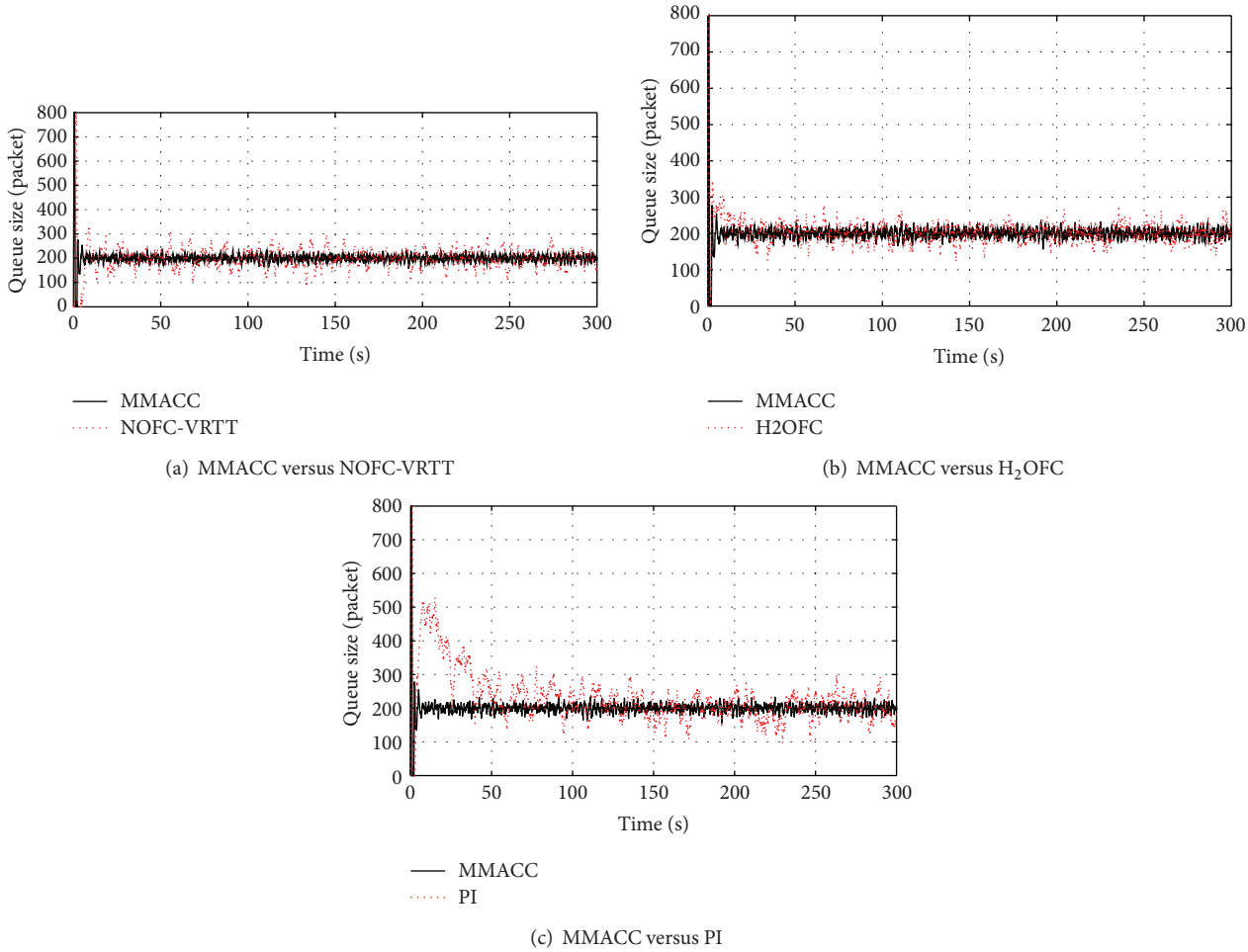

(a) MMACC versus NOFC-VRTT

(b) MMACC versus H_2OFC

(c) MMACC versus PI

Figure 5: Instantaneous queue length in the bottleneck router.

(c) 15 new FTP sources start at 80 s and 15 FTP sources stop at 180 s randomly; (d) UDP/CBR source as noise starts at 80 s and stops at 240 s. Figure 4 shows the instantaneous queue length of the bottleneck router in variable network condition. As depicted in Figure 4, the instantaneous queue length maintains round the equilibrium value. The simulation results show that MMACC has a good robustness when network condition changes or modeling is uncertain.

Experiment 4. MMACC is considered as the linear combination of the NOFC-VRTT, H_2OUT, and PI. In this simulation experiment, we compare the performance of the four congestion controllers. Figure 5 displays the queue length of the bottleneck router adopting the four congestion control strategies. It is indicated that MMACC has well disturbance attenuation and strong convergence. Tables 1 and 2 show that MMACC achieves a lower packet drop ratio and a higher link utilization than the other three congestion controls in variable network conditions. The simulation results show that MMACC provides better network performance and higher quality of service (QoS). On the other hand, PI controller omitted the high frequency part of the fluid model, and NOFC-VRTT controller only gave the range of the control coefficient. So the performance of H_2OFC is much better among the three "local" congestion controllers.

Table 1: Packet drop ratio in variable RTT.

RTT(s)	0.10	0.12	0.14	0.16	0.18	0.20
MMACC	0.393%	0.361%	0.329%	0.303%	0.282%	0.271%
NOFC-VRTT	0.683%	0.628%	0.581%	0.540%	0.492%	0.479%
H_2OFC	0.931%	0.720%	0.630%	0.504%	0.393%	0.372%
PI	1.556%	1.263%	0.989%	0.767%	0.576%	0.497%

Table 2: Link utilization in variable RTT.

RTT(s)	0.10	0.12	0.14	0.16	0.18	0.20
MMACC	95.41%	95.09%	94.83%	94.57%	94.22%	94.07%
NOFC-VRTT	95.27%	94.78%	94.45%	93.92%	93.47%	93.10%
H_2OFC	95.03%	93.68%	92.04%	89.85%	86.76%	85.71%
PI	95.27%	94.72%	94.14%	93.05%	91.63%	89.69%

5. Conclusion

A new AQM method for TCP network based on multiple model adaptive control has been presented in the paper.

Three dynamic models based on the TCP/AQM fluid-flow mode have been designed for the MMAC. Then the proposed adaptive method regulates the weight of the "local" congestion controller. Simulation results demonstrate that the proposed MMACC scheme is able to preserve the queue length efficiently in the bottleneck router around the desired point. In addition, the superior performance of the proposed controller has been illustrated through the results obtained via Ns-2 simulation. In the MMACC, all of the "local" congestion controllers are queue-based AQM scheme. As the rate-based schemes, providing early feedback for congestion, the rate-based "local" congestion controller would improve our MMACC, which is the next step for us.

Conflict of Interests

The authors declare that there is no conflict of interests regarding the publication of this paper.

Acknowledgment

The authors are indebted to the National Natural Science Foundation of China (61203048, 61201212, and 61304047) for financial support.

References

[1] C. Long, B. Zhao, X. Guan, and J. Yang, "The Yellow active queue management algorithm," *Computer Networks*, vol. 47, no. 4, pp. 525–550, 2005.

[2] V. Jacobson, "Congestion avoidance and control," in *Proceeding of the ACM Symposium on Communications Architectures and Protocols (SIGCOMM '88)*, pp. 314–329, ACM, 1988.

[3] M. H. Yaghmaee and H. A. Toosi, "A fuzzy based on active queue management algorithm," in *Proceeding of the International Symposium on Performance Evaluation of Computer and Telecommunication Systems (SPECTS '03)*, pp. 458–462, 2003.

[4] B. Braden, D. D. Clark, and J. Crowcroft, "Recommendations on queue management and congestion avoidance in the internet," IETF RFC 2309, 1998.

[5] S. Floyd and V. Jacobson, "Random early detection gateways for congestion avoidance," *IEEE/ACM Transactions on Networking*, vol. 1, no. 4, pp. 397–413, 1993.

[6] S. Floyd, R. Gummadi, and S. Shenker, "Adaptive RED: an algorithm for increasing the robustness of RED," Tech. Rep., 2001.

[7] K. Ramakrishnan and S. Floyd, "A proposal to add explicit congestion notification (ECN) to IP," IETF RFC2481, 1999.

[8] S. Doran, "RED experience and differentiated queueing," in *Proceeding of the North American Network Operators Group (NANOG '98)*, June 1998.

[9] M. Martin, B. Thomas, and J. C. Bolot, "Analytic evaluation of RED performance," in *Proceeding of the 19th Annual Joint Conference of the IEEE Computer and Communications Societies (INFOCOM '00)*, vol. 3, pp. 1415–1424, Tel Aviv, Israel, March 2000.

[10] W. H. Kwon and H. S. Kim, "A survey of control theoretic approaches in wired and wireless communication networks," in *Proceeding of the Korea-Japan Joint Workshop.*, pp. 30–45, 2000.

[11] M. A. Ardestani and M. T. H. Beheshti, "A robust discrete-time controller for delay sensitive applications," in *Proceeding of the 7th International Conference on Information, Communications and Signal Processing (ICICS '09)*, Macau, December 2009.

[12] L. Tan, W. Zhang, G. Peng, and G. Chen, "Stability of TCP/RED systems in AQM routers," *IEEE Transactions on Automatic Control*, vol. 51, no. 8, pp. 1393–1398, 2006.

[13] C. V. Hollot, V. Misra, D. Towsley, and W. B. Gong, "On designing improved controllers for AQM routers supporting TCP flows," in *Proceeding of the 20th Annual Joint Conference of the IEEE Computer and Communications Societies (INFOCOM '01)*, vol. 3, pp. 1726–1734, Anchorage, Alska, USA, April 2001.

[14] A. Sridharan, S. Moeller, and B. Krishnamachari, "Making distributed rate control using lyapunov drifts a reality in wireless sensor networks," in *Proceeding of the 6th International Symposium on Modeling and Optimization in Mobile, AdHoc, and Wireless Networks (WiOPT '08)*, pp. 452–461, Berlin, Germany, April 2008.

[15] M. Yan, Y. Jing, and Y. An, "Congestion control over internet with uncertainties and input delay based on variable structure control algorithm," in *Proceeding of the IEEE International Conference on Mechatronics and Automation (ICMA '07)*, pp. 1788–1793, Harbin, China, August 2007.

[16] M. F. Firuzi and M. Haeri, "Active queue management in TCP networks based on self tuning control approach," in *Proceeding of the IEEE Conference on Control Applications (CCA '05)*, pp. 904–909, Toronto, Canada, August 2005.

[17] R. R. Chen and K. Khorasani, "A robust adaptive congestion control strategy for large scale networks with differentiated services traffic," *Automatica*, vol. 47, no. 1, pp. 26–38, 2011.

[18] R. Barzamini, M. Shafiee, and A. Dadlani, "Adaptive generalized minimum variance congestion controller for dynamic TCP/AQM networks," *Computer Communications*, vol. 35, no. 2, pp. 170–178, 2012.

[19] J. X. Wang, P. P. Dong, J. Chen et al., "Adaptive explicit congestion control based on bandwidth estimation for high bandwidth-delay product networks," *Computer Communications*, vol. 36, no. 10–11, pp. 1235–1244, 2013.

[20] P. Jacko and B. Sansò, "Optimal anticipative congestion control of flows with time-varying input stream," *Performance Evaluation*, vol. 69, no. 2, pp. 86–101, 2012.

[21] Z. Q. Zhan, J. Zhu, and D. Xu, "Stability analysis in an AVQ model of internet congestion control algorithm," *The Journal of China Universities of Posts and Telecommunications*, vol. 19, no. 4, pp. 22–28, 2012.

[22] M. Radenkovic and A. Grundy, "Efficient and adaptive congestion control for heterogeneous delay-tolerant networks," *Ad Hoc Networks*, vol. 10, no. 7, pp. 1322–1345, 2012.

[23] W. Zhang, L. S. Tan, C. Yuan et al., "Internet primal-dual congestion control: stability and applications," *Control Engineering Practice*, vol. 21, no. 1, pp. 87–95, 2013.

[24] W. Zhang, "Stability of weighted multiple model adaptive control," *Journal of Control Theory and Applications*, vol. 29, no. 12, pp. 1657–1166, 2012.

[25] S. Fekri, M. Athans, and A. Pascoal, "Issues, progress and new results in robust adaptive control," *International Journal of Adaptive Control and Signal Processing*, vol. 20, no. 10, pp. 519–579, 2006.

[26] S. Fekri, M. Athans, and A. Pascoal, "Robust multiple model adaptive control (RMMAC): a case study," *International Journal of Adaptive Control and Signal Processing*, vol. 21, no. 1, pp. 1–30, 2007.

[27] V. Hassani, J. Hespanha, M. Athans, and A. Pascoal, "Stability analysis of robust multiple model adaptive control," in *Proceeding of the 18th International Federation of Automatic Control World Congress (IFAC '11)*, vol. 18, pp. 350–355, 2011.

[28] W. Zhang, "Stable weighted multiple model adaptive control: discrete-time stochastic plant," *International Journal of Adaptive Control and Signal Processing*, vol. 27, no. 7, pp. 562–581, 2013.

[29] V. Misra, W. B. Gong, and D. Towsley, "Fluid-based analysis of a network of AQM routers supporting TCP flows with an application to RED," in *Proceedings of the ACM SIGCOMM Conference (SIGCOMM '00)*, pp. 151–160, ACM, Stockholm, Sweden, September 2000.

[30] C. V. Hollot, V. Misra, D. Towsley, and W. B. Gong, "A control theoretic analysis of RED," in *Proceeding of the 20th Annual Joint Conference of the IEEE Computer and Communications Societies (INFOCOM '01)*, pp. 1510–1519, Anchorage, Alska, USA, April 2001.

[31] K. Thompson, G. J. Miller, and R. Wilder, "Wide-area internet traffic patterns and characteristics," *IEEE Network*, vol. 11, no. 6, pp. 10–23, 1997.

[32] S. Fekri, M. Athans, and A. Pascoal, "Issues, progress and new results in robust adaptive control," *International Journal of Adaptive Control and Signal Processing*, vol. 20, no. 10, pp. 519–579, 2006.

[33] X. H. Yang and Z. Q. Wang, "NOFC-VRTT: nonlinear AQM algorithm based on variable RTT," *Control and Decision*, vol. 25, no. 1, pp. 69–78, 2010.

[34] M. Michele, L. S. Nelson, and C. Jose, "An optimal active queue management controller," in *Proceeding of the IEEE International Conference on Communications (ICC '04)*, vol. 4, pp. 2261–2266, Paris, France, June 2004.

[35] C. V. Hollot, V. Misra, D. Towsley, and W. B. Gong, "On designing improved controllers for AQM routers supporting TCP flows," in *Proceeding of the 20th Annual Joint Conference of the IEEE Computer and Communications Societies (INFOCOM '01)*, vol. 3, pp. 1726–1734, Anchorage, Alska, USA, April 2001.

Hindawi Publishing Corporation
Mathematical Problems in Engineering
Volume 2013, Article ID 841376, 12 pages
http://dx.doi.org/10.1155/2013/841376

Research Article

Obstacle Avoidance for Unmanned Undersea Vehicle in Unknown Unstructured Environment

Zheping Yan,[1] Yufei Zhao,[1] Shuping Hou,[2] Honghan Zhang,[1] and Yalin Zheng[3]

[1] *College of Automation, Harbin Engineering University, Harbin, Heilongjiang 150001, China*
[2] *College of Mechanical and Electrical Engineering, Harbin Engineering University, Harbin, Heilongjiang 150001, China*
[3] *Department of Eye and Vision Science, University of Liverpool, Liverpool, UK*

Correspondence should be addressed to Zheping Yan; yanzheping2013@163.com

Received 3 September 2013; Accepted 7 October 2013

Academic Editor: Zhiguang Feng

To avoid obstacle in the unknown environment for unmanned undersea vehicle (UUV), an obstacle avoiding system based on improved vector field histogram (VFH) is designed. Forward looking sonar is used to detect the environment, and the divisional sonar modal is applied to deal with the measure uncertainty. To adapt to the VFH, rolling occupancy grids are used for the map building, and high accuracy details of local environment are obtained. The threshold is adaptively adjusted by the statistic of obstacles to solve the problem that VFH is sensitive to threshold. To improve the environment adaptability, the hybrid-behaviors strategy is proposed, which selects the optimal avoidance command according to the motion status and environment character. The simulation shows that UUV could avoid the obstacles fast and escape from the U shape obstacles.

1. Introduction

UUV plays an increasingly important role in underwater operations. A major challenge in the development of UUV is obstacle avoidance in unknown, complex, and unstructured environment. This demands UUV to have accurate perception of environment and make decision intelligently. Obstacle detection and avoidance strategy are two key technologies in obstacle avoidance [1, 2].

For obstacle detection, forward looking sonar (FLS) is the primary sensor to obtain the underwater information [3]. Since sonar data are incomplete and time delayed, current information measured is not enough for avoidance decision. A map with historical sonar data is essential for avoidance. Compared with geometric map and topology map, occupancy grids map is more convenient to describe the unstructured obstacle and has better capability to handle measure uncertainty [4]. Meanwhile, global map cannot be used in long voyage, because of the storage and processing constrains. To save the map storage space and improve the mapping speed, local map is widely used, which can quickly create map with accurate details.

For avoidance strategy, there are many popular real-time avoidance approaches, such as, artificial potential field (APF) [5], dynamic window approach (DWA) [6], fuzzy systems [7], expert systems [8], and neural network [9]. However, they all have drawbacks. For instance, APF and DWA are unable to grasp the environmental connectivity and are easily trapped into local minima position. Design of fuzzy system is complex, and it is difficult to determine avoidance rules. The vector field histogram (VFH) is developed based on the concept of APF and certainty grid. There is two-stage data reduction process for computing the desired commands. In the first stage the histogram grid is reduced to one-dimensional polar histogram. Each sector in the polar histogram contains a polar obstacle density (POD). In the second stage, the algorithm selects the most suitable steering direction among all polar histogram sectors with a low POD [10]. VFH and many of its variants (VFH*,VFH+) are computationally efficient and important consideration for real-time operation [10, 11]. It has been used widely in many fields and can be used for UUV avoidance. However, VFH has some shortcomings, which must be solved.

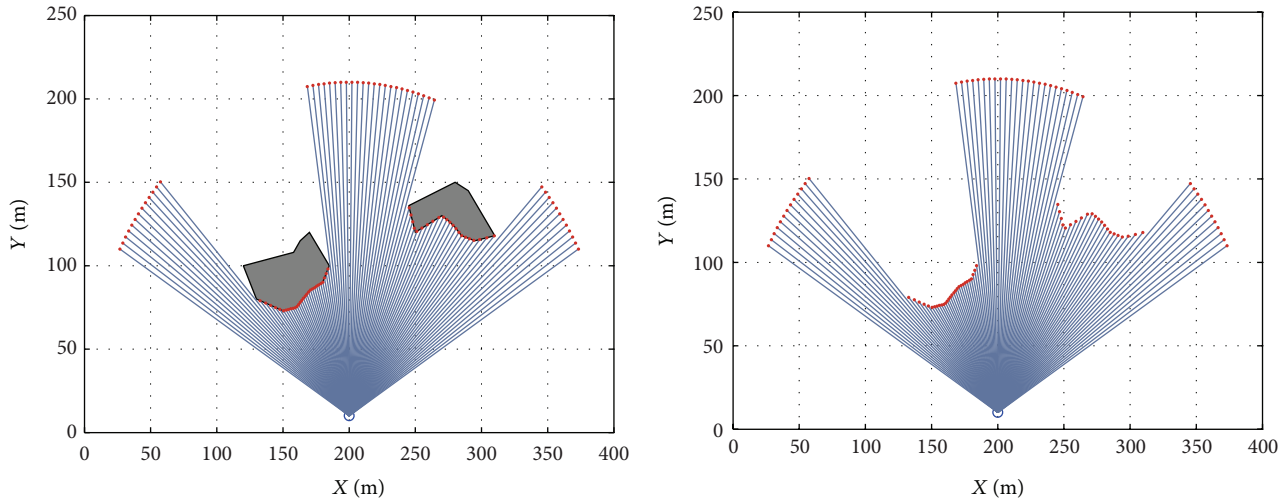

(a) Obstacles detecting by FLS

(b) Obstacles information with FLS

Figure 1: The simulation of sonar detection.

(1) Threshold is sensitive and threshold selection relies heavily on experience. Some algorithms have been studied for adaptive threshold. An adaptive threshold is adjusted according to the distance from the obstacles in [12], and [13] searches for the best threshold in certain interval. However, optimization algorithms are applied in [12, 13], and the computational cost is large.

(2) Adaptability of complex environments: outdoor environment brings up the challenges to the perception and control. Because the calculation of steering direction in the second stage is relatively simple, traditional VFH is unable to adapt to the environment with dense obstacles. Meanwhile, the same as other local planning methods, local minima is the inherent disadvantage of traditional VFH [14]. When sailing near the coast, UUV will be trapped in U shape ports or coasts. Following-wall strategy is widely used to get rid of trap [15, 16]. It is essential to determine when to activate and when to suspend the following-wall, and coordination mechanisms are applied for the integration of following-wall with other avoidance algorithms [16]. In [15], following-wall is combined with virtual force field method and is activated when the vehicle's heading is more than 90° off-target. In [16], following-wall and move-to-goal are combined into the vector polar histogram method. The state memory and position prediction strategies are applied to get better coordination ability.

In this paper, the obstacle avoidance for UUV in unknown unstructured environment is considered. A novel obstacle avoidance system based on VFH is proposed. FLS is used for obstacle detecting. The measures uncertainty is considered in the sonar modal. Storage and processing constrains are considered in the mapping with long voyage. To overcome the problems of traditional VFH and to make UUV more adaptable and robust, the traditional VFH is improved. Behavior-based mechanism is introduced into avoidance process, which can respond to various environments.

The main novelties of this paper are as follows.

(1) To adapt to the VFH, rolling occupancy grids are used for the map building, which can effectively reduce the measure uncertainty and provide high accuracy information for avoidance decision.

(2) To solve the problem that VFH is sensitive to threshold, the threshold is adaptively adjusted by the statistic of POD.

(3) To improve the environment adaptability and get rid of minima position, hybrid-behaviors, straight-to-goal, avoidance-toward-goal, and following-wall, are introduced into the second stage of VFH directly. According to the motion status and environment character, the optimal avoidance command is generated through the switching strategy. Differently from other approaches, no coordination mechanism is applied.

2. Sonar Detection

FLS is used for obstacles detecting and mapping, which is installed in front of UUV. The maximal operating range is 200 m, number of beam is 60, horizontal beam width is 120°, and vertical beam width is 15°. The obstacles are detected in horizontal plane with simulation (see Figure 1).

In this paper, occupancy grids are used for mapping. In occupancy grids map, each cell C has two states: occupied and empty, denoted by OCC and EMP. The probabilistic estimates of two states are $P[s(C) = \text{OCC}]$ and $P[(s(C) = \text{EMP}]$, and the states are exclusive and exhaustive: $\text{OCC} = \neg\text{EMP}$, $P[s(C) = \text{OCC}] + P[s(C) = \text{EMP}] = 1$.

2.1. Coordinate Transform. There are working space and sensing space in the sailing. As shown in Figure 2, polar coordinate is used in the sensing space, and the polar axis is denoted as $\mathbf{O}_s\mathbf{X}_s$. In the 2D plane, the sensing data of sonar have the distance and direction, denoted by (ρ_s, θ_s). Cartesian coordinate *XOY* is used in the working space.

To further analyze the relationship between the two spaces, coordinate transform is solved. The polar coordinates (ρ_s, θ_s) can be converted to the Cartesian coordinate *XOY*. First, (ρ_s, θ_s) is converted to (x_s, y_s) through (1). UUV in the working space is (x_r, y_r, θ), and the angle between polar axis and x-axis is β; then (x_s, y_s) is converted to (x_e, y_e) in *XOY* space through (2). The information in two spaces is unified with the coordinate transform:

$$\begin{bmatrix} x_s \\ y_s \end{bmatrix} = \rho_s \begin{bmatrix} \cos(\theta_s) \\ \sin(\theta_s) \end{bmatrix}, \tag{1}$$

$$\begin{bmatrix} x_e \\ y_e \end{bmatrix} = \begin{bmatrix} \cos(\beta) & -\sin(\beta) \\ \sin(\beta) & \cos(\beta) \end{bmatrix} \begin{bmatrix} x_s \\ y_s \end{bmatrix} + \begin{bmatrix} x_r \\ y_r \end{bmatrix}. \tag{2}$$

2.2. Measure Uncertainty Handling. Due to the poor directionality of FLS and the error in range measurement [3], it is necessary to handle measure uncertainty in sonar model. The previous ideal model does not adapt to complex underwater environment. So, one order gauss probability distribution is applied for the Dolphin sonar in [4]. Divisional sonar modal is proposed in [17, 18], and the effectiveness of proposed modal has been proved.

Here, the divisional sonar modal is applied to handle the measure uncertainty. Figure 3 shows the model of the single sonar beam. In the sensing space, the obstacle detecting data is $r_t = (\rho_s, \theta_s)$ in time t, and covering area can be expressed as one cone, which has range $2\Delta\alpha$ and radius $R_{\max}$. The cone is divided into 3 regions: Region I denotes the empty region, where no obstacle exists; Region II denotes the occupancy region, where the obstacles are found; Region III denotes the unknown region, and it cannot be determined whether there is obstacle [17]. The measure uncertainty of any cell $C = (\rho_i, \theta_j)$ in the covering area is associated with the cell's position. The closer the cell to the axis of beam is, the less noise the raw data has and vice versa. So the occupied probability of cell $P[s(C(\rho_i, \theta_j)) = \text{OCC} \mid r_t]$ can be estimated piecewise according to the region the cell belongs to. The measure distance error is defined as $\Delta\rho$, and $P[s(C(\rho_i, \theta_j)) = \text{OCC} \mid r_t]$ is given by

$$P\left[s\left(C\left(\rho_i, \theta_j\right)\right) = \text{OCC} r_t\right] = \begin{cases} p_{\text{emp}}, & 0 < \rho_i \le \rho_s - \Delta\rho, \\ \left[1 - 0.5\left(\dfrac{|\rho_i - \rho_s|}{\Delta\rho} \times \dfrac{|\theta_j - \theta_s|}{\Delta\alpha}\right)\right] p_{\text{occ}}, & \rho_s - \Delta\rho < \rho_i < \rho_s + \Delta\rho, \\ p_{\text{unk}}, & \rho_s + \Delta\rho \le \rho_i < R_{\max}, \end{cases} \tag{3}$$

where p_{emp}, p_{occ}, and p_{unk} are positive constants, which represent the initial probability of empty state, occupied state, and unknown state, respectively. These values can be $p_{\text{emp}} = 0.3$, $p_{\text{occ}} = 0.9$, and $p_{\text{unk}} = 0.5$, and $R_{\max}$ is the maximal operating range of FLS.

Figure 4 shows a simulation for $P[s(C(\rho_i, \theta_j)) = \text{OCC}]$ in the covering area of single sonar beam. The parameters in (3) choose $\rho_s = 90$ m, $\theta_s = 45^\circ$, $\Delta\rho = 10$ m, and $R_{\max} = 150$ m. In Figure 4, the occupied probability is represented with the color. The light blue region is the empty region, the green region is the unknown region, and the red region is the occupied region. The probabilities in different region have significant difference. The states are distinguished easily and are in accordance with the physical character of sonar.

Always, one grid may be covered by multiple beams and has different states. Information conflicts among multiple beams cause inaccurate map. To obtain high-precision map, grid state needs to be fused and updated. For $s(C_i)$, historical sonar data are $\{r\}_t = \{r_1, r_2, \ldots, r_t\}$ and current state is $P[s(C_i) = \text{OCC} \mid \{r\}_t]$. Given new sonar data r_{t+1} and according to Bayes theory, the grid state can be updated as [4]

$$P\left[s\left(C_i\right) = \text{OCC} \mid \{r\}_{t+1}\right] = \frac{p\left[r_{t+1} \mid s\left(C_i\right) = \text{OCC}\right] P\left[s\left(C_i\right) = \text{OCC} \mid \{r\}_t\right]}{\sum_{s(C_i)} p\left[r_{t+1} \mid s\left(C_i\right)\right] P\left[s\left(C_i\right) \mid \{r\}_t\right]}, \tag{4}$$

where $p[r_{t+1} \mid s(C_i)]$ is the prior probability. Current probability estimation $P[s(C_i) = \text{OCC} \mid \{r\}_t]$ is extracted from the grids map and updated with r_{t+1}; then new $P[r_{t+1} \mid s(C_i) = \text{OCC}]$ is stored in the map.

3. Rolling Occupancy Grids Map

Real-time information storage and processing capacity for UUV are limited. In the long voyage, the environment information increases continuously. If there is no limitation on the mapping, the data will overflow storage capacity and processing time will become longer.

Quad tree model is used in the mapping [19], and there is a map optimization strategy in [20] by cutting the low utilization grids. Here, the rolling occupancy grids map (ROGM) is proposed to adapt the VFH. According to the vision features of UUV, the grids far from UUV have low utilization and will not have impact on the decision-making. On the premise that the information in the active window is complete and accurate, the grids with low utilization can be deleted.

Active window is always centered around the UUV position X_R, and a circular window would be geometrically more appropriate. Active window takes the following form.

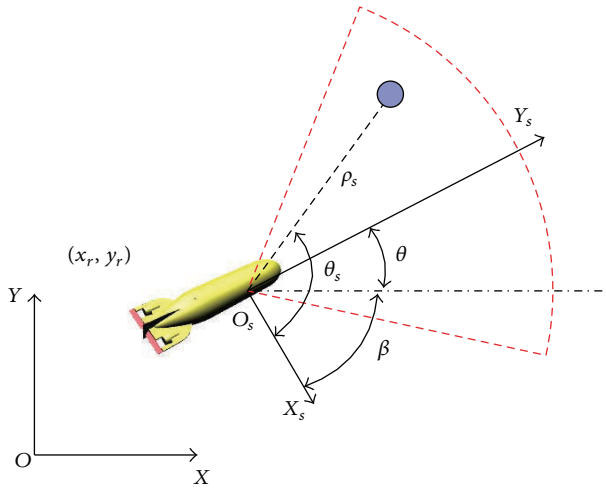

FIGURE 2: The working space and sensing space.

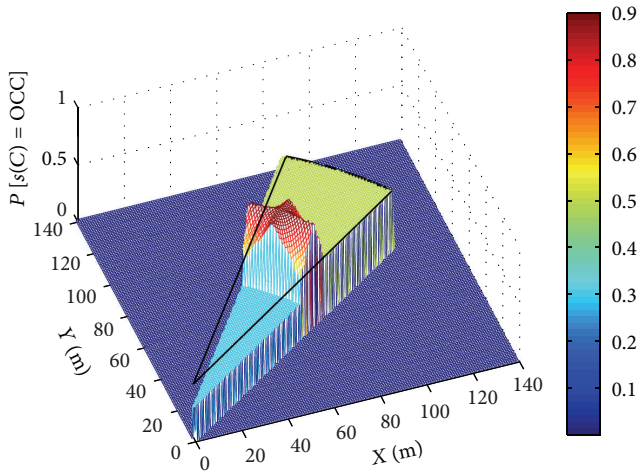

FIGURE 4: Simulation for occupied probability in the covering area of single sonar beam.

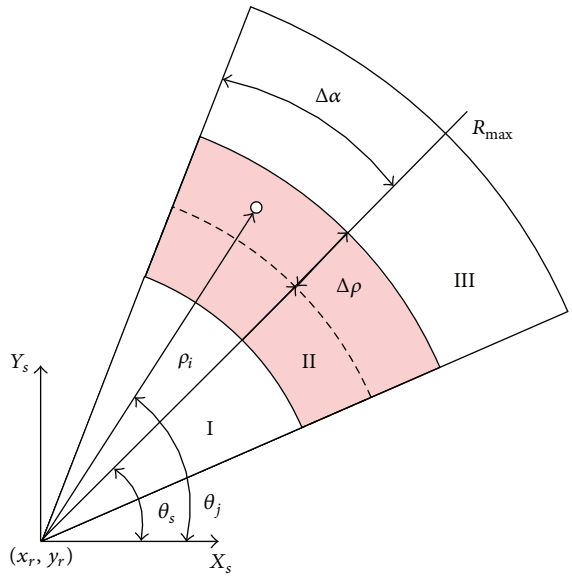

FIGURE 3: The covering area of single sonar beam.

Definition 1. Active window in time t is

$$AW(t) = \{X \mid X \in W, d(X, X_R(t)) < R_w\}, \quad (5)$$

where R_w denotes the radius of $AW(t)$. The size of ROGM must be bigger than active window. It moves with the movement of UUV. A circular window is also used in ROGM, which has radius R_e and is defined as follows.

Definition 2. ROGM in time t is

$$CW(t) = \{X \mid X \in W, d(X, X_M(t)) < R_e\}, \quad (6)$$

where $X_M(t)$ is the center of $CW(t)$; $R_e = \lambda_w R_w$, $(\lambda_w > 1)$, λ_w is the margin coefficient and guarantees that active window is contained in ROGM, so that $AW(t) \subset CW(t)$. In the initial time t_0, the initial ROGM $CW(t_0)$ has the center $X_M(t_0) = X_R(t_0)$, where $X_R(t_0)$ is the initial position of UUV.

Differently from active window, ROGM does not move with UUV on time and only moves when the triggering condition is satisfied. From t to $t + T_{\text{tra}}$, if the travelling distance is bigger than D_{cha}, ROGM will move. It can be described as $\text{Dis}(X_R(t), X_R(t + T_{\text{tra}})) > D_{\text{cha}}$. Here D_{cha} is defined as $R_e - R_w > D_{\text{cha}}$. When moving, $X_M(t)$ will move to $X_M(t + T_{\text{tra}})$. $X_M(t + T_{\text{tra}})$ will be given by the position of closest grid $C_{\text{close}}(t)$ to $X_R(t + T_{\text{tra}})$; thus $X_M(t + T_{\text{tra}}) = X(C_{\text{close}}(t))$. Here, $X(C_{\text{close}}(t)) = \arg\min_{C_i(t)}(\text{Dis}(X_R(t + T_{\text{tra}}), X(C_i(t))))$, $C_i(t) \in CW(t)$.

After moving, The ROGM $CW(t)$ is changed to $CW(t + T_{\text{tra}})$. Some new grids will be expanded into $CW(t+T_{\text{tra}})$, with the state $P[s(C) = \text{OCC}] = 0.5$. If the distance from one grid in $CW(t)$ to $X_R(t + T_{\text{tra}})$ is bigger than R_e, the grid would be deleted from the $CW(t)$.

In $[t, t+T_{tra}]$, the position of $CW(t)$ is static. All the grids in $CW(t)$ are updated in every detection cycle. The update principles of grids in $CW(t)$ are shown as follows.

(A) New sonar data are added into grid map. The sonar data are converted to the working space with (1) and (2). By using (3), the occupied probability of grids is obtained.

(B) The states of overlapping grids are updated following (4).

Because the size of ROGM is constant, unlimited expansion problem of the information can be solved. The speed of mapping is improved, and requirements for VFH are satisfied.

4. Obstacle Avoidance System Design

Based on ROGM, the obstacle avoidance system is designed based on improved VFH. The UUV motion constrains include maximal linear velocity $u_{\max}$, minimum linear velocity $u_{\min}$, maximal yaw angular velocity $w_{\max}$, minimum turning radius $R_{\min}$, and minimum safety distance $d_{\text{safe}} = \lambda_s(R_{\min} + L_r)$.

VFH establishes polar coordinate system with the center of mobile robot and converts the impact of obstacle to POD histogram. The recommended direction is derived from an analysis of POD histogram.

4.1. Polar Histogram. According to the concept of VFH [10], in the active windowAW, the active cell c_{ij} with the center (x_i, y_j) is now treated as an obstacle vector. The direction and magnitude of the obstacle vector can be expressed as

$$\beta_{ij} = \arctan \frac{y_j - y_r^t}{x_i - x_r^t}, \qquad m_{ij} = \left(c_{ij}^*\right)^2 \left(a - bd_{ij}\right). \tag{7}$$

Here, β_{ij} is the direction of obstacle vector; m_{ij} is the magnitude of the obstacle vector; a, b are positive constants and $a - bd_{\max} = 0$; d_{ij} is the distance between active cell c_{ij} and UUV; c_{ij}^* is the occupied probability. As shown in (7), m_{ij} is in inverse proportion to d_{ij}.

The polar histogram $\mathbf{H}$ has an angular resolution α such that $n = 360^\circ/\alpha$ ($\alpha = 10^\circ$). Sector k corresponds to a discrete angle $k\alpha$, $k = 0, 1, \ldots, n-1$, and sector k is established through

$$k = \mathrm{INT}\left(\frac{\beta_{ij}}{\alpha}\right). \tag{8}$$

For each sector k, the POD h_k is calculated as

$$h_k = \sum_{i,j} m_{ij}. \tag{9}$$

Because of the discrete nature of the histogram grid, the result of mapping may appear ragged and cause errors in the selection of steering direction. Therefore, a smoothing function is applied to $\mathbf{H}$, which is defined by

$$h_k' = \frac{h_{k-l} + h_{k-l+1} \cdots + h_k \cdots + h_{k+l-1} + h_{k+l}}{2l+1}. \tag{10}$$

Here, $l = 3$.

4.2. Candidate Heading Set. The safety sector is obtained by the $\mathbf{H}$ and a certain threshold h_{safe}. The sector with POD above the threshold ($h_k' \geq h_{\text{safe}}$) is treated as unsafe sector, and the sector with POD below the threshold ($h_k' < h_{\text{safe}}$) is called safe sector. The consecutive safe sectors are combined as a valley. The valley combined with more than $s_{\max}$ ($s_{\max} = 8$) sectors is considered as wide valley, and other valleys are called narrow valleys [10]. Each valley has two border sectors, left border k_l and right border k_r. If narrow valley has only one sector k, then $k_l = k_r = k$.

The desired heading of the next planning cycle is selected in the candidate valleys. The desired headings generated in each valley compose the candidate heading set $\Omega_{\text{can}} = \{\theta_s^c\}$. The candidate heading should guarantee the safety and smoothness of the movement, which is generated according to valley type in the following discussions.

(1) For narrow valley, candidate heading is selected as the middle direction of the valley, $\theta_s^c = ((k_l + k_r)/2)\alpha$. UUV will maintain a course centered between obstacles.

(2) For wide valley, if the candidate heading is still the middle direction of the valley, sometimes the candidate heading is far from current heading, and UUV would adjust the heading acutely. The best situation is that UUV travel at a proper distance from the obstacle, so there are two candidate headings within the wide valley: $\theta_s^c = (k_l + s_{\max}/2)\alpha$ and $\theta_s^c = (k_r - s_{\max}/2)\alpha$.

4.3. Adaptive Threshold. To reduce the steering frequency, it is not necessary to avoid forane obstacles; meanwhile, the close obstacles should not be neglected. It is important for UUV to find fine-tuned threshold. With the same polar histogram, the bigger the threshold is, the more safe the sectors are selected and vice versa. If the threshold is much too large, UUV is not aware of obstacle and may approach obstacle closely. If threshold is much too low, some potential candidate valleys will be precluded and UUV will not pass through narrow passage [4].

Here, a novel method to get threshold is proposed. The statistics of POD are used for the threshold selection. $h_{\max} = \max(h_k')$, $k = 0, 1, \ldots, n-1$, which represents the closest obstacle to UUV. The average POD of all sectors is $h_{\text{ave}} = \sum_{k=0}^{n-1} h_k'$, which represents obstacles contribution. To some extent, h_{ave} represents the type of obstacles. h_{ave} is large in the narrow passage, and h_{ave} is low in the environment with sparse obstacles. If UUV is requested to pass through a narrow passage, the h_{safe} should be temporarily raised [4]. To obtain potential candidate valleys, h_{safe} is raised with the increase of h_{ave}. The h_{ave} and $h_{\max}$ are considered in the threshold selection, which can be defined by $h_{\text{safe}} = \omega_1 h_{\text{ave}} + \omega_2 h_{\max}$, where $\omega_1, \omega_2 \in [0, 1]$ are weight factors and $\omega_1 + \omega_2 = 1$. Because $h_{\text{ave}} \leq h_{\max}$, we can find $h_{\text{safe}} = \omega_1 h_{\text{ave}} + \omega_2 h_{\max} \leq (\omega_1 + \omega_2) h_{\max} \leq h_{\max}$. So at any time, the sectors with $h_{\max}$ are treated as unsafe sector, and UUV is aware of the close obstacle.

To guarantee the safety, h_{safe} is chosen in the range $[H_{\min}, H_{\max}]$, and the formula for threshold is written by

$$h_{\text{safe}} = \begin{cases} H_{\min} & \text{if } \left(\omega_1 h_{\text{ave}} + \omega_2 h_{\max}\right) < H_{\min} \\ H_{\max} & \text{else if } \left(\omega_1 h_{\text{ave}} + \omega_2 h_{\max}\right) > H_{\max} \\ \omega_1 h_{\text{ave}} + \omega_2 h_{\max} & \text{else.} \end{cases} \tag{11}$$

4.4. Hybrid-Behaviors for Avoidance. Single steering strategy of VFH cannot meet the demand for avoidance in complex environment. So hybrid avoidance strategies are applied. The behaviors of UUV are divided into 3 kinds: straight-to-goal (SG), avoidance-toward-goal (AG), following-wall (FW). SG behavior is traveling to the goal directly without avoidance, AG behavior is the avoidance under the guidance of goal, and FW behavior is the avoidance ignoring the goal. Only one behavior is taken at the same time, and behaviors are triggered according to their triggering conditions.

4.4.1. SG Behavior. When there is no obstacle in the active window or the surrounding obstacles do not affect UUV to sail directly to goal point, SG behavior is triggered. The situation that there is no obstacle in the active window is written by

$$s(X) = \text{EMP}, \quad \forall X \in AW(t). \tag{12}$$

However, in the real application, it is difficult to satisfy (12). Always, there are some obstacles in the active window. We can accept that UUV can take SG behavior if all the sectors are safe. This criterion is defined as follows.

Condition 1. Consider

$$h_k < h_{\text{safe}}, \quad \forall k \in [0, 1, \ldots, n-1]. \tag{13}$$

There is no doubt that Condition 1 must also satisfy (12). Besides, SG behavior should be triggered, if goal is found in active window and there is no unsafe sector within the range of 90° from the target heading. It implies that obstacles have no impact on the target heading. UUV can take SG behavior. It is written as follows.

Condition 2. Consider

$$\begin{aligned} h_k < h_{\text{safe}}, \quad & \forall k \in \left\{k \mid \left|f_{\text{AL}}\left(\theta_g - k\alpha\right)\right| < 90^\circ\right\}, \\ & d\left(X_R(t), X_G\right) < R_w, \end{aligned} \tag{14}$$

where $f_{\text{AL}}(\cdot)$ is the steering angle limitation function, which limits the steering angle in $(-180^\circ, 180^\circ]$

$$f_{\text{AL}}(x) = \begin{cases} x - 360^\circ, & \text{if } x > 180^\circ, \\ x + 360^\circ, & \text{if } x \le -180^\circ. \end{cases} \tag{15}$$

To sum up, SG behavior is triggered if any one of Conditions 1 and 2 is satisfied. The UUV state is $X_r^t = (x_r^t, y_r^t, \theta_r^t)$, the goal point is $X_G = (x_g, y_g)$, and target heading in t is defined by $\theta_g = \arctan(y_g - y_r^t)/(x_g - x_r^t)$. In SG behavior, the desired heading in $t+1$ is given by $\widehat{\theta}_r^{t+1} = \theta_g$, and the desired linear velocity in $t+1$ is implemented by $\widehat{u}_r^{t+1} = u_{\max}$. SG behavior can make UUV approach the goal quickly under safe conditions.

4.4.2. AG Behavior. AG behavior is the main behavior and UUV avoids obstacles under the guidance of goal point. If none of Conditions 1 and 2 is satisfied, obstacles may collide with UUV, and UUV should avoid the obstacles. The relationship between current heading and target heading can be divided into 2 conditions.

Condition 3. Consider

$$\left|f_{\text{AL}}\left(\theta_g - \theta_r^t\right)\right| < 90^\circ. \tag{16}$$

Condition 4. Consider

$$\left|f_{\text{AL}}\left(\theta_g - \theta_r^t\right)\right| \ge 90^\circ. \tag{17}$$

When Condition 3 is satisfied, AG behavior is triggered. Guidance of goal point means that the candidate heading closest to the target heading in Ω_{can} is selected as the desired heading in $t+1$:

$$\widehat{\theta}_r^{t+1} = \arg\min\left(\left|f_{\text{AL}}\left(\theta_g - \theta_s^c\right)\right|, \theta_s^c \in \Omega_{\text{can}}\right). \tag{18}$$

The magnitude of the linear velocity is affected by POD. Bigger POD means that UUV approaches closer to obstacle, so it requires UUV to turn a big direction and slow down to obtain enough time for avoidance. The magnitude of the linear velocity is inversely proportional to the POD, and the desired linear velocity in $t+1$ is

$$\widehat{u}_r^{t+1} = u_{\max}\left(1 - \frac{h_{\text{safe}}}{h_{\max}}\right). \tag{19}$$

4.4.3. FW Behavior. Usually, there is local minima in the working space filled with U shape obstacles or complex obstacles. Local minima is generated under both influence of goal point and local obstacle. UUV may be trapped in the local minima or makes reciprocating traveling along closed route. Following-wall is an effective mechanism to get rid of local minima. Take U shape obstacle as an example; following-wall will give up the guidance of goal temporarily and follow the edges of the U shape obstacle, until UUV escapes from the trap.

When the difference between current heading and target heading is more than 90°, UUV may be trapped in the local minima. It implies that Condition 4 is satisfied; then FW behavior is triggered. In FW behavior, the candidate heading closest to the current heading in Ω_{can} is selected as the desired heading in $t+1$:

$$\widehat{\theta}_r^{t+1} = \arg\min\left(\left|f_{\text{AL}}\left(\theta_c - \theta_s^c\right)\right|, \theta_s^c \in \Omega_{\text{can}}\right). \tag{20}$$

The same with AG, set the desired linear velocity in $t+1$ as (18). To prevent the infinite loop, a watchdog *TickCount* is used. When *TickCount* exceeds the preset number of cycles T_{stop}, FW behavior is terminated and *TickCount* is cleared to zero.

To sum up, the termination condition for FW behavior is defined as

$$\left|f_{\text{AL}}\left(\theta_g - \theta_r^t\right)\right| < 90^\circ \quad \text{or } TickCount \ge T_{\text{stop}}. \tag{21}$$

The switch strategy of the three behaviors is shown in Figure 5.

4.5. UUV Motion. The first-order motion model of UUV moving in two dimensions is

$$X_r^{t+1} = \begin{bmatrix} x_r^t + u_r^t \Delta T \cos\left(\theta_r^t\right) \\ y_r^t + u_r^t \Delta T \sin\left(\theta_r^t\right) \\ \theta_r^t + w_r^t \Delta T \end{bmatrix}. \tag{22}$$

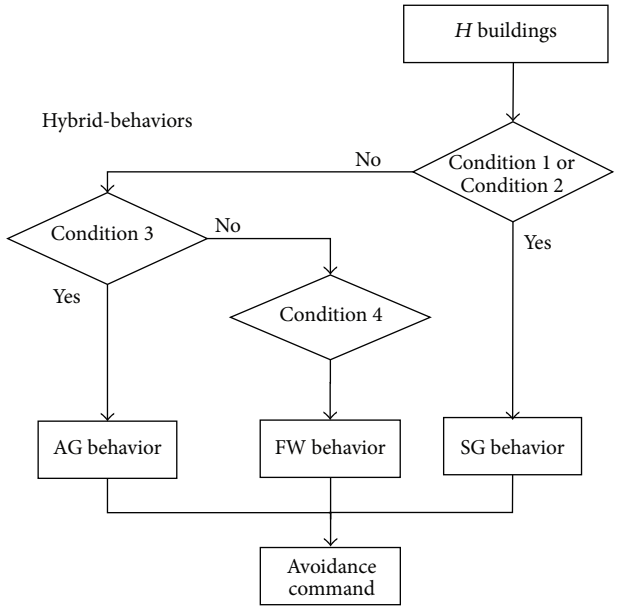

Figure 5: The switch strategy of hybrid-behaviors.

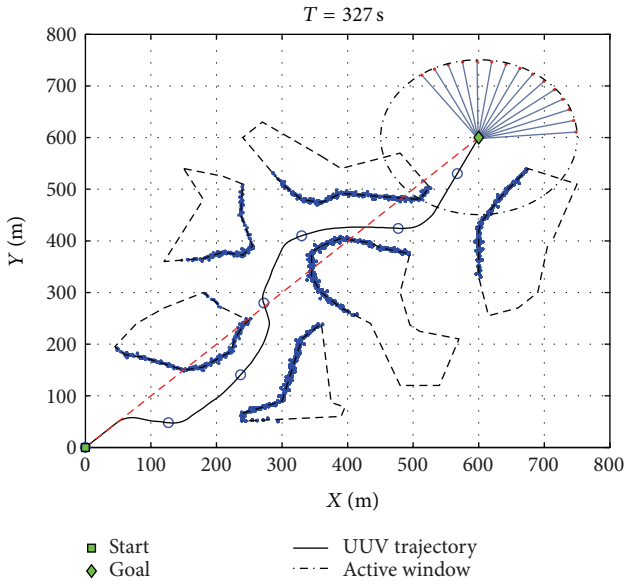

Figure 6: Avoidance result in Case 1.

The linear velocity and yaw velocity satisfy the constrains: $u_{\min} \le |\hat{u}_r^{t+1}| \le u_{\max}$ and $|\hat{\theta}_r^{t+1} - \theta_r^t| \le w_{\max}$. So, the linear velocity and heading in $t+1$ are

$$u_r^{t+1} = \begin{cases} \hat{u}_r^{t+1}, & u_{\min} < \hat{u}_r^{t+1} < u_{\max}, \\ u_{\min}, & \hat{u}_r^{t+1} \le u_{\min}, \\ u_{\max}, & \hat{u}_r^{t+1} \ge u_{\max}, \end{cases}$$

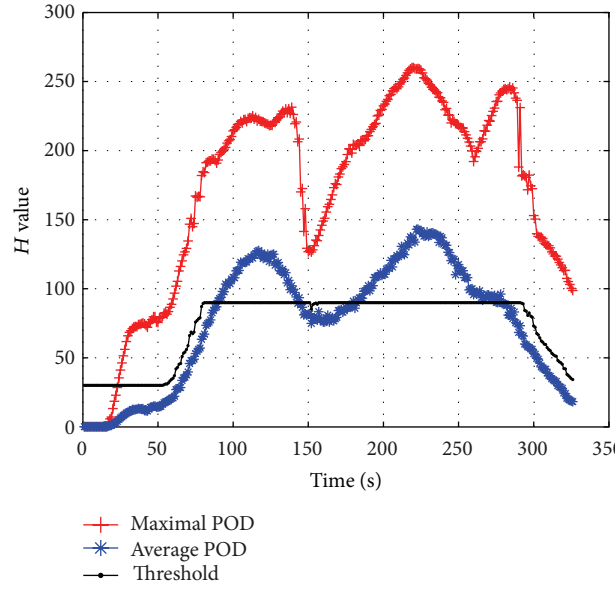

Figure 7: The threshold of VFH in Case 1.

$$\theta_r^{t+1} = \begin{cases} \hat{\theta}_r^{t+1}, & \left|\hat{\theta}_r^{t+1} - \theta_r^t\right| \le w_{\max}, \\ \theta_r^t + \operatorname{sgn}\left(\hat{\theta}_r^{t+1} - \theta_r^t\right) w_{\max}, & \left|\hat{\theta}_r^{t+1} - \theta_r^t\right| > w_{\max}, \end{cases} \tag{23}$$

where $\operatorname{sgn}(\cdot)$ is the symbol function and $\operatorname{sgn}(x) = \begin{cases} -1 & x<0 \\ 0 & x=0 \\ 1 & x>0 \end{cases}$.

4.6. Algorithm Steps. Through the FLS detection and ROGM building, obstacle avoidance algorithm steps are given as follows.

Step 1 (initialization). The initialization includes the motion constrains and the parameters of sonar and map.

Step 2 (sonar detecting). The obstacles are detected by FLS, and the sonar data are converted to the position information in working space by using (1) and (2).

Step 3 (ROGM building). The occupied probability of new data is calculated using (3). The ROGM is updated according to the principle.

Step 4 (**H** building). By using ROGM in Step 3, **H** is built according to (4), (7), (8), (9), and (10).

Step 5 (threshold generation). After average POD and maximal POD are generated according to **H**, the adaptive threshold is calculated through (11).

Step 6 (generation for candidate heading set). Using the threshold generated in Step 5, the valleys are determined. The candidate heading is calculated according to the valley type.

Step 7 (hybrid-behaviors switch). SG, AG, and FW behaviors are chosen according to Conditions 1–4. The desired heading is selected in Ω_{can} generated in Step 6.

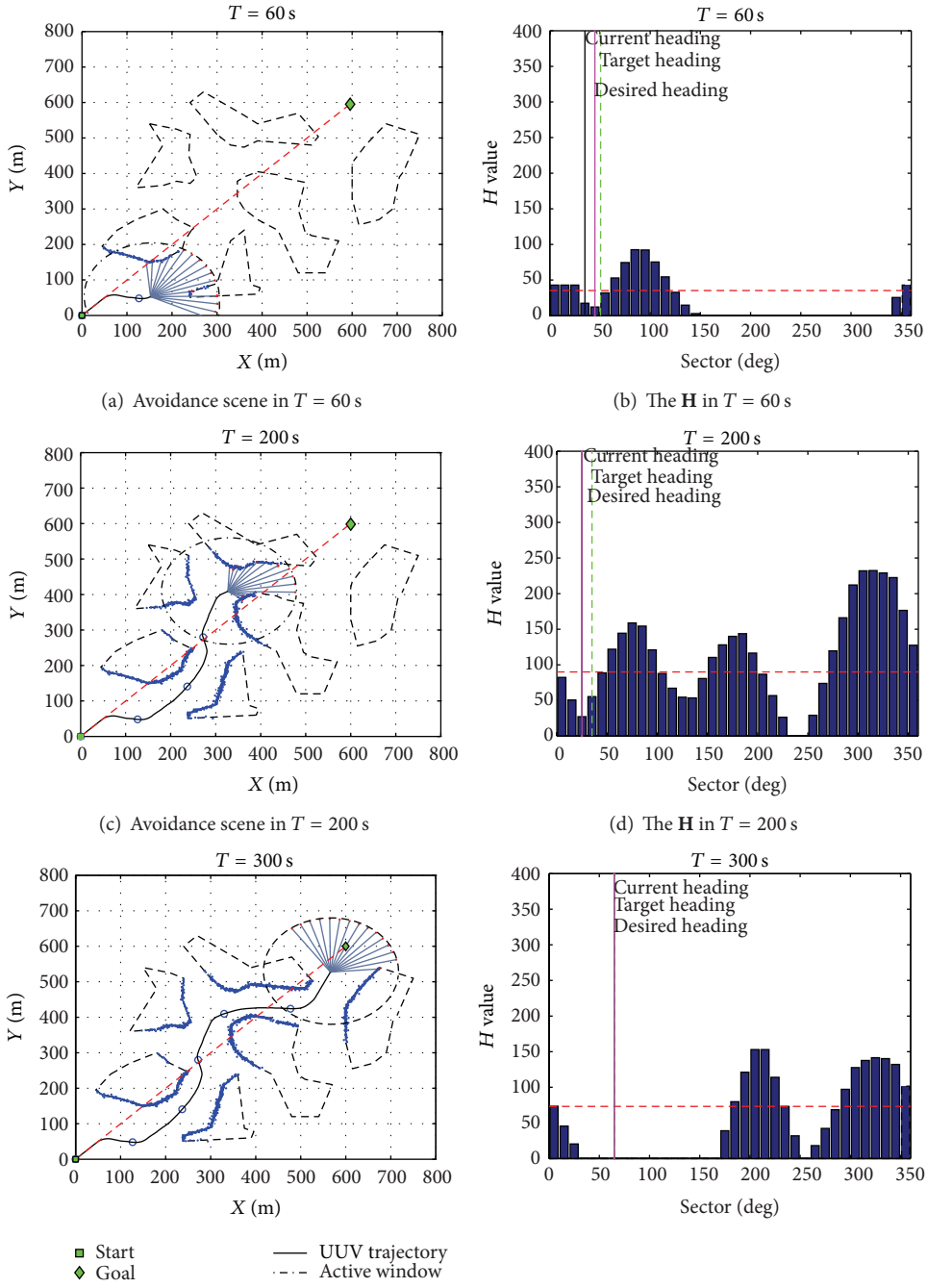

(a) Avoidance scene in $T = 60$ s

(b) The **H** in $T = 60$ s

(c) Avoidance scene in $T = 200$ s

(d) The **H** in $T = 200$ s

(e) Avoidance scene in $T = 300$ s

(f) The **H** in $T = 300$ s

FIGURE 8: Avoidance scenes in different phases and **H** value of Case 1.

Step 8 (UUV state update). Under the new command, the speed and position of UUV are updated by (22). If the goal is arrived, the algorithm quits and else returns to Step 8.

5. Simulation

A simulation framework is developed in Matlab to test proposed method. In the simulation, the size and position of the obstacles are completely unknown, and UUV makes decision relying on the obstacle data detected by FLS. The motion constrains include $u_{\max} = 3$ m/s, $u_{\min} = 0.3$ m/s, $w_{\max} = 5^{\circ}$/s, $R_{\min} = 20$ m, $L_r = 10$ m, $\lambda_s = 1.5$, and $d_{\text{safe}} = \lambda_s(R_{\min} + L_r) = 45$ m. The detecting range of FLS is $R_{\max} = 150$ m, and zero mean Gaussian noise is added into the sensing distance from FLS. The parameters of map are $R_w = 150$ m, $R_e = 180$ m, and $D_{\text{cha}} = 25$ m. According to d_{safe}, the safe threshold interval chooses $H_{\min} = 30$, $H_{\max} = 90$, and the coefficients in (10) choose $\omega_1 = 0.8$, $\omega_2 = 0.2$. Simulations are developed in the map with dense obstacles, narrow passage, and U shape obstacle, respectively.

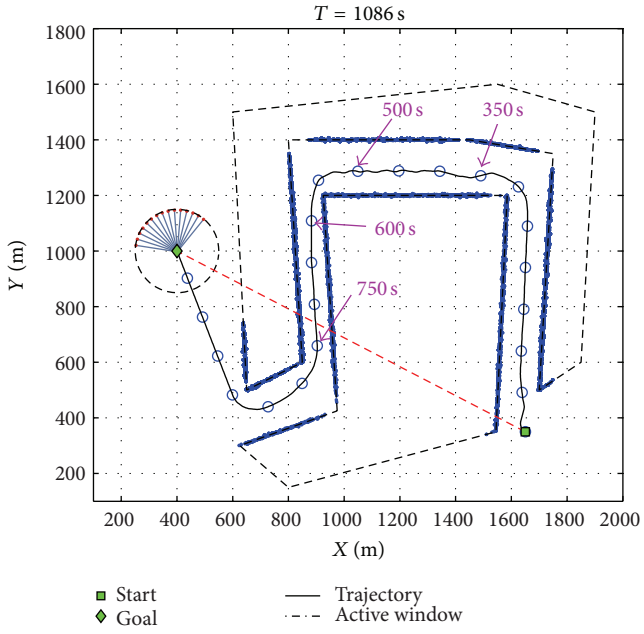

Figure 9: Avoidance result in Case 2.

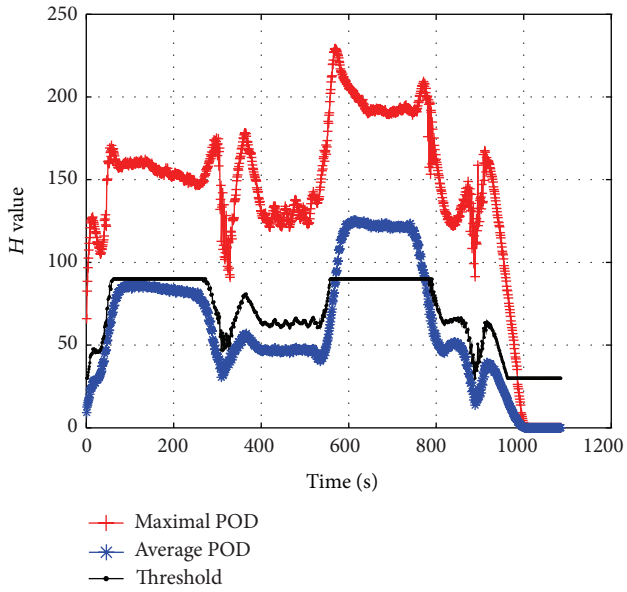

Figure 10: The threshold of VFH in Case 2.

Case 1. Avoidance test with dense obstacles.

In Case 1, 6 obstacles with different size are designed in the map with size of 800 m × 800 m. UUV sails from the start point (0, 0) to goal (600, 600). The total traveling time is 327 s, and Figure 6 shows the map and complete avoidance results for Case 1. Edges of obstacles (dashed line) and the sonar data (blue point) are plotted in the map. The average POD, maximum POD, and adaptive threshold are shown in Figure 7.

Figure 8 shows the avoidance scenes and **H** in 60 s, 200 s, and 300 s. Figure 8(a) shows the avoidance scene in 60 s, and Figure 8(b) shows **H**, current heading (black solid line), target heading (green dashed line), and desired heading (magenta solid line) calculated by the proposed algorithm. As shown in Figure 8(a), when $T = 60$ s, UUV takes AG behavior and chooses the closest candidate heading to target heading. As shown in Figures 8(c) and 8(d), there are 3 narrow valleys in **H** when $T = 200$ s, and UUV takes AG behavior. As shown in Figures 8(e) and 8(f), UUV takes SG behavior when $T = 300$ s. In this test, UUV can pass through the dense obstacles successfully and safely.

Case 2. Avoidance test in passage environment.

Curved passage is designed in the map with size of 2000 m × 1800 m in Case 2. Width of passage is about 200 m, and it is difficult for UUV to traverse. UUV sails from the start point (1650, 350) to goal (400, 1000). Traveling time is 1086 s, and Figure 9 shows the map and complete avoidance results for Case 2. The average POD, maximum POD and adaptive threshold are shown in Figure 10.

As seen from Figures 9 and 10, from 350 s to 500 s, average POD is low while passing through the wide passage and the threshold is low. However, average POD is large when UUV passes through the narrow passage from 600 s to 750 s, and threshold is raised. The adaptive threshold helps UUV to pass through the narrow passage.

Figure 11 shows the avoidance scene and **H** in 290 s, 600 s, and 950 s. In Figure 11(a), when $T = 290$ s, UUV detects the frontal and right obstacles in the corner of the passage, and there are a wide valley and a narrow valley in **H** (see Figure 11(b)); UUV turns left under the guidance of target heading. In Figure 11(c), when $T = 600$ s, the obstacles on the two sides of the passage cause 2 peaks and 2 narrow valleys in the polar histogram (see Figure 11(d)). So, UUV travels in the center path of the passage. In Figure 11(e), when $T = 950$ s, UUV takes SG behavior. In this test, UUV can pass through the narrow passage and has the ability to choose new heading agilely in the complex passage.

Case 3. Avoidance test with U shape obstacle.

A comparison of the improved VFH to traditional VFH is given in Case 3. U shape obstacle is designed in the map with size of 1300 m × 1000 m, and UUV sails from start point (800, 200) to goal (800, 800). Figure 12 shows the map and avoidance results for Case 3. The avoidance result with traditional VFH described in [10] is shown in Figure 12(a), and UUV makes reciprocating traveling along closed route and fails to reach the goal. Figure 12(b) shows the avoidance result by using improved VFH with hybrid-behaviours. The traveling time is 608 s. As seen from Figure 12(b), UUV turns left when the front obstacles are found in 80 s. After a period of sailing, the right obstacles are found, and UUV turns left. UUV takes FW behavior in 125 s and terminates FW behavior in 160 s. Then, UUV takes AG behavior until leaving the obstacles. Compared with Figure 12(a), this test clearly illustrates that UUV chooses right decisions in U shape obstacle and gets rid of the minima trap through following the edges of obstacle.

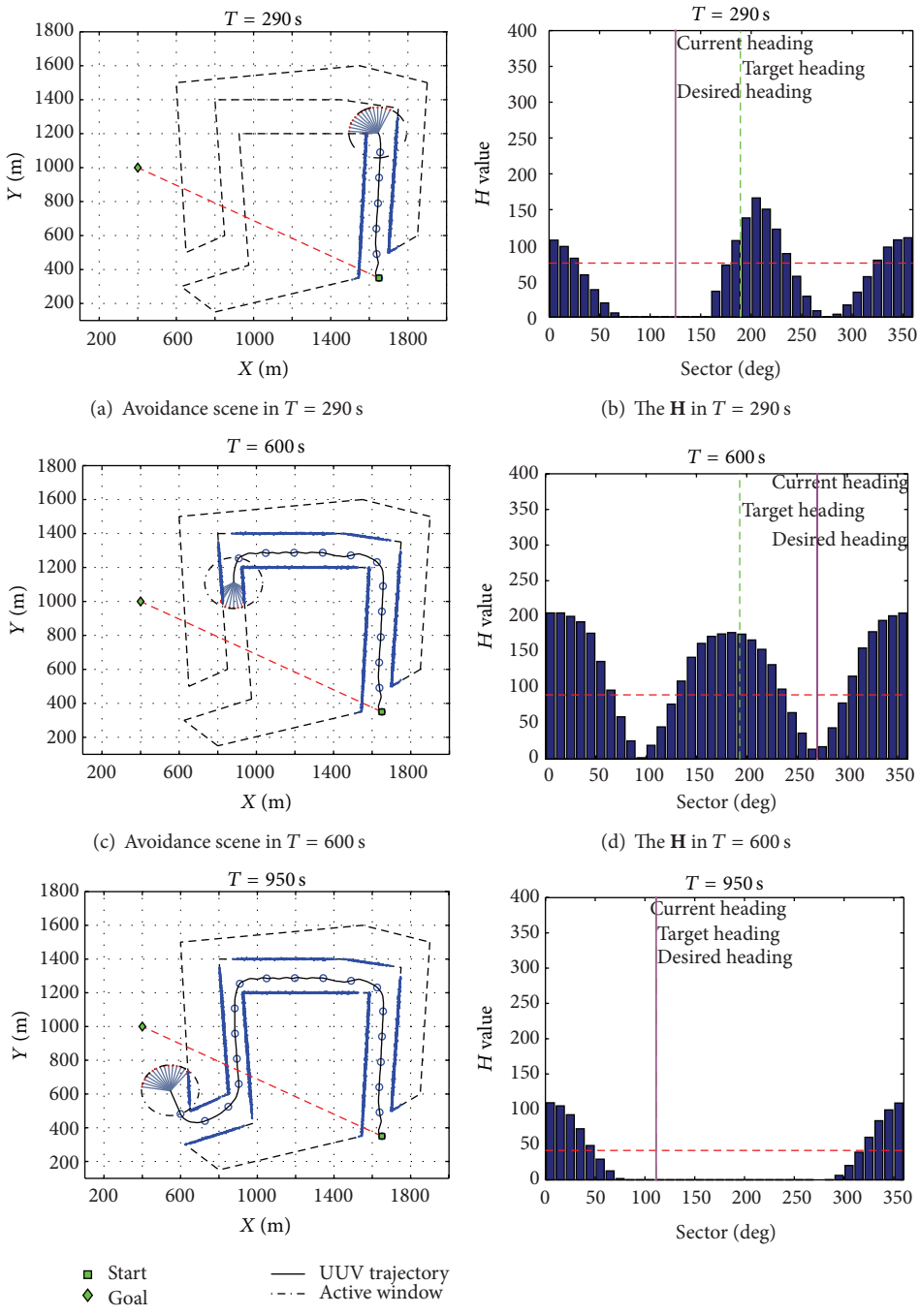

(a) Avoidance scene in $T = 290$ s

(b) The **H** in $T = 290$ s

(c) Avoidance scene in $T = 600$ s

(d) The **H** in $T = 600$ s

(e) Avoidance scene in $T = 950$ s

(f) The **H** in $T = 950$ s

FIGURE 11: Avoidance scenes in different phases and **H** value of Case 2.

6. Conclusions

To improve the avoidance ability of UUV in the unknown unstructured environment, an obstacle avoidance system based on improved VFH is designed. The FLS is used for obstacle detection, and the divisional sonar modal is applied to handle the measures uncertainty. To adapt to the VFH, rolling occupancy grids are used for the map building, which can effectively reduce the measure uncertainty and provide high accuracy information for avoidance decision. There are two main improvements over traditional VFH. First, the threshold is adaptively adjusted by the statistic of POD, which represents the obstacle type and solves the problem that VFH is sensitive to threshold. In narrow passage, threshold is raised adaptively to make UUV pass through. Second, to improve the environment adaptability and get rid of minima position, hybrid-behaviours are proposed into the second stage of VFH, which are straight-to-goal, avoidance-toward-goal,

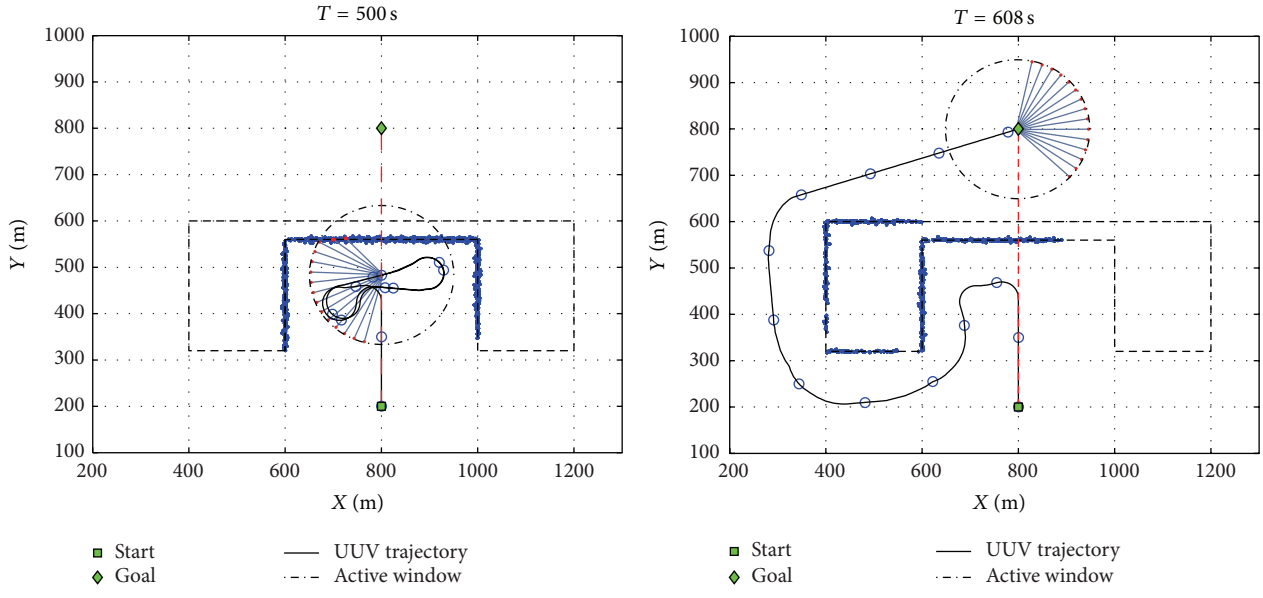

(a) The avoidance result with traditional VFH

(b) The avoidance result with proposed improved VFH

Figure 12: Avoidance results in Case 3.

and following-wall. According to the motion status and environment character, the optimal avoidance command is generated through the switching strategy.

Simulations are developed in three different scenarios. Simulation results illustrate that UUV can avoid the dense obstacles fast, pass through the curved passage, and escape from the U shape obstacles successfully. The proposed approach can help UUV to adapt to various environments. The feasibility of the proposed approach is confirmed. A future extension of this work is a realization of proposed avoidance system in a real UUV.

Conflict of Interests

The authors declare that there is no conflict of interests regarding the publication of this paper.

Acknowledgments

This work is partially supported by the Natural Science Foundation of China (51179038, 51109043), and the Program of New Century Excellent Talents in University (NCET-10-0053).

References

[1] G. Antonelli, S. Chiaverini, R. Finotello, and R. Schiavon, "Real-time path planning and obstacle avoidance for RAIS: an autonomous underwater vehicle," *IEEE Journal of Oceanic Engineering*, vol. 26, no. 2, pp. 216–227, 2001.

[2] K. Teo, K. W. Ong, and H. C. Lai, "Obstacle detection, avoidance and anti collision for MEREDITH AUV," in *MTS/IEEE Biloxi—Marine Technology for Our Future: Global and Local Challenges (OCEANS '09)*, pp. 1–10, October 2009.

[3] Y. Petillot, I. T. Ruiz, and D. M. Lane, "Underwater vehicle obstacle avoidance and path planning using a multi-beam forward looking sonar," *IEEE Journal of Oceanic Engineering*, vol. 26, no. 2, pp. 240–251, 2001.

[4] E. Alberto, *Occupancy grids: a probabilistic framework for robot perception and navigation [Ph.D. thesis]*, Carnegie-Mellon University, 1989.

[5] J.-O. Kim and P. K. Khosla, "Real-time obstacle avoidance using harmonic potential functions," *IEEE Transactions on Robotics and Automation*, vol. 8, no. 3, pp. 338–349, 1992.

[6] P. Ögren and N. E. Leonard, "A convergent dynamic window approach to obstacle avoidance," *IEEE Transactions on Robotics*, vol. 21, no. 2, pp. 188–195, 2005.

[7] P. Reignier, "Fuzzy logic techniques for mobile robot obstacle avoidance," *Robotics and Autonomous Systems*, vol. 12, no. 3-4, pp. 143–153, 1994.

[8] H.-J. Lee and K. P. Rhee, "Development of collision avoidance system by using expert system and search algorithm," *International Shipbuilding Progress*, vol. 48, no. 3, pp. 197–210, 2001.

[9] R. Glasius, A. Komoda, and S. C. A. M. Gielen, "Neural network dynamics for patch planning and obstacle avoidance," *Neural Networks*, vol. 8, no. 1, pp. 125–133, 1995.

[10] J. Borenstein and Y. Koren, "The vector field histogram–Fast obstacle avoidance for mobile robots," *IEEE Transactions on Robotics and Automation*, vol. 7, no. 3, pp. 278–288, 1991.

[11] I. Ulrich and J. Borenstein, "VFH+: reliable obstacle avoidance for fast mobile robots," in *Proceedings of the IEEE International Conference on Robotics and Automation*, pp. 1572–1577, Leuven, Belgium, May 1998.

[12] Y. Xu, C. Zhang, and H. Xu, "A new obstacle avoidance method for mobile robot based on laser range finder," *Robot*, vol. 32, no. 2, pp. 179–183, 2010.

[13] W. Ye, C. Wang, M. Yang, and B. Wang, "Virtual obstacles based path planning for mobile robots," *Robot*, vol. 33, no. 3, pp. 273–286, 2011.

[14] C. Luo, M. Krishnan, M. Paulik, U. Mohammad, and Q. Wang, "Navigating with VFH: a strategy to avoid traps," in *Intelligent Robots and Computer Vision XXIX: Algorithms and Techniques*, pp. 1–11, January 2012.

[15] J. Borenstein and Y. Koren, "High-speed obstacle avoidance for mobile robots," in *Proceedings of the 3rd International Symposium on Intelligent Control*, pp. 382–384, August 1988.

[16] J. Gong, Y. Duan, K. Liu, Y. Chen, G. Xiong, and H. Chen, "A robust multistrategy unmanned ground vehicle navigation method using laser radar," in *IEEE Intelligent Vehicles Symposium*, pp. 417–424, June 2009.

[17] B. K. Ellore, *Dynamically Expanding Occupancy Grids*, Texas Tech University, 2002.

[18] Y. Duan and X.-H. Xu, "Navigation for mobile robot based on uncertainty grid-map," *Control Theory & Applications*, vol. 23, no. 6, pp. 1009–1013, 2006.

[19] L. Guo, *Study on simultaneous localization and mapping of mobile robot in large-scale environments [Ph.D. thesis]*, Tianjin University, Tianjin, China, 2007.

[20] Z. Ma and Z. Yuan, "Real-time navigation and obstacle avoidance based on grids method for fast mobile robot," *Robot*, vol. 18, no. 6, pp. 344–348, 1996.

Hindawi Publishing Corporation
Mathematical Problems in Engineering
Volume 2013, Article ID 163976, 8 pages
http://dx.doi.org/10.1155/2013/163976

Research Article

On Building a Universal and Compact Visual Vocabulary

Jian Hou,[1] Wei-Xue Liu,[1] Xu E,[1] and Hamid Reza Karimi[2]

[1] *School of Information Science and Technology, Bohai University, Jinzhou 121013, China*
[2] *Department of Engineering, Faculty of Engineering and Science, University of Agder, 4898 Grimstad, Norway*

Correspondence should be addressed to Jian Hou; dr.houjian@gmail.com

Received 28 August 2013; Accepted 1 October 2013

Academic Editor: Zhiguang Feng

Bag-of-visual-words has been shown to be a powerful image representation and attained great success in many computer vision and pattern recognition applications. Usually, for a given dataset, researchers choose to build a specific visual vocabulary from the dataset, and the problem of deriving a universal visual vocabulary is rarely addressed. Based on previous work on the classification performance with respect to visual vocabulary sizes, we arrive at a hypothesis that a universal visual vocabulary can be obtained by taking-into account the similarity extent of keypoints represented by one visual word. We then propose to use a similarity threshold-based clustering method to calculate the optimal vocabulary size, where the universal similarity threshold can be obtained empirically. With the optimal vocabulary size, the optimal visual vocabularies of limited sizes from three datasets are shown to be exchangeable and therefore universal. This result indicates that a universal and compact visual vocabulary can be built from a not too small dataset. Our work narrows the gab between bag-of-visual-words and bag-of-words, where a relatively fixed vocabulary can be used with different text datasets.

1. Introduction

Bag-of-visual-words is a powerful and widely used image representation in computer vision and pattern recognition applications. In this approach, salient image regions (keypoints) are detected, described, and then clustered into groups. By treating the centroid of each group as a visual word, we obtain a visual vocabulary composed of all visual words. With this vocabulary, an image can be represented as a histogram of the visual words, namely, a bag-of-visual-words [1]. Since one visual word represents one type of image patterns, a bag-of-visual-words can be regarded as the distribution of various image patterns in an image. The basic bag-of-visual-words representation captures this distribution in the whole image and ignores the spatial relationships among keypoints, and this is shown to weaken the discriminative power of this representation [2, 3]. In order to make use of the spatial information, in [4] the authors proposed to use a spatial pyramidal partition of an image and concentrate the histogram in each partition into one final description. Some other approaches to encode spatial information include [5, 6] considering that some visual words in a visual vocabulary may be more informative than the others in a specific domain, [3, 7, 8] propose to weight visual words accordingly, and [9, 10] present methods to reduce vocabulary size for better efficiency. Furthermore, it was proposed in [7] to build a vocabulary tree by hierarchical k-means clustering to scale to large vocabularies and large datasets.

While the potential of bag-of-visual-words has been explored in various aspects as we briefly reviewed above, the construction of visual vocabularies almost always follows a fixed procedure; that is, randomly selecting some images from the given datasets, extracting keypoints from these images, and building the specific vocabulary by clustering in the keypoints, where the vocabulary size is selected empirically and may range from hundreds to tens of thousands [1, 4, 11, 12]. This practice is quite different from that of bag-of-words in text domain, where a universal and limited vocabulary can be used for different datasets. Noticing that bag-of-words is the counterpart and preceder of bag-of-visual-words, we are interested to find out if it is possible to eliminate this difference and build a universal and compact visual vocabulary. By universal we mean that on different datasets, the visual vocabulary performs comparable to their

specifically trained vocabularies, and thereby removing the necessity to build a specific visual vocabulary for each dataset, and by *compact* we mean that the vocabulary is not so large, in case users feel it is not worthwhile to use a large vocabulary. An earlier version of some works in this paper appeared in [13].

In the literature, the most related works to ours are the ones in [14, 15] which address the problem of deriving a universal visual vocabulary. Specifically, it was empirically found in [14, 15] that the visual vocabularies trained from one dataset can be used on some other datasets without apparently harming the performance, only if the dataset is large enough. In these two papers, the vocabulary sizes are still user-defined and this implies that an inappropriate vocabulary size may lead to a universal vocabulary that performs moderately, which obviously is not what we really expect. On the contrary, in our work, the universal vocabulary is naturally derived from our work on optimal vocabulary size. Furthermore, the universal vocabulary obtained with our approach is optimal and compact, in that it can be used on different datasets to obtain the (near-)best performance, and the vocabulary size is only several thousands. These two important properties are not possessed by the universal vocabularies achieved in [14, 15].

It should be noted that in [16, 17], the term *universal* is used-with different meanings. In [16], a universal vocabulary refers to a large vocabulary which serves as the basis of generating small and optimal vocabularies. Whereas in [17], a universal vocabulary is built from images from all categories, in contrast to the class-specific ones built from one category. On the contrary, in this paper, a vocabulary is universal in that it can be used-with different datasets to achieve the (near-)best performance.

The remainder of this paper is organized as follows. In Section 2, we present details on using a similarity threshold-based clustering method and an optimal similarity threshold to determine the optimal vocabulary size for a given dataset. Then, in Section 3, we test if the optimal vocabulary trained from one dataset can be used to produce the (near-)best performance on other datasets, and thus decide if it can be used as a universal visual vocabulary. Section 4 discusses the experimental results in Sections 2 and 3 and their implications. Finally, Section 5 concludes the paper.

2. Optimal Visual Vocabulary

2.1. Hypothesis. This work originates from the observations from experiments on vocabulary sizes in [3], where it is found that with the increase of vocabulary size, the classification performance of the visual vocabulary rises dramatically until a peak is reached, and after that, the performance levels off or drops mildly. Experiments in [18] also showed that when the vocabulary size reaches a certain value, a larger size does not improve the performance further. These observations imply that the increase in vocabulary size does not definitely improve the classification performance. Instead, their exists an optimal vocabulary size for a given dataset, and the optimal size is smaller than the number of keypoints. This, in turn, indicates that if a set of keypoints are similar enough to each other, they should be represented by one single visual word, not only for efficiency reasons, but also for the best performance. With a descriptor of limited dimension, for example, SIFT, this means that all the possible keypoints can be mapped to a limited number of visual words, which can then be used as a universal visual vocabulary. Here, by optimal we mean that the vocabulary performs the (near-)best and a larger size does not pay off.

We have speculated that there should exist a universal visual vocabulary of limited size. However, it is still not clear how to derive such a visual vocabulary. Noticing that a universal visual vocabulary is the optimal one for any dataset, our solution to universal visual vocabulary derivation is to build an optimal vocabulary from a large and representative dataset, and then test if it is also the optimal ones for other datasets. For a given dataset, the optimal vocabulary is decided by the optimal vocabulary size. We already know that there exists an optimal vocabulary size for a given dataset, but we do not know how to determine the optimal vocabulary size. Empirically selecting such a size is not a good option, because the optimal vocabulary size varies from dataset to dataset, and there are so many sizes to test for each dataset. In fact, we propose to use a similarity threshold-based clustering method and an optimal similarity threshold to determine the optimal vocabulary size for a given dataset. After the optimal vocabularies for some datasets are obtained by k-means clustering, we test if they are also the optimal ones for other datasets to decide if they can be treated as universal visual vocabularies.

Determining the optimal vocabulary size is the key step in building the optimal vocabulary from a given dataset. While [3, 18] show that there exists an optimal vocabulary size smaller than the number of training descriptors for a given dataset, they do not provide the reason behind the observation and provide a solution to find the optimal size. Instead, they just test many sizes and select the best performing one. In this paper, we intend to analyze the reasons behind the observations and then derive a method to determine the optimal visual vocabulary size.

2.2. Similarity Based Clustering Method. With the popular detectors, for example, DoG used in SIFT [19], usually at least hundreds of keypoints can be detected from one image. Therefore, with only hundreds of training images, we can obtain at lease tens of thousands of training keypoints. In this case, using a vocabulary size of several hundreds implies that a large number of keypoints are clustered into one single group and are represented by one single visual word. This often means a large intracluster dissimilarity and leads to little discriminating power of the vocabulary. With the increase of vocabulary size, one visual word tends to represent only similar keypoints and the discriminating power of the vocabulary tends to increase. In this way, a larger vocabulary should performs better until the largest vocabulary size, that is, the number of keypoints, is reached. However, the experiments in [3, 18] show that when the vocabulary size is large enough (i.e., the optimal size observed), a larger size

does not result in performance gain. This further indicates that if a set of keypoints are similar enough, they should be clustered into one single group and represented by one single visual word, instead of many different visual words, respectively. This is a very important conclusion and it serves as the basis of deriving a universal visual vocabulary which is optimal and of limited size. Therefore, in the following, we explain it in a little more detail.

Firstly, at the optimal size, the keypoints represented by one visual word are so similar that they actually describe the same image pattern and their difference is too small to be taken into account. Secondly, the difference in keypoints represented by the same visual word may be caused by noise and thus should be ignored. This viewpoint is also supported by the work on local descriptors matching in [20] and visual words weighting scheme in [3]. In [20], we show that in straightforward local keypoints matching, the number of matched keypoint types is a better image similarity measure than that of the number of matched keypoints. Here, by type, we mean that one type of keypoints are very similar to each other and thus should be regarded as of one type. In [3], experiments on binary weighting and term-frequency weighting indicate that when the vocabulary size is large enough, the count of keypoints in one visual word provides no more useful information than the presence or absence of the visual word. If we regard the keypoints of enough similarity as of one type, all these works lead to the same conclusion that it is better to treat keypoints by types than individually. In other words, in bag-of-visual-words representation, the optimal vocabulary size should be equal to the number of training keypoints types, and not the number of training keypoints. Now what is left for us to do is to define when a set of keypoints can be regarded as of one type and calculate the number of keypoint types among keypoints.

Since the keypoints of one type are similar to each other, we use a similarity threshold to define the notion of keypoint type. Specifically, we regard a set of keypoints as of one type if their similarities with their mean are all above a threshold th_s. In order to calculate the number of keypoint types among training descriptors, we need to do clustering among keypoints where each cluster corresponds to one keypoint type. Besides, we want the number of clusters to be minimized so that all keypoints of one type are really grouped into one cluster. Since the number of clusters is not known beforehand, the k-means-like clustering methods cannot be used here. Based on our previous work [13, 21], we propose to use the following similarity threshold based clustering method.

(1) Label all training keypoints as unclustered.

(2) Label the first unclustered keypoint as the centroid of one cluster.

(3) Compare each unclustered keypoint with the current center, and add it into the current cluster if the similarity is bigger than th_c.

(4) Return to Step 2 until all keypoints are clustered.

(5) Calculate the new centroid of each cluster, and use the count of keypoints in the cluster as the weight.

(6) Sort the centroids by weight in decreasing order.

(7) Compare all keypoints with each centroid in order and add to the corresponding cluster if the similarity is bigger than th_c.

(8) If there are keypoints left unclustered, repeat Step 2 to 3 to cluster them into new clusters.

(9) Repeat Steps 5 to 8 for a certain time.

The above presented is a simple clustering procedure to serve our purpose of obtaining a clustering with minimal clusters and each cluster corresponds to one keypoint type. Although we do not have theoretical evidence that this clustering procedure is guaranteed to converge and minimize the number of clusters, all our experiments show that the number of clusters obtained decreases gradually and tends to be stable after 5 iterations. Recalling that the performance of bag-of-visual-words is not sensitive to small changes in vocabulary size, we stick to this procedure in this paper and use the results after 10 iterations in all experiments.

Different from the traditional clustering methods which strengthen high intracluster similarity and low intercluster similarity, our clustering method requires all clusters to have an identical distribution range determined by the similarity threshold. In other words, our clustering method actually seeks to obtain an even and disjoint partition of the keypoint feature space by a set of hyperspheres whose radii are determined by the similarity threshold. Since the features in each hypersphere are represented by visual words, the visual vocabulary obtained in this way covers the whole feature space and is guaranteed to be of the minimum size. This visual vocabulary can therefore be regarded as a universal one and used-with any datasets. Here, we see that the similarity threshold, based clustering method is not a clustering method in the strict sense, and it is just an approach to find the similarity extent of one visual word in the universal visual vocabulary.

2.3. Optimal Similarity Threshold. In order to determine the optimal vocabulary size, we still need an appropriate selection of the similarity threshold th_s. By definition, th_s decides if a set of keypoints should be treated as of one type. Theoretically deriving such a threshold, if feasible, is out of our scope in this paper as it may involves physiological and psychological issues. Instead, we choose to empirically select the optimal similarity threshold th_s. In the first step, we test several candidates of th_s on different datasets and check if the best performing candidates coincidence with each other. If a unique best performing th_s is identified, the corresponding vocabulary size is then compared with other candidate sizes to see if it is the best performing one. It should be pointed out that in our experiments, the similarity threshold based clustering is only used to determine the vocabulary size, and the vector quantization with all vocabulary sizes is done with k-means clustering method. In this way, we make sure that the performance difference of different vocabulary sizes is not due to different clustering methods.

The experimental setup is as follows. DoG and SIFT [19] is used to detect and describe keypoints, and cosine similarity is selected as the keypoints similarity measure.

We do SVM classification on three diverse datasets: Caltech-101 [22], Scene-15 [4, 23, 24], and Event-8 [25]. With the well known Caltech-101, we randomly select 30 images per class as training and up to 15 images in the remaining as testing. Different from some of the literature using only 101 classes, here we test with all 102 classes. The Scene-15 dataset is composed of images of 15 classes with 200 to 400 images in each class. Following the setup in [4], we use 100 randomly selected images per class in training and all the others in testing. The Event-8 dataset contains images of 8 sports categories and each category has 130 to 250 images. This dataset is challenging for classification, not just in classifying events from static images, but that cluttered and diverse background, and various poses, sizes, and views of foreground objects are involved. We follow the setup in [25], that is, randomly selecting 70 images per class as training and another 60 images as testing.

We build the visual vocabularies of each dataset based on a set of randomly selected images from the dataset. In order to avoid any additional influence on the classification performance, the bag-of-visual-words histograms are built in the whole image, that is, at spatial pyramid level 0. In classification, we use term-frequency weighting scheme to build linear kernels. The multiclass SVM is trained in a one-versus-all setup and the regulation parameter C is fixed to be 1000. For all three datasets, we test with 10 training-testing splits and report the mean results. The performance measure adopted is the mean recognition rate per class. Note that in all our experiments, we use visual words without spatial information or special kernel; therefore, we do not expect to obtain superior classification performance comparable to the state-of-the-art. What is really important here is the trend of recognition rates with respect to the vocabulary sizes.

In the first step, we compare the performance of 4 candidate similarity thresholds 0.7, 0.75, 0.8, and 0.85. We do not adopt larger or smaller candidates as they produce extremely large or small vocabulary sizes that are obviously far from the optimal ones in our experiments. The four sizes calculated with similarity based clustering are 544, 2323, 12593, and 88328 for Caltech-101; 455, 1790, 9208, and 59539 for Event-8; and 560, 2378, 13124, and 92735 for Scene-15. The classification rates are reported in Figure 1, where we use similarity thresholds instead of the specific vocabulary sizes to show the trend more evidently. From this figure, we find that the vocabulary sizes from $\text{th}_c = 0.75$ and $\text{th}_c = 0.8$ perform the best.

We then compare the vocabulary sizes from these two optimal similarity thresholds with other sizes 100, 1000, 10000, 50000, and 100000 to check if they still perform the best. The results are shown in Table 1. As the optimal sizes corresponding to similarity thresholds 0.75 and 0.8 are different for different datasets, in the leftmost column we use $\text{th}_c = 0.75$ and $\text{th}_c = 0.8$ to represent their respective sizes.

It is evident from Table 1 that the vocabulary sizes from $\text{th}_c = 0.75$ and $\text{th}_c = 0.8$ perform the best or near-best among all sizes with three datasets. This confirms that $\text{th}_c = 0.75$ and $\text{th}_c = 0.8$ can be used to produce the optimal vocabulary size. Taking into account the small performance difference and large size difference between thresholds 0.8 and 0.75, we recommend to select 0.75 as the optimal similarity threshold in practical applications. Although Table 1 also indicates that the exact optimal similarity threshold should lie between these two values, we do not bother to seek it and are satisfied with these two candidates. One main consideration is that the performance of a visual vocabulary is not very sensitive to its size, only if the size is not too small. Our experiments indicate that for a common dataset of about the size of Caltech-101, 1000, or 2000, it might be a suitable vocabulary size. Adopting a larger size usually does not pay off.

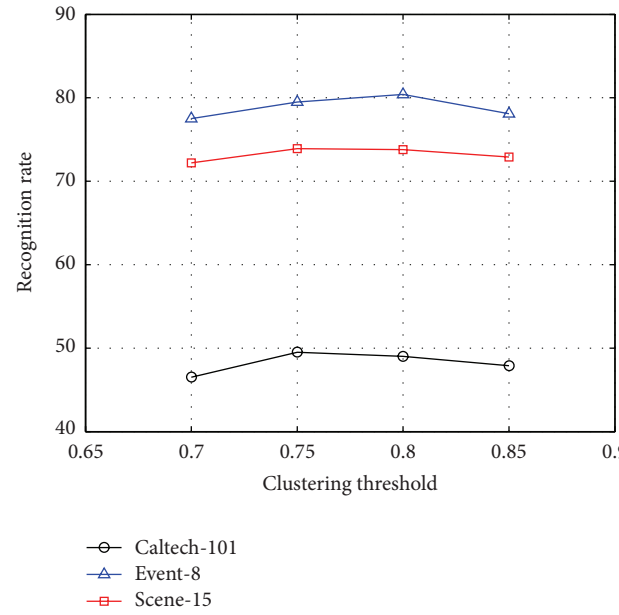

Figure 1: Recognition rates of different similarity thresholds. With all three datasets, the similarity thresholds 0.75 and 0.8 produce the best or near-best performance.

Table 1: Classification rates of different vocabulary sizes on three datasets. The sizes corresponding to similarity thresholds 0.75 and 0.8 produce the best or near-best results in all cases.

	caltech-101	Event-8	Scene-15
100	36.6 ± 1.0	70.7 ± 2.5	65.0 ± 0.4
1000	48.5 ± 1.1	79.3 ± 2.1	73.1 ± 0.7
10000	48.3 ± 1.1	80.0 ± 2.2	**73.9 ± 0.5**
50000	47.1 ± 0.9	78.5 ± 2.1	72.1 ± 0.5
100000	46.5 ± 1.1	78.1 ± 2.0	71.3 ± 0.7
$\text{th}_c = 0.75$	**49.5 ± 0.9**	79.5 ± 2.4	73.9 ± 0.6
$\text{th}_c = 0.8$	49.0 ± 1.0	**80.4 ± 2.5**	73.8 ± 0.5

In this, section we present a similarity threshold based clustering method to determine the optimal vocabulary size for a given dataset. Although the similarity threshold is determined empirically, this method cannot be regarded as just transforming the problem of determining k in k-means to the one of determining th_s. For different datasets the optimal vocabulary sizes are usually different, as shown in Table 1. This implies that one cannot select the optimal vocabulary size from one dataset and apply this size to other datasets.

Whereas with our similarity threshold based clustering method, the different optimal vocabulary sizes from different datasets correspond to a relatively fixed threshold th_s. This means that we can use this threshold to compute the optimal vocabulary size for a newly given dataset. More importantly, the results of this section support our hypothesis that the whole feature space can be mapped to a limited number of visual words, as one visual word is able to represent a set of keypoints that are similar enough. As shown in Section 3, this hypothesis is the basis of obtaining a universal and compact visual vocabulary.

3. Universal Visual Vocabulary

With a given dataset, researchers usually choose to build a specific visual vocabulary, instead of using an existing universal vocabulary. One possible explanation is that researchers tend to believe that the optimal visual vocabulary is data dependent and must be built specifically. However, the existence of an optimal visual vocabulary size smaller than the number of keypoints indicates that if some keypoints are similar enough, they should be grouped into one cluster and represented by one single visual word, but not by different visual words separately. This further implies that all keypoints can be mapped to a limited number of visual words. With the visual vocabulary obtained this way, all image patterns with semantic meanings can be represented with enough precision. This amounts to say that the images from any datasets can be represented accurately by this vocabulary; that is, this vocabulary is universal across datasets.

Recall that the optimal similarity threshold sets a criterion for keypoints to be mapped to one single visual word. Theoretically it is possible to enumerate all the possible visual words with the optimal similarity threshold th_s. However, it is not clear if all these image patterns represented by the vocabulary occur frequently in images or have semantic meanings. In other words, by enumerating all possible image pattern types, we may obtain a visual vocabulary that is complete but of a very large size. Nevertheless, many of these image patterns may rarely appear in real images. This causes unnecessary computation load and reduces the necessity of obtaining a universal vocabulary. Therefore, in this paper, we resort to empirical methods.

In Section 2, we have computed the optimal visual vocabularies for three datasets, which we refer to as voc-caltech, voc-event, and voc-scene, respectively. Here, we interchange the roles of datasets and visual vocabularies to check if different visual vocabularies produce a large performance difference on the same datasets. Take voc-caltech for example, we use it on Event-8 and Scene-15 and see if it performs comparably to voc-event and voc-scene, respectively. The comparison is shown in Figure 2.

Contrary to the traditional viewpoint that a good visual vocabulary is data dependent, we found from the comparison in Figure 2 that with each dataset, the visual vocabularies built with the three datasets perform rather similarly. This seems to imply that the visual vocabularies built from different datasets have a rather larger portion of visual words in common. In order to validate this viewpoint, we calculate the pairwise similarity between three vocabularies. Specifically, for each visual word in one vocabulary, we compute its cosine similarity with its closest counterpart in the other vocabulary. For all the 6 cases, that is, Caltech-Event, Event-Caltech, Caltech-Scene, Scene-Caltech, Event-Scene, and Scene-Event, almost all visual words have $a > 0.9$ similarity with their counterparts in other vocabularies, and over 60% of the visual words have $a > 0.95$ similarity. These results confirm that the three vocabularies are very similar to each other. This is interesting as the descriptors from three diverse datasets are mapped to almost identical vocabularies with our optimal vocabulary sizes. This observation confirms our belief that there does exist a universal visual vocabulary and the difference in appearances of images is only caused by the different distribution of image patterns represented by these visual words in the vocabulary. In other words, the experiments indicate that obtaining a universal visual vocabulary is not only theoretically sound, but practically feasible.

In [14], the authors conclude through experiments that with a given vocabulary size large enough, the visual vocabularies built from different datasets are exchangeable without harming the classification performance evidently. Therefore, a large vocabulary needs to be computed only once and can be used as a universal one. However, it is not clear if the universal visual vocabulary obtained this way is optimal or suboptimal. A vocabulary that is universal but performs ordinarily is not what we need definitely. In this paper, we arrive at much more powerful conclusions. When we say an optimal vocabulary is universal, our meaning is threefold. Firstly, the vocabulary can be used on other datasets to obtain comparable performance as their specific vocabulary. Secondly, our vocabulary is optimal in that it can produce the best or near-best performance on any datasets. Thirdly, our optimal vocabularies are of limited size (1000 to several thousands). This not only means efficiency in classification, but implies that a very large vocabulary may not be necessary at all. To sum up, in this paper, we provide an approach to produce a vocabulary that is universal, optimal, and compact.

Although currently we only test the approach on three datasets, we also note that all the three datasets contain objects of diverse types and large variations, and are thus rather representative. In the next step, we will extend the experiments to more and larger datasets, for example, Caltech-256 [26], Oxford flowers [27], NUS-WIDE [28], and Graz [29], and so forth, in order to finally produce a universal visual vocabulary, which can be used in a large number of datasets for the best or near-best performance.

4. Discussion

Our work in this paper is motivated from the difference between bag-of-words and bag-of-visual-words and also the experiments in [3]. Since bag-of-words is the counterpart and preceder of bag-of-visual-words, we expect them to share some common properties. However, we observe that in text domain, a universal vocabulary of relatively fixed size can

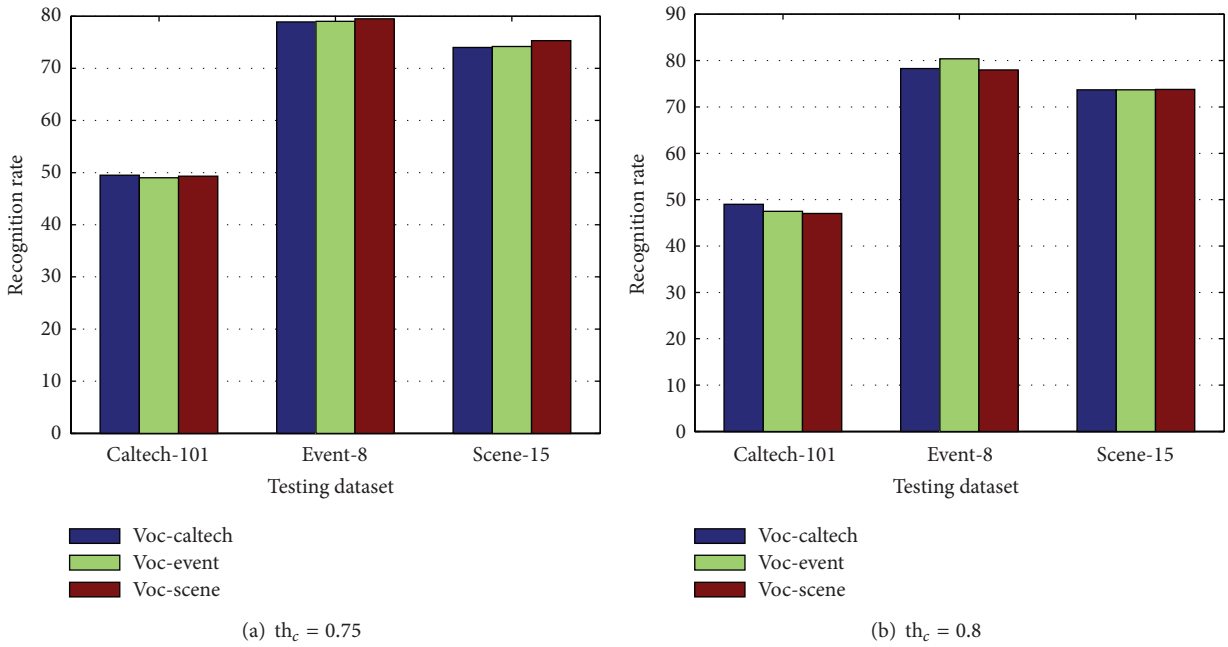

(a) $th_c = 0.75$ (b) $th_c = 0.8$

Figure 2: Recognition rates with vocabularies trained from different datasets. x-axis represents different testing datasets, and the different bars indicate vocabularies trained from different datasets. It is clear that different vocabularies perform similarly on the same datasets.

be used on different datasets, whereas in image domain the visual vocabularies are usually built specifically for given datasets and the vocabulary sizes are user-defined or determined empirically. On the other hand, the experiments in [3, 18] indicate that for an image dataset, the best performing vocabulary size is smaller than the number of keypoints. In other words, if some keypoints are similar enough to each other, they should be represented by one single visual word instead of many different visual words separately in order to obtain the best performance. From this perspective, we see that with any descriptor of limited dimension, all the possible keypoints can be represented by a limited number of visual words. Since this vocabulary of limited size covers the whole feature space, it can be used as a universal visual vocabulary. In Sections 2 and 3, we empirically validate this hypothesis.

The existence of a universal and compact visual vocabulary can be understood as follows. In the text domain, the number of words with semantic meanings is limited and the vocabulary is of a limited size. However, this vocabulary of limited size is able to deliver numerous meanings which we intend to express. The reason, in our opinion, lies in that each word in the vocabulary delivers not just one basic meaning, but also some other meanings similar enough to the basic one. In other words, each word in the vocabulary covers not just one point in the space of semantic meanings, but also the neighborhood of the point. In this way, a vocabulary of limited size is able to cover the whole space of semantic meanings and be used as a universal vocabulary. From this perspective, it is easy to understand why a compact visual vocabulary is able to represent all the image patterns with semantic meanings accurately and is universal across image datasets.

The observation in [3] that a larger size than the optimal may result in performance loss is explained in the following. Theoretically, visual vocabularies of optimal and larger sizes are all able to describe all the possible image patterns and their performances should be identical. However, with the increase of vocabulary sizes, the number of keypoints represented by one visual word tends to decrease. As a result, the calculation of a visual word as the centroid of a group of keypoints is more likely to be influenced by noise, which, in turn, harms the performance of visual vocabularies. Another interesting observation is that the optimal vocabularies from different datasets are of different sizes and they all can be used as the universal one. Our explanation is that when the vocabulary size is large enough, the relatively small variance in vocabulary sizes has little influence on the representation of image content, as illustrated in Table 1.

Based on the above analysis and the experimental results in Sections 2 and 3, we believe we have found out something related to the mechanism of bag-of-visual-words. In the next step, we plan to deepen our work by borrowing ideas and methods from related domains, for example, data-driven approaches [30–35] and psychological research.

5. Conclusion

Bag-of-visual-words is an important image representation and has been widely used in computer vision and pattern recognition problems. While much works have been published surrounding this representation, almost all existing works are based on the implicit assumption that a good visual vocabulary is data dependent. The problem of building a universal visual vocabulary of limited size is rarely touched.

Based on previous works on classification performance with respect to the vocabulary sizes, we arrive at the hypothesis that when features are similar enough, they should be represented by one visual word in order to obtain the best classification results. This further indicates that the whole feature space can be represented by a limited number of visual words, which constitute a universal visual vocabulary of limited size.

Starting from this hypothesis, we proposed to use a similarity threshold based clustering method to calculate the optimal vocabulary size for a given dataset. The optimal vocabulary size is then used to generate the optimal visual vocabulary for the dataset. In the experiments, we found that the three optimal vocabularies of limited sizes (several thousands) built from three datasets separately are very similar to each other, and any of them can be used to generate the best or near-best performance with all three datasets. This encouraging result indicates that with more datasets involved, it is really feasible to obtain a universal and compact visual vocabulary to be used in any datasets to generate (near-)best performance.

We analyzed the reasons behind the existence of a universal and compact visual vocabulary and other related phenomena observed in experiments. Based on the experiments and our analysis, we believe that we have found out something underlying the behavior of the bag-of-visual-words representation. Since in text domain a universal vocabulary is usually used with different datasets, our work narrows the gap between bag-of-visual-words and bag-of-words. This may lead to new approaches to explore the potential of the bag-of-visual-words representation and other image representation methods.

Conflict of Interests

The authors declare that there is no conflict of interests regarding the publication of this paper.

Acknowledgments

This work is supported by the National Natural Science Foundation of China (Grant no. 61304102), the Natural Science Foundation of Liaoning Province of China (Grant no. 2013020002), and the Scientific Research Fund of Liaoning Provincial Education Department of China (Grant nos. L2012400 and L2012397).

References

[1] J. Sivic and A. Zisserman, "Video google: a text retrieval approach to object matching in videos," in *Proceedings of the IEEE International Conference on Computer Vision*, pp. 1470–1477, October 2003.

[2] S. Lazebnik, C. Schmid, and J. Ponce, "A maximum entropy framework for part-based texture and object recognition," in *Proceedings of the 10th IEEE International Conference on Computer Vision (ICCV '05)*, pp. 832–838, October 2005.

[3] J. Yang, Y.-G. Jiang, A. G. Hauptmann, and C.-W. Ngo, "Evaluating bag-of-visual-words representations in scene classification," in *Proceedings of the International workshop on Multimedia Information Retrieval*, pp. 197–206, September 2007.

[4] S. Lazebnik, C. Schmid, and J. Ponce, "Beyond bags of features: spatial pyramid matching for recognizing natural scene categories," in *Proceedings of the IEEE Computer Society Conference on Computer Vision and Pattern Recognition (CVPR '06)*, pp. 2169–2178, June 2006.

[5] M. Marszałek and C. Schmid, "Spatial weighting for bag-of-features," in *Proceedings of the IEEE Computer Society Conference on Computer Vision and Pattern Recognition (CVPR '06)*, pp. 2118–2125, June 2006.

[6] V. Viitaniemi and J. Laaksonen, "Spatial extensions to bag of visual words," in *Proceedings of the ACM International Conference on Image and Video Retrieval (CIVR '09)*, pp. 280–287, July 2009.

[7] D. Nistér and H. Stewénius, "Scalable recognition with a vocabulary tree," in *Proceedings of the IEEE Computer Society Conference on Computer Vision and Pattern Recognition (CVPR '06)*, pp. 2161–2168, June 2006.

[8] H. Cai, F. Yan, and K. Mikolajczyk, "Learning weights for codebook in image classification and retrieval," in *Proceedings of the IEEE Computer Society Conference on Computer Vision and Pattern Recognition (CVPR '10)*, pp. 2320–2327, June 2010.

[9] T. Li, T. Mei, and S. K. In, "Learning optimal compact codebook for efficient object categorization," in *Proceedings of the IEEE Workshop on Applications of Computer Vision (WACV '08)*, pp. 1–6, January 2008.

[10] P. K. Mallapragada, R. Jin, and A. K. Jain, "Online visual vocabulary pruning using pairwise constraints," in *Proceedings of the IEEE Computer Society Conference on Computer Vision and Pattern Recognition (CVPR '10)*, vol. 2, pp. 3073–3080, June 2010.

[11] J. Zhang, M. Marszalek, S. Lazebnik, and C. Schmid, "Local features and kernels for classification of texture and object categories: an in-depth study," Tech. Rep., INRIA, 2003.

[12] W. Zhao, Y. Jiang, and C. Ngo, "Keyframe retrieval by keypoints: can point-to-point matching help?" in *Proceedings of the ACM International Conference on Image and Video Retrieval*, pp. 72–81, 2006.

[13] J. Hou, Z. S. Feng, Y. Yang, and N. M. Qi, "Towards a universal and limited visual vocabulary," in *Proceedings of the International Symposium on Visual Computing*, pp. 414–424, 2011.

[14] C. X. Ries, S. Romberg, and R. Lienhart, "Towards universal visual vocabularies," in *Proceedings of the IEEE International Conference on Multimedia and Expo (ICME '10)*, pp. 1067–1072, July 2010.

[15] J. Hou, W. X. Liu, X. E, Q. Xia, and N. M. Qi, "An experimental study on the universality of visual vocabularies," *Journal of Visual Communication and Image Representation*, vol. 24, pp. 1204–1211, 2013.

[16] J. Winn, A. Criminisi, and T. Minka, "Object categorization by learned universal visual dictionary," in *Proceedings of the 10th IEEE International Conference on Computer Vision (ICCV '05)*, pp. 1800–1807, October 2005.

[17] F. Perronnin, "Universal and adapted vocabularies for generic visual categorization," *IEEE Transactions on Pattern Analysis and Machine Intelligence*, vol. 30, no. 7, pp. 1243–1256, 2008.

[18] T. Deselaers, L. Pimenidis, and H. Ney, "Bag-of-visual-words models for adult image classification and filtering," in *Proceedings of the 19th International Conference on Pattern Recognition (ICPR '08)*, pp. 1–4, December 2008.

[19] D. G. Lowe, "Distinctive image features from scale-invariant keypoints," *International Journal of Computer Vision*, vol. 60, no. 2, pp. 91–110, 2004.

[20] J. Hou, N. M. Qi, and J. X. Kang, "Image matching based on representative local descriptors," in *Proceedings of the International Conference on Multimedia Modeling*, pp. 303–313, 2010.

[21] J. Hou, J. X. Kang, and N. M. Qi, "On vocabulary size in bag-of-visual-words representation," in *Proceedings of the Pacific-Rim Conference on Multimedia*, pp. 414–424, 2010.

[22] L. Fei-Fei, R. Fergus, and P. Perona, "Learning generative visual models from few training examples: an incremental bayesian approach tested on 101 object categories," in *Proceedings of the Workshop on Generative-Model Based Vision (CVPR '04)*, p. 178, 2004.

[23] A. Oliva and A. Torralba, "Modeling the shape of the scene: a holistic representation of the spatial envelope," *International Journal of Computer Vision*, vol. 42, no. 3, pp. 145–175, 2001.

[24] F.-F. Li and P. Perona, "A bayesian hierarchical model for learning natural scene categories," in *Proceedings of the IEEE Computer Society Conference on Computer Vision and Pattern Recognition (CVPR '05)*, vol. 1, pp. 524–531, June 2005.

[25] L. L. Jia and L. Fei-Fei, "What, where and who? Classifying events by scene and object recognition," in *Proceedings of the IEEE 11th International Conference on Computer Vision (ICCV '07)*, pp. 1–8, October 2007.

[26] G. Griffin, A. Holub, and P. Perona, "Caltech-256 object category dataset," Tech. Rep. 7694, Caltech, 2007.

[27] M.-E. Nilsback and A. Zisserman, "A visual vocabulary for flower classification," in *Proceedings of the IEEE Computer Society Conference on Computer Vision and Pattern Recognition (CVPR '06)*, pp. 1447–1454, June 2006.

[28] T.-S. Chua, J. Tang, R. Hong, H. Li, Z. Luo, and Y. Zheng, "NUS-WIDE: a real-world web image database from National University of Singapore," in *Proceedings of the ACM International Conference on Image and Video Retrieval (CIVR '09)*, pp. 1–9, July 2009.

[29] A. Opelt, M. Fussenegger, A. Pinz, and P. Auer, "Weak hypotheses and boosting for generic object detection and recognition," in *Proceedings of the European Conference on Computer Vision*, pp. 71–84, 2004.

[30] S. Yin, X. Yang, and H. R. Karimi, "Data-driven adaptive observer for fault diagnosis," *Mathematical Problems in Engineering*, vol. 2012, Article ID 832836, 21 pages, 2012.

[31] S. Yin, S. Ding, A. Haghani, H. Hao, and P. Zhang, "A comparison study of basic datadriven fault diagnosis and process monitoring methods on the benchmark tennessee eastman process," *Journal of Process Control*, vol. 22, pp. 1567–1581, 2012.

[32] P. Flandrin and P. Goncalves, "Empirical mode decompositions as data-driven wavelet-like expansions," *International Journal of Wavelets, Multiresolution and Information Processing*, vol. 2, pp. 1–20, 2004.

[33] S. Yin, S. Ding, A. Haghani, and H. Hao, "Data-driven monitoring for stochastic systems and its application on batch process," *International Journal of Systems Science*, vol. 44, pp. 1366–1376, 2013.

[34] A. Baak, M. Muller, G. Bharaj, H.-P. Seidel, and C. Theobalt, "A data-driven approach for real-time full body pose reconstruction from a depth camera," in *Proceedings of the IEEE International Conference on Computer Vision (ICCV '11)*, pp. 1092–1099, November 2011.

[35] S. Yin, H. Luo, and S. Ding, "Real-time implementation of fault-tolerant control systems with performance optimization," *IEEE Transactions on Industrial Electronics*, 2013.

Hindawi Publishing Corporation
Mathematical Problems in Engineering
Volume 2013, Article ID 572026, 9 pages
http://dx.doi.org/10.1155/2013/572026

Research Article

A Delta Operator Approach for the Discrete-Time Active Disturbance Rejection Control on Induction Motors

John Cortés-Romero,[1] Alberto Luviano-Juárez,[2] and Hebertt Sira-Ramírez[3]

[1] *Departamento de Ingeniería Eléctrica y Electrónica, Universidad Nacional de Colombia, Carrera 45 No. 26-85, Bogotá, Colombia*
[2] *Unidad Profesional Interdisciplinaria en Ingeniería y Tecnologías Avanzadas (UPIITA)-Instituto Politécnico Nacional 2580, Barrio La Laguna Ticomán, Gustavo A. Madero, 07340 México, DF, Mexico*
[3] *Centro de Investigación y de Estudios Avanzados del Instituto Politécnico Nacional (CINVESTAV-IPN), Avenida Instituto Politécnico Nacional, No. 2508, Departamento de Ingeniería Eléctrica, Sección de Mecatrónica, Colonia San Pedro Zacatenco, A.P. 14740, 07300 México, DF, Mexico*

Correspondence should be addressed to John Cortés-Romero; jacortesr@unal.edu.co

Received 23 August 2013; Accepted 8 October 2013

Academic Editor: Baoyong Zhang

The problem of active disturbance rejection control of induction motors is tackled by means of a generalized PI observer based discrete-time control, using the delta operator approach as the methodology of analyzing the sampled time process. In this scheme, model uncertainties and external disturbances are included in a general additive disturbance input which is to be online estimated and subsequently rejected via the controller actions. The observer carries out the disturbance estimation, thus reducing the complexity of the controller design. The controller efficiency is tested via some experimental results, performing a trajectory tracking task under load variations.

1. Introduction

To obtain high performance control of electric machines there has been a growing interest in the design of controllers based on the discrete-time model of the system. In the case of induction motors, the system is continuous in nature, being necessary to obtain a sampled-time model. Preliminary studies on the sampling of continuous time nonlinear systems can be found in [1]. Many advances have been reported about control of sampled nonlinear systems; see for instance [2, 3] and references therein. Specifically, an analysis about the discretization techniques for the induction motor model can be found in [4].

There exists a variety of control strategies for the induction motor that depend on the difficulty to measure parameters while their closed loop behavior is found to be sensitive to their variations. Generally speaking, the designed feedback control strategies have to exhibit a certain robustness level with respect to unknown bounded additive disturbance, in order to guarantee an acceptable performance. It is possible to (online or offline) obtain estimates of the motor parameters [5], but some of them can be subject to variations when the system is undergoing actual operation. Frequent misbehavior is also due to external and internal disturbances, such as generated heat, that significantly affect some of the system parameter values. An alternative to overcome this situation is to use robust feedback control techniques which take into account these variations as unknown disturbance inputs that need to be online estimated and rejected. One of the first attempts to solve this problem was proposed by Johnson [6], known as disturbance accommodation control, in which external disturbances are given as "waveform functions", proposing an unknown input observer to perform the robust controller. On the other hand, the active disturbance rejection scheme [7–9] considers both external disturbances and internal perturbations, as a lumped generalized additive disturbance functions to be canceled out. The main idea of the controller is the fact that the disturbance observer can estimate the lumped disturbance input, which allows to approximately reduce the original nonlinear tracking control

problem to that of a disturbed input tracking problem, suitable for the application of a simple controller.

One variant of this scheme resorts to a local internal model characterization of the lumped disturbance using a representative element of a family of discrete-time polynomial signals of fixed degree. This results in a local self-updating polynomial model of the uncertainty which can be estimated, in an arbitrarily close manner, via a suitable extended linear observer of generalized proportional integral (GPI) nature [10]. The GPI estimation procedure has been extended for fault tolerant control applications as proposed in [11].

For the case of the induction motor control, we consider a robust controller design based upon a simplified discrete model of the system including additive, completely unknown, disturbance inputs lumping nonlinearities and external disturbances whose effect is to be determined in an online fashion by means of a discrete-time linear observer of the GPI. The gathered knowledge will be used in the appropriate canceling of the assumed disturbances themselves while reducing the underlying control problem to a simple linear feedback control task. The control scheme thus requires knowledge of a reduced set of the motor parameters to be implemented.

The controller design for the induction motor is carried out within the philosophy of the classical field oriented controller scheme and implemented through a flux simulator or reconstructor (see Chiasson [12] and Martín and Rouchon [13]). It is considered a two-stage design procedure for the feedback control scheme of an induction motor which allows one to, simultaneously, regulate the motor shaft angular velocity towards a prespecified reference trajectory and to stabilize the flux magnitude to a desired constant level. The first stage designs a controller for the reference trajectory tracking of the rotor shaft angular velocity. The stator currents are used as auxiliary control input variables within a *field oriented* strategy combined with a load torque elimination executed on the basis of an online close estimation of the load disturbance input.

The control configuration for the first stage inherently includes a *flux reconstructor*, and a discrete-time generalized proportional integral observer based control for the efficient and rather accurate online estimation of the unknown but bounded load torque disturbance input function. The second design stage takes the synthesized rotor currents as reference trajectories to be tracked from the rotor input voltages.

In this case, the sampled time system is not defined purely in terms of the time-shift operator but in terms of the unified operator approach proposed by Goodwin et al. [14]. This operator came up with an alternative to obtain better results in high sampling rates, where most traditional discrete-time algorithms may be ill-conditioned when applied to data taken at sampling rates which are high relative to the dynamics of sampled data [15]. The unified approach developed a strategy capable of unifying both continuous and discrete-time formulations [14]. Moreover, this approach overcomes the unstable sampling zero problem as analyzed in [16] and the procedure for the control gains is enhanced since the stability region increases as sampling time decreases, avoiding extra reparametrizations as the Tustin approach. In this type of approach, the authors proposed the use of an operator called δ-operator defined as follows: $\delta = (q-1)/\Delta$, where q is the forward shift operator in the time domain and Δ is the sampling time.

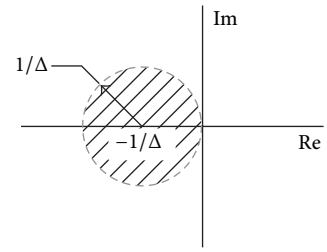

Figure 1: Stability region for delta operator.

Here, the discrete-time GPI control has been proposed using the delta operator approach taking advantages of the high sampling rates and advantages of working directly in the sampled time system with respect to the continuous scheme, such as the faster implementation in a digital controller.

The remainder of the paper is organized as follows. Section 2 introduces the unified operator framework. In Section 3, the induction motor model is introduced, and some considerations regarding the additive disturbances are reported. Section 4.3 presents the problem of disturbance estimation in the context of the discrete-time GPI observer. Section 5 deals with the field oriented control strategy; the angular velocity and stator current controls are presented as a two-stage design procedure involving inner and outer loop controls. Section 6 provides some experimental results in a test bed to show the behavior of the observer-based control. Finally, some conclusions are reported in Section 7.

2. Brief Remarks about the Delta Operator

In this section, some preliminary concepts regarding the δ operator and its properties are introduced; more details concerning the operator and its applications are found in [14, 17, 18].

Definition 1. The domain of possible nonnegative "times" $\Omega^+(\Delta)$ is defined as follows:

$$\Omega^+(\Delta) = \begin{Bmatrix} \mathbb{R}^+ \cup \{0\} & : \Delta = 0, \\ \{0, \Delta, 2\Delta, 3\Delta, \ldots\} & : \Delta \neq 0 \end{Bmatrix}, \quad (1)$$

where Δ denotes the sampling period in discrete time or $\Delta = 0$ for a continuous time framework.

Definition 2. A time function $x(t)$, $t \in \Omega^+(\Delta)$, is, in general, simply a mapping from times, to either the real or the complex set. That is, $x(t) : \Omega^+ \to \mathbb{C}$.

Definition 3. The δ operator is defined as follows:

$$\delta x(t) \triangleq \frac{(q-1)\,x(t)}{\Delta} = \frac{x(t+\Delta) - x(t)}{\Delta} : \Delta \neq 0, \quad (2)$$

where q is the shift operator and

$$\lim_{\Delta \to 0^+} \delta(x(t)) = \frac{dx(t)}{dt}. \tag{3}$$

Definition 4. We will consider ρ as a generalized derivative operator, which will denote d/dt in continuous time or δ in discrete time.

Definition 5. The unified integration operation $\mathbf{S}$ is given as follows:

$$\mathbf{S}_{t_1}^{t_2} x(\tau)\, d\tau = \begin{Bmatrix} \int_{t_1}^{t_2} x(\tau)\, d\tau & : \Delta = 0 \\ \Delta \sum_{l=t_1/\Delta}^{l=t_2/\Delta - 1} x(l\Delta) & : \Delta \neq 0 \end{Bmatrix}, \tag{4}$$

$t_1, t_2 \in \Omega^+$.

The integration operator corresponds to the antiderivative operator.

Definition 6 (generalized matrix exponential). In the case of the unified transform theory, the generalized exponential E is defined as follows:

$$E(A,t,\Delta) = \begin{Bmatrix} e^{At} & : \Delta = 0 \\ (I + A\Delta)^{t/\Delta} & : \Delta \neq 0 \end{Bmatrix}, \tag{5}$$

where $A \in \mathbb{C}^{n\times n}$, I is the identity matrix, and $t \in \Omega^+$. The generalized matrix exponential satisfies to be the fundamental matrix of $\delta x = Ax$, and thus the unique solution to

$$\rho x = Ax, \qquad x(0) = x_0 \tag{6}$$

is $x(t) = E(A,t,\Delta)x_0$. The general solution to:

$$\rho x = Ax + Bu, \qquad x(0) = x_0 \tag{7}$$

is

$$x(t) = E(A,t,\Delta)\, x_0 + \mathbf{S}_0^t E(A, t-\tau-\Delta, \Delta)\, Bu(\tau)\, d\tau. \tag{8}$$

Definition 7 (stability boundary). The solution of (6) is said to be asymptotically stable if and only if, for all x_0, $x(t) \to 0$ as time elapses. The stability arises if and only if $E(A,t,\Delta) \to 0$ as $t \to \infty$ if and only if every eigenvalue of A, denoted as λ_i, $i = 1, \ldots, n$, satisfies the following condition:

$$\mathrm{Re}\{\lambda_i\} + \frac{\Delta}{2}|\lambda_i|^2 < 0. \tag{9}$$

Therefore, the stability boundary is the circle with center $(-1/\Delta, 0)$ and radius $1/\Delta$ (see Figure 1). In particular, consider the following nth degree characteristic equation on the complex variable γ (see Definition 8):

$$\prod_{i=1}^{n} (\gamma - \lambda_i) = \gamma^n + c_{n-1}\gamma^{n-1} + \cdots + c_1\gamma + c_0 = 0. \tag{10}$$

If all the roots λ_i, $i = 1 \ldots, n$, of the last equation satisfy condition (9), then the solution of the associated system to (10) is asymptotically stable.

Definition 8 (Unified Transform Theory). There is a close connection between the forward shift operator q and the Z-transform variable z. Analogously, consider a new transform variable γ associated with the δ operator as $\gamma = (z-1)/\Delta$. From the Z-transform, the delta transform is derived as follows:

$$\mathbf{T}(f(k)) = \Delta F(z)|_{z=\Delta\gamma+1} = \Delta \sum_{k=0}^{\infty} f(k)\,(1+\Delta\gamma)^{-k}. \tag{11}$$

2.1. Transform Properties. We will just point out to the transform properties to be used throughout the work. A more extensive list of the delta transform properties is found in [17].

(i) Linearity. For any scalar α_1, α_2,

$$\mathbf{T}\{\alpha_1 f(t) + \alpha_2 g(t)\} = \alpha_1 \mathbf{T}\{f(t)\} + \alpha_2 \mathbf{T}\{g(t)\}. \tag{12}$$

(ii) Differentiation

$$\mathbf{T}\{\rho[f(t)]\} = \gamma \mathbf{T}\{f(t)\} - f(0^-)(1+\Delta\gamma). \tag{13}$$

(iii) Integration

$$\mathbf{T}\left\{\mathbf{S}_0^t f(\tau)\, d\tau\right\} = \frac{1}{\gamma}\mathbf{T}\{f(t)\}. \tag{14}$$

(iv) Frequency Differentiation

$$\mathbf{T}\{tf(t)\} = -(\Delta\gamma + 1)\frac{d}{d\gamma}[\mathbf{T}\{f(t)\}]. \tag{15}$$

3. System Model and Problem Formulation

Consider the two-phase equivalent mathematical model (a,b) of a three-phase induction motor controlled by the phase voltages represented by the complex input voltage $u_S = u_{Sa} + ju_{Sb} = |u_S|e^{j\theta_u}$. The state variables are given by: θ, which is the rotor angular position, ω denoting the rotor angular velocity, ψ_{R_a} and ψ_{R_b} denote the unmeasured rotor fluxes consolidated by the complex rotor flux: $\psi_R = \psi_{Ra} + j\psi_{Rb} = |\psi_R|e^{j\theta_\psi}$. The variables i_{Sa} and i_{Sb} represent the stator currents, and $i_S = i_{Sa} + ji_{Sb} = |i_S|e^{\theta_i}$ is their corresponding complex armature current. It is assumed that $j = \sqrt{-1}$ is the imaginary unit, $\overline{x}$ is the conjugate of x, $\mathscr{R}_e(x)$ denote the real part of x and $\mathscr{I}_m(x)$ denote the imaginary part of x. From the abovementioned definitions, we have

$$\begin{aligned} \rho\omega &= \mu\, \mathrm{Im}(\overline{\psi}_R i_S) - \frac{B}{J}\omega - \frac{\tau_L}{J}, \\ \rho\psi_R &= -(\eta - jn_p\omega)\psi_R + \eta M i_S, \\ \rho i_S &= \beta(\eta - jn_p\omega)\psi_R - \gamma i_S + \frac{1}{\sigma L_S}u_S, \end{aligned} \tag{16}$$

with ρ the generalized derivative operator, $\eta := R_R/L_R$, $\beta := M/\sigma L_R L_S$, $\mu := n_p M/JL_R$, $\gamma := M^2R_R/\sigma L_R^2 L_S + R_S/\sigma L_S$, and $\sigma := 1 - M^2/L_R L_S$. R_R and R_S are the rotor and stator resistances. The rotor and stator inductance parameters are

given by L_R and L_S, and M is the mutual inductance constant; the moment of inertia is set by J, the friction coefficient is denoted by B, and n_p is the number of pole pairs. The signal τ_L is the unknown load torque disturbance input.

3.1. Flux Observer. A simple way to obtain a discretization of the flux observer is using δ-operator approximation for the derivatives (which is equivalent to Euler's approximation); that is,

$$\dot{\psi}_R(t) \approx \delta\psi_R(t) = \frac{\left[\psi_R(t+\Delta) - \psi_R(t)\right]}{\Delta}. \tag{17}$$

A discretized version of flux dynamics is given by

$$\psi_R(t+\Delta) = \left[1 - \eta\Delta + jn_p\Delta\omega(t)\right]\psi_R(t) + \eta M\Delta i_S(t). \tag{18}$$

An observer for this discretized system is given by

$$\widehat{\psi}_R(t+\Delta) = \left[1 - \eta\Delta + jn_p\Delta\omega(t)\right]\widehat{\psi}_R(t) + \eta M\Delta i_S(t). \tag{19}$$

In order to analyze the stability of the discrete-time flux estimator, the estimation error is defined as: $e_\psi(t+\Delta) = \psi_R(t+\Delta) - \widehat{\psi}_R(t+\Delta)$; these errors satisfy $e_\psi(t+\Delta) = [1 - \eta\Delta + jn_p\Delta\omega(t)]e_\psi(t)$. Consider the Lyapunov function candidate $V(k) = |e_\psi(t)|^2$ under simple algebraic manipulations yields

$$V(t+\Delta) = \alpha(t)\,V(t) \tag{20}$$

with $0 \le \alpha(t) = (1-\eta\Delta)^2 + (n_p\Delta\omega(t))^2$. The stability is guaranteed when $0 \le \alpha(t) < 1$. It is possible to find a condition on the sample period, Δ, and speed, ω, such that the origin of the complex error space, $e_\psi(t) = 0$, is a globally asymptotic equilibrium point for (18):

$$\Delta < \frac{2\eta}{\eta^2 + n_p^2\omega_{\max}^2} \Longrightarrow 0 \le \alpha(t) < 1, \tag{21}$$

where $\omega_{\max}$ is the maximum angular velocity of the motor.

The flux simulator variable, $\widehat{\psi}_R$, will be used, henceforth, in place of the actual flux without further considerations.

3.2. Assumptions

(i) It is assumed that only the shaft's angular position, θ, and the stator currents, i_{Sa}, i_{Sb}, are measured.

(ii) The motor parameters are assumed to be known.

(iii) The load torque $\tau_L(t)$ is assumed to be time-varying but unknown.

(iv) Let us assume that the sampling period Δ is sufficiently small to achieve accurate results when using, as a discretization methodology, the unified operator ρ (the use of Euler methods is in [4] in a difereent context). In particular, Δ is small enough to satisfy (21).

3.3. Problem Formulation. Under the above assumptions, consider the induction motor dynamic model (16). Given a reference trajectory for the motor angular velocity, $\omega^*(t)$, and a reference for the magnitude of the complex flux, $|\psi_R^*|$, the main objective of this paper is to devise multivariable discrete-time feedback control laws for the stator voltages, $u_{Sa}(t)$, $u_{Sb}(t)$, such that they force, in an arbitrary fashion, $\omega(t)$ to track $\omega^*(t)$ and $|\psi_R|$ to track $|\psi_R^*|$ regardless of the values adopted by the time-varying torque, $\tau_L(t)$, the discretization errors resulting from the δ-operator discretization procedure, and eventually parameter uncertainty.

4. Control Strategy

4.1. Simplified Model. The proposed control strategy is based on a simplified vision of the system model (16), which is systematically advocated in the ADRC approach. One adopts the simplified models, defined in terms of complex variables notation:

$$\rho\omega = \mu\,\mathrm{Im}\left(\overline{\psi}_R i_S\right) + \xi_1(t), \tag{22}$$

$$\rho|\psi_R|^2 = -2\eta|\psi_R|^2 + 2\eta M\,\mathrm{Re}\left(\overline{\psi}_R i_S\right), \tag{23}$$

$$\rho\theta_\psi = n_p\omega + \frac{R_r M}{L_r|\psi_R|^2}\,\mathrm{Im}\left(\overline{\psi}_R i_S\right), \tag{24}$$

$$\rho i_S = \frac{1}{\sigma L_S}u_S + \xi_2(t), \tag{25}$$

where $\widetilde{\xi}_1(t)$ is the exogenous disturbance function that takes into account the load torque disturbance term, $-\tau_L(t)/J$, the viscous friction term, $-(B/J)\omega$, and discretization errors due to δ-operator approximation; $\widetilde{\xi}_2(t)$ is the endogenous state dependent disturbance function that represents nonlinear and linear additive dissipation terms, depending on the stator currents, i_{Sa}, i_{Sb}, and the angular velocity, ω, and it also includes discretization errors.

4.2. Field Oriented Control. From (22) and (23), we can obtain an interesting control decoupling property: the angular velocity is governed by $\mathrm{Im}(\overline{\psi}_R i_S)$, while the squared flux magnitude is commanded by $\mathrm{Re}(\overline{\psi}_R i_S)$. Consequently, taking the current, i_S, as auxiliary control input, both constitutive parts of the system can be controlled independently of each other. This classical indirect control decoupling property is equivalent to the field oriented control approach. We use this property to set, with the help of auxiliary input variable, $\nu = \nu_a + j\nu_b$, the following input current field oriented controller:

$$i_S = \left(\frac{\psi_R}{|\psi_R|^2}\right)\nu, \tag{26}$$

yielding the following set of control decoupled linear disturbed systems:

$$\rho\omega = \mu\nu_b + \xi_1(t), \tag{27}$$

$$\rho|\psi_R|^2 = -2\eta|\psi_R|^2 + 2\eta M\nu_a. \tag{28}$$

The control law v should accomplish the simultaneous tracking tasks for $|\psi_R|$ and ω (see (28), (27)) and the control law u_S for the tracking of i_S (see (25)) in a two-stage feedback observer based control configuration. The key observation of this observer based control approach is that the disturbance inputs, ξ_1, ξ_2, involved in (27), (25), can be approximately estimated and then canceled at the controller stage. This procedure goes with the total active disturbance rejection paradigm (see [8]).

4.3. Disturbance Estimation. In this subsection, a methodology of disturbance estimation by means of a delta operator discrete-time observer, which can be associated to an extended Luenberger like linear observer, is developed.

The ideal performance of control systems and its dual estimation is to achieve zero steady-state errors in an asymptotic fashion. Given the uncertainty of unified disturbance signals (regarding external disturbances and the dynamics of the system) involved in the dynamics of the inner and outer loops of the proposed control scheme, it is necessary to make an approach to a generic model for signals. The approximation used and which is simpler to determine the internal model is given by the approximation of the truncated Taylor series. These families of functions with respect to disturbance signals are in agreement with the model $\rho^{m_i}\xi_i = ((q-1)^{m_i}/\Delta^{m_i})\xi_i \approx 0$ with $i = 1, 2$. The approach uses the fact that the disturbance inputs, ξ_i, $i = 1, 2$, can be approximately modeled by

$$\rho^{m_i}\xi_i \approx 0, \tag{29}$$

where m_1, m_2 are integers large enough. So, taking ξ_i, $i = 1, 2$, as augmented variables it is possible to establish generalized state observers (see [19]).

The disturbance inputs ξ_i can be expressed as functions of the output, the input and a finite application of the delta operator on them; therefore, the algebraic observability property is achieved, and a delta operator based observer can be proposed in each equation.

The construction of the delta generalized proportional integral disturbance observer for ξ_1 is described in the following proposition.

Proposition 9. *Define the observation error as* $\widetilde{e}_\theta(t) = \theta(t) - \widehat{\theta}(t)$. *The following system*

$$\begin{aligned}
\widehat{\rho\theta}(t) &= \widehat{\omega}(t) + l_{m_1+1}\widetilde{e}_\theta(t),\\
\widehat{\rho\omega}(t) &= \mu v_b(t) + l_{m_1}\widetilde{e}_\theta(t) + \widehat{z}_{1,1}(t),\\
\widehat{\rho z}_{1,1}(t) &= l_{m_1-1}\widetilde{e}_\theta(t) + \widehat{z}_{1,2}(t),\\
\widehat{\rho z}_{1,2}(t) &= l_{m_1-2}\widetilde{e}_\theta(t) + \widehat{z}_{1,3}(t),\\
&\vdots\\
\widehat{\rho z}_{1,m_1-1}(t) &= l_1\widetilde{e}_\theta(t) + \widehat{z}_{1,m_1}(t),\\
\widehat{\rho z}_{1,m_1}(t) &= l_0\widetilde{e}_\theta(t),
\end{aligned}$$

$$\begin{aligned}
&\widehat{\theta}(0) = \widehat{\omega}(0) = \widehat{z}_{1,1}(0) = \cdots = \widehat{z}_{1,m_1}(0) = 0,\\
&\widehat{\xi}_1(t) = \widehat{z}_{1,1}(t)
\end{aligned} \tag{30}$$

constitutes an asymptotic unified discrete generalized proportional integral observer of order m for the disturbance ξ_1, *where* $l_0, \ldots, l_{m_1+1}$ *are the design constants which regulate the convergence rate of the observation error.*

Proof. The disturbance estimation procedure is the dual counterpart of disturbance rejection mechanism which resides in the application of m_1 discrete-time successive differences; that is, $\rho^{m_1} = \delta^{m_1} = (q-1)^{m_1}/\Delta^{m_1}$ (see (29)).

Let us use (30) in (27) and the internal model of the disturbance input ξ_1. Then, applying the unified operator and some algebraic manipulations in the resulting expression, the observation error satisfies the following disturbed linear dynamics:

$$\begin{aligned}
&\rho^{m_1+2}\widetilde{e}_\theta + l_{m_1+1}\rho^{m_1+1}\widetilde{e}_\theta + l_{m_1}\rho^{m_1}\widetilde{e}_\theta + \cdots + l_1\rho\widetilde{e}_\theta + l_0\widetilde{e}_\theta\\
&\quad = \rho^{m_1}\xi_1(t).
\end{aligned} \tag{31}$$

According to the assumptions, ξ_1; is uniformly bounded, therefore, successive differences of ξ_1, namely, $\rho^{m_1}\xi_1$, remain also uniformly bounded. If $\rho^{m_1}\xi_1(t)$ is uniformly absolutely bounded, by selecting the gain parameters l_j, $j = 0, 1, \ldots, m_1 + 1$, such that the characteristic polynomial in the variable γ, associated to the linear undisturbed part of (31)

$$p_{o,\theta}(\gamma) = \gamma^{m_1+2} + l_{m_1+1}\gamma^{m_1+1} + \cdots + l_1\gamma + l_0, \tag{32}$$

satisfies (9), the estimation error $\widetilde{e}_\theta$ is restricted to a vicinity of zero as time elapses. Thus, $\widehat{\xi}_1(t)$ tends to be located in the neighborhood of $\xi_1(t)$. The size of the vicinity is related to the achieved rank of attenuation in the term $\rho^{m_1}\xi_1(t)$. The parameter m_1 is related to the complexity of the signal to estimate, as in the case of Taylor polynomial approximation [10]. □

Remark 10. ADRC-GPI observer-based controllers use an internal model approximation of the perturbation functions to reconstruct and reject the perturbations. Under this disturbance model approximation setting, several authors have applied it to different areas. Parker and Johnson used a first-order perturbation approximation to model wind speed perturbations in a wind turbine operating in region 3 [20]. Freidovich and Khalil [21] used a first-order perturbation model approximation to estimate the model uncertainty and disturbance on a nonlinear system. Zhao and Gao also used a first-order internal model disturbance approximation to estimate the resonance in two-inertia systems [22] and a first- and second-order approximation to estimate the nonlinearities of an actuator [23]. Zheng et al. also used disturbance model approximation applied to disturbance decoupling control [24].

Remark 11. The parameter m is related to the complexity of the signal to estimate, as in the case of Taylor polynomial

approximation. A first-order perturbation model approximation means that the internal model naturally converges towards a constant disturbance. Equation (30) is a more generalized extension of the internal model perturbation function which provides extra information and increases the ability to track different types of disturbances. For example, $m = 2$ allows convergence to a disturbance with a constant derivative, $m = 3$ allows convergence to a disturbance with a constant acceleration, and so forth.

Remark 12. The ultimate bounded of the estimation errors, produced by the GPI observer, is strongly dependent on the product of poles magnitudes of the dominant characteristic polynomial for the estimation error. Given a desired ultimate value the use of a lager m in the internal model approximation can alleviate the need for high gain related to the observer parameters. In practice, however, m can be small and chosen within the range of 2 to 5. We recall here a quote by J. von Neumann: "With four parameters I can fit an elephant, and with five I can make him wiggle his trunk!"

Remark 13. GPI observers are bandwidth limited by the roots location of the estimation error characteristic polynomial. Generally, the larger the observer bandwidth is, the more accurate the estimation will be. However, a large observer bandwidth will increase noise sensitivity. Then, the selection of the roots of the estimation error characteristic polynomial affects the bandwidth of the GPI observer and also the influence of measurement noises on the estimations. Therefore, GPI observers are usually tuned in a compromise between disturbance estimation performance (set by the internal model approximation degree) and noise sensitivity.

Remark 14. The trajectory tracking problem is formulated in terms of the angular velocity. The disturbance observer, however, is treated in terms of the angular position second-order dynamics. This allows an alternative estimation of the angular velocity, $\widehat{\omega}$.

For the estimation of ξ_2 a similar procedure can be proposed which is synthesized in the following proposition.

Proposition 15. *Consider the observation error $\widetilde{e}_{iS} = i_S - \widehat{i}_S$, and consider the following characteristic polynomial: $p_{o,iS} = \gamma^{m_2+1} + \alpha_{m_2}\gamma^{m_2} + \cdots + \alpha_1\gamma + \alpha_0$, with all the roots into the stable region related to δ operator (see Figure 1); then the system*

$$\begin{aligned}
\widehat{\rho i}_S(t) &= \frac{1}{\sigma L_S}u_S(t) + \alpha_{m_2}\widetilde{e}_\theta(t) + \widehat{z}_{2,1}(t),\\
\widehat{\rho z}_{2,1}(t) &= \alpha_{m_2-1}\widetilde{e}_\theta(t) + \widehat{z}_{2,2}(t),\\
\widehat{\rho z}_{2,2}(t) &= \alpha_{m_2-2}\widetilde{e}_\theta(t) + \widehat{z}_{2,3}(t),\\
&\vdots\\
\widehat{\rho z}_{2,m_2-1}(t) &= \alpha_1\widetilde{e}_\theta(t) + \widehat{z}_{2,m_2}(t),\\
\widehat{\rho z}_{2,m_2}(t) &= \alpha_0\widetilde{e}_\theta(t),
\end{aligned}$$

$$\begin{aligned}
&\widehat{i}_S(0) = \widehat{z}_{2,1}(0) = \cdots = \widehat{z}_{2,m_2}(0) = 0,\\
&\widehat{\xi}_2(t) = \widehat{z}_{2,1}(t)
\end{aligned} \tag{33}$$

constitutes an asymptotic unified discrete generalized proportional integral observer of order m for the disturbance ξ_2, where $\alpha_0, \ldots, \alpha_{m_2}$ are the design constants which regulate the convergence rate of the observation error.

Proof. The proof is similar to that of the previous proposition. □

5. Controller Design

A two-stage feedback control law is considered for this system. In the first stage (outer loop), the angular position of the motor shaft is forced to track a reference signal $\omega^*(t)$, while regulating the flux magnitude towards a given constant value $|\psi_R^*|$. This stage devises a set of desirable current trajectories, which are taken as output references for the second stage. The second stage (inner loop) designs a feedback controller to track the current trajectories from the first stage; in this case, the stator voltages are the control inputs. For both stages, observer based controls will be implemented.

5.1. Outer Loop Design

5.1.1. Flux Magnitude Regulation. Consider again the linear system (27) and (28). According to the problem formulation, for the case of rotor flux magnitude regulation, a simple control law can be proposed:

$$v_a = \frac{|\psi_R^*|^2}{M}. \tag{34}$$

From (34), it is guaranteed that the tracking of the rotor flux modulus approaches to the given reference modulus flux. Indeed, in closed loop, the square modulus of the rotor flux satisfies $\rho(|\psi_R|^2) = -2\eta[|\psi_R|^2 - |\psi_R^*|^2]$, and then $|\psi_R|$ tends to $|\psi_R^*|$ in an exponential asymptotic manner for a constant reference flux modulus. Notice that the partial feedback (28) requires no cancelations of exogenous or endogenous disturbances. In the case of a time variant reference flux modulu, the decoupling property allows one to propose an independent flux magnitude control law. This fact is properly used in [25].

5.1.2. Stator Current Control. Assuming a proper observer behavior related to system (30), accurate estimations for the disturbance input ξ_1 and angular velocity ω are provided. The following observer based control is proposed:

$$v_b = \frac{1}{\mu}\left[\rho\omega^*(t) - k_{0\omega}\left(\widehat{\omega} - \omega^*\right) - \widehat{\xi}_1(t)\right]. \tag{35}$$

The characteristic polynomial of the tracking error, $e_\omega = \omega - \omega^*$, is given by $p_{e_\omega}(\gamma) = \gamma + k_{0\omega} = \gamma + p_k$, where $k_{0\omega} = p_k$ and $\mathrm{Re}\{-p_k\} + (\Delta/2)|p_k|^2 < 0$, to ensure the closed loop stability property.

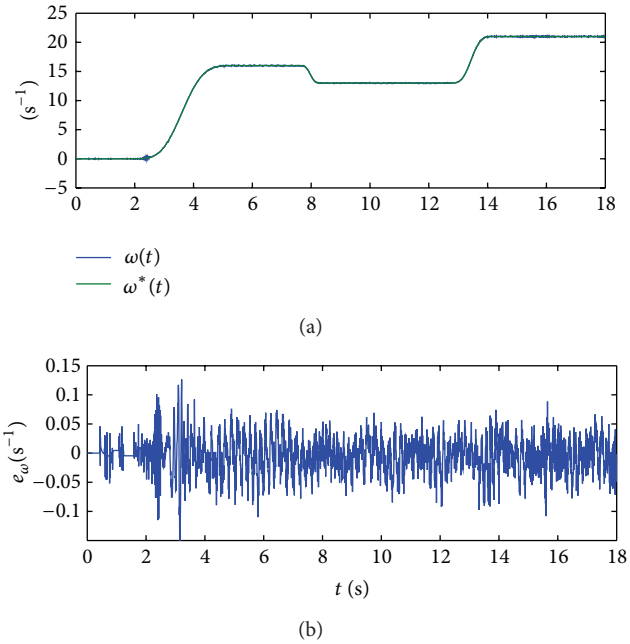

FIGURE 2: Velocity tracking results.

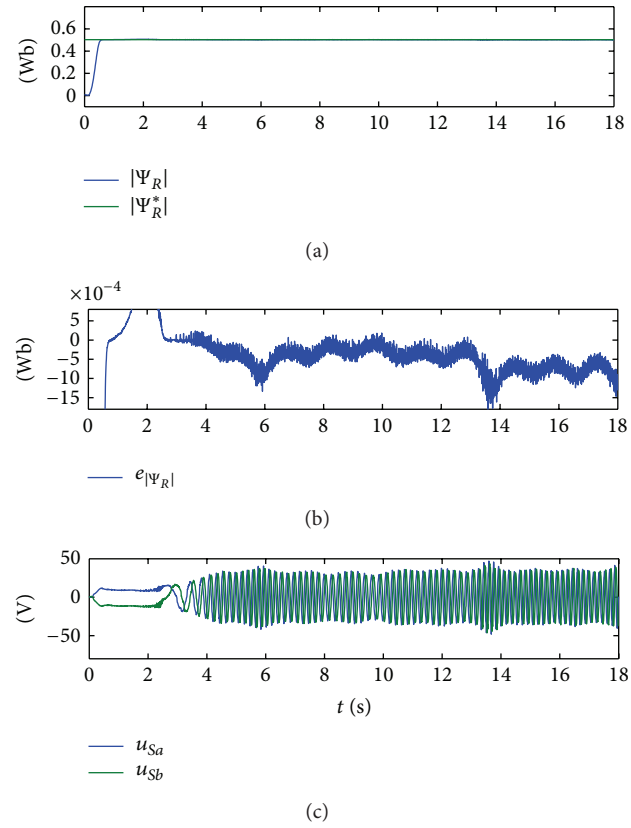

FIGURE 3: Regulation of the flux magnitude and control input.

5.2. Inner Loop Design. Let $i_s^*(t)$ be the desired stator current vector reference trajectory as represented by (26). At this stage, the given structure for the outer loop control is also proposed for the current regulation scheme. We have

$$u_S(t) = \sigma L_s \left[\rho i_S^*(t) - k_{0i} e_{i_S}(t) - \widehat{\xi}_2(t)\right], \tag{36}$$

where $e_{i_S}(t) = i_S(t) - i_S^*(t)$ and the estimation $\widehat{\xi}_2$ is provided by the observer in (33). Finally, the closed loop tracking error for the stator currents is given by $p_{i_S}(\gamma) = \gamma + k_{0i}$.

6. Experimental Results

To assess the control approach, some experiments were carried out in a test bed including a controlled load, by means of a controlled coupled DC motor. The experimental induction motor has the following parameters: $J = 2 \times 10^{-3}$ [Kg·m^2], $n_p = 1$, $M = 0.2374$ [H], $L_R = 0.2505$ [H], $L_S = 0.2505$ [H], $R_S = 4.32$ [Ω], and $R_R = 2.8807$ [Ω]. The flux absolute desired value was selected to maximize the induced torque subject to the nominal current constraints. That is, $\psi_R^* = Mi_{\text{nom}}/\sqrt{2} = 0.5036$ [Wb], for $i_{\text{nom}} = 3$ [A].

The controller was devised in a MATLAB-xPC Target environment using a sampling period of 0.125 [ms]. The communication between the plant and the controller was performed by two data acquisition devises: a National Instruments PCI-6025E data acquisition card for the analog data, and the digital I/O implementation was performed in a National Instruments PCI-6602 data acquisition card. The voltage and current signals are conditioned for acquisition system by means of low pass filters with cut frequency of 1 [kHz].

The reference trajectory of the velocity consisted in a series of rest to rest transitions with values 0, 15, 13, and 21 [rad/s]. The gain parameter associated to the velocity control was $k_{0\omega} = -70.3071$, and the gain constant of the current control was set to be $k_{0i} = -357.7691$. The characteristic polynomial of the disturbance GPI observer in the velocity loop was set to be $(\gamma^2 + 35.96\gamma + 339.23)^2$, and the characteristic polynomial for the disturbance GPI observer of the current control loop was $(\gamma^2 + 98.9\gamma + 2500)^2$. The characteristic polynomial selection was based on the transformation of continuous time transfer functions (s-domain) to the unified operator domain (γ) (further details concerning this procedure are found in [17]). The responses were given in terms of two nested second-order damped responses with damping coefficients 4 and 6 for the velocity and current loops and natural frequencies of 4 and 50, respectively.

Figure 2 shows the behavior of the tracking velocity with respect to the reference value, achieving accurate results. Figure 3 illustrates that the rotor flux magnitude is regulated with an approximate error of about 15×10^{-4} [Wb]. In Figure 4, a precise tracking of the stator currents is depicted. Additionally, to illustrate the robustness of the scheme, a time varying load torque was applied through the manipulation of the DC motor armature current, such that the generated external torque load described a trajectory of a chaotic type, corresponding to the output of a Chua's circuit, respectively. The peak value of the applied torque was 1.7 [N·m]. The

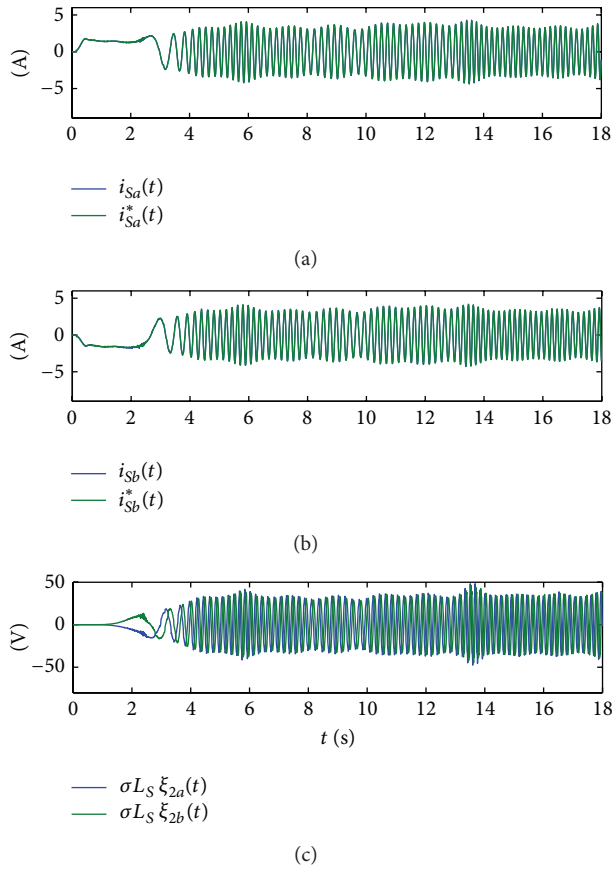

Figure 4: Trajectory tracking of the stator currents and associated disturbance estimations.

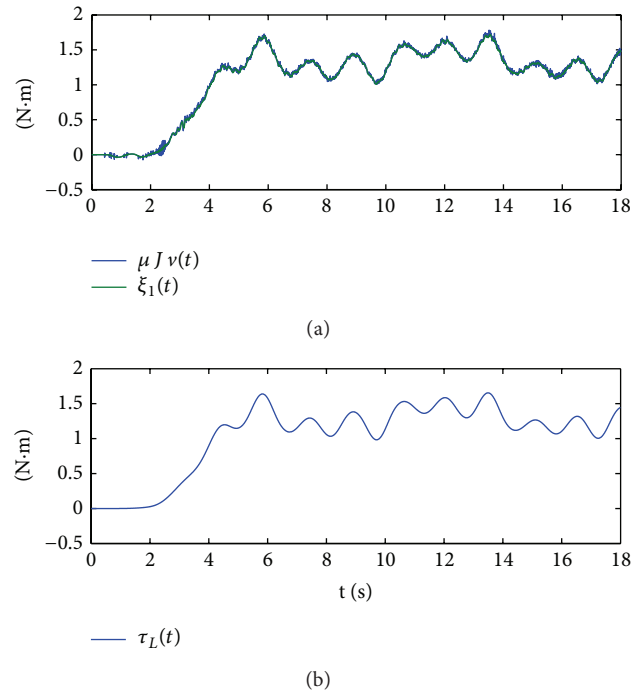

Figure 5: Mechanical lumped disturbance estimation.

estimation of the disturbance, as well as the applied torque, are shown in Figure 5.

The main advantage of the control algorithm, using the xPC target environment, in a single tasking execution mode was the minimization of the execution time; in the case of the discrete-time control scheme, this time was 4.810^{-5} [s], in contrast with a similar control scheme in a continuous time design, which has an execution time of 6.510^{-5} [s].

7. Concluding Remarks

In this work, a discrete-time disturbance observer based control was proposed to solve the problem of controlling an induction motor. The discrete-time process based on the delta operator allows a faster digital control implementation scheme as well as some easy tuning strategies for both control and observer processes in relation to the pole placement for the closed loop tracking (and injection) errors. The presence of the observer in the control loop makes the proposed scheme quite simple and easy to implement. Besides, it is accurate in presence of different nature disturbance inputs.

The degree of polynomial approximation of the disturbance input, denoted by m, depends on the sampling frequency parameter; for high sampling frequencies the approximation needs a smaller degree of polynomial approximation; in particular, the treated case study was satisfied with $m = 2$, which reduces considerably the implementation complexity.

Even though the control loops were proposed for first-order plants, the proposed observer based control can be extended without loss of generality to higher order systems.

References

[1] S. Monaco and D. Normand-Cyrot, "On the sampling of a linear analytic control system," in *Proceedings of the 24th IEEE Conference on Decision and Control*, vol. 24, pp. 1457–1462, 1985.

[2] P. Di Giamberardino, S. Monaco, and D. Normand-Cyrot, "On equivalence and feedback equivalence to finitely computable sampled models," in *Proceedings of the 45th IEEE Conference on Decision and Control*, pp. 5869–5874, December 2006.

[3] S. Monaco and D. Normand-Cyrot, "Issues on nonlinear digital systems," in *Proceedings of the 40th IEEE Conference on Decision and Control*, pp. 160–178, 2001.

[4] A. Elfadili, F. Giri, H. Ouadi, and L. Dugard, "Discrete-time modelling of induction motors with consideration of magnetic saturation," in *Proceedings of the 32nd Annual Conference on IEEE Industrial Electronics (IECON '06)*, pp. 5119–5124, November 2006.

[5] H. A. Toliyat, E. Levi, and M. Raina, "A review of RFO induction motor parameter estimation techniques," *IEEE Transactions on Energy Conversion*, vol. 18, no. 2, pp. 271–283, 2003.

[6] C. D. Johnson, "Control and dynamic systems: advances in theory and applications," in *A Discrete-Time-Accommodating Control Theory for Digital Control of Dynamical Systems*, vol. 18, Academic Press, New York, NY, USA, 1982.

[7] J. Han, "From PID to active disturbance rejection control," *IEEE Transactions on Industrial Electronics*, vol. 56, no. 3, pp. 900–906, 2009.

[8] D. Sun, "Comments on active disturbance rejection control," *IEEE Transactions on Industrial Electronics*, vol. 54, no. 6, pp. 3428–3429, 2007.

[9] Y. Xia, B. Liu, and M. Fu, "Active disturbance rejection control for power plant with a single loop," *Asian Journal of Control*, vol. 14, no. 1, pp. 239–250, 2012.

[10] H. Sira-Ramírez, C. A. Núñez, and N. Visairo, "Robust sigma-delta generalised proportional integral observer based control of a "buck" converter with uncertain loads," *International Journal of Control*, vol. 83, no. 8, pp. 1631–1640, 2010.

[11] D.-J. Zhao, Y.-J. Wang, L. Liu, and Z.-S. Wang, "Robust fault-tolerant control of launch vehicle via GPI observer and integral sliding mode control," *Asian Journal of Control*, vol. 15, no. 2, pp. 614–623, 2013.

[12] J. Chiasson, *Modeling and High-Performance Control of Electric Machines*, John Wiley & Sons, New York, NY, USA, 2005.

[13] P. Mártin and P. Rouchon, "Two simple flux observers for induction motors," *International Journal of Adaptive Control and Signal Processing*, vol. 14, no. 2, pp. 171–175, 2000.

[14] G. C. Goodwin, R. H. Middleton, and H. V. Poor, "High-speed digital signal processing and control," *Proceedings of the IEEE*, vol. 80, no. 2, pp. 240–259, 1992.

[15] J. I. Yuz and G. C. Goodwin, "On sampled-data models for nonlinear systems," *IEEE Transactions on Automatic Control*, vol. 50, no. 10, pp. 1477–1489, 2005.

[16] A. Tesfaye and M. Tomizuka, "Zeros of discretized continuous systems expressed in the Euler operator—an asymptotic analysis," *IEEE Transactions on Automatic Control*, vol. 40, no. 4, pp. 743–747, 1995.

[17] R. H. Middleton and G. C. Goodwin, *Digital Control and Estimation: A Unified Approach*, Prentice Hall, 1990.

[18] G. C. Goodwin, J. I. Yuz, J. C. Agüero, and M. Cea, "Sampling and sampled-data models," in *Proceedings of the American Control Conference (ACC '10)*, pp. 1–20, July 2010.

[19] S. Li, J. Yang, W.-H. Chen, and X. Chen, "Generalized extended state observer based control for systems with mismatched uncertainties," *IEEE Transactions on Industrial Electronics*, vol. 59, no. 12, pp. 4792–4802, 2012.

[20] G. A. Parker and C. D. Johnson, "Improved speed regulation and mitigation of drive-train torsion fatigue in flexible wind turbines, using disturbance utilization control: part two," in *Proceedings of the 41st Southeastern Symposium on System Theory (SSST '09)*, pp. 177–183, March 2009.

[21] L. B. Freidovich and H. K. Khalil, "Performance recovery of feedback-linearization-based designs," *IEEE Transactions on Automatic Control*, vol. 53, no. 10, pp. 2324–2334, 2008.

[22] S. Zhao and Z. Gao, "An active disturbance rejection based approach to vibration suppression in two-inertia systems," in *Proceedings of the American Control Conference (ACC '10)*, pp. 1520–1525, July 2010.

[23] S. Zhao, Q. Zheng, and Z. Gao, "On model free accommodation of actuator nonlinearities," in *Proceedings of the 10th World Congress on Intelligent Control and Automation*, Beijing, China, 2012.

[24] Q. Zheng, Z. Chen, and Z. Gao, "A practical approach to disturbance decoupling control," *Control Engineering Practice*, vol. 17, no. 9, pp. 1016–1025, 2009.

[25] H. Sira-Ramírez, F. González-Montanez, J. A. Cortés-Romero, and A. Luviano-Juárez, "A robust linear field-oriented voltage control for the induction motor: experimental results," *IEEE Transactions on Industrial Electronics*, vol. 60, no. 8, pp. 3025–3033, 2013.

Hindawi Publishing Corporation
Mathematical Problems in Engineering
Volume 2013, Article ID 483913, 7 pages
http://dx.doi.org/10.1155/2013/483913

Research Article

Multitarget Tracking by Improved Particle Filter Based on H_∞ Unscented Transform

Yazhao Wang

The Department of Systems and Control, Beihang University (BUAA), Beijing 100191, China

Correspondence should be addressed to Yazhao Wang; bhbwc2012@126.com

Received 29 August 2013; Accepted 11 October 2013

Academic Editor: Tao Li

This paper considers the problem of multitarget tracking in cluttered environment. To reduce the dependency on the noise priori knowledge, an improved particle filtering (PF) data association approach is presented based on the H_∞ filter (HF). This approach can achieve higher robustness in the condition that the measurement noise prior is unknown. Because of the limitations of the HF in nonlinear tracking, we first present the H_∞ unscented filter (HUF) by embedding the unscented transform (UT) into the H_∞ extended filter (HEF) structure. Then the HUF is incorporated into the Rao-Blackwellized particle filter (RBPF) framework to update the particles. Simulation results are provided to demonstrate the effectiveness of the proposed algorithms in linear and nonlinear multitarget tracking.

1. Introduction

Multitarget tracking is to estimate the targets' current positions from a series of noise-corrupted measurements by filtering methods [1]. In cluttered environment, the foremost difficulty involves the problem of associating the correct measurements with the appropriate tracks. A number of strategies, including the joint probabilistic data association (JPDA) [2, 3], multiple hypothesis tracking (MHT) [4, 5], S-D assignment [6], and the probabilistic hypothesis density filer (PHDF) [7–9], are available to solve this problem.

Recently, the sequential Monte Carlo (SMC) data association approaches are also applied to the tracking and association problems [10, 11]. This paper tackles data association joint with state estimation via a SMC method called Rao-Blackwellized particle filter (RBPF) [12–14]. This particle method can be considered as a generalization of MHT, which represents the data association and state posteriors as a discrete set of hypotheses. Instead of the pure particle strategy, a mixture of Gaussian representation of the joint posterior distribution is used to reduce the estimation variance. In the application of RBPF for nonlinear target tracking, it can replace the Kalman filter (KF) in the data association algorithm by the extended Kalman filter (EKF) or the unscented Kalman filter (UKF) [15]. Although RBPF has shown higher tracking efficiency against the pure particle filtering schemes, there is still weakness lying in the strong assumptions on the system models and noise statistics [16]. That is, the KF or its variants can only be applied in the condition that a perfect system model is known and the process and measurement noise statistics are white and Gaussian with known covariance matrices. In many practical applications, these assumptions can hardly be satisfied, and the performance of the KF based methods may degrade severely when the measurement disturbances are not in definite Gaussian forms. Hence, we need a solution with more robustness against the uncertainties of the noise than the KF. The H_∞ filter (HF), which aims at minimizing the worst possible effects of the disturbances on the estimation errors, can provide an alternative to solve this problem [17–19]. Different from the KF, the only assumption made for HF is that the noise signals have a finite energy but without any statistic assumptions.

The HF techniques have been used in linear-model target tracking. Accordingly, the H_∞ extended filter (HEF) has also been proposed for nonlinear models by using the EKF structure. As another way to approximate the filtering distribution, the unscented transform (UT) can be more

accurate compared to the EKF for it performs a higher order of the Taylor series expansion. By a Gaussian density instead of approximating the nonlinear functions as the EKF, the UT technique has shown its priority in handling nonlinear estimation problems and also been combined with the H_∞ filter [20]. In this paper, we aim to incorporate the HF technique into the framework of RBPF to reduce its dependency on a priori knowledge of the noise statistics in multitarget tracking. In RBPF, the continuous state is estimated using the KF or its variants, while the discrete state or the mode state is estimated using particle filters. Thus, the HF can be embedded into the RBPF structure directly. Because of the limitations of the HF in nonlinear tracking, we present the H_∞ unscented filter (HUF) by embedding the UT into the HEF structure. Since the HUF has the same observer structure as the UKF, it can also be embedded into the RBPF framework to update the continuous states of the particles.

The remainder of this paper is organized as follows. In Section 2, we give a brief introduction of the generic RBPF target tracking approach and the basic H_∞ linear filter structure. The main work is given in Section 3 where the HUF is first presented. Then the HUF is incorporated into the RBPF framework to update the particles. Simulation results are provided in Section 4 to demonstrate the effectiveness of the proposed algorithms in linear and nonlinear multitarget tracking. In Section 5, conclusions are also given to summarize the main works of this paper.

2. Background

2.1. Rao-Blackwellized Particle Filter for Target Tracking. Consider the following time-varying state-space system:

$$\begin{aligned} \mathbf{x}_k &= \mathbf{F}_{k-1}\mathbf{x}_{k-1} + \mathbf{w}_{k-1}, \\ \mathbf{z}_k &= \mathbf{H}_k\mathbf{x}_k + \mathbf{v}_k, \end{aligned} \tag{1}$$

where $\mathbf{x}_k \in \mathbb{R}^n$ and $\mathbf{z}_k \in \mathbb{R}^p$ are the system state and measurement vectors at time step k, respectively. $\mathbf{w}_{k-1} \sim \mathcal{N}(0, \mathbf{Q}_{k-1})$ and $\mathbf{v}_k \sim \mathcal{N}(0, \mathbf{R}_k)$ are zero mean mutually independent Gaussian process noise, and $\mathbf{F}_{k-1}$ and $\mathbf{H}_k$ are matrices with compatible dimensions. Suppose that we are able to form another variable c_k to describe the matrices $\mathbf{F}_{k-1}$ and $\mathbf{H}_k$; then the RBPF algorithm can be applied to estimate the whole state $\{\mathbf{x}_k; c_k\}$ [21]. For space consideration, we omit the details of the RBPF algorithms which can be found in [22, 23]. In the application of RBPF for target tracking, the latent variable c_k is defined to be the data association event indicator [12]. That is, $c_k = 0$ when the measurement is from clutter, and $c_k = j$ when the measurement is from target j ($j = 1, \ldots, T$, where T is number of targets). The predictive probability $p(c_k \mid c_{1:k-1})$ gives the data association prior given the data association results $\{c_{1:k-1}\}$ in the previous $k-1$ time steps. The posterior distribution of c_k is $p(c_k \mid c_{1:k-1}, \mathbf{z}_{1:k})$ which can be calculated by

$$\begin{aligned} &p\left(c_k \mid c_{1:k-1}, \mathbf{z}_{1:k}\right) \\ &\quad \propto p\left(\mathbf{z}_k \mid c_k, c_{1:k-1}, \mathbf{z}_{1:k-1}\right) p\left(c_k \mid c_{1:k-1}\right), \end{aligned} \tag{2}$$

where the data association prior $p(c_k \mid c_{1:k-1})$ is modeled as a recursive Markov chain, which guarantees the association assumption of one target per measurement in each time step. Accordingly, the $p(c_k \mid c_{1:k-1})$ in (2) has been replaced by $p(c_k \mid c_{k-M:k-1})$ [13], and the general form of the joint prior model is given by

$$p\left(c_{k+M-1}, \ldots, c_k\right) = \prod_{m=1}^{M} p\left(c_{k+m} \mid c_k, \ldots, c_{k+m-1}\right). \tag{3}$$

That means if we obtain M measurements in time step k, the mth ($m = 2, \ldots, M$) measurement's association prior $p(c_{k+m-1} \mid c_{k+m-2}, \ldots, c_k)$ only depends on the previous association results $\{c_{k+m-2}, \ldots, c_k\}$ in the kth time step. Note that c_k has the prior $p(c_k)$ if $m = 1$. This RBPF multitarget tracking algorithm is also termed Rao-Blackwellized Monte Carlo data association (RBMCDA) [12]. In this paper, we aim to improve the robustness of the RBPF for target tracking by the H_∞ filter and unscented transform.

2.2. H_∞ Linear Filter. Consider the model given by (1), where the process noise $\mathbf{w}_{k-1}$ and the measurement noise $\mathbf{v}_k$ are assumed to be uncorrelated zero-mean white noise processes with unknown statistical properties. Note that they are also the energy bounded $l_2[0, +\infty]$ signals. Let $\widehat{\mathbf{x}}_{k|k} \triangleq \mathscr{L}\{\mathbf{z}_0, \mathbf{z}_1, \ldots, \mathbf{z}_k\}$ denote the estimation of $\mathbf{x}_k$ given measurements $\mathbf{z}_{0:k}$. We can define the estimation error as $\mathscr{E}_k \triangleq \widehat{\mathbf{x}}_{k|k} - \mathbf{x}_k$ and denote $\mathscr{T}_k(\mathscr{L})$ as the transfer operator that maps the unknown disturbances $\mathbf{x}_0 - \widehat{\mathbf{x}}_{0|0}$, $\mathbf{w}_{0:k-1}$, and $\mathbf{v}_{1:k}$ to the estimation errors $\mathscr{E}_{1:k}$, where $\widehat{\mathbf{x}}_{0|0}$ is a priori estimate of $\mathbf{x}_0$ and $\mathbf{x}_0 - \widehat{\mathbf{x}}_{0|0}$ represents unknown initial estimation error.

In optimal H_∞ filter, it is operated to minimize the possible worst effects of the unknown disturbances on the estimation errors. That is, the estimation strategy $\mathscr{L}$ should be designed so as to minimize the H_∞ norm of the operator $\mathscr{T}_k(\mathscr{L})$. Actually, it is hard to obtain the closed-form solution of the optimal H_∞ filtering except in some specific cases. For example, the desired accuracy of the optimal H_∞ filter can be obtained by iterating the γ^2 of the suboptimal solution [16]. This paper considers the suboptimal solutions that can bound the maximum energy gain from the disturbance to the estimation errors under the prescribed disturbance tolerance level. Given a scalar $\gamma^2 > 0$, find the estimation strategies $\mathscr{L}$ such that the H_∞ norm of $\mathscr{T}_k(\mathscr{L})$ satisfies [24, 25]

$$\begin{aligned} &\left\|\mathscr{T}_k(\mathscr{L})\right\|_\infty \\ &\quad \triangleq \frac{\sup_{\mathbf{x}_0, \mathbf{w}_t, \mathbf{v}_t \in l_2} \left(\sum_{t=1}^{k} \left\|\mathscr{E}_t\right\|_2^2\right)}{\left(\left\|\mathbf{x}_0 - \widehat{\mathbf{x}}_{0|0}\right\|_{\mathbf{P}_{0|0}^{-1}}^2 + \sum_{j=0}^{k} \left\|\mathbf{w}_t\right\|_{\mathbf{Q}_t^{-1}}^2 + \sum_{t=1}^{k} \left\|\mathbf{v}_t\right\|_{\mathbf{R}_t^{-1}}^2\right)} < \gamma^2, \end{aligned} \tag{4}$$

where the notation $||a||_\beta^2$ is defined as the square of the weighted l_2 norm of a, that is, $||a||_\beta^2 = a^T \beta a$. The matrix $\mathbf{P}_{0|0} > 0$ reflects a priori knowledge of how close $\mathbf{x}_0$ is to the initial estimate $\widehat{\mathbf{x}}_{0|0}$. $\mathbf{Q}_t > 0$ and $\mathbf{R}_t > 0$ are weighting matrices, by which the designer can make appropriate choice

to satisfy the performance requirements. The solution to the H_∞ filtering algorithm as shown in [26] is given by

$$\hat{\mathbf{x}}_{k|k-1} = \mathbf{F}_{k-1}\hat{\mathbf{x}}_{k-1|k-1}, \tag{5}$$

$$\mathbf{P}_{k|k-1} = \mathbf{F}_{k-1}\mathbf{P}_{k-1|k-1}\mathbf{F}_{k-1}^T + \mathbf{Q}_{k-1}, \tag{6}$$

$$\hat{\mathbf{x}}_{k|k} = \hat{\mathbf{x}}_{k|k-1} + \mathbf{K}_k\left(\mathbf{z}_k - \mathbf{H}_k\hat{\mathbf{x}}_{k|k-1}\right), \tag{7}$$

$$\mathbf{K}_k = \mathbf{P}_{k|k-1}\mathbf{H}_k^T\left[\mathbf{R}_k + \mathbf{H}_k\mathbf{P}_{k|k-1}\mathbf{H}_k^T\right]^{-1}, \tag{8}$$

$$\mathbf{P}_{k|k} = \mathbf{P}_{k|k-1} - \mathbf{P}_{k|k-1}\left[\mathbf{H}_k^T \;\; I\right]R_{\mathscr{E},k}^{-1}\left[\mathbf{H}_k^T \;\; I\right]^T\mathbf{P}_{k|k-1}, \tag{9}$$

where I is an identity matrix with compatible dimension. The matrix $R_{\mathscr{E},k}$ is given by

$$R_{\mathscr{E},k} = \begin{bmatrix}\mathbf{R}_k & 0\\ 0 & -\gamma^2 I\end{bmatrix} + \begin{bmatrix}\mathbf{H}_k\\ I\end{bmatrix}\mathbf{P}_{k|k-1}\left[\mathbf{H}_k^T \;\; I\right]. \tag{10}$$

3. Improved Rao-Blackwellized Particle Filter

3.1. H_∞ Nonlinear Filter with Unscented Transform. Consider the following discrete-time nonlinear state-space model:

$$\begin{aligned}\mathbf{x}_k &= f\left(\mathbf{x}_{k-1}\right) + \mathbf{w}_{k-1},\\ \mathbf{z}_k &= h\left(\mathbf{x}_k\right) + \mathbf{v}_k.\end{aligned} \tag{11}$$

The HEF just replaces $\mathbf{F}_{k-1}$ and $\mathbf{H}_k$ in (5) and (7) by $f(\hat{\mathbf{x}}_{k-1|k-1})$ and $h(\hat{\mathbf{x}}_{k|k-1})$, respectively. Here, we present the HUF by embedding the UT technique into the HF structure, which can be used to update the continuous-state particles in the RBPF framework. Suppose that $(2n+1)$ sigma points are generated based on the state estimates at time $k-1$,

$$\begin{aligned}\zeta_{k-1|k-1}^0 &= \hat{\mathbf{x}}_{k-1|k-1},\\ \zeta_{k-1|k-1}^s &= \hat{\mathbf{x}}_{k-1|k-1} + \left(\sqrt{(n+\mathscr{D})\,\mathbf{P}_{k-1|k-1}}\right)^s,\\ \zeta_{k-1|k-1}^{s+n} &= \hat{\mathbf{x}}_{k-1|k-1} - \left(\sqrt{(n+\mathscr{D})\,\mathbf{P}_{k-1|k-1}}\right)^s, \quad s = 1,\ldots,n,\end{aligned} \tag{12}$$

where the state estimate $\hat{\mathbf{x}}_{k-1|k-1}$ and its covariance $\mathbf{P}_{k-1|k-1}$ have been obtained at time $k-1$. $\mathscr{D} \in \mathbb{R}$ is a scaling factor, and $(\sqrt{(n+\mathscr{D})\mathbf{P}_{k-1|k-1}})^s$ is the sth row or column of the matrix squares root of $(n+\mathscr{D})\mathbf{P}_{k-1|k-1}$. By implementing the UT into (5) and (6), the predicted mean and covariance can be obtained as follows:

$$\begin{aligned}\zeta_{k|k-1}^s &= f\left(\zeta_{k-1|k-1}^s\right),\\ \hat{\mathbf{x}}_{k|k-1} &= \sum_{s=0}^{2n}\omega^s\zeta_{k|k-1}^s,\\ \mathbf{P}_{k|k-1} &= \sum_{s=0}^{2n}\omega^s\left[\zeta_{k|k-1}^s - \hat{\mathbf{x}}_{k|k-1}\right]\\ &\quad\times\left[\zeta_{k|k-1}^s - \hat{\mathbf{x}}_{k|k-1}\right]^T + \mathbf{Q}_{k-1},\end{aligned} \tag{13}$$

where ω^s is the normalized weight associated with the sth sigma points (see [27, 28]). Since the linearized measurement function $\mathbf{H}_k$ does not exist explicitly under the unscented transform framework, the statistical linear error propagation method [29] is used to reformulate the updated equations. Approximately, the measurement covariance and its cross-correlation covariance can be given by

$$\begin{aligned}\mathbf{P}_{k|k-1}^{zz} &\approx \mathbf{H}_k\mathbf{P}_{k|k-1}\mathbf{H}_k^T,\\ \mathbf{P}_{k|k-1}^{xz} &\approx \mathbf{P}_{k|k-1}\mathbf{H}_k^T.\end{aligned} \tag{14}$$

By using the predicted sigma points, they can be calculated by

$$\begin{aligned}\mathbf{P}_{k|k-1}^{zz} &= \sum_{s=0}^{2n}\omega^s\left[h\left(\zeta_{k|k-1}^s\right) - \hat{\mathbf{z}}_{k|k-1}\right]\\ &\quad\times\left[h\left(\zeta_{k|k-1}^s\right) - \hat{\mathbf{z}}_{k|k-1}\right]^T,\\ \mathbf{P}_{k|k-1}^{xz} &= \sum_{s=0}^{2n}\omega^s\left[\zeta_{k|k-1}^s - \hat{\mathbf{x}}_{k|k-1}\right]\\ &\quad\times\left[h\left(\zeta_{k|k-1}^s\right) - \hat{\mathbf{z}}_{k|k-1}\right]^T,\end{aligned} \tag{15}$$

where

$$\hat{\mathbf{z}}_{k|k-1} = \sum_{s=0}^{2n}\omega^s h\left(\zeta_{k|k-1}^s\right). \tag{16}$$

By substituting (14) into (7)–(10), the filtered estimates can be obtained by

$$\begin{aligned}\hat{\mathbf{x}}_{k|k} &= \hat{\mathbf{x}}_{k|k-1} + \mathbf{P}_{k|k-1}^{xz}\left[\mathbf{R}_k + \mathbf{P}_{k|k-1}^{zz}\right]^{-1}\\ &\quad\times\left(\mathbf{z}_k - \hat{\mathbf{z}}_{k|k-1}\right),\\ \mathbf{P}_{k|k} &= \mathbf{P}_{k|k-1} - \left[\mathbf{P}_{k|k-1}^{xz} \;\; \mathbf{P}_{k|k-1}\right]\\ &\quad\times\mathbf{R}_{\mathscr{E},k}^{-1}\left[\mathbf{P}_{k|k-1}^{xz} \;\; \mathbf{P}_{k|k-1}\right]^T,\end{aligned} \tag{17}$$

where

$$R_{\mathscr{E},k} = \begin{bmatrix}\mathbf{R}_k + \mathbf{P}_{k|k-1}^{zz} & \left[\mathbf{P}_{k|k-1}^{xz}\right]^T\\ \mathbf{P}_{k|k-1}^{xz} & -\gamma^2 I + \mathbf{P}_{k|k-1}\end{bmatrix}. \tag{18}$$

It should be pointed out that the HUF has the same observer structure as that of the UKF, and $\mathbf{Q}_{k-1}$ and $\mathbf{R}_k$ play the same role as the covariance matrices of the process noise and the measurement noise when using the UKF. Hence, the weighting matrices can be adjusted with no conflictions to the framework of KF. For the HUF, it not only outperforms the HEF in accuracy, but also achieves more robustness than the UKF for unknown noise statistics [16].

3.2. H_∞ Unscented Rao-Blackwellized Particle Filter. In this section, the HUF based RBPF multiple target tracking algorithm (HURBPF) is provided. It can be found that

the $p(\mathbf{x}_k \mid c_{i,1:k}, \mathbf{z}_{1:k})$ will not be strictly Gaussian if the system dynamic and (or) measurement function are (is) nonlinear. In this case, the HUF can be a better candidate than HEF or UKF for updating the continuous state within the particle filtering framework. The conditional distribution mentioned above can be chosen as

$$p\left(\mathbf{x}_k \mid c_{i,1:k}, \mathbf{z}_{1:k}\right) = \mathcal{N}\left(\mathbf{x}_k; \widehat{\mathbf{x}}_{i,k|k}, \mathbf{P}_{i,k|k}\right), \tag{19}$$

where $\widehat{\mathbf{x}}_{i,k|k}$ and $\mathbf{P}_{i,k|k}$ are the mean and covariance of $\mathbf{x}_k$ computed by the HUF (17). The main procedure for the HURBPF algorithm is presented as follows (see Algorithm 1). In this algorithm, the target state priors can be represented as a weighted importance sample set

$$p\left(\mathbf{x}_0^{(j)}\right) = \sum_{i=1}^{N_p} \mathbf{w}_{i,0} \mathcal{N}\left(\mathbf{x}_0^{(j)} \mid \mathbf{x}_{i,0}^{(j)}, \mathbf{P}_{i,0}^{(j)}\right), \tag{20}$$

where i ($i = 1, \ldots, N_p$) is the identifier of particle.

Algorithm 1. H_∞ unscented Rao-Blackwellized particle filter.

For $k = 1$ to n do.

Step 1. Do prediction step. For $i = 1, 2, \ldots, N_p$ and $j = 1, 2, \ldots, T$, perform HUF prediction from the mean $\widehat{\mathbf{x}}_{i,k-1|k-1}$ and covariances $\mathbf{P}_{i,k-1|k-1}$ to generate the predicted estimates $\widehat{\mathbf{x}}_{i,k|k-1}^{(j)}$ and $\mathbf{P}_{i,k|k-1}^{(j)}$.

Step 2. Calculate the data association priors $p(c_{i,k} \mid c_{i,1:k-1})$ based on the recursive Markov chain described in [13].

Step 3. For $i = 1, 2, \ldots, N_p$, perform HUF update for each particle to get contemporary filtered estimates $\overline{\mathbf{x}}_{i,k|k}^{(j)}$ and $\overline{\mathbf{P}}_{i,k|k}^{(j)}$.

Step 4. Calculate the posterior distribution of $c_{i,k}$:

$$\begin{aligned} &p\left(c_{i,k} \mid c_{i,1:k-1}, \mathbf{z}_{1:k}\right) \\ &\quad = p\left(\mathbf{z}_k \mid c_{i,k}, c_{i,1:k-1}, \mathbf{z}_{1:k-1}\right) p\left(c_{i,k} \mid c_{i,1:k-1}\right). \end{aligned} \tag{21}$$

Step 5. Sample a new association $c_{i,k} = j$ with probability $\rho_i^{(j)}$:

$$\rho_i^{(j)} = \frac{\widehat{\rho}_i^{(j)}}{\sum_{j'=0}^{T} \widehat{\rho}_i^{(j')}}, \qquad j = 0, \ldots, T, \tag{22}$$

where

$$\begin{aligned} \widehat{\rho}_i^{(0)} &= p\left(c_{i,k} = 0 \mid c_{i,1:k-1}, \mathbf{z}_{1:k}\right), \\ \widehat{\rho}_i^{(j)} &= p\left(c_{i,k} = j \mid c_{i,1:k-1}, \mathbf{z}_{1:k}\right). \end{aligned} \tag{23}$$

Step 6. Calculate the new weights

$$\mathbf{w}_{i,k} \propto \mathbf{w}_{i,k-1} \frac{p\left(\mathbf{z}_k \mid c_{i,k}, c_{i,1:k-1}, \mathbf{z}_{1:k-1}\right) p\left(c_{i,k} \mid c_{i,1:k-1}\right)}{p\left(c_{i,k} \mid c_{i,1:k-1}, \mathbf{z}_{1:k}\right)}. \tag{24}$$

Step 7. Update the jth target according to the new $c_{i,k}$ ($i = 1, 2, \ldots, N_p$). If $c_{i,k} = j$ ($j \neq 0$), then

$$\widehat{\mathbf{x}}_{i,k|k}^{(j)} = \overline{\mathbf{x}}_{i,k|k}^{(j)}, \qquad \mathbf{P}_{i,k|k}^{(j)} = \overline{\mathbf{P}}_{i,k|k}^{(j)}. \tag{25}$$

Step 8. Calculate the target state vectors

$$\widehat{\mathbf{x}}_{k|k}^{(j)} = \sum_{i=1}^{N_p} \mathbf{w}_{i,k} \widehat{\mathbf{x}}_{i,k|k}^{(j)}. \tag{26}$$

End for. (Resample if needed [30–32].)

It should be pointed out that in H_∞ filter the level γ must be selected carefully to guarantee the existence of the HUF, or else the filtering program will fail in the applications of HURBPF approach. To adaptively adjust γ to its minimum at each iteration, we can choose the value of γ_k as [16]

$$\begin{aligned} \gamma_k^2 = \alpha \max\Big\{ &\operatorname{eig}\Big(\mathbf{P}_{k|k-1}^{-1} + \mathbf{P}_{k|k-1}^{-1} \mathbf{P}_{k|k-1}^{xz} \mathbf{R}_{\mathbf{k}}^{-1} \\ &\times \left[\mathbf{P}_{k|k-1}^{-1} \mathbf{P}_{k|k-1}^{xz}\right]^T\Big)^{-1}\Big\}, \end{aligned} \tag{27}$$

where α is a scalar larger than one and $\max\{\operatorname{eig}(A)^{-1}\}$ denotes the maximum eigenvalue of the matrix A^{-1}.

4. Simulation Results

This section presents the two-dimensional (2D) target tracking examples to demonstrate the performance of the proposed tracking algorithms.

Example 1. The targets are modeled with near constant velocity model in Cartesian coordinates. The discrete-time dynamic and measurement models of the jth target have the following form:

$$\begin{aligned} \mathbf{x}_{j,k} &= \mathbf{F}_{j,k-1} \mathbf{x}_{j,k-1} + \mathbf{w}_{k-1}, \\ \mathbf{z}_{j,k} &= \mathbf{H}_{j,k} \mathbf{x}_{j,k} + \mathbf{v}_k, \end{aligned} \tag{28}$$

where

$$\begin{aligned} \mathbf{F}_{j,k-1} &= \begin{pmatrix} 1 & 0 & \delta_t & 0 \\ 0 & 1 & 0 & \delta_t \\ 0 & 0 & 1 & 0 \\ 0 & 0 & 0 & 1 \end{pmatrix}, \\ \mathbf{H}_{j,k} &= \begin{pmatrix} 1 & 0 & 0 & 0 \\ 0 & 1 & 0 & 0 \end{pmatrix}, \end{aligned} \tag{29}$$

$\mathbf{w}_{k-1}$ and $\mathbf{v}_k$ are zero mean Gaussian process noises. The standard process and measurement noise variances are selected as $\sigma_x = 0.001$ km and $\sigma_z = 20$ km, respectively. The sample interval $\delta_t = 1$ and the correct measurements return with a known detection probability $P_d = 1$ (detection missing will not happen). At each time step k, the target is located at coordinates (x_k, y_k) and moves with constant velocity vector $(\dot{x}_k, \dot{y}_k)$, which are combined

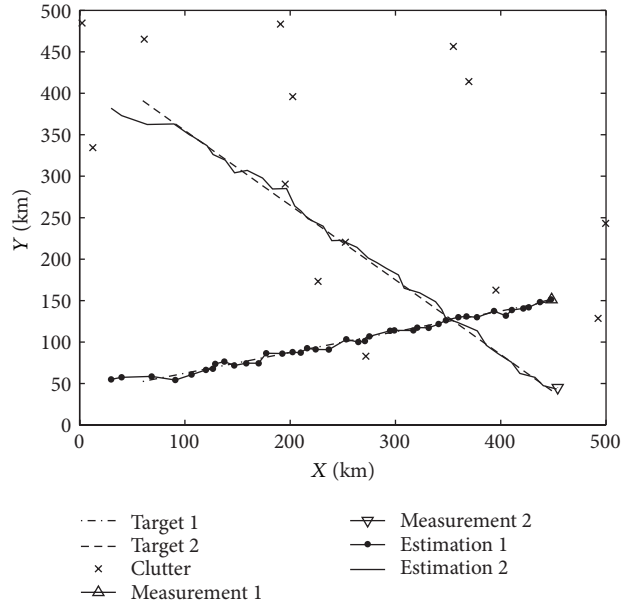

Figure 1: Example of two targets tracking (a successful track by HRBPF).

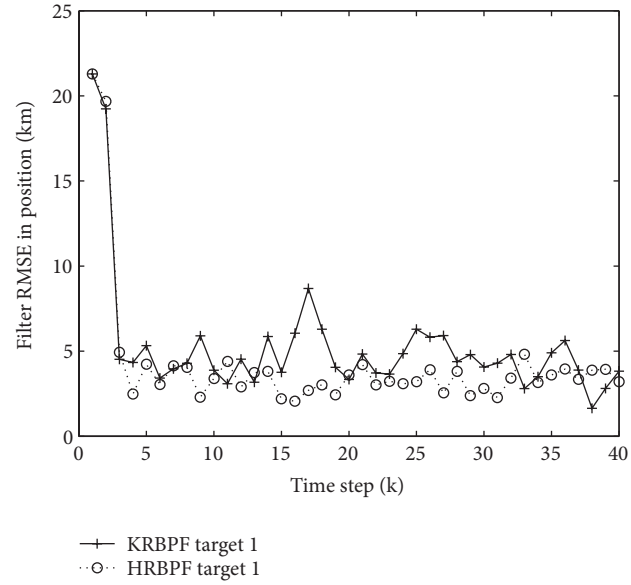

Figure 2: Comparison of the average position estimation errors of target 1.

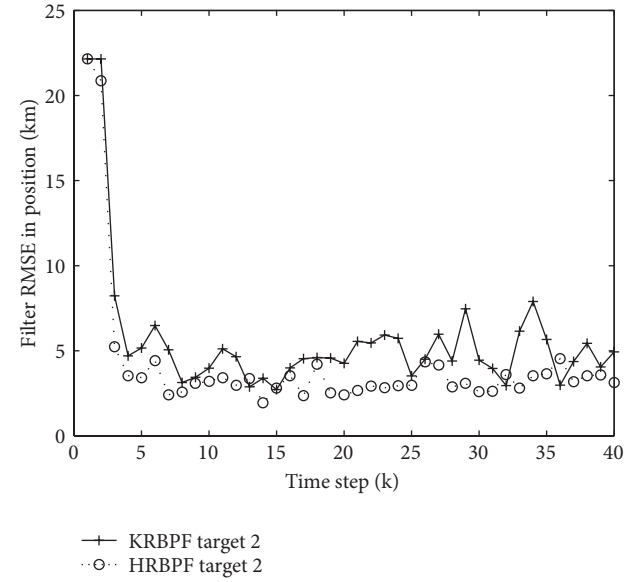

Figure 3: Comparison of the average position estimation errors of target 2.

with the target's state vector $\mathbf{x}_k = (x_k, y_k, \dot{x}_k, \dot{y}_k)^T$. In this two-target-crossing scenario (see Figure 1), target 1 and target 2 begin at $k = 0$ with position-velocity coordinates $\mathbf{x}_0^{(1)} = (50\,\text{km}, 50\,\text{km}, 10\,\text{km/s}, 2.5\,\text{km/s})^T$ and $\mathbf{x}_0^{(2)} = (50\,\text{km}, 400\,\text{km}, 10\,\text{km/s}, -9\,\text{km/s})^T$, respectively. The total number of tracking time steps is 40.

The KRBPF serves as the baseline algorithm, and the proposed HRBPF algorithm is compared with it. Both algorithms are designed based on the same assumptions, and the performance of the two algorithms is evaluated by the average results over Monte Carlo runs. The initial state estimates of the two targets are set to $\hat{\mathbf{x}}_{0|0}^{(1)} = (30\,\text{km}, 50\,\text{km}, 10\,\text{km/s}, 2.5\,\text{km/s})^T$ and $\hat{\mathbf{x}}_{0|0}^{(2)} = (30\,\text{km}, 400\,\text{km}, 10\,\text{km/s}, -9\,\text{km/s})^T$, respectively. The clutter is modeled as independent and identically distributed with uniform spatial distribution in a detection region of the coordinate plane $[0\,\text{km}, 500\,\text{km}] \times [0\,\text{km}, 500\,\text{km}]$, and the number of clutter measurements obeys a Poisson distribution with the Poisson random number $\lambda = 10$ (clutter rate). The number of particles used in the simulation is 100. The standard measurement variance used in both algorithms, KRBPF (Kalman filter based RBPF) and HRBPF (H_∞ filter based RBPF), is $\sigma_z^a = 30\,\text{km}$. The position root mean square errors (RMSEs) of the KRBPF and HRBPF algorithms are illustrated in Figure 2 (target 1) and Figure 3 (target 2). We can see that the overall performance of the proposed HRBPF is significantly better than that of the KRBPF as expected. This is due to the fact that the HF outperforms the KF when the statistics of the noise processes are not known by the filtering algorithms.

Example 2. Consider a scenario of tracking two targets using bearings-only measurements received by two static sensors which are located at $(s_{x,k}^i, s_{y,k}^i)$, $i = 1, 2$ (see Figure 4, where "□" represents the location of the sensor). The dynamic of discrete-time velocity model is the same as (28), and the measurement function is given by

$$z_{j,k}^i = \arctan\left(\frac{y_{j,k} - s_{y,k}^i}{x_{j,k} - s_{x,k}^i}\right) + r_k^i, \tag{30}$$

where $r_k^i \sim N(0, \sigma_z^2)$ with $\sigma_z = 0.01$ rad. Since this measurement model is nonlinear, the URBPF (UKF based RBPF) and HURBPF are employed for tracking. The clutter originated

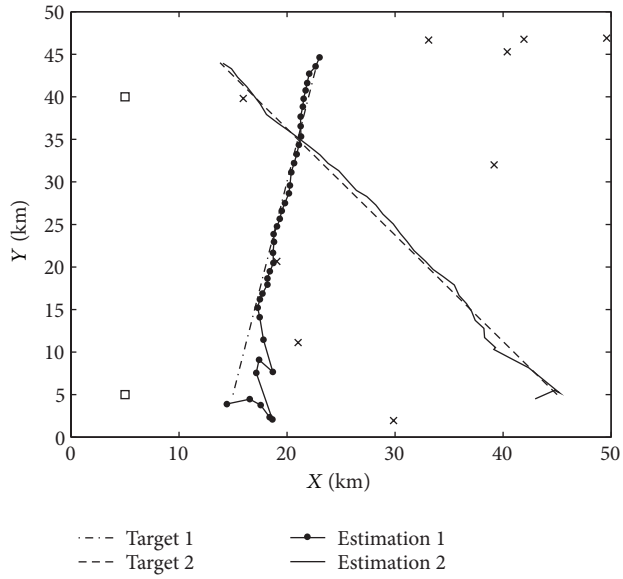

Figure 4: Example of two targets bearings-only tracking (a successful track by HURBPF).

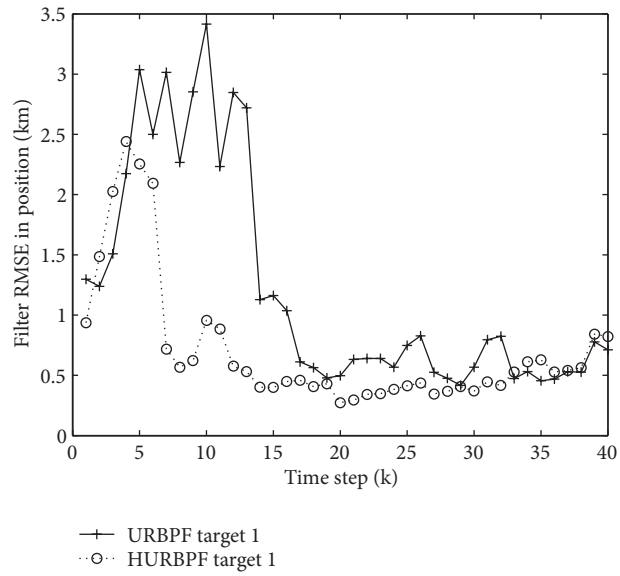

Figure 5: Comparison of the average position estimation errors of target 1.

measurements obey Poisson distribution with clutter rate $\lambda = 5$ in a single time step. The detection region of the coordinated plane is set to be $[0\,\text{km}, 50\,\text{km}] \times [0\,\text{km}, 50\,\text{km}]$. The standard bearings-only measurement variance used in both algorithms is $\sigma_z^a = 0.03$ rad.

The performance of the HURBPF is compared with that of the URBPF using 50 particles. The two targets begin at $k = 0$ with position-velocity coordinates $\mathbf{x}_0^{(1)} = (15\,\text{km}, 5\,\text{km}, 0.2\,\text{km/s}, 1\,\text{km/s})^T$ and $\mathbf{x}_0^{(2)} = (45\,\text{km}, 5\,\text{km}, -0.8\,\text{km/s}, 1\,\text{km/s})^T$, respectively. The total number of tracking time steps is 40. In this example, the initial state

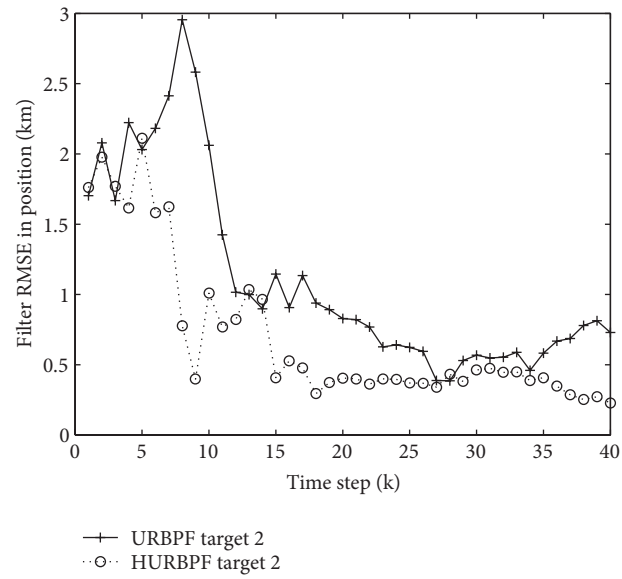

Figure 6: Comparison of the average position estimation errors of target 2.

estimates of the two targets are set to $\hat{\mathbf{x}}_{0|0}^{(1)} = (13\,\text{km}, 3\,\text{km}, 0.05\,\text{km/s}, 0\,\text{km/s})^T$ and $\hat{\mathbf{x}}_{0|0}^{(2)} = (43\,\text{km}, 3\,\text{km}, -0.2\,\text{km/s}, 0\,\text{km/s})^T$.

The tracking performance of the HURBPF and the URBPF in terms of RMSE in position is shown in Figures 5 and 6. It can be seen that the HURBPF also outperforms the URBPF for almost the entire simulation interval since the HURBPF deals with the unknown measurement noises variance priors. By the typical examples demonstrated above, a conclusion can be drawn that the H_∞ based RBPF algorithms show good robustness against unknown noise statistics.

5. Conclusions

In this paper, we present an improved Rao-Blackwellized particle filtering algorithm by using the H_∞ unscented transform. The main benefit lies in it requiring no priori knowledge of the statistical properties of the measurement noise. By decomposing the RBPF filtering distribution, the HRBPF and HURBPF algorithms are developed based on the H_∞ filter for solving the multitarget tracking problems with unknown noise statistics. The proposed algorithms are tested by both the linear and nonlinear tracking experiments. Simulation results show that they can achieve better tracking performance than the standard KF and UKF based RBPF algorithms.

Acknowledgment

The author would like to thank the anonymous reviewers for their helpful comments on this paper.

References

[1] M. Mallick, B. N. Vo, T. Kirubarajan, and S. Arulampalam, "Introduction to the issue on multitarget tracking," *IEEE Journal of Selected Topics in Signal Processing*, vol. 7, no. 3, pp. 373–375, 2013.

[2] Y. Bar-Shalom, F. Daum, and J. Huang, "The probabilistic data association filter: estimation in the presence of measurement origin uncertainty," *IEEE Control Systems Magazine*, vol. 29, no. 6, pp. 82–100, 2009.

[3] J. Liu, C. Han, F. Han, and Y. Hu, "Multiple maneuvering target tracking by improved particle filter based on multiscan JPDA," *Mathematical Problems in Engineering*, vol. 2012, Article ID 372161, 25 pages, 2012.

[4] S. S. Blackman, "Multiple hypothesis tracking for multiple target tracking," *IEEE Aerospace and Electronic Systems Magazine*, vol. 19, no. 1, pp. 5–18, 2004.

[5] T. Sathyan, T. J. Chin, S. Arulampalam, and D. Suter, "A multiple hypothesis tracker for multitarget tracking with multiple simultaneous measurements," *IEEE Journal of Selected Topics in Signal Processing*, vol. 7, no. 3, pp. 448–460, 2013.

[6] R. L. Popp, K. R. Pattipati, and Y. Bar-Shalom, "M-best S-D assignment algorithm with application to multitarget tracking," *IEEE Transactions on Aerospace and Electronic Systems*, vol. 37, no. 1, pp. 22–39, 2001.

[7] R. P. S. Mahler, "Multitarget bayes filtering via first-order multitarget moments," *IEEE Transactions on Aerospace and Electronic Systems*, vol. 39, no. 4, pp. 1152–1178, 2003.

[8] B.-N. Vo and W.-K. Ma, "The Gaussian mixture probability hypothesis density filter," *IEEE Transactions on Signal Processing*, vol. 54, no. 11, pp. 4091–4104, 2006.

[9] O. Cheng, H. Ji, and Y. Tian, "Improved Gaussian mixture CPHD tracker for multitarget tracking," *IEEE Transactions on Aerospace and Electronic Systems*, vol. 49, no. 2, pp. 1177–1191, 2013.

[10] O. Cappé, S. J. Godsill, and E. Moulines, "An overview of existing methods and recent advances in sequential Monte Carlo," *Proceedings of the IEEE*, vol. 95, no. 5, pp. 899–924, 2007.

[11] G. Casella and C. P. Robert, "Rao-Blackwellisation of sampling schemes," *Biometrika*, vol. 83, no. 1, pp. 81–94, 1996.

[12] S. Särkkä, A. Vehtari, and J. Lampinen, "Rao-Blackwellized Monte Carlo data association for multiple target tracking," in *Proceedings of the 7th International Conference on Information Fusion (FUSION '04)*, pp. 583–590, Stockholm, Sweden, July 2004.

[13] S. Särkkä, A. Vehtari, and J. Lampinen, "Rao-Blackwellized particle filter for multiple target tracking," *Information Fusion*, vol. 8, no. 1, pp. 2–15, 2007.

[14] T. Schön, F. Gustafsson, and P.-J. Nordlund, "Marginalized particle filters for mixed linear/nonlinear state-space models," *IEEE Transactions on Signal Processing*, vol. 53, no. 7, pp. 2279–2289, 2005.

[15] S. Julier, J. Uhlmann, and H. F. Durrant-Whyte, "A new method for the nonlinear transformation of means and covariances in filters and estimators," *IEEE Transactions Automatic Control*, vol. 45, no. 3, pp. 477–482, 2000.

[16] W. Li and Y. Jia, "H-infinity filtering for a class of nonlinear discrete-time systems based on unscented transform," *Signal Processing*, vol. 90, no. 12, pp. 3301–3307, 2010.

[17] M. J. Grimble and A. Elsayed, "Solution of the H_∞ optimal linear filtering problem for discrete-time systems," *IEEE Transactions on Acoustics, Speech and Signal Processing*, vol. 38, no. 7, pp. 1092–1104, 1990.

[18] I. Yaesh and U. Shaked, "A transfer function approach to the problems of discrete-time systems: H_∞-optimal linear control and filtering," *IEEE Transactions Automatic Control*, vol. 36, no. 11, p. 1217, 1264–1271, 1991.

[19] B. Hassibi, A. H. Sayed, and T. Kailath, *Indefinite-Quadratic Estimation and Control: A Unified Approach to* H_2 *and* H_∞ *Theories*, SIAM Press, 1999.

[20] J. Chandrasekar, A. J. Ridley, and D. S. Bernstein, "A comparison of the extended and unscented Kalman filters for discrete-time systems with nondifferentiable dynamics," in *Proceedings of the American Control Conference*, pp. 4431–4436, July 2007.

[21] F. Mustière, M. Bolić, and M. Bouchard, "Rao-Blackwellised particle filters: examples of applications," in *Proceedings of the Canadian Conference on Electrical and Computer Engineering (CCECE '06)*, pp. 1196–1200, Ottawa, Canada, May 2006.

[22] A. Doucet, J. D. Freitas, and N. Gordon, *Sequential Monte Carlo Methods in Practice*, Springer, New York, NY, USA, 2001.

[23] A. Giremus, J.-Y. Tourneret, and V. Calmettes, "A particle filtering approach for joint detection/estimation of multipath effects on GPS measurements," *IEEE Transactions on Signal Processing*, vol. 55, no. 4, pp. 1275–1285, 2007.

[24] D. Simon, *Optimal State Estimation: Kalman,* H_∞ *and Nonlinear Approaches*, Wiley Press, 2006.

[25] U. Shaked and N. Berman, "H_∞ nonlinear filtering of discrete-time processes," *IEEE Transactions on Signal Processing*, vol. 43, no. 9, pp. 2205–2209, 1995.

[26] G. A. Einicke and L. B. White, "Robust extended Kalman filtering," *IEEE Transactions on Signal Processing*, vol. 47, no. 9, pp. 2596–2599, 1999.

[27] S. Julier, J. Uhlmann, and H. F. Durrant-Whyte, "A new method for the nonlinear transformation of means and covariances in filters and estimators," *IEEE Transactions Automatic Control*, vol. 45, no. 3, pp. 477–482, 2000.

[28] J. Chandrasekar, A. J. Ridley, and D. S. Bernstein, "A comparison of the extended and unscented Kalman filters for discrete-time systems with nondifferentiable dynamics," in *Proceedings of the American Control Conference (ACC '07)*, pp. 4431–4436, July 2007.

[29] G. Sibley, G. Sukhatme, and L. Matthies, "The iterated sigma point Kalman filter with applications to long range stereo," in *Proceedings of the 2nd Robotics: Science and Systems Conference*, pp. 16–19, Philadelphia, Pa, USA, August 2006.

[30] A. Doucet, S. Godsill, and C. Andrieu, "On sequential Monte Carlo sampling methods for Bayesian filtering," *Statistics and Computing*, vol. 10, no. 3, pp. 197–208, 2000.

[31] G. Kitagawa, "Monte Carlo filter and smoother for non-Gaussian nonlinear state space models," *Journal of Computational and Graphical Statistics*, vol. 5, no. 1, pp. 1–25, 1996.

[32] M. Bolić, P. M. Djurić, and S. Hong, "Resampling algorithms and architectures for distributed particle filters," *IEEE Transactions on Signal Processing*, vol. 53, no. 7, pp. 2442–2450, 2005.

Hindawi Publishing Corporation
Mathematical Problems in Engineering
Volume 2013, Article ID 852502, 9 pages
http://dx.doi.org/10.1155/2013/852502

Research Article

Robust Adaptive Switching Fault-Tolerant Control of a Class of Uncertain Systems against Actuator Faults

Xiao-Zheng Jin

The Key Laboratory of Manufacturing Industrial Integrated Automation, Shenyang University, Shenyang Liaoning 110044, China

Correspondence should be addressed to Xiao-Zheng Jin; jin445118@163.com

Received 18 August 2013; Accepted 16 October 2013

Academic Editor: Bo-Chao Zheng

This paper deals with the fault-tolerant control (FTC) problem for a class of linear time-invariant systems with time-varying actuator faults and uncertainties. For more general consideration, the faults and uncertainties are supposed to depend on the states of systems and unknown constant bounds. For the sake of eliminating the effects of such state-dependent faults and uncertainties automatically, a switching control strategy which is formulated by a sign function is designed to configure controller based on system's states. And some adjustable control parameters are updated via designing adaptive laws. Based on the information from switching function and the adaptive estimation mechanism, the robust adaptive controllers are constructed to compensate for the effects of faults and uncertainties. Through Lyapunov functions and adaptive schemes, the asymptotic stability of the resulting adaptive FTC uncertain system can be achieved. The effectiveness of the proposed design is illustrated via a rocket fairing structural-acoustic model.

1. Introduction

In recent years, the safety, reliability, and validity of practical systems have attracted growing attention. However, during the operation of systems, the occurrence of some critical and unpredictable faults of system components, especially in actuators and sensors, is unavoidable and intolerable. As we know, actuators afford the operating function of the whole system. In the event of an actuator fault, the traditional feedback control design may result in unsatisfactory performance of systems or even cause other catastrophic consequence. Thus, fault-tolerant control (FTC) designs are necessary to make the system have capability of tolerating potential actuator faults and to improve the safety and reliability of systems.

In the existing literatures, there are many valuable research results on fault-tolerant control designs in time-delay systems [1, 2], uncertain systems [3–9], nonlinear systems [10, 11], network control systems [12, 13], and so forth. Among those studies, the FTC design approaches can be generally classified into two types, that is, the passive FTC approach and the active FTC approach. By considering faults as special strong uncertainties without any access of on-line fault information, the passive FTC approach just designs a fixed controller to compensate for the faults and take no additional actions in response to the faults (see, e.g., [14, 15]). Contrarily, active FTC methodologies design adjustable controllers on line and take some response actions to the faults for eliminating the effects of faults. On one hand, the active FTC methods based on fault detection and isolation (FDI) technique can reconfigure or reconstruct controllers by using the real-time fault information provided by the fault diagnosis mechanism [16–18]. But note that some delays of the response action may occur in the procedure of diagnosing the faults, and incorrect decision of FDI mechanism may also happen due to some unexpected factors such as exogenous disturbances and system uncertainties. On the other hand, the active FTC methods based on adaptive technique can regulate controller inputs immediately according to the state changes caused by faults. However, estimating or adjusting parameters by adaptive laws will consume large computation resource, which will make its unavailable in a practical system. Overall, despite the fact that an active FTC approach always causes some drawbacks, it is less conservative and more flexible in dealing with various faults than a passive FTC approach.

Recently, as adaptive technique has capability of quick and automatic response for estimating unknown parameters at each instant, there has been a growing interest in designing active FTC schemes for systems based on adaptive methods.

The faults of loss actuator effectiveness and parameterizable stuck-actuator faults were studied in [19–24] by using indirect adaptive and direct adaptive methods, respectively. Afterward, the unparameterizable stuck-actuator faults were, respectively, dealt with in [25, 26] with indirect adaptive and direct adaptive methods. The problem of bias-/stuck-actuator fault compensation was addressed in [27, 28] via an adaptive sliding-mode design with L_2 gain performance specification. Moreover, for the loss actuator effectiveness faults, the papers [29, 30] combined adaptive technique and linear matrix inequality (LMI) technique to provide the optimization of adaptive H_∞ performance of an FTC system via dynamic output feedback and state feedback designs, respectively. Using the notion of adaptive H_∞ performance in [29, 30], the recent papers [31, 32] gave less conservative methods with mode-dependent Lyapunov functions against unparameterizable stuck-actuator faults. In terms of the above studies, the adaptive methods can deal with the actuator faults covering loss of effectiveness, outage, and bias-/stuck-actuator faults. Motivated by the effectiveness and real-timely of eliminating a variety of actuator faults, we design a novel active FTC methodology based on adaptive technique to automatically accommodate faults in this paper.

It should be mentioned that the compensation of uncertainties have not been fully considered in the existing robust FTC literature, though some works considered the robust fault-tolerant compensation control with external disturbances in [25, 26]. Similar to the studies of some related uncertain systems [33], the uncertainties can always be addressed by the LMI technique [3, 4] and sidling mode control methods [5] in FTC systems. In [6], an adaptive method was proposed to deal with norm bounded uncertainties and actuator faults. Combining the effects of parametric uncertainties, external disturbances, actuator failures, and control input constraints, the authors of [7] developed fuzzy logic and back-stepping techniques to construct an adaptive controller for achieving high attitude performance of aircraft. For uncertain nonlinear systems, the papers [8, 9] utilized Hamilton-Jacobi-inequality-based approach and adaptive diagnostic-based approach to solve the FTC problem, respectively. In those studies, the uncertainties were always considered as norm bounded, sector-bounded, and polytopic-type uncertainties. However, in particular, system's uncertainties may vary along with the changes of system's state, and it will cause huge damage to the systems when the states have big amplitude. Thus, the kind of state-dependent uncertainties should also receive considerable attention.

In this paper, a novel switching adaptive method is proposed to solve the robust fault-tolerant control compensation problem of a class of uncertain linear systems. Similar to the adaptive controllers designed in [25, 26], the proposed adaptive approach can also be used for the general actuator fault model, which covers the cases of normal operation, loss of effectiveness, outage, and unparameterizable bias/stuck faults. But different from [25, 26], a more general state-dependent unparameterizable bias/stuck fault is considered in this paper. Moreover, the state-dependent uncertainties are also addressed in the adaptive controller designs. Here, each control effectiveness and bias/stuck faults are assumed to be unknown, and the rate of dependency of states in uncertainties also needs not to be known. But the maximum degree of dependency states is supposed to be known. Thus, a switching control strategy which is formulated by a sign function is proposed, and, furthermore, some adaptation laws are designed to estimate the unknown controller parameters on line. Based on the switching function and the updated values of these estimations, a class of state feedback controllers is constructed to solve the active FTC problem. Based on the Lyapunov stability theory, the adaptive closed-loop system can be guaranteed to be asymptotically stable in the presence of failures on actuators and uncertainties.

The rest of the paper is organized as follows. The robust fault-tolerant control problem formulation is described in Section 2. In Section 3, the switching adaptive state feedback controllers are developed. Section 4 gives a numerical example of rocket fairing structural-acoustic model and its simulation results. Finally, conclusion is given in Section 5.

2. Preliminaries and Problem Statement

In this paper, we consider that a linear time-invariant uncertain continuous-time model captured the following state-space equation:

$$\dot{x}(t) = \left(A + \Delta_A\right) x(t) + \left(B + \Delta_B\right) u(t), \tag{1}$$

where $x(t) \in R^n$ is the state, $u(t) \in R^m$ is the control input, A, B are known real constant matrices with appropriate dimensions, and Δ_A and Δ_B stand for the system uncertainties described by some bounded nonlinear functions.

Similar to [25], we consider the following mathematic model to formulate actuator faults:

$$u_{ij}^F(t) = \rho_i^j(t)\, u_i(t) + \sigma_i^j u_{si}(t), \quad i = 1, \ldots, m, \ j = 1, \ldots, L, \tag{2}$$

where the index i denotes the ith actuator, j stands for the jth faulty mode, L is the total faulty modes, $u_{ij}^F(t)$ represents the signal from the ith actuator that has failed in the jth faulty mode, $\rho_i^j(t)$ is the unknown time-varying actuator efficiency factor, $\underline{\rho}_i^j$ and $\overline{\rho}_i^j$ represent the known lower and upper bounds of $\rho_i^j(t)$, respectively, satisfying $0 \le \underline{\rho}_i^j \le \rho_i^j \le \overline{\rho}_i^j \le 1$ according to the practical case, and σ_i^j is an unknown constant defined as

$$\sigma_i^j = \begin{cases} 0, & \rho_i^j > 0, \\ 0 \text{ or } 1, & \rho_i^j = 0. \end{cases} \tag{3}$$

$u_{si}(t)$ is the unparametrizable time-varying stuck-actuator fault in the ith actuator satisfying

$$\left\| u_s(t) \right\| \le \alpha \left\| x(t) \right\| + \overline{u}_s, \tag{4}$$

where $\alpha \ge 0$ and $\overline{u}_s > 0$ are unknown constants. Note that the fault model can formulate the faults of actuator outage, loss of effectiveness, and bias and stuck (please see [25] for detail).

Remark 1. According to the practical case, the occurrence of time-varying unparametrizable faults may be related to the current system states. Thus, we assume that the unparametrizable stuck fault in (4) depends on system's states and a positive constant. Obviously, it is a more general assumption on actuator-stuck faults than the norm-bounded unparametrizable stuck faults considered in [25] or parametrizable stuck faults addressed in [21–24]. Setting $\alpha = 0$, the condition reduces to the assumption proposed in [25].

Here, we define the following sets:

$$\Delta_{\rho^j} = \left\{ \rho^j(t) : \rho^j(t) = \operatorname*{diag}_{i=1}^{m}\left[\rho_i^j(t)\right],\ \rho_i^j(t) \in \left[\underline{\rho}_i^j, \overline{\rho}_i^j\right] \right\},$$

$$N_{\rho^j} = \left\{ \rho^j(t) : \rho^j(t) = \operatorname*{diag}_{i=1}^{m}\left[\rho_i^j(t)\right], \right.$$
$$\left. \rho_i^j(t) = \underline{\rho}_i^j \text{ or } \rho_i^j(t) = \overline{\rho}_i^j \right\}, \tag{5}$$

where $i = 1, 2, \ldots, m$, $j = 1, 2, \ldots, L$, and the notation $\operatorname{diag}_{i=1}^{m}[\rho_i^j(t)]$ denotes the block-diagonal matrix with $\rho_i^j(t)$, $i = 1, 2, \ldots, m$ along the diagonal. And, for the sake of convenience description, for all possible faulty modes L, the following uniform actuator fault model is exploited:

$$u^F(t) = \rho(t)\, u(t) + \sigma u_s(t), \tag{6}$$

where $\rho(t) = \operatorname{diag}[\rho_1(t), \ldots, \rho_m(t)] \in \{\rho^1(t), \ldots, \rho^L(t)\}$.

Taking actuator faults (6) into consideration, the actual control inputs $u(t)$ generated by actuators are

$$u^F(t) = u(t) + P(t-T)\left[(\rho(t) - I)\, u(t) + \sigma u_s(t)\right], \tag{7}$$

where $P(t-T) = \operatorname{diag}_{i=1}^{m}[p_i(t-t_i)]$ with $T = [t_1, t_2, \ldots, t_n]^T \in R^n$ denotes the time profiles of faults and t_i, $i = 1, 2, \ldots, m$ is the unknown fault-occurrence time representing the time profile of a fault affecting the ith actuator. Then, the faults with time profiles are modeled as follows:

$$p_i(t - t_i) = \begin{cases} 0, & \text{if } t < t_i, \\ 1 - e^{-a_i(t-t_i)}, & \text{if } t \geq t_i, \end{cases} \tag{8}$$

where the scalar $a_i > 0$ denotes the unknown fault evolution rate. Small values of a_i characterize slowly developing faults, also known as incipient faults. For large values of a_i, the time profile p_i approaches a step function that models abrupt faults. It was worth mentioning that the fault time profile described by (8) denotes only the developing speed of a fault, whereas all its other basic features are defined by the vector $(\rho(t) - I)u(t) + \sigma u_s(t)$.

Hence, considering actuator faults (7), the dynamics of system (1) can be described by

$$\begin{aligned} \dot{x}(t) = {} & \left(A + \Delta_A\right) x(t) \\ & + \left(B + \Delta_B\right)\left(I + P(t-T)\left(\rho(t) - I\right)\right) u(t) \\ & + \left(B + \Delta_B\right) P(t-T)\, \sigma u_s(t). \end{aligned} \tag{9}$$

Here, we consider the case of state-feedback fault-tolerant controller design. Thus, we assume that all the states of system are available at every instant and all pairs $\{A, B\rho(t)\}$, are uniformly completely controllable for any actuator failure mode $\rho(t) \in \{\rho^1(t), \ldots, \rho^L(t)\}$. Moreover, according to the study of [25], for completely compensating the unparametrizable stuck faults, $\operatorname{rank}[B\rho(t)] = \operatorname{rank}[B]$ should be satisfied for any actuator failure mode $\rho(t) \in \{\rho^1(t), \ldots, \rho^L(t)\}$. On the other hand, for an uncertain system (1), the following assumption in FTC design is also assumed to be valid.

Assumption 2. For any vector $x \in R^n$, there exists a positive constant $\eta < 1$ such that

$$\left\| x^T \Delta_B \right\| \leq \eta \left\| x^T B \underline{\rho} \right\|, \tag{10}$$

where $\underline{\rho} = \min(\operatorname{diag}_{i=1}^{m}[\underline{\rho}_i^j]) \in \Delta_{\rho^j}$, $i = 1, 2, \ldots, m$, $j = 1, 2, \ldots, L$. Moreover, Δ_A is a norm bounded matrix satisfying

$$\left\| \Delta_A \right\| \leq \delta_A, \tag{11}$$

where δ_A is an unknown positive constant.

Then, the main objective of this paper is to construct a robust adaptive state feedback controller $u(t)$ such that the closed-loop system (9) can be guaranteed to be asymptotically stable even in the cases of actuator failures and uncertainties.

3. Switching Robust Adaptive FTC System Design

For the sake of eliminating the effects of actuator faults and uncertainties completely, a switching adaptive control strategy is proposed in this section. Some adaptive laws are designed to construct the controller with the estimation signals of the unknown actuator failure parameters and upper bound of uncertainties. Then, the asymptotically stable results of the closed-loop FTC system via state feedback are presented in Theorem 3.

Consider a linear time-invariant uncertain FTC model described by (9) and controller model

$$u(t) = -\operatorname{sgn}\left(x^T B\right)^T \left(\widehat{k}_1(t) + \widehat{k}_2(t) \left\| x^T B \underline{\rho} \right\|\right), \tag{12}$$

where the sign function $\operatorname{sgn}(x^T B)^T = [\operatorname{sgn}(b_1), \operatorname{sgn}(b_2), \ldots, \operatorname{sgn}(b_m)]^T$, b_i, $i = 1, 2, \ldots, m$ is the i element of the vector $x^T B$ and $\operatorname{sgn}(b_i)$ is defined by

$$\operatorname{sgn}(b_i) = \begin{cases} -1, & \text{if } b_i < 0, \\ 1, & \text{if } b_i > 0, \\ 0, & \text{if } b_i = 0; \end{cases} \tag{13}$$

$\widehat{k}_1(t) \in R$ is updated by the following adaptive law:

$$\frac{d\widehat{k}_1(t)}{dt} = \gamma(1 - \eta) \left\| x^T B \underline{\rho} \right\|, \tag{14}$$

where γ is any positive constant and $\widehat{k}_1(t_0)$ is finite, and, from (14), we can see that $\widehat{k}_1(t) \geq 0$ if $\widehat{k}_1(t_0) \geq 0$; $\widehat{k}_2(t) \in R$ is updated by the following adaptive law:

$$\frac{d\widehat{k}_2(t)}{dt} = \kappa(1-\eta)\lambda_{\min}\|x\|^2, \tag{15}$$

where κ is any positive constant, $\lambda_{\min}$ is the smallest eigenvalue of $B\underline{\rho}(B\underline{\rho})^T$, and $\widehat{k}_2(t_0)$ is finite, and, from (15), we can see that $\widehat{k}_2(t) \geq 0$ if $\widehat{k}_2(t_0) \geq 0$.

Therefore, substituting (12) into (9), the closed-loop FTC system model can be written by

$$\begin{aligned}\dot{x}(t) = {} & (A+\Delta_A)x(t) - B(I+P(t-T)(\rho(t)-I)) \\ & \times \operatorname{sgn}\left(x^TB\right)^T\left(\widehat{k}_1(t)+\widehat{k}_2(t)\left\|x^TB\underline{\rho}\right\|\right) \\ & - \Delta_B(I+P(t-T)(\rho(t)-I)) \\ & \times \operatorname{sgn}\left(x^TB\right)^T\left(\widehat{k}_1(t)+\widehat{k}_2(t)\left\|x^TB\underline{\rho}\right\|\right) \\ & + (B+\Delta_B)P(t-T)\sigma u_s(t).\end{aligned} \tag{16}$$

On the other hand, we denote that

$$\begin{aligned}\widetilde{k}_1(t) &= \widehat{k}_1(t) - k_1, \\ \widetilde{k}_2(t) &= \widehat{k}_2(t) - k_2.\end{aligned} \tag{17}$$

Since k_1 and k_2 are unknown constants, we can write the following error system:

$$\begin{aligned}\frac{d\widetilde{k}_1(t)}{dt} &= \gamma(1-\eta)\left\|x^TB\underline{\rho}\right\|, \\ \frac{d\widetilde{k}_2(t)}{dt} &= \kappa(1-\eta)\lambda_{\min}\|x\|^2.\end{aligned} \tag{18}$$

In the following, we denote a solution of the closed-loop system and the error system by $(x, \widetilde{k}_1, \widetilde{k}_2)(t)$. Then, the following main results can be obtained which shows the globally asymptotic stability of the solutions of the adaptive closed-loop system described by (16) and (18).

Theorem 3. *Consider the adaptive closed-loop system described by* (16) *and* (18) *satisfying Assumption 2. The fault-tolerant control system is asymptotically stable for any* $\rho(t) \in \Delta_{\rho^j}$, *if one chooses the controller as* (12) *and determine* $\widehat{k}_3(t)$, $\widehat{k}_4(t)$ *according to the adaptive laws* (14) *and* (15), *respectively.*

Proof. For the adaptive closed-loop system described by (16), we first define a Lyapunov functional candidate as

$$V\left(x, \widetilde{k}_1, \widetilde{k}_2\right) = x^Tx + \gamma^{-1}\widetilde{k}_1^2 + \kappa^{-1}\widetilde{k}_2^2. \tag{19}$$

Then, according to (9), the time derivative of V for $t > 0$ associated with a certain failure mode $\rho \in \Delta_{\rho^j}$ is

$$\begin{aligned}&\frac{dV\left(x, \widetilde{k}_1, \widetilde{k}_2, t\right)}{dt} \\ &= x^T\left[(A+\Delta_A)^T + (A+\Delta_A)\right]x \\ &\quad + 2x^T(B+\Delta_B)(I+P(t-T)(\rho(t)-I))u \\ &\quad + 2x^T(B+\Delta_B)P(t-T)\sigma u_s \\ &\quad + 2\gamma^{-1}\widetilde{k}_1\dot{\widetilde{k}}_1 + 2\kappa^{-1}\widetilde{k}_2\dot{\widetilde{k}}_2 \\ &= 2x^T(A+\Delta_A)^Tx \\ &\quad - 2x^TB(I+P(t-T)(\rho(t)-I)) \\ &\quad \times \operatorname{sgn}\left(x^TB\right)^T\left(\widehat{k}_1 + \left\|x^TB\underline{\rho}\right\|\widehat{k}_2\right) \\ &\quad - 2x^T\Delta_B(I+P(t-T)(\rho(t)-I)) \\ &\quad \times \operatorname{sgn}\left(x^TB\right)^T\left(\widehat{k}_1 + \left\|x^TB\underline{\rho}\right\|\widehat{k}_2\right) \\ &\quad + 2x^T(B+\Delta_B)P(t-T)\sigma u_s \\ &\quad + 2\gamma^{-1}\widetilde{k}_1\dot{\widetilde{k}}_1 + 2\kappa^{-1}\widetilde{k}_2\dot{\widetilde{k}}_2.\end{aligned} \tag{20}$$

According to the definition of $\rho(t)$ and $P(t-T)$ in (2) and (8), respectively, we know that $(I + P(t-T)(\rho(t) - I))$ is a positive diagonal matrix. Then considering the definition of (13), we have the following fact:

$$\left\|x^TBP_\rho\right\| \leq x^TBP_\rho \operatorname{sgn}\left(x^TB\right)^T, \tag{21}$$

where $P_\rho = I + P(t-T)(\rho(t) - I)$.

Thus, by the light of the inequality of (21) and the condition (4), we can rewrite (20) as

$$\begin{aligned}&\frac{dV\left(x, \widetilde{k}_1, \widetilde{k}_2\right)}{dt} \\ &\leq \|x\|^2\|A+\Delta_A\| \\ &\quad - 2\left\|x^TBP_\rho\right\|\widehat{k}_1 - 2\left\|x^TBP_\rho\right\|\left\|x^TB\underline{\rho}\right\|\widehat{k}_2 \\ &\quad + 2\left\|x^T(B+\Delta_B)\right\|\|P(t-T)\sigma\|\|u_s\| \\ &\quad + 2\left\|x^T\Delta_BP_\rho\right\|\widehat{k}_1 + 2\left\|x^T\Delta_BP_\rho\right\|\left\|x^TB\underline{\rho}\right\|\widehat{k}_2 \\ &\quad + 2\gamma^{-1}\widetilde{k}_1\dot{\widetilde{k}}_1 + 2\kappa^{-1}\widetilde{k}_2\dot{\widetilde{k}}_2 \\ &\leq \|x\|^2\|A+\Delta_A\| \\ &\quad - 2\left\|x^TBP_\rho\right\|\widehat{k}_1 - 2\left\|x^TBP_\rho\right\|\left\|x^TB\underline{\rho}\right\|\widehat{k}_2 \\ &\quad + 2\left\|x^T(B+\Delta_B)\right\|\|P(t-T)\sigma\|\left(\alpha\|x(t)\| + \overline{u}_s\right)\end{aligned}$$

$$+ 2\left\|x^T\Delta_B P_\rho\right\|\left\|\widehat{k}_1 + 2\right\|\left\|x^T\Delta_B P_\rho\right\|\left\|x^T B\underline{\rho}\right\|\widehat{k}_2 + 2\gamma^{-1}\widetilde{k}_1\dot{\widetilde{k}}_1 + 2\kappa^{-1}\widetilde{k}_2\dot{\widetilde{k}}_2. \tag{22}$$

Due to the fact that $\underline{\rho} \le I + P(t-T)(\rho - I) \le I$, we have $\|x^T B\underline{\rho}\| \le \|x^T \overline{B} P_\rho\|$ and $\|P_\rho\| \le 1$. Then, following Assumption 2, we can yield

$$\begin{aligned}
&\frac{dV\left(x,\widetilde{k}_1,\widetilde{k}_2\right)}{dt}\\
&\le \|x\|^2\left\|A+\Delta_A\right\| - 2(1-\eta)\left\|x^T B\underline{\rho}\right\|\widehat{k}_1 - 2(1-\eta)\left\|x^T B\underline{\rho}\right\|^2\widehat{k}_2\\
&\quad + 2\left\|x^T\left(B+\Delta_B\right)\right\|\|P(t-T)\sigma\|\alpha\|x(t)\| + 2\left\|x^T\left(B+\Delta_B\right)\right\|\|P(t-T)\sigma\|\overline{u}_s\\
&\quad + 2\gamma^{-1}\widetilde{k}_1\dot{\widetilde{k}}_1 + 2\kappa^{-1}\widetilde{k}_2\dot{\widetilde{k}}_2\\
&\le \|x\|^2\left\|A+\Delta_A\right\| - 2(1-\eta)\left\|x^T B\underline{\rho}\right\|\widehat{k}_1 - 2(1-\eta)\left\|x^T B\underline{\rho}\right\|^2\widehat{k}_2\\
&\quad + 2\|x\|^2\left\|B+\Delta_B\right\|\|P(t-T)\sigma\|\alpha + 2\left\|x^T\left(B+\Delta_B\right)\right\|\|P(t-T)\sigma\|\overline{u}_s\\
&\quad + 2\gamma^{-1}\widetilde{k}_1\dot{\widetilde{k}}_1 + 2\kappa^{-1}\widetilde{k}_2\dot{\widetilde{k}}_2\\
&\le \|x\|^2\left(\left\|A+\Delta_A\right\| + 2\left\|B+\Delta_B\right\|\|P(t-T)\sigma\|\alpha\right) - 2(1-\eta)\left\|x^T B\underline{\rho}\right\|\widehat{k}_1 - 2(1-\eta)\lambda_{\min}\|x\|^2\widehat{k}_2\\
&\quad + 2\left\|x^T\left(B+\Delta_B\right)\right\|\|P(t-T)\sigma\|\overline{u}_s + 2\gamma^{-1}\widetilde{k}_1\dot{\widetilde{k}}_1 + 2\kappa^{-1}\widetilde{k}_2\dot{\widetilde{k}}_2,
\end{aligned} \tag{23}$$

where $\lambda_{\min}$ is the smallest eigenvalue of $B\underline{\rho}(B\underline{\rho})^T$.

On the other hand, according to the definition of (1), (4), and (8), we know that there always exist positive constants k_1 and k_2 such that

$$\begin{aligned}
&(1-\eta)\left\|x^T B\underline{\rho}\right\|k_1 > \left\|x^T\left(B+\Delta_B\right)\right\|\|P(t-T)\sigma\|\overline{u}_s,\\
&(1-\eta)\lambda_{\min}\|x\|^2 k_2 > \|x\|^2\left(\left\|A+\Delta_A\right\| + 2\left\|B+\Delta_B\right\|\|P(t-T)\sigma\|\alpha\right)
\end{aligned} \tag{24}$$

for any $x \neq 0$.

Then, it follows from (22) that, for any $x \neq 0$,

$$\begin{aligned}
&\frac{dV\left(x,\widetilde{k}_1,\widetilde{k}_2\right)}{dt}\\
&< -2(1-\eta)\left\|x^T B\underline{\rho}\right\|\widetilde{k}_1 - 2(1-\eta)\lambda_{\min}\|x\|^2\widetilde{k}_2 + 2\gamma^{-1}\widetilde{k}_1\dot{\widetilde{k}}_1 + 2\kappa^{-1}\widetilde{k}_2\dot{\widetilde{k}}_2\\
&= 0.
\end{aligned} \tag{25}$$

Hence, it is easy to see that $dV(x,\widetilde{k}_1,\widetilde{k}_2)/dt < 0$ for any $x \neq 0$. Thus, the solutions of closed-loop FTC system are uniformly bounded, and the state $x(t)$ converges asymptotically to zero. This ends the proof. □

Theorem 3 indicates that the proposed adaptive switching control scheme can deal with a class of uncertain systems and actuator faults with condition (4) and Assumption 2. Actually, some more relaxant conditions of systems and actuator faults can also be dealt with by the modified adaptive switching control designs. The following theorem is given to illustrate the asymptotic stability results of multidimension state-dependent uncertainties and stuck-actuator faults.

Theorem 4. *Consider uncertain system* (1) *satisfying* (10) *and*

$$\left\|\Delta_A\right\| \le \delta\|x\|^p + \delta_A, \tag{26}$$

where $\delta, \delta_A > 0$*, and actuator faults formulated in* (6) *with*

$$\left\|u_s(t)\right\| \le \alpha\|x(t)\|^q + \overline{u}_s, \tag{27}$$

where p *and* q *are known maximum degree of* $\|x(t)\|$ *denoting the rate of dependency of states using the following controller:*

$$\begin{aligned}
u_i(t) = &-\operatorname{sgn}\left(x^T B\right)^T\\
&\times\left(\widehat{k}_1(t) + \widehat{k}_2(t)\left\|x^T B\underline{\rho}\right\| + \widehat{k}_3(t)\left\|x^T B\underline{\rho}\right\|^{p+1} + \widehat{k}_4(t)\left\|x^T B\underline{\rho}\right\|^q\right),
\end{aligned} \tag{28}$$

where $\widehat{k}_1(t)$ *and* $\widehat{k}_2(t)$ *are updated by adaptive laws* (14) *and* (15) *and* $\widehat{k}_3(t)$ *and* $\widehat{k}_4(t)$ *are adjusted by the following adaptive laws:*

$$\begin{aligned}
\frac{d\widehat{k}_3(t)}{dt} &= \zeta(1-\eta)\|x\|^{p+2},\\
\frac{d\widehat{k}_4(t)}{dt} &= \xi(1-\eta)\lambda_{\min}\|x\|^{q+1},
\end{aligned} \tag{29}$$

where ζ *and* ξ *are any positive constants. Then, the system states are asymptotically convergence to zero within finite time.*

Proof. Similar to the proof of Theorem 3, we first define a Lyapunov functional candidate as:

$$V\left(x,\widetilde{k}_1,\widetilde{k}_2,\widetilde{k}_3,\widetilde{k}_4\right) = x^T x + \gamma^{-1}\widetilde{k}_1^2 + \kappa^{-1}\widetilde{k}_2^2 + \zeta^{-1}\widetilde{k}_3^2 + \xi^{-1}\widetilde{k}_4^2. \tag{30}$$

Then, in terms of (21), the time derivative of V for $t > 0$ associated with a certain failure mode $\rho \in \Delta_{\rho^j}$ is

$$\begin{aligned}
&\frac{dV\left(x,\widetilde{k}_1,\widetilde{k}_2,\widetilde{k}_3,\widetilde{k}_4,t\right)}{dt}\\
&= x^T\left[\left(A+\Delta_A\right)^T+\left(A+\Delta_A\right)\right]x\\
&\quad + 2x^T\left(B+\Delta_B\right)\left(I+P\left(t-T\right)\left(\rho\left(t\right)-I\right)\right)u\\
&\quad + 2x^T\left(B+\Delta_B\right)P\left(t-T\right)\sigma u_s\\
&\quad + 2\gamma^{-1}\widetilde{k}_1\dot{\widetilde{k}}_1 + 2\kappa^{-1}\widetilde{k}_2\dot{\widetilde{k}}_2 + 2\zeta^{-1}\widetilde{k}_3\dot{\widetilde{k}}_3 + 2\xi^{-1}\widetilde{k}_4\dot{\widetilde{k}}_4\\
&\le 2\|x\|^2\left(\|A\|+\left\|\Delta_A\right\|\right)\\
&\quad - 2\left\|x^TBP_\rho\right\|\widehat{k}_1 - 2\left\|x^TBP_\rho\right\|\left\|x^TB\underline{\rho}\right\|\widehat{k}_2\\
&\quad - 2\left\|x^TBP_\rho\right\|\left\|x^TB\underline{\rho}\right\|^{p+1}\widehat{k}_3 - 2\left\|x^TBP_\rho\right\|\left\|x^TB\underline{\rho}\right\|^{q}\widehat{k}_4\\
&\quad + 2\left\|x^T\left(B+\Delta_B\right)\right\|\left\|P\left(t-T\right)\sigma\right\|\left\|u_s\right\|\\
&\quad + 2\left\|x^T\Delta_BP_\rho\right\|\widehat{k}_1 + 2\left\|x^T\Delta_BP_\rho\right\|\left\|x^TB\underline{\rho}\right\|\widehat{k}_2\\
&\quad + 2\left\|x^T\Delta_BP_\rho\right\|\left\|x^TB\underline{\rho}\right\|^{p+1}\widehat{k}_3 + 2\left\|x^T\Delta_BP_\rho\right\|\left\|x^TB\underline{\rho}\right\|^{q}\widehat{k}_4\\
&\quad + 2\gamma^{-1}\widetilde{k}_1\dot{\widetilde{k}}_1 + 2\kappa^{-1}\widetilde{k}_2\dot{\widetilde{k}}_2 + 2\zeta^{-1}\widetilde{k}_3\dot{\widetilde{k}}_3 + 2\xi^{-1}\widetilde{k}_4\dot{\widetilde{k}}_4.
\end{aligned} \tag{31}$$

From the fact of $\|x^TB\underline{\rho}\| \le \|x^TBP_\rho\|$, $\|P_\rho\| \le 1$, and inequalities (10), (26), and (27), we can rewrite (31) as

$$\begin{aligned}
&\frac{dV\left(x,\widetilde{k}_1,\widetilde{k}_2,\widetilde{k}_3,\widetilde{k}_4,t\right)}{dt}\\
&\le 2\|x\|^2\left(\|A\|+\delta\|x\|^p+\delta_A\right)\\
&\quad - 2\left(1-\eta\right)\left\|x^TB\underline{\rho}\right\|\widehat{k}_1 - 2\left(1-\eta\right)\left\|x^TB\underline{\rho}\right\|^2\widehat{k}_2\\
&\quad - 2\left(1-\eta\right)\left\|x^TB\underline{\rho}\right\|^{p+2}\widehat{k}_3 - 2\left(1-\eta\right)\left\|x^TB\underline{\rho}\right\|^{q+1}\widehat{k}_4\\
&\quad + 2\left\|x^T\left(B+\Delta_B\right)\right\|\left\|P\left(t-T\right)\sigma\right\|\left(\alpha\|x\left(t\right)\|^q+\overline{u}_s\right)\\
&\quad + 2\gamma^{-1}\widetilde{k}_1\dot{\widetilde{k}}_1 + 2\kappa^{-1}\widetilde{k}_2\dot{\widetilde{k}}_2 + 2\zeta^{-1}\widetilde{k}_3\dot{\widetilde{k}}_3 + 2\xi^{-1}\widetilde{k}_4\dot{\widetilde{k}}_4\\
&\le 2\|x\|^2\left(\|A\|+\delta_A\right) + 2\delta\|x\|^{p+2}\\
&\quad - 2\left(1-\eta\right)\left\|x^TB\underline{\rho}\right\|\widehat{k}_1 - 2\left(1-\eta\right)\left\|x^TB\underline{\rho}\right\|^2\widehat{k}_2\\
&\quad - 2\left(1-\eta\right)\left\|x^TB\underline{\rho}\right\|^{p+2}\widehat{k}_3 - 2\left(1-\eta\right)\left\|x^TB\underline{\rho}\right\|^{q+1}\widehat{k}_4\\
&\quad + 2\alpha\|x\|^{q+1}\left\|\left(B+\Delta_B\right)\right\|\left\|P\left(t-T\right)\sigma\right\|\\
&\quad + 2\left\|x^T\left(B+\Delta_B\right)\right\|\left\|P\left(t-T\right)\sigma\right\|\overline{u}_s\\
&\quad + 2\gamma^{-1}\widetilde{k}_1\dot{\widetilde{k}}_1 + 2\kappa^{-1}\widetilde{k}_2\dot{\widetilde{k}}_2 + 2\zeta^{-1}\widetilde{k}_3\dot{\widetilde{k}}_3 + 2\xi^{-1}\widetilde{k}_4\dot{\widetilde{k}}_4,
\end{aligned} \tag{32}$$

where $\lambda_{\min}$ is the smallest eigenvalue of $B\underline{\rho}(B\underline{\rho})^T$.

Since δ, α, δ_A, and $\overline{u}_s$ are constants, then there always exist positive constants k_1, k_2, k_3, and k_4 such that

$$\begin{aligned}
\left(1-\eta\right)\left\|x^TB\underline{\rho}\right\|k_1 &> \left\|x^T\left(B+\Delta_B\right)\right\|\left\|P\left(t-T\right)\sigma\right\|\overline{u}_s,\\
\left(1-\eta\right)\lambda_{\min}\|x\|^2k_2 &> \|x\|^2\left(\|A\|+\delta_A\right),\\
\left(1-\eta\right)\lambda_{\min}\|x\|^{p+2}k_3 &> \delta\|x\|^{p+2},\\
\left(1-\eta\right)\lambda_{\min}\|x\|^{q+1}k_4 &> \alpha\|x\|^{q+1}\left\|\left(B+\Delta_B\right)\right\|\left\|P\left(t-T\right)\sigma\right\|
\end{aligned} \tag{33}$$

for any $x \neq 0$.

Then, it follows from (32) that, for any $x \neq 0$,

$$\begin{aligned}
&\frac{dV\left(x,\widetilde{k}_1,\widetilde{k}_2,\widetilde{k}_3,\widetilde{k}_4,t\right)}{dt}\\
&< -2\left(1-\eta\right)\left\|x^TB\underline{\rho}\right\|\widetilde{k}_1 - 2\left(1-\eta\right)\lambda_{\min}\|x\|^2\widetilde{k}_2\\
&\quad - 2\left(1-\eta\right)\lambda_{\min}\|x\|^{p+2}\widetilde{k}_3 - 2\left(1-\eta\right)\lambda_{\min}\|x\|^{q+1}\widetilde{k}_4\\
&\quad + 2\gamma^{-1}\widetilde{k}_1\dot{\widetilde{k}}_1 + 2\kappa^{-1}\widetilde{k}_2\dot{\widetilde{k}}_2 + 2\zeta^{-1}\widetilde{k}_3\dot{\widetilde{k}}_3 + 2\xi^{-1}\widetilde{k}_4\dot{\widetilde{k}}_4\\
&= 0.
\end{aligned} \tag{34}$$

Hence, it indicates that, for any $x \neq 0$, $dV(x,\widetilde{k}_1,\widetilde{k}_2,\widetilde{k}_3,\widetilde{k}_4,t)/dt < 0$. Thus, the global adaptive fault-tolerant compensation problem of uncertain system is solvable. The solutions of closed-loop FTC system are uniformly bounded, and the state $x(t)$ converges asymptotically to zero. □

Remark 5. Theorem 4 has shown that the proposed method can compensate for multidimension state-dependent uncertainties and stuck-actuator faults. However, the dependency rate of states should be known to construct the compensation controllers, which will bring some limitation of this method. On the other hand, inequality (10) is also a conservative condition for uncertainties. Some more effective methods should be investigated to reduce the limitation in future studies.

From Theorems 3 and 4, we know that the multidimension state-dependent uncertainties and unparametrizable stuck-actuator faults can be completely compensated by

the proposed adaptive switching control method. Actually, the proposed adaptive switching compensation control designs are not only suitable for the system's uncertainties, but also suitable for the controller gain uncertainties. The following corollary is given to illustrate the asymptotic stability of such nonfragile systems in the case of additive controller coefficient variations.

Corollary 6. *Consider uncertain system* (1) *satisfying* (10), (26), *and* (27) *using the following controller:*

$$u_i(t) = -\operatorname{sgn}\left(x^T B\right)^T \left(\widehat{k}_1(t) + \Delta_{k1} + \left(\widehat{k}_2(t) + \Delta_{k2}\right)\left\|x^T B\underline{\rho}\right\| + \left(\widehat{k}_3(t) + \Delta_{k3}\right)\left\|x^T B\underline{\rho}\right\|^{p+1} + \left(\widehat{k}_4(t) + \Delta_{k4}\right)\left\|x^T B\underline{\rho}\right\|^{q}\right), \tag{35}$$

where Δ_{k1}, Δ_{k2}, Δ_{k3}, *and* Δ_{k4} *are bounded additive controller coefficient variations satisfying* $|\Delta_{kl}| \le \delta_{kl}$, δ_{kl} *is unknown positive constants,* $l = 1, 2, 3, 4$, *and* $\widehat{k}_1(t)$, $\widehat{k}_2(t)$, $\widehat{k}_3(t)$, *and* $\widehat{k}_4(t)$ *are updated by adaptive laws* (14), (15), *and* (29). *Then, the system states are asymptotically convergence to zero within finite time.*

Proof. The proof of this corollary is omitted. It is quite similar to the one of Theorem 4. □

Remark 7. From Theorems 3 and 4, we can see that the effects of system matrix A have also been eliminated in the designs. Different from other designs to construct a Lyapunov matrix P from system matrices A and B in [25], the method needs not to solve the Lyapunov matrix. Thus, the estimation of K_1 in [25] has also been omitted. And it can reduce the computation burden in the designs. It should also be mentioned that the same design can also be realized by modifying K_2 such as

$$K_2(t) = \frac{-\left(x^T PB\right)^T \beta \left\|x^T PB\right\| \left(\widehat{k}_1(t) + \widehat{k}_2(t)\left\|x^T PB\right\|\right)}{\left\|x^T PB\right\|^2 \alpha} \tag{36}$$

in [25]. In other word, the function of (12) and (36) is the same.

Remark 8. Actually, several methods have been proposed to completely compensate for the effects of time-varying matched perturbations and redundant actuator faults (e.g., [25, 26, 31]). All of the methods have a limitation that chattering phenomenon will occur when the states or tracking errors converge to zero. Note that the limitation still exists in the method proposed in this paper, because of the usage of sign function $\operatorname{sgn}(\cdot)$ in (13). The limitation can be reduced by some improved control strategies such as filtering theory, boundary layer around the switching surface, and switching gain which is proposed in sliding mode control technique [34, 35]. However, a bounded stability result can be achieved rather than asymptotic stability.

4. Numerical Example

Similar to [22, 23], the rocket fairing structural-acoustic model which is also used in [25] is adopted with the following system matrices:

$$A = \begin{bmatrix} 0 & 1 & 0.0802 & 1.0415 \\ -0.1980 & -0.115 & -0.0318 & 0.3 \\ -3.0500 & 1.1880 & -0.4650 & 0.9 \\ 0 & 0.0805 & 1 & 0 \end{bmatrix}, \quad B = \begin{bmatrix} 1 & 1.55 & 0.75 \\ 0.975 & 0.8 & 0.85 \\ 0 & 0 & 0 \\ 0 & 0 & 0 \end{bmatrix}. \tag{37}$$

With the similar simulation of [25], we consider four possible faulty modes as follows.

Normal Mode 1. All the third actuators are normal; that is, $\rho_i^1 = 1$, $\sigma_i^1 = 0$, $a_i = 0$, and $i = 1, 2, 3$.

Fault Mode 2. The first actuator is outage or stuck, the second and the third actuators may be normal or loss of effectiveness; described by $\rho_1^2 = 0$, $b_2 \le \rho_2^2 \le 1$, $b_3 \le \rho_3^2 \le 1$, and $b_2 = 0.3$, and $b_3 = 0.5$, which denotes the maximum loss of effectiveness for the second and the third actuators, and $a_2 = 2$, $a_3 = 3$.

Fault Mode 3. The second actuator is outage or stuck, the first and third actuators may be normal or loss of effectiveness, that is, $\rho_2^3 = 0$, $b_1 \le \rho_1^3 \le 1$, $b_3 \le \rho_3^3 \le 1$, $b_1 = 0.5$, $b_3 = 0.3$, which denotes the maximum loss of effectiveness for the first and the third actuators, and $a_1 = 3$, $a_3 = 2$.

Fault Mode 4. The third actuator is outage or stuck, the first and second actuators may be normal or loss of effectiveness; that is, $\rho_3^4 = 0$, $c_1 \le \rho_1^4 \le 1$, $c_2 \le \rho_2^4 \le 1$, $b_1 = 0.5$, and $b_2 = 0.2$, which denotes the maximum loss of effectiveness for the first and the second actuators, and $a_1 = 1$, $a_2 = 0.5$.

For the sake of verifying the effectiveness of the proposed adaptive method, the simulations are given with the following parameters and initial conditions:

$$\gamma = 50, \quad \kappa = 1, \quad \zeta = 10, \quad \varepsilon = 10, \quad x(0) = [0, 1, 0.5, -1]^T, \quad \widehat{k}_i(0) = 0, \quad i = 1, 2, 3, 4. \tag{38}$$

The following faulty case is considered in the simulations; that is, before 8 second, the systems operate in normal case and the uncertainties $\Delta_A = (-0.3\sin(0.1t)\|x\| + 0.5) \times A$, $\Delta_B = 0.2 \times B$ enter into the system at the beginning ($t \ge 0$). At 8 second, the fault mode 2 has occurred; that is, the first actuator has stuck at $u_{s1}(t) = 2 + 0.5\sin(0.1t) - 0.5\cos(0.5t)\|x\|^2$ and the third actuator loss of effectiveness described by $\rho_3 = 1 - 0.03t$ until loss effectiveness of 50%.

Figure 1 is the response curves of the system's states with robust adaptive state feedback controller in the above-mentioned faulty case. Figure 2 illustrates the estimated curves of controller parameters $\widehat{k}_1(t)$, $\widehat{k}_2(t)$, $\widehat{k}_3(t)$, and $\widehat{k}_4(t)$, respectively. It is easy to see that the estimates can converge

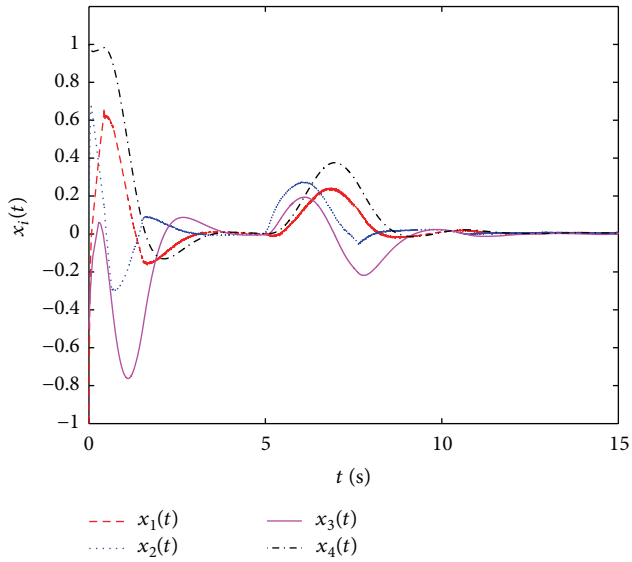

FIGURE 1: Response curves of the system's states $x_i(t)$, $i = 1, 2, 3, 4$ under the proposed adaptive switching controller (28).

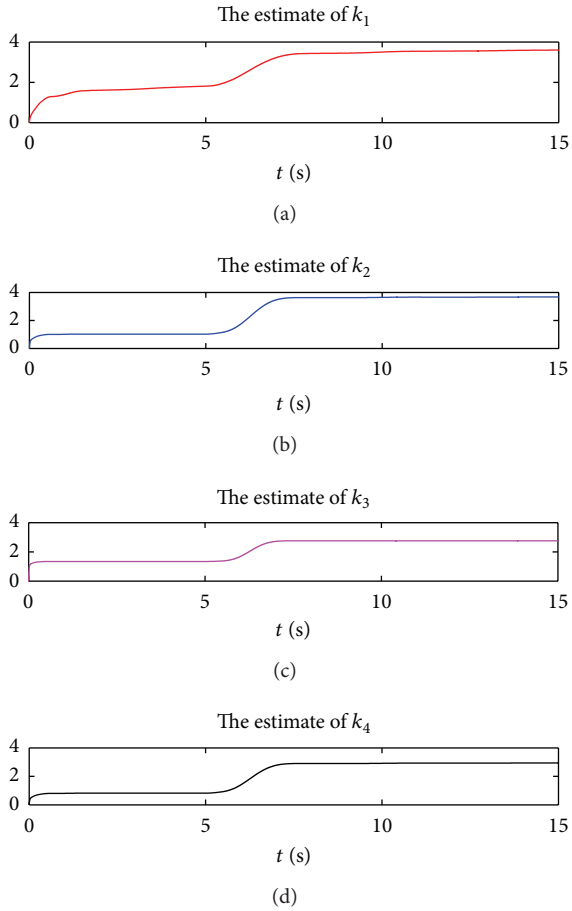

FIGURE 2: Response curves of the adaptive adjustable control parameters $\widehat{k}_1(t)$, $\widehat{k}_2(t)$, $\widehat{k}_3(t)$, and $\widehat{k}_4(t)$, respectively.

and the closed-loop FTC system asymptotically stable in the presence of faults on actuators and uncertainties.

5. Conclusion

This paper presents a switching adaptive method for robust fault-tolerant control problem of actuator faults and compensation in continuous-time linear systems. The fault model of normal operation, loss of effectiveness, outage, and stuck are considered, and the bias-/stuck-actuator faults and system uncertainties are supposed to be satisfying a state-dependent condition. The switching robust adaptive control schemes are constructed based on a sign function and some updating adaptation laws which are used to estimate the controller parameters on line. The proposed state feedback controllers can automatically compensate the fault and uncertainty effects and guarantee the asymptotically stable of the system. A numerical example has shown the effectiveness of the proposed method.

One of the further research topics is to eliminate the assumption of knowing the dependency rate of states p and q and to reduce the condition of (10). Additionally, the chattering problem should be further considered for the sake of application of the proposed method.

Acknowledgments

This work is supported by the National Natural Science Foundation (Grant nos. 61104029, 61273155, and 61203087), Program for Liaoning Excellent Talents in University (LNET) (Grant no. LJQ2013122), the science and technology plan of Liaoning Province (2011219011), the Natural Science Foundation of Liaoning Province (Grant no. 201202156), and the Scientific Research Foundation for Doctor of Liaoning Province (Grant no. 20121040).

References

[1] Z. Mao, B. Jiang, and P. Shi, "Observer-based fault-tolerant control for a class of networked control systems with transfer delays," *Journal of the Franklin Institute*, vol. 348, no. 4, pp. 763–776, 2011.

[2] E. Tian, D. Yue, and C. Peng, "Reliable control for networked control systems with probabilistic actuator fault and random delays," *Journal of the Franklin Institute*, vol. 347, no. 10, pp. 1907–1926, 2010.

[3] C. Cheng and Q. Zhao, "Reliable control of uncertain delayed systems with integral quadratic constraints," *IEE Proceedings of Control Theory and Applications*, vol. 151, no. 6, pp. 790–796, 2004.

[4] S. Ye, Y. Zhang, X. Wang, and B. Jiang, "Fault-tolerant control for a class of uncertain systems with actuator faults," *Tsinghua Science and Technology*, vol. 15, no. 2, pp. 174–183, 2010.

[5] T. Wang, W. Xie, and Y. Zhang, "Sliding mode fault tolerant control dealing with modeling uncertainties and actuator faults," *ISA Transactions*, vol. 51, no. 3, pp. 386–392, 2012.

[6] X. J. Li and G. H. Yang, "Robust adaptive fault-tolerant control for uncertain linear systems with actuator failures," *IET Control Theory & Applications*, vol. 6, no. 10, pp. 1544–1551, 2012.

[7] A.-M. Zou and K. D. Kumar, "Adaptive fuzzy fault-tolerant attitude control of spacecraft," *Control Engineering Practice*, vol. 19, no. 1, pp. 10–21, 2011.

[8] G.-H. Yang, J. L. Wang, and Y. C. Soh, "Reliable guaranteed cost control for uncertain nonlinear systems," *IEEE Transactions on Automatic Control*, vol. 45, no. 11, pp. 2188–2192, 2000.

[9] X. Zhang, T. Parisini, and M. M. Polycarpou, "Adaptive fault-tolerant control of nonlinear uncertain systems: an information-based diagnostic approach," *IEEE Transactions on Automatic Control*, vol. 49, no. 8, pp. 1259–1274, 2004.

[10] S. Varma and K. D. Kumar, "Fault tolerant satellite attitude control using solar radiation pressure based on nonlinear adaptive sliding mode," *Acta Astronautica*, vol. 66, no. 3-4, pp. 486–500, 2010.

[11] Z. Zhang and W. Chen, "Adaptive output feedback control of nonlinear systems with actuator failures," *Information Sciences*, vol. 179, no. 24, pp. 4249–4260, 2009.

[12] C.-X. Yang, Z.-H. Guan, and J. Huang, "Stochastic fault tolerant control of networked control systems," *Journal of the Franklin Institute*, vol. 346, no. 10, pp. 1006–1020, 2009.

[13] H. Zhihong, Z. Yuan, and X. Chang, "A robust fault-tolerant control strategy for networked control systems," *Journal of Network and Computer Applications*, vol. 34, no. 2, pp. 708–714, 2011.

[14] R. J. Veillette, J. B. Medanic, and W. R. Perkins, "Design of reliable control systems," *IEEE Transactions on Automatic Control*, vol. 37, no. 3, pp. 290–304, 1992.

[15] G.-H. Yang, J. L. Wang, and Y. C. Soh, "Reliable H_∞ controller design for linear systems," *Automatica*, vol. 37, no. 5, pp. 717–725, 2001.

[16] K. Zhang, B. Jiang, and P. Shi, "Fast fault estimation and accommodation for dynamical systems," *IET Control Theory and Applications*, vol. 3, no. 2, pp. 189–199, 2009.

[17] H. Alwi and C. Edwards, "Fault detection and fault-tolerant control of a civil aircraft using a sliding-mode-based scheme," *IEEE Transactions on Control Systems Technology*, vol. 16, no. 3, pp. 499–510, 2008.

[18] W. Chen and F. N. Chowdhury, "Analysis and detection of incipient faults in post-fault systems subject to adaptive fault-tolerant control," *International Journal of Adaptive Control and Signal Processing*, vol. 22, no. 9, pp. 815–832, 2008.

[19] J. D. Boskovic and R. K. Mehra, "A robust adaptive reconfigurable flight con-trol scheme for accommodation of control effector failures," in *Proceeding of the American Control Conference*, vol. 2, pp. 1127–1132, Arlington, Va, USA, 2001.

[20] D. Ye and G.-H. Yang, "Adaptive fault-tolerant tracking control against actuator faults with application to flight control," *IEEE Transactions on Control Systems Technology*, vol. 14, no. 6, pp. 1088–1096, 2006.

[21] G. Tao, S. M. Joshi, and X. Ma, "Adaptive state feedback and tracking control of systems with actuator failures," *IEEE Transactions on Automatic Control*, vol. 46, no. 1, pp. 78–95, 2001.

[22] L. F. Wang, B. Huang, and K. C. Tan, "Fault-tolerant vibration control in a networked and embedded rocket fairing system," *IEEE Transactions on Industrial Electronics*, vol. 51, no. 6, pp. 1127–1141, 2004.

[23] X. Tang, G. Tao, L. Wang, and J. A. Stankovic, "Robust and adaptive actuator failure compensation designs for a rocket fairing structural-acoustic model," *IEEE Transactions on Aerospace and Electronic Systems*, vol. 40, no. 4, pp. 1359–1366, 2004.

[24] X. D. Tang, G. Tao, and S. M. Joshi, "Adaptive actuator failure compensation for nonlinear MIMO systems with an aircraft control application," *Automatica*, vol. 43, no. 11, pp. 1869–1883, 2007.

[25] X.-Z. Jin and G.-H. Yang, "Robust adaptive fault-tolerant compensation control with actuator failures and bounded disturbances," *Acta Automatica Sinica*, vol. 35, no. 3, pp. 305–309, 2009.

[26] X. Jin, G. Yang, and Y. Li, "Robust fault-tolerant controller design for linear time-invariant systems with actuator failures: an indirect adaptive method," *Journal of Control Theory and Applications*, vol. 8, no. 4, pp. 471–478, 2010.

[27] Q. Hu, "Robust adaptive sliding-mode fault-tolerant control with L_2-gain performance for flexible spacecraft using redundant reaction wheels," *IET Control Theory and Applications*, vol. 4, no. 6, pp. 1055–1070, 2010.

[28] Q. Hu and B. Xiao, "Adaptive fault tolerant control using integral sliding mode strategy with application to flexible spacecraft," *International Journal of Systems Science*, vol. 44, no. 12, pp. 2273–2286, 2013.

[29] G.-H. Yang and D. Ye, "Adaptive fault-tolerant H_∞ control via dynamic output feedback for linear systems against actuator faults," in *Proceeding of the 45th IEEE Conference on Decision and Control 2006*, pp. 3524–3529, San Diego, Calif, USA, December 2006.

[30] G.-H. Yang and D. Ye, "Reliable H_∞ control of linear systems with adaptive mechanism," *IEEE Transactions on Automatic Control*, vol. 55, no. 1, pp. 242–247, 2010.

[31] X. Z. Jin, G. H. Yang, X. H. Chang, and W. W. Che, "Robust fault-tolerant H_∞ control with adaptive compensation," *Acta Automatica Sinica*, vol. 39, no. 1, pp. 31–42, 2013.

[32] X. Z. Jin, G. H. Yang, and X. H. Chang, "Robust H_∞ and adaptive tracking control against actuator faults with a linearised aircraft application," *International Journal of Systems Sciences*, vol. 44, no. 1, pp. 151–165, 2013.

[33] X. Xie, X. Zhu, and Y. Wang, "Relaxed global asymptotic stability of 2-D state-space digital filters described by Roesser model with polytopic-type uncertainty," *Signal Processing*, vol. 94, no. 1, pp. 102–107, 2014.

[34] W.-J. Cao and J.-X. Xu, "Nonlinear integral-type sliding surface for both matched and unmatched uncertain systems," *IEEE Transactions on Automatic Control*, vol. 49, no. 8, pp. 1355–1360, 2004.

[35] P. Kachroo and M. Tomizuka, "Chattering reduction and error convergence in the sliding-mode control of a class of nonlinear systems," *IEEE Transactions on Automatic Control*, vol. 41, no. 7, pp. 1063–1068, 1996.

Hindawi Publishing Corporation
Mathematical Problems in Engineering
Volume 2013, Article ID 636374, 6 pages
http://dx.doi.org/10.1155/2013/636374

Research Article

Modeling Analysis of Power Transformer Fault Diagnosis Based on Improved Relevance Vector Machine

Lutao Liu[1] and Zujun Ding[2]

[1] *College of Information and Telecommunication, Harbin Engineering University, Harbin 150001, China*
[2] *Department of Electronic and Electrical Engineering, Huaiyin Institute of Technology, Huai'an 223001, China*

Correspondence should be addressed to Zujun Ding; dzj_king@263.net

Received 13 September 2013; Accepted 15 October 2013

Academic Editor: Zhiguang Feng

A new method of transformer fault diagnosis based on relevance vector machine (RVM) is proposed. Bayesian estimation is applied to support vector machine (SVM) in the novel algorithm, which made fault diagnosis system work more effectively. In the paper, the analysis model is presented that the solutions of RVM have the feature of sparsity and RVM can obtain global solutions under finite samples. The process of transformer fault diagnosis for four working statuses is given in experiments and simulations. The results validated that this method has obvious advantages of diagnosis time and accuracy compared with backpropagation (BP) neural networks and general SVM methods.

1. Introduction

Power transformer is one of the key equipment for electric power transmission and distribution, which is a widely distributed, complex, and expensive equipment in the power system. And its safety situation plays a great effect on stability and security level of power system. Therefore, it is of great realistic significance to study the fault diagnosis technology and raise the level of maintenance of power transformers. Dissolved gas analysis (DGA) [1, 2], which provides operation information by detection of certain gases generated in an oil-filled transformer, is the method widely adopted by the utilities. The concentrations of the dissolved gases, their generation rates, ratio of respective gases, or total combustible gases in the oil are the attributes used in the DGA method to interpret a malfunction. Accuracy and reliability of the DGA data are influenced by many factors, so the DGA three-ratio method and its improved ratio methods by classical IEC [3] are considered that limitations are obvious, such that the ratio crosses the coding boundary or codes change sharply [3, 4]. And it cannot offer completely objective, accurate diagnosis for all the faults, such as the low diagnostic accuracy for overheating fault. With the development of artificial intelligence, some solutions [5, 6] based on neural networks are applied to power transformer fault diagnosis process. Though some improved results in faults diagnosis can be obtained, this kind of methods has some inherent disadvantages in application, such as local optimization and danger of overfitting [7, 8]. Support vector machine (SVM) overcomes the drawbacks of neural networks in aspects of convergence and real-time application [9, 10]. In recent years, SVM methods have been applied to fault diagnosis and identification of power transformers [11–13]. However, the input characteristic information during the process of fault diagnosis is large in order that SVM methods take heavy computation to approximate the optimal solution and spend much time in parameter searching [14, 15]. So they are difficult in real-time monitoring and power transformer fault diagnosis.

According to practical situations that there are many uncertainties in the running of transformers and there are finite samples during fault diagnosis process, relevance vector machine is introduced to fault detection and identification of power transformers. RVM, which applies Bayesian estimation model to SVM algorithms [16, 17], can decrease hyperparameters in diagnosis algorithms and bring good adaptive ability in kernel function and model parameters chosen. RVM is a machine learning methodology based on sparse Bayesian learning theory proposed by Tipping in 2000. It absorbs the advantages of wonderful generalization and precision from SVM; meanwhile, it overcomes some inherent

limitations of SVM and possesses advantageous features such as high degree of sparsity, fewer kernel functions, and low computation load. Particularly, the RVM classification can provide posterior probabilities for class memberships, which is suitable to analyse indeterminate problem in power transformer fault diagnosis. By dissolved gas analysis of power transformer oil, fault diagnosis models are established based on RVM in the paper. Through fault diagnosis for several kinds of power transformers, the proposed algorithm is validated to be better than BP neural networks and general SVM methods in the aspects of finite sample size, diagnosing speed, and diagnosing accuracy. It provides a new way of thinking for resolving the transformer fault diagnosis problem in real time. In the future, the research of transformer diagnosis faults based on RVM is real-time implementation for power transformer systems. Recently, data-driven fault diagnosis methods become more popular in many industry sectors [18–21]. So a combination of the proposed method and data-driven methods is the future work to realize large-scale real-time implementation in fault diagnosis of power transformers.

The paper is organized as follows. In the next section, we introduce RVM model of fault diagnosis. Diagnosis process for power transformers is extended in Section 3, which includes fault information preprocessing, diagnosis model training, and fault identification for power transformers. In Section 4, we give the experiment results in application and offer some benchmark comparison with least squares support vector machine (LS-SVM) and BP neutral networks before summarising in Section 5.

2. Analysis of RVM Model for Faults Diagnosis

RVM based on Bayesian learning framework introduces Bayesian theory of Gaussian process in SVM. The results of inference are shown in the form of probability density, and it can be written as

$$y(x) = \sum_{j=1}^{n} h_j \phi_j(x) + h_0, \tag{1}$$

where $\phi_j(x)$ is a nonlinear kernel function and h_j is the weight of the model. For avoiding overfitting of traditional SVM, based on Bayesian framework [22], maximum likelihood method is applied to training of the model weight. RVM defines the prior probability distribution as follows:

$$p\left(h_j \mid a_j\right) = \left(\frac{a_j}{2\pi}\right)^{1/2} \exp\left(-\frac{1}{2} a_j h_j^2\right), \tag{2}$$

where a_j is hyperparameter of the prior distribution. Assuming that input training sample set is $\{x_j, k_j\}_{j=1}^{N}$, target value k_j is independent, and input noise is Gaussian distribution with variance σ^2, the maximum likelihood function of training sampling set correspondingly can be expressed as

$$p\left(\mathbf{k} \mid \mathbf{h}, \sigma^2\right) = \left(2\pi\sigma^2\right)^{-N/2} \exp\left(-\frac{1}{2\sigma^2}\|\mathbf{k} - \mathbf{\Phi h}\|^2\right), \tag{3}$$

where $\mathbf{k} = [k_1, \ldots, k_N]^{\mathbf{T}}$, $\mathbf{h} = [h_1, \ldots, h_N]^{\mathbf{T}}$, and $\mathbf{\Phi} = [1, \Phi_1(x_j), \ldots, \Phi_n(x_j)]^{\mathbf{T}}$ is the response of all kernel functions with input x_j. The posterior distribution of the weight value conditioned on the data is given by combining the likelihood function (3) and the prior probability distribution (2) within Bayesian rule:

$$p\left(\mathbf{h} \mid \mathbf{k}, \mathbf{a}, \sigma^2\right) = \frac{p\left(\mathbf{k} \mid \mathbf{h}, \sigma^2\right) p\left(\mathbf{h} \mid \mathbf{a}\right)}{p\left(\mathbf{k} \mid \mathbf{a}, \sigma^2\right)}, \tag{4}$$

where $\mathbf{a} = [a_1, \ldots, a_n]^{\mathrm{T}}$ denotes the vector of hyperparameters. And the posterior probability distribution over the weights is multivariate Gaussian distribution:

$$p\left(\mathbf{h} \mid \mathbf{k}, \mathbf{a}, \sigma^2\right) \sim N\left(\boldsymbol{\mu}, \mathbf{\Sigma}\right), \tag{5}$$

where $\mathbf{\Sigma} = (\sigma^{-2}\mathbf{\Phi}^{\mathbf{T}}\mathbf{\Phi} + \mathbf{A})^{-1}$ is the posterior covariance of the multivariate Gaussian distribution, $\mathbf{A}$ is defined as diagonal matrix with the elements $(a_1, \ldots, a_n)$, and $\boldsymbol{\mu} = \sigma^{-2}\mathbf{\Sigma}\mathbf{\Phi}^{\mathrm{T}}$ is the mean of the multivariate Gaussian distribution. Integrating the distribution with respect to weight value, the likelihood distribution of training value can be given by

$$p\left(h_j \mid k_j, a_j, \sigma^2\right) = \int p\left(k_j \mid h_j, \sigma^2\right) p\left(h_j \mid a_j\right) \mathrm{d}h_j. \tag{6}$$

Marginalize (6); marginal likelihood distribution of hyperparameters can be written as

$$p\left(\mathbf{k} \mid \mathbf{a}, \sigma^2\right) \sim N\left(\mathbf{0}, \mathbf{C}\right), \tag{7}$$

where $\mathbf{C} = \sigma^2\mathbf{I} + \mathbf{\Phi}\mathbf{A}^{-1}\mathbf{\Phi}^{\mathbf{T}}$. Estimated values of weights in RVM method are given by the means of the posterior probability distribution. Maximum posterior estimation of weights depended on hyperparameter $\mathbf{a}$ and noise variance σ^2, and estimated values $\overline{\mathbf{a}}$ and $\overline{\sigma}^2$ can be computed by the maximum marginal likelihood distribution. Uncertainty of diagnosis model prediction can be represented by the uncertainty of optimum weight, which is shown in the posterior distribution. If input $\mathbf{x}^*$ is given, the corresponding probability distribution of output can be expressed as

$$\begin{aligned} &p\left(k_j \mid x_j^*, \overline{a}_j, \overline{\sigma}^2\right) \\ &\quad = \int p\left(k_j \mid x_j^*, h_j, \overline{\sigma}^2\right) p\left(h_j \mid k_j, \overline{a}_j, \overline{\sigma}^2\right) \mathrm{d}k_j, \end{aligned} \tag{8}$$

and this probability distribution is Gaussian distribution:

$$p\left(\mathbf{k}^* \mid \mathbf{x}^*, \overline{\mathbf{a}}, \overline{\sigma}^2\right) \sim N\left(\mathbf{y}^*, \sigma^{2*}\right). \tag{9}$$

In (9), the predict mean and variance are, respectively,

$$\begin{aligned} \mathbf{y}^* &= \boldsymbol{\mu}^{\mathrm{T}}\mathbf{\Phi}\left(x^*\right), \\ \sigma^{2*} &= \overline{\sigma}^2 + \mathbf{\Phi}^{\mathbf{T}}\left(x^*\right)\mathbf{\Sigma}\mathbf{\Phi}\left(x^*\right). \end{aligned} \tag{10}$$

Using Bayesian theory to compute parameters of fault diagnosis model based on RVM, diagnosis parameters choice can be optimized and application range of the faults diagnosis can be extended.

3. Diagnosis Process of the Transformer Based on RVM

Internal faults of transformers are classified into heat fault and electrical fault. In this paper, RVM method was applied to diagnose four types of working situations in power transformers, which include high energy discharge, low energy discharge, overheating, and normal condition operation. After the following three steps: characteristic information extraction by DGA, diagnosis model training, and faults recognition, the fault of transformer can be identified accurately.

3.1. Fault Information Preprocessing. Through DGA, concentrations of dissolved gases H_2 (hydrogen), CH_4 (methane), C_2H_6 (ethane), C_2H_4 (ethylene), and C_2H_2 (acetylene) could be obtained. The information of concentration of the five dissolved gases can be used to verify the four fault types stated above. So the ratio of each gas can be computed firstly by the following method:

$$x^k = \frac{c^k}{\max_{i=1}^{5}(c^i)}, \tag{11}$$

where $k = 1, 2, \ldots, 5$ is the index of each gas. c^k is the concentration of gas in the unit ppm. Then, we can obtain special character information by computing the maximum concentration of the gas as $x^6 = \log_{10}(\max_{k=1}^{5}(x^k))$, which is used for crosswise comparisons for all groups of test data. The six characteristics of data construct a six-dimension vector $\mathbf{x} = [x^1, x^2, x^3, x^4, x^5]^T$. This fault character information vector can be used to determine the working condition of power transformer: high energy discharge, low energy discharge, overheating, or normal condition.

3.2. Diagnosis Model Training. After faults feature extraction, it is necessary for fault diagnosis that RVM classifiers are trained to identify four possible states: high energy discharge, low energy discharge, overheating, and normal condition. So three diagnosis RVMs should have been set up and trained by all training samples. Each RVM corresponds to one of the fault states in power transformers. Training samples are sent into RVMs for training and identification. The output is assigned to one if the data of identification result is larger than zero. On the contrary, the output is zero if the data is less than zero. Firstly, the RMV1 is trained to overheating identification by the training sample set. Output of RVM1 for overheating samples is set to one, and the output for other fault states remains zero. Secondly, the RVM2 is trained to separate high energy discharge from low energy discharge. The output of RVM2 is set to one when the input is a high energy discharge sample; otherwise output of RVM2 is zero. Finally, RVM3 for low energy discharge is trained. In the same way, the output for low energy discharge samples is set to one; otherwise output is zero. Thus, three RVMs could be obtained to realize binary classification to all the samples for faults diagnosis. In the process, the kernel functions implicated in the three RVMs are all Gaussian radial basis functions. The flowchart of diagnosis model training was shown in Figure 1.

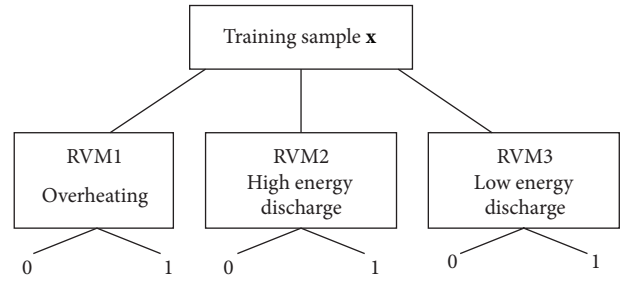

Figure 1: The flowchart of diagnosis model training.

3.3. Fault Identification of Power Transformers. After features extraction of DGA in Section 3.1, the test data with character information are considered as identification samples, which would be input to the RVMs established for faults diagnosis. The three RVMs are used to recognize the fault types. If the output of RVM1 is larger than zero, we could consider that the fault of power transformer is overheating. If the output of RVM1 is less than zero, the sample continues to be sent to RVM2 and RVM3 for recognizing the faults of high energy discharge and low energy discharge in the same way. If the outputs of the three RVMs are all less than zero, the power transformer would be judged in normal working condition. Thus, RVM classifier identifies the four states of transformers after three times of identification process.

4. Experimental Results and Analysis of Faults Diagnosis of Power Transformers

Sixty groups of historical data about gas concentrations in certain power transformer were collected as the training set. The data corresponding to actual fault conditions were known. In the training dataset, there were four working states of the power transformer, which were overheating, high energy discharge, low energy discharge, and normal operation. Each state had 15 samples. Three RVMs (RVM1, RVM2, and RVM3) were constructed by the samples related to each state in the training dataset, separately. And other 10 groups of samples of the running transformer were considered as the test data set; the test samples included 3 overheating samples, 2 high power discharge samples, 3 low power discharge samples, and 2 normal operation samples; see Table 1.

The 10 groups of test data were sent to the three RVMs for faults diagnosis after the preprocessing mentioned above. The output of test data through RVM1 was [4.4361, 0.9235, 3.4215, −8.4312, −7.6557, −9.5236, −4.1404, −2.9146, −6.3237, −8.3624]; then, we could modify the output result of RVM1 as [1, 1, 1, 0, 0, 0, 0, 0, 0, 0], so the first three samples in Table 1 were adjudged as overheating faults by RMV1. In the same way, the test samples were sent to RVM2 for the identification of high energy discharge fault. The output of RVM2 was [−3.7431, −17.2762, −4.0026, 12.7902, 9.2563, −12.5385, −3.0571, −6.7612, −37.6247, −26.6382]. So the result of RVM2 was represented as [0, 0, 0, 1, 1, 0, 0, 0, 0, 0]; samples numbers 4 and 5 were recognized as high energy discharge fault. Finally, the test samples were sent to RVM3, and the outputs were [−10.9261, −0.7481, −7,6892, −3.6297, −2.6589, 1.2792,

Table 1: Sample group of dissolved gases.

No.	Fault type	Data of gas content (unit: ppm)				
		H_2	CH_4	C_2H_6	C_2H_4	C_2H_2
1	Overheating	74	523	142	1200	6
2	Overheating	220	382	82	1019	17
3	Overheating	116	352	90	465	5
4	High energy discharge	295	51	12	117	124
5	High energy discharge	449	83	12	104	176
6	Low energy discharge	566	92	35	46	2
7	Low energy discharge	152	54	32	20	3
8	Low energy discharge	172	78	36	28	6
9	No fault	5	3	2	6	6
10	No fault	6	7	6	13	6

Table 2: Diagnosis comparison of the algorithms.

Diagnosis model	Target error	Training time (s)	Test times (s)	Accuracy diagnosis
BP neutral net	0.01	116.47	0.25	93%
LS-SVM	0.01	1.25	0.107	96%
Proposed RVM	0.01	0.714	0.05	100%

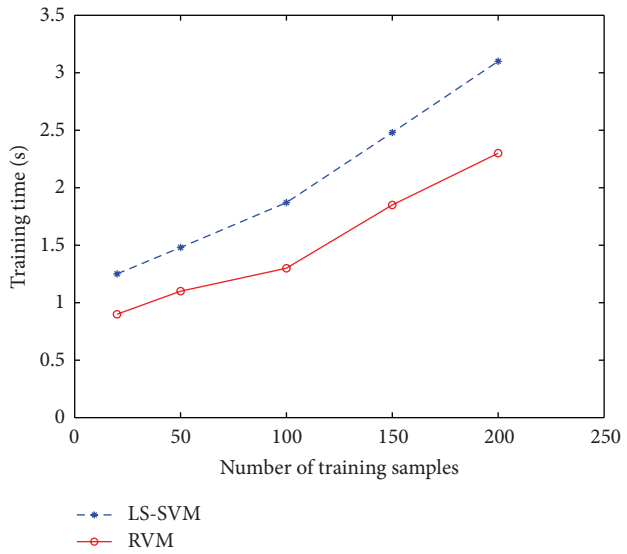

Figure 2: Training time via different numbers of training samples.

3.4769, 4.2915, −6.4163, −5.4794]; the result through RVM3 was written as [0, 0, 0, 0, 0, 1, 1, 1, 0, 0]; we could obtain the decision that low energy discharge happened in samples of numbers 6, 7, and 8. From the whole process of fault diagnosis, we found that the output results of three RVMs were all zeros for the samples numbers 9 and 10, which means that the transformer was in normal condition. From the results of the fault diagnosis by the proposed RVM method in experiments, we concluded that it had the ability for fault detection and identification of power transformers and the identification rate was high.

For evaluation of the proposed fault diagnosis model, we compared three learning models: the proposed RVM, BP neutral network and LS-SVM. There were 6 six input nodes, 44 hidden nodes, and 4 output nodes in BP neutral network, in which target error is 0.01. For LS-SVM, target error is 0.01 with the Gaussian radial basis function as the kernel function. Test parameters included training time, test time, and diagnosis accuracy of three methods in the condition of the same training samples. The test samples were 50 groups of historical data samples of the power transformer. The performance of testing was shown in Table 2. It is shown in Table 2 that the faults diagnosis models of LS-SVM and proposed RVM algorithms are superior to those of BP neutral network in the aspects of training time, test time, and diagnosis accuracy under the same target error. Furthermore, because of application of Bayesian probability model in the proposed RVM algorithm, the number of hyperparameters decreases. So test time and diagnosis accuracy of the proposed algorithm are better compared to those of conventional LS-SVM algorithm. It is more suitable to practical application. Next, the performance of training time, diagnose accuracy, and test time of LS-SVM and the proposed RVM are illuminated. Figures 2 and 3 show the performance of training time and diagnose accuracy in different numbers of training samples. The range of training samples number is from 25 to 200. From Figure 2, we can find that training time obviously become, longer for both of fault diagnosis models with the training sample number increasing. However, training time of the proposed optimum RVM model is much less than that of LS-SVM. In Figure 3, the testing diagnosis accuracy reaches 100% for the proposed method when the number of training samples is larger than 25. The proposed method is also superior to LS-SVM in test time see (Figure 4), in which the training sample number is 200. All the performance described above proves that the proposed RVM algorithm has advantages in the aspects of global optimization and sparsity of the solution. It has a wider range of adaptability than that of conventional SVM model.

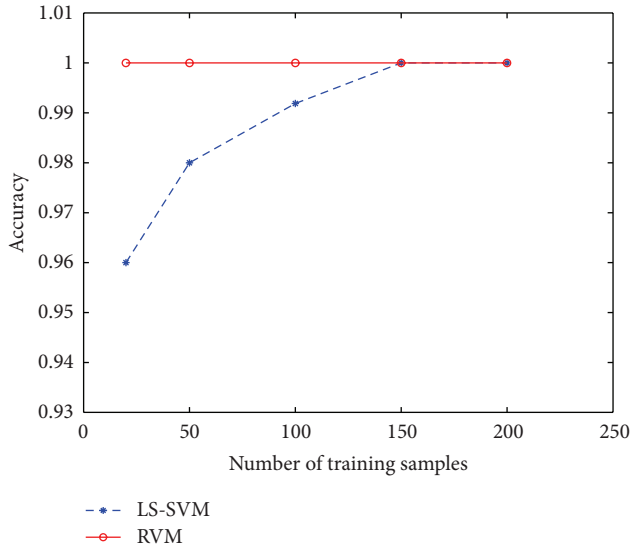

Figure 3: Diagnosis accuracy via different numbers of training samples.

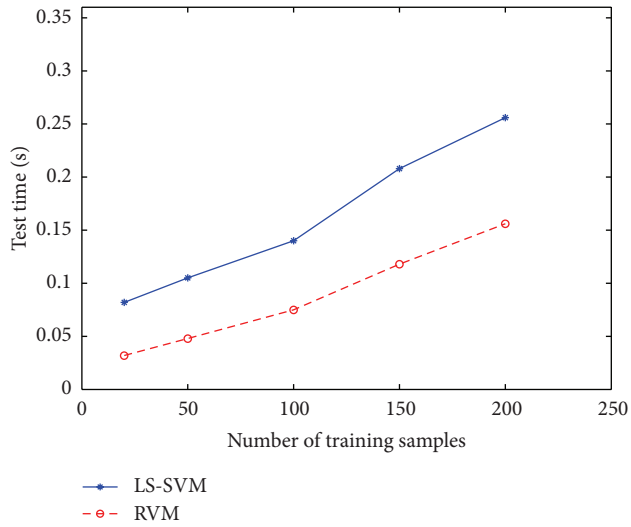

Figure 4: Test time via different numbers of test samples.

From the results of the faults diagnosis model by the RVM algorithm in the experiments, we can conclude that the proposed method can output the probability of working states of power transformers, which supply more useful information for transformer overhaul. The method is superior to conventional diagnosis methods in diagnosis accuracy, response time, and sample number.

5. Conclusion

The novel fault diagnosis model based on RVM for power transformers is proposed in the paper. Bayesian learning framework applied in the model makes hyperparameters decrease and improves the sparsity of the solutions. It overcomes the limitations of some traditional algorithms and enhances applicability of fault diagnosis. The proposed method uses three RVMs to identify the faults of power transforms and brings about good results. The probability statistics of characteristics of the diagnosis model provide the advantages of small sampling, high sparsity, and low computation load. Compared to BP neutral network and LS-SVM, the test time of fault diagnosis is shorter and accuracy of fault diagnosis is much higher. The results of experiments and simulations validate that this diagnosis method is suitable for real-time surveillance and identification of power transformers fault. The study of this issue is quite significant for transformers fault diagnosis application. The future work is to realize real-time implementation in power transformer systems by the proposed method.

Acknowledgments

This research has been supported by the National Natural Science Foundation of China (no. 61201410) and the Natural Science Fund of Jiangsu Province (11KJB470002). The authors are grateful to their colleagues from College of Information and Telecommunication in Harbin Engineering University for providing helpful comments.

References

[1] R. Zhang, R. Guo, H. Li, and Z. Yan, "Feature selection of DGA data based on transformer fault classification," *High Voltage Engineering*, vol. 4, no. 31, pp. 32–33, 2005.

[2] S. Singh and M. Bandyopadhyay, "Dissolved gas analysis technique for incipient fault diagnosis in power transformers: a bibliographic survey," *IEEE Electrical Insulation Magazine*, vol. 26, no. 6, pp. 41–46, 2010.

[3] M. Duval and A. dePablo, "Interpretation of gas-in-oil analysis using new IEC publication 60599 and IEC TC 10 databases," *IEEE Electrical Insulation Magazine*, vol. 17, no. 2, pp. 31–41, 2001.

[4] "IEEE guide for the interpretation of gases generated in oil-immersed transformers," IEEE Standard C57.104-2008, 2009.

[5] M. Hui, C. Ekanayake, and T. K. Saha, "Power transformer fault diagnosis under measurement originated uncertainties," *IEEE Transactions on Dielectrics and Electrical Insulation*, vol. 19, no. 6, 1982.

[6] A. R. Hooshmand, M. Parastegari, and Z. Forghani, "Adaptive neuro-fuzzy inference system approach for simultaneous diagnosis of the type and location of faults in power transformers," *IEEE Electrical Insulation Magazine*, vol. 28, no. 5, pp. 32–42, 2012.

[7] B. Li, G. Godi, and M.-Y. Chow, "Detection of common motor bearing faults using frequency domain vibration signals and a neural network based approach," in *Proceedings of the American Control Conference*, pp. 2032–2036, June 1998.

[8] S. Yin, *Data-Driven Design of Fault Diagnosis Systems*, Fortschritt-Berichte, Dsseldorf, Germany, 2012.

[9] X. G. Zhang, "Introduction to statistical learning theory and support vector machines," *Acta Automatica Sinica*, vol. 26, no. 1, pp. 32–42, 2000.

[10] S. Souahlia, K. Bacha, and A. Chaari, "SVM-based decision for power transformers fault diagnosis using Rogers and Doernenburg ratios DGA," in *Proceedings of the 10th IEEE International Multi-Conference on Systems, Signals & Devices (SSD '13)*, vol. 1, pp. 1–6, Hammamet, Tunisia, March 2013.

[11] V. Miranda, A. R. G. Castro, and S. Lima, "Diagnosing Faults in power transformers with autoassociative neural networks and mean shift," *IEEE Transactions on Power Delivery*, vol. 27, no. 3, pp. 1350–1357, 2012.

[12] D.-H. Liu, J.-P. Bian, and X.-Y. Sun, "The study of fault diagnosis model of DGA for oil-immersed transformer based on fuzzy means Kernel clustering and SVM multi-class object simplified structure," in *Proceedings of the 7th International Conference on Machine Learning and Cybernetics (ICMLC '08)*, pp. 1505–1509, July 2008.

[13] L. V. Ganyun, C. Haozhong, Z. Haibao, and D. Lixin, "Fault diagnosis of power transformer based on multi-layer SVM classifier," *Electric Power Systems Research*, vol. 74, no. 1, pp. 1–7, 2005.

[14] V. N. Vapnik, *The Nature of Statistical Learning Theory*, Springer, New York, NY, USA, 1995.

[15] S. Wen-gang, "Support vector machines based approach for fault diagnosis of valves in reciprocating pumps," *Journal of Mechanical Strength*, vol. 24, no. 3, pp. 362–364, 2002.

[16] M. E. Tipping, "Sparse bayesian learning and the relevance vector machine," *Journal of Machine Learning Research*, vol. 1, no. 3, pp. 211–244, 2001.

[17] M. E. Tipping, *The Relevance Vector Machine*, vol. 12 of *Advances in Neural Information Proceeding Systems*, MIT Press, Cambridge, Mass, USA, 2000.

[18] S. Yin, X. Yang, and H. R. Karimi, "Data-driven adaptive observer for fault diagnosis," *Mathematical Problems in Engineering*, vol. 2012, Article ID 832836, 21 pages, 2012.

[19] S. Yin, S. X. Ding, A. H. A. Sari, and H. Hao, "Data-driven monitoring for stochastic systems and its application on batch process," *International Journal of Systems Science*, vol. 44, no. 7, pp. 1366–1376, 2013.

[20] S. Yin, S. Ding, A. Haghani, H. Hao, and P. Zhang, "A comparison study of basic data-driven fault diagnosis and process monitoring methods on the benchmark Tennessee Eastman process," *Journal of Process Control*, vol. 22, no. 9, pp. 1567–1581, 2012.

[21] S. Yin, S. Ding, and H. Luo, "Real-time implementation of fault tolerant control system with performance optimization," *IEEE Transactions on Industrial Electronics*, vol. 61, no. 5, pp. 2402–2411, 2013.

[22] D. J. MacKay, "Bayesian interpolation," *Neural Compution*, vol. 4, no. 3, pp. 415–447, 1992.

Hindawi Publishing Corporation
Mathematical Problems in Engineering
Volume 2013, Article ID 762385, 8 pages
http://dx.doi.org/10.1155/2013/762385

Research Article

Fault Tolerant Control for Civil Structures Based on LMI Approach

Chunxu Qu, Linsheng Huo, and Hongnan Li

Faculty of Infrastructure Engineering, Dalian University of Technology, Dalian 116024, China

Correspondence should be addressed to Linsheng Huo; lshuo@dlut.edu.cn

Received 18 July 2013; Revised 22 September 2013; Accepted 16 October 2013

Academic Editor: Bo-Chao Zheng

The control system may lose the performance to suppress the structural vibration due to the faults in sensors or actuators. This paper designs the filter to perform the fault detection and isolation (FDI) and then reforms the control strategy to achieve the fault tolerant control (FTC). The dynamic equation of the structure with active mass damper (AMD) is first formulated. Then, an estimated system is built to transform the FDI filter design problem to the static gain optimization problem. The gain is designed to minimize the gap between the estimated system and the practical system, which can be calculated by linear matrix inequality (LMI) approach. The FDI filter is finally used to isolate the sensor faults and reform the FTC strategy. The efficiency of FDI and FTC is validated by the numerical simulation of a three-story structure with AMD system with the consideration of sensor faults. The results show that the proposed FDI filter can detect the sensor faults and FTC controller can effectively tolerate the faults and suppress the structural vibration.

1. Introduction

The structural control system is commonly classified into four types: passive, active, hybrid, and semiactive control [1–9]. An active control system contains sensors, controllers, and actuators. Sensors can measure the structural vibration data that is sent to the controllers. The controllers compute the desired force according to the control strategy and sensor data and then command the control devices to generate control force for vibration reduction. Active control can achieve many control decisions. Therefore, active control is an efficient method to resist external excitation, such as earthquake and strong wind. Control strategy is the key of active control, which is widely studied in recent decades [10–16]. However, there are some controller design problems in civil engineering due to the characteristics of the civil structures, such as large number of degrees of freedom and uncertainties of system parameters, in which many researchers are interested [17–21].

In practical engineering, sensors and actuators may be destroyed due to the lack of maintenance or extreme loading such as strong wind or intense earthquake. These faulty sensors and control devices may degrade the performance of vibration suppressing and even enlarge the structural response. Therefore, the robustness is important for the control system. Fault tolerant control (FTC) technology is an efficient method to promote the system reliability. FTC can tolerate faults caused by the components of control system, such as sensors and actuators, and then guarantee the system performance. FTC can be divided into two categories, passive FTC and active FTC. The difference between them exists if the faults are identified online. Passive FTC cannot detect faults online and cannot be recognized as traditional robust control [22]. The faults in passive FTC are assumed as system model uncertainties. Accordingly, passive FTC has limited tolerance ability because its robustness is only for the estimated faults, and the faults cannot be detected online. On the other hand, active FTC can detect faults online, which is called the fault detection and isolation (FDI) technology, and suppress excessive structural response.

This paper designs a fault detection and isolation (FDI) filter and reforms a fault tolerant controller (FTC) through LMI approach considering sensor faults in civil building structures with active mass damper (AMD). An estimated system is built to facilitate the design of FDI and FTC. In order to make the difference between the estimated and the practical system smaller, an FDI filter is designed, which

can minimize the H∞ norm of the transfer function from all the inputs to the residual of the estimated and practical state. According to the bounded real lemma, solving the FDI filter problem is transformed to solve a matrix inequality, which can be deformed to a linear matrix inequality (LMI) by variable substitution method [23]. LMI problem is convex and can be solved easily. After the FDI filtering, the new data is used to isolate the sensor faults and transmitted to the previous designed controllers so that the control strategy is reformed. The process executes the function of fault tolerant control (FTC). Finally, the numerical example of a three-story building is provided to validate the performance of FDI and FTC.

2. Formulation of AMD Control System

Considering n degrees of freedom civil structural system which is subjected to a unidirectional earthquake with $\ddot{q}_g(t)$ acceleration, the dynamic equation is described as follows:

$$\mathbf{M}\ddot{\mathbf{q}}(t) + \mathbf{C}\dot{\mathbf{q}}(t) + \mathbf{K}\mathbf{q}(t) = \mathbf{T}_g\ddot{q}_g(t) + \mathbf{T}_u\mathbf{u}(t), \quad (1)$$

where $\mathbf{M}$, $\mathbf{C}$, and $\mathbf{K} \in \mathbb{R}^{n\times n}$ are, respectively, mass, damping, and stiffness matrix; $\mathbf{q}(t)$, $\dot{\mathbf{q}}(t)$ and $\ddot{\mathbf{q}}(t) \in \mathbb{R}^{n\times 1}$ are the relative displacement, relative velocity, and relative acceleration vector, respectively; $\mathbf{u}(t) \in \mathbb{R}^{m_u\times 1}$ is the control force vector generated by actuators and $\mathbf{T}_u \in \mathbb{R}^{n\times m_u}$ and $\mathbf{T}_g \in \mathbb{R}^{n\times 1}$ are the location matrices of the control force and earthquake excitation, respectively.

For a structure with an AMD on the top floor as shown in Figure 1, the control force is exerted only on the top floor. The control force location matrix $\mathbf{T}_u$ and earthquake excitation location matrix $\mathbf{T}_g$ are represented as

$$\mathbf{T}_u = \left[\underbrace{0, 0 \ldots, 0,}_{n-1} \ 1\right]^T_{1\times n}, \qquad \mathbf{T}_g = -\mathbf{M}\{\mathbf{1}\}_{n\times 1}. \quad (2)$$

The dynamic equation of the AMD system can be formulated as

$$m_a\left(\ddot{q}_a(t) + \ddot{q}_g(t)\right) + c_a\left(\dot{q}_a(t) - \dot{q}_n(t)\right) + k_a\left(q_a(t) - q_n(t)\right) = F_a(t), \quad (3)$$

where m_a, c_a, and $k_a \in \mathbb{R}^{1\times 1}$ are, respectively, mass, damping, and stiffness of AMD system and $q_a(t)$, $\dot{q}_a(t)$, and $\ddot{q}_a(t) \in \mathbb{R}^{1\times 1}$ are the relative displacement, relative velocity, and relative acceleration of AMD system. $q_n(t)$ and $\dot{q}_n(t) \in \mathbb{R}^{1\times 1}$ are relative displacement and relative velocity of the nth floor, which is also the top floor and can be represented as

$$q_n(t) = \mathbf{T}_n\mathbf{q}(t), \qquad \dot{q}_n(t) = \mathbf{T}_n\dot{\mathbf{q}}(t), \qquad \mathbf{T}_n = \left[\underbrace{0, 0 \ldots, 0,}_{n-1} \ 1\right]_{1\times n}. \quad (4)$$

$F_a(t) \in \mathbb{R}^{1\times 1}$ is the force between structural system and AMD mass. The motion equation of the structural system with AMD can be derived as

$$\mathbf{M}_s\ddot{\mathbf{q}}_s(t) + \mathbf{C}_s\dot{\mathbf{q}}_s(t) + \mathbf{K}_s\mathbf{q}_s(t) = \mathbf{T}_{gs}\ddot{q}_g(t) + \mathbf{T}_{us}F_a(t). \quad (5)$$

The matrices $\mathbf{M}_s$, $\mathbf{C}_s$, $\mathbf{K}_s$, $\mathbf{q}_s$, $\mathbf{T}_{gs}$, and $\mathbf{T}_u$ are denoted as

$$\mathbf{M}_s = \begin{bmatrix}\mathbf{M} & \\ & m_a\end{bmatrix} = \begin{bmatrix} m_1 & & & \\ & \ddots & & \\ & & m_n & \\ & & & m_a\end{bmatrix}_{(n+1)\times(n+1)},$$

$$\mathbf{q}_s = \begin{bmatrix}\mathbf{q} \\ q_a\end{bmatrix} = \begin{bmatrix} q_1 \\ \vdots \\ q_n \\ q_a\end{bmatrix}_{(n+1)\times 1},$$

$$\mathbf{T}_{gs} = \begin{bmatrix}\mathbf{T}_g \\ -m_a\end{bmatrix} = -\mathbf{M}_s\begin{Bmatrix}1 \\ \vdots \\ 1 \\ 1\end{Bmatrix}_{(n+1)\times 1},$$

$$\mathbf{T}_u = \begin{bmatrix}-\mathbf{T}_u \\ 1\end{bmatrix} = \begin{Bmatrix}0 \\ \vdots \\ 0 \\ -1 \\ 1\end{Bmatrix}_{(n+1)\times 1}, \quad (6)$$

$$\mathbf{K}_s = \begin{bmatrix}\mathbf{K} + \mathbf{T}_u k_a \mathbf{T}_n & -\mathbf{T}_u k_a \\ -k_a\mathbf{T}_n & k_a\end{bmatrix} = \begin{bmatrix} k_1 + k_2 & -k_2 & 0 & 0 \\ -k_2 & \ddots & -k_n & 0 \\ 0 & -k_n & k_n + k_a & -k_a \\ 0 & 0 & -k_a & k_a\end{bmatrix}_{(n+1)\times(n+1)},$$

$$\mathbf{C}_s = \begin{bmatrix}\mathbf{C} + \mathbf{T}_u c_a \mathbf{T}_n & -\mathbf{T}_u c_a \\ -c_a\mathbf{T}_n & c_a\end{bmatrix} = \begin{bmatrix} c_1 + c_2 & -c_2 & 0 & 0 \\ -c_2 & \ddots & -c_n & 0 \\ 0 & -c_n & c_n + c_a & -c_a \\ 0 & 0 & -c_a & c_a\end{bmatrix}_{(n+1)\times(n+1)},$$

where m_i, c_i, and k_i are the ith floor mass, damping, and stiffness. Equation (5) can be represented in state space as follows:

$$\dot{\mathbf{X}}_s(\mathbf{t}) = \mathbf{A}_s\mathbf{X}_s(t) + \mathbf{B}_{1s}\ddot{q}_g(t) + \mathbf{B}_{2s}F_a(t), \quad (7)$$

where $\mathbf{A}_s \in \mathbb{R}^{2(n+1)\times 2(n+1)}$, $\mathbf{B}_{1s} \in \mathbb{R}^{2(n+1)\times 1}$, and $\mathbf{B}_{2s} \in \mathbb{R}^{2(n+1)\times 1}$ are system matrix, excitation matrix, and control matrix, respectively.

One can see that

$$\mathbf{A}_s = \begin{bmatrix}[\mathbf{0}]_{(n+1)\times(n+1)} & [\mathbf{I}]_{(n+1)\times(n+1)} \\ -\mathbf{M}_s^{-1}\mathbf{K}_s & -\mathbf{M}_s^{-1}\mathbf{C}_s\end{bmatrix}, \qquad \mathbf{B}_{1s} = \begin{bmatrix}[\mathbf{0}]_{(n+1)\times 1} \\ \mathbf{M}_s^{-1}\mathbf{T}_{gs}\end{bmatrix}, \qquad \mathbf{B}_{2s} = \begin{bmatrix}[\mathbf{0}]_{(n+1)\times 1} \\ \mathbf{M}_s^{-1}\mathbf{T}_{us}\end{bmatrix}. \quad (8)$$

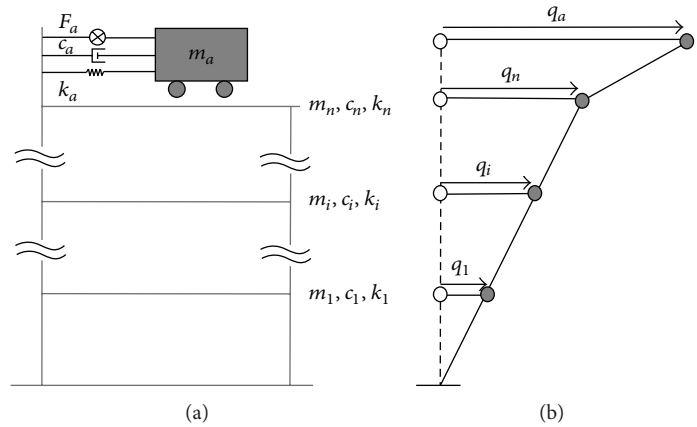

Figure 1: The model of AMD structure system.

$\mathbf{X}_s(t) = [\mathbf{q}_s(t); \dot{\mathbf{q}}_s(t)] \in \mathbb{R}^{2(n+1)\times 1}$ is the state vector, which contains relative displacement and relative velocity. This relative state vector can be transformed to another state vector which consists of interstory drift and interstory velocity as,

$$\mathbf{X}(t) = \left[q_1 \;\; q_2 - q_1 \;\; \cdots \;\; q_n - q_{n-1} \;\; q_a - q_n, \;\; \dot{q}_1 \;\; \dot{q}_2 - \dot{q}_1 \;\; \cdots \;\; \dot{q}_a - \dot{q}_n\right]^T \in \mathbb{R}^{2(n+1)\times 1}. \tag{9}$$

Define a transformation matrix $\mathbf{\Gamma} \in \mathbb{R}^{2(n+1)\times 2(n+1)}$ to obtain $\mathbf{X}(t)$ such that $\mathbf{X}(t) = \mathbf{\Gamma}\mathbf{X}_s(t)$. Substituting $\mathbf{X}_s(t) = \mathbf{\Gamma}^{-1}\mathbf{X}(t)$ into (7) and left-multiplying this equation with $\mathbf{\Gamma}$, the state equation expressed by $\mathbf{X}(t)$ becomes

$$\dot{\mathbf{X}}(t) = \mathbf{A}\mathbf{X}(t) + \mathbf{B}_1\ddot{q}_g(t) + \mathbf{B}_2 F_a(t), \tag{10}$$

where $\mathbf{A} = \mathbf{\Gamma}\mathbf{A}_s\mathbf{\Gamma}^{-1} \in \mathbb{R}^{2(n+1)\times 2(n+1)}$, and $\mathbf{B}_1 = \mathbf{\Gamma}\mathbf{B}_{1s} \in \mathbb{R}^{2(n+1)\times 1}$, $\mathbf{B}_2 = \mathbf{\Gamma}\mathbf{B}_{2s} \in \mathbb{R}^{2(n+1)\times 1}$, and $\mathbf{\Gamma}$ is shown as

$$\mathbf{\Gamma} = \begin{bmatrix} \mathbf{\Gamma}_s & [\mathbf{0}]_{(n+1)\times(n+1)} \\ [\mathbf{0}]_{(n+1)\times(n+1)} & \mathbf{\Gamma}_s \end{bmatrix},$$

$$\mathbf{\Gamma}_s = \begin{bmatrix} 1 & 0 & \cdots & \cdots & 0 \\ -1 & 1 & 0 & \cdots & 0 \\ 0 & \ddots & \ddots & & \vdots \\ \vdots & & \ddots & \ddots & 0 \\ 0 & \cdots & \cdots & -1 & 1 \end{bmatrix}_{(n+1)\times(n+1)}. \tag{11}$$

3. Fault Detection and Isolation and Fault Tolerant Control

A simple and efficient way to design a controller for this structural control system with AMD is to design the H∞ state feedback gain $\mathbf{G}_\infty \in \mathbb{R}^{1\times 2(n+1)}$ [24], such that

$$F_a(t) = \mathbf{G}_\infty \mathbf{X}(t). \tag{12}$$

However, when there are some faults in sensors or actuators, the performance of vibration suppressing may be degraded and even enlarge the structural response. So, it is necessary to detect and isolate faults such that the controller can tolerate the faults. This paper only considers the faults in sensors and designs a fault detection and isolation (FDI) filter. The designed FDI filter is intended to estimate structural system state, which can be used to reappear the structural sensor data with fewer faults. The difference between the measured output data and the estimated output data is the faults. The estimated output data can be used to isolate the faults transmitted to the designed H∞ state feedback gain $\mathbf{G}_\infty$. So, the controller strategy is reformed and can perform the fault tolerant control performance.

For the faults in sensors, the sensor data including faults can be represented as

$$\mathbf{y}_v(t) = \mathbf{C}_y\mathbf{X}(t) + \mathbf{v}(t), \tag{13}$$

where $\mathbf{v}(t) \in \mathbb{R}^{q\times 1}$ is the faults part in sensor data $\mathbf{y}_v(t) \in \mathbb{R}^{q\times 1}$ and $\mathbf{C}_y\mathbf{X}(t)$ is the real part of sensor data, which is the system real output. The faults can be recognized as the additional data into the real sensor data. Combined with (10), the following equation can be derived:

$$\begin{aligned} \dot{\mathbf{X}}(t) &= \mathbf{A}\mathbf{X}(t) + \mathbf{B}_1\ddot{q}_g(t) + \mathbf{B}_2 F_a(t), \\ \mathbf{y}_v(t) &= \mathbf{C}_y\mathbf{X}(t) + \mathbf{v}(t). \end{aligned} \tag{14}$$

The faults estimator is shown in Figure 2 and its state space formulation can be described as

$$\begin{aligned} \dot{\widehat{\mathbf{X}}}(t) &= \mathbf{A}\widehat{\mathbf{X}}(t) + \mathbf{B}_2 F_a(t) + \mathbf{r}(t), \\ \widehat{\mathbf{y}}(t) &= \mathbf{C}_y\widehat{\mathbf{X}}(t), \\ \mathbf{r}(t) &= \mathbf{K}\left(\widehat{\mathbf{y}}(t) - \mathbf{y}_v(t)\right), \end{aligned} \tag{15}$$

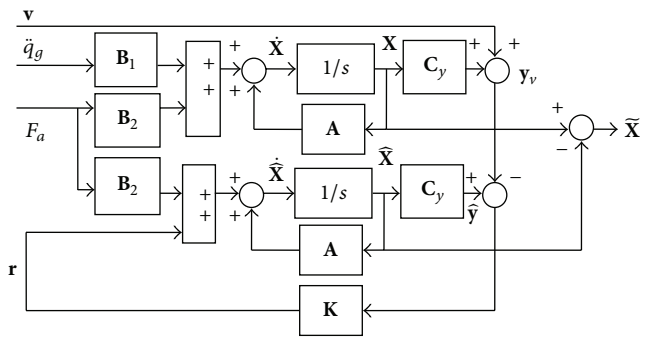

Figure 2: FDI diagram of AMD structure system.

where $\widehat{\mathbf{X}}(t) \in \mathbb{R}^{2(n+1)\times 1}$ is the estimated state for the structural state $\mathbf{X}(t)$, $\widehat{\mathbf{y}}(t) \in \mathbb{R}^{q\times 1}$ is the estimated measurement output for the real part of $\mathbf{y}_v(t) \in \mathbb{R}^{q\times 1}$, that is, $\mathbf{C}_y\mathbf{X}(t)$, $\mathbf{r}(t) \in \mathbb{R}^{2(n+1)\times 1}$ is the adjustment vector for estimated state vector, and $\mathbf{K} \in \mathbb{R}^{2(n+1)\times q}$ is the FDI filter to make the estimated state vector closed with structural system state vector. In this structural system with the sensor faults, the state is estimated so that the sensor data real part $\mathbf{C}_y\mathbf{X}(t)$ can be estimated as $\widehat{\mathbf{y}}(t) = \mathbf{C}_y\widehat{\mathbf{X}}(t)$. The faults in sensor data $\mathbf{y}_v(t) \in \mathbb{R}^{q\times 1}$ can be calculated by $\mathbf{y}_v(t) - \widehat{\mathbf{y}}(t)$ and then can be isolated by replacing $\mathbf{y}_v(t)$ with $\widehat{\mathbf{y}}(t)$. This is the fault detection and isolation (FDI). According to (14) and (15), the residue equation is obtained as follows:

$$\begin{aligned}\dot{\widetilde{\mathbf{X}}}(t) &= \widetilde{\mathbf{A}}\widetilde{\mathbf{X}}(t) + \widetilde{\mathbf{B}}\mathbf{w}(t),\\ \widetilde{\mathbf{Z}}(t) &= \widetilde{\mathbf{C}}\widetilde{\mathbf{X}}(t) + \widetilde{\mathbf{D}}\mathbf{w}(t).\end{aligned} \tag{16}$$

$\widetilde{\mathbf{A}}$, $\widetilde{\mathbf{B}}$, $\widetilde{\mathbf{C}}$, $\widetilde{\mathbf{D}}$, $\widetilde{\mathbf{X}}(t)$, $\widetilde{\mathbf{Z}}(t)$, and $\mathbf{w}(t)$ are defined as

$$\begin{aligned}\widetilde{\mathbf{A}} &= \mathbf{A} + \mathbf{K}\mathbf{C}_y \in \mathbb{R}^{2(n+1)\times 2(n+1)},\\ \widetilde{\mathbf{B}} &= \begin{bmatrix}\mathbf{B}_1 & \mathbf{K}\end{bmatrix} \in \mathbb{R}^{2(n+1)\times(q+1)},\\ \widetilde{\mathbf{C}} &= \mathbf{I} \in \mathbb{R}^{2(n+1)\times 2(n+1)},\\ \widetilde{\mathbf{D}} &= [\mathbf{0}]_{2(n+1)\times(q+1)} \in \mathbb{R}^{2(n+1)\times(q+1)},\end{aligned} \tag{17a}$$

$$\begin{aligned}\widetilde{\mathbf{X}}(t) &= \left(\mathbf{X}(t) - \widehat{\mathbf{X}}(t)\right) \in \mathbb{R}^{2(n+1)\times 1},\\ \widetilde{\mathbf{Z}}(t) &= \widetilde{\mathbf{X}}(t) \in \mathbb{R}^{2(n+1)\times 1},\\ \mathbf{w}(t) &= \left[\ddot{q}_g(t);\ \mathbf{v}(t)\right] \in \mathbb{R}^{(q+1)\times 1},\end{aligned} \tag{17b}$$

where $\widetilde{\mathbf{Z}}(t) = \widetilde{\mathbf{X}}(t) \in \mathbb{R}^{2(n+1)\times 1}$ is the output of the residue equation and $\widetilde{\mathbf{X}}(t)$ is the state of the residue equation.

In order to estimate the system state $\mathbf{X}(t)$ precisely, this paper designs the FDI filter $\mathbf{K}$ in (15) to minimize the H∞ norm of the transfer function from input $\mathbf{w}(t)$ to output $\widetilde{\mathbf{Z}}(t)$. This design can be recognized as H∞ optimization problem. It can be described as designing a static controller $\mathbf{K}$ to stabilize the system (16) such that

$$J = \left\|\mathbf{H}_{\mathbf{zw}}(s)\right\|_\infty = \sup_{\omega,\|\omega(t)\|_2\neq 0}\left(\frac{\left\|\widetilde{\mathbf{Z}}(t)\right\|_2}{\|\mathbf{w}(t)\|_2}\right) < \gamma, \tag{18}$$

where γ is a given scalar. According to the bounded real lemma [25], the following two statements are equivalent:

(1) H∞ norm of the system in (16) is less than γ, and $\widetilde{\mathbf{A}}$ is stable;

(2) There exists a symmetric positive definite matrix $\mathbf{\Phi} \in \mathbb{R}^{2(n+1)\times 2(n+1)}$ such that the following matrix inequality holds:

$$\begin{bmatrix}\widetilde{\mathbf{A}}^T\mathbf{\Phi} + \mathbf{\Phi}\widetilde{\mathbf{A}} & \mathbf{\Phi}\widetilde{\mathbf{B}} & \widetilde{\mathbf{C}}^T\\ \widetilde{\mathbf{B}}^T\mathbf{\Phi} & -\gamma\mathbf{I} & \widetilde{\mathbf{D}}^T\\ \widetilde{\mathbf{C}} & \widetilde{\mathbf{D}} & -\gamma\mathbf{I}\end{bmatrix} < \mathbf{0}. \tag{19}$$

Substituting (17b) into (19),

$$\begin{bmatrix}\left(\mathbf{A}+\mathbf{K}\mathbf{C}_y\right)^T\mathbf{\Phi} + \mathbf{\Phi}\left(\mathbf{A}+\mathbf{K}\mathbf{C}_y\right) & \mathbf{\Phi}[\mathbf{B}_1 \ \ K]_{2(n+1)\times(q+1)} & \mathbf{I}_{2(n+1)\times 2(n+1)}\\ [\mathbf{B}_1 \ \ \mathbf{K}]^T_{(q+1)\times 2(n+1)}\mathbf{\Phi} & -\gamma\mathbf{I}_{(q+1)\times(q+1)} & [\mathbf{0}]_{(q+1)\times 2(n+1)}\\ \mathbf{I}_{2(n+1)\times 2(n+1)} & [\mathbf{0}]_{2(n+1)\times(q+1)} & -\gamma\mathbf{I}_{2(n+1)\times 2(n+1)}\end{bmatrix} < \mathbf{0}. \tag{20}$$

Because both $\mathbf{\Phi}$ and $\mathbf{K}$ are unknown variables and multiplied together, this problem cannot be solved directly. This paper employs variable substitution method [23] to linearize this constraint.

Define a new variable $\mathbf{\Xi} = \mathbf{\Phi}\mathbf{K} \in \mathbb{R}^{2(n+1)\times q}$ and take it into (20)

$$\begin{bmatrix}\mathbf{A}^T\mathbf{\Phi} + \mathbf{\Phi}\mathbf{A} + \mathbf{C}_y^T\mathbf{\Xi}^T + \mathbf{\Xi}\mathbf{C}_y & [\mathbf{\Phi}\mathbf{B}_1]_{2(n+1)\times 1} & \mathbf{\Xi}_{2(n+1)\times q} & \mathbf{I}_{2(n+1)\times 2(n+1)}\\ \left[\mathbf{B}_1^T\mathbf{\Phi}\right]_{1\times 2(n+1)} & -\gamma\mathbf{I}_{1\times 1} & [\mathbf{0}]_{1\times q} & [\mathbf{0}]_{1\times 2(n+1)}\\ \mathbf{\Xi}_{q\times 2(n+1)} & [\mathbf{0}]_{q\times 1} & -\gamma\mathbf{I}_{q\times q} & [\mathbf{0}]_{q\times 2(n+1)}\\ \mathbf{I}_{2(n+1)\times 2(n+1)} & [\mathbf{0}]_{2(n+1)\times 1} & [\mathbf{0}]_{2(n+1)\times q} & -\gamma\mathbf{I}_{2(n+1)\times 2(n+1)}\end{bmatrix} < \mathbf{0}. \tag{21}$$

Equation (21) is a linear matrix inequality with matrix variables $\mathbf{\Phi}$ and Ξ. The optimal values of $\mathbf{\Phi}$ and Ξ can be computed through the solver feasp and mincx in MATLAB LMI toolbox. Then, $\mathbf{K}$ can be obtained from $\mathbf{K} = \mathbf{\Phi}^{-1}\Xi$. So, the FDI filter in (15) is designed.

Through FDI filter, the estimated state $\widehat{\mathbf{X}}(t)$ and the estimated sensor data $\hat{\mathbf{y}}(t) = \mathbf{C}_y\widehat{\mathbf{X}}(t)$ can be very closed to the system state $\mathbf{X}(t)$ and the sensor data real part $\mathbf{C}_y\mathbf{X}(t)$, respectively. The estimated state $\widehat{\mathbf{X}}(t)$ can be recognized as the input of H∞ state feedback gain $\mathbf{G}_\infty$. This reformed control system can be described in Figure 3. The reformed control strategy is different from the one in (12)

$$\overline{F}_a(t) = \mathbf{G}_\infty\widehat{\mathbf{X}}(t). \tag{22}$$

As a summary, when the sensor data has faults, the control system cannot guarantee a good performance. Through FDI filter, the sensor data real part and system state can be estimated. The estimated information can be used to isolate the sensor faults. Then, put the estimated state into the previous designed H∞ state feedback controller to reform the control strategy such that the control system can perform the fault tolerant control (FTC).

4. Numerical Example

Considering a three-story numerical example [26], an AMD control device is set on the top of this structure as shown in Figure 4. Define the structural mass, damping, and stiffness as follows:

$$\mathbf{M} = \begin{bmatrix} 6 & & \\ & 6 & \\ & & 6 \end{bmatrix} \times 10^3\ \text{kg},$$

$$\mathbf{C} = \begin{bmatrix} 12.4 & -5.16 & \\ -5.16 & 12.4 & -4.59 \\ & -4.59 & 7.2 \end{bmatrix} \times 10^3\ \text{N/(m/s)}, \tag{23}$$

$$\mathbf{K} = \begin{bmatrix} 3.4 & -1.8 & \\ -1.8 & 3.4 & -1.6 \\ & -1.6 & 1.6 \end{bmatrix} \times 10^6\ \text{N/m}.$$

AMD control system mass, damping, and stiffness are as follows:

$$m_a = 360\ \text{kg},$$

$$k_a = 18819\ \text{N/m},$$

$$c_a = 365.3910\ \text{N/(m/s)}. \tag{24}$$

Suppose the sensor measurement outputs are the system states. H∞ state feedback control strategy is employed to control this structural system with AMD. The H∞ state feedback gain $\mathbf{G}_\infty$ in (12) can be obtained as follows:

$$\mathbf{G}_\infty = [3.2155\ \ 3.1275\ \ 6.7705\ \ -0.0127\ \ -0.1344\ \ -0.0877\ \ -0.1335\ \ -0.0188] \times 10^6. \tag{25}$$

The El Centro NS earthquake acceleration record $\ddot{q}_g(t)$ with its peak scaled to 200 gal (2 m/s^2) is used as the ground excitation. The response suppression comparisons are shown in Figures 5 and 6 for the bare structure without control, passive tuned mass damper (TMD) structure, and active mass damper (AMD) structure without sensor faults. The bare structure is the structure without actuators. The TMD structure has actuators but does not generate control force. The control strategy for the AMD structure is H∞ state feedback control.

In Figure 6, $\mathbf{G}_\infty$ represents H∞ state feedback controller. Figures 5 and 6 illustrate the relative displacement response on the 3rd floor. The maximum value of the relative displacement for the TMD structure is 24.1% less than the one for the bare structure, while AMD structure is 67.0% off. Therefore, TMD and AMD can both suppress the structural vibration. Furthermore, AMD structure can reduce the vibration 56.5% more than TMD structure.

If there exist some faults in sensors, the faulty signal data $\mathbf{v}(t)$ is supposed to be located in the third floor displacement sensors. And its mean value and variance are zero and 2.5×10^{-5}, respectively. The comparison of the 3rd interstory drift between the AMD structure and the TMD structure is shown in Figure 7.

From Figure 7, AMD structural control system with H∞ state feedback control strategy loses its control performance when there exist faults in the sensors. Accordingly, it is necessary to detect and isolate the faults in the sensors. Through proposed FDI filter design method, the gain $\mathbf{K}$ is obtained as follows:

$$\mathbf{K} = \begin{bmatrix} -6.4162 & -2.4851 & -0.9160 & 0.4926 & -92.0527 & -118.6123 & -28.5338 & -23.9462 \\ -1.0675 & -2.3501 & -0.6025 & 0.1106 & -42.2075 & 93.6605 & -82.5947 & -27.4098 \\ 0.3623 & -0.1068 & -1.8490 & -0.4097 & 39.9383 & -55.9578 & 105.6514 & -90.3240 \end{bmatrix}^T. \tag{26}$$

Taking $\mathbf{K}$ into (15) and putting the estimated state $\widehat{\mathbf{X}}(t)$ into state feedback gain $\mathbf{G}_\infty$, the control strategy is reformed to perform the fault tolerate control.

Figure 8 compares the interstory drift in the top story between the real interstory drift and the estimated drift. The related coefficients are shown in Table 1. From Table 1, the

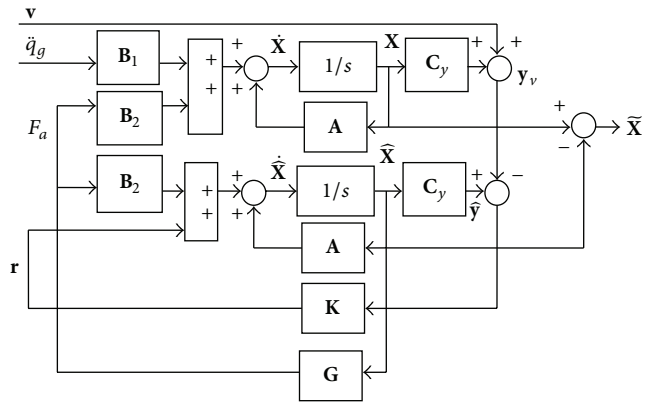

Figure 3: FTC diagram of AMD structure system.

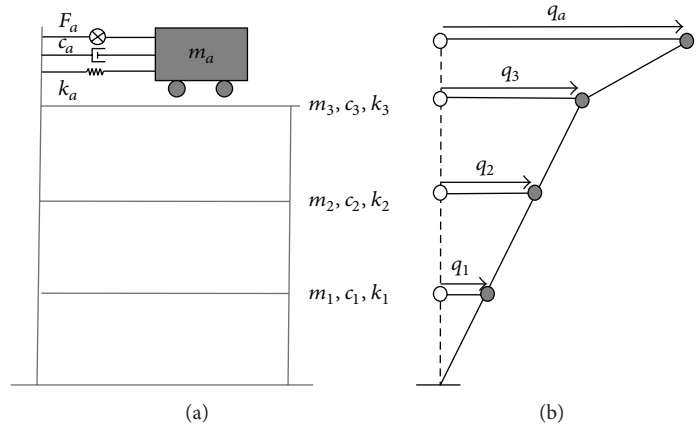

Figure 4: Three-story structure model with AMD system.

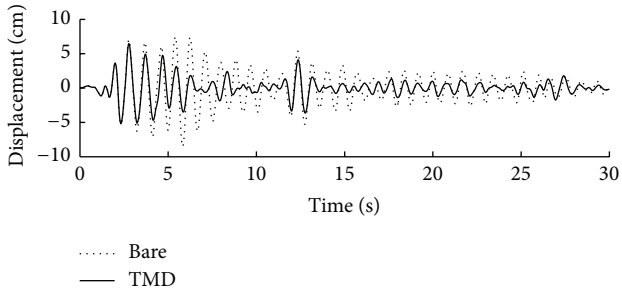

Figure 5: Comparison of the 3rd floor relative displacement between no control and TMD passive control.

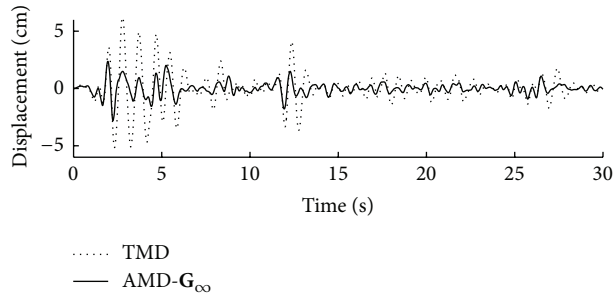

Figure 6: Comparison of the 3rd floor relative displacement between TMD passive control and AMD-H∞ state feedback control.

dash line, which is the real drift, matches the solid line, which is the estimated drift by FDI. From Table 1, the related coefficients (RCs) are almost close to 1, which means that FDI can estimate drift precisely.

Through FTC strategy, the interstory drift is suppressed, and the third story drift is shown in Figures 9 and 10. Table 2 shows some details about vibration suppression effects for other stories.

Figure 9 illustrates the comparison of the interstory drift in the 3rd story between TMD structure and AMD structure considering sensor faults. In AMD structure, the control strategy is FTC. AMD structure can suppress the structural vibration more effectively than TMD structure does. While only using H∞ state feedback control strategy, the vibration is worsened as shown in Figure 7. Figure 10 can illustrate the difference more directly.

From Table 2, the maximum values of all the interstory drifts for AMD structure with H∞ state feedback control strategy are 29.37%, 38.29%, and −46.50% less than the TMD structural drifts, respectively. While using FTC strategy, the drifts are 23.42%, 39.19%, and 54.78% less than the TMD

Table 1: Correlation coefficient between FDI estimated state and the real state.

	Comparison between the states estimated by FDI and structure system real states							
	Interstory drift				Interstory velocity			
	q_1 cm	$q_2 - q_1$ cm	$q_3 - q_2$ cm	$q_a - q_3$ cm	$\dot{q}_1$ cm	$\dot{q}_2 - \dot{q}_1$ cm	$\dot{q}_3 - \dot{q}_2$ cm	$\dot{q}_a - \dot{q}_3$ cm
RC	0.8422	0.8064	0.8584	0.9989	0.7741	0.7483	0.9035	0.9985

Table 2: Suppressing effect comparisons among the bared structure, TMD structure, AMD structure without faults, and AMD H∞ structure with faults.

Systems	q_1 cm	$q_2 - q_1$ cm	$q_3 - q_2$ cm	$q_a - q_3$ cm	$F_a(t)$ kN
Bare system	4.04	2.81	1.68	—	—
TMD system	2.69	2.22	1.57	25.08	—
AMD system without faults using $\mathbf{G}_\infty$	1.88	1.08	0.86	78.38	15.46
AMD system with faults using $\mathbf{G}_\infty$	1.90	1.37	2.30	108.7	209.1
AMD system with faults using FTC	2.06	1.35	0.71	83.36	16.00

$\mathbf{G}_\infty$ represents H∞ state feedback control.

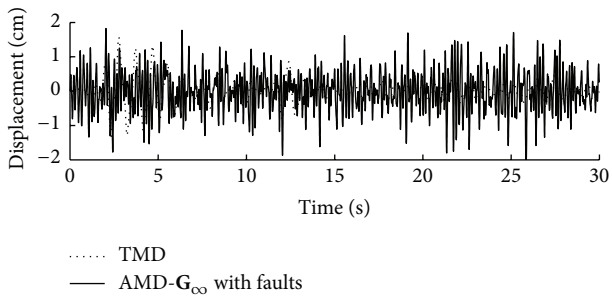

Figure 7: Comparison of the 3rd story interstory drift between TMD and AMD with H∞ state feedback control strategy considering the sensor faults.

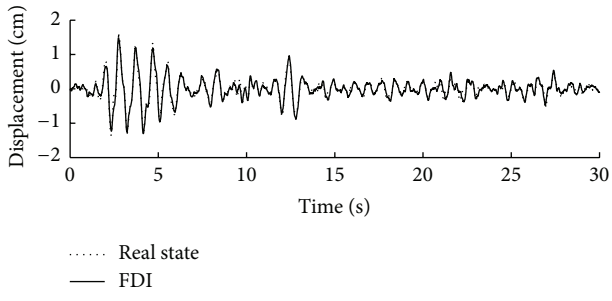

Figure 8: Comparison between the real and FDI estimated interstory drift in the top story.

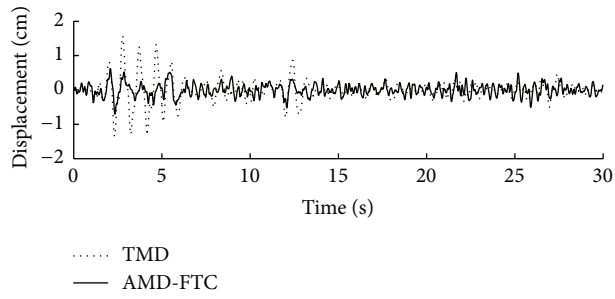

Figure 9: Comparison of the interstory drifts in the 3rd story between the TMD and AMD-FTC control.

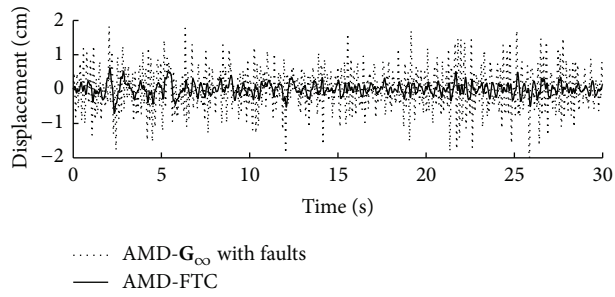

Figure 10: Comparison of the 3rd floor interstory drifts between the AMD-H∞ state feedback control and AMD-FTC control.

structural drifts, respectively. The actuator force $F_a(t)$ saves a lot of energy using FTC strategy than when only using H∞ state feedback control strategy. Therefore, FTC can tolerate faults in sensors and suppress structural vibration efficiently.

5. Conclusions

In practical engineering, structural control system may have faults which can degrade control system performance. This paper presents fault tolerant control (FTC) for civil structures. Considering the faults in sensors, fault detection and isolation (FDI) filter is designed. Transmitting the estimated state to H∞ state feedback controller designed previously, the reformed control strategy is obtained, which is called fault tolerant control (FTC). This paper also presents the derivation of FDI, which transforms the inequality matrix to linear inequality matrix using variable substitution method. A three-story numerical example validates FDI and FTC performance. From this study, there are some conclusions.

(1) When there is no fault in sensors, H∞ state feedback control in AMD structure has better suppressing performance than TMD structure.

(2) When there are faults in sensors, H∞ state feedback control in AMD structure cannot guarantee the control performance and even worsen the vibration.

(3) FDI designed by the proposed method can detect and isolate the faults. It can estimate the system state precisely. According to the estimated state, the measurement output from sensors can also be estimated.

(4) FTC designed by the proposed method can tolerate the faults in sensors. So, it can strengthen the robustness of the control system.

Acknowledgment

The authors are grateful for the support of the National Natural Science Foundation of China (Grant nos. 51121005 and 51261120375).

References

[1] T. T. Soong, *Active Structure Control Theory and Practice*, Longman Scientific & Technical, New York, NY, USA, 1990.

[2] T. T. Soong and G. F. Dargush, *Passive Energy Dissipation Systems in Structural Engineering*, John Wiley & Sons, London, UK, 1997.

[3] J. T. P. Yao, "Concept of structural control," *Journal of Structural Division*, vol. 98, pp. 1567–1574, 1972.

[4] G. Song, P. Qiao, V. Sethi, and A. Prasad, "Active vibration control of a smart pultruded fiber-reinforced polymer I-beam," *Smart Materials and Structures*, vol. 13, no. 4, pp. 819–827, 2004.

[5] G. Song, S. P. Schmidt, and B. N. Agrawal, "Experimental study of active vibration suppression of flexible structure using modular control patch," in *Proceedings of the IEEE Aerospace Conference*, vol. 1, pp. 189–201, March 1998.

[6] G. Song, B. Kelly, and B. N. Agrawal, "Active position control of a shape memory alloy wire actuated composite beam," *Smart Materials and Structures*, vol. 9, no. 5, pp. 711–716, 2000.

[7] V. Sethi, M. A. Franchek, and G. Song, "Active multimodal vibration suppression of a flexible structure with piezoceramic sensor and actuator by using loop shaping," *Journal of Vibration and Control*, vol. 17, no. 13, pp. 1994–2006, 2011.

[8] V. Sethi and G. Song, "Multimodal vibration control of a flexible structure using piezoceramic sensor and actuator," *Journal of Intelligent Material Systems and Structures*, vol. 19, no. 5, pp. 573–582, 2008.

[9] H. Gu and G. Song, "Active vibration suppression of a flexible beam with piezoceramic patches using robust model reference control," *Smart Materials and Structures*, vol. 16, no. 4, pp. 1453–1459, 2007.

[10] L. Huo and H. Li, *Multi-Dimensional Structure Damping Control*, Science Press, Beijing, China, 2008.

[11] G. Song, B. Kelly, B. N. Agrawal, P. C. Lam, and T. S. Srivatsan, "Application of shape memory alloy wire actuator for precision position control of a composite beam," *Journal of Materials Engineering and Performance*, vol. 9, no. 3, pp. 330–333, 2000.

[12] Y. Wang, "Time-delayed dynamic output feedback H_∞ controller design for civil structures: a decentralized approach through homotopic transformation," *Structural Control and Health Monitoring*, vol. 18, no. 2, pp. 121–139, 2011.

[13] Y. Bai and K. M. Grigoriadis, "H_∞ collocated control of structural systems: an analytical bound approach," *Journal of Guidance, Control, and Dynamics*, vol. 28, no. 5, pp. 850–853, 2005.

[14] H. Gu, G. Song, and H. Malki, "Chattering-free fuzzy adaptive robust sliding-mode vibration control of a smart flexible beam," *Smart Materials and Structures*, vol. 17, no. 3, Article ID 035007, 2008.

[15] Y. Bai and K. M. Grigoriadis, "Damping parameter design optimization in structural systems using an explicit H_∞ norm bound," *Journal of Sound and Vibration*, vol. 319, no. 3–5, pp. 795–806, 2009.

[16] H. Gu and G. Song, "Active vibration suppression of a composite I-beam using fuzzy positive position control," *Smart Materials and Structures*, vol. 14, no. 4, pp. 540–547, 2005.

[17] Y. Bai, K. M. Grigoriadis, and G. Song, "Active fault tolerant control of a flexible beam," in *Modeling, Signal Processing, and Control for Smart Structures* ., D. K. Lindner, Ed., vol. 6523 of *Proceedings of SPIE*, 2007.

[18] G. Song, L. Cai, Y. Wang, and R. W. Longman, "A sliding-mode based smooth adaptive robust controller for friction compensation," *International Journal of Robust and Nonlinear Control*, vol. 8, no. 8, pp. 725–739, 1998.

[19] G. Song and N. Ma, "Robust control of a shape memory alloy wire actuated flap," *Smart Materials and Structures*, vol. 16, no. 6, pp. N51–N57, 2007.

[20] G. Song and R. Mukherjee, "A comparative study of conventional nonsmooth time-invariant and smooth time-varying robust compensators," *IEEE Transactions on Control Systems Technology*, vol. 6, no. 4, pp. 571–576, 1998.

[21] L. Li, G. Song, and J. Ou, "Adaptive fuzzy sliding mode based active vibration control of a smart beam with mass uncertainty," *Structural Control and Health Monitoring*, vol. 18, no. 1, pp. 40–52, 2011.

[22] G. E. Stavroulakis, D. G. Marinova, and E. C. Zacharenakis, "Robust control in structural dynamics, taking into account structural uncertainties," in *Proceedings of the 5th GRACM International Congress on Computational Mechanics*, Limassol, Cyprus, 2005.

[23] L. Yu, *Robust Control—Linear Matrix Inequalities Approach*, Tsinghua University Press, Beijing, China, 2002.

[24] Y. Bai, K. M. Grigoriadis, and V. Sethi, "Static output feedback H_∞ control of collocated structural systems," in *Proceedings of the American Control Conference*, vol. 1–12, pp. 828–833, June 2006.

[25] U. Mackenroth, *Robust Control Systems: Theory and Case Studies*, Springer, Berlin, Germany, 2004.

[26] Y. Wang, J. P. Lynch, and K. H. Law, "Decentralized H_∞ controller design for large-scale civil structures," *Earthquake Engineering and Structural Dynamics*, vol. 38, no. 3, pp. 377–401, 2009.

Hindawi Publishing Corporation
Mathematical Problems in Engineering
Volume 2013, Article ID 724918, 13 pages
http://dx.doi.org/10.1155/2013/724918

Research Article

Control Design for Discrete-Time Fuzzy Systems with Disturbance Inputs via Delta Operator Approach

Qi Zhou,[1] Yabin Gao,[1] Hongyi Li,[2] and Hamid Reza Karimi[3]

[1] *College of Information Science and Technology, Bohai University, Jinzhou, Liaoning 121013, China*
[2] *College of Engineering, Bohai University, Jinzhou, Liaoning 121013, China*
[3] *Department of Engineering of the Faculty of Engineering and Science, University of Agder, Grimstad, Norway*

Correspondence should be addressed to Hongyi Li; lihongyi2009@gmail.com

Received 21 August 2013; Accepted 22 September 2013

Academic Editor: Tao Li

This paper is concerned with the problem of passive control design for discrete-time Takagi-Sugeno (T-S) fuzzy systems with time delay and disturbance input via delta operator approach. The discrete-time passive performance index is established in this paper for the control design problem. By constructing a new type of Lyapunov-Krasovskii function (LKF) in delta domain, and utilizing some fuzzy weighing matrices, a new passive performance condition is proposed for the system under consideration. Based on the condition, a state-feedback passive controller is designed to guarantee that the resulting closed-loop system is very-strictly passive. The existence conditions of the controller can be expressed by linear matrix inequalities (LMIs). Finally, a numerical example is provided to demonstrate the feasibility and effectiveness of the proposed method.

1. Introduction

It is well known that the fuzzy logic control [1–4] is one of the most effective approaches to handle complex nonlinear systems. Takagi-Sugeno (T-S) fuzzy model has been proposed in [5] and applied to formulate a complex nonlinear systems into a framework. Some affine local models can be interpolated by a set of fuzzy membership functions in this framework. By T-S fuzzy model, a set of complex nonlinear systems can be possibly described as a weighed sum of some simple linear subsystems. Recently, the problem of stability analysis and controller synthesis of nonlinear systems in T-S fuzzy model has been extensively investigated in [5–18]. Due to the effect of time delay in systems, the problems of T-S fuzzy systems with time delays have got considerable attention in recent years, and some results have been developed in [9, 19–31].

Recently, due to the fact that the passive properties can keep the system internally stable and have been frequently used to improve the stability of control systems. The passivity control has been widely applied in various engineering areas, such as electrical circuits systems, complex networks systems, mechanical systems, and nonlinear systems. The problems of passivity analysis and passive control for systems have been widely investigated [32–38]. The passive control problem has been investigated for fuzzy systems [35, 39, 40]. Among them, the authors in [40] are concerned with the very strict passive controller design problem for T-S fuzzy systems with time-varying delay.

It is well known that the best system performances can be obtained with the shorter sampling period. In [41, 42], the authors pointed out that the excellent finite word length performance can be achieved under fast sampling via delta operator approach. The authors in [43] introduced the transformations between shift operator and delta operator transfer function models. A technique was developed in [44] to obtain an approximate delta operator system for a given continuous system. In [45], a tabular method was presented for real polynomial root distribution with respect to a circle in the complex plane, which is useful in stability of delta operator

formulated discrete-time systems with a sampling time. By using delta operator formulation, the main design features of a loop transfer recovery controller both at input and output have been overviewed in [46]. More recently, many stability analysis and controller synthesis results about delta operator approach have been proposed in [47–49]. To mention a few, the robust stabilization problem was investigated in [47] for delta operator systems with time-varying delays. The authors in [49] investigated the robust H_∞ control problem for a class of T-S fuzzy systems with time delays by using delta operator approach. However, there have been few results on the passive control for T-S fuzzy systems with time delays and disturbance inputs via delta operator approach, which motivates this study.

In this paper, the problem of passive control is investigated for discrete-time T-S fuzzy systems with time delay and disturbance input via delta operator approach. The discrete-time passive performance index is concerned in this paper for the control design problem. A novel type Lyapunov-Krasovskii functional (LKF) is constructed in delta domain to present a new passive performance condition for discrete-time T-S fuzzy systems. Based on the condition, a state-feedback passive controller is designed to guarantee that the resulting closed-loop system is very strictly passive. The controller existence condition can be obtained in terms of linear matrix inequalities (LMIs), which can be solved by the standard software. A numerical example is given to illustrate the effectiveness of the proposed approach.

At first, the T-S fuzzy model is employed to represent the nonlinear systems. By applying the LMIs techniques and LKF in δ-domain, the problem of passive control design for the discrete T-S fuzzy system with time delay and disturbance inputs is chewed. Then a new fuzzy state-feedback controller is designed which guarantees that the closed-loop fuzzy delta operator system with time delay is robustly asymptotically stable and satisfies a prescribed passive performance level. And those are some key points of contribution. It is worthwhile to note that a faster sampling method is utilized, and hence a better control effect by applying delta operator approach than shift operator approach is achieved. Finally, a numerical example is shown to indicate the feasibility and effectiveness of the proposed method.

This paper is organized as follows. The problem to be solved is formulated in Section 2. Main results, including passive analysis and passive controller design, are presented in Section 3. Section 4 provides an illustrative example to show the effectiveness and potential of the proposed design techniques. It is concluded this paper in Section 5.

Notation. The notation used throughout the paper is fairly standard. $L_2[0,\infty)$ denotes the space of square-integrable vector functions over $[0,\infty)$. The notation $X > 0$ (resp., $X \geq 0$), for $X \in \mathbb{R}^{n\times n}$, means that the matrix X is real symmetric positive definite (resp., positive semidefinite). The symbol "$*$" in a matrix $A \in \mathbb{R}^{n\times n}$ stands for the transposed elements in the symmetric positions. The superscripts "T" and "-1" denote the matrix transpose and inverse, respectively. Identity matrices of appropriate dimensions will be denoted by I. The shorthand $\mathrm{diag}\{M_1, M_2, \ldots, M_r\}$ denotes a block diagonal matrix with diagonal blocks being the matrices M_1, M_2,..., M_r. If not explicitly stated, all matrices are assumed to have compatible dimensions for algebraic operations.

2. Problem Formulation

Considering the following fuzzy delta operator system with time delay, which is described by

Plant Rule i. IF $\theta_1(t_k)$ is N_{i1}, and ..., and $\theta_j(t_k)$ is N_{ij}, and ..., and $\theta_p(t_k)$ is N_{ip}, THEN

$$\begin{aligned}
\delta x(t_k) &= A_i x(t_k) + A_{di} x(t_k - d_k) + B_i u(t_k) + B_{wi} w(t_k),\\
z(t_k) &= C_i x(t_k) + C_{di} x(t_k - d_k) + D_i u(t_k) + D_{wi} w(t_k),\\
x(t_k) &= \phi(t_k), \quad t_k = -d_M,\ d_M + T, \ldots, 0,\ i = 1, 2, \ldots, r,
\end{aligned} \tag{1}$$

where $x(t_k) \in \mathbb{R}^n$ is the state variable, $u(t_k) \in \mathbb{R}^m$ is the control input variable, $w(t_k) \in \mathbb{R}^l$ is the disturbance input variable which belongs to $L_2[0,\infty)$, $z(t_k) \in \mathbb{R}^p$ is the control output, and $\phi(t_k)$ is a continuous vector-valued initial function. Let $t_k = kT$ for the convenience in analysis. A_i, A_{di}, B_i, B_{wi}, C_i, C_{di}, D_i, and D_{wi} $(i = 1, 2, \ldots, r)$ are system matrices with appropriate dimensions. The scalar r is the number of IF-THEN rules. $\theta_j(t_k)$ and N_{ij} are the premise variable and the fuzzy set, respectively, for $j = 1, 2, \ldots, p$. The parametric variable $d_k = nT$ which is the bounded time delay in the state and satisfies $0 < d_m \leq d_k \leq d_M$ with $d_m = n_m T$ and $d_M = n_M T$ (n_m and n_M are the known positive and finite integers, and T is a sampling period). $\delta x(t_k)$ is the delta operator of $x(t_k)$, which is defined by

$$\delta x(t_k) = \begin{cases} \dfrac{d}{dt_k} x(t_k), & T = 0,\\ \dfrac{x(t_k + T) - x(t_k)}{T}, & T \neq 0. \end{cases} \tag{2}$$

Then the defuzzified model of system (1) is inferred as follows:

$$\begin{aligned}
\delta x(t_k) &= \sum_{i=1}^{r} h_i(\theta(t_k)) \left[A_i x(t_k) + A_{di} x(t_k - d_k) + B_i u(t_k) + B_{wi} w(t_k)\right],\\
z(t_k) &= \sum_{i=1}^{r} h_i(\theta(t_k)) \left[C_i x(t_k) + C_{di} x(t_k - d_k) + D_i u(t_k) + D_{wi} w(t_k)\right],
\end{aligned} \tag{3}$$

where $h_i(\theta(t_k)) = \mu_i(\theta(t_k)) / \sum_{i=1}^{r} \mu_i(\theta(t_k))$, $\mu_i(\theta(t_k)) = \prod_{j=1}^{p} N_{ij}(\theta_j(t_k))$, and $N_{ij}(\theta_j(t_k))$ is the degree of the membership of $\theta_j(t_k)$ in fuzzy set N_{ij}. It can be assumed that $\mu_i(\theta(t_k)) \geq 0$ (for $i = 1, 2, \ldots, r$) and $\sum_{i=1}^{r} \mu_i(\theta(t_k)) \geq 0$ (for all t_k). Therefore, $h_i(\theta(t_k)) \geq 0$ (for $i = 1, 2, \ldots, r$) and

$\sum_{i=1}^{r} h_i(\theta(t_k)) = 1$. Based on the parallel distributed compensation (PDC), similar to the fuzzy model, the following overall fuzzy control law can be constructed as

$$u(t_k) = \sum_{s=1}^{r} h_s(\theta(t_k)) K_s x(t_k), \tag{4}$$

where K_s $(s = 1, 2, \ldots, r)$ is the local control gain such that closed-loop fuzzy system (3) is asymptotically stable. Then substituting (4) into system (3), the closed-loop fuzzy system can be expressed as

$$\begin{aligned}
\delta x(t_k) &= \sum_{i=1}^{r}\sum_{s=1}^{r} h_i h_s [(A_i + B_i K_s) x(t_k) \\
&\qquad + A_{di} x(t_k - d_k) + B_{wi} w(t_k)], \\
z(t_k) &= \sum_{i=1}^{r}\sum_{s=1}^{r} h_i h_s [(C_i + D_i K_s) x(t_k) \\
&\qquad + C_{di} x(t_k - d_k) + D_{wi} w(t_k)],
\end{aligned} \tag{5}$$

where $\sum_{i=1}^{r} h_i = \sum_{i=1}^{r} h_i(\theta(t_k))$. For the convenience, system (5) can be rewritten as

$$\begin{aligned}
\delta x(t_k) &= A(t_k) x(t_k) + A_d(t_k) x(t_k - d_k) \\
&\qquad + B_w(t_k) w(t_k), \\
z(t_k) &= C(t_k) x(t_k) + C_d(t_k) x(t_k - d_k) \\
&\qquad + D_w(t_k) w(t_k),
\end{aligned} \tag{6}$$

where

$$\begin{aligned}
A(t_k) &= \sum_{i=1}^{r}\sum_{s=1}^{r} h_i h_s (A_i + B_i K_s), \\
A_d(t_k) &= \sum_{i=1}^{r} h_i A_{di}, \qquad B_w(t_k) = \sum_{i=1}^{r} h_i B_{wi}, \\
C(t_k) &= \sum_{i=1}^{r}\sum_{s=1}^{r} h_i h_s (C_i + D_i K_s), \\
C_d(t_k) &= \sum_{i=1}^{r} h_i C_{di}, \qquad D_w(t_k) = \sum_{i=1}^{r} h_i D_{wi}.
\end{aligned} \tag{7}$$

In the next section, the following definitions and lemmas are introduced for developing the main results.

Definition 1 (see [47]). The conditions for the asymptotic stability of a delta operator system hold:

(a) $V(x(t_k)) \geq 0$, with equality if and only if $x(t_k) = 0$,

(b) $\delta V(x(t_k)) = [V(x(t_k + T)) - V(x(t_k))]/T < 0$,

where $V(x(t_k))$ is a Lyapunov function in δ-domain. For Lyapunov function both in s-domain and z-domain, the condition (a) $V(x(t_k)) \geq 0$ in Definition 1 is given. On the other hand for the condition (b), when $T \to 0$, there exists

$$\begin{aligned}
\lim_{T \to 0} \delta V(x(t_k)) &= \lim_{T \to 0} \frac{V(x(t_k + T)) - V(x(t_k))}{T} \\
&= \frac{dV(x(t_k))}{dt_k} < 0,
\end{aligned} \tag{8}$$

and when $T = 1$, there exists

$$\begin{aligned}
\delta V(x(t_k)) &= \frac{[V(x(t_k + 1)) - V(x(t_k))]}{1} \\
&= V(x(t_k + 1)) - V(x(t_k)) < 0.
\end{aligned} \tag{9}$$

Obviously, the Lyapunov function in δ-domain can be reduced to the traditional Lyapunov function in s-domain or z-domain when the sampling period T tends to 0 or is 1.

Definition 2 (see [50]). (i) System (5) is said to be passive if there exists constant ρ such that

$$2\sum_{t_k=0}^{\infty} z^T(t_k) w(t_k) \geq \rho. \tag{10}$$

(ii) System (5) is said to be strictly passive if there exist constants $\zeta > 0$ and ρ such that

$$2\sum_{t_k=0}^{\infty} z^T(t_k) w(t_k) \geq \rho + \zeta \sum_{t_k=0}^{\infty} w^T(t_k) w(t_k). \tag{11}$$

(iii) System (5) is said to be output strictly passive if there exist constants $\varepsilon > 0$ and ρ such that

$$2\sum_{t_k=0}^{\infty} z^T(t_k) w(t_k) \geq \rho + \varepsilon \sum_{t_k=0}^{\infty} z^T(t_k) z(t_k). \tag{12}$$

(iv) System (5) is said to be very strictly passive if there exist constants $\varepsilon > 0, \zeta > 0$, and ρ such that

$$\begin{aligned}
2\sum_{t_k=0}^{\infty} z^T(t_k) w(t_k) &\geq \rho + \varepsilon \sum_{t_k=0}^{\infty} z^T(t_k) z(t_k) \\
&\qquad + \zeta \sum_{t_k=0}^{\infty} w^T(t_k) w(t_k).
\end{aligned} \tag{13}$$

Lemma 3 (see [47]). *For any of the time functions $x(t_k)$ and $y(t_k)$,*

$$\begin{aligned}
\delta(x(t_k) y(t_k)) &= \delta(x(t_k)) y(t_k) + x(t_k) \delta(y(t_k)) \\
&\qquad + T\delta(x(t_k)) \delta(y(t_k)),
\end{aligned} \tag{14}$$

where T is a sampling period.

Lemma 4 (see [51]). *For any of the two positive integers r and r_0, satisfying $1 \leq r_0 \leq r$ holds:*

$$\left[\sum_{i=r_0}^{r} x(i)\right]^T M \left[\sum_{i=r_0}^{r} x(i)\right] \leq (r - r_0 + 1) \sum_{i=r_0}^{r} x^T(i) M x(i), \tag{15}$$

where M is a constant positive semidefinite symmetric matrix.

Lemma 5 (see [52]). *For the given constant matrices G, H and a symmetric constant matrix χ of appropriate dimensions, the following inequality holds:*

$$\chi + GF(t_k)H + H^T F^T(t_k)G^T \le 0, \tag{16}$$

where $F(t_k)$ satisfies $F^T(t_k)F(t_k) \le I$, if and only if for $\xi > 0$ the following inequality holds:

$$\chi + \xi^{-1}H^T H + \xi G G^T \le 0. \tag{17}$$

Lemma 6. *If there exist scalars $\varepsilon > 0, \zeta > 0$, and a differential function $V(x(t_k)) \ge 0$ such that*

$$\begin{aligned}&\delta V(x(t_k)) + \varepsilon z^T(t_k)z(t_k) + \zeta w^T(t_k)w(t_k)\\ &\quad - 2z^T(t_k)w(t_k) \le 0,\end{aligned} \tag{18}$$

then system (5) *is very strictly passive.*

Proof. It follows from (18) that

$$\begin{aligned}2\sum_{t_k=0}^{\infty} z^T(t_k)w(t_k) \ge\ & -V(x(0)) + \varepsilon\sum_{t_k=0}^{\infty} z^T(t_k)z(t_k)\\ &+ \zeta\sum_{t_k=0}^{\infty} w^T(t_k)w(t_k)\\ =\ & \rho + \varepsilon\sum_{t_k=0}^{\infty} z^T(t_k)z(t_k)\\ &+ \zeta\sum_{t_k=0}^{\infty} w^T(t_k)w(t_k),\end{aligned} \tag{19}$$

where $\rho = -V(x(0))$. Then, it can be seen that (13) is equivalent to (18) for very strict passive definition. □

Remark 7. Based on Definition 2, the main objective of this paper is just to prove that T-S fuzzy system (5) is very strictly passive via delta operator approach, which can also satisfy other three indexs. The very strictly passive control for system (5) is shown in the next section.

3. Main Results

This section focuses on designing a sufficient condition for the solvability of the proposed passive control problem and a developed LMI approach for designing the passive controller for fuzzy system (5). Firstly, the passivity analysis criterion is derived for the system (5) in the following theorem.

Theorem 8. *Considering fuzzy delta operator system* (5)*, for a given sampling period $T > 0$, constants d_m, d_M $(0 < d_m \le d_M)$, and matrix K_s $(s = 1, 2, \ldots, r)$, system* (5) *is very strictly passive if there exist scalars $\varepsilon > 0, \zeta > 0$ and symmetric matrices $P > 0$, $R_1 > 0, R_2 > 0, Q_\kappa > 0, S_{1\kappa} > 0$, and $S_{2\kappa} > 0$ $(\kappa = 1, 2, \ldots, r)$ with appropriate dimensions, such that the following LMIs hold for $\kappa, \lambda, \mu, \nu, i, s = 1, 2, \ldots, r$:*

$$\begin{aligned}&\Theta_{\kappa\lambda\mu\nu ii} < 0,\\ &\Theta_{\kappa\lambda\mu\nu is} + \Theta_{\kappa\lambda\mu\nu si} < 0, \quad s \ne i,\end{aligned} \tag{20}$$

where

$$\Theta_{\kappa\lambda\mu\nu is} = \begin{bmatrix}\Omega_{1\kappa\lambda\mu\nu is} & \Omega_{2is}^T\\ * & -\varepsilon I\end{bmatrix}, \qquad \Omega_{2is} = \begin{bmatrix}0 & C_i + D_i K_s & C_{di} & 0 & 0 & D_{wi}\end{bmatrix},$$

$$\Omega_{1\kappa\lambda\mu\nu is} = \begin{bmatrix}\Xi_1 & P(A_i + B_i K_s) & PA_{di} & 0 & 0 & PB_{wi}\\ * & \Xi_{2\kappa is} & PA_{di} & \frac{1}{d_m}R_1 & \frac{1}{d_M}R_2 & \Xi_{3is}\\ * & * & -Q_\lambda & 0 & 0 & -C_{di}\\ * & * & * & -S_{1\mu} - \frac{1}{d_m}R_1 & 0 & 0\\ * & * & * & * & -S_{2\nu} - \frac{1}{d_M}R_2 & 0\\ * & * & * & * & * & \zeta I - D_{wi} - D_{wi}^T\end{bmatrix}, \tag{21}$$

$$\Xi_1 = (T-2)P + d_m R_1 + d_M R_2, \qquad \Xi_{3is} = PB_{wi} - (C_i + D_i K_s)^T,$$

$$\Xi_{2\kappa is} = P(A_i + B_i K_s) + (A_i + B_i K_s)^T P + (d_M - d_m + T + 1)Q_\kappa + S_{1\kappa} + S_{2\kappa} - \frac{1}{d_m}R_1 - \frac{1}{d_M}R_2.$$

Proof. Firstly, in order to simplify the calculation, relevant fuzzy weighing matrices which directly include the membership functions are defined as follows:

$$\breve{Q}(t_k) = \sum_{\kappa=1}^{r} h_\kappa(\theta(t_k)) Q_\kappa, \qquad \breve{S}_1(t_k) = \sum_{\kappa=1}^{r} h_\kappa(\theta(t_k)) S_{1\kappa},$$
$$\breve{S}_2(t_k) = \sum_{\kappa=1}^{r} h_\kappa(\theta(t_k)) S_{2\kappa}. \tag{22}$$

Choose a LKF $V(x(t_k))$ for system (5) as follows:

$$V(x(t_k)) = V_1(x(t_k)) + V_2(x(t_k)) + V_3(x(t_k)) + V_4(x(t_k)) + V_5(x(t_k)), \tag{23}$$

where

$$V_1(x(t_k)) = x^T(t_k) P x(t_k),$$
$$V_2(x(t_k)) = T\sum_{i=1}^{n} x^T(t_k - iT)\breve{Q}(t_k - iT) x(t_k - iT),$$
$$V_3(x(t_k)) = T\sum_{i=1}^{n_m} x^T(t_k - iT)\breve{S}_1(t_k - iT) x(t_k - iT) + T\sum_{i=1}^{n_M} x^T(t_k - iT)\breve{S}_2(t_k - iT) x(t_k - iT),$$
$$V_4(x(t_k)) = T^2\sum_{i=n_m}^{n_M}\sum_{s=1}^{i} x^T(t_k - sT)\breve{Q}(t_k - sT) x(t_k - sT),$$
$$V_5(x(t_k)) = \sum_{i=1}^{n_m}\sum_{s=1}^{i} e^T(t_k - sT) R_1 e(t_k - sT) + \sum_{i=1}^{n_M}\sum_{s=1}^{i} e^T(t_k - sT) R_2 e(t_k - sT), \tag{24}$$

and symmetric matrices $P > 0, R_1 > 0, R_2 > 0, Q_\kappa > 0, S_{1\kappa} > 0, S_{2\kappa} > 0$ (for $\kappa = 1, 2, \ldots, r$), and $e(s) = x(s) - x(s+T)$ from which it can be concluded that there exist $e(t_k - iT) = x(t_k - iT) - x(t_k - (i-1)T)$ and $\delta x(t_k) = -e(t_k)/T$.

Applying Lemma 3 to $V_1(x(t_k))$ and along the trajectory of the system (5), it can be obtained that

$$\begin{aligned}\delta V_1(x(t_k)) &= \delta^T(x(t_k)) P x(t_k) + x^T(t_k) P\delta(x(t_k)) + T\delta^T(x(t_k)) P\delta(x(t_k)) \\ &= x^T(t_k)\left[PA(t_k) + A^T(t_k) P\right] x(t_k) + 2x^T(t_k) PA_d(t_k) x(t_k - d_k) \\ &\quad + 2x^T(t_k) PB_w(t_k) w(t_k) + T\delta^T(x(t_k)) P\delta(x(t_k)).\end{aligned} \tag{25}$$

Similarly, applying the delta operator to $V_2(x(t_k))$, $V_3(x(t_k))$, and $V_4(x(t_k))$, it can be obtained as follows:

$$\begin{aligned}\delta V_2(x(t_k)) &= \frac{1}{T}\left[T\sum_{i=1}^{n} x^T(t_k - iT + T)\breve{Q}(t_k - iT + T) \times x(t_k - iT + T) - T\sum_{i=1}^{n} x^T(t_k - iT)\breve{Q}(t_k - iT) x(t_k - iT)\right] \\ &\le x^T(t_k)\breve{Q}(t_k) x(t_k) - x^T(t_k - d_k)\breve{Q}(t_k - d_k) x(t_k - d_k) + T\sum_{i=n_m}^{n_M} x^T(t_k - iT)\breve{Q}(t_k - iT) x(t_k - iT), \\ \delta V_3(x(t_k)) &= x^T(t_k)\left(\breve{S}_1(t_k) + \breve{S}_2(t_k)\right) x(t_k) - x^T(t_k - d_m)\breve{S}_1(t_k - d_m) x(t_k - d_m) - x^T(t_k - d_M) S_2(t_k - d_M) x(t_k - d_M), \\ \delta V_4(x(t_k)) &= T\left[\sum_{s=1}^{i}\left(x^T(t_k - sT + T)\breve{Q}(t_k - sT + T) \times x(t_k - sT + T)\right) - \sum_{s=1}^{i}\left(x^T(t_k - sT)\breve{Q}(t_k - sT) \times x(t_k - sT)\right)\right] \\ &= (d_M - d_m + T) x^T(t_k)\breve{Q}(t_k) x(t_k) - T\sum_{i=n_m}^{n_M} x^T(t_k - iT)\breve{Q}(t_k - iT) x(t_k - iT).\end{aligned} \tag{26}$$

Applying Lemma 4 to $V_5(x(t_k))$ and along the trajectory of system (5), it can be obtained that

$$\begin{aligned}\delta V_5(x(t_k)) = \frac{1}{T}\Bigg[&\sum_{i=1}^{n_m}\sum_{s=1}^{i} e^T(t_k - sT + T) R_1 e(t_k - sT + T) - \sum_{i=1}^{n_m}\sum_{s=1}^{i} e^T(t_k - sT) R_1 e(t_k - sT) \\ &+ \sum_{i=1}^{n_M}\sum_{s=1}^{i} e^T(t_k - sT + T)\end{aligned}$$

$$\times R_2 e(t_k - sT + T) - \sum_{i=1}^{n_M}\sum_{s=1}^{i} e^T(t_k - sT) R_2 e(t_k - sT)\Bigg]$$
$$= \frac{1}{T}\Bigg[\sum_{i=1}^{n_m} e^T(t_k) R_1 e(t_k) - \sum_{i=1}^{n_m} e^T(t_k - iT) R_1 e(t_k - iT) + \sum_{i=1}^{n_M} e^T(t_k) R_2 e(t_k) - \sum_{i=1}^{n_M} e^T(t_k - iT) R_2 e(t_k - iT)\Bigg]$$
$$\le e^T(t_k)\left(\frac{n_m}{T}R_1 + \frac{n_M}{T}R_2\right) e(t_k) - \frac{1}{n_m T}\left[\sum_{i=1}^{n_m} e(t_k - iT)\right]^T R_1 \times \left[\sum_{i=1}^{n_m} e(t_k - iT)\right] - \frac{1}{n_M T}\left[\sum_{i=1}^{n_M} e(t_k - iT)\right]^T \times R_2 \left[\sum_{i=1}^{n_M} e(t_k - iT)\right]$$
$$= \delta^T(x(t_k))(d_m R_1 + d_M R_2)\delta(x(t_k)) - \frac{1}{d_m}[x(t_k) - x(t_k - d_m)]^T \times R_1 [x(t_k) - x(t_k - d_m)] - \frac{1}{d_M}[x(t_k) - x(t_k - d_M)]^T \times R_2 [x(t_k) - x(t_k - d_M)]. \quad (27)$$

For the real matrix $P > 0$, the following equation is tenable:

$$0 = -2\delta^T(x(t_k)) P[\delta(x(t_k)) - A(t_k)x(t_k) - A_d(t_k)x(t_k - d_k) - B_w(t_k)w(t_k)]$$
$$= -2\delta^T(x(t_k)) P\delta(x(t_k)) + 2\delta^T(x(t_k)) PA(t_k)x(t_k) + 2\delta^T(x(t_k)) PA_d(t_k)x(t_k - d_k) + 2\delta^T(x(t_k)) PB_w(t_k)w(t_k). \quad (28)$$

Generally, considering the passive performance index in Definition 2, which is described as the passivity analysis, performance of system (5) can be established as follows:

$$J = \varepsilon^{-1} z^T(t_k) z(t_k) + \zeta w^T(t_k) w(t_k) - 2z^T(t_k) w(t_k) + \delta V(t_k). \quad (29)$$

By adding (28) into $\delta V(t_k)$ and applying (7), it can be found that

$$J = \varepsilon^{-1} z^T(t_k) z(t_k) + \zeta w^T(t_k) w(t_k) - 2z^T(t_k) w(t_k) + \delta V(t_k) \le \eta^T(t_k) \sum_{\kappa=1}^{r}\sum_{\lambda=1}^{r}\sum_{\mu=1}^{r}\sum_{\nu=1}^{r}\sum_{i=1}^{r}\sum_{s=1}^{r} h_\kappa h_\lambda h_\mu h_\nu h_i h_s \eta^T(t_k) \times \left[\Omega_{1\kappa\lambda\mu\nu is} + \varepsilon^{-1}\Omega_{2is}^T \Omega_{2is}\right]\eta(t_k), \quad (30)$$

where $h_\kappa = h_\kappa(\theta(t_k)), h_\lambda = h_\lambda(\theta(t_k - d_k)), h_\mu = h_\mu(\theta(t_k - d_m)), h_\nu = h_\nu(\theta(t_k - d_M)), h_i = h_i(\theta(t_k)), h_s = h_s(\theta(t_k))$, and

$$\eta^T(t_k) = \left[\delta^T(x(t_k)) \;\; x^T(t_k) \;\; x^T(t_k - d_k) \;\; x^T(t_k - d_m) \;\; x^T(t_k - d_M) \;\; w^T(t_k)\right]. \quad (31)$$

On the other hand, it can be seen from Theorem 8 that

$$\sum_{\kappa=1}^{r}\sum_{\lambda=1}^{r}\sum_{\mu=1}^{r}\sum_{\nu=1}^{r}\sum_{i=1}^{r}\sum_{s=1}^{r} h_\kappa h_\lambda h_\mu h_\nu h_i h_s \Theta_{\kappa\lambda\mu\nu is} = \sum_{\kappa=1}^{r}\sum_{\lambda=1}^{r}\sum_{\mu=1}^{r}\sum_{\nu=1}^{r} h_\kappa h_\lambda h_\mu h_\nu \times \Bigg[\sum_{i=1}^{r} h_i^2 \Theta_{\kappa\lambda\mu\nu ii} + \sum_{i=1}^{r-1}\sum_{s=i+1}^{r} h_i h_s \left(\Theta_{\kappa\lambda\mu\nu is} + \Theta_{\kappa\lambda\mu\nu si}\right)\Bigg] < 0. \quad (32)$$

Applying Schur complement, it can be obtained that

$$J = \varepsilon^{-1} z^T(t_k) z(t_k) + \zeta w^T(t_k) w(t_k) - 2z^T(t_k) w(t_k) + \delta V(t_k) < 0. \quad (33)$$

It can be seen that the LMIs conditions in Theorem 8 satisfy the very strictly passive performance index for the fuzzy delta operator system (5). The proof is completed. □

Based on the conditions in Theorem 8, the state-feedback control gain matrices K_s $(s = 1, 2, \ldots, r)$ will be designed in the following theorem.

Theorem 9. *Considering fuzzy delta operator system* (5)*, for a given sampling period* $T > 0$ *and constants* d_m, d_M $(0 < d_m \leq d_M)$*, system* (5) *is very strictly passive if there exist scalars* $\varepsilon > 0, \zeta > 0$ *and symmetric matrices* $\overline{P} > 0$, $\overline{R}_1 > 0$, $\overline{R}_2 > 0$, $\overline{Q}_\kappa > 0$, $\overline{S}_{1\kappa} > 0$, *and* $\overline{S}_{2\kappa} > 0$ $(\kappa = 1, 2, \ldots, r)$ *with appropriate dimensions, such that the following LMIs hold for* $\kappa, \lambda, \mu, \nu, i, s = 1, 2, \ldots, r$*:*

$$\begin{aligned} \overline{\Theta}_{\kappa\lambda\mu\nu ii} &< 0, \\ \overline{\Theta}_{\kappa\lambda\mu\nu is} + \overline{\Theta}_{\kappa\lambda\mu\nu si} &< 0, \qquad s \neq i, \end{aligned} \tag{34}$$

where

$$\overline{\Theta}_{\kappa\lambda\mu\nu is} = \begin{bmatrix} \overline{\Omega}_{1\kappa\lambda\mu\nu is} & \overline{\Omega}_{2is}^T \\ * & -\varepsilon I \end{bmatrix}, \qquad \overline{\Omega}_{2\lambda\mu\nu is} = \begin{bmatrix} 0 & \overline{C}_i\overline{P} + D_i\overline{K}_s & C_{di}\overline{P} & 0 & 0 & D_{wi} \end{bmatrix},$$

$$\overline{\Omega}_{1\kappa\lambda\mu\nu is} = \begin{bmatrix} \overline{\Xi}_1 & A_i\overline{P} + B_i\overline{K}_s & A_{di}\overline{P} & 0 & 0 & B_{wi} \\ * & \overline{\Xi}_{2\kappa is} & A_{di}\overline{P} & \frac{1}{d_m}\overline{R}_1 & \frac{1}{d_M}\overline{R}_2 & \overline{\Xi}_{3is} \\ * & * & -\overline{Q}_\lambda & 0 & 0 & -\overline{P}C_{di}^T \\ * & * & * & -\overline{S}_{1\mu} - \frac{1}{d_m}\overline{R}_1 & 0 & 0 \\ * & * & * & * & -\overline{S}_{2\nu} - \frac{1}{d_M}\overline{R}_2 & 0 \\ * & * & * & * & * & \zeta I - D_{wi} - D_{wi}^T \end{bmatrix}, \tag{35}$$

$$\overline{\Xi}_1 = (T-2)\,\overline{P} + d_m\overline{R}_1 + d_M\overline{R}_2, \qquad \overline{\Xi}_{3is} = B_{wi} - \overline{P}C_i^T - \overline{K}_s^T D_i^T,$$

$$\overline{\Xi}_{2\kappa is} = A_i\overline{P} + \overline{P}A_i^T + B_i\overline{K}_s + \overline{K}_s^T B_i^T + (d_M - d_m + T + 1)\,\overline{Q}_\kappa + \overline{S}_{1\kappa} + \overline{S}_{2\kappa} - \frac{1}{d_m}\overline{R}_1 - \frac{1}{d_M}\overline{R}_2.$$

The fuzzy sate-feedback controller can be obtained:

$$u(t_k) = \overline{K}_s\overline{P}^{-1}x(t_k). \tag{36}$$

Proof. Premultiplying and postmultiplying (34) by diagonal matrix

$$\operatorname{diag}\left\{\overline{P}^{-1}, \overline{P}^{-1}, \overline{P}^{-1}, \overline{P}^{-1}, \overline{P}^{-1}, I, I\right\} \tag{37}$$

and letting

$$\begin{aligned} P &= \overline{P}^{-1}, \qquad K_s = \overline{K}_s\overline{P}^{-1}, \qquad R_1 = \overline{P}^{-1}\overline{R}_1\overline{P}^{-1}, \\ R_2 &= \overline{P}^{-1}\overline{R}_2\overline{P}^{-1}, \\ Q_i &= \overline{P}^{-1}\overline{Q}_i\overline{P}^{-1}, \qquad S_{1i} = \overline{P}^{-1}\overline{S}_{1i}\overline{P}^{-1}, \\ S_{2i} &= \overline{P}^{-1}\overline{S}_{2i}\overline{P}^{-1}, \end{aligned} \tag{38}$$

for $i = 1, 2, \ldots, r$, it can be found that the conditions (20) hold, which means that system (5) is very strictly passive. The proof is completed. □

Remark 10. In this paper, the modeling uncertainties are not taken into account in system (1). It should be pointed out that the robust passive controller design condition can be presented for uncertain discrete-time T-S fuzzy systems with time delay and disturbance input via delta operator approach.

In order to present the stability and stabilization condition for discrete-time T-S fuzzy systems with time delay via delta operator approach, it is assumed that the disturbance input $w(t_k) = 0$ in fuzzy delta operator system (3), which can be described as

$$\begin{aligned} \delta x(t_k) &= \sum_{i=1}^{r} h_i(\theta(t_k)) \\ &\quad \times \left[A_i x(t_k) + A_{di} x(t_k - d_k) + B_i u(t_k)\right], \\ z(t_k) &= \sum_{i=1}^{r} h_i(\theta(t_k)) \\ &\quad \times \left[C_i x(t_k) + C_{di} x(t_k - d_k) + D_i u(t_k)\right]. \end{aligned} \tag{39}$$

Similar to the proof of Theorems 8 and 9, the following two corollaries can be obtained.

Corollary 11. *For a given sampling period $T > 0$ and constants d_m and d_M ($0 < d_m \le d_M$), system (39) ($u(t_k) = 0$) is asymptotically stable if there exist symmetric matrices $P > 0$, $R_1 > 0, R_2 > 0, Q_\kappa > 0, S_{1\kappa} > 0$, and $S_{2\kappa} > 0$ ($\kappa = 1, 2, \ldots, r$) with appropriate dimensions, such that the following LMIs hold for $\kappa, \lambda, \mu, \nu, i = 1, 2, \ldots, r$:*

$$\breve{\Theta}_{\kappa\lambda\mu\nu i} < 0, \tag{40}$$

where

$$\breve{\Theta}_{\kappa\lambda\mu\nu i} = \begin{bmatrix} \Xi_1 & PA_i & PA_{di} & 0 & 0 \\ * & \breve{\Xi}_{2\kappa i} & PA_{di} & \frac{1}{d_m}R_1 & \frac{1}{d_M}R_2 \\ * & * & -Q_\lambda & 0 & 0 \\ * & * & * & -S_{1\mu} - \frac{1}{d_m}R_1 & 0 \\ * & * & * & * & -S_{2\nu} - \frac{1}{d_M}R_2 \end{bmatrix}, \tag{41}$$

$$\Xi_1 = (T-2)P + d_m R_1 + d_M R_2,$$

$$\breve{\Xi}_{2\kappa i} = PA_i + A_i^T P + (d_M - d_m + T + 1)Q_\kappa + S_{1\kappa} + S_{2\kappa} - \frac{1}{d_m}R_1 - \frac{1}{d_M}R_2.$$

Corollary 12. *System (39) with the controller in (4) is asymptotically stable for a given sampling period $T > 0$ and constants d_m and d_M ($0 < d_m \le d_M$), if there exist symmetric matrices $\overline{P} > 0$, $\overline{R}_1 > 0, \overline{R}_2 > 0, \overline{Q}_\kappa > 0, \overline{S}_{1\kappa} > 0$, and $\overline{S}_{2\kappa} > 0$ ($\kappa = 1, 2, \ldots, r$) with appropriate dimensions, such that the following LMIs hold for $\kappa, \lambda, \mu, \nu, i, s = 1, 2, \ldots, r$:*

$$\begin{aligned} &\widetilde{\Theta}_{\kappa\lambda\mu\nu ii} < 0, \\ &\widetilde{\Theta}_{\kappa\lambda\mu\nu is} + \widetilde{\Theta}_{\kappa\lambda\mu\nu si} < 0, \quad s \ne i, \end{aligned} \tag{42}$$

where

$$\widetilde{\Theta}_{\kappa\lambda\mu\nu is} = \begin{bmatrix} \overline{\Xi}_1 & A_i\overline{P} + B_i\overline{K}_s & A_{di}\overline{P} & 0 & 0 \\ * & \overline{\Xi}_{2\kappa is} & A_{di}\overline{P} & \frac{1}{d_m}\overline{R}_1 & \frac{1}{d_M}\overline{R}_2 \\ * & * & -\overline{Q}_\lambda & 0 & 0 \\ * & * & * & -\overline{S}_{1\mu} - \frac{1}{d_m}\overline{R}_1 & 0 \\ * & * & * & * & -\overline{S}_{2\nu} - \frac{1}{d_M}\overline{R}_2 \end{bmatrix}, \tag{43}$$

$$\overline{\Xi}_{1\kappa} = (T-2)\overline{P} + d_m\overline{R}_1 + d_M\overline{R}_2,$$

$$\overline{\Xi}_{2\kappa is} = A_i\overline{P} + \overline{P}A_i^T + B_i\overline{K}_s + \overline{K}_s^T B_i^T + (d_M - d_m + T + 1)\overline{Q}_\kappa + \overline{S}_{1\kappa} + \overline{S}_{2\kappa} - \frac{1}{d_m}\overline{R}_1 - \frac{1}{d_M}\overline{R}_2.$$

Then, the controller (4) can be designed as

$$u(t_k) = \overline{K}_s\overline{P}^{-1}x(t_k). \tag{44}$$

4. Numerical Example

In this section, one example is presented to demonstrate the effectiveness of the proposed method.

Example 1. Consider the following fuzzy system with time-varying delay and input disturbance:

Plant Rule 1. IF $\theta(t_k)$ is 0, THEN

$$\delta x(t_k) = A_1 x(t_k) + A_{d1} x(t_k - d_k) + B_1 u(t_k) + B_{w1} w(t_k),$$

Table 1: The feasibility of the system with $T = 0.001$.

	d_m	d_M	K_1	K_2
$T = 0.001$	0.01	7.44	[−0.2229 −13.6801]	[−1.7743 −4.5044]

$$z(t_k) = C_1 x(t_k) + C_{d1} x(t_k - d_k) + D_1 u(t_k) + D_{w1} w(t_k). \tag{45}$$

Plant Rule 2. IF $\theta(t_k)$ is $\pm(\pi/2)(|\theta(t_k)| < \pi/2)$, THEN

$$\begin{aligned} \delta x(t_k) &= A_2 x(t_k) + A_{d2} x(t_k - d_k) + B_2 u(t_k) \\ &\quad + B_{w2} w(t_k), \\ z(t_k) &= C_2 x(t_k) + C_{d2} x(t_k - d_k) + D_2 u(t_k) \\ &\quad + D_{w2} w(t_k). \end{aligned} \tag{46}$$

The system matrix parameters in (45) and (46) are given as follows:

$$\begin{aligned} &A_1 = \begin{bmatrix} -2.000 & -0.060 \\ 0.070 & 0.100 \end{bmatrix}, \quad A_2 = \begin{bmatrix} -1.800 & 0.080 \\ -0.050 & 0.100 \end{bmatrix}, \\ &B_1 = \begin{bmatrix} 0.080 \\ 0.050 \end{bmatrix}, \quad B_2 = \begin{bmatrix} 0.080 \\ 0.090 \end{bmatrix}, \\ &A_{d1} = \begin{bmatrix} -0.020 & -0.010 \\ 0.010 & 0.020 \end{bmatrix}, \quad A_{d2} = \begin{bmatrix} -1.800 & 0.080 \\ -0.050 & 0.100 \end{bmatrix}, \\ &B_{w1} = \begin{bmatrix} 0.010 & -0.100 \end{bmatrix}^T, \\ &B_{w2} = \begin{bmatrix} -0.010 & -0.100 \end{bmatrix}^T, \quad C_1 = \begin{bmatrix} -0.010 & 0.010 \end{bmatrix}, \\ &C_2 = \begin{bmatrix} 0.120 & -0.100 \end{bmatrix}, \quad D_1 = 0.010, \\ &C_{d1} = \begin{bmatrix} 0.080 & 0.010 \end{bmatrix}, \quad C_{d2} = \begin{bmatrix} -0.010 & -0.050 \end{bmatrix}, \\ &D_2 = 0.020, \quad D_{w1} = 0.010, \quad D_{w2} = 0.020. \end{aligned} \tag{47}$$

Two membership functions are chosen for Plant Rules 1 and 2 as follows:

$$\begin{aligned} h_1(\theta(t_k)) &= \begin{cases} 1 - \dfrac{2}{\pi}\theta(t_k), & 0 \le \theta(t_k) \le \dfrac{\pi}{2}, \\ 1 + \dfrac{2}{\pi}\theta(t_k), & -\dfrac{\pi}{2} \le \theta(t_k) < 0, \end{cases} \\ h_2(\theta(t_k)) &= 1 - h_1(\theta(t_k)). \end{aligned} \tag{48}$$

And Figure 1 shows the membership functions.

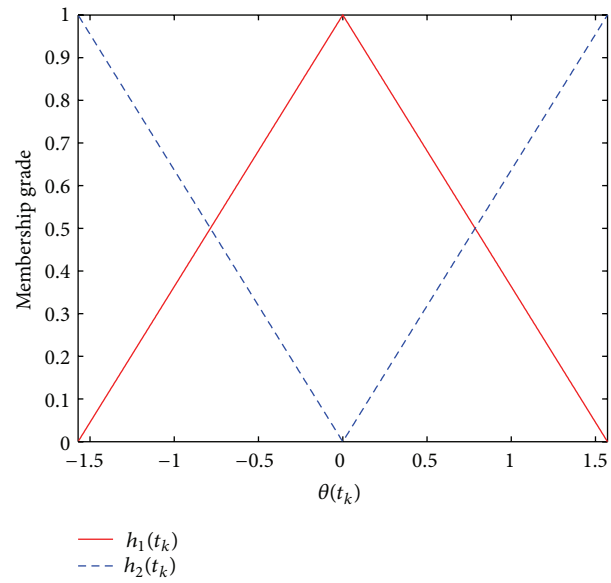

Figure 1: Membership functions of two rules.

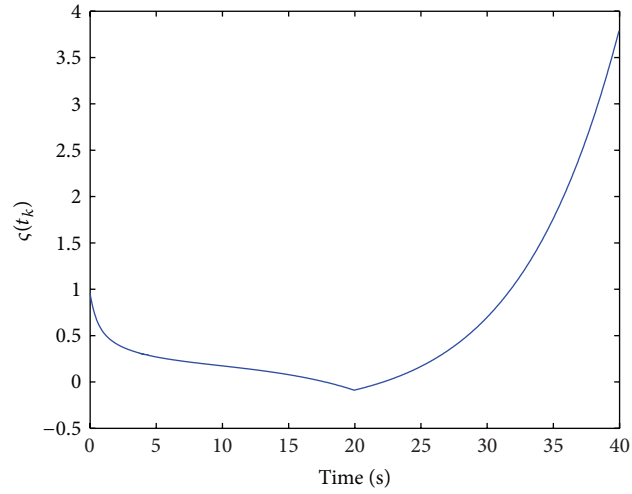

Figure 2: Response of $\varsigma(t_k)$ of the open-loop system.

Define the value range of time delay $d_k = nT$, and choosing the lower bound $d_m = 0.01$, the sampling period T may be assumed as $T = 0.001$ and it can be found from Theorem 9 that the maximum upper bound of time delay d_k and the control gain matrices are listed in Table 1.

Assume that time delay $d_k = nT = 40T$ and the disturbance input $w(t_k) = -1/(2 + t_k)$. It can be calculated

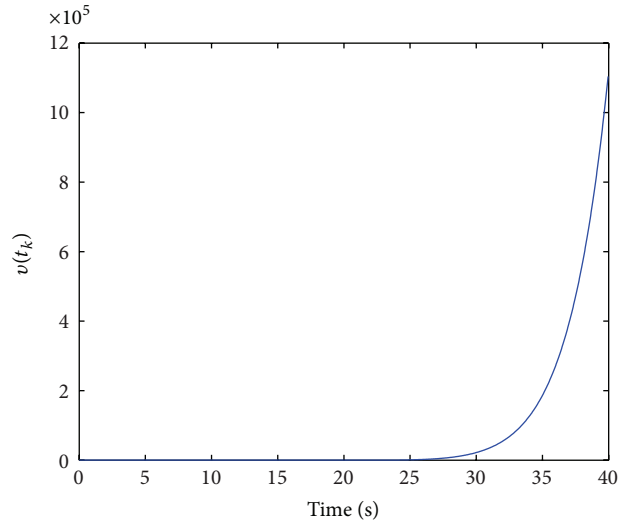

Figure 3: Response of $\upsilon(t_k)$ of the open-loop system.

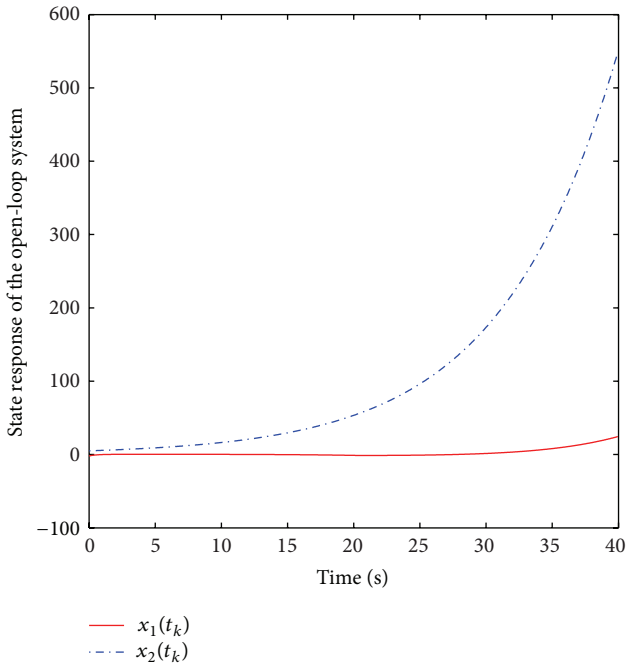

Figure 4: State response of the open-loop system.

that $\sum_{t_k=0}^{\infty} w^T(t_k)w(t_k) = 0.5 < \infty$, which means that $w(t_k) \in L_2[0, \infty)$. Let

$$\upsilon(t_k) = 2\sum_{t_k=0}^{\infty} z^T(t_k)\, w(t_k) - \varepsilon \sum_{t_k=0}^{\infty} z^T(t_k)\, z(t_k) - \zeta \sum_{t_k=0}^{\infty} w^T(t_k)\, w(t_k), \quad (49)$$

$$\varsigma(t_k) = 2\sum_{t_k=0}^{\infty} z^T(t_k)\, w(t_k).$$

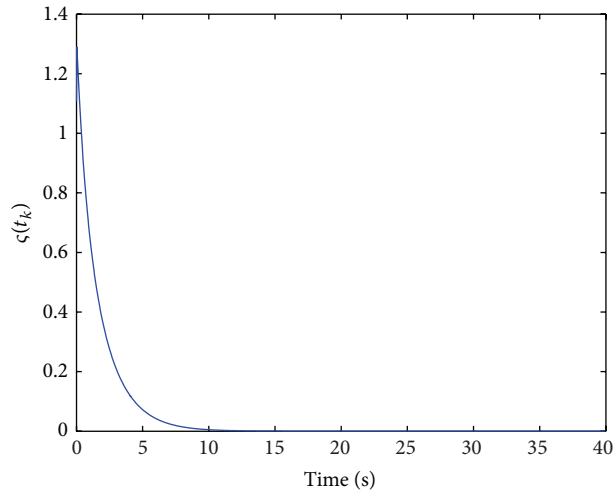

Figure 5: Response of $\varsigma(t_k)$ of the closed-loop system.

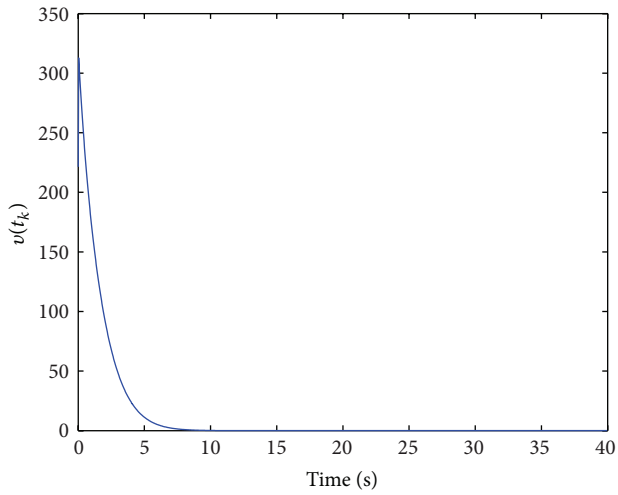

Figure 6: Response of $\upsilon(t_k)$ of the closed-loop system.

In Figure 2, it can be observed that $\varsigma(t_k)$ decreases finally as the time t_k increases, which means that there may not exist a scalar ρ such that $\varsigma(t_k) \geq \rho$ hold for all $t_k \geq 0$ for $T = 0.001$. Furthermore, Figure 3 shows that there may not exist a scalar ρ such that $\upsilon(t_k) \geq \rho$, which means that the open-loop system is not passive in the sense of Definition 2, and it is not very strictly passive. Figure 4 illustrates that the open-loop system is not stable for $T = 0.001$.

Under the control gain matrices in Table 1, Figure 5 plots the responses of $\varsigma(t_k)$ for the closed-loop system for $T = 0.001$. It can be seen that there may exist a scalar ρ such that $\varsigma(t_k) \geq \rho$ holds for all $t_k \geq 0$. It can be seen from Figure 6 that there may exist a scalar ρ such that $\upsilon(t_k) \geq \rho$. Then, it is clear that the closed-loop system is very strictly passive under the control gain matrices in Table 1. In addition, Figure 7 shows that the closed-loop system is stable. Furthermore, Figure 8 depicts the control input responses. These simulation results have demonstrated the effectiveness of the proposed method.

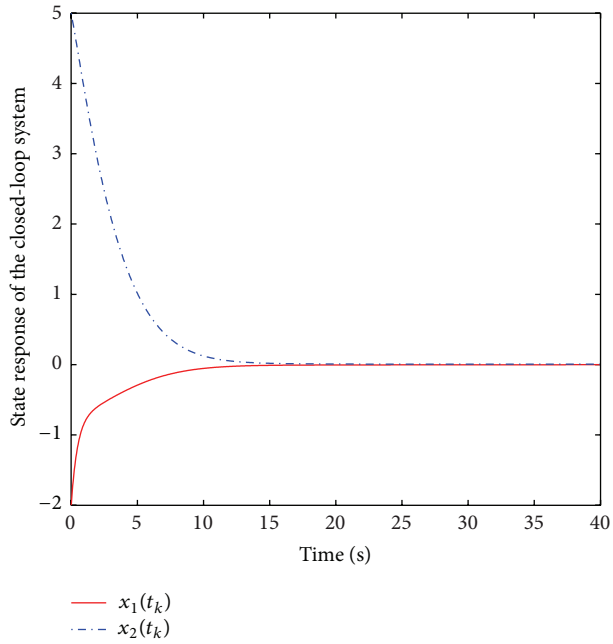

Figure 7: State response of the open-loop system.

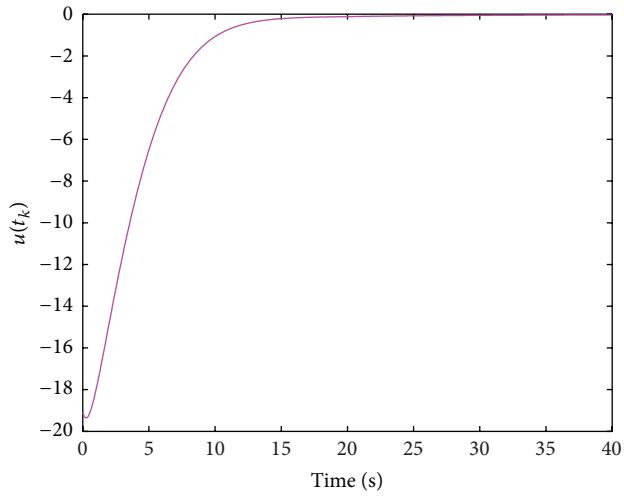

Figure 8: Control signal response of the closed-loop system.

5. Conclusions

In this paper, the problems of passivity analysis and passive control have been investigated for fuzzy delta operator systems with time delay and disturbance input. By applying some new LKF in δ-domain and utilizing some fuzzy weighing matrices, the state-feedback controller has been designed to guarantee that the resulting closed-loop system is very strictly passive. The existence conditions for the controller have been expressed as LMIs. Finally, a numerical example has been included to illustrate the effectiveness of the proposed results. In future work, based on T-S fuzzy control method, the problems of control and monitoring in the data-driven framework [53, 54] could be further studied.

Conflict of Interests

The authors declare that there is no conflict of interests regarding the publication of this paper.

Acknowledgments

This work was partially supported by the National Natural Science Foundation of China (61203002, 61304002, and 61304003), the Program for New Century Excellent Talents in University (NCET-13-0696), the Program for Liaoning Innovative Research Team in University (LT2013023), and the Program for Liaoning Excellent Talents in University (LR2013053).

References

[1] S. Tong, X.-L. He, and H.-G. Zhang, "A combined backstepping and small-gain approach to robust adaptive fuzzy output feedback control," *IEEE Transactions on Fuzzy Systems*, vol. 17, no. 5, pp. 1059–1069, 2009.

[2] S. Tong and Y. Li, "Observer-based fuzzy adaptive control for strict-feedback nonlinear systems," *Fuzzy Sets and Systems*, vol. 160, no. 12, pp. 1749–1764, 2009.

[3] Y. Li, S. Tong, Y. Liu, and T. Li, "Adaptive fuzzy robust output feedback control of nonlinear systems with unknown dead zones based on small-gain approach," *IEEE Transactions on Fuzzy Systems*, 2013.

[4] Y. Li, S. Tong, and T. Li, "Adaptive fuzzy output feedback control of uncertain nonlinear systems with unknown backlash-like hysteresis," *Information Sciences*, vol. 198, pp. 130–146, 2012.

[5] T. Takagi and M. Sugeno, "Fuzzy identification of systems and its applications to modeling and control," *IEEE Transactions on Systems, Man and Cybernetics*, vol. 15, no. 1, pp. 116–132, 1985.

[6] K. Tanaka, T. Hori, and H. O. Wang, "A multiple Lyapunov function approach to stabilization of fuzzy control systems," *IEEE Transactions on Fuzzy Systems*, vol. 11, no. 4, pp. 582–589, 2003.

[7] T. M. Guerra and L. Vermeiren, "LMI-based relaxed nonquadratic stabilization conditions for nonlinear systems in the Takagi-Sugeno's form," *Automatica*, vol. 40, no. 5, pp. 823–829, 2004.

[8] K. Tanaka and H. O. Wang, *Fuzzy Control Systems Design and Analysis. A Linear Matrix Inequality Approach*, John Wiley and Sons, New York, NY, USA, 2001.

[9] G. Feng, "A survey on analysis and design of model-based fuzzy control systems," *IEEE Transactions on Fuzzy Systems*, vol. 14, no. 5, pp. 676–697, 2006.

[10] S. Nguang and P. Shi, "H_∞ fuzzy output feedback control design for nonlinear systems: an LMI approach," *IEEE Transactions on Fuzzy Systems*, vol. 11, no. 3, pp. 331–340, 2003.

[11] S. Nguang, W. Assawinchaichote, and P. Shi, "Robust H_∞ control design for fuzzy singularly perturbed systems with Markovian jumps: an LMI approach," *IET Control Theory and Applications*, vol. 1, no. 4, pp. 893–908, 2007.

[12] B. Jiang, Z. Mao, and P. Shi, "H_∞-filter design for a class of networked control systems via TS fuzzy-model approach," *IEEE Transactions on Fuzzy Systems*, vol. 18, no. 1, pp. 201–208, 2010.

[13] H. Dong, Z. Wang, D. W. C. Ho, and H. Gao, "Robust H_∞ fuzzy output-feedback control with multiple probabilistic delays and

multiple missing measurements," *IEEE Transactions on Fuzzy Systems*, vol. 18, no. 4, pp. 712–725, 2010.

[14] L. Wu, X. Su, P. Shi, and J. Qiu, "Model approximation for discrete-time state-delay systems in the TS fuzzy framework," *IEEE Transactions on Fuzzy Systems*, vol. 19, no. 2, pp. 366–378, 2011.

[15] M. Liu, X. Cao, and P. Shi, "Fault estimation and tolerant control for fuzzy stochastic systems," *IEEE Transactions on Fuzzy Systems*, vol. 21, no. 2, pp. 221–229, 2013.

[16] M. Liu, X. Cao, and P. Shi, "Fuzzy-model-based fault tolerant design for nonlinear stochastic systems against simultaneous sensor and actuator faults," *IEEE Transactions on Fuzzy Systems*, vol. 21, no. 5, pp. 789–799, 2013.

[17] J. Qiu, G. Feng, and H. Gao, "Fuzzy-model-based piecewise H_∞ static-output-feedback controller design for networked nonlinear systems," *IEEE Transactions on Fuzzy Systems*, vol. 18, no. 5, pp. 919–934, 2010.

[18] J. Qiu, G. Feng, and H. Gao, "Asynchronous output-feedback control of networked nonlinear systems with multiple packet dropouts: T-S fuzzy affine model-based approach," *IEEE Transactions on Fuzzy Systems*, vol. 19, no. 6, pp. 1014–1030, 2011.

[19] B. Chen, X. Liu, S. Tong, and C. Lin, "Guaranteed cost control of T-S fuzzy systems with state and input delays," *Fuzzy Sets and Systems*, vol. 158, no. 20, pp. 2251–2267, 2007.

[20] B. Chen, X. Liu, C. Lin, and K. Liu, "Robust H_∞ control of Takagi-Sugeno fuzzy systems with state and input time delays," *Fuzzy Sets and Systems*, vol. 160, no. 4, pp. 403–422, 2009.

[21] S. Xu and J. Lam, "Robust H_∞ control for uncertain discrete-time-delay fuzzy systems via output feedback controllers," *IEEE Transactions on Fuzzy Systems*, vol. 13, no. 1, pp. 82–93, 2005.

[22] C. Lin, G. Wang, and T. Lee, *LMI Approach to Analysis and Control of Takagi-Sugeno Fuzzy Systems with Time Delay*, Springer, New York, NY, USA, 2007.

[23] C. Lin, Q.-G. Wang, and T. H. Lee, "Stabilization of uncertain fuzzy time-delay systems via variable structure control approach," *IEEE Transactions on Fuzzy Systems*, vol. 13, no. 6, pp. 787–798, 2005.

[24] B. Zhang and S. Xu, "Delay-Dependent Robust H_∞ control for uncertain discrete-time fuzzy systems with time-varying delays," *IEEE Transactions on Fuzzy Systems*, vol. 17, no. 4, pp. 809–823, 2009.

[25] B. Zhang, J. Lam, S. Xu, and Z. Shu, "Robust stabilization of uncertain T-S fuzzy time-delay systems with exponential estimates," *Fuzzy Sets and Systems*, vol. 160, no. 12, pp. 1720–1737, 2009.

[26] L. Wu, X. Su, P. Shi, and J. Qiu, "A new approach to stability analysis and stabilization of discrete-time T-S fuzzy time-varying delay systems," *IEEE Transactions on Systems, Man, and Cybernetics B*, vol. 41, no. 1, pp. 273–286, 2011.

[27] H. Li, J. Yu, C. Hilton, and H. Liu, "Adaptive sliding mode control for nonlinear active suspension vehicle systems using T-S fuzzy approach," *IEEE Transactions on Industrial Electronics*, vol. 60, no. 8, pp. 3328–3338, 2013.

[28] H. Li, H. Liu, H. Gao, and P. Shi, "Reliable fuzzy control for active suspension systems with actuator delay and fault," *IEEE Transactions on Fuzzy Systems*, vol. 20, no. 2, pp. 342–357, 2012.

[29] H. K. Lam and J. Lauber, "Membership-function-dependent stability analysis of fuzzy-model-based control systems using fuzzy Lyapunov functions," *Information Sciences*, vol. 232, no. 14, pp. 253–266, 2013.

[30] H. K. Lam and J. C. Lo, "Output regulation of polynomial-fuzzy-model-based control systems," *IEEE Transactions on Fuzzy Systems*, vol. 21, no. 2, pp. 262–274, 2013.

[31] H. K. Lam, "Polynomial fuzzy-model-based control systems: stability analysis via piecewise-linear membership functions," *IEEE Transactions on Fuzzy Systems*, vol. 19, no. 3, pp. 588–593, 2011.

[32] X. Zhao, L. Zhang, P. Shi, and H. R. Karimi, "Novel stability criteria for T-S fuzzy systems," *IEEE Transactions on Fuzzy Systems*, 2013.

[33] L. Wu and W. X. Zheng, "Passivity-based sliding mode control of uncertain singular time-delay systems," *Automatica*, vol. 45, no. 9, pp. 2120–2127, 2009.

[34] H. Gao, T. Chen, and T. Chai, "Passivity and passification for networked control systems," *SIAM Journal on Control and Optimization*, vol. 46, no. 4, pp. 1299–1322, 2007.

[35] S. Xu, W. X. Zheng, and Y. Zou, "Passivity analysis of neural networks with time-varying delays," *IEEE Transactions on Circuits and Systems II*, vol. 56, no. 4, pp. 325–329, 2009.

[36] J. Liang, Z. Wang, and X. Liu, "On passivity and passification of stochastic fuzzy systems with delays: the discrete-time case," *IEEE Transactions on Systems, Man, and Cybernetics B*, vol. 40, no. 3, pp. 964–969, 2010.

[37] C. Wang and Y. Shen, "Passive control for stochastic interval systems with interval time-varying delay," *Asian Journal of Control*, vol. 15, no. 1, pp. 248–259, 2013.

[38] H. Li, H. Gao, and P. Shi, "New passivity analysis for neural networks with discrete and distributed delays," *IEEE Transactions on Neural Networks*, vol. 21, no. 11, pp. 1842–1847, 2010.

[39] Z.-G. Wu, P. Shi, H. Su, and J. Chu, "Passivity analysis for discrete-time stochastic markovian jump neural networks with mixed time delays," *IEEE Transactions on Neural Networks*, vol. 22, no. 10, pp. 1566–1575, 2011.

[40] C. Li, H. Zhang, and X. Liao, "Passivity and passification of fuzzy systems with time delays," *Computers and Mathematics with Applications*, vol. 52, no. 6-7, pp. 1067–1078, 2006.

[41] B. Zhang, W. X. Zheng, and S. Xu, "Passivity analysis and passive control of fuzzy systems with time-varying delays," *Fuzzy Sets and Systems*, vol. 174, no. 1, pp. 83–98, 2011.

[42] G. Goodwin, R. L. Leal, D. Q. Mayne, and R. H. Middleton, "Rapprochement between continuous and discrete model reference adaptive control," *Automatica*, vol. 22, no. 2, pp. 199–207, 1986.

[43] R. Middleton and G. Goodwin, "Improved finite word length characteristics in digital control using delta operators," *IEEE Transactions on Automatic Control*, vol. 31, no. 11, pp. 1015–1021, 1986.

[44] C. P. Neuman, "Transformation between delta and forward shift operator transfer function models," *IEEE Transactions on Systems, Man and Cybernetics*, vol. 23, no. 1, pp. 295–296, 1993.

[45] K. Premaratne, R. Salvi, N. R. Habib, and J. P. LeGall, "Delta-operator formulated discrete-time approximations of continuous-time systems," *IEEE Transactions on Automatic Control*, vol. 39, no. 3, pp. 581–585, 1994.

[46] K. Premaratne and E. Jury, "Tabular method for determining root distribution of delta-operator formulated real polynomials," *IEEE Transactions on Automatic Control*, vol. 39, no. 2, pp. 352–355, 1994.

[47] M. Tadjine, M. M'Saad, and L. Dugard, "Discrete-time compensators with loop transfer recovery," *IEEE Transactions on Automatic Control*, vol. 39, no. 6, pp. 1259–1262, 1994.

[48] J. Qiu, Y. Xia, H. Yang, and J. Zhang, "Robust stabilisation for a class of discrete-time systems with time-varying delays via delta operators," *IET Control Theory and Applications*, vol. 2, no. 1, pp. 87–93, 2008.

[49] H. Yang, Y. Xia, and P. Shi, "Observer-based sliding mode control for a class of discrete systems via delta operator approach," *Journal of the Franklin Institute*, vol. 347, no. 7, pp. 1199–1213, 2010.

[50] H. Yang, P. Shi, J. Zhang, and J. Qiu, "Robust H_∞ control for a class of discrete time fuzzy systems via delta operator approach," *Information Sciences*, vol. 184, no. 1, pp. 230–245, 2012.

[51] B. Brogliato, O. Egeland, R. Lozano, and B. Maschke, *Dissipative Systems Analysis and Control: Theory and Applications*, Springer, London, UK, 2007.

[52] X. Jiang, Q.-L. Han, and X. Yu, "Stability criteria for linear discrete-time systems with interval-like time-varying delay," in *2005 American Control Conference, ACC*, pp. 2817–2822, usa, June 2005.

[53] S. Yin, S. Ding, and H. Luo, "Real-time implementation of fault tolerant control system with performance optimization," *IEEE Transactions on Industrial Electronics*, vol. 61, no. 5, pp. 2402–2411, 2014.

[54] L. Xie, "Output feedback H_∞ control of systems with parameter uncertainty," *International Journal of Control*, vol. 63, no. 4, pp. 741–750, 1996.

Hindawi Publishing Corporation
Mathematical Problems in Engineering
Volume 2013, Article ID 680272, 6 pages
http://dx.doi.org/10.1155/2013/680272

Research Article

Improving Delay-Range-Dependent Stability Condition for Systems with Interval Time-Varying Delay

Wei Qian,[1] Tao Li,[2] and Juan Liu[3]

[1] *School of Electrical Engineering and Automation, Henan Polytechnic University, Jiaozuo, Henan 454000, China*
[2] *School of Automation Engineering, Nanjing University of Aeronautics and Astronautics, Nanjing 210016, China*
[3] *Department of Mathematics and Information Science, Henan Polytechnic University, Jiaozuo, Henan 454000, China*

Correspondence should be addressed to Wei Qian; qwei@hpu.edu.cn

Received 26 August 2013; Accepted 12 October 2013

Academic Editor: Bo-Chao Zheng

This paper discusses the delay-range-dependent stability for systems with interval time-varying delay. Through defining the new Lyapunov-Krasovskii functional and estimating the derivative of the LKF by introducing new vectors, using free matrices and reciprocally convex approach, the new delay-range-dependent stability conditions are obtained. Two well-known examples are given to illustrate the less conservatism of the proposed theoretical results.

1. Introduction

It is well known that time-varying delays are frequently encountered in many practical control systems, and they are usually regarded as a source of instability and poor performance. So the stability issue of time delay systems has received considerable attention [1–16]. In the last years, in order to further reduce conservatism of the stability results, some methods were developed, such as the delay-fraction approach in [1, 2], free weighting matrices method in [3, 4], the convex analysis method in [5, 6], the reciprocally convex approach in [7], LKF constructing method with matrices that depend on the time delays [8], LKF constructing method with triple-integral terms in [9], LKF constructing method with quadruple-integral terms in [10], and simple LKF having quadratic terms multiplied by a higher degree scalar function [11, 12]. These methods reduced the conservatism of the stability results. But when delay is interval time-varying, the information of the delay derivative is not full used, which causes the conservatism of the stability results.

Motivated by recent methods, in this paper, we further discuss the stability of linear systems with interval time-varying delay. Firstly, a novel LKF is introduced. Then, by introducing new vectors, using free matrices and reciprocally convex approach, the derivative of LKF is estimated less conservatively, and as a result, the stability criterion is obtained in terms of LMI. Finally, two examples are given to illustrate the effectiveness of the proposed method.

Throughout the note, the used notations are standard. $\mathbf{R}^n$ denotes the n-dimensional Euclidean space, $\mathbf{R}^{n\times m}$ is a set of $n \times m$ real matrix, A^T is the transpose of A, $P > 0$ ($P < 0$) means symmetric positive (negative) definite matrix, and $*$ in the matrix denotes the symmetric element; I is the identity matrix of appropriate dimensions, $x_t = x(t+\theta), \theta \in [-h, 0]$. Matrices, if their dimensions are not explicitly stated, are assumed to be compatible for algebraic operations.

2. Problem Formulations

Consider the following time-delay system:

$$\begin{aligned} \dot{x}(t) &= Ax(t) + A_1 x(t - h(t)), \\ x(t) &= \phi(t), \quad t \in [-h, 0], \end{aligned} \tag{1}$$

where $x(t) \in \mathbf{R}^n$ is the state vector, the initial condition $\phi(t)$ is a continuously differentiable vector-valued function, $A, A_1 \in \mathbf{R}^{n\times n}$ are known real constant matrices, and $h(t)$ is the time-varying delay satisfying

$$h_1 \le h(t) \le h_2, \qquad \dot{h}(t) \le \mu \le \infty, \tag{2}$$

where h_1, h_2, and μ are constants.

To obtain the main results, the following lemmas are needed.

Lemma 1 (see [9]). *For any symmetric matrix $Z = Z^T \geq 0$, scalars $h_2 > h_1 > 0$ such that the integration is well defined; then*

$$\begin{aligned} &-(h_2 - h_1)\int_{-h_2}^{-h_1}\int_{t+\theta}^{t} x^T(s) Z x(s)\, ds\, d\theta \\ &\quad\leq -\int_{-h_2}^{-h_1}\int_{t+\theta}^{t} x^T(s)\, ds\, d\theta Z \int_{-h_2}^{-h_1}\int_{t+\theta}^{t} x(s)\, ds\, d\theta. \end{aligned} \tag{3}$$

Lemma 2 (see [7]). *Let $f_1, f_2, \ldots, f_N : \mathbf{R}^m \to \mathbf{R}$ have positive values in an open subset $\mathbf{D}$ of $\mathbf{R}^m$. Then, the reciprocally convex combination of f_i over $\mathbf{D}$ satisfies*

$$\begin{aligned} &\min_{\{\alpha_i \mid \alpha_i > 0, \sum \alpha_i = 1\}} \sum_i \frac{1}{\alpha_i} f_i(t) = \sum_i f_i(t) + \max_{g_{ij}(t)} \sum_{i \neq j} g_{ij}(t) \\ &\text{subject to} \quad g_{i,j} : \mathbf{R}^m \longrightarrow \mathbf{R}, \qquad g_{ij}(t) = g_{ji}(t), \\ &\begin{bmatrix} f_i(t) & g_{ij}(t) \\ g_{ij}(t) & f_j(t) \end{bmatrix} \geq 0. \end{aligned} \tag{4}$$

Lemma 3 (see [16]). *The symmetric appropriately dimensional matrices $\Theta > 0, \Xi, \Upsilon$, if $\Xi - \Upsilon\Theta\Upsilon^T < 0$ hold; then there exists a matrix of appropriate dimension Π such that the following LMI holds:*

$$\begin{bmatrix} \Xi + \Upsilon\Pi^T + \Pi\Upsilon^T & \Pi \\ * & -\Theta \end{bmatrix} < 0. \tag{5}$$

3. Main Results

In this section, the stability of system (1) is investigated. Through constructing a novel LKF and estimating the derivative of it, new stability condition is provided.

Firstly, define the following vector as

$$\begin{aligned} \zeta^T(t) &= \left[x^T(t) \quad \int_{t-h_1}^{t} x^T(s)\, ds \right], \\ \xi^T(t) &= \left[\dot{x}^T(t) \quad x^T(t) \right], \end{aligned} \tag{6}$$

and then construct the L-K functional as follows:

$$V(x_t) = \sum_{i=1}^{4} V_i(x_t), \tag{7}$$

where

$$\begin{aligned} V_1(x_t) &= \zeta^T(t) P \zeta(t), \\ V_2(x_t) &= \int_{t-h_1}^{t} x^T(s) Q_1 x(s)\, ds + \int_{t-h(t)}^{t-h_1} x^T(s) Q_2 x(s)\, ds \\ &\quad + \int_{t-h_2}^{t-h(t)} x^T(s) Q_3 x(s)\, ds, \\ V_3(x_t) &= h_1 \int_{-h_1}^{0}\int_{t+\theta}^{t} \xi^T(s) \begin{bmatrix} R_1 & 0 \\ * & R_2 \end{bmatrix} \xi(s)\, ds\, d\theta \\ &\quad + (h_2 - h_1)\int_{-h_2}^{-h_1}\int_{t+\theta}^{t} \xi^T(s) \begin{bmatrix} X_1 & 0 \\ * & X_2 \end{bmatrix} \xi(s)\, ds\, d\theta, \\ V_4(x_t) &= \frac{h_1^2}{2}\int_{-h_1}^{0}\int_{\theta}^{0}\int_{t+\lambda}^{t} \dot{x}^T(s) U_1 \dot{x}(s)\, ds\, d\lambda\, d\theta \\ &\quad + \frac{h_2^2 - h_1^2}{2}\int_{-h_1}^{-h_2}\int_{\theta}^{0}\int_{t+\lambda}^{t} \dot{x}^T(s) U_2 \dot{x}(s)\, ds\, d\lambda\, d\theta \\ &\quad + \frac{1}{2}\int_{t-h_2}^{t-h_1}\int_{\theta}^{t-h_1}\int_{\lambda}^{t} \dot{x}^T(s) U_3 \dot{x}(s)\, ds\, d\lambda\, d\theta, \end{aligned} \tag{8}$$

and matrices $Q_1, Q_2, Q_3, R_1, R_2, X_1, X_2, U_1, U_2, U_3 \in \mathbf{R}^{n\times n} > 0$, $P = [P_{ij}]$ $(1 \leq i \leq j \leq 2) \in \mathbf{R}^{2n\times 2n} > 0$.

In order to make the proof process clear, the following notations are used:

$$\begin{aligned} &\alpha(t) = h(t) - h_1, \qquad \beta(t) = h_2 - h(t), \qquad \varphi(t) = \frac{1}{\alpha(t)}\int_{t-h(t)}^{t-h_1} x^T(s)\, ds, \qquad \phi(t) = \frac{1}{\beta(t)}\int_{t-h_2}^{t-h(t)} x^T(s)\, ds, \\ &\chi^T(t) = \left[x^T(t) \quad x^T(t-h(t)) \quad x^T(t-h_1) \quad x^T(t-h_2) \quad \int_{t-h_1}^{t} x^T(s) \quad \varphi^T(t) \quad \phi^T(t) \quad \dot{x}^T(t) \right] \end{aligned} \tag{9}$$

and block entry matrices e_i $(i = 1, 2, \ldots, 5)$ (e.g., $e_2^T = [0 \ I \ 0 \ 0 \ 0 \ 0 \ 0 \ 0]$).

Then taking the time derivatives of $V_i(x_t)$ along the trajectory of system (1) yields

$$\begin{aligned} \dot{V}_1(x_t) &= 2\zeta^T(t) P \dot{\zeta}(t) = 2\chi^T(t) \left[e_1 \quad e_5 \right] P \left[e_8 \quad e_1 - e_3 \right]^T \chi(t), \\ \dot{V}_2(x_t) &= x^T(t) Q_1 x(t) - x^T(t-h_1)(Q_1 - Q_2) x(t-h_1) \\ &\quad - \left(1 - \dot{h}(t)\right) x^T(t-h(t)) (Q_2 - Q_3) x(t-h(t)) \\ &\quad - x^T(t-h_2) Q_3 x(t-h_2) \\ &\leq \chi^T(t) \left[e_1 Q_1 e_1^T - e_3 (Q_1 - Q_2) e_3^T \right. \\ &\quad \left. - (1-\mu) e_2 (Q_2 - Q_3) e_2^T - e_4 Q_3 e_4^T \right] \chi(t), \end{aligned} \tag{10}$$

where $Q_2 - Q_3 > 0$.

To reduce the conservatism of the main result, by using the Jesen inequality and Lemma 2 with introducing appropriate matrices $Y_1, Y_2 \in \mathbf{R}^{n\times n}$, we can calculate $\dot{V}_3(x_t)$ as

$$\begin{aligned}
\dot{V}_3(x_t) &= h_1^2\xi^T(t)\begin{bmatrix} R_1 & 0 \\ * & R_2 \end{bmatrix}\xi(t) \\
&\quad + (h_2-h_1)^2\xi^T(t)\begin{bmatrix} X_1 & 0 \\ * & X_2 \end{bmatrix}\xi(t) \\
&\quad - h_1\int_{t-h_1}^{t}\xi^T(s)\begin{bmatrix} R_1 & 0 \\ * & R_2 \end{bmatrix}\xi(s)\,ds \\
&\quad - (h_2-h_1)\int_{t-h_2}^{t-h_1}\xi^T(s)\begin{bmatrix} X_1 & 0 \\ * & X_2 \end{bmatrix}\xi(s)\,ds \\
&\le \chi^T(t)\left\{e_8\left[h_1^2R_1 + (h_2-h_1)^2X_1\right]e_8^T\right. \\
&\qquad + e_1\left[h_1^2R_2 + (h_2-h_1)^2X_2\right]e_1^T \\
&\qquad \left. - (e_1-e_3)R_1(e_1-e_3)^T - e_5R_2e_5^T\right\}\chi(t) \\
&\quad - \chi^T(t)\left[e_2-e_3 \;\; e_4-e_2\right] \\
&\quad \times\begin{bmatrix} X_1 & Y_1 \\ * & X_1 \end{bmatrix}\left[e_2-e_3 \;\; e_4-e_2\right]^T\chi(t) - \Gamma_1,
\end{aligned} \tag{11}$$

where by using Lemma 2 with matrix Y_1, one can get

$$\begin{aligned}
&-(h_2-h_1)\int_{t-h_2}^{t-h_1}\dot{x}^T(s)X_1\dot{x}(s)\,ds \\
&\quad = -(h_2-h_1)\int_{t-h(t)}^{t-h_1}\dot{x}^T(s)X_1\dot{x}(s)\,ds \\
&\qquad -(h_2-h_1)\int_{t-h_2}^{t-h(t)}\dot{x}^T(s)X_1\dot{x}(s)\,ds \\
&\quad \le -\begin{bmatrix} x(t-h(t))-x(t-h_1) \\ x(t-h_2)-x(t-h(t)) \end{bmatrix}^T \\
&\qquad \times\begin{bmatrix} X_1 & Y_1 \\ * & X_1 \end{bmatrix}\begin{bmatrix} x(t-h(t))-x(t-h_1) \\ x(t-h_2)-x(t-h(t)) \end{bmatrix} \\
&\quad = -\chi^T(t)\left[e_2-e_3 \;\; e_4-e_2\right]\begin{bmatrix} X_1 & Y_1 \\ * & X_1 \end{bmatrix} \\
&\qquad \times\left[e_2-e_3 \;\; e_4-e_2\right]^T\chi(t),
\end{aligned} \tag{12}$$

and by using Lemma 2 with matrix Y_2, one can get

$$\begin{aligned}
&-(h_2-h_1)\int_{t-h_2}^{t-h_1}x^T(s)X_2x(s)\,ds \\
&\quad = -(h_2-h_1)\int_{t-h(t)}^{t-h_1}x^T(s)X_2x(s)\,ds \\
&\qquad -(h_2-h_1)\int_{t-h_2}^{t-h(t)}x^T(s)X_2x(s)\,ds \\
&\quad \le -\begin{bmatrix} \int_{t-h(t)}^{t-h_1}x(s)ds \\ \int_{t-h_2}^{t-h(t)}x(s)ds \end{bmatrix}^T \\
&\qquad \times\begin{bmatrix} X_2 & Y_2 \\ * & X_2 \end{bmatrix}\begin{bmatrix} \int_{t-h(t)}^{t-h_1}x(s)\,ds \\ \int_{t-h_2}^{t-h(t)}x(s)\,ds \end{bmatrix} = \Gamma_1.
\end{aligned} \tag{13}$$

To the time-derivative of $V_4(x_t)$, it can be calculated as

$$\begin{aligned}
\dot{V}_4(x_t) &= \frac{h_1^4}{4}\dot{x}^T(t)U_1\dot{x}(t) + \frac{\left(h_2^2-h_1^2\right)^2}{4}\dot{x}^T(t)U_2\dot{x}(t) \\
&\quad + \frac{(h_2-h_1)^2}{4}\dot{x}^T(t)U_3\dot{x}(t) \\
&\quad - \frac{h_1^2}{2}\int_{-h_1}^{0}\int_{t+\theta}^{t}\dot{x}^T(s)U_1\dot{x}(s)\,ds\,d\theta \\
&\quad - \frac{h_2^2-h_1^2}{2}\int_{-h_2}^{-h_1}\int_{t+\theta}^{t}\dot{x}^T(s)U_2\dot{x}(s)\,ds\,d\theta \\
&\quad - \frac{1}{2}\int_{t-h_2}^{t-h_1}\int_{\theta}^{t-h_1}\dot{x}^T(s)U_3\dot{x}(s)\,ds\,d\theta \\
&= \chi^T(t)e_8\left[\frac{h_1^2}{2}U_1 + \frac{\left(h_2^2-h_1^2\right)^2}{4}U_2\right. \\
&\qquad \left. + \frac{(h_2-h_1)^2}{4}U_3\right]e_8^T\chi(t) \\
&\quad - \chi^T(t)(h_1e_1-e_5)U_1(h_1e_1-e_5)^T\chi(t) \\
&\quad - \chi^T(t)\left[(e_3-e_6)^TU_3(e_3-e_6)\right. \\
&\qquad \left. - (e_2-e_7)^TU_3(e_2-e_7)\right]\chi(t) - \Gamma_2,
\end{aligned} \tag{14}$$

where by using Lemma 1, we can get

$$\begin{aligned}
&-\frac{h_1^2}{2}\int_{-h_1}^{0}\int_{t+\theta}^{t}\dot{x}^T(s)U_1\dot{x}(s)\,ds\,d\theta \\
&\quad \le -\left[h_1x(t) - \int_{t-h_1}^{t}x(s)\,ds\right]^T \\
&\qquad \times U_1\left[h_1x(t) - \int_{t-h_1}^{t}x(s)\,ds\right] \\
&\quad = -\chi^T(t)(h_1e_1-e_5)U_1(h_1e_1-e_5)^T\chi(t), \\
&-\frac{1}{2}\int_{t-h_2}^{t-h_1}\int_{\theta}^{t-h_1}\dot{x}^T(s)U_3\dot{x}(s)\,ds\,d\theta
\end{aligned}$$

$$
\begin{aligned}
&\le -\frac{1}{2}\int_{t-h(t)}^{t-h_1}\int_{\theta}^{t-h_1}\dot{x}^T(s)U_3\dot{x}(s)\,ds\,d\theta \\
&\quad -\frac{1}{2}\int_{t-h_2}^{t-h(t)}\int_{\theta}^{t-h(t)}\dot{x}^T(s)U_3\dot{x}(s)\,ds\,d\theta \\
&\le -\left[(h(t)-h_1)x(t-h_1)-\int_{t-h(t)}^{t-h_1}x(s)\,ds\right]^T \\
&\quad \times\frac{U_3}{\alpha^2(t)}\left[(h(t)-h_1)x(t-h_1)-\int_{t-h(t)}^{t-h_1}x(s)\,ds\right] \\
&\quad -\left[(h_2-h(t))x(t-h(t))-\int_{t-h_2}^{t-h(t)}x(s)\,ds\right]^T \\
&\quad \times\frac{U_3}{\beta^2(t)}\left[(h_2-h(t))x(t-h(t))-\int_{t-h_2}^{t-h(t)}x(s)\,ds\right] \\
&= -\chi^T(t)\left[(e_3-e_6)^TU_3(e_3-e_6)\right. \\
&\qquad \left.-(e_2-e_7)^TU_3(e_2-e_7)\right]\chi(t).
\end{aligned}
\tag{15}
$$

Similar to the method in (12)-(13), by introducing matrix $Y_3 \in \mathbf{R}^{n\times n}$ and using Lemma 2, we can estimate the following:

$$
\begin{aligned}
&-\frac{h_2^2-h_1^2}{2}\int_{-h_2}^{-h_1}\int_{t+\theta}^{t}\dot{x}^T(s)U_2\dot{x}(s)\,ds\,d\theta \\
&\quad =-\frac{h_2^2-h_1^2}{2}\int_{-h(t)}^{-h_1}\int_{t+\theta}^{t}\dot{x}^T(s)U_2\dot{x}(s)\,ds\,d\theta \\
&\qquad -\frac{h_2^2-h_1^2}{2}\int_{-h_2}^{-h(t)}\int_{t+\theta}^{t}\dot{x}^T(s)U_2\dot{x}(s)\,ds\,d\theta \\
&\quad \le -\begin{bmatrix}(h(t)-h_1)x(t)-\displaystyle\int_{t-h(t)}^{t-h_1}x(s)\,ds\\ (h_2-h(t))x(t)-\displaystyle\int_{t-h_2}^{t-h(t)}x(s)ds\end{bmatrix}^T \\
&\qquad \times\begin{bmatrix}U_2 & Y_3\\ * & U_2\end{bmatrix}\begin{bmatrix}(h(t)-h_1)x(t)-\displaystyle\int_{t-h(t)}^{t-h_1}x(s)\,ds\\ (h_2-h(t))x(t)-\displaystyle\int_{t-h_2}^{t-h(t)}x(s)\,ds\end{bmatrix}=\Gamma_2.
\end{aligned}
\tag{16}
$$

In the last, in order to obtain the stability result base on LMI, we can deal with Γ_1, Γ_2 as follows:

$$
\begin{aligned}
\Gamma_1+\Gamma_2 = &-\chi^T(t)\begin{bmatrix}0&0&0&0&0&\alpha(t)&0&0\\0&0&0&0&0&0&\beta(t)&0\end{bmatrix}^T \\
&\begin{bmatrix}X_2&Y_2\\*&X_2\end{bmatrix}\begin{bmatrix}0&0&0&0&0&\alpha(t)&0&0\\0&0&0&0&0&0&\beta(t)&0\end{bmatrix}\chi(t) \\
&-\chi^T(t)\begin{bmatrix}\alpha(t)&0&0&0&0&-\alpha(t)&0&0\\\beta(t)&0&0&0&0&0&-\beta(t)&0\end{bmatrix}^T \\
&\times\begin{bmatrix}U_2&Y_3\\*&U_2\end{bmatrix} \\
&\times\begin{bmatrix}\alpha(t)&0&0&0&0&-\alpha(t)&0&0\\\beta(t)&0&0&0&0&0&-\beta(t)&0\end{bmatrix}\chi(t) \\
= &-\chi^T(t)\Upsilon(t)\Theta\Upsilon^T(t)\chi(t),
\end{aligned}
\tag{17}
$$

where

$$
\begin{aligned}
\Upsilon^T(t) &= \begin{bmatrix}\alpha(t)&0&0&0&0&-\alpha(t)&0&0\\\beta(t)&0&0&0&0&0&-\beta(t)&0\\0&0&0&0&0&\alpha(t)&0&0\\0&0&0&0&0&0&\beta(t)&0\end{bmatrix}, \\
\Theta &= \begin{bmatrix}U_2&Y_3&0&0\\*&U_2&0&0\\0&0&X_2&Y_2\\0&0&*&X_2\end{bmatrix}.
\end{aligned}
\tag{18}
$$

Also, for appropriate matrices N_1, N_2, one can have

$$
\begin{aligned}
&2\left[x^T(t)N_1+\dot{x}^T(t)N_2\right] \\
&\quad\times\left[Ax(t)+A_1x(t-h(t))-\dot{x}(t)\right]=0.
\end{aligned}
\tag{19}
$$

Therefore, combining (10)–(19), we can obtain

$$
\dot{V}(x_t)=\sum_{i=1}^{4}\dot{V}_i(x_t)\le\chi^T(t)\left[\Xi-\Upsilon(t)\Theta\Upsilon^T(t)\right]\chi(t),
\tag{20}
$$

where

$$
\begin{aligned}
\Xi = &\left[e_1\ \ e_5\right]P\left[e_8\ \ e_1-e_3\right]^T+\left[e_8\ \ e_1-e_3\right]P\left[e_1\ \ e_5\right]^T \\
&-e_3(Q_1-Q_2)e_3^T-(1-\mu)e_2(Q_2-Q_3)e_2^T-e_4Q_3e_4^T \\
&+e_8\left[h_1^2R_1+(h_2-h_1)^2X_1+\frac{h_1^2}{2}U_1\right. \\
&\qquad\left.+\frac{\left(h_2^2-h_1^2\right)^2}{4}U_2+\frac{(h_2-h_1)^2}{4}U_3\right]e_8^T \\
&+e_1\left[Q_1+h_1^2R_2+(h_2-h_1)^2X_2\right]e_1^T \\
&-(e_1-e_3)R_1(e_1-e_3)^T-e_5R_2e_5^T \\
&-\left[e_2-e_3\ \ e_4-e_2\right]\begin{bmatrix}X_1&Y_1\\*&X_1\end{bmatrix}\left[e_2-e_3\ \ e_4-e_2\right]^T \\
&-(h_1e_1-e_5)U_1(h_1e_1-e_5)^T \\
&-(e_3-e_6)^TU_3(e_3-e_6)-(e_2-e_7)^TU_3(e_2-e_7) \\
&+(e_1N_1+e_8N_2)\left(e_1^TA+e_2^TA_1-e_8\right)^T \\
&+\left(e_1^TA+e_2^TA_1-e_8\right)(e_1N_1+e_8N_2)^T.
\end{aligned}
\tag{21}
$$

As we know, if $\Xi - \Upsilon(t)\Theta\Upsilon^T(t) < 0$ holds, then $\dot{V}(x_t) < 0$, which means that system (1) is asymptotically stable. So, by Lemma 3, there exists a matrix of appropriate dimension Π such that the following LMI holds:

$$\begin{bmatrix} \Xi + \Upsilon\Pi^T + \Pi\Upsilon^T & \Pi \\ * & -\Theta \end{bmatrix} < 0. \tag{22}$$

So, we give the main theorem of this paper as follows.

Theorem 4. *The time-delayed system* (1) *having contrains* (2) *is asymptotically stable, if there exist matrices* $Q_1, Q_2, Q_3, R_1, R_2, X_1, X_2, U_1, U_2, U_3 \in \mathbf{R}^{n\times n} > 0$, *matrix* $P \in \mathbf{R}^{2n\times 2n} > 0$, *and appropriate matrices* $Y_1, Y_2, Y_3, N_1, N_2, \Pi$ *such that the following LMIs hold:*

$$\begin{gathered} Q_2 - Q_3 > 0, \\ \begin{bmatrix} \Xi + \Upsilon_1\Pi^T + \Pi\Upsilon_1^T & \Pi \\ * & -\Theta \end{bmatrix} < 0, \\ \begin{bmatrix} \Xi + \Upsilon_2\Pi^T + \Pi\Upsilon_2^T & \Pi \\ * & -\Theta \end{bmatrix} < 0, \end{gathered} \tag{23}$$

where Ξ, Υ, Π, *and* Θ *are defined in* (18) *and* (21).

Proof. From above, one can see that $\Xi + \Upsilon\Pi^T + \Pi\Upsilon^T$ is a convex combination of matrix Π as

$$\begin{aligned} \Xi + \Upsilon\Pi^T + \Pi\Upsilon^T = {} & \Xi + \left(h(t) - h_1\right)\left(\Upsilon_1\Pi^T + \Pi\Upsilon_1^T\right) \\ & + \left(h_2 - h(t)\right)\left(\Upsilon_2\Pi^T + \Pi\Upsilon_2^T\right) < 0. \end{aligned} \tag{24}$$

So (22) can be handled nonconservatively by the two corresponding boundary LMIs:

$$\begin{gathered} \begin{bmatrix} \Xi + \Upsilon_1\Pi^T + \Pi\Upsilon_1^T & \Pi \\ * & -\Theta \end{bmatrix} < 0, \\ \begin{bmatrix} \Xi + \Upsilon_2\Pi^T + \Pi\Upsilon_2^T & \Pi \\ * & -\Theta \end{bmatrix} < 0, \end{gathered} \tag{25}$$

where $\Upsilon_1 = \Upsilon(h(t) - h_1 = 0)$, $\Upsilon_2 = \Upsilon(h_2 - h(t) = 0)$. This completes the proof. □

Remark 5. From (17) and (22), it can be seen that, in order to obtain the less conservative stability condition in terms of LMI, $\alpha(t)$, $\beta(t)$ are used, but free matrices $\Pi = [\Pi_{ij}]$ $(1 \le i \le j \le 8)$ are also introduced, which increases the computational burden; this is a disadvantage of the proposed method.

Remark 6. When $h_1 \le h(t) \le h_2$, $\mu_1 \le \dot{h}(t) \le \mu_2$, let $\Xi_1 = \Xi(\mu = \mu_1), \Xi_2 = \Xi(\mu = \mu_2)$, and using the convex combination again with $\begin{bmatrix} \Xi_1+\Upsilon_1\Pi^T+\Pi\Upsilon_1^T & \Pi \\ * & -\Theta \end{bmatrix} < 0$, $\begin{bmatrix} \Xi_1+\Upsilon_2\Pi^T+\Pi\Upsilon_2^T & \Pi \\ * & -\Theta \end{bmatrix} < 0$, $\begin{bmatrix} \Xi_2+\Upsilon_1\Pi^T+\Pi\Upsilon_1^T & \Pi \\ * & -\Theta \end{bmatrix} < 0$, $\begin{bmatrix} \Xi_2+\Upsilon_2\Pi^T+\Pi\Upsilon_2^T & \Pi \\ * & -\Theta \end{bmatrix} < 0$, the corresponding stability criterion can also be obtained.

4. Numerical Examples

In this section, the effectiveness of the obtained results in this paper is shown by the two well-known numerical examples.

Table 1: Admissible upper bound h_2 for various h_1 and μ in Example 1.

h_1	Methods	$\mu = 0.3$	$\mu = 0.5$	$\mu = 0.9$
2	Shao [6]	2.69	2.50	2.50
	Sun et al. [9]	2.91	2.50	2.50
	Theorem 4	3.00	2.64	2.64
3	Shao [6]	3.25	3.25	3.25
	Sun et al. [9]	3.34	3.34	3.34
	Theorem 4	3.35	3.35	3.35

Table 2: Admissible upper bound h_2 for various h_1 and $\mu = 0.3$ in Example 1.

Methods	h_1	0.3	0.5	0.8	1
Shao [6]	h_2	2.22	2.22	2.23	2.24
Sun et al. [9]	h_2	2.26	2.28	2.30	2.30
Theorem 4	h_2	2.39	2.41	2.42	2.43

Example 1. Consider the linear system (1) with

$$A = \begin{bmatrix} -2 & 0 \\ 0 & -0.9 \end{bmatrix}, \qquad A_1 = \begin{bmatrix} -1 & 0 \\ -1 & -1 \end{bmatrix}. \tag{26}$$

The purpose is to compare the admissible upper bounds h_2 given lower bound h_1 and μ.

For $h_1 = 0$, $\mu = 0.5, 0.9$, in [14], the result is $h_2 = 2.04, 1.37$, in [17], the result is $h_2 = 2.33, 1.87$, and our results are $h_2 = 2.33, 1.87$.

For $h_1 = 1$, $\mu = 0.5, 0.9$, in [14], the result is $h_2 = 2.07, 1.74$, in [17], the result is $h_2 = 2.33, 2.07$, and our results are $h_2 = 2.43, 2.08$.

For $h_1 = 2$, $\mu = 0.5, 0.9$, in [14], the result is $h_2 = 2.43, 2.43$, in [17], the result is $h_2 = 2.61, 2.61$, and our results are $h_2 = 2.64, 2.64$.

For various h_1, μ, the maximum upper bounds on delay h_2 by different methods are also listed in Table 1. It can be seen that the result obtained in this paper is less conservative.

Example 2. Consider the linear system (1) with

$$A = \begin{bmatrix} 0 & 1 \\ -1 & -2 \end{bmatrix}, \qquad A_1 = \begin{bmatrix} 0 & 0 \\ -1 & 1 \end{bmatrix}. \tag{27}$$

The purpose is to compare the admissible upper bounds h_2 which guarantee the asymptotic stability of the above system for given lower bound h_1 and μ. This example is used in many recent papers, such as [6, 9], For $\mu = 0.3$, Table 2 lists the comparison of our results with some recent ones, and it is easy to see that the results obtained in this paper are less conservative.

5. Conclusions

In this note, the stability of interval time-varying delay systems has been discussed. Through constructing a novel LKF and using some new analysis methods, the delay-range-dependent stability criteria were derived. Compared with

some previous stability conditions, the obtained main results in this paper have less conservatism. In the end, numerical examples were given to show the superiority of the obtained criteria and their improvements over the existing results.

Conflict of Interests

The authors declare that there is no conflict of interests regarding the publication of this paper.

Acknowledgments

This work is supported by the National Nature Science Foundation under Grants 61104119, the Science and Technology Innovation Talents Project of Henan University under Grant 13HASTIT044, the Doctoral Foundation from Henan Polytechnic University under Grants B2010-50, and the Young Core Instructor Foundation from the Department of Education of Henan Province under Grant 2011GGJS-054.

References

[1] X. L. Zhu, Y. Wang, and G. H. Yang, "New stability criteria for continuous-time systems with interval time-varying delay," *IET Control Theory & Applications*, vol. 4, no. 6, pp. 1101–1107, 2010.

[2] X. Jiang and Q. L. Han, "New stability criteria for linear systems with interval time-varying delay," *Automatica*, vol. 44, no. 10, pp. 2680–2685, 2008.

[3] Y. He, Q. G. Wang, C. Lin, and M. Wu, "Delay-range-dependent stability for systems with time-varying delay," *Automatica*, vol. 43, no. 2, pp. 371–376, 2007.

[4] M. J. Park, O. M. Kwon, J. H. Park, and S. M. Lee, "A new augmented Lyapunov-Krasovskii functional approach for stability of linear systems with time-varying delays," *Applied Mathematics and Computation*, vol. 217, no. 17, pp. 7197–7209, 2011.

[5] P. Park and J. W. Ko, "Stability and robust stability for systems with a time-varying delay," *Automatica*, vol. 43, no. 10, pp. 1855–1858, 2007.

[6] H. Shao, "New delay-dependent stability criteria for systems with interval delay," *Automatica*, vol. 45, no. 3, pp. 744–749, 2009.

[7] P. Park, J. W. Ko, and C. Jeong, "Reciprocally convex approach to stability of systems with time-varying delays," *Automatica*, vol. 47, no. 1, pp. 235–238, 2011.

[8] E. Fridman, U. Shaked, and K. Liu, "New conditions for delay-derivative-dependent stability," *Automatica*, vol. 45, no. 11, pp. 2723–2727, 2009.

[9] J. Sun, G. P. Liu, J. Chen, and D. Rees, "Improved delay-range-dependent stability criteria for linear systems with time-varying delays," *Automatica*, vol. 46, no. 2, pp. 466–470, 2010.

[10] W. Qian, S. Cong, T. Li, and S. Fei, "Improved stability conditions for systems with interval time-varying delay," *International Journal of Control, Automation, and Systems*, vol. 10, no. 6, pp. 1146–1152, 2012.

[11] J. H. Kim, "Note on stability of linear systems with time-varying delay," *Automatica*, vol. 47, no. 9, pp. 2118–2121, 2011.

[12] M. N. A. Parlakçı, "Extensively augmented Lyapunov functional approach for the stability of neutral time-delay systems," *IET Control Theory & Applications*, vol. 2, no. 5, pp. 431–436, 2008.

[13] X. Nian, H. Pan, W. Gui, and H. Wang, "New stability analysis for linear neutral system via state matrix decomposition," *Applied Mathematics and Computation*, vol. 215, no. 5, pp. 1830–1837, 2009.

[14] T. Li, L. Guo, and L. Wu, "Simplified approach to the asymptotical stability of linear systems with interval time-varying delay," *IET Control Theory & Applications*, vol. 3, no. 2, pp. 252–260, 2009.

[15] Y. Chen, W. X. Zheng, and A. Xue, "A new result on stability analysis for stochastic neutral systems," *Automatica*, vol. 46, no. 12, pp. 2100–2104, 2010.

[16] J. Liu and J. Zhang, "Note on stability of discrete-time time-varying delay systems," *IET Control Theory & Applications*, vol. 6, no. 2, pp. 335–339, 2012.

[17] W. Zhang, X. Cai, and Z. Z. Han, "Robust stability criteria for systems with interval time-varying delay and nonlinear perturbations," *Journal of Computational and Applied Mathematics*, vol. 234, no. 1, pp. 174–180, 2010.

Hindawi Publishing Corporation
Mathematical Problems in Engineering
Volume 2013, Article ID 535437, 13 pages
http://dx.doi.org/10.1155/2013/535437

Research Article

Robust Adaptive PID Control of Robot Manipulator with Bounded Disturbances

Jian Xu and Lei Qiao

Department of Automation, Harbin Engineering University, Harbin 150001, China

Correspondence should be addressed to Lei Qiao; qiaolei2008114106@gmail.com

Received 6 July 2013; Accepted 1 October 2013

Academic Editor: Zhiguang Feng

To solve the strong nonlinearity and coupling problems in robot manipulator control, two novel robust adaptive PID control schemes are proposed in this paper with known or unknown upper bound of the external disturbances. Invoking the two proposed controllers, the unknown bounded external disturbances can be compensated and the global asymptotical stability with respect to the manipulator positions and velocities is able to be guaranteed. As compared with the existing adaptive PD control methods, the designed control laws can enlarge the tolerable external disturbances, enhance the accuracy in finite-time trajectory tracking control, and improve the dynamic performance of the manipulator systems. The stability and convergence properties of the closed-loop system are analytically proved using Lyapunov stability theory and Barbalat's lemma. Simulations are performed for a planner manipulator with two rotary degrees of freedom to illustrate the viability and the advantages of the proposed controllers.

1. Introduction

Robot manipulators play an important part in modern industry by providing lower production cost, enhanced precision, quality, productivity, and efficiency. The control of rigid robot manipulators faces significant difficulties such as highly nonlinear, coupled, and time-varying behaviors. Moreover, there always exist uncertainties in the system's dynamic model, such as the external disturbances and parameter uncertainty, to name a few, which cause unstable performance of the robot manipulator systems.

Since linear control methods are not suitable for strong coupled, nonlinear, and time-varying rigid robot manipulator systems, many nonlinear control schemes based on conventional PID control theory have been proposed to improve the control performance. In [1], the global asymptotic stability of a class of nonlinear PD-type controllers for position and motion control of robot manipulators is analyzed, and a global regulator constrained to deliver torques within prescribed limits of the actuator's capabilities is proposed. This class of controllers, when rule-based or gain scheduling approaches are used, can get high performance control systems. However, it has been shown that although the PD controller is robust with respect to uncertainties on inertial parameters and the global asymptotic stability is guaranteed, uncertainties on the gravity parameters may lead to undesired steady-state errors [2]. A PID control scheme can eliminate the steady-state errors, but it can only ensure local asymptotic stability. Moreover, to guarantee the stability, the gain matrices must satisfy complicated inequalities [3]. In [4], a new variable structure PID control scheme is designed for robot manipulators. Even through the global asymptotic stability of the controlled robot systems is analyzed, the bounds of system parameter matrices need to be known in the controller design.

To further enhance the tracking performance of robot manipulator systems in presence of parametric uncertainties, significant efforts have been made to seek advanced control strategies. Robust and adaptive control schemes of robot manipulators have been the active research topics for many years. Robust control laws are used for external disturbances, unstructured dynamics, and other sources of uncertainties. Leitmann [5] and Corless and Leitmann [6] present a popular approach utilized for designing robust controller for robot manipulators. In an early application of the Corless-Leitmann approach to robot manipulators [7], a simple robust nonlinear control law is derived for n-link robot manipulators using the well-known Lyapunov

based theory of guaranteed stability of uncertain systems. The uncertainty bounds needed to derive the control law and to prove that uniform ultimate boundedness of the tracking errors only depends on the inertia parameters of the robot. Some other robust control methods developed based on [5, 6] are given in [8, 9]. However, disturbances and unmodeled dynamics are not considered in the algorithms in [7–9]. In [10], Spong's method [7] is extended in such a manner that the control law is robust not only to uncertain inertia parameters but also to unmodeled dynamics and disturbances. Another improvement to the Spong's methodology [7] is suggested in [11]. A drawback of a single robust control is that it cannot estimate the uncertainties and disturbances online, which limits the adaptability of the controller to the changed uncertain parameters. Adaptive algorithm provides an effective way to solve this problem; however, most adaptive controls, like most parameter adaptive methods, may exhibit poor robustness to unstructured dynamics and external disturbances. Some related results can be seen in [12–15]. To resolve this, a combination of robust control and adaptive algorithm is investigated in a number of literature sources. In [16], adaptive controllers are designed for robot manipulator systems that yield robust trajectory in spite of the unwanted effects of the external disturbances and fast maneuvering of the manipulator. The convergence rate is improved and the transient oscillation is reduced considerably. In [17], an adaptive control law for continuous-time direct adaptive control of robot manipulator is presented. The algorithm is suitable for swift adaptation to rapidly changing system parameters. And the uniform global asymptotic stability with respect to the manipulator positions and velocities is guaranteed for unknown constant parameters. In [18], a decentralized adaptive robust controller is investigated for trajectory tracking of robot manipulator systems. A disturbance observer (DOB) is introduced in each local controller to compensate for the low-passed coupled uncertainties, and an adaptive sliding mode control term is employed to handle the fast-changing components of the uncertainties beyond the pass band of the DOB. For some other results on robust and adaptive control the reader can refer to [19–22].

Furthermore, other control algorithms such as fuzzy logic, neural networks, and PD control have been adopted to combine with robust and adaptive control to cope with the problems in robot manipulators control. In [23], a robust adaptive compensation scheme is presented for compensation of asymmetric deadzone, dynamic friction, and uncertainty in the direct-drive robot manipulator. The estimation laws of deadzone and friction are proposed to offset both deadzone of joint input torque and friction. A model-free recurrent wavelet cerebellar model articulation controller (RWCMAC) to mimic the ideal control law is employed to overcome some shortcomings of the traditional model-based adaptive controller. In [24], a novel robust decentralized control of electrically driven robot manipulator by adaptive fuzzy estimation and compensation uncertainty is proposed. The controller is designed via voltage control strategy. A fuzzy system is used to estimate and compensate uncertainty. In [25, 26], two adaptive PD control methods are investigated for trajectory tracking control of robot manipulators with known and unknown upper bound of the external disturbances, respectively. Both of the controllers are composed by a nonlinear PD feedback control law and an adaptive algorithm. The PD feedback control law can avoid large initial torque due to the large initial position error, and the adaptive algorithm can make good dynamic performance for the robot manipulator systems. However, the PD feedback control is rarely used in practical control systems. That is because the pure differential element cannot be realized in practice. Moreover, the differential action is very sensitive to system noise; as a result, if the PD control is adopted, any disturbances in each system's element would result in big fluctuation in systems output. Hence, the PD control is indeed of no benefit for the improvement of the system dynamic performance.

In the present study two new robust adaptive PID controllers are introduced for an n degree-of-freedom robot manipulator systems with known or unknown upper bound of the external disturbances based on [1, 25, 26]. The designed controllers are composited by PID control and robust adaptive approach to cope with the external disturbances and unknown constant parameters that can arise. As regards the innovation of this study, an integration element is embedded in both PD control and robust adaptive algorithm based on the existing adaptive PD control laws [25, 26]. With the adoption of the proposed controllers, the tolerable external disturbances are enlarged, and also the dynamic performance of the manipulator systems is improved and the finite-time tracking control accuracy is enhanced in contrast to those obtained with the usage of the adaptive PD controllers [25, 26]. By choosing adequate Lyapunov candidate functions and utilizing Barbalat's lemma, the system's closed-loop stability is proven. Some numerical results are also presented in order to demonstrate the control systems performance.

This paper is organized as follows. The nonlinear dynamics of rigid robot manipulator and some useful properties of dynamic systems are introduced in Section 2. In Section 3, three necessary assumptions for control laws development and systems stability analysis are given, and two robust adaptive PID controllers are designed for trajectory tracking control of robot manipulator with known or unknown upper bound of the external disturbances, respectively. The numerical verification of the controllers and the discussion are presented in Section 4. A short conclusion is given in Section 5.

2. Dynamic Model of Robot Manipulator and Some Properties

2.1. Dynamic Model. Generally, the dynamics of an n degree of freedom (n-DOF) rigid link robot manipulator with rotary joints can be expressed as [27]

$$M(q)\ddot{q} + C(q,\dot{q})\dot{q} + G(q) + u = \tau, \tag{1}$$

where $q(t) \in R^n$ is the vector of joint angles, $M(q) \in R^{n\times n}$ is the inertia matrix of the manipulator, $C(q,\dot{q}) \in R^{n\times n}$ is the matrix of Coriolis and centripetal forces, $G(q) \in R^n$ is

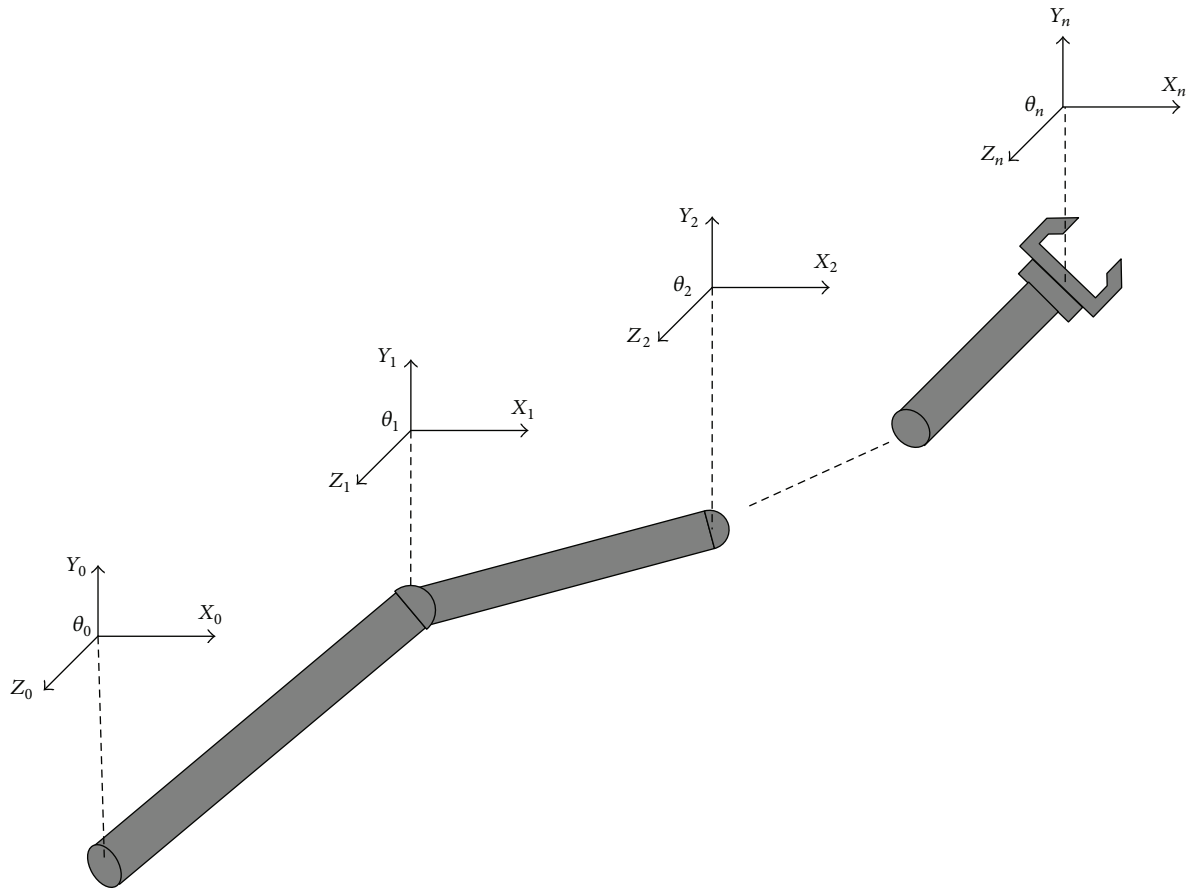

Figure 1: The frames assignment of an n-DOF rigid robot manipulator.

the vector of gravity factor, $\tau \in R^n$ is the vector of input torque, and $u \in R^n$ is the vector of all external disturbances.

Figure 1 presents the conceptual model of an n-DOF rigid robot manipulator. Assume that the manipulator is mounted on a fixed base, so the dynamic coupling between the manipulator and the base is neglected.

2.2. Dynamic System Properties. The dynamic systems given by (1) exhibit the following properties that are utilized in the subsequent control laws development and stability analysis [27].

(B1) The inertial matrix is symmetric and positive definite; that is, $M(q) = M^T(q) > 0$, $\forall q \in R^n$. There are positive constants m_m and m_M such that $m_m\|y\|^2 \leq y^T M(q) y \leq m_M\|y\|^2$, $\forall y \in R^n$.

(B2) $\dot{M}(q) - 2C(q, \dot{q})$ is a skew-symmetric matrix; for example, $s^T[\dot{M}(q) - 2C(q, \dot{q})]s = 0$, $\forall s \in R^n$.

(B3) $M(q)$, $C(q, \dot{q})$, and $G(q)$ meet the linear condition of $M(q)\alpha + C(q, \dot{q})\beta + G(q) = \Psi(q, \dot{q}, \alpha, \beta)P$, where $P \in R^m$ is an unknown constant vector which describes the mass characteristics of the manipulator and $\Psi(q, \dot{q}, \alpha, \beta) \in R^{n\times m}$ is a known regression matrix.

3. Robust Adaptive PID Control of Robot Manipulator

Firstly, the following assumptions are imposed for the manipulator systems.

(C1) The desired trajectory q_d and the time derivatives $\dot{q}_d$ and $\ddot{q}_d$ are available and bounded signals.

(C2) The external disturbances vector u is bounded, and it is confined within the following limit:

$$\|u\| \leq b_1 + b_2\|e\| + b_3\|\dot{e}\| + b_4\left\|\int_0^t e dt\right\|, \tag{2}$$

where b_1, b_2, b_3, and b_4 are positive constants, $e = q - q_d$ and $\dot{e} = \dot{q} - \dot{q}_d$ are the position tracking error and the velocity tracking error, respectively, $\int_0^t e dt = [\int_0^t e_1 dt, \ldots, \int_0^t e_n dt]^T$.

(C3) $\ddot{e}(t) = \ddot{q} - \ddot{q}_d$ is existent and bounded in t.

Here we introduce two variables x and q_k; meanwhile let

$$\begin{aligned} x &= \dot{e} + \gamma e + \int_0^t e dt, \\ \dot{q}_k &= \dot{q}_d - \gamma e - \int_0^t e dt, \end{aligned} \tag{3}$$

where the parameter γ is a positive constant.

With (3) giving

$$\dot{q} - \dot{q}_k = x. \tag{4}$$

With regard to the robot manipulator property (B3), let $\alpha = \ddot{q}_k, \beta = \dot{q}_k$; one obtains

$$M(q)\ddot{q}_k + C(q,\dot{q})\dot{q}_k + G(q) = \Psi(q,\dot{q},\dot{q}_k,\ddot{q}_k)P. \tag{5}$$

Substituting (4) into the above equation yields

$$\begin{aligned} &M(q)\ddot{q} + C(q,\dot{q})\dot{q} + G(q) - M(q)\dot{x} - C(q,\dot{q})x \\ &\quad = \Psi(q,\dot{q},\dot{q}_k,\ddot{q}_k)P. \end{aligned} \tag{6}$$

3.1. Robust Adaptive PID Controller Design with Known Upper Bound of the External Disturbances. For the robot manipulator systems (1), if the upper bound of the external disturbances signals u is known, motivated by [1, 25], the controller which makes the position and the velocity tracking errors asymptotically converge to zero can be designed as follows:

$$\tau = -K_P e - K_D\dot{e} - K_I\left(\int_0^t e dt\right) + \Psi(q,\dot{q},\dot{q}_k,\ddot{q}_k)\widehat{P} + V, \tag{7}$$

$$V = [v_1,\ldots,v_n]^T, \tag{8}$$

$$v_i = -\left(b_1 + b_2\|e\| + b_3\|\dot{e}\| + b_4\left\|\int_0^t e dt\right\|\right)\operatorname{sgn}(x_i), \tag{9}$$

where $\widehat{P}$ is the estimate value of P.

Take the parameter estimation law of $\widehat{P}$ as

$$\dot{\widehat{P}} = -\Phi\Psi^T(q,\dot{q},\dot{q}_k,\ddot{q}_k)x. \tag{10}$$

The gain matrices are given by

$$\begin{aligned} K_P &= \operatorname{diag}[k_{P1},\ldots,k_{Pn}], \\ K_D &= \operatorname{diag}[k_{D1},\ldots,k_{Dn}], \\ K_I &= \operatorname{diag}[k_{I1},\ldots,k_{In}], \end{aligned} \tag{11}$$

where k_{Pi}, k_{Di}, k_{Ii} $(i = 1,2,\ldots,n)$ are all positive constants and $k_{Di} = k_{Ii}$, $\Phi \in R^{m\times m}$ is a positive definite and symmetric matrix.

The framework of the proposed control scheme is shown in Figure 2.

Proof. Considering the Lyapunov function candidate,

$$\begin{aligned} V = \frac{1}{2}\Bigg[&x^T M(q)x + e^T(K_P + \gamma K_D)e \\ &+ \left(\int_0^t e dt\right)^T(K_P + \gamma K_I)\left(\int_0^t e dt\right) + \widetilde{P}^T\Phi^{-1}\widetilde{P}\Bigg] \end{aligned} \tag{12}$$

with $\widetilde{P} = \widehat{P} - P$.

From property (B1) one obtains

$$\begin{aligned} \left(x^T M(q)x\right)' &= \dot{x}^T M(q)x + x^T\dot{M}(q)x + x^T M(q)\dot{x} \\ &= x^T\dot{M}(q)x + 2x^T M(q)\dot{x}. \end{aligned} \tag{13}$$

□

With the positive definite and symmetric matrices K_P, K_D, K_I, and Φ, one gets

$$\begin{aligned} &\left[e^T(K_P + \gamma K_D)e\right]' = 2e^T(K_P + \gamma K_D)\dot{e}, \\ &\left[\left(\int_0^t e dt\right)^T(K_P + \gamma K_I)\left(\int_0^t e dt\right)\right]' \\ &\quad = 2\left(\int_0^t e dt\right)^T(K_P + \gamma K_I)e, \\ &\left(\widetilde{P}^T\Phi^{-1}\widetilde{P}\right)' = 2\widetilde{P}^T\Phi^{-1}\dot{\widetilde{P}}. \end{aligned} \tag{14}$$

Therefore, one obtains

$$\begin{aligned} \dot{V} = &\frac{1}{2}x^T\dot{M}(q)x + x^T M(q)\dot{x} \\ &+ e^T(K_P + \gamma K_D)\dot{e} \\ &+ \left(\int_0^t e dt\right)^T(K_P + \gamma K_I)e + \widetilde{P}^T\Phi^{-1}\dot{\widetilde{P}}. \end{aligned} \tag{15}$$

Using (6) and (7) leads to

$$\begin{aligned} x^T M(q)\dot{x} &= x^T[\tau - u - \Psi(q,\dot{q},\dot{q}_k,\ddot{q}_k)P - C(q,\dot{q})x] \\ &= x^T\left[-K_P e - K_D\dot{e} - K_I\left(\int_0^t e dt\right)\right. \\ &\qquad \left. + \Psi(q,\dot{q},\dot{q}_k,\ddot{q}_k)\widetilde{P} + V - u\right] \\ &\quad - x^T C(q,\dot{q})x. \end{aligned} \tag{16}$$

Considering $x^T = \dot{e}^T + \gamma e^T + (\int_0^t e dt)^T$, one gets

$$\begin{aligned} &x^T\left(-K_P e - K_D\dot{e} - K_I\int_0^t e dt\right) \\ &= \left[\dot{e}^T + \gamma e^T + \left(\int_0^t e dt\right)^T\right]\left[-K_P e - K_D\dot{e} - K_I\left(\int_0^t e dt\right)\right] \\ &= -\dot{e}^T K_P e - \dot{e}^T K_D\dot{e} - \dot{e}^T K_I\left(\int_0^t e dt\right) - \gamma e^T K_P e \\ &\quad - \gamma e^T K_D\dot{e} - \gamma e^T K_I\left(\int_0^t e dt\right) - \left(\int_0^t e dt\right)^T K_P e \\ &\quad - \left(\int_0^t e dt\right)^T K_D\dot{e} - \left(\int_0^t e dt\right)^T K_I\left(\int_0^t e dt\right). \end{aligned} \tag{17}$$

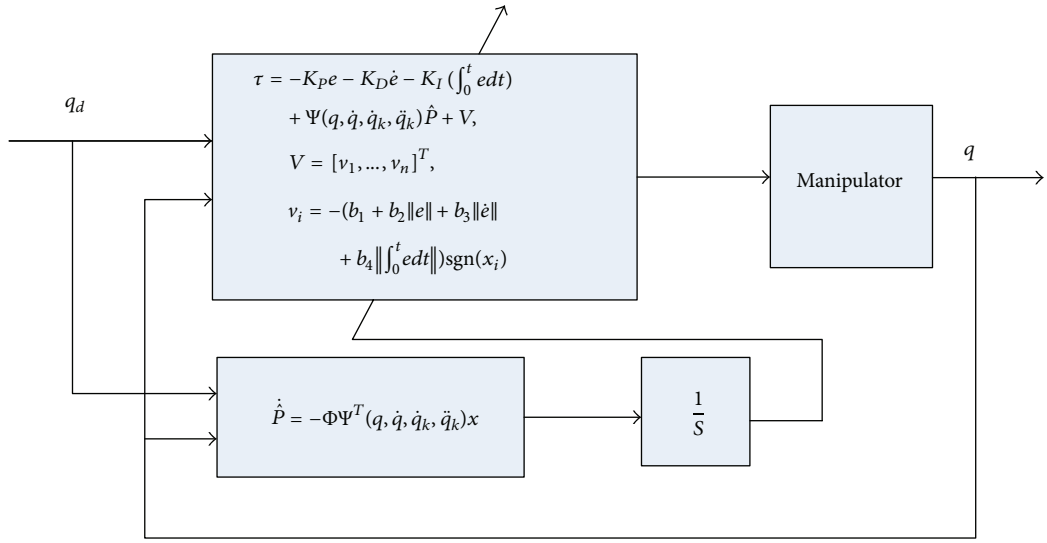

Figure 2: Framework of control law with known upper bound of the disturbances.

Substituting (16) and (17) into (15) yields

$$\begin{aligned}\dot{V} = {} & -\dot{e}^T K_D \dot{e} - \gamma e^T K_P e - \left(\int_0^t e dt\right)^T K_I \left(\int_0^t e dt\right) \\ & - \dot{e}^T (K_D + K_I)\left(\int_0^t e dt\right) + \frac{1}{2}x^T \dot{M}(q)\, x - x^T C(q, \dot{q})\, x \\ & + \tilde{P}^T \Phi^{-1} \dot{\tilde{P}} + x^T \Psi(q, \dot{q}, \dot{q}_k, \ddot{q}_k)\, \tilde{P} + x^T (V - u).\end{aligned} \tag{18}$$

With property (B2) one obtains

$$\frac{1}{2}x^T \dot{M}(q)\, x - x^T C(q, \dot{q})\, x = \frac{1}{2}x^T \left[\dot{M}(q) - 2C(q, \dot{q})\right] x = 0. \tag{19}$$

Note that

$$x^T \Psi(q, \dot{q}, \dot{q}_k, \ddot{q}_k)\, \tilde{P} = \tilde{P}^T \Psi^T(q, \dot{q}, \dot{q}_k, \ddot{q}_k)\, x, \quad \dot{\tilde{P}} = \dot{\hat{P}}, \tag{20}$$

and one gets

$$\begin{aligned}& \tilde{P}^T \Phi^{-1} \dot{\tilde{P}} + x^T \Psi(q, \dot{q}, \dot{q}_k, \ddot{q}_k)\, \tilde{P} \\ & = \tilde{P}^T \Phi^{-1} \left[-\Phi \Psi^T(q, \dot{q}, \dot{q}_k, \ddot{q}_k)\, x\right] \\ & \quad + \tilde{P}^T \Psi^T(q, \dot{q}, \dot{q}_k, \ddot{q}_k)\, x = 0.\end{aligned} \tag{21}$$

Thus, one obtains

$$\begin{aligned}\dot{V} = {} & -\dot{e}^T K_D \dot{e} - \gamma e^T K_P e - \left(\int_0^t e dt\right)^T K_I \left(\int_0^t e dt\right) \\ & - \dot{e}^T (K_D + K_I)\left(\int_0^t e dt\right) + x^T (V - u).\end{aligned} \tag{22}$$

Note that the following equalities and inequalities hold

$$\begin{aligned}& \dot{e}^T K_D \dot{e} = \sum_{i=1}^n k_{Di} \dot{e}_i^2, \qquad \gamma e^T K_P e = \sum_{i=1}^n \gamma k_{Pi} e_i^2, \\ & \left(\int_0^t e dt\right)^T K_I \left(\int_0^t e dt\right) = \sum_{i=1}^n k_{Ii} \left(\int_0^t e_i dt\right)^2, \\ & \dot{e}^T (K_D + K_I)\left(\int_0^t e dt\right) = \sum_{i=1}^n (k_{Di} + k_{Ii})\, \dot{e}_i \left(\int_0^t e_i dt\right), \\ & \qquad - \sum_{i=1}^n (k_{Di} + k_{Ii})\, \dot{e}_i \left(\int_0^t e_i dt\right) \\ & \qquad \le \frac{1}{2}\sum_{i=1}^n (k_{Di} + k_{Ii})\, \dot{e}_i^2 \\ & \qquad + \frac{1}{2}\sum_{i=1}^n (k_{Di} + k_{Ii}) \left(\int_0^t e_i dt\right)^2.\end{aligned} \tag{23}$$

Hence, one gets

$$\begin{aligned}\dot{V} = {} & -\sum_{i=1}^n k_{Di} \dot{e}_i^2 - \sum_{i=1}^n \gamma k_{Pi} e_i^2 - \sum_{i=1}^n k_{Ii} \left(\int_0^t e_i dt\right)^2 \\ & - \sum_{i=1}^n (k_{Di} + k_{Ii})\, \dot{e}_i \left(\int_0^t e_i dt\right) + x^T (V - u) \\ \le {} & -\sum_{i=1}^n k_{Di} \dot{e}_i^2 - \sum_{i=1}^n \gamma k_{Pi} e_i^2 - \sum_{i=1}^n k_{Ii} \left(\int_0^t e_i dt\right)^2 \\ & + \frac{1}{2}\sum_{i=1}^n (k_{Di} + k_{Ii})\, \dot{e}_i^2 + \frac{1}{2}\sum_{i=1}^n (k_{Di} + k_{Ii}) \left(\int_0^t e_i dt\right)^2 \\ & + x^T (V - u)\end{aligned}$$

$$\leq -\sum_{i=1}^{n}\left[k_{Di}-\frac{1}{2}\left(k_{Di}+k_{Ii}\right)\right]\dot{e}_i^2-\sum_{i=1}^{n}\gamma k_{Pi}e_i^2 - \sum_{i=1}^{n}\left[k_{Ii}-\frac{1}{2}\left(k_{Di}+k_{Ii}\right)\right]\left(\int_0^t e_i dt\right)^2+x^T\left(V-u\right). \tag{24}$$

Now considering the term of $x^T(V-u)$,

$$\begin{aligned} x^TV &= \sum_{i=1}^{n}x_i\left[-\left(b_1+b_2\left\|e\right\|+b_3\left\|\dot{e}\right\|+b_4\left\|\int_0^t edt\right\|\right)\operatorname{sgn}\left(x_i\right)\right] \\ &= \sum_{i=1}^{n}\left[-\left(b_1+b_2\left\|e\right\|+b_3\left\|\dot{e}\right\|+b_4\left\|\int_0^t edt\right\|\right)\left|x_i\right|\right] \\ &\leq \sum_{i=1}^{n}\left(-\left\|u\right\|\cdot\left|x_i\right|\right); \end{aligned} \tag{25}$$

here the assumption (C2) has been used.

Note that

$$-x^Tu\leq\left\|x^T\right\|\cdot\left\|u\right\|. \tag{26}$$

Defining $\|x^T\|=\sum_{i=1}^{n}|x_i|$ gives

$$\begin{aligned} \dot{V} &\leq -\sum_{i=1}^{n}\left[k_{Di}-\frac{1}{2}\left(k_{Di}+k_{Ii}\right)\right]\dot{e}_i^2-\sum_{i=1}^{n}\gamma k_{Pi}e_i^2 \\ &\quad -\sum_{i=1}^{n}\left[k_{Ii}-\frac{1}{2}\left(k_{Di}+k_{Ii}\right)\right]\left(\int_0^t e_i dt\right)^2 \\ &\quad +\sum_{i=1}^{n}\left(-\left\|u\right\|\cdot\left|x_i\right|\right)+\left\|x^T\right\|\cdot\left\|u\right\| \\ &\leq -\sum_{i=1}^{n}\left[k_{Di}-\frac{1}{2}\left(k_{Di}+k_{Ii}\right)\right]\dot{e}_i^2-\sum_{i=1}^{n}\gamma k_{Pi}e_i^2 \\ &\quad -\sum_{i=1}^{n}\left[k_{Ii}-\frac{1}{2}\left(k_{Di}+k_{Ii}\right)\right]\left(\int_0^t e_i dt\right)^2. \end{aligned} \tag{27}$$

With $k_{Di}=k_{Ii}>0$ and $k_{Pi}>0$ one obtains

$$\begin{aligned} k_{Di}-\frac{1}{2}\left(k_{Di}+k_{Ii}\right)=0, \qquad \gamma k_{Pi}>0, \\ k_{Ii}-\frac{1}{2}\left(k_{Di}+k_{Ii}\right)=0. \end{aligned} \tag{28}$$

Finally, one gets

$$\dot{V}\leq-\sum_{i=1}^{n}\gamma k_{Pi}e_i^2. \tag{29}$$

From the proof and analysis above we know that the function $\dot{V}$ is negative and vanishes if and only if $e(t)=0$; thus the position tracking error goes to zero as time goes to infinity; namely, $\lim_{t\to\infty}e(t)=0$.

According to the assumption (C3) we obtain that $\dot{e}(t):R^+\to R$ is uniformly continuous [28]. Consider the following formula holds:

$$\begin{aligned} \lim_{t\to\infty}\int_0^t\dot{e}\left(\tau\right)d\tau &= \lim_{t\to\infty}\left[e\left(t\right)-e\left(0\right)\right]=\lim_{t\to\infty}e\left(t\right)-e\left(0\right) \\ &= -e\left(0\right)<\infty \end{aligned} \tag{30}$$

which implies that the limit $\lim_{t\to\infty}\int_0^t\dot{e}(\tau)d\tau$ is existent and bounded. Therefore, it follows from the Barbalat's lemma [29] that $\dot{e}(t)\to 0$ as $t\to\infty$; that is, $\lim_{t\to\infty}\dot{e}(t)=0$.

Hence, the designed controller can guarantee the equilibrium $(e,\dot{e})=(0,0)$ globally asymptotically stable. It is also seen that the parameter vector $\widetilde{P}$ is bounded but does not necessarily converge to zero.

3.2. Robust Adaptive PID Controller Design with Unknown Upper Bound of the External Disturbances. On the other hand, if the upper bound of the external disturbances signals u is unknown, inspired by [1, 26], the controller which ensures the global asymptotical stability of the manipulator positions and velocities can be designed as follows:

$$\tau=-K_Pe-K_D\dot{e}-K_I\left(\int_0^t edt\right)+\Psi\left(q,\dot{q},\dot{q}_k,\ddot{q}_k\right)\widehat{P}+V, \tag{31}$$

$$V=-\frac{\left(\widehat{b}\xi\right)^2}{\left(\widehat{b}\xi\right)\left\|x\right\|+\varepsilon^2}\cdot x, \tag{32}$$

$$\dot{\widehat{b}}=\lambda_1\xi\left\|x\right\|, \qquad \widehat{b}\left(0\right)=0, \tag{33}$$

$$\dot{\varepsilon}=-\lambda_2\varepsilon, \qquad \varepsilon\left(0\right)\neq 0, \tag{34}$$

where $b=b_1+b_2+b_3+b_4$, $\widetilde{b}=b-\widehat{b}$, $\widehat{b}$ is the estimate value of b, $\xi=\max(1,\|e\|,\|\dot{e}\|,\|\int_0^t edt\|)$, λ_1 and λ_2 are the arbitrary positive constants, and other parameters are defined as Section 3.1.

The framework of the proposed control scheme is shown in Figure 3.

Proof. Consider the following Lyapunov function:

$$\begin{aligned} V=\frac{1}{2}\Bigg[&x^TM\left(q\right)x+e^T\left(K_P+\gamma K_D\right)e \\ &+\left(\int_0^t edt\right)^T\left(K_P+\gamma K_I\right)\left(\int_0^t edt\right) \\ &+\widetilde{P}^T\Phi^{-1}\widetilde{P}+\left(\lambda_1^{-1}\widetilde{b}^2+\lambda_2^{-1}\varepsilon^2\right)\Bigg]. \end{aligned} \tag{35}$$

Based on the controller stability analysis with known upper bound of the external disturbances in Section 3.1, according to (24) one gets

$$\dot{V}\leq-\sum_{i=1}^{n}\gamma k_{Pi}e_i^2+x^TV-x^Tu+\lambda_1^{-1}\widetilde{b}\dot{\widetilde{b}}+\lambda_2^{-1}\varepsilon\dot{\varepsilon}. \tag{36}$$

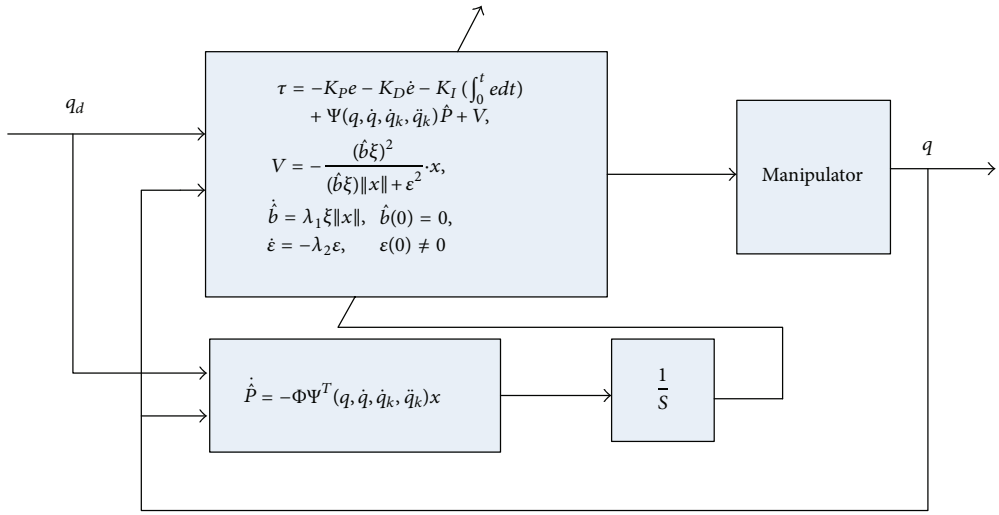

Figure 3: Framework of control law with unknown upper bound of the disturbances.

Substituting (32) and (34) into (36) yields

$$\dot{V} \leq -\sum_{i=1}^{n} \gamma k_{Pi} e_i^2 + x^T \left[-\frac{\left(\hat{b}\xi\right)^2}{\left(\hat{b}\xi\right)\|x\| + \varepsilon^2} \right] x - x^T u + \lambda_1^{-1} \tilde{b}\dot{\tilde{b}} - \varepsilon^2. \tag{37}$$

Take into account that the following equalities and inequalities hold:

$$x^T x = \|x\|^2, \qquad -x^T u \leq \|x\| \cdot \|u\|,$$

$$\|u\| \leq b_1 + b_2 \|e\| + b_3 \|\dot{e}\| + b_4 \left\| \int_0^t e dt \right\| \leq b\xi, \tag{38}$$

$$\dot{\tilde{b}} = -\dot{\hat{b}} = -\lambda_1 \xi \|x\|;$$

here the assumption (C2) and (33) have been used.

Therefore, one obtains

$$\begin{aligned}
\dot{V} &\leq -\sum_{i=1}^{n} \gamma k_{Pi} e_i^2 \\
&\quad - \frac{\left(\hat{b}\xi\right)^2}{\left(\hat{b}\xi\right)\|x\| + \varepsilon^2} \cdot \|x\|^2 + \|x\| \cdot (b\xi) - \tilde{b}\xi\|x\| - \varepsilon^2 \\
&\leq -\sum_{i=1}^{n} \gamma k_{Pi} e_i^2 \\
&\quad + \frac{-\left(\hat{b}\xi\right)^2 \|x\|^2 + \left(\hat{b}\xi\right)^2 \|x\|^2 + \varepsilon^2 \xi \|x\| \hat{b} - \varepsilon^2 \left(\hat{b}\xi\right)\|x\| - \varepsilon^4}{\left(\hat{b}\xi\right)\|x\| + \varepsilon^2} \\
&\leq -\sum_{i=1}^{n} \gamma k_{Pi} e_i^2 - \frac{\varepsilon^4}{\left(\hat{b}\xi\right)\|x\| + \varepsilon^2}.
\end{aligned} \tag{39}$$

From the definitions of (33) and (34), it can be easily verified that $\hat{b} > 0$ and $\varepsilon^2 > 0$ as $t > 0$, and $\varepsilon \to 0$ as $t \to \infty$. Thus the condition $\dot{V} < 0$ is satisfied. According to the Lyapunov stability theory and Barbalat's lemma (see (30)), the convergence of e and $\dot{e}$ to zero is guaranteed, and also the boundedness of the parameter vector $\tilde{P}$ is obtained. □

4. Simulation Experiments and Discussion

In order to illustrate the performance of the proposed robust adaptive PID controllers, simulation results are given by means of MATLAB/SIMULINK. A comparison between the adaptive PD controllers in [25, 26] and the robust adaptive PID controllers derived in this study is carried out. The simulation model is a two-degree-of-freedom planar rigid manipulator with rotary joints. According to (1), its dynamic equation can be described as follows [30]:

$$\begin{aligned}
&\begin{bmatrix} M_{11}(q_2) & M_{12}(q_2) \\ M_{12}(q_2) & M_{22}(q_2) \end{bmatrix} \begin{bmatrix} \ddot{q}_1 \\ \ddot{q}_2 \end{bmatrix} \\
&\quad + \begin{bmatrix} -C_{12}(q_2)\dot{q}_2 & -C_{12}(q_2)(\dot{q}_1 + \dot{q}_2) \\ C_{12}(q_2)\dot{q}_1 & 0 \end{bmatrix} \\
&\quad \cdot \begin{bmatrix} \dot{q}_1 \\ \dot{q}_2 \end{bmatrix} + \begin{bmatrix} G_1(q_1, q_2)\, g \\ G_2(q_1, q_2)\, g \end{bmatrix} = \begin{bmatrix} \tau_1 \\ \tau_2 \end{bmatrix},
\end{aligned} \tag{40}$$

where

$$\begin{aligned}
M_{11}(q_2) &= (m_1 + m_2) r_1^2 + m_2 r_2^2 + 2m_2 r_1 r_2 \cos q_2, \\
M_{12}(q_2) &= m_2 r_2^2 + m_2 r_1 r_2 \cos q_2, \\
M_{22}(q_2) &= m_2 r_2^2, \\
C_{12}(q_2) &= m_2 r_1 r_2 \sin q_2, \\
G_1(q_1, q_2) &= (m_1 + m_2) r_1 \cos q_2 + m_2 r_2 \cos(q_1 + q_2), \\
G_2(q_1, q_2) &= m_2 r_2 \cos(q_1 + q_2).
\end{aligned} \tag{41}$$

At first, linearize (40) and give the parameter matrices Ψ and P.

According to (5) the following equality holds:

$$M(q)\ddot{q}_k + C(q,\dot{q})\dot{q}_k + G(q) = \Psi(q,\dot{q},\dot{q}_k,\ddot{q}_k)P. \quad (42)$$

Let the matrices Ψ and P have the following forms:

$$\Psi = \begin{bmatrix} \psi_{11} & \psi_{12} & \psi_{13} \\ \psi_{21} & \psi_{22} & \psi_{23} \end{bmatrix}, \qquad P = \begin{bmatrix} p_1 & p_2 & p_3 \end{bmatrix}^T. \quad (43)$$

Then the parameters can be derived as below:

$$\begin{aligned} \psi_{11} &= \ddot{q}_{1k} + \left(\frac{g}{r_1}\right)\cos q_2, \qquad \psi_{12} = \ddot{q}_{1k} + \ddot{q}_{2k}, \\ \psi_{13} &= 2\ddot{q}_{1k}\cos q_2 + \ddot{q}_{2k}\cos q_2 - \dot{q}_2\dot{q}_{1k}\sin q_2 \\ &\quad - (\dot{q}_1 + \dot{q}_2)\dot{q}_{2k}\sin q_2 + \left(\frac{g}{r_1}\right)\cos(q_1 + q_2), \\ \psi_{21} &= 0, \qquad \psi_{22} = \psi_{12}, \\ \psi_{23} &= \dot{q}_1\dot{q}_{1k}\sin q_2 + \ddot{q}_{1k}\cos q_2 + \left(\frac{g}{r_1}\right)\cos(q_1 + q_2), \\ p_1 &= (m_1 + m_2)r_1^2, \qquad p_2 = m_2 r_2^2, \qquad p_3 = m_2 r_1 r_2. \end{aligned} \quad (44)$$

The link parameters of robot manipulator are given by $r_1 = 1\,\text{m}$, $r_2 = 0.8\,\text{m}$, $m_1 = 0.5\,\text{kg}$, and $m_2 = 0.5\,\text{kg}$. The upper bound parameters are selected as $b_1 = 2$, $b_2 = 3$, $b_3 = 6$, and $b_4 = 1$. The disturbances vector is chosen as $u = [1.0 \;\; 1.0]^T + 2e + 5\dot{e}$. The reference trajectories are $q_{1d} = \cos(\pi t)$ and $q_{2d} = \cos(\pi t)$. The initial values of manipulator positions and velocities are selected as $[q_1 \;\; \dot{q}_1 \;\; q_2 \;\; \dot{q}_2]^T = [0.6 \;\; 0 \;\; 0.3 \;\; 0]^T$.

Take the gain coefficients of the robust adaptive PID control as

$$\begin{aligned} K_P &= \text{diag}[1000, 400], \qquad K_D = \text{diag}[180, 150], \\ K_I &= K_D, \qquad \gamma = 5, \qquad \Phi = \text{diag}[5.0, 5.0, 5.0]. \end{aligned} \quad (45)$$

The adaptive PD control gains K_P and K_D are determined by [25, 26].

The MATLAB/SIMULINK framework is shown in Figure 4.

In order to show the advantage of the proposed control laws, two simulations are conducted, one with adaptive PD control and the other with robust adaptive PID control. The simulation results are presented in Figures 5–16.

4.1. Simulation Results with Known Upper Bound of the External Disturbances. Adopting the control law described in Section 3.1 to simulate the tracking effects of robot manipulator, the simulation results can be seen from Figures 5, 6, 7, 8, 9, and 10.

4.2. Simulation Results with Unknown Upper Bound of the External Disturbances. Choosing $\lambda_1 = \lambda_2 = 40$ and utilizing the control scheme represented in Section 3.2 to express the tracking capability of robot manipulator, the simulation results are shown in Figures 11, 12, 13, 14, 15, and 16.

5. Discussion

These figures indicate that the robust adaptive PID control schemes can compensate the unknown bounded external disturbances and guarantee the manipulator systems to track the desired position and velocity trajectories accurately with quite small tracking errors in finite time. The adaptive algorithm can effectively estimate the unknown constant vector P which describes the mass characteristics of robot manipulator.

In comparison with the adaptive PD controllers proposed in [25, 26], the robust adaptive PID controllers can provide better control performance. The main reason lies in the incorporation of an integral action within both PD control and robust adaptive algorithm based on the adaptive PD control laws [25, 26]. Concerning the PID control term in the robust adaptive PID controllers, it exhibits the superiority in contrast to the PD one in the adaptive PD controllers [25, 26]. In the case of PD control, the differential element only plays a part in dynamic process, and it has no effect on steady-state process, although the steady-state errors can be smaller by increasing the proportional gain matrix; yet, too large proportional gain may cause the system to be unstable. In addition, from a practical point of view, the pure differential element cannot be realized in practice; furthermore, the differential action is very sensitive to system noise; as a result, any disturbances in each system's element would result in big fluctuation in systems output. Hence, the adoption of PD control is indeed of no benefit for the improvement of system dynamic performance. While the PID control includes an integral element which can raise the indiscrimination degree of the system, so it can enhance the stead-state performance of the closed-loop system. Apart from that, the PID control can also provide one negative real zero, which contributes to improve the dynamic performance of robot manipulator systems. In terms of the adaptation algorithm in this work, different from the one in [25, 26], an integral element acts on the estimation law $\dot{\widehat{P}}$ via the variable x (see (3) and (10)). In this case, note that continuously accumulated position errors under the action of integration element result in a bigger value of $\dot{\widehat{P}}$ than that in [25, 26], which implies that the estimated rate of the estimate vector $\widehat{P}$ is increased. As a consequence, the dynamic performance and the finite-time estimation accuracy of the estimate vector $\widehat{P}$ are improved with comparison to those in [25, 26]. In addition to these, note that assumption (C2) provides a bigger upper bound of the external disturbances than the one which is defined as $\|u\| \le b_1 + b_2\|e\| + b_3\|\dot{e}\|$ in [25, 26]. Because when the two upper bound inequalities of the external disturbances signals u in [25, 26] and this study hold the same parameter values of b_1, b_2, and b_3, an arbitrary positive constant b_4 together with the nonzero accumulated position errors in assumption (C2) can lead to a bigger upper bound value for the external disturbances signals u. However, the enlarged external disturbances can be compensated by the enhanced robust term V (see (3), (9), (32), and (33)). Therefore, greater external disturbances are allowed for this study than the ones tolerated in [25, 26]. Hence, the proposed robust adaptive PID

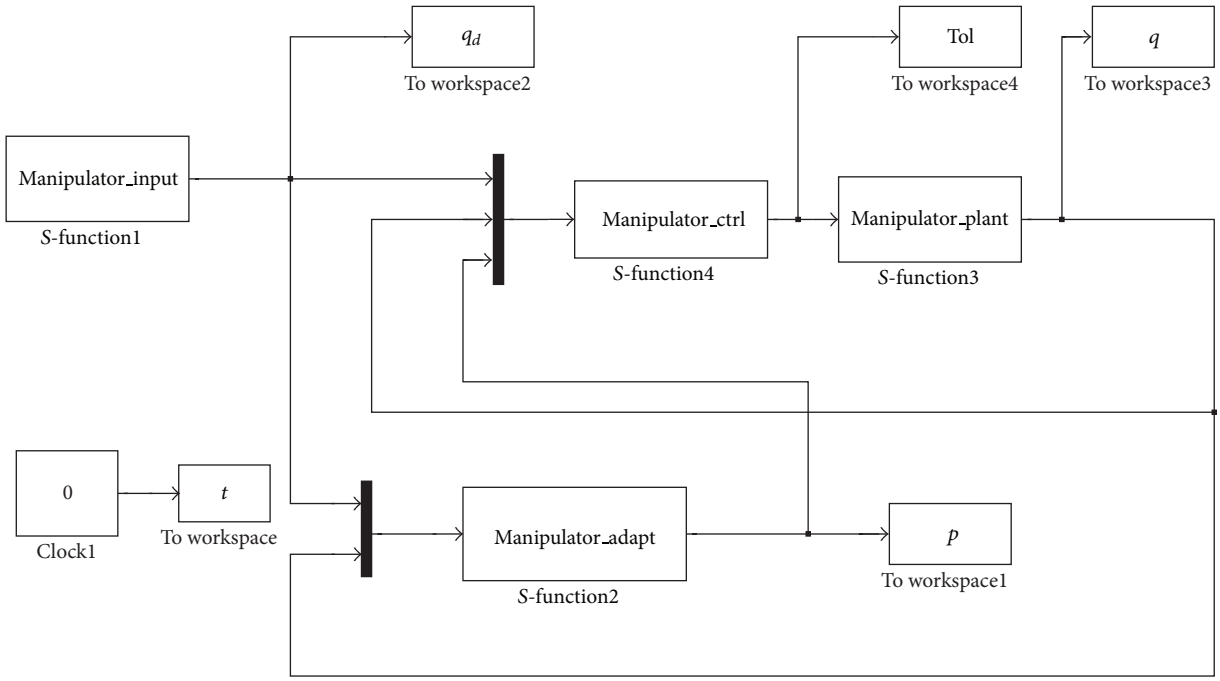

Figure 4: The MATLAB/SIMULINK framework.

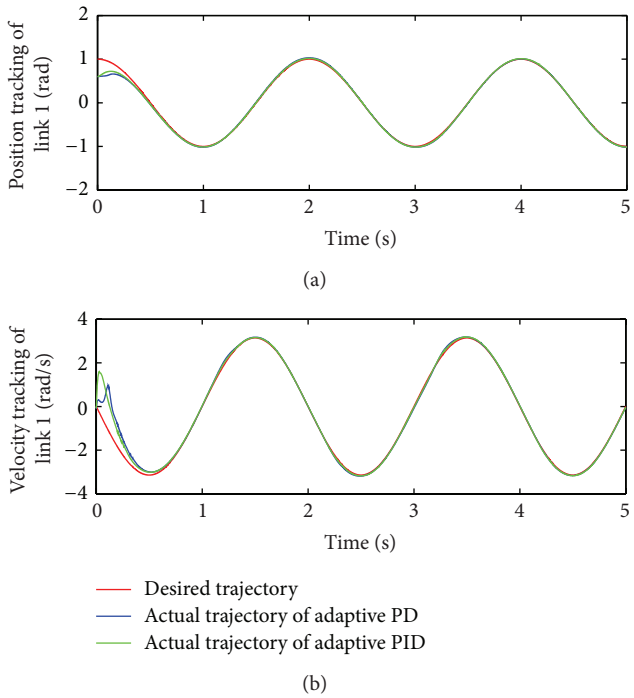

Figure 5: Position and velocity trajectory tracking of link 1.

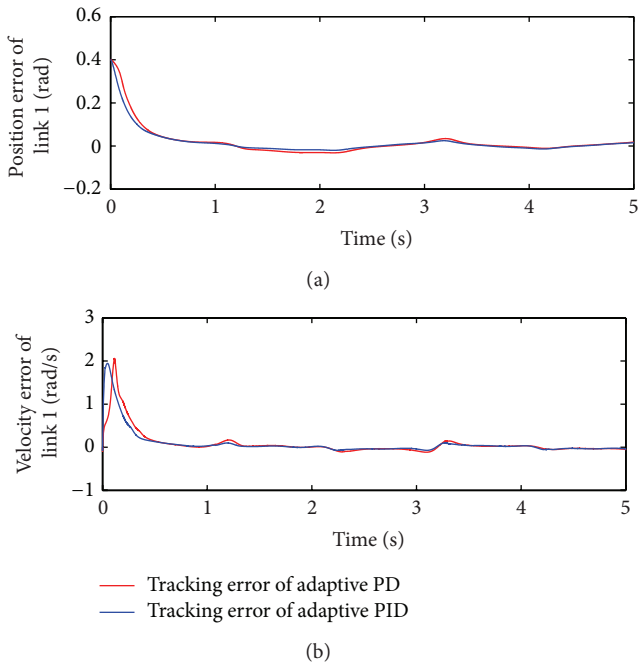

Figure 6: Position and velocity trajectory tracking errors of link 1.

control laws could show their advantages with appropriate control gains in contrast to the adaptive PD ones [25, 26].

However, it should emphasize that the proposed robust adaptive PID controllers can only enhance the finite-time tracking accuracy in contrast to the existing adaptive PD ones [25, 26], because the global asymptotical stability with respect to the manipulator positions and velocities can also be achieved by using the adaptive PD control laws [25, 26], which implies that $e(t) \to 0$ and $\dot{e}(t) \to 0$ as $t \to \infty$ can be guaranteed. Nevertheless, the dynamic performance of the closed-loop system can be improved in the whole process by adopting the robust adaptive PID control laws. In fact, the control procedure is always the finite-time process in

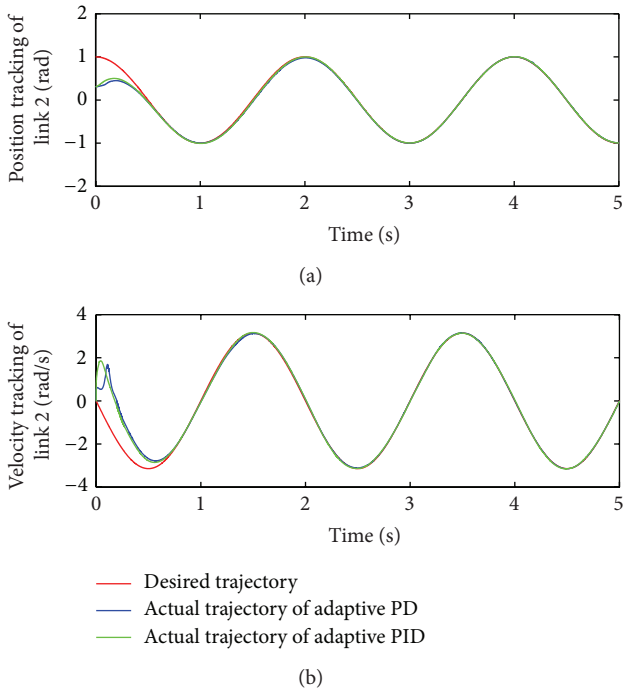

Figure 7: Position and velocity trajectory tracking of link 2.

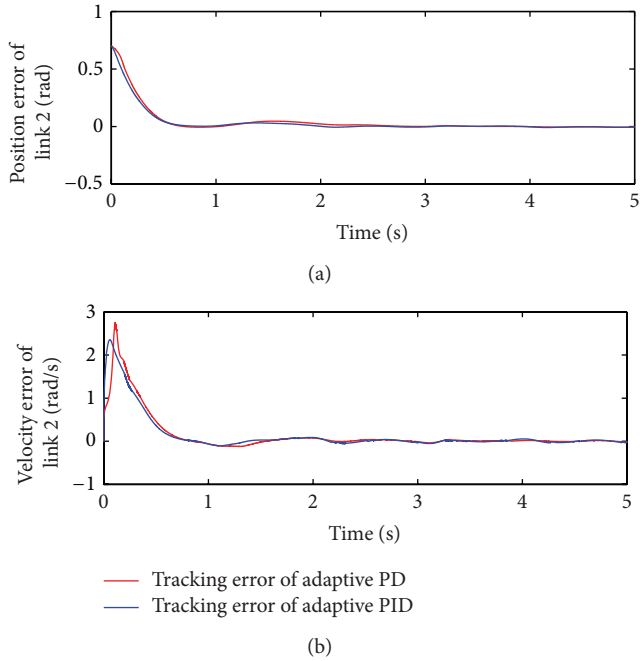

Figure 8: Position and velocity trajectory tracking errors of link 2.

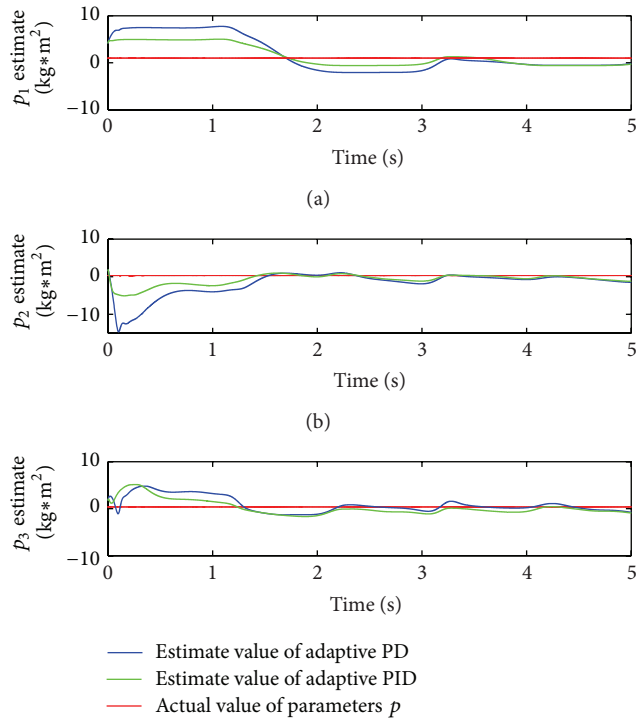

Figure 9: Estimate values of parameters p_1, p_2, and p_3.

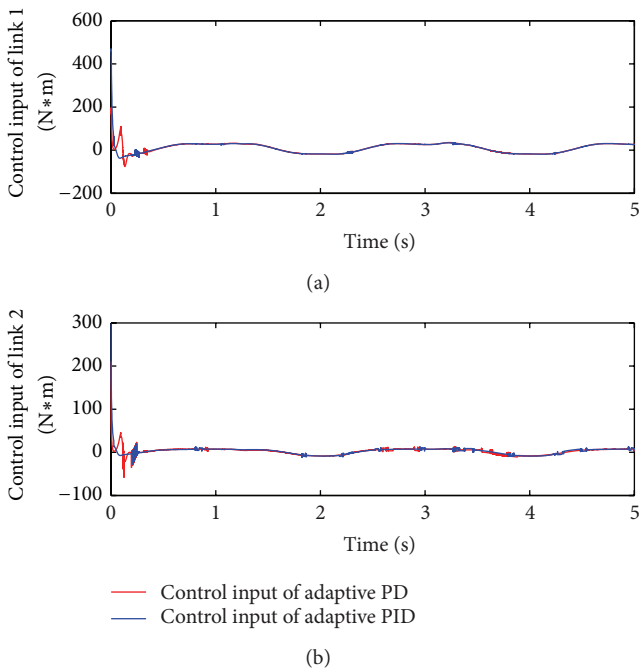

Figure 10: Control inputs of link 1 and link 2.

practical control systems; hence the study of the finite-time control performance improvement of robot manipulator in this work is of practical significance.

Simulation results verify the advantages of the proposed control schemes. The experimental curves show that the robust adaptive PID controllers provide higher accuracy in finite-time position and velocity tracking control than those provided by the adaptive PD ones [25, 26]. Moreover, the robust adaptive PID controllers result in better dynamic performance of the manipulator systems. By observing the experimental figures, it can be verified that the proposed control laws can ensure a faster convergence rate and smaller

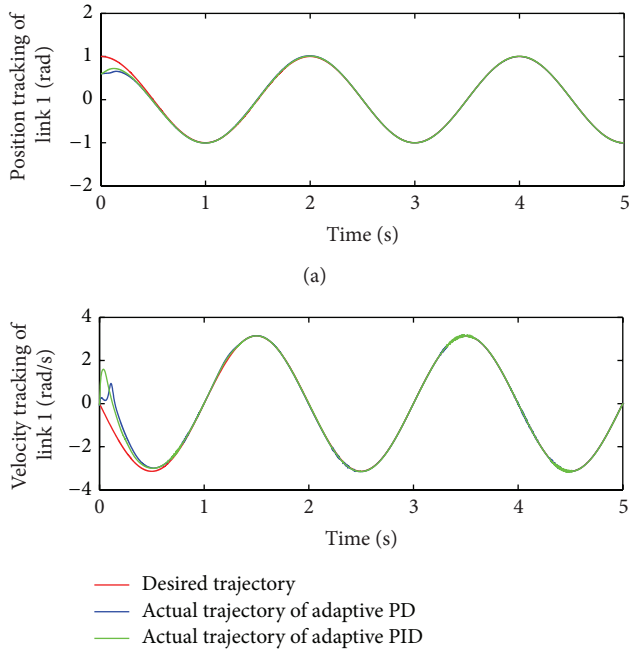

Figure 11: Position and velocity trajectory tracking of link 1.

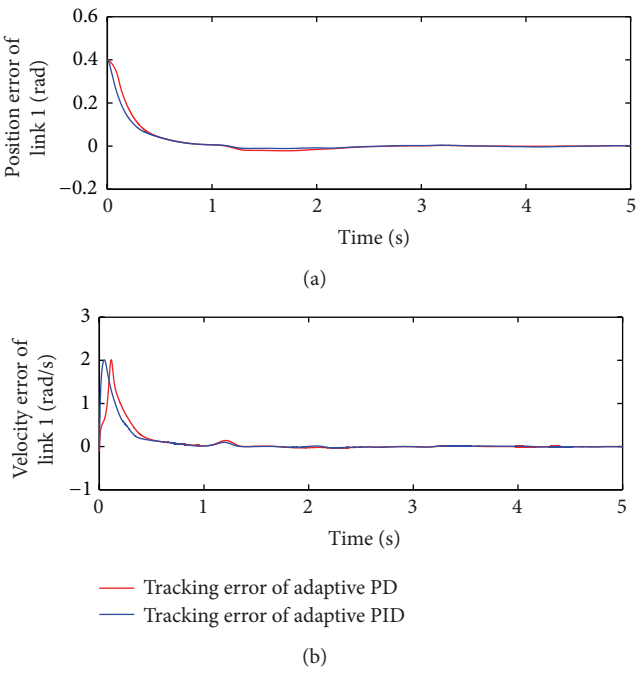

Figure 12: Position and velocity trajectory tracking errors of link 1.

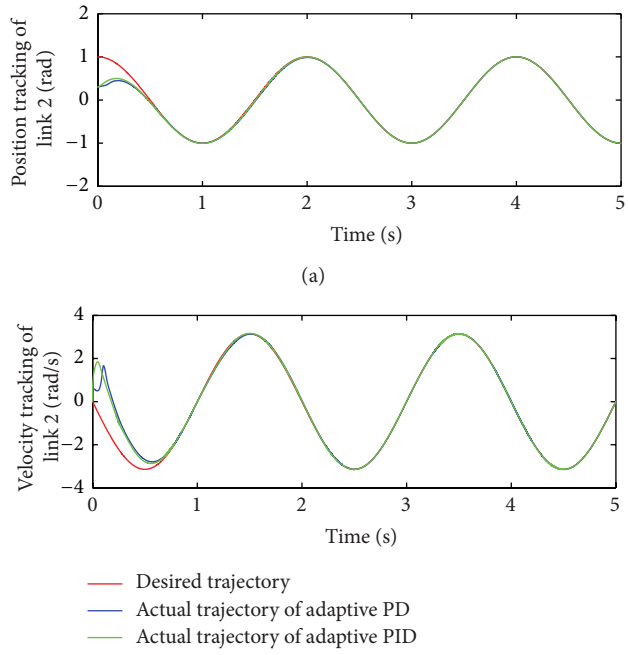

Figure 13: Position and velocity trajectory tracking of link 2.

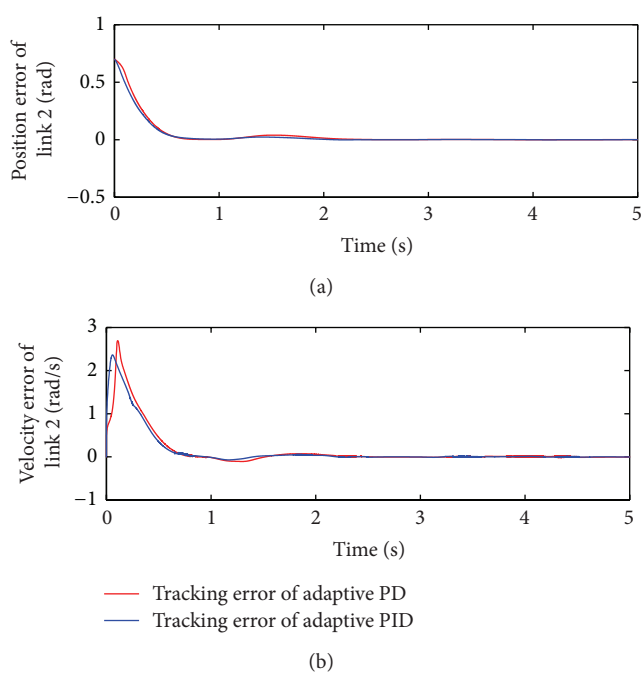

Figure 14: Position and velocity trajectory tracking errors of link 2.

overshoot of the system states tracking to the desired trajectories when compared with the adaptive PD controllers [25, 26]. In terms of the control input, the robust adaptive PID controllers lead to less chattering effect, which is beneficial to prolong the service life of robot manipulator. For the unknown constant vector P, the designed controllers in this study ensure higher finite-time estimation accuracy and significantly lower overshoot.

From the above analysis, the investigation of this work presents more effective control methods for robot manipulator operation under unknown bounded external disturbances.

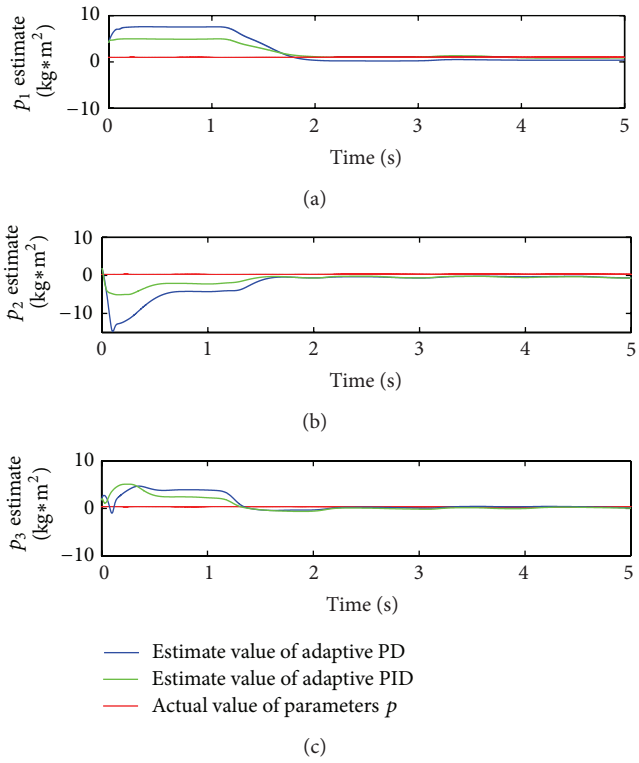

FIGURE 15: Estimate values of parameters p_1, p_2, and p_3.

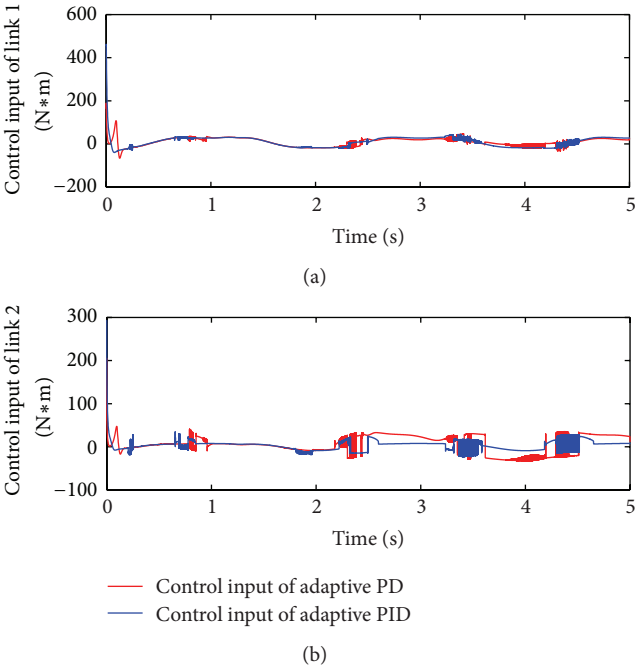

FIGURE 16: Control inputs of link 1 and link 2.

Remark. Both the adaptive PD control laws in [25, 26] and the robust adaptive PID control laws in this study can make the position and the velocity tracking errors of the manipulator systems asymptotically converge to zero, which means $e(t) \to 0$ and $\dot{e}(t) \to 0$ as $t \to \infty$. Therefore, when the control gains chosen for simulation in [25, 26] and this paper simultaneously result in rapid convergence of the manipulator positions and velocities, the advantage of the robust adaptive PID controllers will be tiny with comparison to the adaptive PD controllers [25, 26].

Nevertheless, it is necessary to emphasize that the proposed controllers are unavailable under manipulator actuators fault. However, actuators fault may occur due to infrequent maintenance or limited life cycle, which could cause several damages to the operators and products. In [31], an adaptive variable structure control scheme is proposed for underactuated mechanical manipulators. Reference [32] investigates the basic data-driven methods for process monitoring and fault diagnosis. And [33] discusses two online schemes for an integrated design of fault-tolerant control systems. Based on these current researches, our future work will focus on the fault diagnosis and fault-tolerant control of robot manipulators in case of actuators fault.

6. Conclusion

This paper describes the design and simulation implementation of two new robust adaptive PID controllers for the trajectory tracking control of rigid robot manipulator with known or unknown upper bound of the external disturbances. The main feature of this design is that it combines PID control law with robust adaptive algorithm. The adaptive algorithm is utilized to estimate the unknown constant vector P online, while the robust term and the PID control are used to cope with the unknown bounded external disturbances, adaptive approximation errors, and trajectory tracking errors.

The convergence and stability properties of the closed-loop system are guaranteed. In addition, the tolerable external disturbances are enlarged; besides, the dynamic performance of the manipulator systems is improved and the finite-time tracking control accuracy is enhanced by adopting the proposed control schemes in contrast to those achieved through applying the existing adaptive PD control laws [25, 26]. The control techniques have been finally simulated for a planner manipulator model with two rotary degrees of freedom in MATLAB/SIMULINK toolbox. Simulation results show the advantages of the designed controllers and verify that the proposed strategies are able to cope with both the external disturbances, that can typically arise in practical control, and uncertain constant parameters in system dynamics.

The limitation of the proposed control schemes lies in the requirement of $K_D = K_I$, which in fact constrains the flexibility of the controllers. Currently we are working on the extension of the proposed methods to remove this constraint. Future work will investigate the fault diagnosis and fault-tolerant control of robot manipulator systems with actuators fault.

Acknowledgments

This work was supported by the National Natural Science Foundation of China under Grant 51179038 and the Fundamental Research Funds for the Central Universities of HEUCF041337.

References

[1] R. Kelly and R. Carelli, "A class of nonlinear PD-type controllers for robot manipulators," *Journal of Robotic Systems*, vol. 13, no. 12, pp. 793–802, 1996.

[2] S. Kawamura, F. Miyazaki, and S. Arimoto, "Is a local PD feedback control law effective for trajectory tracking of robot motion?" in *Proceedings of the IEEE International Conference on Robotics and Automation*, vol. 3, pp. 1335–1340, 1988.

[3] S. Arimoto and F. Miyazaki, "Stability and robustness of PID feedback control for robot manipulators of sensory capability," in *Proceedings of the 1st International Symposium on Robotics Research*, pp. 783–799, 1984.

[4] E. M. Jafarov, M. N. A. Parlakçi, and Y. Istefanopulos, "A new variable structure PID-controller design for robot manipulators," *IEEE Transactions on Control Systems Technology*, vol. 13, no. 1, pp. 122–130, 2005.

[5] G. Leitmann, "On the efficacy of nonlinear control in uncertain linear systems," *Journal of Dynamic Systems, Measurement and Control*, vol. 103, no. 2, pp. 95–102, 1981.

[6] M. J. Corless and G. Leitmann, "Continuous state feedback guaranteeing uniform ultimate boundedness for uncertain dynamic systems," *Institute of Electrical and Electronics Engineers*, vol. 26, no. 5, pp. 1139–1144, 1981.

[7] M. W. Spong, "On the robust control of robot manipulators," *Institute of Electrical and Electronics Engineers*, vol. 37, no. 11, pp. 1782–1786, 1992.

[8] E. Yaz, "Commons on "on the robust control of robot manipulators" by M. W. Spong," *IEEE Transactions on Automatic Control*, vol. 38, no. 3, pp. 511–512, 1993.

[9] K.-M. Koo and J.-H. Kim, "Robust control of robot manipulators with parametric uncertainty," *Institute of Electrical and Electronics Engineers*, vol. 39, no. 6, pp. 1230–1233, 1994.

[10] M. Danesh, M. Keshmiri, and F. Sheikholeslam, "Developing a robot control scheme robust to uncertain model parameters and unmodeled dynamics," in *Proceedings of the 1st IEEE Conference on Industrial Electronics and Applications (ICIEA '06)*, pp. 1–6, May 2006.

[11] G. Liu and A. A. Goldenberg, "Uncertainty decomposition-based robust control of robot manipulators," *IEEE Transactions on Control Systems Technology*, vol. 4, no. 4, pp. 384–393, 1996.

[12] J. J. Craig, P. Hsu, and S. S. Sastry, "Adaptive control of mechanical manipulators," *International Journal of Robotics Research*, vol. 6, no. 2, pp. 16–28, 1987.

[13] J.-J. E. Slotine and W. Li, "On the adaptive control of robot manipulators," *International Journal of Robotics Research*, vol. 6, no. 3, pp. 49–59, 1987.

[14] R. Burkan, "Design of an adaptive control law using trigonometric functions for robot manipulators," *Robotica*, vol. 23, no. 1, pp. 93–99, 2005.

[15] R. Burkan, "Modelling of a logarithmic parameter adaptation law for adaptive control of mechanical manipulators," *Robotica*, vol. 24, no. 4, pp. 523–525, 2006.

[16] K. Y. Lim and M. Eslami, "Robust adaptive controller designs for robot manipulator systems," *IEEE Journal of Robotics and Automation*, vol. 3, no. 1, pp. 54–66, 1987.

[17] R. Johansson, "Adaptive control of robot manipulator motion," *IEEE Transactions on Robotics and Automation*, vol. 6, no. 4, pp. 483–490, 1990.

[18] Z. J. Yang, Y. Fukushima, and P. Qin, "Decentralized adaptive robust control of robot manipulators using disturbance observers," *IEEE Transactions on Control Systems Technology*, vol. 20, no. 5, pp. 1357–1365, 2012.

[19] R. Burkan, "Design parameters and uncertainty bound estimation functions for adaptive-robust control of robot manipulators," *Turkish Journal of Electrical Engineering and Computer Sciences*, vol. 20, no. 1, pp. 169–186, 2012.

[20] R. Burkan, "Design of adaptive compensators for the control of robot manipulators robust to unknown structured and unstructured parameters," *Turkish Journal of Electrical Engineering & Computer Sciences*, vol. 21, no. 2, pp. 452–469, 2013.

[21] F. Aghili, "Adaptive control of manipulators forming closed kinematic chain with inaccurate kinematic model," *IEEE/ASME Transactions on Mechatronics*, vol. 8, no. 5, pp. 1544–1554, 2013.

[22] D. J. López-Araujo, A. Zavala-Río, V. Santibáñez, and F. Reyes, "Output-feedback adaptive control for the global regulation of robot manipulators with bounded inputs," *International Journal of Control, Automation, and Systems*, vol. 11, no. 1, pp. 105–115, 2013.

[23] S. I. Han, K. S. Lee, M. G. Park, and J. M. Lee, "Robust adaptive deadzone and friction compensation of robot manipulator using RWCMAC network," *Journal of Mechanical Science and Technology*, vol. 25, no. 6, pp. 1583–1594, 2011.

[24] M. M. Fateh and S. Khorashadizadeh, "Robust control of electrically driven robots by adaptive fuzzy estimation of uncertainty," *Nonlinear Dynamics*, vol. 69, no. 3, pp. 1465–1477, 2012.

[25] H. J. Bai, D. F. Tang, and J. B. Cao, "A robust adaptive PD control method of robot manipulator," *Journal of Mechanical Transmission*, vol. 35, no. 11, pp. 34–40, 2011.

[26] D. Ge and S. Jiang, "Self-adaptive PD control of robot manipulator," in *Proceedings of the 8th ACIS International Conference on Software Engineering, Artificial Intelligence, Networking, and Parallel/Distributed Computing (SNPD '07)*, pp. 605–610, August 2007.

[27] M. W. Spong and M. Vidyasagar, *Robot Dynamics and Control*, John Wiley, New York, NY, USA, 1989.

[28] J. Slotine and W. Li, *Applied Nonlinear Control*, Prentice Hall, New Jersey, NJ, USA, 1991.

[29] H. K. Khalil, *Nonlinear Systems*, Prentice Hall, Upper Saddle River, NJ, USA, 3rd edition, 2003.

[30] C.-Y. Su and T.-P. Leung, "Sliding mode controller with bound estimation for robot manipulators," *IEEE Transactions on Robotics and Automation*, vol. 9, no. 2, pp. 208–214, 1993.

[31] J. H. Yang and K. S. Yang, "An adaptive variable structure control scheme for underactuated mechanical manipulators," *Mathematical Problems in Engineering*, vol. 2013, Article ID 270649, 23 pages, 2012.

[32] S. Yin, S. X. Ding, A. Haghani, H. Hao, and P. zhang, "A comparison study of basic data-driven fault diagnosis and process monitoring methods on the benchmark Tennessee Eastman process," *Journal of Process Control*, vol. 22, no. 9, pp. 1567–1581, 2012.

[33] S. Yin, H. Lou, and S. X. Ding, "Real-time implementation of fault tolerant control system with performance optimization," *IEEE Transactions on Industrial Electronics*, vol. 61, no. 5, pp. 2402–2411, 2014.

Hindawi Publishing Corporation
Mathematical Problems in Engineering
Volume 2013, Article ID 156262, 7 pages
http://dx.doi.org/10.1155/2013/156262

Research Article

Fuzzy Filter-Based FDD Design for Non-Gaussian Stochastic Distribution Processes Using T-S Fuzzy Modeling

Yang Yi, Yue-Yue Zhao, and Song-Yin Cao

College of Information Engineering, Yangzhou University, Yangzhou 225127, China

Correspondence should be addressed to Yang Yi; yiyangcontrol@163.com

Received 22 August 2013; Accepted 12 October 2013

Academic Editor: Tao Li

This paper studies the fuzzy modeling problem and the fault detection and diagnosis (FDD) algorithm for non-Gaussian stochastic distribution systems based on the nonlinear fuzzy filter design. Following spline function approximation for output probability density functions (PDFs), the T-S fuzzy model is built as a nonlinear identifier to describe the dynamic relationship between the control input and the weight vector. By combining the designed filter and the threshold value, the fault in T-S weight model can be detected and the stability of error system can also be guaranteed. Moreover, the novel adaptive fuzzy filter based on stochastic distribution function is designed to estimate the size of system fault. Finally, the simulation results can well verify the effectiveness of the proposed algorithm for the constant fault and the time-varying fault, respectively.

1. Introduction

In order to improve the stability and the security of system, the fault detection and diagnosis (FDD) algorithm for the complex systems has been an important part in the field of control engineering. Many significant approaches have also been presented and applied to practical processes successfully (see [1–4] and references therein). On the other hand, a series of modeling and control strategies which control the shape of output probability density functions (PDFs) for non-Gaussian stochastic processes have received considerable attention (see [5–8]). However, most of the existing FDD results for stochastic systems were only concerned with Gaussian variables, where mean or variance was the objective for optimization and control [9]. Since 2000, the FDD algorithm for non-Gaussian stochastic distribution systems has begun to be discussed based on filter theory [10]. In these results, the modeling problem is often ignored and only linear model or common nonlinear model is considered in FDD (see [10–12]).

In recent years, the well-known T-S fuzzy model was viewed as a popular and powerful modeling tool since it is a powerful solution that bridges the gap between linear and nonlinear control systems (see [13–15]). By introducing a family of fuzzy IF-THEN rules that represent local linear input-output relations of the system, many complex nonlinear models, such as descriptor systems [16], stochastic systems [17], and time-delay model [14], can be described or approximated by T-S fuzzy modeling. Meanwhile, some typical control problems, including dynamic tracking control [14], sliding-mode control [18], and filter design [19, 20], have also been considered through T-S fuzzy modeling.

In this paper, we provide a novel FDD approach for non-Gaussian stochastic distribution systems. Based on B-spline approximation and T-S fuzzy modeling, the concerned FDD problem of the dynamic non-Gaussian systems can be transferred into a special nonlinear FDD problem for deterministic T-S weight dynamics. Instead of common nonlinear observer or filter in [10–12], the nonlinear fuzzy filter and the adaptive filter are conducted by involving the measured output PDFs with the T-S fuzzy weight dynamics. Moreover, by optimizing a series of linear matrix inequalities (LMIs), the fault existing in the stochastic processes can be detected with a defined threshold and the satisfactory estimation value for the size of fault can also be guaranteed. It is noted that the T-S fuzzy model is first applied into the FDD for stochastic distribution systems which solves the nonlinear modeling difficulty in previous results [10–12]. This

represents a significant extension of the previous results that only common linear/nonlinear weight dynamic models are considered and has also an independent significance in the field of fuzzy FDD.

In this paper, for a square matrix M, we denote that $\mathrm{sym}(M) = M + M^T$. The identity and zero matrices are expressed by I and 0, respectively. For a symmetric matrix M, the notation $M > (\geq)0$ is used to denote that M is positive definite (positive semidefinite). The case for $M < (\leq)0$ follows similarly. Moreover, for a vector $v(t)$, define Euclidean norm by $\|v(t)\| = v^T(t)v(t)$.

2. Problem Formulation and T-S Fuzzy Modeling

For a complex non-Gaussian stochastic process, we denote that $u(t) \in R^m$ is the control input, $y(t) \in [a, b]$ is the stochastic output of the concerned system, and F represents the fault to be detected and is supposed as a constant vector. The conditional probability of output $y(t)$ lying inside $[a, \beta]$ can be defined as follows:

$$P\{a \leq y(t) < \beta\} = \int_a^\beta \gamma(z, u(t), F)\, dz, \tag{1}$$

where $\gamma(z, u(t), F)$ stands for the output PDF with fault term under the effect of the control input $u(t)$.

Similarly, with [7, 10, 11], it is supposed that the output PDF $\gamma(z, u(t), F)$, as the control objective, can be measured or estimated. For the PDF $\gamma(z, u(t), F)$, the square root B-spline expansion is given as

$$\sqrt{\gamma(z, u(t), F)} = \sum_{i=1}^{n} v_i(u(t), F)\, b_i(z) + \omega(z, u(t), F), \tag{2}$$

where $b_i(z)$ are the prespecified basis functions and $v_i(u(t), F)$ are the corresponding weight values with fault. $\omega(z, u(t), F)$ represents the model uncertainty or the error term of the approximation of PDFs, which is assumed to satisfy the inequality $\|\omega(z, u(t), F)\| \leq \xi$, where ξ is a known positive constant.

Due to the PDF constraint condition $\int_a^b \gamma(z, u(t), F)dz = 1$, only $n - 1$ weights are independent. Thus, the output PDF can be further expressed as

$$\sqrt{\gamma(z, u(t), F)} = B(z)\, V(u(t), F) + h(V(u(t), F))\, b_n(z) + \omega(z, u(t), F), \tag{3}$$

where $V(u(t), F) = [v_1(u(t), F), \ldots, v_{n-1}(u(t), F)]^T$, $B(z) = [b_1(z), \ldots, b_{n-1}(z)]$. Similarly, with [7], the nonlinear term $h(V(t))$ satisfies the following equality:

$$h(V(t)) = \frac{\sqrt{\Lambda_3 - V^T(t)\Lambda_0 V(t)} - \Lambda_2 V(t)}{\Lambda_3}, \tag{4}$$

where $\Lambda_0 = \Lambda_1 - \Lambda_3^{-1}\Lambda_2^T\Lambda_2$ and

$$\Lambda_1 = \int_a^b B^T(z)\, B(z)\, dz, \qquad \Lambda_2 = \int_a^b B(z)\, b_n(z)\, dz, \qquad \Lambda_3 = \int_a^b b_n^2(z)\, dz \neq 0. \tag{5}$$

It is obvious that the nonlinear term $h(V(t))$ satisfies the Lipschitz condition within its operation region; that is, for any $V_1(t)$ and $V_2(t)$, there exists a known matrix U_1 such that

$$\|h(V_1(t)) - h(V_2(t))\| \leq \|U_1(V_1(t) - V_2(t))\|. \tag{6}$$

In the following, we will find the dynamic relationship between the control input $u(t)$ and the weight vectors $V(u(t), F)$, which corresponds to a further modeling procedure. It is well known that the T-S fuzzy model is a powerful solution for identifying complex nonlinear dynamics by a blending of some local linear system models. Compared with those results that only consider common linear/nonlinear weight dynamic model (see [10–12]), we will use the T-S model to describe the nonlinear weight dynamics and the ith rule of the T-S fuzzy model is of the following form.

Plant Rule i. If θ_1 is μ_{i1}, θ_2 is μ_{i2}, θ_p is μ_{ip}, then

$$\dot{x}(t) = A_i x(t) + G_i x(t - \tau(t)) + H_i u(t) + J_i F, \qquad V(t) = E_i x(t), \tag{7}$$

where $V(t) := V(u(t), F) \in R^{n-1}$ is the independent weight vector. $x(t) \in R^m$ is the unmeasured state and $x(t - \tau(t))$ represents the time-delay state. The time-varying delay $\tau(t)$ is assumed to satisfy $0 < \dot{\tau}(t) < \beta < 1$, where β is a known constant. A_i, G_i, H_i, J_i, and E_i are known constant real matrices of appropriate dimension. θ_j and u_{ij} ($i = 1, \ldots, r$, $j = 1, \ldots, p$) are, respectively, the premise variables and the fuzzy sets, r is the number of the If-Then rules, and p is the number of the premise variables. By fuzzy blending, the overall fuzzy model can be defined as follows:

$$\dot{x}(t) = \sum_{i=1}^{r} h_i(\theta)\left(A_i x(t) + G_i x(t - \tau(t)) + H_i u(t) + J_i F\right), \qquad V(t) = \sum_{i=1}^{r} h_i(\theta) E_i x(t), \tag{8}$$

where

$$\theta = \left[\theta_1, \cdots, \theta_p\right], \qquad h_i(\theta) = \frac{\sigma_i(\theta)}{\sum_{i=1}^{r} \sigma_i(\theta)}, \qquad \sigma_i(\theta) = \prod_{j=1}^{p} \mu_{ij}\left(\theta_j\right). \tag{9}$$

Moreover, we have

$$\sigma_i(\theta) \geq 0, \quad i = 1, \ldots, r, \qquad \sum_{i=1}^{r} \sigma_i(\theta) > 0 \tag{10}$$

for any θ. Hence, $h_i(\theta)$ satisfies

$$h_i(\theta) \geq 0, \quad i = 1, \ldots, r, \qquad \sum_{i=1}^{r} h_i(\theta) = 1. \tag{11}$$

3. Fault Detection for T-S Fuzzy Weight Model

To detect the fault existing in the output stochastic distribution, we construct the following fuzzy filter:

$$\dot{\hat{x}}(t) = \sum_{i=1}^{r} h_i(\theta) \left(A_i \hat{x}(t) + G_i \hat{x}_\tau(t) + H_i u(t) + L\varepsilon(t)\right), \tag{12}$$

where $\hat{x}(t)$ is the estimated state, L is the gain to be determined later, and $\varepsilon(t)$ represents the residual signal and is defined as follows:

$$\begin{aligned} \varepsilon(t) &= \int_a^b \sigma(z) \left(\sqrt{\gamma(z, u(t), F)} - \sqrt{\hat{\gamma}(z, u(t))} \right) dz, \\ \sqrt{\hat{\gamma}(z, u(t))} &= \sum_{i=1}^{r} h_i(\theta) B(z) E_i \hat{x}(t) \\ &\quad + h\left(\sum_{i=1}^{r} h_i(\theta) E_i \hat{x}(t) \right) b_n(z), \end{aligned} \tag{13}$$

where $\sigma(z)$ can be regarded as the prespecified vector defined on $[a, b]$. By defining $e(t) = x(t) - \hat{x}(t)$, $\overline{E} = \sum_{i=1}^{r} h_i(\theta) E_i$, the estimated error system can be expressed as

$$\begin{aligned} \dot{e}(t) = \sum_{i=1}^{r} h_i(\theta) \big[&\left(A_i - L\Gamma_1\right) e(t) + G_i e_\tau(t) \\ &- L\Gamma_2 \left(h\left(\overline{E} x(t)\right) - h\left(\overline{E}\hat{x}(t)\right) \right) \\ &+ J_i F - L\Delta(t) \big], \end{aligned} \tag{14}$$

where

$$\begin{aligned} \Gamma_1 &= \int_a^b \sigma(z) B(z) \overline{E}\, dz, \qquad \Gamma_2 = \int_a^b \sigma(z) b_n\, dz, \\ \Delta(t) &= \int_a^b \sigma(z)\, \omega(z, u(t), F)\, dz. \end{aligned} \tag{15}$$

It can be seen that $\|\Delta(t)\| \leq \widetilde{\xi}$, where $\widetilde{\xi} = \xi \| \int_a^b \sigma(z) dz \|$ is a known constant. Meanwhile, the residual signal can be expressed as

$$\begin{aligned} \varepsilon(t) = &\int_a^b \sigma(z) B(z) \overline{E} e(t)\, dz \\ &+ \int_a^b \sigma(z) \left[h\left(\overline{E} x(t)\right) - h\left(\overline{E}\hat{x}(t)\right) \right] b_n(z)\, dz \\ &+ \int_a^b \sigma(z)\, \omega(z, u(t), F)\, dz \\ = &\Gamma_1 e(t) + \Gamma_2 \left[h\left(\overline{E} x(t)\right) - h\left(\overline{E}\hat{x}(t)\right) \right] + \Delta(t). \end{aligned} \tag{16}$$

In the fault detection phase, our objective is to find the gain L such that the estimated error system (14) is stable if $F = 0$, which can be formulated in the following theorem.

Theorem 1. *For the known parameters $\lambda > 0$, $\eta > 0$, suppose that there exist matrices $P > 0$, $Q > 0$, R, such that the following LMIs*

$$\begin{bmatrix} \Pi_i + \eta I & PG_i & R\Gamma_2 \\ G_i^T P & -(1-\beta) Q + \eta I & 0 \\ \Gamma_2^T R^T & 0 & -\lambda^{-2} I \end{bmatrix} < 0, \quad i = 1, \ldots, r \tag{17}$$

are solvable, where

$$\Pi_i = \text{sym}\left(PA_i - R\Gamma_1\right) + Q + \lambda^{-2} \overline{E}^T U^T U \overline{E}; \tag{18}$$

then the error system (14) is stable when $F = 0$, and, for any $t \in [-\tau(t), +\infty)$, the error variable $e(t)$ satisfies

$$\|e(t)\| \leq \alpha_0 = \max\left\{ \|e_m\|, 2\eta^{-1} \widetilde{\xi} \|R\| \right\}, \tag{19}$$

where the gain L can be computed by $L = P^{-1} R$.

Proof. Denote the Lyapunov function candidate as

$$\begin{aligned} &\Phi(e, x, \hat{x}, t) \\ &= e^T(t) P e(t) + \int_{t-\tau(t)}^{t} e^T(\tau)(t) Q e(\tau)\, d\tau \\ &\quad + \frac{1}{\lambda^2} \int_0^t \left[\left\| U \overline{E} e(\tau) \right\|^2 - \left\| h\left(\overline{E} x(\tau)\right) - h\left(\overline{E} x(\tau)\right) \right\|^2 \right] d\tau, \end{aligned} \tag{20}$$

when $F = 0$, and, based on (14), we can get

$$\begin{aligned} \dot{\Phi} \leq &\sum_{i=1}^{n} h_i(\theta) \left\{ e^T(t) \left(\text{sym}\left(PA_i - R\Gamma_1\right) + Q \right) e(t) \right\} \\ &+ 2 \sum_{i=1}^{r} h_i(\theta)\, e^T P G_i e_\tau(t) - (1-\beta) e_\tau^T(t) Q e_\tau(t) \\ &+ \lambda^{-2} e^T(t) \overline{E}^T U^T U \overline{E} e(t) - 2 e^T(t) P L \Delta(t) \\ &+ \lambda^2 e^T(t) P L \Gamma_2 \Gamma_2^T L^T P e(t) \\ = &\sum_{i=1}^{r} h_i(\theta)\, \xi^T(t)\, \Omega_i \xi(t) - 2 e^T(t) P L \Delta(t), \end{aligned} \tag{21}$$

where $\xi(t) = [e^T(t), e_\tau^T(t)]^T$,

$$\begin{aligned} \Omega_i &= \begin{bmatrix} \Xi_i & PG_i \\ G_i^T P & -(1-\beta) Q \end{bmatrix}, \\ \Xi_i &= \text{sym}\left(PA_i - R\Gamma_1\right) + Q + \lambda^{-2} \overline{E}^T U^T U \overline{E} \\ &\quad + \lambda^2 P L \Gamma_2 \Gamma_2^T L^T P. \end{aligned} \tag{22}$$

By defining $L = P^{-1}R$ and using Schur complement formula with respect to (17), we have

$$\begin{aligned}\dot{\Phi} &\leq -\eta\|e(t)\|^2 + 2\widetilde{\delta}\,\|e(t)\|\,\|R\| \\ &= -\eta\,\|e(t)\|\left(\|e(t)\| - 2\eta^{-1}\,\|R\|\,\widetilde{\delta}\right).\end{aligned} \tag{23}$$

Thus, when $\|e(t)\| > 2\eta^{-1}\|R\|\widetilde{\delta}$, $\dot{\Phi} < 0$ can be guaranteed. So we can get that the system (14) is stable and the estimated error satisfies

$$\|e(t)\| \leq \max\left\{\left\|e_m\right\|, 2\eta^{-1}\widetilde{\xi}\,\|R\|\right\}, \tag{24}$$

where $\|e_m\| = \max_{-\tau(t)<t<0}\|e(t)\|$.

It is noted that Theorem 1 gives a necessary condition for fault detection. Based on the conclusion of Theorem 1, when the fault $F = 0$, the residual error signal satisfies the following inequality:

$$\begin{aligned}\|\varepsilon(t)\| &\leq \left\|\Gamma_1\right\|\|e(t)\| + \left\|\Gamma_2\right\|\|U\|\,\|e(t)\| + \|\Delta(t)\| \\ &\leq \alpha_0\left(\left\|\Gamma_1\right\| + \left\|\Gamma_2\right\|\|U\|\right) + \widetilde{\delta}.\end{aligned} \tag{25}$$

By defining the threshold $\alpha = \alpha_0(\|\Gamma_1\| + \|\Gamma_2\|\|U\|) + \widetilde{\delta}$, we can conclude that the system has no fault, when the residual error signal is less than or equal to the threshold. If the residual signal is greater than the threshold, the system causes the existence of fault. □

4. Fault Diagnosis for T-S Fuzzy Weight Model

Based on the results regarding fault detection, this part will estimate the size of the fault if the system has fault. We construct the following adaptive fuzzy filter:

$$\begin{aligned}&\dot{\hat{x}}(t) \\ &= \sum_{i=1}^{r} h_i(\theta)\left(A_i\hat{x}(t) + G_i\hat{x}_\tau(t) + H_i u(t) + L\varepsilon(t) + J_i\widehat{F}(t)\right), \\ &\dot{\widehat{F}} = -C_1\widehat{F}(t) + C_2\varepsilon(t), \\ &\varepsilon(t) = \int_a^b\left(\sqrt{\gamma(z,u(t),F)} - \sqrt{\widehat{\gamma}(z,u(t))}\right)dz, \\ &\sqrt{\widehat{\gamma}(z,u(t))} = B(z)\,\overline{E}\hat{x}(t) + h\left(\overline{E}\hat{x}(t)\right)b_n(z),\end{aligned} \tag{26}$$

where $\widehat{F}$ is the estimate value of the fault F, $C_i > 0, (i = 1, 2)$ are the designed learning rate. Denoting $e(t) = x(t) - \hat{x}(t)$, $\widetilde{F}(t) = F - \widehat{F}(t)$, the estimated error system can be expressed as follows:

$$\begin{aligned}\dot{e}(t) = \sum_{i=1}^{r} h_i(\theta)\Big[&\left(A_i - L\Gamma_1\right)e(t) + G_i e_\tau(t) \\ &- L\Gamma_2\left(h\left(\overline{E}x(t)\right) - h\left(\overline{E}\hat{x}(t)\right)\right) \\ &+ J_i\widetilde{F} - L\Delta(t)\Big], \\ \dot{\widetilde{F}} = -C_1\widetilde{F} + C_1F - C_2\varepsilon(t).&\end{aligned} \tag{27}$$

Theorem 2. *Suppose that $\|F\| \leq M/2$, $\|\widehat{F}\| \leq M/2$; then one has $\|\widetilde{F}\| \leq M$. For the known parameter $\lambda > 0$ and matrices C_i, $(i = 1, 2)$, there exist matrices $P > 0$, $Q > 0$, R and constants $k_1 > 0$, $\theta_j > 0$, $(j = 1, 2, 3)$ satisfying*

$$\begin{bmatrix} \Pi_{1i} & \Pi_{2i} & PG_i & \overline{E}^T U^T \\ \Pi_{2i}^T & -2C_1^T + \Theta_1^T\Theta_1 & 0 & 0 \\ G_i^T P & 0 & -(1-\beta)Q & 0 \\ U\overline{E} & 0 & 0 & -\theta_3 I \end{bmatrix} < 0, \tag{28}$$

where

$$\begin{aligned}\Pi_{1i} &= \Pi_i + kI + \Theta_2^T\Theta_2 \\ \Pi_{2i} &= PJ_i - \Gamma_1^T C_2^T \\ \Theta_1 &= \begin{bmatrix}\theta_2 C_2 \\ \theta_3 C_2\Gamma_2\end{bmatrix}, \qquad \Theta_2 = \begin{bmatrix}\lambda R\Gamma_2 \\ \theta_1 R\end{bmatrix};\end{aligned} \tag{29}$$

then the error system (27) is stable in the presence of F. The estimation error satisfies

$$\|e(t)\|^2 \leq \max\left\{\left\|e_m\right\|^2, k^{-1}\left(\left(\theta_1^{-2} + \theta_2^{-2}\right)\widetilde{\delta}^2\right) + \left\|C_1\right\|M^2\right\} \tag{30}$$

for all $t \in [-\tau, \infty)$. The gain L of diagnosis filter (26) can be computed by $L = P^{-1}R$.

Proof. Define the Lyapunov function as follows:

$$\Upsilon\left(e, x, \hat{x}, \widetilde{F}, t\right) = \Phi(e, x, \hat{x}, t) + \widetilde{F}^T(t)\,\widetilde{F}(t), \tag{31}$$

where $\Phi(e, x, \hat{x}, t)$ is defined in (20), and it can be concluded that

$$\begin{aligned}\dot{\Phi} \leq &\sum_{i=1}^{r} h_i(\theta)\,\xi_i^T(t)\,\overline{\Omega}_i\xi_i(t) + \theta_1^{-2}\Delta^T(t)\,\Delta(t) \\ &+ 2\sum_{i=1}^{r} h_i(\theta)\,e^T(t)\,PJ_i\widetilde{F}(t),\end{aligned} \tag{32}$$

where

$$\overline{\Omega}_i = \begin{bmatrix}\Xi_i + \theta_1^2 RR^T & PG_i \\ G_i^T P & -(1-\beta)Q\end{bmatrix}. \tag{33}$$

Furthermore, we can get that

$$\begin{aligned}\dot{\Upsilon} &\leq \sum_{i=1}^{r} h_i(\theta)\,\xi_i^T(t)\,\Omega_i\xi_i(t) + \theta_1^{-2}\Delta^T(t)\,\Delta(t) \\ &\quad + 2\sum_{i=1}^{r} h_i(\theta)\,e^T(t)\,PJ_i\widetilde{F}(t) + 2\widetilde{F}^T(t)\,\dot{\widetilde{F}}(t) \\ &\leq \sum_{i=1}^{r} h_i(\theta)\,\overline{\xi}^T(t)\,\Psi_i\overline{\xi}(t) + \left(\theta_1^{-2} + \theta_2^{-2}\right)\widetilde{\delta}^2 \\ &\quad + 2F^T(t)\,C_1^T\widetilde{F}(t),\end{aligned} \tag{34}$$

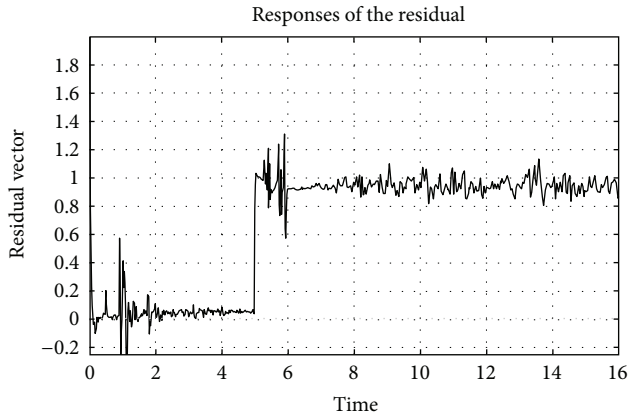

FIGURE 1: The responses of residual signal.

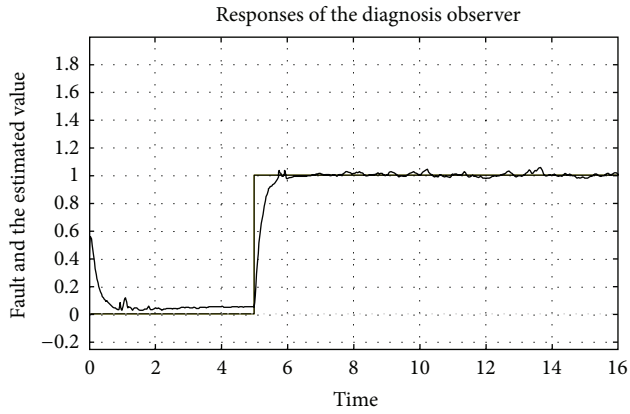

FIGURE 2: Fault and its estimation value.

where

$$\bar{\xi}(t) = \left[e^T(t), e_d^T(t), \widetilde{F}^T(t)\right]^T,$$
$$\varpi = -2C_1^T + \theta_2^2 C_2 C_2^T + \theta_3^2 C_2 \Gamma_2 \Gamma_2^T C_2^T,$$
$$\Psi_i = \begin{bmatrix} \Xi_i + \theta_1^2 RR^T + \theta_3^{-2}\overline{E}^T U^T U \overline{E} & PG_i & \Pi_{13} \\ G_i^T P & (\beta - 1)Q & 0 \\ \Pi_{13}^T & 0 & \varpi \end{bmatrix}. \tag{35}$$

By using Schur complement, the inequality (28) is equivalent to $\Psi_i < \mathrm{diag}\{-kI, 0, 0\}$. Then we can get that

$$\begin{aligned} \dot{\Upsilon} &\le -k\|e(t)\|^2 + \left(\theta_1^{-2} + \theta_2^{-2}\right)\widetilde{\delta}^2 + 2\widetilde{F}^T(t) C_1 \widehat{F}(t) \\ &\le -k\|e(t)\|^2 + \left(\theta_1^{-2} + \theta_2^{-2}\right)\widetilde{\delta}^2 + \|C_1\| M^2. \end{aligned} \tag{36}$$

So $\dot{\Upsilon} < 0$, if $k\|e(t)\|^2 \ge (\theta_1^{-2} + \theta_2^{-2})\widetilde{\delta}^2 + \|C_1\|M^2$ holds. Similarly, with Theorem 1, the estimated error $\|e(t)\|$ satisfies the inequality (30). It can be validated that system (27) is stable in the presence of F, which also implies the good fault diagnosis performance. □

5. An Illustrative Example

Suppose that the output PDFs can be approximated using the following B-spline model:

$$b_i = \begin{cases} |\sin 2\pi z|, & z \in [0.5(i-1), 0.5i] \\ 0, & z \in [0.5(j-1), 0.5j] \end{cases} \quad i \ne j, \tag{37}$$

where $i = 1, 2, 3$, $z \in [0, 1.5]$.

In the simulation, it is supposed that $\widetilde{\delta} = \|\Lambda_1\|^{-1} = 5$. The fault F is defined as

$$F(t) = \begin{cases} 0, & t \le 5 \\ 1, & t > 5. \end{cases} \tag{38}$$

For the T-S fuzzy weight dynamics, the rule $i = 2$ and the model parameters are given as follows:

$$A_1 = \begin{bmatrix} -5 & 1 \\ 1 & -5 \end{bmatrix}, \quad G_1 = \begin{bmatrix} 0 & 1 \\ 1 & 0 \end{bmatrix}, \quad H_1 = H_2 = \begin{bmatrix} 1 \\ 1 \end{bmatrix}, \tag{39}$$

$$A_2 = \begin{bmatrix} -2 & 2 \\ 2 & -2 \end{bmatrix}, \quad G_2 = \begin{bmatrix} 0 & 1 \\ 1 & 0 \end{bmatrix}, \quad E_1 = E_2 = \begin{bmatrix} 4 & 1 \\ 1 & 4 \end{bmatrix}. \tag{40}$$

Furthermore, we choose the following Gaussian type functions as our member functions:

$$M_i = \frac{\exp\left(-(v_2 \pm 1)^2/\sigma^2\right)}{\exp\left(-(v_2 + 1)^2/\sigma^2\right) + \exp\left(-(v_2 - 1)^2/\sigma^2\right)}, \quad i = 1, 2, \tag{41}$$

where $\sigma = 0.8$.

By defining $\lambda = \eta = 1$, $\theta_1 = 0.1$, and $\theta_2 = \theta_3 = 0.05$ and solving LMIs (17), we can get that

$$L = \begin{bmatrix} 6.0672 & 1.5213 \\ 1.6494 & 6.6723 \end{bmatrix}. \tag{42}$$

The responses of the residual signal are shown in Figure 1. It can be clearly seen that when $t > 5$, the fault will occur. Figure 2 is the fault and its estimated value that shows the estimation error can be converged in a small field. Figure 3 shows the 3D mesh plot of the output PDFs and we can find that the fault occurs in front of two peaks. Moreover, when the fault F is redefined as a time-varying function

$$F(t) = \begin{cases} 0, & t \le 5 \\ 1 + 0.2\sin t, & t > 5 \end{cases} \tag{43}$$

the responses of time-varying fault and its estimated value are shown in Figure 4.

6. Conclusions

This paper presents a novel FDD algorithm for non-Gaussian stochastic distribution systems based on T-S fuzzy modeling

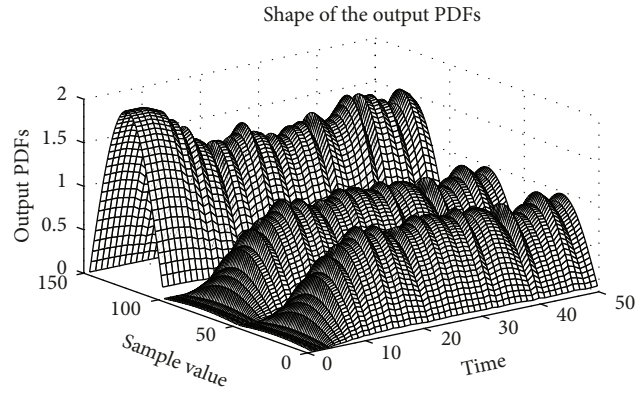

Figure 3: 3D mesh plot of the PDFs.

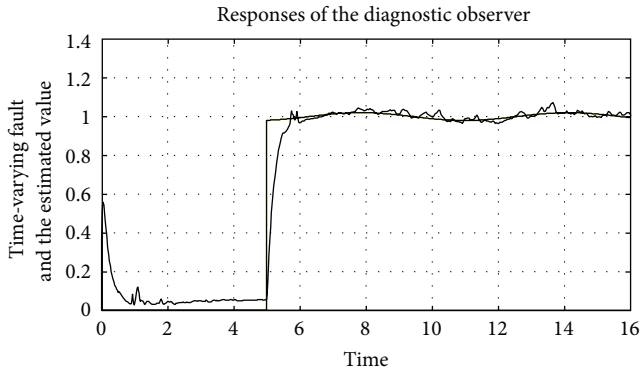

Figure 4: Time-varying fault and its estimation value.

and nonlinear fuzzy filter design. A series of LMIs based solution is presented such that the estimation error system is stable and the fault can be detected through a known threshold. Moreover, the adaptive filter based on the T-S fuzzy model is designed to estimate the size of system fault by optimizing the solutions for the concerned LMIs. Simulations are given to demonstrate the efficiency of the proposed approach.

Conflict of Interests

The authors declare that there is no conflict of interests regarding the publication of this paper.

Acknowledgments

This paper is supported by the National Natural Science Foundation of China under Grants (60904030, 61174046, and 61203195) and China Postdoctoral Science Foundation under Grants (201000470067, 201104541).

References

[1] J. J. Gertler, *Fault Detection and Diagnosis in Engineering Systems*, Marcel Dekker, New York, NY, USA, 1998.

[2] S. X. Ding, *Model-Based Fault Diagnosis Techniques: Design Schemes, Algorithms and Tools*, Springer, Berlin, Germany, 2008.

[3] K. Zhang, B. Jiang, and P. Shi, "Fault estimation observer design for discrete-time takagi-sugeno fuzzy systems based on piecewise lyapunov functions," *IEEE Transactions on Fuzzy Systems*, vol. 20, no. 1, pp. 192–200, 2012.

[4] B. Jiang, K. Zhang, and P. Shi, "Integrated fault estimation and accommodation design for discrete-time takagi-sugeno fuzzy systems with actuator faults," *IEEE Transactions on Fuzzy Systems*, vol. 19, no. 2, pp. 291–304, 2011.

[5] H. Wang, *Bounded Dynamic Stochastic Systems: Modeling and Control*, Springer, London, UK, 2000.

[6] L. Guo and H. Wang, *Stochastic Distribution Control System Design: A Convex Optimization Approach*, Springer, London, UK, 2010.

[7] Y. Yi, L. Guo, and H. Wang, "Constrained PI tracking control for output probability distributions based on two-step neural networks," *IEEE Transactions on Circuits and Systems I*, vol. 56, no. 7, pp. 1416–1426, 2009.

[8] Y. An, Y. Yi, T. P. Zhang, and Q. S. Sun, "PDF shaping control for non-gaussian stochastic distribution systems with time-delay," in *Proceedings of the International Conference on Machine Learning and Computing (ICMLC '12)*, pp. 857–862, Xian, China, July 2012.

[9] R. H. Chen, D. L. Mingori, and J. L. Speyer, "Optimal stochastic fault detection filter," *Automatica*, vol. 39, no. 3, pp. 377–390, 2003.

[10] H. Wang and W. Lin, "Applying observer based FDI techniques to detect faults in dynamic and bounded stochastic distributions," *International Journal of Control*, vol. 73, no. 15, pp. 1424–1436, 2000.

[11] L. Guo and H. Wang, "Fault detection and diagnosis for general stochastic systems using B-spline expansions and nonlinear filters," *IEEE Transactions on Circuits and Systems*, vol. 52, no. 8, pp. 1644–1652, 2005.

[12] T. Li and L. Guo, "Optimal fault-detection filtering for non-gaussian systems via output PDFs," *IEEE Transactions on Systems, Man and Cybernetics A*, vol. 39, no. 2, pp. 476–481, 2009.

[13] T. Takagi and M. Sugeno, "Fuzzy identification of systems and its applications to modeling and control," *IEEE Transactions on Systems, Man and Cybernetics*, vol. 15, no. 1, pp. 116–132, 1985.

[14] C. S. Tseng, "Model reference output feedback fuzzy tracking control design for nonlinear discrete-time systems with time-delay," *IEEE Transactions on Fuzzy Systems*, vol. 14, no. 1, pp. 58–70, 2006.

[15] G. Feng, "A survey on analysis and design of model-based fuzzy control systems," *IEEE Transactions on Fuzzy Systems*, vol. 14, no. 5, pp. 676–697, 2006.

[16] H. B. Zhang, Y. Y. Shen, and G. Feng, "Delay-dependent stability and H_∞ control for a class of fuzzy descriptor systems with time delay," *Fuzzy Sets and Systems*, vol. 160, no. 12, pp. 1689–1707, 2009.

[17] Y. Yi and L. Guo, "Constrained PI tracking control for the output pdfs based on T-S fuzzy mode," *International Journal of Innovative Computing, Information and Control*, vol. 5, no. 2, pp. 349–358, 2009.

[18] W. C. H. Daniel and Y. G. Niu, "Robust fuzzy design for nonlinear uncertain stochastic systems via sliding-mode control," *IEEE Transactions on Fuzzy Systems*, vol. 15, no. 3, pp. 350–358, 2007.

[19] X. J. Su, P. Shi, L. G. Wu, and Y. D. Song, "A novel approach to filter design for T-S fuzzy discrete-time systems with time-varying delay," *IEEE Transactions on Fuzzy Systems*, vol. 20, no. 6, pp. 1114–1129, 2012.

[20] H. G. Zhang, S. X. Lun, and D. R. Liu, "Fuzzy H_{∞} filter design for a class of nonlinear discrete-time systems with multiple time delays," *IEEE Transactions on Fuzzy Systems*, vol. 15, no. 3, pp. 453–469, 2007.

Hindawi Publishing Corporation
Mathematical Problems in Engineering
Volume 2013, Article ID 743716, 9 pages
http://dx.doi.org/10.1155/2013/743716

Research Article

Active Disturbance Rejection with Sliding Mode Control Based Course and Path Following for Underactuated Ships

Ronghui Li,[1] Tieshan Li,[1] Renxiang Bu,[1] Qinling Zheng,[2] and C. L. Philip Chen[3]

[1] *Navigation College, Dalian Maritime University, Dalian 116033, China*
[2] *Department of Electrical and Computer Engineering, Cleveland State University, Cleveland, OH 44115, USA*
[3] *Faculty of Science and Technology, University of Macau, Macau and UMacau Research Institute, Zhuhai, Guangdong 519000, China*

Correspondence should be addressed to Ronghui Li; lironghui@163.com

Received 23 August 2013; Accepted 30 September 2013

Academic Editor: Zhiguang Feng

The compound control of active-disturbance-rejection control (ADRC) with sliding mode is proposed to improve the performance of the closed-loop system and deal with the constraint condition problem of a surface ship. The advantages of ADRC with sliding mode were verified by ship course control simulations. Meanwhile, to solve the path-following problem of underactuated surface ships with uncertainties of internal dynamic and external disturbances, the ADRC controller with sliding mode is introduced to steer the ship to follow the desired path. In order to overcome the cross-track error caused by wind and current, drift angle is compensated in the controller by designing a coordinate transformation equation. Simulations were performed on a nonlinear kinematics model of a training ship to validate the stability and excellent robustness of the proposed path-following controller.

1. Introduction

Control of underactuated ships is an active field due to its important applications such as passenger and goods transportation, environmental surveying, and offshore oil installations. Based on its practical requirement, motion control of an underactuated surface vessel on the horizontal plane can be divided into ship course, path following, and trajectory tracking. Ship course control is mainly concerned with keeping its heading angle to a desired course angle, which is not an underactuated control problem. However, nowadays, by making use of the position feedback signals obtained from a GPS navigation device, a ship guidance system, namely, a tracking control system, can be designed to make the ship track a desired path. Path following is here defined as a control problem of forcing an underactuated ship to follow a specified path at a desired forward speed [1, 2].

Ship control problems are challenging due to the fact that the motion of underactuated surface ships possesses more degrees of freedom to be controlled than the number of the independent controls under some nonintegrable second-order nonholonomic constraints [3]. In particular, underactuated ships do not usually have an actuator in the sway axis on the horizontal plane, whose configuration is by far the most common among marine vessels. Therefore, Brockett's condition indicates that any continuous time-invariant feedback control law does not make a null solution of the underactuated surface ship dynamics asymptotically stable in the sense of Lyapunov. Furthermore, as observed in [3], the underactuated ship system is not transformable into a standard chain system. Consequently, existing control schemes [4] developed for chained systems cannot be applied directly.

Due to the high dependence on the reference model and complicated control laws of the trajectory tracking approach, several researchers have studied the path following problem, which is more suitable for practical implementation. The problem of path following was introduced in [5] where some local results were obtained using linearization techniques. A fourth-order ship model in the Serret-Frenet frame was used in [6] to develop a control strategy to track both a straight line and a circumference under constant ocean current disturbance. A path-following controller was proposed in [7] by using a kinematic model written in polar coordinates, which is inspired by the solution for mobile robots in [8]. However, the controller was designed at the kinematic level with

an assumption of constant ocean current and its direction known to achieve an adjustable boundedness of the path-following error. Since ocean vessels do not have direct control over velocities, a static mapping implementation might result in an unstable closed-loop system due to nonvanishing environmental disturbances. A path-following controller based on a transformation of the ship kinematics to the Serret-Frenet frame, which was used for mobile robot control [9], on the path was proposed in [10], where an acceleration feedback and linearization of ship dynamics were used. Since underactuated surface ships have fewer numbers of actuators than the to be controlled degrees of freedom and are subject to nonintegrable acceleration constraints, their dynamic models are not transformable into a system without drifts. Therefore, the above control scheme is not directly applicable.

The simplest track-keeping system can be designed from a conventional course-keeping autopilot by using information from a positioning system. The whole system approach may be considered as applying "analytical control strategies" dependent techniques including self-tuning control, LQG control, multivariable optimal control, and H_∞ control. The main drawback of analytical control strategies is their dependence on a reliable model. As a matter of fact, a surface ship is strongly influenced by the model internal dynamic uncertainties as well as external disturbances of wind, waves, and ocean current flow. Furthermore, the surface ship motion usually has large inertia, large time lag, nonlinearity, and constraint condition characteristics which reflects in the ship yaw angular rate with a constraint.

In some literature, several methods have been proposed to deal with the uncertainties of the system and the external perturbations. An adaptive robust controller combining the Nussbaum gain technique with a backstepping approach was developed in [11] to cope with ship straight-line tracking control system with parametric uncertainties and unknown control gain coefficients without a priori knowledge of its sign. In [12], a global controller was presented without velocity measurements for feedback. To deal with nonlinear damping coefficients, an adaptive observer was used to estimate the inaccuracies. In order to avoid the need of explicit knowledge of the detailed ship dynamics, application to the marine field of techniques of neural network, fuzzy logic control, and other artificial intelligence (AI) was also investigated in recent years. However, in most of these works, the uncertainty of external perturbation of the nonnegligible ocean current was seldom explicitly involved. These controllers are able to drive the cross-track error to zero in the absence of a constant direction current disturbance. When a surface ship is proceeding under perturbation of a cross ocean constant direction current or wind, it is necessary to maintain a deliberate deviation angle known as "drift angle and leeway." In [13], based on a technique of feedback linearization and backstepping, a control algorithm for a fourth-order ship model was developed with an estimation of the uncertain constant ocean current with known direction to track both line and circumference. However, the assumption and precondition of a priori knowledge of current's direction are very restrictive from a practical point of view.

Based upon the above observations, this paper aims at developing a ship-tracking controller with improved performance in adaptation and robustness by employing the ADRC technique which has been proved to very effective due to its independence of accurate mathematical model of the plant. Aiming specially at the uncertain system, the ADRC technique was proposed by Han [14, 15]. Then, the linear ADRC (LADRC) was developed to achieve the parameterization by Gao [16]. LADRC is a simplified algorithm comparing to nonlinear ADRC, but it also inherits ADRC's advantages; furthermore, it is easy to apply in engineering.

It is well known that the sliding mode control (SMC) has also attractive features to keep the systems insensitive to uncertainties on the sliding surface; its applications have been extensively studied in [17–24]. In this paper, compound control combines the advantages of ADRC and SMC to apply to ship course and path-following control, so that improves the performance of the ship closed-loop systems and makes the parameters of more obvious physical meaning. The cross-track error resulting from constant direction wind and current is removed.

The rest of this paper is organized as follows. The ship model is described in Section 2; three degrees of freedom model for simulation are given. Section 3 proposes the design of ADRC with SMC. Section 4 designs the ship course controller and validates control performance. The ship path-following controller design and simulations are studied in Section 5. Finally, Section 6 contains the main conclusions.

2. Ship Motion Control Model

2.1. The Ship Kinematics Model. The kinematics and dynamics (MMG) model [25] of an underactuated ship moving in surge, sway, and yaw in the earth-fixed and body-fixed frames (Figure 1) can be described as

$$
\begin{aligned}
\dot{x} &= u_r \cos\psi - v_r \sin\psi + V_c \cos\psi_c = V_X \cos\psi - V_Y \sin\psi,\\
\dot{y} &= u_r \sin\psi + v_r \cos\psi + V_c \sin\psi_c = V_X \sin\psi + V_Y \cos\psi,\\
\dot{u}_r &= \dot{V}_X - V_c r \sin\left(\psi_c - \psi\right),\\
\dot{v}_r &= \dot{V}_Y + V_c r \cos\left(\psi_c - \psi\right),\\
\dot{\psi} &= r,\\
&\left(m + m_x\right)\dot{V}_X - \left(m + m_y\right)V_Y r\\
&\quad = X_H + X_P + X_R\left(\delta\right) + X_W\\
&\qquad + \left(m_x - m_y\right)V_c \sin\left(\psi_c - \psi\right) r,\\
&\left(m + m_y\right)\dot{V}_Y + \left(m + m_x\right)V_X r\\
&\quad = Y_H + Y_P + Y_R\left(\delta\right) + Y_W\\
&\qquad - \left(m_x - m_y\right)V_c \cos\left(\psi_c - \psi\right) r,\\
&\left(I_{zz} + J_{ZZ}\right)\dot{r} = N_H + N_P + N_R\left(\delta\right) + N_W,
\end{aligned}
\tag{1}
$$

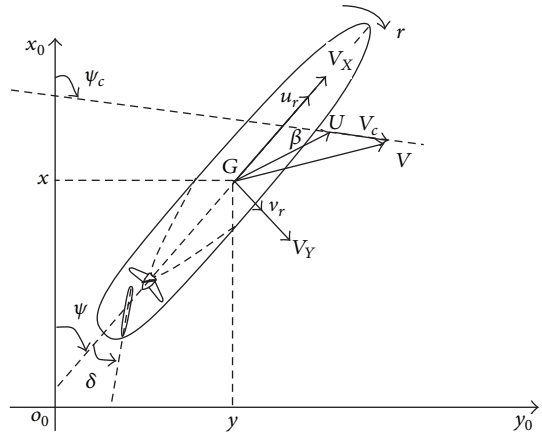

Figure 1: Ship's planimetric position and kinematics with current disturbance.

where x, y, and ψ are the longitudinal displacement, lateral displacement, and heading angle, respectively, in the earth-fixed frame, V_X and V_Y are the longitudinal and lateral velocities over ground, respectively, r is the yaw angular rate in the ship-fixed frame, u_r and v_r denote surge and sway velocities through water, and V_c and ψ_c denote the speed and set of current in the earth-fixed frame. The vector summation of both determines the magnitude and direction of current. δ is rudder angle. m, m_x, m_y, I_{zz}, and J_{zz} denote the ship inertia, added mass, and added moment of inertia. X, Y, and N terms with subscripts H, P, R, and E, respectively, are longitudinal and lateral forces and moments induced by hydrodynamic damping, propeller, rudder, and other external effects except current.

2.2. Ship Course and Path-Following Control Problem. In this paper, in order to design ADRC ship-tracking controller, the following path-following design model derived from (1) is used:

$$\begin{aligned} \dot{y} &= V_x \sin\psi + V_y \cos\psi, \\ \dot{\psi} &= r, \\ \dot{r} &= f(r, w) + b\delta, \end{aligned} \tag{2}$$

where $f(r, w)$ is a multivariable function of both the states and external disturbances as well as time. w is the combined external disturbance from wind and current. $b > 0$ is the control gain which is the design parameter. In the system of (2), the last two equations can be defined as ship course control system which is not an underactuated system.

In practice, when an underactuated surface ship travels at sea, its rudder angle is the only control input used to follow a desired path and to steer a comparatively steady course. However, cross track cannot be regulated to zero by coordinate transformation for the sake of rudder angle under drift caused by wind and current, and it must be compensated by a loxodrome (or sideslip compensation) since no sway control means are available. Because of this, the equilibrium point of the system is not at the origin of transformed coordinates but at a drifting point since the wind and current are time and regional variant. Moreover, the only measurable state variables are the ship's position and heading in earth-fixed coordinates. The path-following problem is rephrased as the stabilization to zero of a suitable scalar path error function based on basic knowledge of the steering feature. The goal of ship path following is to design a robust controller that can force an underactuated surface ship with the abovementioned constraints to follow a desired path.

3. ADRC Controller Design

3.1. ADRC Structure and Its Algorithm. Consider a generally nonlinear time-varying second dynamic system:

$$\ddot{y}(t) = f\left(\dot{y}(t), y(t), d(t)\right) + bu, \tag{3}$$

where y and u are output and input, respectively, and $d(t)$ is the external disturbance. Here, $f(\dot{y}(t), y(t), d(t))$ represents the nonlinear time-varying dynamics of the plant, that is, unknown. b is control gain and unknown, although some knowledge of b can be got; that is, $b \approx b_0$. Rewrite (3) as

$$\begin{aligned} \ddot{y}(t) &= f\left(\dot{y}(t), y(t), d(t)\right) + \left(b - b_0\right)u + b_0 u \\ &= f + b_0 u, \end{aligned} \tag{4}$$

where $f = f(\dot{y}(t), y(t), d(t)) + (b - b_0)u$ is referred to as the generalized disturbance. Assuming that f is differentiable, let $x_3 = f$ and $h = \dot{f}$; (4) can be written in an augmented state space form

$$\begin{aligned} \dot{x}_1 &= x_2, \\ \dot{x}_2 &= x_3 + b_0 u, \\ \dot{x}_3 &= h, \\ y &= x_1, \end{aligned} \tag{5}$$

where $x = [x_1 \;\; x_2 \;\; x_3]^T$. An extended state observer (ESO) of (5) will estimate the derivatives of y and f since (5) is now a state in extended state model. With u and y as inputs of ESO, the ESO of (5) is given as

$$\begin{aligned} \dot{\hat{x}}_1 &= \hat{x}_2 - l_1\left(\hat{x}_1 - x_1\right), \\ \dot{\hat{x}}_2 &= \hat{x}_3 - l_2\left(\hat{x}_1 - x_1\right) + b_0 u, \\ \dot{\hat{x}}_3 &= -l_3\left(\hat{x}_1 - x_1\right), \end{aligned} \tag{6}$$

where $\hat{x} = [\hat{x}_1 \;\; \hat{x}_2 \;\; \hat{x}_3]^T$ is the estimate of the state of (5), and l_i, $i = 1, 2, 3$, are the observer gain parameters to be chosen. The observer gains are chosen such that the characteristic polynomial $s^3 + l_1 s^2 + l_2 s + l_3$ is Hurwitz. For tuning simplicity, all the observer poles are placed at $-\omega_o$. It results in the characteristic polynomial of (6) to be

$$s^3 + l_1 s^2 + l_2 s + l_3 = \left(s + \omega_o\right)^3, \tag{7}$$

where the observer bandwidth ω_o is the sole turning parameter, and $L = [3\omega_o \;\; 3\omega_o^2 \;\; \omega_o^3]^T$.

Generally, the larger the observer bandwidth is, the more accurate the estimation will be. However, a large observer bandwidth will increase noise sensitivity. Therefore, a proper observer bandwidth should be selected in a compromise between the tracking performance and the noise tolerance [16].

Once the observer is designed and well tuned, its outputs will track x_1, x_2, and x_3, respectively. By canceling the effect of f using $\hat{x}_3$, the ADRC actively compensates for f in real time. The ADRC control law is given by

$$u = \frac{-k_p\left(\hat{x}_1 - v\right) - k_d\left(\hat{x}_2 - \dot{v}\right) + \ddot{v} - \hat{x}_3}{b_0}, \tag{8}$$

where v is the reference signal and k_p and k_d are the controller gain parameters selected to make $s^2 + k_d s + k_p$ which is Hurwitz.

The closed-loop system becomes

$$\ddot{y} = \left(f - \hat{x}_3\right) - k_p\left(\hat{x}_1 - v\right) - k_d\left(\hat{x}_2 - \dot{v}\right) + \ddot{v}. \tag{9}$$

Note that with a well-designed ESO, the estimation error in $\hat{x}_i$, $i = 1, 2, 3$, is ignored, and let $e = x_1 - v$. Then, $\hat{x}_1 - v \approx e$ and $\hat{x}_2 - \dot{v} \approx \dot{e}$. The plant (4) is reduced to

$$\ddot{e} = -k_p e - k_d \dot{e} = u_0, \tag{10}$$

which is a classic PD control law.

It is apparent that system (10) is stable, while $t \to \infty$, $e(t) \to 0$.

3.2. Feedback Control Law Design with Linear Sliding Mode. The method of determining k_p and k_d was proposed using the bandwidth idea in [16], but its physical meaning is not clear. Furthermore, the tracking is hard to achieve perfect performance. Therefore, linear sliding mode idea is applicable to the design of error feedback control law in this section.

Letting $k_1 = k_p/k_d$ and $k_2 = k_d$, (10) and (4) become

$$\ddot{e} = -k_2\left(k_1 e + \dot{e}\right). \tag{11}$$

And let

$$\sigma = k_1 e + \dot{e}. \tag{12}$$

While $\sigma \to 0$, $\dot{e}(t) = -k_1 e(t)$, $e(t)$ will converge in index law, and time constant is $1/k_1$. Therefore, σ is the phrase locus of e and $\dot{e}_1$ on the phrase plane. To stabilize system, (11) is the problem of stabilizing σ.

Letting $T = 1/k_1$ and $e(0) = 1$, we have

$$e(t) = e^{-t/T}, \tag{13}$$

where $e(t)$ is an exponential decline curve. Meanwhile, the time constant is T. We have

$$\begin{aligned} e(T) &= 1 - 0.632 = 0.368, \\ e(2T) &= 1 - 0.865 = 0.135, \\ e(3T) &= 1 - 0.95 = 0.05, \\ e(4T) &= 1 - 0.982 = 0.018. \end{aligned} \tag{14}$$

For (12),

$$\dot{\sigma} = k_1\dot{e} + \ddot{e} = k_1\dot{e} + u_0 = k_1\dot{e} - k_d\sigma. \tag{15}$$

Owing to $k_1\dot{e}(t) \to 0$, while $t \to \infty$ and $k_d > 0$, obviously, system (15) is a simple proportion negative feedback system; that is,

$$\dot{\sigma} = -k_d\sigma. \tag{16}$$

The essence of PD control for a second-order system is similar to the design of only one-step sliding mode in form. The control law of (10) is written as

$$u_0 = -k_2\left(k_1 e + \dot{e}\right), \tag{17}$$

where $k_1 > 0$ and $k_2 > 0$ are the design parameters. In addition, $k_2 > k_1$ normally. $1/k_1$ is the system convergence time constant. k_1 is tuned based on how fast we want the output to track the set point. A large k_1 generally increases the response speed, but it may push the system to its limit, leading to oscillations or even instability. So k_1 should be adjusted based on the competing requirements of performance of the actuator. We should consider the limit of the actuator to calculate the value of k_1. For instance, we set the value of k_1 according to the desired turn back time and the limit of ship turning rate. k_2 determines the response speed of control input directly. A large k_2 within a limited range usually increases the rate of change in control signal, but it may lead the system to oscillations or even instability.

3.3. Feedback Control Law Design with Nonlinear Sliding Mode. The important feature of linear sliding is that its projection in each phase plane is a straight line. Linear sliding mode requests the system state has a larger convergence rate when it is at a greater deviation, which can be achieved by higher speed and larger control input. However, in the actual control system, to ensure the control quality of the system when the deviation is large, it often needs to reduce approach speed due to the limited control input, and the cost is to sacrifice the control quality when the deviation is small, where the result is that the system is too slow to be stable. Therefore, linear sliding mode is essentially the same as linear control system, which applies to the small neighborhood of system.

To solve the above problem of linear sliding mode (LSM), the form of nonlinear sliding mode (NLSM) in the phase plane as shown in Figure 2 can be taken. The characteristic of nonlinear sliding mode is that the system has fast convergence rate when the deviation is small, and with the increase of deviation, the convergence rate increases as nonlinear until it tends to a constant, so that the nonlinear sliding mode could ensure good control quality in a wide range.

The actual state of system has constraint condition due to the limitation of control input, so we can select the monotone bounded hyperbolic tangent function as the nonlinear sliding mode function. Let

$$\sigma = k_1 \tanh\left(k_0 e\right) + \dot{e}. \tag{18}$$

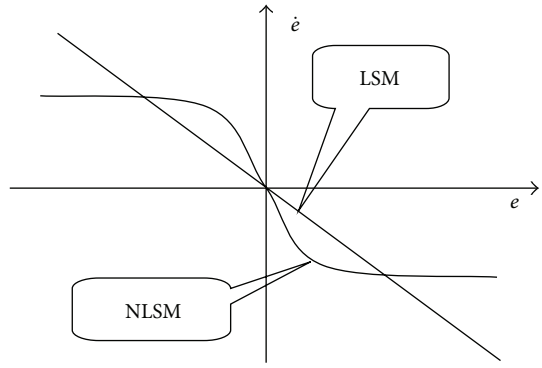

Figure 2: Comparison of linear with nonlinear sliding modes.

The feedback control law of system (10) becomes

$$u_0 = k_2 \left(k_1 \tanh\left(k_0 e\right) + \dot{e}\right), \tag{19}$$

where $k_i \in \mathbb{R}^+$, $i = 0, 1, 2$, are the parameters to be tuned.

If $\sigma \to 0$, then $\dot{e} \to -k_1 \tanh(k_0 e)$, where $\max(|\dot{e}|) \to k_1$ and $-1 < \dot{e} < 1$. That is, the maximum system convergence rate is less than k_1. While e is large enough, e will converge as almost fixed rate k_1. While e is small enough, e will converge as index law. At the same time, k_0 and k_1 determine the slope of sliding mode in phase plane.

4. Ship Course Controller Design and Simulation

4.1. Ship Course Controller Design. For the ship course response model

$$\begin{aligned} \dot{\psi} &= r, \\ \dot{r} &= f\left(r, w\right) + b\delta, \\ \psi &= \psi_d, \end{aligned} \tag{20}$$

where ψ_d is the tracking target, and the meaning of the other symbols is the same as system (2).

Similar to (6), the 3rd-order LESO of the plant (20) can be written as

$$\begin{aligned} \dot{\widehat{\psi}}_1 &= \widehat{\psi}_2 - l_1\left(\widehat{\psi}_1 - \psi\right), \\ \dot{\widehat{\psi}}_2 &= \widehat{f} - l_2\left(\widehat{\psi}_1 - \psi\right) + b_0\delta, \\ \dot{\widehat{f}} &= -l_3\left(\widehat{\psi}_1 - \psi\right), \end{aligned} \tag{21}$$

where $\widehat{\psi}_1$ and $\widehat{\psi}_2$ are the estimators of ψ and $\dot{\psi}$, respectively, and $\widehat{f}$ is the estimator of $f(r, w) + (b - b_0)\delta$, which contains the total uncertainties of internal dynamic and external disturbances.

Similar to (8), the controller is defined as

$$\delta = \frac{u_0 - \widehat{f} + \ddot{\psi}_d}{b_0}. \tag{22}$$

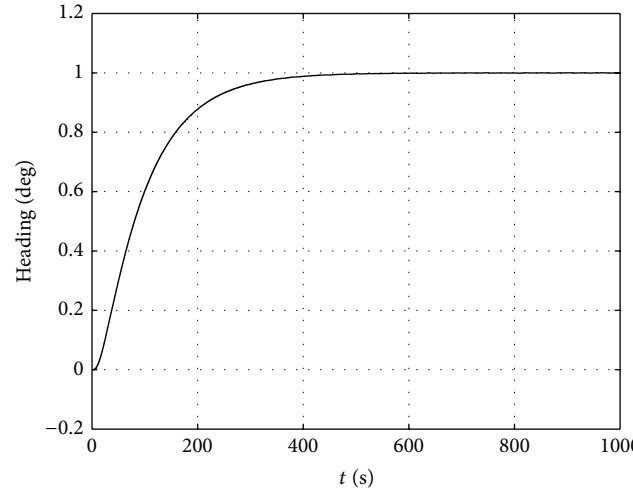

Figure 3: Course (heading) angle with $k_1 = 0.01$.

Similar to (17), linear sliding mode control law is

$$u_0 = -k_2\left(k_1\left(\widehat{\psi}_1 - \psi_d\right) + \left(\widehat{\psi}_2 - \dot{\psi}_d\right)\right). \tag{23}$$

Or similar to (19), nonlinear sliding mode control law is

$$u_0 = -k_2\left(k_1 \tanh\left(k_0\left(\widehat{\psi}_1 - \psi_d\right)\right) + \left(\widehat{\psi}_2 - \dot{\psi}_d\right)\right). \tag{24}$$

4.2. Ship Course Control Simulation. In this section, simulation results are based on an oceangoing training vessel "Yulong" of Dalian Maritime University. The principal particulars are as follows: length of ship is 126 m, beam is 20.8 m, mean draft is 8.80 m, trim is 0, diameter of propeller is 4.6 m, and block coefficient is 0.681.

In this section, a simple ship response model is used to simulate. In the system (20), let

$$f\left(r, w\right) = -\frac{a_1}{T_1} r - \frac{a_3}{T_1} r^3 + w. \tag{25}$$

While the ship speed of Yulong is 7.2 m/s, $T_1 = 216$, $a_1 = 1$, and $a_3 = 30$ [11]. External disturbance w is given as white noise of amplitude 0.001.

First of all, two simulations were based on linear sliding mode feedback control law as (22) and (23).

Case 1. The tracking target $\psi_d = 1$ rad; that is, $\psi_d = 57.3^\circ$. While a linear sliding mode control law was used, the parameters are chosen as $k_1 = 0.01$ and $k_2 = 0.1$, control gain $b_0 = 0.0022$, and the bandwidth of observer $\omega_o = 0.4$. The results were shown in Figures 3 and 4.

Case 2. Let the parameter of linear sliding mode control law $k_1 = 0.02$; the other parameters of controller, observer, control gain, and ship state are the same as Case 1. The results were shown in Figures 5 and 6.

Based on the simulation results of Figures 3, 4, 5, and 6, while $k_1 = 0.01$, the time of ship course reaching designated course is about 400 s which approximately equals

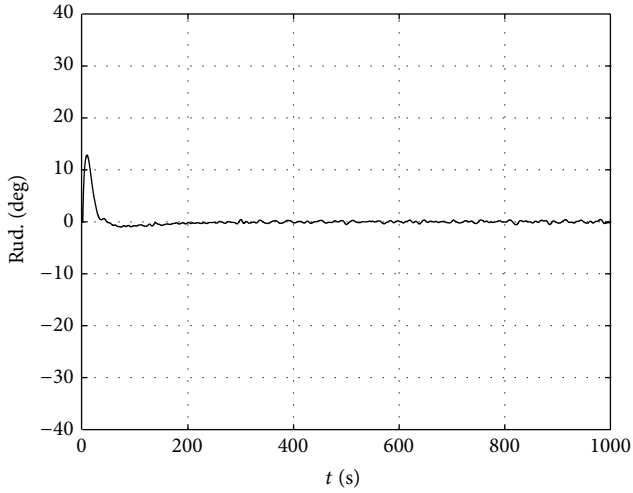

Figure 4: Rudder angle with $k_1 = 0.01$.

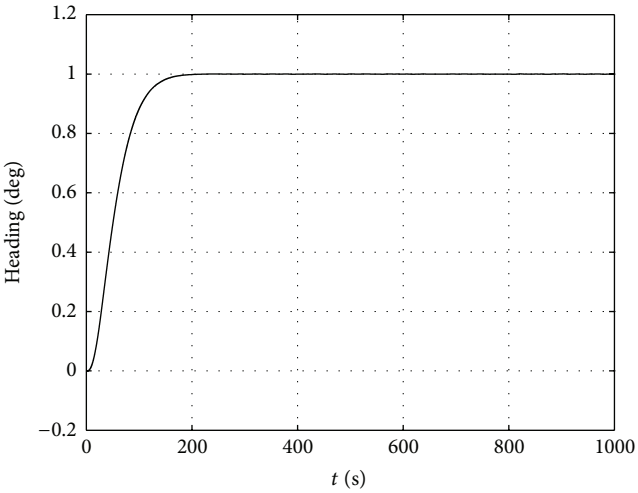

Figure 5: Course angle with $k_1 = 0.02$.

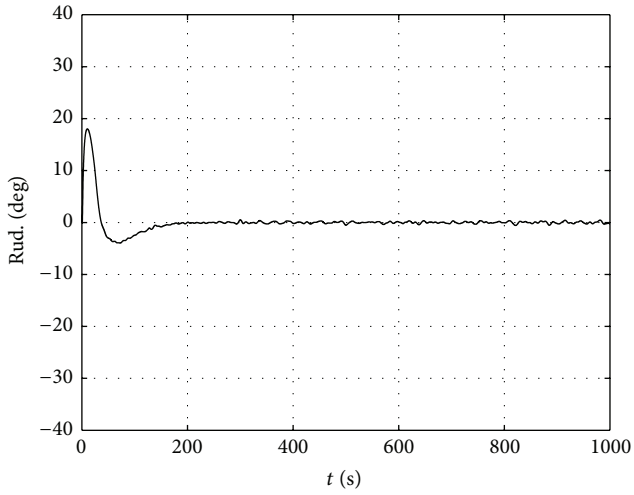

Figure 6: Rudder angle with $k_1 = 0.02$.

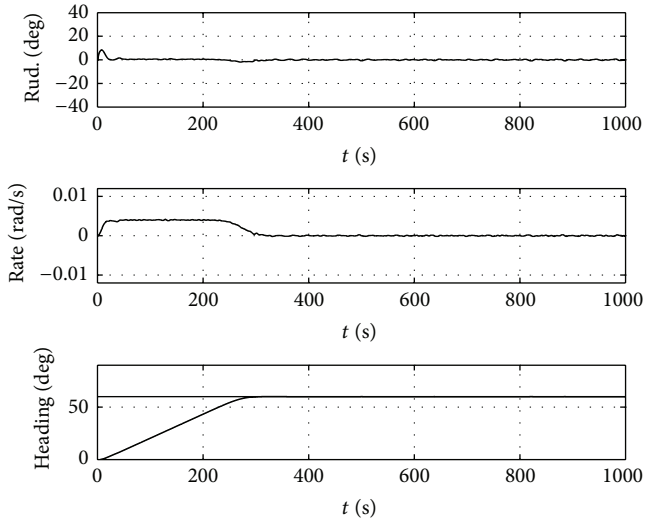

Figure 7: Rudder angle, course rate, and ship course with $k_1 = 0.004$.

$4/k_1$, whereas, while $k_1 = 0.02$, the time of ship course reaching designated course is about 200 s which also equals $4/k_1$. Meanwhile, the rudder angle being used has increased in order to prompt response. The results of simulations validated the meaning of time constant $1/k_1$. In practical work, deck officers can choose the appropriate parameter of k_1 according to the angle of ship course to be changed and the desired time to reach the designated course.

Then, the following two simulations were based on nonlinear sliding mode feedback control law as (22) and (24).

Case 3. The tracking target $\psi_d = 60^\circ$. While nonlinear sliding mode control law was used, the parameters are chosen as $k_0 = 10$, $k_1 = 0.004$, and $k_2 = 0.1$, and the other parameters of observer, control gain, and ship state are the same as Case 1. The results were shown in Figure 7.

We can find the maximum ship turning rate was restricted within 0.004 rad of the range.

Case 4. Let the parameter of nonlinear sliding mode control law $k_1 = 0.01$; the other parameters of controller, observer, control gain, and ship state are the same as Case 3. The results were shown in Figure 8.

We can find that the maximum ship turning rate was restricted within 0.01 rad/s of the range, and the time of reaching the designated course was shortened.

5. ADRC Based Ship Path-Following Controller Design and Simulation

5.1. ADRC Based Ship Path-Following Controller Design. The first formula of system (2) can be written as

$$\dot{y} = V_X \sin\psi + V_Y \cos\psi = \sqrt{V_X^2 + V_Y^2}\sin(\psi + \beta), \quad (26)$$

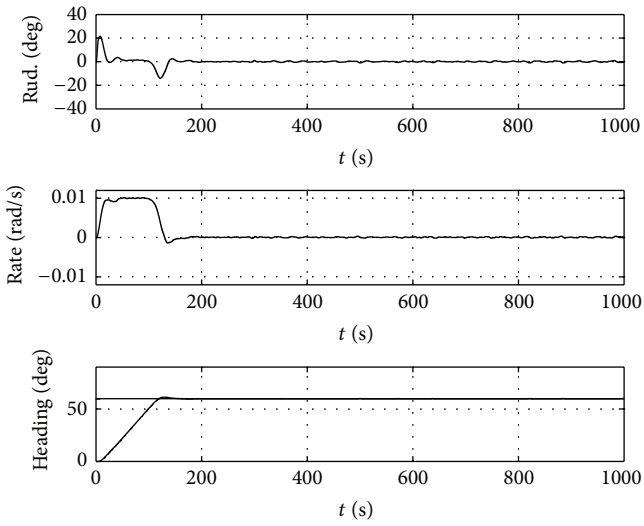

Figure 8: Rudder angle, course rate, and ship course with $k_1 = 0.01$.

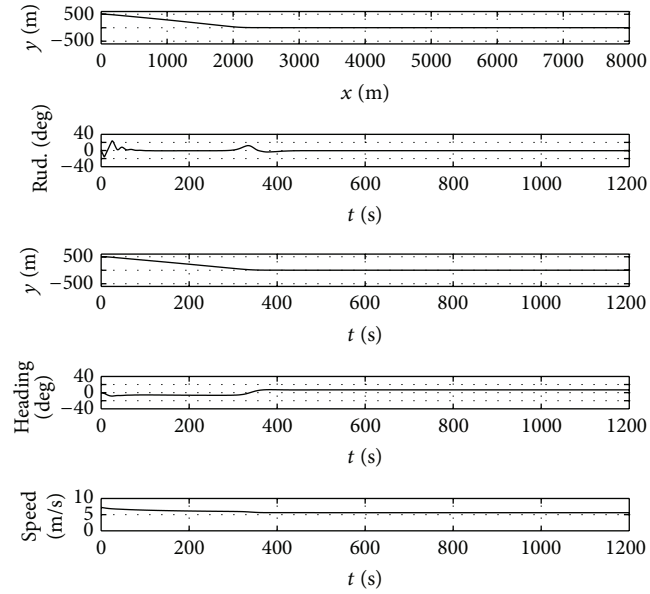

Figure 9: Straight-line path and input-output based on trace tracking method.

where $\beta = \arctan(v/u)$ is called the ship leeway angle or drift angle, as Figure 1, which can be measured by GPS in real time on a modern ship. ψ is also the ship heading angle. $\psi + \beta$ is the ship course over the ground, and it is also called course made good in navigation.

In this paper, a nonlinear function of combining y with $\psi + \beta$ by designing a coordinate transformation equation is defined as

$$z = c_1 \tanh(c_0 y) + \psi + \beta, \tag{27}$$

where $c_0 > 0$ and $\pi > c_1 > 0$ are design parameters.

Theorem 1. *For the system* (2)*, if the nonlinear function* $z \to 0$*, then both* $y \to 0$ *and* $\psi + \beta \to 0$.

Proof. There exists a Lyapunov function $V = (1/2)y^2$; then $\dot{V} = y\dot{y} = y\sqrt{V_X^2 + V_Y^2}\sin(z - c_1\tanh(c_0 y))$; if $z = 0$, then $\dot{V} = y\sqrt{V_X^2 + V_Y^2}\sin(-c_1\tanh(c_0 y))$; while $y > 0$ and $\pi > c_1 > 0$, $-c_1 < -c_1\tanh(c_0 y) < 0$. We have $\sin(-c_1\tanh(c_0 y)) < 0$, so $\dot{V} < 0$.

In addition, while $y < 0$ and $\pi > c_1 > 0$, $\sin(-c_1\tanh(c_0 y)) > 0$, so $\dot{V} < 0$; while $y = 0$, $\dot{V} = 0$. Thus, while $V = (1/2)y^2 \geq 0$, $\dot{V} \leq 0$. While $z \to 0$, $y \to 0$; meanwhile, $\psi + \beta \to 0$. □

In (27), c_0 is used to compress coordinate and c_1 is used to adjust ship track convergence rate. Meanwhile, c_1 can restrict the maximum course angle over ground $\psi + \beta$ to be used when the ship returns to the planned route. Accordingly, the physics meaning of parameters is obvious and parameters would be tuned easily.

Let $\psi^* = -c_1\tanh(c_0(y - y_d)) - \beta$; ψ^* is the desired ship heading angle that makes the ship cross-track error converge to zero. Hence, the ship track control problem is transformed into ship course control. Based on the theory of ship course ADRC with sliding mode control, similar to (20)–(23), path following can be achieved by letting ship heading angle track the desired ship heading angle ψ^* which is regarded as reference signal. The controller can automatically seek "drift angle and leeway" and the input control quantity of rudder angle can remove the cross-track error in real time resulting from wind and current.

5.2. Ship Path-Following Control Simulation

5.2.1. Straight-Line Path Following. To demonstrate the practicality of the design, simulations were performed using the ship *Yulong* based on the kinetic model as (1), and the control law was selected as the form of ADRC with linear sliding mode.

The initial states were chosen to be as follows: the main engine was set to be 103.4 revolutions per minute (RPM), $x = 0$, $y = 500$, $\psi = 0$, and $V_X = 7.2$ m/s. Planned route is a straight line to the north of $y_d = 0$. External disturbances are as the following: constant wind direction of NE with speed 5 m/s and constant current set of SW with velocity of 1 m/s.

The parameters of ADRC below simulations in this paper were chosen as $\omega_o = 0.4$ and $b_0 = 0.0022$; the parameters of linear sliding mode control law were chosen as $k_1 = 0.02$ and $k_2 = 0.1$, where $k_1 = 0.02$ means that the time constant of ship heading angle reaching maximum is 50 seconds; the parameters of the transformation (27) were chosen as, respectively, $c_0 = 0.03$ and $c_1 = \pi/12$, where $c_1 = \pi/12$ indicates that $\max(\psi + \beta) = \pi/12$ will be used before ship is stable.

In Figure 9, when the system is stable, heading angle is not zero because the ship was affected by wind and ocean current.

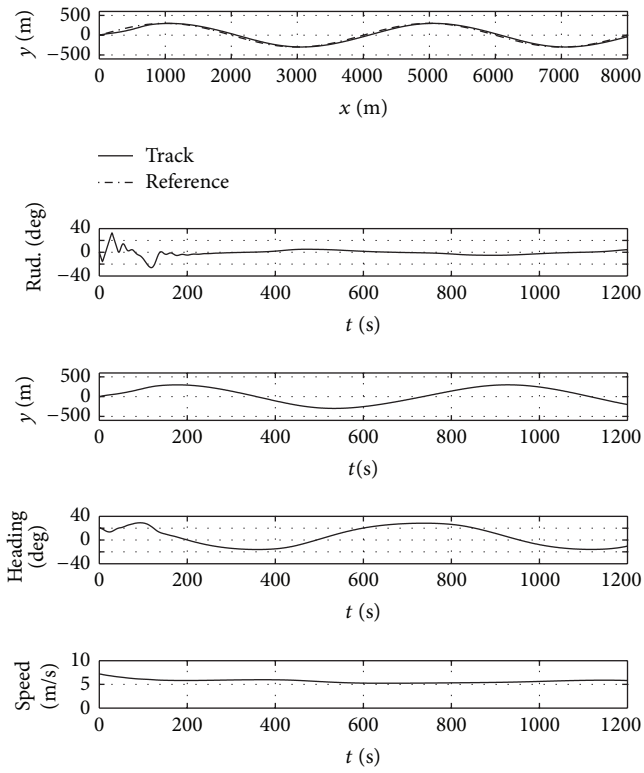

Figure 10: Curve path and input-output based on ship trace tracking method.

5.2.2. Curve Path Following. In the earth-fixed frame, ship initial heading angle and position (ψ_0, x_0, y_0) are $(20^\circ, 0, 0)$, and planned route is a curve of $y_d = 300\sin(0.0005\pi x)$. The others of ship initial state and external disturbances are the same as the above simulation. The parameters of controller are chosen as $k_1 = 0.03$, $k_2 = 0.1$, $c_1 = \pi/6$, and $c_0 = 0.03$. The simulation results are shown in Figure 10.

Remark 2. k_1 and c_1 here are larger than the ones of straight-line path following because faster turning rate and larger heading angle are needed while curve path following.

By analyzing the results of Figures 9 and 10, we can summarize some conclusions as follows.

Firstly, the cross-track error resulting from constant wind and current has been overcome. The tracking control precision is high. Rudder and course response are smooth, and the rudder-turning angle is not large in spite of external disturbances, such as wind and current.

Secondly, the results indicate that the ADRC controller has powerful robustness to the environment and the nonlinearity of ship tracking motion control with constraint condition. And the ship tracking control is fast and smooth with lower energy consumption.

6. Conclusion

This paper has presented a novel path-following control approach to underactuated vessels under environmental disturbances of ocean current and wind. A compound control approach of ADRC with sliding mode has been applied to the design of ship course and path-following control utilizing the characteristic of ADRC independence of the controlled plant's mathematical model. The parameters of controller have more obvious physical meaning; meanwhile, the constraint condition problem of a ship has been solved. The leeway angle was compensated in the controller by means of designing a coordinate transformation equation. The ADRC controller has guaranteed that the cross-track error converges to the planned path, and the parameters of controller can be easily tuned according to the ship's maneuverability. The high precision ship tracking controller is robust to the internal dynamic uncertainties of a ship and the external disturbances.

Acknowledgments

This work was supported in part by the National Natural Science Foundation of China (nos. 51379026, 51179019, and 61374114), the Natural Science Foundation of Liaoning Province (no. 20102012), the Program for Liaoning Excellent Talents in University (LNET) (Grant no. LR 2012016), the Applied Basic Research Program of Ministry of Transport of China (nos. 2011-329-225-390 and 2013-329-225-270), the Fundamental Research Funds for the Central Universities of China (no. 2012QN013), the National Fundamental Research 973 Program of China under Grant no. 2011CB302801, the Macau Science and Technology Development Foundation under Grant no. 008/2010/A1, and Multiyear Research Grants.

References

[1] K. Do and J. Pan, *Control of Ships and Underwater Vehicle-Design for Underactuated and Nonlinear Marine Systems*, Springer, New York, NY, USA, 2009.

[2] J. Wu, H. Peng, K. Ohtsu, G. Kitagawa, and T. Itoh, "Ship's tracking control based on nonlinear time series model," *Applied Ocean Research*, vol. 36, pp. 1–11, 2012.

[3] K. Y. Pettersen, *Exponential Stabilization of Underactuated Vehicles [Ph.D. thesis]*, Norwegian University of Science Technology, Trondheim, Norway, 1996.

[4] Z.-P. Jiang, "Iterative design of time-varying stabilizers for multi-input systems in chained form," *Systems & Control Letters*, vol. 28, no. 5, pp. 255–262, 1996.

[5] I. Kaminer, A. Pascoal, E. Hallberg, and C. Silvestre, "Trajectory tracking for autonomous vehicles: an integrated approach to guidance and control," *Journal of Guidance, Control, and Dynamics*, vol. 21, no. 1, pp. 29–38, 1998.

[6] P. Encarnacao, A. Pacoal, and M. Arcak, "Path following for autonomous marine craft," in *Proceedings of the 5th International Federation of Automatic Control Conference on Manoeuvring and Control of Marine Craft*, pp. 117–122, 2000.

[7] M. Aicardi, G. Casalino, G. Indiveri, A. Aguiar, P. Encarnacao, and A. Pascoal, "A plannar path following controller for underactuated marine vehicles," in *Proceedings of the 9th IEEE Mediterranean Conference on Control and Automation (MED '01)*, Dubrovnik, Croatia, 2001.

[8] M. Aicardi, G. Casalino, A. Bicchi, and A. Balestrino, "Closed loop steering of unicycle-like vehicles via Lyapunov techniques,"

IEEE Robotics and Automation Magazine, vol. 2, no. 1, pp. 27–35, 1995.

[9] C. Samson, "Velocity and torque feedback control of a nonholonomic cart," in *Advanced Robot Control*, C. Canudas de Wit, Ed., Lecture Notes in Control and Information Sciences, pp. 125–151, Springer, Berlin, Germany, 1991.

[10] R. Skjetne and T. I. Fossen, "Nonlinear maneuvering and control of ships," in *Proceedings of OCEANS MTS/IEEE Conference and Exhibition*, pp. 1808–1815, November 2001.

[11] T. Li, Y. Yang, B. Hong, J. Ren, and J. Du, "A robust adaptive nonlinear control approach to ship straight-path tracking design," in *Proceedings of the American Control Conference*, pp. 4016–4021, Portland, Ore, USA, June 2005.

[12] K. D. Do and J. Pan, "Underactuated ships follow smooth paths with integral actions and without velocity measurements for feedback: theory and experiments," *IEEE Transactions on Control Systems Technology*, vol. 14, no. 2, pp. 308–322, 2006.

[13] P. Encarnacao, A. Pacoal, and M. Arcak, "Path following for autonomous marine craft," in *Proceedings of the 5th International Federation of Automatic Control Conference on Manoeuvring and Control of Marine Craft*, pp. 117–122, Aalborg, Denmark, 2000.

[14] J. Han, *Active Disturbance Rejection Control Technique—the Technique For Estimating and Compensating the Uncertainties*, National Defense Industry Press, Beijing, Ghina, 2008.

[15] J. Q. Han, "From PID to active disturbance rejection control," *IEEE Transactions on Industrial Electronics*, vol. 56, no. 3, pp. 900–906, 2009.

[16] Z. Q. Gao, "Scaling and bandwidth-parameterization based controller tuning," in *Proceedings of the American Control Conference*, pp. 4989–4996, Denver, Colo, USA, June 2003.

[17] S. C. Tong and H.-X. Li, "Fuzzy adaptive sliding-mode control for MIMO nonlinear systems," *IEEE Transactions on Fuzzy Systems*, vol. 11, no. 3, pp. 354–360, 2003.

[18] H.-X. Li and S. C. Tong, "A hybrid adaptive fuzzy control for a class of nonlinear MIMO systems," *IEEE Transactions on Fuzzy Systems*, vol. 11, no. 1, pp. 24–34, 2003.

[19] S.-C. Tong, X.-L. He, and H.-G. Zhang, "A combined backstepping and small-gain approach to robust adaptive fuzzy output feedback control," *IEEE Transactions on Fuzzy Systems*, vol. 17, no. 5, pp. 1059–1069, 2009.

[20] S. C. Tong, C. L. Liu, and Y. M. Li, "Fuzzy-adaptive decentralized output-feedback control for large-scale nonlinear systems with dynamical uncertainties," *IEEE Transactions on Fuzzy Systems*, vol. 18, no. 5, pp. 845–861, 2010.

[21] S. C. Tong and Y. M. Li, "Observer-based fuzzy adaptive control for strict-feedback nonlinear systems," *Fuzzy Sets and Systems*, vol. 160, no. 12, pp. 1749–1764, 2009.

[22] Y. Li, S. Tong, and T. Li, "Adaptive fuzzy output feedback control of uncertain nonlinear systems with unknown backlash-like hysteresis," *Information Sciences*, vol. 198, pp. 130–146, 2012.

[23] T. Wang, S. C. Tong, and Y. M. Li, "Robust adaptive fuzzy control for nonlinear system with dynamic uncertainties based on backstepping," *International Journal of Innovative Computing, Information and Control*, vol. 5, no. 9, pp. 2675–2688, 2009.

[24] Y. Q, Xia, M. Y. Fu, Z. H. Deng, and X. M. Ren, "Recent developments in sliding mode control and active disturbance rejection control," *Control Theory & Applications*, vol. 30, no. 2, pp. 137–147, 2013.

[25] X. Jia and Y. Yang, *Ship Motion Mathematical Model-Mechanism Modeling and Identification Modeling*, Dalian Maritime University Press, 1999.

Hindawi Publishing Corporation
Mathematical Problems in Engineering
Volume 2013, Article ID 741908, 6 pages
http://dx.doi.org/10.1155/2013/741908

Research Article

Impulsive Controller Design for Complex Nonlinear Singular Networked Systems with Packet Dropouts

Xian-Lin Zhao,[1,2] Ai-Min Wang,[1] Cun-Li Dai,[2] Xiao-Lin Li,[2] and Wei Lu[2]

[1] *School of Instrument Science and Engineering, Southeast University, Nanjing 210096, China*
[2] *College of Engineering, Nanjing Agricultural University, Nanjing 210031, China*

Correspondence should be addressed to Cun-Li Dai; daicunli@163.com

Received 12 September 2013; Accepted 14 October 2013

Academic Editor: Tao Li

Globally exponential stability of Complex (with coupling) Nonlinear Singular Impulsive Networked Control Systems (CNSINCS) with packet dropouts and time-delay is investigated. Firstly, the mathematic model of CNSINCS is established. Then, by employing the method of Lyapunov functional, exponential stability criteria are obtained and the impulsive controller design method is given. Finally, some simulation results are provided to demonstrate the effectiveness of the proposed method.

1. Introduction

At present, singular system is widely used in the control of spacecraft, flexible robot, complex power, large chemical and wireless transmission system [1–5]. Many results had been achieved for discrete singular system and time-delay singular system. Such as in [6], the nonlinear discrete singular perturbation model was established and the system condition was given. In [7], chattering free sliding mode control for uncertain discrete time-delay singular system was investigated. The asymptotically stable was established, and the chattering problem that appears in traditional variable structure system was eliminated. As for time-delay singular system, the stability of uncertain time-delay singular systems was researched and the asymptotic stability condition was achieved in [8] by using Jensen integral inequality and feedback control method.

On the other hand, singular system has impulsive behavior in many cases [9–14]. So it is very important to discuss the problem of impulsive control. For the stability of the impulsive control system, nonlinear impulsive control was put forward and the concept of asymptotic stability condition was provided in [11]. Asymptotic stability condition for a class of uncertain impulsive system was established through the comparison theorem in [12]. Switch control method was used to research the stability of singular impulsive system, robust stabilization, and H_∞ control problem in [13]. Linear approximation and the LMI method were used, respectively, to study the problem of system stability and the sufficient conditions for asymptotic stability in [14].

In network impulsive control system packet dropouts and time-delay exist which will influence the stability of singular system. It is necessary to analyze stability condition and the method of controller design. That is the problem focussed in this study. According to the Lyapunov function theory and comparison theorem, the sufficient conditions for the global exponential stability of the system is obtained. The detailed design process of impulsive controller is given in the paper. System will be stable in accordance with the decay rate to achieve exponential stability. A numerical example is provided to illustrate the correctness of theoretical and the effectiveness of design method.

2. The Mathematic Model of CNSINCS

The mathematic model of CNSINCS can be described as

$$E\dot{x}_i(t) = Ax_i(t) + f(x_i(t)) + \sum_{j=1}^{N} G_{ij}\Gamma x_j(t - \tau(t)),$$
$$i = 1, \ldots, N,\ t \in (t_{k-1}, t_k]$$

$$x_i\left(t_k^+\right) = c_i x_i\left(t_k\right) + \overline{u}_i\left(t_k\right), \quad t = t_k^+,\ k = 1, 2, \ldots$$
$$x_i\left(t\right) = \varphi_i\left(t\right), \quad t \in [-\overline{\tau}, 0], \tag{1}$$

where $x_i(t) \in R^n$ is the state vector of the ith node. A is a constant matrix of $n \times n$. c_i is known scalar. $E \in R^{n\times n}$ is a singular constant matrix, and $0 < \operatorname{rank} E = r \le n$, without loss of generality; we hypotheses $E = \left[\begin{smallmatrix} I_r & 0 \\ 0 & 0 \end{smallmatrix}\right]$. $f(\cdot)$ is a nonlinear function. Γ is the internal coupling matrix. $G = G_{ij} \in R^{n\times n}$ is the coupling matrix of the whole network structure and weights. $\tau(t)$ is network transmission delay and is assumed to satisfy $0 \le \tau(t) \le \overline{\tau}$.

In the process of data transmitting, the buffer's model can be described as:

$$\overline{u}_i\left(t_k\right) = \begin{cases} u_i\left(t_k\right), & k = 1, 2, \ldots, \text{ if transmitted successfully,} \\ \overline{u}_i\left(t_{k-1}\right), & k = 1, 2, \ldots, \text{ otherwise,} \end{cases}$$

$$\overline{x}_i\left(t_k\right) = \begin{cases} x_i\left(t_k\right), & k = 1, 2, \ldots, \text{if transmitted successfully,} \\ \overline{x}_i\left(t_{k-1}\right), & k = 1, 2, \ldots, \text{ otherwise.} \end{cases} \tag{2}$$

The impulsive controller can be designed as

$$\overline{u}_i\left(t_k\right) = K_i \overline{x}_i\left(t_k\right), \tag{3}$$

where $\overline{u}_i(t_k) \in R^m$. Substituting (2) and (3) into (1), the closed-loop nonlinear singular impulsive networked system model is obtained as follows:

$$\begin{aligned} E\dot{x}_i\left(t\right) &= Ax_i\left(t\right) + f\left(x_i\left(t\right)\right) + \sum_{j=1}^{N} G_{ij}\Gamma x_j\left(t - \tau\left(t\right)\right), \\ &\qquad i = 1, \ldots, N,\ t \in \left(t_{k-1}, t_k\right], \\ x_i\left(t_k^+\right) &= c_i x_i\left(t_k\right) + \left(1 - \sigma_i\left(t_k\right)\right) K_i x_i\left(t_k\right) \\ &\quad + \sigma_i\left(t_k\right) K_i \overline{x}_i\left(t_{k-1}\right), \quad t = t_k^+,\ k = 1, 2, \ldots, \\ x_i\left(t\right) &= \varphi_i\left(t\right), \quad t \in [-\overline{\tau}, 0], \end{aligned} \tag{4}$$

where $\sigma_i(t_k) = 1$ denotes that there are data dropouts and, $\sigma_i(t_k) = 0$, there are no packet dropouts.

Lemma 1. *Let $P \in R^{n\times n}$ be a symmetric positive definite matrix and $P = Q^TQ$. For any $x, y \in R^{n\times n}$ and $A \in R^{n\times n}$, then*

(1) $x^T(A^TPE + E^TP^TA)x \le 2\lambda_{\max}(A)x^TE^TPEx$,

(2) $x^T(A^TP + PA)x \le 2\mu(QAQ^{-1})x^TPx$,

(3) $|x^TPy| \le \sqrt{x^TPx}\sqrt{y^TPy}$.

Lemma 2. *According to the definition of Kronecker product, for a given matrix A, B, and scalar α, the following equality can be achieved:*

(1) $(\alpha A) \otimes B = A \otimes (\alpha B)$,

(2) $(A + B) \otimes C = (A \otimes C) + (B \otimes C)$,

(3) $(A \otimes B) \otimes (C \otimes D) = (AC) \otimes (BD)$.

If $X(t) = (x_1^T(t), \ldots, x_N^T(t))^T$, $C = \operatorname{diag}\{c_1, \ldots, c_N\}$, and $F(X(t)) = (f^T(x_1^T(t), \ldots, f^T(x_N^T(t))^T$, according to Lemma 1, the complex nonlinear singular system can be expressed as

$$\begin{aligned} \left(I_N \otimes E\right)\dot{X}\left(t\right) &= \left(I_N \otimes A\right)X\left(t\right) + F\left(X\left(t\right)\right) \\ &\quad + \left(G \otimes \Gamma\right)X\left(t - \tau\left(t\right)\right), \quad t \in \left(t_{k-1}, t_k\right], \\ X\left(t_k^+\right) &= CX\left(t_k\right) + \left(1 - \sigma\left(t_k\right)\right)KX\left(t_k\right) \\ &\quad + \sigma\left(t_k\right)\overline{X}\left(t_{k-1}\right), \quad t = t_k^+. \end{aligned} \tag{5}$$

Suppose

$$\overline{E} = \begin{bmatrix} E & 0 \\ 0 & 0 \end{bmatrix}, \quad \overline{I}_N = \begin{bmatrix} I_N & 0 \\ 0 & 0 \end{bmatrix}, \quad Z\left(t_k\right) = \begin{bmatrix} X\left(t_k\right) \\ X\left(t_{k-1}\right) \end{bmatrix}, \quad \overline{A} = \begin{bmatrix} A & 0 \\ 0 & 0 \end{bmatrix}. \tag{6}$$

Then (5) is equivalent to the following system:

$$\begin{aligned} \left(\overline{I}_N \otimes \overline{E}\right)\dot{z}\left(t\right) &= \left(\overline{I}_N \otimes \overline{A}\right)z\left(t\right) + \begin{bmatrix} F\left(x\left(t\right)\right) \\ 0 \end{bmatrix} \\ &\quad + \begin{bmatrix} G \otimes \Gamma & 0 \\ 0 & 0 \end{bmatrix} z\left(t - \tau\left(t\right)\right), \\ \left(\overline{I}_N \otimes \overline{E}\right)z\left(t_k^+\right) &= C\left(\overline{I}_N \otimes \overline{E}\right)z\left(t_k\right) \\ &\quad + \begin{bmatrix} \left(1 - \sigma\left(t_k\right)\right)K & \sigma\left(t_k\right)K \\ 0 & 0 \end{bmatrix}\left(\overline{I}_N \otimes \overline{E}\right)z\left(t_k\right). \end{aligned} \tag{7}$$

Lemma 3 (see [15]). *If $L(t, z(t))$ and $U_k(z(t))$ satisfy the Lipchitz condition, there exists a uniqueness of solution to nonlinear singular impulsive differential equation which is written as*

$$\begin{aligned} \dot{z}\left(t\right) &= L\left(x, t\right), \quad t \in \left(t_{k-1}, t_k\right], \\ \Delta z\left(t\right) &= U_k\left(z\left(t\right)\right), \quad t = t_k^+, k = 1, 2, \ldots, \end{aligned} \tag{8}$$

where $z(t) \in R^n, L : R_+ \times R^n \to R^n, U_k : R^n \to R^n$.

3. The Design of CNSINCS

For the nonlinear singular networked impulsive control system (4), we have the following theorem.

Theorem 4. *If there exist* $0 < \rho = \sup_{k\in N}\{t_k - t_{k-1}\} < \infty$ *and a nonsingular matrix* $K \in R^{n\times n}$*, such that*

$$\frac{2\ln\beta}{\rho} + \left(2\lambda_{\max}\left(\overline{A}\right) + 2L\frac{\lambda_{\max}\left(\left(\overline{I}_N\otimes\overline{E}\right)^T P\right)}{\lambda_{\min}\left(\left(\overline{I}_N\otimes\overline{E}\right)^T P\right)} + 1\right) \tag{9}$$

$$+\lambda^2_{\max}(G\otimes\Gamma) < 1$$

$$0 < \beta < 1, \tag{10}$$

where

$$\beta = \left[\lambda^2_{\max}\left(C + \begin{bmatrix}(1-\sigma(t_k))K & \sigma(t_k)K\\ 0 & 0\end{bmatrix}\right)\right]^{1/2} \tag{11}$$

then the nonlinear singular networked impulsive control system (4) *is asymptotically stable:*

$$\|x(t)\| \le \frac{1}{\beta}\sqrt{\frac{\lambda_{\max}(P)}{\lambda_{\min}(P)}}\sup_{-\tau\le\theta\le 0}\left\{\|\phi(\theta)\|\right\}e^{-(\lambda/2)t}, \tag{12}$$

where λ *is the positive solution of* $\lambda + p + qe^{\lambda\overline{\tau}} = 0$*, and* $q > 0, p + q < 0$*:*

$$p = \frac{2\ln\beta}{\rho} + \left(2\lambda_{\max}\left(\overline{A}\right) + 2L\frac{\lambda_{\max}\left(\left(\overline{I}_N\otimes\overline{E}\right)^T P\right)}{\lambda_{\min}\left(\left(\overline{I}_N\otimes\overline{E}\right)^T P\right)} + 1\right) + \lambda^2_{\max}(G\otimes\Gamma). \tag{13}$$

Proof. From [16], we know that $\lambda + p + qe^{\lambda\overline{\tau}} = 0$ must have a solution. Set $V(t) = z^T(t)(\overline{I}_N\otimes\overline{E})^T P(\overline{I}_N\otimes\overline{E})z(t)$, where $(\overline{I}_N\otimes\overline{E})^T P(\overline{I}_N\otimes\overline{E}) \ge 0$.

When $t \in (t_{k-1}, t_k]$, the derivative of $V(t)$ along the trajectories of the CNSINCS (4) is

$$\begin{aligned}\dot V(t) &= \left(\left(\overline{I}_N\otimes\overline{E}\right)\dot z(t)\right)^T P\left(\overline{I}_N\otimes\overline{E}\right)z(t)\\ &\quad + \left(\left(\overline{I}_N\otimes\overline{E}\right)z(t)\right)^T P^T\left(\overline{I}_N\otimes\overline{E}\right)\dot z(t)\\ &= \left(\left(\overline{I}_N\otimes\overline{A}\right)z(t) + \begin{bmatrix}F(x(t))\\ 0\end{bmatrix} + \begin{bmatrix}G\otimes\Gamma & 0\\ 0 & 0\end{bmatrix}\right.\\ &\qquad \left.\times z(t-\tau(t))\right)^T P\left(\overline{I}_N\otimes\overline{E}\right)z(t)\\ &\quad + \left(\left(\overline{I}_N\otimes\overline{E}\right)z(t)\right)^T P\left(\overline{I}_N\otimes\overline{A}\right)z(t)\begin{bmatrix}F(x(t))\\ 0\end{bmatrix}\\ &\quad + \begin{bmatrix}G\otimes\Gamma & 0\\ 0 & 0\end{bmatrix}z(t-\tau(t))\\ &= z^T(t)\left(\overline{A}^T P\left(\overline{I}_N\otimes\overline{E}\right) + \left(\overline{I}_N\otimes\overline{E}\right)^T P^T\overline{A}\right)\\ &\quad \times z(t) + F^T(x(t))P\left(\overline{I}_N\otimes\overline{E}\right)z(t)\\ &\quad + z^T(t)\left(\overline{I}_N\otimes\overline{E}\right)^T PF(x(t))\\ &\quad + z^T(t-\tau(t))G^T PEz(t)\\ &\quad + z^T(t)\left(\overline{I}_N\otimes\overline{E}\right)^T P^T Gz(t-\tau(t)).\end{aligned} \tag{14}$$

According to Lemma 3 we have

$$\begin{aligned}&\dot V(t)\\ &\le 2\lambda_{\max}\left(\overline{A}\right)z^T(t)\left(\overline{I}_N\otimes\overline{E}\right)^T P\left(\overline{I}_N\otimes\overline{E}\right)z(t)\\ &\quad + 2L\lambda\left(\overline{I}_N\otimes\overline{E}\right)^T P\|z(t)\|\\ &\quad + 2\sqrt{z^T(t)P\left(\overline{I}_N\otimes\overline{E}\right)z(t)}\\ &\quad \times\sqrt{z^T(t-\tau(t))(G\otimes\Gamma)^T\left(\overline{I}_N\otimes\overline{E}\right)^T P(G\otimes\Gamma)z(t-\tau(t))}\\ &\le \lambda^2_{\max}(G\otimes\Gamma)z^T(t-\tau(t))\left(\overline{I}_N\otimes\overline{E}\right)^T P\left(\overline{I}_N\otimes\overline{E}\right)z(t-\tau(t))\\ &\quad + 2L\frac{\lambda_{\max}\left(\left(\overline{I}_N\otimes\overline{E}\right)^T P\right)}{\lambda_{\min}\left(\left(\overline{I}_N\otimes\overline{E}\right)^T P\right)}z^T(t)\left(\overline{I}_N\otimes\overline{E}\right)^T P\left(\overline{I}_N\otimes\overline{E}\right)z(t)\\ &\quad + 2\lambda_{\max}\left(\overline{A}\right)z^T(t)\left(\overline{I}_N\otimes\overline{E}\right)^T P\left(\overline{I}_N\otimes\overline{E}\right)z(t)\\ &\quad + z^T(t)\left(\overline{I}_N\otimes\overline{E}\right)^T P\left(\overline{I}_N\otimes\overline{E}\right)z(t).\end{aligned} \tag{15}$$

On the other hand, when $t = t_k^+$,

$$\begin{aligned}\dot V\left(t_k^+\right) &= z^T\left(t_k^+\right)\left(\overline{I}_N\otimes\overline{E}\right)^T P\left(\overline{I}_N\otimes\overline{E}\right)z\left(t_k^+\right)\\ &= z^T\left(t_k^+\right)\left(\overline{I}_N\otimes\overline{E}\right)^T\left(\overline{I}_N\otimes\overline{E}\right)^T\\ &\quad \times P\left(\overline{I}_N\otimes\overline{E}\right)\left(\overline{I}_N\otimes\overline{E}\right)z\left(t_k^+\right)\\ &= \left[\left(\overline{I}_N\otimes\overline{E}\right)z^T\left(t_k^+\right)\right]^T\left(\overline{I}_N\otimes\overline{E}\right)^T P\left(\overline{I}_N\otimes\overline{E}\right)\\ &\quad \times\left[\left(\overline{I}_N\otimes\overline{E}\right)z\left(t_k^+\right)\right]\\ &= \left(C\left(\overline{I}_N\otimes\overline{E}\right)z(t_k)\right.\\ &\qquad \left.+\begin{bmatrix}(1-\sigma(t_k))K & \sigma(t_k)K\\ 0 & 0\end{bmatrix}\left(\overline{I}_N\otimes\overline{E}\right)z(t_k)\right)^T,\\ &\quad \left(\overline{I}_N\otimes\overline{E}\right)^T P\left(\overline{I}_N\otimes\overline{E}\right)\\ &\quad \times\left(C + \begin{bmatrix}(1-\sigma(t_k))K & \sigma(t_k)K\\ 0 & 0\end{bmatrix}\right)\left(\overline{I}_N\otimes\overline{E}\right)z(t_k)\end{aligned}$$

$$
\begin{aligned}
&= z^T(t_k)\left(\bar{I}_N \otimes \bar{E}\right)^T \\
&\quad \times \left(C + \begin{bmatrix} (1-\sigma(t_k))K & \sigma(t_k)K \\ 0 & 0 \end{bmatrix}\right)^T \\
&\quad \times \left(\bar{I}_N \otimes \bar{E}\right)^T, \\
&P\left(\bar{I}_N \otimes \bar{E}\right) z(t_k) \\
&\quad \le \lambda_{\max}^2 \left(C + \begin{bmatrix} (1-\sigma(t_k))K & \sigma(t_k)K \\ 0 & 0 \end{bmatrix}\right) \\
&\quad \times z^T(t_k)\left(\bar{I}_N \otimes \bar{E}\right)^T \left(\bar{I}_N \otimes \bar{E}\right)^T P, \\
&\left(\bar{I}_N \otimes \bar{E}\right)\left(\bar{I}_N \otimes \bar{E}\right) z(t_k) \\
&\quad = \lambda_{\max}^2 \left(C + \begin{bmatrix} (1-\sigma(t_k))K & \sigma(t_k)K \\ 0 & 0 \end{bmatrix}\right) \\
&\quad \times z^T(t_k)\left(\bar{I}_N \otimes \bar{E}\right)^T P \left(\bar{I}_N \otimes \bar{E}\right) z(t_k) \\
&\quad = \beta^2 V(t_k),
\end{aligned}
\tag{16}
$$

where $\beta^2 = \lambda_{\max}^2(C + \left[\begin{smallmatrix} (1-\sigma(t_k))K & \sigma(t_k)K \\ 0 & 0 \end{smallmatrix}\right])$, supposing that $\varepsilon > 0$ is random constant, a comparison system can be established as follows:

$$
\begin{aligned}
\dot{v}(t) &= \left(2\lambda_{\max}\left(\overline{A}\right) + 2L\frac{\lambda_{\max}\left(\left(\bar{I}_N \otimes \bar{E}\right)^T P\right)}{\lambda_{\min}\left(\left(\bar{I}_N \otimes \bar{E}\right)^T P\right)} + 1\right) v(t) \\
&\quad + \lambda_{\max}^2 (G \otimes \Gamma)\, v(t - \tau(t)) + \varepsilon \quad t \ne t_k, \\
v\left(t_k^+\right) &= \beta v(t_k), \quad t = t_k, \\
v(\theta) &= \lambda_{\max}(P)\left\|\phi(\theta)\right\|^2, \quad -\overline{\tau} \le \theta \le 0.
\end{aligned}
\tag{17}
$$

It is clear that $V(t) \le v(t)$ when $-\overline{\tau} \le \theta \le 0$, according to [16], and we have $V(t) \le v(t)$ when $t \ge 0$; the trivial solution of the comparison system is

$$
\begin{aligned}
v(t) &= W(t,0)\, v(0) \\
&\quad + \int_0^t W(t,s)\, \lambda_{\max}^2 (G \otimes \Gamma)\, v(s - \tau(s) + \varepsilon)\, ds, \quad t \ge 0,
\end{aligned}
\tag{18}
$$

where $W(t,s)$ is Cauchy matrix which satisfies

$$
\begin{aligned}
W(t,s) &= \beta^{2\eta(t,s)} \\
&\quad \times e^{\{(2\lambda_{\max}(\overline{A}) + 2L(\lambda_{\max}((\bar{I}_N \otimes \bar{E})^T P)/\lambda_{\min}((\bar{I}_N \otimes \bar{E})^T P)) + 1)(t-s)\}} \\
&\quad \le \beta^{2(t-s/\rho)-1} e^{(p - (2\ln\beta/\rho))(t-s)} \le \beta^{-2} e^{p(t-s)}
\end{aligned}
\tag{19}
$$

in which $\eta(t,s)$ is the number of control impulses in the interval $(s,t]$, $0 < \rho = \sup_{k\in N}\{t_k - t_{k-1}\} < \infty$, for $t \ge 0$; we have

$$
\begin{aligned}
v(t) &\le \beta^{-2}\lambda_{\max}\left(\left(\bar{I}_N \otimes \bar{E}\right)^T P \left(\bar{I}_N \otimes \bar{E}\right)\right)\left\|\varphi(0)\right\|^2 \\
&\quad + \int_0^t \beta^{-2} e^{p(t-s)} \lambda_{\max}^2 (G \otimes \Gamma)\, v(s - \tau(s) + \varepsilon)\, ds \\
&\quad \le \gamma e^{pt} + e^{p(t-s)}(q v(s - \tau(s) + \varepsilon)\, ds,
\end{aligned}
\tag{20}
$$

where

$$
\begin{aligned}
\gamma &= \beta^{-2}\lambda_{\max}\left(\left(\bar{I}_N \otimes \bar{E}\right)^T P \left(\bar{I}_N \otimes \bar{E}\right)\right) \sup_{-\overline{\tau}\le s\le 0}\left\|\varphi(s)\right\|^2 \\
&= \beta^{-2}\lambda_{\max}(P) \sup_{-\overline{\tau}\le s\le 0}\left\|\varphi(s)\right\|^2.
\end{aligned}
\tag{21}
$$

In the following, we will prove that the following inequality holds:

$$
v(t) \le \gamma e^{-\lambda t} - \frac{\varepsilon}{\beta^2 p}, \quad t \ge 0 \tag{22}
$$

Since $\varepsilon > 0$, $p < 0$, so $\varepsilon/\beta^2 p < 0$. If there exists $t^* > 0$ which satisfies

$$
v(t^*) \ge \gamma e^{-\lambda t^*} - \frac{\varepsilon}{\beta^2 p}, \tag{23}
$$

$$
v(t) > \gamma e^{-\lambda t} - \frac{\varepsilon}{\beta^2 p}, \quad t < t^*. \tag{24}
$$

From (16) and (24) we have

$$
\begin{aligned}
&v(t^*) \\
&\le \gamma e^{-\lambda t^*} + \int_0^{t^*} e^{p(t^*-s)}\left[q v(s - \tau(s)) + \varepsilon\right] ds \\
&< e^{pt^*}\left\{\gamma - \frac{\varepsilon}{\beta^2(p+q)}\right. \\
&\qquad \left. + \int_0^{t^*} e^{-ps}\left[\gamma q e^{-\lambda(s-\tau(s))} - \frac{\varepsilon q}{\beta^2(p+q)} + \frac{\varepsilon}{\beta^2}\right] ds\right\} \\
&< e^{pt^*}\left\{\gamma - \frac{\varepsilon}{\beta^2(p+q)} + \gamma q e^{\lambda\tau}\right. \\
&\qquad \left. \times \int_0^{t^*} e^{-(p+\lambda)s} ds + \frac{\varepsilon p}{\beta^2(p+q)} \int_0^{t^*} e^{-ps} ds\right\} \\
&< e^{pt^*}\left\{\gamma - \frac{\varepsilon}{\beta^2(p+q)}\right. \\
&\qquad \left. + \gamma\left[e^{-(p+\lambda)t^*} - 1\right] - \frac{\varepsilon}{\beta^2(p+q)}\left(e^{-pt^*} - 1\right)\right\} \\
&= \gamma e^{-\lambda t^*} - \frac{\varepsilon}{\beta^2(p+q)}
\end{aligned}
\tag{25}
$$

which contradicts with (23), and consequently (22) holds. Let $\varepsilon \to 0$; then

$$V(t) \le v(t) \le \gamma e^{-\lambda t}, \quad t \ge 0. \tag{26}$$

Moreover

$$V(t) \ge \lambda_{\min}(P) \|x(t)\|^2, \quad t \ge 0. \tag{27}$$

Combining the inequality (26) and (27),

$$\|x(t)\| \le \left(\frac{1}{\beta}\right) \sqrt{\frac{\lambda_{\max}(P)}{\lambda_{\min}(P)}} \sup_{-\tau \le \theta \le 0} \{\|\phi(\theta)\|\} e^{-(\lambda/2)t} \tag{28}$$

which implies conclusion (22) and this completes the proof. □

Remark 5. For the case $\beta \ge 1$, we can replace the condition $0 < \rho = \sup_{k\in N}\{t_k - t_{k-1}\} < \infty$ with $0 < \varsigma = \inf_{k\in N}\{t_k - t_{k-1}\} < \infty$; then the conclusion of Theorem 4 still holds except that now inequality (9) becomes

$$\frac{2\ln\beta}{\varsigma} + \left(2\lambda_{\max}\left(\overline{A}\right) + 2L\frac{\lambda_{\max}\left(\left(\overline{I}_N \otimes \overline{E}\right)^T P\right)}{\lambda_{\min}\left(\left(\overline{I}_N \otimes \overline{E}\right)^T P\right)} + 1\right) + \lambda^2_{\max}(G \otimes \Gamma) < 1. \tag{29}$$

For $\beta \ge 1$, we have

$$\left\|x_i(t) - x_j(t)\right\| \le \frac{1}{\sqrt{\beta}} \sup_{-\overline{\tau} \le t \le 0} \{\|\phi(t)\|\} e^{-(\lambda/2)t} \tag{30}$$

in which $\lambda = \max_{k\in N}\{\ln\beta/(t_k - t_{k-1})\}$.

The proof of the above conclusion remains largely the same as Theorem 4, so we omitted it to avoid repetition.

4. Design Procedure of Impulsive Control for Complex Network

According to Theorem 4, the design process of impulsive control is given as follows.

(1) Calculate the parameters L, m.

(2) Choose a matrix P which satisfies $(\overline{I}_N \otimes \overline{E})^T P (\overline{I}_N \otimes \overline{E}) \ge 0$.

(3) For a given parameter λ_0, we can determine the control sequence $\{t_k\}$, $t \in N$ as follows. If $0 < \beta < 1$, let $\Theta := (2\lambda_{\max}(\overline{A}) + 2L(\lambda_{\max}((\overline{I}_N \otimes \overline{E})^T P)/\lambda_{\min}((\overline{I}_N \otimes \overline{E})^T P)) + 1) + \lambda^2_{\max}(G \otimes \Gamma)$; then the upper bounds of time can be taken as $0 < \rho = \sup_{k\in N}\{t_k - t_{k-1}\} = -(\ln\beta)/\Theta$; if $\beta \ge 1$, let $\Theta := (2\lambda_{\max}(\overline{A}) + 2L(\lambda_{\max}((\overline{I}_N \otimes \overline{E})^T P)/\lambda_{\min}((\overline{I}_N \otimes \overline{E})^T P)) + 1) + \lambda^2_{\max}(G \otimes \Gamma)$; then the lower bounds of control intervals is $0 < \varsigma = \inf_{k\in N}\{t_k - t_{k-1}\} = (\ln\beta)/\Theta$.

5. Numerical Simulation

In this section, a numerical example is presented to illustrate the effectiveness of derived results.

Example 6. Consider the following complicated nonlinear singular system:

$$\begin{aligned} E\dot{x}_i(t) &= Ax_i(t) + f(x_i(t)) + \sum_{j=1}^{N} G_{ij}\Gamma x_j(t - \tau(t)), \\ &\qquad i = 1, \ldots, N, \ t \in (t_{k-1}, t_k], \\ x_i(t_k^+) &= c_i x_i(t_k) + (1 - \sigma_i(t_k)) K_i x_i(t_k) \\ &\quad + \sigma_i(t_k) K_i \overline{x}_i(t_{k-1}), \quad t = t_k^+, \ k = 1, 2, \ldots, \\ x_i(t) &= \varphi_i(t), \quad t \in [-\overline{\tau}, 0]. \end{aligned} \tag{31}$$

The parameters are given as follows:

$$E = \begin{bmatrix} 1 & 0 & 0 & 0 \\ 0 & 1 & 0 & 0 \\ 0 & 0 & 1 & 0 \\ 0 & 0 & 0 & 0 \end{bmatrix}, \qquad c_1 = c_2 = 1.2,$$

$$A = \begin{bmatrix} -10 & 10 & 0 & 0 \\ \frac{8}{3} & -1 & 0 & 0 \\ 0 & 0 & \frac{-8}{3} & 0 \\ 0 & 0 & 2 & 1 \end{bmatrix}, \qquad N = 2,$$

$$f(t, x_i(t)) = \left(0\left(-x_{i1}(t)\, x_{i3}(t)\right)^T \left(x_{i1}(t)\, x_{i2}(t)\right)^T 2x_{i3}(t)\right)^T. \tag{32}$$

For simplicity, consider the system with 2 nodes. Assume that the external coupling matrix is $G = \left[\begin{smallmatrix} -7 & 3 \\ 3 & -4 \end{smallmatrix}\right]$ and the internal coupling matrix is

$$\Gamma = \begin{bmatrix} 0.1 & -0.2 & -0.1 & 0 \\ 0 & 0.1 & 0.2 & 0 \\ -0.2 & 0 & 0.1 & 0 \\ 0.1 & 0.2 & 0.1 & -0.1 \end{bmatrix}. \tag{33}$$

Supposing that $\tau(t) = 0.02\sin t$. According to Lemma 1, we can choose $P = I_{8\times 8}$, $T = t_{k+1} - t_k = 0.005$. The region of parameters of chaotic system is $L = 80$, and the gain of impulsive controller is $-1.8653 \le K \le -0.5347$. The state trajectory diagram of system is depicted in Figure 1. For the case of packet dropouts probability is $\Pr(\sigma(k) = 0 \mid 0.8)$ and initial condition is $x_1(t) = [3 \ \ 2 \ \ -1 \ \ 2]^T$, $x_2(t) = [6 \ \ 5 \ \ -4 \ \ 8]^T$, and $t \in (-\tau, 0)$.

Figure 1 shows that the asymptotic stability of the closed-loop uncertain system can be guaranteed using the networked impulsive controller designed in this paper.

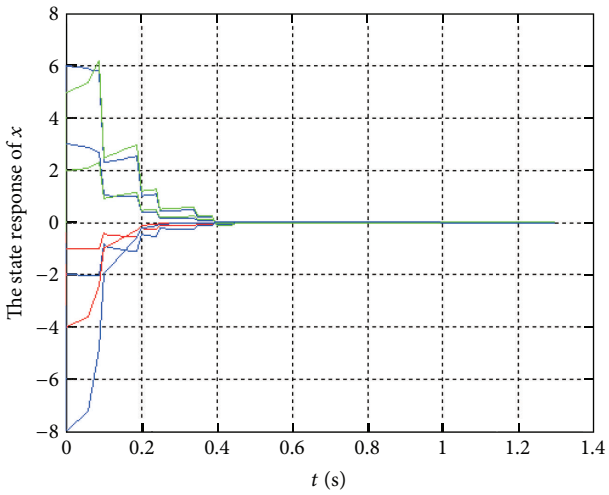

Figure 1: The state response of CNSINCS via impulsive control (color online).

6. Conclusion

In this paper, the global exponential stability CNSINCS via impulsive control is investigated. According to the Lyapunov stability theory, the mathematic model of CNSINCS is established. A general model of network consisting of time-delay and packet dropouts has been formulated and the globally exponential stable sufficient conditions have been established. Impulsive controller, which may ensure the system achieves exponential stability with a given decay rate is designed. Therefore our control scheme is efficient and practical in dealing with problems of data transmission with time-delay and packet dropouts. As an application, a numerical simulation is given to demonstrate the usefulness and practicability of proposed theoretical results.

Acknowledgments

This work was supported by the Jiangsu Planned Projects for Postdoctoral Research Funds under Grants 1202005C and the Jiangsu Natural Science Funds for Young Scholar under Grants BK20130696.

References

[1] D. Yang, C. Sha, and Q. Zhang, "H_2 analysis and parameterized H_2 observer design for descriptor systems," in *Proceedings of the 6th World Congress on Intelligent Control and Automation (WCICA '06)*, vol. 1, pp. 2370–2374, Dalian, China, June 2006.

[2] S. Q. Zhu and N. Ji, *Robust Control for Linear Singular Time-Delay Systems*, School of Mathmetics, Shandong University, 2005.

[3] T. Li, L. Guo, and L. Wu, "Simplified approach to the asymptotical stability of linear systems with interval time-varying delay," *IET Control Theory and Applications*, vol. 3, no. 2, pp. 252–260, 2009.

[4] T. Li and W. X. Zheng, "Networked-based generalised H_∞ fault detection filtering for sensor faults," *International Journal of Systems Science*, 2013.

[5] J. Lin and S. Fei, "Reliable control for a class of uncertain singular systems with interval time-varying delay," *Asian Journal of Control*, vol. 13, no. 4, pp. 542–552, 2011.

[6] B. Sfaihi and Mo. Benrejeb, "On stability analysis of nonlinear discrete singularly perturbed T-S fuzzy models," *International Journal of Dynamics and Control*, vol. 1, no. 1, pp. 20–31, 2013.

[7] J. N. Li, H. Y. Su, Y. B. Zhang, Z. G. Wu, and J. Chu, "Chattering free sliding mode control for uncertain discrete time-delay singular systems," *Asian Journal of Control*, vol. 15, no. 1, pp. 260–269, 2013.

[8] X. Sun, Q.-L. Zhang, C.-Y. Yang, Z. Su, and Y.-Y. Shao, "An improved approach to delay-dependent robust stabilization for uncertain singular time-delay systems," *International Journal of Automation and Computing*, vol. 7, no. 2, pp. 205–212, 2010.

[9] J. A. K. Suykens, T. Yang, and J. L. O. Vandewalle, "Impulsive control and synchronization of chaos," in *Controlling Chaos and Bifurcations in Engineering Systems*, G. Chen, Ed., pp. 275–298, CRC Press, Boca Raton, Fla, USA, 1999.

[10] Z.-H. Guan, J. Huang, and G. Chen, "Stability analysis of networked impulsive control systems," in *Proceedings of the 25th Chinese Control Conference (CCC '06)*, pp. 2041–2044, Harbin, China, August 2006.

[11] J. Yao, Z.-H. Guan, G. Chen, and D. W. C. Ho, "Stability, robust stabilization and H_∞ control of singular-impulsive systems via switching control," *Systems and Control Letters*, vol. 55, no. 11, pp. 879–886, 2006.

[12] T. Yang, "Impulsive control," *IEEE Transactions on Automatic Control*, vol. 44, no. 5, pp. 1081–1083, 1999.

[13] J. Sun, Y. Zhang, and Q. Wu, "Less conservative conditions for asymptotic stability of impulsive control systems," *IEEE Transactions on Automatic Control*, vol. 48, no. 5, pp. 829–831, 2003.

[14] H. Ye, A. N. Michel, and L. Hou, "Stability theory for hybrid dynamical Systems," *IEEE Transactions on Automatic Control*, vol. 43, no. 4, pp. 461–474, 1998.

[15] T. Yang, *Impulsive Control Theory*, Springer, Berlin, Germany, 2001.

[16] Y. Dai, Y. Cai, and X. Xu, "Synchronisation analysis and impulsive control of complex networks with coupling delays," *IET Control Theory and Applications*, vol. 3, no. 9, pp. 1167–1174, 2009.

Hindawi Publishing Corporation
Mathematical Problems in Engineering
Volume 2013, Article ID 679039, 10 pages
http://dx.doi.org/10.1155/2013/679039

Research Article

Robust Adaptive Control for Nonlinear Discrete-Time Systems by Using Multiple Models

Xiao-Li Li, De-Xin Liu, Jiang-Yun Li, and Da-Wei Ding

School of Automation and Electrical Engineering and the Key Laboratory of Advanced Control of Iron and Steel Process (Ministry of Education), University of Science and Technology Beijing, Beijing 100083, China

Correspondence should be addressed to Xiao-Li Li; lixiaoli@hotmail.com

Received 23 August 2013; Accepted 28 September 2013

Academic Editor: Zhiguang Feng

Back propagation (BP) neural network is used to approximate the dynamic character of nonlinear discrete-time system. Considering the unmodeling dynamics of the system, the weights of neural network are updated by using a dead-zone algorithm and a robust adaptive controller based on the BP neural network is proposed. For the situation that jumping change parameters exist, multiple neural networks with multiple weights are built to cover the uncertainty of parameters, and multiple controllers based on these models are set up. At every sample time, a performance index function based on the identification error will be used to choose the optimal model and the corresponding controller. Different kinds of combinations of fixed model and adaptive model will be used for robust multiple models adaptive control (MMAC). The proof of stability and convergence of MMAC are given, and the significant efficacy of the proposed methods is tested by simulation.

1. Introduction

Due to the strong ability of approximation, neural network has been widely used in the identification of nonlinear system. It is also a very useful tool for prediction, pattern recognition, and control [1]. The network structure comprises the interconnected group of nodes and the weight. There are many kinds of neural networks such as back propagation (BP), radial basis function (RBF), cerebellar model articulation controller (CMAC). As the most effective learning algorithm for feedforward networks [2], BP neural network has been the research focus for many years [3–6].

Adaptive control of nonlinear systems using neural network has been an active research area for over two decades [7–9]. The controller will be set up by adjusting the weights of the neural network [10, 11]. But adaptive control using neural network still has the same shortcomings as conventional adaptive control; it is extensively studied in time-invariant system with unknown parameters or time-variant system with slow drifting parameters [12, 13]. While the system has abrupt changes in parameters, the algorithm cannot find the exact identification model and will respond slowly to system parameter variations. To solve this kind of problem, MMAC has been a very useful tool in recent years.

Since MMAC was presented in 1970s, it has attracted a lot of attention of experts [14–17]. MMAC is an effective approach to solve problems such as time variations and uncertainties. It has the ability to improve the transient responses and the control performance. According to the dynamic character of controlled plant, multiple models are set up to cover the uncertainty of parameter. Much research has been done on continuous-time and discrete-time linear systems [18, 19]. For nonlinear system, only a few results have been given. In recent years, the MMAC based on neural network has been considered by some researchers [20, 21]. But in these papers, the nonlinear system has been modeled by the combination of linear model (the main part) and neural network model (the unmodeled dynamics). The multiple models are still multiple linear models with different parameters, and neural network is used only to compensate for the modeling error of linear model. In this case, the nonlinear system should not be very complex, and too big modeling error between the system and linear model is forbidden. The parameter and structure uncertainty of a relatively complex nonlinear system cannot be modeled by this method. This kind of MMAC with neural network still follows the main ideas of linear MMAC.

In this paper, a kind of robust MMAC is proposed for nonlinear system. Multiple BP neural networks with different weights will be used to cover the uncertainty of the parameters of the system. A performance index function based on the identification errors will be used to choose the best model and the corresponding controller. Considering the unmodeling error of neural network, a dead-zone recursive algorithm will be used, and the proof of robust property and stability of the MMAC are given. Different combinations of adaptive models and fixed models will be used for MMAC, and the effectiveness of the proposed method has been tested in simulations.

2. Robust Adaptive Control Using Neural Network

The single-input/single-output nonlinear discrete-time system can be represented as follows:

$$y(k+1) = f_0(\cdot) + g_0(\cdot)\, u(k-d+1), \tag{1}$$

where f_0 and g_0 are infinitely differentiable functions of

$$y(k-n+1), \ldots, y(k), u(k-d-m+1), \ldots, u(k-d), \tag{2}$$

where y is the output, u is the input, $m \le n$, d is the relative degree of the system, and g_0 is bounded away from zero. The arguments of f_0 and g_0 are real variables.

Due to the existence of noncausal problem, normally state transformation should be made first [11], and a causal system as follows can be given:

$$y(k+d) = f_{d-1}[\mathbf{x}(k)] + g_{d-1}[\mathbf{x}(k)]\, u(k). \tag{3}$$

Assumptions 1 and 2 in [11] about $g_0(\mathbf{x}), \ldots, g_{d-1}(\mathbf{x})$ and minimum phase assumption should still be satisfied.

As Assumption 3 in [11], there exist the weights $\mathbf{w}$, $\mathbf{v}$ of neural network; the functions $\widehat{f}_{d-1}[\mathbf{x}(k), \mathbf{w}]$ and $\widehat{g}_{d-1}[\mathbf{x}(k), \mathbf{v}]$ can approximate the functions f_{d-1} and g_{d-1} with any accuracy ϵ.

Plant (3) can be modeled by the neural network.

Consider

$$\widehat{y}(k+d) = \widehat{f}_{d-1}[\mathbf{x}(k), \mathbf{w}] + \widehat{g}_{d-1}[\mathbf{x}(k), \mathbf{v}]\, u(k). \tag{4}$$

The functions $\widehat{f}_{d-1}[\cdot,\cdot]$ and $\widehat{g}_{d-1}[\cdot,\cdot]$ depend on the structure of the neural network and the number of neurons. For example, if $\widehat{f}_{d-1}[\cdot,\cdot]$ and $\widehat{g}_{d-1}[\cdot,\cdot]$ are three-layer neural networks with p and q hidden neurons, respectively, then they can be expressed as

$$\begin{aligned} \widehat{f}_{d-1}[\mathbf{x}(k), \mathbf{w}] &= \sum_{i=1}^{p} w_i H\left(\sum_{j=1}^{m+n+d-1} w_{ij} x_j(k) + \widehat{w}_i \right), \\ \widehat{g}_{d-1}[\mathbf{x}(k), \mathbf{v}] &= \sum_{i=1}^{q} v_i H\left(\sum_{j=1}^{m+n+d-1} v_{ij} x_j(k) + \widehat{v}_i \right), \end{aligned} \tag{5}$$

where H is a hyperbolic tangent function.

Let $\mathbf{w}(k)$ and $\mathbf{v}(k)$ denote the estimates of $\mathbf{w}$ and $\mathbf{v}$ at time k. Rewrite (3) and (4) as follows:

$$\begin{aligned} y(k+1) &= f_{d-1}[\mathbf{x}(k-d+1)] \\ &\quad + g_{d-1}[\mathbf{x}(k-d+1)]\, u(k-d+1), \\ \widehat{y}(k+1) &= \widehat{f}_{d-1}[\mathbf{x}(k-d+1), \mathbf{w}] \\ &\quad + \widehat{g}_{d-1}[\mathbf{x}(k-d+1), \mathbf{v}]\, u(k-d+1). \end{aligned} \tag{6}$$

We have the estimated plant output as:

$$\begin{aligned} y^*(k+1) &= \widehat{f}_{d-1}[\mathbf{x}(k-d+1), \mathbf{w}(k)] \\ &\quad + \widehat{g}_{d-1}[\mathbf{x}(k-d+1), \mathbf{v}(k)]\, u(k-d+1). \end{aligned} \tag{7}$$

Define $e^*(k+1)$ as

$$e^*(k+1) = y^*(k+1) - y(k+1). \tag{8}$$

If the neural network could approximate the nonlinear system with zero error; that is, $\epsilon = 0$, the following weight $\boldsymbol{\Theta} = \left[\begin{smallmatrix} \mathbf{w} \\ \mathbf{v} \end{smallmatrix}\right]$ updating rule can be used:

$$\boldsymbol{\Theta}(k+1) = \boldsymbol{\Theta}(k) - \frac{1}{r(k)} e^*(k+1)\, \mathbf{J}(k-d+1), \tag{9}$$

where

$$\begin{aligned} &\mathbf{J}(k-d+1) \\ &= \left[\left. \frac{\partial y(k+1)^*}{\partial \boldsymbol{\Theta}} \right|_{\boldsymbol{\Theta}(k)} \right]' \\ &= \begin{bmatrix} \left(\left. \dfrac{\partial \widehat{f}_{d-1}[\mathbf{x}(k-d+1), \mathbf{w}]}{\partial \mathbf{w}} \right|_{\mathbf{w}(k)} \right)' \\ \left(\left. \dfrac{\partial \widehat{g}_{d-1}[\mathbf{x}(k-d+1), \mathbf{v}]}{\partial \mathbf{v}} \right|_{\mathbf{v}(k)} \right)' u(k-d+1) \end{bmatrix} \end{aligned} \tag{10}$$

and $r(k)$ is the reference command. One has

$$r(k) = 1 + \mathbf{J}'(k-d+1)\, \mathbf{J}(k-d+1). \tag{11}$$

Due to the existence of unmodeling dynamics $\epsilon > 0$, the design of robust adaptive controller should be considered. A dead-zone algorithm will be used instead of (9) for updating the weights. Therefor,

$$D(e) = \begin{cases} 0, & \text{if } |e| \le d_0, \\ e - d_0, & \text{if } e > d_0, \\ e + d_0, & \text{if } e < -d_0, \end{cases} \tag{12}$$

where d_0 will be the function of ϵ which can be seen in proof procedure of the Theorem 1.

The output of the dead-zone function is used in the following updating rule:

$$\boldsymbol{\Theta}(k+1) = \boldsymbol{\Theta}(k) - \frac{1}{r(k)} D\left(e^*(k+1)\right) \mathbf{J}(k-d+1). \tag{13}$$

Define the parameter error as

$$\widetilde{\mathbf{\Theta}}(k) = \mathbf{\Theta}(k) - \mathbf{\Theta} \tag{14}$$

and give the control $u(k)$ as follows:

$$u(k) = \frac{-\widehat{f}_{d-1}[\mathbf{x}(k), \mathbf{w}(k)] + r(k)}{\widehat{g}_{d-1}[\mathbf{x}(k), \mathbf{v}(k)]}. \tag{15}$$

We have Theorem 1 for the feedback control system.

Theorem 1 (see [11]). *Suppose $|r(k)| \le d_1$ for all $k \ge 0$. Given any constant $\rho > 0$ and any small constant $d_0 > 0$, there exist positive constants $\rho_1 = \rho_1(\rho, d_1)$, $\rho_2 = \rho_2(\rho, d_1)$, $\epsilon^* = \epsilon^*(\rho, d_0, d_1)$, and $\delta^* = \delta^*(\rho, d_0, d_1)$ such that if Assumptions 1 and 3 are satisfied on $S \supset B_{\rho 1}$, with $\epsilon < \epsilon^*$, Assumption 2 is satisfied on $B_{\rho 2}$, $|\mathbf{x}(0)| \le \rho$, and $|\widetilde{\mathbf{\Theta}}(0)| \le \delta < \delta^*$, then*

(1) *the $\mathbf{x}(k)$ and $u(k)$ are bounded for all k,*

(2) *$|\widetilde{\mathbf{\Theta}}(k)|$ will be monotonically nonincreasing, and $\mathbf{\Theta}(k+1) - \mathbf{\Theta}(k)$ will converge to zero,*

(3) $\sum_{k=1}^{\infty}([D(e^*(k+1))]^2/(1+\mathbf{J}'(k-d+1)\mathbf{J}(k-d+1))) \le 0$,

(4) *the tracking error between the plant output and the reference command will converge to a ball of radius d_0 centered at the origin.*

3. Robust Multiple Model Adaptive Control

The conventional adaptive control systems are usually based on a fixed or slowly adaptive model. It cannot react quickly to abrupt changes and will result in large transient errors before convergence. For this kind of problem, MMAC algorithm is presented as a useful tool. The rationale for using MMAC is to ensure that there is at least one model with parameters sufficiently close to those of the unknown plant. By the switching rule, the control strategy is to determine the best model for the current environment at every instant and activate the corresponding controller. The structure of the multiple model adaptive control is shown in Figure 1.

3.1. Architecture of the Control System. Multiple adaptive models can be regarded as an extension of conventional indirect adaptive control. The objective is to make the control error $e^c = r - y$ tend to zero, where r is the desired output. The control system contains N identification models, denoted by $I^{(l)}$, $l \in \{1, 2, \ldots, N\}$ according to (7), operating in parallel. Consider the following:

$$\begin{aligned} I^{(l)} : y^{*(l)}(k+1) = {} & \widehat{f}_{d-1}^{(l)}\left[\mathbf{x}(k-d+1), \mathbf{w}^{(l)}(k)\right] \\ & + \widehat{g}_{d-1}^{(l)}\left[\mathbf{x}(k-d+1), \mathbf{v}^{(l)}(k)\right] \\ & \times u^{(l)}(k-d+1), \end{aligned} \tag{16}$$

where

$$\widehat{f}_{d-1}^{(l)}\left[\mathbf{x}(k), \mathbf{w}^{(l)}(k)\right] = \sum_{i=1}^{p} w_i^{(l)}(k) H\left(\sum_{j=1}^{m+n+d-1} w_{ij}^{(l)}(k) x_j - \widehat{w}_i^{(l)}(k)\right),$$

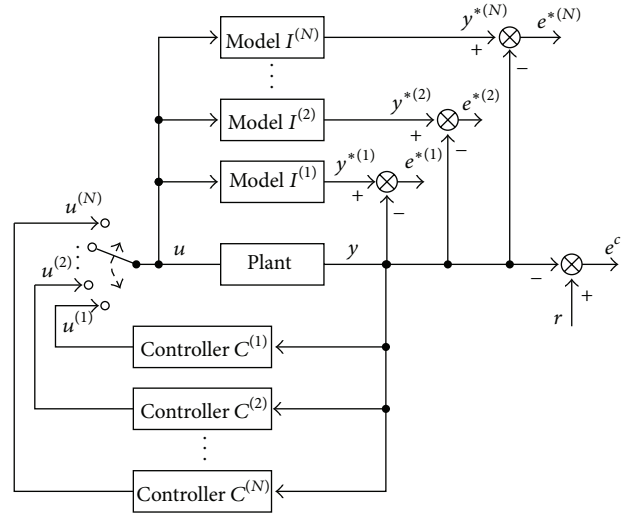

Figure 1: Structure of multiple model adaptive control.

$$\widehat{g}_{d-1}^{(l)}\left[\mathbf{x}(k), \mathbf{v}^{(l)}(k)\right] = \sum_{i=1}^{q} v_i^{(l)}(k) H\left(\sum_{j=1}^{m+n+d-1} v_{ij}^{(l)}(k) x_j - \widehat{v}_i^{(l)}(k)\right). \tag{17}$$

The identification error between the output $y^{*(l)}$ of $I^{(l)}$ and y of the plant is denoted as $e^{*(l)} = y^{*(l)} - y$. Corresponding to each $I^{(l)}$ is a parameterized controller $C^{(l)}$ which achieves the control objective for $I^{(l)}$. The output of $C^{(l)}$ is denoted by $u^{(l)}$.

One has

$$u^{(l)}(k) = \frac{-\widehat{f}_{d-1}^{(l)}\left[\mathbf{x}(k), \mathbf{w}^{(l)}(k)\right] + r(k)}{\widehat{g}_{d-1}^{(l)}\left[\mathbf{x}(k), \mathbf{v}^{(l)}(k)\right]}, \tag{18}$$

where $l \in \{1, 2, \ldots, N\}$, and $r(k)$ is the reference command.

At every instant, one of the models $I^{(l)}$ is selected by a switching rule, and the corresponding control input is used to control the plant.

Given prior knowledge of the different possible environments, the control problem is to determine suitable rules for switching and tuning these parameters to yield the best performance for the given objective while assuring stability.

3.2. Choice of Multiple Models. The following three different combinations have been considered [22].

3.2.1. N Adaptive Models. N adaptive models with different initial parameter values can be viewed as an extension of conventional indirect adaptive control. When the parameters of the plant change abruptly, the change can be detected by identification error. Then, the parameters of models are reset to initial values, and the model with the smallest error is selected. Hence, we can construct multiple adaptive models with different initial parameters which adjust dynamically in any instant. The method was considered in detail in [8, 19].

3.2.2. $N-1$ Fixed Models and One Adaptive Model. The previous method reveals that massive calculation may be produced because each adaptive model needs to adjust dynamically. Hence, if the models are fixed, the same strategy can be used in stationary and time-varying environments. However, fixed models can represent exactly only a finite number of environments. Thus, $N-1$ parallel fixed model and one adaptive model are combined, and the efficiency can be improved by the multiple fixed models and the accuracy can be increased by the adaptive model.

3.2.3. $N-2$ Fixed Models, One Free Running Adaptive Model, and One Reinitialized Adaptive Model. It is commonly accepted that the convergence time of an adaptive model will be large for large initial parametric errors. Hence, in the configuration described above, a large number of fixed models may be needed to keep the transient response under control until the adaptive model has converged. If the fixed model, which is the closest to the given plant, is assumed to be known, faster convergence can be obtained by initiating a new adaptive model from the location of the former. The same objective can be achieved on-line by starting adaptation from the location of each different fixed model that is successively chosen by the switching scheme.

The reinitialized adaptive model I^r included is introduced, and its parameters are determined as follows: if a fixed model $I^{(l)}$, $l \in \{1, 2, \ldots, N-2\}$, is activated by the switching rule at any instant k, then the parameters of I^r are reinitialized to the value of $I^{(l)}$. Thereafter, this adaptive model will be left to adapt until the next reinitialization.

3.3. Choice of the Switching Rule. A natural way to decide when and to which controller one should switch is to determine performance cost indexes for each controller $C^{(l)}$, $l \in \{1, 2, \ldots, N\}$, and switch to the one with the minimum index at every instant. However, since only one control input can be used at any instant, the performance of any candidate controller can be evaluated only after it has been used. On the other hand, the performance of all the identification models can be evaluated in parallel at every instant. Hence, the indexes must be based on the performance of the models rather than the controllers, that is, using identification errors $e^{(l)}$ rather than the control error e^c. From an adaptive control point of view, this rationale extends the principle of certainty equivalence from tuning to switching.

Considering the unmodeling error of neural network and robustness of the adaptive controller, the specific performance index proposed has the form

$$J_m(k) = \sum_{k=1}^{\infty} \frac{\left[D\left(e^*(k+1)\right)\right]^2}{1 + \mathbf{J}'(k-d+1)\,\mathbf{J}(k-d+1)}, \tag{19}$$

where $e^*(k+1) = y^*(k+1) - y(k+1)$.

The switching scheme consists of monitoring the performance indexes $J_m(k)$ at every instant. After every switching, the controller corresponding to the model with the minimum index is chosen (switched) to control the plant.

Theorem 2. *Suppose $|r(k)| < d_1$ for all $k \geq 0$. Given any constant $\rho > 0$, for all the model (adaptive model or fixed model), if $|x(0)| \leq \rho$, $|\widetilde{\boldsymbol{\Theta}}^{(l)}(0)| \leq \delta < \delta^*$, $l = 1, 2, \ldots, N$, and the conditions in Theorem 1 are satisfied, then when index switching (19) is used,*

(1) *all the signals in the system are bounded,*

(2) *the tracking error between $r(k)$ and $y(k+d)$*

$$\lim_{k\to\infty} \left|r(k) - y(k+d)\right| < d_0. \tag{20}$$

3.4. Proof of the Multiple Models Stability

3.4.1. N Adaptive Model. At time k, lth adaptive model will be selected, $l \in \{1, 2, \ldots, N\}$.

The control input

$$r(k) = \widehat{f}_{d-1}\left[\mathbf{x}(k), \mathbf{w}^{(l)}(k)\right] + \widehat{g}_{d-1}\left[\mathbf{x}(k), \mathbf{v}^{(l)}(k)\right] u(k). \tag{21}$$

From Theorem 1, if $|\mathbf{x}(0)| \leq \rho$, $|\widetilde{\boldsymbol{\Theta}}^{(l)}(0)| < \delta < \delta^*$, with control input (21), we can have that $\mathbf{x}(k)$ and $u(k)$ are bounded, for all k, and

$$\begin{aligned} \lim_{k\to\infty} \left|e^{*(l)}(k)\right| &= \lim_{k\to\infty} \left|y^{*(l)}(k) - y(k)\right| < d_0, \\ \lim_{k\to\infty} \left|\widetilde{\boldsymbol{\Theta}}^{(l)}(k)\right| &= \lim_{k\to\infty} \left|\boldsymbol{\Theta}^{(l)}(k+1) - \boldsymbol{\Theta}^{(l)}(k)\right| \longrightarrow 0. \end{aligned} \tag{22}$$

Then, the control error at time k is given by

$$\begin{aligned} \left|y^{*(l)}(k+d) - r(k)\right| \leq{}& \left|\widehat{f}_{d-1}\left[\mathbf{x}(k), \mathbf{w}^{(l)}(k+d-1)\right]\right. \\ &\left. - \widehat{f}_{d-1}\left[\mathbf{x}(k), \mathbf{w}^{(l)}(k)\right]\right| \\ &+ \left|\left\{\widehat{g}_{d-1}\left[\mathbf{x}(k), \mathbf{v}^{(l)}(k+d-1)\right]\right.\right. \\ &\left.\left. - \widehat{g}_{d-1}\left[\mathbf{x}(k), \mathbf{v}^{(l)}(k)\right]\right\} u(k)\right| \\ \leq{}& k\left|\boldsymbol{\Theta}^{(l)}(k-d+1) - \boldsymbol{\Theta}^{(l)}(k)\right| \\ &\longrightarrow 0 \quad \text{as } k \longrightarrow \infty, \end{aligned} \tag{23}$$

$$\begin{aligned} \left|r(k) - y(k+d)\right| ={}& \left|r(k) - y^{*(l)}(k+d)\right. \\ &\left. + y^{*(l)}(k+d) - y(k+d)\right| \\ \leq{}& \left|r(k) - y^{*(l)}(k+d)\right| \\ &+ \left|y^{*(l)}(k+d) - y(k+d)\right| \\ \leq{}& \left|y^{*(l)}(k+d) - y(k+d)\right| \\ <{}& d_0 \quad \text{as } k \longrightarrow \infty. \end{aligned} \tag{24}$$

Let one of N controller be chosen at random, for any instant of time k and any model chosen; then (24) holds.

So we have all the signals in the system bounded, and

(1) $\lim_{k\to\infty}|e^{*(l)}(k)| < d_0$,

(2) $\lim_{k\to\infty}|r(k) - y(k+d)| < d_0$.

3.4.2. $N-1$ Fixed Model and One Adaptive Model. Consider the following index function:

$$J_m^{(l)}(k) = \sum_{k=1}^{\infty} \frac{\left[D^{(l)}\left(e^*(k+1)\right)\right]^2}{1 + \left(\mathbf{J}^{(l)}(k-d+1)\right)' \mathbf{J}^{(l)}(k-d+1)}. \quad (25)$$

At every instant k, model $I^{(l)}$,

$$l = \arg\min_{1\le l\le N} J_m^{(l)}(k), \quad (26)$$

will be selected.

Proof. From Theorem 1, we have that, for adaptive model,

$$\lim_{k\to\infty} J_m^{(a)}(k) = \lim_{k\to\infty} \sum_{k=1}^{\infty} \frac{\left[D^{(a)}\left(e^*(k+1)\right)\right]^2}{1 + \left(\mathbf{J}^{(a)}(k-d+1)\right)' \mathbf{J}^{(a)}(k-d+1)} < \infty. \quad (27)$$

For the fixed models l, $\lim_{k\to\infty} J_m^{(l)}(k)$ is either bounded or ∞, if the performance index $J_m^{(l)}(k)$ tends to ∞; there exist a time t, $J_m^{(a)}(k) < J_m^{(l)}(k)$, $k \ge t$, which implies that the adaptive model will be selected finally.

If $\lim_{k\to\infty} J_{\mathrm{m}}^{(l)}(k)$ is bounded, then

$$\lim_{k\to\infty} \sum_{k=1}^{\infty} \frac{\left[D^{(l)}(e^*(k+1))\right]^2}{1 + \left(\mathbf{J}^{(l)}(k-d+1)\right)' \mathbf{J}^{(l)}(k-d+1)} < \infty, \quad (28)$$

$$\lim_{k\to\infty} \frac{\left[D^{(l)}(e^*(k+1))\right]^2}{1 + \left(\mathbf{J}^{(l)}(k-d+1)\right)' \mathbf{J}^{(l)}(k-d+1)} \longrightarrow 0. \quad (29)$$

If the fixed model is selected, the relationship of ρ, ϵ, δ in Theorem 1 is satisfied; the proof procedure will be similar to that of multiple adaptive controller. We also have the following:

(1) all the signals in the system are bounded,

(2) $\lim_{k\to\infty}|e^{*(l)}(k)| < d_0$,

(3) $\lim_{k\to\infty}|r(k) - y(k+d)| < d_0$.

□

3.4.3. $N-2$ Fixed Model, One Free Running Adaptive Model, and One Reinitialized Adaptive Model. The introduction of the reinitialized adaptive model will not affect the stability of the whole system, and the proof of the stability will be similar to the case of $N-1$ fixed model and one adaptive model.

4. Simulation

4.1. The Problem. PH neutralization is a very important procedure in the chemical industry. Usually, we use the logarithmic behavior to present pH characteristic; the existing nonlinearity always makes the identification and control of pH neutralization more difficult. A strong acid flows into a tank and is thoroughly mixed with a strong base whose inward rate of flow is controlled in such a way to produce a neutral outward flow from the tank. Because the acid and the base are strong, they are completely dissociated, and also the dissociation of the water can be disregarded [23]. The equation describing this model is

$$V\frac{dy}{dk} = F(k)\left(a - y(k)\right) - u(k)\left(b + y(k)\right), \quad (30)$$

where $y(k) = [\mathrm{H}^+] - [\mathrm{pH}^-]$ is the distance from neutrality,

V = volume of the tank,

$F(k)$ = rate of flow of the acid,

a = concentration of the acid,

$u(k)$ = rate of flow of the base,

b = concentration of the base.

Note that pH value can be determined from the $y(k)$, $\mathrm{pH}(k)$ by the following nonlinear transformation:

$$\mathrm{pH}(k) = -\log_{10}\left(\frac{y(k) + \sqrt{(y(k))^2 + 4K_w}}{2}\right), \quad (31)$$

where K_w = water equilibrium constant $\simeq 10^{14}$.

We suppose that $\overline{b}$ and a are fixed and known, that $\overline{F}(k)$ can be measured online, and that $\overline{u}(k)$ can be given assigned values within certain limits.

An approximate discrete-time model can be developed, incorporating measurement and input actuator errors, as follows:

$$y_{k+1} \simeq y_k + \frac{T}{V}\left[F(k)\left(a - y_k\right) - u_k\left(b + y_k\right)\right]. \quad (32)$$

The following values were adopted for the various quantities of interest:

$$0.1 \le F(k) \le 0.125\,\mathrm{l/min}, \qquad 0 \le u(k) \le 0.2\,\mathrm{l/min},$$
$$a = 10^{-3}\,\mathrm{mol/l}, \qquad V = 2\,\mathrm{l}, \quad (33)$$
$$b = 10^{-3}\,\mathrm{mol/l}, \qquad T = 2\,\mathrm{min}.$$

Then our goal is to control the plant as follows:

$$y(k+1) = y(k)\left[1 - 0.5F(k)\right] + 0.5 \times 10^{-3}F(k) - 0.5\left[10^{-3} + y(k)\right]u(k), \quad (34)$$

where $F(x)$ is the variable parameter. And the single-input/single-output nonlinear discrete-time system represented as (1) can be modeled by

$$y^*(k+1) = \widehat{f}\left[y(k), \mathbf{w}(k)\right] + \widehat{g}\left[y(k), \mathbf{v}(k)\right]u(k), \quad (35)$$

where $\widehat{f}$ and $\widehat{g}$ are the output of neural network.

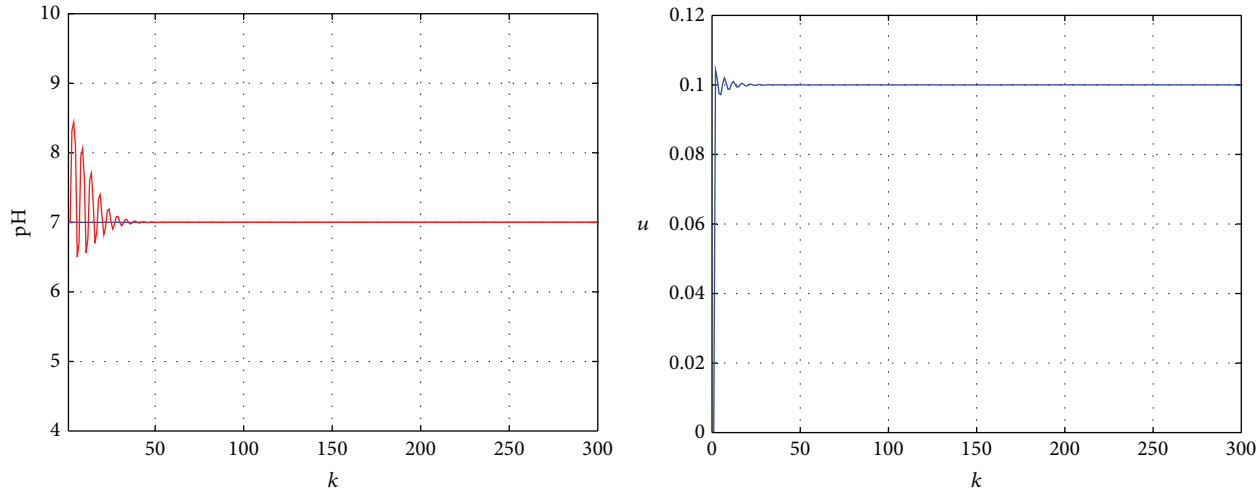

(a) System output pH(k) (b) Control input $u(k)$

Figure 2: One adaptive mode with fixed parameter.

The neural networks $\widehat{f}$ and $\widehat{g}$ are 3 layered with 4 neurons in each hidden layer. Based on the error between the plant output $y(k+1)$ and the model output $y^*(k+1)$, the network parameters $\mathbf{w}(k)$ and $\mathbf{v}(k)$ are updated to $\mathbf{w}(k+1)$ and $\mathbf{v}(k+1)$ using the standard back propagation algorithm.

4.2. Experiments

Adaptive Model Only. In the process of parameter identification, let $F(k) = 0.1$, $d_0 = 0.001$, $y(1) = 0$, $y(2) = 0$, the reference command $r(k) = 0$ (according to (31), pH$(k) = 7$), and $k = 1, 2, \ldots, 300$. The initial weights $\mathbf{w}$ and $\mathbf{v}$ are given a random number in the range $[-1, 1]$. The identification results are shown in Figure 2.

After 300 sample times, the weights will converge to the following values:

$$\begin{aligned}\mathbf{w} = {} & [0.865, 0.799, -0.823, 1.478, 0.232, 0.484,\\ & -0.251, 0.794, 1.052, -0.742, 0.591, -0.019]^T,\\ \mathbf{v} = {} & [-0.483, -0.665, -0.288, -0.767, -0.519, -0.187,\\ & 0.506, -0.236, -0.268, 0.965, 1.201, 0.891]^T.\end{aligned} \tag{36}$$

Now, we consider a worse case of the plant where abruptly changing parameters appear:

$$F(k) = \begin{cases} 0.1, & 1 \le k < 100,\\ 0.113, & 100 \le k < 200,\\ 0.125, & 200 \le k < 300.\end{cases} \tag{37}$$

Given the initial weights as the convergent weights of $\mathbf{w}$ and $\mathbf{v}$ in (36).

As the parameters change at $k = 100$ and $k = 200$, the overshoot of the system is big and the settling time is long. The nonlinear system cannot track the reference trajectory in time (Figure 3). When MMAC is used, the following simulation results can be obtained.

4.2.1. Three Adaptive Models. Three adaptive models $I^{(a1)}$, $I^{(a2)}$, and $I^{(a3)}$ are established. According to the three different values of $F(k)$ obtained ($k = 1, 100, 300$), each group of weights can be got using the same method as that in (36). One has

$$\begin{aligned}\mathbf{w}^{(a1)} &= \mathbf{w}, \qquad \mathbf{v}^{(a1)} = \mathbf{w}\\ \mathbf{w}^{(a2)} &= [-0.423, 0.482, -0.054, 1.023, 0.487, 0.248,\\ &\quad 0.072, 0.825, 0.230, -0.214, -0.678, 0.032]^T,\\ \mathbf{v}^{(a2)} &= [-1.064, -0.103, 0.563, 0.578, -0.439, -0.487,\\ &\quad 0.258, -0.557, -0.820, 0.385, 0.842, 0.831]^T,\\ \mathbf{w}^{(a3)} &= [-0.584, 0.341, 0.376, 0.733, 0.394, 0.476,\\ &\quad 1.067, 1.089, -0.144, -0.577, 0.051, -0.058]^T,\\ \mathbf{v}^{(a3)} &= [0.811, 0.076, -0.532, 0.399, 0.412, -0.268,\\ &\quad 0.897, -0.384, 0.933, -0.131, -0.313, -0.758]^T.\end{aligned} \tag{38}$$

The multiple models based on neural networks are chosen as in (16). Figures 4(a) and 4(b) present the responses of the plant. Switching sequence of controllers is shown in Figure 4(c). Obviously, this method can track the reference trajectory fast and improve the transient response. According to the index function, the system can choose an approximate model to identify the unknown plant. Once the parameters change, the weights and the index functions of neural network models will be initialized and the system will choose the optimal model again to conduct identification. In this way, the overshoot of the system can be decreased and the reference trajectory can be tracked fast at the same time.

4.2.2. Three Fixed Models and One Adaptive Model. In this case, three fixed models $I^{(f1)}$, $I^{(f2)}$, and $I^{(f3)}$ are used to

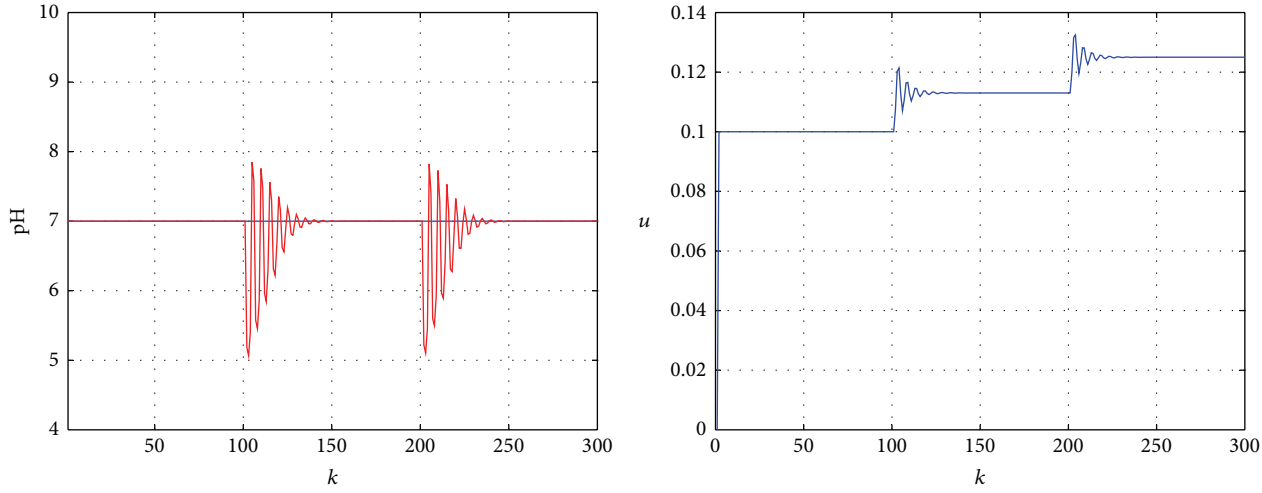

(a) System output pH(k) (b) Control input $u(k)$

Figure 3: One adaptive mode with variable parameter.

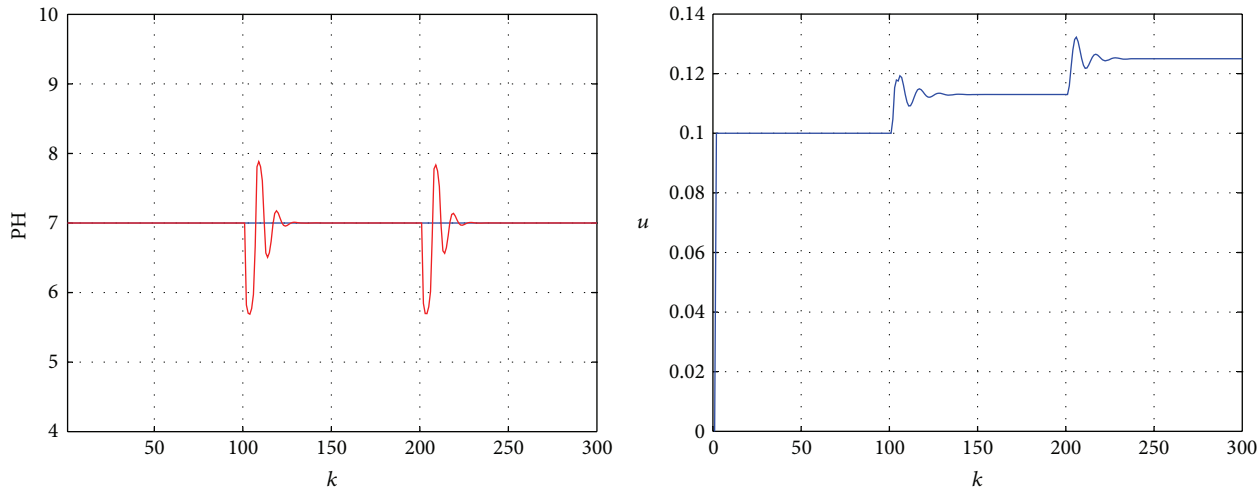

(a) System output pH(k) (b) Control input $u(k)$

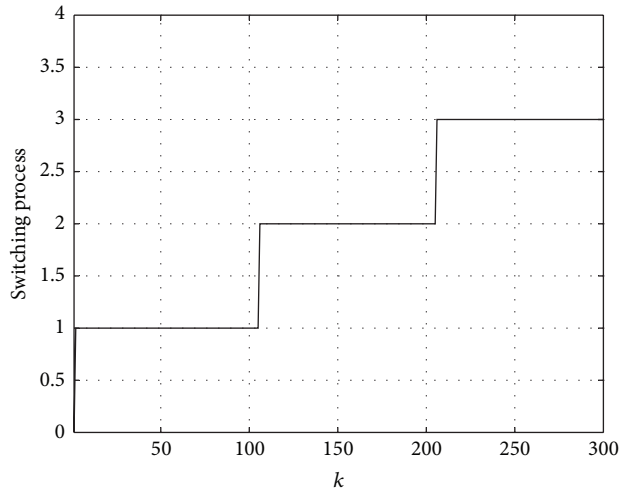

(c) Switching scheme

Figure 4: Three adaptive models.

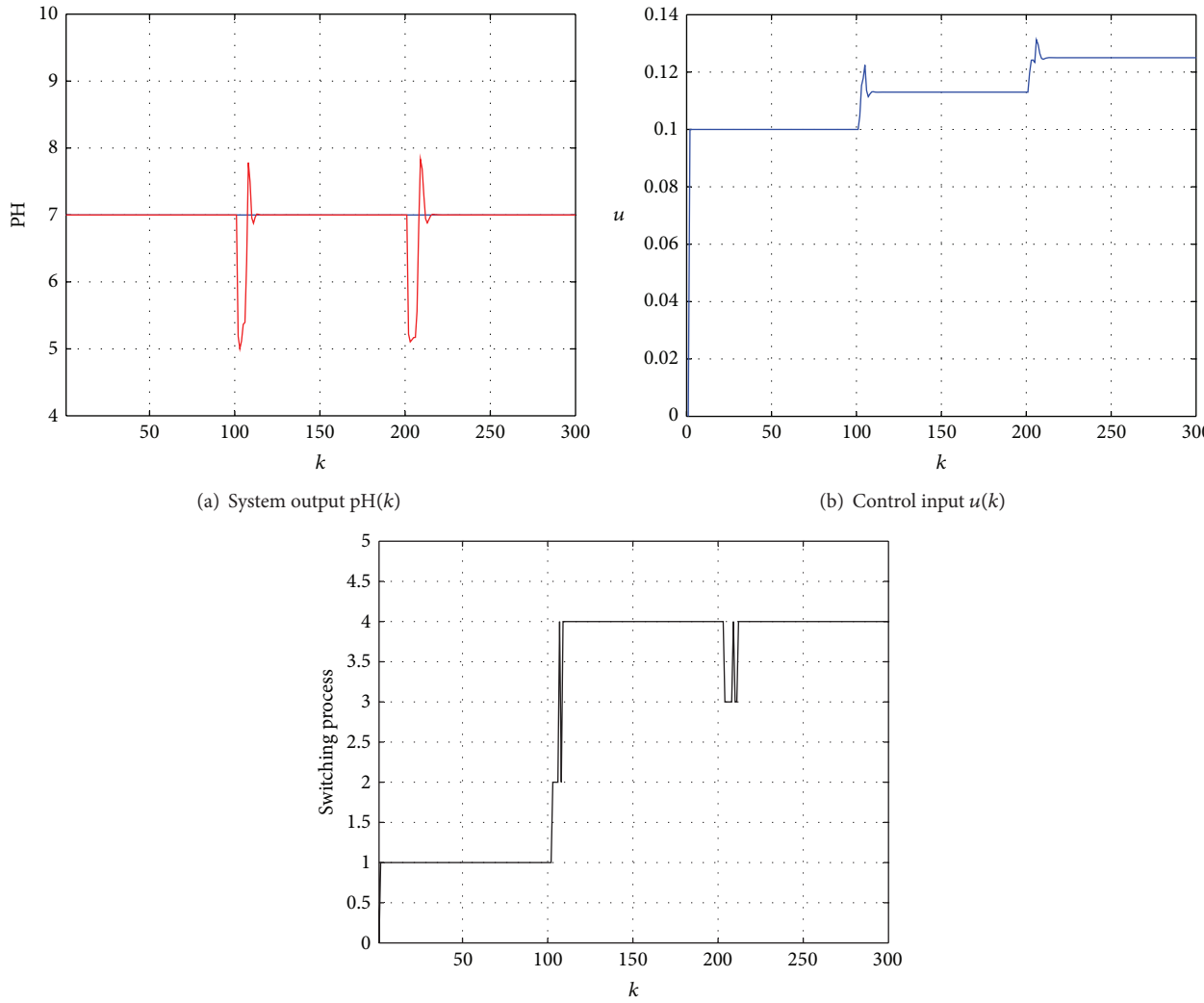

(a) System output pH(k)

(b) Control input $u(k)$

(c) Switching scheme

FIGURE 5: Three fixed models and one adaptive model.

improve the transient response, and one adaptive model $I^{(a4)}$ is used to guarantee the stability. The initial weights of the three fixed models are the same as those of the three adaptive models, and the weights of one adaptive model $I^{(a4)}$ are equal to those of $I^{(f1)}$.

In the process of parameter identification, this method could improve the transient response compared with the conventional adaptive control (Figures 5(a) and 5(b)). Switching sequence of controllers is shown in Figure 5(c). Once the parameter changes abruptly at 100 or 200, the controller will switch to the nearest fixed model $I^{(f2)}$, $I^{(f3)}$ to reduce the error. When the adaptive model gradually converges to the true value, the system will switch to the adaptive model $I^{(a4)}$. Multiple fixed models play a transitional role in the process of identification. This method can reduce massive calculation compared with the case of three adaptive models, but it produces a larger overshoot compared with Figures 4(a) and 4(b).

4.2.3. Three Fixed Models, One Free Running Adaptive Model, and One Reinitialized Adaptive Model. In this case, we establish three fixed models $I^{(f1)}$, $I^{(f2)}$, and $I^{(f3)}$ with different initial weights; $I^{(a4)}$ is the free adaptive model and $I^{(r5)}$ is the reinitialized adaptive model. The reinitialized adaptive model can achieve the initial weights by choosing a set of fixed models based on the past performance of the plant. If at any instant one of them is determined to be the best, the reinitialized adaptive model can be adapted from this model.

From the simulation, we can see that this method can improve the control quality dramatically (Figures 6(a) and 4(b)). Switching sequence of controllers is shown in Figure 6(c). Compared with the other algorithm proposed before, this method show perfect performance in reducing the overshoot and tracking the reference trajectory, and computation time is reduced greatly.

5. Conclusion

In this paper, multiple models are used to establish robust multiple models adaptive controller for a class of nonlinear discrete-time systems by using neural networks. Three kinds of combinations of adaptive model and fixed model are used

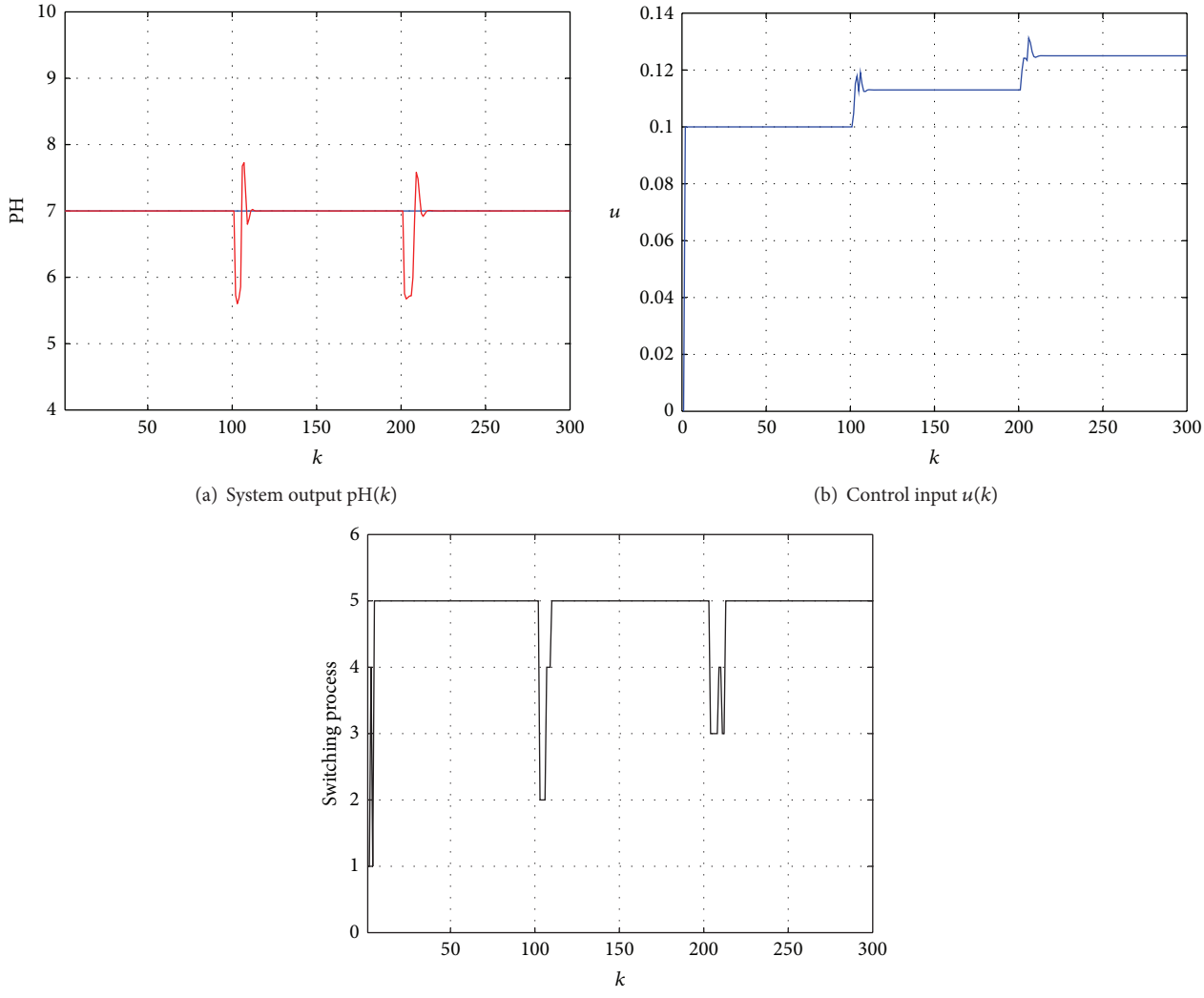

(a) System output pH(k)

(b) Control input $u(k)$

(c) Switching scheme

Figure 6: Three fixed models, one free running adaptive model and one reinitialized adaptive model.

to make the multiple model set, and a switching law is suitably defined to make the decision of the best model. The principal contribution of this paper is the proof of stability of robust MMAC by using neural networks. Multiple neural network models with different weights represent different dynamical characters of the plant when it operates in different environments, which can be described by a mount of input and output data. So the design of the model set can also be regarded as a kind of data driven problem [24, 25]. How to divide the region of data into suitable numbers of subregions which can be represented by multiple neural network models will decide the accuracy of MMAC. A moving or dynamically optimal model set will be an important problem that needs to be solved in the future.

Conflict of Interests

The authors declare that there is no conflict of interests regarding the publication of this paper.

Acknowledgments

This work was supported by the Fundamental Research Funds for the Central Universities under Grant FRF-TP-12-005B, the Program for New Century Excellent Talents in Universities under Grant NCET-11-0578, and the National Natural Science Foundation of China under Grant 61074055.

References

[1] D. Wang and J. Huang, "Adaptive neural network control for a class of uncertain nonlinear systems in pure-feedback form," *Automatica*, vol. 38, no. 8, pp. 1365–1372, 2002.

[2] D. E. Rumelhart, G. E. Hinton, and R. J. Williams, "Learning representations by back-propagating errors," *Nature*, vol. 323, no. 6088, pp. 533–536, 1986.

[3] X. J. Jing and L. Cheng, "An optimal PID control algorithm for training feedforward neural networks," *IEEE Transactions on Industrial Electronics*, vol. 60, no. 6, pp. 2273–2283, 2013.

[4] B. William and L. Stanislao, "Robot navigation control based on monocular images: an image processing algorithm for obstacle avoidance decisions," *Mathematical Problems in Engineering*, vol. 2012, Article ID 240476, 14 pages, 2012.

[5] M. Arvaneh, C. Guan, K. K. Ang, and C. Quek, "Optimizing spatial filters by minimizing within-class dissimilarities in electroencephalogram-based brain—computer interface," *IEEE Transactions on Neural Networks and Learning Systems*, vol. 24, no. 4, pp. 610–619, 2013.

[6] H. A. Talebi and K. Khorasani, "A neural network-based multiplicative actuator fault detection and isolation of nonlinear systems," *IEEE Transactions on Control Systems Technology*, vol. 21, no. 3, pp. 842–851, 2012.

[7] K. J. Astrom and B. Wittenmark, *Adaptive Control*, Addison-Wesley, Longman Publishing, Boston, Mass, USA, 1995.

[8] K. S. Narendra and A. Annaswamy, *Stable Adaptive Systems*, Prentice-Hall, Englewood Cliffs, NJ, USA, 1989.

[9] P. A. Ioannou and J. Sun, *Robust Adaptive Control*, Prentice-Hall, Upper Saddle River, NJ, USA, 1996.

[10] K. S. Narendra and K. Parthasarathy, "Identification and control of dynamical systems using neural networks," *IEEE Transactions on Neural Networks*, vol. 1, no. 1, pp. 4–27, 1990.

[11] F. C. Chen and H. K. Khalil, "Adaptive control of a class of nonlinear discrete-time systems using neural networks," *IEEE Transactions on Automatic Control*, vol. 40, no. 5, pp. 791–801, 1995.

[12] F. C. Chen and H. K. Khalil, "Adaptive control of nonlinear systems using neural networks," *International Journal of Control*, vol. 55, no. 6, pp. 1299–1317, 1992.

[13] G. Kreisselmeier and B. D. O. Anderson, "Robust model reference adaptive control," *IEEE Transactions on Automatic Control*, vol. 31, no. 2, pp. 127–133, 1986.

[14] L. Giovanini, "Robust adaptive control using multiple models, switching and tuning," *IET Control Theory & Applications*, vol. 5, no. 18, pp. 2168–2178, 2011.

[15] W. Wang and X. L. Li, *Multiple Model Adaptive Control*, Science Press, Beijing, China, 2001.

[16] D. T. Magill, "Optimal adaptive estimation of sampled stochastic processes," *IEEE Transactions on Automatic Control*, vol. 10, pp. 434–439, 1965.

[17] D. G. Lainiotis, "Partitioning: a unifying framework for adaptive systems. I. Estimation," vol. 64, no. 8, pp. 1126–1143, 1976.

[18] M. Athans, D. Castanon, K.-P. Dunn et al., "The stochastic control of the F-8C aircraft using a multiple model adaptive control (MMAC) method—part I: equilibrium flight," *IEEE Transactions on Automatic Control*, vol. 22, no. 5, pp. 768–780, 1977.

[19] K. S. Narendra and J. Balakrishnan, "Adaptive control using multiple models," *IEEE Transactions on Automatic Control*, vol. 42, no. 2, pp. 171–187, 1997.

[20] L. Chen and K. S. Narendra, "Nonlinear adaptive control using neural networks and multiple models," *Automatica*, vol. 37, no. 8, pp. 1245–1255, 2001.

[21] Y. Fu and T. Chai, "Nonlinear multivariable adaptive control using multiple models and neural networks," *Automatica*, vol. 43, no. 6, pp. 1101–1110, 2007.

[22] K. S. Narendra and C. Xiang, "Adaptive control of discrete-time systems using multiple models," *IEEE Transactions on Automatic Control*, vol. 45, no. 9, pp. 1669–1686, 2000.

[23] G. C. Goodwin and K. S. Sin, *Adaptive Filtering Prediction and Control*, Prentice-Hall, Englewood Cliffs, NJ, USA, 1984.

[24] S. Yin, S. X. Ding, A. Haghani, H. Y. Hao, and P. Zhang, "A comparison study of basic data-driven fault diagnosis and process monitoring methods on the benchmark Tennessee Eastman process," *Journal of Process Control*, vol. 22, no. 9, pp. 1567–1581, 2012.

[25] S. Yin, H. Luo, and S. X. Ding, "Real-time implementation of fault-tolerant control systems with performance optimization," *IEEE Transactions on Industrial Electronics*, no. 99, p. 1, 2013.

Hindawi Publishing Corporation
Mathematical Problems in Engineering
Volume 2013, Article ID 364726, 9 pages
http://dx.doi.org/10.1155/2013/364726

Research Article

Sliding Sector-Based Variable Structure Control of Continuous-Time Markov Jump Linear Systems Subject to Unknown Transition Rates

Yan-Mei Xue,[1] Jianwei Yang,[1] and Xiao-Mei Liu[2]

[1] *The School of Mathematics & Statistics, Nanjing University of Information Science & Technology, Nanjing, Jiangsu 210044, China*
[2] *The School of Automation, Southeast University, Nanjing, Jiangsu 210096, China*

Correspondence should be addressed to Yan-Mei Xue; ymxue1@163.com

Received 8 August 2013; Accepted 5 October 2013

Academic Editor: Tao Li

Based on sliding sector technique, the variable structure control for a class of uncertain continuous-time Markovian jump linear systems (MJLS) is investigated. The elements in the transition rate matrix include completely known, boundary known, and completely unknown ones. First, the related notions about sliding sector for continuous-time Markov jump linear systems are given; then based on linear matrix inequalities (LMIs) technique, sufficient conditions for the design of the sliding sector are provided. Second, a variable structure control law is presented to guarantee the mean-square quadratic stability of the closed-loop system in spite of the effects of the existing uncertainties and unknown/uncertain transition rates. Finally, an example is given to verify the validity of the theoretical results.

1. Introduction

The subject of this paper is variable structure control of continuous-time Markov jump linear uncertain systems. Control design problems of Markov jump systems are motivated by the fact that these systems represent a class of important stochastic systems which is popular in modeling practical engineering systems subject to failures or changes in structures and parameters. Such as in [1, 2], Markovian switching technique has been used to model the switching action of mobile manipulators. In addition, some important theoretical results have also been published so far; see, for example, [3–9] and the references therein. It is worth noticing that these results require that the transition probabilities/rates must be known precisely. In fact, the likelihood of obtaining the perfect information on all transition probabilities/rates is questionable, and the cost might be expensive in some areas. As a result, the study of control synthesis for Markov jump systems with uncertain or unknown transition probabilities/rates becomes interesting, and some important results have been established. For instance, the robust control designs for MJLS subject to the norm-bounded or polytopic uncertainties in the transition rates were considered in [10, 11]. However, they both require to know the structure and "nominal" terms of the uncertain transition rates. Furthermore, control designs of MJLS with partly unknown transition rates were developed in [12–14], in which the transition rate matrix included two kinds of elements: completely known and completely unknown ones. In fact, besides the two kinds of elements, it might also own boundary known elements in practice, and we will consider this more general case for reducing the conservatism of control design in this paper.

On the other hand, variable structure control is a well-known robust control technique against external disturbances, parameter uncertainties, and unmodeled dynamics [15–17], and thus there are also some remarkable results published on variable structure control of continuous-time MJLS recently [18–22]. In [21], the robust stabilization of variable structure control for continuous-time MJLS with matched uncertainties was first investigated, and then in [22], a singular system approach was introduced for systems with parameter uncertainties and unknown nonlinear function. It is worth mentioning that these works require the transition rates to be

precisely known *a prior*, and to the best of our knowledge, no results have been reported to variable structure control of continuous-time MJLS with unknown transition rates. In addition, one of the disadvantages about variable structure control is that chattering phenomenon might occur on the neighbor of the sliding manifold which is harmful to actuator devices, and thus it is a barrier for the use of the variable structure control strategy [23–25]. In order to avoid the occurrence of chattering phenomenon, it is worth noting that for a class of linear deterministic systems, a variable structure control-based sliding sector is first introduced in [26]. The main feature of the sliding sector-based variable structure control scheme is that zero control input can be used in the sliding sector of the state space and then the chattering phenomenon is avoided.

Motivated by the aforementioned discussion, for a class of continuous-time uncertain MJLS subject to unknown transition rates, a novel robust variable structure control-based sliding sector technique is investigated. The main contribution of this paper is summarized as follows. First, related notions of the sliding sector for MJLS, P_iR_i-sliding sector, simplified P_iR_i-sliding sector, and inner sector and outer sector are given. Second, sufficient conditions for the design of the simplified P_iR_i-sliding sector for the considered Markov jump linear uncertain system are presented in terms of LMI technique. Finally, a variable structure control law is established to drive the state trajectory to converge to the inner sector of the P_iR_i-sliding sector and guarantee mean square quadratic stability of the closed-loop system in spite of the effect of unknown transition rates and system uncertainties.

The rest of this paper is organized as follows. The problem statement and preliminaries are presented in Section 2. The main results are given in Section 3. In Section 4, a numerical example is presented to illustrate the effectiveness of the results, and the conclusions are drawn in Section 5.

Throughout this paper, the following notations are used. $\mathbb{R}^n$ denotes the n-dimensional Euclidean space; A^T stands for the transpose of matrix A; I and 0 represent the identity matrix and zero matrix in appropriate dimension, respectively. In addition, the symbol $\mathrm{He}(X)$ is used to represent $X + X^T$. $P > 0$ ($P \geq 0$) means that P is real symmetric and (semi-) positive definite. $|\cdot|$ denotes the absolute value of a scalar, the standard Euclidean norm of a vector, or the induced norm of a matrix, respectively. In symmetric block matrices, the notation $*$ is used to represent a term that is induced by symmetry.

2. Problem Statement and Preliminaries

Consider the following time-invariant continuous-time linear uncertain system:

$$\dot{x} = \left(A\left(r_t\right) + \Delta A\left(r_t\right)\right)x + \left(B\left(r_t\right) + \Delta B\left(r_t\right)\right)u, \tag{1}$$

where $x(t) \in \mathbb{R}^n$ and $u(t) \in \mathbb{R}$ are state and control input, respectively. ΔAr_t and $\Delta B(r_t)$ are the system uncertainties. $\{r_t, t \geq 0\}$ is a continuous-time Markovian process with right continuous trajectories and taking values in a finite set $\mathcal{S} = \{1, 2, \ldots, \mathbb{N}\}$. It governs the switching among the different system modes with the following mode transition probabilities:

$$\mathrm{Prob}\left\{r_{t+m} = j \mid r_t = i\right\} = \begin{cases} \lambda_{ij}m + o\left(m\right), & \text{if } j \neq i, \\ 1 + \lambda_{ii}m + o\left(m\right), & \text{if } j = i, \end{cases} \tag{2}$$

where $m > 0$, $\lim_{m\to 0}(o(m)/m) = 0$ and $\lambda_{ij} \geq 0\,(i, j \in \mathcal{S}, j \neq i)$ denote the switching rate from mode i at time t to mode j at time $t + m$, and $\lambda_{ii} = -\sum_{j=1, j\neq i}^{\mathbb{N}} \lambda_{ij}$ for each $i \in \mathcal{S}$.

In general, the Markov process transition rate matrix Λ is defined by

$$\Lambda = \left[\lambda_{ij}\right]_{\mathbb{N}\times\mathbb{N}}. \tag{3}$$

In this paper, the transition rates of the jumping process are assumed to be partly available; that is, some elements in Λ have been exactly known; some ones are uncertain but with known boundaries; others may have no information to use. For instance, for system (1) with four operation modes, the transition rate matrix might be described by

$$\Lambda = \begin{bmatrix} ? & \lambda_{12} & \lambda_{13} & ? \\ \lambda_{21} & ? & \lambda_{23} & ? \\ ? & a & ? & \lambda_{34} \\ b & ? & \lambda_{43} & \lambda_{44} \end{bmatrix}, \tag{4}$$

where ? represents the completely unknown element in the transition rate matrix; parameters a and b represent the elements with known lower and upper bounds. That is, $\underline{a} \leq a \leq \overline{a}$ and $\underline{b} \leq b \leq \overline{b}$, where $\underline{a}$, $\overline{a}$, $\underline{b}$, and $\overline{b}$ are known parameters; λ_{ij} denotes the precisely known element.

For clarity, denote $\mathcal{S} = \mathcal{S}^i_{k1} \cup \mathcal{S}^i_{k2} \cup \mathcal{S}^i_{uk}$, $i = 1, 2, \ldots, \mathbb{N}$ by

$$\begin{aligned} \mathcal{S}^i_{k1} &= \left\{j : \lambda_{ij} \text{ is exactly known}\right\}, \\ \mathcal{S}^i_{k2} &= \left\{j : \text{the bounds of } \lambda_{ij} \text{ is known}\right\}, \\ \mathcal{S}^i_{uk} &= \left\{j : \text{there is no information available for } \lambda_{ij}\right\}. \end{aligned} \tag{5}$$

Furthermore, let $\mathcal{S}^i_k = \{j : \underline{\lambda}_{ij} \leq \lambda_{ij} \leq \overline{\lambda}_{ij}\}$; then $\mathcal{S}^i_k = \mathcal{S}^i_{k1} \cup \mathcal{S}^i_{k2}$. Let $\mathcal{S}^i_k = \{\mathcal{K}^i_1, \mathcal{K}^i_2, \ldots, \mathcal{K}^i_{m^i_k}\}$. $\mathcal{S}^i_{uk} = \{\mathbb{K}^i_1, \mathbb{K}^i_2, \ldots, \mathbb{K}^i_{m^i_{uk}}\}$, where $\mathcal{K}^i_{l_1}$ denotes the l_1th element in $\mathcal{S}^i_k$ with the index $\mathcal{K}^i_{l_1}$ in the ith row of the matrix Λ. $\mathbb{K}^i_{l_2}$ denotes the l_2th element in $\mathcal{S}^i_{uk}$ with the index $\mathbb{K}^i_{l_2}$ in the ith row of the matrix Λ. m^i_k and m^i_{uk} represent the number of elements in $\mathcal{S}^i_k$ and $\mathcal{S}^i_{uk}$, respectively.

Remark 1. When $\underline{\lambda}_{ij} = \overline{\lambda}_{ij}$, the transition rates are reduced to the situation in [12]. Obviously, the solving method there can only treat the above known bound case as the completely unknown case, and some conservativeness has been brought in.

For convenience, let $A_i = A(r_t)$, $\Delta A_i = \Delta A(r_t)$, $B_i = B(r_t)$, and $\Delta B_i = \Delta B(r_t)$ for each possible value $r_t = i$, $i \in \mathcal{S}$,

where A_i and B_i are known constant matrices with appropriate dimensions; then system (1) can be described by

$$\dot{x} = \left(A_i + \Delta A_i\right) x + \left(B_i + \Delta B_i\right) u. \tag{6}$$

Throughout this paper, for each i, suppose that the following assumptions are valid.

Assumption 2. The pair (A_i, B_i) is controllable.

Assumption 3. The uncertainties satisfy $\Delta A_i = D_i E_i(t,x) F_i$, $\Delta B_i = B_i \Theta_i(t)$, where D_i and F_i are known constant matrices with appropriate dimensions, $E_i(t,x)$ is time-varying uncertain matrix satisfying $E_i E_i^T \le I$, the parameter $\Theta_i(t)$ satisfies $|\Theta_i(t)| \le \overline{d}_i < 1$, $\overline{d}_i$ is a known positive scalar.

For continuous-time Markov jump linear nominal systems

$$\dot{x} = A_i x + B_i u, \tag{7}$$

some related notions of sliding sector are firstly presented.

Definition 4. The $P_i R_i$-sliding sector is a subset of $\mathbb{R}^n$ defined as

$$\mathcal{S}_i = \left\{ x \mid x^T \left(A_i^T P_i + P_i A_i + \sum_{j=1}^{\mathbb{N}} \lambda_{ij} P_j \right) x \le -x^T R_i x,\ x \in \mathbb{R}^n \right\}, \tag{8}$$

where $P_i \in \mathbb{R}^{n\times n}$ is a positive definite symmetric matrix, $R_i \in \mathbb{R}^{n\times n}$ is a positive semidefinite symmetric matrix, $R_i = C_i^T C_i$, $C_i \in \mathbb{R}^{l_i \times n}$, $l_i \ge 1$, and (C_i, A_i) is an observable pair.

The set of the $P_i R_i$-sliding sector is nonempty since at least zero state stays inside it.

Obviously, while the state of the plant evolves in the $P_i R_i$-sliding sector $\mathcal{S}_i$, the P_i-norm $|x|_{P_i} = x^T P_i x$ of the plant (7) decreases with zero control input since

$$\dot{L}_i = x^T \left(A_i^T P_i + P_i A_i + \sum_{j=1}^{\mathbb{N}} \lambda_{ij} P_j \right) x \le -x^T R_i x \le 0, \quad \forall x \in \mathcal{S}_i,\ x \ne 0, \tag{9}$$

where $L_i = |x|_{P_i}^2$.

Remark 5. When $A_i = A$, $P_i = P$, $R_i = R$, the $P_i R_i$-sliding sector in (8) becomes

$$\mathcal{S} = \left\{ x \mid x^T \left(A^T P + PA \right) x \le -x^T R x,\ x \in \mathbb{R}^n \right\}. \tag{10}$$

The definition of *PR*-sliding sector for linear deterministic systems is introduced in [26].

Definition 6. A simplified $P_i R_i$-sliding sector is a subset of $\mathbb{R}^n$ defined as

$$\mathcal{S}_i = \left\{ x \mid \left| s_i(x) \right| \le \delta_i(x),\ x \in \mathbb{R}^n \right\}, \tag{11}$$

where the linear function $s_i(x)$ and the square root $\delta_i(x)$ of the quadratic function $\delta_i^2(x)$ are determined by

$$\begin{aligned} s_i(x) &= S_i x, \qquad S_i \in \mathbb{R}^{1\times n}, \\ \delta_i(x) &= \sqrt{x^T \Omega_i x}, \quad \Omega_i \in \mathbb{R}^{n\times n},\ \Omega_i \ge 0\ \ (\Omega_i \ne 0). \end{aligned} \tag{12}$$

Remark 7. Suppose that the following inequalities are satisfied:

$$A_i^T P_i + P_i A_i + \sum_{j=1}^{\mathbb{N}} \lambda_{ij} P_j - P_i B_i B_i^T P_i + Q_i < 0, \quad i = 1, 2, \ldots, \mathbb{N}. \tag{13}$$

Then the parameters in the simplified $P_i R_i$-sliding sector P_i, R_i, S_i, and Ω_i can be selected as follows:

$$\Omega_i = r_i Q_i, \qquad R_i = \left(1 - r_i\right) Q_i, \qquad S_i = B_i^T P_i, \tag{14}$$

where $0 < r_i < 1$.

Obviously, while the state of the plant evolves in the simplified $P_i R_i$-sliding sector $\mathcal{S}_i$, the P_i-norm $|x|_{P_i}$ of the plant (7) decreases with zero control input since

$$\begin{aligned} \dot{L}_i &= x^T \left(A_i^T P_i + P_i A_i + \sum_{j=1}^{\mathbb{N}} \lambda_{ij} P_j \right) x \\ &= x^T \left(P_i B_i B_i^T P_i - Q_i \right) x \\ &= s_i^2(x) - \delta_i^2(x) - x^T R_i x \\ &\le -x^T R_i x, \quad \forall x \in \mathcal{S}_i,\ x \ne 0. \end{aligned} \tag{15}$$

In addition, in order to avoid the chattering phenomenon on the boundary of the $P_i R_i$-sliding sector, an inner sector $\mathcal{S}_i^{\text{in}}$ and an outer sector $\mathcal{S}_i^{\text{out}}$ are introduced as subsets of the $P_i R_i$-sliding sector (11):

$$\mathcal{S}_i^{\text{in}} = \left\{ x \mid \left| s_i(x) \right| \le \alpha_i \delta_i(x),\ x \in \mathbb{R}^n \right\}, \tag{16}$$

$$\mathcal{S}_i^{\text{out}} = \left\{ x \mid \alpha_i \delta_i(x) < \left| s_i(x) \right| \le \delta_i(x),\ x \in \mathbb{R}^n \right\}, \tag{17}$$

where the positive scalar α_i satisfies $0 < \alpha_i < 1$. It is not difficult to see that the sets $\mathcal{S}_i^{\text{in}}$ and $\mathcal{S}_i^{\text{out}}$ constitute a partition of the simplified *PR*-sliding sector $\mathcal{S}_i$. That is, $\mathcal{S}_i = \mathcal{S}_i^{\text{in}} \cup \mathcal{S}_i^{\text{out}}$ and $\mathcal{S}_i^{\text{in}} \cap \mathcal{S}_i^{\text{out}} = \emptyset$.

A hysteresis dead-zone function $\sigma_i(s_i(x), \delta_i(x))$ is further introduced for avoiding the chattering. It is defined as

$$\sigma_i\left(s_i(x), \delta_i(x)\right) = \begin{cases} 0, & x \in \mathcal{S}_i^{\text{in}} \\ \text{unchanged}, & x \in \mathcal{S}_i^{\text{out}} \\ 1, & x \overline{\in} \mathcal{S}_i. \end{cases} \tag{18}$$

Lemma 8 (see [20]). *For any given $\lambda_j \geq 0$ and matrices $P_j > 0$ ($P_j \in R^{n\times n}, 1 \leq j \leq \mathbb{N}$), if there exists $Z_i \geq P_j$, then the following inequality holds:*

$$\sum_{j=1}^{\mathbb{N}} \lambda_j P_j \leq \sum_{j=1}^{\mathbb{N}} \lambda_j Z_i. \tag{19}$$

Lemma 9 (see [27]). *Given a symmetric matrix Π and matrices M, N with appropriate dimensions, then $\Pi + MF(t)N + N^T F^T(t) M^T < 0$ for all $F(t)$ satisfying $F^T(t)F(t) \leq I$, if and only if there exists a scalar $\varepsilon > 0$ such that the following inequality holds:*

$$\Pi + \varepsilon M M^T + \varepsilon^{-1} N^T N < 0. \tag{20}$$

Lemma 10 (see [28]). *For symmetric and positive definite matrices X and Y, if $X \geq Y > 0$, then $Y^{-1} \geq X^{-1} > 0$.*

3. Main Results

First, we present the design of the simplified $P_i R_i$-sliding sector for the considered continuous-time Markov jump linear uncertain system (6). Second, the controller design for mean-square quadratic stability of the continuous-time Markov jump linear uncertain system is developed.

3.1. The Design of the Simplified $P_i R_i$-Sliding Sector

Theorem 11. *For continuous-time Markov jump linear uncertain system (6), there exist symmetric and positive definite matrices X_i, Z_i, and Y_i satisfying the following LMIs:*

$$i \in \mathcal{S}_k^i, \begin{cases} \begin{bmatrix} \Gamma_{11i} & \Gamma_{12i} & \Gamma_{13i} & X_i & X_i F_i \\ * & -\Gamma_{22i} & 0 & 0 & 0 \\ * & * & -Z_i & 0 & 0 \\ * & * & * & -Y_i & 0 \\ * & * & * & * & -\varepsilon_i I \end{bmatrix} < 0, \\ Z_i \leq X_j, \ j \in \mathcal{S}_{uk}^i, \ j \neq i \end{cases} \tag{21}$$

$$i \in \mathcal{S}_{uk}^i, \begin{cases} \begin{bmatrix} \Phi_{11i} & \Phi_{12i} & X_i & X_i F_i \\ * & -X_j & 0 & 0 \\ * & * & -Y_i & 0 \\ * & * & * & -\varepsilon_i I \end{bmatrix} < 0, \\ X_i \leq X_j, \ j \in \mathcal{S}_{uk}^i, \ j \neq i, \end{cases} \tag{22}$$

where

$$\begin{aligned} \Gamma_{11i} &= \mathrm{He}\,(A_i X_i) + \overline{\lambda}_{ii} X_i - B_i B_i^T + \varepsilon_i D_i D_i^T, \\ \Gamma_{12i} &= \left[\sqrt{\overline{\lambda}_{i\mathcal{K}_1^i}} X_i, \sqrt{\overline{\lambda}_{i\mathcal{K}_2^i}} X_i, \ldots, \sqrt{\overline{\lambda}_{i\mathcal{K}_{m_k^i}^i}} X_i \right], \\ \Gamma_{22i} &= \mathrm{diag}\left\{ -X_{\mathcal{K}_1^i}, -X_{\mathcal{K}_2^i}, \ldots, -X_{\mathcal{K}_{m_k^i}^i} \right\}, \\ \Gamma_{13i} &= \sqrt{-\left(\sum_{j\in\mathcal{S}_k^i, j\neq i} \underline{\lambda}_{ij} + \underline{\lambda}_{ii} \right)} X_i, \\ \Phi_{11i} &= \mathrm{He}\,(A_i X_i) - \sum_{j\in\mathcal{S}_k^i, j\neq i} \underline{\lambda}_{ij} X_i - B_i B_i^T + \varepsilon_i D_i D_i^T, \\ \Phi_{12i} &= \left[\sqrt{\overline{\lambda}_{i\mathcal{K}_1^i}} X_i, \sqrt{\overline{\lambda}_{i\mathcal{K}_2^i}} X_i, \ldots, \sqrt{\overline{\lambda}_{i\mathcal{K}_{m_k^i}^i}} X_i \right], \\ \Phi_{22i} &= \mathrm{diag}\left\{ -X_{\mathcal{K}_1^i}, -X_{\mathcal{K}_2^i}, \ldots, -X_{\mathcal{K}_{m_k^i}^i} \right\}; \end{aligned} \tag{23}$$

then the parameters of $P_i R_i$-sliding sector in (14) can be designed as $P_i = X_i^{-1}$, $Q_i = Y_i^{-1}$, $\Omega_i = r_i Y_i^{-1}$, $R_i = (1 - r_i) Y_i^{-1}$, and $S_i = B_i^T X_i^{-1}$.

Proof. For system (6), for all ΔA_i, $i = 1, 2, \ldots, \mathbb{N}$, the conditions in (13) are equal to

$$\begin{aligned} &(A_i + \Delta A_i)^T P_i + P_i (A_i + \Delta A_i) \\ &\quad + \sum_{j\in\mathcal{S}_k^i, j\neq i} \lambda_{ij} P_j + \sum_{j\in\mathcal{S}_{uk}^i, j\neq i} \lambda_{ij} P_j \\ &\quad + \lambda_{ii} P_i - P_i B_i B_i^T P_i + Q_i < 0. \end{aligned} \tag{24}$$

In the following, we consider two cases: $i \in \mathcal{S}_k^i$ and $i \in \mathcal{S}_{uk}^i$ in the proof.

Case I ($i \in \mathcal{S}_k^i$). In this case, the conditions in (24) can be guaranteed when for $i = 1, 2, \ldots, \mathbb{N}$, the following inequalities:

$$\begin{aligned} &\mathrm{He}\left((A_i + \Delta A_i)^T P_i \right) + \sum_{j\in\mathcal{S}_k^i, j\neq i} \lambda_{ij} P_j \\ &\quad + \sum_{j\in\mathcal{S}_{uk}^i, j\neq i} \lambda_{ij} W_i + \lambda_{ii} P_i \\ &\quad - P_i B_i B_i^T P_i + Q_i < 0, \\ &\quad P_j \leq W_i, \ j \in \mathcal{S}_{uk}^i, \end{aligned} \tag{25}$$

are satisfied. Substituting $\sum_{j\in\mathcal{S}_{uk}^i, j\neq i} \lambda_{ij} = -\sum_{j\in\mathcal{S}_k^i, j\neq i} \lambda_{ij} - \lambda_{ii}$ into the first inequality above and utilizing the boundary information of λ_{ij}, one can see that the above inequalities can be guaranteed by

$$\begin{aligned} &\mathrm{He}\left((A_i + \Delta A_i)^T P_i \right) \\ &\quad + \sum_{j\in\mathcal{S}_k^i, j\neq i} \overline{\lambda}_{ij} P_j - \left(\sum_{j\in\mathcal{S}_k^i, j\neq i} \underline{\lambda}_{ij} + \underline{\lambda}_{ii} \right) W_i \\ &\quad + \overline{\lambda}_{ii} P_i - P_i B_i B_i^T P_i + Q_i < 0, \\ &\quad P_j \leq W_i, \ j \in \mathcal{S}_{uk}^i. \end{aligned} \tag{26}$$

Pre- and postmultiplying P_i^{-1} on both sides of the first inequality in above inequalities and letting $X_i = P_i^{-1}$, one has

$$\begin{aligned} &\mathrm{He}\left((A_i + \Delta A_i) X_i \right) + \sum_{j\in\mathcal{S}_k^i, j\neq i} \overline{\lambda}_{ij} X_i X_j^{-1} X_i \\ &\quad - \left(\sum_{j\in\mathcal{S}_k^i, j\neq i} \underline{\lambda}_{ij} + \underline{\lambda}_{ii} \right) X_i W_i X_i + \overline{\lambda}_{ii} X_i \\ &\quad - B_i B_i^T + X_i Q_i X_i < 0. \end{aligned} \tag{27}$$

Let $Y_i = Q_i^{-1}$, $Z_i = W_i^{-1}$, and applying Schur-complement technique and Lemma 9, one can obtain the first LMI condition in (21).

In addition, by using Lemma 10, one can see that the second inequality in (26) can be converted into the second LMI condition in (21).

Case II ($i \in \mathcal{S}_{uk}^i$). In this case, substituting $\lambda_{ii} = -\sum_{j\in\mathcal{S}_k^i, j\neq i}\lambda_{ij} - \sum_{j\in\mathcal{S}_{uk}^i, j\neq i}\lambda_{ij}$ into (24), one has

$$\begin{aligned}&\mathrm{He}\left(\left(A_i+\Delta A_i\right)^T P_i\right) + \sum_{j\in\mathcal{S}_k^i, j\neq i}\lambda_{ij}P_j \\ &+ \sum_{j\in\mathcal{S}_{uk}^i, j\neq i}\lambda_{ij}P_j - \left(\sum_{j\in\mathcal{S}_k^i, j\neq i}\lambda_{ij} + \sum_{j\in\mathcal{S}_{uk}^i, j\neq i}\lambda_{ij}\right)P_i \\ &- P_iB_iB_i^TP_i + Q_i < 0, \\ &\quad i = 1,2,\ldots,\mathbb{N}.\end{aligned} \tag{28}$$

The conditions in (28) can be guaranteed provided that for $i = 1, 2, \ldots, \mathbb{N}$, one has

$$\begin{aligned}&\mathrm{He}\left(\left(A_i+\Delta A_i\right)^T P_i\right) + \sum_{j\in\mathcal{S}_k^i, j\neq i}\lambda_{ij}P_j \\ &- \sum_{j\in\mathcal{S}_k^i, j\neq i}\lambda_{ij}P_i - P_iB_iB_i^TP_i + Q_i < 0, \\ &\quad P_j \le P_i,\ \ j\in\mathcal{S}_{uk}^i,\ \ j\neq i.\end{aligned} \tag{29}$$

Taking use of the boundary information of λ_{ij}, one can see that the above inequalities can be guaranteed by

$$\begin{aligned}&\mathrm{He}\left(\left(A_i+\Delta A_i\right)^T P_i\right) + \sum_{j\in\mathcal{S}_k^i, j\neq i}\overline{\lambda}_{ij}P_j \\ &- \sum_{j\in\mathcal{S}_k^i, j\neq i}\underline{\lambda}_{ij}P_i - P_iB_iB_i^TP_i + Q_i < 0, \\ &\quad P_j \le P_i,\ \ j\in\mathcal{S}_{uk}^i,\ \ j\neq i.\end{aligned} \tag{30}$$

Pre- and postmultiplying P_i^{-1} on both sides of the first inequality in above inequalities and letting $X_i = P_i^{-1}$ and $Y_i = Q_i^{-1}$, one has

$$\begin{aligned}&\mathrm{He}\left(\left(A_i+\Delta A_i\right)X_i\right) + \sum_{j\in\mathcal{S}_k^i, j\neq i}\overline{\lambda}_{ij}X_iX_j^{-1}X_i \\ &- \sum_{j\in\mathcal{S}_k^i, j\neq i}\underline{\lambda}_{ij}X_i - B_iB_i^T + X_i\overline{Q}_i^{-1}X_i < 0.\end{aligned} \tag{31}$$

Applying Schur-complement technique and Lemma 9 again, the above inequality (31) can be converted into the first LMI condition in (22).

Applying Lemma 10, one can see that the second inequality in (30) can be converted into the second condition in (22). By the design of the parameters of PR-sliding sector in (14), the proof of Theorem 11 is completed. □

3.2. Variable Structure Control Design

Theorem 12. *Considering the simplified P_iR_i-sliding sector $\mathcal{S}_i$ (11) with the inner sector $\mathcal{S}_i^{in}$ (16) and the outer sector $\mathcal{S}_i^{out}$ (17), the following variable structure controller is designed to ensure that the state trajectories of the plant (6) enter into the inner sector from the outside of P_iR_i-sliding sector and obtain mean-square quadratic stability of the closed-loop system. Consider*

$$u = u_{i1} + u_{i2}, \tag{32}$$

where

$$u_{i1} = -\sigma_i\left(s_i(x), \delta_i(x)\right)\left(S_iB_i\right)^{-1}\left(S_iA_ix + K_is_i(x)\right), \tag{33}$$

$$\begin{aligned}u_{i2} = &-\frac{1}{1-\overline{d}_i}\sigma_i\left(s_i(x), \delta_i(x)\right) \\ &\times \left(S_iB_i\right)^{-1}\mathrm{sign}\left(s_i(x)\right)\rho_i,\end{aligned} \tag{34}$$

$\rho_i = |S_i||D_i||F_i||x| + \overline{d}_i|S_iA_i||x| + \overline{d}_iK_i|s_i(x)|$ *and the parameter* $K_i > \max\{S_iB_i/2, H_i\}$ *satisfies the following inequality:*

$$2H_i\alpha_i^2r_iQ_i + S_i^TS_iA_i + A_i^TS_i^TS_i > 0. \tag{35}$$

Proof. It is assumed that the initial state of the plant lies outside the P_iR_i-sliding sector. In this case, we have $\sigma_i(s_i(x), \delta_i(x)) = 1$ and $u_{i1} = -(S_iB_i)^{-1}(S_iA_ix + K_is_i(x))$. It can be easily checked that

$$\begin{aligned}s_i(x)\dot{s}_i(x) = &-K_is_i^2(x) + s_i(x)S_i\Delta A_ix \\ &+ s_i(x)S_iB_iu_{i2} + s_i(x)S_i\Delta B_iu.\end{aligned} \tag{36}$$

Noting that $\Delta B_i = B_i\Theta_i$ and $|\Theta| \le \overline{d}_i < 1$, we have

$$\begin{aligned}s_i(x)\dot{s}_i(x) \le &-K_is_i^2(x) + s_i(x)S_iB_iu_{i2} \\ &+ \left|s_i(x)\right|\left|S_i\right|\left|\Delta A_i\right|\left|x\right| + \overline{d}_i\left|s_i(x)\right|\left|S_iB_i\right|\left|u\right|.\end{aligned} \tag{37}$$

In view of $u = u_{i1} + u_{i2}$, it is easy to check that

$$\begin{aligned}s_i(x)\dot{s}_i(x) \le &-K_is_i^2(x) + s_i(x)S_iB_iu_{i2} \\ &+ \left|s_i(x)\right|\left|S_i\right|\left|\Delta A_i\right|\left|x\right| + \overline{d}_i\left|s_i(x)\right| \\ &\times \left|S_iB_i\right|\left|u_{i1}\right| + \overline{d}_i\left|s_i(x)\right|\left|S_iB_i\right|\left|u_{i2}\right|.\end{aligned} \tag{38}$$

Substituting $u_{i1} = -(S_iB_i)^{-1}(S_iA_ix + K_is_i(x))$ into the above inequality and noting that $S_iB_i = B_i^TP_iB_i > 0$, one can see that

$$\begin{aligned}&s_i(x)\dot{s}_i(x) \\ &\le -\left(1-\overline{d}_i\right)K_is_i^2(x) + \left(1-\overline{d}_i\right)s_i(x)S_iB_iu_{i2} \\ &\quad + \left|s_i(x)\right|\left|S_i\right|\left|\Delta A_i\right|\left|x\right| + \overline{d}_i\left|s_i(x)\right|\left|S_iA_i\right| \\ &\quad \times |x| + \overline{d}_is_i(x)S_iB_iu_{i2} + \overline{d}_i\left|s_i(x)\right|\left|S_iB_i\right|\left|u_{i2}\right|.\end{aligned} \tag{39}$$

Taking use of u_{i2} in (34) where $\rho_i = |S_i||D_i||F_i||x| + \overline{d}_i|S_iA_i||x| + \overline{d}_iK_i|s_i(x)| > \overline{d}_i|S_iA_i||x| + \overline{d}_iK_i|s_i(x)|$, one can see that

$$\begin{aligned} s_i(x)\,\dot{s}_i(x) \le -K_i s_i^2(x) + \overline{d}_i s_i(x)\,S_iB_iu_{i2} \\ + \overline{d}_i\left|s_i(x)\right|\left|S_iB_i\right|\left|u_{i2}\right|. \end{aligned} \tag{40}$$

According to the design of u_{i2} again, one can easily observe that

$$\begin{aligned} & s_i(x)\,S_iB_iu_{i2} + \left|s_i(x)\right|\left|S_iB_i\right|\left|u_{i2}\right| \\ & \le -\frac{1}{1-\overline{d}_i}\left|s_i(x)\right|\rho_i + \frac{1}{1-\overline{d}_i}\left|s_i(x)\right| \\ & \quad \times \left|S_iB_i\right|\left|\left(S_iB_i\right)^{-1}\right|\left|\operatorname{sign}\left(s_i(x)\right)\right|\rho_i = 0. \end{aligned} \tag{41}$$

It follows from (40) and (41) that

$$s_i(x)\,\dot{s}_i(x) \le -K_i s_i^2(x). \tag{42}$$

Thus the state trajectory of the closed-loop system will be driven into the inner sector of the P_iR_i-sliding sector.

In the following, we will prove that the P_i-norm keeps decreasing. Consider

$$\begin{aligned} \dot{L}_i(t) &= x^T\left\{\left(A_i+\Delta A_i\right)^TP + P\left(A_i+\Delta A_i\right) + \sum_{j=1}^{\mathbb{N}}\lambda_{ij}P_j\right\}x \\ &\quad + 2x^TP_i\left(B_i+\Delta B_i\right)u \\ &\le s_i^2(x) - \delta_i^2(x) - x^TR_ix + 2x^TP_i\left(B_i+\Delta B_i\right)u. \end{aligned} \tag{43}$$

Noting that $\Delta B_i = B_i\Theta_i$ and $S_i = B_i^TP_i$, one can see that

$$\begin{aligned} \dot{L}_i(t) \le s_i^2(x) - \delta_i^2(x) - x^TR_ix + 2s_i(x)\,u_{i1} \\ + 2s_i(x)\,u_{i2} + 2s_i(x)\,\Theta_i\left(u_{i1}+u_{i2}\right). \end{aligned} \tag{44}$$

In the following, we first prove that

$$s_i(x)\,u_{i2} + \overline{d}_i\left|s_i(x)\right|\left|u_{i1}+u_{i2}\right| \le 0. \tag{45}$$

Substituting (33) and (34) into the left side of above inequality, one has

$$\begin{aligned} & s_i(x)\,u_{i2} + \overline{d}_i\left|s_i(x)\right|\left|u_{i1}+u_{i2}\right| \\ & = -\frac{1}{1-\overline{d}_i}\left(S_iB_i\right)^{-1}\left|s_i(x)\right|\rho_i + \overline{d}_i\left|s_i(x)\right| \\ & \quad \times \left|\left(S_iB_i\right)^{-1}S_iA_ix + K_i\left(S_iB_i\right)^{-1}s_i(x)\right. \\ & \quad \left. + \frac{1}{1-\overline{d}_i}\left(S_iB_i\right)^{-1}\operatorname{sign}\left(s_i(x)\right)\rho_i\right|. \end{aligned} \tag{46}$$

Noting that $S_iB_i = B_i^TP_iB_i > 0$ and $\overline{d}_i < 1$, we have

$$\begin{aligned} & s_i(x)\,u_{i2} + \overline{d}_i\left|s_i(x)\right|\left|u_{i1}+u_{i2}\right| \\ & \le -\left(S_iB_i\right)^{-1}\left|s_i(x)\right|\rho_i + \overline{d}_i\left(S_iB_i\right)^{-1}\left|s_i(x)\right| \\ & \quad \times \left|S_iA_ix + K_is_i(x)\right|. \end{aligned} \tag{47}$$

Since $\rho_i = |S_i||D_i||F_i||x| + \overline{d}_i|S_iA_i||x| + \overline{d}_iK_i|s_i(x)|$, it is easy to check that

$$\rho_i \ge \overline{d}_i\left|S_iA_ix + K_is_i(x)\right|. \tag{48}$$

It follows from (47) and (48) that (45) is established. Thus we have

$$\dot{L}_i(t) \le s_i^2(x) - \delta_i^2(x) - x^TR_ix + 2s_i(x)\,u_{i1}. \tag{49}$$

Substituting (33) into the above inequality (49) and noting that $K_i > (S_iB_i/2)$, $2K_i\alpha_i^2r_iQ_i + S_i^TS_iA_i + A_i^TS_i^TS_i > 0$ and $s_i^2(x) \ge \alpha_i\delta_i^2(x)$, one can see that

$$\begin{aligned} \dot{L}_i(t) &\le s_i^2(x) - \delta_i^2(x) - x^TR_ix + 2s_i(x) \\ &\quad \times \left(-\left(S_iB_i\right)^{-1}S_iA_ix - K_i\left(S_iB_i\right)^{-1}s_i(x)\right) \\ &= -\left(S_iB_i\right)^{-1}x^T\left(2K_i\alpha_i^2r_iQ_i + S_i^TS_iA_i + A_i^TS_i^TS_i\right)x \\ &\quad - x^TR_ix \\ &< -x^TR_ix. \end{aligned} \tag{50}$$

After being forced into the inner sector of the P_iR_i-sliding sector and before moving out of the P_iR_i-sliding sector, the control input $u(t)$ is set equal to zero with $\sigma_i(s_i(x), \delta_i(x)) = 0$. In this case, $|s_i(x)| \le \delta_i(x)$ and

$$\begin{aligned} \dot{L}_i(t) &= x^T\left\{\left(A_i+\Delta A_i\right)^TP + P\left(A_i+\Delta A_i\right) + \sum_{j=1}^{\mathbb{N}}\lambda_{ij}P_j\right\}x \\ &\le s_i^2(x) - \delta_i^2(x) - x^TR_ix \le -x^TR_ix. \quad \forall x \in \mathcal{S}_i. \end{aligned} \tag{51}$$

Once the state trajectory of the plant runs out of the P_iR_i-sliding sector with zero control input, the control input (32)–(34) will make it move back to the inside of the inner sector again, while the P_i-norm $|x|_{P_i}$ keeps decreasing.

Thus, from the above proof, one can see that it guarantees that the state trajectory of the plant moves from the outside of the P_iR_i-sliding sector into the inside of the inner sector and the Lyapunov function $L_i(x) = x^TP_ix$ keeps decreasing in the whole state space; then mean-square quadratic stability of the closed-loop system is established. □

4. Illustrative Example

Consider the Markov jump linear system with four operation modes:

$$A_1 = \begin{bmatrix} 1 & 0 \\ 2 & 3 \end{bmatrix}, \quad A_2 = \begin{bmatrix} 0 & 1 \\ 1 & -2 \end{bmatrix},$$
$$A_3 = \begin{bmatrix} 2 & 0 \\ 0 & -1 \end{bmatrix}, \quad A_4 = \begin{bmatrix} 3 & 1 \\ -1 & 2 \end{bmatrix},$$
$$B_1 = \begin{bmatrix} 1 \\ 1 \end{bmatrix}, \quad B_2 = \begin{bmatrix} 1 \\ 1 \end{bmatrix},$$
$$B_3 = \begin{bmatrix} 2 \\ 1 \end{bmatrix}, \quad B_4 = \begin{bmatrix} 2 \\ 3 \end{bmatrix}, \tag{52}$$
$$D_1 = \begin{bmatrix} 0.1 \\ 0 \end{bmatrix}, \quad D_2 = \begin{bmatrix} 0.2 \\ 0.5 \end{bmatrix}$$
$$D_3 = \begin{bmatrix} 0.2 \\ 0.6 \end{bmatrix}, \quad D_4 = \begin{bmatrix} 0.1 \\ 0.5 \end{bmatrix},$$
$$F_1 = \begin{bmatrix} 0 & -0.1 \end{bmatrix}, \quad F_2 = \begin{bmatrix} 1 & 0.3 \end{bmatrix},$$
$$F_3 = \begin{bmatrix} 0.2 & 0.5 \end{bmatrix}, \quad F_4 = \begin{bmatrix} 0.1 & 0.1 \end{bmatrix}.$$

For simulation, we take $E_1(t,x) = 0.1\sin(t)$, $E_2(t,x) = 0.1\sin(2t)$, $E_3(t,x) = 0.5\sin(t)$, $E_4(t,x) = 0.4\sin(2t)$, $\Theta_1 = 0.2\sin(2)$, $\Theta_2 = 0.3\cos(2t)$, $\Theta_3 = 0.2\cos(t)$, and $\Theta_4 = 0.2\sin(2t)$.

The transition rates matrix is

$$\Lambda = \begin{bmatrix} -1.5 & 0.2 & ? & ? \\ ? & ? & 0.5 & 0.9 \\ 1 & ? & -2 & ? \\ 0.1 & \alpha & ? & \beta \end{bmatrix}, \tag{53}$$

where $0.5 \le \alpha \le 2$ and $-0.8 \le \beta \le -0.1$. Since there exist the completely unknown transition rates "?" and boundary known transition rates α and β, the reported methods in [21, 22] cannot work. Solving the LMIs conditions (21)-(22) in Theorem 11, one can obtain that positive definite matrices are as follows:

$$P_1 = \begin{bmatrix} 6.2534 & -6.4840 \\ -6.4840 & 18.4380 \end{bmatrix}, \quad P_2 = \begin{bmatrix} 6.8785 & -7.1343 \\ -7.1343 & 20.0458 \end{bmatrix},$$
$$P_3 = \begin{bmatrix} 8.5811 & -9.6120 \\ -9.6120 & 15.6407 \end{bmatrix}, \quad P_4 = \begin{bmatrix} 6.1859 & -1.5374 \\ -1.5374 & 1.1026 \end{bmatrix},$$
$$Q_1 = \begin{bmatrix} 6.9519 & -7.5088 \\ -7.5088 & 22.4304 \end{bmatrix},$$
$$Q_2 = \begin{bmatrix} 13.4209 & -14.1627 \\ -14.1627 & 40.0263 \end{bmatrix}$$
$$Q_3 = \begin{bmatrix} 11.4377 & -11.6823 \\ -11.6823 & 18.2712 \end{bmatrix},$$
$$Q_4 = \begin{bmatrix} 10.3808 & -2.6205 \\ -2.6205 & 2.0926 \end{bmatrix}. \tag{54}$$

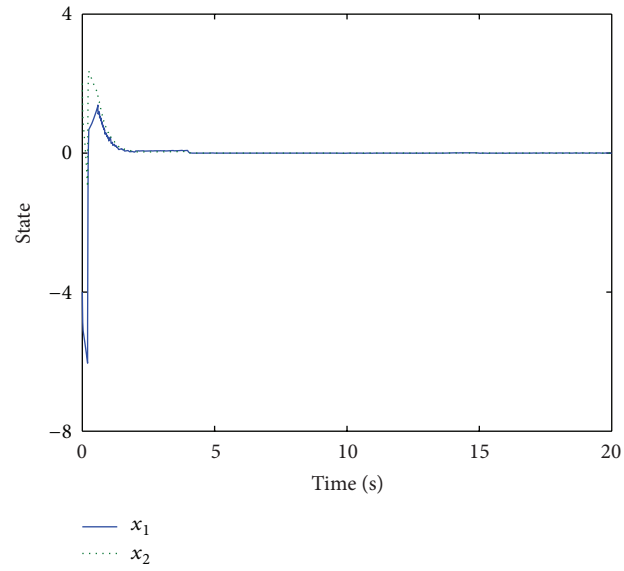

Figure 1: The response curves of the system states.

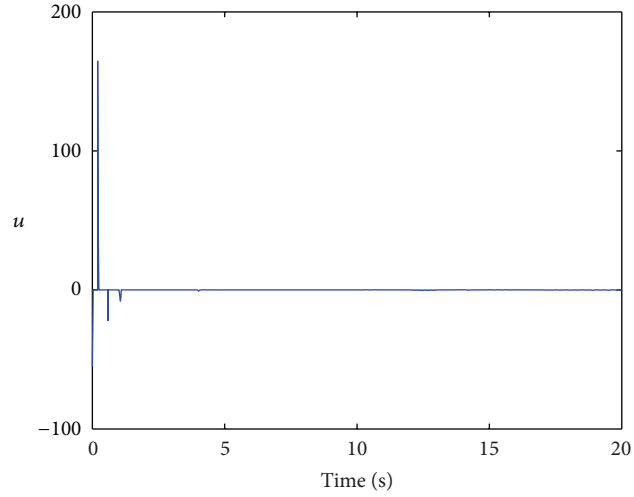

Figure 2: The response curve of the control input.

Selecting $\alpha_1 = 0.8$, $\alpha_2 = 0.9$, $\alpha_3 = 0.6$, $\alpha_4 = 0.6$, $r_1 = 0.8$, $r_2 = 0.9$, $r_3 = 0.8$, $r_4 = 0.8$, $K_1 = 20$, $K_2 = 120$, $K_3 = 40$, $K_4 = 50$, then the condition in Theorem 12 is satisfied. For the purpose of simulation, let $\overline{d}_1 = 0.2$, $\overline{d}_2 = 0.3$, $\overline{d}_3 = 0.2$, and $\overline{d}_4 = 0.2$. Using these data, a simulation program has been done in Matlab. The simulation results are presented in Figures 1–3. It can be seen from Figure 1 that the system state can converge to the equilibrium point in less than 5 seconds. Figure 2 shows the response curve of the control input. One can easily see that no chattering phenomenon happens in the whole control process. The transition modes of system are given in Figure 3. It can be seen that the considered continuous-time Markov jump linear uncertain system is stochastic quadratic stable in spite of mismatched uncertainty and the transition rate matrix which covers completely known, boundary unknown, and completely unknown elements.

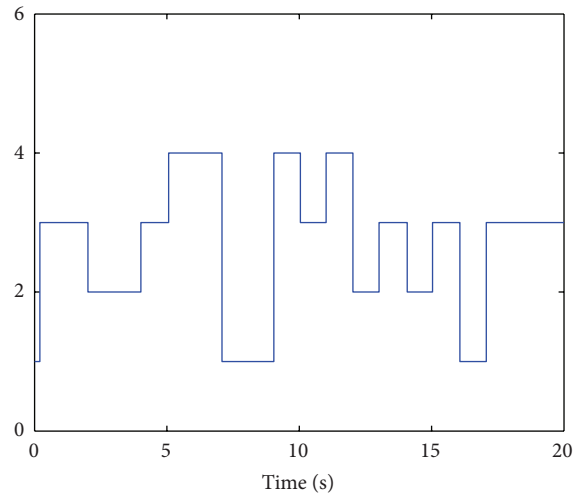

Figure 3: The response curve of the transition modes.

5. Conclusions

In this paper, the problem of designing sliding sector-based variable structure controllers is considered for Markov jump linear uncertain continuous-time time-invariant systems with unknown transition rates. First, the related notions about sliding sector for continuous-time MJLSs are presented and sufficient conditions for the design of the sliding sector are given by LMIs. Second, the variable structure control law is presented to ensure the mean-square quadratic stability of the closed-loop system, and simulation results finally have verified the effectiveness of the proposed method. In our future research, how to design dynamic output feedback variable structure controller based on sliding sector technique and considering the applying of the sliding sector technique in industrial robotic systems are interesting work. Finally, the authors would like to thank the associate editor and all the reviewers for their constructive comments and suggestions for improving this paper.

Acknowledgments

This work was supported in part by the Funds of National Science of China (nos. 11301276, 61104123), the Natural Science Funds of Jiangsu Province (BK20130984, BK20131000), the Scientific Research Foundation of Nanjing University of Information Science & Technology (S8112075001, S8112081001), and Laboratory Open Fund of Nanjing University of Information Science & Technology (N1081005112).

References

[1] L. Dai, D. Huang, and Z. Li, "Sliding mode control of hybrid joints for wheeled mobile manipulators with Markovian switching and bounded torques," *Intelligent Robotics and Applications*, vol. 6424, no. 1, pp. 171–182, 2010.

[2] L. Ding, H. Gao, K. Xia, Z. Liu, J. Tao, and Y. Liu, "Adaptive sliding mode control of mobile manipulators with markovian switching joints," *Journal of Applied Mathematics*, vol. 2012, Article ID 414315, 24 pages, 2012.

[3] E. K. Boukas, *Stochastic Switching Systems: Analysis and Design*, Birkhauser, Berlin, Germany, 2005.

[4] E. K. Boukas and H. Yang, "Stability of discrete-time linear systems with Markovian jumping parameters," *Mathematics of Control, Signals, and Systems*, vol. 8, no. 4, pp. 390–402, 1995.

[5] J. X. Dong and G.-H. Yang, "Robust H_2 control of continuous-time Markov jump linear systems," *Automatica*, vol. 44, no. 5, pp. 1431–1436, 2008.

[6] M. G. Todorov and M. D. Fragoso, "On the stability radii of continuous-time infinite Markov jump linear systems," *Mathematics of Control, Signals, and Systems*, vol. 22, no. 1, pp. 23–38, 2010.

[7] O. L. V. Costa and E. K. Boukas, "Necessary and sufficient condition for robust stability and stabilizability of continuous-time linear systems with Markovian jumps," *Journal of Optimization Theory and Applications*, vol. 99, no. 2, pp. 359–379, 1998.

[8] Z. Wang, J. Lam, and X. Liu, "Exponential filtering for uncertain Markovian jump time-delay systems with nonlinear disturbances," *IEEE Transactions on Circuits and Systems II*, vol. 51, no. 5, pp. 262–268, 2004.

[9] S. Xu, T. Chen, and J. Lam, "Robust H_∞ filtering for uncertain Markovian jump systems with mode-dependent time delays," *IEEE Transactions on Automatic Control*, vol. 48, no. 5, pp. 900–907, 2003.

[10] M. Karan, P. Shi, and C. Y. Kaya, "Transition probability bounds for the stochastic stability robustness of continuous- and discrete-time Markovian jump linear systems," *Automatica*, vol. 42, no. 12, pp. 2159–2168, 2006.

[11] J. L. Xiong, J. Lam, H. J. Gao, and W. C. Daniel, "On robust stabilization of Markovian jump systems with uncertain switching probabilities," *Automatica*, vol. 41, no. 5, pp. 897–903, 2005.

[12] L. Zhang, E.-K. Boukas, and J. Lam, "Analysis and synthesis of Markov jump linear systems with time-varying delays and partially known transition probabilities," *IEEE Transactions on Automatic Control*, vol. 53, no. 10, pp. 2458–2464, 2008.

[13] L. Zhang and E.-K. Boukas, "Stability and stabilization of Markovian jump linear systems with partly unknown transition probabilities," *Automatica*, vol. 45, no. 2, pp. 463–468, 2009.

[14] L. Zhang and J. Lam, "Necessary and sufficient conditions for analysis and synthesis of markov jump linear systems with incomplete transition descriptions," *IEEE Transactions on Automatic Control*, vol. 55, no. 7, pp. 1695–1701, 2010.

[15] P. Y. Richard, H. Cormerais, and J. Buisson, "A generic design methodology for sliding mode control of switched systems," *Nonlinear Analysis: Theory, Methods and Applications*, vol. 65, no. 9, pp. 1751–1772, 2006.

[16] G. S. Tombul, S. P. Banks, and N. Akturk, "Sliding mode control for a class of non-affine nonlinear systems," *Nonlinear Analysis: Theory, Methods and Applications*, vol. 71, pp. 1589–1597, 2009.

[17] M. Roopaei and M. Z. Jahromi, "Chattering-free fuzzy sliding mode control in MIMO uncertain systems," *Nonlinear Analysis: Theory, Methods and Applications*, vol. 71, no. 10, pp. 4430–4437, 2009.

[18] Y. Niu, D. W. C. Ho, and J. Lam, "Robust integral sliding mode control for uncertain stochastic systems with time-varying delay," *Automatica*, vol. 41, no. 5, pp. 873–880, 2005.

[19] Y. Niu, D. W. C. Ho, and X. Wang, "Sliding mode control for Itô stochastic systems with Markovian switching," *Automatica*, vol. 43, no. 10, pp. 1784–1790, 2007.

[20] B. C. Zheng and G. H. Yang, "Sliding mode control for Markov jump linear uncertain systems with partly unknown transition rates," *International Journal of Systems Science*, 2013.

[21] P. Shi, Y. Xia, G. P. Liu, and D. Rees, "On designing of sliding-mode control for stochastic jump systems," *IEEE Transactions on Automatic Control*, vol. 51, no. 1, pp. 97–103, 2006.

[22] S. Ma and E.-K. Boukas, "A singular system approach to robust sliding mode control for uncertain Markov jump systems," *Automatica*, vol. 45, no. 11, pp. 2707–2713, 2009.

[23] C. Edwards and S. K. Spurgeon, *Sliding Mode Control: Theory and Applications*, Taylor and Francis, London, UK, 1998.

[24] J. Y. Hung, W. B. Gao, and J. C. Hung, "Variable structure control: a survey," *IEEE Transactions on Industrial Electronics*, vol. 40, no. 1, pp. 2–22, 1993.

[25] V. I. Utkin, *Sliding Modes in Control and Optimization*, Springer, Berlin, Germany, 1992.

[26] K. Furuta and Y. Pan, "Variable structure control with sliding sector," *Automatica*, vol. 36, no. 2, pp. 211–228, 2000.

[27] I. R. Petersen, "A stabilization algorithm for a class of uncertain linear systems," *Systems and Control Letters*, vol. 8, no. 4, pp. 351–357, 1987.

[28] R. A. Horn and C. R. Johnson, *Matrix Analysis*, Cambridge University Press, 1985.

Hindawi Publishing Corporation
Mathematical Problems in Engineering
Volume 2013, Article ID 157063, 8 pages
http://dx.doi.org/10.1155/2013/157063

Research Article

Fault Detection for Quantized Networked Control Systems

Wei-Wei Che,[1] Zhi-Yong Mei,[2] and Yu-Long Wang[3]

[1] *Key Laboratory of Manufacturing Industrial Integrated Automation, Shenyang University, Shenyang 110044, China*
[2] *Institute of Information, Shenyang University, Shenyang 110044, China*
[3] *School of Electronics and Information, University of Science and Technology, Zhenjiang 212003, China*

Correspondence should be addressed to Wei-Wei Che; cwwemail1980@126.com

Received 21 August 2013; Accepted 5 October 2013

Academic Editor: Tao Li

The fault detection problem in the finite frequency domain for networked control systems with signal quantization is considered. With the logarithmic quantizer consideration, a quantized fault detection observer is designed by employing a performance index which is used to increase the fault sensitivity in finite frequency domain. The quantized measurement signals are dealt with by utilizing the sector bound method, in which the quantization error is treated as sector-bounded uncertainty. By using the Kalman-Yakubovich-Popov (GKYP) Lemma, an iterative LMI-based optimization algorithm is developed for designing the quantized fault detection observer. And a numerical example is given to illustrate the effectiveness of the proposed method.

1. Introduction

Recently, due to many advantages of networked control systems, such as lower cost, easier installation and maintenance, and higher reliability, NCSs have been found successfully industrial applications in automobiles, manufacturing plants, aircraft, HVAC, systems and unmanned vehicles. However, the insertion of the communication channels results in discrepancies between the data information to be transmitted and their associated remotely transmitted images, hence raising new interesting and challenging problems such as quantization, packet losses, and time delays. As is well known to all, quantization always exists in bandwidth limited networked systems and the performance of NCSs will be inevitably subject to the effect of quantization error. Hence, the quantization problem of NCSs has long been studied and many important results have been reported in [1–10] and the references therein. Two most pertinent references to this paper are the work [2] and the following work [3]. In [2], the problem of quadratic stabilization of discrete-time single-input single-output (SISO) linear time-invariant systems using quantized feedback is studied. In [3], the work of [2] is generalized to general multi-input multi-output (MIMO) systems and to control problems requiring performances. This is done using the so-called sector bound method, which is based on using a simple sector bound to model the quantization error. This method has been employed by quite a few researchers and many results have been given correspondingly [4–7] and so on.

On the other hand, fault detection (FD) is a very significant problem and has attracted a lot of attention in the past two decades. A fault is defined as an unpermitted deviation of at least one characteristic property of a variable from an acceptable behaviour. Such a fault disturbs the normal operation of an automatic system, thus causing an unacceptable deterioration of the performance of the system [11, 12]. To detect the fault, an observer is usually designed which generates the residual signal, and, by satisfying certain performances, the observer parameters are then determined. Up to now, the studies on the FD are mainly categorized into two classes depending on the fault frequency domain. There are many results that study the FD problem in the full frequency domain, such as [13, 14]. Recently, there are many studies considering the fault in finite frequency domain which much more accords with practice. Because in practice, faults are usually in the finite frequency domain; for example, for an incipient fault signal, the fault information is contained within a low frequency band as the fault development is slow as stated in [15]. Another important finite frequency fault is the actuator stuck fault whose frequency is zero. The stuck

fault occurs when an aircraft control surface (such as the rudder or an aileron) is stuck at some fixed value as stated in [16]. And the stuck fault is also considered for the F-16 aircraft in [17]. So, the finite frequency domain method to FD has been paid more attention to many new results occur successively [18–20]. In networked control systems, FD problem also exists and is unavoidably. So far, there have been some studies on the FD problem of the networked control systems [21, 22]. But to the best of the authors' knowledge, there has been no work considering the quantized FD problem in finite frequency domain for networked control systems.

Motivated by the above-mentioned reason, in this paper, the quantized FD observer design problem for networked control systems with logarithmic quantizers is studied. The quantization errors are modeled as sector-bounded uncertainties. By employing the GKYP method, a quantized FD observer design method is proposed with an iterative LMI-based optimization algorithm. Finally, a numerical example is given to show the effectiveness of the proposed method.

The organization of this paper is as follows. Section 2 presents the problem under consideration and some preliminaries. Section 3 gives design methods of quantized FD observer design strategies. In Section 4, an example is presented to illustrate the effectiveness of the proposed methods. Finally, Section 5 gives some concluding remarks.

Notation. For a matrix E, E^T, $E^\perp$, and E^* denote its transpose, orthogonal complement, and complex conjugate transpose, respectively. And $A^\dagger = A^T(AA^T)^{-1}$ denotes its Moore-Penrose inverse. I denotes the identity matrix with an appropriate dimension. For a symmetric matrix, $A > (\geq)\ 0$ and $A < (\leq)\ 0$ denote positive (semi-) definiteness and negative (semi-) definiteness. The Hermitian part of a square matrix M is denoted by $He(M) := M + M^*$. The symbol H_n stands for the set of $n \times n$ Hermitian matrices. The symbol "$*$" within a matrix represents the symmetric entries. $\sigma_{\max}(G)$ and $\sigma_{\min}(G)$ denote maximum and minimum singular value of the transfer matrix G, respectively.

2. Problem Statement and Preliminaries

2.1. Problem Statement. Consider an LTI discrete-time system as

$$\begin{aligned} x(k+1) &= Ax(k) + B_1 f(k) + B_2 u_c(k), \\ y(k) &= Cx(k) + D_1 f(k), \end{aligned} \tag{1}$$

where $x(k) \in R^n$ is the state, $u_c(k) \in R^u$ is the control input, and $f(k) \in R^f$ is the fault input vector, respectively. A, B_1, B_2, C, and D_1 are known constant matrices of appropriate dimensions. Without loss of generality, assume that (A, C) is observable and B_1 is of full column rank.

To formulate the quantized FD problem, consider the quantized FD observer with the following form.

Consider a dynamic observer-based control strategy for (1) with observer given by

$$\begin{aligned} \widehat{x}(k+1) &= A\widehat{x}(k) + B_2 u_c(k) + L\left(y_c(k) - \overline{y}_c(k)\right) \\ \overline{y}_c(k) &= C\widehat{x}(k), \\ u_c(k) &= K\widehat{x}(k), \\ r(k) &= y_c(k) - \overline{y}_c(k), \end{aligned} \tag{2}$$

where $\overline{y}_c(k) \in R^y$ is the observer output, $\widehat{x}(k) \in R^n$ is the state estimation of system (1), and $r(k) \in R^r$ is the residual signal. L is the observer gain to be designed. Due to the insertion of the communication channel, the measurement signals will be quantized before they are transmitted to the filter through the network. The quantizer is denoted as $q[\cdot] = [q_1[\cdot], q_2[\cdot], \ldots, q_y[\cdot]]^T$, which is assumed to be symmetric; that is, $q_j[-\varepsilon] = -q_j[\varepsilon]$, $j = 1, 2, \ldots, y$. In this paper, the quantizer is selected as a logarithmic one, and, for each $q_j[\cdot]$, the quantization levels are given by

$$\begin{aligned} V_j = \left\{\pm\nu_i^{(j)} : \nu_i^{(j)} = \rho_j^i \nu_0^{(j)},\ i = 0, \pm1, \pm2, \ldots\right\} \cup \{0\}, \\ \nu_0^{(j)} > 0,\ 0 < \rho_j < 1. \end{aligned} \tag{3}$$

As in [3, 4], the associated quantizer is defined as follows:

$$q_j[\varepsilon] = \begin{cases} \rho_j^i \nu_0^j, & \text{if } \dfrac{1}{1+\delta_j}\rho_j^i\nu_0^j < \varepsilon < \dfrac{1}{1-\delta_j}\rho_j^i\nu_0^j, \varepsilon > 0 \\ 0, & \text{if } \varepsilon = 0, \\ -q_j[-\varepsilon], & \text{if } \varepsilon < 0, \end{cases} \tag{4}$$

$$\delta_j = \frac{1-\rho_j}{1+\rho_j}. \tag{5}$$

Then, based on the quantizer (4), the measurement signal at the filter end is with the form as

$$y_c(k) = q\left(y(k)\right) = \begin{bmatrix} q_1\left(y_1(k)\right) \\ \vdots \\ q_y\left(y_y(k)\right) \end{bmatrix} = \left(I + \Delta(k)\right) y(k), \tag{6}$$

where

$$\begin{aligned} \Delta(k) = \operatorname{diag}\left\{\Delta_1(k), \Delta_2(k), \ldots, \Delta_y(k)\right\}, \\ \Delta_i(k) \in \left[-\delta_i, \delta_i\right]. \end{aligned} \tag{7}$$

Combining FD observer (2) with system (1) and the quantized measurement (6), the following quantized error dynamic system is obtained:

$$\begin{aligned} x(k+1) &= \left(A + B_2K\right)x(k) + B_1 f(k) - B_2 K e(k), \\ e(k+1) &= (A - LC)\,e(k) - L\Delta(k)Cx(k) \\ &\quad + \left(B_1 - L\Delta(k)D_1\right)f(k), \\ r(k) &= Ce(k) + \Delta(k)Cx(k) + \left(I + \Delta(k)\right)D_1 f(k), \end{aligned} \tag{8}$$

where $e(k) = x(k) - \widehat{x}(k)$.

Facilitating the presentation, (8) can be rewritten as

$$\begin{aligned} x_e(k+1) &= \overline{A}x_e(k) + \overline{B}_1 f(k) \\ r(k) &= \overline{C}x_e(k) + \overline{D}_1 f(k), \end{aligned} \tag{9}$$

where $x_e(k) = \left[\begin{smallmatrix} e(k) \\ x(k) \end{smallmatrix}\right]$ and

$$\begin{aligned} \overline{A} &= \begin{bmatrix} A - LC & -L\Delta(k)C \\ -B_2K & A + B_2K \end{bmatrix}, \\ \overline{B}_1 &= \begin{bmatrix} B_1 - L(I + \Delta(k))D_1 \\ B_1 \end{bmatrix}, \\ \overline{C} &= \begin{bmatrix} C & \Delta(k)C \end{bmatrix}, \qquad \overline{D}_1 = (I + \Delta(k))D_1. \end{aligned} \tag{10}$$

Note that the dynamics of the residual signal depends on the fault $f(k)$, to detect the fault effects; quantized observer (2) is designed in this work such that the following conditions are satisfied:

$$\begin{aligned} &\text{(i)}: \overline{A} = \begin{bmatrix} A - LC & -L\Delta(k)C \\ -B_2K & A + B_2K \end{bmatrix} \text{ is stable,} \\ &\text{(ii)}: \inf \sigma_{\min}\left(G_{rf}\left(e^{j\theta}\right)\right) > \gamma, \quad \forall\theta \in [\upsilon_1, \upsilon_2], \end{aligned} \tag{11}$$

where

$$G_{rf}\left(e^{j\theta}\right) := \overline{C}\left(e^{j\theta}I - \overline{A}\right)^{-1}\left(\overline{B}_1 - L\overline{D}_1\right) + \overline{D}_1. \tag{12}$$

Remark 1. Condition (ii) is a finite frequency performance index used to increase the fault sensitivity. Note that υ_1, υ_2 are given scalars which reflects the frequency range of faults.

The problem addressed in this paper is as follows.

Quantized FD Control Problem. Considering the effects of the quantization, design a quantized FD observer such that the error system (8) is with high fault sensitivity in finite frequency domain.

2.2. Preliminaries. The following lemma presented will be used in this paper.

Lemma 2 (see [23]). *Consider a transfer function matrix $G(e^{j\theta}) := C(e^{j\theta}I - A)^{-1}B + D$; let a symmetric matrix Π and scalars ν_1, ν_2 be given; the following statements are equivalent.*

(i) The finite frequency inequality

$$\begin{bmatrix} G\left(e^{j\theta}\right) \\ I \end{bmatrix}^* \Pi \begin{bmatrix} G\left(e^{j\theta}\right) \\ I \end{bmatrix} < 0, \quad \forall\theta \in [\nu_1, \nu_2]. \tag{13}$$

(ii) There exist matrices $P, Q \in \mathbf{H}_n$ of appropriate dimensions, satisfying $Q > 0$, and

$$\begin{bmatrix} A & B \\ I & 0 \end{bmatrix}^* \Xi \begin{bmatrix} A & B \\ I & 0 \end{bmatrix} + \begin{bmatrix} C & D \\ 0 & I \end{bmatrix}^* \Pi \begin{bmatrix} C & D \\ 0 & I \end{bmatrix} < 0, \tag{14}$$

where

$$\Xi = \begin{bmatrix} -P & e^{j(\nu_1+\nu_2)/2}Q \\ e^{-j(\nu_1+\nu_2)/2}Q & P - \left(2\cos\left(\left(\nu_2 - \nu_1\right)/2\right)\right)Q \end{bmatrix}. \tag{15}$$

Lemma 3 (Finsler's Lemma). *Let $x \in R^n$, $Q \in R^{n\times n}$, and $U \in R^{n\times m}$. Let $U^\perp$ be any matrix such that $U^\perp U = 0$. The following statements are equivalent:*

(i) $x^*Qx < 0$, *for all* $U^*x = 0, x \neq 0$,

(ii) $U^\perp Q U^{\perp^*} = 0$,

(iii) $\exists\mu \in R : Q - \mu UU^* < 0$,

(iv) $\exists y \in R^{m\times n} : Q + UY + Y^*U^* < 0$.

Lemma 4 (Projection Lemma). *Let Γ, Λ, Θ and be given. There exists a matrix F satisfying $\Gamma F\Lambda + (\Gamma F\Lambda)^T + \Theta < 0$ if and only if the following two conditions hold:*

$$\Gamma^\perp\Theta < 0, \quad \Lambda^{T^\perp}\Theta\Lambda^{T^{\perp^T}} < 0. \tag{16}$$

Lemma 5 (see [24]). *For any real matrices Y, M, F, and E with compatible dimensions and $F^TF \leq \delta^2 I$, where $\delta > 0$ is a scalar, then*

$$Y + MFE + (MFE)^T < 0 \tag{17}$$

holds if and only if there exists a scalar $\varepsilon > 0$, such that

$$Y + \frac{1}{\varepsilon}MM^T + \varepsilon\delta^2 E^TE < 0. \tag{18}$$

3. Quantized FD Observer Design

In this section, an inequality for the stability condition (i) is given first. Then, considering the fault sensitivity problem, an inequality is given for the fault sensitivity condition (ii).

Firstly, considering the stability condition (i), we have the following lemma.

Lemma 6. *Consider system* (9) *if there exists a matrix $\overline{X} = \left[\begin{smallmatrix} X & 0 \\ 0 & X \end{smallmatrix}\right] > 0$ such that the following inequality holds:*

$$\begin{bmatrix} -X & * & * & * & * & * \\ 0 & -X & * & * & * & * \\ XA - \Gamma^TC & 0 & -X & * & * & * \\ -XB_2K & XA + XB_2K & 0 & -X & * & * \\ 0 & 0 & -\Gamma & 0 & -\varepsilon I & * \\ 0 & \delta_a\varepsilon C & 0 & 0 & 0 & -\varepsilon I \end{bmatrix} < 0, \tag{19}$$

where $\Gamma = L^TX$.

Proof. It is easy to know that (i) holds if there exists $\overline{X} > 0$, such that

$$\overline{A}^T\overline{X}\,\overline{A} - \overline{X} < 0. \tag{20}$$

By using the Schur complement lemma, we have that

$$\begin{bmatrix} -\overline{X} & \overline{A}^T\overline{X} \\ \overline{X}\,\overline{A} & -\overline{X} \end{bmatrix} < 0. \tag{21}$$

Equation (21) can be converted into

$$\begin{bmatrix} -X & * & * & * & * & * \\ 0 & -X & * & * & * & * \\ XA-\Gamma^T C & -XL\Delta(k)C & -X & * & * & * \\ -XB_2K & XA+XB_2K & 0 & -X & * & * \\ 0 & 0 & -\Gamma & 0 & -\varepsilon I & * \\ 0 & \delta_a \varepsilon C & 0 & 0 & 0 & -\varepsilon I \end{bmatrix} < 0. \tag{22}$$

Obviously, (22) can be rewritten as

$$\begin{aligned} &\begin{bmatrix} -X & * & * & * & * & * \\ 0 & -X & * & * & * & * \\ XA-\Gamma^T C & 0 & -X & * & * & * \\ -XB_2K & XA+XB_2K & 0 & -X & * & * \\ 0 & 0 & -\Gamma & 0 & -\varepsilon I & * \\ 0 & \delta_a \varepsilon C & 0 & 0 & 0 & -\varepsilon I \end{bmatrix} \\ &+ \begin{bmatrix} 0 \\ 0 \\ -\Gamma \\ 0 \end{bmatrix} \Delta(k) \begin{bmatrix} 0 & C & 0 & 0 \end{bmatrix} \\ &+ \left(\begin{bmatrix} 0 \\ 0 \\ -\Gamma \\ 0 \end{bmatrix} \Delta(k) \begin{bmatrix} 0 & C & 0 & 0 \end{bmatrix} \right)^T < 0. \end{aligned} \tag{23}$$

By using Lemma 5, (19) holds, which shows that condition (i) holds if (19) holds. This completes the proof □

In the following, the fault sensitivity problem is studied. Considering system (9), the following lemma is presented to give the fault sensitivity condition.

Lemma 7. *Let real matrix $\overline{A}$, $\overline{B}_1$, $\overline{C}$, $\overline{D}_1$, a symmetric matrix $\Pi = \begin{bmatrix} -I & 0 \\ 0 & \gamma^2 I \end{bmatrix}$, and scalars ϑ_1, ϑ_2 be given; consider system* (9)*, then the following conditions are equivalent.*

(i) The following finite frequency inequality

$$\sigma_{\min}\left(G_{rf}\left(e^{j\theta}\right)\right) > \gamma, \quad \forall \theta \in [\vartheta_1, \vartheta_2] \tag{24}$$

holds, where $G_{rf}(e^{j\theta}) = \overline{C}(e^{j\theta} I - \overline{A})^{-1}\overline{B}_1 + \overline{D}_1$ is the transfer function matrix from $f(k)$ to $r(k)$.

(ii) There exist $2n \times 2n$ Hermitian matrices P and Q satisfying $Q > 0$, and

$$\begin{bmatrix} \overline{A} & \overline{B} \\ I & 0 \end{bmatrix}^* \Xi \begin{bmatrix} \overline{A} & \overline{B}_1 \\ I & 0 \end{bmatrix} + \begin{bmatrix} \overline{C} & \overline{D}_1 \\ 0 & I \end{bmatrix}^* \Pi \begin{bmatrix} \overline{C} & \overline{D}_1 \\ 0 & I \end{bmatrix} < 0, \tag{25}$$

where

$$\Xi = \begin{bmatrix} -P & e^{j(\nu_1+\nu_1)/2} Q \\ e^{-j(\nu_1+\nu_1)/2} Q & P - \left(2\cos\dfrac{\nu_1 - \nu_1}{2}\right) Q \end{bmatrix}. \tag{26}$$

Note that condition (25) in Lemma 7 can be rewritten as

$$\begin{bmatrix} \Upsilon & I \end{bmatrix} T \begin{bmatrix} \Xi & 0 \\ 0 & \Pi \end{bmatrix} T^* \begin{bmatrix} \Upsilon & I \end{bmatrix}^* < 0, \tag{27}$$

where

$$\Upsilon = \begin{bmatrix} A^T - C^T L^T & -K^T B_2^T & C^T \\ -C^T \Delta(k) L^T & A^T + K^T B_2^T & \Delta(k) C^T \\ B_1^T - D_1^T (I + \Delta(k))^T L^T & B_1^T & D_1^T (I + \Delta(k))^T \end{bmatrix}, \tag{28}$$

and T is the permutation matrix defined as

$$\begin{bmatrix} N_1 & N_2 & N_3 & N_4 & N_5 & N_6 \end{bmatrix} T = \begin{bmatrix} N_1 & N_2 & N_5 & N_3 & N_4 & N_6 \end{bmatrix}. \tag{29}$$

By using Lemma 3, we have that (27) is equivalent to the existence of a multiplier $\mathcal{X}$ such that

$$T \begin{bmatrix} \Xi & 0 \\ 0 & \Pi \end{bmatrix} T^* < He \begin{bmatrix} I \\ \Upsilon \end{bmatrix} \mathcal{X}. \tag{30}$$

Obviously, Υ can be rewritten as

$$\begin{aligned} \Upsilon &= \begin{bmatrix} A^T & -K^T B_2^T & C^T \\ 0 & A^T + K^T B_2^T & \Delta(k) C^T \\ B_1^T & B_1^T & D_1^T (I + \Delta(k))^T \end{bmatrix} \\ &+ \begin{bmatrix} -C^T \\ -C^T \Delta(k) \\ -D_1^T (I + \Delta(k))^T \end{bmatrix} L^T \begin{bmatrix} I & 0 & 0 \end{bmatrix} = \mathscr{A} + \mathscr{B} L^T \mathscr{C}. \end{aligned} \tag{31}$$

To facilitate dealing with the problem, restrict $\mathcal{X}$ with the following structure:

$$\mathcal{X} = \left\{ \mathscr{C}^\dagger X R + \left(I - \mathscr{C}^\dagger \mathscr{C}\right) V \mid X \in \mathbb{R}^{n \times n}, \det X \neq 0 \right\}, \tag{32}$$

where R is a matrix to be specified later, X, V are matrix variables.

Then, we have

$$\begin{aligned} \Upsilon \mathcal{X} &= \left(\mathscr{A} + \mathscr{B} L^T \mathscr{C}\right) \left(\mathscr{C}^\dagger X R + \left(I - \mathscr{C}^\dagger \mathscr{C}\right) V\right) \\ &= \mathscr{A} \mathcal{X} + \mathscr{B} \Gamma R. \end{aligned} \tag{33}$$

Then the following lemma is given to show that the restriction of $\Upsilon\mathcal{X}$ does not introduce conservatism if the matrix R is specified appropriately.

Lemma 8. *Consider system* (9)*, let R and Π be with appropriate dimensions, and let $Q > 0$; then the following statements are equivalent.*

(i) There exists a gain matrix L such that condition (25) *and*

$$\left(SR^*\right)^\perp S T \begin{bmatrix} \Xi & 0 \\ 0 & \Pi \end{bmatrix} T^* S^* \left(SR^*\right)^{\perp *} < 0 \tag{34}$$

hold, where

$$S = \begin{bmatrix} A^T - C^T L^T & -K^T B_2^T & C^T & I & 0 & 0 \\ -C^T \Delta(k) L^T & A^T + K^T B_2^T & \Delta(k) C^T & 0 & I & 0 \\ B_1^T - D_1^T (I + \Delta(k))^T L^T & B_1^T & D_1^T (I + \Delta(k))^T & 0 & 0 & I \\ I & 0 & 0 & 0 & 0 & 0 \\ 0 & I & 0 & 0 & 0 & 0 \end{bmatrix}. \tag{35}$$

(ii) There exists matrix variable $\Gamma = L^T X$ such that

$$T \begin{bmatrix} \Xi & 0 \\ 0 & \Pi \end{bmatrix} T^* < He \begin{bmatrix} \mathcal{X} \\ -\mathscr{A}\mathcal{X} - \mathscr{B}\Gamma R \end{bmatrix}. \tag{36}$$

Proof. The proof is similar to the proof of Lemma 5 in [20], it is omitted here. □

Then, combining Lemmas 7 and 8, the following theorem is presented.

Denote

$$F_{a1} = \begin{bmatrix} 0 & 0 & 0 & 0 \\ 0 & 0 & 0 & 0 \\ 0 & 0 & 0 & 0 \\ 0 & 0 & 0 & 0 \\ I & -C^T & 0 & 0 \\ 0 & 0 & -D_1^T & -D_1^T \end{bmatrix},$$

$$F_{a2} = \begin{bmatrix} C^T V_{c1} & C^T V_{c2} & C^T V_{c3} & C^T V_{c4} & C^T V_{c5} & C^T V_{c6} \\ \Gamma & \Gamma & 0 & 0 & \Gamma & -\Gamma B_1 \\ V_{c1} & V_{c2} & V_{c3} & V_{c4} & V_{c5} & V_{c6} \\ \Gamma & \Gamma & 0 & 0 & \Gamma & -\Gamma B_1 \end{bmatrix}, \tag{37}$$

$$\Lambda = \begin{bmatrix} -P_{11} - X - X^T & * & * & * & * & * \\ -P_{21} - V_{b1} - X^T & -P_{22} - V_{b2} - V_{b2}^T & * & * & * & * \\ e^{-j\vartheta_c} Q_{11} - V_{c1} & e^{-j\vartheta_c} Q_{12} - V_{c2} V_{b3} & \Phi & * & * & * \\ \Phi_1 & \Phi_2 & \Phi_3 & \Phi_4 & * & * \\ \Phi_5 & \Phi_6 & \Phi_7 & \Phi_8 & \Phi_9 & * \\ \Phi_{10} & \Phi_{11} & \Phi_{12} & \Phi_{13} & \Phi_{14} & \Phi_{15} \end{bmatrix}, \tag{38}$$

where

$$\Phi = P_{12} - 2\cos\vartheta_w Q_{12} - V_{c3} - V_{c3}^T,$$

$$\Phi_1 = e^{-j\vartheta_c} Q_{12}^T + A^T X - K^T B_2^T V_{b1} + C^T V_{c1} - C^T \Gamma - X^T,$$

$$\Phi_2 = e^{-j\vartheta_c} Q_{22}^T + A^T X - K^T B_2^T V_{b2} - C^T V_{c3} + C^T \Gamma - V_{b4}^T,$$

$$\Phi_3 = P_{12} 2\cos\vartheta_w Q_{22} - K^T B_2^T V_{b3} + C^T V_3 + V_{c4}^T,$$

$$\Phi_4 = -K^T B_2^T V_{b4} + C^T V_{c4} - \left(K^T B_2^T V_{b4} - C^T V_{c4}\right)^T,$$

$$\Phi_5 = \left(A^T + K^T B_2^T\right) V_{b1} - X^T,$$

$$\Phi_6 = \left(A^T + K^T B_2^T\right) V_{b2} - V_{b5},$$

$$\Phi_7 = \left(A^T + K^T B_2^T\right) V_{b3} - V_{c5},$$

$$\Phi_8 = -I + \left(A^T + K^T B_2^T\right) V_{b4} + V_{c5}^T + X^T A - V_{b5}^T B_2 K - \Gamma^T C,$$

$$\Phi_9 = \left(A^T + K^T B_2^T\right) V_{b5} - V_{b5}^T \left(A + B_2 K\right),$$

$$\Phi_{10} = B_1^T X + B_1^T V_{b1} + B_1^T X^T - D_1^T V_{c1} - D_1^T \Gamma,$$

$$\Phi_{11} = B_1^T X + B_1^T V_{b2} - V_{b6}^T - D_1^T V_{c2} - D_1^T \Gamma,$$

$$\Phi_{12} = B_1^T V_{b3} - V_{c6} - D_1^T V_{c3},$$

$$\Phi_{13} = B_1^T V_{b4} + \left[A^T X B_1 - K^T B_2^T V_{b6} + C^T V_{c6} + C^T \Gamma B_1\right]^T - D_1^T V_{c4},$$

$$\Phi_{14} = B_1^T X + B_1^T V_{b5} + \left[A^T + K^T B_2^T V_{b6}\right]^T - D_1^T V_{c5} - D_1^T \Gamma,$$

$$\Phi_{15} = B_1^T X B_1 - B_1^T V_{b6} + \left[B_1^T X B_1 - B_1^T V_{b6}\right]^T - D_1^T V_{c6} + D_1^T \Gamma B_1, \tag{39}$$

with

$$\vartheta_c = \frac{(\vartheta_1 + \vartheta_2)}{2}, \qquad \vartheta_\omega = \frac{(\vartheta_2 - \vartheta_1)}{2}. \tag{40}$$

Theorem 9. *Consider system* (9)*; let* $\gamma > 0$ *and* $\delta_a > 0$ *be given constants and*

$$\Pi := \begin{bmatrix} -I & 0 \\ 0 & \gamma^2 I \end{bmatrix}, \quad P, Q \in H_n \tag{41}$$

and $Q > 0$*. Provided that* $R = [I \quad I \quad 0 \quad 0 \quad -B_1]$*, then*

$$\sigma_{\min} G_{rf}\left(e^{j\theta}\right) > \gamma, \quad \forall \theta \in [\vartheta_2, \vartheta_2], \tag{42}$$

holds if there exist matrix variables V_{bi}, V_{ci}, $i = 1, \ldots, 6$, X, *and scalars* ϑ_1, ϑ_2, *and* ε *such that*

$$\begin{bmatrix} \Lambda & F_{a1} & \delta_a \varepsilon F_{a2}^T \\ * & -\varepsilon I & 0 \\ * & * & -\varepsilon I \end{bmatrix} < 0. \tag{43}$$

Proof. By Lemmas 7 and 8, we have that (42) holds if inequality (36) holds. Similar to the proof of Theorem 1 in [20], since $\mathscr{C} = [I \quad 0 \quad 0]$, we know that

$$\mathscr{C}^\dagger = \begin{bmatrix} I \\ 0 \\ 0 \end{bmatrix}. \tag{44}$$

Then from (32) we have

$$\mathscr{X} = \begin{bmatrix} I \\ 0 \\ 0 \end{bmatrix} XR + \begin{bmatrix} 0 & 0 & 0 \\ 0 & I & 0 \\ 0 & 0 & I \end{bmatrix} V. \tag{45}$$

Partition V as $V = \begin{bmatrix} V_a \\ V_b \\ V_c \end{bmatrix}$; then we get

$$\mathscr{X} = \begin{bmatrix} XR \\ V_b \\ V_c \end{bmatrix}. \tag{46}$$

So, (36) can be written as

$$T \begin{bmatrix} \Xi & 0 \\ 0 & \Pi \end{bmatrix} T^* < He \begin{bmatrix} I & 0 & 0 & 0 \\ 0 & I & 0 & 0 \\ 0 & 0 & I & 0 \\ -A^T & K^T B_2^T & -C^T & C^T \\ 0 & -A^T - K^T B_2^T & -\Delta(k) C^T & C^T \Delta(k) \\ -B_1^T & -B_1^T & D_1^T (I + \Delta(k)) & D_1^T (I + \Delta(k)) \end{bmatrix} \times \begin{bmatrix} XR \\ V_b \\ V_c \\ \Gamma R \end{bmatrix}. \tag{47}$$

Let $V_b = [V_{b1} - V_{b6}]$, $V_c = [V_{c1} - V_{c6}]$, and partition P and Q as $P = \begin{bmatrix} P_{11} & P_{12} \\ P_{21} & P_{22} \end{bmatrix}$, $Q = \begin{bmatrix} Q_{11} & Q_{12} \\ Q_{12}^T & Q_{22} \end{bmatrix} > 0$; then we have

$$\begin{aligned} &\Lambda + F_{a1} \operatorname{diag}\{\Delta(k), \Delta(k), \Delta(k), \Delta(k)\} F_{a2} \\ &\quad + \left(F_{a1} \operatorname{diag}\{\Delta(k), \Delta(k), \Delta(k), \Delta(k)\} F_{a2}\right)^T < 0, \end{aligned} \tag{48}$$

where $\Delta(k)$ satisfyies (7). By using Lemma 5, we can obtain that (43) holds. So, it concludes that (42) holds if (43) holds, which completes the proof. □

Combining Lemma 6 and Theorem 9, we have the following theorem.

Theorem 10. *Consider system* (1)*, and let* $\gamma > 0$ *and* $\delta_a > 0$ *be given constants; there exists a quantized fault detection observer* (2) *such that error closed-loop system* (9) *is stable and with the finite frequency performance*

$$\sigma_{\min} G_{rf}\left(e^{j\theta}\right) > \gamma, \quad \forall \theta \in [\vartheta_2, \vartheta_2] \tag{49}$$

if there exist matrix variables Γ, V_{bi}, V_{ci}, $i = 1, \ldots, 6$, $\overline{X} = \begin{bmatrix} X & 0 \\ 0 & X \end{bmatrix} > 0$, $P = \begin{bmatrix} P_{11} & P_{12} \\ P_{21} & P_{22} \end{bmatrix}$, *and* $Q = \begin{bmatrix} Q_{11} & Q_{12} \\ Q_{12}^T & Q_{22} \end{bmatrix} > 0$ *and scalars* ϑ_1, ϑ_2, ε_1, *and* ε_2 *such that the following inequalities hold:*

$$\begin{bmatrix} -X & * & * & * & * & * \\ 0 & -X & * & * & * & * \\ XA - \Gamma^T C & 0 & -X & * & * & * \\ -XB_2K & XA + XB_2K & 0 & -X & * & * \\ 0 & 0 & -\Gamma & 0 & -\varepsilon_1 I & * \\ 0 & \delta_a \varepsilon_1 C & 0 & 0 & 0 & -\varepsilon_1 I \end{bmatrix} < 0$$

$$\begin{bmatrix} \Lambda & F_{a1} & \delta_a \varepsilon_2 F_{a2}^T \\ * & -\varepsilon_2 I & 0 \\ * & * & -\varepsilon_2 I \end{bmatrix} < 0, \tag{50}$$

where $\delta_a = \max\{\delta_i, i = 1, \ldots, y\}$ *and* Λ *is defined by* (38)*, and the observer gain* L *is obtained as* $L^T = \Gamma X^{-1}$.

Remark 11. Note that, due to the existence of the unknown controller gain, the conditions given in Theorem 10 are not convex. In order to solve this problem, we design a controller gain by state feedback method as follows:

$$\begin{bmatrix} -X & XA^T + \overline{K}^T B_2^T \\ AX + B_2 \overline{K} & -X \end{bmatrix} < 0, \tag{51}$$

for $X > 0$, and the controller gain is given as $K = \overline{K} X^{-1}$. Then use the state feedback controller gain as the initial value to obtain the observer gain L. So the following algorithm is given.

Algorithm 12. Let $\delta_a > 0$ be given scalars and $\zeta > 0$ a given small constant specifying a convergence criterion.

Step 1. By (51), we obtain the initial solutions K^{ini}; go to Step 2.

Step 2. Letting $K = K^{\text{ini}}$,

$$\begin{aligned} &\max \quad \gamma \\ &\text{s.t.} \quad (50), \end{aligned} \tag{52}$$

we obtain Γ, X, V_{bi}, $i = 1, \ldots, 6$, and γ_{ini}; then go to Step 3.

Step 3. Let $X_{\text{ini}} = X$, $V_{bi}^{\text{ini}} = V_{bi}$, $i = 1, \ldots, 6$,

$$\begin{aligned} &\max \quad \gamma \\ &\text{s.t.} \quad (50). \end{aligned} \tag{53}$$

γ and K are obtained. Then if $\|\gamma - \gamma_{\text{ini}}\| < \zeta$, stop, and $L^T = \Gamma X^{-1}$, else, let $K = K$ and $\gamma_{\text{ini}} = \gamma$; return to Step 2.

Remark 13. $\varepsilon_1, \varepsilon_2$ in (50) can be obtained by searching method to guarantee that the performance γ is maximum.

4. Example

In this section, an example is given to illustrate the effectiveness of the developed theory. Consider a linear system of form (1) with

$$\begin{aligned} A &= \begin{bmatrix} 0.9673 & 0 & 0.12 \\ 0.0293 & 0.8763 & -0.4 \\ 0.0259 & 0 & 0.9032 \end{bmatrix}, \\ B_1 &= \begin{bmatrix} 0.1 & 0 \\ 0.5 & 0.06 \\ -0.2 & 0.15 \end{bmatrix}, \qquad B_2 = \begin{bmatrix} 1 & 0.04 \\ 0 & 0.3 \\ 0 & 0.05 \end{bmatrix}, \\ D_1 &= \begin{bmatrix} 0.1 & 0 \\ 0.5 & 12 \end{bmatrix}, \qquad D_2 = \begin{bmatrix} 1 & 0 \\ 0.5 & 0.1 \end{bmatrix}, \\ C &= \begin{bmatrix} 0.1 & 0 & 0 \\ 1 & 1 & 0 \end{bmatrix}. \end{aligned} \tag{54}$$

For this example, set the quantization densities as $\rho_1 = \rho_2 = 0.91$. Assume that the frequency range of faults is known as $\theta \in [0, 0.5]$. Let $\varepsilon_1 = 0.9899$, $\varepsilon_2 = 1.1299$; by Algorithm 12, we obtain the fault sensitivity performance index $\gamma = 1.2131$, and, correspondingly, the quantized fault detection observer gain matrix L_{finite} is obtained as

$$L_{\text{finite}} = \begin{bmatrix} 0.1452 & 0.0541 \\ -0.0145 & -0.2156 \\ -0.5421 & 0.3741 \end{bmatrix}. \tag{55}$$

In order to study the effects of fault on residual of the quantized detection observer, the fault signal is selected as

$$f(k) = \begin{cases} \begin{bmatrix} 1 & 0.9 \end{bmatrix}^T, & k \geq 20, \\ \begin{bmatrix} 0 & 0 \end{bmatrix}^T, & \text{otherwise.} \end{cases} \tag{56}$$

Using the observer gain matrix L_{finite} given in (48), the two residual outputs are denoted by the solid lines of Figures 1 and 2, respectively, from which we can see that the faulty cases are well discriminated from the fault free cases in presence of the disturbance effects.

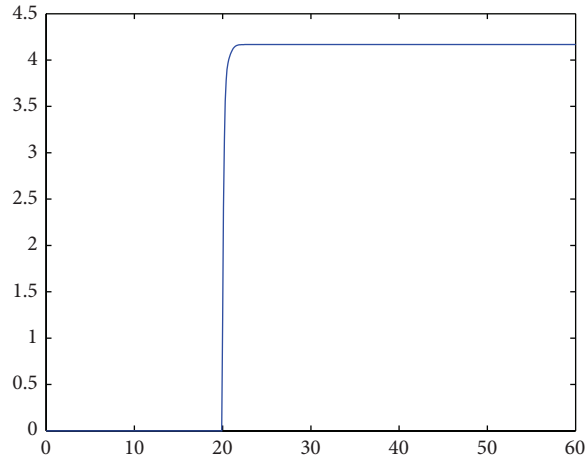

Figure 1: Residual output signal.

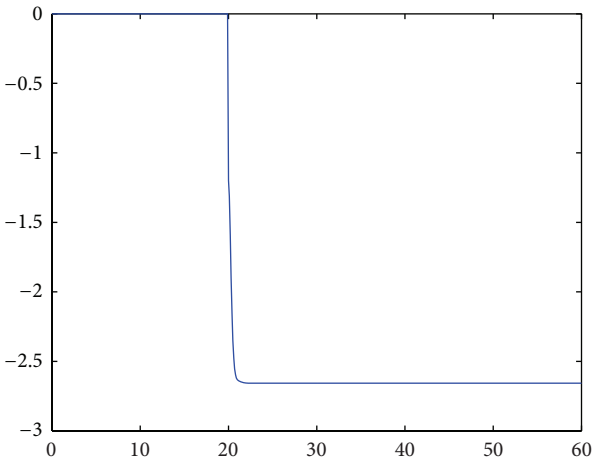

Figure 2: Residual output signal.

5. Conclusion

This paper considers the fault detection problem in the finite frequency domain for networked control systems with signal quantization. A quantized fault detection observer is designed by employing a performance index which is used to increase the fault sensitivity in finite frequency domain. By using the logarithmic quantizer method, the quantized measurement signals are dealt with by utilizing the sector bound method, in which the quantization error is treated as sector-bounded uncertainty. Further, By using the GKYP Lemma, an iterative LMI-based optimization algorithm is developed to design the quantized fault detection observer. Finally, a numerical example is given to illustrate the the effectiveness of the proposed method.

Conflict of Interests

One of the authors declares that there is no conflict of interests regarding the publication of this paper.

Acknowledgments

This work is partially supported by the Funds of National Science of China (Grant nos. 61104106 and 61104029), the Natural Science Foundation of Liaoning Province (Grant nos. 201202156 and 2013020144), and by Program for Liaoning Excellent Talents in University (LNET) (LJQ2012100).

References

[1] D. F. Delchamps, "Stabilizing a linear system with quantized state feedback," *Institute of Electrical and Electronics Engineers*, vol. 35, no. 8, pp. 916–924, 1990.

[2] N. Elia and S. K. Mitter, "Stabilization of linear systems with limited information," *Institute of Electrical and Electronics Engineers*, vol. 46, no. 9, pp. 1384–1400, 2001.

[3] M. Fu and L. Xie, "The sector bound approach to quantized feedback control," *Institute of Electrical and Electronics Engineers*, vol. 50, no. 11, pp. 1698–1711, 2005.

[4] H. Gao and T. Chen, "H_∞estimation for uncertain systems with limited communication capacity," *Institute of Electrical and Electronics Engineers*, vol. 52, no. 11, pp. 2070–2084, 2007.

[5] M. Fu and L. Xie, "Quantized feedback control for linear uncertain systems," *International Journal of Robust and Nonlinear Control*, vol. 20, no. 8, pp. 843–857, 2010.

[6] X. Yao, L. Wu, and W. X. Zheng, "Quantized H_∞ filtering for Markovian jump LPV systems with intermittent measurements," *International Journal of Robust and Nonlinear Control*, vol. 23, no. 1, pp. 1–14, 2013.

[7] Y. Niu, T. Jia, X. Wang, and F. Yang, "Output-feedback control design for NCSs subject to quantization and dropout," *Information Sciences*, vol. 179, no. 21, pp. 3804–3813, 2009.

[8] W.-W. Che and G.-H. Yang, "Quantised H_∞ filter design for discrete-time systems," *International Journal of Control*, vol. 82, no. 2, pp. 195–206, 2009.

[9] W.-W. Che, J.-L. Wang, and G.-H. Yang, "Quantised H_∞ filtering for networked systems with random sensor packet losses," *IET Control Theory & Applications*, vol. 4, no. 8, pp. 1339–1352, 2010.

[10] W. W. Che, J. L. Wang, and G. H. Yang, "H_∞ control for networked control systems with limited communication," *European Journal of Control*, vol. 18, no. 2, pp. 103–118, 2012.

[11] R. Isermann, "Supervision, fault-detection and fault-diagnosis methods—an introduction," *Control Engineering Practice*, vol. 5, no. 5, pp. 639–652, 1997.

[12] J. J. Gertler, *Fault Detection and Diagnosis in Engineering Systems*, Marcel Dekker, New York, NY, USA, 1998.

[13] I. M. Jaimoukha, Z. Li, and V. Papakos, "A matrix factorization solution to the H_-/H_∞ fault detection problem," *Automatica*, vol. 42, no. 11, pp. 1907–1912, 2006.

[14] M. Zhong, S. X. Ding, B. Tang, P. Zhang, and T. Jeinsch, "An LMI approach to robust fault detection filter design for discrete-time systems with model uncertainty," in *Proceedings of the 40th IEEE Conference on Decision and Control (CDC '01)*, pp. 3613–3618, December 2001.

[15] J. Chen and R. Patton, *Robust Model-Based Fault Diagnosis for Dynamic Systems*, Kluwer Academic, Dordrecht, The Netherlands, 1999.

[16] G. Tao, S. M. Joshi, and X. Ma, "Adaptive state feedback and tracking control of systems with actuator failures," *Institute of*

Electrical and Electronics Engineers, vol. 46, no. 1, pp. 78–95, 2001.

[17] F. Liao, J. L. Wang, and G. H. Yang, "Reliable robust flight tracking control: an LMI Approach," *IEEE Transactions on Control Systems Technology*, vol. 10, pp. 76–89, 2002.

[18] H. Wang, J. Wang, and J. Lam, "An optimization approach for worst-case fault detection observer design," in *Proceedings of the American Control Conference (AAC '04)*, pp. 2475–2480, July 2004.

[19] H. Wang, J. Wang, J. Liu, and J. Lam, "Iterative LMI approach for robust fault detection observer design," in *Proceedings of the 42nd IEEE Conference on Decision and Control*, pp. 1974–1979, December 2003.

[20] H. Wang and G.-H. Yang, "A finite frequency domain approach to fault detection for linear discrete-time systems," *International Journal of Control*, vol. 81, no. 7, pp. 1162–1171, 2008.

[21] Z. Mao, B. Jiang, and P. Shi, "Protocol and fault detection design for nonlinear networked control systems," *IEEE Transactions on Circuits and Systems II*, vol. 56, no. 3, pp. 255–259, 2009.

[22] D. Huang and S. K. Nguang, "Robust fault estimator design for uncertain networked control systems with random time delays: an ILMI approach," *Information Sciences*, vol. 180, no. 3, pp. 465–480, 2010.

[23] T. Iwasaki and S. Hara, "Generalized KYP lemma: unified frequency domain inequalities with design applications," *Institute of Electrical and Electronics Engineers*, vol. 50, no. 1, pp. 41–59, 2005.

[24] I. R. Petersen, "A stabilization algorithm for a class of uncertain linear systems," *Systems & Control Letters*, vol. 8, no. 4, pp. 351–357, 1987.

Hindawi Publishing Corporation
Mathematical Problems in Engineering
Volume 2013, Article ID 430630, 10 pages
http://dx.doi.org/10.1155/2013/430630

Research Article

An LMI-Based H_∞ Control Approach for Networked Control Systems with Deadband Scheduling Scheme

Hui-ying Chen, Zu-xin Li, and Yan-feng Wang

School of Information & Engineering, Huzhou Teachers College, Zhejiang 313000, China

Correspondence should be addressed to Hui-ying Chen; hychen@hutc.zj.cn

Received 20 July 2013; Revised 16 September 2013; Accepted 16 September 2013

Academic Editor: Baoyong Zhang

Due to the bandwidth constraints in the networked control systems (NCSs), a deadband scheduling strategy is proposed to reduce the data transmission rate of network nodes. A discrete-time model of NCSs is established with both deadband scheduling and network-induced time-delay. By employing the Lyapunov functional and LMI approach, a state feedback H_∞ controller is designed to ensure the closed-loop system asymptotically to be stable with H_∞ performance index. Simulation results show that the introduced deadband scheduling strategy can ensure the control performance of the system and effectively reduce the node's data transmission rate.

1. Introduction

Networked control systems (NCSs) are control systems in which the control loop is closed over a wired or wireless communication network. They have received a great deal of attention in the recent years owing to their successful applications in a wide range of areas such as industrial automation, aerospace, and nuclear power station [1, 2]. Compared with the traditional point-to-point communication, NCSs have advantages of low cost, easy installation and maintenance, great reliability, and so forth. However, due to the introduction of the communication networks, they also incur some new issues such as network-induced delays, packet dropouts, and limited bandwidth resources, which make the analysis and design of NCSs become more complex [3, 4].

Many results for NCSs have been reported to handle network-induced delays, packet dropouts and communication constraints in the literature; see [5–12] and the references therein. It should be pointed out that most of the available results make use of time-driven sampling and communication scheme since it is relatively easy to implement, and there is a well-established system theory for periodic signals. However, time-driven communication scheme is not desirable in many control applications. For example, in the NCSs with limited bandwidth resources, frequent data transmission will increase the network collision probability when there are many nodes on the network, thereby increasing the communication delay and data dropouts and leading to the poor performance and instability of the systems [3]. On the other hand, as is well-known, in the wireless networked control systems (WNCSs), a main constraint of wireless devices is the limited battery life, and wireless transmission consumes significantly more energy than internal computation [13]; thus reducing the data transmission rate is particularly important in the WNCSs. For the above two cases, time-driven communication scheme is not suitable since its transmission rate is generally high which results in inefficient utilization of the limited resources, such as network bandwidth and energy. Therefore, how to design a reasonable scheduling strategy to reduce the use of constrained resources and ensure the performance of NCSs becomes one of the research hotspots.

Not only deadband scheduling techniques (i.e., by setting transmission deadband for the network node, the node will not transmit a new message if the node signal or signal change is within the deadband), which can effectively reduce the use of network bandwidth and energy consumption, but also the algorithms which are easy to realize have received an increasing attention in the recent years [14–18]. Besides, numerous other concepts have been proposed in the literature, such as send-on-delta sampling [19–21], event-based

sampling [22–24], and event-triggered sampling [25, 26]. Despite the existence of many names, the basic principle is the same. In [14], a deadband method was introduced into the NCSs for the first time, in which the transmission deadbands were set in the sensor and controller to reduce the data transmission rate, and the deadband threshold optimization problem was also discussed. In [15], the relationship between the deadband threshold and the control performance was analyzed by simulation. The paper [23] used the deviation of two adjacent states beyond the deadband threshold to drive the nodes' data transmission and a dynamically selected deadband threshold value in accordance with the round-trip delay. In [16, 17], the stability of the system with deadband scheduling was investigated, but the network delay was not considered in [16] the nodes should be synchronized and the network delay should be measurable in [17]. The paper [18] proposed a signal difference-based transmission deadband scheduling strategy, a continuous-time model of WNCSs was established with both the probability distribution of delay and parametric uncertainties, and the H_∞ controller was designed. In [26], for a class of uncertain continuous-time NCSs with quantizations, the codesign for controller and event-triggering scheme was proposed by using a delay system approach.

Until now, although some important pieces of work have been reported on deadband scheduling schemes in NCSs, which have a great significance on both theoretical development and practical applications in NCSs, it is worth noting that the obtained results on deadband scheduling in NCSs mostly focus on the system simulation and performance analysis; few papers have solved the problems of controller design and synthesis, which are more useful and challenging than the issue of performance analysis. In addition, to the best of our knowledge, few related results have been established for discrete-time NCSs with deadband scheduling, which motivates the work of this paper.

In this paper, we propose a deadband scheduling scheme to save the limited bandwidth resources while guaranteeing the desired H_∞ control performance. Considering the influence of uncertain short time-delay, the NCSs with both deadband scheduling and time-delay is modeled as a discrete-time system with parameter uncertainties. By the Lyapunov functional and LMI approach, the H_∞ control problem is investigated. Finally, a numerical example is given to show the usefulness of the derived results.

The rest of this paper is organized as follows. Section 2 gives a discrete-time model of the closed-loop system. In Section 3, a state feedback H_∞ controller is designed to ensure the closed-loop system asymptotically to be stable with H_∞ performance index. Section 4 demonstrates the validness of the proposed method through a numerical example. Conclusions are given in Section 5.

Notation. The notations used throughout this paper are fairly standard. $\mathbb{R}^n$ denotes the n-dimensional Euclidean space. $\|\cdot\|_2$ refers to the Euclidean vector norm. $l_2[0,\infty)$ is the space of square summable infinite sequence. I and 0 represent the identity matrix and zero matrix with appropriate dimensions, respectively. diag$\{\cdots\}$ stands for a diagonal matrix.

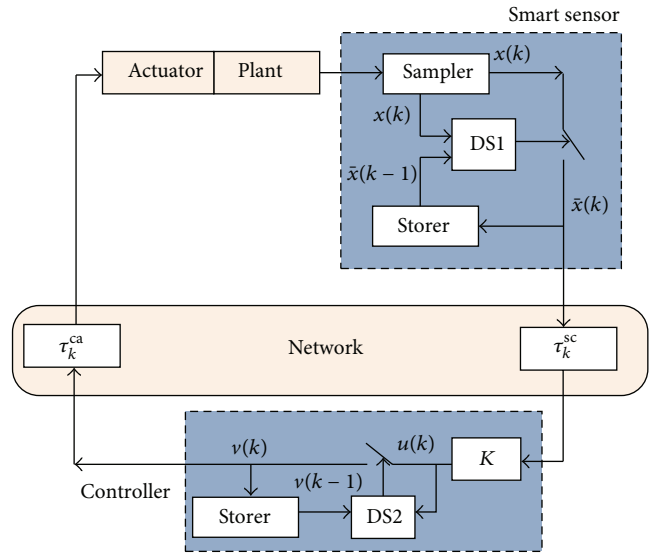

Figure 1: Model of networked control system with deadband scheduling.

The superscripts "T" and "-1" represent matrix transpose and inverse, and "$*$" denotes the term that is induced by symmetry.

2. Problem Description and Modeling

The networked control system with deadband scheduling in this paper is shown in Figure 1, where deadband schedulers (DS1, DS2) are set in the sensor and controller, respectively, τ_k^{sc} is sensor-to-controller delay, and τ_k^{ca} is controller-to-actuator delay.

Consider the following continuous plant model:

$$\begin{aligned} \dot{x}(t) &= Ax(t) + B_1 v(t) + B_2 w(t), \\ y(t) &= Cx(t), \end{aligned} \tag{1}$$

where $x(t) \in \mathbb{R}^n$ is the state vector of plant, $v(t) \in \mathbb{R}^p$ is the input vector, $y(t) \in \mathbb{R}^q$ is the output vector, and $w(t) \in \mathbb{R}^p$ is the disturbance input. A, B_1, B_2, and C are known real constant matrices with appropriate dimensions.

Make the following assumptions for the system.

(1) In the smart sensor, the sampler is time-driven, with a sampling period h; both the controller and actuator are event-driven.

(2) The total network-induced time-delay $\tau_k = \tau_k^{sc} + \tau_k^{ca}$ is time varying and nondeterministic, which satisfies $0 \le \tau_k \le h$.

Thus, the discretized equation of plant can be described as [27]

$$\begin{aligned} x(k+1) = {} & Gx(k) + H_0(\tau_k) v(k) \\ & + H_1(\tau_k) v(k-1) + H_w w(k), \\ y(k) = {} & Cx(k), \end{aligned} \tag{2}$$

where $G = e^{Ah}$, $H_0(\tau_k) = \int_0^{h-\tau_k} e^{At}dtB_1$, $H_1(\tau_k) = \int_{h-\tau_k}^{h} e^{At}dtB_1$, and $H_w = \int_0^h e^{At}dtB_2$. By mathematical transformation, $H_0(\tau_k)$, $H_1(\tau_k)$ can be expressed as

$$\begin{aligned} H_0(\tau_k) &= H_0 + DF(\tau_k')E, \\ H_1(\tau_k) &= H_1 - DF(\tau_k')E, \end{aligned} \tag{3}$$

where

$$\begin{aligned} &H_0 = \int_0^{h/2} e^{As}ds \cdot B, \qquad H_1 = \int_{h/2}^{h} e^{As}ds \cdot B, \\ &\delta = \max_{\tau_k'} \left\| \int_0^{-\tau_k'} e^{As}ds \right\|_2 = \left\| \int_0^{h/2} e^{As}ds \right\|_2, \\ &D = \delta e^{A(h/2)}, \qquad E = B, \qquad \tau_k' \in \left[-\frac{h}{2}, \frac{h}{2}\right], \\ &F^T(\tau_k')F(\tau_k') \le I. \end{aligned} \tag{4}$$

Remark 1. Limited by space, the detailed discretization process for system (1) with uncertain short time-delay is omitted in this paper and can be found in [27]. From (2) and (3), we know that the continuous plant with uncertain short time-delay in NCSs can be modeled as a discrete linear system with parameter uncertainties.

2.1. Description of Deadband Schedulers. The signal will be transmitted only when the difference between the current signal and the previous transmission signal is greater than the error threshold. According to this, the deadband schedulers designed in this paper are the error threshold-based deterministic schedulers. The working mechanism of the deadband scheduler 1(DS1) in the sensor can be described as

$$\overline{x}_i(k) = \begin{cases} x_i(k), & \left|\overline{x}_i(k-1) - x_i(k)\right| > \delta_i \left|x_i(k)\right|, \\ \overline{x}_i(k-1), & \left|\overline{x}_i(k-1) - x_i(k)\right| \le \delta_i \left|x_i(k)\right|, \end{cases} \tag{5}$$

where $i = 1, 2, \ldots, n$; $\delta_i \in [0, 1]$, $\overline{x}_i(k)$, and $x_i(k)$ are given error threshold values, output signals, and input signals of DS1, respectively.

Set $\Lambda_1 = \text{diag}\{\delta_1, \delta_2, \ldots, \delta_n\}$, $F_1(k) = \text{diag}\{f_{11}(k), f_{12}(k), \ldots, f_{1n}(k)\}$, $f_{1i}(k) \in [-1, 1]$, $i = 1, 2, \ldots, n$; then from (5), the input-output relationship of DS1 can be converted to

$$\overline{x}(k) = x(k) + \Lambda_1 F_1(k)\, x(k), \tag{6}$$

where $F_1^T(k)F_1(k) \le I$.

Remark 2. In this paper, the effect of active packet dropouts under the deadband scheduling scheme is modeled as a bounded uncertain item of the transmission signal. The main advantages of this modeling method are as follows: (1) a non-linear relationship between the input and output of the deadband scheduler is converted to a linear relationship with uncertain parameters; (2) due to the bounded ranges of uncertain parameters related to the deadband threshold values, it is easier to merge scheduling policy parameters into the system model.

Similarly, the working mechanism of deadband scheduler 2(DS2) in the controller can be described as:

$$v_j(k) = \begin{cases} u_j(k), & \left|v_j(k-1) - u_j(k)\right| > \sigma_j \left|u_j(k)\right|, \\ v_j(k-1), & \left|v_j(k-1) - u_j(k)\right| \le \sigma_j \left|u_j(k)\right|, \end{cases} \tag{7}$$

where $j = 1, 2, \ldots, p$; $\sigma_j \in [0, 1]$, $v_j(k)$ and $u_j(k)$ are given error threshold values, output signals and input signals of DS2, respectively.

Set $\Lambda_2 = \text{diag}\{\sigma_1, \sigma_2, \ldots \sigma_p\}$, $F_2(k) = \text{diag}\{f_{21}(k), f_{22}(k), \ldots, f_{2p}(k)\}$, $f_{2j}(k) \in [-1, 1]$, $j = 1, 2, \ldots, p$, then from (7) the input-output relationship of DS2 can be converted to:

$$v(k) = u(k) + \Lambda_2 F_2(k)\, u(k), \tag{8}$$

where $F_2^T(k)F_2(k) \le I$.

From the above, we know that after the introduction of deadband schedulers into NCSs, the signals do not need to be transmitted at each sampling period so as to achieve the purpose of reducing data transmission rate and the effect of bandwidth constraints on the system. In addition, the principles of the considered schedulers are simple, which do not require a lot of computing and data storage.

2.2. The Model of Closed-Loop System. Employ a memoryless state feedback controller

$$u(k) = K\overline{x}(k), \tag{9}$$

where $\overline{x}(k) \in \mathbb{R}^n$, $u(k) \in \mathbb{R}^p$, and K is the state feedback gain with appropriate dimensions.

Selecting the augmented vector $z(k) = \left[x^T(k) \;\; v^T(k-1)\right]^T$ and synthesizing (2), (3), (6), (8), and (9), the closed-loop system can be described as

$$\begin{aligned} z(k+1) &= \Phi_k z(k) + \overline{H}_w w(k), \\ y(k) &= \overline{C} z(k), \end{aligned} \tag{10}$$

where

$$\begin{aligned}\Phi_k &= \begin{bmatrix} G + \left(H_0 + DF\left(\tau_k'\right)E\right)\left(I + \Lambda_2 F_2(k)\right)K\left(I + \Lambda_1 F_1(k)\right) & H_1 - DF\left(\tau_k'\right)E \\ \left(I + \Lambda_2 F_2(k)\right)K\left(I + \Lambda_1 F_1(k)\right) & 0 \end{bmatrix} \\ &= \overline{G} + \overline{H}K_1\overline{I} + \overline{D}F\left(\tau_k'\right)EK_1\overline{I} + \overline{D}F\left(\tau_k'\right)\overline{E},\end{aligned} \tag{11}$$

where

$$\begin{aligned}\overline{G} &= \begin{bmatrix} G & H_1 \\ 0 & 0 \end{bmatrix}, \qquad \overline{C} = \begin{bmatrix} C & 0 \end{bmatrix}, \\ \overline{H} &= \begin{bmatrix} H_0 \\ I \end{bmatrix}, \qquad \overline{D} = \begin{bmatrix} D \\ 0 \end{bmatrix}, \\ \overline{I} &= \begin{bmatrix} I & 0 \end{bmatrix}, \qquad \overline{E} = \begin{bmatrix} 0 & -E \end{bmatrix}, \\ \overline{H}_w &= \begin{bmatrix} H_w \\ 0 \end{bmatrix}, \qquad K_1 = \left(I + \Lambda_2 F_2(k)\right)K\left(I + \Lambda_1 F_1(k)\right).\end{aligned} \tag{12}$$

3. Design of H_∞ Controller

In this section, we will investigate H_∞ control problem for the closed-loop system (10). Throughout this paper, we will use the following lemmas.

3.1. Related Lemmas

Lemma 3 (see [28]). *For the given matrices A, $Q = Q^T$, and $P = P^T > 0$, $A^TPA + Q < 0$ hold if and only if*

$$\begin{bmatrix} Q & A^T \\ A & -P^{-1} \end{bmatrix} < 0, \qquad \begin{bmatrix} -P^{-1} & A \\ A^T & Q \end{bmatrix} < 0. \tag{13}$$

Lemma 4 (see [28]). *Let W, M, N, $F(k)$ be real matrices of appropriate dimensions with $F^T(k)F(k) \le I$ and $W = W^T$; then*

$$W + MF(k)N + N^TF^T(k)M^T < 0 \tag{14}$$

holds if and only if there exists a real scalar $\varepsilon > 0$, satisfying

$$W + \varepsilon MM^T + \varepsilon^{-1}N^TN < 0. \tag{15}$$

More especially, when $F(k)$ is a diagonal matrix, there also exists the following lemma.

Lemma 5 (see [29]). *Let W, M, N be real matrices of appropriate dimensions, let $F(k)$ be a diagonal matrix with $F^T(k)F(k) \le I$ and $W = W^T$; then the following two conditions are equivalent:*

(1) $W + MF(k)N + N^TF^T(k)M^T < 0$

(2) *there exists a matrix $S = S^T > 0$, satisfying $W + MSM^T + N^TS^{-1}N < 0$.*

Remark 6. Due to the introduction of a symmetric positive-definite matrix instead of a scalar in Lemma 5, problem solving is expected to have a less conservatism compared with Lemma 4.

We are now in a position to formulate H_∞ control problem for NCSs with both deadband scheduling and uncertain short time-delay. More specifically, given a disturbance attenuation level γ, we design a state feedback controller of the form (9) such that the closed-loop system (10) with $w(k) = 0$ is asymptotically stable and under zero initial condition; the output $y(k)$ satisfies $\|y\|_2 \le \gamma\|w\|_2$ for all nonzero $w(k) \in l_2[0, \infty)$.

3.2. Main Results.

Based on Lyapunov functional method and H_∞ theory [28], the following conclusions can be obtained.

Theorem 7. *For a given scalar $\gamma > 0$, under the given deadband scheduling schemes (5) and (7), the closed-loop system (10) is asymptotically stable with H_∞ performance γ if there exist symmetric positive-definite matrices P, W_1, W_2, feedback gain matrix K, and scalar $\varepsilon_1 > 0$ such that*

$$\begin{bmatrix} \Pi_{11} & \overline{G} + \overline{H}K\overline{I} & \overline{H}_w & \Pi_{14} & \overline{H}K\Lambda_1 & 0 \\ * & \Pi_{22} & 0 & \left(EK\overline{I} + \overline{E}\right)^T & 0 & \left(K\overline{I}\right)^T \\ * & * & -\gamma^2 I & 0 & 0 & 0 \\ * & * & * & \Pi_{44} & EK\Lambda_1 & 0 \\ * & * & * & * & -W_1 & \left(K\Lambda_1\right)^T \\ * & * & * & * & * & -W_2 \end{bmatrix} < 0, \tag{16}$$

where

$$\begin{aligned}\Pi_{11} &= -P^{-1} + \varepsilon_1\overline{D}\,\overline{D}^T + \left(\overline{H}\Lambda_2\right)W_2\left(\overline{H}\Lambda_2\right)^T, \\ \Pi_{14} &= \left(\overline{H}\Lambda_2\right)W_2(E\Lambda_2)^T, \\ \Pi_{22} &= -P + \overline{C}^T\overline{C} + \overline{I}^TW_1\overline{I}, \\ \Pi_{44} &= -\varepsilon_1 I + \left(E\Lambda_2\right)W_2\left(E\Lambda_2\right)^T.\end{aligned} \tag{17}$$

Proof. (i) We first show that system (10) with $w(k) = 0$ is asymptotically stable. To the end, defining a Lyapunov functional as $V(k) = z^T(k)Pz(k)$, we have that

$$\begin{aligned}\Delta V(k) &= V(k+1) - V(k) \\ &= z^T(k+1)Pz(k+1) - z^T(k)Pz(k) \\ &= z^T(k)\Phi_k^TP\Phi_kz(k) - z^T(k)Pz(k) \\ &= z^T(k)\left(\Phi_k^TP\Phi_k - P\right)z(k).\end{aligned} \tag{18}$$

Obviously, if $\Phi_k^T P \Phi_k - P < 0$, then $\Delta V(k) < 0$, and the closed-loop system (10) is asymptotically stable.

(ii) Next, we prove that system (10) has H_∞ performance γ. Define

$$\begin{aligned} J &= \sum_{k=0}^{\infty} \left[y^T(k)\, y(k) - \gamma^2 w^T(k)\, w(k) \right] \\ &= \sum_{k=0}^{\infty} \left[y^T(k)\, y(k) - \gamma^2 w^T(k)\, w(k) + \Delta V(k) \right] \\ &\quad - V(\infty) + V(0). \end{aligned} \tag{19}$$

Under zero initial conditions, we have that $V(0) = 0$, but $V(\infty) \geq 0$; therefore,

$$\begin{aligned} J &\leq \sum_{k=0}^{\infty} \left[y^T(k)\, y(k) - \gamma^2 w^T(k)\, w(k) + \Delta V(k) \right] \\ &= \sum_{k=0}^{\infty} \left[z^T(k) \;\; w^T(k) \right] \Pi \begin{bmatrix} z(k) \\ w(k) \end{bmatrix}, \end{aligned} \tag{20}$$

where

$$\Pi = \begin{bmatrix} \Phi_k^T P \Phi_k + \overline{C}^T \overline{C} - P & \Phi_k^T P \overline{H}_w \\ * & \overline{H}_w^T P \overline{H}_w - \gamma^2 I \end{bmatrix}. \tag{21}$$

If $\Pi < 0$, then $\Phi_k^T P \Phi_k + \overline{C}^T \overline{C} - P < 0$; therefore, $\Phi_k^T P \Phi_k - P < -\overline{C}^T \overline{C} < 0$; the condition in (i) holds, and system (10) with $w(k) = 0$ is asymptotically stable. In addition, If $\Pi < 0$, then $J < 0$; therefore, $\|y\|_2^2 = \sum_{k=0}^{\infty} y^T(k) y(k) < \gamma^2 \sum_{k=0}^{\infty} w^T(k) w(k) = \gamma^2 \|w\|_2^2$.

According to $\Pi < 0$, substituting $\Phi_k = \overline{G} + \overline{H} K_1 \overline{I} + \overline{D} F(\tau_k') E K_1 \overline{I} + \overline{D} F(\tau_k') \overline{E}$ into (21) and applying Lemma 3, we have that

$$\begin{aligned} &\begin{bmatrix} -P^{-1} & \overline{G} + \overline{H} K_1 \overline{I} & \overline{H}_w \\ * & -P + \overline{C}^T \overline{C} & 0 \\ * & * & -\gamma^2 I \end{bmatrix} + \begin{bmatrix} \overline{D} \\ 0 \\ 0 \end{bmatrix} F(\tau_k') \begin{bmatrix} 0 & E K_1 \overline{I} + \overline{E} & 0 \end{bmatrix} \\ &\quad + \begin{bmatrix} 0 & E K_1 \overline{I} + \overline{E} & 0 \end{bmatrix}^T F^T(\tau_k') \begin{bmatrix} \overline{D} \\ 0 \\ 0 \end{bmatrix}^T < 0. \end{aligned} \tag{22}$$

Due to $F^T(\tau_k') F(\tau_k') \leq I$ and by the use of Lemma 4, we can get that

$$\begin{aligned} &\begin{bmatrix} -P^{-1} & \overline{G} + \overline{H} K_1 \overline{I} & \overline{H}_w \\ * & -P + \overline{C}^T \overline{C} & 0 \\ * & * & -\gamma^2 I \end{bmatrix} + \varepsilon_1 \begin{bmatrix} \overline{D} \\ 0 \\ 0 \end{bmatrix} \begin{bmatrix} \overline{D} \\ 0 \\ 0 \end{bmatrix}^T \\ &\quad + \varepsilon_1^{-1} \begin{bmatrix} 0 & E K_1 \overline{I} + \overline{E} & 0 \end{bmatrix}^T \begin{bmatrix} 0 & E K_1 \overline{I} + \overline{E} & 0 \end{bmatrix} < 0. \end{aligned} \tag{23}$$

According to Lemma 3, (23) is equivalent to

$$\begin{bmatrix} -P^{-1} + \varepsilon_1 \overline{D}\, \overline{D}^T & \overline{G} + \overline{H} K_1 \overline{I} & \overline{H}_w & 0 \\ * & -P + \overline{C}^T \overline{C} & 0 & \left(E K_1 \overline{I} + \overline{E} \right)^T \\ * & * & -\gamma^2 I & 0 \\ * & * & * & -\varepsilon_1 I \end{bmatrix} < 0. \tag{24}$$

Substituting $K_1 = (I + \Lambda_2 F_2(k)) K (I + \Lambda_1 F_1(k))$ into (24), we have that

$$\begin{aligned} &\begin{bmatrix} -P^{-1} + \varepsilon_1 \overline{D}\, \overline{D}^T & \overline{G} + \overline{H} \left(I + \Lambda_2 F_2(k) \right) K \overline{I} & \overline{H}_w & 0 \\ * & -P + \overline{C}^T \overline{C} & 0 & \left(E \left(I + \Lambda_2 F_2(k) \right) K \overline{I} + \overline{E} \right)^T \\ * & * & -\gamma^2 I & 0 \\ * & * & * & -\varepsilon_1 I \end{bmatrix} \\ &\quad + \begin{bmatrix} \overline{H} \left(I + \Lambda_2 F_2(k) \right) K \Lambda_1 \\ 0 \\ 0 \\ E \left(I + \Lambda_2 F_2(k) \right) K \Lambda_1 \end{bmatrix} F_1(k) \begin{bmatrix} 0 & \overline{I} & 0 & 0 \end{bmatrix} + \begin{bmatrix} 0 & \overline{I} & 0 & 0 \end{bmatrix}^T F_1^T(k) \begin{bmatrix} \overline{H} \left(I + \Lambda_2 F_2(k) \right) K \Lambda_1 \\ 0 \\ 0 \\ E \left(I + \Lambda_2 F_2(k) \right) K \Lambda_1 \end{bmatrix}^T < 0. \end{aligned} \tag{25}$$

Considering that $F_1(k)$ is a diagonal matrix with $F_1^T(k) F_1(k) \leq I$, and so employing Lemma 5, we can get that

$$\begin{bmatrix} -P^{-1}+\varepsilon_1\overline{D}\,\overline{D}^T & \overline{G}+\overline{H}\left(I+\Lambda_2F_2(k)\right)K\overline{I} & \overline{H}_w & 0 \\ * & -P+\overline{C}^T\overline{C} & 0 & \left(E\left(I+\Lambda_2F_2(k)\right)K\overline{I}+\overline{E}\right)^T \\ * & * & -\gamma^2 I & 0 \\ * & * & * & -\varepsilon_1 I \end{bmatrix} + \begin{bmatrix} \overline{H}\left(I+\Lambda_2F_2(k)\right)K\Lambda_1 \\ 0 \\ 0 \\ E\left(I+\Lambda_2F_2(k)\right)K\Lambda_1 \end{bmatrix} W_1^{-1} \begin{bmatrix} \overline{H}\left(I+\Lambda_2F_2(k)\right)K\Lambda_1 \\ 0 \\ 0 \\ E\left(I+\Lambda_2F_2(k)\right)K\Lambda_1 \end{bmatrix}^T + \begin{bmatrix} 0 & \overline{I} & 0 & 0 \end{bmatrix}^T W_1 \begin{bmatrix} 0 & \overline{I} & 0 & 0 \end{bmatrix} < 0. \tag{26}$$

According to Lemma 3, (26) is equivalent to

$$\begin{bmatrix} -P^{-1}+\varepsilon_1\overline{D}\,\overline{D}^T & \overline{G}+\overline{H}\left(I+\Lambda_2F_2(k)\right)K\overline{I} & \overline{H}_w & 0 & \overline{H}\left(I+\Lambda_2F_2(k)\right)K\Lambda_1 \\ * & -P+\overline{C}^T\overline{C}+\overline{I}^TW_1\overline{I}_1 & 0 & \left(E\left(I+\Lambda_2F_2(k)\right)K\overline{I}+\overline{E}\right)^T & 0 \\ * & * & -\gamma^2 I & 0 & 0 \\ * & * & * & -\varepsilon_1 I & E\left(I+\Lambda_2F_2(k)\right)K\Lambda_1 \\ * & * & * & * & -W_1 \end{bmatrix} < 0. \tag{27}$$

Similarly, we can eliminate $F_2(k)$. By use of Lemma 5, we have that

$$\begin{bmatrix} -P^{-1}+\varepsilon_1\overline{D}\,\overline{D}^T & \overline{G}+\overline{H}K\overline{I} & \overline{H}_w & 0 & \overline{H}K\Lambda_1 \\ * & -P+\overline{C}^T\overline{C}+\overline{I}^TW_1\overline{I}_1 & 0 & \left(EK\overline{I}+\overline{E}\right)^T & 0 \\ * & * & -\gamma^2 I & 0 & 0 \\ * & * & * & -\varepsilon_1 I & EK\Lambda_1 \\ * & * & * & * & -W_1 \end{bmatrix} + \begin{bmatrix} \overline{H}\Lambda_2 \\ 0 \\ 0 \\ E\Lambda_2 \\ 0 \end{bmatrix} W_2 \begin{bmatrix} \overline{H}\Lambda_2 \\ 0 \\ 0 \\ E\Lambda_2 \\ 0 \end{bmatrix}^T + \begin{bmatrix} 0 & K\overline{I} & 0 & 0 & K\Lambda_1 \end{bmatrix}^T W_2^{-1} \begin{bmatrix} 0 & K\overline{I} & 0 & 0 & K\Lambda_1 \end{bmatrix} < 0. \tag{28}$$

Furthermore, applying Lemma 3, (28) can be converted to (16).

The proof is completed. □

Remark 8. Notice that the matrix inequality (16) in Theorem 7 is a bilinear matrix inequality due to the existence of P^{-1}. Generally, it can be solved by the linear approach [30] or the cone complementarity linearization (CCL) method [31]. By contrast, the CCL result is less conservative [32] and so is employed in this paper.

Corollary 9. *The bilinear matrix inequality* (16) *can be transformed to the following objective function minimization problems by the CCL method.*

Find

$$
\begin{gathered}
P > 0, \qquad X > 0, \qquad W_1 > 0, \\
W_2 > 0, \qquad \varepsilon_1 > 0, K \\
\min \qquad \text{Trace}\,(PX) \\
\text{s.t.} \quad \begin{bmatrix}
\widehat{\Pi}_{11} & \overline{G} + \overline{H}K\overline{I} & \overline{H}_w & \Pi_{14} & \overline{H}K\Lambda_1 & 0 \\
* & \Pi_{22} & 0 & \left(EK\overline{I} + \overline{E}\right)^T & 0 & \left(K\overline{I}\right)^T \\
* & * & -\gamma^2 I & 0 & 0 & 0 \\
* & * & * & \Pi_{44} & EK\Lambda_1 & 0 \\
* & * & * & * & -W_1 & \left(K\Lambda_1\right)^T \\
* & * & * & * & * & -W_2
\end{bmatrix} < 0, \\
\begin{bmatrix} P & I \\ I & X \end{bmatrix} \geq 0,
\end{gathered}
\tag{29}
$$

where $\widehat{\Pi}_{11} = -X + \varepsilon_1 \overline{D}\,\overline{D}^T + (\overline{H}\Lambda_2) W_2 (\overline{H}\Lambda_2)^T$.

Since Corollary 9 has turned the nonconvex feasibility problem of Theorem 7 into a minimization problem of nonlinear objective function with linear matrix inequalities constraints, it can be solved by the following iterative algorithm.

Algorithm 10.

Step 1. Find a set of feasible solutions $\Xi_0 = \{P_0, X_0, W_{10}, W_{20}, \varepsilon_{10}, K_0\}$, which satisfyies (29), and set the iterative number $l = 0$.

Step 2. Use LMI toolbox of mincx solver to solve the following linear objective function minimization problem:

$$
\begin{gathered}
\min \quad \text{Trace}\left(P_l X + P X_l\right) \\
\text{s.t.} \qquad (29).
\end{gathered}
\tag{30}
$$

The solutions are set $\Xi^* = \{P^*, X^*, W_1^*, W_2^*, \varepsilon_1^*, K^*\}$.

Step 3. Substituting the solutions Ξ^* into the matrix inequality (16) in Theorem 7 to check if (16) is satisfied, then K^* becomes the state feedback gain matrix and the iteration terminates. Otherwise, enter into Step 4.

Step 4. If the iterative number satisfies $l \leq L$ (L is a predetermined iterative number upper bound), set $\Xi_{l+1} = \Xi^*$, $l = l + 1$, and return to Step 2 for the next iteration. Otherwise, enter into Step 1 and reselect a set of feasible solutions Ξ_0 to calculate.

Thus, a state feedback H_∞ controller can be obtained for NCSs with both deadband scheduling and uncertain short time-delay. More especially, if there are no deadband schedulers in the NCSs shown in Figure 1, the closed-loop system in (10) reads

$$
\begin{gathered}
z(k+1) = \Phi_k z(k) + \overline{H}_w w(k), \\
y(k) = \overline{C} z(k),
\end{gathered}
\tag{31}
$$

where

$$
\begin{aligned}
\Phi_k &= \begin{bmatrix} G + \left(H_0 + DF\left(\tau_k'\right)E\right)K & H_1 - DF\left(\tau_k'\right)E \\ K & 0 \end{bmatrix} \\
&= \overline{G} + \overline{H}K\overline{I} + \overline{D}F\left(\tau_k'\right)EK\overline{I} + \overline{D}F\left(\tau_k'\right)\overline{E}.
\end{aligned}
\tag{32}
$$

Then, we have the following corollary, which can be proved along similar lines as in the proof of Theorem 7.

Corollary 11. *Consider the NCSs in Figure 1, but without the deadband schedulers. For a given scalar $\gamma > 0$, the closed-loop system* (31) *is asymptotically stable with H_∞ performance γ if there exist symmetric positive-definite matrix P, feedback gain matrix K, and scalar $\varepsilon_1 > 0$ such that*

$$
\begin{bmatrix}
-P^{-1} + \varepsilon_1 \overline{D}\,\overline{D}^T & \overline{G} + \overline{H}K\overline{I} & \overline{H}_w & 0 \\
* & -P + \overline{C}^T\overline{C} & 0 & \left(EK\overline{I} + \overline{E}\right)^T \\
* & * & -\gamma^2 I & 0 \\
* & * & * & -\varepsilon_1 I
\end{bmatrix} < 0.
\tag{33}
$$

Similarly, the bilinear matrix inequality (33) *can be solved by the above CCL method and the iterative algorithm in Corollary 9 and is thus omitted.*

4. Numerical Example

In this section, a numerical example is introduced to demonstrate the effectiveness of the proposed method. Consider a ball and beam system with [33]

$$
\begin{gathered}
\dot{x}(t) = \begin{bmatrix} 0 & 1 \\ 0 & 0 \end{bmatrix} x(t) + \begin{bmatrix} 0 \\ 1 \end{bmatrix} u(t) + \begin{bmatrix} 0 \\ 1 \end{bmatrix} w(t), \\
y(t) = \begin{bmatrix} 1 & 0 \end{bmatrix} x(t).
\end{gathered}
\tag{34}
$$

Table 1: The feedback gain matrix K values for various Λ_1, Λ_2.

Case	Λ_1	Λ_2	K
1	Without scheduling	Without scheduling	$K = [-0.5462 \quad -1.0978]$
2	$[0.02 \quad 0; 0 \quad 0.02]$	0.02	$K = [-0.4942 \quad -1.0314]$
3	$[0.05 \quad 0; 0 \quad 0.05]$	0.05	$K = [-0.4393 \quad -0.9733]$
4	$[0.07 \quad 0; 0 \quad 0.07]$	0.05	$K = [-0.4185 \quad -0.9605]$
5	$[0.1 \quad 0; 0 \quad 0.1]$	0.07	No solution

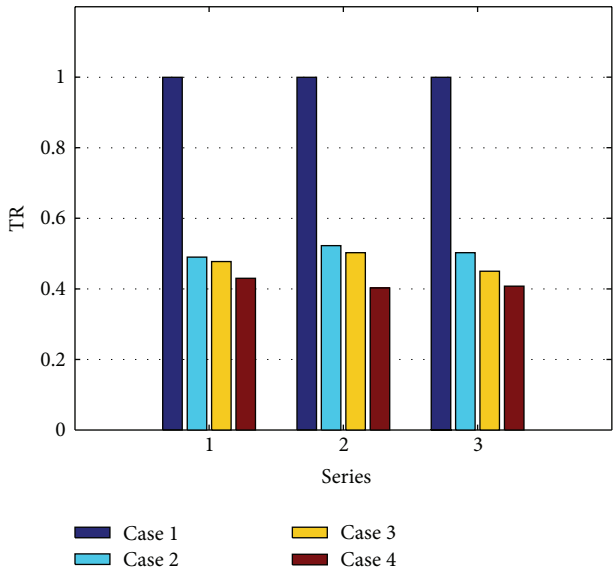

Figure 2: The performance of MTR.

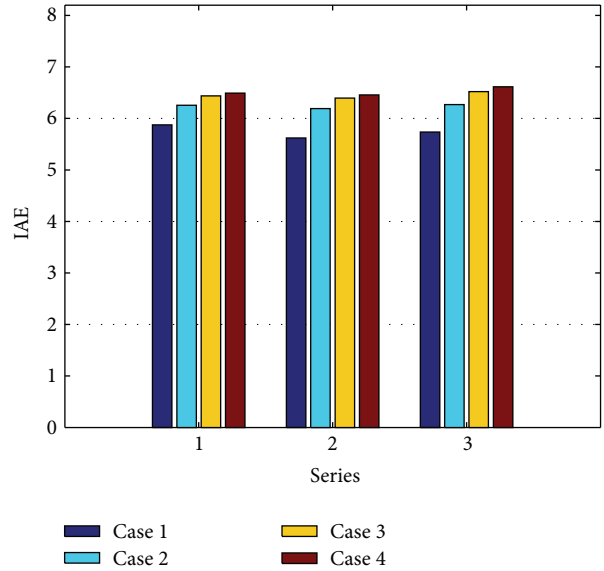

Figure 3: The performance of IAE.

In this example, we choose $h = 0.5s$, and $\tau_k \in [0, h]$ is time varying and nondeterministic. According to (2) and (3), we have that

$$G = \begin{bmatrix} 1 & 0.5 \\ 0 & 1 \end{bmatrix}, \quad H_0 = \begin{bmatrix} 0.0313 \\ 0.25 \end{bmatrix},$$
$$H_1 = \begin{bmatrix} 0.0938 \\ 0.25 \end{bmatrix}, \quad D = \begin{bmatrix} 0.2661 & 0.0665 \\ 0 & 0.2661 \end{bmatrix}, \tag{35}$$
$$E = \begin{bmatrix} 0 \\ 1 \end{bmatrix}, \quad H_w = \begin{bmatrix} 0.125 \\ 0.5 \end{bmatrix}.$$

For a given disturbance attenuation level $\gamma = 5$, based on the LMI toolbox, and applying Corollaries 9 and 11, the feedback gain matrix K values are given with different error threshold values Λ_1, Λ_2 in Table 1. It is obvious from Table 1 that for a given level γ we can find the feasible feedback gain matrix K values when Λ_1, Λ_2 are within certain ranges.

In addition, we choose the initial value $x_0 = [2 \quad -0.5]^T$, the disturbance

$$w(k) = \begin{cases} 0.1, & 50 \le k \le 60, \\ 0, & \text{other}, \end{cases} \tag{36}$$

and the total runtime 100 seconds. Define MTR $= n_{\text{sent}}/n_{\text{total}}$ and IAE $= \sum \|e(k)\|_2 \cdot h$, in which MTR denotes the mean data transmission rate (n_{sent} and n_{total} denote the number of data transmitted with and without deadband schedulers in the runtime, respectively.) and IAE denotes the control performance of the system. Under three different random time-delay sequences, the performance of MTR and IAE is shown for the system with the above four error threshold values in Figures 2 and 3, respectively. It can be easily seen that compared with the system without deadband schedulers (case 1), although the control performance of the system by using deadband scheduling scheme (case 2–case 4) is slightly worse (in Figure 3), the mean data transmission rate of the system is greatly reduced (in Figure 2).

Figures 4–6 show the simulation results for the system in which the error threshold values take $\Lambda_1 = \text{diag}\{0.07, 0.07\}$, $\Lambda_2 = 0.05$, the feedback gain matrix $K = [-0.4185 \quad -0.9605]$ according to Table 1, and the time-delay takes the first series. It can be seen that the closed-loop system is asymptotically stable (in Figure 4), and only part of the sampled data and control signal are transmitted with the proposed deadband scheduling scheme (in Figures 5 and 6, here the transmission interval of $\bar{x}_2(k)$ is similar to $\bar{x}_1(k)$ in DS1 and is thus omitted).

Furthermore, under zero initial conditions, we get that $\|y\|_2 = 0.7310$, $\|w\|_2 = 0.3317$, which yields $\gamma^* = 2.20$. It means that the practical disturbance attenuation level

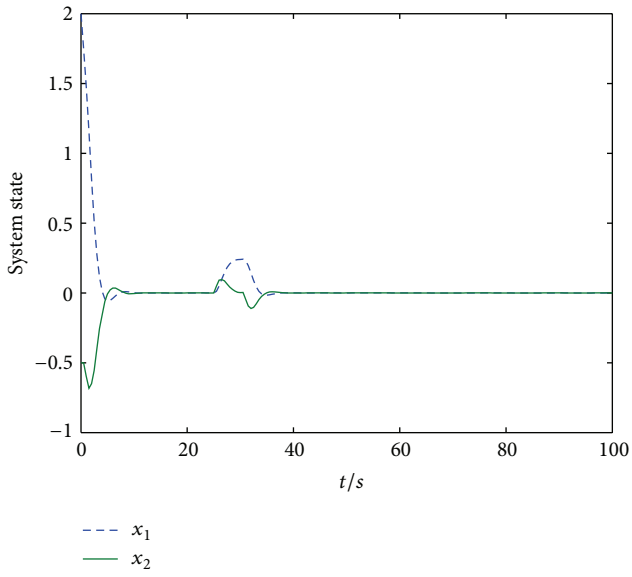

Figure 4: State response curves of the closed-loop system.

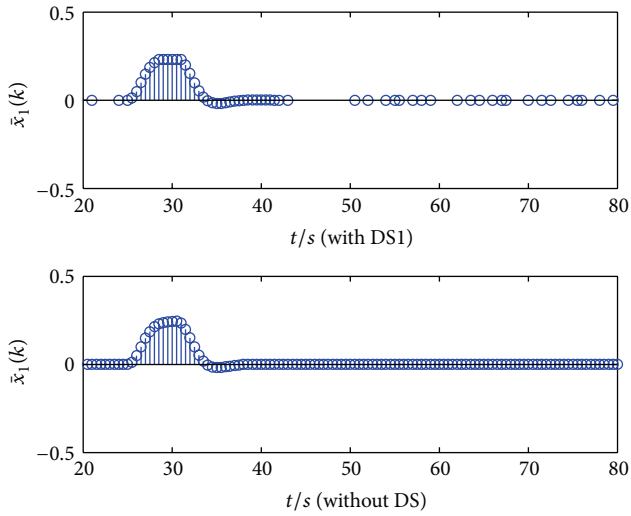

Figure 5: Comparisons of the transmission interval of $\bar{x}_1(k)$.

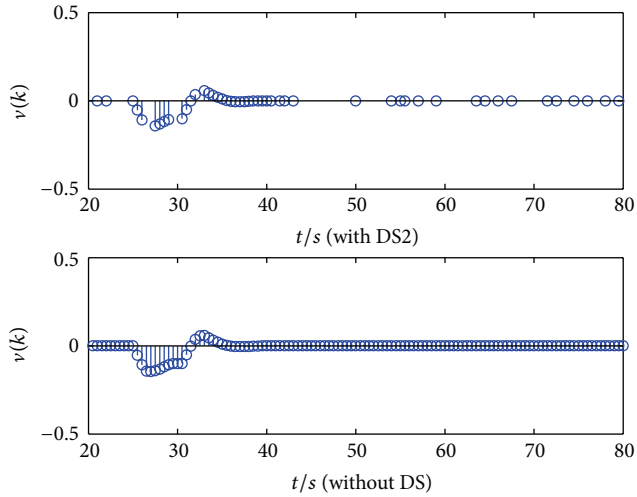

Figure 6: Comparisons of the transmission interval of $v(k)$.

is smaller than the given level $\gamma = 5$, which shows the effectiveness of the proposed H_∞ controller design method.

5. Conclusions

In this paper, a discrete-time model for NCSs with both deadband scheduling and time-delay has been established and the H_∞ control problem has been investigated. Based on the LMI approach, a state feedback H_∞ controller has been designed to ensure the closed-loop system asymptotically to be stable with H_∞ performance index. A numerical example has been provided to show the validness of the derived results. Since the principles and algorithms of deadband schedulers in this paper are very simple, the smart sensor and controller are easy to implement. In addition, simulation results show that it can effectively reduce the node's data transmission rate, so it is very suitable for applying in the NCSs with limited bandwidth resources.

Acknowledgments

The authors thank the reviewers for their very helpful comments and suggestions, which have improved the presentation of this paper. This study is supported by the National Natural Science Foundation of China under Grant 61174029, the Key Project of Chinese Ministry of Education under Grant 211067 and the Zhejiang Provincial Natural Science Foundation of China under Grant Y1110944.

References

[1] J. P. Hespanha, P. Naghshtabrizi, and Y. Xu, "A survey of recent results in networked control systems," *Proceedings of the IEEE*, vol. 95, no. 1, pp. 138–172, 2007.

[2] H. Gao and T. Chen, "H_∞ estimation for uncertain systems with limited communication capacity," *IEEE Transactions on Automatic Control*, vol. 52, no. 11, pp. 2070–2084, 2007.

[3] P. Antsaklis and J. Baillieul, "Special issue on networked control systems," *IEEE Transactions on Automatic Control*, vol. 49, no. 9, pp. 1421–1423, 2004.

[4] R. A. Gupta and M.-Y. Chow, "Networked control system: overview and research trends," *IEEE Transactions on Industrial Electronics*, vol. 57, no. 7, pp. 2527–2535, 2010.

[5] W.-A. Zhang and L. Yu, "A robust control approach to stabilization of networked control systems with time-varying delays," *Automatica*, vol. 45, no. 10, pp. 2440–2445, 2009.

[6] B. Zhang and S. Xu, "Delay-dependent robust H_∞ control for uncertain discrete-time fuzzy systems with time-varying delays," *IEEE Transactions on Fuzzy Systems*, vol. 17, no. 4, pp. 809–823, 2009.

[7] B. Zhang, S. Xu, Y. Chu, and G. Zong, "Delay-dependent stability for Markovian genetic regulatory networks with time-varying delays," *Asian Journal of Control*, vol. 14, no. 5, pp. 1403–1406, 2012.

[8] Y. Li, S. Fei, B. Zhang, and Y. Chu, "Decentralized $L_2 - L_\infty$ filtering for interconnected Markovian jump systems with delays," *Circuits, Systems, and Signal Processing*, vol. 31, no. 3, pp. 889–909, 2012.

[9] B. Y. Zhang, W. X. Zheng, and S. Y. Xu, "Filtering of Markovian jump delay systems based on a new performance index," *IEEE Transactions on Circuits and Systems I*, vol. 60, no. 5, pp. 1250–1263, 2013.

[10] B. Zhang and W. X. Zheng, "H_∞ filter design for nonlinear networked control systems with uncertain packet-loss probability," *Signal Processing*, vol. 92, no. 6, pp. 1499–1507, 2012.

[11] Q. Lu, L. Zhang, M. Basin, and H. Tian, "Analysis and synthesis for networked control systems with uncertain rate of packet losses," *Journal of the Franklin Institute*, vol. 349, no. 7, pp. 2500–2514, 2012.

[12] W.-A. Zhang, L. Yu, and G. Feng, "Optimal linear estimation for networked systems with communication constraints," *Automatica*, vol. 47, no. 9, pp. 1992–2000, 2011.

[13] L. M. Feeney and M. Nilsson, "Investigating the energy consumption of a wireless network interface in an ad hoc networking environment," in *Proceedings of the 20th Annual Joint Conference of the IEEE Computer and Communications Societies (INFOCOM '01)*, pp. 1548–1557, Anchorage, Alaska, USA, April 2001.

[14] P. G. Otanez, J. R. Moyne, and D. M. Tilbury, "Using deadbands to reduce communication in networked control systems," in *Proceedings of the American Control Conference*, pp. 3015–3020, Piscataway, NJ, USA, May 2002.

[15] X.-M. Tang, K. Qian, and J.-S. Yu, "Dynamic deadband feedback scheduling in networked control systems," *Journal of East China University of Science and Technology*, vol. 33, no. 5, pp. 716–721, 2007.

[16] H. Y. Chen, W. L. Wang, and Z. X. Li, "Communication scheduling of networked control system based on error threshold," *Information and Control*, vol. 38, no. 5, pp. 580–584, 2009.

[17] Y.-B. Zhao, G.-P. Liu, and D. Rees, "Packet-based deadband control for internet-based networked control systems," *IEEE Transactions on Control Systems Technology*, vol. 18, no. 5, pp. 1057–1067, 2010.

[18] Z. N. Gao, R. H. Xie, W. H. Fan, and Q. W. Chen, "H_∞ control of wireless networked control systems with signal-difference-based deadband scheduling," *Control and Decision*, vol. 27, no. 9, pp. 1301–1307, 2012.

[19] M. Miskowicz, "Send-on-delta concept: an event-based data reporting strategy," *Sensors*, vol. 6, no. 1, pp. 49–63, 2006.

[20] Y. S. Suh, "Send-on-delta sensor data transmission with a linear predictor," *Sensors*, vol. 7, no. 4, pp. 537–547, 2007.

[21] Y. S. Suh, V. H. Nguyen, and Y. S. Ro, "Modified Kalman filter for networked monitoring systems employing a send-on-delta method," *Automatica*, vol. 43, no. 2, pp. 332–338, 2007.

[22] M. Miskowicz, "Efficiency of event-based sampling according to error energy criterion," *Sensors*, vol. 10, no. 3, pp. 2242–2261, 2010.

[23] A. D. McKernan and G. W. Irwin, "Event-based sampling for wireless network control systems with QoS," in *Proceedings of the American Control Conference (ACC '10)*, pp. 1841–1846, Baltimore, Md, USA, July 2010.

[24] J. Lunze and D. Lehmann, "A state-feedback approach to event-based control," *Automatica*, vol. 46, no. 1, pp. 211–215, 2010.

[25] S. Li, D. Sauter, and B. Xu, "Fault isolation filter for networked control system with event-triggered sampling scheme," *Sensors*, vol. 11, no. 1, pp. 557–572, 2011.

[26] S. Hu and D. Yue, "Event-triggered control design of linear networked systems with quantizations," *ISA Transactions*, vol. 51, no. 1, pp. 153–162, 2012.

[27] W. G. Ma and C. Shao, "Stochastic stability for networked control system," *Acta Automatic Sinica*, vol. 38, no. 8, pp. 378–382, 2007.

[28] L. Yu, *Robust Control—The Method of Linear Matrix Inequalities*, Tsinghua University Press, Beijing, China, 2002.

[29] W. Wang and F. W. Yang, "Robust and non-fragile H_∞ control for linear interval system," *Journal of Jimei University*, vol. 10, no. 2, pp. 109–113, 2005.

[30] H. Gao, T. Chen, and J. Lam, "A new delay system approach to network-based control," *Automatica*, vol. 44, no. 1, pp. 39–52, 2008.

[31] W.-A. Zhang and L. Yu, "Output feedback stabilization of networked control systems with packet dropouts," *IEEE Transactions on Automatic Control*, vol. 52, no. 9, pp. 1705–1710, 2007.

[32] H. Zhao, *Analysis and Design of Networked Control System Based on Free-Weighting Matrices*, Central South University, Changsha, China, 2011.

[33] G. Xie and L. Wang, "Stabilization of NCSs with time-varying transmission period," in *Proceedings of the IEEE International Conference on Systems, Man and Cybernetics*, pp. 3759–3763, Waikoloa, Hawaii, USA, October 2005.

Hindawi Publishing Corporation
Mathematical Problems in Engineering
Volume 2013, Article ID 871674, 6 pages
http://dx.doi.org/10.1155/2013/871674

Research Article

Modeling and Backstepping Control of the Electronic Throttle System

Rui Bai,[1] Shaocheng Tong,[1] and Hamid Reza Karimi[2]

[1] *School of Electrical Engineering, Liaoning University of Technology, Jinzhou 121001, China*
[2] *Department of Engineering, Faculty of Engineering and Science, University of Agder, 4898 Grimstad, Norway*

Correspondence should be addressed to Rui Bai; broffice@126.com

Received 20 August 2013; Accepted 22 September 2013

Academic Editor: Tao Li

Electronic throttle is widely used in modern automotive engines. An electronic throttle system regulates the throttle plate angle by using a DC servo motor to adjust the inlet airflow rate of an internal combustion engine. Its application leads to improvements in vehicle drivability, fuel economy, and emissions. In this paper, by taking into account the dynamical behavior of the electronic throttle, the mechanism model is first built, and then the mechanism model is transformed into the state-space model. Based on the state-space model and using the backstepping design technique, a new backstepping controller is developed for the electronic throttle. The proposed controller can make the actual angle of the electronic throttle track its set point with the satisfactory performance. Finally, a computer simulation is performed, and simulation results verify that the proposed control system can achieve favorable tracking performance.

1. Introduction

In recent years, many functions of modern automobiles are shifting from a purely mechanical to an electromechanical implementation. These functions are implemented by using the so-called "x-by-wire" systems, including drive-by-wire and steer-by-wire systems [1]. "X-by-wire" systems act as an interface between the driver and the targeted mechanical subsystem of the vehicle. Now, advanced control strategies, including the data-driven control [2], fuzzy control [3, 4], and neural network control [5, 6], have been widely applied in the process industry and automobile industry, for example, the Tennessee Eastman process [7], the suspension control system [8, 9], the electronic throttle control system [10, 11], and so on. In this paper, we focus on the control strategy of the electronic throttle system, which is one of the important drive-by-wire systems in the automobile industry.

In automotive spark ignition engines, the air coming into the intake manifold and therefore the power generated strongly depend on the angular position of a throttle valve [12]. In traditional systems, the throttle position is actuated by a mechanical link with the accelerator pedal, directly operated by the driver. The traditional mechanical throttle is difficult to achieve the accurate control result. Therefore, the vehicle drivability, fuel economy, and emissions are not satisfactory by using the traditional mechanical throttle. In recent years, new and increasing requirements in terms of emissions control, drivability, and safety have led to the development of electronic throttle system. The electronic throttle is essentially a DC-motor-driven valve that regulates air inflow into the vehicle's combustion system, and the mechanical linkage between accelerator pedal and the throttle is replaced by an electronic connection [13]. Recently, several control strategies for electronic throttle have been presented. In [10], a new intelligent fuzzy controller is proposed. It can handle the nonlinear hysteretic of electronic throttle. In [11], the controller synthesis is performed in discrete time by solving a constrained time-optimal control problem of the throttle. In [12], a robust position controller for motorized throttle body in automotive applications is presented. Complexity of the control problem is explained and control architecture is also presented. In [13], a process to design the control strategy is proposed for a vehicle with the electronic throttle control and the automatic transmission, and the dynamic programming

(DP) technique is also used to obtain the optimal gear shift and throttle opening angular which maximizes fuel economy while satisfying the power demand. In [14], the nonlinear hysteretic characteristic of the electronic throttle is described and the variable structure control method is proposed to control the electronic throttle. In [15], an adaptive control strategy for the electronic throttle is introduced. In [16], an integrated control strategy is proposed, which consists of a proportional-integral-derivative (PID) controller and a feedback compensator for friction and limp-home effects. In [17], a novel nonlinear controller for the electronic throttle valve is presented, which uses the approximate model method and support vector machine (SVM) modeling. Although the abovementioned control methods can achieve the acceptable control performance, these control methods have complex structure and algorithm. As we know, the controller complex design process often leads to the difficulty of its realization in the actual automotive manufacturing industry. Therefore, more attention has been paid to backstepping design technique because of its systematic design and the excellent transient performance of the closed-loop system. Backstepping design technique is a recursive and systematic design scheme first presented by Kanellakopoulos et al. in 1991 [18]. The main idea is to decompose a complex system into multiple small-scale subsystems, then to design recursively control Lyapunov function and virtual controller for each subsystem, and finally obtain the original control law and realize the global regulation and tracking for the controlled system [19–21]. For the systematic design process, backstepping control scheme is easy to be realized, and it has been applied in many cases, such as induction motor [22], chemical process [23, 24], ship course [25], and robot manipulator [26].

Motivated by the advantage of the backstepping design method, this paper investigates the backstepping control problem of the electronic throttle. Since the backstepping design technique is a typical model-based design method, the dynamical model of the electronic throttle is first built in this paper. Based on the proposed dynamical model, the backstepping control design method for the electronic throttle is presented. The proposed backstepping controller can achieve the satisfactory performance; that is, the actual angular of the electronic throttle can track its set point. Finally, a computer simulation is performed, and simulation results verify the effectiveness of the proposed control method.

This paper is organized as follows. Section 2 describes the mathematical model of the electronic throttle. Section 3 designs the electronic throttle controller by using the backstepping method. Section 4 illustrates the simulation results and finally Section 5 shows the conclusion of this paper.

2. Mathematic Model of the Electronic Throttle

There are some symbols in this section. At first, definitions of these symbols are described as follows:

θ^*: Set point of the valve plate angular

$\theta(t)$: Actual angular of the valve plate

θ_0: Static angular of the valve plate

$\omega(t)$: Angular speed of the valve plate

$i_a(t)$: Armature current

R_a: Armature resistance

$U_a(t)$: Input voltage of the motor

$U_b(t)$: Electromotive force

U_{bat}: Supply voltage

$D(t)$: Duty cycle of the bipolar chopper

$T_e(t)$: Electromagnetism torque

$T_s(t)$: Return spring torque

$T_f(t)$: Friction torque

K_t: Torque constant

K_s: Elastic coefficient

K_m: Torque compensation coefficient

K_d: Friction coefficient

J: Moment of inertia

j: Gear ratio.

The schematic of a typical electronic throttle control system is shown in Figure 1.

There are a controller, a bipolar chopper, and an electronic throttle body (ETB) in Figure 1. ETB consists of a DC drive powered by the bipolar chopper, a gearbox, a valve plate, a return spring, and a position sensor. When the valve plate angular is regulated, the air inflow into the vehicle's combustion system can also be regulated. The control objective of the electronic throttle is to control the valve plate angular tracking its set point with the satisfactory performance.

At first, we build the motion equation for the electronic throttle system. The motion equation is

$$jT_e(t) - T_s(t) - T_f(t) = j^2 J \frac{d\omega(t)}{dt}. \tag{1}$$

The relation between current $i_a(t)$ and input voltage $U_a(t)$ in the armature circuit is described as

$$i_a(t) R_a = U_a(t) - U_b(t), \tag{2}$$

where

$$\begin{aligned} U_a(t) &= U_{\text{bat}} \times D(t), \\ U_b(t) &= K_t \times j \times \omega(t). \end{aligned} \tag{3}$$

By substituting (3) into (2), we have

$$i_a(t) = \frac{U_{\text{bat}} \times D(t) - K_t \times j \times \omega(t)}{R_a}. \tag{4}$$

Computation formula of $T_e(t)$ is

$$T_e(t) = K_t i_a(t). \tag{5}$$

By substituting (4) into (5), we get

$$T_e(t) = K_t \frac{U_{\text{bat}} \times D(t) - K_t \times j \times \omega(t)}{R_a}. \tag{6}$$

Return spring torque $T_s(t)$ and friction torque $T_f(t)$ are

$$\begin{aligned} T_s(t) &= K_s(\theta(t) - \theta_0) + K_m, \\ T_f(t) &= K_d \omega(t). \end{aligned} \tag{7}$$

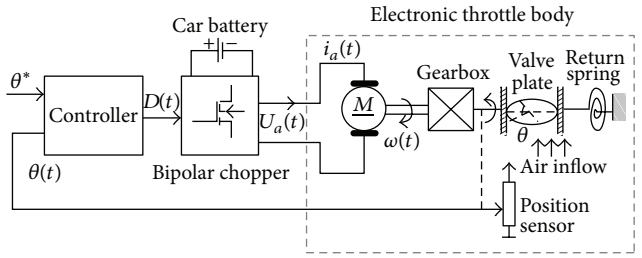

Figure 1: Electronic throttle control system.

By substituting (6) and (7) into (1), we get

$$\frac{d\omega(t)}{dt} = -\frac{K_s}{j^2 \times J} \times \theta(t) - \left(\frac{K_t^2}{JR_a} + \frac{K_d}{j^2 \times J}\right)\omega(t) + \frac{K_t \times U_{\text{bat}}}{j \times J \times R_a} D(t) + \frac{K_s\theta_0 - K_m}{j^2 \times J}. \tag{8}$$

Equation (8) is the mechanism model of the electronic throttle.

Defining state variables $x_1(t) = \theta(t)$, $x_2(t) = \omega(t)$, input variable $u(t) = D(t)$, and the output variable $y(t) = \theta(t)$, (8) can be rewritten as

$$\dot{x}_1(t) = x_2(t), \tag{9}$$

$$\dot{x}_2(t) = -\frac{K_s}{j^2 \times J} \times x_1(t) - \left(\frac{K_t^{\,2}}{JR_a} + \frac{K_d}{j^2 \times J}\right)x_2(t) + \frac{K_t \times U_{bat}}{j \times J \times R_a} u(t) + \frac{K_s\theta_0 - K_m}{j^2 \times J}, \tag{10}$$

$$y(t) = x_1(t). \tag{11}$$

Equations (9)–(11) are the state-space model of the electronic throttle.

3. Backstepping Control Design and Stability Analysis

The control objective of this paper is to design a backstepping control system such that the output $y(t)$ of the system shown in (11) to track its set point x_d asymptotically. The proposed backstepping control procedure is described step by step as follows.

Step 1. For the position-tracking objective, define the tracking error as

$$z_1(t) = x_1(t) - x_d. \tag{12}$$

Taking $\alpha(t)$ as a virtual control and defining

$$z_2(t) = x_2(t) - \alpha(t), \tag{13}$$

consider the following Lyapunov function candidate:

$$V_1(t) = \frac{1}{2} z_1^2(t). \tag{14}$$

The time derivative of $V_1(t)$ is

$$\dot{V}_1(t) = z_1(t)\,\dot{z}_1(t). \tag{15}$$

From (12) and (13), we obtain

$$\begin{aligned}\dot{z}_1(t) &= \dot{x}_1(t)\\ &= x_2(t)\\ &= -z_1(t) + z_1(t) + x_2(t) - \alpha(t) + \alpha(t)\\ &= -z_1(t) + x_2(t) - \alpha(t) + z_1(t) + \alpha(t)\\ &= -z_1(t) + z_2(t) + z_1(t) + \alpha(t).\end{aligned} \tag{16}$$

Choosing the virtual control function $\alpha(t)$

$$\alpha(t) = -z_1(t). \tag{17}$$

By substituting (17) into (16), we have

$$\dot{z}_1(t) = -z_1(t) + z_2(t). \tag{18}$$

By using (18) and (15), we get

$$\begin{aligned}\dot{V}_1(t) &= z_1(t)\,\dot{z}_1(t)\\ &= z_1(t)\left(-z_1(t) + z_2(t)\right)\\ &= -z_1^2(t) + z_1(t)\,z_2(t).\end{aligned} \tag{19}$$

From (19), we know if $z_2(t)$ is equal to zero, the time derivative of $V_1(t)$ will be smaller than or equal to zero. If $\dot{V}_1(t) \le 0$, we know that $z_1(t)$ will converge to zero, and $x_1(t)$ will converge to the set point x_d. Therefore, in the next step, we will design a controller $u(t)$ to make $z_2(t)$ converge to zero.

Step 2. Consider the following Lyapunov function candidate $V_2(t)$:

$$V_2(t) = \frac{1}{2} z_2^2(t) + V_1(t). \tag{20}$$

The time derivative of $V_2(t)$ is

$$\begin{aligned}\dot{V}_2(t) &= z_2(t)\,\dot{z}_2(t) + \dot{V}_1(t)\\ &= z_2(t)\,\dot{z}_2(t) - z_1^2(t) + z_1(t)\,z_2(t)\end{aligned} \tag{21}$$

From (10), (13), and (17), we have

$$\begin{aligned}\dot{z}_2(t) &= \dot{x}_2(t) - \dot{\alpha}(t)\\ &= \mu_0 u(t) - \mu_1 x_1(t) - \mu_2 x_2(t) + F - \dot{\alpha}(t),\end{aligned} \tag{22}$$

where $\mu_0 = K_t/(j \times J \times R_a)$, $\mu_1 = K_s/(j^2 \times J)$, and $\mu_2 = K_b \times K_t/JR_a + K_d/j^2 \times J$ and $F = (K_s\theta_0 - K_m)/(j^2 \times J)$.

Note that

$$\begin{aligned}\dot{\alpha}(t) &= -\dot{z}_1(t)\\ &= -\dot{x}_1(t)\\ &= -x_2(t).\end{aligned} \tag{23}$$

Table 1: Parameter values.

$j = 20$	$J = 0.02\,\text{Kg·m}^2$	$R = 2.1\,\Omega$
$K_b = 0.075\,\text{N·m/A}$	$K_t = 0.072\,\text{N·m/A}$	$K_m = 0.34\,\text{N·m}$
$K_s = 0.01\,\text{N·m/rad}$	$K_d = 5 \times 10^{-6}\,\text{N·m·s/rad}$	$\theta_0 = 0.16\,\text{rad}$

By substituting (23) into (22), we have

$$\begin{aligned}\dot{z}_2(t) &= \mu_0 u(t) - \mu_1 x_1(t) - \mu_2 x_2(t) + F + x_2(t)\\ &= \mu_0 u(t) - \mu_1 \left[x_1(t) - x_d + x_d\right]\\ &\quad - \mu_2 \left[x_2(t) - \alpha(t) + \alpha(t)\right] + F + x_2(t)\\ &= \mu_0 u(t) - \mu_1 z_1(t) - \mu_1 x_d - \mu_2 z_2(t)\\ &\quad - \mu_2 \alpha(t) + F + x_2(t)\\ &= \mu_0 u(t) - \mu_1 z_1(t) - \mu_1 x_d - \mu_2 z_2(t)\\ &\quad + \mu_2 z_1(t) + F + x_2(t).\end{aligned} \tag{24}$$

Choosing the control function $u(t)$

$$\begin{aligned}u(t) = \frac{1}{\mu_0}\{&(\mu_1 - 1) z_1(t) + (\mu_2 - 1) z_2(t)\\ &+\mu_1 x_d - \mu_2 z_1(t) - F - x_2(t)\}.\end{aligned} \tag{25}$$

From (25) and (24), we have

$$\dot{z}_2(t) = -z_1(t) - z_2(t) \tag{26}$$

Substituting (26) into (21) results in

$$\begin{aligned}\dot{V}_2(t) &= z_2(t)\dot{z}_2(t) - z_1^2(t) + z_1(t) z_2(t)\\ &= z_2(t)\left[-z_1(t) - z_2(t)\right]\\ &\quad - z_1^2(t) + z_1(t) z_2(t)\\ &= -z_1^2(t) - z_2^2(t) \le 0.\end{aligned} \tag{27}$$

Equation (27) means that $\dot{V}_2(t) \le 0$. Therefore, it is obtained that the variables $z_1(t)$ and $z_2(t)$ converge to zero; that is, the output $y(t) = x_1(t)$ of the system shown in (11) can track its set point x_d asymptotically.

4. Simulation Experiments

In this section, we perform simulation experiment to confirm the effectiveness of the proposed backstepping control. The values of the parameters in the electronic throttle system are given in Table 1. All these parameters are obtained from the experiment platform of the electronic throttle in our laboratory.

Simulation results are shown in Figures 2–5. Figure 2 shows the set point of the electronic throttle angular, that is, x_d. Figure 3 shows the input voltage of the DC servo motor. Figure 4 shows the actual angular of the electronic throttle, that is, $x_1(t)$. Figure 5 shows the actual angular speed of the electronic throttle, that is, $x_2(t)$. In Figure 2, set point x_d is

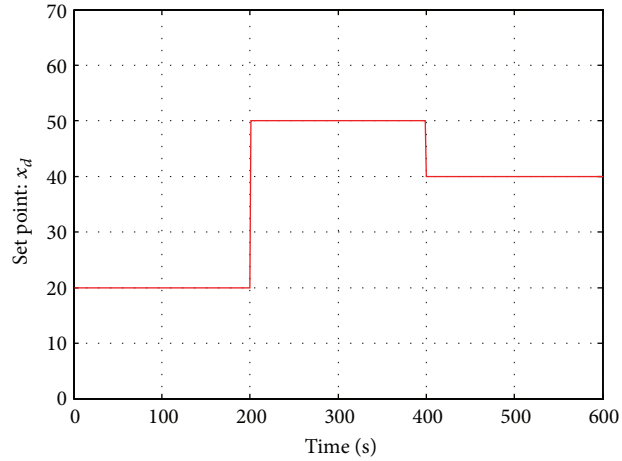

Figure 2: Set point of the valve plate angular.

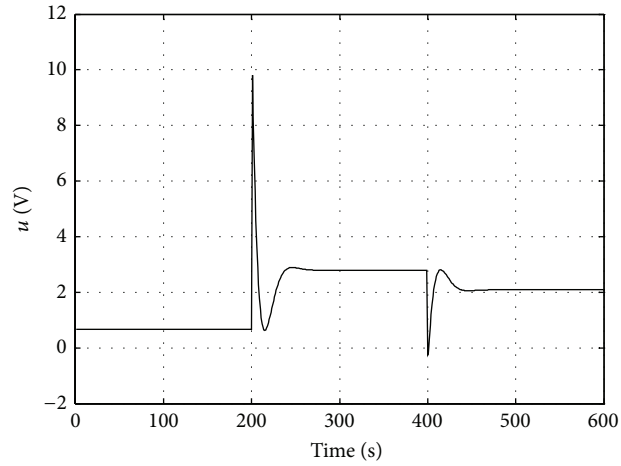

Figure 3: Input voltage of the motor.

20 degrees during 0 to 200 seconds. After 200 seconds, x_d is increased from 20 to 50 degrees, and after 400 seconds, x_d is decreased from 50 to 40 degrees.

At 200 seconds, x_d is increased. In order to increase the actual angular $x_1(t)$, the input voltage should be increased. From Figure 3, at first, the input voltage is increased when time is 200 seconds. Increase of the input voltage $u(t)$ leads to the increase of the angular speed $x_2(t)$, which is shown in Figure 5. When the angular speed $x_2(t)$ is increased, the actual angular of the electronic throttle $x_1(t)$ will be also increased, which is shown in Figure 4. Therefore, the actual angular $x_1(t)$ is regulated to track its set point. When the dynamical regulation process is finished, the input voltage $u(t)$ is a new stable value, and $x_2(t)$ is controlled to zero.

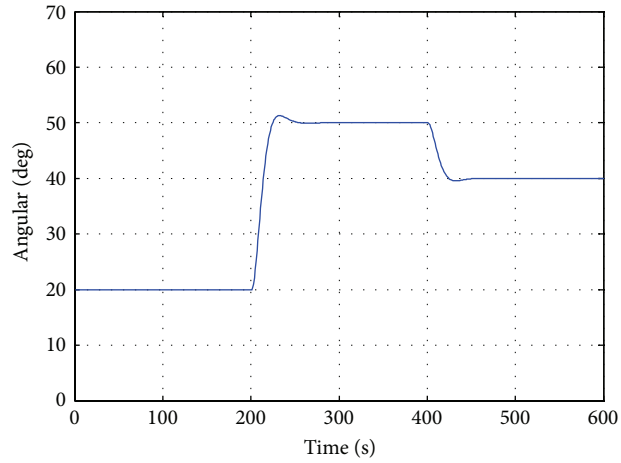

Figure 4: Actual angular of the valve plate.

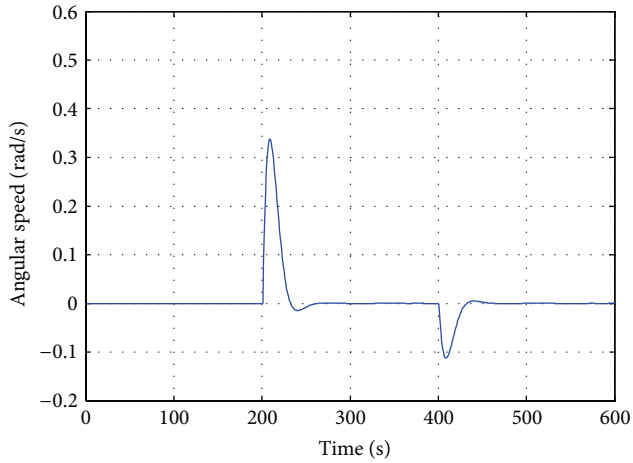

Figure 5: Angular speed of the valve plate.

At 400 seconds, x_d is decreased. When x_d is decreased, in order to decrease the actual angular $x_1(t)$, the input voltage should be decreased. From Figure 3, at first, the input voltage is decreased when time is 400 seconds. For the decrease of the input voltage, the angular speed $x_2(t)$ is also decreased, which is shown in Figure 5. When the $x_2(t)$ is decreased, the actual angular of the electronic throttle $x_1(t)$ will be decreased, which is shown in Figure 4. Therefore, the actual angular $x_1(t)$ is regulated to track its set point. When the dynamical regulation process is finished, the input voltage is a new stable value, and $x_2(t)$ is controlled to zero.

From Figures 2–5, we know that the dynamical process of the simulation experiment is right for the electronic throttle, and the tracking performance is also satisfactory.

5. Conclusions

In this paper, the model and control method on the electronic throttle is considered. The dynamical mechanism model and state-space model of the electronic throttle are presented. Based on the state-space model, a backstepping controller is developed. The proposed controller can make the actual angular of the throttle plate track its set point with the satisfactory performance. Simulation experiment is implemented, and the simulation results confirm the effectiveness of the proposed control method.

Conflict of Interests

None of the authors of the paper has declared any conflict of interests.

Acknowledgments

This work was supported by the National Natural Science Foundation of China (no. 61074014), Natural Science Fundamental of Liaoning Province (201102089), Program for Liaoning Excellent Talents in University (LJQ2011062), and the State Key Laboratory of Synthetic Automation for Process Industries.

References

[1] U. Kiencke and L. Nielsen, *Automotive Control Systems*, Springer, Berlin, Germany, 2005.

[2] S. Yin, S. X. Ding, A. H. A. Sari, and H. Hao, "Data-driven monitoring for stochastic systems and its application on batch process," *International Journal of Systems Science*, vol. 44, no. 7, pp. 1366–1376, 2013.

[3] Q. Zhou, P. Shi, J. Lu, and S. Xu, "Adaptive output-feedback fuzzy tracking control for a class of nonlinear systems," *IEEE Transactions on Fuzzy Systems*, vol. 19, no. 5, pp. 972–982, 2011.

[4] Q. Zhou, P. Shi, S. Y. Xu, and H. Y. Li, "Adaptive output feedback control for nonlinear time-delay systems by fuzzy approximation approach," *IEEE Transactions on Fuzzy Systems*, vol. 21, no. 2, pp. 301–313, 2013.

[5] Q. Zhou, P. Shi, H. H. Liu, and S. Y. Xu, "Neural network based decentralized adaptive output-feedback control for large-scale stochastic nonlinear systems," *IEEE Transactions on Systems, Man, and Cybernetics*, vol. 42, no. 6, pp. 1608–1619, 2012.

[6] T. Li, W. X. Zheng, and C. Lin, "Delay-slope-dependent stability results of recurrent neural networks," *IEEE Transactions on Neural Networks*, vol. 22, no. 12, pp. 2138–2143, 2011.

[7] S. Yin, S. Ding, A. Haghani, H. Hao, and P. Zhang, "A comparison study of basic data-driven fault diagnosis and process monitoring methods on the benchmark Tennessee Eastman process," *Journal of Process Control*, vol. 22, no. 9, pp. 1567–1581, 2012.

[8] H. Li, H. Liu, H. Gao, and P. Shi, "Reliable fuzzy control for active suspension systems with actuator delay and fault," *IEEE Transactions on Fuzzy Systems*, vol. 20, no. 2, pp. 342–357, 2012.

[9] H. Li, J. Yu, H. Liu, and C. Hilton, "Adaptive sliding mode control for nonlinear active suspension vehicle systems using T-S fuzzy approach," *IEEE Transactions on Industrial Electronics*, vol. 60, no. 8, pp. 3328–3338, 2013.

[10] C. H. Wang and D. Y. Huang, "A New intelligent fuzzy controller for nonlinear hysteretic electronic throttle in modern intelligent automobiles," *IEEE Transaction Industrial Electronics*, vol. 60, no. 6, pp. 2332–2345, 2013.

[11] M. Vašak, M. Baotić, I. Petrović, and N. Perić, "Hybrid theory-based time-optimal control of an electronic throttle," *IEEE Transaction Industrial Electronics*, vol. 54, no. 3, pp. 1483–1494, 2008.

[12] C. Rossi, A. Tilli, and A. Tonielli, "Robust control of a throttle body for drive by wire operation of automotive engines," *IEEE Transactions on Control Systems Technology*, vol. 8, no. 6, pp. 993–1002, 2000.

[13] D. Kim, H. Peng, S. Bai, and J. M. Maguire, "Control of integrated powertrain with electronic throttle and automatic transmission," *IEEE Transactions on Control Systems Technology*, vol. 15, no. 3, pp. 474–482, 2007.

[14] Y. Pan, Ü. Özguner, and O. H. Dağci, "Variable-structure control of electronic throttle valve," *IEEE Transactions on Industrial Electronics*, vol. 55, no. 11, pp. 3899–3907, 2008.

[15] D. Pavković, J. Deur, M. Jansz, and N. Perić, "Adaptive control of automotive electronic throttle," *Control Engineering Practice*, vol. 14, no. 2, pp. 121–136, 2006.

[16] J. Deur, D. Pavković, N. Perić, M. Jansz, and D. Hrovat, "An electronic throttle control strategy including compensation of friction and limp-home effects," *IEEE Transactions on Industry Applications*, vol. 40, no. 3, pp. 821–834, 2004.

[17] X. Yuan, Y. Wang, and L. Wu, "SVM-based approximate model control for electronic throttle valve," *IEEE Transactions on Vehicular Technology*, vol. 57, no. 5, pp. 2747–2756, 2008.

[18] I. Kanellakopoulos, P. V. Kokotović, and A. S. Morse, "Systematic design of adaptive controllers for feedback linearizable systems," *Institute of Electrical and Electronics Engineers*, vol. 36, no. 11, pp. 1241–1253, 1991.

[19] T. Wang, S. Tong, and Y. Li, "Robust adaptive fuzzy control for nonlinear system with dynamic uncertainties based on backstepping," *International Journal of Innovative Computing, Information and Control*, vol. 5, no. 9, pp. 2675–2688, 2009.

[20] S.-C. Tong, X.-L. He, and H.-G. Zhang, "A combined backstepping and small-gain approach to robust adaptive fuzzy output feedback control," *IEEE Transactions on Fuzzy Systems*, vol. 17, no. 5, pp. 1059–1069, 2009.

[21] T. Shaocheng, L. Changying, and L. Yongming, "Fuzzy adaptive observer backstepping control for MIMO nonlinear systems," *Fuzzy Sets and Systems*, vol. 160, no. 19, pp. 2755–2775, 2009.

[22] F.-J. Lin, C.-K. Chang, and P.-K. Huang, "FPGA-based adaptive backstepping sliding-mode control for linear induction motor drive," *IEEE Transactions on Power Electronics*, vol. 22, no. 4, pp. 1222–1231, 2007.

[23] B. Chen and X. Liu, "Fuzzy approximate disturbance decoupling of MIMO nonlinear systems by backstepping and application to chemical processes," *IEEE Transactions on Fuzzy Systems*, vol. 13, no. 6, pp. 832–847, 2005.

[24] D. M. Bošković and M. Krstić, "Backstepping control of chemical tubular reactors," *Computers and Chemical Engineering*, vol. 26, no. 7-8, pp. 1077–1085, 2002.

[25] A. Witkowska and R. Smierzchalski, "Nonlinear backstepping ship course controller," *International Journal of Automation and Computing*, vol. 6, no. 3, pp. 277–284, 2009.

[26] Y. Li, S. Tong, and T. Li, "Adaptive fuzzy output feedback control for a single-link flexible robot manipulator driven DC motor via backstepping," *Nonlinear Analysis. Real World Applications*, vol. 14, no. 1, pp. 483–494, 2013.

Hindawi Publishing Corporation
Mathematical Problems in Engineering
Volume 2013, Article ID 719474, 9 pages
http://dx.doi.org/10.1155/2013/719474

Research Article

Robust Tracking Control of Robot Manipulators Using Only Joint Position Measurements

Ancai Zhang,[1] Jinhua She,[2] Xuzhi Lai,[3] Min Wu,[3] Jianlong Qiu,[4] and Xiangyong Chen[4]

[1] *School of Automobile Engineering, Linyi University, Linyi, Shandong 276005, China*
[2] *School of Computer Science, Tokyo University of Technology, Hachioji, Tokyo 192-0982, Japan*
[3] *School of Information Science and Engineering, Central South University, Changsha, Hunan 410083, China*
[4] *School of Science, Linyi University, Linyi, Shandong 276005, China*

Correspondence should be addressed to Jinhua She; she@stf.teu.ac.jp

Received 13 August 2013; Accepted 23 September 2013

Academic Editor: Bo-Chao Zheng

This paper concerns the tracking control of a robot manipulator with unknown uncertainties and disturbances. It presents a new control method that uses only joint position measurements to design a tracking controller. The controller has two parts. One is based on a feedback linearization technique; it makes the nominal model of a manipulator asymptotically track a desired trajectory. The other is based on the idea of equivalent input disturbance (EID); it compensates for uncertainties and disturbances. Together they enable a robot manipulator to precisely track the desired trajectory. The new control algorithm is applied to a two-link robot manipulator, and simulation results demonstrate the validity of this method.

1. Introduction

Robot manipulators are widely used in many fields. They are especially useful in areas where it is impractical or undesirable for a human to go, for example, undersea exploration, radioactive environments, and defusing explosive devices. Interest in the control of robot manipulators has been increasing over the past few years [1–3], and it is now a central issue in robotics.

If an exact dynamic model of a robot manipulator is known, the motion control problem is easy to solve by the computed-torque-control (CTC) method [4]. It uses nonlinear state feedback to cancel the nonlinear terms and a simple PD controller for motion control. Although this method is simple and effective, the requirement of an exact model limits its practicality because it is usually impossible to obtain an exact, or even reasonably accurate, dynamic model in practical applications. For example, an actual plant inevitably contains structured and unstructured uncertainties, and a robot manipulator may be influenced by unpredictable external disturbances when the operating environment changes. Since these uncertainties and disturbances may greatly affect control performance, it is necessary to consider their effects in the study of the motion control of robot manipulators.

A number of strategies have been developed to solve the problem of controlling the motion of a robot manipulator with uncertainties and disturbances. They include a Lyapunov-based method [5], a neural-network-based method [6, 7], an adaptive neural network H_∞ strategy [8], an adaptive switching learning PD (ASL-PD) method [9], a parameter-dependent nonlinear observer approach [10], and a variable-structure PID control method [11]. However, all of them require measurement of both the displacement and velocity of joints.

Generally speaking, joint displacement can be accurately measured with an encoder. However, velocity is typically measured with a tachometer, and the results usually contain noise, which can affect the control precision and performance of a closed-loop system. So, both practically and theoretically, it is meaningful to devise a motion control method for robot manipulators which relies only on the measurement of joint position. Various strategies have been developed to solve this challenging problem. One is a controller-observer combination strategy. It has a two-step design procedure:

(1) construct an observer for a robot manipulator based on joint information and (2) use joint displacement and the state of the observer to design a state feedback controller. Many control methods based on this strategy have been reported [12–14]. The problem with it is that the stability of both the observer and the controller is of a local nature. Another strategy [15–17] involves using a linear or nonlinear compensator to obtain substitutes for the velocity variables. It enables the global tracking control of a robot manipulator, but the addition of external state variables complicates the design of the control system. A third is an adaptive tracking control strategy that includes an output feedback scheme (OFS) [18] and an iterative learning scheme (ILS) [19], but the OFS-based controller only locally ensures the asymptotic stability of the joint position error, and the ILS-based controller makes the system only track the same task iteratively.

This paper presents a new tracking control approach for a robot manipulator with unknown uncertainties and disturbances. Its advantage is that the design of the tracking controller relies only on the measurements of joint position, not velocity, and the tracking control is global. It is based on the concept of an equivalent input disturbance (EID), which was first presented in [20] to deal with disturbance rejection in a linear servo system. The EID approach has been validated through application to several mechatronic systems [20–22]. In this study, it was used to design a global robust tracking controller for a robot manipulator. The controller has two parts: one makes the nominal model of a manipulator asymptotically track a desired trajectory and the other compensates for uncertainties and disturbances. Together they enable a robot manipulator with unknown uncertainties and disturbances to precisely track the desired trajectory.

The rest of this paper is organized as follows. Section 2 describes the model and formulates the problem. Section 3 explains the design of an EID-based tracking controller. Section 4 discusses a numerical example for a two-link robot manipulator. Finally, Section 5 presents some concluding remarks.

2. Model Description and Problem Formulation

For a robot manipulator with n serial links, we take $\ddot{q}, \dot{q}, q \in \mathbb{R}^n$ to be the acceleration, velocity, and position vectors, respectively, of the joints. Choose the Lagrangian of the robot system to be

$$L(q,\dot{q}) = \frac{1}{2}\dot{q}^T M(q)\dot{q} - P(q), \tag{1}$$

where $M(q) \in \mathbb{R}^{n\times n}$ is a positive-definite symmetric inertia matrix and $P(q)$ is the potential energy of the system. The equation of motion of the manipulator is obtained from the Euler-Lagrange equation:

$$\frac{d}{dt}\left[\frac{\partial L(q,\dot{q})}{\partial \dot{q}}\right] - \frac{\partial L(q,\dot{q})}{\partial q} = \tau - \tau_f + \tau_{\text{ext}}, \tag{2}$$

where $\tau \in \mathbb{R}^{n\times 1}$ is the vector of control torques, $\tau_f \in \mathbb{R}^{n\times 1}$ is the vector of friction torques, and $\tau_{\text{ext}} \in \mathbb{R}^{n\times 1}$ is the vector of the external disturbances imposed on the joints. We rewrite (2) in the general form

$$M(q)\ddot{q} + H(q,\dot{q}) + N(q) = \tau - \tau_f + \tau_{\text{ext}}, \tag{3}$$

where $H(q,\dot{q}) \in \mathbb{R}^{n\times 1}$ is the vector of Coriolis and centrifugal forces and $N(q) \in \mathbb{R}^{n\times 1}$ is the gravity vector.

Due to the unmodeled dynamics, measurement error, and changes in environment, it is difficult to obtain precise values for the masses and lengths of the links, the moments of inertia of the links, and other physical parameters. The measured values of these parameters are usually not very accurate. Thus, the values of the matrices $M(q)$, $H(q,\dot{q})$, and $N(q)$ in (3) are

$$\begin{aligned} M(q) &= M_0(q) + \Delta M(q), \\ H(q,\dot{q}) &= H_0(q,\dot{q}) + \Delta H(q,\dot{q}), \\ N(q) &= N_0(q) + \Delta N(q), \end{aligned} \tag{4}$$

where $M_0(q)$, $H_0(q,\dot{q})$, and $N_0(q)$ are the nominal values of $M(q)$, $H(q,\dot{q})$, and $N(q)$, respectively, and $\Delta M(q)$, $\Delta H(q,\dot{q})$, and $\Delta N(q)$ are the corresponding additive uncertain terms. Consequently, (3) becomes

$$M_0(q)\ddot{q} + H_0(q,\dot{q}) + N_0(q) = \tau + d, \tag{5}$$

where

$$d = \tau_{\text{ext}} - \Delta M(q)\ddot{q} - \Delta H(q,\dot{q}) - \Delta N(q) - \tau_f. \tag{6}$$

We assume that there is no prior information about $\Delta M(q)$, $\Delta H(q,\dot{q})$, $\Delta N(q)$, τ_f, or τ_{ext}. Thus, d is an unknown disturbance of the nonlinear system (5).

Let $q_r \in \mathbb{R}^{n\times 1}$ be the desired trajectory of the manipulator, and let $e = q - q_r$ be the tracking error of the trajectory. If we take the control law, τ, in (5) to be

$$\begin{aligned} \tau_0 = {} & M_0(q)\left[\ddot{q}_r - K_D(\dot{q} - \dot{q}_r) - K_P(q - q_r)\right] \\ & + H_0(q,\dot{q}) + N_0(q), \end{aligned} \tag{7}$$

where K_P and $K_D \in \mathbb{R}^{n\times n}$ are two given positive-definite diagonal matrices, then (5) and (7) give

$$\ddot{e} + K_D\dot{e} + K_P e - M_0^{-1}(q)\, d = 0. \tag{8}$$

Assume that $\Delta M(q)$, $\Delta H(q,\dot{q})$, $\Delta N(q)$, τ_f, and τ_{ext} are all zero, which means that there are no parameter perturbations and external disturbances acting on the manipulator. Then, combining (6) and (8) yields

$$\ddot{e} + K_D\dot{e} + K_P e = 0. \tag{9}$$

It is easy to obtain $\lim_{t\to\infty} e = 0$ and $\lim_{t\to\infty} \dot{e} = 0$ for (9). So, the state variables of the system, $[q^T, \dot{q}^T]$, asymptotically approach the desired trajectory, $[q_r^T, \dot{q}_r^T]$, for this case.

However, in practice it is difficult to acquire exact knowledge of a robot manipulator; uncertainties and disturbances can greatly reduce the tracking precision. So, we need to consider the tracking control problem for the perturbed robot system (5). This paper presents an EID-based tracking controller for (5) that relies only on measured joint position, q.

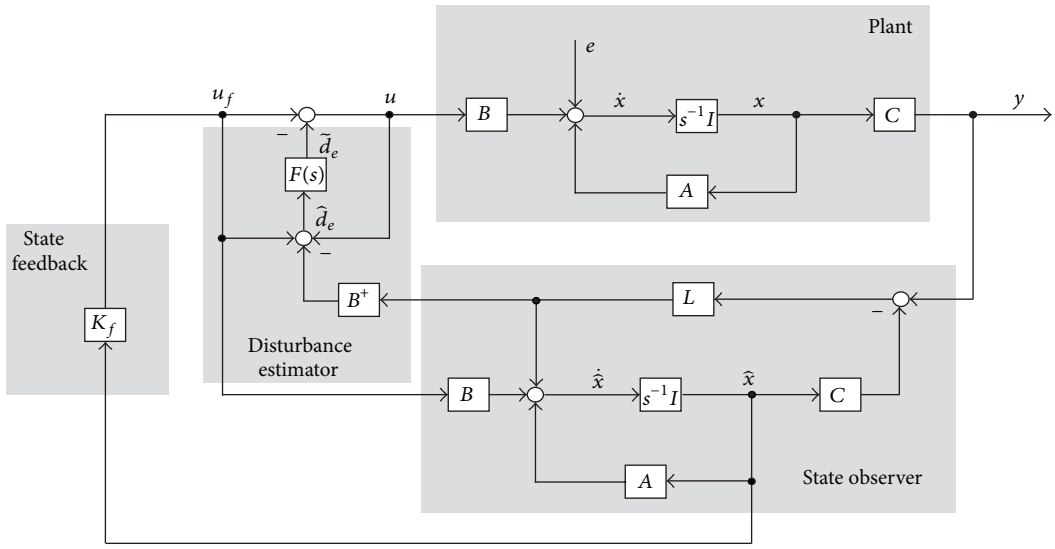

Figure 1: Configuration of an EID-based control system.

3. Design of EID-Based Tracking Controller

For the nonlinear system (5), we take

$$\tau = \tau_0 + M_0(q)\,\widetilde{B}u, \tag{10}$$

where τ_0 is defined in (7); $\widetilde{B} = [b_1, b_2, \ldots, b_n]^T \in \mathbb{R}^{n\times 1}$, b_i ($i = 1, 2, \ldots, n$) are constants; and $u \in \mathbb{R}$ is a new input that is used to compensate for the disturbance, d. Combining (5) and (10) yields

$$\ddot{e} = -K_D\dot{e} - K_P e + \widetilde{B}u + M_0^{-1}(q)\,d. \tag{11}$$

Let $x = [e^T, \dot{e}^T]^T \in \mathbb{R}^{2n\times 1}$; the state space form of (11) is

$$\dot{x} = Ax + Bu + \varepsilon, \tag{12}$$

where

$$A = \begin{bmatrix} 0_{n\times n} & I_n \\ -K_P & -K_D \end{bmatrix}, \qquad B = \begin{bmatrix} 0_{n\times 1} \\ \widetilde{B} \end{bmatrix}, \qquad \varepsilon = \begin{bmatrix} 0_{n\times 1} \\ M_0^{-1}(q)\,d \end{bmatrix}, \tag{13}$$

where I_n is the $n \times n$ identity matrix and $0_{i\times j}$ is an $i \times j$ zero matrix for positive integers i and j.

Since only the measured q is available, we take the output of (12) to be

$$y = Cx = e, \quad C = [I_n, 0_{n\times n}]. \tag{14}$$

It is easy to verify that (C, A) is observable. If we denote

$$\Phi(s) = \left[K_P + (sI_n + K_D)\,sI_n\right]^{-1}, \tag{15}$$

then

$$\begin{aligned} C(sI - A)^{-1}B &= [I_n, 0_{n\times n}] \\ &\quad \times \begin{bmatrix} -\Phi(s)(sI_n + K_D) & \Phi(s) \\ -I_n - sI_n\Phi(s)(sI_n + K_D) & sI_n\Phi(s) \end{bmatrix} B \\ &= \left[-\Phi(s)(sI_n + K_D), \Phi(s)\right] B \\ &= \left[0_{n\times 1}, -\Phi(s)\,\widetilde{B}\right]. \end{aligned} \tag{16}$$

Equation (16) tells us that (A, B, C) has no zeros on the imaginary axis because

$$\Phi(s)\,\widetilde{B} = \left[\frac{b_1}{\phi_1(s)}, \frac{b_2}{\phi_2(s)}, \ldots, \frac{b_n}{\phi_n(s)}\right]^T, \tag{17}$$

where $\phi_i(s) = s^2 + K_{di}s + K_{pi}$ ($i = 1, 2, \ldots, n$), and K_{pi} and K_{di} are the diagonal elements of the matrices K_P and K_D, respectively.

In addition, we choose b_i in $\widetilde{B}$ such that (A, B) is controllable. Then, as shown in [20], there always exists an EID, d_e, on the control input channel. It produces the same effect on the output, y, as the disturbance, ε, does. The perturbed plant (12) and (14) can be considered to be an EID-based plant:

$$\begin{aligned} \dot{x} &= Ax + B\left[u + d_e\right], \\ y &= Cx. \end{aligned} \tag{18}$$

In the configuration of the EID-based control system (see Figure 1), K_f is the feedback gain; L is the observer gain; $\hat{d}_e$ is an estimate of the EID, d_e; and $F(s)$ is a low-pass filter that limits the angular frequency band of the disturbance estimate. Their design is discussed below.

3.1. Estimation of Equivalent Input Disturbance. First, we construct a full-order Luenberger observer for (18):

$$\dot{\hat{x}} = A\hat{x} + Bu_f + L\left(y - C\hat{x}\right), \tag{19}$$

where $u_f = u + d_e$. Letting

$$\Delta x = \hat{x} - x \tag{20}$$

and substituting that into (18) yield

$$\dot{\hat{x}} = A\hat{x} + B\left[u + \hat{d}_e\right], \tag{21}$$

where

$$\begin{aligned} \hat{d}_e &= d_e + \Delta d, \\ B\Delta d &= \Delta\dot{x} - A\Delta x. \end{aligned} \tag{22}$$

Note that (21) has the same form as (18). We take $\hat{d}_e$ to be an estimate of the actual EID, d_e. From (18), (21), and (22), it is clear that the difference between the state of the plant and that of the observer is equivalent to the difference between d_e and $\hat{d}_e$. Combining (19) and (21) yields

$$B\left(u + \hat{d}_e - u_f\right) = L\left(y - C\hat{x}\right). \tag{23}$$

We solve (23) for $\hat{d}_e$ and obtain a least-squares solution:

$$\hat{d}_e = B^{+}L\left(y - C\hat{x}\right) + u_f - u, \tag{24}$$

where

$$B^{+} = \left[B^T B\right]^{-1} B^T. \tag{25}$$

To ensure the estimation accuracy, the low-pass filter

$$F(s) = \frac{1}{Ts + 1} \tag{26}$$

is used to select the angular frequency band for disturbance estimation, where T is the time constant. The filtered disturbance estimate, $\tilde{d}_e$, is given by

$$\widetilde{D}_e(s) = F(s)\,\widehat{D}_e(s), \tag{27}$$

where $\widetilde{D}_e(s)$ and $\widehat{D}_e(s)$ are the Laplace transforms of $\tilde{d}_e$ and $\hat{d}_e$, respectively.

We take control law u to be

$$u = u_f - \tilde{d}_e, \tag{28}$$

$$u_f = K_f\hat{x}, \tag{29}$$

where K_f is a feedback gain that makes $A + BK_f$ stable. Assume that the observer (19) is stable. Then, control law (29) makes the output of plant (18) asymptotically converge to zero. According to the definition of EID, control law (28) asymptotically stabilizes the output of (12), which is e, at the origin. Thus, the tracking control objective of system (12) is achieved.

Remark 1. From (7) and (10), the velocity, $\dot{q}$, is needed to calculate the control input, τ. Since we assume that the measured value of $\dot{q}$ is unavailable, we use information of the observer (19) to obtain a substitute for $\dot{q}$ in (7):

$$\dot{q} = \hat{x}_2 + \dot{q}_r, \tag{30}$$

where $\hat{x}_2 \in \mathbb{R}^n$, $\hat{x} = [\hat{x}_1^T, \hat{x}_2^T]^T$ is the state vector of the observer (19), and $\hat{x}_1 \in \mathbb{R}^n$.

3.2. Design of State Observer. Since the separation theorem holds for an EID-based control system [20], we can separately design the feedback gain K_f and the observer gain L. Since (A, B) is controllable, it is easy to design a K_f by any appropriate method (pole placement, optimal control, etc.). So, here we focus on the design of L.

The design of L should first ensure the stability of the state observer (19). We take

$$\begin{aligned} L &= K_\rho^T, \\ K_\rho &= R_L^{-1}CS, \\ AS + SA^T - SC^T R_L^{-1} CS + \rho Q_L &= 0, \end{aligned} \tag{31}$$

where Q_L and R_L are two given positive-definite matrices and ρ is a positive scalar. Since (C, A) is observable, (C^T, A^T) is controllable. Thus, the observer gain, L, designed in (31) makes $A - LC$ stable, which means that the state observer (19) is stable.

On the other hand, we tackle the stability issue by first letting $d = 0$. From (19), (21), and (22), we have

$$\Delta\dot{x} = (A - LC)\,\Delta x + B\tilde{d}_e. \tag{32}$$

Combining (24) and (10) yields

$$\hat{d}_e = -B^{+}LC\Delta x + \tilde{d}_e. \tag{33}$$

From (32) and (24), we obtain the transfer function from $\tilde{d}_e$ to $\hat{d}_e$:

$$\begin{aligned} G(s) &= 1 - B^{+}LC[sI - (A - LC)]^{-1}B \\ &= B^{+}(sI - A)\,[sI - (A - LC)]^{-1}B. \end{aligned} \tag{34}$$

Note that the transfer function from $\hat{d}_e$ to $\tilde{d}_e$ is $F(s)$ (Figure 2). The small-gain theorem [23] tells us that the condition

$$\|GF\|_\infty < 1 \tag{35}$$

must be satisfied to guarantee the stability of the control system, where $\|GF\|_\infty := \sup_{0\le\omega\le\infty}\sigma_{\max}[G(j\omega)F(j\omega)]$ and $\sigma_{\max}(\cdot)$ is the maximum singular-value function.

Since the number of inputs of the plant (A^T, C^T, B^T) is not less than the number of outputs, and since $A^T - C^T K_\rho$ is stable, according to [24, Theorems 1 and 3], we have

$$\lim_{\rho\to\infty}\left\{\left[sI - \left(A - K_\rho^T C\right)\right]^{-1}B\right\}^T = 0. \tag{36}$$

Note that $[sI - (A - K_\rho^T C)]^{-1}B$ is part of $G(s)$. So, for a given $F(s)$ in (26), the observer gain, L, designed in (31) makes the condition (35) true provided that ρ is large enough.

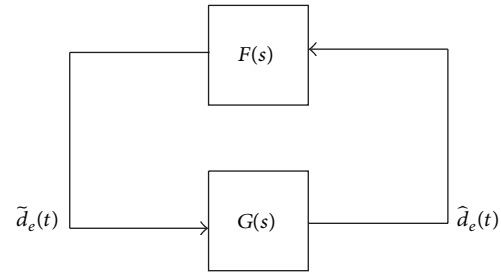

Figure 2: Stability condition (35).

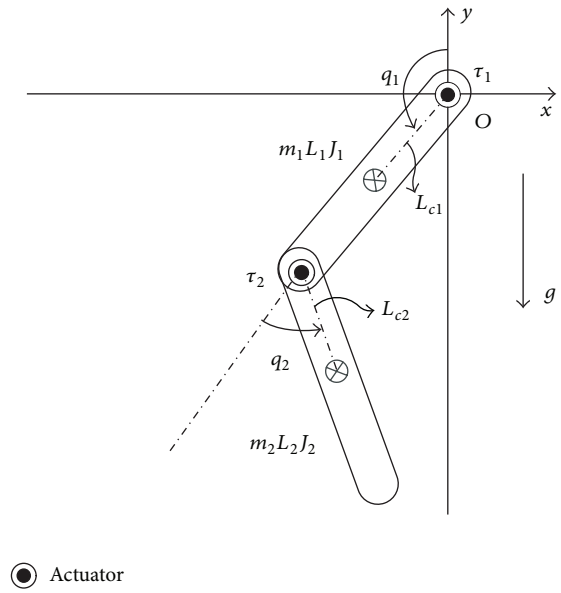

Figure 3: Two-link robot manipulator.

4. Numerical Example

We applied the EID-based tracking control strategy to a two-link rigid robot manipulator (Figure 3) to demonstrate its validity.

The simulations employed the parameters (Table 1) of a PUMA 560 manipulator [7]. The matrices for the dynamics of the nominal model are

$$M_0(q) = \begin{bmatrix} a_1 + a_2 + 2a_3\cos q_2 & a_2 + a_3\cos q_2 \\ a_2 + a_3\cos q_2 & a_2 \end{bmatrix},$$

$$H_0(q,\dot{q}) = \begin{bmatrix} -a_3\left(2\dot{q}_1 + \dot{q}_2\right)\dot{q}_2\sin q_2 \\ a_3\dot{q}_1^2\sin q_2 \end{bmatrix}, \tag{37}$$

$$N_0(q) = \begin{bmatrix} -b_1\sin q_1 - b_2\sin\left(q_1 + q_2\right) \\ -b_2\sin\left(q_1 + q_2\right) \end{bmatrix},$$

Table 1: Parameters of the two-link manipulator for simulations.

Link i	m_i (kg)	L_i (m)	L_{ci} (m)	J_i (kg·m^2)
$i = 1$	31.20	1.05	0.43	0.41
$i = 2$	22.53	0.78	0.32	0.35

where

$$\begin{aligned} a_1 &:= m_1L_{c1}^2 + m_2L_1^2 + J_1, \\ a_2 &:= m_2L_{c2}^2 + J_2, \\ a_3 &:= m_2L_1L_{c2}, \\ b_1 &:= \left(m_1L_{c1} + m_2L_1\right)g, \\ b_2 &:= m_2L_{c2}g, \end{aligned} \tag{38}$$

q_1 is the angle of the first link relative to the vertical, q_2 is the angle of the second link relative to the first link, m_i is the mass of the ith link ($i = 1,2$), L_i is the length of the ith link ($i = 1,2$), L_{ci} is the distance from the ith joint to the center of mass (COM) of the ith link ($i = 1,2$), J_i is the moment of inertia around the COM of the ith link ($i = 1,2$), τ_i is the torque applied to the ith joint ($i = 1,2$), and g is the gravitational constant (9.80665 m/s^2).

Let the desired trajectory $q_r = [q_{1r}, q_{2r}]^T$ be

$$\begin{aligned} q_{1r} &= 0.5\cos t + 0.2\sin 3t, \\ q_{2r} &= -0.2\sin 2t - 0.5\cos t. \end{aligned} \tag{39}$$

First, when $d = 0$, we choose

$$K_P = \begin{bmatrix} 1 & 0 \\ 0 & 1 \end{bmatrix}, \qquad K_D = \begin{bmatrix} 2 & 0 \\ 0 & 1 \end{bmatrix} \tag{40}$$

for (7) and (9). Figure 4 shows the tracking control results for the initial condition

$$\left[q_1, q_2, \dot{q}_1, \dot{q}_2\right]^T = [\pi, 0, 0, 0]^T. \tag{41}$$

Notice that the actual trajectories converge to the desired trajectories in less than 10 seconds.

Next, we consider the uncertainties in the physical parameters by letting m_1 and L_{c2} be 5% larger than their nominal values, letting m_2 and L_{c1} be 5% smaller than their nominal values, and letting J_1 and J_2 be 10% larger than their nominal values. We also added two types of torques to the joints of the manipulator: (a) a viscous friction torque, $\tau_f = [\tau_{1f}, \tau_{2f}]^T$:

$$\tau_{1f} = 0.5\dot{q}_1, \qquad \tau_{2f} = 0.5\dot{q}_2, \tag{42}$$

and (b) an external disturbance torque, $\tau_{\text{ext}} = [\tau_{1\text{ext}}, \tau_{2\text{ext}}]^T$ (Figure 5):

$$\begin{aligned} \tau_{1\text{ext}} &= 0.5\left(\sin 4\pi t + \cos 2\pi t\right), \\ \tau_{2\text{ext}} &= 0.5\left(\sin \pi t + \cos 0.5\pi t\right). \end{aligned} \tag{43}$$

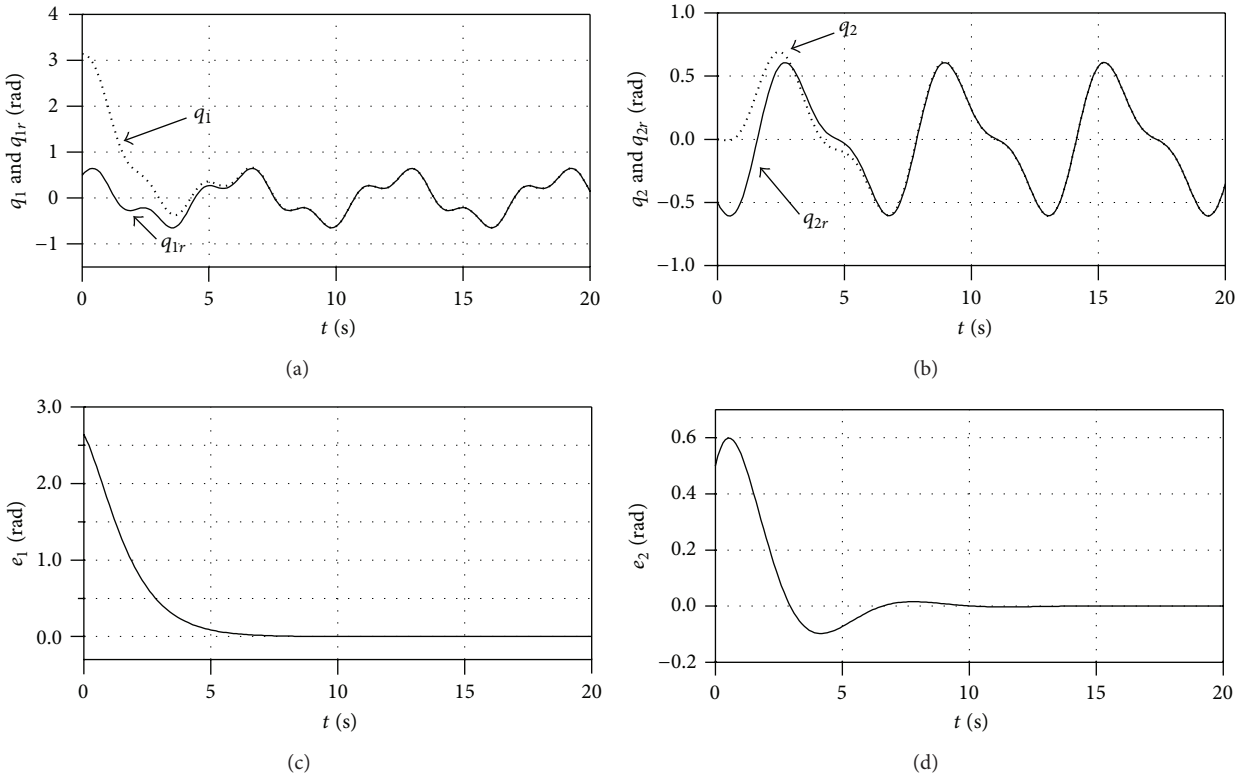

Figure 4: Tracking control results without uncertainties or disturbances.

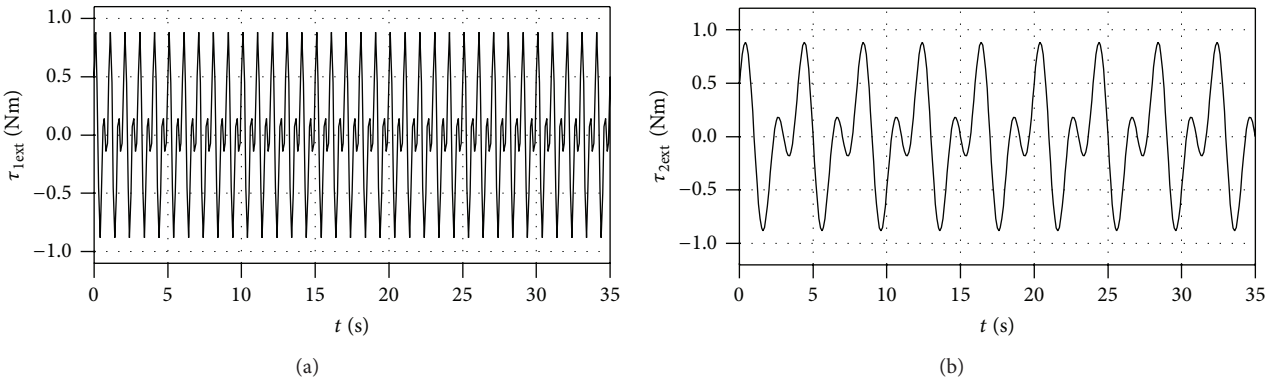

Figure 5: Disturbance to torque of joints added to the two-link manipulator.

The simulation results (Figure 6) for (5), (7), (40), and (41) show that the tracking performance was much worse, and a large steady-state tracking error appeared. That means that control law (7) by itself does not force the robot manipulator to track the desired trajectory when uncertainties and disturbances are present.

Finally, we applied the EID-based control strategy. We chose $\widetilde{B} = [10, 10]$. It is easy to verify that (A, B) is controllable. Letting all of the poles of $A + BK_f$ be -2.5 yields the feedback gain

$$K_f = [-2.3625, -1.4437, -1.8563, 1.1563]. \quad (44)$$

The design parameters for (26) and (31) were chosen to be

$$T = 0.1, \quad Q_L = 10I_4, \quad R_L = 50I_2, \quad \rho = 10^6. \quad (45)$$

That gave

$$L = \begin{bmatrix} 447.4463 & 0 & 104.1078 & 0 \\ 0 & 447.6245 & 0 & 183.8319 \end{bmatrix}^T, \quad \|GF\|_\infty = 0.9186 < 1. \quad (46)$$

The simulation results (Figure 7) for (5), (10), (28), (40), (41), and (45) show that the tracking performance was much

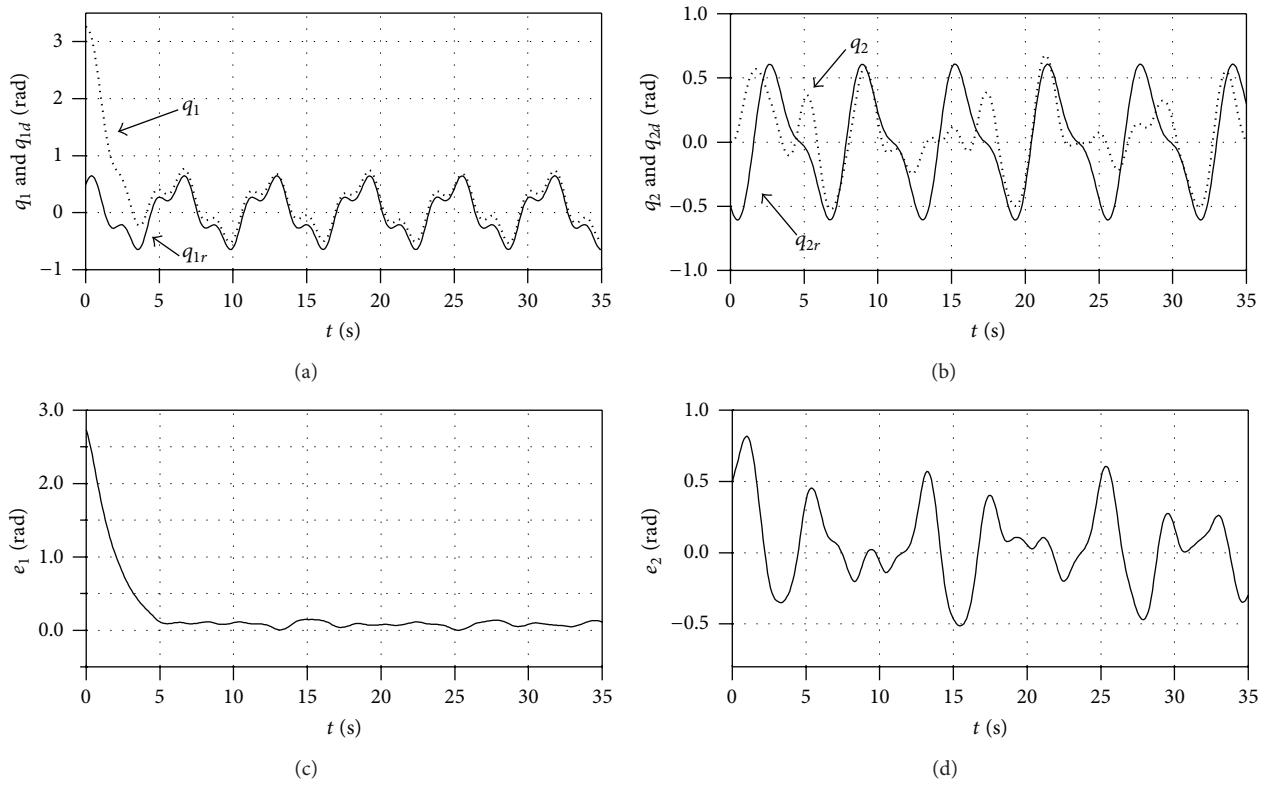

Figure 6: Simulation results for control law (7) when uncertainties and disturbances are present.

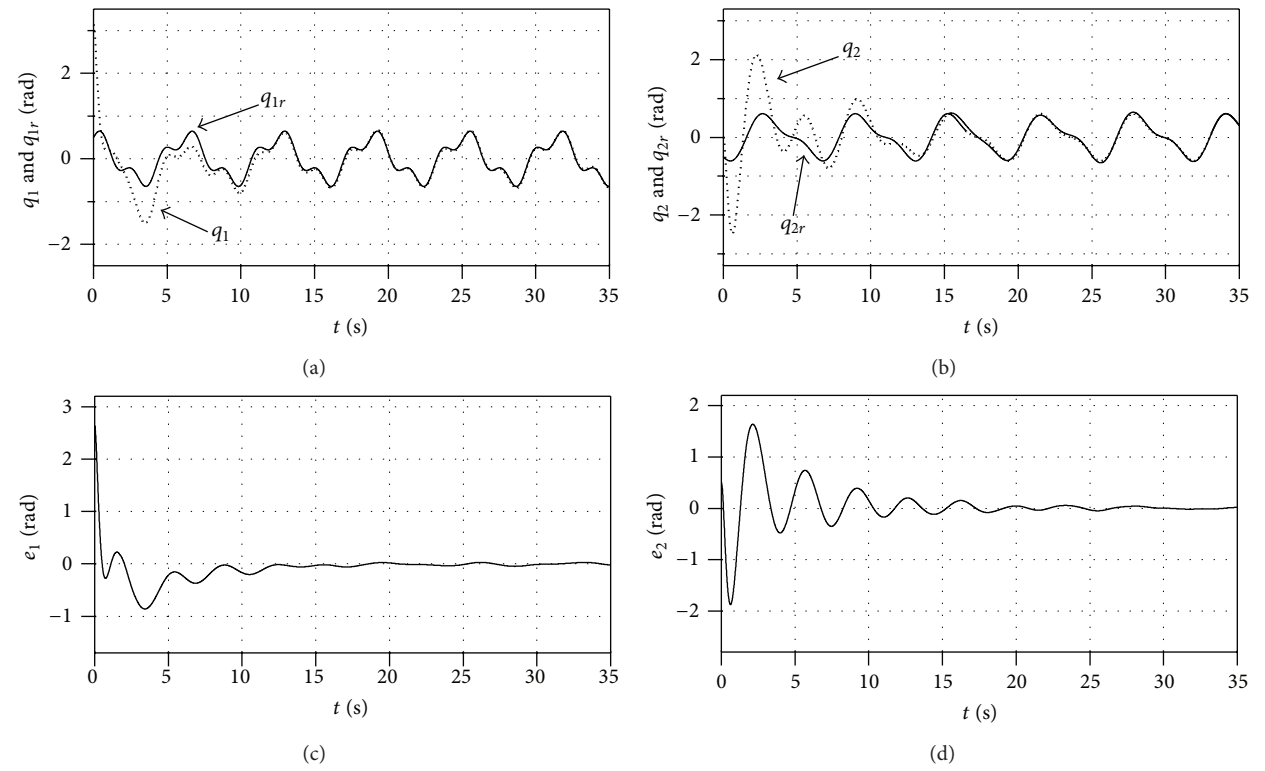

Figure 7: Simulation results for EID-based control when uncertainties and disturbances are present.

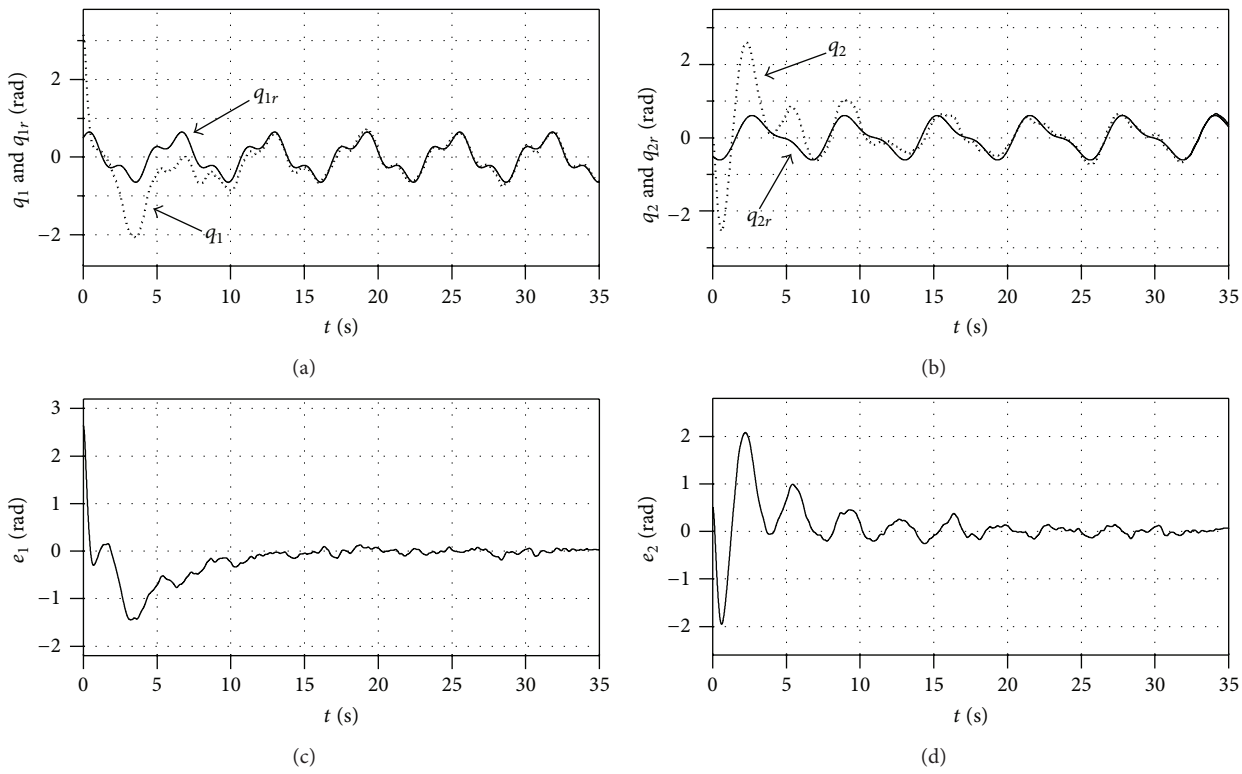

Figure 8: Simulation results for EID-based control when uncertainties, disturbances, and measurement white noise are present.

better than that in Figure 6. The EID-based controller (28) almost completely rejects the effect of the uncertainties and disturbances. So, the perturbed manipulator system (3) precisely tracks the desired trajectory. Since measurement noise is very common in actual control engineering applications, we also added white noise (peak value: ±0.2) to the measured q. The simulation results (Figure 8) show that the robot manipulator precisely tracks the desired trajectory even in this case.

5. Conclusion

This paper presents an EID-based control strategy that solves the tracking control problem for a robot manipulator with unknown uncertainties and disturbances. It uses only joint position measurements in the design of the tracking controller. The controller has two parts: one part uses an exact linearization technique to guarantee the asymptotical stability of the nominal model and the other is based on the idea of EID, which compensates for the effects of parameter uncertainties and exogenous disturbances. The combination makes a robot manipulator precisely track the desired trajectory. Simulation results show the validity of this control strategy.

Acknowledgments

This work was supported in part by the National Science Foundation of China under Grants nos. 61304023, 61273012 and 61074112, by the Project of Shandong Province Higher Educational Science and Technology Program under Grant nos. J12LI58 and J13LI11, and by the Applied Mathematics Enhancement Program of Linyi University. The authors declare that there is no conflict of interests regarding the publication of this paper.

References

[1] B. Jayawardhana and G. Weiss, "Tracking and disturbance rejection for fully actuated mechanical systems," *Automatica*, vol. 44, no. 11, pp. 2863–2868, 2008.

[2] C. Canudas-de-Wit and R. Kelly, "Passivity analysis of a motion control for robot manipulators with dynamic friction," *Asian Journal of Control*, vol. 9, no. 1, pp. 30–36, 2007.

[3] M. Homayounzade and M. Keshmiri, "On the robust tracking control of kinematically constrained robot manipulators," in *Proceedings of the IEEE International Conference on Mechatronics (ICM '11)*, pp. 248–253, Istanbul, Turkey, April 2011.

[4] R. H. Middleton and G. C. Goodwin, "Adaptive computed torque control for rigid link manipulations," *Systems and Control Letters*, vol. 10, no. 1, pp. 9–16, 1988.

[5] M. W. Spong, "On the robust control of robot manipulators," *IEEE Transactions on Automatic Control*, vol. 37, no. 11, pp. 1782–1786, 1992.

[6] R.-J. Wai, "Tracking control based on neural network strategy for robot manipulator," *Neurocomputing*, vol. 51, pp. 425–445, 2003.

[7] Y. Zuo, Y. Wang, X. Liu et al., "Neural network robust H_∞ tracking control strategy for robot manipulators," *Applied Mathematical Modelling*, vol. 34, no. 7, pp. 1823–1838, 2010.

[8] Y.-C. Chang and B.-S. Chen, "A nonlinear adaptive H_∞ tracking control design in robotic systems via neural networks," *IEEE Transactions on Control Systems Technology*, vol. 5, no. 1, pp. 13–29, 1997.

[9] P. R. Ouyang, W. J. Zhang, and M. M. Gupta, "An adaptive switching learning control method for trajectory tracking of robot manipulators," *Mechatronics*, vol. 16, no. 1, pp. 51–61, 2006.

[10] X. Wang, Y. Yao, and F. He, "Control design for harmonic disturbance rejection for robot manipulators with bounded inputs," in *Proceedings of the Chinese Control and Decision Conference (CCDC '09)*, pp. 2323–2328, Guilin, China, June 2009.

[11] E. M. Jafarov, M. N. A. Parlakçi, and Y. Istefanopulos, "A new variable structure PID-controller design for robot manipulators," *IEEE Transactions on Control Systems Technology*, vol. 13, no. 1, pp. 122–130, 2005.

[12] S. Nicosia and P. Tomei, "Robot control by using only joint position measurements," *IEEE Transactions on Automatic Control*, vol. 35, no. 9, pp. 1058–1061, 1990.

[13] C. C. de Wit, N. Fixot, and K. J. Astrom, "Trajectory tracking in robot manipulators via nonlinear estimated state feedback," *IEEE Transactions on Robotics and Automation*, vol. 8, no. 1, pp. 138–144, 1992.

[14] M. Homayounzade, M. Keshmiri, and M. Danesh, "An observer-based state feedback controller design for robot manipulators considering actuators' dynamic," in *Proceedings of the 15th International Conference on Methods and Models in Automation and Robotics (MMAR '10)*, pp. 240–248, Miedzyzdroje, Poland, August 2010.

[15] J. Alvarez-Ramirez, R. Kelly, and I. Cervantes, "Stable output feedback position control with integral action for robot manipulators," *Asian Journal of Control*, vol. 5, no. 2, pp. 230–241, 2003.

[16] H. Berghuis and H. Nijmeijer, "Robust control of robots via linear estimated state feedback," *IEEE Transactions on Automatic Control*, vol. 39, no. 10, pp. 2159–2162, 1994.

[17] A. Zavala-Río, E. Aguiñaga-Ruiz, and V. Santibáñez, "Global trajectory tracking through output feedback for robot manipulators with bounded inputs," *Asian Journal of Control*, vol. 13, no. 3, pp. 430–438, 2011.

[18] S. Purwar, I. N. Kar, and A. N. Jha, "Adaptive output feedback tracking control of robot manipulators using position measurements only," *Expert Systems with Applications*, vol. 34, no. 4, pp. 2789–2798, 2008.

[19] S. Islam and P. X. Liu, "Adaptive iterative learning control for robot manipulators without using velocity signals," in *Proceedings of the IEEE/ASME International Conference on Advanced Intelligent Mechatronics (AIM '10)*, pp. 1293–1298, Montreal, Canada, July 2010.

[20] J.-H. She, M. Fang, Y. Ohyama, H. Hashimoto, and M. Wu, "Improving disturbance-rejection performance based on an equivalent-input-disturbance approach," *IEEE Transactions on Industrial Electronics*, vol. 55, no. 1, pp. 380–389, 2008.

[21] J.-H. She, X. Xin, and Y. Ohyama, "Estimation of equivalent input disturbance improves vehicular steering control," *IEEE Transactions on Vehicular Technology*, vol. 56, no. 6, pp. 3722–3731, 2007.

[22] J.-H. She, X. Xin, and Y. Pan, "Equivalent-input-disturbance approachanalysis and application to disturbance rejection in dual-stage feed drive control system," *IEEE/ASME Transactions on Mechatronics*, vol. 16, no. 2, pp. 330–340, 2011.

[23] K. Zhou, J. Doyle, and K. Glover, *Robust and Optical Control*, Prentice Hall, Englewood Cliffs, NJ, USA, 1996.

[24] H. Kimura, "A new approach to the perfect regulation and the bounded peaking in linear multivariable control systems," *IEEE Transactions on Automatic Control*, vol. 26, no. 1, pp. 253–270, 1981.

Hindawi Publishing Corporation
Mathematical Problems in Engineering
Volume 2013, Article ID 718012, 17 pages
http://dx.doi.org/10.1155/2013/718012

Research Article

Underwater Environment SDAP Method Using Multi Single-Beam Sonars

Zheping Yan,[1] Dongnan Chi,[1] Shuping Hou,[2] and Yalin Zheng[3]

[1] *College of Automation, Harbin Engineering University, Harbin, Heilongjiang 150001, China*
[2] *College of Mechanical and Electrical Engineering, Harbin Engineering University, Harbin, Heilongjiang 150001, China*
[3] *Department of Eye and Vision Science, University of Liverpool, L69 3GA Liverpool, UK*

Correspondence should be addressed to Zheping Yan; yanzheping2013@163.com

Received 22 August 2013; Accepted 30 August 2013

Academic Editor: Zhiguang Feng

A new autopilot system for unmanned underwater vehicle (UUV) using multi-single-beam sonars is proposed for environmental exploration. The proposed autopilot system is known as simultaneous detection and patrolling (SDAP), which addresses two fundamental challenges: autonomous guidance and control. Autonomous guidance, autonomous path planning, and target tracking are based on the desired reference path which is reconstructed from the sonar data collected from the environmental contour with the predefined safety distance. The reference path is first estimated by using a support vector clustering inertia method and then refined by Bézier curves in order to satisfy the inertia property of the UUV. Differential geometry feedback linearization method is used to guide the vehicle entering into the predefined path while finite predictive stable inversion control algorithm is employed for autonomous target approaching. The experimental results from sea trials have demonstrated that the proposed system can provide satisfactory performance implying its great potential for future underwater exploration tasks.

1. Introduction

Underwater exploration often encounters environment that is difficult or even impossible for humans to access due to their physical constraints such as deep depth, narrow spaces, and severe working conditions. Unmanned underwater vehicle has a number of advantages for exploring underwater environments, such as autonomous control ability and self-sufficient energy supply. Autopilot of UUV often relies on the information or characteristics (e.g., geometrical information) of the surrounding environment, reflected by data collected from sensors such as sonars.

When in operation, sonar sends out an acoustic beam and the returned (usually the fastest) beam from the environment is collected to determine the distance and location of the environment. This means that it can detect the point on the contour that has the shortest distance from the sonar. Therefore, sonar data can be used to plan the desired path of the UUV and control it by changing thruster forces and rudder angles of the UUV to approach the target. An important issue for designing UUV control systems is the strength of the signal observed from sonar. It is weak primarily due to the random effect caused by complicated marine disturbance; other interferences between received beams can be due to delay and scattering effect.

In this paper a new autopilot system, known as simultaneous detection and patrolling (SDAP), is proposed to address this challenge. Autonomous guidance and control are implemented synchronously where the reconstructed environment contour is used as the guidance path for UUV navigation. For the environment contour reconstruction, the major focus of research is on simultaneous localization and mapping (SLAM) [1], where navigation is the key issue to be addressed. With the advances in control theory, UUV control systems have rapidly evolved from classic control theory to modern control models, including PID [2, 3], backstepping [4–7], fuzzy theory [8, 9], neutral network [10–13], sliding model [14, 15], model prediction control [16, 17], and feedback linearization [18–23]. In particular, Zou has proposed an optimal inversion-based output tracking approach for the guidance of a vertical takeoff and landing (VTOL) aircraft problem [21]. Song has further improved this approach

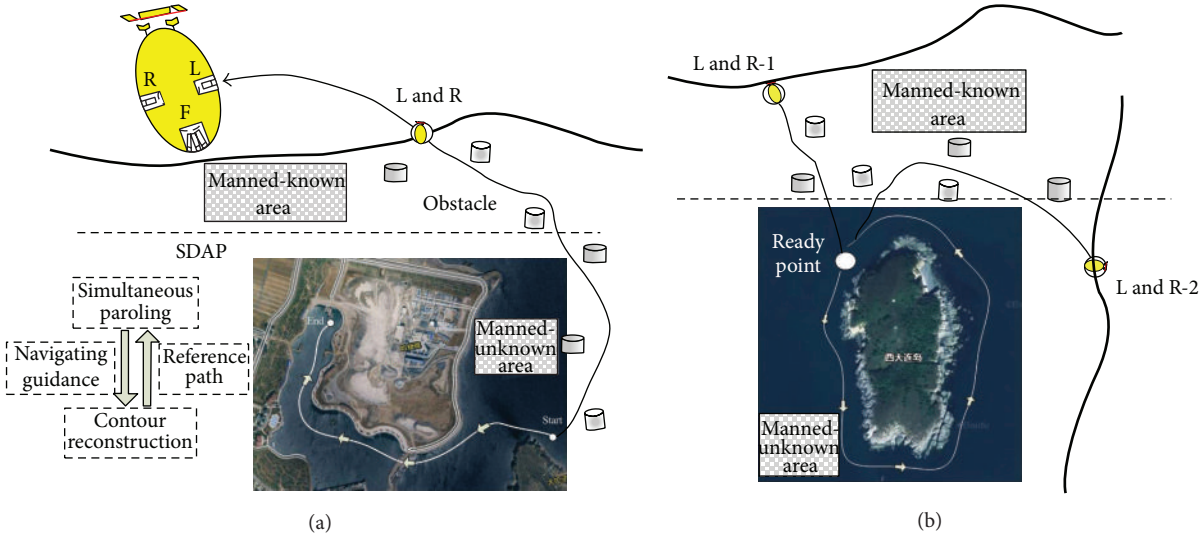

Figure 1: Illustration of the proposed SDAP system for different environments.

with better convergence property such that a second order convergence can be achieved even with aggressive trajectories and strong nonlinearities [20]. Given that stable inversion technique has shown excellent performance for achieving stable control inputs, it is chosen to be implemented in the controllers for accuracy, efficiency, and cost effectiveness.

In this paper autopilot of UUV for both closed and open environments is considered, as shown in Figure 1. In the closed port (Figure 1(a)), there is only one entrance and the UUV has to be able to navigate to the only ready point from any launch and recovery position (L&R). For the open island (Figure 1(b)), there are theoretically infinite numbers of possible entrance points around the island. With consideration of the disturbances such as current direction, an appropriate ready point has to be chosen to guide the UUV to enter into the manned-unknown area. In the manned-known areas, accurate predefined path is applied for the UUV to follow in order to reduce the cost and risks. The main issue addressed in the paper is the navigation using autonomous guidance and control is implemented in manned-unknown areas or area inaccessible for humans where the contour has to be reconstructed in real time. Although in reality, the environment is semiclosed where there is more than one entrance, it is not discussed explicitly here as it can be addressed by applying the strategy for closed environment in an iterative manner.

The main novelties of this paper are as follows.

(1) To address the weak sonar data, a wavelet transform is applied to preprocess the original data so as to eliminate possible outliers in the original sonar data. To reduce the information loss in the preprocessing, the wavelet coefficient values of the current time are estimated using those coefficients estimated in the past times and the original sonar data. All the estimated wavelet coefficients are then regarded as the data resource for the contour reconstruction processes.

(2) A support vector clustering (SVC) inertia algorithm is proposed to cluster the data into different classes so as to determine the property of the original sonar data and obtain the boundaries of the classes (also known as contour). The resulting contour after this step is composed of successively connected lines.

(3) To satisfy the inertia property of the UUV path, the initial contour is smoothed using different order Bézier curves which are automatically determined by the local properties of the structural environments.

(4) With the information of the smoothed contour as the reference path and a predefined safety distance, an improved inversion algorithm, finite predictive stable inversion is proposed to control vehicle navigation.

The remainder of this paper is organized as follows: in Section 2, weak observable sonar data is preprocessed using the wavelet transform and represented as a collection of wavelet coefficients. In Section 3, the wavelet coefficients together with the data confidence limit and DVL information are used to estimate the contour of the environment structure by a support vector clustering inertia method. Addressing the inertia requirement of the vehicle, in Section 4 different order Bézier curves are introduced to smooth the initial contour and automatic decision strategy is made to generate the reference path according to the local properties of the structural environment. In Section 5 details on the controller design methods are presented, and employed for predictive trading during detection mission. The validation experiment design and results are presented in Section 6. Section 7 concludes this paper with some insightful discussions.

2. Preprocessing of Sonar Data Using Wavelet Transform

2.1. Collection of Sonar Data. In this paper five single-beam sonars are configured on the vehicle in order to automatically

Table 1: Metrics to categorize obstacles.

E_t	$E_{\Delta t}$	L_t change	Class
1	1	No	TO
1	1	Yes	GLTO
1	0	No contour	Noise or SLTO

detect the underwater environment: three sonars in the front to detect local environment characteristics and two on the left and the right side for contour reconstruction. The three front sonars are deployed in a way where the middle one is located on the axis of the vehicle surge direction and the other two are installed on the left and right of the middle one with an angle of 7.5 degree, respectively.

Data collected from sonars often include useful data describing obstacles and noise from random outliers. To address the "false alarm" problem in vehicle navigation, those outliers have to be detected and eliminated as much as possible. Outliers can be divided into noise patches and objects (e.g., fish swarm) that have less or no threats to the vehicle. Therefore, three different types of objects are defined as follows.

(a) *Threaten Obstacle* (*TO*). They are obstacles existing in the environment that can be detected by sonar and have threats to the vehicle, including wreck, reef, and iceberg.

(b) *Low Threaten Obstacle* (*LTO*). They are obstacles existing in the environment that can be detected by sonar but have low level of threat to the vehicle, such as suspensions, and fish swarms. LTO can be further fractionized to single LTO (SLTO) distributing as single isolated objects and group LTO (GLTO) with unfixed contour.

(c) *Noise.* Data is collected from sonar that denotes non-obstacles.

With the above definitions, data describing TO is considered to be useful while LTO and noise are regarded as outliers in this paper. Let E_t and $E_{\Delta t}$ be data distribution at instants t and $(t + \Delta t)$, respectively, and the values of 1 and 0 describe data existence and nonexistence, respectively; L_t express the contour of data class at time t, and the sonar data can be classified as Table 1.

2.2. Preprocessing of Weak Observable Data Using Wavelet Transform Modulus Maxima. Outliers mixed in the dataset can be described as singularities by estimating local Lipchitz exponent using wavelet transforms. Defined either at a certain time instant or in an interval, Lipschitz exponent can be calculated by numerical methods. A wavelet transform modulus maximum (WTMM) is introduced to preprocess the sonar data.

Let $x(t)$ and $\psi(t)$ be the sonar data and a certain function (introduced next) at instant t, respectively; the wavelet transform can be defined as $Wx(b,a) = (1/\sqrt{a}) \int_{-\infty}^{\infty} x(t) \cdot \overline{\psi}((t-b)/a)dt$, where $^-$ is complex conjugation and a and b describe scale element and shift coefficient, respectively.

Mathematically the local regularity indicated by Lipschitz exponent is the precondition for data reconstruction using wavelet transform. Owing to the relationship between the WTMM and Lipschitz exponent, the pattern of change in WTMM at different scales is of great importance for the preprocessing of weak data. At a certain scale, if the maximum modulus exists at some time point, search along the scale decrease direction within the cone of influence will find a singular point or a peak point close to the zero scale, which can be determined by the Lipschitz exponent.

2.2.1. Estimation of Wavelet Coefficients and Compensation of Lost Data. In order to remedy the eliminated sonar data and to guarantee the continuity of the reconstructed contour, the wavelet coefficient estimation method proposed by Liu and Mao [24] is used. More specifically, the original sonar data in previous five instants and the wavelet coefficients in the previous six instants are used for the estimation as follows:

$$\begin{aligned} Wx(kT,f) = \sqrt{fT}\,\{&\delta_1 x[(k-1)T,f] \\ &+ \delta_2 x[(k-2)T,f] \\ &+ \delta_3 x[(k-3)T,f] \\ &+ \delta_4 x[(k-4)T,f] \\ &+ \delta_5 x[(k-5)T,f] \\ &- \lambda_1 Wx[(k-1)T,f] \\ &- \lambda_2 Wx[(k-2)T,f] \\ &- \lambda_3 Wx[(k-3)T,f] \\ &- \lambda_4 Wx[(k-4)T,f] \\ &- \lambda_5 Wx[(k-5)T,f] \\ &- \lambda_6 Wx[(k-6)T,f]\}, \end{aligned} \tag{1}$$

where

$$\begin{aligned} \varepsilon &= e^{-fT(\sigma - iw_0)}, \\ \lambda_1 &= -6\varepsilon, \\ \delta_1 &= \left[\frac{(\sigma fT)^3}{3} - \frac{(\sigma fT)^4}{4} + \frac{(\sigma fT)^5}{5}\right]\varepsilon, \\ \delta_2 &= \left[\frac{2(\sigma fT)^3}{3} - \frac{5(\sigma fT)^4}{3} + \frac{26(\sigma fT)^5}{15}\right]\varepsilon^2, \\ \lambda_2 &= 15\varepsilon^2, \\ \lambda_3 &= -20\varepsilon^3, \end{aligned}$$

$$\delta_3 = \left[\frac{22\cdot(\sigma f T)^5}{5} - 2(\sigma f T)^3\right]\varepsilon^3,$$

$$\delta_4 = \left[\frac{2\cdot(\sigma f T)^3}{3} + \frac{5\cdot(\sigma f T)^4}{3} + \frac{26\cdot(\sigma f T)^5}{15}\right]\varepsilon^4,$$

$$\lambda_4 = 15\varepsilon^4,$$

$$\lambda_5 = -6\varepsilon^5,$$

$$\lambda_6 = \varepsilon^6,$$

$$\delta_5 = \left[\frac{(\sigma f T)^3}{3} + \frac{(\sigma f T)^4}{6} + \frac{(\sigma f T)^5}{15}\right]\varepsilon^5. \quad (2)$$

2.2.2. Confidence Limit of a Single-Beam Sonar Data. Confidence limit is introduced to assess the degree of match between the wavelet coefficients and the model calculated using the data. Hypothesis test is used to estimate this confidence limit.

Assume that M is the calculated model built using Hidden Markov Model [24]; the null hypothesis H_0 and alternative hypothesis H_1 are as the follows.

H_0: WT is valid data and equals the data calculated using the model. This means the original sonar data are the true signal from threatening obstacles.

H_1: WT is an outlier and its corresponding original sonar data are from either low threatening obstacles or noise.

The tracking evaluation function is introduced to estimate the confidence limit,

$$Ev(WT, H_0, H_1) = \frac{P\{WT \mid H_0\}}{P\{WT \mid H_1\}}, \quad (3)$$

where $P\{WT \mid \cdot\}$ is the probability to obtain the same model data with WT in corresponding hypothesis.

If $T_{\min}$ is defined as the acceptable minimum threshold, the ratio between the evaluation function value and $T_{\min}$ is used to determine the class property of the data; see Table 2.

3. Initial Contour Reconstruction

The preprocess sonar data by using the wavelet transform can locally amplify abnormal signals or outliers. This observation helps detect and eliminate potential outliers in order to reconstruct the contour of environmental structure. Support vector clustering (SVC) inertial algorithm was used to achieve the initial contour reconstruction.

Table 2: Determination of class types.

Ratio	Class type
≥1	Outliers
<1	Valid data

Table 3: Criterion of clustering.

Class	Condition	Conclusion
Nonbounded support vector	$\vartheta_i = 0, 0 < \alpha_i < P$	Class contour
Bounded support vector	$\vartheta_i > 0, \alpha_i = P$	Outliers
Data class	$\alpha_i = 0$	Class data

3.1. Structural Environment Construction Using SVC Algorithm. The main idea of SVC is to project sonar data $\{x_1, x_2, \ldots, x_N\}$ into high-dimension hypersphere space with a minimum radius using nonlinear mapping $H = \{\Phi(x_i) \mid 1 \le i \le N\}$. For the mapping data in hypersphere, it holds that $\|\Phi(x_i) - a\|^2 \le R^2$ where a and R denote the center and radius of the sphere. The objective function is described as [25],

$$\max\left\{\sum_{i=1}^{N} K(x_i, x_i)\alpha_i - \sum_{i,j=1}^{N}\alpha_i\alpha_j K(x_i, x_j)\right\}. \quad (4)$$

In high dimension space, the distance from x to the sphere center a, $R^2 = \|\Phi(x) - a\|^2$ is adapted as

$$R^2 = K(x,x) - 2\sum_{i=1}^{N}\alpha_i K(x_i, x) + \sum_{i,j=1}^{N}\alpha_i\alpha_j K(x_i, x_j), \quad (5)$$

where hypersphere radius $R = \sum_i R(\alpha_i^*)/N$, a support vector α_i^*, and the number of support vector N. Class bound of dataset will be collected

$$\{x \mid R(x) = R\}. \quad (6)$$

Outliers are defined as

$$\{x \mid R(x) > R\}. \quad (7)$$

After the clustering, the sonar data are separated into three classes according to the position with respect to the class bound, shown in Table 3. ϑ and P are the relaxation factor and penalty coefficient to balance the performance.

Adjacency matrix $A = (A_{ij})_{N\times N}$ is included to determine type of classes with the distance as its elements:

$$A_{ij} = \begin{cases} 1 & \forall t \in \text{seg}(x_i, x_j), R(t) \le R \\ 0 & \text{other,} \end{cases} \quad (8)$$

where $\text{seg}(x_i, x_j)$ expresses the line segment between x_i and x_j. If the line is either inside or outside the hypersphere, x_i and x_j are then attributed to the same class. A three-step implementation is as follows.

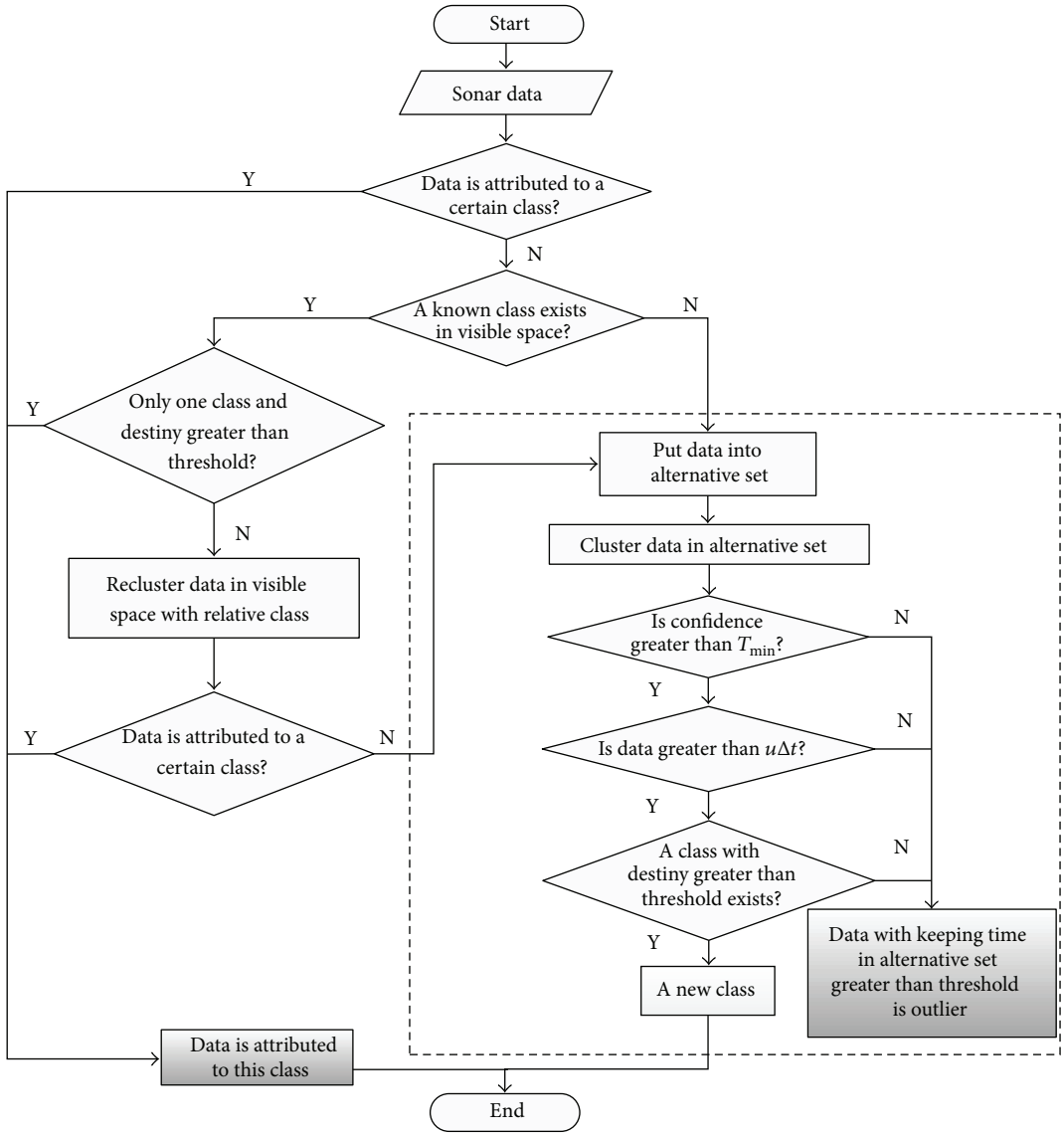

Figure 2: Flow chart of outlier inertia detection for preprocessed data.

Step 1. k-average interpolation is applied on the line between x_i and x_j.

Step 2. Compute $x = \|x_i - x_j\| \cdot l/k$, and let Δx be regarded as the determinant distance and l is the number of lines inside or on the hypersphere.

Step 3. If $x \geq \Delta x$, x_i and x_j are attributed to the same class; otherwise they are from different classes and will have to be further differentiated in the next subsection.

3.2. Inertia Algorithm for Improving Construction. Inertia algorithm is a common action delay method proposed to avoid unnecessary actions of the UUV in order to escape from potentially threatening obstacles [25]. This idea is adopted here to determine the classes of those data that has not been successfully classified. Outliers determined by the SVC algorithm are regarded as candidate outliers. Inertia method is used to determine the class label of those data that have not been explicitly classified. After this step the sonar data are separated into three classes: data class, class bound data, and outliers by using inertia algorithm. The flowchart of inertia algorithm is illustrated in Figure 2.

Let k and ρ_T, respectively, denote the number of classes and a preset minimum constant threshold. $\forall i \geq 1$, if it is satisfied that

$$\exists \bigcup_k \{x_k \mid k > \rho_T\} \subseteq C_i. \tag{9}$$

C_i is regard as a *known class*. An alternative set is introduced to temporarily place preoutliers, denoted as *AlS*.

The conditions for classifying the sonar data into the alternative set can be described as follows.

(1) There is not any known class.

At the beginning of path planning, there is not enough sonar data to be clustered and to clearly indicate any obstacles.

The data x is placed into alternative set AlS. If there is more sonar data in the visible range of x and the density increases to ρ_T, it means that the dataset constitutes the first class C_1. If the density is still lower than ρ_T with time evolution of Δt, x will be determined as LTO or noise and will not be used to reconstruct the contour of the environment.

(2) If any C_i exists with $i \geq 1$, $i \in \mathbf{N}^+$, the class may include class data, class bound data, and/or outliers and thus cannot be directly determined. Let X be an arbitrary dataset and described as

$$X = \left\{ \bigcup_{j=1}^{m} x_j \mid m < \rho_T, x_j \notin C_{\text{any}} \right\}, \tag{10}$$

where C_{any} denotes any known class. It implies that once the destiny of sonar data is less than ρ_T, it will be placed into AlS for further assessment.

Assume that N_c is the number of known classes, and Class set C is defined as

$$C = \bigcup_{i \in M} C_i = \{x : \exists i \in N_c, \text{with } x \in C_i\}. \tag{11}$$

Outlier set is symbol by O, including the outliers and the data with density less than the preset threshold ρ_T.

Criterion 1. For any sonar data x, if it is satisfied that $x \in L_i$, $1 \leq i \leq M$, where L_i is the bound of known class C_i, we will have $x \in C_i$.

For arbitrary data x, Criterion 1 is utilized to identify whether it belongs to any known class. If it just falls into bound L_i, x is assigned to C_i directly and $x \in C_i$; otherwise, go to the next criterion. In order to determine the properties of the data, visible space is defined as follows.

Visible space is an artificial sphere space centered at x with a radius of r. It is used to estimate distribution density near x. In the visible space, if the density of sonar data is larger than a predefined threshold, we can determine that it is a valid class.

Criterion 2. $\forall x, x \notin C_i$, x does not belong to any known class. Assume that $V = \{x \mid |x - x_a| < r\}$, with x_a as a point in the visible range of x. If the number of data satisfying the condition $x_a \in C_i$ is not less than ρ_T, then C_i is a known class in x's visible range.

Criterion 3. If the number of data in C_i is larger than ρ_T, and C_i is the unique known class of x, it can be ascertained that $x \in C_i$ directly.

To determine the property of any x that has not been successfully classified by using Criterion 1, Criterion 3 is important to ensure whether it can be assigned to a unique known class. If it fails, reclustering has to be performed.

It is observed that the objects for reclustering C_{Re} only contain the classes including the data point and those in its visible range, and therefore the effectiveness of algorithm can be increased:

$$C_{\text{Re}} = \left\{ x \mid x \notin C_i \bigcap |x - x_a| < r \right\} \bigcup \{x_a \mid x_a \in C_i\}. \tag{12}$$

Sonar data x with unknown class in its visible range will be located in the alternative set AlS. Similarly, those data that can still not be classified by reclustering are also placed into AlS for further analysis.

Criterion 4. $\forall 1 \leq i \leq M, \exists x_i \in AlS$, SVC algorithm is applied to cluster and class C_r is obtained. If the density ρ_R of C_r is larger than ρ_T, it is considered that $C_r \subseteq C$. The total number of M increases by 1. Otherwise, data x (or dataset X) exist which satisfies the following condition:

$$\begin{gathered} \{x \mid t > t_T\} \subseteq O \\ \{X \mid \text{Total number of } X < \rho_T, t > t_T\} \subseteq O, \end{gathered} \tag{13}$$

where t shows the time related to the data x (or set X).

In environmental structure detection, data gradually accumulates. Through preprocessing using wavelet transform and clustering by SVC inertia algorithm, an initial contour can be reconstructed with data class bound as reference. The initial contour consists of several successively connected lines.

4. Smoothing Initial Contour Based on Local Environment Characters

4.1. Extraction of Local Environmental Characteristics. Based on the assumption that the data collected from the 5 sonars are accurate, three different local environmental characteristics can be determined, and they are described as follows.

4.1.1. Line Path. Figure 3 shows two scenarios where the vehicle is located on the right (Figure 3(a)) and left side (Figure 3(b)) of a local linear environment, respectively. l_1, l_2, and l_3 denote the data collected from the left, middle, and right sonars in the front of the vehicle, respectively, while l_l and l_r are the data collected from the left and right side sonars.

If the left (resp., right) side sonar data is valid and the right (resp., left) one shows maximum effective distance, then the vehicle is on a line path and on the right (resp., left) side of the contour. Remark: energy carried with an UUV is often limited. When there is no obstacle on one side of the vehicle, the sonar on that side can be turned off in order to conserve energy and extend the working time for the mission.

4.1.2. Narrow Path. If the distance between the environment contours on both sides of the path is not wide enough for the vehicle to turn safely, the vehicle is in a narrow path. Figure 4 illustrates this scenario where the distances l_{12} and l_{23} are calculated by using the data from the three front sonars. If the sonar data from the left and right side are effective and $l_{12} + l_{23} < 2d_c$ where d_c is the predefined minimum turning radius, the vehicle is in a narrow turning path.

Proof. The triangle inequality theorem states that any one side of a triangle is always shorter than the sum of the other two sides. For the triangle with l_{12}, l_{23}, and l_{13} as its sides, it holds that

$$l_{12} + l_{23} > l_{13}. \tag{14}$$

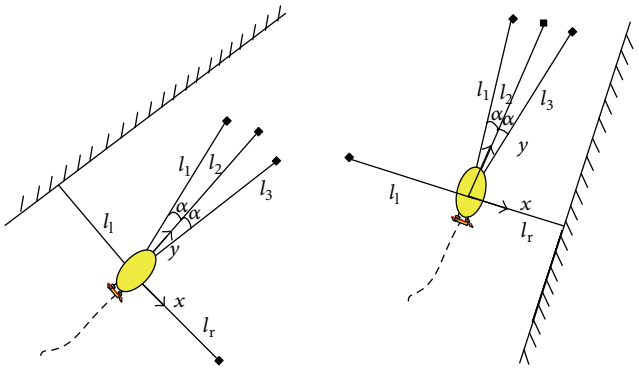

Figure 3: Diagram illustrating line path.

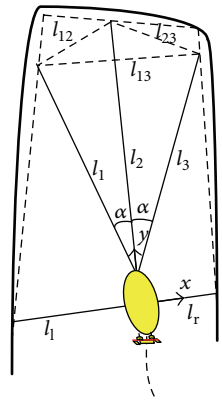

Figure 4: Diagram illustrating narrow turn path.

Let l_0 be the line connecting the two sides of the contours; it also holds that

$$l_{13} \geq l_0. \tag{15}$$

Then we have

$$l_0 \leq l_{13} < l_{12} + l_{23}. \tag{16}$$

If $l_{12} + l_{23} < 2d_c$ is satisfied, it holds that $l_0 < 2d_c$. That is, the line is smaller than the turning radius, and the vehicle cannot steer out of this narrow turning environment by normal turning motion. Theorem holds. □

4.1.3. Regular Turning Path. The determination of regular turning path is similar to the narrow turning path. If the left side sonar data is effective, the vehicle in regular turning path can be separated into two situations according to the data from the 3 sonars at the front; see Figure 5. The left front sonar beam is located on the previous path, with the middle and right ones being located on the rear path in Figure 5(a). The difference between (b) and (a) is the left and middle sonar beam located on the previous path, with the right sonar beam being on the rear path. The stage of UUV turning is reflected. If the sonar data on one side is effective and the other side is ineffective or has the maximum value (this is different to narrow turning path), it can be determined that the vehicle is in a regular turning path.

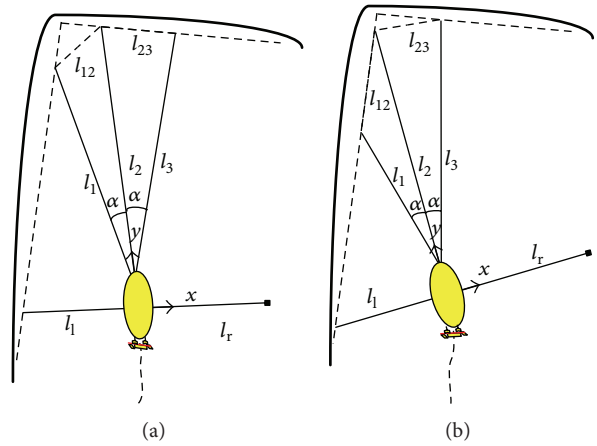

Figure 5: Diagram illustrating normal turn paths.

4.2. Smoothness of the Local Environmental Contour. The initial contour reconstructed by using the SVC inertia algorithm comprises lines that are successively connected. Due to the inertia property of the underwater vehicle, this cannot be used as the reference path for tracking. In this paper, Bézier curve is introduced to smooth the initial contour in order to extract a reference path that can be used for navigation.

Given a set of control points $P_0, P_1, \ldots, P_n$, $\forall t \in [0, 1]$, nth-order Bézier curve can be defined as $B(t) = \sum_{i=0}^{n} P_i b_{i,n}(t)$, with Bernstein Polynomial $b_{i,n}(t) = \begin{bmatrix} n \\ i \end{bmatrix}^T t^i (1-t)^{n-i}$, $i = 0, 1, \ldots, n$. Different order Bézier curves are chosen to smooth the initial contour. To determine the curve orders, control points are located first. Considering navigation requirement and the contour characteristics, it is intrinsic that the starting point, end point, and intersection point between turning paths should be the control points. Moreover, the width of the local environment is another significant issue to be considered for the order of Bézier curve.

Based on Section 4.1, the local environmental characteristics are separated into line and turning paths, and then the orders of different characteristics are classified. It has been proved that 2nd-order Bézier curve is sufficient for turning path restriction [26], and as such Bézier curves used here must satisfy C^2 continuity condition.

C^k continuity condition: Bézier curves $P(t)$ and $Q(t)$ in C^k continuous at t_0 are,

$$\begin{aligned} P(t_0) &= Q(t_0) \\ \dot{P}(t_0) &= \dot{Q}(t_0) \\ &\vdots \\ P^{(k)}(t_0) &= Q^{(k)}(t_0). \end{aligned} \tag{17}$$

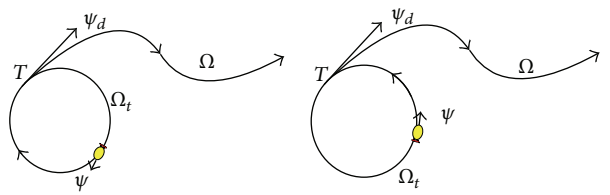

Figure 6: Rolling path with different orientations to find initial points on reference path.

Based on the definition of C^k continuity condition, smoothness conditions for n segments can be shown as

$$\begin{aligned} {}^{i-1}P_{n_{i-1}} &= {}^{i}P_0 \\ n_{i-1}\left({}^{i-1}P_{n_{i-1}} - {}^{i-1}P_{n_{i-1}-1}\right) &= n_i\left({}^{i}P_1 - {}^{i}P_0\right) \\ n_{i-1}\left(n_{i-1}-1\right)\left({}^{i-1}P_{n_i-1} - 2\cdot {}^{i-1}P_{n_{i-1}-1} + {}^{i-1}P_{n_{i-1}-2}\right) &= n_i\left(n_i-1\right)\left({}^{i}P_2 - 2\cdot {}^{i}P_1 + {}^{i}P_0\right), \end{aligned} \tag{18}$$

where $i = 2, 3, \ldots, 2N-3$, and n_i is the number of control points for the ith Bézier subcurves. The first and last segments are special cases and their orders are discussed first and followed by those ones in the middle.

4.2.1. First and Last Segments. For the first and last segments, ${}^{1}B(t)$ and ${}^{2N-3}B(t)$, with the known control points $W_1 = {}^{1}P_0$ and $W_N = {}^{2N-3}P_4$. To find the orders of these curves, the following must hold.

Condition 1. The heading ψ_0 and ψ_f at control points W_1 and W_N must be guaranteed as follows:

$$\begin{aligned} {}^{1}p_1 &= W_1 + c_0\left[\cos\psi_0 \;\; \sin\psi_0\right]^T, \quad c_0 \in \mathbf{R}^+, \\ {}^{2N-3}p_3 &= W_N - c_f\left[\cos\psi_f \;\; \sin\psi_f\right]^T, \quad c_f \in \mathbf{R}^+, \end{aligned} \tag{19}$$

where c_0 and c_f are constant parameters. To satisfy Condition 1, ${}^{1}P_0$ and ${}^{1}P_1$ of the first segment, as well as ${}^{2N-3}P_3$ and ${}^{2N-3}P_4$ of the final segment must be known.

Condition 2. C^2 continuity condition with contiguous subcurves must be guaranteed. Therefore, the points ${}^{i-1}P_{n_{i-1}}$, ${}^{i-1}P_{n_{i-1}-1}$, and ${}^{i-1}P_{n_{i-1}-2}$ should be known in (18).

Given all the above conditions, the total number of the control points required to be known is 5 for the first and last segment, respectively. This implies that 4th-order Bézier curves are needed for both of them.

4.2.2. Middle Segments. To guarantee C^2 continuity condition, for each middle segment it has 6 control points in total: three control points, respectively, from the previous segment (including ${}^{i}P_2$, ${}^{i}P_1$ and ${}^{i}P_0$) and the segment after (including ${}^{i-1}P_{n_{i-1}}$, $P_{n_{i-1}-1}$, and $P_{n_{i-1}-2}$) are known (see (30)). Therefore, the order of Bézier subcurves is 5 for the middle segments, ${}^{i}B(t)$, $i = 3, 5, \ldots, 2N-5$. Table 4 summarizes the order selection for different local environment characters.

Table 4: Orders of Bézier curve.

Local environment character	Order of Bézier curve
Turning	2nd-order
Start and final segments	4th-order
Middle segments	5th-order

5. Path Tracking Control

Two types of feedback linearization methods are used for path tracking control: differential geometry feedback linearization and stable inversion, which can be used for exactly automatic target approaching in known region and contour reconstruction in unknown region, two stages of the navigating process. This will be detailed in this section.

The path tracking control model for a UUV can be described with state vectors as follows:

$$\begin{aligned} \dot{x}(t) &= f(x) + g(x)\,\mu(t), \\ y(t) &= \left[y_1 \;\; y_2 \;\; y_3\right]^T = h(x(t)), \end{aligned} \tag{20}$$

where $x(t) = \left[x \;\; y \;\; \psi \;\; u \;\; v \;\; r\right]^T \in \mathbf{R}^6$ denotes states, $\mu(t) = \left[\tau_u \;\; \tau_r\right]^T \in \mathbf{R}^2$ denotes input variable matrix, mapping $f(\cdot): \mathbf{R}^6 \to \mathbf{R}^6$, $g(\cdot): \mathbf{R}^6 \to \mathbf{R}^{6\times 2}$, and $h(\cdot): \mathbf{R}^6 \to \mathbf{R}^3$ is smooth enough. f and g are nonlinear items and input coefficient items given in the following:

$$\begin{aligned} f &= \begin{bmatrix} u\cos\psi - v\sin\psi + \tau_{du} \\ u\sin\psi + v\cos\psi + \tau_{dv} \\ r + \tau_{dr} \\ p_1 vr + p_2 u \\ p_4 ur + p_5 v \\ p_7 uv + p_8 r \end{bmatrix}, \\ g &= \begin{bmatrix} 0 & 0 \\ 0 & 0 \\ 0 & 0 \\ p_3 & 0 \\ 0 & 0 \\ 0 & p_9 \end{bmatrix}, \end{aligned} \tag{21}$$

where $p_1 = m_{22}/m_{11}$, $p_2 = (-X_u - X_{u|u|}|u|)/m_{11}$, $p_3 = 1/m_{11}$, $p_4 = m_{11}/m_{22}$, $p_5 = (-Y_v - Y_{v|v|}|v|)/m_{22}$, $p_6 = 1/m_{22}$, $p_7 = (m_{11} - m_{22})/m_{33}$, $p_8 = (-N_r - N_{r|r|}|r|)/m_{33}$, $p_9 = 1/m_{33}$, $m_{11} = m - X_{\dot{u}}$, $m_{22} = m - Y_{\dot{v}}$, and $m_{33} = I_z - N_{\dot{r}}$. m is the mass of the UVV; $X(\cdot)$, $Y(\cdot)$, and $N(\cdot)$ are the derivatives of the hydrodynamic coefficients related to the added mass; I_z denotes the initial moment of the UUV under body coordinate system, τ_u and τ_r are the input force, and moment τ_{du}, τ_{dv}, and τ_{dr} are the disturbance at those corresponding directions.

5.1. Autonomous Arriving Based on Differential Geometry Feedback Linearization. The UUV is diving underwater with arbitrary states (including heading and position) at any point

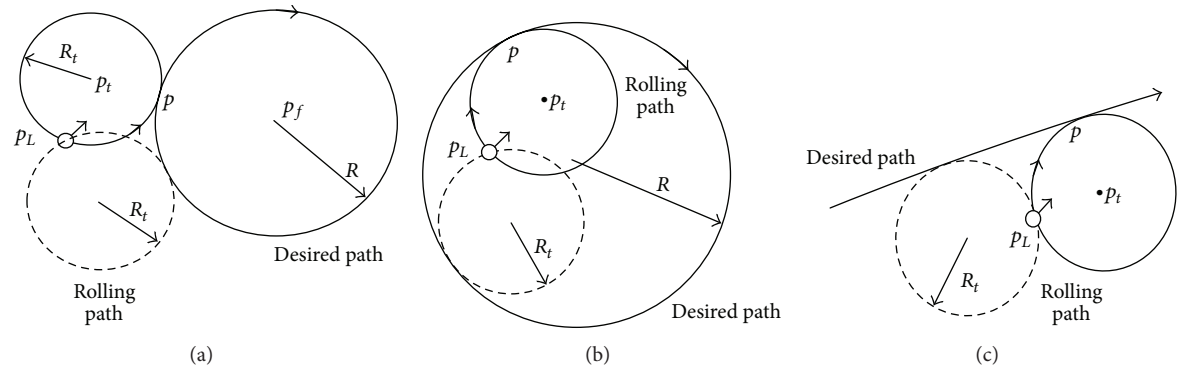

Figure 7: Rolling path generation for three different situations. (a) UUV is outside circle path. (b) UUV is outside circle path. (c) UUV is outside line path.

and has to be able to navigate towards a preset target near the structural environment. This is known as *Autonomous Arriving*. A differential geometry feedback linearization control algorithm with rolling path guidance is proposed to achieve accurate tracking. Figure 6 illustrates how to find the initial points: circle arc is used to represent rolling path according to the initial heading and orientation of the vehicle, Ω and Ω_t represent the desired path and rolling path, respectively, ψ and ψ_d are the current heading direction and desired heading direction, respectively, and T denotes the tangent point of Ω and Ω_t, which is the initial point on Ω for the vehicle. Note, the UUVs in Figure 6 have the same initial positions but different headings (upward and downward in Figures 6(a) and 6(b), resp.). Given the desired orientation and the inertia of the vehicle, the vehicle is unable to turn at T in the scenario as shown in Figure 6(b). Further analysis is required and detailed as follows.

Let model output be $\eta = [\eta_1 \ \ \eta_2]^T$, η_1 is the distance of the chosen path, and $\eta_2 = \psi$.

It has been proved that any nonlinear path can be reconstructed by circular arcs and lines [27]. Therefore, with circle and line as example, rolling paths are generated as the desired path for the guidance of the UUV.

(1) Circle Path. Assume that $p_f(x_f, y_f)$ is the center of a circle path and the radius of the circle path R_f is a constant; then the output can be given as

$$\eta_1 = \sqrt{\left(x - x_f\right)^2 + \left(y - y_f\right)^2} - R, \tag{22}$$

where $p_L(x, y)$ is the actual initial position of the vehicle. From the equation above, $|\eta_1|$ is the minimum distance between p_L and the circle path.

According to the position between the desired path and the current position of the vehicle, radius of a rolling path can be derived as follows:

(a) when the initial position of the UUV is outside of the circular path (see Figure 7(a)) and ϖ is a constant

$$R_t = \begin{cases} \eta_1 + \varpi R & \eta_1 > \dfrac{R}{2} \\ R & \text{others,} \end{cases} \tag{23}$$

(b) when the initial position of the UUV is inside of the circular path (see Figure 7(b))

$$R_t = \begin{cases} \dfrac{\eta_1 + 2R}{2} - \varpi R & p_L \neq p_f \\ \dfrac{R}{2} & \text{others.} \end{cases} \tag{24}$$

(2) Line Path. With line path $Ax + By + C = 0$, the output η_1 is given as follows,

$$\eta_1 = \frac{\left(Ax + By + C\right)}{\sqrt{A^2 + B^2}}, \tag{25}$$

where $A^2 + B^2 \neq 0$. In this case $R_t = \varpi\eta_1 + R_0$ and R_0 is a constant.

Assumption 1. UUV tracking system satisfies $m_{11} < m_{22}$ and the surge and yaw velocity are nonobservable.

Figure 7 illustrates how the rolling path is generated in three different cases as discussed above. The solid and dashed circles are tangent to the rolling circular path across the vehicle position p_L. According to the consistency between the heading direction of the vehicle and the desired path, the solid arc $\widehat{p_L p}$ will be chosen as the rolling path while the orientation of the vehicle becomes close to the direction of the desired path. Once a rolling path is generated as above, a feedback linearization controller can be designed for automatic arriving.

Theorem 1. *Assume (i) the mass, added mass, and damping coefficients are diagonal matrixes; (ii) Assumption 1 is satisfied. For the nonlinear tracking model* (20)*, according to the relative position between the vehicle and the originally desired path, if a circular arc rolling path with radius R_t is chosen in real time with suitable parameters (k_{11},k_{12}) and (k_{21},k_{22}), the controller can be designed.*

Proof. The lines and circular arcs can be combined to form any nonlinear path; therefore, the proof is established from the following two aspects.

(1) Desired path is a circle path.

Obtaining a direct relationship between the output η and the input vector,

$$\begin{aligned}
\dot{\eta}_1 &= \frac{1}{\sqrt{\left(x-x_f\right)^2+\left(y-y_f\right)^2}} \\
&\quad\cdot\left[\left(x-x_f\right)\left(\dot{x}-\dot{x}_f\right)+\left(y-y_f\right)\left(\dot{y}-\dot{y}_f\right)\right] \\
\dot{\eta}_2 &= \dot{\psi} \\
\ddot{\eta}_1 &= -0.5e_k^3 \\
&\quad\times\left[\left(x-x_f\right)\left(\dot{x}-\dot{x}_f\right)+\left(y-y_f\right)\left(\dot{y}-\dot{y}_f\right)\right]^2 \\
&\quad+e_k\left[\left(\dot{x}-\dot{x}_f\right)^2+\left(x-x_f\right)\left(\ddot{x}-\ddot{x}_f\right)\right] \\
&\quad+e_k\left[\left(\dot{y}-\dot{y}_f\right)^2+\left(y-y_f\right)\left(\ddot{y}-\ddot{y}_f\right)\right] \\
\ddot{\eta}_2 &= \dot{r},
\end{aligned} \tag{26}$$

where

$$e_k = \frac{1}{\sqrt{\left(x-x_f\right)^2+\left(y-y_f\right)^2}}. \tag{27}$$

Define state function $h = \begin{bmatrix} h_1 & h_2 \end{bmatrix}^T$, and

$$\begin{aligned}
u_1 &= p_1 vr + p_2 u + p_3\tau_{du} \\
v_1 &= p_4 ur + p_5 v + p_6\tau_{dv} \\
h_1 &= -0.5e_k^{\,3} \\
&\quad\times\left[\left(\dot{x}-\dot{x}_f\right)\left(x-x_f\right)+\left(\dot{y}-\dot{y}_f\right)\left(y-y_f\right)\right]^2 \\
&\quad+\left(x-x_f\right)\left(u_1\cos\psi-ur\sin\psi\right. \\
&\qquad\left.-v_1\sin\psi-vr\cos\psi-\ddot{x}_f\right) \\
&\quad+e_k\cdot\left\{\left(\dot{x}-\dot{x}_f\right)^2+\left(\dot{y}-\dot{y}_f\right)^2\right. \\
&\qquad+\left(y-y_f\right)\left(u_1\sin\psi+ur\cos\psi\right. \\
&\qquad\left.\left.+v_1\cos\psi-vr\sin\psi-\ddot{y}_f\right)\right\} \\
h_2 &= p_7 uv + p_8 r + p_9\tau_{dr} \\
\ddot{\eta} &= h + \begin{bmatrix} e_k\cdot\left(p_3\tau_u\left(\left(x-x_f\right)\cos\psi+\left(y-y_f\right)\sin\psi\right)\right) \\ p_9\tau_r \end{bmatrix}.
\end{aligned} \tag{28}$$

Choose a new input $\mu = \begin{bmatrix} \nu_1 & \nu_2 \end{bmatrix}^T$ and neglect nonlinear portion; let $e = \sqrt{(x-x_f)^2+(x-x_f)^2} - R$ be the tracking error, and the input vector can be derived as follows:

$$\begin{aligned}
\nu_1 &= -k_{11}e_1 - k_{12}\dot{e}_1 = -k_{11} \\
&\quad\times\left(\sqrt{\left(x-x_f\right)^2+\left(y-y_f\right)^2}-R\right) \\
&\quad-k_{12}\left[\frac{1}{\sqrt{\left(x-x_f\right)^2+\left(y-y_f\right)^2}}\right] \\
&\quad\cdot\left[\left(x-x_f\right)\left(\dot{x}-\dot{x}_f\right)+\left(y-y_f\right)\left(\dot{y}-\dot{y}_f\right)\right] \\
\nu_2 &= \ddot{\eta}_{2d} - k_{21}e_2 - k_{22}\dot{e}_2 \\
&= \ddot{\psi}_d - k_{21}\left(\psi-\psi_d\right) - k_{22}\left(\dot{\psi}-\dot{\psi}_d\right),
\end{aligned} \tag{29}$$

where k_{11}, k_{12}, k_{21}, and k_{22} are constants, $\eta_{2d} = \psi_d$.

The input vector can be shown as

$$\begin{aligned}
\tau_u &= \frac{\left(\nu_1-h_1\right)}{p_3 e_k\left[\left(x-x_f\right)\cos\psi+\left(y-y_f\right)\sin\psi\right]} \\
\tau_r &= \frac{\left(\nu_2-h_2\right)}{p_9}.
\end{aligned} \tag{30}$$

(2) Desired path is line path.

The proving process is similar to the above:

$$\begin{aligned}
\dot{\eta}_1 &= \frac{\left(A\dot{x}+B\dot{y}+C\right)}{\sqrt{A^2+B^2}} \\
\dot{\eta}_2 &= \dot{\psi} \\
\ddot{\eta}_1 &= \frac{\dot{u}\left(A\cos\psi+B\sin\psi\right)+\dot{v}\left(B\cos\psi-A\sin\psi\right)}{\sqrt{A^2+B^2}} \\
&\quad+\frac{A\left(-ur\sin\psi-vr\cos\psi\right)}{\sqrt{A^2+B^2}} \\
&\quad+\frac{B\left(ur\cos\psi-vr\sin\psi\right)+C}{\sqrt{A^2+B^2}} \\
\ddot{\eta}_2 &= \dot{r} \\
h_1 &= t_k\left[A\left(-ur\sin\psi-vr\cos\psi\right)\right. \\
&\quad+B\left(ur\cos\psi-vr\sin\psi\right)+C \\
&\quad+u_1\left(A\cos\psi+B\sin\psi\right) \\
&\quad\left.+v_1\left(B\cos\psi-A\sin\psi\right)\right] \\
h_2 &= p_7 uv + p_8 r + p_9\tau_{dr} \\
\ddot{\eta} &= h + \begin{bmatrix} t_k p_3\left(A\cos\psi+B\sin\psi\right)\tau_u \\ p_9\tau_r \end{bmatrix}
\end{aligned} \tag{31}$$

with $t_k = 1/\sqrt{A^2+B^2}$.

Let $e_1 = t_k(Ax + By + C)$ be the tracking error and $e_2 = \eta_{2d} - \eta_2$ the heading error; the new inputs are described as

$$\begin{aligned}\nu_1 &= -k_{11}e_1 - k_{21}\dot{e}_1 \\ &= -k_{11}t_k\left(Ax + By + C\right) \\ &\quad - k_{21}t_k\left(A\dot{x} + B\dot{y}\right) \\ \nu_2 &= \dot{\eta}_{d2} - k_{12}e_2 - k_{22}\dot{e}_2 \\ &= \ddot{\psi}_d - k_{12}\left(\psi - \psi_d\right) - k_{22}\left(\dot{\psi} - \dot{\psi}_d\right).\end{aligned} \tag{32}$$

The control output can be shown as

$$\begin{aligned}\tau_u &= \frac{\left(\nu_1 - h_1\right)}{\left[p_3 t_k\left(A\cos\psi + B\sin\psi\right)\right]} \\ \tau_r &= \frac{\left(\nu_2 - h_2\right)}{p_9}\end{aligned} \tag{33}$$

□

5.2. Contour Reconstruction Based on Finite Predictive Stable Inversion. For $\forall\varepsilon > 0$, a predictive time instant T_p can be found to obtain stable input $\mu_d(t_c)$ using future output $y_d(t)$, $t \in [t_c, t_c + T_p]$. It satisfies

$$\left\|\mu_d\left(t_c\right) - \mu_p\left(t_c\right)\right\| \le \varepsilon, \tag{34}$$

where $\mu_p(t_c)$ is the desired input. The inner dynamic condition is given as

$$L \triangleq \begin{bmatrix} L_s\left(t_c\right) \\ L_u\left(t_f\right)\end{bmatrix} \triangleq \begin{bmatrix} \sigma_s\left(t_c\right) \\ \sigma_u\left(t_f\right)\end{bmatrix}, \qquad t_f = t_c + T_p. \tag{35}$$

A finite predictive path is regarded as known variables in the time window $[t_c, t_c + T_p]$. The desired output in this time window is utilized to describe the stable and unstable part of the inner dynamics. Picard iteration method [10] is introduced to solve the bounded solution of both parts.

Given the nonlinear tracking model (20), the linearity item of inner dynamics $\sigma(t)$ is extracted to obtain a bounded solution.

Let $A_\sigma = \partial s(\sigma, Y_d)/\partial\sigma|_{Y_d=0,\sigma=0}$, and the linearity part $\dot{\bar{\sigma}}$ can be resolved from $\sigma(t)$ as $\dot{\bar{\sigma}} = A_\sigma\sigma$. The inner dynamics can be described as

$$\begin{aligned}\dot{\sigma}\left(t\right) &= A_\sigma\sigma\left(t\right) + \left[s\left(\sigma\left(t\right), Y_d\left(t\right)\right) - A_\sigma\sigma\left(t\right)\right] \\ &\triangleq A_\sigma\sigma\left(t\right) + \Psi\left(\sigma\left(t\right), Y_d\left(t\right)\right).\end{aligned} \tag{36}$$

A_σ can be further separated into a stable part A_s and an unstable part A_u, which, respectively, denote the characteristic values in the left and right planes of the imaginary axis of the complex plane. Thus, the inner dynamics equations can be rewritten as

$$\begin{aligned}\dot{\sigma}_s &= A_s\sigma_s + I_s\Psi_s\left(\left[\sigma_s \;\; \sigma_u\right]^T, Y_d\right) \\ &\triangleq A_s\sigma_s + \Psi_s\left(\sigma_s, \sigma_u, Y_d\right) \\ \dot{\sigma}_u &= A_u\sigma_u + I_u\Psi_u\left(\left[\sigma_u \;\; \sigma_u\right]^T, Y_d\right) \\ &\triangleq A_u\sigma_u + \Psi_u\left(\sigma_s, \sigma_u, Y_d\right).\end{aligned} \tag{37}$$

With Picard iteration method, the bounded solution for both parts of the inner dynamic can be derived as

$$\begin{aligned}\dot{\sigma}_{s,k}\left(t\right) &= A_s\sigma_{s,k}\left(t\right) \\ &\quad + \Psi_s\left(\sigma_{s,k-1}\left(t\right), \sigma_{u,k-1}\left(t\right), Y_d\left(t\right)\right) \\ \dot{\sigma}_{u,k}\left(t\right) &= A_u\sigma_{u,k}\left(t\right) \\ &\quad + \Psi_u\left(\sigma_{s,k-1}\left(t\right), \sigma_{u,k-1}\left(t\right), Y_d\left(t\right)\right).\end{aligned} \tag{38}$$

For any $t \in [t_c, t_f]$, the bounded solution can be described as follows:

(1) Initial solution is shown with $k = 0$,

$$\sigma_0\left(t\right) = \begin{bmatrix} e^{A_s(t-t_c)}L_s\left(t_c\right) \\ e^{-A_u(t_f-t)}L_u\left(t_f\right)\end{bmatrix}. \tag{39}$$

(2) With $k \ge 1$,

$$\begin{aligned}&\sigma_k\left(t\right) \\ &= \begin{bmatrix}\sigma_{s,k}\left(t\right) \\ \sigma_{u,k}\left(t\right)\end{bmatrix} \\ &= \begin{bmatrix} e^{A_s(t-t_c)}L_s\left(t_c\right) + \int_{t_c}^{t} e^{A_s(t-\tau)}\Psi_s\left(\sigma_{s,k-1}\left(\tau\right), \sigma_{u,k-1}\left(\tau\right), Y_d\left(\tau\right)\right)d\tau \\ e^{-A_u(t_f-t)}L_u\left(t_f\right) - \int_{t}^{t_f} e^{-A_u(\tau-t)}\Psi_u\left(\sigma_{s,k-1}\left(\tau\right), \sigma_{u,k-1}\left(\tau\right), Y_d\left(\tau\right)\right)d\tau\end{bmatrix} \\ &\triangleq S_M\left(\sigma_{k-1}\left(\cdot\right), Y_d\left(\cdot\right), L\right)\left(t\right).\end{aligned} \tag{40}$$

It is clear that the integration operation for the stable and unstable inner dynamics are from current time instant t_c to t forward and backward, respectively.

Assumption 2. Inner dynamics character $\Psi(\cdot,\cdot)$ is a nonlinear item, and it is satisfied that local Lipschitz condition at origin with any constants (K_1, K_2) and any small positive constant σ_0 hold that, for any $t \in \mathbf{R}$, a bounded function exists

$$\begin{aligned}&\left\|\Psi\left(\sigma\left(t\right), Y\left(t\right)\right) - \Psi\left(\overline{\sigma}\left(t\right), \overline{Y}\left(t\right)\right)\right\|_\infty \\ &\leq K_1\left\|\sigma\left(t\right) - \overline{\sigma}\left(t\right)\right\|_\infty + K_2\left\|Y\left(t\right) - \overline{Y}\left(t\right)\right\|_\infty,\end{aligned} \tag{41}$$

where

$$\begin{aligned}\left\|Y\left(\cdot\right)\right\|_\infty &< \sigma_0, \\ \left\|\overline{Y}\left(\cdot\right)\right\|_\infty &< \sigma_0, \\ \left\|\overline{\sigma}\left(\cdot\right)\right\|_\infty &< \sigma_0, \\ \left\|\sigma\left(\cdot\right)\right\|_\infty &< \sigma_0.\end{aligned} \tag{42}$$

Remark. Nonlinearity for inner dynamics will decrease with the decrease of Lipchitz constants K_1 and K_2. If $\Psi(\cdot,\cdot)$ is continuous and differentiable, the locally Lipchitz condition is satisfied.

Assumption 3. A positive constant K exists to hold that

$$\begin{aligned}\left\|\Phi_s\left(t, t_0\right)\right\|_\infty &\leq Ke^{-\alpha(t-t_0)} \quad \forall t_0 \leq t \leq t_f \\ \left\|\Phi_u\left(t_f, t\right)\right\|_\infty &\leq Ke^{-\beta(t_f-t)} \quad \forall t_0 \leq t \leq t_f,\end{aligned} \tag{43}$$

where α and β are minimum character values of A_s and A_u, respectively,

$$\begin{aligned}\alpha &< \inf_i \left|\mathrm{Re}\left(\lambda_i\left(A_s\right)\right)\right| \\ \beta &< \inf_i \left|\mathrm{Re}\left(\lambda_i\left(A_u\right)\right)\right|,\end{aligned} \tag{44}$$

where "inf" denotes the lower bound, "Re" means the real part, and $\lambda_i(A_s)$ and $\lambda_i(A_u)$ are characteristic values of A_s and A_u, respectively.

Remark. The large α and β are, the further is the distance from dynamics poles to the imaginary axis implying stronger hyperbolic properties.

Theorem 2. *If Assumptions 1 and 2 are satisfied and there exist positive constants K_y and K_σ, it holds that*

$$\begin{aligned}&\left\|\mu_d\left(\sigma\left(t\right), Y\left(t\right)\right) - \mu_d\left(\overline{\sigma}\left(t\right), \overline{Y}\left(t\right)\right)\right\|_\infty \\ &\leq K_y\left\|Y\left(t\right) - \overline{Y}\left(t\right)\right\|_\infty \\ &\quad + K_\sigma\left\|\sigma\left(t\right) - \overline{\sigma}\left(t\right)\right\|_\infty.\end{aligned} \tag{45}$$

If Lipchitz constants K_1 and K_2 in (41) satisfy $(K_1 + K_2)/2 < 1$, there is only one fixed point $\sigma^*(\cdot)$ to hold that $\sigma^*(t) = s[\sigma^*(\cdot), Y_d(\cdot)](t)$ for any $\forall t \in [t_c, t_c + T_p]$. The error between the desired input $\mu_{e,d}(t_c)$ and the input $\mu_{d,m}(t_c)$ derived from finite predictive inversion can be quantitated as

$$\begin{aligned}e_{d,m}\left(t_c\right) &\triangleq \left\|\mu_{e,d}\left(t_c\right) - \mu_{d,m}\left(t_c\right)\right\|_\infty \\ &\leq K_\sigma K K_{\alpha\beta}\left[\frac{2KK_{\alpha\beta}}{K_2} + \frac{e^{-\widehat{\beta}T_p}}{1-\delta_\beta}\right]\left\|Y_d\left(\cdot\right)\right\|_\infty,\end{aligned} \tag{46}$$

where

$$\begin{aligned}K_{\alpha\beta} &= \frac{K_{\alpha\beta,2}}{\left(1 - K_{\alpha\beta,1}\right)} \\ K_{\alpha\beta,1} &= KK_1 \max\left\{\left(1/\alpha\right), \left(1/\beta\right)\right\} \\ K_{\alpha\beta,2} &= KK_2 \max\left\{\left(1/\alpha\right), \left(1/\beta\right)\right\}.\end{aligned} \tag{47}$$

The proof is not included here due to space limit. The reader is referred to the original paper for details [21]. According to Theorem 2, the parameter T_p can be optimized and thus the time window.

6. Evaluations and Results

6.1. Evaluation Criteria. Evaluation criteria are set out for assessing the contour accuracy and predictive controlperformance towards detection mission using the UUV under weak observable conditions, respectively.

6.1.1. Evaluation Criterion for Contour Accuracy. Errors between the reconstructed contour and the environment model are computed in order to evaluate the accuracy of the contour reconstruction (only the contours estimated using the SVC inertia algorithm are evaluated here). Considering the characteristics of the environment, "accumulate error" and "overall error" are proposed. Figure 8 illustrates how these errors are computed where the solid lines express the actual contours of the environment model while the dashed lines indicate the contour reconstructed by using the SVC inertia algorithm.

(1) *Accumulative Error Δd_a.* The error between the contour of the environment model and the reconstructed one can accumulate over time, and the accumulative error is used to evaluate this trend.

As shown in Figure 8, d_1, d_3, and d_5 are the deflections between the environment contours and the reconstructed smooth path at the starting point of each segment. d_2, d_4, and d_6 are the deflections at the end point of each segment. Assume that d_s is the safe distance, and the errors of each segment Δd_{a1}, Δd_{a2}, and Δd_{a3} are described as follows:

$$\begin{aligned}\Delta d_{a1} &= \left(d_2 - d_s\right) - \left(d_1 - d_s\right) = d_2 - d_1 \\ \Delta d_{a2} &= \left(d_4 - d_s\right) - \left(d_3 - d_s\right) = d_4 - d_3 \\ \Delta d_{a3} &= \left(d_6 - d_s\right) - \left(d_5 - d_s\right) = d_6 - d_5.\end{aligned} \tag{48}$$

The accumulative error can be defined as follows:

$$\Delta d_a = \sum_{i=1}^{N} \Delta d_{ai}/N \quad i = 1, 2, 3. \tag{49}$$

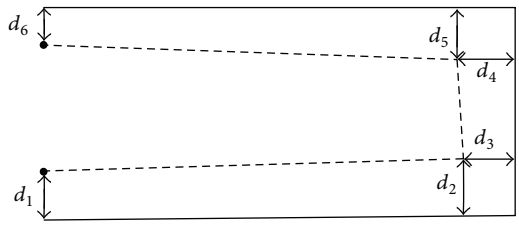

Figure 8: Illustration of the accumulate error and overall error.

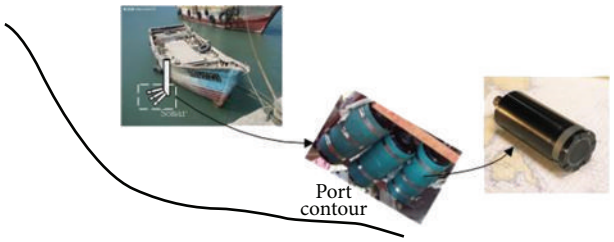

Figure 9: Deployment of the sonars.

(2) *Overall Error* Δd_w. The entire environment contour is reconstructed and the overall error Δd_w at the end point is defined as

$$\Delta d_w = d_6 - d_s. \tag{50}$$

Remark. Both Δd_a and Δd_w have signed values. A positive value means the deflection is larger than the safe distance while a negative value means the deflection is smaller than the safe distance implying a threat to the vehicle navigation.

6.1.2. Evaluation Criteria for Autonomous Tracking Control. To estimate the performance of autonomous tracking control, the error is defined as $e_k = y(k) - \hat{y}(k)$ where $y(k)$ is the navigating path of the vehicle and $\hat{y}(k)$ the smoothed contour from reconstruction. More specifically, the error at the k instant is the minimum distance from the vehicle position to the contour, that is, the tangent point on the contour. Three measures are proposed to analyze the errors.

(1) *Zero Mean Value.* Define $\bar{e} = (1/n)\sum_{k=1}^{n} e_k$ as the estimated value of error serial $\{e_k\}$. To guarantee the zero mean value, for any $n \in \mathbf{Z}^+$, it is satisfied that $\bar{e} \to 0$. From the definition of error, it will be affected by the estimated mean values of the output $\tilde{y}$; therefore, reestimation of the mean value $\bar{e} = \tilde{e}/\tilde{y} < e_T$ is needed. e_T is preset on the basis of accuracy requirement.

(2) *Validity*. It is defined as the degree of deflection between the error serial $\{e_k\}$ and the zero mean value. Standard deviation $\sigma = \sqrt{(1/(n-1))\sum_{k=1}^{n}(e_k - \bar{e})^2}$ is introduced to estimate the data validity.

(3) *Independence*. The error serial describes the error between the real navigating path and the smoothed contour after subtracting the safe distance. Error variables are regarded as random variables and thus the independence describes the randomness. Autocorrelation coefficient r_p is used to describe the independence as follows:

$$r_p = \frac{1}{(n-p-1)}\sum_{k=1}^{n-p}\left(\Delta e_k \Delta e_{p+k}\right), \tag{51}$$

where $\Delta e_k = e_k - \bar{e}_k$. In this paper the autocorrelation coefficient is rewritten as $\rho_p = r_p/r_0$, and the relation between $\rho_p - k$ will be plotted for demonstration. If autocorrelation coefficients are in the Independence Confidence Limit Interval $(-\sigma, \sigma)$, the error serial is not correlated and vice versa.

(a) (b)

Figure 10: Sonar data collection in sea trial.

Figure 11: Sea trial in islands environment.

6.2. Validation Using Sea Trial Data. The performance of the proposed model is verified with the data collected from a sea trial operated at Xiaoping Island in Dalian, China, in August 2009. We choose sonar data collected from two different environments, respectively, a port and two islands. The single-beam sonars were assembled on one side of a fishing boat to simulate UUV sonars. To guarantee the number of sonar data satisfying the clustering requirement, 3 single beam sonars were fixed in the boat side; see Figure 9. The sonars used in the sea trial are manufactured by Kongsberg, Norway. The boat was steered along the contour with acoustic beam vertically acting on environment. The sonars were deployed below the bottom of the boat to avoid acoustic beam to project onto the boat. The boat sails at a velocity of 2 m/s.

Sonar data are collected during the boat navigating along islands horizontally in real time. To verify the effectiveness of the proposed control algorithm in disturbance situation, synthetic disturbance noise is added: $t_{du} = 40 \times (1 + \text{rand}(\cdot))$,

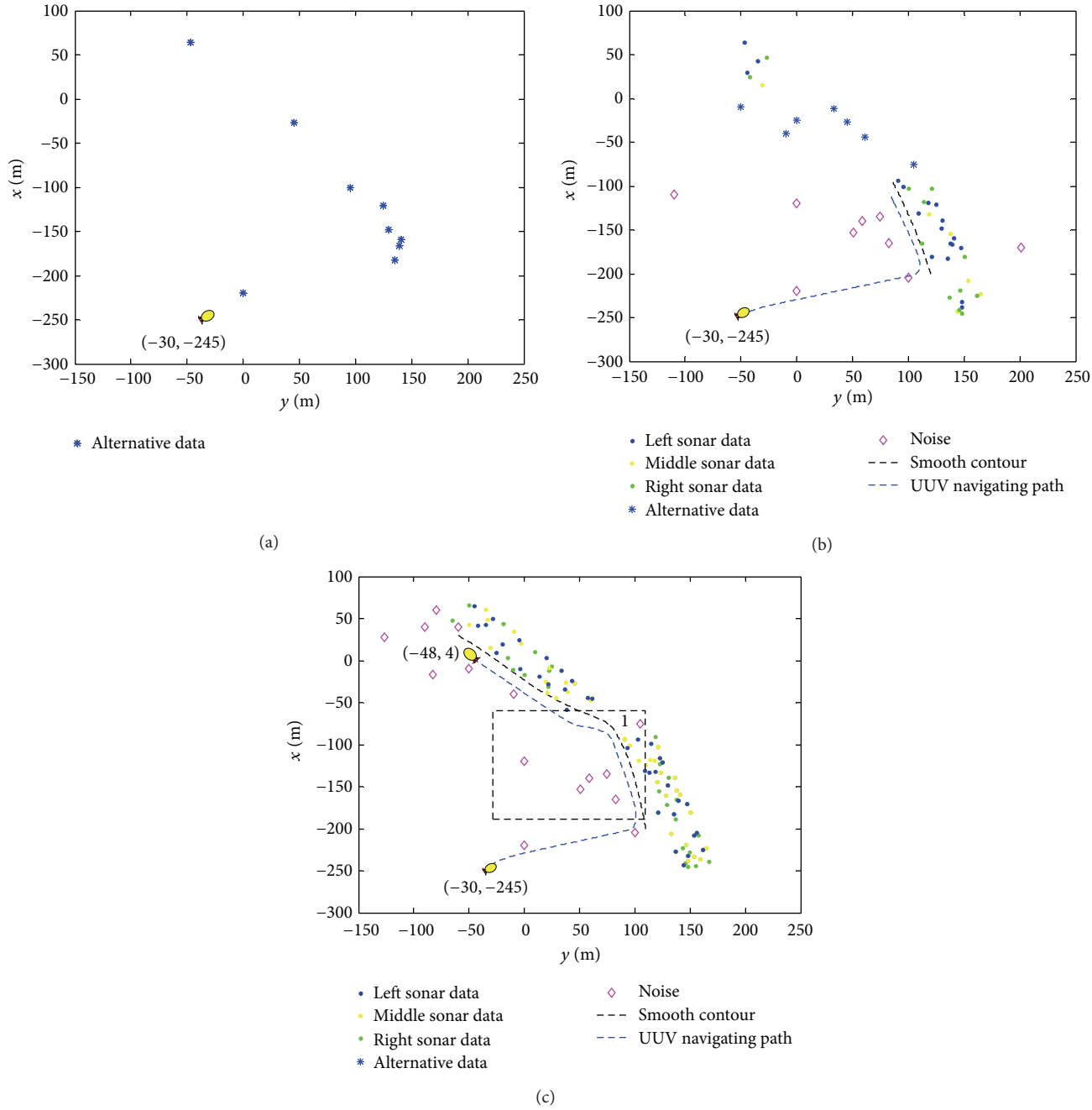

Figure 12: Islands contour construction and patrolling.

$\tau_{dv} = 35 \times (1 + \text{rand}(\cdot))$, $\tau_{dr} = 40 \times (1 + \text{rand}(\cdot))$, with rand$(\cdot)$ denoting zero-mean Gaussian random noise. From Figure 10 the sonar assembly in the sea can be seen, with diving in the water as Figure 10(a) and navigating as Figure 10(b).

6.2.1. Path Following Validation Using Data from Islands. In the first experiment, the boat navigates between two small islands in order to move close to them (see Figure 11). We record the data from initial point A (−30, −245) with heading of 60 degree. The effective distance of sonars is 200 m. Figure 12 shows the process of data clustering. At the beginning, the number of data is too small to construct accurate data class; therefore, data are placed into alternative set; see Figure 12(a). With the number of sonar data increasing, data with the same property, including data in alternative set, are clustered in corresponding class contours with support vectors distributed on. Sonar data determined by the rules in Section 3 are eliminated as outliers (see Figures 12(b) and 12(c)). The contours close to UUV, determined by normal line and distance, connected with lines successively, are regarded as preliminary contour, waiting for postprocessing.

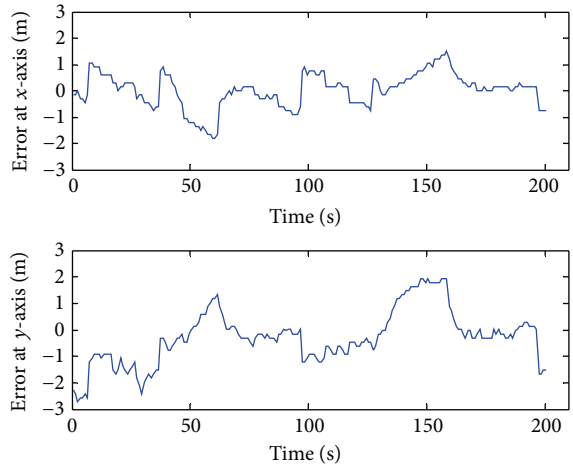

Figure 13: Patrolling errors at x- and y-axis in islands contour.

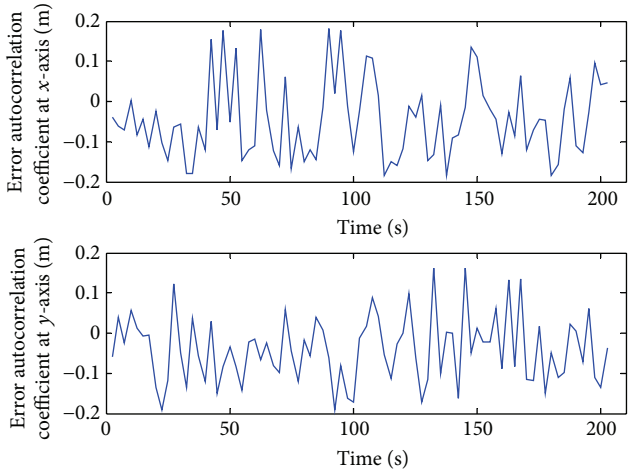

Figure 14: Error autocorrelation coefficients of error serials.

On the basis of initial contour (see solid green line in Figures 12(b) and 12(c)), the smoothing method described in Section 4.2 is applied and a reasonable desired reference path (dash black curves) for vehicle navigation can be achieved. When the vehicle is close to the island on the right less than 200 m, sonar data returned is collected to construct the contour in real time which is regarded as the guidance for the vehicle to navigate, keeping a fixed distance (set to 10 m in this paper) as the safe distance. The optimal time window parameter is $T_p \geq 3$ s. Considering the control period 0.5 s, $T_p = 3$ s satisfies the requirement (5 original sonar data and 6 wavelet coefficients) to estimate wavelet coefficients at any time. According to Section 6.1, the error series denoting the deflection between the actual navigation path and the reconstructed contour is computed; see Figure 13.

The mean (standard deviation) value along x- and y-axis is 0.15 (0.37) m and 0.98 (0.30) m, respectively. According to evaluation criterion for contour accuracy in Section 6.1.1, the accumulated error for island contour is 1.45 m, and overall error is 1.74 m. The negative deflection values are much smaller than the safe distance; this means that the UUV can safely complete the detection mission as designed. The maximum absolute value of the autocorrelation coefficients at x-axis and y-axis is 0.14 and 0.16, respectively, while the respective standard deviations are 0.37 and 0.30 (see Figure 14). This confirms that the error series is independent without influence from the designed controller. This means that the designed controller using finite predictive stable inversion algorithm can control the vehicle to follow a path predicted in real time.

6.2.2. Path Tracking Validation Using Data from Port. With the same deployment and trial methods as above, sonar data was collected in a port as Figure 15 with its environment pictures at the right. The initial position of the boat was (−1605, −688). Owing to the port area is wide and safe distance is set to 30 m. Figure 16 demonstrates the autonomous tracking of the boat in the port. From Figure 16, it can be seen that the smoothed path illustrated by black solid is reconstructed using data from 3 sonars and guides the vehicle to approach the target. The noise in the data is detected and eliminated to guarantee the accuracy of the contour.

Figure 17 illustrates the error of the smoothed path reconstructed and the actual path without consideration of the safe distance. Figure 18 shows the autocorrelation coefficients of the tracking error series to assess whether the errors are from the control method or stochastic disturbance. The maximum absolute value of autocorrelation coefficients at x-axis and y-axis are 0.20 and 0.20, within the range of standard deviations, respectively, (−0.26, 0.26) and (−0.38, 0.38) (see Figure 17). Therefore, it is true that error series are caused stochastically. Moreover, the accumulated error for island contour tracking is 1.50 m, and overall error is 1.20 m, respectively.

7. Conclusions

A new autopilot system, known as SDAP, is proposed for the exploration of underwater environments using UUV equipped with multiple single-beam sonars. The main issue studied is the control problem in detection process which is separated into two stages according to different requirements of the mission, accurate tracking and autonomous tracking. A rolling path generation method is present to guide the vehicle to follow a preset path accurately. For autonomous tracking stage, wavelet transform is introduced to preprocess weak observable data and the wavelet coefficients obtained are used to reconstruct the contour of the environment using the SVC inertia algorithm. To satisfy the inertia property of the UUV which requires a smooth reference path, different order Bézier curves are included to fit the initial contours for the desired reference path by considering a fixed safety distance. Finite predictive stable inversion method is applied to control the vehicle in order to follow the predictive path in real time. Data collected from a sea trial is used to validate the proposed technique, and the results have demonstrated that the algorithms are able to control vehicle navigating along the desired paths that are either preset or predicted automatically.

Figure 15: Sea trial in port environment.

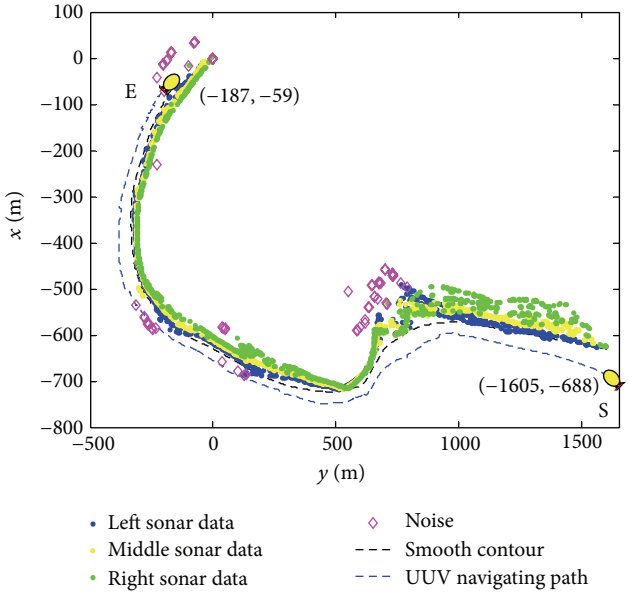

Figure 16: Port contour construction and tracking.

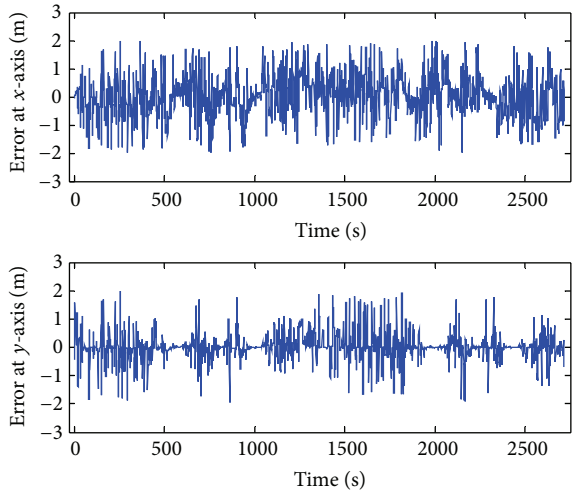

Figure 17: Path error serials at x- and y-axis for patrolling port contour.

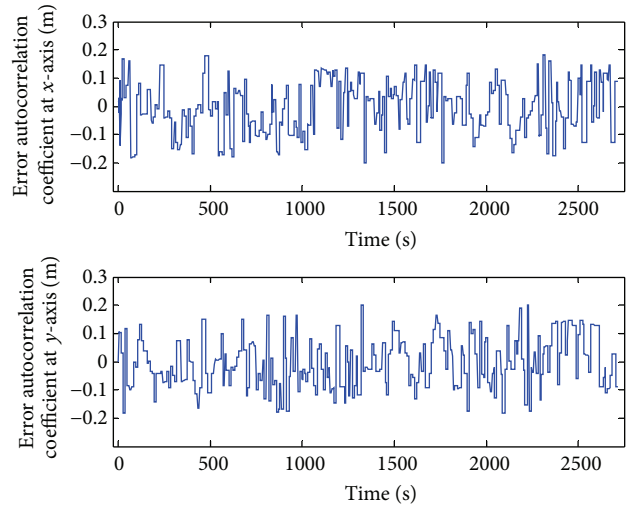

Figure 18: Error autocorrelation coefficients of error serials.

It has laid a solid foundation for using UUV to perform SDAP mission.

During environment detection, the accuracy of environment information obtained is vital to guide UUV steering safely. With the insight, the navigation error will affect the environment outline constructed. In this paper, it is assumed that the navigation error is not considered in the UUV steering. In the future study, it is necessary to include navigation error into the SDAP issue for completeness. Otherwise, the further verification should be implemented through inserting the algorithms into UUV and executing mission in the real environment underwater.

Acknowledgments

This work is partially supported by the Natural Science Foundation of China (51179038), the Program of New Century Excellent Talents in University (NCET-10-0053), and Fundamental Research Funds for the Central Universities (HEUCF041323).

References

[1] A. Chatterjee and F. Matsuno, "A Geese PSO tuned fuzzy supervisor for EKF based solutions of simultaneous localization and mapping (SLAM) problems in mobile robots," *Expert Systems with Applications*, vol. 37, no. 8, pp. 5542–5548, 2010.

[2] O. Calvo, A. Rozenfeld, A. Souza, F. Valenciaga, P. F. Puleston, and G. Acosta, "Experimental results on smooth path tracking with application to pipe surveying on inexpensive AUV," in *Proceedings of the IEEE/RSJ International Conference on Intelligent Robots and Systems (IROS '09)*, pp. 3647–3653, September 2008.

[3] Y. Gan, L. Wan, W. Li et al., "Research on path following of underwater vehicle without rudder and fin," *The Ocean Engineering*, vol. 25, no. 1, pp. 70–75, 2007.

[4] P. Encarnação and A. Pascoal, "3D path following for autonomous underwater vehicle," in *Proceedings of the 39th IEEE Confernce on Decision and Control*, pp. 2977–2982, December 2000.

[5] L. Lapierre and D. Soetanto, "Nonlinear path-following control of an AUV," *The Ocean Engineering*, vol. 34, no. 11-12, pp. 1734–1744, 2007.

[6] L. Lapierre, D. Soetanto, and A. Pascoal, "Nonlinear path following with applications to the control of autonomous underwater vehicles," in *Proceedings of the 42nd IEEE Conference on Decision and Control*, pp. 1256–1261, December 2003.

[7] X. Xiang, *Research on Path following and coordinated control for second-order nonholonomic AUVs [doctor dissertation]*, Huazhong University of Science and Technology, Wuhan, China, 2010.

[8] H. Ren, L. Li, and X. Bian, "Research on fuzzy heading guidance based track keeping method for AUV," *Applied Science and Technology*, vol. 31, no. 9, pp. 43–45, 2004.

[9] J. Zhao, *AUV Fuzzy Neural Network Hybrid Learning Algorithm Control*, Harbin Engineering University, Harbin, China, 2007.

[10] L. Ćirić, A. Rafiq, and N. Cakić, "On Picard iterations for strongly accretive and strongly pseudo-contractive Lipschitz mappings," *Nonlinear Analysis: Theory, Methods and Applications*, vol. 70, no. 12, pp. 4332–4337, 2009.

[11] K. D. Do, "Global robust and adaptive output feedback dynamic positioning of surface ships," *Journal of Marine Science and Application*, vol. 10, no. 3, pp. 325–332, 2011.

[12] R. Amin, A. A. Khayyat, and K. G. Osgouie, "Neural networks modeling of autonomous underwater vehicle," in *Proceedings of the IEEE/ASME International Conference on Mechatronic and Embedded Systems and Applications (MESA '10)*, pp. 14–19, July 2010.

[13] I. Astrov and A. Pedai, "Multirate depth control of an AUV by neural network predictive controller for enhanced situational awareness," in *Proceedings of the 5th International Symposium on Computational Intelligence and Intelligent Informatics (ISCIII '11)*, pp. 47–52, Floriana, Malta, September 2011.

[14] K. Maček, R. Philippsen, and R. Siegwart, "Path following for autonomous vehicle navigation with inherent safety and dynamics margin," in *Proceedings of the IEEE Intelligent Vehicles Symposium*, vol. 6, pp. 108–113, June 2008.

[15] Z. Wang, X. Peng, and D. Wang, "Path following robust output control of underactuated ship under Serret-Frenet frame," *Ship Engineering*, vol. 32, no. 3, pp. 24–32, 2010.

[16] M.-J. Zhang, P. Gao, and J.-A. Xu, "Neural-network-based generalized predictive control for autonomous underwater vehicles," *Robot*, vol. 30, no. 1, pp. 91–96, 2008.

[17] S.-R. Oh and J. Sun, "Path following of underactuated marine surface vessels using line-of-sight based model predictive control," *The Ocean Engineering*, vol. 37, no. 2-3, pp. 289–295, 2010.

[18] Y. Jiang, *Neural Network Based Feedback Linearization Control of an Unmanned Aerial Vehicle*, Ottawa-Carleton Institute for Mechanical and Aerospace Engineering University, Ottawa, Canada, 2005.

[19] Y. Han, Y. Sun, and H. Mo, "Design of nonlinear robust controller for underwater high-speed vehicle," *Journal of Wuhan University of Technology*, vol. 34, no. 2, pp. 221–232, 2010.

[20] J. SONG, *Research on control of supercavitating vehicle based on feedback linearization [master dissertation]*, HarbinHarbin Institute of Technology, 2011.

[21] Q. Zou, *Preview-based systems-inversion for output- tracking: theory and application [doctor dissertation]*, University of Washington, Washington, DC, USA, 2003.

[22] Q. Zou and S. Devasia, "Precision preview-based stable-inversion for nonlinear nonminimum-phase systems: the VTOL example," *Automatica*, vol. 43, no. 1, pp. 117–127, 2007.

[23] Z. Jianhong and Z. Ping, "Precise decoupling tracking of airspeed and altitude for UAV based on causal solution of stable inversion," *Chinese Journal of Aeronautics*, vol. 22, no. 3, pp. 307–315, 2009.

[24] F. Liu and Z.-Z. Mao, "Outlier detection for control process data based on wavelet-HMM methods," *Control and Decision*, vol. 26, no. 8, pp. 1187–1196, 2011.

[25] Z. Yan, D. Chi, Z. Zhao et al., "Outlier inertia detection of UUV obstacles based on support vector clustering," *Journal of Harbin Engineering University*, vol. 33, no. 11, pp. 1377–1383, 2012.

[26] J.-W. Choi, R. E. Curry, and G. H. Elkaim, "Curvature-continuous trajectory generation with corridor constraint for autonomous ground vehicles," in *Proceedings of the 49th IEEE Conference on Decision and Control (CDC '10)*, pp. 7166–7171, Hilton Atlanta Hotel, Atlanta, Ga, USA, December 2010.

[27] J. A. Reeds and L. A. Shepp, "Optimal paths for a car that goes both forwards and backwards," *Pacific Journal of Mathematics*, vol. 145, no. 2, pp. 367–393, 1990.

Hindawi Publishing Corporation
Mathematical Problems in Engineering
Volume 2013, Article ID 230413, 12 pages
http://dx.doi.org/10.1155/2013/230413

Research Article

State-Feedback Sampled-Data Control Design for Nonlinear Systems via Passive Theory

Chengming Yang,[1] Qi Zhou,[2] H. R. Karimi,[3] and Huanqing Wang[4]

[1] *College of Engineering, Bohai University, Jinzhou, Liaoning 121013, China*
[2] *College of Information Technology and Science, Jinzhou, Liaoning 121013, China*
[3] *Department of Engineering of the Faculty of Engineering and Science, University of Agder, 4898 Grimstad, Norway*
[4] *School of Mathematics and Physics, Bohai University, Jinzhou, Liaoning 121013, China*

Correspondence should be addressed to Qi Zhou; zhouqi2009@gmail.com

Received 30 August 2013; Accepted 6 September 2013

Academic Editor: Zhiguang Feng

This paper investigates the problem of passive controller design for a class of nonlinear systems under variable sampling. The Takagi-Sugeno (T-S) fuzzy modeling method is utilized to represent the nonlinear systems. Attention is focused on the design of passive controller for the T-S fuzzy systems via sampled-data control approach. Under the concept of very-strict passivity, a novel time-dependent Lyapunov functional is constructed to develop passive analysis criteria and passive controller synthesis conditions. A new sampled-data controller is designed to guarantee that the resulting closed-loop system is very-strictly passive. These conditions are formulated in the form of linear matrix inequalities (LMIs), which can be solved by convex optimization approach. Finally, an application example is given to demonstrate the feasibility and effectiveness of the proposed results.

1. Introduction

Recently, it is well known that the fuzzy logic control [1–6] is one of effective approaches to handle complex nonlinear systems and has some applications in various real systems. It is well known that the Takagi-Sugeno (T-S) [7] fuzzy model has become a popular and effective method to control complex nonlinear systems. T-S fuzzy model is described as a weighted sum of some simple linear subsystems and thus are easily analyzable. During the past few decades, the problem of stability analysis and controller synthesis of nonlinear systems in Takagi-Sugeno (T-S) [7–10] fuzzy model has been extensively studied and some stability analysis and controller synthesis results have been reported, see, for instance, [11–18] and the references therein. To mention a few, the book [11] proposed fuzzy control systems design and analysis results via linear matrix inequality (LMI) approach [19–26] and the paper [12] presented a survey on the state-of-the-art and recent developments of the art of analysis and design of model-based fuzzy control systems. In addition, due to the effect of time delay in systems, the study of T-S fuzzy systems with time delays has received considerable attention in recent years and the results have been developed in [27–35]. The authors in [35] dealt with the problem of reliable fuzzy H_∞ controller design for uncertain active suspension systems with actuator delay and fault.

In practical control systems, it is important to investigate the controller design problem for sampled-data systems [36, 37]. Recently, the researchers in [38–43] discussed two main methods to develop stability analysis and control synthesis for sampled-data systems. The first one is to model a sampled data system as a discrete-time system [44], in which a sampled data system with a delay is modeled as a discrete-time system and a stability condition is derived. However, it should be mentioned that this method is very difficult to analyze or synthesize for complex systems. The second one is a delayed control input method by modeling the sampled-data system as a continuous-time system with a delayed

control input, which was proposed in [41] and later used in [42, 45]. More recently, many sampled-data analysis and synthesis results have been reported for T-S fuzzy systems [46–50]. Among these results, the state-feedback control design method has been used in [47–51] and observed-based control approach has been used in [46]. Using input delay approach, the stabilization of nonuniform sampling fuzzy control systems have been investigated in [48–52], where the systems are regarded as ordinary continuous-time systems with a fast-varying delay. The authors in [51] used the time-dependent delay Lyapunov-Krasovskii functional idea [42] and introduced some slack matrices to improve the sampled-data control results about stabilization for fuzzy systems [48, 52]. However, these slack matrices may lead to a significant increase in the computational demand.

The passive properties of a system can keep the system internally stable and is frequently used in control systems to prove the stability of systems. There are extensive applications for passivity problem in various engineering areas such as electrical circuits, complex networks, mechanical systems, and nonlinear systems. The problems of passivity analysis and passive control have been extensively applied in many areas such as signal processing, fuzzy control, sliding mode control [53], and networked control systems [54]. More recently, the passive control problem has been studied for fuzzy systems [55–57]. In [57], the authors considered the passive control problems for a class of continuous-time T-S fuzzy systems with both state and input delays. The state-feedback fuzzy controller was designed such that the resulting closed-loop system is very-strictly passive. To the best of the authors' knowledge, so far no attempt has been made towards solving the problem of passive control design results for nonlinear systems with variable sampling. This problem still remains challenging, which motivates this study.

In this paper, the passive controller design problem is investigated for a class of nonlinear systems under variable sampling. Firstly, the T-S fuzzy model is employed to represent the nonlinear systems. By using the input delay approach, the T-S fuzzy system with variable uncertain sampling is transformed into a continuous-time T-S fuzzy system with a delay in the state. Secondly, by constructing a novel time-dependent Lyapunov functional, under the concept of very-strict passivity, new passive analysis criteria are proposed and then novel sampled-data controller is designed to guarantee that the resulting closed-loop system is very-strictly passive. The existence conditions of the obtained controller can be expressed as linear matrix inequalities (LMIs), which can be solved using standard numerical software. Finally, an application example is given to illustrate the feasibility and effectiveness of the proposed passive control approach. The remainder of this paper is organized as follows. The problem to be solved is formulated in Section 2. Main results, including passive analysis and passive controller design are presented in Section 3. Section 4 provides an illustrative example to show the effectiveness and potential of the proposed design techniques. We conclude this paper in Section 4.

Notation. The notation used throughout the paper is fairly standard. The notation $X > 0$ (resp., $X \geq 0$), for $X \in \mathbb{R}^{n\times n}$ means that the matrix X is real symmetric positive definite (resp., positive semidefinite). Identity matrices, of appropriate dimensions, will be denoted by I. If not explicitly stated, all matrices are assumed to have compatible dimensions for algebraic operations. The symbol "$*$" in a matrix $A \in \mathbb{R}^{n\times n}$ stands for the transposed elements in the symmetric positions. The superscripts "T" and "-1" denote the matrix transpose and inverse, respectively.

2. Problem Formulation

In this paper, we consider the following nonlinear system:

$$\dot{x}(t) = f(x(t), u(t)), \tag{1}$$

where $x(t) \in \mathbb{R}^n$ is the state, $u(t) \in \mathbb{R}^n$ denotes the control input, and $f(x(t), u(t))$ is a known nonlinear continuous function and satisfies $f(0,0) = 0$. In order to consider the passive controller design problem, under the concept of sector nonlinearity, the nonlinear system in (1) can be represented by the following T-S fuzzy systems.

Plant Rule i. If $\theta_1(t)$ is N_{i1} and $\cdots \theta_p(t)$ is N_{ip}, then

$$\begin{aligned} \dot{x}(t) &= A_i x(t) + B_i u(t) + B_{wi} w(t), \\ z(t) &= C_i x(t) + D_i u(t) + D_{wi} w(t), \end{aligned} \tag{2}$$

where $z(t) \in \mathbb{R}^p$ is the control output and $w(t) \in \mathbb{R}^p$ is the disturbance input. A_i, B_i, B_{wi}, C_i, D_i, and D_{wi} are system matrices with appropriate dimensions. $i \in 1, 2, \ldots, r$, the scalar r is the number of IF-Then rules. $\theta_j(t)$ and N_{ij} are the premise variable and the fuzzy set, respectively, $j = 1, 2, \ldots, p$. The defuzzified output of system (2) is inferred as follows:

$$\begin{aligned} \dot{x}(t) &= \sum_{i=1}^{r} h_i(\theta(t)) \left[A_i x(t) + B_i u(t) + B_{wi} w(t)\right], \\ z(t) &= \sum_{i=1}^{r} h_i(\theta(t)) \left[C_i x(t) + D_i u(t) + D_{wi} w(t)\right], \end{aligned} \tag{3}$$

where $h_i(\theta(t)) = \mu_i(\theta(t)) / \sum_{i=1}^{r} \mu_i(\theta(t))$, $\mu_i(\theta(t)) = \prod_{j=1}^{p} N_{ij}(\theta_j(t))$, and $N_{ij}(\theta_j(t))$ is the degree of the membership of $\theta_j(t)$ in fuzzy set N_{ij}. In this paper, we assume that $\mu_i(\theta(t)) \geq 0$ for $i = 1, 2, \ldots, k$ and $\sum_{i=1}^{r} \mu_i(\theta(t)) > 0$ for all t. Therefore, $h_i(\theta(t)) \geq 0$ (for $i = 1, 2, \ldots, k$) and $\sum_{i=1}^{r} h_i(\theta(t)) = 1$. Suppose that the updating signal successfully transmitted signal from the sampler to the controller and to the Zero-Order Hold (ZOH) at the instant t_k. We assume that the sampling intervals are bounded

$$t_{k+1} - t_k \leq h, \quad k = 0, 1, 2 \ldots. \tag{4}$$

Here h denotes the maximum time span between the time t_k at which the state is sampled and the time t_{k+1} at which the next update arrives at the destination. The initial conditions of $x(t)$ and $u(t)$ are given as $x(t) = \varphi(t)$ and $u(t) = 0$ for $t \in [t_0 - h, t_0]$, where $\varphi(t)$ is a differentiable function. Similar

to the fuzzy model, the same fuzz rule is used to construct the following overall fuzzy control law:

$$u(t) = \sum_{s=1}^{r} h_s(\theta(t_k)) K_s x(t_k), \quad t_k \le t < t_{k+1}, \quad k = 0, 1, 2, \ldots, \tag{5}$$

where t_k ($k = 0, 1, 2, \ldots$) denotes the kth sampling instant, $t_0 \ge 0$, and $\lim_{k\to\infty} t_k = \infty$. K_s ($s = 1, 2, \ldots, r$) are the local control gains and t_{k+1} is the next updating instant time of the ZOH after t_k. Denote $d(t) = t - t_k$ for $t_k \le t < t_{k+1}$. It is clear that $0 \le d(t) < t_{k+1} - t_k \le h$. It can be seen that $d(t)$ is sawtooth structure, that is, piecewise-linear with derivative $\dot{d}(t) = 1$, $t \ne t_k$. Then, from (5), we have

$$u(t) = \sum_{s=1}^{r} h_s(\theta(t_k)) K_s x(t - d(t)), \quad t_k \le t < t_{k+1}, \quad k = 0, 1, 2, \ldots. \tag{6}$$

Then, substituting (6) into (3) yields

$$\begin{aligned} \dot{x}(t) &= \sum_{i=1}^{r}\sum_{s=1}^{r} h_i h_s^k \left[A_i x(t) + B_i K_s x(t - d(t)) + B_{wi} w(t)\right], \\ z(t) &= \sum_{i=1}^{r}\sum_{s=1}^{r} h_i h_s^k \left[C_i x(t) + D_i K_s x(t - d(t)) + D_{wi} w(t)\right], \end{aligned} \tag{7}$$

where h_i and h_s^k stand for $h_i(\theta(t))$ and $h_s(\theta(t_k))$, respectively.

In order to develop the main results in the next section, the following definition is introduced.

Definition 1 (see [58]). Consider the following.

(D1) System (7) is said to be passive if there exists constant ρ such that

$$2\int_0^t z^T(s) w(s)\, ds \ge \rho \tag{8}$$

holds for all $t \ge 0$.

(D2) System (7) is said to be strictly passive if there exist constants $\delta > 0$ and ρ such that

$$2\int_0^t z^T(s) w(s)\, ds \ge \rho + \delta \int_0^t w^T(s) w(s)\, ds \tag{9}$$

holds for all $t \ge 0$.

(D3) System (7) is said to be output strictly passive if there exist constants $\varepsilon > 0$ and ρ such that

$$2\int_0^t z^T(s) w(s)\, ds \ge \rho + \varepsilon \int_0^t z^T(s) z(s)\, ds \tag{10}$$

holds for all $t \ge 0$.

(D4) System (7) is said to be very-strictly passive if there exist constants $\varepsilon > 0$, $\delta > 0$ and ρ such that

$$2\int_0^t z^T(s) w(s)\, ds \ge \rho + \varepsilon \int_0^t z^T(s) z(s)\, ds + \delta \int_0^t w^T(s) w(s)\, ds \tag{11}$$

holds for all $t \ge 0$.

The main objective of this paper is to give the novel sampled-data control conditions for T-S fuzzy system in (7) via passive control method. The controller is designed to guarantee that the resulting closed-loop system is very-strictly passive.

2.1. Main Results. This section focuses on designing the passive controller for fuzzy system (7). Firstly, the passivity analysis criterion is established for system (7) in the following theorem.

Theorem 2. *Consider system in* (7)*, for given constant* h *and matrix* K_s*, system* (7) *is very-strictly passive if there exist scalars* $\varepsilon > 0$, $\delta > 0$, *matrices* $P > 0$, $Q_{is} > 0$, $R_{is} > 0$, $Z_1 > 0$, *and* $Z_2 > 0$ *with appropriate dimensions, such that the following LMIs hold for* $i, s = 1, 2, \ldots, r$,

$$\begin{bmatrix} \Xi_{11is} + \Theta_{1is} & \Xi_{12is}^T & \Xi_{13is}^T \\ * & \Xi_{22is} & 0 \\ * & * & \Xi_{33} \end{bmatrix} < 0, \tag{12}$$

$$\begin{bmatrix} \Xi_{11is} + \Theta_{2is} & \Xi_{12is}^T \\ * & \Xi_{22is} \end{bmatrix} < 0, \tag{13}$$

$$Q_{si} < R_{is}, \tag{14}$$

where

$$\Xi_{11is} = \begin{bmatrix} PA_i + A_i^T P - Q_{is} - \frac{1}{h}Z_1 - Z_2 & PB_iK_s + Q_{is} + \frac{1}{h}Z_1 + Z_2 & 0 & PB_{wi} - C_i^T \\ * & -2Q_{is} - \frac{1}{h}Z_1 - Z_2 & Q_{is} & -K_s^T D_i^T \\ * & * & -Q_{is} & 0 \\ * & * & * & \delta I - D_{wi} - D_{wi}^T \end{bmatrix},$$

$$\Xi_{12is} = \begin{bmatrix} C_i & D_iK_s & 0 & D_{wi} \\ hR_{is}A_i & hR_{is}B_iK_s & 0 & hR_{is}B_{wi} \end{bmatrix}, \qquad \Xi_{22is} = \operatorname{diag}\{-\varepsilon I, -R_{is}\},$$

$$\Theta_{1is} = \begin{bmatrix} -Q_{is} & Q_{is} & 0 & 0 \\ * & -Q_{is} & 0 & 0 \\ * & * & 0 & 0 \\ * & * & * & 0 \end{bmatrix}, \qquad \Theta_{2is} = \begin{bmatrix} 0 & 0 & 0 & 0 \\ * & -Q_{is} & Q_{is} & 0 \\ * & * & -Q_{is} & 0 \\ * & * & * & 0 \end{bmatrix},$$

$$\Xi_{13is} = \begin{bmatrix} hZ_2 & -hZ_2 & 0 & 0 \\ hA_i & hB_iK_s & 0 & hB_{wi} \\ hZ_1A_i & hZ_1B_iK_s & 0 & hZ_1B_{wi} \end{bmatrix}, \qquad \Xi_{33} = \operatorname{diag}\{-hI, -hI, -hZ_1\}. \tag{15}$$

Proof. Now, define a Lyapunov-Krasovskii function for system (7) as follows:

$$\begin{aligned} V(x(t)) &= V_1(x(t)) + V_2(x(t)) + V_3(x(t)), \\ V_1(x(t)) &= x^T(t) P x(t), \\ V_2(x(t)) &= h\int_{-h}^{0}\int_{t+\theta}^{t} \dot{x}^T(s) R(s) \dot{x}(s)\, \mathrm{d}s\, \mathrm{d}\theta, \\ V_3(x(t)) &= (h - d(t)) \int_{t-d(t)}^{t} \dot{x}^T(s) Z_1 \dot{x}(s)\, \mathrm{d}s \\ &\quad + (h - d(t))\, \vartheta^T(t) Z_2 \vartheta(t), \end{aligned} \tag{16}$$

where $P > 0$, $R(t) = \sum_{i=1}^{r}\sum_{s=1}^{r} h_i h_s^k R_{is} > 0$, $Z_1 > 0$ and $Z_2 > 0$, $\vartheta(t) = (x(t) - x(t - d(t)))$, $t_k \le t < t_{k+1}$. It can be found that the term $V_3(x(t))$ vanishes after the jumps because $x(t)_{|t=t_k} = x(t - d(t))_{|t=t_k}$. Hence $V(x(t)) > 0$ and is continuous in time. The time-derivative of $V_1(x(t))$, $V_2(x(t))$, and $V_3(x(t))$ can be obtained as

$$\begin{aligned} \dot{V}_1(x(t)) &= 2x^T(t) P \dot{x}(t), \\ \dot{V}_2(x(t)) &= h^2 \dot{x}^T(t) R(t) \dot{x}(t) \\ &\quad - h\int_{t-h}^{t} \dot{x}^T(s) R(s) \dot{x}(s)\, \mathrm{d}s, \\ \dot{V}_3(x(t)) &= -\int_{t-d(t)}^{t} \dot{x}^T(s) Z_1 \dot{x}(s)\, \mathrm{d}s \\ &\quad + (h - d(t))\, \dot{x}^T(t) Z_1 \dot{x}(t) \\ &\quad - \vartheta^T(t) Z_2 \vartheta(t) + 2(h - d(t))\, \vartheta^T(t) Z_2 \dot{x}(t). \end{aligned} \tag{17}$$

From the condition in (14), we have $Q(t) = \sum_{i=1}^{r}\sum_{s=1}^{r} h_i h_s^k Q_{is} < R(t)$. According to Jensen's inequality and the second term in $\dot{V}_2(x(t))$, we can have the following inequalities:

$$\begin{aligned} &-h\int_{t-h}^{t} \dot{x}^T(s) R(s) \dot{x}(s)\, \mathrm{d}s \\ &< -h\int_{t-h}^{t} \dot{x}^T(s) Q(t) \dot{x}(s)\, \mathrm{d}s \\ &= -h\int_{t-d(t)}^{t} \dot{x}^T(s) Q(t) \dot{x}(s)\, \mathrm{d}s \\ &\quad - h\int_{t-h}^{t-d(t)} \dot{x}^T(s) Q(t) \dot{x}(s)\, \mathrm{d}s \\ &= -(h - d(t)) \int_{t-d(t)}^{t} \dot{x}^T(s) Q(t) \dot{x}(s)\, \mathrm{d}s \\ &\quad - d(t)\int_{t-d(t)}^{t} \dot{x}^T(s) Q(t) \dot{x}(s)\, \mathrm{d}s \\ &\quad - (h - d(t)) \int_{t-h}^{t-d(t)} \dot{x}^T(s) Q(t) \dot{x}(s)\, \mathrm{d}s \\ &\quad - d(t)\int_{t-h}^{t-d(t)} \dot{x}^T(s) Q(t) \dot{x}(s)\, \mathrm{d}s \\ &\le -\frac{(h - d(t))}{h} \zeta_1^T(t) Q(t) \zeta_1(t) - \zeta_1^T(t) Q(t) \zeta_1(t) \\ &\quad - \zeta_2^T(t) Q(t) \zeta_2(t) - \frac{d(t)}{h} \zeta_2^T(t) Q(t) \zeta_2(t) \\ &= \zeta_3^T(t) \begin{bmatrix} -Q(t) & Q(t) & 0 \\ Q(t) & -2Q(t) & Q(t) \\ 0 & Q(t) & -Q(t) \end{bmatrix} \zeta_3(t) \end{aligned}$$

$$+\frac{(h-d(t))}{h}\zeta_3^T(t)\begin{bmatrix}-Q(t) & Q(t) & 0\\ Q(t) & -Q(t) & 0\\ 0 & 0 & 0\end{bmatrix}\zeta_3(t)$$
$$+\frac{d(t)}{h}\zeta_3^T(t)\begin{bmatrix}0 & 0 & 0\\ 0 & -Q(t) & Q(t)\\ 0 & Q(t) & -Q(t)\end{bmatrix}\zeta_3(t), \tag{18}$$

where

$$\zeta_1(t)=\int_{t-d(t)}^{t}\dot{x}(s)\,ds,\qquad \zeta_2(t)=\int_{t-h}^{t-d(t)}\dot{x}(s)\,ds,$$
$$\zeta_3^T(t)=\left[x^T(t)\quad x^T(t-d(t))\quad x^T(t-h)\right]. \tag{19}$$

Similarly, for the first term in $\dot{V}_3(x(t))$, we can have the following inequalities,

$$-\int_{t-d(t)}^{t}\dot{x}^T(s)Z_1\dot{x}(s)\,ds\le\zeta_4^T(t)\begin{bmatrix}-\frac{1}{h}Z_1 & \frac{1}{h}Z_1\\ \frac{1}{h}Z_1 & -\frac{1}{h}Z_1\end{bmatrix}\zeta_4(t), \tag{20}$$

where

$$\zeta_4^T(t)=\left[x^T(t)\quad x^T(t-d(t))\right]. \tag{21}$$

For the last term in $\dot{V}_3(x(t))$, it can be found that

$$2(h-d(t))\vartheta^T(t)Z_2\dot{x}(t)\le\frac{(h-d(t))}{h}\left[h\vartheta^T(t)Z_2Z_2\vartheta(t)+h\dot{x}^T(t)\dot{x}(t)\right]. \tag{22}$$

In addition,

$$\begin{aligned}z^T(t)z(t)&=\left\{\sum_{i=1}^{r}\sum_{s=1}^{r}h_ih_s^k\left[C_ix(t)+D_iK_sx(t-d(t))+D_{wi}w(t)\right]\right\}^T\\&\quad\times\left\{\sum_{i=1}^{r}\sum_{s=1}^{r}h_ih_s^k\left[C_ix(t)+D_iK_sx(t-d(t))+D_{wi}w(t)\right]\right\}\\&\le\sum_{i=1}^{r}\sum_{s=1}^{r}h_ih_s^k\left[C_ix(t)+D_iK_sx(t-d(t))+D_{wi}w(t)\right]^T\\&\qquad\times\left[C_ix(t)+D_iK_sx(t-d(t))+D_{wi}w(t)\right].\end{aligned} \tag{23}$$

Then, we establish the passivity analysis performance of system in (7),

$$\begin{aligned}&\dot{V}(x(t))+\varepsilon^{-1}z^T(t)z(t)+\delta w^T(t)w(t)-2z^T(t)w(t)\\&\le\sum_{i=1}^{r}\sum_{s=1}^{r}h_ih_s^k\eta^T(t)\\&\qquad\times\left[\Xi_{11is}-\Xi_{12is}^T\Xi_{22is}^{-1}\Xi_{12is}+\frac{(h-d(t))}{h}\right.\\&\qquad\left.\times\left(\Theta_{1is}-\Xi_{13is}^T\Xi_{33}^{-1}\Xi_{13is}\right)+\frac{d(t)}{h}\Theta_{2is}\right]\eta(t)\\&=\sum_{i=1}^{r}\sum_{s=1}^{r}h_ih_s^k\eta^T(t)\\&\qquad\times\left[\frac{(h-d(t))}{h}\left(\Xi_{11is}-\Xi_{12is}^T\Xi_{22is}^{-1}\Xi_{12is}\right.\right.\\&\qquad\left.+\Theta_{1is}-\Xi_{13is}^T\Xi_{33}^{-1}\Xi_{13is}\right)+\frac{d(t)}{h}\\&\qquad\left.\times\left(\Xi_{11is}-\Xi_{12is}^T\Xi_{22is}^{-1}\Xi_{12is}+\Theta_{2is}\right)\right]\eta(t),\end{aligned} \tag{24}$$

where

$$\eta^T(t)=\left[x^T(t)\quad x^T(t-d(t))\quad x^T(t-h)\quad w^T(t)\right]. \tag{25}$$

It follows from Theorem 2 and $(h-d(t))/h+d(t)/h=1$; it is derived that

$$\dot{V}(x(t))+\varepsilon^{-1}z^T(t)z(t)+\delta w^T(t)w(t)-2z^T(t)w(t)\le 0. \tag{26}$$

Integrating both sides of (26) yields

$$\begin{aligned}2\int_0^t z^T(s)w(s)\,ds&\ge V(x(t))-V(x(0))\\&\quad+\varepsilon\int_0^t z^T(s)z(s)\,ds+\delta\int_0^t w^T(s)w(s)\,ds\\&\ge\rho+\varepsilon\int_0^t z^T(s)z(s)\,ds+\delta\int_0^t w^T(s)w(s)\,ds,\end{aligned} \tag{27}$$

where $\rho=-V(x(0))$. Then, it can be seen from Definition 1 that system (7) is very-strictly passive. The proof is finished. □

Remark 3. In the proof of Theorem 2, we construct a new time-dependent and membership-dependent Lyapunov functional and use the advance methods to present the passivity analysis conditions, resulting in less number of slack variable being introduced in Theorem 2.

Based on the passivity analysis condition in Theorem 2, the controller is derived in the form of (6) for the system in (7).

Theorem 4. *Consider system in* (7)*, for given positive scalars* h*,* $\nu_{R_{is}}$*,* ν_{Z_1}*, and* ν_{Z_2}*, system* (7) *is very-strictly passive if there exist scalars* $\varepsilon > 0$*,* $\delta > 0$*, matrices* $\overline{P} > 0$*,* $\overline{Q}_{is} > 0$*,* $\overline{R}_{is} > 0$*,* $\overline{Z}_1 > 0$ *and* $\overline{K}_s$ *with appropriate dimensions, such that the following LMIs hold for* $i, s = 1, 2, \ldots, r$*,*

$$\begin{bmatrix} \overline{\Xi}_{11is} + \overline{\Theta}_{1is} & \overline{\Xi}_{12is}^T & \overline{\Xi}_{13is}^T \\ * & \overline{\Xi}_{22is} & 0 \\ * & * & \overline{\Xi}_{33} \end{bmatrix} < 0, \tag{28}$$

$$\begin{bmatrix} \overline{\Xi}_{11is} + \overline{\Theta}_{2is} & \overline{\Xi}_{12is}^T \\ * & \overline{\Xi}_{22is} \end{bmatrix} < 0, \tag{29}$$

$$\overline{Q}_{si} < \overline{R}_{is}, \tag{30}$$

where

$$\overline{\Xi}_{11is} = \begin{bmatrix} A_i\overline{P} + \overline{P}A_i^T - \overline{Q}_{is} - \frac{1}{h}\overline{Z}_1 - \nu_{Z_2}\overline{P} & B_i\overline{K}_s + \overline{Q}_{is} + \frac{1}{h}\overline{Z}_1 + \nu_{Z_2}\overline{P} & 0 & B_{wi} - \overline{P}C_i^T \\ * & -2\overline{Q}_{is} - \frac{1}{h}\overline{Z}_1 - \nu_{Z_2}\overline{P} & \overline{Q}_{is} & -\overline{K}_s^T D_i^T \\ * & * & -\overline{Q}_{is} & 0 \\ * & * & * & \delta I - D_{wi} - D_{wi}^T \end{bmatrix},$$

$$\overline{\Xi}_{12is} = \begin{bmatrix} C_i\overline{P} & D_i\overline{K}_s & 0 & D_{wi} \\ hA_i\overline{P} & hB_i\overline{K}_s & 0 & hB_{wi} \end{bmatrix}, \qquad \overline{\Xi}_{22is} = \operatorname{diag}\left\{-\varepsilon I, \nu_{R_{is}}^2\overline{R}_{is} - 2\nu_{R_{is}}\overline{P}\right\},$$

$$\overline{\Theta}_{1is} = \begin{bmatrix} -\overline{Q}_{is} & \overline{Q}_{is} & 0 & 0 \\ * & -\overline{Q}_{is} & 0 & 0 \\ * & * & 0 & 0 \\ * & * & * & 0 \end{bmatrix}, \qquad \overline{\Theta}_{2is} = \begin{bmatrix} 0 & 0 & 0 & 0 \\ * & -\overline{Q}_{is} & \overline{Q}_{is} & 0 \\ * & * & -\overline{Q}_{is} & 0 \\ * & * & * & 0 \end{bmatrix},$$

$$\overline{\Xi}_{13is} = \begin{bmatrix} h\nu_{Z_2}I & -h\nu_{Z_2}I & 0 & 0 \\ hA_i\overline{P} & hB_i\overline{K}_s & 0 & hB_{wi} \\ hA_i\overline{P} & hB_i\overline{K}_s & 0 & hB_{wi} \end{bmatrix}, \qquad \overline{\Xi}_{33} = \operatorname{diag}\left\{-hI, -hI, h\left(\nu_{Z_1}^2\overline{Z}_1 - 2\nu_{Z_1}\overline{P}\right)\right\}. \tag{31}$$

Then, the control gain matrix is $K_s = \overline{K}_s\overline{P}^{-1}$*.*

Proof. Firstly, it can be seen that the two inequalities $-\overline{P}\,\overline{R}_{is}^{-1}\overline{P} \le \nu_{R_{is}}^2\overline{R}_{is} - 2\nu_{R_{is}}\overline{P}$ and $-\overline{P}\,\overline{Z}_1^{-1}\overline{P} \le \nu_{Z_1}^2\overline{Z}_1 - 2\nu_{Z_1}\overline{P}$ hold for positive scalars $\nu_{R_{is}}$ and ν_{Z_1} due to the following two inequalities:

$$\begin{aligned} \left(\nu_{R_{is}}\overline{R}_{is} - \overline{P}\right)\overline{R}_{is}^{-1}\left(\nu_{R_{is}}\overline{R}_{is} - \overline{P}\right) \ge 0, \\ \left(\nu_{Z_1}\overline{Z}_1 - \overline{P}\right)\overline{Z}_1^{-1}\left(\nu_{Z_1}\overline{Z}_1 - \overline{P}\right) \ge 0. \end{aligned} \tag{32}$$

Then, define the variables as $P = \overline{P}^{-1}$, $Q_{is} = \overline{P}^{-1}\overline{Q}_{is}\overline{P}^{-1}$, $R_{is} = \overline{P}^{-1}\overline{R}_{is}\overline{P}^{-1}$, $Z_1 = \overline{P}^{-1}\overline{Z}_1\overline{P}^{-1}$, and $Z_2 = \nu_{Z_2}\overline{P}^{-1}$, and replace the terms $\nu_{R_{is}}^2\overline{R}_{is} - 2\nu_{R_{is}}\overline{P}$ and $\nu_{Z_1}^2\overline{Z}_1 - 2\nu_{Z_1}\overline{P}$ with $-\overline{P}\,\overline{R}_{is}^{-1}\overline{P}$ and $-\overline{P}\,\overline{Z}_1^{-1}\overline{P}$ in (28) and (29). We perform congruence transformation to (28) and (29) by

$$\begin{aligned} &\operatorname{diag}\left\{P \;\; P \;\; P \;\; I \;\; I \;\; R_{is} \;\; I \;\; I \;\; Z_1\right\}, \\ &\operatorname{diag}\left\{P \;\; P \;\; P \;\; I \;\; I \;\; R_{is}\right\}, \end{aligned} \tag{33}$$

respectively. We can see that the LMIs conditions in (12) and (13) hold. Therefore, all the conditions in Theorem 2 are satisfied. The proof is completed. □

If the assumption $\dot{d}(t) = 1$ is removed, which means that Lyapunov functional candidate (16) does not include the term $V_3(x(t))$. Similar to the proof of Theorems 2 and 4, we have the following corollaries.

Corollary 5. *Consider system in* (7)*, for given constant* h *and matrix* K_s*, system* (7) *is very-strictly passive if there exist scalars*

$\varepsilon > 0$, $\delta > 0$, *matrices* $P > 0$, $Q_{is} > 0$, *and* $R_{is} > 0$ *with appropriate dimensions, such that the following LMIs hold for* $i, s = 1, 2, \ldots, r$,

$$\begin{bmatrix} \Xi_{11is} + \Theta_{1is} & \Xi_{12is}^T \\ * & \Xi_{22is} \end{bmatrix} < 0, \qquad \begin{bmatrix} \Xi_{11is} + \Theta_{2is} & \Xi_{12is}^T \\ * & \Xi_{22is} \end{bmatrix} < 0, \qquad Q_{si} < R_{is}, \tag{34}$$

where

$$\Xi_{11is} = \begin{bmatrix} PA_i + A_i^T P - Q_{is} & PB_i K_s + Q_{is} & 0 & PB_{wi} - C_i^T \\ * & -2Q_{is} & Q_{is} & -K_s^T D_i^T \\ * & * & -Q_{is} & 0 \\ * & * & * & \delta I - D_{wi} - D_{wi}^T \end{bmatrix},$$

$$\Xi_{12is} = \begin{bmatrix} C_i & D_i K_s & 0 & D_{wi} \\ hR_{is}A_i & hR_{is}B_i K_s & 0 & hR_{is}B_{wi} \end{bmatrix}, \qquad \Xi_{22is} = \operatorname{diag}\{-\varepsilon I, -R_{is}\}, \tag{35}$$

$$\Theta_{1is} = \begin{bmatrix} -Q_{is} & Q_{is} & 0 & 0 \\ * & -Q_{is} & 0 & 0 \\ * & * & 0 & 0 \\ * & * & * & 0 \end{bmatrix}, \qquad \Theta_{2is} = \begin{bmatrix} 0 & 0 & 0 & 0 \\ * & -Q_{is} & Q_{is} & 0 \\ * & * & -Q_{is} & 0 \\ * & * & * & 0 \end{bmatrix}.$$

Corollary 6. *Consider system in* (7)*, for given positive scalars* h, $\nu_{R_{is}}$, ν_{Z_1}, *and* ν_{Z_2}, *system* (7) *is very-strictly passive if there exist scalars* $\varepsilon > 0$, $\delta > 0$, *matrices* $\overline{P} > 0$, $\overline{Q}_{is} > 0$, $\overline{R}_{is} > 0$, $\overline{Z}_1 > 0$, *and* $\overline{K}_s$ *with appropriate dimensions, such that the following LMIs hold for* $i, s = 1, 2, \ldots, r$,

$$\begin{bmatrix} \overline{\Xi}_{11is} + \overline{\Theta}_{1is} & \overline{\Xi}_{12is}^T \\ * & \overline{\Xi}_{22is} \end{bmatrix} < 0, \qquad \begin{bmatrix} \overline{\Xi}_{11is} + \overline{\Theta}_{2is} & \overline{\Xi}_{12is}^T \\ * & \overline{\Xi}_{22is} \end{bmatrix} < 0, \qquad \overline{Q}_{si} < \overline{R}_{is}, \tag{36}$$

where

$$\overline{\Xi}_{11is} = \begin{bmatrix} A_i\overline{P} + \overline{P}A_i^T - \overline{Q}_{is} & B_i\overline{K}_s + \overline{Q}_{is} & 0 & B_{wi} - \overline{P}C_i^T \\ * & -2\overline{Q}_{is} & \overline{Q}_{is} & -\overline{K}_s^T D_i \\ * & * & -\overline{Q}_{is} & 0 \\ * & * & * & \delta I - D_{wi} - D_{wi}^T \end{bmatrix},$$

$$\overline{\Xi}_{12is} = \begin{bmatrix} C_i\overline{P} & D_i\overline{K}_s & 0 & D_{wi} \\ hA_i\overline{P} & hB_i\overline{K}_s & 0 & hB_{wi} \end{bmatrix}, \qquad \overline{\Xi}_{22is} = \operatorname{diag}\left\{-\varepsilon I, \nu_{R_{is}}^2 \overline{R}_{is} - 2\nu_{R_{is}}\overline{P}\right\},$$

$$\overline{\Theta}_{1is} = \begin{bmatrix} -\overline{Q}_{is} & \overline{Q}_{is} & 0 & 0 \\ * & -\overline{Q}_{is} & 0 & 0 \\ * & * & 0 & 0 \\ * & * & * & 0 \end{bmatrix}, \quad \overline{\Theta}_{2is} = \begin{bmatrix} 0 & 0 & 0 & 0 \\ * & -\overline{Q}_{is} & \overline{Q}_{is} & 0 \\ * & * & -\overline{Q}_{is} & 0 \\ * & * & * & 0 \end{bmatrix}. \tag{37}$$

The control gain matrix is computed as $K_s = \overline{K}_s \overline{P}^{-1}$.

3. Simulation Results

In this section, an application example is used to demonstrate the applicability of the controller design method proposed in this paper.

Example 7. Consider the problem of balancing and swing-up of an inverted pendulum on a cart. The equations of the pendulum motion are given by [4]:

$$\begin{aligned} \dot{x}_1(t) &= x_2(t), \\ \dot{x}_2(t) &= \left(g \sin(x_1(t)) - \frac{\text{aml}\, x_2^2(t) \sin(2x_1(t))}{2} \right. \\ &\quad \left. - a \cos(x_1(t)) u(t) \right) \\ &\quad \times \left(\frac{4l}{3} - \text{aml} \cos^2(x_1(t)) \right)^{-1}, \end{aligned} \tag{38}$$

where $x_1(t)$ stands for the angle (in radians) of the pendulum from the vertical, $x_2(t)$ denotes the angular velocity, and $u(t)$ is the force applied to the cart (in newtons). $g = 9.8\,\text{m/s}^2$ is the gravity constant, m denotes the mass of the pendulum, M stands for the mass of the cart, $2l$ is the length of the pendulum, and $a = 1/(m + M)$. Here, we choose $m = 2.0\,\text{kg}$, $M = 8.0\,\text{kg}$, and $2l = 1.0\,\text{m}$ in simulations [3].

The control objective here is to balance the inverted pendulum for the approximate range $x_1(t) \in (-(\pi/2), (\pi/2))$ through a sampled-data control approach. First, we represent the system in (38) by a two-rule Takagi-Sugenofuzzy model [39].

Plant Rule 1. If $x_1(t)$ is 0, then

$$\dot{x}(t) = A_1 x(t) + B_1 u(t), \tag{39}$$

Plant Rule 2. If $x_1(t)$ is $\pm(\pi/2)(|x_1(t)| < \pi/2)$, then

$$\dot{x}(t) = A_2 x(t) + B_2 u(t), \tag{40}$$

where

$$\begin{aligned} A_1 &= \begin{bmatrix} 0 & 1 \\ \dfrac{g}{4l/3 - \text{aml}} & 0 \end{bmatrix}, \quad B_1 = \begin{bmatrix} 0 \\ -\dfrac{a}{4l/3 - \text{aml}} \end{bmatrix}, \\ A_2 &= \begin{bmatrix} 0 & 1 \\ \dfrac{2g}{\pi(4l/3 - \text{aml}\beta^2)} & 0 \end{bmatrix}, \\ B_2 &= \begin{bmatrix} 0 \\ -\dfrac{a\beta}{\pi 4l/3 - \text{aml}\beta^2} \end{bmatrix}, \end{aligned} \tag{41}$$

and $\beta = \cos(88^\circ)$ (notice that when $x_1(t) = \pm(\pi/2)$, the system is uncontrollable). Membership functions for Rules 1 and 2 are listed below:

$$h_1(\theta(t)) = \begin{cases} 1 - \dfrac{2}{\pi}\theta(t), & \text{if } 0 \le \theta(t) < \dfrac{\pi}{2}, \\ 1 + \dfrac{2}{\pi}\theta(t), & \text{if } -\dfrac{\pi}{2} \le \theta(t) < 0, \end{cases} \tag{42}$$

and $h_2(\theta(t)) = 1 - h_1(\theta(t))$, where $\theta(t) = x_1(t)$. Figure 1 shows the membership functions.

In order to demonstrate the effectiveness of the proposed passive control design method, we consider the system in (38) and other parameters in system (2):

$$\begin{aligned} B_{w1} &= [-0.01 \;\; 0.01]^T, \quad B_{w2} = [0.01 \;\; -0.01]^T, \\ C_1 &= [0.1 \;\; 0.01], \quad C_2 = [-0.01 \;\; 0.1], \\ D_1 &= -0.01, \quad D_2 = 0.02, \\ D_{w1} &= 0.01, \quad D_{w2} = 0.02. \end{aligned} \tag{43}$$

We choose the disturbance input $w(t) = -1/(2 + t)$. It can be calculated that $\int_0^\infty w^T(t) w(t) \mathrm{d}t = 0.5 < \infty$, which means $w(t) \in L_2[0, \infty)$. Let

$$\begin{aligned} \varrho(t) &= 2 \int_0^t z^T(s) w(s) \mathrm{d}s \\ &\quad - \varepsilon \int_0^t z^T(s) z(s) \mathrm{d}s - \delta \int_0^t w^T(s) w(s) \mathrm{d}s. \end{aligned} \tag{44}$$

In Figure 2, it can be observed that $2\int_0^\infty z^T(t) w(t) \mathrm{d}t$ decreases as the time t increases, which means that there may

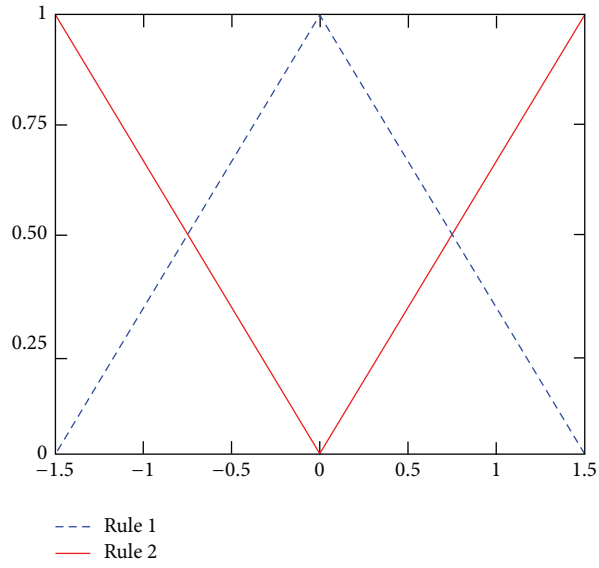

Figure 1: Membership functions of two rules.

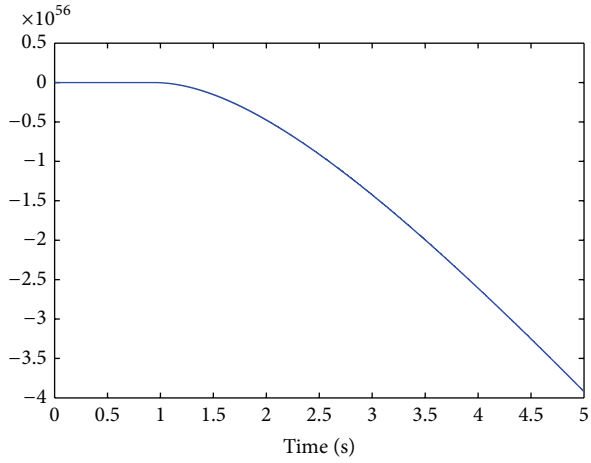

Figure 2: Response of $2\int_0^\infty z^T(t)w(t)\mathrm{d}t$ of the open-loop system.

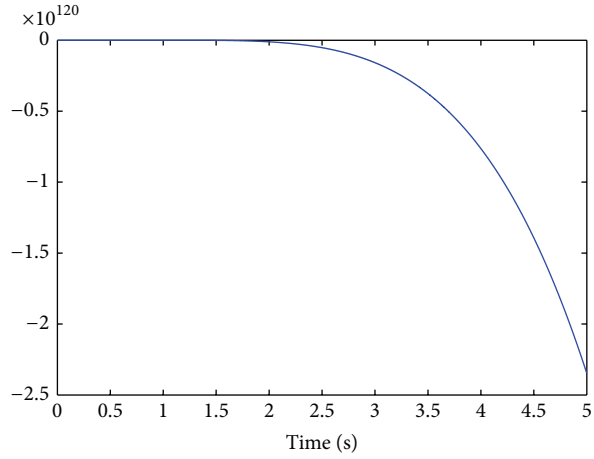

Figure 3: Response of $\varrho(t)$ of the open-loop system.

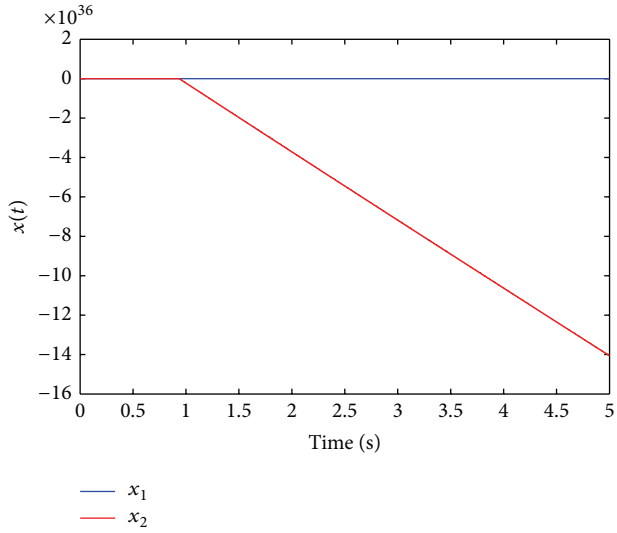

Figure 4: State response of the open-loop system.

not exist a scalar ρ such $2\int_0^\infty z^T(t)w(t)\mathrm{d}t \geq \rho$ holds for all $t \geq 0$. In addition, Figure 3 still holds that there may not exist a scalar ρ such that $\varrho(t) \geq \rho$, which means that the open-loop system is not passive in the sense of Definition 1, and it is not very-strictly passive. Figure 4 demonstrates that the open-loop system is not stable.

In Theorem 4, letting $\nu_{R_{11}} = 0.01$, $\nu_{R_{12}} = 0.02$, $\nu_{R_{21}} = 0.02$, $\nu_{R_{22}} = 0.01$, $\nu_{Z_1} = 10$, and $\nu_{Z_2} = 1$, it can be found that the closed-loop system is very-strictly passive for the allowable upper bound of $h = 9$ ms. The control gain matrices are listed below:

$$K_1 = \begin{bmatrix} 279.1851 & 74.3281 \end{bmatrix},$$
$$K_2 = \begin{bmatrix} 3363.479 & 1083.6839 \end{bmatrix}. \quad (45)$$

Under the control gain matrices in (45), Figure 5 plots the responses of $2\int_0^\infty z^T(t)w(t)\mathrm{d}t$ for the closed-loop system, which means that there may exist a scalar ρ such $2\int_0^\infty z^T(t)w(t)\mathrm{d}t \geq \rho$ holds for all $t \geq 0$. In Figure 6, it can be seen that there may exist a scalar ρ such that $\varrho(t) \geq \rho$. Then, one can know that the closed-loop system is very-strictly passive under the control gain matrices in (45). In addition, Figure 7 shows that the closed-loop system is stable. The computed control inputs arriving at the ZOH are shown in Figure 8, in which we can see that the piecewise continuous holding behavior of the control inputs.

According to the above observation, these simulation results can demonstrate that the designed sampled-data controller meets the specified design requirements.

4. Conclusions

In this paper, the problems of passivity analysis and passive control have been investigated for nonlinear systems under variable sampling. By using the nonlinear sector method, the T-S fuzzy model was established to describe the nonlinear

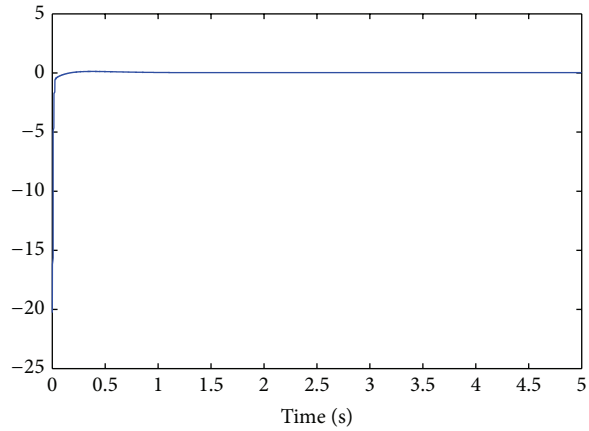

Figure 5: Response of $2\int_0^\infty z^T(t)w(t)\mathrm{d}t$ of the closed-loop system.

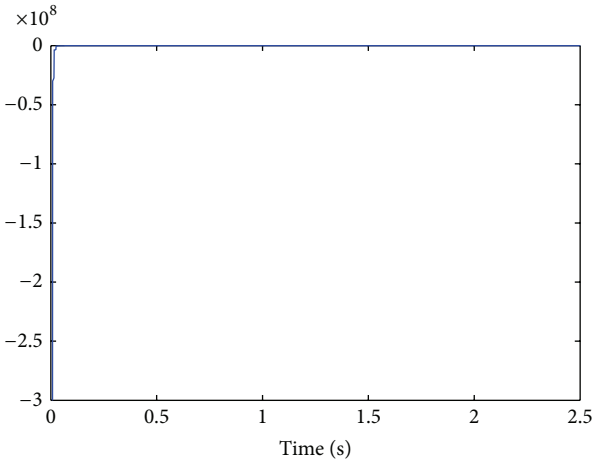

Figure 6: Response of $\varrho(t)$ of the closed-loop system.

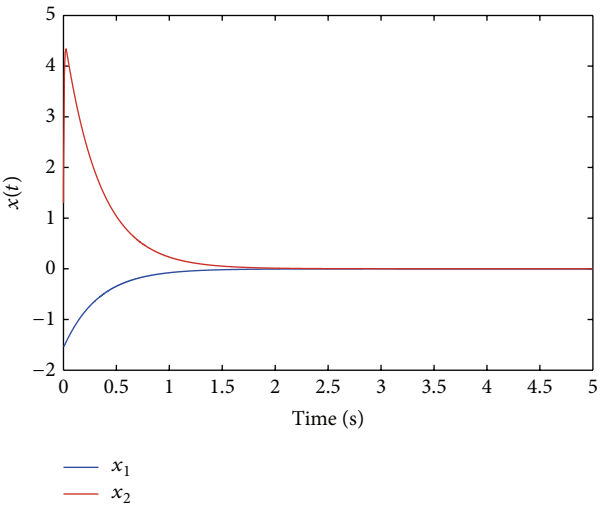

Figure 7: State response of the closed-loop system.

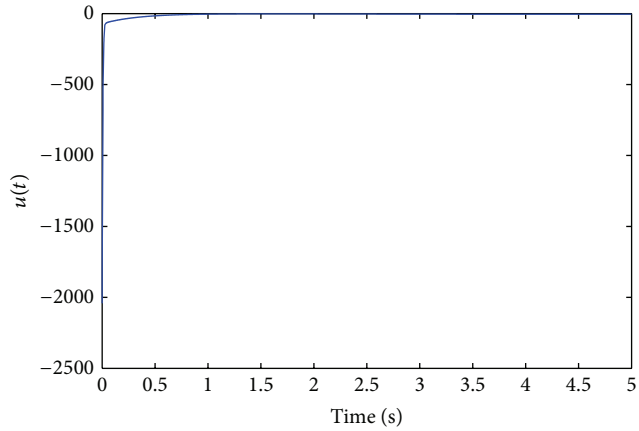

Figure 8: Control signal response of the closed-loop system

systems. Based on the input delay approach, the T-S fuzzy system with variable uncertain sampling was transformed into a continuous-time T-S fuzzy system with a delay in the state. By constructing a novel time-dependent Lyapunov functional, sampled-data controller was designed to guarantee that the resulting closed-loop system is very-strictly passive. The controller existence conditions were expressed as LMIs. This paper has taken into account the main characteristics of sampled-data systems via defining a novel time-dependent Lyapunov functional. An example has been included to demonstrate the advantages of the theoretic results obtained. This paper talks about passivity analysis and passive control for nonlinear systems under variable sampling. In order to achieve more practical oriented results, further work could be considered under data-driven (measurements) framework [59, 60]. The future topics, for example, control [61] and fault tolerant scheme [62] in the identical framework, seem more interesting from both academic and industrial domains.

Conflict of Interests

The authors declare that there is no conflict of interests regarding the publication of this paper.

Acknowledgments

This work was partially supported by the National Natural Science Foundation of China under Grants (61304002, 61304003), the Program for Liaoning Excellent Talents in University (LR2013053), and the Education Department of Liaoning Province under the general project research Grant no. L2013424.

References

[1] S. Tong and H.-X. Li, "Fuzzy adaptive sliding-mode control for MIMO nonlinear systems," *IEEE Transactions on Fuzzy Systems*, vol. 11, no. 3, pp. 354–360, 2003.

[2] S.-C. Tong, X.-L. He, and H.-G. Zhang, "A combined backstepping and small-gain approach to robust adaptive fuzzy output

feedback control," *IEEE Transactions on Fuzzy Systems*, vol. 17, no. 5, pp. 1059–1069, 2009.

[3] S. Tong and Y. Li, "Observer-based fuzzy adaptive control for strict-feedback nonlinear systems," *Fuzzy Sets and Systems*, vol. 160, no. 12, pp. 1749–1764, 2009.

[4] Y. Li, S. Tong, and T. Li, "Adaptive fuzzy output feedback control of uncertain nonlinear systems with unknown backlash-like hysteresis," *Information Sciences*, vol. 198, pp. 130–146, 2012.

[5] H. Li, J. Yu, C. Hilton, and H. Liu, "Adaptive sliding mode control for nonlinear active suspension vehicle systems using ts fuzzy approach," *IEEE Transactions on Industrial Electronics*, vol. 60, no. 8, pp. 3328–3338, 2013.

[6] Y.-J. Liu, S. Tong, and C. Chen, "Adaptive fuzzy control via observer design for uncertain nonlinear systems with unmodeled dynamics," *IEEE Transactions on Fuzzy Systems*, vol. 21, no. 2, pp. 275–288, 2013.

[7] T. Takagi and M. Sugeno, "Fuzzy identification of systems and its applications to modeling and control," *IEEE Transactions on Systems, Man and Cybernetics*, vol. 15, no. 1, pp. 116–132, 1985.

[8] S.-G. Cao, N. W. Rees, and G. Feng, "Analysis and design of fuzzy control systems using dynamic fuzzy-state space models," *IEEE Transactions on Fuzzy Systems*, vol. 7, no. 2, pp. 192–200, 1999.

[9] S. G. Cao, N. W. Rees, and G. Feng, "H_∞ control of uncertain fuzzy continuous-time systems," *Fuzzy Sets and Systems*, vol. 115, no. 2, pp. 171–190, 2000.

[10] K. Tanaka, T. Hori, and H. O. Wang, "A multiple *Lyapunov* function approach to stabilization of fuzzy control systems," *IEEE Transactions on Fuzzy Systems*, vol. 11, no. 4, pp. 582–589, 2003.

[11] K. Tanaka and H. O. Wang, *Fuzzy Control Systems Design and Analysis: A Linear Matrix Inequality Approach*, John Wiley & Sons, New York, NY, USA, 2001.

[12] G. Feng, "A survey on analysis and design of model-based fuzzy control systems," *IEEE Transactions on Fuzzy Systems*, vol. 14, no. 5, pp. 676–697, 2006.

[13] S. K. Nguang and P. Shi, "H_∞ fuzzy output feedback control design for nonlinear systems: an LMI approach," *IEEE Transactions on Fuzzy Systems*, vol. 11, no. 3, pp. 331–340, 2003.

[14] H. K. Lam, "Stabilization of nonlinear systems using sampled-data output-feedback fuzzy controller based on polynomial-fuzzy-model-based control approach," *IEEE Transactions on Systems, Man, and Cybernetics B*, vol. 42, no. 1, pp. 258–267, 2012.

[15] H. Dong, Z. Wang, D. W. C. Ho, and H. Gao, "Robust H_∞ fuzzy output-feedback control with multiple probabilistic delays and multiple missing measurements," *IEEE Transactions on Fuzzy Systems*, vol. 18, no. 4, pp. 712–725, 2010.

[16] L. Wu, X. Su, P. Shi, and J. Qiu, "Model approximation for discrete-time state-delay systems in the T-S fuzzy framework," *IEEE Transactions on Fuzzy Systems*, vol. 19, no. 2, pp. 366–378, 2011.

[17] M. Liu, X. Cao, and P. Shi, "Fault estimation and tolerant control for fuzzy stochastic systems," *IEEE Transactions on Fuzzy Systems*, vol. 21, no. 2, pp. 221–229, 2013.

[18] M. Liu, X. Cao, and P. Shi, "Fuzzy-model-based fault tolerant design for nonlinear stochastic systems against simultaneous sensor and actuator faults," *IEEE Transactions on Fuzzy Systems*, 2012.

[19] P. Gahinet, A. Nemirovskii, A. J. Laub, and M. Chilali, "The LMI control toolbox," in *Proceedings of the 33rd IEEE Conference on Decision and Control*, vol. 3, pp. 2038–2041, IEEE, 1994.

[20] X. Xie, S. Yin, H. Gao, and O. Kaynak, "Asymptotic stability and stabilisation of uncertain delta operator systems with time-varying delays," *IET Control Theory & Applications*, vol. 7, no. 8, pp. 1071–1078, 2013.

[21] T. Li, W. X. Zheng, and C. Lin, "Delay-slope-dependent stability results of recurrent neural networks," *IEEE Transactions on Neural Networks*, vol. 22, no. 12, pp. 2138–2143, 2011.

[22] H. Gao, T. Chen, and J. Lam, "A new delay system approach to network-based control," *Automatica*, vol. 44, no. 1, pp. 39–52, 2008.

[23] H. Li, H. Gao, and P. Shi, "New passivity analysis for neural networks with discrete and distributed delays," *IEEE Transactions on Neural Networks*, vol. 21, no. 11, pp. 1842–1847, 2010.

[24] H. Li, X. Jing, and H. Karimi, "Output-feedback based h-infinity control for active suspension systems with control delay," *IEEE Transactions on Industrial Electronics*, vol. 61, no. 1, pp. 436–446, 2014.

[25] B. Shen, Z. Wang, and Y. S. Hung, "Distributed H_∞-consensus filtering in sensor networks with multiple missing measurements: the finite-horizon case," *Automatica*, vol. 46, no. 10, pp. 1682–1688, 2010.

[26] B. Shen, Z. Wang, H. Shu, and G. Wei, "On nonlinear H_∞ filtering for discrete-time stochastic systems with missing measurements," *IEEE Transactions on Automatic Control*, vol. 53, no. 9, pp. 2170–2180, 2008.

[27] B. Chen, X. Liu, S. Tong, and C. Lin, "Guaranteed cost control of T-S fuzzy systems with state and input delays," *Fuzzy Sets and Systems*, vol. 158, no. 20, pp. 2251–2267, 2007.

[28] S. Xu and J. Lam, "Robust H_∞ control for uncertain discrete-time-delay fuzzy systems via output feedback controllers," *IEEE Transactions on Fuzzy Systems*, vol. 13, no. 1, pp. 82–93, 2005.

[29] C. Lin, Q.-G. Wang, T. H. Lee, and Y. He, *LMI Approach to Analysis and Control of Takagi-Sugeno Fuzzy Systems with Time Delay*, vol. 351 of *Lecture Notes in Control and Information Sciences*, Springer, Berlin, Germany, 2007.

[30] C. Lin, Q.-G. Wang, and T. H. Lee, "Stabilization of uncertain fuzzy time-delay systems via variable structure control approach," *IEEE Transactions on Fuzzy Systems*, vol. 13, no. 6, pp. 787–798, 2005.

[31] B. Zhang and S. Xu, "Delay-dependent robust H_∞ control for uncertain discrete-time fuzzy systems with time-varying delays," *IEEE Transactions on Fuzzy Systems*, vol. 17, no. 4, pp. 809–823, 2009.

[32] B. Zhang, J. Lam, S. Xu, and Z. Shu, "Robust stabilization of uncertain T-S fuzzy time-delay systems with exponential estimates," *Fuzzy Sets and Systems*, vol. 160, no. 12, pp. 1720–1737, 2009.

[33] L. Wu and W. X. Zheng, "L_2-L_∞ control of nonlinear fuzzy itô stochastic delay systems via dynamic output feedback," *IEEE Transactions on Systems, Man, and Cybernetics B*, vol. 39, no. 5, pp. 1308–1315, 2009.

[34] L. Wu, X. Su, P. Shi, and J. Qiu, "A new approach to stability analysis and stabilization of discrete-time T-S fuzzy time-varying delay systems," *IEEE Transactions on Systems, Man, and Cybernetics B*, vol. 41, no. 1, pp. 273–286, 2011.

[35] H. Li, H. Liu, H. Gao, and P. Shi, "Reliable fuzzy control for active suspension systems with actuator delay and fault," *IEEE Transactions on Fuzzy Systems*, vol. 20, no. 2, pp. 342–357, 2012.

[36] T. Chen and B. Francis, *Optimal Sampled-Data Control Systems*, Springer, London, UK, 1995.

[37] R. Kalman, "Nonlinear aspects of sampled-data control systems," in *Proceedings of the Symposium on Nonlinear Circuit Analysis*, vol. 6, pp. 273–313, 1956.

[38] B. Bamieh, J. B. Pearson, B. A. Francis, and A. Tannenbaum, "A lifting technique for linear periodic systems with applications to sampled-data control," *Systems and Control Letters*, vol. 17, no. 2, pp. 79–88, 1991.

[39] T. Chen and L. Qiu, "H_∞ design of general multirate sampled-data control systems," *Automatica*, vol. 30, no. 7, pp. 1139–1152, 1994.

[40] S. K. Nguang and P. Shi, "Nonlinear H_∞ filtering of sampled-data systems," *Automatica*, vol. 36, no. 2, pp. 303–310, 2000.

[41] E. Fridman, A. Seuret, and J.-P. Richard, "Robust sampled-data stabilization of linear systems: an input delay approach," *Automatica*, vol. 40, no. 8, pp. 1441–1446, 2004.

[42] E. Fridman, "A refined input delay approach to sampled-data control," *Automatica*, vol. 46, no. 2, pp. 421–427, 2010.

[43] L.-S. Hu, T. Bai, P. Shi, and Z. Wu, "Sampled-data control of networked linear control systems," *Automatica*, vol. 43, no. 5, pp. 903–911, 2007.

[44] W. Zhang, M. S. Branicky, and S. M. Phillips, "Stability of networked control systems," *IEEE Control Systems Magazine*, vol. 21, no. 1, pp. 84–97, 2001.

[45] H. Gao, J. Wu, and P. Shi, "Robust sampled-data H_∞ control with stochastic sampling," *Automatica*, vol. 45, no. 7, pp. 1729–1736, 2009.

[46] S. K. Nguang and P. Shi, "Fuzzy H_∞ output feedback control of nonlinear systems under sampled measurements," *Automatica*, vol. 39, no. 12, pp. 2169–2174, 2003.

[47] H. Katayama and A. Ichikawa, "H_∞ control for sampled-data nonlinear systems described by Takagi-Sugeno fuzzy systems," *Fuzzy Sets and Systems*, vol. 148, no. 3, pp. 431–452, 2004.

[48] H. Gao and T. Chen, "Stabilization of nonlinear systems under variable sampling: a fuzzy control approach," *IEEE Transactions on Fuzzy Systems*, vol. 15, no. 5, pp. 972–983, 2007.

[49] H. K. Lam and F. H. F. Leung, "Sampled-data fuzzy controller for time-delay nonlinear systems: fuzzy-model-based LMI approach," *IEEE Transactions on Systems, Man, and Cybernetics B*, vol. 37, no. 3, pp. 617–629, 2007.

[50] H. K. Lam, "Sampled-data fuzzy-model-based control systems: stability analysis with consideration of analogue-to-digital converter and digital-to-analogue converter," *IET Control Theory and Applications*, vol. 4, no. 7, pp. 1131–1144, 2010.

[51] X.-L. Zhu, B. Chen, D. Yue, and Y. Wang, "An improved input delay approach to stabilization of fuzzy systems under variable sampling," *IEEE Transactions on Fuzzy Systems*, vol. 20, no. 2, pp. 330–341, 2012.

[52] J. Yoneyama, "Robust H_∞ control of uncertain fuzzy systems under time-varying sampling," *Fuzzy Sets and Systems*, vol. 161, no. 6, pp. 859–871, 2010.

[53] L. Wu and W. X. Zheng, "Passivity-based sliding mode control of uncertain singular time-delay systems," *Automatica*, vol. 45, no. 9, pp. 2120–2127, 2009.

[54] H. Gao, T. Chen, and T. Chai, "Passivity and passification for networked control systems," *SIAM Journal on Control and Optimization*, vol. 46, no. 4, pp. 1299–1322, 2007.

[55] C. Li, H. Zhang, and X. Liao, "Passivity and passification of fuzzy systems with time delays," *Computers and Mathematics with Applications*, vol. 52, no. 6-7, pp. 1067–1078, 2006.

[56] J. Liang, Z. Wang, and X. Liu, "Robust passivity and passification of stochastic fuzzy time-delay systems," *Information Sciences*, vol. 180, no. 9, pp. 1725–1737, 2010.

[57] B. Zhang, W. X. Zheng, and S. Xu, "Passivity analysis and passive control of fuzzy systems with time-varying delays," *Fuzzy Sets and Systems*, vol. 174, no. 1, pp. 83–98, 2011.

[58] B. Brogliato, R. Lozano, B. Maschke, and O. Egeland, *Dissipative Systems Analysis and Control: Theory and Applications*, Communications and Control Engineering Series, Springer, London, UK, 2nd edition, 2007.

[59] S. Yin, S. Ding, A. Haghani, H. Hao, and P. Zhang, "A comparison study of basic data-driven fault diagnosis and process monitoring methods on the benchmark Tennessee Eastman process," *Journal of Process Control*, vol. 22, no. 9, pp. 1567–1581, 2012.

[60] S. Yin, S. X. Ding, A. H. A. Sari, and H. Hao, "Data-driven monitoring for stochastic systems and its application on batch process," *International Journal of Systems Science*, vol. 44, no. 7, pp. 1366–1376, 2013.

[61] S. Yin, S. Ding, and H. Luo, "Real-time implementation of fault tolerant control system with performance optimization," *IEEE Transactions on Industrial Electronics*, 2013.

[62] S. Yin, X. Yang, and H. R. Karimi, "Data-driven adaptive observer for fault diagnosis," *Mathematical Problems in Engineering*, vol. 2012, Article ID 832836, 21 pages, 2012.

Hindawi Publishing Corporation
Mathematical Problems in Engineering
Volume 2013, Article ID 597195, 8 pages
http://dx.doi.org/10.1155/2013/597195

Research Article

Robust Coordinated Control Algorithm for Multiple Marine Vessels with External Disturbances

Weixue Liu,[1] Jianfang Jiao,[1] Hamid Reza Karimi,[2] and Jian Jiao[3]

[1] *Bohai University, Jinzhou 121013, China*
[2] *Department of Engineering, Faculty of Engineering and Science, University of Agder, 4898 Grimstad, Norway*
[3] *No. 803 Research Institute of Shanghai Academy of Spaceflight Technology, No. 710 Yishan Road, Shanghai 200233, China*

Correspondence should be addressed to Jianfang Jiao; jiaojianfangheu@163.com

Received 16 August 2013; Accepted 23 September 2013

Academic Editor: Zhiguang Feng

The problem of coordinated control for multiple marine vessels in the presence of external disturbances is considered in this paper. A robust coordinated control algorithm is proposed for multiple marine vessels. The proposed robust coordinated control algorithm is divided into two parts. The first part develops an extended state observer to estimate the disturbances of marine vessels. The second part presents a robust coordinated control algorithm based on the output of the extended state observer. Furthermore, the robust coordinated control algorithm is designed using the dynamic surface control method. In light of the leader-follower strategy, the trajectory for each vessel is defined according to the desired trajectory of the assigned leader and the relative distance with respect to the leader. The effectiveness of the proposed coordination algorithm is demonstrated by the simulation results.

1. Introduction

In recent years, coordinated control of multiple vehicles has received increasing attention as an emerging technology [1]. Multiple vehicles can perform many complex tasks effectively with less time and lower cost than a single vehicle. And multiple vehicles can accomplish some tasks which cannot be executable by a single one. In order to perform these complicated practical tasks, it is necessary for these vehicles to move collectively as a whole formation. In practice, many relevant applications of coordinated control can be found on the land, in the sea, and in the air [2]. For instance, in the operations of underway replenishment by a fleet of surface vessels, it is required that the replenished vehicle should maintain a fixed relative position with respect to the replenishing one, in order to ensure the replenishment operation performed safely and effectively.

The problem of coordinated formation control has been reported in a large number of recent publications. Basic approaches of the coordinated control include leader-follower approach [3–5], behavioral approach [6, 7], and virtual structures approach [8, 9]. In the leader-follower approach, some agents are considered as the leaders, and the rest ones are considered as the followers. The followers will track the leaders, and the leaders will track the predefined desired trajectories. This method is easy to be manipulated and implemented. However, the main criticism of the leader-follower approach is that it depends heavily on the leader to achieve the goal of the formation task which may be undesirable [3–5]. In the behavioral approach, the collision avoidance/obstacle avoidance and the target tracking are prescribed for each agent, and the whole formation is achieved by calculating the weight of the relative importance of each behavior. However, it is difficult to analyze the stability of the group behavior using such approach [6, 7]. In the virtual-structure approach, each member in the formation is considered as a particle embedded in a rigid geometric structure, but the relative applications are limited when the formation structure is time-varying or needs to be frequently reconfigured [8, 9].

Some advanced approaches including graph theory [10], passivity-based control [11, 12], and hybrid control [13] are also used for coordinated control of multiple marine vessels. Most results about the coordinated control problem addressed in the earlier papers are on the assumption that marine vessels are free from environmental disturbances.

However, coordinated control for multiple surface vessels encountering exogenous disturbances adds a new level of complexity to the problem. Other advanced methods are proposed to solve the robust coordinated formation control problem, for example, the Lagrangian approach [14], the nonlinear model predictive control [15], the adaptive control [16], and the sliding mode control [17]. In addition, the fault tolerant control and the fault diagnosis are studied in references [18–20]. In particular, the problem of coordinated path following multiple vessels has also been discussed in the related literature studies [21, 22]. The robustness to environmental disturbances is highly important when performing practical marine and offshore tasks for surface vessels, which is also the concerned issue in this paper. The core of the extended state observer is that the disturbances and the unknown dynamics can be considered as extend state, and then the detailed values can be estimated by designed observer. The correlative applications can be found in literature studies [23–26]. The stability of the extended state observer is analyzed in [27–29]. The robust coordination control algorithm for multiple surface vessels based on extend state observer and robust control technology is studied in this paper. The designed controller is useful for the practical marine operations.

In this paper, we consider the problem of coordinated formation control of multiple surface vessels in the presence of exogenous disturbances. The coordinated formation controller is proposed by combining the extended state observer and dynamic surface control using the leader-follower strategy. The extended state observer is developed to estimate the external disturbances of the surface vessels. The coordinated control algorithm is accomplished based on the output of the extended state observer. Furthermore, the trajectory of each vessel is defined using the desired trajectory of the assigned leader and the relative distance with respect to the leader. This paper is organized as follows. In Section 2, the vessel model is established. Section 3 contains a detailed algorithm of the coordination formation control for multiple vessels. Simulation is carried out in Section 4, and we draw conclusions in Section 5.

2. Preliminaries

The vessel model can be divided into two parts: the kinematics and nonlinear dynamics. Generally, only the motion in the horizontal plane is considered for the surface vessel. The elements corresponding to heave, roll, and pitch are neglected. The dynamic model for the ith surface vessel can be represented by the following 3 degrees of freedom (DOF) [30]:

$$\dot{\eta}_i = \mathbf{R}_i(\psi_i)\,\mathbf{v}_i, \tag{1}$$

$$\mathbf{M}_i\dot{\mathbf{v}}_i + \mathrm{C}_i(\mathbf{v}_i)\,\mathbf{v}_i + \mathbf{D}_i(\mathbf{v}_i)\,\mathbf{v}_i = \tau_i + \tau_{di}, \tag{2}$$

where $\eta_i = [n_i, e_i, \psi_i]^T$ denotes the north position, east position, and orientation which are decomposed in the Earth-fixed reference frame, $\mathbf{v}_i = [u_i, v_i, r_i]^T$ denotes the linear surge velocity, sway velocity, and angular velocity which are decomposed in the body-fixed reference frame. $\mathbf{R}_i(\psi_i)$ is the transformations matrix from the body-fixed reference frame to the Earth-fixed reference frame, the form of which is as follows:

$$\mathbf{R}_i(\psi_i) = \begin{bmatrix} \cos(\psi_i) & -\sin(\psi_i) & 0 \\ \sin(\psi_i) & \cos(\psi_i) & 0 \\ 0 & 0 & 1 \end{bmatrix}. \tag{3}$$

The transformations matrix satisfies $\mathbf{R}_i^{-1}(\psi_i) = \mathbf{R}_i^T(\psi_i)$, for all ψ_i. $\mathbf{M}_i$ denotes the system inertia mass matrix including added mass which is positive definite. $\mathbf{C}_i(\mathbf{v}_i)$ and $\mathbf{D}_i(\mathbf{v}_i)$ denote the Coriolis-centripetal matrix and damping matrix, respectively. The detailed representation of the above three system matrices can be found in reference [30]. $\tau_i = [\tau_{ui} \quad \tau_{vi} \quad \tau_{ri}]^T$ is the vector of forces and torques input from the thruster system. τ_{di} is the vector of external environment forces and torques input which is generated by wind, wave, and current.

In order to design the backstepping sliding mode controller, we transform the vessel model as follows:

$$\mathbf{v}_i = \mathbf{R}_i^{-1}(\psi_i)\,\dot{\eta}_i, \tag{4}$$

because $\dot{\mathbf{R}}_i(\psi_i) = \mathbf{R}_i(\psi_i)S$, where

$$S = \begin{bmatrix} 0 & -r_i & 0 \\ r_i & 0 & 0 \\ 0 & 0 & 0 \end{bmatrix} = -S^T \tag{5}$$

with r_i being the angular velocity in the body-fixed reference frame. We can obtain that

$$\begin{aligned} \dot{\mathbf{v}}_i &= \dot{\mathbf{R}}_i^{-1}(\psi_i)\,\dot{\eta}_i + \mathbf{R}_i^{-1}(\psi_i)\,\ddot{\eta}_i \\ &= -\mathbf{R}_i^{-1}(\psi_i)\,\dot{\mathbf{R}}_i(\psi_i)\,\mathbf{R}_i^{-1}(\psi_i)\,\dot{\eta}_i + \mathbf{R}_i^{-1}(\psi_i)\,\ddot{\eta}_i. \end{aligned} \tag{6}$$

Taking (4) and (6) into the vessel dynamic model (2) yields

$$\begin{aligned} &\mathbf{M}_i\mathbf{R}_i^{-1}(\psi_i)\,\ddot{\eta}_i - \mathbf{M}_i\mathbf{R}_i^{-1}(\psi_i)\,\dot{\mathbf{R}}_i(\psi_i)\,\mathbf{R}_i^{-1}(\psi_i)\,\dot{\eta}_i \\ &\quad + \mathbf{C}_i(\mathbf{v}_i)\,\mathbf{R}_i^{-1}(\psi_i)\,\dot{\eta}_i + \mathbf{D}_i(\mathbf{v}_i)\,\mathbf{R}_i^{-1}(\psi_i)\,\dot{\eta}_i = \tau_i + \tau_{di}. \end{aligned} \tag{7}$$

The above equation can be written as

$$\mathbf{M}_{ni}(\eta_i)\,\ddot{\eta}_i + \mathbf{C}_{ni}(\eta_i, \dot{\eta}_i)\,\dot{\eta}_i + \mathbf{D}_{ni}(\eta_i, \dot{\eta}_i)\,\dot{\eta}_i = \tau_i + \tau_{di}, \tag{8}$$

where

$$\begin{aligned} \mathbf{M}_{ni}(\eta_i) &= \mathbf{M}_i\mathbf{R}_i^{-1}(\psi_i); \\ \mathbf{C}_{ni}(\eta_i, \dot{\eta}_i) &= \left[\mathbf{C}_i(\mathbf{v}_i) - \mathbf{M}_i\mathbf{R}_i^{-1}(\psi_i)\,\dot{\mathbf{R}}_i(\psi_i)\right]\mathbf{R}_i^{-1}(\psi_i); \\ \mathbf{D}_{ni}(\eta_i, \dot{\eta}_i) &= \mathbf{D}_i(\mathbf{v}_i)\,\mathbf{R}_i^{-1}(\psi_i). \end{aligned} \tag{9}$$

3. Coordinated Formation Controller Design

In this section, the controller is designed from two inspects. One is the extended state observer design for each vessel, and the other is the coordinated controller for multiple vessels based on the output of the extended state observer.

3.1. Extended State Observer Design. In this section, we design the extended state observer for each vessel to estimate the disturbances.

Let $\dot{\eta}_i = \mathbf{v}_{ni}$, and then (8) can be written as

$$\mathbf{M}_{ni}(\eta_i)\dot{\mathbf{v}}_{ni} + \mathbf{C}_{ni}(\eta_i, \mathbf{v}_{ni})\mathbf{v}_{ni} + \mathbf{D}_{ni}(\eta_i, \mathbf{v}_{ni})\mathbf{v}_{ni} = \tau_i + \tau_{di}. \tag{10}$$

Then we have

$$\begin{aligned} \dot{\eta}_i &= \mathbf{v}_{ni}, \\ \dot{\mathbf{v}}_{ni} &= \mathbf{M}_{ni}^{-1}(\eta_i)\tau_i \\ &\quad + \mathbf{M}_{ni}^{-1}(\eta_i)\left(-\mathbf{C}_{ni}(\eta_i, \mathbf{v}_{ni})\mathbf{v}_{ni} - \mathbf{D}_{ni}(\eta_i, \mathbf{v}_{ni})\mathbf{v}_{ni} + \tau_{di}\right). \end{aligned} \tag{11}$$

Let $\mathbf{K}_i = \mathbf{M}_{ni}^{-1}(\eta_i)(-\mathbf{C}_{ni}(\eta_i, \mathbf{v}_{ni})\mathbf{v}_{ni} - \mathbf{D}_{ni}(\eta_i, \mathbf{v}_{ni})\mathbf{v}_{ni} + \tau_{di})$, $\mathbf{u}_i = \mathbf{M}_{ni}^{-1}(\eta_i)\tau_i$. Then the above equation can be rewritten as

$$\begin{aligned} \dot{\eta}_i &= \mathbf{v}_{ni}, \\ \dot{\mathbf{v}}_{ni} &= \mathbf{K}_i + \mathbf{u}_i. \end{aligned} \tag{12}$$

Here $\mathbf{K}_i$ is assumed to be unknown. We assume that $\mathbf{K}_i$ is an extended state. However, $\mathbf{K}_i$ can be estimated using an extended state observer. Then the disturbances are observed and compensated by the designed controller.

The extended state observer is designed as

$$\begin{aligned} \mathbf{z}_{1\mathrm{i}} &= \eta_i - \widehat{\eta}_i, \\ \dot{\widehat{\eta}}_i &= \widehat{\mathbf{v}}_{ni} + \beta_1 \mathrm{fal}_1(\mathbf{z}_{1i}, \alpha, \delta), \\ \dot{\widehat{\mathbf{v}}}_{ni} &= \widehat{\mathbf{K}}_i + \beta_2 \mathrm{fal}_2(\mathbf{z}_{1i}, \alpha, \delta) + \mathbf{u}_i, \\ \dot{\widehat{\mathbf{K}}}_i &= \beta_3 \mathrm{fal}_3(\mathbf{z}_{1i}, \alpha, \delta), \end{aligned} \tag{13}$$

where

$$\mathrm{fal}(\mathbf{z}_{1i}, \alpha, \delta) = \begin{cases} |\mathbf{z}_{1i}|^{\alpha} \operatorname{sign}(\mathbf{z}_{1i}), & |\mathbf{z}_{1i}| > \delta, \\ \dfrac{\mathbf{z}_{1i}}{\delta^{\alpha-1}}, & |\mathbf{z}_{1i}| \le \delta. \end{cases} \tag{14}$$

And $\delta > 0$, $0 < \alpha < 1$.

Set $\mathbf{z}_{1i} = \eta_i - \widehat{\eta}_i$, $\mathbf{z}_{2i} = \mathbf{v}_{ni} - \widehat{\mathbf{v}}_{ni}$, $\mathbf{z}_{3i} = \mathbf{K}_i - \widehat{\mathbf{K}}_i$. $\widehat{\eta}_i, \widehat{\mathbf{v}}_{ni}, \widehat{\mathbf{K}}_i$ are the estimated values of $\eta_i, \mathbf{v}_{ni}, \mathbf{K}_i$, respectively. Taking the derivative of $\mathbf{z}_{1i}, \mathbf{z}_{2i}, \mathbf{z}_{3i}$, respectively, we can obtain that

$$\begin{aligned} \dot{\mathbf{z}}_{1i} &= \widehat{\mathbf{v}}_{ni} + \mathbf{z}_{2i} - \widehat{\mathbf{v}}_{ni} - \beta_1 \mathrm{fal}_1(\mathbf{e}_i, \alpha, \delta) \\ &= \mathbf{z}_{2i} - \beta_1 \mathrm{fal}_1(\mathbf{z}_{1i}, \alpha, \delta) \end{aligned} \tag{15}$$

$$\begin{aligned} \dot{\mathbf{z}}_{2i} &= \mathbf{K}_i + \mathbf{u}_i - \widehat{\mathbf{K}}_i - \beta_2 \mathrm{fal}_2(\mathbf{z}_{1i}, \alpha, \delta) - \mathbf{u}_i \\ &= \mathbf{z}_{3i} - \beta_2 \mathrm{fal}_2(\mathbf{z}_{1i}, \alpha, \delta) \end{aligned} \tag{16}$$

$$\dot{\mathbf{z}}_{3i} = \dot{\mathbf{K}}_i - \beta_3 \mathrm{fal}_3(\mathbf{z}_{1i}, \alpha, \delta). \tag{17}$$

The following assumptions are presumed.

(1) The possibly unknown function $\mathbf{K}_i$ is continuously differentiable with respect to their variables. $|\dot{\mathbf{K}}_i| \le M$ for all $t > 0$, where M is a positive constant.

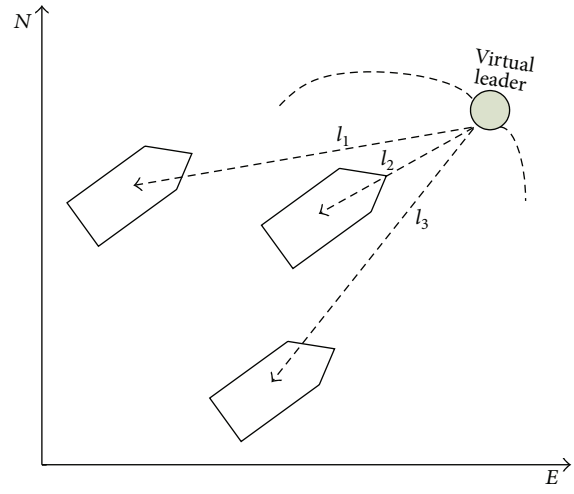

Figure 1: The formation of these vessels.

(2) Let $\mathbf{z} = [\mathbf{z}_1, \mathbf{z}_2, \mathbf{z}_3]^T$, and $\|\bullet\|$ denotes the Euclid norm of $\mathbb{R}^9$. There exist positive definite constants λ_i $(i = 1, 2, 3, 4)$, α and continuous differentiable functions $V, W : \mathbb{R}^9 \to \mathbb{R}$ such that

(i) $\lambda_1\|\mathbf{z}\|^2 \le \mathbf{V}(\mathbf{z}) \le \lambda_2\|\mathbf{z}\|^2$, $\lambda_3\|\mathbf{z}\|^2 \le \mathbf{W}(\mathbf{z}) \le \lambda_4\|\mathbf{z}\|^2$,

(ii) $(\partial V/\partial \mathbf{z}_1)(\mathbf{z}_2 - f_1(\mathbf{z}_1)) + (\partial V/\partial \mathbf{z}_2)(\mathbf{z}_2 - f_2(\mathbf{z}_1)) + (\partial V/\partial \mathbf{z}_3) f_3(\mathbf{z}_1) \le -W(\mathbf{z})$,

(iii) $\|\partial V/\partial \mathbf{z}_3\| \le \alpha\|\mathbf{z}\|$.

The stability for the extended state observer is analyzed in [24]. Then we can obtain $\widehat{\eta}_i \to \eta_i$, $\widehat{\mathbf{v}}_{ni} \to \mathbf{v}_{ni}$, $\widehat{\mathbf{K}}_i \to \mathbf{K}_i$.

3.2. Coordinated Controller Design

3.2.1. Formation Setup. This paper considers a fleet of n vessels to perform the desired coordination formation task. Each vessel in the formation is identified by the index set $I = [1, 2, \ldots, n]$. The desired formation is established using the leader-follower strategy as shown in Figure 1. Furthermore, the leader is a virtual vessel. If we assume the desired trajectory of the leader vessel is denoted as η_d, where $\eta_d = [n_d(t), e_d(t), \psi_d(t)]^T$, $n_d(t)$, $e_d(t)$ are sufficiently smooth functions, and $\psi_d(t) = \arctan(\dot{e}_d(t)/\dot{n}_d(t))$. That means the vessel direction is chosen as the tangential vector of the respective desired trajectory. If we define the relative distance between the follower vessel and the leader vessel as $\mathbf{l}_i = [x_{0i}, y_{0i}, \psi_{0i}]^T$, then the desired trajectory of the follower vessel is denoted as $\eta_{di} = \eta_d + \mathbf{R}(\psi_d)\mathbf{l}_i$.

3.2.2. Controller Design. Define the first dynamic surface as

$$\mathbf{S}_{1i} = \widehat{\eta}_i - \eta_{di}. \tag{18}$$

Taking the derivative of the first surface, with (13), we obtain

$$\begin{aligned} \dot{\mathbf{S}}_{1i} &= \dot{\widehat{\eta}}_i - \dot{\eta}_{di} \\ &= \widehat{\mathbf{v}}_{ni} + \beta_1 \mathrm{fal}_1(\mathbf{z}_{1i}, \alpha, \delta) - \dot{\eta}_{di}. \end{aligned} \tag{19}$$

Define a virtual velocity $\mathbf{v}_{ri}$ as follows:

$$\mathbf{v}_{ri} = \dot{\eta}_{di} - \beta_1 \mathrm{fal}_1\left(\mathbf{z}_{1i}, \alpha, \delta\right) - \mathbf{\Lambda}_1 \mathbf{S}_{1i}, \tag{20}$$

where $\mathbf{\Lambda}_1$ is a positive definite matrix. With this definition, if $\mathbf{v}_{ri} = \hat{\mathbf{v}}_{ni}$, then $\dot{\mathbf{S}}_{1i} = -\mathbf{\Lambda}_1 \mathbf{S}_{1i}$. Then $\mathbf{S}_{1i} \to 0$ with a convergence rate determined by the choice of $\mathbf{\Lambda}_1$. Because of the definition of $\mathbf{S}_{1i}$, this will also guarantee that $\hat{\eta}_i \to \eta_i \to \eta_{di}$.

$\mathbf{v}_{ri}$ is passed through a first order filter in order to avoid the problem existed in the backstepping scheme:

$$\mathbf{T}\dot{\mathbf{v}}_{di} + \mathbf{v}_{di} = \mathbf{v}_{ri}, \tag{21}$$

where $\mathbf{T}$ is a diagonal matrix of the filter time constants which are chosen to be as small as possible. Because $\hat{\mathbf{v}}_{ni} \to \mathbf{v}_{ni}$, then we can define the second sliding surface as

$$\mathbf{S}_{2i} = \hat{\mathbf{v}}_{ni} - \mathbf{v}_{di}, \tag{22}$$

where $\mathbf{v}_{di}$ is the estimated value of $\mathbf{v}_{ri}$; take the derivative of $\mathbf{v}_{di}$, then we have

$$\dot{\mathbf{v}}_{di} = \mathbf{T}^{-1}\left(\mathbf{v}_{ri} - \mathbf{v}_{di}\right). \tag{23}$$

Taking the derivative of the second surface, with (13), we have

$$\begin{aligned}\dot{\mathbf{S}}_{2i} &= \dot{\hat{\mathbf{v}}}_{ni} - \dot{\mathbf{v}}_{di} \\ &= \widehat{\mathbf{K}}_i + \beta_2 \mathrm{fal}_2\left(\mathbf{z}_{1i}, \alpha, \delta\right) + \mathbf{u}_i - \dot{\mathbf{v}}_{di}.\end{aligned} \tag{24}$$

We consider the following Lyapunov function candidate:

$$\mathbf{V}_{1i} = \frac{1}{2}\mathbf{S}_{2i}^T \mathbf{S}_{2i}. \tag{25}$$

We take the time derivative of (25):

$$\dot{\mathbf{V}}_{1i} = \mathbf{S}_{2i}^T\left(\widehat{\mathbf{K}}_i + \beta_2 \mathrm{fal}_2\left(\mathbf{z}_{1i}, \alpha, \delta\right) + \mathbf{u}_i - \dot{\mathbf{v}}_{di}\right). \tag{26}$$

So we choose the control input as $\mathbf{u}_i = \dot{\mathbf{v}}_{di} - \widehat{\mathbf{K}}_i - \beta_2 \mathrm{fal}_2(\mathbf{z}_{1i}, \alpha, \delta) - \mathbf{K}_D \mathbf{S}_{2i}$.

The control input of the vessel is $\tau_i = \mathbf{M}_{ni}(\eta_i)\mathbf{u}_i$. So the control force input τ is selected as

$$\tau_i = \mathbf{M}_{ni}\left(\eta_i\right)\left(\dot{\mathbf{v}}_{di} - \widehat{\mathbf{K}}_i - \beta_2 \mathrm{fal}_2\left(\mathbf{z}_{1i}, \alpha, \delta\right) - \mathbf{K}_D \mathbf{S}_{2i}\right). \tag{27}$$

Theorem 1. *Consider the vessel with the nonlinear model as in* (1), (2), *and* (8), *with the control law* (27), *and then one can guarantee that the vessels approach the desired trajectory ultimately while holding the desired formation structure.*

Proof. With the definition of the second surface, (19) can be rewrite as

$$\dot{\mathbf{S}}_{1i} = \mathbf{S}_{2i} + \mathbf{v}_{di} - \beta_1 \mathrm{fal}_1\left(\mathbf{z}_{1i}, \alpha, \delta\right) - \dot{\eta}_{di}. \tag{28}$$

Define the estimated error of the first order filter as

$$\mathbf{S}_{3i} = -\mathbf{T}\dot{\mathbf{v}}_{di} = \mathbf{v}_{di} - \mathbf{v}_{ri}. \tag{29}$$

Taking the derivative of $\mathbf{S}_{3i}$ yields

$$\begin{aligned}\dot{\mathbf{S}}_{3i} &= \dot{\mathbf{v}}_{di} - \mathbf{v}_{ri} \\ &= \dot{\mathbf{v}}_{di} + \beta_1 \frac{d\mathrm{fal}_1\left(\mathbf{z}_{1i}, \alpha, \delta\right)}{dt} + \mathbf{\Lambda}_1 \dot{\mathbf{S}}_{1i} - \ddot{\eta}_{di} \\ &= -\frac{\mathbf{S}_{3i}}{\mathbf{T}} + \beta_1 \frac{d\mathrm{fal}_1\left(\mathbf{z}_{1i}, \alpha, \delta\right)}{dt} + \mathbf{\Lambda}_1 \dot{\mathbf{S}}_{1i} - \ddot{\eta}_{di} \\ &= -\frac{\mathbf{S}_{3i}}{\mathbf{T}} + g\left(\beta_1, \mathbf{z}_{1i}, \alpha, \delta, \dot{\mathbf{z}}_{1i}, \ddot{\eta}_{di}, \dot{\mathbf{S}}_{1i}\right).\end{aligned} \tag{30}$$

With (19) and (21), we obtain

$$\dot{\mathbf{S}}_{1i} = \mathbf{S}_{2i} + \mathbf{S}_{3i} - \mathbf{\Lambda}_{1i}\mathbf{S}_{1i}. \tag{31}$$

Define the Lyapunov function as

$$\mathbf{V}_i = \frac{1}{2}\mathbf{S}_{1i}^T \mathbf{S}_{1i} + \frac{1}{2}\mathbf{S}_{2i}^T \mathbf{S}_{2i} + \frac{1}{2}\mathbf{S}_{3i}^T \mathbf{S}_{3i}. \tag{32}$$

Differentiating the above equation yields

$$\begin{aligned}\dot{\mathbf{V}}_i &= \mathbf{S}_{1i}^T \dot{\mathbf{S}}_{1i} + \mathbf{S}_{2i}^T \dot{\mathbf{S}}_{2i} + \mathbf{S}_{3i}^T \dot{\mathbf{S}}_{3i} \\ &= \mathbf{S}_{1i}^T\left(\mathbf{S}_{2i} + \mathbf{S}_{3i} - \mathbf{\Lambda}_1 \mathbf{S}_{1i}\right) - \mathbf{S}_{2i}^T \mathbf{K}_D \mathbf{S}_{2i} + \mathbf{S}_{3i}^T \\ &\quad \times \left(-\frac{\mathbf{S}_{3i}}{\mathbf{T}} + g\left(\beta_1, \mathbf{z}_{1i}, \alpha, \delta, \dot{\mathbf{z}}_{1i}, \ddot{\eta}_{di}, \dot{\mathbf{S}}_{1i}\right)\right) \\ &= -\mathbf{S}_{1i}^T \mathbf{\Lambda}_1 \mathbf{S}_{1i} + \mathbf{S}_{1i}^T \mathbf{S}_{2i} + \mathbf{S}_{1i}^T \mathbf{S}_{3i} \\ &\quad - \mathbf{S}_{2i}^T \mathbf{K}_D \mathbf{S}_{2i} - \frac{\mathbf{S}_{3i}^T \mathbf{S}_{3i}}{\mathbf{T}} \\ &\quad + \mathbf{S}_{3i}^T g\left(\beta_1, \mathbf{z}_{1i}, \alpha, \delta, \dot{\mathbf{z}}_{1i}, \ddot{\eta}_{di}, \dot{\mathbf{S}}_{1i}\right).\end{aligned} \tag{33}$$

If we define the maximum of $g(\beta_1, \mathbf{z}_{1i}, \alpha, \delta, \dot{\mathbf{z}}_{1i}, \ddot{\eta}_{di}, \dot{\mathbf{S}}_{1i})$ is $g_{\max}$, we can know that $\mathbf{S}_{1i}^T \mathbf{S}_{1i} + \mathbf{S}_{2i}^T \mathbf{M} \mathbf{S}_{2i} + \mathbf{S}_{3i}^T \mathbf{S}_{3i} \le 2p$, p is a positive constant. Then we can obtain that $V_i \le p$. Let $\mathbf{\Lambda}_1 = \mathbf{K}_D = \alpha_0 + 2I_3$, and the filter time constant can be chosen as $\mathbf{T} = (I_3 + (g_{\max}^T g_{\max}/2\varepsilon I_3) + \alpha_0)^{-1}$; then we can obtain that

$$\begin{aligned}\dot{\mathbf{V}}_i = &-\mathbf{S}_{1i}^T\left(\alpha_0 + 2I_3\right)\mathbf{S}_{1i} - \mathbf{S}_{2i}^T\left(\alpha_0 + 2I_3\right)\mathbf{S}_{2i} \\ &- \mathbf{S}_{3i}^T\left(I_3 + \left(\frac{g_{\max}^2}{2\varepsilon I_3}\right) + \alpha_0\right)\mathbf{S}_{3i} \\ &+ \mathbf{S}_{1i}^T \mathbf{S}_{2i} + \mathbf{S}_{1i}^T \mathbf{S}_{3i} + \mathbf{S}_{3i}^T g \\ \le &-\mathbf{S}_{1i}^T\left(\alpha_0 + 2I_3\right)\mathbf{S}_{1i} - \mathbf{S}_{2i}^T\left(\alpha_0 + 2I_3\right)\mathbf{S}_{2i} \\ &+ \frac{2\mathbf{S}_{1i}^T \mathbf{S}_{1i} + \mathbf{S}_{2i}^T \mathbf{S}_{2i} + \mathbf{S}_{3i}^T \mathbf{S}_{3i}}{2} \\ &- \mathbf{S}_{3i}^T \mathbf{S}_{3i} - \mathbf{S}_{3i}^T \alpha_0 \mathbf{S}_{3i} - \mathbf{S}_{3i}^T\left(\frac{g_{\max}^T g_{\max}}{2\varepsilon I_3}\right)\mathbf{S}_{3i} \\ &+ \frac{g_{\max}^2 \mathbf{S}_{3i}^T \mathbf{S}_{3i}}{2\varepsilon I_3}\frac{g^T g}{g_{\max}^2} + \frac{\varepsilon}{2} \\ \le &-2\alpha_0 \mathbf{V}_i + \frac{\varepsilon}{2}.\end{aligned} \tag{34}$$

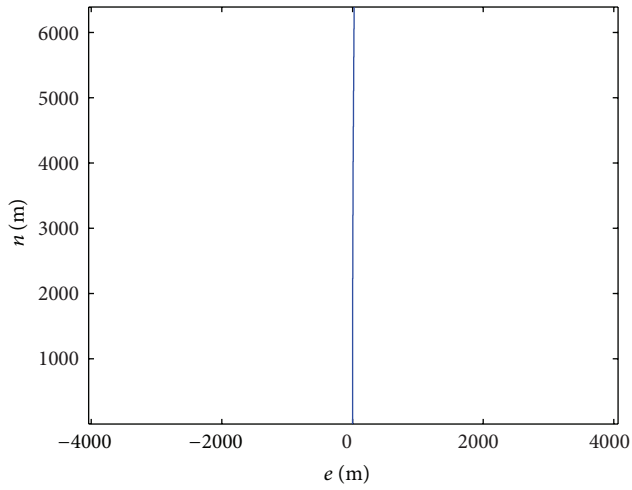

Figure 2: The movement of the vessel in the plane.

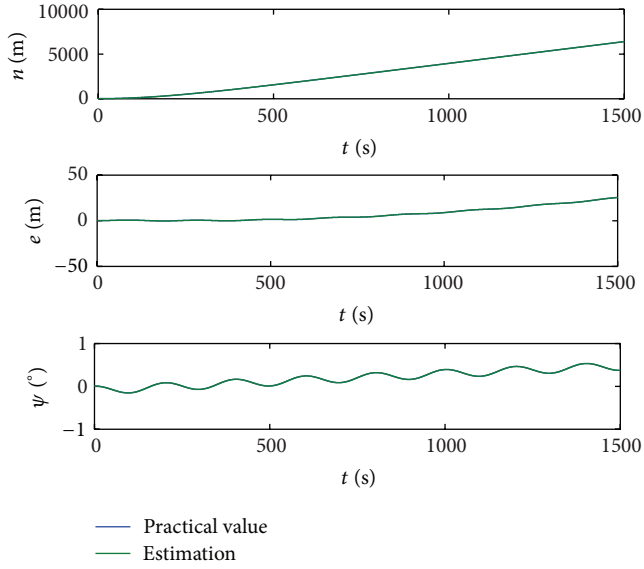

Figure 3: The practical value and estimated value of the positions.

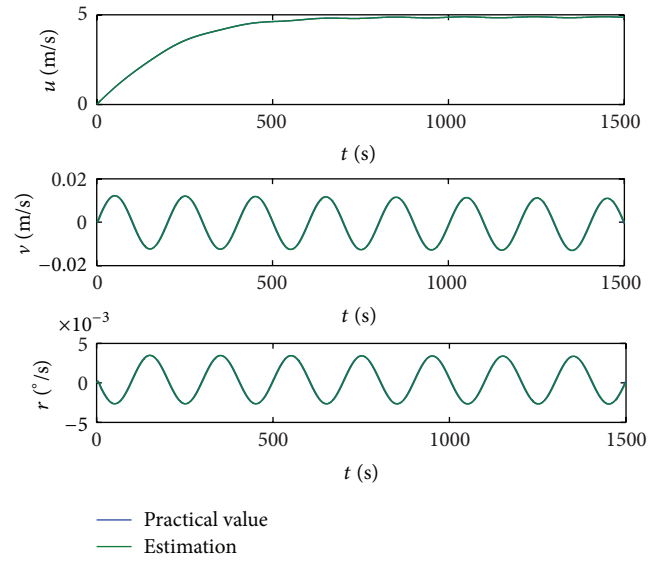

Figure 4: The practical value and estimated value of the velocities.

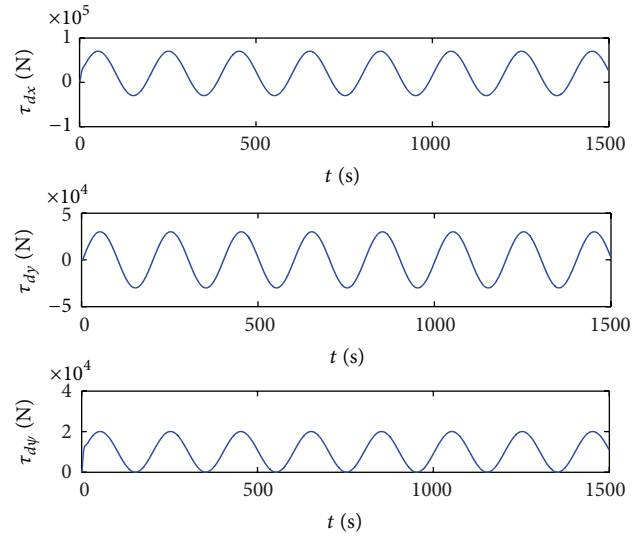

Figure 5: The estimated value of the disturbances.

If we choose $\alpha_0 > \varepsilon/2p$, then $\dot{V}_i < 0$. We can guarantee that $\mathbf{S}_{2i} \to 0$. This implies $\hat{\mathbf{v}}_{ni} \to \mathbf{v}_{ni} \to \mathbf{v}_{di}$, in turn, $\mathbf{S}_{1i} \to 0$ and $\hat{\eta}_i \to \eta_i \to \eta_{di}$. □

4. Simulation Results

In this section, experimental simulations are carried out to evaluate the effectiveness of the proposed coordinated formation control algorithm. The detailed parameters of the vessel are presented in the literature [11]. At the beginning, the proposed extended state observer of one vessel is evaluated by the simulation. Similarly, the performance of the extended state observer of other vessels is achieved. Compare with the existing literature studies, we let the initial position of the vessel is $\eta = [0, 0, 0]^T$. The vessel moves in a beeline northward. assume that the vessels encounter the wind, wave, and current. The wind is assumed to be fixed direction and fixed velocity, and then the disturbance of wind is a constant; the wave and current are assumed to be the sine wave with a fixed frequency at one time. The external disturbances can be chosen as

$$\tau_d = 10^6 * [0.05 \sin(\pi t/100) + 0.02, \; 0.03 \sin(\pi t/100), \; 0.01 \sin(\pi t/100) + 0.01]^T (N). \quad (35)$$

In the simulation, we assume that the external disturbances are unknown. The proposed observer parameters are selected as $\beta_1 = 30$, $\beta_2 = 15$, $\beta_3 = 5$, $\alpha = 0.25$, and $\delta = 0.1$.

The simulation results are shown in Figures 2 to 5. Figure 2 shows the movements for the vessel in the plane. The practical value and estimated value of the north position, east

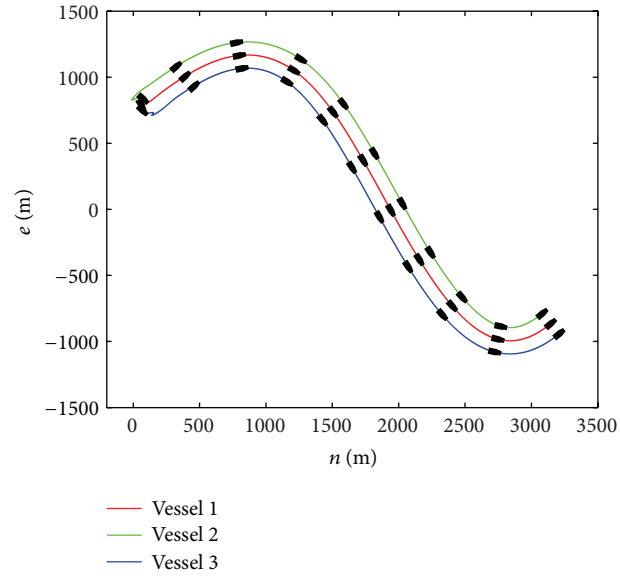

Figure 6: Coordinated trajectory tracking of the vessels.

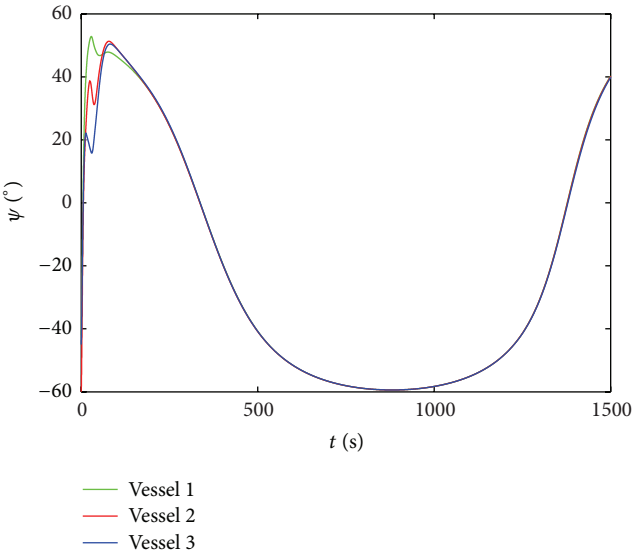

Figure 7: Heading change of the vessels.

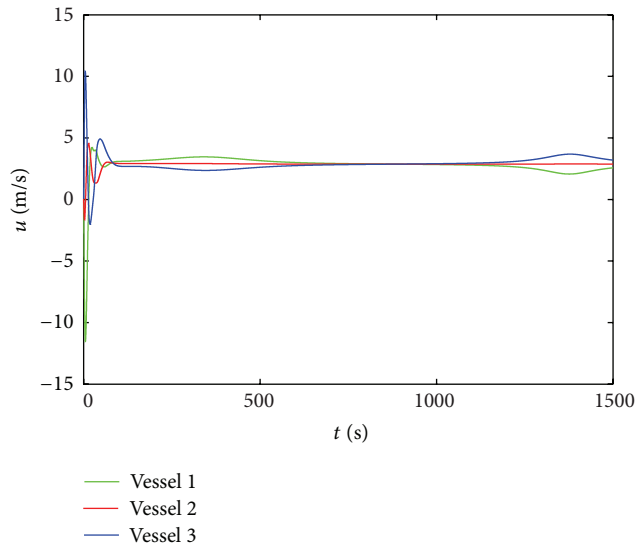

Figure 8: Surge velocity change of the vessels.

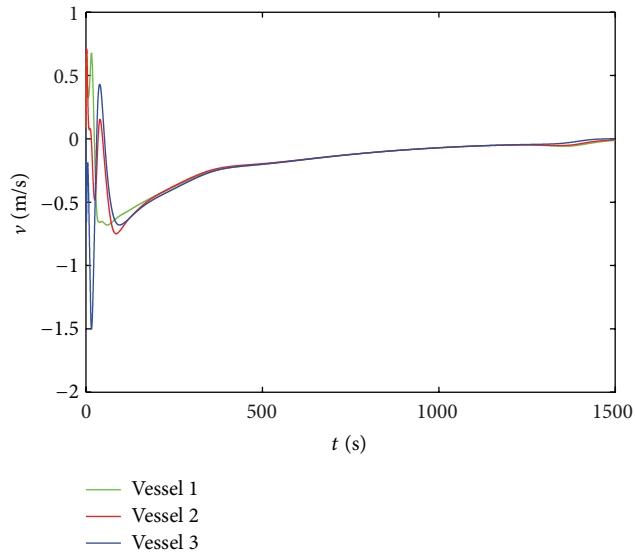

Figure 9: Sway velocity change of the vessels.

position, and heading change curve of the vessel are shown in Figure 3. Figure 4 shows the practical value and estimated value of the surge velocity, sway velocity, and angular velocity of the vessel. The estimated value of the external disturbances are shown in Figure 5. In the simulation experiment, there is no measurement noise in the kinematics and nonlinear dynamics. So the practical value and estimated value of the position and velocity are consensus in a way. What's more, the external disturbances can be estimated through introducing the extended state.

Then we evaluate the effectiveness of the proposed robust coordinated formation control algorithm. Three surface vessels are considered to perform the coordinated tracking task. The initial positions of the three vessels are $\eta_1 = [65 \quad 782 \quad -\pi/3]^T$, $\eta_2 = [80 \quad 831 \quad -7\pi/30]^T$, and $\eta_3 = [75 \quad 743 \quad -\pi/4]^T$, respectively. In order to evaluate the performance of the coordinated tracking, the desired formation pattern of the coordinated formation controller is described by $\mathbf{l}_1 = [0 \quad 0 \quad 0]^T$, $\mathbf{l}_2 = [0 \quad -100 \quad 0]^T$, and $\mathbf{l}_3 = [0 \quad 100 \quad 0]^T$. The desired trajectory for the assigned leader is chosen as $\eta_d(t) = [n_d \quad e_d \quad \psi_d]^T$, and the detailed forms are $n_d = t$, $e_d = 1000\sin(t/600)$, $\psi_d = \arctan(\dot{e}_d/\dot{n}_d)$. The proposed controller parameters are selected as $\mathbf{\Lambda}_1 = \text{diag}(0.05, 0.05, 0.05)$, $\mathbf{T} = \text{diag}(0.1, 0.1, 0.1)$, and $\mathbf{K}_D = 10^4 * \text{diag}(6.5, 6.5, 6.5)$.

The simulation results are shown in Figures 6 to 10. Figure 6 shows the movements for these vessels in the plane. The heading change curve of each vessel is shown in Figure 7. Figures 8, 9, and 10 show the surge velocity, the sway velocity, and the angular velocity of each vessel during the coordinated control process, respectively. We can see that

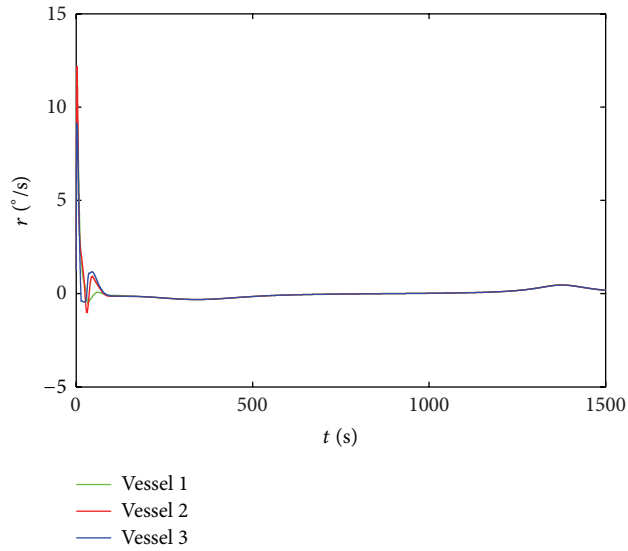

Figure 10: Angular velocity change of the vessels.

these vessels realized the coordinated tracking task from Figures 6 and 7. From Figures 8, 9, and 10, the velocities of these vessels achieve consensus as a whole, and the velocities cannot achieve consensus absolutely when the vessels move to the inflexion of the curves. With the analysis of the simulation results, we can conclude that these vessels can accomplish coordinated trajectory tracking task while keeping the desired formation. It means that the proposed coordination control algorithm is effective.

5. Conclusion

This paper has proposed a new robust coordinated formation control algorithm for multiple surface vessels in the presence of external environmental disturbances. The proposed coordinated formation controller for these vessels is designed by combining the extended state observer and the dynamic surface control together. The extended state observer is designed to estimate the external disturbances of the surface vessels. The coordinated formation is realized based on the leader-follower strategy. The desired trajectory of each vessel is defined using the desired trajectory of the assigned leader and relative distance with respect to the leader. The controller is designed based on the output of the extended state observer and using the dynamic surface control method. The proposed coordinated controller is robust to the external disturbances. Finally, the effectiveness of the proposed robust coordination control algorithm is demonstrated by the simulation results.

Conflict of Interests

The authors declare that there is no conflict of interests regarding the publication of this paper.

Acknowledgment

The authors would like to acknowledge the support of the Natural Science Grant of Liaoning Province (2013020002).

References

[1] W. Ren, R. W. Beard, and E. M. Atkins, "A survey of consensus problems in multi-agent coordination," in *Proceedings of the American Control Conference*, pp. 1859–1864, June 2005.

[2] A. Aguiar, J. Almeida, M. Bayat et al., "Cooperative autonomous marine vehicle motion control in the scope of the EU GREX Project: theory and practice," in *Proceedings of the IEEE Bremen: Balancing Technology with Future Needs (OCEANS '09)*, pp. 1–10, May 2009.

[3] P. K. C. Wang, "Navigation strategies for multiple autonomous mobile robots moving in formation," *Journal of Robotic Systems*, vol. 8, no. 2, pp. 177–195, 1991.

[4] J. K. Hedrick, M. Tomizuka, and P. Varaiya, "Control issues in automated highway systems," *IEEE Control Systems Magazine*, vol. 14, no. 6, pp. 21–32, 1994.

[5] M. Breivik, V. E. Hovstein, and T. I. Fossen, "Ship formation control: a guided leader-follower approach," in *Proceedings of the 17th World Congress, International Federation of Automatic Control (IFAC '08)*, pp. 16008–16014, July 2008.

[6] G. Antonelli, F. Arrichiello, and S. Chiaverini, "Experiments of formation control with collisions avoidance using the null-space-based behavioral control," in *Proceedings of the 14th Mediterranean Conference on Control and Automation (MED '06)*, pp. 1–6, June 2006.

[7] J. R. T. Lawton, R. W. Beard, and B. J. Young, "A decentralized approach to formation maneuvers," *IEEE Transactions on Robotics and Automation*, vol. 19, no. 6, pp. 933–941, 2003.

[8] M. A. Lewis and K.-H. Tan, "High precision formation control of mobile robots using virtual structures," *Autonomous Robots*, vol. 4, no. 4, pp. 387–403, 1997.

[9] W. Ren and R. W. Beard, "Decentralized scheme for spacecraft formation flying via the virtual structure approach," *Journal of Guidance, Control, and Dynamics*, vol. 27, no. 1, pp. 73–82, 2004.

[10] J. Almeida, C. Silvestre, and A. M. Pascoal, "Cooperative control of multiple surface vessels with discrete-time periodic communications," *International Journal of Robust and Nonlinear Control*, vol. 22, no. 4, pp. 398–419, 2012.

[11] C. Thorvaldsen and R. Skjetne, "Formation control of fully-actuated marine vessels using group agreement protocols," in *Proceedings the 50th IEEE Conference on Decision and Control and European Control Conference*, pp. 4132–4139, 2011.

[12] Y. Wang, W. Yan, and J. Li, "Passivity-based formation control of autonomous underwater vehicles," *IET Control Theory & Applications*, vol. 6, no. 4, pp. 518–525, 2012.

[13] M. Fu and J. Jiao, "A hybrid approach for coordinated formation control of multiple surface vessels," *Mathematical Problems in Engineering*, vol. 2013, Article ID 794284, 8 pages, 2013.

[14] I.-A. F. Ihle, J. Jouffroy, and T. I. Fossen, "Formation control of marine surface craft: a lagrangian approach," *IEEE Journal of Oceanic Engineering*, vol. 31, no. 4, pp. 922–934, 2006.

[15] F. Fahimi, "Non-linear model predictive formation control for groups of autonomous surface vessels," *International Journal of Control*, vol. 80, no. 8, pp. 1248–1259, 2007.

[16] J. Almeida, C. Silvestre, and A. Pascoal, "Cooperative control of multiple surface vessels in the presence of ocean currents and parametric model uncertainty," *International Journal of Robust and Nonlinear Control*, vol. 20, no. 14, pp. 1549–1565, 2010.

[17] F. Fahimi, "Sliding-mode formation control for underactuated surface vessels," *IEEE Transactions on Robotics*, vol. 23, no. 3, pp. 617–622, 2007.

[18] S. Yin, S. Ding, and H. Luo, "Real-time implementation of fault tolerant control system with performance optimization," in *Proceedings of the IEEE Transactions on Industrial Electronics*, vol. 61, no. 5, 2013.

[19] S. Yin, S. Ding, A. Haghani, H. Hao, and P. Zhang, "A comparison study of basic data-driven fault diagnosis and process monitoring methods on the benchmark Tennessee Eastman process," *Journal of Process Control*, vol. 22, no. 9, pp. 1567–1581, 2012.

[20] S. Yin, S. X. Ding, A. H. A. Sari, and H. Hao, "Data-driven monitoring for stochastic systems and its application on batch process," *International Journal of Systems Science*, vol. 44, no. 7, pp. 1366–1376, 2013.

[21] E. Børhaug, A. Pavlov, E. Panteley, and K. Y. Pettersen, "Straight line path following for formations of underactuated marine surface vessels," *IEEE Transactions on Control Systems Technology*, vol. 19, no. 3, pp. 493–506, 2011.

[22] J. Ghommam and F. Mnif, "Coordinated path-following control for a group of underactuated surface vessels," *IEEE Transactions on Industrial Electronics*, vol. 56, no. 10, pp. 3951–3963, 2009.

[23] X. P. Shi, S. R. Liu, and F. Liu, "New robust control strategy for module manipulators via sliding mode control with an extended state observer," *Proceedings of the Institution of Mechanical Engineers I*, vol. 224, no. 5, pp. 545–555, 2010.

[24] Y. Xia, Z. Zhu, and M. Fu, "Back-stepping sliding mode control for missile systems based on an extended state observer," *IET Control Theory & Applications*, vol. 5, no. 1, pp. 93–102, 2011.

[25] S. E. Talole, J. P. Kolhe, and S. B. Phadke, "Extended-state-observer-based control of flexible-joint system with experimental validation," *IEEE Transactions on Industrial Electronics*, vol. 57, no. 4, pp. 1411–1419, 2010.

[26] M. Fu, J. Jiao, and L. Hao, "A coordinated dyanmic positioning control algorithm based on active disturbance rejection control," in *Proceedings of IEEE International Joint Conference on Computational Sciences and Optimization*, pp. 67–71, 2012.

[27] B.-Z. Guo and Z.-l. Zhao, "On the convergence of an extended state observer for nonlinear systems with uncertainty," *Systems & Control Letters*, vol. 60, no. 6, pp. 420–430, 2011.

[28] B.-Z. Guo and Z.-L. Zhao, "On convergence of non-linear extended state observer for multi-input multi-output systems with uncertainty," *IET Control Theory & Applications*, vol. 6, no. 15, pp. 2375–2386, 2012.

[29] B.-Z. Guo and Z.-L. Zhao, "On convergence of the nonlinear active disturbance rejection control for MIMO systems," *SIAM Journal on Control and Optimization*, vol. 51, no. 2, pp. 1727–1757, 2013.

[30] T. Fossen, *Marine Control Systems: Guidance, Navigation and Control of Ships, Rigs and Underwater Vehicles*, Marine Cybernetics, Trondheim, Norway, 2002.

Hindawi Publishing Corporation
Mathematical Problems in Engineering
Volume 2013, Article ID 145396, 5 pages
http://dx.doi.org/10.1155/2013/145396

Research Article

H_∞ Control Theory Using in the Air Pollution Control System

Tingya Yang,[1] Zhenyu Lu,[2] and Junhao Hu[3]

[1] *Jiangsu Meteorological Observatory, Nanjing 210008, China*
[2] *College of Electrical and Information Engineering, Nanjing University of Information Science and Technology, Nanjing 210044, China*
[3] *College of Mathematics and Statistics, South-Central University for Nationalities, Wuhan 430074, China*

Correspondence should be addressed to Junhao Hu; junhaomath@163.com

Received 5 August 2013; Accepted 23 September 2013

Academic Editor: Bo-chao Zheng

In recent years, air pollution control has caused great concern. This paper focuses on the primary pollutant SO_2 in the atmosphere for analysis and control. Two indicators are introduced, which are the concentration of SO_2 in the emissions (PSO_2) and the concentration of SO_2 in the atmosphere (ASO_2). If the ASO_2 is higher than the certain threshold, then this shows that the air is polluted. According to the uncertainty of the air pollution control systems model, H_∞ control theory for the air pollution control systems is used in this paper, which can change the PSO_2 with the method of improving the level of pollution processing or decreasing the emissions, so that air pollution system can maintain robust stability and the indicators ASO_2 are always operated within the desired target.

1. Introduction

The main feature of the H_∞ control theory is based on the frequency design method of using the state-space model, and this theory presents an effective method to solve the uncertainty problem of external disturbance to the system. In order to overcome the drawbacks of the classical control theory and the modern control theory, H_∞ control theory established technology and method of the loop shaping in the frequency domain, which combines the classic frequency-domain and the modern state-space method. The design problem of the control system is converted to the H_∞ control problem, which made the system closer to the actual situation and meet the actual needs. So it gives the robust control system design method, which obtains H_∞ controller by solving two Riccati equations. This method fully considered the impact of system uncertainty, which not only can ensure the robust stability of the control system, but also can optimize some performance indices. It is the optimal control theory in frequency domain, and the parameters design of H_∞ controller is more effective than optimal regulator [1].

So the H_∞ control theory for the air pollution control systems can solve the uncertainty of the air pollution control systems model, which can get the control strategy to change the PSO_2, so that air pollution system can maintain robust stability and the indicators ASO_2 are always operated within the desired target.

2. Standard H_∞ Control Problem

2.1. Problem Description. The standard H_∞ control problem is shown in Figure 1, which consists of G and K. G is a generalized control target which is a given part of the system. K is H_∞ controller, and it needs to be designed.

It is supposed that G and K are described as the transfer function matrix of the linear time invariant system [2]. Then, $G(s)$ and $K(s)$ are proper rational matrices, Decomposing $G(s)$ as

$$G = \begin{bmatrix} G_{11} & G_{12} \\ G_{21} & G_{22} \end{bmatrix}. \tag{1}$$

Its state-space realization is

$$\begin{aligned} \dot{x} &= Ax + B_1\omega + B_2u, \\ z &= C_1x + D_{11}\omega + D_{12}u, \\ y &= C_2x + D_{21}\omega + D_{22}u. \end{aligned} \tag{2}$$

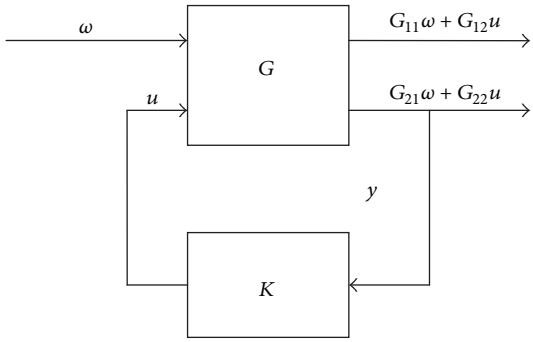

Figure 1: The diagram of the standard H_∞ control problem.

It is denoted as:

$$G = \begin{bmatrix} A & B_1 & B_2 \\ C_1 & D_{11} & D_{12} \\ C_2 & D_{21} & D_{22} \end{bmatrix}, \tag{3}$$

where $x \in R^n$ is the state vector, ω is the external input, u is the control input, z is the controlled output, and y is the measured output. They are all vector signals. To compare (1) and (3), we can obtain

$$G_{ij} = C_i(sI - A)^{-1}B_j + D_{ij}, \quad i, j = 1, 2. \tag{4}$$

Obviously, the closed-loop transfer function matrix from ω to z can be expressed as

$$T_{z\omega}(s) = G_{11} + G_{12}K\left(I - G_{22}K\right)^{-1}G_{21} = F_l(G, K). \tag{5}$$

The problem of H_∞ optimal control theory is to find a proper rational controller K for closed-loop control system, and make the closed-loop control system internally stabile, and then minimize the H_∞ norm of closed-loop transfer function matrix $T_{z\omega}(s)$ [3]:

$$\min_{K \text{ stability } G} \left\| F_l(G, K) \right\|_\infty < 1. \tag{6}$$

2.2. State-Space H_∞ Output-Feedback Control. We assume that the state-space representation of the generalized controlled object G state-space representation is (2), where $x \in R^n, \omega \in R^{m_1}, u \in R^{m_2}, z \in R^{p_1}, y \in R^{P_2}, A \in R^{n\times n}, B_1 \in R^{n\times m_1}, B_2 \in R^{n\times m_2}, C_1 \in R^{p_1\times n}, C_2 \in R^{p_2\times n}$, D_{21} and D_{22} are the corresponding dimension of the real matrix, and controller K is dynamic output feedback compensator [4].

Consider that G have a special form:

$$G = \begin{bmatrix} A & B_1 & B_2 \\ C_1 & 0 & D_{12} \\ \begin{bmatrix} I \\ 0 \end{bmatrix} & \begin{bmatrix} 0 \\ I \end{bmatrix} & \begin{bmatrix} 0 \\ 0 \end{bmatrix} \end{bmatrix}, \tag{7}$$

which satisfies the following conditions:

(1) (A, B_1) is stabilizable, and (C_1, A) is detectable;

(2) (A, B_2) is stabilizable;

(3) $D_{12}^T \begin{bmatrix} C_1 & D_{12} \end{bmatrix} = \begin{bmatrix} 0 & I \end{bmatrix}$.

Obviously, $y = \begin{bmatrix} x \\ \omega \end{bmatrix}$; that is, the state x of generalized control object and the external input signal ω could be measured; then, it can be directly used to constitute control law.

As the result, we can obtain Theorem 1.

Theorem 1. *If and only if $H_\infty \in \mathrm{dom}(\mathrm{Ric})$, $X_\infty = \mathrm{Ric}(\mathrm{H}_\infty) \geq 0$, there exists H_∞ controller*

$$u = -B_2^T X_\infty x + Q(s)\left(\omega - \gamma^{-2}B_1^T X_\infty x\right). \tag{8}$$

That is,

$$K(s) = \left[-B_2^T X_\infty - Q(s)\gamma^{-2}B_1^T X_\infty Q(s)\right], \tag{9}$$

where $Q(s) \in RH_\infty$, $\|Q(s)\|_\infty < \gamma$, which is made to stabilize the closed-loop control system, and the closed-loop transfer function matrix $T_{z\omega}(s)$ from ω to z is satisfied as $\|T_{z\omega}(s)\|_\infty < \gamma$.

Proof. If Hamilton matrix H_∞ was considered, there exist $X_\infty = \mathrm{Ric}(H_\infty)$, and then the derivative of $x^T(t)X_\infty x(t)$ can be achieved, such that

$$\frac{d}{dt}x^T X_\infty x = \dot{x}^T X_\infty x + x^T X_\infty \dot{x}. \tag{10}$$

Substituting (2) into (10) and considering Riccati equation (11) and orthogonality condition

$$\begin{aligned} A^T X_\infty + X_\infty A + \gamma^{-2}X_\infty B_1 B_1^T X_\infty \\ - X_\infty B_2 B_2^T X_\infty + C_1^T C_1 = 0. \end{aligned} \tag{11}$$

So the following formula can be achieved:

$$\begin{aligned} \frac{d}{dt}x^T X_\infty x &= x^T\left(A^T X_\infty + X_\infty A\right)x \\ &\quad + \omega^T\left(B_1^T X_\infty x\right) + \left(B_1^T X_\infty x\right)^T\omega \\ &\quad + u^T\left(B_2^T X_\infty x\right) + \left(B_2^T X_\infty x\right)^T u \\ &= -\left\|C_1 x\right\|^2 - \gamma^{-2}\left\|B_1^T X_\infty x\right\|^2 \\ &\quad + \left\|B_2^T X_\infty x\right\|^2 + \omega^T\left(B_1^T X_\infty x\right) + \left(B_1^T X_\infty x\right)^T\omega \\ &\quad + u^T\left(B_2^T X_\infty x\right) + \left(B_2^T X_\infty x\right)^T u \\ &= -\|z\|^2 + \gamma^2\|\omega\|^2 - \gamma^2\left\|\omega - \gamma^{-2}B_1^T X_\infty x\right\|^2 \\ &\quad + \left\|u + B_2^T X_\infty x\right\|^2. \end{aligned} \tag{12}$$

If $x(0) = x(\infty) = 0$, $\omega \in L_2[0, +\infty)$, to integral above equation from $t = 0$ to $t = \infty$, then

$$\begin{aligned} &\|z\|_2^2 - \gamma^2\|\omega\|_2^2 \\ &\quad = \left\|u + B_2^T X_\infty x\right\|_2^2 - \gamma^2\left\|\omega - \gamma^{-2}B_1^T X_\infty x\right\|_2^2. \end{aligned} \tag{13}$$

According to the equivalence relation,

$$\left\|T_{z\omega}(s)\right\|_\infty < \gamma \Longleftrightarrow \|z\|_2^2 < \gamma^2 \|\omega\|_2^2. \tag{14}$$

Form (12) and (13), we can get that

$$\begin{aligned} \left\|T_{z\omega}(s)\right\|_\infty < \gamma &\Longleftrightarrow \left\|u + B_2^T X_\infty x\right\|_2^2 \\ &< \gamma^2 \left\|\omega - \gamma^{-2} B_1^T X_\infty x\right\|_2^2 \\ &\Longleftrightarrow u + B_2^T X_\infty x \\ &= Q(s)\left(\omega - \gamma^{-2} B_1^T X_\infty x\right), \end{aligned} \tag{15}$$

where $\|\bullet\|$ represent Euclidean norm.

Hence, $u = -B_2^T X_\infty x + Q(s)(\omega - \gamma^{-2} B_1^T X_\infty x)$; the proof is completed. □

u is the input to ensure $\|T_{z\omega}(s)\|_\infty < \gamma$, where $Q(s)(\omega - \gamma^{-2} B_1^T X_\infty x)$ is the output of the transfer system $Q(s)$ by the input $(\omega - \gamma^{-2} B_1^T X_\infty x)$. From (12), the decay of $x^T(t) X_\infty x(t) \geq 0$ is the slowest when $\omega = \gamma^{-2} B_1^T X_\infty x$. Then for this kind of disturbance, we can stabilize (12) by using control strategy u.

3. Analysis and Synthesis of Air Pollution Control System

Atmospheric quality management is essentially the process of the analysis and synthesis to the air pollution control system. So-called atmospheric system analysis is qualitative and quantitative research for an atmospheric area system or facilities system, which include that to evaluate the current situation, to find out the main environment problems, to put a series of optional target projects, and to establish the quantitative relation between emission and the quality of the permissive atmosphere [5]. The systems synthesis means the plan and design of an air pollution control system on the basis of system analysis to determine the target and to determine a management method of a system, in other words, in order to achieve certain environmental goal to select the optimal planning scheme, to optimal design, to find the optimal management method, and so forth. So the process of the synthesis should include three main steps: determine the target, form better feasibility scheme of system, and optimization decision [6].

Usually, the atmosphere has certain self-purification ability; namely, the atmospheric environment has a certain capacity. It refers to the permissible pollutant emissions within the natural purification capacity, which reach the limiting quantity in order not to destruct the nature material circulation [7]. We can make the quantity of pollutant discharged that meets a certain environmental goal to be permissible total emission. Only when the pollutant emissions beyond atmospheric self-purification ability, namely, exceeds the environmental capacity, there may be air pollution [8].

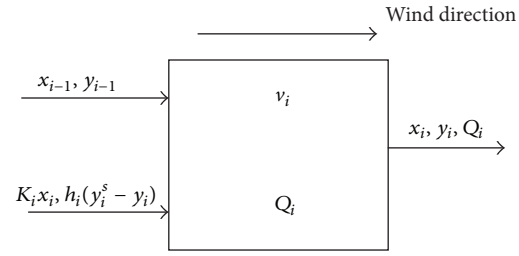

Figure 2: The stirred reactor model of an ideal atmosphere section.

In this paper, the objective of applying the H_∞ control theory in air pollution control system is to find out regularity, to make full use of atmospheric environmental self-purification ability; we cannot only develop production but also protect the environment.

4. H_∞ Control of Air Pollution

In recent years, air pollution control has caused great concern. This paper focuses on primary pollutant SO_2 in the atmosphere for analysis and control, which is mainly pollutant of the PM2.5. We introduced two indicators, which are the concentration of SO_2 in the emissions (PSO_2) and the concentration of SO_2 in the atmosphere (ASO_2). Meanwhile, we can change the content of SO_2 in the emissions (with the method of improving the methods of processing), with the aim of returning atmospheric quality back to the desired value.

4.1. The Mathematical Model of Air Pollution. A certain volume of air mainly accepted the controlled pollutants which discharged from certain purification equipments. In addition, considering that the atmospheric self-purification ability is mainly affected by wind and other meteorological factors, a certain volume of air can be defined as atmospheric section. Thus, we can put forward a second order state-space equation; it describes the relationship between PSO_2 and ASO_2 on an average point of the atmospheric section [9]. The basic idea of modeling is to consider each section as ideal stirred reactor, as shown in Figure 2. So, the parameters and variables of the whole section are consistent, and the output concentration of PSO_2 and ASO_2 is equal to the counterpart concentration in this section. Hence, from the point of view of the mass balance, we can get the following equation.

PSO_2 balance equation:

$$\dot{x}_i = -k_i x_i + \frac{Q_{i-1}}{v_i} x_{i-1} - \frac{Q_i + Q_E}{v_i} x_i. \tag{16}$$

ASO_2 balance equation:

$$\dot{y}_i = h_i\left(y_i^s - y_i\right) + \frac{Q_{i-1}}{v_i} y_{i-1} - \frac{Q_i + Q_E}{v_i} y_i - k_i x_i, \tag{17}$$

where x_i, x_{i-1} are the PSO_2 of Section i and Section $i-1$ (mg/m^3), v_i is the atmospheric capacity of Section i (m^3);

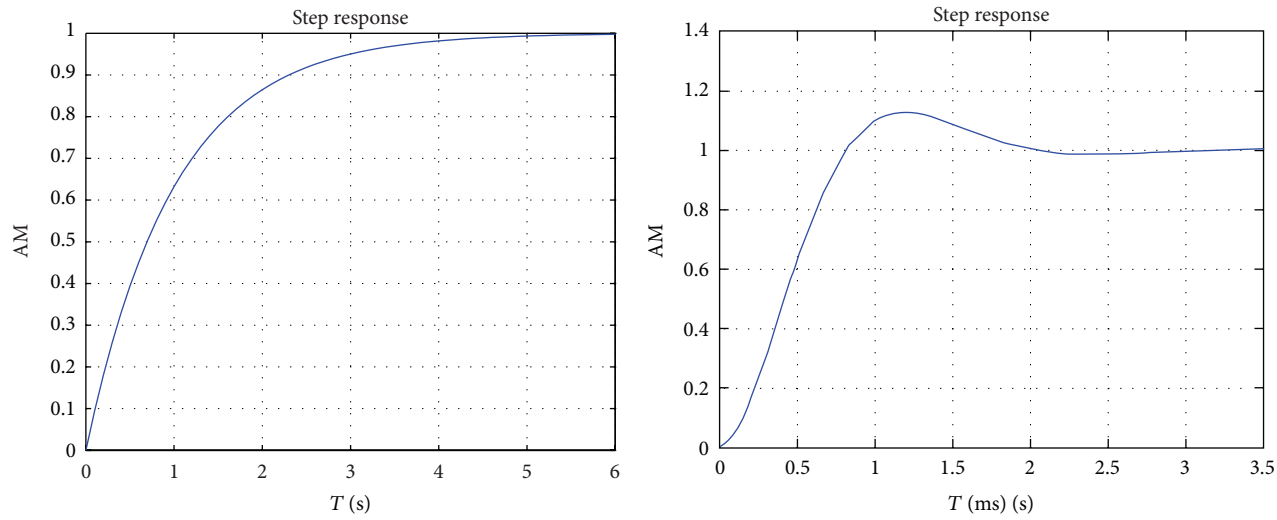

(a) The original closed-loop system

(b) The closed-loop system with H_∞ control strategy

FIGURE 3: The system step response.

Q_E is PSO_2 gas flow rate of Section i (m^3/d), y_i, y_{i-1} are ASO_2 of Section i and Section $i-1$ (mg/m^3), k_i, h_i are daily decay rate of PSO_2 of Section i and supply rate of ASO_2 of Section i, Q_i, Q_{i-1} are atmosphere gas flow rates of Section i and Section $i-1$ (m^3/d), and y_i^s is saturating capacity of SO_2 of Section i (mg/m^3).

From [5], we can conclude that it is advisable to take the following values as the coefficients in above equations:

$$k_i = 0.32/\text{day}, \qquad h_i = 0.2/\text{day}, \qquad y_i^s = 0.36\,\text{mg/m}^3,$$
$$\frac{Q_E}{v_i} = 0.1, \qquad \frac{Q_i}{v_i}, \frac{Q_{i-1}}{v_i} = 0.9. \tag{18}$$

Thus, the mathematical model of Section i air pollution is

$$\begin{bmatrix} \dot{x}_i \\ \dot{y}_i \end{bmatrix} = \begin{bmatrix} -1.32 & 0 \\ -0.32 & -1.2 \end{bmatrix} \begin{bmatrix} x_i \\ y_i \end{bmatrix} + \begin{bmatrix} 0.1 \\ 0 \end{bmatrix} u + \begin{bmatrix} 0.9x_{i-1} \\ 0.9y_{i-1} + 1.9 \end{bmatrix}, \tag{19}$$

where u is control strategy.

4.2. Simulation of Air Pollution H_∞ Control. H_∞ control problem of air pollution is basically how to control emissions of pollutants in the best way, in order to properly handle the cost of cleaning and the price we pay for too much atmospheric pollution. Using H_∞ control theory can better achieve this goal, which not only saves investment but also is easy to be realized [10].

In this paper, the simulation object is two sections of the H_∞ control of atmospheric pollution, the state-space equation is described as

$$\begin{bmatrix} \dot{x}_1 \\ \dot{y}_1 \\ \dot{x}_2 \\ \dot{y}_2 \end{bmatrix} = \begin{bmatrix} -1.32 & 0 & 0 & 0 \\ -0.32 & -1.2 & 0 & 0 \\ 0.9 & 0 & -1.32 & 0 \\ 0 & 0.9 & -0.32 & -1.2 \end{bmatrix} \begin{bmatrix} x_1 \\ y_1 \\ x_2 \\ y_2 \end{bmatrix} + \begin{bmatrix} 0.1 \\ 0 \\ 0.1 \\ 0 \end{bmatrix} u + \begin{bmatrix} 5.35 \\ 1.09 \\ 4.19 \\ 1.9 \end{bmatrix}. \tag{20}$$

Using the MATLAB to simulate [11], we can conclude the step response curve of the air pollution control system. We have

$$u(s) = \frac{570613.9602\,(s+7.702)\,(s+1.32)^2(s+1.2)^2}{(s+4012)\,(s+1.77)\,(s^2+2.5s+1.563)\,(s^2+2.4s+1.44)}, \tag{21}$$

$$K(s) = \begin{bmatrix} -0.67 & -1.77 & -2.32 & -1.52 & -0.4 & 0.1 \\ 0.1 & 0 & 0 & 0 & 0 & 0 \\ 0 & 0.1 & 0 & 0 & 0 & 0 \\ 0 & 0 & 0.1 & 0 & 0 & 0 \\ 0 & 0 & 0 & 0.1 & 0 & 0 \\ 8.63 & 4.36 & 8.24 & 6.92 & 2.18 & 0.14 \end{bmatrix} Q(s), \tag{22}$$

which is the transfer function and the state-space expression of robust H_∞ control strategy.

It could be seen from Figure 3, that the response time of the original system is 3.6 s, while the response time of closed

loop system is 0.026 s by using H_∞ control strategy. It means that H_∞ control strategy makes the step response of the atmosphere system with an improvement; the response time is greatly reduced. Therefore, H_∞ control strategy is a practical control strategy, which can ensure that air pollution control system is operating steadily within the desired target [12].

5. Conclusion

In this paper, the H_∞ control theory and methods have a great application value on air pollution control system. It can help the environmental protection departments at various levels to analyze the air pollution system, which can ensure the atmosphere quality steady work within the desired target value. Of course, the analysis and control of a large-scale air pollution system that introduced other influencing factors will be very complicated, which will be the focus of the study in this field.

Acknowledgments

This work was supported by National Natural Science Foundation of China (Grants nos. 61104062, 61374085, and 61174077), Jiangsu Qing Lan Project, and PAPD.

References

[1] H. Akashi and H. Kumamoto, "Optimal sulfur dioxide gas discharge control for Osaka City, Japan," *Automatica*, vol. 15, no. 3, pp. 331–337, 1979.

[2] G. R. Cass, "Sulfate air quality control strategy design," *Atmospheric Environment A*, vol. 15, no. 7, pp. 1227–1249, 1981.

[3] E. J. Croke and S. G. Booras, "The design of an air pollution incident control plan," in *Proceedings of the Air Pollution Control Assoc 62nd APCA Annual Meeting*, Paper No. 69-99, New York, NY, USA, 1969.

[4] P. J. Dejax and D. C. Gazis, "Optimal dispatch of electric power with ambient air quality constraints," *IEEE Transactions on Automatic Control*, vol. AC-21, no. 2, pp. 227–233, 1976.

[5] R. E. KaHN, "A mathematical programming model for air pollution control," *School Science and Mathematics*, pp. 487–494, 1969.

[6] R. E. Kohn, *A Linear Programming Model for Air Pollution Control*, MIT Press, Cambridge, Mass, USA, 1978.

[7] C. P. Kyan and J. H. Seinfeld, "Determination of optimal multiyear air pollution control policies," *Journal of Dynamic Systems, Measurement and Control, Transactions of the ASME*, vol. 94, no. 3, pp. 266–274, 1972.

[8] C. P. Kyan and J. H. Seinfeld, "Real-time control of air pollution," *AIChE Journal*, vol. 19, no. 3, pp. 579–589, 1973.

[9] M. Wu and W. Gui, *Modern Robust Control*, The Press of Central South University, 1998.

[10] W. Jiang, W. Cao, and R. Jiang, *The Meteorology of the Air Pollution*, The Meteorology Press, 1993.

[11] M. B. Beck, *The application of control and system theory to problems of river pollution control [Ph.D. thesis]*, Cambridge University, New York, NY, USA, 1974.

[12] Z. Lu and D. Xiao, "The most optimum means of controlling the vehicle exhaust pollution in municipal," *The Journal of Hubei University*, vol. 7, pp. 104–107, 2001.

Hindawi Publishing Corporation
Mathematical Problems in Engineering
Volume 2013, Article ID 202969, 8 pages
http://dx.doi.org/10.1155/2013/202969

Research Article

Dissipativity Analysis and Synthesis for a Class of Nonlinear Stochastic Impulsive Systems

Guici Chen,[1,2] Jianzhong Zhou,[1] and Yongchuan Zhang[1]

[1] *School of Hydropower & Information Engineering, Huazhong University of Science and Technology, Wuhan 430074, China*
[2] *Hubei Province Key Lab of Systems Science in Metallurgical Process, Wuhan University of Science and Technology, Wuhan 430081, China*

Correspondence should be addressed to Guici Chen; gcichen@aliyun.com

Received 1 August 2013; Accepted 6 September 2013

Academic Editor: Tao Li

The dissipativity analysis and control problems for a class of nonlinear stochastic impulsive systems (NSISs) are studied. The systems are subject to the nonlinear disturbance, stochastic disturbance, and impulsive effects, which often exist in a wide variety of industrial processes and the sources of instability. Our aim is to analyse the dissipativity and to design the state-feedback controller and impulsive controller based on the dissipativity such that the nonlinear stochastic impulsive systems are stochastic stable and strictly (Q, S, R)-dissipative. The sufficient conditions are obtained in terms of linear matrix inequality (LMI), and a numerical example with simulation is given to show the correctness of the derived results and the effectiveness of the proposed method.

1. Introduction

As we all know that many real-world systems may be disturbed by stochastic factors. Thus, stochastic differential systems appear as a natural description of many observed phenomena of real world. In the past few years, much research effort has paid to the stability analysis and robust control problems for stochastic systems which have been come to play an important role in many fields including population dynamics, macroeconomics, chemical reactor control, communication network, image processes, and mobile robot localization. So far, plenty of significant results also have been published; see, for example, [1–8] and the references therein.

Recent years, there are many real-world systems and natural processes which display some kind of dynamic behavior in a style of both continuous and discrete characteristics; we called "impulsive effects," which exist widely in many evolution process, particularly some biological system such as biological neural networks and bursting rhythm models in pathology as well as optimal control models in economics, frequency-modulated signal processing system, fly object motions, and so on [9, 10]. Impulsive dynamical systems are characterized by the occurrence of abrupt changes in the state of the system occurring at certain time instants. The stability and control problems of impulsive dynamical systems have attracted considerable interest in science and engineering during the past decades including stability analysis of stochastic impulsive systems or with time delay [11–14], robust control of impulsive systems with time delay [15, 16], and robust control and filtering of stochastic impulsive systems with time delay [17].

On the other hand, since the notation of dissipative dynamical system was introduced by Willems [18], dissipative systems have been of particular interest to researchers in areas of systems, circuits, networks, control, and so forth. Now, dissipative theory has wide-ranging implications and applications in control theory. For instance, dissipativeness was crucially used in the stability analysis of nonlinear system [19], and the theory of dissipative systems generalizes basic tools including the passivity theory, bounded real lemma, Kalman Yakubovich lemma, and the circle criterion [20]. Among the relevant topics are the passivity analysis and synthesis for time-delay systems [21, 22]. These results show that the passivity-based methods are highly effective in designing the robust controller.

The stability and stabilization [11–13, 19, 23], controllability [14], robust control [15, 16, 20, 22], robust filtering [17], and reliable dissipative control [24] problems have been extensively studied. However, the dissipative analysis and synthesis for nonlinear stochastic impulsive system have not been fully discussed and remains challenging. In this paper, we mainly study the dissipativity analysis and control problems for a class of nonlinear stochastic impulsive systems (NSISs). The systems are subject to the nonlinear disturbance, stochastic disturbance, and impulsive effects, which often exist in a wide variety of industrial processes and the sources of instability. Here, our aim is to analysis the dissipativity and to design the state-feedback controller and impulsive controller based on the dissipativity such that the nonlinear stochastic impulsive systems are stochastic stable and strictly (Q, S, R)-dissipative.

Notations. Throughout this paper, if not explicitly stated, matrices are assumed to have compatible dimensions. For symmetric matrices X and Y, the notation $X \geq Y$ (resp., $X > Y$) means that the matrix $X - Y$ is positive semidefinite (resp., positive definite). I is a identity matrix with appropriate dimensions; the subscript "T" represents the transposition. $E(\cdot)$ denotes the expectation operator with respect to some probability measure P. $L_2[0, \infty)$ is the space of square integrable vector functions over $[0, \infty)$; let (Ω, F, P) be a complete probability space which relates to an increasing family $(F_t)_{t>0}$ of σ algebras $(F_t)_{t>0} \subset F$, where Ω is the samples space, F is σ algebra of subsets of the sample space, and P is the probability measure on F. R^n and $R^{n\times m}$ denote the n dimensional Euclidean space and the set of all $n \times m$ real matrices, respectively. For any $0 < T < \infty$, we write $[0, T]$ for the closure of the open interval $(0, T)$ in R and denote by $L_2^n([0, T]; L^2(\Omega, K^k))$ the space of the nonanticipative stochastic processes $y(\cdot) = (y(\cdot))_{t\in[0,T]}$ with respect to $(F_t)_{t\in[0,T]}$ satisfying $\|y(\cdot)\|_{L_2^n}^2 = E(\int_0^T \|y(t)\|^2 \mathrm{d}t) = \int_0^T E(\|y(t)\|^2)\mathrm{d}t < \infty$. $\lambda_{\min}(\cdot)$ and $\lambda_{\max}(\cdot)$ describe the minimum and maximum eigenvalue, respectively.

2. A Class of Nonlinear Stochastic Impulsive Systems

In this paper, we mainly consider the following nonlinear stochastic impulsive systems (NSISs):

$$\begin{aligned} \mathrm{d}x(t) = {} & \left[Ax(t) + Bu(t) + f(t, x(t)) + Dv(t)\right]\mathrm{d}t \\ & + \sigma(t, x(t))\,\mathrm{d}w(t), \quad t \in (t_{k-1}, t_k], \\ \Delta x(t_k^+) = {} & \left(E_k + \overline{E}_k\right) x(t_k), \quad t = t_k, \\ z(t) = {} & Cx(t), \\ x(t_0^+) = {} & x_0, \end{aligned} \tag{1}$$

where $x(t) \in R^n$ is the system state, $u(t) \in R^l$ is the control input, $v(t) \in R^q$ is the exogenous disturbance input of the systems which belong to $L_2[0, \infty)$, $z(t) \in R^r$ is the system control output, and $w(t)$ is a zero mean real scalar Weiner processes on a probability space (Ω, F, P) relative to an increase family $(F_t)_{t>0}$ of σ algebras $(F_t)_{t>0} \subset F$. A, B, C, and D are the known real constant matrices with appropriate dimensions. Moreover, we assume that

$$E(\mathrm{d}w(t)) = 0, \qquad E\left((\mathrm{d}w(t))^2\right) = \mathrm{d}t. \tag{2}$$

The sequence, $\{t_k, E_k x(t_k)\}$ and $\{t_k, \overline{E}_k x(t_k)\}$ in the systems describe the impulsive effect and impulsive control, respectively, where E_k, $\overline{E}_k$ are known real-valued matrices with appropriate dimensions, which have the effect of suddenly changing the state of the system at the point t_k. $\Delta x(t_k) = x(t_k^+) - x(t_k^-)$, where $x(t_k^-) = \lim_{h\to 0^+} x(t_k - h)$, $x(t_k^+) = \lim_{h\to 0^+} x(t_k + h)$ with discontinuity instants $t_0 < t_1 < t_2 < \cdots < t_k < \cdots$, $\lim_{k\to\infty} t_k = \infty$; for convenience, let $t_0 = 0$ and $h > 0$ be sufficiently small. Without loss of generality, it is assumed that $x(t_k) = x(t_k^-) = \lim_{h\to 0^+} x(t_k - h)$.

$f(\cdot, \cdot) : R_+ \times R^n \to R^n$ is an unknown nonlinear function which describes the system nonlinearity satisfying the following condition:

$$f(0, 0) = 0, \qquad \|f(t, x(t))\| \leq \beta \|x(t)\|, \tag{3}$$

for a positive constant β. Equivalently stated, condition (3) implies that there exists a scalar $\kappa > 0$ such that

$$\kappa\left(\beta^2 x^T(t) x(t) - f^T(t, x(t)) f(t, x(t))\right) \geq 0. \tag{4}$$

$\sigma(\cdot, \cdot) : R_+ \times R^n \to R^n$ also is an unknown nonlinear function which describes the stochastic nonlinearity satisfying

$$\sigma^T(t, x(t))\,\sigma(t, x(t)) \leq x^T(t) G^T G x(t), \tag{5}$$

where G is a known real constant matrices with approximate dimension.

3. Preliminaries

In this section, some definitions and lemmas are given.

Definition 1. For systems in (1) with $v(t) = 0$, if there exists a constant $c > 0$ satisfying $E\int_0^\infty \|x(t)\|^2 \mathrm{d}t \leq c\|x_0\|^2$, $x_0 \in R^n$, systems in (1) are said to be stochastically stable.

Before giving the following definition, we firstly give the definition of quadratic energy supply function associated with systems in (1) as follows:

$$\begin{aligned} & \Psi(v, z, T) \\ & = E\int_0^T \left(z^T(t) Q z(t) + 2v^T(t) S z(t) + v^T(t) R v(t)\right)\mathrm{d}t, \end{aligned} \tag{6}$$

where Q, S, and R are real matrices with appropriate dimensions and Q and R are symmetrical.

Definition 2. Systems in (1) are called (Q, S, R)-dissipative if for any $T > 0$, under zero initial state, the following condition is satisfied:

$$\Psi(v, z, T) \geq 0, \quad \forall T \geq 0. \tag{7}$$

Furthermore, if for a scalar $\alpha > 0$, such that

$$\Psi(v, z, T) \geq \alpha E \int_0^T v^T(t)\, v(t)\, \mathrm{d}t, \quad \forall T \geq 0, \tag{8}$$

systems in (1) are called strictly (Q, S, R)-dissipative.

Lemma 3 (Schur complement lemma (see [25])). *For a given matrix* $S = \begin{pmatrix} S_1 & S_3 \\ * & S_2 \end{pmatrix}$ *with* $S_1^T = S_1$, $S_2^T = S_2$, *then the following conditions are equivalent:*

(1) $S < 0$,

(2) $S_2 < 0$, $S_1 - S_3 S_2^{-1} S_3^T < 0$,

(3) $S_1 < 0$, $S_2 - S_3 S_1^{-1} S_3^T < 0$.

Lemma 4 (see [26]). *For any* $x \in R^n$, *if* $P \in R^{n\times n}$ *is a positive definite matrix,* $Q \in R^{n\times n}$ *is a symmetric matrix, then*

$$\lambda_{\min}\left(P^{-1}Q\right) x^T P x \leq x^T Q x \leq \lambda_{\max}\left(P^{-1}Q\right) x^T P x. \tag{9}$$

In this paper, our aim is to develop dissipativity criteria for systems in (1) based on Definition 2 and subsequently design the feedback dissipative controller $u(t) = Kx(t)$.

4. Main Results and Proofs

4.1. Dissipativity Analysis of NSISs. For dissipativity analysis for NSISs, we treat the free systems as follows:

$$\begin{aligned} \mathrm{d}x(t) = {} & \left[Ax(t) + f(t, x(t)) + Dv(t)\right] \mathrm{d}t \\ & + \sigma(t, x(t))\, \mathrm{d}\omega(t), \quad t \in \left(t_{k-1}, t_k\right], \\ \Delta x\left(t_k^+\right) = {} & \left(E_k + \overline{E}_k\right) x\left(t_k\right), \quad t = t_k, \\ z(t) = {} & Cx(t), \\ x\left(t_0^+\right) = {} & x_0. \end{aligned} \tag{10}$$

Theorem 5. *Given a real matrix* S, *the positive matrices* $R, Z > 0$ *and a negative semidefinite matrix* $Q \leq 0$, *if there exist a scalar* $\delta > 0$ *and a positive definite matrix* $P > 0$, *such that the following inequalities hold:*

$$\Xi = \begin{pmatrix} \Delta & PD - C^T S & P \\ * & -R & 0 \\ * & * & -\kappa I \end{pmatrix} < 0, \tag{11}$$

$$\beta_k = \lambda_{\max}\left(P^{-1}\left(I + E_k + \overline{E}_k\right)^T P \left(I + E_k + \overline{E}_k\right)\right) < 1, \tag{12}$$

where $\Delta = A^T P + PA + G^T P G + \kappa\beta^2 I - C^T Q C + \delta Z$. *Then the NSISs in* (10) *are stochastic stable and strictly* (Q, S, R)*-dissipative.*

Proof. Construct a simple Lyapunov function $V(\cdot, \cdot) : R^n \times R_+ \to R_+$ as follows:

$$V(x(t), t) = x^T(t) P x(t). \tag{13}$$

For $t \in (t_{k-1}, t_k]$, $k = 1, 2, \ldots$, according to the Itô formula, along with the solution of systems in (10), we have

$$\begin{aligned} LV(x(t), t) = {} & 2x^T(t) P \left[Ax(t) + f(t, x(t)) + Dv(t)\right] \\ & + \sigma^T(t, x(t)) P \sigma(t, x(t)). \end{aligned} \tag{14}$$

Applying (3)–(5), we get that

$$\begin{aligned} LV(x(t), t) &= x^T(t)\left(A^T P + PA\right) x(t) + 2x^T(t) P f(t, x(t)) \\ &\quad + 2x^T(t) PDv(t) + \sigma^T(t, x(t)) P \sigma(t, x(t)) \\ &\leq x^T(t)\left(A^T P + PA + G^T P G + \kappa\beta^2 I\right) x(t) \\ &\quad + 2x^T(t) P f(t, x(t)) + 2x^T(t) PDv(t) \\ &\quad - k f^T(t, x(t)) f(t, x(t)) \\ &= \chi^T(t)\, \Theta\, \chi(t), \end{aligned} \tag{15}$$

where

$$\begin{aligned} \chi(t) &= \left(x^T(t) \quad v^T(t) \quad f^T\right)^T, \\ \Theta &= \begin{pmatrix} A^T P + PA + G^T P G + \kappa\beta^2 I & PD & P \\ * & 0 & 0 \\ * & * & -\kappa I \end{pmatrix}. \end{aligned} \tag{16}$$

So

$$LV(x(t), t) - z^T Q z - 2z^T S v - v^T R v \leq \chi^T(t)\, \Theta' \chi(t), \tag{17}$$

where

$$\begin{aligned} \Theta' &= \begin{pmatrix} \Sigma' & PD - C^T S & P \\ * & -R & 0 \\ * & * & -\kappa I \end{pmatrix}, \\ \Sigma' &= A^T P + PA + G^T P G + \kappa\beta^2 I - C^T Q C. \end{aligned} \tag{18}$$

By Lemma 3, if (17) holds, then (11) holds. Since $R > 0$, there exists a sufficient small $\alpha > 0$ such that $R - \alpha I > 0$. Together with (11), we have

$$\Xi + \mathrm{diag}(0, \alpha I, 0) < 0. \tag{19}$$

In the following section, we firstly consider the stability of NSISs in (10). Setting $v(t) = 0$, by (11) and Lemma 4, we have

$$LV(x(t), t) - z^T Q z - 2z^T S v - v^T R v \leq \alpha v^T v, \tag{20}$$

which leads to

$$\begin{aligned} LV(x(t), t) &\leq x^T\left(C^T Q C - \delta Z\right) x \\ &\leq -\mu x^T P x = -\mu V(x(t), t), \end{aligned} \tag{21}$$

where $\mu = \lambda_{\min} P^{-1}(\delta Z - C^T Q C) > 0$.

Applying Dynkin formula and Grownwall-Bellman inequality, together with (21), for $t \in (t_{k-1}, t_k]$, $k = 1, 2, \ldots$, we have

$$E\{V(x(t), t)\} \le V\left(x\left(t_{k-1}^{+}\right), t_{k-1}^{+}\right) e^{-\mu(t-t_{k-1})}. \tag{22}$$

By Lemma 4 and (10), it follows that

$$\begin{aligned} V\left(x\left(t_{k-1}^{+}\right), t_{k-1}^{+}\right) &= x^T\left(t_{k-1}^{+}\right) P x\left(t_{k-1}^{+}\right) \\ &= x^T\left(t_{k-1}\right)\left[I + E_{k-1} + \overline{E}_{k-1}\right]^T \\ &\quad \times P\left[I + E_{k-1} + \overline{E}_{k-1}\right] x\left(t_{k-1}\right) \\ &\le \beta_{k-1} x^T\left(t_{k-1}\right) P x\left(t_{k-1}\right) \\ &= \beta_{k-1} V\left(x\left(t_{k-1}\right), t_{k-1}\right). \end{aligned} \tag{23}$$

For $t \in (t_0, t_1]$, it follows from (22) and (23) that

$$E\{V(x(t), t)\} \le V\left(x\left(t_0\right), t_0^{+}\right) e^{-\mu(t-t_0)}, \tag{24}$$

which leads to

$$\begin{aligned} E\{V\left(x\left(t_1\right), t_1\right)\} &\le V\left(x\left(t_0\right), t_0^{+}\right) e^{-\mu(t_1-t_0)}, \\ E\{V\left(x\left(t_1\right), t_1^{+}\right)\} &\le \beta_1 V\left(x\left(t_0\right), t_0^{+}\right) e^{-\mu(t_1-t_0)}. \end{aligned} \tag{25}$$

Hence, for $t \in (t_{k-1}, t_k]$, it follows from (22)–(25) that

$$\begin{aligned} E\{V(x(t), t)\} &\le V\left(x\left(t_{k-1}^{+}\right), t_{k-1}^{+}\right) e^{-\mu(t-t_{k-1})} \\ &\le \beta_{k-1} V\left(x\left(t_{k-1}\right), t_{k-1}\right) e^{-\mu(t-t_{k-1})} \\ &\le \beta_{k-1} V\left(x\left(t_{k-2}\right), t_{k-2}^{+}\right) e^{-\mu(-t_{k-1}-t_{k-2})} \\ &\quad \times e^{-\mu(t-t_{k-1})} \le \cdots \\ &\le \beta_{k-1}\beta_{k-2}\cdots\beta_1 V\left(x\left(t_0\right), t_0^{+}\right) e^{-\mu(t-t_0)}. \end{aligned} \tag{26}$$

We know that

$$\begin{aligned} &E\int_{t_0^{+}}^{t_1} V(x(t), t)\, dt \\ &\quad \le E\int_{t_0^{+}}^{t_1} V\left(x\left(t_0\right), t_0^{+}\right) e^{-\mu(t-t_0)} dt \\ &\quad = -\frac{1}{\mu} E\{V\left(x\left(t_0\right), t_0^{+}\right)\}\left[e^{-\mu(t_1-t_0)} - 1\right], \\ &E\int_{t_{k-1}^{+}}^{t_k} V(x(t), t)\, dt \\ &\quad \le E\int_{t_{k-1}^{+}}^{t_k} V\left(x\left(t_{k-1}\right), t_{k-1}^{+}\right) \\ &\qquad \times e^{-\mu(t-t_{k-1})} dt \\ &\quad = -\frac{1}{\mu} E\{V(x(t_{k-1}), t_{k-1}^{+})\} \\ &\qquad \times \left[e^{-\mu(t_k-t_{k-1})} - 1\right] \\ &\quad \le -\frac{1}{\mu} E\{V\left(x\left(t_{k-1}\right), t_{k-1}^{+}\right)\} \\ &\qquad \times \left[e^{-\mu(t_k-t_{k-1})} - 1\right] \\ &\quad \le -\frac{1}{\mu}\beta_{k-1} E\{V\left(x\left(t_{k-2}\right), t_{k-2}^{+}\right)\} \\ &\qquad \times \left[e^{-\mu(t_{k-1}-t_{k-2})}\right]\left[e^{-\mu(t_k-t_{k-1})} - 1\right] \\ &\quad \le \cdots \le -\frac{1}{\mu}\beta_{k-1}\beta_{k-2}\cdots\beta_1 \\ &\qquad \times E\{V\left(x\left(t_0\right), t_0^{+}\right)\} \\ &\qquad \times \left[e^{-\mu(t_k-t_0)} - e^{-\mu(t_{k-1}-t_0)}\right]. \end{aligned} \tag{27}$$

In summary, we obtain that

$$E\int_{t_0^{+}}^{T} V(x(t), t)\, dt \le -\frac{1}{\mu} E\{V\left(x\left(t_0\right), t_0^{+}\right)\}\theta, \tag{28}$$

where $\theta = [e^{-\mu(t_1-t_0)} - 1] + \beta_1[e^{-\mu(t_2-t_0)} - e^{-\mu(t_1-t_0)}] + \cdots + \beta_k\beta_{k-1}\cdots\beta_1[e^{-\mu(T-t_0)} - e^{-\mu(t_k-t_0)}]$; let $\overline{\beta} = \max\{\beta_1, \beta_2, \ldots, \beta_k\}$, and we have

$$e^{-\mu(t_1-t_0)} - 1 - e^{-\mu(t_1-t_0)}\frac{\overline{\beta}}{1-\overline{\beta}} < \theta < e^{-\mu(t_1-t_0)} - 1 < 0. \tag{29}$$

Therefore, we get

$$E\int_{t_0^{+}}^{T} V(x(t), t)\, dt \le -\frac{1}{\mu} E\{V\left(x\left(t_0\right), t_0^{+}\right)\}\theta = -\frac{\theta}{\mu} x_0^T P x_0. \tag{30}$$

Then, there exists a constant $c = -\theta\lambda_{\max}(P)/\mu\lambda_{\min}(P) > 0$, such that

$$\lim_{T\to\infty}\left\{E\int_{t_0}^{T} V(x(t), t)\, dt\right\} \le c x_0^T x_0, \quad x_0 \in R^n, \ t \ge t_0. \tag{31}$$

Hence, the NSISs in (10) are stochastic stable.

Secondly, we consider the (Q,S,R)-dissipativity of NSISs in (10). When $x(t_0)=0$, setting $v(t)\neq 0$, from (11) and (12), we have

$$\begin{aligned}
&E\int_{t_0}^{T}\left[z^T(s)Qz(s)+2z^T(s)Sv(s)+v^T(s)(R-\alpha I)v(s)\right]\mathrm{d}s\\
&\quad>E\int_{t_0}^{T}LV(x(s),s)\,\mathrm{d}s=E\int_{t_0}^{t_1}LV(x(s),s)\,\mathrm{d}s\\
&\qquad+E\int_{t_1^+}^{t_2}LV(x(s),s)\,\mathrm{d}s\\
&\qquad+\cdots+E\int_{t_k^+}^{T}LV(x(s),s)\,\mathrm{d}s\\
&\quad=EV(x(t_1),t_1)-EV(x(t_0),t_0)+EV(x(t_2),t_2)\\
&\qquad-EV(x(t_1^+),t_1^+)+\cdots+EV(x(T),T)\\
&\qquad-EV(x(t_k^+),t_k^+)\\
&\quad\geq\sum_{i=1}^{k}(1-\beta_i)EV(x(t_i),t_i)+EV(x(T),T)\\
&\qquad-EV(x(t_0),t_0)\geq EV(x(T),T)>0.
\end{aligned}\tag{32}$$

So it follows that (8) holds; thus the NSISs in (10) are strictly (Q,S,R)-dissipative according to Definition 2. The proof is complete. □

Remark 6. From (12), we see that $\beta_k=\lambda_{\max}(P^{-1}(I+E_k+\overline{E}_k)^TP(I+E_k+\overline{E}_k))<1$ is not a LMI; it is difficult to obtain the feasible solution, so by schur complement lemma, which is implied by a matrix inequality,

$$\begin{pmatrix}P & \left(I+E_k+\overline{E}_k\right)^T\\ * & P^{-1}\end{pmatrix}>0.\tag{33}$$

4.2. State-Feedback Dissipative Control of NSISs. We are now ready to design the state-feedback controller $u(t)=Kx(t)$ for the closed-loop NSISs in (1), and the NSISs in (1) can be rewritten as

$$\begin{aligned}
\mathrm{d}x(t)=&\left[(A+BK)x(t)+f(t,x(t))+Dv(t)\right]\mathrm{d}t\\
&+\sigma(t,x(t))\,\mathrm{d}w(t),\quad t\in(t_{k-1},t_k],\\
\Delta x(t_k^+)=&\left(E_k+\overline{E}_k\right)x(t_k),\quad t=t_k,\\
z(t)=&Cx(t),\\
x(t_0^+)=&x_0.
\end{aligned}\tag{34}$$

Then, we have the following results.

Theorem 7. *Given a real matrix S, a positive definite matrices $R>0$ and a negative semidefinite matrix $Q\leq 0$, if there exist a scalar $\delta>0$, and three matrices $X>0$, Y, and $\widetilde{Z}$, such that the following linear matrices inequalities (LMIs)*

$$\Sigma=\begin{pmatrix}\Sigma_1 & D-XC^TS & \Sigma_2\\ * & -R & 0\\ * & * & \Sigma_3\end{pmatrix}<0,\tag{35}$$

$$\begin{pmatrix}X & X\left(I+E_k\right)^T+Y_k^T\\ * & X\end{pmatrix}>0\tag{36}$$

have a feasible solution, then the NSISs in (34) *are stochastic stable and strictly (Q,S,R)-dissipative, the feedback gain is $K=YX^{-1}$, and the impulsive controller gain is $\overline{E}_k=Y_kX^{-1}$, where $\Sigma_1=XA^T+AX+\delta\widetilde{Z}+Y^TB^T+BY$, $\Sigma_2=\begin{pmatrix}I & XG^T & XC^T & \kappa\beta X\end{pmatrix}$, $\Sigma_3=\mathrm{diag}(-\kappa I,-X,Q^{-1},-\kappa I)$.*

Proof. For NSISs in (34), applying Theorem 5 and Lemma 3, we have

$$\begin{pmatrix}\Sigma_1' & PD-C^TS & P & G^T & C^T & \kappa\beta I\\ * & -R & 0 & 0 & 0 & 0\\ * & * & -\kappa I & 0 & 0 & 0\\ * & * & * & -P^{-1} & 0 & 0\\ * & * & * & * & Q^{-1} & 0\\ * & * & * & * & * & -\kappa I\end{pmatrix}<0,\tag{37}$$

where $\Sigma_1'=(A+BK)^TP+P(A+BK)+\delta Z$.

Applying the congruent transformation $T_1=\mathrm{diag}(X,I,I,I,I,I)$ and $T_2=\mathrm{diag}(X,I)$, $X=P^{-1}$ to (37) and (33), respectively, introducing the linearization $\widetilde{Z}=XZX$, and using $KX=Y$, $\overline{E}_kX=Y_k$, LMIs (35) and (36) hold. The proof is complete. □

Remark 8. When $Q=-I$, $S=0$, and $R=\gamma^2I$, strictly (Q,S,R)-dissipative reduces to the H_∞ performance level. When $Q=0$, $S=I$, and $R=\gamma I$, strictly (Q,S,R)-dissipative reduces to the strictly passivity.

Remark 9. If $\beta_k=\lambda_{\max}(P^{-1}(I+E_k)^TP(I+E_k))<1$, then let $\overline{E}_k=0$, which means that there is no need for any impulsive controller for NSIS (1). If $\beta_k=\lambda_{\max}(P^{-1}(I+E_k)^TP(I+E_k))>1$, then choose appropriate $\overline{E}_k$ such that $\beta_k=\lambda_{\max}(P^{-1}(I+E_k+\overline{E}_k)^TP(I+E_k+\overline{E}_k))<1$, which means that there is need of impulsive controller with gain $\overline{E}_k$ for NSISs in (1).

Corollary 10. *If there exist a scalar $\delta>0$ and three matrices $X>0$, Y, and $\widetilde{Z}$, such that the inequalities*

$$\begin{pmatrix}\Sigma_1 & D & I & XG^T & XC^T & \kappa\beta X\\ * & -\gamma^2I & 0 & 0 & 0 & 0\\ * & * & -\kappa I & 0 & 0 & 0\\ * & * & * & -X & 0 & 0\\ * & * & * & * & -I & 0\\ * & * & * & * & * & -\kappa I\end{pmatrix}<0\tag{38}$$

and (36) *have a feasible solution, then the NSISs in* (34) *are stochastic stable with H_∞ performance level, and the feedback gain is $K=YX^{-1}$.*

Corollary 11. *If there exist a scalar $\delta > 0$ and three matrices $X > 0$, Y, and $\widetilde{Z}$, such that the inequalities*

$$\begin{pmatrix} \Sigma_1 & D - XC^T & I & XG^T & \kappa\beta X \\ * & -\gamma I & 0 & 0 & 0 \\ * & * & -\kappa I & 0 & 0 \\ * & * & * & -X & 0 \\ * & * & * & * & -\kappa I \end{pmatrix} < 0 \tag{39}$$

and (36) *have a feasible solution, then the NSISs* (34) *are stochastic strictly passive, and the feedback gain is $K = YX^{-1}$.*

5. Numerical Example with Simulation

In this section, we will give an example to show the correctness of the derived results and the effectiveness of the proposed methods. Considering NSISs in (1), the system parameters are given as follows:

$$A = \begin{pmatrix} -1.5 & 1 & 0 & 1 \\ 2 & 4 & 2.5 & 0 \\ -1 & -1.5 & 5 & 0 \\ 0 & 0 & 2 & -5 \end{pmatrix}, \quad B = \begin{pmatrix} 0 & 1 \\ -0.5 & 0 \\ -0.2 & 0 \\ 0 & 0.2 \end{pmatrix},$$

$$C = \begin{pmatrix} 1 & 2 & 0 & 0 \\ 0 & 0.5 & 0 & 0 \\ 0 & 0 & 1 & 0 \\ 0 & 0 & 0.2 & 1 \end{pmatrix}, \quad D = \begin{pmatrix} 0.4 & 0.2 & 0.1 & 0 \\ 0.5 & 0.1 & 0.5 & 0.2 \\ 0 & 0.1 & 0 & 1 \\ 0.1 & 0 & 1 & 0.1 \end{pmatrix},$$

$$E = \begin{pmatrix} -0.2 & 0 & 0 & 0 \\ 0 & -0.1 & 0 & 0 \\ 0 & 0 & -0.3 & 0 \\ 0 & 0 & 0 & -0.2 \end{pmatrix},$$

$$f(x) = \begin{pmatrix} 0.1x_1 \sin x_3 \\ 0.2x_2 \cos x_2 \\ 0.1x_3 \sin x_3 \\ 0.3x_4 \cos x_1 \end{pmatrix},$$

$$\sigma(t, x(t)) = \begin{pmatrix} 0.5x_1 \sin x_1 \\ \dfrac{t}{1+t} x_2 \\ 0.5x_3 \cos x_3 \\ \dfrac{0.2t}{t+2} x_4 \end{pmatrix},$$

$$v(t) = \begin{pmatrix} 0.5 \sin 0.8t \\ e^{-0.2t} \cos t \\ 0.3 \cos 0.5t \\ e^{-t} \sin t \end{pmatrix}, \quad -Q = R = S = I. \tag{40}$$

From Figure 1, we can see that the uncontrolled NSISs in (1) are not stable; from (3)–(5), we can easily calculate that $\beta = 0.3$, $G = \mathrm{diag}(0.5, 1, 0.5, 0.2)$, and we choose $\kappa = 1$. Applying Theorem 7 to this example with $\widetilde{Z} = 0.2I$, then we have

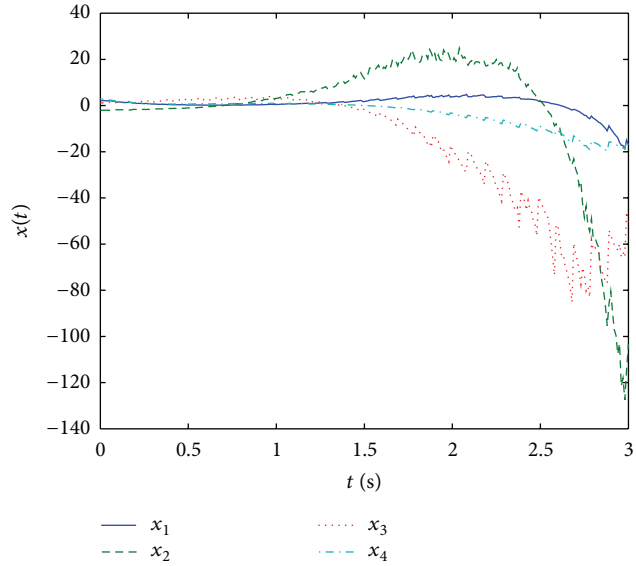

Figure 1: The state curves of the uncontrolled NSISs in (1) with $x(0) = (2 \ -2 \ 1 \ 3)^T$.

$$X = \begin{pmatrix} 218.4915 & -78.3446 & -28.6536 & 41.2314 \\ -78.3446 & 61.9663 & 23.7252 & -14.7112 \\ -28.6536 & 23.7252 & 9.2450 & -5.2351 \\ 41.2314 & -14.7112 & -5.2351 & 11.9250 \end{pmatrix},$$

$$Y = 1.0e+004 * \begin{pmatrix} -0.0840 & 1.4332 & 0.5742 & -0.0115 \\ -1.0921 & 0.1494 & 0.0621 & -0.2110 \end{pmatrix}. \tag{41}$$

So the controller parameters can be calculated as follows:

$$K = 1.0e+003 * \begin{pmatrix} 0.1421 & 0.2444 & 0.4278 & -0.0116 \\ -0.0786 & -0.4984 & 1.0753 & -0.0478 \end{pmatrix},$$

$$E_k = \begin{pmatrix} -0.8 & 0 & 0 & 0 \\ 0 & -0.9 & 0 & 0 \\ 0 & 0 & -0.7 & 0 \\ 0 & 0 & 0 & -0.8 \end{pmatrix}. \tag{42}$$

The state curves and the output curves of closed-loop NSISs in (1) can be seen in Figures 2 and 3.

From Figure 4, we can see that the closed-loop NSISs in (1) are strictly (Q, S, R)-dissipative, and Figure 5 shows the variation of α in $\Psi(v, z, T) \geq \alpha E \int_0^T v^T(t)v(t)\mathrm{d}t$, for all $T \geq 0$.

6. Conclusions

In this paper, the dissipativity analysis and control problems for a class of nonlinear stochastic impulsive systems (NSISs) have been investigated. The systems are subject to the nonlinear disturbance, stochastic disturbance, and impulsive effects,

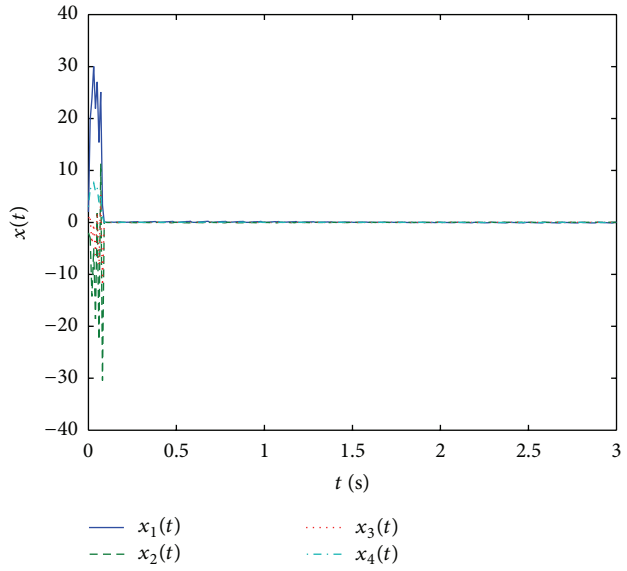

Figure 2: The state curves of the NSISs in (1) under state-feedback control and impulsive control with $x(0) = \begin{pmatrix} 2 & -2 & 1 & 3 \end{pmatrix}^T$.

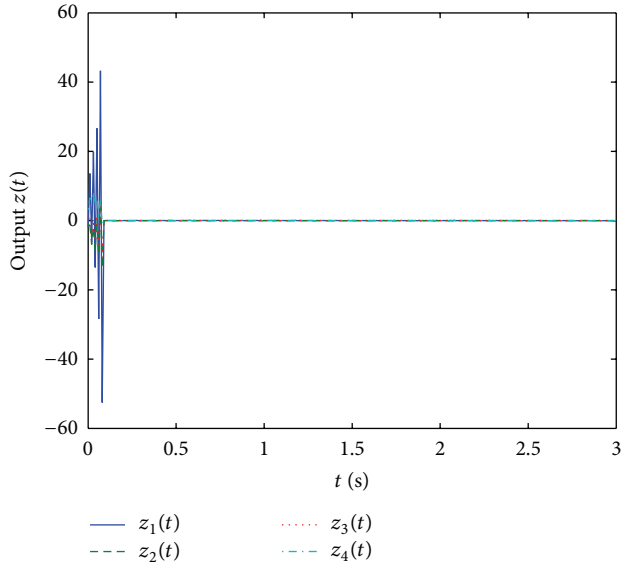

Figure 3: The output curves of the NSISs in (1) under state-feedback control and impulsive control with $x(0) = \begin{pmatrix} 2 & -2 & 1 & 3 \end{pmatrix}^T$.

which often exist in a wide variety of industrial processes and the sources of instability. Based on the dissipativity, the state-feedback controller and impulsive controller, such that the nonlinear stochastic impulsive systems are stochastic stable and strictly (Q, S, R)-dissipative, have been designed. The sufficient conditions have been obtained in terms of linear matrix inequalities (LMIs), and the given numerical example with simulation shows the correctness of the derived results and the effectiveness of the proposed method.

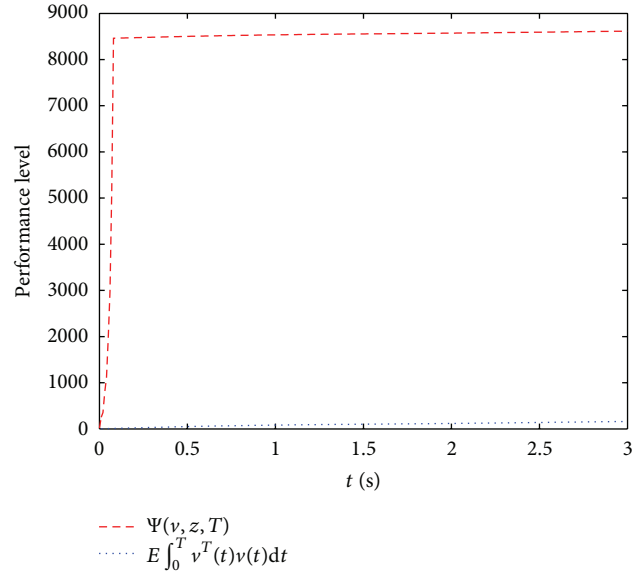

Figure 4: The curves of performance level $\Psi(v, z, T)$ and $E\int_0^T v^T(t)v(t)\mathrm{d}t$ of the NSISs in (1).

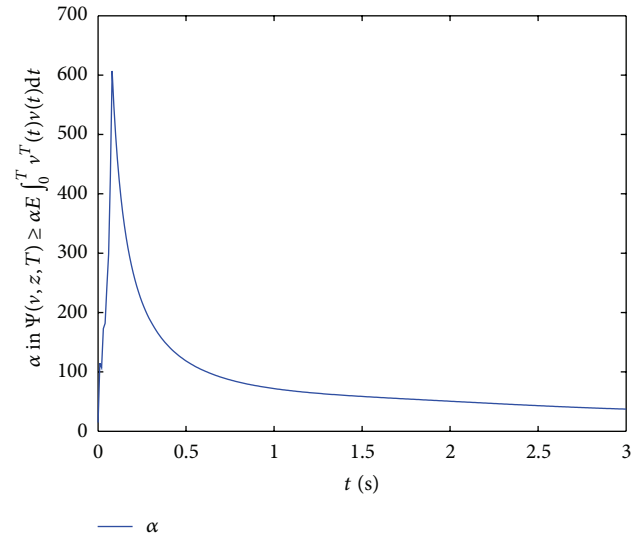

Figure 5: The variation curve of α in $\Psi(v, z, T) \geq \alpha E\int_0^T v^T(t)v(t)\mathrm{d}t$ in the NSISs in (1).

Conflict of Interests

The authors declare that there is no conflict of interests regarding the publication of this paper.

Acknowledgments

This work is supported by National Science Foundation of China (NSFC) under Grant nos. 61104127, 51079057, and 61134012, China Postdoctoral Science Foundation with Grant no. 2012M521428, and Hubei Province Key Laboratory of

Systems Science in Metallurgical Process (Wuhan University of Science and Technology) under Grant no. Y201101.

References

[1] Y. Shen and J. Wang, "An improved algebraic criterion for global exponential stability of recurrent neural networks with time-varying delays," *IEEE Transactions on Neural Networks*, vol. 19, no. 3, pp. 528–531, 2008.

[2] V. Kolmanovskii and A. Myshkis, *Introduction to the Theory and Applications of Functional-Differential Equations*, vol. 463 of *Mathematics and Its Applications*, Kluwer Academic Publishers, Dordrecht, The Netherlands, 1999.

[3] Y. Shen and J. Wang, "Robustness analysis of global exponential stability of recurrent neural networks in the presence of time delays and random disturbances," *IEEE Transactions on Neural Networks and Learning Systems*, vol. 23, no. 1, pp. 87–96, 2012.

[4] G. Chen and Y. Shen, "Robust reliable H_∞ control for nonlinear stochastic Markovian jump systems," *Mathematical Problems in Engineering*, vol. 2012, Article ID 431576, 16 pages, 2012.

[5] T. Li, W. X. Zheng, and C. Lin, "Delay-slope-dependent stability results of recurrent neural networks," *IEEE Transactions on Neural Networks*, vol. 22, no. 12, pp. 2138–2143, 2011.

[6] T. Li and Y. Zhang, "Fault detection and diagnosis for stochastic systems via output PDFs," *Journal of the Franklin Institute*, vol. 348, no. 6, pp. 1140–1152, 2011.

[7] B. Zhang, S. Xu, G. Zong, and Y. Zou, "Delay-dependent stabilization for stochastic fuzzy systems with time delays," *Fuzzy Sets and Systems*, vol. 158, no. 20, pp. 2238–2250, 2007.

[8] B. Zhang, S. Xu, and Y. Zou, "Output feedback stabilization for delayed large-scale stochastic systems with Markovian jumping parameters," *Asian Journal of Control*, vol. 11, no. 4, pp. 457–460, 2009.

[9] V. Lakshmikantham, D. D. Baĭnov, and P. S. Simeonov, *Theory of Impulsive Differential Equations*, vol. 6 of *Series in Modern Applied Mathematics*, World Scientific Publishing, Teaneck, NJ, USA, 1989.

[10] D. D. Baĭnov and P. S. Simeonov, *Systems with Impulse Effect: Stability, Theory and Applications*, Ellis Horwood Series: Mathematics and Its Applications, Ellis Horwood, New York, NY, USA, 1989.

[11] C. Li, J. Sun, and R. Sun, "Stability analysis of a class of stochastic differential delay equations with nonlinear impulsive effects," *Journal of the Franklin Institute*, vol. 347, no. 7, pp. 1186–1198, 2010.

[12] B. Li, D. S. Li, and D. Y. Xu, "Stability analysis of impulsive stochastic delay differential equations with markovian switching," *Journal of the Franklin Institute*, vol. 350, no. 7, pp. 1848–1864, 2013.

[13] L. Pan and J. Cao, "Exponential stability of impulsive stochastic functional differential equations," *Journal of Mathematical Analysis and Applications*, vol. 382, no. 2, pp. 672–685, 2011.

[14] L. Shen, J. Sun, and Q. Wu, "Controllability of linear impulsive stochastic systems in Hilbert spaces," *Automatica A*, vol. 49, no. 4, pp. 1026–1030, 2013.

[15] W.-H. Chen and W. X. Zheng, "Robust stability and H_∞-control of uncertain impulsive systems with time-delay," *Automatica A*, vol. 45, no. 1, pp. 109–117, 2009.

[16] X. Li and R. Rakkiyappan, "Impulse controller design for exponential synchronization of chaotic neural networks with mixed delays," *Communications in Nonlinear Science and Numerical Simulation*, vol. 18, no. 6, pp. 1515–1523, 2013.

[17] S. Xu and T. Chen, "Robust H_∞ filtering for uncertain impulsive stochastic systems under sampled measurements," *Automatica A*, vol. 39, no. 3, pp. 509–516, 2003.

[18] J. C. Willems, "Dissipative dynamical systems. I. General theory," *Archive for Rational Mechanics and Analysis*, vol. 45, no. 5, pp. 321–351, 1972.

[19] D. Hill and P. Moylan, "The stability of nonlinear dissipative systems," *IEEE Transactions on Automatic Control*, vol. 21, no. 5, pp. 708–711, 1976.

[20] Z. Tan, Y. C. Soh, and L. Xie, "Dissipative control for linear discrete-time systems," *Automatica A*, vol. 35, no. 9, pp. 1557–1564, 1999.

[21] M. S. Mahmoud and A. Ismail, "Passivity and passification of time-delay systems," *Journal of Mathematical Analysis and Applications*, vol. 292, no. 1, pp. 247–258, 2004.

[22] M. S. Mahmoud, Y. Shi, and F. M. AL-Sunni, "Dissipativity analysis and synthesis of a class of nonlinear systems with time-varying delays," *Journal of the Franklin Institute*, vol. 346, no. 6, pp. 570–592, 2009.

[23] H. Zhang, H. Yan, and Q. Chen, "Stability and dissipative analysis for a class of stochastic system with time-delay," *Journal of the Franklin Institute*, vol. 347, no. 5, pp. 882–893, 2010.

[24] H. Zhang, Z.-H. Guan, and G. Feng, "Reliable dissipative control for stochastic impulsive systems," *Automatica A*, vol. 44, no. 4, pp. 1004–1010, 2008.

[25] S. Boyd, L. El Ghaoui, E. Feron, and V. Balakrishnan, *Linear Matrix Inequalities in System and Control Theory*, vol. 15 of *SIAM Studies in Applied Mathematics*, SIAM, Philadelphia, Pa, USA, 1994.

[26] L. Huang, *Linear Algebra in Systems and Control Theory*, Science Press, Beijing, China, 1984.

Hindawi Publishing Corporation
Mathematical Problems in Engineering
Volume 2013, Article ID 741216, 9 pages
http://dx.doi.org/10.1155/2013/741216

Research Article

State Tracking of MRAC Systems in the Presence of Controller Temporary Failure Based on a Switching Method

Caiyun Wu[1,2] and Jun Zhao[1]

[1] *State Key Laboratory of Synthetical Automation for Process Industries, Northeastern University, Shenyang 110819, China*
[2] *School of Equipment Engineering, Shenyang Ligong University, Shenyang 110159, China*

Correspondence should be addressed to Jun Zhao; zhaojun@mail.neu.edu.cn

Received 19 July 2013; Accepted 5 September 2013

Academic Editor: Bochao Zheng

The state tracking problem for a class of model reference adaptive control (MRAC) systems in the presence of controller temporary failures is studied. Due to the controller temporary failure, the considered system is viewed as an error switched system. The properties of Lyapunov function candidates without switching are described. Then the notion of global practical stability of switched systems is presented, and sufficient conditions for global practical stability of the error system under the restrictions of controller failure frequency and unavailability rate are provided. An example is presented to demonstrate the feasibility and effectiveness of the proposed method.

1. Introduction

There are often parameter, structural, and environment uncertainties in practical systems [1–4]. Model reference adaptive control (MRAC) has been used as an important control approach for such uncertain systems [5, 6]. Closed-loop signal boundedness and asymptotic tracking can be ensured by a state feedback controller and adaptive laws in MRAC systems [7].

On the other hand, controller temporary failures are often encountered in real control systems due to various environment factors during operation. Some motivations of studying controller failures are summarized in [8]. The reasons can be roughly classified into two categories: passive and positive ones. A typical passive reason is that the signals are not transmitted perfectly or the controller itself is not available for some reasons. For instance, the packet dropout phenomenon in networked control systems leads to controller failure, which is inevitable because of unreliable transmission paths. In contrast to passive reasons, a typical positive reason is that the controller is purposefully suspended from time to time for an economic or system life consideration [9]. Apparently, controller failures may lead to severe performance deterioration of systems. Especially, for adaptive control systems, the controller failure may cause the tracking error divergence due to the uncertainties of systems. Therefore, it is both theoretically and practically important to develop some new techniques to deal with the case of controller temporary failure of adaptive systems.

Recently, there are rapidly growing interests in switched systems and switching control in the control community [10–13]. In the study of stability of switched systems, one of the effective tools is the average dwell time approach [14–16]. Based on this approach, exponential stability is guaranteed if the unavailability rate of the controller is smaller than a specified constant and the average time interval between controller failures is large enough [9, 17, 18]. In [8], this result was further extended to symmetric linear time-invariant system. The concept of controller failure frequency was first introduced in [9], and the cases of controller temporary failure for a class of time-varying delay systems were analyzed in [19]. Interestingly, a nonswitched MRAC system in the presence of controller temporary failure can be viewed as a switched system with a switching signal depending on the time interval between controller failures. Thus, theories and methods of switched systems may be applicable to the study of the state tracking problem for nonswitched MRAC systems with controller temporary failure. However, this issue has been rarely explored so far.

In this paper, we study the state tracking problem for MRAC systems in the presence of controller temporary failure. As in [8], the controller temporary failure means that the controller itself is not available or the controller signals are not transmitted perfectly within a certain time interval. Furthermore, we assume that the parameter estimation is "frozen" in the instant of the controller temporary failure until the controller works normally. There are two main issues to be addressed in this paper. One is to describe a tradition MRAC system in the presence of controller temporary failure as an error switched system with two subsystems: the normal error subsystem which stands for the case without controller failure and the unstable error subsystem which describes the case of controller failure. The other issue is the stability analysis for the error switched system. To address the second issue, we analyze the properties of Lyapunov function candidates without switching and introduce the notions of global practical stability, failure frequency, and unavailability rate.

The results in this paper have three features. First of all, MRAC systems in the presence of controller temporary failure are first considered. Secondly, the state tracking problem is studied from a switched system point of view. Finally, the global practical stability criterion is given for the considered system under the condition of controller failure frequency and unavailability rate.

The organization of the paper is as follows. The state tracking problem in the presence of controller failure is formulated in Section 2. In Section 3, we present an error switched system. Section 4 gives three lemmas and the main result. An example is given to illustrate the effectiveness of the proposed method in Section 5. Finally, the conclusions are presented in Section 6.

The notation is standard. Consider the following:

$\lambda_{\max}(A)$ ($\lambda_{\min}(A)$): the largest (smallest) eigenvalue of matrix A;

$\|A\| = \sqrt{\lambda_{\max}(AA^T)}$: the norm of matrix A;

$\|x\| = \sqrt{(\sum_{i=1}^{n} |x_i|^2)}$: the norm of a vector $x = (x_1, x_2, \ldots, x_n)^T \in R^n$;

$\mathrm{tr}[A]$: the trace of a square matrix A.

2. Problem Statement

Consider a system

$$\dot{x}(t) = \Theta f(x) + Bu(t), \tag{1}$$

where $B \in R^{n\times n}$ is input matrix, $x(t) \in R^n$ is the state, $u(t) \in R^n$ is the control input, $\Theta \in R^{n\times p}$ is an uncertain constant parameter matrix with a bounded δ_Θ, that is, $\|\Theta\| \le \delta_\Theta$, and $f(x) \in R^p$ is a vector which can be described as $f(x) = Fx + g(x)$, where $F \in R^{p\times n}$ is a constant parameter matrix and $\|g(x)\| \le M$ for some $M \ge 0$.

The classical state tracking problem is to design a controller such that the state $x(t)$ of the system (1) tracks a given reference state $x_m(t)$ generated from the reference model system

$$\dot{x}_m(t) = A_m x_m(t) + B_m r(t), \tag{2}$$

where $A_m \in R^{n\times n}$ is a constant Hurwitz matrix, $B_m \in R^{n\times n}$ is a constant input matrix, and $r(t) \in R^n$ is a bounded and piecewise continuous reference input.

Suppose that there exist matrices R, T, and W^* such that the following matching equations are satisfied:

$$A_m = BR, \qquad B_m = BT, \qquad BW^* = \Theta, \tag{3}$$

where W^* is an unknown matrix due to uncertain constant parameter matrix Θ.

Define the tracking error $e(t) = x_m(t) - x(t)$. To solve the state tracking problem, we use the controller structure [20]

$$u(t) = \psi\omega, \tag{4}$$

where $\psi = \begin{bmatrix} R & \widehat{W}(t) & T \end{bmatrix}$ and $\omega = \begin{bmatrix} x^T \\ -f^T(x) \\ r^T \end{bmatrix}$, $\widehat{W}(t)$ is the estimate of unknown matrix W^*, and $\|\widehat{W}(t)\| \le \delta_{\widehat{W}}$.

Apply a parameter projection adaptive law

$$\dot{\widehat{W}}(t) = -\Gamma B^T P_1 e(t) f^T(x) + F_s, \tag{5}$$

where $\Gamma = \mathrm{diag}\{\Gamma_1, \Gamma_2, \ldots, \Gamma_i, \ldots, \Gamma_M\}$ with positive constants Γ_i, P_1 is a symmetric positive definite matrix satisfying $A_m^T P_1 + P_1 A_m < 0$, and F_s is a vector satisfying

$$F_s = \begin{cases} 0, & \text{if } \left\|\widehat{W}(t)\right\| \le \delta_{\widehat{W}}, \\ \Gamma B^T P_1 e(t) f^T(t), & \text{if } \left\|\widehat{W}(t)\right\| > \delta_{\widehat{W}}. \end{cases} \tag{6}$$

Then, the closed-loop system is

$$\dot{x}(t) = A_m x(t) + B_m r(t) + B\widetilde{W}(t) f(x), \tag{7}$$

where $\widetilde{W}(t) = W^* - \widehat{W}(t)$.

From [5, 20, 21], $x(t)$ converges asymptotically to $x_m(t)$ under the controller (4) and the adaptive law (5), that is, $\lim_{t\to\infty} e(t) = 0$.

We now consider the case of controller temporary failure depicted in Figure 1. Controller failures occur when the controller (a) itself is not available or when the signals are not transmitted perfectly on the route (b). Suppose that the time interval of the controller failures is not more than a specified constant T_s, which means the designed controller can be recovered within a finite time interval [19]. Also, the failed controller implies the complete breakdown of the controller ($u(t) = 0$) in its failure time interval [8]. Hence, the system (1) with the controller temporary failure is dominated by the following piecewise differential equations:

$$\dot{x}(t) = \begin{cases} \Theta f(t) + Bu(t), & \text{when the controller works,} \\ \Theta f(t), & \text{when the controller fails.} \end{cases} \tag{8}$$

We introduce the following definitions which will play key roles in deriving our main results.

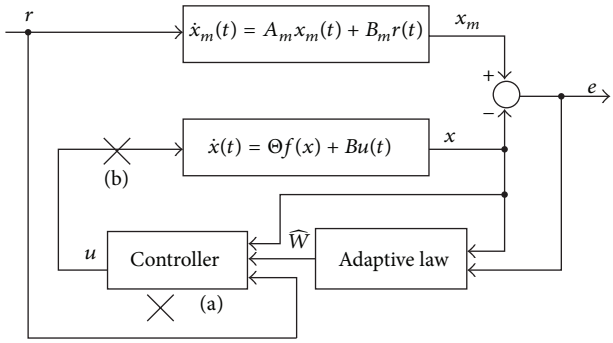

Figure 1: Controller failures occur in MRAC systems.

Definition 1 (see [8]). For any $T_2 > T_1$, denote $T^+(T_1, T_2)$ as the total time interval of controller failure during (T_1, T_2), and call the ratio $T^+(T_1, T_2)/(T_2 - T_1)$ the unavailability rate of the controller in the system.

Definition 2 (see [9]). For any $T_2 > T_1 \geq 0$, let $N_f(T_1, T_2)$ denote the number of control failure in the time interval (T_1, T_2). $F_f(T_1, T_2) = N_f(T_1, T_2)/(T_2 - T_1)$ is referred to as the controller failure frequency in the time interval (T_1, T_2).

In this paper, our objective is to develop conditions under which $x(t)$ tracks $x_m(t)$ subject to controller temporary failure.

3. Error Switched System

From the closed-loop system (7), we have a normal error system

$$\dot{e}(t) = A_m e(t) - B\widetilde{W}(t) f(x). \tag{9}$$

When controller fails, we obtain an unstable error system

$$\dot{e}(t) = A_m e(t) + A_m x(t) + B_m r - \Theta f(x). \tag{10}$$

In this condition, we choose the adaptive law

$$\dot{\widehat{W}}(t) = 0. \tag{11}$$

Remark 3. When controller fails, because the adaptive parameter $\widehat{W}(t)$ has no influence on the tracking error $e(t)$, it is proper that the parameter estimation $\widehat{W}(t)$ is "frozen" in the instants of the controller temporary failure until the controller works normally.

Based on (5), (9), (10), and (11), $e(t)$ is governed by the following error switched system:

$$\dot{e}(t) = A_m e(t) + \Phi_\sigma(t), \tag{12}$$

where $\sigma(t) : [0, +\infty) \to M = \{1, 2\}$, $\Phi_1 = -B\widetilde{W}(t) f(x)$, and $\Phi_2 = A_m x(t) B_m r - \Theta f(x)$.

Meanwhile, we have a switching adaptive law of the following form:

$$\dot{\widehat{W}}(t) = \left(-\Gamma B^T P_1 e(t) f^T(x) + F_s\right) \Psi_\sigma, \tag{13}$$

where $\Psi_1 = I_{p\times p}$ and $\Psi_2 = 0_{p\times p}$.

When $\sigma = 1$, the normal error subsystem is active, which corresponds to the case of no controller failure; when $\sigma = 2$, the unstable error subsystem is active, which denotes that the controller fails.

Therefore, the problem of state tracking in the presence of controller temporary failure can be handled by means of analyzing the stability of the error switched system (12) with the switching adaptive law (13).

To analyze the stability of the error switched system (12), we introduce the following definition.

Definition 4 (see [22]). Consider system (12). Given a constant $r^* > 0$, the system (12) is said to be globally practically stable with respect to r^* if there exist a switching law $\sigma(t)$ and a constant $T = T(e(t_0), r^*) \geq 0$ which depends on $e(t_0)$ and r^* such that $e(t; t_0, e(t_0)) \in S(r^*) \triangleq \{e \mid \|e\| \leq r^*\}$ for $t \geq t_0 + T$.

Remark 5. Unlike the ε-practical stability concept [23], the initial error in Definition 4 is not required to be bounded. If the initial error is constrained by $e(t_0) \in B(r^*)$, then the global practical stability, given by Definition 4, degenerates into ε-practical stability [22]. Global practical stability stated here expresses a global version of the existing practical stability concept. Obviously, Definition 4 covers the ε-practical stability as a special case.

4. Main Result

In this section, firstly, we give three lemmas to analyze the properties of Lyapunov function candidates without switching. Secondly, we present a theorem to give some conditions under which the error switched system (12) is globally practically stable. Let

$$z(t) = \left[e^T(t), \widetilde{w}_1^T(t), \ldots \widetilde{w}_n^T(t), \ldots \widetilde{w}_p^T(t)\right]^T \in R^{n+n\times p}, \tag{14}$$

where $\widetilde{w}_i(t) \in R^n$ is the ith column of $\widetilde{W}(t), i = 1, 2, \ldots, p$; that is,

$$\widetilde{W}(t) = \left[\widetilde{w}_1(t), \ldots, \widetilde{w}_p(t)\right] \in R^{n\times p}. \tag{15}$$

According to [21], we have

$$\mathrm{tr}\left[\widetilde{W}^T \Gamma^{-1} F_s\right] \leq 0. \tag{16}$$

Note that the parameter estimates $\widehat{W}$ are bounded; thus there exists a constant $l > 0$ defined as

$$l = \max\left(\mathrm{tr}\left[\widetilde{W}^T \Gamma^{-1} \widetilde{W}\right]\right). \tag{17}$$

Consider the situation of the system (1) without controller failure. A Lyapunov functional candidate of the normal error subsystem of (12) is chosen as

$$V_1(z(t)) = e^T(t) P_1 e(t) + \mathrm{tr}\left[\widetilde{W}^T(t) \Gamma^{-1} \widetilde{W}(t)\right]. \tag{18}$$

Differentiating V_1 along the trajectory of the normal error subsystem of (12) and the adaptive law (13) gives

$$\dot{V}_1(z(t)) = e^T(t)\left(A_m^T P_1 + P_1 A_m\right) e(t) + 2\mathrm{tr}\left[\widetilde{W}^T \Gamma^{-1} F_s\right]. \tag{19}$$

The following lemma gives the estimate of the convergence rate of V_1 along the trajectory of the normal error subsystem of (12).

Lemma 6. *Consider the normal error subsystem of* (12). *For any given* $r_1 > \sqrt{l/\lambda_{\min}(P_1)}$, *denote* $S(r_1) = \{e \mid \|e\| < r_1\}$. *If* $e(t) \in R^n/S(r_1)$, *then the inequality*

$$V(z(t)) \le \exp\left(-2\lambda_1 (t - t_0)\right) V_1(z(t_0)) \tag{20}$$

holds for any λ_1 *satisfying* $0 < \lambda_1 \le (\overline{\lambda_1}/2)(1-(l/r_1^2\lambda_{\min}(P_1)))$.

Proof. From (17) and (18), it is easy to get

$$e^T(t) P_1 e(t) \le V_1(z(t)) \le e^T(t) P_1 e(t) + l. \tag{21}$$

It is obvious that

$$\lambda_{\min}(P_1) \|e(t)\|^2 \le V_1(z(t)) \le \lambda_{\max}(P_1) \|e(t)\|^2 + l. \tag{22}$$

From (16) and (19), it holds that

$$\dot{V}_1(z(t)) \le e^T \left(A_m^T P_1 + P_1 A_m\right) e < 0. \tag{23}$$

Since A_m is Hurwitz matrix, there exists a scalar $\overline{\lambda_1} > 0$ such that $A_m^T P_1 + P_1 A_m + \overline{\lambda_1} P_1 < 0$.

With the help of (21)– (23), we have

$$\begin{aligned}
&\dot{V}_1(z(t)) \\
&\le -\overline{\lambda_1} V_1(z(t)) + \overline{\lambda_1}\, l \\
&= -2\lambda_1 V_1(z(t)) - \left(\overline{\lambda_1} - 2\lambda_1\right) V_1(z(t)) + \overline{\lambda_1}\, l \\
&\le -2\lambda_1 V_1(z(t)) - \lambda_{\min}(P_1)\left(\overline{\lambda_1} - 2\lambda_1\right)\|e(t)\|^2 + \overline{\lambda_1}\, l.
\end{aligned} \tag{24}$$

Given that $r_1 > \sqrt{l/\lambda_{\min}(P_1)}$, when $e(t) \in R^n/S(r_1)$, applying (24) leads to $\dot{V}_1(z(t)) \le -2\lambda_1 V_1(z(t))$ that is, $V(z(t)) \le \exp(-2\lambda_1(t - t_0))V_1(z(t_0))$; for any λ_1 satisfying $0 < \lambda_1 \le (\overline{\lambda_1}/2)(1 - (l/r_1^2\lambda_{\min}(P_1)))$.

This completes the proof. □

When the controller fails, for the unstable error subsystem of (12), we choose another Lyapunov functional candidate of the following form:

$$V_2(z(t)) = e^T(t) P_2 e(t) + tr\left[\widetilde{W}^T(t) \Gamma^{-1} \widetilde{W}(t)\right], \tag{25}$$

where P_2 is a positive definite matrix.

Differentiating V_2 along the trajectory of the normal error subsystem of (12) and the adaptive law (13) gives

$$\dot{V}_2(z(t)) = \dot{e}(t) P_2 e(t) + e(t) P_2 \dot{e}(t). \tag{26}$$

Then, in the following lemma, we estimate the divergence rate of V_2 along the trajectory of the unstable error subsystem of (12).

Lemma 7. *Consider the unstable error subsystem of* (12). *For any given* $r_2 > 0$, *denote* $S(r_2) = \{e \mid \|e\| < r_2\}$. *If* $e(t) \in R^n/S(r_2)$, *then the inequality*

$$V(z(t)) \le \exp\left(2\lambda_2 (t - t_0)\right) V_2(z(t_0)) \tag{27}$$

holds for any λ_2 *satisfying* $0 < \lambda_2 \le (1/2\lambda_{\min}(P_2))((\beta_2/r_2) + \beta_1)$.

Proof. From (17), we have

$$e^T(t) P_2 e(t) \le V_2(z(t)) \le e^T(t) P_2 e(t) + l. \tag{28}$$

It is obvious that

$$\lambda_{\min}(P_2) \|e(t)\|^2 \le V_2(z(t)) \le \lambda_{\max}(P_2) \|e(t)\|^2 + l. \tag{29}$$

From (10) and (26), we have

$$\begin{aligned}
\dot{V}_2(z(t)) &= e^T(t)\left(A_m^T P_2 + P_2 A_m\right) e(t) \\
&\quad + 2e^T(t) P_2 \left(A_m x_m + B_m r(t) - \Theta f(x)\right) \\
&= e^T(t)\left(A_m^T P_2 - P_2 A_m + 2\Theta F\right) e(t) \\
&\quad + 2e^T(t) P_2 \left(\left(A_m - \Theta F\right) x_m + B_m r(t) - \Theta g(x)\right) \\
&= e^T(t) P_3 e(t) + e^T(t)\xi_1 - e^T(t) P_2 \Theta g(x),
\end{aligned} \tag{30}$$

where $P_3 \triangleq A_m^T P_2 - P_2 A_m + 2\Theta F$ and $\xi_1 \triangleq 2P_2(A_m - \Theta F)x_m + B_m r(t)$.

Since Θ and $r(t)$ are bounded, we have

$$\begin{aligned}
\dot{V}_2(z(t)) &\le \|e(t)\|^2 \|P_3\| + \|e(t)\| \|\xi_1\| \\
&\quad + \|e(t)\| \|P_2\| \ \|\Theta\| \|g(x)\| \\
&\le \|e(t)\|^2 \|P_3\| + \|e(t)\| \|\xi_1\| \\
&\quad + M \|e(t)\| \|P_2\| \|\Theta\| \\
&\le \|e(t)\|^2 \|P_3\| + \|e(t)\| \left(\|\xi_1\| + M \|P_2\| \|\Theta\|\right).
\end{aligned} \tag{31}$$

Then, it holds that

$$\dot{V}_2(z(t)) \le \beta_1 \|e(t)\|^2 + \beta_2 \|e(t)\|, \tag{32}$$

where $\beta_1 = \|P_3\|$ and $\beta_2 = \|\xi_1\| + M\|P_2\|\|\Theta\|$.

Therefore, for any $r_2 > 0$, when $e(t) \in R^n/S(r_2)$, then the inequality $\dot{V}_2(z(t)) \le 2\lambda_2 V_2(z(t))$, that is, $V(z(t)) \le \exp(2\lambda_2(t-t_0))V_2(z(t_0))$, holds for any λ_2 satisfying $0 < \lambda_2 \le (1/2\lambda_{\min}(P_2))((\beta_2/r_2) + \beta_1)$.

This completes the proof. □

Based on Lemmas 6 and 7, we have the following lemma.

Lemma 8. *Consider the subsystems of* (12). *For any* $r_3 > 0$, *if* $e(t) \in R^n/S(r_3)$, *then the inequality*

$$\eta_1 \|e(t)\|^2 \le V_i(z(t)) \le \eta_3 \|e(t)\|^2, \tag{33}$$

holds for $\eta_1 = \min\{\lambda_{\min}(P_1), \lambda_{\min}(P_2)\}$, $\eta_2 = \max\{\lambda_{\max}(P_1), \lambda_{\max}(P_2)\}$, *and* $\eta_3 = \eta_2 + (l/r_3^2)$.

Proof. Form (22) and (29), we have

$$e^T(t)P_i e(t) \le V_i(z(t)) \le e^T(t)P_i e(t) + l. \quad (34)$$

Denote that $\eta_1 = \min\{\lambda_{\min}(P_1), \lambda_{\min}(P_2)\}$ and $\eta_2 = \max\{\lambda_{\max}(P_1), \lambda_{\max}(P_2)\}$. Then, we have

$$\eta_1 \|e(t)\|^2 \le V_i(z(t)) \le \eta_2 \|e(t)\|^2 + l. \quad (35)$$

For any $r_3 > 0$, when $e(t) \in R^n/S(r_3)$, we can find a constant $\eta_3 = \eta_2 + (l/r_3^2)$ such that $\eta_1\|e(t)\|^2 \le V_i(z(t)) \le \eta_3\|e(t)\|^2$.

This completes the proof. □

Furthermore, according to Lemmas 6–8, for any given $r_0' = \max\{r_1, r_2, r_3\}$ and $t > t_0$, if $e(t) \in R^n/S(r_0')$, it is true that

$$V(z(t)) \le \begin{cases} \exp(-2\lambda_1(t-t_0))V_1(z(t_0)) & \text{when the controller works,} \\ \exp(2\lambda_2(t-t_0))V_2(z(t_0)) & \text{when the controller fails.} \end{cases} \quad (36)$$

For (18) and (25), it is obvious that there exists $\mu = \eta_3/\eta_1$ such that

$$V_i(z(t)) \le \mu V_j(z(t)) \quad (i, j = 1, 2). \quad (37)$$

Without loss of generality, for $k = 0, 1, \ldots$, we assume that the controller works during $[t_{2k}, t_{2k+1})$, which means that the first subsystem is active on $[t_{2k}, t_{2k+1})$, while the controller fails during $[t_{2k+1}, t_{2k+2})$, which denotes that the second subsystem is active on $[t_{2k+1}, t_{2k+2})$.

When $e(t_{2k}) \in S(r_1)$, from (22), we have $e(t_{2k+1}) \in S(r_1')$ for any given $r_1' \ge \sqrt{(r_1^2\lambda_{\max}(P_1) + l)/\lambda_{\min}(P_1)}$. It is obvious that (36) and (37) still hold for $r_0 \ge \max\{r_1', r_0'\}$.

Remark 9. Because of the uncertainties of the systems, the properties of the Lyapunov function candidates are restricted outside the ball with the radius r_0 as described as in Lemmas 6–8.

Now, we are in the position to give the main result of this paper.

Theorem 10. *Consider the error switched system* (12) *with the adaptive control law* (13). *For* $k = 0, 1, \ldots$, *if the switching law* $\sigma(t)$ *satisfies the following two conditions:*

Condition 1

$$\frac{T^+(t_{2k}, t)}{(t - t_{2k})} \le \frac{(\lambda_1 - \lambda^*)}{(\lambda_1 + \lambda_2)} \quad (38)$$

holds for some scalar $\lambda^* \in (0, \lambda_1)$,

Condition 2

$$F_f(t_{2k}, t) \le F_f^* = \frac{\lambda}{\ln \mu} \quad (39)$$

holds for some scalar $\lambda \in (0, \lambda^*)$, *then, the error switched system* (12) *is globally practically stable.*

Proof. For any given $r_0 \ge \max\{r_1', r_0'\}$, denote

$$r^* = \exp[\|\Theta\|\|F\|(T_s)] \cdot r_0 + \frac{(\kappa + M\|\Theta\|)[\exp(\|\Theta\|\|F\|(T_s)) - 1]}{\|\Theta\|\|F\|}, \quad (40)$$

where $\kappa \ge \|(A_m - \Theta F)x_m(t) + B_m r(t)\|$ for some $\kappa > 0$. When the initial error $e(t_0) \in R^n$, we will show that there exists a constant $T = T(e(t_0), r^*) \ge 0$, concerned with $e(t_0)$ and r^* such that $e(t; t_0, e(t_0)) \in S(r^*)$ for $t \ge t_0 + T$ under the switching law $\sigma(t)$ satisfying Conditions 1-2. To this end, we will prove the theorem in three cases.

(a) For $e(t_{2k}) \in S(r_0)$, we will show that $e(t_{2k+2}) \in S(r^*)$.

(b) For $e(t_{2k}) \in R^n/S(r_0)$, we will prove that there exists $T_{2k} = T_{2k}(e(t_{2k}), r_0) \ge 0$ such that $\|e(t_{2k} + T_{2k})\| = r_0$ for $e(t) \in R^n/S(r_0)$ and $t \in [t_{2k}, T_{2k})$.

(c) When the initial error $e(t_0) \in R^n$, we will show that there exists a constant $T = T(e(t_0), r^*) \ge 0$ such that $e(t; t_0, e(t_0)) \in S(r^*)$ for $t \ge t_0 + T$ under the switching law $\sigma(t)$ satisfying Conditions 1 and 2.

We first prove (a). Consider $e(t_{2k}) \in S(r_0)$. Because of the asymptotical stability of the normal subsystem of (12), it is obvious that $e(t_{2k+1}) \in S(r_0)$. When $t \in [t_{2k+1}, t_{2k+2})$, the second subsystem is active. From (10), we have

$$\dot{e}(t) = \Theta F e(t) + (A_m - \Theta F)x_m + B_m r - \Theta g(x); \quad (41)$$

then, the trajectory of the error switched system (12) satisfies

$$e(t_{2k+2}) = \exp[\Theta F(t_{2k+2} - t_{2k+1})]e(t_{2k+1}) + \int_{t_{2k+1}}^{t_{2k+2}} \{\exp[\Theta F(t_{2k+2} - t)] \times [(A_m - \Theta F)x_m(t) + B_m r(t) - \Theta g(x(t))]\} dt. \quad (42)$$

With the help of $\|e^A\| \le e^{\|A\|}$, it is obvious that

$$\begin{aligned} &\|e(t_{2k+2})\| \\ &\le \exp[\|\Theta\|\|F\| \cdot (t_{2k+2} - t_{2k+1})]\|e(t_{2k+1})\| \\ &\quad + \int_{t_{2k+1}}^{t_{2k+2}} \{\exp[\|\Theta\|\|F\| \cdot (t_{2k+2} - \tau)] \\ &\qquad \times [\|(A_m - \Theta F)x_m(\tau) + B_m r(\tau)\| \\ &\qquad + \|\Theta\|\|g(x(\tau))\|]\} d\tau \end{aligned}$$

$$\begin{aligned}
&\le \exp\left[\|\Theta\|\,\|F\|\left(t_{2k+2}-t_{2k+1}\right)\right]\left\|e\left(t_{2k+1}\right)\right\| \\
&\quad+\int_{t_{2k+1}}^{t_{2k+2}}\left\{\left(\Lambda+M\|\Theta\|\right)\exp\left[\|\Theta\|\,\|F\|\left(t_{2k+2}-\tau\right)\right]\right\}d\tau \\
&=\exp\left[\|\Theta\|\,\|F\|\left(t_{2k+2}-t_{2k+1}\right)\right]\left\|e\left(t_{2k+1}\right)\right\| \\
&\quad+\frac{\left(\Lambda+M\|\Theta\|\right)\left[\exp\left(\|\Theta\|\,\|F\|\left(t_{2k+2}-t_{2k+1}\right)\right)-1\right]}{\|\Theta\|\,\|F\|}.
\end{aligned} \tag{43}$$

Because $T_s=\max_k\{t_{2k+2}-t_{2k+1}\}$, we have

$$\begin{aligned}
\left\|e\left(t_{2k+2}\right)\right\| &\le \left\|e\left(t_{2k+1}+T_s\right)\right\| \\
&=\exp\left[\|\Theta\|\,\|F\|\left(T_s\right)\right]\left\|e\left(t_{2k+1}\right)\right\| \\
&\quad+\frac{\left(\kappa+M\|\Theta\|\right)\left[\exp\left(\|\Theta\|\,\|F\|\left(T_s\right)\right)-1\right]}{\|\Theta\|\,\|F\|}.
\end{aligned} \tag{44}$$

Note that r_0 is the maximum value of $\|e(t_{2k+1})\|$; thus we have

$$\begin{aligned}
\left\|e\left(t_{2k+2}\right)\right\| &\le r^* \\
&=\exp\left[\|\Theta\|\,\|F\|\left(T_s\right)\right]\ r_0 \\
&\quad+\frac{\left(\kappa+M\|\Theta\|\right)\left[\exp\left(\|\Theta\|\,\|F\|\left(T_s\right)\right)-1\right]}{\|\Theta\|\,\|F\|}.
\end{aligned} \tag{45}$$

Because of $r^*>r_0$, we have $e(t_{2k+2})\in S(r^*)$ when $e(t_{2k})\in S(r_0)$.

Then, we prove (b). For $e(t_{2k})\in R^n/S(r_0)$, obviously, we only need to consider the trajectory $e(t)$ being totally outside $S(r_0)$. We discuss two cases for $t\ge t_{2k}$. One is $t\in[t_{2j},t_{2j+1})$, and the other is $t\in[t_{2j+1},t_{2j+2})$, where $j=k,\ k+1,\ldots$.

Thus, from Lemmas 6 and 7, it is true that

$$\begin{aligned}
&V\left(z\left(\tau\right)\right) \\
&\le\begin{cases}\exp\left(-2\lambda_1\left(\tau-t_{2k}\right)\right)V_1\left(z\left(t_{2k}\right)\right), & \text{if } t_{2k}\le\tau<t_{2k+1}\\ \exp\left(2\lambda_2\left(\tau-t_{2k+1}\right)\right)V_2\left(z\left(t_{2k+1}\right)\right), & \text{if } t_{2k+1}\le\tau<t_{2k+2}.\end{cases}
\end{aligned} \tag{46}$$

If $t\in[t_{2j},t_{2j+1})$, according to (37) and (46), it holds that

$$\begin{aligned}
V\left(z\left(t\right)\right) &\le \exp\left(-2\lambda_1\left(t-t_{2j}\right)\right)V_1\left(z\left(t_{2j}\right)\right) \\
&\le \exp\left(-2\lambda_1\left(t-t_{2j}\right)\right)\mu V_2\left(z\left(t_{2j}\right)\right) \\
&\le \mu\exp\left(-2\lambda_1\left(t-t_{2j}\right)\right)\exp\left(2\lambda_2\left(t_{2j}-t_{2j-1}\right)\right) \\
&\quad\times V_2\left(z\left(t_{2j-1}\right)\right) \\
&\le \mu^2\exp\left(-2\lambda_1\left(t-t_{2j}\right)\right)\exp\left(2\lambda_2\left(t_{2j}-t_{2j-1}\right)\right) \\
&\quad\times V_1\left(z\left(t_{2j-1}\right)\right) \\
&\le \mu^2\exp\left(-2\lambda_1\left(t-t_{2j}\right)\right)\exp\left(2\lambda_2\left(t_{2j}-t_{2j-1}\right)\right) \\
&\quad\times\exp\left(-2\lambda_1\left(t_{2j-1}-t_{2j-2}\right)\right)V_1\left(z\left(t_{2j-2}\right)\right) \\
&\le\cdots\le \mu^{2(j-k)}\exp\left(-2\lambda_1\left(t-t_{2k}-T^+\left(t_{2k},t\right)\right)\right) \\
&\quad\times\exp\left(2\lambda_2T^+\left(t_{2k},t\right)\right)V_1\left(z\left(t_{2k}\right)\right).
\end{aligned} \tag{47}$$

If $t\in[t_{2j+1},t_{2j+2})$, again from (37) and (46), we have

$$\begin{aligned}
V\left(z\left(t\right)\right) &\le \exp\left(2\lambda_2\left(t-t_{2j+1}\right)\right)V_2\left(z\left(t_{2j+1}\right)\right) \\
&\le \exp\left(2\lambda_2\left(t-t_{2j+1}\right)\right)\mu V_1\left(z\left(t_{2j+1}\right)\right) \\
&\le \mu\exp\left(2\lambda_2\left(t-t_{2j+1}\right)\right)\exp\left(-2\lambda_1\left(t_{2j+1}-t_{2j}\right)\right) \\
&\quad\times V_1\left(z\left(t_{2j}\right)\right) \\
&\le \mu^2\exp\left(2\lambda_2\left(t-t_{2j+1}\right)\right)\exp\left(-2\lambda_1\left(t_{2j+1}-t_{2j}\right)\right) \\
&\quad\times V_2\left(z\left(t_{2j}\right)\right) \\
&\le \mu^2\exp\left(2\lambda_2\left(t-t_{2j+1}\right)\right)\exp\left(-2\lambda_1\left(t_{2j+1}-t_{2j}\right)\right) \\
&\quad\times\exp\left(2\lambda_2\left(t_{2j}-t_{2j-1}\right)\right)V_2\left(z\left(t_{2j-1}\right)\right) \\
&\le\cdots\le \mu^{2(j-k)+1}\exp\left(-2\lambda_1\left(t-t_{2k}-T^+\left(t_{2k},t\right)\right)\right) \\
&\quad\times\exp\left(2\lambda_2T^+\left(t_{2k},t\right)\right)V_1\left(z\left(t_{2k}\right)\right).
\end{aligned} \tag{48}$$

By Definition 2, we know $N_f(t_{2k},t)=2(j-k)$ for $t\in[t_{2j},t_{2j+1})$ and $N_f(t_{2k},t)=2(j-k)+1$ for $t\in[t_{2j+1},t_{2j+2})$. Thus, for any $t\in[t_{2j+1},t_{2(j+1)})$, from (47) and (48), we can obtain

$$\begin{aligned}
V\left(z\left(t\right)\right) &\le \mu^{N_f\left(t_{2k},t\right)}\exp\left(-2\lambda_1\left(t-t_{2k}-T^+\left(t_{2k},t\right)\right)\right) \\
&\quad\times\exp\left(2\lambda_2T^+\left(t_{2k},t\right)\right)V_1\left(z\left(t_{2k}\right)\right).
\end{aligned} \tag{49}$$

With the help of Lemma 8, it holds that

$$\begin{aligned}
\left\|e\left(z\left(t\right)\right)\right\| &\le \sqrt{\frac{\eta_2}{\eta_1}}\ \exp\left(N_f\left(t_{2k},t\right)\ln\mu\right) \\
&\quad\times\exp\left(-\lambda_1\left(t-t_{2k}-T^+\left(t_{2k},t\right)\right)\right) \\
&\quad\times\exp\left(\lambda_2T^+\left(t_{2k},t\right)\right)\left\|e\left(z\left(t_{2k}\right)\right)\right\|.
\end{aligned} \tag{50}$$

Applying Condition 1 gives

$$\begin{aligned}
&\exp\left(-\lambda_1\left(t-t_{2k}-T^+\left(t_{2k},t\right)\right)+\lambda_2T^+\left(t_{2k},t\right)\right) \\
&\quad\le\exp\left(-\lambda^*\left(t-t_{2k}\right)\right).
\end{aligned} \tag{51}$$

From Condition 2 and Definition 1, we have

$$\exp\left(N_f\left(t_{2k},t\right)\ln\mu\right)\le\exp\left(\lambda\left(t-t_{2k}\right)\right). \tag{52}$$

Using (49), (51), and (52) results in

$$\begin{aligned}&\left\|e\left(z\left(t;t_{2k},e\left(t_{2k}\right)\right)\right)\right\|\\&\quad\le \exp\left(-\left(\lambda^{*}-\lambda\right)\left(t-t_{2k}\right)\right)\left\|e\left(z\left(t_{2k}\right)\right)\right\|.\end{aligned}\tag{53}$$

Therefore, when $e(t_{2k}) \in R^n/S(r_0)$, there exists $T_{2k} = T_{2k}(e(t_{2k}), r_0) \ge 0$ such that $\|e(t_{2k} + T_{2k})\| = r_0$ under the switching law $\sigma(t)$ satisfying Conditions 1-2. Obviously, $\{T_{2k}\}$ is a decreasing sequence, and thus $T_0 = \max_k\{T_{2k}\}$.

Finally, we prove (c). If $e(t_0) \in R^n/S(r^*)$, by applying (a), (b), and $r^* > r_0$, there exists a positive constant $T = T(e(t_0), r^*) < T_0$ such that $e(t; t_0, e(t_0)) \in S(r^*)$ for $t \ge t_0 + T$. If $e(t_0) \in S(r^*)$, the result remains true with $T = 0$.

This completes the proof. □

Remark 11. When the initial error $e(t_0) \in S(r^*)$, the error switched system is ε-practical stability [23].

Remark 12. The error switched system (12) is globally practically stable if the controller fails only for a short time interval and with a low frequency of occurrence.

5. Example

In this section, we present an example to demonstrate the effectiveness of the proposed method in this paper.

Consider the system (1) with

$$\begin{aligned}&\Theta=\begin{bmatrix}1&3\\1&2\end{bmatrix},\qquad F=\begin{bmatrix}1&0\\0&1\end{bmatrix},\\&g(x)=\begin{bmatrix}\sin x_1\\\cos x_2\end{bmatrix},\qquad B=\begin{bmatrix}1&0\\0&2\end{bmatrix}.\end{aligned}\tag{54}$$

The reference state x_m is generated by the reference model (2) with $A_m = \left[\begin{smallmatrix}-2&0\\0&-3\end{smallmatrix}\right]$, $B_m = \left[\begin{smallmatrix}1\\1\end{smallmatrix}\right]$, and the reference input is $r = 1$.

Choose $R = \left[\begin{smallmatrix}-2&0\\0&-1.5\end{smallmatrix}\right]$, $T = \left[\begin{smallmatrix}1\\0.5\end{smallmatrix}\right]$, $P_1 = P_2 = \left[\begin{smallmatrix}0.4449&0\\0&0.2862\end{smallmatrix}\right]$, and $\Gamma = \left[\begin{smallmatrix}20&0\\0&20\end{smallmatrix}\right]$. We have $r^* = 6.8147$ when $r_0 = 5$. Then, according to (38) and (39), we obtain $T^{+}(t_{2k}, t)/(t - t_{2k}) \le 0.0302$ and $F_f(t_{2k}, t) \le F_f^* = 0.548$. The switching signal is chosen as

$$\sigma(t)=\begin{cases}1, & t\in\Pi,\\ 2, & t\in\dfrac{[0,+\infty)}{\Pi},\end{cases}\tag{55}$$

where $\Pi = [15k, 15k + 1.95) \cup [15k + 2, 15k + 4) \cup [15k + 4.05, 15k + 6.35) \cup [15k + 6.4, 15k + 8.85) \cup [15k + 8.9, 15k + 11.55) \cup [15k + 11.6, 15k + 14.55) \cup [15k + 14.6, 15k + 15)$, $k = 0, 1, 2, \ldots$, which is described in Figure 2. It is easy to verify that $\sigma(t)$ satisfies Conditions 1-2 of Theorem 10.

When $x_m(t_0) = [0, 0]^T$ and $x(t_0) = [5, 6]^T$, the norm of the tracking error of (12) with and without controller failures is shown in Figures 3 and 4, respectively.

Simulations are carried out for $\|e(t_0)\| = 7.81 \ge r_0$ and $\|e(t_0)\| = 2.236 < r^*$. The results are depicted in Figures 5 and 6.

From Figures 5 and 6, we can conclude that whether $\|e(t_0)\| \ge r_0$ or not, the states of the system (1) with controller temporary failure track the reference signal $x_m(t)$ well under the switching signal $\sigma(t)$, and the tracking error $\|e(t)\|$ is small in the sense of r^*. Simulation illustrates the effectiveness of the proposed method.

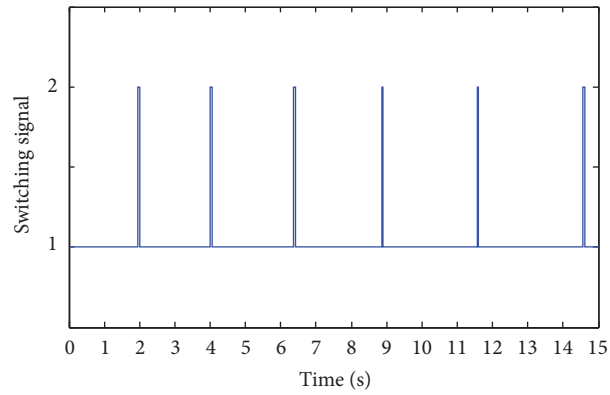

Figure 2: Switching signal.

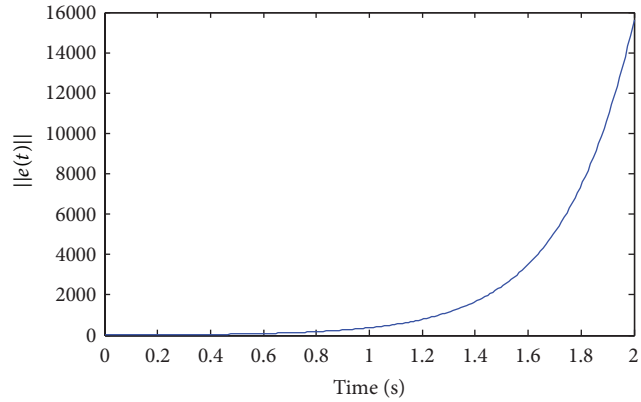

Figure 3: The norm of the tracking error of (12) when controller fails.

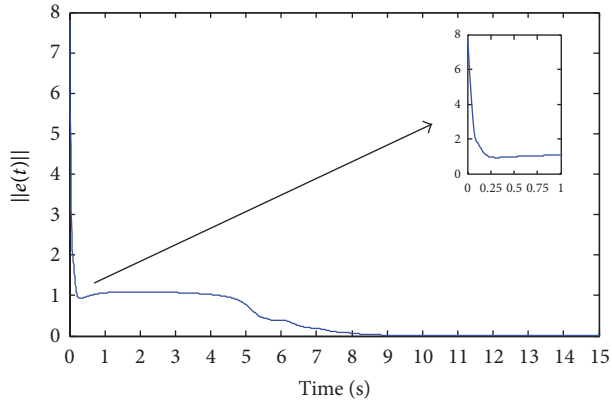

Figure 4: The norm of the tracking error of (12) without controller failure.

6. Conclusion

This paper has considered the state tracking problem for a class of MRAC systems in the presence of controller

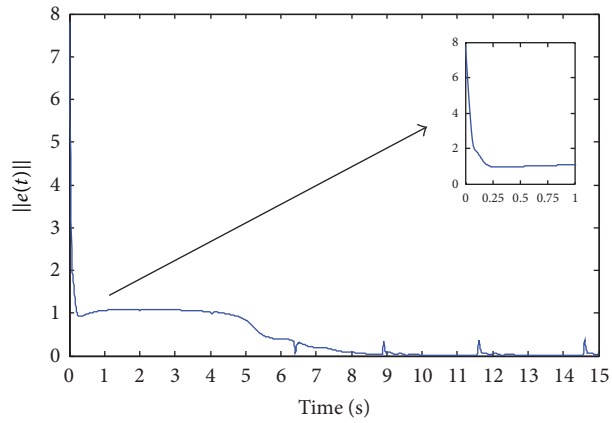

FIGURE 5: The norm of the tracking error of (12) under $\sigma(t)(\|e(t_0)\| = 7.81)$.

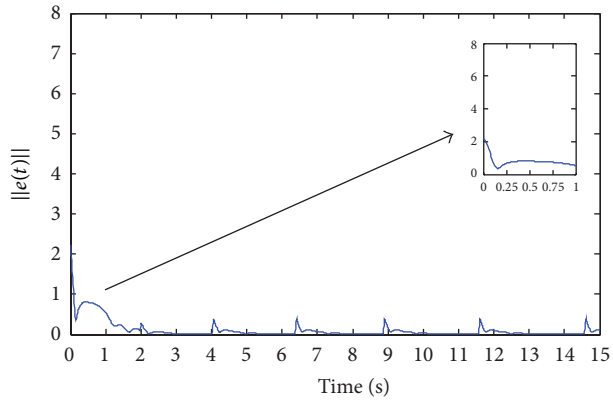

FIGURE 6: The norm of the tracking error of (12) under $\sigma(t)(\|e(t_0)\| = 2.236)$.

temporary failure. A key point is to describe such a system as an error switched system. The properties of Lyapunov function candidates without switching have been given. Then, the global practical stability of the error switched system can be ensured by the proposed scheme, providing that the controller suffers from failures only for a relatively short time interval and with a low frequency of occurrence. It is an interesting topic to extend the results for the output tracking problem of adaptive systems.

Conflict of Interests

The authors declare that there is no conflict of interests regarding the publication of this paper.

Acknowledgments

This work was supported by the Chinese National Fundamental Research Program under Grant 2009CB320601 and National Natural Science Foundation of China under Grants 61233002 and 61174073.

References

[1] H. K. Khalil, "Adaptive output feedback control of nonlinear systems represented by input-output models," *IEEE Transactions on Automatic Control*, vol. 41, no. 2, pp. 177–188, 1996.

[2] S. Yin, X. Yang, and H. R. Karimi, "Data-driven adaptive observer for fault diagnosis," *Mathematical Problems in Engineering*, vol. 2012, Article ID 832836, 21 pages, 2012.

[3] Q. Sang and G. Tao, "Adaptive control of piecewise linear systems with state feedback for output tracking," *Asian Journal of Control*, vol. 15, no. 4, pp. 933–943, 2013.

[4] M. di Bernardo, U. Montanaro, and S. Santini, "Hybrid model reference adaptive control of piecewise affine systems," *IEEE Transactions on Automatic Control*, vol. 58, no. 2, pp. 304–316, 2013.

[5] P. A. Ioannou and J. Sun, *Robust Adaptive Control*, Prentice Hall, Englewood Cliffs, NJ, USA, 1996.

[6] B. M. Mirkin and P.-O. Gutman, "Adaptive coordinated decentralized control of state delayed systems with actuator failures," *Asian Journal of Control*, vol. 8, no. 4, pp. 441–448, 2006.

[7] G. Tao, *Adaptive Control Design and Analysis*, Adaptive and Learning Systems for Signal Processing, Communications, and Control, John Wiley & Sons, Hoboken, NJ, USA, 2003.

[8] G. Zhai and H. Lin, "Controller failure time analysis for symmetric H_∞ control systems," *International Journal of Control*, vol. 77, no. 6, pp. 598–605, 2004.

[9] X. M. Sun, G. P. Liu, D. Rees, and W. Wang, "Stability of systems with controller failure and time-varying delay," *IEEE Transactions on Automatic Control*, vol. 53, no. 10, pp. 2391–2396, 2008.

[10] D. Liberzon, *Switching in Systems and Control*, Systems & Control: Foundations & Applications, Birkhäuser, Boston, Mass, USA, 2003.

[11] J. Zhao and D. J. Hill, "Dissipativity theory for switched systems," *IEEE Transactions on Automatic Control*, vol. 53, no. 4, pp. 941–953, 2008.

[12] J. Li, Q. Su, and L. Sun, "Fault detection for nonlinear impulsive switched systems," *Mathematical Problems in Engineering*, vol. 2013, Article ID 815329, 12 pages, 2013.

[13] B. Niu and J. Zhao, "Barrier Lyapunov functions for the output tracking control of constrained nonlinear switched systems," *Systems & Control Letters*, vol. 62, no. 10, pp. 963–971, 2013.

[14] J. P. Hespanha and A. S. Morse, "Stability of switched systems with average dwell-time," in *Proceedings of the 38th IEEE Conference on Decision and Control*, pp. 2655–2660, 1999.

[15] L. I. Allerhand and U. Shaked, "Robust stability and stabilization of linear switched systems with dwell time," *IEEE Transactions on Automatic Control*, vol. 56, no. 2, pp. 381–386, 2011.

[16] G. S. Zhai, B. Hu, K. Yasuda, and A. N. Michel, "Stability analysis of switched systems with stable and unstable subsystems: an average dwell time approach," *International Journal of Systems Science*, vol. 32, no. 8, pp. 1055–1061, 2001.

[17] G. S. Zhai, X. Chen, S. Takai, and K. Yasuda, "Controller failure time analysis for H-infinity control systems," in *Proceedings of the 40th IEEE Conference on Decision and Control (CDC '01)*, pp. 1029–1030, December 2001.

[18] G. S. Zhai, B. Hu, K. Yasuda, and A. N. Michel, "Piecewise lyapunov functions for switched systems with average dwell time," *Asian Journal of Control*, vol. 2, no. 3, pp. 192–197, 2008.

[19] X. M. Sun, G. P. Liu, W. Wang, and D. Rees, "L2-gainof systems with input delays and controller temporary failure: zero-order

hold model," *IEEE Transactions on Control Systems Technology*, vol. 19, no. 3, pp. 699–706, 2011.

[20] X. Wang, J. Zhao, and Y. Tang, "State tracking model reference adaptive control for switched nonlinear systems with linear uncertain parameters," *Journal of Control Theory and Applications*, vol. 10, no. 3, pp. 354–358, 2012.

[21] Q. Sang and G. Tao, "Adaptive control of piecewise linear systems: the state tracking case," in *Proceedings of the American Control Conference (ACC '10)*, pp. 4040–4045, July 2010.

[22] C. Wu, C. Li, and J. Zhao, "Switching-based state tracking of model reference adaptive control systems in the presence of intermittent failures of all actuators," *International Journal of Adaptive Control and Signal Processing*, 2013.

[23] X. P. Xu and G. S. Zhai, "On practical stability and stabilization of hybrid and switched systems," in *Proceeding of the 7th International Workshop on Hybrid Systems: Computation and Control (HSCC '04)*, vol. 2993 of *Lecture Notes in Computer Science*, pp. 615–630, Berlin, Germany, 2004.

Hindawi Publishing Corporation
Mathematical Problems in Engineering
Volume 2013, Article ID 930927, 9 pages
http://dx.doi.org/10.1155/2013/930927

Research Article

Delay-Probability-Distribution-Dependent $\mathscr{H}_\infty$ FIR Filtering Design with Envelope Constraints

Cheng Peng,[1] Zhandong Yu,[2] Hamid Reza Karimi,[3] Weizhi Wang,[1] and Nan Wang[1]

[1] *The Research Institute of Intelligent Control and Systems, Harbin Institute of Technology, Harbin 150001, China*
[2] *The Bohai University, Jinzhou 121013, China*
[3] *The Department of Engineering, Faculty of Engineering and Science, University of Agder, 4898 Grimstad, Norway*

Correspondence should be addressed to Cheng Peng; hitpech@gmail.com

Received 23 August 2013; Accepted 11 September 2013

Academic Editor: Zhiguang Feng

This paper studies the problem of $\mathscr{H}_\infty$ finite-impulse response (FIR) filtering design of time-delay system. The time-delay considered here is time-varying meanwhile with a certain stochastic characteristic, and the probability of delay distribution is assumed to be known. Furthermore, the requirement of pulse-shape is also considered in filter design. Employing the information about the size and probability distribution of delay, a delay-probability-distribution-dependent criterion is proposed for the filtering error system. Based on a Lyapunov-Krasovskii functional, a set of linear matrix inequalities (LMIs) are formulated to solve the problem. At last, a numerical example is used to demonstrate the effectiveness of the filter design approach proposed in the paper.

1. Introduction

In the studies about filtering problem, one most significant approach frequently applied in the past decades is Kalman filtering, the main idea of which is to minimize the variance of the estimation error assuming considered system dynamics to be exactly known and the external disturbances to be stationary Gaussian noises with known statistical properties [1, 2]. However, in many practical engineering applications, the statistical details about external noise are not available [3–8]. In these cases, many approaches are introduced to improve systems' robustness, such as $\mathscr{H}_\infty$, $\mathscr{H}_2$, and mixed $\mathscr{H}_\infty/\mathscr{H}_2$ filtering [2, 9–13]. In this paper, the $\mathscr{H}_\infty$ filtering approach is utilized.

On the other hand, time-delays are frequently encountered in practical engineering systems, such as manufacturing systems, power systems, and networked control systems [14–17]. Existence of delay makes the analysis and synthesis of systems a much more difficult task; meanwhile it is also the source of instability and poor performance in many cases [13, 18–20]. The main approaches to solve delay problems can be classified into delay-dependent approach and delay-independent approach. It has been shown in [21, 22] that the results obtained using delay-dependent approaches are generally less conservative than the delay-independent approaches ones [23]. Acknowledging this fact, the delay-dependent approach is applied in this paper.

In fact, the variation of delay may often stick to some probability distribution in spite of its varying and underivable property [24, 25]. Furthermore, in many real systems such as networked control systems, the time-varying delay may have some abrupt burst, leading to very large delay with a very small probability [26]. In this sense, the discussion about time-delay should not only depend on its size but also on its probability distribution. In this paper, a new filter design approach and new stability criteria for the filtering error system taking the stochastic characteristic of time-varying delay into account is proposed.

While an $\mathscr{H}_\infty$ optimal filter can catch the frequency-domain property, the time-domain constraints such as envelope constraints or bounds on signals cannot be handled by this frequency-domain approach [27]. Among various time-domain specifications, envelope constraints, which make requirement on the pulse-shape, have significant applications in many practical engineering systems, such as communication systems, radar, sonar systems, and signal processing

systems [28–31]. For instance, in deconvolution filtering and data channel equalization problems, it is extremely important to achieve a desired pulse-shape through designing an appropriate filter [27].

Therefore, aiming at incorporating both frequency-domain and time-domain constraints into the problem, we intend to design a filter satisfying the $\mathscr{H}_\infty$ performance and subject to envelope constraints in outputs. Meanwhile, time-varying delays with certain stochastic characteristics in the transmission channel are also taken into account. With the proposed filter design approach, a more general condition of time-varying delay problem can be solved. As in most situations, although detailed and exact information about delay cannot be achieved, the delay's probability distribution characteristics can be predicted or observed relatively easily. Once the probability information is gotten, the filter design approach can be developed.

In this paper, based on a Lyapunov-Krasovskii functional, we first present an $\mathscr{H}_\infty$ optimal solution to the design of a finite-impulse response (FIR) filter using information about the range of time-varying delay and its probability distribution. Then, the envelope constraints are taken into consideration. The resultant filter is called an $\mathscr{H}_\infty$ optimal Envelope-Constrained FIR (ECFIR) filter. We obtain the solution via solving an LMI optimization problem. At last, a numerical example is presented to illustrate the effectiveness of the proposed filtering design approach.

2. Problem Formulation and Preliminaries

Consider a filtering system shown in Figure 1, where Σ_l represents a linear dynamic system with state-space realization given by

$$\Sigma_l : \begin{cases} x_l(k+1) = A_l x_l(k) + B_l w(k) \\ s(k) = C_l x_l(k), \end{cases} \tag{1}$$

where $x_l(k) \in \mathfrak{R}^{n_l}$ is the model state vector, $w(k) \in \mathfrak{R}^{n_w}$ is the input signal, $s(k) \in \mathfrak{R}^{n_s}$ is the source signal generated by the model, and A_l, B_l, C_l are known constant matrices with appropriate dimensions. Then the output $s(k)$ is transmitted through a channel with time-varying delay modeled by

$$\Sigma_c : \begin{cases} x_c(k+1) = A_c x_c(k) + A_d s(k - d(k)) + B_c v(k) \\ y(k) = C_c x_c(k) + C_d s(k - d(k)) + D_c v(k), \end{cases} \tag{2}$$

where $x_c(k) \in \mathfrak{R}^{n_c}$ is the channel state vector, $d(k) \in [0, d_2]$ is the time-varying delay with an upper bound of d_2, $y(k)$ is the output of the channel, and $v(k)$ is the disturbance input; A_c, A_d, B_c, C_c, C_d, D_c are all known constant system matrices with appropriate dimensions. As is shown in (2), the source signal $s(k)$ suffers from influence of time-varying delay $d(k)$ and disturbance from the environment represented by $v(k)$. The output of transmission channel is $y(k)$, which is also the input signal of the filter. We are going to use the corrupted signal $y(k)$ to reconstruct original source signal.

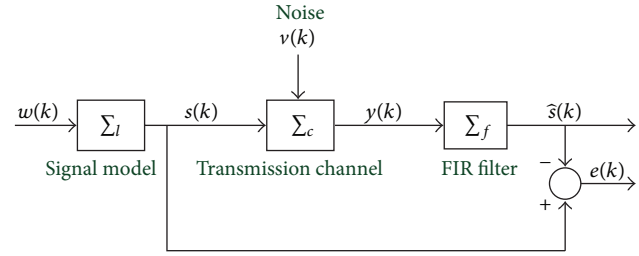

Figure 1: Filtering system.

Assumption 1. $d(k)$ changes randomly and for a constant $d_1 \in [0, d_2]$, and the probability of $d(k) \in [0, d_1)$ and $d(k) \in [d_1, d_2]$ can be known. The following sets and functions are defined:

$$\begin{aligned} \Omega_1 &= \{k : d(k) \in [0, d_1)\}, \\ \Omega_2 &= \{k : d(k) \in [d_1, d_2]\}, \\ d_1(k) &= \begin{cases} d(k), & \text{for } k \in \Omega_1 \\ 0 & \text{for } k \notin \Omega_1, \end{cases} \\ d_2(k) &= \begin{cases} d(k), & \text{for } k \in \Omega_2 \\ d_1, & \text{for } k \notin \Omega_2. \end{cases} \end{aligned} \tag{3}$$

Obviously, it can be seen from the definition that $k \in \Omega_1$ is equal to the occurrence of event $d(k) \in [0, d_1)$ and $k \in \Omega_2$ means that the event $d(k) \in [d_1, d_2]$ occurs. Therefore, a stochastic variable $\beta(k)$ can be defined as

$$\beta(k) = \begin{cases} 1, & k \in \Omega_1 \\ 0, & k \in \Omega_2. \end{cases} \tag{4}$$

Assumption 2. $\beta(k)$ is a Bernoulli distributed sequence with

$$\begin{aligned} \text{Prob}\{\beta(k) = 1\} &= \mathbb{E}\{\beta(k)\} = \beta_0, \\ \text{Prob}\{\beta(k) = 0\} &= 1 - \mathbb{E}\{\beta(k)\} = 1 - \beta_0, \end{aligned} \tag{5}$$

where $0 \le \beta_0 \le 1$ is a constant.

Remark 3. From Assumption 2, it is easy to see that $\mathbb{E}\{\beta(k) - \beta_0\} = 0$ and $\mathbb{E}\{(\beta(k) - \beta_0)^2\} = \beta_0(1 - \beta_0)$. As $\text{Prob}\{d(k) \in [0, d_1)\} = \text{Prob}\{\beta(k) = 1\} = \beta_0$ and $\text{Prob}\{d(k) \in [d_1, d_2]\} = \text{Prob}\{\beta(k) = 0\} = 1 - \beta_0$, β_0 and $1 - \beta_0$ also denote the probability of $d(k)$ taking values in $[0, d_1)$ and $[d_1, d_2]$, respectively.

According to Assumptions 1 and 2, the system model described by (2) can be rewritten as

$$\begin{aligned} x_c(k+1) &= A_c x_c(k) + \beta(k) A_d s(k - d_1(k)) \\ &\quad + (1 - \beta(k)) A_d s(k - d_2(k)) + B_c v(k), \\ y(k) &= C_c x_c(k) + \beta(k) C_d s(k - d_1(k)) \\ &\quad + (1 - \beta(k)) C_d s(k - d_2(k)) + D_c v(k). \end{aligned} \tag{6}$$

At the receiving end, we are interested in designing a linear filter with state-realization as follows:

$$\Sigma_f : \begin{cases} x_f(k+1) = A_f x_f(k) + B_f y(k) \\ \hat{s}(k) = C_f x_f(k) + D_f y(k), \end{cases} \tag{7}$$

where $x_f(k) \in \Re^{n_f}$ is the filter state vector, $\hat{s}(k)$, is the estimated signal of source signal $s(k)$ and A_f, B_f, C_f, D_f have the following form:

$$A_f = \begin{bmatrix} 0 & 1 & 0 & \cdots & 0 \\ 0 & 0 & 1 & \cdots & 0 \\ \vdots & \vdots & \vdots & \ddots & \vdots \\ 0 & 0 & 0 & \cdots & 1 \\ 0 & 0 & 0 & \cdots & 0 \end{bmatrix}_{n_f \times n_f}, \quad B_f = \begin{bmatrix} 0 \\ 0 \\ \vdots \\ 0 \\ 1 \end{bmatrix}_{n_f \times 1},$$
$$C_f = \begin{bmatrix} f(n_f) & f(n_f - 1) & \cdots & f(1) \end{bmatrix} D_f = f(0). \tag{8}$$

The transfer function of the filter is given by

$$\begin{aligned} \Phi_f(z) &= C_f \left(zI - A_f\right)^{-1} B_f + D_f \\ &= f(0) + f(1) z^{-1} + f(2) z^{-2} + \cdots + f(n_f) z^{-n_f}, \end{aligned} \tag{9}$$

where $f(0)$, $f(1), \ldots$, and $f(n_f)$ are parameters to be determined. Define the filtering error as $e(k) = s(k) - \hat{s}(k)$. Then, via augmenting the models Σ_l and Σ_c, the filtering error system is given as follows:

$$\Sigma_e : \begin{cases} x_e(k+1) = A_e x_e(k) \\ \quad + \beta(k) A_{ed} x_e(k - d_1(k)) \\ \quad + (1 - \beta(k)) A_{ed} x_e(k - d_2(k)) + B_e w_e(k) \\ e(k) \\ = C_e x_e + \beta(k) C_{ed} x_e(k - d_1(k)) \\ \quad + (1 - \beta(k)) C_{ed} x_e(k - d_2(k)) + D_e w_e(k), \end{cases} \tag{10}$$

where

$$x_e^T(k) = \begin{bmatrix} x_l^T(k) & x_c^T(k) & x_f^T(k) \end{bmatrix}^T,$$
$$w_e(k) = \begin{bmatrix} w^T(k) & v^T(k) \end{bmatrix}^T,$$
$$A_e = \begin{bmatrix} A_l & 0 & 0 \\ 0 & A_c & 0 \\ 0 & B_f C_c & A_f \end{bmatrix}, \quad B_e = \begin{bmatrix} B_l & 0 \\ 0 & B_c \\ 0 & B_f D_c \end{bmatrix},$$
$$C_e = \begin{bmatrix} C_l & -D_f C_c & -C_f \end{bmatrix},$$
$$D_e = \begin{bmatrix} 0 & -D_f D_c \end{bmatrix},$$
$$A_{ed} = \begin{bmatrix} 0 & 0 & 0 \\ A_d C_l & 0 & 0 \\ B_f C_d C_l & 0 & 0 \end{bmatrix}, \quad C_{ed} = \begin{bmatrix} -D_f C_d C_l & 0 & 0 \end{bmatrix}. \tag{11}$$

Before giving the main results, we need following definitions at first.

Definition 4. For a given function $V(x(k))$, its stochastic difference operator is defined as

$$\Delta V(x(k)) = \mathbb{E}\{V(x(k+1)) \mid x(k)\} - V(x(k)). \tag{12}$$

Definition 5 (see [32]). The filtering error system in (10) is said to be stochastically stable if for any initial condition $x_e(0)$ and zero exogenous noise $w_e(k)$, there exists a positive definite W independent of $x_e(0)$, such that the following condition is satisfied:

$$\mathbb{E}\left\{\sum_{k=0}^{\infty} |x_e(k)|^2 \mid x_e(0)\right\} < x_e^T(0) W x_e(0). \tag{13}$$

Definition 6. System (10) is said to be stochastically stable with an $\mathscr{H}_\infty$ norm bound γ, if the following conditions hold.

(1) The filtering error system with $w_e(k) = 0$ is stochastically stable.

(2) For all nonzero $w_e(k) \in l_2[0, \infty)$ and under zero initial conditions, the following inequality holds:

$$\|e(k)\|_2 \leq \gamma \|w_e(k)\|_2. \tag{14}$$

Now, with the definitions above, we present the objective of this paper.

Given the filtering system shown in Figure 1, we are interested in designing a filter in the form of (7)-(8) such that

(a) the filtering error system (10) is asymptotically stable in the stochastic sense;

(b) the filtering error system (10) possesses a minimized $\mathscr{H}_\infty$ performance level γ;

(c) a time-domain envelope constraint is imposed on the output signal $\hat{s}(k)$ as follows:

$$l(k) \leq \hat{s}(k) \leq u(k), \tag{15}$$

where $l(k)$ and $u(k)$ are the lower and upper bounds of the time-domain mask, respectively.

3. Main Results

In this section, based on the Lyapunov-Krasovskii stability theorem, a delay-probability-distribution-dependent approach is proposed to solve the $\mathscr{H}_\infty$ FIR filter design problem subject to envelope constraints described in (15). First, a stability criterion for the filtering error system described in (10) is proposed. Then the envelope constraints are taken into consideration. An $\mathscr{H}_\infty$ optimal ECFIR filter design approach is given at last.

Theorem 7. *Given the system in Figure 1, for some given constants* $0 \leq d_1 \leq d_2$, β_0, *and* γ, *the filtering error system* (10)

is stochastically stable with $\mathscr{H}_\infty$ performance γ if there exist matrices $P > 0$, $Q_1 > 0$, $Q_2 > 0$, $R_1 > 0$, $R_2 > 0$ of appropriate dimensions such that the following optimization problem has solutions,

$$\min_{P>0,Q_1>0,Q_2>0,R_1>0,R_2>0,f} \gamma, \tag{16}$$

subject to the following LMI constraint:

$$\Xi = \begin{bmatrix} \Xi_{11} & \Xi_{12} & \Xi_{13} \\ * & \Xi_{22} & \Xi_{23} \\ * & * & \Xi_{33} \end{bmatrix} < 0, \tag{17}$$

where

$$\begin{aligned}
\Xi_{11} &= \begin{bmatrix} -P & PA_e & \beta_0 PA_{ed} \\ * & Q - P - \dfrac{1}{d_1}R_1 & \dfrac{1}{d_1}R_1 \\ * & * & -Q_1 - \dfrac{1}{d_1}R_1 - \dfrac{1}{d_2 - d_1}R_2 \end{bmatrix}, \\
\Xi_{12} &= \begin{bmatrix} (1-\beta_0)PB_e & PB_e & 0 \\ 0 & 0 & \sqrt{d_1}\left(A_e^T - I\right)R_1 \\ \dfrac{1}{d_2 - d_1}R_2 & 0 & \sqrt{d_1}\beta_0 A_{ed}^T R_1 \end{bmatrix}, \\
\Xi_{13} &= \begin{bmatrix} 0 & 0 \\ \sqrt{d_2 - d_1}\left(A_e^T - I\right)R_2 & C_e^T \\ \beta_0\sqrt{d_2 - d_1}A_{ed}^T R_2 & \beta_0 C_{ed}^T \end{bmatrix}, \\
\Xi_{22} &= \begin{vmatrix} -Q_2 - \dfrac{1}{d_2 - d_1}R_2 & 0 & \sqrt{d_1}(1-\beta_0)A_{ed}^T R_1 \\ * & -\gamma^2 I & \sqrt{d_1}B_e^T R_1 \\ * & * & -R_1 \end{vmatrix}, \\
\Xi_{23} &= \begin{bmatrix} \sqrt{d_2 - d_1}(1-\beta_0)A_{ed}^T R_2 & (1-\beta_0)C_{ed}^T \\ \sqrt{d_2 - d_1}B_e^T R_2 & D_e^T \\ 0 & 0 \end{bmatrix}, \\
\Xi_{33} &= \begin{bmatrix} -R_2 & 0 \\ * & -I \end{bmatrix}, \\
Q &= (1 + d_1)Q_1 + (d_2 - d_1 + 1)Q_2,
\end{aligned} \tag{18}$$

and A_e, A_{ed}, B_e, C_e, C_{ed}, and D_e are defined in (11).

Proof. First, define a Lyapunov-Krasovskii functional as follows:

$$V(k) \triangleq V_1(k) + V_2(k) + V_3(k) + V_4(k), \tag{19}$$

where

$$\begin{aligned}
V_1(k) &\triangleq x_e^T(k)Px_e(k), \\
V_2(k) &\triangleq \sum_{i=k-d_1(k)}^{k-1} x_e^T(i)Q_1x_e(i) \\
&\quad + \sum_{i=k-d_2(k)}^{k-1} x_e^T(i)Q_2x_e(i), \\
V_3(k) &\triangleq \sum_{i=-d_1+2}^{-1}\sum_{j=k+i-1}^{k-1} x_e^T(j)Q_1x_e(j) \\
&\quad + \sum_{i=-d_2+2}^{-d_1+1}\sum_{j=k+i-1}^{k-1} x_e^T(j)Q_2x_e(j), \\
V_4(k) &\triangleq \sum_{i=k-d_1}^{k-1}\sum_{j=i}^{k-1}\delta^T(j)R_1\delta(j) \\
&\quad + \sum_{i=k-d_2}^{k-d_1-1}\sum_{j=i}^{k-1}\delta^T(j)R_2\delta(j), \\
\delta(j) &\triangleq x_e(j+1) - x_e(j),
\end{aligned} \tag{20}$$

and $P = P^T > 0$, $Q_1 = Q_1^T > 0$, $Q_2 = Q_2^T > 0$, $R_1 = R_1^T > 0$, and $R_2 = R_2^T > 0$ are Lyapunov matrices to be determined.

Then using the stochastic difference operator defined in (12), we obtain

$$\begin{aligned}
\Delta V_1(k) &= \left[x_e^T(k)A_e^T + \beta_0 x_e^T(k - d_1(k))A_{ed}^T\right. \\
&\quad \left. + (1-\beta_0)x_e^T(k - d_2(k))A_{ed}^T + w_e^T(k)B_e^T\right] \\
&\quad \times P\left[A_e x_e(k) + \beta_0 A_{ed}x_e(k - d_1(k))\right. \\
&\quad \left. + (1-\beta_0)A_{ed}x_e(k - d_2(k)) + B_e w_e(k)\right] \\
&\quad - x_e^T(k)Px_e(k), \\
\Delta V_2(k) &= x_e^T(k)(Q_1 + Q_2)x_e(k) - x_e^T(k - d_1(k)) \\
&\quad \times Q_1 x_e(k - d_1(k)) \\
&\quad - x_e^T(k - d_2(k))Q_2 x_e(k - d_2(k)) \\
&\quad + \sum_{i=k+1-d_1(k+1)}^{k-1} x_e^T(i)Q_1x_e(i) \\
&\quad - \sum_{i=k-d_1(k)+1}^{k-1} x_e^T(i)Q_1x_e(i) \\
&\quad + \sum_{i=k+1-d_2(k+1)}^{k-1} x_e^T(i)Q_2x_e(i) \\
&\quad - \sum_{i=k-d_2(k)+1}^{k-1} x_e^T(i)Q_2x_e(i)
\end{aligned}$$

$$\begin{aligned}
&\le x_e^T(k)(Q_1+Q_2)x_e(k) - x_e^T(k-d_1(k)) \\
&\quad \times Q_1 x_e(k-d_1(k)) \\
&\quad - x_e^T(k-d_2(k))Q_2 x_e(k-d_2(k)) \\
&\quad + \sum_{i=k-d_1+1}^{k} x_e^T(i)Q_1 x_e(i) + \sum_{k-d_2+1}^{k-d_1} x_e^T(i)Q_2 x_e(i), \\
\Delta V_3(k) &= d_1 x_e^T(k)Q_1 x_e(k) + (d_2-d_1)x_e^T(k)Q_2 x_e(k) \\
&\quad - \sum_{i=k-d_1+1}^{k} x_e^T(i)Q_1 x_e(i) - \sum_{i=k-d_2+1}^{k-d_1} x_e^T(i)Q_2 x_e(i), \\
\Delta V_4(k) &= d_1 \delta^T(k)R_1\delta(k) + (d_2-d_1)\delta^T(k)R_2\delta(k) \\
&\quad - \sum_{i=k-d_1}^{k-1} \delta^T(i)R_1\delta(i) - \sum_{i=k-d_2}^{k-d_1-1} \delta^T(i)R_2\delta(i) \\
&\le d_1\delta^T(k)R_1\delta(k) + (d_2-d_1)\delta^T(k)R_2\delta(k) \\
&\quad - \sum_{i=k-d_1(k)}^{k-1} \delta^T(i)R_1\delta(i) - \sum_{i=k-d_2(k)}^{k-d_1-1} \delta^T(i)R_2\delta(i).
\end{aligned} \tag{21}$$

Using the Jensen inequality [33], the following expressions are obtained:

$$\begin{aligned}
&- \sum_{i=k-d_1(k)}^{k-1} \delta^T(i)R_1\delta(i) \\
&\le -\frac{1}{d_1(k)}\left(\sum_{i=k-d_1(k)}^{k-1}\delta^T(i)\right)R_1\left(\sum_{i=k-d_1(k)}^{k-1}\delta(i)\right) \\
&\le -\frac{1}{d_1}\left(\sum_{i=k-d_1(k)}^{k-1}\delta^T(i)\right)R_1\left(\sum_{i=k-d_1(k)}^{k-1}\delta(i)\right), \\
&- \sum_{i=k-d_2(k)}^{k-d_1-1} \delta^T(i)R_2\delta(i) \\
&\le -\frac{1}{d_2(k)-d_1}\left(\sum_{i=k-d_2(k)}^{k-d_1-1}\delta^T(i)\right)R_2\left(\sum_{i=k-d_2(k)}^{k-d_1-1}\delta(i)\right) \\
&\le -\frac{1}{d_2-d_1}\left(\sum_{i=k-d_2(k)}^{k-d_1-1}\delta^T(i)\right)R_2\left(\sum_{i=k-d_2(k)}^{k-d_1-1}\delta(i)\right).
\end{aligned} \tag{22}$$

Thus, we have

$$\begin{aligned}
\Delta V_4(k) &\le \delta^T(k)\left[d_1R_1 + (d_2-d_1)R_2\right]\delta(k) \\
&\quad - \frac{1}{d_1}\left[x_e^T(k) - x_e^T(k-d_1(k))\right] \\
&\quad \times R_1\left[x_e(k) - x_e(k-d_1(k))\right] \\
&\quad - \frac{1}{d_2-d_1}\left[x_e^T(k-d_1(k)) - x_e^T(k-d_2(k))\right] \\
&\quad \times R_1\left[x_e(k-d_1(k)) - x_e(k-d_2(k))\right].
\end{aligned} \tag{23}$$

Thus, we obtain

$$\begin{aligned}
\Delta V(k) &= \Delta V_1(k) + \Delta V_2(k) + \Delta V_3(k) \\
&\quad + \Delta V_4(k) \le \eta^T(k)\Upsilon\eta(k),
\end{aligned} \tag{24}$$

where

$$\begin{aligned}
\eta^T(k) &= \left[x_e^T(k) \;\; x_e^T(k-d_1(k)) \;\; x_e^T(k-d_2(k)) \;\; w_e^T(k)\right], \\
\Upsilon &= \begin{bmatrix} \Upsilon_{11} & \Upsilon_{12} & \Upsilon_{13} & \Upsilon_{14} \\ * & \Upsilon_{22} & \Upsilon_{23} & \Upsilon_{24} \\ * & * & \Upsilon_{33} & \Upsilon_{34} \\ * & * & * & \Upsilon_{44} \end{bmatrix}, \\
\Upsilon_{11} &= A_e^T P A_e + \left(A_e^T - I\right)R\left(A_e - I\right) + Q - P - \frac{1}{d_1}R_1, \\
\Upsilon_{12} &= \beta_0 A_e^T P A_{ed} + \beta_0\left(A_e^T - I\right)RA_{ed} + \frac{1}{d_1}R_1, \\
\Upsilon_{13} &= (1-\beta_0)A_e^T P A_{ed} + (1-\beta_0)\left(A_e^T - I\right)RA_{ed}, \\
\Upsilon_{14} &= A_e^T P B_e + \left(A_e^T - I\right)RB_e^T, \\
\Upsilon_{22} &= \beta_0^2 A_{ed}^T(P+R)A_{ed} - Q_1 - \frac{1}{d_1}R_1 - \frac{1}{d_2-d_1}R_2, \\
\Upsilon_{23} &= \beta_0(1-\beta_0)A_{ed}^T(P+R)A_{ed} + \frac{1}{d_2-d_1}R_2, \\
\Upsilon_{24} &= \beta_0 A_{ed}^T(P+R)B_e, \\
\Upsilon_{33} &= (1-\beta_0)^2 A_{ed}^T(P+R)A_{ed} - Q_2 - \frac{1}{d_2-d_1}R_2, \\
\Upsilon_{34} &= (1-\beta_0)A_{ed}^T(P+R)B_e, \\
\Upsilon_{44} &= B_e^T(P+R)B_e, \\
R &= d_1R_1 + (d_2-d_1)R_2.
\end{aligned} \tag{25}$$

By Schur complement, it can be concluded from (17) that $\Upsilon < 0$. By similar lines as in [32], the stochastic stability can be guaranteed if condition (17) holds.

Then, define the performance index as follows:

$$J = \sum_{k=0}^{\infty}\left[e^T(k)e(k) - \gamma^2 w_e^T(k)w_e(k)\right]. \tag{26}$$

Considering the fact that $V(k) \geq 0$, under the zero initial condition, we have

$$J \leq \sum_{k=0}^{\infty} \left[e^T(k)\, e(k) - \gamma^2 w_e^T(k)\, w_e(k) \right] + V(\infty) - V(0)$$
$$= \sum_{k=0}^{\infty} \left[e^T(k)\, e(k) - \gamma^2 w_e^T(k)\, w_e(k) + \Delta V(k) \right]. \tag{27}$$

Thus, $J < 0$ is equal to

$$\eta^T(k)\,(\Theta + \Upsilon)\,\eta(k) < 0, \tag{28}$$

where

$$\Theta = \begin{bmatrix} C_e^T C_e & \beta_0 C_e^T C_{ed} & (1-\beta_0) C_e^T C_{ed} & C_e^T D_e \\ * & \beta_0^2 C_{ed}^T C_{ed} & \beta_0 (1-\beta_0) C_{ed}^T C_{ed} & \beta_0 C_{ed}^T D_e \\ * & * & (1-\beta_0)^2 C_{ed}^T C_{ed} & (1-\beta_0) C_{ed}^T D_e \\ * & * & * & D_e^T D_e - \gamma^2 I \end{bmatrix}. \tag{29}$$

Through applying Schur complement, it is shown that $(\Theta + \Upsilon) < 0$ can be guaranteed by condition (17). That is to say, once (17) is satisfied, the $\mathscr{H}_\infty$ performance can be guaranteed to be less than γ. Thus, the proof is completed.

At this point, the second desired property of the system will be considered, which is the envelope constraints demand. First, some notations are introduced [34]:

$$y = \begin{bmatrix} y(0) \\ y(1) \\ \vdots \\ y(m) \end{bmatrix}, \qquad l = \begin{bmatrix} l(0) \\ l(1) \\ \vdots \\ l(n) \end{bmatrix},$$
$$u = \begin{bmatrix} u(0) \\ u(1) \\ \vdots \\ u(n) \end{bmatrix}, \qquad f = \begin{bmatrix} f(0) \\ f(1) \\ \vdots \\ f(n_f) \end{bmatrix}, \tag{30}$$
$$Y = \begin{bmatrix} y(0) & 0 & \cdots & 0 \\ y(1) & y(0) & \cdots & 0 \\ \vdots & y(1) & \cdots & \vdots \\ y(m) & \vdots & & y(0) \\ 0 & y(m) & \vdots & y(1) \\ \vdots & \vdots & & \vdots \\ 0 & 0 & \cdots & y(m) \end{bmatrix},$$

where Y is an $n \times (n_f + 1)$ matrix, $n = m + n_f + 1$,

$$\{y(0)\ \ y(1)\ \ \cdots\ \ y(m)\ \ 0\ \ 0\ \ \cdots\} \tag{31}$$

is a given signal, and

$$\{l(0)\ \ l(1)\ \ \cdots\ \ l(m)\},$$
$$\{u(0)\ \ u(1)\ \ \cdots\ \ u(m)\} \tag{32}$$

Are, respectively, the upper and lower bounds. Therefore, the constraint of (15) is equal to

$$\operatorname{diag}(l) \leq \operatorname{diag}(Yf) \leq \operatorname{diag}(u), \tag{33}$$

where diag(•) denotes a conversion from a vertical vector to a diagonal matrix.

Based on Theorem 7 and (33), we can establish another theorem to determine the filter that satisfies the envelope constraint meanwhile possessing optimal $\mathscr{H}_\infty$ performance. □

Theorem 8. *An $\mathscr{H}_\infty$ optimal filter of the form* (7)-(8) *satisfying envelope constraint in* (15) *can be obtained by solving the following LMI optimization problem:*

$$\min_{P>0, Q_1>0, Q_2>0, R_1>0, R_2>0, f} \gamma, \tag{34}$$

subject to

$$\Xi = \begin{bmatrix} \Xi_{11} & \Xi_{12} & \Xi_{13} \\ * & \Xi_{22} & \Xi_{23} \\ * & * & \Xi_{33} \end{bmatrix} < 0,$$
$$\operatorname{diag}(l) \leq \operatorname{diag}(Yf), \tag{35}$$
$$\operatorname{diag}(Yf) \leq \operatorname{diag}(u),$$

where Ξ is defined in (17).

4. An Illustrative Example

In this section, an example is given to support the filter design method proposed in the paper. Consider a filtering system as shown in Figure 1. The parameters for Σ_l are given by

$$A_l = \begin{bmatrix} -2.3060 & -2.9625 & -2.2590 & -1.0922 & -0.3009 & -0.0325 \\ 1 & 0 & 0 & 0 & 0 & 0 \\ 0 & 1 & 0 & 0 & 0 & 0 \\ 0 & 0 & 1 & 0 & 0 & 0 \\ 0 & 0 & 0 & 1 & 0 & 0 \\ 0 & 0 & 0 & 0 & 1 & 0 \end{bmatrix},$$
$$B_l = \begin{bmatrix} 1 \\ 0 \\ 0 \\ 0 \\ 0 \\ 0 \end{bmatrix},$$
$$C_l = [0\ \ 0\ \ 0\ \ 0\ \ 0.0062\ \ 0.2170]. \tag{36}$$

The parameters for the delay channel Σ_c are given by

$$A_c = \begin{bmatrix} 0 & 1 \\ 0 & -0.1 \end{bmatrix}, \qquad A_d = \begin{bmatrix} 0 \\ 0.1 \end{bmatrix}, \qquad B_c = \begin{bmatrix} 0.1 \\ 0.1 \end{bmatrix},$$
$$C_c = [0\ \ 1], \qquad C_{cd} = 0.2, \qquad D_c = 1, \tag{37}$$
$$d_1 = 2, \qquad d_2 = 3, \qquad \beta_0 = 0.7.$$

Using Theorem 8, the $\mathscr{H}_\infty$ optimal filter is obtained via using the LMI toolbox of MATLAB with n_f chosen to be 5. The

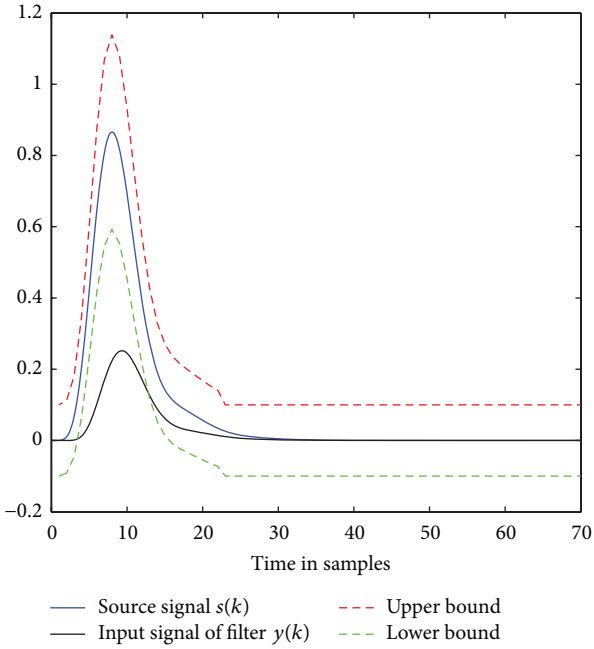

Figure 2: Source signal $s(k)$, filter input signal $y(k)$, and envelope bounds.

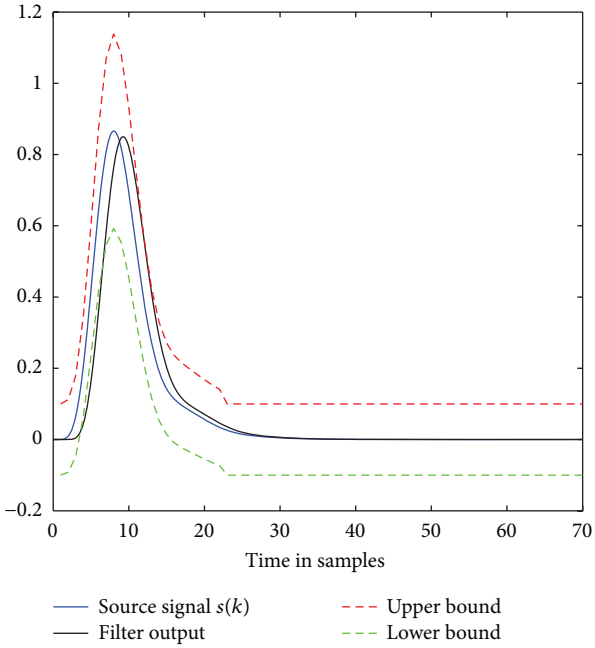

Figure 3: Output of the filter without disturbance.

resultant optimal γ is 8.5057 and filter gains are given as follows:

$$C_f = \begin{bmatrix} 0.0437 & -0.3344 & -0.4023 & 0.2045 & -0.5089 \end{bmatrix}, \quad D_f = 4.3664. \tag{38}$$

The expected envelope constraints and $s(k)$ (the output of Σ_l) corresponding to a particular case where input signal $w(k)$ is chosen to be unit impulse signal are shown in Figure 2. The transmitted signal $y(k)$ through Σ_c which is generated with no noise added is also given in the figure. The filter output $\hat{s}(k)$ and filtering error $e(k)$ are given in Figures 3 and 4, respectively.

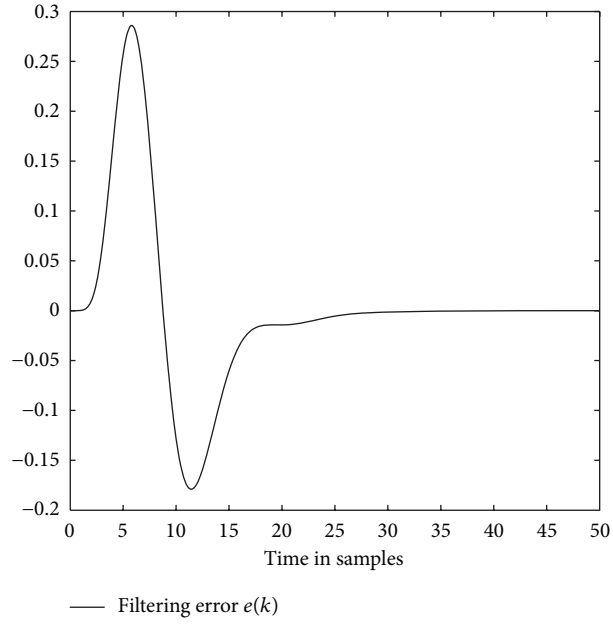

Figure 4: Filtering error $e(k)$ without disturbance.

Furthermore, to illustrate the performance of the designed filter, we add the disturbance signal $v(k)$ chosen as white noise with mean of zero and variance of 1×10^{-3} into the system. The resultant filter output and filtering error are shown in Figures 5 and 6, respectively. It is shown that the designed filter is effective.

5. Conclusions

In this paper, we have solved the filtering design problem of time-delay system. The time-delay considered here is time-varying meanwhile with a certain stochastic characteristic, and the probability of delay distribution is assumed to be known. Furthermore, the envelope constraints are also considered in the process of filtering design. The delay-distribution-dependent criterion is formed for the filtering error system, employing the information about not only the size of delay but also its probability distribution. A set of linear matrix inequalities (LMIs) are formulated to solve the problem. Through solving the LMI optimization problem, the $\mathscr{H}_\infty$ performance is minimized and pulse-shape demand imposed by envelope constraints is satisfied. Finally, an illustrative example is presented to demonstrate the effectiveness of the filtering design approach. For future research directions, extending the filter design approach proposed in this paper to networked control systems and distributed systems is an interesting issue. Besides, more general filter

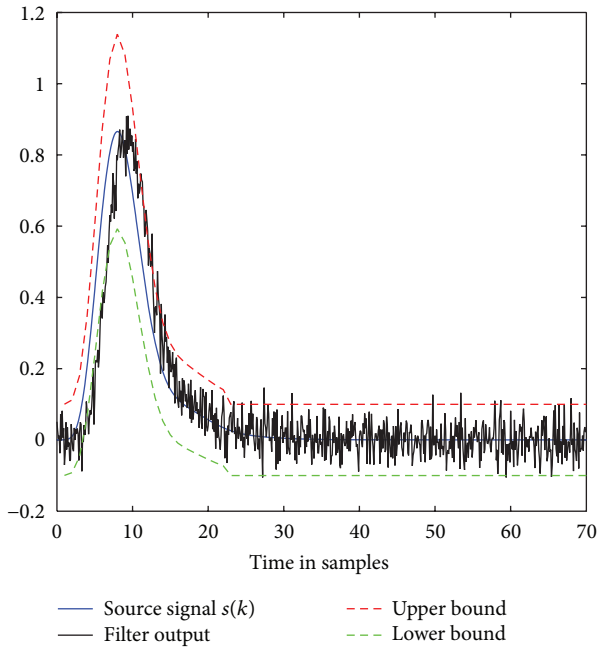

Figure 5: Output of the filter with disturbance.

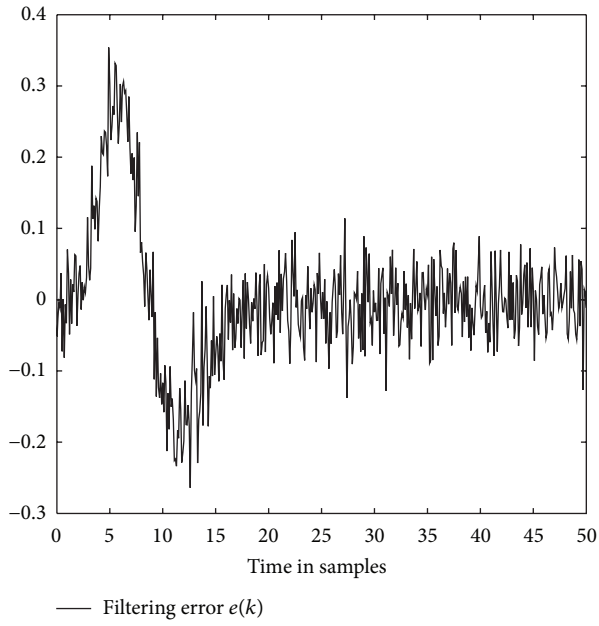

Figure 6: Filtering error $e(k)$ with disturbance.

design approaches considering delays in different forms with different characteristics also deserve further investigation.

Acknowledgments

The authors are grateful to the associate editor and anonymous reviewers for their constructive comments based on which the presentation of this paper has been greatly improved.

References

[1] R. E. Kalman, "A new approach to linear filtering and prediction problems," *Transanctions of the ASME: Journal of Basic Engineering*, vol. 82, no. 1, pp. 35–45, 1960.

[2] B. D. O. Anderson and J. B. Moore, *Optimal Filtering*, Prentice-Hall, Englewood Cliffs, NJ, USA, 1979.

[3] S. Yin, S. Ding, and H. Luo, "Real-time implementation of fault tolerant control system with performance optimization," *IEEE Transactions on Industrial Electronics*, 2013.

[4] S. Yin, S. Ding, A. Haghani, H. Hao, and P. Zhang, "A comparison study of basic data-driven fault diagnosis and process monitoring methods on the benchmark Tennessee Eastman process," *Journal of Process Control*, vol. 22, no. 9, pp. 1567–1581, 2012.

[5] S. Yin, S. X. Ding, A. H. A. Sari, and H. Hao, "Data-driven monitoring for stochastic systems and its application on batch process," *International Journal of Systems Science*, vol. 44, no. 7, pp. 1366–1376, 2013.

[6] S. Tong, Y. Li, Y. Li, and Y. Liu, "Observer-based adaptive fuzzy backstepping control for a class of stochastic nonlinear strict-feedback systems," *IEEE Transactions on Systems, Man, and Cybernetics B*, vol. 41, no. 6, pp. 1693–1704, 2011.

[7] S. Tong and Y. Li, "Observer-based fuzzy adaptive control for strict-feedback nonlinear systems," *Fuzzy Sets and Systems*, vol. 160, no. 12, pp. 1749–1764, 2009.

[8] Y. Li, S. Tong, and T. Li, "Adaptive fuzzy output feedback control of uncertain nonlinear systems with unknown backlash-like hysteresis," *Information Sciences*, vol. 198, pp. 130–146, 2012.

[9] L. Xie, C. E. de Souza, and M. Fu, "$\mathcal{H}_\infty$ estimation for discrete-time linear uncertain systems," *International Journal of Robust and Nonlinear Control*, vol. 1, no. 2, pp. 111–123, 1991.

[10] R. M. Palhares and P. L. D. Peres, "Robust filtering with guaranteed energy-to-peak performance—an *LMI* approach," *Automatica*, vol. 36, no. 6, pp. 851–858, 2000.

[11] H. D. Tuan, P. Apkarian, and T. Q. Nguyen, "Robust and reduced-order filtering: new LMI-based characterizations and methods," *IEEE Transactions on Signal Processing*, vol. 49, no. 12, pp. 2975–2984, 2001.

[12] H. Gao, J. Lam, L. Xie, and C. Wang, "New approach to mixed $\mathcal{H}_2/\mathcal{H}_\infty$ filtering for polytopic discrete-time systems," *IEEE Transactions on Signal Processing*, vol. 53, no. 8, part 2, pp. 3183–3192, 2005.

[13] J. Qiu, G. Feng, and J. Yang, "Delay-dependent non-synchronized robust $\mathcal{H}_\infty$ state estimation for discrete-time piecewise linear delay systems," *International Journal of Adaptive Control and Signal Processing*, vol. 23, no. 12, pp. 1082–1096, 2009.

[14] R. Zhang, T. Li, and L. Guo, "$\mathcal{H}_\infty$ control for flexible spacecraft with time-varying input delay," *Mathematical Problems in Engineering*, vol. 2013, Article ID 839108, 6 pages, 2013.

[15] T. Li, K. Zhang, and B. Zheng, "Fault detection for non-Gaussian stochastic systems with timevarying delay," *Mathematical Problems in Engineering*, vol. 2013, Article ID 958954, 8 pages, 2013.

[16] B. Zhang and W. X. Zheng, "$\mathcal{H}_\infty$ filter design for nonlinear networked control systems with uncertain packet-loss probability," *Signal Processing*, vol. 92, no. 6, pp. 1499–1507, 2012.

[17] J. Qiu, G. Feng, and J. Yang, "A new design of delay-dependent robust $\mathcal{H}_\infty$ filtering for discrete-time T-S fuzzy systems with time-varying delay," *IEEE Transactions on Fuzzy Systems*, vol. 17, no. 5, pp. 1044–1058, 2009.

[18] Z. Feng and J. Lam, "Robust reliable dissipative filtering for discrete delay singular systems," *Signal Processing*, vol. 92, no. 12, pp. 3010–3025, 2012.

[19] Z. Feng, J. Lam, and H. Gao, "Delay-dependent robust $\mathscr{H}_\infty$ controller synthesis for discrete singular delay systems," *International Journal of Robust and Nonlinear Control*, vol. 21, no. 16, pp. 1880–1902, 2011.

[20] S. Tong, W. Wang, and L. Qu, "Decentralized robust control for uncertain T-S fuzzy large-scale systems with time-delay," *International Journal of Innovative Computing, Information and Control*, vol. 3, no. 3, pp. 657–672, 2007.

[21] H. Gao and C. Wang, "Delay-dependent robust $\mathscr{H}_\infty$ and $\mathscr{L}_2 - \mathscr{L}_\infty$ filtering for a class of uncertain nonlinear time-delay systems," *IEEE Transactions on Automatic Control*, vol. 48, no. 9, pp. 1661–1666, 2003.

[22] J. Qiu, G. Feng, and J. Yang, "Improved delay-dependent $\mathscr{H}_\infty$ filtering design for discrete-time polytopic linear delay systems," *IEEE Transactions on Circuits and Systems II*, vol. 55, no. 2, pp. 178–182, 2008.

[23] C. E. de Souza, R. M. Palhares, and P. L. D. Peres, "Robust $\mathscr{H}_\infty$ filter design for uncertain linear systems with multiple time-varying state delays," *IEEE Transactions on Signal Processing*, vol. 49, no. 3, pp. 569–576, 2001.

[24] S. Wang, R. Nathuji, R. Bettati, and W. Zhao, "Providing statistical delay guarantees in wireless networks," in *Proceedings of the 24th International Conference on Distributed Computing Systems*, pp. 48–55, Tokyo, Japan, March 2004.

[25] Y. Wei, M. Wang, and J. Qiu, "A new approach to delay-dependent $\mathscr{H}_\infty$ filtering for discretetime Markovian jump systems with time-varying delay and incomplete transition descriptions," *IET Control Theory and Applications*, vol. 7, no. 5, pp. 684–696, 2013.

[26] J. Liu, D. Yue, Z. Gu, and E. Tian, "$\mathscr{H}_\infty$ filtering for systems with time-varying delay satisfying a certain stochastic characteristic," *IET Signal Processing*, vol. 5, no. 8, pp. 757–766, 2011.

[27] Z. Tan, Y. C. Soh, and L. Xie, "Envelope-constrained $\mathscr{H}_\infty$FIR filter design," *IEEE Transactions on Circuits and Systems II*, vol. 47, no. 1, pp. 79–82, 2000.

[28] K. L. Teo, A. Cantoni, and X. G. Lin, "New approach to the optimization of envelope-constrained filters with uncertain input," *IEEE Transactions on Signal Processing*, vol. 42, no. 2, pp. 426–429, 1994.

[29] R. J. Evans, T. E. Fortmann, and A. Cantoni, "Envelope-constrained filters. I. Theory and applications," *IEEE Transactions on Information Theory*, vol. IT-23, no. 4, pp. 421–434, 1977.

[30] R. J. Evans, A. Cantoni, and K. M. Ahmed, "Envelope-constrained filters with uncertain input," *Circuits, Systems, and Signal Processing*, vol. 2, no. 2, pp. 131–154, 1983.

[31] B. N. Vo, A. Cantoni, and K. L. Teo, "Envelope constrained filter with linear interpolator," *IEEE Transactions on Signal Processing*, vol. 45, no. 6, pp. 1405–1414, 1997.

[32] H. Gao, T. Chen, and L. Wang, "Robust fault detection with missing measurements," *International Journal of Control*, vol. 81, no. 5, pp. 804–819, 2008.

[33] K. Gu, "An integral inequality in the stability problem of time-delay systems," in *Proceedings of the 39th IEEE Confernce on Decision and Control*, pp. 2805–2810, Sydney, Australia, December 2000.

[34] Z. Tan, Y. Soh, and L. Xie, "$\mathscr{H}_\infty$ optimal envelope-constrained FIR filter design: an LMI approach," in *Proceedings of the 5th International Symposium on Signal Processing and Its Applications*, pp. 951–954, Brisbane, Australia, 1999.

Hindawi Publishing Corporation
Mathematical Problems in Engineering
Volume 2013, Article ID 197845, 14 pages
http://dx.doi.org/10.1155/2013/197845

Research Article

Robust Fuzzy H_∞ Output Feedback Control for a Class of Nonlinear Uncertain Systems with Mixed Time Delays

Xiaona Song and Shanzhong Liu

Electronic and Information Engineering College, Henan University of Science and Technology, Luoyang 471023, China

Correspondence should be addressed to Xiaona Song; xiaona_97@163.com

Received 25 June 2013; Accepted 18 August 2013

Academic Editor: Baoyong Zhang

This paper studies the problem of delay-dependent robust H_∞ output feedback control for a class of uncertain fuzzy neutral systems with both discrete and distributed delays. The system is described by a state-space Takagi-Sugeno fuzzy model with distributed delays and norm-bounded parameter uncertainties. The purpose is to design a fuzzy dynamic output feedback controller which ensures the robust asymptotic stability of the closed-loop fuzzy neutral system and satisfies an H_∞ norm bound constraint for all admissible uncertainties. In terms of linear matrix inequalities, sufficient conditions for the solvability of this problem are presented. Finally, a numerical example is included to demonstrate the effectiveness of the proposed method.

1. Introduction

Fuzzy control, as a promising way to approach nonlinear control problems, has had an impact on the control community [1–4]. Furthermore, the Takagi-Sugeno (*T*-*S*) fuzzy dynamic model [5–9] is nonlinear system described by fuzzy IF-THEN rules which give local linear representations of the underlying systems [10, 11]. It has been shown that such models can describe a wide class of nonlinear systems. Hence it is important to investigate their stability analysis and controller design problems, and in the past two decades many stability and control issues related to the *T*-*S* fuzzy systems have been studied; see, for example, [12–15] and the references cited therein.

On the other hand, time delays exist commonly in dynamic systems due to measurement, transmission, transport lags, and so forth [16], which have been generally regarded as a main source of instability and poor performance. Thus the analysis of time delay systems and controller design for them is very important [17–20]. Recently, *T*-*S* fuzzy systems with time delays have attracted a great deal of interests. For example, in [21], the stability analysis and stabilization problems for *T*-*S* fuzzy delay systems were considered, and state feedback fuzzy controllers and fuzzy observers were designed. The robust H_∞ control problem for *T*-*S* fuzzy systems with time delays was investigated in [22, 23], and state feedback fuzzy controllers were designed; the corresponding results for the discrete case can be found in [24, 25], while in [26, 27], the robust H_∞ output feedback controllers were designed for the continuous and discrete fuzzy time-delay systems, respectively.

Quite recently, *T*-*S* fuzzy time-delay systems of neutral type were introduced in [28], where both the stabilization and H_∞ control problems were studied. It should be point out that distributed delays were not taken into account. While in [29], authors considered the problems of robust stabilization and robust H_∞ control for uncertain *T*-*S* fuzzy neutral systems with both discrete and distributed time delays. However, the results in [28, 29] were all delay-independent. It is known that delay-dependent results are less conservative than delay-independent ones, especially in the case when the size of the delay is small. On the other hand, these obtained results, however, are mainly dealt with through a state feedback controller design method that requires all state variables to be available. In many cases, this condition is too restrictive. So it is meaningful to investigate the output feedback control method. To the best of our knowledge, so far, there are no results of delay-dependent robust H_∞ output feedback control for uncertain fuzzy neutral systems with both discrete and distributed delays. This motives the present studies.

In this paper, we consider the delay-dependent robust H_∞ output feedback control problem for fuzzy neutral systems with both discrete and distributed delays. The system to be considered is described by a state-space T-S fuzzy model with mixed delays and norm-bounded parameter uncertainties. The distributed delays are assumed to appear in the state equation, and the uncertainties are allowed to be time varying but norm bounded. The aim of this paper is to design a full-order fuzzy dynamic output feedback controller such that the resulting closed-loop system is robustly asymptotically stable while satisfying an H_∞ norm condition with a prescribed level irrespective of the parameter uncertainties. A sufficient condition for the solvability of this problem is proposed in terms of linear matrix inequalities (LMIs). When these LMIs are feasible, an explicit expression of a desired output feedback controller is also given.

Notation. Throughout this paper, for real symmetric matrices X and Y, the notation $X \geq Y$ (resp., $X > Y$) means that the matrix $X - Y$ is positive semidefinite (resp., positive definite). I is an identity matrix with appropriate dimension. $\mathbb{N}$ is the set of natural numbers. $\mathscr{L}_2[0,\infty)$ refers to the space of square summable infinite vector sequences. $\|\cdot\|_2$ stands for the usual $\mathscr{L}_2[0,\infty)$ norm. The notation M^T represents the transpose of the matrix M. Matrices, if not explicitly stated, are assumed to have compatible dimensions. "$*$" is used as an ellipsis for terms induced by symmetry.

2. Problem Formulation

A continuous T-S fuzzy neutral model with distributed delays and parameter uncertainties can be described by the following.

Plant Rule i: if $s_1(t)$ is μ_{i1} and $\cdots$ and $s_p(t)$ is μ_{ip}, then

$$\begin{aligned}
\dot{x}(t) = {} & \left[A_i + \Delta A_i(t)\right] x(t) + \left[A_{1i} + \Delta A_{1i}(t)\right] x\left(t-\tau_1\right) \\
& + \left[A_{2i} + \Delta A_{2i}(t)\right] \dot{x}\left(t-\tau_2\right) \\
& + \left[A_{3i} + \Delta A_{3i}(t)\right] \int_{t-\tau_3}^{t} x(s)\, ds \\
& + \left[B_i + \Delta B_i(t)\right] u(t) + D_{1i} w(t), \\
y(t) = {} & \left[C_i + \Delta C_i(t)\right] x(t) + C_{1i} x\left(t-\tau_1\right) + D_{2i} w(t), \\
z(t) = {} & E_i x(t) + E_{1i} x\left(t-\tau_1\right) + G_i u(t), \\
x(t) = {} & \phi(t) \quad \forall t \in [-\overline{\tau}, 0], \ i = 1, 2, \ldots, r,
\end{aligned} \tag{1}$$

where μ_{ij} is the fuzzy set, r is the number of IF-THEN rules, and $s_1(t), \ldots, s_p(t)$ are the premise variables. Throughout this paper, it is assumed that the premise variables do not depend on control variables; $x(t) \in \mathbb{R}^n$ is the state; $u(t) \in \mathbb{R}^m$ is the control input; $y(t) \in \mathbb{R}^s$ is the measured output; $z(t) \in \mathbb{R}^q$ is the controlled output; $w(t) \in \mathbb{R}^p$ is the noise signal; $\tau_i > 0$ $(i = 1, 2, 3)$ are integers representing the time delay of the fuzzy systems; $\overline{\tau} = \max\{\tau_1, \tau_2, \tau_3\}$; A_i, A_{1i}, A_{2i}, A_{3i}, B_i, C_i, C_{1i}, D_{1i}, D_{2i}, E_i, E_{2i}, and G_i are known real constant matrices; $\Delta A_i(t)$, $\Delta A_{1i}(t)$, $\Delta A_{2i}(t)$, $\Delta A_{3i}(t)$, $\Delta B_i(t)$, and $\Delta C_i(t)$ are real-valued unknown matrices representing time-varying parameter uncertainties and are assumed to be of the form

$$\begin{aligned}
&\left[\Delta A_i(t) \ \ \Delta A_{1i}(t) \ \ \Delta A_{2i}(t) \ \ \Delta A_{3i}(t) \ \ \Delta B_i(t) \ \ \Delta C_i(t)\right] \\
&\quad = M_i F_i(t) \left[N_{0i} \ \ N_{1i} \ \ N_{2i} \ \ N_{3i} \ \ N_{4i} \ \ N_{5i}\right] \quad i = 1, 2, \ldots, r,
\end{aligned} \tag{2}$$

where M_i, N_{0i}, N_{1i}, N_{2i}, N_{3i}, N_{4i}, and N_{5i} are known real constant matrices and $F_i(\cdot) : \mathbb{N} \to \mathbb{R}^{I_1 \times I_2}$ are unknown time-varying matrix function satisfying

$$F_i(t)^T F_i(t) \leq I, \quad \forall t. \tag{3}$$

The parameter uncertainties $\Delta A_i(t)$, $\Delta A_{1i}(t)$, $\Delta A_{2i}(t)$, $\Delta A_{3i}(t)$, $\Delta B_i(t)$, and $\Delta C_i(t)$ are said to be admissible if both (2) and (3) hold.

Then the final output of the fuzzy neutral system is inferred as follows:

$$\begin{aligned}
\dot{x}(t) = {} & \sum_{i=1}^{r} h_i(s(t)) \Big\{ \left[A_i + \Delta A_i(t)\right] x(t) \\
& + \left[A_{1i} + \Delta A_{1i}(t)\right] x\left(t-\tau_1\right) \\
& + \left[A_{2i} + \Delta A_{2i}(t)\right] \dot{x}\left(t-\tau_2\right) \\
& + \left[A_{3i} + \Delta A_{3i}(t) \int_{t-\tau_3}^{t} x(s)\, ds\right] \\
& + \left[B_i + \Delta B_i(t)\right] u(t) + D_{1i} w(t) \Big\}, \\
y(t) = {} & \sum_{i=1}^{r} h_i(s(t)) \left\{ \left[C_i + \Delta C_i(t)\right] x(t) \right. \\
& \left. + C_{1i} x\left(t-\tau_1\right) + D_{2i} w(t) \right\}, \\
z(t) = {} & \sum_{i=1}^{r} h_i(s(t)) \left[E_i x(t) + E_{1i} x\left(t-\tau_1\right) + G_i u(t)\right],
\end{aligned} \tag{4}$$

where

$$\begin{aligned}
h_i(s(t)) &= \frac{\varpi_i(s(t))}{\sum_{i=1}^{r} \varpi_i(s(t))}, \\
\varpi_i(s(t)) &= \prod_{j=1}^{p} \mu_{ij}\left(s_j(t)\right), \\
s(t) &= \left[s_1(t) \ \ s_2(t) \ \ \cdots \ \ s_p(t)\right],
\end{aligned} \tag{5}$$

in which $\mu_{ij}(s_j(t))$ is the grade of membership of $s_j(t)$ in μ_{ij}. Then, it can be seen that

$$\begin{aligned}
&\varpi_i(s(t)) \geq 0, \quad i = 1, \ldots, r, \\
&\sum_{i=1}^{r} \varpi_i(s(t)) > 0,
\end{aligned} \tag{6}$$

for all t. Therefore, for all t,

$$h_i(s(t)) \geq 0, \quad i = 1, \ldots, r,$$
$$\sum_{i=1}^{r} h_i(s(t)) = 1, \quad \forall t. \tag{7}$$

Now, by the parallel distributed compensation (PDC), the following full-order fuzzy dynamic output feedback controller for the fuzzy neutral system in (4) is considered.

Control Rule i: if $s_1(t)$ is μ_{i1} and $\cdots$ and $s_p(t)$ is μ_{ip}, then

$$\dot{\hat{x}}(t) = A_{ki}\hat{x}(t) + B_{ki}y(t), \tag{8}$$
$$u(t) = C_{ki}\hat{x}(t), \quad i = 1, 2, \ldots, r, \tag{9}$$
$$\hat{x}(t) = 0, \quad t \leq 0, \tag{10}$$

where $\hat{x}(t) \in \mathbb{R}^n$ is the controller state and A_{ki}, B_{ki}, and C_{ki} are matrices to be determined later. Then, the overall fuzzy output feedback controller is given by

$$\dot{\hat{x}}(t) = \sum_{i=1}^{r} h_i(s(t)) \left[A_{ki}\hat{x}(t) + B_{ki}y(t)\right], \tag{11}$$
$$u(t) = \sum_{i=1}^{r} h_i(s(t)) C_{ki}\hat{x}(t), \quad i = 1, 2, \ldots, r. \tag{12}$$

From (4) and (11), one can obtain the closed-loop system as

$$\begin{aligned}\dot{e}(t) = \sum_{i=1}^{r}\sum_{j=1}^{r} h_i(s(t)) h_j(s(t)) \\ \times \Bigg\{ \left[A_{ij} + \Delta A_{ij}(t)\right] e(t) \\ + \left[A_{1ij} + \Delta\widetilde{A}_{1i}(t)\right] e(t-\tau_1) \\ + \left[\widetilde{A}_{2i} + \Delta\widetilde{A}_{2i}(t)\right] \dot{e}(t-\tau_2) \\ + \left[\widetilde{A}_{3i} + \Delta\widetilde{A}_{3i}(t)\right] \\ \times \int_{t-\tau_3}^{t} e(s)\, ds + D_{ij}w(t) \Bigg\},\end{aligned} \tag{13}$$

$$z(t) = \sum_{i=1}^{r}\sum_{j=1}^{r} h_i(s(t)) h_j(s(t)) \left[E_{ij}e(t) + \widetilde{E}_{1i}e(t-\tau_1)\right], \tag{14}$$

where

$$\dot{e}(t) = \begin{bmatrix}\dot{x}(t) \\ \dot{\hat{x}}(t)\end{bmatrix},$$
$$A_{ij} = \begin{bmatrix}A_i & B_iC_{kj} \\ B_{kj}C_i & A_{kj}\end{bmatrix},$$
$$\Delta A_{ij}(t) = \begin{bmatrix}\Delta A_i(t) & \Delta B_i(t) C_{kj} \\ B_{kj}\Delta C_i(t) & 0\end{bmatrix},$$
$$A_{1ij} = \begin{bmatrix}A_{1i} & 0 \\ B_{kj}C_{1i} & 0\end{bmatrix}, \qquad \Delta\widetilde{A}_{1i}(t) = \begin{bmatrix}\Delta A_{1i}(t) & 0 \\ 0 & 0\end{bmatrix},$$
$$\widetilde{A}_{2i} = \begin{bmatrix}A_{2i} & 0 \\ 0 & 0\end{bmatrix}, \qquad \Delta\widetilde{A}_{2i}(t) = \begin{bmatrix}\Delta A_{2i}(t) & 0 \\ 0 & 0\end{bmatrix},$$
$$\widetilde{A}_{3i} = \begin{bmatrix}A_{3i} & 0 \\ 0 & 0\end{bmatrix}, \qquad \Delta\widetilde{A}_{3i}(t) = \begin{bmatrix}\Delta A_{3i}(t) & 0 \\ 0 & 0\end{bmatrix},$$
$$D_{ij} = \begin{bmatrix}D_{1i} \\ B_{kj}D_{2i}\end{bmatrix}, \qquad E_{ij} = \begin{bmatrix}E_i & G_iC_{kj}\end{bmatrix},$$
$$\widetilde{E}_{1i} = \begin{bmatrix}E_{1i} & 0\end{bmatrix}. \tag{15}$$

Then, the problem of robust fuzzy H_∞ control problem to be addressed in the previous is formulated as follows: given an uncertain distributed delay fuzzy neutral system in (4) and a scalar $\gamma > 0$, determine a dynamic output feedback fuzzy controller in the form of (8) and (9) such that the closed-loop system in (13) and (14) is robustly asymptotically stable when $w(t) = 0$ and

$$\|z\|_2 < \gamma\|w\|_2, \tag{16}$$

under zero-initial conditions for any nonzero $w(t) \in \mathscr{L}_2[0, \infty)$ and all admissible uncertainties.

3. Main Results

In this section, an LMI approach will be developed to solve the problem of robust output feedback H_∞ control of uncertain distributed delay fuzzy neutral systems formulated in the previous section. We first give the following results which will be used in the proof of our main results.

Lemma 1 (see [30]). *Let $\mathscr{A}$, $\mathscr{D}$, $\mathscr{S}$, $\mathscr{W}$, and F be real matrices of appropriate dimensions with $\mathscr{W} > 0$ and F satisfying $F^TF \leq I$. Then one has the following.*

(1) *For any scalar $\epsilon > 0$ and vectors x, $y \in \mathbb{R}^n$,*

$$2x^T\mathscr{D}\mathscr{F}\mathscr{S}y \leq \epsilon^{-1}x^T\mathscr{D}\mathscr{D}^Tx + \epsilon y^T\mathscr{S}^T\mathscr{S}y. \tag{17}$$

(2) *For any scalar $\epsilon > 0$ such that $\mathscr{W} - \epsilon\mathscr{D}\mathscr{D}^T > 0$,*

$$\begin{aligned}(\mathscr{A} + \mathscr{D}\mathscr{F}\mathscr{S})^T\mathscr{W}^{-1}(\mathscr{A} + \mathscr{D}\mathscr{F}\mathscr{S}) \\ \leq \mathscr{A}^T\left(\mathscr{W} - \epsilon\mathscr{D}\mathscr{D}^{\mathscr{T}}\right)^{-1}\mathscr{A} + \epsilon^{-1}\mathscr{S}^T\mathscr{S}.\end{aligned} \tag{18}$$

Lemma 2 (see [31]). *Given any matrices $\mathcal{X}$, $\mathcal{Y}$, and $\mathcal{Z}$ with appropriate dimensions such that $\mathcal{Y} > 0$, then, one has*

$$\mathcal{X}^T\mathcal{Z} + \mathcal{Z}^T\mathcal{X} \le \mathcal{X}^T\mathcal{Y}\mathcal{X} + \mathcal{Z}^T\mathcal{Y}^{-1}\mathcal{Z}. \tag{19}$$

Theorem 3. *The uncertain fuzzy neutral delay system in* (13) *and* (14) *is asymptotically stable, and* (16) *is satisfied if there exist matrices $P > 0$, $P_1 > 0$, $P_2 > 0$, $Q_1 > 0$, $Q_2 > 0$, R_1, and R_2 and scalars $\epsilon_{ij} > 0$, $1 \le i \le j \le r$, such that the following LMIs hold:*

$$\begin{bmatrix}
\Pi_{1ii} & \Pi_{2ii} & P\widetilde{A}_{2i} & P\widetilde{A}_{3i} & PD_{ii} & \tau_1 R_1 & E_{ii}^T & \Gamma_{ii} & PM_{ii} & N_{ii}^T \\
* & J_1 & 0 & 0 & 0 & \tau_1 R_2 & E_{1i}^T & \Gamma_{1ii} & 0 & 0 \\
* & * & -P_2 & 0 & 0 & 0 & 0 & \Gamma_{2i} & 0 & 0 \\
* & * & * & -Q_2 & 0 & 0 & 0 & \Gamma_{3i} & 0 & 0 \\
* & * & * & * & -\gamma^2 I & 0 & 0 & \Gamma_{4ii} & 0 & 0 \\
* & * & * & * & * & -\tau_1 Q_1 & 0 & 0 & 0 & 0 \\
* & * & * & * & * & * & -I & 0 & 0 & 0 \\
* & * & * & * & * & * & * & -J_2^T & J_2^T M_{ii} & 0 \\
* & * & * & * & * & * & * & * & -\epsilon_{ii} I & 0 \\
* & * & * & * & * & * & * & * & * & -\epsilon_{ii}^{-1} I
\end{bmatrix} < 0, \quad 1 \le i \le r,$$

$$\begin{bmatrix}
\Lambda_{1ij} & \Lambda_{2ij} & \Lambda_{3ij} \\
* & \Lambda_{4ij} & \Lambda_{5ij} \\
* & * & \Lambda_{6ij}
\end{bmatrix} < 0, \quad 1 \le i < j \le r, \tag{20}$$

where

$$\Lambda_{1ij} = \begin{bmatrix}
\Pi_{1ij} + \Pi_{1ji} & \Pi_{2ij} + \Pi_{2ji} & P\widetilde{A}_{2i} + P\widetilde{A}_{2j} & P\widetilde{A}_{3i} + P\widetilde{A}_{3j} \\
* & 2J_1 & 0 & 0 \\
* & * & -2P_2 & 0 \\
* & * & * & -2Q_2
\end{bmatrix},$$

$$\Lambda_{2ij} = \begin{bmatrix}
PD_{ij} + PD_{ji} & 2\tau_1 R_1 & E_{ij}^T + E_{ji}^T & \Gamma_{ij} + \Gamma_{ji} \\
0 & 2\tau_1 R_2 & \widetilde{E}_{1i}^T + \widetilde{E}_{1j}^T & \Gamma_{1ij} + \Gamma_{1ji} \\
0 & 0 & 0 & \Gamma_{2i} + \Gamma_{2j} \\
0 & 0 & 0 & \Gamma_{3i} + \Gamma_{3j}
\end{bmatrix},$$

$$\Lambda_{3ij} = \begin{bmatrix}
PM_{ij} & PM_{ji} & N_{ij}^T & N_{ji}^T \\
0 & 0 & \widetilde{N}_{1i}^T & \widetilde{N}_{1j}^T \\
0 & 0 & \widetilde{N}_{2i}^T & \widetilde{N}_{2j}^T \\
0 & 0 & \widetilde{N}_{3i}^T & \widetilde{N}_{3j}^T
\end{bmatrix},$$

$$\Lambda_{4ij} = \begin{bmatrix}
-2\gamma^2 I & 0 & 0 & \Gamma_{4ij} + \Gamma_{4ji} \\
* & -2\tau_1 Q_1 & 0 & 0 \\
* & * & -2I & 0 \\
* & * & * & -2J_2^T
\end{bmatrix},$$

$$\Lambda_{5ij} = \begin{bmatrix}
0 & 0 & 0 & 0 \\
0 & 0 & 0 & 0 \\
0 & 0 & 0 & 0 \\
J_2^T M_{ij} & J_2^T M_{ji} & 0 & 0
\end{bmatrix},$$

$$\Lambda_{6ij} = \begin{bmatrix}
-\epsilon_{ij} I & 0 & 0 & 0 \\
* & -\epsilon_{ji} I & 0 & 0 \\
* & * & -\epsilon_{ij}^{-1} I & 0 \\
* & * & * & -\epsilon_{ji}^{-1} I
\end{bmatrix},$$

$$\begin{aligned}
\Upsilon_1 &= H^T\left(P_1 + \tau_3^2 Q_2 - R_1 - R_1^T\right)H, \\
\Pi_{1ij} &= \Upsilon_1 + PA_{ij} + A_{ij}^T P, \\
\Upsilon_2 &= H^T\left(R_1 - R_2^T\right), \qquad \Pi_{2ij} = \Upsilon_2 + PA_{1ij}, \\
\Gamma_{ij} &= A_{ij}^T\left(P_2 + \tau_1 Q_1\right), \\
\Gamma_{1ij} &= A_{1ij}^T\left(P_2 + \tau_1 Q_1\right), \qquad \Gamma_{2i} = \widetilde{A}_{2i}^T\left(P_2 + \tau_1 Q_1\right), \\
\Gamma_{3i} &= \widetilde{A}_{3i}^T\left(P_2 + \tau_1 Q_1\right), \qquad \Gamma_{4ij} = D_{ij}^T\left(P_2 + \tau_1 Q_1\right), \\
J_1 &= -P_1 + R_2 + R_2^T, \qquad J_2 = P_2 + \tau_1 Q_1, \\
M_{ij} &= \begin{bmatrix} M_i & 0 \\ 0 & B_{kj} M_i \end{bmatrix}, \qquad \widetilde{F}_i(t) = \begin{bmatrix} F_i(t) & 0 \\ 0 & F_i(t) \end{bmatrix}, \\
N_{ij} &= \begin{bmatrix} N_{0i} & N_{3i} C_{kj} \\ N_{4i} & 0 \end{bmatrix}, \qquad \widetilde{N}_{1i} = \begin{bmatrix} N_{1i} & 0 \\ 0 & 0 \end{bmatrix}, \\
\widetilde{N}_{2i} &= \begin{bmatrix} N_{2i} & 0 \\ 0 & 0 \end{bmatrix}, \qquad \widetilde{N}_{3i} = \begin{bmatrix} N_{3i} & 0 \\ 0 & 0 \end{bmatrix}.
\end{aligned} \tag{21}$$

Proof. To establish the robust stability of the system in (13), we consider (13) with $w(t) \equiv 0$; that is,

$$\begin{aligned}
\dot{e}(t) = \sum_{i=1}^{r}\sum_{j=1}^{r} & h_i(s(t))\, h_j(s(t)) \\
& \times \Big\{ \left[A_{ij} + \Delta A_{ij}(t)\right] e(t) \\
& + \left[A_{1ij} + \Delta\widetilde{A}_{1i}(t)\right] e(t - \tau_1) \\
& + \left[\widetilde{A}_{2i} + \Delta\widetilde{A}_{2i}(t)\right] \dot{e}(t - \tau_2) \\
& + \left[\widetilde{A}_{3i} + \Delta\widetilde{A}_{3i}(t)\right] \int_{t-\tau_3}^{t} e(s)\, ds \Big\}.
\end{aligned} \tag{22}$$

For this system, we define the following Lyapunov function candidate:

$$V(t) = V_1(t) + V_2(t) + V_3(t) + V_4(t) + V_5(t) + V_6(t), \tag{23}$$

where

$$\begin{aligned} V_1(t) &= e(t)^T P e(t), \\ V_2(t) &= \int_{t-\tau_1}^{t} e(s)^T P_1 e(s)\, ds, \\ V_3(t) &= \int_{t-\tau_2}^{t} \dot{e}(s)^T P_2 \dot{e}(s)\, ds, \\ V_4(t) &= \int_{-\tau_1}^{0} \int_{t+\beta}^{t} \dot{e}(\alpha)^T Q_1 \dot{e}(\alpha)\, d\alpha\, d\beta, \\ V_5(t) &= \int_{t-\tau_3}^{t} \left[\int_{s}^{t} e(\theta)^T d\theta \right] Q_2 \left[\int_{s}^{t} e(\theta)\, d\theta \right] ds, \\ V_6(t) &= \int_{0}^{\tau_3} ds \int_{t-\beta}^{t} (\theta - t + \beta)\, e(\alpha)^T Q_2 e(\alpha)\, d\alpha\, d\beta. \end{aligned} \tag{24}$$

The time derivative of $V(t)$ is given by

$$\dot{V}(t) = \dot{V}_1(t) + \dot{V}_2(t) + \dot{V}_3(t) + \dot{V}_4(t) + \dot{V}_5(t) + \dot{V}_6(t), \tag{25}$$

where

$$\begin{aligned} \dot{V}_1(t) &= 2e(t)^T P \dot{e}(t), \\ \dot{V}_2(t) &= e(t)^T P_1 e(t) - e(t-\tau_1)^T P_1 e(t-\tau_1), \\ \dot{V}_3(t) &= \dot{e}(t)^T P_2 \dot{e}(t) - \dot{e}(t-\tau_2)^T P_2 \dot{e}(t-\tau_2), \\ \dot{V}_4(t) &= \tau_1 \dot{e}(t)^T Q_1 \dot{e}(t) - \int_{t-\tau_1}^{t} \dot{e}(\alpha)^T Q_1 \dot{e}(\alpha)\, d\alpha, \\ \dot{V}_5(t) &= 2 \int_{t-\tau_3}^{t} (\theta - t + \tau_3)\, e(t)^T Q_2 e(\theta)\, d\theta \\ &\quad - \left[\int_{t-\tau_3}^{t} e(\theta)^T d\theta \right] Q_2 \left[\int_{t-\tau_3}^{t} e(\theta)\, d\theta \right], \\ \dot{V}_6(t) &= \frac{1}{2}\tau_3^2 e(t)^T Q_2 e(t) - \int_{t-\tau_3}^{t} (\theta - t + \tau_3)\, e(\theta)^T Q_2 e(\theta)\, d\theta. \end{aligned} \tag{26}$$

Now, by Lemma 1, it can be shown that

$$2e(t)^T Q_2 e(\theta) \le e(t)^T Q_2 e(t) + e(\theta)^T Q_2 e(\theta). \tag{27}$$

Therefore

$$\begin{aligned} \dot{V}_5(t) \le{}& \frac{1}{2}\tau_3^2 e(t)^T Q_2 e(t) \\ &+ \int_{t-\tau_3}^{t} (\theta - t + \tau_3)\, e(\theta)^T Q_2 e(\theta)\, d\theta \\ &- \left[\int_{t-\tau_3}^{t} e(\theta)^T d\theta \right] Q_2 \left[\int_{t-\tau_3}^{t} e(\theta)\, d\theta \right]. \end{aligned} \tag{28}$$

This together with (26) implies

$$\dot{V}_5(t) + \dot{V}_6(t) \le \tau_3^2 e(t)^T Q_2 e(t) - \alpha(t)^T Q_2 \alpha(t), \tag{29}$$

where

$$\alpha(t) = \int_{t-\tau_3}^{t} e(\theta)\, d\theta. \tag{30}$$

Then, there holds

$$\begin{aligned} \dot{V}(t) \le{}& 2e(t)^T P \dot{e}(t) \\ &+ e(t)^T P_1 e(t) - e(t-\tau_1)^T P_1 e(t-\tau_1) \\ &+ \dot{e}(t)^T P_2 \dot{e}(t) - \dot{e}(t-\tau_2)^T P_2 \dot{e}(t-\tau_2) \\ &+ \tau_1 \dot{e}(t)^T Q_1 \dot{e}(t) - \int_{t-\tau_1}^{t} \dot{e}(\alpha)^T Q_1 \dot{e}(\alpha)\, d\alpha \\ &+ \tau_3^2 e(t)^T Q_2 e(t) - \alpha(t)^T Q_2 \alpha(t) \\ &+ 2e(t)^T R_1 \int_{t-\tau_1}^{t} \dot{e}(\alpha)\, d\alpha \\ &- 2e(t)^T R_1 \left[e(t) - e(t-\tau_1) \right] \\ &+ 2e(t-\tau_1)^T R_2 \int_{t-\tau_1}^{t} \dot{e}(\alpha)\, d\alpha \\ &- 2e(t-\tau_1)^T R_2 \left[e(t) - e(t-\tau_1) \right]. \end{aligned} \tag{31}$$

It follows from (22) and Lemma 2 that

$$\begin{aligned} &2e(t)^T P \dot{e}(t) \\ &= 2e(t)^T P \sum_{i=1}^{r} \sum_{j=1}^{r} h_i(s(t))\, h_j(s(t)) \\ &\qquad \times \left\{ \left[A_{ij} + \Delta A_{ij}(t) \right] e(t) \right. \\ &\qquad\quad + \left[A_{1ij} + \Delta \widetilde{A}_{1i}(t) \right] e(t-\tau_1) \\ &\qquad\quad + \left[\widetilde{A}_{2i} + \Delta \widetilde{A}_{2i}(t) \right] \dot{e}(t-\tau_2) \\ &\qquad\quad \left. + \left[\widetilde{A}_{3i} + \Delta \widetilde{A}_{3i}(t) \right] \int_{t-\tau_3}^{t} e(s)\, ds \right\} \\ &\le 2 \sum_{i=1}^{r} \sum_{j=1}^{r} h_i(s(t))\, h_j(s(t))\, e(t)^T P \overline{A}_{ij} \beta(t) \\ &\quad + \sum_{i=1}^{r} \sum_{j=1}^{r} h_i(s(t))\, h_j(s(t)) \\ &\qquad \times \left[\varepsilon_{1ij}^{-1} e(t)^T P M_{ij} M_{ij}^T P e(t) \right. \\ &\qquad\quad \left. + \varepsilon_{1ij} \beta(t)^T \widetilde{N}_{ij}^T \widetilde{N}_{ij} \beta(t) \right], \end{aligned} \tag{32}$$

where

$$\begin{aligned} \overline{A}_{ij} &= \left[A_{ij} \;\; A_{1ij} \;\; \widetilde{A}_{2i} \;\; \widetilde{A}_{3i} \right], \\ \beta(t) &= \left[e(t)^T \;\; e(t-\tau_1)^T \;\; \dot{e}(t-\tau_2)^T \;\; \alpha(t)^T \;\; \dot{e}(\alpha)^T \right], \\ \widetilde{N}_{ij} &= \left[N_{ij} \;\; \widetilde{N}_{1i} \;\; \widetilde{N}_{2i} \;\; \widetilde{N}_{3i} \right]. \end{aligned} \tag{33}$$

It also can be verified that

$$\begin{aligned}
&\dot{e}(t)^T P_2 \dot{e}(t) \\
&= \frac{1}{2}\sum_{i=1}^{r}\sum_{j=1}^{r}\sum_{u=1}^{r}\sum_{v=1}^{r} h_i(s(t))\, h_j(s(t))\, h_u(s(t))\, h_v(s(t))\, \beta(t)^T \\
&\qquad \times \left\{\left[\overline{A}_{ij} + M_{ij}\widetilde{F}_i(t)\widetilde{N}_{ij}\right]^T \right. \\
&\qquad\quad \times P_2\left[\overline{A}_{uv} + M_{uv}\widetilde{F}_u(t)\,\widetilde{N}_{uv}\right] \\
&\qquad\quad + \left[\overline{A}_{uv} + M_{uv}\widetilde{F}_u(t)\,\widetilde{N}_{uv}\right]^T \\
&\qquad\quad \left. \times P_2\left[\overline{A}_{ij} + M_{ij}\widetilde{F}_i(t)\,\widetilde{N}_{ij}\right]\right\}\beta(t) \\
&\le \sum_{i=1}^{r}\sum_{j=1}^{r} h_i(s(t))\, h_j(s(t))\, \beta(t)^T \\
&\qquad \times \left[\overline{A}_{ij} + M_{ij}\widetilde{F}_i(t)\,\widetilde{N}_{ij}\right]^T P_2\left[\overline{A}_{ij} + M_{ij}\widetilde{F}_i(t)\,\widetilde{N}_{ij}\right] \\
&\le \sum_{i=1}^{r}\sum_{j=1}^{r} h_i(s(t))\, h_j(s(t))\, \beta(t)^T \\
&\qquad \times \left[\overline{A}_{ij}^T\left(P_2^{-1} - \varepsilon_{2ij}^{-1}M_{ij}M_{ij}^T\right)^{-1}\overline{A}_{ij} + \varepsilon_{2ij}\widetilde{N}_{ij}^T\widetilde{N}_{ij}\right]\beta(t), \\
&\tau_1\dot{e}(t)^T Q_1 \dot{e}(t) \\
&\le \sum_{i=1}^{r}\sum_{j=1}^{r} h_i(s(t))\, h_j(s(t))\, \beta(t)^T \\
&\qquad \times \left\{\overline{A}_{ij}^T\left[(\tau_1 Q_1)^{-1} - \varepsilon_{3ij}^{-1}M_{ij}M_{ij}^T\right]^{-1}\overline{A}_{ij} \right. \\
&\qquad\quad \left. + \varepsilon_{3ij}\widetilde{N}_{ij}^T\widetilde{N}_{ij}\right\}\beta(t).
\end{aligned} \tag{34}$$

Hence, with the support of the above conditions, we have

$$\begin{aligned}
\dot{V}(t) &\le 2e(t)^T P\dot{e}(t) + \dot{e}(t)^T P_2\dot{e}(t) \\
&\quad + \tau_1\dot{e}(t)^T Q_1\dot{e}(t) + e(t)^T\left(P_1 + \tau_3^2 Q_2\right)e(t) \\
&\quad - e(t-\tau_1)^T P_1 e(t-\tau_1) \\
&\quad - \dot{e}(t-\tau_2)^T P_2\dot{e}(t-\tau_2) - \int_{t-\tau_1}^{t}\dot{e}(\alpha)^T Q_1\dot{e}(\alpha)\,d\alpha \\
&\quad - \alpha(t)^T Q_2\alpha(t) + 2e(t)^T R_1\int_{t-\tau_1}^{t}\dot{e}(\alpha)\,d\alpha \\
&\quad - 2e(t)^T R_1\left[e(t) - e(t-\tau_1)\right] \\
&\quad + 2e(t-\tau_1)^T R_2\int_{t-\tau_1}^{t}\dot{e}(\alpha)\,d\alpha - 2e(t-\tau_1)^T \\
&\quad \times R_2\left[e(t) - e(t-\tau_1)\right] \\
&= \sum_{i=1}^{r}\sum_{j=1}^{r} h_i(s(t))\, h_j(s(t))\, \beta(t)^T \\
&\quad \times \left[\Xi_{ij} + \overline{A}_{ij}\left(P_2^{-1} - \varepsilon_{2ij}^{-1}M_{ij}M_{ij}^T\right)^{-1}\overline{A}_{ij}\right. \\
&\quad \left. + \overline{A}_{ij}\left(\tau_1^{-1}Q_1^{-1} - \varepsilon_{3ij}^{-1}M_{ij}M_{ij}^T\right)^{-1}\overline{A}_{ij} + \delta_{ij}\widetilde{N}_{ij}^T\widetilde{N}_{ij}\right]\beta(t),
\end{aligned} \tag{35}$$

where

$$\Xi_{ij} = \begin{bmatrix}
\Sigma_{ij} & PA_{1ij} + R_1 - R_2^T & P\widetilde{A}_{2i} & P\widetilde{A}_{3i} & \tau_1 R_1 \\
* & -P_1 + R_2 + R_2^T & 0 & 0 & \tau_1 R_2 \\
* & * & -P_2 & 0 & 0 \\
* & * & * & -Q_2 & 0 \\
* & * & * & * & -\tau_1 Q_1
\end{bmatrix},$$

$$\Sigma_{ij} = PA_{ij} + A_{ij}^T P + P_1 + \tau_3^2 Q_2 - R_1 - R_1^T + \varepsilon_{1ij}^{-1}PM_{ij}M_{ij}^T P, \tag{36}$$

for $1 \le i \le j \le r$. On the other hand, by applying the Schur complement formula to (20), we have that for $1 \le i < j \le r$,

$$\Gamma_{ij} < 0, \tag{37}$$

and from this and (7), we have that $\dot{V}(t) < 0$ for all $\beta(t) \neq 0$. Therefore, the system in (13) is robustly asymptotically stable.

This completes the proof. □

Next, we will establish the robust H_∞ performance of the system in (13) and (14) under the zero initial condition. To this end, we introduce

$$J(t) = \int_0^t \left[z(s)^T z(s) - \gamma^2 w(s)^T w(s)\right]ds, \tag{38}$$

where $t > 0$. Noting the zero initial condition, it can be shown that for any nonzero $w(t) \in \mathscr{L}_2[0,\infty)$ and $t > 0$,

$$\begin{aligned}
J(t) &= \int_0^t \left[z(s)^T z(s) - \gamma^2 w(s)^T w(s) + \dot{V}(s)\right]ds - V(t) \\
&\le \int_0^t \left[z(s)^T z(s) - \gamma^2 w(s)^T w(s) + \dot{V}(s)\right]ds,
\end{aligned} \tag{39}$$

where $V(s)$ is defined in (23), and then we have

$$\begin{aligned}
\dot{V}(t) &= \sum_{i=1}^{r}\sum_{j=1}^{r} h_i(s(t))\, h_j(s(t)) \\
&\quad \times \left\{2e(t)^T P\left[A_{ij}(t)\,e(t) + A_{1ij}(t)\,e(t-\tau_1)\right.\right. \\
&\quad + A_{2i}(t)\,\dot{e}(t-\tau_2) \\
&\quad \left.\left. + A_{3i}(t)\,\alpha(t) + D_{ij}w(t)\right]\right\}
\end{aligned}$$

$$
\begin{aligned}
&+ e(t)^T P_1 e(t) - e(t-\tau_1)^T P_1 e(t-\tau_1) \\
&+ \dot{e}(t)^T P_2 \dot{e}(t) - \dot{e}(t-\tau_2)^T P_2 \dot{e}(t-\tau_2) \\
&+ \tau_1 \dot{e}(t)^T Q_1 \dot{e}(t) \\
&- \int_{t-\tau_1}^{t} \dot{e}(t)^T Q_1 \dot{e}(\alpha)\, d\alpha + \tau_3^2 e(t)^T Q_2 e(t) \\
&- \alpha(t)^T Q_2 \alpha(t) \\
&+ 2e(t)^T R_1 \int_{t-\tau_1}^{t} \dot{e}(\alpha)\, d\alpha - 2e(t)^T \\
&\times R_1 \left[e(t) - e(t-\tau_1)\right] \\
&+ 2e(t-\tau_1)^T R_2 \int_{t-\tau_1}^{t} \dot{e}(\alpha)\, d\alpha - 2e(t-\tau_1)^T \\
&\times R_2 \left[e(t) - e(t-\tau_1)\right].
\end{aligned} \tag{40}
$$

Then, by noting (14) and using Lemma 2, we have

$$
\begin{aligned}
z(s)^T z(s) &= \sum_{i=1}^{r}\sum_{j=1}^{r}\sum_{u=1}^{r}\sum_{v=1}^{r} h_i(s(s))\, h_j(s(s))\, h_u(s(s)) \\
&\quad \times h_v(s(s))\, \zeta(s)^T \widetilde{E}_{ij}^T \widetilde{E}_{uv} \zeta(s) \\
&\le \sum_{i=1}^{r}\sum_{j=1}^{r} h_i(s(s))\, h_j(s(s))\, \zeta(s)^T \widetilde{E}_{ij}^T \widetilde{E}_{ij} \zeta(s).
\end{aligned} \tag{41}
$$

It can be deduced that

$$
\begin{aligned}
&z(s)^T z(s) - \gamma^2 w(s)^T w(s) + \dot{V}(s) \\
&\quad \le \sum_{i=1}^{r}\sum_{j=1}^{r} h_i(s(s))\, h_j(s(s))\, \zeta(s)^T \Pi_{1ij} \zeta(s) \\
&\quad = \sum_{i=1}^{r} h_i(s(s))^2 \zeta(s)^T \Xi_{1ii} \zeta(s) \\
&\qquad + 2 \sum_{i,j=1, i<j}^{r} h_i(s(s))\, h_j(s(s))\, \zeta(s)^T \frac{\Xi_{1ij} + \Xi_{1ji}}{2} \zeta(s),
\end{aligned} \tag{42}
$$

where

$$
\Xi_{1ij} = \begin{bmatrix}
\Sigma_{ij} & PA_{1ij}(t) + R_1 - R_2^T & PA_{2i}(t) & PA_{3i}(t) & PD_{ij} & \tau_1 R_1 & E_{ij}^T & A_{ij}^T(t)\left(P_2 + \tau_1 Q_1\right) \\
* & J_1 & 0 & 0 & 0 & \tau_1 R_2 & \widetilde{E}_{1i}^T & A_{1ij}^T(t)\left(P_2 + \tau_1 Q_1\right) \\
* & * & -P_2 & 0 & 0 & 0 & 0 & A_{2i}^T(t)\left(P_2 + \tau_1 Q_1\right) \\
* & * & * & -Q_2 & 0 & 0 & 0 & A_{3i}^T(t)\left(P_2 + \tau_1 Q_1\right) \\
* & * & * & * & -\gamma^2 I & 0 & 0 & D_{ij}^T\left(P_2 + \tau_1 Q_1\right) \\
* & * & * & * & * & -\tau_1 Q_2 & 0 & 0 \\
* & * & * & * & * & * & -I & 0 \\
* & * & * & * & * & * & * & -\left(P_2 + \tau_1 Q_1\right)^T
\end{bmatrix}, \tag{43}
$$

$$
\zeta(s) = \left[e(t)^T \;\; e(t-\tau_1)^T \;\; \dot{e}(t-\tau_2)^T \;\; \alpha(t)^T \;\; w(t)^T \;\; \dot{e}(\alpha)^T\right]^T,
$$

$$
\widetilde{E}_{ij} = \left[E_{ij} \;\; \widetilde{E}_{1i} \;\; 0 \;\; 0 \;\; 0 \;\; 0\right],
$$

for $1 \le i < j \le r$. Similar to the previous section, applying the Schur complement formula to the LMI in (20) results in $\Xi_{1ij} < 0, 1 \le i < j \le r$, which together with (39) gives $J(t) < 0$ for any nonzero $w(t) \in \mathscr{L}_2[0, \infty)$ and $t > 0$. Therefore, we have $\|z\|_2 < \gamma \|w\|_2$.

Now, we are in a position to present a solution to the robust output feedback H_∞ control problem.

Theorem 4. *Consider the uncertain fuzzy neutral delay system in* (1)*, and let $\gamma > 0$ be a prescribed constant scalar. The robust H_∞ problem is solvable if there exist matrices $X > 0$, $Y > 0$, Q_1, Q_2, Φ_i, Ψ_i, and Ω_i and scalars ϵ_{ij}, $1 \le i \le j \le r$, such that the following LMIs hold:*

$$
\begin{bmatrix}
\Sigma_{ii} & \Sigma_{1ii} & \Sigma_{2ii} & \Sigma_{3ii} & R_5 \\
* & -R_{11} & R_{2ii} & 0 & 0 \\
* & * & R_{3ii} & 0 & R_{6ii} \\
* & * & * & -R_4 & 0 \\
* & * & * & * & -R_7
\end{bmatrix} < 0, \quad 1 \le i \le r, \tag{44}
$$

$$\begin{bmatrix} \Sigma_{ij}+\Sigma_{ji} & \Sigma_{1ij}+\Sigma_{1ji} & \widetilde{\Sigma}_{2ij} & \Sigma_{4ij} & \Sigma_{5ij} & \Sigma_{6ij} & 0 \\ * & -2R_{11} & \widetilde{R}_{2ij} & 0 & 0 & 0 & 0 \\ * & * & \widetilde{R}_{3ij} & 0 & 0 & 0 & \widetilde{R}_{6ij} \\ * & * & * & -I & 0 & 0 & 0 \\ * & * & * & * & -R_8 & 0 & 0 \\ * & * & * & * & * & -I & 0 \\ * & * & * & * & * & * & -I \end{bmatrix} < 0, \quad 1 \le i < j \le r, \tag{45}$$

$$\begin{bmatrix} -Y & -I \\ -I & -X \end{bmatrix} < 0, \tag{46}$$

where

$$\Theta_{ij} = \begin{bmatrix} A_iX + XA_i^T + B_i\Psi_j + \Psi_j^TB_i^T & A_i + \Omega_i^T \\ A_i^T + \Omega_i & YA_i + A_i^TY + \Phi_jC_i + C_i^T\Phi_j^T \end{bmatrix} - R_1 - R_1^T,$$

$$\Theta_{1ij} = \begin{bmatrix} A_{1i}X & A_{1i} \\ 0 & YA_{1i} + \Phi_jC_{1i} \end{bmatrix} + R_1 - R_2^T,$$

$$\Theta_{2i} = \begin{bmatrix} A_{2i} & 0 \\ YA_{2i} & 0 \end{bmatrix}, \qquad \Theta_{3i} = \begin{bmatrix} A_{3i} & 0 \\ YA_{3i} & 0 \end{bmatrix},$$

$$\Theta_{4ij} = \begin{bmatrix} D_{1i} \\ YD_{1i} + \Phi_jD_{2i} \end{bmatrix}, \qquad \Theta_{5ij} = \begin{bmatrix} XE_i^T + \Psi_j^TG_i^T \\ E_i^T \end{bmatrix},$$

$$\Theta_{6ij} = \begin{bmatrix} XA_i^T + \Psi_j^TB_i^T & \Omega_j^T \\ A_i^T & A_i^TY + C_i^T\Phi_j^T \end{bmatrix},$$

$$\Theta_{7ij} = \begin{bmatrix} M_i & 0 \\ YM_i & \Phi_jM_i \end{bmatrix},$$

$$\Theta_{8ij} = \begin{bmatrix} XN_{0i}^T + \Psi_j^TN_{4i}^T & XN_{5i}^T \\ N_{0i}^T & N_{5i}^T \end{bmatrix}, \qquad J_{3i} = \begin{bmatrix} XE_{1i}^T \\ E_{1i}^T \end{bmatrix},$$

$$J_{4ij} = \begin{bmatrix} XA_{1i} & 0 \\ A_{1i} & A_{1i}Y + C_{1i}^T\Phi_j^T \end{bmatrix},$$

$$J_{5i} = \begin{bmatrix} XN_{1i}^T & 0 \\ N_{1i}^T & 0 \end{bmatrix}, \qquad J_{6i} = \begin{bmatrix} A_{2i}^T & A_{2i}^TY \\ 0 & 0 \end{bmatrix},$$

$$J_{7i} = \begin{bmatrix} A_{3i}^T & A_{3i}^TY \\ 0 & 0 \end{bmatrix},$$

$$J_{8ij} = \begin{bmatrix} D_{1i}^T & D_{1i}^TY + D_{2i}^T\Phi_j^T \end{bmatrix},$$

$$J_9 = \Pi_2^T + \Pi_2 - P_2 - \tau_1Q_1,$$

$$J_{10ij} = \begin{bmatrix} M_i & 0 \\ YM_i & \Phi_jM_i \end{bmatrix},$$

$$\Sigma_{ij} = \begin{bmatrix} \Theta_{ij} & \Theta_{1ij} & \Theta_{2i} \\ * & -U + R_2 + R_2^T & 0 \\ * & * & -P_2 \end{bmatrix},$$

$$\Sigma_{1ij} = \begin{bmatrix} \Theta_{3i} & \Theta_{4ij} & \tau_1R_1 \\ 0 & 0 & \tau_1R_2 \\ 0 & 0 & 0 \end{bmatrix},$$

$$\Sigma_{2ij} = \begin{bmatrix} \Theta_{5ij} & \Theta_{6ij} & \Theta_{7ij} & \Theta_{8ij} \\ J_{3i} & J_{4ij} & 0 & J_{5i} \\ 0 & J_{6i} & 0 & \widetilde{N}_{2i}^T \end{bmatrix},$$

$$\widetilde{\Sigma}_{2ij} = \begin{bmatrix} \Theta_{5ij} + \Theta_{5ji} & \Theta_{6ij} + \Theta_{6ji} & \Theta_{7ij} & \Theta_{7ji} & \Theta_{8ij} & \Theta_{8ji} \\ J_{3i} + J_{3j} & J_{4ij} + J_{4ji} & 0 & 0 & J_{5i} & J_{5j} \\ 0 & J_{6i} + J_{6j} & 0 & 0 & \widetilde{N}_{2i}^T & \widetilde{N}_{2j}^T \end{bmatrix},$$

$$\Sigma_{3ij} = \begin{bmatrix} \Pi_1^T & \tau_3\Pi_1^T & T_{ij} \\ 0 & 0 & 0 \\ 0 & 0 & 0 \end{bmatrix}, \qquad T_{ij} = \begin{bmatrix} 0 \\ YA_{1i} + \Phi_jC_{1i} \end{bmatrix},$$

$$R_5 = \begin{bmatrix} 0 & 0 & 0 \\ T_1 & T_1 & 0 \\ 0 & 0 & 0 \end{bmatrix},$$

$$T_1 = \begin{bmatrix} x \\ 0 \end{bmatrix}, \qquad \Sigma_{4ij} = \begin{bmatrix} T_{2ij} & T_{3ij} & T_{4ij} & T_{5ij} \\ 0 & 0 & 0 & 0 \\ 0 & 0 & 0 & 0 \end{bmatrix},$$

$$T_{2ij} = \begin{bmatrix} \left(C_ix - C_jx\right)^T \\ 0 \end{bmatrix},$$

$$T_{3ij} = \begin{bmatrix} 0 \\ \Phi_j - \Phi_i \end{bmatrix}, \qquad T_{4ij} = \begin{bmatrix} \left(\Psi_j - \Psi_i\right)^T \\ 0 \end{bmatrix},$$

$$T_{5ij} = \begin{bmatrix} 0 \\ YB_i - YB_j \end{bmatrix},$$

$$\Sigma_{5ij} = \begin{bmatrix} \Pi_1^T & \tau_3\Pi_1^T & T_{ij} & 0 \\ 0 & 0 & 0 & T_1 \\ 0 & 0 & 0 & 0 \end{bmatrix},$$

$$\Sigma_{6ij} = \begin{bmatrix} T_{ji} & 0 & T_4 & T_2 \\ 0 & T_1 & 0 & 0 \\ 0 & 0 & 0 & 0 \end{bmatrix},$$

$$R_{11} = \operatorname{diag}\left(Q_2 \;\; \gamma^2 I \;\; V\right), \qquad R_{2ij} = \begin{bmatrix} 0 & J_{7i} & 0 & \widetilde{N}_{3i}^T \\ 0 & J_{8ij} & 0 & 0 \\ 0 & 0 & 0 & 0 \end{bmatrix},$$

$$\widetilde{R}_{2ij} = \begin{bmatrix} 0 & J_{7i} + J_{7j} & 0 & 0 & \widetilde{N}_{3i}^T & \widetilde{N}_{3j}^T \\ 0 & J_{8ij} + J_{8ji} & 0 & 0 & 0 & 0 \\ 0 & 0 & 0 & 0 & 0 & 0 \end{bmatrix},$$

$$R_{3ij} = \begin{bmatrix} -I & 0 & 0 & 0 \\ * & -J_9 & J_{10ij} & 0 \\ * & * & -\epsilon_{ij} I & 0 \\ * & * & * & -\epsilon_{ij}^{-1} I \end{bmatrix},$$

$$\widetilde{R}_{3ij} = \begin{bmatrix} -2I & 0 & 0 & 0 & 0 & 0 \\ * & -2J_9 & J_{10ij} & J_{10ji} & 0 & 0 \\ * & * & -\epsilon_{ij} I & 0 & 0 & 0 \\ * & * & * & -\epsilon_{ji} I & 0 & 0 \\ * & * & * & * & -\epsilon_{ij}^{-1} I & 0 \\ * & * & * & * & * & -\epsilon_{ji}^{-1} I \end{bmatrix},$$

$$R_4 = \operatorname{diag}\left(P_1^{-1} \;\; Q_2^{-1} \;\; I\right),$$

$$R_{6ij} = \begin{bmatrix} 0 & 0 & 0 \\ 0 & 0 & T_{6ij} \\ 0 & 0 & 0 \\ 0 & 0 & 0 \end{bmatrix}, \qquad \widetilde{R}_{6ij} = \begin{bmatrix} 0 & 0 \\ T_{5ij} & T_{3ij} \\ 0 & 0 \\ 0 & 0 \\ 0 & 0 \\ 0 & 0 \end{bmatrix},$$

$$T_{6ij} = \begin{bmatrix} 0 \\ YA_{1i}^T + \Phi_j C_{1i} \end{bmatrix},$$

$$R_7 = \operatorname{diag}\left(I \;\; I \;\; I\right), \qquad R_8 = \operatorname{diag}\left(\frac{1}{2}P_1^{-1} \;\; \frac{1}{2}Q_2^{-1} \;\; I \;\; I\right),$$

$$\Pi_1 = \begin{bmatrix} X & I \\ X & 0 \end{bmatrix}, \qquad \Pi_2 = \begin{bmatrix} X & I \\ X & 0 \end{bmatrix}. \tag{47}$$

Furthermore a desired robust dynamic output feedback controller is given in the form of (11) *with parameters as follows:*

$$A_{Ki} = \left(X^{-1} - Y\right)^{-1} \left(\Omega_i - YA_iX - YB_i\Psi_i - \Phi_i C_i X\right) X^{-1},$$

$$B_{Ki} = \left(X^{-1} - Y\right)^{-1} \Phi_i, \quad C_{Ki} = \Psi_i X^{-1}, \quad 1 \le i \le r. \tag{48}$$

Proof. Applying the Schur complements formula to (44) and (45) and using Lemma 2 result in

$$\begin{bmatrix} \widetilde{\Sigma}_{ii} & \Sigma_{1ii} & \widehat{\Sigma}_{2ii} \\ * & -R_{11} & R_{2ii} \\ * & * & R_{3ii} \end{bmatrix} < 0, \quad 1 \le i \le r,$$

$$\begin{bmatrix} \widehat{\Sigma}_{ij} & \Sigma_{1ij} + \Sigma_{1ji} & \overline{\Sigma}_{2ij} \\ * & -2R_{11} & \widetilde{R}_{2ij} \\ * & * & \widetilde{R}_{3ij} \end{bmatrix} < 0, \quad 1 \le i < j \le r, \tag{49}$$

where

$$\widetilde{\Sigma}_{ij} = \begin{bmatrix} \Theta_{ij} + \Pi_1^T P_1 \Pi_1 + \left(\tau_3 \Pi_1\right)^T Q_2 \left(\tau_3 \Pi_1\right) & \Theta_{1ij} + \begin{bmatrix} 0 & 0 \\ \left(YA_{1i} + \Phi_j C_{1i}\right) X & 0 \end{bmatrix} & \Theta_{2i} \\ * & -U + R_2 + R_2^T & 0 \\ * & * & -P_2 \end{bmatrix},$$

$$\widehat{\Sigma}_{2ij} = \begin{bmatrix} \Theta_{5ij} & \Theta_{6ij} & \Theta_{7ij} & \Theta_{8ij} \\ J_{3i} & J_{4ij} + \begin{bmatrix} 0 & X\left(A_{1i}Y + C_{1i}^T \Phi_j^T\right) \\ 0 & 0 \end{bmatrix} & 0 & J_{5i} \\ 0 & J_{6i} & 0 & \widetilde{N}_{2i}^T \end{bmatrix},$$

$$\widehat{\Sigma}_{ij} = \widetilde{\Sigma}_{ij} + \widetilde{\Sigma}_{ji} + \begin{bmatrix} 0 & \left(C_iX - C_jX\right)^T \left(\Phi_j - \Phi_i\right)^T + \left(\Psi_j - \Psi_i\right)^T \left(YB_i - YB_j\right)^T & 0 & 0 & 0 \\ * & 0 & 0 & 0 & 0 \\ * & * & 0 & 0 & 0 \\ * & * & * & 0 & 0 \\ * & * & * & * & 0 \end{bmatrix},$$

$$\overline{\Sigma}_{2ij} = \widetilde{\Sigma}_{2ij} + \begin{bmatrix} 0 & \left(\Psi_j^T - \Psi_i^T\right)\left(B_i^T Y - B_j^T Y\right) + \left(XC_i^T - XC_j^T\right)\left(\Phi_j^T - \Phi_i^T\right) & 0 & 0 & 0 & 0 \\ 0 & 0 & 0 & 0 & 0 & 0 \\ 0 & 0 & 0 & 0 & 0 & 0 \end{bmatrix}. \tag{50}$$

Note that

$$\Pi_2^T + \Pi_2 - P_2 - \tau_1 Q_1 \le \Pi_2^T (P_2 + \tau_1 Q_1)^{-1} \Pi_2. \quad (51)$$

Then, by this inequality, it follows from (49) that

$$\begin{bmatrix} \widetilde{\Sigma}_{ii} & \Sigma_{1ii} & \widehat{\Sigma}_{2ii} \\ * & -R_{11} & R_{2ii} \\ * & * & \widehat{R}_{3ii} \end{bmatrix} < 0, \quad 1 \le i \le r,$$

$$\begin{bmatrix} \widehat{\Sigma}_{ij} & \Sigma_{1ij} + \Sigma_{1ji} & \overline{\Sigma}_{2ij} \\ * & -2R_{11} & \widetilde{R}_{2ij} \\ * & * & \overline{R}_{3ij} \end{bmatrix} < 0, \quad 1 \le i < j \le r, \quad (52)$$

where

$$\widehat{R}_{3ij} = \begin{bmatrix} -I & 0 & 0 & 0 \\ * & -\Pi_2^T (P_2 + \tau_1 Q_1)^{-1} \Pi_2 & J_{10ij} & 0 \\ * & * & -\epsilon_{ij} I & 0 \\ * & * & * & -\epsilon_{ij}^{-1} I \end{bmatrix},$$

$$\overline{R}_{3ij} = \begin{bmatrix} -2I & 0 & 0 & 0 & 0 & 0 \\ * & -2\Pi_2^T (P_2 + \tau_1 Q_1)^{-1} \Pi_2 & J_{10ij} & J_{10ji} & 0 & 0 \\ * & * & -\epsilon_{ij} I & 0 & 0 & 0 \\ * & * & * & -\epsilon_{ji} I & 0 & 0 \\ * & * & * & * & -\epsilon_{ij}^{-1} I & 0 \\ * & * & * & * & * & -\epsilon_{ji}^{-1} I \end{bmatrix}. \quad (53)$$

Now, set

$$\widetilde{P} = \Pi_2 \Pi_1^{-1}. \quad (54)$$

Then, by (46), it can be verified that $\widetilde{P} > 0$. Noting the parameters in (48) and pre- and postmultiplying (3) by

$$\operatorname{diag}\left(\Pi_1^{-T}, \Pi_1^{-T}, I, I, I, \Pi_1^{-T}, I, \Pi_2^{-T}, I, \ldots, I\right) \quad (55)$$

and its transpose, respectively, we have

$$\begin{bmatrix} \widetilde{\Pi}_{1ii} & \widetilde{\Pi}_{2ii} & P\widetilde{A}_{2i} & P\widetilde{A}_{3i} & PD_{ii} & \tau_1 \widetilde{R}_1 & E_{ii}^T & \Gamma_{ii} & PM_{ii} & N_{ii}^T \\ * & J_1 & 0 & 0 & 0 & \tau_1 \widetilde{R}_2 & E_{1i}^T & \Gamma_{1ii} & 0 & 0 \\ * & * & -P_2 & 0 & 0 & 0 & 0 & \Gamma_{2i} & 0 & 0 \\ * & * & * & -Q_2 & 0 & 0 & 0 & \Gamma_{3i} & 0 & 0 \\ * & * & * & * & -\gamma^2 I & 0 & 0 & \Gamma_{4ii} & 0 & 0 \\ * & * & * & * & * & -\tau_1 Q_1 & 0 & 0 & 0 & 0 \\ * & * & * & * & * & * & -I & 0 & 0 & 0 \\ * & * & * & * & * & * & * & -J_2^T & J_2^T M_{ii} & 0 \\ * & * & * & * & * & * & * & * & -\epsilon_{ii} I & 0 \\ * & * & * & * & * & * & * & * & * & -\epsilon_{ii}^{-1} I \end{bmatrix} < 0, \quad 1 \le i \le r,$$

$$\begin{bmatrix} \Lambda_{1ij} & \Lambda_{2ij} & \Lambda_{3ij} \\ * & \Lambda_{4ij} & \Lambda_{5ij} \\ * & * & \Lambda_{6ij} \end{bmatrix} < 0, \quad 1 \le i < j \le r, \quad (56)$$

where

$$\widetilde{\Lambda}_1 = H^T \left(P_1 + \tau_3^2 Q_2 - \widetilde{R}_1 - \widetilde{R}_1^T\right) H,$$

$$\widetilde{\Pi}_{1ij} = \widetilde{\Lambda}_1 + PA_{ij} + A_{ij}^T P,$$

$$\widetilde{\Lambda}_2 = H^T \left(\widetilde{R}_1 - \widetilde{R}_2^T\right),$$

$$\widetilde{\Pi}_{2ij} = \widetilde{\Lambda}_2 + PA_{1ij},$$

$$\widetilde{R}_1 = \Pi_1^T R_1 \Pi_1. \quad (57)$$

Finally, by Theorem 3, the desired result follows immediately. □

Remark 5. Theorem 4 provides a sufficient condition for the solvability of the robust H_∞ output feedback control problem for uncertain fuzzy neutral systems with both discrete and distributed delays. It is worth pointing out that the result in Theorem 4 can be readily extended to the case with multiple delays.

Remark 6. In Theorem 4, if we set $A_{21} = 0$, $M_i = 0$, and $N_{2i} = 0$ $(i = 1, 2, \ldots r)$, then the results in [32] are included in our paper. Also, the controller design method in our paper can be the reference for designing the observer-based output feedback controllers and so forth.

4. Simulation Example

In this section, we provide one example to illustrate the output feedback H_∞ controller design approach developed in this paper.

The uncertain fuzzy system with distributed delays considered in this example is with two rules.

Plant Rule 1: if $x_1(t)$ is μ_1, then

$$\begin{aligned}
\dot{x}(t) = {} & \left[A_1 + \Delta A_1(t)\right] x(t) + \left[A_{11} + \Delta A_{11}(t)\right] x\left(t - \tau_1\right) \\
& + \left[A_{21} + \Delta A_{21}(t)\right] \dot{x}\left(t - \tau_2\right) \\
& + \left[A_{31} + \Delta A_{31}(t)\right] \int_{t-\tau_3}^{t} x(s)\, ds \\
& + \left[B_1 + \Delta B_1(t)\right] u(t) + D_{1i} w(t), \\
y(t) = {} & \left[C_1 + \Delta C_1(t)\right] x(t) + C_{11} x\left(t - \tau_1\right) + D_{21} w(t), \\
z(t) = {} & E_1 x(t) + E_{11} x\left(t - \tau_1\right) + G_1 u(t).
\end{aligned} \tag{58}$$

Plant Rule 2: if $x_1(t)$ is μ_2, then

$$\begin{aligned}
\dot{x}(t) = {} & \left[A_2 + \Delta A_2(t)\right] x(t) + \left[A_{12} + \Delta A_{12}(t)\right] x\left(t - \tau_1\right) \\
& + \left[A_{22} + \Delta A_{22}(t)\right] \dot{x}\left(t - \tau_2\right) \\
& + \left[A_{32} + \Delta A_{32}(t)\right] \int_{t-\tau_3}^{t} x(s)\, ds \\
& + \left[B_2 + \Delta B_2(t)\right] u(t) + D_{12} w(t), \\
y(t) = {} & \left[C_2 + \Delta C_2(t)\right] x(t) + C_{12} x\left(t - \tau_1\right) + D_{22} w(t), \\
z(t) = {} & E_2 x(t) + E_{12} x\left(t - \tau_1\right) + G_2 u(t),
\end{aligned} \tag{59}$$

where

$$\begin{gathered}
A_1 = \begin{bmatrix} 0.05 & 0 \\ -0.2 & -0.06 \end{bmatrix}, \qquad A_{11} = \begin{bmatrix} 0.05 & 0.02 \\ -0.05 & 0.01 \end{bmatrix}, \\
A_{21} = \begin{bmatrix} -0.002 & 0.008 \\ 0.006 & 0 \end{bmatrix}, \\
A_{31} = \begin{bmatrix} -0.05 & 0.08 \\ 0.06 & 0 \end{bmatrix}, \qquad B_1 = \begin{bmatrix} 0.01 & 0 \\ 0.03 & 0.06 \end{bmatrix}, \\
C_1 = \begin{bmatrix} -0.03 & -0.1 \\ 0.2 & 0.02 \end{bmatrix}, \qquad C_{11} = \begin{bmatrix} -0.03 & -0.01 \\ 0.02 & 0.02 \end{bmatrix}, \\
D_{11} = \begin{bmatrix} 0.03 \\ 0.06 \end{bmatrix}, \qquad D_{21} = \begin{bmatrix} -0.5 \\ 0 \end{bmatrix}, \\
E_1 = \begin{bmatrix} -0.2 & 0 \end{bmatrix}, \qquad E_{11} = \begin{bmatrix} -0.02 & 0 \end{bmatrix}, \\
G_1 = \begin{bmatrix} 0 & -0.03 \end{bmatrix}, \\
A_2 = \begin{bmatrix} -0.05 & 0 \\ -0.2 & -0.06 \end{bmatrix}, \qquad A_{12} = \begin{bmatrix} -0.05 & 0.2 \\ -0.5 & 0.01 \end{bmatrix}, \\
A_{22} = \begin{bmatrix} 0.008 & -0.002 \\ -0.003 & 0.02 \end{bmatrix}, \\
A_{32} = \begin{bmatrix} 0.05 & -0.2 \\ -0.3 & 0.2 \end{bmatrix}, \qquad B_2 = \begin{bmatrix} 0.01 & -0.08 \\ 0.02 & 0.05 \end{bmatrix}, \\
C_2 = \begin{bmatrix} 0.03 & -0.1 \\ 0.2 & 0.02 \end{bmatrix}, \\
C_{12} = \begin{bmatrix} -0.03 & -0.01 \\ 0.02 & 0.2 \end{bmatrix}, \qquad D_{12} = \begin{bmatrix} -0.01 \\ 0.02 \end{bmatrix}, \\
D_{22} = \begin{bmatrix} -0.3 \\ 0 \end{bmatrix}, \\
E_2 = \begin{bmatrix} -0.01 & 0 \end{bmatrix}, \qquad E_{12} = \begin{bmatrix} -0.01 & 0 \end{bmatrix}, \\
G_2 = \begin{bmatrix} 0 & 0.02 \end{bmatrix},
\end{gathered} \tag{60}$$

and $\Delta A_i(t)$, $\Delta A_{1i}(t)$, $\Delta A_{2i}(t)$, $\Delta A_{3i}(t)$, $\Delta B_i(t)$, $\Delta C_i(t)$ $(i = 1, 2)$ can be represented in the form of (2) and (3) with

$$\begin{gathered}
M_1 = \begin{bmatrix} -0.02 \\ 0 \end{bmatrix}, \qquad N_{01} = \begin{bmatrix} -0.2 & 0.1 \end{bmatrix}, \\
N_{11} = \begin{bmatrix} -0.2 & 0.2 \end{bmatrix}, \\
N_{21} = \begin{bmatrix} -0.02 & 0.01 \end{bmatrix}, \qquad N_{31} = \begin{bmatrix} -0.02 & 0.01 \end{bmatrix}, \\
N_{41} = \begin{bmatrix} -0.02 & 0.01 \end{bmatrix}, \\
N_{51} = \begin{bmatrix} -0.02 & 0.01 \end{bmatrix}, \qquad M_2 = \begin{bmatrix} 0.03 \\ 0 \end{bmatrix}, \\
N_{02} = N_{01}, \qquad N_{12} = N_{11}, \\
N_{22} = N_{21}, \qquad N_{32} = N_{31}, \\
N_{42} = N_{41}, \qquad N_{52} = N_{51}.
\end{gathered} \tag{61}$$

Then, the final outputs of the fuzzy systems are inferred as follows:

$$\begin{aligned}\dot{x}(t) &= \sum_{i=1}^{2} h_i(s(t)) \\ &\quad \times \{[A_i + \Delta A_i(t)]x(t) \\ &\quad + [A_{1i} + \Delta A_{1i}(t)]x(t-\tau_1) \\ &\quad + [A_{2i} + \Delta A_{2i}(t)]\dot{x}(t-\tau_2) \\ &\quad + [A_{3i} + \Delta A_{3i}(t)]\int_{t-\tau_3}^{t} x(s)\,ds \\ &\quad + [B_i + \Delta B_i(t)]u(t) + D_{1i}w(t)\}, \\ y(t) &= \sum_{i=1}^{2} h_i(s(t)) \\ &\quad \times \{[C_i + \Delta C_i(t)]x(t) \\ &\quad + C_{1i}x(t-\tau_1) + D_{2i}w(t)\}, \\ z(t) &= \sum_{i=1}^{2} h_i(s(t))\{E_i x(t) + E_{1i}x(t-\tau_1) + G_i u(t)\},\end{aligned} \tag{62}$$

where

$$h_1(x_1(t)) = \begin{cases} \frac{1}{3}, & \text{for } x_1 < -1, \\ \frac{2}{3} + \frac{1}{3}x_1, & \text{for } |x_1| \le 1, \\ 1, & \text{for } x_1 > 1, \end{cases}$$
$$h_2(x_1(t)) = \begin{cases} \frac{2}{3}, & \text{for } x_1 < -1, \\ \frac{1}{3} - \frac{1}{3}x_1, & \text{for } |x_1| \le 1, \\ 0, & \text{for } x_1 > 1. \end{cases} \tag{63}$$

In this example, we choose the H_∞ performance level $\gamma = 3$.

In order to design a fuzzy H_∞ output feedback controller for the T-S model, we first choose the initial condition that is $x(0) = [0.3 \ \ -0.1]^T$, and the disturbance input $w(t)$ is assumed to be

$$w(t) = \frac{1}{t + 0.1}, \quad t \ge 0. \tag{64}$$

Then, solving the LMIs in (44), (45), and (46), we obtain the solution as follows:

$$\begin{aligned} X &= \begin{bmatrix} 0.9868 & 0.6071 \\ 0.6071 & 1.3948 \end{bmatrix}, \\ Y &= \begin{bmatrix} 12.9348 & 0.1814 \\ 0.1814 & 6.3384 \end{bmatrix}, \\ \Omega_1 &= \begin{bmatrix} -1.6069 & -1.6112 \\ -0.0417 & -3.2117 \end{bmatrix}, \\ \Omega_2 &= \begin{bmatrix} 8.2076 & -3.7031 \\ -5.8461 & 5.3292 \end{bmatrix}, \\ \Phi_1 &= \begin{bmatrix} 3.1848 & 0.0758 \\ -0.1899 & -2.5282 \end{bmatrix}, \\ \Phi_2 &= \begin{bmatrix} 2.0547 & 0.1643 \\ -0.2930 & -0.7113 \end{bmatrix}, \\ \psi_1 &= \begin{bmatrix} -140.1869 & -27.8001 \\ 5.7867 & -77.8562 \end{bmatrix}, \\ \psi_2 &= \begin{bmatrix} -79.1853 & -88.2601 \\ -88.1012 & -95.7242 \end{bmatrix}. \end{aligned} \tag{65}$$

Now, by Theorem 4, a desired fuzzy output feedback controller can be constructed as in (11) and (12) with

$$\begin{aligned} A_{k1} &= \begin{bmatrix} 87.3277 & -68.0397 \\ 139.9266 & -107.2394 \end{bmatrix}, \\ A_{k2} &= \begin{bmatrix} -24.9856 & 15.8880 \\ 11.1983 & -12.2840 \end{bmatrix}, \\ B_{k1} &= \begin{bmatrix} 10.9115 & -0.3725 \\ 16.5830 & 1.9936 \end{bmatrix}, \\ B_{k2} &= \begin{bmatrix} 1.4642 & -0.0212 \\ 3.1940 & 0.5922 \end{bmatrix}, \\ C_{k1} &= \begin{bmatrix} -16.0423 & 12.7577 \\ 20.2647 & -14.8918 \end{bmatrix}, \\ C_{k2} &= \begin{bmatrix} 14.2596 & -10.4929 \\ 3.2304 & -1.1934 \end{bmatrix}. \end{aligned} \tag{66}$$

With the output feedback fuzzy controller, the simulation results of the state response of the nonlinear system are given in Figure 1. Figure 2 shows the control input, while Figures 3 and 4 present the corresponding measured output and the controlled output, respectively.

From these simulation results, it can be seen that the designed fuzzy output feedback controller ensures the robust asymptotic stability of the uncertain fuzzy neutral system and guarantees a prescribed H_∞ performance level.

5. Conclusion and Future Work

The problem of delay-dependent robust output feedback H_∞ control for uncertain T-S fuzzy neutral systems with parameter uncertainties and distributed delays has been studied. In

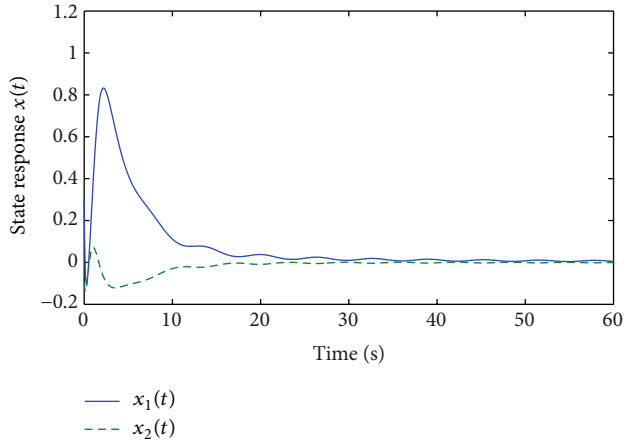

FIGURE 1: State response $x_1(t)$ (continuous line) and $x_2(t)$ (dashed line).

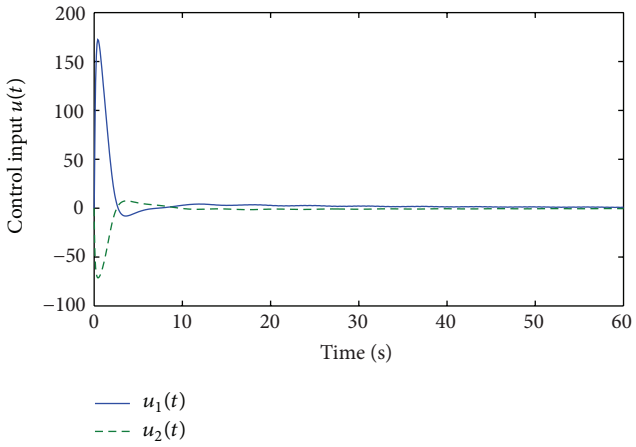

FIGURE 2: Control input $u_1(t)$ (continuous line) and $u_2(t)$ (dashed line).

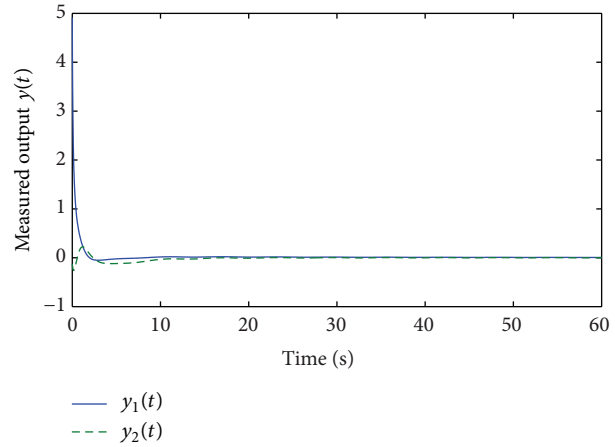

FIGURE 3: Measured output $y_1(t)$ (continuous line) and $y_2(t)$ (dashed line).

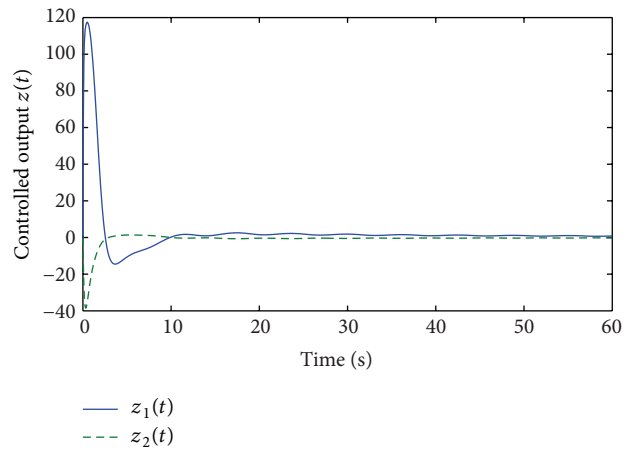

FIGURE 4: Controlled output $z_1(t)$ (continuous line) and $z_2(t)$ (dashed line).

terms of LMIs, a sufficient condition for the existence of a full-order fuzzy dynamic output feedback controller, which robustly stabilizes the uncertain fuzzy neutral delay systems and guarantees a prescribed level on disturbance attenuation, has been obtained.

Future work will mainly cover the problem of robust output feedback H_∞ control for uncertain fractional-order (FO) T-S fuzzy neutral systems with state and distributed delays. Firstly, investigate the robust output feedback H_∞ control for FO T-S fuzzy systems with state delays; then, study the robust output feedback H_∞ control for FO T-S fuzzy systems with both state and distributed delays; finally, obtain the results about the robust output feedback H_∞ control for uncertain FO T-S fuzzy neutral systems with state and distributed delays.

Acknowledgments

This work is supported by the National Natural Science Foundation of China under Grant 61203047, the China Postdoctoral Science Foundation under Grant 2013T60670, and the Projects of International Technology Cooperation under Grant 2011DFA10440.

References

[1] T. Wang, S. Tong, and Y. Li, "Robust adaptive fuzzy control for nonlinear system with dynamic uncertainties based on backstepping," *International Journal of Innovative Computing, Information and Control*, vol. 5, no. 9, pp. 2675–2688, 2009.

[2] S. Tong and Y. Li, "Observer-based fuzzy adaptive control for strict-feedback nonlinear systems," *Fuzzy Sets and Systems*, vol. 160, no. 12, pp. 1749–1764, 2009.

[3] Y. Li, S. Tong, and T. Li, "Adaptive fuzzy output feedback control of uncertain nonlinear systems with unknown backlash-like hysteresis," *Information Sciences*, vol. 198, pp. 130–146, 2012.

[4] S. Tong, X. He, and H. Zhang, "A combined backstepping and small-gain approach to robust adaptive fuzzy output feedback control," *IEEE Transactions on Fuzzy Systems*, vol. 17, no. 5, pp. 1059–1069, 2009.

[5] T. Takagi and M. Sugeno, "Fuzzy identification of systems and its applications to modeling and control," *IEEE Transactions on Systems, Man and Cybernetics*, vol. 15, no. 1, pp. 116–132, 1985.

[6] K. Tanaka and M. Sano, "On the concepts of regulator and observer of fuzzy control systems," in *Proceedings of the 3rd IEEE International Conference on Fuzzy Systems*, pp. 767–772, 1994.

[7] J. Yoneyama, M. Nishikawa, H. Katayama, and A. Ichikawa, "Output stabilization of Takagi-Sugeno fuzzy systems," *Fuzzy Sets and Systems*, vol. 111, no. 2, pp. 253–266, 2000.

[8] B. Zhang, J. Lam, S. Xu, and Z. Shu, "Robust stabilization of uncertain T-S fuzzy time-delay systems with exponential estimates," *Fuzzy Sets and Systems*, vol. 160, no. 12, pp. 1720–1737, 2009.

[9] H. Shen, S. Xu, J. Zhou, and J. Lu, "Fuzzy H_∞ filtering for nonlinear Markovian jump neutral systems," *International Journal of Systems Science*, vol. 42, no. 5, pp. 767–780, 2011.

[10] Y. Niu, J. Lam, X. Wang, and D. W. C. Ho, "Adaptive H_∞ control using backstepping design and neural networks," *Journal of Dynamic Systems, Measurement and Control*, vol. 127, no. 3, pp. 478–485, 2004.

[11] K. Tanaka and M. Sugeno, "Stability analysis and design of fuzzy control systems," *Fuzzy Sets and Systems*, vol. 45, no. 2, pp. 135–156, 1992.

[12] X. Ban, X. Gao, X. Huang, and H. Yin, "Stability analysis of the simplest Takagi-Sugeno fuzzy control system using popov criterion," *International Journal of Innovative Computing, Information and Control*, vol. 3, no. 5, pp. 1087–1096, 2007.

[13] S. Tong, W. Wang, and L. Qu, "Decentralized robust control for uncertain T-S fuzzy large-scale systems with time-delay," *International Journal of Innovative Computing, Information and Control*, vol. 3, no. 3, pp. 657–672, 2007.

[14] S. Zhou, G. Feng, J. Lam, and S. Xu, "Robust H_∞ control for discrete-time fuzzy systems via basis-dependent Lyapunov functions," *Information Sciences*, vol. 174, no. 3-4, pp. 197–217, 2005.

[15] B. Zhang, S. Xu, G. Zong, and Y. Zou, "Delay-dependent stabilization for stochastic fuzzy systems with time delays," *Fuzzy Sets and Systems*, vol. 158, no. 20, pp. 2238–2250, 2007.

[16] H. Gao, J. Lam, C. Wang, and Y. Wang, "Delay-dependent output-feedback stabilisation of discrete-time systems with time-varying state delay," *IEE Proceedings—Control Theory and Applications*, vol. 151, pp. 691–698, 2004.

[17] B. Zhang, W. X. Zheng, and S. Xu, "On robust H_∞ filtering of uncertain Markovian jump time-delay systems," *International Journal of Adaptive Control and Signal Processing*, vol. 26, no. 2, pp. 138–157, 2012.

[18] B. Zhang, W. X. Zheng, and S. Xu, "Filtering of Markovian jump delay systems based on a new performance index," *IEEE Transactions on Circuits and Systems I*, vol. 60, pp. 1250–1263, 2013.

[19] H. Shen, S. Xu, J. Lu, and J. Zhou, "Passivity-based control for uncertain stochastic jumping systems with mode-dependent round-trip time delays," *Journal of the Franklin Institute*, vol. 349, no. 5, pp. 1665–1680, 2012.

[20] H. Shen, S. Xu, J. Lu, and J. Zhou, "Fuzzy dissipative control for nonlinear Markovian jump systems via retarded feedback," *Journal of the Franklin Institute*, 2013.

[21] Y.-Y. Cao and P. Frank, "Analysis and synthesis of nonlinear time-delay systems via fuzzy control approach," *IEEE Transactions on Fuzzy Systems*, vol. 8, no. 2, pp. 200–211, 2000.

[22] K. R. Lee, E. T. Jeung, and H. B. Park, "Robust fuzzy H_∞ control for uncertain nonlinear systems via state feedback: an LMI approach," *Fuzzy Sets and Systems*, vol. 120, no. 1, pp. 123–134, 2001.

[23] B. Zhang, S. Zhou, and T. Li, "A new approach to robust and non-fragile H_∞ control for uncertain fuzzy systems," *Information Sciences*, vol. 177, no. 22, pp. 5118–5133, 2007.

[24] Y.-Y. Cao and P. M. Frank, "Robust H_∞ disturbance attenuation for a class of uncertain discrete-time fuzzy systems," *IEEE Transactions on Fuzzy Systems*, vol. 8, no. 4, pp. 406–415, 2000.

[25] B. Zhang and S. Xu, "Delay-dependent robust H_∞ control for uncertain discrete-time fuzzy systems with time-varying delays," *IEEE Transactions on Fuzzy Systems*, vol. 17, no. 4, pp. 809–823, 2009.

[26] K. R. Lee, J. H. Kim, E. T. Jeung, and H. B. Park, "Output feedback robust H_∞ control of uncertain fuzzy dynamic systems with time-varying delay," *IEEE Transactions on Fuzzy Systems*, vol. 8, no. 6, pp. 657–664, 2000.

[27] S. Xu and J. Lam, "Robust H_∞ control for uncertain discrete-time-delay fuzzy systems via output feedback controllers," *IEEE Transactions on Fuzzy Systems*, vol. 13, no. 1, pp. 82–93, 2005.

[28] S. Xu, J. Lam, and B. Chen, "Robust H_∞ control for uncertain fuzzy neutral delay systems," *European Journal of Control*, vol. 10, no. 4, pp. 365–385, 2004.

[29] Y. Li, S. Xu, B. Zhang, and Y. Chu, "Robust stabilization and H_∞ control for uncertain fuzzy neutral systems with mixed time delays," *Fuzzy Sets and Systems*, vol. 159, no. 20, pp. 2730–2748, 2008.

[30] Y. Wang, L. Xie, and C. E. de Souza, "Robust control of a class of uncertain nonlinear systems," *Systems & Control Letters*, vol. 19, no. 2, pp. 139–149, 1992.

[31] L. Xie and C. E. de Souza, "Robust H_∞ control for linear systems with norm-bounded time-varying uncertainty," *IEEE Transactions on Automatic Control*, vol. 37, no. 8, pp. 1188–1191, 1992.

[32] X. Song, S. Xu, and H. Shen, "Robust H_∞ control for uncertain fuzzy systems with distributed delays via output feedback controllers," *Information Sciences*, vol. 178, no. 22, pp. 4341–4356, 2008.

Hindawi Publishing Corporation
Mathematical Problems in Engineering
Volume 2013, Article ID 804754, 9 pages
http://dx.doi.org/10.1155/2013/804754

Research Article

Antidisturbance Fault Tolerant Control of Attitude Control Systems for Microsatellite with Unknown Input Delay

Jianzhong Qiao[1] and Lei Guo[1,2]

[1] *School of Instrumentation Science and Opto-Electronics Engineering, Beihang University, Beijing 100191, China*
[2] *Science and Technology on Aircraft Control Laboratory, Beihang University, Beijing 100191, China*

Correspondence should be addressed to Jianzhong Qiao; qiaojianzhong83@163.com

Received 23 August 2013; Accepted 24 September 2013

Academic Editor: Tao Li

The antidisturbance fault tolerant control problem of attitude control systems for microsatellite is investigated in the presence of unknown input delay, stuck faults from the reaction wheel and the multiple disturbances. The multiple disturbances are supposed to include the vibration disturbance torque from the reaction wheel and modeling uncertainties. The fault diagnosis observer and disturbance observer are constructed to estimate stuck faults and vibration disturbance torque from the reaction wheel, respectively. A composite fault tolerant controller is designed by combining a PID controller, the fault accommodation estimation based on the fault diagnosis observer, and the disturbance compensator based on the disturbance observer. The controller and observer gains can be easily obtained via a set of linear matrix inequalities. Simulation results are given to show that the faults can be accommodated readily, and the disturbances can be rejected and attenuated simultaneously.

1. Introduction

Microsatellite, which is a kind of modern small satellites with mass below 100 kg, plays more and more important roles in position location, earth observation, atmospheric data collection, space science, and other space missions because of its advantages of cost, risk, and manufacturing time. The reaction wheel had been widely used for microsatellite attitude control as a kind of momentum exchange device owing to its great decrease in size and weight. In order to pursue designated space missions, the reaction wheel works on a high-speed rotational state sometimes; it raises the probability of faults to occur inevitably (see [1, 2]). Moreover, the wheel produces a disturbance torque and force as by products; the effects of wheel disturbances on the microsatellite's attitude error and stability are so critical that the influence of disturbances on the quality of the attitude control should be analyzed prior to the application of the wheels for microsatellite (see [3–6]). In addition, it is well known that time-delay is a common phenomenon in many industrial and engineering system and is one of the instability sources for dynamical systems (see [7–9]). With an impending requirement on reliability and stability of attitude control systems, time delay must be considered when designing the control algorithm. All these aspects in a realistic environment create considerable difficulty in the design of attitude control systems for adequate performance and stability, especially when all these issues are treated simultaneously.

In the past several decades, one way to improve the reliability is that enhancing the fault tolerance of the system. More and more attention had been paid to the development of methodologies to detect and isolate faults so that measures could be taken to accommodate these faults (see [10–13]). In [14], a simple and effective fault tolerant control method for satellites with four reaction wheels has been proposed based on dynamic inversion and time-delay control theory. In [15], a nonlinear fault detection and isolation strategy for redundant reaction wheels in the attitude control subsystem for a satellite has been attempted. However, the strategy for redundant reaction wheels is unfeasible for microsatellite because of its size and weight.

To remedy this problem, more and more attention had been focused on model-based methodologies. In [16], an interactive bank of unscented Kalman filters has been developed for fault detection and isolation in reaction wheel actuators of satellite attitude control systems. In [17], an unsupervised algorithm of kernel fuzzy c-means-based fault diagnosis method for unknown faults in satellite reaction wheels has been presented. Because of continued presence of disturbance, the fault tolerant control (FTC) problem of attitude control systems for microsatellite with multiple disturbances will be more complicated.

To overcome these obstacles, some approaches have been provided and applied. In [18], a robust adaptive FTC approach for attitude tracking of flexible spacecraft is proposed for use in situations when there are reaction wheels/actuator failures, external disturbances, and time-varying inertia-parameter uncertainties. In [19], a FTC design technique against actuator stuck faults with application to spacecraft attitude maneuvering control systems has been proposed via designing an integral-type sliding mode attitude controller to compensate for the effects of stuck actuators and system parameters and external disturbances. In [20], a robust adaptive controller has been provided with the utilization of fuzzy logic and backstepping techniques. The authors investigate the problem of spacecraft in the presence of unknown mass moment of inertia matrix, external disturbances, actuator failures, and control input constraints. Overall, some robust control techniques had been applied in most existing literature for the disturbances are assumed to be norm bounded. However, in practical engineering, the disturbance may originate from various sources and can be described by a composite form rather than a single variable. In this case, the robust control may be too conservative to provide highly accurate control performance. As such, disturbance attenuation and rejection for linear (or nonlinear) control systems is a challenging objective in the control area. Analysis and synthesis for control systems with disturbances have been one of the most active research fields in the past few decades. The idea of disturbance-observer-based control (DOBC) is to construct an observer to estimate and compensate some external disturbances (see [21–27]). And it has been shown that DOBC approach has a good performance to reject the various unknown disturbances. However, none of these methods has dealt with multiple disturbances as well as unknown input delay simultaneously.

In this paper, a composite fault tolerant controller is firstly addressed for the attitude control systems for microsatellite with stuck faults from reaction wheel, multiple disturbances and unknown input delay based on fault diagnosis observer, disturbance observer and PID state-feedback controller. Fault diagnosis observer can estimate the stuck faults from reaction wheel real time. Disturbance observer can estimate the effect of vibration from the reaction wheel. PID state-feedback controller can attenuate the influence of the norm bounded disturbances and the estimation errors. Simulation results for a microsatellite are given to show the efficiency of the proposed approach.

The remainder of this paper is organized as follows. In Section 2, the dynamic model for microsatellite and control problem formulation is presented. In Section 3, the fault diagnosis observer and disturbance observer are designed. In Section 4, the stabilization of the attitude control systems under the given controller is analyzed, and the solution of the controller is resolved. In Section 5, the proposed control algorithm is confirmed by numerical simulation. Section 6 contains conclusions.

2. Problem Formulation

When the Euler angle is very small, the attitude dynamics equation for microsatellite can be described by the following matrix form:

$$\begin{aligned} I_1\ddot{\gamma} - \omega\left(I_1 - I_2 + I_3\right)\dot{\theta} + 4\omega^2\left(I_2 - I_3\right)\gamma &= u_1\left(t - \Delta\left(t\right)\right) + F_1 + M_{d1}, \\ I_2\ddot{\varphi} + 3\omega^2\left(I_1 - I_3\right)\varphi &= u_2\left(t - \Delta\left(t\right)\right) + F_2 + M_{d2}, \\ I_3\ddot{\theta} + \omega\left(I_1 - I_2 + I_3\right)\dot{\gamma} + \omega^2\left(I_2 - I_1\right)\theta &= u_3\left(t - \Delta\left(t\right)\right) + F_3 + M_{d3}, \end{aligned} \tag{1}$$

where γ, φ, and θ are the yaw angle, pitch angle, and rolling angle, respectively. I_i $(i = 1, 2, 3)$ is the inertia matrix, and ω is the velocity of the orbital reference frame with respect to the inertial frame expressed in the body-fixed reference frame. $\Delta(t)$ is an unknown control input delay, and the control input torque is supposed to be $u_i(t - \Delta(t))$. $\Delta(t)$ satisfies $0 \le \Delta(t) \le \tau < \infty$ and $\dot{\Delta}(t) \le \overline{d} < 1$. M_{di} and F_i are the disturbance torques and fault input vector, respectively.

Since the microsatellite rarely performs a large angle maneuver, the linear model is reasonably accurate and acceptable to be used in attitude controller design. So, the attitude dynamics equation can be rewritten as follows:

$$\begin{aligned} &M\ddot{p}\left(t\right) + C\dot{p}\left(t\right) + Kp\left(t\right) \\ &\quad = B_u\left(u\left(t - \Delta\left(t\right)\right) + F\left(t\right) + d_1\left(t\right)\right) + B_w d_2\left(t\right), \end{aligned} \tag{2}$$

where $p(t) = [\gamma, \varphi, \theta]^T$ is the state vector of Euler angles, $\dot{p}(t)$ is the Euler angular velocity, and $\ddot{p}(t)$ is the Euler angles acceleration. $F(t)$ is the stuck fault from reaction wheel, and it is supposed to be time varying, but its derivative is supposed to be bounded. $d_1(t)$ is the disturbance which represents the vibration disturbance torque from reaction wheel. $d_2(t)$ is the merged disturbance from space environmental disturbances, moment-of-inertia uncertainty, and noises from sensors and actuators. Considering

$$M = \begin{bmatrix} I_1 & 0 & 0 \\ 0 & I_2 & 0 \\ 0 & 0 & I_3 \end{bmatrix}, \tag{3}$$

$$C = \begin{bmatrix} 0 & 0 & -\omega\left(I_1 - I_2 + I_3\right) \\ 0 & 0 & 0 \\ \omega\left(I_1 - I_2 + I_3\right) & 0 & 0 \end{bmatrix}, \tag{4}$$

$$K = \begin{bmatrix} 4\omega^2 (I_2 - I_3) & 0 & 0 \\ 0 & 3\omega^2 (I_1 - I_3) & 0 \\ 0 & 0 & -\omega^2 (I_1 - I_2) \end{bmatrix}, \quad (5)$$

$$B_u = B_w = \begin{bmatrix} 1 & 0 & 0 \\ 0 & 1 & 0 \\ 0 & 0 & 1 \end{bmatrix}. \quad (6)$$

Define $x(t) = [\int_0^t p(\tau)d\tau, p(t), \dot{p}(t)]^T$ and then transform the attitude dynamics equation into state space model, which can be written as

$$\dot{x}(t) = Ax(t) + B_1 \left(u(t - \Delta(t)) + F(t) + d_1(t)\right) + B_2 d_2(t), \quad (7)$$

where

$$A = \begin{bmatrix} 0 & I \\ -M^{-1}K & -M^{-1}C \end{bmatrix}, \quad B_1 = \begin{bmatrix} 0 \\ M^{-1}B_u \end{bmatrix}, \quad B_2 = \begin{bmatrix} 0 \\ M^{-1}B_w \end{bmatrix}. \quad (8)$$

The vibration disturbance torque $d_1(t)$ is supposed to be described by

$$d_1(t) = \sum_{i=1}^{n} C_i f_{rwa}^2 \sin\left(2\pi h_i f_{rwa} t + \phi_i\right), \quad (9)$$

where n is the number of harmonics included in the model, C_i is the amplitude of the ith harmonic, f_{rwa} is the wheel speed in Hz, h_i is the ith harmonic number, and ϕ_i is a random phase (assumed to be uniform over $[0, 2\pi]$) (see [5, 6]). However, it is impossible to obtain the information of C_i and ϕ_i except f_{rwa} when the reaction wheel works on a high-speed rotational state. The disturbance force or torque $d_1(t)$ can be rewritten as the following matrix form:

$$d_1(t) = Vw(t), \quad \dot{w}(t) = Ww(t) + B_3\delta(t), \quad (10)$$

where $w(t)$ is the state variable, and $\delta(t)$ is the additional disturbance that results from the perturbations and uncertainties in the exogenous system. W is the vibration frequency of reaction wheel, and V and B_3 are the known parameter matrices of the exogenous system with proper dimension.

Assumption 1. (A, B_1) is controllable; (W, B_1V) is observable.

In the next section, the objective is to design fault diagnosis observer and disturbance observer, with which the fault can be accommodated, and the modeled disturbance can be rejected.

3. Fault Diagnosis Observer and Disturbance Observer Design

3.1. Fault Diagnosis Observer Design. Fault diagnosis needs to be accomplished in order to reconfigure system and improve its reliability. For this purpose, the following fault diagnosis observer is constructed to diagnose the stuck faults from the reaction wheel

$$\begin{aligned} \widehat{F}(t) &= \varepsilon(t) - Kx(t), \\ \dot{\varepsilon}(t) &= KB_1(\varepsilon(t) - Kx(t)) \\ &\quad + K\left[Ax(t) + B_1u(t - \Delta(t)) + B_1\widehat{d}_1(t)\right], \end{aligned} \quad (11)$$

where $\varepsilon(t)$ is the auxiliary variable, and $\widehat{F}(t)$ is the estimation of $F(t)$. K is the fault diagnosis observer gain to be determined later. $\widehat{d}_1(t)$ is the estimation of $d_1(t)$ which will be designed in next subsection.

3.2. Disturbance Observer Design. Disturbance observer is designed in this subsection in order to reject the modeled external disturbance, and the disturbance observer is formulated as

$$\begin{aligned} \widehat{d}_1(t) &= V\widehat{w}(t), \\ \widehat{w}(t) &= \nu(t) - Lx(t), \\ \dot{\nu}(t) &= \left(W + LB_1V\right)(\nu(t) - Lx(t)) \\ &\quad + L\left[Ax(t) + B_1u(t - \Delta(t)) + B_1\widehat{F}(t)\right], \end{aligned} \quad (12)$$

where $\nu(t)$ is the auxiliary variable, and $\widehat{w}(t)$ is the estimation of $w(t)$. L is the disturbance observer gain to be determined later.

The error of disturbance observer and fault diagnosis observer are defined as

$$e_w(t) = w(t) - \widehat{w}(t - \Delta(t)), \quad e_F(t) = F(t) - \widehat{F}(t - \Delta(t)). \quad (13)$$

Then

$$\begin{aligned} \dot{e}(t) &= W_1e(t) + NB_1Ee(t - \Delta(t)) \\ &\quad + NB_2d_2(t - \Delta(t)) + H_3\delta(t) + H_1\dot{F}(t), \end{aligned} \quad (14)$$

where

$$e(t) = \begin{bmatrix} e_w(t) \\ e_F(t) \end{bmatrix}, \quad N = \begin{bmatrix} L \\ K \end{bmatrix}, \quad E = \begin{bmatrix} V & I \end{bmatrix}, \quad H_3 = \begin{bmatrix} B_3 \\ 0 \end{bmatrix}, \quad H_1 = \begin{bmatrix} 0 \\ 1 \end{bmatrix}, \quad W_1 = \begin{bmatrix} W & 0 \\ 0 & 0 \end{bmatrix}. \quad (15)$$

In this section, fault diagnosis observer and disturbance observer are designed for fault estimation and disturbance estimation, respectively. In the next section, a composite time-delay fault tolerant controller should be determined for reconfiguring the systems with disturbance rejection and attenuation performance.

4. Composite Fault Tolerant Controller

In this section, a composite fault tolerant controller is designed to guarantee system (7) stability in the presence of

stuck faults and disturbances simultaneously. A composite fault tolerant controller is presented as

$$u(t) = Mx(t) - \hat{d}_1(t) - \hat{F}(t), \tag{16}$$

where M is the state feedback controller gain to be determined later. Substituting (16) into (7), and it is possible to obtain the augmented system

$$\begin{aligned}\begin{bmatrix} \dot{x}(t) \\ \dot{e}(t) \end{bmatrix} &= \begin{bmatrix} A & B_1E \\ 0 & W_1 \end{bmatrix} \begin{bmatrix} x(t) \\ e(t) \end{bmatrix} \\ &+ \begin{bmatrix} B_1M & 0 \\ 0 & NB_1E \end{bmatrix} \begin{bmatrix} x(t-\Delta(t)) \\ e(t-\Delta(t)) \end{bmatrix} \\ &+ \begin{bmatrix} B_2 & 0 & 0 \\ 0 & NB_2 & H_3 \end{bmatrix} \begin{bmatrix} d_2(t) \\ d_2(t-\Delta(t)) \\ \delta(t) \end{bmatrix} \\ &+ \begin{bmatrix} 0 \\ H_1 \end{bmatrix} \dot{F}(t). \end{aligned} \tag{17}$$

Then the reference output equation in the H_∞ preference index can be described as

$$z(t) = \begin{bmatrix} C_{11} & C_{12} \end{bmatrix} \begin{bmatrix} x(t) \\ e(t) \end{bmatrix} + \begin{bmatrix} C_{21} & C_{22} \end{bmatrix} \begin{bmatrix} x(t-\Delta(t)) \\ e(t-\Delta(t)) \end{bmatrix}. \tag{18}$$

Denoting $\overline{x}(t) = \begin{bmatrix} x(t) & e(t) \end{bmatrix}^T$, then (17) and (18) can be described as

$$\begin{aligned} \dot{\overline{x}}(t) &= A_0\overline{x}(t) + A_d\overline{x}(t-\Delta(t)) + B_0\overline{w}_0(t) + B_F\dot{F}(t), \\ z(t) &= C_1\overline{x}(t) + C_2\overline{x}(t-\Delta(t)), \end{aligned} \tag{19}$$

where

$$A_0 = \begin{bmatrix} A & B_1E \\ 0 & W_1 \end{bmatrix}, \qquad A_d = \begin{bmatrix} B_1M & 0 \\ 0 & NB_1E \end{bmatrix},$$
$$B_0 = \begin{bmatrix} B_2 & 0 & 0 \\ 0 & NB_2 & H_3 \end{bmatrix}, \qquad B_F = \begin{bmatrix} 0 \\ H_1 \end{bmatrix},$$
$$\overline{w}_0 = \begin{bmatrix} d_2(t) & d_2(t-\Delta(t)) & \delta(t) \end{bmatrix}^T, \tag{20}$$
$$C_1 = \begin{bmatrix} C_{11} & C_{12} \end{bmatrix}, \qquad C_2 = \begin{bmatrix} C_{21} & C_{22} \end{bmatrix}.$$

At this stage, the objective is to find K, L, and M such that system (17) is robustly asymptotically stable and satisfies the generalized H_∞ performance. We give the following theorem for the concerned robust fault diagnosis problem.

Lemma 2. *For composite system* (21)*, the parameters* $\gamma_1 > 0$*,* $\gamma_2 > 0$*, if there exist matrices* $P > 0$*,* $Q > 0$*,* $S > 0$*, and* $S \le P^{-1}$*, satisfying*

$$\begin{bmatrix} \Phi_{11} & 0 & PB_0 & PB_F & \tau A_0^T & \tau PA_d & C_1^T \\ * & -\sigma Q & 0 & 0 & \tau A_d^T & 0 & C_2^T \\ * & * & -\gamma_0^2 I & 0 & \tau B_0^T & 0 & 0 \\ * & * & * & -\gamma_1^2 I & \tau B_F^T & 0 & 0 \\ * & * & * & * & -\tau S & 0 & 0 \\ * & * & * & * & * & -\tau\sigma P & 0 \\ * & * & * & * & * & * & -I \end{bmatrix} < 0, \tag{21}$$

where $\Phi_{11} = sym[P(A_0 + A_d)] + Q$*,* $\sigma = 1 - \overline{d}$*, then the composite system* (21) *is robustly asymptotically stable and satisfies* $\|z(t)\|_2^2 < \gamma_0^2\|w_0(t)\|_2^2 + \gamma_1^2\|w_F(t)\|_2^2$.

Proof. First, we prove the stability of the control system, according to the Schur complement formula and $S \le P^{-1}$, the linear matrix inequalities (21) can be transformed into

$$\Theta_1 = \begin{bmatrix} \Pi_{11} & \tau A_0^T S^{-1} A_d + C_1^T C_2 & PB_0 + \tau A_0^T S^{-1} B_0 & PB_F + \tau A_0^T S^{-1} B_F \\ * & -(1-\overline{d})Q + \tau A_d^T S^{-1} A_d + C_2^T C_2 & \tau A_d^T S^{-1} B_0 & \tau A_D^T S^{-1} B_F \\ * & * & -\gamma_0^2 I + \tau B_0^T S^{-1} B_0 & \tau B_0^T S^{-1} B_F \\ * & * & * & -\gamma_1^2 I + \tau B_F^T S^{-1} B_F \end{bmatrix} < 0, \tag{22}$$

where

$$\begin{aligned} \Pi_{11} = {} & \mathrm{sym}\left[P(A + A_d)\right] + Q + \tau A_0^T S^{-1} A_0 \\ & + \tau\left(1-\overline{d}\right)^{-1} PA_d S A_d^T P + C_1^T C_1. \end{aligned} \tag{23}$$

Define

$$x_d(t) = x(t-\Delta(t)) = x(t) - \int_{t-\Delta(t)}^{t} \xi(s)\, ds, \tag{24}$$

where

$$\xi(s) = Ax(s) + A_d x_d(s) + B_0 w_0(s) + B_F w_F(s). \tag{25}$$

A Lyapunov function candidate for system (21) is chosen as

$$\begin{aligned} V(x,t) = {} & x^T(t) Px(t) + \int_{t-\Delta(t)}^{t} x^T(s) Qx(s)\, ds \\ & + \int_{-\Delta(t)}^{0} \int_{t+\beta}^{t} \xi^T(s) S^{-1} \xi(s)\, ds\, d\beta. \end{aligned} \tag{26}$$

It can be shown that

$$\begin{aligned} & \dot{V}(x(t), t) \\ & = \dot{x}^T(t) Px(t) + x^T(t) P\dot{x}(t) \\ & \quad + x^T(t) Qx(t) - \left[\left(1 - \dot{\Delta}(t)\right)\right] x_d^T(t) Qx_d(t) \\ & \quad + \dot{\Delta}(t) \int_{t-\Delta(t)}^{t} \xi^T(s) S^{-1} \xi(s)\, ds + \Delta(t)\, \xi^T(t) S^{-1} \xi(t) \end{aligned}$$

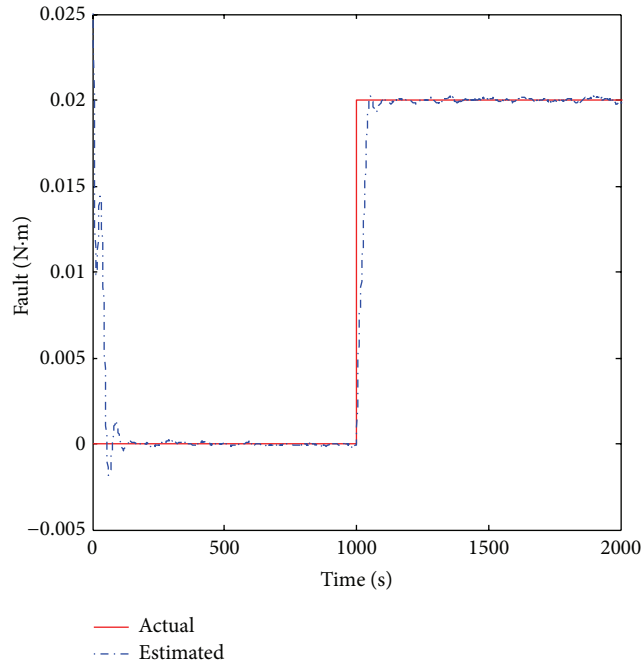

Figure 1: Curves of stuck fault and its estimation.

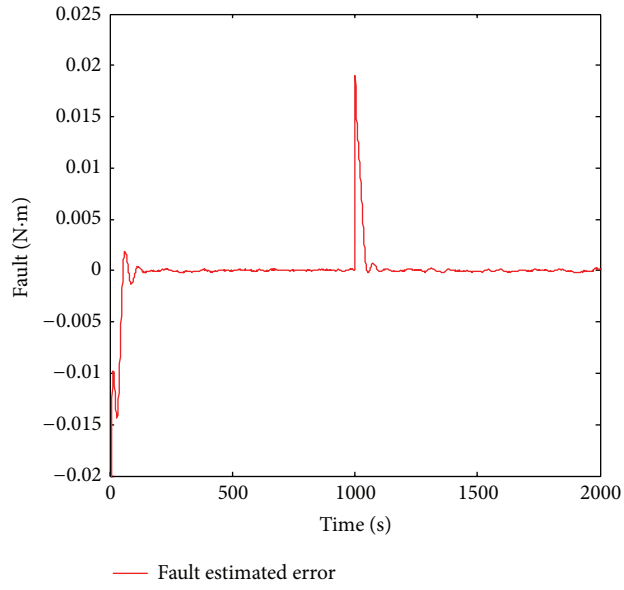

Figure 2: Curves of the estimation error of stuck faults.

$$-\int_{-\Delta(t)}^{0}\xi^{T}(t+\beta)S^{-1}\xi(t+\beta)\,d\beta \le \alpha^{T}(t)(\Theta_1-\Theta_2)\alpha(t), \tag{27}$$

where

$$\alpha(t)=\begin{bmatrix} x(t) \\ x_d(t) \\ w_0(t) \\ w_F(t) \end{bmatrix},$$

$$\Theta_2=\begin{bmatrix} C_1^TC_1 & C_1^TC_2 & 0 & 0 \\ * & C_2^TC_2 & 0 & 0 \\ * & * & -\gamma_0^2 I & 0 \\ * & * & * & -\gamma_1^2 I \end{bmatrix}. \tag{28}$$

By using Schur complement formula that $\Theta_1 < 0$ leads to $\Theta_1 - \Theta_2 < 0$, it can be obtained that $\dot{V}(x(t),t) \le 0$,

which implies that the system (17) is robustly asymptotically stable.

The next step is to prove the robustness of the system. Consider an auxiliary function as the performance index

$$J(x(t)) = V(x(t),t) + \int_0^t \|z(s)\|_2^2 - \gamma_0^2\|w_0(s)\|_2^2 - \gamma_1^2\|w_F(s)\|_2^2 ds, \tag{29}$$

which satisfies the zero initial condition. Similar to the proof of the stability, from (21) we have

$$\dot{J}(x(t) = \dot{V}(x(t),t) + \|z(t)\|_2^2 - \gamma_0^2\|w_0(t)\|_2^2 - \gamma_1^2\|w_F(t)\|_2^2 \le \alpha^T(t)(\Theta_1 - \Theta_2)\alpha(t) < 0. \tag{30}$$

Then, we can draw a conclusion that $J(x(t)) < 0$ under the zero initial condition which further leads to $\|z(t)\|_2^2 < \gamma_0^2\|w_0(t)\|_2^2 + \gamma_1^2\|w_F(t)\|_2^2$. The proof is completed. □

Theorem 3. *For composite system* (18)*, the parameters* $\gamma_0 > 0$*,* $\gamma_1 > 0$*,* $\gamma_2 > 0$*, and* $\gamma_3 > 0$*, if there exist matrices* $X > 0$*,* $Y > 0$*,* $P_2 > 0$*,* $Q_2 > 0$*,* $T > 0$*,* $S_1 > 0$*, and* $S_1 < X$*,* $T < P_2$*, satisfying*

$$\begin{bmatrix}
\phi_{11} & B_1E & 0 & 0 & B_2 & 0 & 0 & 0 & \tau XA^T & 0 & \tau B_1R_1 & 0 & XC_{11}^T \\
* & \phi_{22} & 0 & 0 & 0 & R_2B_2 & P_2H_3 & P_2H_1 & \tau E^TB_1^T & \tau W_1^TP_2 & 0 & R_2B_1E & C_{12}^T \\
* & * & -\sigma Y & 0 & 0 & 0 & 0 & 0 & \tau R_1^TB_1^T & 0 & 0 & 0 & XC_{21}^T \\
* & * & * & -\sigma Q_2 & 0 & 0 & 0 & 0 & 0 & \tau E^TB_1^TR_2^T & 0 & 0 & C_{22}^T \\
* & * & * & * & -\gamma_0^2 I & 0 & 0 & 0 & \tau B_2^T & 0 & 0 & 0 & 0 \\
* & * & * & * & * & -\gamma_1^2 I & 0 & 0 & 0 & \tau B_2^TR_2^T & 0 & 0 & 0 \\
* & * & * & * & * & * & -\gamma_2^2 I & 0 & 0 & \tau H_3^TP_2 & 0 & 0 & 0 \\
* & * & * & * & * & * & * & -\gamma_3^2 I & 0 & \tau H_1^TP_2 & 0 & 0 & 0 \\
* & * & * & * & * & * & * & * & -\tau S_1 & 0 & 0 & 0 & 0 \\
* & * & * & * & * & * & * & * & * & -\tau T & 0 & 0 & 0 \\
* & * & * & * & * & * & * & * & * & * & -\tau\sigma X & 0 & 0 \\
* & * & * & * & * & * & * & * & * & * & * & -\tau\sigma P_2 & 0 \\
* & * & * & * & * & * & * & * & * & * & * & * & -I
\end{bmatrix} < 0, \tag{31}$$

where $\phi_{11} = sym(AX + B_1R_1) + Y$*,* $\phi_{22} = sym(P_2W_1 + R_2B_1E) + Q_2$*, then the composite system* (18) *with controller gain* $M = R_1X^{-1}$ *and observer gain* $\begin{bmatrix} L \\ K \end{bmatrix} = {P_2}^{-1}R_2$ *is robustly asymptotically stable and satisfies*

$$\|z(t)\|_2^2 < \gamma_0^2\|d_2(t)\|_2^2 + \gamma_1^2\|d_2(t-\Delta(t))\|_2^2 + \gamma_2^2\|\delta(t)\|_2^2 + \gamma_3^2\left\|\dot{F}(t)\right\|_2^2. \tag{32}$$

Proof. According to the system (18), denoting

$$P = \begin{bmatrix} P_1 & 0 \\ 0 & P_2 \end{bmatrix}, \qquad Q = \begin{bmatrix} Q_1 & 0 \\ 0 & Q_2 \end{bmatrix}, \qquad S = \begin{bmatrix} S_1 & 0 \\ 0 & S_2 \end{bmatrix}. \tag{33}$$

Substituting the related matrix into Lemma 2, we can get

$$\begin{bmatrix}
\varphi_{11} & P_1B_1E & 0 & 0 & P_1B_2 & 0 & 0 & 0 & \tau A^T & 0 & \tau P_1B_1N & 0 & C_{11}^T \\
* & \varphi_{22} & 0 & 0 & 0 & R_2B_2 & P_2H_3 & P_2H_1 & \tau E^TB_1^T & \tau W_1^T & 0 & R_2B_1E & C_{12}^T \\
* & * & -\sigma Y & 0 & 0 & 0 & 0 & 0 & \tau M^TB_1^T & 0 & 0 & 0 & C_{21}^T \\
* & * & * & -\sigma Q_2 & 0 & 0 & 0 & 0 & 0 & \tau E^TB_1^TN^T & 0 & 0 & C_{22}^T \\
* & * & * & * & -\gamma_0^2 I & 0 & 0 & 0 & \tau B_2^T & 0 & 0 & 0 & 0 \\
* & * & * & * & * & -\gamma_1^2 I & 0 & 0 & 0 & \tau B_2^TN^T & 0 & 0 & 0 \\
* & * & * & * & * & * & -\gamma_2^2 I & 0 & 0 & \tau H_3^T & 0 & 0 & 0 \\
* & * & * & * & * & * & * & -\gamma_3^2 I & 0 & \tau H_1^T & 0 & 0 & 0 \\
* & * & * & * & * & * & * & * & -\tau S_1 & 0 & 0 & 0 & 0 \\
* & * & * & * & * & * & * & * & * & -\tau S_2 & 0 & 0 & 0 \\
* & * & * & * & * & * & * & * & * & * & -\tau\sigma P_1 & 0 & 0 \\
* & * & * & * & * & * & * & * & * & * & * & -\tau\sigma P_2 & 0 \\
* & * & * & * & * & * & * & * & * & * & * & * & -I
\end{bmatrix} < 0, \tag{34}$$

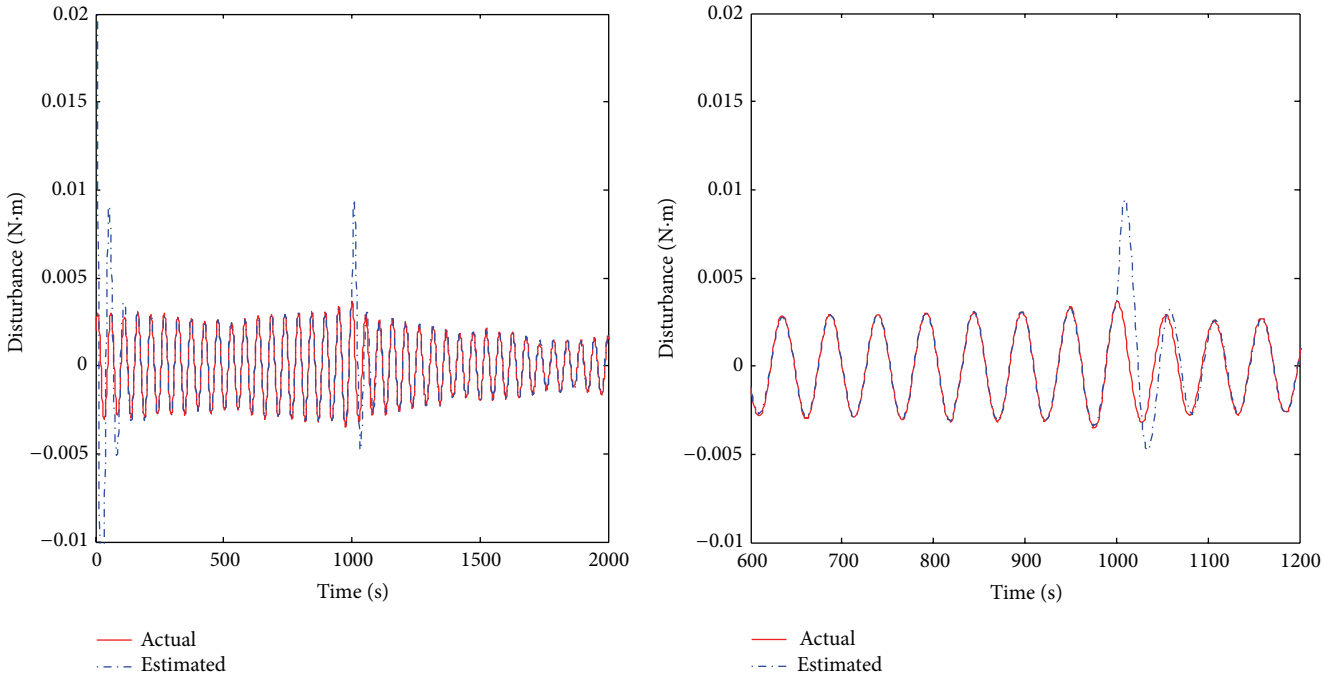

(a) Time responses of vibration and vibration observed

(b) Partial amplification of (a)

Figure 3: Curves of vibration estimation of disturbance observer.

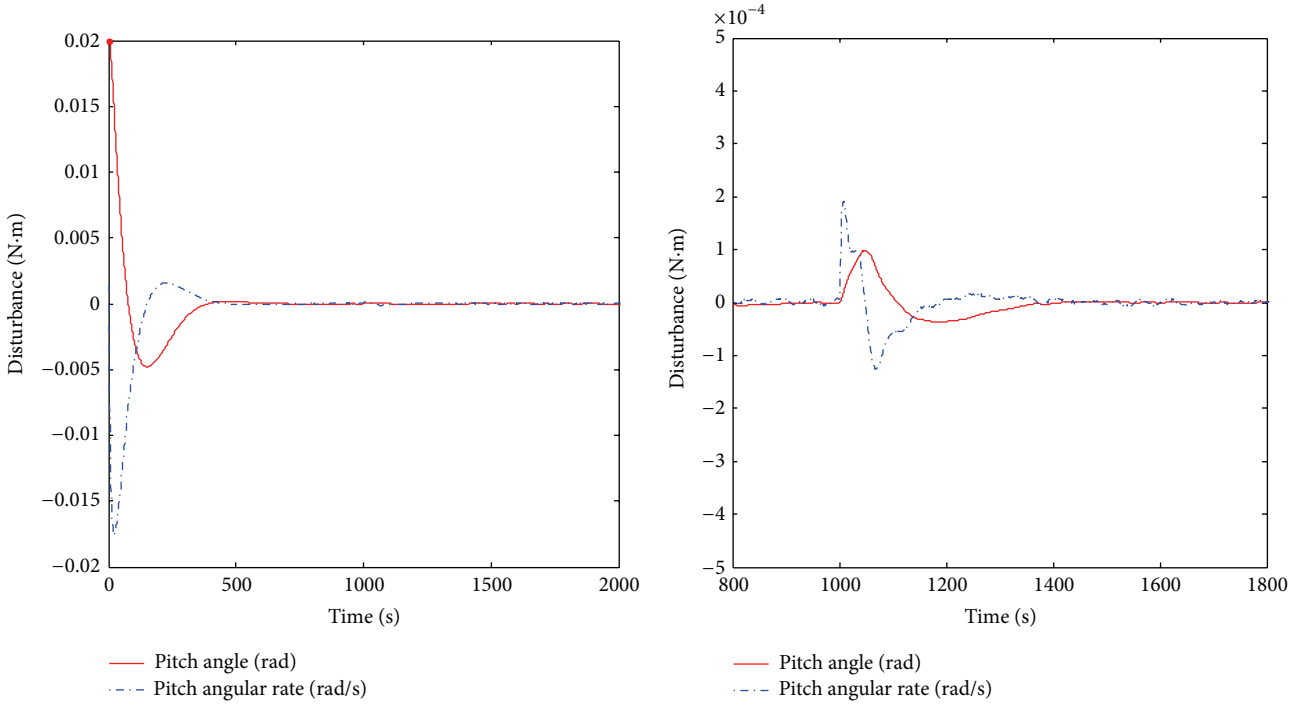

(a) Time responses of attitude angle and attitude angular velocity

(b) Partial amplification of (a)

Figure 4: Time responses of attitude angle and attitude angular velocity.

where $\varphi_{11} = \mathrm{sym}(P_1A + B_1M) + Q_1$, $\varphi_{22} = \mathrm{sym}(P_2W_1 + R_2B_1E) + Q_2$, premultiply and postmultiply $\mathrm{diag}\{X, I, X, I, I, I, I, I, P_2, X, I, I\}$ simultaneously to the left and right sides of (34), and then defining $X = P_1^{-1}$, $R_1 = MP_1^{-1} = MX$, $R_2 = P_2N$, $Y = XQ_1X$, and $T = P_2S_2P_2$ then (31) is obtained. Furthermore, $S_1 \le P_1^{-1} = X$ and $S_2 \le P_2^{-1}$ are equivalent to $T \le P_2$. So, the composite system (18) with controller gain $M = R_1X^{-1}$ and $N = P_2^{-1}R_2$ is robustly asymptotically stable and satisfies $\|z(t)\|_2^2 < \gamma_0^2\|d_2(t)\|_2^2 + \gamma_1^2\|d_2(t-\Delta(t))\|_2^2 + \gamma_2^2\|\delta(t)\|_2^2 + \gamma_3^2\|\dot{F}(t)\|_2^2$. □

5. Simulation Example

In order to demonstrate the effectiveness of the proposed control algorithm, numerical simulations will be performed in this section. The composite controller will be applied for the attitude control of a microsatellite with unknown input delay, reaction wheel's faults, and vibration disturbance torque from reaction wheel simultaneously.

In this paper, we only consider the attitude in the pitch channel. Select the upper bound $\tau = 30$ ms, and $\overline{d} = 0.1$. The microsatellite is supposed to move in a circular orbit with the altitude of 900 km; then the orbit rate $n = 0.0011$ rad/s. $J = 6.14\,\mathrm{kg{\cdot}m^2}$ is the nominal principal moment of inertia of pitch axis. The initial pitch attitudes of the microsatellite are $\theta = 0.02$ rad and $\dot{\theta} = 0.002$ rad/s. Periodic disturbances $d_1(t)$ caused by reaction wheel are described by (10) with $W = \left[\begin{smallmatrix} 0 & 6 \\ -6 & 0 \end{smallmatrix}\right]$, $V = [5 \;\; 0]$. We select $\delta(t)$ as the random signal with upper 2-norm bound 1. $d_2(t)$ can also be considered as the random signal with bounded upper 2-norm. For the reference output, it is denoted that $C_{11} = [0.2 \;\; 0.2 \;\; 0.2]$, $C_{12} = [0.8 \;\; 0.2 \;\; 0]$, $C_{21} = [0 \;\; 0.2 \;\; 0.8]$, and $C_{22} = [0.8 \;\; 0.2 \;\; 0]$. For $\sigma = 0.9$ and $\gamma_0 = 1$, $\gamma_1 = 2$, $\gamma_2 = 0.5$, and $\gamma_3 = 1.2$. It can be solved via LMI related to (17) that the gain of fault diagnosis observer (11) is

$$K = [0 \;\; 0 \;\; -20.4023], \tag{35}$$

the gain of disturbance observer (12) is

$$L = \begin{bmatrix} 0 & 0 & -4.3713 \\ 0 & 0 & -2.3608 \end{bmatrix}, \tag{36}$$

and the gain of state feedback controller is

$$M = [-17.2607 \;\; -37.7208 \;\; -38.7539]. \tag{37}$$

The stuck fault of reaction wheel is supposed to occur at the 1000th second as $F = 0.02\,\mathrm{N{\cdot}m}$. The estimation of stuck faults is demonstrated in Figure 1, where the solid line represents the real fault signal and the dash-dot line stands for their estimation. Fault estimation error is shown in Figure 2. From Figures 1 and 2, it can be seen that the proposed fault diagnosis method has respectable estimation ability.

When the disturbance observer is constructed based on (12), Figure 3(a) shows the actual value, and estimated value of the disturbance caused by the reaction wheel. Figure 3(b) is obtained by partially amplifying Figure 3(a). From both figures, we can see that the main disturbance can be estimated and rejected accurately by the proposed disturbance observer.

Figures 4(a) and 4(b) show that the composite controller is capable of compensating the effect of stuck faults and vibration disturbance torque from reaction wheel actively and can improve the reliability and stability of the microsatellite in the presence of the model uncertainty and space environmental disturbances.

6. Conclusion

In this paper, the fault diagnosis problem is addressed for microsatellite with unknown input delay. The following features of the proposed algorithm are compared with the previous results. Firstly, a uniform fault diagnosis observer is constructed for the attitude control systems. Secondly, the disturbances considered in this paper are assumed to include vibration disturbance torque from reaction wheel and norm bounded uncertain disturbance. A disturbance observer is constructed to estimate the vibration disturbance. Thirdly, a new composite controller is designed which can attenuate the influence of the norm bounded disturbances and the estimation errors and correspondingly guarantee the robust stability against other disturbances. Finally, simulations for a microsatellite are given to show the efficiency of the proposed approach. Although numerical simulations have shown that enhanced robustness can be achieved by using the proposed method, more general theoretical research and experimental simulations need to be carried out in the future to ensure the reliability and stability of attitude control systems for microsatellite.

Conflict of Interests

There is no conflict of interests regarding the publication of this paper.

Acknowledgments

This work was supported by the National 973 Program (Grant no. 2012CB720003), and the National Natural Science Foundation of China (NSFC) (Grants no. 60925012, 61127007, 91016004, and 61121003).

References

[1] M. Tafazoli, "A study of on-orbit spacecraft failures," *Acta Astronautica*, vol. 64, no. 2-3, pp. 195–205, 2009.

[2] J.-F. Castet and J. H. Saleh, "Beyond reliability, multi-state failure analysis of satellite subsystems: a statistical approach," *Reliability Engineering and System Safety*, vol. 95, no. 4, pp. 311–322, 2010.

[3] W.-Y. Zhou, G. S. Aglietti, and Z. Zhang, "Modelling and testing of a soft suspension design for a reaction/momentum wheel assembly," *Journal of Sound and Vibration*, vol. 330, no. 18-19, pp. 4596–4610, 2011.

[4] S. Taniwaki and Y. Ohkami, "Experimental and numerical analysis of reaction wheel disturbances," *JSME International Journal C*, vol. 46, no. 2, pp. 519–526, 2003.

[5] H.-S. Oh and D.-I. Cheon, "Precision measurements of reaction wheel disturbances with frequency compensation process," *Journal of Mechanical Science and Technology*, vol. 19, no. 1, pp. 136–143, 2005.

[6] R. A. Masterson, D. W. Miller, and R. L. Grogan, "Development and validation of reaction wheel disturbance models: empirical model," *Journal of Sound and Vibration*, vol. 249, no. 3, pp. 575–598, 2002.

[7] C.-Y. Kao and A. Rantzer, "Stability analysis of systems with uncertain time-varying delays," *Automatica*, vol. 43, no. 6, pp. 959–970, 2007.

[8] J. Lam, H. Gao, and C. Wang, "Stability analysis for continuous systems with two additive time-varying delay components," *Systems and Control Letters*, vol. 56, no. 1, pp. 16–24, 2007.

[9] M. Blanke, M. Kinnaert, M. Lunze et al., *Diagnosis and Fault Tolerant Control*, Springer, New York, NY, USA, 2003.

[10] M. Zhong, H. Ye, S. X. Ding, and G. Wang, "Observer-based fast rate fault detection for a class of multirate sampled-data systems," *IEEE Transactions on Automatic Control*, vol. 52, no. 3, pp. 520–525, 2007.

[11] W. Wang, D. H. Zhou, and Z. Li, "Robust state estimation and fault diagnosis for uncertain hybrid systems," *Nonlinear Analysis: Theory, Methods and Applications*, vol. 65, no. 12, pp. 2193–2215, 2006.

[12] L. Guo, Y.-M. Zhang, H. Wang, and J.-C. Fang, "Observer-based optimal fault detection and diagnosis using conditional probability distributions," *IEEE Transactions on Signal Processing*, vol. 54, no. 10, pp. 3712–3719, 2006.

[13] Z. Gao and S. X. Ding, "Actuator fault robust estimation and fault-tolerant control for a class of nonlinear descriptor systems," *Automatica*, vol. 43, no. 5, pp. 912–920, 2007.

[14] J. Jin, S. Ko, and C.-K. Ryoo, "Fault tolerant control for satellites with four reaction wheels," *Control Engineering Practice*, vol. 16, no. 10, pp. 1250–1258, 2008.

[15] N. Meskin and K. Khorasani, "Fault detection and isolation in a redundant reaction wheels configuration of a satellite," in *Proceedings of the IEEE International Conference on Systems, Man, and Cybernetics (SMC '07)*, pp. 3153–3158, October 2007.

[16] N. Tudoroiu, E. Sobhani-Tehrani, and K. Khorasani, "Interactive bank of unscented Kalman filters for fault detection and isolation in reaction wheel actuators of satellite attitude control system," in *Proceedings of the 32nd Annual Conference on IEEE Industrial Electronics (IECON '06)*, pp. 264–269, November 2006.

[17] D. Hu, A. Sarosh, and Y.-F. Dong, "A novel KFCM based fault diagnosis method for unknown faults in satellite reaction wheels," *ISA Transactions*, vol. 51, no. 2, pp. 309–316, 2012.

[18] Q. Hu, "Robust adaptive sliding-mode fault-tolerant control with L2-gain performance for flexible spacecraft using redundant reaction wheels," *IET Control Theory and Applications*, vol. 4, no. 6, pp. 1055–1070, 2010.

[19] Q. Hu, Y. Zhang, X. Huo, and B. Xiao, "Adaptive integral-type sliding mode control for spacecraft attitude maneuvering under actuator stuck failures," *Chinese Journal of Aeronautics*, vol. 24, no. 1, pp. 32–45, 2011.

[20] A.-M. Zou and K. D. Kumar, "Adaptive fuzzy fault-tolerant attitude control of spacecraft," *Control Engineering Practice*, vol. 19, no. 1, pp. 10–21, 2011.

[21] L. Guo and W.-H. Chen, "Disturbance attenuation and rejection for systems with nonlinearity via DOBC approach," *International Journal of Robust and Nonlinear Control*, vol. 15, no. 3, pp. 109–125, 2005.

[22] L. Guo, C. B. Feng, and W. H. Chen, "A survey of disturbance-observer-based control for dynamic nonlinear system," *Dynamics of Continuous Discrete and Impulsive System B*, vol. 13E, pp. 79–84, 2006.

[23] S. Cao, L. Guo, and X. Wen, "Fault tolerant control with disturbance rejection and attenuation performance for systems with multiple disturbances," *Asian Journal of Control*, vol. 13, no. 6, pp. 1056–1064, 2011.

[24] L. Guo, "Composite Hierarchical Anti-Disturbance Control (CHADC) for systems with multiple disturbances: Survey and overview," in *Proceedings of the 30th Chinese Control Conference (CCC '11)*, pp. 6193–6198, July 2011.

[25] H. Liu, L. Guo, and Y. Zhang, "An anti-disturbance PD control scheme for attitude control and stabilization of flexible spacecrafts," *Nonlinear Dynamics*, vol. 67, no. 3, pp. 2081–2088, 2012.

[26] H. Liu, L. Guo, and Y. Zhang, "Composite attitude control for flexible spacecraft with simultaneous disturbance attenuation and rejection performance," *Proceedings of the Institution of Mechanical Engineers I*, vol. 226, no. 2, pp. 154–161, 2012.

[27] J. Z. Qiao, L. Guo, Y. J. Lei et al., "Subtle anti-disturbance tolerant control of attitude control systems for microsatellites," *Scientia Sinica Informationis*, vol. 42, pp. 1327–1337, 2012.

Hindawi Publishing Corporation
Mathematical Problems in Engineering
Volume 2013, Article ID 782617, 11 pages
http://dx.doi.org/10.1155/2013/782617

Research Article

Fault Tolerant Control in Redundant Inertial Navigation System

Xiaoqiang Dai, Lin Zhao, and Zhen Shi

College of Automation, Harbin Engineering University, Harbin 150001, China

Correspondence should be addressed to Xiaoqiang Dai; dxq_just@163.com

Received 25 July 2013; Accepted 1 September 2013

Academic Editor: Zhiguang Feng

Conventional fault detection and isolation technology cannot fully ensure system redundancy features when sensors experience drift in a redundant inertial navigation system. A new fault tolerant control method employs state estimation and state feedback techniques to compensate the sensor drift. However, the method is sensitive to measurement noise characteristics, and the performance of the method nearly depends on the feedback gain. This paper proposes an improved fault tolerant control algorithm, which employs an adaptive extended Kalman particle filter (AEKPF) to deal with unknown noise characteristics and model inaccuracies. In addition, a drift factor is introduced in the improved fault tolerant controlin order to reduce the dependence of compensation system on the feedback gain. Simulation results show that the improved fault tolerant control algorithm can effectively correct the faulty sensor even when the multiple erroneous sensors are producing faulty outputs simultaneously. Meanwhile, the AEKPF is able to solve the problem of unknown non-Gaussian noise characteristics. Moreover, the feedback gain is significantly improved by the drift factor.

1. Introduction

The reliability of inertial sensor affects the reliability of the entire inertial navigation system. A redundant technology is applied to improve the precision and reliability of the inertial navigation system, that is, by means of increasing numbers of gyro and accelerometer [1–3]. In order to monitor a redundant system, an effective fault detection and isolation scheme has to be designed to detect and isolate the fault in time once a sensor failure occurs [4–8]. For the redundant strapdown inertial navigation system usually working in dynamic environments, the performance of fault detection depends not only on the detecting method but also on the constraint from errors of inertial sensors. Nowadays, many fault detection and isolation techniques are constructed based on the geometric redundancy and parity space approach, involving identical inertial sensors deployed at various locations to establish algebraic equations for each inertial sensor output [1, 9–11]. These equations are referred to as either parity equations or voting equations. The erroneous sensor unit can be identified by such equations and excluded from the sensor array. As far as the parity space approach is concerned, the fault identification is solved by some voting equations [9, 10]. Both the threshold value and observation period should be set up to watchdog the contaminated outputs by noise. When outputs from the voting equations exceed the threshold value at the end of an observation period, a faulty sensor recognition is active [12]. However, the parity space approach has following faults: (1) the threshold value and the observation period are empirical, and the inappropriate values will lead to failure of fault detection system, (2) the need for an observation period indicates that this approach cannot be done in real time [6], and (3) the redundant inertial navigation system would lose its redundancy easily.

Conventional fault-identification algorithms are difficult to maintain the redundancy of the redundant inertial navigation system. This is simply because each sensor in a sensor array is drifting from time to time due to the nature of the drift. Moreover, after the first few drifting sensors are identified and excluded from the sensor array, the system would lose its redundancy and identify other drifting sensors. Therefore, the redundant inertial navigation system should have the capability of self-repairing to maintain its redundancy.

A fault tolerant control algorithm for fault-tolerant sensor systems was proposed by Chen and You in [12]. The state

estimation and state feedback techniques were used in fault tolerant control algorithm. Due to its capability of the real time fault correction, the fault tolerant control algorithm is able to compensate sensor fault drifts. The sensor which has experienced fault drift is no longer isolated, but compensated in real time. Therefore, it maintains the system's redundancy [12–14]. However, the fault tolerant control algorithm is sensitive to the priori knowledge of the measured noise and the feedback gain. Inappropriate measurement of the noise covariance and the feedback gain will cause the compensation algorithm invalidity. Meanwhile, it requires that the measured noise must be white Gaussian noise. Moreover, the range of its feedback gain is narrow, and a lot of experiments should be done to determine the feedback gain.

This paper proposes an improved fault tolerant control algorithm based on the work [12], which employs an AEKPF to deal with unknown noise characteristics and model inaccuracies, and a drift factor is introduced in the improved fault tolerant control to reduce the dependence of compensation system on the feedback gain. The algorithm has the following advantages. First, the drift sensors are compensated in real time. Secondly, the improved algorithm does not need the threshold value and the observation period. Thirdly, the improved algorithm uses the AEKPF to solve the problem of unknown noise characteristics and model inaccuracies. Fourthly, the improved fault tolerant control algorithm is insensitive to the feedback gain, and it can enlarge the range of feedback gain due to the drift factor. Last but not the least, the redundant inertial navigation system with the improved fault tolerant control is unconditionally stable, even if all inertial sensors have experienced drift at certain circumstances.

This paper is arranged as follows. The basic theory of the fault tolerant control algorithm is introduced in Section 2. The proposed improved fault tolerant control algorithm is explained in Section 3. Simulation results of the improved fault tolerant control algorithm are shown in Section 4. Section 5 discusses both the certain circumstances and the unique features of the improved fault tolerant control algorithm. Finally, Section 6 concludes the paper.

2. The Basic Theory of the Fault Tolerant Control Algorithm

A reasonable redundant configuration of inertial sensors can improve the reliability of the inertial navigation system. Assuming that there are n similar inertial sensors in the redundant inertial navigation system, the measurement equation is given by

$$m = H\omega + \varepsilon, \tag{1}$$

where m is a vector of sensor measurements, H is measurement matrix, ω is the state vector to be measured by sensors, and ε is the sensor noise with zero mean. Let H^* be the transpose conjugate of H and let V be the null space of H^*; then,

$$V^*H = 0. \tag{2}$$

The parity equations are defined as

$$P = V^*m. \tag{3}$$

As shows in previous researches [1–6], if there are n gyroscopes to measure three angular rates in redundant inertial navigation system, the navigation system can form $n-3$ parity equations. Assuming that only one faulty sensor exists in a sensor array, the system needs at least two parity equations to locate it [12, 13]. This means that one state needs at least three sensors to measure it if the system needs to locate the faulty sensor. So the number of parity equation must be more than or equal to 2; that is, $n-3 \geq 2$. These $n-3$ parity equations are often converted into n equations in linear transformation. In other words, the matrix V can be converted into a $n \times n$ matrix where all of the diagonal terms are equal to zeros while nonzero elsewhere. The newly formed equations are referred to as voting equations with an associated voting matrix to distinguish them from the parity equations. Furthermore, the voting matrix is derived from the $n-3$ parity equations, resulting in a rank of $n-3$.

The voting equations are defined as

$$Q = C_v m = C_v \begin{bmatrix} m_1 & \cdots & m_n \end{bmatrix}^T, \tag{4}$$

$$C_v = \begin{bmatrix} 0 & C_{12} & \cdots & C_{1,n} \\ C_{21} & 0 & \cdots & C_{2,n} \\ \vdots & & & \vdots \\ C_{n,1} & \cdots & C_{n,n-1} & 0 \end{bmatrix} = \begin{bmatrix} C_{v1} \\ C_{v2} \\ \vdots \\ C_{vn} \end{bmatrix}, \tag{5}$$

where $m_1, \ldots, m_n$ represent measurements from the n sensors, and $C_{v1}, \ldots, C_{vn}$ are the row vectors of C_v. The voting equation (5) is derived from the parity equations of (3). By means of linear transformations, the parity equations can be converted into voting equation. A faulty sensor can be more easily identified from voting equations than from parity equations. For example, if the output of the first voting equation is zero but the rest are non-zeros, one can determine that sensor m_1 is faulty. When sensor measurements are contaminated by noise, the above fault-finding method cannot be done in real time, since at any time instant, none of the voting equation outputs is zero. In addition, the above method cannot be used in the system when incorporated sensors experience sensor drifts, because every sensor in a sensor array is drifting, and thus the assumption of only one faulty sensor in a sensor array can hardly be satisfied [12].

3. The Improved Fault Tolerant Control Algorithm

The improved fault tolerant control algorithm is designed under the condition when outputs of incorporated sensors are contaminated by noise and signal drifts. This is done by formulating the conventional fault-identification algorithm into a real time state estimation and state compensation algorithm.

3.1. Real Time Sensor Drifts Estimation. The state estimation techniques are used to identify sensor drifts in sensor outputs,

and the drift of sensor is separated from sensor measurements and modeled as a system which meets

$$m_{di} = m_i + d_i, \quad i = 1, \ldots, n, \tag{6}$$

where d_i is the drift of sensor i, m_{di} is the sensor output with drift and white noise, and m_i is the sensor output with white noise. When these drifts are treated as system states, their governing equations can be written as

$$\dot{d}_i = \delta, \quad i = 1, \ldots, n, \tag{7}$$

where δ is the change of drift.

From a system observability point of view, the above system needs n output equations to observe n states. These $n-3$ parity equations, which are used to describe the relations between outputs of n sensors, can be processed to obtain $n-3$ output equations for the estimation. They can be arbitrary chosen from $n-3$ row vectors in the voting matrix, such as Z_1 shown as

$$\begin{aligned} Z_1 &\triangleq \begin{bmatrix} C_{v1} \\ \vdots \\ C_{vn-3} \end{bmatrix} \begin{bmatrix} d_1 \\ \vdots \\ d_n \end{bmatrix} = \begin{bmatrix} C_{v1} \\ \vdots \\ C_{vn-3} \end{bmatrix} \begin{bmatrix} m_{d1} - m_1 \\ \vdots \\ m_{dn} - m_n \end{bmatrix} \\ &= \begin{bmatrix} C_{v1} \\ \vdots \\ C_{vn-3} \end{bmatrix} \begin{bmatrix} m_{d1} \\ \vdots \\ m_{dn} \end{bmatrix}. \end{aligned} \tag{8}$$

There are only $n-3$ equations in (8), so the system at least need is 3 equations which are not linear correlation with (8) in addition. As stated as before, assuming that there is only one fault sensor existed in the sensor array, the remaining output equations can written as

$$\begin{aligned} Z_2 &\triangleq \begin{bmatrix} C_{v1}d & 0 & 0 \\ 0 & \ddots & 0 \\ 0 & 0 & C_{vn}d \end{bmatrix} d = \begin{bmatrix} C_{v1}d & 0 & 0 \\ 0 & \ddots & 0 \\ 0 & 0 & C_{vn}d \end{bmatrix} \begin{bmatrix} d_1 \\ \vdots \\ d_n \end{bmatrix} \\ &= \begin{bmatrix} C_{v1}dd_1 \\ \vdots \\ C_{vn}dd_n \end{bmatrix} = \begin{bmatrix} 0 + C_{12}d_2d_1 + \cdots + C_{1n}d_nd_1 \\ \vdots \\ C_{n1}d_1d_n + C_{n2}d_2d_n + \cdots + 0 \end{bmatrix}. \end{aligned} \tag{9}$$

Equation (9) also implements the constraint of only one faulty sensor array. For example, the multiplication of any two drifts is equal to zero ($d_i \times d_j = 0, i \neq j$). If only one faulty sensor existed in the sensor array, the row vector Z_2 is a zero vector; otherwise, Z_2 is not a zero vector. With both the system governing equations (7) and the output equations (8) and (9), one can estimate these drifts in real time by constructing a state observer. Since the associated output equations Z_2 are nonlinear, a nonlinear filter should be chosen to serve as the state observer [12, 13].

In fact, the expression of δ is hard to get since sensor drifts are random. In order to facilitate the establishment of system model, the governing equations can be written as $\dot{d}_i = 0, i = 1, \ldots, n$ if assuming $\delta(t) = 0$, which means that all of drifts are assumed as dc offset. However, when the sensor errors are drifting, the real time drifts estimation would fail because the new governing equation is incapable of describing time-varying signals. In this case, the estimation failure would be attributed to the system modeling error. Some "fading memory" techniques [15–17] were developed to ensure the state convergence in the presence of model error. These techniques were applied to ensure the state convergence by eliminating the effect of older data from current state estimation if they are no longer valid [12]. If the measurement noise is non-Gaussian noise in a variety of applications, the performance and convergence of adaptive extended Kalman filter cannot be ensured. This paper uses an AEKPF to solve the problem that the measurement noise is not white Gaussian noise and the system model is inaccurate.

Assume that the state equation and measurement equation of estimation system can be written as

$$\begin{aligned} d_{k+1} &= d_k + W_k, \\ z_k &= h(d) = \begin{bmatrix} Z_1 \\ Z_2 \end{bmatrix}. \end{aligned} \tag{10}$$

The AEKPF algorithm is expressed by following steps.

(1) *Initialize the Particles.* The particle number is initialized as N. The particle d_0^i is sampled from the proposal distribution $p(d_0)$, $X = \{(d_0^i, \omega_0^i) \mid i = 1, 2, \ldots, N\}$; at the same time, the particle weights are set as $\omega_0^i = 1/N$. That is, $d_0^i \sim p(d_0)$.

(2) *Sequential Importance Sampling.* Every particle with EKF is updated firstly. The project error covariance $P_{k+1/k}$ is

$$P_{k+1/k} = \lambda_k P_k. \tag{11}$$

The Kalman gain is

$$L_{k+1} = P_{k+1/k} H_{k+1}^T \left(H_{k+1} P_{k+1/k} H_{k+1}^T + R_{k+1} \right)^{-1}. \tag{12}$$

The update error covariance is

$$P_{k+1} = \left(I - L_{k+1} H_{k+1} \right) P_{k+1/k}. \tag{13}$$

The update estimates is

$$\hat{d}_{k+1} = \hat{d}_k + L_{k+1} \left(z_{k+1} - h\left(\hat{d}_k \right) \right). \tag{14}$$

The observation matrix is

$$H_{k+1} = \frac{\partial}{\partial d} h(d) \mid_{d=\hat{d}_k}, \tag{15}$$

where $\hat{d}_k$ is the estimated value of d_k, λ_k is the fading factor, L_k is the observer gain, P_k is the state covariance matrix, R_k is the measurement noise covariance matrix, and $h(\cdot)$ is the output equation for sensor measurements. If

$$\begin{aligned} M_k &= H_{k+1} P_k H_{k+1}^T + R_k, \\ N_k &= \left[z_{k+1} - h\left(\hat{d}_k \right) \right] \left[z_{k+1} - h\left(\hat{d}_k \right) \right]^T. \end{aligned} \tag{16}$$

The fading factor is

$$\lambda_k = \max\left\{1, \frac{\operatorname{trace}(N_k)}{\operatorname{trace}(M_k)}\right\}. \tag{17}$$

With above equations, we can deduce the mean value d_k^{-i} and variance P_k^i of the particles $\{\widehat{d}_k^i\}_{i=1}^N$ and sample particles d_k^i from the importance density function $q(d_k^i \mid d_{k-1}^i, z_{1:k}) = N(\widehat{d}_k^i; d_k^{-i}, P_k^i)$.

Secondly, the particle weights are updated. If the importance density is a first-order Markov process and expressed in a recursively form, the expression of the particle weights can be written as

$$\omega_k^i = \omega_{k-1}^i \frac{p(z_k \mid d_k)\, p\left(d_k^i \mid d_{k-1}^i\right)}{q\left(d_k^i \mid d_{k-1}^i, z_{1:k}\right)}. \tag{18}$$

The particle weights are normalized as

$$\omega_k^i = \frac{\omega_k^i}{\sum_{i=1}^N \omega_k^i}. \tag{19}$$

(3) *Resample the Particles*. The effective particle number is given by

$$\widehat{N}_{\text{eff}} = \frac{1}{\sum_{i=1}^N \left(\omega_k^i\right)^2}. \tag{20}$$

If $\widehat{N}_{\text{eff}} < N_{\text{th}}$ (here N_{th} is the threshold of effective particle number, i.e., $N_{\text{th}} = 2N/3$), then the particles $\{\widehat{d}_k^i\}_{i=1}^N$ and the new particles are determined by

$$\begin{aligned} &\left\{d_k^i\right\}_{i=1}^N, \qquad P\left(d_k^i = \widehat{d}_k^i\right) = \omega_k^i, \\ &d_k^i \sim \left(d_k^i, \omega_k^i\right), \quad \omega_k^i = \frac{1}{N}. \end{aligned} \tag{21}$$

By means of the resampling operation, those particles with larger weights will be reserved, and those with smaller weights be killed.

(4) *Output.* The expectation is assumed as

$$\widehat{d}_k = \sum_{i=1}^N d_k^i \omega_k^i. \tag{22}$$

And the covariance is

$$P_k^i = E\left[\left(\widehat{d}_k - d_k^i\right)\left(\widehat{d}_k - d_k^i\right)^T\right]. \tag{23}$$

(5) *Replace* $k = k + 1$ *and Return to Step* (2).

3.2. Real Time Sensor Drifts Compensation. Once the drift in each sensor output is estimated in real time, the drift compensation can be done by the state feedback technique, as

$$\dot{d} = u, \tag{24}$$

$$u = -K\alpha\widehat{d}. \tag{25}$$

Equations (24) and (25) can also be written in a discrete time form as

$$d_k = \widehat{d}_{k-1} + u_{k-1} \tag{24a}$$

$$u_{k-1} = -K\alpha_{k-1}\widehat{d}_{k-1}, \tag{25a}$$

where K is the feedback gain, and α_k is the drift factor.

Since the drift is changed by the estimated drift in the compensation system, the output equations, namely, (8) and (9) which are used in the drift estimation system, are no longer valid. The output values of output equations for the compensation system are obtained by processing the compensated drift values to obtain compensated sensor outputs, as the m_{cik} shown in the following:

$$\begin{aligned} m_{cik} &= m_{ik} + d_{cik} = m_{ik} + d_{ik} - K\sum_{\tau=0}^{k} \alpha_{i\tau}\widehat{d}_{i\tau} \\ &= m_{dik} - K\sum_{\tau=0}^{k} \alpha_{i\tau}\widehat{d}_{i\tau} = m_{dik} - D_{ik}, \end{aligned} \tag{27}$$

and then m_{cik} should be replaced by m_{dik} in (8) to obtain new Z_1 equations, the new Z_2 equations remain the same as shown in (9), where d_{cik} is the drift value after compensation, d_{ik} is the drift value, D_{ik} is compensated drift values, K is the feedback gain, and α_{ik} is the drift factor, and m_{dik} is discrete time form of m_{di} in (8). As shown in (27), the compensated drift values D_{ik} is

$$D_{ik} = K\sum_{\tau=0}^{k} \alpha_{i\tau}\widehat{d}_{i\tau}. \tag{28}$$

As shown before, the state feedback technique is chosen for the real time sensor fault drift compensation system, and the compensation system is stated as discrete time form. Figure 9 shows the block diagram of compensation system. In the compensation system, the system feedback value is the compensated drift values D_{ik}; the input of estimation system is the compensated sensor outputs m_{cik}. This approach is very similar to the conventional linear quadratic Gaussian methods; the only difference is that the Kalman filter is replaced by the AEKPF [13].

Since Z_2 equations are incorrect in the compensation system, the compensation system is no longer restricted to the constraint of only on faulty sensor in a sensor array. In turn, the proposed compensation algorithm can process multiple erroneous sensors especially when they produce faulty outputs simultaneously.

3.3. The Drift Factor. The performance of real time compensation algorithm largely depends on the choice of feedback

gain since the inappropriate feedback gain will lead to the system failure [12]. Due to lack of a guiding theorem and method, the choice of feedback gain relies on empirical values. The feedback gain which is selected by experience cannot always guarantee the system validation along with the environmental change. Moreover, the feedback gain is not only related to system features and drift characteristics but also related to noise characteristics. The feedback gains of some sensors are interrelated to each other. Therefore, the choice of feedback gain is a complex problem. This paper introduces a drift factor, which can increase and reduce the sensitivity of real time compensation system to the feedback gain. The drift factor makes compensation system less dependent on feedback gain. It includes the prior drift factor and the current drift factor.

(1) *The Prior Drift Factor.* The prior drift factor represents the change of sensor drift in previous. The greater the rate of change of predrift is, the greater the prior drift factor is. The rate of change of sensor predrift is given by

$$\delta_{ik} = D_{ik} - D_{ik-1} = K\sum_{\tau=0}^{k}\alpha_{i\tau}\widehat{d}_{i\tau} - K\sum_{\tau=0}^{k-1}\alpha_{i\tau}\widehat{d}_{i\tau} = K\alpha_{ik}\widehat{d}_{ik}. \tag{29}$$

And the change of sensor predrift is

$$\beta_{ik} = \frac{\sum_{\tau=0}^{k}\left|\delta_{i\tau}\right|}{k} = \frac{\sum_{\tau=0}^{k}K\alpha_{ik}\left|\widehat{d}_{ik}\right|}{k} = \frac{K\sum_{\tau=0}^{k}\alpha_{ik}\left|\widehat{d}_{ik}\right|}{k}. \tag{30}$$

Here β_{ik} is normalized as

$$\beta_{ik} = \frac{\beta_{ik}}{\sum_{i=1}^{n}\beta_{ik}}. \tag{31}$$

(2) *The Current Drift Factor.* The current drift factor represents the change of sensor drift currently, which relates with the amplitude and the rate of change of the current drift. The greater the amplitude and the rate of change of the current drift, the greater the current drift factor. The current drift factor is given by

$$\gamma_{ik} = D_{ik}\widehat{d}_{ik}. \tag{32}$$

Here γ_{ik} is normalized as

$$\gamma_{ik} = \frac{\gamma_{ik}}{\sum_{i=1}^{n}\gamma_{ik}}. \tag{33}$$

(3) *The Drift Factor.* The drift factor is defined as

$$\alpha_{ik} = \beta_{ik}\gamma_{ik}. \tag{34}$$

Here α_{ik} is normalized as

$$\alpha_{ik} = \frac{\alpha_{ik}}{\sum_{i=1}^{n}\alpha_{ik}}. \tag{35}$$

If $\alpha_{ik} < 0.01$, then $\alpha_{ik} = 0.01$. Therefore, the drift factor is

$$\alpha_k = \operatorname{diag}\left(\alpha_{1k}\ \ \alpha_{2k}\ \ \ldots\ \ \alpha_{nk}\right). \tag{36}$$

4. Simulation Results

A six-sensor configuration is preferred in the strap-down inertial navigation system because of its powerful error calibration and fault detection capabilities. In this configuration, six sensors are mounted on a regular polyhedron with 12 faces, which is a specific symmetric structure. All the sensors have an angle of $2\alpha = 63^{\circ}26'5.8''$ to each other, and each two measurement axes are in one orthogonal plane of the reference coordinate [1–4]. Taking the gyros as an example, the measurement equation can be written as

$$m = \begin{bmatrix} m_1 \\ m_2 \\ m_3 \\ m_4 \\ m_5 \\ m_6 \end{bmatrix} = H\omega = \begin{bmatrix} \cos\alpha & \sin\alpha & 0 \\ \cos\alpha & -\sin\alpha & 0 \\ 0 & \cos\alpha & \sin\alpha \\ 0 & \cos\alpha & -\sin\alpha \\ \sin\alpha & 0 & \cos\alpha \\ -\sin\alpha & 0 & \cos\alpha \end{bmatrix} \begin{bmatrix} \omega_x \\ \omega_y \\ \omega_z \end{bmatrix}, \tag{37}$$

where $m_1 \sim m_6$ represent measurements from the six gyros, H is measurement matrix, and $\omega_x, \omega_y, \omega_z$ represent the three angular velocities. The three parity equations can be found from H. Assuming that

$$V^* = \begin{bmatrix} 0 & 0 & -\cos\alpha & \cos\alpha & \sin\alpha & \sin\alpha \\ -\sin\alpha & -\sin\alpha & 0 & 0 & \cos\alpha & -\cos\alpha \\ \cos\alpha & -\cos\alpha & -\sin\alpha & -\sin\alpha & 0 & 0 \end{bmatrix}, \tag{38}$$

then $V^*H = 0$. According to (3), the parity equation can be written as

$$P = V^*m = V^*\begin{bmatrix} m_1 & \cdots & m_6 \end{bmatrix}^T. \tag{39}$$

In this configuration, there are six gyros to measure three angular velocities. The three parity equations, which are used to describe the relations between outputs of six gyros, can be processed to obtain three output equations for estimation. Let $C_v' = V^*$; the output matrix can be written as

$$C_v' = \begin{bmatrix} C_{v1} \\ C_{v2} \\ C_{v3} \end{bmatrix} = V = \begin{bmatrix} 0 & 0 & -\cos\alpha & \cos\alpha & \sin\alpha & \sin\alpha \\ -\sin\alpha & -\sin\alpha & 0 & 0 & \cos\alpha & -\cos\alpha \\ \cos\alpha & -\cos\alpha & -\sin\alpha & -\sin\alpha & 0 & 0 \end{bmatrix}. \tag{40}$$

In order to get the associated output equations Z_2, the output matrix C_v' can be converted into C_v. The associated output matrix C_v is defined as

$$C_v = \begin{bmatrix} C_{v1} \\ C_{v1} \\ C_{v2} \\ C_{v2} \\ C_{v3} \\ C_{v3} \end{bmatrix}. \tag{41}$$

The system measurement equation is

$$z_k = h(d) = \begin{bmatrix} Z_1 \\ Z_2 \end{bmatrix}, \tag{42}$$

where Z_1 and Z_2 are

$$Z_1 = \begin{bmatrix} C_{v1} \\ C_{v2} \\ C_{v3} \end{bmatrix} \begin{bmatrix} d_1 \\ \vdots \\ d_6 \end{bmatrix} = \begin{bmatrix} C_{v1} \\ C_{v2} \\ C_{v3} \end{bmatrix} \begin{bmatrix} m_{d1} \\ \vdots \\ m_{d6} \end{bmatrix}, \tag{43}$$

$$\begin{aligned} Z_2 &= \operatorname{diag}\left(C_{v1}d, C_{v1}d, C_{v2}d, C_{v2}d, C_{v3}d, C_{v3}d\right) d \\ &= \begin{bmatrix} C_{v1}dd_1 \\ \vdots \\ C_{v3}dd_6 \end{bmatrix}, \end{aligned} \tag{44}$$

respectively.

Assume that the measurement noise is glint noise which describes the long-tailed nature of noise distribution. The model of glint noise is expressed by a mixture of two Gaussian components. One Gaussian component has a large variance and a small occurring probability, and the other has a small variance but a large occurring probability. The weighting coefficient (glint probability) in the mixture (percentage of contamination) is used to the non-Gaussian nature of the glint spikes. Further, assuming that the Gaussian terms are denoted by $N(x; \mu_1, P_1)$ and $N(x; \mu_2, P_2)$, then the mixture distribution has the following form [18, 19]:

$$P(x) = (1 - \varepsilon) N\left(x; \mu_1, P_1\right) + \varepsilon N\left(x; \mu_2, P_2\right), \tag{45}$$

where ε is a small positive value, $\varepsilon \in [0, 1]$. μ_1, μ_2 represent the means, and P_1, P_2 represent the variances. The measurement noise is expressed by a mixture of $N(x; 0, 0.05)$ and $N(x; 0, 0.01)$, and the weighting coefficient ε is 0.4. The feedback gain in the compensation algorithm is 40, and the particle number is 100. Three experiments were done as follows.

Experiment 1. Six gyros outputs are all drifting and these drifts are initialed at different time instant. The drifting signal with the gyro m_1 is $2 - 0.5 \sin 0.5t$ starting at the 2nd second. The drifting signal with the gyro m_2 is $-e^{0.01t}$ starting at the 6th second. The dc offset with the gyro m_3 is 2 starting at the 12th second. The dc offset with the gyro m_4 is -2 starting at the 20th second. The dc offset with the gyro m_5 is 2 starting at the 26th second. The drifting signal with the gyro m_6 is $3 - 0.6 \sin t$ starting at the 32nd second. Simulation results are shown in Figures 1 and 2.

Experiment 2. The drifting signals with the gyros $m_1 \sim m_4$, m_6 are the same as Experiment 1. The drifting signal with the gyro m_5 is $2 - 0.6 \sin t$ starting at the 26th second. Simulation results are shown in Figures 3 and 4.

Experiment 3. The drifting signals with the gyros $m_1 \sim m_6$ are the same as Experiment 1. When the feedback gains K are 5, 10, 40, 60, 80, and 120, respectively, the outputs of gyro m_2 are shown in Figures 5 and 6.

5. Discussion

The real time sensor drift estimation algorithm (Section 3.1) can estimate the dc offset value when the faulty sensor is experiencing dc offset. The feedback compensated values are constant due to the constant dc offsets. Those sensors experiencing dc offset can be considered as not experienced drift when the dc offset is compensated by real time sensor drifts compensation algorithm (Section 3.2). Since the inertial navigation system requires at least three of gyroscope to measure three-directional speed of rotation, there are at least three sensors that do not experience fault drift to measure speed of rotation in the navigation system. If multisensors experience fault drift, the system should have at least three sensors that do not experience fault drift, otherwise the navigation system cannot work. The proposed algorithm can correct the faulty sensor. The substance of the proposed algorithm is used to estimate the fault drift value of the faulty sensor by the measurement of other sensors. If two sensors break down at the same time, parity equations would failure. In this situation, the algorithm cannot estimate the fault drift of the sensors. All in all, to ensure the effectiveness of the compensation algorithm, the sensors should not fail simultaneously, but the fault drift can exist at the same time. The impact of both drift and the feedback gain on the compensation system and the estimation of the error signal will be discussed one by one.

(1) *The Impact of Drift on the Compensation System.* As shown in Figures 1 and 2, all drifts of gyros $m_1 \sim m_6$ are compensated. Can we draw the conclusion that the proposed fault tolerant control algorithm can correct all these drifting gyros in the redundant inertial navigation system? The answer is obviously not. As shown in Figures 3 and 4, the proposed improved fault tolerant control algorithm can correct the drifting gyros $m_1 \sim m_5$. However, the improved fault tolerant control algorithm fails when the gyro m_6 starts drift at the 32nd second. That implies that the improved fault tolerant controlalgorithm cannot correct all these drifting gyros. Now the upcoming issue is under what circumstances, that the improved fault tolerant control algorithm can correct all these drifting gyros. According to the simulation results of Experiments 1 and 2, when a sensor starts drift, the sensor can be corrected by the improved fault tolerant control algorithm if the sum of the number of the sensor that did not experience drift and the sensor experienced dc offset but had been corrected is not less than three sensors. For example, the drifting gyros $m_1 \sim m_3$ were corrected by the improved fault tolerant control algorithm in Figures 1 and 3. More than three gyros did not drift when the gyros $m_1 \sim m_3$ experienced drift. In Figures 2 and 4, the drifting gyros m_4 were corrected by the proposed algorithm due to the gyros m_5, m_6 which did not drift and the gyro m_3 which experienced dc offset but had been corrected when gyros m_4 started drift. The drifting gyros m_5 were corrected by the proposed algorithm due to the gyros m_6 which did not drift and the gyro m_3, m_4 which experienced dc offset but had been corrected when gyros m_5 started drift.

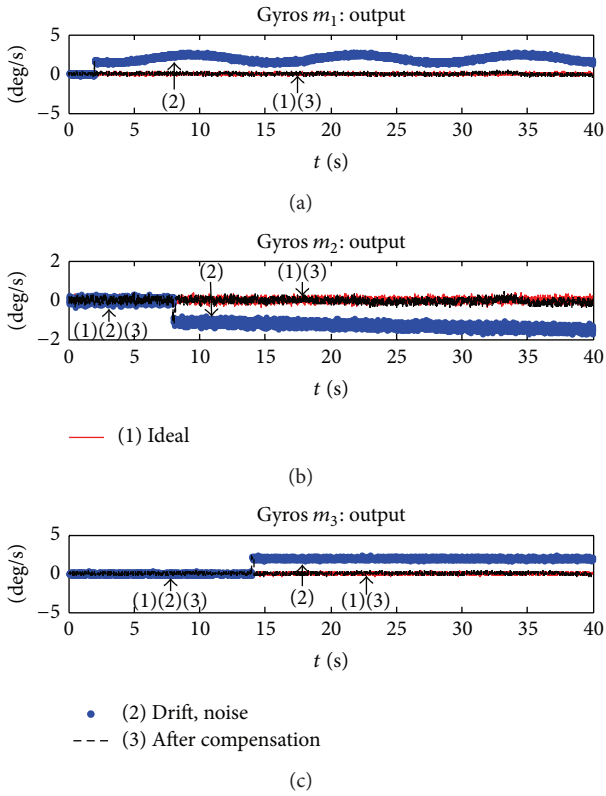

Figure 1: Experiment 1: No. 1–3 Gyro output.

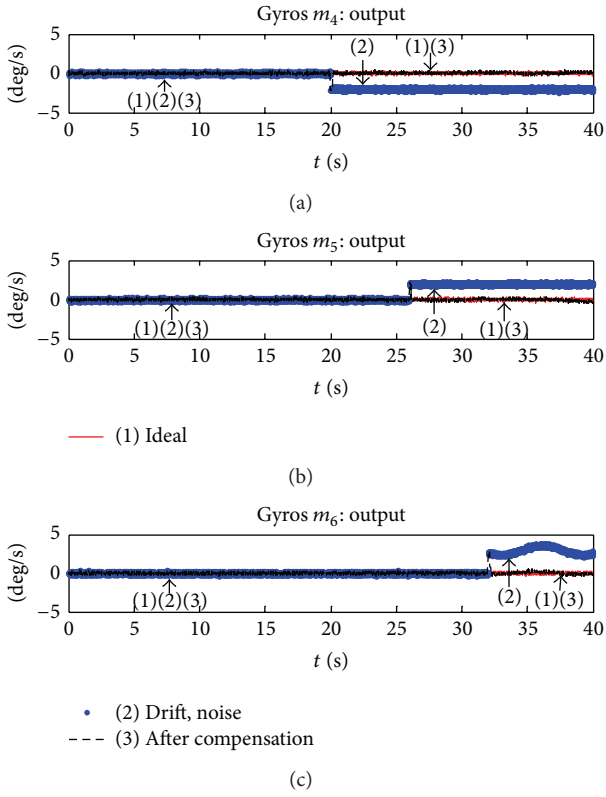

Figure 2: Experiment 1: No. 4–6 Gyro output.

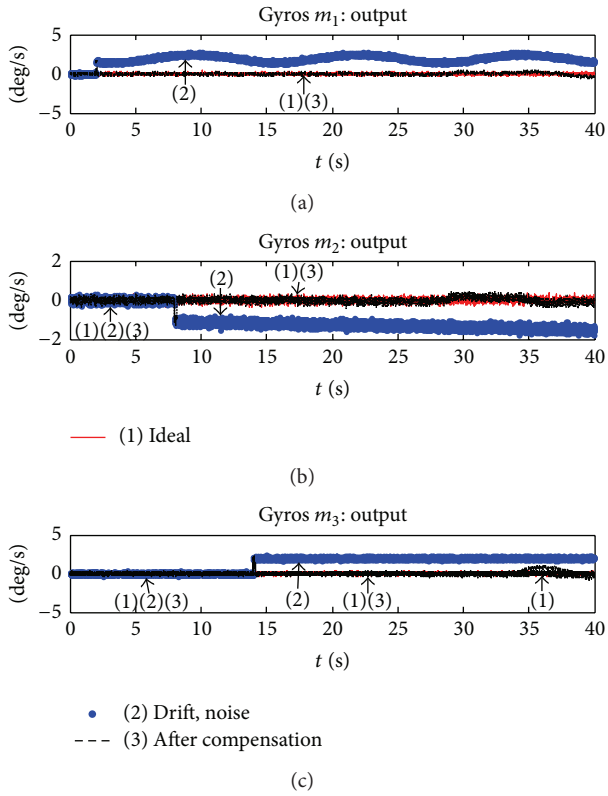

Figure 3: Experiment 2: No. 1–3 Gyro output.

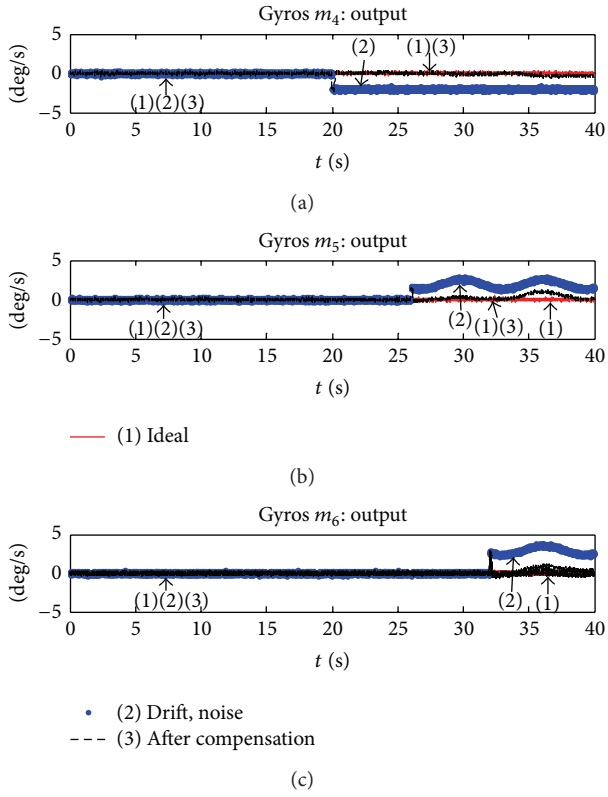

Figure 4: Experiment 2: No. 4–6 Gyro output.

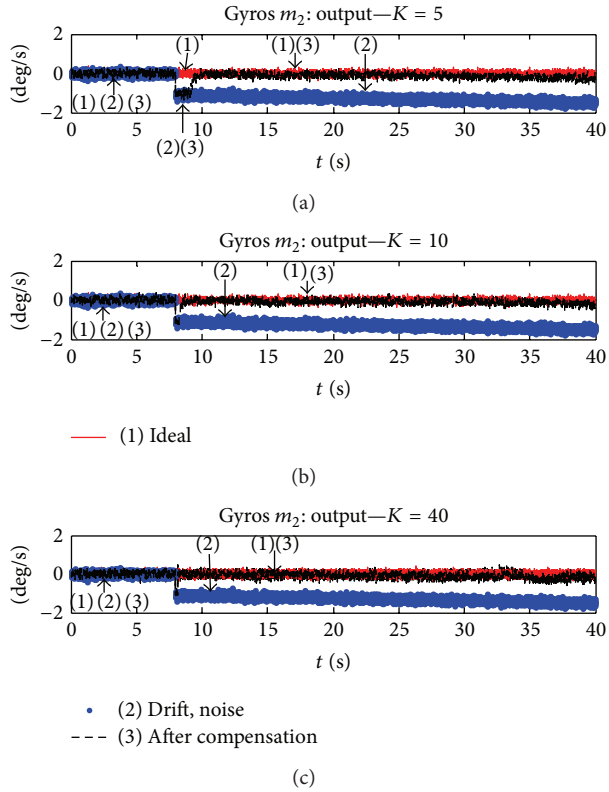

Figure 5: Experiment 3: No. 2 Gyro output by different feedback gain.

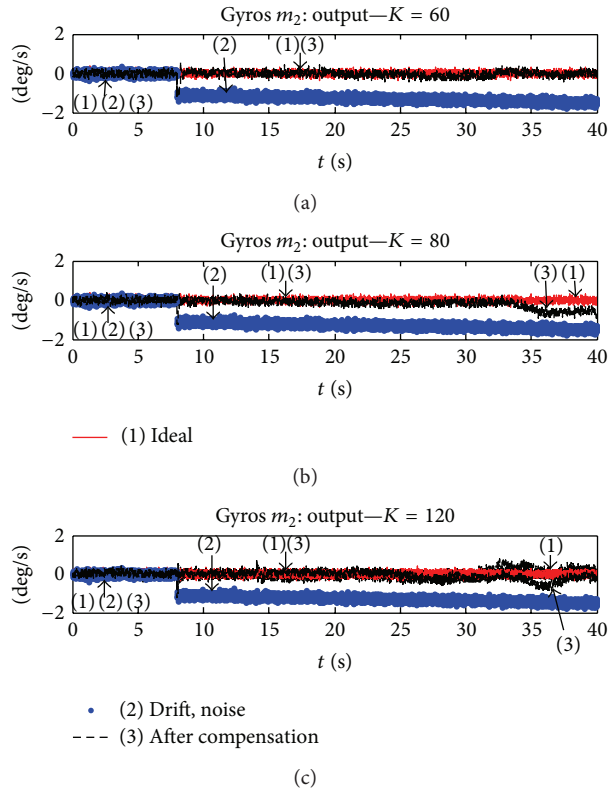

Figure 6: Experiment 3: No. 2 Gyro output by different feedback gain.

The drifting gyros m_6 were corrected by the improved fault tolerant control algorithm in Figure 2 due to the gyro $m_3 \sim m_5$ which experienced dc offset but had been corrected when gyros m_6 started drift. However, the improved fault tolerant control algorithm was failure when gyros m_6 started drift in Figure 4. This is because there were only two gyros m_3 and m_4 which experienced dc offset and had been corrected when gyros m_6 started drift. Therefore, the conclusion is that the improved fault tolerant control algorithm can correct the drifting sensor if the sum of the number of the sensor that did not drift and the sensor that experienced dc offset but had been corrected is not less than three.

(2) *The Impact of the Feedback Gain on the Compensation System.* Figures 5 and 6 show the convergence of gyro m_2 outputs used in the improved fault tolerant control algorithm for various feedback gains, ranging from 5 to 120. According to the simulation results shown in Figure 5, the feedback gain of 5 is too small to reduce sensor errors quickly. It needs 3 seconds to eliminate gyro m_2 error when the feedback gain is 5. Intuitively, a large feedback gain in this compensation algorithm is preferred for two reasons. It can compensate for the fast changing drift signals, and it can quickly decrease the magnitudes of current errors, so that the constraint of local stability can be satisfied for the incoming sensor errors. On the other hand, the large feedback gain may lead to the oscillation of the system, and this oscillation would be beyond the stability region and stability constraint. This is the case of feedback gain 80 and 120, as shown in Figure 6.

The performance of the fault tolerant control algorithm largely depends on the choice of feedback gain. The inappropriate feedback gain will lead to the system failure [12]. The drift factor in the improved fault tolerant control algorithm is introduced, which can eliminate the dependence of the feedback gain in fault tolerant control system. As shown in the Figures 5 and 6, the improved fault tolerant control algorithm can correctly compensate the drift for the sensor m_2 when the feedback gain K is 5, 10, 40, or 60. However, only the case with feedback gain of 8 can correctly compensate for the sensor drifts in the compensation algorithm proposed by Chen and You [12].

(3) *The Estimation of the Error Signal.* Figure 7 shows the estimation of the error signal of the adaptive extended Kalman particle filter (AEKPF) and the traditional particle filter (TPF). The particle number is 800 in the TPF. As shown in plot, the AEKPF and the TPF can correctly estimate the drift for each sensor when the sensors do not experience fault drifts. The TPF cannot work well when the sensors experience fault drift, but the AEKPF can correctly estimate the drift for each sensor in real time.

Figure 8 shows the estimation error of the error signal for both the AEKPF and TPF. As shown in plot, the average estimation error of the AEKPF is nearly half of that of the TPF when the particle number of the AEKPF is 1/8 of TPF. As

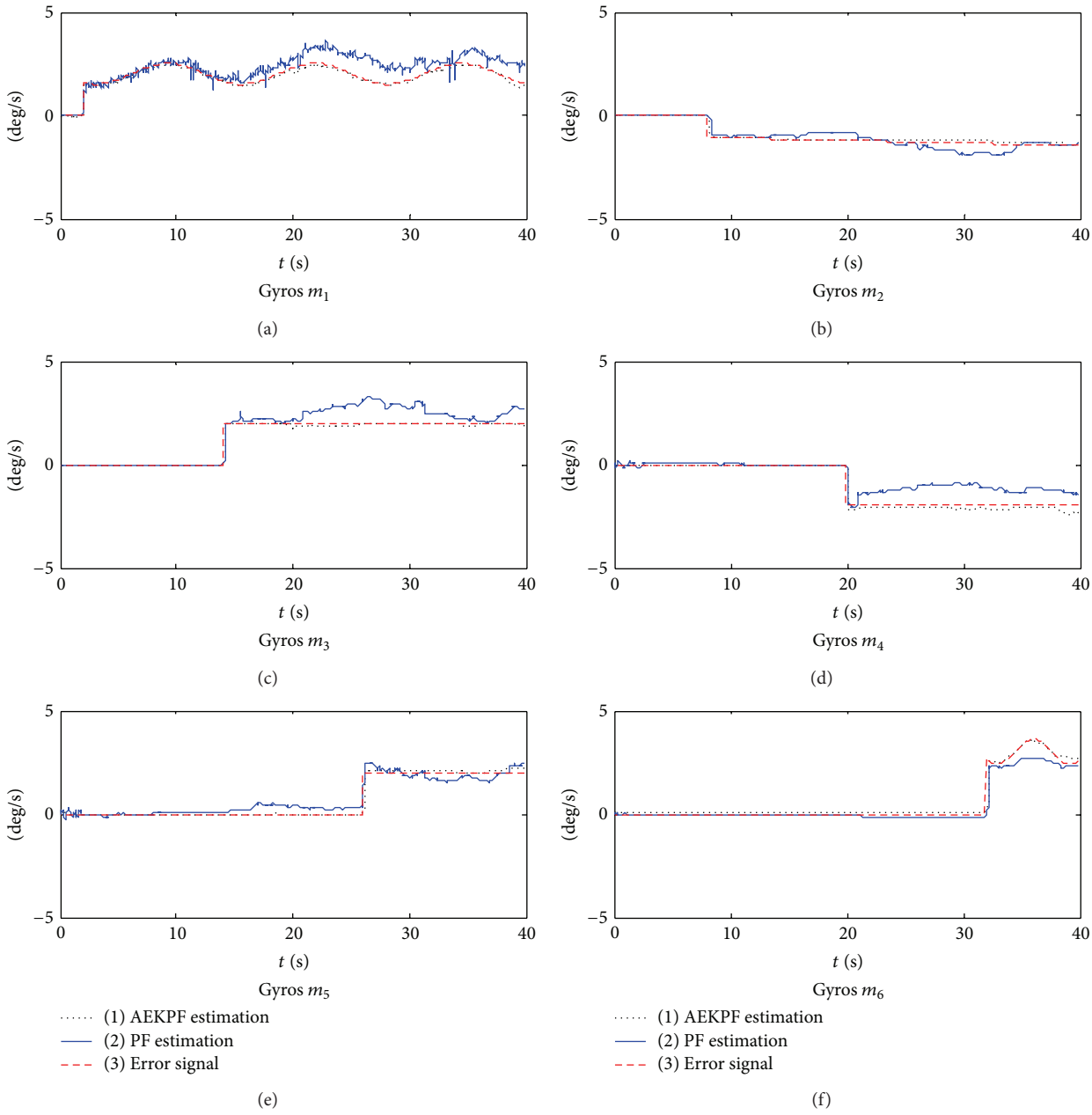

Figure 7: The estimation of the error signal for the AEKPF and TPF.

show in Table 1, the average estimation error of the AEKPF is [0.1053, 0.1540, 0.1770, 0.1758, 0.1294, 0.1993] when the particle number is 100, and the average estimation error of the TPF is [0.2738, 0.3845, 0.2517, 0.2471, 0.2253, 0.2754] when the particle number is 800.

The fault tolerant control system uses the real time estimation techniques to estimate the error signal and then compensates the error according to the estimated value. However, the estimated value of the error signal is not being very accurate due to the difference between the measured noise and the system model. The fault tolerant control algorithm can reduce the error signal but the error signal may not decrease to zero. Therefore, better results are expected when the calibration and other offline methods are used to further reduce the signal error further.

6. Conclusion

This paper presents an improved fault tolerant control algorithm for the redundant inertial navigation system. The improved fault tolerant control algorithm employs the state estimation techniques to estimate the values of error signals and the state feedback technique to eliminate the error signals in real time. To overcome the shortcomings of the fault tolerant control algorithm proposed by Chen, the improved fault tolerant control algorithm applies an AEKPF to deal

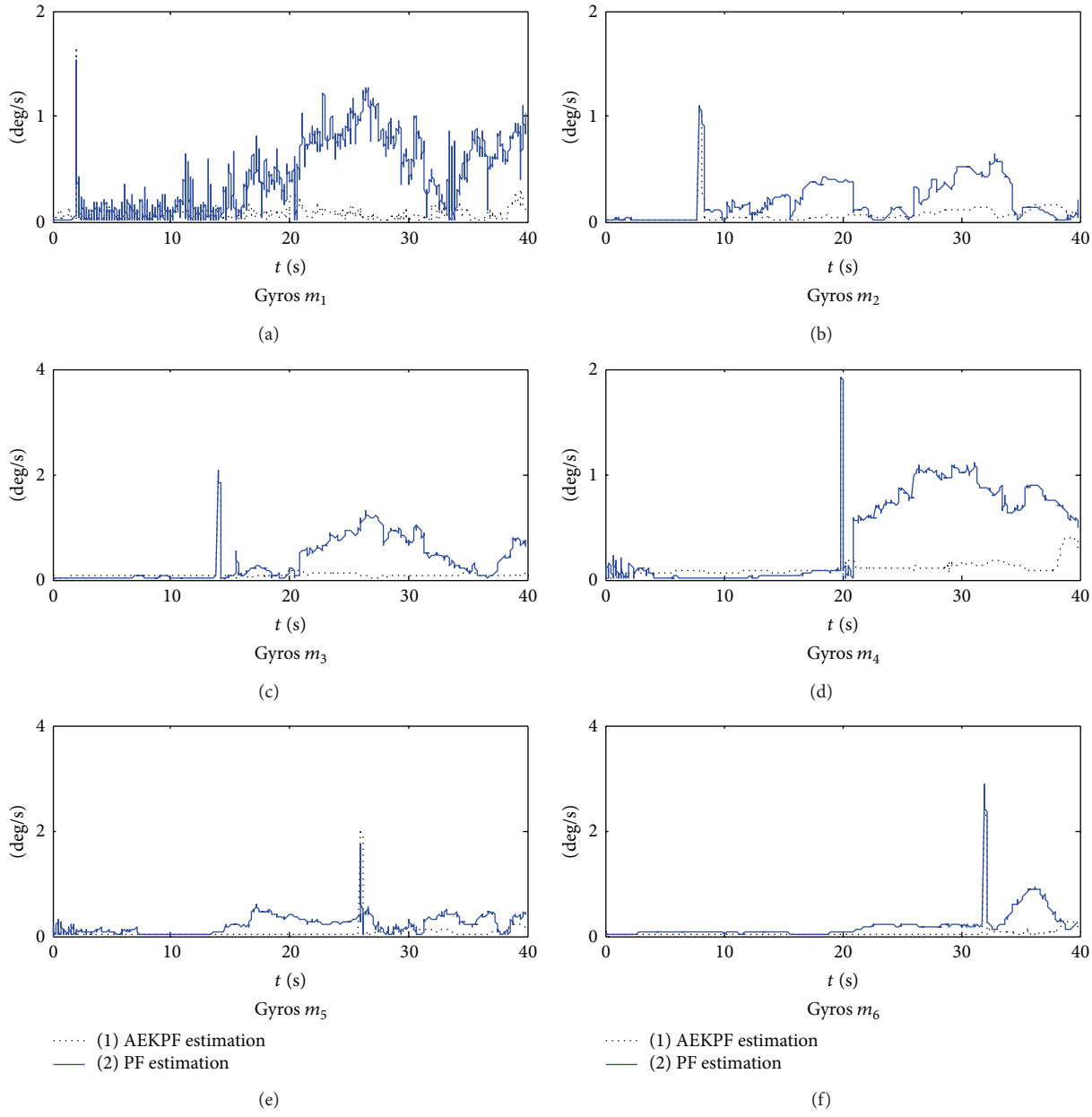

Figure 8: The estimation error of the error signal for the AEKPF and TPF.

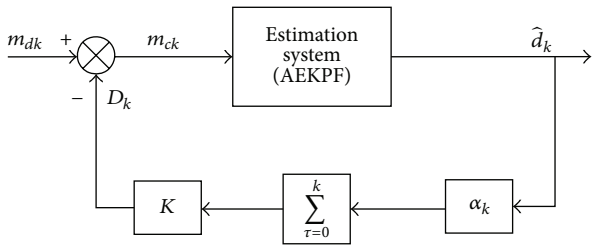

Figure 9: The block diagram of compensated system.

with the problem of non-Gaussian measurement noise and the problem of inaccurate system model. In addition, a drift factor is introduced in order to enlarge range of choice of the feedback gain. In short, the improved fault tolerant control algorithm can compensate the sensor drifts effectively and improve the robustness and reliability of the redundant inertial navigation system. Of course, the AEKPF which involved in this paper is not the only way to solve the problem of unknown noise characteristics. If the characteristics of the measurement noise and system noise can be identified at same time, the adaptive Kalman filter also can estimate sensor drifts in real time. The autocovariance least squares (ALSs) technique can estimate the measurement noise and system noise characteristics, but there are a variety of problems in ALS technique itself, such as the positive definiteness of ALS result, and time-varying noise. In this manuscript, the

Table 1: The average estimation error of the error signal for the AEKPF and TPF.

The particle number N	AEKPF 100	TPF 800
The average estimation error		
m_1	0.1035	0.2738
m_2	0.1540	0.3845
m_3	0.1770	0.2517
m_4	0.1758	0.2471
m_5	0.1294	0.2253
m_6	0.1993	0.2754

drift factor get from the normalized product of prior drift factor and current drift factor. However, the drift factor also can get from other method, such as fuzzy method. With the development of estimation techniques, the fault tolerant control algorithm can be improved by other methods.

Conflict of Interests

The authors declare that there is no conflict of interests regarding the publication of this paper.

Acknowledgment

The paper is supported by the National Natural Science Foundation of China (no.60974104/F03030).

References

[1] J. E. Potter and M. C. Suman, "Thresholdlless redundancy management with arrays of skewed instruments, Integrity in Electronic Flight Control Systems," *AGARDograph*, no. 224, pp. 15–25, 1977.

[2] S. Y. Cho and C. G. Park, "A calibration technique for a redundant IMU containing low-grade inertial sensors," *ETRI Journal*, vol. 27, no. 4, pp. 418–425, 2005.

[3] A. J. Pejsa, "Optimum skewed redundant inertial navigators," in *Proceedings of the AIAA Guidance and Control Conference*, pp. 256–264, Key Biscayne, Fla, USA, 1973.

[4] D.-S. Shim and C.-K. Yang, "Geometric FDI based on SVD for redundant inertial sensor systems," in *Proceedings of the 5th Asian Control Conference*, pp. 1094–1100, July 2004.

[5] C.-L. Wei and H.-Y. Zhang, "Parity vector compensation for multi-sensor fault detection," *Journal of Beijing University of Aeronautics and Astronautics*, vol. 27, no. 6, pp. 698–701, 2001.

[6] A. D. Pouliezous and G. S. Stavrakakis, *Real Time Fault Monitoring of Industrial Processes*, Kluwer Academic Publishers, 1994.

[7] S. Kim, Y. Kim, C. Park, and I. Jung, "Hybrid fault detection and isolation techniques for aircraft inertial measurement sensors," in *Proceedings of the AIAA Guidance, Navigation, and Control Conference*, pp. 3399–3417, August 2004.

[8] D. Yan and H. Zhang, "Design of optimal robustness analytical redundancy," *Acta Automatica Sinica*, vol. 23, no. 1, pp. 9–15, 1997.

[9] U. K. Krogmann, "Failure management in spatio-temporal redundant, integrated navigation and flight control reference-systems," in *Proceedings of the IEEE Position Location and Navigation Symposium*, pp. 330–337, March 1990.

[10] J. Gilmore and R. McKern, "A redundant strapdown inertial reference unit (SIRC)," *Journal of Spacecraft and Rocket*, vol. 9, no. 1, pp. 39–47, 1972.

[11] A. Ray and R. Luck, "An introduction to sensor signal validation in redundant measurement systems," *IEEE Control Systems Magazine*, vol. 11, no. 2, pp. 44–49, 1991.

[12] T. L. Chen and R. Z. You, "A novel fault-tolerant sensor system for sensor drift compensation," *Sensors and Actuators A*, vol. 147, no. 2, pp. 623–632, 2008.

[13] T.-L. Chen, "Design and analysis of a fault-tolerant coplanar gyro-free inertial measurement unit," *Journal of Microelectromechanical Systems*, vol. 17, no. 1, pp. 201–212, 2008.

[14] Y.-R. Lin, S.-Y. Guo, and G.-Y. Zhang, "Fault detection method applied to a redundant strapdown inertial navigation system," *Advanced Materials Research*, vol. 179-180, pp. 1242–1247, 2011.

[15] S. Zhangguo and Q. Feng, "Adaptive Kalman filtering algorithm based on exponent fading factor," *Electronic Measurement Technology*, vol. 33, no. 1, pp. 40–42, 2010.

[16] K.-H. Kim, G.-I. Jee, C.-G. Park, and J.-G. Lee, "The stability analysis of the adaptive fading extended kalman filter using the innovation covariance," *International Journal of Control, Automation and Systems*, vol. 7, no. 1, pp. 49–56, 2009.

[17] Y. Geng and J. Wang, "Adaptive estimation of multiple fading factors in Kalman filter for navigation applications," *GPS Solutions*, vol. 12, no. 4, pp. 273–279, 2008.

[18] H. Hu, Z. Jing, A. Li, S. Hu, and H. Tian, "Target tracking in glint noise using a MCMC particle filter," *Journal of Systems Engineering and Electronics*, vol. 16, no. 2, pp. 305–309, 2005.

[19] W. U. Wen-Rong, "Maximum likelihood identification of glint noise," *IEEE Transactions on Aerospace and Electronic Systems*, vol. 32, no. 1, pp. 41–51, 1996.

Hindawi Publishing Corporation
Mathematical Problems in Engineering
Volume 2013, Article ID 283426, 10 pages
http://dx.doi.org/10.1155/2013/283426

Research Article

Output Feedback Control of Discrete Impulsive Switched Systems with State Delays and Missing Measurements

Xia Li,[1] Hamid Reza Karimi,[2] and Zhengrong Xiang[1]

[1] *School of Automation, Nanjing University of Science and Technology, Nanjing 210094, China*
[2] *Department of Engineering, Faculty of Engineering and Science, University of Agder, 4898 Grimstad, Norway*

Correspondence should be addressed to Zhengrong Xiang; xiangzr@mail.njust.edu.cn

Received 7 July 2013; Revised 31 July 2013; Accepted 19 August 2013

Academic Editor: Tao Li

This paper is concerned with the problem of dynamic output feedback (DOF) control for a class of uncertain discrete impulsive switched systems with state delays and missing measurements. The missing measurements are modeled as a binary switch sequence specified by a conditional probability distribution. The problem addressed is to design an output feedback controller such that for all admissible uncertainties, the closed-loop system is exponentially stable in mean square sense. By using the average dwell time approach and the piecewise Lyapunov function technique, some sufficient conditions for the existence of a desired DOF controller are derived, then an explicit expression of the desired controller is given. Finally, a numerical example is given to illustrate the effectiveness of the proposed method.

1. Introduction

Due to their wide applications, switched systems which are an important class of hybrid systems have drawn considerable attention in the last decade [1, 2]. During these years, there have been increasing research activities in the field of stability analysis for such systems (see [3–6], and the references cited therein). Recently, impulsive switched systems as a class of special switched systems have gained research attention. This is because impulsive switched systems can represent some practical switched systems that exhibit impulsive dynamical behavior due to sudden changes in the state of the system at certain instants of switching. Some problems on impulsive switched systems with and without delays have been successfully investigated, and a rich body of the literatures is now available [7–10].

On the other hand, control synthesis is one of the important issues in system theory. State feedback control as an effective control strategy has been widely used in various complex dynamical systems. For instance, some state feedback control problems for switched systems have been extensively studied in [11, 12]. The adaptive control for a class of nonlinear systems via backstepping method was studied in [13]. The authors in [14] considered an optimal state feedback control problem for impulsive switched systems. In [15–18], some controller design methods for impulsive switched systems were developed. In addition, output feedback control has been considered as an effective control method when the states of the system are not all measurable in practice. At present, many results on the output feedback controller design for nonlinear systems or switched systems have been obtained (see [19–24]), and less work has been done for impulsive switched systems.

In almost all the works mentioned above, the assumption of consecutive measurements has been made implicitly. Unfortunately, in many practical applications, such an assumption does not hold. For example, due to sensor temporal failure or network transmission delay/loss, at certain time points, the system measurement may contain noise only, indicating that the real signal is missing. One of the most popular ways to describe the missing measurement is to view it as a Bernoulli distributed (binary switching) white sequence specified by a conditional probability distribution in the output equation. The Bernoulli distribution description was first proposed in [25] to deal with the optimal recursive filtering problem and then has been used in [26–29] for

various control and filtering problems of linear systems with probabilistic missing measurements. It is worth pointing out that the references mentioned above did not consider the effect of impulse. However, the missing measurements and impulsive jumps happening simultaneously in the systems will bring some challenges and difficulties for the analysis and synthesis. To the best of our knowledge, the issue of dynamic output feedback controller design with missing measurements for impulsive switched systems has not been fully investigated, which motivates our present study.

In this paper, we will focus our interest on the problem of dynamic output feedback (DOF) control for a class of uncertain discrete impulsive switched systems with state delays and missing measurements. The main contributions of the paper are as follows: (1) a DOF controller is proposed for discrete impulsive switched systems, and the controller contains impulsive jumps, which is different from most of the existing ones, for example, those in [20–23]; (2) sufficient conditions for the existence of a DOF controller are developed such that the resulting closed-loop system is exponentially stable in mean square sense.

The remainder of the paper is organized as follows. In Section 2, problem formulation and some necessary preliminaries are given. In Section 3, the main results are presented. Section 4 gives a numerical example to illustrate the effectiveness of the proposed approach. Concluding remarks are given in Section 5.

Notations. Throughout this paper, the superscript "T" denotes the transpose, and the notation $X \geq Y$ ($X > Y$) means that matrix $X - Y$ is positive semidefinite (positive definite, resp.). $\|\cdot\|$ denotes the Euclidean norm. $\varepsilon\{\cdot\}$ stands for the mathematical expectation, and Prob$\{\cdot\}$ means the occurrence probability of the event "$\cdot$". I represents the identity matrix and diag$\{a_i\}$ denotes a diagonal matrix with the diagonal elements a_i, $i = 1, 2, \ldots, n$. X^{-1} denotes the inverse of X. The asterisk $*$ in a matrix is used to denote a term that is induced by symmetry. The set of all positive integers is represented by Z^+.

2. Problem Formulation and Preliminaries

Consider the following uncertain discrete impulsive switched systems with state delay:

$$\begin{aligned} x(k+1) &= \widehat{A}_{\sigma(k)} x(k) + \widehat{A}_{d\sigma(k)} x(k-d) \\ &\quad + B_{\sigma(k)} u(k), \quad k \neq k_b - 1,\ b \in Z^+, \end{aligned} \tag{1a}$$

$$x(k+1) = E_{\sigma(k+1)\sigma(k)} x(k), \quad k = k_b - 1,\ b \in Z^+, \tag{1b}$$

$$y(k) = C_{\sigma(k)} x(k), \tag{1c}$$

$$x(k_0 + \theta) = \phi(\theta), \quad \theta \in [-d, 0], \tag{1d}$$

where $x(k) \in R^n$ is the state vector, $u(k) \in R^m$ is the control input, $y(k) \in R^p$ is the output vector, and $\phi(\theta)$ is a discrete vector-valued initial function on interval $[-d, 0]$. d is the discrete time delay. $\sigma(k)$ is a switching signal which takes its values in the finite set $\underline{N} := \{1, \ldots, N\}$, N denotes the number of subsystems. k_0 is the initial time and k_b ($b \in Z^+$) denotes the bth switching instant. Moreover, $\sigma(k) = i \in \underline{N}$ means that the ith subsystem is activated.

The measurement output which may contain missing data is described by

$$\tilde{y}(k) = r(k)\, y(k) = r(k)\, C_{\sigma(k)} x(k), \tag{2}$$

where $\tilde{y}(k) \in R^q$ is the measurement output vector and C_i ($i \in \underline{N}$) are known real constant matrices with appropriate dimensions. The stochastic variable $r(k) \in R$ is a Bernoulli distributed white sequence taking the values of 0 and 1 with

$$\text{Prob}\{r(k) = 1\} = \varepsilon\{r(k)\} = \bar{r}, \tag{3a}$$

$$\text{Prob}\{r(k) = 0\} = 1 - \varepsilon\{r(k)\} = 1 - \bar{r}, \tag{3b}$$

where $\bar{r} \in R$ is a known positive scalar. From (3a)-(3b), we obtain that

$$\tau = \varepsilon\left\{(r(k) - \bar{r})^2\right\} = (1 - \bar{r})\,\bar{r}. \tag{4}$$

For each $i \in \underline{N}$, $\widehat{A}_i$ and $\widehat{A}_{di}$ are uncertain real-valued matrices with appropriate dimensions. We assume that these uncertainties are norm-bounded and satisfy

$$\left[\widehat{A}_i \quad \widehat{A}_{di}\right] = \left[A_i \quad A_{di}\right] + H_i F_i(k) \left[M_{1i} \quad M_{2i}\right], \tag{5}$$

where A_i, A_{di}, H_i, M_{1i}, and M_{2i}, $i \in \underline{N}$, are known real constant matrices with appropriate dimensions. $F_i(k)$ are unknown and are possibly time-varying matrices with Lebesgue measurable elements and satisfy

$$F_i^T(k) F_i(k) \leq I. \tag{6}$$

Here, we are interested in designing a DOF switched controller described by

$$\begin{aligned} x_c(k+1) &= A_{c\sigma(k)} x_c(k) + B_{c\sigma(k)} \tilde{y}(k), \\ &\quad k \neq k_b - 1, \quad b \in Z^+, \end{aligned} \tag{7a}$$

$$\begin{aligned} x_c(k+1) &= G_{\sigma(k+1)\sigma(k)} x_c(k), \\ &\quad k = k_b - 1, \quad b \in Z^+, \end{aligned} \tag{7b}$$

$$u(k) = C_{c\sigma(k)} x_c(k), \tag{7c}$$

$$x_c(k_0 + \theta) = 0, \quad \theta \in [-d, 0], \tag{7d}$$

where $x_c(k) \in R^{n_c}$ is the controller state vector; A_{ci}, B_{ci}, and C_{ci} are constant matrices to be determined later.

Remark 1. Different from the existing DOF controllers proposed in [20–23], the controller proposed here contains (7b), which coincides with the structure of system (1a), (1b), (1c), and (1d).

Now, define a new state vector,

$$\xi(k) = \left[x^T(k) \quad x_c^T(k)\right]^T \in R^{n+n_c}. \tag{8}$$

The combination of the previous DOF controller (7a), (7b), (7c), and (7d) and system (1a), (1b), (1c), and (1d) yields the following closed-loop system:

$$\begin{aligned}\xi(k+1) &= \overline{A}_{\sigma(k)}\xi(k) + (r(k)-\overline{r})\,\overline{A}_{m\sigma(k)}\xi(k) \\ &\quad + \overline{A}_{d\sigma(k)}\xi(k-d), \quad k \neq k_b - 1,\end{aligned} \tag{9a}$$

$$\xi(k+1) = \overline{E}_{\sigma(k+1)\sigma(k)}\xi(k), \quad k = k_b - 1, \tag{9b}$$

$$\xi(k_0+\theta) = \varphi(\theta), \quad \theta \in [-d, 0], \tag{9c}$$

where

$$\begin{aligned}\overline{A}_i &= \begin{bmatrix} \widehat{A}_i & B_i C_{ci} \\ \overline{r} B_{ci} C_i & A_{ci} \end{bmatrix}, \qquad \overline{A}_{di} = \begin{bmatrix} \widehat{A}_{di} & 0 \\ 0 & 0 \end{bmatrix}, \\ \overline{A}_{mi} &= \begin{bmatrix} 0 & 0 \\ B_{ci} C_i & 0 \end{bmatrix}, \qquad \overline{E}_{ij} = \begin{bmatrix} E_{ij} & 0 \\ 0 & G_{ij} \end{bmatrix}, \\ \varphi(\theta) &= \begin{bmatrix} \phi(\theta) \\ 0 \end{bmatrix}, \quad i, j \in \underline{N},\ i \neq j.\end{aligned} \tag{10}$$

The following definitions and lemmas will be essential for our later development.

Definition 2 (see [30]). For any $k > k_0 \geq 0$, let $N_\sigma(k_0, k)$ denote the switching number of $\sigma(k)$ during the interval $[k_0, k)$. If there exist $N_0 \geq 0$ and $\tau_a \geq 0$ such that

$$N_\sigma(k_0, k) \leq N_0 + \frac{k - k_0}{\tau_a}, \quad \forall k \geq k_0, \tag{11}$$

then τ_a and N_0 are called the average dwell time and the chatter bound, respectively.

Remark 3. In this paper, the average dwell time method is used to restrict the switching number during a time interval such that the stability of system (9a), (9b), and (9c) can be guaranteed.

Definition 4 (see [27]). System (9a), (9b), and (9c) is said to be exponentially stable in mean square sense under the switching signal $\sigma(k)$, if there exist constants $\gamma \geq 0$ and $\rho \in (0, 1)$, such that the trajectory of system (9a), (9b), and (9c) satisfies

$$\varepsilon\left\{\left\|\xi(k)\right\|^2\right\} \leq \gamma \rho^{k-k_0} \sup_{-d \leq \theta \leq 0} \varepsilon\left\{\left\|\xi(k_0+\theta)\right\|^2\right\}, \quad k \geq k_0. \tag{12}$$

Lemma 5 (see [31]). *For a given matrix $S = \begin{bmatrix} S_{11} & S_{12} \\ S_{12}^T & S_{22} \end{bmatrix}$, where S_{11} and S_{22} are square matrices, the following conditions are equivalent:*

(i) $S < 0$;

(ii) $S_{11} < 0$, $S_{22} - S_{12}^T S_{11}^{-1} S_{12} < 0$;

(iii) $S_{22} < 0$, $S_{11} - S_{12} S_{22}^{-1} S_{12}^T < 0$.

Lemma 6 (see [32]). *Let U, V, W, and X be real matrices of appropriate dimensions with X satisfying $X = X^T$, then for all $V^T V \leq I$, $X + UVW + W^T V^T U^T < 0$, if and only if there exists a scalar β such that $X + \beta U U^T + \beta^{-1} W^T W < 0$.*

3. Main Results

3.1. Stability Analysis. The following theorem provides sufficient conditions under which the exponential stability of system (9a), (9b), and (9c) can be guaranteed in mean square sense.

Theorem 7. *Consider system* (9a), (9b), *and* (9c), *for a given scalar $0 < \alpha < 1$, if there exist positive definite symmetric matrices R_i and P_i ($i \in \underline{N}$) with appropriatedimensions, such that*

$$\begin{bmatrix} R_i - \alpha P_i & 0 & \overline{A}_i^T P_i & \tau \overline{A}_{mi}^T P_i \\ * & -\alpha^d R_i & \overline{A}_{di}^T P_i & 0 \\ * & * & -P_i & 0 \\ * & * & * & -\tau P_i \end{bmatrix} < 0, \tag{13}$$

where $\tau = (1-\overline{r})\overline{r}$, then, under the following average dwell time scheme

$$\tau_a > \tau_a^* = -\frac{\ln \mu}{\ln \alpha} + 1, \tag{14}$$

system (9a), (9b), *and* (9c) *is exponentially stable in mean square sense, where $\mu \geq 1$ satisfies*

$$\begin{aligned}&\begin{bmatrix} R_i - \mu P_j & \overline{E}_{ij}^T P_i \\ * & -P_i \end{bmatrix} < 0, \\ &\alpha R_i < \mu R_j, \quad (i, j \in \underline{N}, i \neq j).\end{aligned} \tag{15}$$

Proof. Choose a piecewise Lyapunov function candidate for system (9a), (9b), and (9c) of the form

$$V(k) = V_{\sigma(k)}(x(k)) = V_{\sigma(k)}(k), \tag{16}$$

the form of $V_{\sigma(k)}(k)$ is given by

$$V_{\sigma(k)}(k) = V_{1\sigma(k)}(k) + V_{2\sigma(k)}(k), \tag{17}$$

where

$$\begin{aligned}V_{1i}(k) &= \xi^T(k) P_i \xi(k), \\ V_{2i}(k) &= \sum_{r=k-d}^{k-1} \xi^T(r) R_i \xi(r) \alpha^{k-r-1}, \quad i \in \underline{N}.\end{aligned} \tag{18}$$

When $k \in [k_b, k_{b+1}-1)$, we let $\sigma(k) = \sigma(k+1) = i$ ($i \in \underline{N}$). Then along the trajectory of system (9a), (9b), and (9c), we have

$$\begin{aligned}
\Delta V_{1i}(k) &= \varepsilon\{V_{1i}(k+1)\} - \alpha\varepsilon\{V_{1i}(k)\} \\
&= \xi^T(k)\left(\overline{A}_i^T P_i \overline{A}_i - \alpha P_i\right)\xi(k) \\
&\quad + 2\varepsilon\{(r(k)-\overline{r})\}\xi^T(k)\overline{A}_i^T P_i \overline{A}_{mi}\xi(k) \\
&\quad + 2\xi^T(k)\overline{A}_i^T P_i \overline{A}_{di}\xi(k-d) \\
&\quad + \varepsilon\left\{(r(k)-\overline{r})^2\right\}\xi^T(k)\overline{A}_{mi}^T P_i \overline{A}_{mi}\xi(k) \\
&\quad + \xi^T(k-d)\overline{A}_{di}^T P_i \overline{A}_{di}\xi(k-d) \\
&\quad + 2\varepsilon\{(r(k)-\overline{r})\}\xi^T(k)\overline{A}_{mi}^T P_i \overline{A}_{di}\xi(k-d), \\
\Delta V_{2i}(k) &= \varepsilon\{V_{2i}(k+1)\} - \alpha\varepsilon\{V_{2i}(k)\} \\
&= \sum_{r=k+1-d}^{k} \xi^T(r) R_i \xi(r)\alpha^{k-r} \\
&\quad - \sum_{r=k-d}^{k-1} \xi^T(r) R_i \xi(r)\alpha^{k-r} \\
&= \xi^T(k) R_i \xi(k) - \alpha^d \xi^T(k-d) R_i \xi(k-d).
\end{aligned} \tag{19}$$

Notice that

$$\varepsilon\{r(k)-\overline{r}\} = 0, \qquad \tau = \varepsilon\left\{(r(k)-\overline{r})^2\right\} = (1-\overline{r})\overline{r}. \tag{20}$$

Thus we obtain

$$\begin{aligned}
\Delta V_i(k) &= \varepsilon\{V_i(k+1)\} - \alpha\varepsilon\{V_i(k)\} = X^T(k)\varphi_i X(k), \\
\varphi_i &= \begin{bmatrix} R_i - \alpha P_i & 0 \\ 0 & -\alpha^d R_i \end{bmatrix} + \begin{bmatrix} \overline{A}_i^T \\ \overline{A}_{di}^T \end{bmatrix} P_i \begin{bmatrix} \overline{A}_i & \overline{A}_{di} \end{bmatrix} \\
&\quad + \begin{bmatrix} \tau\overline{A}_{mi}^T P_i \overline{A}_{mi} & 0 \\ 0 & 0 \end{bmatrix},
\end{aligned} \tag{21}$$

where $X^T(k) = \left[\begin{array}{cc} \xi^T(k) & \xi^T(k-d) \end{array}\right]$.

Applying Lemma 5, it is easy to get that inequality (13) is equivalent to $\varphi_i < 0$. Thus we can obtain from (13) that

$$\varepsilon\{V_i(k+1)\} < \alpha\varepsilon\{V_i(k)\}, \quad 0 < \alpha < 1. \tag{22}$$

When $k = k_b - 1$, we let $\sigma(k_b - 1) = j$. Along the trajectory of system (9a), (9b), and (9c), we have

$$\begin{aligned}
&\varepsilon\{V_i(x(k_b))\} - \mu\varepsilon\left\{V_j(x(k_b-1))\right\} \\
&\quad = x^T(k_b-1)\left(\overline{E}_{ij}^T P_i \overline{E}_{ij} - \mu P_j\right)x(k_b-1) \\
&\qquad + \sum_{r=k_b-d}^{k_b-1} x^T(r) R_i x(r)\alpha^{k_b-r-1} \\
&\qquad - \mu\sum_{r=k_b-1-d}^{k_b-2} x^T(r) R_j x(r)\alpha^{k_b-r-2} \\
&\quad = x^T(k_b-1)\left(\overline{E}_{ij}^T P_i \overline{E}_{ij} - \mu P_j + R_i\right)x(k_b-1) \\
&\qquad - \mu x^T(k_b-1-d) R_j x(k_b-1-d)\alpha^{d-1} \\
&\qquad + \sum_{r=k_b-d}^{k_b-2} \alpha^{k_b-r-2} x^T(r)\left(\alpha R_i - \mu R_j\right)x(r).
\end{aligned} \tag{23}$$

It can be obtained from (15) that

$$\begin{aligned}
\overline{E}_{ij}^T P_i \overline{E}_{ij} - \mu P_j + R_i < 0, \\
\alpha R_i - \mu R_j < 0.
\end{aligned} \tag{24}$$

It follows that

$$\varepsilon\left\{V_{\sigma(k_b)}(x(k_b))\right\} < \mu\varepsilon\left\{V_{\sigma(k_b-1)}(x(k_b-1))\right\}. \tag{25}$$

Thus, for $k \in [k_b, k_{b+1})$, we have

$$\begin{aligned}
\varepsilon\left\{V_{\sigma(k)}(x(k))\right\} &< \alpha^{k-k_b}\varepsilon\left\{V_{\sigma(k_b)}(x(k_b))\right\} \\
&< \mu\alpha^{k-k_b}\varepsilon\left\{V_{\sigma(k_b-1)}(x(k_b-1))\right\}.
\end{aligned} \tag{26}$$

Repeating the previous manipulation, one has that

$$\begin{aligned}
&\varepsilon\left\{V_{\sigma(k)}(x(k))\right\} \\
&\quad < \alpha^{k-k_b}\varepsilon\left\{V_{\sigma(k_b)}(x(k_b))\right\} \\
&\quad < \mu\alpha^{k-k_b}\varepsilon\left\{V_{\sigma(k_b-1)}(x(k_b-1))\right\} \\
&\quad < \mu\alpha^{k-k_{b-1}-1}\varepsilon\left\{V_{\sigma(k_{b-1})}(x(k_{b-1}))\right\} \\
&\quad < \mu^2\alpha^{k-k_{b-1}-1}\varepsilon\left\{V_{\sigma(k_{b-1}-1)}(x(k_{b-1}-1))\right\} \\
&\quad < \cdots \\
&\quad < \mu^b\alpha^{k-k_0-b}\varepsilon\left\{V_{\sigma(k_0)}(x(k_0))\right\}.
\end{aligned} \tag{27}$$

From Definition 2, we get that $b = N_\sigma(k_0, k) \le N_0 + (k - k_0)/\tau_a$, where b denotes the switching number of $\sigma(k)$ during the interval $[k_0, k)$, then it follows that

$$\begin{aligned}
&\varepsilon\left\{V_{\sigma(k)}\left(x\left(k\right)\right)\right\}\\
&\quad< \left(\mu\alpha^{-1}\right)^{N_0+(k-k_0)/\tau_a}\alpha^{k-k_0}\varepsilon\left\{V_{\sigma(k_0)}\left(x\left(k_0\right)\right)\right\}\\
&\quad< \left(\mu\alpha^{-1}\right)^{N_0}e^{((k-k_0)/\tau_a)(\ln\mu-\ln\alpha)}e^{(k-k_0)\ln\alpha}\varepsilon\left\{V_{\sigma(k_0)}\left(x\left(k_0\right)\right)\right\}\\
&\quad< \left(\mu\alpha^{-1}\right)^{N_0}e^{((\ln\mu-\ln\alpha)/\tau_a+\ln\alpha)(k-k_0)}\varepsilon\left\{V_{\sigma(k_0)}\left(x\left(k_0\right)\right)\right\}.
\end{aligned} \tag{28}$$

Notice that

$$\begin{aligned}
&\min_{i\in\underline{N}}\left\{\lambda_{\min}\left(P_i\right)\right\}\varepsilon\left\{\left\|\xi\left(k\right)\right\|^2\right\} \le \varepsilon\left\{V_{\sigma(k)}\left(x\left(k\right)\right)\right\},\\
&\varepsilon\left\{V\left(x\left(k_0\right)\right)\right\}\\
&\quad\le \max_{i\in\underline{N}}\left\{\lambda_{\max}\left(P_i\right)+d\lambda_{\max}\left(R_i\right)\right\}\sup_{-d\le\theta\le0}\varepsilon\left\{\left\|\xi\left(k_0+\theta\right)\right\|^2\right\}.
\end{aligned} \tag{29}$$

Then, one obtains

$$\varepsilon\left\{\left\|\xi\left(k\right)\right\|^2\right\} < \gamma\rho^{(k-k_0)}\sup_{-d\le\theta\le0}\varepsilon\left\{\left\|\xi\left(k_0+\theta\right)\right\|^2\right\}, \quad \forall k \ge k_0, \tag{30}$$

where

$$\begin{aligned}
\gamma &= \left(\mu\alpha^{-1}\right)^{N_0}\frac{\max_{i\in\underline{N}}\left\{\lambda_{\max}\left(P_i\right)+d\lambda_{\max}\left(R_i\right)\right\}}{\min_{i\in\underline{N}}\left\{\lambda_{\min}\left(P_i\right)\right\}},\\
\rho &= e^{(\ln\mu-\ln\alpha)/\tau_a+\ln\alpha}.
\end{aligned} \tag{31}$$

Then under the average dwell time scheme (14), it is easy to get that $0 < \rho < 1$, which implies that system (9a), (9b), and (9c) is exponentially stable in mean square sense.

This completes the proof. □

Remark 8. Compared with the existing results presented in [16–18], we get sufficient conditions of exponential stability in mean square sense. In addition, the paper takes the missing measurement into consideration, which yields different results from those of [16–18], where the missing measurement is not considered.

3.2. Design of DOF Controller. This section will give some LMIs conditions for the controller design.

Theorem 9. *Consider system* (1a), (1b), (1c), *and* (1d) *for a given positive scalar* $0 < \alpha < 1$, *if there exist positive-definite symmetric matrices* $\overline{S}_{11i}$, P_{11i}, R_{11i}, *and* $\widetilde{Y}_i'$, *any matrices* Σ_i, Y_i', *and* $\overline{Z}_i'$ *with appropriate dimensions, and positive scalars* ε_i *and* δ_i $(i \in \underline{N})$, *such that*

$$\begin{bmatrix}
\Phi_i & \Lambda_i & 0 & 0 & \theta_i & \Sigma_i & 0 & \tau C_i^T Z_i^T & \varepsilon_i M_{1i}^T & 0 & \delta_i M_{1i}^T & 0\\
* & \Upsilon_i & 0 & 0 & A_i^T\overline{S}_{11i} & \Theta_i & 0 & \tau C_i^T Z_i^T & \varepsilon_i M_{1i}^T & 0 & \delta_i M_{1i}^T & 0\\
* & * & \Xi_i & \Omega_i & A_{di}^T\overline{S}_{11i} & A_{di}^T P_{11i} & 0 & 0 & \varepsilon_i M_{2i}^T & 0 & \delta_i M_{2i}^T & 0\\
* & * & * & -\alpha^d R_{11i} & A_{di}^T\overline{S}_{11i} & A_{di}^T P_{11i} & 0 & 0 & \varepsilon_i M_{2i}^T & 0 & \delta_i M_{2i}^T & 0\\
* & * & * & * & -\overline{S}_{11i} & -I & 0 & 0 & 0 & \overline{S}_{11i}H_i & 0 & 0\\
* & * & * & * & * & -P_{11i} & 0 & 0 & 0 & 0 & 0 & P_{11i}H_i\\
* & * & * & * & * & * & -\tau\overline{S}_{11i} & -\tau\overline{S}_{11i} & 0 & 0 & 0 & 0\\
* & * & * & * & * & * & * & -\tau P_{11i} & 0 & 0 & 0 & 0\\
* & * & * & * & * & * & * & * & -\varepsilon_i I & 0 & 0 & 0\\
* & * & * & * & * & * & * & * & * & -\varepsilon_i I & 0 & 0\\
* & * & * & * & * & * & * & * & * & * & -\delta_i I & 0\\
* & * & * & * & * & * & * & * & * & * & * & -\delta_i I
\end{bmatrix} < 0, \tag{32a}$$

where $\tau = (1-\overline{r})\overline{r}$, $\Phi_i = R_{11i} + Y_i' + (Y_i')^T + \widetilde{Y}_i' - \alpha\overline{S}_{11i}$, $\Upsilon_i = R_{11i} - \alpha P_{11i}$, $\Lambda_i = R_{11i} + Y_i' - \alpha\overline{S}_{11i}$, $\theta_i = A_i^T\overline{S}_{11i} + (\overline{Z}_i')^T$, $\Theta_i = A_i^T P_{11i} + \overline{r}C_i^T Z_i^T$, $\Xi_i = -\alpha^d R_{11i} - \alpha^d Y_i' - \alpha^d(Y_i')^T - \alpha^d\widetilde{Y}_i'$, $\Omega_i = -\alpha^d R_{11i} - \alpha^d Y_i'$.

Then, there exists a DOF controller (7a), (7b), (7c), *and* (7d) *such that the closed-loop system* (9a), (9b), *and* (9c) *is exponentially stable in mean square sense for any switching signals with average dwell time scheme* (14), *where* $\mu \ge 1$ *satisfies*

$$\begin{bmatrix} R_i - \mu P_j & \overline{E}_{ij}^T P_i \\ * & -P_i \end{bmatrix} < 0, \tag{32b}$$

$$\alpha R_i < \mu R_j, \quad (i, j \in \underline{N}), \tag{32c}$$

where

$$P_i = \begin{bmatrix} P_{11i} & P_{12i} \\ * & P_{22i} \end{bmatrix}, \qquad R_i = \begin{bmatrix} R_{11i} & R_{12i} \\ * & R_{22i} \end{bmatrix}, \tag{33}$$

$$P_{11i}\overline{S}_{11i}^{-1} + P_{12i}S_{12i}^T = I, \qquad P_{12i}^T\overline{S}_{11i}^{-1} + P_{22i}S_{12i}^T = 0, \tag{34a}$$

$$R_{12i} = \left(Y_i'\right)^T\overline{S}_{11i}^{-1}S_{12i}^{-T}, \qquad R_{22i} = S_{12i}^{-1}\overline{S}_{11i}^{-1}\widetilde{Y}_i'\overline{S}_{11i}^{-1}S_{12i}^{-T}. \tag{34b}$$

Moreover, if the previous LMI conditions are feasible, then the desired dynamic output feedback controller parameters can be designed as

$$A_{ci} = P_{12i}^{-1}\left(\Sigma_i^T - P_{11i}A_i - \overline{r}Z_iC_i - P_{11i}\overline{S}_{11i}^{-1}\widetilde{Z}_i'\right)\overline{S}_{11i}^{-1}S_{12i}^{-T}, \tag{35a}$$

$$B_{ci} = P_{12i}^{-1}Z_i, \qquad C_{ci} = B_i^{-1}\overline{S}_{11i}^{-1}\widetilde{Z}_i'\overline{S}_{11i}^{-1}S_{12i}^{-T}. \tag{35b}$$

Proof. Let the matrix P_i^{-1} be partitioned as follows:

$$P_i^{-1} = \begin{bmatrix} S_{11i} & S_{12i} \\ * & S_{22i} \end{bmatrix}, \tag{36}$$

where $S_{11i} \in R^{n\times n}$.

By $P_iP_i^{-1} = I$ and from (34a) and (36), we have

$$P_{11i}S_{11i} + P_{12i}S_{12i}^T = I, \qquad P_{12i}^TS_{11i} + P_{22i}S_{12i}^T = 0. \tag{37}$$

Define the following matrices:

$$J_i = \begin{bmatrix} S_{11i} & I \\ S_{12i}^T & 0 \end{bmatrix}, \qquad \widetilde{J}_i = \begin{bmatrix} I & P_{11i} \\ 0 & P_{12i}^T \end{bmatrix}. \tag{38}$$

Then we have

$$P_iJ_i = \widetilde{J}_i,$$

$$J_i^TP_i\overline{A}_iJ_i = \begin{bmatrix} \widehat{A}_iS_{11i} + B_iC_{ci}S_{12i}^T & \widehat{A}_i \\ \Psi_{1i} & P_{11i}\widehat{A}_i + \overline{r}P_{12i}B_{ci}C_i \end{bmatrix},$$

$$J_i^TP_i\overline{A}_{mi}J_i = \begin{bmatrix} 0 & 0 \\ P_{12i}B_{ci}C_iS_{11i} & P_{12i}B_{ci}C_i \end{bmatrix},$$

$$J_i^TP_i\overline{A}_{di}J_i = \begin{bmatrix} \widehat{A}_{di}S_{11i} & \widehat{A}_{di} \\ P_{11i}\widehat{A}_{di}S_{11i} & P_{11i}\widehat{A}_{di} \end{bmatrix},$$

$$J_i^TP_iJ_i = \begin{bmatrix} S_{11i} & I \\ I & P_{11i} \end{bmatrix}, \tag{39}$$

$$J_i^TR_iJ_i = \begin{bmatrix} \Psi_{2i} & S_{11i}R_{11i} + S_{12i}R_{12i}^T \\ R_{11i}S_{11i} + R_{12i}S_{12i}^T & R_{11i} \end{bmatrix},$$

$$\Psi_{1i} = P_{11i}\widehat{A}_iS_{11i} + \overline{r}P_{12i}B_{ci}C_iS_{11i} + P_{11i}B_iC_{ci}S_{12i}^T + P_{12i}A_{ci}S_{12i}^T,$$

$$\Psi_{2i} = S_{11i}R_{11i}S_{11i} + S_{12i}R_{12i}^TS_{11i} + S_{11i}R_{12i}S_{12i}^T + S_{12i}R_{22i}S_{12i}^T.$$

Use $\mathrm{diag}\{J_i^T, J_i^T, J_i^T, J_i^T\}$ to premultiply and $\mathrm{diag}\{J_i, J_i, J_i, J_i\}$ to postmultiply the left-hand term of (13), and denote

$$Z_i = P_{12i}B_{ci}, \qquad \widetilde{Z}_i = C_{ci}S_{12i}^T,$$
$$Y_i = S_{12i}R_{12i}^T, \qquad \widetilde{Y}_i = S_{12i}R_{22i}S_{12i}^T. \tag{40}$$

Then, we can obtain that (13) is equivalent to the following inequality:

$$\begin{bmatrix} \Phi_{i1} & \Lambda_{i1} & 0 & 0 & \widehat{\theta}_{i1} & \widehat{\Sigma}_{i1} & 0 & \tau S_{11i}C_i^TZ_i^T \\ * & \Upsilon_{i1} & 0 & 0 & \widehat{A}_i^T & \widehat{\Theta}_{i1} & 0 & \tau C_i^TZ_i^T \\ * & * & \Xi_{i1} & \Omega_{i1} & S_{11i}\widehat{A}_{di}^T & S_{11i}\widehat{A}_{di}^TP_{11i} & 0 & 0 \\ * & * & * & -\alpha^dR_{11i} & \widehat{A}_{di}^T & \widehat{A}_{di}^TP_{11i} & 0 & 0 \\ * & * & * & * & -S_{11i} & -I & 0 & 0 \\ * & * & * & * & * & -P_{11i} & 0 & 0 \\ * & * & * & * & * & * & -\tau S_{11i} & -\tau I \\ * & * & * & * & * & * & * & -\tau P_{11i} \end{bmatrix} < 0, \tag{41}$$

where

$$\begin{aligned}
\Phi_{i1} &= S_{11i}R_{11i}S_{11i} + Y_iS_{11i} + S_{11i}Y_i^T + \widetilde{Y}_i - \alpha S_{11i},\\
\Lambda_{i1} &= S_{11i}R_{11i} + Y_i - \alpha I,\\
\Upsilon_{i1} &= R_{11i} - \alpha P_{11i},\\
\widehat{\Sigma}_{i1} &= S_{11i}\widehat{A}_i^T P_{11i} + \overline{r}S_{11i}C_i^T Z_i^T\\
&\quad + \widetilde{Z}_i^T B_i^T P_{11i} + \left(P_{12i}A_{ci}S_{12i}^T\right)^T,\\
\widehat{\theta}_{i1} &= S_{11i}\widehat{A}_i^T + \widetilde{Z}_i^T B_i^T,\\
\Xi_{i1} &= -\alpha^d S_{11i}R_{11i}S_{11i} - \alpha^d Y_iS_{11i} - \alpha^d S_{11i}Y_i^T - \alpha^d\widetilde{Y}_i,\\
\widehat{\Theta}_{i1} &= \widehat{A}_i^T P_{11i} + \overline{r}C_i^T Z_i^T,\\
\Omega_{i1} &= -\alpha^d S_{11i}R_{11i} - \alpha^d Y_i.
\end{aligned} \tag{42}$$

Using $\mathrm{diag}\{S_{11i}^{-1}, I, S_{11i}^{-1}, I, S_{11i}^{-1}, I, S_{11i}^{-1}, I\}$ to pre- and post-multiply the left-hand term of (41) and denoting

$$\begin{gathered}
\widetilde{Z}_i' = S_{11i}^{-1}B_i\widetilde{Z}_iS_{11i}^{-1}, \qquad Y_i' = S_{11i}^{-1}Y_i,\\
\widetilde{Y}_i' = S_{11i}^{-1}\widetilde{Y}_iS_{11i}^{-1},
\end{gathered} \tag{43}$$

one obtains

$$\begin{bmatrix}
\Phi_i & \Lambda_i & 0 & 0 & \widehat{\theta}_i & \widehat{\Sigma}_i & 0 & \tau C_i^T Z_i^T\\
* & \Upsilon_i & 0 & 0 & \widehat{A}_i^T S_{11i}^{-1} & \widehat{\Theta}_i & 0 & \tau C_i^T Z_i^T\\
* & * & \Xi_i & \Omega_i & \widehat{A}_{di}^T S_{11i}^{-1} & \widehat{A}_{di}^T P_{11i} & 0 & 0\\
* & * & * & -\alpha^d R_{11i} & \widehat{A}_{di}^T S_{11i}^{-1} & \widehat{A}_{di}^T P_{11i} & 0 & 0\\
* & * & * & * & -S_{11i}^{-1} & -I & 0 & 0\\
* & * & * & * & * & -P_{11i} & 0 & 0\\
* & * & * & * & * & * & -\tau S_{11i}^{-1} & -\tau S_{11i}^{-1}\\
* & * & * & * & * & * & * & -\tau P_{11i}
\end{bmatrix} < 0, \tag{44}$$

where

$$\begin{aligned}
\Phi_i &= R_{11i} + Y_i' + \left(Y_i'\right)^T + \widetilde{Y}_i' - \alpha S_{11i}^{-1},\\
\widehat{\Theta}_i &= \widehat{A}_i^T P_{11i} + \overline{r}C_i^T Z_i^T,\\
\Lambda_i &= R_{11i} + Y_i' - \alpha S_{11i}^{-1},\\
\widehat{\theta}_i &= \widehat{A}_i^T S_{11i}^{-1} + \left(\widetilde{Z}_i'\right)^T,\\
\widehat{\Sigma}_i &= \widehat{A}_i^T P_{11i} + \overline{r}C_i^T Z_i^T + \left(\widetilde{Z}_i'\right)^T S_{11i}P_{11i} + S_{11i}^{-1}\left(P_{12i}A_{ci}S_{12i}^T\right)^T,\\
\Upsilon_i &= R_{11i} - \alpha P_{11i},\\
\Xi_i &= -\alpha^d R_{11i} - \alpha^d Y_i' - \alpha^d\left(Y_i'\right)^T - \alpha^d\widetilde{Y}_i',\\
\Omega_i &= -\alpha^d R_{11i} - \alpha^d Y_i'.
\end{aligned} \tag{45}$$

Then combining (5) with (44), one has

$$\widehat{T}_i = T_i + \Delta T_i < 0$$

$$T_i = \begin{bmatrix}
\Phi_i & \Lambda_i & 0 & 0 & \theta_i & \Sigma_i & 0 & \tau C_i^T Z_i^T\\
* & \Upsilon_i & 0 & 0 & A_i^T S_{11i}^{-1} & \Theta_i & 0 & \tau C_i^T Z_i^T\\
* & * & \Xi_i & \Omega_i & A_{di}^T S_{11i}^{-1} & A_{di}^T P_{11i} & 0 & 0\\
* & * & * & -\alpha^d R_{11i} & A_{di}^T S_{11i}^{-1} & A_{di}^T P_{11i} & 0 & 0\\
* & * & * & * & -S_{11i}^{-1} & -I & 0 & 0\\
* & * & * & * & * & -P_{11i} & 0 & 0\\
* & * & * & * & * & * & -\tau S_{11i}^{-1} & -\tau S_{11i}^{-1}\\
* & * & * & * & * & * & * & -\tau P_{11i}
\end{bmatrix}, \tag{46}$$

where

$$\begin{aligned}
\Theta_i &= A_i^T P_{11i} + \overline{r}C_i^T Z_i^T,\\
\theta_i &= A_i^T S_{11i}^{-1} + \left(\widetilde{Z}_i'\right)^T,\\
\Sigma_i &= A_i^T P_{11i} + \overline{r}C_i^T Z_i^T + \left(\widetilde{Z}_i'\right)^T S_{11i}P_{11i} + S_{11i}^{-1}\left(P_{12i}A_{ci}S_{12i}^T\right)^T,\\
\Delta T_i &= \overline{M}_iF_i(k)^T\overline{H}_i + \left(\overline{M}_iF_i(k)^T\overline{H}_i\right)^T\\
&\quad + \overline{M}_iF_i(k)^T\widetilde{H}_i + \left(\overline{M}_iF_i(k)^T\overline{H}_i\right)^T,\\
\overline{M}_i^T &= \begin{bmatrix} M_{1i} & M_{1i} & M_{2i} & M_{2i} & 0 & 0 & 0 & 0\end{bmatrix},\\
\overline{H}_i &= \begin{bmatrix} 0 & 0 & 0 & 0 & H_i^T S_{11i}^{-1} & 0 & 0 & 0\end{bmatrix},\\
\widetilde{H}_i &= \begin{bmatrix} 0 & 0 & 0 & 0 & 0 & H_i^T P_{11i} & 0 & 0\end{bmatrix}.
\end{aligned} \tag{47}$$

By Lemma 6, (46) is equivalent to

$$T_i + \varepsilon_i\overline{M}_i\overline{M}_i^T + \varepsilon_i^{-1}\overline{H}_i^T\overline{H}_i + \delta_i\overline{M}_i\overline{M}_i^T + \delta_i^{-1}\widetilde{H}_i^T\widetilde{H}_i < 0, \tag{48}$$

where ε_i and δ_i are positive scalars.

Using Lemma 5, we have

$$\begin{bmatrix}
\Phi_i & \Lambda_i & 0 & 0 & \theta_i & \Sigma_i & 0 & \tau C_i^T Z_i^T & M_{1i}^T & 0 & M_{1i}^T & 0 \\
* & \Upsilon_i & 0 & 0 & A_i^T S_{11i}^{-1} & \Theta_i & 0 & \tau C_i^T Z_i^T & M_{1i}^T & 0 & M_{1i}^T & 0 \\
* & * & \Xi_i & \Omega_i & A_{di}^T S_{11i}^{-1} & A_{di}^T P_{11i} & 0 & 0 & M_{2i}^T & 0 & M_{2i}^T & 0 \\
* & * & * & -\alpha^d R_{11i} & A_{di}^T S_{11i}^{-1} & A_{di}^T P_{11i} & 0 & 0 & M_{2i}^T & 0 & M_{2i}^T & 0 \\
* & * & * & * & -S_{11i}^{-1} & -I & 0 & 0 & 0 & S_{11i}^{-1} H_i & 0 & 0 \\
* & * & * & * & * & -P_{11i} & 0 & 0 & 0 & 0 & 0 & P_{11i} H_i \\
* & * & * & * & * & * & -\tau S_{11i}^{-1} & -\tau S_{11i}^{-1} & 0 & 0 & 0 & 0 \\
* & * & * & * & * & * & * & -\tau P_{11i} & 0 & 0 & 0 & 0 \\
* & * & * & * & * & * & * & * & -\varepsilon_i^{-1} I & 0 & 0 & 0 \\
* & * & * & * & * & * & * & * & * & -\varepsilon_i I & 0 & 0 \\
* & * & * & * & * & * & * & * & * & 0 & -\delta_i^{-1} I & 0 \\
* & * & * & * & * & * & * & * & * & 0 & * & -\delta_i I
\end{bmatrix} < 0. \tag{49}$$

Using $\mathrm{diag}\{I, I, I, I, I, I, I, I, \varepsilon_i, I, \delta_i, I\}$ to pre- and postmultiply the left-hand term of (49) and denoting $\overline{S}_{11i} = S_{11i}^{-1}$ we can obtain that (32a) is equivalent to (49), that is to say, (32a) guarantees that (13) is tenable.

The proof is completed. □

Remark 10. From Theorem 9, it is easy to see that a larger α will be favorable to the solvability of inequality (32a), (32b), and (32c) which leads to a larger value of τ_a^*. Considering these, we can first select a larger α to guarantee the feasibility of inequality (32a), (32b), and (32c), and then decrease α to obtain a smaller τ_a^*.

Based on Theorem 9, we present an algorithm for the design of dynamic output controller.

Algorithm 11.

Step 1. Given the system matrices and a constant $0 < \alpha < 1$; by solving (32a), we can get the feasible solution of positive definite symmetric matrices $\overline{S}_{11i}$, P_{11i}, R_{11i}, $\widetilde{Y}_i'$, matrices Σ_i, Y_i', $\widetilde{Z}_i'$, and positive scalars ε_i, δ_i.

Step 2. Applying singular value decomposition to the first equation of (34a), we can obtain square and nonsingular matrices P_{12i} and S_{12i}. Then we can get P_{22i}, R_{12i}, and R_{22i} by (34a) and (34b).

Step 3. By substituting matrices P_{11i}, P_{12i}, P_{22i}, R_{11i}, R_{12i}, and R_{22i} into (32b)-(32c) and solving them, we can get μ and τ_a^* by (14).

Step 4. Determine the DOF controller parameters A_{ci}, B_{ci}, and C_{ci} based on (35a) and (35b).

4. Numerical Example

In this section, we present an example to illustrate the effectiveness of the proposed approach. Consider system (1a), (1b), (1c), and (1d) with parameters as follows:

$$\begin{aligned}
A_1 &= \begin{bmatrix} -0.5 & 0.6 \\ -0.19 & -0.6 \end{bmatrix}, \quad A_{d1} = \begin{bmatrix} 0.03 & -0.053 \\ -0.044 & 0.012 \end{bmatrix}, \\
B_1 &= \begin{bmatrix} 0.025 & -0.012 \\ -0.041 & 0.051 \end{bmatrix}, \quad C_1 = \begin{bmatrix} -0.3 & 0.14 \\ -0.2 & -0.5 \end{bmatrix}, \\
H_1 &= \begin{bmatrix} 0.033 & 0.052 \\ -0.041 & -0.06 \end{bmatrix}, \quad M_{11} = \begin{bmatrix} 0.012 & -0.04 \\ 0.025 & -0.06 \end{bmatrix}, \\
M_{21} &= \begin{bmatrix} -0.25 & 0.08 \\ -0.077 & 0.055 \end{bmatrix}, \\
F_1(k) &= \begin{bmatrix} \dfrac{e^{-0.1k}}{1+0.5k}\cos(k) & 0 \\ 0 & \sin(k) \end{bmatrix}, \\
A_2 &= \begin{bmatrix} -0.8 & -0.43 \\ 0.35 & -0.4 \end{bmatrix}, \quad A_{d2} = \begin{bmatrix} -0.035 & 0.037 \\ 0.027 & -0.063 \end{bmatrix}, \\
B_2 &= \begin{bmatrix} -0.041 & 0.051 \\ 0.025 & -0.012 \end{bmatrix}, \quad C_2 = \begin{bmatrix} -0.1 & 0.25 \\ 0.18 & 0.25 \end{bmatrix}, \\
H_2 &= \begin{bmatrix} -0.01 & -0.033 \\ 0.073 & 0.03 \end{bmatrix}, \quad M_{12} = \begin{bmatrix} -0.025 & 0.02 \\ -0.015 & 0.074 \end{bmatrix}, \\
M_{22} &= \begin{bmatrix} 0.4 & -0.05 \\ 0.046 & -0.062 \end{bmatrix}, \\
F_2(k) &= \begin{bmatrix} \sin(k) & 0 \\ 0 & \dfrac{e^{-0.1k}}{1+0.5k}\cos(k) \end{bmatrix}.
\end{aligned} \tag{50}$$

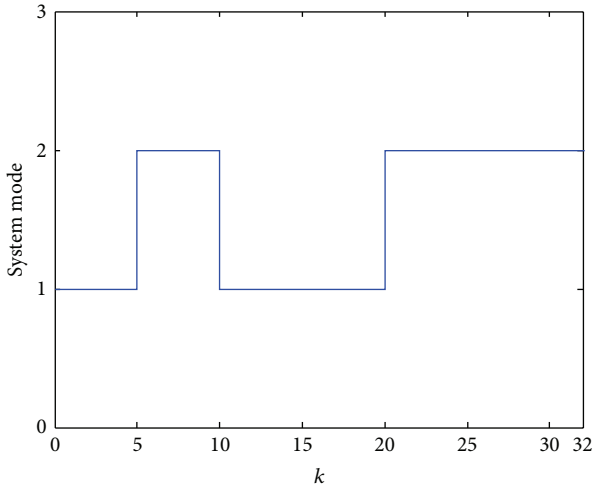

Figure 1: Switching signal.

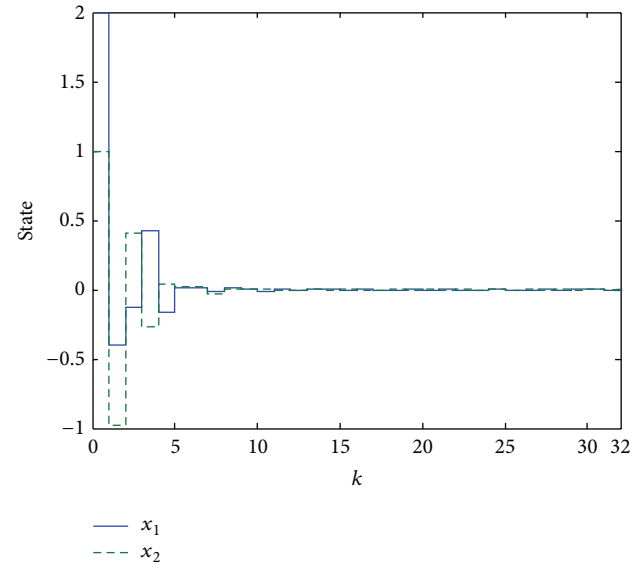

Figure 2: State responses of the resulting closed-loop system.

Let $\alpha = 0.788$, $d = 2$, and $\bar{r} = 0.7$, then by solving the matrix inequalities in Theorem 9, we can get the DOF controller parameters

$$A_{c1} = \begin{bmatrix} 0.2203 & 0.0818 \\ -0.1621 & 0.1568 \end{bmatrix}, \quad B_{c1} = \begin{bmatrix} 0.4072 & -2.0364 \\ -2.1032 & 0.7452 \end{bmatrix},$$
$$C_{c1} = \begin{bmatrix} 10.2067 & -13.1427 \\ 5.4233 & -11.6044 \end{bmatrix}, \quad A_{c2} = \begin{bmatrix} 0.1868 & -0.0881 \\ 0.1339 & 0.1329 \end{bmatrix},$$
$$B_{c2} = \begin{bmatrix} 1.4037 & 2.2041 \\ -2.6439 & 3.7189 \end{bmatrix}, \quad C_{c2} = \begin{bmatrix} -16.7083 & 19.4157 \\ -22.2824 & 11.7057 \end{bmatrix}. \tag{51}$$

Let

$$\overline{E}_{1,2} = \begin{bmatrix} 0.8 & 0 & 0 & 0 \\ 0 & 1.15 & 0 & 0 \\ 0 & 0 & 1.2 & 0 \\ 0 & 0 & 0 & 1.08 \end{bmatrix},$$
$$\overline{E}_{2,1} = \begin{bmatrix} 1.16 & 0 & 0 & 0 \\ 0 & 0.9 & 0 & 0 \\ 0 & 0 & 0.9 & 0 \\ 0 & 0 & 0 & 1.12 \end{bmatrix}. \tag{52}$$

According to (32a), (32b), and (32c), we get $\mu = 5.4319$. From (14), it can be obtained that $\tau_a^* = 7.1028$. Choosing $\tau_a = 8$, simulation results are shown in Figures 1 and 2, where the initial conditions are $x(0) = [2 \ 1]^T$, $x(\theta) = 0$, $\theta \in [-d, 0)$, and $x_c(\theta) = 0$, $\theta \in [-d, 0]$. Figure 1 depicts the switching signal. Under this switching signal and dynamic output feedback controller, the state responses of the resulting closed-loop system are shown in Figure 2. From Figure 1, we can see that the switching signal satisfies $\tau_a = 8$. Furthermore, it can be observed from Figure 2 that the resulting closed-loop system is exponentially stable in mean square sense. This indicates that the designed controller is effective although there exist missing measurements.

5. Conclusions

This paper has presented a solution to the problem of dynamic output feedback controller design for a class of uncertain discrete impulsive switched systems with state delay and missing measurements. By employing the average dwell time approach, a sufficient condition for the existence of a DOF controller is presented such that the exponential stability in mean square sense of the resulting closed-loop system is ensured. An example is given to illustrate the applicability of the proposed approach. Our future work will focus on studying the problem of asynchronous control for discrete impulsive switched systems with state delay and missing measurements.

Acknowledgments

This work was supported by the National Natural Science Foundation of China under Grant no. 61273120 and the Alexander von Humboldt Foundation in Germany.

References

[1] D. Liberzon, *Switching in Systems and Control*, Systems & Control: Foundations & Applications, Birkhäuser, Boston, Mass, USA, 2003.

[2] D. Liberzon and A. S. Morse, "Basic problems in stability and design of switched systems," *IEEE Control Systems Magazine*, vol. 19, no. 5, pp. 59–70, 1999.

[3] J. P. Hespanha and A. S. Morse, "Stability of switched systems with average dwell-time," in *Proceedings of the 38th IEEE Conference on Decision and Control (CDC '99)*, pp. 2655–2660, December 1999.

[4] W.-A. Zhang and L. Yu, "Stability analysis for discrete-time switched time-delay systems," *Automatica*, vol. 45, no. 10, pp. 2265–2271, 2009.

[5] L. Zhang and B. Jiang, "Stability of a class of switched linear systems with uncertainties and average dwell time switching," *International Journal of Innovative Computing, Information and Control*, vol. 6, no. 2, pp. 667–676, 2010.

[6] P. Yan and H. Özbay, "Stability analysis of switched time delay systems," *SIAM Journal on Control and Optimization*, vol. 47, no. 2, pp. 936–949, 2008.

[7] Z.-H. Guan, D. J. Hill, and X. Shen, "On hybrid impulsive and switching systems and application to nonlinear control," *IEEE Transactions on Automatic Control*, vol. 50, no. 7, pp. 1058–1062, 2005.

[8] B. Liu and H. J. Marquez, "Controllability and observability for a class of controlled switching impulsive systems," *IEEE Transactions on Automatic Control*, vol. 53, no. 10, pp. 2360–2366, 2008.

[9] H. Ye, A. N. Michel, and L. Hou, "Stability analysis of systems with impulse effects," *IEEE Transactions on Automatic Control*, vol. 43, no. 12, pp. 1719–1723, 1998.

[10] S.-H. Lee and J.-T. Lim, "Stability analysis of switched systems with impulse effects," in *Proceedings of the IEEE International Symposium on Intelligent Control, Intelligent Systems and Semiotics*, pp. 79–83, Semiotics, Cambridge, UK, September 1999.

[11] J. C. Geromel and P. Colaneri, "H_∞ and dwell time specifications of switched linear systems," in *Proceedings of the 47th IEEE Conference on Decision and Control (CDC '08)*, pp. 5318–5323, Cancun, Mexico, December 2008.

[12] J. C. Geromel and G. S. Deaecto, "Switched state feedback control for continuous-time uncertain systems," *Automatica*, vol. 45, no. 2, pp. 593–597, 2009.

[13] S. Tong and Y. Li, "Observer-based fuzzy adaptive control for strict-feedback nonlinear systems," *Fuzzy Sets and Systems*, vol. 160, no. 12, pp. 1749–1764, 2009.

[14] R. Li, Z. G. Feng, K. L. Teo, and G. R. Duan, "Optimal piecewise state feedback control for impulsive switched systems," *Mathematical and Computer Modelling*, vol. 48, no. 3-4, pp. 468–479, 2008.

[15] F. Long and S. Fei, "Neural networks stabilization and disturbance attenuation for nonlinear switched impulsive systems," *Neurocomputing*, vol. 71, no. 7–9, pp. 1741–1747, 2008.

[16] W. Xiang and J. Xiao, "Stability analysis and control synthesis of switched impulsive systems," *International Journal of Robust and Nonlinear Control*, vol. 22, no. 13, pp. 1440–1459, 2012.

[17] X. Li, H. R. Karimi, and Z. Xiang, "Robust reliable control of uncertain discrete impulsive switched systems with state delays," *Mathematical Problems in Engineering*, vol. 2013, Article ID 197819, 8 pages, 2013.

[18] X. Li, Z. Xiang, and H. R. Karimi, "Asynchronously switched control of discrete impulsive switched systems with time delays," *Information Sciences*, vol. 249, pp. 132–142, 2013.

[19] S.-C. Tong, X.-L. He, and H.-G. Zhang, "A combined backstepping and small-gain approach to robust adaptive fuzzy output feedback control," *IEEE Transactions on Fuzzy Systems*, vol. 17, no. 5, pp. 1059–1069, 2009.

[20] D.-W. Ding and G.-H. Yang, "H_∞ static output feedback control for discrete-time switched linear systems with average dwell time," *IET Control Theory & Applications*, vol. 4, no. 3, pp. 381–390, 2010.

[21] L. Wu, T. Qi, and Z. Feng, "Average dwell time approach to $L_2 - L_\infty$ control of switched delay systems via dynamic output feedback," *IET Control Theory & Applications*, vol. 3, no. 10, pp. 1425–1436, 2009.

[22] J. C. Geromel, P. Colaneri, and P. Bolzern, "Dynamic output feedback control of switched linear systems," *IEEE Transactions on Automatic Control*, vol. 53, no. 3, pp. 720–733, 2008.

[23] L. Galbusera, P. Bolzern, G. S. Deaecto, and J. C. Geromel, "State and output feedback H_∞ control of time-delay switched linear systems," *International Journal of Robust and Nonlinear Control*, vol. 22, no. 15, pp. 1674–1690, 2012.

[24] S. Cong, Y. Zou, and Y. Zhang, "Stability and output feedback stabilization for systems with Markovian switching and impulse effects," *Journal of Control Theory and Applications*, vol. 8, no. 4, pp. 453–456, 2010.

[25] N. E. Nahi, "Optimal recursive estimation with uncertain observation," *IEEE Transactions on Information Theory*, vol. 15, no. 4, pp. 457–462, 1969.

[26] Z. Wang, D. W. C. Ho, Y. Liu, and X. Liu, "Robust H_∞ control for a class of nonlinear discrete time-delay stochastic systems with missing measurements," *Automatica*, vol. 45, no. 3, pp. 684–691, 2009.

[27] Z. Wang, F. Yang, D. W. C. Ho, and X. Liu, "Robust H_∞ filtering for stochastic time-delay systems with missing measurements," *IEEE Transactions on Signal Processing*, vol. 54, no. 7, pp. 2579–2587, 2006.

[28] X. He and D. Zhou, "Robust H-infinity filtering for time-delay systems with missing measurements: a parameter-dependent approach," *Journal of Control Theory and Applications*, vol. 5, no. 4, pp. 336–344, 2007.

[29] H. Zhang, Q. Chen, H. Yan, and J. Liu, "Robust H_∞ filtering for switched stochastic system with missing measurements," *IEEE Transactions on Signal Processing*, vol. 57, no. 9, pp. 3466–3474, 2009.

[30] A. Mahmoudi, A. Momeni, A. G. Aghdam, and P. Gohari, "On observer design for a class of impulsive switched systems," in *Proceedings of the American Control Conference (ACC '08)*, pp. 4633–4639, Seattle, Wash, USA, June 2008.

[31] S. Boyd, L. El Ghaoui, E. Feron, and V. Balakrishnan, *Linear Matrix Inequalities in System and Control Theory*, vol. 15 of *SIAM Studies in Applied Mathematics*, SIAM, Philadelphia, Pa, USA, 1994.

[32] L. Xie, "Output feedback H_∞ control of systems with parameter uncertainty," *International Journal of Control*, vol. 63, no. 4, pp. 741–750, 1996.

Hindawi Publishing Corporation
Mathematical Problems in Engineering
Volume 2013, Article ID 298268, 11 pages
http://dx.doi.org/10.1155/2013/298268

Research Article

A Novel Approach to ℓ_2-ℓ_∞ Filter Design for T-S Fuzzy Systems with Multiple Time-Varying Delays

Xiaoyu Zhang,[1] Cheng Gong,[2] and Zhen Zeng[3]

[1] *College of Automation, Harbin Engineering University, Harbin 150001, China*
[2] *College of Nuclear Science and Technology, Harbin Engineering University, Harbin 150001, China*
[3] *College of Aerospace and Civil Engineering, Harbin Engineering University, Harbin 150001, China*

Correspondence should be addressed to Cheng Gong; gongcheng2004@126.com

Received 6 June 2013; Accepted 14 August 2013

Academic Editor: Zhiguang Feng

This paper investigates the ℓ_2-ℓ_∞ filtering problem of T-S fuzzy systems with multiple time-varying delays. First, by the Lyapunov-Krasovskii functional approach and free-weighting matrix method, a delay-dependent sufficient condition on ℓ_2-ℓ_∞-disturbance attenuation is presented, in which both stability and prescribed ℓ_2-ℓ_∞ performance are required to be achieved for the filtering-error systems. Then, based on the condition, the full-order and reduced-order delay-dependent ℓ_2-ℓ_∞ filter design schemes for T-S fuzzy multiple time-varying delays systems are developed in terms of linear matrix inequality (LMI). Finally, an example is given to illustrate the effectiveness of the result.

1. Introduction

Time delay arises frequently in many engineering areas of the real world, which is usually a source of instability. Therefore, the stability analysis and synthesis for time-delay system have been one of a most hot research area in the control community over the past years [1–9]. To research the nonlinear time-delay system, the scholars considered the Takagi-Sugeno (T-S) fuzzy time-delay model which is a kind of effective representation, and many analysis and synthesis methods for T-S fuzzy time-delay systems have been developed over the past years [10–13].

Since the state variables in control systems are not always available, filtering or state estimation of a dynamic system through an available measurement state is one of the fundamental problems in signal processing, communications, and control application [14–22]. There are many works that appeared to cope with the nonlinear filtering problem for T-S fuzzy systems with time delays [23–31]. For example, in [23, 24], a delay-dependent $\mathscr{H}_\infty$ filter design via continuous-time T-S fuzzy model approach is proposed in terms of linear matrix inequalities. In [25], by using a basis-dependent Lyapunov function, a delay-dependent result on the $\mathscr{H}_\infty$ performance of the discrete filtering error system is presented. Based on the similar Lyapunov function combined with Finslers Lemma, [26] researched the delay-dependent robust $\mathscr{H}_\infty$ filtering problem for a class of uncertain discrete-time T-S fuzzy systems with interval-like time-varying state delay. Reference [27] proposed the delay-dependent approach to robust $\mathscr{H}_\infty$ and ℓ_2-ℓ_∞ filtering for a class of uncertain nonlinear time-delayed systems. References [28, 29] investigated delay-dependent $\mathscr{H}_\infty$ filter design problems for discrete-time T-S fuzzy time-delayed systems and continuous-time T-S fuzzy time-delayed systems, respectively, which were both based on a delay-dependent piecewise Lyapunov-Krasovskii functional.

Several $\mathscr{H}_\infty$ filtering approaches for T-S fuzzy systems with multiple delays have been developed over the past few years [32–36]. For instance [32] studied the $\mathscr{H}_\infty$ filter design problem for discrete-time T-S fuzzy systems with multiple time delays. In [33], a robust mixed $\mathscr{H}_2/\mathscr{H}_\infty$ filtering problem for continuous-time T-S fuzzy systems with multiple time-varying delays in state variables was addressed.

While the time-varying delay functions above mentioned were all assumed slow-varying (the derivative of delay function is less than one) or fast-varying (the derivative of delay function is unknown). Reference [34] dealt with the fuzzy $\mathscr{H}_\infty$ filter design problem for discrete-time T-S fuzzy systems

with multiple time delays in the state variables. Reference [35] introduced a decentralized $\mathscr{H}_\infty$ fuzzy filter design for nonlinear interconnected systems with multiple constant delays via T-S fuzzy models. Reference [36] addressed the problem of ℓ_2-ℓ_∞ filter design for T-S fuzzy systems with multiple time-varying delays, but the derivative of delay functions must be less than one.

To the best of our knowledge, the problem of ℓ_2-ℓ_∞ filter design for T-S fuzzy systems with multiple time-varying delays has not been fully investigated in the literature. As is well known, time delays usually exist in many physical systems and result in unsatisfactory performance, and the derivative of delay function may vary from $-\infty$ to $+\infty$. So, the research on T-S fuzzy systems with multiple time-varying delays is of great practical and theoretical significance. This motivates the research in this paper.

In summary, the purpose of this paper is to develop an ℓ_2-ℓ_∞ filter for T-S fuzzy systems with multiple time-varying delays. Based on the Lyapunov-Krasovskii functional approach and free-weighting matrix method, a delay-dependent sufficient condition on ℓ_2-ℓ_∞-disturbance attenuation is presented. Then, the full-order and reduced-order delay-dependent ℓ_2-ℓ_∞ filter design schemes for T-S fuzzy multiple time-varying-delays systems are developed in terms of LMI. The example illustrates the effectiveness of the result.

This paper is organized as follows. In Section 2, the T-S fuzzy model and corresponding filter are formulated. In Section 3 we give the sufficient condition to assure asymptotic stability and the ℓ_2-ℓ_∞ noise-attenuation level bound for the T-S fuzzy filtering-error systems. Based on the condition in Section 3, we present a stable fuzzy filter in terms of LMIs. Section 4 provides illustrative examples to demonstrate the effectiveness of the proposed method. Conclusions are given in Section 5.

Notations. The notations used throughout this paper are fairly standard. The superscript "T" stands for matrix transpose, and the notation $P > 0$ ($P \geq 0$) means that matrix P is real symmetric and positive (or being positive semidefinite). I and 0 and are used to denote identity matrix and zero matrix with appropriate dimension, respectively. The notation $*$ in a symmetric matrix always denotes the symmetric block in the matrix. The parameter diag$\{\cdots\}$ denotes a block-diagonal matrix. Matrices, if not explicitly stated, are assumed to have compatible dimensions for algebraic operations.

2. System Descriptions and Preliminaries

Consider the nonlinear system with multiple state delays that is described by the following T-S model.

2.1. Plant Form

Rule i. IF $s_1(t)$ is F_{i1}, $s_2(t)$ is F_{i2}, and $s_n(t)$ is F_{in}, then

$$\begin{aligned}
\dot{x}(t) &= A_i x(t) + \sum_{k=1}^{q} A_{dik} x\left(t - d_k(t)\right) + B_i \omega(t), \\
y(t) &= C_i x(t) + \sum_{k=1}^{q} C_{dik} x\left(t - d_k(t)\right) + D_i \omega(t), \\
z(t) &= E_i x(t), \\
x(t) &= \phi(t), \quad t \in [-h, 0], \\
h &= \max\{h_k\}, \quad k = 1, 2, \ldots, q,
\end{aligned} \tag{1}$$

where $s_1(t), s_2(t), \ldots,$ and $s_n(t)$ are the premise variables that are measurable, and each F_{ij} ($j = 1, 2, \ldots, n$) is a fuzzy set. $x(t) \in R^n$ is the state variables. $y(t) \in R^m$ is the measured output of the system. $z(t) \in R^p$ is the signal to be estimated. $\omega(t) \in R^b$ is the disturbance input. r is the number of IF-THEN rules. Also $0 \leq d_k(t) \leq h_k$ is the time-varying delay in the state, and it is assumed that $\dot{d}_k(t) \leq d_k$. That is, the derivative of time-varying delay function is continuous and bounded. q is the number of time delays. $\phi(t)$ is a vector-valued initial continuous function.

By using center-average defuzzifier, product inference, and singleton fuzzifier, the dynamic fuzzy model (1) can be expressed by the following global model:

$$\begin{aligned}
\dot{x}(t) &= \sum_{i=1}^{r} u_i(s(t)) \left[A_i x(t) + \sum_{k=1}^{q} A_{dik} x\left(t - d_k(t)\right) + B_i \omega(t) \right] \\
&= A(t) x(t) + \sum_{k=1}^{q} A_{dk} x\left(t - d_k(t)\right) + B(t) \omega(t), \\
y(t) &= \sum_{i=1}^{r} u_i(s(t)) \left[C_i x(t) + \sum_{k=1}^{q} C_{dik} x\left(t - d_k(t)\right) + D_i \omega(t) \right] \\
&= C(t) x(t) + \sum_{k=1}^{q} C_{dk} x\left(t - d_k(t)\right) + D(t) \omega(t), \\
z(t) &= \sum_{i=1}^{r} u_i(s(t)) \left[E_i x(t) \right] \\
&= E(t) x(t)
\end{aligned} \tag{2}$$

with

$$u_i(s(t)) = \frac{\alpha_i(s(t))}{\sum_{i=1}^{r} \alpha_i(s(t))}, \qquad \alpha_i(s(t)) = \prod_{j=1}^{n} F_{ij}\left(s_j(t)\right), \tag{3}$$

in which $F_{ij}(s_j(t))$ is the grade of membership of $s_j(t)$ in F_{ij}. It is assumed that $\alpha_i(s(t)) \geq 0$, $i = 1, 2, \ldots, r$, $\sum_{i=1}^{r} \alpha_i(s(t)) > 0$ for all t. Therefore, $u_i(s(t)) \geq 0$ and $\sum_{i=1}^{r} u_i(s(t)) = 1$ for all t. In this paper, we study the following filter form of order l ($l = n$ for full-order filter, and $1 \leq l < n$ for reduced-order filter):

$$\begin{aligned}
\dot{x}_f(t) &= \sum_{i=1}^{r} u_i(s(t)) \left[A_{fi} x(t) + B_{fi} y(t) \right], \\
z_f(t) &= \sum_{i=1}^{r} C_{fi} x_f(t),
\end{aligned} \tag{4}$$

where the A_{fi}, B_{fi}, and C_{fi} are the filter parameters to be designed. Combining (2) and (4) and defining $\xi(t) = [x^T(t), x_f^T(t)]^T$, $e(t) = z(t) - z_f(t)$, and $K = [I_{n\times n}\ 0_{n\times l}]$, we have the filtering-error system:

$$\dot{\xi}(t) = \overline{A}(t)\xi(t) + \sum_{k=1}^{q}\overline{A}_{dk}(t)K\xi\left(t - d_k(t)\right) + \overline{B}(t)\omega(t),$$
$$e(t) = \overline{E}(t)\xi(t), \tag{5}$$

where $\xi(t) \doteq [\phi^T(t), 0]^T$ for $t \in [-h, 0]$ and

$$\begin{aligned}
\overline{A}(t) &= \begin{bmatrix} A(t) & 0 \\ B_f(t)C(t) & A_f(t) \end{bmatrix} \\
&= \sum_{i=1}^{r}\sum_{j=1}^{r} u_i(s(t))u_j(s(t)) \begin{bmatrix} A_j & 0 \\ B_{fi}C_j & A_{fi} \end{bmatrix}, \\
\overline{A}_{dk}(t) &= \begin{bmatrix} A_{dk}(t) \\ B_f(t)C_d(t) \end{bmatrix} \\
&= \sum_{i=1}^{r}\sum_{j=1}^{r} u_i(s(t))u_j(s(t)) \begin{bmatrix} A_{djk} \\ B_{fi}C_{dj} \end{bmatrix}, \\
\overline{B}(t) &= \begin{bmatrix} B(t) \\ B_f(t)D(t) \end{bmatrix} \\
&= \sum_{i=1}^{r}\sum_{j=1}^{r} u_i(s(t))u_j(s(t)) \begin{bmatrix} B_j \\ B_{fi}D_j \end{bmatrix}, \\
\overline{E}(t) &= [E(t)\ \ -C_f(t)] \\
&= \sum_{i=1}^{r}\sum_{i=1}^{r} u_i(s(t))u_j(s(t)) [E_j\ \ -C_{fi}].
\end{aligned} \tag{6}$$

Before ending this section, we introduce the following definition, which will be used in the derivation of our main results.

Definition 1 (ℓ_2-ℓ_∞ performance). Given a scalar $\gamma > 0$, the system (1) is said to be with ℓ_2-ℓ_∞ performance if the system (1) is asymptotically stable and the output $z(t)$ satisfies

$$\|z(t)\|_\infty \le \gamma\|\omega(t)\|_2 \tag{7}$$

for all nonzero $\omega \in \ell_2[0, +\infty]$ under zero-initial condition, where,

$$\begin{aligned}
\|\omega(t)\|_2 &= \sqrt{\int_0^\infty \omega^T(t)\omega(t)}, \\
\|z(t)\|_\infty &= \sqrt{\sup_t \{z^T(t)z(t)\}}.
\end{aligned} \tag{8}$$

Here, we want to design a suitable filter (4) for the system (1) with a ℓ_2-ℓ_∞ performance.

3. Main Results

In this section, the conditions to assure the system (1) asymptotically stable with ℓ_2-ℓ_∞ performance γ for the T-S fuzzy filtering-error systems are presented (Lemmas 2 and 3). Then, based on the conditions, a filter is given in terms of LMIs.

Lemma 2. *Given $\gamma > 0$, if there exist common matrices $0 < P \in R^{(n+l)\times(n+l)}$, $0 < Q_k \in R^{n\times n}$, $0 < R_k \in R^{n\times n}$, $Y_k(t) \in R^{n\times n}$, $T_k(t) \in R^{n\times n}$, $U_k \in R^{b\times n}$, $k = 1, 2, \ldots, q$, and $A_f(t)$, $B_f(t)$, and $C_f(t)$ satisfying*

$$\begin{bmatrix} \Xi_{11} & \Xi_{12} & \Xi_{13} \\ * & -\Xi_{22} & 0 \\ * & * & -\Xi_{33} \end{bmatrix} < 0, \tag{9}$$

$$\begin{bmatrix} P & \overline{E}^T(t) \\ * & \gamma^2 I \end{bmatrix} > 0, \tag{10}$$

where

$$\Xi_{11} = \begin{bmatrix} \Pi_0 & \Pi_1 & \cdots & \Pi_q & \Pi_{q+1} \\ * & -(1-d_1)Q_1 - T_1(t) - T_1^T(t) & 0 & 0 & -U_1^T(t) \\ * & * & \ddots & \vdots & \vdots \\ * & * & * & -(1-d_q)Q_q - T_q(t) - T_q^T(t) & -U_q^T(t) \\ * & * & * & * & -I \end{bmatrix},$$

$$\Pi_0 = \overline{A}^T(t)P + P\overline{A}(t) + \sum_{k=1}^{q}\left(K^TQ_kK + K^TY_k(t)K + K^TY_k^T(t)K\right),$$

$$\Pi_1 = P\overline{A}_{d1}(t) - K^TY_1(t) + K^TT_1^T(t),$$

$$\Pi_q = P\overline{A}_{dq}(t) - K^TY_q(t) + K^TT_q^T(t),$$

$$\Pi_{q+1} = P\overline{B}(t) + K^T U_q^T(t),$$

$$\Xi_{12} = \begin{bmatrix} \sqrt{h_1}\overline{A}^T(t)K^T R_1 & \cdots & \sqrt{h_q}\overline{A}^T(t)K^T R_q \\ \sqrt{h_1}\overline{A}_{d1}^T(t)K^T R_1 & \cdots & \sqrt{h_q}\overline{A}_{d1}^T(t)K^T R_q \\ \vdots & \vdots & \vdots \\ \sqrt{h_1}\overline{A}_{dq}^T(t)K^T R_1 & \cdots & \sqrt{h_q}\overline{A}_{dq}^T(t)K^T R_q \\ \sqrt{h_1}\overline{B}^T(t)K^T R_1 & \cdots & \sqrt{h_q}\overline{B}^T(t)K^T R_q \end{bmatrix},$$

$$\Xi_{13} = \begin{bmatrix} \sqrt{h_1}K^T Y_1(t) & \cdots & \sqrt{h_q}K^T Y_q(t) \\ \sqrt{h_1}T_1(t) & \cdots & 0 \\ \vdots & \ddots & \vdots \\ 0 & \cdots & \sqrt{h_q}T_q(t) \\ \sqrt{h_1}U_1(t) & \cdots & \sqrt{h_q}U_q(t) \end{bmatrix},$$

$$\Xi_{22} = \Xi_{33} = \operatorname{diag}\left\{R_1, \ldots, R_q\right\}, \tag{11}$$

then the system (5) is asymptotically stable with an ℓ_2-ℓ_∞ performance γ.

Proof. Choose a Lyapunov-Krasovskii functional candidate as

$$V(t) = V_1(t) + V_2(t) + V_3(t), \tag{12}$$

where

$$V_1(t) = \xi^T(t)P\xi(t),$$

$$V_2(t) = \sum_{j=1}^{q}\int_{t-d_j(t)}^{t}\xi^T(s)K^T Q_j K\xi(s)\,ds, \tag{13}$$

$$V_3(t) = \sum_{j=1}^{q}\int_{-h_j}^{0}\int_{t+\theta}^{t}\dot{\xi}^T(s)K^T R_j K\dot{\xi}(s)\,ds.$$

The time derivative of $V(t)$ along the solution of (5) is computed as follows:

$$\begin{aligned}\dot{V}_1(t) &= \dot{\xi}^T(t)P\xi(t) + \xi^T(t)P\dot{\xi}(t) \\ &= \left(\overline{A}(t)\xi(t) + \sum_{k=1}^{q}\overline{A}_{dk}K\xi\left(t-d_k(t)\right) + \overline{B}(t)\omega(t)\right)^T P\xi(t) \\ &\quad + \xi^T(t)P\left(\overline{A}(t)\xi(t) + \sum_{k=1}^{q}\overline{A}_{dk}K\xi\left(t-d_k(t)\right) + \overline{B}(t)\omega(t)\right),\end{aligned} \tag{14}$$

$$\begin{aligned}\dot{V}_2(t) \le \sum_{k=1}^{q}\Big\{&\xi^T(t)K^T Q_k K\xi(t) \\ &- \left(1-d_k\right)\xi^T\left(t-d_k(t)\right)K^T Q_k K\xi\left(t-d_k(t)\right)\Big\},\end{aligned} \tag{15}$$

$$\begin{aligned}\dot{V}_3(t) = &\sum_{k=1}^{q}h_k\dot{\xi}^T(t)K^T R_k K\dot{\xi}(t) \\ &- \sum_{k=1}^{q}\int_{t-d_k(t)}^{t}\dot{\xi}^T(s)K^T R_k K\dot{\xi}(s)\,ds.\end{aligned} \tag{16}$$

Applying free-weighting matrix method [37], using the Newton-Leibniz formula that

$$\begin{aligned}0 = 2\Big[&\xi^T(t)K^T Y_k(t) + \xi^T\left(t-d_k(t)\right)K^T T_k(t) \\ &+\omega^T(t)U_k(t)\Big] \\ &\times\left[K\xi(t) - K\xi\left(t-d_k(t)\right) - \int_{t-d_k(t)}^{t}K\dot{\xi}(s)\,ds\right], \\ &k = 1, 2, \ldots, q,\end{aligned} \tag{17}$$

and defining

$$\eta_k^T(t) = \left[\xi^T(t), \xi^T(t-d_k(t))K^T, \omega^T(t)\right], \quad k = 1,2,\ldots,q,$$
$$\eta^T(t) = \left[\xi^T(t), \xi^T(t-d_1(t))K^T, \ldots, \xi^T\left(t-d_q(t)\right)K^T, \omega^T(t)\right], \tag{18}$$
$$M^T(t) = \left[Y^T(t), T^T(t), U^T(t)\right],$$

we can know that

$$\begin{aligned}
&-\int_{t-d_k(t)}^{t} \dot{\xi}^T(s) K^T R_k K \dot{\xi}(s)\, ds \\
&= -\int_{t-d_k(t)}^{t} \dot{\xi}^T(s) K^T R_k K \dot{\xi}(s)\, ds \\
&\quad + 2\left[\xi^T(t) K^T Y_k(t) + \xi^T(t-d_k(t)) K^T T_k(t) + \omega^T(t) U_k(t)\right] \\
&\quad \times \left[K\xi(t) - K\xi(t-d_k(t)) - \int_{t-d_k(t)}^{t} K\dot{\xi}(s)\, ds\right] \\
&\le h_k \eta_k^T M(t) R_k^{-1} M^T(t) \eta_k \\
&\quad - \int_{t-d_k(t)}^{t} \left[\eta_k^T M(t) + \dot{\xi}^T(s) K^T R_k\right] \\
&\qquad \times R_k^{-1}\left[M^T(t)\eta_k + R_k K\dot{\xi}(s)\right] ds \\
&\quad + 2\left[\xi^T(t) K^T Y_k(t) + \xi^T(t-d_k(t)) K^T T_k(t) + \omega^T(t) K^T U_k(t)\right] \\
&\quad \times \left[K\xi(t) - K\xi(t-d_k(t))\right].
\end{aligned} \tag{19}$$

Consider the index

$$J \triangleq V(t) - \int_0^t \omega^T(s)\omega(s)\, ds. \tag{20}$$

Then for any nonzero $\omega \in \ell_2[0,+\infty]$ under zero-initial condition,

$$J \triangleq \int_0^t \left(\dot{V}(s) - \omega^T(s)\omega(s)\right) ds. \tag{21}$$

After substitution of $\dot{\xi}(t)$ into (16) with (5). and taking into consideration (19), one has from (14), (15), and (16) that

$$J \le \eta^T(t)\left\{\Xi_{11} + \Xi_{12}\Xi_{22}^{-1}\Xi_{12}^T + \Xi_{13}\Xi_{33}^{-1}\Xi_{13}^T\right\}\eta(t). \tag{22}$$

Applying the Schur complement to (22), we know that (9) guarantees $J < 0$, which implies that

$$\xi^T(t) P \xi(t) \le V(t) < \int_0^t \omega^T(s)\omega(s)\, ds. \tag{23}$$

On the other hand, using the Schur complement to (10), we can know that $\overline{E}^T(t)\overline{E}(t) < \gamma^2 P$. Then it can be easily got that for all $t \ge 0$

$$\begin{aligned}
e^T(t) e(t) &= \xi^T(t)\overline{E}^T(t)\overline{E}(t)\xi(t) < \gamma^2 \xi^T(t) P \xi(t) \\
&< \gamma^2 \int_0^t \omega^T(s)\omega(s)\, ds \\
&< \gamma^2 \int_0^\infty \omega^T(s)\omega(s)\, ds.
\end{aligned} \tag{24}$$

Taking the supremum over $t \ge 0$ yields $\|e(t)\|_\infty^2 < \gamma^2 \|\omega(t)\|_2^2$ for all nonzero $\omega \in \ell_2[0,+\infty]$.

Next, we prove the asymptotic stability of system (5) when $\omega = 0$. Choose a Lyapunov-Krasovskii functional $V(\xi_t)$ as in (12), where $\xi_t = \xi(t-\alpha)$, $\alpha \in [-h, 0]$. It is easy to find that there exist two scalars $c_1 > 0$ and $c_2 > 0$ such that

$$c_1|\xi|^2 \le V \le c_2 \sup_{\alpha\in[-h,0]} |\xi_t|^2. \tag{25}$$

Similar to the above deduction, we can know from (9) that the time derivative of V along the solution of (5) with $\omega = 0$ satisfies $\dot{V} < 0$. This proves the asymptotic stability of system (5) with $\omega = 0$ according to the same method of [19]. This completes the proof. □

Lemma 2 is the sufficient condition for the ℓ_2-ℓ_∞ filter design which contains the coupled matrix variables in the matrix inequality. Using the decoupling technique as follows, we can transform Lemma 2 into another form.

Lemma 3. *Given $\gamma > 0$, if there exist common matrices $0 < P \in R^{(n+l)\times(n+l)}$, $0 < Q_k \in R^{n\times n}$, $0 < R_k \in R^{n\times n}$, $Y_k(t) \in R^{n\times n}$, $T_k(t) \in R^{n\times n}$, $U_k \in R^{b\times n}$, $k = 1,2,\ldots,q$, and $A_f(t)$, $B_f(t)$, and $C_f(t)$, such that* (9), (10) *hold if and only if there exist matrices $0 < \Omega$, $0 < F$, $0 < Q_k$, $Y_k(t)$, $T_k(t)$, $U_k(t)$, $k = 1,2,\ldots,q$, and $\widehat{A}_f(t)$, $\widehat{B}_f(t)$, and $\widehat{C}_f(t)$ such that the following inequalities hold:*

$$\Sigma(t) < 0, \tag{26}$$
$$\begin{bmatrix} \Omega & EF & E^T(t) \\ * & F & -\widehat{C}_f^T(t) \\ * & * & \gamma^2 I \end{bmatrix} > 0, \tag{27}$$

where

$$\Sigma(t) = \begin{bmatrix} \Sigma_{11} & \Sigma_{12} & \Sigma_{13} \\ * & -\Sigma_{22} & 0 \\ * & * & -\Sigma_{33} \end{bmatrix},$$

$$\Sigma_{11}=\begin{bmatrix}\Phi_0 & \Phi_1 & \cdots & \Phi_q & \Phi_{q+1}\\ * & -(1-d_1)Q_1-T_1(t)-T_1^T(t) & 0 & 0 & -U_1^T(t)\\ * & * & \ddots & \vdots & \vdots\\ * & * & * & -(1-d_q)Q_q-T_q(t)-T_q^T(t) & -U_q^T(t)\\ * & * & * & * & -I\end{bmatrix},$$

$$\Phi_0=\begin{bmatrix}\Omega A(t)+E\widehat{B}_f(t)C(t) & E\widehat{A}_f(t)\\ FE^TA(t)+\widehat{B}_f(t)C(t) & \widehat{A}_f(t)\end{bmatrix}+\begin{bmatrix}\Omega A(t)+E\widehat{B}_f(t)C(t) & E\widehat{A}_f(t)\\ FE^TA(t)+\widehat{B}_f(t)C(t) & \widehat{A}_f(t)\end{bmatrix}^T+\sum_{k=1}^{q}\left(K^TQ_kK+K^TY_k(t)K+K^TY_k^T(t)K\right),$$

$$\Phi_1=\begin{bmatrix}\Omega A_{d1}(t)+E\widehat{B}_f(t)C_{d1}(t)\\ FE^TA_{d1}(t)+\widehat{B}_f(t)C_{d1}(t)\end{bmatrix}-K^TY_1(t)+K^TT_1^T(t),$$

$$\Phi_q=\begin{bmatrix}\Omega A_{dq}(t)+E\widehat{B}_f(t)C_{dq}(t)\\ FE^TA_{dq}(t)+\widehat{B}_f(t)C_{dq}(t)\end{bmatrix}-K^TY_q(t)+K^TT_q^T(t),$$

$$\Phi_{q+1}=\begin{bmatrix}\Omega B(t)+E\widehat{B}_f(t)D(t)\\ FE^TB(t)+\widehat{B}_f(t)D(t)\end{bmatrix}+K^TU_q^T(t),$$

$$\Sigma_{12}=\begin{bmatrix}\sqrt{h_1}\overline{A}^T(t)K^TR_1 & \cdots & \sqrt{h_q}\overline{A}^T(t)K^TR_q\\ \sqrt{h_1}\overline{A}_{d1}^T(t)R_1 & \cdots & \sqrt{h_q}\overline{A}_{d1}^T(t)R_q\\ \vdots & \vdots & \vdots\\ \sqrt{h_1}\overline{A}_{dq}^T(t)R_1 & \cdots & \sqrt{h_q}\overline{A}_{dq}^T(t)R_q\\ \sqrt{h_1}\overline{B}^T(t)R_1 & \cdots & \sqrt{h_q}\overline{B}^T(t)R_q\end{bmatrix},$$

$$\Sigma_{13}=\begin{bmatrix}\sqrt{h_1}K^TY_1(t) & \cdots & \sqrt{h_q}K^TY_q(t)\\ \sqrt{h_1}T_1(t) & \cdots & 0\\ \vdots & \ddots & \vdots\\ 0 & \cdots & \sqrt{h_q}T_q(t)\\ \sqrt{h_1}U_1(t) & \cdots & \sqrt{h_q}U_q(t)\end{bmatrix},$$

$$\Sigma_{22}=\Sigma_{33}=\operatorname{diag}\left\{R_1,\ldots,R_q\right\},\qquad E=\left[I_{l\times l}\ 0_{l\times(n-l)}\right],\tag{28}$$

then the system (5) is asymptotically stable with an ℓ_2-ℓ_∞ performance γ.

Proof. Necessity. Suppose (9), (10) hold. Partition as

$$P=\begin{bmatrix}\Omega & ES\\ S^TE^T & W\end{bmatrix},\tag{29}$$

where $\Omega>0$, $W>0$, and S is invertible. Let

$$H=\begin{bmatrix}I & 0\\ 0 & SW^{-1}\end{bmatrix}.\tag{30}$$

We pre- and postmultiply D and its transpose to (9) and (10), respectively, where

$$D=\operatorname{diag}\{H,I,I,I,I,I,I,I,I,I\}.\tag{31}$$

Apply the changes of variables such that

$$F=SW^{-1}S^T,\qquad \widehat{A}_f(t)=SA_f(t)W^{-1}S^T,$$
$$\widehat{B}_f(t)=SB_f(t),\qquad \widehat{C}(t)=C_f(t)W^{-1}S^T.\tag{32}$$

Then we obtain (26) and (27).

Sufficiency. Suppose that (26) and (27) hold for $\Omega > 0$, $F > 0$, $Q_k > 0$, $Y_k(t)$, $T_k(t)$, $U_k(t)$, $k = 1, 2, \ldots, q$, and $\widehat{A}_f(t)$, $\widehat{B}_f(t)$, and $\widehat{C}_f(t)$. Choose two matrices with $W > 0$ and S being invertible such that $F = SW^{-1}S^T$. Let P and H be defined as in (29) and (30). Then $P > 0$ is concluded from (27). Pre- and postmultiply D^{-1} and D^{-T} to (26) and (27), respectively. We can get (9) and (10) with the changes of variables as

$$A_f(t) = S^{-1}\widehat{A}_f(t)S^{-T}W, \qquad B_f(t) = S^{-1}\widehat{B}_f(t), \qquad C_f(t) = \widehat{C}_f(t)S^{-T}W. \tag{33}$$

This completes the proof. □

Theorem 4. *Given $\gamma > 0$, if there exist common matrices $\Omega > 0$, $F > 0$, $Q_k > 0$, T_{ki}, Y_{ki}, U_{ki}, $k = 1, 2, \ldots, q$, and $\widehat{A}_{fi}$, $\widehat{B}_{fi}$, and $\widehat{C}_{fi}$ such that the following inequalities hold:*

$$\Theta_{ij} + \Theta_{ji} < 0, \quad i \le j \le r, \tag{34}$$

$$\begin{bmatrix} \Omega & EF & E_i^T \\ * & F & -\widehat{C}_{fi}^T \\ * & * & \gamma^2 I \end{bmatrix} > 0, \tag{35}$$

then ℓ_2-ℓ_∞ filter parameters in (4) *are given by*

$$A_{fi} = F^{-1}\widehat{A}_{fi}, \qquad B_{fi} = F^{-1}\widehat{B}_{fi}, \qquad C_{fi} = \widehat{C}_{fi}, \tag{36}$$

where

$$\Theta_{ij} = \begin{bmatrix} \Psi_{11} & \Psi_{12} & \Psi_{13} \\ * & -\Psi_{22} & 0 \\ * & * & -\Psi_{13} \end{bmatrix},$$

$$\Psi_{11} = \begin{bmatrix} \Phi_0 & \Phi_1 & \cdots & \Phi_q & \Phi_{q+1} \\ * & -(1-d_k)Q_1 - T_{1i} - T_{1i}^T & 0 & 0 & -U_{1i}^T \\ * & * & \ddots & \vdots & \vdots \\ * & * & * & -(1-d_q)Q_q - T_{qi} - T_{qi}^T & -U_{qi}^T \\ * & * & * & * & -I \end{bmatrix},$$

$$\Phi_0 = \begin{bmatrix} \Omega A_i + E\widehat{B}_{fj}C_i & E\widehat{A}_{fj} \\ FE^T A_i + \widehat{B}_{fj}C_i & \widehat{A}_{fj} \end{bmatrix} + \begin{bmatrix} \Omega A_i + E\widehat{B}_{fj}C_i & E\widehat{A}_{fj} \\ FE^T A_i + \widehat{B}_{fj}C_i & \widehat{A}_{fj} \end{bmatrix}^T + \sum_{k=1}^{q}\left(K^T Q_k K + K^T Y_{ki} K + K^T Y_{ki}^T K\right),$$

$$\Phi_1 = \begin{bmatrix} \Omega A_{d1i} + E\widehat{B}_{fj}C_{d1i} \\ FE^T A_{d1i} + \widehat{B}_{fj}C_{d1i} \end{bmatrix} - K^T Y_{1i} + K^T T_{1i}^T,$$

$$\Phi_q = \begin{bmatrix} \Omega A_{dqi} + E\widehat{B}_{fj}C_{dqi} \\ FE^T A_{dqi} + \widehat{B}_{fj}C_{dqi} \end{bmatrix} - K^T Y_{qi} + K^T T_{qi}^T,$$

$$\Phi_{q+1} = \begin{bmatrix} \Omega B_i + E\widehat{B}_{fj}D_i \\ FE^T B_i + \widehat{B}_{fj}D_i \end{bmatrix} + K^T U_{qi}^T,$$

$$\Psi_{12} = \begin{bmatrix} \sqrt{h_1}(A_i K)^T R_1 & \cdots & \sqrt{h_q}(A_i K)^T R_q \\ \sqrt{h_1}A_{d1i}^T R_1 & \cdots & \sqrt{h_q}A_{d1i}^T R_q \\ \vdots & \vdots & \vdots \\ \sqrt{h_1}A_{dqi}^T R_1 & \cdots & \sqrt{h_q}A_{dqi}^T R_q \\ \sqrt{h_1}B_i^T R_1 & \cdots & \sqrt{h_q}B_i^T R_q \end{bmatrix},$$

$$\Psi_{13} = \begin{bmatrix} \sqrt{h_1}K^T Y_{1i} & \cdots & \sqrt{h_q}K^T Y_{qi} \\ \sqrt{h_1}T_{1i} & \cdots & 0 \\ \vdots & \ddots & \vdots \\ 0 & \cdots & \sqrt{h_q}T_{qi} \\ \sqrt{h_1}U_{1i} & \cdots & \sqrt{h_q}U_{qi} \end{bmatrix},$$

$$\Psi_{22} = \Psi_{33} = \operatorname{diag}\left\{R_1, \ldots, R_q\right\}, \qquad E = \left[I_{l\times l}\ 0_{l\times(n-l)}\right]. \tag{37}$$

Proof. By considering (6),we know that $\Sigma(t)$ in (26) and the Θ_{ij} in (34) satisfy

$$\begin{aligned} \Sigma(t) &= \sum_{i=1}^{r}\sum_{j=1}^{r} u_i(s(t))\, u_j(s(t))\, \Theta_{ij} \\ &= \sum_{i=1}^{r} u_i^2(s(t))\, \Theta_{ii} \\ &\quad + \sum_{i<j}^{r} u_i(s(t))\, u_j(s(t)) \left(\Theta_{ij} + \Theta_{ji}\right). \end{aligned} \tag{38}$$

Based on Lemmas 2 and 3, the ℓ_2-ℓ_∞ filter matrices are given by (33). Under the transformation $S^{-T}Wx_f(t)$, the filter matrices functions can be of the following forms:

$$\begin{aligned} A_f(t) &= S^{-T}W\left(S^{-1}\widehat{A}_f(t)\, S^{-T}W\right)W^{-1}S^T, \\ B_f(t) &= S^{-T}W\left(S^{-1}\widehat{B}_f(t)\right), \\ C_f(t) &= \left(\widehat{C}_f(t)\, S^{-T}W\right)W^{-1}S^T. \end{aligned} \tag{39}$$

Hence, the filter in (4) can be got by (36). This completes the proof. □

4. Simulation

In this section, we give a numerical example to illustrate the use of the present method. Consider the system of the form (1) with two plants ($r = 2$) and two delays ($q = 2$), where

$$A_1 = \begin{bmatrix} -2.1 & 0.1 \\ 1 & -2 \end{bmatrix}, \qquad A_{d11} = \begin{bmatrix} -1.1 & 0.1 \\ -0.8 & -0.9 \end{bmatrix},$$

$$A_{d21} = \begin{bmatrix} -0.1 & 0.1 \\ -0.1 & -0.3 \end{bmatrix},$$

$$A_2 = \begin{bmatrix} -1.9 & 0 \\ -0.2 & -1.1 \end{bmatrix}, \qquad A_{d12} = \begin{bmatrix} -0.9 & 0 \\ -1.1 & -1.2 \end{bmatrix},$$

$$A_{d22} = \begin{bmatrix} -0.1 & 0 \\ -0.2 & -0.2 \end{bmatrix},$$

$$B_1 = \begin{bmatrix} 1 \\ -0.2 \end{bmatrix}, \qquad C_1 = \begin{bmatrix} 1 & 0 \end{bmatrix},$$

$$C_{d11} = \begin{bmatrix} -0.8 & 0.6 \end{bmatrix},$$

$$C_{d21} = \begin{bmatrix} -0.1 & 0.2 \end{bmatrix}, \qquad D_1 = 0.3,$$

$$E_1 = \begin{bmatrix} 1 & -0.5 \end{bmatrix},$$

$$B_2 = \begin{bmatrix} 0.3 \\ 0.1 \end{bmatrix}, \qquad C_2 = \begin{bmatrix} 0.5 & -0.6 \end{bmatrix},$$

$$C_{d12} = \begin{bmatrix} -0.1 & 0.1 \end{bmatrix},$$

$$C_{d22} = \begin{bmatrix} -0.1 & 0.1 \end{bmatrix}, \qquad D_2 = -0.6,$$

$$E_2 = \begin{bmatrix} -0.2 & 0.3 \end{bmatrix}. \tag{40}$$

Here, we only consider the full-order filter design. First, we set $h_1 = 0.5$, $h_2 = 0.3$. Figure 1 shows the ℓ_2-ℓ_∞ gain bound got from Theorem 4 in pointwise manner, where the derivatives of time-varying delay function bound $d_1 \in [0\ 1.9]$, $d_2 \in [0\ 1.9]$. We can find that the maximum ℓ_2-ℓ_∞ gain is $\gamma = 0.3714$ at the point $d_1 = 1.9$, $d_2 = 1.9$. The minimum ℓ_2-ℓ_∞ gain is $\gamma = 0.3358$ at the point $d_1 = 0$, $d_2 = 0$.

Then, we set $d_1 = 0.4$, $d_2 = 0.4$. Figure 2 shows the ℓ_2-ℓ_∞ gain bound got from Theorem 4 in pointwise manner, where the time-varying delay function bound $h_1 \in [0\ 1.1]$, $h_2 \in [0\ 1.1]$. We can find that the maximum ℓ_2-ℓ_∞ gain is $\gamma = 0.5257$ at the point $h_1 = 1.1$, $h_2 = 1.1$. The minimum ℓ_2-ℓ_∞ gain is $\gamma = 0.0055$ at the point $h_1 = 0$, $h_2 = 0$.

Now, We choose both time-varying delays to be $0.4\sin(t) + 0.7$ which gives $h_1 = 1.1$, $h_2 = 1.1$, $d_1 = 0.4$, and $d_2 = 0.4$, and we get a set of feasible solutions to Theorem 4 with the ℓ_2-ℓ_∞ gain $\gamma = 0.5257$ and

$$F = \begin{bmatrix} 3.8096 & -1.2607 \\ -1.2607 & 0.6116 \end{bmatrix},$$

$$\widehat{A}_{f1} = \begin{bmatrix} -12.9071 & 1.8516 \\ 5.1902 & -1.1454 \end{bmatrix},$$

$$\widehat{A}_{f2} = \begin{bmatrix} -10.0276 & 4.2653 \\ 3.0519 & -1.5986 \end{bmatrix}, \qquad \widehat{B}_{f1} = \begin{bmatrix} -5.0266 \\ 1.9199 \end{bmatrix},$$

$$\widehat{B}_{f2} = \begin{bmatrix} -4.1959 \\ 1.8120 \end{bmatrix},$$

$$\widehat{C}_{f1} = \begin{bmatrix} 0.8524 & -0.3426 \end{bmatrix}, \qquad \widehat{C}_{f2} = \begin{bmatrix} -0.2629 & 0.1428 \end{bmatrix}. \tag{41}$$

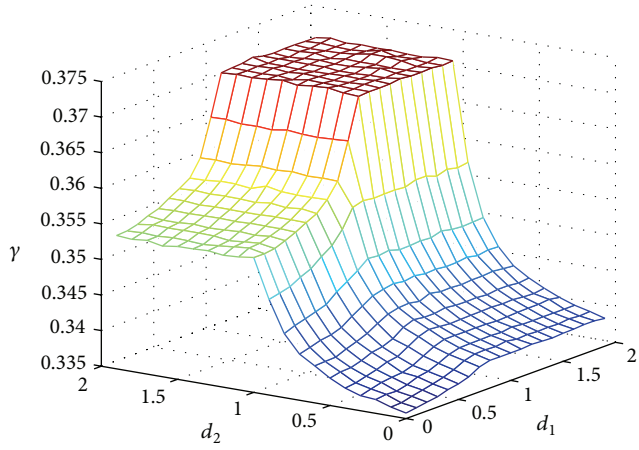

FIGURE 1: ℓ_2-ℓ_∞ gain bound from Theorem 4 with $h_1 = 0.5$ and $h_2 = 0.3$.

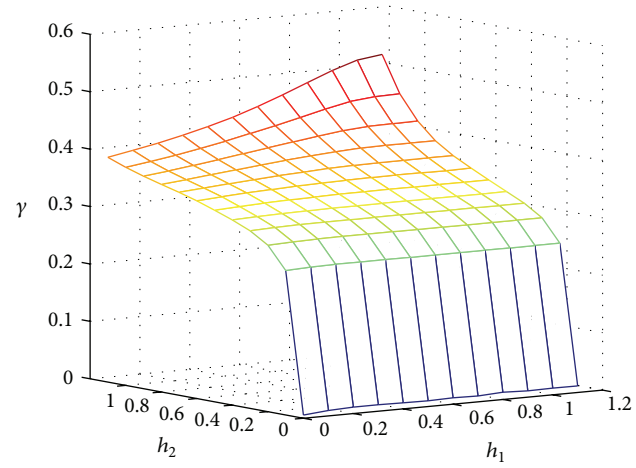

FIGURE 2: ℓ_2-ℓ_∞ gain bound from Theorem 4 with $d_1 = 0.4$ and $d_2 = 0.4$.

Therefore, we can solve the corresponding filter from (36) as

$$A_{f1} = \begin{bmatrix} -1.8241 & -0.4206 \\ 4.7259 & -2.7398 \end{bmatrix},$$

$$A_{f2} = \begin{bmatrix} -3.0858 & 0.8012 \\ -1.3706 & -0.9622 \end{bmatrix},$$

$$B_{f1} = \begin{bmatrix} -0.8829 \\ 1.3191 \end{bmatrix}, \quad (42)$$

$$B_{f2} = \begin{bmatrix} -0.3806 \\ 2.1781 \end{bmatrix}, \qquad C_{f1} = \begin{bmatrix} 0.8524 & -0.3426 \end{bmatrix},$$

$$C_{f2} = \begin{bmatrix} -0.2629 & 0.1428 \end{bmatrix}.$$

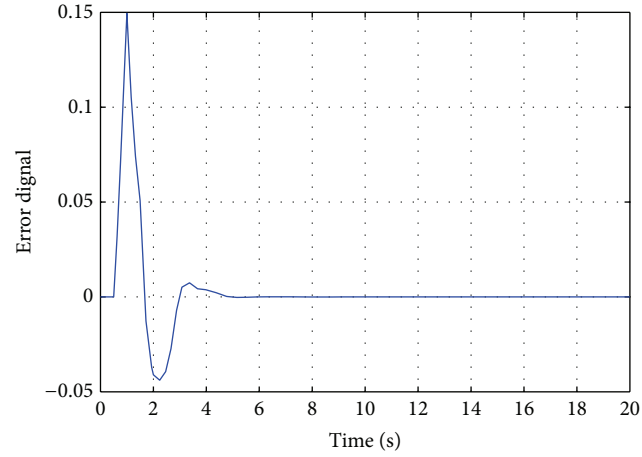

FIGURE 3: The signal $e(t)$.

To illustrate the performance of the designed filter, we assume zero initial condition and the disturbance $\omega(t)$ as follows:

$$\omega(t) = \begin{cases} 1, & 0.5 \le t \le 1 \\ -1, & 1.5 \le t \le 2 \\ 0, & \text{otherwise.} \end{cases} \quad (43)$$

The simulation result of signal $e(t)$ is given in Figure 3.

The resulting output ℓ_∞-norm of the filtering-error system is about 0.15, while $\|\omega(t)\|_2 = 1$. Simulation result for the ratio of the output ℓ_∞-norm to the disturbance ℓ_2-norm is 0.15, and $0.15 < \gamma = 0.5257$ with $h_1 = 1.1$, $h_2 = 1.1$, $d_1 = 0.4$, and $d_2 = 0.4$.

5. Conclusion

The problem on ℓ_2-ℓ_∞ filter design has been addressed for a class of TCS fuzzy-model-based systems with multiple time-varying delays. Based on the Lyapunov-Krasovskii functional approach and free-weighting matrix method, a sufficient condition for the existence of ℓ_2-ℓ_∞ filter, which stabilizes the T-S fuzzy-model-based filtering-error systems and guarantees a prescribed level on disturbance attenuation, has been obtained in terms of LMI form. The numerical example has shown the effectiveness of the proposed method. In addition, the basis-dependent Lyapunov-Krasovskii functional approach for filtering problems of T-S fuzzy delayed systems is also challenging, and could be our further work.

Acknowledgments

This work was supported in part by the National Natural Science Foundation of China (61203005), in part by Harbin Engineering University Central University Foundation Research Special Fund (HEUCFR1024), and in part by Postdoctoral Science-Research Developmental Foundation of Heilongjiang Province (LBH-Q12130) and Heilongjiang Province Natural Science Foundation (F201221).

References

[1] Y.-Y. Cao, Y.-X. Sun, and C. Cheng, "Delay-dependent robust stabilization of uncertain systems with multiple state delays," *IEEE Transactions on Automatic Control*, vol. 43, no. 11, pp. 1608–1612, 1998.

[2] H. Gao, J. Lam, C. Wang, and Y. Wang, "Delay-dependent output-feedback stabilization of discrete-time systems with time-varying state delay," *IEE Proceedings: Control Theory and Applications*, vol. 151, no. 6, pp. 691–698, 2004.

[3] L. Wu and W. X. Zheng, "Weighted $\mathscr{H}_\infty$ model reduction for linear switched systems with time-varying delay," *Automatica*, vol. 45, no. 1, pp. 186–193, 2009.

[4] P. Liu, "Delay-dependent robust exponential stabilization criteria for uncertain time-varying delay singular systems," *International Journal of Innovative Computing, Information and Control*, vol. 9, no. 1, pp. 165–178, 2013.

[5] L. Wu, X. Su, and P. Shi, "Sliding mode control with bounded ℓ_2 gain performance of Markovian jump singular time-delay systems," *Automatica*, vol. 48, no. 8, pp. 1929–1933, 2012.

[6] P. Shi, E.-K. Boukas, Y. Shi, and R. K. Agarwal, "Optimal guaranteed cost control of uncertain discrete time-delay systems," *Journal of Computational and Applied Mathematics*, vol. 157, no. 2, pp. 435–451, 2003.

[7] L. Wu, X. Su, P. Shi, and J. Qiu, "Model approximation for discrete-time state-delay systems in the T-S fuzzy framework," *IEEE Transactions on Fuzzy Systems*, vol. 19, no. 2, pp. 366–378, 2011.

[8] L. Wu, X. Su, P. Shi, and J. Qiu, "A new approach to stability analysis and stabilization of discrete-time T-S fuzzy time-varying delay systems," *IEEE Transactions on Systems, Man, and Cybernetics B*, vol. 41, no. 1, pp. 273–286, 2011.

[9] R. Yang, P. Shi, G.-P. Liu, and H. Gao, "Network-based feedback control for systems with mixed delays based on quantization and dropout compensation," *Automatica*, vol. 47, no. 12, pp. 2805–2809, 2011.

[10] Y.-Y. Cao and P. M. Frank, "Analysis and synthesis of nonlinear time-delay systems via fuzzy control approach," *IEEE Transactions on Fuzzy Systems*, vol. 8, no. 2, pp. 200–211, 2000.

[11] X. Song, J. Lu, S. Xu, H. Shen, and J. Lu, "Robust stabilization of state delayed T-S fuzzy systems with input saturation via dynamic anti-windup fuzzy design," *International Journal of Innovative Computing, Information and Control*, vol. 7, no. 12, pp. 6665–6676, 2011.

[12] L. Wu, X. Su, P. Shi, and J. Qiu, "Model approximation for discrete-time state-delay systems in the T-S fuzzy framework," *IEEE Transactions on Fuzzy Systems*, vol. 19, no. 2, pp. 366–378, 2011.

[13] L. Wu, X. Su, P. Shi, and J. Qiu, "A new approach to stability analysis and stabilization of discrete-time T-S fuzzy time-varying delay systems," *IEEE Transactions on Systems, Man, and Cybernetics B*, vol. 41, no. 1, pp. 273–286, 2011.

[14] F. Li and X. Zhang, "Delay-range-dependent robust $\mathscr{H}_\infty$ filtering for singular LPV systems with time variant delay," *International Journal of Innovative Computing, Information and Control*, vol. 9, no. 1, pp. 339–353, 2013.

[15] D. A. Wilson, "Convolution and Hankel operator norms for linear systems," *IEEE Transactions on Automatic Control*, vol. 34, no. 1, pp. 94–97, 1989.

[16] H. Gao and C. Wang, "Robust ℓ_2-ℓ_∞ filtering for uncertain systems with multiple time-varying state delays," *IEEE Transactions on Circuits and Systems I*, vol. 50, no. 4, pp. 594–599, 2003.

[17] Z. Wang and F. Yang, "Robust filtering for uncertain linear systems with delayed states and outputs," *IEEE Transactions on Circuits and Systems I*, vol. 49, no. 1, pp. 125–130, 2002.

[18] J. Qiu, G. Feng, and J. Yang, "Improved delay-dependent $\mathscr{H}_\infty$ filtering design for discrete-time polytopic linear delay systems," *IEEE Transactions on Circuits and Systems II*, vol. 55, no. 2, pp. 178–182, 2008.

[19] J. Qiu, G. Feng, and J. Yang, "New results on robust $\mathscr{H}_\infty$ filtering design for discrete-time piecewise linear delay systems," *International Journal of Control*, vol. 82, no. 1, pp. 183–194, 2009.

[20] X. Chen, J. Lam, H. Gao, and S. Zhou, "Stability analysis and control design for 2-D fuzzy systems via basis-dependent Lyapunov functions," *Multidimensional Systems and Signal Processing*, pp. 1–21, 2011.

[21] X. Yao, L. Wu, W. X. Zheng, and C. Wang, "Robust $\mathscr{H}_\infty$ filtering of Markovian jump stochastic systems with uncertain transition probabilities," *International Journal of Systems Science*, vol. 42, no. 7, pp. 1219–1230, 2011.

[22] X. Yao, L. Wu, and W. X. Zheng, "Fault detection filter design for Markovian jump singular systems with intermittent measurements," *IEEE Transactions on Signal Processing*, vol. 59, no. 7, pp. 3099–3109, 2011.

[23] C. Lin, Q.-G. Wang, T. H. Lee, and B. Chen, "$\mathscr{H}_\infty$ filter design for nonlinear systems with time-delay through T-S fuzzy model approach," *IEEE Transactions on Fuzzy Systems*, vol. 16, no. 3, pp. 739–746, 2008.

[24] Y. Su, B. Chen, and C. Lin, "Delay-dependent $\mathscr{H}_\infty$ filtering for nonlinear systems via T-S fuzzy model approach," in *Proceedings of the Chinese Control and Decision Conference (CCDC '09)*, pp. 221–226, June 2009.

[25] J. Li, S. Zhou, L. Chai, and Y. Zhang, "$\mathscr{H}_\infty$ filter design for discrete-time-delay T-S fuzzy systems," in *Proceedings of the 16th IEEE International Conference on Control Applications, (CCA '07)*, pp. 1557–1560, October 2007.

[26] J. Qiu, G. Feng, and J. Yang, "A new design of delay-dependent robust $\mathscr{H}_\infty$ filtering for discrete-time T-S fuzzy systems with time-varying delay," *IEEE Transactions on Fuzzy Systems*, vol. 17, no. 5, pp. 1044–1058, 2009.

[27] H. Gao and C. Wang, "Delay-dependent robust $\mathscr{H}_\infty$ and ℓ_2-ℓ_∞ filtering for a class of uncertain nonlinear time-delay systems," *Institute of Electrical and Electronics Engineers*, vol. 48, no. 9, pp. 1661–1666, 2003.

[28] M. Chen, G. Feng, and H. Ma, "A delay-dependent approach to $\mathscr{H}_\infty$ filtering for fuzzy time-varying delayed systems," in *Proceedings of the IEEE International Conference on Fuzzy Systems (FUZZY '07)*, July 2007.

[29] H. Liu, C. Chen, X. Guan, and X. Wu, "$\mathscr{H}_\infty$ piecewise filtering for continuous T-S fuzzy systems with time delays," in *Proceedings of the IEEE International Conference on Fuzzy Systems (FUZZ '08)*, pp. 1012–1017, June 2008.

[30] G. Feng, "Robust $\mathscr{H}_\infty$ filtering of fuzzy dynamic systems," *IEEE Transactions on Aerospace and Electronic Systems*, vol. 41, no. 2, pp. 658–670, 2005.

[31] L. Wu and Z. Wang, "Fuzzy filtering of nonlinear fuzzy stochastic systems with time-varying delay," *Signal Processing*, vol. 89, no. 9, pp. 1739–1753, 2009.

[32] S. Lun, H. Zhang, and D. Liu, "Fuzzy $\mathscr{H}_\infty$ filtering of discrete-time nonlinear systems with multiple time delays," in *Proceedings of the 20th IEEE International Symposium on Intelligent Control, ISIC '05 and the13th Mediterranean Conference on Control and Automation (MED '05)*, pp. 1023–1028, June 2005.

[33] Y.-C. Lin and J.-C. Lo, "Robust mixed $\mathscr{H}_2/\mathscr{H}_\infty$ filtering for time-delay fuzzy systems," *IEEE Transactions on Signal Processing*, vol. 54, no. 8, pp. 2897–2909, 2006.

[34] H. Zhang, S. Lun, and D. Liu, "Fuzzy $\mathscr{H}_\infty$ filter design for a class of nonlinear discrete-time systems with multiple time delays," *IEEE Transactions on Fuzzy Systems*, vol. 15, no. 3, pp. 453–469, 2007.

[35] H. Zhang, C. Dang, and J. Zhang, "Decentralized fuzzy $\mathscr{H}_\infty$ filtering for nonlinear interconnected systems with multiple time delays," *IEEE Transactions on Systems, Man, and Cybernetics B*, vol. 40, no. 4, pp. 1197–1203, 2010.

[36] C. Gong and B. Su, "Robust ℓ_2-ℓ_∞ filtering of convex polyhedral uncertain time-delay fuzzy systems," *International Journal of Innovative Computing, Information and Control*, vol. 4, no. 4, pp. 793–802, 2008.

[37] Y. He, M. Wu, J.-H. She, and G.-P. Liu, "Parameter-dependent Lyapunov functional for stability of time-delay systems with polytopic-type uncertainties," *IEEE Transactions on Automatic Control*, vol. 49, no. 5, pp. 828–832, 2004.

Hindawi Publishing Corporation
Mathematical Problems in Engineering
Volume 2013, Article ID 874890, 11 pages
http://dx.doi.org/10.1155/2013/874890

Research Article

NN-Based Approximate Model Control for the EAF Electrode Regulator System

Hongge Zhao

Shandong Water Polytechnic, Rizhao 276826, China

Correspondence should be addressed to Hongge Zhao; lipower06@163.com

Received 25 May 2013; Revised 30 July 2013; Accepted 14 August 2013

Academic Editor: Zhiguang Feng

This paper proposes a robust adaptive neural network controller (RANNC) for electrode regulator system. According to the characteristics of electrode regulator system, an affine-like equivalent model is first derived. Then, the nonlinear control law is derived directly based on the affine-like equivalent model identified with neural networks, which avoids complex control development and intensive computation. The control scheme is simple enough that it can be implemented on an automotive microcontroller system, and the performance meets the system requirements. The stability of the system is established by the Lyapunov method. Several simulations illustrate the effectiveness of the controller.

1. Introduction

Electric arc furnaces (EAF) are widely used in the steel industry for melting scrap. The most important part of EAF is the electrode regulator system. Its performance affects not only the power utilisation efficiency of the furnace but also the electrode and refractory wear costs. A fast controller response is required to optimise the power utilisation efficiency, but where overshoot of the required electrode position is caused, the results are increased refractory and electrode wear and also, possibly, the injection of unwanted carbon into the steel in the case of a molten bath. Thus, the controller should be designed to meet the requirements of fast response without overshoot. However, the demands are difficult to accomplish since the electrode regulator system is burdened with strong nonlinearity and strong coupling among three phases. Moreover, the control strategy should be simple enough to be implemented on an automotive microcontroller system, while it has to be robust to plant parameter variations.

Several control strategies have been considered and/or applied to furnaces in the past few decades. As early as 1977, Billings and Nicholson proposed a temperature-weighting adaptive controller [1], which uses ambient arc temperature as an additional control parameter to weigh the error feedback. However, the conditions of continuous temperature measurement are not easy to achieve. Zhizhong and Jian pointed that the arc gain can be estimated by the energy applied into the furnace [2], to avoid the problem of continuous temperature measurement, and proposed an adaptive feedback controller for the electrode regulator system, but they did not give an expression for calculating the arc gain. Several of the existing control designs use a linear model of the process and derive a state feedback decoupling controller [3]; however, the controller is only effective around the operating points and has some limitations in the practical applications. Intelligent methods such as fuzzy control and neural network control were also applied in the electrode regulator system [4–9]. Staib et al. proposed to utilize the neural network to control the electrode, which can learn online during the smelt process [4, 5]. In [7–9], an adaptive inverse control algorithm based on RBF NN is presented, which identifies real-time decoupling by RBF NN online, but the control law computation is too much and needs a high-speed acquisition and processing system. Variable structure control with the sliding mode is an effective method for the control of the nonlinear plant with a parameter uncertainty, and it has also been applied in the electrode regulator system in [6]; however, the stability analysis of the closed-loop system was not given in [6]. In [10], a direct adaptive controller is designed. However, the computation is

too much and the control scheme is difficult to be applied in practice.

The principal aim of this paper is to present a practice-oriented robust adaptive neural network controller for electrode regulator system. The control strategy is achieved based on approximate model method and the Taylor expansion technology, which avoids complex control development and intensive computation. So, it is easily implemented in practice. Moreover, the decoupling among the three phases is also realized and the controller has a good performance with respect to parameters varying and falling scrap, which can be illustrated by simulation results.

The proposed controller is acceptable in engineering practice, as it can meet the following requirements. (1) The proposed control scheme is simple enough that it can be implemented on an automotive microcontroller system for practical application. (2) The performance of the closed-loop system satisfies the requirements, that is, a fast transient response without overshoot. (3) Robustness of the control system with respect to variations of process parameters is required, which can be caused by production deviations and variations of external conditions. (4) Stability of the closed-loop system is rigorously established.

This paper is organized as follows. In Section 2, the nonlinear discrete-time dynamics of electrode regulator system is derived. In Section 3, the input-output approximate model is directly derived via the Taylor expansion and nonlinear control law is implemented using NRBFNN modeling. In Section 4, the robustness of the stability is rigorously established by the Lyapunov method. Finally, several simulations and experiments are presented to illustrate the effectiveness of the proposed nonlinear controller.

2. Model Construction

As shown in Figure 1, the electrode regulator system of EAF consists of controller, hydraulic system, and EAF main circuit. In this paper, the hydraulic system and the EAF main circuit are considered to be a generalized plant.

2.1. Hydraulic System. Since we focus on the electrode regulator system, the hydraulic system of EAF is approximated as a third-order system as in [10, 11]. The transfer function can be written as

$$G_s(s) = \frac{b_0 s + b_1}{a_0 s^3 + a_1 s^2 + a_2 s}. \tag{1}$$

2.2. EAF Main Circuit. A typical power supply system of EAF consists of high-voltage power distribution system, EAF transformer, short net, and electric arc. The equivalent circuit of main circuit is presented in Figure 2, where $\dot{U}_j$, $(j = A, B, C)$ is the primary voltage, $\dot{U}_j$, $(j = a, b, c)$ is the secondary voltage, $\dot{I}_j$, $(j = A, B, C)$ is the primary current, $\dot{I}_j$, $(j = a, b, c)$ is the secondary current, R_d is the short net resistance, X_d is the short net reactance, and Z_{jarc}, $(j = a, b, c)$ is the impedance of the arc. In the furnace there is also electrical conduction between the electrodes. However, according to [12], these currents are nearly 1% of the phase currents and we focus on the electrode regulator system. So, these mutual inductances will be neglected for simplicity, and we assume that the parameters of the three phases are the same to each other.

In order to obtain a simpler arc model, Köhle proposed to represent the arc as an equivalent linear circuit element constituted by a resistive and a reactive part [13]. In his model, Köhle defines the arc reactance X_L as a function of its resistance as follows: $X_L = aR_L + bR_L^2$, where the first term represents the influences of low frequency fluctuations and the second represents the influences of harmonics. The values of a and b vary during the melting process.

The primary coils and the secondary coils of the EAF transformer are star connected and delta connected, respectively (as shown in Figure 2). According to the Kirchoff's law, we can obtain the electrode-to-neutral currents as follows:

$$\begin{aligned} i_a &= \left\| \frac{\dot{U}_A\left(Z_k/3n - nZ_b\right) - \dot{U}_B\left(Z_k/3n - nZ_c\right)}{Z_{Kabc}} \right\|, \\ i_b &= \left\| \frac{\dot{U}_B\left(Z_k/3n - nZ_c\right) - \dot{U}_C\left(Z_k/3n - nZ_a\right)}{Z_{Kabc}} \right\|, \\ i_c &= \left\| \frac{\dot{U}_C\left(Z_k/3n - nZ_a\right) - \dot{U}_A\left(Z_k/3n - nZ_b\right)}{Z_{Kabc}} \right\|, \end{aligned} \tag{2}$$

where $Z_{Kabc} = (Z_k/3n - nZ_a)(Z_k/3n - nZ_b) + (Z_k/3n - nZ_a)(Z_k/3n - nZ_c) + (Z_k/3n - nZ_b)(Z_k/3n - nZ_c)$, $Z_j = R_d + jX_d + l_j R_{\text{per}} + j(al_j R_{\text{per}} + b(l_j * R_{\text{per}})^2)$, $(j = a, b, c)$. R_d is the short net resistance, X_d is the short net reactance, and n is the transformer ratio.

By using the n-order approximation method [14], one has $Ti_j^{(1)} = i_j(k+1) - i_j(k)$, $T^2 i_j^{(2)} = i_j(k+1) - 2i_j(k) + i_j(k-1)$, $T^3 i_j^{(3)} = i_j(k+1) - 3i_j(k) + 3i_j(k-1) - i_j(k-2)$, $(j = a, b, c)$ with T being the sampling period. This way, according to (1) and (2), the generalized control plant can be described in the discrete system as

$$i(k+1) = f\left[\omega(k), u(k)\right], \tag{3}$$

where $i(k+1) = [i_a(k+1), i_b(k+1), i_c(k+1)]^T$, $\omega(k) = [i_a(k), i_a(k-1), i_a(k-2), i_b(k), i_b(k-1), i_b(k-2), i_c(k), i_c(k-1), i_c(k-2)]^T$, $u(k) = [u_a(k), u_b(k), u_c(k)]^T$, and $f(\cdot) = [f_a(\cdot), f_b(\cdot), f_c(\cdot)]^T$, where $f(\cdot)$ is a vector-valued nonlinear function and $f_j(\cdot)$, $(j = a, b, c)$ is regarded as nonlinear mapping.

3. Control Strategy Design

In this section, a novel nonlinear controller is proposed based on the approximate method, which avoids complex control development and intensive computation.

3.1. Analysis of the Controlled Object. As $\|Z_{Kabc}\| > 0$ always holds for Z_{Kabc} in (2), it is easy to validate that f_j, $(j = a, b, c)$

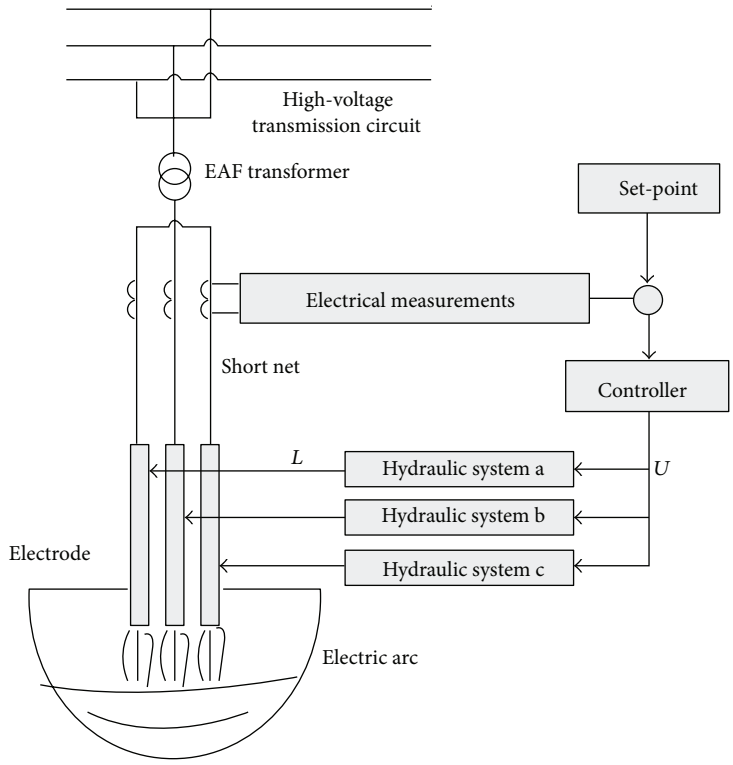

Figure 1: Schematic diagram of EAF electrode regulator system.

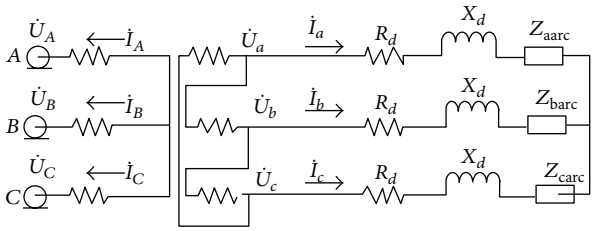

Figure 2: Schematic diagram of EAF main circuit.

is derivable. For the nonlinear autoregressive moving average (NARMA) model (3), a Taylor expansion of the plant gives

$$\begin{aligned} i_j(k+1) = {} & f_j\left[\omega(k-1), u_j(k-1)\right] \\ & + \sum \frac{1}{r!} \frac{\partial^r f_j\left[\omega(k-1), u_j(k-1)\right]}{\partial u_j^r(k-1)} \left[\Delta u_j(k)\right]^r \\ & + \sum \frac{1}{r!} \frac{\partial^r f_j\left[\omega(k-1), u_j(k-1)\right]}{\partial \omega^r(k-1)} \left[\Delta\omega(k)\right]^r, \end{aligned} \tag{4}$$

where $\Delta u_j(k) = u_j(k) - u_j(k-1)$, $\Delta\omega(k) = \omega(k) - \omega(k-1)$, and $(j = a, b, c)$.

The output $i_j(k+1)$ is highly sensitive to control input $u_j(k)$ in the operating region; that is, [15],

$$\begin{aligned} & \left| \frac{\partial f_j\left[\omega(k-1), u_j(k-1)\right]}{\partial u_j(k-1)} \right| \\ & \gg \left| \left(\sum \frac{1}{r!} \frac{\partial^r f_j\left[\omega(k-1), u_j(k-1)\right]}{\partial \omega^r(k-1)} \right.\right. \\ & \left.\left. \times \left[\Delta\omega(k)\right]^r \right) \times \left(\Delta u_j(k)\right)^{-1} \right|, \end{aligned} \tag{5}$$

where Δ is the increment operator.

From (5), we can drop the third term on the right-hand side of (4) to represent model (3) by

$$\begin{aligned} i_j(k+1) = {} & i_j(k) + f_j^1(k)\,\Delta u_j(k) \\ & + R_j\left[\omega(k-1), u_j(k-1), \Delta u_j(k)\right], \end{aligned} \tag{6}$$

where $f_j^1(k) = \partial f_j[\omega(k), u_j(k)]/\partial u_j(k)|_{u_j(k)=u_j(k-1),\,\omega(k)=\omega(k-1)}$, $(j = a, b, c)$.

Theorem 1 (see [16]). *The remainder term $R_j[\omega(k-1), u_j(k-1), \Delta u_j(k)]$ in (6) approaches zero at a faster rate than $\Delta u_j(k)$*

approaches zero, and there exists a variable $\tau_j(k) \in (0, +\infty]$ *such that*

$$\left| \frac{R_j\left[\omega(k-1), u_j(k-1), \Delta u_j(k)\right]}{\Delta u_j(k-1)} \right| \ll \left| f_j^1(k) \right|, \quad (7)$$

whenever $|\Delta u_j(k)| \in [0, \tau_j(k)]$, $(j = a, b, c)$.

According to the Taylor expansion theory, as $|\Delta u_j(k)| \in [0, \tau_j(k)]$, then the remainder $R_j(k)$ in (6) is bounded as follows: $|R_j(k)| \le 1/2 R_j^0 \tau_j^2(k)$, with R_j^0 being a finite positive number. From (4)–(7), the input-output approximate model of the plant can be derived by neglecting the term $R_j(k)$, and thus, (3) can be simplified into

$$i_j(k+1) = i_j(k) + f_j^1(k)\,\Delta u_j(k) \quad (j = a, b, c). \quad (8)$$

From (8), the control law can be determined directly since the increment $\Delta u_j(k)$ of the control signal appears linearly. Before the computation of the control law, an assumption is given.

Assumption 2. Controller output is bounded; that is, $|\Delta u_j(k)| \le \delta_j(k)$ with $\delta_j(k)$ being a finite positive number, which considers constraints on physical variable.

Remark 3. According to Assumption 2, $\Delta u_j(k)$ should not be too large in order to limit the approximation error of (8). In electrode regulator system, this is reasonable because the output of the hydraulic system (actuator) cannot change too fast within a small time interval.

3.2. Derivation of Control Law. From (8), it requires precise information about $f_j^1(k)$ to compute $u_j(k)$. However, $f_j^1(k)$ exists but is unknown. In order to get the nonlinear function $f_j^1(k)$, a normalized radial basis function neural network (NRBFNN) is used to identify the input-output representation model (3) at first. And then, the nonlinear function $f_j^1(k)$ can be estimated from the NN model and is referred to as $\hat{f}_j^1(k)$.

Evolved from radial basis function neural network (RBFNN), the NRBFNN has the same structure as shown in Figure 3. For the NARMA model (3), the output of the NRBFNN is

$$\begin{aligned} \hat{i}_j(k+1) &= \overline{nn}\left(\omega(k), u_j(k)\right) \\ &= \Theta^T \Phi(x) = \sum_{i=1}^{L} \theta_i \phi_i(x), \end{aligned} \quad (9)$$

where $x = [\omega^T(k), u_j(k)]$ is the input vector, $\Theta = [\theta_1 \cdots \theta_L]^T$ is the weight vector, and $\Phi(x) = [\phi_1(x) \cdots \phi_L(x)]^T$ with $\phi_i(x)$ being a normalized activation function to node i and being expressed as follows

$$\phi_i(x) = \frac{\exp\left(-\|x - C_i\|^2 / 2s^2\right)}{\sum_{j=1}^{L} \exp\left(-\|x - C_i\|^2 / 2s^2\right)}, \quad (10)$$

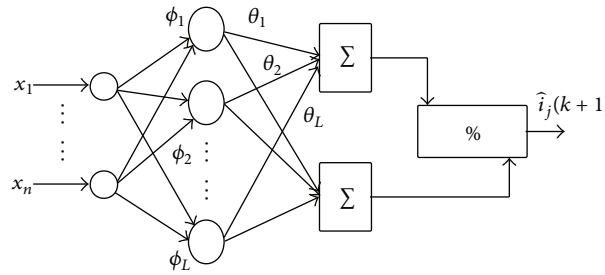

Figure 3: Structure of an NRBFNN.

where $C_i = [c_{i1} \cdots c_{in}]$ denotes the centroid vector, L denotes the NN node number, and s is the spread. The NRBFNN can improve function approximation with a minimal number of weights [17]. In (10), the kernel function is very similar to RBF neural network, except that the kernel output is divided by the sum of all the kernel outputs. Therefore, the outputs of all the kernels add up to one; that is, $\sum_{i=1}^{L} \phi_i(x) = 1$. As the output of every hidden node is less than 1, we can get that the hidden output vector has the properties $0 < \|\Phi(x)\| \le 1$. These properties will be used in Section 4 for the stability analysis of the closed-loop system.

To formulate a well-posed adaptive control problem, we make the following assumptions. Similar assumptions are used in [18, 19].

Assumption 4 (see [15]). An optimal weight vector Θ_j^o for a trained NRBFNN exists, and the corresponding optimal estimation error $e_j^o(k) = \hat{i}_j^o(k) - i_j(k)$ has a known finite upper bound $[e_j^o]_{\max}$, accordingly

$$\left| \hat{i}_j^o(k) - i_j(k) \right| = \left| e_j^o(k) \right| < \left[e_j^o \right]_{\max}. \quad (11)$$

Remark 5. The NRBFNN has been theoretically proven to be capable of universal approximation in a satisfactory sense [20]. Assumption 4 shows that a perfect function estimation can be achieved if enough radial basis functions are used. However, more hidden nodes means more computation. There should be a trade-off between the computation burden and approximation errors. In the electrode regulator system, 20 hidden nodes can meet the requirement of the estimation errors.

The parameter update rule must be robust with respect to modeling errors because these errors can prevent the convergence of the weights of the neural network and thereby destabilize the closed-loop system. One of the approaches to ensure convergence of neural network weights is through a "deadzone," which suspends parameter adaption whenever estimation error becomes small. The corresponding weights updated law as follows:

$$\Theta_j(k+1) = \Theta_j(k) - \rho_j(k)\,\eta_j(k) \left[\frac{e_j(k+1)\,\Phi_j(k)}{1 + \left\|\Phi_j(k)\right\|^2} \right], \quad (12)$$

where $\rho_j(k)$ is the adaptive rate, and $0 < \rho_j(k) \leq [\rho_j]_{\max} < 2$, and

$$\eta_j(k) = \begin{cases} 1, & \text{if } \left|e_j(k+1)\right| > \dfrac{2\left[e_j^o\right]_{\max}}{2 - \left[\rho_j\right]_{\max}}, \\ 0, & \text{otherwise.} \end{cases} \quad (13)$$

We have a gradient descent parameter update rule with a deadzone, where $e_j(k+1)$ is the estimation error at the time $k+1$ and $e_j(k+1) = \widehat{i}_j(k+1) - i_j(k+1)$. Their other parameters such as centroids and spreads can be found in [18, 19] and thus are not discussed here.

Based on the NRBFNN model (9), we can get $\widehat{f}_j^1(k)$; that is,

$$\widehat{f}_j^1(k) = \left.\frac{\partial \overline{nn}\left[\omega(k), u_j(k)\right]}{\partial u_j(k)}\right|_{u_j(k)=u_j(k-1),\, \omega(k)=\omega(k-1)}. \quad (14)$$

And according to Assumptions 2 and 4, the control law can be determined straigthforwardly from (8) as follows:

$$u_j(k) = u_j(k-1) + \Delta u_j(k), \quad (j = a, b, c), \quad (15)$$

where

$$\Delta u_j(k) = \frac{r_j(k+1) - i_j(k)}{\left[\widehat{f}_j^1(k)\right]^2 + \alpha}\widehat{f}_j^1(k) \quad \text{if } \left|\Delta u_j(k)\right| \leq \delta_j,$$
$$\Delta u_j(k) = \delta_j \operatorname{sign}\left|\Delta u_j(k)\right| \quad \text{if } \left|\Delta u_j(k)\right| > \delta_j, \quad (16)$$

where α and δ_j are given finite positive constants and $r_j(k)$ is the reference current.

Define the tracking error at the time k as

$$\left[e_c\right]_j(k) = r_j(k) - i_j(k), \quad (j = a, b, c). \quad (17)$$

4. Stability Analysis of RANNC

Stability and performance of the closed-loop system with NN adaptive control (15) and weight updating law (12) are given in Theorem 6.

Theorem 6. *For given $|r_j(k) - r_j(k-1)| \leq \Delta r$, using the NN control law* (15) *with NN weight updating law* (12)*, then the solution of the error system* (17) *is uniformly ultimately bounded (UUB) [21] for all k with ultimate bound $\lim_{k\to\infty}|[e_c]_j(k)| \leq (k_2/(1-k_1))$, where $k_1 = |(1 - s_j(k)([\widehat{f}_j^1(k)]^2/([\widehat{f}_j^1(k)]^2+\alpha)))|$ and $k_2 = k_1 \cdot r_0 + 2[e_j^o]_{\max}/(2 - [\rho_j]_{\max})$, in which $0 < s_j(k) \leq 1$, α, r_0, $[e_j^o]_{\max}$ and $[\rho_j]_{\max}$ are the same as those defined above, $(j = a, b, c)$.*

Proof. See Appendix. □

5. Simulations and Experiment

5.1. Simulations. This section shows the MATLAB simulations of the proposed approximate model control strategy on the electrode regulator system. The parameter values are selected as follows.

(1) Hydraulic system: $b_0 = 5$, $b_1 = 95$, $a_0 = 1$, $a_1 = 9$, and $a_2 = 110$.

(2) EAF transformer: $\dot{U}_A = 35000\,\text{V}$, $\dot{U}_B = \dot{U}_A e^{-j(2/3)\pi}$, $\dot{U}_C = \dot{U}_A e^{j(2/3)\pi}$, $Z_K = (0.0069 + j0.076)\,\Omega$, and $n = 80$.

(3) Electric arc: $a = 0.12$, $b = 0.02$, and $R_{\text{per}} = 0.000058\,\Omega/\text{mm}$.

(4) Short net: $(Z_d = 0.0003 + j8.3292e - 006)\Omega$.

(5) Controller parameters: $\alpha = 0.01$, $[e_j^0]_{\max} = 50\,\text{A}$, $\delta_j = 3.5\,\text{V}$, $\rho_j = 1$, and $s = 0.6$.

Here, three controllers' (including the PID controller (PIDC), inverse neural network controller (INNC), Robust adaptive neural network controller (RANNC)) capability of following set-point, restraining parameters varying and falling scrap is studied by simulation.

There are strong coupling among three phases in the electrode regulator system. To validate the decoupling performance of the proposed controller, several set-point trackings are performed with different operating points and reference changes. Figure 4 shows the simulation results of the current A and current B. We can know from figures that the RANNC is better in respect of tracking the set value, and the current B is almost not influenced by the changes of current A. Approximate decoupling is realized. When the PIDC and INNC are used, the system has slower response and larger overshoot, and its performance is worse than RANNC.

In the smelting process, production deviation and variations of external condition can cause the variation of process parameters, and falling scrap is also common. In order to make the proposed control strategy more acceptable in practice, we simulate these situations and the parameters change at 25 s and 50 s, respectively. The simulation results are illustrated in Figure 5. We can know from figures that the RANNC preserves important performance measures, like fast response, the little overshoot, and accuracy within the measurement resolution.

Three phase electrodes discharge to molten steel, forming star connection, so there are strong coupling among three phases. In PIDC system, there is three controllers for three phases individually and the coupling effects are not considered. The performance of INNC is better than that of PIDC as the coupling effects are regarded as disturbances in INNC system. However, the complete decoupling is still not achieved. In RANNC system, the control law is directly derived from the approximate model, which fully reflects the coupling effects among the three phases. Approximate complete decoupling can be realized. From Figures 4 and 5, we can get that the performance of the RANNC is better than that of PIDC and INNC.

5.2. Experiment. The experiment apparatus is shown in Figure 6, and our robust adaptive neural network controller is implemented on SIEMENS CPU414-2. The parts of the experiment system include arc model Machine, programmer, HMI, electrode PLC, master PLC, and other models Machine, and they communicate via industry ethernet. Long-distance

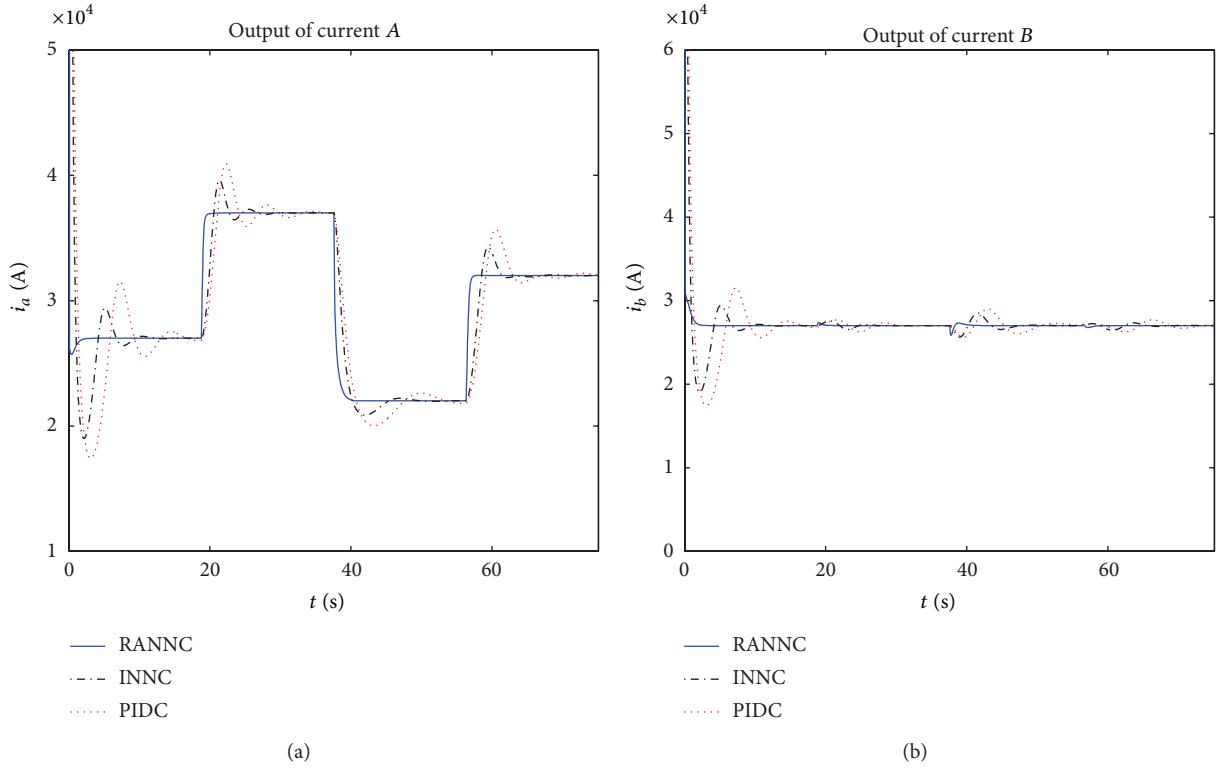

Figure 4: Comparison of decoupling control.

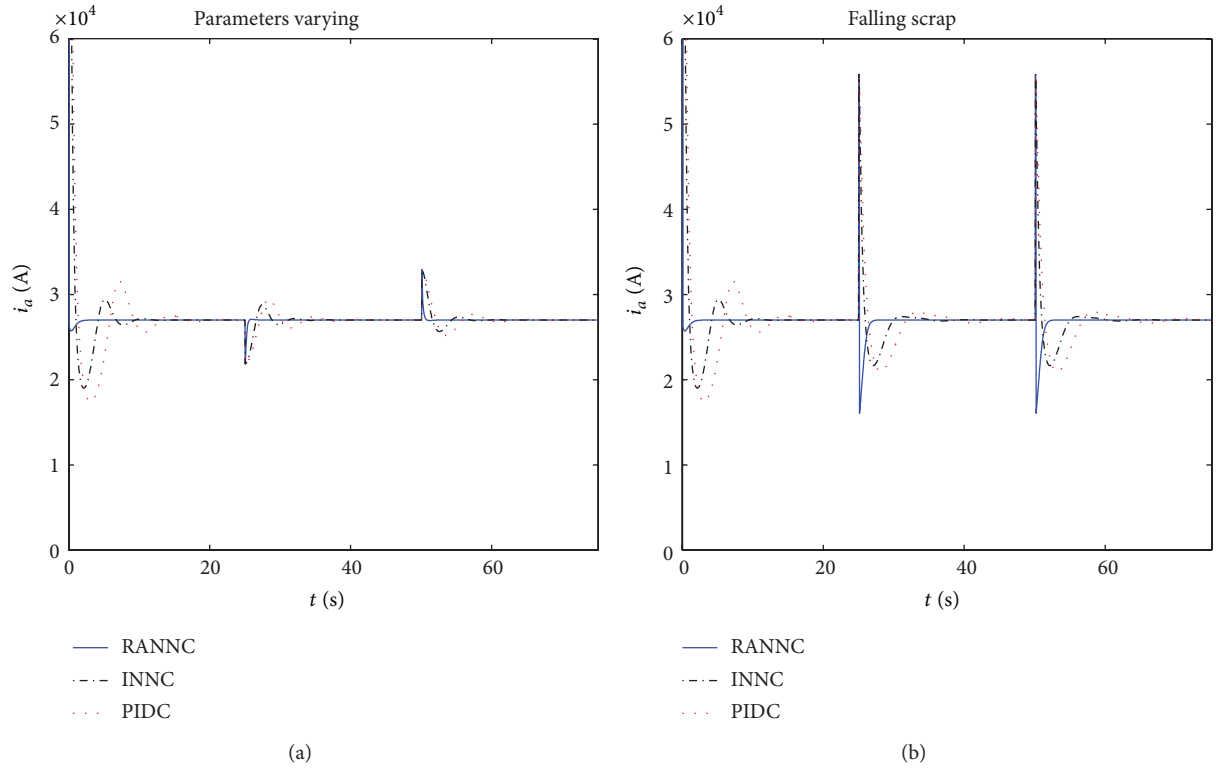

Figure 5: Comparison of robustness and falling scrap.

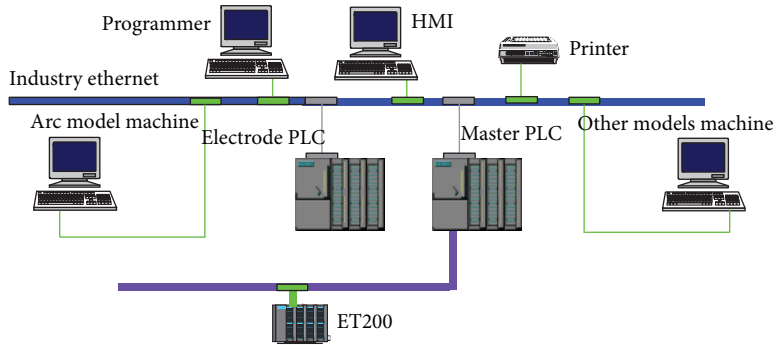

Figure 6: Schematic diagram of EAF electrode system.

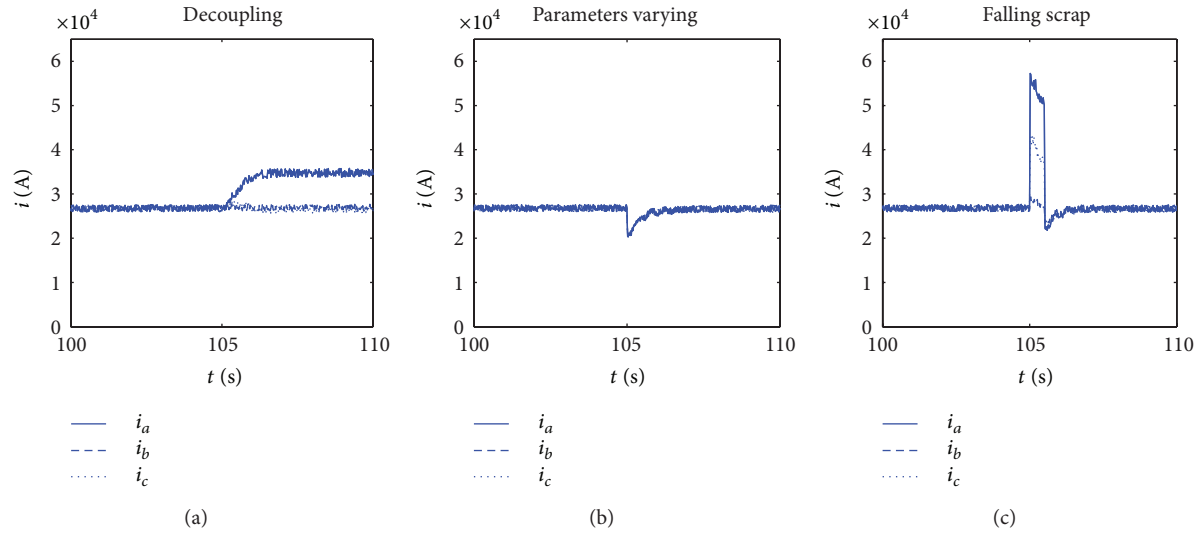

Figure 7: Output of the currents.

I/O interface ET200M is connected with Master PLC with Profibus DP. The power module is PS407, and the analog input module and analog output module are AI431 and AO432; digital input module and digital output module are DI321 and DO322, respectively. Similar to the simulations, we verify the effectiveness of the controller via decoupling performance, robustness, and antidisturbance ability. The results are shown in Figure 7.

The corresponding parameters are changed at 105 s. Figure 7 shows experimental results of the three phase currents when only RANNC is used. As is shown in Figure 7, the RANNC has a good performance, that is, faster response and smaller overshoot, which means more power utilisation efficiency and less refractory and electrode wear. From the experiments, we can come to the following conclusions.

(i) As the coupling effects by other two phases are considered in the approximate model, the coupling among three phases is decreased greatly. Real-time decoupling and control scheme are realized for the electrode regulator system.

(ii) In our proposed controller, small nodes of NRBFNN are chosen, which renders our control scheme possible application in real-time control of electric arc furnace.

6. Conclusion

Many nonlinear discrete systems can be described by NARMA model. In this paper, a generalized model for electrode regulator system on NARMA form is established. With a novel I/O approximation proposed for the NARMA model, a robust adaptive controller is derived directly from the approximation being and it can be implemented straightforwardly by using neural network. The controller design method can be also applied on other systems such as electronic throttle valve and distributed curing process etc., in which the approximation model can be derived by the similar procedure. The design of the proposed nonlinear controller is simple and practical. Simulation results illustrate the good performance of this controller.

Appendix

We will prove, one by one in the order of the NN weights, the estimation error and the tracking error are bounded.

(1) Boundedness of the weights: Choose a Lyapunov candidate $V_j(k, \widetilde{\Theta}_j(k)) = \widetilde{\Theta}_j^T(k)\widetilde{\Theta}_j(k)$, where $\widetilde{\Theta}_j(k) = \Theta_j(k) - \Theta_j^o$, Θ_j^o is the optimal weight vector as in Assumption 4; then

$$\begin{aligned}\Delta V_j\left(k+1, \widetilde{\Theta}_j(k+1)\right) &= V_j\left(k+1, \widetilde{\Theta}_j(k+1)\right) - V\left(k, \widetilde{\Theta}_j(k)\right) \\ &= \widetilde{\Theta}_j^T(k+1)\,\widetilde{\Theta}_j(k+1) - \widetilde{\Theta}_j^T(k)\,\widetilde{\Theta}_j(k).\end{aligned} \tag{A.1}$$

According to [15]

$$\begin{aligned}\Delta V_j\left(k+1, \widetilde{\Theta}_j(k+1)\right) &= 2\widetilde{\Theta}_j^T(k)\cdot\left[\Delta\widetilde{\Theta}_j(k+1)\right] \\ &\quad + \left[\Delta\widetilde{\Theta}_j(k+1)\right]^T\cdot\Delta\widetilde{\Theta}_j(k+1),\end{aligned} \tag{A.2}$$

where $\Delta\widetilde{\Theta}_j(k+1) = \widetilde{\Theta}_j(k+1) - \widetilde{\Theta}_j(k)$, and from (12), we get

$$\Delta\widetilde{\Theta}_j(k+1) = -\rho_j(k)\,\eta_j(k)\left[\frac{e_j(k+1)\,\Phi_j(k)}{1+\left\|\Phi_j(k)\right\|^2}\right]. \tag{A.3}$$

Note that the estimation error is

$$\begin{aligned}e_j(k+1) &= \hat{i}_j(k+1) - i_j(k+1) \\ &= \widetilde{\Theta}_j^T(k)\cdot\Phi_j(k) + e_j^o(k+1).\end{aligned} \tag{A.4}$$

We consider two cases associated with (A.3) separately.

Case 1 ($|e_j(k+1)| \le 2[e_j^o]_{\max}/(2-[\rho_j]_{\max})$). Equation (A.3) implies $\widetilde{\Theta}_j(k+1) = \widetilde{\Theta}_j(k)$, therefore, $\Delta V_j(k+1, \widetilde{\Theta}_j(k+1)) = 0$.

Case 2 ($|e_j(k+1)| > 2[e_j^o]_{\max}/(2-[\rho_j]_{\max})$). Equation (A.3) implies

$$\begin{aligned}\Delta\widetilde{\Theta}_j(k+1) &= \widetilde{\Theta}_j(k+1) - \widetilde{\Theta}_j(k) \\ &= -\rho_j(k)\left[\frac{e_j(k+1)\,\Phi_j(k)}{1+\left\|\Phi_j(k)\right\|^2}\right].\end{aligned} \tag{A.5}$$

From (A.4)

$$\widetilde{\Theta}_j^T(k)\cdot\Phi_j(k) = e_j(k+1) - e_j^o(k+1). \tag{A.6}$$

Therefore, substituting for $\widetilde{\Theta}_j^T(k)$ and $\Delta\widetilde{\Theta}_j(k+1)$ in (A.2) gives

$$\begin{aligned}&\Delta V_j\left(k+1, \widetilde{\Theta}_j(k+1)\right) \\ &\quad= 2\left[e_j(k+1) - e_j^o(k+1)\right]\cdot\left[-\rho_j(k)\,\frac{e_j(k+1)}{1+\left\|\Phi_j(k)\right\|^2}\right] \\ &\qquad+\left[-\rho_j(k)\,\frac{e_j(k+1)\,\Phi_j(k)}{1+\left\|\Phi_j(k)\right\|^2}\right] \\ &\qquad\cdot\left[-\rho_j(k)\,\frac{e_j(k+1)\,\Phi_j(k)}{1+\left\|\Phi_j(k)\right\|^2}\right].\end{aligned} \tag{A.7}$$

This implies

$$\begin{aligned}&\Delta V_j\left(k+1, \widetilde{\Theta}_j(k+1)\right) \\ &\quad= -\rho_j(k)\left[\frac{e_j^2(k+1)}{1+\left\|\Phi_j(k)\right\|^2}\right] \\ &\qquad\cdot\left[2\left(1-\frac{e_j^o(k+1)}{e_j(k+1)}\right) - \rho_j(k)\,\frac{\left\|\Phi_j(k)\right\|^2}{1+\left\|\Phi_j(k)\right\|^2}\right].\end{aligned} \tag{A.8}$$

Using the fact that $|e_j(k+1)| > 2[e_j^o]_{\max}/(2-[\rho_j]_{\max})$ and $0 < \rho_j(k) \le [\rho_j]_{\max} < 2$, simple algebraic manipulations of (A.8) can be used to show that $\Delta V_j(k) \le 0$.

Clearly, the system must operate under Cases 1 or 2 or alternate between both cases. Since $\Delta V_j(k) \le 0$, for Cases 1 and 2, then $\Delta V_j(k) \le 0$ for $k = 0, 1, 2, \ldots$. This implies

$$V_j\left(k, \widetilde{\Theta}_j(k)\right) = \left\|\widetilde{\Theta}_j(k)\right\|^2 \le \left\|\widetilde{\Theta}_j(0)\right\|^2, \quad \text{for } k = 0, 1, 2, \ldots. \tag{A.9}$$

This proves that $\widetilde{\Theta}_j(k)$ is uniformly bounded. Since $\|\widetilde{\Theta}_j(k)\|$ is uniformly bounded and $\widetilde{\Theta}_j(k) = \Theta_j(k) - \Theta_j^o$, where Θ_j^o is a constant, then $\|\Theta_j(k)\|$ is uniformly bounded.

(2) Boundedness of the estimation error: since $V_j(k, \widetilde{\Theta}_j(k))$ converges

$$\lim_{k\to\infty}\Delta V_j\left(k, \widetilde{\Theta}_j(k)\right) = 0. \tag{A.10}$$

Clearly, this can only happen if there exists some k_0, such that

$$\left|e_j(k+1)\right| \le \frac{2\left[e_j^o\right]_{\max}}{2-\left[\rho_j\right]_{\max}}, \quad \text{for } k = k_0, k_0+1, k_0+2, \ldots. \tag{A.11}$$

This implies

$$\widetilde{\Theta}_j(k+1) = \widetilde{\Theta}_j(k), \quad \text{for } k = k_0, k_0+1, k_0+2, \ldots \tag{A.12}$$

which, in turn, implies

$$\Delta V_j\left(k, \widetilde{\Theta}_j(k)\right) = 0, \quad \text{for } k = k_0, k_0+1, k_0+2, \ldots. \tag{A.13}$$

The fact that k_0 exists is proven by contradiction as shown below. If k_0 described above does not exist, we consider subsequence $t_k(i), i = 1, 2, \ldots$ of instants $k = 0, 1, 2, \ldots$, when weights of the neural network are updated; that is,

$$t_k = \left\{ k : \left|e_j(k+1)\right| > \frac{2\left[e_j^0\right]_{\max}}{2 - \left[\rho_j(k)\right]_{\max}} \right\}. \tag{A.14}$$

Under this case,

$$\begin{aligned}
&\Delta V_j\left(t_k+1, \widetilde{\Theta}_j(t_k+1)\right) \\
&\quad = -\rho_j(k)\left[\frac{e_j^2(t_k+1)}{1+\left\|\Phi_j(t_k)\right\|^2}\right] \\
&\qquad \cdot \left[2\left(1 - \frac{e_j^o(t_k+1)}{e_j(t_k+1)}\right) - \rho_j(k)\frac{\left\|\Phi_j(t_k)\right\|^2}{1+\left\|\Phi_j(t_k)\right\|}\right].
\end{aligned} \tag{A.15}$$

From (A.8),

$$\begin{aligned}
V_j\left(r, \widetilde{\Theta}_j(r)\right) &= V_j\left(0, \widetilde{\Theta}_j(0)\right) \\
&\quad + \sum_{k=1}^{r} -\rho_j(k)\left[\frac{e_j^2(k+1)}{1+\left\|\Phi_j(k)\right\|^2}\right] \\
&\qquad \cdot \left[2\left(1 - \frac{e_j^o(k+1)}{e_j(k+1)}\right)\right. \\
&\qquad\quad \left. -\rho_j(k)\frac{\left\|\Phi_j(k)\right\|^2}{1+\left\|\Phi_j(k)\right\|}\right] \\
&\le V_j\left(0, \widetilde{\Theta}(0)\right) \\
&\quad - \lambda\sum_{k=1}^{r}\left[\frac{e_j^2(k+1)}{1+\left\|\Phi_j(k)\right\|^2}\right] \quad \text{for } \lambda > 0.
\end{aligned} \tag{A.16}$$

Hence

$$\sum_{k=1}^{r}\frac{e_j^2(k+1)}{1+\left\|\Phi_j(k)\right\|^2} \le \frac{1}{\lambda}\left[V\left(0, \widetilde{\Theta}_j(0)\right) - V\left(r, \widetilde{\Theta}_j(r)\right)\right]. \tag{A.17}$$

When $r \to \infty$, we get

$$\sum_{k=1}^{\infty}\frac{e_j^2(k+1)}{1+\left\|\Phi_j(k)\right\|^2} < \infty. \tag{A.18}$$

In other words, sequence $e_j^2(k+1)/(1+\|\Phi_j(k)\|^2)$ converges. Normalized error $e_j(k+1)/\sqrt{1+\|\Phi_j(k)\|^2}$ is squared summable, and it follows that

$$\lim_{k\to\infty}\frac{e_j^2(k+1)}{1+\left\|\Phi_j(k)\right\|^2} = 0. \tag{A.19}$$

Then, from $0 < \|\Phi_j(k)\|^2 \le 1$, this implies

$$\frac{e_j^2(k+1)}{1+1} \le \frac{e_j^2(k+1)}{1+\left\|\Phi_j(k)\right\|^2} \tag{A.20}$$

or

$$e_j^2(k+1) \le 2\frac{e_j^2(k+1)}{1+\left\|\Phi_j(k)\right\|^2}. \tag{A.21}$$

In the limit as $k \to \infty$, the right-hand side of (A.21) converges zero which results in

$$\lim_{k\to\infty} e_j(k) = 0. \tag{A.22}$$

This conclusion clearly contradicts the assumption that $|e_j(t_k+1)| > 2[e_j^o]_{\max}/(2 - [\rho_j]_{\max})$ for all t_k. Therefore, the only possibility is that an integer k_0 exists such that

$$\left|\widehat{i}_j(k+1) - i_j(k+1)\right| = \left|e_j(k+1)\right| \le \frac{2\left[e_j^o\right]_{\max}}{2 - \left[\rho_j\right]_{\max}} \tag{A.23}$$

for $k = k_0, k_0+1, k_0+2, \ldots$ which implies

$$\lim_{k\to\infty}\left|e_j(k)\right| = \lim_{k\to\infty}\left|\widehat{i}_j(k) - i_j(k)\right| \le \frac{2\left[e_j^o\right]_{\max}}{2 - \left[\rho_j\right]_{\max}}. \tag{A.24}$$

(3) Boundness of the tracking error: define a variable $s_j(k)$, where $0 < s_j(k) \le 1$ for all k. The control law (15) is equivalently expressed as

$$\Delta u_j(k) = s_j(k)\frac{r_j(k+1) - i_j(k)}{\left[\widehat{f}_j^1(k)\right]^2 + \alpha}\widehat{f}_j^1(k), \tag{A.25}$$

where $s_j(k) = 1$ if $|\Delta u_j(k)| < \delta_j$, and $0 < s_j(k) < 1$ if $|\Delta u_j(k)| > \delta$. Using (A.25), one has

$$\begin{aligned}
\left[e_c\right]_j(k+1) &= r_j(k+1) - i_j(k+1) \\
&= r_j(k+1) - i_j(k) - f_j^1(k)\Delta u_j(k)
\end{aligned}$$

$$
\begin{aligned}
&= r_j(k+1) - i_j(k) \\
&\quad - \widehat{f}_j^1(k)\,\Delta u_j(k) + e_j(k+1) \\
&= r_j(k+1) - i_j(k) \\
&\quad - s_j(k)\left[\widehat{f}_j^1(k)\right]^2 \frac{r_j(k+1) - i_j(k)}{\left[\widehat{f}_j^1(k)\right]^2 + \alpha} \\
&\quad + e_j(k+1) \\
&= \left(1 - s_j(k)\,\frac{\left[\widehat{f}_j^1(k)\right]^2}{\left[\widehat{f}_j^1(k)\right]^2 + \alpha}\right) \\
&\quad \times \left(r_j(k+1) - i_j(k)\right) + e_j(k+1) \\
&= \left(1 - s_j(k)\,\frac{\left[\widehat{f}_j^1(k)\right]^2}{\left[\widehat{f}_j^1(k)\right]^2 + \alpha}\right) \\
&\quad \times \left(\Delta r_j(k+1) + \left[e_c\right]_j(k)\right) + e_j(k+1).
\end{aligned}
\tag{A.26}
$$

Therefore

$$
\begin{aligned}
&\left|\left[e_c\right]_j(k+1)\right| \\
&\quad = \left|\left(1 - s_j(k)\,\frac{\left[\widehat{f}_j^1(k)\right]^2}{\left[\widehat{f}_j^1(k)\right]^2 + \alpha}\right)\right. \\
&\qquad \left. \times \left(\Delta r_j(k+1) + \left[e_c\right]_j(k)\right) + e_j(k+1)\right| \\
&\quad \le \left|\left[e_c\right]_j(k)\left(1 - s_j(k)\,\frac{\left[\widehat{f}_j^1(k)\right]^2}{\left[\widehat{f}_j^1(k)\right]^2 + \alpha}\right)\right| \\
&\qquad + \left|\Delta r_j(k+1)\left(1 - s_j(k)\,\frac{\left[\widehat{f}_j^1(k)\right]^2}{\left[\widehat{f}_j^1(k)\right]^2 + \alpha}\right)\right. \\
&\qquad \left. + e_j(k+1)\right| \\
&\quad \le \left|\left[e_c\right]_j(k)\right| \cdot \left|1 - s_j(k)\,\frac{\left[\widehat{f}_j^1(k)\right]^2}{\left[\widehat{f}_j^1(k)\right]^2 + \alpha}\right| \\
&\qquad + |\Delta r| \cdot \left|1 - s_j(k)\,\frac{\left[\widehat{f}_j^1(k)\right]^2}{\left[\widehat{f}_j^1(k)\right]^2 + \alpha}\right| \\
&\qquad + \left|e_j(k+1)\right|.
\end{aligned}
\tag{A.27}
$$

From (A.24), one has

$$
\begin{aligned}
\left|\left[e_c\right]_j(k+1)\right| &\le \left|\left[e_c\right]_j(k)\right| \cdot \left|1 - s_j(k)\,\frac{\left[\widehat{f}_j^1(k)\right]^2}{\left[\widehat{f}_j^1(k)\right]^2 + \alpha}\right| \\
&\quad + r_0 \cdot \left|1 - s_j(k)\,\frac{\left[\widehat{f}_j^1(k)\right]^2}{\left[\widehat{f}_j^1(k)\right]^2 + \alpha}\right| \\
&\quad + \frac{2\left[e_j^o\right]_{\max}}{2 - \left[\rho_j\right]_{\max}} \\
&= k_1\left|\left[e_c\right]_j(k)\right| + k_2.
\end{aligned}
\tag{A.28}
$$

Since $0 \le k_1 < 1$ and k_2 is bounded, according to [14, Lemma 13.1], one concludes that, using the control law (15), the solutions of error system (17) are UUB for all k with ultimate bound $\lim_{k\to\infty}|[e_c]_j(k)| \le (k_2/(1-k_1))$.

References

[1] S. A. Billings and H. Nicholson, "Temperature weighting adaptive controller for electric arc furnaces," *Ironmaking and Steelmaking*, vol. 4, no. 4, pp. 216–221, 1977.

[2] M. Zhizhong and L. Jian, "Adaptive controller of an electric arc furnace with feedforward," *Journal of Northeastern University*, vol. 17, no. 1, pp. 65–68, 1996.

[3] A. S. Hauksdóttir, A. Gestsson, and A. Vésteinsson, "Current control of a three-phase submerged arc ferrosilicon furnace," *Control Engineering Practice*, vol. 10, no. 4, pp. 457–463, 2002.

[4] W. E. Staib and R. R. Staib, "The Intelligence arc furnace controller: a neural network electrode position optimization system for the electric arc furnace," in *Proceedings of the IEEE International Joint Conference on Neural Network*, vol. 3, pp. 1–9, Baltimore, Md, USA.

[5] W. E. Staib and N. G. Bliss, "Neural network control system for electric arc furnaces," *Metallurgical Plant and Technology International*, vol. 18, no. 2, p. 3, 1995.

[6] G. Ping, J.-C. Li, and X.-H. Liu, "Direct adaptive fuzzy sliding mode control of Arc furnace electrode regulator system," in *Proceedings of the Chinese Control and Decision Conference (CCDC '09)*, pp. 2776–2781, Guilin, China, June 2009.

[7] S.-D. Zhang, "Decoupling control for electrode system in electric arc furnace based on neural network inverse identification," in *Proceedings of the 6th International Conference on Intelligent Systems Design and Applications (ISDA '06)*, pp. 112–116, Jinan, China, October 2006.

[8] S. Zhang, K. Li, P. Li, and Z. Zhang, "Application of the electrode system intelligent controller for ladle furnace," in *Proceedings of the IEEE International Conference on Mechatronics and Automation (ICMA '07)*, pp. 2570–2574, Harbin, China, August 2007.

[9] S. Zhang and X. Zheng, "Application of double model control scheme based on RBF inverse identification in electrode system of electrical arc furnace," in *Proceedings of the IEEE International Conference on Automation and Logistics (ICAL '07)*, pp. 485–489, Jinan, China, August 2007.

[10] L. Li and Z. Mao, "A direct adaptive controller for EAF electrode regulator system using neural networks," *Neurocomputing*, vol. 82, pp. 91–98, 2012.

[11] C. Xinming, "The dynamic analysis for hydraulic system of EAF," *Industrial Heating*, vol. 3, pp. 1–5, 1980.

[12] A. M. Valderhaug, *Modelling and control of submerged-arc ferrosilicon furnaces [Ph.D. thesis]*, Norwegian Institute of Technology, Trondheim, Norway, report 92-81-W, 1992.

[13] R. P. Paiva, "Modelling and control of an electirc arc furance," Department of Automatic Control Lund Institute of Technology, Lund, Sweden, 1996.

[14] S. S. Ge, J. Zhang, and T. H. Lee, "Adaptive MNN control for a class of non-affine NARMAX systems with disturbances," *Systems & Control Letters*, vol. 53, no. 1, pp. 1–12, 2004.

[15] O. Adetona, S. Sathananthan, and L. H. Keel, "Robust adaptive control of nonaffine nonlinear plants with small input signal changes," *IEEE Transactions on Neural Networks*, vol. 15, no. 2, pp. 408–416, 2004.

[16] O. Adetona, E. Garcia, and L. H. Keel, "A new method for the control of discrete nonlinear dynamic systems using neural networks," *IEEE Transactions on Neural Networks*, vol. 11, no. 1, pp. 102–112, 2000.

[17] D. Schroder, *Intelligence Observer and Control Design for Nonlinear Systems*, Springer, Berlin, Germany, 2000.

[18] M. R. Cowper, B. Mulgrew, and C. P. Unsworth, "Nonlinear prediction of chaotic signals using a normalised radial basis function network," *Signal Processing*, vol. 82, no. 5, pp. 775–789, 2002.

[19] G. Bugmann, "Normalized Gaussian radial basis function networks," *Neurocomputing*, vol. 20, no. 1–3, pp. 97–110, 1998.

[20] M. Benaim, "On the functional approximation with normalized Gaussian units," *Neural Computation*, vol. 6, no. 2, pp. 314–333, 1994.

[21] J. T. Spooner, M. Maggiore, and K. M. Passino, *Stable Adaptive Control and Estimation for Nonlinear Systems*, Wiley, New York, NY, USA, 2002.

Hindawi Publishing Corporation
Mathematical Problems in Engineering
Volume 2013, Article ID 382016, 10 pages
http://dx.doi.org/10.1155/2013/382016

Research Article

A Nonlinear Robust Controller Design of Lower-Triangular Systems Based on Dissipation Theory

Bing Wang and Yue Yuan

College of Energy and Electrical Engineering, Hohai University, Nanjing 211100, China

Correspondence should be addressed to Bing Wang; icekingking@ustc.edu

Received 16 May 2013; Revised 11 July 2013; Accepted 21 July 2013

Academic Editor: Baoyong Zhang

Based on dissipation theory, a novel robust control is proposed for the lower-triangular nonlinear systems, which include strict-feedback systems and high-order lower-triangular systems. Some important concepts in dissipation theory are integrated into the recursive design, which are used to dominate the uncertain disturbance and construct the robust controller. The gotten controller renders the closed-loop system finite-gain L_2 stable in the presence of disturbance and asymptotically stable in the absence of disturbance. Especially, the controller has its advantage in regulating large disturbance. Finally, one example and one application are given to show the effectiveness of the design method. Moreover, by comparing with another robust controller, the characteristic of the proposed controller is illustrated in the simulations.

1. Introduction

Over the last decade, the lower-triangular systems are researched widely in the field of nonlinear systems [1–4]. This class of systems is not only important theoretically, but a lot of practical systems can conform to or be transformed into its form, such as the power generators [5], aircraft control system [6], and mobile robots [7]. It is well known that backstepping design [8, 9] is proposed to design the strict-feedback systems, which hold the simplest triangular structure. For different types of triangular systems, the condition for existence of control laws is investigated in [10, 11], and the explicit constructions of controllers are provided in [12, 13]. Then, a power integrator technique is given to design the high-order lower-triangular systems, which are neither feedback linearizable nor affine in the control input [4, 14]. Moreover, the robust control problem of lower-triangular systems has attracted a lot of attention [15–18] for overcoming the hurdle of disturbance, which possibly comes from model simplification, external disturbance, or other unknown factors.

In this paper, based on dissipation theory, a novel design method is proposed to solve the robust control problem of lower-triangular nonlinear systems in the presence of uncertain disturbance. This approach constructs the storage function and designs the controller recursively, which ensures that the closed-loop system satisfies the dissipation inequality having L_2-gain performance. The technique is firstly used in the strict-feedback system. Then, it is extended to the high-order lower-triangular system. Finally, one example of lower-triangular system and one application of synchronous generator system are given to illustrate the effectiveness of the robust control.

For the lower-triangular system with uncertain disturbance, this work uses the frame of dissipation property theory to solve the problem of disturbance rejection. First of all, the appropriate function of supply rate is chosen, which is used to gather the disturbance inputs in the recursive design. Next, the storage function and robust controller are constructed recursively to guarantee that the result at each step satisfies the dissipation property. During the design, by using feedback domination technique [4, 14], the disturbed parts are dominated by the functions of system states and disturbances. Then, the function of disturbances is regarded as the input of supply rate, which satisfies the dissipation inequality ensuring finite-gain L_2 stability. The effect of this method can be summarized as two aspects. Firstly, the restriction of uncertain disturbance is relaxed, and the only assumption of uncertain disturbance is bounded.

So, no information about disturbance is required in the gotten control law, which means that certain controller can regulate uncertain disturbance. Secondly, compared with some previous robust controllers only applicable for small disturbances, the proposed robust controller is effective for all cases of bounded disturbance, especially for large disturbance.

The structure of this paper is as follows: Section 2 describes the problem and offers key lemma; Section 3 gives the robust controller design for strict-feedback systems; Section 4 extends the design method to high-order lower-triangular systems; Section 5 provides an example and application to illustrate the effectiveness of design approach. The conclusion is contained in Section 6.

2. Problem Formulation and Key Lemma

In this paper, we focus on the problem of constructing robust controller for the lower-triangular system, which is described by the following differential equations:

$$\begin{aligned}
\dot{x}_1 &= f_1(x_1) + x_2^{p_1} + \omega_1(t) \\
\dot{x}_2 &= f_2(X_2) + x_3^{p_2} + \omega_2(t) \\
&\vdots \\
\dot{x}_n &= f_n(X_n) + u^{p_n} + \omega_n(t) \\
y &= x_1,
\end{aligned} \tag{1}$$

where for $i = 1, 2, \ldots, n$, the state $X_i = (x_1, \ldots, x_i)^T \in \mathbb{R}^i$, the input $u \in \mathbb{R}$, the output $y \in \mathbb{R}$, the uncertain disturbance vector $\omega = [\omega_1, \omega_2, \ldots, \omega_n]^T$, $\omega_i(t)$ is unknown nonlinear function, which denotes external disturbance with unknown bound, $f_i : \mathbb{R}^i \mapsto \mathbb{R}$ is a smooth function, and $f_i(0) = 0$. About the system (1), one hypothesis is given as follows.

Assumption 1. $p_i \geq 1$ $(i = 1, 2, \ldots, n)$ is odd integer, and p_1 is maximum of them.

Compared with the corresponding assumption in [4, 14], Assumption 1 relaxes the condition of p_i. Next, the main definitions of dissipation theory are given as follows.

Definition 2 (see [1]). The general systems are described in the following form:

$$\begin{aligned}
\dot{x}(t) &= f(x, u_0) \\
y_0(t) &= h(x, u_0),
\end{aligned} \tag{2}$$

where the state $x \in \mathbb{R}^n$, the input $u_0 \in \mathbb{R}^p$, and the output $y_0 \in \mathbb{R}^q$. Let the function $s(u_0, y_0) : \mathbb{R}^p \times \mathbb{R}^q \mapsto \mathbb{R}$ if there exists $V(x) \geq 0$, $V : \mathbb{R}^n \mapsto \mathbb{R}^+$, such that

$$V(x(\tau)) \leq V(x(0)) + \int_0^\tau s(u_0, y_0)\, dt; \tag{3}$$

for any $x(0)$ and τ, the system (3) is dissipative about $s(u_0, y_0)$. And $s(u_0, y_0)$ is the supply rate, and $V(x)$ is the storage function.

Remark 3. The supply rate $s(u_0, y_0)$ in Definition 2 is selectable. And there are some optional functions. The most commonly used are two options: one is $s(u_0, y_0) = u_0^T y_0$, and the other is $s(u_0, y_0) = \Upsilon^2 \|u_0\|^2 - \|y_0\|^2$, $\Upsilon > 0$. In this paper, when the uncertain disturbance $\omega = [\omega_1, \omega_2, \ldots, \omega_n]^T$ is regarded as the input of the system (3), the latter is chosen as the supply rate. And if the closed-loop system is dissipative, we have

$$V(x(\tau)) - V(x(0)) \leq \int_0^\tau \left(\Upsilon^2 \|\omega\|^2 - \|y_0\|^2\right) dt. \tag{4}$$

That is, the gain of the system is not more than Υ for the uncertain disturbance.

Definition 4 (see [1]). A mapping $H : L_e^m \to L_e^q$ is finite-gain L stable if there exist nonnegative constants Υ_L and β_L, such that

$$\|(Hv)_\tau\|_L \leq \Upsilon_L \|v_\tau\|_L + \beta_L, \tag{5}$$

for $v \in L_e^m$ and $\tau \in [0, \infty)$.

Young's inequality is an important tool used in the recursive design, and Lemma 6 is one direct consequence of Young's inequality.

Lemma 5 (Young's inequality). *For any two vectors $\overline{x}$ and $\overline{y}$, the following holds*

$$\overline{x}^T \overline{y} \leq \frac{\varepsilon^p}{p} \|\overline{x}\|^p + \frac{1}{q\varepsilon^q} \|\overline{y}\|^q, \tag{6}$$

where $\varepsilon > 0$ and the constants $p > 1$ and $q > 1$ satisfy $(p - 1)(q - 1) = 1$.

Lemma 6 (see [19]). *For real numbers $a \geq 0$, $b \geq 0$, and $m \geq 1$, the following inequality holds:*

$$a \leq b + \left(\frac{a}{m}\right)^m \left(\frac{m-1}{b}\right)^{m-1}. \tag{7}$$

3. Robust Controller Design of Strict-Feedback Systems

The strict-feedback system is described by the following equations

$$\begin{aligned}
\dot{x}_1 &= f_1(x_1) + x_2 + \omega_1(t) \\
\dot{x}_2 &= f_2(X_2) + x_3 + \omega_2(t) \\
&\vdots \\
\dot{x}_n &= f_n(X_n) + u + \omega_n(t) \\
y &= x_1.
\end{aligned} \tag{8}$$

Based on the dissipation theory, the novel robust controller design is proposed step by step. For $i = 1, 2, \ldots, n$, firstly set the design parameter $C_i > 0$.

Step 1. Let $z_1 = x_1$. The storage function is constructed as $V_1 = z_1^2/2$, whose derivative is

$$\dot{V}_1 = z_1\dot{z}_1 = z_1\left(f_1(x_1) + x_2\right) + z_1\omega_1. \tag{9}$$

For the above equation, according to the technique of adding one power integrator [4, 14], by using Young's inequality (6) with $p = q = 2$ and $\varepsilon = \sqrt{n}/\gamma$, the term $z_1\omega_1$ is dominated by $(n/2\gamma^2)z_1^2 + (\gamma^2/2n)\omega_1^2$, where the disturbance attenuation coefficient $\gamma > 0$. Taking it into formula (9) yields

$$\dot{V}_1 \le z_1\left[x_2 + f_1(x_1) + \left(\frac{1}{2} + \frac{n}{2\gamma^2}\right)z_1\right] + \frac{\gamma^2}{2n}\omega_1^2 - \frac{z_1^2}{2}. \tag{10}$$

Design the smooth virtual control as

$$\alpha_2 = -C_1z_1 - f_1(x_1) - \frac{1}{2}\left(1 + \frac{n}{\gamma^2}\right)z_1. \tag{11}$$

Taking controller (11) into formula (10) results in

$$\dot{V}_1 \le -C_1z_1^2 + z_1(x_2 - \alpha_2) + \frac{\gamma^2}{2n}\omega_1^2 - \frac{1}{2}z_1^2. \tag{12}$$

Step k. Through $k-1$ steps, a group of virtual controllers are $z_1 = x_1$, $z_2 = x_2 - \alpha_2$,..., $z_{k-1} = x_{k-1} - \alpha_{k-1}$, and the storage function is $V_{k-1} = \sum_{i=1}^{k-1}(z_i^2/2)$, whose derivative is

$$\dot{V}_{k-1} \le -\sum_{i=1}^{k-1}C_iz_i^2 + z_{k-1}(x_k - \alpha_k) + \frac{\gamma^2}{2}\sum_{j=1}^{k-1}\frac{k-j}{n+1-j}\omega_j^2 - \frac{z_1^2}{2}. \tag{13}$$

Let $z_k = x_k - \alpha_k$, and the storage function is changed into $V_k = V_{k-1} + z_k^2/2$; its derivative is obtained as

$$\begin{aligned}\dot{V}_k &= \dot{V}_{k-1} + z_k\dot{z}_k \\ &\le -\sum_{i=1}^{k-1}C_iz_i^2 + \frac{\gamma^2}{2}\sum_{j=1}^{k-1}\frac{k-j}{n+1-j}\omega_j^2 - \frac{z_1^2}{2} + z_k\omega_k \\ &\quad - z_k\sum_{m=1}^{k-1}\frac{\partial\alpha_k}{\partial x_m}\omega_m + z_k\Bigg[f_k(X_k) + x_{k+1} + z_{k-1} \\ &\qquad - \sum_{m=1}^{k-1}\frac{\partial\alpha_k}{\partial x_m}\left(f_m(X_m) + x_{m+1}\right)\Bigg].\end{aligned} \tag{14}$$

By using Young's inequality, we have

$$\begin{aligned}\dot{V}_k &\le -\sum_{i=1}^{k-1}C_iz_i^2 + \frac{\gamma^2}{2}\sum_{j=1}^{k-1}\frac{k-j}{n+1-j}\omega_j^2 - \frac{z_1^2}{2} \\ &\quad + \frac{\gamma^2}{2(n+1-k)}\omega_k^2 + \frac{\gamma^2}{2}\sum_{m=1}^{k-1}\frac{\omega_m^2}{n+1-m} \\ &\quad + z_k\Bigg[f_k(X_k) + x_{k+1} + z_{k-1} + \frac{n+1-k}{2\gamma^2}z_k \\ &\qquad + \frac{z_k}{2\gamma^2}\sum_{m=1}^{k-1}(n+1-m)\left(\frac{\partial\alpha_k}{\partial x_m}\right)^2 \\ &\qquad - \sum_{m=1}^{k-1}\frac{\partial\alpha_k}{\partial x_m}\left(f_m(X_m) + x_{m+1}\right)\Bigg].\end{aligned} \tag{15}$$

In this step, the smooth virtual controller is taken as follows:

$$\begin{aligned}\alpha_{k+1} &= -C_kz_k - f_k(X_k) - z_{k-1} - \frac{n+1-k}{2\gamma^2}z_k \\ &\quad - \frac{z_k}{2\gamma^2}\sum_{m=1}^{k-1}(n+1-m)\left(\frac{\partial\alpha_k}{\partial x_m}\right)^2 \\ &\quad + \sum_{m=1}^{k-1}\frac{\partial\alpha_k}{\partial x_m}\left(f_m(X_m) + x_{m+1}\right).\end{aligned} \tag{16}$$

Under the action of the above controller, formula (15) is turned into

$$\dot{V}_k \le -\sum_{i=1}^{k}C_iz_i^2 + z_k(x_{k+1} - \alpha_{k+1}) + \frac{\gamma^2}{2}\sum_{j=1}^{k}\frac{k+1-j}{n+1-j}\omega_j^2 - \frac{z_1^2}{2}. \tag{17}$$

Step n. Let $z_n = x_n - \alpha_n$, and the storage function is $V = V_n = V_{n-1} + z_n^2/2 = (1/2)\sum_{i=1}^{n}z_i^2$. The nonlinear robust controller is designed as

$$\begin{aligned}u &= -C_nz_n - f_n(X_n) - z_{n-1} - \frac{z_n}{2\gamma^2} \\ &\quad - \frac{z_n}{2\gamma^2}\sum_{m=1}^{n-1}(n+1-m)\left(\frac{\partial\alpha_n}{\partial x_m}\right)^2 \\ &\quad + \sum_{m=1}^{n-1}\frac{\partial\alpha_n}{\partial x_m}\left(f_m(X_m) + x_{m+1}\right).\end{aligned} \tag{18}$$

Now, the derivative of the storage function is

$$\dot{V}_n \le -\sum_{i=1}^{n}C_iz_i^2 + \frac{\gamma^2}{2}\sum_{j=1}^{n}\omega_j^2 - \frac{z_1^2}{2}. \tag{19}$$

From system (8), it is known that the uncertain disturbance vector $\omega = [\omega_1, \omega_2, \ldots, \omega_n]^T$ and the output $y = x_1 = z_1$. So, we have

$$\dot{V}_n \le -\sum_{i=1}^{n}C_iz_i^2 + \frac{\gamma^2}{2}\|\omega\|_2^2 - \frac{1}{2}\|y\|_2^2 \le \frac{1}{2}\left(\gamma^2\|\omega\|_2^2 - \|y\|_2^2\right). \tag{20}$$

Based on dissipation theory, the robust controller (18) makes the closed-loop system dissipative with the uncertain disturbance, and the supply rate $s(\omega, y) = \gamma^2\|\omega\|_2^2 - \|y\|_2^2$. Furthermore, the finite-gain L_2 stability of the closed-loop system is concluded in the following theorem.

Theorem 7. *Consider the strict-feedback system with disturbance* (8)*. There exists the smooth robust controller* (18)*, such that the closed-loop system is finite-gain L_2 stable and the L_2 gain is no more than γ. Moreover, when the disturbance input $\omega = [\omega_1, \omega_2, \ldots, \omega_n]^T = 0$, the closed-loop system is asymptotically stable.*

Proof. From (20), we have $\dot{V} = \dot{V}_n \leq (1/2)(\gamma^2\|\omega\|_2^2 - \|y\|_2^2)$. Integrating it yields the following inequality:

$$V(x(\tau)) - V(x(0)) \leq \frac{1}{2}\int_0^\tau \left(\gamma^2\|\omega\|_2^2 - \|y\|_2^2\right)dt. \tag{21}$$

Due to $V(x) \geq 0$, we obtain

$$\int_0^\tau \|y\|_2^2 dt \leq \gamma^2 \int_0^\tau \|\omega\|_2^2 dt + 2V(x(0)). \tag{22}$$

Taking the square roots and using the inequality $\sqrt{a^2+b^2} \leq a + b$ for nonnegative numbers a and b, one obtains

$$\|y_\tau\|_{L_2} \leq \gamma\|\omega_\tau\|_{L_2} + \sqrt{2V(x(0))}. \tag{23}$$

Therefore, based on Definition 4, It is known that the system is finite-gain L_2 stable and the gain from disturbance input to system output is no more than γ.

Moreover, when $\omega = 0$, from (20) we have

$$\dot{V} = \dot{V}_n \leq \frac{\gamma^2}{2}\|\omega\|^2 - \frac{1}{2}\|y\|^2 \leq -\frac{1}{2}\|y\|^2 \leq 0, \tag{24}$$

and the storage function $V = (1/2)\sum_{i=1}^n z_i^2$ is positive definite. According to the invariance principle [1], we need to find $S = \{X_n \in \mathbb{R}^n \mid \dot{V} = 0\}$. Note that

$$\dot{V} = 0 \Longrightarrow y = 0 \Longrightarrow x_1 = 0. \tag{25}$$

Hence, $S = \{X_n \in \mathbb{R}^n \mid x_1 = 0\}$. Let $X_n(t)$ be a solution that belongs identically to S. From the system (8), we can deduce that

$$x_1 \equiv 0 \Longrightarrow \dot{x}_1 \equiv 0 \Longrightarrow x_2 \equiv 0 \Longrightarrow \dot{x}_2 \equiv 0 \Longrightarrow \cdots \Longrightarrow x_n \equiv 0. \tag{26}$$

Therefore, the only solution that can stay identically in S is the trivial solution $X_n(t) \equiv 0$. Thus, the closed-loop system is asymptotically stable in the case of $\omega = 0$. □

Remark 8. About the proposed method, there are the following opinions.

(1) This method integrates the idea of dissipation property into the recursive design. In the frame of dissipation theory, by using the feedback domination technology, the unknown disturbance is decoupled from the known state and gathered together to satisfy the dissipation inequality, which leads to the result of disturbance rejection and finite-gain L_2 stability.

(2) In the previous research of lower-triangular system (1), some assumption is needed for the uncertain disturbance, such as boundary condition and functional constraint. In this paper, the assumption is relaxed to be bounded, which can ensure that the closed-loop system is finite-gain L_2 stable. On the other hand, just for there is no constraint about the uncertain disturbance, the result is only finite-gain L_2 stable.

(3) It is interesting to note that the external disturbance ω_i can be generalized to more general uncertainties $\Delta_i(X_i, t)$, which satisfies the condition $|\Delta_i(X_i, t)| \leq \omega_i(t)\phi_i(X_i)$, with $\phi_i(X_i)$ being a known smooth function and $\omega_i(t)$ being the unknown bound. The proposed method is still applicable for the more general case.

4. Robust Controller Design of Lower-Triangular Systems

The robust control law of lower-triangular systems (1) is designed in this section. Similarly, for $i = 1, 2, \ldots, n$, the design parameter $C_i > 0$.

Step 1. Let $z_1 = x_1$. Due to Assumption 1, the storage function is constructed as $V_1 = z_1^{p_1 - p_1 + 2}/(p_1 - p_1 + 2) = z_1^2/2$, and its derivative is

$$\dot{V}_1 = z_1\dot{z}_1 = z_1\left(f_1(x_1) + x_2^{p_1}\right) + z_1\omega_1. \tag{27}$$

Similar to the design of strict-feedback systems, one obtains:

$$\dot{V}_1 \leq z_1\left[x_2^{p_1} + f_1(x_1) + \left(\frac{1}{2} + \frac{n}{2\gamma^2}\right)z_1\right] + \frac{\gamma^2}{2n}\omega_1^2 - \frac{z_1^2}{2}. \tag{28}$$

Owing to (7), for any positive real number $\sigma > 0$, let $b = \sigma$, $a = |z_1[f_1 + ((1/2) + (n/2\gamma^2))z_1]|$, and $m = p_1 + 1$. We have

$$\left|z_1\left[f_1 + \left(\frac{1}{2} + \frac{n}{2\gamma^2}\right)z_1\right]\right| \leq \sigma + z_1^{p_1+1}\rho_1(z_1), \tag{29}$$

where $\rho_1(z_1) = (1/(p_1+1))[p_1/(p_1+1)\sigma]^{p_1}(f_1 + z_1/2 + nz_1/2\gamma^2)^{p_1+1} \geq 0$.

Substituting (29) into (28) yields

$$\dot{V}_1 \leq z_1 x_2^{p_1} + z_1^{p_1+1}\rho_1(z_1) + \frac{\gamma^2}{2n}\omega_1^2 - \frac{z_1^2}{2} + \sigma. \tag{30}$$

Paying attention to Assumption 1, we design the smooth virtual control as

$$\alpha_2 = -z_1\left(C_1 + 1 + \rho_1(z_1)\right)^{1/p_1}. \tag{31}$$

Taking the controller (31) into (30) results in

$$\dot{V}_1 \leq -(C_1 + 1)z_1^{p_1+1} + z_1\left(x_2^{p_1} - \alpha_2^{p_1}\right) + \frac{\gamma^2}{2n}\omega_1^2 - \frac{z_1^2}{2} + \sigma. \tag{32}$$

Step k. Through $k-1$ steps, a group of virtual controllers are $z_1 = x_1$, $z_2 = x_2 - \alpha_2, \ldots, z_{k-1} = x_{k-1} - \alpha_{k-1}$, and the storage function is $V_{k-1} = \sum_{i=1}^{k-1}(z_i^{p_1-p_i+2}/(p_1-p_i+2))$, whose derivative is

$$\begin{aligned}\dot{V}_{k-1} \le & -\sum_{i=1}^{k-1} C_i z_i^{p_1+1} - z_{k-1}^{p_1+1} + z_{k-1}^{p_1-p_{k-1}+1}\left(x_k^{p_{k-1}} - \alpha_k^{p_{k-1}}\right) \\ & + \frac{\gamma^2}{2}\sum_{j=1}^{k-1}\frac{k-j}{n+1-j}\omega_j^2 - \frac{z_1^2}{2} + (k-1)\sigma.\end{aligned} \tag{33}$$

Let $z_k = x_k - \alpha_k$, and consider the storage function $V_k = V_{k-1} + z_k^{p_1-p_k+2}/(p_1-p_k+2)$; its derivative is obtained as

$$\begin{aligned}\dot{V}_k &= \dot{V}_{k-1} + z_k^{p_1-p_k+1}\dot{z}_k \\ &\le -\sum_{i=1}^{k-1} C_i z_i^{p_1+1} - z_{k-1}^{p_1+1} + z_{k-1}^{p_1-p_{k-1}+1}\left(x_k^{p_{k-1}} - \alpha_k^{p_{k-1}}\right) \\ &\quad + \frac{\gamma^2}{2}\sum_{j=1}^{k}\frac{k+1-j}{n+1-j}\omega_j^2 - \frac{z_1^2}{2} + (k-1)\sigma \\ &\quad + z_k^{p_1-p_k+1}\left[x_{k+1}^{p_k} + f_k(X_k) + \frac{n+1-k}{2\gamma^2}z_k^{p_1-p_k+1}\right. \\ &\qquad + \frac{z_k^{p_1-p_k+1}}{2\gamma^2}\sum_{m=1}^{k-1}(n+1-m)\left(\frac{\partial\alpha_k}{\partial x_m}\right)^2 \\ &\qquad \left. - \sum_{m=1}^{k-1}\frac{\partial\alpha_k}{\partial x_m}\left(f_m + x_{m+1}^{p_m}\right)\right].\end{aligned} \tag{34}$$

Due to Young's inequality, there exists the smooth function $\overline{\rho}_k(z_1, \ldots, z_k)$, such that

$$\left|z_{k-1}^{p_1-p_{k-1}+1}\left(x_k^{p_{k-1}} - \alpha_k^{p_{k-1}}\right)\right| \le z_{k-1}^{p_1+1} + z_k^{p_1+1}\overline{\rho}_k(z_1, \ldots, z_k), \tag{35}$$

where

$$\begin{aligned}&\overline{\rho}_k(z_1, \ldots, z_k) \\ &= \frac{p_{k-1}}{p_1+1}\left(2^{p_{k-1}-2}p_{k-1}\right)^{(p_1+1)/p_{k-1}} \\ &\quad \times \left[\frac{2(p_1-p_{k-1}+1)}{p_1+1}\right]^{(p_1-p_{k-1}+1)/p_{k-1}} \\ &\quad + \frac{1}{p_1+1}\left[\left(1+2^{p_{k-1}-2}\right)p_{k-1}\right. \\ &\qquad \left. \times \left(C_{k-1}+1+\rho_{k-1}\right)^{(p_{k-1}-1)/p_{k-1}}\right]^{p_1+1} \\ &\quad \times \left(\frac{2p_1}{p_1+1}\right)^{p_1},\end{aligned} \tag{36}$$

and the construction of $\overline{\rho}_k(z_1, \ldots, z_k)$ can refer to [19].

Then, we define a smooth function as follows:

$$\begin{aligned}D_k(z_1, \ldots, z_k) &= f_k(X_k) + \frac{n+1-k}{2\gamma^2}z_k^{p_1-p_k+1} \\ &\quad + \frac{z_k^{p_1-p_k+1}}{2\gamma^2}\sum_{m=1}^{k-1}(n+1-m)\left(\frac{\partial\alpha_k}{\partial x_m}\right)^2 \\ &\quad - \sum_{m=1}^{k-1}\frac{\partial\alpha_k}{\partial x_m}\left(f_m + x_{m+1}^{p_m}\right).\end{aligned} \tag{37}$$

Similar to Step 1, we obtain

$$\left|z_k^{p_1-p_k+1}D_k(z_1, \ldots, z_k)\right| \le \sigma + z_k^{p_1+1}\rho_k(z_1, \ldots, z_k). \tag{38}$$

Taking (35) and (38) into (34) yields

$$\begin{aligned}\dot{V}_k \le & -\sum_{i=1}^{k-1} C_i z_i^{p_1+1} + z_k^{p_1-p_k+1}x_{k+1}^{p_k} + z_k^{p_1+1}\left(\overline{\rho}_k(\cdot) + \rho_k(\cdot)\right) \\ & + \frac{\gamma^2}{2}\sum_{j=1}^{k}\frac{k+1-j}{n+1-j}\omega_j^2 - \frac{z_1^2}{2} + k\sigma.\end{aligned} \tag{39}$$

Design the following virtual control law

$$\alpha_{k+1} = -z_k\left(C_k + 1 + \overline{\rho}_k(z_1, \ldots, z_k) + \rho_k(z_1, \ldots, z_k)\right)^{1/p_k}, \tag{40}$$

which renders

$$\begin{aligned}\dot{V}_k \le & -\sum_{i=1}^{k} C_i z_i^{p_1+1} - z_k^{p_1+1} + z_k^{p_1-p_k+1}\left(x_{k+1}^{p_k} - \alpha_{k+1}^{p_k}\right) \\ & + \frac{\gamma^2}{2}\sum_{j=1}^{k}\frac{k+1-j}{n+1-j}\omega_j^2 - \frac{z_1^2}{2} + k\sigma.\end{aligned} \tag{41}$$

Step n. In the end, for the storage function, $V = V_n = \sum_{i=1}^{n}(z_i^{p_1-p_i+2}/(p_1-p_i+2))$, where $z_n = x_n - \alpha_n$. There exists the smooth controller

$$\begin{aligned}u(z_1, \ldots, z_n) = -z_n\left(C_n + \overline{\rho}_n(z_1, \ldots, z_n)\right. \\ \left. + \rho_n(z_1, \ldots, z_n)\right)^{1/p_n},\end{aligned} \tag{42}$$

such that

$$\dot{V}_n \le -\sum_{i=1}^{n} C_i z_i^{p_1+1} + \frac{\gamma^2}{2}\sum_{j=1}^{n}\omega_j^2 - \frac{z_1^2}{2} + n\sigma. \tag{43}$$

Similar to Section 3, we finish this section with the following theorem.

Theorem 9. *Consider the lower-triangular system with disturbance* (1)*. There exists the smooth robust controller* (42)*, such that the closed-loop system is finite-gain L_2 stable and the L_2 gain is no more than γ.*

Proof. The proof of this theorem is similar to Theorem 7, which is omitted. □

5. Example and Application

Example 1. Consider the stabilization problem of a lower-triangular system as follows:

$$\begin{aligned}\dot{x}_1 &= x_1^2 + x_2^3 + \omega_1\\ \dot{x}_2 &= x_1 x_2^2 + x_2 e^{x_2} + u^3 + \omega_2\\ y &= x_1,\end{aligned} \tag{44}$$

where ω_1 and ω_2 are bounded unknown disturbance.

Firstly, let $z_1 = x_1$, and construct the storage function $V_1 = z_1^2/2$. According to the design steps, the virtual control is obtained as

$$\alpha_2 = -z_1\left(C_1 + 1 + \rho_1(z_1)\right)^{1/3}, \tag{45}$$

where $\rho_1(z_1) = (27/256\sigma^3)(x_1^2 + x_1/2 + x_1/\gamma^2)^4$, and the positive parameters σ and γ can be adjusted according to the requirements.

Secondly, let $z_2 = x_2 - \alpha_2$ and $V_2 = V_1 + z_2^2/2$. Based on the design process, the robust controller is taken as

$$u = -z_2\left(C_2 + \rho_2(z_1, z_2) + \overline{\rho}_2(z_1, z_2)\right)^{1/3}, \tag{46}$$

where

$$\begin{aligned}\rho_2(z_1, z_2) = \frac{1}{4}\left(\frac{3}{4\sigma}\right)^3 \Bigg[& x_1 x_2^2 + x_2 e^{x_2} + \frac{z_2}{\gamma^2}\left(\frac{\partial \alpha_2}{\partial x_1}\right)^2\\ & - \frac{\partial \alpha_2}{\partial x_1}\left(x_1^2 + x_2\right)\Bigg]^4\end{aligned} \tag{47}$$

$$\overline{\rho}_2(z_1, z_2) = \frac{9}{2}\sqrt[3]{3} + \frac{27}{32}\left[9\left(C_1 + 1 + \rho_1(z_1)\right)^{2/3}\right]^4.$$

According to Theorem 9, it is known that the solutions of the system are globally bounded and the closed-loop system is finite-gain L_2 stable.

In the simulation, the system parameters are given as follows: $C_1 = 1$, $C_2 = 1$, $\sigma = 2$, and $\gamma = 2$. When the disturbances are $\omega_1 = 5$, $\omega_2 = 4\sin t$, the state curves are shown as Figure 1, and the control law is in Figure 2. From them, we know that the closed-loop system is finite-gain L_2 stable and the gain is no more than $\gamma = 2$.

Example 2. Consider one machine connected to an infinite bus system which is shown in Figure 3. The dynamic model of synchronous generator can be described as follows:

$$\begin{aligned}\dot{\delta} &= \omega - \omega_0\\ \dot{\omega} &= -\frac{D}{H}(\omega - \omega_0) + \frac{\omega_0}{H}(P_m - P_e) + \omega_1\\ \dot{P}_m &= -\frac{P_m}{T_{H\Sigma}} + \frac{P_{m0}}{T_{H\Sigma}} + \frac{C}{T_{H\Sigma}}\mu + \omega_2,\end{aligned} \tag{48}$$

where

$$P_e = \frac{E'_q V_s}{X'_{d\Sigma}}\sin\delta + \frac{V_s^2}{2}\left(\frac{X'_{d\Sigma} - X_{q\Sigma}}{X'_{d\Sigma} X_{q\Sigma}}\right)\sin 2\delta, \tag{49}$$

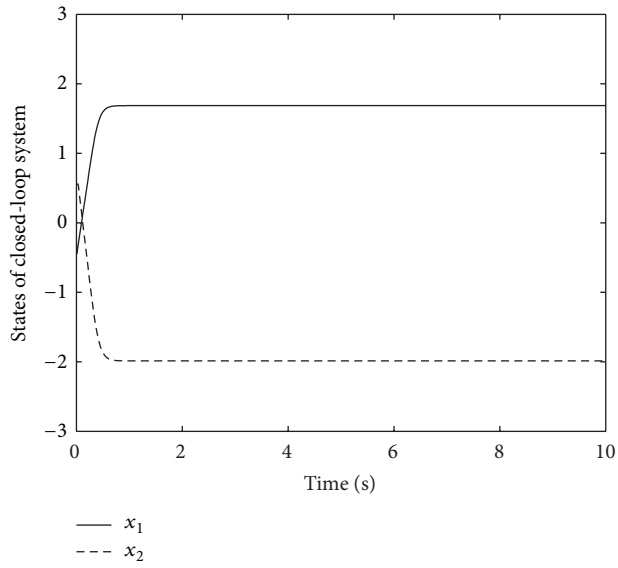

Figure 1: State response curves.

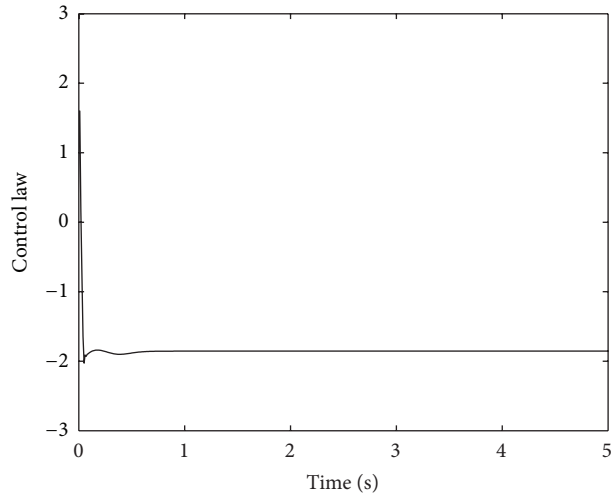

Figure 2: Curve of control law.

δ is the power angle; δ_0 is the operating point of power angle; ω is the relative speed; ω_0 is the synchronous machine speed; P_m is the mechanical input power; P_{m0} is the operating point of mechanical input power; P_e is the electromagnetic power; μ is the steam-valving controller; the uncertain disturbances ω_1 and ω_2 are bounded.

Let $(\delta_0, \omega_0, P_{m0})$ be the operating point, and define state variables by $x_1 = \delta - \delta_0$, $x_2 = \omega - \omega_0$, and $x_3 = P_m - P_{m0}$; then, system (48) and (49) is represented by

$$\begin{aligned}\dot{x}_1 &= x_2\\ \dot{x}_2 &= -\frac{D}{H}x_2 - \frac{\omega_0}{H}\Delta P_e + \frac{\omega_0}{H}x_3 + \omega_1\\ \dot{x}_3 &= -\frac{1}{T_{H\Sigma}}x_3 + \frac{C}{T_{H\Sigma}}\mu + \omega_2,\end{aligned} \tag{50}$$

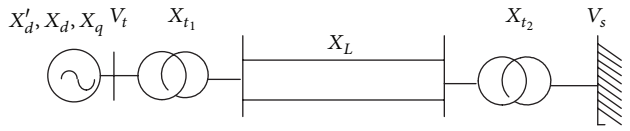

Figure 3: One-machine to infinite-bus circuit.

where

$$\Delta P_e = \frac{E'_q V_s}{X'_{d\Sigma}} \left[\sin\left(\delta_0 + x_1\right) - \sin\delta_0\right] + \frac{V_s^2}{2}\left(\frac{X'_{d\Sigma} - X_{q\Sigma}}{X'_{d\Sigma} X_{q\Sigma}}\right)\left[\sin 2\left(\delta_0 + x_1\right) - \sin 2\delta_0\right]. \tag{51}$$

From the model (50) and (51), we know that this is a strict-feedback system. According to the design process in Section 3, the robust controller is obtained as follows:

$$\mu = T_{H\Sigma}\left\{-C_3 z_3 + \frac{x_3}{T_{H\Sigma}} - z_2 - \frac{z_2}{2\gamma^2} \times \left[1 + 3\left(\frac{\partial\alpha_3}{\partial x_1}\right)^2 + 2\left(\frac{\partial\alpha_3}{\partial x_2}\right)^2\right] + \frac{\partial\alpha_3}{\partial x_1}x_2 + \frac{\partial\alpha_3}{\partial x_2}\left(-\frac{D}{H}x_2 - \frac{\omega_0}{H}\Delta P_e + x_3\right)\right\}, \tag{52}$$

where $z_1 = x_1$, $z_2 = x_2 - \alpha_2$, $z_3 = x_3 - \alpha_3$, $\alpha_2 = -(C_1 + 1/2 + 3/2\gamma^2)z_1$,

$$\alpha_3 = \frac{H}{\omega_0}\left[-C_2 z_2 + \frac{D}{H}x_2 + \frac{\omega_0}{H}\Delta P_e - z_1 - \frac{3z_2}{2\gamma^2}\left(\frac{\partial\alpha_2}{\partial x_1}\right)^2 - \frac{z_2}{\gamma^2} + \frac{\partial\alpha_2}{\partial x_1}x_2\right]. \tag{53}$$

In order to verify the viability and effectiveness of the control law (52), the computer simulation is performed with the following parameters: $D = 8$, $H = 2$, $C = 1$, $V_s = 1$, $T_{H\Sigma} = 0.35$, and $P_{m0} = 0.87455$ (see Figures 4, 5, 6, and 7).

In the presence of external disturbances $\omega_1 = 10$ and $\omega_2 = 15\cos t$, the state responses and control law are shown in Figures 4 and 5, respectively. In the absence of disturbance, the simulation results are given in Figures 6 and 7. It is obvious that the proposed controller is effective for bounded disturbance and the closed-loop system can achieve finite-gain L_2 stable. And, with the reduction of disturbance, the L_2 gain decreases. At last, when the disturbance vanishes, the closed-loop system is asymptotically stable as shown in Figure 6.

Moreover, in order to demonstrate the superiority of the proposed controller, we compare it with another robust

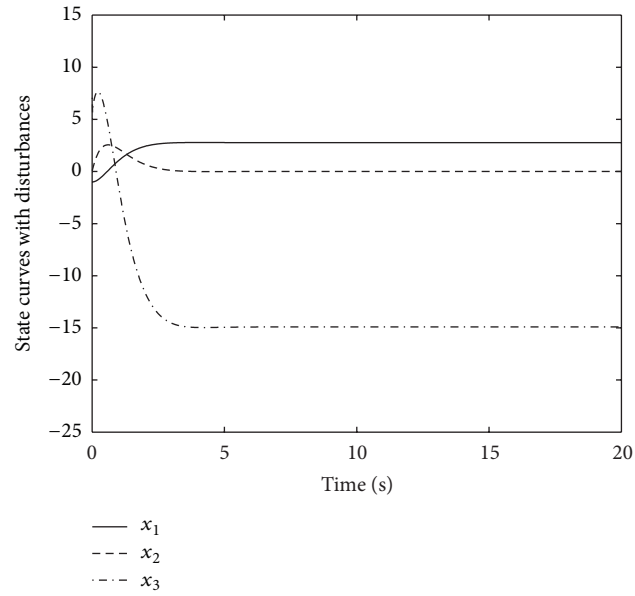

Figure 4: State curves with disturbances.

controller designed based on Hamiltonian function method [20].

Firstly, Hamilton energy function is constructed as

$$H = \frac{E'_q V_s}{X'_{d\Sigma}}(1 - \cos\delta) + \frac{V_s^2}{2}\left(\frac{X_{q\Sigma} - X'_{d\Sigma}}{X'_{d\Sigma} X_{q\Sigma}}\right)\cos^2\delta + H\frac{(\Delta\omega)^2}{2\omega_0} + \frac{1}{2}\left(P_m - P_{m0}\right)^2 + P_{m0}(\pi - \delta). \tag{54}$$

Then, the model (48) in Hamilton form is rewritten into

$$\begin{bmatrix}\dot\delta\\ \Delta\dot\omega\\ \dot P_m\end{bmatrix} = \begin{bmatrix}0 & \frac{\omega_0}{H} & 0\\ -\frac{\omega_0}{H} & -\frac{D\omega_0}{H^2} & \frac{\omega_0}{H}\\ 0 & 0 & -\frac{1}{T_{H\Sigma}}\end{bmatrix}\nabla H + \begin{bmatrix}0\\ 0\\ \frac{C}{T_{H\Sigma}}\end{bmatrix}\mu + \begin{bmatrix}0\\ \omega_1\\ \omega_2\end{bmatrix}. \tag{55}$$

Based on Hamiltonian function method, the robust controller is designed as

$$\mu = \mu_0 - \Gamma G^T \nabla H = -\frac{T_{H\Sigma}}{C}\Delta\omega - \Gamma\frac{C}{T_{H\Sigma}}\left(P_m - P_{m0}\right), \tag{56}$$

where $\mu_0 = -(T_{H\Sigma}/C)\Delta\omega$ is pre-feedback control and $\Gamma \in \mathbb{R}$ is design parameter.

Next, two methods are compared by the simulations. Figures 8, 10, and 12 are the controlled results with Hamiltonian function method; Figures 9, 11, and 13 are the controlled results with dissipation theory method.

In the absence of disturbance, from Figures 8 and 9, it is known that both of them are effective for the generator

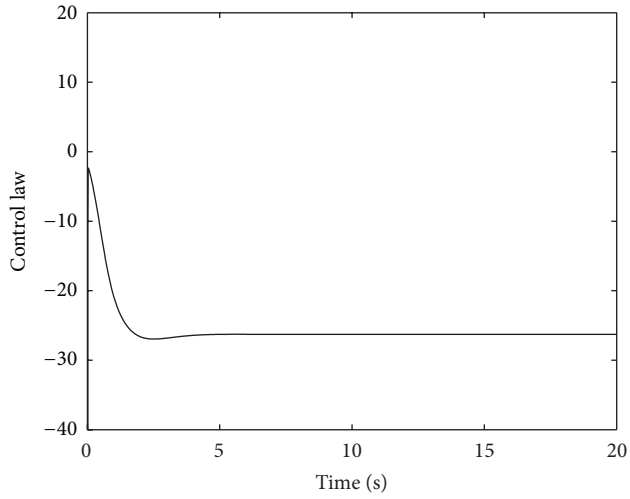

Figure 5: Control law with disturbances.

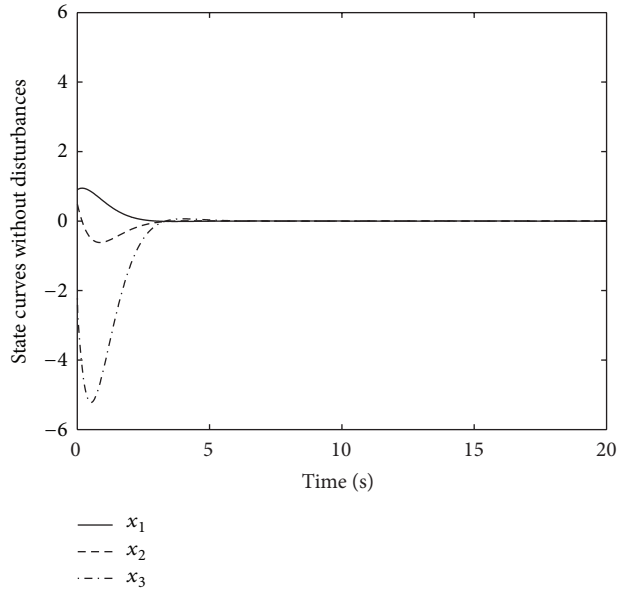

Figure 6: State curves without disturbances.

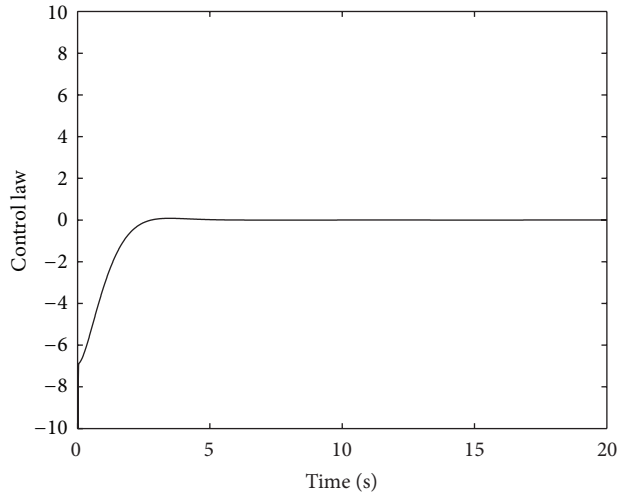

Figure 7: Control law without disturbances.

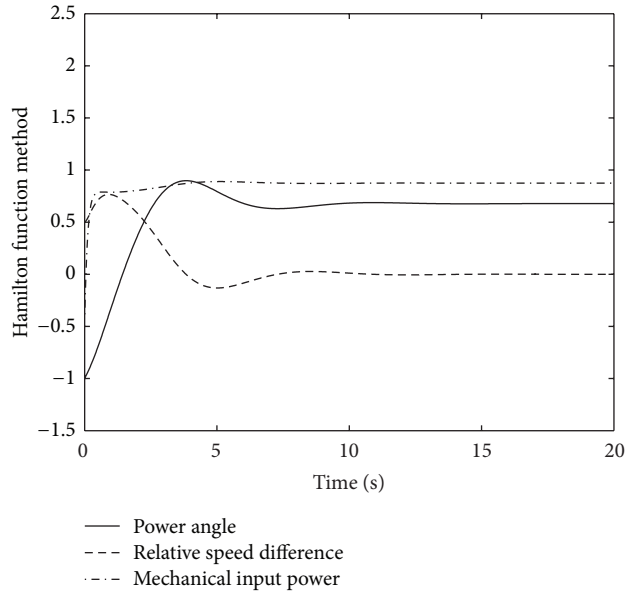

Figure 8: Response curves of Hamiltonian function method without disturbances.

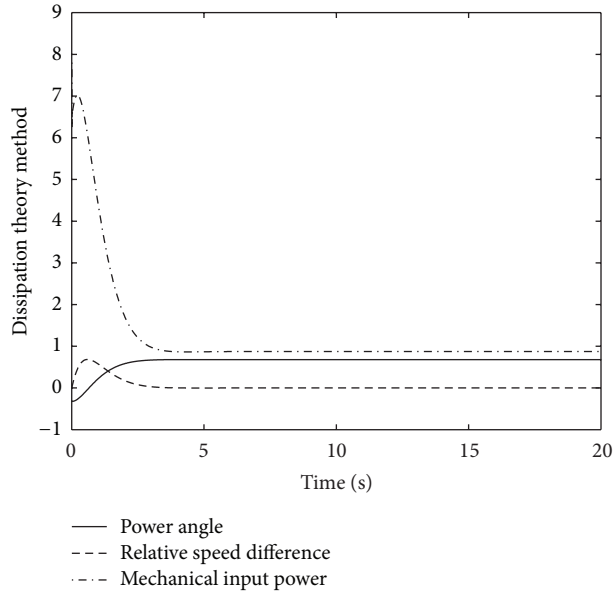

Figure 9: Response curves of dissipation theory method without disturbances.

system. From the dynamic process, it is seen that overshooting of Hamiltonian function method is less than that of dissipation theory method, and settling time of Hamiltonian function method is longer than that of dissipation. Then, in the presence of small disturbances with $\omega_1 = 1$, $\omega_2 = 1$, the simulation results are shown in Figures 10 and 11. It is shown that both of closed-loop systems are stable and the robust controller is effective. Next, with the enlargement of disturbances ($\omega_1 = 10$, $\omega_2 = 10$), the response curves are shown in Figures 12 and 13, where the controlled system of Hamiltonian function method is unstable and the power

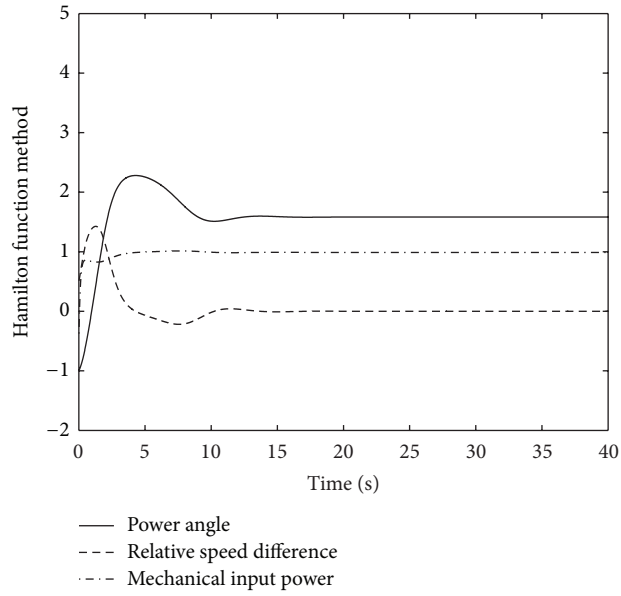

Figure 10: Response curves of Hamiltonian function method with small disturbances.

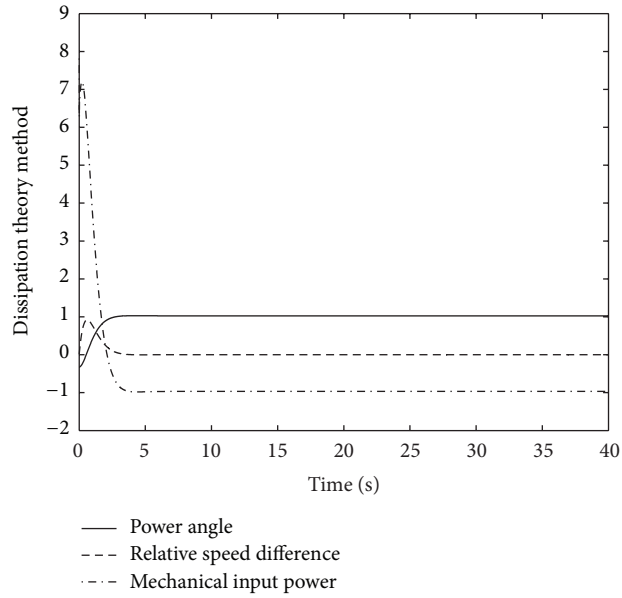

Figure 11: Response curves of dissipation theory method with small disturbances.

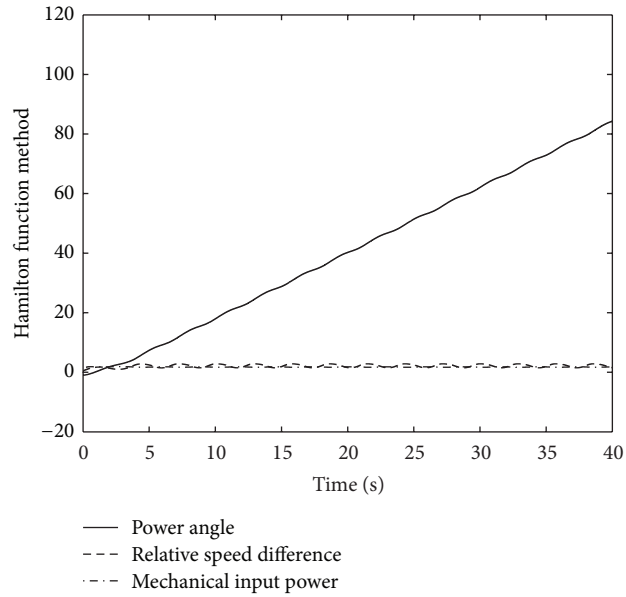

Figure 12: Response curves of Hamiltonian function method with large disturbances.

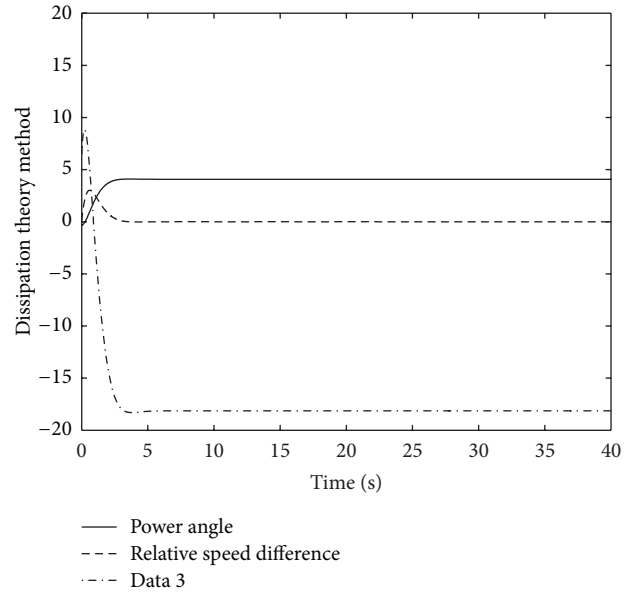

Figure 13: Response curves of dissipation theory method with large disturbances.

angle is out of control, while that of dissipation theory method is still stable, and the closed-loop system is L_2 stable.

In summary, based on Hamiltonian function method, the design process is concise, and the gotten controller (56) is simple, which is effective for the generator system in the presence of no disturbance or small disturbance. By using dissipation theory method, the construction of robust controller is relatively complex. However, it can guarantee that the closed-loop system is L_2 stable in all cases involving no disturbance, small disturbance, or large disturbance. Therefore, the proposed robust controller is more effective for the system with uncertain disturbance, especially for large disturbance.

6. Conclusions

In lower-triangular nonlinear systems, strict-feedback systems and high-order lower-triangular systems are two classes of main mathematical models. In this paper, the dissipation-based nonlinear controller is proposed to solve the robust control problem of these two systems. Uncertain disturbance

is dominated by the supply rate, and the stability analysis is based on the storage function. The design method integrates the energy supply, energy storage, and energy dissipation into the recursive construction of robust controller. The simulations illustrate that the gotten controller is effective and has the advantage in regulating large disturbance. In the future research, the dissipation-based idea can be expanded to the robust controller design for more nonlinear systems.

Acknowledgment

This work is supported by the National Natural Science Foundation of China (Grant no. 51007019).

References

[1] H. K. Khalil, *Nonlinear Systems*, Prentice-Hall, Upper Saddle River, NJ, USA, 3rd edition, 2002.

[2] M. Krstic, I. Kanellakopoulos, and P. V. Kokotovic, *Nonlinear and Adaptive Control Design*, Wiley, New York, NY, USA, 1995.

[3] R. Sepulchre, M. Jankovic, and P. V. Kokotovic, *Constructive Nonlinear Control*, Springer, New York, NY, USA, 1997.

[4] W. Lin and C. Qian, "Adding one power integrator: a tool for global stabilization of high-order lower-triangular systems," *Systems and Control Letters*, vol. 39, no. 5, pp. 339–351, 2000.

[5] H. Chen, H.-B. Ji, B. Wang, and H.-S. Xi, "Coordinated passivation techniques for the dual-excited and steam-valving control of synchronous generators," *IEE Proceedings: Control Theory and Applications*, vol. 153, no. 1, pp. 69–73, 2006.

[6] K. D. Do, Z. P. Jiang, and J. Pan, "On global tracking control of a VTOL aircraft without velocity measurements," *IEEE Transactions on Automatic Control*, vol. 48, no. 12, pp. 2212–2217, 2003.

[7] Z.-G. Hou, A.-M. Zou, L. Cheng, and M. Tan, "Adaptive control of an electrically driven nonholonomic mobile robot via backstepping and fuzzy approach," *IEEE Transactions on Control Systems Technology*, vol. 17, no. 4, pp. 803–815, 2009.

[8] C. I. Byrnes and A. Isidori, "New results and examples in nonlinear feedback stabilization," *Systems and Control Letters*, vol. 12, no. 5, pp. 437–442, 1989.

[9] J. Tsinias, "Sufficient Lyapunov-like conditions for stabilization," *Mathematics of Control, Signals, and Systems*, vol. 2, no. 4, pp. 343–357, 1989.

[10] J. Tsinias, "Triangular systems: a global extension of the coron-praly theorem on the existence of feedback-integrator stabilisers," *European Journal of Control*, vol. 3, no. 1, pp. 37–46, 1997.

[11] J.-M. Coron and L. Praly, "Adding an integrator for the stabilization problem," *Systems and Control Letters*, vol. 17, no. 2, pp. 89–104, 1991.

[12] S. Celikovsky and E. Aranda-Bricaire, "Constructive nonsmooth stabilization of triangular systems," *Systems and Control Letters*, vol. 36, no. 1, pp. 21–37, 1999.

[13] M. Tzamtzi and J. Tsinias, "Explicit formulas of feedback stabilizers for a class of triangular systems with uncontrollable linearization," *Systems and Control Letters*, vol. 38, no. 2, pp. 115–126, 1999.

[14] W. Lin and C. Qian, "Adaptive regulation of high-order lower-triangular systems: an adding a power integrator technique," *Systems and Control Letters*, vol. 39, no. 5, pp. 353–364, 2000.

[15] L. Liu, Z. Chen, and J. Huang, "Global disturbance rejection of lower triangular systems with an unknown linear exosystem," *IEEE Transactions on Automatic Control*, vol. 56, no. 7, pp. 1690–1695, 2011.

[16] C. Wen, J. Zhou, Z. Liu, and H. Su, "Robust adaptive control of uncertain nonlinear systems in the presence of input saturation and external disturbance," *IEEE Transactions on Automatic Control*, vol. 56, no. 7, pp. 1672–1678, 2011.

[17] Y. Yu and Y. Zhong, "Semi-global robust output tracking for non-linear uncertain systems in strict-feedback form," *IET Control Theory and Applications*, vol. 6, no. 5, pp. 751–759, 2012.

[18] R. Wang, G. Jin, and J. Zhao, "Robust fault-tolerant control for a class of switched nonlinear systems in lower triangular form," *Asian Journal of Control*, vol. 9, no. 1, pp. 68–72, 2007.

[19] C. Qian and W. Lin, "Practical output tracking of nonlinear systems with uncontrollable unstable linearization," *IEEE Transactions on Automatic Control*, vol. 47, no. 1, pp. 21–36, 2002.

[20] Z. Xi, D. Cheng, Q. Lu, and S. Mei, "Nonlinear decentralized controller design for multimachine power systems using Hamiltonian function method," *Automatica*, vol. 38, no. 3, pp. 527–534, 2002.

Hindawi Publishing Corporation
Mathematical Problems in Engineering
Volume 2013, Article ID 183279, 10 pages
http://dx.doi.org/10.1155/2013/183279

Research Article

Robust Adaptive Control and L_2 Disturbance Attenuation for Uncertain Hamiltonian Systems with Time Delay

Weiwei Sun,[1,2] Guochen Pang,[3] Pan Wang,[1] and Lianghong Peng[1]

[1] *Institute of Automation, Qufu Normal University, Qufu 273165, China*
[2] *School of Electrical Information and Automation, Qufu Normal University, Rizhao 276826, China*
[3] *Department of Automation, Southeast University, Nanjing 210096, China*

Correspondence should be addressed to Weiwei Sun; wwsun@hotmail.com

Received 20 June 2013; Accepted 8 July 2013

Academic Editor: Tao Li

This paper deals with the robust stabilizability and L_2 disturbance attenuation for a class of time-delay Hamiltonian control systems with uncertainties and external disturbances. Firstly, the robust stability of the given systems is studied, and delay-dependent criteria are established based on the dissipative structural properties of the Hamiltonian systems and the Lyapunov-Krasovskii (L-K) functional approach. Secondly, the problem of L_2 disturbance attenuation is considered for the Hamiltonian systems subject to external disturbances. An adaptive control law is designed corresponding to the time-varying delay pattern involved in the systems. It is shown that the closed-loop systems under the feedback control law can guarantee the γ-dissipative inequalities be satisfied. Finally, two numerical examples are provided to illustrate the theoretical developments.

1. Introduction

Systems with unknown delayed states are often encountered in practice, such as communication systems, engineering systems, and process control systems. For this reason, robust stability analysis for uncertain time-delay control systems has attracted a considerable amount of interests in recent years [1–9]. The Lyapunov-Krasovskii (L-K) method is always employed, and the results are often obtained in the form of linear matrix inequalities (LMIs). However, robust stabilization of nonlinear systems with time delays has been a challenging problem. As is well known, the control design of nonlinear systems is a difficult process. The existence of time delay in nonlinear systems further degrades the control performance and sometimes makes the closed-loop stabilization difficult [10–12]. More recently, Mahmoud and El Ferik obtained some new results on dissipative analysis and state feedback synthesis for a class of nonlinear systems with time-varying delays and convex polytypic uncertainties [12]. This class consists of linear time-delay systems subject to nonlinear cone-bounded perturbations. Hu et al. in [10] integrated the sliding mode control method with the robust H_∞ technique and developed a discrete-time sliding mode controller for a class of time-delay uncertain systems with stochastic nonlinearities. The nonlinearities are described by statistical means.

On the other hand, for affine nonlinear systems with disturbances, the L_2-gain analysis and the L_2 disturbance attenuation are always important issues [13]. Almost all these studies deal with the existence of solutions to some partial differential inequality, which reflects the dissipative behavior of the system under consideration for a certain supply rate which is called passivity-based control design method. This kind of method is used to achieve a γ-dissipative inequality which not only guarantees asymptotic stability but also renders the L_2-gain from disturbance to the penalty signal less than or equal to a given level $\gamma > 0$. The key to solve the problem of L_2 disturbance attenuation is to find a proper storage function that ensures the γ-dissipative inequality holding.

As an important class of nonlinear systems, port-controlled Hamiltonian systems (PCH) proposed by [14, 15] have attracted increasing attentions in the field of nonlinear control theory [16–18]. The Hamilton function in a PCH

system is considered as the sum of potential energy (excluding gravitational potential energy) and kinetic energy in physical systems, and it can be used as a good candidate of Lyapunov functions for many physical systems. Due to this and its nice structure with clear physical meaning, the PCH system has drawn a good deal of attention in practical control designs [19–23]. In [21], with a proper penalty signal, the γ-dissipativity was achieved by making a sufficiently large damping injection in the design stage. Wang et al. in [23] proposed an energy-based adaptive L_2 disturbance attenuation control scheme for the power systems with superconducting magnetic energy storage (SMES) units. Besides, Hamiltonian systems with time delay also have been studied [24–27]. Reference [25] addresses the stabilization problem of a class of Hamiltonian systems with state time delay and input saturation. The problem of L_2-disturbance attenuation for time-delay port-controlled Hamiltonian systems is studied in [26]. The case that there are time-invariant uncertainties belonging to some convex bounded polytypic domains is also considered in [26], and an L_2 disturbance attenuation control law is proposed. In practice, dynamic uncertainties often arise from many different control engineering applications. The inevitable uncertainties may enter a nonlinear system in a much more complex way. In addition to polytypic uncertainties, systems may encounter modeling error, parameter perturbations, and external disturbances. However, to the best of our knowledge, the analysis and synthesis for time-delay Hamiltonian systems with parametric perturbations have not been discussed yet. It is well worth pointing out that with the help of Hamiltonian realization [28, 29], the control problem of a large class of time-delay nonlinear systems with uncertainties can be solved via the Hamiltonian system framework. Thus, study of time-delay Hamiltonian control systems with uncertainties and disturbances is a meaningful topic.

Motivated by the above observations, in this paper we study a class of time-delay Hamiltonian systems model with uncertainties and external disturbances. We derive sufficient condition for which the uncertain time-delay Hamiltonian system along with the proposed feedback controller is robustly stable for all admissible uncertainties. The condition is given in terms of linear matrix inequalities. Furthermore, the problem of L_2 disturbance attenuation is examined using the parametric adaptive methodology for delay-dependent case. The L_2 feedback adaptive control law can guarantee that the closed-loop time-delay Hamiltonian system is asymptotically stable and the L_2 performance is achieved. The effectiveness of the proposed methods in this paper is illustrated by numerical examples.

The paper is organized as follows. Section 2 presents the problem formulation and some preliminaries. The main results are proposed in Section 3. Section 4 illustrates the obtained results by several numerical examples, which is followed by the conclusion in Section 5.

Notations. $\mathbb{R}^n$ denotes the n-dimension Euclidean space, and $\mathbb{R}^{n\times m}$ is the real matrices with dimension $n \times m$; $\|\cdot\|$ stands for either the Euclidean vector norm or the induced matrix 2-norm; $\|x\|_{\mathscr{C}} = \max_{t-h\leqslant\varphi\leqslant t}\|x(\varphi)\|$, where $\mathscr{C} = \mathscr{C}([-h, 0], \mathbb{R}^n)$ denotes the Banach space of continuous functions mapping the interval $[-h, 0]$ into $\mathbb{R}^n$; $L_2^n[0,\infty)$ denotes the set of all measurable functions $x : [0,\infty) \to \mathbb{R}^n$ that satisfy $\int_0^\infty |x(t)|^2 dt < \infty$. $\mathbb{C}^i$ denotes the set of all functions with continuous ith partial derivatives. The notation $X \geqslant Y$ (resp., $X > Y$) where X and Y are symmetric matrices means that the matrix $X - Y$ is positive semidefinite (resp., positive definite); $\lambda_{\max}(A)$ and $\lambda_{\min}(A)$ denote the maximum and the minimum of eigenvalue of a real symmetric matrix A. The notation $*$ represents the elements below the main diagonal of a symmetric matrix; A^{T} denotes the transposed matrix of A; $(\cdot)'$ and $[\cdot]'$ denote the derivative of the variable inside the brackets. What is more, for the sake of simplicity, throughout the paper, we denote $\partial H/\partial x$ by ∇H.

2. Problem Statement and Preliminaries

Consider the following class of time-delay Hamiltonian systems with parametric uncertainties and external disturbances:

$$\begin{aligned}\dot{x}(t) = {} & \left[J(x,p) - R(x,p)\right]\nabla H(x,p) \\ & + \left[J^*(x_\tau) - R^*(x_\tau)\right]\nabla H(x_\tau) + g_1 u(t) + g_2\omega(t),\end{aligned} \tag{1}$$

where $x(t) \in \mathbb{R}^n$ is the state; $x_\tau := x(t - d(t)) \in \mathscr{C}$ stands for the delayed state; $u \in \mathbb{R}^s$ is the control input; $\omega \in L_2^m[0,\infty)$ is the disturbance input; $H(x) : \mathbb{R}^n \to \mathbb{R}$ is the Hamilton function which satisfies $H(x) \geqslant 0$, $H(0) = 0$; p is an unknown constant vector and denotes the disturbance parameter; $J(x,p), J^*(x_\tau) \in \mathbb{R}^{n\times n}$ are skew-symmetric structure matrices; $R(x,p), R^*(x_\tau) \in \mathbb{R}^{n\times n}$ are positive semidefinite symmetric matrices; g_1 and g_2 are gain matrices of appropriate dimensions; $g_1 g_1^{\mathrm{T}}$ is nonsingular.

The delay $d(t)$ is a time-varying continuous function which satisfies

$$\begin{aligned} & 0 \leqslant d(t) \leqslant h, \\ & \dot{d}(t) \leqslant \mu < 1, \end{aligned} \tag{2}$$

where the bounds h and μ are known positive scalars.

The initial condition is $x(t) = \phi(t)$, $t \in [-h, 0]$.

Throughout the paper, we suppose that the following assumptions are satisfied.

Assumption 1. The matrices $R(x,p)$ and $R^*(x_\tau)$ satisfy

$$R(x,p) \geqslant \overline{R}, \qquad R^*(x_\tau) \geqslant \overline{R}^*, \tag{3}$$

where $\overline{R}, \overline{R}^* \geqslant 0$ are known constant matrices.

Assumption 1 means that $R(x,p)$ and $R^*(x_\tau)$ are unknown, but they are bounded by known nonnegative constant matrices. To illustrate that this assumption is reasonable, an example is given below.

Example 2. Consider two functional matrices

$$R_1(x,p) = \begin{pmatrix} \left(1+p^2x_1^2\right)^2 + x_2^2 & x_2 \\ x_2 & 2 \end{pmatrix},$$
$$R_2(x_\tau) = \begin{pmatrix} 2+x_1^2(t-\tau) & 0 & 0 \\ 0 & \sin^2(x_2(t-\tau)) & 0 \\ 0 & 0 & 0 \end{pmatrix}, \tag{4}$$

where p is unknown constant and τ is the time delay.

It is easy to find two corresponding matrices

$$\overline{R} = \begin{pmatrix} 1 & 0 \\ 0 & 1 \end{pmatrix},$$
$$\overline{R}^* = \begin{pmatrix} 2 & 0 & 0 \\ 0 & 0 & 0 \\ 0 & 0 & 0 \end{pmatrix}, \tag{5}$$

which satisfy $R_1(x,p) \geqslant \overline{R}$ and $R_2(x_\tau) \geqslant \overline{R}^*$.

Assumption 3. The Hamilton function $H(x)$ and its gradient $\nabla H(x)$ satisfy

(A1) $H(x) \in \mathbb{C}^2$,

(A2) $\varepsilon_1(\|x\|) \leqslant H(x) \leqslant \varepsilon_2(\|x\|)$,

(A3) $\epsilon_1(\|x\|) \leqslant \nabla^{\mathrm{T}} H(x) \cdot \nabla H(x) \leqslant \epsilon_2(\|x\|)$,

(A4) $\pi_1(\|x\|) \leqslant [(\nabla H(x))']^{\mathrm{T}} \cdot [\nabla H(x)]' \leqslant \pi_2(\|x\|)$,

where $\varepsilon_1, \varepsilon_2, \epsilon_1, \epsilon_2, \pi_1, \pi_2$ all belong to $\mathscr{K}$-class functions.

Remark 4. Assumption 3 not only guarantees the existence of $\nabla H(x)$ and $[\nabla H(x)]'$ but also guarantees that $H(x)$, $\nabla H(x)$, and $[\nabla H(x)]'$ are bounded in terms of x. We shall note that the assumption is not very conservative to Hamilton functions and the majority of Hamilton functions in Hamiltonian systems can easily satisfy these conditions.

Assumption 5. There exists a function $\Phi(x)$ such that

$$[J(x,p) - R(x,p)]\,\Delta_H(x,p) = g_1\Phi(x)\theta \tag{6}$$

holds for all $x \in \mathbb{R}^n$, where $\theta \in \mathbb{R}^s$ denotes an unknown parametric vector, $\Delta_H(x,p) = \nabla H(x,p) - \nabla H(x,0)$.

In what follows, we shall address the problems of robust stability and the disturbance attenuation of system (1). Specifically, the objective of this paper can be summarized as follows.

(i) Robust Stability Problem. In the absence of disturbances ω, develop LMI-based conditions, and find an adaptive control law of the form

$$u = \alpha\left(x,\widehat{\theta}\right), \qquad \dot{\widehat{\theta}} = \varsigma(x) \tag{7}$$

so that the closed-loop system under the control law can be asymptotically stable.

(ii) L_2 Disturbance Attenuation Problem. Given a penalty signal $z = q(x)$ and a disturbance attenuation level $\gamma > 0$, find an adaptive feedback control law

$$u = \beta\left(x,\widehat{\theta}\right), \qquad \dot{\widehat{\theta}} = \rho(x) \tag{8}$$

and a positive storage function $V(x,x_\tau,\widetilde{\theta})$ such that the γ-dissipation inequality

$$\dot{V}\left(x,x_\tau,\widetilde{\theta}\right) + Q(x,x_\tau) \leqslant \frac{1}{2}\left\{\gamma^2\|\omega\|^2 - \|z\|^2\right\}, \quad \forall\omega \in L_2^m[0,\infty) \tag{9}$$

holds along the closed-loop systems consisting of (1) and the feedback law, where $Q(x,x_\tau)$ is a nonnegative definite symmetric matrix.

We conclude this section by recalling an auxiliary result to be used in this paper.

Lemma 6 (see [30]). *For given matrices $Y = Y^{\mathrm{T}}$, D and E with appropriate dimensions,*

$$Y + DF(t)E + E^{\mathrm{T}}F^{\mathrm{T}}(t)D^{\mathrm{T}} < 0 \tag{10}$$

holds for all $F(t)$ satisfying $F^{\mathrm{T}}(t)F(t) \leqslant I$ if and only if there exists $c > 0$ such that

$$Y + c^{-1}DD^{\mathrm{T}} + cE^{\mathrm{T}}E < 0. \tag{11}$$

3. Main Results

3.1. Robust Stabilization. In the absence of external disturbances, namely, $\omega = 0$, and under Assumption 5, system (1) can be transformed into

$$\dot{x} = [J(x,p) - R(x,p)]\nabla H(x) + [J^*(x_\tau) - R^*(x_\tau)]\nabla H(x_\tau) + g_1\Phi(x)\theta + g_1u. \tag{12}$$

In this subsection, we will put forward a robust stabilization result for system (12). Delay-dependent criteria are developed as follows.

Theorem 7. *Consider system* (12). *Suppose that Assumptions 1 and 3 hold. If there exist matrices*

$$0 < P_1 = P_1^{\mathrm{T}}, \qquad 0 < Z_1 = Z_1^{\mathrm{T}}, \qquad 0 < M_1 = M_1^{\mathrm{T}},$$
$$0 \leqslant X = X^{\mathrm{T}} = \begin{pmatrix} X_{11} & X_{12} & X_{13} \\ X_{21} & X_{22} & X_{23} \\ X_{31} & X_{32} & X_{33} \end{pmatrix}, \tag{13}$$

any appropriately dimensioned matrices E, F, T, B_1, B_2, and a scalar $\varepsilon > 0$ such that the following conditions hold:

$$J^*(x_\tau) - R^*(x_\tau) = E\Delta(x_\tau)F + T, \tag{14}$$

$$\Xi_1 = \begin{pmatrix} -\overline{R} - \overline{R}^* & \frac{B_1^{\mathrm{T}}}{2} + hX_{12} & \frac{B_2^{\mathrm{T}}}{2} + hX_{13} \\ * & \Phi_{22} & -\frac{B_2^{\mathrm{T}}}{2} + hX_{23} \\ * & * & -M_1 + hZ_1 + hX_{33} \end{pmatrix} < 0, \tag{15}$$

$$\Theta = \begin{pmatrix} X_{11} + \varepsilon^{-1}EE^{\mathrm{T}} & X_{12} & X_{13} & \frac{1}{2}T \\ * & X_{22} & X_{23} & \frac{1}{2}B_1 \\ * & * & X_{33} & \frac{1}{2}B_2 \\ * & * & * & Z_1 + \varepsilon^{-1}F^{\mathrm{T}}F \end{pmatrix} \geqslant 0, \tag{16}$$

where

$$\begin{aligned} &\Delta^{\mathrm{T}}(x_\tau)\Delta(x_\tau) \leqslant I, \\ &\Phi_{22} = -(1-\mu)P_1 - \frac{B_1}{2} - \frac{B_1^{\mathrm{T}}}{2} + hX_{22}, \end{aligned} \tag{17}$$

then the closed-loop systems under the feedback control law

$$\begin{aligned} u = & -g_1^{\mathrm{T}}\left(g_1 g_1^{\mathrm{T}}\right)^{-1}\Big\{(P_1 + hX_{11})\nabla H(x) - \Phi(x)\widehat{\theta} \\ & + \left[\nabla^{\mathrm{T}}H(x)\cdot\nabla H(x)\right]^{-1}\nabla H(x) \\ & \times\left[(\nabla H(x(t)))'\right]^{\mathrm{T}}M_1[\nabla H(x(t))]'\Big\}, \\ \dot{\widehat{\theta}} = & K_1\Phi^{\mathrm{T}}(x)\, g_1^{\mathrm{T}}\nabla H(x) \end{aligned} \tag{18}$$

is asymptotically stable, where $K_1 > 0$ is an adaptive gain matrix with appropriate dimension.

Proof. Substituting (18) into (12) yields

$$\begin{aligned} \dot{x} = & \left[J(x,p) - R(x,p)\right]\nabla H(x) \\ & + \left[J^*(x_\tau) - R^*(x_\tau)\right]\nabla H(x_\tau) \\ & + g_1\Phi(x)\left(\theta - \widehat{\theta}\right) - (P_1 + hX_{11})\nabla H(x) \\ & - \left[\nabla^{\mathrm{T}}H(x)\nabla H(x)\right]^{-1}\nabla H(x)\left[(\nabla H(x(t)))'\right]^{\mathrm{T}} \\ & \times M_1[\nabla H(x(t))]', \\ & \dot{\widehat{\theta}} = K_1\Phi^{\mathrm{T}}(x)\, g_1^{\mathrm{T}}\nabla H(x). \end{aligned} \tag{19}$$

Choose a Lyapunov functional described as

$$\begin{aligned} V_1\left(x, x_\tau, \widetilde{\theta}\right) = & H(x) + \frac{1}{2}\widetilde{\theta}^{\mathrm{T}}K_1^{-1}\widetilde{\theta} \\ & + \int_{t-d(t)}^{t}\nabla^{\mathrm{T}}H(x(\varphi))\, P_1\nabla H(x(\varphi))\, d\varphi \\ & + \int_{-h}^{0}\int_{t+\beta}^{t}\left[(\nabla H(x(\alpha)))'\right]^{\mathrm{T}} \\ & \times Z_1[\nabla H(x(\alpha))]'\, d\alpha\, d\beta, \end{aligned} \tag{20}$$

where $\widetilde{\theta} = \theta - \widehat{\theta}$.

Since $H(x) \in \mathbb{C}^2$, $P_1 > 0$, $Z_1 > 0$, and (A3) in Assumption 3 holds, we have the following inequalities:

$$\begin{aligned} & \int_{t-d(t)}^{t}\nabla^{\mathrm{T}}H(x(\varphi))\, P_1\nabla H(x(\varphi))\, d\varphi \\ & \leqslant \int_{t-d(t)}^{t}\left\|\nabla^{\mathrm{T}}H(x(\varphi))\, P_1\nabla H(x(\varphi))\right\| d\varphi \\ & \leqslant \iota_p\int_{t-d(t)}^{t}\epsilon_2\left(\max\|x(\varphi)\|\right)d\varphi \\ & = h\iota_p\epsilon_2\left(\|x\|_{\mathscr{C}}\right), \end{aligned} \tag{21}$$

where $\iota_p = \lambda_{\max}(P_1) > 0$.

Moreover, according to (A4) in Assumption 3, we have

$$\begin{aligned} & \int_{-h}^{0}\int_{t+\beta}^{t}\left[(\nabla H(x(\alpha)))'\right]^{\mathrm{T}}Z_1[\nabla H(x(\alpha))]'\, d\alpha\, d\beta \\ & \leqslant \int_{-h}^{0}\int_{t+\beta}^{t}\iota_z\pi_2(\|x(\alpha)\|)\, d\alpha\, d\beta \\ & = \frac{1}{2}h^2\iota_z\pi_2\left(\|x\|_{\mathscr{C}}\right), \end{aligned} \tag{22}$$

where $\iota_z = \lambda_{\max}(Z_1) > 0$.

Combining (21) and (22), from (A2) in Assumption 3, we obtain

$$\begin{aligned} V_1\left(x, x_\tau, \widetilde{\theta}\right) \leqslant & \varepsilon_2(\|x\|) + \kappa\left\|\widetilde{\theta}\right\|^2 \\ & + h\iota_p\epsilon_2\left(\|x\|_{\mathscr{C}}\right) + \frac{1}{2}h^2\iota_z\pi_2\left(\|x\|_{\mathscr{C}}\right), \end{aligned} \tag{23}$$

where $\kappa = \lambda_{\max}(K_1^{-1}) > 0$.

Let $\nu(\|\chi\|_{\mathscr{C}}) = \varepsilon_2(\|x\|) + \kappa\|\widetilde{\theta}\|^2 + h\iota_p\epsilon_2(\|x\|_{\mathscr{C}}) + (1/2)h^2\iota_z\pi_2(\|x\|_{\mathscr{C}})$, $\chi = \left[x^{\mathrm{T}}\ \ x_\tau^{\mathrm{T}}\ \ \widetilde{\theta}^{\mathrm{T}}\right]^{\mathrm{T}}$. Obviously, it belongs to $\mathscr{K}$-class function. So, we obtain

$$\varepsilon_1\left(\|\chi(0)\|\right) \leqslant V_1\left(x, x_\tau, \widetilde{\theta}\right) \leqslant \nu\left(\|\chi\|_{\mathscr{C}}\right). \tag{24}$$

According to the Newton-Leibnitz formula, it follows that

$$\nabla H(x) - \int_{t-d(t)}^{t}[\nabla H(x(\alpha))]'\, d\alpha - \nabla H(x_\tau) = 0; \tag{25}$$

then for any matrices B_1 and B_2 with appropriate dimensions, we have

$$\begin{aligned}&\left\{\nabla^{\mathrm{T}}H(x)\left[J^{*}(x_\tau)-R^{*}(x_\tau)\right]+\nabla^{\mathrm{T}}H(x_\tau)B_1\right.\\&\left.+[\nabla H(x(t))]'B_2\right\}\\&\cdot\left[\nabla H(x)-\nabla H(x_\tau)-\int_{t-d(t)}^{t}[\nabla H(x(\alpha))]'d\alpha\right]\equiv 0.\end{aligned}\tag{26}$$

As is well known, for any positive definite matrix $X \geqslant 0$ and a vector function η, the following inequality holds:

$$h\eta^{\mathrm{T}}(t)X\eta(t)-\int_{t-d(t)}^{t}\eta^{\mathrm{T}}(t)X\eta(t)\,d\alpha\geqslant 0.\tag{27}$$

Noting that

$$\begin{aligned}&\nabla^{\mathrm{T}}H(x)J(x,p)\nabla H(x)\\&\quad=\frac{1}{2}\nabla^{\mathrm{T}}H(x)\left[J(x,p)+J^{\mathrm{T}}(x,p)\right]\nabla H(x)=0\end{aligned}\tag{28}$$

and combining (26) and (27) and using Assumption 1, we can evaluate the derivative of $V_1(x,x_\tau,\widetilde{\theta})$ along the trajectory of the closed-loop system (19) as follows:

$$\begin{aligned}&\dot{V}_1\left(x,x_\tau,\widetilde{\theta}\right)\\&\quad=\nabla^{\mathrm{T}}H(x)\left[J(x,p)-R(x,p)\right]\nabla H(x)\\&\qquad+\nabla^{\mathrm{T}}H(x)\left[J^{*}(x_\tau)-R^{*}(x_\tau)\right]\nabla H(x_\tau)\\&\qquad+\nabla^{\mathrm{T}}H(x)g_1\Phi(x)\widetilde{\theta}+\nabla^{\mathrm{T}}H(x)P_1\nabla H(x)\\&\qquad-\nabla^{\mathrm{T}}H(x)\left(P_1+hX_{11}\right)\nabla H(x)\\&\qquad-\left[(\nabla H(x(t)))'\right]^{\mathrm{T}}M_1[\nabla H(x(t))]'\\&\qquad-\left(1-\dot{d}(t)\right)\nabla^{\mathrm{T}}H(x_\tau)P_1\nabla H(x_\tau)\\&\qquad-\widetilde{\theta}^{\mathrm{T}}\Phi^{\mathrm{T}}(x)g_1^{\mathrm{T}}\nabla H(x)\\&\qquad+h\left[(\nabla H(x(t)))'\right]^{\mathrm{T}}Z_1[\nabla H(x(t))]'\\&\qquad-\int_{t-h}^{t}\left[(\nabla H(x(\alpha)))'\right]^{\mathrm{T}}Z_1[\nabla H(x(\alpha))]'d\alpha\\&\quad\leqslant-\nabla^{\mathrm{T}}H(x)\overline{R}\nabla H(x)-h\nabla^{\mathrm{T}}H(x)X_{11}\nabla H(x)\\&\qquad-\left[(\nabla H(x(t)))'\right]^{\mathrm{T}}M_1[\nabla H(x(t))]'\\&\qquad-(1-\mu)\nabla^{\mathrm{T}}H(x_\tau)P_1\nabla H(x_\tau)\\&\qquad-\int_{t-d(t)}^{t}\left[(\nabla H(x(\alpha)))'\right]^{\mathrm{T}}Z_1[\nabla H(x(\alpha))]'d\alpha\\&\qquad+h\left[(\nabla H(x(t)))'\right]^{\mathrm{T}}Z_1[\nabla H(x(t))]'\\&\qquad-\nabla^{\mathrm{T}}H(x)\overline{R}^{*}\nabla H(x)\\&\qquad+\nabla^{\mathrm{T}}H(x_\tau)B_1\nabla H(x)-\nabla^{\mathrm{T}}H(x_\tau)B_1\nabla H(x_\tau)\\&\qquad+\left[(\nabla H(x(t)))'\right]^{\mathrm{T}}B_2\nabla H(x)\\&\qquad-\left[(\nabla H(x(t)))'\right]^{\mathrm{T}}B_2\nabla H(x_\tau)\\&\qquad-\int_{t-d(t)}^{t}\nabla^{\mathrm{T}}H(x)\left[E\Delta(x_\tau)F+T\right][\nabla H(x(\alpha))]'d\alpha\\&\qquad-\int_{t-d(t)}^{t}\nabla^{\mathrm{T}}H(x_\tau)B_1[\nabla H(x(\alpha))]'d\alpha\\&\qquad-\int_{t-d(t)}^{t}\left[(\nabla H(x(t)))'\right]^{\mathrm{T}}\\&\qquad\quad\times B_2[\nabla H(x(\alpha))]'d\alpha+h\eta_1^{\mathrm{T}}X\eta_1\\&\qquad-\int_{t-d(t)}^{t}\eta_1^{\mathrm{T}}(t)X\eta_1(t)\,d\alpha,\end{aligned}\tag{29}$$

where $\eta_1=\left[\nabla^{\mathrm{T}}H(x)\ \ \nabla^{\mathrm{T}}H(x_\tau)\ \ [(\nabla H(x(t)))']^{\mathrm{T}}\right]^{\mathrm{T}}$.

Let

$$\begin{aligned}&\eta_2\\&=\left[\nabla^{\mathrm{T}}H(x)\ \ \nabla^{\mathrm{T}}H(x_\tau)\ \ \left[(\nabla H(x(t)))'\right]^{\mathrm{T}}\ \ \left[(\nabla H(x(\alpha)))'\right]^{\mathrm{T}}\right]^{\mathrm{T}};\end{aligned}\tag{30}$$

according to (15)-(16) and using Lemma 6, we get that

$$\dot{V}_1\left(x,x_\tau,\widetilde{\theta}\right)\leqslant\eta_1^{\mathrm{T}}\Xi_1\eta_1-\int_{t-d(t)}^{t}\eta_2^{\mathrm{T}}\Theta\eta_2 d\alpha\leqslant\eta_1^{\mathrm{T}}\Xi_1\eta_1.\tag{31}$$

Furthermore, since $\Xi_1 < 0$, according to Assumption 3, there exists a continuous nondecreasing function $\epsilon(\|\chi\|)$, $\chi=[x^{\mathrm{T}}\ \ x_\tau^{\mathrm{T}}\ \ \widetilde{\theta}^{\mathrm{T}}]^{\mathrm{T}}$ such that

$$\dot{V}_1\left(x,x_\tau,\widetilde{\theta}\right)\leqslant-\epsilon\left(\|\chi(0)\|\right).\tag{32}$$

According to the Lyapunov-Krasovskii stability theorem, we can conclude that the closed-loop system (19) consisting of system (12) and the control law (18) is asymptotically stable. This completes the proof. □

3.2. L_2 Disturbance Attenuation. In what follows, we consider the L_2 disturbance attenuation problem of systems (1). Given

a disturbance attenuation level $\gamma > 0$, choose the following penalty function:

$$z = h(x)\, g_1^{\mathrm{T}} \nabla H(x), \tag{33}$$

where $h(x) \in \mathbb{R}^{q\times s}$ is weighing matrix.

For time delay $d(t)$ satisfying (2), we have the following result.

Theorem 8. *Consider system* (1). *Suppose that Assumptions 1–5 hold. If there exist matrices*

$$0 < P_2 = P_2^{\mathrm{T}}, \qquad 0 < Z_2 = Z_2^{\mathrm{T}}, \qquad 0 < M_2 = M_2^{\mathrm{T}}, \tag{34}$$

$$0 \leqslant \overline{X} = \begin{pmatrix} \overline{X}_{11} & \overline{X}_{12} & \overline{X}_{13} \\ \overline{X}_{21} & \overline{X}_{22} & \overline{X}_{23} \\ \overline{X}_{31} & \overline{X}_{32} & \overline{X}_{33} \end{pmatrix}, \tag{35}$$

any appropriately dimensioned matrices E, F, T, B_3, B_4 and a scalar $\varepsilon > 0$ such that (14) *and the following conditions hold*

$$\Xi_2 = \begin{pmatrix} \overline{\Phi}_{11} = -\overline{R} - \overline{R}^* - \dfrac{1}{2\gamma^2}\left(g_1 g_1^{\mathrm{T}} - g_2 g_2^{\mathrm{T}}\right) & \dfrac{B_3^{\mathrm{T}}}{2} + h\overline{X}_{12} & \dfrac{B_4^{\mathrm{T}}}{2} + h\overline{X}_{13} \\ * & -(1-\mu)P_2 - \dfrac{B_3}{2} - \dfrac{B_3^{\mathrm{T}}}{2} + h\overline{X}_{22} & -\dfrac{B_4^{\mathrm{T}}}{2} + h\overline{X}_{23} \\ * & * & -M_2 + hZ_2 + h\overline{X}_{33} \end{pmatrix} < 0,$$

$$\overline{\Theta} = \begin{pmatrix} \overline{X}_{11} + \varepsilon^{-1}EE^{\mathrm{T}} & \overline{X}_{12} & \overline{X}_{13} & \dfrac{1}{2}T \\ * & \overline{X}_{22} & \overline{X}_{23} & \dfrac{1}{2}B_3 \\ * & * & \overline{X}_{33} & \dfrac{1}{2}B_4 \\ * & * & * & Z_2 + \varepsilon F^{\mathrm{T}}F \end{pmatrix} \geqslant 0, \tag{36}$$

then the L_2 disturbance attenuation problem of system (1) *can be solved by the feedback control law:*

$$\begin{aligned} u = & -g_1^{\mathrm{T}}\left(g_1 g_1^{\mathrm{T}}\right)^{-1}\left\{\left(P_2 + h\overline{X}_{11}\right)\nabla H(x) - \Phi(x)\,\widehat{\theta}\right. \\ & + \left[\nabla^{\mathrm{T}} H(x)\,\nabla H(x)\right]^{-1}\nabla H(x) \\ & \left.\times\left[(\nabla H(x(t)))'\right]^{\mathrm{T}} M_2[\nabla H(x(t))]'\right\} \\ & -\left[\frac{1}{2}h^{\mathrm{T}}(x)\,h(x) + \frac{1}{2\gamma^2}I_m\right] g_1^{\mathrm{T}}\nabla H(x), \\ & \dot{\widehat{\theta}} = K_2\Phi^{\mathrm{T}}(x)\, g_1^{\mathrm{T}}\nabla H(x), \end{aligned} \tag{37}$$

where $K_2 > 0$ is an adaptive gain matrix with appropriate dimension.

Moreover, the γ-dissipation inequality

$$V_2\left(x, x_\tau, \widetilde{\theta}\right) + Q(x, x_\tau) \leqslant \frac{1}{2}\left\{\gamma^2\|\omega\|^2 - \|z\|^2\right\} \tag{38}$$

holds along the trajectories of the closed-loop systems consisting of (1) *and* (37), *where*

$$Q(x, x_\tau) = -\eta_1^{\mathrm{T}}\Xi_2\eta_1 + \int_{t-d(t)}^{t}\eta_2^{\mathrm{T}}\overline{\Theta}\eta_2 d\alpha \tag{39}$$

with

$$\begin{aligned} \eta_1 &= \left[\nabla^{\mathrm{T}}H(x) \;\; \nabla^{\mathrm{T}}H(x_\tau) \;\; \left[(\nabla H(x(t)))'\right]^{\mathrm{T}}\right]^{\mathrm{T}}, \\ \eta_2 &= \left[\nabla^{\mathrm{T}}H(x) \;\; \nabla^{\mathrm{T}}H(x_\tau) \;\; \left[(\nabla H(x(t)))'\right]^{\mathrm{T}} \;\; \left[(\nabla H(x(\alpha)))'\right]^{\mathrm{T}}\right]^{\mathrm{T}}. \end{aligned} \tag{40}$$

The storage function is given as

$$\begin{aligned} & V_2\left(x, x_\tau, \widetilde{\theta}\right) \\ & = H(x) + \int_{t-d(t)}^{t}\nabla^{\mathrm{T}}H(x(\varphi))\,P_2\nabla H(x(\varphi))\,d\varphi \\ & \quad + \int_{-h}^{0}\int_{t-d(t)}^{t}\left[\nabla^{\mathrm{T}}H(x(\alpha))\right]' Z_2[\nabla H(x(\alpha))]'\,d\alpha\,d\beta \\ & \quad + \frac{1}{2}\widetilde{\theta}^{\mathrm{T}}K_2^{-1}\widetilde{\theta}. \end{aligned} \tag{41}$$

Proof. Substituting (37) into (1) yields

$$\begin{aligned}\dot{x} = {} & [J(x,p) - R(x,p)]\nabla H(x) \\ & + [J^*(x_\tau) - R^*(x_\tau)]\nabla H(x_\tau) \\ & - \left(P_2 + h\overline{X}_{11}\right)\nabla H(x) + g_2\omega \\ & - \left[\nabla^{\mathrm{T}} H(x)\nabla H(x)\right]^{-1}\nabla H(x) \\ & \times \left[(\nabla H(x(t)))'\right]^{\mathrm{T}} M_2 [\nabla H(x(t))]' \\ & + g_1\Phi(x)\left(\theta - \widehat{\theta}\right) \\ & - g_1\left[\frac{1}{2}h^{\mathrm{T}}(x)h(x) + \frac{1}{2\gamma^2}I_m\right] g_1^{\mathrm{T}}\nabla H(x), \\ \dot{\widehat{\theta}} = {} & K_2\Phi^{\mathrm{T}}(x) g_1^{\mathrm{T}}\nabla H(x). \end{aligned} \tag{42}$$

Evaluating the derivative of (41) along the trajectory of system (42) and using (26), (27), and Assumption 1, we get

$$\begin{aligned}\dot{V}_2 & \left(x, x_\tau, \widetilde{\theta}\right) \\ = {} & \nabla^{\mathrm{T}} H(x)[J(x,p) - R(x,p)]\nabla H(x) \\ & + \nabla^{\mathrm{T}} H(x)[J^*(x_\tau) - R^*(x_\tau)]\nabla H(x_\tau) \\ & - h\nabla^{\mathrm{T}} H(x)\overline{X}_{11}\nabla H(x) + \nabla^{\mathrm{T}} H(x) g_2\omega \\ & - \left[(\nabla H(x(t)))'\right]^{\mathrm{T}} M_2[\nabla H(x(t))]' \\ & - \nabla^{\mathrm{T}} H(x) g_1\left[\frac{1}{2}h^{\mathrm{T}}(x)h(x) + \frac{1}{2\gamma^2}I_m\right] g_1^{\mathrm{T}}\nabla H(x) \\ & - \left(1 - \dot{d}(t)\right)\nabla^{\mathrm{T}} H(x_\tau) P_2\nabla H(x_\tau) \\ & + h\left[(\nabla H(x(t)))'\right]^{\mathrm{T}} Z_2[\nabla H(x(t))]' \\ & - \int_{t-h}^{t}\left[(\nabla H(x(\alpha)))'\right]^{\mathrm{T}} Z_2[\nabla H(x(\alpha))]' d\alpha \\ \leqslant {} & -\nabla^{\mathrm{T}} H(x)\overline{R}\nabla H(x) - h\nabla^{\mathrm{T}} H(x)\overline{X}_{11}\nabla H(x) \\ & - \left[(\nabla H(x(t)))'\right]^{\mathrm{T}} M_2[\nabla H(x(t))]' \\ & - (1-\mu)\nabla^{\mathrm{T}} H(x_\tau) P_2\nabla H(x_\tau) \\ & + h\left[(\nabla H(x(t)))'\right]^{\mathrm{T}} Z_2[\nabla H(x(t))]' \\ & - \int_{t-h}^{t}\left[(\nabla H(x(\alpha)))'\right]^{\mathrm{T}} Z_2[\nabla H(x(\alpha))]' d\alpha \\ & + \nabla^{\mathrm{T}} H(x)[J^*(x_\tau) - R^*(x_\tau)]\nabla H(x) \\ & + \nabla^{\mathrm{T}} H(x_\tau) B_3\nabla H(x) \\ & - \nabla^{\mathrm{T}} H(x_\tau) B_3\nabla H(x_\tau) + \left[(\nabla H(x(t)))'\right]^{\mathrm{T}} B_4\nabla H(x) \\ & - \int_{t-d(t)}^{t}\nabla^{\mathrm{T}} H(x)[J^*(x_\tau) - R^*(x_\tau)][\nabla H(x(\alpha))]' d\alpha \\ & - \int_{t-d(t)}^{t}\nabla^{\mathrm{T}} H(x_\tau) B_3[\nabla H(x(\alpha))]' d\alpha \\ & - \left[(\nabla H(x(t)))'\right]^{\mathrm{T}} B_4\nabla H(x_\tau) \\ & - \int_{t-d(t)}^{t}\left[(\nabla H(x(t)))'\right]^{\mathrm{T}} B_4[\nabla H(x(\alpha))]' d\alpha \\ & + h\eta_1^{\mathrm{T}}\overline{X}\eta_1 \\ & - \int_{t-d(t)}^{t}\eta_1^{\mathrm{T}}(t)\overline{X}\eta_1(t) d\alpha \\ & - \frac{1}{2}\left\|\gamma\omega - \frac{1}{\gamma}\nabla^{\mathrm{T}} H(x) g_2\right\|^2 \\ & - \nabla^{\mathrm{T}} H(x) g_1\left[\frac{1}{2}h^{\mathrm{T}}(x)h(x) + \frac{1}{2\gamma^2}I_m\right] g_1^{\mathrm{T}}\nabla H(x) \\ & + \frac{1}{2\gamma^2}\nabla^{\mathrm{T}} H(x) g_2 g_2^{\mathrm{T}}\nabla H(x) \\ & + \frac{1}{2}\left\{\gamma^2\|\omega\|^2 - \|z\|^2\right\} \\ & + \frac{1}{2}\nabla^{\mathrm{T}} H(x) g_1 h^{\mathrm{T}}(x) h(x) g_1^{\mathrm{T}}\nabla H(x). \end{aligned} \tag{43}$$

According to (35), (36), and Lemma 6, we have

$$\dot{V}_2\left(x, x_\tau, \widetilde{\theta}\right) - \eta_1^{\mathrm{T}}\Xi_2\eta_1 + \int_{t-d(t)}^{t}\eta_2^{\mathrm{T}}\overline{\Theta}\eta_2 d\alpha \leqslant \frac{1}{2}\left\{\gamma^2\|\omega\|^2 - \|z\|^2\right\}. \tag{44}$$

It is obvious that the γ-dissipation inequality (38) holds along the closed-loop system (42) which consist of (1) and (37). This completes the proof. □

4. Illustrative Examples

In this section, we give some examples to show how to apply the results proposed in this paper to investigate the robust stabilization and the L_2 disturbance attenuation for a class of time-delay nonlinear control systems with uncertainties and disturbances.

Let us consider the following 2-dimensional time-delay nonlinear control systems with parametric uncertainties and external disturbances:

$$\begin{aligned}\dot{x}_1(t) = {} & -4x_1^3(t) - 4x_1^3(t - d(t)) + 2u, \\ \dot{x}_2(t) = {} & -2x_1^3(t) - \left(2 + 3p + p^2\right)x_2(t) - 2x_1^3(t - d(t)) \\ & - 2x_2(t - d(t)) - x_2(t - d(t))\sin\left(x_2(t - d(t))\right) \\ & + 3u + 0.5\omega, \\ x_1(t_0) = {} & \phi_1(t_0), \quad x_2(t_0) = \phi_2(t_0), \quad t_0 \in [-h, 0], \end{aligned} \tag{45}$$

where $d(t)$ is a time varying delay of the system (45); p is an unknown constant, $0 < p < 1$; ω is the disturbance input.

The system (45) can be realized into the following Hamiltonian system form:

$$\begin{aligned}\dot{x} = {} & [J(x,p) - R(x,p)]\nabla H(x,p) \\ & + [J^*(x_\tau) - R^*(x_\tau)]\nabla H(x_\tau) + g_1 u + g_2 \omega, \\ & x(t_0) = \phi(t_0), \quad t_0 \in [-h, 0]\end{aligned} \tag{46}$$

with

$$\begin{aligned} J(x,p) &= \begin{pmatrix} 0 & 0.5 \\ -0.5 & 0 \end{pmatrix}, \qquad R(x,p) = \begin{pmatrix} 2 & 0.5 \\ 0.5 & 2+p \end{pmatrix}, \\ J^*(x_\tau) &= \begin{pmatrix} 0 & 0.5 \\ -0.5 & 0 \end{pmatrix}, \\ R^*(x_\tau) &= \begin{pmatrix} 2 & 0.5 \\ 0.5 & 2 + \sin x_2(t - d(t)) \end{pmatrix}, \\ g_1 &= \begin{pmatrix} 2 \\ 3 \end{pmatrix}, \qquad g_2 = \begin{pmatrix} 0 \\ 0.5 \end{pmatrix}, \\ x &= \begin{pmatrix} x_1 \\ x_2 \end{pmatrix}, \qquad \phi = \begin{pmatrix} \phi_1 \\ \phi_2 \end{pmatrix}, \\ H(x,p) &= 0.5\left(x_1^4 + (1+p)x_2^2\right), \\ H(x_\tau) &= 0.5\left(x_1^4(t - d(t))\right) + x_2^2(t - d(t)). \end{aligned} \tag{47, 48}$$

Let $E = F = \left(\begin{smallmatrix} 1 & 0 \\ 0 & 1 \end{smallmatrix}\right)$, $T = \left(\begin{smallmatrix} -2 & 0 \\ -1 & -2 \end{smallmatrix}\right)$, $\Delta(x_\tau) = \left(\begin{smallmatrix} 0 & 0 \\ 0 & -\sin x_2(t-d(t)) \end{smallmatrix}\right)$, $\theta = (-1 - 0.5p)p$ and $\Phi(x) = x_2$. It is easy to verify that system (46) with the above values satisfies Assumptions 1–5 and the condition (14) of Theorem 7.

Firstly, we demonstrate the application of Theorem 7 by using LMI solver [31].

Set $\mu = 0.25$ and $h = 1$. Using the LMI control toolbox of MATLAB, the LMIs in Theorem 7 are solved to find the following matrices:

$$\begin{aligned} P_1 &= \begin{pmatrix} 2.3387 & -0.0187 \\ -0.0187 & 2.3387 \end{pmatrix}, \qquad Z_1 = \begin{pmatrix} 0.3770 & 0.0447 \\ 0.0447 & 0.2949 \end{pmatrix}, \\ M_1 &= \begin{pmatrix} 1.0000 & 0.0000 \\ 0.0000 & 1.0000 \end{pmatrix}, \qquad B_1 = \begin{pmatrix} 0.7608 & 0.0232 \\ 0.0232 & 0.7653 \end{pmatrix}, \\ X_{11} &= \begin{pmatrix} 1.4363 & 0.0957 \\ 0.0957 & 1.4842 \end{pmatrix}, \qquad X_{12} = \begin{pmatrix} -0.1565 & -0.0155 \\ -0.0155 & -0.1583 \end{pmatrix}, \\ X_{22} &= \begin{pmatrix} 1.3787 & 0.0070 \\ 0.0070 & 1.3801 \end{pmatrix}, \qquad X_{33} = \begin{pmatrix} 0.5258 & -0.0203 \\ -0.0203 & 0.5359 \end{pmatrix}, \\ B_2 &= X_{13} = X_{23} = \begin{pmatrix} 0 & 0 \\ 0 & 0 \end{pmatrix}. \end{aligned} \tag{49}$$

Thus a robust stabilizing controller is obtained as

$$u = -3.8229x_2 - x_2\left(\dot{x}_1^4 + \dot{x}_2^2\right)\left(x_1^4 + x_2^2\right)^{-1} - 0.0770x_1^3 - x_2\widehat{\theta}. \tag{50}$$

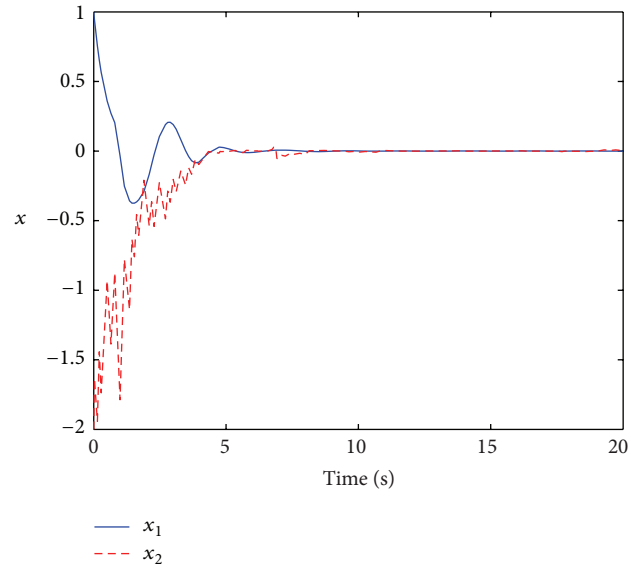

Figure 1: Responses of state x.

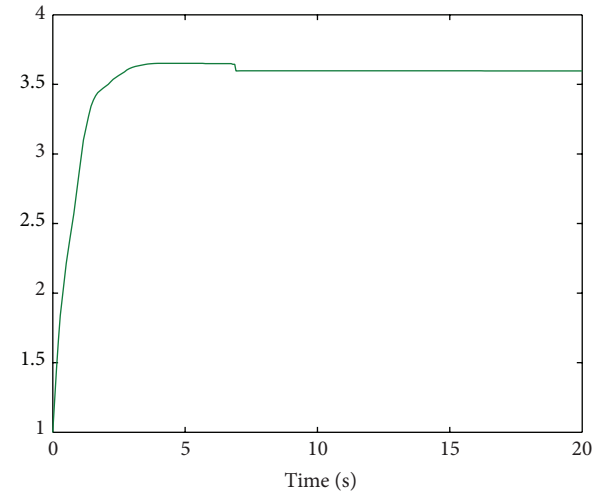

Figure 2: Parameter estimation $\widehat{\theta}$.

The simulation with the initial condition $x(0) = \phi(0) = [1 \quad -2]^T$ is given in Figures 1 and 2. It is clear that under the delay-dependent conditions, system (46) along with the controller (50) is asymptotically stable.

Next, we demonstrate the application of Theorem 8. We will check whether the designed L_2 disturbance attenuation controller according to Theorem 8 is effective in stabilizing the given time-delay Hamiltonian system (46) and has strong robustness against external disturbances.

Given a disturbance attenuation level γ, choose

$$z = h(x)\, g_1^T \nabla H(x) \tag{51}$$

as the penalty function, where $h = [0.1 \quad 0.1]^T$.

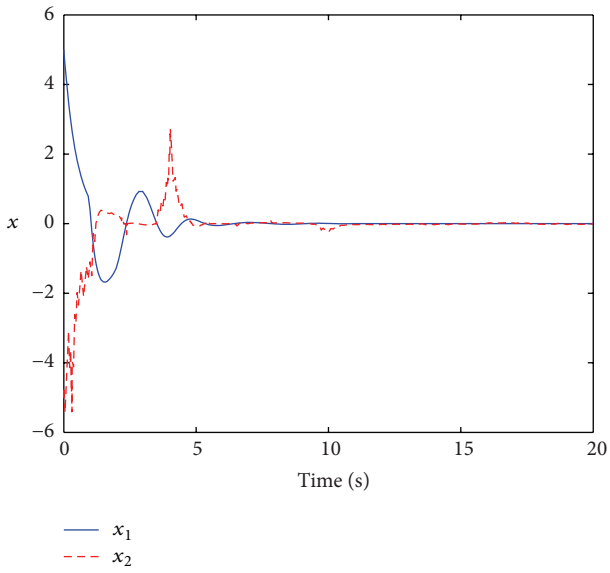

Figure 3: Responses of state x.

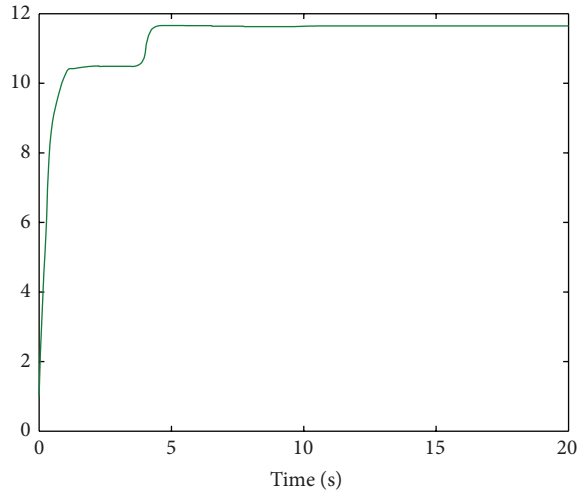

Figure 4: Parameter estimation $\widehat{\theta}$.

Using the LMI control toolbox, the LMIs in Theorem 8 are solved to find the following matrices with $\mu = 0.25, h = 1$:

$$P_2 = \begin{pmatrix} 2.4230 & -0.0178 \\ -0.0178 & 2.4230 \end{pmatrix}, \quad Z_2 = \begin{pmatrix} 0.3136 & 0.0426 \\ 0.0426 & 0.2926 \end{pmatrix},$$
$$M_2 = \begin{pmatrix} 1.0000 & 0.0000 \\ 0.0000 & 1.0000 \end{pmatrix}, \quad B_3 = \begin{pmatrix} 0.7859 & 0.0223 \\ 0.0223 & 0.7939 \end{pmatrix},$$
$$\overline{X}_{11} = \begin{pmatrix} 1.4799 & 0.0894 \\ 0.0894 & 1.5238 \end{pmatrix}, \quad \overline{X}_{12} = \begin{pmatrix} -0.1568 & -0.0160 \\ -0.0160 & -0.1551 \end{pmatrix},$$
$$\overline{X}_{22} = \begin{pmatrix} 1.4275 & 0.0069 \\ 0.0069 & 1.4304 \end{pmatrix}, \quad \overline{X}_{33} = \begin{pmatrix} 0.5382 & -0.0194 \\ -0.0194 & 0.5477 \end{pmatrix},$$
$$B_4 = \overline{X}_{13} = \overline{X}_{23} = \begin{pmatrix} 0 & 0 \\ 0 & 0 \end{pmatrix}. \tag{52}$$

Then according to Theorem 8, a feedback adaptive controller can be obtained as

$$u = -4.4041x_2 - x_2\left(\dot{x}_1^4 + \dot{x}_2^2\right)\left(x_1^4 + x_2^2\right)^{-1} - 0.0716x_1^3 - x_2\widehat{\theta}. \tag{53}$$

To illustrate the effectiveness of the adaptive control law (53), we carry simulation result with the following choices: the disturbance signal $\omega = \sin t$; the initial condition is $x(0) = \phi(0) = [5 \quad -5]^{\mathrm{T}}$; the disturbance attenuation level is chosen by $\gamma = 0.9$. The simulation results are shown in Figures 3 and 4, which are responses of the system's state and the parameter estimation, respectively. It can be seen from the simulation that the time-delay system converges to its equilibrium very quickly under the controller (53).

In general, from the simulations, we can conclude that the results presented in this paper are very practicable and effective in stabilization analysis and L_2 disturbance attenuation of time-delay Hamiltonian systems with parametric uncertainties and external disturbances. What is more, by using the result presented in this paper, we may solve the stability and control problem of some classes of time-delay nonlinear systems which can be realized into Hamiltonian systems form.

5. Conclusions

In this paper, the robust asymptotical stability and L_2 disturbance attenuation problem of a class of time-delay Hamiltonian control systems with parametric uncertainties and external disturbances have been investigated. Delay-dependent criteria are established. The proposed adaptive feedback control law, by which the asymptotic stability and the L_2 performance of the close-loop system is guaranteed, is determined by linear matrix inequalities constraints. Simulations show the effectiveness of the proposed method.

Acknowledgments

This work was supported in part by the National Natural Science Foundation of China under Grant 61203013 and 61004013 and in part by the Outstanding Middle-age and Young Scientist Award Foundation of Shandong Province under Grant BS2011DX012.

References

[1] C. E. de Souza and X. Li, "Delay-dependent robust H_∞ control of uncertain linear state-delayed systems," *Automatica*, vol. 35, no. 7, pp. 1313–1321, 1999.

[2] E. Fridman, "Stability of systems with uncertain delays: a new "complete" Lyapunov-Krasovskii functional," *IEEE Transactions on Automatic Control*, vol. 51, no. 5, pp. 885–890, 2006.

[3] Y. S. Lee, Y. S. Moon, W. H. Kwon, and P. G. Park, "Delay-dependent robust H_∞ control for uncertain systems with a state-delay," *Automatica*, vol. 40, no. 1, pp. 65–72, 2004.

[4] X. Li and H. Gao, "A new model transformation of discrete-time systems with time-varying delay and its application to stability analysis," *IEEE Transactions on Automatic Control*, vol. 56, no. 9, pp. 2172–2178, 2011.

[5] Y. Liu, Z. Wang, and X. Liu, "Stability analysis for a class of neutral-type neural networks with Markovian jumping parameters and mode-dependent mixed delays," *Neurocomputing*, vol. 94, pp. 46–53, 2012.

[6] C. Peng and Y.-C. Tian, "Delay-dependent robust H_∞ control for uncertain systems with time-varying delay," *Information Sciences*, vol. 179, no. 18, pp. 3187–3197, 2009.

[7] F. Souza and R. Palhares, "New delay-interval stability condition," *International Journal of Systems Science*, 2012.

[8] M. Wu, Y. He, and J.-H. She, *Stability Analysis and Robust Control of Time-Delay Systems*, Science Press Beijing, Beijing, China, 2010.

[9] S. Xu, J. Lam, and Y. Zou, "New results on delay-dependent robust H_∞ control for systems with time-varying delays," *Automatica*, vol. 42, no. 2, pp. 343–348, 2006.

[10] J. Hu, Z. Wang, H. Gao, and L. K. Stergioulas, "Robust H_∞ sliding mode control for discrete time-delay systems with stochastic nonlinearities," *Journal of the Franklin Institute*, vol. 349, no. 4, pp. 1459–1479, 2012.

[11] X. Jiao and T. Shen, "Adaptive feedback control of nonlinear time-delay systems: the LaSalle-Razumikhin-based approach," *IEEE Transactions on Automatic Control*, vol. 50, no. 11, pp. 1909–1913, 2005.

[12] M. S. Mahmoud and S. A. El Ferik, "New stability and stabilization methods for nonlinear systems with time-varying delays," *Optimal Control Applications & Methods*, vol. 31, no. 3, pp. 273–287, 2010.

[13] A. van der Schaft, *L_2-Gain and Passivity Techniques in Nonlinear Control*, Communications and Control Engineering Series, Springer, London, UK, 2nd edition, 2000.

[14] B. M. Maschke and A. J. vander Schaft, "Port-controlled Hamiltonian systems: modeling origins and system theoretic properties," in *Proceedings of the IFAC symposium on NOLCOS*, pp. 282–288, Bordeaux, France, 1992.

[15] A. J. van der Schaft and B. Maschke, "The Hamiltonian formulation of energy conserving physical systems with external ports," *Archive für Elektronik und übertragungstechnik*, vol. 49, no. 5-6, pp. 362–371, 1995.

[16] K. Fujimoto, K. Sakurama, and T. Sugie, "Trajectory tracking control of port-controlled Hamiltonian systems via generalized canonical transformations," *Automatica*, vol. 39, no. 12, pp. 2059–2069, 2003.

[17] R. Ortega, A. van der Schaft, B. Maschke, and G. Escobar, "Interconnection and damping assignment passivity-based control of port-controlled Hamiltonian systems," *Automatica*, vol. 38, no. 4, pp. 585–596, 2002.

[18] L. Sun and Y. Wang, "H_∞ control of a class of nonlinear Hamiltonian descriptor systems," *Science China. Information Sciences*, vol. 53, no. 11, pp. 2195–2204, 2010.

[19] S. Mei, F. Liu, Y. Chen, and Q. Lu, "Co-ordinated H_∞ control of excitation and governor of hydroturbo-generator sets: a Hamiltonian approach," *International Journal of Robust and Nonlinear Control*, vol. 14, no. 9-10, pp. 807–832, 2004.

[20] M. Schöberl, H. Ennsbrunner, and K. Schlacher, "Modelling of piezoelectric structures—a Hamiltonian approach," *Mathematical and Computer Modelling of Dynamcial Systems*, vol. 14, no. 3, pp. 179–193, 2008.

[21] T. Shen, R. Ortega, Q. Lu, S. Mei, and K. Tamura, "Adaptive L_2 disturbance attenuation of Hamiltonian systems with parametric perturbation and application to power systems," in *Proceedings of the 39th IEEE Confernce on Decision and Control*, vol. 5, pp. 4939–4944, Sydney, Australia, December 2000.

[22] W.-W. Sun, Z. Lin, and Y.-Z. Wang, "Global asymptotic and finite-gain L_2 stabilisation of port-controlled Hamiltonian systems subject to actuator saturation," *International Journal of Modelling, Identification and Control*, vol. 12, no. 3, pp. 304–310, 2011.

[23] Y. Wang, G. Feng, D. Cheng, and Y. Liu, "Adaptive L_2 disturbance attenuation control of multi-machine power systems with SMES units," *Automatica*, vol. 42, no. 7, pp. 1121–1132, 2006.

[24] R. Pasumarthy and C.-Y. Kao, "On stability of time delay hamiltonian systems," in *Proceedings of American Control Conference (ACC '09)*, pp. 4909–4914, St. Louis, Mo, USA, June 2009.

[25] W. W. Sun, "Stabilization analysis of time-delay Hamiltonian systems in the presence of saturation," *Applied Mathematics and Computation*, vol. 217, no. 23, pp. 9625–9634, 2011.

[26] W. Sun, Y. Wang, and R. Yang, "L_2 disturbance attenuation for a class of time-delay Hamiltonian systems," *Journal of Systems Science & Complexity*, vol. 24, no. 4, pp. 672–682, 2011.

[27] R. Yang and Y. Wang, "Finite-time stability analysis and H_∞ control for a class of nonlinear time-delay Hamiltonian systems," *Automatica*, vol. 49, no. 2, pp. 390–401, 2013.

[28] Y. Wang, D. Cheng, and X. Hu, "Problems on time-varying port-controlled Hamiltonian systems: geometric structure and dissipative realization," *Automatica*, vol. 41, no. 4, pp. 717–723, 2005.

[29] R. Yang and Y. Wang, "Stability for a class of nonlinear time-delay systems via Hamiltonian functional method," *Science China. Information Sciences*, vol. 55, no. 5, pp. 1218–1228, 2012.

[30] I. R. Petersen and C. V. Hollot, "A Riccati equation approach to the stabilization of uncertain linear systems," *Automatica*, vol. 22, no. 4, pp. 397–411, 1986.

[31] P. Gahinet, A. Nemirovskii, A. J. Laub et al., *LMI Control Toolbox*, The MathWorks, Natick, Mass, USA, 1995.

Hindawi Publishing Corporation
Mathematical Problems in Engineering
Volume 2013, Article ID 749798, 15 pages
http://dx.doi.org/10.1155/2013/749798

Research Article

Global Harmonic Current Rejection of Nonlinear Backstepping Control with Multivariable Adaptive Internal Model Principle for Grid-Connected Inverter under Distorted Grid Voltage

Yang Yu, Zengqiang Mi, Yiming Che, Tong Zhao, and Yikun Xu

State Key Laboratory of Alternate Electrical Power System with Renewable Energy Sources, North China Electric Power University, Baoding 071003, China

Correspondence should be addressed to Yang Yu; ncepu_yy@163.com

Received 28 May 2013; Accepted 8 July 2013

Academic Editor: Zhiguang Feng

Based on a brief review on current harmonics generation mechanism for grid-connected inverter under distorted grid voltage, the harmonic disturbances and uncertain items are immersed into the original state-space differential equation of grid-connected inverter. A new algorithm of global current harmonic rejection based on nonlinear backstepping control with multivariable internal model principle is proposed for grid-connected inverter with exogenous disturbances and uncertainties. A type of multivariable internal model for a class of nonlinear harmonic disturbances is constructed. Based on application of backstepping control law of the nominal system, a multivariable adaptive state feedback controller combined with multivariable internal model and adaptive control law is designed to guarantee the closed-loop system globally uniformly bounded, which is proved by a constructed Lyapunov function. The presented algorithm extends rejection of nonlinear single-input systems to multivariable globally defined normal form, the correctness and effectiveness of which are verified by the simulation results.

1. Introduction

Along with the strong demand of electric power energy, conventional fossil fuels are gradually reduced. The exploiting of renewable energy is an inevitable route for development of sustainable society. According to the planning of EU Commission, the renewable energy goal is achieving 20% of energy consumption from sustainable sources by 2020 [1].

Renewable energy sources include wind (onshore and offshore), solar PV, hydroenergy, biomass energy, geothermal energy, and tidal energy. Currently, two of main utilization approaches of renewable energy are off-grid power generation and connected to utility grid. In the past decade, the renewable energy sources connected to utility grid have achieved a considerable growth with the forceful needs of electric power energy [2]. Grid-connected inverter, which is one of the key technologies, supports renewable energy to be transmitted to the utility grid. In design, pulse width modulation (PWM) and the corresponding inverter control system require grid voltage as an ideal sine wave. Actually, it is difficult to keep a perfect sine wave of grid voltage under a variety of nonlinear loads and unexpected network failures. Furthermore, the existing researches have shown distorted grid voltage, such as dips [3], asymmetry [4], and harmonics [5], which will have a significantly adverse influence to grid power quality. In other words, rejection of current harmonics for grid-connected inverter under distorted grid voltage is a useful work for the normal operation of power networks [6].

The rejection solutions of current harmonics for grid-connected inverter mainly consist of two categories: hardware implementation and software programming. A simple and practical scheme of hardware implementation is adding filters to inverter's output. The aim of adding filters is to compensate for the fluctuations of grid voltage. In [7], LCL filters are designed for grid-connected converters. However, the application of LCL filters may encounter the resonance problem. Close by the resonant frequency, the impedance of the filters is small, and the harmonic current in corresponding frequency would be amplified, even beyond the harmonic standard [8]. In addition, new hardware will

certainly increase the investment of the system. One of the rejection ways for software programming is to design a proportional resonant (PR) controller to improve the gain in background harmonic [9]. Nevertheless, with the increasing of the background harmonic frequency, the PR controller can reduce the phase margin of the system [10]. The other one is application of feedforward control of grid voltage to increase output impedance of the system. The feedforward control has no impact on phase margin of the system [11], but the scheme, which only depends on the proportion feedforward to regulation, cannot eliminate the influence of background harmonic [12].

For the disadvantages of the above methods, some scholars attempt to apply modern control theory to improve the capability of harmonics disturbance rejection. The nonlinear control methods, such as repetitive control [13, 14], H_∞ control [15, 16], prediction control [17–19], backstepping control [20–22], and fuzzy-adaptive control [23–26], can deal with the nonlinearity and uncertainty of nonlinear models better. However, these preexisting rejection control methods have the following problems more or less.

(1) The harmonics rejection algorithms are concerned primarily with the single-input field; the research of multiple-input field is rarely mentioned.

(2) For an operating grid-connected system, the parameters of resistance and inductance for the system are often time varying and cannot be measured accurately. Hence, these proportional-integral-based controllers, which take no account of the time-varying characteristics of the parameters, cannot work very efficiently.

(3) The parameter design of robust controller is relatively complicated and needs large amount of calculations.

In the paper, a multivariable state feedback control algorithm based on nonlinear backstepping control with multivariable internal model principle (MIMP) and adaptive control law (ACL) for grid-connected inverter is proposed to reject the harmonic disturbance produced by a class of exosystem and uncertainties related with system states caused by modeling perturbations, parameter uncertainty or actuator end disturbance. The main contributions in the paper are the following.

(1) A new harmonic rejection algorithm based on nonlinear backstepping control with MIMP and ACL is proposed in the paper, which extends the disturbance rejection of the nonlinear single-input system to multivariable globally defined normal form in contrast with the previous literatures.

(2) A new type of nonlinear multivariable internal model for a class of nonlinear harmonic disturbances and uncertain items related with system states is constructed.

(3) The proposed algorithm is practically applied to reject current harmonic disturbances for grid-connected inverter under distorted grid voltage.

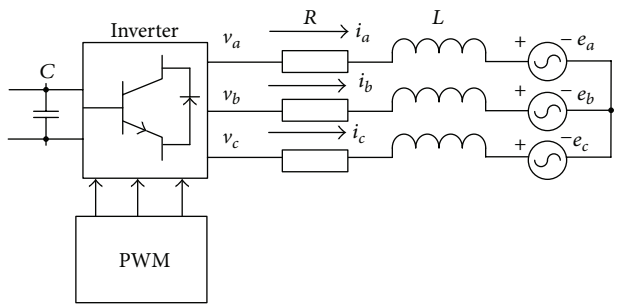

Figure 1: Modeling of grid-connected inverter.

The paper is organized as the following: it starts with an introduction to the research status of current harmonics rejection for grid-connected inverter in Section 1. The modeling of state differential equation for grid-connected inverter is constructed and an analysis of current harmonics generation mechanism is given in Section 2. In addition, Section 2 describes the control and mathematical problem concerned in the paper. Nonlinear multivariable internal model is presented and designed in Section 3. In Section 4, nonlinear multivariable adaptive state feedback controller is proposed and the global robust stabilization is demonstrated. Section 5 gives the results of numerical simulation. Finally, the conclusions are summarized in Section 6.

2. Problem Formulation

2.1. Modeling of Grid-Connected Inverter. The model of grid-connected inverter can be shown in Figure 1. In Figure 1, R and L represent the equivalent series resistance and inductor, respectively, C is the capacitance, v_{abc} and i_{abc} are three-phase output voltage and grid current of three-phase inverter, and e_{abc} represents three-phase grid voltage.

In terms of Figure 1, the voltage equations of three-phase grid-connected inverter in stationary *abc* reference frame can be written as

$$\begin{aligned} v_a &= Ri_a + L\frac{di_a}{dt} + e_a, \\ v_b &= Ri_b + L\frac{di_b}{dt} + e_b, \\ v_c &= Ri_c + L\frac{di_c}{dt} + e_c. \end{aligned} \tag{1}$$

Application of the park transformation to (1) in rotating dq reference frame equation (1) is converted into

$$\begin{aligned} v_d &= Ri_d + L\frac{di_d}{dt} - \omega Li_q + e_d, \\ v_q &= Ri_q + L\frac{di_q}{dt} + \omega Li_d + e_q; \end{aligned} \tag{2}$$

namely,

$$\begin{bmatrix} \frac{di_d}{dt} \\ \frac{di_q}{dt} \end{bmatrix} = \begin{bmatrix} -\frac{R}{L} & \omega \\ -\omega & -\frac{R}{L} \end{bmatrix} \begin{bmatrix} i_d \\ i_q \end{bmatrix} + \begin{bmatrix} \frac{1}{L} & 0 \\ 0 & \frac{1}{L} \end{bmatrix} \begin{bmatrix} v_d & -e_d \\ v_q & -e_q \end{bmatrix}, \quad (3)$$

where v_{dq} and i_{dq} represent the voltage and current of grid-connected inverter in rotating dq reference frame, e_{dq} is the grid voltage in dq reference frame, and ω is the synchronous angular velocity of the grid.

Rearrange (2) in the form of state space as follows:

$$\begin{aligned} \dot{\mathbf{x}} &= \mathbf{A}\mathbf{x} + \mathbf{B}(\mathbf{v} - \mathbf{e}), \\ \mathbf{y} &= \mathbf{C}\mathbf{x}, \end{aligned} \quad (4)$$

where $\mathbf{x}$, $\mathbf{v}$, and $\mathbf{y}$ are the state vector, the control input vector, and the output vector, respectively, $\mathbf{e}$ is the voltage vector of the grid, $\mathbf{x} = [i_d \quad i_q]^T$, $\mathbf{v} = [v_d \quad v_q]^T$, $\mathbf{y} = \mathbf{x}$, $\mathbf{e} = [e_d \quad e_q]^T$, $\mathbf{A} = \begin{bmatrix} -R/L & \omega \\ -\omega & -R/L \end{bmatrix}$, $\mathbf{B} = \begin{bmatrix} 1/L & 0 \\ 0 & 1/L \end{bmatrix}$, and $\mathbf{C} = \begin{bmatrix} 1 & 0 \\ 0 & 1 \end{bmatrix}$.

2.2. Current Harmonics Generation Mechanism for Grid-Connected Inverter. In terms of Figure 1, the harmonic voltage equations of three-phase grid-connected inverter instationary *abc* reference frame can be written as

$$\mathbf{v}_{abck} = R\mathbf{i}_{abck} + L\frac{d\mathbf{i}_{abck}}{dt} + \mathbf{e}_{abck}, \quad (5)$$

where k is the harmonic order, $\mathbf{v}_{abck}$ is the control voltage vector, $\mathbf{i}_{abck}$ is the current vector of harmonics, and $\mathbf{e}_{abck}$ is the unbalanced harmonic voltage vector of the grid.

Assume that the distorted voltage of the network contains the 5th and 7th harmonics. In stationary *abc* reference frame, the rotating direction of the 5th harmonics is contrary to fundamental harmonics, and its rotating electrical angular velocity is -5ω. However, the rotating direction of the 7th harmonics is the same as the fundamental harmonics, and its rotating electrical angular velocity is 7ω. Indeed, the distorted voltage of the network may include more harmonics in addition to the 5th and 7th harmonics, such as the 3rd, 11th, and 13th. The rotating direction of the 11th harmonics is exactly identical to the 5th, except that the rotating electrical angular velocity is -11ω. A similar relationship exists in the 7th and 13th harmonics. In order to reveal the essence of the problem more simply, consider only the 5th and 7th harmonics and construct multiple synchronous rotating reference frames shown in Figure 2. For convenience, in what follows, +/− in superscript represents +/− rotating direction, respectively; 5 and 7 in superscript describe the rotating direction of the 5th and 7th harmonics, respectively; 1, 5, and 7 in subscript demonstrate the 1st, 5th, and 7th harmonics, respectively.

In rotating dq reference frame of the 5th harmonics, the voltage equation of the 5th harmonics can be written as

$$\mathbf{v}_{dq5} = R\mathbf{i}_{dq5} + L\frac{d\mathbf{i}_{dq5}}{dt} + \mathbf{e}_{dq5} - j5\omega L i_{dq5}, \quad (6)$$

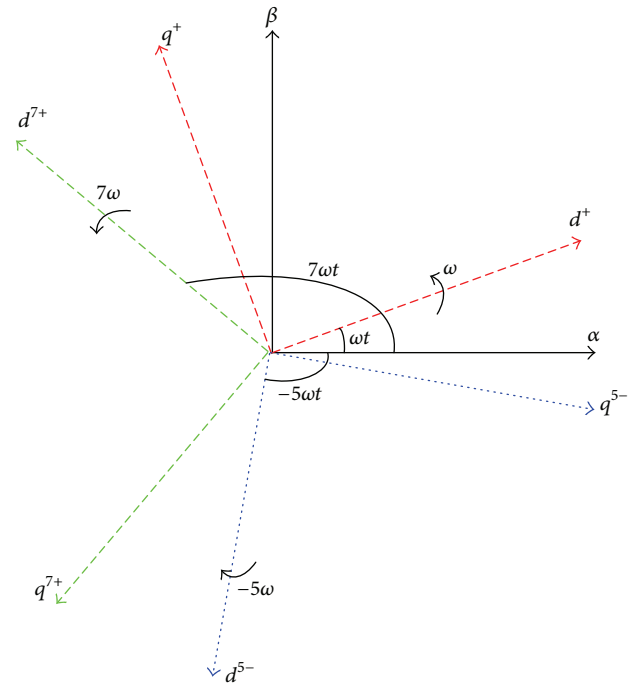

Figure 2: Multiple synchronous rotating reference frames.

where

$$\begin{aligned} \mathbf{v}_{dq5} &= \mathbf{v}^+_{dq1}e^{j6\omega t} + \mathbf{v}^{5-}_{dq5} + \mathbf{v}^{7+}_{dq7}e^{j12\omega t}, \\ \mathbf{i}_{dq7} &= \mathbf{i}^+_{dq1}e^{j6\omega t} + \mathbf{i}^{5-}_{dq5} + \mathbf{i}^{7+}_{dq7}e^{j12\omega t}, \\ \mathbf{e}_{dq5} &= \mathbf{e}^+_{dq1}e^{j6\omega t} + \mathbf{e}^{5-}_{dq5} + \mathbf{e}^{7+}_{dq7}e^{j12\omega t}. \end{aligned} \quad (7)$$

Equation (7) indicates that only voltage and current components of the 5th harmonics are DC signals in rotating dq reference frame of the 5th harmonics. Voltage and current components of the remaining harmonics are AC signals. One other thing to note is that all of the harmonic components in rotating dq reference frame of fundamental wave are AC signals.

In a similar way, the voltage equation of the 7th harmonics can be written as

$$\mathbf{v}_{dq7} = R\mathbf{i}_{dq7} + L\frac{d\mathbf{i}_{dq7}}{dt} + \mathbf{e}_{dq7} + j7\omega L i_{dq7}. \quad (8)$$

Equations (6) and (8) demonstrate that once the grid voltage becomes unbalance, the controller designed by the principle of ideal sine wave will not be able to compensate for harmonic voltage, and the current waveform of the grid will be distorted.

2.3. Control Problem Description. Use $\mathbf{D}(\mathbf{w})$ and $\boldsymbol{\delta}(\mathbf{x}, t)$ to describe the exogenous disturbance of voltage harmonics and the uncertain items related with system states caused by modeling perturbations, parameter uncertainties, or actuator

end disturbances, respectively, then the state equation in (4) can be rewritten as a multivariable system as follows:

$$\begin{aligned}\dot{\mathbf{x}} &= \mathbf{A}\mathbf{x} + \mathbf{B}\left(\mathbf{v} - \mathbf{e}_0 - \mathbf{D}(\mathbf{w}) + \boldsymbol{\delta}(\mathbf{x},t)\right)\\ &= \mathbf{f}(\mathbf{x}) + \sum_{i=1}^{2}\mathbf{g}_i(\mathbf{x})\left(v_i - e_{i0} - D_i(\mathbf{w}) + \delta_i(\mathbf{x},t)\right), \qquad (9)\\ &\qquad\qquad 1 \le i \le 2,\end{aligned}$$

where $\mathbf{x} = [x_1, x_2]^T = [i_d, i_q]^T$, $\mathbf{f}(\mathbf{x}) = \begin{bmatrix} -(R/L)x_1 + \omega x_2 \\ -\omega x_1 - (R/L)x_2 \end{bmatrix} = \begin{bmatrix} -(R/L)i_d + \omega i_q \\ -\omega i_d - (R/L)i_q \end{bmatrix}$, $\mathbf{g}_1(\mathbf{x}) = \mathbf{g}_2(\mathbf{x}) = 1/L$, $\mathbf{v} = [v_1, v_2]^T = [v_d, v_q]^T$, $[e_{10}, e_{20}] = [e_{d0}, e_{q0}]$, and e_{d0} and e_{q0} are network voltages of fundamental wave in dq reference frame. For a specific network, e_{d0} and e_{q0} can be determined easily. The uncertain item $\boldsymbol{\delta}(\mathbf{x},t)$ in the control input channel satisfies the matching condition. In the paper, the range of variable i is (1,2). For convenience and conciseness, in what follows, the range of variable i is no longer written.

Assumption 1. $\mathbf{w} \in \mathbf{R}^q$ is an exogenous signal generated by the following exosystem:

$$\dot{\mathbf{w}} = \mathbf{W}_i\mathbf{w}, \qquad (10)$$

where $\mathbf{W}_i$ is a pending matrix depending on the exogenous signal.

Assumption 2. Considering disturbance-free and no modeling perturbations, the nominal system of (9) can be written as:

$$\dot{\mathbf{x}} = \mathbf{f}(\mathbf{x}) + \sum_{i=1}^{2}\mathbf{g}_i(\mathbf{x})\left(v_i - e_{i0}\right) \qquad (11)$$

there exists a control law of state feedback a follows:

$$v_i' = v_i - e_{i0} = \alpha_i(\mathbf{x}), \qquad (12)$$

let (11) be asymptotically stable. In addition, there exists a Lyapunov function $V(\mathbf{x})$ which satisfies:

$$\underline{d}(\|\mathbf{x}\|) \le V(\mathbf{x}) \le \overline{d}(\|\mathbf{x}\|), \qquad (13)$$

$$\frac{\partial V(\mathbf{x})}{\partial \mathbf{x}}\left(\mathbf{f}(\mathbf{x}) + \sum_{i=1}^{2}\mathbf{g}_i(\mathbf{x})\alpha_i(\mathbf{x})\right) \le -d_0(\|\mathbf{x}\|), \qquad (14)$$

$$\left|\frac{\partial V(\mathbf{x})}{\partial \mathbf{x}}\sum_{i=1}^{2}\mathbf{g}_i(\mathbf{x})\right|^2 \le d_0(\|\mathbf{x}\|), \qquad (15)$$

where $\underline{d}$, $\overline{d}$, and d_0 are all of class K_∞ functions.

Assumption 3. There exist smooth functions $r_i(x) : \mathbf{R}^n \to \mathbf{R}^q$ which make

$$\frac{\partial r_i(\mathbf{x})}{\partial \mathbf{x}}\mathbf{g}_i(\mathbf{x}) = \mathbf{K}_i, \qquad (16)$$

where $\mathbf{K}_i$ are nonzero constant vectors defined in $\mathbf{R}^q$.

Assumption 4. There exist a constant m_i and a known smooth bounded function $p_i(\mathbf{x})$ making the uncertain item $\boldsymbol{\delta}(\mathbf{x},t)$ satisfy

$$\left|\delta_i(\mathbf{x},t)\right| \le m_i p_i(\mathbf{x}). \qquad (17)$$

Remark 5. Similar to the uncertain item $\boldsymbol{\delta}(\mathbf{x},t)$, the disturbance $\mathbf{D}(\mathbf{w})$ also satisfies the matching condition and can be injected in the input path. Nevertheless, a method of iterative design, such as adaptive backstepping, can extend the presented algorithm to more general instance of strict feedback. Therefore, the matching condition is not critical, and application of the assumption is reasonable.

Remark 6. One of the research points in the paper is stability problem for multivariable input system. Currently, some literatures focus on the point of stability problem, but the focused attention of these literatures is the field of single input and single output [27] or semiglobal stability [28]. For the multivariable system, the research of stability problem will be more challenging, and the core is to transform the stability problem from multivariable system to multiple single-input system [29].

Remark 7. For Assumption 2, (13) and (14) automatically hold when the closed-loop system is asymptotically stable. Equation (15) holds when the closed-loop system is exponentially stable. Nevertheless, Assumption 2 is not a sufficient condition to make the closed-loop system exponentially stable [30].

Remark 8. For Assumption 3, if $\mathbf{g}_i(\mathbf{x})$ is a nonzero constant vector, it will be easy to find a solution of $(\partial r_i(\mathbf{x})/\partial \mathbf{x})\mathbf{g}_i(\mathbf{x}) = \mathbf{K}_i$ for a non-zero constant vector $\mathbf{K}_i$. For a nonconstant vector $\mathbf{g}_i(\mathbf{x})$, the solutions can be found more complex with the help of geometric tool [31].

Remark 9. Assumption 4 is to guarantee the boundedness of the uncertain item $\boldsymbol{\delta}(\mathbf{x},t)$ relative to the system state vector $\mathbf{x}$. For instance, if $\delta_1(\mathbf{x},t) = x_1\sin(x_1 t)$, m_1 and $p_1(\mathbf{x})$ can be chosen as 1 and x_1, respectively.

The problem solved in the paper can be described by the following theorem.

Definition 10. For any given compact set $\mathbf{D}_\mathbf{w} \in \mathbf{R}^q$, state feedback controller v_i can always be found to ensure the solution of closed-loop system (9) existing under arbitrary initial conditions for all $\mathbf{w}(\mathbf{0}) \in \mathbf{D}_\mathbf{w}$ and $t \ge 0$ and to reject exogenous disturbances and uncertain items.

3. Design of Nonlinear Multivariable Internal Model

Application of internal model principle (IMP) to reject the exogenous disturbance $\mathbf{D}(\mathbf{w})$ and uncertain item $\boldsymbol{\delta}(\mathbf{x},t)$ in the paper is chosen as an indirect method. In other words, an appropriate equation of internal model should be constructed to estimate the nonlinear disturbances and uncertain items.

The nonlinear equation of exogenous disturbance internal model is designed as

$$\widehat{D}_i(\mathbf{w}) = \mathbf{V}_i \widehat{\mathbf{w}}_i(t), \tag{18}$$

$$\widehat{\mathbf{w}}_i(t) = \widehat{\boldsymbol{\eta}}_i(t) + \mathbf{r}_i(\mathbf{x}), \tag{19}$$

$$\begin{aligned}\dot{\widehat{\boldsymbol{\eta}}}_i(t) = {} & \left(\mathbf{W}_i - \mathbf{K}_i\mathbf{V}_i\right)\left(\widehat{\boldsymbol{\eta}}_i(t) + \mathbf{r}_i(\mathbf{x})\right) \\ & - \mathbf{K}_i v_i'(\mathbf{x}) - \frac{\partial \mathbf{r}_i(\mathbf{x})}{\partial \mathbf{x}}\mathbf{f}(\mathbf{x}),\end{aligned} \tag{20}$$

where $\widehat{\mathbf{w}}(t)$ is the estimation value of exogenous signal $\mathbf{w}(t)$, $\widehat{\boldsymbol{\eta}}_i$ is the introduced auxiliary vector, $\widehat{\boldsymbol{\eta}}_i = [\widehat{\eta}_{i1} \quad \widehat{\eta}_{i2} \cdots \widehat{\eta}_{ip}]$, $\mathbf{r}_i(\mathbf{x})$ is a vector constructed by the smooth functions $r_i(\mathbf{x})$, $\mathbf{r}_i(\mathbf{x}) = [r_i(\mathbf{x}) \quad 0 \cdots 0]_{1\times p}$, and the matrix $\mathbf{K}_i \in \mathbf{R}^q$ is selected satisfying Assumption 3 and makes the matrix $(\mathbf{W}_i - \mathbf{K}_i\mathbf{V}_i)$ be Hurwitz; that is, positive definite matrices $\mathbf{P}_i$ and $\mathbf{Q}_i$ are always existing and satisfy

$$\mathbf{P}_i\left(\mathbf{W}_i - \mathbf{K}_i\mathbf{V}_i\right) + \left(\mathbf{W}_i - \mathbf{K}_i\mathbf{V}_i\right)^T\mathbf{P}_i = -\mathbf{Q}_i. \tag{21}$$

In terms of Assumption 4, the adaptive internal model of uncertain item is devised as

$$\widehat{\delta}_i(\mathbf{x}, t) = m_i\mathbf{K}_i p_i(\mathbf{x}) \tanh\left(\frac{\widehat{\eta}_i^T\mathbf{P}_i^T\mathbf{K}_i p_i(\mathbf{x})}{\lambda_i}\right), \tag{22}$$

where m_i and $p_i(\mathbf{x})$ indicate a constant and a known smooth function defined in Assumption 4, respectively, and λ_i is a designed constant.

Define an auxiliary error vector as follows:

$$er_i(t) = \mathbf{w}_i(t) - \widehat{\mathbf{w}}_i(t). \tag{23}$$

With the derivative of (23) along with (9), (10) and (19), we can obtain

$$\begin{aligned}\dot{er}_i(t) &= \dot{\mathbf{w}}_i(t) - \dot{\widehat{\mathbf{w}}}_i(t) = \mathbf{W}_i\mathbf{w}_i - \dot{\widehat{\boldsymbol{\eta}}}_i(t) - \frac{\partial \mathbf{r}_i(\mathbf{x})}{\partial \mathbf{x}}\frac{\partial \mathbf{x}}{\partial t} \\ &= \mathbf{W}_i\mathbf{w}_i - \left(\mathbf{W}_i - \mathbf{K}_i\mathbf{V}_i\right)\left(\widehat{\boldsymbol{\eta}}_i(t) + \mathbf{r}_i(\mathbf{x})\right) \\ &\quad + \mathbf{K}_i\mathbf{v}_i'(\mathbf{x}) + \frac{\partial \mathbf{r}_i(\mathbf{x})}{\partial x}\mathbf{f}(\mathbf{x}) - \frac{\partial \mathbf{r}_i(\mathbf{x})}{\partial x} \\ &\quad \times \left(\mathbf{f}(\mathbf{x}) + \mathbf{g}_i(\mathbf{x})\left(v_i - e_{i0} - D_i(\mathbf{w}) \quad + \delta_i(\mathbf{x},t)\right)\right) \\ &= \mathbf{W}_i\mathbf{w}_i - \left(\mathbf{W}_i - \mathbf{K}_i\mathbf{V}_i\right)\left(\widehat{\boldsymbol{\eta}}_i(t) + \mathbf{r}_i(\mathbf{x})\right) + \mathbf{K}_i v_i'(x) \\ &\quad - \frac{\partial \mathbf{r}_i(\mathbf{x})}{\partial x}\mathbf{g}_i(\mathbf{x})\left(v_i - e_{i0} - D_i(\mathbf{w}) + \delta_i(\mathbf{x},t)\right) \\ &= \mathbf{W}_i\mathbf{w}_i - \left(\mathbf{W}_i - \mathbf{K}_i\mathbf{V}_i\right)\left(\widehat{\boldsymbol{\eta}}_i(t) + \mathbf{r}_i(\mathbf{x})\right) + \mathbf{K}_i v_i'(\mathbf{x}) \\ &\quad - \mathbf{K}_i\left(v_i - e_{i0} - D_i(\mathbf{w}) + \delta_i(\mathbf{x},t)\right) \\ &= \mathbf{W}_i\mathbf{w}_i - \left(\mathbf{W}_i - \mathbf{K}_i\mathbf{V}_i\right)\widehat{\mathbf{w}}_i(t) + \mathbf{K}_i v_i'(\mathbf{x}) \\ &\quad - \mathbf{K}_i\left(v_i - e_{i0} - \mathbf{V}_i\mathbf{w}(t) + \delta_i(\mathbf{x},t)\right) \\ &= \mathbf{W}_i\mathbf{w}_i - \left(\mathbf{W}_i - \mathbf{K}_i\mathbf{V}_i\right)\widehat{\mathbf{w}}(t) + \mathbf{K}_i V_i\mathbf{w}(t) - \mathbf{K}_i\delta_i(\mathbf{x},t) \\ &= \left(\mathbf{W}_i - \mathbf{K}_i\mathbf{V}_i\right)er_i(t) - \mathbf{K}_i\delta_i(\mathbf{x},t).\end{aligned} \tag{24}$$

4. Design of Nonlinear State Feedback Controller

In comparison with the nominal system (11), the original system (9) adds two items: exogenous disturbance $\mathbf{D}(\mathbf{w})$ and uncertain items $\boldsymbol{\delta}(\mathbf{x}, t)$. On the basis of control law of the nominal system, nonlinear state feedback controller of the original system (9) should add two items to compensate for $\mathbf{D}(\mathbf{w})$ and $\boldsymbol{\delta}(\mathbf{x}, t)$. In terms of the idea, nonlinear state feedback controller of the original system (9) is designed as

$$v_i' = \alpha_i(\mathbf{x}) - \widehat{D}_i(\mathbf{w}) + \theta_i(\cdot), \tag{25}$$

where $\theta(\cdot)$ is a pending design function to compensate for an uncertain item such as modeling perturbation.

Apparently, designing of nonlinear internal model $\widehat{D}_i(\mathbf{w})$ is accomplished in Section 3. In what follows, we complete the design of v_i' in two steps. The first step is application of backstepping theory to devise $\alpha_i(\mathbf{x})$, and the second is to complete an adaptive solution of $\theta(\cdot)$ to reject uncertain item $\boldsymbol{\delta}(\mathbf{x}, t)$.

(1) Designing of $\alpha_i(\mathbf{x})$. It is assumed that the parameters of grid-connected inverter are known and invariant. The control target of designing $\alpha_i(\mathbf{x})$ is to regulate $i_d(x_1)$ and $i_q(x_2)$ to track the respective reference value $x_{1\text{ref}}$ and $x_{2\text{ref}}$.

Firstly, we define the errors as follows:

$$\begin{aligned}ez_1 &= x_1 - x_{1\text{ref}}, \\ ez_2 &= x_2 - x_{2\text{ref}};\end{aligned} \tag{26}$$

the dynamics derived from (26), we can get with

$$\begin{aligned}\dot{ez}_1 &= \dot{x}_1 - \dot{x}_{1\text{ref}}, \\ \dot{ez}_2 &= \dot{x}_2 - \dot{x}_{2\text{ref}}.\end{aligned} \tag{27}$$

Substituting (9) into (27), we obtain

$$\dot{ez}_1 = \dot{x}_1 - \dot{x}_{1\text{ref}} = -\frac{R}{L}x_1 + \omega x_2 + \frac{1}{L}\alpha_1(\mathbf{x}) - \dot{x}_{1\text{ref}}, \tag{28}$$

$$\dot{ez}_2 = \dot{x}_2 - \dot{x}_{2\text{ref}} = -\frac{R}{L}x_2 - \omega x_1 + \frac{1}{L}\alpha_2(\mathbf{x}) - \dot{x}_{2\text{ref}}. \tag{29}$$

Define a quadratic function as the following:

$$Q_1 = \frac{1}{2}c_1 ez_1^2, \tag{30}$$

where c_1 is a positive real number.

Derivative of Q_1 along (28) can be written as

$$\dot{Q}_1 = c_1 ez_1\dot{ez}_1 = c_1 ez_1\left(-\frac{R}{L}x_1 + \omega x_2 + \frac{1}{L}\alpha_1(\mathbf{x}) - \dot{x}_{1\text{ref}}\right). \tag{31}$$

Assume that

$$-\frac{R}{L}x_1 + \omega x_2 + \frac{1}{L}\alpha_1(\mathbf{x}) - \dot{x}_{1\text{ref}} = -\frac{ez_1}{c_1}. \tag{32}$$

That is,

$$\alpha_1(\mathbf{x}) = -\frac{Lez_1}{c_1} + Rx_1 - L\omega x_2 + L\dot{x}_{1\text{ref}}. \tag{33}$$

Replacing (33) into (31), the derivative of Q_1 is given by

$$\dot{Q}_1 = c_1 ez_1 \dot{ez}_1 = -ez_1^2 \le 0. \tag{34}$$

Define another quadratic function as the following:

$$Q_2 = \frac{1}{2} c_2 ez_2^2, \tag{35}$$

where c_2 is also a positive real number.

Derivative of Q_2 along (29) is given by

$$\dot{Q}_2 = c_2 ez_2 \dot{ez}_2 = c_2 z_2 \left(-\frac{R}{L}x_2 - \omega x_1 + \frac{1}{L}\alpha_2(x) - \dot{x}_{2\text{ref}}\right). \tag{36}$$

Suppose that

$$-\frac{R}{L}x_2 - \omega x_1 + \frac{1}{L}\alpha_2(x) - \dot{x}_{2\text{ref}} = -\frac{ez_2}{c_2}; \tag{37}$$

that is,

$$\alpha_2(\mathbf{x}) = -\frac{Lez_2}{c_2} + Rx_2 + L\omega x_1 + L\dot{x}_{2\text{ref}}. \tag{38}$$

Replacing (38) into (36), the derivative of Q_2 can be written as

$$\dot{Q}_2 = c_2 ez_2 \dot{ez}_2 = -ez_2^2 \le 0. \tag{39}$$

Now, from (30) and (35), the Lyapunov function $V(\mathbf{x})$ defined in Assumption 2 can be written as

$$V(\mathbf{x}) = Q_1 + Q_2 = \frac{1}{2}c_1 ez_1^2 + \frac{1}{2}c_2 ez_2^2. \tag{40}$$

Hence, from (34) and (39), we can see that the controllers $\alpha_1(\mathbf{x})$ shown in (33) and $\alpha_2(\mathbf{x})$ shown in (38) can stabilize the disturbance-free closed-loop system.

(2) Designing of $\theta(\cdot)$. Under the actual operating environments, the parameters of grid-connected inverter are not always known and invariant. For instance, the inductance L varies with the environment temperature, and the resistance R changes nonlinearly with heating. Hence, the parametric uncertainties in the process of system modeling should be considered to reflect the real condition of the operating system. Due to the uncertainty of modeling perturbations, $\theta(\cdot)$ should be an adaptive controller to reject the perturbations. In terms of the internal model of uncertain items shown in (22), the controller is devised as

$$\theta_i(\mathbf{x}, t) = m_i p_i(\mathbf{x}) \tanh\left(\frac{(\partial V(\mathbf{x})/\partial x)\, g_i(\mathbf{x})\, p_i(\mathbf{x})}{\xi_i}\right), \tag{41}$$

where ξ_i is the designed constant.

Convergence Proof of the Proposed Controller. For a start, we give a lemma as the following.

Lemma 11. *For any positive number* $\varepsilon > 0$*, there exists a smooth function* h *making the inequality* $|x| \le xh(x) + \varepsilon$*, for all* $x \in R$ *hold, and* $f(0) = 0$.

Remark 12. If we choose $h(x) = (1/4\varepsilon)x$, for all $x \in R$, the above inequality holds obviously. In [32], another function meeting the above requirements is given as $h(x) = \tanh(\beta x/\varepsilon)$, for all $x \in R$, where $\beta = e^{-(\beta+1)}$ and $\beta > 0$, hence $\beta < 1/2$.

In terms of (23) and (40), construct a new Lyapunov function as

$$W = V(\mathbf{x}) + \sum_{i=1}^{2} er_i^T P_i er_i. \tag{42}$$

With the derivative of (42) along the system (9), (24), and (25), we obtain

$$\begin{aligned}
\dot{W} &= \frac{\partial V(\mathbf{x})}{\partial \mathbf{x}}\left(\mathbf{f}(\mathbf{x}) + \sum_{i=1}^{2}\mathbf{g}_i(\mathbf{x})\left(\nu_i - e_{i0} - D_i(\mathbf{w}) + \delta_i(\mathbf{x}, t)\right)\right) \\
&\quad + \sum_{i=1}^{2}\left(er_i^T\left(\mathbf{P}_i\left(\mathbf{W}_i - \mathbf{K}_i\mathbf{V}_i\right) + \left(\mathbf{W}_i - \mathbf{K}_i\mathbf{V}_i\right)^T\mathbf{P}_i\right)er_i\right) \\
&\quad + 2\sum_{i=1}^{2}\left(er_i^T\mathbf{P}_i\left(-\mathbf{K}_i\delta_i(\mathbf{x}, t)\right)\right) \\
&= \frac{\partial V(\mathbf{x})}{\partial \mathbf{x}}\left(\mathbf{f}(\mathbf{x}) + \sum_{i=1}^{2}\mathbf{g}_i(\mathbf{x})\alpha_i(\mathbf{x})\right) \\
&\quad + \frac{\partial V(\mathbf{x})}{\partial \mathbf{x}}\sum_{i=1}^{2}\mathbf{g}_i(\mathbf{x})\left(\widehat{D}_i(\mathbf{w}) - D_i(\mathbf{w})\right) \\
&\quad - \frac{\partial V(\mathbf{x})}{\partial \mathbf{x}}\sum_{i=1}^{2}\mathbf{g}_i(\mathbf{x})\left(\theta_i(\mathbf{x}, t) - \delta_i(\mathbf{x}, t)\right) \\
&\quad - \sum_{i=1}^{m}\left(er_i^T\mathbf{Q}_i er_i\right) + 2\sum_{i=1}^{2}\left(er_i^T\mathbf{P}_i\left(-\mathbf{K}_i\delta_i(\mathbf{x}, t)\right)\right) \\
&= \frac{\partial V(\mathbf{x})}{\partial \mathbf{x}}\left(\mathbf{f}(\mathbf{x}) + \sum_{i=1}^{2}\mathbf{g}_i(\mathbf{x})\alpha_i(\mathbf{x})\right) \\
&\quad + \frac{\partial V(\mathbf{x})}{\partial \mathbf{x}}\sum_{i=1}^{2}\mathbf{g}_i(\mathbf{x})\left(\mathbf{V}_i\widehat{\mathbf{w}}(t) - V_i\mathbf{w}(t)\right) \\
&\quad - \frac{\partial V(\mathbf{x})}{\partial \mathbf{x}}\sum_{i=1}^{2}\mathbf{g}_i(\mathbf{x})\left(m_i p_i(\mathbf{x})\tanh\right. \\
&\qquad \left.\times\left(\frac{(\partial V(\mathbf{x})/\partial \mathbf{x})\,\mathbf{g}_i(\mathbf{x})\,p_i(\mathbf{x})}{\xi_i}\right) - \delta_i(\mathbf{x}, t)\right) \\
&\quad - \sum_{i=1}^{m}\left(er_i^T\mathbf{Q}_i er_i\right) - 2\sum_{i=1}^{2}\left(er_i^T\mathbf{P}_i\left(\mathbf{K}_i\delta_i(\mathbf{x}, t)\right)\right).
\end{aligned} \tag{43}$$

In terms of Assumption 4, (43) can be rewritten as

$$\begin{aligned}\dot{W} \le{}& \frac{\partial V(\mathbf{x})}{\partial \mathbf{x}}\left(\mathbf{f}(\mathbf{x})+\sum_{i=1}^{2}\mathbf{g}_i(\mathbf{x})\alpha_i(\mathbf{x})\right)+\frac{\partial V(\mathbf{x})}{\partial \mathbf{x}}\sum_{i=1}^{2}\mathbf{g}_i(\mathbf{x})\left(\mathbf{V}_i er_i(t)\right)\\ &-\frac{\partial V(\mathbf{x})}{\partial \mathbf{x}}\sum_{i=1}^{2}\mathbf{g}_i(\mathbf{x})\left(m_i p_i(\mathbf{x})\tanh\left(\frac{(\partial V(\mathbf{x})/\partial \mathbf{x})\,\mathbf{g}_i(\mathbf{x})\,p_i(\mathbf{x})}{\xi_i}\right)-\left|m_i p_i(\mathbf{x})\right|\right)\\ &-\sum_{i=1}^{m}\left(er_i^T\mathbf{Q}_i er_i\right)-2\sum_{i=1}^{2}\left(er_i^T\mathbf{P}_i\left(\mathbf{K}_i\delta_i(\mathbf{x},t)\right)\right)\\ ={}& \frac{\partial V(\mathbf{x})}{\partial \mathbf{x}}\left(\mathbf{f}(\mathbf{x})+\sum_{i=1}^{2}\mathbf{g}_i(\mathbf{x})\alpha_i(\mathbf{x})\right)+\frac{\partial V(\mathbf{x})}{\partial \mathbf{x}}\sum_{i=1}^{2}\mathbf{g}_i(\mathbf{x})\left(\mathbf{V}_i er_i(t)\right)\\ &+m_i\sum_{i=1}^{2}\begin{pmatrix}\dfrac{\partial V(\mathbf{x})}{\partial \mathbf{x}}\mathbf{g}_i(\mathbf{x})\left|p_i(\mathbf{x})\right|\\ -\dfrac{\partial V(\mathbf{x})}{\partial \mathbf{x}}\mathbf{g}_i(\mathbf{x})\,p_i(\mathbf{x})\tanh\left(\dfrac{(\partial V(\mathbf{x})/\partial x)\,\mathbf{g}_i(\mathbf{x})\,p_i(\mathbf{x})}{\xi_i}\right)\end{pmatrix}\\ &-\sum_{i=1}^{m}\left(er_i^T\mathbf{Q}_i er_i\right)-2\sum_{i=1}^{2}\left(er_i^T\mathbf{P}_i\left(\mathbf{K}_i\delta_i(\mathbf{x},t)\right)\right).\end{aligned} \tag{44}$$

According to Lemma 11, the following inequality holds:

$$0 \le |x| - x\tanh\left(\frac{x}{\varepsilon}\right) \le \frac{1}{2}\varepsilon. \tag{45}$$

That is,

$$\begin{aligned}&\frac{\partial V(\mathbf{x})}{\partial \mathbf{x}}\mathbf{g}_i(\mathbf{x})\left|p_i(\mathbf{x})\right|\\ &-\frac{\partial V(\mathbf{x})}{\partial \mathbf{x}}\mathbf{g}_i(\mathbf{x})\,p_i(\mathbf{x})\tanh\left(\frac{(\partial V(x)/\partial x)\,\mathbf{g}_i(\mathbf{x})\,p_i(\mathbf{x})}{\xi_i}\right)\\ &\le \frac{1}{2}\xi_i.\end{aligned} \tag{46}$$

Substituting (46) into (44), we can get

$$\begin{aligned}\dot{W} \le{}& \frac{\partial V(\mathbf{x})}{\partial \mathbf{x}}\left(\mathbf{f}(\mathbf{x})+\sum_{i=1}^{2}\mathbf{g}_i(\mathbf{x})\alpha_i(\mathbf{x})\right)\\ &+\frac{\partial V(\mathbf{x})}{\partial \mathbf{x}}\sum_{i=1}^{2}\mathbf{g}_i(\mathbf{x})\left(\mathbf{V}_i er_i(t)\right)+m_i\frac{1}{2}\xi_i\\ &-\sum_{i=1}^{m}\left(er_i^T\mathbf{Q}_i er_i\right)-2\sum_{i=1}^{2}\left(er_i^T\mathbf{P}_i\left(\mathbf{K}_i\delta_i(\mathbf{x},t)\right)\right).\end{aligned} \tag{47}$$

With the application of (14) in Assumption 2 into (47), we can obtain

$$\begin{aligned}\dot{W} \le{}& -d_0(\|\mathbf{x}\|)+\frac{\partial V(\mathbf{x})}{\partial \mathbf{x}}\sum_{i=1}^{2}\mathbf{g}_i(\mathbf{x})\left(\mathbf{V}_i er_i(t)\right)\\ &+m_i\frac{1}{2}\xi_i-\sum_{i=1}^{m}\left(er_i^T\mathbf{Q}_i er_i\right)\\ &-2\sum_{i=1}^{2}\left(er_i^T\mathbf{P}_i\left(\mathbf{K}_i\delta_i(\mathbf{x},t)\right)\right)\\ \le{}& -d_0(\|\mathbf{x}\|)+\left|\frac{\partial V(\mathbf{x})}{\partial \mathbf{x}}\sum_{i=1}^{2}\mathbf{g}_i(\mathbf{x})\right|^2\left|\mathbf{V}_i er_i(t)\right|\\ &+m_i\frac{1}{2}\xi_i-\sum_{i=1}^{m}\left(er_i^T\mathbf{Q}_i er_i\right)\\ &-2\sum_{i=1}^{2}\left(er_i^T\mathbf{P}_i\left(\mathbf{K}_i\delta_i(\mathbf{x},t)\right)\right).\end{aligned} \tag{48}$$

Assuming that $\lambda_{\min}(\mathbf{Q}_i)$ represent the minimal eigenvalue of the matrix $\mathbf{Q}_i$, (48) can be given by

$$\begin{aligned}\dot{W} \le{}& -d_0(\|\mathbf{x}\|)+\left|\frac{\partial V(\mathbf{x})}{\partial \mathbf{x}}\sum_{i=1}^{2}\mathbf{g}_i(\mathbf{x})\right|^2\left|\mathbf{V}_i er_i(t)\right|\\ &+m_i\frac{1}{2}\xi_i-\sum_{i=1}^{m}\lambda_{\min}(\mathbf{Q}_i)\left\|er_i\right\|^2\\ &+\sum_{i=1}^{2}\left(2\mu_i\left\|\mathbf{P}_i\mathbf{K}_i\right\|^2\left\|er_i^T\right\|^2+\frac{1}{2\mu_i}\left|m_i p_i(\mathbf{x})\right|^2\right),\end{aligned} \tag{49}$$

where μ_i is a positive number.

In terms of permanent establishment inequality $2ab \le ca^2 + c^{-1}b^2$, (49) is rewritten as

$$\begin{aligned}\dot{W} \le & -d_0(\|\mathbf{x}\|) + \left(\left| \frac{\partial V(\mathbf{x})}{\partial \mathbf{x}} \sum_{i=1}^{2} \mathbf{g}_i(\mathbf{x}) \right|^2 + \frac{1}{4} \sum_{i=1}^{2} \|\mathbf{V}_i\|^2 \|er_i\|^2 \right) \\ & + m_i \frac{1}{2} \xi_i - \sum_{i=1}^{2} \lambda_{\min}(\mathbf{Q}_i) \|er_i\|^2 \\ & + \sum_{i=1}^{2} \left(2\mu_i \|\mathbf{P}_i \mathbf{K}_i\|^2 \|er_i^T\|^2 + \frac{1}{2\mu_i} |m_i p_i(\mathbf{x})|^2 \right).\end{aligned} \tag{50}$$

With the application of (15) in Assumption 2 into (50), we can obtain

$$\begin{aligned}\dot{W} \le & -d_0(\|\mathbf{x}\|) + \left(d_0(\|\mathbf{x}\|) + \frac{1}{4} \sum_{i=1}^{2} \|\mathbf{V}_i\|^2 \|er_i\|^2 \right) \\ & + m_i \frac{1}{2} \xi_i - \sum_{i=1}^{2} \lambda_{\min}(\mathbf{Q}_i) \|er_i\|^2 \\ & + \sum_{i=1}^{2} \left(2\mu_i \|\mathbf{P}_i \mathbf{K}_i\|^2 \|er_i^T\|^2 + \frac{1}{2\mu_i} |m_i p_i(\mathbf{x})|^2 \right) \\ = & \frac{1}{4} \sum_{i=1}^{2} \|\mathbf{V}_i\|^2 \|er_i\|^2 + m_i \frac{1}{2} \xi_i - \sum_{i=1}^{2} \lambda_{\min}(\mathbf{Q}_i) \|er_i\|^2 \\ & + \sum_{i=1}^{2} \left(2\mu_i \|\mathbf{P}_i \mathbf{K}_i\|^2 \|er_i^T\|^2 + \frac{1}{2\mu_i} |m_i p_i(\mathbf{x})|^2 \right) \\ \le & \frac{1}{4} \sum_{i=1}^{2} \|\mathbf{V}_i\|^2 \|er_i\|^2 - \sum_{i=1}^{2} \lambda_{\min}(\mathbf{Q}_i) \|er_i\|^2 \\ & + m_i \frac{1}{2} \xi_i + \sum_{i=1}^{2} \left(2\mu_i \|\mathbf{P}_i \mathbf{K}_i\|^2 \|er_i^T\|^2 + \frac{m_i}{2\mu_i} |p_{\max}|^2 \right),\end{aligned} \tag{51}$$

where $|p_{\max}|$ indicates the maximum value of $|p_i(x)|$.

Suppose that $d_i = \lambda_{\min}(\mathbf{Q}_i) - (1/4)\|V_i\|^2 - 2\mu_i \|\mathbf{P}_i \mathbf{K}_i\|^2 > 0$ and choose proper ξ_i to satisfy

$$\dot{W} \le -\sum_{i=1}^{m} d_i \|\mathbf{e}_i\|^2 + m_i \frac{1}{2} \xi_i + \sum_{i=1}^{2} \left(\frac{m_i}{2\mu_i} |p_{\max}|^2 \right) \le 0. \tag{52}$$

As can be seen above, the proposed controller can ensure all the signals of the closed-loop system uniformly bounded. Consequently, the paper comes to the following conclusion.

Theorem 13. *There exist positive definite matrices $\mathbf{P}_i$ and $\mathbf{Q}_i$ satisfying formula* (21) *and nonzero constant vector $\mathbf{K}_i \in \mathbf{R}^q$ satisfying Assumption 3, such that the matrix $\mathbf{W}_i - \mathbf{K}_i \mathbf{V}_i$ is Hurwitz. Furthermore, the formula* (52) *holds. For the multivariable nonlinear system* (9) *and exosystem* (10) *satisfying the Assumptions* (1) *to* (5)*, the nonlinear multivariable internal models* (18) *and* (22) *and the input feedback control* (25) *can make the closed-loop system globally uniformly bounded.*

5. Numerical Simulations and Analysis

To illustrate the performance of the present control algorithm, some numerical simulations are performed in the section. The whole simulation time is 5 seconds with the sampling interval 0.001 s. The simulation parameters are chosen as follows.

For the grid, the rms value of network voltage $e_0 = 380$ V the synchronous angular velocity $\omega = 100\pi$ rad/s. For the three-phase grid-connected inverters, the filter inductance $L = 1.0$ mH and equivalent series resistance $R = 0.02\ \Omega$.

Substituting the relevant parameters into the original state equation (9), the nonlinear system (9) can be described by

$$\dot{\mathbf{x}} = \mathbf{f}(\mathbf{x}) + \sum_{i=1}^{2} \mathbf{g}_i(\mathbf{x}) \left(\mathbf{v}_i - \mathbf{e}_{i0} - D_i(\mathbf{w}) + \delta_i(\mathbf{x}, t) \right), \quad 1 \le i \le 2, \tag{53}$$

where $\mathbf{x} = [x_1, x_2]^T$, $\mathbf{f}(\mathbf{x}) = \begin{bmatrix} -20x_1 + 100\pi x_2 \\ -100\pi x_1 - 20x_2 \end{bmatrix}$, $\mathbf{g}_1(\mathbf{x}) = \mathbf{g}_2(\mathbf{x}) = 1000$, and $[e_{10}, e_{20}] = [380, 0]$. The control input $\mathbf{v} = [v_1, v_2]^T$. It is thus clear that the system (53) has two-variable input, and the conventional single-input algorithm cannot solve the problem.

Example 14. The network is immersed 3% 3rd harmonics to fundamental wave.

The exosystem matrices for exogenous disturbance $\mathbf{D}(\mathbf{w})$ represented in (10) and (18) are given as $\mathbf{W}_1 = \mathbf{W}_2 = \begin{bmatrix} 0 & 2\omega \\ -2\omega & 0 \end{bmatrix}$, $\mathbf{V}_1 = \mathbf{V}_2 = [11.4 \quad 0]$, and the uncertain items satisfy

$$\delta_1(\mathbf{x}, t) = x_1 \sin(x_1 t), \qquad \delta_2(\mathbf{x}, t) = x_2 \sin(x_2 t). \tag{54}$$

It is worth noticing that the rotating electrical angular velocity of the 3rd harmonics in stationary *abc* reference frame is in accordance with that of the 2nd harmonics in rotating *dq* reference frame of fundamental wave. Hence, $\mathbf{W}_1 = \mathbf{W}_2 = \begin{bmatrix} 0 & 2\omega \\ -2\omega & 0 \end{bmatrix}$ in *dq* coordinated system represents the 3rd harmonics in stationary *abc* coordinated system. Furthermore, the values of $\mathbf{V}_1$ and $\mathbf{V}_2$ represent that the network is immersed 3% 3rd harmonics to fundamental wave.

In terms of (33) and (38), the control law of the nominal system is given by

$$\begin{aligned}\alpha_1(\mathbf{x}) &= -Lz_1 + Rx_1 - L\omega x_2 + L\dot{x}_{1\text{ref}} \\ &= -0.001(x_1 - x_{1\text{ref}}) + 0.02x_1 - 0.1\pi x_2 + 0.001\dot{x}_{1\text{ref}}, \\ \alpha_2(\mathbf{x}) &= -Lez_2 + Rx_2 + L\omega x_1 + L\dot{x}_{2\text{ref}} \\ &= -0.001(x_2 - x_{2\text{ref}}) + 0.02x_1 + 0.1\pi x_2 + 0.001\dot{x}_{2\text{ref}}.\end{aligned} \tag{55}$$

Supposing that

$$V(\mathbf{x}) = \frac{1}{2} c_1 (x_1 - x_{1\text{ref}})^2 + \frac{1}{2} c_2 (x_2 - x_{2\text{ref}})^2, \tag{56}$$

we can obtain

$$\frac{\partial V(\mathbf{x})}{\partial \mathbf{x}}\left(\mathbf{f}(\mathbf{x})+\sum_{i=1}^{2}\mathbf{g}_i(\mathbf{x})\boldsymbol{\alpha}_i\right) = -(x_1-x_{1\mathrm{ref}})^2-(x_2-x_{2\mathrm{ref}})^2, \tag{57}$$

$$\frac{\partial \mathbf{V}(\mathbf{x})}{\partial \mathbf{x}}\sum_{i=1}^{2}\mathbf{g}_i(\mathbf{x}) = \frac{c_1(x_1-x_{1\mathrm{ref}})}{L}+\frac{c_2(x_2-x_{2\mathrm{ref}})}{L}. \tag{58}$$

Supposing $\mathbf{x}' = [(x_1-x_{1\mathrm{ref}}) \quad (x_2-x_{2\mathrm{ref}})^T]$, in terms of (56), (57) and (58), and choosing $c_1 = L$ and $c_2 = L$ make the following inequalities hold

$$\begin{aligned}
&\frac{1}{2}L\left\|\mathbf{x}'\right\|^2 \le V(\mathbf{x}) \le L\left\|\mathbf{x}'\right\|^2,\\
&\frac{\partial V(\mathbf{x})}{\partial \mathbf{x}}\left(\mathbf{f}(\mathbf{x})+\sum_{i=1}^{2}\mathbf{g}_i(\mathbf{x})\alpha_i\right) \le -\left\|\mathbf{x}'\right\|^2,\\
&\left|\frac{\partial \mathbf{V}(\mathbf{x})}{\partial \mathbf{x}}\sum_{i=1}^{m}\mathbf{g}_i(\mathbf{x})\right|^2 \le \left\|\mathbf{x}'\right\|^2.
\end{aligned} \tag{59}$$

That is, Assumption 2 is satisfied.

Choosing

$$r_1(\mathbf{x}) = 9Lx_1, \qquad r_2(\mathbf{x}) = 9Lx_1, \tag{60}$$

we can obtain

$$\begin{aligned}
\mathbf{K}_1 &= \frac{\partial r_1(\mathbf{x})}{\partial \mathbf{x}}\mathbf{g}_1(\mathbf{x}) = \begin{bmatrix}9 & 0\end{bmatrix}^T,\\
\mathbf{K}_2 &= \frac{\partial r_2(\mathbf{x})}{\partial \mathbf{x}}\mathbf{g}_2(\mathbf{x}) = \begin{bmatrix}9 & 0\end{bmatrix}^T.
\end{aligned} \tag{61}$$

Therefore, Assumption 3 holds.

According to (61), we can obtain

$$\mathbf{W}_1-\mathbf{K}_1\mathbf{V}_1 = \begin{bmatrix}-102.6000 & 628.3185\\ -628.3185 & 0\end{bmatrix}, \tag{62}$$

$$\mathbf{W}_2-\mathbf{K}_2\mathbf{V}_2 = \begin{bmatrix}-102.6000 & 628.3185\\ -628.3185 & 0\end{bmatrix}. \tag{63}$$

Furthermore, let $\mathbf{P}_1 = \mathbf{P}_2 = \left[\begin{smallmatrix}4 & -2\\ 2 & 4\end{smallmatrix}\right]$; substituting (62) and (63) into (21), respectively, we obtain

$$\begin{aligned}
\mathbf{Q}_1 &= \begin{bmatrix}820.8000 & -205.2000\\ 205.2000 & 0\end{bmatrix},\\
\mathbf{Q}_2 &= \begin{bmatrix}820.8000 & -205.2000\\ 205.2000 & 0\end{bmatrix}.
\end{aligned} \tag{64}$$

Let $\mu_1 = \mu_2 = 0.005$; substituting $\mathbf{Q}_i$, $\mathbf{V}_i$, $\mathbf{P}_i$, $\mathbf{K}_i$, and μ_i into (52), through some arithmetical operations, we can obtain

$$\begin{aligned}
d_1 &= \lambda_{\min}(\mathbf{Q}_1) - \frac{1}{4}\left\|\mathbf{V}_1\right\|^2 - 2\mu_1\left\|\mathbf{P}_1\mathbf{K}_1\right\|^2\\
&= 54.9832 - \frac{1}{4}\times 129.9600 - 2\mu_1\times 1620 > 0,\\
d_2 &= \lambda_{\min}(\mathbf{Q}_2) - \frac{1}{4}\left\|\mathbf{V}_2\right\|^2 - 2\mu_2\left\|\mathbf{P}_2\mathbf{K}_2\right\|^2\\
&= 54.9832 - \frac{1}{4}\times 129.9600 - 2\mu_2\times 1620 > 0.
\end{aligned} \tag{65}$$

Hence, through the presented algorithm, the final internal models of disturbance and uncertain items are given by

$$\begin{aligned}
&\widehat{D}_1(\mathbf{w}) = \mathbf{V}_1\widehat{\mathbf{w}}_1(t), \qquad \widehat{D}_2(\mathbf{w}) = \mathbf{V}_2\widehat{\mathbf{w}}_2(t),\\
&\widehat{\mathbf{w}}_1(t) = \widehat{\boldsymbol{\eta}}_1(t)+\mathbf{r}_1(x), \qquad \widehat{\mathbf{w}}_2(t) = \widehat{\boldsymbol{\eta}}_2(t)+\mathbf{r}_2(\mathbf{x}),\\
&\dot{\widehat{\eta}}_{11}(t) = -102.6\widehat{\eta}_{11}(t) - 0.7434x_1\\
&\qquad + 628.3185\widehat{\eta}_{12}(t) - 9u_1 - 2.8274x_2,\\
&\dot{\widehat{\eta}}_{12}(t) = -628.3185\widehat{\eta}_{11} - 5.6549x_1,\\
&\dot{\widehat{\eta}}_{21}(t) = -102.6\widehat{\eta}_{21}(t) + 628.3185\widehat{\eta}_{22}(t) - 9u_1\\
&\qquad + 1.9036x_1 + 0.18x_2,\\
&\dot{\widehat{\eta}}_{22}(t) = -628.3185\widehat{\eta}_{21} - 5.6549x_1,
\end{aligned} \tag{66}$$

$$\begin{aligned}
\widehat{\delta}_1(\mathbf{x},t) &= m_1\mathbf{K}_1 p_1(\mathbf{x})\tanh\left(\frac{\left[\widehat{\eta}_{11} \quad \widehat{\eta}_{12}\right]\mathbf{P}_1^T\mathbf{K}_1 p_1(\mathbf{x})}{\lambda_1}\right)\\
&= \begin{bmatrix}9\tanh\left(\dfrac{(36\widehat{\eta}_{11}-18\widehat{\eta}_{12})x_1}{\lambda_1}\right)\\ 0\end{bmatrix},\\
\widehat{\delta}_2(\mathbf{x},t) &= m_2\mathbf{K}_2 p_2(\mathbf{x})\tanh\left(\frac{\left[\widehat{\eta}_3 \quad \widehat{\eta}_4\right]\mathbf{P}_2^T\mathbf{K}_2 p_2(\mathbf{x})}{\lambda_2}\right)\\
&= \begin{bmatrix}9\tanh\left(\dfrac{(36\widehat{\eta}_{21}-18\widehat{\eta}_{22})x_2}{\lambda_2}\right)\\ 0\end{bmatrix}.
\end{aligned} \tag{67}$$

Choosing $m_1 = m_2 = 1$, $\xi_1 = \xi_2 = 0.1$, the controller is designed as

$$\begin{aligned}
\alpha_1(\mathbf{x}) &= -\frac{Lez_1}{c_1} + Rx_1 - L\omega x_2 + L\dot{x}_{1\mathrm{ref}}\\
&= -(x_1-x_{1\mathrm{ref}}) + 0.02x_1 - 0.3142x_2,\\
\alpha_2(\mathbf{x}) &= -\frac{Lez_2}{c_2} + Rx_2 + L\omega x_1 + L\dot{x}_{2\mathrm{ref}}\\
&= -(x_2-x_{2\mathrm{ref}}) + 0.02x_2 + 0.3142x_1,
\end{aligned}$$

$$
\begin{aligned}
v_1' &= \alpha_1(\mathbf{x}) - \widehat{D}_1(\mathbf{w}) \\
&\quad + m_1 p_1(\mathbf{x}) \tanh\left(\frac{(\partial V(\mathbf{x})/\partial x)\, g_1(\mathbf{x})\, p_1(\mathbf{x})}{\xi_1}\right) \\
&= -(x_1 - x_{1\mathrm{ref}}) + 0.02x_1 - 0.3142x_2 \\
&\quad - 11.4(\widehat{\eta}_{11}(t) + 0.009x_1) \\
&\quad + x_1 \tanh\left(\frac{(x_1 - x_{1\mathrm{ref}})\, x_1}{\xi_1}\right) - 380, \\
v_2' &= \alpha_2(\mathbf{x}) - \widehat{D}_2(\mathbf{w}) \\
&\quad + m_2 p_2(\mathbf{x}) \tanh\left(\frac{(\partial V(\mathbf{x})/\partial x)\, g_2(\mathbf{x})\, p_2(\mathbf{x})}{\xi_2}\right) \\
&= -(x_2 - x_{2\mathrm{ref}}) + 0.02x_2 + 0.3142x_1 \\
&\quad - 11.4(\widehat{\eta}_{21}(t) + 0.009x_1) \\
&\quad + x_2 \tanh\left(\frac{(x_2 - x_{2\mathrm{ref}})\, x_2}{\xi_2}\right).
\end{aligned} \tag{68}
$$

Let the initial condition of the simulation be $x(0) = [0 \quad 0]^T$, $\widehat{\eta}(0) = [0 \quad 0 \quad 0 \quad 0]^T$, $\widehat{w}(0) = [1 \quad 0]^T$. The reference values of the output current are chosen as $x_{\mathrm{ref}} = [4, 0]^T$. Figures 3, 4, 5, and 6 show the simulation results. Figure 3 demonstrates the system states (output currents in dq reference frame). Figure 4 indicates the control inputs in dq axis, respectively. The disturbances produced by the exosystem and their estimates are shown in Figure 5. Figure 6 demonstrates the estimating errors under the existence of exosystem disturbances and uncertain items. As shown in Figure 3, the system states are asymptotically convergence to the expected references under the existence of exogenous disturbances and uncertain modeling perturbations. Figures 5 and 6 also indicate that the designed internal models can produce the exogenous disturbance successfully and the estimating errors converge to zero.

Example 15. The network is immersed 1.5% 3rd harmonics and 1% 5th harmonics to fundamental wave.

The exosystem matrices for exogenous disturbance $\mathbf{D}(w)$ represented in (10) and (18) are given as $\mathbf{W} = \begin{bmatrix} 0 & 2\omega & 0 & 0 \\ -2\omega & 0 & 0 & 0 \\ 0 & 0 & 0 & 4\omega \\ 0 & 0 & -4\omega & 0 \end{bmatrix}$, $\mathbf{V}_1 = \mathbf{V}_2 = [5.7 \quad 0 \quad 3.8 \quad 0]$, and the uncertain items also satisfy

$$
\delta_1(\mathbf{x}, t) = x_1 \sin(x_1 t), \qquad \delta_2(\mathbf{x}, t) = x_2 \sin(x_2 t). \tag{69}
$$

The design of the nominal system and the verification of Assumption 2 are the same as in Example 14, their derivation processes are no longer described in detail.

Choosing

$$
r_1(\mathbf{x}) = r_2(\mathbf{x}) = \begin{bmatrix} 9Lx_1 & 9Lx_1 \end{bmatrix}^T, \tag{70}
$$

we can obtain:

$$
K_1 = K_2 = \frac{\partial r_1(\mathbf{x})}{\partial x}\mathbf{g}_1(\mathbf{x}) = [9 \quad 0 \quad 9 \quad 0]^T. \tag{71}
$$

Therefore, Assumption 3 holds.

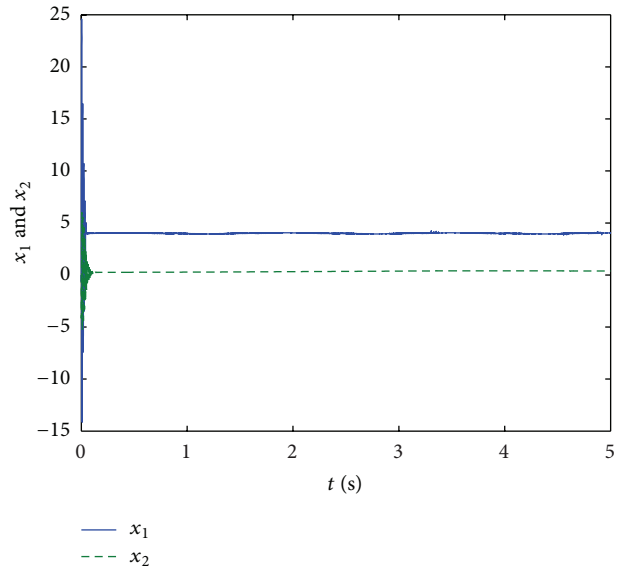

Figure 3: System states (output currents in dq reference frame).

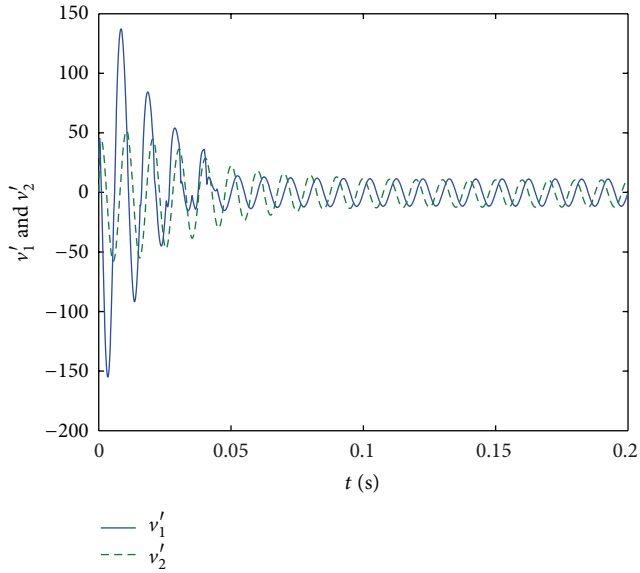

Figure 4: Control inputs in dq axis, respectively.

In terms of (71), we can obtain

$$
\begin{aligned}
&\mathbf{W}_1 - \mathbf{K}_1\mathbf{V}_1 \\
&\quad = \mathbf{W}_2 - \mathbf{K}_2\mathbf{V}_2 \\
&\quad = \begin{bmatrix} -51.3000 & 628.3185 & -34.2000 & 0 \\ -628.3185 & 0 & 0 & 0 \\ -51.3000 & 0 & -34.2000 & 1256.637 \\ 0 & 0 & -1256.637 & 0 \end{bmatrix}.
\end{aligned} \tag{72}
$$

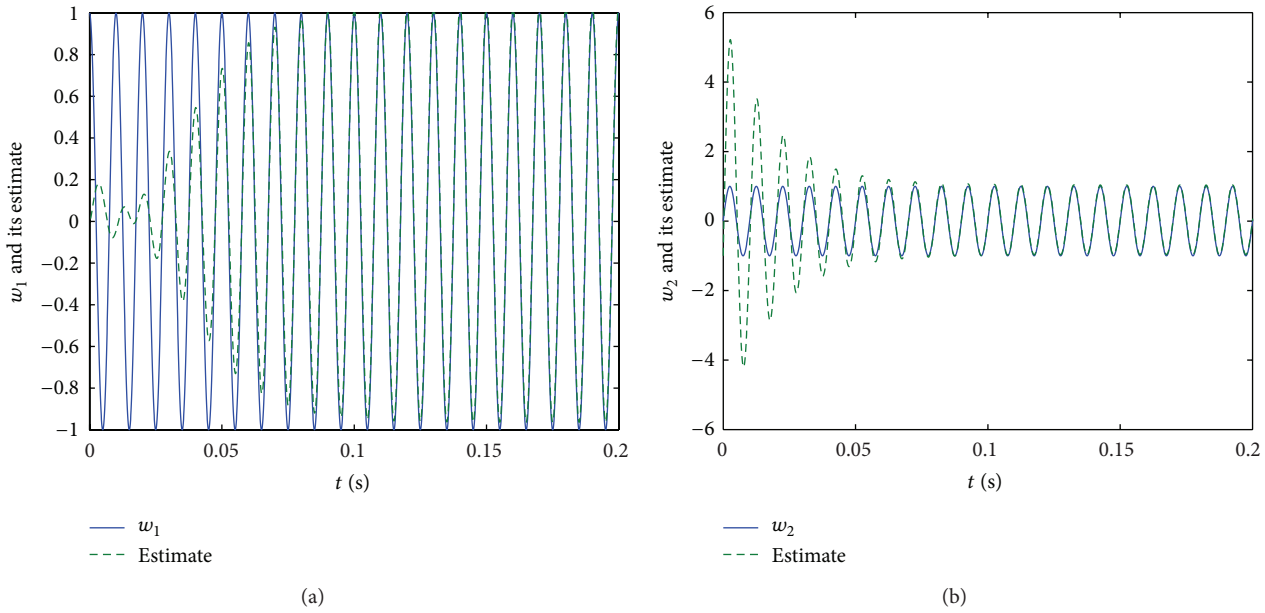

Figure 5: Exogenous disturbances of w_1 and w_2 and their estimates.

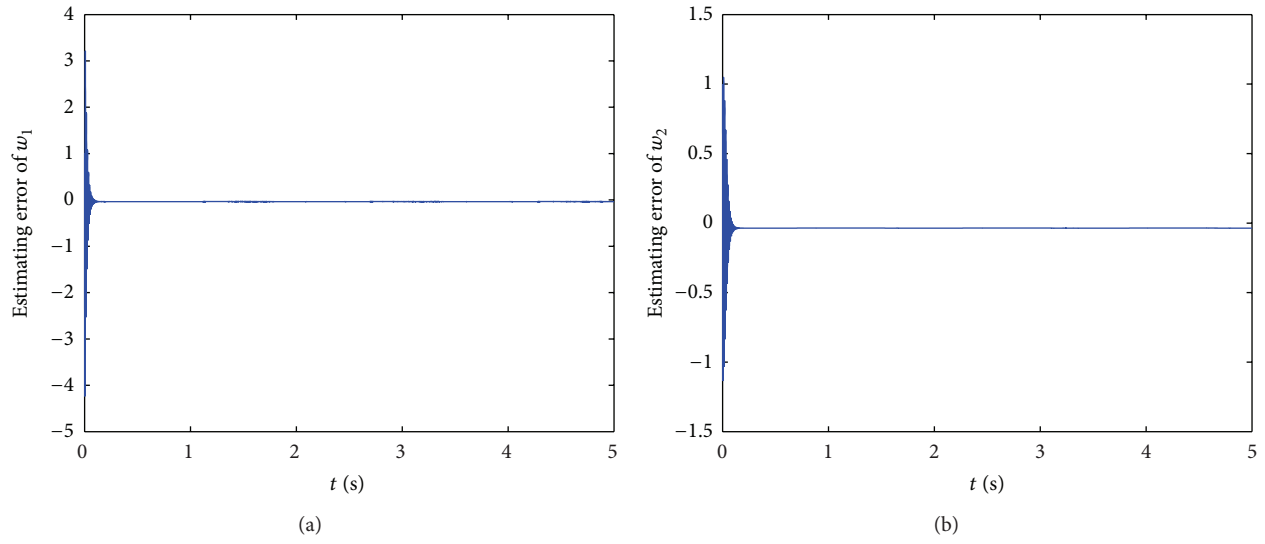

Figure 6: Estimating errors of w_1 and w_2.

Let

$$\mathbf{P}_1 = \mathbf{P}_2 = \begin{bmatrix} 3.970777 & -0.159154 & -0.072142 & -0.300626 \\ -0.159154 & 4.137151 & 0.070735 & 0.045912 \\ -0.072142 & 0.070735 & 5.920095 & -0.079577 \\ -0.300626 & 0.045912 & -0.07957 & 6.010020 \end{bmatrix}; \tag{73}$$

substituting (73) into (21), we obtain

$$\mathbf{Q}_1 = \mathbf{Q}_2 = \begin{bmatrix} 200.0011 & 100.0000 & 99.9996 & 99.9993 \\ 100.0000 & 199.9988 & 99.9989 & 100.0007 \\ 99.9996 & 99.9989 & 200.0100 & 100.0001 \\ 99.9996 & 100.0007 & 100.0004 & 199.9900 \end{bmatrix}. \tag{74}$$

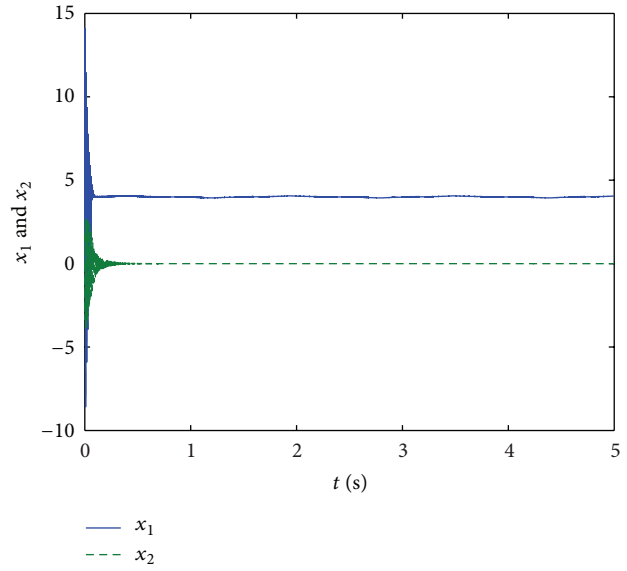

Figure 7: System states (output currents in dq reference frame).

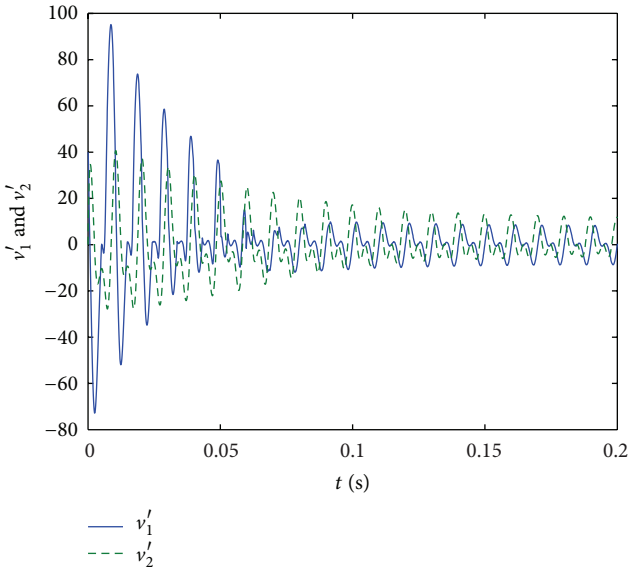

Figure 8: Control inputs in dq axis, respectively.

Let $\mu_1 = \mu_2 = 0.01$; substituting $\mathbf{Q}_i$, $\mathbf{V}_i$, $\mathbf{P}_i$, $\mathbf{K}_i$, and μ_i into (52), through some arithmetical operations, we can obtain

$$\begin{aligned} d_1 &= \lambda_{\min}(\mathbf{Q}_1) - \frac{1}{4}\|\mathbf{V}_1\|^2 - 2\mu_1\|P_1K_1\|^2 \\ &= 99.9924 - \frac{1}{4}\times 46.93 - 2\mu_1 \times 4013.57 > 0, \\ d_2 &= \lambda_{\min}(\mathbf{Q}_2) - \frac{1}{4}\|\mathbf{V}_2\|^2 - 2\mu_2\|\mathbf{P}_2\mathbf{K}_2\|^2 \\ &= 99.9924 - \frac{1}{4}\times 46.93 - 2\mu_1 \times 4013.57 > 0. \end{aligned} \tag{75}$$

Hence, through the presented algorithm, the final internal models of disturbance and uncertain items are given by

$$\begin{aligned} &\widehat{D}_1(\mathbf{w}) = \mathbf{V}_1\widehat{\mathbf{w}}_1(t), \qquad \widehat{D}_2(\mathbf{w}) = \mathbf{V}_2\widehat{\mathbf{w}}_2(t), \\ &\widehat{\mathbf{w}}_1(t) = \widehat{\boldsymbol{\eta}}_1(t) + \mathbf{r}_1(x), \qquad \widehat{\mathbf{w}}_2(t) = \widehat{\boldsymbol{\eta}}_2(t) + \mathbf{r}_2(\mathbf{x}), \\ &\dot{\widehat{\eta}}_{11}(t) = -51.3\widehat{\eta}_{11} + 628.3185\widehat{\eta}_{12} - 34.2\widehat{\eta}_{13} \\ &\qquad - 9u_1 + 5.3731x_1 - 2.8274x_2, \\ &\dot{\widehat{\eta}}_{12}(t) = -628.3185\widehat{\eta}_{11} - 5.6549x_1, \\ &\dot{\widehat{\eta}}_{13}(t) = -51.3\widehat{\eta}_{11} - 34.2\widehat{\eta}_{13} + 1256.637\widehat{\eta}_{14} \\ &\qquad - 9u_1 - 0.2817x_1 - 2.8274x_2, \\ &\dot{\widehat{\eta}}_{14}(t) = -1256.637\widehat{\eta}_{13}, \\ &\dot{\widehat{\eta}}_{21}(t) = -51.3\widehat{\eta}_{21} + 628.3185\widehat{\eta}_{22} - 34.2\widehat{\eta}_{23} \\ &\qquad - 9u_2 + 2.3657x_1 + 0.18x_2, \\ &\dot{\widehat{\eta}}_{22}(t) = -628.3185\widehat{\eta}_{21} - 5.6549x_1, \\ &\dot{\widehat{\eta}}_{23}(t) = -51.3\widehat{\eta}_{21} - 34.2\widehat{\eta}_{23} + 1256.637\widehat{\eta}_{24} \\ &\qquad - 9u_2 + 2.3657x_1 + 0.18x_2, \\ &\dot{\widehat{\eta}}_{24}(t) = -1256.637\widehat{\eta}_{23}, \\ &\widehat{\delta}_1(\mathbf{x},t) = m_1\mathbf{K}_1 p_1(\mathbf{x}) \tanh \\ &\qquad \times\left(\frac{[\widehat{\eta}_{11} \quad \widehat{\eta}_{12} \quad \widehat{\eta}_{13} \quad \widehat{\eta}_{14}]\,\mathbf{P}_1^T\mathbf{K}_1 p_1(\mathbf{x})}{\lambda_1}\right) \\ &\qquad = \begin{bmatrix} 9\tanh\left(\frac{\left(\begin{smallmatrix}35.0877\widehat{\eta}_{11}-0.7958\widehat{\eta}_{12}\\ +52.6316\widehat{\eta}_{13}-3.4218\widehat{\eta}_{14}\end{smallmatrix}\right)x_1}{\lambda_1}\right) \\ 0 \\ 9\tanh\left(\frac{\left(\begin{smallmatrix}35.0877\widehat{\eta}_{11}-0.7958\widehat{\eta}_{12}\\ +52.6316\widehat{\eta}_{13}-3.4218\widehat{\eta}_{14}\end{smallmatrix}\right)x_1}{\lambda_1}\right) \\ 0 \end{bmatrix}, \\ &\widehat{\delta}_2(\mathbf{x},t) = m_2\mathbf{K}_2 p_2(\mathbf{x}) \tanh \\ &\qquad \times\left(\frac{[\widehat{\eta}_{21} \quad \widehat{\eta}_{22} \quad \widehat{\eta}_{23} \quad \widehat{\eta}_{24}]\,\mathbf{P}_2^T\mathbf{K}_2 p_2(\mathbf{x})}{\lambda_2}\right) \\ &\qquad = \begin{bmatrix} 9\tanh\left(\frac{\left(\begin{smallmatrix}35.0877\widehat{\eta}_{21}-0.7958\widehat{\eta}_{22}\\ +52.6316\widehat{\eta}_{23}-3.4218\widehat{\eta}_{24}\end{smallmatrix}\right)x_2}{\lambda_2}\right) \\ 0 \\ 9\tanh\left(\frac{\left(\begin{smallmatrix}35.0877\widehat{\eta}_{21}-0.7958\widehat{\eta}_{22}\\ +52.6316\widehat{\eta}_{23}-3.4218\widehat{\eta}_{24}\end{smallmatrix}\right)x_2}{\lambda_2}\right) \\ 0 \end{bmatrix}. \end{aligned} \tag{76}$$

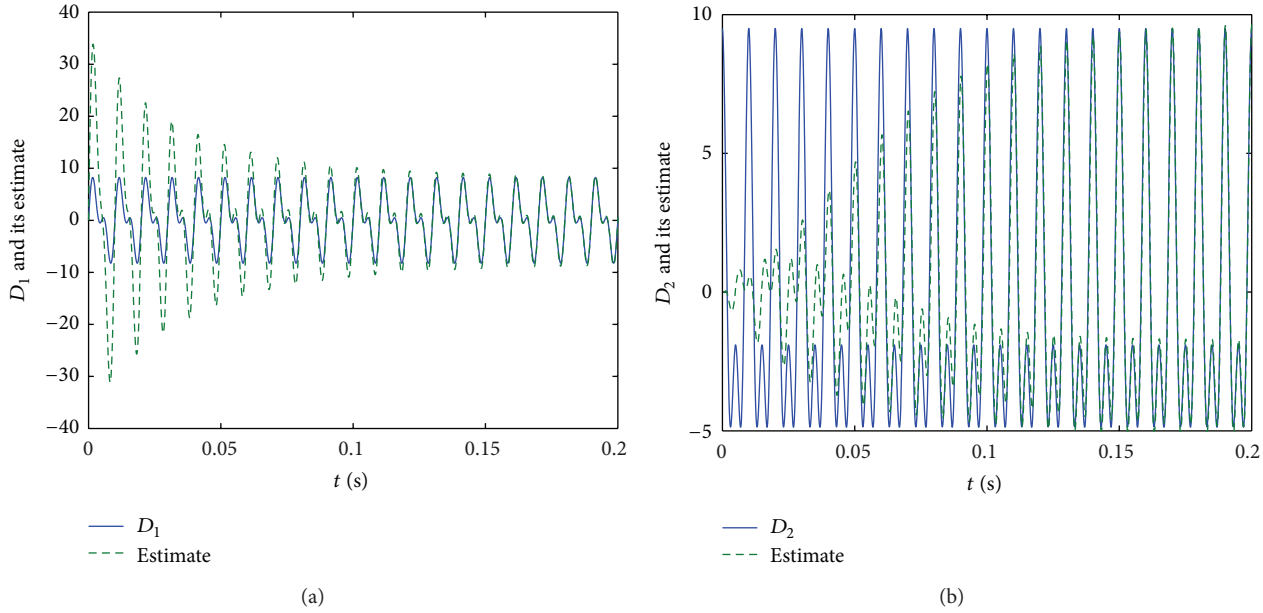

FIGURE 9: Exogenous disturbances of w_1 and w_2 and their estimates.

Choosing $m_1 = m_2 = 1$, $\xi_1 = \xi_2 = 0.1$, the controller is designed as

$$\begin{aligned} v_1' &= \alpha_1(\mathbf{x}) - \widehat{D}_1(\mathbf{w}) \\ &\quad + m_1 p_1(\mathbf{x}) \tanh\left(\frac{(\partial V(\mathbf{x})/\partial x)\,\mathbf{g}_1(\mathbf{x})\,p_1(\mathbf{x})}{\xi_1}\right) \\ &= -(x_1 - x_{1\mathrm{ref}}) + 0.02x_1 - 0.31415x_2 \\ &\quad - 5.7(\widehat{\eta}_{11}(t) + 0.009x_1) - 3.8\widehat{\eta}_{13}(t) \\ &\quad + x_1 \tanh\left(\frac{(x_1 - x_{1\mathrm{ref}})\,x_1}{\xi_1}\right) - 380, \\ v_2' &= \alpha_2(\mathbf{x}) - \widehat{D}_2(\mathbf{w}) \\ &\quad + m_2 p_2(\mathbf{x}) \tanh\left(\frac{(\partial V(x)/\partial x)\,\mathbf{g}_2(\mathbf{x})\,p_2(\mathbf{x})}{\xi_2}\right) \\ &= -(x_2 - x_{2\mathrm{ref}}) + 0.02x_2 + 0.31415x_1 \\ &\quad - 5.7(\widehat{\eta}_{21}(t) + 0.009x_1) - 3.8\widehat{\eta}_{23}(t) \\ &\quad + x_2 \tanh\left(\frac{(x_2 - x_{2\mathrm{ref}})\,x_2}{\xi_2}\right). \end{aligned} \tag{77}$$

Let the initial condition of the simulation be $x(0) = [0 \quad 0]^T$, $\widehat{\eta}(0) = [0 \quad 0 \quad 0 \quad 0 \quad 0 \quad 0 \quad 0 \quad 0]^T$, and $\widehat{w}(0) = [1 \quad 0 \quad 1 \quad 0]^T$. The reference values of the output current are also chosen as $x_{\mathrm{ref}} = [4, 0]^T$. Figures 7, 8, 9, and 10 show the simulation results. Figure 7 display that the system states are asymptotically convergence to the expected references under the existence of exogenous disturbances and uncertain modeling perturbations. Figures 9 and 10 also indicate that the designed internal models can produce the exogenous disturbances successfully.

6. Conclusions

In this paper, a nonlinear backstepping control with multivariable adaptive internal model principle for grid-connected inverter is proposed to reject the harmonic disturbance produced by a class of exosystems under the existence of uncertain items related with system states. Due to the nonlinearity and multiple variables for the original system, a nonlinear and multivariable internal model is constructed. In addition, in order to compensate for the effect of bounded uncertain items, an adaptive control law is designed to realize the real-time estimation of the perturbation. Based on the backstepping control law of the nominal system, a state feedback controller combined with the multivariable internal model and the adaptive control law is designed. A Lyapunov function is constructed and theoretically proves that all the signals of the multivariable closed-loop system are global boundedness. The simulation results show that the proposed control algorithm can guarantee the closed-loop system asymptotically converge to expected references quickly and the designed internal model can produce the exogenous disturbances successfully.

Restricted by the actual problem of grid-connected inverter control under distorted grid voltage, the proposed algorithm in the research aims at rejection of harmonic disturbances, and without considering the nonharmonic disturbances. However, the nonharmonic disturbances may induce adverse impacts, for example, noise and precision reduction. The future research should extend the algorithm to reject the nonharmonic disturbances.

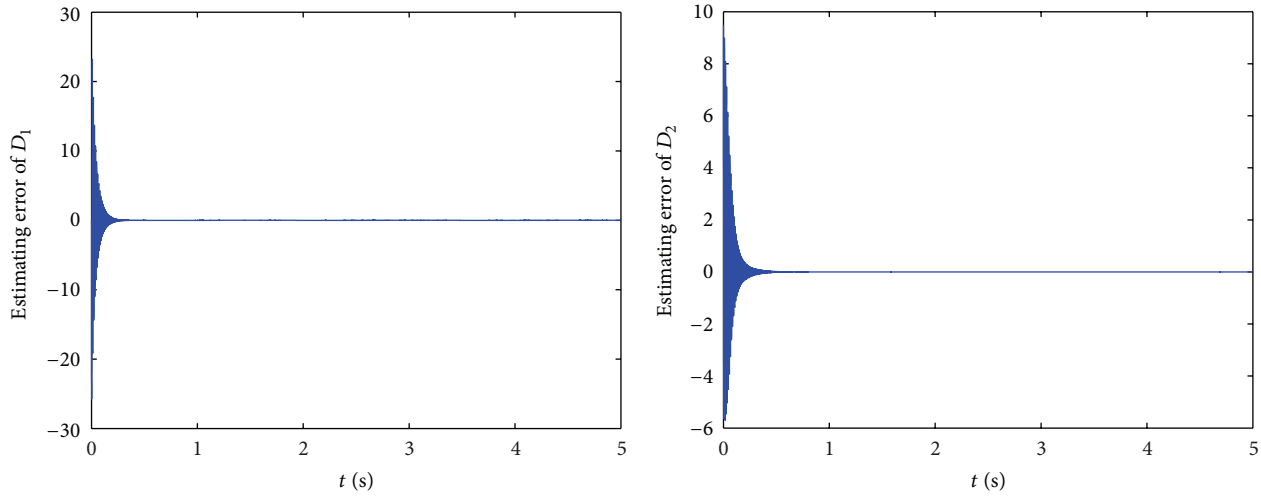

FIGURE 10: Estimating errors of D_1 and D_2.

Acknowledgments

This research is supported by the Specialized Research Fund for the Doctoral Program of Higher Education of China under Grant no. 20120036130001, the Fundamental Research Funds for the Central Universities of China under Grant no. 11MG40, and the Independent Research Funds of State Key Laboratory of Alternate Electrical Power System with Renewable Energy Sources of China under Grant no. 201209.

References

[1] H. Lund, "Renewable energy strategies for sustainable development," *Energy*, vol. 32, no. 6, pp. 912–919, 2007.

[2] T. J. Hammons, "Integrating renewable energy sources into European grids," *International Journal of Electrical Power & Energy Systems*, vol. 30, no. 8, pp. 462–475, 2008.

[3] J. López, P. Sanchis, X. Roboam, and L. Marroyo, "Dynamic behavior of the doubly fed induction generator during three-phase voltage dips," *IEEE Transactions on Energy Conversion*, vol. 22, no. 3, pp. 709–717, 2007.

[4] L. Xu and Y. Wang, "Dynamic modeling and control of DFIG-based wind turbines under unbalanced network conditions," *IEEE Transactions on Power Systems*, vol. 22, no. 1, pp. 314–323, 2007.

[5] L. L. Fan, S. Yuvarajan, and R. Kavasseri, "Harmonic analysis of a DFIG for a wind energy conversion system," *IEEE Transactions on Energy Conversion*, vol. 25, no. 1, pp. 181–190, 2010.

[6] J. Hu, H. Nian, H. Xu, and Y. He, "Dynamic modeling and improved control of DFIG under distorted grid voltage conditions," *IEEE Transactions on Energy Conversion*, vol. 26, no. 1, pp. 163–175, 2011.

[7] H. R. Karshenas and H. Saghafi, "Basic criteria in designing LCL filters for grid connected converters," in *Proceedings of IEEE International Symposium on Industrial Electronics (ISIE '06)*, pp. 1996–2000, Montreal, Canada, July 2006.

[8] W. Gullvik, L. Norum, and R. Nilsen, "Active damping of resonance oscillations in LCL-filters based on virtual flux and virtual resistor," in *Proceedings of the European Conference on Power Electronics and Applications*, pp. 1–10, Aalborg, Denmark, September 2007.

[9] F. Blaabjerg, M. Liserre, P. C. Loh, and R. Teodorescu, "Proportional-resonant controllers and filters for grid-connected voltage-source converters," *IEE Proceedings*, vol. 153, no. 5, pp. 750–762, 2006.

[10] P. F. Hu, D. Z. Jiang, Y. B. Zhou, J. Guo, and Z. Y. Lin, "Study of the proportional resonant control based modular multilevel converter," in *Proceedings of the 3rd International Conference on Digital Manufacturing and Automation*, pp. 810–813, Hangzhou, China, 2012.

[11] M. Liserre, R. Teodorescu, and F. Blaabjerg, "Stability of photovoltaic and wind turbine grid-connected inverters for a large set of grid impedance values," *IEEE Transactions on Power Electronics*, vol. 21, no. 1, pp. 263–272, 2006.

[12] F. Blaabjerg, Z. Chen, and S. B. Kjaer, "Power electronics as efficient interface in dispersed power generation systems," *IEEE Transactions on Power Electronics*, vol. 19, no. 5, pp. 1184–1194, 2004.

[13] C. Dong, J. M. Zhang, and Z. M. Qian, "An improved repetitive control scheme for grid-connected inverter with frequency-adaptive capability," *IEEE Transactions on Industrial Electronics*, vol. 60, no. 2, pp. 814–823, 2013.

[14] Y. Y. Tzou, S. L. Jung, and H. C. Yeh, "Adaptive repetitive control of PWM inverters for very low THD AC-voltage regulation with unknown loads," *IEEE Transactions on Power Electronics*, vol. 14, no. 5, pp. 973–981, 1999.

[15] T. S. Lee, S. J. Chiang, and J. M. Chang, "H_∞ loop-shaping controller designs for the single-phase UPS inverters," *IEEE Transactions on Power Electronics*, vol. 16, no. 4, pp. 473–481, 2001.

[16] G. Weiss, Q. C. Zhong, T. C. Green, and J. Liang, "H^∞ repetitive control of DC-AC converters in microgrids," *IEEE Transactions on Power Electronics*, vol. 19, no. 1, pp. 219–230, 2004.

[17] J. I. Ha, "Current prediction in vector-controlled PWM inverters using single DC-link current sensor," *IEEE Transactions on Industrial Electronics*, vol. 57, no. 2, pp. 716–726, 2010.

[18] G. H. Bode, P. C. Loh, M. J. Newman, and D. G. Holmes, "An improved robust predictive current regulation algorithm," *IEEE Transactions on Industry Applications*, vol. 41, no. 6, pp. 1720–1733, 2005.

[19] S. Thielemans, T. J. Vyncke, and J. Melkebeek, "Weight factor selection for model-based predictive control of a four-level flying-capacitor inverter," *IET Power Electronics*, vol. 5, no. 3, pp. 323–333, 2012.

[20] T. Wang, S. C. Tong, and Y. M. Li, "Robust adaptive fuzzy control for nonlinear system with dynamic uncertainties based on backstepping," *International Journal of Innovative Computing, Information and Control*, vol. 5, no. 9, pp. 2675–2688, 2009.

[21] S. C. Tong, Y. M. Li, and P. Shi, "Fuzzy adaptive backstepping robust control for SISO nonlinear system with dynamic uncertainties," *Information Sciences*, vol. 179, no. 9, pp. 1319–1332, 2009.

[22] F. Zouari, K. S. Ben, and M. Benrejeb, "Robust adaptive control for a class of nonlinear systems using the backstepping method," *International Journal of Advanced Robotic Systems*, vol. 10, pp. 1–12, 2013.

[23] Y. J. Liu, W. Wang, S. C. Tong, and Y. S. Liu, "Robust adaptive tracking control for nonlinear systems based on bounds of fuzzy approximation parameters," *IEEE Transactions on Systems, Man, and Cybernetics A*, vol. 40, no. 1, pp. 170–184, 2010.

[24] R. Ketata, Y. Rezgui, and N. Derbel, "Stability and robustness of fuzzy adaptive control of nonlinear systems," *Applied Soft Computing*, vol. 11, no. 1, pp. 166–178, 2011.

[25] S. Tong, C. Liu, and Y. Li, "Fuzzy-adaptive decentralized output-feedback control for large-scale nonlinear systems with dynamical uncertainties," *IEEE Transactions on Fuzzy Systems*, vol. 18, no. 5, pp. 845–861, 2010.

[26] Y. J. Liu and W. Wang, "Adaptive fuzzy control for a class of uncertain nonaffine nonlinear systems," *Information Sciences*, vol. 177, no. 18, pp. 3901–3917, 2007.

[27] S. T. Liu, Y. Jiang, and P. Liu, "Rejection of nonharmonic disturbances in nonlinear systems," *Kybernetika*, vol. 46, no. 5, pp. 785–798, 2010.

[28] C. L. Chen, Z. T. Ding, and B. Lennox, "Rejection of non-harmonic disturbances in nonlinear systems with semi-global stability," *IEEE Transactions on Circuit System*, vol. 55, no. 12, pp. 1289–1293, 2008.

[29] Z. W. Ping and J. Huang, "Global robust output regulation for a class of multivariable systems and its application to a motor drive system," in *Proceedings of the American Control Conference (ACC '11)*, pp. 4560–4565, San Francisco, Calif, USA, June-July 2011.

[30] H. K. Khalil, *Nonlinear Systems*, Prentice-Hall, New Jersey, NJ, USA, 3rd edition, 2002.

[31] A. Isidori, *Nonlinear Control Systems*, Springer, New York, NY, USA, 3rd edition, 1995.

[32] M. M. Polycarpou and P. A. Ioannou, "A robust adaptive nonlinear control design," *Automatica*, vol. 32, no. 3, pp. 423–427, 1996.

Hindawi Publishing Corporation
Mathematical Problems in Engineering
Volume 2013, Article ID 426271, 9 pages
http://dx.doi.org/10.1155/2013/426271

Research Article

H_2 Control for the Continuous-Time Markovian Jump Linear Uncertain Systems with Partly Known Transition Rates and Input Quantization

Xin-Gang Zhao,[1] Dan Ye,[1,2] and Jian-Da Han[1]

[1] *State Key Laboratory of Robotics, Shenyang Institute of Automation, Chinese Academy of Sciences, Shenyang 110016, China*
[2] *College of Information Science and Engineering, Northeastern University, Shenyang 110189, China*

Correspondence should be addressed to Dan Ye; yedan@ise.neu.edu.cn

Received 22 May 2013; Accepted 19 July 2013

Academic Editor: Bochao Zheng

For a class of continuous-time Markovian jump linear uncertain systems with partly known transition rates and input quantization, the H_2 state-feedback control design is considered. The elements in the transition rates matrix include completely known, boundary known, and completely unknown ones. First, an H_2 cost index for Markovian jump linear uncertain systems is introduced; then by introducing a new matrix inequality condition, sufficient conditions are formulated in terms of linear matrix inequalities (LMIs) for the H_2 control of the Markovian jump linear uncertain systems. Less conservativeness is achieved than the result obtained with the existing technique. Finally, a numerical example is given to verify the validity of the theoretical results.

1. Introduction

Recently, much attention has been devoted to the study of the stochastic stability for the Markovian jump systems, and many important results have been published [1–4]. This is because the Markovian jump systems have been widely employed to model many practical systems, such as manufacturing systems, the power systems, and the economic systems in which they may experience abrupt changes in their structures and parameters [5, 6]. It is worth noticing that these results require that the transition probabilities/rates must be known *a priori*. However, in many practical engineering applications, the likelihood for obtaining the perfect information on all transition probabilities/rates elements is questionable, and the cost might be expensive in some cases. Therefore, the study of the stabilization of the Markovian jump systems with partly known transition probabilities/rates becomes interesting, and some well-known results have been published. The idea for the stochastic stability of the Markovian jump linear uncertain systems with partly known transition probabilities/rates is developed in Zhang et al. [7]. It is then applied to the H_∞ control design in Zhang and Boukas [8]. In those papers, the feature of the information about the transition probabilities/rates matrix considered includes two kinds of elements: completely known and completely unknown ones. As a matter of fact, the transition probabilities matrix might involve completely known, completely unknown, and boundary known elements. In Shen and Yang [9], an H_2 state-feedback controller design method is proposed for the continuous-time Markovian jump linear uncertain systems with the three kinds of transition rates matrix elements. In order to yield the design condition for analysis and synthesis, a matrix inequality is introduced to present LMIs conditions. In this paper, less conservative design conditions will be formulated by introducing a new relaxed matrix inequality condition.

On the other hand, in many modern engineering practices, all kinds of information processing devices, such as analog-to-digital and digital-to-analog converters, have been widely used. By the utilization of such information processing

devices, some advantages have been brought, for example, lower cost, reduced weight and power, simple installation, and maintenance. However, some new phenomena have also been induced, which might cause server deterioration of system performance or even lead to system instability. Signal quantization is one of the important aspects that should be fully considered in such cases, which always exists in computer-based control systems. Nowadays, many well-known results have been published on quantized feedback control. For example, the feedback stabilization problem is considered by utilizing dynamic quantizers [10–13] and static quantizers [14–17]. In addition, the filter design [18] and the H_∞ control design [19] are also investigated. Specially, quantization errors have adverse effects on the network control systems which can often be modeled as Markovian jump systems. In Xiao et al. [20], the stabilization problem for single-input discrete Markovian jump linear uncertain systems via mode-dependent quantized state-feedback is addressed, but the transition rates are assumed to be completely known.

To the best of our knowledge, no result has been presented for the control design of the continuous-time Markovian jump linear uncertain systems with partly known transition rates and input signal quantization. In this paper, the H_2 control for a class of continuous-time Markovian jump linear uncertain systems with respect to partly known transition rates and input signal quantization is addressed. The structure of the controller consists of two parts: the nonlinear part is provided to eliminate the effect of input quantization, and the linear part is obtained by solving LMIs for achieving the H_2 performance against unknown transition rates and model uncertainties. In comparison with the design utilizing the LMIs technique in Shen and Yang [9], the design method has less conservativeness by introducing a relaxed inequality condition.

The rest of this paper is organized as follows. The problem statement and preliminaries are presented in Section 2. The main results are given in Section 3. In Section 4, a numerical example is presented to illustrate the effectiveness of the results, and the conclusions are drawn in Section 5.

Notations. Throughout this paper, the following notations are used. R^n denotes the n-dimensional Euclidean space; A^T denotes the transpose of matrix A; I and 0 represent the identity matrix and a zero matrix in appropriate dimensions, respectively; $\mathbb{E}\{\cdot\}$ denotes the mathematical expectation operator; $X > Y$ $(X \geq Y)$, where X and Y are symmetric matrices, means that $X - Y$ is positive definite (positive semi-definite); $|x|_p$ denotes the p-norm of the vector x; that is, $|x|_p = (|x_1|^p + |x_2|^p + \cdots + |x_n|^p)^{1/p}$, where $p \geq 1$. When $p = \infty$, $|x|_\infty = \max_{1\leq i\leq n}|x_i|$. For matrix $X \in R^{m\times n}$, $|X|_p$ is used to present the matrix p-norm: $|X|_p = \sup_{y\neq 0}(|Xy|_p/|y|_p)$. The notation $|\cdot|$, in particular denotes the absolute value of a scalar, the standard Euclidean norm of a vector, and the induced norm of a matrix, respectively. In symmetric block matrices, an $*$ is used to represent a term that is induced by symmetry. Finally, the symbol $He(X)$ is used to represent $X + X^T$.

2. Problem Statement and Preliminaries

Consider a class of the continuous-time Markovian jump linear uncertain systems in the following probability space $(\Omega, \mathcal{F}, \mathcal{P})$:

$$\dot{x}(t) = \left(A(r_t) + \Delta A(r_t)\right)x(t) + \left(B(r_t) + \Delta B(r_t)\right)q(u(t)),$$
$$x_0 = x(0), \qquad r_0 = r(0), \tag{1}$$

where $x(t) \in R^n$ is the system state and $u(t) \in R^m$ is the control input. $\{r_t, t \geq 0\}$ is a continuous-time Markovian process with right continuous trajectories taking values in the finite set $\mathcal{S} = \{1, 2, \ldots, \mathbb{N}\}$. It governs the switching among the different system modes with the following mode transition probabilities:

$$\Pr\{r_{t+h} = j \mid r_t = i\} = \begin{cases} \lambda_{ij}h + o(h), & \text{if } j \neq i, \\ 1 + \lambda_{ii}h + o(h), & \text{if } j = i, \end{cases} \tag{2}$$

where $h > 0$, $\lim_{h\to 0}(o(h)/h) = 0$, and $\lambda_{ij} \geq 0$ $(i, j \in \mathcal{S}; j \neq i)$ denote the switching rate from mode i at time t to mode j at time $t + h$ and that $\lambda_{ii} = -\sum_{j=1, j\neq i}^{\mathbb{N}} \lambda_{ij}$ for each $i \in \mathcal{S}$.

In general, the Markovian process transition rates matrix Λ is defined by:

$$\Lambda = \begin{bmatrix} \lambda_{11} & \lambda_{12} & \cdots & \lambda_{1\mathbb{N}} \\ \lambda_{21} & \lambda_{22} & \cdots & \lambda_{2\mathbb{N}} \\ \vdots & \cdots & \ddots & \vdots \\ \lambda_{\mathbb{N}1} & \cdots & \cdots & \lambda_{\mathbb{N}\mathbb{N}} \end{bmatrix}. \tag{3}$$

In this paper, the transition rates of the jumping process are assumed to be partly available; that is, some elements in matrix Λ have been exactly known, some ones have been merely known with lower and upper bounds, and others may have no information to use. For instance, for the system (1) with four operation modes, the transition rates matrix might be described by

$$\Lambda = \begin{bmatrix} \lambda_{11} & ? & ? & \lambda_{14} \\ ? & ? & \lambda_{23} & ? \\ ? & ? & \beta & ? \\ \alpha & ? & \lambda_{43} & \lambda_{44} \end{bmatrix}, \tag{4}$$

where ? represents the completely unknown element of the transition rates matrix and the parameters α and β represent the elements with known lower and upper bounds. That is, $\underline{\alpha} \leq \alpha \leq \overline{\alpha}$, and $\underline{\beta} \leq \beta \leq \overline{\beta}$, where $\underline{\alpha}$, $\overline{\alpha}$, $\underline{\beta}$, and $\overline{\beta}$ are known parameters; λ_{ij} denotes the precisely known element.

For clarity, we denote that $\mathcal{S} = \mathcal{S}^i_{k1} \cup \mathcal{S}^i_{k2} \cup \mathcal{S}^i_{uk}$, $i = 1, 2, \ldots, \mathbb{N}$, with

$$\begin{aligned} \mathcal{S}^i_{k1} &= \left\{j : \lambda_{ij} \text{ is exactly known}\right\}, \\ \mathcal{S}^i_{k2} &= \left\{j : \text{the bounds of } \lambda_{ij} \text{ are known}\right\}, \\ \mathcal{S}^i_{uk} &= \left\{j : \text{there is no information available for } \lambda_{ij}\right\}. \end{aligned} \tag{5}$$

Furthermore, let $\mathcal{S}_k^i = \{j : \underline{\lambda}_{ij} \le \lambda_{ij} \le \overline{\lambda}_{ij}\}$; then one can obtain $\mathcal{S}_k^i = \mathcal{S}_{k1}^i \cup \mathcal{S}_{k2}^i$. If $\mathcal{S}_k^i \neq \emptyset$, it can be described as

$$\mathcal{S}_k^i = \left\{\mathcal{K}_1^i, \mathcal{K}_2^i, \ldots, \mathcal{K}_{m_k^i}^i\right\}. \tag{6}$$

Similarly, if $\mathcal{S}_{uk}^i \neq \emptyset$, let us denote that

$$\mathcal{S}_{uk}^i = \left\{\mathbb{K}_1^i, \mathbb{K}_2^i, \ldots, \mathbb{K}_{m_{uk}^i}^i\right\}, \tag{7}$$

where $\mathcal{K}_{l_1}^i$ denotes the l_1th element in $\mathcal{S}_k^i$ with the index $\mathcal{K}_{l_1}^i$ in the ith row of the matrix Λ. $\mathbb{K}_{l_2}^i$ denotes the l_2th completely unknown element with the index $\mathbb{K}_{l_2}^i$ in the ith row of the matrix Λ. m_k^i and m_{uk}^i represent the number of elements in $\mathcal{S}_k^i$ and $\mathcal{S}_{uk}^i$, respectively. For example, considering the transition rates matrix (4), one can easily check that $\mathcal{S}_k^4 = \{\mathcal{K}_1^4, \mathcal{K}_2^4, \mathcal{K}_3^4\}$ with $\mathcal{K}_1^4 = 1$, $\mathcal{K}_2^4 = 3$, $\mathcal{K}_3^4 = 4$, $\mathcal{S}_{uk}^4 = \{\mathbb{K}_1^4\}$ with $\mathbb{K}_1^4 = 2$, $m_k^4 = 3$, and $m_{uk}^4 = 1$.

Remark 1. When the lower and upper bounds of the elements in $\mathcal{S}_{k2}^i$ are equal, the transition rates matrix is reduced to the considered case in Zhang et al. [7]. It is obvious that the solving method there can only treat $j \in \mathcal{S}_{k2}^i$ as the completely unknown case which can result in some conservativeness.

For convenience, the notations $A_i = A(r_t)$, $B_i = B(r_t)$, $\Delta A_i = \Delta A(r_t)$, and $\Delta B_i = \Delta B(r_t)$ are used for each possible value $r_i = i, i \in \mathcal{S}$, where A_i and B_i are known constant matrices with appropriate dimensions. Then, the system (1) can be described by

$$\begin{aligned} \dot{x}(t) &= \left(A_i + \Delta A_i\right) x(t) + \left(B_i + \Delta B_i\right) q(u(t)), \\ x_0 &= x(0), \qquad r_0 = r(0). \end{aligned} \tag{8}$$

The following assumptions are assumed to be valid.

Assumption 1. The pair (A_i, B_i) is controllable.

Assumption 2. Consider the following: $\Delta A_i = D_i E_i(t) F_i$, $\Delta B_i = B_i M_i \Xi_i(t) N_i$, and $|M_i \Xi_i(t) N_i|_\infty \le \psi_i$, where D_i, F_i, M_i, and N_i are known constant matrices with appropriate dimensions, $E_i(t)$ and $\Xi_i(t)$ are time-varying uncertain matrices satisfying $E_i E_i^T \le I$ and $\Xi_i \Xi_i^T \le I$, and the parameter ψ_i satisfies $0 \le \psi_i < 1$.

In addition, the quantizer $q(\cdot)$ is defined by an operator function round$(\cdot)$ that rounds towards the nearest integer; that is,

$$q(u(t)) = \mu \cdot \text{round}\left(\frac{u(t)}{\mu}\right), \tag{9}$$

where $\mu(>0)$ is called a quantizing level of the quantizer. In computer-based control systems, the value of μ depends on the sampling accuracy and is known *a priori*. $q(\cdot)$ is the uniform quantizer with the fixed level μ. Define $e_\mu = q(u(t)) - u(t)$, since each component of e_μ is bounded by the half of the quantizing level μ; thus, we have $|e_\mu|_\infty \le \mu/2$.

The objective of this paper is to design the state-feedback control law

$$u(t) = K_i x + u_{ic}, \quad K_i = K\left(r_t\right), \text{ when } r_t = i, \tag{10}$$

such that the resulting closed-loop system is stochastically stable and obtains as small value of the H_2 cost index for the Markovian jump linear uncertain systems given in the following as possible

$$\begin{aligned} \mathcal{J}(t) = \mathbb{E}\Bigg[\int_t^\infty \Big\{ & x^T(\tau) Q\left(r_\tau\right) x(\tau) \\ & + x^T(\tau) K^T\left(r_\tau\right) R\left(r_\tau\right) K\left(r_\tau\right) x(\tau)\Big\} d\tau \mid r_0\Bigg], \end{aligned} \tag{11}$$

where $Q(r_t)$ and $R(r_t)$ are positive definite matrices. The nonlinear part of the controller u_{ic} is designed against the effect of signal quantization, and the linear part $K_i x$ is proposed to deal with model uncertainties and to unknown transition rates and achieve optimal H_2 performance.

Remark 2. When $Q(r_t) = Q > 0$, $R(r_t) = R > 0$, and $K(r_t) = K$, the above H_2 cost index is reduced to the following, (12) which is given in Yun et al. [17]:

$$\mathcal{J}(t) = \int_t^\infty \left\{x^T(\tau) Q x(\tau) + x^T(\tau) K^T R K x(\tau)\right\} d\tau. \tag{12}$$

Some useful lemmas are firstly presented before formulating the main result.

Lemma 3 (see [21]). *Given a symmetric matrix Π and matrices M and N with appropriate dimensions, then $\Pi + MF(t)N + N^T F^T(t) M^T < 0$ for all $F(t)$ satisfying $F^T(t)F(t) \le I$, if and only if there exists a scalar $\varepsilon > 0$ such that the following inequality holds:*

$$\Pi + \varepsilon M M^T + \varepsilon^{-1} N^T N < 0. \tag{13}$$

Lemma 4. *For any given $\lambda_j \ge 0$ and matrices $P_j > 0$ ($P_j \in R^{n\times n}$, $1 \le j \le \mathbb{N}$), if there exists $Z_i \ge P_j$, then the following inequality holds:*

$$\sum_{j=1}^{\mathbb{N}} \lambda_j P_j \le \sum_{j=1}^{\mathbb{N}} \lambda_j Z_i. \tag{14}$$

Proof. According to $Z_i \ge P_j$ and $\lambda_j \ge 0$, one can obtain that $\lambda_j Z_i \ge \lambda_j P_j$, which further imply that inequality (14) holds. □

Remark 5. In Shen and Yang [9], the inequality $\sum_{j=1}^{\mathbb{N}} \lambda_j P_j \le (\sum_{j=1}^{\mathbb{N}} \lambda_j)(\sum_{j=1}^{\mathbb{N}} P_j)$ is introduced to obtain design conditions. It is clear that the utilization of Lemma 4 will result in less conservativeness since $\max\{P_1, P_2, \ldots, P_{\mathbb{N}}\} < \sum_{j=1}^{\mathbb{N}} P_j$ for any $P_i > 0$.

Lemma 6. *For $\alpha, \beta \in R^n$, $p \ge 1$, and $q \ge 1$, the following inequality holds:*

$$\left|\alpha^T \beta\right| \le |\alpha|_p |\beta|_q, \quad p^{-1} + q^{-1} = 1. \tag{15}$$

Lemma 7 (see [22]). *For the symmetric and positive definite matrices P and Q, if $P \ge Q > 0$, then $Q^{-1} \ge P^{-1} > 0$.*

3. Main Results

Theorem 8. *For the system* (1) *subject to Assumptions 1 and 2, suppose that there exist the symmetric positive definite matrices* X_i, *general matrices* Y_i, *and positive scalars* ε_i, δ_i, *and* γ *such that*

$$\begin{bmatrix} \Gamma_{11} & X_iF_i^T & Y_i^TN_i^T & \Gamma_{14} & \Gamma_{15} & X_i & Y_i \\ * & -\varepsilon_iI & 0 & 0 & 0 & 0 & 0 \\ * & * & -\delta_iI & 0 & 0 & 0 & 0 \\ * & * & * & \Gamma_{44} & 0 & 0 & 0 \\ * & * & * & * & -Z_i & 0 & 0 \\ * & * & * & * & * & -Q_i^{-1} & 0 \\ * & * & * & * & * & * & -R_i^{-1} \end{bmatrix} < 0, \tag{16}$$

$$Z_i \le X_j, \quad j \in \mathcal{S}_{uk}^i,$$

$$\begin{bmatrix} \Phi_{11} & X_iF_i^T & Y_i^TN_i^T & \Phi_{14} & X_i & Y_i^T \\ * & -\varepsilon_iI & 0 & 0 & 0 & 0 \\ * & * & -\delta_iI & 0 & 0 & 0 \\ * & * & * & \Phi_{44} & 0 & 0 \\ * & * & * & * & -Q_i^{-1} & 0 \\ * & * & * & * & * & -R_i^{-1} \end{bmatrix} < 0, \tag{17}$$

$$X_i \le X_j, \quad j \in \mathcal{S}_{uk}^i,$$

$$\begin{bmatrix} \gamma & x_0^T \\ x_0 & X_i \end{bmatrix} > 0, \tag{18}$$

where

$$\begin{aligned} \Gamma_{11} &= He\left(A_iX_i\right) + He\left(B_iY_i\right) + \varepsilon_iD_iD_i^T + \delta_iB_iM_iM_i^TB_i^T \\ &\quad + \overline{\lambda}_{ii}X_i, \\ \Gamma_{14} &= \left[\sqrt{\overline{\lambda}_{i\mathcal{K}_1^i}}X_i, \sqrt{\overline{\lambda}_{i\mathcal{K}_2^i}}X_i, \ldots, \sqrt{\overline{\lambda}_{i\mathcal{K}_{m_k^i}^i}}X_i\right], \\ \Gamma_{44} &= \operatorname{diag}\left\{-X_{\mathcal{K}_1^i}, -X_{\mathcal{K}_2^i}, \ldots, -X_{\mathcal{K}_{m_k^i}^i}\right\}, \\ \Gamma_{15} &= \sqrt{-\sum_{j\in\mathcal{S}_k^i}\underline{\lambda}_{ij}}X_i, \\ \Phi_{11} &= He\left(A_iX_i\right) + He\left(B_iY_i\right) + \varepsilon_iD_iD_i^T + \delta_iB_iM_iM_i^TB_i^T \\ &\quad - \sum_{j\in\mathcal{S}_k^i}\underline{\lambda}_{ij}X_i, \\ \Phi_{14} &= \left[\sqrt{\overline{\lambda}_{i\mathcal{K}_1^i}}X_i, \sqrt{\overline{\lambda}_{i\mathcal{K}_2^i}}X_i, \ldots, \sqrt{\overline{\lambda}_{i\mathcal{K}_{m_k^i}^i}}X_i\right], \\ \Phi_{44} &= \operatorname{diag}\left\{-X_{\mathcal{K}_1^i}, -X_{\mathcal{K}_2^i}, \ldots, -X_{\mathcal{K}_{m_k^i}^i}\right\}. \end{aligned} \tag{19}$$

Then, the controller designed as

$$u\left(t\right) = K_ix\left(t\right) + u_{ic}\left(t\right) \tag{20}$$

can drive the state trajectory to the origin asymptotically and can obtain the H_2 *cost by the minimum of* r, *where* $K_i = Y_iX_i^{-1}$, $P_i = X_i^{-1}$, *and* $u_{ic} = (-(1+\psi)\mu/2(1-\psi))\operatorname{sign}(x^TP_iB_i)$.

Proof. Take the Lyapunov function candidate $V = x^TP_ix$; then, along the system trajectory of plant (1), the weak infinitesimal operator $\mathfrak{T}_a^x[\cdot]$ of the process $\{x(t), r_t, t \ge 0\}$ for plant (8) at the point $\{t, x, i\}$ is given by Kushner [23] as follows:

$$\begin{aligned} \mathfrak{T}_a^x\left[V\right] &= \dot{x}^TP_ix + x^TP_i\dot{x} + x^T\sum_{j=1}^{\mathbb{N}}\lambda_{ij}P_jx \\ &= \left[\left(A_i + \Delta A_i\right)x + \left(B_i + \Delta B_i\right)\left(K_ix + u_{ic} + e_\mu\right)\right]^TP_ix \\ &\quad + x^TP_i\left[\left(A_i + \Delta A_i\right)x + \left(B_i + \Delta B_i\right)\left(K_ix + u_{ic} + e_\mu\right)\right] \\ &\quad + x^T\sum_{j=1}^{\mathbb{N}}\lambda_{ij}P_jx \\ &= x^T\left[\left(A_i + \Delta A_i\right)^TP_i + P_i\left(A_i + \Delta A_i\right)\right. \\ &\qquad \left. + P_i\left(B_i + \Delta B_i\right)K_i + K_i^T\left(B_i + \Delta B_i\right)^TP_i\right]x \\ &\quad + 2x^TP_i\left(B_i + \Delta B_i\right)\left(u_{ic} + e_\mu\right) + x^T\sum_{j=1}^{\mathbb{N}}\lambda_{ij}P_jx. \end{aligned} \tag{21}$$

According to Assumption 2, u_{ic} in Theorem 8, and Lemma 7, one can obtain that

$$\begin{aligned} &2x^TP_i\left(B_i + \Delta B_i\right)\left(u_{ic} + e_\mu\right) \\ &= 2x^TP_iB_iu_{ic} + 2x^TP_i\Delta B_i\left(u_{ic} + e_\mu\right) + 2x^TP_iB_ie_\mu \\ &= 2x^TP_iB_iu_{ic} + 2x^TP_iB_iM_i\Xi_i\left(t\right)N_i\left(u_{ic} + e_\mu\right) \\ &\quad + 2x^TP_iB_ie_\mu \\ &\le 2x^TP_iB_iu_{ic} + 2\left|x^TP_iB_i\right|_1\left|M_i\Xi_i\left(t\right)N_i\right|_\infty\left(\left|u_{ic}\right|_\infty + \frac{\mu}{2}\right) \\ &\quad + 2\left|x^TP_iB_i\right|_1\frac{\mu}{2} \\ &= 2x^TP_iB_iu_{ic} + 2\left|x^TP_iB_i\right|_1\psi\left(\left|u_{ic}\right|_\infty + \frac{\mu}{2}\right) \\ &\quad + \left|x^TP_iB_i\right|_1\mu \\ &= 2x^TP_iB_iu_{ic} + \left(1+\psi\right)\left|x^TP_iB_i\right|_1\mu \\ &\quad + 2\psi\left|x^TP_iB_i\right|_1\left|u_{ic}\right|_\infty \\ &= -\frac{\left(1+\psi\right)\mu}{1-\psi}\left|x^TP_iB_i\right|_1 + \left(1+\psi\right)\left|x^TP_iB_i\right|_1\mu \\ &\quad + \frac{\psi\left(1+\psi\right)\mu}{1-\psi}\left|x^TP_iB_i\right|_1 = 0. \end{aligned} \tag{22}$$

It follows from (21) and (22) that

$$\begin{aligned}\mathfrak{F}_a^x[V] \le x^T &\left[(A_i+\Delta A_i)^T P_i + P_i(A_i+\Delta A_i)\right.\\ &\left.+P_i(B_i+\Delta B_i)K_i + K_i^T(B_i+\Delta B_i)^T P_i\right]x\\ &+x^T\sum_{j=1}^{\mathbb{N}}\lambda_{ij}P_j x.\end{aligned} \tag{23}$$

Furthermore, consider the following inequality:

$$\begin{aligned}&(A_i+\Delta A_i)^T P_i + P_i(A_i+\Delta A_i) + P_i(B_i+\Delta B_i)K_i\\ &\quad+K_i^T(B_i+\Delta B_i)^T P+\sum_{j=1}^{\mathbb{N}}\lambda_{ij}P_j+Q_i+K_i^T R_i K_i<0.\end{aligned} \tag{24}$$

Since $\Delta B_i = B_i M_i \Xi_i(t) N_i$ and $\Delta A_i = D_i E_i(t) F_i$, the above inequality can be rewritten as

$$\begin{aligned}&A_i^T P_i + P_i A_i + P_i D_i E_i(t) F_i + F_i^T E_i^T(t) D_i^T P_i + P_i B_i K_i\\ &\quad+K_i^T B_i^T P_i + P_i B_i M_i \Xi_i(t) N_i K_i\\ &\quad+K_i^T N_i^T \Xi_i^T(t) M_i^T B_i^T P_i + \sum_{j=1}^{\mathbb{N}}\lambda_{ij}P_j + Q_i + K_i^T R_i K_i<0.\end{aligned} \tag{25}$$

Using Lemma 3, it is equivalent to

$$\begin{aligned}&A_i^T P_i + P_i A_i + \varepsilon_i P_i D_i D_i^T P_i + \frac{1}{\varepsilon_i}F_i^T F_i + P_i B_i K_i + K_i^T B_i^T P_i\\ &\quad+\delta_i P_i B_i M_i M_i^T B_i^T P_i + \frac{1}{\delta_i}K_i^T N_i^T N_i K_i\\ &\quad+\sum_{j=1}^{\mathbb{N}}\lambda_{ij}P_j + Q_i + K_i^T R_i K_i<0.\end{aligned} \tag{26}$$

That is,

$$\begin{aligned}&He\left(A_i^T P_i\right) + He\left(P_i B_i K_i\right) + \varepsilon_i P_i D_i D_i^T P_i + \frac{1}{\varepsilon_i}F_i^T F_i\\ &\quad+\delta_i P_i B_i M_i M_i^T B_i^T P_i + \frac{1}{\delta_i}K_i^T N_i^T N_i K_i + \sum_{j\in\mathcal{S}_k^i, j\neq i}\lambda_{ij}P_j\\ &\quad+\sum_{j\in\mathcal{S}_{uk}^i, j\neq i}\lambda_{ij}P_j + \lambda_{ii}P_i + Q_i + K_i^T R_i K_i<0.\end{aligned} \tag{27}$$

Two cases will be considered.

Case 1 ($\lambda_{ii} \in \mathcal{S}_k^i$). In this case, using Lemma 4, one can see that

$$\begin{aligned}&He\left(A_i^T P_i\right) + He\left(P_i B_i K_i\right) + \varepsilon_i P_i D_i D_i^T P_i\\ &\quad+\frac{1}{\varepsilon_i}F_i^T F_i + \delta_i P_i B_i M_i M_i^T B_i^T P_i + \frac{1}{\delta_i}K_i^T N_i^T N_i K_i\\ &\quad+\sum_{j\in\mathcal{S}_k^i, j\neq i}\lambda_{ij}P_j + \sum_{j\in\mathcal{S}_{uk}^i, j\neq i}\lambda_{ij}W_i + \lambda_{ii}P_i\\ &\quad+Q_i + K_i^T R_i K_i<0,\\ &\qquad P_j \le W_i, \quad j\in\mathcal{S}_{uk}^i.\end{aligned} \tag{28}$$

Substituting $\sum_{j\in\mathcal{S}_{uk}^i, j\neq i}\lambda_{ij} = -\sum_{j\in\mathcal{S}_k^i, j\neq i}\lambda_{ij} - \lambda_{ii}$ into the first inequality in (22) and using the boundary information of the elements of the transition rates matrix, one can achieve that

$$\begin{aligned}&He\left(A_i^T P_i\right) + He\left(P_i B_i K_i\right) + \varepsilon_i P_i D_i D_i^T P_i\\ &\quad+\frac{1}{\varepsilon_i}F_i^T F_i + \delta_i P_i B_i M_i M_i^T B_i^T P_i + \frac{1}{\delta_i}K_i^T N_i^T N_i K_i\\ &\quad+\sum_{j\in\mathcal{S}_k^i, j\neq i}\overline{\lambda}_{ij}P_j - \left(\sum_{j\in\mathcal{S}_k^i, j\neq i}\underline{\lambda}_{ij} + \underline{\lambda}_{ii}\right)W_i\\ &\quad+\overline{\lambda}_{ii}P_i + Q_i + K_i^T R_i K_i<0,\\ &\qquad P_j \le W_i, \quad j\in\mathcal{S}_{uk}^i.\end{aligned} \tag{29}$$

Case 2 ($\lambda_{ii} \in \mathcal{S}_{uk}^i$; namely, it is completely unknown). In such case, let us take $\lambda_{ii} = -\sum_{j\in\mathcal{S}_k^i}\lambda_{ij} - \sum_{j\in\mathcal{S}_{uk}^i, j\neq i}\lambda_{ij}$ into (21); then, one can see that

$$\begin{aligned}&A_i^T P_i + P_i A_i + \varepsilon_i P_i D_i D_i^T P_i + \frac{1}{\varepsilon_i}F_i^T F_i + P_i B_i K_i\\ &\quad+K_i^T B_i^T P_i + \delta_i P_i B_i M_i M_i^T B_i^T P_i\\ &\quad+\frac{1}{\delta_i}K_i^T N_i^T N_i K_i + \sum_{j\in\mathcal{S}_k^i}\lambda_{ij}P_j + \sum_{j\in\mathcal{S}_{uk}^i, j\neq i}\lambda_{ij}P_j\\ &\quad+\left(-\sum_{j\in\mathcal{S}_k^i}\lambda_{ij} - \sum_{j\in\mathcal{S}_{uk}^i, j\neq i}\lambda_{ij}\right)P_i + Q_i + K_i^T R_i K_i<0.\end{aligned} \tag{30}$$

Then, the stochastic stability can be guaranteed when

$$\begin{aligned}&He\left(A_i^T P_i\right) + He\left(P_i B_i K_i\right) + \varepsilon_i P_i D_i D_i^T P_i + \frac{1}{\varepsilon_i}F_i^T F_i\\ &\quad+\delta_i P_i B_i M_i M_i^T B_i^T P_i + \frac{1}{\delta_i}K_i^T N_i^T N_i K_i + \sum_{j\in\mathcal{S}_k^i}\overline{\lambda}_{ij}P_j\\ &\quad-\sum_{j\in\mathcal{S}_k^i, j\neq i}\underline{\lambda}_{ij}P_i + Q_i + K_i^T R_i K_i<0,\\ &\qquad P_j \le P_i, \quad j\in\mathcal{S}_{uk}^i.\end{aligned} \tag{31}$$

For Case 1, pre- and postmultiplying P_i^{-1} in the first inequality in (27) and using Lemma 7 in the second inequality in (21), one can get that

$$\begin{aligned} &He\left(P_i^{-1}A_i^T\right) + He\left(B_iK_iP_i^{-1}\right) + \varepsilon_iD_iD_i^T + \frac{1}{\varepsilon_i}P_i^{-1}F_i^TF_iP_i^{-1} \\ &\quad + \delta_iB_iM_iM_i^TB_i^T + \frac{1}{\delta_i}P_i^{-1}K_i^TN_i^TN_iK_iP_i^{-1} \\ &\quad + \sum_{j\in\mathcal{S}_k^i, j\neq i}\overline{\lambda}_{ij}P_i^{-1}P_jP_i^{-1} - \sum_{j\in\mathcal{S}_k^i}\underline{\lambda}_{ij}P_i^{-1}W_iP_i^{-1} \\ &\quad + \overline{\lambda}_{ii}P_i^{-1} + P_i^{-1}Q_iP_i^{-1} + P_i^{-1}K_i^TR_iK_iP_i^{-1} < 0, \\ &\qquad W_i^{-1} \le P_j^{-1}, \quad j \in \mathcal{S}_{uk}^i. \end{aligned} \tag{32}$$

Let $X_i = P_i^{-1}$, $Y_i = K_iP_i^{-1}$, and $Z_i = W_i^{-1}$; then, we have

$$\begin{aligned} &He\left(A_iX_i\right) + He\left(B_iY_i\right) + \varepsilon_iD_iD_i^T + \frac{1}{\varepsilon_i}X_iF_i^TF_iX_i \\ &\quad + \delta_iB_iM_iM_i^TB_i^T + \frac{1}{\delta_i}Y_i^TN_i^TN_iY_i + \sum_{j\in\mathcal{S}_k^i, j\neq i}\overline{\lambda}_{ij}X_iX_j^{-1}X_i \\ &\quad - \sum_{j\in\mathcal{S}_k^i}\underline{\lambda}_{ij}X_iZ_i^{-1}X_i + \overline{\lambda}_{ii}X_i + X_iQ_iX_i + Y_i^TR_iY_i < 0, \\ &\qquad Z_i \le X_j, \quad j \in \mathcal{S}_{uk}^i. \end{aligned} \tag{33}$$

Applying the Schur complement formula, one can get (16).

For Case 2, pre- and postmultiplying P_i^{-1} in the first inequality in (28) and applying Lemma 7 to the second inequality in (28), one can obtain that

$$\begin{aligned} &He\left(P_i^{-1}A_i^T\right) + He\left(B_iK_iP_i^{-1}\right) + \varepsilon_iD_iD_i^T + \frac{1}{\varepsilon_i}P_i^{-1}F_i^TF_iP_i^{-1} \\ &\quad + \delta_iB_iM_iM_i^TB_i^T + \frac{1}{\delta_i}P_i^{-1}K_i^TN_i^TN_iK_iP_i^{-1} \\ &\quad + \sum_{j\in\mathcal{S}_k^i}\overline{\lambda}_{ij}P_i^{-1}P_jP_i^{-1} - \sum_{j\in\mathcal{S}_k^i}\underline{\lambda}_{ij}P_i^{-1} + P_i^{-1}Q_iP_i^{-1} \\ &\quad + P_i^{-1}K_i^TR_iK_iP_i^{-1} < 0, \\ &\qquad P_i^{-1} \le P_j^{-1}, \quad j \in \mathcal{S}_{uk}^i. \end{aligned} \tag{34}$$

Let $X_i = P_i^{-1}$ and $Y_i = K_iP_i^{-1}$; then, one can see that

$$\begin{aligned} &He\left(A_iX_i\right) + He\left(B_iY_i\right) + \varepsilon_iD_iD_i^T + \frac{1}{\varepsilon_i}X_iF_i^TF_iX_i \\ &\quad + \delta_iB_iM_iM_i^TB_i^T + \frac{1}{\delta_i}Y_i^TN_i^TN_iY_i \\ &\quad + \sum_{j\in\mathcal{S}_k^i}\overline{\lambda}_{ij}X_iX_j^{-1}X_i - \sum_{j\in\mathcal{S}_k^i}\underline{\lambda}_{ij}X_i \\ &\quad + X_iQ_iX_i + Y_i^TR_iY_i < 0, \\ &\qquad X_i \le X_j, \quad j \in \mathcal{S}_{uk}^i. \end{aligned} \tag{35}$$

Thus, the LMIs in (17) are derived by using the Schur complement formula.

From the above proof, one can see that

$$\mathfrak{F}_a^x[V] < -x^TQ_ix - x^TK_i^TR_iK_ix. \tag{36}$$

It follows from Kushner [23] that

$$\begin{aligned} &\mathbb{E}\left[V(t,x,i) \mid r_0\right] - V\left(x_0,r_0\right) \\ &\quad \le -\mathbb{E}\left[\int_0^t \left\{x^T(\tau)Q_ix(\tau) - x^T(\tau)K_i^TR_iK_ix(\tau)\right\}d\tau\right]. \end{aligned} \tag{37}$$

Since $\mathbb{E}[V(t,x,i) \mid r_0] \ge 0$, by some simple calculation, one can achieve that

$$\mathcal{J}(t) \le \mathcal{J}(0) \le V\left(x_0,r_0\right) = x_0^TP_ix_0 \le \gamma. \tag{38}$$

Therefore, the minimum cost can be obtained by minimizing γ. Thus, the proof is achieved. □

Remark 9. The merit of the proposed results lies in that the transition rates of the jumping process are assumed to be more general, which means that some elements in the transition rates matrix have been exactly known, some ones have been merely known with lower and upper bounds, and others may have no information to use. Dealing with the unknown transition rates, a less conservative method is used. At the same time, the impact of the input signal quantization on the system is also considered. Finally, the controller design conditions are presented in the framework of LMIs.

In order to make comparison with the design method using the LMIs technique in Shen and Yang [9], we present the conditions designed by the utilization of Lemma 2 there.

Proposition 10. *For the system* (1) *subject to Assumptions 1 and 2, suppose that there exist symmetric positive definite matrices X_i, general matrices Y_i, and positive scalars ε_i, δ_i, and γ such that*

$$\begin{bmatrix} \Gamma_{11} & X_iF_i^T & Y_i^TN_i^T & \Gamma_{14} & \Gamma_{15} & X_i & Y_i \\ * & -\varepsilon_iI & 0 & 0 & 0 & 0 & 0 \\ * & * & -\delta_iI & 0 & 0 & 0 & 0 \\ * & * & * & \Gamma_{44} & 0 & 0 & 0 \\ * & * & * & * & -\Gamma_{55} & 0 & 0 \\ * & * & * & * & * & -Q_i^{-1} & 0 \\ * & * & * & * & * & * & -R_i^{-1} \end{bmatrix} < 0, \tag{39}$$

$$Z_i \le X_j, \quad j \in \mathcal{S}_{uk}^i,$$

$$\begin{bmatrix} \Phi_{11} & X_iF_i^T & Y_i^TN_i^T & \Phi_{14} & X_i & Y_i^T \\ * & -\varepsilon_iI & 0 & 0 & 0 & 0 \\ * & * & -\delta_iI & 0 & 0 & 0 \\ * & * & * & \Phi_{44} & 0 & 0 \\ * & * & * & * & -Q_i^{-1} & 0 \\ * & * & * & * & * & -R_i^{-1} \end{bmatrix} < 0, \tag{40}$$

$$X_i \le X_j, \quad j \in \mathcal{S}_{uk}^i,$$

$$\begin{bmatrix} \gamma & x_0^T \\ x_0 & X_i \end{bmatrix} > 0, \tag{41}$$

where

$$\Gamma_{11} = He\left(A_iX_i\right) + He\left(B_iY_i\right) + \varepsilon_iD_iD_i^T + \delta_iB_iM_iM_i^TB_i^T + \overline{\lambda}_{ii}X_i,$$

$$\Gamma_{14} = \left[\sqrt{\overline{\lambda}_{i\mathcal{K}_1^i}}X_i,\ \sqrt{\overline{\lambda}_{i\mathcal{K}_2^i}}X_i, \ldots,\ \sqrt{\overline{\lambda}_{i\mathcal{K}_{m_k^i}^i}}X_i\right],$$

$$\Gamma_{44} = \operatorname{diag}\left\{-X_{\mathcal{K}_1^i},\ -X_{\mathcal{K}_2^i},\ \ldots,\ -X_{\mathcal{K}_{m_k^i}^i}\right\},$$

$$\Gamma_{15} = \left[\sqrt{-\sum_{j\in\mathcal{S}_k^i}\underline{\lambda}_{ij}}X_i,\ \sqrt{-\sum_{j\in\mathcal{S}_k^i}\underline{\lambda}_{ij}}X_i, \ldots,\ \sqrt{-\sum_{j\in\mathcal{S}_k^i}\underline{\lambda}_{ij}}X_i\right],$$

$$\Gamma_{55} = \operatorname{diag}\left\{-X_{\mathbb{K}_1^i},\ -X_{\mathbb{K}_2^i}, \ldots, -X_{\mathbb{K}_{m_{uk}^i}^i}\right\},$$

$$\Phi_{11} = He\left(A_iX_i\right) + He\left(B_iY_i\right) + \varepsilon_iD_iD_i^T + \delta_iB_iM_iM_i^TB_i^T - \sum_{j\in\mathcal{S}_k^i}\underline{\lambda}_{ij}X_i,$$

$$\Phi_{14} = \left[\sqrt{\overline{\lambda}_{i\mathcal{K}_1^i}}X_i,\ \sqrt{\overline{\lambda}_{i\mathcal{K}_2^i}}X_i, \ldots,\ \sqrt{\overline{\lambda}_{i\mathcal{K}_{m_k^i}^i}}X_i\right],$$

$$\Phi_{44} = \operatorname{diag}\left\{-X_{\mathcal{K}_1^i},\ -X_{\mathcal{K}_2^i}, \ldots, -X_{\mathcal{K}_{m_k^i}^i}\right\}. \tag{42}$$

Then, the controller designed as

$$u(t) = K_ix(t) + u_{ic}(t) \tag{43}$$

can drive the state trajectory to the origin asymptotically and can obtain the H_2 cost by minimizing r, where $K_i = Y_iX_i^{-1}$, $P_i = X_i^{-1}$, and $u_{ic} = (-(1+\psi)\mu/2(1-\psi))\operatorname{sign}(x^TP_iB_i)$.

Proof. The proof process is similar to that in Theorem 8 but with replacing $P_j \le W_i$, $j \in \mathcal{S}_{uk}^i$, and $\sum_{j\in\mathcal{S}_{uk}^i, j\neq i}\lambda_{ij}W_j$ with $(\sum_{j\in\mathcal{S}_{uk}^i, j\neq i}\lambda_{ij})(\sum_{j\in\mathcal{S}_{uk}^i, j\neq i}P_j)$ in (22). The details are omitted here for space limitation. □

4. Numerical Example

An example is presented to illustrate the effectiveness of the proposed method.

Consider the MJLSs with four operation modes as follows:

$$A_1 = \begin{bmatrix}1 & 0.2\\ 0.4 & -4\end{bmatrix},\quad A_2 = \begin{bmatrix}-1.5 & 1.2\\ 1.4 & -5\end{bmatrix},$$

$$A_3 = \begin{bmatrix}-1 & 3\\ 2 & -2\end{bmatrix},\quad A_4 = \begin{bmatrix}0 & 3\\ 4 & 0\end{bmatrix},$$

$$B_1 = \begin{bmatrix}0.5\\ 0.2\end{bmatrix},\quad B_2 = \begin{bmatrix}0.1\\ 0.3\end{bmatrix},$$

$$B_3 = \begin{bmatrix}0\\ 1\end{bmatrix},\quad B_4 = \begin{bmatrix}0\\ 1\end{bmatrix},$$

Table 1: Comparison of optimal γ.

Theorem 8	Proposition 10
1.4518	2.4567

$$D_1 = \begin{bmatrix}0\\ 2\end{bmatrix},\quad D_2 = \begin{bmatrix}1\\ 0\end{bmatrix},$$

$$D_3 = \begin{bmatrix}0.4\\ 0.8\end{bmatrix},\quad D_4 = \begin{bmatrix}-0.5\\ 0.5\end{bmatrix},$$

$$F_1 = \begin{bmatrix}1 & 0\end{bmatrix},\quad F_2 = \begin{bmatrix}0.5 & 1\end{bmatrix},$$

$$F_3 = \begin{bmatrix}0 & 0.3\end{bmatrix},\quad F_4 = \begin{bmatrix}0.5 & 0.8\end{bmatrix},$$

$$M_1 = 0.4,\quad M_2 = 0.6,\quad M_3 = 0.5,\quad M_4 = 1,$$

$$N_1 = 0.8,\quad N_2 = 0.2,\quad N_3 = 0.1,\quad N_4 = 0.5. \tag{44}$$

The considered transition rates matrix is given as follows:

$$\Lambda = \begin{bmatrix}-1.3 & 0.2 & ? & ?\\ ? & \alpha_1 & 0.3 & 0.3\\ 0.6 & ? & ? & ?\\ 0.4 & \alpha_2 & ? & \alpha_3\end{bmatrix}, \tag{45}$$

where $-1.2 \le \alpha_1 \le -0.8$, $0.6 \le \alpha_2 \le 0.8$, and $-2 \le \alpha_3 \le -1.5$. Choosing $x_0 = [1; -0.5]$ and solving (16)–(18) in Theorem 8 and (34)–(38) in Proposition 10, one can obtain the optimal H_2 performance indices shown in Table 1. It can be seen that less conservativeness is obtained by the proposed method in Theorem 8.

For simulation, one can obtain the controller gains by solving the LMIs in Theorem 8 as follows:

$K_1 = [-5.2949\ \ -0.5848]$, $K_2 = [-2.4332\ \ -1.6826]$, $K_3 = [-4.0556\ \ -4.6580]$, and $K_4 = [-14.2188\ \ -12.4624]$ and by considering the positive definite matrices

$$P_1 = \begin{bmatrix}1.5153 & 0.1052\\ 0.1052 & 0.1670\end{bmatrix},\quad P_2 = \begin{bmatrix}1.1640 & 0.5337\\ 0.5337 & 0.4595\end{bmatrix},$$

$$P_3 = \begin{bmatrix}0.7788 & 0.4269\\ 0.4269 & 0.4903\end{bmatrix},\quad P_4 = \begin{bmatrix}3.6726 & 2.8438\\ 2.8438 & 2.4925\end{bmatrix}. \tag{46}$$

The following parameters are used in the simulation: $\mu = 0.3$, $E_1(t) = 0.2\cos(t)$, $E_2(t) = 0.05\sin(t)$, $E_3(t) = 0.8\cos(3t)$, $E_4(t) = 0.4\sin(t)$, $\Xi_1(t) = 0.5\cos(3t)$, $\Xi_2(t) = 0.6\cos(2t)$, $\Xi_3(t) = 0.2\sin(t)$, and $\Xi_4(t) = 0.05\cos(2t)$. In order to reduce the chattering effects induced by u_{ic}, $\operatorname{sign}(x^TP_iB_i)$ is substituted by $\operatorname{sat}(x^TP_iB_i/\delta_i)$, where $\delta_1 = 0.0015$, $\delta_2 = 0.0004$, $\delta_3 = 0.0015$, and $\delta_4 = 0.0004$.

The switching mode, the control input, and the response curves of the system states are presented in Figures 1, 2, and 3, respectively. Among them, Figure 1 shows a possible system modes evolution which meets the transition rates given in this example. As shown in Figure 1, the system has 4 modes and is in different modes at a different time. Figure 2 shows the curve of the control input $u(t)$. With this controller, Figure 3 depicts the state response curves of the closed-loop system.

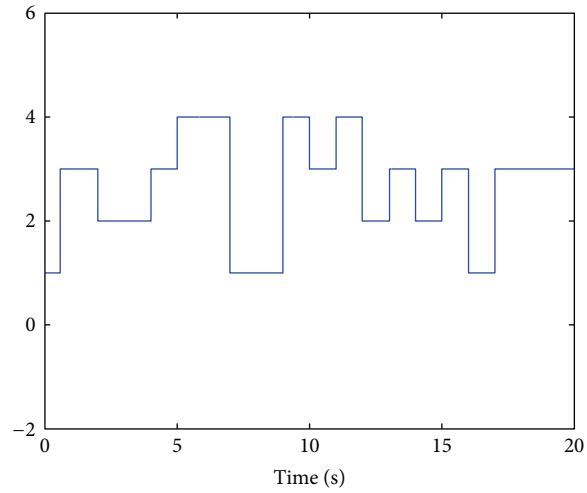

Figure 1: Evolution of the system mode.

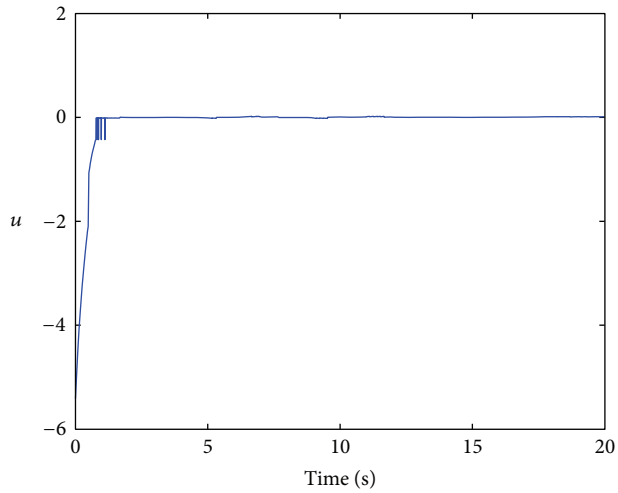

Figure 2: The curve of the control input $u(t)$.

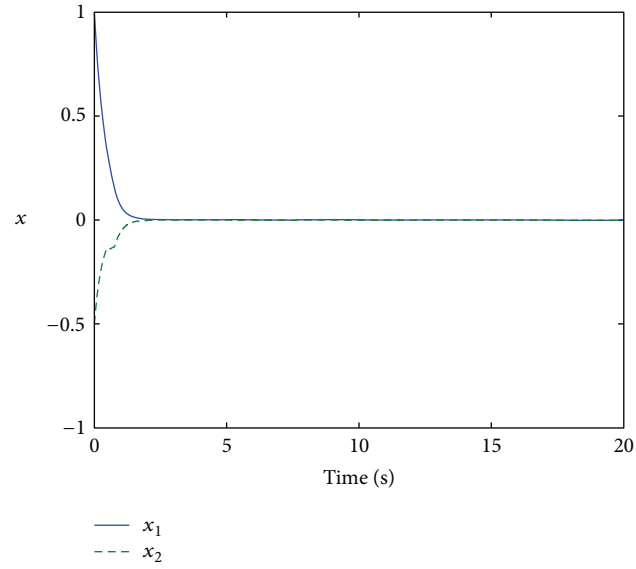

Figure 3: The response curve of the state x.

It can be seen that the considered continuous-time Markovian jump linear uncertain system is stochastically stable in spite of mismatched uncertainty, the input signal quantization, and the partly known transition rates covering the completely known, the boundary unknown, and the completely unknown elements in the transition rates matrix.

5. Conclusions

H_2 control design for a class of the continuous-time Markovian jump linear uncertain systems with partly unknown transition rates and input quantization has been investigated. The H_2 cost index for the Markovian jump systems is first introduced, and then sufficient conditions of the H_2 control for the Markovian jump linear uncertain systems with unknown transition rates have been presented. The controller is constructed by two parts. The nonlinear part is proposed to eliminate the effect of input quantization. The linear part is designed by solving the LMIs conditions for achieving the H_2 performance against model uncertainties and unknown transition rates. In comparison with the existing result in the literature, less conservativeness has been obtained by introducing new relaxed inequality conditions. Finally, a numerical example is given to show the effectiveness of the proposed design method.

Acknowledgments

This work is supported by the National Natural Science Foundation of China (Grants nos. 61273155, 61273355, 61322312, and 61273356), the Foundation of State Key Laboratory of Robotics (Grant no. Z2013-06), the New Century Excellent Talents in the University (Grant no. NCET-11-0083), a Foundation for the Author of National Excellent Doctoral Dissertation of PR China (Grant no. 201157), the Fundamental Research Funds for the Central Universities (Grant no. N120504003).

References

[1] E.-K. Boukas, *Stochastic Switching Systems: Analysis and Design*, Control Engineering, Birkhäuser, Boston, Mass, USA, 2006.

[2] S. Ma and E.-K. Boukas, "A singular system approach to robust sliding mode control for uncertain Markov jump systems," *Automatica*, vol. 45, no. 11, pp. 2707–2713, 2009.

[3] P. Shi, Y. Xia, G. P. Liu, and D. Rees, "On designing of sliding-mode control for stochastic jump systems," *IEEE Transactions on Automatic Control*, vol. 51, no. 1, pp. 97–103, 2006.

[4] L. Wu, P. Shi, and H. Gao, "State estimation and sliding-mode control of Markovian jump singular systems," *IEEE Transactions on Automatic Control*, vol. 55, no. 5, pp. 1213–1219, 2010.

[5] W. Li, H. Su, D. Wei, and K. Wang, "Global stability of coupled nonlinear systems with Markovian switching," *Communications in Nonlinear Science and Numerical Simulation*, vol. 17, no. 6, pp. 2609–2616, 2012.

[6] E. F. Costa and J. B. R. do Val, "On the observability and detectability of continuous-time Markov jump linear systems," *SIAM Journal on Control and Optimization*, vol. 41, no. 4, pp. 1295–1314, 2002.

[7] L. Zhang, E.-K. Boukas, and J. Lam, "Analysis and synthesis of Markov jump linear systems with time-varying delays and partially known transition probabilities," *IEEE Transactions on Automatic Control*, vol. 53, no. 10, pp. 2458–2464, 2008.

[8] L. Zhang and E.-K. Boukas, "H_∞ control of a class of extended Markov jump linear systems," *IET Control Theory & Applications*, vol. 3, no. 7, pp. 834–842, 2009.

[9] M. Shen and G.-H. Yang, "H_2 state feedback controller design for continuous Markov jump linear systems with partly known information," *International Journal of Systems Science*, vol. 43, no. 4, pp. 786–796, 2012.

[10] R. W. Brockett and D. Liberzon, "Quantized feedback stabilization of linear systems," *IEEE Transactions on Automatic Control*, vol. 45, no. 7, pp. 1279–1289, 2000.

[11] D. Liberzon, "Hybrid feedback stabilization of systems with quantized signals," *Automatica*, vol. 39, no. 9, pp. 1543–1554, 2003.

[12] B.-C. Zheng and G.-H. Yang, "Quantised feedback stabilisation of planar systems via switching-based sliding-mode control," *IET Control Theory & Applications*, vol. 6, no. 1, pp. 149–156, 2012.

[13] B.-C. Zheng and G.-H. Yang, "Decentralized sliding mode quantized feedback control for a class of uncertain large-scale systems with dead-zone input," *Nonlinear Dynamics*, vol. 71, no. 3, pp. 417–427, 2013.

[14] M. Fu and L. Xie, "The sector bound approach to quantized feedback control," *IEEE Transactions on Automatic Control*, vol. 50, no. 11, pp. 1698–1711, 2005.

[15] M. Fu and L. Xie, "Quantized feedback control for linear uncertain systems," *International Journal of Robust and Nonlinear Control*, vol. 20, no. 8, pp. 843–857, 2010.

[16] E. Tian, D. Yue, and X. Zhao, "Quantised control design for networked control systems," *IET Control Theory and Applications*, vol. 1, no. 6, pp. 1693–1699, 2007.

[17] S. W. Yun, Y. J. Choi, and P. Park, "$\mathcal{H}_2$ control of continuous-time uncertain linear systems with input quantization and matched disturbances," *Automatica*, vol. 45, no. 10, pp. 2435–2439, 2009.

[18] W.-W. Che and G.-H. Yang, "Quantised H_∞ filter design for discrete-time systems," *International Journal of Control*, vol. 82, no. 2, pp. 195–206, 2009.

[19] C. Peng and Y.-C. Tian, "Networked H_∞ control of linear systems with state quantization," *Information Sciences*, vol. 177, no. 24, pp. 5763–5774, 2007.

[20] N. Xiao, L. Xie, and M. Fu, "Stabilization of Markov jump linear systems using quantized state feedback," *Automatica*, vol. 46, no. 10, pp. 1696–1702, 2010.

[21] I. R. Petersen, "A stabilization algorithm for a class of uncertain linear systems," *Systems & Control Letters*, vol. 8, no. 4, pp. 351–357, 1987.

[22] R. A. Horn and C. R. Johnson, *Matrix Analysis*, Cambridge University Press, Cambridge, UK, 1985.

[23] H. J. Kushner, *Stochastic Stability and Control*, Mathematics in Science and Engineering, vol. 33, Academic Press, New York, NY, USA, 1967.

Hindawi Publishing Corporation
Mathematical Problems in Engineering
Volume 2013, Article ID 945705, 7 pages
http://dx.doi.org/10.1155/2013/945705

Research Article

H_∞ Filter Design for Large-Scale Systems with Missing Measurements

Ying Zhou,[1] Shuming Yang,[1] and Qiang Zang[2]

[1] *College of Automation, Nanjing University of Posts and Telecommunications, Nanjing 210003, China*
[2] *School of Information and Control Engineering, Nanjing University of Information Science & Technology, Nanjing 210044, China*

Correspondence should be addressed to Ying Zhou; zhouying@njupt.edu.cn

Received 29 May 2013; Accepted 22 July 2013

Academic Editor: Bochao Zheng

This paper is concerned with H_∞ filter design problem for large-scale systems with missing measurements. The occurrence of missing measurements is assumed to be a Bernoulli distributed sequence with known probability. The new full-dimensional filter is designed to make the filter error system exponentially mean-square stable and achieve a prescribed H_∞ performance. Sufficient conditions are derived in terms of linear matrix inequality (LMI) for the existence of the filter, and the parameters of filter are obtained by solving the LMI. Finally, the numerical simulation results illustrate the effectiveness of the proposed scheme.

1. Introduction

In many practical applications, due to the limitations imposed by the network, missing measurements often occur due to the network link transmission errors, network congestion, and so forth. Currently, the research of filter and controller design for systems with missing measurements has attracted more attention [1–7]. In [1], the robust control problem with missing measurements was investigated, where the missing measurements were described by a binary switch sequence satisfied conditional probability distribution. The similar model was employed in [2–4], where the filtering problem was investigated in [2, 3], and the distributed state estimation problem was studied in [4]. In [5], the quantized H_∞ control problem is investigated for a class of nonlinear stochastic time-delay network-based systems with probabilistic data missing. In [6], the filtering problem with packet loss was considered using Markov chains to describe probabilistic losses. The problem of robust H_∞ filtering for discrete-time switched systems with missing measurements under asynchronous switching is considered in [7].

Most of the existing research is focused on general linear or nonlinear discrete system. However, many actual systems are large-scale systems which are composed of interconnected subsystems. Although ideas of decentralized control of large-scale systems have attracted much attention in the literature during the past two decades, the research about large-scale systems with missing measurements is seldom. In [8], a decentralized H_∞ controller design for a class of large-scale systems with missing measurements is considered. In [9], a state feedback H_∞ controller is designed for a class of linear discrete-time large-scale system with both measurement data and control data missing simultaneously.

In this paper, H_∞ filter is considered for a class of large-scale systems with missing measurements. We apply Bernoulli distributed sequence to describe the occurrence of missing measurements, and the linear discrete-time large-scale system is modeled as interconnection of N subsystems with missing measurements. Then, we design a new decentralized filter. Sufficient conditions are derived in terms of linear matrix inequality (LMI) which is easy to be solved by using MATLAB LMI Toolbox for the decentralized stabilization of this class of large-scale system.

2. Problem Formulation

Consider the linear discrete-time large-scale system comprising N subsystems Ξ_i, $i = 1, 2, \ldots, N$; the dynamics of the ith subsystem is described by

$$\Xi_i : \begin{cases} x_i(k+1) = A_i x_i(k) + B_i w_i(k) + \sum_{\substack{j=1 \\ j\neq i}}^{N} G_{ij} x_j(k) \\ z_i(k) = C_i x_i(k) + D_i w_i(k) \\ y_i(k) = x_i(k), \end{cases} \tag{1}$$

where $x_i(k) \in R^{n_i}$ is the state vector of the ith subsystem at time k, $y_i(k) \in R^{q_i}$ is the measurement output, $z_i(k) \in R^{p_i}$ is the controlled output, $w_i(k) \in R^{r_i}$ is the disturbance vector belonging to $l_2[0,\infty)$, A_i, B_i, C_i, and D_i are known real constant matrices with appropriate dimensions, and $G_{ij} \in R^{n_i \times n_j}$ is the interconnection matrix of the subsystem of j and i.

The measurement with missing data can be characterized by

$$\overline{x}_i(k) = \alpha_i(k)\, x_i(k), \tag{2}$$

where $\overline{x}_i(k) \in R^{m_i}$ is the actual measured state, the stochastic variable $\alpha_i(k) \in R$ is a Bernoulli distributed white noise sequence taking the values of 0 and 1 with certain probability

$$\begin{aligned} \operatorname{prob}\{\alpha_i(k) = 1\} &= E\{\alpha_i(k)\} := \overline{\alpha}_i, \\ \operatorname{prob}\{\alpha_i(k) = 0\} &= 1 - E\{\alpha_i(k)\} := 1 - \overline{\alpha}_i, \end{aligned} \tag{3}$$

and $0 < \overline{\alpha}_i < 1$ is a known positive constant.

In order to observe the states of the system (1), we consider the following filter of order n described by

$$\begin{aligned} \widehat{x}_i(k+1) &= A_i \widehat{x}_i(k) + \sum_{\substack{j=1 \\ j\neq i}}^{N} G_{ij} \widehat{x}_j(k) + K_i\left(\overline{\alpha}_i \widehat{x}_i(k) - \overline{x}_i(k)\right), \\ \widehat{z}_i(k) &= C_i \widehat{x}_i(k), \\ \widehat{y}_i(k) &= \widehat{x}_i(k), \end{aligned} \tag{4}$$

where $\widehat{x}_i(k) \in R^{n_i}$ is the state estimate of system (1) and K_i is the observer gain to be determined later.

Define the state estimation error by

$$\varepsilon_i(k) = x_i(k) - \widehat{x}_i(k), \tag{5}$$

and the filter error output is denoted by

$$e_i(k) = z_i(k) - \widehat{z}_i(k). \tag{6}$$

Then it follows from (1), (2), and (4) that

$$\begin{aligned} \varepsilon_i(k+1) = {} & \left(A_i + \overline{\alpha}_i K_i\right)\varepsilon_i(k) + \sum_{\substack{j=1 \\ j\neq i}}^{N} G_{ij}\varepsilon_j(k) \\ & + \left(\alpha_i(k) - \overline{\alpha}_i\right) K_i x_i(k) + B_i w_i(k), \end{aligned} \tag{7}$$

$$e_i(k) = z_i(k) - \widehat{z}_i(k) = C_i \varepsilon_i(k) + D_i w_i(k). \tag{8}$$

Since it contains stochastic quantities $\alpha_i(k)$, the filter error system (8) is actually a stochastic parameter system. Then we use the following definition.

Definition 1 (see [10]). The filter error system (8) is said to be exponentially mean-square asymptotically stable if with $w(k) = 0$, there exist constants $\kappa > 0$ and $0 < \tau < 1$, such that

$$E\left\{\|e(k)\|^2\right\} < \kappa \tau^k E\left\{\|e(0)\|^2\right\}, \quad \forall e(k) \neq 0, \tag{9}$$

where $e(k) = \left[e_1^T(k) \ \cdots \ e_N^T(k)\right]^T$ and $w(k) = \left[w_1^T(k) \ \cdots \ w_N^T(k)\right]^T$.

With this definition, our objective is to design the full-order filter of form (4), such that

(1) the filter error system (8) is exponentially mean-square asymptotically stable with $w(k) = 0$;

(2) under zero-initial condition, the filter error $e(k)$ satisfies

$$\sum_{k=0}^{\infty} E\left\{\|e(k)\|^2\right\} < \gamma^2 \sum_{k=0}^{\infty} E\left\{\|w(k)\|^2\right\}, \tag{10}$$

where γ is a given positive constant.

3. Main Results

For investigating the stability conditions of the filter error system (8), the following lemma is needed.

Lemma 2 (see [10]). *Let $V(\eta(k))$ be a Lyapunov functional. If there exist constants $\lambda \geq 0$, $\mu > 0$, $\nu > 0$, and $0 < \psi < 1$ such that*

$$\begin{aligned} \mu\|\eta(k)\|^2 &\leq V(\eta(k)) \leq \nu\|\eta(k)\|^2, \\ E\{V(\eta(k+1) \mid \eta(k))\} - V(\eta(k)) &\leq \lambda - \psi V(\eta(k)), \end{aligned} \tag{11}$$

then the sequence $\eta(k)$ satisfies

$$E\left\{\left\|\eta(k)^2\right\|\right\} \leq \frac{\nu}{\mu}\|\eta(0)\|^2 (1-\psi)^k + \frac{\lambda}{\mu\psi}. \tag{12}$$

The main results are concluded into the following theorems.

Theorem 3. *Given $0 < \overline{\alpha}_i < 1$ and $w(k) = 0$, the filter error system (8) is exponentially mean-square asymptotically stable if there exist positive definite matrices $P_{1i} = P_{1i}^T$, $P_{2i} = P_{2i}^T$ and gain matrix $K_i, i = 1, 2, \ldots, N$, satisfying*

$$\begin{bmatrix} -P_1 & 0 & Q_1^T + \overline{\alpha}K & 0 & 0 \\ 0 & -P_2 & 0 & Q_1^T & K \\ Q_1 + \overline{\alpha}K & 0 & -P_1^{-1} & 0 & 0 \\ 0 & Q_1 & 0 & -P_2^{-1} & 0 \\ 0 & K & 0 & 0 & -\beta^2 P_1^{-1} \end{bmatrix} < 0, \tag{13}$$

where

$$Q_1 = \begin{bmatrix} A_1 & G_{12} & \cdots & G_{1N} \\ G_{21} & A_2 & \cdots & G_{2N} \\ \vdots & \vdots & \ddots & \vdots \\ G_{N1} & G_{N2} & \cdots & A_N \end{bmatrix},$$

$$P_1 = \operatorname{diag}\{P_{11}, P_{12}, \ldots, P_{1N}\},$$

$$P_2 = \operatorname{diag}\{P_{21}, P_{22}, \ldots, P_{2N}\},$$

$$K = \operatorname{diag}\{K_1, K_2, \ldots, K_N\}, \qquad \beta = \operatorname{diag}\{\beta_1, \beta_2, \ldots, \beta_N\},$$

$$\beta_i = \left((1-\overline{\alpha}_i)\,\overline{\alpha}_i\right)^{1/2}, \quad i = 1, 2, \ldots, N,$$

$$\overline{\alpha} = \operatorname{diag}\{\overline{\alpha}_1, \overline{\alpha}_2, \ldots, \overline{\alpha}_N\}. \tag{14}$$

Proof. When $w(k) = 0$, define the Lyapunov functional

$$V(k) = \sum_{i=1}^{N} \varepsilon_i^T(k) P_{1i} \varepsilon_i(k) + \sum_{i=1}^{N} x_i^T(k) P_{2i} x_i(k), \tag{15}$$

where $P_{1i} = P_{1i}^T$, $P_{2i} = P_{2i}^T$ are positive definite matrices. It follows from (8) that

$$\begin{aligned} &V(k+1) - V(k) \\ &= \sum_{i=1}^{N} \Bigg(\left(A_i + \overline{\alpha}_i K_i\right) \varepsilon_i(k) \\ &\qquad + \sum_{\substack{j=1 \\ j\neq i}}^{N} G_{ij}\varepsilon_j(k) + \left(\alpha_i(k) - \overline{\alpha}_i\right) K_i x_i(k) \Bigg)^T P_{1i} \\ &\qquad \times \Bigg(\left(A_i + \overline{\alpha}_i K_i\right) \varepsilon_i(k) \\ &\qquad + \sum_{\substack{j=1 \\ j\neq i}}^{N} G_{ij}\varepsilon_j(k) + \left(\alpha_i(k) - \overline{\alpha}_i\right) K_i x_i(k) \Bigg) \\ &\qquad + \sum_{i=1}^{N} \left(A_i x_i(k) + \sum_{\substack{j=1 \\ j\neq i}}^{N} G_{ij} x_j(k) \right)^T P_{2i} \\ &\qquad \times \left(A_i x_i(k) + \sum_{\substack{j=1 \\ j\neq i}}^{N} G_{ij} x_j(k) \right) \\ &\qquad - \sum_{i=1}^{N} \varepsilon_i^T(k) P_{1i} \varepsilon_i(k) - \sum_{i=1}^{N} x_i^T(k) P_{2i} x_i(k). \end{aligned} \tag{16}$$

Noting that $E\{\alpha_i(k) - \overline{\alpha}_i\} = 0$, $E\{(\alpha_i(k) - \overline{\alpha}_i)^2\} = (1-\overline{\alpha}_i)\overline{\alpha}_i \triangleq \beta_i^2$, we have

$$\begin{aligned} &E\{V(k+1)\} - V(k) \\ &\quad = \sum_{i=1}^{N} \left(\left(A_i + \overline{\alpha}_i K_i\right) \varepsilon_i(k) + \sum_{\substack{j=1 \\ j\neq i}}^{N} G_{ij}\varepsilon_j(k) \right)^T P_{1i} \\ &\qquad \times \left(\left(A_i + \overline{\alpha}_i K_i\right) \varepsilon_i(k) + \sum_{\substack{j=1 \\ j\neq i}}^{N} G_{ij}\varepsilon_j(k) \right) \\ &\qquad + \sum_{i=1}^{N} \left(A_i x_i(k) + \sum_{\substack{j=1 \\ j\neq i}}^{N} G_{ij} x_j(k) \right)^T P_{2i} \\ &\qquad \times \left(A_i x_i(k) + \sum_{\substack{j=1 \\ j\neq i}}^{N} G_{ij} x_j(k) \right) \\ &\qquad + \sum_{i=1}^{N} \beta_i^2 \left(K_i x_i(k)\right)^T P_{1i} \left(K_i x_i(k)\right) \\ &\qquad - \sum_{i=1}^{N} \varepsilon_i^T(k) P_{1i} \varepsilon_i(k) - \sum_{i=1}^{N} x_i^T(k) P_{2i} x_i(k) \\ &\quad = \eta^T(k) \theta_1 \eta(k), \end{aligned} \tag{17}$$

where $x(k) = \left[x_1^T(k) \ \cdots \ x_N^T(k)\right]^T$, $\varepsilon(k) = \left[\varepsilon_1^T(k) \ \cdots \ \varepsilon_N^T(k)\right]^T$, and $\eta(k) = \left[\varepsilon^T(k), x^T(k)\right]^T$.

By Schur complement, inequality (13) implies $\theta_1 < 0$. Then we have

$$\begin{aligned} E\{V(k+1)\} - V(k) &= \eta^T(k) \theta_1 \eta(k) \\ &\leq -\lambda_{\min}\left(-\theta_1\right) \eta^T(k) \eta(k) \\ &< -\gamma \eta^T(k) \eta(k), \end{aligned} \tag{18}$$

where $0 < \gamma < \min\{\lambda_{\min}(-\theta_1), \sigma\}$, and then from (18), we get

$$\begin{aligned} E\{V(k+1)\} - V(k) &< -\gamma \eta^T(k) \eta(k) \\ &< -\frac{\gamma}{\sigma} V\left(\eta(k)\right) = -\psi V\left(\eta(k)\right), \end{aligned} \tag{19}$$

where $\psi = \gamma/\sigma \in (0, 1)$.

From Definition 1 and Lemma 2, we can conclude that the filter error system (8) is exponentially mean-square asymptotically stable. This completes the proof. □

In the sequel, we further provide method for solving matrix inequality (13) that is not a linear matrix inequality (LMI).

Theorem 4. *Given $0 < \overline{\alpha}_i < 1$ if there exist positive definite matrices $M_1 = M_1^T$, $M_2 = M_2^T$ and gain matrices N_1, N_2 that satisfy linear matrix inequality*

$$\left[\begin{array}{cc|ccc} -M_1 & 0 & M_1Q_1^T + \overline{\alpha}N_1 & 0 & 0 \\ 0 & -M_2 & 0 & M_2Q_1^T & \beta N_2 \\ \hline Q_1M_1 + \overline{\alpha}N_1 & 0 & -M_1 & 0 & 0 \\ 0 & Q_1M_2 & 0 & -M_2 & 0 \\ 0 & \beta N_2 & 0 & 0 & -M_1 \end{array}\right] < 0 \quad (20)$$

and equation

$$N_1P_1 = N_2P_2 = K, \quad (21)$$

where $M_1 = P_1^{-1}$, $M_2 = P_2^{-1}$, $N_1 = KP_1^{-1}$, and $N_2 = KP_2^{-1}$, then the error system (8) *is exponentially mean-square asymptotically stable.*

Proof. Through left- and right-multiplying (13) by $\mathrm{diag}\{P_1^{-1}, P_2^{-1}, I, I, \beta I\}$, we have

$$\left[\begin{array}{cc|ccc} -P_1^{-1} & 0 & P_1^{-1}(Q_1 + \overline{\alpha}K)^T & 0 & 0 \\ 0 & -P_2^{-1} & 0 & P_2^{-1}Q_1^T & \beta P_2^{-1}K \\ \hline (Q_1 + \overline{\alpha}K)P_1^{-1} & 0 & -P_1^{-1} & 0 & 0 \\ 0 & Q_1P_2^{-1} & 0 & -P_2^{-1} & 0 \\ 0 & \beta KP_2^{-1} & 0 & 0 & -P_1^{-1} \end{array}\right] < 0. \quad (22)$$

For the definitions of the matrices M_1, M_2, N_1, and N_2, the matrix inequality (13) is equivalent to (20) and (21). This completes the proof. □

By solving the linear matrix inequality (20) and (21), we have M_1, M_2 and N_1, N_2. Moreover, the matrices are given by $P_1 = M_1^{-1}$, $P_2 = M_2^{-1}$, and $K = N_1P_1 = N_2P_2$.

Theorem 5. *Given $0 < \overline{\alpha}_i < 1$ if there exist positive definite matrices $P_{1i} = P_{1i}^T$, $P_{2i} = P_{2i}^T$ and gain matrix $K_i, i = 1, 2, \ldots, N$, that satisfy the following linear matrix inequality:*

$$\left[\begin{array}{ccccccc} -P_1 & * & * & * & * & * & * \\ 0 & -P_2 & * & * & * & * & * \\ 0 & 0 & -\gamma^2 I & * & * & * & * \\ Q_1 + \overline{\alpha}K & 0 & B & -P_1^{-1} & * & * & * \\ 0 & Q_1 & B & 0 & -P_2^{-1} & * & * \\ 0 & K & 0 & 0 & 0 & -\beta^2 P_1^{-1} & * \\ C & 0 & D & 0 & 0 & 0 & -I \end{array}\right] < 0, \quad (23)$$

where $C = \mathrm{diag}\{C_1, C_2, \ldots, C_N\}$, $D = \mathrm{diag}\{D_1, D_2, \ldots, D_N\}$, $B = \mathrm{diag}\{B_1, B_2, \ldots, B_N\}$, and Q_1, P_1, P_2, K, $\overline{\alpha}$, β_i, and β are the same as (13)*, then the filter error system* (8) *is exponentially mean-square asymptotically stable and achieves the prescribed H_∞ performance.*

Proof. When $w(k) = 0$, (23) is equivalent to (13), so the filter error system is exponentially mean-square asymptotically stable.

When $w(k) \neq 0$, define the Lyapunov functional as

$$V(k) = \sum_{i=1}^{N} \varepsilon_i^T(k) P_{1i} \varepsilon_i(k) + \sum_{i=1}^{N} x_i^T(k) P_{2i} x_i(k), \quad (24)$$

then

$$\begin{aligned} &E\{V(k+1)\} - V(k) \\ &\quad + E\left\{e^T(k)\, e(k)\right\} - \gamma^2 E\left\{w^T(k)\, w(k)\right\} \\ &\quad = \sum_{i=1}^{N} \left(\left(A_i + \overline{\alpha}_i K_i\right) \varepsilon_i(k) + \sum_{\substack{j=1 \\ j \neq i}}^{N} G_{ij} \varepsilon_j(k) + B_i w_i(k) \right)^T \\ &\qquad \times P_{1i} \\ &\qquad \times \left(\left(A_i + \overline{\alpha}_i K_i\right) \varepsilon_i(k) + \sum_{\substack{j=1 \\ j \neq i}}^{N} G_{ij} \varepsilon_j(k) + B_i w_i(k) \right) \\ &\qquad + \sum_{i=1}^{N} \left(A_i x_i(k) + \sum_{\substack{j=1 \\ j \neq i}}^{N} G_{ij} x_j(k) + B_i w_i(k) \right)^T P_{2i} \\ &\qquad \times \left(A_i x_i(k) + \sum_{\substack{j=1 \\ j \neq i}}^{N} G_{ij} x_j(k) + B_i w_i(k) \right) \\ &\qquad + \beta_i^2 \sum_{i=1}^{N} \left(K_i x_i(k)\right)^T P_{1i} \left(K_i x_i(k)\right) \\ &\qquad + E\left\{ \sum_{i=1}^{N} \left(C_i \varepsilon_i(k) + D_i w_i(k)\right)^T \right. \\ &\qquad\qquad \left. \times \left(C_i \varepsilon_i(k) + D_i w_i(k)\right) \right\} \\ &\qquad - \sum_{i=1}^{N} \varepsilon_i^T(k) P_{1i} \varepsilon_i(k) \\ &\qquad - \sum_{i=1}^{N} x_i^T(k) P_{2i} x_i(k) - \gamma^2 E\left\{w^T(k)\, w(k)\right\} \\ &\quad = \overline{\eta}^T(k) \theta_2 \overline{\eta}(k), \end{aligned} \quad (25)$$

where $\overline{\eta}(k) = [\varepsilon^T(k), x^T(k), w^T(k)]^T$. By the Schur complement, inequality (23) implies $\theta_2 < 0$, and then we have

$$\begin{aligned} &E\{V(k+1)\} - V(k) + E\left\{e^T(k)\, e(k)\right\} \\ &\qquad - \gamma^2 E\left\{w^T(k)\, w(k)\right\} < 0, \\ &\sum_{k=0}^{\infty} E\left\{e^T(k)\, e(k)\right\} < \gamma^2 \sum_{k=0}^{\infty} E\left\{w^T(k)\, w(k)\right\} \\ &\qquad + E\{V(0)\} - E\{V(\infty)\}. \end{aligned} \quad (26)$$

Since the system is exponentially mean-square asymptotically stable, it is straightforward to see that

$$\sum_{k=0}^{\infty} E\left\{\|e(k)\|^2\right\} < \gamma^2 \sum_{k=0}^{\infty} E\left\{\|w(k)\|^2\right\}, \tag{27}$$

under the zero-initial condition. This completes the proof. □

In the sequel, we further present how to convert the matrix inequality (23) into an LMI with matrix equality constraint.

Theorem 6. *Given* $0 < \overline{\alpha}_i < 1$ *if there exist positive definite matrices* $M_1^T = M_1$, $M_2^T = M_2$ *and gain matrices* N_1, N_2 *that satisfy the following linear matrix inequality*

$$\begin{bmatrix} -M_1 & * & * & * & * & * & * \\ 0 & -M_2 & * & * & * & * & * \\ 0 & 0 & -\gamma^2 I & * & * & * & * \\ Q_1 M_1 + \overline{\alpha} N_1 & 0 & B & -M_1 & * & * & * \\ 0 & Q_1 M_2 & B & 0 & -M_2 & * & * \\ 0 & \beta N_2 & 0 & 0 & 0 & -M_1 & * \\ CM_1 & 0 & D & 0 & 0 & 0 & -I \end{bmatrix} < 0,$$
$$K = N_1 P_1 = N_2 P_2, \tag{28}$$

then the filter error system (8) *is exponentially mean-square asymptotically stable and achieves the prescribed* H_∞ *performance.*

Proof. Through left- and right-multiplying (23) by $\mathrm{diag}\{P_1^{-1}, P_2^{-1}, I, I, I, \beta I, I\} > 0$, we have

$$\begin{bmatrix} -P_1^{-1} & * & * & * & * & * & * \\ 0 & -P_2^{-1} & * & * & * & * & * \\ 0 & 0 & -\gamma^2 I & * & * & * & * \\ (Q_1 + \alpha K) P_1^{-1} & 0 & B & -P_1^{-1} & * & * & * \\ 0 & Q_1 P_2^{-1} & B & 0 & -P_2^{-1} & * & * \\ 0 & \beta K P_2^{-1} & 0 & 0 & 0 & -P_1^{-1} & * \\ CP_1^{-1} & 0 & D & 0 & 0 & 0 & -I \end{bmatrix}$$
$$< 0. \tag{29}$$

Similar to the proof of Theorem 4, we define $M_1 = P_1^{-1}$, $M_2 = P_2^{-1}$, $N_1 = KP_1^{-1}$, and $N_2 = KP_2^{-1}$. Then the matrix inequality (29) is equivalent to (23). From Theorem 5, we can conclude that the filter error system (8) is exponentially mean-square asymptotically stable and achieves the prescribed H_∞ performance. The proof is completed. □

4. Numerical Simulations

Consider a linear discrete-time large-scale system which consists of two interconnected subsystems:

$$\begin{aligned} x_1(k+1) &= \begin{bmatrix} -1 & 3 \\ 0 & -0.1 \end{bmatrix} x_1(k) + \begin{bmatrix} 0.2 & 0.3 \\ 0.1 & 0.2 \end{bmatrix} x_2(k) \\ &\quad + \begin{bmatrix} 1 & 0 \\ 0 & 1 \end{bmatrix} w_1(k) \\ &= A_1 x_1(k) + G_{12} x_2(k) + E_1 w_1(k), \\ z_1 &= \begin{bmatrix} 1 & 0 \\ -1 & 0.8 \end{bmatrix} x_1(k) + \begin{bmatrix} 1 & 1 \\ 1 & 0 \end{bmatrix} w_1(k) \\ &= C_1 x_1(k) + D_1(k) w_1(k), \\ y_1(k) &= x_1(k), \\ x_2(k+1) &= \begin{bmatrix} -1 & 1 \\ 0 & -0.2 \end{bmatrix} x_2(k) + \begin{bmatrix} 0.3 & 0.1 \\ 0.2 & 0.2 \end{bmatrix} x_1(k) \\ &\quad + \begin{bmatrix} 1 & 0 \\ 0 & 1 \end{bmatrix} w_2(k) \\ &= A_2 x_2(k) + G_{21} x_1(k) + E_2 w_2(k), \\ z_2 &= \begin{bmatrix} 1 & 0 \\ 1 & -0.8 \end{bmatrix} x_2(k) + \begin{bmatrix} 1 & 1 \\ 0 & 1 \end{bmatrix} w_2(k) \\ &= C_2 x_2(k) + D_2(k) w_2(k), \\ y_2(k) &= x_2(k). \end{aligned} \tag{30}$$

Choose the disturbance input $w_1(k) = w_2(k) = 0.01 \begin{bmatrix} \sin(100k) \\ \sin(100k) \end{bmatrix}$. The initial state values of original system and its observer are $x_1(0) = \begin{bmatrix} 2 \\ 1 \end{bmatrix}$, $x_2(0) = \begin{bmatrix} 2 \\ 2 \end{bmatrix}$ and $\widehat{x}_1(0) = \begin{bmatrix} 0 \\ 0 \end{bmatrix}$, $x_2(0) = \begin{bmatrix} -1 \\ 0 \end{bmatrix}$, respectively. Suppose that stochastic sequence obeys Bernoulli distribution with probability $E\{\alpha_1(k) \mid \alpha_1(k) = 1\} = E\{\alpha_2(k) \mid \alpha_2(k) = 1\} = 0.996$, given $\gamma = 1$. For simplicity, let $M = P_1^{-1} = P_2^{-1}$ and $N = KP_1^{-1} = KP_2^{-1}$. We can obtain the following parameters in Theorem 6 by using the MATLAB YALMIP Toolbox:

$$\begin{aligned} M_1 &= \begin{bmatrix} 1.3549 & 0.4014 \\ 0.4014 & 0.3819 \end{bmatrix}, \qquad M_2 = \begin{bmatrix} 1.1058 & 0.7881 \\ 0.7881 & 1.6449 \end{bmatrix}, \\ N_1 &= \begin{bmatrix} 0.1755 & -0.3232 \\ -0.3232 & 0.0041 \end{bmatrix}, \qquad N_2 = \begin{bmatrix} 0.2464 & -0.3847 \\ -0.3847 & 0.3580 \end{bmatrix}. \end{aligned} \tag{31}$$

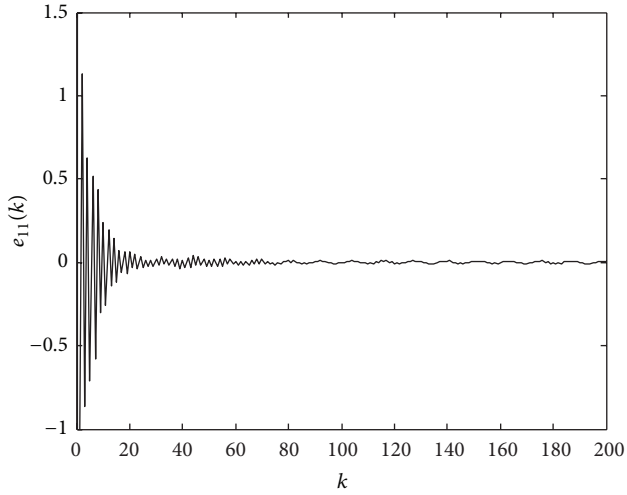

Figure 1: Filter error $e_{11}(k)$.

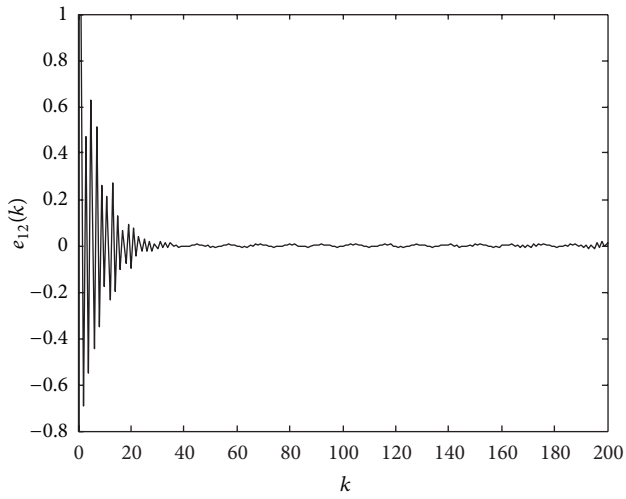

Figure 2: Filter error $e_{12}(k)$.

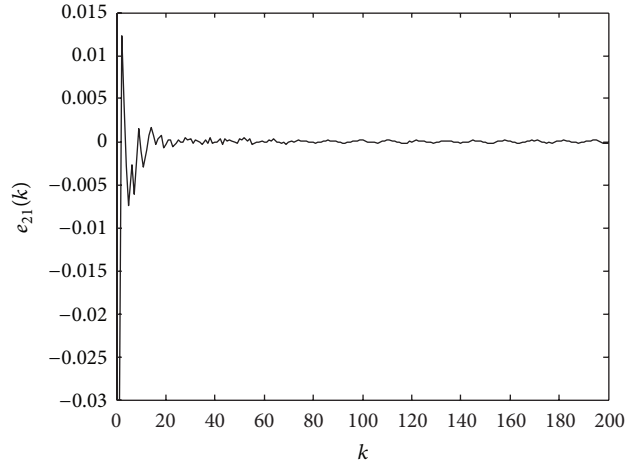

Figure 3: Filter error $e_{21}(k)$.

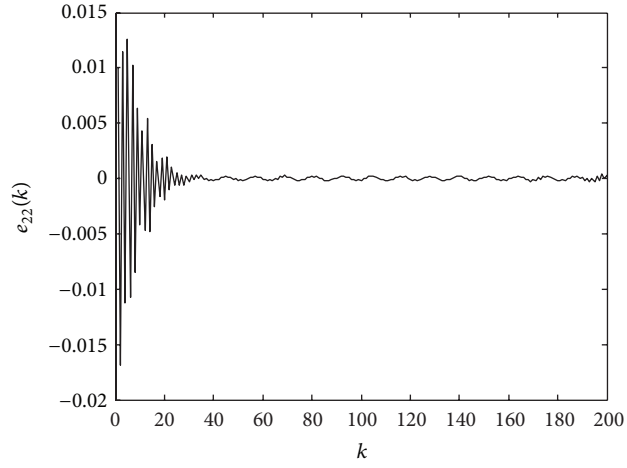

Figure 4: Filter error $e_{22}(k)$.

The Lyapunov function solution matrices and observer parameter are given by

$$P_{11} = P_{21} = M_1^{-1} = \begin{bmatrix} 1.0718 & -1.1264 \\ -1.1264 & 3.8021 \end{bmatrix},$$

$$P_{12} = P_{22} = M_2^{-1} = \begin{bmatrix} 1.3732 & -0.6579 \\ -0.6579 & 0.9231 \end{bmatrix},$$

$$K_1 = N_1 P_1 = \begin{bmatrix} 0.5521 & -1.4264 \\ -0.3510 & 0.3789 \end{bmatrix}, \quad (32)$$

$$K_2 = N_2 P_2 = \begin{bmatrix} 0.5919 & -0.5172 \\ -0.7637 & 0.5835 \end{bmatrix}.$$

The simulation results are shown in Figures 1, 2, 3, and 4.

It can be verified that $\sum_{k=0}^{\infty} E\{\|e(k)\|^2\} < \gamma^2 \sum_{k=0}^{\infty}\{\|w(k)\|^2\}$ and the filter error system satisfies the prescribed H_∞ performance.

5. Conclusion

In this paper, the H_∞ filter for a class of linear discrete-time large-scale system has been designed, where the measurements are probably missing. The missing probability is assumed to obey Bernoulli distribution. By employing the Lyapunov stability theory combined with stochastic analysis method, a filter is designed to reconstruct the states of original system such that the filter error system is exponentially stable in the sense of mean square and achieves the prescribed H_∞ performance.

Acknowledgments

This work is supported by the National Natural Science Foundation of China (61104103, 60904025, 61203028); Natural Science Foundation of Jiangsu Province of China (BK2011826); Jiangsu Government Scholarship for Overseas Studies; Natural Science Foundation for Colleges and Universities in

Jiangsu Province (10KJB120001); Climbing Program of Nanjing University of Telecommunications and Posts (NY210013, NY210014).

References

[1] F. W. Yang, Z. D. Wang, D. W. C. Ho, and M. Gani, "Robust H_∞ control with missing measurements and time delays," *IEEE Transactions on Automatic Control*, vol. 52, no. 9, pp. 1666–1672, 2007.

[2] B. Shen, Z. D. Wang, H. S. Shu, and G. L. Wei, "On nonlinear H_∞ filtering for discrete-time stochastic systems with missing measurements," *IEEE Transactions on Automatic Control*, vol. 53, no. 9, pp. 2170–2180, 2008.

[3] H. Zhang, Q. J. Chen, H. C. Yan, and J. Liu, "Robust H_∞ filtering for switched stochastic system with missing measurements," *IEEE Transactions on Signal Processing*, vol. 57, no. 9, pp. 3466–3474, 2009.

[4] J. L. Liang, Z. d. Wang, and X. H. Liu, "Distributed state estimation for discrete-time sensor networks with randomly varying nonlinearities and missing measurements," *IEEE Transactions on Neural Networks*, vol. 22, no. 3, pp. 486–496, 2011.

[5] Z. D. Wang, B. Shen, H. S. Shu, and G. L. Wei, "Quantized H_∞ control for nonlinear stochastic time-delay systems with missing measurements," *IEEE Transactions on Automatic Control*, vol. 57, no. 6, pp. 1431–1444, 2012.

[6] B. F. Wang and G. Guo, "State estimation for discrete-time systems with Markovian time-delay and packet loss," *Control Theory and Applications*, vol. 26, no. 12, pp. 1331–1336, 2009.

[7] Z. R. Xiang, C. Y. Liang, and M. S. Mahmoud, "Robust H_∞ filtering for discrete-time switched time-delay systems with missing measurements and asynchronous switching," *Transactions of the Institute of Measurement and Control*, vol. 35, no. 2, pp. 200–211, 2012.

[8] Y. Zhou, F. W. Yang, and C. X. Fan, "Robust H_∞ control for large-scale systems with missing measurements," *Control and Decision*, vol. 27, no. 7, pp. 1109–1112, 2012.

[9] Y. Zhou, C. X. Fan, F. W. Yang, and Q. Zang, "Network-based robust H_∞ control for large-scale systems," *Journal of Systems Science and Mathematical Sciences*, vol. 31, no. 6, pp. 709–719, 2011.

[10] F. W. Yang, Z. D. Wang, Y. S. Hung, and M. Gani, "H_∞ control for networked systems with random communication delays," *IEEE Transactions on Automatic Control*, vol. 51, no. 3, pp. 511–518, 2006.

Hindawi Publishing Corporation
Mathematical Problems in Engineering
Volume 2013, Article ID 659457, 6 pages
http://dx.doi.org/10.1155/2013/659457

Research Article

Path Planning for Spray Painting Robot of Workpiece Surfaces

Wei Chen and Dean Zhao

School of Electrical and Information Engineering, Jiangsu University, Zhenjiang 212013, China

Correspondence should be addressed to Dean Zhao; dazhao@ujs.edu.cn

Received 27 May 2013; Revised 3 July 2013; Accepted 7 July 2013

Academic Editor: Baoyong Zhang

A new optimization algorithm of the path planning for spray painting robot of workpiece surfaces is proposed. This paper first provides the paint deposition rate function on a plane according to the experiment data. And the model of film thickness on surface is discussed. A multiobjective constraint optimization problem is formulated. An optimal tool path with an optimal time and film quantity deviation is generated. And the min-max method is adopted here to calculate the values. A workpiece, which is a free-form surface, is used to test the scheme. The results of experiments have shown that the path optimization algorithm achieves satisfactory performance. This algorithm can also be extended to other applications.

1. Introduction

Painting robot is a kind of important and advanced spray equipment. It is widely used in automotive manufacturing. The figure of a product and the tool parameters can strongly influence the quality of painting. In order to achieve the new spraying operation standards, new painting models and tool planning algorithms are active research for many years. Automated tool path generation is the key technology of robotic offline programming method. At present, generating paint gun trajectories for plane and regular surfaces have achieved satisfactory results [1, 2]. However, it is very difficult to get the optimal tool trajectory with an optimal time and film quantity deviation for a free-form surface in practice. Due to the complex geometry of free-form surfaces, it is still a challenge to generate optimization trajectories of spray gun that satisfies paint uniformity requirements. Currently, automated tool planning has always caused a bottleneck for spray painting. Hence, it is essential to develop new automated tool path planning to replace past tool path planning. This challenging research topic has been receiving more and more attention from academia and industry [3–5]. Some researchers developed modeling methods to model the material deposition for the spraying processes, such as parabolic, Gaussian, Cauchy, and Beta models. Since the spray painting process is much more complicated than the spray forming process, these models may not generate satisfactory paint paths to satisfy the paint distribution requirements [6–9]. Chen et al. [10–13] developed an automatic tool path planning for a free-form surface. However, due to that the process is complex and very timeconsuming, their algorithms could not resolve robot trajectory optimization problem. The paint thickness function for free-form surfaces is not considered, and the optimal time is not satisfying.

In this paper, the paint thickness function for free-form surfaces is given. A multiobjective constraint optimization problem is formulated. An optimal tool trajectory with an optimal time and film quantity deviation is generated. And the min-max method is adopted here to calculate the values. The spray painting experiment demonstrates the feasibility and availability of the optimization algorithm.

2. The Path Planning on a Plane

In this paper, a model of paint deposition rate is established according to the experimental data. And assuming that the shape of spray painting from the gun is a cone, and the distribution model of spray is shown in [14].

The tool path can be defined as a series of points. There is a feasible method for determining the tool path. Firstly, the nonoptimal path and orientation of the tool should be designed. Then, the problem is transformed into how to find the optimal time sequence along this path when the objectives

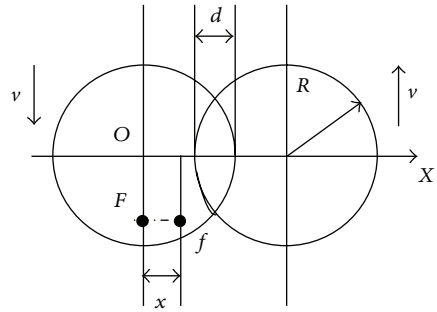

Figure 1: Paint accumulation on a plane.

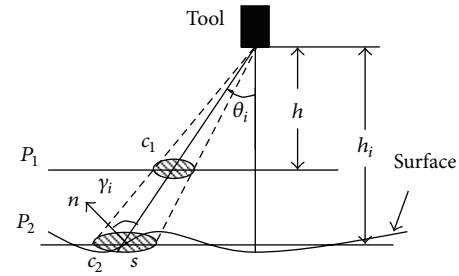

Figure 2: Paint accumulation on a free-form surface.

can be optimal. Therefore, the variable parameters which are six (the position and orientation of the paint gun) in path optimization problem are reduced to one. The key factor of this method is d which is the overlap distance of the two spray painting optimization paths.

Figure 1 shows the paint accumulation on a plane. x is the distance of a point f in the spray cone radius to the first path. F is the projection of the point f. O is the projection of gun center. The material thickness of the point f can be calculated as

$$q_f(x) = \begin{cases} q_1(x), & 0 \le x \le R-d, \\ q_1(x) + q_2(x), & R-d < x \le R, \\ q_2(x), & R < x \le 2R-d, \end{cases} \quad (1)$$

where $q_1(x)$ and $q_2(x)$ are the material thickness of the point f when the tool sprays on two adjacent paths. $q_1(x)$ and $q_2(x)$ can be calculated as

$$\begin{aligned} q_1(x) &= 2\int_0^{t_1} f(r_1)\,dt, \quad 0 \le x \le R, \\ q_2(x) &= 2\int_0^{t_2} f(r_2)\,dt, \quad R-d \le x \le 2R-d, \\ t_1 &= \frac{\sqrt{R^2-x^2}}{v}; \qquad t_2 = \frac{\sqrt{R^2-(2R-d-x)^2}}{v}, \\ r_1 &= \sqrt{(vt)^2+x^2}; \qquad r_2 = \sqrt{(vt)^2+(2R-d-x)^2}, \end{aligned} \quad (2)$$

where t_1 and t_2 are the half time of the tool spraying on two adjacent paths. r_1 and r_2 are the distance of a point f to the projection of gun center. t is the time for the gun moving from the point O to F. By (2), it can be calculated as $q_f(x,d,v) = (1/v)J(x,d)$, where J is a function of x and d. To find optimal velocity v and overlap distance d, the mean square error of the thickness deviation from the average thickness q_d must be minimized:

$$\min_{d\in[0,R],v} E(d,v) = \int_0^{2R-d} \left(q_d - q_s(x,d,v)\right)^2 dx. \quad (3)$$

A golden section method [15] is adopted here to calculate their values.

3. The Path Planning on a Surface

There are many methods to model a surface in CAD, such as Bezier method and B-splines method. But these methods are too complicated to model a free-form surface [16]. In order to obtain uniform material thickness on a free-form surface, it can use "*bounding box*" method to design nonoptimal path as follows.

(1) A triangular approximation of a free-form surface is adopted in CAD modeling.

(2) The initial normal vector of each triangle is found. A seed triangle is chosen as the first triangle of a patch. Before adding a new neighbor triangle, a maximum deviation angle is calculated. After all triangles are found, they are taken as seeds, and new triangles are added into the patch. The process is repeated until no more neighbor triangles can be added into the patch.

(3) The overlap distance of the two spray painting optimization paths is calculated. And the non-optimal tool paths are planned.

Paths planning must consider the free-form surface geometric features. For example, the tool paths should parallel to the boundary of the patch. Sheng et al. [5] presented the rules of non-optimal tool paths planning.

Figure 2 shows paint accumulation on a surface. P_1 is a reference plane, and P_2 is a parallel plane which pass the point s; θ_i is the angle of gun axis and the line of the point s to gun center; h_i is the actual tool height; h is the desired tool height. Suppose the material sprayed on a small area c_1 is projected to the area c_2. The relationship between the two areas is

$$S_{c_2} = \left(\frac{h_i}{h}\right)^2 S_{c_1}, \quad (4)$$

where S_{c_1} and S_{c_2} are the areas of c_1 and c_2. Based on the assumption, the material thickness on c_2 can be expressed as follows:

$$q_2 = q_f\left(\frac{h}{h_i}\right)^2, \quad (5)$$

where q_f and q_2 are the material thickness on c_1 and c_2, respectively.

Figure 3(a) shows a circle c_3, which is perpendicular to the material emission direction. The material on c_3 is projected

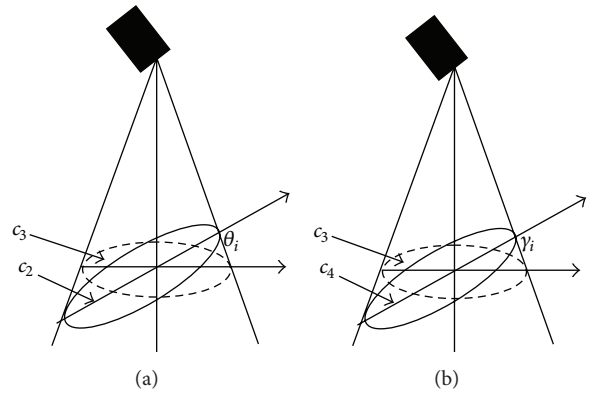

Figure 3: Material projection.

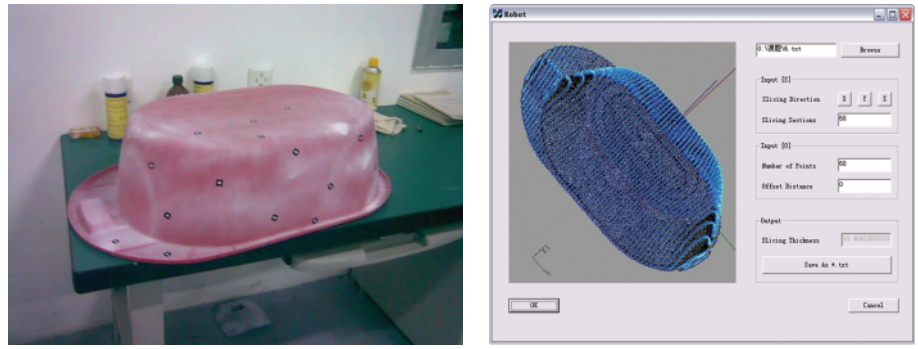

Figure 4: (a) The workpiece. (b) The triangular approximation of the workpiece.

to the free-from surface with deviation angle γ_i, as shown in Figure 4(b). The material thickness on c_3 and c_4 can be expressed as:

$$q_3 = \frac{q_2}{\cos\theta_i},$$
$$q_s = q_3 \cos\gamma_i. \tag{6}$$

Based on (5), (6), the material thickness on the free-form surface can be obtained as

$$q_s = q_f \left(\frac{h}{h_i}\right)^2 \frac{\cos\gamma_i}{\cos\theta_i}. \tag{7}$$

If the distance from the tool to the point s is l_i, $h_i = l_i \cos\theta_i$. When the deviation angle $\gamma_i \geq 90^\circ$, there is no material sprayed on a surface. Therefore, the material thickness on a free-form surface can be modeled as

$$q_s = \begin{cases} q_f \left(\dfrac{h}{l_i}\right)^2 \dfrac{\cos\gamma_i}{\cos\theta_i}, & \gamma_i < 90^\circ, \\ 0, & \gamma_i \geq 90^\circ. \end{cases} \tag{8}$$

Since there are many parameters that need optimizing, such as time, material thickness uniformity, and material waste. The process optimization of surface manufacturing is a multiobject optimization problem. The proposed technique for solving the optimal process planning problem is based on approximating the optimization parameters as a piecewise constant functions. Therefore, the path is divided into P segments. For each segment, we continue to divide the segment into m smaller segments and assume the parameters in the smaller segment do not change too much. d_k is the length of each segment; t_k is the spraying time on the kth segment. In the derivative of (8),

$$\frac{dq_s}{dt} = \frac{dq_f}{dt}\left(\frac{h}{l_i}\right)^2 \frac{\cos\gamma_i}{\cos^3\theta_i} = f(r_i)\left(\frac{h}{l_i}\right)^2 \frac{\cos\gamma_i}{\cos^3\theta_i}, \tag{9}$$

with $r_i = h\tan\theta_i$. Suppose for each smaller segment, the spray angle θ_i and deviation angel γ_i do not change too much. Then, for the jth triangle on a free-form surface, its material thickness due to the kth segment can be written as

$$q_{jk} = \sum_{i=1}^{m} f(h\tan\theta_i)\left(\frac{h}{l_i}\right)^2 \frac{\cos\gamma_i}{\cos^3\theta_i} t_k', \tag{10}$$

where t_k' is the spraying time on each segment. Thus, material thickness for the ith triangle is

$$q_j = \sum_{k=1}^{p}\sum_{i=1}^{m} f(h\tan\theta_i)\left(\frac{h}{l_i}\right)^2 \frac{\cos\gamma_i}{\cos^3\theta_i}\frac{t_k}{m}. \tag{11}$$

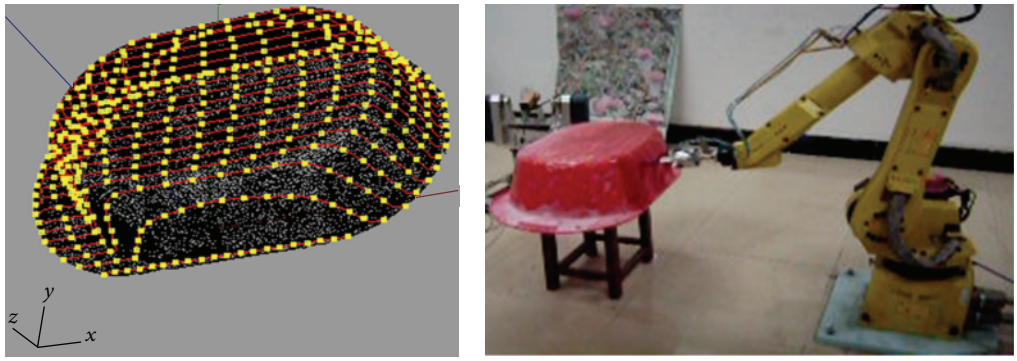

(a) (b)

Figure 5: (a) The part of generated gun path of the workpiece. (b) Robotic spray painting experiment.

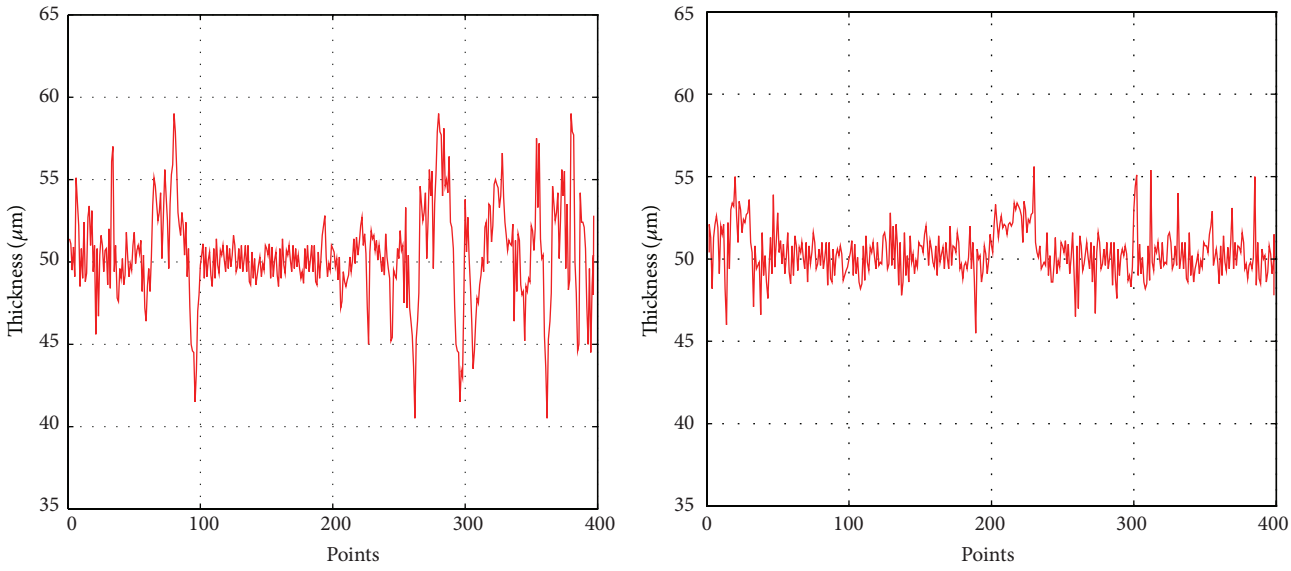

(a) (b)

Figure 6: Material thickness of random chosen points on the workpiece: (a) nonoptimal tool path planning; (b) optimal tool path planning.

This equation can be written as

$$q_j = \sum_{k=1}^{p} \frac{d_k}{m v_k} \sum_{i=1}^{m} f\left(h \tan\theta_i\right) \left(\frac{h}{l_i}\right)^2 \frac{\cos\gamma_i}{\cos^3\theta_i}. \tag{12}$$

The total time to spray the free-form surface is

$$T = \sum_{k=1}^{p} t_k = \sum_{k=1}^{p} \frac{d_k}{v_k}. \tag{13}$$

For a given free-form surface, find the minimum time to spray the surface such that the given constraints are satisfied and material deviation from the required material thickness is minimized. Suppose the required average material thickness is q_d, and the max material thickness deviation is q_w. Then, the tool path optimization problems can be formulated as

$$\begin{aligned} &\min \quad L = \left(L_1, L_2\right), \\ &\text{s.t.} \quad \left|q_j - q_d\right| \le q_w, \end{aligned} \tag{14}$$

where

$$\begin{aligned} L_1 &= \sum_{k=1}^{p} \frac{d_k}{v_k}, \qquad L_2 = \sum_{j=1}^{N} \left(q_j - q_d\right)^2, \\ q_j &= \sum_{k=1}^{p} \frac{d_k}{m v_k} \sum_{i=1}^{m} f\left(h \tan\theta_i\right) \left(\frac{h}{l_i}\right)^2 \frac{\cos\gamma_i}{\cos^3\theta_i}. \end{aligned} \tag{15}$$

This is a constraint multi-objective optimization problem. There are different ways to perform multi-objective optimization problems, such as weighted-sum approach, nonlinear approach, and min-max approach. In order to reduce the calculation procedure, we use min-max approach to solve the problem as follows.

Step 1. Weights are given. $\omega_i > 0$ and $\sum_{i=1}^{2} \omega_i = 1$.

Step 2. Non-linear programming problem is solved. Variable parameter v is introduced, $v > 0$; v is $(i = 1, 2)$ a common

Table 1: The results of non-optimal and optimal tool path planning.

	Optimal	Non-optimal
Average (μm)	49.3	48.8
Maximum (μm)	55.6	58.8
Minimum (μm)	45.8	41.5
Process time (S)	49.6	57.8

upper bound of $\omega_i f_i(x)$. The following auxiliary problem can be formulated as

$$\begin{aligned} &\min \ v; \\ &\text{s.t.} \quad \omega_i f_i(x) \le v \quad (i = 1, 2), \ x \in D, \end{aligned} \tag{16}$$

where D is the feasible region for x. Then, the optimal solution (x^*, v^*) can be obtained.

4. Experimental Verification

Suppose the required average material thickness is $q_d = 50\,\mu$m, and the max material thickness deviation is $q_w = 10\,\mu$m. The spray radius $R = 60$ mm. The material deposition rate is $f(r) = (1/15)(R^2 - r^2)\,\mu$m/s.

After optimizing the spray process on a plane, the tool velocity and the overlap distance are calculated as $v = 256.6$ mm/s, $d = 50.2$ mm.

The workpiece, shown in Figure 4(a), is used to test the algorithm. The triangular approximation of the workpiece is shown in Figure 4(b). The parameters in the algorithm are as follows: $q_w = 10 \times 10^{-6}$ mm; $R = 60$ mm; $h = 100$ mm; $N = 586$; $P = 192$; $d_k = 50$ mm; $m = 10$; $\omega = (0.5, 0.5)^{\mathrm{T}}$. The non-optimal tool path is generated using "*bounding box*" method. The part of generated gun path is shown in Figure 5(a). And Figure 5(b) shows the robotic spray painting experiment.

The material thickness of random chosen points on the workpiece are measured by coating thickness gauge. Figure 6(a) shows the result for non-optimal tool path planning. Figure 6(b) shows the result for optimal tool path planning. The results for non-optimal and optimal tool path planning are summarized in Table 1.

5. Conclusion

A general framework for optimal tool path planning on surfaces has been developed. A multiobjective constraint optimization problem has been formulated. Experiments are performed to measure the material thickness on a free-form surface for both optimal and non-optimal tool path. Experimental results show that the optimal tool path takes less process time compared with the non-optimal tool path. And the results demonstrate the advantages of the optimal path planning algorithm. This algorithm can also be extended to other applications such as optimal tool path for free-form surface of cleaning robot or grinding robot.

Acknowledgment

This project is supported by National Natural Science Foundation of China (Grant no. 60875052).

References

[1] W. H. Huang, "Optimal line-sweep-based decompositions for coverage algorithms," in *Proceedings of the 2001 IEEE International Conference on Robotics and Automation (ICRA '01)*, pp. 27–32, Seoul, Korea, May 2001.

[2] W. Sheng, N. Xi, H. Chen, Y. Chen, and M. Song, "Suface partitioning in automated CAD guided tool planning for additive manufacturing," in *Proceedings of the 2003 IEEE/RSJ International Conference on Intelligent Robots and Systems*, pp. 2072–2077, Las Vegas, Nev, USA, October 2003.

[3] H. Choset, "Coverage of known spaces: the boustrophedon cellular decomposition," *Autonomous Robots*, vol. 9, no. 3, pp. 247–253, 2000.

[4] P. N. Atkar, H. Choset, and A. A. Rizzi, "Toward optimal coverage of 2-dimensional surfaces embedded in r3: choice of start curve," in *Proceedings of the 2003 IEEE/RSJ International Conference on Intelligent Robots and Systems*, pp. 3581–3587, Las Vegas, Nev, USA, October 2003.

[5] W. Sheng, H. Chen, N. Xi, and Y. Chen, "Tool path planning for compound surfaces in spray forming processes," *IEEE Transactions on Automation Science and Engineering*, vol. 2, no. 3, pp. 240–249, 2005.

[6] D. C. Conner, A. Greenfield, P. N. Atkar, A. A. Rizzi, and H. Choset, "Paint deposition modeling for trajectory planning on automotive surfaces," *IEEE Transactions on Automation Science and Engineering*, vol. 2, no. 4, pp. 381–391, 2005.

[7] R. C. Luo and J. H. Tzou, "Investigation of a linear 2-D planar motor based rapid tooling system," in *Proceedings of the IEEE International Conference on Robotics and Automation*, pp. 1471–1476, Washington, DC, USA, May 2002.

[8] P. N. Atkar, A. Greenfield, D. C. Conner, H. Choset, and A. A. Rizzi, "Uniform coverage of automotive surface patches," *International Journal of Robotics Research*, vol. 24, no. 11, pp. 883–898, 2005.

[9] J. Li, J. Xiao, Y. Huang, and H. H. Lou, "Integrated process and product analysis: a multiscale approach to paint spray," *AIChE Journal*, vol. 53, no. 11, pp. 2841–2857, 2007.

[10] H. Chen, F. Thomas, and L. Xiongzi, "Automated industrial robot path planning for spray painting a process: a review," in *Proceedings of the 4th IEEE Conference on Automation Science and Engineering (CASE '08)*, pp. 522–527, Washington, DC, USA, August 2008.

[11] L. Xiongzi, O. A. Landsnes, and C. Heping, "Automatic trajectory generation for robotic painting application," in *Proceedings of the 41st International Symposium on Robotics and 2010 6th German Conference on Robotics*, pp. 1–6, Berlin, Germany, 2010.

[12] S. Yu and L. Cao, "Modeling and prediction of paint film deposition rate for robotic spray painting," in *Proceedings of the 2011 IEEE International Conference on Mechatronics and Automation (ICMA '11)*, pp. 1445–1450, Beijing, China, August 2011.

[13] P. J. From, J. Gunnar, and J. T. Gravdahl, "Optimal paint gun orientation in spray paint applications—experimental results," *IEEE Transactions on Automation Science and Engineering*, vol. 8, no. 2, pp. 438–442, 2011.

[14] C. Wei and Z. Dean, "Tool trajectory optimization of robotic spray painting," in *Proceedings of the 2nd International Conference on Intelligent Computing Technology and Automation, ICICTA 2009*, pp. 419–422, Changsha, China, October 2009.

[15] H. Hong-Xuan and H. Ji-Ye, *Mathematical Programming*, Tsinghua University Press, 2006.

[16] J. Y. Lai and D. J. Wang, "A strategy for finish cutting path generation of compound surfaces," *Computers in Industry*, vol. 25, no. 2, pp. 189–209, 1994.

Hindawi Publishing Corporation
Mathematical Problems in Engineering
Volume 2013, Article ID 784013, 8 pages
http://dx.doi.org/10.1155/2013/784013

Research Article

Invertibility of Nonlinear Differential-Algebraic-Equation Subsystems with Application to Power Systems

Qiang Zang,[1,2] Kaifeng Zhang,[2] Xianzhong Dai,[2] and Ying Zhou[3]

[1] *School of Information and Control Engineering, Nanjing University of Information Science & Technology, Nanjing 210044, China*
[2] *Key Laboratory of Measurement and Control of Complex Systems of Engineering, Ministry of Education, Southeast University, Nanjing 210096, China*
[3] *College of Automation, Nanjing University of Posts and Telecommunications, Nanjing 210003, China*

Correspondence should be addressed to Qiang Zang; zangq@nuist.edu.cn

Received 28 May 2013; Accepted 7 July 2013

Academic Editor: Baoyong Zhang

For nonlinear differential-algebraic-equation subsystems, whose index is one and interconnection input is locally measurable, the problem of invertibility is discussed and the results are applied to the power systems component decentralized control. The inverse systems' definitions for such a class of differential-algebraic-equation subsystems are put forward. A recursive algorithm is proposed to judge whether the controlled systems are invertible. Then physically feasible α-order integral right inverse systems are constructed, with which the composite systems are linearizaed and decoupled. Finally, decentralized excitation and valve coordinative control for one synchronous generator within multimachine power systems are studied and the simulation results based on MATLAB demonstrate the effectiveness of the control scheme proposed in this paper.

1. Introduction

A number of physical systems such as power systems, economic systems, and constrained robot systems are mathematically described by differential-algebraic-equation (DAE) systems [1]. Various concepts, theories, and methods of ordinary-differential-equation (ODE) systems are extended and great progress has been made for DAE systems [2–6]. In [2], for linear DAE systems with input saturation, the composite nonlinear feedback control problem was considered through introducing the generalized Lyapunov function. In [3], the state-feedback stabilization *is considered* for nonlinear discrete DAE large-scale control systems using Lyapunov matrix equation. H_∞ Observer was designed for a class of continuous time nonlinear DAE systems in [4], where necessary and sufficient condition for observer existence was established under the worst conditions. In [5], the traditional Kalman filter was improved and a recursive state estimation method is presented for nonlinear DAE systems. In [6], the output feedback compensation problem was considered by coupling the design of controller and observer instead of separation principle.

In order to provide a measure of the difference between DAE systems and ODE systems, the notion of differential index is commonly used, which corresponds to the minimum number of differentiations of the algebraic equations required to obtain equivalent ODE systems [7]. Among nonlinear DAE systems, the systems of index one represent an important class of physical systems such as power systems and electric circuits. In [8], the Lyapunov method of nonlinear ODE systems was extended to nonlinear DAE systems of index one and the sufficient conditions of stability are presented. In [9], still for such a class of nonlinear DAE systems, an explicit constructing method was given and the state space order-reduction realization was achieved with application to power systems control.

In most existing results, the controlled systems are treated as isolated ones. However, in many practical applications, controlled systems are subsystems within large-scale systems and there exist mutual influence and constraint between the

controlled systems and the rest of the large-scale systems. Typically, a so-called "power systems component structural model" put forward in [10, 11] for power systems component decentralized control problem just falls into this category. At the same time, it should be noted that DAE subsystems control problems are common not only for power systems but also for large-scale systems of others areas [12]. As far as the authors know, the research about nonlinear DAE subsystems is seldom found.

Among various nonlinear control methods, the invertibility of systems plays an important role in linearization and decoupling of general nonlinear systems (not restricted to affine form) [13]. The research on invertibility of nonlinear DAE systems can be traced to [14, 15], where the invertibility of continuous and discrete DAE systems was discussed, respectively.

In this paper, for nonlinear DAE systems whose index is one and interconnection inputs are locally measurable and bounded, the invertibility is studied and the results are applied to power systems component decentralized control. The structure of this paper is as follows. Firstly, the definitions of unit right inverse systems and α-order integral right inverse systems are given. Secondly, a recursive algorithm is proposed with which to determine whether the controlled nonlinear DAE subsystems are invertible. If the controlled systems are invertible, physically realizable α-order integral right inverse systems are constructed through state-feedback and dynamic compensation, with which the decoupling and linearization of the composite systems are both achieved so that various linear control methods and theories can be applied. At last, decentralized excitation and valve coordinative controller are designed for one synchronous generator set within multimachine power systems. The simulation is conducted based on MATLAB and the simulation results illustrate the effectiveness of the proposed scheme in this paper.

2. System Description and Problem Formulation

We consider general nonlinear DAE subsystems as follows:

$$\begin{aligned} \dot{x}_i &= f_i\left(x_i, z_i, u_i, \overline{v}_i\right), \\ g_i\left(x_i, z_i, u_i, \overline{v}_i\right) &= 0, \\ y_i &= h_i\left(x_i, z_i, u_i, \overline{v}_i\right), \quad i = 1, \ldots, N, \end{aligned} \tag{1}$$

where $x_i \in N_0^i \subset R^{n_i}$, $z_i \in M_0^i \subset R^{l_i}$, $u_i \in L_0^i \subset R^{m_i}$, $y_i \in K_0^i \subset R^{m_i}$, $\overline{v}_i \in S_0^i \subset R^{s_i}$ are differential variable, algebraic variable, manipulated input, controlled output, and interconnection input, respectively. $\overline{v}_i$ reflects the influence of the rest of the large-scale systems on controlled systems (1). $f_i \in R^{n_i}$, $g_i \in R^{l_i}$, $h_i \in R^{m_i}$ are smooth vector fields. For the sake of simplicity, we will omit the subscript i of (1) in the remainder of this paper. Let $X_0 = (x_0, u_0, z_0, y_0, \overline{v}_0) \in U_0$ is compatible initial conditions, that is, $g(x_0, z_0, u_0, \overline{v}_0) = 0$ where $U_0 = [N_0, M_0, L_0, K_0, S_0]$ [8].

Throughout this paper, the following basic hypotheses are made for (1).

(H1) The Jacobian matrix of $g(x, z, u, \overline{v})$ with respect to z has constant full rank on U_0:

$$\operatorname{rank}\left(\frac{\partial g}{\partial z}\right) = l, \quad \forall\left(x, z, u, y, \overline{v}\right) \in U_0, \tag{2}$$

that is, (1) is of index one.

(H2) The interconnection input $\overline{v}$ and its sufficient order derivatives are locally measurable and bounded.

Remark 1. Above basic hypotheses hold for power systems components under normal operating conditions.

In sequel we will give inverse systems definition of nonlinear DAE subsystems (1), including unit right inverse systems and α-order integral right inverse systems.

The controlled output $y(t)$ of nonlinear DAE subsystems (1) is determined together by the interconnection input $\overline{v}$, manipulated input $u(t)$ and initial conditions. From the functional point of view, nonlinear DAE subsystems (1) can be regarded as an operator (marked by θ) which maps the manipulated input $u(t)$, and interconnection input $\overline{v}(t)$ to control output $y(t)$, that is,

$$y = \theta\left(u, \overline{v}\right). \tag{3}$$

Definition 2. Suppose there exist systems $\overline{\Sigma}$ which bear input-output mapping relationship: $\widehat{y} = \overline{\theta}(r, \overline{v})$, where the input $r(t) = (r_1, \ldots, r_m)^T$ is a smooth vector. For nonlinear DAE subsystems (1), if $u(t) = \widehat{y}(t)$, we have $y(t) = r(t)$, and then the systems Σ are the unit right inverse systems of nonlinear DAE subsystems (1). We call systems (1) are invertible.

Definition 3. Suppose there exist systems $\overline{\Sigma}_\alpha$ which bear input-output mapping relationship: $\widehat{y} = \overline{\theta}_\alpha(\varphi, \overline{v})$ where the input $\varphi(t) = (\varphi_1, \ldots, \varphi_m)^T = r^{(\alpha)} = (r_1^{(\alpha_1)}, \ldots, r_m^{(\alpha_m)})^T$ is a continuous vector. For nonlinear DAE subsystems (1), if $u(t) = \widehat{y}(t)$, we have $y^{(\alpha)} = \varphi$ where $y^{(\alpha)} = (y_1^{(\alpha_1)}, \ldots, y_m^{(\alpha_m)})^T$ (i.e., $y_i^{(\alpha_i)} = \varphi_i$, $i = 1, \ldots, m$), and then the systems Σ are the unit right inverse systems of nonlinear DAE subsystems (1). We call systems (1) are invertible.

The aim of this paper is to study the invertibility of nonlinear DAE subsystems (1) satisfying (H1) and (H2). The linearization and decoupling of the composite systems can be achieved if the controlled systems (1) are invertible. As a result, various linear control theorems and methods can be applied.

3. Recursive Algorithm and Invertibility of Nonlinear DAE Subsystems

We will give a recursive algorithm, with which to determine the invertibility of nonlinear DAE subsystems (1).

From (2) we know that $(\partial g/\partial z)^{-1}$ exist on U_0. We use the following operator $E_\xi(\cdot)$:

$$E_\xi(F) \triangleq \left.\frac{\partial F}{\partial \xi}\right|_{0=g(x,z,u,\overline{v})} = \frac{\partial F}{\partial \xi} - \frac{\partial F}{\partial z}\left(\frac{\partial g}{\partial z}\right)^{-1}\frac{\partial g}{\partial \xi} \tag{4}$$

to denote the Jacobian matrix of vector function $F(x,z,u,y,\ldots,y^{(k)},\overline{v},\ldots,\overline{v}^{(k)})$ with respect to some variable $\xi \in (x,u,\overline{v})$ under the algebraic constraint $0 = g(x,z,u,\overline{v})$. For the limit of space, only the procedure of step k is presented.

Step k ($k = 1,2,\ldots$). Suppose that, until to step k, we can get a sequence of nonnegative integers $\gamma_0,\ldots,\gamma_{k-2},\gamma_{k-1}$ and the distribution Δ_{k-1} with X_0^{k-1} is the regular point. Around X_0^{k-1} we have $\operatorname{rank} E_u(h_{k-1}) = \gamma_{k-1}$ where $h_{k-1} = \begin{bmatrix} H_{k-2} \\ \widehat{h}_{k-1} \end{bmatrix}$. Obviously $\gamma_{k-1} \geq \gamma_{k-2}$, and let $\widehat{h}_{k-1,1}$ denote $\gamma_{k-1} - \gamma_{k-2}$ rows chosen from $\widehat{h}_{k-1}$ such that $\operatorname{rank} E_u(\begin{bmatrix} H_{k-2} \\ \widehat{h}_{k-1,1} \end{bmatrix}) = \gamma_{k-1}$. Let $H_{k-1} = \begin{bmatrix} H_{k-2} \\ \widehat{h}_{k-1,1} \end{bmatrix}$ and $\widehat{h}_{k-1,2}$ denote the rest rows of $\widehat{h}_{k-1}$. Then there exist neighborhood $\overline{U}_k = [N_k, M_k, L_k, \overline{K}_k, \overline{S}_k] \subseteq U_{k-1}$ and smooth mapping $\lambda_{k-1}(x,z,u,y,\ldots,y^{(k-1)},\overline{v},\ldots,\overline{v}^{(k-1)})$ such that

$$E_u\left(\widehat{h}_{k-1,2}\right) = \lambda_{k-1}(\cdot)\, E_u\left(H_{k-1}\right), \tag{5}$$

where

$$\begin{aligned}
N_k &= \{x \mid x \in N_{k-1}, \operatorname{rank}\left(E_u\left(h_{k-1}\right)\right) = \gamma_{k-1}\} \\
M_k &= \{z \mid z \in M_{k-1}, \operatorname{rank}\left(E_u\left(h_{k-1}\right)\right) = \gamma_{k-1}\} \\
L_k &= \{u \mid u \in L_{k-1}, \operatorname{rank}\left(E_u\left(h_{k-1}\right)\right) = \gamma_{k-1}\} \\
\overline{K}_k &= \left\{\left(y,\ldots,y^{(k-1)}\right) \mid \left(y,\ldots,y^{(k-1)}\right) \in K_{k-1}, \right. \\
&\qquad \left. \operatorname{rank}\left(E_u\left(h_{k-1}\right)\right) = \gamma_{k-1}\right\} \\
\overline{S}_k &= \left\{\left(\overline{v},\ldots,\overline{v}^{(k-1)}\right) \mid \left(\overline{v},\ldots,\overline{v}^{(k-1)}\right) \in S_{k-1}, \right. \\
&\qquad \left. \operatorname{rank}\left(E_u\left(h_{k-1}\right)\right) = \gamma_{k-1}\right\}.
\end{aligned} \tag{6}$$

Remark 4. If $E_u(hk-1,2) = 0$, then we only need to set $\lambda_{k-1}(\cdot) = 0$.

Let

$$\begin{aligned}
\widehat{h}_k &= \widehat{h}_k\left(x,z,u,y,\ldots,y^{(k)},\overline{v},\ldots,\overline{v}^{(k)}\right) \\
&= \left[E_x\left(\widehat{h}_{k-1,2}\right) - \lambda_{k-1}(\cdot)\, E_x\left(H_{k-1}\right)\right]\dot{x} \\
&\quad + \sum_{i=0}^{k-1}\left[\frac{\partial \widehat{h}_{k-1,2}}{\partial y^{(i)}} - \lambda_{k-1}(\cdot)\frac{\partial H_{k-1}}{\partial y^{(i)}}\right] y^{(i+1)} \\
&\quad + \left[E_{\overline{v}}\left(\widehat{h}_{k-1,2}\right) - \lambda_{k-1}(\cdot)\, E_{\overline{v}}\left(H_{k-1}\right)\right]\dot{\overline{v}} \\
&\quad + \sum_{i=1}^{k-1}\left[\frac{\partial \widehat{h}_{k-1,2}}{\partial \overline{v}^{(i)}} - \lambda_{k-1}(\cdot)\frac{\partial H_{k-1}}{\partial \overline{v}^{(i)}}\right] \overline{v}^{(i+1)}
\end{aligned} \tag{7}$$

and define recursively

$$h_k\left(x,z,u,y,\ldots,y^{(k)},\overline{v},\ldots,\overline{v}^{(k)}\right) = \begin{bmatrix} H_{k-1} \\ \widehat{h}_k \end{bmatrix} = 0. \tag{8}$$

Let $U_k = [N_k, M_k, L_k, K_k, S_k]$, where $K_k = [\overline{K}_k, \widehat{K}_k]$, $S_k = [\overline{S}_k, \widehat{S}_k]$, and $\widehat{K}_k, \widehat{S}_k$ are the value region of $y^{(k)}$ and $\overline{v}^{(k)}$, respectively, when $x \in N_{k-1}$, $z \in M_{k-1}$, $u \in L_{k-1}$, $(y,\ldots,y^{(k-1)}) \in \overline{K}_{k-1}$, $(\overline{v},\ldots,\overline{v}^{(k-1)}) \in \overline{S}_{k-1}$. Accordingly we get the point $X_0^k = (x_0, z_0, u_0, y_0,\ldots,y_0^{(k)},\overline{v}_0,\ldots,\overline{v}_0^{(k)})$ and let Δ_k denote the distribution generated by the row vectors of $E_u(h_k)$. If X_0^k is the regular point of Δ_k, that is, the matrix $E_u(h_k)$ has constant rank γ_k at some neighborhood of X_0^k. If $\gamma_k = m$, then algorithm stops; if $\gamma_k < m$, then algorithm enters next step.

In the above construction we produce a sequence of nonnegative integers $\gamma_1, \gamma_2, \ldots$ which satisfy $0 \leq \gamma_1 \leq \gamma_2 \leq \gamma_3 \leq \cdots \leq m$.

Definition 5. The relative order ρ for the nonlinear DAE subsystems (1) is the least positive integer k such that $\gamma_k = m$ or $\rho = \infty$ if $\gamma_k < m$ for all $k = 1,2,\ldots$.

The main results of this paper can be concluded into the following theorems.

Theorem 6. *Consider the nonlinear DAE subsystems* (1) *with relative order* θ. *If* $\theta < \infty$, *then there exist unit right inverse systems of nonlinear DAE subsystems* (1).

Proof. According to the recursive algorithm, at step θ we can get the following equation:

$$h_\theta\left(x,z,u,y,\ldots,y^{(\theta)},\overline{v},\ldots,\overline{v}^{(\theta)}\right) = 0 \tag{9}$$

with $\operatorname{rank}(E_u(h_\theta)) = \gamma_\theta = m$. By the virtue of the *Implicit Function Theorem*, (9) determines a unique solution about u:

$$u = h_\theta^{-1}\left(x,z,y,\ldots,y^{(\theta)},\overline{v},\ldots,\overline{v}^{(\theta)}\right). \tag{10}$$

Denote $\overline{v}_k = (\overline{v}^T,\ldots,(\overline{v}^{(k)})^T)^T$, $k = 0,1,\ldots,\theta$ and construct the following systems:

$$\begin{aligned}
\dot{\widehat{x}} &= f\left(\widehat{x},\widehat{z},h_\theta^{-1}\left(\widehat{x},\widehat{z},r,\ldots,r^{(\theta)},\overline{v}_\theta\right),\overline{v}\right), \\
&\quad \left(\widehat{x}\left(t_0\right),\widehat{z}\left(t_0\right)\right) = \left(x\left(t_0\right),z\left(t_0\right)\right) \\
0 &= g\left(\widehat{x},\widehat{z},h_\theta^{-1}\left(\widehat{x},\widehat{z},r,\ldots,r^{(\theta)},\overline{v}_\theta\right),\overline{v}\right), \\
\widehat{y} &= h_\theta^{-1}\left(\widehat{x},\widehat{z},r,\ldots,r^{(\theta)},\overline{v}_\theta\right),
\end{aligned} \tag{11}$$

where $\widehat{x} \in R^n$, $\widehat{z} \in R^l$, $r \in R^m$ and $\widehat{y} \in R^m$, are differential variables, algebraic variables, manipulated input, and controlled output, respectively. Systems (11) are unit right inverse systems of nonlinear DAE subsystems (1), and conclusion can be proved as follows.

By virtue of the recursive algorithm, there exists a row transmit matrix $\Pi_k = \begin{bmatrix} I_{r_{k-1}} & 0 \\ 0 & \widehat{\Pi}_{k1} \\ 0 & \widehat{\Pi}_{k2} \end{bmatrix}$, $k = 1,\ldots,\theta-1$ where

$\widehat{\Pi}_{k1} \in R^{(\gamma_k-\gamma_{k-1})\times(m-\gamma_{k-1})}$ and $\widehat{\Pi}_{k2} \in R^{(m-\gamma_k)\times(m-\gamma_{k-1})}$ such that $\begin{bmatrix} H_{k-1} \\ \hat{h}_{k,1} \end{bmatrix} = \Pi_k \cdot h_k$, that is,

$$H_k = \begin{bmatrix} H_{k-1} \\ \hat{h}_{k,1} \end{bmatrix} = \begin{bmatrix} H_{k-1} \\ \widehat{\Pi}_{k1}\left(\frac{d}{dt}\hat{h}_{k-1,2} - \lambda_k \frac{d}{dt}H_{k-1}\right) \end{bmatrix}, \qquad \hat{h}_{k,2} = \widehat{\Pi}_{k2}\left(\frac{d}{dt}\hat{h}_{k-1,2} - \lambda_k \frac{d}{dt}H_{k-1}\right). \tag{12}$$

For h_0 especially, we have $\begin{bmatrix} H_0 \\ \hat{h}_0 \end{bmatrix} = \begin{bmatrix} \widehat{\Pi}_{01} \\ \widehat{\Pi}_{02} \end{bmatrix} h_0$, where $\widehat{\Pi}_{01} \in R^{r_0\times m}$ and $\widehat{\Pi}_{k2} \in R^{(m-\gamma_0)\times m}$.

When the manipulated input of nonlinear DAE subsystems (1) is set to $u(t) = \hat{y}(t)$, the states $(x(t), z(t))$ satisfy

$$\begin{aligned} \dot{x} &= f\left(x, z, \hat{y}, \overline{v}\right), \\ 0 &= g\left(x, z, \hat{y}, \overline{v}\right). \end{aligned} \tag{13}$$

From (11) we have $\dot{\hat{x}} = f(\hat{x}, \hat{z}, \hat{y}, \overline{v})$, $0 = g(\hat{x}, \hat{z}, \hat{y}, \overline{v})$ as well as $(\hat{x}(t_0), \hat{z}(t_0)) = (x(t_0), z(t_0))$; thus, we have $(\hat{x}, \hat{z}) = (x, z)$.

Define $\overline{y}_0 = \widehat{\Pi}_{0,1} y$, $\hat{y}_0 = \widehat{\Pi}_{0,2} y$ and let $\overline{y}_k = \widehat{\Pi}_{k,1}\hat{y}_{k-1}$, $\hat{y}_k = \widehat{\Pi}_{k,2}\hat{y}_{k-1}$, $k = 1, \ldots, \theta - 1$. It can be proved that if the manipulated input $r(t) \in C^n(R)$ of systems (11) satisfies $h_\alpha(\hat{x}, \hat{z}, \hat{y}, r, \ldots, r^{(\alpha)}, \overline{v}_\theta) = 0$ and

$$\begin{aligned} &H_k\left(x, z, u, r, \ldots, r^{(k)}, \overline{v}_k\right) \\ &\quad = H_k\left(x, z, u, y, \ldots, y^{(k)}, \overline{v}_k\right), \quad k = 1, \ldots, \theta - 1 \end{aligned} \tag{14}$$

as well as initial conditions satisfying

$$\begin{aligned} &\hat{h}_{k,2}\left(x(t_0), z(t_0), u(t_0), r(t_0), \ldots, r^{(k)}(t_0), \overline{v}_k(t_0)\right) \\ &\quad = \hat{h}_{k,2}\left(x(t_0), z(t_0), u(t_0), y(t_0), \ldots, \right. \\ &\qquad \left. y^{(k)}(t_0), \overline{v}_k(t_0)\right), \end{aligned} \tag{15}$$

then we have $y(t) = r(t)$ where $y(t)$ is the controlled output of nonlinear DAE subsystems (1). From Definition 2, systems (11) are unit right inverse systems of nonlinear DAE subsystems (1). This completes the proof. □

Since $(\hat{x}, \hat{z}) = (x, z)$, unit right inverse systems (11) can be realized by directly feedbacking states (x, z) of nonlinear DAE subsystems (1). The composite systems will be linearized and decoupled when (11) is series connected before (1).

It should be noted that there exist differential operator in above realization (11), which is difficult to be realized in physics. For this we have the following theorem.

Theorem 7. *Consider the nonlinear DAE subsystems* (1) *with relative order* θ. *If* $\theta < \infty$, *then there exist* α*-order integral right inverse systems of nonlinear DAE subsystems* (1).

Proof. Replace y of (10) with r:

$$u = h_\theta^{-1}\left(x, z, r, \ldots, r^{(\theta)}, \overline{v}, \ldots, \overline{v}^{(\theta)}\right). \tag{16}$$

Let the highest and lowest order derivative of r_i $(i = 1, \ldots, m)$ are $r_i^{(\beta_i)}$ and $r_i^{(\alpha_i)}$, respectively. Define

$$\begin{aligned} \varphi &= (\varphi_1, \ldots, \varphi_m)^T = \left(r_1^{(\alpha_1)}, \ldots, r_m^{(\alpha_m)}\right)^T, \\ \xi_i &= \left(r_i^{(\beta_i)}, r_i^{(\beta_i+1)}, \ldots, r_i^{(\alpha_i-1)}\right)^T, \quad i = 1, \ldots, m \end{aligned} \tag{17}$$

and construct the following systems $\overline{\Sigma}_\alpha$:

$$\begin{aligned} \dot{\xi}_i &= A_i\xi_i + B_i\varphi_i, \quad i = 1, \ldots, m \\ \hat{y} &= h_\alpha^{-1}\left(x, z, \xi, \varphi, \overline{v}_\alpha\right), \end{aligned} \tag{18}$$

where

$$A_i = \begin{pmatrix} 0 & 1 & & \\ & \ddots & \ddots & \\ & & \ddots & 1 \\ & & & 0 \end{pmatrix}_{(\alpha_i-\beta_i)\times(\alpha_i-\beta_i)}$$

$$B_i = \begin{pmatrix} 0 \\ \vdots \\ 0 \\ 1 \end{pmatrix}_{(\alpha_i-\beta_i)\times 1}, \tag{19}$$

$$\xi = \left(\xi_1^T, \ldots, \xi_m^T\right)^T, \qquad \overline{v}_\theta = \left(\overline{v}^T, \ldots, (\overline{v}^{(\theta)})^T\right)^T.$$

If $r(t) \in C^\theta(R)$ of (18) satisfies

$$\begin{aligned} &h_\theta\left(x, z, u, r, \ldots, r^{(\theta)}, \overline{v}_\theta\right) = 0, \\ &H_k\left(x, z, u, r, \ldots, r^{(k)}, \overline{v}_k\right) \\ &\quad = H_k\left(x, z, u, y, \ldots, y^{(k)}, \overline{v}_k\right), \quad k = 1, \ldots, \theta - 1. \end{aligned} \tag{20}$$

Meanwhile initial conditions satisfy

$$\begin{aligned} &\hat{h}_{k,2}\left(x(t_0), z(t_0), u(t_0), r(t_0), \ldots, r^{(k)}(t_0), \overline{v}_k(t_0)\right) \\ &\quad = \hat{h}_{k,2}\left(x(t_0), z(t_0), u(t_0), y(t_0), \ldots, \right. \\ &\qquad \left. y^{(k)}(t_0), \overline{v}_k(t_0)\right) \end{aligned} \tag{21}$$

when $\varphi = (r_1^{(\alpha_1)}, \ldots, r_m^{(\alpha_m)})^T$, $\xi_i(t_0) = (r_i^{(\beta_i)}(t_0), \ldots, r_i^{(\alpha_i-1)}(t_0))^T$ $(i = 1, \ldots, m)$, we have output of nonlinear DAE subsystems satisfies $y_i^{(\alpha_i)}(t) = \varphi_i(t)$, $i = 1, \ldots, m$ (where φ is new control input to be designed). By Definition 3, systems (18) are α-order integral right inverse systems realized by state-feedback and dynamic compensation. This completes the proof. □

There are two possible difficulties existing in realization of inverse systems: The one hand, the proposed method depends on the exact model of the controlled systems and sensitive to the perturbation of parameters or variation of structure. On the other hand, analysis solution of manipulated control

may be difficult to be obtained. Inspired by [16], we may use the excellent approximation ability of Neural Networks to overcome the imprecise model and unknown analysis solution of manipulated control. This will be the next work we will undertake.

4. Decentralized Excitation and Valve Coordinative Control of Synchronous Generator

Excitation and valve coordinative control is studied for one synchronous generator based on the scheme proposed in this paper. For the sake of simplicity, the subscript i is still omitted.

The mathematical model of synchronous generator excitation and valve coordinative control is described by the following two-input two-output nonlinear DAE subsystems [10]:

$$\begin{aligned}
\dot{\delta} &= f_1(\cdot) = \omega - \omega_0 \\
\dot{\omega} &= f_2(\cdot) = \frac{\omega_0}{H}\left\{P_H + C_{ML}P_{m0} - \frac{D}{\omega_0}(\omega - \omega_0)\right. \\
&\qquad \left. - \left[E'_q + \left(x_q - x'_d\right) I_d\right] I_q\right\} \\
\dot{E}'_q &= f_3(\cdot) = \frac{1}{T'_{d0}}\left[E_f - E'_q - \left(x_q - x'_d\right) I_d\right] \\
\dot{P}_H &= f_4(\cdot) = \frac{1}{T_{H\Sigma}}\left(-P_H + C_H P_{m0} + C_H U_c\right) \\
g(x, z, u, \overline{v}) &= 0,
\end{aligned} \tag{22}$$

where

$$g(x, z, u, \overline{v}) = \begin{pmatrix} P_t - \left[E'_q + \left(x_q - x'_d\right) I_d\right] I_q + r_a\left(I_d^2 + I_q^2\right) \\ \theta_U - \delta + \operatorname{arc}ctg\dfrac{x_q I_q - r_a I_d}{E'_q - x'_d I_d - r_a I_q} \\ I_t - \sqrt{I_d^2 + I_q^2} \\ Q_t - E'_q I_d + x_q I_q^2 + x'_d I_d^2 \end{pmatrix}, \tag{23}$$

where the differential variables $x = (\delta, \omega, E'_q, P_H)^T$ are relative power angle between G1 and G4, rotate speed deviation of G1, q-axis transient potential, and the high pressure mechanical power, respectively, the algebraic variables $z = (P_t, \theta_U, I_d, I_q)^T$ are active power, the angle of voltage, the d-axis current, and the q-axis current, respectively, and the interconnection input $\overline{v} = (I_t, Q_t)^T$ are the generator stator current and the reactive power, respectively. The manipulated input $u = (E_f, U_c)^T$ are induction electromotive force and the governor position, respectively. The controlled output y is chosen as voltage and rotate speed deviation, respectively:

$$y = h(\cdot) = \begin{pmatrix} V_t \\ \omega \end{pmatrix} = \begin{pmatrix} \dfrac{\sqrt{P_t^2 + Q_t^2}}{I_t} \\ \omega \end{pmatrix}. \tag{24}$$

The others are the systems parameters.

The Jacobian matrix of $g(x, z, u, \overline{v})$ with respect to z is

$$\begin{aligned}
\frac{\partial g}{\partial z} &= \begin{pmatrix} 1 & 0 & \left(x_q - x'_d\right) I_q + 2r_a I_d & \left(x_q - x'_d\right) I_d + 2r_a I_q \\ 0 & 1 & \dfrac{-1}{1 + A^2}\dfrac{\partial A}{\partial I_d} & \dfrac{-1}{1 + A^2}\dfrac{\partial A}{\partial I_q} \\ 0 & 0 & \dfrac{I_d}{I_t} & -\dfrac{I_q}{I_t} \\ 0 & 0 & -E'_q + 2x'_d I_d & 2x_q I_q \end{pmatrix} \\
&\triangleq \begin{pmatrix} 1 & 0 & a_{13} & a_{14} \\ 0 & 1 & a_{23} & a_{24} \\ 0 & 0 & a_{33} & a_{34} \\ 0 & 0 & a_{43} & a_{44} \end{pmatrix},
\end{aligned} \tag{25}$$

where $A = (x_q I_q - r_a I_d)/(E'_q - x'_d I_d - r_a I_q)$. It can be verified that under the normal operating condition, the following equation $\det(\partial g/\partial z) = -(1/I_t)(2x_q I_d I_q + E'_q I_q - 2x'_d I_d I_q) \neq 0$ holds, that is, matrix $\partial g/\partial z$ is of full rank and generator is of index one.

From (22) and (23), we can get the differential equation of z as follows:

$$\dot{z} = -\left(\frac{\partial g}{\partial z}\right)^{-1}\left(\frac{\partial g}{\partial x}\right) f - \left(\frac{\partial g}{\partial z}\right)^{-1}\left(\frac{\partial g}{\partial \overline{v}}\right)\dot{\overline{v}}, \tag{26}$$

where

$$\begin{aligned}
\left(\frac{\partial g}{\partial z}\right)^{-1} &= \begin{pmatrix} 1 & 0 & b_1 & c_1 \\ 0 & 1 & b_2 & c_2 \\ 0 & 0 & b_3 & c_3 \\ 0 & 0 & -a_{33}^{-1}a_{43} & 1 \end{pmatrix}, \\
b_1 &= -a_{33}^{-1}a_{13} - a_{33}^{-1}a_{43}c_1, \qquad b_2 = -a_{33}^{-1}a_{23} - a_{33}^{-1}a_{43}c_2, \\
b_3 &= 1 - a_{33}^{-1}a_{43}c_3, \qquad c_1 = -c_4^{-1}a_{14} + a_{33}^{-1}c_4^{-1}a_{13}a_{34}, \\
c_2 &= -c_4^{-1}a_{24} + a_{33}^{-1}c_4^{-1}a_{23}a_{34}, \\
c_3 &= c_4^{-1}a_{34}, \qquad c_4 = a_{44} - a_{33}^{-1}a_{34}a_{43}.
\end{aligned} \tag{27}$$

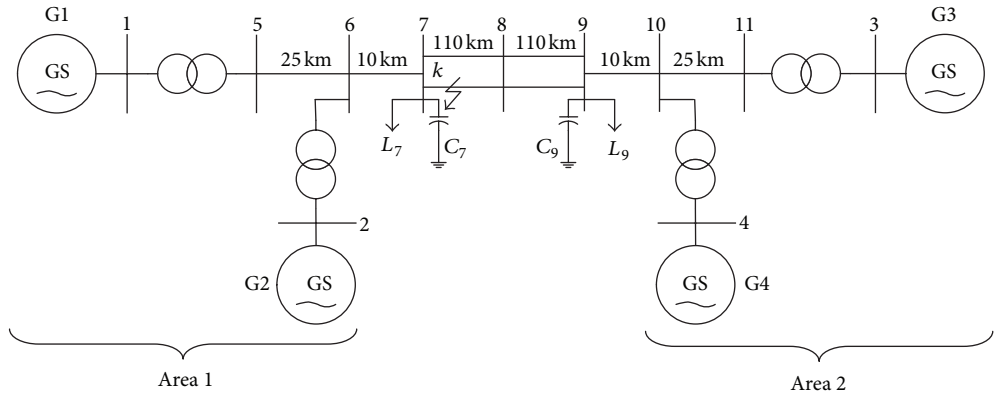

Figure 1: Two-area four-machine power system.

The Jacobian matrix of g with respect to x and interconnection input $\overline{v}$ are

$$\frac{\partial g}{\partial x} = \begin{pmatrix} 0 & 0 & -I_q & 0 \\ -1 & 0 & \dfrac{-1}{1+A^2}\dfrac{\partial A}{\partial E'_q} & 0 \\ 0 & 0 & 0 & 0 \\ 0 & 0 & -I_d & 0 \end{pmatrix}, \qquad \frac{\partial g}{\partial \overline{v}} = \begin{pmatrix} 0 & 0 \\ 0 & 0 \\ 1 & 0 \\ 0 & 1 \end{pmatrix}. \tag{28}$$

According to the recursive algorithm, the relative degree of (22) is 2 and the solution of u can be derived as follows:

$$\begin{aligned} E_f = {} & \frac{T'_{d_0}}{-I_q - c_1 I_d} \\ & \times \left\{ \frac{1}{P_t}\left[\frac{1}{I_t}\sqrt{P_t^2+Q_t^2}\left(I_t^2 \dot{y}_1 + \dot{I}_t\sqrt{P_t^2+Q_t^2}\right) - Q_t\dot{Q}_t \right] \right. \\ & \left. + b_1\dot{I}_t + c_1\dot{Q}_t \right\} + E'_q + \left(x_d - x'_d\right) I_d, \\ U_c = {} & \frac{\omega_0 C_H}{HT_{H\Sigma}} \\ & \times \left\{ \ddot{y}_2 - \frac{\omega_0}{HT_{H\Sigma}}\left(-P_H + C_H P_{m0}\right) \right. \\ & - \frac{D}{\omega_0} f_2 - I_q f_3 - \left(x_q - x'_d\right) c_3 I_d I_q f_3 \\ & + \left(x_q - x'_d\right) b_3 I_q \dot{I}_t + \left(x_q - x'_d\right) c_3 I_q \dot{Q}_t \\ & - E'_q I_d f_3 + a_{33}^{-1} a_{43} E'_q \dot{I}_t + E'_q \dot{Q}_t \\ & - \left(x_q - x'_d\right) I_d^2 f_3 + a_{33}^{-1} a_{43}\left(x_q - x'_d\right) I_d \dot{I}_i \\ & \left. + \left(x_q - x'_d\right) I_d \dot{Q}_t \right\}. \end{aligned} \tag{29}$$

According to (18), the $(1,2)$-order integral right inverse systems for synchronous generator (22) can be constructed, with which the decoupling and linearization of the composed systems can be achieved.

The simulation is conducted based on a two-area four-machine power systems (as shown in Figure 1).

The parameters of each generator and transformer are the same and the other parameters can be found in [17]. Systems operating condition is as follows: at first systems operate under double circuit stable state, then a three-phase symmetrical earth fault happens at k point at line 7-8 on 0.5 second and the ground reactance of the failure point is 0.0001 pu.The fault is cut on 0.65 second and the systems return to original operating condition. Generators G1, G3 both adopted inverse excitation and valve controller and the closed-loop φ_1, φ_2 adopted *PID* controller where φ_1 only adopts proportion part equal to 10 and φ_2 adopt proportion part equal to 30 and differential part equal to 5. The other generators adopt traditional linear controller. The simulation is based-on MATLAB and the results are shown in Figure 2.

As shown in Figure 2, when generators G1 and G3 both equipped excitation and valve coordinative inverse controller, both interarea oscillation and area oscillation are improved dramatically.

With noting that x_d, x_q cannot be measured online. To overcome this difficulty, we can adopt the method proposed in [16] to replace the x_d, x_q with local measured signals.

5. Conclusion

In this paper, the problem of invertibility for a special class of nonlinear DAE subsystems is studied. The definitions of inverse systems for nonlinear DAE subsystems are put forward. Then a recursive algorithm is given, with which to determine the invertibility of nonlinear DAE subsystems. Physically realizable right inverse systems are constructed

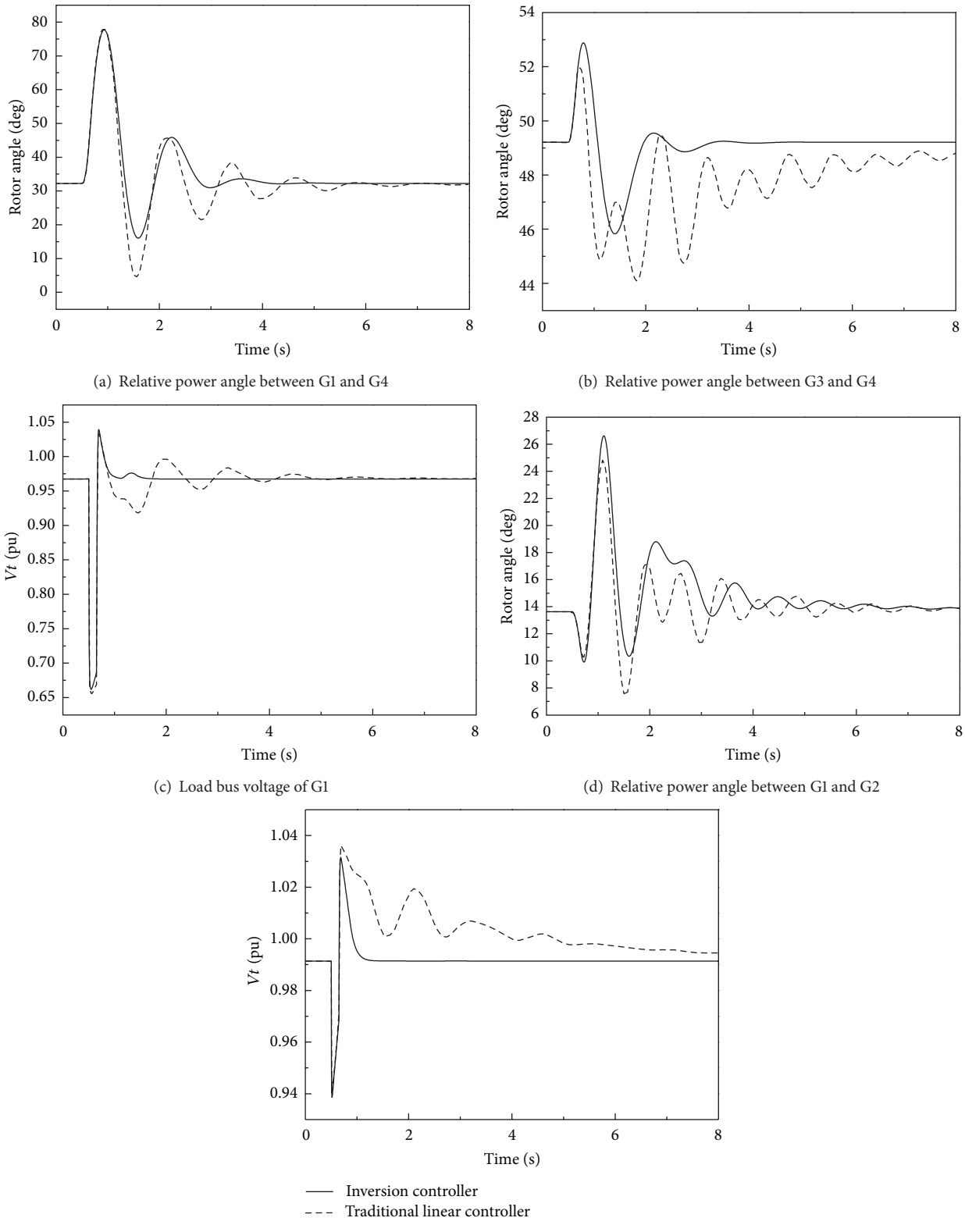

(a) Relative power angle between G1 and G4

(b) Relative power angle between G3 and G4

(c) Load bus voltage of G1

(d) Relative power angle between G1 and G2

(e) Load bus voltage of G3

Figure 2: Simulation results of G1 and G3.

through state-feedback and dynamic compensation, with which the decoupling and linearization of composite systems are achieved so that various linear control theorems and methods can be applied. Not restricted to power systems components decentralized control, the result of this paper is also meaningful to decentralized control of other areas of large-scale systems.

Acknowledgments

This work is supported by the National Natural Science Foundation of China (61004001, 61104103, 51177019), Natural Science Foundation of Jiangsu Province of China (BK2011826), Jiangsu Government Scholarship for Overseas Studies, Open Project of Key Laboratory of Measurement and Control of Complex Systems of Engineering, Ministry of Education, Southeast University (MCCSE2012A07), and State Grid Corporation of China, Major Projects on Planning and Operation Control of Large Scale Grid (SGCC-MPLG022-2012).

References

[1] S. L. Campbell, N. K. Nichols, and W. J. Terrell, "Duality, observability, and controllability for linear time-varying descriptor systems," *Circuits Systems and Signal Processing*, vol. 10, no. 4, pp. 455–470, 1991.

[2] D. Lin, W. Lan, and M. Li, "Composite nonlinear feedback control for linear singular systems with input saturation," *Systems and Control Letters*, vol. 60, no. 10, pp. 825–831, 2011.

[3] S. L. Sun and Y. Y. Chen, "Stabilization of a kind of nonlinear discrete singular large-scale control systems," *Advance in Natural Science*, vol. 5, no. 2, pp. 10–13, 2012.

[4] M. Darouach, L. Boutat-Baddas, and M. Zerrougui, "H_∞ observers design for a class of nonlinear singular systems," *Automatica*, vol. 47, no. 11, pp. 2517–2525, 2011.

[5] R. K. Mandela, R. Rengaswamy, S. Narasimhan, and L. N. Sridhar, "Recursive state estimation techniques for nonlinear differential algebraic systems," *Chemical Engineering Science*, vol. 65, no. 16, pp. 4548–4556, 2010.

[6] Q. Zang and X.-Z. Dai, "Output feedback stabilization control for nonlinear differential-algebraic equation systems," *Acta Automatica Sinica*, vol. 35, no. 9, pp. 1244–1248, 2009 (Chinese).

[7] L. Petzold, "Differential/algebraic equations are not ode's," *SIAM Journal on Scientific and Statistical Computing*, vol. 3, no. 3, pp. 367–384, 1982.

[8] D. J. Hill and I. M. Y. Mareels, "Stability theory for differential/algebraic systems with application to power systems," *IEEE transactions on circuits and systems*, vol. 37, no. 11, pp. 1416–1423, 1990.

[9] A. R. Ríos and M. L. López, "Order-reduction strategy of nonlinear differential-algebraic equation models with application on power systems," *Electric Power Components & Systems*, vol. 40, no. 15, pp. 1690–1707, 2012.

[10] X.-Z. Dai and K.-F. Zhang, "Interface concept and structural model of complex power systems," *Proceedings of the Chinese Society of Electrical Engineering*, vol. 27, no. 7, pp. 7–12, 2007 (Chinese).

[11] X.-Z. Dai, K.-F. Zhang, and Q. Zang, "Nonlinear decentralized control method of power systems based on component structural model," *Proceedings of the Chinese Society of Electrical Engineering*, vol. 28, no. 22, pp. 15–22, 2008 (Chinese).

[12] M. T. Frye, Y. L. lu, and C. J. Qian, "Decentralized output feedback control of large-scale nonlinear systems interconnected by unmeasurable states," *Proceeding of the American Control Conference*, vol. 5, pp. 4267–4272, 2004.

[13] R. M. Hirschorn, "lnvertibility of multivariable nonlinear control systems," *IEEE Transactions on Automatic Control*, vol. 24, no. 6, pp. 855–865, 1979.

[14] S. Tan and J. Vandewalle, "Inversion of singular systems," *IEEE transactions on circuits and systems*, vol. 35, no. 5, pp. 583–587, 1988.

[15] M. El-Tohami, V. Lovass-Nagy, and P. D. L. Powers D. L., "On minimal order inverse of discrete-time descriptor systems," *International Journal of Control*, vol. 41, no. 4, pp. 991–1004, 1985.

[16] X. Dai, D. He, T. Zhang, and K. Zhang, "ANN generalised inversion for the linearisation and decoupling control of nonlinear systems," *IEE Proceedings*, vol. 150, no. 3, pp. 267–277, 2003.

[17] P. Kundur, *Power System Stability and Control*, McGraw-Hill, 1994.

Hindawi Publishing Corporation
Mathematical Problems in Engineering
Volume 2013, Article ID 352198, 7 pages
http://dx.doi.org/10.1155/2013/352198

Research Article

Full-Order Disturbance-Observer-Based Control for Singular Hybrid System

Xiuming Yao,[1,2] Ze Dong,[1] and Dongfeng Wang[1]

[1] *Hebei Engineering Research Center of Simulation & Optimized Control for Power Generation, North China Electric Power University, Baoding 071003, China*
[2] *National Key Laboratory on Aircraft Control Technology, Beihang University, Beijing 100191, China*

Correspondence should be addressed to Xiuming Yao; xiumingyao@gmail.com

Received 22 May 2013; Accepted 24 June 2013

Academic Editor: Zhiguang Feng

The problem of the disturbance-observer-based control for singular hybrid system with two types of disturbances is addressed in this paper. Under the assumption that the system states are, unavailable, full-order observers (for both system states and the disturbance) and a nonlinear control scheme are constructed, such that the composite system can be guaranteed to be stochastically admissible, and the two types of disturbances can be attenuated and rejected, simultaneously. Based on the Lyapunov stability theory, sufficient conditions for the existence of the desired full-order disturbance-observer-based controllers are established in terms of linear matrix inequalities (LMIs). Finally, a numerical example is provided to show the effectiveness of the proposed approaches.

1. Introduction

Singular systems, which are also referred to as implicit systems, descriptor systems, are widely used to model various engineering systems, such as electrical networks, power systems, networked control systems, and robotics, due to the fact that such systems can provide a more general representation than standard state-space systems in the sense of modeling [1]. A great number of fundamental results based on the theory of state-space systems have been successfully extended to singular systems. For some fundamental work on this subject, we refer the reader to [2–7].

Disturbance-observer-based control has been proven to be an effective strategy to reject the disturbance which can be modeled by an exogenous system [8–13]. Recently, its applications have been found in the robotic systems [8], table drive systems [12], missile system [11], and so on. The essential idea of the disturbance-observer-based control scheme is to design a disturbance observer to estimate the matched disturbance and cancel the effect of the matched disturbance by applying the estimation information into the control law. On another research front line, singular Markovian jump system which includes the dynamics of both singular system and Markovian jump system has attracted great attention from researchers, and recently some results are available in the publication: sliding control problem for continuous Markovian jump singular system is investigated in [14, 15], where the necessary and sufficient condition for the admissibility of the nominal system is presented. ℓ_2-ℓ_∞ filter problem is designed for discrete-time singular Markovian jump systems in [16]. Notice that in the above-mentioned publications, the disturbance considered in the plant has been assumed to be norm-bounded one. In this paper, we will consider a wider case: the plant is subject to multiple disturbances (one is norm-bounded disturbance, and the other is the disturbance that can be modeled by the exogenous system).

Based on the previous reasons, in this paper, we will investigate the disturbance-observer-based control problem for a class of singular systems with Markovian switching parameters and multiple disturbances. With the proposed nonlinear control scheme and by choosing a proper stochastic Lyapunov-Krasovskii functional, sufficient conditions for the existence of the desired controllers in terms of LMIs [17, 18] are presented, such that the composite system is stochastically admissible and meets certain performance requirements. Finally, a numerical example is used to illustrate the efficiency of the developed results.

The remainder of this paper is organized as follows. Section 2 describes the problem and preliminaries. Section 3 presents the main theoretical results. A numerical example is given in Section 4. Finally, we conclude the paper in Section 5.

2. Problem Statement and Preliminaries

Fix a probability space $(\Omega, \mathcal{F}, \mathcal{P})$, where Ω is the sample space, $\mathcal{F}$ is the σ-algebra of subsets of the sample space, and $\mathcal{P}$ is the probability measure on $\mathcal{F}$. Under this probability space, we consider the following singular MJLs:

$$E\dot{x}(t) = A(r_t)x(t) + G(r_t)\left[u(t) + d_1(t)\right] + H(r_t)d_2(t), \tag{1a}$$

$$y(t) = D_1(r_t)x(t) + D_2(r_t)d_1(t), \tag{1b}$$

where $x(t) \in \mathbb{R}^n$ is the semistate vector, $u(t) \in \mathbb{R}^m$ is the control input, $y(t) \in \mathbb{R}^s$ is the output measurement and $d_1(t) \in \mathbb{R}^m$ is supposed to satisfy conditions described as Assumption 1, which can represent the constant and harmonic noises. $d_2(t) \in \mathbb{R}^q$ is another disturbance which is assumed to be an arbitrary signal in $\mathcal{L}_2[0,\infty)$. The matrix $E \in \mathbb{R}^{n\times n}$ is singular with $\operatorname{rank}(E) = r < n$, and the matrices $A_i \triangleq A(r_t = i)$, $G_i \triangleq G(r_t = i)$, $H_i \triangleq H(r_t = i)$, $D_{1i} \triangleq D_1(r_t = i)$, and $D_{2i} \triangleq D_2(r_t = i)$ are known real constant matrices of appropriate dimensions. $\{r_t\}$ is a continuous-time Markov process with right continuous trajectories and taking values in a finite set $\mathcal{S} = \{1, 2, \ldots, \mathcal{N}\}$ with transition probability matrix $\Pi \triangleq \{\pi_{ij}\}$ given by

$$\Pr\{r_{t+\Delta} = j \mid r_t = i\} = \begin{cases} \pi_{ij}\Delta + o(\Delta) & \text{if } j \neq i, \\ 1 + \pi_{ii}\Delta + o(\Delta) & \text{if } j = i, \end{cases} \tag{2}$$

where $\Delta > 0$, $\lim_{\Delta\to 0}(o(\Delta)/\Delta) = 0$, $\pi_{ij} \geq 0$ is the transition rate from i at time t to j at time $t + \Delta$, and $\pi_{ii} = -\sum_{j=1, j\neq i}^{\mathcal{N}} \pi_{ij}$.

Assumption 1. The disturbance $d_1(t)$ can be formulated by the following exogenous system:

$$\begin{aligned} \dot{\omega}(t) &= W_i\omega(t) + M_i d_3(t), \\ d_1(t) &= V_i\omega(t), \end{aligned} \tag{3}$$

where W_i, M_i, and V_i are known matrices with proper dimensions. $d_3(t)$ is the additional disturbance belonging to $\mathcal{L}_2[0,\infty)$.

The following assumptions are necessary conditions for the disturbance-observer-based control problem.

Assumption 2. (E, A_i, D_{1i}) is impulse observable [19].

Assumption 3. (E, A_i, G_i) is impulse controllable, and (W_i, G_iV_i) is observable.

The free singular system with Markovian switching of (1a) and (1b) with $u(t) = 0$, $d_1(t) = 0$, and $d_2(t) = 0$ can be described as

$$E\dot{x}(t) = A_i x(t). \tag{4}$$

We give the following definition for the singular Markovian jump system (4).

Definition 4 (Dai [2]). The singular Markovian jump system (4) or the pair (E, A_i) is said to be

(i) regular if, for each $i \in \mathcal{S}$, $\det(sE - A_i)$ is not identically zero;

(ii) impulse-free if, for each $i \in \mathcal{S}$, $\deg(\det(sE - A_i)) = \operatorname{rank}(E)$;

(iii) stochastically admissible if it is regular, impulse-free, and stochastically stable.

In this section, we suppose that all of the states in (1a), (1b), and (3) are unavailable. Then, we need to estimate $x(t)$ and $\omega(t)$, respectively. Here, we construct full-order observers for the whole states, and then based on the estimated states, we design a composite controller such that the resulting composite system is stochastically admissible with $\mathcal{H}_\infty$ performance γ. For this purpose, Assumptions 2 and 3 are needed.

By augmenting the states of the system (1a) and (1b) by the disturbance dynamics (3), we obtain the following augmented model:

$$\overline{E}\dot{\xi}(t) = \overline{A}_i\xi(t) + \overline{H}_i d(t) + \overline{G}_i u(t), \tag{5a}$$

$$y(t) = \overline{D}_i\xi(t) \tag{5b}$$

with $\xi(t) \triangleq \left[x(t)^T \;\; \omega(t)^T\right]^T$, $d(t) \triangleq \left[d_2(t)^T \;\; d_3(t)^T\right]^T$, and

$$\begin{aligned} \overline{A}_i &\triangleq \begin{bmatrix} A_i & G_iV_i \\ 0 & W_i \end{bmatrix}, \qquad \overline{E} \triangleq \begin{bmatrix} E & 0 \\ 0 & I \end{bmatrix}, \\ \overline{H}_i &\triangleq \begin{bmatrix} H_i & 0 \\ 0 & M_i \end{bmatrix}, \qquad \overline{D}_i \triangleq \begin{bmatrix} D_{1i} & D_{2i}V_i \end{bmatrix}. \end{aligned} \tag{6}$$

The full-order observer for both $x(t)$ and $\omega(t)$ is designed as

$$\overline{E}\dot{\hat{\xi}}(t) = \overline{A}_i\hat{\xi}(t) + \overline{G}_i u(t) + L_i\left(\hat{y}(t) - y(t)\right), \tag{7a}$$

$$\hat{y}(t) = \overline{D}_i\hat{\xi}(t) \tag{7b}$$

with $\hat{\xi}(t) \triangleq \left[\hat{x}(t)^T \;\; \hat{\omega}(t)^T\right]^T$, and L_i is the observer gain to be determined.

Define

$$e(t) \triangleq \xi(t) - \hat{\xi}(t) \triangleq \begin{bmatrix} e_x(t) \\ e_\omega(t) \end{bmatrix} \triangleq \begin{bmatrix} x(t) - \hat{x}(t) \\ \omega(t) - \hat{\omega}(t) \end{bmatrix} \tag{8}$$

as the estimation error.

Based on (5a), (5b), (7a), and (7b), we obtain the estimation error dynamics as follows:

$$\overline{E}\dot{e}(t) = \left(\overline{A}_i + L_i\overline{D}_i\right)e(t) + \overline{H}_i d(t). \tag{9}$$

In the DOBC scheme, the control can be constructed as

$$u(t) = -\hat{d}_1(t) + K_i\hat{x}(t), \tag{10}$$

where $\widehat{d}_1(t) \triangleq V_i\widehat{\omega}(t)$ is the estimation of $d_1(t)$ and K_i is the controller gain. Combining the estimation error equation (9) with system (1a) and (1b) yields

$$\widetilde{E}\dot{\eta}(t) = \widetilde{A}_i\eta(t) + \widetilde{H}_i d(t) \tag{11}$$

with $\eta(t) \triangleq \left[x(t)^T \;\; e(t)^T\right]^T$ and

$$\widetilde{E} \triangleq \begin{bmatrix} E & 0 \\ 0 & \overline{E} \end{bmatrix}, \qquad \widetilde{A}_i \triangleq \begin{bmatrix} A_i + G_iK_i & \overline{B}_i \\ 0 & \overline{A}_i + L_i\overline{D}_i \end{bmatrix},$$
$$\widetilde{H}_i \triangleq \begin{bmatrix} H_i & 0 \\ 0 & \overline{H}_i \end{bmatrix}, \qquad \overline{B}_i \triangleq \left[-G_iK_i \;\; G_iV_i\right], \tag{12}$$

where $\overline{E}$, $\overline{A}_i$, $\overline{F}_i$, $\overline{H}_i$, and $\overline{D}_i$ are defined in (5a) and (5b).

The reference output is set to be

$$z(t) = C_i x(t) \triangleq \widetilde{C}_i\eta(t) \tag{13}$$

with $\widetilde{C}_i \triangleq [C_i \;\; 0]$.

Therefore, the disturbance-observer-based control problem based on full-order observer (7a) and (7b) for system (1a) and (1b) with (3) can be formulated as follows.

Disturbance-Observer-Based Control Problem. Given the Markovian jump singular system (1a) and (1b) with (3), design full-order observer of the form (7a) and (7b) and controller of the form (10) such that the following requirements are satisfied:

(R1) the composite system in (11) and (13) with $d(t) = 0$ is stochastically admissible;

(R2) under the zero initial conditions, the following inequality holds:

$$\|z(t)\|_2 < \gamma\|d(t)\|_2 \tag{14}$$

for all nonzero $d(t) \in \mathscr{L}_2[0,\infty)$, where $\gamma > 0$ is a prescribed scalar and $\|z(t)\|_2 = \int_0^\infty z^T(t)z(t)dt$.

3. Main Results

Under Assumptions 2 and 3, suppose that K_i and L_i are given, and we first present the bounded real lemma for the composite system in (11) and (13) in terms of LMIs.

Lemma 5. *Given the controller gains K_i, the observer gains L_i, parameters $\lambda_{1i} > 0$, $\lambda_{2i} > 0$, and $\gamma > 0$, the composite system in* (11) *and* (13) *is stochastically admissible and satisfies the $\mathscr{H}_\infty$ performance inequalities* (14) *if there exist matrices P_i such that for $i = 1, 2, \ldots, \mathscr{N}$,*

$$\widetilde{E}^T P_i = P_i^T\widetilde{E} \geq 0, \tag{15a}$$

$$\begin{bmatrix} \Xi_i & P_i^T\widetilde{H}_i \\ \star & -\gamma^2 I \end{bmatrix} < 0 \tag{15b}$$

with

$$\Xi_i \triangleq \widetilde{E}^T\overline{P}_i + P_i^T\widetilde{A}_i + \widetilde{A}_i^T P_i + \widetilde{C}_i^T\widetilde{C}_i,$$
$$\overline{P}_i \triangleq \sum_{j=1}^{\mathscr{N}} \pi_{ij}P_j. \tag{16}$$

Proof. Define a Lyapunov functional candidate as follows:

$$V(\eta(t), r_t, t) \triangleq \eta^T(t)\widetilde{E}^T P_i\eta(t). \tag{17}$$

Let $\mathscr{A}$ be the weak infinitesimal generator of the random process $\{\xi(t), r_t\}$. Then, for each $r_t = i$, $i \in \mathscr{S}$, it can be shown that

$$\begin{aligned} &\mathscr{A}V(\eta(t), i, t) \\ &\quad = 2\eta^T(t)P_i^T\left(\widetilde{A}_i\eta(t) + \widetilde{H}_i d(t)\right) + \eta^T(t)\widetilde{E}^T\overline{P}_i\eta(t) \\ &\quad = \zeta^T(t)\begin{bmatrix} \overline{\Xi}_i & P_i^T\widetilde{H}_i \\ \star & 0 \end{bmatrix}\zeta(t) \end{aligned} \tag{18}$$

with $\zeta(t) \triangleq \left[\eta^T(t) \;\; d^T(t)\right]^T$ and

$$\overline{\Xi}_i \triangleq \widetilde{E}^T\overline{P}_i + P_i^T\widetilde{A}_i + \widetilde{A}_i^T P_i. \tag{19}$$

Consider the following index:

$$J(T) \triangleq \mathbf{E}\left\{\int_0^T \left[z^T(t)z(t) - \gamma^2 d^T(t)d(t)\right]dt\right\}. \tag{20}$$

Then, under the zero initial conditions, it follows from (13) and (18) that

$$\begin{aligned} &J(T) \\ &= \mathbf{E}\left\{\int_0^T \left[z^T(t)z(t) - \gamma^2 d^T(t)d(t)\right]dt\right\} + \mathbf{E}V(\eta(T), i, T) \\ &= \mathbf{E}\left\{\int_0^T \left[z^T(t)z(t) - \gamma^2 d^T(t)d(t) + \mathscr{A}V(\eta(t), r_t = i)\right]dt\right\} \\ &= \mathbf{E}\left\{\int_0^T \zeta^T(t)\Omega_i\zeta(t)\,dt\right\} \end{aligned} \tag{21}$$

with

$$\Omega_i \triangleq \begin{bmatrix} \overline{\Xi}_i + \widetilde{C}_i^T\widetilde{C}_i & P_i^T\overline{H}_i \\ \star & -\gamma^2 I \end{bmatrix}. \tag{22}$$

Based on (15b), we can derive $J(T) \leq 0$ by taking (21) into account. Thus, under the zero initial conditions and for any nonzero $d(t) \in \mathscr{L}_2(0,\infty)$, letting $T \to \infty$, we obtain $\|z(t)\|_2 \leq \gamma\|d(t)\|_2$. The proof is completed. □

Now, we are in a position to present a solution to the *composite DOBC and $\mathscr{H}_\infty$ control problem* formulated in this section.

Theorem 6. *Consider system* (1a) *and* (1b) *with the disturbance* (3) *under Assumptions 2 and 3. Given parameters $\lambda_{1i} > 0$, $\lambda_{2i} > 0$, and $\gamma > 0$, there exists a full-order observer in the form of* (7a) *and* (7b) *and there exists a controller in the form of* (10) *such that the augmented system in* (11) *and* (13) *is stochastically admissible and satisfies the $\mathscr{H}_\infty$ performance*

inequalities (14) *if there exist parameters* $\alpha_i > 0$, *matrices* $P_{1i} > 0$, P_{2i}, $Q_i > 0$, X_i, *and* Y_i *such that for* $i = 1, 2, \ldots, \mathcal{N}$,

$$Q_i E^T = E Q_i \geq 0, \tag{23a}$$

$$Q_i E^T \leq \alpha_i I, \tag{23b}$$

$$\overline{E}^T P_{2i} = P_{2i}^T \overline{E} \geq 0, \tag{23c}$$

$$\begin{bmatrix} \Pi_{1i} & 0 & H_i & 0 & Q_i C_i^T & G_i X_i & G_i V_i & W_i \\ \star & \Pi_{2i} \overline{F}_i & 0 & P_{2i}^T \overline{H}_i & 0 & 0 & 0 & 0 \\ \star & \star & 0 & 0 & 0 & 0 & 0 & 0 \\ \star & \star & 0 & 0 & 0 & 0 & 0 & 0 \\ \star & \star & -\gamma^2 I & 0 & 0 & 0 & 0 & 0 \\ \star & \star & \star & -\gamma^2 I & 0 & 0 & 0 & 0 \\ \star & \star & \star & \star & 0 & 0 & 0 & 0 \\ \star & \star & \star & \star & -I & 0 & 0 & 0 \\ \star & \star & \star & \star & \star & -Q_i & 0 & 0 \\ \star & \star & \star & \star & \star & \star & -I & 0 \\ \star & \star & \star & \star & \star & \star & \star & -\Lambda_i \end{bmatrix} < 0, \tag{23d}$$

$$P_{1i} Q_i = I, \tag{23e}$$

where λ_i *is defined in* (15a) *and* (15b) *and*

$$W_i \triangleq \left[\sqrt{\pi_{i1}} Q_i \ \cdots \ \sqrt{\pi_{ij}} Q_i \ \cdots \ \sqrt{\pi_{i\mathcal{N}}} Q_i^T \right]_{j \neq i},$$

$$\Lambda_i \triangleq \operatorname{diag} \left\{ 2Q_1 - \alpha_1 I, \ldots, 2Q_j - \alpha_j I, \ldots, 2Q_{\mathcal{N}} - \alpha_{\mathcal{N}} I \right\}_{j \neq i},$$

$$\Pi_{1i} \triangleq A_i Q_i + G_i X_i + \left(A_i Q_i + G_i X_i \right)^T + \pi_{ii} Q_i E^T,$$

$$\Pi_{2i} \triangleq P_{2i}^T \overline{A}_i + Y_i \overline{D}_i + \left(P_{2i}^T \overline{A}_i + Y_i \overline{D}_i \right)^T + \overline{E}^T \overline{P}_{2i} + \operatorname{diag} \{ P_{1i}, I \},$$

$$\overline{P}_{2i} \triangleq \sum_{j=1}^{\mathcal{N}} \pi_{ij} P_{2j}. \tag{24}$$

Moreover, if the previous conditions are feasible, the gains of the desired observer in the form of (7a) *and* (7b) *and the desired controller in the form of* (10) *are given by*

$$K_i = X_i Q_i^{-1}, \qquad L_i = P_{2i}^{-T} Y_i. \tag{25}$$

Proof. Define

$$P_i \triangleq \begin{bmatrix} P_{1i} & 0 \\ 0 & P_{2i} \end{bmatrix} \tag{26}$$

with $P_{1i} > 0$.

Substituting $\widetilde{A}_i$, $\widetilde{H}_i$ defined in (11), $\widetilde{C}_i$ defined in (13), and P_i defined in (26) into (15a) and (15b) of Lemma 5 and based on the process of the proof of Lemma 5, we can draw a conclusion that the system in (11) and (13) is stochastically admissible with $\mathscr{H}_\infty$ performance γ if (23c) and the following equalities and inequalities hold:

$$E^T P_{1i} = P_{1i} E \geq 0, \tag{27a}$$

$$\zeta^T (t) \begin{bmatrix} \Gamma_{1i} & 0 & P_{1i} H_i & 0 \\ \star & \Gamma_{3i} & 0 & P_{2i}^T \overline{H}_i \\ \star & \star & -\gamma^2 I & 0 \\ \star & \star & \star & -\gamma^2 I \end{bmatrix} \zeta (t) + 2x^T (t) \Gamma_{2i} e (t) < 0, \tag{27b}$$

where $\overline{P}_{2i}$ is defined in (25) and

$$\begin{aligned} \Gamma_{1i} &\triangleq P_{1i} \left(A_i + G_i K_i \right) + \left(A_i + G_i K_i \right)^T P_{1i} + E^T \overline{P}_{1i} + C_i^T C_i, \\ \Gamma_{2i} &\triangleq P_{1i} \left[-G_i K_i \ \ G_i V_i \right], \\ \Gamma_{3i} &\triangleq P_{2i}^T \left(\overline{A}_i + L_i \overline{D}_i \right) + \left(\overline{A}_i + L_i \overline{D}_i \right)^T P_{2i} + \overline{E}^T \overline{P}_{2i}, \\ \overline{P}_{1i} &\triangleq \sum_{j=1}^{\mathcal{N}} \pi_{ij} P_{1j}. \end{aligned} \tag{28}$$

Note that

$$\begin{aligned} &2x^T (t) \Gamma_{2i} e (t) \\ &\quad = -2x^T (t) P_{1i}^T G_i K_i e_x (t) + 2x^T (t) P_{1i}^T G_i V_i e_\omega (t) \\ &\quad \leq x^T (t) P_{1i} G_i K_i P_{1i}^{-1} K_i^T G_i^T P_{1i} x (t) + e_x^T (t) P_{1i} e_x (t) \\ &\qquad + x^T (t) P_{1i} G_i V_i V_i^T G_i^T P_{1i} x (t) + e_\omega^T (t) e_\omega (t). \end{aligned} \tag{29}$$

Considering (27b) and (29) and using Schur complement, we can see that if the following equalities (30) hold, then (27b) holds as follows:

$$\begin{bmatrix} \Gamma_{1i} & 0 & P_{1i} H_i & 0 & C_i^T & P_{1i} G_i K_i P_{1i}^{-1} & P_{1i} G_i V_i \\ \star & \Gamma_{3i} + R & 0 & P_{2i}^T \overline{H}_i & 0 & 0 & 0 \\ \star & \star & -\gamma^2 I & 0 & 0 & 0 & 0 \\ \star & \star & \star & -\gamma^2 I & 0 & 0 & 0 \\ \star & \star & \star & \star & -I & 0 & 0 \\ \star & \star & \star & \star & \star & -P_{1i}^{-1} & 0 \\ \star & \star & \star & \star & \star & \star & -I \end{bmatrix} < 0 \tag{30}$$

with $R \triangleq \operatorname{diag}\{P_{1i}, I\}$.

Define

$$Q_i \triangleq P_{1i}^{-1}, \qquad X_i \triangleq K_i P_{1i}^{-1}, \qquad Y_i \triangleq P_{2i} L_i. \tag{31}$$

Performing a congruence transformation to (30) by $\operatorname{diag}\{Q_i, I, I, I, I, I, I\}$, we obtain

$$\begin{bmatrix} \overline{\Pi}_{1i} & 0 & H_i & 0 & Q_i C_i^T & G_i X_i & G_i V_i \\ \star & \Pi_{2i} & 0 & P_{2i}^T \overline{H}_i & 0 & 0 & 0 \\ \star & \star & -\gamma^2 I & 0 & 0 & 0 & 0 \\ \star & \star & \star & -\gamma^2 I & 0 & 0 & 0 \\ \star & \star & \star & \star & -I & 0 & 0 \\ \star & \star & \star & \star & \star & -Q_i & 0 \\ \star & \star & \star & \star & \star & \star & -I \end{bmatrix} < 0 \tag{32}$$

with $\overline{\Pi}_{1i} \triangleq A_iQ_i + G_iX_i + (A_iQ_i + G_iX_i)^T + \pi_{ii}Q_iE^T + \sum_{j=1,j\neq i}^{\mathcal{N}} \pi_{ij}Q_iE^TQ_j^{-1}Q_i$.

Performing a congruence transformation to (23a) and (23b) by Q_i^{-1}, respectively, we can readily get (27a) and

$$E^TQ_i^{-1} \leq \alpha_iQ_i^{-1}Q_i^{-1}. \tag{33}$$

By Schur complement to (32) and based on (33), we can conclude that if the following inequalities (34) hold, then (32) holds as follows:

$$\begin{bmatrix} \widetilde{\Pi}_{1i} & 0 & F_i & 0 & H_i & 0 & Q_iU_i^T & Q_iC_i^T & G_iX_i & G_iV_i \\ \star & \Pi_{2i} & 0 & P_{2i}^T\overline{F}_i & 0 & P_{2i}^T\overline{H}_i & 0 & 0 & 0 & 0 \\ \star & \star & -\lambda_iI & 0 & 0 & 0 & 0 & 0 & 0 & 0 \\ \star & \star & \star & -\lambda_iI & 0 & 0 & 0 & 0 & 0 & 0 \\ \star & \star & \star & \star & -\gamma^2I & 0 & 0 & 0 & 0 & 0 \\ \star & \star & \star & \star & \star & -\gamma^2I & 0 & 0 & 0 & 0 \\ \star & \star & \star & \star & \star & \star & -\lambda_{1i}^2I & 0 & 0 & 0 \\ \star & \star & \star & \star & \star & \star & \star & -I & 0 & 0 \\ \star & \star & \star & \star & \star & \star & \star & \star & -Q_i & 0 \\ \star & \star & \star & \star & \star & \star & \star & \star & \star & -I \end{bmatrix} < 0 \tag{34}$$

with $\widetilde{\Pi}_{1i} \triangleq A_iQ_i + G_iX_i + (A_iQ_i + G_iX_i)^T + \pi_{ii}Q_iE^T + \sum_{j=1,j\neq i}^{\mathcal{N}} \pi_{ij}Q_i\alpha_jQ_j^{-1}Q_j^{-1}Q_i$.

By Schur complement to (34), we have

$$\begin{bmatrix} \Pi_{1i} & 0 & H_i & 0 & Q_iC_i^T & G_iX_i & G_iV_i & W_i \\ \star & \Pi_{2i} & 0 & P_{2i}^T\overline{H}_i & 0 & 0 & 0 & 0 \\ \star & \star & -\gamma^2I & 0 & 0 & 0 & 0 & 0 \\ \star & \star & \star & -\gamma^2I & 0 & 0 & 0 & 0 \\ \star & \star & \star & \star & -I & 0 & 0 & 0 \\ \star & \star & \star & \star & \star & -Q_i & 0 & 0 \\ \star & \star & \star & \star & \star & \star & -I & 0 \\ \star & \star & \star & \star & \star & \star & \star & -\overline{\Lambda}_i \end{bmatrix} < 0 \tag{35}$$

with

$$\overline{\Lambda}_i \triangleq \operatorname{diag}\left\{\alpha_1^{-1}Q_1^2, \ldots, \alpha_j^{-1}Q_j^2, \ldots, \alpha_{\mathcal{N}}^{-1}Q_{\mathcal{N}}^2\right\}_{j\neq i}. \tag{36}$$

By using the fact that

$$\alpha_j^{-1}Q_j^2 \geq 2Q_j - \alpha_jI, \tag{37}$$

we can show that if (23d) holds, then (34) holds, and thus (27b) holds. The proof is completed. □

Corollary 7. *Note that the conditions* (23d) *given in Theorem 6 are not strict LMI conditions due to* (23e)*. However, with the result of [20], one can solve these nonconvex feasibility problems by formulating them into some sequential optimization problems subject to LMI constraints. By making the cone complementary linearization (CCL) [20], instead of dealing with the original nonconvex feasibility problem formulated in* (23d) *of Theorem 6, one may consider solving the following minimization problem involving LMI conditions* (23d)*:*

$$\begin{aligned} \min \quad & \operatorname{trace}\left\{\sum_{i=1}^{\mathcal{N}} Q_iP_{1i}\right\}, \\ s.t. \quad & (23a)\text{–}(23d) \quad \text{for } i = 1, 2, \ldots, \mathcal{N}, \\ & \begin{bmatrix} P_{1i} & I \\ I & Q_i \end{bmatrix} \geq 0. \end{aligned} \tag{38}$$

Now, similar to Section 3, we consider the following case: system (1a) and (1b) under Assumptions 1–3 is without jumping parameters (that is $N = 1$), and thus the observer in (7a) and (7b) and the controller in (10) are mode independent. For such a case, the composite system in (11) and (13) becomes singular system effectively operating at one of the subsystems all the time, and it can be described by

$$\widetilde{E}\dot{\eta}(t) = \widetilde{A}\eta(t) + \widetilde{H}d(t), \tag{39a}$$

$$z(t) = \widetilde{C}\eta(t) \tag{39b}$$

with

$$\widetilde{A} \triangleq \begin{bmatrix} A + GK & \overline{B} \\ 0 & \overline{A} + L\overline{D} \end{bmatrix}, \qquad \overline{A} \triangleq \begin{bmatrix} A & GV \\ 0 & W \end{bmatrix},$$

$$\widetilde{H} \triangleq \begin{bmatrix} H & 0 \\ 0 & \overline{H} \end{bmatrix}, \qquad \overline{B} \triangleq \begin{bmatrix} -GK & GV \end{bmatrix}, \qquad \widetilde{C} \triangleq \begin{bmatrix} C & 0 \end{bmatrix},$$

$$\overline{H} \triangleq \begin{bmatrix} H & 0 \\ 0 & M \end{bmatrix}, \qquad \overline{D} \triangleq \begin{bmatrix} D_1 & D_2V \end{bmatrix}. \tag{40}$$

Corollary 8. *Consider system* (1a) *and* (1b) *under Assumptions 1–3 without jumping parameters. Given parameters* $\lambda_1 > 0$, $\lambda_2 > 0$, *and* $\gamma > 0$, *there exists a full-order observer in the form of* (7a) *and* (7b) *without jumping parameters and there exists a controller in the form of* (10) *without jumping parameters such that the composite system in* (39a) *and* (39b) *is admissible and satisfies the* $\mathscr{H}_\infty$ *performance inequalities* (14) *if there exist matrices* $P_1 > 0$, P_2, $Q > 0$, X, *and* Y *such that*

$$\begin{aligned} \min \quad & \operatorname{trace}\ \{QP_1\}, \\ s.t. \quad & (42a), (42b), (42c), (42d) \end{aligned} \tag{41}$$

$$QE^T = EQ \geq 0, \tag{42a}$$

$$\overline{E}^TP_2 = P_2^T\overline{E} \geq 0, \tag{42b}$$

$$\begin{bmatrix} \Pi_1 & 0 & H & 0 & QC^T & GX & GV \\ \star & \Pi_2 & 0 & P_2^T\overline{H} & 0 & 0 & 0 \\ \star & \star & -\gamma^2I & 0 & 0 & 0 & 0 \\ \star & \star & \star & -\gamma^2I & 0 & 0 & 0 \\ \star & \star & \star & \star & -I & 0 & 0 \\ \star & \star & \star & \star & \star & -Q & 0 \\ \star & \star & \star & \star & \star & \star & -I \end{bmatrix} < 0, \tag{42c}$$

$$\begin{bmatrix} P_1 & I \\ I & Q \end{bmatrix} \geq 0 \tag{42d}$$

with

$$\begin{aligned}\Pi_1 &\triangleq AQ + GX + (AQ + GX)^T,\\ \Pi_2 &\triangleq P_2^T\overline{A} + Y\overline{D} + \left(P_2^T\overline{A} + Y\overline{D}\right)^T + \operatorname{diag}\{P_1, I\}.\end{aligned} \tag{43}$$

Moreover, if the previous conditions are feasible, the gains of the desired observer in the form of (7a) *and* (7b) *without jumping parameters and the desired controller in the form of* (10) *without jumping parameters are given by*

$$K = XQ^{-1}, \qquad L = P_2^{-T}Y. \tag{44}$$

Remark 9. To the best of the authors' knowledge, this is also the first time that the full-order disturbance-observer-based control strategy is applied in the singular system with multiple disturbances.

4. Numerical Example

In this section, a numerical example is given to illustrate the effectiveness of the proposed approaches. Consider the systems in (1a), (1b), and (3) with the following parameters:

$$\begin{aligned}A_1 &= \begin{bmatrix}-2.2 & 1.2\\ -0.9 & -0.2\end{bmatrix}, \quad G_1 = \begin{bmatrix}-0.1\\ 0.1\end{bmatrix},\\ H_1 &= \begin{bmatrix}0.2\\ 0.1\end{bmatrix}, \quad E = \begin{bmatrix}1.0 & 0\\ 0 & 0\end{bmatrix},\\ C_1 &= \begin{bmatrix}0.1 & 0.1\end{bmatrix}, \quad D_{11} = \begin{bmatrix}0.1 & 0\\ 0 & 0.1\end{bmatrix},\\ D_{21} &= \begin{bmatrix}0.1\\ 0.1\end{bmatrix}, \quad W_1 = \begin{bmatrix}0 & 0.2\\ -0.2 & 0\end{bmatrix},\\ V_1 &= \begin{bmatrix}3.0 & 0\end{bmatrix}, \quad M_1 = \begin{bmatrix}0.2\\ 0.4\end{bmatrix},\\ A_2 &= \begin{bmatrix}-1.2 & 0.5\\ 0.2 & -0.8\end{bmatrix}, \quad G_2 = \begin{bmatrix}0.1\\ 0.3\end{bmatrix},\\ C_2 &= \begin{bmatrix}0.2 & 0.1\end{bmatrix}, \quad D_{12} = \begin{bmatrix}0.05 & 0\\ 0 & 0.1\end{bmatrix},\\ D_{22} &= \begin{bmatrix}0.1\\ 0.1\end{bmatrix}, \quad H_2 = \begin{bmatrix}0.2\\ 1.0\end{bmatrix},\\ W_2 &= \begin{bmatrix}0 & 0.5\\ -0.5 & 0\end{bmatrix}, \quad V_2 = \begin{bmatrix}1.0 & 0\end{bmatrix}, \quad M_2 = \begin{bmatrix}0.1\\ 0.3\end{bmatrix}.\end{aligned} \tag{45}$$

The transition probability matrix is assumed to be $\Pi = \left[\begin{smallmatrix}-0.5 & 0.5\\ 1.0 & -1.0\end{smallmatrix}\right]$, and γ is set to be $\gamma = 1$. Our intention here is to design reduced-order-observer-based controller in the form of (7a), (7b), and (10), such that the composite system is stochastically admissible and satisfies prescribed $\mathscr{H}_\infty$ performance. We resort to the LMI Toolbox in MATLAB to solve the problems established in (38), and the gains of the desired observer and controller are given by

$$\begin{aligned}K_1 &= \begin{bmatrix}0.5657 & -9.2561\end{bmatrix}, \qquad K_2 = \begin{bmatrix}-0.0461 & -3.2981\end{bmatrix},\\ L_1 &= \begin{bmatrix}-1.7020 & 2.8579\\ -4.2366 & 2.7401\\ -3.9409 & -4.4407\\ -5.3114 & -10.7753\end{bmatrix},\\ L_2 &= \begin{bmatrix}35.2258 & -19.4542\\ 119.1428 & -95.2410\\ -22.2709 & -0.0573\\ -42.1632 & -0.2238\end{bmatrix}.\end{aligned} \tag{46}$$

5. Conclusion

The problem of disturbance-observer-based control for Markovian jump singular systems with multiple disturbance has been studied. Full-order observer- (both disturbance and system states) based controller has been constructed. The explicit expression of the desired disturbance-observer-based controller has also been presented. Finally, the proposed methods have been verified by a numerical example.

Acknowledgments

This work was supported in part by the Major State Basic Research Development Program of China (973 Program) under Grant 2012CB720003, by the National Natural Science Foundation of China under Grants 61203041, 61127007, and 61121003, by the Chinese National Postdoctor Science Foundation under Grants 2011M500217 and 2012T50036, by the Doctoral Fund of Ministry of Education of China under Grant 20120036120013, and by the Fundamental Research Funds for the Central Universities under Grant 11QG70.

References

[1] E. Uezato and M. Ikeda, "Strict LMI conditions for stability, robust stabilization, and $\mathscr{H}_\infty$ control of descriptor systems," in *Proceedings of the 38th IEEE Conference on Decision and Control (CDC '99)*, pp. 4092–4097, Phoenix, Ariz, USA, December 1999.

[2] L. Dai, *Singular Control Systems*, vol. 118 of *Lecture Notes in Control and Information Sciences*, Springer, Berlin, Germany, 1989.

[3] Z. Wu, H. Su, P. Shi, and J. Chu, *Analysis and Synthesis of Singular Systems with Time-Delays*, Springer, Berlin, Germany, 2013.

[4] S. Xu, P. Van Dooren, R. Ştefan, and J. Lam, "Robust stability and stabilization for singular systems with state delay and parameter uncertainty," *Institute of Electrical and Electronics Engineers*, vol. 47, no. 7, pp. 1122–1128, 2002.

[5] S. Xu and C. Yang, "$\mathscr{H}_\infty$ state feedback control for discrete singular systems," *Institute of Electrical and Electronics Engineers*, vol. 45, no. 7, pp. 1405–1409, 2000.

[6] S. Xu and J. Lam, *Robust Control and Filtering of Singular Systems*, vol. 332 of *Lecture Notes in Control and Information Sciences*, Springer, Berlin, Germany, 2006.

[7] S. Xu and J. Lam, "Robust stability and stabilization of discrete singular systems: an equivalent characterization," *Institute of Electrical and Electronics Engineers*, vol. 49, no. 4, pp. 568–574, 2004.

[8] W.-H. Chen, "Disturbance observer based control for nonlinear systems," *IEEE/ASME Transactions on Mechatronics*, vol. 9, no. 4, pp. 706–710, 2004.

[9] W.-H. Chen, "Nonlinear disturbance observer-enhanced dynamic inversion control of missiles," *Journal of Guidance, Control, and Dynamics*, vol. 26, no. 1, pp. 161–166, 2003.

[10] L. Guo and W.-H. Chen, "Disturbance attenuation and rejection for systems with nonlinearity via DOBC approach," *International Journal of Robust and Nonlinear Control*, vol. 15, no. 3, pp. 109–125, 2005.

[11] L. Guo and X.-Y. Wen, "Hierarchical anti-disturbance adaptive control for non-linear systems with composite disturbances and applications to missile systems," *Transactions of the Institute of Measurement and Control*, vol. 33, no. 8, pp. 942–956, 2011.

[12] M. Iwasaki, T. Shibata, and N. Matsui, "Disturbance-observer-based nonlinear friction compensation in table drive system," *IEEE/ASME Transactions on Mechatronics*, vol. 4, no. 1, pp. 3–8, 1999.

[13] R. Zhang, L. Tao, and L. Guo, "Disturbance observer based $\mathscr{H}_\infty$ control for flexible spacecraft with time-varying input delay," *Advances in Difference Equations*, vol. 2013, article 142, 2013.

[14] L. Wu, P. Shi, and H. Gao, "State estimation and sliding-mode control of Markovian jump singular systems," *Institute of Electrical and Electronics Engineers*, vol. 55, no. 5, pp. 1213–1219, 2010.

[15] L. Wu, X. Su, and P. Shi, "Sliding mode control with bounded $\mathscr{L}_2$ gain performance of Markovian jump singular time-delay systems," *Automatica*, vol. 48, no. 8, pp. 1929–1933, 2012.

[16] Z.-G. Wu, P. Shi, H. Su, and J. Chu, "l_2-l_∞ filter design for discrete-time singular Markovian jump systems with time-varying delays," *Information Sciences*, vol. 181, no. 24, pp. 5534–5547, 2011.

[17] T. Li, L. Guo, C. Sun, and C. Lin, "Further results on delay-dependent stability criteria of neural networks with time-varying delays," *IEEE Transactions on Neural Networks*, vol. 19, no. 4, pp. 726–730, 2008.

[18] T. Li and L. Guo, "Optimal fault-detection filtering for non-Gaussian systems via output PDFs," *IEEE Transactions on Systems, Man, and Cybernetics Part A*, vol. 39, no. 2, pp. 476–481, 2009.

[19] M. Darouach, L. Boutat-Baddas, and M. Zerrougui, "$\mathscr{H}_\infty$ observers design for a class of nonlinear singular systems," *Automatica*, vol. 47, no. 11, pp. 2517–2525, 2011.

[20] L. El Ghaoui, F. Oustry, and M. AitRami, "A cone complementarity linearization algorithm for static output-feedback and related problems," *Institute of Electrical and Electronics Engineers*, vol. 42, no. 8, pp. 1171–1176, 1997.

Hindawi Publishing Corporation
Mathematical Problems in Engineering
Volume 2013, Article ID 494218, 7 pages
http://dx.doi.org/10.1155/2013/494218

Research Article

Robust Adaptive Synchronization of the Energy Resource System with Constraint

Duo Meng

School of Civil and Architectural Engineering, Liaoning University of Technology, Jinzhou 121001, China

Correspondence should be addressed to Duo Meng; mengduo2004@163.com

Received 18 May 2013; Accepted 5 June 2013

Academic Editor: Tao Li

Two different chaos synchronization methods are proposed for a class of energy resource demand supply-system with input constraint. Firstly, chaotic synchronization is achieved for a class of energy resource demand supply system with known system parameters based on the Lyapunov theory. Secondly, an adaptive control approach is investigated for a class of energy resource demand supply system with input constraint, and the parameters of the system are unknown based on the Lyapunov stability and robust adaptive theory. To address the input constraint, new auxiliary signals and design systems are employed. Numerical simulations are provided to illustrate the effectiveness of the proposed approach.

1. Introduction

Energy resource system is a kind of complex nonlinear system. Energy resource including coal, petroleum, natural gas, water and electricity, and nuclear power can be classified as renewable energy and nonrenewable energy according to the capability of sustainable utilization. The issue of energy supply and demand has been valued worldwide with increasing development of economy. One of the most noticeable problems in the field of energy resource is how to study energy resource system deeply through nonlinear dynamics, which is currently a rapid developing method [1].

Reference [2] established a three-dimensional energy resource demand-supply system based on the real energy resources demand-supply in the East and the West of China. Furthermore, by adding a new variable to consider the renewable resources, a four-dimensional energy resource system was proposed in [3]. The dynamics behaviors of the four-dimensional energy resource system have been analyzed by means of the Lyapunov exponents and bifurcation diagrams. Also the same as the above-mentioned power systems, this four-dimensional energy resource system is with rich chaos behaviors. The problem of chaotic control for the energy resource system was considered in [1]. Feedback control and adaptive control methods were used to suppress chaos to unstable equilibrium or unstable periodic orbits, where only three of the system's parameters were supposed to be unknown. Reference [4] investigated the robust chaos synchronization problem for the four-dimensional energy resource systems based on the sliding mode control technique. The control of energy resource chaotic system was investigated by time delayed feedback control method in [5]. Based on stability criterion of linear system and Lyapunov stability theory, respectively, the chaos synchronization problems for energy resource demand-supply system were discussed using two novel different control methods in [6].

Although the adaptive synchronization control has achieved a great progress, the aforementioned control approaches assume that all the components of the considered energy resource demand-supply systems are in good operating conditions. As we know, many control systems have constraints on their inputs in the forms of input saturation or dead zone [7–17]. In practice, input saturation constraint is one of the most important input constraints which usually appear in many industries control systems. There are two main motivations for the saturation studies. One is that saturation is a potential problem for actuators of control systems. It often severely degrades the system performance, gives rise to undesirable inaccuracy, or even affects system stability. The other is that the control actions are usually limited in energy or magnitude; the saturation of the control output is necessary in practice.

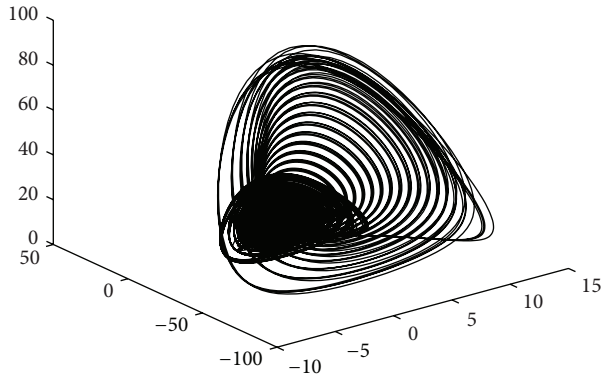

Figure 1: Energy resource attractor.

Motivated by the above observations, two different chaos synchronization control methods are proposed for a class of energy resource demand-supply system with input constraint. Based on Lyapunov stability and robust adaptive theory, on the assumption that all the parameters of the system are known and unknown, nonadaptive and adaptive control approaches are proposed to make the states of two chaotic systems asymptotic synchronization. The main contributions of the proposed algorithm are that (i) the problems of the input constraint are solved by employing a new auxiliary system; (ii) the stability of the energy resource demand-supply system is guaranteed based on the Lyapunov theory.

2. Energy Resource Chaotic System

In the paper, we consider the following energy resource system (see [2, 6]):

$$\begin{aligned} \dot{x} &= a_1 x\left(1-\frac{x}{M}\right)-a_2\left(y+z\right), \\ \dot{y} &= -b_1 y-b_2 z+b_3 x\left[N-\left(x-z\right)\right], \\ \dot{z} &= c_1 z\left(c_2 x-c_3\right), \end{aligned} \tag{1}$$

where $x(t)$ is the energy resource shortage in A region, $y(t)$ is the energy resource supply increment in B region, and $z(t)$ is the energy resource import in A region; M, N, a_i, b_j ($i = 1, 2$, $j = 1, 2, 3$) are parameters that are all positive real.

Similar to [6], when the system parameters are taken as the following values, this system exhibits chaotic behavior: $M = 1.8$, $N = 1$, $a_1 = 0.09$, $a_2 = 0.15$, $b_1 = 0.06$, $b_2 = 0.082$, $b_3 = 0.07$, $c_1 = 0.2$, $c_2 = 0.5$, and $c_3 = 0.4$. Without the particular statement, these values are adopted in this whole paper. Figure 1 shows the phase portrait with initial conditions of $x(0) = 0.82$, $y(0) = 0.29$, and $z(0) = 0.48$.

3. Synchronization of the Energy Resource System

In this section, we will design a controller in order to make the response system trace the drive system. In order to obtain synchronization of the energy resource system (1), the drive system with subscript 1 is written as

$$\begin{aligned} \dot{x}_1 &= a_1 x_1\left(1-\frac{x_1}{M}\right)-a_2\left(y_1+z_1\right), \\ \dot{y}_1 &= -b_1 y_1-b_2 z_1+b_3 x_1\left[N-\left(x_1-z_1\right)\right], \\ \dot{z}_1 &= c_1 z_1\left(c_2 x_1-c_3\right). \end{aligned} \tag{2}$$

The controlled response system with subscript 2 can be expressed as

$$\begin{aligned} \dot{x}_2 &= a_1 x_2\left(1-\frac{x_2}{M}\right)-a_2\left(y_2+z_2\right)+u_1\left(v_1\left(t\right)\right), \\ \dot{y}_2 &= -b_1 y_2-b_2 z_2+b_3 x_2\left[N-\left(x_2-z_2\right)\right]+u_2\left(v_2\left(t\right)\right), \\ \dot{z}_2 &= c_1 z_2\left(c_2 x_2-c_3\right)+u_3\left(v_3\left(t\right)\right), \end{aligned} \tag{3}$$

where v_i ($i = 1, 2, 3$) is the controller inputs to be designed, $u_i(v_i(t))$ ($i = 1, 2, 3$) denotes the plant input subject to saturation type nonlinearly.

Remark 1. If no input saturation (i.e., $u_i(v_i(t)) = v_i(t)$) ($i = 1, 2, 3$) is included in (3), then (3) becomes the chaotic systems studied widely; see [2, 6].

$u(v(t))$ is described by

$$\begin{aligned} u_i\left(v_i\left(t\right)\right) &= \operatorname{sat}\left(v_i\left(t\right)\right) \\ &= \begin{cases} \operatorname{sign}\left(v_i\left(t\right)\right)u_M, & \left|v_i\left(t\right)\right| \geq u_{iM}, \\ v_i\left(t\right), & \left|v_i\left(t\right)\right| < u_{iM}, \end{cases} \end{aligned} \tag{4}$$

where u_{iM} is a known bound of $u_i(v_i(t))$. Clearly, the relationship between the applied control $u_i(v_i(t))$ and the control input $v_i(t)$ has a sharp corner when $|v_i(t)| = u_{iM}$. Similar to [15], define

$$\begin{aligned} e_1 &= x_2-x_1-h_1, \\ e_2 &= y_2-y_1-h_2, \\ e_3 &= z_2-z_1-h_3, \end{aligned} \tag{5}$$

where h_i ($i = 1, 2, 3$) are filter signals and will be given later.

By using (2), (3), and (5), the error dynamical system can be written as

$$\begin{aligned} \dot{e}_1 &= -\dot{h}_1+a_1 e_1-a_2\left(e_2+e_3\right)-\frac{a_1 x_2^2}{M}+\frac{a_1 x_1^2}{M} \\ &\quad +a_1 h_1+a_2\left(h_2+h_3\right)+u_1\left(v_1\left(t\right)\right), \\ \dot{e}_2 &= -\dot{h}_2-b_1 e_2-b_2 e_3+b_3 N e_1-b_3 x_2^2 \\ &\quad +b_3 x_1^2+b_3 x_2 z_2-b_3 x_1 z_1+b_1 h_2 \\ &\quad +b_2 h_3-b_3 N h_1+u_2\left(v_2\left(t\right)\right), \\ \dot{e}_3 &= -\dot{h}_3-c_1 c_3 e_3+c_1 c_2 x_2 z_2 \\ &\quad -c_1 c_2 x_1 z_1+c_1 c_3 h_3+u_3\left(v_3\left(t\right)\right). \end{aligned} \tag{6}$$

Similar to [18, 19], choose Lyapunov function candidate V as

$$V = \frac{1}{2}e_1^2 + \frac{1}{2}e_2^2 + \frac{1}{2}e_3^2. \tag{7}$$

The time derivative of V is

$$\dot{V} = e_1\dot{e}_1 + e_2\dot{e}_2 + e_3\dot{e}_3. \tag{8}$$

Define the dynamic system as

$$\dot{h}_i = -h_i + (u_i - v_i), \quad i = 1, 2, 3. \tag{9}$$

Substituting (6) and (9) into (8) results in

$$\begin{aligned}\dot{V} = {} & e_1\left[h_1 + v_1 + a_1e_1 - a_2(e_2 + e_3) - \frac{a_1x_2^2}{M}\right.\\ & \left. + \frac{a_1x_1^2}{M} + a_1h_1 + a_2(h_2 + h_3)\right]\\ & + e_2\left[h_2 + v_2 - b_1e_2 - b_2e_3 + b_3Ne_1\right.\\ & - b_3x_2^2 + b_3x_1^2 + b_3x_2z_2 - b_3x_1z_1\\ & \left. + b_1h_2 + b_2h_3 - b_3Nh_1 + u_2\right]\\ & + e_3\left[h_3 + v_3 - c_1c_3e_3 + c_1c_2x_2z_2\right.\\ & \left. - c_1c_2x_1z_1 + c_1c_3h_3\right].\end{aligned} \tag{10}$$

By using Young's inequality, we have

$$\begin{aligned}-a_2e_1(e_2 + e_3) &\le a_2^2e_1^2 + \frac{1}{2}e_2^2 + \frac{1}{2}e_3^2,\\ e_2\left[-b_2e_3 + b_3Ne_1\right] &\le \frac{b_2^2 + b_3^2N^2}{2}e_2^2 + \frac{1}{2}e_3^2 + \frac{1}{2}e_1^2.\end{aligned} \tag{11}$$

Substituting (11) into (10) results in

$$\begin{aligned}\dot{V} \le {} & \left(a_1 + a_2^2 + \frac{1}{2}\right)e_1^2 + \left(b_1 + \frac{1}{2} + \frac{b_2^2 + b_3^2N^2}{2}\right)e_2^2\\ & + (1 - c_1c_3)e_3^2\\ & + e_1\left[h_1 + v_1 - \frac{a_1x_2^2}{M} + \frac{a_1x_1^2}{M} + a_1h_1 + a_2(h_2 + h_3)\right]\\ & + e_2\left[h_2 + v_2 - b_3x_2^2 + b_3x_1^2 + b_3x_2z_2 - b_3x_1z_1\right.\\ & \left. + b_1h_2 + b_2h_3 - b_3Nh_1\right]\\ & + e_3\left[h_3 + v_3 + c_1c_2x_2z_2 - c_1c_2x_1z_1 + c_1c_3h_3\right].\end{aligned} \tag{12}$$

Choose the actual controllers v_i

$$\begin{aligned}v_1 = {} & -l_1e_1 - h_1 + \frac{a_1x_2^2}{M} - \frac{a_1x_1^2}{M} - a_1h_1 - a_2(h_2 + h_3),\\ v_2 = {} & -l_2e_2 - h_2 + b_3x_2^2 - b_3x_1^2 - b_3x_2z_2\\ & + b_3x_1z_1 - b_1h_2 - b_2h_3 + b_3Nh_1,\\ v_3 = {} & -l_3e_3 - h_3 - c_1c_2x_2z_2 + c_1c_2x_1z_1 - c_1c_3h_3,\end{aligned} \tag{13}$$

where l_i $(i = 1, 2, 3)$ are positive design parameters. Substituting (13) into (12) results in

$$\begin{aligned}\dot{V} \le {} & -\left(l_1 - a_1 - a_2^2 - \frac{1}{2}\right)e_1^2\\ & - \left(l_2 - b_1 - \frac{1}{2} - \frac{b_2^2 + b_3^2N^2}{2}\right)e_2^2 - (l_3 + c_1c_3 - 1)e_3^2.\end{aligned} \tag{14}$$

Let l_i satisfy $l_1 > a_1 + a_2^2 + 1/2$, $l_2 > b_1 + 1/2 + (b_2^2 + b_3^2N^2)/2$, and $l_3 + c_1c_3 > 1$. We can obtain $\dot{V} \le 0$, and it is concluded that e_1, e_2, and e_3 converge to zero as time t tends to infinity. Therefore, the synchronization of response systems (3) and the drive system (2) is finally achieved.

Remark 2. It is noted that the controller in [6] was designed by using the stability criterion of linear system, not based on Lyapunov stability theory. However, this paper designed the control laws based on Lyapunov method. This paper can use a constructive way to obtain the control laws for this class of energy resource demand-supply system. In addition, the control laws' design parameters of this paper have fewer restrictions compared to [6].

4. Simulation Results 1

In this section, the initial values of are chosen as $x_1(0) = 0.82$, $y_1(0) = 0.29$, $z_1(0) = 0.48$, $x_2(0) = 0.69$, $y_2(0) = -0.03$, $z_2(0) = 1.25$. The saturation values are $u_{1M} = 0.5$, $u_{2M} = 2$, and $u_{3M} = 2$. The design parameters in controllers are chosen as $l_1 = 20$, $l_2 = 10$, and $l_3 = 10$. The simulation results are shown in Figures 2, 3, 4, and 5.

5. Adaptive Synchronization of the Energy Resource System

In this section, we assume that all the parameters of the energy resource system are unknown. For convenience, we define $a_3 = a_1/M$, $b_4 = b_3N$, $d_1 = c_1c_2$, and $d_2 = c_1c_3$. The energy resource system (1) can be rewritten as:

$$\begin{aligned}\dot{x} &= a_1x - a_2(y + z) - a_3x^2,\\ \dot{y} &= -b_1y - b_2z - b_3x(x - z) + b_4x,\\ \dot{z} &= d_1xz - d_2z\end{aligned} \tag{15}$$

and the drive system can be also rewritten as

$$\begin{aligned}\dot{x}_1 &= a_1x_1 - a_2(y_1 + z_1) - a_3x_1^2,\\ \dot{y}_1 &= -b_1y_1 - b_2z_1 - b_3x_1(x_1 - z_1) + b_4x_1,\\ \dot{z}_1 &= d_1x_1z_1 - d_2z_1.\end{aligned} \tag{16}$$

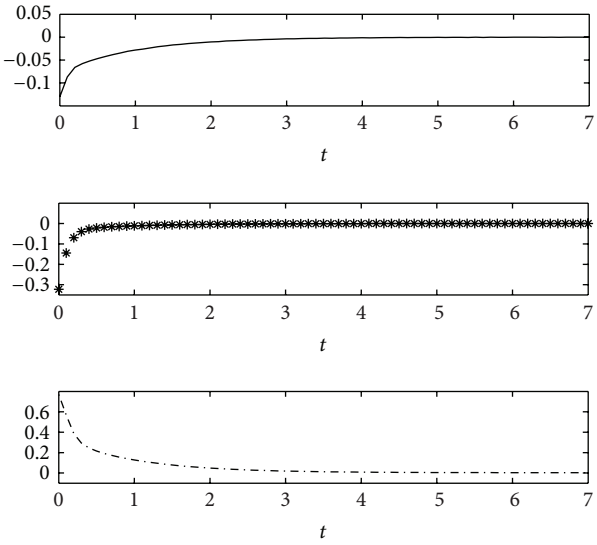

Figure 2: The trajectories of e_1 (solid line), e_2 (star line), and e_3 (dash-dotted line).

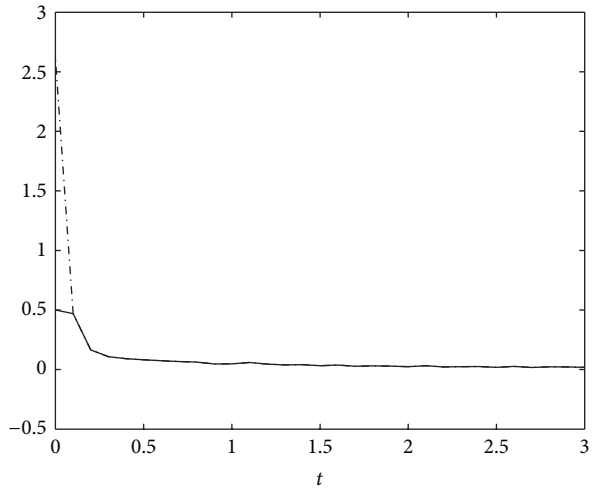

Figure 3: The trajectories of v_1 (solid line) and u_1 (dash-dotted line).

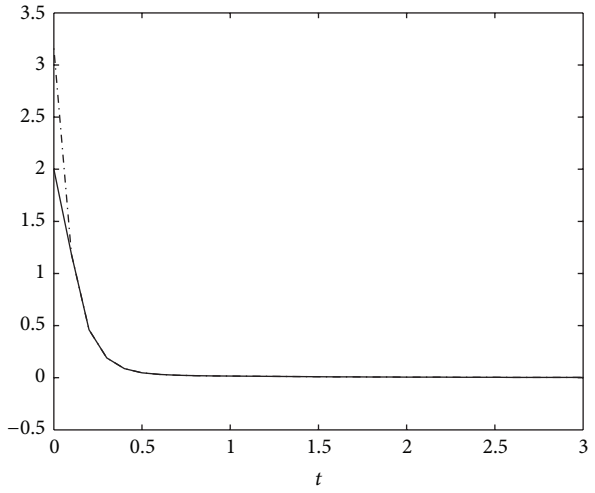

Figure 4: The trajectories of v_2 (solid line) and u_2 (dash-dotted line).

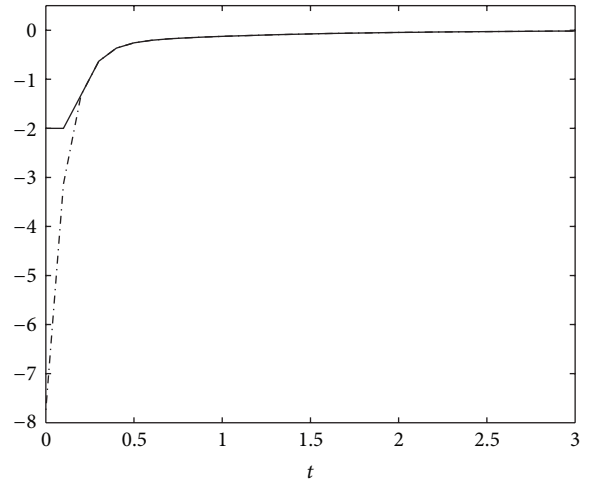

Figure 5: The trajectories of v_3 (solid line) and u_3 (dash-dotted line).

The response system can be expressed as

$$\begin{aligned}\dot{x}_2 &= a_1 x_2 - a_2 (y_2 + z_2) - a_3 x_2^2 + u_1 (v_1(t)),\\ \dot{y}_2 &= -b_1 y_2 - b_2 z_2 - b_3 x_2 (x_2 - z_2) + b_4 x_2 + u_2 (v_2(t)),\\ \dot{z}_2 &= d_1 x_2 z_2 - d_2 z_2 + u_3 (v_3(t)).\end{aligned} \tag{17}$$

Choose the same errors e_i as (5) and the same filter signals h_i as (9), and we have

$$\begin{aligned}\dot{e}_1 = {} & -\dot{h}_1 + a_1 e_1 - a_2 (e_2 + e_3) - a_3 x_2^2 + a_3 x_1^2\\ & + a_1 h_1 + a_2 (h_2 + h_3) + u_1 (v_1(t)),\\ \dot{e}_2 = {} & -\dot{h}_2 - b_1 e_2 - b_2 e_3 + b_4 e_1 - b_3 x_2^2 + b_3 x_1^2 + b_3 x_2 z_2\\ & - b_3 x_1 z_1 + b_1 h_2 + b_2 h_3 - b_4 h_1 + u_2 (v_2(t)),\\ \dot{e}_3 = {} & -\dot{h}_3 - d_2 e_3 + d_1 x_2 z_2 - d_2 x_1 z_1 + d_1 h_3 + u_3 (v_3(t)).\end{aligned} \tag{18}$$

Choose the Lyapunov function candidate $\overline{V}$ as

$$\begin{aligned}\overline{V} = \frac{1}{2} \Big(& e_1^2 + e_2^2 + e_3^2 + \widetilde{a}_1^2 + \widetilde{a}_2^2 + \widetilde{a}_3^2 + \widetilde{b}_1^2 + \widetilde{b}_2^2\\ & + \widetilde{b}_3^2 + \widetilde{b}_4^2 + \widetilde{d}_1^2 + \widetilde{d}_2^2 \Big),\end{aligned} \tag{19}$$

where $\widetilde{a}_i = a_i - \widehat{a}_i$ $(i = 1, 2, 3)$, $\widetilde{b}_j = b_j - \widehat{b}_j$ $(j = 1, 2, 3, 4)$, and $\widetilde{d}_k = d_k - \widehat{d}_k$ $(k = 1, 2)$.

The time derivative of $\overline{V}$ along with the solution of (18) is

$$\begin{aligned}\dot{\overline{V}} = {} & e_1 \left[h_1 + v_1 + \widehat{a}_1 e_1 - \widehat{a}_2 (e_2 + e_3) - \widehat{a}_3 x_2^2 \right.\\ & \left. + \widehat{a}_3 x_1^2 + \widehat{a}_1 h_1 + \widehat{a}_2 (h_2 + h_3) \right]\\ & + e_2 \left[h_2 + v_2 - \widehat{b}_1 e_2 - \widehat{b}_2 e_3 + \widehat{b}_4 e_1 - \widehat{b}_3 x_2^2 \right.\\ & \left. + \widehat{b}_3 x_1^2 + \widehat{b}_3 x_2 z_2 - \widehat{b}_3 x_1 z_1 + \widehat{b}_1 h_2 + \widehat{b}_2 h_3 - \widehat{b}_4 h_1 \right]\\ & + e_3 \left[h_3 + v_3 - \widehat{d}_2 e_3 + \widehat{d}_1 x_2 z_2 - \widehat{d}_2 x_1 z_1 + \widehat{d}_1 h_3 \right]\end{aligned}$$

$$
\begin{aligned}
&+ \tilde{a}_1 \left(e_1 h_1 + e_1^2 - \dot{\hat{a}}_1\right) \\
&+ \tilde{a}_2 \left(-\left(e_2 + e_3\right) e_1 + \left(h_2 + h_3\right) e_1 - \dot{\hat{a}}_2\right) \\
&+ \tilde{a}_3 \left(-e_1 x_2^2 + e_1 x_1^2 + e_1 h_1 + e_1 \left(h_2 + h_3\right) - \dot{\hat{a}}_3\right) \\
&+ \tilde{b}_1 \left(-e_2^2 + e_2 h_2 - \dot{\hat{b}}_1\right) + \tilde{b}_2 \left(-e_2 e_3 + e_2 h_3 - \dot{\hat{b}}_2\right) \\
&+ \tilde{b}_3 \left(-e_2 x_2^2 + e_2 x_1^2 + e_2 x_2 z_2 - e_2 x_1 z_1 - \dot{\hat{b}}_3\right) \\
&+ \tilde{b}_4 \left(e_1 e_2 - e_2 h_1 - \dot{\hat{b}}_4\right) \\
&+ \tilde{d}_1 \left(e_3 x_2 z_2 + e_3 h_3 - \dot{\hat{d}}_1\right) + \tilde{d}_2 \left(-e_3^2 - e_3 x_1 z_1 - \dot{\hat{d}}_2\right).
\end{aligned} \tag{20}
$$

Choose the actual controllers v_i and update the laws of $\hat{a}_i$ ($i = 1, 2, 3$), $\hat{b}_j$ ($j = 1, 2, 3, 4$), and $\hat{d}_k$ ($k = 1, 2$) as follows:

$$
\begin{aligned}
v_1 = & -\bar{l}_1 e_1 - h_1 - \hat{a}_1 e_1 + \hat{a}_2 \left(e_2 + e_3\right) \\
& + \hat{a}_3 x_2^2 - \hat{a}_3 x_1^2 - \hat{a}_1 h_1 - \hat{a}_2 \left(h_2 + h_3\right), \\
v_2 = & -\bar{l}_2 e_2 - h_2 + \hat{b}_1 e_2 + \hat{b}_2 e_3 - \hat{b}_4 e_1 + \hat{b}_3 x_2^2 - \hat{b}_3 x_1^2 \\
& - \hat{b}_3 x_2 z_2 + \hat{b}_3 x_1 z_1 - \hat{b}_1 h_2 - \hat{b}_2 h_3 + \hat{b}_4 h_1, \\
v_3 = & -\bar{l}_3 e_3 - h_3 + \hat{d}_2 e_3 - \hat{d}_1 x_2 z_2 + \hat{d}_2 x_1 z_1 - \hat{d}_1 h_3,
\end{aligned} \tag{21}
$$

where $\bar{l}_i$ ($i = 1, 2, 3$) are positive design parameters:

$$
\begin{aligned}
\dot{\hat{a}}_1 &= e_1 h_1 + e_1^2, \\
\dot{\hat{a}}_2 &= -\left(e_2 + e_3\right) e_1 + \left(h_2 + h_3\right) e_1, \\
\dot{\hat{a}}_3 &= -e_1 x_2^2 + e_1 x_1^2 + e_1 h_1 + e_1 \left(h_2 + h_3\right), \\
\dot{\hat{b}}_1 &= -e_2^2 + e_2 h_2, \\
\dot{\hat{b}}_2 &= -e_2 e_3 + e_2 h_3, \\
\dot{\hat{b}}_3 &= -e_2 x_2^2 + e_2 x_1^2 + e_2 x_2 z_2 - e_2 x_1 z_1, \\
\dot{\hat{b}}_4 &= e_1 e_2 - e_2 h_1, \\
\dot{\hat{d}}_1 &= e_3 x_2 z_2 + e_3 h_3, \\
\dot{\hat{d}}_2 &= -e_3^2 - e_3 x_1 z_1.
\end{aligned} \tag{22}
$$

Substituting (21) and (22) into (20) results in

$$
\dot{\bar{V}} = -\bar{l}_1 e_1^2 - \bar{l}_2 e_2^2 - \bar{l}_3 e_3^2. \tag{23}
$$

From (23), we can conclude that the states x_2, y_2, and z_2 of response system (17) and the states x_1, y_1, and z_1 of drive system (16) are ultimately synchronized asymptotically.

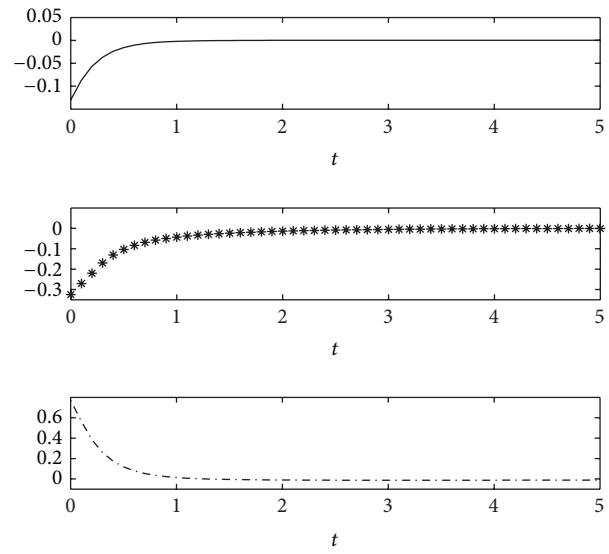

Figure 6: The trajectories of e_1 (solid line), e_2 (star line), and e_3 (dash-dotted line).

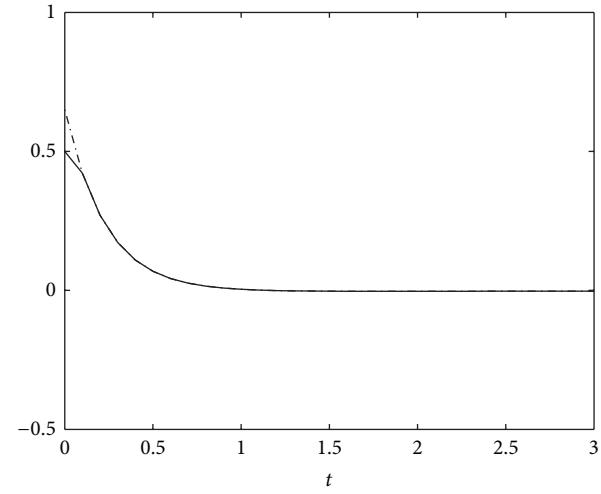

Figure 7: The trajectories of v_1 (solid line) and u_1 (dash-dotted line).

6. Simulation Results 2

In this section, the initial values are chosen as $x_1(0) = 0.82$, $y_1(0) = 0.29$, $z_1(0) = 0.48$, $x_2(0) = 0.69$, $y_2(0) = -0.03$, and $z_2(0) = 1.25$, and the other initial values are chosen as zeros. The saturation values are $u_{1M} = 0.5$, $u_{2M} = 0.5$, and $u_{3M} = 2$. The design parameters in controllers are $\bar{l}_1 = 5$, $\bar{l}_2 = 4$, and $\bar{l}_3 = 4$. The simulation results are shown in Figures 6, 7, 8, and 9.

7. Conclusions

For a class of known and unknown parameters for energy resource demand-supply system with input constraints, the chaos synchronization problems have been discussed using two different control methods, respectively. The main features

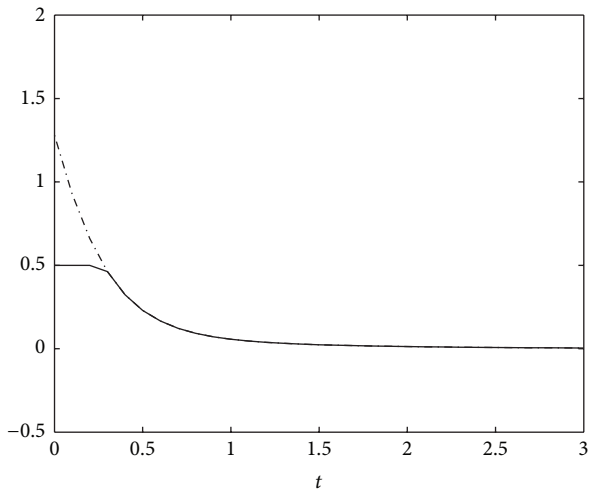

Figure 8: The trajectories of v_2 (solid line) and u_2 (dash-dotted line).

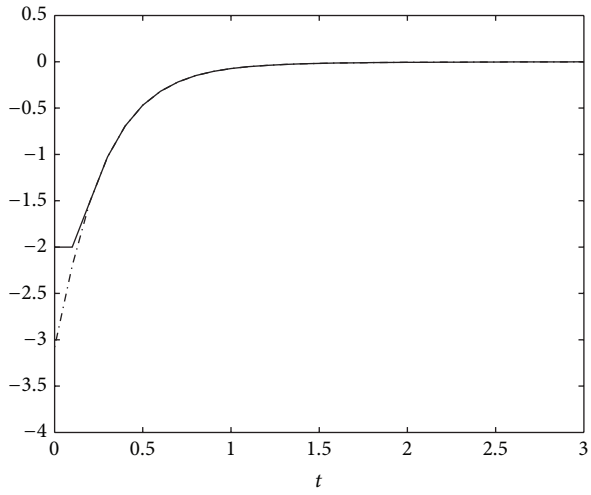

Figure 9: The trajectories of v_3 (solid line) and u_3 (dash-dotted line).

of the proposed algorithm are that (i) the problems of the input constraint have been solved by employing a new auxiliary system; (ii) the stability of the energy resource demand-supply system has been guaranteed based on Lyapunov theory. The results all have demonstrated the validity and feasibility of the proposed approaches.

Acknowledgment

This work was supported by the Foundation of Liaoning Educational Committee (no. L2012225).

References

[1] M. Sun, L. Tian, Y. Fu, and W. Qian, "Dynamics and adaptive synchronization of the energy resource system," *Chaos, Solitons and Fractals*, vol. 31, no. 4, pp. 879–888, 2007.

[2] M. Sun, L. Tian, and Y. Fu, "An energy resources demand-supply system and its dynamical analysis," *Chaos, Solitons and Fractals*, vol. 32, no. 1, pp. 168–180, 2007.

[3] M. Sun, Q. Jia, and L. Tian, "A new four-dimensional energy resources system and its linear feedback control," *Chaos, Solitons and Fractals*, vol. 39, no. 1, pp. 101–108, 2009.

[4] C. Huang, K. Cheng, and J. Yan, "Robust chaos synchronization of four-dimensional energy resource systems subject to unmatched uncertainties," *Communications in Nonlinear Science and Numerical Simulation*, vol. 14, no. 6, pp. 2784–2792, 2009.

[5] M. Sun, L. Tian, and J. Xu, "Time-delayed feedback control of the energy resource chaotic system," *International Journal of Nonlinear Science*, vol. 1, no. 3, pp. 172–177, 2006.

[6] X. Li, W. Xu, and R. Li, "Chaos synchronization of the energy resource system," *Chaos, Solitons and Fractals*, vol. 40, no. 2, pp. 642–652, 2009.

[7] A. Boulkroune, M. M'Saad, and M. Farza, "Adaptive fuzzy controller for multivariable nonlinear state time-varying delay systems subject to input nonlinearities," *Fuzzy Sets and Systems*, vol. 164, no. 1, pp. 45–65, 2011.

[8] C. Wen, J. Zhou, Z. Liu, and H. Su, "Robust adaptive control of uncertain nonlinear systems in the presence of input saturation and external disturbance," *Institute of Electrical and Electronics Engineers*, vol. 56, no. 7, pp. 1672–1678, 2011.

[9] C.-S. Ting, "A robust fuzzy control approach to stabilization of nonlinear time-delay systems with saturating inputs," *International Journal of Fuzzy Systems*, vol. 10, no. 1, pp. 50–60, 2008.

[10] S. C. Tong and Y. M. Li, "Adaptive fuzzy output feedback control of MIMO nonlinear systems with unknown dead-zone input," *IEEE Transactions on Fuzzy Systems*, vol. 21, no. 1, pp. 134–146, 2013.

[11] S. Tong and Y. Li, "Adaptive fuzzy output feedback tracking backstepping control of strict-feedback nonlinear systems with unknown dead zones," *IEEE Transactions on Fuzzy Systems*, vol. 20, no. 1, pp. 168–180, 2012.

[12] T. Li, J. Yu, and Z. Wang, "Delay-range-dependent synchronization criterion for Lur'e cprime e systems with delay feedback control," *Communications in Nonlinear Science and Numerical Simulation*, vol. 14, no. 5, pp. 1796–1803, 2009.

[13] T. Li and W. X. Zheng, "New stability criterion for fixed-point state-space digital filters with generalized overflow arithmetic," *IEEE Transactions on Circuits and Systems B*, vol. 59, no. 7, pp. 443–447, 2012.

[14] Y. Li, S. Tong, and T. Li, "Adaptive fuzzy output feedback control of uncertain nonlinear systems with unknown backlash-like hysteresis," *Information Sciences*, vol. 198, pp. 130–146, 2012.

[15] Y. M. Li, T. S. Li, and X. J. Jing, "Indirect adaptive fuzzy control for input and output constrained nonlinear systems using a barrier Lyapunov function," *International Journal of Adaptive Control and Signal Processing*, 2013.

[16] J. H. Pérez-Cruz, E. Ruiz-Velázquez, J. J. Rubio, and C. A. de Alba-Padilla, "Robust adaptive neurocontrol of SISO nonlinear systems preceded by unknown deadzone," *Mathematical Problems in Engineering*, vol. 2013, Article ID 342739, 23 pages, 2012.

[17] H. W. Zhu, G. Z. Qin, Y. X. Yan, Z. C. Jiang, and Z. S. Duan, "Delayed antiwindup control using a decoupling structure," *Mathematical Problems in Engineering*, vol. 2013, Article ID 248153, 7 pages, 2013.

[18] T. Wang, S. Tong, and Y. Li, "Robust adaptive fuzzy control for nonlinear system with dynamic uncertainties based on backstepping," *International Journal of Innovative Computing, Information and Control*, vol. 5, no. 9, pp. 2675–2688, 2009.

[19] S. Tong and Y. Li, "Observer-based fuzzy adaptive control for strict-feedback nonlinear systems," *Fuzzy Sets and Systems*, vol. 160, no. 12, pp. 1749–1764, 2009.